REVIEWS

Generation of Cytotoxic Agents by Targeted Enzymes†

Peter D. Senter,* Philip M. Wallace, Håkan P. Svensson, Vivekananda M. Vrudhula, David E. Kerr, Ingegerd Hellström, and Karl Erik Hellström

Bristol-Myers Squibb Pharmaceutical Research Institute, 3005 First Avenue, Seattle, Washington 98121.
Received July 14, 1992

A major limitation in the chemotherapeutic treatment of cancer is that anticancer drugs generally act on metabolically active or rapidly dividing cells and cannot easily distinguish between neoplastic and normal tissues (*1*). As a result, toxicities to nontarget tissues limit the amount of drug that can be administered, and cures are rarely obtained for the more common forms of cancers in adults.

Many approaches are currently being explored to improve the effectiveness and specificity of cancer chemotherapy. One method involves drug targeting, in which an anticancer agent is conjugated to a monoclonal antibody (mAb) or some other molecule that binds to antigens or receptors preferentially expressed on tumor cells (*2–6*). Although very promising results have been obtained in model studies using mAb conjugates for cancer therapy, a number of factors may limit their efficacies in the treatment of solid tumors in man. These include the heterogeneity of tumor-associated antigen expression, poor penetration of the conjugate within solid tumor masses, inefficient release of the cytotoxic agent from the carrier, and low levels of intratumoral conjugate accumulation (*4–11*).

The heterogeneous uptake of conjugates in tumors is illustrated in Figure 1, which shows histological sections of surgically removed melanoma tumors from patients who earlier received the radiolabeled antimelanoma antibody [^{131}I]-9.2.27 (*8*). The autoradiograms indicate that mAb binding was uneven, diffuse (Figure 1A), and restricted to regions in the tumor mass that were near vascular structures (Figure 1B). The fact that mAb distribution varied by as much as 17-fold within a single tumor (Figure 1B) might lead to the prediction that a great deal of variability in antitumor activity would be obtained by using conjugates that require physical contact with the cells they are intended to eliminate.

An alternative strategy is to use mAbs as delivery agents for enzymes that are capable of generating low molecular weight cytotoxic drugs from relatively noncytotoxic precursors within tumor masses (Figure 2). The drugs generated in this manner would be expected to readily diffuse. This is supported by recent studies showing that tumor interstitial transport of low molecular weight agents is quite facile compared to that of high molecular weight macromolecules (*12*). Thus, not only could enzymatic activation result in a large number of drugs generated per conjugate molecule, but the drugs formed in this manner may be able to diffuse to tumor regions that are inaccessible to the conjugate. This review will describe some of the approaches and advances in the use of targeted enzymes for the site-specific generation of cytotoxic agents.

ENZYMATIC FORMATION OF REDUCED OXYGEN SPECIES

The production of reduced oxygen species has been shown to play a role in the antineoplastic activities of chemotherapeutic agents (*13, 14*), radiation therapy (*15*), and cellular defense mechanisms (*16*). The cytotoxic agents implicated in these processes include superoxide radicals, hydroxyl radicals, and hydrogen peroxide. High-energy species such as these can also be generated under physiological conditions through the activities of certain enzymes. This has provided the basis for much research with glucose oxidase and xanthine oxidase.

The first example of a targeted enzyme that was used to generate cytotoxic agents was reported by Philpott and co-workers before the advent of mAb technology (*17*). Glucose oxidase, an enzyme that generates H_2O_2 through the oxidation of glucose, was covalently bound to a polyclonal antihapten antibody. Very little, if any, cytotoxic activity was observed on hapten-substituted cells that were treated only with the anti-hapten-glucose oxidase conjugate in media containing glucose. This might have been due to low enzyme activity or insensitivity of the target cells to H_2O_2, since other workers (*18, 19*) have shown that glucose oxidase conjugates are cytotoxic. However, when the glucose oxidase reaction was coupled to lactoperoxidase and iodide, iodine was formed, cells were iodinated, and a significant level of cytotoxicity was observed (*17*). Cellular iodination and cytotoxicity occurred in an immunologically specific manner, since nonhaptenated cells were not as sensitive to this combination of enzymes and substrates.

One of the most intriguing findings in this work was that a higher proportion of hapten-substituted cells were killed when mixed cultures originally containing equal numbers of hapten-substituted and unsubstituted cells were treated with targeted glucose oxidase, lactoperoxidase, and their respective substrates. The authors proposed that the cytotoxic entity that formed remained localized or was rapidly consumed before it could migrate to the nonconjugate-bearing bystander cells. Assuming this to be the case under in vivo conditions, it would be expected that antigen negative tumor cells or cells that are inaccessible to the conjugate in solid tumor masses might not be influenced by the cytotoxic agents formed by these enzymes. This drawback might detract from the value of targeted glucose oxidase for in vivo tumor therapy. However, it may actually prove to be advantageous for applications where a very high degree of selectivity is desired. For example, in bone marrow transplantation, it is necessary to purge the T cells from the graft marrow in the presence of myeloid precursors. Ito and co-workers

* To whom correspondence should be sent.

† Dedicated to Professor Fritz Eckstein on the occasion of his 60th birthday.

1043-1802/93/2904-0003$04.00/0 © 1993 American Chemical Society

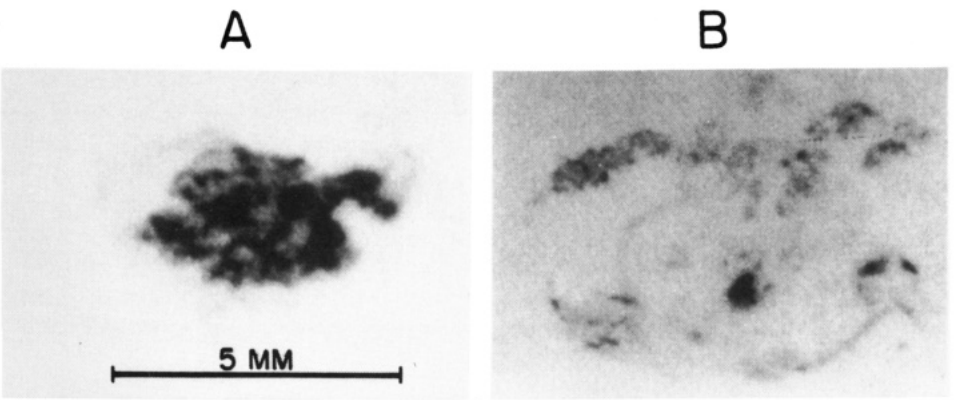


Figure 1. Heterogeneity of mAb binding. Autoradiograms obtained from histological sections of melanoma tumors from patients that received [^{131}I]-9.2.27 prior to surgery. The dark areas indicate regions of high mAb uptake (from ref 8).

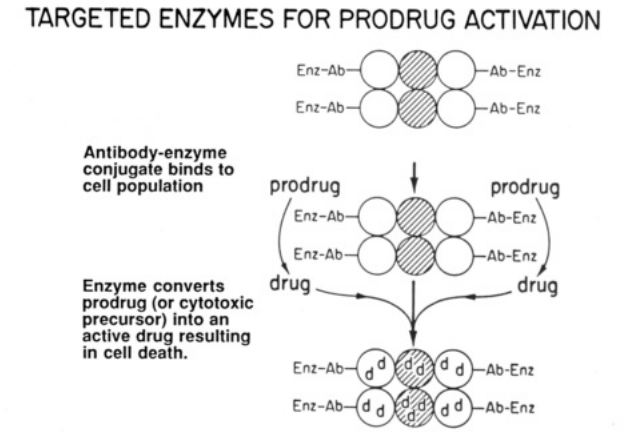


Figure 2. Generation of cytotoxic agents by targeted enzymes. Hatched circles represent cells that have not bound antibody–enzyme conjugate, and internalized drug is abbreviated with the letter "d".

covalently linked glucose oxidase and lactoperoxidase to 097, a pan-leukocyte specific mAb, and showed that the combination of conjugates with glucose and iodide was strongly cytotoxic to T cells (*20*). At low conjugate concentrations, 99.4% of the T cells were eliminated in 2 h. Significantly, the conjugates together with their substrates were noncytotoxic to myeloid precursors in human bone marrow (*20*, *21*). This is consistent with the suggestion made by Philpott and co-workers (*17*) that the product of this particular enzyme system does not migrate far from its site of formation.

Xanthine oxidase, like glucose oxidase, is also known to generate reduced oxygen species. Superoxide, H_2O_2 and under some conditions hydroxyl radical are formed when xanthine oxidase catalyzes the oxidation of hypoxanthine and xanthine (*22*, *23*). Xanthine oxidase was covalently attached to 8A, a mAb that recognizes an antigen on human plasma cells (*24*, *25*). The conjugate, together with hypoxanthine, was cytotoxic to target plasma cells and noncytotoxic to human myeloid precursors. There is evidence that the cytotoxic activity was due to the formation of reactive oxygen species, since the serum proteins, catalase and superoxide dismutase, neutralized the effects of the xanthine oxidase conjugate.

The neutralizing effect of catalase was also observed with a mAb–glucose oxidase conjugate (*18*). This could limit the utility of such conjugates as therapeutic reagents in vivo. However, glucose oxidase conjugates that are active in the presence of catalase have been reported (*26*). The insensitivity of this particular conjugate to catalase neutralization might be due to the generation of H_2O_2 intracellularly or in environments that are inaccessible to serum enzymes (*19*, *27*). Interestingly, the protective effects of catalase against H_2O_2 cytotoxicity have provided the basis for positive immunoselective procedures, in which cells that can bind antibody–catalase conjugates are spared from the toxic effects of H_2O_2 (*28*, *29*).

In summary, it appears that significant levels of cytotoxic activity can be obtained with targeted glucose oxidase and xanthine oxidase in the presence and, in some cases, in the absence of peroxidase and halide. There are indications that the toxic molecules formed exert activity in close proximity to where they are generated, and that the activity can be neutralized by serum proteins. Finally, conjugates of glucose oxidase and xanthine oxidase show promise for the selective elimination of T cells from bone marrow.

ACTIVATION OF ANTICANCER PRODRUGS

A great deal of research has been directed toward the discovery of pharmacologically inactive drug precursors (prodrugs) that can be selectively activated at tumor sites (*30–32*). This area of research has proven to be quite challenging due to similarities between neoplastic and normal tissues and the resulting difficulties in finding tumor-associated enzymes or physiological conditions for specific prodrug activation. An approach to overcome this problem has recently been described in which mAbs are used to deliver enzymes to tumor cell surfaces (*33*). The enzymes are selected for their abilities to convert relatively noncytotoxic prodrugs into active anticancer drugs. This approach is wider in scope than the previously described work with glucose and xanthine oxidases, since a variety of enzymes can be used to release a multitude of mechanistically different anticancer agents. Furthermore, since the prodrug is administered in a separate step, the timing and duration of drug release is controllable, in contrast to the oxidase systems where the substrates are normally present in the blood.

Alkaline Phosphatase. The feasibility of using mAb–enzyme conjugates for the site-specific formation of a clinically used anticancer drug was first demonstrated with the prodrug etoposide phosphate (Figure 3) and mAb conjugates of alkaline phosphatase (*34*). Etoposide phosphate, which was derived from the anticancer drug etoposide by phosphorylation, was much less cytotoxic than etoposide against H3347 human colon carcinoma (*34*), H2981 human lung adenocarcinoma (*35*), and the SW1398 human colon carcinoma (*36*) cell lines. Alkaline phosphatase rapidly converted etoposide phosphate back to etoposide.

Significant levels of antitumor activity have been obtained in vitro (*34–36*) and in vivo (*34*) with etoposide

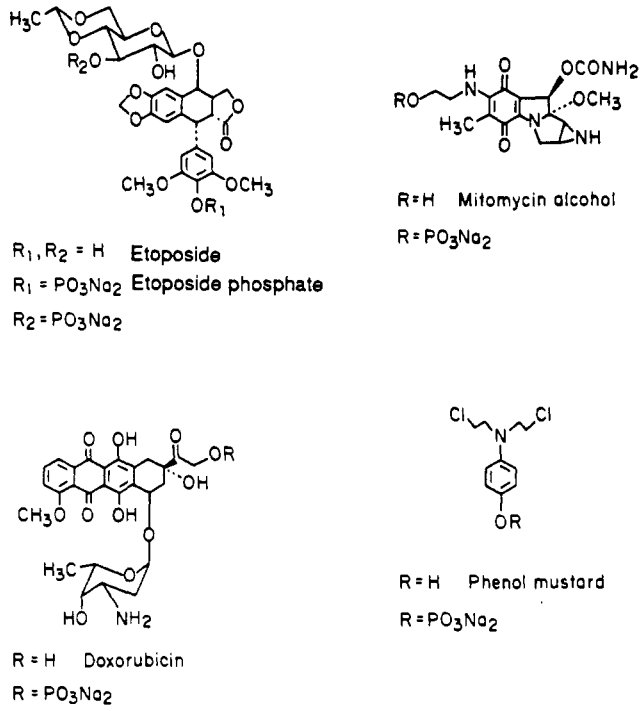


Figure 3. Structures of some anticancer drugs (R = H) and their corresponding phosphate derivatives (R = PO_3Na_2) (from refs 33–38).

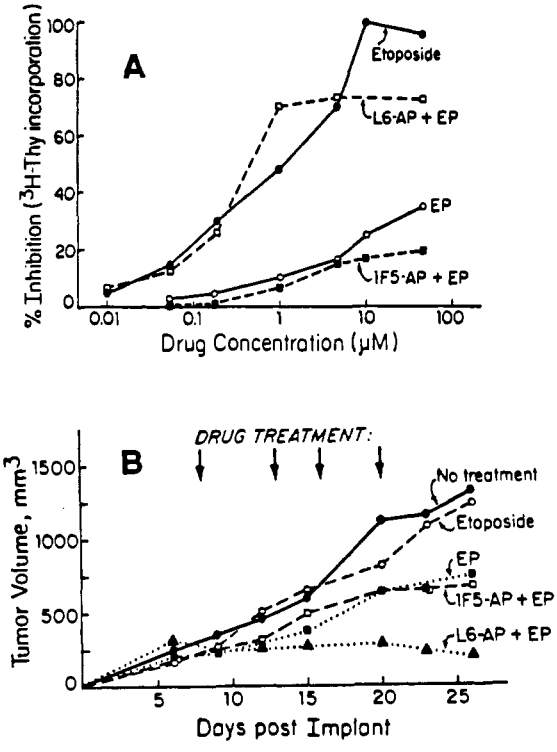


Figure 4. (A) Cytotoxic effects of etoposide and etoposide phosphate (EP) ± mAb–alkaline phosphatase conjugates on H3347 colon carcinoma cells. (B) Effects of etoposide and etoposide phosphate (EP) ± mAb–alkaline phosphatase conjugates on the growth of subcutaneous H3347 tumors in nude mice. Conjugates were administered 24 h prior to etoposide phosphate (from ref 34).

phosphate and mAb–alkaline phosphatase conjugates. The in vitro effects on H3347 cells (L6 antigen positive, 1F5 antigen negative) are illustrated in Figure 4A, which shows the activation of etoposide phosphate by the mAb conjugates, L6–alkaline phosphatase and 1F5–alkaline phosphatase. The cytotoxic activity of etoposide phosphate

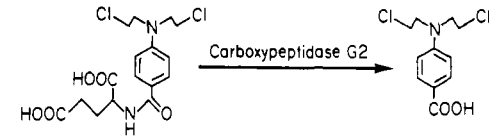


Figure 5. Structures of the prodrug substrate (on left) for carboxypeptidase G2 and the drug, benzoic acid mustard (on right) (from ref 39).

on cells that were pretreated with L6–alkaline phosphatase was equal to that of etoposide. Prodrug activation occurred in an immunologically specific manner, since the nonbinding control conjugate did not enhance prodrug activity. In vivo studies indicated that significant antitumor activities could be obtained in mice that were treated with the combination of L6–alkaline phosphatase and etoposide phosphate (Figure 4B). The effects of this treatment protocol were immunologically specific and superior to therapy with prodrug or drug without prior conjugate administration. These results provided the first evidence that mAb–enzyme conjugates could kill antigen-positive tumor cells when combined with a prodrug derived from an approved anticancer drug.

Several other phosphorylated prodrugs were shown to be substrates for mAb–alkaline phosphatase conjugates (Figure 3), and their in vitro and in vivo effects were analogous to those observed for etoposide phosphate (*35*, *37*). Thus, a single mAb–enzyme conjugate has been used to generate therapeutically effective doses of mechanistically distinct anticancer agents. This illustrates the potential of using a single mAb–enzyme conjugate for combination chemotherapy.

One of the theoretical advantages that this targeting strategy has over direct mAb–drug conjugates is that not all of the tumor cells in a given population need to bind the enzyme conjugate to be affected by the released drug. This was demonstrated in vitro with a bifunctional mAb that could bind to both alkaline phosphatase and to antigens present on a Hodgkin's lymphoma cell line (*38*). A significant level of cytotoxic activity was exerted on antigen-negative cells that were cocultured with antigen-positive cells, and then treated with the bifunctional mAb, alkaline phosphatase and mitomycin phosphate (Figure 3). These results are in contrast to those mentioned earlier for glucose oxidase, in which antigen-negative cells were largely unaffected by cytotoxins released in their vicinity by conjugate that was bound to antigen-positive cells (*17*).

Alkaline phosphatase is not an ideal enzyme for this targeting strategy since it is present in many biological tissues and substantial amounts of the phosphorylated prodrug can undergo activation before reaching the tumor. To circumvent this limitation, much attention has been directed toward the use of enzymes that can carry out reactions not ordinarily occurring in the body. Relatively nontoxic prodrug substrates for such enzymes would be stable in vivo until they contact the targeted enzyme, thus enabling large doses to be administered.

Carboxypeptidase G2. Bagshawe and co-workers have investigated the use of carboxypeptidase G2 for the activation of the glutamic acid derivative of benzoic acid mustard (Figure 5). A conjugate of carboxypeptidase G2 (*Pseudomonas* sp., cloned and expressed in *Escherichia coli*) was prepared by chemically linking the enzyme to the $F(ab')_2$ fragment of W14, an antibody that is directed to the β-subunit of human chorionic gonadotropin (*39*). The prodrug was much less toxic to human choriocarcinoma cells than either the parent drug, benzoic acid mustard, or the combination of carboxypeptidase G2 with the prodrug. Similar results have since been reported for

Table I. Distribution of W14-Carboxypeptidase G2, Drug, and Prodrug in Mice Bearing CC3 Choriocarcinoma Xenografts (W14-Antigen Positive)[a]

tissue	enzyme activity (% injected dose/g of tissue)[b]	drug/prodrug (ratio area under the curves after 4 h)[c]	drug (μg/g of tissue, 1 h post prodrug administration)[c]
tumor	3.80	29	0.84
kidney	0.45	5.5	3.17
liver	0.10	4.2	3.83
lung	2.60	1.3	1.32
plasma	0.10	0.9	3.35

[a] Data from ref 42. Structures of the drug and prodrug are shown in Figure 5. [b] Measured 56 h after iv injection of W14-carboxypeptidase G2 (500 units/kg). [c] Mice were injected iv with W14-carboxypeptidase G2 (1000 units/kg). After 72 h, prodrug (16 mg/kg) was administered, and the amounts of prodrug and active drug were determined for up to 4 h.

the mono- and bis-mesyloxy analogues of the nitrogen mustard prodrug (*40*).

The in vivo activities of the nitrogen mustard prodrug (Figure 5) in combination with W14–carboxypeptidase G2 were determined in nude mice bearing subcutaneous choriocarcinoma xenografts (*39*). This tumor was shown to be resistant to a panel of clinically approved anticancer drugs, benzoic acid mustard, and the glutamic acid containing prodrug. Pronounced antitumor activity was observed in groups of mice receiving the conjugate prior to prodrug administration. Similar results were obtained using the mono-mesyloxy prodrug in combination with W14–carboxypeptidase G2 (*41*).

Insight into the mechanism of activity was obtained by measurement of prodrug, drug, and enzyme levels in the tumors and normal tissues of mice treated with conjugate and the nitrogen mustard prodrug (*39, 42*). The relative levels of carboxypeptidase G2 activity (% injected dose/g of tissue) was higher in tumors than in other tissues when measured 56 h post conjugate administration (Table I). Consistent with this was the finding that the active drug to prodrug ratio was highest in tumors of mice that received conjugate followed 72 h later by prodrug. In fact, the tumor was the only tissue where the level of prodrug was found to be below the limit of detection. These studies provide evidence that active drug is generated intratumorally by mAb–carboxypeptidase G2 conjugate that is bound to cell-surface antigens and may account for the antitumor activity of the enzyme/prodrug combination.

The data presented in Table I illustrate a potential weakness of the general strategy described here. The fact that the tumor did not have the highest absolute level of active drug indicates that a significant proportion of the prodrug was hydrolyzed at other sites. It is likely that higher intratumoral drug concentrations could be realized by further reducing the amount of conjugate that is nontumor associated. This might be accomplished through the use of better mAbs, lower molecular weight mAb fragments, or clearance of circulating conjugate in a separate step prior to prodrug administration. Indeed, Sharma and co-workers have shown that higher tumor to blood conjugate ratios could be obtained by clearing the circulating conjugate with a glycosylated antienzyme mAb (*43, 44*). Other methods for clearance might include plasmapheresis (*45*), the use of avidin to clear biotinylated conjugate (*46*), or the use of antiidiotypic antibodies. Further experiments are required to determine whether a separate clearance step is necessary to achieve optimal therapeutic effects.

Survey of the Methodology. Several enzyme/prodrug combinations have now been reported and are listed in Table II. The diversity of the approach is apparent from the spectrum of cytotoxic agents that can be generated. These range from clinically approved anticancer drugs such as etoposide (*34–36*), doxorubicin (*33, 47*), methotrexate (*48–50*), 5-fluorouracil (*51*), and melphalan (*47*), to highly toxic or unstable agents such as cyanide (*52*), phenol mustard (*37, 53, 54*), phenylenediamine mustard (*55, 56*), and palytoxin (*57*). It should be possible to make use of many other potent cytotoxic agents that have either failed or would most likely fail in the clinic due to systemic toxicity, providing that the prodrug forms are significantly less toxic and have appropriate biological distributions.

Some of the enzyme/prodrug combinations have additional features that should be noted. A mAb–β-glucuronidase conjugate has been shown to hydrolyze a relatively nontoxic nitrogen mustard derivative (*53, 54*). Since some mammalian tissues have high levels of uridine 5′-diphosphoglucuronyl transferase, a detoxification enzyme that catalyzes the reverse reaction of β-glucuronidase (*58*), the prodrug could potentially be regenerated in vivo from drug that is not taken up by tumor cells (*53, 54*). β-Lactamases are of interest since a variety of enzymes are available that have high turnover rates and broad substrate specificities. Cephalosporin-containing prodrugs have been developed that undergo drug elimination according to the fragmentation mechanism shown in Figure 6 (*55, 56, 59–61*). One of the advantages of this approach is that since the β-lactam ring is distal to where the drug is appended, many different anticancer drugs can be released upon enzymatic hydrolysis. Finally, the in vitro activities of a mAb–penicillin-G amidase conjugate in combination with a palytoxin prodrug illustrate that this methodology can be used to release one of the most cytotoxic drugs known (*57*).

Limitations and Considerations For Optimized Therapy. *a. Immunogenicity.* Several phase I clinical trials for solid tumor therapy have been performed utilizing immunotoxins consisting of plant or microbial proteins conjugated to mouse mAbs. The vast majority of patients developed antibody responses against both the toxin and antibody moieties of the immunoconjugates (*4, 62, 63*). Similar immune responses have recently been reported in patients that were treated with a mAb–carboxypeptidase G2 conjugate followed by the nitrogen mustard prodrug shown in Figure 5 (*64*). Clearly, this is likely to limit therapeutic efficacy by reducing serum half life and tumor uptake of the conjugate or by entirely precluding extended therapy. It may be possible to partially overcome the host immune response by using humanized antibodies and enzymes of human origin. Alternative methods to minimize immune reactions might involve coadministration of immunosuppressive agents, such as cyclosporin A (*65*) or 15-deoxyspergualin (*66*), or by chemically modifying the immunoconjugates to make them less immunogenic (*67*). Finally, catalytic antibodies (*68*) designed to activate prodrugs and bind to tumor-associated antigens are not likely to be highly immunogenic, and may have potential in this targeting strategy.

b. Conjugate Heterogeneity. With only a single exception (*38*), the conjugates described to this point have been prepared using chemical cross-linking reagents that react with amino acid side chains on each of the individual proteins. The lack of specificity displayed by these reagents (*69*) results in the formation of heterogeneous mixtures of conjugates which presumably have varying degrees of binding and enzymatic activities. Recombinant DNA technology provides a means to construct conjugates having uniform and well-defined properties. Indeed, such

Table II. Targeted Enzymes for Prodrug Activation

enzyme	prodrug	released drug	ref(s)
alkaline phosphatase	doxorubicin phosphate	doxorubicin	33
	etoposide phosphate	etoposide	34–36
	mitomycin phosphate	mitomycin	35,38
	phenol mustard phosphate	phenol mustard	37
carboxypeptidase A	methotrexate–alanine	methotrexate	48–50
carboxypeptidase G2	benzoic acid mustard(s)– glutamic acid	benzoic acid mustard(s)	39–44
cytosine deaminase	5-fluorocytosine	5-fluorouracil	51
β-glucosidase	amygdalin	cyanide	52
β-glucuronidase	phenol mustard glucuronide	phenol mustard	53,54
β-lactamase			
(*E. cloacae*)	vinca–cephalosporin	vinca alkaloid	59–61
(*E. cloacae*)	nitrogen mustard(s)– cephalosporin	nitrogen mustard(s)	55
(*B. cereus* and *E. coli*)	phenylenediamine mustard–cephalosporin	phenylenediamine mustard	56
penicillin amidase	doxorubicin–phenoxyacetamide	doxorubicin	47
	melphalan–phenoxyacetamide	melphalan	47
	palytoxin–4-hydroxyphenylacetamide	palytoxin	57

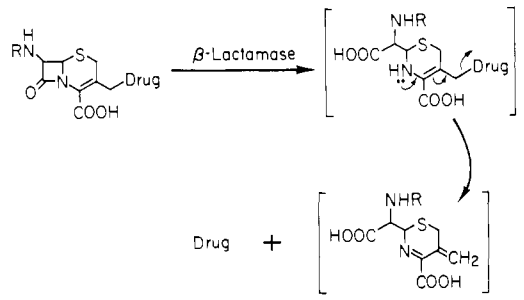


Figure 6. Mechanism of drug release catalyzed by β-lactamase.

methods have been used with encouraging results for the construction of mAb–plasminogen activator fusion proteins (*70–72*). Recently, Bosslet and co-workers have reported the preparation and properties of a recombinant mAb–β-glucuronidase fusion protein (*73*). The conjugate, which was comprised of a humanized F(ab') mAb fragment and human β-glucuronidase, appeared to have unimpaired binding avidity and significant levels of enzyme activity. Because of the relatively uniform composition and potentially low immunogenicity of the conjugate, as well as the availability of suitable prodrug substrates (*53, 54*), fusion molecules such as these warrant investigation for prodrug activation.

c. Pharmacokinetics. The therapeutic efficacy of targeted enzymes for prodrug activation will be significantly influenced by the biodistribution and pharmacokinetics of the conjugates, the prodrug substrates, and the released drugs. A pharmacokinetic model that evaluates the effects that conjugate localization, binding affinity, and enzyme kinetics have on intratumoral drug concentrations has recently been reported (*74*). This model emphasizes the necessity of having prodrugs that are nontoxic and that are not rapidly converted to active drugs in the serum. Furthermore, the model predicts that under some circumstances, enzymes with relatively high K_m and V_{max} values will lead to high tumor to blood drug ratios. It may be possible to test these hypotheses using conjugates of β-lactamase (*55, 56, 59–61*), since site-specific mutations on the enzyme have been shown to dramatically alter their kinetic properties (*75, 76*). Studies along these lines may prove to be invaluable for the selection of an enzyme having optimal properties for in vivo therapy.

CONCLUSIONS

Several mAb–enzyme conjugates have now been developed for the site-specific formation of cytotoxic agents. The principle advantage of this approach compared to those involving the direct attachment of a cytotoxic agent to a mAb is that the targeted enzyme can greatly amplify the number of drug molecules delivered to each tumor cell. Furthermore, the cytotoxic effect may not be restricted to only those tumor cells that have bound the conjugate, since the drug is released extracellularly and may be able to migrate to neighboring tumor cells. The principle disadvantage lies in the approach's inherent complexity, since two separate agents and an appropriate time interval between their respective administrations are required for therapeutic efficacy.

As indicated here, mAb–enzyme conjugates can release a vast array of cytotoxins ranging from clinically approved anticancer drugs to highly potent agents that would have little chance for success in the clinic if given systemically. Several groups have demonstrated that significant in vitro and in vivo antitumor activities can be obtained using this approach, and clinical studies are now underway. Further refinements in the technology, such as the use of recombinant fusion proteins comprised of relatively nonimmunogenic components, the development of prodrugs with optimal pharmacological distributions and minimal toxicities, and strategies to achieve high tumor to normal tissue conjugate ratios, may provide the basis for making this approach clinically useful.

ACKNOWLEDGMENT

We thank the co-workers from our laboratory (whose names appear in the references) for their contributions to the work described here, Ana Wieman for her assistance in the preparation of the manuscript, and Carina V. Olsson for her helpful comments on the manuscript.

LITERATURE CITED

(1) Zubrod, C. G. (1982) Principles of Chemotherapy. *Cancer Med.* (J. F. Holland, and E. Frei, Eds.) pp 627–632, Lea and Febiger, Philadelphia.

(2) Thorpe, P. E. (1985) Antibody carriers of cytotoxic agents in cancer therapy. A review. *Monoclonal Antibodies '84: Biological And Clinical Applications* (A. Pinchera, G. Doria, F. Dammacco, and A. Bargellesi, Eds.) pp 475–506, Editrice Kurtis, Milan.

(3) Vitetta, E. S., Fulton, R. J., May, T. D., Till, M., and Uhr, J. W. (1987) Redesigning nature's poisons to create anti-tumor reagents. *Science 238*, 1098–1104.

(4) Wawrzynczak, E. J. (1991) Systemic immunotoxin therapy of cancer: advances and prospects. *Br. J. Cancer 64*, 624–630.

(5) Pimm, M. V. (1988) Drug-monoclonal antibody conjugates for cancer therapy: potential and limitations. *CRC Crit. Rev. Ther. Drug Carrier Syst. 5*, 189–227.

(6) Koppel, G. A. (1990) Recent advances with monoclonal antibody drug targeting for the treatment of human cancer. *Bioconjugate Chem. 1*, 13–23.

(7) Weinstein, J. N., and van Osdol, W. (1992) Early intervention in cancer using monoclonal antibodies and other biological ligands: Micropharmacology and the "binding site barrier". *Cancer Res. 52*, 2747s–2751s.

(8) Del Vecchio, S., Reynolds, J. C., Carrasquillo, J. A., Blasberg, R. G., Neumann, R. D., Lotze, M. T., Bryant, G. J., Farkas, R. J., and Larson, S. M. (1989) Local distribution and concentration of intravenously injected ^{131}I-9.2.27 monoclonal antibody in human malignant melanoma. *Cancer Res. 49*, 2783–2789.

(9) Del Vecchio, S., Reynolds, J. C., Blasberg, R. G., Neumann, R. D., Carrasquillo, J. A., Hellström, I., and Larson, S. M. (1988) Measurement of local M_r 97,000 and 250,000 protein antigen concentration in sections of human melanoma tumor using in vitro quantitative autoradiography. *Cancer Res. 48*, 5475–5481.

(10) Shockley, T. R., Lin, K., Nagy, J. A., Tompkins, R. G., Yarmush, M. L., and Dvorak, H. F. (1992) Spatial distribution of tumor-specific monoclonal antibodies in human melanoma xenografts. *Cancer Res. 52*, 367–376.

(11) Jain, R. K., and Baxter, L. T. (1988) Mechanisms of heterogeneous distribution of monoclonal antibodies and other macromolecules in tumors: Significance of elevated interstitial pressure. *Cancer Res. 48*, 7022–7032.

(12) Clauss, M. A. and Jain, R. K. (1990) Interstitial transport of rabbit and sheep antibodies in normal and neoplastic tissues. *Cancer Res. 50*, 3487–3492.

(13) Mimnaugh, E. G., Dusre, L., Atwell, J., and Myers, C. E. (1989) Differential oxygen radical susceptibility of adriamycin-sensitive and -resistant MCF-7 human breast tumor cells. *Cancer Res. 49*, 8–15.

(14) Sartorelli, A. C. (1986) The role of mitomycin antibiotics in the chemotherapy of solid tumors. *Biochem. Pharmacol. 35*, 67–69.

(15) Oberley, L. W., Lindgren, L. A., Baker, S. A., and Stevens, R. H. (1976) Superoxide ion as the cause of the oxygen effect. *Radiat. Res. 68*, 320–328.

(16) Rossi, F. (1986) The O_2-forming NADPH oxidase of the phagocytes: nature, mechanisms of activation and function. *Biochim. Biophys. Acta 853*, 69–89.

(17) Philpott, G. W., Shearer, W. T., Bower, R. W., and Parker, C. W. (1973) Selective cytotoxicity of hapten-substituted cells with an antibody-enzyme conjugate. *J. Immunol. 111*, 921–929.

(18) Stanislawski, M., Rousseau, V., Goavec, M., and Ito, H. (1989) Immunotoxins containing glucose oxidase and lactoperoxidase with tumoricidal properties: in vitro killing effectiveness in a mouse plasmacytoma cell model. *Cancer Res. 49*, 5497–5504.

(19) Muzykantov, V. R., and Danilov, S. M. (1991) Glucose oxidase conjugated with anti-endothelial monoclonal antibodies: *in vitro* and *in vivo* studies. *Int. J. Radiat. Biol. 60*, 11–15.

(20) Ito, H., Morizet, J., Coulombel, L., Goavec, M., Rousseau, V., Bernard, A., and Stanislawski, M. (1989) An immunotoxin system intended for bone marrow purging composed of glucose oxidase and lactoperoxidase coupled to monoclonal antibody 097. *Bone Marrow Transplant. 4*, 519–527.

(21) Ito, H., Morizet, J., Coulombel, L., and Stanislawski, M. (1990) T cell depletion of human bone marrow using an oxidase-peroxidase enzyme immunotoxin. *Bone Marrow Transplant. 6*, 395–398.

(22) Kuppusamy, P., and Zweier, J. L. (1989) Characterization of free radical generation by xanthine oxidase. *J. Biol. Chem. 264*, 9880–9884.

(23) Britigan, B. E., Pou, S., Rosen, G. M., Lilleg, D. M., and Buettner, G. R. (1990) Hydroxyl radical is not a product of the reaction of xanthine oxidase and xanthine. *J. Biol. Chem. 265*, 17533–17538.

(24) Battelli, M. G., Abbondanza, A., Tazzari, P. L., Dinota, A., Rizzi, S., Grassi, G., Gobbi, M., and Stirpe, F. (1988) Selective cytotoxicity of an oxygen-radical-generating enzyme conjugated to a monoclonal antibody. *Clin. Exp. Immunol. 73*, 128–133.

(25) Dinota, A., Tazzari, P. L., Abbondanza, A., Battelli, M. G., Gobbi, M., and Stirpe, F. (1990) Bone marrow purging by a xanthine oxidase-antibody conjugate. *Bone Marrow Transplant. 6*, 31–36.

(26) Muzykantov, V. R., Sakharov, D. V., Sinitsyn, V. V., Domogatsky, S. P., Goncharov, N. V., and Danilov, S. M. (1988) Specific killing of human endothelial cells by antibody-conjugated glucose oxidase. *Anal. Chem. 169*, 383–389.

(27) Muzykantov, V. R., Trubetskaya, O. V., Puchnina, E. A., Sakharov, D. V., and Domogatsky, S. P. (1990) Cytotoxicity of glucose oxidase conjugated with antibodies to target cells: Killing efficiency depends on the conjugate internalization. *Biochim. Biophys. Acta 1053*, 27–31.

(28) Basch, R. S., Lakow, E., Teng, M., and Buxbaum, J. N. (1984) Isolation of highly malignant Thy-1-positive revertants from cultured cloned Thy-1-negative lymphoma cells of low tumorigenicity. *Somatic Cell Mol. Genet. 10*, 37–44.

(29) Sakharov, D. V., Muzykantov, V. R., Domogatsky, S. P., and Danilov, S. M. (1987) Protection of cultured endothelial cells from hydrogen peroxide-induced injury by antibody-conjugated catalase. *Biochim. Biophys. Acta 930*, 140–144.

(30) Wilman, D. E. V. (1986) Prodrugs in cancer chemotherapy. *Biochem. Soc. Trans. 14*, 375–382.

(31) Denny, W. A. (1988) New directions in the design and evaluation of anti-cancer drugs. *Drug Des. Del. 3*, 99–124.

(32) Conners, T. A. (1986) Prodrugs in cancer chemotherapy. *Xenobiotica 16*, 975–988.

(33) Senter, P. D. (1990) Activation of prodrugs by antibody-enzyme conjugates: A new approach to cancer therapy. *FASEB 4*, 188–193.

(34) Senter, P. D., Saulnier, M. G., Schreiber, G. J., Hirschberg, D. L., Brown, J. P., Hellström, I., and Hellström, K. E. (1988) Anti-tumor effects of antibody-alkaline phosphatase conjugates in combination with etoposide phosphate. *Proc. Natl. Acad. Sci. U.S.A. 85*, 4842–4846.

(35) Senter, P. D., Schreiber, G. J., Hirschberg, D. L., Ashe, S. A., Hellström, K. E., and Hellström, I. (1989) Enhancement of the in vitro and in vivo antitumor activities of phosphorylated mitomycin c and etoposide derivatives by monoclonal antibody-alkaline phosphatase conjugates. *Cancer Res. 49*, 5789–5792.

(36) Haisma, H. J., Boven, E., van Muijen, M., De Vries, R., and Pinedo, H. M. (1992) Analysis of a conjugate between anti-carcinoembryonic antigen monoclonal antibody and alkaline phosphatase for specific activation of the prodrug etoposide phosphate. *Cancer Immunol. Immunother. 34*, 343–348.

(37) Wallace, P. M., and Senter, P. D. (1991) In vitro and in vivo activities of monoclonal antibody-alkaline phosphatase conjugates in combination with phenol mustard phosphate. *Bioconjugate Chem. 2*, 349–352.

(38) Sahin, U., Hartmann, F., Senter, P., Pohl, C., Engert, A., Diehl, V., and Pfreundschuh, M. (1990) Specific activation of the prodrug mitomycin phosphate by a bispecific anti-CD30/anti-alkaline phosphatase monoclonal antibody. *Cancer Res. 50*, 6944–6948.

(39) Bagshawe, K. D., Springer, C. J., Searle, F., Antoniw, P., Sharma, S. K., Melton, R. G., and Sherwood, R. F. (1988) A cytotoxic agent can be generated selectively at cancer sites. *Br. J. Cancer 58*, 700–703.

(40) Springer, C. J., Antoniw, P., Bagshawe, K. D., Searle, F., Bisset, G. M. F., and Jarman, M. (1990) Novel prodrugs which are activated to cytotoxic alkylating agents by carboxypeptidase G2. *J. Med. Chem. 33*, 677–681.

(41) Springer, C. J., Bagshawe, K. D., Sharma, S. K., Searle, F., Boden, J. A., Antoniw, P., Burke, P. J., Rogers, G. T., Sherwood, R. F., and Melton, R. G. (1991) Ablation of human choriocarcinoma xenografts in nude mice by antibody-directed enzyme prodrug therapy (ADEPT) with three novel compounds. *Eur. J. Cancer 27*, 1361–1366.

(42) Antoniw, P., Springer, C. J., Bagshawe, K. D., Searle, F., Melton, R. G., Rogers, G. T., Burke, P. J., and Sherwood, R. F. (1990) Disposition of the prodrug 4-(bis(2-chloroethyl)-amino)benzoyl-L-glutamic acid and its active parent drug in mice. *Br. J. Cancer 62*, 909–914.

(43) Sharma, S. K., Bagshawe, K. D., Burke, P. J., Boden, R. W., and Rogers, G. T. (1990) Inactivation and clearance of an anti-CEA carboxypeptidase G2 conjugate in blood after localisation in a xenograft model. *Br. J. Cancer 61*, 659–662.
(44) Sharma, S. K., Bagshawe, K. D., Springer, C. J., Burke, P. J., Rogers, G. T., Boden, J. A., Antoniw, P., Melton, R. G., and Sherwood, R. F. (1991) Antibody directed enzyme prodrug therapy (ADEPT): A three phase system. *Dis. Markers 9*, 225–231.
(45) Williams, C., Buskard, N., and Bussel, J. (1990) Plasma exchange in idiopathic thrombocytopenic purpura. *Curr. Stud. Hematol. Blood Transfus. 57*, 131–151.
(46) Sinitsyn, V. V., Mamontova, A. G., Checkneva, Y. Y., Shnyra, A. A., and Domogatsky, S. P. (1989) Rapid blood clearance of biotinylated lgG after infusion of avidin. *J. Nucl. Med. 30*, 66–69.
(47) Kerr, D. E., Senter, P. D., Burnett, W. V., Hirschberg, D. L., Hellström, I., and Hellström, K. E. (1990) Antibody-penicillin-V-amidase conjugates kill antigen-positive tumor cells when combined with doxorubicin phenoxyacetamide. *Cancer Immunol. Immunother. 31*, 202–206.
(48) Haenseler, E., Esswein, A., Vitols, K. S., Montejano, Y., Mueller, B. M., Reisfeld, R. A., and Huennekens, F. M. (1992) Activation of methotrexate-α-alanine by carboxypeptidase A-monoclonal antibody conjugate. *Biochemistry 31*, 891–897.
(49) Kuefner, U., Lohrmann, U., Montejano, Y. D., Vitols, K. S., and Huennekens, F. M. (1989) Carboxypeptidase-mediated release of methotrexate from methotrexate-α-peptides. *Biochemistry 28*, 2288–2297.
(50) Esswein, A., Hanseler, E., Montejano, Y., Vitols, K. S., and Huennekens, F. M. (1991) Construction and chemotherapeutic potential of carboxypeptidase-A/monoclonal antibody conjugate. *Adv. Enzyme Regul. 31*, 3–12.
(51) Senter, P. D., Su, P. C. D., Katsuragi, T., Sakai, T., Cosand, W. L., Hellström, I., and Hellström, K. E. (1991) Generation of 5-fluorouracil from 5-fluorocytosine by monoclonal antibody-cytosine deaminase conjugates. *Bioconjugate Chem. 2*, 447–451.
(52) Rowlinson-Busza, G., Bamias, A., Krausz, T., and Epenetos, A. A. (1992) Antibody-guided enzyme nitrile therapy (Agent): in vitro cytotoxicity and in vivo tumour localisation. *Monoclonal Antibodies. Applications in Clinical Oncology*, (A. A. Epenetos, Ed.) Chapman and Hall, London.
(53) Roffler, S. R., Wang, S.-M., Chern, J.-W., Yeh, M.-Y., and Tung, E. (1991) Anti-neoplastic glucuronide prodrug treatment of human tumor cells targeted with a monoclonal antibody-enzyme conjugate. *Biochem. Pharmacol. 42*, 2062–2065.
(54) Wang, S.-M., Chern, J.-W., Yeh, M.-Y., Ng, J. C., Tung, E., and Roffler, S. R. (1992) Specific activation of glucuronide prodrugs by antibody-targeted enzyme conjugates for cancer therapy. *Cancer Res. 52*, 4484–4491.
(55) Alexander, R. P., Beeley, N. R. A., O'Driscoll, M., O'Neill, F. P., Millican, T. A., Pratt, A. J., and Willenbrock, F. W. (1991) Cephalosporin nitrogen mustard carbamate prodrugs for "ADEPT". *Tetrahedron Letts. 32*, 3269–3272.
(56) Svensson, H. P., Kadow, J. F., Vrudhula, V. M., Wallace, P. M., and Senter, P. D. (1992) Monoclonal antibody-β-lactamase conjugates for the activation of a cephalosporin mustard prodrug. *Bioconjugate Chem. 3*, 176–181.
(57) Bignami, G. S., Senter, P. D., Grothaus, P. G., Fischer, K. J., Humphreys, T., and Wallace, P. M. (1992) N-(4′-Hydroxyphenylacetyl)palytoxin: A palytoxin prodrug that can be activated by a monoclonal antibody-penicillin-G amidase conjugate, *Cancer Res.*, in press.
(58) Bock, K. W. (1991) Roles of UDP-glucuronosyltransferases in chemical carcinogenisis. *Crit. Rev. Biochem. Mol. Biol. 26*, 129–150.
(59) Shepherd, T. A., Jungheim, L. N., Meyer, D. L., and Starling, J. J. (1991) A novel targeted delivery system utilizing a cephalosporinoncolytic prodrug activated by an antibody β-lactamase conjugate for the treatment of cancer. *Bioorg. Med. Chem. Letts. 1*, 21–26.
(60) Meyer, D. L., Jungheim, L. N., Mikolajczyk, S. D., Shepherd, T. A., Starling, J. J., and Ahlem, C. (1992) Preparation and characterization of β-lactamase-Fab′ conjugates for the site specific activation of oncolytic agents. *Bioconjugate Chem. 3*, 42–48.
(61) Jungheim, L. N., Shepherd, T. A., and Meyer, D. L. (1992) Synthesis of acylhydrazido-substituted cephems. Design of cephalosporin-vinca alkaloid prodrugs: Substrates for an antibody-targeted enzyme. *J. Org. Chem. 57*, 2334–2340.
(62) Byers, V. S., Rodvien, R., Grant, K., Durrant, L. G., Hudson, K. H., Baldwin, R. W., and Scannon, P. J. (1989) Phase I study of monoclonal antibody-ricin A chain immunotoxin XomaZyme-791 in patients with metastatic colon cancer. *Cancer Res. 49*, 6153–6160.
(63) Oratz, R., Speyer, J. L., Wernz, J. C., Hochster, H., Meyers, M., Mischak, R., and Spitler, L. E. (1990) Anti-melanoma monoclonal antibody-ricin A chain immunoconjugate (XMMME-001-RTA) plus cyclophosphamide in the treatment of metastatic malignant melanoma: Results of a phase II trial. *J. Biol. Respons. Mod. 9*, 345–354.
(64) Bagshawe, K. D., Sharma, S. K., Springer, C. J., Antoniw, P., Rogers, G. T., Burke, P. J., Melton, R., and Sherwood, R. (1991) Antibody-enzyme conjugates can generate cytoxic drugs from inactive precursors at tumor sites. *Antibody Imm. Radiopharm. 4*, 915–922.
(65) Lederman, J. A., Begent, R. H. J., Bagshawe, K. D., Riggs, S. J., Searle, F., Glaser, M. G., Green, A. J., and Dale, R. G. (1988) Repeated anti-tumor antibody therapy in man with suppression of the host response by cyclosporin A. *Br. J. Cancer 58*, 654–657.
(66) Pai, L. H., Fitzgerald, D. J., Tepper, M., Schacter, B., Spitalny, G., and Pastan, I. (1990) Inhibition of antibody response to Pseudomonas exotoxin and an immunotoxin containing Pseudomonas exotoxin by 15-deoxyspergualin in mice. *Cancer Res. 50*, 7750–7753.
(67) Sehon, A. H. (1989) Modulation of antibody responses by conjugates of antigens with monomethoxypolyethylene glycol. *Adv. Exp. Med. Biol. 251*, 341–351.
(68) Schultz, P. G., Lerner, R. A., and Benkovic, S. J. (1990) Catalytic antibodies. *Chem. Eng. News 68*, May 28, 26–40.
(69) Brinkley, M. (1992) A brief survey of methods for preparing protein conjugates with dyes, haptens, and cross-linking reagents. *Bioconjugate Chem. 3*, 2–13.
(70) Dewerchin, M., and Collen, D. (1991) Enhancement of the thrombolytic potency of plasminogen activators by conjugation with clot-specific monoclonal antibodies. *Bioconjugate Chem. 2*, 293–300.
(71) Hayzer, D. J., Lubin, I. M., and Runge, M. S. (1991) Conjugation of plasminogen activators and fibrin-specific antibodies to improve thrombolytic therapeutic agents. *Bioconjugate Chem. 2*, 301–308.
(72) Haber, E., Quertermous, T., Matsueda, G. R., and Runge, M. S. (1989) Innovative approaches to plasminogen activator therapy. *Science 243*, 51–56.
(73) Bosslet, K., Czech, J., Lorenz, P., Sedlacek, H. H., Schuermann, M., and Seemann, G. (1992) Molecular and functional characterisation of a fusion protein suited for tumour specific prodrug activation. *Br. J. Cancer 65*, 234–238.
(74) Yuan, F., Baxter, L. T., and Jain, R. K. (1991) Pharmacokinetic analysis of two-step approaches using bifunctional and enzyme-conjugated antibodies. *Cancer Res. 51*, 3119–3130.
(75) Sowek, J. A., Singer, S. B., Ohringer, S., Malley, M. F., Dougherty, T. J., Gougoutas, J. Z., and Bush, K. (1991) Substitution of lysine at position 104 or 240 of TEM-pTZ18R β-lactamase enhances the effect of serine-164 substitution on hydrolysis or affinity for cephalosporins and the monobactam aztreonam. *Biochemistry 30*, 3179–3188.
(76) Dube, D. K. and Loeb, L. A. (1989) Mutants generated by the insertion of random oligonucleotides into the active site of the β-lactamase gene. *Biochemistry 28*, 5703–5707.

ARTICLES

Enhanced in Vitro Tumor Cell Retention and Internalization of Antibody Derivatized with Synthetic Peptides

D. C. Anderson,* R. Manger, J. Schroeder, D. Woodle, M. Barry, A. C. Morgan, and A. R. Fritzberg

NeoRx Corporation, 410 West Harrison, Seattle, Washington 98119. Received January 31, 1992

The Fab fragments of two antitumor monoclonal antibodies, NR-ML-05 and NR-LU-10, have been covalently derivatized with synthetic peptides designed to provide secondary sites of attachment to enhance their retention on tumor cells. Analogs of the peptide "GALA", an amphipathic peptide previously reported to interact with uncharged lipid bilayers, gave antibody conjugates of different molecular weight and bound peptide stoichiometry when attached to Fab fragments using the heterobifunctional cross-linker sulfo-SMCC. This attached peptide enhanced the retention and internalization of Fab fragments of NR-ML-05 on FEMX human melanoma cells, but not of NR-LU-10 on HT-29 human colon carcinoma cells, indicating that this effect might be specific for individual tumor antigen–antibody systems. This peptide appeared to increase nonspecific interactions of the conjugate with antigen-negative cells. Other membrane-active peptides were also tested. None were as effective as the "GALA" analogs. A synthetic ion channel peptide attached to NR-ML-05 Fab exhibited the greatest enhanced internalization of these tested peptides.

INTRODUCTION

An enhanced internalization of therapeutics such as cytotoxic antitumor agents (*1*) or potentially highly specific agents such as ribozymes into target cells, or an improved retention of such agents on the surface of target cells for slow release (the "depot" effect, ref 2), may be therapeutically beneficial. An example in the area of radioimmunotherapy might include radiolabeled antibodies, which were first reported to localize in tumors by Pressman in 1957 (*3*) and are currently under development for imaging and therapy of cancer. A major shortcoming of these antibodies in humans is the low fraction of antibody actually localized in tumors, a percent injected dose per gram of ca. 0.005% or less in most cases. This amount may be 10-fold too low for effective therapy (*4*, *5*). Changes which may improve tumor retention include enhancing antibody affinity for tumor-associated antigen, increasing the kinetics of antibody uptake from the circulation, or decreasing desorption from the tumor site. An example of this is the use of aryl carbohydrate adducts of a radioiodinated antibody to increase intracellular retention (*6*). This area may thus be a good model system for exploring the effects of agents designed to increase the cell surface retention or internalization of therapeutics.

To explore another general approach to increasing internalization or cellular retention, we have selected Fab fragments from two antitumor IgG_{2b} antibodies, the anti-melanoma antibody NR-ML-05 (*7*) and the pan-carcinoma antibody NR-LU-10 (*8*), for chemical attachment of analogs of the peptide "GALA" (*9*, *10*). This peptide reversibly forms an amphipathic α helix at pH values below 5, and has been shown to interact with bilayers and induce fusion of small vesicles. Analogs of this peptide are intended to enhance the retention of a therapeutic antibody Fab fragment at the tumor by addition of a secondary interaction in addition to antigen binding to the cell. We have also attached and tested three other peptides, which either are soluble in membrane bilayers or bind to a cell surface receptor. These include an analog of an amphipathic synthetic ion channel designed originally by DeGrado (*11*), a fragment of a viral fusion protein (*12*), and MSH_a, a ligand for α-MSH receptors (*13*). Fab fragments have been chosen for testing since addition of a secondary interaction to their monovalent binding of antigen may cause a more noticeable change in their tumor retention than for a bivalent whole antibody. Additionally, Fab fragments may be superior to whole antibodies as radiotherapeutic agents due to enhanced diffusion within a tumor (*6*).

Here we report the properties of analogs of "GALA", the separation and characterization of conjugates with antibody Fab fragments, and the effect of these peptides on tumor retention and internalization of the Fab fragment of the monoclonal antibody NR-ML-05. On the basis of in vitro experiments with these peptides, we have observed increases in both the cell surface retention of the Fab conjugate on FEMX human melanoma cells and the apparent internalization of these conjugates into tumor cells.

EXPERIMENTAL PROCEDURES

Peptide Synthesis and Radiolabeling. Peptides were synthesized on *p*-methylbenzhydrylamine resin (0.6 mequiv/g) with an Applied Biosystems 430A peptide synthesizer using standard Boc-benzyl cycles. The coupling yields were monitored by ninhydrin using resin collected automatically, and were all above 99.3% for the parent peptide 1, which has the sequence

* Address correspondence to this author at the following address: Somatogen, Inc., 5797 Central Ave., Boulder, CO 80301.

[1] Abbreviations used: sulfo-SMCC, sulfosuccinimidyl 4-(*N*-maleimidomethyl)cyclohexane-1-carboxylate, DTT, dithiothreitol; ELISA enzyme-linked immunosorption assay; PBS, phosphate-buffered saline; DTNB, 5,5′-dithiobis(2-nitrobenzoic acid); MSH, α-melanocyte stimulating hormone; MSH_a, the peptide SYS(Nle)EH(D-Phe)RWGKPV-amide.

1043-1802/93/2904-0010$04.00/0 © 1993 American Chemical Society

$$\underset{1}{\text{CGEAAL(AEAL)}_5\text{EALAA-amide}}$$

The sequence of this peptide was based on the sequence of "GALA" (*9*), WEAAL(AEAL)$_2$(AEHL)(AEAL)$_2$EALAA-amide. The N terminus was changed to allow chemically specific conjugation to a maleimide cross-linking reagent, and the W (Trp) and H (His) were replaced to decrease potential problems during the hydrofluoric acid cleavage. Coupling yields were similar for the other peptides. To ascertain the stoichiometry of peptide bound to Fab conjugates, 8.9 mg of peptide was labeled at the N-terminus with [^{14}C]acetic anhydride (1 mCi, 11.3 mCi/mmol, ICN), which was added and shaken for 2.5 h. A 5-fold molar excess of diisopropylethylamine was added and N-acetylation was continued for 30 min. The peptide resin was sealed in a 1-in. square polypropylene mesh bag which contained the resin but allowed access of chemical reagents (*14*). The resin was washed several times with 4 mL/bag of methylene chloride and then 5% diisopropylethylamine in methylene chloride and finally shaken with 10% v/v cold acetic anhydride in methylene chloride for 30 min to finish N-acetylation. Excess [^{14}C]acetic anhydride was washed from the resin by 2 × 1 min consecutive rinses (4 mL/bag) of methylene chloride, dimethyl formamide, isopropyl alcohol, methylene chloride, and methanol, and the labeled resin was then dried under vacuum.

The peptide was cleaved from the resin while still in polypropylene bags, in 10:1:1:0.2 by volume hydrofluoric acid–anisole–dimethyl sulfide–*p*-thiocresol for 1 h at −5 to 0 °C using a multiple-HF cleavage apparatus (*14*). This was followed by extraction of the resin with 7 mL of methylene chloride and then 2 × 5 mL of 0.2 M sodium bicarbonate, pH 8.0. Lyophilization for 2 days gave peptide as a white powder which was purified by reverse-phase chromatography using a Hewlett-Packard 1090M HPLC equipped with diode-array detection, on a Vydac C4 analytical column eluted with a linear gradient of 5 mM, pH 6.7 phosphate buffer to 100% acetonitrile in 30 min, after 5 min of isocratic elution in the first buffer. The peptide was eluted at ca. 80% acetonitrile, and its final specific activity was 2.85 mCi/mmol. A fast atom bombardment mass spectrum was obtained of the purified peptide from the University of Washington Department of Chemistry Mass Spectrometer Lab. The mass spectrum was analyzed using MacProMass v. 1.0, a program obtained from Terry Lee of the Beckman Research Institute of the City of Hope, Duarte, CA.

Attachment of Peptides to Antibodies with Sulfo-SMCC. Fab fragments from the mouse hybridoma-derived melanoma-reactive antibody NR-ML-05 (*7*) and the pan-carcinoma antibody NR-LU-10 (*8*) were prepared by papain immobilized on agarose beads using conditions similar to those discussed by Parham (*15*). The digestion supernatant was eluted over a Pharmacia Q Sepharose column equilibrated with pH 8.0, 5 mM sodium phosphate plus 0.1 M NaCl. Undigested antibody remained bound to the column while pure Fab fragments were eluted as a single peak.

Peptides were cross-linked to the Fab fragments using the water-soluble heterobifunctional cross-linker sulfo-SMCC, obtained from Pierce Chemical Co. Sulfo-SMCC was chosen to cross-link Fab amino groups to the unique N-terminal cysteine of the peptides. Sulfo-SMCC was reacted with Fab at pH 6.0 at 20 °C in 0.1 M phosphate buffer for 45 min, followed by centrifugation with a Centricon (Amicon, Inc.) 10 kDa exclusion centrifuge filtration apparatus to remove unreacted SMCC.

Prior to reaction with Fab–SMCC, peptide 1 was first reduced by 0.1 M DTT, separated from the DTT by gel filtration on Sephadex G-10, and assayed for its thiol content using DTNB with detection at 412 nm (*16*) and for its concentration using the biscinchoninic acid protein assay (*17*). Reagents for this assay were supplied by Pierce Chemical Co. For the reaction of peptide 1 and Fab–SMCC used for the separations in Figure 2, 36 mg of NR-ML-05 Fab–SMCC at a final concentration of 8 μM was reacted with a 6-fold excess of peptide 1 (final concentration 48 μM) in pH 6.0, 0.1 M sodium phosphate for 16 h. The free peptide was separated from the conjugate, and individual conjugate peaks were separated from each other, by repeated gel filtration runs on a Du Pont Zorbax GF-250 XL column.

Sulfo-SMCC incorporation was assayed in two ways. In the first method a 100-fold excess of [^{35}S]cysteine was reacted with maleimide-labeled antibody for at least 2 h at room temperature, the mixture was subjected to centrifugation–ultrafiltration as above for multiple cycles, and the remaining Fab was counted. In a similar procedure, reaction of 6.7×10^{-4} M 2-mercaptoethylamine with SMCC-labeled alkaline phosphatase at pH 6 was complete after 20 min (*18*); thus the 2-h time taken here for reaction of [^{35}S]cysteine with 2×10^{-5} M maleiimide-labeled Fab should be adequate for complete reaction. In the second, a 10-fold excess of [^{14}C]peptide was reacted with Fab-SMCC and purified by gel filtration over a Sephadex G-10 column, and the Fab-SMCC–peptide complex was counted to determine the number of attached peptides, and thus the number of incorporated reactive SMCC molecules per Fab. Using the [^{35}S]cysteine assay, reaction of NRML-05 Fab in separate experiments with a range of 10–30-fold molar excess of sulfo-SMCC (pH 7.5 in PBS, 3 mg/mL Fab) resulted in incorporation of from 1.6 to 4.0 mol of [^{35}S]cysteine/Fab in this range. There was no loss of antigen binding in these different reactions as measured by competition ELISA. Using the [^{14}C]peptide assay for SMCC incorporation, Fab reacting with a range of 1–15 mol of sulfo-SMCC/mol of Fab incorporated a corresponding range of 0.3–5.5 mol of [^{14}C]peptide/mol of Fab.

Radioiodination of the Peptide–Fab Conjugates. Conjugates of NRML-05 Fab, sulfo-SMCC, and peptide were radioiodinated for subsequent in vitro testing. This was done using purified succinimidyl *p*-iodobenzoate and the protocol of Wilbur et al. (*19*) or iodogen (*20*). The NR-ML-05–SMCC–peptide 1 conjugates in peaks 1, 2, and 3 were iodinated for in vitro studies using the iodogen method. Four nanomoles of each conjugate peak was added to glass vials coated with 46 nmol of iodogen (Pierce Chemical Co.) and a total of 314, 187, and 103 μCi of Na^{125}I was added to the above conjugates, respectively. After reaction for 10 min in the pH 6.8, 0.2 M sodium phosphate buffer, the conjugate was separated from unreacted Na^{125}I by gel filtration over a PD-10 column. The radiochemical purity of the iodinated conjugate was checked by TLC using silica gel impregnated glass-fiber strips (*19*) and was 80% or above.

In Vitro Assays of Tumor Cell Retention. The interaction in vitro of iodinated conjugates with either FEMX human melanoma cells, which express the NRML-05 antigen, or human HT-29 colon carcinoma cells, which express the NRLU-10 antigen on their surface, was monitored using the method of Press et al. (*21*). Briefly, cells were incubated with the appropriate antibody on ice for 1 h, washed with PBS at 4 °C, and incubated in fresh medium at 37 °C for various times up to 24 h before harvesting. At harvest, the overlaying supernatant (shed component) was collected. This component contains

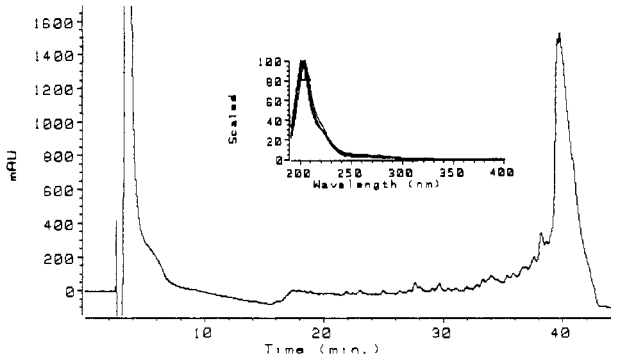


Figure 1. Reversed-phase HPLC purification of peptide 1. N-Acetylated crude peptide was chromatographed on a Vydac analytical C4 column with an elution gradient of 2% acetonitrile/min starting from 100% water and a flow rate of 1 mL/min. The peptide elutes at ca. 40 min, at 80% acetonitrile–20% pH 6.7, 5 mM phosphate buffer. Inset: overlaid spectra of the eluted peak taken during elution at 39.4, 39.7, and 40.8 min. See text for details.

unbound conjugate. The cells were collected by centrifugation and treated using two consecutive washes with a pH 2.5 solution of 2.5 mg/mL chymopapain. Surface-bound conjugates which were removed are referred to as the cell surface component, and remaining conjugates are referred to as the internalized component.

Antigen Binding. Antigen binding of free and peptide-derivatized NR-ML-05 Fab was examined by competition ELISA (*22*). Briefly, a 0.1% Nonidet NP-40 extract of A375 met-mix melanoma cells containing the tumor antigen for NR-ML-05 was used to coat the ELISA plates. The test conjugate was then mixed with biotin-labeled NR-ML-05 whole antibody, varying in concentration from 0.9 to 70 nM, and both were equilibrated in the ELISA wells. After washing, bound conjugates were detected by the loss of NR-ML-05 binding, which was detected with streptavidin–horse radish peroxidase. The apparent inhibition constants are the concentration of test conjugate which half-inhibited whole antibody binding. A similar protocol was used to quantitate NR-LU-10 Fab conjugate binding to antigen extracted from LS174 colon carcinoma cells.

RESULTS

Characterization of Peptide 1. Figure 1 shows the reversed-phase elution from a C4 column of peptide 1 as a single peak at 80% acetonitrile. More common elution conditions incorporating 0.1% trifluoroacetic acid as an ion pairing agent were not used since the peptide was insoluble at pH 2. Of the 1.04×10^6 ^{14}C cpm injected, 77% were recovered in the main peak. The peptide peak eluting at 40 min appears somewhat asymmetrical, which could be due to multiple factors such as the presence of an impurity, multisite attachment of this 31mer to the column matrix (*23*), or aggregation such as that known to occur with the similar peptide "GALA" (*9*). The inset shows overlaid UV spectra taken during elution of the 40-min peak on the leading and trailing edges, and at the apex of the peak. These spectra are quite similar, and the lack of significant absorbance in the range of 260–280 nm suggests little derivatization by benzyl carbonium ions or anisylation of glutamates has occurred during the hydrofluoric acid cleavage. A fast atom bombardment mass spectrum showed a single parent ion at $m/z = 2983$. This is consistent with the presence of a single main species eluting in this peak with the predicted mass of N-acetylated peptide 1-amide, and shows that the N-terminal cysteine was not stably modified during the hydrofluoric acid cleavage. The lack of a peak at $m/z = 2940$ suggests that the peptide was fully N-acetylated.

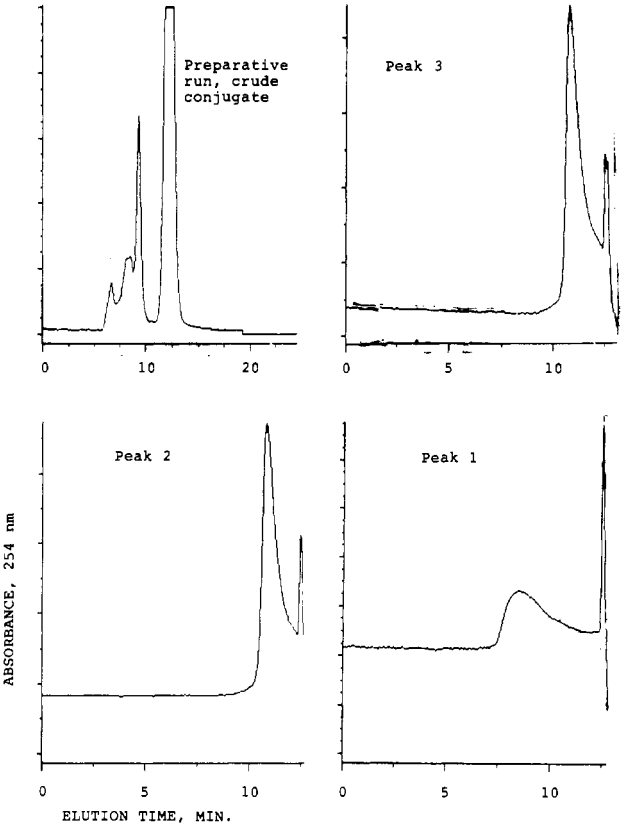


Figure 2. Isolation of three NR-ML-05 Fab–SMCC–peptide 1 conjugate peaks from two preparative gel filtration runs. An example of a preparative run is shown in the upper left panel; rechromatography of three different peaks isolated from two of these runs is shown in the other three panels. Small molecules elute after about 12 min and unmodified Fab elutes at an apparent molecular weight of 34 kDa (10.9 min). These three peaks represent the conjugates studied in Figures 3–6.

Preparation and Separation of Conjugates of Varying Molecular Weight and Peptide Stoichiometry. Based on the linear dose–response curve obtained for reaction of peptide 1 with Fab-SMCC, a defined conjugate with ca. 3 peptides/Fab was purified from free peptide by gel filtration. Samples (2 mL) of conjugate stocks from two separate reactions were eluted in pH 6.8, 0.2 M sodium phosphate buffer on a Du Pont Zorbax GF-250XL 2.1 × 25 cm gel filtration column at 5 mL/min. The peaks from 14 such injections were pooled and rechromatographed (Figure 2). Incorporation of peptide was monitored by counting the attached N-[^{14}C]peptide. Figure 2 (top left) shows that this conjugate was composed of at least three molecular species. From two combined scaled-up reactions, three rechromatographed peaks were selected for further testing (Figure 2). They had apparent molecular weights of 286, 34, and 34 kDa (the apparent molecular weight of unconjugated Fab) and contained a ratio of 3.7, 3.7, and 1.4 peptides/NR-ML-05 Fab. The final specific activities of peaks 1, 2, and 3 were 0.75, 0.65, and 0.36 μCi/μg, respectively, and the concentrations of NR-ML-05 Fab in each were, respectively, 81, 90, and 69 μg/mL after radioiodination and purification by gel filtration on PD-10 columns. Final specific activity of other peptide conjugates was in the range of 0.2–0.9 mCi/mg.

The highest molecular weight peak is broader than the two smaller peaks, suggesting its greater heterogeneity. In the absence of any effect of conjugate asymmetry on its

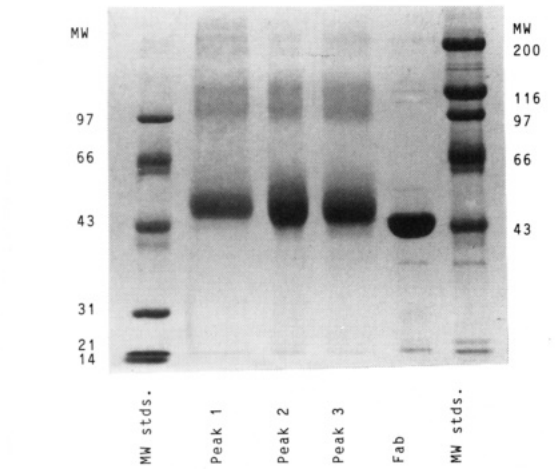


Figure 3. Peptide 1–Fab complexes examined by 10% nonreducing SDS-PAGE. Complexes are those shown in Figure 2, and appear at a slightly higher molecular weight than the Fab standard. Ten micrograms are loaded in each lane; staining is with Coomassie Blue R250. Faint bands are seen at 2–3 times the molecular weight of the heavy and light chains, which may represent a low level of aggregates.

apparent hydrodynamic molecular weight (*24*), the size of peak 1 is roughly consistent with a complex of six Fab fragments (each of apparent molecular weight 34 kDa) and ca. 3.7 times as many attached peptides. If this conjugate is asymmetric in its molecular dimensions, fewer than six Fab fragments would likely be involved in the complex. The stability of peak 1 upon rechromatography suggests strong interactions are involved in this apparent aggregate.

Derivatization of NR-ML-05 Fab with sulfo-SMCC and then with peptide 1 does not appear to significantly compromise its antigen binding. Using competition ELISA, the apparent inhibition constants for NR-ML-05 whole antibody, NR-ML-05 Fab, and conjugate peaks 1 (MW_{app} = 286 kDa) and 2 (3.7 peptides/Fab) were 33, 14, 26, and 24 nM, respectively.

Covalency of Peptide Attachment. No change was observed in the gel-filtration chromatogram of a conjugate of peptide 1 with NR-ML-05 Fab (4.1 peptides/Fab) after incubation with either 13 mM DTT for 2 h or 0.5 M, pH 7.4 sodium phosphate or 3 M guanidine hydrochloride for 3 hours. This suggests that strong interactions bind the higher molecular weight conjugate together, that the Fab fragments are not linked through disulfide bonds, and that any peptide 1 causing the higher molecular weight is also not attached to Fab by a readily reducible disulfide bond.

Since this class of amphipathic peptide has been hypothesized to aggregate (*9*), and peptide 1 sticks tightly to reversed-phase HPLC columns (Figure 1), we evaluated the covalent nature of the interaction of peptide 1 with NR-ML-05 Fab–SMCC using two methods. First, the conjugates isolated by gel filtration above were examined by nonreducing SDS-PAGE (Figure 3). Compared with the Fab standard (MW_{app} = 43 kDa), the conjugate peaks 1–3 appear to run at a slightly higher molecular weight (MW_{app} = 46, 47, and 48 kDa, respectively) and to give slightly broader bands. Since sample preparation for the SDS gels involved boiling in 1% SDS for 3 min, this is consistent with a high-temperature and SDS-resistant derivatization of the Fab by the peptide.

Second, aliquots of each peak were incubated with 0.1 M DTT and 7.5 M urea at room temperature for 2 h and then subjected to reversed-phase chromatography. Peptide and Fab fractions were located by running standards.

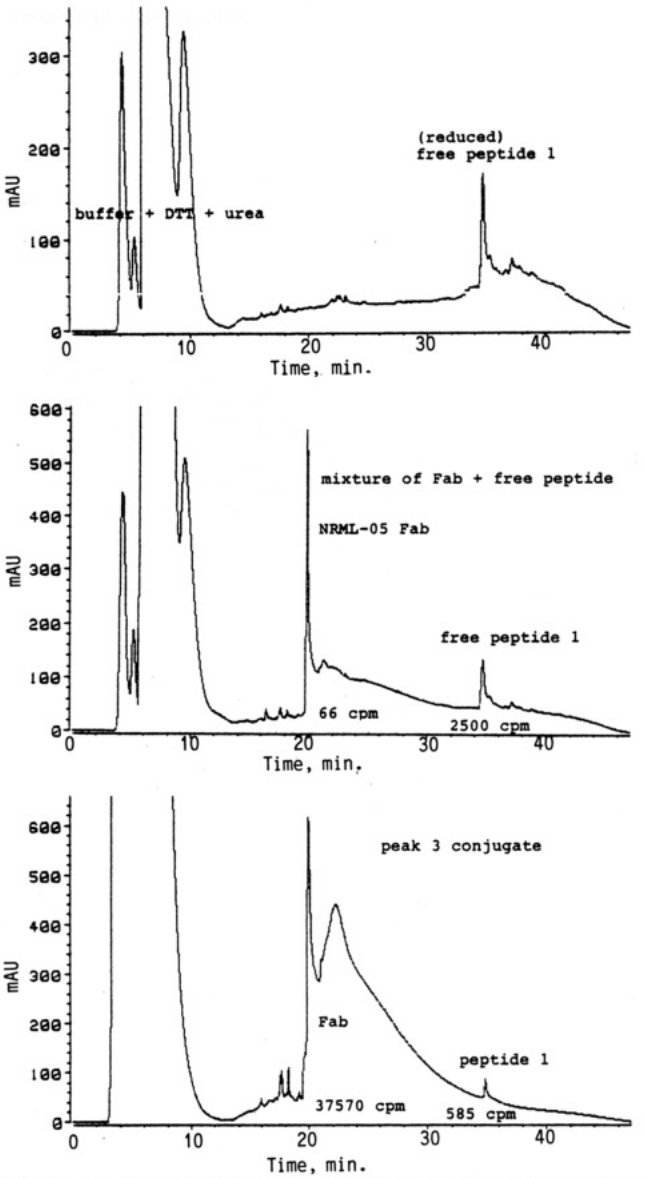


Figure 4. C4 reversed-phase chromatographic separation of peptide 1 from its conjugate. Chromatography at pH 7.0 separated a mixture of free peptide (eluting at 35 min) from free Fab (eluting at 20 min) when both were dissolved in 7.5 M urea + 0.1 M DTT. This assay was used to quantitate peptide 1 bound noncovalently to Fab. Each chromatogram represents a separate experiment. Chromatography was done at pH 7.0 to keep peptide 1 soluble.

Figure 4 shows a chromatogram of free peptide 1 dissolved in 7.5 M urea and 0.1 M DTT which elutes at 82% acetonitrile. NR-ML-05 Fab alone eluted in the range of 50–60% acetonitrile in two peaks. Also shown in a separate experiment is elution of free Fab and peptide 1 without prior cross-linking. This indicates that the broad Fab peaks and the sharp peptide peak are well separated and that free peptide does not appear to bind to Fab under these conditions. Elution of the purified peak 3 conjugate (bottom panel) is shown for comparison. The Fab area appears to be significantly broadened, due perhaps to covalent derivatization with one or more molecules of cross-linker and peptide. Counting the Fab and peptide peaks for each of the three conjugates studied here (peaks 1, 2, and 3) gave only 1.1%, 2.0% and 1.5% of the total ^{14}C cpm eluting in the free peptide region, out of a total of 74 000, 265 000, and 37 600 cpm, respectively.

Characterization of Peptide 1 Aggregation. In view of the high molecular weight peaks apparent in the

Table I. Apparent Molecular Weight of Peptide Analogs under Different Conditions

peptide	pH	buffer	MW_{app}[a]
1	4.5	0.2 M phosphate–10% DMSO adjusted with acetic acid	2 800
	6.8	0.2 M phosphate	32 500 + 133 000
2	5.0	0.1 M phosphate adjusted with acetic acid	3 100
	6.7	0.2 M phosphate	77 000 + 514 000[b]
	7.4	0.5 M phosphate	6 500

[a] Molecular weight was measured by gel filtration on a Du Pont Zorbax GF-250 column and calculated from a plot of log (molecular weight) vs elution time for Bio-Rad molecular weight standards. The molecular weights of peptides 1 and 2 calculated from their amino acid compositions are, respectively, 2937 and 3320 Da. Peptides 1 and 2 were injected onto the column at concentrations of 375 and 300 μM, respectively. At pH 4.5 the peptide 1 stock solution was somewhat cloudy, as was that for peptide 2 at pH 5.0; thus their concentrations were likely lower at these pH values. [b] Molecular weights were not affected by the presence of 10 mm DTT.

peptide–Fab conjugates discussed above, the molecular weights of peptide 1 and a longer analog, peptide 2, were

CGEAAL(AEAL)$_7$EALAA-amide
2

investigated by gel filtration under different solution conditions (Table I). The peptides appear to have their expected molecular weights at pH 4.5–5.0. Both appear to form more than one higher molecular weight species at pH 6.7–6.8 unless the ionic strength is very high. Since conjugate peaks 2 and 3 appear to have the same molecular weight by gel filtration, while they have different bound stoichiometries of peptide (3.7 and 1.4, respectively), the bound peptides do not appear to significantly affect the molecular weight of these particular conjugates. However, they may contribute to the formation of conjugate peak 1 (MW_{app} = 286 kDa) since the Fab fragment alone has an apparent molecular weight of about 34 kDa by gel filtration.

Interaction of Conjugates with Melanoma Cells. Interaction of peptide 1–NR-ML-05 Fab conjugates with melanoma tumor cells was examined by coincubation at 0 °C for 1 h followed by incubation at 37 °C for up to 24 h and classification of conjugate into unbound, cell-surface, and internalized fractions. Figure 5 shows the time courses resulting from these incubations. About 5% of the NR-ML-05 Fab control bound to cells after 1 h, while 1–2% appears to be internalized. The peak 3 conjugate (1.4 peptides/Fab) gave very similar results. The peak 2 conjugate (3.7 peptides/Fab, MW_{app} same as for Fab) showed enhanced cellular retention. After 1 h, about 12% of the conjugate remained cell surface associated, and ca. 5% was internalized. Thus both conjugate cell surface counts and internalization appear increased for peak 2.

The peak 1 conjugate (MW_{app} = 286 kDa, 3.7 peptides/Fab) showed the most dramatic increase in its cellular interaction. The cell surface component of this conjugate increased over 2-fold, and was internalized 6–9-fold more (to ca. 14%) than the control Fab at times greater than 1 h. As a control, SMCC-derivatized Fab was reacted with 100-fold excess cysteine (the N-terminal peptide residue) to prevent unwanted reaction of the SMCC with any cell surface thiols. Fab–SMCC–Cys did not show any enhanced retention (data not shown). Thus peptide 1 causes some Fab aggregation, and increases antibody retention and internalization by melanoma cells.

Since these conjugates appear to have enhanced cell retention, it was of interest to further probe the role of the peptide in this phenomenon. In a separate experiment, the cellular retention/internalization of peptide 1-derivatized Fab (1.8 peptides/Fab) was compared on HT-29 colon carcinoma cells lacking the antigen for this antibody at 0, 2, and 5 h (Figure 6). Antigen specificity is shown in the top panel for cell-surface-associated Fab. The ratio of bound conjugate for the antigen positive to the antigen-negative cells ranges from 70 at 0 h of incubation to 12 after 2 h. For the Fab–peptide 1 conjugate shown in the bottom panel, this ratio is 4–5 at 0, 2, and 5 h. Thus peptide 1 itself appears to enhance nonspecific binding of conjugate to cells.

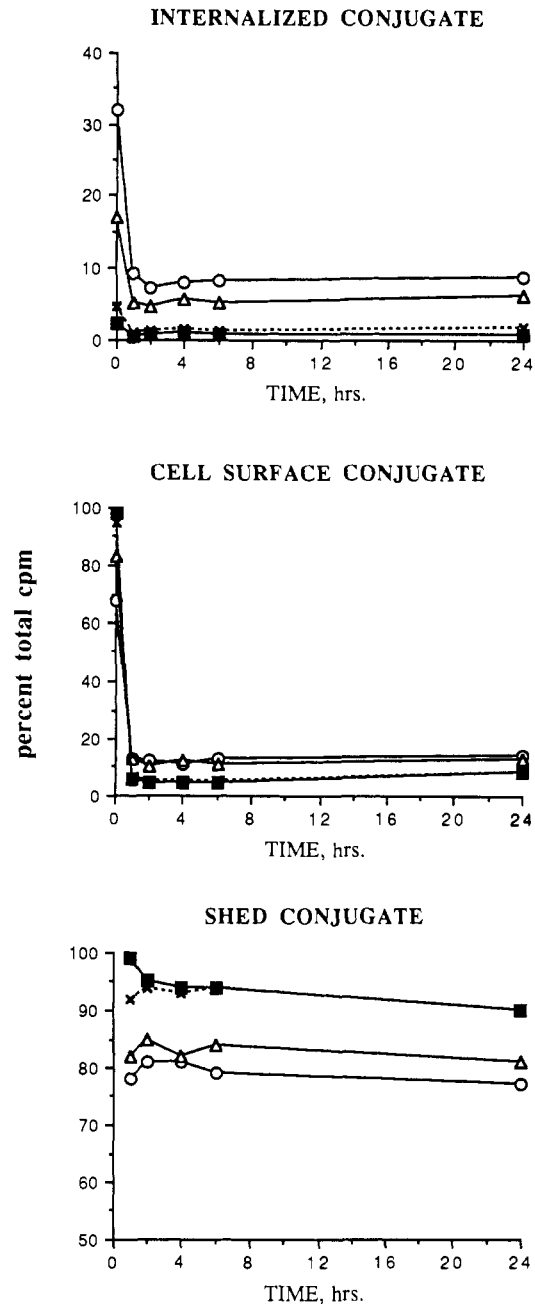


Figure 5. Cell-surface association and internalization of NR-ML-05 Fab–SMCC–peptide 1 conjugate peaks 1, 2, and 3 from Figure 2. All three conjugates were labeled with ^{125}I. Shed cpm appear in the supernatant, cell-surface cpm are released from pelleted FEMX ascites cells by two consecutive pH 2.5 chymopapain washes, and internalized cpm remain with the pellet after this treatment. The properties of the radiolabeled Fab are shown for comparison. Filled squares represent Fab; open circles, peak 1 conjugate; open triangles, peak 2 conjugates; and crosses, peak 3 conjugates.

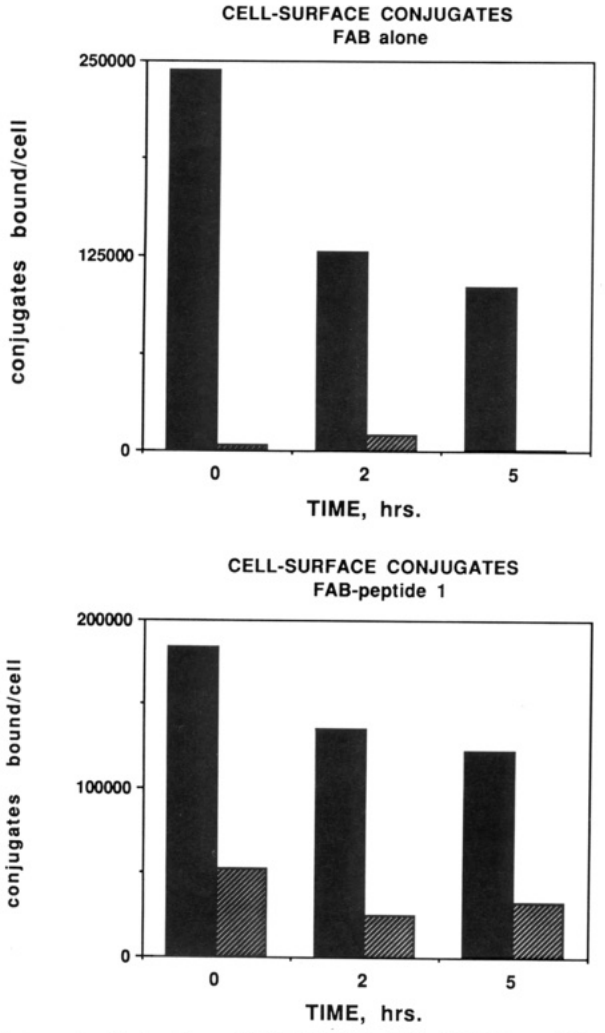


Figure 6. Retention of NR-ML-05 Fab–SMCC–peptide 1 conjugate on antigen-positive and antigen-negative cells. A conjugate with 1.8 peptides/Fab was tested on both antigen-positive A375 met-mix melanoma cells (solid bars) and on antigen-negative HT-29 colon carcinoma cells (hatched bars). The number of conjugates bound/cell was calculated from the bound ^{125}I cpm, the specific activity of radiolabeled Fab (0.37 μCi/μg) and Fab–peptide 1 (0.20 μCi/μg), and the number of cells (10^6). NR-ML-05 Fab alone is poorly retained on antigen-negative cells relative to antigen-positive cells (top panel), but this retention is increased by conjugation to peptide 1 (bottom panel).

Tumor Cell Retention of Conjugates with Peptide 2. To examine whether the apparent added retention due to peptide 1 can be modified or enhanced, an analog of peptide 1 (peptide **2**) was also tested (Figure 6). This analog contains two additional four-residue (AEAL) internal repeats and is thus eight residues longer than peptide 1. A conjugate of 2.9 mol of peptide **2**/mol of NR-ML-05 Fab appeared to have significantly improved early internalization relative to that of Fab alone (20- and 15-fold increases at 0–1.5 h, 3–5-fold increases thereafter to 24 h). This gives a preliminary indication that this longer peptide might work as well as or better than peptide 1.

Tumor Cell Retention of Conjugates with Other Membrane-Active Peptides. To investigate whether other peptides might enhance tumor cell retention or internalization in a similar fashion to peptides **1** and **2**, several peptides known to interact with cell membranes or a membrane-bound receptor were synthesized and their conjugates chromatographed and assayed. Initial experiments with conjugates of these peptides showed little effect on retention or internalization (data not shown), so an N-terminal spacer was fused to these peptides to possibly allow better steric access to the cell surface membrane. The spacer was designed with a somewhat irregular alternation of polar and charged residues, to remain soluble but to avoid β sheet formation. If extended by charge repulsion in the spacer region at pH 7.4, these peptides would have a length of ca. 40–50 Å in addition to the 11 Å of the SMCC cross-linker. The peptides included a synthetic ion channel peptide (with the spacer sequence shown at the N-terminus) CDNDNDDNDD-NGGGLSSLLSLLSSLLSLLSSLLSL-amide (*11*), a Sendai virus fusion peptide CDNDNDDNDDNGGG-GAV-IGTIALGVATATAAQIT-amide (*12*), and the MSH analog MH_a (*13*), CDNDNDDNDDNGGGGGG-SYS(Nle)EH-(d-Phe)RWGKPV-amide. The unmodified ion channel peptide conducts H^+, Na^+, K^+, and guanidinium ions (*11*), and the MSH_a analog binds human melanoma cells with a K_d = 2 nM (*13*).

The bound peptide stoichiometry and antigen binding constants for the Fab conjugate of this ion channel peptide were 4.0 peptides/Fab and K_i(app) = 21 nM. For the viral fusion peptide conjugate they were 1.4 peptides/Fab and K_i(app) = 23 nM, and for the MSHa conjugate they were 2.7 peptides/Fab and K_i(app) = 27 nM. The apparent inhibition constants measured by competition ELISA were 3.3 nM for whole NR-ML-05 and 16 nM for the Fab fragment. Gel filtration of the viral fusion peptide conjugate gave a single Fab-sized peak, while conjugates of the other two peptides gave peaks at higher apparent molecular weights. Thus Fab aggregation may also be a problem with other conjugates made using membrane-active peptides.

Figure 7 shows the tumor cell retention of these unfractionated conjugates. For all three peptide derivatives, the kinetics of internalization appear different than for peptides **1** and **2**, with a slow continual increase in internalized counts over 24 h. The largest increase at 24 h (ca. 4-fold) was due to the spacer–ion channel peptide, and this was less than the 6–9-fold increase of the peak 1 conjugate of peptide 1. Cell surface retention of all conjugates was comparable to or less than that of underivatized Fab. The marked internalization seen previously with peptides **1** and **2** does not appear to be due merely to derivatization of Fab-SMCC with a membrane-binding peptide since two of the conjugates shown in Figure 7 are internalized significantly less than conjugates of peptides 1 and 2.

Retention/Internalization Studies of Peptide Conjugates with NRLU-10 Fab. To examine whether the enhanced retention/internalization observed with NR-ML-05 conjugates can be generalized to other Fab fragments, peptides **1** and **2** were similarly attached to NR-LU-10 Fab, a pan-carcinoma antibody directed to a 39 kDa antigen (*8*). Conjugates were constructed similarly to those detailed above, with stoichiometries of bound peptide of 3.8 and 4.4, respectively. Antigen binding of the resulting unfractionated complexes to HT-29 colon carcinoma cells was essentially unchanged. Neither conjugate showed retention or internalization enhanced beyond that of NR-LU-10 Fab alone (data not shown).

DISCUSSION

This work examines several different peptides for their ability to enhance the cellular retention or internalization of attached therapeutic agents. As an example we have used conjugates with antibody Fab fragments, and have demonstrated that analogs of the peptide "GALA" are capable of increasing the internalization and apparent cell

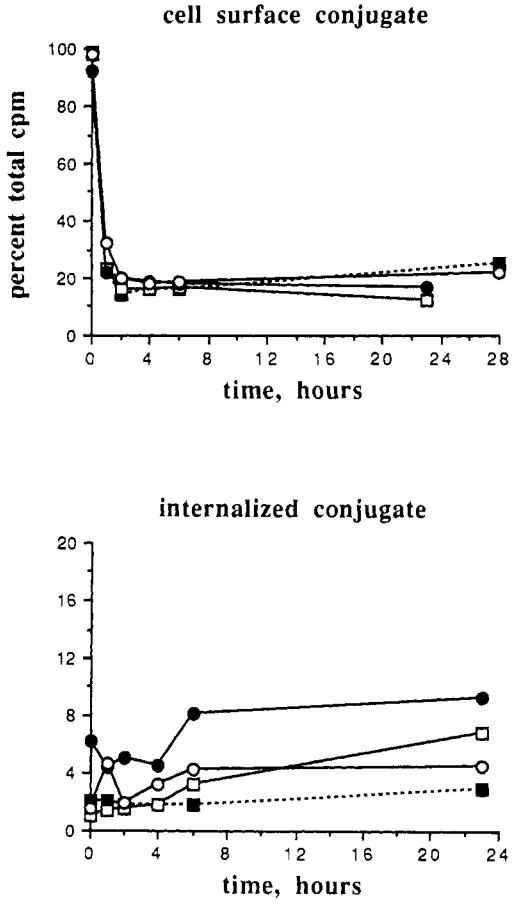


Figure 7. Internalization and cell surface binding of NR-ML-05 Fab alone (solid squares, dashed line) and conjugates with attached spacer-synthetic ion channel peptide (solid circles) (*11*), spacer-Sendai virus fusion peptide (open squares) (*12*), or spacer-MSH_a analog (open circles) (*13*). The peptides were attached to the antibody fragment via the cross-linker SMCC (see the text for details). The *y*-axis scale is expanded for the internalized conjugates for clarity.

surface binding of this 50 kDa protein. Since this approach might be applied to any targeting antibody or protein, results beyond this preliminary work might also be applicable to the internalization of drug-delivery vehicles or other therapeutic proteins. Other approaches in this area include engineering antibodies for increased affinity (see ref 26, for example), addition of nonmetabolizable compounds for radioisotope retention in cells (*6*), or methods for screening large numbers of antibodies for desired properties (*27*). Enhanced tumor localization may also be obtained by the use of antibodies directed to nuclear antigens such as histones, which occur at the necrotic core of solid tumors (*28*). Retention or internalization of toxin conjugates has previously been examined by the inclusion of receptor-mediated internalizing moieties in the conjugates such as transferrin (*29*), an internalizing monoclonal antibody or epidermal growth factor (*30*), transforming growth factor α (*31*), melanocyte simulating hormone (*32*) including chimeric fusion proteins (*33*), or a tight-binding MSH analog (*13*). In this work we examined synthetic peptides for enhancing retention by chemically cross-linking these different peptides to targeting Fab fragments. With the exception of MSH_a, these peptides exhibit no receptor-mediated internalization of which we are aware.

We derivatized Fab fragments rather than whole antibodies since Fab fragments are hypothesized to have enhanced diffusion within a tumor (*5*), enhanced blood clearance which would limit the radiation dose to nontumor tissue, and reduced tumor retention and internalization in vivo. They thus represent a target for which enhanced retention without large increases in molecular weight would be desirable. Due to the diminished retention of Fab fragments, the efficacy of a retention agent should be more readily apparent when attached to a Fab than to a whole antibody.

Conjugates represented as peaks 1 and 2 showed an increased apparent internalization of ca. 6- and 3–4-fold, respectively, over underivatized Fab. The time course of disappearance of ^{125}I from the internal compartment may reflect metabolism of the labeled antibody and excretion of ^{125}I to the cell culture medium as seen by Press et al. (*21*) in similar experiments, and may thus lead to an underestimation of the amount of conjugate internalized and an overestimation of the amount of shed component.

Comparison of the attached peptide stoichiometry of conjugate peaks 2 and 3 (3.7/Fab and 1.4/Fab, respectively) suggests that the increased number of attached peptides in peak 2 may be responsible for its enhanced retention/internalization. Although free peptide 1 appears to aggregate at pH 6.8 (Table I), gel filtration at pH 6.8 (Figure 2) shows that both complexes appear to be unaggregated. The fact that the apparent inhibition constants of Fab binding of the conjugate peaks, as measured by ELISA at pH 7.4, are essentially the same as that for underivatized Fab suggests that the enhanced tumor cell retention at pH 7.4 of conjugate peaks 1 and 2 is not due only to enhanced affinity for the cells. One possible explanation for the enhanced retention and internalization due to peptide 1 would thus include peptide-mediated aggregation of Fab's without a change in the apparent binding affinity to the cells, essentially causing bivalent or multivalent Fab attachment which results in internalization or tight surface retention. If this occurred, and retention were due only to additional Fab-antigen interactions in an aggregated conjugate such as peak 1, one would not expect enhanced retention on antigen negative cells as seen in Figure 6. Another explanation would rely on a direct interaction of the attached peptides with the cell to increase retention/internalization. This could also involve bivalent or multivalent attachment of the conjugate, and might explain the increased retention and internalization seen with antigen negative cells.

The enhanced retention of the peak 1 and 2 complexes of NR-ML-05 Fab–SMCC–peptide 1 is not seen with NR-LU-10 Fab–SMCC–peptide 1 when it is derivatized with a similar number of peptides and a similar protocol. Thus any maleimide unreacted after an overnight incubation with a 6-fold excess of the peptide is not likely to account for the enhanced retention of peaks 1 and 2. Since the maleimide moiety of sulfo-SMCC is stable in aqueous solution at pH 7.0 and 4 °C for only about 64 h (*34*), and preparation and isolation of the peak 1, 2, and 3 conjugates required 8 days, the maleimide moiety may not have been available for further reaction after this time.

The enhanced retention/internalization associated with the above peptide 1 complexes is not exhibited by Fab–SMCC–cysteine. However, a residual retention of the peptide 1 conjugates beyond the retention of Fab alone is seen on antigen-negative cells. Thus the peptide itself appears to contribute this retention. Since the enhancement is not seen when the Fab fragment of NR-LU-10 is derivatized with peptide 1, it may only occur for appropriate antigen–antibody combinations. The A375 metmix melanoma cells on which significant NR-ML-05–SMCC–peptide 1 retention was observed have 1–3 × 10^5 NR-ML-05 whole antibody binding sites/cell, while the

HT-29 colon carcinoma cells used for measurements of NR-LU-10–SMCC–peptide 1 retention have 3×10^6 binding sites/cell for NR-LU-10 Fab (*35*). Thus the NR-ML-05 Fab conjugate which exhibits enhanced in vitro tumor cell retention relative to the NR-LU-10 conjugate of the same peptide has target cells with a 10-fold lower antigen density than those of NR-LU-10 conjugate. It is thus possible that more enhancement of tumor retention due to the attached peptide may be observed at a lower antigen density, although the exact mechanism is unknown.

The enhanced cellular retention which appears to be due to peptide 1 probably cannot be assigned to a single derivatized species, since each conjugate is likely composed of a population of Fabs with variable numbers of lysines derivatized by the heterobifunctional cross-linker sulfo-SMCC. This is consistent with broadened bands seen on SDS gels (Figure 3). We have confined the conjugates examined here to a range of one to four bound peptides, since stoichiometries of peptide below this range have given results similar to underivatized Fab, and higher stoichiometries may interfere with antigen binding. On the basis of its variable region sequences and the constant region consensus sequence for IgG_{2b} antibodies (*36*), NR-ML-05 Fab appears to have only one of about 21 total lysines in its hypervariable loops, loop 2 of the heavy chain. This may explain why antigen binding is not substantially weakened upon derivatization of three or four lysines.

The original parent peptide "GALA", WEAAL$(AEAL)_2$-$(AEHL)(AEAL)_2$EALAA-amide, has been shown to have some helical content at pH 7.5 in 35 mM TES buffer and a higher helical content at pH 5.1 (*10*). Assuming a limiting molar ellipticity for 100% α helix of −38 500 (*25*), the helical content at pH 7.6 and 5.0 can be calculated as 10% and 35%, respectively. This helical content increased with increasing ionic strength at pH 6.5 (*10*). A high helical content of "GALA" would indicate a more compact (lower apparent molecular weight) peptide. Peptide 1, if fully α helical, would be expected to be about 48 Å long, while fully extended it would be about 115 Å. Our data obtained under conditions where "GALA" appeared less helical (pH 4.5 or high ionic strength at pH 7) showed a higher apparent molecular weight for peptide 1 (32 kDa) and peptide 2 (77 kDa). This may be due to nonhelical (extended) forms of the peptide, which are as long or longer than the approximate diameter of a Fab fragment.

We also observe additional higher molecular weight peaks for peptide 1 (130 kDa) and peptide 2 (500 kDa) at pH 6.7–6.8 in lower salt (Table I). If the 32 and 77 kDa peaks are due to extended forms of peptides 1 and 2, the highest molecular weight free peptide peaks may be due to some other structure, such as an aggregated form containing more than one peptide.

The activity of peptide 1 may be somewhat enhanced by lengthening its sequence by eight internal residues. The mechanism by which peptide 1 acts is currently unknown, although peptide 1 bound to a large protein such as a Fab fragment may act by a different mechanism than the low-pH-induced amphipathic helix formation hypothesized to occur for the analogous free peptide (*9*, *10*). The internalization may in fact be dominated by the properties of the antibody–antigen complex, and only modified by addition of peptide to antibody. Alternatively, due to the length of peptides 1 and 2 when extended, peptide-mediated internalization could be due to action as an extended polyanion. These possibilities might be most easily addressed with peptide analogs designed to vary the α helical potential but not the charge distribution or overall hydrophobicity or amphiphilicity, the total negative charge on the peptide, the spacing of the charges, and the hydrophobic moment and amphiphilicity of the peptide.

We have also examined conjugates of other membrane-active peptides to see if we could enhance or generalize this approach. In contrast to conjugates of peptides 1 and 2, all three conjugates gave a slowly increasing internalized fraction over 24 h, although the fractions internalized were less than for peptides 1 and 2. In the case of NR-ML-05 Fab, attachment of a Sendai virus fusion peptide with a spacer region had little effect, even though peptide 1 is an analog of a peptide designed to mimic the activity of a pH-dependent viral fusion protein (*9*, *10*). Enhanced activity was seen with a spacer region fused to an ion channel peptide, but not with the spacer-viral fusion peptide. Thus this spacer sequence does not itself appear to be solely responsible for the activity seen when it is fused to other peptides. Since conjugates of these peptides without the spacer region did not exhibit enhanced retention/internalization, the combination of spacer and membrane-active peptide appears to be necessary for the effect of the ion channel peptide and perhaps the slight effect seen with the MSH_a analog. Although one could speculate that increased accessibility due to the spacer region may account for this effect, the molecular details are currently unknown.

Further applications to radioimmunotherapy using chemical derivatization with particular peptides such as the analogs of "GALA" studied here, which form complex higher molecular weight species with its Fab conjugates, may be limited, since (1) the aggregated species may not be suitable for in vivo use and the active lower molecular weight species such as peak 2 require significant prior purification before use, (2) peptides 1 and 2 failed to enhance cellular retention of a second, different antibody, suggesting their effect on tumor retention may not be generally applicable, and (3) the attachment of peptide 1 to Fab may decrease its specificity of interaction with tumor cells at the same time retention and internalization are enhanced. To avoid the heterogeneity apparent with the chemical derivatization approach, it may be preferable to produce recombinant proteins with the retention sequence of interest fused to the N- or C-terminus, or perhaps in surface ω loops remote from the antibody hypervariable loops.

Peptides such as the "GALA" analogs studied here, which do appear to enhance the internalization of a relatively large protein such as a Fab fragment, may be more useful when combined with more specific therapeutics which thus may need less targeting, such as ribozymes or agents targeted to specific intracellular pathogens.

ACKNOWLEDGMENT

We thank NeoRx Corp. and Dr. Paul Abrams for support of this work and its publication, Dr. Mike Bjorn for helpful suggestions and discussions about retention mechanisms of toxin conjugates, and Jeff Parkins for data on antigen densities of several tumor cell lines.

LITERATURE CITED

(1) Garnett, M. C., and Baldwin, R. W. (1986) An improved synthesis of a methotrexate–albumin–791T/36 monoclonal antibody conjugate cytotoxic to osteogenic sarcoma cell lines. *Cancer Res. 46*, 2407.

(2) Ghose, T., and Blair, A. H. The design of cytotoxic agent-antibody conjugates. In *CRC Critical Reviews in Therapeutic Drug Carrier Systems*, Vol. 3, p 263, CRC Press Inc., Boca Raton, FL.
(3) Pressman, D. (1957) Radiolabeled Antibodies. *Ann. N.Y. Acad. Sci. 69*, 644–650.
(4) Dykes, P. W., Bradwell, A. R., Chapman, C. E., and Vaughan, A. T. M. (1987) Radioimmunotherapy of cancer: Clinical studies and limiting factors. *Cancer Treat. Rev. 14*, 87–106.
(5) Hnatowich, D. J. (1990) Antibody radiolabeling, problems and promises. *Nucl. Med. Biol. 17*, 49–55.
(6) Ali, S. A., Warren, S. D., Richter, K. Y., Badger, C. C., Eary, J. F., Press, O. W., Krohn, K. A., Bernstein, I. D., and Nelp, W. (1990) Improving the tumor retention of radioiodinated antibody: aryl carbohydrate adducts. *Cancer Res. (Suppl.) 50*, 783s–788s.
(7) Woodhouse, C. S., Bordonaro, J. P., Beaumier, P. L., and Morgan, A. C. (1990) Second generation monoclonal antibodies to a human melanoma-associated proteoglycan. In *Human Melanoma, from Basic Research to Clinical Application* (S. Ferrone, et al., eds.) pp 413–429, Springer-Verlag, New York.
(8) Varki, N. M., Reisfeld, R. A. and Walker, L. E. (1984) Antigens associated with a human lung adenocarcinoma defined by monoclonal antibodies. *Cancer Res. 44*, 681–687.
(9) Subbarao, N. K., Parente, R. A., Szoka, F. C., Nadasdi, L., and Pongracz, K. (1987) pH-dependent bilayer stabilization by an amphipathic peptide. *Biochemistry 26*, 2964–2972.
(10) Parente, R. A., Nir, S., and Szoka, F. C. (1988) pH-dependent fusion of phosphatidylcholine small vesicles. Induction by a synthetic amphipathic peptide. *J. Biol. Chem. 263*, 4724–4730.
(11) Lear, J. D., Wasserman, Z. R., and deGrado, W. F. (1988) Synthetic amphiphilic peptide models for protein ion channels. *Science 240*, 1177–1181.
(12) Taken from Varsanyi, T. M., Jornvall, H., and Norrby, E. (1985) Isolation and characterization of the measles virus F1 polypeptide: Comparison with other paramyxovirus fusion proteins. *Virology 147*, 110–117.
(13) Liu, M. A., Nussbaum, S. R., and Eisen, H. N. (1988) Hormone conjugated with antibody to CD3 mediates cytotoxic T cell lysis of human melanoma cells. *Science 239*, 395–398.
(14) Houghten, R. A., DeGraw, S. T., Bray, M. K., Hoffmann, S. R. and Frizzell, N. D. (1986) Simultaneous multiple peptide synthesis: the rapid preparation of large numbers of discrete peptides for biological, immunological and methodological studies. *Biotechniques 4*, 522–528.
(15) Parham, P. (1986) In *Handbook of Experimental Immunology. Volume 1. Immunochemistry* (D. M. Weir, Ed.) Chapter 14, Blackwell Scientific Publications, London.
(16) Ellman, G. L. (1958) A colorimetric method for determining low concentrations of mercaptans. *Arch. Biochem. Biophys. 74*, 443.
(17) Smith, P. K., Krohn, R. I., Hermanson, G. T., Mallia, A. K., et al. (1985) Measurement of protein using biscinchoninic acid. *Anal. Biochem. 150*, 76–85.
(18) *Sulfo-SMCC Handbook*, (1988) Pierce Chemical Co., Rockford, IL.
(19) Wilbur, D. S., Hadley, S. W., Hylarides, M. D., Abrams, P. G., Beaumier, P. A., Morgan, A. C., Reno, J. M., and Fritzberg, A. R. (1989) Development of a stable radioiodinating reagent to label monoclonal antibodies for radiotherapy of cancer. *J. Nucl. Med. 30*, 216–226.
(20) Fraker, P. J. and Speck, J. C., Jr. (1978) Protein and cell membrane iodinations with a sparingly soluble chloramide, 1,3,4,6-tetrachloro-3a,6a-diphenylglycouril. *Biochim. Biophys. Res. Commun. 80*, 849–857.
(21) Press, O., Hansen, J. A., Farr, A., and Martin, P. D. (1988) Endocytosis and degradation of murine anti-human CD3 monoclonal antibodies by normal and malignant T-lymphocytes. *Cancer Res. 48*, 2249–2257.
(22) Marchitto, K. S., Kindsvogal, W. R., Beaumier, P. L., Fine, S. K., Gilbert, T., Levin, S. D., Woodhouse, C. S., and Morgan, A. C. (1989) Characterization of a human-mouse chimeric antibody reactive with a human melanoma-associated antigen. In *Immunity to Cancer*, Vol. 2, pp 101–105, Alan R. Liss, New York.
(23) Hearn, M. T. W. (1984) Reversed-phase high-performance liquid chromatography. *Methods Enzymol. 104*, 190–212.
(24) Tanford, C. (1961) *Physical Chemistry of Macromolecules*, pp 336–346, John Wiley and Sons, Inc., New York.
(25) Merutka, G. and Stellwagen, E. (1989) Analysis of peptides for helical prediction. *Biochemistry 28*, 352–357.
(26) Houghton, A. N. (1988) Building a better monoclonal antibody. *Immunol. Today 9*, 265–267.
(27) Huse, W. D., Sastry, L., Everson, S. A., Kang, A. S., Alting-Mees, M., Burton, D. R., Benkovic, S. J. and Lerner, R. A. (1989) Generation of a large combinatorial library of the immunoglobulin repertoire in phage lambda. *Science 246*, 1275–1281.
(28) Chen, F. M., Epstein, A. L., Li, Z., and Taylor, C. R. (1990) A comparative autoradiographic study demonstrating differential intratumor localization of monoclonal antibodies to cell surface (Lym-1) and intracellular (TNT-1) antigens. *J. Nucl. Med. 31*, 1059–1066.
(29) Raso, V. and Basala, M. (1984) A highly cytotoxic human transferrin-ricin A chain conjugate used to select receptor-modified cells. *J. Biol. Chem. 259*, 1143–1149.
(30) Vollmar, A. M., Banker, D. E., Mendelsohn, J., and Herschman, H. R. (1987) Toxicity of ligand and antibody-directed ricin A-chain conjugates recognizing the epidermal growth factor receptor. *J. Cell. Physiol. 131*, 418–25.
(31) Chaudhary, V. K., FitzGerald, D. J., Adhya, S., and Pastan, I. (1987) Activity of a recombinant fusion protein between transforming growth factor type alpha and Pseudomonas toxin. *Proc. Natl. Acad. Sci. U.S.A. 84*, 4538–4542.
(32) Murphy, J. R., Bishai, W., Borowski, M., Miyanohara, A., Boyd, J., and Nagle, S. (1986) Genetic construction, expression, and melanoma-selective cytotoxicity of a diphtheria toxin-related alpha-melanocyte-stimulating hormone fusion protein. *Proc. Natl. Acad. Sci. U.S.A. 83*, 8258–8262.
(33) Murphy, J. R., Bishai, W., Williams, D., Bacha, P., Borowski, M., Parker, K., Boyd, J., Waters, C., and Strom, T. (1987) Genetic assembly and selective toxicity of diphtheria-toxin-related polypeptide hormone fusion proteins. *Biochem. Soc. Symp. 53*, 9–23.
(34) *ImmunoTechnology Handbook and Catalog* (1990) Vol. 1, p E7, Pierce Chemical Company, Rockford, IL.
(35) Jeff Parkins, personal communication.
(36) Burton, D. R. (1985) Immunoglobulin G: Functional Sites. *Mol. Immunol. 22*, 161.

Synthesis of Protein-Reactive (Aminostyryl)pyridinium Dyes

Anthony C. Stevens,† Rogelio P. Frutos,‡ Daniel F. Harvey,*,‡ and Adrienne A. Brian*,†

Department of Chemistry and Cancer Center, University of California, San Diego, La Jolla, California 92093-0506.
Received June 29, 1992

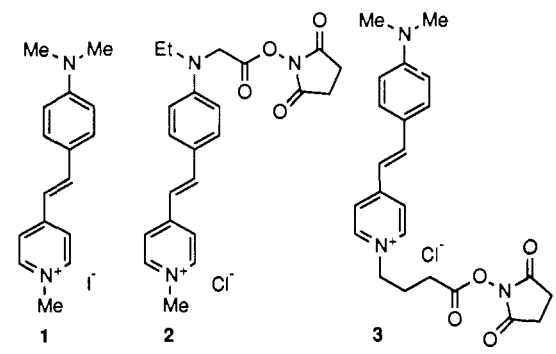
The synthesis of two protein reactive (aminostyryl)pyridinium fluorescent dyes, *N*-ethyl-*N*-[4-[2-[4-(1-methylpyridinio)]ethenyl]phenyl]glycine chloride *N*-hydroxysuccinimide ester (SuASP, **2**) and 4-[4-[2-[4-(*N*,*N*-dimethylamino)phenyl]ethenyl]pyridinio]butyrate *N*-hydroxysuccinimide ester (ASPSu, **3**), is reported. Both form amide linkage through the activated succinimidyl ester with primary amines. The two analogues differ by the position of the pyridinium positive charge relative to the activated ester. SuASP forms an amide linkage that positions the positive charge distal to the protein surface, while ASPSu places the positive charge proximal. The synthesis of SuASP utilizes a palladium coupling reaction for the arylation of 4-vinylpyridine, while the major connection for ASPSu is accomplished through an aldol condensation between 4-(*N*,*N*-dimethylamino)benzaldehyde and picoline. Both reagents are shown to label covalently bovine serum albumin.

INTRODUCTION

Extrinsic covalently attached fluorophores have been widely used in many different avenues of biological research (*1*), including localization of specific proteins in cell organelles (*2*), the determination of rotational and translational diffusion coefficients of proteins (*3*), and the measurement of distances between binding sites on proteins (*4*). Of particular interest are fluorophores that exhibit high environmental sensitivity (*5*). A fluorophore is considered environmentally sensitive when substantial changes in emission intensity and/or wavelength occur in solvents of different polarity. This is generally a good indication that spectral changes will be observed upon interaction of the fluorophore with a biological molecule or upon a change in the environment or structure of a protein to which it is attached. The covalent attachment of an environment-sensitive dye to a protein or peptide can thus provide structural and chemical information about the protein or peptide, as well as information about other molecules that might interact with the protein or peptide near the sight of attachment.

A particularly interesting example of environment sensitivity is the group of (aminostyryl)pyridinium (ASP) dyes (see 1 below) developed by Loew et al. (*6*). The spectral properties of the ASP fluorophore have been observed to be sensitive to static electric potentials through an electrochromic mechanism. This has been demonstrated by measuring the spectral response of the membrane-bound probe as a function of potential applied across the membrane (*6a*). The electrochromic behavior of ASP dyes is the result of the colinearity of its transition dipole and its permanent dipole, essentially producing a migration of the pyridinium positive charge to the aniline nitrogen upon excitation (*6b*). This characteristic of the ASP moiety is probably the cause of its high environmental sensitivity. A 50-nm blue shift and 100-fold increase in the intensity of its emission maximum has been observed upon changing from water to egg lecithin vesicles (*6a*).

We sought to prepare two derivatives of 1 that would permit the covalent attachment of the ASP moiety to a protein or peptide. The environmental sensitivity of this group might then provide information about the environment local to the point of attachment. The two derivatives were sought in order to determine if there is an orientational dependence on the environmental sensitivity of this fluorophore.



Besides the interesting spectral properties of ASP, this fluorophore has several other novel features that suggest its suitability for covalent attachment to a protein or peptide. The relatively small size and positive charge make it water soluble and thus less apt to induce changes in the structure and/or bulk properties of the labeled protein or peptide. It has an excitation maximum of 475 nm (in H_2O), making it nearly coincident with the 488-nm emission line of an argon ion laser, providing a source for measurements that demand high sensitivity.

The ASP derivatives **2** and **3** were prepared by using modifications of the procedures previously developed by Hassner and Loew (*6d*). The key step in the preparation of **3** is a base-catalyzed condensation of 4-(dimethylamino)-benzaldehyde with 4-picoline while a Heck coupling of an aryl bromide with 4-vinylpyridine is used in the preparation of **2**.

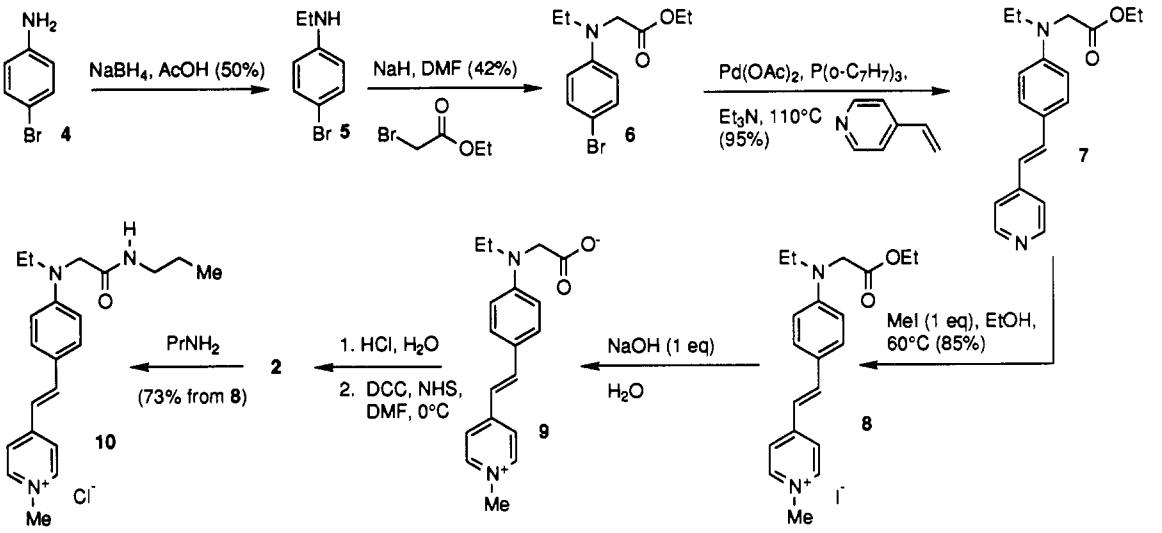
RESULTS AND DISCUSSION

The preparation of SuASP (**2**) required the generation of an unsymmetrical dialkylaniline system. This was accomplished as outlined in Scheme I. Reductive amination of 4-bromoaniline with $NaBH_4$ in AcOH using the procedure developed independently by Gribble et al. (*7*) and Marchini, et al. (*8*) gave *N*-ethylaniline derivative **5** (*9*) in 50% yield. Alkylation of **5** with ethyl bromoacetate gave ethyl ester **6** in 42% yield. The procedure previously

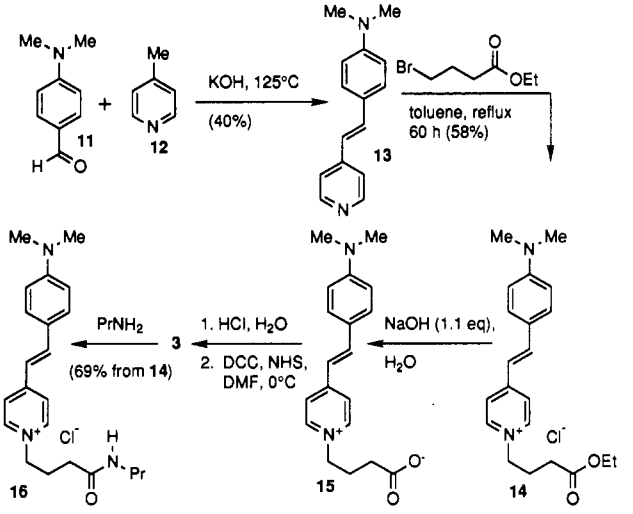
† Department of Chemistry and Cancer Center.
‡ Department of Chemistry.

1043-1802/93/2904-0019$04.00/0 © 1993 American Chemical Society

Scheme I



Scheme II



developed by Heck (*6d*, *10*), palladium-mediated coupling of aryl bromide **6** with 4-vinylpyridine, gave the desired 4-styrylpyridine derivative **7** in 95% yield. The assignment of *trans*-olefin stereochemistry to **7** was based on the observed ^{1}H-NMR coupling constant of 16 Hz between the two olefinic hydrogens. Subsequent pyridine methylation with MeI in ethanol at 60 °C gave pyridinium cation **8**. Careful saponification of **8** with 1.0 equiv of NaOH in an 8:2 mixture of acetone and H_2O gave carboxylate **9**. With greater than 1.0 equiv of base, decomposition/polymerization of **8** was observed, presumably via reaction of the excess base with the pyridinium cation. Protonation of the carboxylate with HCl, followed by treatment with 1,3-dicyclohexylcarbodiimide and *N*-hydroxysuccinimide in DMF, gave the desired *N*-hydroxysuccinimide ester **2**.

The preparation of **3** began with styrylpyridine **13**, prepared by the KOH-catalyzed condensation of 4-(dimethylamino)benzaldehyde (**11**) with 4-picoline (**12**) (Scheme II) (*11*). Alkylation with ethyl 4-bromobutyrate (toluene, reflux) gave pyridinium salt **14** in 58% yield. The butyrate group was the shortest feasible tether because of problems associated with shorter tethers upon exposure to strong base. The relatively low pK_a of the α-hydrogens of 2-pyridinium acetates (*12*) and the prospect of β-elimination with propionate derivatives made them inappropriate for use in this instance. Careful saponification of the ester **14** with NaOH in water gave pyridinium carboxylate **15**. Subsequent protonation with HCl, followed by treatment with 1,3-dicyclohexylcarbodiimide and *N*-hydroxysuccinimide in DMF at 0 °C, gave ASPSu **3**.

Because of their hygroscopic nature and sensitivity toward hydrolysis, difficulties were encountered in the isolation of the pure *N*-hydroxysuccinimide esters **2** and **3**. To confirm the structure of these reagents, both were treated with propylamine to give the corresponding amides **10** and **16** in 73 and 69% yield, respectively, from the corresponding ester.

To demonstrate that **2** and **3** are capable of functioning as protein reactive reagents, each was subjected to labeling conditions in the presence of bovine serum albumin (BSA). A 20:1 molar excess of **2** or **3** to BSA in pH 8.5 $NaHCO_3$ buffer produced a highly colored protein fraction that was readily separable from free label by gel filtration chromatography. Measurements of the UV/vis absorption indicated that >5 equiv of the label were attached to BSA with both **2** and **3**.

To confirm that the above results were due to the covalent modification of BSA with **2** and **3**, and not a result of noncovalent adsorption of the corresponding carboxylates **9** and **15**, several control experiments were carried out. When **9** and **15** were mixed with BSA under the same labeling conditions described above, gel-filtration chromatography resolved a colorless BSA fraction and a highly colored salt fraction (Figure 1a,b). Samples of labeled BSA, previously separated from the unreacted fluorophore by the above gel filtration method, were dissolved in 1% sodium dodecyl sulfate, heated to reflux for 5 min, and purified by gel-filtration chromatography. All of the fluorophore eluted as a sharp peak in the BSA fraction, indicating that all of the fluorophore was covalently bound to the protein (Figure 1c).

The emission and excitation spectra of the parent compound **1** and the amide derivatives **10** and **16** are shown in Figure 2. The emission spectra of these compounds are very similar and structureless, the largest difference being a 20-nm blue shift of **10**, with respect to **1** and **16**. The excitation spectra exhibit two subbands, one at 440 nm (α) and the other at approximately 480 nm (β). Similar structure is also present in the absorption spectra (data not shown). The relative intensities of the two subbands differ between the three compounds. The β-subband is more intense for the two dimethylaniline derivatives (**1** and **16**), while **10** has its excitation maximum at the α-subband.

When **2** and **3** are conjugated to BSA the emission spectra remain structureless and are blue shifted 10 and 20 nm,

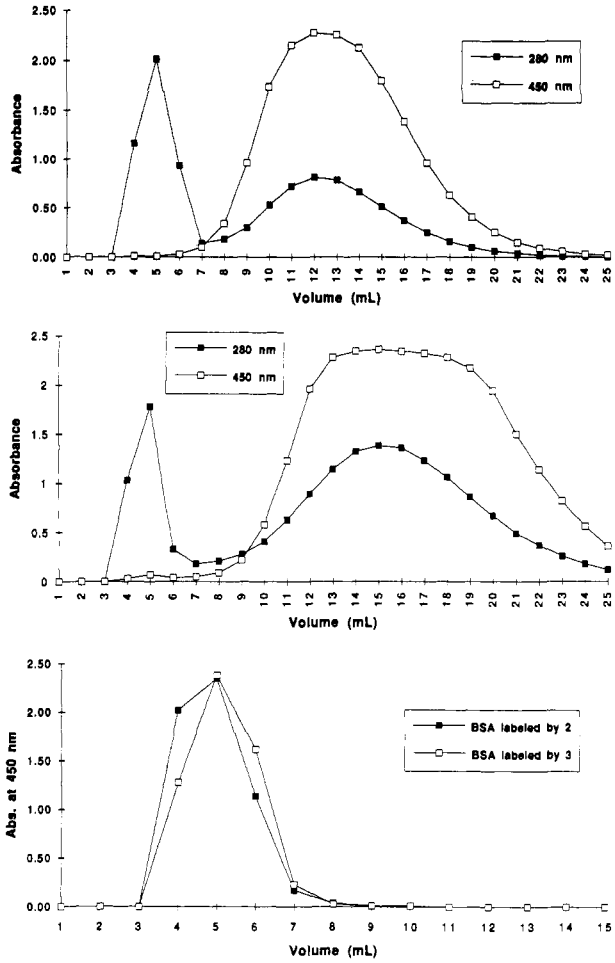


Figure 1. Gel-filtration chromatograms demonstrating covalent labeling of BSA by **2** and **3**. (a) Mixtures of BSA and **9**. (b) Mixture of BSA and **15**. (c) Labeled BSA after reflux in 1% sodium dodecyl sulfate.

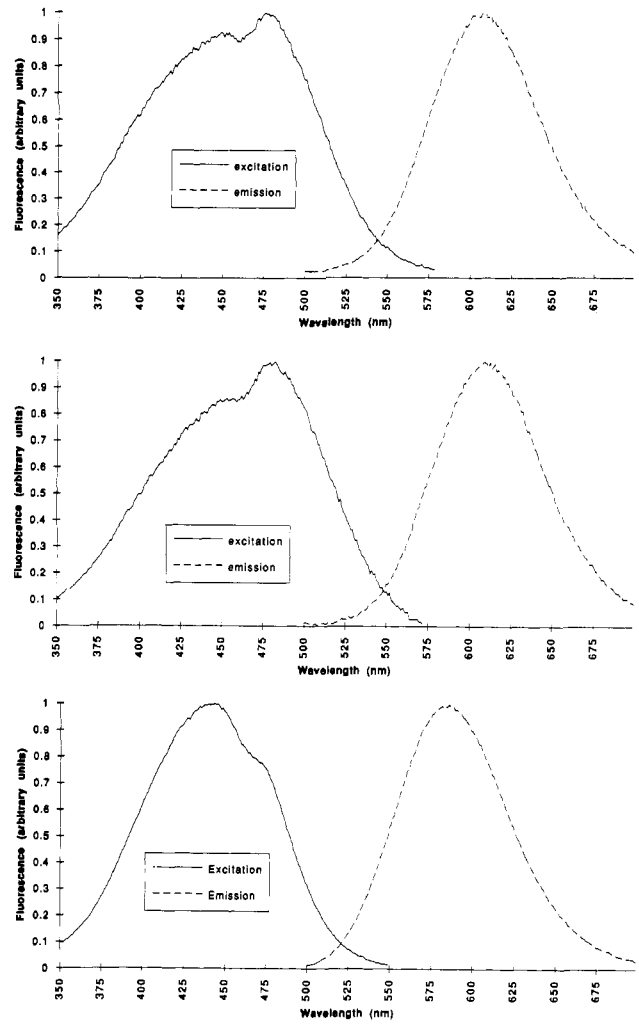


Figure 2. Excitation and emission spectra of unbound (aminostyryl)pyridinium probes in phosphate-buffered saline (PBS), pH 7.4: (a) parent compound **1**, (b) ASPSu propylamide derivative **16**, (c) SuASP propylamide derivative **10**.

respectively (Figure 3). The excitation spectra for both of the BSA conjugates are red shifted and show an increase in the β-subband with respect to the α-subband. In Table I the spectral characteristics of the free (aminostyryl)-pyridiniums and their respective BSA conjugates are compared. A large differene in the sensitivity of absorbance maximum in going from the free to the protein-bound state for **2** and **3** is indicated, where **3**–BSA produces a much larger red shift than **2**-BSA. There also appears to be greater sensitivity of the emission maximum for **3**. The quantum yields of the protein bound and free forms are quite different. The **3**-BSA and **2**-BSA conjugates have a 120- and 12-fold increase in the fluorescence efficiency, respectively.

Since the spectral properties of the two unbound probes behave in a similar fashion within a series of different solvents (*13*), the (aminostyryl)pyridiniums in **2**-BSA and **3**-BSA may reside in different environments. If one interprets the data with respect to the behavior of the free probes in bulk solvents of different polarity, then the trends in spectral properties suggest that the probes are in a hydrophobic environment relative to bulk aqueous solution, with **3**-BSA being more hydrophobic than **2**-BSA. If **2** and **3**, on average, react with the same lysine ϵ-amino groups on BSA, these results suggest that the probe with the pyridinium positive charge distal from the protein surface (**2**-BSA) is more accessible to the bulk solvent than when the positive charge is proximal to the protein surface (**3**-BSA). Table I also shows the differences in spectral characteristics when the label density of **2** and **3** are varied from one to multiple sites on BSA. Interpreting the data in terms of the behavior of the probes in solvents of different polarity, the changes in spectral properties are in the direction of a less hydrophobic environment (with exception to the absorbance maximum of **2**-BSA, which is red shifted further). This may indicate that the probes **2** and **3** react more efficiently with the lysine ϵ-amino groups in hydrophobic sites. Alternatively, the self-interaction of the fluorophores with neighboring fluorophores could be responsible for the observed behavior.

In conclusion, two protein-reactive (aminostyryl)pyridinium reagents have been prepared and shown to covalently label BSA. The spectral properties of the two fluorophore/protein conjugates are different and show a dependence on the density of fluorophore on the protein. Studies of the interactions of (aminostyryl)pyridinium dyes with protein environments and the nature of the observed spectral changes are currently in progress.

EXPERIMENTAL PROCEDURES

General Experimental. Melting points are uncorrected and were obtained using a Mel-Temp II melting point apparatus. The 90-MHz ^{1}H-NMR spectra were obtained using a Varian EM-390. A QE-300 (G.E.) NMR spectrometer was used for the 300-MHz ^{1}H-NMR spectra. Infrared spectra were collected using a Galaxy 2020 (Mattson) FT-IR spectrometer. High- and low-resolution

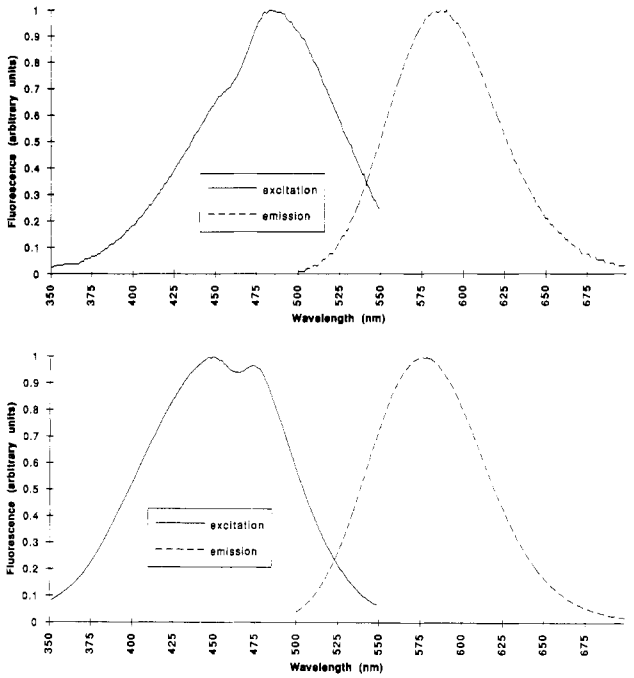


Figure 3. Excitation and emission spectra of BSA conjugates. (a) **3**-BSA. (b) **2**-BSA.

Table I. Spectral Data of Free and BSA-Bound (Aminostyryl)pyridiniums

compd/conjug	absorbance max (nm)	emission max (nm)	quantum yield
1	443	605	0.001
16	452	608	0.001
10	435	586	0.01
2-BSA[a]	438	576	0.12
2-BSA[b]	442	580	0.07
3-BSA[a]	473	587	0.12
3-BSA[b]	466	592	0.04

[a] Labeling under 1:1 (**2** and **3** to BSA) conditions. These conditions produced 0.4 probes/BSA for **2**-BSA and 0.8 probes/BSA for **3**-BSA. [b] Labeling under 20:1 conditions. These conditions produced 6 probes/BSA for **2**-BSA and 8 probes/BSA for **3**-BSA.

mass spectra were obtained through the mass spectrometry facility at the University of California, Riverside. Reported mass spectra were derived by using a FAB ionization source in all cases except **5**, **6**, **10**, and **16**, which were obtained with an electron impact source (20 eV). UV/vis measurements were done on a Perkin-Elmer Lambda 3A UV/vis spectrophotometer. Excitation and emission spectra were measured using a SLM-AMINCO SPF-500C spectrofluorometer. All cation-exchange chromatography separations were done using CM Bio-Gel A (Bio-Rad) resins in the sodium form. The parent compound **1** was purchased from Molecular Probes and used without further purification. Quantum yields were determined according to the method of the National Bureau of Standards (*14*) using quinine sulfate in 0.1 M $HClO_4$ as a standard.

4-Bromo-*N*-ethylaniline (5). Using a procedure similar to Gribble's (*7*), a stirred solution of 4-bromoaniline (**4**, 3.44 g, 20.0 mmol) in AcOH (150 mL) was treated with $NaBH_4$ (3.40 g, 89 mmol) in small portions while the reaction mixture was kept between 20 and 25 °C. During the addition, subsequent portions were added only after gas evolution had ceased. After the addition was complete the reaction mixture was stirred at room temperature for 24 h. After addition of $CHCl_3$ (100 mL) and extraction with 2 N NaOH solution (2 × 100 mL), the organic phase was dried (Na_2SO_4) and concentrated in vacuo to give a light brown oil. Chromatography on silica gel (9:1 petroleum ether/methanol) gave 4-bromo-*N*-ethylaniline (**5**, 2.0 g, 50%) as a colorless oil. ^1H NMR ($CDCl_3$, 90 MHz): δ 7.26 (d, J = 9 Hz, 2 H), 6.48 (d, J = 9 Hz, 2 H), 3.49 (s, 1 H), 3.08 (q, J = 7 Hz, 2 H), 1.21 (t, J = 7 Hz, 3 H). IR (neat): 3410, 2977, 2872, 1595, 1498, 1319, 1177, 811 cm^{-1}. LRMS: *m/e* (relative intensity) 201 (56, M^+), 199 (59), 186 (99), 184 (100). HRMS ($C_8H_{10}NBr$): calcd, 285.0364; found, 285.0378. UV/vis: λ_{max}(EtOH) = 254 nm, ϵ = 17 500.

***N*-Ethyl-*N*-(4-bromophenyl)glycine Ethyl Ester (6).** A solution of 4-bromo-*N*-ethylaniline (**5**, 1.00 g, 5.0 mmol) in DMF (1.0 mL) was treated with NaH (0.12 g, 5.0 mmol) and heated at 60 °C. After gas evolution had ceased, ethyl bromoacetate (0.90 mL, 7.3 mmol) was added, and the reaction mixture was heated at 50–60 °C for 12 h. After addition of $CHCl_3$ (100 mL) and extraction with H_2O (2 × 100 mL), the organic layer was dried (Na_2SO_4) and concentrated in vacuo to give a yellow oil. Chromatography on silica gel (95:5 petroleum ether/acetone) gave ethyl 2-[*N*-ethyl-*N*-(4-bromophenyl)amino]acetate (**6**, 0.60 g, 42%) as a yellow oil. ^1H NMR ($CDCl_3$, 90 MHz) δ 7.26 (d, J = 9 Hz, 2 H), 6.45 (d, J = 9 Hz, 2 H), 4.15 (q, J = 7 Hz, 2 H), 3.96 (s, 2 H), 3.39 (q, J = 7 Hz, 2 H), 1.4–1.1 (m, 6 H). IR (neat): 2976, 1745, 1592, 1499, 1375, 1191, 1034, 807 cm^{-1}. LRMS: *m/e* (relative intensity) 287 (20, M^+), 285 (21), 214 (94), 212 (100). HRMS ($C_{12}H_{16}NO_2Br$): calcd, 285.0364; found, 285.0378. UV/vis: λ_{max}(EtOH) = 257 nm, ϵ = 16 700.

***N*-Ethyl-*N*-[4-[2-(4-pyridyl)ethenyl]phenyl]glycine Ethyl Ester (7).** Following the procedure of Hassner and Loew (*6d*), a solution of **6** (3.50 g, 12.0 mmol), 4-vinylpyridine (1.66 g, 15.0 mmol), $Pd(OAc)_2$ (27 mg, 0.12 mmol), and tri-*o*-tolylphosphine (72.0 mg, 2.4 mmol) in Et_3N (6.0 mL) under N_2 was heated in a sealed vial at 110 °C for 72 h. After cooling to room temperature and addition of $CHCl_3$ (100 mL), the reaction mixture was extracted with H_2O (2 × 100 mL), dried (Na_2SO_4), and concentrated in vacuo to give a yellow solid. Recrystallization from a hot EtOH/H_2O mixture gave **7** (3.5 g, 95%). Mp: 122–125 °C. ^1H NMR ($CDCl_3$, 300 MHz): δ 8.49 (d, J = 6 Hz, 2 H), 7.39 (d, J = 9 Hz, 2 H), 7.29 (d, J = 6 Hz, 2 H), 7.20 (d, J = 16 Hz, 1 H), 6.77 (d, J = 16 Hz, 1 H), 6.62 (d, J = 9 Hz, 2 H), 4.19 (q, J = 7 Hz, 2 H), 4.03 (s, 2 H), 3.49 (q, J = 7 Hz, 2 H), 1.23 (t, J = 7 Hz, 3 H), 1.20 (t, J = 7 Hz, 3 H). IR (KBr): 1742, 1602, 1523, 1184 cm^{-1}. LRMS: *m/e* (relative intensity) 311 (100, MH^+), 310 (58, M^+), 237 (55), 209 (20). HRMS ($C_{19}H_{23}N_2O_2$): calcd, 311.1759; found, 311.1777. UV/vis: λ_{max}(EtOH) = 370 nm, ϵ = 20 200.

***N*-Ethyl-*N*-[4-[2-[4-(1-methylpyridinio)]ethenyl]phenyl]glycine Iodide Ethyl Ester (8).** To a solution of **7** (0.1 g, 0.32 mmol) in warm EtOH (50 °C, 1.0 mL) was added MeI (20 μL, 0.32 mmol). The reaction mixture was sealed and heated to 60 °C for 8 h. During the reaction dark red crystals appeared. After addition of petroleum ether (5 mL), the red solid was filtered and washed with toluene to give **8** (0.12 g, 81%). Mp: 146–148 °C. ^1H NMR (d_6-DMSO, 300 MHz): δ 8.68 (d, J = 7 Hz, 2 H), 8.04 (d, J = 7 Hz, 2 H), 7.88 (d, J = 16 Hz, 1 H), 7.56 (d, J = 9 Hz, 2 H), 7.16 (d, J = 16 Hz, 1 H), 6.69 (d, J = 9 Hz, 2 H), 4.25 (s, 2 H), 4.17 (s, 3 H), 4.12 (q, J = 7 Hz, 2 H), 3.50 (q, J = 7 Hz, 2 H), 1.19 (t, J = 7 Hz, 3 H), 1.12 (t, J = 7 Hz, 3 H). IR (KBr): 1744, 1643, 1618, 1588, 1524, 1177 cm^{-1}. LRMS: *m/e* (relative intensity) 326 (25, MH^+), 325 (100, M^+). HRMS ($C_{20}H_{25}N_2O_2$): calcd, 325.1916; found, 325.1924. UV/vis: λ_{max}(EtOH) = 469 nm, ϵ = 37 700. Anal. Calcd for $C_{20}H_{25}N_2O_2I$: C, 53.10; H, 5.53; N, 6.19. Found: C, 52.52; H, 5.44; N, 5.94.

***N*-Ethyl-*N*-[4-[2-[4-(1-methylpyridinio)]ethenyl]-phenyl]glycinate Inner Salt (9).** To a solution of ester 8 (32 mg, 70 μmol) in acetone (0.8 mL) and H_2O (0.2 mL) was added a 10 N solution of NaOH (7 μL, 70 μmol). After 30 min, the reaction mixture was diluted with H_2O (5 mL) and passed over a cation-exchange resin (CM Bio-Gel A, Bio-Rad) pre-equilibrated with deionized H_2O. Unreacted ester remained bound to the resin and the carboxylate 9 passed through. Carboxylate 9 was collected and dried in vacuo (20 mg, 96% crude yield). This material was used directly in subsequent transformations without further purification. Mp: 159–162 °C. ^{1}H NMR (CD_3OD, 300 MHz): δ 8.42 (d, J = 7 Hz, 2 H), 7.86 (d, J = 7 Hz, 2 H), 7.74 (d, J = 16 Hz, 1 H), 7.51 (d, J = 9 Hz, 2 H), 6.98 (d, J = 16 Hz, 1 H), 6.68 (d, J = 9 Hz, 2 H), 4.18 (s, 3 H), 3.87 (s, 2 H), 3.56 (q, J = 8 Hz, 2 H), 1.22 (t, J = 8 Hz, 3 H). IR (KBr): 1628, 1586, 1526, 1389, 1339, 1175 cm^{-1}. LRMS: m/e (relative intensity) 297 (70, MH^+), 237 (22), 223 (39), 155 (36), 138 (49), 137 (87). UV/vis: λ_{max}(EtOH) = 503 nm, ε = 70 700.

***N*-Ethyl-*N*-[4-[2-[4-(1-methylpyridinio)]ethenyl]-phenyl]glycine Chloride *N*-Hydroxysuccinimide Ester (2).** Carboxylate 9 (generated from 70 μmol of 8) was treated with 1.0 M HCl (70 μL, 70 μmol) at room temperature. After concentration in vacuo at 50 °C, this salt was dissolved in DMF (2.0 mL), cooled to 0 °C, and treated with *N*-hydroxysuccinimide (10 mg, 91 μmol) and 1,3-dicyclohexylcarbodiimide (17 mg, 82 μmol). After 12 h at 0 °C the precipitated *N*,*N*-dicyclohexylurea was removed by centrifugation and washed with DMF (2 × 0.25 mL). The resulting combined DMF solution of *N*-hydroxysuccinimide ester 2 could be used directly or concentrated in vacuo at 70 °C. Alternatively, the NHS ester and any free acid could be separated from excess DCC by precipitation and washing with petroleum ether. Because of the hydroscopic nature of this salt, it was used directly without further purification or characterization.

2-[*N*-Ethyl-*N*-[4-[2-[4-(1-methylpyridinio)]ethenyl]-phenyl]amino]-*N*-propylacetamide Chloride (10). To the *N*-hydroxysuccinimide ester 2 (product of 70 μmol of 8) in DMF (2.5 mL) was added propylamine (12 μL, 140 μmol). After 1 h, the reaction mixture was diluted with water (10 mL) and filtered. The filtrate was passed over a CM Bio-Gel A cation-exchange column in which the bound propylamide 10 was eluted using NaCl (1 M). The propylamide/NaCl solution was dried in vacuo, resuspended in CH_2Cl_2, filtered, and washed with CH_2Cl_2. The CH_2Cl_2 was removed in vacuo to give propylamide 10 (19 mg, 73% yield). Mp: 164–167 °C. ^{1}H NMR (CD_3OD, 300 MHz): δ 8.54 (d, J = 7 Hz, 2 H), 7.99 (d, J = 7 Hz, 2 H), 7.84 (d, J = 16 Hz, 1 H), 7.62 (d, J = 9 Hz, 2 H), 7.13 (d, J = 16 Hz, 1 H), 6.75 (d, J = 9 Hz, 2 H), 4.23 (s, 3 H), 4.00 (s, 2 H), 3.58 (q, J = 7 Hz, 2 H), 3.17 (t, J = 7 Hz, 2 H), 1.50 (sextet, J = 7 Hz, 2 H), 1.24 (t, J = 7 Hz, 3 H), 0.88 (t, J = 7 Hz, 3 H). IR (KBr): 1645, 1587, 1523, 1175. LRMS: m/e (relative intensity) 338 (100, M^+), 289 (23), 239 (30), 155 (36), 138 (40), 137 (78), 107 (25). HRMS ($C_{21}H_{28}N_3O$): calcd, 338.2232; found, 338.2236. UV/vis λ_{max}(EtOH) = 466 nm, ε = 26 000.

4-[2-[4-(*N*,*N*-Dimethylamino)phenyl]ethenyl]pyridine (13). A mixture of *p*-(dimethylaminobenzaldehyde (11, 4.0 g, 26.8 mmol), 4-picoline (12, 5.2 mL, 53.5 mmol), and KOH (1.5 g) was heated at reflux (125 °C) for 1 h. After cooling to room temperature, cold (0 °C) water was added and a yellow solid precipitated. Filtration and recrysallization of this crude precipitate from hot EtOH gave styrylpyridine 13 (2.4 g, 40%) (*11*).

4-[4-[2-[4-(*N*,*N*-Dimethylamino)phenyl]ethenyl]pyridinio]butyrate Chloride Ethyl Ester (14). A solution of 13 (0.25 g, 1.1 mmol) and ethyl 4-bromobutyrate (315 μL, 2.2 mmol) in toluene (12 mL) was heated at reflux for 60 h, cooled to room temperature, and concentrated in vacuo. The crude product was dissolved in H_2O, filtered, and passed over a CM Bio-Gel cation-exchange column. The ethyl ester was eluted using 1.0 M NaCl. The pyridinium chloride/NaCl solution was dried (50 °C) in vacuo and resuspended in CH_2Cl_2. The CH_2Cl_2 solution was filtered and dried in vacuo to give 14 (0.24 g, 58%). Mp: 204–206 °C. ^{1}H NMR ($CDCl_3$, 300 MHz) δ 9.02 (d, J = 6 Hz, 2 H), 7.82 (d, J = 6 Hz, 2 H), 7.60 (d, J = 16 Hz, 1 H), 7.52 (d, J = 9 Hz, 2 H), 6.85 (d, J = 16 Hz, 1 H), 6.67 (d, J = 9 Hz, 2 H), 4.81 (t, J = 7 Hz, 2 H), 4.09 (q, J = 7 Hz, 2 H), 3.03 (s, 6 H), 2.53 (t, J = 7 Hz, 2 H), 2.30 (pentet, J = 7 Hz, 2 H), 1.24 (t, J = 7 Hz, 3 H). IR (KBr): 1720, 1695, 1585, 1527, 1366, 1163 cm^{-1}. LRMS: m/e (relative intensity) 340 (27, MH^+), 339 (100, M^+), 155 (20), 138 (25), 137 (52). HRMS ($C_{21}H_{27}N_2O_2$): calcd, 339.2072; found, 339.2056. UV/vis: λ_{max}(EtOH) = 486 nm, ε = 40 000. Anal. Calcd for $C_{21}H_{27}N_2O_2Cl$: C, 67.2; H, 7.20; N, 7.47; Cl, 9.47. Found: C, 66.13; H, 7.09; N, 7.23; Cl, 9.14.

4-[4-[2-[4-(*N*,*N*-Dimethylamino)phenyl]ethenyl]pyridinio]butyrate Inner Salt (15). To a solution of ester 14 (25 mg, 67 μmol) in H_2O (10 mL) was added a 10 N solution of NaOH (7 μL, 70 μmol). After 30 min at room temperature the reaction mixture was passed over a CM Bio-Gel A cation-exchange resin (pre-equilibrated in deionized H_2O) from which the carboxylate 15 was collected (unreacted ester remained bound) and dried in vacuo (20 mg, 96% crude yield). This material was used directly in subsequent transformations without further purification. Mp: 188–191 °C. ^{1}H NMR (CD_3OD, 300 MHz): δ 8.58 (d, J = 7 Hz, 2 H), 7.96 (d, J = 7 Hz, 2 H), 7.83 (d, J = 16 Hz, 1 H), 7.60 (d, J = 9 Hz, 2 H), 7.08 (d, J = 16 Hz, 1 H), 6.77 (d, J = 9 Hz, 2 H), 4.44 (t, J = 7 Hz, 2 H), 3.06 (s, 6 H), 2.21–2.18 (m, 4 H). IR (KBr): 1586, 1528, 1367, 1164, 821 cm^{-1}. HRMS ($C_{19}H_{23}N_2O_2$): calcd, 311.1759; found, 311.1743. UV/vis: λ_{max}(EtOH) = 475 nm, ε = 34 000.

4-[4-[2-[4-(*N*,*N*-Dimethylamino)phenyl]ethenyl]pyridinio]butyrate *N*-Hydroxysuccinimide Ester (3). Carboxylate 15 (product of 67 μmol of 14) in H_2O (1 mL) was treated with 1.0 N HCl (60 μL) to give the corresponding acid and concentrated in vacuo at 50 °C. This acid was dissolved in DMF (2.0 mL), cooled to 0 °C, and treated with *N*-hydroxysuccinimide (9 mg, 78 μmol) and 1,3-dicyclohexylcarbodiimide (15 mg, 75 μmol). After 12 h, *N*,*N*-dicyclohexylurea was removed by centrifugation and washed with DMF (2 × 0.25 mL). The resulting *N*-hydroxysuccinimide ester could be used directly as a DMF solution or concentrated in vacuo at 70 °C. Alternatively, the NHS ester and any free acid could be separated from excess DCC by precipitation and washing with petroleum ether. Because of the hydroscopic nature of this salt, it was used directly without further purification or characterization.

***N*-Propyl-4-[4-[2-[4-(*N*,*N*-dimethylamino)phenyl]-ethenyl]pyridinio]butyramide Chloride (16).** *N*-Hydroxysuccinimide ester 3 (generated from 67 μmol of 14) in DMF (2.5 mL) was treated with propylamine (10 μL, 122 μmol). After 1 h, the reaction mixture was diluted in H_2O (10 mL), filtered, and washed with H_2O. The filtrate was passed over a CM Bio-Gel A cation-exchange column in which the propylamide was eluted with 1.0 M NaCl. The amide/NaCl solution was dried (50 °C) in vacuo

and resuspended in CH_2Cl_2. The CH_2Cl_2 solution was filtered and dried in vacuo to give **16** (18 mg, 69%). Mp: 170–174 °C. ^1H NMR (d_6-DMSO, 300 MHz): δ 8.80 (d, J = 6 Hz, 2 H), 8.02 (d, J = 6 Hz, 2 H), 7.99 (br s, 1 H), 7.95 (d, J = 16 Hz, 1 H), 7.61 (d, J = 9 Hz, 2 H), 7.19 (d, J = 16 Hz, 1 H), 6.78 (d, J = 9 Hz, 2 H), 4.55–4.38 (m, 2 H), 3.05 (s, 6 H), 2.93 (q, J = 6 Hz, 2 H), 2.3–2.1 (m, 4 H), 1.36 (sextet, J = 7 Hz, 2 H), 0.82 (t, J = 7 Hz, 3 H). IR (KBr): 1655, 1589, 1528, 1261, 1167, 1093, 1026, 804 cm^{-1}. LRMS: m/e (relative intensity) 353 (16, MH^+), 225 (25), 224 (100), 223 (36), 134 (22). HRMS ($C_{22}H_{31}N_3O$): calcd, 353.2467; found, 353.2472. UV/vis: λ_{max}(EtOH) = 485 nm, ϵ = 37 100.

Bovine Serum Albumin (BSA)–ASP Conjugates. To a 1.0 mL $NaHCO_3$ (50 mM, pH 8.5) solution of BSA (5 mg, 75 nmol) was added 70 μL of **2** (0.022 M in DMF) or 55 μL of **3** (0.027 M in DMF) and the mixture stirred at room temperature for 2 h. The labeled protein was separated from unreacted ASP by gel-filtration chromatography on a G-25 (PD-10, Pharmacia) column. The ratio of ASP to BSA was determined by measuring the relative concentrations of both in the protein fraction using UV/vis spectroscopy. BSA concentration was determined using ϵ_{max}(280 nm) of 44 200 and taking the difference of ASP absorbance at 280 nm [ϵ(280 nm, H_2O) = 6000]. ASP concentration was determined by using $\epsilon_{max}(H_2O)$ for **8** (450 nm) and **14** (465 nm) of 30 000 and 25 000, respectively. It was found that 6 equiv of ASP (from **2**) and 8 equiv of ASP (from **3**) were incorporated into each equivalent of BSA. The above incorporation results are typical of labeling reactions carried out with these reagents and many other proteins (ovalbumin, ribonuclease A, lysozyme, trypsin, chymotrypsin, etc.).

ACKNOWLEDGMENT

This work was supported by the American Cancer Society (Junior Faculty Research Award to D.F.H.), the National Institutes of Health (GM39056), and the Rita Allen Foundation (A.A.B.).

Supplementary Material Available: 300-MHz ^1H NMR spectra for **7–10** and **14–16** (7 pages). Ordering information is given on any current masthead page.

LITERATURE CITED

(1) See: Rousseau, D. L. (1984) *Optical Techniques in Biological Research*, Chapter 4, Academic Press, New York.
(2) Thieringe, R., Shio, H., Han, Y. S., Cohen, G., and Lazarow, P. B. (1991) *Mol. Cell. Biol. 11*, 510–522.
(3) Weber, G. (1953) *Adv. Protein Chem. 8*, 415–459.
(4) Wu, C. W., and Stryer, L. (1972) *Proc. Natl. Acad. Sci., U.S.A. 69*, 1104–1108.
(5) Lakowicz, J. R. (1983) *Principles of Fluorescence Spectroscopy*, Chapter 7, Plenum Press, New York.
(6) (a) Loew, L. M., Simpson, L., Hassner, A., and Alexanian, V. (1979) *J. Am. Chem. Soc. 101*, 5439–5440. (b) Loew, L. M., Scully, S., Simpson, L., and Waggoner, A. S. (1979) *Nature 281*, 497. (c) Loew, L. M., Bonneville, G. W., and Surow, J. (1978) *Biochemistry 17*, 4065–4071. (d) Hassner, A., Birnbaum, D., and Loew, L. M. (1984) *J. Org. Chem. 49*, 2546–2551.
(7) Gribble, G. W., Lord, P. D., Skotnicki, J., Dietz, S. E., Eation, J. T., and Johnson, J. L. (1974) *J. Am. Chem. Soc. 96*, 7812–7814.
(8) Marchini, P., Liso, G., Reho, A., Liberatore, F., and Moracci, F. M. (1975) *J. Org. Chem. 40*, 3453–3456.
(9) Kakinami, T., Kondo, M., Nakamura, H., Inoue, K., Fujikawa, M., Okamoto, T., and Kajigaeshi, S. (1989) *Ube Kogyo Koto Senmon Gakko Kenkyu Hokoku 35*, 37–45.
(10) Heck, R. F. (1982) *Org. React. 27*, 345–390.
(11) This simple one-pot procedure was found in our hands to be the most reproducible and time-efficient method for the preparation of 13. We thank Professor Jay Siegel for bringing this method to our attention. For other methods for the preparation of 13, see: (a) Pentimalli, L. (1961) *Gazz. Chim. Acta 91*, 991–1004. (b) Kost, A. N., Sheinkman, A. K., and Rozenberg, A. N. (1964) *Zh. Obschch. Khim. 34*, 4046–4054. (c) Sheinkman, A. K., Kost, A. N., Sheichenko, V. I., and Rozenberg, A. N. (1967) *Ukr. Khim. Zh. 33*, 941–946. (d) Kuo, K. T. (1979) *J. Chin. Chem. Soc. 25*, 131–139. (e) Lu, T. H., Lee, T. J., Wong, C., and Kuo, K. T. (1979) *Chin. Chem. Soc. 26*, 53–56.
(12) (a) Krönke, F. (1963) *Angew. Chem., Int. Ed. Engl. 2*, 225–238. (b) Bapat, J. B., Epsztajn, J., Katritzky, A. R., and Plau, B. (1977) *J. Chem. Soc., Perkin Trans. 1*, 1692–1697.
(13) In a series of water/ethanol solvents, the following are the differences in going from 0% to 100% ethanol for ethyl esters 8 and 14. Absorbance max.: (8) 25 nm blue, (14) 33 nm blue. Emission max.: (8) 6 nm red, (14) 5 nm blue. Quantum yield: (8) 9-fold enhancement, (14) 7-fold enhancement.
(14) Velapoldi, R. A. A Fluorescence Standard Reference Material: Quinine Sulfate Dihydrate. *Standard Reference Materials, No. 64.* U.S. Dept. of Commerce, National Bureau of Standards, Washington, DC.

Influence of Carrier on Biodistribution and in Vitro Cytotoxicity of Methotrexate–Branched Polypeptide Conjugates†

F. Hudecz,*,‡ J. A. Clegg,§ J. Kajtár,∥ M. J. Embleton,§ M. V. Pimm,§ M. Szekerke,‡ and R. W. Baldwin§

Research Group for Peptide Chemistry, Hungarian Academy of Science, and the Institute of Organic Chemistry, Eötvös L. University, Budapest 112, P.O. Box 32, H-1518 Hungary, and Cancer Research Campaign Laboratories, University of Nottingham, University Park, Nottingham NG7 2RD, United Kingdom. Received June 29, 1992

Methotrexate (MTX) has been conjugated to various structurally related, synthetic, branched polypeptides containing a poly(L-Lys) backbone by the aid of water-soluble carbodiimide. The average degree of MTX incorporated was found to be dependent on the size of the polymer and on the identity of the terminal amino acid residue of the side chains. Consequently the average molar substitution ratio was in the range of 4.9–72.0 MTX per carrier molecule. CD spectra of conjugates showed significant differences in solution conformation correlating with the identity of the side-chain-terminating amino acid. Polycationic conjugates XAK–MTX (X = Leu or D-Leu) assumed essentially ordered (helical) secondary structure, while the CD spectrum of the amphoteric conjugate (X = Glu) corresponded to only a partially ordered conformation in PBS. The covalent attachment of MTX to branched polypeptides results in a reduction of drug in vitro cytotoxicity influenced by the carrier structure. Conjugation to amphoteric polymers, depending on the configuration and position of glutamic acid (XAK–MTX vs AXK–MTX type conjugates) resulted in a decrease of anti-791T cell activity. However polycationic conjugates bearing L-Leu at the side chain terminal position (LAK–MTX) produced a compound with cytotoxicity only about 60 times less effective than free MTX. The biodistribution in mice has been characterized by blood clearance, whole-body retention, and tissue distribution 24 h after iv administration. Blood clearance of MTX-branched polypeptides could be significantly prolonged by incorporation of glutamic acid into the side chain. The presence of a D-amino acid in the terminal position of the side chain (D-LAK–MTX vs LAK–MTX) or adjacent to the polylysine backbone (a-D-ek–MTX vs aek–MTX) resulted in an elevated whole-body survival. Interestingly enough, the retarded blood survival of amphoteric or polycationic conjugates did not implicate similar tissue distribution. Polycationic carriers were directed predominantly to spleen, liver, and kidney, while conjugates with Glu in the side chain were taken up by the lung, kidney, and liver. It was demonstrated that branched polypeptide–MTX conjugates constructed from a polycationic or even amphoteric carrier can (a) sustain the cytotoxic activity of MTX at a level comparable to that of the frequently used HSA-MTX and (b) be present in the circulation (amphoteric conjugates) and/or in the body (both amphoteric and polycationic conjugates) for a much longer period of time than HSA–MTX or free drug. This study suggests that it is feasible to alter beneficially the body distribution and in vitro toxicity of MTX by logical combination of side-chain sequence, configuration, and identity of amino acid X in the branches of the carrier molecule.

INTRODUCTION

Methotrexate (MTX),[1] a folate antimetabolite, has been in clinical use for more than 35 years. It is a potent anticancer agent of proven benefit in the treatment of acute leukemia, osteogenic sarcoma (*1*), and of rheumatological disorders (*2*). Recently its inhibitory potential has been demonstrated against a group of intracellular parasites (Leishmania) of macrophages (*3*).

MTX was also the subject of early attempts to synthesize drug–carrier conjugates to improve its therapeutic index, including attempts at site-specific targeting or providing controlled release of MTX by using biopolymers like poly- and monoclonal antibodies (*4–8*), serum albumins (*9–15*), neoglycoproteins (*16*), chitosan (*17*), SPDP-modified HSA (*12*), and maleylated BSA (*18*).

Methotrexate has also been linked to various synthetic macromolecules such as poly(Lys) (*6, 19–21*), poly(D-Lys) (*22*), poly(Orn) (*23*), (carboxymethyl)cellulose (*21*), poly(iminoethylene) (*21*), poly(vinyl alcohol) (*21*), dextran (*6, 9, 10, 24*), aminodextran (*25*), or poly(divinyl ether-*co*-maleic anhydride) (*21*). Some of these conjugates like those with HSA (*13, 14*), dextran (*24*), aminodextran (*25*),

† Presented in part at the 32nd Annual Meeting of the British Association of Cancer Research, Manchester, UK, April 14–17, 1991, and at the ACS Symposium on Advances in Bioconjugate Chemistry, San Francisco, CA, April 9–10, 1992.

* Author to whom all correspondence and reprint requests should be addressed.

‡ Research Group for Peptide Chemistry, Hungarian Academy of Sciences.

§ Cancer Research Campaign Laboratories, University of Nottingham.

∥ Institute of Organic Chemistry, Eötvös L. University.

[1] Abbreviations used (in order of appearance in the text): MTX, methotrexate; SPDP, *N*-succinimidyl 3-(2-pyridyldithio)-propionate; EDC, *N*-ethyl-*N'*-[3-(dimethylamino)propyl]carbodiimide hydrochloride; CMC, *N*-cyclohexyl-*N'*-(2-*N*-morpholinoethyl)carbodiimide methyl *p*-toluenesulfonate; HSA, human serum albumin; BSA, bovine serum albumin; XAK, poly[Lys-(X_i-DL-Ala_m)], X = Glu, D-Glu, Leu, D-Leu, or Pro; AXK, poly[Lys-(DL-Ala_m-X_i)], X = Pro, Glu, or D-Glu; AK, poly[Lys-(DL-Ala_m)]; $\overline{DP}_n$, number average of the degree of polymerization; CD, circular dichroism; PBS, phosphate-buffered saline, pH 7.3; $\overline{DS}$, average degree of substitution; MTX–XAK, poly[Lys-(MTX_j-X_i-DL-Ala_m)], X = Glu, D-Glu, Leu, D-Leu, or Pro; MTX–AXK, poly[Lys-(MTX_j-DL-Ala_m-X_i)], X = Pro, Glu, or D-Glu; WBS, whole-body survival; AUC, area under the curve.

1043-1802/93/2904-0025$04.00/0 © 1993 American Chemical Society

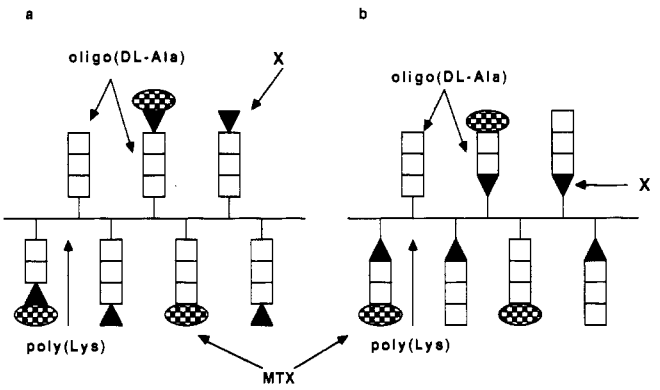


Figure 1. Schematic representation of branched polypeptide–methotrexate (MTX) conjugates: (a) poly[Lys-(MTX$_j$-X$_i$-DL-Ala$_m$)], (XAK-MTX) and (b) poly[Lys-(MTX$_j$-DL-Ala$_m$-X$_i$)], (AXK-MTX).

and the derivatives of HSA (*12*) have been used for coupling to target specific poly- or monoclonal antibodies. MTX–polylysines were used successfully in studying the mechanism of action of cellular uptake by pinocytosis (*19*, *22*).

The methods for conjugation of methotrexate to carriers have involved predominantly the glutamic acid moiety. Activation of α- and γ-carboxyl groups has been achieved by (a) *N*,*N*′-dicyclohexylcarbodiimides like EDC (*7–11*, *16*, *17*, *25*) and CMC (*21*), (b) ester formation with *N*-hydroxysuccinimide (*5*, *7*, *14*, *19*, *25*), or (c) synthesis of the mixed anhydride (*7*, *8*, *26*). MTX hydrazide was also examined for the introduction of a hydrazone bond with the carbohydrate moieties in IgG (*27*). (None of the above reported methods has been used for selective derivatization of α- or γ-carboxyl groups of MTX (*5*).) Even though the 2- and 4-amino groups of the pteridine ring of the drug are not proven to be nucleophilic, it is postulated that the aminodextran conjugate of MTX was linked through the amines (*24*). Conjugates have also been synthesized by incorporation of cysteine or 2-mercaptoethylamine (*28*), tetrapeptide (Leu-Ala-Leu-Ala) (*29*), and of (Glu)$_n$, where n = 2–5 oligopeptides (*30*) as spacers.

In the past decade two new groups of branched polypeptides with the general formula poly[Lys-(X$_i$-DL-Ala$_m$)] (XAK) or poly[Lys-(DL-Ala$_m$-X$_i$)] (AXK), where $i < 1$ and $m \sim 3$, have been synthesized (*31–34*), characterized (*33–35*), and used as biodegradable (*36*) macromolecular carriers for targeting of drug (*37*, *38*), as immunomodulatory peptides (*39*), or as construction materials for synthetic antigens with T or B cell epitopes (*40*, *41*). The aim of the present work was to provide a rational approach for selection of synthetic branched polypeptide carriers for methotrexate. In order to achieve this, MTX has been attached to various related polymeric polypeptides with different primary (*33*, *34*) and secondary structure (*33*, *34*) and immunological (*42–44*) and pharmacological (*45*, *46*) properties.

In this paper we describe the synthesis and conformation analysis of methotrexate-branched polypeptide conjugates (Figure 1) in which MTX molecules are attached to the carrier by amide bonds. In order to determine predominant structural features of the carrier polypeptide influencing the conjugate's biodistribution (blood-clearance profile, whole-body survival, tissue distribution) and in vitro cytotoxicity, we performed comparative studies on a range of MTX conjugates with different side-chain characteristics. Conjugates have been tested and compared with the free drug and other conjugates like MTX–HSA.

EXPERIMENTAL PROCEDURES

Abbreviations used in this paper follow the rules of the IUPAC–IUB Commission of Biochemical Nomenclature (*47*) in accord with the recommended nomenclature of graft polymers (*48*).

Methotrexate was obtained from Lederle Laboratories (Gosport, UK); *N*-ethyl-*N*′-[3-(dimethylamino)propyl]-carbodiimide hydrochloride (EDC) was obtained from Pierce (UK).

Branched polypeptides used in these studies were synthesized in our laboratory as described previously (*33*, *34*). Briefly, poly(Lys) was prepared by the polymerization of N^{α}-carboxy-N^{ϵ}-(benzyloxycarbonyl)lysine anhydride under conditions that allowed an average degree of polymerization ($\overline{DP}_n$) of approximately either 80–120 or 400–500. After cleavage of protecting groups from poly-[Lys(Z)], either poly[Lys-(DL-Ala$_m$)] (AK) was prepared by grafting of short oligomeric DL-Ala side chains onto the ϵ-amino groups of poly(Lys) or poly[Lys-(X$_i$)] was produced by coupling protected amino acid by the active ester method. Poly[Lys-(X$_i$-DL-Ala$_m$)] (XAK) was synthesized by reacting a suitably protected amino acid pentachlorophenyl ester to the α-amino groups of AK. Blocking groups were removed completely with HBr in glacial acetic acid, as confirmed by UV spectroscopy at 254 nm. Poly-[Lys-(DL-Ala$_m$-X$_i$)] (AXK) was prepared by the introduction of DL-Ala oligomers to the previously deprotected α- and ϵ-amino groups of poly[Lys-(X$_i$)] by the aid of *N*-carboxy-DL-Ala anhydride. The primary structures of polypeptides were studied by amino acid analysis, by the identification of the branch-terminating amino acid residue (*49*), and by the determination of the enantiomer composition of the side chains (*50*). The size of these compounds was analyzed by sedimentation analysis and gel chromatography (*31*).

Coupling of Methotrexate to Branched Polypeptides. Coupling was performed with *N*-ethyl-*N*′-[3-(dimethylamino)propyl]carbodiimide hydrochloride (EDC) in PBS at pH 9.0 using a 1.5 times molar excess of carbodiimide. Briefly, dried methotrexate (10.0 mg, 22 μmol) was dissolved in 0.05 N NaOH (1 mL) before use. A 136–680-μL portion (3.0–15.0 μmol) of this solution was added dropwise to 20 mg (0.1–0.5 μmol) of polypeptide in 10 mL of 0.01 M PBS. The mixture was stirred and treated with 4.5–22.5 μmol (0.9–4.3 mg) of EDC in 90–430 μL of water and the pH was adjusted to 9.0. The reaction mixture was stirred for 1 h at room temperature and allowed to react for 16 h at 4 °C in the dark. The final concentration of polypeptide was 1.5 mg/mL. The input molar ratio of MTX to polypeptide was between 30:1 and 135:1. After conjugation, the reaction mixture was applied to a Sephadex G-25 M column (15 × 1.6 cm) equilibrated with PBS. The appropriate macromolecular peak as defined by UV detection at 275 nm was collected. The average degree of molar substitution (DS) was estimated by amino acid analysis and spectrophotometrically at 373 nm assuming that the extinction coefficient of methotrexate at 373 nm is 7800 M^{-1} cm^{-1}. Analytical data on the conjugates are presented in Table I.

HPLC Analysis of Branched Polypeptide–MTX Conjugates. *Instrumentation.* The HPLC system consisted of one Model 302 and one Model 303 liquid delivery modules, a Model HM/HPLC Holochrome UV–vis detector, a Model 811 dynamic mixer, a Model 802 manometric module, a Model N1 recorder (all from Gilson France SA), a Model 7125 injector valve, and 100- and 200-μL sample loops (Rheodyne Inc, Cotati, CA). A 25 cm × 4.6 mm column in a 3 cm × 4.6 mm Aquapore RP-

300 guard column (Brownlee Labs Inc, Santa Clara, CA) were used. Both columns contained spherical 7-μm silica (300-Å pore size) with a hydrophobic bonded phase.

Conditions. The mobile phase consisted of 0.1 M sodium acetate buffer (pH 4.8) and of acetonitrile (10:90 v/v). Sodium acetate buffer was prepared daily using high-purity (Analar) components and deionized water and was mixed with acetonitrile 20 min before use. The injection volume was 100 μL containing 0.9–1.5 μg (2.0 pmol–3.3 nmol) of methotrexate dissolved in eluent immediately before application or 200 μL containing 0.8–3.0 μg (1.8–6.4 nmol) of MTX coupled to polypeptides in PBS, pH 7.3, and diluted with eluent before use. Free MTX was run as standard and its retention time was determined. UV absorbance was monitored at a wavelength of 313 nm (0.01–0.05 AUFS). Quantitative analysis of conjugates was performed using peak-area measurement calibrated with appropriate standards. All analyses were carried out at ambient temperature with a flow rate of 1.0 mL/min.

Spectroscopic Measurements. Absorption spectra were recorded on an ultraviolet–visible spectrophotometer (Unicam-Pye) in PBS at pH 7.3. Conformations of the conjugates were studied by CD spectroscopy. CD spectra were recorded using a Roussel-Jouan Model III dichrograph (Jobin-Yvon, Longjumeau, France) in quartz cells with optical paths of 0.5 and 0.02 cm at room temperature under constant nitrogen flush. The dichrograph was calibrated with epiandrosterone at 304 nm and D-(−)-pantoyllactone at 220 nm (*51*). The concentrations of solutions was approximately 0.5 mg/mL. CD band intensities are expressed as $\Delta\epsilon$ values related either to one lysine residue in the main chain including a whole side chain (in the range of the spectrum between 190 and 250 nm) or to the MTX content of the conjugate (in the 250–420-nm absorption range). Interpretation of CD spectra was based on the secondary structure analysis of the well-characterized poly(Lys) (*33–34*).

Cytotoxicity Assay. Osteogenic sarcoma cell line 791T was grown in monolayer culture in Eagle's minimum essential medium supplemented with 10% newborn calf serum (MEM + NBCS). It was harvested for routine passage and for cytotoxicity assays with a mixture of 0.25% trypsin and 0.1% ethylenediaminetetraacetic acid in phosphate-buffered saline, adjusted to pH 7.2. Cells suspended in MEM + NBCS were adjusted to a concentration of 5×10^4/mL and plated at 100 μL (5×10^3 cells)/well in 96-well flat-bottom tissue culture grade microtiter plates (Falcon 3072). They were incubated at 37 °C for 4 h until fully adherent. MTX and conjugates in PBS were diluted in MEM + NBCS to twice the desired final concentration and a range of 10-fold dilutions prepared. Each dilution was added in 100 μL to quadruplicate wells, the concentrations stated in the Results being the final concentrations in the wells at this point. Control wells were treated with 100 μL of MEM + NBCS alone. The cells were incubated and then labeled with [^{75}Se]selenomethionine (Amersham International plc, Amersham, UK) as reported previously (*37*). The radioactivity of the wells was measured as counts per minute (cpm) in a γ spectrometer. Percent cytotoxicity was calculated by the following formula:

$$\frac{\text{mean cpm of controls} - \text{mean cpm of treated wells}}{\text{mean cpm of controls}} \times 100$$

Radioiodination of Branched Polypeptide–MTX Conjugates. Branched polypeptide–MTX conjugates were labeled with *N*-succinimidyl 3-(4-hydroxy-5-[^{125}I]-iodophenyl propionate (Amersham International plc, Amersham, UK) using the Bolton–Hunter procedure (*52*) as described earlier (*37*). The ^{125}I-labeled conjugate was purified on a G-25 Sephadex gel column using 0.066 M phosphate buffer, pH 7.6, containing 0.25% gelatin as eluent. Electrophoresis on native polyacrylamide gel with a continuous 8 to 25% gradient (PhastGel gradient 8–25, Pharmacia-LKB, Uppsala, Sweden) was applied to assess the low molecular weight labeled product content of the preparation.

Blood-Clearance and Tissue-Distribution Studies. Balb/mice (Bantin and Kingman, Hull, UK) were used throughout these studies. Drinking water was supplemented with 0.1% w/v sodium iodide. All experimental procedures were carried out with appropriate licences from the UK Home Office and with due consideration for animal welfare.

Groups of mice (n = 3) received a single injection (0.2 mL) of ^{125}I-labeled conjugate via a tail vein. Serial blood samples (10 μL) were taken from the tail tip up to 24 h after injection. At this time the mice were killed and dissected. The blood samples, visceral organs, and residual carcasses were weighed and assayed for radioactivity. Results of the blood-clearance study were expressed as a percentage of the zero-time count rate assuming the blood volume of the mouse (mL) to be 11.2% of the body weight (g) (*53*). Area under the blood concentration–time curve up to 6 h following injection was calculated by the trapezoidal rule (*54*). Results of the tissue-distribution analyses were expressed as (i) a percentage of the injected dose of radioactivity/gram of tissue or blood and (ii) ratios of radioactivity/gram of tissue to radioactivity/gram of blood (tissue to blood). Levels of statistical difference between groups of animals were assessed by Student's t-test.

RESULTS

Synthesis and Chemical Characterization of MTX-Branched Polypeptide Conjugates. The coupling of MTX to branched polypeptides was achieved by a carbodiimide method in which one carboxyl group of the molecule was linked to the α-amino group of the terminal amino acid to provide covalent α-amide bonding. The carboxyl groups of MTX were activated by water-soluble carbodiimide using a 1.5 times molar excess of carbodiimide. It should be noted that no precipitate was detected during the synthesis of conjugates under these conditions. The MTX–XAK/AXK preparations were purified by gel filtration and free MTX content was assessed by reversed-phase HPLC. Characteristic values of the conjugates (MTX content, M_w) are summarized in Table I. The results presented in this table indicate that the amount of MTX incorporated into the polypeptide conjugate depends on the size of the polymer and on the identity of the terminal amino acid residue of the side chain.

The average molar substitution ratio was in the range of 4.9–18.3 MTX per carrier molecule in the case of small relative molar mass polypeptides ($\overline{DP}_n$ = 100) or in the range of 20.3–72.0 in the case of large relative molar mass polymers ($\overline{DP}_n$ = 450). Thus the total number of MTX molecules in conjugates was found to be in correlation with the size of the carrier polypeptide. In order to compare the coupling efficacy in conjugate groups of different size, the average degree of MTX substitution ($\overline{DS}$) has been also calculated and expressed as percent of modified side chains in the conjugates. Interestingly enough no marked differences have been observed be-

Table I. Characteristics of Branched Polypeptide–Methotrexate Conjugates

conjugate	abbreviation[a]	MTX:polypeptide molar ratio	$\overline{DS}$[b] (%)	$\overline{M_w}$[c] ± 5%	% free of[d] MTX
poly[Lys-(MTX$_j$-DL-Ala$_{2.94}$)]	ak–MTX	18.3	18.3	41 400	0.8
poly[Lys-(MTX$_j$-DL-Ala$_{3.1}$)]	AK–MTX	70.2	15.6	186 800	0.7
poly[Lys-(MTX$_j$-Leu$_{0.81}$-DL-Ala$_{2.94}$)]	lak–MTX	6.0	6.0	45 400	0.5
poly[Lys-(MTX$_j$-Leu$_{0.98}$-DL-Ala$_{3.1}$)]	LAK–MTX	36.0	8.0	222 300	0.6
poly[Lys-(MTX$_j$-D-Leu$_{0.98}$-DL-Ala$_{3.1}$)]	D-LAK–MTX	20.3	4.5	215 400	<0.5
poly[Lys-(MTX$_j$-DL-Ala$_{3.8}$-Pro$_{0.95}$)]	apk–MTX	4.9	4.9	51 100	nt[e]
poly[Lys-(MTX$_j$-Pro$_{0.94}$-DL-Ala$_{2.94}$)]	pak–MTX	14.0	14.0	48 900	0.6
poly[Lys-(MTX$_j$-Pro$_{0.96}$-DL-Ala$_{3.1}$)]	PAK–MTX	72.0	16.0	223 000	<0.5
poly[Lys-(MTX$_j$-Glu$_{0.93}$-DL-Ala$_{2.94}$)]	eak–MTX	8.1	8.1	49 200	0.5
poly[Lys-(MTX$_j$-DL-Ala$_{2.67}$-Glu$_{1.0}$)]	aek–MTX	10.0	10.0	49 000	<0.5
poly[Lys-(MTX$_j$-DL-Ala$_{3.1}$-D-Glu$_{0.98}$)]	a-D-ek–MTX	6.2	6.2	50 200	<0.5
poly[Lys-(MTX$_j$-Glu$_{0.96}$-DL-Ala$_{3.1}$)]	EAK–MTX	41.4	9.2	230 500	<0.5
poly[Lys-(MTX$_j$-D-Glu$_{0.95}$-DL-Ala$_{3.1}$)]	D-EAK–MTX	49.9	11.1	229 000	nt[e]

[a] Based on one-letter symbols of amino acids and abbreviation of methotrexate. Capital or small letters denote the size of the conjugates. [b] Average degree of substitution, expressed as percentage of side chains modified with MTX. [c] Calculated from the average degree of polymerization of poly(L-Lys) and of the side-chain composition as described in the Experimental Procedures. [d] Determined by reversed-phase HPLC as described in the Experimental Procedures. [e] nt = not tested.

tween the respective $\overline{DS}$ values of low ($\overline{DP}_n$ = 100) and high ($\overline{DP}_n$ = 450) relative molar mass polypeptide pairs [$\overline{DS}$ for poly[Lys-(MTX$_j$-Leu$_{0.81}$-DL-Ala$_{2.94}$)] (lak–MTX), 6.0%, for poly[Lys-(MTX$_j$-Leu$_{0.98}$-DL-Ala$_{3.1}$)]-(LAK–MTX), 8.0%, for poly[Lys-(MTX$_j$-Glu$_{0.93}$-DL-Ala$_{2.94}$)](eak–MTX), 8.1%, and for poly[Lys-(MTX$_j$-Glu$_{0.96}$-DL-Ala$_{3.1}$)](EAK–MTX), 9.2%].

The choice of carrier polypeptide could also influence the composition of the conjugates. The highest coupling efficacy was obtained with polypeptides containing only oligo(DL-Ala) side chains or Pro at the terminal positions of the side chains ($\overline{DS}_{AK}$ = 15.6%, $\overline{DS}_{PAK}$ = 16.0%). Under identical conditions EDC-mediated synthesis of conjugates made of branched polypeptides with N-terminal Leu/D-Leu could lead to lower $\overline{DS}$ values (e.g., $\overline{DS}_{lak}$ = 6.0% or $\overline{DS}_{D\text{-}LAK}$ = 4.5%).

Quantitative analysis, performed on a reversed-phase HPLC column (pore size of 300 Å, isocratic elution), indicated less than 1% of MTX in the conjugates samples using peak-area measurement calibrated with appropriate standards.

Conformation of Branched Polypeptide–MTX Conjugates. The conformation of the conjugates in water solution was studied by CD spectroscopy in the wavelength region 190–250 nm. The CD curves of LAK–MTX, poly-[Lys-(MTX$_j$-D-Leu$_{0.98}$-DL-Ala$_{3.1}$)] (D-LAK–MTX), and poly[Lys-(MTX$_j$-D-Glu$_{0.95}$-DL-Ala$_{3.1}$)] (D-EAK–MTX) conjugates in PBS at pH 7.3 are shown in Figure 2. In this wavelength region, the circular dichroic spectra indicate the formation of a helical secondary structure for LAK and D-LAK, but only partially ordered conformation for D-EAK conjugates (Figure 2A). The CD signals in this range originate from the optical activity of amide bonds and from the contribution of the MTX moiety. In order to consider this, the $\Delta\epsilon$ are related to the one lysine residue in the main chain including a whole MTX-substituted side chain. Considering the relatively low MTX content of the conjugates (4.5–18.3%), the CD contribution of MTX proved to be negligeble. It should be noted that the CD spectrum of the unconjugated polypeptide LAK corresponds to a highly ordered helical conformation, while D-LAK is partially ordered and D-EAK (*35*) assumes no ordered structure under identical circumstances. These conjugates as well as the free drug also have optical activity in the 250–400 nm absorption range, which is distinct from the amide chromophores and corresponds only to the structure of MTX. Therefore this range of the CD spectra is suitable for monitoring covalently coupled drug and

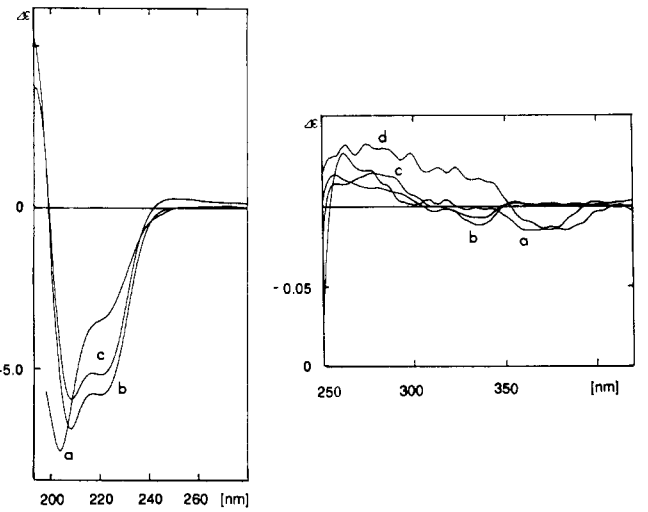


Figure 2. CD spectra of branched polypeptide–MTX conjugates and MTX in PBS of pH 7.3: (a) LAK–MTX, (b) D-LAK–MTX, (c) D-EAK–MTX, and (d) MTX.

Table II. Cytotoxicity of Methotrexate and Branched Polypeptide–MTX Conjugates against 791T Osteogenic Sarcoma Cells

compd	IC_{50}[a] (pmol/mL)	compd	IC_{50}[a] (pmol/mL)
MTX	9.0×10^0	PAK–MTX	6.1×10^3
ak–MTX	1.2×10^3	eak–MTX	6.2×10^3
AK–MTX	3.4×10^3	aek–MTX	2.1×10^3
LAK–MTX	5.4×10^2	a-D-ek–MTX	1.0×10^4
D-LAK–MTX	1.1×10^3	EAK–MTX	6.2×10^3
apk–MTX	3.7×10^3	D-EAK–MTX	9.5×10^3
pak–MTX	5.8×10^3	HSA–MTX	1.2×10^3

[a] Concentration is expressed in terms of molar MTX content of conjugates

local alterations in conjugate structures. CD spectra in the region of 250–400 nm demonstrate the presence of methotrexate moieties (Figure 2B), but no further information could be obtained from this part of the spectra.

Cytotoxicity against Tumor Cells in Vitro. As shown in Table II and Figure 3, conjugation of MTX to branched polypeptide carriers resulted in a marked overall reduction in its cytotoxicity for 791T cells. The poly[Lys-(MTX$_j$-DL-Ala$_{2.94}$)] (ak–MTX) and poly[Lys-(MTX$_j$-DL-Ala$_{3.1}$)] (AK–MTX) conjugates were about 2 orders of magnitude less active, in terms of their MTX content, than the free drug (Figure 3). However, there was only a 2–3-fold difference in cytotoxicity between ak–MTX and AK–

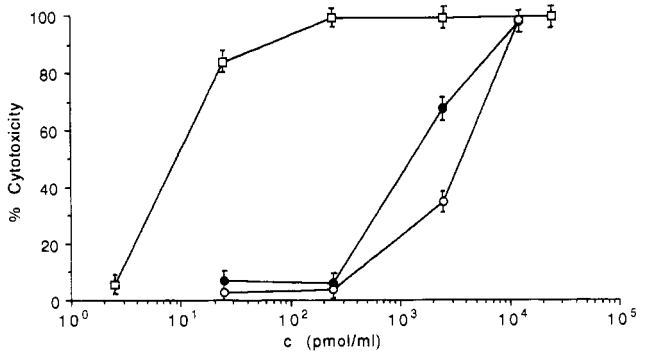


Figure 3. Molecular size of the polypeptide carrier molecule in relation to methotrexate cytotoxicity, and comparison with free drug: (□) free methotrexate, (●) ak-MTX, and (○) AK-MTX.

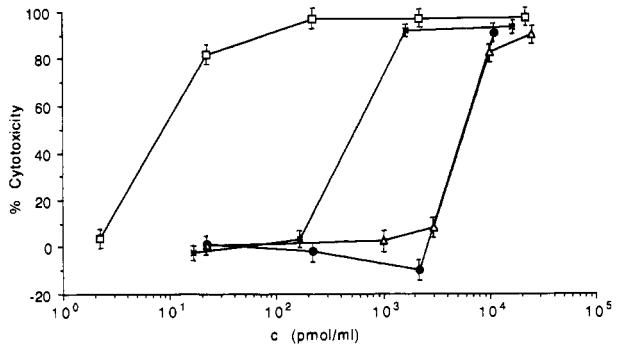


Figure 4. Influence of different side chain terminal amino acids on cytotoxicity of polypeptide-methotrexate conjugates: (□) MTX, (●) PAK-MTX, (△) EAK-MTX, and (X) LAK-MTX.

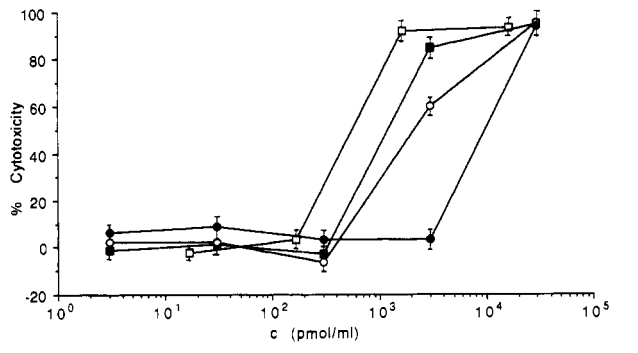


Figure 5. Influence of amino acid configuration of the side chain terminal on cytoxicity of polypeptide-methotrexate conjugates: (○) aek-MTX, (●) a-D-ek-MTX, (□) LAK-MTX, and (■) D-LAK-MTX.

MTX, suggesting that for any given type of polypeptide the conjugation rather than the relative size of the carrier was the primary factor influencing drug activity.

However, the identity of the terminal amino acid on the side chains had more effect than did molecular size. Two conjugates, the polycationic poly[Lys-(MTX_j-$Pro_{0.96}$-DL-$Ala_{3.1}$)] (PAK-MTX) and the amphoteric EAK-MTX were approximately 10 times less cytotoxic than the polycationic LAK-MTX, although compared with each other their cytotoxicity was virtually identical (Figure 4). LAK-MTX was only about 60 times less effective than free MTX in this experiment.

The configuration of the terminal or subterminal amino acid also had a small effect on cytotoxicity. As shown in Figure 5, poly[Lys-(MTX_j-DL-$Ala_{2.67}$-$Glu_{1.0}$)] (aek-MTX) was about 10 times less toxic than LAK-MTX, and in both cases substitution of one amino acid from the L isomer to the D form (aek-MTX) to poly[Lys-(MTX_j-DL-$Ala_{3.1}$-D-$Glu_{0.98}$)] (a-D-ek-MTX) produced a further 4–5-fold

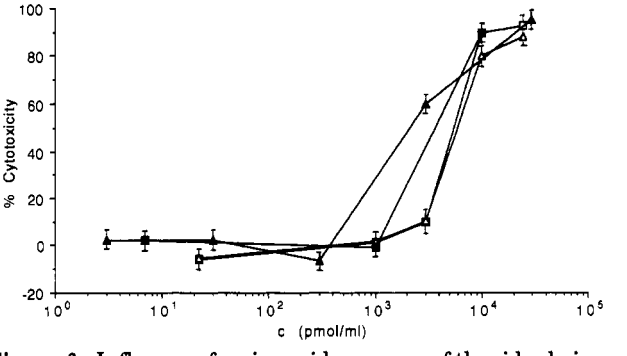


Figure 6. Influence of amino acid sequence of the side chain on cytotoxicity of polypeptide-methotrexate conjugates: (□) pak-MTX, (■) apk-MTX, (△) eak-MTX, and (▲) aek-MTX.

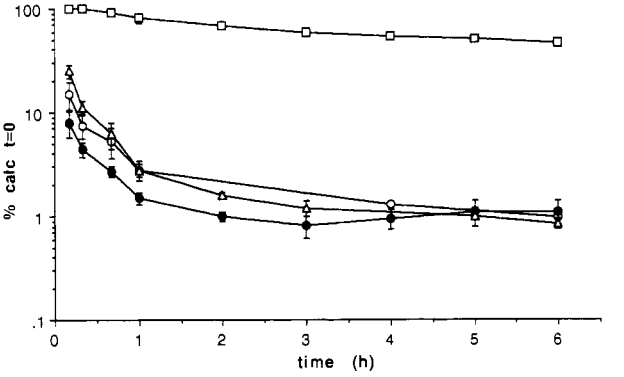


Figure 7. Blood-clearance profiles of ^{125}I-branched polypeptide-MTX conjugates following iv administration to Balb/c mice. AUC_{0-6h} calculated from these data are given in Table III. Results are expressed as mean ± standard deviation for groups of three animals: (○) ak-MTX, (●) AK-MTX, (□) eak-MTX, and (△) pak-MTX.

reduction in activity. Similarly, the sequence of the amino acids in the side chain had a slight influence on cytotoxic efficacy. Thus, while poly[Lys-(MTX_j-$Pro_{0.94}$-DL-$Ala_{2.94}$)] (pak-MTX) and eak-MTX were approximately 500-fold less effective than MTX, moving the alanine residue to the terminal position to make poly[Lys-(MTX_j-DL-$Ala_{3.8}$-$Pro_{0.95}$)] (apk-MTX) and aek-MTX produced a 2–3-fold increase in their activity (Figure 6). These modifications had only a very modest effect in comparison with the overall influence of drug conjugation per se.

Biodistribution of Branched Polypeptide-MTX Conjugates. The blood clearance profile of labeled alanylated polylysine-MTX conjugates after iv administration is depicted in Figure 7. There was no significant difference in the area under the curve (AUC_{0-6h}) for conjugates prepared with either lower (ak-MTX) or higher (AK-MTX) relative molecular mass branched polypeptide. The whole body survival (WBS) 24 h after injection was somewhat elevated for ak-MTX (12.3 ± 0.7% injected dose vs 7.7 ± 0.9% injected dose for AK-MTX). Besides an increased lung uptake of ak-MTX, the tissue-distribution profiles of these conjugates were similar (Figure 8), both compounds being taken up predominantly by spleen and liver. Interestingly enough, alterations in the identity of the side-chain terminating amino acid of the conjugate resulted in marked changes in their biodistribution pattern. The presence of glutamic acid at the end of the branches significantly prolonged blood survival (Figure 7) with a 16-fold increase in the AUC_{0-6h} for eak-MTX compared to that for ak-MTX. The percent injected dose values after 24 h were 1.6–1.8 higher for all three conjugates (eak-MTX, lak-MTX, pak-MTX) than for ak-MTX (Table III). The 24-h tissue distributions of xak-

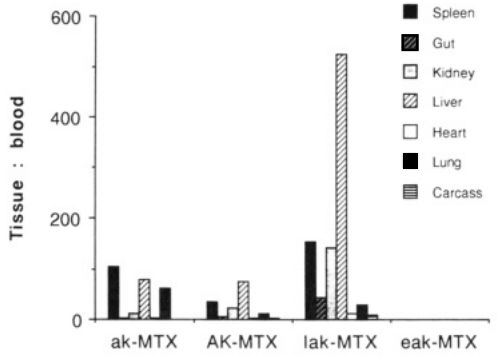


Figure 8. Tissue distribution of ^{125}I-branched polypeptide–MTX conjugates in Balb/c mice 24 h after iv administration. Results are expressed as mean for groups of three animals.

Table III. Biodistribution Parameters of Branched Polypeptide–MTX Conjugates

conjugate	AUC_{0-6h} (% calc t = 0 cpm·h, mean ± SD)	WBS at t = 24 h (% injected dose, mean ± SD)	% dose/g blood at t = 24 h (mean ± SD)
ak–MTX	<25	12.3 ± 0.7	0.1 ± 0.02
AK–MTX	<20	7.7 ± 0.9	0.06 ± 0.01
lak–MTX	ND[a]	20.1 ± 1.9	0.03 ± 0.01
LAK–MTX	ND	12.8 ± 1.4	0.06 ± 0.03
D-LAK–MTX	20.6 ± 1.1	30.1 ± 0.9	0.04 ± 0.01
apk–MTX	<25	21.9 ± 2.4	0.2 ± 0.02
pak–MTX	<25	19.6 ± 0.5	0.12 ± 0.01
eak–MTX	394.3 ± 27.4	22.9 ± 1.5	12.9 ± 1.9
aek–MTX	171.0 ± 3.9	9.7 ± 0.5	4.8 ± 0.2
a-D-ek–MTX	259.3 ± 14.6	36.1 ± 2.0	16.5 ± 2.4
EAK–MTX	265.1 ± 4.6	16.9 ± 1.7	6.5 ± 0.6
D-EAK–MTX	206.3 ± 13.2	13.6 ± 0.6	9.4 ± 3.2
HSA–MTX	ND	5.6 ± 2.2	0.25 ± 0.06

[a] ND = not determined.

MTX (where X = Leu or Glu) are shown in Figure 8. Although the WBS values were very similar for these conjugates and for pak–MTX, tissue to blood ratios for spleen, liver, and kidney were different. Polycationic lak–MTX had a highly increased tissue to blood ratio (>150 for all three tissues mentioned above). However, tissue to blood ratios for eak–MTX were less than 0.25, with the percent dose/gram of blood at t = 24 h being 100 times greater than for ak–MTX or xak–MTX, where X = Leu or Pro.

Replacement of the L-amino acid by its D-isomer at the side chain terminal position had no significant effect on the biodistribution of the Glu-containing conjugates (Figure 9) and only minor changes could be observed in AUC_{0-6h} and in WBS values (Table III). In contrast, for conjugates studied, when Glu was adjacent to the polylysine backbone, the blood survival and the WBS of the two conjugates differed markedly. The conjugate with D-Glu (a-D-ek–MTX) had a 1.5-fold elevated AUC_{0-6h} and 3.7-fold increased WBS compared to the respective values of aek–MTX. In the case of polycationic conjugates, the same tendency was observed, namely D-LAK–MTX had significantly higher WBS than LAK–MTX (Table III). Twenty-four hours following iv administration the tissue-distribution profiles of each pair were very similar (Figure 10). Both LAK–MTX and D-LAK–MTX, and also lak–MTX (Figure 8), were taken up predominantly into liver, spleen, and kidney. In contrast EAK–MTX and D-EAK–MTX (Figure 10) or aek–MTX (Figure 12) had tissue to blood ratios less than 0.4 for all tissues.

The effect of changing the side-chain amino acid sequence of the branched polypeptides on the biodistribution of carrier–MTX conjugates is illustrated in Figures

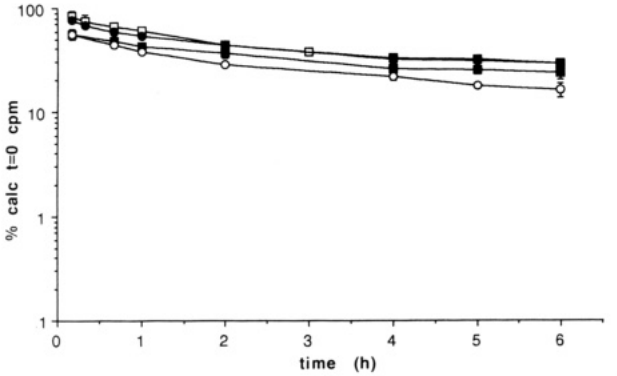


Figure 9. A comparison of the blood clearance of ^{125}I-labeled EAK–MTX and D-EAK–MTX and of ^{125}I-labeled aek–MTX and a-D-ek–MTX in Balb/c mice following iv administration. AUC_{0-6h} calculated from these data are given in Table III. Results are expressed as mean ± standard deviation for groups of three mice: (□) EAK–MTX, (■) D-EAK–MTX, (○) aek–MTX, and (●) a-D-ek–MTX.

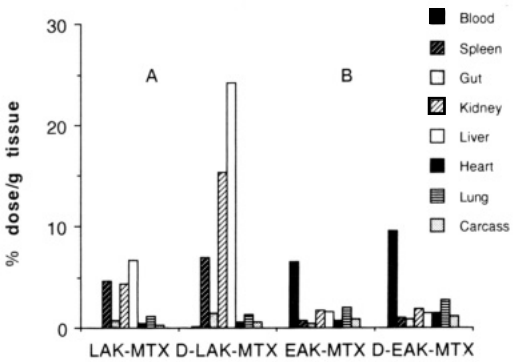


Figure 10. Effect of absolute configuration of amino acid X in the side chain on tissue distribution of ^{125}I-labeled branched polypeptide–MTX conjugates in Balb/c mice 24 h after administration: (a) LAK–MTX and D-LAK–MTX and (b) EAK–MTX and D-EAK–MTX. Results are the mean of three animals.

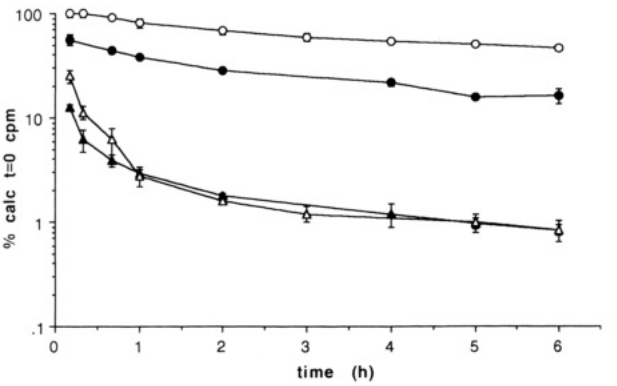


Figure 11. Effect of side-chain sequence on blood survival of ^{125}I-labeled branched polypeptide–MTX conjugates following iv administration to Balb/c mice. AUC_{0-6h} calculated from these data are given in Table III: (○) eak–MTX, (●) aek–MTX, (△) pak–MTX, and (▲) apk–MTX.

11 and 12 and was not the same for polycationic and amphoteric conjugates. In the former case, when proline was next to the polylysine backbone, the blood clearance of its MTX derivative (apk–MTX) was almost identical with that of the pak–MTX conjugate. In contrast to amphoteric conjugates investigated, when Glu was present adjacent to the polylysine backbone, the blood survival of the conjugate (aek–MTX) was decreased with 2-fold reduction in AUC_{0-6h} (Table III) compared to a conjugate containing Glu at the end of the branches. Figure 12 shows that although the WBS was much lower than for eak–

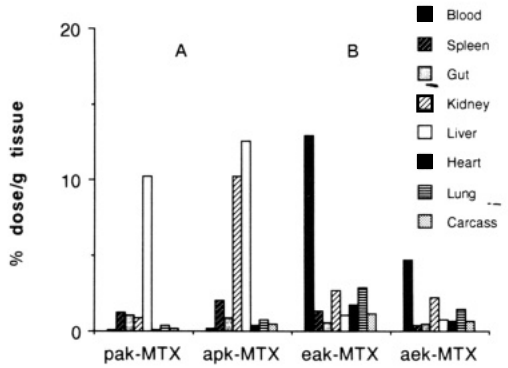


Figure 12. Effect of side-chain sequence on the tissue distribution of ^{125}I-labeled branched polypeptide–MTX conjugates in Balb/c mice 24 h after iv administration: (a) pak–MTX and apk–MTX and (b) eak–MTX and aek–MTX. Data shown are the mean of three mice.

MTX, the tissue-distribution patterns of these two conjugates were very similar, with a tissue to blood ratio of less than 0.5.

DISCUSSION

For the construction of macromolecule–drug conjugates it is important to provide a rational basis to the selection of an appropriate carrier. To this end we have reported data on the synthesis, biodistribution, and in vitro cytotoxicity of daunomycin-branched polypeptide conjugates (*37*). In this contribution we extended our studies by the investigation of the synthesis and properties of another group of branched-polypeptide-based conjugates containing an antimetabolite antitumor drug, methotrexate. These conjugates have been produced with the aid of water-soluble carbodiimide, ensuring the same type of methotrexate–polymer bond in all compounds prepared. Two groups of polypeptides with essentially identical side-chain composition but different size (*45*) were used for the synthesis. As a result of a standardized coupling procedure, the respective MTX–polypeptide conjugates representing the two different size groups had a similar average degree of molar substitution (Table I), allowing the analysis of the size effect. With respect to the importance of the side-chain structure and charge of the branched polypeptides in formation of ordered conformation in solution (*33*, *34*) and immunological (*41*, *46*) and pharmacological (*45*, *46*) properties, we have studied the conformation, the biodistribution, and the in vitro cytotoxicity of MTX–carrier conjugates with polypeptides containing amino acids of different identity and/or configuration (e.g., Leu, D-Leu, Pro, Glu, D-Glu) at the end of the branches (XAK type) or adjacent to the polylysine backbone (AXK type).

CD spectra of conjugates showed significant differences correlating with the identity of the side-chain terminating amino acid, but only minor changes could be related to the replacement of L-amino acid by its D-isomer. Polycationic conjugates (LAK–MTX or D-LAK–MTX) investigated assumed essentially ordered (helical) secondary structure, while the CD spectrum of the amphoteric conjugate corresponded to only a partially ordered conformation. It should be noted that the conformational properties of LAK–MTX are very similar to those of unconjugated polypeptide, while in the case of D-LAK–MTX or D-EAK–MTX an expressed tendency could be demonstrated in the formation of ordered structure as compared to the respective free polypeptides. Consequently, the incorporation of methotrexate molecules even with an average degree of substitution of up to 18.5% could have an effect on the solution conformation of the free carrier by promoting its transition toward ordered secondary structure.

The data summarized in this report indicate that the covalent attachment of methotrexate to branched polypeptides results in a reduction in drug cytotoxicity. Similar phenomena have been observed for several protein or polymer conjugates of antitumor drugs (*5*), including our previous results on daunomycin–branched polypeptide compounds (*37*).

The reduction of cytotoxic activity was found to be essentially independent of the relative size of the carrier. The sequence of the amino acids in the side chain and the configuration of amino acid X at the terminal or adjacent to the polylysine backbone positions have a modest influence on cytotoxic efficacy with up to 1.5–4.8-fold differences in IC_{50} values (Table III). In contrast, the identity of the terminal amino acid in the side chains has a more pronounced effect on the cytotoxic potential of MTX. Conjugation to amphoteric polymers, depending on the configuration and position of amino acid X (where X = Glu or D = Glu), resulted in roughly a 500-fold reduction of anti-791T cell activity. However, polycationic conjugates bearing L-Leu at the side chain terminal position (LAK–MTX) produced a compound with cytotoxicity only about 60 times less effective than free MTX. This observation might be explained by the hydrophobic character of leucine's side chain and the proper steric orientation of the MTX molecule in the ordered L-Leu-containing conjugate, which could provide preferred hydrophobic interaction with enzymes during the degradation of the conjugate within the cell.

The biodistribution of MTX–branched polypeptides in mice have been characterized by blood clearance, whole-body distribution and tissue distribution 24 h after iv administration. The disappearance of conjugates from the circulation and their tissue-distribution profiles revealed no significant correlation with the average molecular mass. In contrast, blood survival of these compounds could be significantly prolonged by incorporation of glutamic acid residue into the side chain, producing amphoteric conjugates. The effect of the configuration of amino acid X onto the fate of the conjugate was found to be dependent on its identity or position in the branches. The presence of D-amino acid in the terminal position of the side chain (D-LAK–MTX vs LAK–MTX) or adjacent to the polylysine backbone (a-D-ek–MTX vs aek–MTX) resulted in an elevated whole-body survival, while the introduction of D- or L-Glu at the terminal position had no marked influence on WBS. Interestingly enough the prolonged blood survival of amphoteric or polycationic conjugates did not result in similar tissue distribution. In agreement with our results of branched polypeptide–daunomycin conjugates (*37*), compounds with a polycationic carrier were directed predominantly to spleen, liver, and kidney while conjugates with glutamic acid in the side chain were taken up by the lung, kidney, and liver.

In conclusion, these studies have indicated that synthetic branched polypeptides can be considered as potential candidates for constructing suitable conjugates for not only daunomycin (*37*) but also methotrexate delivery. The proper combination of elements of the primary/secondary structure of the branched polypeptide carrier molecule can result in conjugates with increased whole-body survival and prolonged half-life in the blood. In this paper we showed that (a) a branched polypeptide–methotrexate conjugate constructed from a polycationic or even an amphoteric carrier can sustain the cytotoxic activity of MTX comparable with the frequently used HSA–MTX

construct (Table II) and (b) branched polypeptide conjugates can be present in the circulation (amphoteric conjugates) and/or in the body (both amphoteric and polycationic conjugates) for a much longer period of time than HSA-MTX (Table III) or free drug (*55*). In comparative experiments MTX immunoconjugates produced less impressive responses in vitro and in vivo than similar conjugates of doxorubicin, daunomycin, or mitomycin C (*56*). Taken together, our study suggests that it is feasible to alter beneficially the body distribution and the in vitro toxicity of methotrexate and of daunomycin (*37*) by logical combination of side-chain sequence, configuration, and identity of amino acid X in the branches of the carrier molecule. We are currently studying the therapeutic efficacy in tumor-bearing mice of the conjugates reported here.

ACKNOWLEDGMENT

This work was supported partly by a grant from the Ministry of Health (T-240/1990), Budapest, Hungary, and partly by the Cancer Research Campaign, London, UK.

LITERATURE CITED

(1) Embleton, M. J., and Garnett, M. C. (1985) Antibody targeting of anticancer agents. In *Monoclonal antibodies for cancer detection and therapy* (R. W. Baldwin, and V. S. Byers, Eds.) pp 317–344, Academic Press, London.

(2) Furst, D. E., and Kremer, J. M. (1988) Methotrexate in rheumatoid arthritis. *Arthritis Rheum. 31*, 305–314.

(3) Mukhopadhyay, A., Chaudhuri, G., Arora, S. K., Sehgal, S., and Basu, S. K. (1989) Receptor mediated drug delivery to macrophages in chemotherapy of leishmaniasis. *Science 244*, 705–707.

(4) Ghose, T., Blair, A. H., Kralovec, J., Mammen, M., and Uadia, P. O. (1988) Synthesis and testing of antibody-antifolate conjugates for drug testing. In *Antibody-Mediated Delivery Systems* (J. D. Rodwell, Ed.) pp 81–122, Marcel Dekker Inc., New York.

(5) Upeslacis, J., and Hinman, L. (1988) Chemical modification of antibodies for cancer chemotherapy. *Annual Reports in Medical Chemistry* (N. Saltzman, Ed.) pp 151–160. Academic Press, New York.

(6) Endo, N., Takeda, Y., Umemoto, N., Kishida, K., Watanabe, K., Saito, M., Kato, Y., and Hara, T. (1988) Nature of linkage and mode of action of methotrexate conjugated with antitumour antibodies: Implications for future preparation of conjugates. *Cancer Res. 48*, 3330–3335.

(7) Burnstein, S., and Knapp, R. (1977) Cheomtherapy of murine ovarian carcinoma by methotrexate–antibody conjugates. *J. Med. Chem. 20*, 950–952.

(8) Kulkarni, P. N., Blair, A. H., and Ghose, T. I. (1981) Covalent binding of methotrexate to immunoglobulins and the effect of antibody linked drug on tumour growth in vivo. *Cancer Res. 41*, 2700–2706.

(9) Harding, N. G. L. (1971) Amethopterin linked covalently to water-soluble macromolecules. *Ann. N. Y. Acad. Sci. 186*, 270–283.

(10) Chu, B. C. F., and Whiteley, J. M. (1977) High molecular weight derivatives of methotrexate as chemotherapeutic agents. *Mol. Pharmacol. 13*, 80–88.

(11) Halbert, G. W., Florence, A. T., and Stuart, J. F. B. (1987) Characterization of in vivo drug release and biological activity of methotrexate-bovine serum albumin conjugates. *J. Pharm. Pharmacol. 39*, 871–876.

(12) Garnett, M. C., Embleton, M. J., Jacobs, E., and Baldwin, R. W. (1983) Preparation and properties of a drug–carrier–antibody conjugate showing selective antibody-directed cytotoxicity in vitro. *Int. J. Cancer 31*, 661–670.

(13) Garnett, M. C., and Baldwin, R. W. (1986) An improved synthesis of a methotrexate–albumin–791T/36 monoclonal antibody conjugate cytotoxic to human osteogenic sarcoma cell lines. *Cancer Res. 46*, 2407–2412.

(14) Endo, N., Kato, Y., Takeda, Y., Saito, M., Umemoto, N., Kisida, K., and Hara, T. (1987) In vitro cytotoxicity of human serum albumin-mediated conjugated of methotrexate with anti-MM46 monoclonal antibody. *Cancer Res. 47*, 1076–1080.

(15) Bures, I., Lichy, A., Bostik, J., and Spundova, M. (1990) The use of protein as a carrier of methotrexate for experimental cancer chemotherapy. Alternative method for preparation of serum albumin-methotrexate derivative. *Neoplasma 37*, 225–231.

(16) Chakraborty, P., Bhaduri, A. N., and Das, P. K. (1990) Sugar receptor mediated drug delivery to macrophages in the therapy of experimental visceral leishmaniasis. *Biochem. Biophys. Res. Commun. 166*, 404–410.

(17) Sanzgiri, Y., Blaton, C. D., and Gallo, J. M. (1990) Synthesis, characterisation and in vitro stability of chitosan-methotrexate conjugates. *Pharm. Res. 7*, 418–421.

(18) Chaudhuri, G., Mukhopadhyay, A., and Basu, S. K. (1989) Selective delivery of drugs to macrophages through a highly specific receptor. An efficient chemotherapeutic approach against leishmaniasis. *Biochem. Pharmacol. 38*, 2995–3002.

(19) Ryser, H. J. P., and Shen, W. C. (1978) Conjugation of methotrexate to poly(L-Lysine) increases drug transport and overcomes drug resistance in cultured cells. *Proc. Natl. Acad. Sci. U.S.A. 75*, 3867–3870.

(20) Arnold, L. J., Jr. (1985) Polylysine–drug conjugates. *Methods Enzymol. 112*, 270–285.

(21) Przybylski, M., Fell, E., Ringsdorf, H., and Zaharki, D. S. (1978) Synthesis and characterization of polymeric derivatives of the antitumour agent methotrexate. *Makromol. Chem. 179*, 1719–1733.

(22) Galivan, J., Balinska, M., and Whiteley, J. M. (1982) Interaction of methotrexate–poly(L-Lys) with transformed hepatic cells in culture. *Arch. Biochem. Biophys. 216*, 544–550.

(23) McGuire, J. J., and Russell, C. A. (1990) A human leukemia cell culture system for testing new antifols: Differential sensitivity of lymphoid and non-lymphoid cell lines to unconjugated and methotrexate conjugated polymers of basic amino acids. *Leukemia 4*, 48–52.

(24) Manabe, Y., Tsubota, T., Haruta, Y., Kataoka, K., Okazaki, M., Haisa, S., Nakamura, K., and Kimura, I. (1984) Production of a monoclonal antibody-methotrexate conjugate utilizing dextran T-40 and its biological activity. *J. Lab. Clin. Med. 104*, 445–454.

(25) Shih, L. B., Sharkey, R. M., Primus, F. J., and Goldenberg, D. M. (1988) Site-specific linkage of methotrexate to monoclonal antibodies using an intermediate carrier. *Int. J. Cancer 41*, 832–839.

(26) Ghose, M. K., Kildsig, D. O., and Mitra, A. K. (1989) Preparation and characterisation of methotrexate-immunoglobulin conjugates. *Drugs Des. Delivery 4*, 13–25.

(27) Kralovec, J., Singh, M., Mammen, M., Blair, A. H., and Ghose, T. (1989) Synthesis of site-specific methotrexate-IgG conjugates. *Cancer Immunol. Immunother. 29*, 293–302.

(28) Umemoto, N., Kato, Y., and Hara, T. (1989) Cytotoxicities of two disulfide-bound-linked conjugates of methotrexate with monoclonal anti-MM46 antibody. *Cancer Immunol. Immunother. 28*, 9–16.

(29) Umemoto, N., Kato, Y., Endo, N., Takeda, Y., and Hara, T. (1989) Preparation and in vitro toxicity of a MTX-anti-MM46 monoclonal antibody conjugate via an oligopeptide spacer. *Int. J. Cancer 43*, 677–684.

(30) Abraham, A., Nair, M. G., Kisliuk, R. L., Gaumont, Y., and Galivan, J. (1990) Folate analogues. 33. Synthesis of folate and antifolate poly-gamma-glutamates by [(9-fluorenylmethoxy)oxy]carbonyl chemistry and biological evaluation of certain methotrexate polyglutamate polylysine conjugates as inhibitors of the growth of H35 hepatoma cells. *J. Med. Chem. 33*, 711–717.

(31) Hudecz, F., and Szekerke, M. (1980) Investigation of drug-protein interactions and the drug-carrier concept by the use of branched polypeptides as model systems. Synthesis and characterization of the model peptides. *Collect. Czech. Chem. Commun. 45*, 933–940.

(32) Hudecz, F., and Szekerke, M. (1985) Synthesis of new branched polypeptides with polylysine backbone. *Collect. Czech. Chem. Commun. 50*, 103–113.
(33) Hudecz, F., Votavova, H., Gaál, D., Sponar, J., Kajtár, J., Blaha, K., and Szekerke, M. (1985) Branched polypeptides with poly(L-lysine) backbone: synthesis, conformation and immunomodulation. In *Polymeric Materials in Medication* (Ch. G. Gebelein, and Ch. E. Carraher, Eds.) pp 265–289, Plenum Press, New York.
(34) Mezö, G., Hudecz, F., Kajtár, J., Szókán, Gy., and Szekerke, M. (1989) The influence of the side chain sequence on the structure–activity correlations of immunomodulatory branched polypeptides. *Biopolymers 28*, 1801–1826.
(35) Votavova, H., Hudecz, F., Kajtár, J., Sponar, J., Blaha, K., and Szekerke, M. (1985) Conformation of branched polypeptides based on poly(L-lysine): The effect of terminal amino acids in the branches. *Collect. Czech. Chem. Commun. 50*, 228–244.
(36) Hudecz, F., Kutassi-Kovács, S., Mezö, G., and Szekerke, M. (1989) Biodegradability of synthetic branched polypeptide with poly/L-lysine/backbone. *Biol. Chem. Hoppe-Seyler 370*, 1019–1026.
(37) Hudecz, F., Clégg, J. A., Kajtár, J., Embleton, M. J., Szekerke, M., and Baldwin, R. W. (1992) Synthesis, conformation, biodistribution and in vitro cytotoxicity of daunomycin–branched polypeptide conjugates. *Bioconjugate Chem. 3*, 49–57.
(38) Clegg, J. A., Hudecz, F., Embleton, M. J., and Baldwin, R. W. (1991) In vitro cytotoxicity and biodistribution studies with synthetic branched polypeptide–methotrexate conjugates. *Br. J. Cancer 63*, Suppl. XIII, 44.
(39) Mezö, G., Kajtár, J., Szókán, Gy., Sármay, G., Gergely, J., and Szekerke, M. (1991) Branched polypeptides as carriers of tuftsin analogs: synthesis, structure and immunostimulatory activity. In *Peptides 1990* (E. Giralt, and D. Andreu, Eds.) pp 244–246, ESCOM Sci., Leiden.
(40) Rajnavölgyi, É., Lányi, Á., Hudecz, F., Kurucz, I., Kiss, K., László, G., Szekerke, M., and Gergely, J. (1989) Structural characteristics influencing the carrier function of synthetic branched polypeptides based on poly[Lys-(DL-Ala)$_3$] backbone. *Mol. Immunol. 26*, 949–958.
(41) Rajnavölgyi, É., Hudecz, F., Mezö, G., Watari, E., Heber-Katz, E., Gaál, D., Kurucz, I., Szekerke, M., and Gergely, J. (1990) Synthetic branched polypeptides as carriers for low-molecular weight antigens: Correlation between chemical structure and biological functions. *Chim. Oggi 8*, 21–28.
(42) Rajnavölgyi, É., Hudecz, F., Mezö, G., Szekerke, M., and Gergely, J. (1986) Isotype distribution and fine specificity of the antibody response on inbred mouse strains to four compounds belonging to a new group of synthetic branched polypeptides. *Mol. Immunol. 23*, 27–37.
(43) Gaál, D., Hudecz, F., and Szekerke, M. (1984) Immunomodulatory effect of synthetic branched polypeptides. *J. Biol. Response Modif. 3*, 174–184.
(44) Gaál, D., Hudecz, F., Kovács, A. L., and Szekerke, M. (1986) Immunomodulatory effect of synthetic branched polypeptides II. *J. Biol. Response Modif. 5*, 148–159.
(45) Clegg, J. A., Hudecz, F., Pimm, M. V., and Baldwin, R. W. (1990) Drug-carrier design: Biodistribution of branched polypeptides with poly-L-lysine backbone. *Bioconjugate Chem. 2*, 425–430.
(46) Hudecz, F., Gaál, D., Lányi, Á., Kurucz, I., Kovács, A. L., Mezö, G., Rajnavölgyi, É., and Szekerke, M. (1992) Carrier design: Cytotoxicity and immunogenicity of branched polypeptides with polylysine backbone. *J. Controlled Release 19*, 231–244.
(47) IUPAC–IUB Commission on Biochemical Nomenclature (1972) *Biochem. J. 127*, 753–756.
(48) IUPAC–IUB Commission on Biochemical Nomenclature (1984) *Eur. J. Biochem. 138*, 9–37.
(49) Hudecz, F., and Szókán, Gy. (1985) Structure analysis of branched chain poly- and isopeptides based on HPLC of their dansyl derivatives. In *Chromatography, the State of the Art* (H. Kalász, and L. S. Ettre, Eds.) pp 273–286, Akadémiai Kiadó, Budapest.
(50) Szókán, Gy., Mezö, G., and Hudecz, F. (1988) Application of Marfey's reagent in racemization studies of amino acids and peptides. *J. Chromatogr. 444*, 115–122.
(51) Schippers, P. H., and Dekkers, H. P. J. (1981) Direct determination of absolute circular dichroism data and calibration of commercial instruments. *Anal. Chem. 53*, 778–782.
(52) Bolton, A. E., and Hunter, W. M. (1973) The labelling of proteins to high specific radioactivities by conjugation to a ^{125}I-containing acylating agent. *Biochem. J. 133*, 529–539.
(53) Pimm, M. V., Clegg, J. A., and Baldwin, R. W. (1987) *Eur. J. Cancer Clin. Oncol. 23*, 521.
(54) Rowland, M., and Tozer, T. N. (1989) *Clinical Pharmacokinetics, Concepts and Application.* 2nd ed., pp 459–463, Lea and Fibiger, Philadelphia.
(55) Stock, J. A. (1966) Antimetabolites. In *Experimental Chemotherapy* (R. F. Sohnitzer, and F. Hawking, Eds.) Vol. IV, pp 79–377, Academic Press, New York.
(56) Dillman, R. O., Johnson, D. W., Ogden, J., and Beidler, D. (1989) Significance of antigen, drug and tumour cell targets in the preclinical evaluation of doxorubicin, daunomycin, methotrexate and mitomycin-C monoclonal antibody immunoconjugates. *Mol. Biother. 1*, 250–255.

Bead-Based Sandwich Hybridization Characteristics of Oligonucleotide–Alkaline Phosphatase Conjugates and Their Potential for Quantitating Target RNA Sequences

Jennifer K. Ishii and Soumitra S. Ghosh*

Life Sciences Research Laboratory, Baxter Diagnostics Inc., San Diego, California 92121. Received July 15, 1992

The hybridization characteristics of oligonucleotide–alkaline phosphatase conjugate probes were examined in bead-based sandwich hybridization reactions using single-stranded nucleic acid targets and oligonucleotide–polystyrene capture beads. Enzymatic activity was monitored using a chemiluminescent substrate and calibration plots of chemiluminescent signal versus conjugate concentration were used to estimate the sandwich hybridization efficiencies. Improved hybridization behavior was noted using glycerol as an additive and by increasing the length of the probe and alkyl spacer of the conjugates. The chemiluminescent assay is at least as sensitive as those employing ^{32}P-labeled probes and can detect as little as 10–20 amol of target RNA. The linear relationship of chemiluminescent signal versus target assayed provides a method for quantitating unknown target samples. A single human immunodeficiency virus type 1 infected cell in a background of 10^6 uninfected cells is facilely detected when this enzyme-based detection assay is prefaced with a self-sustained sequence-replication amplification reaction.

During the past decade, nucleic acid hybridization techniques have become increasingly important for the clinical diagnosis of infectious diseases (*1*) and genetic disorders (*2*). The application of these methodologies have been immensely facilitated by the development of in vitro nucleic acid amplification procedures (*3–5*), which have dramatically improved the sensitivity of detection of target DNA or RNA sequences (*6*). Traditionally, radioisotope-labeled probes have been favored in hybridization methods because of their sensitivity and ease of quantitation, despite issues such as safety and short lifetimes. However, with the advent of a number of powerful nonisotopic detection systems (*7*) which rival ^{32}P in sensitivity, attention has been steadily shifting toward the use of these alternative detection methods. One such promising nonisotopic approach utilizes enzyme-linked oligonucleotide conjugate probes wherein signal amplification is achieved by rapid turnover of substrate to a colored, fluorescent, or chemiluminescent product (*8–14*). In particular, alkaline phosphatase has emerged as the reporter molecule of choice in such conjugates because of the exquisite sensitivity of detection possible using chemiluminescent (CL)[1] dioxetane-based substrates (*12–14*). Recently, detection of as little as 0.001 amol of the enzyme have been reported using 4-methoxy-4-(3-phosphonophenyl)spiro[1,2-dioxetane-3,2′-adamantane] (*15*, *16*).

A current focus in viral diagnostics has been on developing quantitative hybridization methods for the detection of viral pathogens in clinical samples (*17*, *18*). Such assays are critical for assessing the viral load in an infected patient over the time span of the disease, following the expression of specific viral and host genes, and for monitoring changes in viral titers to determine the efficacy of drug therapy regimens. Our choice of a sandwich hybridization approach (*19–21*) employing oligonucleotide–alkaline phosphatase conjugates and oligonucleotide-linked polystyrene beads (*22*) was dictated by the following features: (1) the rapid kinetics of hybridization obtained by using short oligonucleotide probe sequences, (2) the approximation of the conditions of solution hybridization when capture oligonucleotides are covalently end-attached, via spacer arms, to the solid support, (3) the enhanced specificity in target detection derived from two independent hybridization events of the nucleic acid analyte with the capture and detection oligonucleotides, and (4) the sensitivity of CL detection afforded by oligonucleotide–alkaline phosphatase conjugates and the numerical readout of the CL signal for quantitative analysis.

This paper describes the sandwich hybridization behavior of the conjugates in bead-based sandwich hybridization (BBSH) reactions with RNA targets (Figure 1), parameters for improving its hybridization efficiencies, and the quantitative potential of the assay. The efficacy of this BBSH system is demonstrated in its ability to detect RNA products generated by self-sustained sequence replication (3SR) amplification reactions (*5*) of samples containing low titers of human immunodeficiency virus type 1 (HIV-1).

EXPERIMENTAL PROCEDURES

Calf intestine alkaline phosphatase (EC 3.1.3.1, enzyme immunoassay grade) was purchased from Boehringer Mannheim, and [γ-^{32}P]ATP and [γ-^{32}P]CTP were from ICN. T4 polynucleotide kinase was obtained from New England Biolabs. Sodium dodecyl sulfate (SDS), polyvinylpyrrolidone (PVP), and glycerol were from Sigma, and Ficoll was from Pharmacia. LumiPhos 530, a formulation of the dioxetane substrate 4-methoxy-4-(3-phosphonophenyl)spiro[1,2-dioxetane-3,2′-adamantane], was purchased from Lumigen, Inc., and CML latex beads (0.807 μm size) were obtained from Seradyn, Inc. Presiliconized Eppendorf tubes were obtained were Denville Scientific, Inc. Radioactivity was measured by Cerenkov counting

* Author to whom correspondence should be addressed: Life Sciences Research Laboratory, Baxter Diagnostics, Inc., 4245 Sorrento Valley Boulevard, San Diego, CA 92121. Phone: (619) 622-9726. FAX: (619) 597-2935.

[1] Abbreviations used: BBSH, bead-based sandwich hybridization; CL, chemiluminescent; HIV-1, human immunodeficiency virus type 1; SDS, sodium dodecyl sulfate; PVP, polyvinylpyrrolidone; DTT, dithiothreitol; TEAC, triethylammonium acetate; EDTA, etylenediaminetetraacetic acid; HEPES, *N*-(2-hydroxyethyl)piperazine-*N*′-ethanesulfonic acid; BSA, bovine serum albumin fraction V; 3SR, self-sustained sequence replication.

1043-1802/93/2904-0034$04.00/0 © 1993 American Chemical Society

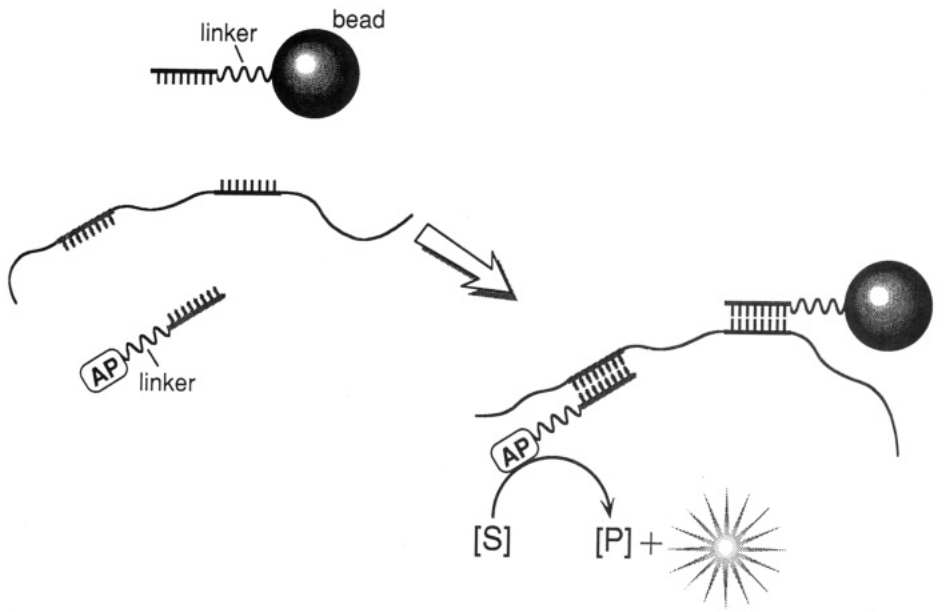


Figure 1. Scheme for enzyme-based BBSH detection.

Table I. Sequences of HIV-1 *env*-Region Oligonucleotide Probes and Primers[a]

86–272	5′TCTAATTACTACCTCTTCTTCTGCTAGACT3′
86–273	5′AGTCTACGAGAAGAAGAGGTAGTAATTAGA3′
86–274	5′TGTACTATTATGGTTTTAGCATTGTCTGTG3′
86–275	5′CACAGACAATGCTAAAACCATAATAGTACA3′
88–211	5′AATTTAATACGACTCACTATA**GGGA**TCTATTG-TGCCCCGCGGGTTTTGCGATTCTA3′
88–297	5′TGGCCTAATTCCATGTGTACATTGTACTGT3′
88–347	5′AATTTAATACGACTCACTATA**GGGA**TGTACTA-TTATGGTTTTAGCATTGTCTGTGA3′
89–255	5′TTATTGTGCCCCGGCTGGTTTTGCGATTCTA3′
90–066	5′TTACAATTTCTGGGTCCCCTCCTGAGGA3′
90–374	5′AATTTAATACGACTCACTATA**GGGA**TTTTT-CTTGTATTGTTGTTGGGTCTTGTAC3′
90–422	5′AATTAGGCCAGTAGTATCAACTCAACTGCT3′
90–673	5′AGAAGAGGTAGTAATTAGATCTGCCAATTT3′
90–675	5′CATGGAATTAGGCCAGTAGTATCAACTCAAC-TGCT3′

[a] Underlined bases in the oligonucleotide sequences denote the presence of a T7 promoter at the 5′ ends (*5*, *24*). Transcription initiation sequences are in boldface.

using a Beckman LS 7800 liquid scintillation system. Oligonucleotides and their alkaline phosphatase conjugates were quantitated on the basis of their 260/280 absorbances using a Beckman DU 40 spectrophotometer. CL signals were measured with a Monolight 2010 luminometer (Advanced Luminescence Laboratory) equipped with a photon-counting device with 20-ns resolution and a spectral sensitivity range of 360–620 nm. Linear regresson analysis of the data was carried out using the KaleidaGraph program (Abelbeck Software).

Reagent Preparation. (*a*) *Selection and Synthesis of Oligonucleotides.* The sequences (*23*) of the detection and capture oligonucleotides used to detect the *env* region of HIV-1 RNA and the 3SR primer oligonucleotides utilized in the 3SR amplification and T7 RNA polymerase transcription reactions are shown in Table I. Figure 2 illustrates the location of these sequences relative to the HIV-1 *env*-region map. With the exception of primer oligonucleotide 89–255, the 3SR primer oligonucleotides 88–211*, 88–347*, and 90–374* contain a T7 promoter sequence at their 5′ end (*5*, *24*) (asterisks denote presence of T7 promoters).

Oligonucleotides were synthesized on an Applied Biosystems 380A DNA synthesizer. The detection oligonucleotide sequences 86–272T, 90–422T, and 90–675T contain a hexylthiol group at their 5′ termini which was incorporated using a C6 thiol-modifier phosphoramidite reagent (Amersham, Inc.) in the last coupling step of the synthesis. The capture oligonucleotides sequences 86–273, 88–297, 90–673, and 86–275 contain a 5′ terminal aminohexyl group and were synthesized by using the Aminolink 2 reagent (Applied Biosystems, Inc.) in the last coupling step of the automated synthesis.

The tritylated oligonucleotides were purified as described elsewhere (*25*). Prior to their use, the purified tritylated thiol oligonucleotides were deprotected using a two-step Ag^+/dithiothreitol (DTT) procedure (*26*). Crude deprotected 5′-aminohexyl oligonucleotides were taken up in 0.1 M triethylammonium acetate (TEAC), pH 8.5, and purified by reverse-phase HPLC (C8 column, 1 × 25 cm) using a gradient of 7–25% acetonitrile in 0.1 M TEAC, pH 6.8. Following purification, all the oligonucleotides were stored in 0.2 M HEPES, pH 7.7, at −20 °C. The purified oligonucleotides migrated as single bands on a 15% denaturing polyacrylamide gel. Detection oligonucleotide sequences 86–272 and 90–422 were phosphorylated at the 5′ terminus using T4 polynucleotide kinase and cold ATP or [γ-^{32}P]ATP (*27*). Oligonucleotide Trisacryl (90–66) support was prepared according to the method described by Davis et al. (*28*).

(*b*) *Preparation of Oligonucleotide–Alkaline Phosphatase Conjugate Detection Probes.* Calf intestine alkaline phosphatase was covalently attached to the oligonucleotides 86–272, 90–422, or 90–675 by a thioether linkage as described elsewhere (*8*). The oligonucleotides in these conjugates are separated from the reporter enzyme by a two-carbon spacer. Conjugates with hexyl linkers were synthesized by the same method using the sequences 86–272T, 90–422T, and 90–675T. The conjugates are stable for at least 1 year when stored at 4 °C. The conjugate concentrations were determined by spectrophotometric analysis (*8*, *11*). The two sets of conjugates, which differ in the length of the spacer, were equivalent in their sensitivity of detection of nitrocellulose-filter-bound complementary HIV-1 target using a dye precipitation assay (*8*) and in their specific activities. Prior to using the conjugates in sandwich hybridization assays, they were diluted in 50 mM NaCl, 10 mM $MgCl_2$, 0.1% gelatin, 0.1 M TrisHCl, pH 7.5 (dilution buffer), such that 10–100 fmol of each probe were delivered in a volume not exceeding 15 μL for the hybridization reaction.

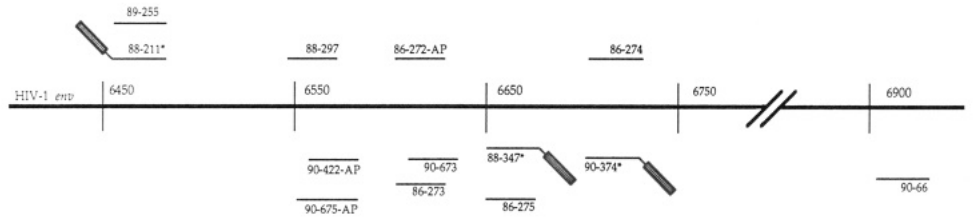


Figure 2. Map of the *env* region of HIV-1 illustrating the positions of detection and capture oligonucleotides as well as positions of oligonucleotide primers. Sequence which are shown above the center line are complementary to the sense strand of HIV-1 RNA, while those below the line are complementary to the antisense strand.

(*c*) *Preparation of the Capture Oligonucleotide–Polystyrene Support.* Sequences 86–273, 88–297, 90–673, and 86–275 5′-aminohexyl oligonucleotides were covalently attached to carboxylated polystyrene beads using 1-ethyl-3-[3-(dimethylamino)propyl]diimide hydrochloride as the coupling reagent (*22*). The capture oligonucleotide–polystyrene beads were diluted in 5X SSC (*27*), 5X PVP/Ficoll, 0.5% SDS, and 0.02 μg/μL calf thymus DNA prior to their use in the hybridization reaction.

(*d*) *Preparation of RNA Transcripts.* Some of the RNA transcripts used in the BBSH assays were obtained from single promoter 3SR reactions (*29*) using primers 89–255 and either 88–347* or 90–374*. The other RNA target was a product of a 3SR amplification reaction using the primer combination 88–211*/88–347*. All targets and transcripts were quantitated by BBSH using ^{32}P-labeled oligonucleotide detection probes and Trisacryl–oligonucleotide supports (*28*).

A T7 promoter-containing PCR product was synthesized using the primer pair 88–211* and 86–274. This PCR product was used as a template for a T7 RNA polymerase transcription reaction using 200 units of T7 RNA polymerase, 25 μM of unlabeled rCTP supplemented with 25 μCi of [α-^{32}P]CTP, and 0.4 mM of the other rNTPs in 100 μL of transcription buffer (40 mM TrisHCl, pH 8.1, 8 mM $MgCl_2$, 25 mM NaCl, 2 mM spermidine, 5 mM DTT, and 80 mg of nuclease-free BSA). The reaction mixture was incubated at 37 °C, following which the transcript was separated from unincorporated nucleotides by passage through a G-50 spin column. Quantitation of the ^{32}P-labeled transcript was based on the amount of label incorporated in the nucleic acid. The size and integrity of the transcript was evaluated by electrophoresis on a 6% denaturing polyacrylamide gel.

Bead-Based Sandwich Hybridization. Presiliconized Eppendorf tubes were used in the BBSH assays to minimize nonspecific binding of the conjugates to the reaction tubes. Prior to use, the tubes were washed with 70% ethanol and then dried at 55–60 °C for 30 min. RNase-mediated degradation of the target or control RNA was inhibited by preparing buffer solutions in diethyl pyrocarbonate-treated water (*27*).

In a typical assay, oligonucleotide–polystyrene beads (50 μg) were suspended in prehybridization reaction buffer (5X SSC, 0.5% SDS, 0.02 μg/μL calf thymus DNA) and then pelleted by centrifugation for 5 min at 14 000 rpm. The supernatant was removed and a 25-μL aliquot of 2X optimized hybridization buffer (10X SSC, 1% SDS, 0.04 μg/μL calf thymus DNA, 5% glycerol), prewarmed to 50 °C, was added to the pellet. The target or negative control RNA was diluted in TE buffer (10 mM TrisHCl, 1 mM EDTA, pH 8.1) so that a requisite amount of nucleic acid was delivered in 5–10 μL and added to the beads. The oligonucleotide–alkaline phosphatase conjugate probe was added to the beads in a volume ranging from 15 to 20 μL, resulting in a total reaction of 50 μL. The tubes were vortexed, and the hybridization reaction was allowed to proceed for 1 h at 50 °C. After the incubation period, a 50-μL aliquot of wash solution (0.1X SSC, 0.1% SDS) was added and the mixture was allowed to stand for 3 min at room temperature before centrifugation at 14 000 rpm for 5 min. The supernatant was removed and the bead pellet was washed two times with 50 μL each of wash solution before addition of the chemiluminescent substrate.

Chemiluminescent Detection of the BBSH Complex. A 200-μL aliquot of Lumi-Phos 530 was added to the bead–target–probe complex from the BBSH reaction and gently vortexed. The alkaline phosphatase-catalyzed dephosphorylation of the dioxetane substrate was allowed to proceed in the dark for 1 h at room temperature. The mixture was then transferred to a cuvette and the CL signal was measured by luminometer.

RESULTS

Correlation Curves of CL Signal and Oligonucleotide–Alkaline Phosphatase Conjugate. Various amounts of the 86–272–alkaline phosphatase conjugate detection probe (86–272–AP), which is complementary to the sense strand of the HIV-1 *env* region, were incubated at 42 or 50 °C for 1 h in buffer containing 5X SSC, 5X PVP/Ficoll, 0.5% SDS, and 0.02 μg/μL calf thymus DNA. The mixtures were diluted 100-fold, and then aliquots corresponding to amounts ranging from 10^{-16} to 10^{-19} mol of conjugate were assayed for enzymatic activity using the dioxetane substrate LumiPhos 530. As seen in Figure 3, increasing the incubation temperature from 42 to 50 °C resulted in a 34% decrease in CL signal generated by the conjugate probe. The addition of 2.5% glycerol to the hybridization solution stabilized the conjugate, and the signal increase compensated for the enzyme activity lost with the increase in temperature. Calibration curves plotting measured CL signal versus conjugate concentration from data such as those obtained above were used to estimate bound conjugate in sandwich hybridization complexes (see below). It should be noted that the enzymatic activity of the conjugate was unaltered in the presence of 0.8-μm polystyrene beads (50 μg) in the assay.

Optimization of BSSH Assays using Oligonucleotide–Alkaline Phosphatase Conjugates. (*a*) *Influence of Temperature on Hybridization Efficiencies.* A range of concentrations of a ^{32}P-labeled 218 base length RNA target transcript (see Experimental Procedures) was assayed with 88–297–polystyrene beads and 86–272–AP conjugate probe at different hybridization temperatures. The hybridization buffer for these BBSH reactions contained 5X SSC, 5X PVP/Ficoll, 0.5% SDS, and 0.02 μg/μL calf thymus DNA. Calibration curves plotting CL signal versus conjugate concentrations (see previous section) were used to quantitate the conjugate probe bound in the sandwich complex and estimate the sandwich hybridization efficiencies. The efficiency of the capture step was determined from the amount of radiolabel associated with the beads. The results of the BBSH assays are summarized in Table II. The signals obtained in assays performed at 50 °C were higher than those at 42 °C, a result of increased hybridization efficiency at 50 °C. When

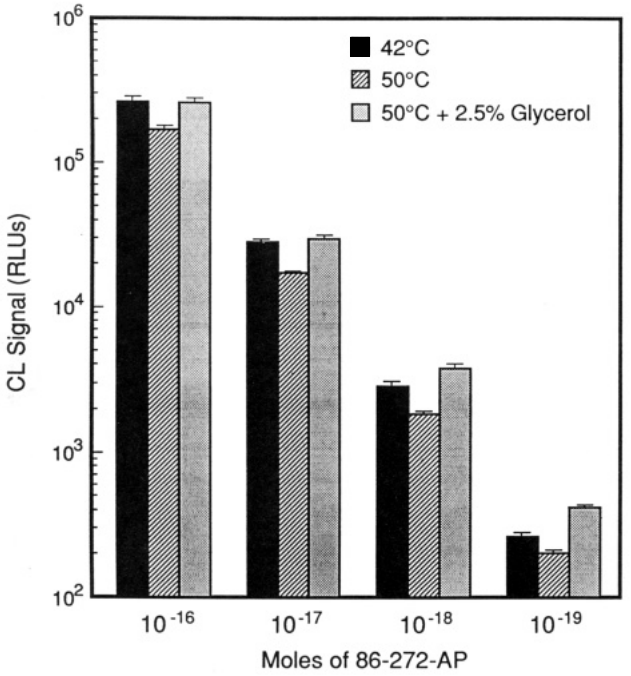


Figure 3. Effect of hybridization temperatures and glycerol on the enzymatic activity of 86–272–AP conjugate probe. The 86–272–AP conjugate probe was subjected to hybridization conditions for 1 hour at 42 °C (solid bar), 50 °C (striped bar), and 50 °C in the presence of 2.5% glycerol (dotted bar). Aliquots (in triplicates) of the conjugate corresponding to amounts ranging from 10^{-16} to 10^{-19} mol were then incubated for 1 hour at room temperature with the dioxetane substrate, and chemiluminescence was detected using a single photon counting device. The CL signal is reported in relative light units (RLU) and has been corrected for the CL value of the substrate alone (42 °C, 1009 RLU; 50 °C 845 RLU; 50 °C and glycerol, 1055 RLU).

the hybridization mixture was supplemented with 2.5% glycerol, a further improvement in sensitivity was observed. In the presence of the additive, the conjugate probe was capable of detecting 20 amol of the RNA target with a 4:1 signal/negative control ratio when the assay was performed at 50 °C.

(*b*) *Effect of Reaction Components on Sandwich Hybridizations.* The influence of the various hybridization reaction buffer components was examined in BBSH reactions of 86–273–polystyrene beads and 90–422–AP conjugate with a 236-base, antisense HIV-1 *env*-region RNA target. An antisense HIV-1 *pol* 3SR-generated product was used as a negative control for these reactions. Exclusion of SDS from reaction buffer resulted in a 35-fold increase in nonspecific binding, as seen in the hybridization reaction of the probe with the noncomplementary *pol* target (Figure 4A) thus obscuring the hybridization signal obtained in hybridization of the probe to the *env* target. Removal of PVP/Ficoll had little effect on the signal obtained in hybridization of the probe to the *env* target or in nonspecific hybridization of the probe to the *pol* target. However, removal of SDS/PVP/Ficoll resulted in a marked increase in the signal generated in the hybridization reaction with the negative control *pol* target.

(*c*) *Effect of Time on BBSH Reactions.* The optimal time for sandwich hybridization of 90–422–AP conjugate probe and 86–273–polystyrene beads to the 236-base *env*-region RNA target was investigated. The hybridization reactions were performed at 50 °C in optimized buffer (5X SSC, 0.5% SDS, 0.2 μg/μL calf thymus DNA, 2.5% glycerol). Figure 4B shows that the maximum CL signal was observed when the hybridization period was between 60 and 90 min. The signal/negative control ratio was not significantly enhanced by increasing the time of hybridization beyond 60 min. It should be noted that a 10% loss of enzymatic activity was observed when the incubation time of the conjugate in the hybridization reaction buffer was increased from 60 to 120 min, and a 40% loss after 150 min (data not shown).

(*d*) *Influence of Conjugate Probe Concentration on BBSH Detection.* A constant amount of a 236-base, HIV-1 *env*-region RNA target (1 fmol) was assayed under the BBSH conditions with 86–273–polystyrene beads and 10–100 fmol of 90–422–AP probe. Figure 4C shows that there was an increase in CL signal with increasing amounts of detection probe, up to approximately 50 fmol of 90–422–AP.

(*e*) *Influence of Length of Alkyl Spacer in Conjugate on BBSH Detection.* The maleimide–thiol coupling reaction (*8*) was used to synthesize two sets of oligonucleotide–alkaline phosphatase conjugates, in which the enzyme moiety was separated from the nucleic acid by ethylene and hexylene spacers. The conjugates of oligonucleotide sequence 86–272 were complementary to the sense strand of *env* HIV-1 RNA, whereas the 90–422–AP conjugates were specific probes for the antisense strand of *env* HIV-1 RNA. As shown in Figure 5A, a two-fold increase in signal-to-background ratio was observed for the detection of the sense strand with 86–272T–AP probe, which has a six-carbon spacer between the oligonucleotide and the enzyme. The same trend was observed with the 90–422–AP probes, where a 3-fold increase in signal-to-background ratio was obtained upon increasing the length of the spacer.

(*f*) *Effect of Probe Length on BBSH Detection.* Conjugate probes 90–422–AP and 90–675–AP having six-carbon spacers were used in combination with 86–273–, 90–673– or 86–275–polystyrene beads to detect a 268 base length antisense, *env*-region HIV-1 RNA target in BBSH assays. Conjugate probe 90–675–AP were identical in sequence to 90–422, but had an additional five bases complementary to the target sequence appended at the 5′ end. Oligonucleotides 90–673 and 86–275 were shifted 11 bases and 41 bases downstream from 86–273, respectively. Figure 5B illustrates a uniform trend of increased signal-to-background ratios using 90–675–AP probe with all beads compared to 90–422–AP conjugate with the same beads. However, extending the spatial distance between the detection and capture probes, as in the case with 86–275 polystyrene beads, was found to be detrimental for hybridization.

Comparison of Sensitivities of Chemiluminescence and ^{32}P-Detection Systems. Various amounts of sense, 3SR-amplified, HIV-1 *env*-region product were detected by BBSH using 86–297–polystyrene beads and 86–272–AP probe. A parallel set of experiments was conducted with ^{32}P-labeled 86–272 oligonucleotide as probe under the same hybridization conditions. Figure 6a shows that enzyme-based chemiluminescence detection was equivalent in sensitivity to ^{32}P detection. However, when a similar comparison was made in BBSH assays of antisense HIV-1 *env*-region RNA transcripts using 86–273–polystyrene beads and 90–422 detection probes, the CL assay was 10-fold more sensitive than ^{32}P detection (Figure 6B).

Correlation of CL Signal to Amount of 3SR-Amplified Antisense HIV RNA Target. Figure 6A shows a plot of CL signal versus HIV-1 *env*-region RNA target obtained from BBSH assays of a range of target concentrations with 90–422–AP probe and 86–273–polystyrene beads. Linear regression analysis of the data indicate a direct correlation of the signal with target amounts ranging between 10^{-17} and 10^{-14} mol (see Figure 7A inset). The deviation from linearity observed in the

Table II. Influence of Temperature on BBSH Efficiencies

^{32}P-labeled transcript (mol)[a,b]	42 °C signal[c,d]	42 °C BBSH efficiency (%)	50 °C signal[c,d]	50 °C BBSH efficiency (%)	50 °C signal[c,d]	50 °C + glycerol: BBSH efficiency (%)
5.0×10^{-15}	400 695	3.4	885 863	11.2	over range[e]	over range
1.0×10^{-15}	63 924	2.5	201 511	13.1	690 826	27.0
1.0×10^{-16}			24 273	17.3	70 264	29.7
5.0×10^{-17}					36 609	31.5
2.0×10^{-17}					14 548	35.2

[a] A ^{32}P-labeled, 218 base HIV-1 envelope region RNA transcript was used as target, and was generated from a T-7 RNA polymerase transcription reaction of a T-7 promoter-containing PCR product using [α-^{32}P]CTP as one of the substrates. The target was quantitated by correlating the radioactivity incorporated in the RNA transcript with the specific activity of [α-^{32}P]CTP. The primers used in the PCR reaction were 88–211* and 86–274 (see Table I and Figure 1 for sequences and locations). [b] Capture efficiencies for the target were as follows: at 42 °C, 5 fmol (29.2%), 1 fmol (21.9%); at 50 °C, 5 fmol (67.6%), 1 fmol (67.5%); at 50 °C with 2.5% glycerol, 1 fmol (69.8%). [c] The data is presented as the averages of triplicates in relative light units, and is corrected for the substrate background (at 42 °C, 1000; at 50 °C, 850; at 50 °C with 2.5% glycerol, 1260). [d] The averaged background signals for the *pol*-region HIV-1 RNA transcript were as follows: at 42 °C, 4262; at 50 °C, 1527; at 50 °C with 2.5% glycerol, 4458. [e] The signal was above the dynamic range of the instrument.

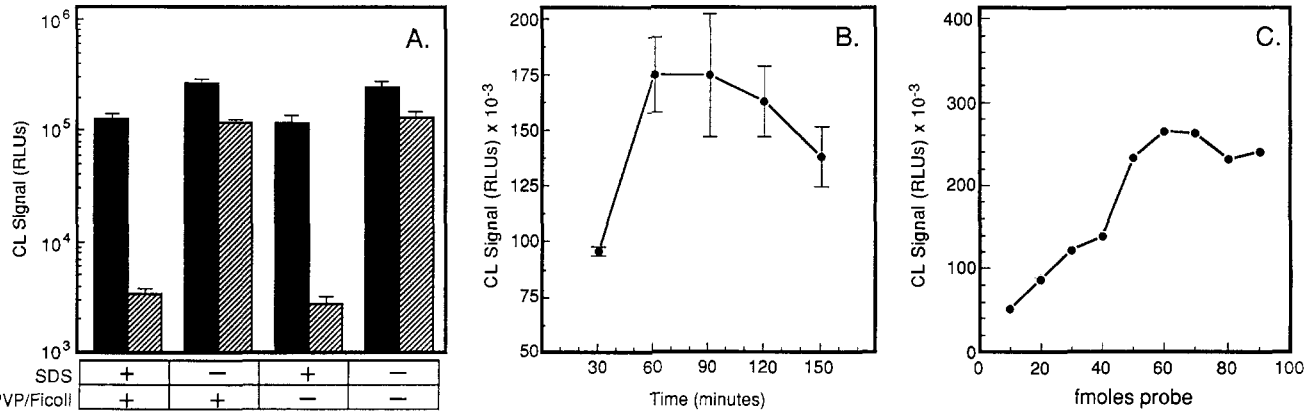


Figure 4. Optimization of conditions for BBSH. The target was a 236-base, antisense HIV-1 *env*-region RNA, which was generated by a 3SR amplification reaction of HIV-1 RNA using primers 88–211* and 88–347*. The CL value obtained with substrate alone was subtracted from all the test values obtained with the target and negative control RNA. (A) Effect of hybridization components on the detection of 2 fmol of target RNA (solid bar) using 10 fmol of 90–422 conjugate probe and 86–273–polystyrene beads. The hybridization reactions were carried out in duplicate. 1X Hyb buffer contains 5X SSC, 5X PVP/Ficoll, 0.5% SDS, 0.02 μg/μL calf thymus DNA, and 2.5% glycerol. Two femtomoles of antisense HIV-1 *pol*-region RNA (striped bar) were used as negative control (B) Effect of hybridization time on BBSH detection of 3 fmol of target RNA using 10 fmol of 90–422–AP conjugate probe and 86–273–polystyrene beads. The hybridization reactions for each timepoint were carried out in triplicate. Background CL signals obtained with negative control antisense HIV-1 *pol*-region RNA for each timepoint ranged from 500 to 1700 RLU. (C) Effect of increasing concentrations of 90–422 conjugate probe in BBSH reactions with 1 fmol of target RNA and 86–273–polystyrene beads. For B and C PVP/Ficoll were not used as components in the hybridization buffer.

calibration curve for higher target concentrations arises because the target is in excess of the 90–422–AP conjugate probe used in the assay.

Detection of HIV-1 (LAV) Infected CEM Cells. Serial dilutions of HIV-1 (LAV) infected CEM cells in a background of 10^6 uninfected PBMCs were lysed using guanidinium isothiocyanate, and the HIV-1 RNA was isolated by affinity purification using oligonucleotide Trisacryl (90–66) support (*28*). The RNA was then amplified in the presence of the capture beads using the 3SR reaction, and the products were detected by BBSH using 86–273–polystyrene beads and 90–422T–AP conjugate probe. The amplified products were quantitated by correlation of the CL signal to a calibration curve generated with known amounts of HIV-1 *env*-region RNA (see Figure 7A inset). Figure 7B shows that the conjugate probe easily detects one HIV-1-infected CEM cell when the BBSH assay is prefaced with a 3SR amplification reaction.

DISCUSSION

The hybridization characteristics of oligonucleotide–alkaline phosphatase conjugates in BBSH reactions were investigated using a CL detection format. Single photon counting luminometers afforded exquisite sensitivities and wide dynamic range in the measurement of the emitted light signals and as little as 60 000 molecules of oligonucleotide–alkaline phosphatase conjugate were facilely detected (Figure 3). Calibration curve plotting CL signal versus conjugate spanning four log concentrations were generated and used to quantitate conjugate associated in a sandwich complex after a BBSH reaction (Table II).

The BBSH reaction with target RNA was more efficient at 50 °C than at 42 °C, presumably because the secondary structures of both the probe and the target nucleic acids are more relaxed at the elevated temperature (Table II). Although the conjugate's enzymatic activity was depressed at 50 °C, inclusion of glycerol in the hybridization solution was found to restore the enzymatic activity (Figure 3). The stabilization of the conjugate in the presence of glycerol only partially accounted for the increase in signal for BBSH reactions at 50 °C, since there was also an unexpected improvement in hybridization efficiency in the presence of the additive (Table II). The nature of the effect of glycerol in the BBSH reaction is at present unknown. A critical requirement in the BBSH assay was the inclusion of SDS in the hybridization buffer, as this reagent was extremely effective in reducing nonspecific hybridization of the conjugate probe (Figure 4A).

It was noted that the sandwich hybridization efficiencies for ^{32}P-labeled probes were significantly higher than those obtained with conjugates, and approached 60% for the detection of unlabeled RNA target with the 86–272/88–297 BBSH detection system (results not shown). It was reasoned that the lower BBSH efficiencies observed for the conjugates (Table II) may be due to unfavorable steric

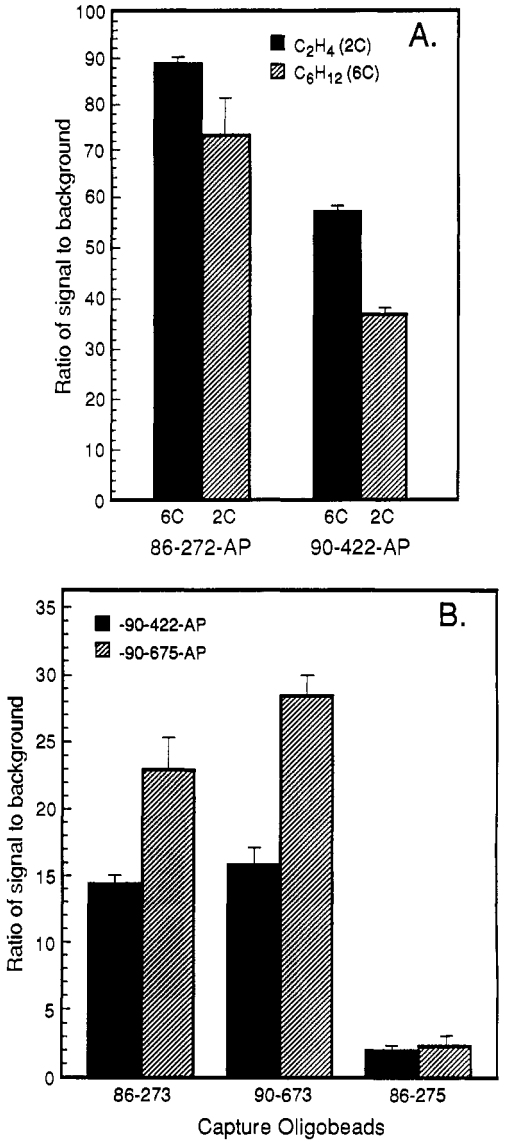


Figure 5. (A) Effect of alkyl spacer length in oligonucleotide–AP conjugate probes on BBSH detection of target RNA. 86–272–AP probe and 88–297–polystyrene beads were used to detect 0.25 fmol of 218-base, sense HIV-1 *env*-region RNA, while 90–422–AP conjugate probe and 86–273–polystyrene beads were used to detect 2.5 fmol of 236-base, antisense HIV-1 *env*-region RNA. The conjugate probes were synthesized using ethylene (2C, striped bar) and hexylene (6C, solid bar) linkers, respectively. The 218-base sense RNA target was generated from a 3SR amplification reaction using primers 88–211* and 86–274. The hybridization reactions were carried out in triplicate. The CL value obtained with substrate alone was subtracted from the test values. The background signals (RLU) generated from nontarget samples were as follows: 86–272–AP (6C), 1137–1421; 86–272–AP (2C), 485–1070; 90–422–AP (6C), 755–1471; 90–422–AP (2C), 191–238. (B) Effect of probe length and spatial distance between the capture and detection probes on BBSH detection. 90–422–AP (solid bar) or 90–675–AP (striped bar) conjugate probe, each having a six-carbon spacer, was used in combination with 86–273;–, 90–673–, and 86–275–polystyrene beads for detecting 1 fmol of 268-base, antisense HIV-1 *env*-region RNA target, generated from 3SR amplification of HIV-1 using the primer pair 89–255 and 90–374*. The hybridization reactions were carried out in triplicate. The 90–675 sequence has an extra five bases appended to the 5′ end of the 90–422 sequence. The CL value obtained with substrate alone was substracted from the test values.

interactions. This could arise due to the inadequate length of the ethylene spacer between alkaline phosphatase and the oligonucleotide in the conjugate, as well as the proximity of the conjugate to the immobilized capture oligonucleotide (see Figures 1 and 2). Therefore, the

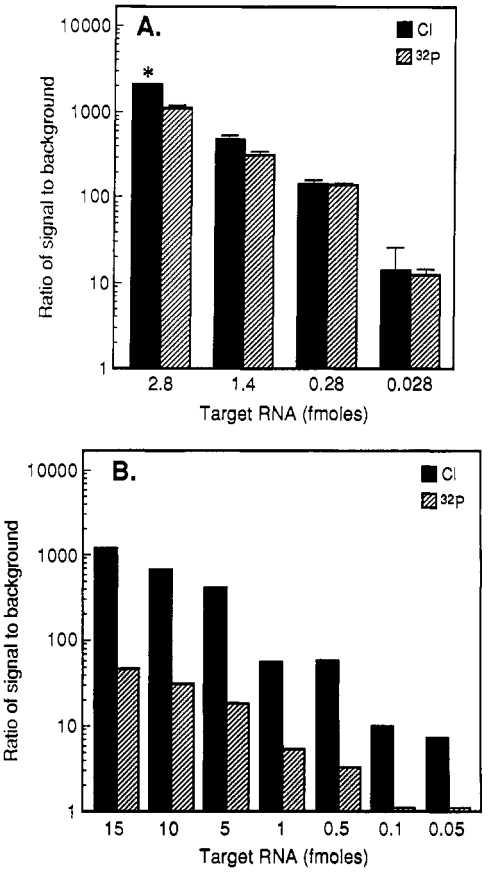


Figure 6. Direct comparison of CL and ^{32}P detection in a BSSH format. A range of concentrations of 3SR-amplified, sense and antisense HIV-1 *env*-region RNA were assayed using alkaline phosphatase conjugate and ^{32}P-radiolabeled oligonucleotide probes. An antisense HIV-1 *pol*-region RNA was used as a negative control. The CL value obtained with substrate alone was subtracted from the test values. Figure A shows signal-to-background ratios for detecting 3SR-amplified, 218-base, sense HIV-1 *env*-region RNA using 86–272–AP (solid bar) or ^{32}P–86–272 (striped bar) detection probe (specific activity: 6×10^6 cpm/pmol) and 88–297–polystyrene beads. The asterisk on solid bar indicates estimate since signal was over range. The hybridization reactions were carried out in duplicate. Figure B shows signal-to-background ratios for detecting 3SR-amplfied, 236-base, antisense RNA with 90–422–AP (solid bar) or ^{32}P–90–422 (striped bar) detection probe (specific activity: 2.5×10^6 cpm/pmol) and 86–273–polystyrene beads.

influence of the following variables was investigated to further characterize the behavior of a conjugate-based BBSH system: (1) probe concentrations in the hybridization reaction, (2) alkyl spacer length in the conjugates, (3) length of probe sequence, and (4) the spatial distance between the capture and detection probes.

A concomitant increase in signal was observed upon increasing the probe concentration in the BBSH reaction (Figure 4C). This suggested that increasing the probe/target ratio drives the kinetics of duplex formation and results in higher hybridization efficiencies of the conjugate with its RNA target. From these observations and other similar assays, 50 fmol was found to be the optimal amount of conjugate for assaying 10 fmol or less of target.

It was envisioned that increasing the spatial separation between the nucleic acid and alkaline phosphatase would minimize the steric interference of the enzyme moiety in the hybridization reaction of the oligonucleotide component with its complementary target. This hypothesis was borne out by the trend of elevated signal-to-background ratios observed with conjugates which had a six-carbon spacer between the oligonucleotide and alkaline phosphatase (Figure 5A).

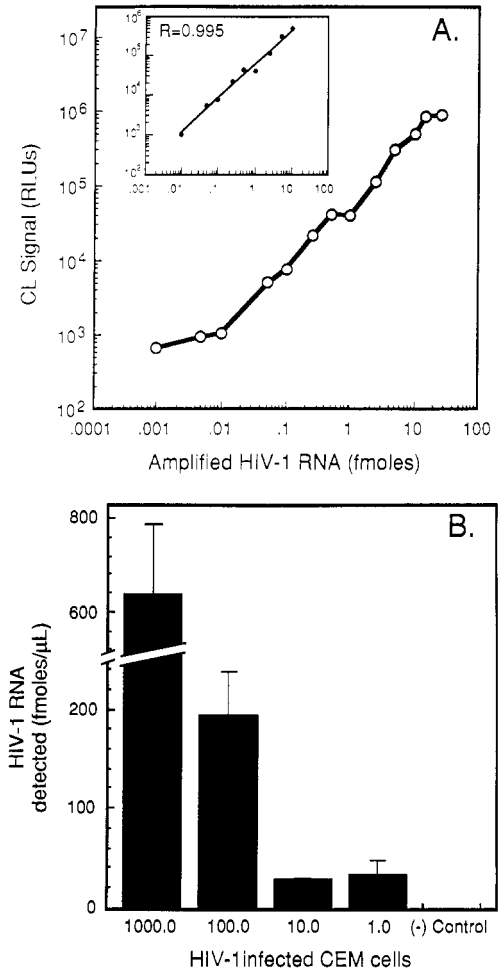


Figure 7. (A) Plot of CL signal versus quantitated amounts of 3SR-amplified target RNA. A range of concentrations of 3SR-amplified, antisense HIV-1 *env*-region RNA generated using primers 89–255 and 88–347* was assayed with 10 fmol of 90–422–AP conjugate probe and 86–273–polystyrene beads. Inset: linear portion of the curve spanning 10^{-17}–10^{-14} mol of target. (B) Detection and quantitation of HIV-1-infected cells using a coupled 3SR/BBSH assay. HIV-1 (LAV) infected CEM cells in a background of 10^{-6} uninfected PBMCs were lysed in 6 M guanidinium isothiocyanate/0.1 M β-mercaptoethanol and then added to 20 mg of 90–66–Trisacryl oligobeads (*28*) for capture of the HIV-1 RNA at room temperature for 90 min. The oligobeads were washed three times each with 1 mL of 0.3 M NaCl followed by two times with 1 mL each of 3SR reaction buffer. Amplification of the *env* region was performed in the presence of the oligobeads using primers 88–211*/88–347* in a 3SR reaction. The resulting products were detected by BBSH in duplicate reactions using 90–422–AP conjugate probe and 86–273–polystyrene beads. The 3SR-amplified products were quantitated by correlating the observed CL signals with the linear segment of a calibration curve described above, and reported as fmol/μL of 3SR amplified product. The 3SR-amplified products were also independently quantitated using a BBSH assay employing ^{32}P-labeled 90–422 detection probe and 86–273–Trisacryl oligobeads. On the basis of specific activity of the detection probe (2.5×10^6 cpm/pmol), 456.0, 117.0, 29.0, and 21.0 fmol/μL of 3SR product were obtained from 1000, 100, 10, and 1 HIV-1-infected cell samples, respectively.

The oligonucleotide sequence of 90–422–AP conjugate was extended to ascertain if the extra bases of the resulting 90–675–AP conjugate would enhance its efficiency of hybridization with its complementary target. Further, the conjugates were used in combination with different capture beads to examine the effect of greater spatial distance between the capture and detection probes. An improvement in overall hybridization efficiency was observed using longer detection probes (Figure 4B). However, increasing the distance between the capture and detection sequences did not afford higher signal-to-background ratios. This unexpected result may reflect poor capture efficiency of the 86–275–polystyrene beads due to a higher degree of secondary structure of the RNA target near its region of homology.

From the studies discussed above, the accessibility of the probe-complementary regions of the RNA target emerges as a critical factor and is dependent on the secondary structure adopted by the target under the pseudosolution hybridization conditions of the BBSH reaction. It is likely that the differences observed in the sensitivity of detection of the two RNA targets using either conjugates or ^{32}P-labeled oligonucleotides (Figures 5A, 6) arise from differences in the complexity of the secondary structure of the targets. Further, local secondary structure may account for differences observed in the sensitivity of detection of a common RNA target with different capture bead/conjugate probe combinations (Figure 5B). The effect of secondary structure is minimized in filter-based assays these probes, since the target is immobilized in denatured form. While temperatures higher than 50 °C facilitate denaturation of target, such conditions would be detrimental to the enzymatic activity of the conjugates in BBSH assays.

The conjugate-based detection system is at least as sensitive as ^{32}P detection in BBSH assays (Figure 6). Typically, a manual assay employing 18 tubes requires 3 h for assay setup, hybridization reaction, and centrifugation steps, followed by detection. The CL BBSH assay for experiments performed in quadruplicate is quite reproducible and the variability, expressed by percent ratio of standard deviation/signal, is typically 10% or less. However, the day-to-day variability appears to be somewhat higher (~15%) (data not shown). Due to the inherent variability of the detection system and the day-to-day variability, an alternate approach was adopted for quantitation of unknown target using standard curves plotting BBSH signal against known amounts of target HIV-1 RNA (Figure 7A). Such calibration curves were utilized for reliable quantitation of products from 3SR amplification reactions.

Following target amplification using the 3SR reaction, the BBSH assay is easily capable of detection one HIV-1 (LAV) infected CEM cell in a background of 10^6 uninfected cells (Figure 7B). A calibration curve (Figure 7A) was used to quantitate the CL signals obtained in the BBSH assays of the 3SR amplified products. As seen in Figure 7B, there was no correlation of 3SR product detected with the number of HIV-1-infected cells present in the samples. In particular, equivalent amounts of 3SR amplification product were detected by the CL assay for the 10- and one-infected-cell samples, which was also noted in BBSH assays using ^{32}P detection (see legend for Figure 7). This lack of correlation is presumably due to the variability associated with sample preparation step, as well as differences in amplification efficiencies of the 1 h 3SR reaction with the extracted target RNA. It has been shown that between 20 and 35 min of the 3SR reaction, there is a linear relationship between 3SR-generated product and amount of initial target nucleic acid for target amounts ranging from 10^2 to 10^4 molecules (*30*). Beyond this time interval, the product accumulation curves converge and the linear relationship no longer holds when total 3SR product synthesized exceeds approximately 50 fmol/μL. Thus, meaningful quantitation of HIV-1 present in infected-cell samples requires reproducible and efficient sample preparation, and BBSH detection of 3SR-generated products which are obtained at reaction timepoints where the efficiency of amplification is independent of starting target amounts. Our current efforts are directed

toward addressing these issues in order to successfully apply the 3SR/enzyme-based BBSH system for quantitative DNA diagnostics.

ACKNOWLEDGMENT

We are grateful to K. Blumeyer, K. Fearon, L. Beninsig, K. Stringer, L. DiMichele, and W. Walker, for technical assistance, and to G. Davis, D. Kwoh, and T. Gingeras, for critical reading of the manuscript. This work was supported by funds from Baxter Diagnostics, Inc.

LITERATURE CITED

(1) Landry, M. L. (1990) Nucleic acid hybridization in viral diagnosis. *Clin. Biochem.* **23**, 267–277.

(2) Dawson, D. B. (1990) Use of nucleic acid probes in genetic tests. *Clin. Biochem. 23*, 279–285.

(3) Saiki, R. K., Scharf, S., Faloona, F. A., Mullis, K. B., Horn, C. T., Erlich, H. A., and Arnheim, N. (1985) Enzymatic amplification of β-globin genomic sequences and restriction site analysis for diagnosis of sickle cell anemia. *Science 230*, 1350–1354.

(4) Barany, F. (1991) Genetic disease detection and RNA amplification using cloned thermostable ligase. *Proc. Natl. Acad. Sci. U.S.A. 88*, 189–193.

(5) Guatelli, J. C., Whitfield, K. M., Kwoh, D. Y., Barringer, K. J., Richman, D. D., and Gingeras, T. R. (1990) Isothermal in vitro amplification of nucleic acids by a multienzyme reaction modeled after retroviral replication. *Proc. Natl. Acad. Sci. U.S.A. 87*, 1874–1878.

(6) Bej, A. K., Mahbubani, M. H., and Atlas, R. M. (1991) Amplification of nucleic acids by polymerase chain reaction (PCR) and other methods and their applications. *Crit. Rev. Biochem. Mol. Biol. 26* (3/4), 301–334.

(7) Matthews, J. A., and Kricka, L. J. (1988) Analytical strategies for the use of DNA probes. *Anal. Biochem. 169*, 1–25.

(8) Ghosh, S. S., Kao, P. M., McCue, A. W., and Chappelle, H. L. (1990) Use of maleimide–thiol coupling chemistry for efficient syntheses of oligonucleotide–enzyme conjugate hybridization probes. *Bioconjugate Chem. 1*, 71–76.

(9) Ghosh, S. S., Kao, P. M., and Kwoh, D. Y. (1989) Synthesis of 5′-oligonucleotide hydrazide derivatives and their use in preparation of enzyme–nucleic acid hybridization probes. *Anal. Biochem. 178*, 43–51.

(10) Jablonski, E., Moomaw, E. W., Tullis, R. H., and Ruth, J. L. (1986) Preparation of oligodeoxynucleotide–alkaline phosphatase conjugates and their use as hybridization probes. *Nucleic Acids Res. 14*, 6115–6128.

(11) Li, P., Medon, P. P., Skingle, D. C., Lanser, J. A., and Symons, R. H. (1987) Enzyme-linked synthetic oligonucleotide probes: Non-radioactive detection of enterotoxigenic *Escherichia coli* in faecal specimens. *Nucleic Acids Res. 15*, 5275–5287.

(12) Urdea, M. S., Kolberg, J., Clyne, J., Running, J. A., Bessemer, D., Warner, B., and Sanchez-Pescador, R. (1989) Application of a rapid non-radioisotopic nucleic acid analysis system to the detection of sexually transmitted disease-causing organisms and their associated antimicrobial resistances. *Clin. Chem. 35*, 1571–1575.

(13) Bronstein, I., Voyta, J. C., and Edwards, B. (1989) A comparison of chemiluminescent and colormetric substrates in a hepatitis B virus DNA hybridization assay. *Anal. Biochem. 180*, 95–99.

(14) Pollard-Knight, D., Simmonds, A. C., Schaap, A. P., Akhavan, H. and Brady, M. A. (1990) Nonradioactive DNA detection on Southern blots by enzymatically triggered chemiluminescence. *Anal. Biochem. 185*, 353–358.

(15) Schapp, A. P., Akhavan, H. and Romano, L. J. (1989) Chemiluminescent substrates for alkaline phosphatase: application to ultrasensitive enzyme-linked immunoassays and DNA probes. *Clin. Chem. 35*, 1863–1864.

(16) Bronstein, I., Edwards, B., and Voyta, J. C. (1988) Novel chemiluminescent enzyme substrates and their applications in immunoassays [Abstract]. *J. Biolumin. Chem. 2*, 186.

(17) Thompson, J. D., and Gillespie, D. (1990) Current concepts in quantitative molecular hybridization. *Clin. Biochem. 23*, 261–266.

(18) Kwoh, D. Y., and Gingeras, T. R. (1991) The use of transcription-based amplification systems in the diagnosis of HIV-1 infections. *App. Virol. Res.* (in press).

(19) Ranki, M., Palva, A., Virtanen, M., Laaksonen, M., and Söderland, H. (1983) Sandwich hybridization as a convenient method for detection of nucleic acids in crude samples. *Gene 21*, 77–85.

(20) Kwoh, D. Y., Davis, G. R., Whitfield, K. M., Chappelle, H. L., DiMechele, L. J., and Gingeras, T. R. (1989) Transcription-based amplification system and detection of amplified human immunodeficiency virus type 1 with a bead-based sandwich hybridization format. *Proc. Natl. Acad. Sci. U.S.A. 86*, 1173–1177.

(21) Dahlén, P. O., Iitiä, A. J., Skagius, G., Frostell, A., Nunn, M. F., and Kwiatkowski, M. (1991) Detection of human immunodeficiency virus type 1 by using the polymerase chain reaction and a time-resolved fluorescence-based hybridization assay. *J. Clin. Microbiol. 29*, 798–804.

(22) Bush, C. E., Donovan, R. M., Peterson, W. R., Jennings, M. B., Bolton, V., Sherman, D. G., Vanden Brink, K. M., Beninsig, L. A., and Godsey, J. H. (1992) Detection of human immunodeficiency virus type 1 RNA in plasma from high-risk pediatric patients by using the self-sustained sequence replication reaction. *J. Clin. Microbiol. 30*, 281–286.

(23) GenBank Release Notes 67.0. Accession K02013 (IntelliGenetics, Inc.).

(24) Bailey, J. N., Klement, J. F., and McAllister, W. T. (1983) Relationship between promoter structure and template specificities exhibited by the bacteriophage T3 and T7 RNA polymerases. *Proc. Natl. Acad. Sci. U.S.A. 80*, 2814–2818.

(25) Ghosh, S. S., and Musso, G. M. (1987) Covalent attachment of oligonucleotides to solid supports. *Nucleic Acids Res. 15*, 5353–5372.

(26) Connolly, B. A., and Rider, P. (1985) Chemical synthesis of oligonucleotides containing a free sulfhydryl group and subsequent attachment of thiol specific probes. *Nucleic Acid Res. 13*, 4485–4502.

(27) Sambrook, J., Fritsch, E. F., and Maniatis, T. (1989) *Molecular Cloning: A Laboratory Manual*, Cold Spring Harbor Laboratory Press, Cold Spring Harbor.

(28) Davis, G. R., Blumeyer, K., DiMichele, L. J., Whitfield, K. M., Chappelle, H., Riggs, N., Ghosh, S. S., Kao, P. M., Fahy, E., Kwoh, D. Y., Guatelli, J. C., Spector, S. A., Richman, D. D., and Gingeras, T. R. (1990) Detection of human immunodeficiency virus type 1 in AIDS patients using amplification mediated hybridization analysis: Reproducibility and quantitative limitations. *J. Infect Dis. 162*, 13–20.

(29) Fahy, E., Kwoh, D. Y., and Gingeras, T. R. (1991) Self-sustained sequence replication (3SR): An isothermal transcription-based amplification system alternative to PCR. *PCR Methods Appl. 1*, 25–33.

(30) Gingeras, T. R., and Kwoh, D. Y. (1992) In vitro nucleic acid target amplification techniques: issues and benefits. *Jahrbuch Biotechnologie Band 4* (P. Präve, M. Schlingmann, K. Esser, R. Thauer, and F. Wagner, Eds.) pp 403–429.

Registry No. Alkaline phosphatase, 9001-78-9; glycerol, 56-81-5; polystyrene, 9003-53-6.

Temperature-Responsive Bioconjugates. 1. Synthesis of Temperature-Responsive Oligomers with Reactive End Groups and Their Coupling to Biomolecules†

Yoshiyuki G. Takei, Takashi Aoki, Kohei Sanui, Naoya Ogata, Teruo Okano,*,‡ and Yasuhisa Sakurai‡

Department of Chemistry, Faculty of Science and Technology, Sophia University, 7-1 Kioi-cho, Chiyoda, Tokyo 102, Japan, and Institute of Biomedical Engineering, Tokyo Women's Medical College, 8-1 Kawada-cho, Shinjuku, Tokyo 162, Japan. Received July 27, 1992

Using 3-mercaptopropionic acid (MPA) as a chain-transfer agent, the radical oligomerization of *N*-isopropylacrylamie (IPAAm) was carried out with varying molar ratios of MPA to IPAAm in DMF. The molecular weight of oligo-IPAAm (OIPAAm) could be controlled by the ratio of MPA to IPAAm. The OIPAAm was confirmed to average one carboxyl end group per chain. All OIPAAms samples were highly water-soluble at lower temperatures and exhibited phase separation near 32 °C. The optical transmittance of the OIPAAms aqueous solutions changed drastically at 32 °C which was independent of OIPAAms molecular weight. In aqueous solutions of OIPAAm having concentrations higher than 1 wt % and molecular weight of 6100, the oligomers were precipitated and recovered in 85 wt % yield of their original content. Further, OIPAAm was grafted to atelo collagen by activated ester–amine coupling. The OIPAAm–collagen conjugates were able to dissolved in cold water and precipitated at 34 °C. Temperature-responsive OIPAAm–collagen conjugates are expected to maintain native collagen funtionality in the solution state, react at lower temperatures, and be easily removed from the system with small temperature increases.

INTRODUCTION

Poly(*N*-isopropylacrylamide) (PIPAAm) is well-known to change its structure in response to temperature in aqueous solutions (*1*, *2*). Polymer chains of IPAAm hydrate to form expanded structures in water at lower solution temperatures (<32 °C). At temperatures above 32 °C, however, the chains form compact structures by dehydration manifested as a lower critical solution temperature (LCST) (*2*). Temperature-responsive PIPAAm hydrogels are capable of controlling drug-release rates by temperature, demonstrating a potential to realize an intelligent drug-delivery system. Pulsatile drug delivery in response to temperature using temperature-responsive IPAAm hydrogels has been studied in detail (*3–5*).

Telomerization chemistry is expected to control oligomer molecular weight and create synthetic routes to semitelechelic oligomers averaging one functional end group per oligomer chain (*6*). Thiol compounds having functional groups as telogens are known to be effective in introducing functional groups to the ends of growing polymeric chains and regulating polymer molecular weight by radical telomerization via chain-transfer reactions (*7*). Oligomers with reactive end groups allow facile synthesis not only of block and graft copolymers but also of oligomer-modified biomolecules. If biomolecules such as enzymes, antigens, antibodies, and nucleotides can be modified while retaining their bioactivity, new macromolecular bioconjugates with an array of potential applications would become available. In this case, semitelechelic oligomers would be expected to avoid nonspecific aggregation problems associated with the process of biomolecule conjugation because they possess one reactive end group per oligomer.

Abuchowski et al. (*8*) have modified various proteins and enzymes using monomethoxypoly(ethylene oxide) (PEO). PEO–biomolecule conjugates showed high solubility and stability in blood, with loss of immunogenicity, and demonstrated increased solubility in organic solvents. PEO-modified biomolecules can scarcely control the reactivity of biomolecules by external stimuli. OIPAAm–biomolecule conjugates should be water-soluble at lower temperatures and precipitate at higher temperatures. These conjugates are expected to be bioactive in aqueous solution with an intrinsic ability to be conveniently separated from reactive products with small temperature increases. This strategy introduces temperature-responsive activities into biomolecules, and may lead to development of "intelligent bioconjugates".

This paper reports the synthesis of OIPAAms as semitelechelic oligomers containing carboxyl end groups. We have investigated the control of chain length, the activity of end-standing carboxyl groups, and temperature-responsive phase-transition phenomena of the oligomers. A model intelligent biomolecule conjugate, OIPAAm–collagen, was synthesized to introduce temperature-responsive functions into collagen. From these results, new synthesis techniques and potential characteristics of OIPAAm–biomolecule conjugates were discovered.

EXPERIMENTAL PROCEDURES

Materials. *N*-Isopropylacrylamide (IPAAm; provided by Kohjin, Tokyo, Japan) was purified by recrystallization from toluene–petroleum ether and dried at room temperature in vacuo (*2*). 3-Mercaptopropionic acid (MPA; Aldrich, Milwaukee, WI) was distilled under reduced pressure and the fraction boiling at 95 °C (5 mmHg) was used. *N*,*N*′-Azobisisobutyronitrile (AIBN), *N*,*N*′-dimethylformamide (DMF), and ethyl acetate (EtOAc) were

† Abbreviations used: IPAAm, *N*-isopropylacrylamide; PIPAAm, poly-IPAAm; OIPAAm, oligo-IPAAm; MPA, 3-mercaptopropionic acid; AIBN, *N*,*N*′-azobisisobutylonitrile; DMF, *N*,*N*-dimethylformamide; Ic, semitelechelic OIPAAm with a carboxyl end group; EtOAc, ethyl acetate; HOSu, *N*-hydroxysuccinimide; DCC, dicyclohexylcarbodiimide, [S], chain-transfer agent (MPA) concentration; [M], monomer concentration.

* Author to whom correspondence should be addressed.
‡ Tokyo Women's Medical College.

1043-1802/93/2904-0042$04.00/0 © 1993 American Chemical Society

Table I. Preparation and Analysis of IPAAm Oligomers[a]

code	[S]/[M][b]	conversion (%)	molecular weight from analysis of end group[d]	$\overline{M}_n$[c]	$\overline{M}_w$[c]	average number COOH/molecule[d]
Ic-10	0.099	76.0	1300	1140	1400	1.03
Ic-20	0.055	63.2	2600	2150	2700	0.97
Ic-30	0.033	83.4	3800	3340	4000	0.86
Ic-40	0.028	84.7	4270	4000	4800	1.02
Ic-50	0.022	84.2	4500	4500	6100	0.91
Ic-70	0.014	76.0	5100	5000	9700	1.04
Ic-100	0.010	68.4	7500	7600	12300	0.97

[a] OIPAAm, in DMF (1.0 mol/L at 70 ± 1 °C); AIBN, 0.4 mol/L; reaction time, 300 min. [b] [S] chain-transfer agent (3-mercaptopropionic acid) concentration; [M], monomer concentration. [c] GPC in THF at 40 °C. [d] Average (n = 3).

obtained from Wako Pure Chemicals (Tokyo, Japan) and purified by conventional methods. Atelo collagen was provided by Koken (Tokyo, Japan). Ultrapure water used for sample solutions was provided by a commercial water-purification device (Toray, Model LV-10T). Other reagents and solvents were commercially obtained and used without further purification.

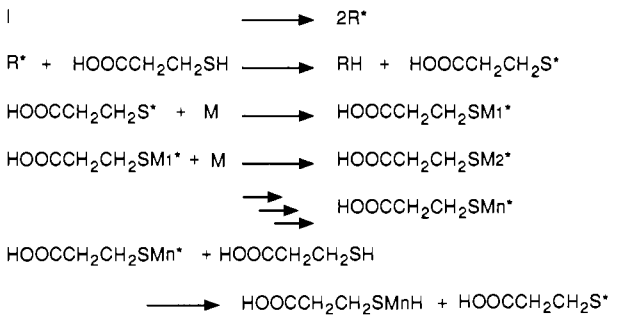
Oligomerization Procedure. Semitelechelic OIPAAm (Ic-X; X denotes the number of IPAAms in the oligomer vs in the preparation) was prepared by radical oligomerization of IPAAm with MPA using AIBN as an initiator in DMF at 70 ± 1 °C for 5 h (*7*). After evaporation, the reactant was poured into diethyl ether to precipitate the oligomers. The oligomer was purified by repeated precipitations from DMF–diethyl ether.

Measurement of Molecular Weight. Oligomer molecular weights were determined by gel permeation chromatography (GPC, Shimadzu; Model C-R4AX, Shodex; KF-80M × 2) in tetrahydrofuran at 40 °C (polystyrene standard; Polyscience Inc., Warrington, PA). The molecular weight of oligomers was also determined by end-group titration using 0.01 M NaOH and phenolphthalein at 4 °C, which detects the carboxyl group at the end of oligomer molecules.

Transmittance Measurements. Optical transmittance of oligomer solutions (1 wt %) at various temperatures was carried out by monitoring transmittance at 500 nm using a spectrophotometer (Shimadzu, UV-240). The observation cell was thermostated by a circular water jacket (Iuchi, Model HT-01C).

Modification of Collagen. The oligomer, Ic-50, was activated by *N*-hydroxysuccinimide (HOSu) with dicyclohexylcarbodiimide (DCC) in dry EtOAc at 4 °C for 16 h in a molecular ratio in 1:1:2:1.2, respectively. After evaporation, the reactant was precipitated from diethyl ether. Activated-ester groups were confirmed by infrared and ultraviolet spectrometry (*9*). The protocol used to synthesize the collagen–Ic-50 conjugate was based on the method of Bückmann et al. (*10*). The solution was adjusted to pH 3.0 with 0.1 M HCl and maintained at pH 3.0 during the course of the reaction. All steps were carried out at 4 °C. Atelo collagen (M_w = 300 000, 500 mg) was macerated in 90 mL of cold distilled water. After collagen was completely dissolved, the solution was diluted 30-fold with distilled water to about 0.3 wt %. Then, 140 mg of activated Ic-50 was dissolved in 4 mL of dry DMF and added to the collagen solution. This process was repeated five more times at 30-min intervals. The total amount of activated Ic-50 added was 700 mg (molar ratio = 1:30). The reactant solution was then gently stirred for 16 h. The solution was dialyzed (cellulose, 10 000 molecular weight cutoff) against distilled water/HCl, pH 3.0, and lyophilized. The resulting collagen–Ic-50 conjugate molecular weight was measured by GPC and its transmittance change in aqueous solution (0.3 wt %) recorded as a function of temperature as described for OIPAAm oligomers above.

Scheme I. Telomerization of IPAAm Using MPA as a Chain-Transfer Agent



Aggregation of Oligomers. Diluted OIPAAm aqueous solutions and collagen–Ic-50 conjugate aqueous solutions (0.3 wt %) were maintained at 37 °C for 10 min, vigorously shaken for 30 s, and then held at 37 °C for 5 min. After filtration of the supernatant, the aggregates were lyophilized and recovered. Alternatively, the samples were centrifugated for 5 min at 37 °C, and the oligomers were recovered by the same method.

RESULTS AND DISCUSSION

Synthesis of IPAAm Oligomers. Kitano et al. (*11*) recently reported the synthesis of semitelechelic OIPAAm averaging one carboxyl end group per polymer chain. Porous glass beads were modified by these semitelechelic oligomers to achieve temperature-modulated reactions trapped inside the aqueous interstices of the glass beads. However, the telomerization chemistry was not discussed in detail.

We have investigated the telomerization of IPAAm with MPA as a chain-transfer agent. The objective was to regulate oligomer molecular weight and functional-group incorporation. Table I shows the preparation conditions and analysis of IPAAm oligomerization with MPA resulting in semitelechelic OIPAAm with carboxyl end groups. Molecular weights calculated from the carboxyl group analysis assuming one carboxyl group per OIPAAm molecule were approximately equivalent to those determined from GPC data. All data were consistent with one OIPAAm molecule averaging one carboxyl end group per polymer chain. The polymerization mechanism is assumed to follow the telomerization shown in Scheme I.

Oligomer chain length was controlled by varying the ratio of MPA to the monomer. Short chain length oligomers were obtained using large amounts of MPA. Chain-transfer constants (C_s) for MPA with IPAAm in these experiments were determined from the equation of Mayo (*12*), yielding a value of 6.62×10^{-3}. Other C_s values for MPA with methyl methacrylate and styrene monomers were 0.38×10^{-4} and 9.4×10^{-4}, respectively (*13*). As MPA shows a large chain transfer constant value, it would

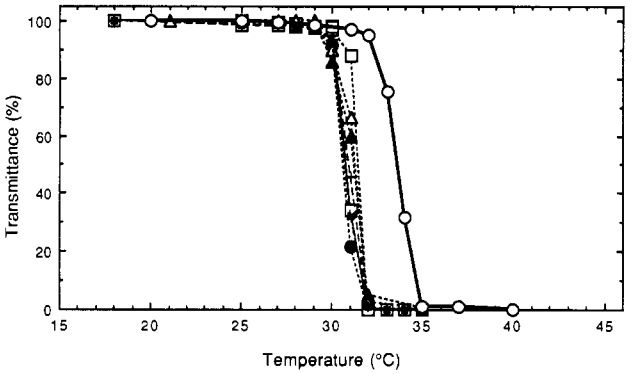


Figure 1. Temperature dependence of optical transmittance for aqueous solutions of (+) Ic-10, (×) Ic-20, (●) Ic-30, (▦) Ic-40, (□) Ic-50, (▲) Ic-70, (△) Ic-100, and (○) collagen–Ic-50 conjugate (OIPAAm, 1 wt % solution; conjugate, 0.3 wt % solution; λ = 500 nm).

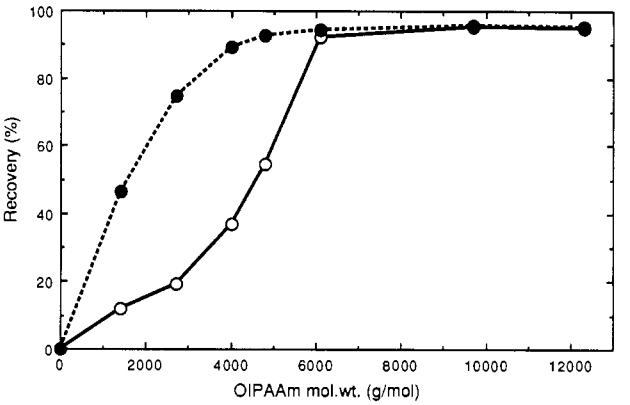


Figure 2. Recovery of OIPAAm from aqueous medium as a function of molecular weight (○, 1 wt %; ●, 10 wt %).

typically require correction using the equation of Kice (*14*). However, a plot of 1/Pn against [S]/[M] is found to be nearly linear by applying the equation of Mayo to OIPAAm samples obtained in these experiments.

Phase Transition of IPAAm Oligomers. The series of OIPAAm samples in aqueous solution was examined for optical transmittance change at various temperatures (Figure 1). Phase-transition behavior was readily detectable in these experiments. OIPAAm exhibits an LCST at approximately 32 °C independent of oligomer molecular weight. Coil–globule transition phenomena for the polymer chains was followed by aggregation of individual chain molecules due to intermolecular interactions between hydrophobic groups distributed across the surfaces of the resulting polymer globular particles in the aqueous medium (*15*). The aggregation kinetics of OIPAAm depends on the molecular chain length and its concentration in solution. All OIPAAm samples demonstrated an LCST near 32 °C as 1 wt % aqueous solutions. OIPAAm oligomers of small molecular weight clearly exhibited a phase transition from soluble species, resulting in precipitation and aggregation. In the case of concentrated polymer solutions (500 wt %), the OIPAAm LCST shifts to a higher temperature range, influenced by the enriched presence of hydrophilic end group moieties (*11*). Since aqueous solutions in our experiments were dilute (1 wt %), LCST behavior was scarcely effected by hydrophilic end group moieties. Precipitated oligomers forming microaggregates were assumed to disperse in the water medium.

Collagen–OIPAAm Conjugates. Carboxyl end groups of semitelechelic OIPAAm were activated using HOSu/DCC. Succinimidylated oligomers show a new peak in the IR spectrum at 1780 cm^{-1} corresponding to the C=O stretching mode of the succinimidyl group. The activated ester also showed ultraviolet absorption at 260 nm in NH_4-OH corresponding to the succinimidyl anion (*9*). In general, the succinimidylation of the carboxyl group reacts quantitatively and the analytical data confirmed that OIPAAm had been completely activated. Chen et al. also reported polymer–protein conjugates using PIPAAm (*16, 17*). They synthesized IPAAm copolymers with *N*-(acryloxy)succinimide as a comonomer and conjugated the copolymer with various proteins. Proteins randomly coupled to copolymers are capable of aggregation during preparation. Moreover, conjugation of copolymer with proteins may inhibit the mobility of polymer chains. We synthesized semitelechelic OIPAAm while controlling its chain length, so we would be able to introduce the PIPAAm sequence into one biomolecule. The resulting collagen–Ic-50 conjugate exhibited a molecular weight of 452 000, that is, about 24 molecules of oligomer were grafted to a molecule of collagen. The conjugates showed water solubility at room temperature regardless of isotonic conditions, and were able to dissolve in polar organic solvents such as ethanol and DMF. Transmittance changes in aqueous solutions of collagen–Ic-50 conjugates are shown in Figure 1. Unconjugated collagen solutions showed no such changes. Collagen–Ic-50 conjugates, however, precipitated with increasing temperature. Precipitates were identified as collagen–Ic-50 conjugates having a molecular weight of about 450 000. Because the soluble collagen precipitated during the phase transition of the grafted OIPAAm, the collagen–Ic-50 conjugate maintains properties of both the collagen and the PIPAAm homopolymers.

Although OIPAAm alone shows a LCST near 32 °C in aqueous systems, the collagen–Ic-50 conjugate showed a temperature response at 34 °C, which is higher than the LCST of the oligomer. Precipitation of freely soluble collagen of molecular weight 300 000 requires a significant hydrophobic driving force. Hence, a significant amount of OIPAAm grafting is required to obtain this response. Therefore, the LCST for the conjugate system is shifted to a higher temperature range, reflecting the energy change required for sufficient dehydration of OIPAAm to precipitate conjugates. Collagen–Ic-50 conjugate aqueous solutions heated over 44 °C become partly insolubilized due to collagen denaturation. Solutions under these conditions do not gel. OIPAAm carboxyl group coupling reactions, however, yield temperature-sensitive biomolecule conjugates without any undesired aggregation and cross-linking.

Temperature-Modulated Precipitation. Because of the LCST phenomena, OIPAAm can be recovered from aqueous solution by increasing temperature above a critical point. After filtration of supernatant, the aggregates were lyophilized. Once precipitated, dispersed OIPAAm microaggregates in water medium tend to form larger aggregates under vigorous shaking. Figure 2 shows the recovery efficiencies for OIPAAms after incubation and shaking at 37 °C in dilute aqueous solutions as a function of chain length. Only 20 wt % of the oligomers, Ic-10 (M_w = 1400) and Ic-20 (M_w = 2700), were recovered from 1 wt % aqueous solutions. The oligomers having higher molecular weight were recovered to over 90 wt % of their original content. Phase transitions for OIPAAm molecules in aqueous solution is schematically illustrated in Figure 3.

Oligomers having higher molecular weight are more readily precipitated and aggregate into large particles.

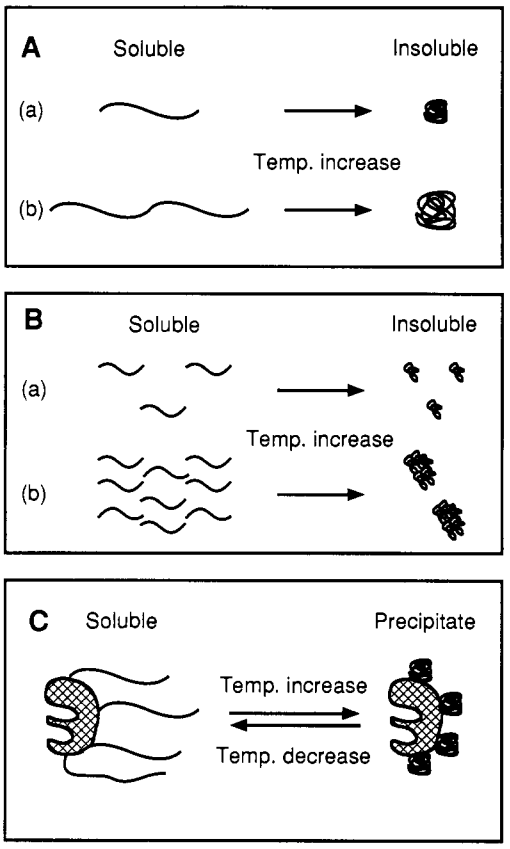


Figure 3. Illustration of the phase transition corresponding to the temperature response of OIPAAm: (A) molecular chain length dependence, (B) concentration of aqueous solution dependence, (C) collagen–Ic-50 conjugate.

Precipitated aggregates grow and gather larger aggregates (Figure 3A). Although the aggregates of the lower molecular weight oligomers are insufficiently aggregated to be separated from supernatant, sufficiently strong phase transitions are present for detection by transmittance changes shown in Figure 1. In solutions of lower concentration, oligomers having short chain lengths precipitate in small units, failing to aggregate to larger particles. In the case of higher solution concentrations, however, the Ic oligomers are easily aggregated and precipitated. For concentrated solutions, OIPAAm oligomers of shorter chain lengths aggregate via increased intermolecular interactions (Figure 3B). While transmittance changes for aqueous solutions of each of the oligomers were independent of molecular weight, aggregation properties of the OIPAAms separated from aqueous systems seem to be related to solution concentration and OIPAAm molecular weight.

Figure 4 shows the results for centrifugation recovery of OIPAAm oligomers and a collagen–Ic-50 conjugates as a function of a centrifugal force. Recovery of OIPAAm from aqueous solution by temperature increases is over 80% efficient for Ic-10 (M_w = 1400) and Ic-20 (M_w = 2700). In contrast to the flocculation recovery methods, oligomers having short chain lengths and the oligomers in diluted solution are readily recovered by centrifugation. Collagen–Ic-50 conjugates aggregated into large particles at 37 °C, and 87% by weight was recovered from 0.3 wt % aqueous solutions. Precipitated conjugates aggregated easily because collagen–Ic-50 conjugates have a very high molecular weight (near 450 000). OIPAAm molecules having long chain lengths are advantageous for the effective precipitation of OIPAAm-grafted biomolecules (Figure 3C). Multiple grafts per biomolecule are required when using

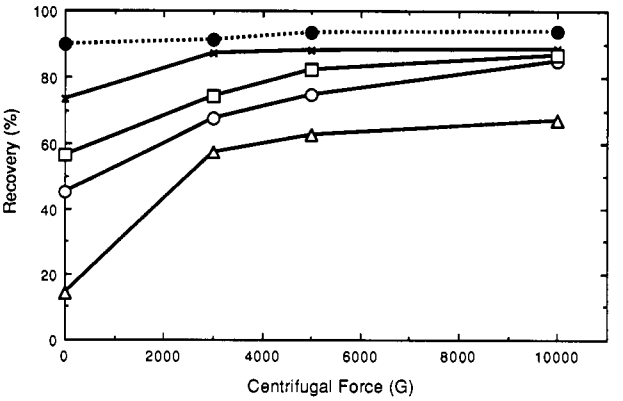


Figure 4. Recovery of OIPAAms and OIPAAm–collagen conjugates from aqueous media as a function of centrifugal force (○, Ic-10 of 10 wt %; △, Ic-20 of 1 wt %; ×, Ic-20 of 10 wt %; □, Ic-40 of 1 wt %; ●, collagen conjugate).

OIPAAm of short chain lengths. While the chemical coupling specificity between biomolecules and OIPAAm has not been investigated, previous studies indicated that there are no demonstratable effects of grafting on the bioactive recognition site in immunoglobulin G-PEO (M_w = 5000) conjugates (*8*). It was thought that increased polymer chain length and degree of substitution would enhanced the temperature-response due to the increase in the temperature-responsive segments of PIPAAm associated with the bioconjugates. Although there is a possibility that the mobility of long polymer chains and a high degree of substitution may denature biomolecule structures and destroy the reactivity of biomolecules due to steric hindrance, there should be an optimum length and substitution for each enzyme. The mobility of the long polymer chains in aqueous medium may also elicit some effect on the bioactivity of the biomolecule conjugates. Further studies are warranted in this regard.

Collagen is an essential component for diagnostic assays and cell-culture media. Modified soluble collagens will contribute to improved cell culture and the development of biofunctional materials. It is expected that temperature-responsive bioconjugates promote the efficiency of the whole system to actualize homogeneous reaction and to maintain the activity of biomolecules in aqueous media compared with immobilized enzymes. Once bioconjugates are reacted in aqueous media at a lower temperature, small temperture increases easily induce precipitation, which can be utilized as a new method for recovery; namely, bioconjugates can be separated from the aqueous media easily after desirable reaction. Moreover, temperature-responsive bioconjugates, with a designated precipitation temperature, may enable targeting of drugs by heating of localized sites in the body. Our results demonstrate the potential for initiating soluble–insoluble changes of biomolecule–OIPAAm conjugates with small temperature changes in physiologically relevant regimes. This method can be applied to a wide variety of other bioactive enzymes and proteins. We have prepared other IPAAm cooligomers with reactive end groups and modified biomolecules demonstrating LCST around 37 °C; the details of how to control the LCST of the bioconjugates will be reported in a forthcoming paper.

CONCLUSIONS

(i) Temperature-responsive semitelechelic oligomers with carboxyl end-groups were synthesized by the radical telomerization of IPAAm using MPA as a chain-transfer agent.

(ii) This synthetic strategy is capable of regulating the chain length of the oligomers by varying the molar ratio of MPA to IPAAm.

(iii) All OIPAAm products demonstrated a LCST in the same temperature range as homogeneous PIPAAm. This property is independent of both molecular weight and the presence of the hydrophilic moiety at the end of the polymer chain.

(iv) OIPAAms, especially Ic-50 (M_w = 6100), are separated from aqueous media by centrifugation at temperatures above the LCST.

(v) Collagen–Ic-50 conjugates demonstrate water solubility and precipitate near 34 °C. The conjugates are separated from aqueous systems as precipitates with over 90% recovery efficiency.

ACKNOWLEDGMENT

The authors are sincerely grateful to Dr. David W. Grainger, Oregon Graduate Institute of Science and Technology, and Dr. Glen S. Kwon, International Center for Biomaterial Science, Tokyo Women's Medical College, for their valuable discussions.

LITERATURE CITED

(1) Bae, Y. H., Okano, T., and Kim, S. W. (1990) Temperature dependance of swelling of crosslinked poly(N,N′-alkyl substituted acrylamides) in water. *J. Polym. Sci. Polym. Phys. 28*, 923–936.

(2) Heskins, M., Guillet, J. E., and James E., (1968) Solution properties of poly(N-isopropylacrylamide). *J. Macromol. Sci. Chem. A2*, 1441–1455.

(3) Okano, T., Bae, Y. H., Jacobs, H., and Kim, S. W. (1990) Thermally on-off switching polymers for drug permeation and release. *J. Controlled Release 11*, 255–265.

(4) Yoshida, R., Sakai, K., Okano, T., Sakurai, Y., Bae, Y. H., and Kim, S. W. (1991) Surface-modulated skin layers of thermal responsive hydrogels as on-off switches: I. Drug release. *J. Biomater. Sci. Polym. Ed. 3*, 155–162.

(5) Yoshida, R., Sakai, K., Okano, T., and Sakurai, Y. (1992) Surface-modulated skin layers of thermal responsive hydrogels as on-off switches: II. Drug permeation. *J. Biomater. Sci. Polym. Ed. 3*, 243–252.

(6) Starks, C. M. (1974) *Free Radical Telomerization*, Academic Press Inc., New York.

(7) Okano, T., Katayama, M., and Shinohara, I. (1978) The influence of hydrophilic and hydrophobic domains on water wettability of 2-hydroxylethyl methacrylate–styrene copolymers. *J. Appl. Polym. Sci. 22*, 369–377.

(8) Abuchowski, A., van Es, T., Palczuk, N. C., and Davis F. F. (1977) Alteration of immunological properties of bovine serum albumin by covalent attachment of polyethylene glycol. *J. Biol. Chem. 252*, 3578–3581.

(9) Miron, T., and Wilchek, M. (1982) A spectrophotometric assay for soluble and immobilized N-hydroxysuccinimide esters. *Anal. Biochem. 126*, 433–435.

(10) Bückmann, A. F., and Morr, M. (1981) Functionalization of poly(ethylene glycol) and monomethoxy-poly(ethylene glycol). *Makromol. Chem. 182*, 1379–1384.

(11) Gewehr, M., Nakamura, K., Ise, N., and Kitano, H. (1992) Gel permeation chromatography using porous beads modified with temperature-responsive polymers. *Makromol. Chem. 193*, 249–256.

(12) Mayo, F. R., Lewis, F. M., and Walling, C. (1948) Copolymerization: VIII. The relation between structure and reactivity of monomers in copolymerization. *J. Am. Chem. Soc. 70*, 1529–1533.

(13) *Polymer Handbook* (J. Braudrup, and E. H. Immergut, Ed.) pp 92–95, John Wiley & Sons, New York.

(14) Kice, J. L. (1956) Inhibition of polymerization II. Methyl acetate. *J. Polymer Sci. 19*, 123–140.

(15) Fujishige, S., Kubota, K., and Ando, I. (1989) Phase transition of aqueous solutions of poly(N-isopropylacrylamide) and poly(N-isopropylmethacrylamide). *J. Phys. Chem. 93*, 3311–3313.

(16) Chen, J. P., Yang, H. J., and Hoffman, A. S., (1990) Polymer-protein conjugates I. Effect of protein conjugation on the cloud point of poly(N-isopropylacrylamide). *Biomaterials 11*, 625–630.

(17) Chen, J. P., and Hoffman, A. S., (1990) Polymer-protein conjugates II. Affinity precipitation separation of human immunogammaglobulin by a poly(N-isopropylacrylamide)–protein A conjugates. *Biomaterials 11*, 631–634.

^1H and ^{13}C NMR of 3-O and 4-O Conjugates of Dopamine and Other Catecholamines[1]

Delbert D. Mueller,*,† Thomas D. Morgan,‡ James D. Wassenberg,† Theodore L. Hopkins,§ and Karl J. Kramer†,‡

Departments of Biochemistry and Entomology, Kansas State University, Manhattan, Kansas 66506, and U.S. Grain Marketing Research Laboratory, Agricultural Research Service, U.S. Department of Agriculture, Manhattan, Kansas 66502. Received July 31, 1992

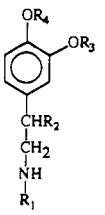
Dopamine and its conjugates are widely distributed among biological species and are utilized for a variety of functions. Insects metabolize dopamine for cuticle melanization and sclerotization. Among the most abundant dopamines found in the larval and pupal development stages of *Manduca sexta*, the tobacco hornworm, are *N*-acetyldopamine and *N*-β-alanyldopamine. In addition, glycosylated derivatives of these dopamines are found mainly in the hemolymph just prior to cuticulogenesis. The ^1H and ^{13}C NMR resonances of dopamine, its 3-*O*-methyl, 4-*O*-methyl, *N*-acetyl, and *N*-β-alanyl derivatives, norepinephrine, 4-*O*-(β-D-glucuronopyranosyl)dopamine, and the glycosylated products of *N*-β-alanyldopamine and dopamine have largely been assigned. Assignments were based on one- and two-dimensional NMR analyses of the above compounds combined with that of specifically enriched [C7-^{13}C]dopamine. ^1H NMR showed that the major glycosylated natural product isolated from *M. sexta* pupal hemolymph was a 3-*O*-glycosyl derivative of *N*-β-alanyldopamine. ^{13}C NMR confirmed that the carbohydrate was D-glucose probably in a β-linkage. ^1H NMR of the aromatic ring protons provided the most definitive method to distinguish 3-O- from 4-O-derivatives of dopamine. In addition, the 3-*O*-glucosyl conjugate of *N*-β-alanyldopamine had unique chemical shifts and coupling patterns compared to those of 4-*O*-(β-D-glucuronosyl)- and 3-*O*-(β-D-glucopyranosyl)dopamine.

INTRODUCTION

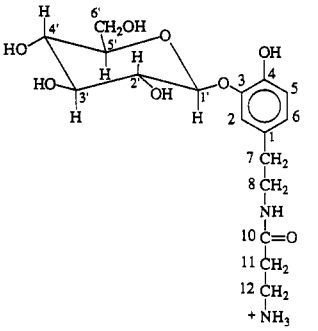
Dopamine and related catecholamines (Chart I) are involved in a host of biological functions. One of the most widely recognized and studied functions is neurotransmission (*1*). In insects, dopamine and/or substituted dopamines are also utilized in cuticle sclerotization (hardening) resulting in an insoluble, heterogeneous skeletal complex of proteins, lipids, catecholamines, polysaccharides, and water (*2–4*). Recent solid-state NMR studies have begun to elucidate some of the chemical reaction products that form during sclerotization (*5, 6*). Apparently insects do not use dopamine directly for sclerotization, but form *N*-acyl derivatives with acetate or β-alanine from the hemolymph before incorporation into the cuticle (*4*). Glucoside or sulfate conjugates of the *N*-acylcatecholamines often accumulate in the hemolymph before sclerotization.

Conjugates of catecholamines often are assigned a protective and possibly a transport role in the regulation of substrate availability for cuticle tanning (*7*). One of the most abundant dopamine adducts in pharate pupa of the tobacco hornworm, *Manduca sexta*, is NBAD[2] (*8–10*). Other conjugated dopamines isolated from *M. sexta* larval hemolymph (*8*), the left colleterial gland of the praying mantis, *Hierodula patellifera* (*11*), and whole body extracts of *Drosophila melanogaster* (*12*), *Calliphora vomitoria* (*13*), and *Bombyx mori* (*14*) include NBAD and NADA, as well as other catecholamines, glycosylated at a ring hydroxyl group. In addition, *O*-(β-D-glucopyranosyl)-L-tyrosine was found in several insect species (*15*) and in the seeds of *Entada pursaetha*, which also contained a 3-*O*-dopamine glucoside (*16*). This paper concerns the use of ^1H- and ^{13}C-NMR solution spectroscopy to identify and characterize some of thse dopamine derivatives. These analyses resulted in the determination of the structure of a glucoside of NBAD which serves as a precursor for protein cross-linking agents in the cuticle of the tobacco hornworm. This glucoside exhibited atypical chemical shifts and spin–spin coupling patterns compared to other catecholamines.

Chart I. Structure I: Generic Representation for Dopamine and Its Derivatives. Structure II: 3-*O*-(β-D-Glucopyranosyl)-*N*-β-alanyldopamine



I



II

EXPERIMENTAL PROCEDURES

The chemical shift reference compounds, *N*-β-alaninamide, dopamine, 3-*O*- and 4-*O*-methyldopamine, NADA, and norepinephrine, were obtained from Sigma Chemical

[1] This research was supported in part by the National Science Foundation research grant DCB90-19400 and conducted by the Kansas Agricultural Experiment Station (Contribution No. 93-38-j) in cooperation with the Agricultural Research Service, U.S. Department of Agriculture.

* To whom correspondence should be addressed.
† Department of Biochemistry, Kansas State University.
‡ U.S. Department of Agriculture.
§ Department of Entomology, Kansas State University.

[2] Abbreviations used: NBAD, *N*-β-alanyldopamine; NBAD-glucoside, 3-*O*-(β-D-glucopyranosyl)-*N*-β-alanyldopamine; NADA, *N*-acetyldopamine; dopamine glucoside, 3-*O*-(β-D-glucopyranosyl)dopamine.

1043-1802/93/2904-0047$04.00/0 © 1993 American Chemical Society

Table I. ^{1}H-NMR Chemical Shifts and Coupling Constants[a] (in parentheses) of Catecholamines and Related Compounds

compd[b]	2-H	5-H	6-H	3-OCH_3	4-OCH_3	7-CHR_2	8-CH_2	10-CH_3	11-CH_2	12-CH_2
dopamine	6.833	6.894	6.746			2.863	3.216			
$R_1 = R_2 = H$	(8.11)	(8.09)				(7.22a)	(7.23)			
$R_3 = R_4 = H$	(1.64)		(1.46)							
[C7-^{13}C]dopamine	6.833	6.896	6.747			2.864	3.218			
		(8.08)	(8.03)			(7.22a)	(7.18)			
	(2.10)		(2.10a)							
[^{13}C-^{1}H J]	(4.21)		(4.16a)			(128.98)	(3.36)			
3-*O*-methyldopamine	6.902	6.829	6.740	3.793		2.851	3.171			
$R_1 = R_2 = R_4 = H$; $R_3 = CH_3$		(8.05)	(8.07)			(7.20a)	(7.23)			
	(1.97)		(2.02a)							
3-*O*-(β-D-glucopyranosyl)dopamine	7.089	6.96e	6.93e			2.928	3.249			
$R_1 = R_2 = R_4 = H$		(7.1e)	(7.5e)			(7.22a)	(7.08a)			
R_3 = β-D-glucopyranosyl	(2.10)	(2.1e)	(nd)							
4-*O*-methyldopamine	6.778	6.949	6.776		3.789	2.823	3.163			
$R_1 = R_2 = R_3 = H$		(8.80)	(8.80)			(7.23a)	(7.24)			
$R_4 = CH_3$	(2.00)		(2.18a)							
4-*O*-(β-D-glucuronosyl)dopamine	6.858	7.130	6.796			2.875	3.212			
$R_1 = R_2 = R_3 = H$	(8.29)		(8.33)			(7.15a)	(7.16a)			
R_4 = β-D-glucuronopyranosyl	(1.99)		(2.01a)							
N-acetyldopamine	6.780	6.846	6.687			2.668	3.356	1.748		
$R_2 = R_3 = R_4 = H$		(8.07)	(8.08)			(6.85a)	(6.84)			
$R_1 = C(O)CH_3$	(1.93)		(1.94a)							
norepinephrine	6.946	6.846	6.860			4.871	3.253c			
$R_1 = R_3 = R_4 = H$							3.190t			
$R_2 = OH$		(8.12)	(8.24)			(8.45)	(13.05)			
	(2.18)		(2.05)			(4.39a)	(8.48)			
							(4.37)			
N-β-alanylnorepinephrine[c]	6.906	6.903	6.821			4.713	3.464t		2.625	3.200
$R_3 = R_4 = H$							3.434c			
$R_2 = OH$		(7.90)	(8.16)			(nd)	(12.87)		(6.78)	(6.71)
$R_1 = C(O)CH_2CH_2NH_2$	(1.90)		(1.84a)			(nd)	(6.67)			
							(4.88)			
N-β-alaninamide[d]									2.706	3.260
									(6.64)	(6.63)
N-β-alanyldopamine	[6.72]	[6.78]	[6.63]			[2.62]	[3.34]		[2.50]	[3.09]
$R_2 = R_3 = R_4 = H$		(8.03)	(8.35)			(6.73a)	(6.74)		(6.87)	(6.82)
$R_1 = C(O)CH_2CH_2NH_2$	(1.90)		(1.84a)							
3-*O*-(β-D-glucopyransoyl)-*N*-β-alanyldopamine	6.992	6.865	6.824			2.687	3.389s		2.514	3.105
							3.367s			
(Chart I, structure II)		(8.09)	(8.46)			(6.69a)	(−14.35)s		(6.83)	(6.83)
	(1.50)		(nd)				(7.15)s			
							(6.80)s			

[a] An a after a coupling constant means that it is an average from two or more sets of peaks, an s following a shift or a coupling constant means that the value was obtained by simulation, and an e means it was estimated. Shifts in brackets were referenced to the solvent HOD peak (4.745 ppm). nd means not detected. [b] See Chart 1, structure I, for R_1–R_4 positions. [c] Aliphatic hydrogen assignments given in ref 28. [d] Assignments from Sadtler *Standard NMR Spectra*, compound 10221M.

Co. and used without further purification. The 99.99 atom percent ^2H_2O was from Aldrich Chemical Co. Purification of NBAD and *N*-β-alanylnorepinephrine followed established procedures (*9*) and the NBAD and dopamine glucosides were purified from hemolymph of the tobacco hornworm using HPLC and gel filtration chromatography.[3] [C7-^{13}C]Dopamine that was 99% labeled was obtained from MSD Isotopes (Montreal, Canada) and 4-*O*-(β-D-glucuronopyranosyl)dopamine was a gift from Dr. Cyrus Creveling, Laboratory of Bioorganic Chemistry, NIDDK, National Institutes of Health, Bethesda, MD.

NMR spectra were acquired in 99.98% ^2H_2O on a Bruker WM-400 or a Varian UNITY 600-MHz spectrometer. Typical ^{1}H-NMR acquisitions at 400 MHz used a 60° pulse width, a 4000-Hz sweep width, and 16K data points which were transformed after applying a 0.1-Hz line broadening and zero-filling to 32K points. A 6000-Hz sweep width and 32K data points were used for the 600-MHz acquisitions. The ^{1}H shifts were referenced to the methyl signal of sodium 3-(trimethylsilyl)propionate in ^2H_2O taken as 0 ppm. The ^{1}H-decoupled ^{13}C-NMR spectral parameters were the same as those for ^{1}H NMR expect that the sweep width was 23810 Hz and the line broadening 1.5 Hz, and the shifts were referenced to *p*-dioxane in ^2H_2O taken as 67.4 ppm relative to tetramethylsilane. 2-D NMR homonuclear COSY (*12*) spectra were obtained at 400 MHz using 512 t_1 increments of 1K data points over a 2392.3-Hz spectral width. A symmetrized, absolute value spectrum was obtained after processing the time domain data with a sine-bell function and zero-filling to 1K in F_1 and 2K in F_2 before Fourier transformation. A heteronuclear COSY spectrum was acquired and processed similarly on 0.5 mL of a 40 mg/mL ^2H_2O solution 3-*O*-methyldopamine, except that the spectral width was 10416.7 Hz. All acquisitions were at 30 °C except for NBAD-glucoside, which was also acquired at 45–50 °C.

[3] Hopkins, T. L., Morgan, T. D., Kramer, K. J., and Tomer, K. B., unpublished data.

RESULTS

^{1}H-NMR Assignments. The proton assignments leading to the identification of the metabolite NBAD-glucoside were based on comparison to literature values and data from authentic model compounds, using specific resonance decoupling as well as homonuclear and heteronuclear COSY methods. The authentic compounds were dopamine, 3-*O*-methyldopamine, 4-*O*-methyldopamine, 4-*O*-(β-D-glucuronopyranosyl)dopamine, NADA, β-alaninamide, norepinephrine, and NBAD.

Table II. ^{13}C-NMR Chemical Shifts and Assignments of Catecholamines and Related Compounds

compd[a]	C1	C2	C3	C4	C5	C6	C7	C8	10-CH_3	10-C=O	C11	C12
dopamine $R_1 = R_2 = R_3 = R_4 = H$	130.27	117.56	145.19	143.98	117.53	122.18	32.93	41.62				
dopamine[b]	128.9	117.2	151.1	148.7	116.2	118.6	34.7	42.2				
[C7-^{13}C]dopamine							32.90					
3-*O*-methyldopamine $R_1 = R_2 = R_4 = H$ $R_3 = CH_3$	130.00	113.91	148.47	144.71	116.60	122.55	33.12	41.52	(56.79)[c]			
4-*O*-methyldopamine $R_1 = R_2 = R_3 = H$ $R_4 = CH_3$	130.65	113.81	144.71	145.90	116.76	121.92	32.84	41.44	(56.89)[c]			
4-*O*-(β-D-glucuronopyranosyl)dopamine $R_1 = R_2 = R_3 = H$ R_4 = β-D-glucuronopyranosyl	133.35	118.17	144.56	146.70	117.34	122.11	32.90	41.35				
N-acetyldopamine $R_2 = R_3 = R_4 = H$ $R_1 = C(O)CH_3$	132.94	117.41	144.68	143.11	117.03	121.92	34.52	41.52	22.59	174.73		
N-β-alaninamide										175.90	32.19	36.48
N-β-alanyldopamine $R_2 = R_3 = R_4 = H$ $R_1 = C(O)CH_2CH_2NH_2$	132.77	117.40	144.72	143.17	116.96	121.85	34.46	41.27		172.65	32.88	36.62
3-*O*-(β-D-glucopyranosyl)-*N*-β-alanyldopamine $R_2 = R_4 = H$ $R_1 = C(O)CH_2CH_2NH_2$ R_3 = β-D-glucopyranosyl	132.92	118.01	145.35	144.86	117.86	125.16	34.79	41.36		172.74	32.96	36.75

[a] See Chart I, structure I, for R_1–R_4 positions. [b] Reference 19. [c] Shift for ring OCH_3.

Reasonable assignments for the dopamine aromatic and aliphatic ^{1}H resonances can be made by inspection. These were confirmed in the ^{1}H spectrum of [C7-^{13}C]dopamine in which the three-bond ^{13}C–^{1}H couplings of 4.2 Hz to the ring 2H and 6H protons as well as the two-bond couplings of 3.4 Hz to the aliphatic C8 protons were well-resolved. This unambiguously confirmed that the long range ^{1}H–^{1}H aromatic ring coupling of 2.1 Hz normally observed in dopamine spectra was meta coupling. Similar 1.5–2.1 Hz couplings were seen in almost all the catecholamines investigated and were observed in the proton spectra of 3-*O*- and 4-*O*-sulfates of dopamine and norepinephrine (*17*, *18*). Enrichment at C7 also allowed direct assignment of that resonance (Tables I and II).

Once the dopamine protons were assigned, the two methylene resonances of *N*-acetyldopamine were identifiable, as was the methyl signal. In turn, the *N*-acetyldopamine shifts were used to help assign the four aliphatic protons in NBAD (Table I), which has a similar amide bond. Further confirmation of the assignments of the penultimate methylene resonances of NBAD was obtained through comparison of its ^{1}H-NMR spectrum to that of β-alaninamide and COSY connectivities.

The site of glycosylation of NBAD was investigated by comparison of its aromatic region ^{1}H spectrum to those of authentic 4-*O*- and 3-*O*-methyldopamine. Compared to dopamine (Figure 1A), 3-O-methylation (Figure 1B) interchanged the chemical shifts of H2 and H5 by way of comparable downfield and upfield shifts, respectively, while 6H shifted upfield slightly. In contrast, 4-*O*-methyl substitution (Figure 1D) produced larger shifts for H2 and H5 that were opposite directions from those of the 3-O compound. Consequently, 5H became the most downfield resonance and 2H moved upfield to nearly overlap with the slightly downfield shifted 6H peaks. Strong couplings also were apparent among the aromatic protons of 4-*O*-methyldopamine due to the near equivalence of the H2 and H6 chemical shifts. That overall pattern, without evidence of strong coupling, was preserved in the 4-*O*-glucuronic acid derivative (Figure 1E). However, all three aromatic ring protons were shifted downfield from those of 4-*O*-methyldopamine. Comparison of the 3-O and 4-O shift patterns in the aromatic ring protons to those for NBAD-glucoside (Figure 1C) strongly suggested that the site of attachment was 3-O. Glycosylation at the O-3 position also was compatible with the recovery of 4-*O*-methyldopamine after methylation of the conjugate and subsequent acid hydrolysis[3] (*11*). A ^{1}H spectrum of dopamine glycoside (Table I) showed a similar pattern of aromatic ring hydrogen shifts except that H6 was slightly downfield of H5 and the coupling was stronger. This indicated that dopamine glycoside also was 3-O bonded.

The overall effect of 3-O-glycosylation of dopamine and NBAD was to shift all the aromatic protons downfield relative to their positions in 3-*O*-mthyldopamine, just as observed with 4-*O*-glucuronic acid conjugation. Upon 3-*O*-glycoside formation, however, H2 and H6 shifted even farther downfield while H5 moved less upfield than for 3-*O*-methyldopamine. Downfield shifts relative to the respective *O*-methyl compounds also occurred for 3-*O*- and 4-*O*-sulfates of dopamine and norepinephrine and, unlike the aromatic protons of 4-*O*-methyldopamine, all three resonances of the 4-*O*-sulfates were well-resolved (*18*) as they were in the 4-*O*-glucuronide (Figure 1E).

^{13}C-NMR Assignments. Identification of the glycosyl group and the orientation of the 3-*O*-glycosidic bond was established by ^{13}C NMR. Assignment of most of the NBAD-glycoside catecholamine carbons was also possible. Procedures similar to those for the ^{1}H assignments were followed except that ^{13}C assignments for dopamine (*19*), homoveratrylamine (*20*), and *O*-(β-D-glucopyranosyl)-L-tyrosine (*21*) also were available. Table II lists the catecholamine resonances and Table III gives the glucoside shifts. Comparison of the ^{13}C shifts to those of *O*-(β-D-glucopyranosyl)-L-tyrosine (Table III) indicated that the carbohydrate was glucose and that the anomeric linkage probably was β based on the differences in C1′ shifts between the α- and β-configurations of other aromatic ring glucopyranosides.

Assignments of the unsubstituted carbons of the aromatic ring and the ethylamine group for 3-*O*-methyldopamine were obtained from a heteronuclear ^{13}C–^{1}H COSY spectrum (data not shown), in combination with the ^{1}H assignments described above. Methylation of the 3-hydroxyl of dopamine substantially shifted C2 and C3 and slightly shifted the other aromatic ring carbons (Figure

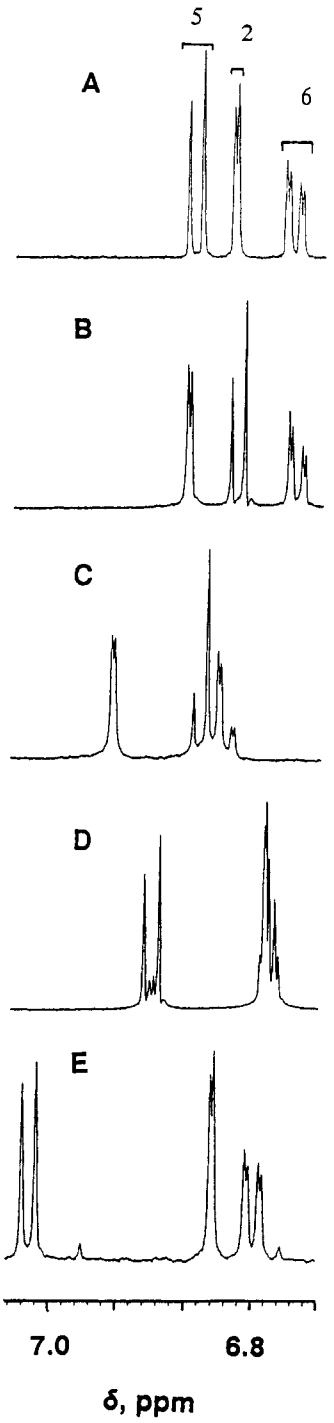


Figure 1. 400-MHz aromatic region ^{1}H-NMR spectra obtained over a 6098.1-Hz sweep width using a 60° flip angle, either 32K data points or 16K with zero-filling, 2.72- or 1.36-s acquisition times, respectively, with a 1.0–1.6-s delay between scans on 0.5-mL ^2H_2O solutions containing 3–8 mg of sample, pH (meter readings) 5–8: (A) dopamine, 32 scans (the numbers above the peaks refer to carbon atom numbers given in Chart I, structure II), (B) 3-*O*-methyldopamine, 16 scans, (C) 3-*O*-(β-D-glucopyranosyl)-*N*-β-alanyldopamine, 32 scans, (D) 4-*O*-methyldopamine, 16 scans, (E) 4-*O*-(β-D-glucuronopyranosyl)dopamine, 64 scans. The two low-intensity peaks at 6.76 and 7.05 ppm are due to an unidentified contaminant.

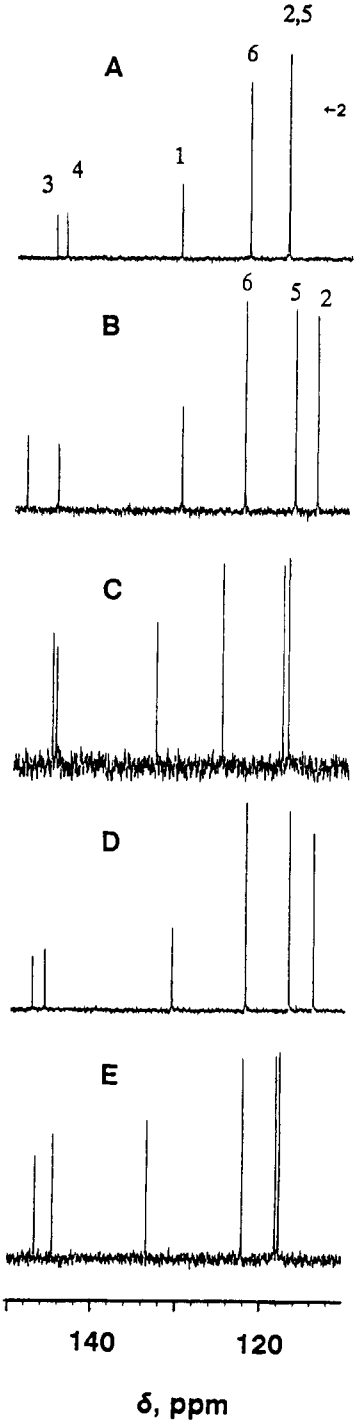


Figure 2. 100.6-MHz aromatic region ^{13}C-NMR spectra for the same samples as in Figure 1 from spectra obtained over a 23809.5-Hz spectral region using 16K data points with zero-filling to 32K, 60° flip angle, 0.344-s acquisition time, and a 2.656-s relaxation delay: (A) dopamine, 9688 scans (the numbers above the peaks refer to carbon atom numbers given in Chart I, structure II), (B) 3-*O*-methyldopamine, 13810 scans, (C) 3-*O*-(β-D-glucopoyranosyl)-*N*-β-alanyldopamine, 4896 scans, (D) 4-*O*-methyldopamine, 13016 scans, (E) 4-*O*-(β-D-glucuronopyranosyl)dopamine, 10856 scans.

2B), producing clearly resolved C2 and C5 peaks. 3-*O*-Glucosyl substitution also shifted the ring carbons but quite differently from those due to methyl substitution (compare parts B and C of Figure 2). Similar differences between shifts resulting from 4-*O*-methyl- and 4-*O*-glucuronosyl substitutions were also apparent (compare parts D and E of Figure 2). In keeping with the apparent 3.28 ppm downfield shift of C3 upon O-methylation (Table II), the most downfield peak in 4-*O*-methyldopamine was tentatively assigned to C4 and, thereby, represented a 1.92 ppm downfield shift from C4 of dopamine. Overall, howver, no clear predictive patterns of hydroxyl substitution shifts have been extracted, partly because unambiguous assignments of C3 and C4 have yet to be made for any of the dopamines. Furthermore, for compounds other

Table III. Glucosyl ^{13}C-NMR Shifts of Catecholamine Conjugates and Related Compounds

	C1′	C2′	C3′	C4′	C5′	C6′
NBAD-glucoside[a]	102.09	73.81	76.45	70.37	77.14	61.49
O-(β-D-glucopyransoyl)-L-tyrosine[b]	101.1	73.8	76.4	70.2	77.0	61.4
p-nitrophenyl α-D-glucopyranoside[c]	100.45	74.1	76.9	72.5	75.75	63.45
p-nitrophenyl β-D-glucopyranoside[c]	102.7	75.95	80.05	72.4	79.3	63.55
4-*O*-(β-D-glucuronopyranosyl)dopamine	101.96	73.53	76.13	72.56	77.19	179.14

[a] Chart I, structure II. [b] From ref 21. [c] From ref 29.

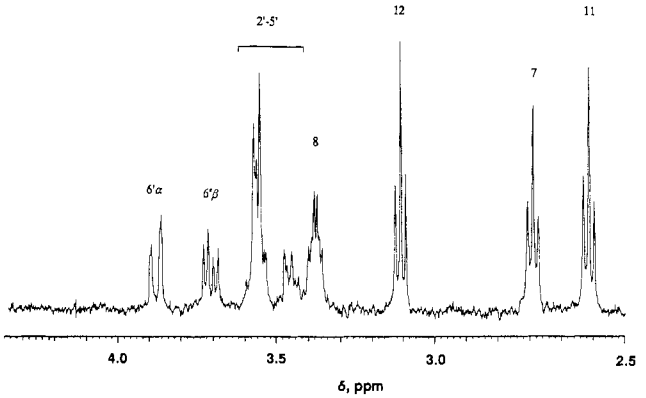


Figure 3. 400-MHz ^{1}H NMR of the aliphatic region of 3-*O*-(β-D-glucopyranosyl)-*N*-β-alanyldopamine using 4.8 mg in 0.5 mL of ^2H_2O, pH 8.17. See Figure 1 for the spectral conditions. Peak numbers refer to the carbon atom numbers given in Chart I, structure II. (6′α and 6′β refer to nonequivalent methylene protons, not anomeric carbon configurations.)

than 3-*O*-methyldopamine, the only compound for which the hydrogen-bearing ring carbons were definitively assigned, the shifts for C2 and C5 were very similar and the tentative assignments listed in Table II might be reversed.

A possible distinction between 3-*O*- and 4-*O*-glycosides based on ^{13}C NMR is seen in the separation of the hydroxylated aromatic ring carbons. With the O-3 position glycosylated, carbons 3 and 4 were separated by only 0.5 ppm (Figure 2C), whereas in the 4-*O*-glucuronide compound the separation was nearly 2.2 ppm (Figure 2E). (That pattern, however, was reversed in the 3-*O*- and 4-*O*-methyl derivatives.) Generally, the ring carbon shifts appeared quite sensitive to both the position and nature of the hydroxyl substituent. Thus, the shift patterns seen in Figure 2, parts C and E, probaby can be used to uniquely identify 3-*O*- versus 4-*O*-(β-D-glucoside) substitution of dopamines.

Unique ^{1}H-NMR Spectrum of *N*-β-Alanyldopamine Glucoside. Figure 3 shows the upfield portion of the ^{1}H spectrum of the NBAD-glucoside. The aromatic ring protons (Figure 1C), the aliphatic methylene protons H7, H11, and H12 as well as those for glucose 6′ appear normal, whereas those for the glucose ring, 2′–5′, are complex and/or largely unresolved, and the H8 methylene resonances show a multiplet pattern. The H8 multiplet pattern was not seen in NBAD, dopamine glycoside, or in the 4-*O*-glucuronic acid derivative of dopamine, but a slight distortion of the normal triplet as apparent at H8 in NADA at 400 MHz.

In the 1-D spectrum of the NBAD 3-*O*-glucosyl compound, the H8 multiplet integrated to essentially two protons. Homonuclear COSY of the conjugate (data not shown) gave clear crosspeaks for the H7–H8 and H11–H12 coupled pairs, which corroborated the initial assignments. Importantly, no connectivity was apparent between the H8 multiplet centered at 3.38 ppm and any resonance other than H7. Specific resonance decoupling of H8 also showed no effect other than collapse of the H7 triplet and vice versa.

An eight-peak multiplet such as that for H8, combined with a normal triplet pattern for H7, suggested an ABX_2 type of coupling in which $J_{AX} \sim J_{BX}$, and for the H8 protons, $\delta_A - \delta_B \sim J_{AB} + J_{AX}$. Strong coupling between the H8 protons along with normal vicinal coupling to the H7 protons would be expected to give an intensity-distorted triplet of a doublet for each of the nonequivalent protons, H8A and H8B. This could occur if rotation about the C8–N bond was slow in NBAD-gluoside while rotation about C7–C8 remained fast (*23*, *24*).

ABX_2 couplings give rise to 22 possible transitions for the A, B, and X protons, several of which are degenerate, especially when $J_{AX} \sim J_{BX}$. Analysis of the spectrum in these terms, using Varian's simulation software and assigning a negative value to J_{AB}, gave δ(H8A) = 3.3890 and δ(H8B) = 3.3667 ppm as well as $J_{AB} = -14.35$ Hz, $J_{AX} = 7.15$ Hz, and $J_{BX} = 6.80$ Hz. The simulated and observed 600-MHz spectra are compared in Figure 4, parts A and B, respectively. Overall the agreement was quite good.

For the glucoside portion of the NBAD conjugate, the homonuclear COSY spectrum showed connectivity between H1′ at 5.09 ppm and the large multiplet at 3.62 ppm, which in the 1-D spectrum had integrated to essentially three hydrogens. Relatively intense crosspeaks between H6′β at 3.763 ppm and the same multiplet were also apparent slightly upfield from where H1′ had connected. Less intense crosspeaks to the same part of the multiplet were observed from H6′α as well. Thus, the 3.62 ppm, set of resonances includes at least the H2′ and H5′ protons. In turn, the peaks centered at 3.62 ppm were coupled to a multiplet between 3.49 and 3.54 ppm, which had integrated to essentially one hydrogen, indicating that either H3′ or H4′ appeared at ca. 3.52 ppm. On the basis of integrated intensities the remaining proton (H4′ or H3′) was part of the three-proton complex at 3.62 ppm. The H4′ (H3′) proton at 3.52 ppm, however, showed a more complex pattern than anticipated for a doublet of a doublet. It seems likely that strong coupling between at least H2′ and H3′ is responsible for the distorted H1′ doublet (Figure 5A) as reflected in the extra peak(s). This interpretation is even more likely since the ^{13}C spectrum of NBAD-glucoside gave no extraneous peaks and uniform line widths for all resonances. In contrast, the glycosyl substituents in the 400-MHz ^{1}H spectra of *O*-(β-D-glucopyranosyl)-L-tyrosine (*15*, *22*), dopamine glycoside, and 4-*O*-(β-D-glucuronopyranosyl)dopamine (Figure 5B) gave normal H1′ doublets. The H2′–H5′ resonances were not well-resolved in these compounds either (data not shown), but were more representative of other aromatic ring substituted monosaccharides (*25*). Unlike the tyrosine and 4-*O*-glycosides, the dopamine glycoside metabolite showed a similar well-separated upfield-shifted resonance (probably H4′) centered at 3.52 ppm as NBAD-glucoside. The nearly identical shfts and couplings among the aromatic ring and glycosyl ^{1}H resonances of NBAD-glycoside and dopamine glycoside suggest that the latter is 3-*O*-(β-D-glucopyranosyl)dopamine.

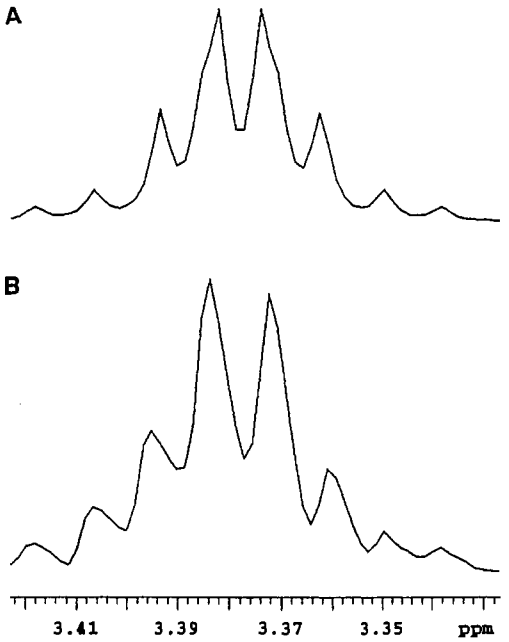


Figure 4. (A) Simulated 600-MHz ^{1}H ABX_2 coupled system. (B) Expansion of the H8 multiplet of 3-*O*-(β-D-glucopyranosyl)-*N*-β-alanyldopamine from a spectrum acquired at 600 MHz under conditions nearly identical to those described in Figure 1. See the text for details.

DISCUSSION

Through ^{1}H- and ^{13}C-NMR analyses it was possible to establish that the major NBAD-glucoside from pharate pupal hemolymph of *M. sexta* was 3-*O*-(β-D-glucopyranosyl)-*N*-β-alanyldopamine, in agreement with chemial evidence[3] (*8*, *26*) and that the dopamine glycoside also was 3-*O*-glucoside. The spectrum of the NBAD 3-O-metabolite at either 400 or 600 MHz, however, showed some unique features relative to the 3-*O*-glucoside of dopamine. Specifically, the H8 multiplet (Figures 3 and 4B) and the extra splitting of H1′ (FIgure 5A) were unique to the NBAD-glucoside. These features were reproducible with two preparations of NBAD-glucoside, were independent of concentration and temperature (up to 45–50 °C, data not shown), and persisted at 600 MHz (Figure 4B for H8). Thus, nonequivalence of the H8 methylene protons and the distorted H1′ doublet were related to the presence of the *N*-β-alanyl group. These data suggest a specific interaction or steric effect involving the 3-*O*-glucosyl group of NBAD-glucoside that slows rotation about the C8–NH bond sufficiently to make the methylene protons magnetically nonequivalent and render some of the H2′–H5′ shifts sufficiently equivalent to relay the strong coupling effects to H1′.

Alternatively, the presence of complex multiple peaks could relfect chemical shift microheterogeneity resulting from slowly interconverting conformers. However, there was only a single peak for each carbon and the line widths were very uniform. For similar differential shifts, ^{13}C NMR is more sensitive to slow interconversion among conformers than ^{1}H NMR. Consequently, for the observed multiple peaks to reflect slow exchange rates, the shifts for the affected protons would have to be considerably greater than those of the carbons to which they are bonded. That seems unlikely. Furthermore, in support of the slow-rotation argument, ABX_2 simulation for the H8 protons (Figure 4A and 4B) successfully reproduced the observed multiplet. In regard to possible reasons for the hindered rotation about the C8 bond, models show that the amide NH group can H-bond to the C3′ oxygen, or that the C9

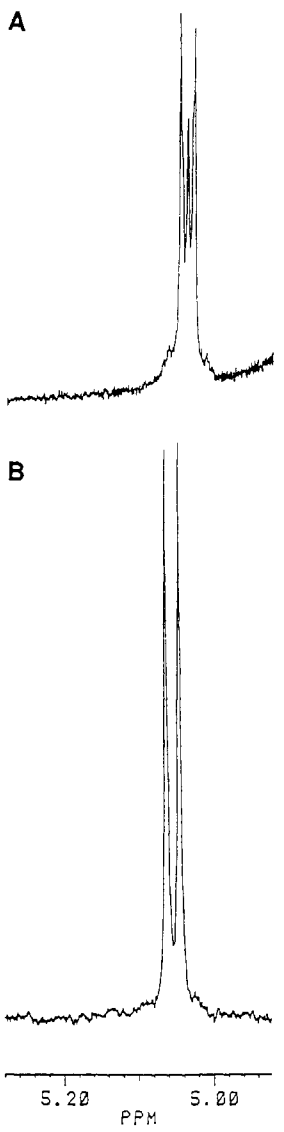


Figure 5. Anomeric proton region of (A) 3-*O*-(β-D-glucopyranosyl)-*N*-β-alanyldopamine and (B) 4-*O*-(β-D-glucuronopyranosyl)dopamine. Spectral conditions are described in Figure 1.

amide carbonyl oxygen can H-bond to the C4′, or C6′, hydroxyl groups. Such interactions could restrict rotations about the C8 bonds and introduce nonequivalence into the 8H protons. All the remaining methylene groups demonstrate typical time-averaged vicinal coupling constants (Table I).

In regard to the anomalous H1′ multiplet, it appears to have resulted from strongly coupled glucose ring protons. However, the ^{1}H homonuclear COSY spectrum did not show evidene of strong coupling in that all the expected connectivities were represented by single sets of crosspeaks of typical intensity. Apparently, if second-order effects were responsible for the anomalous H1′ multiplet, they were not strong enough to distort the COSY spectrum under the acquisitions conditions used. A coupling pattern with an extra center peak for the "X" resonance can ocur for ABX couplings (A = H3′ and B = H2′) when $\nu_A - \nu_B = 0$, J_{AB} = 2 Hz, J_{AX} = 1 Hz, and J_{BX} = 4 Hz (*27*). The couplings in the NBAD glucosyl substituent, however, may be more complex than ABX. In any event, the apparent couplings are quite different from those in methyl-β-D-glucose, for which $\delta_{H3'} - \delta_{H2'}$ = 0.23 ppm, J_{BX} ($J_{H1'-H2'}$) = 8.2 Hz, and J_{AB} ($J_{H2'-H3'}$) = 9.6 Hz (*25*).

Such a change might occur if side-chain interactions alter the orientation of the glucose ring relative to that of

dopamine, which would give different ring current effects in the 3-O-conjugates than for the 4-O-derivative of dopamine, the *O*-glucoside of tyrosine, or the 3-*O*-dopamine glucoside. In that case, the same interaction(s) would be responsible for slow rotation about C8–NH and for the anomalous ^{1}H glucosyl spectrum in NBAD-glucoside.

SUMMARY

^{1}H-NMR data of the aromatic ring protons confirmed that the glycosylated catecholamines isolated from pharate pupal hemolymph of *M. sexta* were bonded at the 3-hydroxyl. For NBAD-glucoside, ^{13}C NMR confirmed the identity of the sugar as glucose, probably bonded through C1′ in the β-configuration. Comparisons of ^{1}H- and ^{13}C-NMR data of model compounds showed that the catecholamine portions of these metabolites were NBAD and dopamine. Thus, the isolated metabolites most probably were 3-*O*-(β-D-glucopyranosyl)dopamine and 3-*O*-(β-D-glucopyranosyl)-*N*-β-alanyldopamine. Furthermore, apparent slow rotation about the C8–NH bond and strong coupling effects among the glucosyl group protons of NBAD-glucoside generated unique ^{1}H spectral features which also might prove useful in distinguishing 3-*O*- and 4-*O*-carbohydrate derivatives of NBAD since para substituents apparently do not interact.

ACKNOWLEDGMENT

The authors are indebted to Dr. Cyrus Creveling, Laboratory of Bioorganic Chemistry, NIDDK, NIH, Bethesda, MD, for the generous gift of 4-*O*-(β-D-glucuronopyranosyl)dopamine, to Dr. Jeff Kao, Department of Chemistry, Washington University, St. Louis, MO, for acquisition and processing help with the 600-MHz spectrum, and to Dr. John S. A. Taylor of the same department for helpful discussions. One of the authors (D.D.M.) wishes to thank the Department of Chemistry, Washington University, St. Louis, MO, and Professor Jacob Schaefer, in particular, for their encouragement and support during a sabbatical leave.

LITERATURE CITED

(1) Snyder, S. H. (1990) *Nature 347*, 121–122.
(2) Hepburn, H. R. (1985) *Comprehensive Insect Physiology, Biochemistry, Pharmacology* (G. A. Kerkut, L. I. Gilbert, Eds.) Vol. 3, pp 1–58, Pergamon Press, Oxford.
(3) Hopkins, T. L., and Kramer, K. J. (1992) *Annu. Rev. Entomol. 37*, 273–302.
(4) Hopkins, T. L., and Kramer, K. J. (1991) In *Physiology of the Insect Epidermis* (K. Binnington, A. Retnakaran, Eds.) pp 213–239, CSIRO, Melbourne.
(5) Schaefer, J., Kramer, K. J., Garbow, J. R., Jacob, G. S., Stejskal, E. O., Hopkins, T. L., and Speirs, R. D. (1987) *Science 235*, 1200–1204.
(6) Christensen, A. M., Schaefer, J., Kramer, K. J., Morgan, T. D., and Hopkins, T. L. (1991) *J. Am. Chem. Soc. 113*, 6799–6802.
(7) Brunet, P. C. J. (1980) *Insect Biochem. 10*, 467–500.
(8) Hopkins, T. L., Morgan, T. D., and Kramer, K. J. (1984) *Insect Biochem. 14*, 533–540
(9) Morgan, T. D., Hopkins, T. L., Kramer, K. J., Roseland, C. R., Czapla, T. H., Tomer, K. B., and Crow, F. W. (1987) *Insect Biochem. 17*, 255–263.
(10) Krueger, R. A., Kramer, K. J., Hopkins, T. L., and Speirs, R. D. (1989) *Insect Biochem. 19*, 169–181.
(11) Yago, M., and Kawasaki, H. (1984) *Insect Biochem. 14*, 487–489.
(12) Okubo, S. (1958) *Med. J. Osaka Univ. 9*, 327–337.
(13) Karlson, P., and Sekeris, C. E. (1962) *Biochim. Biophys. Acta 63*, 489–495.
(14) Tomens, S. (1965) *J. Insect Physiol. 11*, 581–590.
(15) Kramer, K. J., Hopkins, T. L., Ahmed, R. I., Mueller, D. D., and Lookhart, G. (1980) *Arch. Biochem. Biophys. 205*, 146–155.
(16) Larsen, P. D., Pedersen, E., Sorensen, H., and Sorup, P. (1973) *Phytochemistry 12*, 2243–2247.
(17) Kenzl, E., and Eichinger, K. (1988) *J. Chromatogr. 430*, 263–269.
(18) Stoble, G., Werle, E., Helfinger, H., Griebel, D., and Weicher, H. (1988) *Eur. J. Biochem. 176*, 397–402.
(19) Haran, R., Nepveir-Juras, F., and Laurent, J. P. (1979) *Org. Magn. Reson. 12*, 153–158.
(20) Shamma, M., and Hindenlang, D. M. (1979) *Carbon-13 NMR Shift Assignments of Amines and Alkaloids*, p 111, Plenum Press, New York.
(21) Lu, P. W.; Kramer, K. J., Seib, P. A., Mueller, D. D., Ahmed, R., and Hopkins, T. L. (1982) *Insect Biochem. 12*, 377–381.
(22) Psarianos, C. G., Marmaras, V. J., and Vournakis, J. N. (1985) *Insect Biochem. 15*, 129–135.
(23) Pople, J. A., Schneider, W. G., and Bernstein, H. J. (1959) *High-Resolution Nuclear Magnetic Resonance*, McGraw-Hill, New York.
(24) Emsley, J. W., Feeney, J., and Sutcliffe, L. H. (1965) *High Resolution NMR Spectroscopy*, 1st ed., pp 388–391, Pergamon Press, New York.
(25) Bock, K., and Thoegersen, H. (1982) *Annu. Rep. NMR Spectrosc. 13*, 1–57.
(26) Hopkins, T. L., Morgan, T. D., Aso, Y., and Kramer, K. J. (1982) *Science 217*, 364–366.
(27) Bovey, F. A. (1988) *Nuclear Magnetic Resonances Spectroscopy*, p 560 Academic Press, Inc., New York.
(28) Rembold, H., Rascher, J., Eder, J., and Umebachi, Y. (1978) *Z. Naturforsch. 33c*, 498–503.
(29) Rosenthal, S. N., and Fendler, J. H. (1976) ^{13}C NMR Spectroscopy in Macromolecular Systems of Biochemical Interest. In *Advances in Physical Organic Chemistry* (V. Gold, and D. Bethell, Eds.) Vol. 13, p 289, Academic Press, New York.

Copolymers of Lysine and Polyethylene Glycol: A New Family of Functionalized Drug Carriers

Aruna Nathan, Samuel Zalipsky,*,† Sylvie I. Ertel, Spiro N. Agathos,‡ Martin L. Yarmush,§ and Joachim Kohn*,∥

Department of Chemistry, Rutgers—The State University of New Jersey, New Brunswick, New Jersey 08903.
Received August 14, 1992

Poly(PEG-Lys), a new, water-soluble poly(ether urethane), derived from L-lysine and poly(ethylene glycol) was investigated as a precursor for the preparation of polymeric drug conjugates. To facilitate a wide variety of coupling chemistries, the pendent carboxyl groups of poly(PEG-Lys) were converted to other reactive functional groups (amino, hydroxyl, active ester, and aldehyde) in high yield. These reactive pendent chains were then used as anchors for the covalent attachment of penicillin V and cephradine, two clinically used antimicrobial agents. Coupling to the carrier was achieved in good yields and the chemical versatility of this system was demonstrated by the preparation of conjugates having antibiotic ligands linked via biostable or biodegradable linkages to the carrier, either directly or via a spacer. Conjugate 4, poly(PEG-Lys–penicillin V ester), was obtained by linking penicillin V to the polymer backbone via hydrolytically labile ester bonds. This conjugate exhibited activity similar to that of the parent drug against three clinically important strains of bacteria. Drug activity coincided with the release of the drug from the carrier. Hydrolytically stable cephradine-containing conjugates were prepared by three different coupling methods but showed no antibiotic activity. ^{14}C-labeled poly(PEG-Lys) was injected into mice and its biodistribution was monitored for 48 h. The carrier showed no preferential uptake by liver, spleen, or kidney. No signs of acute toxicity were evident in mice or rats when poly(PEG-Lys) was administered iv and ip at doses up to 10 g/kg. These results indicate that poly(PEG-Lys) is a promising precursor for the preparation of soluble drug conjugates.

INTRODUCTION

Attachment of a drug to macromolecular carriers can be used to manipulate biodistribution, permeability through biological barriers, and pharmacokinetics (*1*). Since attachment of a small drug to a macromolecule will slow the rate of drug excretion, drug–polymer conjugates can be used not only for drug targeting but also for the sustained release of a drug over time. Numerous polymers, such as poly(amino acids), polysaccharides, poly(vinyl alcohols), polyvinylpyrrolidinone, polyphosphazenes, and poly(acrylic acid) derivatives have been explored as potential carriers for pharmacologically active agents (*1*).

Due to its recognized biocompatibility, PEG[1] is one of the most widely investigated drug carriers (*2*, *3*). Attachment of PEG to various drugs, proteins, and liposomes has been reported to delay clearance by the reticuloendothelial system (*4–6*). However, PEG has only two reactive groups (the hydroxyl groups at the ends of the chain) that can be used either directly (*5*, *7–9*) or after suitable functionalization (*2*, *5*, *7*, *8*) for covalent attachment of ligands. This severely limits not only the drug "loading" of such conjugates but also the design options for PEG-based drug-carrier systems. To circumvent this limitation, PEG-containing polymers were prepared that bear reactive pendent groups along the polymer backbone. However, the properties of such functionalized polymers are often quite different from those of PEG itself (*10*, *11*). In a different approach, copolymers of PEG and amino acids were explored as biomaterials. These materials were usually prepared by the polymerization of α-amino acid *N*-carboxy anhydrides of γ-benzyl-L-glutamate (*12*), β-benzyl-L-aspartate (*13*), N^{ϵ}-(benzyloxycarbonyl)-L-lysine (*14*), proline (*15*), and phenylalanine (*16*) using amino-PEG as an initiator. This approach led to block copolymers of the general formula ABA (*12*, *15*, *16*) or AB (*13*, *14*), where the A block is composed of homopolypeptide and PEG is the B block. In some instances such block copolymers were further polymerized by enzymatic (*16*) and chemical (*17*) methods yielding multiblock copolymers of higher molecular weights. Potentially useful drug carriers, obtained by oligocondensations of PEG-diamine or PEG-disuccinate with *N*,*N*′-bis(L-phenylalanyl)hexamethylenediamine or *N*,*N*′-adipoylbis(L-phenylalanine), were described by Ulbrich et al. (*18*).

In contrast to the previously known PEG/amino acid block copolymers, the polymers described here are strictly alternating polymers of the general structure: –(PEG-Lys)$_n$–, in which PEG chains of variable molecular weights are linked to the α- and ϵ-amino groups of lysine through stable urethane linkages (2). Such copolymers retain the desirable properties of PEG, while providing reactive pendent groups (the carboxylic acid groups of lysine) at strictly controlled, predetermined intervals along the

† To whom correspondence should be addressed at Liposome Technology, Inc., 1050 Hamilton Ct, Menlo Park, CA 94025.

‡ Waksman Institute of Microbiology and Department of Chemical and Biochemical Engineering, Rutgers University.

§ Department of Chemical and Biochemical Engineering, Rutgers University.

∥ To whom correspondence should be addressed at Department of Chemistry, Rutgers University, P.O. Box 939, Piscataway, NJ 08855.

[1] Abbreviations used: PEG, polyethylene glycol; BSC-PEG, bis(succinimidyl carbonate) of PEG; HOSu, *N*-hydroxysuccinimide; EDC, 1-ethyl-3-[3-(dimethylamino)propyl]carbodiimide; DCC, dicyclohexylcarbodiimide; DCU, dicyclohexyl urea; GPC, gel permeation chromatography; γ-ABA, γ-aminobutyric acid; DMAP, 4-(dimethylamino)pyridine; MIC, minimum inhibitory concentration. A schematic notation is used throughout the text to refer to polymeric products. Similar notations were used in previous publications; see for example ref 19. Figures 1–5 provide the exact chemical structures of all polymeric products.

1043-1802/93/2904-0054$04.00/0 © 1993 American Chemical Society

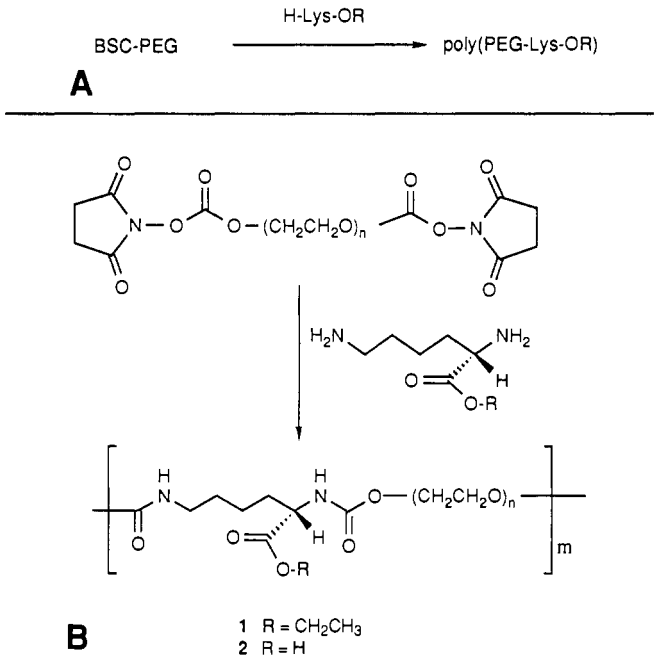


Figure 1. Preparation of poly(PEG-Lys) copolymers: (A) schematic representation, (B) detailed chemical structures.

polymer chain. The reactive pendent groups can be used for derivatization, cross-linking, or conjugation with other molecules. Recently we reported on the usefulness of this new class of polymers for preparation of hydrogels (*19*). The present paper describes some of the biological properties of poly(PEG-Lys) and explores the synthesis of polymeric conjugates with pharmacologically active substances.

RESULTS AND DISCUSSION

Polymer Synthesis. Succinimidyl carbonates (SC) of PEG were recently used by Zalipsky et al. (*20, 21*) for covalent modification and cross-linking of proteins. The high reactivity of SC-activated polymers toward amines as well as their ease of preparation and excellent storage stability prompted our use of bis(succinimidyl carbonates) of PEG (BSC-PEG) as starting materials for the preparation of alternating PEG-lysine polyurethanes (Figure 1). While the previously described interfacial polymerization of BSC-PEG with L-lysine ethyl ester yielded high molecular weight polymers (1) (*19*), the aqueous solution polymerization of BSC-PEG and lysine produced polymers (2) of molecular weights suitable for use as drug carriers ($M_w \leq 50\,000$). The solution polymerization procedure was also conveniently applied for the preparation of radiolabeled carriers using [^{14}C]lysine.

Functionalization. The amount of free carboxyl groups present on 2 or obtained after hydrolysis of the ethyl ester groups of 1 was determined quantitatively by titration with sodium methoxide. In both cases the content of free carboxyl groups was essentially as expected from calculations of the polymer composition. Although carboxyl groups can be used directly for the covalent attachment of drug molecules via amide and ester linkages, transformations of the carboxyl groups to other reactive functional groups were also investigated (Figure 2).

First, we explored the attachment of ligands via amide bonds, using glycine ethyl ester as a simple model compound and EDC as the condensation reagent. Amino acid analysis of conjugate 3 (Figure 3) revealed a Gly:Lys ratio of 0.95/1, indicating that about 95% of all free carboxyl groups had reacted with glycine ethyl ester. The loading of glycine was calculated to be $4.4 \cdot 10^{-4}$ equiv/g of polymer. Similarly, activation of the carboxyl groups with EDC or pivaloyl chloride was used for attachment of ethanolamine and ethylene diamine residues to the polymer, thus introducing primary hydroxyl and amino groups, respectively (derivatives 4 and 5). In these reactions cross-linking is possible. When a diamine was added to the pivaloyl chloride-activated polymer, an insoluble gel was obtained. However, when the order of addition was reversed, e.g., the activated polymer was added into a large excess of diamine (see Experimental Section), the obtained product remained soluble.

The reaction of poly(PEG-Lys) with DCC and HOSu in methylene chloride was found to be the most convenient way for the introduction of active esters into the polymeric backbone. Quantitation of active acyl groups (22) showed that over 95% of the carboxyl groups could be converted into active HOSu ester residues by this reaction. The polymeric active ester derivative (6) proved most useful for direct attachment of primary-amine-containing drugs or spacer residues such as γ-aminobutyric acid (derivative 7).

The derivative having reactive aldehyde groups (9) was prepared using a modification of the method of Vandoorne et al. (*23*). In the first step, derivative 8 was obtained via reaction of 3-amino-1,2-propanediol with the HOSu ester 6. Alternatively, 8 could be prepared by the EDC-mediated coupling of 3-amino-1,2-propanediol to 2. In the second step, the mild oxidation of the 1,2-diol moieties with periodate produced aldehyde groups. Derivative 9 had a tendency to form an insoluble polymer during attempts to isolate and dry the material. Most likely, cross-links were formed due to aldol condensation or formation of acetals as a result of the reaction between newly introduced aldehyde groups (≈70% of the repeat units) and remaining diol residues (≈30% of the repeat units). Derivative 9 was therefore kept in an aqueous solution at 4 °C, which was assayed for aldehyde content with 2,4-dinitrophenylhydrazine (*24*) and used directly for drug-attachment reactions.

Attachment of Drugs. Two antimicrobial agents (penicillin V and cephradine) were chosen for the initial evaluation of poly(PEG-Lys) as a drug carrier. Previously, a number of macromolecular derivatives of β-lactam antibiotics had been prepared and evaluated (*25*). Here, penicillin V was linked to the hydroxyl groups of 4 via hydrolytically labile ester bonds yielding derivative 10 using DCC/DMAP according to a previously reported procedure (Figure 4) (*8, 9*).

The extent of drug incorporation was 66% as determined by NMR and elemental analysis of sulfur. In another series of experiments, cephradine was linked to the poly(PEG-Lys) backbone via three different attachment strategies leading to conjugates 11–13 (Figure 5). In the first conjugate (11), the drug was attached to the carrier directly via an amide bond. In conjugate 12, similarly obtained from an HOSu ester intermediate, cephradine was positioned at a 5-atom distance from the polymer backbone. In an alternative coupling scheme, cephradine was attached to the polymer via stable secondary amine linkages, derived from the reaction of the aldehyde pendent chains of derivative 9 with the primary amine of the drug under reducing conditions. This scheme led to the attachment of cephradine at ≈40% of the repeat units. Considering that only ≈70% of lysine residues of the polymer 9 were bearing aldehyde groups, the efficiency of the reductive amination step was comparable to the formation of amide bonds in derivatives 11 and 12. The

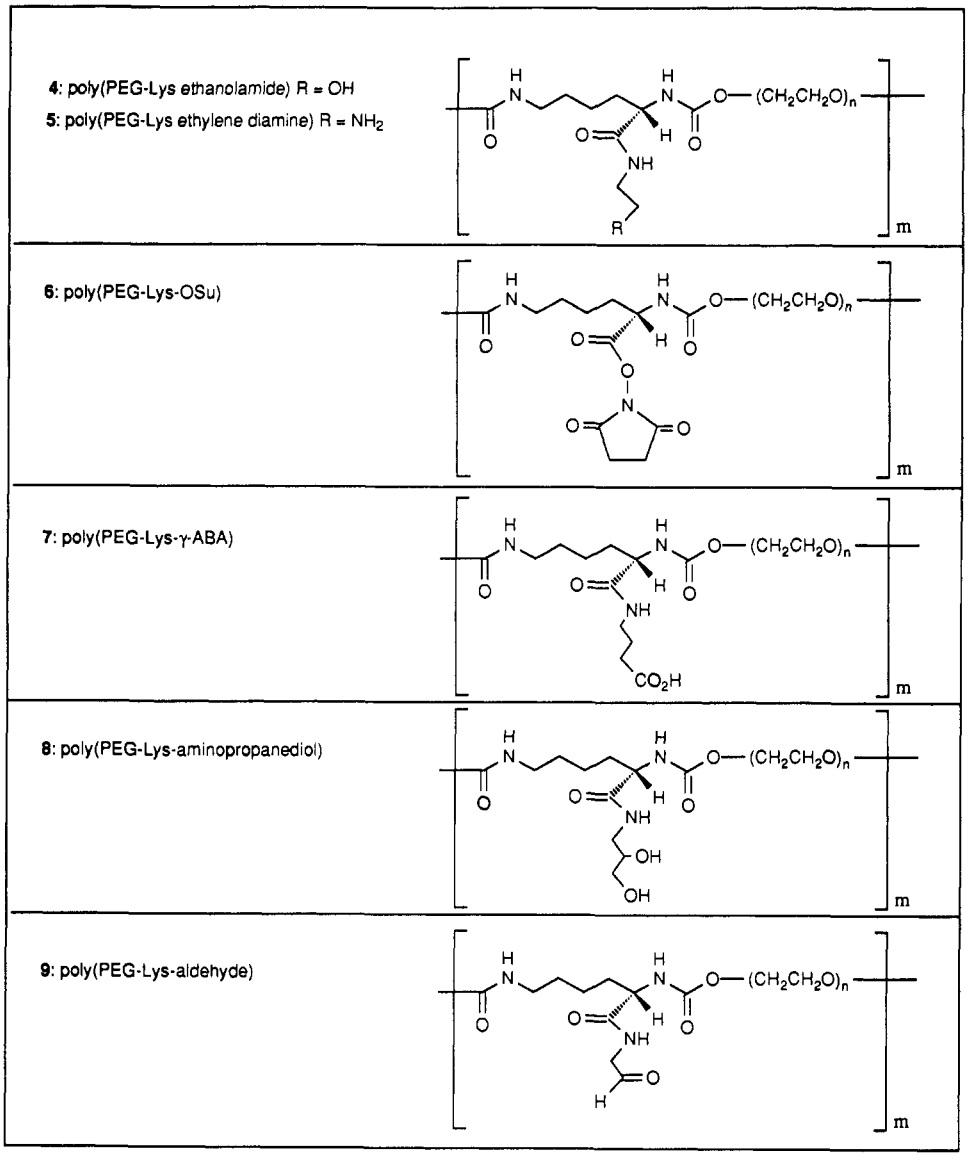
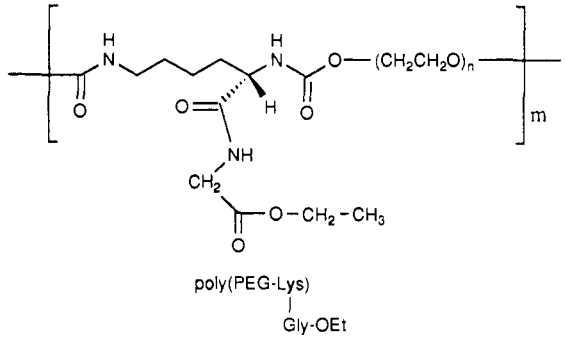


Figure 2. Detailed chemical structures for derivatives of poly(PEG-Lys). Starting from free pendent carboxylic acid groups, derivatives were prepared with pendent hydroxyl groups (**4**), pendent amino groups (**5**), pendent *N*-hydroxysuccinimide active ester groups (**6**), and pendent diol groups (**8**). Further derivatization reactions yielded the γ-aminobutyric acid (γ-ABA) derivative (**7**) and the aldehyde derivative (**9**). See Experimental Procedures for details.



3

Figure 3. Detailed chemical structure of the glycine ethyl ester (Gly-OEt) conjugate of poly(PEG-Lys).

advantage of coupling via reductive amination is that conjugate **13** preserved the positive charge of the amino group of cephradine, considered to be of importance for its antimicrobial activity (*26*). In all penicillin and cephradine conjugates, the integrity of the labile β-lactam unit was confirmed by a selective, quantitative iodometric assay (*27*). These model reactions established the feasibility of linking chemically sensitive drugs to the polymer backbone via a variety of mild coupling protocols.

In the attachment reaction of penicillin V, the carboxyl groups of penicillin, which are essential for antimicrobial activity, were tied up by ester bonds. Penicillin bound in this way should be biologically inactive. However, the gradual hydrolysis of the ester bonds under physiological conditions, should result in the release of penicillin V in biologically active form. In order to test this hypothesis, the activity of poly(PEG-Lys–penicillin V ester) (**10**) was tested against clinically important strains of bacteria (Table I). During these experiments, the release of free penicillin from **10** was monitored spectrophotometrically. Since 95% of all bound penicillin V was released from the conjugate within 24 h, we concluded that the activity of **10** was indeed due to the presence of free penicillin V (Figure 6). On the other hand, none of the cephradine containing conjugates (**11**–**13**) inhibited the growth of cephradine-sensitive microorganisms, even when applied at doses up to 10 times the MIC of free cephradine. This unexpected observation is currently under further investigation.

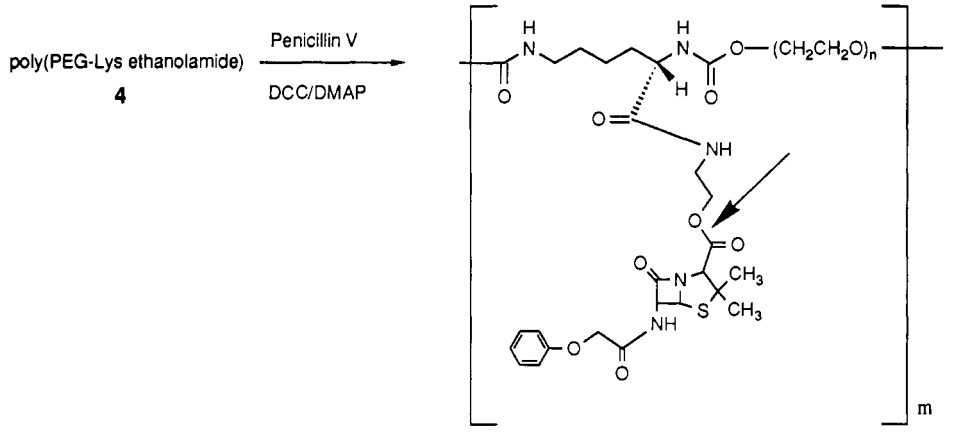


Figure 4. Preparation of the penicillin V conjugate (**10**) from the hydroxyl derivative poly(PEG-Lys-ethanolamide) (**4**). See Experimental Procedures for details. This scheme resulted in the attachment of penicillin V via a hydrolyzable ester linkage to the ethanolamide spacer. Cleavage of the ester bond (marked by an arrow) was shown to restore biologically active, free penicillin V.

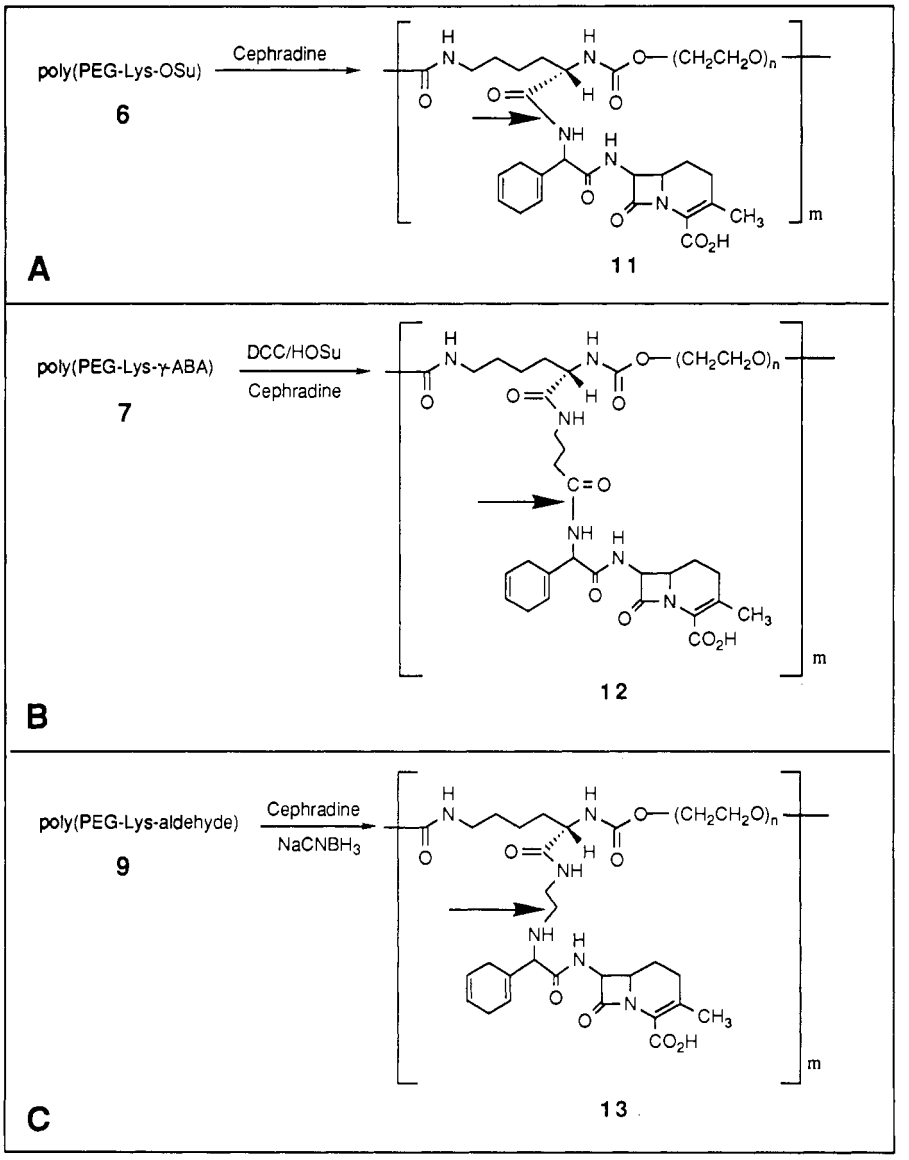


Figure 5. Preparation and chemical structures of different conjugates of cephradine: (A) attachment of cephradine via the *N*-hydroxysuccinimide active ester, poly(PEG-Lys-OSu), through an amide linkage (arrow); (B) attachment of cephradine via the γ-aminobutyric acid derivative, poly(PEG-Lys-γ-ABA), through an amide linkage (arrow); (C) attachment of cephradine via the aldehyde derivative, poly(PEG-Lys-aldehyde), through a secondary amine linkage (arrow). See Experimental Procedures for details.

Biological Properties of Poly(PEG-Lys). The stability of ^{14}C-radiolabeled poly(PEG-Lys) over a period of 48 h was determined by incubation in human plasma at 37 °C, followed by GPC analysis of the polymer molecular

Table I. Growth Inhibition by Free Penicillin V and Polymer-Bound Penicillin V

microorganism (MIC[a])	control experiments[b]				Free Pen V[b]		poly(PEG-Lys-Pen-V)[b]	
	neat growth medium	PEG	PEG-Lys	PEG-Lys-spacer	at MIC	at 10 × MIC	at MIC	at 10 × MIC
E. coli (>200)	+	+	+	+	X	X	X	X
K. pneumoniae (>200)	+	+	+	+	X	X	X	X
S. aureus (3)	+	+	+	+	–	–	–	–
E. faecalis (30)	+	+	+	+	–	–	–	–
S. pyogenes (50)	+	+	+	+	–	–	–	–

[a] MIC, the minimum inhibitory concentration of penicillin V in μg/mL, is given in parentheses for each microorganism. [b] Growth index: +, growth; –, no growth; X, these strains are resistant to penicillin V at 200 μg/mL, the highest concentration tested.

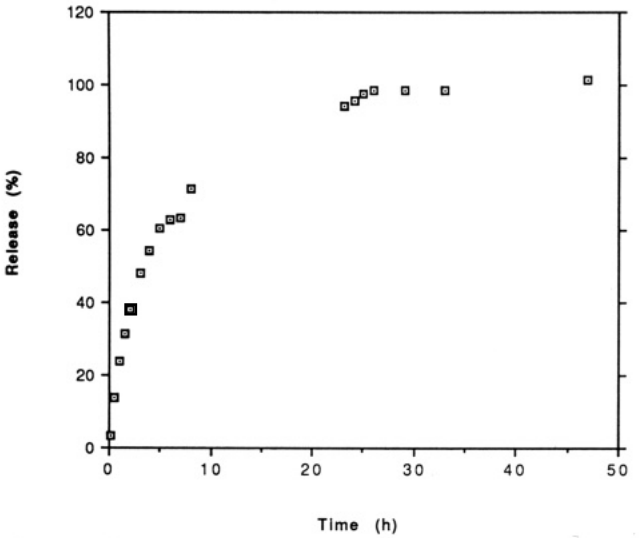


Figure 6. Release of penicillin V from poly(PEG-Lys–penicillin V) in physiological phosphate buffer at 25 °C. The amount of penicillin V released was determined spectrophotometrically (λ_{max} = 260 nm).

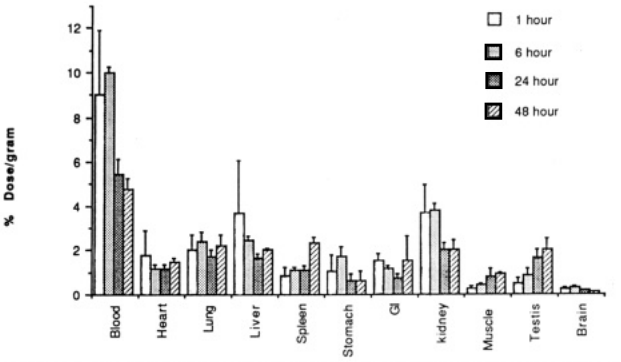


Figure 7. Biodistribution of poly(PEG-^{14}C-Lys) in CD-1 male mice.

weight at predetermined intervals of time. Since the distribution of radioactivity in the analyzed aliquots did not change, we concluded that the backbone of poly(PEG-Lys) is stable in human plasma for at least 48 h. Similarly, when poly(PEG-Lys) was incubated in phosphate buffer, no change in molecular weight was detected by GPC analysis of polymer aliquots extracted from the phosphate buffer solution over up to 48 h. These observations are in agreement with the previously reported stability of aliphatic urethanes toward acidic, basic, and enzymatic hydrolysis (*28*, *29*).

The in vivo distribution of the radiolabeled polymer was determined in CD1 male mice in the usual fashion. Briefly, a sample of poly(PEG-^{14}C-Lys) was injected and the polymer content of selected body fluids and tissues was measured at various time intervals by quantitative β-counting. These experiments showed that most of the radioactivity is located in the circulating blood and is uniformly distributed throughout the different tissues (Figure 7). Specifically, when the results were calculated in terms of dose per organ, no excess uptake of radioactivity by the liver, spleen, or kidney was observed. Excretion of the polymer appears to be primarily through the kidney and the GI tract.

The parent polymer carrying nonreactive ethyl ester pendent chains (1) was subjected to acute toxicity tests in mice and rats. Using both iv and ip injections of polymer solutions in physiological saline, up to 10 g/kg body weight of 1, were administered. Even at this high dose level, no signs of acute toxicity or histopathological changes in liver or kidney were observed and polymer 1 was classified as nontoxic under the conditions of this test assay.

Summary and Conclusions. In this paper we describe the functionalization of poly(PEG-Lys), a new, water-soluble poly(ether urethane). This polymer retains many of the favorable properties of PEG, while providing multiple attachment sites along the polymeric backbone at equal distances from each other. Several pathways for the introduction of reactive functional groups onto the polymer backbone were developed. The corresponding, functionalized derivatives were used for the convenient attachment of various ligands, either directly or via an appropriate spacer. The resulting conjugates had both biologically stable or labile bonds. The distance between neighboring attachment sites can be readily controlled by the length of the PEG monomer used in the synthesis of the poly(PEG-Lys) chain, while the final length of the poly(PEG-Lys) chain can be controlled by the polymerization conditions such as reaction time, concentration of monomers, and stirring rate (*19*). The chemical versatility of this new class of polymers for preparation of various drug conjugates represents a significant advantage over previously reported drug-carrier systems. Preliminary studies of the acute toxicity, plasma stability and biodistribution suggest a wide range of potential applications for PEG-Lys-derived polymeric drugs.

EXPERIMENTAL PROCEDURES

Materials and Methods. Cephradine and penicillin V were obtained from Sigma; [^{14}C]lysine was from NEN Research Products; PEG-2000 and phosgene solution (20%) in toluene (Fluka) were used for preparation of BSC-PEG according to the previously published procedure (*19–21*). Additional chemicals from common commercial sources were used without purification. HPLC-grade solvents were used for synthesis and for GPC. ^{1}H and ^{13}C NMR spectra were recorded on a Varian XL-200 spectrometer at room temperature using $CDCl_3$ and D_2O as solvents. FT-IR spectra were recorded on a Mattson Cygnus 100 spectrophotometer. UV/vis spectra were recorded on a Perkin-Elmer Lambda 3B spectrophotometer. GPC (relative to PEG standards) (*30*) was performed using an HPLC system consisting of a Perkin-Elmer series

410 LC pump, a Waters 410 RI detector, and a Perkin Elmer DEC 3000 data station. DMF containing 0.1% (w/v) of LiBr was used as the mobile phase, at a flow rate of 1 mL/min on two PL-gel columns (300 mm × 7.7 mm; particle size, 5 μm; pore size, 10^3 and 10^5 A, respectively) connected in series. For aqueous GPC, 0.1 M acetate buffer (pH 5.4) was used as the mobile phase at a flow rate of 0.7 mL/min and TSK Gel-2000 and -4000 columns were used in series. The amount of free carboxylic acid groups in poly(PEG-Lys) was determined by nonaqueous titration with sodium methoxide in methanol/toluene using thymol blue as the indicator. The amount of active ester in poly(PEG-Lys-OSu) was determined by a modification of the published titration method (*22*). β-Lactam content in the polymer–antibiotic conjugates was determined by iodometric titrations as described by Alicino (*27*). Amino acid analysis was performed according to the procedure of Meltzer (*31*). Dialysis against distilled water using a Spectrapor membrane with molecular weight cutoff of 12 000–14 000 was routinely used for removal of low molecular weight compounds, including free drugs, from polymer conjugates.

Poly(PEG-Lys-OEt) (1) was prepared by interfacial polymerization (methylene chloride/aqueous solution at pH 8) as described in detail elsewhere (*19*).

Preparation of Poly(PEG-Lys) (2). L-Lysine (0.032 g, 0.22 mmol) was dissolved in 5 mL of 0.1 M borate buffer (pH = 9.3). To this solution was added BSC-PEG (0.5 g, 0.22 mequiv). The reaction mixture was stirred at room temperature for 15 min and then dialyzed against distilled water. The product was recovered by lyophilization to yield 0.36 g (72%). M_w = 47 000 Da, was determined by GPC (in 0.1 M acetate buffer, TSK columns, relative to PEG standards). FT-IR (film on NaCl, cm^{-1}): ν 2870 (CH), 1719 (C=O of urethane), shoulder at 1740 (C=O of acid), 1105 (C—O). ^1H NMR (D_2O): δ 4.06 (4 H, t, terminal CH_2 of PEG), 3.56 (173 H, PEG overlapping with α-C*H*NH), 2.98 (2 H, m, ε-CH_2NH), 1.15–1.76 (6 H, br m, CH_2 of Lys) ppm. ^{13}C NMR ($CDCl_3$): δ 173.45 (C=O of acid), 156.50 (C=O of α-NH urethane), 155.93 (C=O of ε-NH urethane), 63.90–70.48 (CH_2 of PEG), 53.44, 40.39, 31.91, 29.17, 21.98 (CH_2 of Lys) ppm. An identical procedure was used for the preparation of ^{14}C-labeled poly(PEG-Lys) using ^{14}C-Lys (250 μCi in 0.032 g). Alternatively **2** was obtained by mild alkaline hydrolysis of **1** (*19*).

Preparation of Poly(PEG-Lys-Gly-OEt) (3). Poly(PEG-Lys) (0.4 g, 0.18 mequiv) was dissolved in H_2O (40 mL). To this solution was added Gly-OEt·HCl (5.58 g, 0.04 mol). The pH was adjusted to 4.8 and EDC (0.77 g, 4.0 mmol) was added. The pH was maintained at 4.8 by the addition of 0.1 N HCl. After 3 h the reaction mixture was acidified with 0.1 N HCl to pH 4 and the product was extracted with methylene chloride (3 × 50 mL). The combined extracts were washed with saturated brine, dried over anhydrous $MgSO_4$, concentrated to 10 mL, and poured into cold ether (50 mL). The polymer was collected by filtration, washed with cold ether, and dried in vacuo. It was further purified by dialysis followed by lyophilization. Yield: 0.3 g (73%). ^1H NMR ($CDCl_3$): similar to that of poly(PEG-Lys) except that additional absorptions at δ 1.25 (3 H, t, CH_3), 3.98 (2 H, d, CH_2 of glycine), 4.09–4.27 (6 H, terminal CH_2 of PEG + CH_2CH_3), 6.76 (1 H, m, CON*H*CH_2) ppm were observed. Amino acid analysis [according to the procedure of Meltzer (*31*)] of the product showed a lysine to glycine ratio of 1:0.95, indicating that 95% of the side chains had reacted with Gly-OEt.

Preparation of Poly(PEG-Lys-ethanolamide) (4). Poly(PEG-Lys) (1 g, 0.45 mequiv) was dissolved in methylene chloride (10 mL). To this solution was added triethylamine (0.09 mL, 0.68 mmol). The flask was cooled in an ice-water bath and pivaloyl chloride (0.08 g, 0.68 mmol) was added. The reaction mixture was stirred for 2 h and cooled again to 0 °C and dry ethanolamine (0.08 g, 1.36 mmol) was added. After stirring for 24 h, triethylamine hydrochloride was removed by filtration and the filtrate was added into ether (50 mL). The crude material was collected by filtration and purified by recrystallization from 2-propanol. Yield: 0.82 g (80.5%). FT-IR (film on NaCl, cm^{-1}): ν 2888 (CH), 1720 (C=O of urethane), 1671 (C=O of amide), 1109 (C—O). ^1H NMR ($CDCl_3$): δ 6.96 (1 H, m, CONH), 5.76 (1 H, d, α-NH of Lys), 5.25 (1 H, m, ε-NH of Lys), 4.17 (4 H, terminal CH_2 of PEG), 3.61 (175 H, PEG overlapping with α-C*H*NH and HCH_2OH), 3.37 (2 H, m, CH_2NHCO), 3.12 (2 H, m, ε-CH_2NH), 1.25–1.91 (6 H, br m, CH_2 of Lys) ppm.

Preparation of Poly(PEG-Lys-ethylenediamine) (5). Poly(PEG-Lys) (0.8 g, 0.36 mequiv) was dissolved in methylene chloride (15 mL). To this solution was added triethylamine (0.08 mL, 0.63 mmol). The flask was cooled in an ice-water bath and pivaloyl chloride (0.074 g, 0.63 mmol) was added. The reaction mixture was stirred for 2 h, cooled again to 0 °C and added to dry ethylenediamine (0.216 g, 3.6 mmol) in methylene chloride (5 mL) cooled in an ice bath. After stirring for 24 h, triethylamine hydrochloride was removed by filtration and the filtrate was concentrated and added into ether (50 mL). After stirring for 2 h, the ether layer was decanted and fresh ether was added to remove unreacted impurities. The precipitate was then collected by filtration and further purified by recrystallization from 2-propanol. Yield: 0.61 g (75%). FT-IR (film on NaCl, cm^{-1}): ν 2888 (CH), 1720 (C=O of urethane), 1672 (C=O of amide), 1109 (C—O). ^1H NMR ($CDCl_3$): δ 7.15 (1 H, m, CONH), 5.75 (1 H, d, α-NH of Lys), 5.37 (1 H, m, ε-NH of Lys), 4.13 (4 H, terminal CH_2 of PEG), 3.58 (173 H, PEG overlapping with α-C*H*-NH), 3.30 (2 H, m, CH_2NHCO), 3.10 (2 H, m, ε-CH_2-NH), 2.75 (2 H, m, CH_2NH_2), 1.21–1.91 (6 H, br m, CH_2 of Lys) ppm.

Preparation of poly(PEG-Lys-OSu) (6) was as previously reported (*19*).

Preparation of Poly(PEG-Lys-γ ABA) (7). γ-Amino butyric acid (0.25 g, 2.43 mmol) was dissolved in phosphate buffer (10 mL, pH = 7.4). To this solution was added **6** (0.98 g, 0.43 mequiv). The reaction mixture was stirred at room temperature for 0.5 h and dialyzed against distilled water. The product was isolated by lyophilization. TLC (toluene–acetic acid–water 5:5:1) showed absence of free γ-ABA (visualization using ninhydrin). Yield: 0.85 g (85%). ^1H NMR (D_2O): δ 4.07 (4 H, t, terminal CH_2 of PEG), 3.57 (173 H, PEG overlapping with α-C*H*NH), 2.91–3.10 (4 H, m, ε-CH_2NH overlapping with CH_2NHCO), 1.12–1.82 (8 H, br m, CH_2 of Lys overlapping with CH_2CH_2-COOH) ppm.

Preparation of Poly(PEG-Lys-aminopropanediol) (8). Poly(PEG-Lys-OSu) (2 g, 0.87 mequiv) was dissolved in methylene chloride (20 mL). To this solution was added 3-amino-1,2-propanediol (0.29 g, 4.36 mmol). The reaction mixture was stirred at room temperature for 2 h and the product precipitated in ether (100 mL). After cooling to 4 °C the crude product was collected by filtration, dissolved in H_2O, and purified further by dialysis. The product was recovered by lyophilization. Yield: 1.7 g (80%). FT-IR (film on NaCl, cm^{-1}): ν 2885 (CH), 1719 (C=O of urethane), 1674 (C=O of amide), 1110 (C—O). ^1H NMR ($CDCl_3$): δ 7.14 (1 H, m, CONH), 5.80 (1 H, d, α-NH of Lys), 5.26 (1 H, m, ε-NH of Lys), 4.16 (4 H, terminal CH_2 of PEG),

3.60 (176 H, PEG overlapping with α-C*H*NH, C*H*OH, and CH_2OH), 3.37 (2 H, m, CH_2NHCO), 3.13 (2 H, m, ε-CH_2-NH), 1.26–1.94 (6 H, br m, CH_2 of Lys) ppm.

Preparation of Poly(PEG-Lys-aldehyde) (9). Poly-(PEG-Lys-aminopropanediol) (1.2 g, 0.53 mequiv) was dissolved in water (15 mL) and treated for 1 h with sodium periodate (0.11 g, 0.53 mmol) at 4 °C, in the dark. The reaction mixture was dialyzed against distilled water. The aldehyde content of the product determined with 2,4-dinitrophenylhydrazine (*24*) was 0.32 mmol/g, corresponding to 68% of the maximal theoretical value. The aqueous solution of the product was stored at 4 °C and used directly in conjugation reactions.

Preparation of Poly(PEG-Lys-penicillin V) (10). Penicillin V (0.094 g, 0.267 mmol) and 4-(dimethylamino)-pyridine (0.008 g, 0.065 mmol) were added to a solution of 4 (0.400 g, 0.178 mequiv) in methylene chloride (4 mL). The solution was cooled and treated with DCC (0.048 g, 0.232 mmol). The reaction mixture was stirred at 4 °C, for 4 days. The DCU was removed by filtration and the product precipitated with cold ether. The crude product (0.25 g) was further purified on a Sephadex LH-20 column using methanol as the eluant. TLC (methanol) showed absence of free drug in the product. FT-IR (film on NaCl, cm^{-1}): ν 2882 (CH), 1785 (C=O of β-lactam), 1706 (C=O of urethane), shoulder at 1630 (C=O of amide), 1110 (C—O). ^{1}H NMR ($CDCl_3$): δ 6.82–7.1 (3 H, m, meta and para H's of the phenyl group), 7.2–7.4 (2 H, m, ortho H's of the phenyl group), 5.59 (1 H, m, COC*H*NH), 5.41 (1 H, d, α-NH of Lys), 5.3 (1 H, d, C*H*NH), 5.09 (1 H, m, ε-NH of Lys), 4.53 (2 H, s, OCH_2CO), 4.45 (1 H, s, C*H*COOH), 4.16 (4 H, t, terminal CH_2 of PEG), 3.61 (173 H, PEG overlapping with α-C*H*-NH), 3.28 (2 H, m, CH_2NHCO), 3.15 (2 H, m, ε-CH_2NH), 1.31–1.91 (12 H, br peak due to CH_2 of Lys) overlapping with 1.46 and 1.49 (2 s, CH_3 of Pen V) ppm. Anal. Calcd for poly(PEG-Lys-penicillin V): S, 1.15 (for drug attachment to 100% of the side chains). Found: S, 0.87 (corresponding to drug attachment to 66% of the side chains).

Preparation of Poly(PEG-Lys-cephradine) (11). Cephradine (0.15 g, 0.43 mmol) was dissolved in a mixture of water (4.5 mL) and dioxane (2 mL). To this solution was added 6 (0.50 g, 0.22 mequiv) followed by a dropwise addition of $NaHCO_3$ solution (0.055 g in 1 mL of H_2O). The solution (pH ~ 7.5) was stirred at 25 °C for 1 h, acidified to pH ~ 6.5 and the product was extracted with methylene chloride (3 × 25 mL). The extracts were combined and washed with brine, dried ($MgSO_4$), and concentrated to 10 mL. The concentrated solution was added slowly into cold ether (50 mL), causing the drug–polymer conjugate to precipitate. After cooling to 4 °C for several hours the product was collected by filtration, washed with cold ether, and dried in vacuo, yielding 0.36 g (71%). The product was further purified by dialysis against distilled water and recovered by lyophilization (0.27 g). TLC (methanol) showed absence of free drug (visualization using UV and ninhydrin). FT-IR (film on NaCl, cm^{-1}): ν 2882 (CH), 1782 (C=O of β-lactam), 1719 (C=O of urethane), shoulder at 1670 (C=O of both amides), 1113 (C—O). ^{1}H NMR (D_2O): δ 5.75 (1 H, m, CH=C), 5.60 (2 H, s, CH_2S), 5.49 (1 H, m, CH=C*H*CH_2C), 4.98 (1 H, m, C*H*=CHCH_2C), 4.75 (1 H, m, C*H*NHCO), 4.05 (4 H, t, terminal CH_2 of PEG), 3.55 (174 H, PEG overlapping with α-C*H*NH and C*H*CHS), 2.98 (3 H, m, ε-CH_2NH overlapping with CHS), 2.4 to 2.7 (4 H, br m, CH_2's of cyclohexadiene), 1.95 (3 H, s, CH_3), 1.1–1.8 (6 H, br m, CH_2 of Lys) ppm. Anal. Calcd for poly(PEG-Lys–cephradine): S, 1.26 (for drug attachment to 100% of the side chains). Found: S, 0.75 (corresponding to drug attachment to 60% of the side chains).

Preparation of Poly(PEG-Lys-γABA-OSu). Poly-(PEG-Lys-γABA) (0.86 g, 0.35 mequiv) was dissolved in methylene chloride (10 mL). To this solution was added dry and finely powdered HOSu (0.20 g, 1.75 mmol). The flask was cooled in an ice–water bath and DCC (0.10 g, 0.50 mmol) was added. The reaction mixture was stirred at 4 °C for 1 h and at 25 °C for 24 h. The precipitated DCU was removed by filtration and the filtrate was added with stirring to ether (50 mL). After cooling to 4 °C the precipitate was collected by filtration and purified by two recrystallizations from 2-propanol, yielding 0.63 g (75%) of the product. FT-IR (film on NaCl, cm^{-1}): ν 2882 (CH), 1812 and 1781 (C=O of succinimide), 1734 (C=O of ester), 1718 (C=O of urethane), 1653 (C=O of amide), 1113 (C—O). ^{1}H NMR ($CDCl_3$): similar to that of poly(PEG-Lys-γABA) except that an additional absorption at 2.81 ppm (4 H, s, succinimide) was observed.

Preparation of Poly(PEG-Lys–cephradine) (12). Cephradine (0.30 g, 0.86 mmol) was dissolved in a mixture of water (4 mL) and dioxane (6 mL) and treated with poly(PEG-Lys-γABA-OSu) (1.0 g, 0.44 mequiv) followed by the dropwise addition of $NaHCO_3$ solution (0.10 g dissolved in 2 mL of H_2O). The solution (pH ~ 7.5) was stirred at 25 °C for 1 h, acidified to pH ~ 6.5 with 0.1 N HCl, and extracted with methylene chloride (3 × 25 mL). The extracts were combined, washed with brine, dried ($MgSO_4$), concentrated to 10 mL and poured slowly into cold ether (50 mL). After cooling to 4 °C for several hours the precipitated product was collected by filtration, washed with cold ether, and dried in vacuo. The crude product was dissolved in water, extensively dialyzed, and recovered by lyophilization. Yield: 0.71 g (65%). TLC (methanol) showed absence of free drug (visualization using UV and ninhydrin). FT-IR (film on NaCl, cm^{-1}): ν 2885 (CH), 1778 (C=O of β-lactam), 1720 (C=O of urethane), 1660 (C=O of both amides) and 1111 (C—O). ^{1}H NMR (D_2O): δ 5.79 (1 H, m, CH=C), 5.63 (2 H, s, CH_2S), 5.47 (1 H, m, CH=C*H*CH_2C), 4.94 (1 H, m, C*H*=CHCH_2C), 4.75 (1 H, C*H*NHCO overlapping with the D_2O peak), 4.08 (4 H, t, terminal CH_2 of PEG), 3.57 (174 H, PEG overlapping with α-C*H*NH and C*H*CHS), 2.98–3.18 (5 H, br m, ε-CH_2NHCO overlapping with CH_2NHCO and CHS), 2.45–2.77 (4 H, br m, CH_2's of cyclohexadiene), 2.12 (2 H, t, CH_2CONH), 1.80 (3 H, s, CH_3), 1.07–1.75 (8 H, br m, CH_2 of Lys overlapping with CH_2CH_2CONH) ppm. Anal. Calcd for poly(PEG-Lys–cephradine): S, 1.22 (for drug attachment to 100% of the side chains). Found: S, 0.73 (corresponding to drug attachment to 60% of the side chains).

Preparation of Poly(PEG-Lys–cephradine) (13). To a solution of 9 (1.0 g, 0.045 mequiv) in 4 mL of water was added cephradine (0.312 g, 0.89 mmol) and sodium cyanoborohydride (0.028 g, 0.045 mmol). The reaction mixture was stirred for 18 h and the product extracted with methylene chloride (3 × 10 mL). The extracts were combined, washed with saturated brine, dried ($MgSO_4$), and poured into cold ether (50 mL). The precipitated polymer was collected by filtration, washed with cold ether, and dried in vacuo. The product was further purified by dialysis and recovered by lyophilization. Yield: 0.65 g (57%). TLC (methanol) showed absence of free drug (visualization using UV and ninhydrin). FT-IR (film on NaCl, cm^{-1}): ν characteristic bands at 2885 (CH), 1759 (C=O of β-lactam), 1714 (C=O of urethane), 1676 (C=O of amides) and 1111 (C—O). ^{1}H NMR (D_2O): δ 6.00 (1 H, m, CH=C), 5.60 (2 H, s, CH_2S), 5.45–5.48 (1 H, m, CH=C*H*CH_2C), 4.91–4.94 (1 H, m, C*H*=CHCH_2C), 4.29

(1 H, CHNHCO), 4.06 (4 H, t, terminal CH_2 of PEG), 3.55 (174 H, PEG overlapping with α-CHNH and CHCHS), 3.19 (2 H, t, CH_2NHCO), 2.96 (3 H, m, ϵ-CH_2NHCO overlapping with CHS), 2.45–2.77 (4 H, br m, CH_2's of cyclohexadiene), 1.76 (3 H, s, CH_3), 1.12–1.73 (6 H, br m, CH_2 of Lys) ppm. Anal. Calcd for poly(PEG-Lys–cephradine): S, 1.256 (for drug attachment to 100% of the side chains). Found: S, 0.50 (corresponding to drug attachment to 40% of the side chains).

Antimicrobial Activity. Five microorganisms, *Klebsiella pneumonae* (#10031), *Escherichia coli* (#8739), *Staphylococcus aureus* (#6538P), *Streptococcus pyogenes* group A (#8668), and *Enterococcus faecalis* (#29212) were purchased from the American Tissue Culture Collection. The microorganisms were suspended in nutrient broth (Difco #000301-6). The first three microorganisms were then seeded on Difco #0001-01-8 agar slants. The last two microorganisms were seeded on BBL trypticase soy agar, Becton Dickinson #11043, supplemented with 5% defibrinated sheep blood (Fisher B11946). The slants were incubated for 1 day at 37 °C and stored at −4 °C. They were used within 1 month of preparation. The microorganisms were collected with a wire loop from the slants (two loopfulls) and introduced in 50 mL of nutrient broth (which was supplemented with 5% defibrinated sheep blood in the case of *S. pyogenes* and *E. faecalis*). The suspensions were incubated for 1 day, except for *S. pyogenes* and *E. faecalis*, which were incubated for 2 days, prior to the experiment. Then, the suspensions were diluted 5000-fold in the appropriate drug/polymer solutions in nutrient broth. To evaluate growth in a qualitative fashion (yes/no), the suspensions were visually checked for turbidity for up to 1 week. The formation of turbidity was taken as an indication of bacterial growth.

Plasma Stability Study on Poly(PEG-^{14}C-Lys). A sample of human blood (5 mL) was centrifuged (Beckman GPR centrifuge, 3500 rpm for 10 min) to separate cells from plasma. The plasma was filtered through a syringe filter (pore size, 0.2 μm) into a sterile plastic tube. Poly(PEG-^{14}C-Lys) (1.2 mg, 4.3 μCi) was incubated in freshly prepared plasma (600 μL) at 37 °C for predetermined intervals of time. Aliquots were taken at 0, 1, 3, 6, 24 and 48 h and analyzed by GPC (TSK 3000 SW column using 10 mM phosphate buffer as the mobile phase at a flow rate of 1 mL/min). A total of 20 fractions of 1 mL each were collected, and the distribution of radioactivity in the fractions was determined by β-counting.

Biodistribution Study on Poly(PEG-^{14}C-Lys). CD1 male mice were injected intravenously with a sample of poly(PEG-^{14}C-Lys) (5 μCi). At different time intervals after injection (1, 6, 24 and 48 h) the animals were sacrificed and blood (0.2 mL) together with the heart, lung, liver, spleen, stomach, GI, kidney, muscle, testis, and brain were removed and weighed (blood was removed using a heparinized syringe to prevent clotting). A small piece of each tissue was then reweighed, solubilized using tissue-dissolving fluid, and bleached with H_2O_2. After addition of the scintillation cocktail the amount of radioactivity in each tissue was determined by β-counting. As a control, the above procedure was repeated using different amounts of (nonradioactive) tissue to which a known amount of radioactivity was added.

Acute Toxicity Testing. The acute toxicity of poly(PEG-Lys-OEt) was tested according to Good Laboratory Practice Regulations by an independent contract testing facility (Pharmakon Research International). Using rats and mice as animal models, up to 10 g/kg of poly(PEG-Lys-OEt) was administered by ip or iv injection, followed by detailed observation and histopathological examination of all major organs.

ACKNOWLEDGMENT

This work was supported by a research grant from Enzon, Inc. J.K. acknowledges the receipt of NIH Research Career Development Award GM00550.

LITERATURE CITED

(1) Duncan, R., and Kopecek, J. (1984) Soluble synthetic polymers as potential drug carriers. *Adv. Polym. Sci. 57*, 53–101.
(2) Topchieva, I. N. (1990) Synthesis of biologically active polyethylene glycol derivatives. A review. *Polym. Sci. USSR 32*, 833–851.
(3) Zalipsky, S., and Lee, C. (1992) Use of functionalized polyethylene glycols for modification of polypeptides. *Poly(ethylene glycol) Chemistry: Biotechnical and Biomedical Applications* (J. M. Harris, Ed.) pp 347–370, Plenum Press, New York.
(4) Papahadjopoulos, D., Allen, T. M., Gabizon, A., Mayhew, E., Matthay, K., Huang, S. K., Lee, K.-D., Woodle, M. C., Lasic, D. D., Redemann, C., and Martin, F. J. (1991) Sterically stabilized liposomes: Improvements in pharmacokinetics and antitumor therapeutic efficacy. *Proc. Natl. Acad. Sci. U.S.A. 88*, 11460–11464.
(5) Ouchi, T., Yuyama, H., and Vogl, O. (1987) Synthesis of 5-fluorouracil-terminated monomethoxypoly(ethylene glycol)s, their hydrolysis behavior, and their antitumor activities. *J. Macromol. Sci.-Chem. A24*, 1011–1032.
(6) Knauf, M. J., Bell, D. P., Hirtzer, P., Luo, Z.-P., Young, J. D., and Katre, N. V. (1988) Relationship of effective molecular size to systemic clearance in rats of recombinant interlukin-2 chemically modified with water-soluble polymers. *J. Biol. Chem. 263*, 15064–15070.
(7) Harris, J. M. (1985) Laboratory synthesis of polyethylene glycol derivatives. *J. Macromol. Sci., Rev. Macromol. Chem. Phys. C25*, 325–373.
(8) Zalipsky, S., Gilon, C., and Zilkha, A. (1983) Attachment of drugs to polyethylene glycols. *Eur. Polym. J. 19*, 1177–1183.
(9) Zalipsky, S., Gilon, C., and Zilkha, A. (1984) Esterification of polyethylene glycols. *J. Macromol. Sci.-Chem. A21*, 839–845.
(10) Vaze, S., and Tirrell, D. A. (1986) Preparation of poly[(3-bromopropyl)oxirane]: A reactive derivative of poly(ethylene oxide). *J. Bioact. Compat. Polym. 1*, 79–83.
(11) Murouchi, S., Hasebe, Y., and Tsuruta, T. (1990) Synthesis of a polyether containing pendant oxirane rings. Regioselectivity of a chair type organozinc complex. *Makromol. Chem. Rapid Commun. 11*, 129–134.
(12) Nishimura, T., Sato, Y., Yokoyama, M., Okuya, M., and Inoue, S. (1984) Adhesion behavior of rat lymphocytes on poly(γ-benzyl L-glutamate) derivatives having hydroxyl groups or poly(ethylene glycol) chains. *Makromol. Chem. 185*, 2109–2116.
(13) Yokoyama, M., Inoue, S., Kataoka, K., Yui, N., Okano, T., and Sakurai, Y. (1989) Molecular design for missile drug: Synthesis of adriamycin conjugated with immunoglobulin G using poly(ethylene glycol)-block-poly(aspartic acid) as intermediate carrier. *Makromol. Chem. 190*, 2041–2054.
(14) Pratten, M. K., Lloyd, J. B., Horpel, G., and Ringsdorf, H. (1985) Micelle-forming block copolymers: Pinocytosis by macrophages and interaction with model membranes. *Makromol. Chem. 186*, 725–733.
(15) Jeon, S. H., Park, S. M., and Ree, T. (1989) Preparation and complexation of an A-B-A type triblock copolymer consisting of helical poly(L-proline) and random-coil poly(ethylene oxide). *J. Polym. Sci. Part A: Polym. Chem. 27*, 1721–1730.
(16) Leonhardt, A., Gutzler, F., and Wegner, G. (1982) Synthesis of multiblock copolymers from oligo(ethylene oxide) and oligopeptide segments catalyzed by chymotrypsin. *Makromol. Chem. Rapid Commun. 3*, 461–466.

(17) Yokoyama, M., Anazawa, H., Takahashi, A., Inoue, S., Kataoka, K., Yui, N., and Sakurai, Y. (1990) Synthesis and permeation behavior of membranes from segmented multiblock copolymers containing poly(ethylene oxide) and poly(β-benzyl L-aspartate) blocks. *Makromol. Chem. 191*, 301–311.

(18) Ulbrich, K., Strohalm, J., and Kopecek, J. (1986) Poly(ethylene glycol)s containing enzymatically degradable bonds. *Makromol. Chem. 187*, 1131–1144.

(19) Nathan, A., Bolikal, D., Vyavahare, N., Zalipsky, S., and Kohn, J. (1992) Hydrogels based on water-soluble poly(ether urethanes) derived from L-lysine and poly(ethylene glycol). *Macromolecules 25*, 4476–4484.

(20) Zalipsky, S., Seltzer, R., and Nho, K. (1991) Succinimidyl carbonates of polyethylene glycol: Useful reactive polymers for preparation of protein conjugates. *Polymeric Drugs and Drug Delivery Systems* (R. L. Dunn, and R. M. Ottenbrite, Eds.) pp 91–100, American Chemical Society, Washington, DC.

(21) Zalipsky, S., Seltzer, R., and Menon-Rudolph, S. (1992) Evaluation of a New Reagent for Covalent Attachment of Polyethylene Glycol to Proteins. *Biotechnol. Appl. Biochem. 15*, 100–114.

(22) Kalir, R., Fridkin, M., and Patchornik, A. (1974) (4-Hydroxy-3-nitro)benzylated polystyrene: An improved polymeric nitrophenol derivative for peptide synthesis. *Eur. J. Biochem. 42*, 151–156.

(23) Vandoorne, F., Loccufier, J., and Schacht, E. (1989) Functionalization of α-hydrogen-ω-methoxypoly(oxyethylene), 1: A new method for the conversion of hydroxyl end groups into aldehyde groups. *Makromol. Chem. Rapid Commun. 10*, 271–275.

(24) Fields, R., and Dixon, H. B. F. (1971) Micro method for determination of reactive carbonyl groups in proteins and peptides, using 2,4-dinitrophenylhydrazine. *Biochem. J. 121*, 587–589.

(25) Panarin, E. F., and Solovskij, M. V. (1989) Polymer derivatives of β-lactam antibiotics of the penicillin series. *J. Controlled Release 10*, 119–129.

(26) Toth, I., Hughes, R. A., Ward, P., Baldwin, M. A., Welham, K. J., McColm, A. M., Cox, D. M., and Gibbons, W. A. (1991) Lipidic peptides. IV. Penicillin and cephalosporin amide conjugates with lipidic amino acids and their oligomers. *Int. J. Pharm. 73*, 259–266.

(27) Alicino, J. F. (1961) Iodometric assay of natural and synthetic penicillins, 6-aminopenicillanic acid and cephalosporin C. *Anal. Chem. 33*, 648–649.

(28) Chapman, T. M. (1989) Models for polyurethane hydrolysis under moderately acidic conditions: A comparative study of hydrolysis rates of urethanes, ureas and amides. *J. Polym. Sci. Part A. Polym. Chem. 27*, 1993–2005.

(29) Larwood, D. J., and Szoka, F. C. (1984) Synthesis, characterization, and in vivo disposition of iodinatable polyethylene glycol derivatives: Differences in vivo as a function of chain length. *J. Labelled Compd. Radiopharm. 21*, 603–614.

(30) Li, C., and Kohn, J. (1989) Synthesis of poly(iminocarbonates): Degradable polymers with potential applications as disposable plastics and as biomaterials. *Macromolecules 22*, 2029–2036.

(31) Meltzer, N. M., Tous, G. I., Gruber, S., and Stein, S. (1987) Gas-phase hydrolysis of proteins and peptides. *Anal. Biochem. 160*, 356–361.

Affinity Purification and Characterization of Anti-Tac(Fv)-C3-PE38KDEL: A Highly Potent Cytotoxic Agent Specific to Cells Bearing IL-2 Receptors

Cheryl Spence,† Michele Nachman,† Maurice K. Gately,‡ Robert J. Kreitman,§ Ira Pastan,§ and Pascal Bailon*,†

Protein Biochemistry and Immunopharmacology Departments, Hoffmann-La Roche, Inc., Nutley, New Jersey 07110, and Laboratory of Molecular Biology, National Institutes of Health, Bethesda, Maryland 20892. Received August 14, 1992

A chimeric, single chain antibody fused immunotoxin, denoted anti-Tac(Fv)-C3-PE38KDEL, was engineered and expressed in *Escherichia coli*. The microbially expressed anti-Tac(Fv)-C3-PE38KDEL was solubilized from inclusion bodies using guanidine hydrochloride, and subsequently refolded in a redox buffer via thiol/disulfide exchange. The recombinant immunotoxin from the crude extract was purified employing receptor-affinity chromatography, which is based upon biological function and involved the immobilized p55 subunit of human IL-2 receptor. The cytotoxic activity of this immunotoxin was measured by the IL-2 dependent phytohemagglutinin (PHA) blast proliferation inhibition and HUT-102 protein synthesis inhibition assays, in which the IC_{50} values were 41.5 and 0.8 pM, respectively. The biochemical homogeneity and authenticity of the purified material were determined by gel permeation chromatography, amino acid composition and N-terminal sequence analyses, SDS–PAGE, isoelectric focusing, and Western blotting. The receptor-affinity-purified immunotoxin was shown to be highly effective in specifically killing cells bearing IL-2 receptors. Anti-Tac(Fv)-C3-PE38KDEL is a powerful immunosuppressant which may be a potentially useful therapeutic agent in the prevention of allograft rejection and in the treatment of autoimmune diseases. Another anticipated application of this fusion protein is as a chemotoxin in the treatment of some forms of cancer.

INTRODUCTION

Immunotoxins are cytotoxic agents that are designed to selectively kill cells bearing targeted antigens or receptors. The potential clinical applications of immunotoxins include their use as immunosuppressants in the prevention of allograft rejection and in the treatment of autoimmune diseases (*1–3*). Another emerging application of immunotoxins is their use as chemotherapeutic agents in the treatment of cancer, AIDS, and immunological disorders (*4, 5*).

Recombinant DNA technology has allowed the production of chimeric toxins consisting of growth factors, lymphokines, or antibodies linked to modified diphtheria toxin, *Pseudomonas* exotoxin (PE), or other toxins. Recently, a hybrid immunotoxin, denoted anti-Tac(Fv)-PE40, has been constructed (*6*). This immunotoxin consists of peptide-linked variable domains of the heavy and light chains of anti-Tac [monoclonal antibody to the low-affinity p55 subunit of human interleukin-2 (IL-2) receptor] fused to a truncated form of *Pseudomonas* exotoxin, which lacks the binding domain. To increase cytoplasmic delivery and hence toxin activity, anti-Tac-(Fv)-PE40 has been further modified to include the characteristic endoplasmic reticulum retention sequence, KDEL, in place of the C-terminal sequence, REDLK, in PE40 (*7*). Deletion of amino acids 365–380 in PE40KDEL, which removes a disulfide bond but does not decrease activity (*8*), yielded anti-Tac(Fv)-PE38KDEL. The effects of these and other changes in anti-Tac(Fv)-PE40 were recently studied (*9*). Finally an additional peptide connector, C3 (ASGGPE), is used to connect the light chain (Fv) to PE, resulting in anti-Tac(Fv)-C3-PE38KDEL. This connector resulted in improved renaturation yields in B3-(Fv)-PE38KDEL (*10*). This recombinant immunotoxin is a 62.7-kDa protein containing 587 amino acids. Here, we report the purification of this immunotoxin employing receptor-affinity chromatography (RAC), as well as the biochemical characterization of the purified molecule.

EXPERIMENTAL PROCEDURES

Plasmid Construction and Protein Expression. Plasmids encoding anti-Tac(Fv)-C3-PE38KDEL were expressed after transforming them into BL21 (λDE3) *E. coli*, as described (*9–13*). The cultures of *E. coli* were grown in a 10-L fermentor at 37 °C to an A_{650} of 6–8 and induced with isopropyl β-D-thio galactoside to a final concentration of 1 mM, for 90 min at 37 °C.

Bioassays. *Protein Synthesis Inhibition Assay.* Cytotoxic activity of the purified immunotoxin was determined by its inhibition of protein synthesis in HUT-102 cells as measured by the [^{3}H]leucine incorporation as described (*12*).

IL-2 Dependent PHA Blast Proliferation Inhibition Assay. In this assay, cytotoxicity is measured by the decrease in thymidine incorporation into cellular DNA as described in detail elsewhere (*12*). A reference anti-Tac-(Fv)-C3-PE38KDEL, which has been assigned to activity of 400 unit/μg, was used as a standard. Using this standard, 1 unit/mL of anti-Tac(Fv)-C3-PE38KDEL routinely caused approximately 50% inhibition in the assay.

Preparation of Receptor-Affinity Adsorbent. The production and purification procedures of a soluble form of human IL-2 receptor (p55), denoted IL-2RΔNae, have

* Author to whom correspondence should be addressed.
† Protein Biochemistry Department, Hoffmann-La Roche, Inc.
‡ Immunopharmacology Department, Hoffmann-La Roche, Inc.
§ National Institutes of Health.

1043-1802/93/2904-0063$04.00/0 © 1993 American Chemical Society

been described elsewhere (*14*). The purified IL-2R was immobilized on NuGel-Polyaldehyde (500 Å, 40–60 μm, Separation Industries; Metuchen, NJ) according to the following procedure. Fifty grams (100 mL) of dry gel was washed three times in a sintered-glass funnel with 100 mL of ice-cold water. The gel was transferred to a stoppered 500-mL Erlenmeyer flask, containing 100 mL of a 2.0 mg/mL IL-2R solution in phosphate-buffered saline (PBS, pH 7.4). Six hundred milligrams of sodium cyanoborohydride was added to the gel suspension to a final concentration 0.05 M. The mixture was shaken for 16 h at 4 °C. The uncoupled IL-2R was collected by filtration. The gel was washed twice with 100 mL of PBS. The filtrate and washes were pooled and a small aliquot was dialyzed against PBS. The gel was then treated for 2 h with 100 mL of 1.0 M ethanolamine, pH 7.0, in the presence of 0.05 M sodium cyanoborohydride. It was washed with PBS and stored in 0.02% sodium azide at 4 °C. The volume of the uncoupled protein solution was noted and the protein content was determined from its UV absorbance at 280 nm, using the A_{280} value of 1.65 for a 1 mg/mL IL-2R solution. The difference between the amount of IL-2R present in the starting reaction mixture and the amount remaining after coupling, divided by the volume of the gel (100 mL), gave the IL-2R coupling density (mg/mL of gel).

Solubilization and Renaturation of Anti-Tac(Fv)-C3-PE38KDEL from *E. coli*. All operations were carried out at 2–8 °C unless otherwise noted. The frozen *E. coli* cell paste was washed twice in 4 volumes (4 mL/g of cells) of 100 mM Tris-HCl, pH 8.0, containing 5 mM EDTA, and during the washings the pH was adjusted to 8.0, if necessary. The supernatant and pellet were collected by centrifugation at 17000*g* for 20 min. The pellet was uniformly suspended in 20 mM Tris-HCl, pH 8.0, containing 0.2% sarkosyl and 1.5 mM EDTA. The supernatant and pellet were collected as before. The pellet was suspended in 5 volumes (5 mL/g of cells) of 6 M guanidine hydrochloride (Gu·HCl) in 100 mM Tris-HCl, pH 8.0, 1.5 mM EDTA, 1 mM reduced glutathione (GSH), and 0.1 mM oxidized glutathione (GSSG). The suspension was pulse-sonicated six times for 30 s, at 50% power, with a Vibra Cell Sonicator (Sonics and Materials, Inc.; Danbury, CT). The homogenate was stirred for 60 min at room temperature. The supernatant containing the solubilized anti-Tac(Fv)-C3-PE38KDEL was collected by centrifugation at 31000*g* for 30 min. It was then rapidly added to 19 volumes (20-fold dilution) of a vigorously stirring 20 mM Tris-HCl, pH 8.0 buffer, containing EDTA, GSH, and GSSG (redox buffer) at concentrations as described before. The pH was maintained at 8.0. The diluted extract was stirred for 60 min and allowed to stand for 3–4 days. The extract was clarified by centrifugation at 17000*g*, followed by filtration through a 0.8/0.2 μm filter (Sartorius; Yauco, Puerto Rico). This was the starting material used for the receptor-affinity purification of anti-Tac(Fv)-C3-PE38KDEL.

Receptor-Affinity Chromatography. One hundred milliliters of immobilized IL-2R gel were packed into an Amicon G-44 × 250 column fitted with two adapters. The column was equilibrated with PBS buffer and 20 L of the clarified extract (obtained from 200 g of cells) was applied to the column at a flow rate of 10 mL/min. The column effluents were monitored by a Gilson 111b UV detector and recorded by a Kipp and Zonen recorder. The column was washed with PBS until the UV absorbance at 280 nm returned to base-line. The specifically adsorbed anti-Tac(Fv)-C3-PE38KDEL was then eluted from the receptor column with 3 M potassium thiocyanate in PBS buffer. The eluate was dialyzed against PBS buffer.

Gel Permeation Chromatography. A Pharmacia K50/100 cm column was packed with Sephacryl S-200 HR (Pharmacia LKB Biotechnology; Piscataway, NJ) to a height of 95 cm. The column was equilibrated with PBS buffer at a flow rate of 0.85 mL/min and calibrated with standard high and low molecular weight marker proteins (Pharmacia LKB Biotechnology). The concentrated anti-Tac(Fv)-C3-PE38KDEL (40–50 mL) was applied onto the column and developed with the equilibration buffer. The column operations were monitored as described in the affinity purification step. Four-minute fractions were collected using the LKB Ultra Rac-7000 fraction collector. The peak corresponding to the monomer (~63 kDa) was collected, filtered through a 0.2 μm filter, and stored at 4 °C.

Protein Determination. Protein content was determined by the Bradford method (*15*) using bovine serum albumin as the standard, and the values were confirmed by quantitative amino acid analysis (*16*).

SDS–PAGE Analysis, Isoelectric Focusing, and Western Blotting. The immunotoxin from various stages of the purification scheme was analyzed by sodium dodecyl (lauryl) sulfate/polyacrylamide (12%) gel electrophoresis (SDS–PAGE) under nonreducing conditions according to the methods of Laemmli (*17*). The isoelectric focusing of anti-Tac(Fv)-C3-PE38KDEL was performed with LKB's isoelectric focusing unit, using 3–10 p*I* range ampholytes according to the manufacturer's instructions. Western blotting of the purified immunotoxin at concentrations ranging from 0.05 to 0.2 μg was carried out by transferring anti-Tac(Fv)-C3-PE38KDEL to nitrocellulose paper following SDS–PAGE, according to standard procedures. In two separate experiments, blotting was performed with antibodies against murine IgG (H and L chains) and with antibody to *Pseudomonas* exotoxin A. The respective detection antibodies were conjugated with horseradish peroxidase.

Amino Acid Analysis. Amino acid analyses were performed with a postcolumn fluorescamine amino acid analzyer (*16*). Samples were hydrolyzed in 6 N HCl containing 4% thioglycolic acid at 110 °C for 20–24 h in vacuo.

RESULTS

Solubilization of Immunotoxin from Inclusion Bodies. Prior to disrupting the transfected *E. coli* cells by sonication to release the inclusion bodies, the cells were washed sequentially in Tris and sarkosyl buffers. These initial washes removed significant amounts of unwanted soluble proteins from the cell pellet (Figure 1, lanes 1–3). When the Gu·HCl extract was analyzed by SDS–PAGE, a prominent, ~63-kDa band was observed, which corresponded to the expected molecular weight of the immunotoxin (Figure 1, Lane 4).

Receptor-Affinity Purification. A soluble form of the low-affinity p55 subunit of IL-2R was chemically coupled to silica-based NuGel-Polyaldehyde via reductive amination, at a coupling density of 1.35 mg/mL gel. The coupling efficiency was 40%. The affinity sorbent's binding capacity for anti-Tac(Fv)-C3-PE38KDEL was experimentally determined as described (*18*) and found to be 1.65 mg/mL of gel, which translates into a binding efficiency of 47%. The receptor affinity column (100 mL) used in this study had an immunotoxin binding capacity of 165 mg.

Immunotoxin was purified from dilute, crude extract employing receptor-affinity chromatography (RAC, *18*).

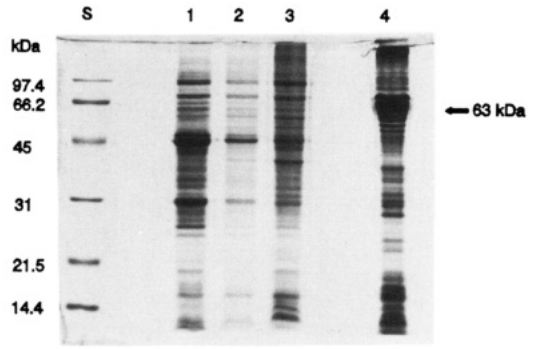


Figure 1. SDS–PAGE analysis of *E. coli* cell washings and Gu·HCl extract under nonreducing conditions: lane S, standard molecular weight marker proteins; lane 1, Tris wash 1; lane 2, Tris wash 2; lane 3, Sarkosyl wash; lane 4, Gu·HCl extract (neat).

The protein contents and activities of immunotoxin obtained from 200 g *E. coli* cell paste at various stages of the purification scheme are listed in Table I. The immunotoxin recoveries were 146 mg (100%) after RAC. Protein recoveries after GPC were 31 mg (21%), 9 mg (2%), and 57 mg (39%), respectively, for GPC peaks 1, 2, and 3. The GPC protein values account only for the major portion of the peaks and exclude the overlapping parts (see Figure 3), thereby reducing the percentage of the protein recoveries. The SDS–PAGE profile of the RAC-purified material indicated a major band around 63 kDa (Figure 2, lane 3). However, upon gel permeation chromatography (GPC), the RAC-purified material yielded three peaks (Figure 3), whose SDS–PAGE profiles under nonreducing conditions are shown in Figure 4. Peaks 1 and 2 corresponded to high molecular weight aggregates, >400 and ~250 kDa (determined from molecular weight standard curves), respectively, yet all three peaks contained the ~63-kDa band expected for the monomeric protein.

An IL-2 dependent PHA blast proliferation inhibition assay was used to determine the bioactivities of the immunotoxin at various stages of the purification scheme (Table I). The 18.1×10^6 units of activity found in the RAC eluate, with a specific activity of 1.26×10^5 units/mg, was taken as 100%. The specific activities of GPC peaks 1, 2, and 3 were 0.26×10^5, 2.54×10^5, and 4.0×10^5 units/mg, respectively. The recovery data indicates that the total activity present in the final product (monomer) is 126% of the activity in the starting material (RAC eluate).

In Table II, the bioactivity of anti-Tac(Fv)-C3-PE38KDEL is compared with that of anti-Tac(Fv)-C3-PE40 (the parent immunotoxin with the C3 linker) and IL2-PE66^{4Glu} (the most cytotoxic IL2-PE construct to date, *19*). In both assays, anti-Tac(Fv)-C3-PE38KDEL was the most active immunotoxin construct, with IC_{50} values of 41.5 and 0.8 pM for the PHA and HUT-102 assays, respectively. The anti-Tac(Fv)-C3-PE40 construct had intermediate activity and the IL2-PE66^{4Glu} had the least cytotoxic activity.

Biochemical Characterization. SDS–PAGE analysis of the monomer under nonreducing conditions indicated a single ~63-kDa protein, devoid of any dimers, oligomers, or degradation products (Figure 4, lane 3). Similarly, isoelectric focusing results indicate a major band with a p*I* of 5.4 (Figure 5). Western blotting with antibodies to murine IgG and PE both show a prominent band at ~63 kDa (Figure 6). However, blotting with anti-PE also indicated the presence of two additional minor bands (<63 kDa), which may be cleavage products containing the PE portion of the original molecule.

The purified anti-Tac(Fv)-C3-PE38KDEL was subjected to amino acid sequence and composition analyses. The experimentally determined N-terminal sequence of the immunotoxin monomer was identical to the unique sequence of the encoded immunotoxin (data not shown). In addition, all molecules contained N-terminal methionine. Finally, the amino acid composition results (Table III) agreed well with the expected values.

DISCUSSION

Anti-Tac(Fv)-C3-PE38KDEL is expressed in *E. coli* as an insoluble form within the inclusion bodies, which necessitates the use of a strong denaturant such as 6 M Gu·HCl for its solubilization. Sonication in the presence of 6 M Gu·HCl not only disrupts the cell wall and membrane, resulting in the release of the inclusion bodies, but also helps to solubilize the immunotoxin (Figure 1, lane 4). Since the Gu·HCl-solubilized immunotoxin has been denatured, it must be renatured. This requires either a substantial reduction in the concentration of Gu·HCl or its complete removal. It has been shown previously that optimal protein refolding occurs at or below the micromolar range (*20*). For this purpose and for the reduction of Gu·HCl concentration, the extract was diluted 20-fold. A redox buffer was chosen for dilution, because previous studies have indicated that S–S bond formation (i.e., protein folding) could be initiated and maintained via thiol/disulfide exchange between the naturally occurring protein sulfhydryl groups and a redox buffer environment (*21*).

The receptor-affinity purification of anti-Tac(Fv)-C3-PE38KDEL is based upon the specific and reversible interaction between the immobilized IL-2R (Tac) and the freely available anti-Tac in the fusion protein. The receptor-affinity sorbent is capable of preferentially binding correctly folded monomers from a heterogeneous population of molecules (*22*). Hence, in the RAC purified immunotoxin, at least the anti-Tac(Fv) portion is expected to be completely renatured.

Gel permeation chromatography is essential for the separation of the desired monomeric form of immunotoxin from the inactive high molecular weight aggregates. It should be pointed out that GPC under aseptic conditions is an ideal tool for the exchange of biotherapeutics such as anti-Tac(Fv)-C3-PE38KDEL into the final storage or formulation buffer. It also serves the purpose of removing trace contaminants such as endotoxins, *E. coli proteins*, degradation products, and salts, among others. In general, GPC is an integral part of any purification scheme used for the preparation of preclinical and clinical-grade protein therapeutics.

The apparent discrepancy between the appearance of high molecular weight peaks in the GPC profile (Figure 3) and their obvious monomeric content as seen on SDS–PAGE (Figure 4) suggests that some dissociation of the aggregates may have occurred upon their exposure to SDS. The receptor-affinity adsorbent's demonstrated preference for binding correctly folded monomers (*22*) lead us to believe that the RAC-purified material was originally monomeric. The high molecular weight aggregates observed during GPC might have been formed during dialysis and concentration, before application onto the gel filtration column.

The bioactivities of the extract and RAC flowthrough materials (Table I) could not be reliably determined in the IL-2 dependent PHA blast proliferation inhibition assay due to their extremely dilute nature as well as the possible presence of interfering substances. Regardless, since the amount of immunotoxin (146 mg) passed through the column did not exceed the total binding capacity (160 mg) of the affinity column, no activity was expected to

Table I. Purification Results of Anti-Tac(Fv)-C3-PE38KDEL[a]

sample	volume (mL)	protein (mg)	units ($\times 10^6$)	specific activity ($\times 10^5$ units/mg)	% recovery	
					protein	activity
extract	20000	6842				
RAC/FT	20000	6650				
RAC/eluate	250	146	18.1	1.24	100	100
GPC-PK1	110	31	0.8	0.26	21	4
GPC-PK2	118	9	2.3	2.54	6	13
GPC-PK3 (monomer)	137	57	22.8	4.00	39	126

[a] Starting material = 200 g of *E. coli* cell paste. RAC = receptor-affinity chromatography. FT = flowthrough. GPC-PK = gel permeation chromatography peak (Figure 3). The activity of anti-Tac(Fv)-PE38KDEL was measured by its ability to inhibit IL-2 dependent PHA blast proliferation. See the text for details.

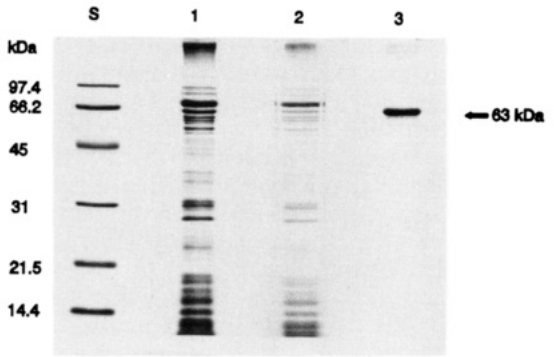


Figure 2. SDS–PAGE analysis (nonreducing conditions) of anti-Tac(Fv)-C3-PE38KDEL at various stages of the purification scheme: lane S, standard molecular weight marker proteins; lane 1, diluted and clarified extract (RAC load); lane 2, RAC flowthrough; lane 3, RAC eluate.

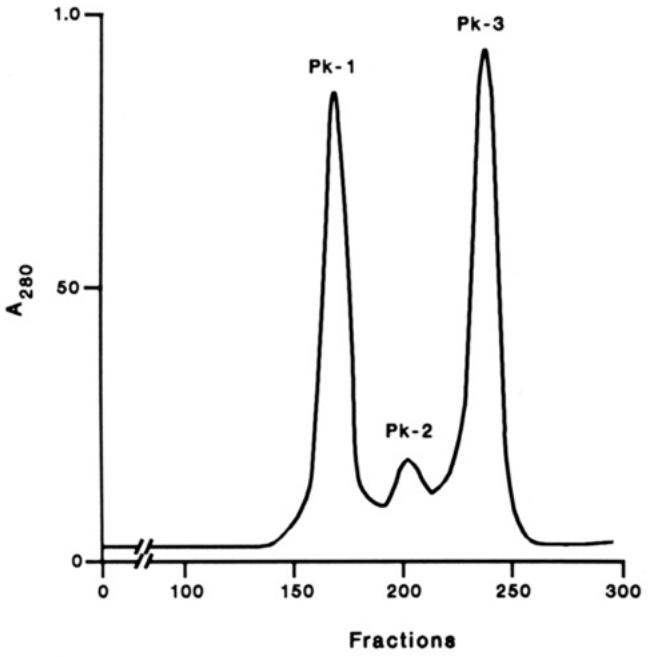


Figure 3. Gel permeation profile of RAC-purified anti-Tac-(Fv)-C3-PE38KDEL. Conditions: 5 × 95 cm column packed with Sephacryl S-200 HR; mobile phase PBS; 39 mL of RAC eluate containing 133 mg immunotoxin was applied at a flow rate of 0.85 mL/min and 4-min fractions were collected.

remain in the flowthrough material. The anomalous increase in total activity observed for the monomer (Table I, 126%) is probably the result of further dissociation of the aggregates into the highly active monomer during GPC. Another possibility is that separation of the high molecular weight aggregates (which did bind to p55) from the monomer eliminates the potential competition between the highly active monomer and the inactive aggregate.

Table II. Comparison of Cytotoxic Activities of Various Immunotoxin Constructs

immunotoxin	IC_{50}[a] IL-2 dependent PHA blast proliferation inhibition assay		IC_{50}[a] HUT-102 protrein synthesis inhibition assay	
	ng/mL	pM	ng/mL	pM
anti-Tac(Fv)-C3-PE38KDEL (62.7 kDa)	2.6	41.5	0.05	0.8
anti-Tac(Fv)-C3-PE40 (64.3 kDa)	6.0	93.3	0.11	1.7
IL2-PE66^{4Glu} (81 kDa)	135.0	1667.0	2.00	24.7

[a] IC_{50} is the concentration of toxin which inhibits 50% of cell proliferation or protein synthesis, as compared to the control in which no toxin is added. See the text for details.

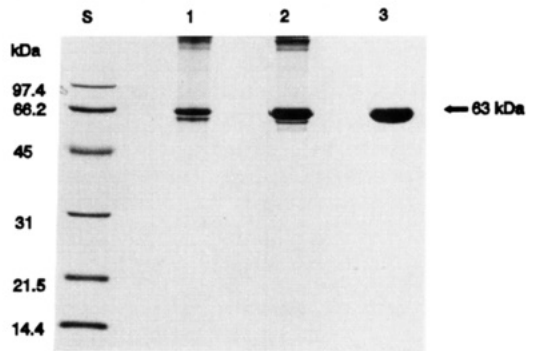


Figure 4. SDS–PAGE analysis (nonreducing conditions) of RAC purified immunotoxin following GPC: lane S, standard molecular weight marker proteins; lane 1, GPC-PK-1; lane 2, GPC-PK-2; lane 3, GPC-PK-3 (monomer).

The end result is an increase in the specific activity of the monomer.

The various biochemical analyses performed on the purified immunotoxin all pointed to a homogeneous and authentic preparation. Purity of the anti-Tac(Fv)-C3-PE38KDEL monomer is demonstrated by a single ~63-kDa band on SDS–PAGE (Figure 4, lane 3). Neither high molecular weight aggregates nor contaminant bands were observed. The fact that Western blotting with antibodies to both portions of the fusion protein yielded the same major band of ~63 kDa (Figure 6), confirms the authenticity of the anti-Tac-PE toxin. The two additional minor bands of <63 kDa in the anti-PE immunoblot were not seen in the anti-murine IgG immunoblot, nor during SDS–PAGE, even at 10-μg protein loading in the latter. Apparently, the aforementioned minor bands are degradation products containing the PE portion of the immunotoxin, and these may have been produced upon storage.

Finally, the amino acid sequence and composition analyses provide further evidence for the homogeneity of the anti-Tac(Fv)-C3-PE38KDEL preparation.

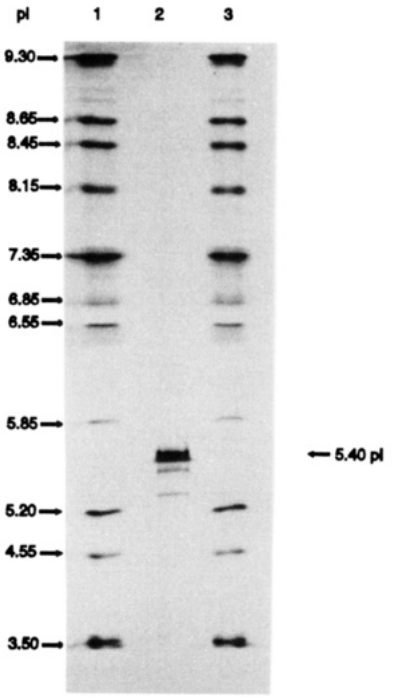


Figure 5. Isoelectric focusing of anti-Tac(Fv)-C3-PE38KDEL. Pharmacia's broad p*I* calibration kit, run on a 5% PA gel containing Pharmalyte 3-10, was used.

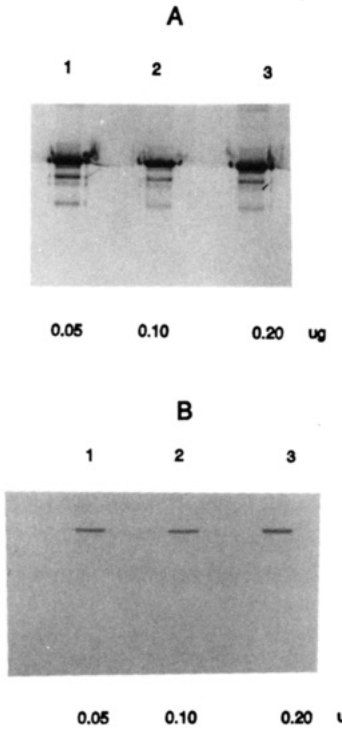


Figure 6. Western blotting of anti-Tac(Fv)-C3-PE38KDEL with anti-PE (panel A) and anti-murine IgG (panel B). Lanes 1, 2, and 3: 0.05, 0.1, and 0.2 μg of immunotoxin, respectively.

Since this is the first reported instance where the immunotoxin is purified based upon biological function rather than charge and size, as in conventional chromatographic methods, it is of interest to compare these two methods. It should be pointed out that only analytical scale purification was carried out with the conventional method. Since the cells used in each of the purification method were produced under different conditions, in terms of fermentation scale, induction conditions, as well as expression levels, a direct comparison of final yield could not be made. However, the absence of immunotoxin in the RAC flowthrough material (Figure 2, lane 2) indicates that the RAC column quantitively adsorbs the immunotoxin from the extract.

Table III. Amino Acid Composition of Anti-Tac(Fv)-C3-FE38KDEL

amino acid	obsd	calcd	amino acid	obsd	calcd
alanine	61.8	61.0	leucine	51.5	52.0
arginine	34.6	35.0	lysine	16.7	16.0
asparagine	37.6	10.0	mthionine	7.6	6.0
aspartic acid		24.0	phenyllalanine	17.3	16.0
cysteine	ND[a]	6.0	proline	ND	35.0
glutamic acid	69.5	35.0	serine	47.7	55.0
glutamine		33.0	threonine	39.4	39.0
glycine	73.7	72.0	tryptophan	ND	10.0
histidine	11.6	9.0	tyrosine	19.0	26.0
isoleucine	21.4	21.0	valine	26.6	26.0
			total	536.0[b]	587.0

[a] ND = not determined. [b] Incomplete.

Another aspect of the purification scheme which requires comparison is the solubilization procedure. The conventional method involves preparation of spheroplasts using osmotic shock lysis, purification of inclusion bodies by lysozyme treatment, and extensive washings and centrifugations, followed by dilution and renaturation. Moreover, the extract must be dialyzed against low ionic strength buffers to render them suitable for application on ion-exchange columns. In contrast, the extract used in RAC is prepared directly from inclusion bodies and does not require dialysis. In summary, the conventional method is labor-intensive, time-consuming, and not readily scalable. RAC-purified immunotoxin is fully characterized, endotoxin-free, and suitable for preclinical studies. Immunotoxin purified by both methods have similar bioactivities.

Due to advances made in recombinant DNA technology, sufficient quantities of a soluble form of IL-2R are available for immobilization. The fast-adsorption kinetics afforded by RAC allows high throughput, resulting in high productivity (*18*). The RAC column is extremely stable during long-term use (no impairment in functionality is observed during 100 cycles of operation, data not shown). Therefore, an affinity column consisting of 100–200 mg of IL-2R is sufficient for producing gram quantities of the anti-Tac-(Fv)-C3-PE38KDEL immunotoxin.

SUMMARY AND CONCLUSIONS

We have developed efficient methods for the solubilization, renaturation, and purification of a biochemically well-defined preparation of anti-Tac(Fv)-C3-PE38KDEL. The key purification step is RAC, which utilizes the interaction between the matrix-bound IL-2R (Tac) and the freely exposed anti-Tac(Fv) region of the soluble immunotoxin. The readily accessible anti-Tac(Fv) portion of the immunotoxin renders RAC an ideal method for the purification of anti-Tac(Fv)-C3-PE38KDEL. Inclusion of a GPC step in the purification scheme enabled the preparation of a monomeric form of the immunotoxin which is suitable for preclinical studies. The biochemical characterization results presented in this manuscript demonstrate the high purity and homogeneity of the final anti-Tac(Fv)-C3-PE38KDEL preparation.

ACKNOWLEDGMENT

We thank Ronald Keeney for preparing the *E. coli* extract, Doreen Waddington and Yu-Ching Pan for performing the amino acid analyses, Maureen Costello and Beatrice Akhabue for isoelectric focusing, and Elcin

Korkmaz for immunoblotting. We are grateful to Dennis Tighe for the graphics, Lisa Nieves for typing the manuscript, and Jill Porter for critically reviewing the manuscript.

LITERATURE CITED

(1) Lorberboum-Galski, H., Barret, L. V., Kirkman, R. L., Ogata, M., Willingham, M. C., Fitzgerald, D. J., and Pastan, I. (1989) Cardiac allografts survival in mice treated with IL-2-PE40. *Proc. Natl. Acad. Sci. U.S.A. 86*, 1008–1012.

(2) Roberge, F. G., Loberboum-Galski, H., Lehoang, P., de Smet, M., Chan, C. C., Fitzgerald, D., and Pastan, I. (1989) Selective immunosuppression of activated T cells with the chimeric toxin IL-2-PE40. Inhibition of experimental autoimmune Uveoretinitis (EAU). *J. Immunol. 143*, 3498–3502.

(3) Case, J. P., Lorberboum-Galski, H., Lafyatis, R., Fitgerald, D., Wilder, R. L., and Pastan, I. (1989) Chimeric cytotoxin IL-2-PE40 delays and mitigates adjuvant-induced arthritis in rats. *Proc. Natl. Acad. Sci. U.S.A. 86*, 287–291.

(4) Pastan, I., Willingham, M. C., and Fitzgerald, D. J. P. (1986) Immunotoxins. *Cell 47*, 641–648.

(5) Vitetta, E. S., Fulton, R. J., May, R. D., Till, M., and Uhr, J. W. (1987) Redesigning nature's poisons to create anti-tumor agents. *Science 238*, 1098–1104.

(6) Chaudhary, V. K., Queen, C., Junghans, R. P., Waldmann, T. A., Fitgerald, D. J., and Pastan, I. (1989) A recombinant immunotoxin consisting of two antibody variable domains fused to pseudomans exotoxin. *Nature 339*, 394–397.

(7) Seetharam, S. Chaudhary, V. K., Fitgerald, D., and Pastan, I. (1991) Increased cytotoxic activity of *Pseudomonas* exotoxin and two chimeric toxins ending in KDEL. *J. Biol. Chem. 266*, 17376–17381.

(8) Siegall, C. B., Chaudhary, V. K., Fitgerald, D. J., and Pastan, I. (1989) Functional analysis of domains II, 1b and III of *Pseudomonas* exotoxin. *J. Biol. Chem. 264*, 14256–14261.

(9) Kreitman, R. J., Batra, J. K., Seetharam, S., Chaudhary, V. K., Fitzgerald, D. J., and Pastan, I. (1993) Single-chain immunotoxin fusions between anti-Tac and *Pseudomonas* exotoxin which differ in the toxin disulfides bonds and at this carboxyl terminus. *Biocongjugate Chem.*, in press.

(10) Brinkmann, U., Buchner, J., and Pastan, I. (1992) Independent domain folding of *Pseudomonas* exotoxin and single-chain immunotoxins: Influence of interdomain connections. *Proc. Natl. Acad. Sci. U.S.A. 89*, 3075–3079.

(11) Kreitman, R. J., Schneider, W. P., Queen, C., Tsudo, M., Fitgerald, D. J. P., Waldmann, T. A., and Pastan, I. (1992) Mik-β1(Fv)-PE40, A recombinant immunotoxin cytotoxic toward cells bearing the β-chain of the IL-2R. *J. Immunol.*, in press.

(12) Batra, J. K., Fitzgerald, D., Gately, M., Chaudhary, V. J., and Pastan, I. (1990) Anti-Tac(Fv)-PE40, Single chain antibody *Pseudomonas* exotoxin fusion protein directed at interleukin 2 receptor bearing cells. *J. Biol. Chem. 265*, 15198–15202.

(13) Chaudhary, V. K., Jinno, Y., Fitgerald, D., and Pastan, I. (1990) *Pseudomonas* exotoxin contains a specific sequence at the carboxyl terminus that is required for cytotoxicity. *Proc. Natl. Acad. Sci. U.S.A. 87*, 308–312.

(14) Weber, D. V., Keeney, R. F., Familletti, and Bailon, P. (1988) Medium-scale ligand-affinity purification of two soluble forms of human interleukin-2 receptor. *J. Chromatogr. Biomed. Appl. 431*, 55–63.

(15) Bradford, M. M. (1976) A rapid and sensitive method for the quantitation of microgram quantities of protein utilizing the principle of protein-dye binding. *Anal. Biochem. 72*, 248–254.

(16) Pan, Y.-C. E., and Stein, S. (1986) Amino acid analysis with post-column fluorescent derivatization. *Methods of Protein Microcharacterization* (J. E. Shively, Ed.) pp 105–119, The Humana Press Inc., Clifton, NJ.

(17) Laemmli, U. K. (1970) Cleavage of structural protein during assembly of the head bacteriophase T4. *Nature 227*, 680–685.

(18) Nachman, M., Azad, A. R. M., and Bailon, P. (1992) Membrane-based receptor affinity chromatography. *J. Chromatogr. Biomed. Appl.* (Syposium edition of the 9th International Symposium on Affinity Chromatography and Biological Recognition) *597*, 155–166.

(19) Lorberboum-Galski, H., Garsia, R. J., Gately, M., Brown, P. S., Clark, R. E., Waldmann, T. A., Chaudhary, V. K., Fitzgerald, D. J. P., and Pastan, I. (1990) IL2-PE66^{4Glu}, A new chimeric protein cytotoxic to human-activated T lymphocytes. *J. Biol. Chem. 265*, 16311–16317.

(20) Light, A. (1985) Protein solubility, protein modifications and protein folding. *BioTechniques 3*, 298–306.

(21) Gilbert, H. F. (1984) Redox control of enzyme activities by thiol/disulfide exchange. *Methods in Enzymology* (F. Wold, and K. Moldave, Eds.) Vol. 107, pp 330–351, Academic Press, Inc., Orlando, FL.

(22) Bailon, P., and Weber, D. V. (1988) Receptor affinity chromatography. *Nature 335*, 839–840.

Nuclease Activity of 1,10-Phenanthroline–Copper. New Conjugates with Low Molecular Weight Targeting Ligands

Chi-hong B. Chen, Abhijit Mazumder, Jean-Francois Constant, and David S. Sigman*

Department of Biological Chemistry, School of Medicine, Department of Chemistry and Biochemistry, and Molecular Biology Institute, University of California, Los Angeles, Los Angeles, California 90024. Received September 2, 1992

The chemical nuclease activity of 1,10-phenanthroline–copper depends on DNA sequence because the coordination complex has affinity for DNA. In order to target this efficient nucleolytic activity, it is essential to override its inherent specificity. The minimal size of ligands capable of redirecting the specificity has been investigated. A conjugate (HOP) prepared by alkylating Hoechst dye 33258 with 5-(iodoacetamido)-1,10-phenanthroline has a greater preference for A-T-rich regions than the unsubstituted 1,10-phenanthroline–copper complex, reflecting the specificity of this A-T-specific minor-groove binder. However, since quaternizing the dye with 5-(iodoacetamido)-1,10-phenanthroline increases its affinity for DNA, the specificity of cleavage by the conjugate is less than the binding selectivity of the dye. Linking 1,10-phenanthroline with the peptide of the helix–turn–helix domain of the Trp repressor specificity results in a conjugate with greater reactivity for the operator sequence than the unsubstituted complex. The intrinsic affinity of the 1,10-phenanthroline–Cu can only be partially overridden by the conformationally unstable peptide. Attachment of 1,10-phenanthroline to a deoxyoligonucleotide complementary to a single-stranded loop of RNA successfully targets the scission of the chemical nuclease. Cleavage sites are observed not only contiguous to the site of hybridization but also at nonadjacent sequence positions. The latter set of sites must be close in space to the 5′ end of the hybridized deoxyoligonucleotide.

INTRODUCTION

1,10-Phenanthroline–copper ion in the presence of thiol and hydrogen peroxide efficiently nicks DNA and RNA by oxidative attack on the (deoxy)ribose moiety (*1*, *2*). The kinetic mechanism involves the following sequence of steps (eq 1): (a) the reversible binding of the tetrahedral

$$(OP)_2Cu^+ + DNA \underset{}{\overset{K_d}{\longleftrightarrow}} (OP)_2Cu^+\text{–DNA} \xrightarrow[k_{cat}]{H_2O_2} \text{scission products} \quad (1)$$

2:1 1,10-phenanthroline–cuprous complex to DNA or RNA (*3*); (b) the one-electron oxidation of the nucleic acid-bound coordination complex (*4*, *5*), (c) attack by the oxidative species generated on the (deoxy)ribose (*6*, *7*), and (d) a series of elimination reactions leading to strand scission (*8*).

Recent studies have demonstrated that ascorbic acid activates the scission chemistry more efficiently than mercaptopropionic acid, which may decrease the concentration of the reactive 2:1 1,10-phenanthroline–cuprous complex (*9*, *10*). The second phenanthroline converts the 1:1 complex to an efficient nucleolytic agent because it generates a hydrophobic cation with high affinity for DNA and RNA (*4*).

Substitution at the 5-position of phenanthroline of functionalities such as phenyl, methyl, bromo, nitro, amino, acetamido, and glycinamido have modest effects on the rate of scission of DNA. The scission patterns obtained for copper complexes of these phenanthroline derivatives are comparable to those obtained with the copper complex of the unsubstituted phenanthroline. Variations in the rate of scission can be attributed to the stability of the noncovalent complex or differences in the rate of oxidation of the cuprous complex by hydrogen peroxide (*3*). In contrast, the copper complexes of 1,10-phenanthrolines derivatized at the 2 position with a methyl, carboxyl, carboxamide, or carbinol group do not cleave DNA. The lack of reactivity is due to a slow rate of oxidation of the cuprous complex attributable to steric hindrance involving the ortho substituents in the square planar cupric complexes (*3*). In fact, 2,9-dimethyl-1,10-phenanthroline quenches the scission reaction because it sequesters copper ion as the redox-stable cuprous complex (*5*).

The specificity and the nuclease activity of 1,10-phenanthroline–copper has been altered by conjugating the ligand at its 5-position to proteins, peptides, and nucleic acids (*2*). The most general method for the preparation of the bioconjugates has been the alkylation of sulfhydryl groups of the carrier with 5-(iodoacetamido)-1,10-phenanthroline (*11–15*). Coupling 5-glycinamido-1,10-phenanthroline to the terminal phosphates of an oligonucleotide has also been successful (*16*). If the carrier ligand has high affinity for one aspect of nucleic acid structure, the reactivity of the bioconjugate will reflect its binding specificity and not that of the hydrophobic cation, 1,10-phenanthroline–copper.

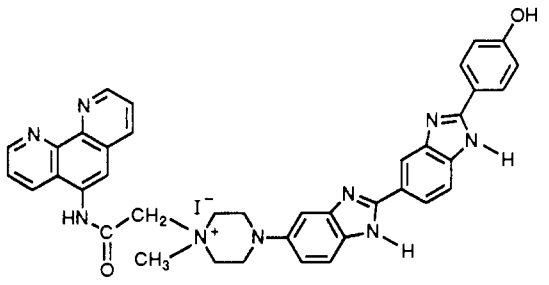
The minimal size, conformational stability, and specificity of carrier ligands which are capable of redirecting the intrinsic scission specificity of the nuclease activity of 1,10-phenanthroline–copper (OP–Cu) have not been defined. They have been investigated in the present report because OP–Cu has significant advantages relative to ferrous EDTA as a scission reagent. Unlike ferrous EDTA, which has been widely used to accomplish the chemical cleavage of the phosphodiester backbone, OP–Cu does not generate diffusible hydroxyl radicals. Therefore nonlabeled DNA or tRNA does not have to be included in reaction mixtures as a free-radical trap to visualize site-

* Address correspondence to this author at the Molecular Biology Institute.

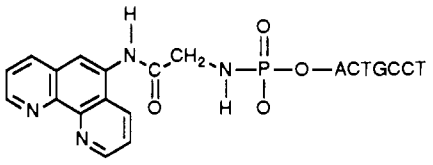
1043-1802/93/2904-0069$04.00/0 © 1993 American Chemical Society

specific scission. Avoiding these extraneous nucleic acids would be essential for a range of applications for chimeric cutters. However, the problem with linking OP–Cu to any carrier is that it is not clear upon conjugation of 1,-10-phenanthroline to a ligand whether the specificity of 1,10-phenanthroline or its carrier will dominate or whether the conjugate will demonstrate an entirely new specificity arising from the influence of the binding elements on one another.

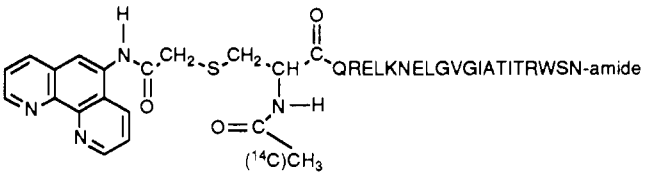
The goal of this study was to address this issue by examining the reactivity of bioconjugates prepared by tethering 1,10-phenanthroline to carrier ligands of modest affinity and specificity for different aspects of nucleic acid structure. These included (a) Hoechst dye 33258, a fluorescent cytological stain with specificity for the minor groove of A-T-rich regions of DNA (*17–19*); (b) the helix–turn–helix of a peptide derived from the *Escherichia coli* Trp repressor, a protein which had previously been converted into a site-specific DNA scission reagent (*11*); and (c) a heptamer 5′-ACTGCCT-3′- which is complementary to a single-stranded loop of a lac-operon-derived RNA fragment (*20*). The structures of conjugates prepared from Hoechst 33258 (HOP), the helix–turn–helix peptide (P-2), and the heptamer (OP–5′-ACTGCCT-3′) are indicated below.



HOP



OP–heptamer



P-2

The synthesis of HOP was prompted by an interest to target (or restrict) the scission chemistry of 1,10-phenanthroline–copper to A-T-rich regions. Although A-T-rich regions are effectively cleaved by the unsubstituted reagent, it also attacks G-T-rich sequences as well (*21, 22*). In view of the use of Hoechst 33258 as a fluorescent stain for metaphase chromosomes (*23*), a scission reagent that reflected the binding specificity of the dye to specific chromosomal regions could prove useful in mapping experiments.

P-2 was studied to determine if the helix–turn–helix peptide of the *E. coli* Trp repressor linked to OP–Cu would exhibit similar scission to the intact protein which had been converted into a site-specific nuclease by modification of lysyl residues with 1,10-phenanthroline (*11*).

The reactivity of 1,10-phenanthroline–copper linked to short deoxyoligonucleotides (up to seven bases long) complementary to single-stranded loops of RNA has not been previously studied. An earlier study (*24*) had demonstrated that a deoxyoligonucleotide linked to phenanthroline at the 5′ end and complementary to sequence positions 1–21 of a lac mRNA fragment cleaved its target at sequence positions 20–25 after denaturation and annealing. Potential applications of short 1,10-phenanthroline-linked conjugates would be to use the scission pattern to identify nucleotides adjacent in space to a single-stranded loop of *native* RNAs.

EXPERIMENTAL SECTION

HOP. Synthesis. A 100-mg portion of Hoechst 33258 (0.236 mmol) was suspended in 1 mL of dry DMF under a nitrogen atmosphere. The resulting solution was heated at 75 °C and then triethylamine (100 μL, 0.717 mmol) was added to obtain the free base form of the dye. Then, 5-(iodoacetamido)-1,10-phenanthroline (*25*) (100 mg, 1.24 times excess) was added and the reaction allowed to proceed for at least 6 h at 75 °C. The mixture is then analyzed on TLC (silica gel) by using successively two different solvents. In the first solvent, pure methanol, Hoechst 33258, and 5-(iodoacetamido)-OP moved close to the solvent front, but the product HOP moved only slightly. In the second solvent, MeOH/NH_4OH 95/5, HOP moves significantly (R_f about 0.15). More NH_4OH increases the R_f but causes smearing. The product can be purified by paper chromatography using 3M paper and 2-propanol, H_2O, and NH_4OH (8/1/1). The slowest fluorescent band (R_f = 0.13) was cut out, and the paper diced into small pieces and covered with 20% acetic acid with heating at 65 °C for 1 h. The products are isolated after filtering on Celite and evaporating to dryness. Alternatively, the product can be purified by silica gel chromatography (methanol/NH_4OH 8/2). It exhibited fluorescence characteristic of the dye and formed a deep red color with ferrous ion typical of the phenanthroline nucleus. The structure of the product was supported by fast-atom bombardment mass spectrometry [FAB MS: *m/e* 660 (M^+)], NMR [^1H NMR (360 MHz, TFA-*d*): δ 9.45–8.00 (m, 12 H, aromatics), 7.35 (d, J = 9 Hz, 1 H, 33258), 5.25 (s, 2 H, CH_2N^+), 4.90 (t, 2 H, 2 NH), 4.40–4.80 (m, 8 H, 4 CH_2), 4.10 (s, 4 H, PhOH), 4.00 (s, 3 H, CH_3)], and UV–vis spectrometry. Dye concentration can also be determined spectroscopically in 5 mM HEPES, 100 mM sodium chloride, pH 7.0. The extinction coefficient is 4.2 × 10^4 M^{-1} cm^{-1} at 338 nm.

Isolation and Labeling of Lac UV-5 and μ_m Terminator Fragment. Conditions for the preparation of the lac UV-5 and μ_m terminator fragment have been previously described (*26, 27*).

Scission Conditions for HOP–Cu and OP–Cu. A solution containing 2.5 μM HOP and 0.5 μM Cu^{2+} was diluted to concentrations of HOP ranging from 0.05 to 0.01 μM. The scission chemistry was activated by the addition of 2.9 mM 3-mercaptopropionic acid (MPA), carried out for 20 h at 37 °C, and then quenched by the addition of 2,9-dimethyl-1,10-phenanthroline. The data for unsubstituted 1,10-phenanthroline–Cu^{2+} was obtained using 5 μM OP and 1.2 μM Cu^{2+}. This reaction was initiated by addition of 2.9 mM MPA, incubated for 1.5 h, and then quenched with 2 mM 2,9-dimethyl-1,10-phenanthroline. After ethanol precipitation, each sample was redissolved in loading buffer composed of 80% deionized formamide, 0.1% bromophenol blue, 0.1% xylene cyanol, and 1 mM EDTA and analyzed on a 10%

polyacrylamide/8.3 M urea sequencing gel. Exposure of the resulting gel to X-ray film produced the autoradiogram displayed.

To obtain footprints of Hoechst 33258, 5 pmol of end-labeled lac operator DNA in 20 μL of 50 mM Tris–Ac (pH 8.0), 1.0 mM $MgCl_2$, and 100 mM KCl were incubated with 10 μM of the DNA ligand for 30 min at 22 °C in the dark. The footprinting reaction was initiated by adding 200 μM OP and 45 μM $CuSO_4$ following by 5.8 mM 3-mercaptopropionic acid.

Peptide Derived from the Helix–Turn–Helix of the Trp Repressor. The peptide synthesized (P-2) has the following sequence:

OP-*N*-[^{14}C]acetyl-Cys-Gln-Arg-Glu-Leu-Lys-Asn-Glu-Leu-Gly-$\underset{77}{\text{Val}}$-Gly-Ile-Ala-Thr-Ile-Thr-Arg-$\underset{85}{\text{Trp}}$-Ser-Asn-$CONH_2$

It was synthesized on an Applied Biosystem Peptide Synthesizer using standard solid-phase methodology (*28*). The N-terminus was acetylated with [^{14}C]acetic anhydride. P-2 (5 mg) was dissolved in 2 mL of phosphate buffer (0.05 M, pH 8, containing 10 mM β-mercaptoethanol). After standing overnight at 4 °C, the peptide was separated from β-mercaptoethanol by passage through a G-25 spin column. Tritiated 5-(iodoacetamido)-1,10-phenanthroline (250 μL of 4 mg/mL, 0.1 mCi/mmol) was added to the eluant of the spin column. The reaction mixture was incubated for 3–4 h at 4 °C, concentrated on the speed vac, and then redissolved in water (final volume of 1 mL). Peptide was separated from excess 5-(iodoacetamido)-1,-10-phenanthroline by two passes through a spin column. The modification of the peptide was assayed by HPLC analysis on a reverse-phase C-18 column and the ^{14}C/^{3}H ratio of the collected eluant.

Footprinting and Cleavage Conditions for 1,10-Phenanthroline-Derivatized Trp Repressor and Derived Peptides. A solution of 3′-labeled *aroH* fragment (*11*) (0.01–0.05 pmol), 1,10-phenanthroline-derivatized peptide (5, 25, and 100 μM), and L-tryptophan (10 mM) was incubated at room temperature for 5 min in 10 μL of Tris-HCl (30 mM, pH 8.0), KCl (100 mM), and $MgCl_2$ (3 mM). The cleavage reactions were initiated by adding 1 μL of $CuSO_4$ (200 μM) and 1 μL of MPA (58 mM) and then incubated for 2 h at 37 °C. The reactions were quenched by 2,9-dimethyl-1,10-phenanthroline. In each case, 1,-10-phenanthroline-derivatized Trp repressor (100 nM) was used as a positive control for the peptide-targeted scission reaction.

Targeted Scission of RNA. RNA substrates derived from the *E. coli* lac operon were prepared and 3′-labeled as described previously (*20*).

Purification of an Heptameric Deoxyribooligonucleotide. The heptamer of sequence 5′-ACTGCCT-3′ was synthesized on an automated DNA synthesizer. The 5′-terminal trityl group was not removed so that the oligonucleotide could be purified on a C18 reversed-phase HPLC column. After equilibration of the column with 85% 50 mM triethylammonium acetate, pH 7, and 15% acetonitrile, the deoxyoligonucleotide was eluted with a linear gradient from 15% to 35% acetonitrile over 12 min. The solution containing the heptamer was evaporated to dryness and redissolved in 1 mL of 80% acetic acid to remove the dimethoxytrityl group.

Synthesis of 5′-(5-Glycinamido-1,10-phenanthroline)-ACTGCCT. This product was prepared using the water-soluble-carbodiimide method of Chu et al. (*29*). This procedure had been previously used in the synthesis of a 1,10-phenanthroline derivative of a 21 base long deoxyoligonucleotide (*24*).

RNA Scission by 5′-(5-Glycinamido-1,10-phenanthroline)-ACTGCCT (OP–ACTGCCT). Two procedures were used to explore the scission of the RNA by the heptamer. Both gave equivalent results. Condition A: a 10-μL solution of lac RNA (0.25 μM) and OP–heptamer (10 μM) in 50 mM Tris, pH 8.0/50 mM NaCl was incubated for 1 h. The cleavage reaction was then initiated by adding 1 μL of $CuSO_4$ (20 μM) and 1 μL of MPA (58 mM) at 4 °C. After overnight at 4 °C, the reaction was quenched with 2,9-dimethyl-1,10-phenanthroline. Condition B: lac RNA (0.25 μM) and OP–heptamer (10 μM) were mixed in 20 μL of buffer containing 25 mM of Tris–Cl (pH 6.5), NaCl (70 mM), $MgCl_2$ (20 mM), and 0.4 mM of spermine at either 4 °C or room temperature. The cleavage reaction was initiated as described above and carried out at either 4 °C or room temperature.

Quenching, Precipitation, and Electrophoresis. Cleavage reactions were quenched by the addition of 2,9-dimethyl-OP to a final concentration of 1 mM. The reactions were precipitated by the addition of 0.1 volume of 3 M sodium acetate and 2.5 volumes of ethanol for 2 h at −80 °C. The reactions were centrifuged, and the pellet was washed with 60 μL of 70% ethanol. The reactions were again centrifuged and evaporated to dryness. The pellet was redissolved in 10 μL of urea dyes (10 M urea, 1 mM EDTA, 0.1% xylene cyanol, and 0.1% bromophenol blue), heated at 90 °C for 3 min, and subjected to polyacrylamide gel electrophoresis on a 10% denaturing gel. The gel was run at 50 W for 2.5 h. Autoradiography was performed overnight at −20 °C.

RNase H Cleavage of RNA–DNA Hybrids. RNA (50 000 dpm) was dissolved in the same buffer as above. After the heptamer was added to a final concentration of 4 μM, hybridization was allowed to proceed as before at 22, 30, or 37 °C. Dithiothreitol was added to a final concentration of 0.1 mM. Ribonuclease H (2 units) was then added and the reaction was incubated for 20 min. The reaction was stopped by the addition of EDTA to a final concentration of 30 mM. The reactions were then precipitated and electrophoresed as described in the previous section.

RESULTS AND DISCUSSION

Specificity of DNA Scission by HOP–Cu. Hoechst dye 33258 is a structurally constrained ligand and, with its crescent shape, preorganized to bind to the minor groove (*17–19*). Given the minor groove reactivity of 1,10-phenanthroline–copper, a very efficient chemical nuclease activity might be expected by conjugation to Hoechst 33258. In addition to the configuration of the dye, three factors should contribute to the high-affinity binding of HOP to the minor groove of DNA. First, Hoechst 33258 binds tightly to A-T-rich regions of the minor groove; second, OP–Cu itself binds preferentially to the minor groove (*30*); finally, quaternization of the piperazine adds additional positive charge to HOP.

Two DNA sequences, the *E. coli* lac UV-5 promoter/operator and the transcription termination region of the mouse immunoglobulin μ_m gene, were used to assay the sequence specificity of the chemical nuclease activity of HOP. Both the 5′-labeled template strand and 3′-labeled nontemplate strand of the lac UV-5 fragment were used to monitor the cleavage chemistry. Histograms summarizing the cleavage sites for both HOP–Cu and the unsubstituted OP–Cu for both strands of lac UV-5 are presented in Figure 1a,b. Hoechst 33258 modifies the

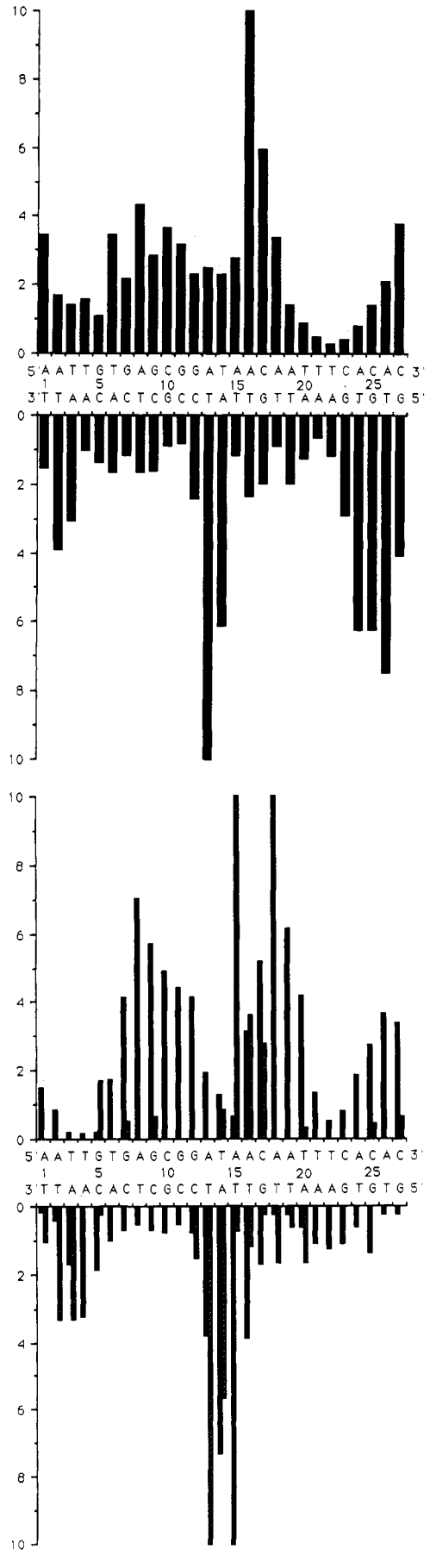


Figure 1. Scission pattern of lac promoter/operator by OP–Cu (a, top) and by HOP–Cu (b, bottom). In 1b, the stippled lines indicate the binding site of Hoechst 33258 determined using OP–Cu footprinting.

cleavage specificity of 1,10-phenanthroline–copper. The sites of HOP scission correspond to a strong binding site of Hoechst 33258 on both strands that has been identified using OP–Cu footprinting. Specifically, the strong sites of cleavage evident at positions 13–15 on the lower (template) strand and 16–20 on the upper (nontemplate) strand are associated with a binding site indicated by the stippled bar. The scission sites of HOP–Cu evident from 1–4 appear to be associated with a binding site that is visualized primarily on the lower strand using OP–Cu also represented by stippled bars. In contrast to OP–Cu, where 5 μM ligand and 1.2 μM metal ion were used, only 0.01 μM HOP–Cu^{2+} was required for scission. Both sets of cleavage sites exhibit a 3′ stagger indicative of minor-groove scission (*31*).

The sequence GTGTG extending from 23 to 27 is effectively cut by OP–Cu but not by HOP–Cu because it lacks runs of A-T. Generally, the results with the lac fragment indicate that, to a first approximation, the conjugation of Hoechst 33258 to phenanthroline restricts the specificity of the phenanthroline scission and concentrates it adjacent to A-T-rich regions. However, the specificity of HOP–Cu for these regions is clearly not stringent. The reason for the asymmetric binding and reactivity of Hoechst and HOP–Cu at the upstream binding site is not apparent. Both HOP–Cu and OP–Cu cut at all nucleotides as would be expected from deoxyribose-based chemistry.

The second DNA fragment that was used as a substrate for HOP–Cu was derived from the region of transcription termination of the μ_m gene of the mouse IgM locus. This A-T-rich DNA fragment contains the binding site for a nuclear protein that may facilitate termination as well as the polyadenylation signal, AAATAAA, and the site of polyadenylation (*26*). Comparison of the scission pattern of the nontemplate strand by HOP–Cu and OP–Cu again indicates that the primary sequence specificity of the two reagents differ (Figure 2a,b). With this fragment, there is preferential cutting near A-T-rich regions, but this sequence preference is relaxed. The increased hydrophobicity and positive charge resulting from the alkylation of Hoechst 33258 by 5-(iodoacetamido)-1,10-phenanthroline may increase the nonspecific binding affinity of HOP–Cu and diminish the bias for A-T-rich regions that would be expected solely on the basis of the specificity of Hoechst 33258. Conjugating 1,10-phenanthroline to other DNA-binding drugs is likely to lead to parallel results, especially if they are minor-groove ligands. Although the increased affinity of the chimeras diminish their specificity, it may make them useful intracellular footprinting reagents.

Specificity of Scission by a 1,10-Phenanthroline-Linked Helix–Turn–Helix Peptide. The *E. coli* Trp repressor has been converted into a site-specific nuclease by chemically modifying all the lysyl residues of the protein with iminothiolane and then alkylating the resulting thio groups with 5-(iodoacetamido)-1,10-phenanthroline (*11*). This derivatized protein cleaved both the *aroH* and *trpEDCBA* operators. This experiment raised the interesting possibility that the helix–turn–helix domain of this protein alone might also be capable of targeting the nuclease activity of 1,10-phenanthroline–copper. To investigate this question, P-2 was synthesized. The sequence of P-2 is presented below along with that of the helix–turn–helix domain of the wild-type repressor (P-1). The sequence of P-2 differs from that of P-1 in two amino acid residues. To conform with the sequence of a mutant Trp superrepressor (*32*), a valine residue has been substituted for an alanine residue at sequence position 77 of the loop

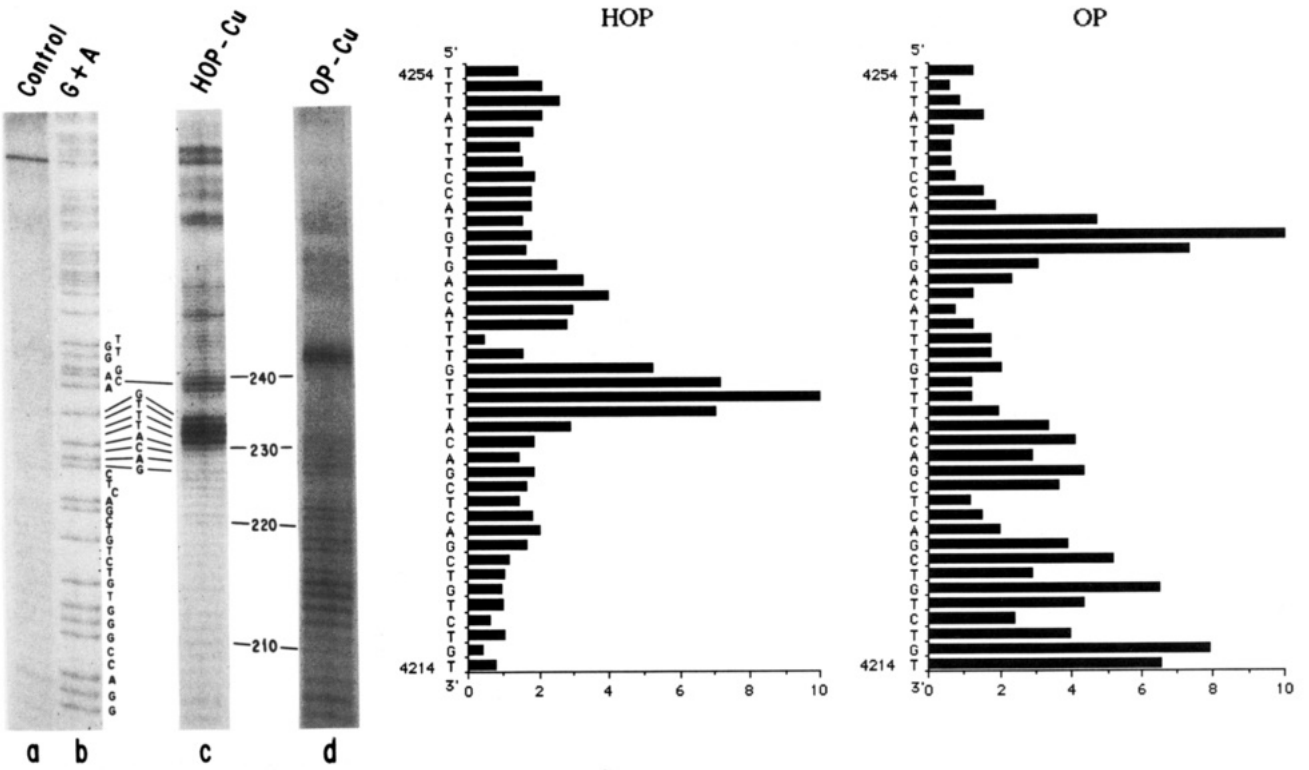


Figure 2. Scission pattern of μm transcription termination. (a, left) Lane a, control; lane b, G + A sequencing lane; lane c, scission by 0.01 μM HOP–Cu; lane d, scission by OP–Cu ([OP] = 5 μM, [Cu] = 1.2 μM). Reaction was carried out in 50 mM Tris–Ac (pH 8.0), 10 mM $MgCl_2$ and 100 mM KCl for 1.5 h at 37 °C for OP–Cu and for 20 h at 37 °C for HOP–Cu. (b, right) Densitometric scan of lanes c and d of panel 2a. For additional sequence information see Law et al. (*26*).

region. In addition, a tryptophan has replaced a glycine residue at position 85 because structural studies have shown that the corepressor tryptophan binds adjacent to this glycine and possibly contributes to the stability of the helix–turn–helix format (*33–36*). An *N*-[^{14}C]acetylcysteinyl residue has been added at the N-terminus of P-2 to provide a convenient site of attachment of 5-(iodoacetamido)-1,10-phenanthroline. In contrast to the rigid preorganized structure of Hoechst 33258, the helix–turn–helix peptide (P-2) derived from the *E. coli* Trp repressor is a flexible, random coil in solution. Circular dichroism studies demonstrated that P-2 lacked a stable secondary structure.

P–2

77

OP-*N*-[^{14}C]acetyl-Cys-Gln-Arg-Glu-Leu-Lys-Asn-Glu-Leu-Gly-Val-Gly-Ile-

85

Ala-Thr-Ile-Thr-Arg-Trp-Ser-Asn-$CONH_2$

P–1

77

Gln-Arg-Glu-Leu-Lys-Asn-Glu-Leu-Gly-Ala-Gly-Ile-Ala-Thr-Ile-Thr-Arg-

85

Gly-Ser-Asn-$CONH_2$

DNase I footprinting (*37*) fails to detect sequence-specific binding of P-2 to the *aroH* operator at the concentrations where the native protein gives a clear footprint. The DNase footprints are presented in Figure 3a (lanes a–d). These experiments, in agreement with circular dichroism studies, indicate that the helix–turn–helix conformational format evident in the native protein is unstable in solution but does not exclude the possibility that selective scission might be obtained if sequence-specific contacts between the operator DNA and peptide transitorily stabilize P-2 in a helix–turn–helix format. This possibility is incorporated in the reaction scheme below in which P-2 exists free in solution as a random coil but can also exist in a helix–turn–helix format characteristic of the native protein when bound to DNA (Scheme I).

When P-2 was used to cleave *aroH*, its pattern of scission was dramatically different from that obtained with the chemically modified wild-type *E. coli* Trp repressor. Instead of a restricted number of discrete sites that were observed with the Trp repressor, multiple products were obtained in the cleavage of *aroH* by the peptide. As a control for the scission of *aroH* by P-2, the identical DNA fragment was cleaved by OP–Cu and the products separated simultaneously on the same sequencing gel. Analysis of the scission products of *aroH* produced by P-2 and OP–Cu by densitometry indicated that a different product distribution was generated, exactly where the products of the protein targeted scission migrated. In the other regions, the product distribution of the P-2 and OP–Cu scission were equivalent.

Two parallel reactions are responsible for the product distribution observed with P-2. One is nonspecific and can be attributed to the background scission of the labeled DNA substrate by OP–Cu substituted with a nonspecific 5 substituent (i.e. a phenyl group or a random peptide) as in the kinetic mechanism summarized in eq 1. *This reaction cannot be quenched by carrier DNA or RNA traps in solution because this cleavage reaction involves the binding of the OP–Cu complexes to the DNA.* Since the cleavage pattern of OP–Cu is not sensitive to substituents at the 5-position lacking a specific affinity for DNA (*3*), this background scission is similar to that observed with OP–Cu. The second reaction which leads to the same products as that observed with the 1,10-phenanthroline-derivatized wild-type repressor must be due to the reaction of the peptide stabilized in the helix–turn–helix format on the surface of the DNA. The complete kinetic scheme for the scission of *aroH* by P-2 is summarized in Scheme II. The most important con-

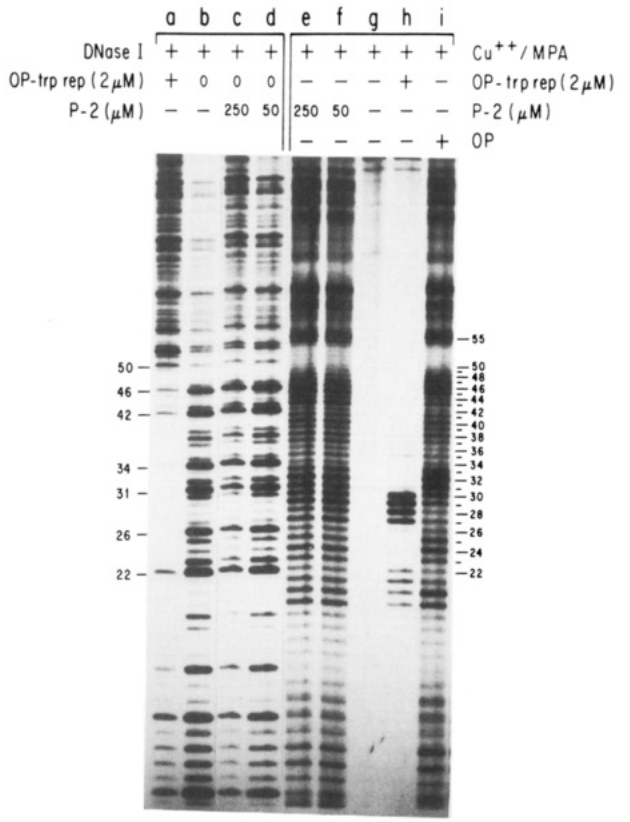
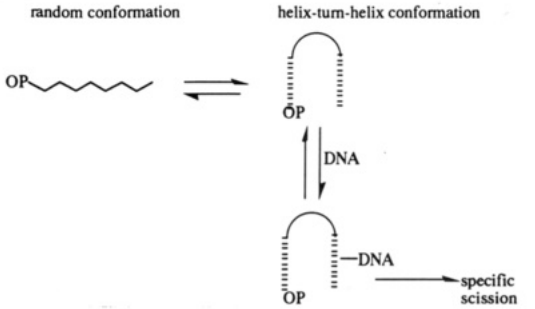
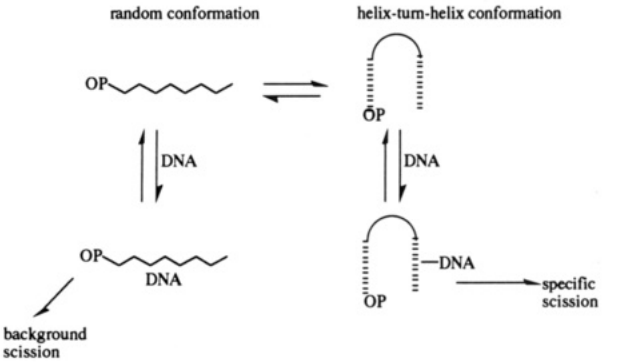


Figure 3. (a, top) Binding of TrpR-derived peptide to *aroH* operator measured by targeted scission and DNase I footprinting. All reactions were carried out using 3′-labeled restriction fragment containing the *aroH* operator (1 nM), 10 mM L-tryptophan in a Tris–HCl buffer (30 mM, pH 8.0) with 100 mM KCl and 3 mM $MgCl_2$ at 25 °C. Reaction volumes were 20 μL. DNase I footprinting was carried out for 5 min at room temperature using 0.04 units of enzyme. The nuclease activity of OP–Cu and P-2 was activated by adding 1 μL of $CuSO_4$ and 1 μL of MPA (58 mM) and then incubated for 2 h at 37 °C. Reactions were quenched by the addition of 2,9-dimethyl-1,10-phenanthroline. (b, bottom) Panels A, B, and C are densitometric scans of lanes f, h, and i, respectively.

Scheme I



Scheme II



clusion of our studies using the helix–turn–helix peptide domain to target cleavage is that *the binding energy available in sequence-specific contacts between DNA and peptide can stabilize a peptide in a functional conformation characteristic of the parent protein.* This, however, does not exclude the stabilization of the helix–turn–helix conformation by other domains of the proteins, as has been recently suggested by Carey and her colleagues (*38*).

Site-Specific Scission by 5′-OP–ATCCGCT-3′. Previous work has demonstrated that deoxyoligonucleotides linked at the 5′ end to 1,10-phenanthroline can nick the target RNA following hybridization when the chemical nuclease is activated by addition of thiol and hydrogen peroxide; they can also direct the scission of the complementary sequence by RNase H (*24*). In those studies, the RNA (the same lac fragment used in the present studies; see Figure 4a), was heat denatured and reannealed in the presence of the scission reagent. In the present case, 5′-OP–ATCCGCT-3′, the heptamer, was simply mixed with the lac RNA without disrupting its structure or causing strand displacement as would be the case following denaturation.

The 5′-OP–ATCCGCT-3′-directed RNase H hydrolysis of the loop confirms the formation of the heteroduplex. However, activation of the chemical nuclease activity by addition of Cu^{2+} and 3-mercaptopropionic acid not only cleaves the RNA at sequence position 13–15 *but also at positions 3–5* (Figure 4b). Although positions 13–15 are adjacent in the linear sequence to the complementary sequence of ATCCGCT, positions 3–5 are not. Nicking of the phosphodiester backbone at these positions can be attributed to the proximity in space of the ribose moieties to the OP at the 5′ end of the hybridized heptamer. If single-stranded M-13 DNA is used as the substrate, scission is not observed at sequence positions 3–5 but only adjacent to the complementary sequence (e.g. sequence positions 13–15). This result is consistent with the lack of stability of stem-loop structures of DNA. The scission efficiency of 5′-OP-AT^{me}C^{me}CG^{me}CT-3′ with the lac RNA is indistinguishable from that of 5′-OP–ATCCGCT-3′.

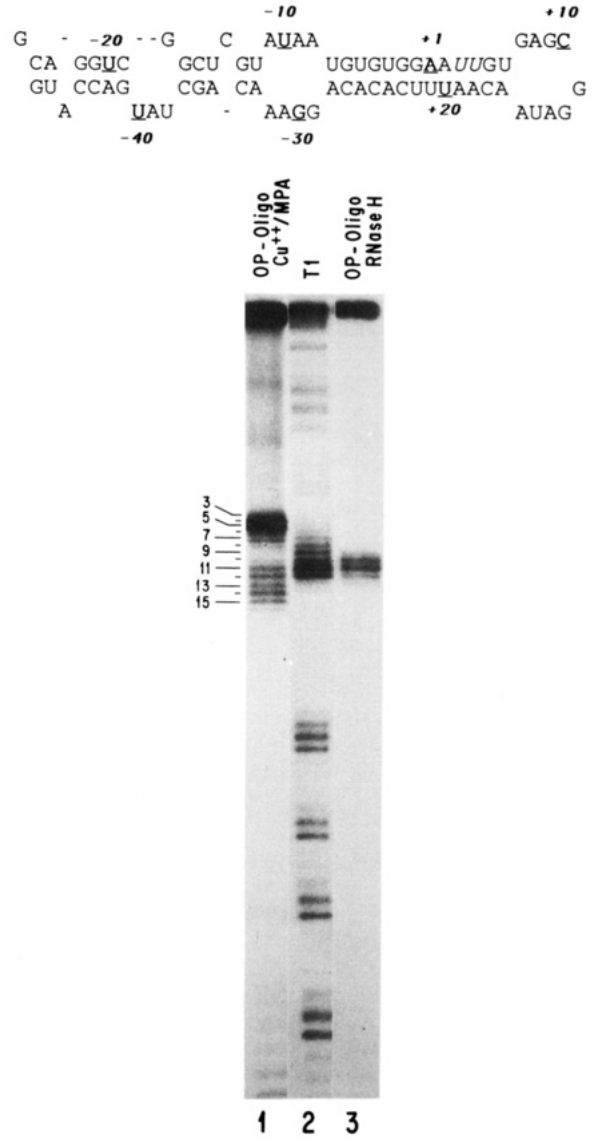


Figure 4. Scission of a single-stranded RNA loop by OP-linked heptamer. (a, top) Secondary structure of lac RNA used as substrate. (b, bottom) Scission of lac RNA fragment by 5′-OP-ATCCGCT-3′. 5′-OP-ATCCGCT-3′ (10 μM) was incubated with 0.25 μM lac RNA in 10 μL of 50 mM Tris, pH 8.0/50 mM NaCl for 1 h at 4 °C. The scission reaction was then initiated by adding 1 μL of $CuSO_4$ (20 μM) and 1 μL of MPA (58 mM). After overnight reaction, the products were analyzed on a sequencing gel.

In effect, conjugates composed of OP and short deoxyoligonucleotides complementary to single-stranded RNA loops can act as a cross-linking reagent and assist in defining the three-dimensional conformation of RNAs. In this application, they are unique. Although OP-linked deoxyoligonucleotides can also be used for the identification of single-stranded loops, this structural information can alternatively be obtained using base-specific chemical reagents (*39*), deoxyoligonucleotide-directed RNase H scission (*40*), or the deoxyoligonucleotide suppression of OP–Cu scission of single-stranded loops (*41*).

A novel use of an OP-linked RNA to probe the three-dimensional structure of the HIV TAR hairpin loop has recently been reported (*42*). In this experiment (Figure 5), the OP-linked ribonucleotide (L1-17) was hybridized with the HIV TAR hairpin loop. Scission sites at C-19 and U-40 provide evidence for the formation of the L1-17–HIV TAR complex presented in Figure 5. Although cleavage at U-40 is predictable from the primary sequence of the two RNAs, scission at C-19 is not and therefore is supportive of the postulated complex. Mapping the

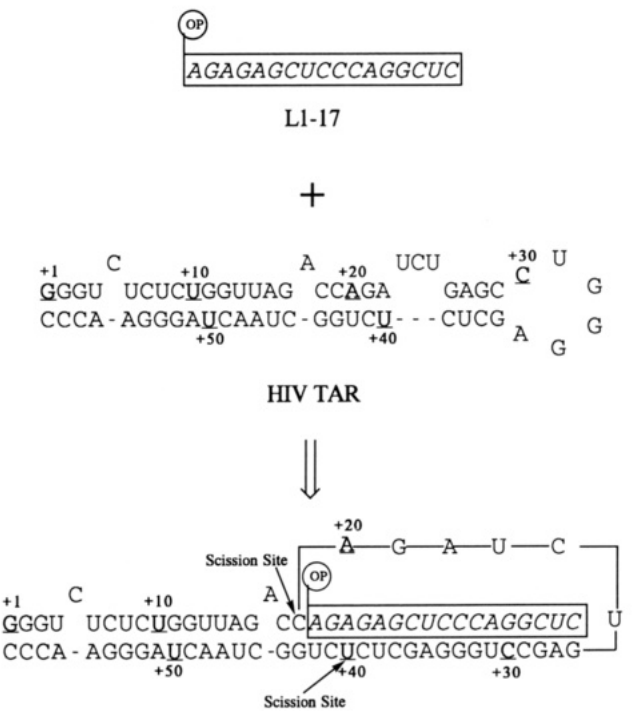


Figure 5. Probing the conformation of a pseudo-half-knot using an OP–Cu-linked RNA (*42*).

guanosine binding site of the *Tetrahymena* ribozymes using an EDTA derivative of this nucleoside is another example of the use of chemical nucleases in probing the conformation of an RNA (*43*).

CONCLUSIONS

The goal of these studies has been to identify new classes of targeting ligands which could modify or redirect the nuclease activity of 1,10-phenanthroline–copper. On the basis of the independence of the specificity on the experimental ratio of copper ion to the 1,10-phenanthroline-derivatized carrier, the reactive complex must consist of one copper per phenanthroline. In all previous cases of the targeting of the nuclease activity of 1,10-phenanthroline–copper (*11*, *12*, *14*, *16*, *24*), a second phenanthroline is not necessary when affinity for nucleic acid is provided by the carrier.

The conclusions of these studies can be summarized as follows.

(1) HOP–Cu has proven to be an efficient scission reagent with different scission specificity than OP–Cu, but its specificity is not rigidly directed to A-T-rich regions. Hoechst dye 33258 is the first abiological functionality linked to the 5-position of phenanthroline which can alter the specificity of the chemical nuclease. Generally, 1,-10-phenanthroline may diminish the binding specificity of an organic ligand (e.g. Hoechst dye 33258) upon conjugation because it will increase the nonspecific binding affinity of the chimera. However, the new reagent may have novel and useful new specificity. HOP–Cu, because of its high binding affinity, may be useful in the analysis of chromatin structure given the competition of Hoechst 33258 with high mobility group (HMG I) nonhistone chromosomal proteins (*44*).

(2) P-2 nicks the *aroH* operator in the same sequence region as the protein conjugate. These results indicate that the binding energy of the DNA–peptide interaction can stabilize the peptide in the helix–turn–helix confor-

mational format. However, significant cleavage is observed at flanking sequences because of the intrinsic affinity of 1,10-phenanthroline–copper for the minor groove of DNA. Therefore, conjugating peptides derived from DNA binding domains to OP–Cu will not generate efficient and specific scission reagents if the peptides exist as random coils. Other studies of peptide–DNA interactions using circular dichroism, tryptic digestion, and infrared spectroscopy have demonstrated the ability of DNA binding to stabilize the structure of a peptide (*45–47*). This is the first study to demonstrate this phenomenon at the level of nucleotide resolution.

(3) Of the three targeting systems studied, only the deoxyoligonucleotide was capable of overriding the intrinsic specificity of 1,10-phenanthroline–copper in its reaction with RNA. Nucleotides adjacent in space, as well in sequence, to single-stranded loops in RNA can be identified using short complementary deoxyoligonucleotides linked to OP–Cu. These reagents therefore are useful in mapping the 3-D structure of RNA. However, the scission may not be sufficiently robust to enhance the efficiency of these deoxyoligonucleotides as antisense reagents.

ACKNOWLEDGMENT

This research was supported by USPHS GM 21199 and Office of Naval Research Grant N00014-86-K5024. We acknowledge useful conversations with Theodore B. Thederahn and the assistance of Eva Chun in the preparation of this manuscript.

LITERATURE CITED

(1) Sigman, D. S. (1990) Chemical Nucleases. *Biochemistry 29*, 9097–9105.

(2) Sigman, D. S., and Chen, C.-h.B. (1990) Chemical Nucleases: New Reagents in Molecular Biology. *Ann. Rev. Biochem. 59*, 207–236.

(3) Thederahn, T. B., Kuwabara, M. D., Larsen, T. A., and Sigman, D. S. (1989) Nuclease Activity of1,10-Phenanthroline-copper: Kinetic Mechanism. *J. Am. Chem. Soc. 111*, 4941–4946.

(4) Marshall, L. E., Graham, D. R., Reich, K. A., and Sigman, D. S. (1981) Cleavage of Deoxyribonucleic Acid by the 1,10-Phenanthroline-cuprous Complex. Hydrogen Peroxide Requirement and Primary and Secondary Structure Specificity. *Biochemistry, 20*, 244–250.

(5) Sigman, D. S., Graham, D. R., D'Aurora, V., and Stern, A. M. (1979) Oxygen-dependent Cleavage of DNA by the 1,10-Phenanthroline–cuprous Complex. Inhibition of *Escherichia coli* DNA Polymerase I. *J. Biol. Chem. 254*, 12269–12272.

(6) Kuwabara, M., Yoon, C., Goyne, T. E., Thederahn, T., and Sigman, D. S. (1986) Nuclease Activity of 1,10-Phenanthroline-copper Ion: Reaction with CGCGAATTCGCG and Its Complexes with Netropsin and *Eco*RI. *Biochemistry 25*, 7401–7408.

(7) Sigman, D. S. (1986) Nuclease Activity of 1,10-Phenanthroline-copper Ion. *Acc. Chem. Res. 19*, 180–186.

(8) Goyne, T. E., and Sigman, D. S. (1987) Nuclease Activity of 1,10-Phenanthroline-copper Ion. Chemistry of Deoxyribose Oxidation. *J. Am. Chem. Soc. 109*, 2846–2848.

(9) Veal, J. M., Merchant, K., and Rill, R. L. (1991) The influence of reducing agent and 1,10-phenanthroline concentration on DNA cleavage by phenanthroline + copper. *Nucleic Acids Res. 19*, 3383–3388.

(10) Veal, J. M., and Rill, R. L. (1991) Noncovalent DNA Binding of Bis(1,10-phenanthroline)copper(I) and Related Compounds. *Biochemistry 30*, 1132–1140.

(11) Chen, C.-h. B., and Sigman, D. S. (1987) Chemical Conversion of a DNA-binding Protein into a Site-specific Nuclease. *Science 237*, 1197–1201.

(12) Bruice, T. W., Wise, J., Rosser, D. S. E., and Sigman, D. S. (1991) Conversion of Lambda Phage Cro into an Operator-Specific Nuclease. *J. Am. Chem. Soc. 113*, 5446–5447.

(13) Sutton, C., Mazumder, A., Chen, C.-h. B., and Sigman, D. S. (1992) Transforming the *E. coli* Trp Repressor into a Site-Specific Nuclease. *Biochemistry*, submitted.

(14) Ebright, R. H., Ebright, Y. W., Pendergast, P. S., and Gunasekera, A. (1990) Conversion of a helix-turn-helix motif sequence-specific DNA binding protein into a site-specific DNA cleavage agent. *Proc. Natl. Acad. Sci. U.S.A. 87*, 2882–2886.

(15) Jayasena, S. D., and Johnston, B. H. (1992) Site-Specific Cleavage of HIV TAR RNA Using a Tat-Based Chemical Nuclease. *Proc. Natl. Acad. Sci. U.S.A. 89*, 3526–30.

(16) Chen, C.-h. B., and Sigman, D. S. (1986) Nuclease Activity of 1,10-Phenanthroline–copper: Sequence-specific Targeting. *Proc. Natl. Acad. Sci. U.S.A. 83*, 7147–7151.

(17) Pjura, P. E., Grezeskowiak, K., and Dickerson, R. E. (1987) The Binding of Hoeschst 33258 to the Minor Groove of B-DNA. *J. Mol. Biol. 197*, 257–271.

(18) Quintana, J. R., Lipanov, A. A., and Dickerson, R. E. (1991) Low-Temperature Crystallographic Analyses of the Binding of Hoechst 33258 to the Double-Helical DNA Dodecamer C-G-C-G-A-A-T-T-C-G-C-G. *Biochemistry 30*, 10294–10306.

(19) Teng, M.-K., Usman, N., Frederick, C. A., and Wang, A. H.-J. (1988) The Molecular Structure of the Complex of Heochst 33258 and the DNA Dodecamer d(CGCGAATTCGCG). *Nucleic Acids Res. 16*, 2671–2690.

(20) Murakawa, G. J., Chen, C.-h. B., Kuwabara, M. D., Nierlich, D., and Sigman, D. S. (1989) Scission of RNA by the Chemical Nuclease 1,10-Phenanthroline–copper. Preference for Single Stranded Loops. *Nucleic Acids Res. 17*, 5361–5369.

(21) Yoon, C., Kuwabara, M. D., Law, R., Wall, R., and Sigman, D. S. (1988) Sequence-dependent Variability of DNA Structure. *J. Biol. Chem. 263*, 8458–8463.

(22) Yoon, C., Kuwabara, M. D., Spassky, A., and Sigman, D. S. (1990) Sequence Specificity of the Deoxyribonuclease Activity of 1,10-Phenanthroline-Copper Ion. *Biochemistry 29*, 2116–2121.

(23) Latt, S. A., Lalande, M., Kunkel, L. M., Schreck, R., and Tantravahi, U. (1985) Applications of Fluorescence Spectroscopy to Molecular Cytogenetics. *Biopolymers 24*, 77–95.

(24) Chen, C.-h. B., and Sigma, D. S. (1988) Sequence-Specific Scission of RNA by 1,10-Phenanthroline-Copper Linked to Deoxyoligonucleotides. *J. Am. Chem. Soc. 110*, 6570–6572.

(25) Sigman, D. S., Kuwabara, M. D., Chen, C.-h. B., and Bruice, T. W. (1991) Nuclease Activity of 1,10-Phenanthroline-Copper in the Study of Protein-DNA Interactions. *Methods Enzymol. 208*, 414–433.

(26) Law, R., Kuwabara, M. D., Briskin, M., Fasel, N., Hermanson, G., Sigman, D. S., and Wall, R. (1987) Protein-binding Site at the Immunoglobulin $\mu_{membrane}$ Polyadenylylation Signal: Possible Role in Transcription Termination. *Proc. Natl. Acad. Sci. U.S.A 84*, 9160–9164.

(27) Kuwabara, M. D., and Sigman, D. S. (1987) Footprinting DNA-Protein Complexes in Situ following Gel Retardation Assays Using 1,10-Phenanthroline-copper Ion: Escherichia coli RNA Polymerase–*lac* Promoter Complexes. *Biochemistry 26*, 7234–7238.

(28) Stewart, J., and Young, J. D. (1984) Solid Phase Peptide Synthesis, 2nd ed, Pierce Chemical Company, San Francisco.

(29) Chu, B. C. F., Wahl, G. M., and Orgel, L. E. (1983) Derivatization of Unprotected Polynucleotides. *Nucleic Acids Res. 11*, 6513–6529.

(30) Graham, D. R., and Sigman, D. S. (1984) Zinc Ion in *E. coli* DNA Polymerase: A Reinvestigation. *Inorg. Chem. 23*, 4188–4191.

(31) Drew, H. R. (1984) Structural Specificities of Five Commonly Used DNA Nucleases. *J. Mol. Biol. 176*, 535–557.

(32) Kelley, R. L., and Yanofsky, C. (1985) Mutational Studies with the *trp* Repressor of *Escherichia coli* Support the Helix-turn-helix Model of Repressor Recognition of Operator DNA. *Proc. Natl. Acad. Sci. U.S.A. 82*, 483–487.

(33) Schevitz, R. W., Otwinowski, Z., Joachimiak, A., Lawson, C. L., and Sigler, P. B. (1985) The Three-dimensional Structure of *Trp* Repressor. *Nature 317*, 782–786.

(34) Otwinowski, Z., Schevitz, R. W., Zhang, R. G., Lawson, C. L., Joachimiak, A., Marmorstein, R. Q., Luisi, B. F., and Sigler, P. B. (1988) Crystal Structure of *Trp* Repressor/Operator Complex at Atomic Resolution. *Nature 335*, 321–329.
(35) Marmorstein, R. Q., Joachimiak, A., Sprinzl, M., and Sigler, P. B. (1987) The Structural Basis for the Interaction between L-Tryptophan and the *E. coli* trp Aporepressor. *J. Biol. Chem. 262*, 4922–4927.
(36) Zhang, R. G., Joachimiak, A., Lawson, C. L., Schevitz, R. W., Otwinowski, Z., and Sigler, P. B. (1987) The Crystal Structure of trp Aporepressor at 1.8 Å Shows How Binding Tryptophan Enhances DNA Affinity. *Nature 327*, 591–597.
(37) Galas, D. J., and Schmitz, A. (1978) DNase Footprinting: A Simple Method for the Detection of Protein DNA Binding Specificity. *Nucleic Acids Res. 5*, 3157–3170.
(38) Tasayco, M. L., and Carey, J. (1991) Ordered Self-Assembly of Polypeptide Fragments Leading to Nativelike Dimeric trp Repressor. *Science 255*, 594–597.
(39) Peattie, D. A., and Gilbert, W. (1980) Chemical Probes for Higher-order Structure in RNA. *Proc. Natl. Acad. Sci. U.S.A. 77*, 4679–4682.
(40) Noller, H. (1991) Ribosomal RNA and Translation. *Annu. Rev. Biochem. 60*, 191–228.
(41) Mazumder, A., Chen, C.-h. B., Gaynor, R. B., and Sigman, D. S. (1992) Probing RNA Conformation and Ligand Binding with the Chemical Nuclease of 1,10-Phenanthroline-Copper, A Footprinting Reagent for Single-stranded Regions of RNAs. *Biochem. Biophys. Res. Commun. 187*, 1503–1509.
(42) Ecker, D. J., Vickers, T., Bruice, T. W., Freier, S. M., Jenison, R. D., Manoharan, M., and Zounes, M. (1992) Pseudo-Half-Knot Formation with RNA. *Science 257*, 958–961.
(43) Wang, J.-F., and Cech, T. R. (1992) Tertiary Structure Around the Guanosine-Binding Site of the *Tetrahymena* Ribozyme. *Science 256*, 526–529.
(44) Reeves, R., and Nissen, M. S. (1990) The A-T-DNA-Binding Domain of Mammalian High Mobility Group I Chromosomal Proteins. *J. Biol. Chem. 265*, 8573–8582.
(45) O'Neil, K. T., Shuman, J. D., Ampe, C., and DeGrado, W. F. (1991) DNA-Induced Increase in the alpha-Helical Content of C/EBP and GCN4. *Biochemistry 30*, 9030–9034.
(46) Walters, L., and Kaiser, E. T. (1985) Design of DNA-binding Peptides: Stabilization of α-Helical Structure by DNA. *J. Am. Chem. Soc. 107*, 6422–6424.
(47) Talanian, R. V., McKnight, C. J., and Kim, P. S. (1990) Sequence-Specific DNA Binding by a Short Peptide Dimer. *Science 249*, 769–771

Radioiodination of Proteins Using *N*-Succinimidyl 4-Hydroxy-3-iodobenzoate

Ganesan Vaidyanathan, Donna J. Affleck, and Michael R. Zalutsky*

Department of Radiology, Duke University Medical Center, Durham, North Carolina 27710.
Received September 23, 1992

N-Succinimidyl 4-hydroxy-3-[^{131}I]iodobenzoate ([^{131}I]SHIB) was synthesized from 4-hydroxybenzoic acid in two steps. The overall radiochemical yield was 40–56%. A monoclonal antibody (mAb) was labeled in 10–15% yield by reaction with [^{131}I]SHIB. The specific binding of [^{131}I]SHIB mAb to tumor homogenates in vivo was 78 ± 3%, compared to 84 ± 3% for the same mAb labeled using *N*-succinimidyl 3-[^{125}I]iodobenzoate ([^{125}I]SIB). Paired-label studies in normal mice demonstrated similar tissue distributions of ^{131}I and ^{125}I except in thyroid. In thyroid, uptake of the two isotopes was similar on day 1; however, ^{131}I levels increased gradually to 2–3 times those of ^{125}I by day 6. Our results indicate that loss of label in vivo from mAbs labeled using SHIB is somewhat higher than seen with SIB but significantly lower than that observed when direct iodination methods are used.

INTRODUCTION

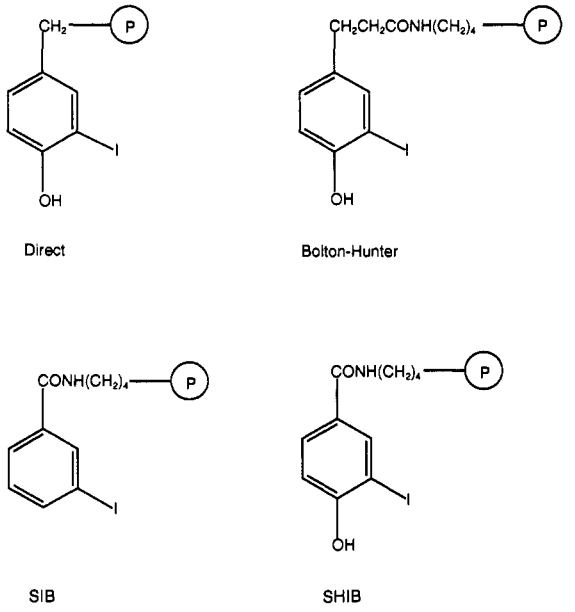
Monoclonal antibodies (mAbs[1]) and other proteins labeled with isotopes such as ^{131}I, ^{125}I, ^{124}I, and ^{123}I have been utilized in a wide variety of basic and clinical investigations (*1–3*). In these studies, the method most commonly used for a protein radioiodination is direct iodination using an oxidant such as Iodogen or Chloramine-T (*4, 5*), generally resulting in the formation of iodinated tyrosine residues (Chart I).

Proteins labeled by direct iodination are ideal for most in vitro applications; however, proteins labeled by this approach frequently undergo extensive deiodination in vivo (*6*). Loss of label is reflected by accumulation of radioiodine in thyroid and stomach and with mAbs, a diminished pool of activity available for tumor uptake (*7*). Since direct iodination results in the formation of iodotyrosine residues on the protein, we hypothesized that the action of deiodinases involved in thyroid hormone metabolism (*8*) might be responsible for the deiodination of mAbs in vivo (*9*).

In order to circumvent the action of these enzymes, we developed an approach for labeling mAbs using the acylation agent *N*-succinimidyl 3-iodobenzoate (SIB), a reagent synthesized via the electrophilic destannylation of *N*-succinimidyl 3-(tri-*n*-butylstannyl)benzoate (*9*). This method involves coupling to lysine residues and, unlike iodotyrosine, does not result in the substitution of the iodine ortho to a hydroxyl group on an aromatic ring (Chart I). Paired-label studies demonstrated that mAbs and F(ab')$_2$ fragments labeled using SIB exhibited 40–100-fold lower levels of thyroid uptake, reflecting a greater inertness to dehalogenation compared to mAbs labeled directly (*10, 11*). Similar results have been obtained by Wilbur et al. (*12*) using the para isomer of SIB.

The current study is directed at refining our understanding of the structural requirements needed for a protein iodination site in order to inhibit deiodination in vivo, particularly with regard to the role played by the *o*-hydroxyl group. In a previous report (*13*), we evaluated the utility of the Bolton–Hunter reagent, *N*-succinimidyl 3-(4-hydroxy-3-iodophenyl)propionate, for in vivo applications of labeled mAbs. Even though labeling proteins via the Bolton–Hunter reagent involves substitution of the radioiodine ortho to a hydroxyl group (Chart I), paired-label experiments demonstrated that mAbs labeled using the Bolton–Hunter method exhibited 1 order of magnitude lower deiodination than directly labeled mAb and a thyroid uptake only twice that observed for mAb labeled using SIB. In addition to the presence or absence of the *o*-hydroxyl group, the iodination site on mAbs labeled using SIB and the Bolton–Hunter agent differ with regard to another structural factor: SIB lacks the two-carbon spacer between the aromatic ring and the active ester moiety. To determine whether this two-carbon spacer was an important factor in reducing dehalogenation, we embarked on this study evaluating the utility of *N*-succinimidyl 4-hydroxy-3-iodobenzoate (SHIB) for mAb labeling. As shown

Chart I. Structure and Attachment Site of Iodinated Moieties of Radioiodinated Proteins: Direct vs Conjugation Methods



* Address correspondence to Michael R. Zalutsky, Ph.D., Department of Radiology, Duke University Medical Center, Durham, North Carolina 27710. FAX: (919) 684-4211.

[1] Abbreviations used: mAbs, monoclonal antibodies; SHIB, *N*-succinimidyl 4-hydroxy-3-iodobenzoate; HIBA, 4-hydroxy-3-iodobenzoic acid; SIB, *N*-succinimidyl 3-iodobenzoate; IBA, 3-iodobenzoic acid.

1043-1802/93/2904-0078$04.00/0 © 1993 American Chemical Society

in Chart I, SHIB differs from SIB only in the presence of the *o*-hydroxyl group. The secondary motivation of this study was more pragmatic in nature. If the SHIB reagent yielded a labeled protein resistant to deiodination in vivo, this labeling method would obviate the need for the synthesis and purification of an *N*-succinimidyl (trialkylstannyl)benzoate precursor and only commercially available compounds would be required. Our results indicate that mAbs can be labeled with SHIB with retention of immunoreactivity and that loss of label in vivo is somewhat higher than seen with SIB but considerably lower than that observed with direct iodination methods.

EXPERIMENTAL PROCEDURES

General. NMR spectra were obtained in appropriate solvents with a General Electric Midfield GN-300 spectrometer. For organic solvents, the proton chemical shifts were reported in ppm downfield from internal TMS (0.00 ppm); where NaOD solution was used, the HOD peak (4.75 ppm) was used as the reference. No chemical shift reference was used for carbon-13 NMR. IR spectra were obtained on a BOMEM MB-100 variable-resolution FTIR spectrophotometer. Mass spectral data were obtained on a VG-705 (VG Analytical, Danvers, MA) or on a Hewlett-Packard GC/MS/DS Model HP-5988A instrument. Melting points were determined on a Haake Buchler variable-heat apparatus or on a Fisher Johns melting point apparatus and are uncorrected.

All reagents were of reagent grade or better. The tin precursor for SIB preparation, *N*-succinimidyl 3-(tri-*n*-butylstannyl)benzoate, was prepared and radioiodinated using previously described procedures (*14*).

Sodium [^{125}I]iodide and sodium [^{131}I]iodide were obtained from Du Pont–New England Nuclear (North Bellerica, MA) in 0.1 N NaOH solution. Monoclonal antibody 81C6 is of the IgG_{2b} isotype and reacts with an epitope of the extracellular matrix antigen tenascin (*15*). This mAb was obtained as a gift from Dr. Darell Bigner, Department of Pathology, Duke University Medical Center.

Thin-layer chromatography was performed on EM Science analytical silica plates. Flash chromatography was done with 230–400 mesh silica gel from VWR scientific, Marietta, GA. High-pressure liquid chromatography (HPLC) was conducted with two systems. For standards and lipophilicity measurements, a Perkin-Elmer series 4 liquid chromatograph was used. The peaks were detected with Perkin-Elmer LC-95 UV/visible spectrophotometer detector. For radioiodinated compounds, HPLC was done with two LKB Model 2150 pumps, an LKB Model 2152 control system, an LKB Model 2138 fixed-wavelength UV detector, and a Beckman Model 170 radioisotope detector. With this system, peak analysis was performed with a Nelson Analytical software package on an IBM computer. An Alltech 250 × 4.6 mm Adsorbosphere 10-micron C18 column and an Alltech 250 × 4.6 mm partisil 10-micron column were used for reverse-phase and normal-phase HPLC, respectively. Depending on the activity level, radioactivity was measured with a Capintec CRC-7 radioisotope calibrator or with a LKB 1282 dual-channel γ counter.

Preparation of *N*-Succinimidyl 4-Hydroxy-3-iodobenzoate. 4-Hydroxybenzoic acid was iodinated following a literature procedure (*16*) for the preparation of 3-(4′-hydroxy-3′-iodophenyl)propanoic acid. Starting from 3.3 g (24 mmol) of 4-hydroxybenzoic acid, 5.6 g (89%) of crude 4-hydroxy-3-iodobenzoic acid (HIBA) was obtained. The product was purified by crystallizing twice from 50% ethanol (38% yield): mp 170–173 °C. [lit. mp 175–176 °C (*17*); 169–173 °C (*18*)]. HPLC and TLC demonstrated the presence of 4-hydroxybenzoic acid; however, this did not interfere with the next step.

The HIBA (254 mg, 1.0 mmol) was dissolved in 3 mL of dry THF, and 150 mg (1.3 mmol) of *N*-hydroxysuccinimide and 204 mg (1 mmol) dicyclohexylcarbodiimide were added. The mixture was stirred overnight under argon at room temperature. The precipitated dicyclohexylurea was filtered and the precipitate was washed with THF. The combined filtrate was evaporated, yielding 362 mg of an off-white solid. This was purified by silica gel chromatography using ethyl acetate as the solvent to yield 120 mg (34%) of a white solid: mp 189–191 °C; TLC (EtOAc) R_f = 0.69; IR (KBr) cm^{-1} 3242, 1756, 1719; NMR (CD_3CN) δ 1.93 (m, residual protons from the solvent), 2.82 (s, 4 H), 7.02 (d, 1 H, J = 9 Hz), 7.80 (m, 1 H), 8.44 (d, 1 H, J = 24 Hz); MS m/z (FAB) 362, 247, 138, 121, 107, 93, 77; HRMS calcd for $C_{11}H_9INO_5$ ($M + H^+$) 361.9525, found 361.9534.

Preparation of Glycine Conjugate of 3-Iodobenzoic Acid. *N*-Succinimidyl 3-iodobenzoate (prepared from 3-iodobenzoic acid and *N*-hydroxysuccinimide; 139 mg, 0.4 mmol) in 2.5 mL of THF was added to glycine (30.2 mg, 0.4 mmol) in 1.25 mL of 0.1 M borate buffer, pH = 8.5. After stirring for 2 h at room temperature, the hazy reaction mixture turned homogenous. Since TLC (25% MeOH/EtOAc) performed 1 h later showed the presence of unreacted ester, 50–60 mg of glycine was added to the above mixture with periodic addition of buffer and THF to keep the reaction mixture homogenous. After two days of stirring at room temperature, the reaction mixture was made alkaline with 1 N NaOH and the unreacted ester was extracted into ethyl acetate. The aqueous layer was acidified and the resultant white crystalline precipitate was extracted with ethyl acetate. After washing with brine, the ethyl acetate layer was dried with sodium sulfate and evaporated to give 67 mg (55%) of a white solid: mp 154–156 °C [lit. mp 156.3 °C (*19*)]; IR (KBr) cm^{-1} 3280, 1741, 1620, 1549, 1201; NMR (NaOD) δ 4.75 (HOD), 3.87 (s, 2 H), 7.21 (t, 1 H, J = 8 Hz), 7.70 (d, 1 H, J = 8 Hz), 7.85 (d, 1 H, J = 8 Hz), 8.09 (s, 1 H); ^{13}C NMR-APT (NaOD) δ 31.92 (CH_2), 81.85 (*C*I), 114.31 (*C*H), 118.34 (*C*H), 122.99 (*C*CO), 123.94 (*C*H), 156.20 (*C*ONH), 164.46 (*C*OOH).

Preparation of Glycine Conjugate of 4-Hydroxy-3-iodobenzoic Acid. This compound was prepared in an identical fashion as above. Starting with 274 mg (0.74 mmol) of SHIB, 330 mg of crude product was obtained. A portion (200 mg) of this was purified by preparative TLC using 50:50 ethyl acetate/methanol to yield 141 mg of a glassy solid: mp 88–90 °C; TLC (50:50 ethyl acetate/methanol) R_f = 0.38; IR (KBr) cm^{-1} 3629, 3545, 3139 (v br), 1730, 1645, 1572, 1500, 1407, 1214, 764; NMR (NaOD) δ 4.75 (HOD), 3.09 (s, 2 H), 6.40 (d, 1 H, J = 8.6 Hz), 7.37 (dd, 1 H, J = 2.5 and 8.6 Hz), 7.97 (d, 1 H, J = 2.5 Hz); ^{13}C NMR-APT (NaOD) δ 32.13 (CH_2), 79.66 (*C*I), 105.45 (*C*H), 107.67 (*C*CO), 117.67 (*C*H), 126.59 (*C*H), 157.27 (*C*OH), 158.54 (*C*ONH), 165.64 (*C*OOH); MS m/z (CI) 339 ($M + NH_4^+$), 322 ($M + H^+$), 281, 264, 220, 196, 180, 138; HRMS (FAB) calcd for $C_9H_9INO_4$ ($M + H^+$) 321.9576, found 321.9575.

Preparation of Radiolabeled 4-Hydroxy-3-iodobenzoic Acid and Its NHS Ester. To a solution of 4-hydroxybenzoic acid (5 μL; 3.8 mg in 4 mL of 0.05 N NaOH) was added 1–2 μL of ^{131}I (or ^{125}I) in 0.1 N NaOH (0.2–1.0 mCi) followed by 5 μL of chloramine-T solution (10 mg/mL in 0.1 M borate, pH = 8.5). After 10-min reaction at room temperature, 7 μL of sodium bisulfite (40

mg/mL in borate buffer) was added. The reaction mixture was injected onto a HPLC (C18, 110:89:1 MeOH/H_2O/HOAc; 0.5 mL/min). Retention time for 4-hydroxybenzoic acid was 9.8 min and that for the iodinated product was 15.8 min. More than 80% of the injected activity eluted with the retention time of [^{131}I]HIBA. A small amount of a coeluting impurity was seen in the UV profile; however, by excluding the first 1 mL of the peak, [^{131}I]HIBA could be isolated from this impurity.

Most of the methanol from the HPLC fraction containing the [^{131}I]HIBA was evaporated with an argon stream, and the activity in the residual aqueous solution was extracted into ethyl acetate (3 × 500 μL). The ethyl acetate solution was dried with sodium sulfate and evaporated to about 100 μL, transferred to a $^1/_2$-dram vial, and evaporated to dryness. *N*-Hydroxysuccinimide and dicyclohexylcarbodiimide (3 μmol in each of 30 μL of THF) were added to the above activity, and the mixture was left at room temperature for 2–3 h. The reaction mixture was injected onto HPLC (silica) and eluted with 50:50:2 (v/v/v) ethyl acetate/hexane/acetic acid at 1 mL/min. The product (t_R = 10.8 min) was isolated in 50–70% radiochemical yield.

Coupling of [^{131}I]SHIB to 81C6. Most of the solvent from the HPLC fraction containing [^{131}I]SHIB was evaporated with argon and transferred to a $^1/_2$-dram vial and the solvent was further evaporated to dryness. To the above activity was added a solution (75 μL, 5 mg/mL) of mAb 81C6 in borate buffer (0.1 M, pH = 9.0). The mixture was incubated at room temperature for 1 h. The reaction was terminated by the addition of 0.3 mL of 0.2 M glycine. The labeled mAb was purified by passage through a Sephadex G-25 column and eluted with phosphate-buffered saline (PBS). The protein-associated activity was measured by TCA precipitation and compared to that of 81C6 labeled using [^{125}I]SIB in a paired-label fashion. Trichloroacetic acid precipitable activity was 98.9 ± 0.3% and 99.7 ± 0.1% for 81C6 labeled using [^{131}I]-SHIB and [^{125}I]SIB, respectively.

In Vitro Specific Binding Measurements. About 100 ng each of 81C6 labeled via [^{125}I]SIB and [^{131}I]SHIB were added in triplicate to 250 mg of both antigen-positive D-54 MG human glioma and antigen-negative rat liver homogenates. The homogenates were incubated overnight at 4 °C, washed three times, and counted for ^{131}I and ^{125}I activity. Specific binding in this single point assay was defined as the percentage of activity bound to tumor minus the percentage bound to liver.

Tissue Distribution Measurements. These studies were performed in paired-label format in normal male BALB/c mice weighing 22–30 g. Groups of five or six animals were injected in the tail vein with a mixture of both preparations and sacrificed by ether overdose at selected time points. Tissues of interest were removed, washed with saline, and weighed. A dual-channel γ counter was used to determine tissue activity levels of ^{131}I and ^{125}I. The percent injected dose per organ was calculated by comparison to standards of appropriate count rate.

The first set of experiments compared the tissue distribution of [^{131}I]HIBA and [^{125}I]IBA, compounds which are potential labeled catabolites of mAbs labeled using [^{131}I]SHIB and [^{125}I]SIB, respectively. [^{131}I]HIBA was prepared as described above and its purity was greater than 99% as confirmed by TLC. To prepare [^{125}I]IBA, [^{125}I]SIB was incubated with 1 mL of 1 N NaOH for 1 h at room temperature. This solution was acidified with 250–300 μL of 6 N HCl. The activity was extracted into ethyl acetate (3 × 500 μL). The ethyl acetate solution was washed with brine and dried with sodium sulfate, and the ethyl acetate was evaporated. Little or no activity was lost in this step. The dried activity was reconstituted in PBS. TLC of hydrolyzed products was run using 1% acetic acid in ethyl acetate as the eluent. More than 97% coeluted with an authentic IBA standard and 0.50% was retained at the origin. Mice were injected with 7 μCi of [^{131}I]HIBA and 5 μCi of [^{125}I]IBA and groups of animals were sacrificed at 30 min and 1 and 2 h.

In a similar study, blood and urine samples were obtained 1 and 2 h after injection of [^{131}I]HIBA and [^{125}I]-IBA for HPLC analysis. In each case, samples were pooled from three to five animals. Urine samples were diluted with phosphate-buffered saline and passed through a 0.2-μm syringe filter (Acrodisc, Gelman Sciences). Blood samples were centrifuged, and sera were passed through a 10-kD cutoff Centricon (Amicon, Danvers, MA). Samples were analyzed using a reverse-phase HPLC system described in a previous publication (*20*).

The second set of paired-label biodistribution measurements were performed to compare the distribution of radioactivity following the administration of mAb radioiodinated using SHIB and SIB. Animals were injected via the tail vein with 8 μg (3 μCi) of 81C6 labeled with [^{131}I]SHIB and 3 μg (4 μCi) of 81C6 labeled with [^{125}I]-SIB. Groups of animals were studied at 1, 2, 5, 6, and 7 days after injection.

Lipophilicity Measurement. The relative lipophilicities of the two potential catabolites were measured by a reverse-phase HPLC system (*21*). The retention times of the two compounds were determined by using an Alltech Adsorbosphere C18 10-micron column and 59.4:39.6:1 (v/v/v) H_2O/MeOH/HOAc as the eluent at a flow rate of 1 mL/min. The capacity factor k' was calculated for each compound and was used as an indicator of relative lipophilicity.

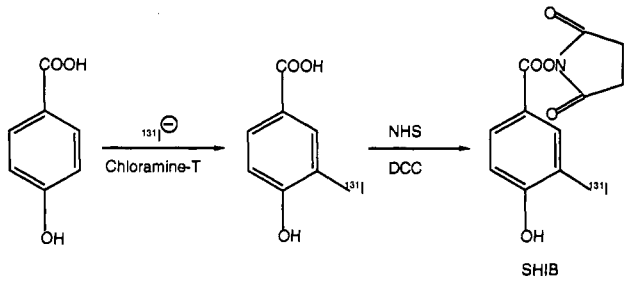
Statistical Analysis. Since the tissue-distribution experiments were performed in a paired-label format, with each animal serving as its own control, a paired t test was used to compare the biodistribution of the two radioiodinated mAbs as well as that of the potential catabolites.

RESULTS AND DISCUSSION

When evaluating potential methods for the radioiodination of mAbs, a number of factors must be considered. First, the mAb should be labeled in reasonable radiochemical yield with retention of antigen-binding capacity. Second, the bond between the radioiodine and the mAb should be stable in vivo. Third, the labeled species generated by the catabolism of the mAb should be excreted rapidly. The potential utility of SHIB as an acylation agent for labeling mAbs was evaluated using the anti-glioma mAb 81C6 IgG because of the availability of data for this mAb using a variety of radioiodination methods (*11*, *13*, *20*).

A potential advantage of SHIB compared to SIB is that due to the presence of the hydroxyl group, iodination via electrophilic substitution should proceed in reasonable yield. Thus, SHIB can be labeled from commercially available compounds and the synthesis, and purification of an *N*-succinimidyl (trialkylstannyl)benzoate precursor is not required. Initially, the labeling of SHIB in one step by reaction of *N*-succinimidyl 4-hydroxybenzoate with chloramine-T and ^{131}I was attempted. Since only modest yields were obtained and separation of SHIB from unreacted radioiodine and excess starting ester was problematic, the two-step procedure outlined in Scheme I was adopted.

Scheme I. Synthesis of *N*-Succinimidyl 4-Hydroxy-3-[^{131}I]iodobenzoate



In the first step, 4-hydroxy-3-[^{131}I]iodobenzoic acid was prepared by reaction of sodium [^{131}I]iodide with 4-hydroxybenzoic acid using chloramine-T as the oxidant. Yields of more than 80% were obtained and the product could be purified using reverse-phase HPLC. A 2–3-h reaction of the labeled acid with *N*-hydroxysuccinimide and dicyclohexylcarbodiimide gave the desired product, [^{131}I]SHIB, in 50–70% yield. The [^{131}I]SHIB acylation agent was purified using normal-phase HPLC prior to reaction with mAb.

An important advantage of SIB compared to the Bolton–Hunter reagent is that its mAb coupling efficiency is about 2-fold higher (*12*). This difference was considered to be related to the higher rate of competitive hydrolysis imparted by the two-carbon spacer between the ester moiety and the aromatic ring present in the Bolton–Hunter reagent (Chart I). Since SHIB also lacks this spacer, it might be expected that protein coupling should proceed in good yield with this reagent. However, even with a reaction time of 60 min and a relatively high pH (9.0) and protein concentration (5 mg/mL), the coupling efficiency of SHIB to mAb 81C6 was only 10–15%; even poorer yields were obtained with shorter reaction times. In comparison, after only a 15–20-min reaction, more than 70% of SIB could be coupled to mAb 81C6 and yields for the Bolton–Hunter reagent were 25–30% (*13*).

We believe that the low mAb coupling efficiency for SHIB can be attributed to the presence of the hydroxyl group para to the ester. Unlike the case with the Bolton–Hunter reagent, this *p*-hydroxyl group enhances the resonance stabilization of the ground state, thereby reducing the rate of nucleophilic attack at the carboxyl carbon (*22*). This ground-state stabilization is also reflected by the fact that HIBA is a weaker acid than IBA (*23*).

A potential advantage of SHIB for labeling mAbs is that like other conjugation methods, direct exposure of the mAb to oxidants is avoided. Using a single-point assay, the specific binding in vitro of mAb 81C6 labeled using [^{131}I]SHIB was 78 ± 3%, a value comparable to that observed in parallel studies with mAb labeled using [^{125}I]-SIB (84 ± 3%). The specific binding percentages for mAb labeled with both acylation agents are significantly higher than those reported previously for the same mAb labeled with ^{131}I using Iodogen (*24*).

The tissue distribution of HIBA and IBA were compared in normal mice in order to evaluate the effect of the hydroxyl group on the tissue distribution of radioiodine. In addition, the distribution of these labeled acids are of interest because they are likely catabolites of mAbs labeled using SHIB and SIB. Because of the proclivity of iodide for the thyroid, uptake of activity in this tissue is used frequently as an indicator of deiodination. As shown in Figure 1, thyroid uptake was quite low after injection for both HIBA and SIB. Thyroid accumulation of HIBA increased from 0.13 ± 0.02% injected dose at 30 min to

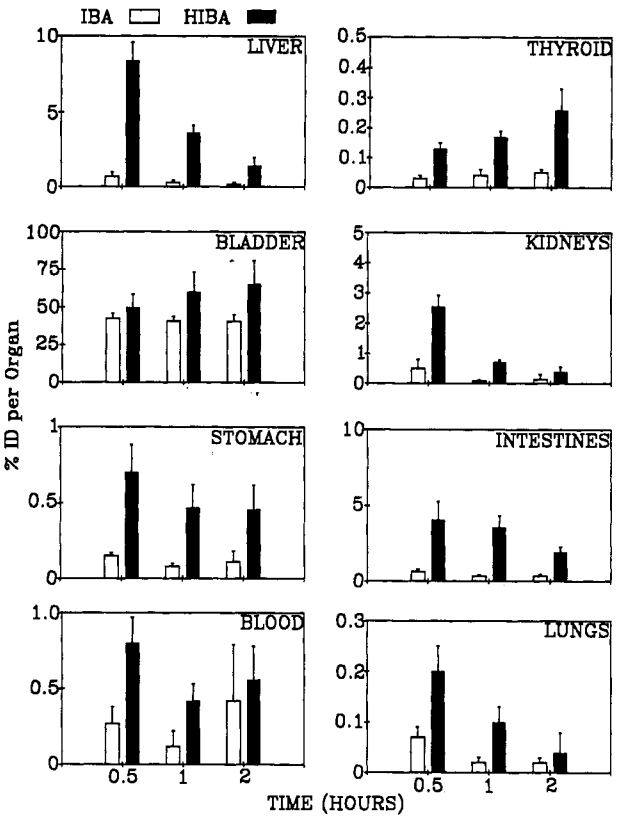


Figure 1. Comparative tissue uptake in mice following the coadministration of [^{131}I]HIBA and [^{125}I]IBA.

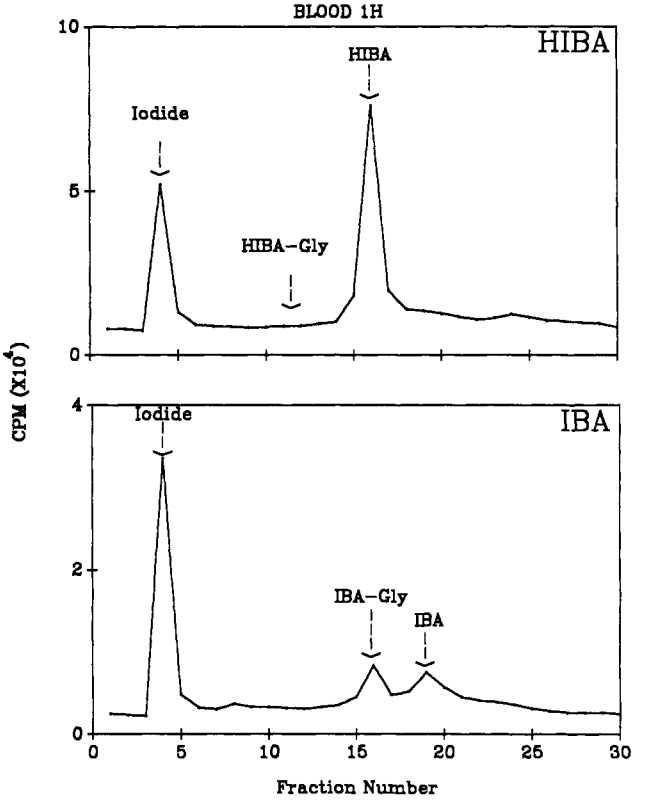


Figure 2. Reverse-phase HPLC chromatogram of blood sample obtained 1 h after coadministration of [^{131}I]HIBA and [^{125}I]IBA.

0.26 ± 0.07% at 2 h. In comparison, thyroid uptake of IBA was significantly lower ($P < 0.005$), ranging from 0.03 ± 0.01% to 0.05 ± 0.01% over the same time period. Although these results suggest 4–5-fold greater dehalogenation of HIBA compared to IBA, it should be noted

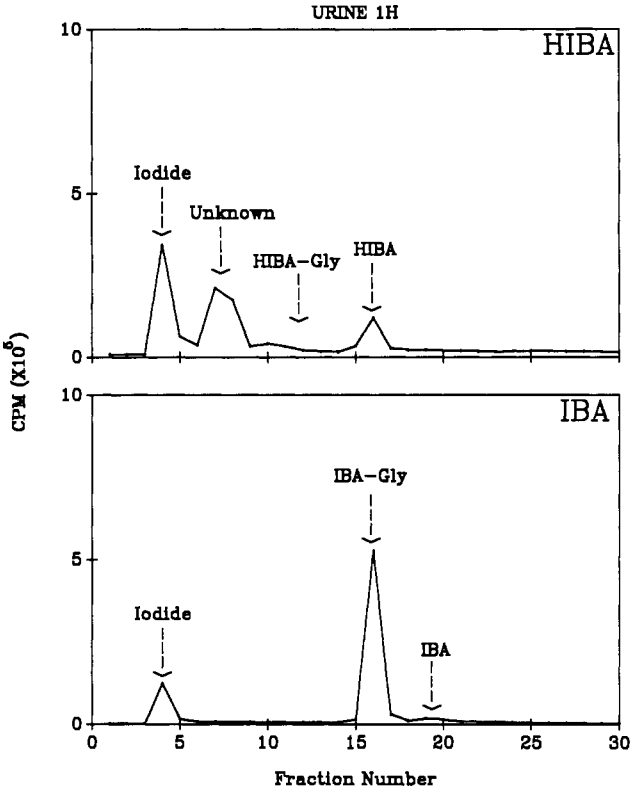


Figure 3. Reverse-phase HPLC chromatogram of urine obtained 1 h after coadministration of [^{131}I]HIBA and [^{125}I]IBA.

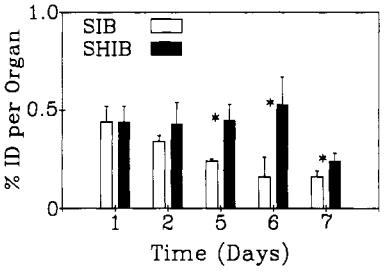


Figure 4. Thyroid uptake in mice following the coadministration of 81C6 mAb labeled with ^{131}I using [^{131}I]SHIB and with ^{125}I using [^{125}I]SIB. Statistically significant differences ($P < 0.01$) indicated by asterisk.

that subtle but indistinguishable levels of free iodide in the two preparations (both about 0.5–0.9%) could also account for the 0.1–0.2% differences in thyroid uptake of HIBA and IBA.

Although metabolic cages were not used to insure complete urine collection, data obtained for activity in urine and bladder at death indicate that excretion of HIBA is significantly greater than for IBA (Figure 1). For example, 1 h after injection, bladder and urine activity was 60.1 ± 13.1% for HIBA, a value significantly higher than that observed for IBA (40.9 ± 3.1%, $P < 0.01$). The more rapid urinary excretion of HIBA may be related to its lower lipophilicity. When the lipophilicities of HIBA and IBA were measured by reverse-phase HPLC, the k' value for HIBA was 3.31 compared to 4.59 for IBA. Liver uptake of HIBA was about 5 times higher than that of IBA at all time points, an observation that might appear to be discordant with the lower lipophilicity of HIBA. However, higher liver selectivity for hydrophilic compounds has been reported (*25*) and the metabolism of HIBA may differ from that of IBA due to the presence of the hydroxyl group (see below). In general, the tissue distribution observed for IBA is in good agreement with previously published results (*10*), with the exception that somewhat lower activity levels were seen in blood in the current study. This may be related to the more stringent conditions used to hydrolyze SIB to IBA. If small amounts of unreacted SIB were present due to incomplete hydrolysis, labeling of serum proteins in vivo might be possible, since incubation of mouse serum with incompletely hydrolyzed SIB resulted in protein labeling in vitro (data not shown).

Previous studies have shown that mAbs labeled by reaction with SIB are excreted via the urine primarily as glycine conjugates (*20*). However, due to the resonance stabilization of SHIB as hypothesized earlier, formation of HIBA–glycine conjugates might not be favorable. One hour after injection, conversion of IBA to its glycine conjugate was observed in blood (Figure 2) and urine (Figure 3) while the HIBA–glycine conjugate was not seen in these same animals. About 40–45% of the HIBA was present in urine as an unknown metabolite with an elution time that indicated that it was more hydrophilic than the HIBA–glycine conjugate. This unidentified compound was not seen in blood. The HPLC pattern at 2 h was similar for both blood and urine except the amount of free iodide and IBA–glycine conjugate in urine was roughly equal.

Excretion of aromatic acids via glycine conjugate formation has been shown to depend on a number of factors including species (*26*), dose, and any coadministered substances (*27*). In the case of salicyclic acid, benzoate (*28*) and *p*-aminobenzoic acid (*29*) have suppressed the formation of glycine conjugates. In rabbits, *o*-(salicyclic acid) and *m*-hydroxybenzoic acids were eliminated essentially unchanged (*30*); however, about 33% of the para isomer was eliminated as the glycine conjugate (*31*).

Table I. Paired-Label Tissue Distribution of Radioiodine in Normal Mice following Injection of 81C6 Labeled with [^{125}I]SIB and with [^{131}I]SHIB

	% injected dose per organ[a]					
	1 day		5 days		6 days	
organ	SIB	SHIB	SIB	SHIB	SIB	SHIB
liver	5.16 ± 1.01	4.88 ± 0.97	1.85 ± 0.36	2.12 ± 0.37	1.16 ± 0.34	1.40 ± 0.44
spleen	0.36 ± 0.04	0.32 ± 0.04	0.14 ± 0.02	0.14 ± 0.02	0.10 ± 0.01	0.11 ± 0.01
lungs	2.69 ± 0.83	2.59 ± 0.81	1.64 ± 0.48	1.95 ± 0.60	0.45 ± 0.07	0.55 ± 0.07
heart	0.57 ± 0.06	0.53 ± 0.06	0.24 ± 0.07	0.27 ± 0.08	0.13 ± 0.05	0.16 ± 0.06
kidneys	2.18 ± 0.25	2.37 ± 0.29	0.86 ± 0.10	1.16 ± 0.10	0.57 ± 0.14	0.87 ± 0.18
stomach	0.61 ± 0.08	0.56 ± 0.08	0.22 ± 0.06	0.25 ± 0.07	0.15 ± 0.06	0.18 ± 0.07
sm int	3.26 ± 0.12	3.07 ± 0.10	1.15 ± 0.19	1.35 ± 0.20	0.62 ± 0.18	0.76 ± 0.23
lg int	1.44 ± 0.13	1.41 ± 0.12	0.61 ± 0.10	0.75 ± 0.13	0.31 ± 0.10	0.42 ± 0.16
muscle	13.85 ± 1.65	12.57 ± 1.68	6.24 ± 0.76	6.84 ± 0.84	4.79 ± 0.47	5.60 ± 0.56
blood	28.65 ± 4.26	29.14 ± 4.49	10.24 ± 1.49	12.54 ± 1.63	6.26 ± 2.22	8.08 ± 3.02
brain	0.15 ± 0.02	0.15 ± 0.02	0.07 ± 0.01	0.07 ± 0.01	0.04 ± 0.01	0.05 ± 0.02

[a] Mean ± SD (n = 5).

Identification of the unknown peak found in urine has not been attempted at this time. This species could be the glucuronide or sulfate, other common metabolites of aromatic acids (*27*).

Paired-label studies were performed in normal mice to compare the in vivo distribution of radioiodine from mAb 81C6 IgG labeled by reaction with [^{131}I]SHIB and [^{125}I]-SIB. In thyroid, uptake of ^{131}I (Figure 4) suggested that, at early time points, the presence of the hydroxyl group does not increase deiodination. However, with time thyroid uptake of ^{131}I becomes 1.7–2.9 times higher than ^{125}I with these differences considered to be statistically significant ($P < 0.01$) on days 5–7. As summarized in Table I, the tissue distribution of both nuclides was quite similar in other tissues. At later time points, retention of radioiodine from mAb appears to be somewhat higher in kidney ($P < 0.01$, days 5 and 6) and several other tissues when labeling was performed using SHIB. Although these differences are small, and generally not significant, these trends are not inconsistent with the differences observed in the in vivo behavior of the potential catabolites HIBA and IBA.

The thyroid uptake levels determined in this study for 81C6 labeled using SIB are in excellent agreement with those obtained previously with this mAb in normal mice (*13*, *20*) but again are 2–3-fold higher than those observed in athymic mice (*11*). This underscores the importance in evaluating various labeling methods in paired-label format in order to eliminate effects related to species and metabolic and nutritional status. The results of this study can be evaluated most effectively by comparison to other paired-label experiments performed with mAb 81C6, and several conclusions regarding the effect of iodination site on deiodination can be made. SHIB lacks a two-carbon spacer between the aromatic ring and the active ester and the Bolton–Hunter reagent contains this spacer, yet both exhibited about 2-fold higher thyroid uptake than SIB (*13*). Although this two-carbon spacer increases the structural difference between the labeling site and that found on mAbs labeled on tyrosine residues, it does not appear to influence the deiodination of mAbs labeled using the Bolton–Hunter reagent.

Thyroid uptake of HIBA was only 0.13–0.26% of injected dose and that of its mAb conjugate was generally less than 0.5%. In comparison, when mAb 81C6 was labeled using Iodogen, 1 order of magnitude higher thyroid uptake was seen (*13*). This suggests that the deiodinases thought to be responsible for the deiodination of tyrosine residues on directly labeled mAbs are enzymes with a high degree of specificity. This is supported by the fact that other molecules containing a hydroxyl group ortho to the site of iodination also exhibit relatively low accumulation in thyroid (*32–34*). Nonetheless, it is important to note that the thyroid uptake of IBA and its mAb conjugate are somewhat lower than observed for HIBA and its mAb conjugate. Deiodination levels are quite low with both acylation agents, possibly reflecting the fact that deiodinases do not play a major role in the loss of label from either compound. In that case, differences in the stability of HIBA and IBA might be due to the lower carbon–iodine bond strength imparted by the hydroxyl group (*35*). In conclusion, although SIB appears to remain the reagent of choice for labeling mAbs, the presence or absence of a hydroxyl group ortho to the iodination site is not the only factor to be considered in the design of mAb radioiodination methods.

ACKNOWLEDGMENT

The excellent technical assistance of Susan Slade is greatly appreciated. The authors are grateful to Sandra Gatling for help in preparing this manuscript. This research was supported by National Institutes of Health Grants CA 42324, NS 20023, CA 14236, and by Grant DEFG05-89ER60789 from the Department of Energy.

LITERATURE CITED

(1) Bolton, A. E., and Hunter, W. M. (1973) The labelling of proteins to high specific radioactivities by conjugation to a ^{125}I-containing acylating agent. *Biochem. J. 133*, 529–539.
(2) Larson, S. M., and Carrasquillo, J. A. (1988) Advantages of radioiodine over radioindium labeled monoclonal antibodies for imaging solid tumors. *Nucl. Med. Biol. 15*, 231.
(3) Eary, J. F., Krohn, K. A., Kishore, R. and Nelp, W. B. (1989) Radiochemistry of halogenated antibodies. In *Antibodies in Radiodiagnosis and Therapy* (M. R. Zalutsky Ed.) Chapter 5, p 83, CRC Press, Boca Raton, FL.
(4) Hunter, W. M., and Greenwood, F. C. (1962) Preparation of iodine-131 labelled human growth hormone of high specific activity. *Nature. 194*, 495–496.
(5) Fraker, P. J., and Speck, J. C. (1978) Protein and cell membrane iodinations with a sparingly soluble chloramide 1,3,4,6-tetrachloro-3α-6α-diphenylglycouril. *Biochem. Biophys. Res. Commun. 80*, 849.
(6) Carasquillo, J. A. (1989) Radioimmunoscintigraphy with polyclonal and monoclonal antibodies. In *Antibodies in Radiodiagnosis and Therapy* (M. R. Zalutsky, Ed.) pp 169–198, CRC Press, Boca Raton, FL.
(7) Hayes, D. F., Zalutsky, M. R., Kaplan, W., Noska, M., Rhor, A., Colcher, D., Schlom, J., and Kufe, D. (1986) Pharmacokinetics of radiolabeled monoclonal antibody B6.2 in patients with metastatic breast cancer. *Cancer Res. 46*, 3157–3163.
(8) Gershengorn, M. C., Glinoer, D., and Robbins, J. (1980) Transport and Metabolism of Thyroid Hormones. In *The Thyroid Gland* (M. DeVisscher, Ed) pp 81–121, Raven Press, New York.
(9) Zalutsky, M. R., and Narula, A. S. (1987) A method for the radiohalogenation of proteins resulting in decreased thyroid uptake of radioiodine. *Appl. Radiat. Isot. 38*, 1051–1055.
(10) Zalutsky, M. R., and Narula, A. S. (1988) Radiohalogenation of a monoclonal antibody using an N-succinimidyl 3-(tri-*n*-butylstannyl)benzoate intermediate. *Cancer Res. 48*, 1446–1450.
(11) Zalutsky, M. R., Noska, M. A., Colapinto, E. V., Garg, P. K., and Bigner, D. D. (1989) Enhanced tumor localization and in vivo stability of a monoclonal antibody radioiodinated using *N*-succinimidyl-3-(tri-*n*-butylstannyl)benzoate. *Cancer Res. 49*, 5543–5549.
(12) Wilbur, D. S., Hadley, S. W., Hylarides, M. D., Abrams, P. G., Beaumier, P. A., Morgan, A. C., Reno, J. M., and Fritzberg, A. R. (1989) Development of a stable radioiodinating reagent to label monoclonal antibodies for radiotherapy of cancer. *J. Nucl. Med. 30*, 216–226.
(13) Vaidyanathan, G., and Zalutsky, M. R. (1990) Protein radiohalogenation: Observations on the design of *N*-succinimidyl ester acylation agents. *Bioconjugate Chem. 1*, 269–273.
(14) Garg, P. K., Archer, G. E., Bigner, D. D., and Zalutsky, M. R. (1989) Synthesis of radioiodinated *N*-succinimidyl iodobenzoate: Optimization for use in antibody labelling. *Appl. Radiat. Isot. 40*, 485–490.
(15) Bourdon, M. A., Wikstrand, C. J., Furthmayr, H., Mathews, T. J. and Bigner, D. D. (1983) Human glioma-mesenchymal extracellular matrix defined by monoclonal antibody. *Cancer Res. 43*, 2796–2805.
(16) Michelot, R., Gozlaw, H., Beaujounaw, J.-C., Besson, M.-J.; Torrens, Y., and Glowinski, J. (1980) Synthesis and biological activities of substance P iodinated derivatives. *Biochem. Biophys. Res. Commun. 95*, 491–498.
(17) Edgar, K. J., and Falling, S. N. (1990) An efficient method for the preparation of iodophenols. *J. Org. Chem. 55*, 5287–5291.

(18) Katzenellenbogen, J. A., Tatee, T., and Robertson, D. W. (1980) Preparation of tritium-labeled 4-hydroxy-α-[p-(2-CN-pyrrolidinyl)ethoxy)phenyl]-α′-nitrostilbene (CN-928), a biologically-important metabolite of the antiestrogen CI-628. *J. Labelled Compd. Radiopharm. 18*, 865–879.

(19) Elias, H., Arnold, C. H., and Kloss, G. (1973) Preparation of ^{131}I-labeled *m*-iodohippuric acid and its behaviour in kidney function studies compared to *o*-iodohippuric acid. *Int. J. Appl. Radiat. Isot. 24*, 463–469.

(20) Garg, P. K., Slade, S. K., Harrison, C. L., and Zalutsky, M. R. (1989) Labeling proteins using aryl iodide acylation agents: Influence of *meta vs para* substitution on *in vivo* stability. *Nucl. Med. Biol. 16*, 669–673.

(21) Nunn, A. D., Loberg, M. D., and Conley, R. A. (1983) Structure–Distribution-Relationship approach leading to the development of Tc-99m mebrofenin: An improved cholescintigraphic agent. *J. Nucl. Med. 24*, 423–430.

(22) Euranto, E. K. (1969) Esterification and ester hydrolysis. In *The Chemistry of Carboxylic Acid and Esters* (S. Patai, Ed.) Chapter 11, p 505, Interscience publishers, New York.

(23) Kalfus, K., Kroupa, J., Vecera, and Exner, O. (1975) Additivity of substituent effects in *meta*- and *para*-substituted benzoic acids. *Coll. Czech. Chem. Commun. 40*, 3009–3019.

(24) Zalutsky, M. R., Moseley, R. P., Coakham, H. B., Coleman, R. E., and Bigner, D. D. (1989) Pharmacokinetics and tumor localization of ^{131}I-labeled anti-tenascin monoclonal antibody 81C6 in patients with gliomas and other intracranial malignancies. *Cancer Res. 49*, 2807–2813.

(25) Roth, B. D., Bocaw, M. A. T., Blankley, C. J., Chucholowski, A. W., Creger, P. L., Creswell, M. W., Ferguson, E., Newton, R. S., O'Brien, P., Picard, J. A., Roark, W. H., Sekerke, C. S., Sliskovic, D. R., and Wilson, M. W. (1991) Relationship between tissue selectivity and lipophilicity for inhibitors of HMG-CoA reductase. *J. Med. Chem. 34*, 463–466.

(26) Williams, R. T. (1971) Species variations in drug biotransformations. In *Fundamentals of Drug Metabolism and Drug Disposition* (B. N. La Du, H. G. Mandel, and E. L. Way, Eds.) Chapter 11, pp 187–205, The Williams & Wilkins Company, Baltimore.

(27) Mandel, H. G. (1971) Pathways of drug transformation: Biochemical conjugations. In *Fundamentals of Drug Metabolism and Drug Disposition* (B. N. La Du, H. G. Mandel, and E. L. Way, Eds.) Chapter 10, pp 149–186, The Williams & Wilkins Company, Baltimore.

(28) Levy, G., and Amsel, L. P. (1966) Kinetics of competitive inhibition of salicylic acid conjugation with glycine in man. *Biochem. Pharmacol. 15*, 1033–1038.

(29) Salassa, R. M., Bollman, J. L., and Dry, T. J. (1948) The effect of *para*-aminobenzoic acid on the metabolism and excretion of salicylate. *J. Lab. Clin. Med. 33*, 1393–1401.

(30) Bray, H. G., Ryman, B. E., and Thorpe, W. V. (1948) The fate of certain organic acids and amides in the rabbit. 5. *o* and *m*-hydroxybenzoic acids and amides. *Biochem. J. 43*, 561–567.

(31) Bray, H. G., Ryman, B. E., and Thorpe, W. V. (1947) The fate of certain organic acids and amides in the rabbit. 2. *p*-Hydroxybenzoic acid and its amide. *Biochem. J. 41*, 212–218.

(32) Dumas, P. (1979) Dehalogenation of a variety of iodinated phenol derivatives in normal and thyrodectomized rats. *Biochem. Pharmacol. 22*, 1599–1605.

(33) Lee, H., Inbasekaran, M. N., Wieland, D. M., Sherman, P. S., Fisher, S. J., Mangner, T. J., Rogers, W. L., and Clinthorne, N. H. (1986) Development of a kit-form analog of metaiodobenzylguanidine. *J. Nucl. Med. 27*, 156–167.

(34) Patel, H. B., Hosain, F., Spencer, R. P., Scharf, H.D., Skulski, M. S., and Jansujwicz, A. (1991) Radioiodination and biodistribution of analogs of a calichemicin constituent. *Nucl. Med. Biol. 18*, 445–447.

(35) Vedeneyev, V. I., Gurvich, L. V., Kondrat'yev, V. A., Medvedev, V. A., and Frankevich, Y. L. (1966) *Bond Energies, Ionization Potentials, and Electron Affinities*, p 63, Edward Arnold, London.

Synthesis and Characterization of a Trigalactosylated Bisacridine Compound To Target DNA to Hepatocytes

Jean Haensler and Francis C. Szoka, Jr.*

School of Pharmacy, University of California, San Francisco, California 94143-0446. Received September 28, 1992

We have synthesized three bisacridine intercalators containing a galactose residue(s) to target DNA to cell surface receptors for use in gene-delivery systems. Each of the bisacridines could intercalate into DNA with micromolar dissociation constants. Bisacridines containing a single galactose on either a three- or six-carbon spacer from the secondary amine of spermidine–bisacridine could mediate binding of DNA to the soluble galactose receptor *Ricinus communis* lectin (RCA I), but not to the asialoglycoprotein receptor on primary hepatocytes. A trigalactosyl dilysyl bisacridine [$(Gal\text{-}6)_3Lys_2$-bA] compound could mediate the binding of DNA to both the ricin lectin and to primary hepatocytes. Binding of the $(Gal\text{-}6)_3Lys_2$-bA–DNA to the hepatocytes could be blocked by asialoorosomucoid. On the basis of luciferase expression, $(Gal\text{-}6)_3Lys_2$-bA did not induce transfection of the hepatocytes when attached to the pCLUC4 plasmid encoding the firefly luciferase gene.

INTRODUCTION

The increasing knowledge of the molecular basis of disease has opened the way for correction of pathology using gene therapy. Success in this goal depends, to a large degree, on the development of safe and efficient carriers for selective gene delivery to the target cells. Although viral vectors currently are the most efficient systems for gene transfer into eucaryotic cells (*1*), a concern exists that the use of viruses for gene therapy might lead to deleterious side effects (*2*). This concern has encouraged the development of gene transfer techniques that do not use viruses.

A nonviral gene carrier will have to surmount all the barriers that viruses have evolved to overcome: The carrier will have to persist in the biophase long enough to gain access to the target cell. It will have to recognize the target cell and mediate entry of the gene into the cell. Finally, the gene will have to find its way into the nucleus, where the genetic information can be transcribed. Our aim is to use biochemical and biophysical principles to design and synthesize nonviral gene-delivery systems that have the characteristics necessary to achieve a high level of gene delivery into the nucleus of cells.

Viruses take advantage of specific cell surface molecules, viral receptors, to bind to the host cells. The initial binding of the virus to its receptor is also essential for viral entry and infection. Binding allows close contact with the host cell surface, which is necessary for membrane fusion or triggers receptor-mediated endocytosis (*3*). To mimic the binding and entry functions of viruses one can exploit the specificity and efficiency afforded by receptor-mediated endocytosis to deliver recombinant DNA (e.g. plasmids) via attached ligands. Methods for the noncovalent attachment of cell-specific ligands to DNA using polycationic anchors or an ethidium homodimer anchor have been devised (*4–6*). Polylysine–ligand conjugates which tightly bind to DNA by forming a charge complex have been used to carry foreign DNA into selected target cells and/or organs expressing the cognate receptor (*4–17*).

As an alternative to these high molecular weight polylysine–ligand carriers, we propose novel bimolecular conjugates that consist of a low molecular weight targeting ligand covalently attached to a chemically well-defined DNA intercalator. We have applied this approach to create a new carrier system for selective gene delivery to the liver, wherein we attach galactose, a targeting ligand for hepatocytes, to a DNA bis-intercalator. We describe here the synthesis and characterization of a series of compounds obtained by attaching thiogalactosyl residues to the central amino group of spermidine–bisacridine via various spacer arms. The binding constant of the bisacridine compounds for DNA, as well as their ability to mediate binding of a 5 kb plasmid to a soluble receptor for galactose (*Ricinus communis* agglutinin, RCA-I)[1] or to the asialoglycoprotein receptor of isolated rat hepatocytes, is described in this paper.

EXPERIMENTAL PROCEDURES

Radioactive $Na^{125}I$ was obtained from Du Pont–New England Nuclear (North Bilerica, MA). [^{125}I]Iodo-2′-deoxycytidine 5′-triphosphate (^{125}I-dCTP) was obtained from Amersham Co. (Arlington Heights, IL). The plasmid pCLUC4 (*18*) was a generous gift from Dr. E. Wagner (Institute of Molecular Pathology, Vienna, Austria). It was radiolabeled with ^{125}I-dCTP using a nick translation kit (Bethesda Research Laboratories, Gaithersburg, MD). Asialoorosomucoid (AsOR), prepared from human orosomucoid by neuraminidase treatment, was a generous gift from Dr. S. Oie (UCSF) and was radioiodinated using Enzymobead radioiodination reagent (Bio-Rad Chemical Division, Richmond, CA). Freshly isolated rat hepatocytes were obtained from Dr. M. Bissel (Liver Center, UCSF). The silica gel for column chromatography (grade 60, 230–400 mesh, 60 Å; Merck) and all chemicals (unless otherwise specified) were from Aldrich Chemical Co. (Milwaukee, WI). Organic solvents were obtained from Fisher Scientific Co. (Santa Clara, CA). Thin-layer chromatography (TLC) was carried out on analytical silica gel 60-Å precoated glass plates (Whatman) supplied by Baxter Scientific Products

* Address correspondence to this author.

[1] Abbreviations used: AsOR, human asialoorosomucoid; DCC, *N,N′*-dicyclohexylcarbodiimide; FCS, fetal calf serum; HEPES, *N*-(2-hydroxyethyl)piperazine-*N′*-(2-ethanesulfonic acid); MEM, minimal essential Eagle's medium; PBS, phosphate-buffered saline; RCA-I, *Ricinus communis* agglutinin; TFA, trifluoroacetic acid; TMS, tetramethylsilane; Tris, tris(hydroxymethyl)aminomethane.

1043-1802/93/2904-0085$04.00/0 © 1993 American Chemical Society

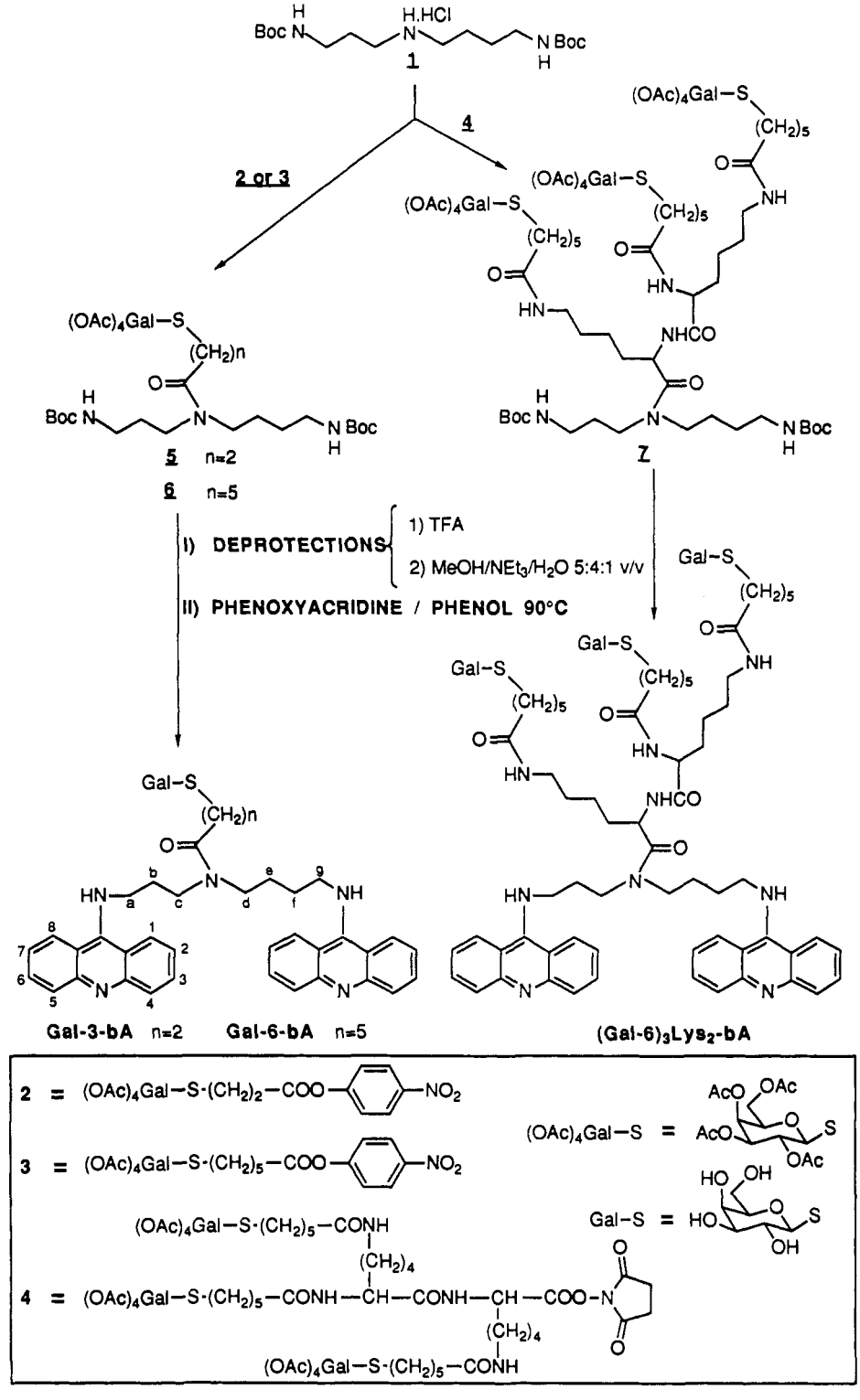


Figure 1. Synthetic schemes for galactosyl bisacridines.

(McGaw Park, IL). Proton NMR were obtained on General Electric GN 500 and QE 300 spectrometers (Fremont, CA). Spectra were recorded on samples diluted in deuterated methanol containing TMS. Proton chemical shifts are reported in ppm downfield from internal TMS (0.00 ppm). Liquid secondary ion mass spectrometry (LSIMS) measurements were made in the positive-ion mode with a Kratos MS-50 mass spectrometer (Ramsey, NJ) at the UCSF mass spectrometry facility. Samples were run in a thioglycerol matrix.

Chemical Synthesis. The synthetic scheme for preparation of the bisacridine targeting ligands is shown in Figure 1. N^1,N^8-Bis(*tert*-butoxycarbonyl)spermidine hydrochloride (1), a substrate for selective N^4-acylation of spermidine, was prepared according to published methods (*19*, *20*). The intermediate N^4-benzylspermidine (*19*) is commercially available (Sigma Chemical Co., St Louis, MO).

L-Lysyl-L-lysine bis(trifluoroacetate), for the synthesis of the branched galactosyl ligand, was obtained by standard peptide chemistry by reacting N^{ϵ}-(*tert*-butoxycarbonyl)-L-lysine (Bachem, Torrance, CA) with 2 equiv of N,N^{ϵ}-bis(*tert*-butoxycarbonyl)-L-lysine *p*-nitrophenyl ester (Bachem) in *N*-methylmorpholine containing *N*,*N*-diiso-

propylethylamine (1.5 equiv). The resulting protected lysine dimer was purified on a silica gel column eluted with the system chloroform/methanol/water 90:10:1 and was further deprotected in TFA.

3-(2,3,4,6-Tetra-*O*-acetyl-1-thio-β-D-galactopyranosyl)-propionate was prepared from 2-*S*-(2,3,4,6-tetra-*O*-acetyl-β-D-galactopyranosyl)-2-thiopseudourea hydrobromide (*21*) and 3-iodopropionic acid as previously described (*22*). 6-(2,3,4,6-Tetra-*O*-acetyl-1-thio-β-D-galactopyranosyl)hexanoate was prepared similarly from 2-*S*-(2,3,4,6-tetra-*O*-acetyl-β-D-galactopyranosyl)-2-thiopseudourea hydrobromide and 6-bromohexanoic acid. These acid-functionalized galactose derivatives were transformed into the corresponding activated esters (respectively **2** and **3**) by esterification with *p*-nitrophenol according to published procedures (*22*, *23*). N^{α}-[N^{α},N^{ϵ}-Bis[6-(2,3,4,6-tetra-*O*-acetyl-1-thio-β-D-galactopyranosyl)hexanoyl]-L-lysyl]-N^{ϵ}-[(6-(2,3,4,6-tetra-*O*-acetyl-1-thio-β-D-galactopyranosyl)-hexanoyl]-L-lysine was synthesized from compound **3** and L-lysyl-L-lysine bis(trifluoroacetate) according to the method of Ponpipom and co-workers (*23*). This derivative was activated by esterification with *N*-hydroxysuccinimide (1.1 equiv) in the presence of DCC (1.1 equiv) in anhydrous dichloromethane to yield the activated ester **4**.

Acylation of N^1,N^8-Bis(tert-butoxycarbonyl)spermidine Hydrochloride with the p-Nitrophenyl Esters 2 and 3. In a typical reaction, 1 mmol of acylating agent (557 mg of compound **2** or 599 mg of compound **3**) in 10 mL of acetonitrile was added dropwise under argon to a stirred solution of 0.7 mmol of N^1,N^8-bis(*tert*-butoxycarbonyl)-spermidine hydrochloride (**1**; 270 mg) in 10 mL of acetonitrile containing 140 μL of triethylamine (1 mmol). After the addition was completed, the reaction mixture was further stirred for 36 h under argon and evaporated in vacuo to a residue. This residue was redissolved in 50 mL of ethyl acetate, washed with 3% hydrochloric acid (3 × 10 mL), water (3 × 10 mL), 5% sodium hydrogen carbonate (3 × 10 mL), and water (3 × 10 mL), dried over $MgSO_4$, and evaporated to a syrup. This crude product was further purified on a silica gel column eluted with ethyl acetate/dichloromethane (1:1 v/v) to afford the desired conjugate (**5** or **6**) as a pale yellow syrup with an average yield from 30 to 40%.

Acylation of N^1,N^8-Bis(tert-butoxycarbonyl)spermidine Hydrochloride with the N-Hydroxysuccinimide Ester 4. A solution containing 400 mg of **4** (0.23 mmol) in 5 mL of acetonitrile was added dropwise to a stirred solution of 80 mg of N^1,N^8-Bis(*tert*-butoxycarbonyl)-spermidine hydrochloride (**1**; 0.22 mmol) in 5 mL of acetonitrile containing 42 μL of triethylamine (0.3 mmol). The reaction mixture was further stirred for 48 h under argon and evaporated in vacuo to a crude product which was chromatographed on a silica gel column eluted with chloroform/methanol/water (90:10:1 v/v) to afford the desired conjugate **7** as a syrup in 45% yield.

Deprotection of Compounds 5–7. In the first step, the *tert*-butoxycarbonyl protecting groups were quantitatively removed from the N^1 and N^8 atoms of the spermidine linker by a 30-min treatment with TFA according to the procedure described in ref 20. In the second step, the acetyl protecting groups were removed from the galactosyl headgroups by an overnight treatment with a mixture of methanol/water/NEt_3 (5:4:1), according to a procedure from reference 23. After the deprotections were completed, the dried residues of galactosylated spermidines were redissolved in water and passed through small Bio-Rad AG 1 × 2 (OH^-) columns in order to convert the salts into the corresponding free amines. The flow-through products from the columns were lyophylized. Spermidine–bisacridine and galactosylated derivatives were synthesized according to a procedure adapted from the general method of Barbet and co-workers (*24*) for the preparation of acridine dimers.

Spermidine–Bisacridine Trihydrochloride (bA·3HCl). 9-Chloroacridine (4.27 g, 20 mmol) and spermidine free base (1.45 g, 1.57 mL, 10 mmol) were dissolved in 30 mL of phenol at 80 °C. The temperature was raised to 130 °C and the solution stirred under argon. After stirring for 1.5 h, the resulting dark solution was cooled to ca. 40 °C and poured into 60 mL of 1 N NaOH. The precipitate was collected by filtration and washed on the filter with 1 N NaOH and water. The solid was redissolved in methanol and purified on a silica gel column eluted with increasing amounts of diethylamine in methanol (0%, 0.25%, 0.5%, 1%, and 2% v/v). The column chromatography separates spermidine–bisacridine from the mono- and trisubstituted byproducts and from the unreacted or degraded starting materials. The fractions containing the acridine dimer, found in the 0.5–2% diethylamine wash, were pooled together and evaporated to dryness in vacuo. The residue was redissolved in boiling methanol and crystallized as a trihydrochloride by dropwise addition of concentrated HCl. The crystals were collected and recrystallization from methanol yielded 1.77 g of the title compound (yield 29%).

Galactosylated Spermidine–Bisacridines Diacetates [(Gal-3-bA, Gal-6-bA and $(Gal\text{-}6)_3Lys_2$-bA)]. Bisacridine derivatives of the galactosylated spermidines were prepared by a modification of the procedure described for spermidine–bisacridine. 9-Phenoxyacridine was used as reagent instead of 9-chloroacridine. It was prepared from 9-chloroacridine according to the procedure of Dupré and Robinson (*25*). In a typical reaction, 0.2 mmol of 9-phenoxyacridine (54.2 mg) and 0.1 mmol of a galactosylated spermidine derivative were dissolved in 3 mL of phenol at 80 °C. This reaction mixture was further stirred under argon at 80–85 °C. After stirring for 2 h, the dark solution was cooled to ca. 40 °C and poured into 30 mL of diethyl ether. The precipitate was isolated by filtration, washed on the filter with diethyl ether, and redissolved in a mixture of *n*-butanol/methanol (3:1 v/v). The resulting solution was concentrated in vacuo and chromatographed on a column of silica gel eluted with n-butanol/pyridine/acetic acid/water (6:2:1:2 v/v) in order to separate the desired bisacridine from the monosubstituted byproduct and from the unreacted or degraded starting materials. The fractions containing the bisacridines were pooled together and evaporated in vacuo to yellow residues.

This method led to the diacetate salts of the expected bisacridines with yields averaging from 25 to 35%. These compounds, used for the targeting study, were stored at 4 °C as concentrated stock solutions in ethanol. The exact concentration of these solutions were determinated from the absorbance at 412 nm using a spermidine–bisacridine standard. TLC analysis after a 6-month storage period showed a slight degradation (ca. 10%) of the diacridines into the corresponding monoacridines.

bA·3HCl. ^1H NMR (CD_3OD) δ (ppm): 8.64–8.55 (dd, J = 8.5 Hz, 4 H, acr H-1 and H-8), 7.99–7.95 (m, 4 H, acr H-4 and H-5), 7.84–7.81 (m, 4 H, acr H-3 and H-6), 7.62–7.56 (m, 4 H, acr H-2 and H-7), 4.32 (t, J = 7.1 Hz, 2 H, spermidine CH_2-a), 4.23 (t, J = 6.8 Hz, 2 H, spermidine CH_2-g), 3.23 (t, J = 7.4 Hz, 2 H, spermidine CH_2-c), 3.15 (t, J = 7.6 Hz, 2 H, spermidine CH_2-d), 2.43 (q, J = 7.1 Hz, 2 H, spermidine CH_2-b), 2.12 (q, J = 7.4 Hz, 2 H, spermidine CH_2-f), 1.92 (q, J = 7.2 Hz, 2 H, spermidine CH_2-e). LSIMS: m/z = 500 (M + H). R_f (*n*-butanol/

acetic acid/pyridine/water 4:1:2:1) = 0.12 (R_f of the monoacridine homolog = 0.02).

Gal-3-bA. ^{1}H NMR (CD_3OD) δ (ppm): 8.55–8.48 (dd, J = 8.5 Hz, 4 H, acr H-1 and H-8), 7.98–7.90 (m, 4 H, acr H-4 and H-5), 7.85–7.78 (m, 4 H, acr H-3 and H-6), 7.56–7.48 (m, 4 H, acr H-2 and H-7), 4.28 (d, J = 10 Hz, 1 H, gal. H-1, β-configuration), 4.20 (t, J = 7.1 Hz, 2 H, spermidine CH_2-a), 4.11 (t, J = 6.5 Hz, 2 H, spermidine CH_2-g), 3.85 (d, J = 3.2, 1 H, gal. H-4), 3.75–3.60 (m, 4 H, spermidine CH_2-c and CH_2-d), 3.54–3.38 (m, 5 H, gal. H-2, H-3, H-5, H-6a, and H6-b), 3.02–2.93 (m, 2 H, spacer arm SCH_2), 2.85–2.70 (m, 2 H, spacer arm CH_2CONR_2), 2.24–2.10 (m, 2 H, spermidine CH_2-b), 2.06–1.94 (m, 2 H, spermidine CH_2-f), 1.90–1.70 (m, 2 H, spermidine CH_2-e). LSIMS: m/z = 750.4 (M + H). R_f (n-butanol/acetic acid/pyridine/water 4:1:2:1) = 0.22 (R_f of the monoacridine homolog = 0.10).

Gal-6-bA. ^{1}H NMR (CD_3OD) δ (ppm): 8.48–8.45 (dd, J = 8.5 Hz, 4 H, acr H-1 and H-8), 7.93–7.88 (m, 4 H, acr H-4 and H-5), 7.85–7.79 (m, 4 H, acr H-3 and H-6), 7.54–7.48 (m, 4 H, acr H-2 and H-7), 4.26 (d, J = 10 Hz, 1 H, gal. H-1, β-configuration), 4.18 (t, J = 7.1 Hz, 2 H, spermidine CH_2-a), 4.05 (t, J = 6.5 Hz, 2 H, spermidine CH_2-g), 3.90 (d, J = 3.2, 1 H, gal. H-4), 3.76–3.66 (m, 4 H, spermidine CH_2-c and CH_2-d), 3.58–3.38 (m, 5 H, gal. H-2, H-3, H-5, H-6a, and H-6b), 2.74–2.54 (m, 2 H, spacer arm SCH_2), 2.28 (t, J = 7.2, 2 H, spacer arm CH_2CONR_2), 2.20–2.14 (m, 2 H, spermidine CH_2-b), 2.01–1.94 (m, 2 H, spermidine CH_2-f), 1.93–1.70 (m, 2 H, spermidine CH_2-e), 1.6–1.0 (bm, spacer arm CH_2). LSIMS: m/z = 792.5 (M + H). R_f (n-butanol/acetic acid/pyridine/water 4:1:2:1) = 0.26 (R_f of the monoacridine homolog = 0.14).

(Gal-6)$_3$Lys$_2$-bA. ^{1}H NMR (CD_3OD) δ (ppm): 8.55–8.45 (m, 4 H, acr H-1 and H-8), 7.98–7.90 (m, 4 H, acr H-4 and H-5), 7.85–7.82 (m, 4 H, acr H-3 and H-6), 7.60–7.52 (m, 4 H, acr H-2 and H-7), 4.33–4.17 (m, 7 H, gal. H-1, spermidine CH_2-a and CH_2-g), 4.15–4.07 (m, 1 H, Lys αCH), 4.05–3.95 (m, 1 H, Lys αCH), 3.87 (m, 3 H, gal. H-4), 3.76–3.34 (bm, 19 H, spermidine CH_2-c and CH_2-d, gal. H-2, H-3, H-5, H-6a, and H-6b), 3.29–2.95 (bm, 4 H, Lys ϵCH_2), 2.78–2.57 (m, 6 H, spacer arm SCH_2), 2.27–2.10 (bm, 8 H, spacer arm CH_2CONHR, spermidine CH_2-b), 2.06–1.80 (bm, spermidine CH_2-f, and CH_2-e, acetate), 1.80–1.00 (bm, spacer arm CH_2). LSIMS: m/z = 1632.8 (M + H), m/z = 1654.8 (M + Na). R_f (n-butanol/acetic acid/pyridine/water 4:1:2:1) = 0.18 (R_f of the monoacridine homolog = 0.08).

Ethidium Bromide Displacement Assay. Ethidium bromide (19 μM) was mixed with calf thymus DNA (5.7 μM as nucleotide equivalents) in a 10 mM Tris-HCl buffer, 0.2 M NaCl, pH 7.4. Then increasing amounts of bA·3HCl, Gal-3-bA, Gal-6-bA, or (Gal-6)$_3$Lys$_2$-bA were added in order to displace ethidium bromide from DNA (*26, 27*). This competitive displacement was monitored by recording the decrease of ethidium bromide fluorescence (excitation = 540 nm; emission = 610 nm). To provide values for the decrease of the fluorescence of the ethidium–DNA complex alone, that of free ethidium was subtracted. Fluorescence values are displayed as a percentage of the maximum (fluorescence of ethidium–DNA complex alone). The intrinsic fluorescence of the bisacridine occurs at 450 nm and does not contribute to the fluorescence signal at 610 nm.

Gel Retardation Assay. Samples of pCLUC4 plasmid (200 ng, 300 pmol base pair equivalents) in 5 μL of water were mixed with 21 pmol of Gal-3-bA, Gal-6-bA, or Gal$_3$-Lys$_2$-bA in 5 μL of water. The intercalator to plasmid ratio is 300:1. When indicated, 33.3 pmol of RCA-I (Boehringer-Mannheim) in 1 μL of a 5 mM phosphate buffer, 0.2 M NaCl, pH 7.2, was added. After 20-min incubation, the samples were electrophoresed through a 0.8% agarose gel using a 40 mM Tris–acetate buffer system (pH 8.0) and stained with ethidium bromide to visualize DNA.

Binding and Uptake of AsOR by Isolated Rat Hepatocytes. The assays on rat hepatocytes in suspension were performed within 2 h after cell isolation. The assays on adherent cells were performed 24 h after cell isolation. AsOR binding was determined using (0.6–0.7) × 10^6 viable hepatocytes incubated in 1.5-mL polypropylene tubes in 0.5 mL of binding medium [Eagle's minimal essential medium (MEM), 20 mM HEPES, pH 7.5] containing 0.1–3 μg of ^{125}I-AsOR/mL (10^6 dpm/μg). The cells were kept in suspension on a rotator for 2 h at 4 °C in the presence of the ligand. At the end of the incubation, the cells were centrifuged and the cell pellets were washed with ice-cold PBS (containing 0.1 g/L $CaCl_2$ and 0.1 g/L $MgCl_2$·$6H_2O$). This was repeated three times. The pellets were counted for radioactivity in a γ scintillation spectrometer (Beckman Gamma 8000) and lysed in 1 mL of 1 N NaOH prior to protein determination using a Bradford dye-binding protein assay (Bio-Rad protein assay kit). The time course of AsOR uptake was determined similarly using ^{125}I-AsOR (10^6 dpm/μg) at a concentration of 1 μg/mL in 0.5 mL of binding medium containing (0.6–0.7) × 10^6 cells rotated for increasing periods of time (0.5, 1, 2, 3, and 4 h) at 37 °C (Figure 5A). AsOR uptake by adherent hepatocytes was determined under the conditions given below for the plasmid uptake assay using 1 μg of ^{125}I-AsOR/mL of medium. Nonspecific binding and uptake were determined in the presence of a 100-fold excess of unlabeled ligand. The amount of cell-associated AsOR is expressed as nanograms of AsOR per milligram of cell protein.

Inhibition of AsOR Binding to Hepatocytes. Increasing amounts of (Gal-6)$_3$Lys$_2$-bA, free or complexed to the plasmid pCLUC4 (500 intercalators per plasmid), and 10 ng of ^{125}I-AsOR (3.6 × 10^5 dpm) in a total volume of 50 μL of phosphate buffer, pH 7.2, were added in duplicate to 0.5 mL of a suspension of freshly isolated rat hepatocytes (1.25 × 10^6 cells) in binding medium in 1.5-mL polypropylene tubes. After incubation for 2 h at 4 °C with rotation, 200 μL of the cell suspension was centrifuged over 200 μL of 4:1 silicone/light mineral oil at 10^4g for 30 s. The radioactivity associated with the cell pellets was measured. The percent cell-associated AsOR was computed as the radioactivity in the presence of inhibitor divided by the radioactivity in the absence of inhibitor times 100.

Uptake of Targeted Plasmids by Isolated Rat Hepatocytes. *Cells in suspension.* Freshly isolated rat hepatocytes (10^6 cells) were kept in suspension in 0.5 mL of binding medium in 1.5-mL polypropylene tubes. Ten microliters of water containing 200 ng of ^{125}I-pCLUC4 plasmid (8 × 10^4 dpm), complexed or not with (Gal-6)$_3$-Lys$_2$-bA (500 bisacridines per plasmid), was added to the tubes in duplicates. The tubes were rotated for different periods at 37 °C (0.5, 1, 2, and 3 h), and the cell suspensions were centrifuged over 0.5 mL of 4:1 silicone/light mineral oil at 10^4g for 30 s. The cell pellets were counted for radioactivity and lysed in 0.5 mL of 1 N NaOH for subsequent protein determination as described above. Cell-associated plasmid is expressed as nanograms of plasmid per milligram of cell protein.

Adherent cells. Freshly isolated rat hepatocytes (10^6 cells) were plated in 60-mm petri dishes in 3 mL of MEM containing 5% fetal calf serum (FCS) and antibiotics (penicillin, 100 units/mL; streptomycin, 100 μg/mL; gen-

tamycin, 25 μg/mL). After 18 h at 37 °C, the medium was removed and replaced with 1 mL of serum-free MEM. One microgram of ^{125}I-pCLUC4 plasmid complexed to bA·3HCl, Gal-3-bA, Gal-6-bA, or $(Gal\text{-}6)_3Lys_2$-bA in 100 μL of water was added in duplicate (with 150 μg of AsOR, when indicated). The bisacridine to plasmid ratio was 500:1 or 100:1. The cells were further incubated for 1 h at 37 °C and then rinsed and digested in 1 mL of 1 N NaOH. The cell lysates were counted for radioactivity and protein was measured as described above.

Transfection Assay. The cells were plated and grown as described above. After 18 h at 37 °C, the medium was removed and replaced with 2 mL of serum-free MEM. Then 4 μg of pCLUC4 plasmid complexed to $(Gal\text{-}6)_3Lys_2$-bA at a ratio of 500 intercalators per plasmid in 100 μL of water was added. After 5-h incubation at 37 °C, the medium was removed and replaced with 3 mL of fresh MEM containing 5% FCS and antibiotics. The cells were grown for an additional 48 h at 37 °C and tested for luciferase activity as described previously (*28*).

RESULTS

Synthesis of Bisacridine Intercalators for Use as DNA Targeting Ligands. To create a targeting system for directing DNA to hepatocytes we have synthesized bifunctional molecular conjugates consisting of a targeting ligand for hepatocytes (galactose) that is covalently attached via spacer arms of various lengths to the DNA bis-intercalator spermidine–bisacridine. The synthesis of the delivery system is based upon the trifunctionalization of the N^1, N^4, and N^8 atoms of spermidine (Figure 1) and involves a selective N^4-acylation starting with N^1,N^8-bis(*tert*-butoxycarbonyl)spermidine hydrochloride as proposed by Bergeron and colleagues (*20*). The acylating agents are the mono (linear) or branched acetyl-protected galactosides **2**–**4** terminated by an activated carboxylic acid function and prepared as described in refs 22 and 23. The acylation of N^1,N^8-bis(*tert*-butoxycarbonyl)spermidine hydrochloride with these agents gives the protected galactose–spermidine conjugates **5**–**7**. The N^4-acylation step is followed by deprotection and subsequent reaction of the primary N^1 and N^8 atoms with 9-phenoxyacridine. This final reaction leads to the desired galactose–spermidine–bisacridine conjugates [Gal-3-bA, Gal-6-bA, and $(Gal\text{-}6)_3Lys_2$-bA]. This chemistry is versatile and can easily be used to attach other carbohydrates or any similarly functionalized targeting ligand to a bisacridine anchor. For instance, a similar strategy has been used by Nielson and co-workers to link nitrobenzamido ligands to a 1,5-bis(9-acridinylamino)-3-azapentane anchor (*29*).

Binding of Intercalators to DNA. Intercalation of the bisacridine conjugates into DNA was demonstrated by an ethidium bromide displacement assay (*26*, *27*). This assay is based upon the marked fluorescence enhancement seen when ethidium bromide intercalates into DNA. This property is used here for spectrofluorometric quantitation of ethidium displacement from its intercalation sites. As shown in Figure 2, the acridine dimers competitively displace ethidium bromide from calf thymus DNA. The binding constants of the bisacridines are calculated from this assay by using a computation method described by Wolfe and Meehan (*30*) and an intrinsic dissociation constant of 6.7×10^{-6} M for ethidium bromide (*31*).

As a result of the loss of one positive charge, a slight but significant decrease in affinity is observed when spermidine–bisacridine is N^4-acylated by the galactosyl derivatives. An additional small decrease in affinity is observed when the size and hydrophilicity of the targeting moiety

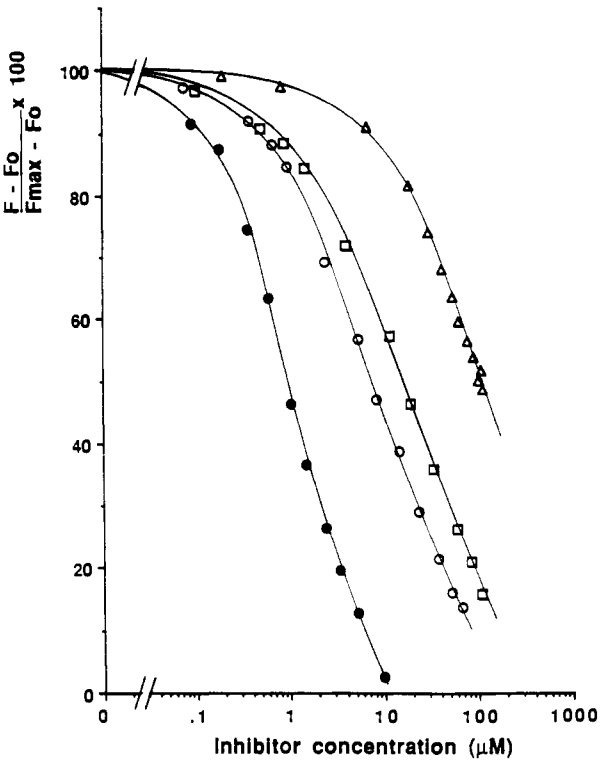


Figure 2. Displacement of ethidium bromide from calf thymus DNA by the bisacridine derivatives. The decrease of the fluorescence of the ethidium–DNA complex was recorded as described in the Experimental Procedures. Fo, fluorescence of free ethidium bromide (19 μM); Fmax, fluorescence of the ethidium–DNA complex alone (19 μM ethidium, 5.7 μM nucleotide); F, fluorescence of the ethidium–DNA complex in the presence of the bisacridine derivative. (●) bA·3HCl, $K_d = 4.31 \times 10^{-8}$ M; (○) Gal-3-bA, $K_d = 5.42 \times 10^{-7}$ M; (□) Gal-6-bA, $K_d = 1.2 \times 10^{-6}$ M; (△) $(Gal\text{-}6)_3Lys_2$-bA), $K_d = 8.64 \times 10^{-6}$ M.

are increased [K_d (bA·3HCl) = 4.31×10^{-8} M, K_d (Gal-3-bA) = 5.42×10^{-7} M, K_d (Gal-6-bA) = 1.2×10^{-6} M, K_d [$(Gal\text{-}6)_3Lys_2$-bA)] = 8.64×10^{-6} M].

Interaction of DNA Ligands with a Soluble Receptor. DNA binding of the galactosylated intercalators and subsequent interaction of the intercalated galactosyl ligands with a soluble receptor, RCA-I, is shown by a gel-mobility-shift assay with the 5 kb plasmid pCLUC4 (Figure 3). Binding of intercalating agents extends the double helix, which leads to a relaxation of the supercoiling of circular DNA (*32*, *33*). As a result, a shift in the electrophoretic mobility of the plasmid–intercalator complex is observed. Intercalation of Gal-3-bA, Gal-6-bA, and $(Gal\text{-}6)_3Lys_3$-bA into pCLUC4 is shown by the retardation of the DNA movement observed in Figure 3, lanes 2, 4, and 6. Intercalation of the conjugates into the plasmid results in the expected relaxation of the supercoiled form to a relaxed circular form, which migrates slower. Due to their higher affinity for DNA, Gal-3-bA and Gal-6-bA are more potent in producing this shift in mobility of the plasmid than $(Gal\text{-}6)_3Lys_2$-bA. The capability of Gal-3-bA, Gal-6-bA, and $(Gal\text{-}6)_3Lys_2$-bA to bind pCLUC4 to a soluble receptor for galactose is shown by the complete retardation of the complexes in the presence of RCA-I (Figure 3, lanes 3, 5, and 7). The lectin RCA-I is a tetramer selective for terminal β-D-galactose residues and is able to cross-link galactosylated particles via four binding sites (*34*). As a consequence of this property, the ability of Gal-3-bA, Gal-6-bA, and $(Gal\text{-}6)_3Lys_2$-bA to promote the binding of pCLUC4 to RCA-I results in the formation of large plasmid aggregates which do not penetrate the gel.

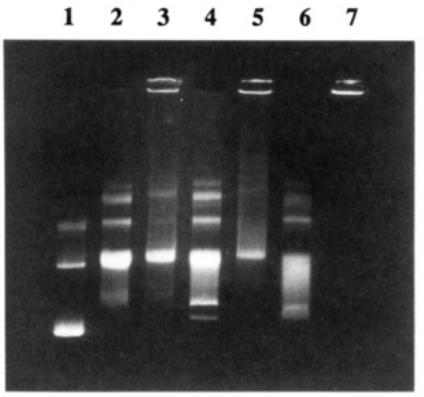


Figure 3. Effect of Gal-3-bA, Gal-6-bA, and $(Gal\text{-}6)_3Lys_2$-bA on plasmid DNA electrophoretic migration in the presence and absence of ricin lectin RCA-I. Electrophoresis was performed as described in the Experimental Procedures. Lane 1, pCLUC4; lane 2, pCLUC4 + Gal-3-bA; lane 3, pCLUC4 + Gal-3-bA + RCA-I; lane 4, pCLUC4 + Gal-6-bA; lane 5, pCLUC4 + Gal-6-bA + RCA-I; lane 6, pCLUC4 + $(Gal\text{-}6)_3Lys_2$-bA; lane 7, pCLUC4 + $(Gal\text{-}6)_3Lys_2$-bA + RCA-I.

Despite its lower affinity for DNA, $(Gal\text{-}6)_3Lys_2$-bA is more efficient (Figure 3, lane 7) in promoting RCA-I-induced plasmid–plasmid aggregation than Gal-3-bA or Gal-6-bA (Figure 3, lanes 3 and 5). The efficiency of RCA-I-mediated plasmid aggregation is limited by the accessibility of the attached galactosyl ligand and by the electrostatic repulsion between adjacent plasmids. Thus interaction between RCA-I and the ligands on the DNA should be favored by increasing the spacing between the plasmid and the attached galactosyl ligands; the gel retardation results are consistent with this expectation. As a result of a multivalent interaction, the plasmid aggregates formed by RCA-I are quite stable. No visible dissociation occurred when a 100-fold excess of free galactose was added and incubated with the aggregates (data not shown).

Interaction of Galactose-Targeted DNA with Hepatocytes. The interaction of the targeted plasmid with cells expressing a receptor for galactose was studied in vitro with isolated rat hepatocytes. Mammalian hepatocytes express a well-characterized asialoglycoprotein receptor which binds and internalizes glycoproteins exposing terminal galactosyl residues (*35*).

To ensure that the receptor was not damaged during the hepatocyte isolation procedure, the cells were checked for specific AsOR binding and uptake using the conditions of Harris and co-workers (*36*). The binding of AsOR is saturable with an apparent K_d of about 10^{-9} M (Figure 4A). The time course of ^{125}I-AsOR uptake is shown in Figure 5A; ^{125}I-AsOR uptake saturates at about 2 h after addition and is efficiently inhibited in the presence of a 100-fold excess of the unlabeled protein. These results are in agreement with published data (*36*) and confirm the presence of a functional receptor for galactose on the isolated cells. Interestingly, when the uptake study was performed on adherent cells 24 h after isolation, the 1-h specific uptake decreased from 133.1 ng/mg of cell protein to 52.6 ng/mg of cell protein. Under these conditions the total uptake is about 2 times greater than the nonspecific uptake, indicating a down regulation of the receptor upon culturing of the cells.

We examined the interaction of the galactose-targeted plasmids with both adherent (Table I) and suspension cells (Figures 4B and 5B). In adherent cells, $(Gal\text{-}6)_3Lys_2$-bA mediates a saturable uptake that can be inhibited by a 100-fold AsOR excess over the targeting ligand concentration. The other ligands tested do not mediate targeting

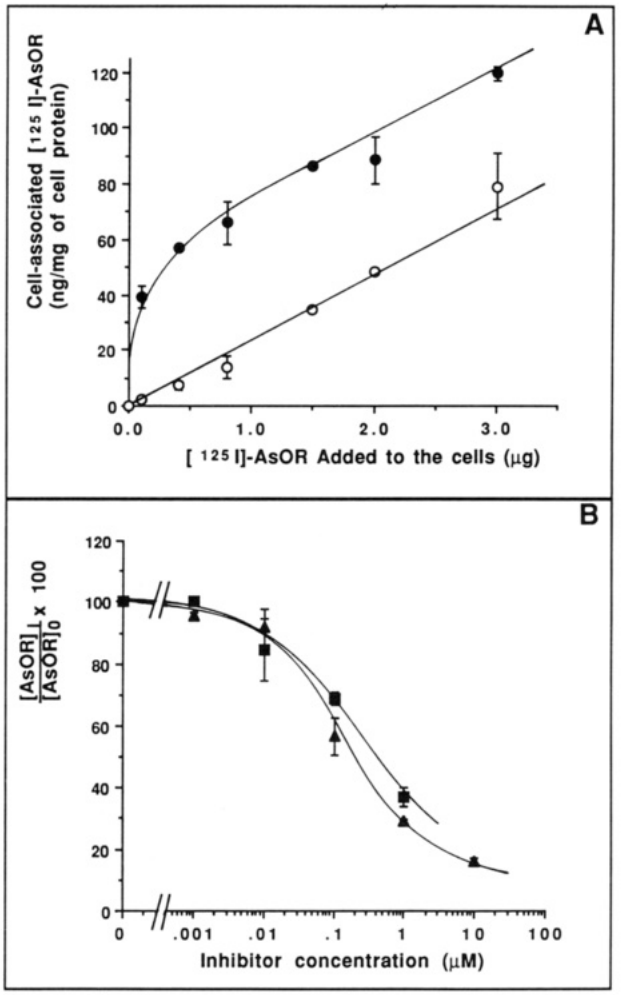


Figure 4. Binding of ^{125}I-AsOR to rat hepatocytes in a suspension in the presence and absence of galactosylated ligands. Panel A: cell-associated ^{125}I-AsOR after 2-h incubation at 4 °C with increasing concentrations of the radiolabeled ligand. Each value is the mean of duplicate determinations that agreed to within 10%; (●) total binding, (○) nonspecific binding in the presence of a 100-fold excess of nonlabeled AsOR as described in the experimental procedures. Panel B: cell-associated ^{125}I-AsOR after 2-h incubation with 20 ng/mL of the radiolabeled ligand and in the presence of increasing concentrations of free $(Gal\text{-}6)_3Lys_2bA$ (▲) or $(Gal\text{-}6)_3Lys_2bA$ complexed to pCLUC4 (■, 500 bisacridines per plasmid). The values are the mean of duplicate measurements that agreed to within 10%. $[AsOR]_i$ = cell-associated ^{125}I-AsOR in the presence of the inhibitor; $[AsOR]_0$ = cell-associated ^{125}I-AsOR in the absence of the inhibitor.

Table I. Plasmid Uptake by Adherent Rat Hepatocytes

complexing agent	ng ^{125}I-pCLUC4/mg of cell protein[a]	
	−AsOR	+AsOR
none	10.5 ± 0.1	10.4 ± 0.1
bA·3HCl (500:1)	9.9 ± 1.8	ND
Gal-3-bA (500:1)	10.7 ± 1.7	ND
Gal-6-bA (500:1)	11..1 ± 1.8	ND
$(Gal\text{-}6)_3Lys_2$-bA (500:1)	17.0 ± 1.2	9.9 ± 0.6
$(Gal\text{-}6)_3Lys_2$-bA (100:1)	14.5 ± 0.6	ND

[a] The cells were incubated with 1 μg of ^{125}I-pCLUC4 plasmid in the presence or absence of the bisacridine derivatives and of an excess of AsOR. The ratio of bis-intercalator to plasmid is shown in parentheses. The amount of plasmid that became cell-associated was determined as described in the Experimental Procedures. The values are the mean of duplicates that agreed within 10%. (ND, not determined).

and do not increase cell-associated plasmid over that found in the absence of ligand (Table I). The targeting is also sensitive to the density of ligand. At a ratio of 500 (Gal-

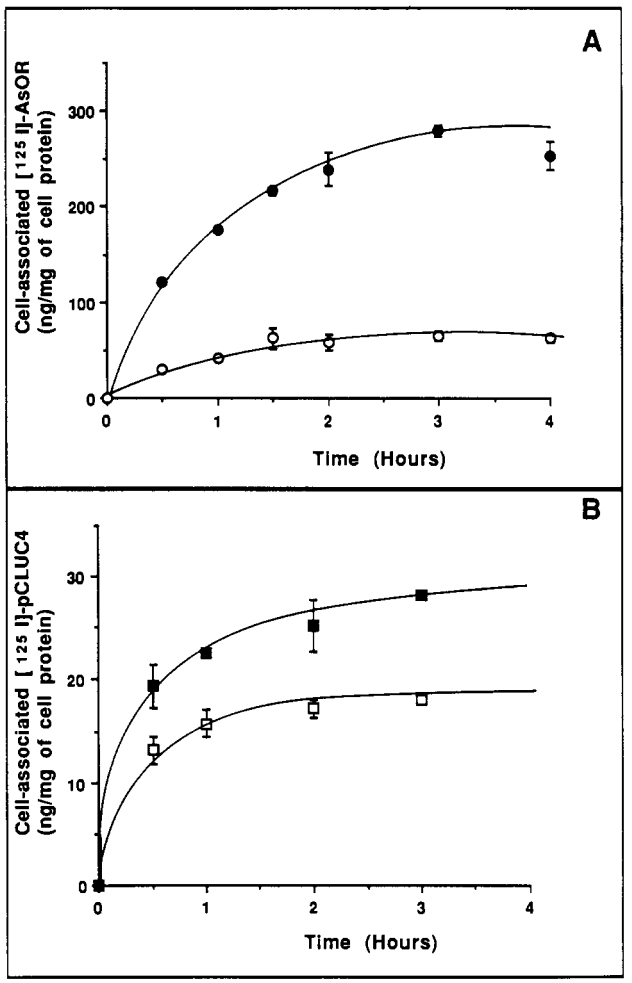


Figure 5. Time course of uptake of ^{125}I-AsOR and of targeted plasmid DNA by freshly isolated rat hepatocytes in suspension. Panel A: the cells were incubated with 1 μg/mL of ^{125}I-AsOR and the amount of ligand that became cell-associated was determined as a function of time as described in the Experimental Procedures. Each value is the mean and the range of duplicates agreed within 10%; (●) total uptake, (○) nonspecific uptake in presence of 100 μg of nonlabeled AsOR. Panel B: the cells were incubated with 200 ng of ^{125}I-pCLUC4 plasmid and the amount of DNA that became cell-associated in presence and absence of the targeting ligand (Gal-6)$_3$Lys$_2$-bA was determined as a function of time as described in the Experimental Procedures. Each value is the mean and the range of duplicates agreed within 10%; (■) plasmid with (Gal-6)$_3$Lys$_2$-bA (500 bisacridines per plasmid), (□) plasmid without (Gal-6)$_3$Lys$_2$-bA.

6)$_3$Lys$_2$-bA per plasmid, the specific plasmid–cell association corresponds to 6.5 ng of DNA/mg of cell protein. (Gal-6)$_3$Lys$_2$-bA was found to be less potent at a reduced conjugate to plasmid ratio. At a ratio of 100:1, the specific association was reduced to 4 ng/mg of cell protein.

In suspension cells, binding of AsOR was inhibited by the targeting ligand (Gal-6)$_3$Lys$_2$-bA with an apparent IC_{50} of about 5×10^{-7} M. Only a slight increase of the IC_{50} to 10^{-6} M was observed when (Gal-6)$_3$Lys$_2$-bA was attached to plasmid DNA (Figure 4B). In addition, (Gal-6)$_3$Lys$_2$-bA mediates a 2-fold increase in plasmid uptake by the cells (Figure 5B). Taken together, these results suggest that the conjugate (Gal-6)$_3$Lys$_2$-bA is able to target plasmid DNA to the asialoglycoprotein receptor of isolated rat hepatocytes.

In spite of AsOR-inhibitable binding of the plasmid to the hepatocytes, no expression of luciferase could be detected from the cells treated with the (Gal-6)$_3$Lys$_2$-bA–pCLUC4 complex and subsequently cultured for 48 h. This is due either to the inability of the plasmid to escape degradation in the lysosomes and/or cross the membrane to enter the cell after its interaction with the asialoglycoprotein receptor.

DISCUSSION

We have designed, synthesized, and characterized a low molecular weight conjugate useful for targeting of DNA to the galactose receptor of various cells including hepatocytes. The design of this conjugate was motivated by recent reports showing that the AsOR–polylysine conjugates can be used for selective and efficient gene delivery to hepatocytes via a receptor-mediated endocytosis pathway (*4*, *7–10*). Related to previous work, our aim was to separate the binding function from the membrane destabilizing function of the targeting complex. Polylysine has at least two effects when used to attach ligands to DNA. The obvious one is the attachment of the ligand. A less obvious one relates to polylysine's ability to introduce DNA into cells in a nonspecific fashion (*37*). Our strategy is based upon the attachment of a synthetic galactosyl ligand to a DNA intercalator. A synthetic approach was selected in order to create a low molecular weight and well-defined system.

We have evaluated the ability of three synthetic conjugates, Gal-3-bA, Gal-6-bA, and (Gal-6)$_3$Lys$_2$-bA, to complex to DNA and subsequently promote binding to a soluble or a cell-surface-localized galactose-binding protein. These conjugates consist of thiogalactosyl head groups that are covalently attached to spermidine–bisacridine via variable spacer arms. The selection of spermidine–bisacridine as a DNA anchor for the targeting ligands was motivated by the following criteria: (1) Spermidine can be functionalized stepwise and without ambiguity as to the stoichiometry of the targeting ligands and the acridines. (2) Acridines and related compounds are used for the treatment of malignant and parasitic deseases in humans (*38*) and thus are a reasonable starting point for a novel human therapeutic. (3) Spermidine–bisacridine is a known DNA bis-intercalator (*33*). Bis-intercalation provides tight binding and slow off-rate (*39*, *40*), two important considerations for the formation of stable noncovalent complexes.

Intercalation of the targeting conjugates into DNA was demonstrated by competitive displacement of ethidium bromide. The dissociation constants of monoacridines from DNA are in the viscinity of 10^{-3}–10^{-4} M whereas the dissociation constants of bisacridines, capable of bis-intercalation, are about 3–4 orders of magnitude smaller (*27*). The high binding affinities of the targeting conjugates for DNA strongly support their binding via bis-intercalation. Since the length of the spermidine linker (10.2 Å) is sufficient to encompass two successive base pairs in the DNA double helix, a model has been proposed where spermidine–bisacridine spans two base pairs of the helix (*33*). Thus, and in further agreement with the neighboring site exclusion principle (*41*), a single spermidine–bisacridine molecule excludes a total of four adjacent base pairs. As a consequence, a maximum of 1225 targeting conjugates can be attached to a 5 kb plasmid. The intercalation of the targeting conjugates into DNA results in both helix extension and distortion, which produced the relaxation of supercoiled plasmid DNA seen on the gel (Figure 3). This ability of the intercalators to distort the helical structure of DNA may be a disadvantage in the use of these compounds for gene transfer since condensation of DNA has been observed by a number of groups to promote transfection activity of various cationic facilitators (*37*)

and intercalators oppose DNA condensation (*32*, *33*). The helix extension subsequent to intercalation may render the plasmid too large for efficient inclusion in a 100–200-nm endosome. It is also conceivable that intercalation of the bisacridines could interfere with the transcription process. However, we have not observed this to be the case in experiments where transfection from bisacridine-containing plasmids was compared to that of unmodified plasmids subsequent to their microinjection into the nucleus of cultured cells (unpublished observation).

Modulation of the spacer arm between the galactosyl ligands and their bisacridine anchors allowed us to examine some structural parameters which are important for receptor binding. All three conjugates tested promoted to some extent the interaction of plasmid DNA with the galactose-binding lectin from RCA-I (gel shift). However, only $(Gal\text{-}6)_3Lys_2$-bA was able to efficiently bind the plasmid both to the soluble lectin and to the cellular galactose receptor of hepatocytes as shown in the competition experiments with AsOR (Figure 4B and Table I). The hepatic asialoglycoprotein receptor is known to have very stringent structural requirements for high-affinity ligand binding (*42*). Thus, improved accessibility and optimal ligand clustering provided by the branched spacer arm in $(Gal\text{-}6)_3Lys_2$-bA may account for its efficient binding.

It is not surprising that targeting the DNA to the galactose receptor did not lead to transfection since this bisacridine construct provides no membrane destabilizing functions, such as provided by defective adenovirus particles in the endosome, to help the DNA enter the cytoplasm (*13*). Although we have not yet studied the fate of the cell-associated DNA, we suspect it is internalized via endocytosis and ultimately degraded in the lysosome. Thus the bisacridine–ligands differ from the polycation–ligands which can bind to DNA as well as mediate transfection.

One can envision a collection of effectors conjugated to intercalators that could be combined to create a tailor-made gene-delivery system. These effectors might include DNA masking molecules, membrane-destabilizing peptides, targeting ligands, and nuclear localization peptides. The galactosyl bisacridines provide an example of the flexibility and robustness of bisacridine chemistry for such a synthesis.

ACKNOWLEDGMENT

The authors are grateful to Dr. Anthony Shaw, Dr. Alan Wolfe, Dr. Jean-Yves Legendre, Gary Green, and Kun-Bee Chang for helpful discussions and technical assistance. Thanks are also extended to the UCSF mass spectrometry facility supported by the NIH Division of Research Resources, Grant RR01614, and to the UCSF Liver Center, Grant POAM26743A-08. This work was supported by NIH Grant GM 26691.

LITERATURE CITED

(1) Gilboa, E., Eglitis, M. A., Kantoff, P. W., and Anderson, W. F. (1986) Transfer and expression of cloned genes using retroviral vectors. *Biotechniques 4*, 504–512.

(2) Felgner, P. L., and Rhodes, G. (1991) Gene therapeutics. *Nature 349*, 351–352.

(3) Marsh, M., and Helenius, A. (1989) Virus entry into animal cells. *Adv. Virus Res. 36*, 107–151.

(4) Wu, G., and Wu, C. H. (1988) Evidence for targeted gene delivery to HepG2 hepatoma cells *in vitro*. *Biochemistry 27*, 887–892.

(5) Wagner, E., Zenke, M., Cotten, M., Beug, H., and Birnstiel, M. L. (1990) Transferrin-polycation conjugates as carriers for DNA uptake into cells. *Proc. Natl. Acad. Sci. U.S.A. 87*, 3410–3414.

(6) Wagner, E., Cotten, M., Mechtler, K., Kirlappos, H., and Birnstiel, M. L. (1991) DNA-binding transferrin conjugates as functional gene-delivery agents: Synthesis by linkage of polylysine or ethidium homodimer to the transferrin carbohydrate moiety. *Bioconjugate Chem. 2*, 226–231.

(7) Wu, G. Y., and Wu, C. H. (1988) Receptor-mediated gene delivery and expression *in vivo*. *J. Biol. Chem. 263*, 14621–14624.

(8) Wu, G. Y., Wilson, J. M., and Wu, C. H. (1989) Targeting genes: Delivery and persistent expression of a foreign gene driven by mammalian regulatory elements *in vivo*. *J. Biol. Chem. 264*, 16985–16987.

(9) Wu, G. Y., Wilson, J. M., Shalaby, F., Grossman, M., Shafritz, D. A., and Wu, C. H. (1991) Receptor-mediated gene delivery *in vivo*—Partial correction of genetic analbuminemia in nagase rats. *J. Biol. Chem. 266*, 14338–14342.

(10) Wilson, J. M., Grossman, M., Wu, C. H., Roy Chowdhury, N., and Roy Chowdhury, J. (1992) Hepatocyte directed gene transfer *in vivo* leads to transient improvement of hypercholesterolemia in low density lipoprotein receptor-deficient rabbits. *J. Biol. Chem. 267*, 963–967.

(11) Zenke, M., Steinlein, P., Wagner, E., Cotten, M., Beug, H., and Birnstiel, M. L. (1990) Receptor-mediated endocytosis of transferrin-polycation conjugates: An efficient way to introduce DNA into hematopoietic cells. *Proc. Natl. Acad. Sci. U.S.A. 87*, 3655–3659.

(12) Cotten, M., Langle-Rouault, F., Kirlappos, H., Wagner, E., Mechtler, K., Zenke, M., Beug, H., and Birnstiel, M. L. (1990) Transferrin–polycation-mediated introduction of DNA into human leukemic cells: Stimulation by agents that affect the survival of transfected DNA or modulate transferrin receptor levels. *Proc. Natl. Acad. Sci. U.S.A. 87*, 4033–4037.

(13) Cotten, M., Wagner, E., Zatloukal, K., Phillips, S., Curiel, D. T., and Birnstiel, M. L. (1992) High efficiency receptor-mediated delivery of small and large (48Kb) gene constructs using the endosome disruption activity of defective or chemically-inactivated adenovirus particles. *Proc. Natl. Acad. Sci. U.S.A. 89*, 6094–6098.

(14) Curiel, D. T., Agarwal, S., Romer, M. U., Wagner, E., Cotten, M., Birnstiel, M. L., and Boucher, R. C. (1992) Gene transfer to respiratory epithelial cells via the receptor-mediated endocytosis pathway. *Am. J. Respir. Cell Mol. Biol. 6*, 247–252.

(15) Huckett, B., Ariatti, M., and Hawtrey, A. O. (1990) Evidence for targeted gene transfer by receptor-mediated endocytosis: Stable expression following insulin-directed entry of neo into HepG2 cells. *Biochem. Pharmacol. 40*, 253–263.

(16) Rozenkrantz, A. A., Yachmenev, S. V., Jans, D. A., Serebryakova, N. V., Murav'ev, V. I., Peters, R., and Sobolev, A. (1992) Receptor-mediated endocytosis and nuclear transport of a transfecting DNA construct. *Exp. Cell Res. 199*, 323–329.

(17) Trubetskoy, V. S., Tortchilin, V. P., Kennel, S. J., and Huang, L. (1992) Use of N-terminal modified poly(L-lysine)–antibody conjugate as a carrier for targeted gene delivery in mouse lung endothelial cells. *Bioconjugate Chem. 3*, 323–327.

(18) De Wet, J. R., Wood, K. V., De Luca, M., Helinsky, D. R., and Subramani, S. (1987) Firefly luciferase gene: Structure and expression in mammalian cells. Mol. Cell Biol. *7*, 725–737.

(19) Bergeron, R. J., Stolovwitch, N. J., and Porter, C. W. (1982) Reagents for the selective secondary N-acylation of linear triamines. *Synthesis* 689–692.

(20) Bergeron, R. J., McGovern, K. A., Channing, M. A., and Burton, P. S. (1979) Synthesis of N4-acylated N1,N8-Bis(acyl)spermidines: An approach to the synthesis of siderophores. *J. Org. Chem. 45*, 1589–1592.

(21) Chipowsky, S., and Lee, Y. C. (1973) Synthesis of 1-thioaldosides having an amino group at the aglycon terminal. *Carbohydr. Res. 31*, 339–346.

(22) Haensler, J., and Schuber, F. (1991) Influence of the galactosyl ligand structure on the interaction of galactosylated liposomes with mouse peritoneal macrophages. *Glycoconjugate J. 8*, 116–124.

(23) Ponpipom, M. M., Bugianesi, R. L., Robbins, J. C., Doebber, T. W., and Shen, T. Y. (1981) Cell-specific ligands for selective drug delivery to tissues and organs. *J. Med. Chem. 24*, 1388–1395.

(24) Barbet, J., Roques, B. P., and Le Pecq, J-B. (1975) Compounds for polyintercalation of DNA: Synthesis of acridine dimers. *C. R. Acad. Sci., Paris 281*, D 851–853.

(25) Dupré, D. J., and Robinson, F. A. (1945) N-substituted 5-aminoacridines. *J. Chem. Soc.* 549–551.

(26) Cain, B. F., Baguley, B. C., and Denny, W. A. (1978) Potential antitumor agents. 28. Deoxyribonucleic acid polyintercalating agents. *J. Med. Chem. 21*, 658–668.

(27) Nielsen, P. E. (1982) Photoaffinity labeling of chromatin. Synthesis and properties of arylazido derivatives of 9-aminoacridine: Potential photolabels for chromatin studies. *Eur. J. Biochem. 122*, 283–289.

(28) Legendre, J.-Y., and Szoka, F. C. (1992) Delivery of plasmid DNA into mammalian cell-lines using pH-sensitive liposomes: Comparison with cationic liposomes. *Pharm. Res. 9*, 1235–1242.

(29) Nielsen, P. E., Egholm, M., Koch, T., Christensen, J. B., and Buchardt, O. (1991) Photolytic cleavage of DNA by nitrobenzamido ligands linked to 9-aminoacridines gives DNA polymerase substrates in a wavelength-dependent reaction. *Bioconjugate Chem. 2*, 57–66.

(30) Wolfe, A. R., and Meehan, T. (1992) Use of binding site neighbor-effect parameters to evaluate the interactions between adjacent ligands on a linear lattice. Effects on ligand–lattice association. *J. Mol. Biol. 223*, 1063–1087.

(31) Reinhardt, C. G., and Krugh, T. R. (1978) A comparative study of ethidium bromide complexes with dinucleotides and DNA: Direct evidence for intercalation and nucleic acid sequence preferences. *Biochemistry 17*, 4845–4854.

(32) Bauer, W., and Vinograd, J. (1970) Interaction of closed circular DNA with intercalative dyes II. The free energy of superhelix formation in SV40 DNA. *J. Mol. Biol. 47*, 419–435.

(33) Wright, R. G. McR., Wakelin, L. P. G., Fieldes, A., Acheson, R. M., and Waring, M. J. (1980) Effect of ring substituents and linker chains on the bifunctional intercalation of diacridines into deoxyribonucleic acid. *Biochemistry 19*, 5825–5836.

(34) Nicholson, G. L., Blaustein, J., and Etzler, M. E. (1974) Characterization of two plant lectins from *Ricinus communis* and their quantitative interaction with a murine lymphoma. *Biochemistry 13*, 196–204.

(35) Ashwell, C., and Morell, A. G. (1974) The role of surface carbohydrates in the hepatic recognition and transport of circulating glycoproteins. *Adv. Enzymol. 41*, 99–128.

(36) Harris, L., Preat, V., and Farber, E. (1987) Patterns of ligand binding to normal, regenerating, preneoplastic, and neoplastic rat hepatocytes. *Cancer Res. 47*, 3954–3958.

(37) Felgner, P. L. (1990) Particulate systems and polymers for *in vitro* and *in vivo* delivery of polynucleotides. *Adv. Drug Delivery Rev. 5*, 163–187.

(38) Denny, W. A., Baguley, B. C., Cain, B. F., and Waring, M. J. (1983) Antitumor Acridines. In *Molecular Aspects of Anti-Cancer Drug Action*, (S. Neidle, and M. J. Waring, Eds.) Topics in Molecular and Structural Biology, Vol. 3, pp 1–34, Macmillan, London.

(39) Capelle, N., Barbet, J., Dessen, P., Blanquet, S., Roques, B. P., and Le Pecq, J-B. (1979) Deoxyribonucleic acid bifunctional intercalators: Kinetic investigation of the binding of several acridine dimers to deoxyribonucleic acid. *Biochemistry 18*, 3354–3362.

(40) Markovits, J., Garbay-Jaureguyberry, C., Roques, B. P., and Le Pecq, J-B. (1989) Acridine dimers: influence of the intercalating ring and of the linking-chain nature on the equilibrium and kinetic DNA-binding parameters. *Eur. J. Biochem. 180*, 359–366.

(41) Von Hippel, P. H., and McGhee, J. D. (1972) DNA-protein interactions. *A. Rev. Biochem. 41*, 231–300.

(42) Lodish, H. F. (1991) Recognition of complex oligosaccharides by the multisubunit asialoglycoprotein receptor. *Trends Biol. Sci. 6*, 374–377.

Specific Recognition of Antibody–Oligonucleotide Conjugates by Radiolabeled Antisense Nucleotides: A Novel Approach for Two-Step Radioimmunotherapy of Cancer

Will H. A. Kuijpers,* Ebo S. Bos, Frans M. Kaspersen, Gerrit H. Veeneman, and Constant A. A. van Boeckel

AKZO Pharma Division, Organon International BV, P.O. Box 20, 5340 BH Oss, The Netherlands.
Received July 9, 1992

One of the major challenges in radioimmunotherapy is the specific delivery of radioisotopes to tumor cells while minimizing normal tissue radiation. In this respect, the application of two-step pretargeting schemes generally leads to more favorable tumor to normal tissue uptake ratios than direct administration of radioimmunoconjugates. In this study, we present the specific hybridization of complementary DNA fragments as a novel recognition mechanism in pretargeting. Briefly, our strategy involves first administration of antibody–DNA conjugate, followed by targeting with radiolabeled complementary DNA (antisense DNA). Complementary oligodeoxynucleotides (14-mers, T_m = 57 °C), in which part of the phosphodiesters has been replaced by methylphosphonates (to ensure stability against nucleases), were prepared on a DNA synthesizer. The oligonucleotides were further derivatized via a uridine moiety at their 5′-end in such a way that radiolabeling or conjugation with antibodies could be accomplished. Both a murine IgG (anti-hCG) and the human anti-tumor IgM 16.88 were conjugated with one to three oligonucleotides via the heterobifunctional cross-linker SMCC. Incubation of these immunoconjugates with the radiolabeled antisense DNA revealed specific hybridization with the antibody-linked oligonucleotides. Antigen binding studies performed with antigen-coated matrices showed that the immunoreactivity of the antibody–DNA conjugate is preserved. Moreover, it is demonstrated that the radiolabeled DNA is still capable of hybridizing selectively with the oligonucleotides of the immunoconjugate, when the latter is bound to its antigen.

INTRODUCTION

Radiolabeled monoclonal antibodies (radioimmunoconjugates) against tumor-associated antigens have received much attention in cancer research during the last decade since they offer a unique opportunity to specifically target tumor cells (*1*). Unfortunately, the slow passage of the antibody through physiological barriers as well as blood clearance and uptake of the radioimmunoconjugate by the reticuloendothelial system (liver, spleen) results in a very low tumor uptake (0.001%–0.01% of injected dose/gram of tumor tissue) (*2*). In tumor diagnosis, the slow pharmacokinetics and low tumor uptake serve no serious problems, since a low radiation dose is sufficient to image tumor sites, once an optimal tumor to normal tissue uptake ratio has been reached (*3*). In radioimmunotherapy, however, a high radiation dose is required in order to kill the tumor cells (*4*). As long as the percentage uptake by the tumor is very low, the majority of the radioactivity administered will cause serious radiation damage to healthy tissue. Due to this poor tumor to normal tissue ratio, the application of radiolabeled monoclonal antibodies in cancer therapy has been limited up to now mainly to tumors which can be treated by intracavitary administration (e.g. in non-Hodgkin's lymphoma and ovarian carcinoma) (*5*, *6*).

An elegant way to circumvent the limitations described above is offered by a "pretargeting" strategy (*7*). In this two-step approach the radioisotope is targeted to the tumor site after prelocalization of a functionalized antibody, with specificity for both the tumor and a radioactive ligand. At the time the optimal tumor to normal tissue uptake of the antibody has been reached, the radioisotope–ligand, displaying relatively fast kinetics, is administered.

Several pretargeting schemes have already been investigated, among them the use of bifunctional antibodies with specificity for both tumor antigens and radiolabeled chelates (*8*, *9*). Early experiments with the latter system have not been encouraging, the main problem being low affinity of the antibody for the radiolabeled chelate (*10*). In another approach the interaction between biotin and avidin is used (*11*, *12*). Although high binding affinities were found, this strategy suffers from immunological responses since avidin conjugates are identified as foreign determinants by the patient's immune system (*13*). Despite these drawbacks, both approaches have recently been shown to provide better tumor contrasts in clinical imaging studies than conventional immunoscintigraphy (*13–15*).

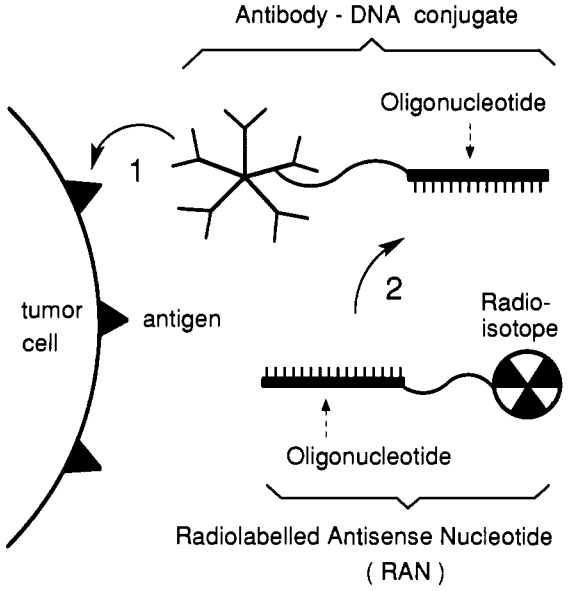
We reasoned that hybridization between two complementary DNA[1] fragments can serve as an ideal recognition mechanism to ensure specificity of the antibody for the radioisotope. In practice, this approach implies targeting of tumor cells with antibody–oligonucleotide[1] conjugates (step 1, Scheme I). As oligonucleotides are naturally occurring highly charged molecules, they are not likely to evoke an immunological response. Once an optimal tumor to normal tissue uptake ratio has been established, the complementary oligonucleotide carrying the radioisotope should be administered (step 2, Scheme I). In contrast to the bulky radioimmunoconjugates, these relatively small radiolabeled DNA fragments are expected to show fast pharmacokinetics as well as a rapid clearance from the blood.

As naturally occurring oligonucleotides are rapidly degraded in serum by nucleases (*16*), modification of the

[1] In this article the terms DNA and oligonucleotide refer to oligodeoxynucleotides.

1043-1802/93/2904-0094$04.00/0 © 1993 American Chemical Society

Scheme I. Principle of DNA–DNA Pretargeting.



DNA fragments is required for the application of DNA–DNA pretargeting. Up to now, several classes of modified oligonucleotides have been described, merely as agents in the so-called antisense oligonucleotide strategy (*17*). In this approach, modified DNA or RNA fragments are targeted to complementary sequences (DNA or mRNA) *inside* cells. Target sequences for future therapies comprise, among others, oncogenes in tumor cells and viral genes, e.g., in HIV-infected cells (*18*, *19*). In the DNA–DNA pretargeting strategy, contrary to antisense therapy, the target sequences for the "antisense" nucleotide are located *outside* the tumor cells, where the antibody–oligonucleotide conjugates are bound. Nevertheless, both the oligonucleotide conjugated to the antibody and the radiolabeled complementary strand essentially have to meet the same criteria as antisense oligonucleotides such as nuclease resistance, duplex stability, and good solubility in serum. In this respect, a choice can be made out of a large variety of backbone modifications including phosphorothioates (*20*), methylphosphonates (*21*), and alkyl phosphotriesters (*22*), as well as substitutes (e.g., methylene acetal or peptide backbones) (*23*, *24*). However, since the DNA–DNA hybridization in pretargeting takes place extracellularly, the oligonucleotides do not have to be as extensively modified as in antisense therapy, where efficient cell penetration is an essential requirement.

Although several modified antisense oligonucleotides have been shown to selectively inhibit gene expression in vitro, only little information is available concerning the in vivo disposition and stability of modified oligonucleotides (*25*, *26*). Preliminary studies in this area indicate that 3′-end modified DNA fragments display in vivo pharmacokinetics suitable for application in DNA–DNA pretargeting: In a mouse model a rapid clearance from the circulation with a half-life of 10 min, excretion into urine (20–30% in 8 h), and uptake in tissues (stable for at least 8 h) was observed (*27*).

In this paper we present the results of a study directed toward the feasibility of the DNA–DNA pretargeting strategy. Methods are described for the preparation of antibody–oligonucleotide conjugates and the radiolabeled "antisense" nucleotides (RANs[2]). Hybridization between the antibody-linked oligonucleotides and the radioactive complementary strand is investigated as well as the immunoreactivity of the antibody–DNA conjugate. Finally, the viability of the two-step regimen, involving incubation with conjugate followed by targeting with RAN, is clearly illustrated in a series of experiments with antigen-coated Sepharose beads.

EXPERIMENTAL PROCEDURES

General Procedures. Analytical HPLC was conducted on a Waters 600E (system controller) single-pump gradient system, equipped with a Waters Model 484 variable-wavelength UV detector and a Waters Model 741 data module under the following conditions: Pharmacia FPLC ion-exchange column MonoQ HR 5/5; buffer A, 0.02 M KH_2PO_4 (pH = 5.5, 25% acetonitrile); buffer B, 0.02 M KH_2PO_4 and 2.0 M KCl (pH = 5.5, 25% acetonitrile); gradient, 0–20 min linear 0 → 64% B; flow rate 1.0 mL/min; detection at 254 nm. IEF was carried out in a Phast electrophoresis system (Pharmacia LKB, Sweden) on a polyacrylamide gel at pH 3.0–9.0, according to the manufacturer's instructions. Gels were stained with Coommassie Brilliant Blue using the programmed staining procedure in the same equipment. SDS–PAGE was performed in a V16 vertical gel electrophoresis system (BRL, Bethesda, MD). Proteins were separated in a linear gradient gel (T = 4–26%, C = 3%) with a spacer (T = 3%, C = 3%) using the discontinuous buffer system of Laemmli (*28*). The thickness of the gel was 1.5 mm. Electrophoresis was performed under nonreducing conditions for 13–15 h at 15 mA at ambient temperature. A prestained protein mixture (Amersham) was used as molecular marker solution, containing myosin (200 kDa), phosphorylase B (94 kDa), serum albumin (68 kDa), ovalbumin (45 kDa), carbonic anhydrase (30 kDa), trypsin inhibitor (21 kDa), and lysozyme (14 kDa) as components. Gels were stained with Coommassie Brilliant Blue G250. Radioactivity was measured in a MINAXI-γ autogamma counter type 5000 (Packard).

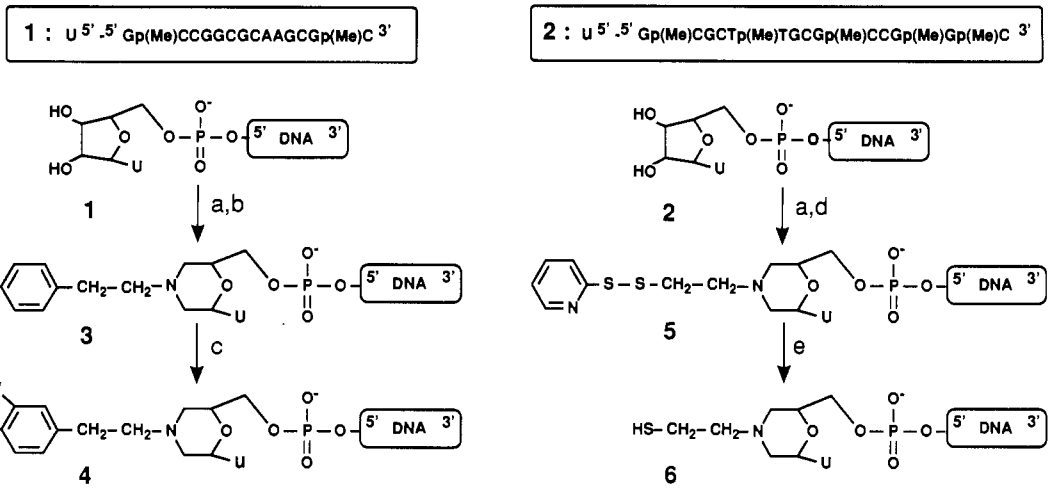
Monoclonal Antibodies. Monoclonal antibody 130A, a murine IgG_1 against human chorionic gonadotropin (hCG), was produced for diagnostic purposes according to the classical Köhler–Milstein fusion procedure. This mAb has a p*I* of 4.8–5.3.

Monoclonal antibody 16.88 is a colon tumor-reactive antibody produced by an immortalized B cell from an ASI patient (*29*). Purified 16.88 was obtained from Organon Teknika Corp. BRI (Rockville, MD). It is directed to CTA*1, a complex of modified cytokeratins 8, 18, 19 that was isolated from HT29 cells (*30*).

Oligonucleotide Synthesis. Oligodeoxynucleotides **1** and **2** (Scheme II), bearing methylphosphonates at defined positions and a 5′–5′ linked uridine fragment at their 5′-ends, were prepared on a fully automated DNA synthesizer (Pharmacia, Gene Assembler). The standard dimethoxytrityl nucleoside phosphoramidite coupling method was used on a 10-μmol CPG support column (*31*). Methylphosphonate linkages were incorporated by applying methylphosphonamidites of suitably protected thymidine and deoxyguanosine nucleosides (*32*). These amidites were prepared by phosphitylation of commer-

[2] Abbreviations used: CPG, controlled-pore glass; DTE, dithioerythritol; DTT, dithiothreitol; hCG, human chorionic gonadotropin; IEF, isoelectric focusing; mAb, monoclonal antibody; PVDF, polyvinylidene difluoride; RAN, radiolabeled antisense nucleotide; SDS–PAGE, polyacrylamide gel electrophoresis in the presence of sodium dodecyl sulfate; SMCC, succinimidyl 4-(maleimidomethyl)cyclohexane-1-carboxylate; SPDP, succinimidyl 3-(pyridyldithio)propionate; SSC, saline–sodium citrate buffer (pH = 6.8); TEAB, triethylammonium bicarbonate buffer (pH = 7.8); T_m, melting temperature.

Scheme II. Oligonucleotide Sequences and Synthesis of RAN 4 and Thiol-Derivatized Oligonucleotide 6[a]



[a] Positions of the methylphosphonate linkages in the oligonucleotides are denoted with p(Me). Reagents: (a) $NaIO_4$, (b) tyramine, $NaCNBH_3$, (c) Iodogen, $Na^{125}I$, (d) *S*-pyridylcysteamine hydrochloride, $NaCNBH_3$, (e) tributylphosphine.

cially available 5′-*O*-(dimethoxytrityl)thymidine and *N*-2-isobutyryl-5′-*O*-(dimethoxytrityl)-2′-deoxyguanosine, respectively, with bis(*N*,*N*-diisopropylamino)methylphosphine and collidine hydrochloride as catalyst. Introduction of the 5′–5′ linked uridine moiety was accomplished using 2′,3′-di-*O*-acetyluridine 5′-(2-cyanoethyl *N*,*N*-diisopropylphosphoramidite). This reagent was prepared starting from known 2′,3′-di-*O*-acetyluridine by phosphitylation with (2-cyanoethyl)-*N*,*N*-diisopropylaminochlorophosphine (*33*).

After completion of the solid-phase synthesis, cleavage of the oligonucleotide from the solid support and removal of protecting groups were carried out by incubation in saturated dry ammonia/methanol solution (20 mL) in a sealed flask for 72 h at 50 °C. The support was removed by filtration and the filtrate was evaporated under reduced pressure. The crude unprotected DNA fragments were chromatographed on Sephadex S-100 (HiLoad HR) (2 cm^2 × 150 cm) with TEAB buffer (0.05 M). The appropriate fractions (as monitored with HPLC) were pooled, concentrated to a small volume, and lyophilized. The oligonucleotides were converted into the Na^+ form by passing them through a column of Dowex 50W X4 cation-exchange resin. The resulting UV-positive fractions were pooled and again lyophilized. Both oligonucleotides were found to be homogeneous according to HPLC analysis (MonoQ HR 5/5).

Determination of Duplex Stability. The stability of the duplex between the complementary oligodeoxynucleotides **1** and **2** was determined by measuring UV hyperchromicity at 260 nm as a function of temperature using a Beckman DU-8 spectrophotometer equipped with a T_m analysis system, consisting of a temperature-controlled sample holder, temperature controller, and T_m Compuset module. Duplexes were made by mixing equimolar amounts of the two complementary strands to a concentration of 1.10^{-5} M per strand in 0.01 M Tris·HCl (pH = 7.0) adjusted to 0.1 M sodium concentration with NaCl. The solution was heated to 90 °C for 10 min to destroy any secondary structures and then cooled to ambient temperature. Absorbance of the oligonucleotide solution at 260 nm was measured every 0.5 °C from 20 to 90 °C. The melting temperature (T_m) was obtained from the maximum value of the first derivative plot of absorbance vs temperature.

Preparation of Tyramine-Derivatized Oligonucleotide 3. Oligonucleotide **1** (2.4 mg, 0.5 μmol) was incubated in an ice-cold solution of sodium periodate (125 μL, 0.05 M) in 0.1 M sodium acetate buffer (pH = 4.75). The oxidation was allowed to proceed for 30 min at 0 °C in the dark. The reaction mixture was applied to a Sephadex G-10 column (1 cm × 10 cm) and eluted with water. The DNA-containing fractions were pooled and concentrated by lyophilization to ca. 50 μL. This solution was diluted with 0.1 M phosphate buffer (pH = 7.5)/methanol (2:1 v/v) (250 μL), followed by the addition of 0.05 M tyramine (300 μL) in 0.1 M phosphate buffer (pH = 6.9)/methanol (2:1 v/v), to give a final pH of 8.5. After 30 min of incubation, a freshly prepared 0.1 M solution of sodium cyanoborohydride (150 μL) was added. The mixture was left overnight at room temperature. After addition of an additional portion of 0.1 M sodium cyanoborohydride in methanol (150 μL), the reaction mixture was maintained at room temperature for 1 h, followed by removal of methanol by evaporation. The mixture was applied to a Sephadex G-25 column (1 cm × 45 cm) and eluted with 0.05 M TEAB (pH = 7.8). The eluted fractions were monitored by absorbance at 254 nm and checked for purity with HPLC (MonoQ) analysis. The first peak fractions, containing derivatized DNA, were pooled and lyophilized. The oligonucleotide **3** was stored at −20 °C.

Preparation of Radiolabeled Antisense Nucleotide (RAN) 4. Iodogen (*34*) was dissolved in dichloromethane at a concentration of 2 mg/mL. An aliquot of 25 μL was transferred to an Eppendorf reaction tube. The solvent was allowed to evaporate under a stream of dry nitrogen. Oligonucleotide **3** (10 μg in 110 μL of PBS) was transferred to the Iodogen-coated tube and 2 mCi of $Na^{125}I$ [3] was added. The mixture was vortexed and incubated for 15 min at room temperature. Unbound radioiodide was separated by gel filtration on Sephadex G-25 (PD-10 column, Pharmacia) using water as eluent. Fractions (0.5 mL) were collected and checked for radioactivity. The appropriate fractions were pooled to give a final concentration of 3 μg DNA/mL with a specific activity of 35 μCi/μg.

Preparation of Thiol-Protected Oligonucleotide 5. To a solution of oligonucleotide **2** (2.8 mg, 0.5 μmol) in 0.1 M ice-cold sodium acetate buffer (pH = 4.75, 100 μL) was added 0.05 M sodium periodate (125 μL) in the same

[3] In this study, the ^{125}I isotope was merely applied as a tracer to get a proof of principle for the DNA–DNA pretargeting; of course, for future therapy other isotopes (e.g. ^{131}I,^{90}Y) should be used.

acetate buffer. Methanol (100 μL) was added to give a clear solution. The reaction mixture was incubated for 45 min at 0 °C in the dark, followed by chromatography on a Sephadex G-10 column (1 cm × 10 cm) using water as eluent. DNA-containing fractions were pooled and concentrated to a volume of ca. 50 μL. To this solution were added, respectively, 0.1 M phosphate buffer (pH = 8.0)/methanol (2:1 v/v) (100 μL), 0.04 M *S*-pyridylcysteamine hydrochloride in the same phosphate buffer/methanol mixture (300 μL), and, after 30 min, freshly prepared 0.1 M sodium cyanoborohydride in methanol (25 μL). The clear solution with a final pH of 8.0 was incubated overnight at room temperature. An additional portion of freshly prepared sodium cyanoborohydride (0.1 M in methanol, 50 μL) was added and the reaction mixture was incubated for another 1.5 h at room temperature. After removal of methanol by evaporation, reagents were separated from the derivatized DNA by chromatography on Sephadex G-25 (1 cm × 45 cm) using 0.05 M TEAB buffer (pH = 7.8) as eluent. The elution profile was monitored by UV absorbance at 254 nm. The fractions containing DNA, as established by HPLC (MonoQ), were collected and lyophilized twice with water. The oligonucleotide was stored at −20 °C.

Determination of *S*-Pyridyl Content of 5. Oligonucleotide **5** was dissolved in 0.1 M phosphate buffer (pH = 8.0)/methanol (2:1 v/v) to a concentration of ca. 20 μM. The oligonucleotide concentration was determined by measuring absorbance at 260 nm ($\epsilon_{DNA,260}$ = 126 000 $M^{-1}\cdot cm^{-1}$). To this solution was added 50 mM dithioerythritol (DTE) in the above phosphate buffer/methanol mixture to a final concentration of 500 μM. The difference in absorbances at 343 and 400 nm (reference) was determined before and after DTE addition. The increase of this value is ascribed to release of pyridinethione (ϵ_{343} = 8080 $M^{-1}\cdot cm^{-1}$) (*35*).

Derivatization of Monoclonal Antibodies with SMCC. To a solution of mAb (1–2 mg of IgG; 5–10 mg of IgM) in 2.5 mL of 50 mM phosphate buffer (pH = 7.5) was added 0.05 M SMCC (*36*) in dimethylformamide (50 equiv for IgG, 20 equiv for IgM). The reaction mixture was incubated for 90 min at room temperature in the dark. Excess SMCC was removed by gel filtration on Sephadex G-25 (PD-10 column, Pharmacia) in 50 mM phosphate buffer (pH = 6.0), containing 0.1 M NaCl and 5 mM EDTA. The mAb concentration in the resulting solution was determined by measuring absorbance at 280 nm (1 mg/mL = 1.4 absorbance units).

The number of maleimide groups incorporated onto the mAb was determined as follows: a small portion (500 μL) of maleimide-derivatized mAb was reacted with 50 mM cysteamine (200 μL) in the phosphate buffer (pH = 6.0) for 10 min. Unreacted cysteamine was back titrated with 5,5′-dithiobis(2-nitrobenzoic acid) (DTNB) (*37*) and quantified spectrophotometrically at 412 nm after 15 min (ϵ_{412} = 13 600 $M^{-1}\cdot cm^{-1}$). As a reference cysteamine oxidation with DTNB in the absence of maleimide was determined. Under the conditions described, typically 8–10 maleimide groups were incorporated per antibody molecule.

Conjugation of Maleimide–mAb with Oligonucleotide 5. Oligonucleotide **5** was dissolved in 0.1 M phosphate buffer (pH = 8.0)/methanol (2:1 v/v), which had been thoroughly degassed with nitrogen, to a concentration of 250 μM. Under a nitrogen atmosphere, 5 mM tributylphosphine in 2-propanol was added (0.75 equiv with respect to the total amount of DNA, i.e. equimolar relative to the pyridyl disulfide present). The reduction was allowed to proceed for 15 min at room temperature. Meanwhile, a solution of maleimide-derivatized mAb in buffer containing 50 mM phosphate, 0.1 M NaCl, and 5 mM EDTA at pH 6.0 (0.5 mg mAb/mL) was similarly degassed and the reduced DNA solution was added under nitrogen to the functionalized antibody at a concentration of 4 molar equiv of (total) oligonucleotide per maleimide group. Conjugation was allowed to proceed overnight at 4 °C. Finally, unreacted maleimide groups were blocked by the addition of cysteamine (0.01 M) in water (100 μL). Following another 2 h at room temperature, the mixture was applied to a Sephacryl S-100 HR column (1.6 cm × 50 cm) using PBS as eluent in order to remove unreacted oligonucleotide. Chromatography was performed at 4 °C. The eluate was monitored at 280 nm. The fractions which contained antibody conjugate were collected and stored at 4 °C.

Determination of Conjugation Ratio. The number of oligonucleotides conjugated to mAb was quantified spectrophotometrically by determination of the absorbance of conjugate in PBS both at 260 and 280 nm. The degree of conjugation is derived from the A_{260}/A_{280} ratio as follows. Assuming that conjugation does not influence extinction coefficients, Beer's equations were formulated at 260 and 280 nm using following extinction coefficients: $\epsilon_{mAb,280} = 2.24\cdot10^5$ $M^{-1}\cdot cm^{-1}$ for IgG, $1.26\cdot10^6$ $M^{-1}\cdot cm^{-1}$ for IgM; $\epsilon_{DNA,260} = 1.26\cdot10^5$ $M^{-1}\cdot cm^{-1}$; A_{260}/A_{280} (free mAb; PBS) = 0.57; A_{260}/A_{280} (free DNA; PBS) = 1.55. With these data a relation can be derived between A_{260}/A_{280} (measured) and the conjugation ratio (Z):

$$Z = \frac{\epsilon_{mAb,280}}{\epsilon_{DNA,260}}\left(\frac{A_{260}/A_{280} - 0.57}{1 - (A_{260}/A_{280})/1.55}\right)$$

Hybridization of mAb–DNA Conjugate and RAN. Antibody–oligonucleotide conjugates in PBS (80 μL of 0.25 mg/mL 130A–DNA or 350 μL of 0.68 mg/mL 16.88–DNA) were diluted to 1.5 mL with 2× SCC hybridization buffer (pH = 6.8). RAN 4 in 2× SCC buffer was added (2 equiv with respect to antibody-linked oligonucleotides). Hybridization was allowed to proceed for 1 h at room temperature. Part of the hybridization mixture (500 μL) was kept apart to be used for an antigen binding study with antigen-coated Sepharose beads (see below). The remainder was applied on a S-100 HR column (1.6 × 50 cm) and eluted at 4 °C with PBS buffer at a flow rate of 1 mL/min. The eluate was monitored at 280 nm, and fractions were collected every 4 min. Presence of RAN in the eluted fractions was checked by measuring radioactivity. In the control experiments similar amounts of unmodified mAb in 2× SCC buffer were incubated with RAN 4 and treated as above.

Antigen Binding Study of 130A–DNA Conjugate with hCG-Sepharose Beads. Tresyl-activated Sepharose 4B (Pharmacia) (0.35 g) was suspended in 1 mM HCl (10 mL) and washed on a glass filter with 1 mM HCl (500 mL) over a period of 1 h. The beads were then washed with 0.1 M $NaHCO_3$, 0.5 M NaCl (100 mL). The gel was transferred to a polypropylene tube and hCG (10 mg) dissolved in 0.5 M $NaHCO_3$ (1.5 mL) was added. The suspension was incubated overnight at 4 °C with mixing. The beads were filtered off and washed with 0.1 M $NaHCO_3$, 0.5 M NaCl (50 mL). Absorbance at 280 nm of the eluate was measured to determine unbound hCG (1 mg/mL = 0.36 absorbance units). Resulting free tresyl groups on the beads were blocked by treatment with 0.1 M Tris·HCl (pH = 8.0) (5 mL) during 4 h at 4 °C. The gel was washed alternately with 0.1 M Tris·HCl, 0.5 M NaCl (pH = 8.0), and 0.1 M NaAc, 0.5 M NaCl (pH = 4.0) (three times each) and finally stored in PBS containing

0.05% sodium azide at 4 °C. For the batch described here a hCG loading of ca. 4.5 mg of hCG/mL of gel was found, as determined by subtraction of the amount of unbound hCG from the starting amount of hCG.

The hybridization mixture (500 μL; see above) was added to hCG-coated Sepharose beads (100 μL of gel in PBS) and incubated with mixing for 1.5 h at room temperature. Occasionally, the mixture was vortexed. After centrifugation, the supernatant was removed and the beads were washed thoroughly with 2× SSC buffer (500 μL). This procedure was repeated three times before the solid-phase-bound radioactivity was determined. In addition, radioactivity in the supernatant fractions was measured. The control experiment was carried out in exactly the same manner using a mixture of 130A and RAN. The following levels of radioactivity were measured: for 130A–DNA/RAN 4.1 μCi on the beads and 9.0 μCi in the supernatant; for 130A/RAN (control): 0.025 μCi on the beads and 13.7 μCi in the supernatant.

Dot Blot Hybridization of RAN with 16.88–DNA Conjugate. Two-fold dilutions of 16.88–DNA (lanes 1 and 3, Figure 3) and the unmodified antibody (lane 2) were transferred onto Immobilon PVDF membranes in a Bio-Rad dot blot apparatus. Excess protein binding sites were blocked by immersing the membrane in Blotto (5% skim milk in PBS/Tween) for 2 h at 37 °C. After several washes with 2× SSC buffer, the dot blots were incubated with RAN 4 (with or without a 100-fold excess of cold DNA 3) for 2 h at room temperature. The blots were subsequently washed six times with PBS/Tween and once with distilled water. After air-drying, autoradiography was performed for 24 h using a Kodak Royal X-omat film.

Antigen Binding Studies of 16.88–DNA Conjugate with CTA*1-Sepharose Beads. CTA*1-coated Sepharose was prepared essentially as described for the hCG-coated beads. Thus, Tresyl-Sepharose 4B (2.5 g) was, after washing, incubated with CTA*1 (3.2 mg) in 0.1 M $NaHCO_3$, 0.5 M NaCl (2.5 mL). The total amount of antigen bound to Sepharose is expected to be much smaller as compared with the hCG loading, since due to the size of CTA*1 only the outer surface of the beads will be coated with antigen. After blocking of free tresyl groups and several washings, beads were obtained with a loading of ca. 150 μg of CTA*1/mL of gel, as derived from determination of the amount of unbound CTA*1 in the eluates by UV spectroscopy (1 mg of CTA*1/mL = 1.0 absorbance units).

Sepharose beads coated with CTA*1 (gel volume, 3 mL) were washed three times with 0.2 M boric acid buffer (pH = 7.5). The hybridization mixture of 16.88–DNA conjugate and RAN 4 in 2× SSC buffer (75 μL, containing 12 μg of conjugate and 0.13 μg of 4; 190 nCi) was added, followed by the addition of 225 μL of 0.2 M boric acid (pH = 7.5). Incubation was allowed to proceed overnight at 4 °C with mixing. The beads were washed thoroughly with boric acid buffer (5 mL), followed by centrifugation and removal of the supernatant. This procedure was repeated five times in order to remove all the unbound conjugate and RAN. Finally, the matrix-bound radioactivity was determined. In the control experiment a same gel volume of CTA*1-Sepharose beads was incubated with a mixture of 16.88 (12 μg) and RAN 4 (0.13 μg, 190 nCi) in 2× SSC buffer and treated as above. For the 16.88–DNA/RAN experiment 17.5-fold higher radioactivity on the beads (11.5 nCi) was found as compared to the 16.88/RAN control (0.65 nCi).

In the "pretargeting" experiment CTA*1-Sepharose beads (four portions of 1 mL of gel volume) were, after equilibration with 0.2 M boric acid buffer (pH = 7.4), incubated overnight with 16.88–DNA conjugate (4.5 μg, 5 pmol) or an equal amount of 16.88 (control tubes) in 100 μL of the above boric acid buffer at 4 °C with mixing. The gel was washed twice with 0.2 M boric acid buffer (pH = 7.4) followed by three washings with 2× SSC buffer. Then, RAN 4 (0.1 μg, 20 pmol) in 100 μL of 2× SSC buffer was added to a 16.88–DNA and 16.88 tube, respectively. The other two tubes were incubated with a same amount of RAN (0.1 μg) and a 100-fold excess of unlabeled oligonucleotide 3 (10 μg) in the SSC buffer (100 μL). Hybridization was allowed to proceed for 2.5 h at room temperature with mixing. The beads in all four tubes were thoroughly washed with 700-μL portions of 0.2 M boric acid buffer (10 times) to remove all unhybridized oligonucleotides. Finally, the remaining radioactivity on the beads was determined and expressed relative to the 16.88 control incubated with 100-fold of 3 (see Table I).

RESULTS AND DISCUSSION

A successful DNA–DNA pretargeting necessitates that both the DNA fragment conjugated to the antibody and the RAN are modified to protect them against nuclease degradation (*16*). The main nuclease activity in the blood originates from 3′-exonucleases (*38*). Therefore, modification at the 3′-end of the oligonucleotide is considered to be essential in order to guarantee sufficient metabolic stability. As the oligonucleotide bound to the antibody should survive for quite a long period (2–3 days), this fragment should preferably be more extensively protected against nucleases than the RAN. On the other hand, care should be taken that the antibody-linked DNA fragment is not modified to such an extent that the conjugate becomes immunogenic. For our purposes, we chose the methylphosphonate modification (*21*). Methylphosphonates are stable toward the chemical conditions necessary for conjugation and radiolabeling and, in addition, we expected that introduction of neutral internucleoside linkages would diminish nonspecific binding of the oligonucleotides to positively charged blood proteins.

Two complementary chimeric phosphodiester/methylphosphonate DNA fragments 1 and 2 (Scheme II), bearing two and five methylphosphonate linkages, respectively, were prepared on a fully automated DNA synthesizer, using the phosphoramidite coupling chemistry (*31*). Methylphosphonates were incorporated by applying methylphosphonamidites instead of the standard cyanoethyl phosphoramidite building blocks (*32*). Similarly, at the 5′-end of both fragments a 2′,3′-di-*O*-acetyluridine nucleotide was introduced, linked in a 5′–5′ fashion. When synthesis was completed, the fully protected oligonucleotides were deprotected in methanolic ammonia and further purified.

The unprotected uridine moiety at the 5′-end offers, after oxidation of the 2′,3′ cis diol, an opportunity to incorporate various amino-containing linkers via reductive amination (*39*, *40*). This flexibility was our main reason for choosing the "uridine" concept instead of the direct introduction of specific linker groups at the oligonucleotide.

The ability of two complementary DNA strands to hybridize is generally not expressed in terms of affinity constants, as is the case for protein–substrate interactions, but formulated as a melting temperature T_m, at which half of the duplex is lost. This temperature can be monitored by measuring the absorbance at 260 nm as a function of temperature. The T_m value for the DNA duplex between 1 and 2 (0.1 M NaCl, 0.01 M Tris·HCl, pH = 7.0) was found to be 57 °C. Thus, it is assumed that effective hybridization is ensured under physiological conditions in vivo (37 °C).

Starting from oligonucleotide **1**, we prepared a radiolabeled DNA fragment (RAN **4**) in the following manner. Oxidation of **1** with sodium periodate afforded an intermediate dialdehyde which was derivatized with tyramine under reductive amination conditions to give oligonucleotide **3**. The (*p*-hydroxyphenyl)ethyl moiety of oligonucleotide **3** could be labeled in a standard iodination procedure with $Na^{125}I$ in the presence of Iodogen (*34*). After removal of free iodide by gel filtration, RAN **4** was obtained with a specific activity of 35 μCi/μg.

Likewise, oligonucleotide **2** had to be functionalized in such a way that conjugation with antibodies could be accomplished. A common strategy in preparing protein conjugates is the use of 2-pyridyl disulfide containing linkers (such as the commercially available SPDP) (*35*). Under reductive conditions, a free thiol group is generated which can be reacted with either a second thiol function (usually activated as 2-pyridyl disulfide) to afford a disulfide bond or a maleimide group, thus forming a thioether. In our approach, the uridine nucleotide allows, subsequent to oxidation, the incorporation of such protected thiol functions on the oligonucleotide. Thus, after oxidation of **2**, reductive amination with *S*-pyridylcysteamine was performed, yielding **5** containing a 2-pyridyl disulfide group. The efficiency of this set of reactions could be determined by treatment of a small aliquot of **5** with excess dithioerythritol (DTE). According to UV absorbance of the pyridinethione released (343 nm), approximately 45% of the oligonucleotide contained the protected thiol linker. Since HPLC analysis (MonoQ) revealed that during conversion of **2** into **5** the oligonucleotide chain remained fully intact, it may be concluded that the underivatized material results from incomplete oxidation or reductive amination of the uridine moiety. Therefore, the oligonucleotide material was not further purified, but used as such for antibody conjugation.

As disulfide-linked protein–DNA conjugates may be insufficiently stable under in vivo conditions (e.g. due to disulfide bond reduction by endogeneous thiols) (*41*), we focused on the maleimide coupling strategy. In this approach, the antibody is derivatized with maleimide groups by treatment of the protein with succinimidyl 4-(*N*-maleimidomethyl)cyclohexane-1-carboxylate (SMCC) (*36*). In our experience, monoclonal antibodies can be functionalized with 10–15 maleimide groups without significant reduction in immunoreactivity (*42*). Subsequently, a conjugate with free thiol containing oligonucleotides can be formed via a stable thioether linkage. To achieve this goal, oligonucleotide **5** was reduced with tributylphosphine to obtain a free thiol group. This reagent is advantageous relative to DTT or DTE since the reaction with tributylphosphine drives to completion when only equimolar amounts are used (*43*). As a result, the reduced oligonucleotide (**6**) can be added immediately to the functionalized antibody without performing an additional purification step. Since at that stage all tributylphosphine is oxidized, disulfide bonds in the antibody remain intact during conjugation.

We successfully prepared antibody–oligonucleotide conjugates for both a murine IgG (anti-hCG 130A) and a human IgM (antitumor 16.88).

Experiments with Anti-hCG IgG 130A. Monoclonal antibody 130A is a murine IgG_1 directed against complete hCG and does not react with either of the subunits separately. The mAb was derivatized by treatment with 60 equiv of SMCC to give an average of 10 maleimide groups per mAb molecule. Reduction of the 2-pyridyl disulfide protected oligonucleotide **5** was effected by

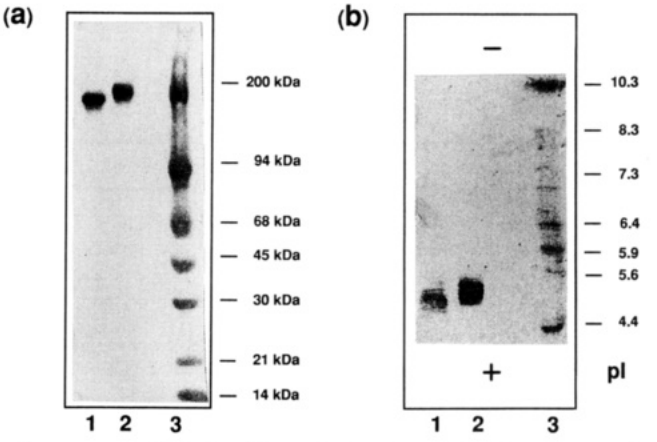
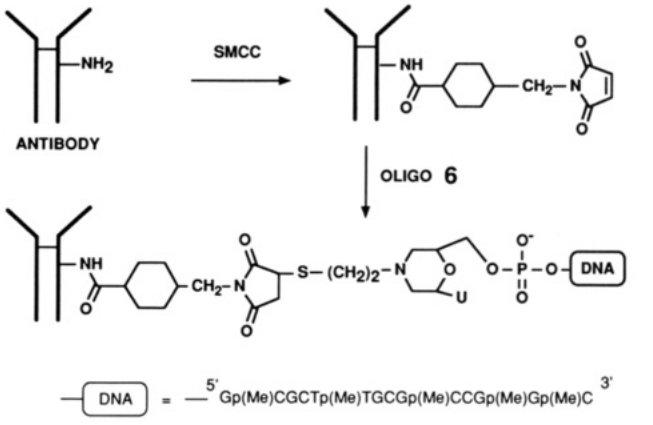


Figure 1. (a) SDS–PAGE analysis of 130A–DNA conjugate. A 4–26% polyacrylamide gel gradient under nonreducing conditions was used: lane 1, 130A control; lane 2, 130A–DNA conjugate; lane 3, molecular weight marker. (b) IEF of 130A–DNA conjugate on polyacrylamide gel at pH 3.0–9.0: lane 1, 130A–DNA conjugate; lane 2, 130A control; lane 3, IEF marker.

Scheme III. Preparation of Antibody–Oligonucleotide Conjugate



treatment with tributylphosphine, affording a free thiol containing DNA fragment which was reacted immediately with the maleimide-derivatized antibody (Scheme III). Conjugation was allowed to proceed overnight at 4 °C, prior to blocking of unreacted maleimide groups with cysteamine.

At this stage, the presence of covalently attached oligonucleotides in the conjugate preparation could be unambiguously demonstrated by isoelectric focusing (IEF) and SDS–PAGE. In IEF a shift of the isoelectric point toward lower pH value was observed, and SDS–PAGE showed a 10% increase in molecular size in comparison with unconjugated IgG 130A, indicating an average attachment of 2–3 oligonucleotides/mol of antibody (Figure 1).

Excess of unreacted oligonucleotide could be removed from antibody conjugate by gel filtration on Sephacryl S-100. The composition of the conjugate was quantified more precisely by determining the 260 nm/280 nm absorbance ratio in the UV spectrum of the purified conjugate. On the basis of this value for the 130A–DNA conjugate (0.99) an average conjugation ratio of 2 oligonucleotides/antibody was found.

It was of interest to find out whether hybridization would occur between the RAN and the oligonucleotides of the antibody conjugate. Thus, RAN **4** was incubated with 130A–DNA conjugate in hybridization buffer. Only a slight excess (ca. 1.8 equiv) of RAN was used in comparison with the total amount of conjugated DNA fragments. After

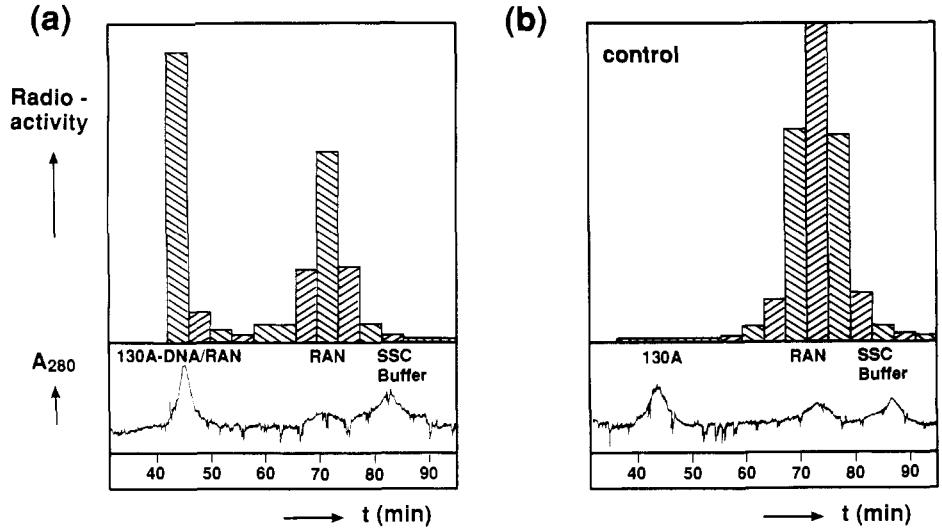


Figure 2. Sephacryl S-100 elution profile in PBS at 4 °C of (a) the hybridization mixture of 130A–DNA conjugate and RAN 4, (b) the control mixture of 130A and RAN 4.

1 h of hybridization at room temperature, the mixture was applied on a Sephacryl S-100 column in order to separate unhybridized RAN from the conjugate/RAN complex. The elution profile (Figure 2a) showed radioactivity in both the conjugate peak and RAN peak. Approximately 45% of the eluted radioactivity was present in the peak containing the antibody conjugate, indicating that efficient hybridization had occurred. In order to exclude the possibility of nonspecific binding of RAN to antibody, a control experiment was carried out in which underivatized IgG 130A was incubated with RAN in hybridization buffer. Gel filtration of this mixture revealed that less than 0.1% of the registered radioactivity was present in the antibody fraction (Figure 2b). Thus, under the conditions used the binding of RAN to antibody–conjugate in a nonspecific manner is negligible. These experiments clearly demonstrate that the RAN is indeed capable of recognizing the complementary sequence on the antibody via a specific hybridization mechanism.

The next question to be answered was whether the antibody–oligonucleotide conjugate had retained its antigen binding properties. To elucidate this issue, part of the hybridization mixture (see above) was incubated with hCG-coated Sepharose beads. After 90 min at room temperature, the mixture was centrifuged and the supernatant was removed. The beads were washed several times with hybridization buffer before the remaining radioactivity on the beads was determined. More than 150-fold higher radioactivity was measured relative to the control experiment, in which hCG-Sepharose beads were incubated with a mixture of RAN and IgG 130A and treated as above. This again illustrates that nonspecific binding of the RAN to the antibody (or beads) does not occur. Moreover, these antigen binding studies clearly prove that the antibody after conjugation with the oligonucleotide has retained its ability to bind specifically to its cognate antigen.

Experiments with the Human Antitumor IgM 16.88. Encouraged by the promising results with the IgG 130A, we focused our efforts on the human monoclonal antibody 16.88. This IgM has been obtained in large quantities through immunization of colon carcinoma patients with autologous tumor cells (active specific immunotherapy, ASI) and subsequent immortalization of their peripheral blood lymphocytes (*29*). IgM 16.88 reacts with an intracellular tumor-associated antigen consisting of modified cytokeratins (*30*). This mAb is currently being evaluated in radioimmunotherapy of various tumors.

IgM 16.88 was activated with maleimide groups by treatment with SMCC as described for the 130A antibody. Since an IgM has more reactive sites than an IgG, 17 equiv of SMCC turned out to be sufficient to obtain an average derivatization with 8.5 maleimide groups, as was determined spectrophotometrically. The activated antibody was reacted immediately with freshly reduced (tributylphosphine treatment) oligonucleotide **6**. After conjugation, the antibody–oligonucleotide conjugate was separated from excess oligonucleotide and other reagents on a Sephacryl S-100 column. In the UV spectrum of the purified conjugate a shift in the 260 nm/280 nm absorbance ratio (0.63) was observed in comparison with IgM 16.88 (0.57). In this case, a precise quantification of the number of conjugated oligonucleotides was more difficult, due to the dominating UV absorbance of the protein. On the basis of our experience with the 130A antibody, however, we estimate a mean conjugation ratio of 1 oligonucleotide/antibody. In more recent conjugations we were able to introduce as many as 6 oligonucleotides/antibody. In these cases significant shifts in the A_{260}/A_{280} ratio were observed.

In analogy with the IgG 130A experiments, the IgM 16.88–DNA conjugate was incubated with RAN (ca. 2 equiv with respect to the conjugate) to allow hybridization of the complementary DNA fragments. After a hybridization period of 1 h at room temperature, a S-100 column was used to separate the antibody-containing fraction from unhybridized RAN, to give an elution profile similar to that for 130A–DNA in Figure 2. Determination of radioactivity in both fractions revealed that 16% of the eluted counts was present in the antibody conjugate fraction. As with IgG 130A, the control experiment, in which RAN and IgM 16.88 were incubated and subsequently separated, showed that negligible nonspecific binding of RAN to IgM 16.88 had occurred: 0.2% of eluted radioactivity was present in the antibody peak.

These findings were confirmed by a series of dot blot hybridization experiments. In this assay a dilution series of the IgM 16.88–DNA conjugate was immobilized on a PVDF membrane and incubated with RAN. Autoradiography of the membrane, after several washings, showed a nice dilution pattern (Figure 3, lane 1). In a parallel experiment, a similar dilution series of IgM 16.88–DNA conjugate was treated with an equal amount of RAN

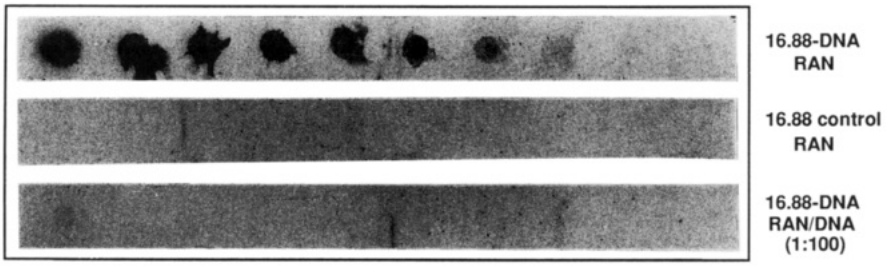


Figure 3. Dot blot hybridization assay with immobilized 16.88–DNA conjugate on a PVDF membrane in a 2-fold dilution series: lane 1, 16.88–DNA conjugate incubated with RAN **4**; lane 2, 16.88 control incubated with RAN **4**; lane 3, 16.88–DNA conjugate incubated with RAN **4** and 100-fold excess of oligonucleotide **3**. The intensity of the first spot in this lane corresponds with 100-fold dilution in lane 1.

Table I. "Pretargeting" Binding Assay on CTA*1-Coated Sepharose Beads

step 1	step 2	relative radioactivity
16.88–DNA	RAN **4**	10.6
16.88 (control)	RAN **4**	1.8
16.88–DNA	RAN **4**/DNA **3** (1:100)	1.4
16.88 (control)	RAN **4**/DNA **3** (1:100)	1

diluted 100-fold with unlabeled oligonucleotide **3**. The radioactivity spotted in this series (Figure 3, lane 3) perfectly matched the pattern for 100-fold dilution in the first experiment. In the control experiment, in which a membrane immobilized with IgM 16.88 was incubated with RAN, only background radioactivity was detected (Figure 3, lane 2). In summary, these results prove that despite of the huge dimensions of the IgM antibody as compared to the oligonucleotide, the RAN is still capable of interacting specifically with the conjugated oligonucleotides.

As in case of the IgG 130A conjugate, the antigen binding capacity of the IgM 16.88–DNA conjugate was examined by incubation of Sepharose beads coated with CTA*1, the cognate antigen of IgM 16.88 with a hybridization mixture of conjugate and RAN. In comparison with the control IgM 16.88/RAN mixture, 17.5-fold radioactivity on the CTA-coated beads was measured. Apart from this experiment, in which RAN was hybridized with the conjugate before the latter had bound to the antigen, an additional test was carried out mimicking the pretargeting "binding sequence". Thus, first CTA-coated beads were incubated with IgM 16.88–DNA conjugate (step 1). After removal of excess conjugate and several washings, the beads were incubated with RAN during 2.5 h at room temperature in hybridization buffer (step 2). Likewise, a competition experiment was performed including hybridization with the same amount of RAN, diluted 100-fold with unlabeled oligonucleotide **3**. Subsequent to removal of the supernatant and several washings, the remaining radioactivity on the beads was determined. The results of these experiments are summarized in Table I. As expected, the highest radioactivity is found for the pretargeting experiment with undiluted RAN. Moreover, the data clearly demonstrate the competitive behavior of the unlabeled oligonucleotides **3**. These experiments (with CTA-coated beads acting as a model for antigen expressing tumor cells) illustrate that a radiolabeled oligonucleotide is able to recognize its complementary sequence on an antibody conjugate, even when the latter is bound to its antigen.

In conclusion, on the basis of the results described here we have fulfilled two essential criteria for an effective DNA–DNA pretargeting therapy, i.e. the conservation of immunoreactivity in the antibody–oligonucleotide conjugate and the specific hybridization of the antisense nucleotides with the antibody-conjugated oligonucleotides. In this manner, pretargeting based on DNA hybridization has been shown to be successful in the testtube phase. One of the key issues in in vivo application of this pretargeting approach is the amount of RAN needed for efficient hybridization. This question will be addressed with high priority since it will give us the definite answer on the applicability of DNA–DNA pretargeting for therapy. Preliminary experiments with microspheroids of tumor cells, targeted with mAb–oligonucleotide conjugates, showed efficient hybridization of RAN as well. The results of these in vitro studies will be published soon.

ACKNOWLEDGMENT

The authors wish to thank Hans van den Elst and Prof. Dr. Jacques van Boom (Rijksuniversiteit Leiden, The Netherlands) for their contributions in the solid-phase DNA synthesis. The competent technical assistance of Irene Schlachter, Diep Pham, and Peter Loeffen (Organon, Oss) is greatly acknowledged.

LITERATURE CITED

(1) Blumenthal, R. D., Sharkey, R. M., and Goldenberg, D. M. (1990) Current perspectives and challenges in the use of monoclonal antibodies as imaging and therapeutic agents. *Adv. Drug. Delivery Rev. 4*, 279–318.

(2) Sands, H. (1988) Radioimmunoconjugates: An overview of problems and promises. *Antibody, Immunoconjugates, Radiopharm. 1*, 213–226.

(3) Larson, S. M. (1990) Clinical radioimmunodetection, 1978–1988: Overview and suggestions for standardization of clinical trials. *Cancer Res. 50*, 892–898.

(4) Buchsbaum, D. J., and Lawrence, T. S. (1991) Tumor therapy with radiolabeled monoclonal antibodies. *Antibody, Immunoconjugates, Radiopharm. 4*, 245–272.

(5) Press, O. W., Eary, J. F., Badger, C. C., Martin, P. J., Appelbaum, F. R., Levy, R., Miller, R., Brown, S., Nelp, W. B., Krohn, K. A., Fisher, D., DeSantes, K., Porter, B., Kidd, P., Thomas, E. D., and Bernstein, I. D. (1989) Treatment of refractory non-Hodgkin's lymphoma with radiolabeled MB-1 (anti-CD37) antibody. *J. Clin. Oncol. 7*, 1027–1038.

(6) Stewart, J. S. W., Hird, V., Snook, D., Sullivan, M., Hooker, G., Courtnay-Luck, N., Sivolapenko, G., Griffiths, M., Myers, M. J., Lambert, H. E., Munro, A. J., and Epenetos, A. A. (1988) Intraperitoneal radioimmunotherapy for ovarian cancer: Pharmacokinetics, toxicity and efficacy of I-131 labelled monoclonal antibodies. *Int. J. Radiat. Oncol. Biol. Phys. 16*, 405–413.

(7) Goodwin, D. A. (1991) Strategies for antibody targeting. *Antibody, Immunoconjugates, Radiopharm. 4*, 427–434.

(8) Stickney, D. R., Slater, J. B., Kirk, G. A., Ahlem, C., Chang, C-H., and Frincke, J. M. (1989) Bifunctional antibody: ZCE/CHA ^{111}Indium BLEDTA-IV clinical imaging in colorectal carcinoma. *Antibody, Immunoconjugates, Radiopharm. 2*, 1–13.

(9) Goodwin, D. A., Meares, C. F., McCall, M. J., McTigue, M., and Chaovapong, W. (1988) Pretargeted immunoscintigraphy of murine tumors with Indium-111-labeled bifunctional haptens. *J. Nucl. Med. 29*, 226–234.

(10) Anderson, L. D., Meyer, D. L., Battersby, T. R., Frincke, J. M., Mackensen, D., Lowe, S., and Connoly, P. (1988)

Optimization of ligand structure for imaging with a bifunctional antibody. *J. Nucl. Med. 29*, 835.
(11) Paganelli, G., Riva, P., Deleide, G., Clivio, A., Chiolerio, F., Scassellati, G. A., Malcovati, M., and Siccardi, A. G. (1988) In vivo labelling of biotinylated monoclonal antibodies by radioactive avidin: a strategy to increase tumor radiolocalisation. *Int. J. Cancer (Suppl. 2)*, 121–125.
(12) Hnatowitch, D. J., Virzi, F., and Ruscokowski, M. (1987) Investigations of avidin and biotin for imaging applications. *J. Nucl. Med. 28*, 1294–1302.
(13) Paganelli, G., Magnani, P., Zito, F., Villa, E., Sudati, F., Lopalco, L., Rossetti, C., Malcovati, M., Chiolerio, F., Seccamani, E., Siccardi, A. G., and Fazio, F. (1991) Three-step monoclonal antibody tumor targeting in carcinoembryonic antigen-positive patients. *Cancer Res. 51*, 5960–5966.
(14) Stickney, D. R., Anderson, L. D., Slater, J. B., Ahlem, C. N., Kirk, G. A., Schweighardt, S. A., and Frincke, J. M. (1991) Bifunctional antibody: A binary radiopharmaceutical delivery system for imaging colorectal carcinoma. *Cancer Res. 51*, 6650–6655.
(15) Le Doussal, J-M., Gruaz-Guyon, A., Martin, M., Gautherot, E., Delaage, M., and Barbet, J. (1990) Targeting of Indium 111-labeled bivalent hapten to human melanoma mediated by bispecific monoclonal antibody conjugates: Imaging of tumors hosted in nude mice. *Cancer Res. 50*, 3445–3452.
(16) Wickstrom, E. (1986) Oligodeoxynucleotide stability in subcellular extracts and culture media. *J. Biochem. Biophys. Methods 13*, 97–102.
(17) Uhlmann, E., and Peyman, A. (1990) Antisense oligonucleotides: A new therapeutic principle. *Chem. Rev. 90*, 544–584.
(18) Crooke, S. T. (1991) Antisense technology. *Curr. Opinion Biotechnol. 2*, 282–287.
(19) Agrawal, S., and Sarin, P. S. (1991) Antisense oligonucleotides: Gene regulation and chemotherapy of AIDS. *Adv. Drug Delivery Rev. 6*, 251–270.
(20) (a) Eckstein, F. (1985) Nucleoside phosphorthioates. *Annu. Rev. Biochem. 54*, 367–402. (b) Stein, C. A. (1989) Phosphorothioate oligodeoxynucleotide analogues. In *Oligodeoxynucleotides, Antisense Inhibitors of Gene Expression* (J. Cohen, Ed.) pp 97–117, Macmillan Press, London.
(21) (a) Miller, P. S., Yano, J., Yano, E., Carroll, C., Jayaraman, K., and Ts'O,P.O.P. (1979) Nonionic nucleic acid analogues. Synthesis and characterization of dideoxyribonucleoside methylphosphonates. *Biochemistry 18*, 5134–5143. (b) Miller, P. S. (1989) Non-ionic antisense oligonucleotides. In *Oligodeoxynucleotides, Antisense Inhibitors of Gene Expression* (J. Cohen, Ed.) pp 79–96, Macmillan Press, London.
(22) (a) Stec, W., Zon, G., Gallo, K. A., and Byrd, R. A. (1985) Synthesis and absolute configuration of P-chiral O-isopropyl oligonucleotide triesters. *Tetrahedron Lett. 26*, 2191–2194. (b) Kuijpers, W. H. A., Huskens, J., Koole, L. H., and van Boeckel, C. A. A. (1990) Synthesis of well-defined phosphate-methylated DNA fragments: the application of potassium carbonate in methanol as deprotecting reagent. *Nucleic Acids Res. 18*, 5197–5205.
(23) (a) Veeneman, G. H., van der Marel, G. A., van den Elst, H., and van Boom, J. H. (1991) An efficient approach to the synthesis of thymine derivatives containing phosphate-isosteric methylene acetal linkages. *Tetrahedron 47*, 1547–1562. (b) Matteucci, M., Lin, K-Y., Butcher, S., and Moulds, C. (1991) Deoxyoligonucleotides bearing neutral analogues of phosphodiester linkages recognize duplex DNA via triple-helix formation. *J. Am. Chem. Soc. 113*, 7767–7768.
(24) Egholm, M., Buchardt, O., Nielsen, P., and Berg, R. H. (1992) Peptide nucleic acids (PNA). Oligonucleotide analogues with an achiral peptide backbone. *J. Am. Chem. Soc. 114*, 1895–1897.
(25) Agrawal, S., Temsamani, J., and Tang, J. Y. (1991) Pharmacokinetics, biodistribution, and stability of oligodeoxynucleotide phosphorthioates in mice. *Proc. Natl. Acad. Sci. U.S.A. 88*, 7595–7599.
(26) Chem, T-L., Miller, P. S., Ts'O,P.O.P., and Colvin, O. M. (1990) Disposition and metabolism of oligodeoxynucleoside methylphosphonates following a single iv injection in mice. *Drug Metab. Dispos. 18*, 815–818.
(27) Zendegui, J. G., Vasquez, K. M., Tinsley, J. H., Kessler, D. J., and Hogan, M. E. (1992) In vivo stability and kinetics of absorption and diposition of 3′ phosphopropyl amine oligonucleotides. *Nucleic Acids Res. 20*, 307–314.
(28) Laemmli, U. K. (1970) Cleavage of structural proteins during the assembly of the head of bacteriophage T4. *Nature 27*, 680–685.
(29) Haspel, M. V., McCabe, R. P., Pomato, N., Janesch, N. J., Knowlton, J. V., Peters, L. C., Hoover, H. C., Jr., and Hanna, M. G., Jr. (1985) Generation of tumor cell-reactive human monoclonal antibodies using peripheral blood lymphocytes from actively immunized colorectal carcinoma patients. *Cancer Res. 45*, 3951–3961.
(30) Pomato, N., Murray, J. H., Bos, E. S., Haspel, M. V., McCabe, R. P., and Hanna, M. G., Jr. (1989) Identification and characterization of a human colon tumor-associated antigen, CTAA 16.88, recognized by a human monoclonal antibody. In *Human tumor antigens and specific tumor therapy* pp 127–136, Alan R. Liss Inc., New York.
(31) Matteucci, M. D., and Caruthers, M. H. (1981) Synthesis of deoxyoligonucleotides on a polymer support. *J. Am. Chem. Soc. 103*, 3185–3191.
(32) (a) Jäger, A., and Engels, J. (1984) Synthesis of deoxynucleoside methylphosphonates via a phosphonamidite approach. *Tetrahedron Lett. 25*, 1437–1440. (b) Agrawal, S., and Goodchild, J. (1987) Oligodeoxynucleoside methylphosphonates: Synthesis and enzymic degradation. *Tetrahedron Lett. 28*, 3539–3542.
(33) Sinha, N. D., Biernat, J., McManus, J., and Köster, H. (1984) Polymer support oligonucleotide synthesis XVIII: Use of β-cyanoethyl-N,N-dialkylamino/N-morpholino phosphoramidite of deoxynucleosides for the synthesis of DNA fragments simplifying deprotection and isolation of the final product. *Nucleic Acids Res. 12*, 4539–4557.
(34) Fraker, P. J., and Speck, J. C. (1978) Protein and cell membrane iodinations with a sparingly soluble chloramide, 1,3,4,6-tetrachloro-3a,6a-diphenylglycoluril. *Biochem. Biophys. Res. Commun. 80*, 849–857.
(35) Carlsson, J., Drevin, H., and Axen, R. (1978) Protein thiolation and reversible protein–protein conjugation. N-succinimidyl 3-(2-pyridyldithio)propionate, a new heterobifunctional reagent. *Biochem. J. 173*, 723–737.
(36) Yoshitake, S., Yamada, Y., Ishikawa, E., and Masseyeff, R. (1979) Conjugation of glucose oxidase from *Aspergillus niger* and rabbit antibodies using N-hydroxysuccinimide ester of N-(4-carboxycyclohexylmethyl)maleimide. *Eur. J. Biochem. 101*, 395–399.
(37) Ellman, G. L. (1959) Tissue sulfhydryl groups. *Arch. Biochem. Biophys. 82*, 70–77.
(38) Shaw, J-P., Kent, K., Bird, J., Fishback, J., and Froehler, B. (1991) Modified deoxyoligonucleotides stable to exonuclease degradation in serum. *Nucleic Acids Res. 19*, 747–750.
(39) Agrawal, S., Christodoulou, C., and Gait, M. J. (1986) Efficient methods for attaching nonradioactive labels to the 5′-end of synthetic oligodeoxyribonucleotides. *Nucleic Acids Res. 14*, 6227–6245.
(40) Lemaitre, M., Bayard, B., and Leblue, B. (1987) Specific antiviral activity of a poly-(L-lysine)-conjugated oligodeoxyribonucleotide sequence complementary to vesicular stomatitis virus N protein mRNA initiation site. *Proc. Natl. Acad. Sci. U.S.A. 84*, 648–652.
(41) Thorpe, P. E., Wallace, P. M., Knowles, P. P., Relf, M. G., Brown, A. N. F., Watson, G. J., Knyba, R. E., Wawrzynczak, E. J., and Blakey, D. C. (1987) New coupling agents for the synthesis of immunotoxins containing a hindered disulfide bond with improved stability in vivo. *Cancer Res. 47*, 5924–5931.
(42) Bos, E. S., unpublished results.
(43) Ruegg, U. Th., and Rudinger, J. (1977) Reductive cleavage of cystine disulfides with tributylphosphine. *Methods Enzymol. 47*, 111–116.

CORRECTIONS

Volume 3, Number 4, July/August 1992

PREPARATION OF MICELLE-FORMING POLYMER–DRUG CONJUGATES

Masayuki Yokoyama,* Glenn S. Kwon, Teruo Okano, Yasuhisa Sakurai, Takashi Seto, and Kazunori Kataoka*

Page 298. In footnote *a* of Table III, each value 9.1×10^{-4} mol should read 4.31×10^{-5} mol.

1043-1802/93/2904-0103$04.00/0 © 1993 American Chemical Society

Bioconjugate Chemistry

MARCH/APRIL 1993
Volume 4, Number 2

© Copyright 1993 by the American Chemical Society

ARTICLES

Cyanine Dye Labeling Reagents: Sulfoindocyanine Succinimidyl Esters

Ratnakar B. Mujumdar, Lauren A. Ernst,† Swati R. Mujumdar, Christopher J. Lewis, and Alan S. Waggoner*

Department of Biological Sciences and Center for Light Microscope Imaging and Biotechnology, Carnegie Mellon University, Pittsburgh, Pennsylvania 15213, and Biological Detection Systems, Inc., 4617 Winthrop Street, Pittsburgh, Pennsylvania 15213. Received July 10, 1992

A series of new fluorescent labeling reagents based on sulfoindocyanine dyes has been developed. We describe the synthesis and properties of these reagents. They contain succinimidyl ester reactive groups and can be readily conjugated to antibodies, avidin, DNA, lipids, polymers, and other amino-group-containing materials. The labeling reagents are water soluble, pH insensitive, and show much reduced dye aggregation under labeling conditions. One of the reagents, Cy3, can be excited with the 488-, 514- and 532-nm laser lines and is optimally excited with the 546-nm mercury arc line. Another, Cy5, can be excited with the 633-nm HeNe and 647-nm Kr laser lines available with many flow cytometers and confocal laser-scanning microscopes. New laser diodes emitting near 650 nm should also be excellent excitation sources for Cy5.

INTRODUCTION

The use of fluorescent labels with antibodies, DNA probes, biochemical analogs, lipids, drugs, cytokines, cells, and polymers has expanded rapidly in recent years. The wider use of fluorescent probes results partly from the evolution of advanced detection instrumentation, particularly electronic imaging microscopes (*1*) and flow cytometers (*2*), and partly from the availability of new fluorescent labeling reagents (*3, 4*). Nevertheless, further progress depends on the availability of fluorescent tags with increased fluorescence brightness, improved photostability, reduced phototoxicity, lower nonspecific binding, and excitation and emission wavelengths better matched to instrumentation light sources and detectors.

Earlier papers (*5–7*) from this laboratory introduced a new class of biological labeling reagents based on cyanine dyes with iodoacetamide, isothiocyanate, and succinimidyl ester as reactive groups. These reagents have large extinction coefficients (130 000–250 000 L/mol cm) and fluorescence covering a wide spectral range (500–750 nm). However, their quantum yields and water solubilities are not optimal. In this paper we report the syntheses of amino-reactive cyanine dyes that contain a negatively charged sulfonate group on the aromatic nucleus of the indocyanine fluorophore. These sulfoindocyanine dyes are highly water soluble and can be used to prepare brightly fluorescent materials, which show low nonspecific binding to cellular constituent (*8*). The different sulfoindocyanines fluoresce in the visible and near-infrared region of the spectrum, well separated from the shorter-wavelength autofluorescence, which is characteristic of many biological specimens.

* Please address correspondence to Alan S. Waggoner, Center for Light Microscope Imaging and Biotechnology, Carnegie Mellon University, Pittsburgh, PA 15213. Telephone: (412) 268-3459. Fax: (412) 268-6571.

† Biological Detection Systems, Inc.

1043-1802/93/2904-0105$04.00/0 © 1993 American Chemical Society

EXPERIMENTAL PROCEDURES

Chemicals. 1,3,3-Trimethoxypropene, *p*-hydrazinobenzenesulfonic acid, and iodoethane were purchased from Eastman Kodak Co., Rochester, NY. Disuccinimidyl carbonate (DSC), triethyl orthoformate, 1,4-butanesultone, 6-bromohexanoic acid, and *N,N'*-diphenylformamidine were purchased from Aldrich Chemical Co., Milwaukee, WI. Glutaconaldehyde dianil hydrochloride was purchased from Fairmount Chemical Co., Newark, NJ. Malonaldehyde dianil hydrochloride was prepared from malonaldehyde bis(dimethyl acetal) and aniline (*9*). Sheep γ-globulins (IgG) was purchased from Sigma Chemical Co. Dry solvents, diethyl ether, and ethyl acetate were purchased from Aldrich Chemical Co. All other solvents were purchased from Fisher Scientific, Pittsburgh, PA.

Purification and Spectroscopic Analysis. Purification of dyes was performed on a Spectra-Physics Model SP8700 analytical HPLC unit equipped with a C8-RP column, on a Water associates Model Prep/LC 500 preparative HPLC unit equipped with a C18-RP column. Purification could also be achieved by conventional or flash column chromatography on C18-RP powder (Analtech, Newark, DE). Water–methanol mixtures were used for elution in all experiments. Dyes were recovered from the fractions with a rotary evaporator at 60–70 °C without appreciable loss. Although these purification procedures isolate the fluorophore from various intermediates and precursors, these multi-ionic dyes typically associate with alkali metal cations, halide anions, and water of hydration in nonstoichiometric amounts. Therefore, it is essential to obtain the final products in a form that is chemically well-defined for elemental and mass spectrometric analysis. This was accomplished by passing the dye with unknown counterion composition through a Dowex-50W hydrogen, strongly acidic cation-exchange column that has been previously washed with 0.1 N sulfuric acid and then distilled water. For example, a sample of Cy5.18 contained 1.29% potassium by microanalysis before ion-exchange and 0.00% afterward. The same sample after ion-exchange gave a high-resolution mass spectrum in 3-nitrobenzyl alcohol (CsI-glycerol as a standard) with *m/e* 743.267 for $C_{37}H_{47}N_2S_2O_{10}$ (calcd, $C_{37}H_{46}N_2S_2O_{10}$ + H). Mass spectral determinations were made at the Midwest Center for Mass Spectrometry at the University of Nebraska—Lincoln, Lincoln, NE, with the partial support from NSF Grant #DIR9017262. Elemental analyses (C, H, N, S, and K) were performed by Atlantic Microlab, Inc., Atlanta, GA. Ultraviolet–visible spectra were measured on a Hewlett-Packard HP 8452 diode-array spectrophotometer. The proton NMR spectra were obtained on an IBM 300 FT-NMR spectrometer. NMR signals are described by use of s for singlet, d for doublet, t for triplet, q for quartet, and m for multiplet and are expressed in δ with TMS as internal standard. Fluorescence measurements were performed using a Spex Fluorolog 2 system. Quantum yields were determined as previously described (*7*). Extinction coefficients were determined from absorbance values of weighed samples of dried material and their estimated molecular weights. Extinction coefficients in Table II were determined from absorbance values of HPLC-purified, ion-exchange-purified (see below), weighed samples of dried material and their molecular weights.

General Synthesis. Seven new cyanine dyes were synthesized using modifications of methods described previously (*5–7, 10*).

2,3,3-Trimethylindoleninium-5-sulfonate (I). This intermediate was synthesized by conventional Fisher indole synthesis (*11, 12*). To a 2-L three-necked flask equipped with mechanical stirrer and reflux condenser were added acetic acid (300 mL), 3-methyl-2-butanone (168 mL, 1.6 mol), and *p*-hydrazinobenzenesulfonic acid (100 g, 0.53 mol). The mixture was heated to reflux for 3 h and then cooled for several hours when a pink solid separated (93 g, mp 290–95 °C, yield 73%). ^{1}H NMR (D_2O) δ 7.13 (s, 1 H, aromatic 4-H), 7.1 (dd, 1 H, J = 7.0, 1.2 Hz, aromatic 6-H), 6.5 (d, 1 H, J = 7 Hz, aromatic 7-H), 1.4 (s, 6 H, $C(CH_3)_2$). Singlet for 2-methyl did not appear in D_2O, but appeared when NMR was recorded in DMSO-d_6. Product was converted to the potassium salt by stirring its solution in methanol with a saturated solution of potassium hydroxide in 2-propanol. The alkaline solution turns yellow and the potassium salt of the sulfoindole precipitated as yellow solid almost quantitatively: ^{1}H NMR (D_2O) δ 7.13 (s, 1 H, aromatic 4-H), 7.1 (dd, 1 H, J = 7.0, 1.2 Hz, aromatic 6-H), 6.5 (d, 1 H, J = 7 Hz, aromatic 7-H), 2.2 (s, 3 H, CCH_3), 1.4 (s, 6 H, $C(CH_3)_2$); R_f = 0.5 (RP-C18, water).

1-Ethyl-2,3,3-trimethylindoleninium-5-sulfonate (II). A mixture of potassium salt of indoleninium sulfonate I (11 g, 0.04 mol) and a large excess of ethyl iodide (40 mL) was heated to boiling for 24 h. The reaction mixture was cooled, excess ethyl iodide was decanted, and the light purple color solid was triturated with acetone (3 × 50 mL) to remove potassium iodide. The light purple powder was used in further experiments without additional purification: λ_{max} (water) = 228, 274 nm; ^{1}H NMR (D_2O) δ 8.13 (s, 1 H, 4-H), 8.03 (dd, 1 H, J = 9.0, 1.1 Hz, 6-H), 7.2 (d, 1 H, J = 9 Hz, 7-H), 4.51 (q, 2 H, J = 7.5 Hz, α-CH_2), 1.59 (t, 3 H, β-CH_3), 1.61 (s, 6 H, $(CH_3)_2$); R_f = 0.16 (RP-C18, water).

1-(ε-Carboxypentynyl)-2,3,3-trimethylindoleninium-5-sulfonate (III). The potassium salt of 2,3,3-trimethylindoleninium-5-sulfonate (I) (11 g, 0.04 mol) and 6-bromohexanoic acid (9.8 g, 0.05 mol) were mixed in 1,2-dichlorobenzene (100 mL) and heated at 110 °C for 12 h under nitrogen. The mixture was cooled, 1,2-dichlorobenzene was decanted, and the solid was triturated with 2-propanol until free powder was obtained: λ_{max} (water) = 274 nm; ^{1}H NMR (D_2O) δ 8.13 (s, 1 H, 4-H), 8.03 (dd, 1 H, J = 9.0, 1.1 Hz, 6-H), 7.2 (d, 1 H, J = 9 Hz, 7-H), 4.51 (t, 2 H, J = 7.5 Hz, α-CH_2), 2.25 (t, 2 H, J = 7.5 Hz, ε-CH_2), 1.99 (m, 2 H, β-CH_2), 1.35–1.66 (m, 4 H, γ- and δ-CH_2), 1.61 (s, 6 H, $(CH_3)_2$); R_f = 0.27 (RP-C18, water).

1-(δ-Sulfonatobutyl)-2,3,3-trimethylindoleninium-5-sulfonate (IV). The potassium salt of 2,3,3-trimethylindoleninium-5-sulfonate (I) (11 g, 0.04 mol) and 1,4-butanesultone (6.5 g, 0.048 mol) were mixed in 1,2-dichlorobenzene (50 mL) and heated at 110 °C for 12 h. The mixture was cooled, 1,2-dichlorobenzene was decanted, and the solid was triturated with 2-propanol until free powder was obtained: λ_{max} (water) = 274 nm; ^{1}H NMR (D_2O) δ 8.13 (s, 1 H, 4-H), 8.03 (dd, 1 H, J = 9, 1.1 Hz, 6-H), 7.2 (d, 1 H, J = 9 Hz, 7-H), 4.51 (t, 2 H, J = 7.5 Hz, α-CH_2), 2.25 (t, 2 H, J = 7.5 Hz, δ-CH_2), 1.99 (m, 2 H, β-CH_2), 1.35–1.66 (m, 2 H, γ-CH_2), 1.61 (s, 6 H, $(CH_3)_2$); R_f = 0.58 (RP-C18, water–methanol 1:1).

CY3.18.OH (IX). Intermediate III (10 g, 0.028 mol) was dissolved in pyridine (50 mL) in a 250-mL round-bottom flask equipped with a reflux condenser. The solution was heated to reflux. Triethyl orthoformate (8.3 mL, 0.05 mol) was added slowly (1 mL at a time, every 15 min). The solution was heated for an additional 2 h. A 4-fold excess of triethyl orthoformate was essential for completion of the reaction. The mixture was cooled and diluted with several volumes of diethyl ether. A product separated in the form of a red powder from which the

supernatant fluid was removed by decantation. It was dissolved in methanol (40 mL) and reprecipitated with addition of 2-propanol. The product was collected on filter paper and dried (17.5 g, yield 80%). Cy3.18.OH made by this method showed two spots on TLC [RP-C18, methanol–water 25:75; R_f = 0.8 (major spot) and 0.21 (minor spot)]. Crude dye (5.0 g) was dissolved in water (30 mL) and chromatographed on a reversed-phase C18 column (70 g). Pure dye obtained as the pyridinium salt (2.5 g, yield 40%) was converted into its potassium salt: ^{1}H NMR (D_2O) δ 8.45 (t, 1 H, J = 14 Hz, β proton of the bridge), 7.9 (s, 2 H, 4-H, 4′-H), 7.8 (d, 2 H, J = 7.7 Hz, 6-H, 6′-H), 7.4 (d, 2 H, J = 7.7 Hz, 7-H, 7′-H), 6.45 (d, 2 H, J = 14 Hz, α, α' protons of the bridge), 4.05 (t, 4 H, J = 7.5 Hz, α-, α'-CH_2), 2.25 (t, 4 H, J = 7.5 Hz, ϵ-, ϵ'-CH_2), 1.99 (m, 4 H, β-, β'-CH_2), 1.35–1.66 (m, 8 H, γ-, γ'-, δ-, δ'-CH_2), 1.71 (s, 12 H, s $(CH_3)_2$); R_f = 0.24 (RP C18, methanol–water 1.7:8.3).

Cy3.29.OH (XI). This unsymmetrical indocarbocyanine was synthesized in two steps.

(*a*) *Intermediate 415 (V).* A mixture of the quaternary salt of indolenine II (4 g, 0.015 mol) and *N,N′*-diphenylformamidine (3.3 g, 0.017 mol) in acetic acid (20 mL) was heated to reflux. The completion of the reaction was monitored by absorption spectra in methanol, which showed that as the reaction progressed the absorption maximum at 286 nm declined almost to the vanishing point and the absorption at 415 nm rose correspondingly (about 3–4 h). Extended heating produced some symmetrical dye (<5%). Acetic acid was removed on a rotary evaporator and the product was triturated with a mixture of ethyl acetate and water (50:50). Excess *N,N′*-diphenylformamidine was dissolved in ethyl acetate while water removed any symmetrical dye and unreacted intermediate II. The crude orange powder (1.8 g, 30%) thus obtained was immediately used in the next reaction: λ_{max} (water) = 415 nm; ^{1}H NMR (D_2O) δ 8.15 (s, 1 H, 4-H), 8.0 (d, 2 H, J = 7.0 Hz, 6-H), 7.9 (d, 1 H, J = 7 Hz, 7-H), 7.1–7.55 (m, 7 H, two vinyl and five aromatic protons of aniline), 4.51 (q, 2 H, J = 7.5 Hz, α-CH_2), 1.35–1.6 (s merged in t, 9 H, β-CH_3 and $(CH_3)_2$); R_f = 0.81 (RP-C18, methanol–water 3.7:6.3).

(*b*) *Preparation of Dye.* The intermediate V (4.7 g, 0.013 mol) was redissolved in an acetic anhydride (25 mL) and pyridine (25 mL) mixture. A UV/vis spectrum showed that the absorption at 415 nm disappeared almost immediately and a new band appeared at 385 nm. Indolenine salt III (5.3 g, 0.015 mol) was added and the mixture was heated at 110 °C until the absorption maxima at 385 nm almost vanished. The mixture was cooled and the dye precipitated with ethyl ether. After washing with 2-propanol (3 × 10 mL) the solid was recovered by filtration and purified by HPLC on reverse-phase C18 using a water–methanol mixture as eluent (2.3 g, yield 25%): ^{1}H NMR (D_2O) δ 8.4 (t, 1 H, J = 14 Hz, β proton of the bridge), 7.8 (s, 2 H, 4-H, 4′-H), 7.6 (d, 2 H, J = 12 Hz, 6-H, 6′-H), 7.3 (m, 2 H, 7-H, 7′-H), 6.3–6.1 (m, 2 H, α, α' protons of the bridge), 4.1 (m, 4 H, α-, α'-CH_2), 2.9 (t, 2 H, J = 7 Hz, CH_2COOH), 1.4–2.0 (m, 21 H, 3 CH_2, 1 CH_3, and 2 $(CH_3)_2$); R_f = 0.51 (RP-C18, methanol–water 2.5:7.5).

Cy3.19.OH (X). This unsymmetrical dye was prepared by condensation of intermediates VI and III following the procedure of Cy3.29.OH (yield 5%): ^{1}H NMR (D_2O) δ 8.4 (t, 1 H, J = 13 Hz, β proton of the bridge), 7.75 (s, 2 H, 4-H, 4′-H), 7.6 (d, 2 H, J = 12 Hz, 6-H, 6′-H), 7.3 (m, 2 H, 7-H, 7′-H), 6.3 and 6.2 (2 d of 1 H each, J = 13 Hz, α, α' protons of the bridge), 4.1 (m, 4 H, α-, α'-CH_2), 2.9 (t, 2 H, J = 7 Hz, CH_2SO_3), 2.5 (t, 2 H, J = 7.5 Hz, CH_2COOH), 1.4–2.0 (m, 22 H, 5 CH_2 groups, with s at 1.6 for 2 $(CH_3)_2$); R_f = 0.23 (RP C18, water–methanol 9:1).

CY5.18.OH (XII). A mixture of indoleniniumsulfonate II (10 g, 0.028 mol), potassium acetate (1.4 g, 0.014 mol), and methanol (60 mL) was refluxed at 60 °C for 2.5 h. 1,3,3-Trimethoxypropene (2 mL) was added every 30 min for 2 h (total 8 mL). At the end of the reaction, the mixture was filtered to remove the potassium acetate. The filtrate was kept at 0–4 °C for 15–18 h. The crystalline dye obtained was filtered and washed with 2-propanol (3 × 50 mL) and dried under vacuum (8.1 g, yield 75%): ^{1}H NMR (D_2O) δ 7.9 (t, 2 H, J = 14 Hz, β, β' protons of the bridge), 7.7 (s, 2 H, 4-H, 4′-H), 7.6 (d, 2 H, J = 8 Hz, 6-H, 6′-H), 7.4 (d, 2 H, J = 7.6 Hz, 7-H, 7′-H), 6.4 (t, 1 H, J = 15 Hz, γ proton of the bridge), 6.0 (d, 2 H, J = 15 Hz, α, α' protons of the bridge), 3.9 (t, 4 H, J = 7.5 Hz, α-, α'-CH_2), 2.15 (t, 4 H, J = 7.5 Hz, ϵ-, ϵ'-CH_2), 1.7 (m, 4 H, β-, β'-CH_2), 1.3–1.66 (m, 8 H, γ-, γ'-, δ-, δ'-CH_2), 1.51 (s, 12 H, 2 $(CH_3)_2$); R_f = 0.58 (RP-C18, methanol–water 2.5:7.5).

Cy5.29.OH (XIV). (*a*) *Intermediate 445 (VII).* A solution of indolenine II (4 g, 0.015 mol) and malonaldehyde dianil hydrochloride (4.4 g, 0.017 mol) in a mixture of acetic acid (20 mL) and acetic anhydride (20 mL) was heated to reflux. The completion of the reaction was monitored by absorption spectra in methanol, which showed that as the reaction progressed the absorption maximum at 286 nm declined almost to the vanishing point and the absorption at 445 nm rose correspondingly (approximately 4 h). Some symmetrical dye (<5%) was always formed if heating was continued for a long time. Acetic acid was removed with a rotary evaporator and the product was washed with ethyl acetate to remove excess malonaldehyde dianil hydrochloride. The crude product thus obtained was used in the next reaction. The intermediate decomposed on standing (UV/vis in water—additional bands at 485 and 515 nm). However this hydrolyzed product can be used in the next reaction: ^{1}H NMR (D_2O) δ 8.15 (s, 1 H, 4-H), 8.0 (d, 2 H, J = 7.0 Hz, 6-H), 7.9 (d, 1 H, J = 7.0 Hz), 7.1–7.55 (m, 7 H, 2 vinyl and 5 aromatic protons of aniline), 4.51 (q, 2 H, J = 7.5 Hz, α-CH_2), 1.35–1.6 (s, m, 9 H, β-CH_3 and $(CH_3)_2$); R_f = 0.48 (RP-C18, water–methanol 1:1).

(*b*) *Preparation of Dye.* The intermediate VII was dissolved in an acetic anhydride and pyridine mixture. The UV spectra of the mixture was recorded to ensure an absorbance at 445 nm for the acetate form of the intermediate. Indolenine III (5.3 g, 0.015 mol) was added and reaction mixture was heated at 110 °C until the absorption maxima at 445 nm almost vanished. The mixture was cooled and the dye precipitated with ethyl acetate. The gummy product was washed with 2-propanol (3 × 10 mL). The crude solid was reverse-phase (C18) chromatographed using a water–methanol mixture as eluent: ^{1}H NMR (D_2O) δ 9.1 (d, 2 H), 8.7 (t, 1 H), and 8.4 (t, 2 H) (pyridine protons); 7.9–8.2 (m, 6 H, 4-H, 4′-H, 6-H, 6′-H, β, β' protons of the bridge), 7.5 (m, 2 H, 7-H, 7′-H), 6.7 (t, 1 H, J = 13 Hz, γ proton of the bridge), 6.2 (m, 2 H, α, α' protons of the bridge), 4.0–4.2 (m, 4 H, α-, α'-CH_2), 2.9 (t, 2 H, J = 7 Hz, CH_2COOH), 1.4–2.0 (m, 21 H, 3 CH_2 groups, 1 CH_3 with s at 1.6 for 2 $(CH_3)_2$); R_f = 0.56 (RP C18, methanol–water 3.7:6.3).

Cy5.19.OH (XIII). This unsymmetrical dye was prepared by condensation of intermediates VIII and III following the procedure of Cy5.29 (yield 5%): ^{1}H NMR (D_2O) δ 7.95 (t, 2 H, J = 13.2 Hz, β, β' protons of bridge), 7.8 (s, 2 H, 4 and 4′-H), 7.65 (d, 2 H, J = 7.7 Hz, 6-H, 6′-H), 7.3–7.4 (2 d, 2 H, 6-H, 6′-H), 6.5 (t, 1 H, J = 13 Hz, γ-H), 6.2 (2 d, 2 H, J = 13 Hz, α-H, α'-H), 4.1 (m, 4 H, α-, α'-

CH_2), 2.9 (t, 2 H, J = 7 Hz, CH_2SO_4), 2.45 (t, 2 H, J = 7.5 Hz, CH_2COOH), 1.4–2.0 (m, 22 H, 5 CH_2 groups, with s at 1.6 for 2 $(CH_3)_2$); R_f = 0.75 (RP C18 water–methanol 7.5:2.5).

Cy7.18.OH (XV). Glutaconaldehyde dianil hydrochloride (143 mg, 0.5 mmol) was dissolved in a heated mixture of acetic anhydride (4 mL) and pyridine (1 mL). Intermediate III (353 mg, 1 mmol) was added and mixture was heated to reflux for additional 10 min and then cooled. The dye was precipitated with diethyl ether. The supernatant liquid was separated. Solid was redissolved in a minimum volume of methanol and reprecipitated with 2-propanol. The bright purple solid was collected on filter paper and dried (164 mg, yield 20%). It was converted into its potassium salt and then purified by HPLC (RP-C18) with a water–methanol mixture as eluent: λ_{max} = 750 nm; ^{1}H NMR (D_2O) δ 7.75 (m, 6 H, 4-H, 4′-H, 6-H, 6′-H, and γ, γ' protons of the bridge), 7.4 (t, 1 H, J = 13 Hz, δ proton of the bridge), 7.2 (d, 2 H, J = 7.7 Hz, 7-H, 7′-H), 6.35 (t, 2 H, J = 13 Hz, β, β' protons of the bridge), 6.15 (d, 2 H, J = 7 Hz, α-, α'-H), 4.1 (br, 4 H, α-, α'-CH_2), 2.2 (t, 2 H, J = 7.5 Hz, CH_2COOH), 1.2–1.7 (m, 24 H, 6 CH_2 groups, with s at 1.5 for 2 $(CH_3)_2$); R_f = 0.25 (RP-C18, water–methanol 7.5:2.5).

Succinimidyl Esters of (Carboxyalkyl)cyanine Dyes. A procedure for making succinimidyl active esters using disuccinimidyl carbonate (DSC) has been described by Ogura et al. (*13*). It was modified for sulfocyanines. In a typical experiment (carboxyalkyl)sulfocyanine was dissolved in a mixture of dry DMF (2 mL/100 mg of dye) and dry pyridine (0.1 mL/100 mg of dye). Disuccinimidyl carbonate (DSC) (1.5 equiv/carboxyl group) was added and the mixture was stirred at 55–60 °C for 90 min under nitrogen. After diluting the mixture with dry ethyl acetate, the supernatant was decanted. The product was either washed repeatedly with solvent or dissolved in DMF and reprecipitated. Nearly quantitative yields of cyanine active esters were obtained.

The formation of the active ester was confirmed by its reaction with benzylamine in DMF or its reaction with taurine in a pH 9.4 bicarbonate buffer. Reversed-phase C18 TLC plates were spotted with the conjugate and the OSu and hydrolyzed carboxylate product for comparison and developed with a water–methanol mixture. Since activation was sometimes incomplete, reverse-phase HPLC was also used to determine the percentage of fluorochrome in the active ester form. The sample was eluted through an Alltech Econosphere 250 mm × 4.6 mm C18 RP column using a mixture of 25% acetonitrile and 75% water containing 0.1% trifluoroacetic acid. The percentages of activated and unactivated cyanine fluorophore were determined by integration of the absorbance signals from a Varian UV/vis detector.

Stability of the Active Ester in Aqueous Buffers. Hydrolysis rates of Cy5.29.OSu (XIX) in aqueous buffers were determined as follows. Reactions were started by adding 200 μL of aqueous phosphate buffer (at pH 7.0, 7.5, 8.0, 8.5 and 9.4) to tubes containing 1 mg of Cy5.29.OSu. At each time interval following initiation of the reaction, 25 μL of the reaction solution was loaded as a small strip on a C18-reversed-phase, 5 × 10 cm TLC plate. The plate was developed using acetonitrile–water 2.5:7.5 containing 0.1% trifluoroacetic acid. The band containing dye in the carboxylic acid form (R_f = 0.88) and the band containing unhydrolyzed succinimidyl ester (R_f = 0.2) were scraped from the TLC plate and extracted in methanol (5 mL). The absorbance of each extract was measured at 650 nm and the fraction of hydrolyzed dye was calculated from the relative absorbances of the two extracts.

General Protein Labeling Procedures. Stock solutions of the sulfoindocyanine succinimidyl active esters were made in dry DMF (1 mg/100 μL) and are stable for days when stored at 4 °C in a desiccator. The active esters are also stable in distilled water for several hours provided the pH of the solution is not basic. Aqueous solutions of the dyes can be used for labeling antibodies if use of DMF is not suitable for certain antibodies. The concentration of the reactive dye in the stock solution was determined by measuring the absorbance of an aliquot of the appropriately diluted stock solution in phosphate-buffered saline (PBS) and using the extinction coefficient of the dye (Table II). Generally, antibody labeling was carried out in 0.1 M carbonate–bicarbonate buffer (pH 9.4) for 15 min at room temperature. One milligram of sheep IgG (6.45 mM) was dissolved in 0.25–1 mL of buffer solution and the desired amount of dye (e.g. 20 μL of the 1 mg/100 μL stock solution) was added during vigorous vortex mixing. Unconjugated dye was separated from the labeled protein by gel permeation chromatography (0.7 × 20 cm column of Sephadex G-50) using pH 7 buffer solution as eluent (*8*).

Protein Labeling Rates at Different pH Values. A series of labeling reactions were set up as described in the general protein labeling procedure above, except that the reactions were carried out at pH 7.0, 7.5, 8.0, 8.5, and 9.4 with 1 mg of antibody per 250 μL of buffer. Aliquots of the reactions were removed at time points and labeled antibody was separated from unreacted dye as described above. The dye-to-protein ratio for each sample was determined as described below.

Determination of Dye-to-Antibody Ratios. A simple method for estimating dye/protein (D/P) ratios involves direct measurement of the protein absorbance at 280 nm and dye absorbance at the absorption maximum. Specifically, the dye/protein ratio is calculated using the equation below with measured values of the absorbance of the

$$\mathrm{D/P} = \frac{A_{dye}E_{prot}}{(A_{280} - 0.05A_{dye})E_{dye}}$$

labeled dye (Cy3 at 550 nm or Cy5 at 650 nm) and the absorbance of protein at 280 nm. The extinction coefficient of the dye is obtained from Table II and the extinction coefficient of the IgG antibody at 280 nm was taken to be 170 000 L/mol cm. The factor of 0.05 (used for both Cy3 and Cy5) in the denominator accounts for dye absorption at 280 nm, which is 5% of the absorption of the dye at its maximum absorption (A_{dye}).

A more accurate method is needed when the labeling reagent shows significant spectral changes when bound to the antibody molecule. For example, this approach is needed when both dimers and monomers of dye, which have different absorption peaks and different extinction coefficients, are present on the protein at higher D/P ratios. In this case, the labeled protein is dissolved in formamide for absorption spectroscopy, and the extinction coefficients of the dye are determined independently for the calculation.

RESULTS

Names of the New Labeling Reagents. The basic structure of the sulfoindocyanine dyes developed in this work is shown in Figure 1. Following the naming scheme for reactive polymethine dyes used in the previous papers (*5–7*) of this series, these dyes will be referenced as Cy3.18.OSu (XVI) or as Cy5.29.OSu (XIX). In these

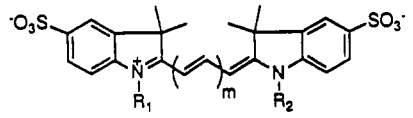
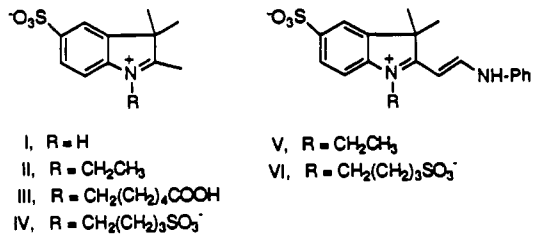


Figure 1. Structure of cyanine dye.



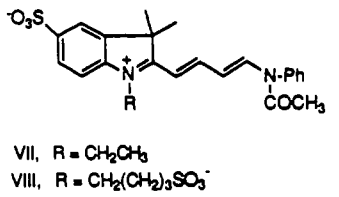


Figure 2. Structures of key intermediates used in the synthesis of symmetrical and unsymmetrical sulfocyanines.

Table I. Structures of Sulfoindocyanine Dyes

dye				
no.	designation	m	R_1	R_2
IX	Cy3.18.OH	1	$(CH_2)_5COOH$	$(CH_2)_5COOH$
X	Cy3.19.OH	1	$(CH_2)_5COOH$	$(CH_2)_4SO_3$
XI	Cy3.29.OH	1	$(CH_2)_5COOH$	CH_2CH_3
XII	Cy5.18.OH	2	$(CH_2)_5COOH$	$(CH_2)_5COOH$
XIII	Cy5.19.OH	2	$(CH_2)_5COOH$	$(CH_2)_4SO_3$
XIV	Cy5.29.OH	2	$(CH_2)_5COOH$	CH_2CH_3
XV	Cy7.18.OH	3	$(CH_2)_5COOH$	$(CH_2)_5COOH$
XVI	Cy3.18.OSu	1	$(CH_2)_5COOSu$	$(CH_2)_5COOSu$
XVII	Cy3.29.OSu	1	$(CH_2)_5COOSu$	CH_2CH_3
XVIII	Cy5.18.OSu	2	$(CH_2)_5COOSu$	$(CH_2)_5COOSu$
XIX	Cy5.29.OSu	2	$(CH_2)_5COOSu$	CH_2CH_3

names, the "Cy" portion indicates that they are cyanine dyes while OSu indicates that the compounds have succinimidyl ester reactive groups. The number immediately after the "Cy" indicates the number of bridge carbons (i.e. Cy3, m = 1; Cy5, m = 2). The number following the decimal point indicates a unique dye structure, which is determined by the substituents (R_1, R_2) on the structure.

Syntheses of Sulfoindocyanine Labeling Reagents. The sulfoindocyanine dyes developed in this work are shown in Table I. The reactivity, the charges, and the solubility properties of basic indolenine dye can be readily controlled by placing appropriate substituents at R_1, R_2, and benzene rings of the nucleus. The sulfoindocyanines have SO_3^- groups at the 5 and 5′ positions to increase water solubility. The R_1 and R_2 substituents consist of one or two carboxyl alkyl groups that can be activated to form succinimidyl esters. Succinimidyl esters readily react with primary amines at basic pH, and less readily with hydroxyl-containing materials. The number of double bonds in the polymethine chain between the heterocyclic nuclei allows control of the color of the fluorochrome.

The synthesis schemes using the intermediate structures of Figure 2 are analogous to those described in earlier papers from this laboratory (*5–7*). Generally, a fluorescent cyanine dye is formed when a quaternized indolenine nucleus, which contains a carboxyl alkyl group for later activation of the fluorophore, is linked to a second identical (or different) indolenine nucleus through a polymethine chain of three, five, or seven conjugated methine carbon atoms. After purification of the resulting fluorophore, the carboxyl group(s) is(are) activated to produce the cyanine dye labeling reagent.

The key intermediate, indoleninium-5-sulfonate required to produce the new group of labeling reagents is prepared from *p*-hydrazinobenzenesulfonic acid and 3-methyl-2-butanone by conventional Fisher indole synthesis (*11*). Indolenine thus obtained is converted into a potassium salt before quaternization. We attempted to increase the water solubility of the reagents by incorporating fewer methyl groups between the OSu group and the indole ring nitrogen. However, quaternization of the sulfoindole nucleus with bromoacetic acid proved difficult and sulfoindocyanines bearing a propionic acid group produced low yields of active esters. Ultimately, we found that sulfoindocyanines derived from nuclei bearing a five-carbon carboxylic acid (hexanoic acid) attached to the nitrogen could be prepared without significant difficulty, and a number of the useful labeling reagents reported in this paper have this group as a linker for formation of the active ester.

Monoreactive Cy3.19.OH (X) and Cy5.19.OH (XIII) dyes bearing a sulfonatobutyl group [R_1 = $(CH_2)_4SO_3^-$ and R_2 = $(CH_2)_5COOH$] were obtained in poor yields and were difficult to activate. When the sulfonatobutyl group is replaced by an ethyl group (R_1 = C_2H_5), the resulting dyes Cy3.29.OH (XI) and Cy5.29.OH (XIV), were obtained in good yield and provided excellent protein labeling. This study reveals that various combinations of charged groups and length of alkyl chains affect the preparation and labeling efficiency of succinimidyl esters.

Counterions also play a role in the synthesis of the ester. All (carboxyethyl)- and (carboxypentyl)sulfoindocyanines were obtained as monopyridinium salts where pyridine was used as solvent. It was observed that these pyridinium salts do not form the active esters readily and had to be converted into monopotassium salts before activation was successful.

Absorption and Fluorescence of the Basic Fluorophores. Direct attachment of the sulfonic acid group to the aromatic system of the chromophore does not appreciably change the basic indocyanine dye absorption and emission wavelengths. The absorption spectra of carboxylic acid-containing cyanines and their active esters have narrow absorption and emission bands and low vibronic shoulders on the short-wavelength sides of the absorption peaks (Figure 3). With the introduction of the two sulfonate groups, these dyes dissolve easily in water, even at millimolar concentrations, with no evidence of new absorption bands that are indicative of dimers and other dye–dye interactions (*14*).

Use of the Sulfoindole Reagent To Label Amino-Containing Materials. Sulfoindocyanine succinimidyl esters react easily with material containing neutral primary amino groups (pH > pK_a ~ 9–10, typically). Figure 4b shows that antibody labeling is very fast at pH greater than 8. Interestingly, the final D/P ratio reached in less than 1 h is higher at high pH, possibly because the ϵ-aminolysine groups in acidic environments of the antibody are not deprotonated until a higher pH is reached, or alternatively, because there may be a pH-dependent conformational change that exposes new amino groups at high pH. It is also clear from these experiments that adequate labeling can take place at neutral pH, provided that the labeling reaction is given a few hours. Figure 4a

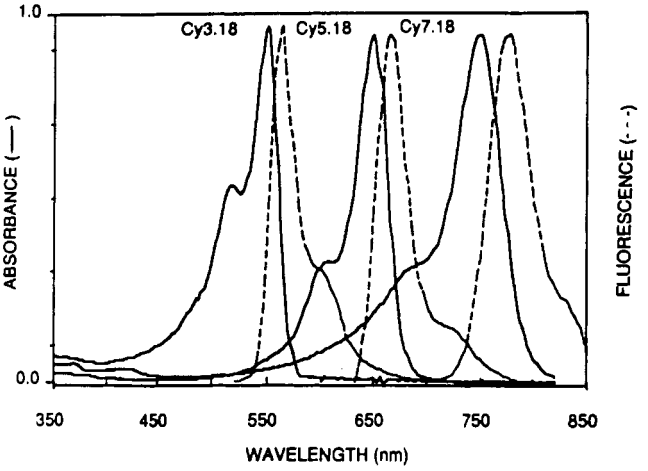


Figure 3. Absorption (—) and emission (- -) spectra of Cy3.18, Cy5.18, and Cy7.18 in PBS.

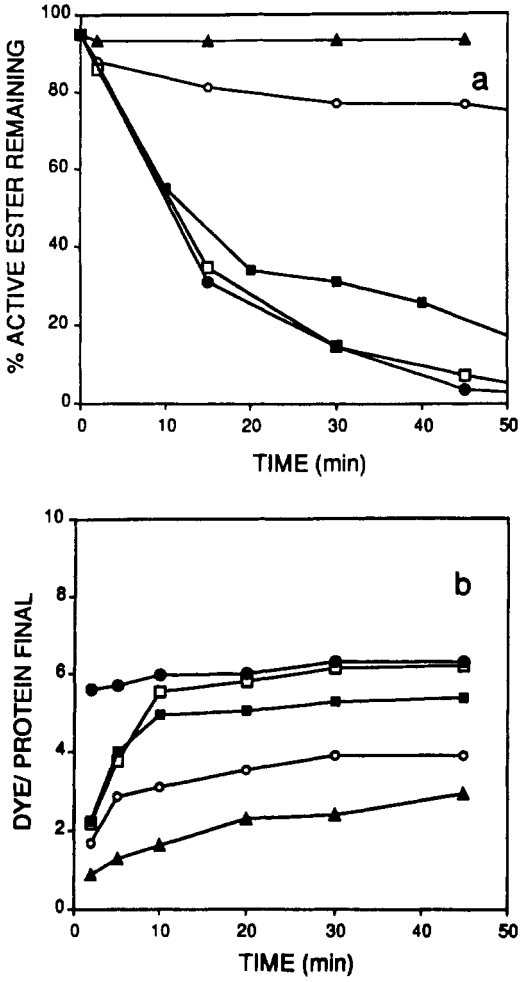


Figure 4. (a) Stability of succinimidyl active ester over time in buffer solutions (see methods) at pH 7.0 (▲), pH 7.5 (○), pH 8.0 (■), pH 8.5 (□), and pH 9.4 (●). (b) Extent of labeling of sheep IgG with Cy5.29.OSu over time in buffer solutions at pH 7.0 (▲), pH 7.5 (○), pH 8.0 (■), pH 8.5 (□), and pH 9.4 (●).

clearly shows that, for aqueous buffers in the pH range 7–9.4, the rate of protein labeling (at 1 mg of protein/250 μL) is at least 10 times faster than the rate of hydrolysis of the succinimidyl ester.

Absorption and Fluorescence of Labeled Amines. Table II shows absorption and emission properties of the cyanine succinimidyl esters that have been reacted with low molecular weight alkylamines. There is minimal dependence of solvent on the absorption and emission

Table II. Spectral Properties of Key Sulfoindocyanine Dyes

dye	solvent	abs max	em max	ϕ	ϵ^d (L/mol cm)
Cy3.18	ethanol	560	575	0.09[a]	150 000
	formamide	558			
	PBS[c]	550	565	0.04	150 000
	glycerol (25 °C)	558	571	0.52	
	glycerol (8 °C)	558	569	0.51	
Cy5.18	ethanol	658	677	0.40[b]	250 000
	formamide	656			
	PBS	650	667	0.27	250 000
	glycerol (25 °C)	656	674	0.39	
	glycerol (8 °C)	658	672	0.43	
Cy5.29	ethanol	658	677	0.30	
	formamide	658			
	PBS	650	666	0.20	
Cy5.29–taurine	PBS (pH 7)	650	665	0.20	
	PBS (pH 9.4)	650	665	0.22	
Cy7.18	ethanol	758	789	–	200 000
	formamide	764	–		
	PBS	750	777	–	200 000

[a] Based on rhodamine-6G quantum yield in ethanol as standard. [b] Based on Di-S-C2-(5) as standard (22). [c] Phosphate-buffered saline. [d] Estimated error range error = +5%.

wavelengths. However, the quantum yields of Cy3 and Cy5 dyes are somewhat higher in organic solvents. The quantum yields of Cy5 derivatives, and especially the Cy3-labeled amines, depend strongly on solvent viscosity. For example, Table II shows that Cy3 is ~10 times more fluorescent in glycerol at 8 °C than it is in water at room temperature.

DISCUSSION

We developed a series of fluorescent labeling reagents that contain negatively charged sulfonate groups directly attached to the indocyanine nuclei. These dyes are intrinsically much more water soluble than cyanines without aryl sulfonate groups (*7*). This property makes these labeling reagents very easy to use because they dissolve rapidly into aqueous buffers with no aggregation under normal labeling conditions. Presumably, because of the location of the sulfonic acid groups on the ring structure of the fluorophore, these labeling reagents have less affinity for one another on the protein surface, and as a result, sulfoindocyanines activated with succinimidyl ester groups can be used to tag antibodies and other proteins with significantly less dimer formation and much greater fluorescence (*8*). Sulfoindocyanines have been used to produce highly fluorescent antibodies (*15*, *16*), phycoerythrin (*17*), transferrin (*18*), dextrans (*14*), and 5′-amino-modified oligonucleotides (*19*).

The speed of the labeling reaction depends on the concentration of the reactive dye, the concentration of the target, and the pH of the reaction medium. Generally, procedures for the labeling proteins with isothiocyanates and succinimidyl esters call for 1–24 h of incubation in aqueous buffer at pH 8.5–9.5 (*20*). We find that less than 10 min is sufficient at pH 8.5–9.4 with the succinimidyl esters of sulfoindocyanines. At the higher pH value, the labeling produces a greater D/P ratio for antibody labeling (Figure 4b). Since the sulfoindocyanine OSu reagents hydrolyze only slowly in aqueous buffers at pH 7, it is also possible to label pH-sensitive materials at neutral pH by increasing the incubation time to several hours. In labeling reactions, the buffering agent should not contain primary amino groups, or other good nucleophiles.

The absorption maximum, extinction coefficient, quantum yield, and fluorescence wavelength of Cy3.18 and Cy5.18 bound to low molecular weight primary amines

are essentially the same as for the corresponding carboxylic acid forms of Cy3.18 and Cy5.18. The quantum yields are somewhat higher in organic solvents but do not depend on pH over the range of 4–10. Highly viscous solvents (e.g., cold glycerol, Table II) that reduce the conformational flexibility of Cy3 increase its quantum yield (*21*). The fluorescence-enhancing effect of a rigid microenvironment may explain the remarkable increase in quantum yield of Cy3 when it is conjugated to antibodies. It is plausible that the use of polymeric microscope slide mounting media might produce a higher Cy3 fluorescence. Cy5-labeled material, on the other hand, shows only a minimal dependence of quantum yield on environmental rigidity.

The reactive cyanines have one or two OSu groups. Symmetrical dyes with two OSu groups are easier to synthesize but may cross-link different amino groups on the same target or on different targets. We have found that labeling of antibody at 1 mg/mL produces almost no cross-linking (*7*). Cross-linking between amino groups on different proteins can occur, however, when both protein and dye concentrations are high.

The emission maxima for members of the series range from 575 to 780 nm. The carbocyanine reagent Cy3.18 can be excited with the 488-, 514-, and 532-nm laser lines and is optimally excited with the 546-nm mercury arc line. Because the extinction coefficient of Cy3.18 on the blue shoulder at 488 nm is still about 25% (22 000 L/mol cm) of its maximum at 550 nm, it is even possible to perform two-color flow cytometry using Cy3.18-labeled antibodies with fluorescein-labeled antibodies. Our preliminary observations indicate that the photostability of Cy3 is comparable to that of rhodamines (*16*) and significantly greater than that of fluorescein and also that Cy3.18 and Cy5.18 produce conjugated antibodies with less nonspecific binding than those obtained using TRITC and other nonsulfonated cyanines. Because of its brightness, water solubility, photostability, and low nonspecific binding, Cy3 may be considered an ideal substitute for tetramethylrhodamine isothiocyanate (TRITC).

The red-fluorescing Cy5.18 can be excited with the 633-nm HeNe laser line and the 647-nm line of a Kr laser. Excitation with these long-wavelength laser lines produces less autofluorescence than with short-wavelength excitation, and as a result, Cy5.18-labeled antibodies can be detected even on macrophages by flow cytometry. In most cases adequate signals can be obtained in flow cytometry and laser confocal scanning microscopes using inexpensive HeNe lasers. The photostability of Cy5 derivatives is comparable to, or somewhat better than that of fluorescein. The labeling reagent Cy5.18.OSu may be considered as a low molecular weight, easy to use alternative to allophycocyanine (*8*).

The near-IR fluorescing Cy7.18.OH can be excited in the 700–750-nm range and emits maximally near 780 nm. Antibodies labeled with Cy7.18 are not as bright and photostable as those generated with Cy3.18 and Cy5.18, but useable images can be obtained when the antigen density is sufficiently high and a cooled CCD camera is used to acquire the images.

ACKNOWLEDGMENT

The authors gratefully acknowledge the assistance of Ms. Jean Chao and Mr. Marc Wagner in the labeling of antibodies and their spectroscopic analysis. This work was supported by Grants NIH NS 19353 and NSF DIR 8920118 and the Western Pennsylvania Advanced Technology Center through Pennsylvania's Ben Franklin Partnership Program.

LITERATURE CITED

(1) Wang, L., and Taylor, D. L., Eds. (1989) Fluorescence Microscopy of Living Cells in Culture. *Methods in Cell Biology*, Vol. 29, Academic Press, Inc., New York.

(2) Melamed, M. R., Lindmo, T., and Mendelsohn, M. L., Eds. (1990) *Flow Cytometry and Sorting*, 2nd ed.; Wiley-Liss, Inc., New York.

(3) Haugland, R. P. (1989) *Handbook of Fluorescent Probes and Research Chemicals*, Molecular Probes, Inc., Eugene, OR 97402.

(4) Tsien, R., and Waggoner, A. S. (1990) *Fluorophores* for confocal microscopy. Photophysics and Photochemistry. *Handbook of Biological Confocal Microscopy*. (J. B. Pawley, Ed.) pp 169–178, Plenum Publishing Corp., New York.

(5) Ernst, L. A., Gupta, R. K., Mujumdar, R. B., and Waggoner, A. S. (1989) Cyanine dye labeling reagents for sulfhydryl groups. *Cytometry 10*, 3–10.

(6) Mujumdar, R. B., Ernst, L. A., Mujumdar, S. R., and Waggoner, A. S. (1989) Cyanine dye labeling reagents containing isothiocyanate groups. *Cytometry 10*, 11–19.

(7) Southwick, P. L., Ernst, L. A., Tauriello, E. W., Stephen, R. P., Mujumdar, R. B., Mujumdar, S. R., Clever, H. A., and Waggoner, A. S. (1990) Cyanine dye labeling reagents—Carboxymethylindocyanine succinimidyl esters. *Cytometry 11*, 418–430.

(8) Mujumdar, R. B., Ernst, L. A., Mujumdar, S. R., Chao, J., Wagner, M., and Waggoner, A. S. (1993) Antibody labeling with multicolor fluorescent cyanine dyes. (submitted).

(9) Jelinek, C. F., and Kleinschmidt, R. F. (1951) Preparation of Malonaldehyde Dianils. U.S. Patent 2,549,097.

(10) Hamer, F. M. (1964) *The Cyanine Dyes and Related Compounds*. Wiley, New York.

(11) Illy, H., and Funderburk, L. (1968). Fisher Indole Synthesis, Direction of Cyclization of Isopropylmethyl Ketone Phenylhydrazone. *J. Org. Chem. 33*, 4283.

(12) Adachi, Kalo, E., Inoue, N., and Tetsurou, K. (1981) Photographic Light sensitive materials having dye lasers. U.S. Patent 4268,622.

(13) Ogura, H., Kobayashi, T., Keiko, S., Kawabe, K., and Takeda, K. (1979) A novel active ester synthesis reagent (N,N'-Disuccinimidyl Carbonate). *Tetrahedron Lett.* 4745–4746.

(14) West, W., and Pearce, S. (1965) The Dimeric State of Cyanine Dyes. *J. Phys. Chem. 69* (6), 1894–1903.

(15) Dauber, J. H., Wagner, M., Brunsvold, S., Ernst, L. A., and Waggoner, A. S. (1992) Flow Cytometric Analysis of Lymphocyte Phenotypes in Bronchoalveolar Lavage Fluid. *Am. J. Resp. Cell Mol. Biol. 7*, 531–541.

(16) Wessendorf, M. W., and Brelje, T. C. (1992) Which fluorophore is brightest? A comparison of the staining obtained using fluorescein, tetramethylrhodamine, lissamine rhodamine, Texas Red and cyanine 3.18. *Histochemistry 98*, 81–86.

(17) Lansdorp, P. M., Smith, C., Safford, M., Terstappen, L. W. M. M., and Thomas T. E. (1991) Single laser three color immunofluorescence staining procedures based on energy transfer between phycoerythrin and cyanine 5. *Cytometry 12*, 723–730.

(18) Cain, C. C., Wilson, R. B., and Murphy, R. F. (1991) Isolation by fluorescence-activated cell sorting of chinese hamster ovary cell lines with pleiotropic, temperature-conditional defects in receptor recycling. *J. Biol. Chem. 266*, 11746–11752.

(19) Yu, H., Ernst, L. E., Wagner, M., and Waggoner, A. S. (1992) Sensitive detection of RNA's in single cells by flow cytometry. *Nucleic Acids Res. 20*, 83–88.

(20) dePetris, S. (1978) Immunoelectron Microscopy and Immunofluorescence in Membrane Biology. *Methods Membr. Biol. 9*, 1–201.

(21) Luby-Phelps, K., Guss, K. A., Ernst, L. E., Mujumdar, R. B., Mujumdar, S. R., and Waggoner, A. S. (1988) The solvent viscosity of the cytometrix as measured by ratio imaging. *J. Cell Biol. 107* (6, Part 3), a59.

(22) Sims, P. J., Waggoner, A. S., Wang, C. H., and Hoffman, J. F. (1974) Studies on the mechanism by which cyanine dyes measure membrane potential in red blood cells and phosphatidylcholine vesicles. *Biochemistry 13*, 3315–3330.

Single-Chain Immunotoxin Fusions between Anti-Tac and *Pseudomonas* Exotoxin: Relative Importance of the Two Toxin Disulfide Bonds

Robert J. Kreitman, Janendra K. Batra,† Saraswathy Seetharam,‡ Vijay K. Chaudhary,§ David J. FitzGerald, and Ira Pastan*

Laboratory of Molecular Biology, Division of Cancer Biology, Diagnosis and Centers, National Cancer Institute, National Institutes of Health, 9000 Rockville Pike, 37/4E16, Bethesda, Maryland 20892. Received August 10, 1992

Anti-Tac(Fv)-PE40 is a recombinant single-chain immunotoxin in which the variable heavy and light domains of the anti-IL2 receptor antibody, anti-Tac, are connected to each other by a peptide linker and then fused to PE40, a truncated form of *Pseudomonas* exotoxin (PE). This fusion protein has four disulfide bonds: one in each of the two variables domains, one in domain II (Cys 265–287), and one in domain Ib (Cys 372–379) of PE. To study the importance of the disulfide bonds of the toxin to the activity of single-chain immunotoxins, we constructed mutants in which either the cysteines in the toxin were changed to alanines or the amino acids 365–380 of PE were deleted. We began this study with anti-Tac(Fv)-PE40 and a more active variant, anti-Tac(Fv)-PE40KDEL, in which the carbonyl terminus is changed from REDLK to KDEL. From these proteins we made anti-Tac(Fv)-PE40^{4A} and anti-Tac(Fv)-PE40KDEL^{4A}, respectively, by converting cysteins at amino acids 265, 287, 372, and 379 of PE to alanines. This change resulted in a 20–100-fold loss of activity toward human target cells, but no significant change in binding affinity to p55. To determine the importance of the second toxin disulfide bond, we removed amino acids 365–380 from anti-Tac(Fv)-PE40, anti-Tac(Fv)-PE40KDEL, and anti-Tac(Fv)-PE40KDEL^{4A}, resulting in anti-Tac(Fv)-PE38, anti-Tac(Fv)-PE38KDEL, and anti-Tac(Fv)-PE38KDEL^{2A}, respectively. This deletion resulted in a slight increase in cytotoxicity toward some target cells. Anti-Tac(Fv)-PE38KDEL and anti-Tac(Fv)-PE40KDEL were up to 300-fold more cytotoxic than their respective mutants which contained alanines only at positions 265 and 287. Thus the first disulfide bond of the toxin (Cys 265–287) is much more important for cytotoxicity than the second one (Cys 372–379). We found that anti-Tac(Fv)-PE40KDEL and anti-Tac(Fv)-PE38KDEL were the most active agents in vitro and had the same half-life in mice and the maximum tolerated dose was also the same for each.

INTRODUCTION

Single-chain antibodies, made from the fusion of the variable heavy and light chain regions of an antibody through a peptide linker, have become candidates for the therapy and diagnosis of human disease. They can be used alone (*1*, *2*) or conjugated to radioactive ligands (*3*) or like Fab fragments, to protein toxins (*4*, *5*). We have recently reported that the single-chain version of the anti-Tac antibody, anti-Tac(Fv), can be genetically fused to derivatives of either *Pseudomonas* exotoxin (*4*) or diphtheria toxin (*6*). The resulting proteins, anti-Tac(Fv)-PE40 and DT388-anti-Tac(Fv), were specifically cytotoxic toward cells expressing the p55 subunit of the IL2 receptor (*4*, *6–8*). Single-chain recombinant immunotoxins have been made from other antibodies as well (*9–12*).

Pseudomonas exotoxin (PE) is a 66-kDa 613 amino acid protein consisting of three major domains (*13*). Domain Ia (amino acids 1–252) binds to the PE receptor on normal cells. Domain II (amino acids 253–364) undergoes proteolytic cleavage and mediates translocation of the 37-kDa carboxyl terminal segment of PE into the cytoplasm. Domain III (amino acids 400–613) contains the enzyme which ADP ribosylates elongation factor 2 (EF-2) and causes cell death (*14*, *15*). The function of domain Ib (amino acids 365–399), which lies between domains II and III in the three-dimensional structure of PE, is unclear. To remove the cell binding activity of PE, we have deleted domain Ia. By fusing the resultant protein, PE40, to other ligands, chimeric toxins have been made which are specifically cytotoxic to appropriate target cells (*16*).

Two studies have previously examined the importance of the disulfide bonds in PE40-containing chimeric toxins. Both studies dealt with the activity of TGFα-PE40. One study found that TGFα-PE38, made by deletion of amino acids 365–380, which includes a disulfide bond, was not less cytotoxic than TGFα-PE40. In contrast, mutating cysteines at positions 265 and 287 decreased cytotoxicity 10-fold (*17*). In another study, replacement of cysteines with alanines at positions 265 and 287 decreased cytotoxicity 18-fold, while the same mutations at positions 372 and 379 decreased cytotoxicity 2.5-fold (*18*). Binding studies showed that cytotoxicity of the TGFα-toxin mutants did not correlate with binding to the EGF receptor. However, since TGFα contains three disulfide bonds and TGFα-PE40 is a heterogeneous mixture with respect to disulfide bonding (*18*), it was not clear that the cytotoxicity differences were independent of folding interactions between TGFα and the toxin.

For several reasons, we desired to study the importance of each disulfide bond of PE40 when it was fused to a single-chain antibody like anti-Tac(Fv). Of technical concern was the low yield of renatured monomer (typically 0.5–2% of total recombinant protein) and the possibility that removal of one of the four disulfide bonds in the

* Author to whom correspondence should be sent.
§ Current address: Department of Biochemistry, University of Delhi South Campus, Benito Juarez Road, New Delhi 110021, India.
† Current address: National Institute of Immunology, N.I.I. Campus, J.N.U. Complex, Shahid Jeet Singh Marg, New Delhi 110067, India.
‡ Current address: Department of Genetics (MC669), University of Illinois College of Medicine, 808 South Wood Street, Chicago, IL 60612.

1043-1802/93/2904-0112$04.00/0 © 1993 American Chemical Society

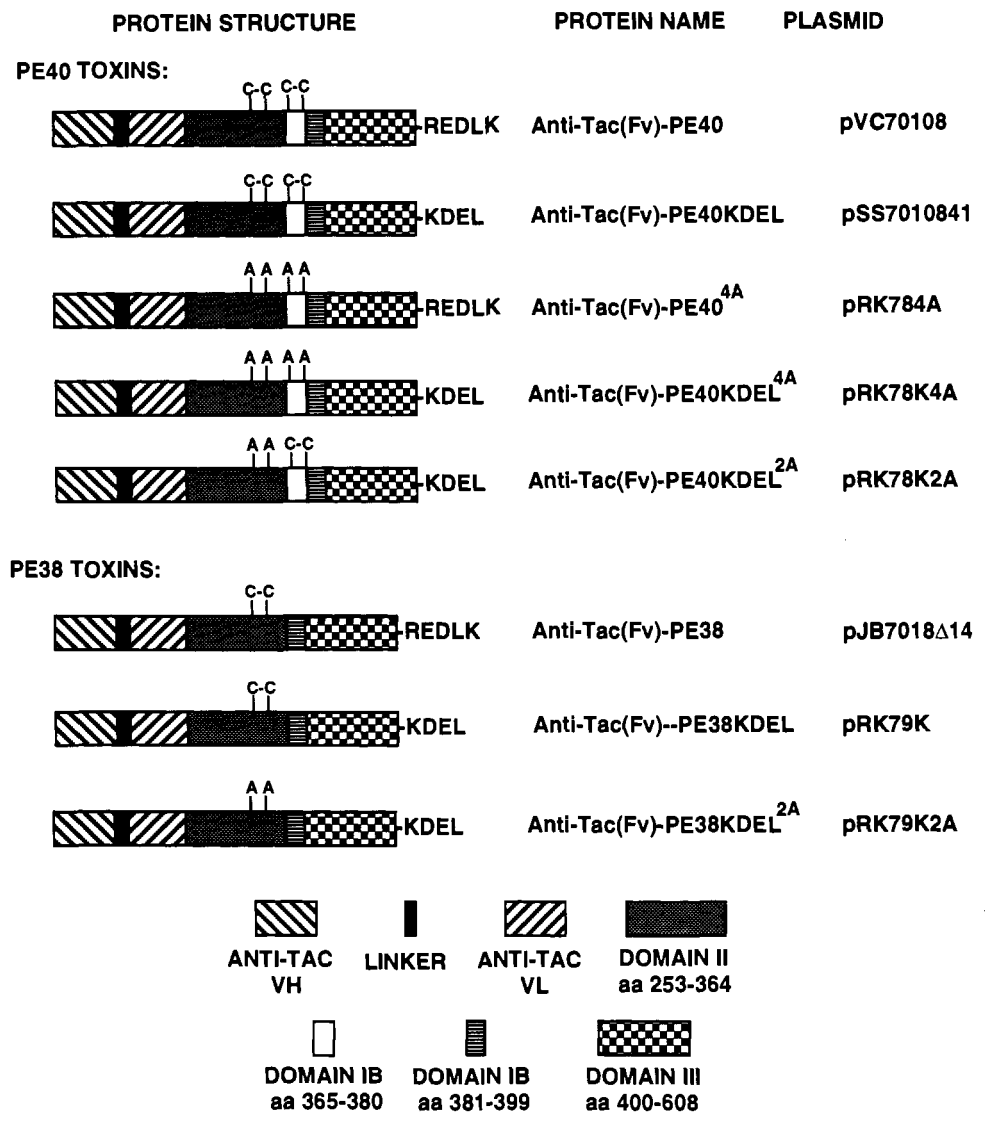


Figure 1. Anti-Tac immunotoxin mutants used in the present study, with the names of the plasmids encoding them. All of the plasmids contain unique *Sal*I, *Bam*HI, *Eco*RI, and *Asp*700 restriction sites, which were used for subcloning. In all plasmids *Sal*I is located at PE codon 308 (domain II), *Bam*HI at codon 492 (domain III), *Eco*RI at the 3′ side of the termination codon, and *Asp*700 several hundred base pairs 3′ to the *Eco*RI site. All plasmids contain a *Hin*dIII site between anti-Tac(Fv) and toxin encoding regions except pVC70108 and pSS7010841.

immunotoxin might improve protein folding. Of biologic interest was whether the disulfide bonds of PE40 had effects on cytotoxicity that were due to toxin activity and independent of the ligand. Anti-Tac(Fv)-PE40 seemed appropriate to study, since in contrast to TGFα-PE40, which had up to 100-fold poorer binding than TGFα (*18*), anti-Tac(Fv)-PE40 bound with over 30% of the affinity of the intact anti-Tac antibody (*4*). Another important biologic issue was the influence of the 365–380 deletion on half-life and nonspecific toxicity. These issues could not be addressed with the TGFα-toxins, since their major toxicity is due to specific toxin binding to EGF receptor-bearing hepatocytes, and such binding markedly affects drug disappearance from the serum. A third biological issue was whether the process by which the disulfide bonds influence cytotoxicity was independent of that by which the KDEL carboxyl terminal mutation influences cytotoxicity (*19*).

To determine the relative importance of the two disulfide bonds within the toxin portion of anti-Tac(Fv)-PE40 and its more active mutant anti-Tac(Fv)-PE40KDEL (*4*, *20*), we either removed the second disulfide bond by deleting amino acids 365–380 or changed cysteines to alanines. The anti-Tac(Fv) chimeric toxins were tested against several malignant cell lines, activated human lymphocytes, and peripheral blood mononuclear cells from an adult T-cell leukemia (ATL) patient. The most active mutants were tested for toxicity in animals, and their pharmacokinetic behavior was also determined.

MATERIALS AND METHODS

Plasmids. All the constructs were made using standard cloning techniques involving restriction enzyme digestions and separation of fragments on low melting point agarose gels, followed by in-gel ligations. The plasmids and the immunotoxins they encode are shown in Figure 1.

pVC70108 (*4*) and pSS7010841 (*20*) encode anti-Tac(Fv)-PE40 and anti-Tac(Fv)-PE40KDEL, respectively. pRK79K, encoding anti-Tac(Fv)-PE38KDEL, was obtained by ligating the 0.9-kb *Sal*I–*Eco*RI fragment of pRK39K (*12*) to the 3.9-kb *Eco*RI–*Sal*I fragment of p7018 (*7*). The 0.9-kb *Sal*I–*Eco*RI fragment encodes amino acids 308–364 and 381–608 of PE, followed by KDEL. pJB-7018Δ14, encoding anti-Tac(Fv)-PE38, was obtained by ligating the 1.0-kb *Sal*I–*Eco*RI fragment of pCS10 (*17*) to the 3.9-kb *Eco*RI–*Sal*II fragment of p7018. This 1.0-kb

*Sal*I–*Eco*RI fragment encodes amino acids 308–364 and 381–613 of PE, which includes the native carboxyl terminus REDLK.

To make the plasmids encoding alanine mutants, we used pTAC TGF57-PE40 (*21*), which encodes TGFα-PE40δcys. The 1.2-kb *Nco*I–*Eco*RI fragment of this plasmid encodes PE40 containing alanines rather than cysteins at positions 265, 287, 372, and 379. Since pTP39, which encodes IGF-I-PE40 (*22*) and p7018, which encodes anti-Tac(Fv)-PE40 (*7*), each contain a *Hin*dIII site between the ligand and PE40 encoding regions, we used a short *Hin*dIII–*Nco*I connector. Two oligonucleotides, of sequence 5′-A-GCT-TTC-GGT-GGT-GGC-TCT-GC-3′ and 5′-CAT-GGC-AGA-GCC-ACC-ACC-GAA-3′, were synthesized and annealed. The duplex and the 1.2-kb *Nco*I–*Eco*RI fragment of pTAC TGF57-PE40 were ligated to the 3.2-kb *Eco*RI–*Hin*dIII fragment of pTP39, resulting in pTP47, which encodes IGF-I-PE40^{4A}. pRK784A, encoding anti-Tac(Fv)-PE40^{4A}, was obtained by ligating the 1.2-kb *Hin*dIII–*Eco*RI fragment of pTP47 to the 3.7-kb *Eco*RI-*Hin*dIII fragment of p7018. pRK78K4A, encoding anti-Tac(Fv)-PE40KDEL^{4A}, was obtained by ligating the 0.37-kb *Bam*HI–*Eco*RI fragment of pCS64GK (*12*) to the 4.5-kb *Eco*RI–*Bam*HI fragment of pRK784A. The 0.35-kb *Bam*HI–*Eco*RI fragment encodes amino acids 492–608 of PE, followed by KDEL. pRK79K2A, encoding anti-Tac(Fv)-PE38KDEL^{2A}, was obtained by ligating the 0.9-kb *Sal*I–*Eco*RI fragment of pRK39K to the 3.9-kb *Eco*RI–*Sal*I frament of pRK784A. pRK78K2A, encoding anti-Tac(Fv)-PE40KDEL^{2A}, was obtained by ligating the 0.95-kb *Sal*I–*Eco*RI fragment of p7018K to the 3.9-kb *Eco*RI–*Sal*I fragment of pRK79K2A. The 0.95-kb *Sal*I–*Eco*RI fragment encodes amino acids 492–608 of PE, followed by KDEL. pRK7018K, a high copy number plasmid encoding anti-Tac(Fv)-PE40KDEL, was obtained by ligating the 0.37-kb *Bam*HI–*Eco*RI fragment of pRK79K to the 4.5-kb *Eco*RI–*Bam*HI fragment of p7018.

We used PCR to design pRK768K, a plasmid encoding anti-Tac(Fv)-PE40KDEL which contains the same *Hin*dIII–*Nco*I connector (encoding the amino acids GGGSAMAEE) which connects anti-Tac(Fv) with PE40^{4A}, PE40KDEL^{4A}, PE40KDEL^{2A}, or PE38KDEL^{2A}. The oligonucleotides BK-62 (5′-ACC-AAG-CTG-GCC-ATG-GCC-GAA-GAG-GGC-GGC-AGC-CTG-GCC-GCG-CTG-3′) and BK-63 (3′-CCG-TGC-GTC-TTG-ACC-TGC-CAC-5′) obtained from Bioserve (College Park, MD), were used to amplify PE codons 253–419 from p7018. The optimal conditions for amplification included a dissociation temperatue of 94 °C for 1 min, an annealing temperature of 40 °C for 2 min, and a polymerization temperature of 72 °C for 3 min with a 10 s/cycle extension, for a total of 30 cycles. Adequate amplification required 10% formamide. PCR reagents were included in the Perkin-Elmer Gene Amp kit obtained from USB (Cleveland, OH). The 0.52-kb amplified DNA fragment was digested with *Nco*I and *Sac*II and the restricted 0.49-kb fragment ligated to the 4.4-kb *Sac*II–*Nco*I fragment of pRK79K2A.

Expression and Purification of Proteins. Plasmids encoding recombinant proteins were expressed as described previously (*7*) and were purified from the denatured and renatured inclusion bodies by Q-Sepharose, Mono-Q and gel filtration chromatography as described previously (*6*). Purified protein was quantitated by Bradford assay using bovine serum albumin as a standard (Bio-Rad, Richmond, CA or Pierce, Rockford, IL), which agreed with values obtained on selected proteins by amino acid analysis (*20*). Humanized anti-Tac monoclonal antibody was furnished by Hazelton Labs (Vienna, VA) and Hoffman-La Roche (Nutley, NJ).

Cells and Cytotoxicity Assays. The origin and maintenance of the cell lines used were described previously (*4*, *23*). Cell lines were washed with media (RPMI + 10% FBS), resuspended with media at a cell density of 8×10^5/mL and added to 96-well plates at 50 μL/well. Fifty microliters of chimeric toxins or controls, diluted in media, were mixed into each well and the cells incubated at 37 °C for 20–24 h. The cells were then pulsed with 1 μCi [^{3}H]leucine (diluted to 50 μL with leucine-free RPMI) per well for 2–4 h, and the incorporated radioactivity was harvested on glass-fiber filters and quantitated on a Betaplate scintillation counter (Pharmacia-LKB, Gaithersburg, MD). Normal human lymphocytes were activated by either phytohemagglutinin-P (PHA-P) (Sigma, St. Louis, MO) or the mixed lymphocyte reaction (MLR) generally as previously described (*7*). During lymphocyte activation by either technique, the tissue culture media (TCM) consisted of RPMI–DMEM (1:1) containing 5% human AB serum, 0.1 mM nonessential amino acids, 60 μg/mL L-arginine, mM HEPES 10, 4 mM L-glutamine, 100 units/mL penicillin, 100 μg/mL streptomycin, 50 μM β-mercaptoethanol, and 1 mg/mL dextrose. PHA (10–25 μg/mL) was used for lymphocyte activation. During the cytotoxicity assay, the assay media used consisted of leucine-free RPMI containing 5% FBS, 1 mM sodium pyruvate, 0.1 mM nonessential amino acids, 2 mM L-glutamine, 100 units/mL penicillin, 100 μg/mL streptomycin, 100 μg/mL gentamycin, and 10 units/mL recombinant IL2 (Cetus, Emeryville, CA). The activated lymphocytes were incubated with toxins or controls using the same volumes and cell densities as for the cell lines, but the incubation time was prolonged to 40–60 h and a 6-h pulse was performed using 2 μCi of [^{3}H]leucine per well.

For the adult T-cell leukemia (ATL) patient sample, anticoagulated blood was obtained from an ATL patient and after Ficoll centrifugation, the washed mononuclear cells were cultured with toxins or controls in 96-well plates. The final cell density was 1×10^6/mL in culture media consisting of RPMI, leucine-free RPMI, and FBS (2:88:10). The remainder of the assay was performed as for the MLR and PHA assays. In all cytotoxicity assays, experiments were performed in triplicate and values within each triplicate usually varied from the median by less than 10%.

Binding Studies. ATac-4 cells were obtained by transfecting a gene encoding human p55 into the human epidermoid line A431 (Chaudhary et al., manuscript in preparation). Cells were cultured in DMEM media containing 5% FBS and G418 (750 μg/mL) (GIBCO-BRL, Gaithersburg, MD). Cells (5×10^4) in 1-mL aliquots were plated in 24-well plates. Twenty-four hours later, the cells were washed twice in binding buffer (DMEM containing bovine serum 1 mg/mL albumin and 50 mM BES, pH 6.8). Aliquots (0.2 mL) of binding buffer containing 3 ng of [^{3}H]anti-Tac with various concentrations of the recombinant toxins or controls were added. After equilibrating for 2 h at 4 °C, the cells were washed three times in cold binding buffer and dissolved in 0.2 mL of 1 M NaOH. After diluting with 0.1 mL of 0.1 M NaOH and neutralizing with 1 mL of 0.4 M AcOH, the bound [^{3}H]anti-Tac was measured by a scintillation counter. For the cytotoxicity and binding assays, data reported are from one of several confirmatory assays.

Animal Toxicity. Maximum tolerated doses of the most cytotoxic recombinant proteins were determined. The toxins, diluted in 0.5 mL of PBS containing 0.2%

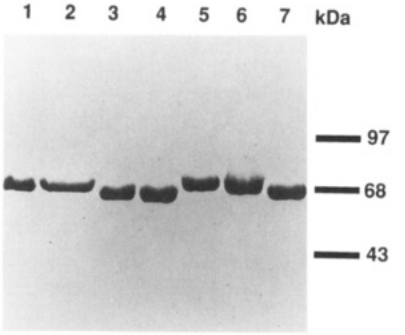


Figure 2. 10% SDS–PAGE reducing gel showing the purity and relative molecular weights of the immunotoxins used in the present study. Lanes 1 and 2 are anti-Tac(Fv)-PE40KDEL and anti-Tac(Fv)-PE40, respectively, each 66 kDa. Lanes 3 and 4 are anti-Tac(Fv)-PE38KDEL and anti-Tac(Fv)-PE38, respectively, which are 64 kDa because the loss of 16 amino acids (amino acids 365-380). Lanes 5 and 6 are anti-Tac(Fv)-PE40KDEL^{4A} and anti-Tac(Fv)-PE40^{4A}, respectively, which are 67 kDa, slightly higher than anti-Tac(Fv)-PE40 because of the nine extra amino acids between anti-Tac(Fv) and the toxin. Lane 7 is anti-Tac(Fv)-PE38KDEL^{2A}, and its molecular weight is 2 kDa less than anti-Tac(Fv)-PE40^{4A} due to the loss of amino acids 365–380.

human serum albumin (HSA–PBS), were administered intraperitoneally (ip) to white Balb/c female 4–6-week-old mice obtained from the NCI at Frederick, MD. Mice typically weighed 16–20 g. Lethal toxicity was defined as death or toxicity preventing the animal from obtaining food (which would require euthanasia) within 72 h following injection.

Measurement of Serum Levels. Balb/c mice were given tail vein injections of recombinant immunotoxin (1 μg in 0.2 mL of 0.2% HSA–PBS). At 1-, 5-, 10-, 20-, 30-, 40-, and 90-min time points, 0.05–0.1 mL of blood was withdrawn from the orbital vein. Each time point was the average of several mice. The serum was collected and the active toxin therein quantitated by measuring the cytotoxicity of serial dilutions of serum on HUT-102 cells. For quantitation, a standard curve using purified toxin was employed.

RESULTS

Single-chain recombinant antibodies have proven useful in targeting toxins to kill specific cells. While these single-chain immunotoxins are nearly as small as growth factor fusion toxins, they may be more versatile since they can target nongrowth factor antigens as well as growth factor receptors. Also, PE40, the truncated toxin portion originally used to make single-chain immunotoxins, can be made smaller or mutations can be introduced without inactivating the toxin (*17*, *18*). We decided to study the importance of the disulfide bonds in the toxin to determine the best derivative of PE40 to fuse to anti-Tac(Fv). We began with anti-Tac(Fv)-PE40 and anti-Tac(Fv)-PE40KDEL (*4*, *20*) and either mutated the cysteines in PE40 to alanines or deleted amino acids 365–380 from domain Ib which contain the second disulfide bond. The structures of the proteins studied are shown schematically in Figure 1.

Purification of Recombinant Immunotoxins. All recombinant proteins were expressed in *Escherichia coli* and purified from inclusion bodies as monomers. The seven chimeric toxins used in the present study were purified to near homogeneity as demonstrated by SDS–PAGE (Figure 2). From 0.5 L of culture, induced with IPTG at an OD_{650} of 2.0, we obtained 100–150 mg of total recombinant protein in an insoluble form in inclusion bodies. The yield of purified monomer ranged from 0.5 to 2 mg. The yield was similar for all of the molecules shown in Figure 1. Purified recombinant immunotoxins were used in all cytotoxicity, binding, and in vivo studies.

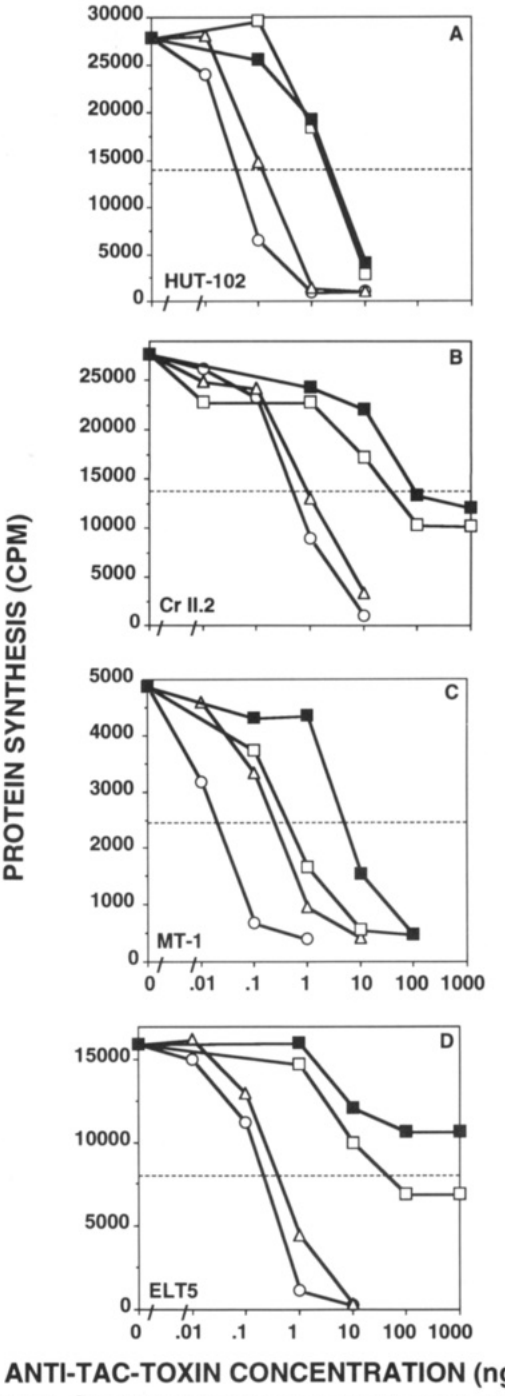


Figure 3. Sensitivity of cell lines to anti-Tac(Fv)-PE40KDEL (○), anti-Tac(Fv)-PE40 (△), anti-Tac(Fv)-PE40KDEL^{4A}, (□) and anti-Tac(Fv)-PE40^{4A} (■).

Cytotoxic Effect of Removing Both Disulfide Bonds. To determine the effect of eliminating both disulfide bonds from the toxin portion of anti-Tac(Fv)-PE40 and anti-Tac(Fv)-PE40KDEL, all four cysteines of the toxin portion were changed to alanines. Figure 3 and Table I indicate that anti-Tac(Fv)PE40^{4A} and anti-Tac(Fv)-PE40KDEL^{4A} were significantly less cytotoxic compared to anti-Tac(Fv)-PE40 and anti-Tac(Fv)-PE40KDEL, respectively. In HUT-102 cells (Figure 3A), the IC_{50} increased from 0.14 ng/mL for anti-Tac(Fv)-PE40 to 2.0 ng/mL for anti-Tac(Fv)-PE40^{4A}. Anti-Tac(Fv)-PE40 and anti-Tac(Fv)-PE40KDEL were 20–100-fold more cytotoxic than anti-Tac(Fv)-PE40^{4A} and anti-Tac(Fv)-PE40KDEL^{4A},

Table I. Activity of Anti-Tac(Fv) Toxins against Cell Lines Containing p55

cell line origin	human HUT-102	human Cr II.2	human MT-1	mouse: ELT5
	Receptor Type[a]			
human p55	+	+	+	+
human p75	+	+	−	−
mouse p75	−	−	−	+
	IC_{50}[b] (ng/mL)			
anti-Tac(Fv)-PE40KDEL	0.04	0.6	0.02	0.2
anti-Tac(Fv)-PE38KDEL	0.03	0.7	0.02	0.18
anti-Tac(Fv)-PE40	0.14	0.9	0.2	0.4
anti-Tac(Fv)-PE38	0.04	0.8	0.2	0.2
anti-Tac(Fv)-PE40KDEL^{4A}	3	30	0.4	40
anti-Tac(Fv)-PE40^{4A}	2.0	90	5	>1000
anti-Tac(Fv)-PE40KDEL^{2A}	1.3	45	0.7	60
anti-Tac(Fv)-PE38KDEL^{2A}	1.7	20	0.4	60

[a] Taken from Chaudhary (*4*) and Lorberboum-Galski (*23*). [b] The IC_{50}'s for each cytotoxicity assay were the concentrations of toxin required to inhibit protein synthesis by 50%. Ten-fold dilutions of each chimeric toxin or control were used, and the median of three triplicates (which generally varied less than 5% of the mean) was used for calculations. Toward all targets, anti-Tac at 2500 ng/mL was noncytotoxic and in excess could compete for the cytotoxicity of recombinant immunotoxin.

Table II. Activity of Anti-Tac(Fv) Toxins against Activated Human Lymphocytes or against Malignant Lymphocytes from a Patient with Adult T-cell Leukemia

	IC_{50} (ng/mL)			
	MLR	PHA	ATL	normal lymphocytes
anti-Tac(Fv)-PE40KDEL	0.03	0.1	0.2	>1000
anti-Tac(Fv)-PE38KDEL	0.06	0.025	<0.1	>1000
anti-Tac(Fv)-PE40	0.05	0.11	0.64	>1000
anti-Tac(Fv)-PE38	0.09	0.09	0.23	>1000
anti-Tac(Fv)-PE40KDEL^{4A}	1.3	1.4	10	>1000
anti-Tac(Fv)-PE40^{4A}	4	3	55	>1000
anti-Tac(Fv)-PE40KDEL^{2A}		2.8		>1000
anti-Tac(Fv)-PE38KDEL^{2A}	0.5	1	6	>1000

respectively, toward Cr II.2 and MT-1 cells (Figure 3B,C, Table I). In murine ELT5 cells (Figure 3D, Table I), the loss of activity was more substantial, with an increase in IC_{50} of at least 200-fold when either anti-Tac(Fv)-PE40 or anti-Tac(Fv)-PE40KDEL was compared to anti-Tac(Fv)-PE40^{4A} or anti-Tac(Fv)-PE40KDEL^{4A}, respectively. In normal human lymphocytes activated by mixed lymphocyte reaction (MLR) or phytohemagglutinin (PHA), anti-Tac(Fv)-PE40 and anti-Tac(Fv)-PE40KDEL were 12–80-fold more cytotoxic than anti-Tac(Fv)-PE40^{4A} and anti-Tac(Fv)-PE40KDEL^{4A}, respectively (Table II). Similar differences were seen with fresh cells from a patient with adult T-cell leukemia. Thus, by removing both disulfide bonds from the toxin, the recombinant immunotoxins lost significant activity but were still active on all human target cells tested.

Cytotoxic Effect of Removing the Second Disulfide Bond. To test the effect of removing only the second disulfide bond within the toxin portion of anti-Tac(Fv)-PE40, we deleted the first half of domain Ib (PE amino acids 365–380) from both anti-Tac(Fv)-PE40 and anti-Tac(Fv)-PE40KDEL. The cytotoxic activities of the resulting proteins, anti-Tac(Fv)-PE38 and anti-Tac(Fv)-PE38KDEL, respectively, were compared to those of anti-Tac(Fv)-PE40 and anti-Tac(Fv)-PE40KDEL in Figure 4. The IC_{50}'s are listed in Tables I and II. In each of the target cells, anti-Tac(Fv)-PE40KDEL and anti-Tac(Fv)-PE40 were similar to anti-Tac(Fv)-PE38KDEL and anti-Tac(Fv)-PE38, respectively. Cells from the patient with ATL were over 2-fold more sensitive to anti-Tac(Fv)-PE38KDEL and anti-Tac(Fv)-PE38 than to anti-Tac(Fv)-PE40KDEL and anti-Tac(Fv)-PE40, respectively. Thus, removal of the second disulfide bond of PE40 did not reduce cytotoxicity. We did not attempt to delete the region containing the first disulfide bond as we did for the second disulfide bond of the toxin; we have previously shown that even small deletions in that region inactivate the toxin (*15*, *17*).

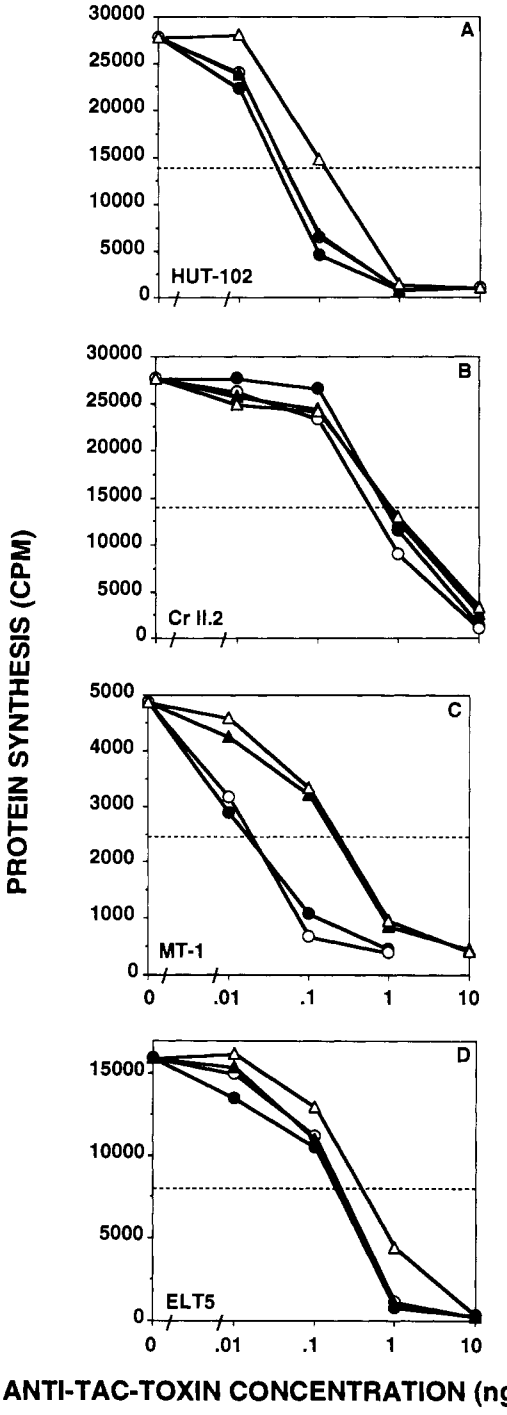


Figure 4. Cytotoxicity on cell lines of anti-Tac(Fv)-PE40 (△), anti-Tac(Fv)-PE38 (▲), anti-Tac(Fv)-PE40KDEL (○), and anti-Tac(Fv)-PE38KDEL (●).

Effect of Removing the First Disulfide Bond. To determine the cytotoxic effect of loss of the first toxin disulfide bond of the immunotoxin, we compared the cytotoxic activity of anti-Tac(Fv)-PE40KDEL and anti-Tac(Fv)-PE38KDEL with that of anti-Tac(Fv)-PE-

40KDEL^{2A} and anti-Tac(Fv)-PE38KDEL^{2A}, respectively. Table I shows that anti-Tac(Fv)-PE38KDEL was 55-, 30-, 20-, and 300-fold more cytotoxic than anti-Tac(Fv)-PE38KDEL^{2A} toward HUT-102, Cr II.2, MT-1, and ELT5 cells, respectively. Similarly, anti-Tac(Fv)-PE40KDEL was 30–300-fold more cytotoxic than anti-Tac(Fv)-PE40KDEL^{2A}. Toward the activated lymphocytes, removal of the first disulfide bond of the toxin decreased the immunotoxin activity 8–28-fold (Table II). Finally, the ATL cells were over 60-fold more sensitive to anti-Tac(Fv)-PE38KDEL than to anti-Tac(Fv)-PE38KDEL^{2A}. Thus, the first disulfide bond of the toxin is very important for cytotoxic activity, whether or not the second disulfide bond is present.

Effect of Toxin Disulfide Bonds on Anti-Tac(Fv) Binding. To determine whether the recombinant immunotoxins without a disulfide bond in domain II were less cytotoxic because of impaired binding to p55, we performed [^{3}H]anti-Tac displacement assays. To facilitate these studies, we transfected the adherent epidermoid cell line A431 with human p55. The sensitivity of the resulting ATac-4 cells to the recombinant toxins in Figure 1 resembles that of HUT-102 cells and will be described in detail elsewhere (Chaudhary et al., manuscript in preparation). The cells were allowed to adhere to plastic wells and were exposed at 4 °C to 1, 3, 9, 27, or 81 ng of [^{3}H]-anti-Tac in the presence and absence of a 1000-fold excess of anti-Tac. The Scatchard plot showing percent versus total [^{3}H]anti-Tac specifically bound to ATac-4 cells is depicted in Figure 5B. The data show there are 1.9×10^5 sites/cell with a K_d of 4×10^{-10} M. We then exposed the cells to 3 ng of [^{3}H]anti-Tac combined with various concentrations of several of the recombinant toxins shown in Figure 1. The data in Figures 5C and D show that the immunotoxins containing anti-Tac(Fv) bound with nearly equal affinity to p55. Thus, the loss of either disulfide bond of the toxin moiety of the immunotoxins did not significantly alter the affinity of the nearby Fv region for p55.

LD_{50} Studies in Mice. To determine the animal toxicity of the most cytotoxic mutants of anti-Tac(Fv)-PE40, we administered three of the single-chain immunotoxins, anti-Tac(Fv)-PE40KDEL, anti-Tac(Fv)-PE38KDEL, and anti-Tac(Fv)-PE38, to mice. Anti-Tac(Fv)-PE40KDEL and anti-Tac(Fv)-PE38KDEL appeared identical in their toxicity to mice with LD_{50}'s near 800 μg/kg (Table III). We found that anti-Tac(Fv)-PE38 was 2–4-fold less toxic than anti-Tac(Fv)-PE38KDEL, which is similar to the difference in animal toxicity between anti-Tac(Fv)-PE40 and anti-Tac(Fv)-PE40KDEL (*20*). Thus, loss of the second disulfide bond of anti-Tac(Fv)-PE40 and anti-Tac(Fv)-PE40KDEL results in no marked change in animal toxicity.

Serum Pharmacokinetics. To determine if the presence or absence of the second disulfide bond of the toxin would affect the stability of the immunotoxin in vivo, we administered them intravenously to mice. The disappearance curves of anti-Tac(Fv)-PE40KDEL and anti-Tac(Fv)-PE38KDEL are shown in Figure 6. We measured serum levels at the indicated times on the basis of cytotoxic activity, which would quantitate only intact immunotoxin. Using an RSTRIP program, the serum levels of anti-Tac-(Fv)-PE40KDEL and anti-Tac(Fv)-PE38KDEL were fitted to monoexponential decay curves (r^2 = 0.99 and 0.98, respectively), with calculated half-lives of 24.8 and 24.4 min, respectively. These values were similar to the calculated β half-lives for each agent, but the α phase was too short to determine accurately by blood draws at 1, 5, and 10 min. Nevertheless, there was no significant difference in overall serum disappearance, indicating that the loss of the second toxin disulfide bond does not alter serum stability, an important factor affecting drug delivery to tumors in vivo.

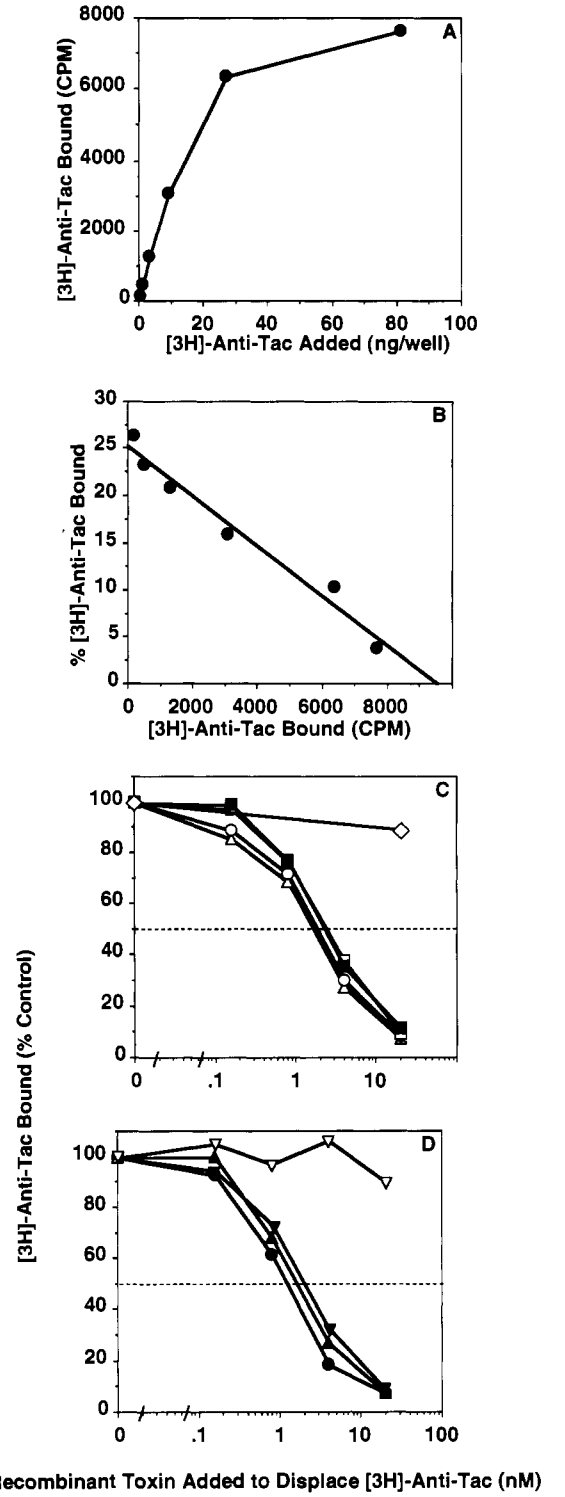


Figure 5. Binding and displacement assays using [^{3}H]anti-Tac (2700 cpm/ng) and ATac-4 cells. In A, Specific [^{3}H]anti-Tac bound (●) is shown when 0.3, 1, 3, 9, 27, or 81 ng is added to ATac-4 cells. The Scatchard plot of this data is shown in B. In C and D, [^{3}H]anti-Tac (0.01 nM) is displaced by either 0.16, 0.8, 4, or 20 nM anti-Tac(Fv)-PE40KDEL (○), anti-Tac(Fv)-PE40 (△), anti-Tac(Fv)-PE40KDEL^{4A} (□), anti-Tac(Fv)-PE40^{4A} (■), anti-Tac(Fv)-PE38 (▲), anti-Tac(Fv)-PE38KDEL (○), and anti-Tac(Fv)-PE38KDEL^{2A} (▼). The negative controls, Mikβ1(Fv)-PE40 (◇) and human IgG (▽), are shown in C and D, respectively.

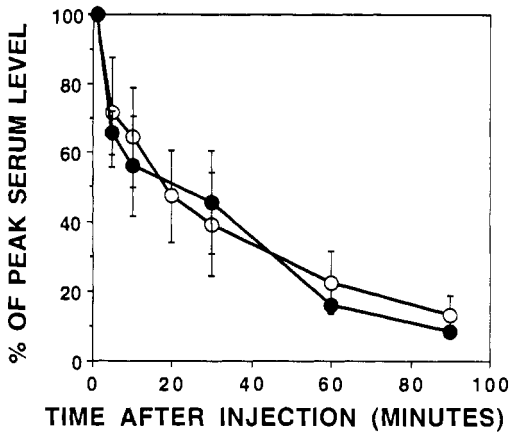


Figure 6. Disappearance of recombinant toxins from serum after iv injection. One microgram of either anti-Tac(Fv)-PE40KDEL (○) or anti-Tac(Fv)-PE38KDEL (●) was injected iv into Balb/c mice and serum was obtained 1, 5, 10, 20, 30, 60, and 90 min later. Levels were determined by cytotoxicity assay on HUT-102 cells using standard curves employing purified recombinant toxin. The serum level for each time point shown represents the mean of values from several mice. Error bars show standard deviations and are not visible if the standard deviation was smaller than the size of the point symbol.

Table III. LD_{50} of Anti-Tac(Fv) Toxins in Mice

	deaths/total		
dose (μg/kg, ip)	anti-Tac(Fv)-PE40KDEL	anti-Tac(Fv)-PE38KDEL	anti-Tac(Fv)-PE38
100		0/2	0/2
200		0/2	0/2
400	0/2	0/2	0/2
800	1/2	1/2	0/2
1600	2/2	2/2	0/2
3200			2/2

DISCUSSION

Our goal in the present study was to examine the binding and cytotoxic behavior of a series of mutants of single-chain immunotoxins which are missing one or more of the disulfide bonds in the toxin. We found that while all mutants were cytotoxic toward target cells, those with an intact disulfide bond in domain II were far more active than those without this bond. In contrast with TGFα-PE40 (*18*), the presence of the disulfide bond in domain II of anti-Tac(Fv)-PE40 did not decrease ligand binding. We also found that the second disulfide bond of the toxin which resides in domain Ib can be removed without impairing cytotoxicity, antigen binding, animal toxicity, or pharmacokinetics in mice.

Importance of the Disulfide Bond in Domain II. Since the region surrounding the disulfide bond in domain II cannot be deleted without completely inactivating the toxin (*15, 17*), we removed it by replacing the cysteines at positions 265 and 287 with alanines, as had been done previously with TGFα-PE40 (*17, 18, 21*). These cysteines in domain II of whole PE had also been replaced with serines and the mutant was 80-fold less cytotoxic than PE (*24*). Similarly, in this study we found in the single-chain antibody toxins that eliminating this disulfide bond greatly affected cytotoxic activity, although in its absence the immunotoxins were still active. For cloning purposes, anti-Tac(Fv)-PE40^{4A}, anti-Tac(Fv)-PE40KDEL^{4A}, anti-Tac(Fv)-PE40KDEL^{2A}, and anti-Tac(Fv)-PE38KDEL^{2A} each contain a short connector between anti-Tac(Fv) and the toxin, resulting in the nine additional amino acids (GGGSAMAEE) compared to the other immunotoxins shown in Figure 1. To ensure that this connector was not responsible for the decreased cytotoxicity of the alanine mutants, we constructed the plasmid pRK768K, encoding a derivative of anti-Tac(Fv)-PE40KDEL containing the same connector. The cytotoxic activity of anti-Tac(Fv)-PE40KDEL was the same with or without this connector (data not shown). This finding agrees with previous studies showing that different connectors linking Fv's with truncated PE do not alter cytotoxicity (*6, 25*). Moreover, our data clearly indicate the important role of the first disulfide bond for cytotoxicity.

Our binding data shows no significant effect of the disulfide bond in domain II on binding to p55. Since all recombinant toxins used here have identical enzymatic domains (amino acids 400–602), our previous data would indicate they have equal ADP-ribosylation activity (*17, 19*). Therefore, the disulfide bond must facilitate a postbinding step necessary for the ultimate translocation of the toxin to the cytosol. We have recently found that after the PE is processed between amino acids 279 and 280, the 37-kDa fragment containing ADP-ribosylation activity translocates to the cytosol (*26*). The translocated fragment would be 35 kDa in the case of anti-Tac(Fv)-PE38KDEL and anti-Tac(Fv)-PE38KDEL^{2A}. After processing, the 35-kDa fragment of these two immunotoxins, which vary markedly in cytotoxicity, should be identical. Therefore, the function of the disulfide bond in domain II is probably to facilitate proteolytic processing. The protease is evidently 10–100-fold less active against the toxin without this disulfide bond. The X-ray crystallographic structure of PE indicates that disulfide loop 265–287 is significantly exposed (*13*). It was previously observed that replacement of amino acids 265 and 287 in whole PE with serines results in a molecule which more readily undergoes conformational change with detergent, exposing hydrophobic residues (*24*). We would hence speculate that the function of the domain II disulfide bond is to stabilize the proteolytic processing site of PE (position 279–280) so that production of the necessary 37-kDa active C-terminal fragment of PE from the whole toxin or from a chimeric toxin can proceed efficiently. More definite determination of the function of this disulfide bond of PE will require identification and purification of the processing protease.

Importance of the Domain Ib Disulfide. In contrast to the first disulfide bond of PE40, the loss of the second did not significantly impair cytotoxicity. In fact, toward some target cells such as HUT-102, PHA-activated lymphocytes, and fresh cells from an ATL patient, at least 3-fold improvements in cytotoxicity were observed after removal of this disulfide bond from anti-Tac(Fv)-PE40 or anti-Tac(Fv)-PE40KDEL (Tables I and II). A slight improvement in cytotoxicity was also seen when this disulfide bond was removed from TGFα-PE40 (*17*), but it was not clear whether the small difference was due to improved TGFα folding. While this disulfide bond is not needed for ADP-ribosylation activity (*19*), it is within the 37-kDa fragment of PE40 or PE40KDEL that translocates to the cytosol. Thus, in some situations intracellular routing or translocation might be facilitated by its absence.

Effect of the KDEL Carboxyl Terminus. We have previously shown that the mutation of REDLK to KDEL at the carboxyl terminus of PE improves chimeric toxin activity, probably by improved routing of the carboxyl terminal fragment of PE to where it can translocate to the cytosol (*19, 20*). In our study, anti-Tac(Fv)-PE40KDEL, anti-Tac(Fv)-PE38KDEL, and anti-Tac(Fv)-PE40KDEL^{4A} were always more active than anti-Tac(Fv)-PE40, anti-Tac(Fv)-PE38, and anti-Tac(Fv)-PE40^{4A}, respectively,

although toward some cell lines the differences were small. Nevertheless, the improved cytotoxicity (Tables I and II) and increased toxicity (Table III) with KDEL were preserved regardless of changes in the disulfide bonds. Thus, the function of KDEL is distinct from that of the disulfide bonds of PE40.

Purification of Mutant Immunotoxins. In essentially all of the recombinant single-chain immunotoxins purified to date, the yield of purified monomeric immunotoxin has been only 0.5–2 mg from about 5 g (wet weight) of bacterial cells which contain 100–150 mg of total recombinant protein (*4*, *7*, *9*–*12*). We believe a significant percentage of the total recombinant protein aggregates due to mismatched disulfide pairing, which would expose non-native surface residues. As in previous reports, in this study the percentage of total recombinant protein renaturing as monomer was less than 2% of starting material and did not seem to vary with the type of mutation. We were surprised by this result, since recent increases in the yield of another recombinant immunotoxin by redox shuffling of disulfide bonds (*27*) suggested that a decrease in the number of disulfide bonds would improve renaturation. By the use of redox reshuffling, we found a several-fold improvement in the yield of renaturation, but no difference between anti-Tac(Fv)-PE40 and anti-Tac(Fv)-PE38 (data not shown). On the basis of these results, we would speculate that the limiting factor in refolding is not folding of the toxin, which is part of a natural protein, but refolding of the Fv domain, which is not a native protein.

In summary, we have examined mutants of the single-chain antibody toxin anti-Tac(Fv)-PE40 differing in the two disulfide bonds of the toxin. While the loss of the first of these bonds markedly impairs cytotoxicity, the loss of the second does not decrease cytotoxicity and may give slight to modest improvements in cytotoxicity toward some cells. Moreover, loss of the second disulfide bond of the toxin in domain Ib does not worsen animal toxicity nor impair binding or serum stability of the recombinant immunotoxin. Anti-Tac(Fv)-PE38KDEL, which is missing the second but not the first disulfide bond of the toxin, appears to be the most active molecule toward several target cells.

ACKNOWLEDGMENT

We thank T. Prior and C. Siegall for plasmid contributions. We acknowledge Hoffmann-La Roche and CETUS for contributing anti-Tac and IL2, respectively. We are grateful to R. Kozak for supplying radiolabeled anti-Tac. We thank A. Harris and B. Lovelace for cell culture assistance and A. Jackson and E. Gott for editorial assistance.

LITERATURE CITED

(1) Houston, J. S., Levinson, D., Mudgett-Hunter, M., Tai, M., Novotny, J., Margolies, M. N., Ridge, R. J., Bruccoleri, R. E., Haber, E., Crea, R., and Oppermann, H. (1988) Protein Engineering of antibody binding sites: Recovery of specific activity in an anti-digoxin single-chain Fv analogue produced in *Escherichia coli*. *Proc. Natl. Acad. Sci. U.S.A. 85*, 5879–5883.

(2) Bird, R. E., Hardman, K. D., Jacobson, J. W., Johnson, S., Kaufman, B. M., Lee, S., Lee, T., Pope, S. H., Riordan, G. S., and Whitlow, M. (1988) Single-chain antigen-binding proteins. *Science 242*, 423–426.

(3) Colcher, D., Bird, R., Roselli, M., Hardman, K. D., Johnson, S., Pope, S., Dodd, S. W., Pantoliano, M. W., Milenic, D. E., and Schlom, J. (1990) In vivo tumor targeting of a recombinant single-chain antigen-binding protein. *J. Natl. Cancer Inst. 82*, 1191–1197.

(4) Chaudhary, V. K., Queen, C., Junghans, R. P., Waldmann, T. A., FitzGerald, D. J., and Pastan, I. (1989) A recombinant immunotoxin consisting of two antibody variable domains fused to *Pseudomonas* exotoxin. *Nature 339*, 394–397.

(5) Chovnick, A., Schneider, W. P., Tso, J. Y., Queen, C., and Chang, C. N. (1991) A recombinant, membrane-acting immunotoxin. *Cancer Res. 51*, 465–467.

(6) Chaudhary, V. K., Gallo, M. G., FitzGerald, D. J., and Pastan, I. (1990) A recombinant single-chain immunotoxin composed of anti-Tac variable regions and a truncated diphtheria toxin. *Proc. Natl. Acad. Sci. U.S.A. 87*, 9491–9494.

(7) Batra, J. K., FitzGerald, D., Gately, M., Chaudhary, V. K., and Pastan, I. (1990) Anti-Tac(Fv)-PE40: A single chain antibody *Pseudomonas* fusion protein directed at interleukin 2 receptor bearing cells. *J. Biol. Chem. 265*, 15198–15202.

(8) Kreitman, R. J., Chaudhary, V. K., Waldmann, T., Willingham, M. C., FitzGerald, D. J., and Pastan, I. (1990) The recombinant immunotoxin anti-Tac(Fv)-*Pseudomonas* exotoxin 40 is cytotoxic toward peripheral blood malignant cells from patients with adult T-cell leukemia. *Proc. Natl. Acad. Sci. U.S.A. 87*, 8291–8295.

(9) Chaudhary, V. K., Batra, J. K., Gallo, M. G., Willingham, M. C., FitzGerald, D. J., and Pastan, I. (1990) A rapid method of cloning functional variable-region antibody genes in *Escherichia coli* as single-chain immunotoxins. *Proc. Natl. Acad. Sci. U.S.A. 87*, 1066–1070.

(10) Batra, J. K., FitzGerald, D. J., Chaudhary, V. K., and Pastan, I. (1991) Single-chain immunotoxins directed at the human transferrin receptor containing *Pseudomonas* exotoxin A or diphtheria toxin: Anti-TFR(Fv)-PE40 and DT388-anti-TFR(Fv). *Mol. Cell. Biol. 11*, 2200–2205.

(11) Brinkmann, U., Pai, L. H., FitzGerald, D. J., Willingham, M., and Pastan, I. (1991) B3(Fv)-PE38KDEL, a single-chain immunotoxin that causes complete regression of a human carcinoma in mice. *Proc. Natl. Acad. Sci. U.S.A. 88*, 8616–8620.

(12) Kreitman, R. J., Schneider, W. P., Queen, C., Tsudo, M., FitzGerald, D. J. P., Waldmann, T. A., and Pastan, I. (1992) Mikβ1(Fv)-PE40, a recombinant immunotoxin cytotoxic toward cells bearing the β-chain of the IL-2 receptor. *J. Immunol. 149*, 2810–2815.

(13) Allured, V. S., Collier, R. J., Carroll, S. F., and McKay, D. B. (1986) Structure of exotoxin A of *Pseudomonas aeruginosa* at 3.0-Ångstrom resolution. *Proc. Natl. Acad. Sci. U.S.A. 83*, 1320–1324.

(14) Hwang, J., FitzGerald, D. J., Adhya, S., and Pastan, I. (1987) Functional domains of Pseudomonas exotoxin identified by deletion analysis of the gene expressed in E. coli. *Cell 48*, 129–136.

(15) Ogata, M., Chaudhary, V. K., Pastan, I., and FitzGerald, D. J. (1990) Processing of *Pseudomonas* exotoxin by a cellular protease results in the generation of a 37,000-Da toxin fragment that is translocated to the cytosol. *J. Biol. Chem. 265*, 20678–20685.

(16) Pastan, I., and FitzGerald, D. (1991) Recombinant toxins for cancer treatment. *Science 254*, 1173–1177.

(17) Siegall, C. B., Chaudhary, V. K., FitzGerald, D. J., and Pastan, I. (1989) Functional analysis of domains II, Ib and III of *Pseudomonas* exotoxin. *J. Biol. Chem. 264*, 14256–14261.

(18) Edwards, G. M., DeFeo-Jones, D., Tai, J. Y., Vuocolo, G. A., Patrick, D. R., Heimbrook, D. C., and Oliff, A. (1989) Epidermal growth factor receptor binding is affected by structural determinants in the toxin domain of transforming growth factor-alpha-*Pseudomonas* exotoxin fusion proteins. *Mol. Cell. Biol. 9*, 2860–2867.

(19) Chaudhary, V. K., Jinno, Y., FitzGerald, D., and Pastan, I. (1990) *Pseudomonas* exotoxin contains a specific sequence at the carboxyl terminus that is required for cytotoxicity. *Proc. Natl. Acad. Sci. U.S.A. 87*, 308–312.

(20) Seetharam, S., Chaudhary, V. K., FitzGerald, D., and Pastan, I. (1991) Increased cytotoxic activity of *Pseudomonas* exotoxin and two chimeric toxins ending in KDEL. *J. Biol. Chem. 266*, 17376–17381.

(21) Heimbrook, D. C., Stirdivant, S. M., Ahern, J. D., Balishin, N. L., Patrick, D. R., Edwards, G. M., DeFeo-Jones, D., FitzGerald, D. J., Pastan, I., and Oliff, A. (1990) Transforming

growth factor-α-*Pseudomonas* exotoxin fusion protein prolongs survival of nude mice bearing tumor xenografts. *Proc. Natl. Acad. Sci. U.S.A. 87*, 4697–4701.

(22) Prior, T. I., Helman, L. J., FitzGerald, D. J., and Pastan, I. (1991) Cytotoxic activity of a recombinant fusion protein between insulin-like growth factor I and *Pseudomonas* exotoxin. *Cancer Res. 51*, 174–180.

(23) Lorberboum-Galski, H., Garsia, R. J., Gately, M., Brown, P. S., Clark, R. E., Waldmann, T. A., Chaudhary, V. K., FitzGerald, D. J. P., and Pastan, I. (1990) IL2-PE66^{4Glu}, a new chimeric protein cytotoxic to human-activated T lymphocytes. *J. Biol. Chem. 265*, 16311–16317.

(24) Madshus, I. H., and Collier, R. J. (1989) Effects of eliminating a disulfide bridge within domain II of *Pseudomonas aeruginosa* exotoxin A. *Infect. Immun. 57*, 1873–1878.

(25) Brinkmann, U., Buchner, J., and Pastan, I. (1992) Independent domain folding of *Pseudomonas* exotoxin and single-chain immunotoxins: influence of interdomain connections. *Proc. Natl. Acad. Sci. U.S.A. 89*, 3075–3079.

(26) Ogata, M., Fryling, C. M., Pastan, I., and FitzGerald, D. J. (1992) Cell-mediated cleavage of *Pseudomonas* exotoxin between Arg279 and Gly280 generates the enzymatically active fragment which translocates to the cytosol. *J. Biol. Chem. 267*, 25396–25401.

(27) Buchner, J., Pastan, I., and Brinkmann, U. (1992) A method for increasing the yield of properly folded recombinant fusion proteins: Single-chain immunotoxins from renaturation of bacterial inclusion bodies. *Anal. Biochem. 205*, 263–270.

Chemoimmunoconjugate Development for Ovarian Carcinoma Therapy: Preclinical Studies with Vinca Alkaloid–Monoclonal Antibody Constructs

L. D. Apelgren,* D. L. Bailey, S. L. Briggs, R. L. Barton, D. Guttman-Carlisle, G. A. Koppel, C. L. Nichols, W. L. Scott, T. D. Lindstrom, A. L. Baker, and T. F. Bumol

Lilly Research Laboratories, Indianapolis, Indiana 46285. Received September 4, 1992

Preclinical efficacy studies are presented in a human ovarian carcinoma model utilizing several novel conjugation strategies with the KS1/4 monoclonal antibody and derivatives of the vinca alkaloid desacetylvinblastine hydrazide. The chemoimmunoconjugates KS1/4–β-alanine–methylenemalonic acid ethyl ester–4-decacetylvinblastine 23-hydrazide (KS1/4–BAMME-DAVLB-HY), KS1/4–β-alanine–5-formylpyrrole-2-carboxylic acid–4-desacetylvinblastine 23-hydrazide (KS1/4-BAP-DAVLB-HY), and KS1/4–4-desacetylvinblastine 23-hydrazide were explored in the OVCAR-3 human ovarian carcinoma xenograft model. These conjugates, constructed with variable linker stability between the vinca alkaloid and the antibody, were studied by comparing the route of administration and the treatment schedule. Under these conditions a mean survival time from 28 to 35 days in untreated control animals was observed. Significant increases in survival (i.e. 3–9-fold over untreated control animals) were observed with all the immunoconjugates tested but with varying potency and efficacy dependent on linker strategy. Parallel therapy with equivalent doses of free DAVLB-HY or a non-antigen-binding immunoconjugate did not significantly increase the survival of the animals. These results suggest several chemoimmunoconjugate strategies for site-directed therapy of human ovarian cancer.

INTRODUCTION

Human ovarian cancer is the fourth most frequent cause of cancer death in women and is the leading cause of death among patients in the United States with gynecologic malignancies (*1*, *2*). Surgery followed by chemotherapy and/or radiation therapy are the current treatments for this disease, which result in about 50% of patients having recurrent disease with survival falling sharply with each advancing of the disease. Ovarian cancer is confined to the peritoneal cavity throughout most of its course, although extra-abdominal metastases can occur. This fact has led to various attempts of intracavitary therapy for ovarian cancer with chemotherapeutic agents (*3*) or radioactive colloids (*4*) which generally have been ineffective.

Monoclonal antibodies have been used in the monitoring (*5*,*6*) and therapy (*7*) of gynecological carcinomas. Intraperitoneal therapy with monoclonal antibody–drug or monoclonal antibody–toxin immunoconjugates has been suggested by a number of investigators (*8*,*9*). Previously, our laboratory demonstrated that the monoclonal antibody–vinca alkaloid immunoconjugate LY203725 (KS1/4–4-desacetylvinblastine 23-hydrazide) significantly prolonged the survival of tumor-bearing animals in the OVCAR-3 human ovarian carcinoma xenograft model (*10*). In this immunoconjugate, the vinca alkaloid moiety was linked to oxidized carbohydrate residues on the monoclonal antibody through a hydrazone linkage. These linkages possess the ability to release active drug by virtue of their inherent hydrolytic instability under physiological conditions (*11*, *12*).

Extending previous studies in the OVCAR-3 xenograft model, this report describes two novel conjugation strategies in the preparation of monoclonal antibody–vinca alkaloid immunoconjugates which vary the chemical linker to potentially optimize delivery of the potent vinca alkaloid moiety. In this study, we have chemically introduced aldehyde or methylenemalonate groups onto the lysine residues of the monoclonal antibody to provide the use of hydrazone- or enamide-based chemistry for conjugation. This modification theoretically achieves more control over the release properties of these linkages to antibodies through enhanced chemical stability. These studies with the OVCAR-3 human ovarian carcinoma model compare intravenous therapy and intraperitoneal therapy for these varied immunoconjugates and report efficacy results as survival advantages for each chemical linker between a common antibody and vinca alkaloid species. The data demonstrate the importance of linker chemistry strategy in structure–activity relationships in the preclinical development of chemoimmunoconjugates for ovarian cancer.

EXPERIMENTAL PROCEDURES

Cell Lines. The human ovarian cancer cell line OVCAR-3 (*8*, *13*) was maintained in vivo by serial passage of ascites fluid in female athymic nude mice (outbred CD1; Charles Rivers). The animals were housed in isolator cages (Lab Products, Maywood, NJ) and all handling of the animals was done under laminar-flow hoods in an AALAC approved facility. The KS1/4 and 9.2.27 hybridoma cell lines were originally obtained from Dr. Ralph A. Reisfeld, Scripps Clinic and Research Foundation, and were maintained as previously described (*10*).

Preparation of Monoclonal Antibodies. The monoclonal antibodies KS1/4, which defines an adenocarcinoma-associated antigen highly expressed in ovarian carcinomas (*14*), and 9.2.27, which recognizes a chondroitan sulfate proteoglycan with high expression in human melanomas (*15*), were purified as described previously (*10*).

Preparation of KS1/4-DAVLB-HY Immunoconjugate. KS1/4–4-desacetylvinblastine 23-hydrazide (KS1/4-DAVLB-HY, Lilly Research Labs serial number LY203725) is a covalent conjugate of the monoclonal antibody KS1/4 and 4-desacetylvinblastine 23-hydrazide,

* Author to whom correspondence should be addressed.

1043-1802/93/2904-0121$04.00/0 © 1993 American Chemical Society

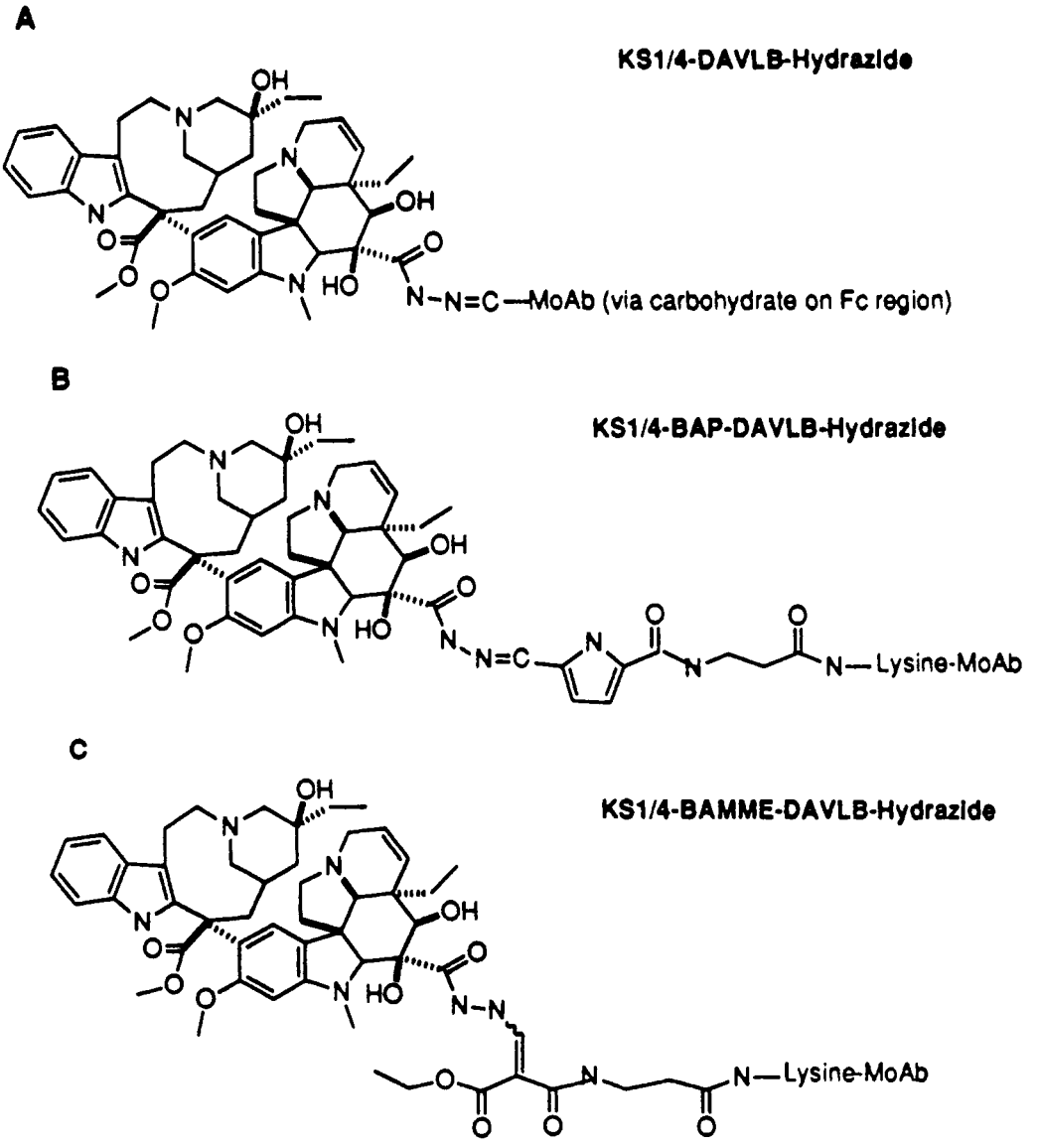


Figure 1. Structures of the monoclonal antibody–vinca alkaloid chemoimmunoconjugates, KS1/4-DAVLB-HY (A), KS1/4-BAP-DAVLB-HY (B), and KS1/4-BAMME-DAVLB-HY (C).

a derivative of the vinca alkaloid vinblastine (*11*). This conjugate was prepared as previously described by the coupling of the vinca alkaloid to the monoclonal antibody through a hydrazone linkage to oxidized carbohydrate residues located in the Fc portion of the antibody (*12*) (Figure 1A). These linkages possess the ability to release active drug by virtue of their hydrolytic instability. In general, immunoconjugates with an average molar conjugation ratio (CR) of 4.5 mol of vinca alkaloid/mol of antibody were utilized.

Preparation of KS1/4-BAP-DAVLB-HY Immunoconjugate. KS1/4–β-alanine–5-formylpyrrole-2-carboxylic acid–DAVLB-hydrazide (KS1/4-BAP-DAVLB-HY) was prepared as follows: to a 33-mL solution of KS1/4 (12.3 mg/mL, 406 mg, 2.7 μmol) in 0.34 M borate buffer, pH 8.6, was added 5 mg (16 μmol) of the N-hydroxysuccinimide active ester of β-alanine–5-formylpyrrole-2-carboxylic acid dissolved in 1 mL of acetonitrile. After stirring gently for 1 h at room temperature, the reaction mixture was chromatographed on a Sephadex G-25 column equilibrated wtih 0.1 M sodium acetate, pH 5.6. The derivatized antibody fraction was collected. To this was added 260 mg (0.3 mmol) of 4-desacetylvinblastine 23-hydrazide sulfate and the reaction mixture stirred at room temperature overnight. The product was isolated by chromatography over a Sephadex G-25 column equilibrated and eluted with PBS, pH 7.4. The protein fractions were pooled and concentrated in an Amicon stirred cell. Drug and protein content were determined by spectrophotometric analysis resulting, on average, in immunoconjugates with a CR of approximately 3.0. The reversible coupling of the vinca alkaloid to the monoclonal antibody occurs through aldehyde groups introduced onto lysine residues in the monoclonal antibody (Figure 1B).

Preparation of KS1/4-BAMME-DAVLB-HY and 9.2.27-BAMME-DAVLB-HY Immunoconjugates. KS1/4–β-alanine–2-methylenemalonic acid ethyl ester–4-desacetylvinblastine 23-hydrazide (KS1/4-BAMME-DAVLB-HY) was prepared as follows: the KS1/4 monoclonal antibody at a concentration of 15–20 mg/mL in 0.34 M sodium borate buffer, pH 8.6, was stirred with the addition over several minutes of NHS-BAMME-DAVLB-HY in dry *N*,*N*-dimethylformamide (DMF). The DMF solution is prepared at a concentration to deliver NHS-BAMME-DAVLB-HY at a molar input ratio (active ester: antibody) of 8:1–12:1 and give a final conjugation reaction mixture of 7.5% DMF cosolvent. The reaction mixture is stirred slowly at 25 °C for 20 min after which it is centrifuged for 10 min to separate suspended precipitate. The supernate is then injected onto an appropriately sized

Table I. Properties of the Chemoimmunoconjugates Utilized

abbrev	IC_{50} (ng/mL)[a]	ave CR[b]	ave % IR[c]	DAVLB-HY release rate (μg/h)[d]
KS1/4-DAVLB-HY	17	4.5	98	0.122
KS1/4-BAP-DAVLB-HY	63	3	92	0.082
KS1/4-BAMME-DAVLB-HY	128	4.5	96	0.004
DAVLB-HY (free drug)	5			

[a] The IC_{50} was measured in a tissue culture microtiter proliferation assay as described in Experimental Procedures. [b] Average CR is the molar conjugation ratio which is the moles of vinca alkaloid per mole of antibody. [c] Average IR is the average immunoreactivity of the immunoconjugate measured by flow cytometry compared to unconjugated KS1/4 antibody. [d] Average release of DAVLB-HY from 0.5 mg/mL conjugate in rat plasma as determined by HPLC analysis.

hydrophobic interaction phenyl-Sepharose column (Pharmacia FPLC) which is equilibrated with 15% acetonitrile, 85% 0.1 M phosphate, pH 6.10. The column is eluted with 10 column volumes of the same buffer followed by a step to 5 column volumes of 40% acetonitrile/60% phosphate. Fractions from the 15% CH_3CN eluent containing antibody, conjugate, and free BAMME-DAVLB-HY were pooled and injected onto a Sephadex G-25M desalting column (Pharmacia FPLC). Fractions containing immunoconjugate were pooled, concentrated, and filtered (Millex GV 0.22-μm filters, sterile). The coupling of the vinca alkaloid to the monoclonal antibody occurs in this strategy by attaching the hydrazide function of the DAVLB-HY to the linker via an enamide-like bond and attaching the linker to the monoclonal antibody by amide formation with the ε–amino groups of the lysine residues (Figure 1C). 9.2.27-BAMME-DAVLB-HY was prepared as described above for the KS1/4-BAMME-DAVLB-HY. In general, immunoconjugates with a CR of approximately 4.5 were utilized.

Immunoreactivity of the Immunoconjugates. The antigen-binding capacity of the above-mentioned immunoconjugates was measured by flow cytometry with OVCAR-3 target cells as reported previously (*10*). The control immunoconjugate 9.2.27-BAMME-DAVLB-HY did not react with the OVCAR-3 target cells in this assay but retained good immunoreactivity toward antigen-positive human melanoma cells in separate experiments.

In Vitro Cytotoxicity Assay. A tissue culture microtiter proliferation assay (*16*) was used to assess the in vitro potency of the immunoconjugates. For each immunoconjugate and the free vinca alkaloid, the percent growth inhibition values were calculated by comparison with the media control group (% inhibition = [(control – treated)/control] × 100). A series of percent growth inhibitions was plotted against the corresponding drug concentrations, and the concentration inhibiting 50% of the cell growth (IC_{50}) was estimated.

Stability Studies. Samples of the above conjugates (0.5 mg/mL) in rat plasma were incubated at 37 °C and aliquots were taken at various times. Samples were assayed for free vinca alkaloid by HPLC with electrochemical detection as an approximation of in vivo stability.

Survival Experiments. In our previous study, we documented the optimal parameters for the use of vinca alkaloid chemoimmunoconjugates under stringent conditions for efficacy in the OVCAR-3 xenograft model where free DAVLB-HY and an irrelevant monoclonal antibody conjugate were inactive (*10*). Dosing schedules using three of our four treatments with the immunoconjugates listed below, free drug, or a non-antigen-binding immunoconjugate were employed and are indicated in Results. Under these conditions, untreated control animals have a mean survival of 28–35 days after inoculation. Treatment was by intraperitoneal (ip) or intravenous (iv) injection of the immunoconjugate in 0.2 mL of PBS as indicated in the text. The date each experiment was terminated is indicated in Results. Statistical evaluation was performed on all in vivo experiments using the Kaplan–Meier survival curve analysis (*17*, *18*).

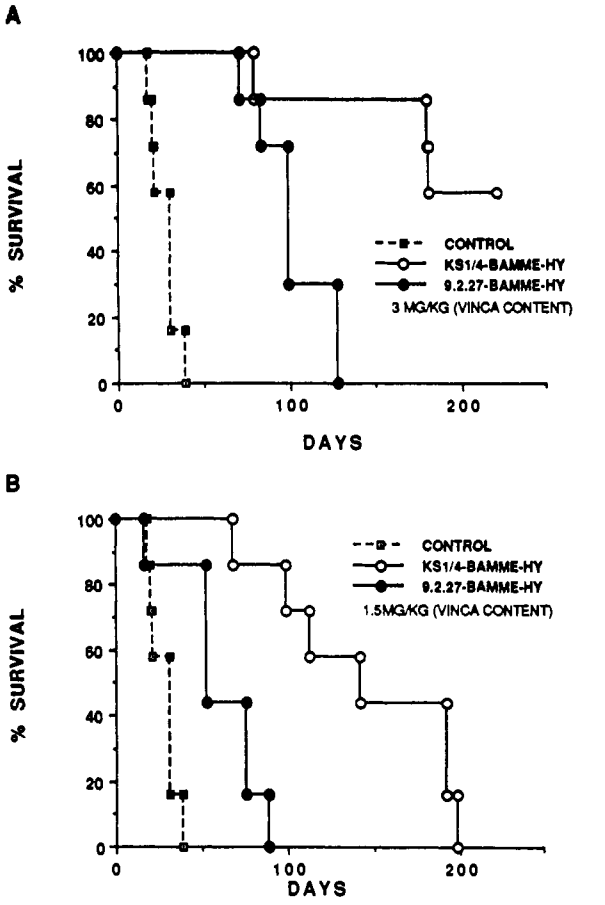


Figure 2. Comparison of KS1/4-BAMME-DAVLB-HY and 9.2.27-BAMME-DAVLB-HY against OVCAR-3 ovarian carcinoma with a three dose treatment protocol. After OVCAR-3 tumor implantation on day 0, the animals (n = 7) were treated ip with a 3.0 [A] or 1.5 mg/kg [B] (vinca content) dose on days 11, 14, and 17. This experiment is summarized in Table II, experiment 1.

RESULTS

In Vitro Properties of Various Chemoimmunoconjugates. Various in vitro parameters of the three chemoimmunoconjugates utilized in this study are presented in Table I. The immunoreactivity of the conjugates to the OVCAR-3 target cell are comparable and display ≥92% immunoreactivity as compared to unmodified KS1/4. In contrast, the varied conjugation strategies displayed variable in vitro cytotoxicity profiles toward human adenocarcinoma target cells. KS1/4-DAVLB-HY (IC_{50}, 17 ng/mL) is approximately 3-fold less potent than the free drug while KS1/4-BAP-DAVLB-HY (IC_{50} = 63 ng/mL) is approximately 12-fold less potent. KS1/4-BAMME-DAVLB-HY (IC_{50} = 128 ng/mL) is 25-fold less potent than the free drug and 2–6 times less potent than the other immunoconjugates tested. The rank order of in vitro potency in this assay is DAVLB-HY > KS1/4-DAVLB-HY > KS1/4-BAP-DAVLB-HY > KS1/4-BAMME-DAVLB-HY. This ranking also correlates with preliminary immunoconjugate stability studies in rat plasma which indicate that KS1/4-DAVLB-HY is the least stable whereas

Table II. Inhibition of OVCAR-3 Xenografts by Immunoconjugates

exp.	treatment[d]	route	dose (mg/kg)	treatment schedule (day)[a]	mean survival (days)[b]	day of termination[c]
1	control	ip		11, 14, 17	27 ± 8	220
	KS1/4-BAMME-DAVLB-HY	ip	3.0		157 ± 85*	
	KS1/4-BAMME-DAVLB-HY	ip	1.5		143 ± 52*	
	9.2.27-BAMME-DAVLB-HY	ip	3.0		101 ± 21*	
	9.2.27-BAMME-DAVLB-HY	ip	1.5		60 ± 24	
2	control	ip		8, 10, 13, 15	28 ± 7	404
	KS1/4-BAP-DAVLB-HY	ip	1.5		228 ± 129*	
	KS1/4-BAP-DAVLB-HY	ip	0.75		340 ± 65*	
	KS1/4-BAP-DAVLB-HY	ip	0.375		219 ± 127*	
	DAVLB-HY	ip	1.5		16 ± 2	
	DAVLB-HY	ip	0.75		84 ± 53	
3	control	ip		8, 11, 15, 18	35 ± 4	300
	KS1/4-DAVLB-HY	ip	0.75		266 ± 72*	
	KS1/4-DAVLB-HY	iv	0.75		172 ± 81*	
	KS1/4-BAP-DAVLB-HY	ip	0.75		226 ± 107*	
	KS1/4-BAP-DAVLB-HY	iv	0.75		254 ± 58*	
	KS1/4-BAMME-DAVLB-HY	ip	0.75		131 ± 25*	
	KS1/4-BAMME-DAVLB-HY	iv	0.75		72 ± 46	
	DAVLB-HY	iv	0.75		39 ± 4	

[a] Days after implant of OVCAR-3 cells. [b] An asterisk indicates a $p < 0.01$ as compared to control in a χ^2 paired analysis. [c] On the day of termination, all surviving animals were sacrificed and survival was statistically evaluated. [d] Each animal was given an ip injection of 6×10^7 Ovar-3 cells on day 0. The animals ($n = 7$) were treated on the days indicated in the treatment schedule. The dose received was in mg/kg based on the vinca content of the immunoconjugate. Inhibition of xenograft growth was determined by increased survival time of the treated animals compared to the untreated control animals.

KS1/4-BAMME-DAVLB-HY is the most stable conjugate exhibiting minimal release of vinca alkaloid (Table I). The corresponding structures of the three chemoimmunoconjugates utilized in this study are shown in Figure 1.

In Vivo Comparison of KS1/4-BAMME-DAVLB-HY and 9.2.27-BAMME-DAVLB-HY. To evaluate the conjugate-mediated effect of KS1/4-BAMME-DAVLB-HY in the OVCAR-3 ovarian carcinoma nude mouse model, a non-antigen-binding, subisotype-equivalent immunoconjugate, 9.2.27-BAMME-DAVLB-HY, was tested. Since KS1/4-BAMME-DAVLB-HY was the least potent chemoimmunoconjugate evaluated (Table I), dose selection was adjusted upward from previous studies (*10*) to 3.0 mg/kg vinca content for this immunoconjugate (based on milligrams of vinca alkaloid per kilogram of animal body weight). When the immunoconjugates 9.2.27-BAMME-DAVLB-HY and KS1/4-BAMME-DAVLB-HY were administered ip with a three dose treatment schedule, a significant increase in survival was obtained with KS1/4-BAMME-DAVLB-HY at 1.5 and 3.0 mg/kg (Figure 2). A significant increase in survival was not observed at 1.5 mg/kg with the irrelevant conjugate 9.2.27-BAMME-DAVLB-HY, but improvement was seen at 3.0 mg/kg with this therapy schedule. These data indicate that a 2–3-fold increase in survival time is obtained with KS1/4-BAMME-DAVLB-HY therapy over that with the irrelevant conjugate 9.2.27-BAMME-DAVLB-HY at the 1.5 mg/kg dose level compared to untreated control animals. A statistical summary of this experiment is shown in Table II.

In Vivo Efficacy of KS1/4-BAP-DAVLB-HY. The in vivo efficacy of KS1/4-BAP-DAVLB-HY was evaluated in the OVCAR-3 human ovarian carcinoma xenograft model. The in vitro cytotoxicity profile of KS1/4-BAP-DALVB-HY was similar to that of KS1/4-DAVLB-HY (Table I), suggesting a lower dose strategy. The mice were given ip injections of the immunoconjugates and free DAVLB-HY at doses of 1.5, 0.75, and 0.375 mg/kg on days 8, 10, 13, and 15 after inoculation with the OVCAR-3 cells (Figure 3). Significant survival was observed with this conjugate at the dose levels used compared to untreated control animals. The free drug, DAVLB-HY, was not effective in increasing the survival of the animals at the

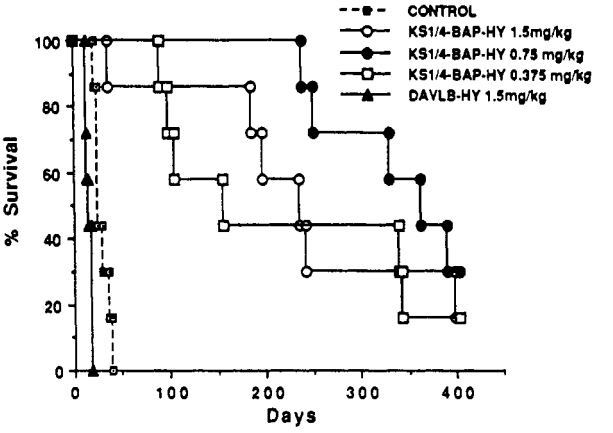


Figure 3. Evaluation of ip administration of KS1/4-BAP-DAVLB-HY and DAVLB-HY against OVCAR-3 ovarian carcinoma. After OVCAR-3 tumor implantation on day 0, the animals ($n = 7$) were treated ip on days 8, 10, 13, and 15 with a 1.5, 0.75, or 0.375 mg/kg (vinca content) dose. This experiment is summarized in Table II, experiment 2.

1.5 mg/kg dose level, indicating a therapeutic advantage with this immunoconjugate. A statistical summary of the results is shown in Table II. The 0.75 mg/kg (vinca content) dose demonstrated optimal survival efficacy in this test, which suggests that this dose may reflect an optimal therapeutic index for this conjugation strategy. The results indicate that a 4–9-fold increase in survival time with KS1/4-BAP-DAVLB-HY was obtained over that with free DAVLB-HY, compared to control animals.

In Vivo Comparison of Intraperitoneal and Intravenous Therapy with KS1/4-DAVLB-HY, KS1/4-BAP-DAVLB-HY, and KS1/4-BAMME-DAVLB-HY. In order to compare the various linker strategies and the effect of the route of administration in the OVCAR-3 ovarian carcinoma nude mouse model, KS1/4-DAVLB-HY, KS1/4-BAP-DAVLB-HY, and KS1/4-BAMME-DAVLB-HY were administered at 0.75 mg/kg (vinca alkaloid content), either ip or iv, on days 8, 11, 15, and 18 after inoculation with OVCAR-3 cells (Figure 4). Both routes of administration produced significant survival of the test groups over the untreated control animals with the KS1/4-DAVLB-HY and KS1/4-BAP-DAVLB-HY

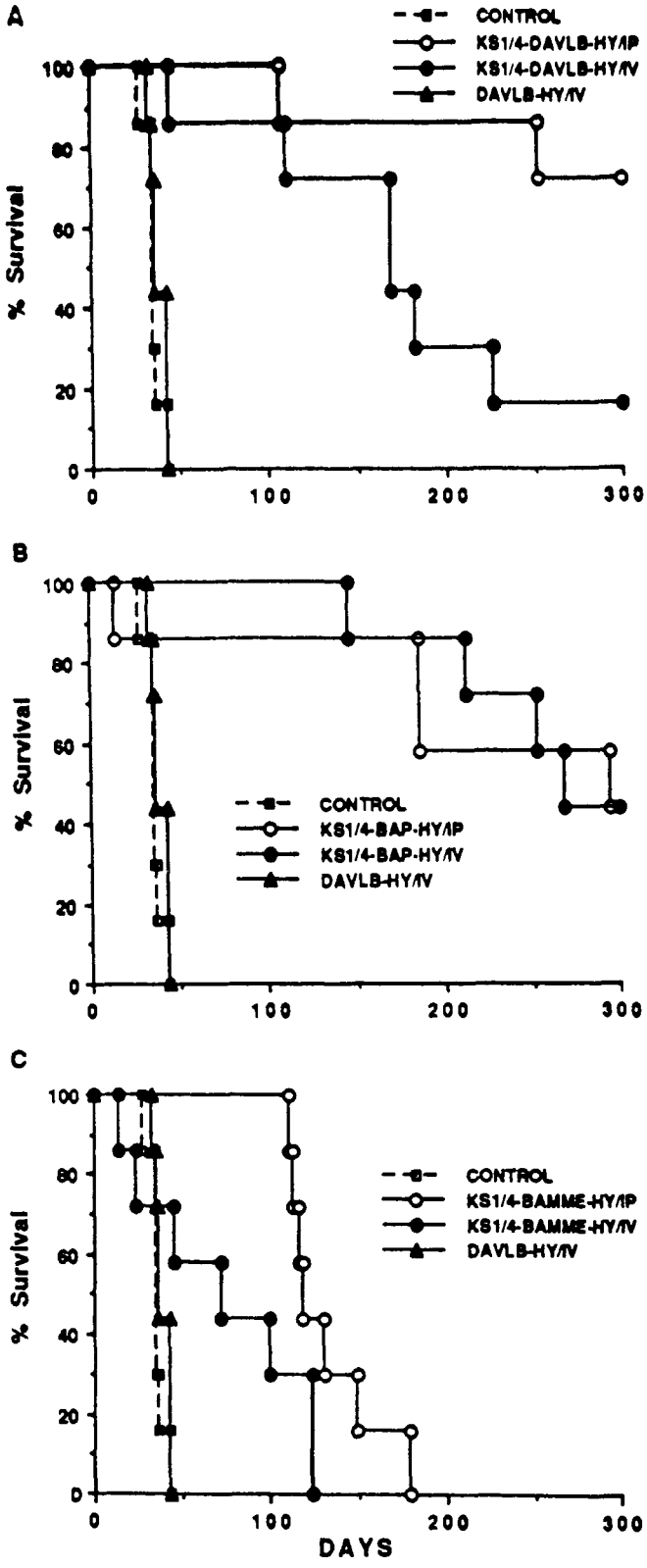


Figure 4. Comparison of iv and ip administration of KS1/4-DAVLB-HY (A), KS1/4-BAP-DAVLB-HY (B) and KS1/4-BAMME-DAVLB-HY (C) against OVCAR-3 ovarian carcinoma. After OVCAR-3 tumor implantation on day 0, the animals (n = 7) were treated eith ip or iv, on days 11, 15, and 18 at 0.75 mg/kg (vinca content). This experiment is summarized in Table II, experiment 3.

conjugates, but only ip therapy was successful with the KS1/4-BAMME-DAVLB-HY conjugate at this dose level. These results in total demonstrate a 3–5-fold increase in survival with either route of therapy, compared to untreated control animals, with the sole exception of the KS1/4-BAMME conjugate administered iv, which did not demonstrate a survival advantage. A statistical summary of the results is shown in Table II.

DISCUSSION

This report examines the preclinical antitumor activity of several chemoimmunoconjugates constructed by varying the chemical linker between the monoclonal antibody KS1/4 to the vinca alkaloid DAVLB-HY. A critical factor in the antitumor activity of a conjugate will be its ability to release drug in an active form after tumor localization has been accomplished. The activity of KS1/4-DAVLB-HY reported earlier (*10*) may reflect this property. In this conjugate, hydrazone linkages are thought to be formed when hydrazide-functionalized drugs are linked to oxidized carbohydrate residues. These linkages possess the ability to release active drug by virtue of their hydrolytic instability, in this case liberating DAVLB-HY, a highly cytotoxic vinca alkaloid (*12*). The heterogeneous nature of carbohydrate residues on the antibody glycoprotein inherently limits our ability to control the conjugate chemistry or the chemical properties of the linkages. Our assumption has been that the hydrolytic instability of hydrazone conjugates is an important factor in moAb targeted drug delivery and the control over this parameter is desirable for more effective chemoimmunoconjugate-based tumor therapy. In this report, we have employed alternative strategies to chemically introduce aldehyde or enamide groups onto lysine residues of the antibody to afford linking chemistries with differential stabilities. The β-alanine–pyrrole ("BAP") chemistry is an example of the successful application of the aldehyde/hydrazone-based approach. Alternatively, β-alanine–2-methylenemalonic acid ethyl ester ("BAMME") was developed to release free DAVLB-HY by a hydrolytically cleavable enamide type linkage. These resulting two conjugates demonstrated excellent immunoreactivity and differential stability of the drug–monoclonal antibody linker, and their antitumor activity was compared to that established with KS1/4-DAVLB-HY (*10*). However, additional studies are warranted to establish potential toxicities associated with these alternative conjugation strategies to determine true therapeutic indices.

This differential in vitro stability correlated with the differential in vitro cytotoxicity profiles of the KS1/4-DAVLB-HY (IC_{50} = 17 ng/mL), KS1/4-BAP-DAVLB-HY (IC_{50} = 63 ng/mL), and KS1/4-BAMME-DAVLB-HY (IC_{50} = 128 ng/mL) chemoimmunoconjugates. All three chemoimmunoconjugates demonstrated significant survival advantages in vivo under varied conditions in the OVCAR-3 human xenograft model. The KS1/4-DAVLB-HY and KS1/4-BAP-DAVLB-HY conjugates had comparable in vivo efficacy. These data suggest that our observed 3.7-fold drop in in vitro potency between these two conjugates did not translate to a comparable decrease in in vivo antitumor activity. The increased stability of the chemical linker of KS1/4-BAP-DAVLB-HY over KS1/4-DAVLB-HY could be an important factor when considering this agent for future studies, as clinical trials with KS1/4-DAVLB-HY have resulted in some patients developing peripheral neuropathies, a possible consequence of inappropriate kinetics of release of vinca alkaloid (*19*). A more stable covalent bond between the drug moiety and the antibody and an increase in serum half-life may translate to more effective tumor localization and drug delivery.

The least potent conjugate in vitro, KS1/4-BAMME-DAVLB-HY, was also the least effective agent in vivo in

increasing the overall survival of the animals. Route of administration did not alter the efficacy of the KS1/4-DAVLB-HY and KS1/4-BAP-DAVLB-HY conjugates. However, ip therapy with the KS1/4-BAMME-DAVLB-HY conjugate was significantly more effective than iv administration at the 0.75 mg/kg vinca content dose. At this time, this differential activity between iv and ip administration of KS1/4-BAMME-DAVLB-HY is not understood. Intraperitoneal therapy may provide a prolonged residence of the conjugate in the peritoneal cavity when administered as an intracavitary agent. In addition, both KS1/4-BAMME-DAVLB-HY and the non-antigen-binding, subisotype-equivalent immunoconjugate 9.2.27-BAMME-DAVLB-HY demonstrated efficacy at the 3 mg/kg dose level after ip administration. This non-antigen-mediated efficacy of 9.2.27-BAMME-DAVLB-HY may reflect a nonspecific drug depot effect in the peritoneal cavity with this immunoconjugate at this high dose. This study did demonstrate antigen-mediated tumor efficacy at the 1.5 mg/kg (vinca content) dose level with the KS1/4-BAMME-DAVLB-HY conjugate where 9.2.27-BAMME-DAVLB-HY was inactive. Further studies of the biodistribution and/or catabolism of the conjugates after iv or ip administration are necessary to correlate efficacy, route of administration, and chemical linker employed. This result does suggest that the conjugate could have overall utility as an intracavitary agent where enhanced conjugate stability would be advantageous (*20*). The two novel conjugates introduced by this study, KS1/4-BAP-DAVLB-HY and KS1/4-BAMME-DAVLB-HY, provide alternatives for further preclinical and clinical evaluation to determine their tumor saturation and drug-release characteristics.

This report summarizes the initial characterization of two chemoimmunoconjugates of the KS1/4 monoclonal antibody with the potent vinca alkaloid DAVLB-HY. They were compared to the chemimmunoconjugate KS1/4-DALVB-HY, which had been shown previously to have excellent in vivo activity (*10*). The alternative chemical linkers reported here, i.e. BAMME and BAP, resulted in a more chemically stable chemoimmunoconjugate than KS1/4-DAVLB-HY. All of the conjugates examined demonstrated significant survival advantages in the OVCAR-3 human xenograft model under conditions where unmodified DAVLB-HY is inactive. These data suggest that the KS1/4 antigenic system represents a therapeutic target for human ovarian cancer when the KS1/4 monoclonal antibody is covalently conjugated to vinca alkaloid by several diverse linker chemistries. In addition, the BAMME and BAP linker chemistries may be utilized for the conjugation of drug moieties other than vinca alkaloids to other antibodies or proteins where the hydrazone- or enamide-based chemistries are applicable, providing flexibility in future design of chemoimmunoconjugates for site directed therapy.

LITERATURE CITED

(1) Richardson, G. S., Scully, R. E., Nikrui, N., and Nelson, J. H., Jr. (1985) Medical progress: Common epithelial cancer of the ovary. *N. Engl. J. Med. 312*, 415–424.

(2) Young, R. C., Knapp, R. C., Fuks, Z., and DiSaia, P. J. (1985) Cancer of the ovary. In *Cancer Principles and Practice of Oncology* (V. T. Devita, Jr., S. Hellman, and S. A. Rosenberg, Eds.) Vol. 1, p 1083, JB Lippincott, Philadelphia.

(3) Markman, M. (1984) Medical principles of intraperitoneal and intrapleural chemotherapy. In *Intra-arterial and intracavitary cancer chemotherapy* Howell, (S. B. Ed.) pp 1–69, Nijhoff, Boston.

(4) Rosenshein, N. B., Leichner, P. K., and Vogelsang, G. (1979) Radiocolloids in the treatment of ovarian cancer. *Obstet. Gynecol. Surv. 34*, 708–720.

(5) Bast, R. C., and Knapp, R. C. (1987) The Emerging Role of Monoclonal Antibodies in the Clinical Management of Epithelial Ovarian Carcinoma. In *Important Advances in Oncology* (V. T. Devita, Jr. Ed.) pp 39–53, J. B. Lippincott Company, Philadelphia.

(6) Simpson, J., and Schlom, J. (1988) The Use of Monoclonal Antibody B72.3 in the Management of Gynecologic Malignancies. *Yale J. Biol. Med. 61*, 351–366.

(7) Riva, P., Marangolo, M., Lazzari, S., Agostini, M., Sarti, G., Moscatelli, G., Franceschi, G., Spinelli, A., and Vecchietti, G. (1989) Locoregional immunotherapy of human ovarian cancer: Preliminary results. *Nucl. Med. Biol.* **16**, 659–666.

(8) Pastan, I., Willingham, M. C., and Fitzgerald, D. J. (1986) *Immunotoxins Cell 47*, 641–648.

(9) Pimm, M. V. (1988) Drug-Monoclonal antibody conjugates for Cancer Therapy: Potentials and Limitations. *Crit. Rev. Ther. Drug Carrier Syst. 5*, 189–226.

(10) Apelgren, L. D., Zimmerman, D. L., Briggs, S. L., and Bumol, T. F. (1990) Antitumor Activity of the Monoclonal Antibody–Vinca Alkaloid Immunoconjugate LY203725 (KS1/4-4-Desacetylvinblastine-3-carboxhydrazide) in a Nude Mouse Model of Human Ovarian Cancer. *Cancer Res. 50*, 3540–3544.

(11) Laguzza, B. C., Nichols, C. L., Briggs, S. L., Cullinan, G. J., Johnson, D. A., Starling, J. J., Baker, A. L., and Bumol, T. F. (1989) New Antitumor Monoclonal Antibody–Vinca Conjugates LY203725 and Related Compounds: Design, Preparation, and Representative In Vivo Activity. *J. Med. Chem. 32*, 548–555.

(12) Lindstrom, T. D., Althaus, W. A., Rutherbories, K. J., and Kau, D. (1989) Pharmacokinetics and disposition of the KS1/4 monoclonal antibody-desacetylvinblastine hydrazide conjugate LY203725 in rats and monkeys. *J. Pharmacol. Exp. Ther. 252*, 1117–1124.

(13) Hamilton, T. C., Young, R. C., Louie, K. G., Behrens, B. C., McCoy, W. M., Grotzinger, K. R., and Ozols, R. F. (1984) Characterization of a Xenograft Model of Human Ovarian Carcinoma Which Produces Ascites and Intraabdominal Carcinomatosis in Mice. *Cancer Res. 44*, 5286–5290.

(14) Varki, N. M., Reisfeld, R. A., and Walker, L. E. (1984) Antigens associated with a human lung adenocarcinoma defined by monoclonal antibodies. *Cancer Res. 44*, 681–686.

(15) Bumol, T. F., and Reisfeld, R. A. (1982) Unique glycoprotein-proteoglycan complex defined by monoclonal antibody on human melanoma cells. *Proc. Natl. Acad. Sci. U.S.A. 79*, 1245–1249.

(16) Mirabelli, C. K., Bartus, H., Bartus, J. O. L., Johnson, R., Mong, S. M., Sung, C. P., and Crooke, S. T. (1985) Application of a tissue culture microtiter test for the detection of cytotoxic agents from natural products. *J. Antibiot. 38*, 758–766.

(17) Thomas, D. G., Breslow, N., and Gart, J. J. (1977) Trend analysis and homogeneity analyses of proportions and life table data. *Comput. Biomed. Res. 10*, 373–381.

(18) Kaplan, E. L., and Meier, P. (1958) Non-parametric estimation from incomplete observations. *J. Am. Stat. Assoc. 53*, 457–481.

(19) Schneck, D., Butler, F., Dugan, W., Littrell, D., Petersen, B., Bowsher, R., Delong, A., and Dorrbecker, S. (1990) Disposition of a murine monoclonal antibody vinca conjugate (KS1/4-DAVLB) in patients with adenocarcinomas. *Clin. Pharmacol. Ther. 47*, 36–41.

(20) Schlom, J. Horan Hand, P., Gerteiner, J. W., Colcher, D., Shrivastav, S., Carrasquillo, J. A., Reynolds, J. C., Larson, S. M., and Raubitschek, A. (1990) Innovations That Influence the pharmacology of Monoclonal Antibody Guided Tumor Targeting. *Cancer Res. (Suppl.) 50*, 820s–827s.

Photodegradation of the Cytosine Nucleosides Family by Water-Soluble Iron(III) Porphyrins

Yoshikatsu Ito

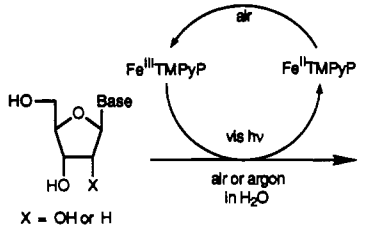
Department of Synthetic Chemistry, Faculty of Engineering, Kyoto University, Kyoto 606, Japan. Received September 23, 1992

Aqueous solutions of cytosine nucleosides such as cytidine (C), 2′-deoxycytidine (dC), 2′,3′-dideoxycytidine (ddC), and 1-β-D-arabinofuranosylcytosine (*ara*-C) were irradiated with visible light in the presence of a water-soluble iron(III) porphyrin photocatalyst (Fe^{III}TMPyP or Fe^{III}TSPP) in air or under an argon atmosphere. HPLC analyses revealed release of cytosine as a dominant reaction. In the case of the irradiations of isomeric C and *ara*-C, their interconversion was also observed as a minor reaction. Under an argon atmosphere, a stoichiometric reduction of the catalyst into Fe^{II}TMPyP or Fe^{II}TSPP was observable by UV-vis spectroscopy. Quantum yields for the cytosine release and the catalyst reduction (Φ_{cyt} and $\Phi_{Fe^{II}}$) were very much dependent both on the presence and the stereochemistry of the 2′-OH group. For the Fe^{III}TMPyP case, for example, (a) Φ_{cyt} and $\Phi_{Fe^{II}}$ decreased in the order C > *ara*-C > dC > ddC and (b) oxygen lowered the Φ_{cyt} of dC and ddC but not Φ_{cyt} of C and *ara*-C. These results strongly support the previously proposed mechanism, i.e., C and *ara*-C undergo the reaction via a C2′ carbon radical (e.g., eq 4) and dC and ddC undergo the reaction via a C1′ or C4′ carbon radical (e.g., eq 3). The observed effects of 2-propanol and solution pH suggest that a main reactive species photogenerated from FeTSPP is a free hydroxyl radical (•OH), while that photogenerated from FeTMPyP is probably an iron-coordinated active oxygen species (crypto-OH or Fe=O).

INTRODUCTION

In connection with the tumor phototherapy with hematoporphyrin derivatives, a number of works have been done about photochemical DNA cleavage by porphyrins (*1–6*). We have been studying the photocatalytic activities of water-soluble metalloporphyrins having redox-active central metals, since they are relatively little studied from the viewpoint of organic photochemistry (*7–11*). Unlike non-redox-active metalloporphyrins such as zinc porphyrin, which can cause only simple photochemical electron or energy transfer reactions (*12*), novel photochemical oxidation–reduction reactivities are expected.

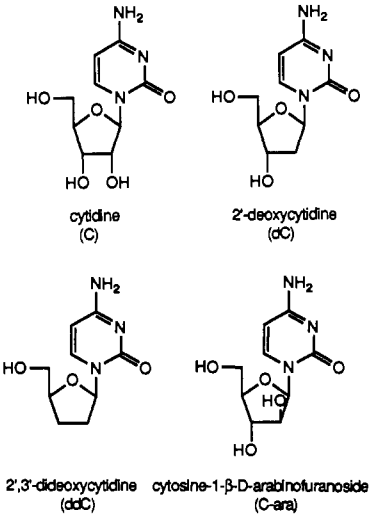
Recently we have found that [*meso*-tetrakis(1-methyl-4-pyridiniumyl)porphyrinato]iron(III), Fe^{III}TMPyP, photocatalyzes the selective release of bases from nucleosides and their derivatives in aerated aqueous solution (e.g., eq 1) (*11*). Ribonucleosides afforded much higher yields of



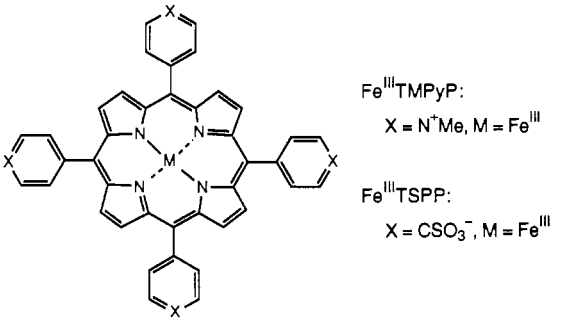
(1)

free base than the corresponding deoxyribonucleosides. The yields decreased in the following order among the ribonucleosides studied: cytidine (C) > uridine (U) ≈ ribosylthymine (T) > adenosine (A) ≈ guanosine (G). This does not correlate with the order of oxidation potentials for the bases: uracil > cytosine > thymine > adenine > guanine. The free base release was a predominant reaction in all cases except for G and 2′-deoxyguanosine (dG), where decomposition of the guanine ring occurred in much preference to the release of guanine. The quantum yield for the disappearance of G or dG is found to be comparable to that for cytosine released from C. Under an argon atmosphere, virtually quantitative reduction of Fe^{III}TMPyP into Fe^{II}TMPyP by C or 2′-deoxycytidine (dC) was observed in addition to the nearly stoichiometric release of cytosine and the reduction was much more effective by C than by dC. The increased reactivity (in both base release and iron reduction) for the ribonucleoside relative to that for the deoxyribonucleoside was ascribed to the difference in their binding strength to the porphyrin catalyst and to a facile base-releasing degradation of only the ribonucleoside from its C2′ carbon radical.

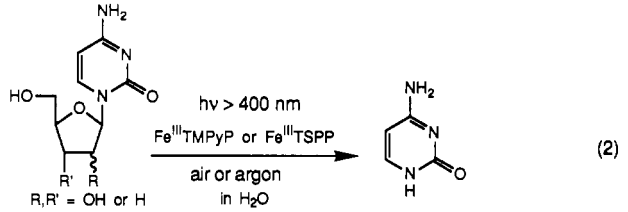
In order to obtain more detailed information about the reaction mechanism, I noted the most reactive cytidine as a substrate for further study. Here, the release of cytosine from cytidine (C), 2′-deoxycytidine (dC), 2′,3′-dideoxycytidine (ddC), and 1-β-D-arabinofuranosylcytosine (*ara*-C) photocatalyzed by iron(III) complexes of *meso*-tetrakis(1-methyl-4-pyridiniumyl)porphyrin (Fe^{III}TMPyP) and



1043-1802/93/2904-0127$04.00/0 © 1993 American Chemical Society



meso-tetrakis(4-sulfonatophenyl)porphyrin (Fe^{III}TSPP) will be reported (eq 2). Quantum yields for the release of



(2)

cytosine (both in air and under an argon atmosphere) and for the reduction of the Fe^{III} complexes into the Fe^{II} ones (under an argon atmosphere) were estimated. Photochemical interconversion between isomeric C and *ara*-C with a low efficiency was also observed to occur.

EXPERIMENTAL PROCEDURES

Conditions for high-performance liquid chromatography (HPLC) analyses were described in a previous paper (*11*). Preparative HPLC was done with a Waters chromatographic system by using a Cosmosil 5C$_{18}$ column (20 mm i.d. × 250 mm) and H$_2$O/MeOH (97:3 v/v) as solvent. UV–vis spectra were measured on a JASCO UVIDEC-610 spectrometer. NMR and mass spectra were recorded on Varian Gemini-200 and JEOL JMS-DX 300 spectrometers, respectively. Cytosine nucleosides C, dC, ddC, and *ara*-C were purchased from Yamasa, Sigma, Aldrich, and Wako, respectively. Water (distilled, HPLC grade) was obtained from Wako. Fe^{III}TMPyP was previously prepared (*7*). Fe^{III}TSPP was prepared according to the published procedure (*13*).

Photolysis. Neutralized stock solutions of the iron(III) porphyrins (2.5 × 10^{-4} M) were diluted to the one-half concentration with an appropriate nucleoside aqueous solution. The solution pH was adjusted by using an aqueous NaOH or HCl solution when necessary. Each sample solution was placed either (a) in a Pyrex tube for photolyses in the presence of air (5 mL) or (b) in a UV cell (path length, 1 mm) with a two-way stopcock for photolyses under an argon atmosphere (0.5 mL). Irradiations of these samples were performed with a 400-W high pressure mercury lamp through a 15% NaNO$_2$ filter solution (>400 nm) for a suitable time (vide infra).

(*a*) *Photolysis in the Presence of Air.* In the experiments in Table I, irradiations were done for a long time (20 h) to obtain high product yields (cytosine yield <2290% based on the catalyst employed, Table I). For quantum yield measurements (Table II (air) and Figures 3–5), irradiations were carried out on an usual merry-go-round apparatus, being stopped at low conversions (cytosine yield <200%). Yields of nucleoside degradation products and porphyrin recoveries were determined by HPLC and UV–vis analyses, respectively.

(*b*) *Photolysis under an Argon Atmosphere.* Each solution placed in the UV cell was purged by bubbling with argon for 10 min and then irradiated. Absorption spectral changes accompanying the photoreduction of Fe^{III} into Fe^{II} were checked from time to time until no further spectral changes were observed (e.g., Figure 1). In the case of ddC, the reduction was so slow that a complete reduction could not be reached within 11 h of irradiation. After the photolysis, oxygen was bubbled through the solution for 10 min. In all cases, the original absorption due to the Fe^{III} porphyrin was almost quantitatively (>97%) recovered. The nucleoside degradation products were analyzed by HPLC before and after the introduction of oxygen.

Increase of the iron(II) porphyrin yield with irradiation time (Figure 2) was determined from the above absorption spectral data (e.g., Figure 1). Since the photoreductions of iron(III) porphyrins by ddC were slow, the final spectra after the complete photoreduction were postulated to be the same as those for the dC case. Relative quantum yields for the Fe^{II} production (Table II (argon)) were estimated from Figure 2, by comparing the irradiation time required to obtain 30–40% yield of Fe^{II}. As is evident from inspection of Figure 2, these values may be subject to considerable errors.

Preparative Photolysis. A neutral solution containing 254 mg (1.04 mmol, 1.23 × 10^{-2} M) of C and 3.6 × 10^{-4} M of Fe^{III}TMPyP in 85 mL of water was placed in a large Pyrex tube and was externally irradiated under air. The reaction was followed by HPLC and UV–vis. After 175 h of photolysis, the reaction mixture which still contained undecomposed Fe^{III}TMPyP (38% recovery) was concentrated to a volume of ca. 5 mL and was then subjected to reverse-phase column chromatography (Cosmosil 75C$_{18}$-OPN 10 g, eluted with water) to remove colored materials. The resultant colorless reaction mixture was separated by preparative HPLC to afford 54 mg (46%) of cytosine, 130 mg (51%) of C, and 8 mg (3%) of *ara*-C. A small amount (3 mg) of material, which was eluted before cytosine, was obtained, but judging from the NMR, UV–vis, mass, and HPLC analyses, it does not seem to be a pure compound.

RESULTS AND DISCUSSION

The cytosine nucleosides family C, dC, ddC, and *ara*-C was irradiated with visible light in the presence of Fe^{III}-TMPyP or Fe^{III}TSPP in aerated water. HPLC analyses revealed cytosine as a dominant product. In the case of the irradiations of isomeric C and *ara*-C their interconversion was also observed as a minor reaction. The results are summarized in Table I.

A large-scale photolysis of C in the presence of FeTMPyP was performed under conditions similar to run 2 in Table I. As was previously reported (*11*), HPLC analysis of the reaction mixture displayed five peaks: two major peaks at 2.5 (cytosine) and 4.6 (C) min and three small peaks at 2, 3.8, and 5.8 (*ara*-C) min. The products were separated by preparative HPLC to afford 46% of cytosine, 3% of *ara*-C, and 51% of recovered C (the yields are based on C employed). Since the sum of these yields amounts to 100%, degradation of the cytosine ring under the present reaction conditions must be negligible. The substance at 3.8 min turned into a complex mixture during the separation procedures (column chromatography and preparative HPLC). The substance at 2 min was separated by preparative HPLC, but its NMR and other spectroscopic evidences indicate that it is still a mixture. Thus, final degradation products derived from the sugar moiety of C are as yet unidentified. A large-scale photolysis of C and FeTSPP was not done. However, judging from the HPLC analyses of irradiated solutions for analytical

Table I. Photodegradation of Cytidine (C), 2'-Deoxycytidine (dC), 2',3'-Dideoxycytidine (ddC), and 1-β-D-Arabinofuranosylcytosine (*ara*-C) by Fe^{III}TMPyP and Fe^{III}TSPP[d]

run	substrate	solvent[b]	% products[a] cytosine	*ara*-C or C	% recovered porphyrin
		(A) Fe^{III}TMPyP			
1	C	H_2O, pH 11.4 (5.8)	2290	160	37
2	C	H_2O, pH 7.2 (5.1)	1680	230	29
3	C	50 mM sodium phosphate buffer, pH 7.3 (7.3)	1080	190	65
4	dC	H_2O, pH 7	54		nd[c]
5	ddC	H_2O, pH 7.5 (7.4)	21		91
6	*ara*-C	H_2O, pH 7	390	19	nd[c]
		(B) Fe^{III}TSPP			
7	C	H_2O, pH 11.2 (9.7)	610	25	77
8	C	H_2O, pH 7.2 (6.6)	350	64	77

[a] (Product/catalyst) × 100%. [b] The solution pH before irradiation is listed; pH after irradiation is in parentheses. [c] Not determined. [d] [FeP] = 1.3×10^{-4} M, [nucleoside] = 1.3×10^{-2} M; irradiated at >400 nm for 20 h in aerated solvent.

experiments, the specificity in photoproduct formation should be the same as with FeTMPyP, except at high pH (pH > 12), where the HPLC charts became somewhat complex in the case of FeTSPP.

Table I demonstrates that the cytosine yield is highly dependent on the sugar structures of the nucleosides; i.e., it decreased in the order C > *ara*-C > dC > ddC, ranging from 1680 to 21% under the corresponding reaction conditions (runs 2 and 4–6); the yields are calculated on the basis of the catalyst employed. The solution pH, which also affected the cytosine yield, was lowered during the irradiation (see runs 1, 2, 7, and 8), but the use of neutral phosphate buffer retarded the reaction (run 3). Coordination of the phosphate ion to the iron atom may be decreasing the photocatalytic activity of FeTMPyP (*11*). FeTMPyP was appreciably more efficient than FeTSPP in photocatalyzing the degradation of C (compare runs 1 and 2 with runs 7 and 8).

Quantum yields for the Fe^{III}TMPyP- or Fe^{III}TSPP-photocatalyzed decomposition of C, dC, ddC and *ara*-C under air were measured by a merry-go-round technique. Relative values for quantum yields for the liberation of cytosine (Φ_{cyt}) and for the interconversion of C and *ara*-C into each other (Φ_{isom}) are summarized in Table II. The absolute value for Φ_{cyt} for the Fe^{III}TMPyP-photocatalyzed cytosine release from C was estimated as 0.0010 on the basis of the Fe^{III}TMPyP-photocatalyzed carbon–carbon bond cleavage of *meso*-hydrobenzoin (*7*).

When the photolyses were carried out in a UV cell under an argon atmosphere, a quantitative reduction of the iron(III) catalysts into the iron(II) species (Fe^{II}TMPyP and Fe^{II}TSPP) was spectrally observed. After enough irradiation times, the absorption bands for the Fe^{III} species were invisible, indicating complete conversion of Fe^{III} into Fe^{II}. The spectral changes obtained from reduction of Fe^{III}TMPyP by C and dC were already shown in a previous paper (*11*), and similar spectral changes were observed in other cases (e.g., Figure 1). From these spectral changes, the time-courses for the iron(II) formation were calculated and they are displayed in Figure 2. From this figure, relative quantum yields for the reduction $Fe^{III} \rightarrow Fe^{II}$ ($\Phi_{Fe^{II}}$) were estimated.

After a complete photoreduction of Fe^{III} into Fe^{II} under an argon atmosphere, oxygen was introduced into the UV cell by bubbling through the solution, which readily resulted in more than 97% recovery of the Fe^{III} absorption

Table II. Quantum Yields for the Fe^{III}TMPyP- or Fe^{III}TSPP-Photocatalyzed Decomposition of Cytosine Nucleosides C, dC, ddC, and *ara*-C in the Presence of Air or under an Argon Atmosphere[d]

substrate	air Φ_{cyt}^{rel}	air Φ_{isom}^{rel}	argon $\Phi_{Fe^{II}}^{rel}$	argon $\Phi_{cyt}^{rel\,a}$	argon $\Phi_{isom}^{rel\,b}$
		(A) Fe^{III}TMPyP			
C	1.00[c]	0.13	3.7	0.92	0.17
dC	0.026		0.33	0.14	
ddC	0.013		0.18	0.10	
ara-C	0.13	0.0062	0.76	0.16	0.02
		(B) Fe^{III}TSPP			
C	0.31	0.042	3.1	0.26	0.03
dC	0.043		0.31	0.17	
ddC	0.025		0.23	0.11	
ara-C	1.2	0.033	0.59	0.053	0.01

[a] The relative value for Φ_{cyt} under argon was calculated by $\Phi_{cyt}^{rel} = \Phi_{Fe^{II}}^{rel} \times$ (the catalyst-based yield of cytosine after a complete conversion of Fe^{III} into Fe^{II}). [b] The relative value for Φ_{isom} under argon was calculated by $\Phi_{isom}^{rel} = \Phi_{Fe^{II}}^{rel} \times$ (the catalyst-based yield of *ara*-C or C after a complete conversion of Fe^{III} into Fe^{II}). [c] The absolute value for Φ_{cyt} (Φ_{cyt}^{abs}) is estimated as 0.0010 on the basis of the photocleavage of *meso*-hydrobenzoin by Fe^{III}TMPyP (7). [d] [FeP] = 1.3×10^{-4} M, [nucleoside] = 1.3×10^{-2} M, in H_2O (pH 7).

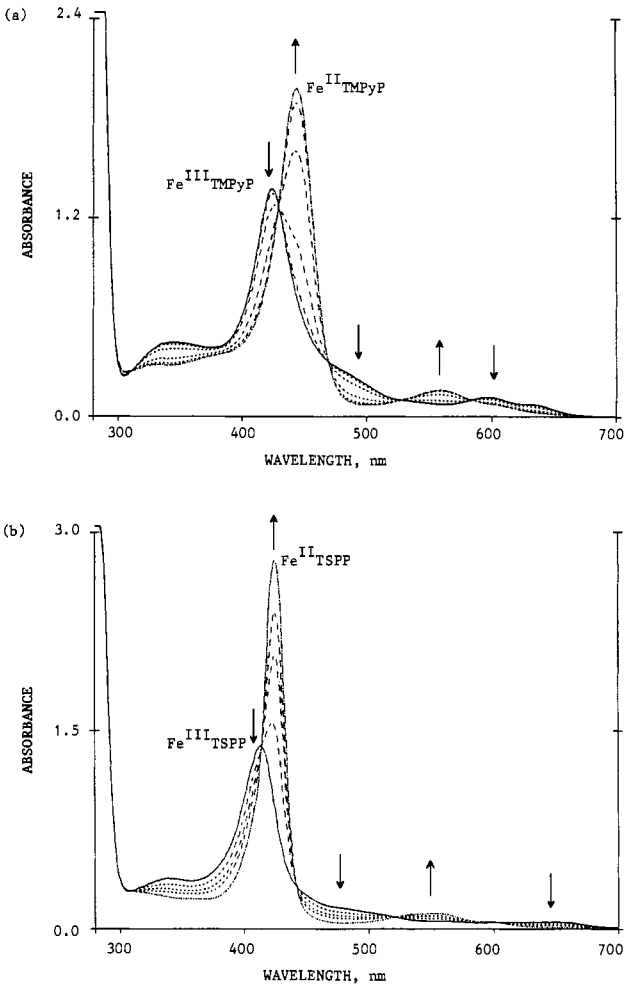


Figure 1. Spectral changes from visible light photolyses of Fe^{III}TMPyP or Fe^{III}TSPP with cytosine nucleosides under an argon atmosphere: [FeP] = 1.3×10^{-4} M, [nucleoside] = 1.3×10^{-2} M, in H_2O (pH 7); path length 1 mm. (a) Fe^{III}TMPyP/*ara*-C; the spectra were taken at t = 0, 0.1, 0.3, 1, 2.5 and 4 h. (b) Fe^{III}TSPP/C; the spectra were taken at t = 0, 0.1, 0.2, 0.3 and 1 h.

in all cases. HPLC analyses were done before and after the oxygen bubbling, and it was found that the yields for the released cytosine (cytosine nucleoside → cytosine) and for the isomers (C → *ara*-C or *ara*-C → C) were essentially

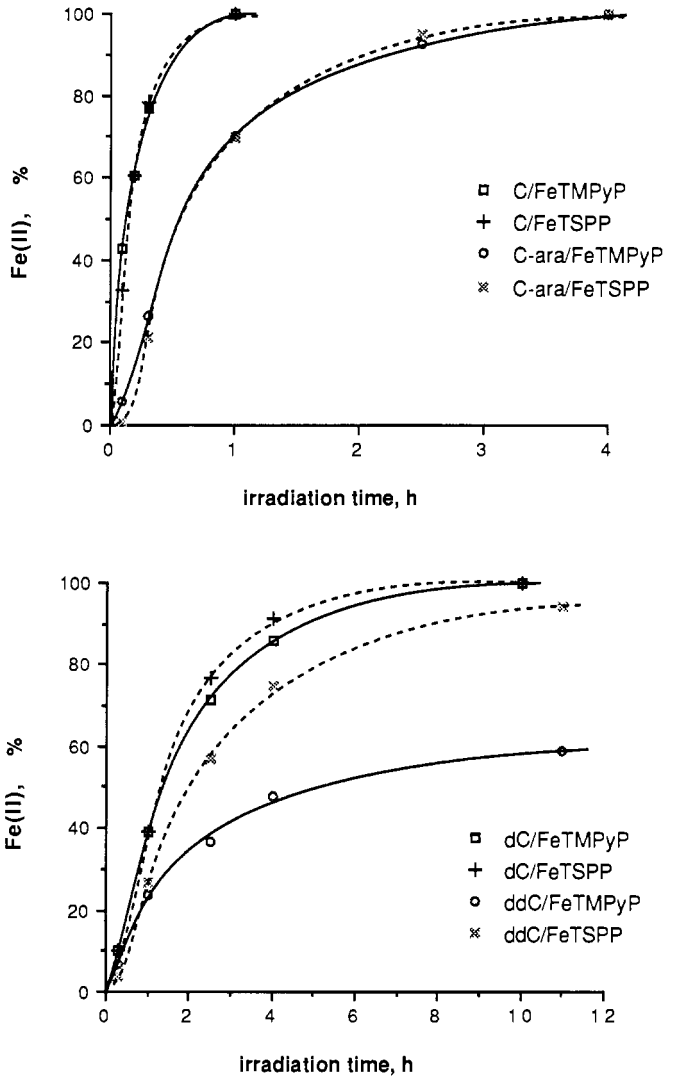
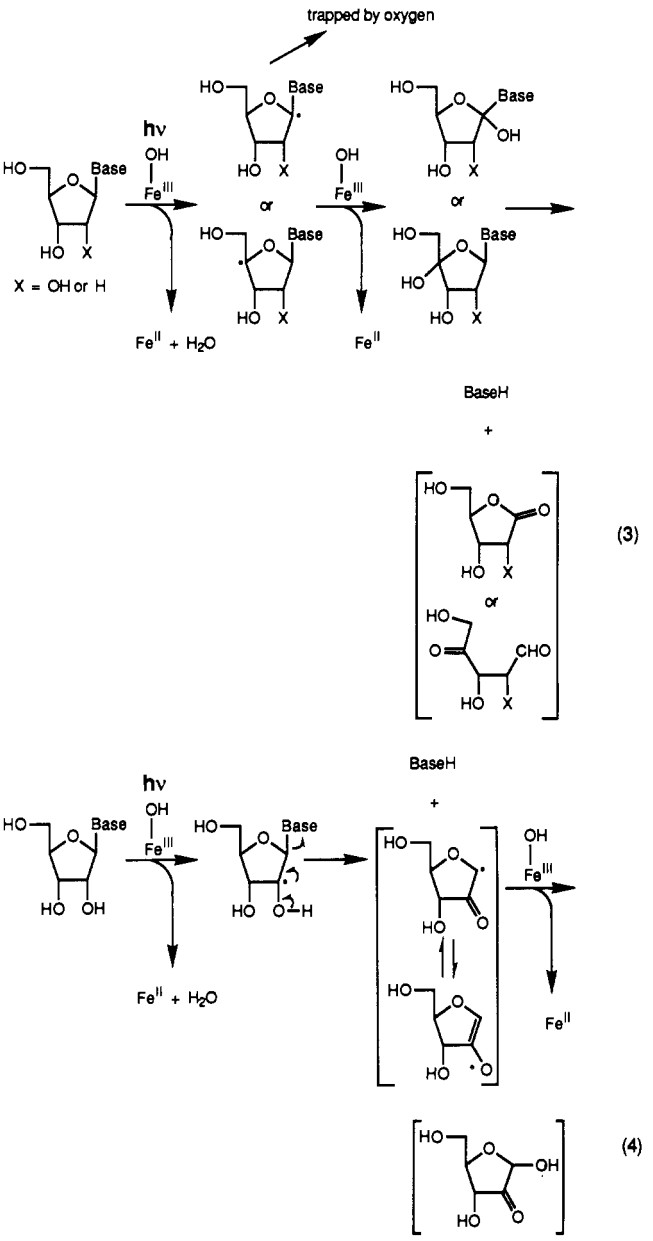


Figure 2. Increase of the iron(II) porphyrin yield with the irradiation time from visible light photolyses of Fe^{III}TMPyP or Fe^{III}TSPP with cytosine nucleosides C, dC, ddC, and *ara*-C under an argon atmosphere: reaction conditions, see the legend in Figure 1.

unaltered by the oxygen bubbling. On the basis of these yields and $\Phi_{Fe^{II}}$ obtained above, quantum yields for cytosine (Φ_{cyt}) and for the isomerization (Φ_{isom}) under an argon atmosphere were estimated. Relative values for $\Phi_{Fe^{II}}$, Φ_{cyt}, and Φ_{isom} under an argon atmosphere are listed in Table II, together with those for Φ_{cyt} and Φ_{isom} under air.

Previously (*11*), we have proposed two tentative mechanisms for the release of base from ribo- and deoxyribonucleosides (eqs 3 and 4). Eq 3 is a mechanism involving a C1′ or C4′ radical intermediate and may be disturbed by molecular oxygen in aerated aqueous solution, since the C1′ and C4′ carbon radicals may be competitively trapped by a porphyrin and an oxygen molecule ([porphyrin] ≈ $[O_2] \approx 10^{-4}$ M under the present reaction conditions). Eq 4 is applicable only for ribonucleosides. This mechanism involves a C2′ radical intermediate, which may rapidly release base without being obstructed by oxygen (*14*). In aqueous solution, Fe^{III}TMPyP and Fe^{III}TSPP undergo acid–base and dimerization equilibria that depend on concentration, ionic strength, and pH (*15*). The identifications of the species relevant to these equilibria are still unsettled. However, since the aqua or hydroxo complexes appear to be main species in neutral aqueous solution at concentrations of the present experiments (*7*, *15*), the porphyrin catalysts are written as a hydroxo species Fe^{III}–



OH in eqs 3 and 4. It is assumed in eqs 3 and 4 that two molecules of Fe^{III}–OH are consumed for the release of one molecule of base. In the presence of oxygen, however, Fe^{II} will be oxidized to regenerate Fe^{III}–OH (eq 5) (*16*) and the

$$Fe^{II} + O_2 \longrightarrow Fe^{III}\text{-}O\text{-}O\cdot \xrightarrow{Fe^{II}} Fe^{III}\text{-}O\text{-}O\text{-}Fe^{III} \longrightarrow 2\,Fe^{IV}{=}O \longrightarrow 2\,Fe^{III}\text{-}OH \quad (5)$$

reaction will become catalytic as was actually observed (Table I).

A possible hydrogen-abstracting species in the first step of eqs 3 and 4 is a hydroxyl radical (•OH), which may be generated by photolysis of Fe^{III}–OH (eq 6) (*8*, *10*, *17*, *18*),

$$Fe^{III}\text{-}OH \xrightarrow{h\nu} Fe^{II} + \cdot OH \text{ (or crypto-OH or Fe=O)} \quad (6)$$

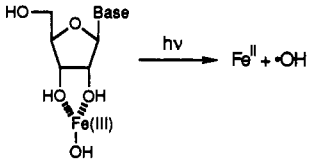
a hydroxyl radical coordinated to the iron atom (crypto-OH) (*19*, *20*), or a high-valent iron-oxo species Fe=O (*21*, *22*). Crypto-OH and Fe=O may be considered equivalent species (*20*, *21*), since they are potentially in equilibration as shown in, for example, eq 7. The ferryl oxide Fe^{IV}=O

$$Fe^{III} + {}^{\bullet}OH \rightleftharpoons Fe^{IV}\text{-}OH \rightleftharpoons Fe^{IV}{=}O + H^{+} \quad (7)$$
(crypto-OH)

is not a powerful hydrogen-abstracting agent, unlike the Fe^{V}=O species in cytochrome P-450 models (*23*), but can be under illumination conditions (*24*). The C2′ radical intermediate in eq 4 may be generated via cytosine OH adduct radicals that are formed either by the addition of water to a radical cation of the cytosine moiety or by the addition of ·OH to the double bond of the cytosine moiety (*25*). However, I have previously (*11*) shown some experimental evidences that nucleobase radical cations do not participate in the present base-releasing reactions. In fact, C liberated undecomposed cytosine in a quantitative yield (vide supra).

Variations in quantum yields in Table II can be well explained by taking eqs 3 and 4 into account, in the following ways.

First, except for the unusually large relative Φ_{cyt} (=1.2) for *ara*-C/FeTSPP under air, the Φ_{cyt} and $\Phi_{Fe^{II}}$ values for C are much larger than those for *ara*-C, dC, and ddC under the corresponding reaction conditions. The only difference in structure between C and *ara*-C is a configuration of the 2′-OH group. dC and ddC do not carry a 2′-OH group. The observed much larger Φ_{cyt} and $\Phi_{Fe^{II}}$ values for C relative to those for dC and ddC indicate a crucial role of the 2′-OH group in releasing cytosine from C. Furthermore, the striking difference in Φ_{cyt} and $\Phi_{Fe^{II}}$ values between C and *ara*-C indicates that the 2′-OH stereochemistry also controls the efficiency of the cytosine release. These facts support that the cytosine release from C takes place according to eq 4, since it comprises the C2′ carbon radical as a key intermediate. The fact that $\Phi_{Fe^{II}}$ for C is by far the largest as compared with that for *ara*-C, dC, and ddC implies a promoted photoreduction of Fe^{III} into Fe^{II} as a result of cis-coordination of C through the 2′- and 3′-OH groups in the molecule (eq 8).



(8)

Second, under an argon atmosphere, $\Phi_{Fe^{II}} \approx 2(\Phi_{cyt})$ for dC and ddC. This means that 1 equiv of cytosine release from dC or ddC corresponds to 2 equiv of Fe^{II} production, just as eq 3 predicts. By contrast, in the cases of C and *ara*-C, where $\Phi_{Fe^{II}} \approx$ 4-12(Φ_{cyt}) under an argon atmosphere, the cytosine release corresponds to production of 4–12 equiv of Fe^{II}. Hence, the Fe^{III} reduction into Fe^{II} occurred more than predicted from eq 3 or 4. The carbon–carbon bonds of 1,2-diols are known to be photochemically cleaved by Fe^{III}TMPyP (*7*). Therefore, the wastage of the Fe^{III} reduction observed for C and *ara*-C may be partly ascribed to the C2′–C3′ bond cleavage in their ribose moiety.

Third, in the case of dC and ddC, Φ_{cyt} under air is much smaller than Φ_{cyt} under argon; i.e., the cytosine release was strongly disturbed by oxygen, as expected from eq 3. In the cases of C and *ara*-C, except for *ara*-C/FeTSPP, Φ_{cyt} under air is approximately equal to Φ_{cyt} under argon, i.e., the inhibitory effect of oxygen is unobservable, as predicted from eq 4. In other words, for C and *ara*-C the cytosine release according to eq 3 is negligible. In the case of *ara*-C/FeTSPP, where Φ_{cyt} under air is much larger than Φ_{cyt} under argon, oxygen has an accelerating effect. This finding is interesting, but is unable to be understood at this stage.

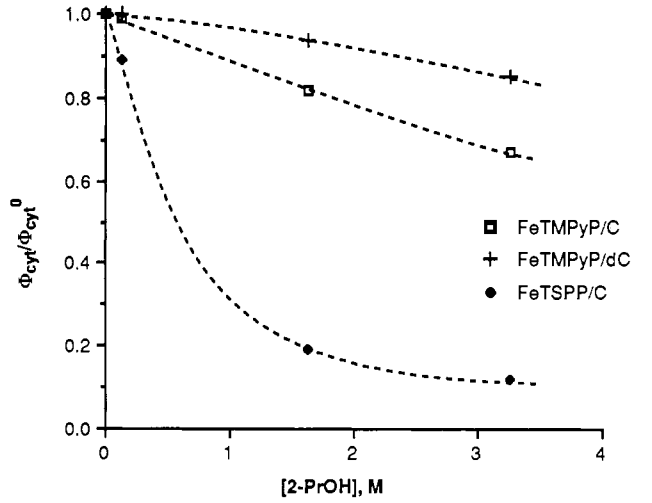


Figure 3. Quenching by 2-propanol of the Fe^{III}TMPyP- and Fe^{III}TSPP-photocatalyzed cytosine release from C or dC in the presence of air: [FeP] = 1.3×10^{-4} M, [nucleoside] = 1.3×10^{-2} M, in 25 mM sodium phosphate buffer (pH 7.3). Φ_{cyt}^{0} is Φ_{cyt} in the absence of 2-propanol.

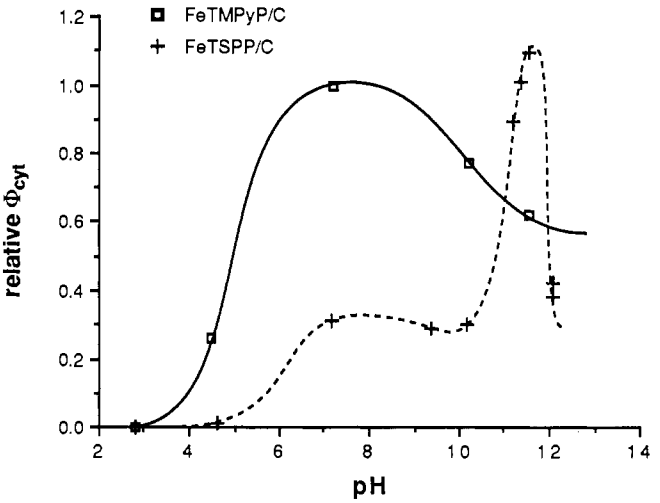


Figure 4. Relative Φ_{cyt} vs pH for the Fe^{III}TMPyP- and Fe^{III}-TSPP-photocatalyzed cytosine release from C in the presence of air: [FeP] = 1.3×10^{-4} M, [C] = 1.3×10^{-2} M, in H_2O; pH was adjusted by NaOH/HCl.

Finally, the observed inefficient epimerization of C and *ara*-C (Φ_{isom} in Table II) may have occurred through intermediacy of a planar or a rapidly inverting C2′ carbon radical in eq 4.

Figure 3 shows the effect of 2-propanol (0.16–3.3 M) on the photocatalytic release of cytosine from C or dC. The FeTSPP-photocatalyzed release was quenched by 2-propanol much more efficiently than the FeTMPyP-photocatalyzed one was: the difference between their quenching efficiencies was especially remarkable at lower concentrations of 2-propanol. Since 2-propanol is a good quencher for the hydroxyl radical ($k_q = 1.3 \times 10^9$ M^{-1} s^{-1}) (*26*), this result indicates that a main active oxidant in the FeTSPP-photocatalyzed reactions is ·OH, while that for FeTMPyP may be other species such as high-valent iron-oxo complexes or crypto-OH.

The photocatalytic release of cytosine from C strongly depended on the solution pH, and this dependence was dramatically different between FeTMPyP and FeTSPP (Figure 4). Although the reaction is very slow at acidic pH in both cases (i.e., Φ_{cyt} is virtually zero at pH 2), Φ_{cyt} for the FeTMPyP case reached a maximum value at pH 7 and that for the FeTSPP case reached a plateau at pH

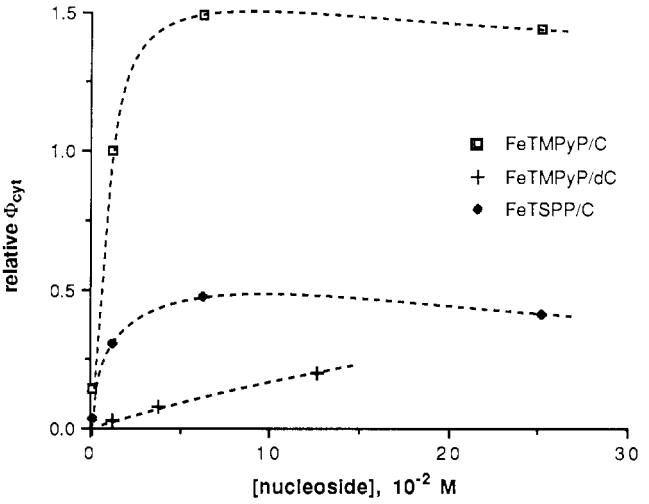


Figure 5. Relative Φ_{cyt} vs nucleoside concentration for the Fe^{III}-TMPyP- and Fe^{III}TSPP-photocatalyzed cytosine release from C or dC in the presence of air: [FeP] = 1.3×10^{-4} M, [nucleoside] = $0.13–25.2 \times 10^{-2}$ M, in H_2O (pH 7).

7, then abruptly increased around pH 11, and suddenly dropped above pH 12. This characteristic pH effect observed in the FeTSPP photocatalysis may also be explained in terms of formation of a reactive hydroxyl radical, since (a) Fe^{III}TSPP in aqueous solution is known to be able to photogenerate •OH with an efficiency that is higher above pH 11 (*17*) and (b) most of the hydroxyl radical deprotonates above pH 12 ($•OH \rightleftarrows O^{•-} + H^+$, $pK_a = 11.9$) (*27*). It has recently been reported that •OH reacts faster than $O^{•-}$ with the nucleosides by a factor of 6–7 (*28*).

Incidentally, it is very interesting to note that the radiolysis-generated hydroxyl radical exhibits little selectivity in reactions with various nucleosides (*29*). For example, U and 2′-deoxyuridine (dU) undergo a base release with similar efficiencies and, furthermore, the base release accounts for only less than 20% of the total reaction (at pH 9) in either case. These results are quite different from the high selectivities observed here for the FeTMPyP-photocatalyzed reactions (also see ref 11).

Effect of the nucleoside concentration (0.0013–0.25 M) on the efficiency of the photocatalytic release of cytosine from C or dC was examined (Figure 5). In the case of C/FeTMPyP and C/FeTSPP, Φ_{cyt} increased up to ca. 0.05 M and then nearly leveled off at higher concentrations. In the case of dC/FeTMPyP, Φ_{cyt} almost uniformly increased up to 0.13 M. These facts may imply that C binds to the iron(III) porphyrins more strongly than dC. Probably, the 2′-OH group of the sugar moiety in C (dC lacks 2′-OH) is acting as a coordinating ligand (cf. eq 8). The different binding strength of C and dC toward Fe^{III}TMPyP was previously (*11*) inferred from both absorption spectral studies and the increased reactivity of C relative to dC (see Table II; Φ_{cyt} and $\Phi_{Fe^{II}}$ are larger for C than for dC).

CONCLUSION

A main reactive species involved in the Fe^{III}TSPP-photocatalyzed cytosine releases from cytosine nucleosides C, dC, ddC, and *ara*-C is a free hydroxyl radical (•OH), while that involved in the Fe^{III}TMPyP-photocatalyzed ones is presumably an iron-coordinated active oxygen species (crypto-OH or Fe=O). It appears that C and *ara*-C undergo the reaction via a C2′ carbon radical (e.g., eq 4), dC and ddC undergo the reaction via a C1′ or C4′ carbon radical (e.g., eq 3), and that the 2′-OH group of the ribose moiety in C promotes the cytosine release via the C2′ carbon radical. Relatively large Φ_{cyt} and $\Phi_{Fe^{II}}$ values observed for C are also likely due to favorable coordination of C onto the central iron(III) atom of the porphyrin through the 2′- and 3′-OH groups.

LITERATURE CITED

(1) Gutter, B., Speck, W. T., and Rosenkranz, H. S. (1977) The Photodynamic Modification of DNA by Hematoporphyrin. *Biochim. Biophys. Acta 475*, 307–314.

(2) Fiel, R. J., Datta-Gupta, N., Mark, E. H., and Howard, J. C. (1981) Induction of DNA Damage by Porphyrin Photosensitizers. *Cancer Res. 41*, 3543–3545.

(3) Kelly, J. M., Murphy, M. J., McConnell, D. J., and OhUigin, C. (1985) A Comparative Study of the Interaction of 5,10,-15,20-Tetrakis(N-methylpyridinium-4-yl)porphyrin and its Zinc Complex with DNA Using Fluorescence Spectroscopy and Topoisomerisation. *Nucleic Acids Res. 13*, 167–184.

(4) Praseuth, D., Gaudemer, A., Verlhac, J., Kraljic, I., Sissoeff, I., and Guille, E. (1986) Photocleavage of DNA in the Presence of Synthetic Water-Soluble Porphyrins. *Photochem. Photobiol. 44*, 717–724.

(5) Le Doan, T., Praseuth, D., Perrouault, L., Chassignol, M., Thuong, N. T., and Hélène, C. (1990) Sequence-Targeted Photochemical Modifications of Nucleic Acids by Complementary Oligonucleotides Covalently Linked to Porphyrins. *Bioconjugate Chem. 1*, 108–113.

(6) Komiyama, M., Kobayashi, M., Harada, M. (1991) Pheophorbide as Efficient Sensitizer for DNA Photocleavage. An Implication to its Role in Photodynamic Cancer Therapy. *Chem. Lett.* 2123–2126.

(7) Ito, Y. (1991) Photochemical Cleavage of 1,2-Diphenylethane-1,2-diol by Water-Soluble Fe^{III}(tmpyp). *J. Chem. Soc., Chem. Commun.* 622–624.

(8) Ito, Y., Kunimoto, K., Miyachi, S., and Kako, T. (1991) Photocatalytic Cleavage of 1,2-Diols by a Cofacially Hindered Water-Soluble Iron(III) Porphyrin. *Tetrahedron Lett. 32*, 4007–4010.

(9) Ito, Y., Matsuoka, G. Solid-State Air-oxidation of Benzhydryl Ethers Catalyzed by Silica Gel-Supported Iron(III) Porphyrins. *Oxid. Commun.*, in press.

(10) Ito, Y. Solid-State Photooxidation of Alkenes and Other Compounds by Silica Gel-Supported Porphyrins. *Oxid. Commun.*, in press.

(11) Ito, Y., and Miyachi, S. (1992) Photochemical Release of Bases from Nucleosides and Their Derivatives by Water-Soluble Iron(III) Porphyrins. *J. Photochem. Photobiol. B: Biol. 13*, 29–37.

(12) Wasielewski, M. R. (1992) Photoinduced Electron Transfer in Supramolecular Systems for Artificial Photosynthesis. *Chem. Rev. 92*, 435–461.

(13) Fleischer, E. B., Palmer, J. M., Srivastava, T. S., and Chatterjee, A. (1971) Thermodynamic and Kinetic Properties of an Iron-Porphyrin System. *J. Am. Chem. Soc. 93*, 3162–3167.

(14) Hildenbrand, K., and Schulte-Frohlinde, D. (1989) E.s.r. Studies on the Mechanism of Hydroxy Radical-Induced Strand Breakage of Polyuridylic Acid. *Int. J. Radiat. Biol. 55*, 725–738.

(15) Ivanca, M. A., Lappin, A. G., and Scheidt, W. R. (1991) Water-Soluble Ferric Porphyrinates: Solution and Solid-State Species. *Inorg. Chem. 30*, 711–718, and references cited therein.

(16) Balch, A. L., LaMar, G. N., Latos-Grazynski, L., Renner, M. W., and Thanabal, V. (1985) Nuclear Magnetic Resonance Studies of Axial Amine Coordination in Synthetic Ferryl, $(Fe^{IV}O)^{2+}$, Porphyrin complexes and in Ferryl Myoglobin. *J. Am. Chem. Soc. 107*, 3003–3007, and their previous papers of this series.

(17) Faraggi, M., Carmichael, A., and Riesz, P. (1984) OH Radical Formation by Photolysis of Aqueous Porphyrin Solution. A Spin Trapping and e.s.r. Study. *Int. J. Radiat. Biol. 46*, 703–713.

(18) Maldotti, A., Bartocci, C., Amadelli, R., Polo, E., Battioni, P., and Mansuy, D. (1991) Oxidation of Alkanes by Dioxygen

Catalyzed by Photoactivated Iron Porphyrins. *J. Chem. Soc., Chem. Commun.*, 1487–1489.
(19) Johnson, G. R. A., and Nazhat, N. B. (1987) Kinetics and Mechanism of the Reaction of the Bis(1,10-phenanthroline)-copper(I) ion with Hydrogen Peroxide in Aqueous Solution. *J. Am. Chem. Soc. 109*, 1990–1994.
(20) Sigman, D. S. (1986) Nuclease Activity of 1,10-Phenanthroline-Copper Ion. *Acc. Chem. Res. 19*, 180–186.
(21) Stubbe, J., and Kozarich, J. W. (1987) Mechanisms of Bleomycin-Induced DNA Degradation. *Chem. Rev. 87*, 1107–1136.
(22) Meunier, B. (1986) Metalloporphyrin-Catalyzed Oxygenation of Hydrocarbons. *Bull. Soc. Chim. Fr.* 578–594.
(23) Suslick, K. S., and Watson, R. A. (1991) Photochemical Reduction of Nitrate and Nitrite by Manganese and Iron Porphyrins. *Inorg. Chem. 30*, 912–919.
(24) Mizutani, Y., Hashimoto, S., Tatsuno, Y., and Kitagawa, T. (1990) Resonance Raman Pursuit of the Change from Fe^{II}-O_2 to Fe^{III}-OH via Fe^{IV}=O in the Autoxidation of Ferrous Iron-Porphyrin. *J. Am. Chem. Soc. 112*, 6809–6814.
(25) Schulte-Frohlinde, D., Simic, M. G., and Görner, H. (1990) Laser-Induced Strand Break Formation in DNA and Polynucleotides. *Photochem. Photobiol. 52*, 1137–1151.
(26) Ingold, K. U. (1973) Rate Constants for Free Radical Reactions in Solution. *Free Radicals* (J. K. Kochi, Ed.) Vol. 1, pp 37–112, Wiley, New York.
(27) Rabani, J., and Matheson, M. S. (1966) The Pulse Radiolysis of Aqueous Solutions of Potassium Ferrocyanide. *J. Phys. Chem. 70*, 761–769.
(28) Scholes, M. L., Schuchmann, M. N., and von Sonntag, C. (1992) Enhancement of Radiation-Induced Base Release from Nucleosides in Alkaline Solution: Essential Role of the $O^{\bullet-}$ Radical. *Int. J. Radiat. Biol. 61*, 443–449.
(29) Fujita, S. (1984) Radiolysis of Nucleosides in Aqueous Solutions: Base Liberation by the Base Attack Mechanism. *Int. J. Radiat. Biol. 45*, 371–377.

Peroxidase-Linked Anti-Basic Fibroblast Growth Factor Monoclonal Antibody Fab' Conjugates: Application for Two-Site Enzyme Immunoassay and Immunohistochemical Detection

Masayuki Kurobe,[†,‡] Yoshifumi Takei,[†] Takashi Fukatsu,[§] Akemi Kato,[†] and Kyozo Hayashi*[,†]

Department of Molecular Biology, Gifu Pharmaceutical University, Gifu 502, Japan, Department of Clinical Biochemistry, Gifu College of Medical Technology, Seki, Gifu 501-32, Japan, and Gifu Prefecture Tajimi Hospital, Tajimi, Gifu 507, Japan. Received June 30, 1992

After conjugating thiol groups in the hinge region of monoclonal antibody (mAb) Fab' fragments specific for basic fibroblast growth factor (bFGF) with maleimido-horseradish peroxidase HRP) complexes synthesized by incubation of HRP with the heterobifunctional reagent *N*-succinimidyl-4-(maleimidomethyl)cyclohexane-1-carboxylate, we developed a fluorometric enzyme immunoassay method based on the sandwiching of the factor between anti-bFGF IgG-coated polystyrene beads and the conjugates, and also an immunohistochemical method for detection of the location of the factor. The discriminatory detection limit by the developed enzyme immunoassay (EIA) was as low as 30 pg/mL. The reproducibility of within- and between-assay series was 6.07–9.18% and 6.28–6.82%, respectively, and the recovery of exogenous bFGF from serum was approximately 98%. The curves generated by the concentrated fraction that eluted at the same position as standard bFGF by size-exclusion chromatography on a TSK 2000SW column were parallel to the curve for standard bFGF. From these results, we consider the developed EIA method to be acceptable in regard to sensitivity, precision, and specificity. Also, without the introduction of any additional signal amplification system, positive immunohistochemical reactions were successfully detected by the HRP-linked anti-bFGF mAb Fab' in fibroblastic and endothelial cells, which have already been shown to synthesize and secrete bFGF, indicating that these conjugates provide a useful means for direct immunohistochemical detection of the factor.

INTRODUCTION

Basic fibroblast growth factor (bFGF), which is a single chain protein composed of 146 amino acid residues (*1*), is identified in a variety of normal and malignant tissues (*2*) and characterized as an exclusive mesodermal and neuroectodermal cell mitogen (*3, 4*). The biological functions of bFGF are mediated by a specific cell-surface receptor, a 130-kDa polypeptide with an extracellular domain that binds bFGF and an intracellular domain that contains intrinsic tyrosine-kinase activity (*5–7*), pointing to an extracellular mechanism of action of bFGF. However, all forms of its primary translational products lack of hydrophobic signal sequence (*8, 9*), which would direct their secretion through the classical secretory pathway. Recently, the oncogenic character of FGF has been pointed out in view of its highly conserved homology with the FGF family, which includes *int*-2 (*10, 11*), *hst*-1 (*12*), and a oncogene obtained from Kaposi's sarcoma (*13*). Two cDNAs encoding the human FGF receptor were isolated and found to be closely related to the oncogene *bek* (*14–16*). In mammalian cells, the expression of bFGF cDNA results in the transformation of the host cells (*17*, 18).

Despite many investigations, the precise molecular mechanism by which bFGF is exported out of the cell and the pathophysiological mechanism including the tumorigenesis elicited by it remain unexplained. Knowledge of the exact distribution of bFGF and its alterations in the bFGF-producing cells may aid in further understanding of the yet poorly defined role of this factor. In order to study these unique biochemical and pathophysiological features of bFGF, it is necessary to develop a sensitive and specific assay and immunohistochemical methods for detection of the factor. In this paper we describe the preparation of HRP-linked anti-bFGF monoclonal antibody (mAb) Fab' conjugate and its efficiency for development of a monoclonal antibody-based two-site enzyme immunoassay method and also for immunohistochemical detection of the factor. The developed enzyme immunoassay (EIA) method for bFGF was deemed acceptable in regard to sensitivity, precision, and specificity. Without any amplification step, the positive reactions were successfully detected by the conjugates in fibroblastic and endothelial cells in unfixed and frozen sections of thyroid gland (histologically normal).

EXPERIMENTAL PROCEDURES

Materials. Bovine serum albumin (Fr. V) was purchased from Armour Pharmaeutical Co. (Kankakee, IL); pepsin (EC 3.4.23.1), from Calibiochem-Behring Co. (San Diego, CA); peroxidase (HRP, EC 1.11.1.7), from Sigma Chemical Co. (St. Louis, MO). Sephadex G-25, and G-100 were obtained from Pharmacia Fine Laboratories (Uppsala, Sweden). An Affigel Protein A MAPS kit was purchased from Bio-Rad Laboratories (Richmond, CA). *N*-Succinimidyl 4-(maleimidomethyl)cyclohexane-1-carboxylate (SMCC) was bought from Pierce Chemical Co. (Rockford, IL); 3-(*p*-hydroxyphenyl)propionic acid (HPPA), from Sigma Chemical Co. (St. Louis, MO). All other chemicals were from Wako Pure Chemical Ind. Ltd. (Osaka, Japan).

Polystyrene beads (3.2 mm in diameter) were obtained from Wako Pure Chemical Ind., Ltd. (Osaka, Japan).

* Correspondence and reprint requests should be addressed to Kyozo Hayashi, Ph.D., Gifu Pharmaceutical University, Department of Molecular Biology, Mitahora-higashi, Gifu 502, Japan. Phone: 0582-(37)-3931, Ext. 318. Telefax: 0582-(37)-5844.

† Gifu Pharmaceutical University.

‡ Gifu College of Medicinal Technology.

§ Gifu Prefecture Tajimi Hospital.

1043-1802/93/2904-0134$04.00/0 © 1993 American Chemical Society

bFGF and mAbs against bFGF. Two monoclonal antibodies (mAbs 12 and 98) (*19*) and recombinant human bFGF (*20*) used for the standard were generously provided by the Takeda Chemical Ind., Ltd. Immunological properties of the mAbs such as specificity were characterized in detail by Seno et al. (*19*).

Preparation of HRP-Linked Anti-bFGF mAb Fab' Conjugates. The procedures for synthesis of HRP-linked anti-bFGF mAb Fab' conjugates were similar to those described earlier (*21*). Briefly, the IgG fraction of mAb 98 (subclass of IgG_1) against bFGF was purified from mouse ascites by affinity chromatography with an Affigel Protein A MAPS kit according to the manual published by Bio-Rad Laboratories, Co. From the purified IgG thus obtained, we prepared the Fab' fragments by digestion of the IgG fraction with pepsin following reduction with 2-mercaptoethylamine. On the other hand, HRP was treated with SMCC to introduce maleimido groups, and the maleimido–HRP thus obtained was allowed to react with thiol groups in the hinge region of the Fab' fragments. The HRP-linked anti-bFGF mAb Fab' conjugates were finally purified by gel filtration on an Ultrogel AcA 44 column equilibrated and developed with 0.1 mol/L phosphate buffer, pH 6.5.

The presence of a thiol group was determined by using 4,4'-dithiodipyridine.

Because of batch-to-batch variation, a preliminary test was necessary to assess the optimal magnitude of dilution of the stock conjugate solution in the assay.

Preparation of Anti-bFGF mAb IgG-Coated Polystyrene Beads. The method for coating polystyrene beads was similar to that described earlier (*21*). One hundred beads were immersed in a solution of the affinity-purified mAb 12 (subclass IgG_1; 200 μg/mL) in 20 mL of 50 mmol/L Tris-HCl buffer, pH 8.5, overnight at 4 °C. The coated beads were stored in buffer A (0.1 mol/L phosphate buffer, pH 7.0, containing 0.1% BSA, 0.3 mol/L NaCl, 0.1% NaN_3, and 1 mmol/L $MgCl_2$) at 4 °C until used.

Two-Site Enzyme Immunoassay Method. For all dilutions buffer A was used. The typical assay procedure is as follows: an aliquot of the standard in buffer A or the samples (100 μL) and buffer A (150 μL) were added to each tube containing one mAb IgG-coated bead. After incubation at 4 °C overnight the aqueous solution was aspirated off and the beads were extensively washed with buffer B (0.1 mol/L phosphate buffer, pH 7.0, containing 0.1% BSA). The beads were next incubatd at 4 °C overnight with HRP-linked anti-bFGF mAb Fab' conjugate in 250 μL of buffer B (300-fold dilution of the stock conjugate solution). After extensively washing of the beads with buffer B, they were transferred to clean tubes.

HRP activity fixed on the beads was fluorophotometrically measured by use of HPPA as coupling reagent as described earlier (*21*).

In any assay of samples, a series of standard solution was always assayed together with the samples. Experiments were carried out in duplicate except where noted otherwise.

Blood Samples. Serum and plasma (anticoagulated with heparin) samples collected from normal subjects were generously donated by Ms. K. Tanno of the Gifu Red-Cross Blood Bank.

Immunohistochemical Staining. Unfixed frozen sections of thyroid gland (histologically normal) were stained as a model tissue. Histopathological diagnoses were made by Dr. Tetsuro Nagasaka, a histopathologist at the Department of Laboratory Medicine, Nagoya University School of Medicine (Nagoya, Japan).

Sections of thyroid gland freshly obtained surgically were directly fixed with phosphate-buffered saline (PBS) containing 4% paraformaldehyde for 10 min at room temperature. The specimens were incubated with PBS containing 0.3% hydrogen peroxide for 3–5 h in order to block endogenous peroxidase, and then with PBS containing the HRP-linked anti-bFGF mAb Fab' conjugates overnight at 4 °C. Between each step, the specimens were washed four times with PBS. Peroxidase activity, indicating antigen location, was visualized by incubation of the slides for 10 min with a freshly prepared solution of 0.02% 3,3'-diaminobenzidine (DAB) in PBS containing 0.005% hydrogen peroxide. The specimens were counterstained with Mayer's hematoxylin.

RESULTS AND DISCUSSION

Thiol groups in the hinge region of the mAb Fab' fragments prepared by digestion of the purified IgG with pepsin followed by reduction with 2-mercaptoethylamine were conjugated with the maleimido–HRP complexes by using the Fab' and the modified HRP at a molar ratio of 1:2. The maleimido–HRP complexes were synthesized by incubation of HRP (2 mg, 50 nmol) in 0.1 mol/L phosphate buffer, pH 6.0, containing a molar excess of the heterobifunctional reagent SMCC (1.3 mg, 5 mmol). Under the same conditions as described earlier (*21*), pepsin digestion of the anti-bFGF mAb 98 IgG fraction (subclass IgG_1) was found to have been further hydrolyzed into smaller peptide fragments. To obtain a higher yield of the $F(ab')_2$ fragments, we digested the antibody by 1/50 (w/w) pepsin for 4 h. Under the optimized reaction conditions, recovery after this step was estimated to be 85–90%.

The number of thiol group in the molecule of Fab' prepared was estimated to be 1.09 (range = 1.07–1.12, n = 3). Within 24 h of incubation in 0.1 mol/L phosphate buffer, pH 6.0, containing 5 mmol/L EDTA, the number of thiol groups of Fab' decreased less than 3%. When HRP was allowed to react with SMCC, the average number of maleimido groups introduced per enzyme molecule was 1.67 (range = 1.40–1.93, n = 3). The enzyme activity after the reaction was 98.6% (range = 96.5–101.5, n = 3) of that before the reaction.

At the last step, the HRP-linked Fab' conjugates were purified by gel filtration on an Ultrogel AcA 44 column. Elution profiles of the protein and the enzyme activity (data not shown) indicated that free forms of HRP and Fab' were almost completely separated from the conjugates, since HRP and Fab' were not polymerized during the conjugation reaction. Fractions eluted at higher molecular weight region containing both immune and enzyme activities were stored at 4 °C in the presence of 0.1% BSA and 0.0015% merthiolate.

The molar ratio of Fab' to the enzyme in the conjugates obtained was calculated to be 0.92 based on the molar extinction coefficients at 403 and 280 nm of Fab' and the enzyme, respectively. The ratio of absorbance at 403 nm to that at 280 nm for the enzyme used was 3.1 (*22*). And the enzyme activity decreased about 20% upon conjugation with Fab'. We did not systematically examine a change in the binding ability of antibody, e.g. the affinity constant, during the conjugation reaction. Overall yield of the conjugates was approximately 40%.

In order to develop a sensitive and valid EIA for bFGF requiring fewer mAbs, we chose the method of sandwiching

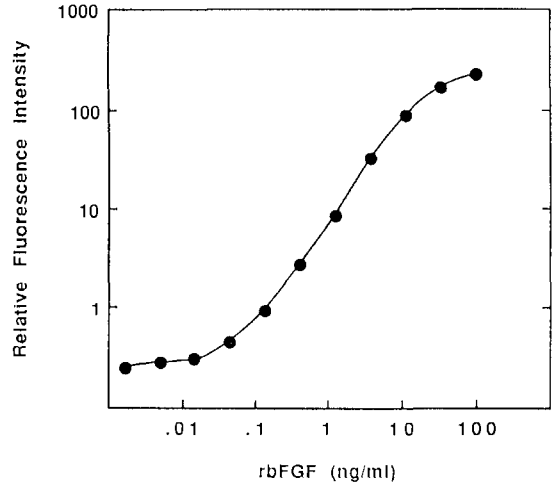


Figure 1. Dose–response curve of recombinant bFGF by sandwich EIA. Fluorescence intensity of specifically bound peroxidase activity was calculated by subtraction of fluorescence intensity obtained in the presence of bFGF from that in its absence (background). Each point indicates the mean of duplicate assays.

Table I. Within- and Between-Assay Variations

assay	bFGF level (pg/mL)	coefficient of variation (%)
	Within-Assay Variations	
serum 1 (n = 10)	110.2 ● 10.12	9.18
serum 2 (n = 10)	127.7 ± 7.75	6.07
	Between-Assay Variations	
serum 1 (n = 5)	110.6 ± 7.54	6.28
serum 2 (n = 5)	133.4 ± 8.38	6.82

the antigen between HRP-labeled Fab' conjugates and mAb IgG-coated polystyrene beads and the use of HPPA as a coupling reagent, to detect HRP activity.

To assess its sensitivity and validity as a two-site monoclonal antibody-based enzyme immunoassay system, we initially prepared a calibration curve with recombinant bFGF in buffer A used as a standard. Typical procedures used for the fluorometrical two-site enzyme immunoassay were the same as those described earlier (*21*). When 100-μL aliquots of various concentrations of recombinant bFGF as a standard were assayed, the dose–response curve (Figure 1) was obtained. When the fluorescence intensity of 1 μg/mL quinine in 50 mmol/L H_2SO_4 was adjusted to a scale of 100, relative fluorescence intensity obtained in the complete absence of bFGF (background) was measured to be 14.51 ± 0.20 (mean ± SD, n = 10). As shown in Figure 1, the linearity of the curve was observed in between 30 pg/mL and 10 ng/mL. Thus the sensitivity is great enough to measure the concentration of bFGF in human body fluids such as serum and urine.

In proportion to the length of the incubation time, the fluorescence intensity increased. An incubation at 4 °C overnight was sufficient to obtain constant formation of each immune complex. The anti-bFGF antibody IgG-coated beads stored in buffer A at 4 °C for at least 3 months gave almost the same calibration curve, and also the HRP-linked anti-bFGF mAb Fab' conjugates stored at 4 °C for the same time gave the same results, demonstrating that the beads and the conjugates can be stored safely for at least that period of time.

Reproducibility of the developed EIA was tested by use of clinically available normal sera. As shown in Table I, the coefficients of variation of within- and between-assay series were 6.07–9.18% (n = 10) and 6.28–6.82% (n = 5), respectively.

Table II. Recovery of Exogenous bFGF from Serum[a]

	endogenous bFGF (pg/mL)	exogenous bFGF added (pg)	increase in bFGF over endogenous (pg)	% recovery
serum 1	152.3	100	105.5	105.5
serum 2	195.0	100	91.2	91.2
serum 3	210.5	100	89.9	89.9
serum 4	160.5	100	108.8	108.8
serum 5	180.3	100	93.5	93.5

[a] Assay conditions are as follows: a 900-μL volume of serum from normal subjects and a 100-μL volume of the standard bFGF (1000 pg/mL) in buffer A were mixed and incubated at 4 °C overnight. A 100-μL volume of serum or a 100-μL volume of the sample added the standard bFGF was assayed by our EIA system, and each recovery value was calculated.

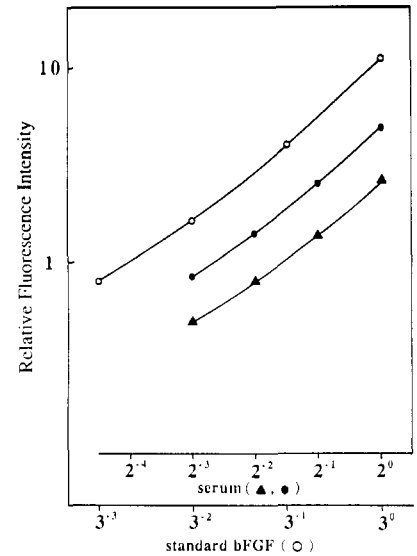


Figure 2. Dilution curve of each fraction of immunoreactive bFGF obtained by HPLC size-exclusion chromatography of human serum on a TSK 2000SW column. Each fraction that eluted at the same positions as standard bFGF was pooled and concentrated. Each concentrated solution (serum 1, bFGF level of 850 pg/mL, ●; or serum 2, bFGF level of 400 pg/mL, ▲) was serially diluted 2-fold with buffer A and a 100-μL volume of each diluent was assayed. The standard bFGF solution in the above buffer (bFGF level of 2000 pg/mL, ○) was diluted 3-fold with the above buffer and a 100-μL volume of each diluent was used for assay.

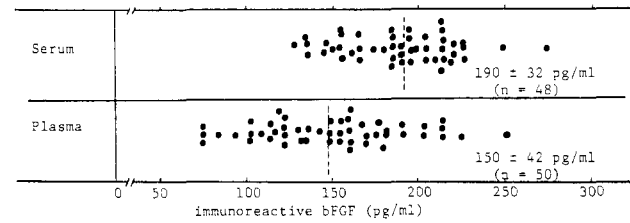


Figure 3. Levels of immunoreactive bFGF in normal serum and plasma. A 100-μL volume of each serum or plasma from normal subjects was assayed. Each point indicates the mean of duplicate assays, and the dotted lines indicate the average level of immunoreactive bFGF of the samples.

Percent "recovery" of exogenously added recombinant bFGF from sera containing different levels of endogenous immunoreactive bFGF was measured. As shown in Table II, recoveries of exogenous bFGF from serum were 89.9–108.8% (mean ± SD = 97.8 ± 8.7%, n = 5), suggesting that there appears to be no interfering substances in serum. In order to examine the immunochemical properties of bFGF in serum, we generated a dilution curve of the pooled and concentrated fraction that coeluted with the standard bFGF by HPLC size-exclusion chromatography on a TSK

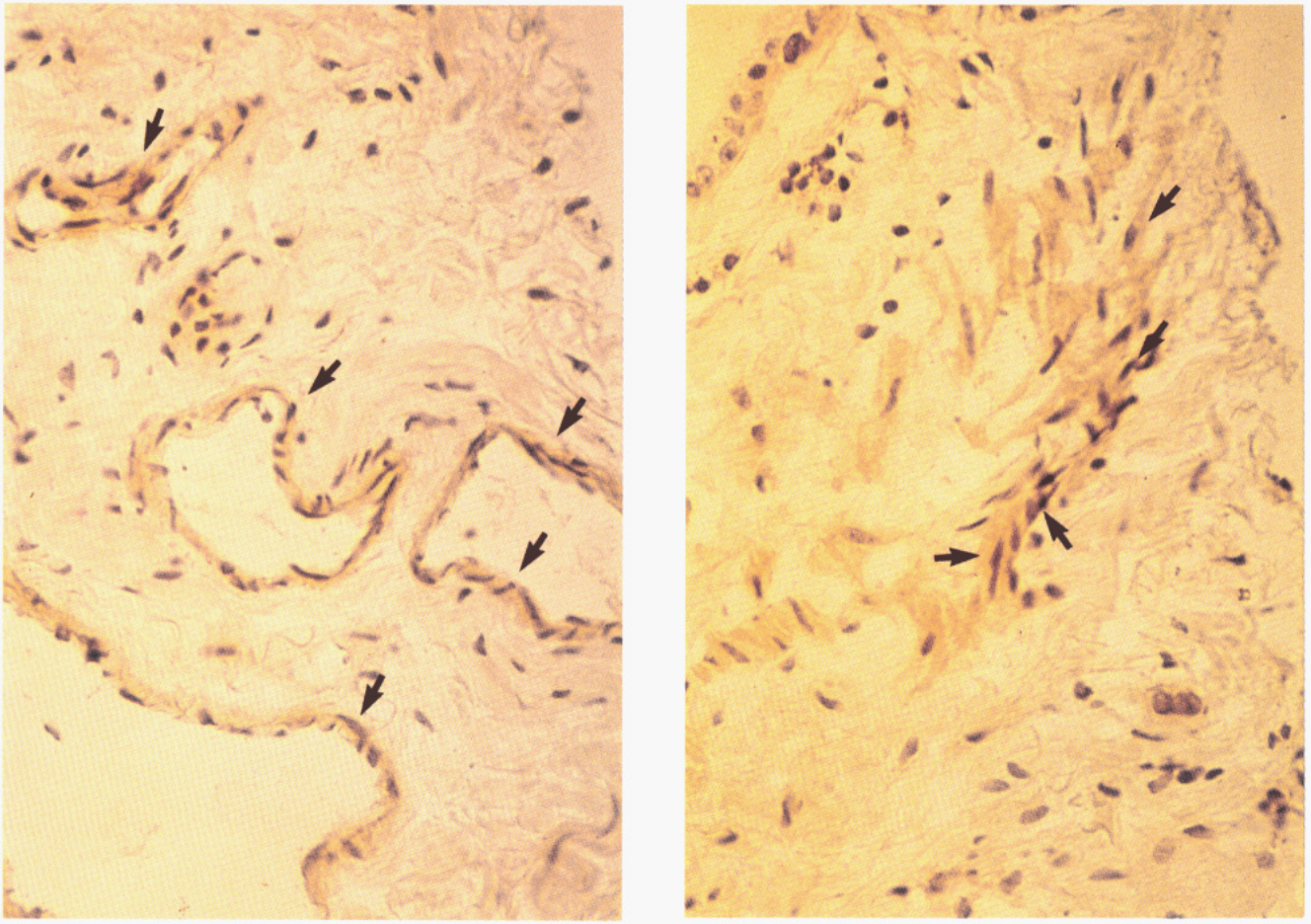


Figure 4. Immunohistochemical staining of normal region of ectomized thyroid gland. Unfixed specimens of normal thyroid tissue showing scattered bFGF-positive reactions that appear diffusely in the cytoplasm of capillary endothelial cells (arrows in A, left) and of fibroblast cells (arrows in B, right) × 100.

2000 SW column. As shown in Figure 2, the slope of the curves were parallel to the slope of the curve for standard bFGF in buffer A, indicating that the antigenicity is similar. From these results, we consider the developed EIA to be acceptable in regard to linearity, sensitivity, recovery from the serum, and precision.

Next, we applied this EIA method for the estimation of bFGF levels in serum and plasma of normal subjects. The results are seen Figure 3. As shown in Figure 3, the level of immunoreactive bFGF in normal serum was 190 ± 32 pg/mL (mean ± SD, $n = 48$), which agrees with the range of 30–206 pg/mL reported by Watanabe et al. (*23*). We further measured the immunoreactive bFGF level in normal plasma (anticoagulated with heparin) and found it to be 150 ± 42 pg/mL ($n = 50$), not significantly different from the serum value.

Structurally, there existed an amino terminal truncated form of bFGF. The sites in the bFGF molecule recognized by the mAb 12 used for coating the beads was located within the sequence of the first nine amino acids of the N-terminal region (*19*). Thus, our EIA would not detect any N-terminal truncated form(s) of bFGF that might retain biological activity.

Conventionally, methods for immunohistochemical detection of antigens employing monoclonal antibodies include an additional signal amplification step such as the peroxidase–antiperoxidase (PAP) or avidin–biotin complex (ABC) system. As a model, we examined an application of the HRP conjugates for immunohistochemical detection of the antigen in the sections of normal organs and tissues. As shown in Figure 4, a diffuse positive reaction was observed in the cytoplasm of capillary endothelial cells and of fibroblastic cells located in normal parts of unfixed frozen sections of thyroid gland surgically obtained. The reaction product varied in density even on the same slide. These results are clearly in support of the numerous reports on production and secretion of bFGF by endothelial cells (24–27). Neutralization of the conjugates with an excess molar amount of recombinant bFGF resulted in a disappearance of the positive reactions (data not shown). From these results, it is apparent that HRP-linked mAb Fab' conjugates specific for bFGF could detect the antigen in sections of tissues and organs without introduction of any additional signal amplification system.

Studies on the distribution and levels of biologically active substances found in only minute amounts in tissues require sensitive, quantitative, and specific analytic methods. The earliest method to detect bFGF was based on its biological activity, i.e., enhanced uptake of ^{3}H-labeled thymidine (*28*), and the radioreceptor assay (RRA) method (*29*). The RRA method, however, has various inherent disadvantages such as less specificity and sensitivity, less stability of radioactive materials, and requirement of comparatively expensive equipment. And the biological method is not specific and sensitive enough to measure endogenous bFGF in various tissues and body fluids including serum. Recently, Watanabe et al. (*23*) established an EIA method for bFGF, the principle of which is based on sandwiching of the factor between a mixture of two mAb IgGs fixed on the surface of wells of a multiwell

plate and HRP-linked mAb conjugates, and found an increased level of bFGF in sera of patients with renal cell carcinoma.

The discriminatory detection limit of bFGF, being as low as 30 pg/mL, is thought to be adequate for measurement of the concentration of endogenous bFGF in human body fluids such as serum, plasma, and urine. Sixteen out of 20 patients with benign mammary gland carcinoma showed generally a higher level of immunoreactive bFGF in their serum (range = 125–1080 pg/mL) than that found in the normal subjects (Figure 3).

Although it appears that bFGF may act exclusively as an autocrine or paracrine factor functioning as an angiogenic and mitogenic factor (*4*), details of the mechanism of these actions remain to be elucidated. Our immunoassay system for bFGF using the HRP-linked anti-bFGF Fab' conjugates described here provides a useful means for detection of bFGF in various fluids, and the conjugates can also be used directly for immunohistochemical detection of the factor.

ACKNOWLEDGMENT

The authors wish to thank the Takeda Chemical Ind. Ltd., for generously providing ascites fluids containing each mAb. We also would like to thank Ms. K. Tanno of the Gifu Red-Cross Blood Bank, for providing sera and plasma of normal subjects, and Dr. T. Nagasaka of the Department of Laboratory Medicine, Nagoya University School of Medicine (Nagoya), for generously donating specimens of thyroid gland.

LITERATURE CITED

(1) Esch, F., Baird, A., Ling, N., Ueno, N., Hill, F., Denoroy, L., Klepper, R., Gospodarowicz, D., Bohlen, P., and Guillmin, P. (1985) Primary structure of bovine pituitary basic fibroblast growth factor (FGF) and comparison with the amino terminal sequence of bovine brain acidic FGF. *Proc. Natl. Acad. Sci. U.S.A. 83*, 6507–6511.

(2) Gospodarowicz, D., Ferrara, N., Schweigerer, L., and Neufeld, G. (1987) Structural characterization and biological functions of fibroblast growth factor. *Endocr. Rev. 8*, 95–114.

(3) Burgess, W. H., and Maciag, T. (1989) The heparin-binding (fibroblast) growth factor family of proteins. *Ann. Rev. Biochem. 58*, 575–606.

(4) Gospodarowicz, D., Neufeld, G., and Schweigerer, L. (1986) Molecular and biological characterization of fibroblast growth factor, and angiogenic factor which also controls the proliferation and differentiation of mesoderm and neuroectoderm derived cells. *Cell Differ. 19*, 1–17.

(5) Lee, P. L., Johnson, D. E., Cousens, L. S., Fried, V. A., and Williams, L. T. (1989) Purification and complementary DNA cloning of a receptor for basic fibroblast growth factor. *Science 245*, 57–60.

(6) Mansukhani, A., Moscatelli, D., Talarico, D., Levytska, V., and Basilico, C. (1990) A murine fibroblast growth factor (FGF) receptor expressed in CHO cells is activated by basic FGF and Kaposi FGF. *Proc. Natl. Acad. Sci. U.S.A. 87*, 4378–4382.

(7) Keegan, K., Johnson D. E., Williams, L. T., and Hyman, M. (1991) Isolation of an additional number of the fibroblast growth factor receptor family, FGFR-3. *Proc. Natl. Acad. Sci. U.S.A. 88*, 1095–1099.

(8) Jaye, M., Howk, R., Burgess, W., Ricca, G. A., Chiu, I. M., Ravera, M. W., O'Brien, S. J., Modi, W. E., Maciag, T., and Drohan, W. N. (1986) Human endothelial cell growth factor. *Science 233*, 541–545.

(9) Schweigerer, L., Neufeld, G., Friedmann, J., Abraham, J. A., Fiddes, J. C., and Gospodarowicz, D. (1987) Capillary endothelial cells express basic fibroblast growth factor, a mitogen that promotes their own growth. *Nature 325*, 257–259.

(10) Dickson, C., and Peters, G. (1987) Potential oncogene product related to growth factors. *Nature 326*, 833.

(11) Moore, R., Casey, G., Brookes S., Dixon, M., Peters, G., and Dickson, C. (1986) Sequence, topography and protein coding potential of mouse int-2: A putative oncogene activated by mouse mammary tumor virus. *EMBO J. 5*, 919–924.

(12) Taira, M., Yoshida, T., Miyagawa, K., and Sakamoto, H. (1987) cDNA sequence of human transforming gene *hst* and identification of the coding sequence required for transforming activity. *Proc. Natl. Acad. Sci. U.S.A. 84*, 2980–2984.

(13) Delli Bovi, P., Curatola, A. M., Kern, F. G., Greco, A., Ittman, M., and Basillico, C. (1987) An oncogene isolated by transfection of Kaposi's sarcoma DNA encodes a growth factor that is a member of the FGF family. *Cell 50*, 729–737.

(14) Dionne, C. A., Crumley, G., Bellot, F., Kaplow, J. M., Searfoss, G., Ruta, M., Burgess, W. H., Jaye, M., and Schlessinger, J. (1990) Cloning and expression of two distinct high-affinity receptors cross-reacting with acidic and basic fibroblast growth factors. *EMBO J. 9*, 2685–2693.

(15) Kornbluth, S., Paulson, K. E., and Hanafusa, H. (1988) Novel tyrosine kinase identified by phosphotyrosine antibody screening of cDNA libraries. *Mol. Cell Biol. 8*, 5541–5544.

(16) Seno, M., Sasada, R., Watanabe, T., Ishimura, K., and Igarashi, K. (1991) Two cDNAs encoding novel human FGF receptor. *Biochem. Biophys. Acta 1089*, 244–246.

(17) Rogelj, S., Weiberg, R. A., Fanning, P., and Klagsbrun, M. (1988) Basic fibroblast growth factor fused to a signal peptide transform cells. *Nature 33*, 173–175.

(18) Sasada, R., Kurokawa, K., Iwane, M., and Igarashi, K. (1988) Transformation of mouse BALB/c3T3 cells with human basic fibroblast growth factor cDNA. *Mol. Cell Biol. 8*, 588–594.

(19) Seno, M., Iwane, M., Sasada, R., Moriya, N., Kurokawa, T., and Igarashi, K. (1989) Monoclonal antibodies against basic fibroblast growth factor. *Hybridoma 8*, 209–221.

(20) Iwane, M., Kurokawa, T., Sasada, R., Seno, M., Nakagawa, S., and Igarashi, K. (1987) Expression of cDNA encoding human fibroblast growth factor in E. coli. *Biochem. Biophys. Res. Commun. 146*, 470–477.

(21) Kurobe, M., Kono, M., Yoshida, M., and Hayashi, K. (1988) A sensitive two-site enzyme immunoassay for human pancreatic secretory trypsin inhibitor (PSTI) using monoclonal antibodies. *Clin. Chim. Acta 178*, 205–214.

(22) Yoshitake, S., Imagawa, M., and Ishikawa, E. (1982) Efficient preparation of rabbit Fab'-horseradish peroxidase conjugates using maleimide compounds and its use for enzyme immunoassay. *Anal. Lett. 15*, 147–160.

(23) Watanabe, H., Hori, A., Seno, M., Kozai, Y., Igarashi, K., Ichimori, Y., and Kondo, K. (1991) A sensitive enzyme immunoassay for human basic fibroblast growth factor. *Biochem. Biophys. Res. Commun. 175*, 229–235.

(24) Shing, Y., Folkman, J., Sullivan, R., Butterfield, C., Murray, J., and Klangsbrun, M. (1984) Heparin affinity: purification of a tumor-derived capillary endothelial cell growth factor. *Science 223*, 1296–1299.

(25) Gospodarowicz, D., Morgan, M., Braun, D, and Birdwell, C. R. (1976) Clonal growth of bovine vascular endothelial cells: fibroblast growth factor as a survival agent. *Proc. Natl. Acad. Sci. U.S.A. 73*, 4120–4124.

(26) Klagsbrun, M., and Shing, Y. (1985) Heparin affinity of anionic and cationic capillary endothelial cell growth factors: analysis of hypothalamus-derived growth factors and fibroblast growth factors. *Proc. Natl. Acad. Sci. U.S.A. 82*, 805–809.

(27) Klagsbrun, M., Sasse, J., Sullivan, R., and Smith J. A (1986) Human tumor cells synthesize an endothelial cell growth factor that is structurally related to basic fibroblast growth factor. *Proc. Natl. Acad. Sci. U.S.A. 83*, 2448–2452.

(28) Gospodarowicz, D. (1975) Purification of a fibroblast growth factor from bovine pituitary. *J. Biol. Chem. 250*, 2515–2520.

(29) Baird, A., Florkiewicz, R. Z., Maher, P. A., Kaner, R. J., and Hajjar, D. P. (1990) Mediation of virion penetration into vascular cells by association of basic fibroblast growth factor with herpes simplex virus type 1. *Nature 348*, 344–346.

Synthesis, in Vitro Kinetics, and in Vivo Studies on Protein Conjugates of AZT: Evaluation as a Transport System To Increase Brain Delivery

B. Mitra Tadayoni,† Phillip M. Friden, Lee R. Walus, and Gary F. Musso*

Alkermes Inc., 64 Sidney Street, Cambridge, Massachusetts 02139. Received September 28, 1992

One method to increase the delivery of polar drugs to the central nervous system is via drug–protein conjugates with proteins that interact with and cross brain capillary endothelial cells. As a model for drugs containing a reactive hydroxyl group, AZT was conjugated via a succinate linker to two such protein carriers, the highly cationic histone H1 and an anti-transferrin receptor antibody, OX-26. The protein carriers were selected on the basis of their ability to interact with brain capillary endothelial cells by absorptive or receptor-mediated events, respectively. An in vitro pH profile of the rate of AZT release indicated that the observed hydrolysis proceeds by a specific base-catalysis mechanism. At 37 °C, the release of AZT proceeded at a rate approximately 10-fold faster ($K_{obs} \sim 8 \times 10^{-4}$ min^{-1}) than expected for a simple ester (AZT succinate; $K_{obs} \sim 1.25 \times 10^{-4}$ min^{-1}). Using simple model systems, product analysis revealed that intramolecular cyclization of the succinate linker accounts for the observed rate enhancement. Drug delivery in vivo was assessed using immunohistochemical techniques and quantitative brain uptake measurements with singly and doubly labeled AZT–OX-26 conjugates. Immunohistochemical staining of brain sections showed the colocalization of AZT and OX-26 in the brain vasculature. Therefore, drug can be linked to the antibody without affecting the targeting property of the antibody. Furthermore, an in vivo time course using radiolabeled conjugate showed that AZT is delivered to the brain capillaries but is not transported into the brain parenchyma with the antibody. These results demonstrate that drugs conjugated via a succinate linker to the anti-transferrin receptor antibody OX-26 could provide a useful method of selective drug delivery to brain capillary endothelial cells.

INTRODUCTION

The delivery of polar drugs to the brain does not generally occur in sufficient levels to achieve a therapeutic benefit due to the presence of a restrictive membrane barrier isolating the brain from the remainder of the body. The anatomical basis for this barrier is the endothelial cell layer which separates the bloodstream from the cellular environment of the brain (*2*). Because of this blood–brain barrier (BBB), most drugs do not gain access to the brain unless they can utilize a specific transport mechanism or the drug has been sufficiently modified to enhance its lipophilic properties. An alternative method to increase brain delivery of drugs is to tether the drug to a macromolecular carrier via a specific linkage strategy (*3*). In this scenario, the specific targeting property of the carrier is used to selectively ferry the drug to the brain.

In our laboratory, we have shown that, upon intravenous administration in rats, the anti-transferrin receptor antibody OX-26 binds brain capillary endothelial cells and crosses the BBB in a time-dependent receptor-mediated fashion. Approximately 0.5–1% of the total injected dose of OX-26 was delivered to the brain parenchyma via bolus intravenous administration (*6*). As it had been reported that cationized proteins display enhanced transport across the BBB via absorptive-mediated transcytosis (*1*, *7*), we chose to explore this phenomenon with an endogenously cationic protein, histone H1. Histone H1 has 25% lysine residues which allowed for high drug loading while maintaining its native cationic character.

Our interests were to explore the feasibility of increasing the delivery of 3′-azido-3′-deoxythymidine (AZT) to the brain as a model for other therapeutic drugs containing hydroxyl groups and to explore the properties of these conjugates for drug release in vitro and in vivo. For this, we developed conjugation strategies with histone and OX-26 as drug carriers. It has been assumed that AZT traverses the cell membrane by a nonfacilitated diffusion mechanism (*8*), although systemically administered AZT does not penetrate the BBB in high levels (*9*, *10*). For conjugation, a succinate linkage was initially selected with the thought that release of AZT could be facilitated through the action of esterases either in the capillary endothelial cells (*11*) or in the brain parenchyma. AZT was succinylated by treatment with succinic anhydride. Activation of the carbonyl group of 5′-AZT succinate with *N*-hydroxysuccinimide allowed the facile preparation of drug conjugates. We then explored in vitro and in vivo properties of these conjugates. Here we detail our findings concerning the kinetics and mechanism of the release pathway of the succinate-linked drug. In addition, we describe our findings on the effectiveness of AZT delivery in an in vivo model system.

EXPERIMENTAL PROCEDURES

Material and Methods. AZT, succinic anhydride, dicyclohexylcarbodiimide (DCC), and *N*-hydroxysuccinimide were obtained from Aldrich. [^{14}C]AZT (50 mCi/mmol) was purchased from Sigma. Nuclear magnetic resonance spectra were recorded with a Bruker AC-250 spectrometer. Infrared spectra were performed with a thin film on NaCl plates using a Mattson Sirius 100 FT-IR spectrometer. UV spectra were obtained with a Beckman DU-65 spectrophotometer. High-performance liquid chromatography (HPLC) were performed on Hewlett-Packard 1090M system equipped with a diode-array detector and temperature-controlled autosampler. Elemental analyses were performed by Galbraith Laboratories (Knoxville, TN). The monoclonal antibody OX-26 was purified by protein A-agarose chromatography (*12*).

* Address correspondence to this author at Alkermes, Inc., 64 Sidney St., Cambridge, MA 02139.

† Current address: ImmunoGen, Inc., 148 Sidney St., Cambridge, MA 02139.

1043-1802/93/2904-0139$04.00/0 © 1993 American Chemical Society

The eluted material was analyzed by sodium dodecyl sulfate–polyacrylamide gel electrophoresis (SDS–PAGE) and enzyme-linked immunoabsorbent assay (ELISA). Histone H1 (bovine, lysine-rich) was purchased from U.S. Biochem and checked by SDS–PAGE. Protein concentrations were determined by the method of Lowry (*13*). Both H1 histone and OX-26 yielded standard curves comparable to bovine serum albumin by this method. All other chemicals and solvents used in this study were reagent or HPLC grade.

AZT Succinate, 2. To a solution of 267 mg (1.00 mmol) of AZT (1), 31 mg (0.25 mmol) of 4-(dimethylamino)-pyridine (DMAP), and 100 mg of Na_2SO_4 in 10 mL of freshly distilled pyridine was added 120 mg (1.2 mmol) of succinic anhydride. The resulting slurry was stirred under argon at room temperature for 3 h. The reaction mixture was then filtered and the filtrate was concentrated in vacuo to give a yellow oil. The oil was diluted with H_2O (45 mL) and applied to a DEAE-Sephedex A-50 column (2.5 × 7.5 cm) using linear gradient of H_2O (500 mL) and 0.20 M triethylammonium bicarbonate (500 mL). The major band (AZT succinate) was eluted with 0.1 M triethylammonium bicarbonate. The eluate was concentrated and collected on a Sep-pack C_{18} cartridge. After washing with water, the AZT succinate was eluted with 80:20 CH_3CN/0.1% aqueous trifluoroacetic acid. The title compound was obtained in 80% yield as a flaky powder: mp = 35 °C; ^{1}H NMR ($CDCl_3$) δ 1.91 (3 H, s), 2.41 (t, 2 H, J = 4 Hz), 2.5–2.7 (m, 4 H), 4.15 (q, 1 H), 4.35–4.80 (m, 3 H), 5.98 (t, 1 H, J = 9 Hz), 7.47 (s, 1 H); IR 3184–2930 (br), 1734–1635, 1472, 1272, 1162, 1099 cm^{-1}.

NHS Ester of AZT Succinate, 3. A solution of 180 mg (0.48 mmol) of AZT succinate **2** and 56.0 mg (0.48 mmol) of *N*-hydroxysuccinimide in 8 mL of freshly distilled tetrahydrofuran (THF) was cooled to 4 °C. To this solution was added 100 mg (0.48 mmol) of dicyclohexylcarbodiimide and the mixture stirred at 4 °C for 2 h. The reaction mixture was concentrated in vacuo to yield a white solid. Purification by flash chromatography (1.25 cm × 15 cm silica gel, eluted with 70:20:10 ethyl acetate/hexanes/methanol) followed by recrystallization from CH_2Cl_2/hexanes yielded the title compound: ^{1}H NMR (CD_3OD) δ 1.93 (s, 3 H), 2.43 (t, 2 H, J = 6.0 Hz), 3.05 (t, 2 H, J = 6 Hz), 4.10 (m, 1 H), 4.4 (m, 3 H), 6.08 (t, 2 H, J = 6.6 Hz), 7.20 (s, 1 H); IR 3328–2851, 1734, 1646, 1558, 1456, 1271, 1205, 1096 cm^{-1}.

AZT–histone H1. To a precooled solution (4 °C) of AZT–NHS ester **3** (0.23 mg, 500.0 nmol) in 100 μL of dioxane was added 0.375 mg (25.0 nmol) histone H1, which was dissolved in 1 mL of 0.1 M of *N*-(2-hydroxyethyl)-*N*-(2-ethanesulfonic acid) sodium salt buffer (HEPES), pH 7.5, and the mixture-stirred at 4 °C for 2 h. The protein conjugate was isolated from the crude reaction mixture by chromatography on Sephadex G-25 (Pharmacia PD-10), equilibrated, and eluted with phosphate/saline buffer, pH 7.4 at room temperature. Fractions of 1.0 mL were collected and analyzed at 266 nm for the AZT. The desired protein conjugate was collected in fractions 4 and 5 whereas free drug was observed in fractions 10 and 11. The conjugates were adjusted to pH 5.0 with acetic acid and stored at −20 °C until use. Each conjugate was further characterized by its mobility on SDS–PAGE minigels (12% acrylamide). The conjugates migrated as a broad band slightly higher than the native protein standard.

AZT–OX-26. For the preparation of AZT conjugates to the antibody OX-26, buffer and reaction conditions similar to those employed for the histone conjugation were used. The amount of the activated AZT derivative was adjusted so as to prepare conjugates of lower drug to protein ratios, as it was found that high drug loading on lysine residues of this antibody (>12:1) altered its ability to recognize antigen (data not shown). Thus, a maximum of 10 equiv of AZT actived ester **3** was added to the antibody solution for preparation of these conjugates. Conjugates were purified and characterized in a manner analogous to that used for the histone conjugates except that SDS–PAGE electrophoresis was conducted using 8% acrylamide gels. The conjugate solutions were adjusted to pH 5.0 with acetic acid and stored at −20 °C until use.

[3-[(Phenethylamino)carbonyl]-1-oxopropoxy]-AZT, 4. A solution of 116 mg (0.25 mmol) of NHS ester in 5 mL of freshly distilled THF was cooled to 4 °C. To this solution was added 30.0 μL (0.25 mmol) of phenethylamine and the mixture stirred overnight under Ar. The solvent was removed in vacuo to yield a white solid. Purification by flash chromatography (1.25 cm × 15 cm silica gel, eluted with 50:50 ethyl acetate/hexanes) gave the title compound in 60% yield: mp = 105 °C; ^{1}H NMR ($CDCl_3$) δ 1.93 (s, 3 H), 2.46–2.73 (m, 6 H), 2.80 (t, 2 H, J = 7.0 Hz), 3.46 (q, 2 H, J_1 = 5 Hz, J_2 = 7.3 Hz), 4.00 (m, 1 H), 4.20–4.50 (m, 3 H), 5.71 (t, 1 H, J = 5.2 Hz), 6.16 (t, 1 H, J = 6.3 Hz), 7.17–7.34 (m, 5 H), 9.2 (s, 1 H); IR 3322–2929, 1688 (br), 1545, 1468, 1437, 1363, 1271, 1161, 1049 cm^{-1}; HRMS calcd for $C_{22}H_{26}O_6N_6$, (M^+) 470.1914, found 470.1884.

***N*-Phenethylsuccinimide 6.** A sample of 100 mg (1.00 mmol) of succinic anhydride was dissolved in 5 mL of freshly distilled pyridine. To this mixture was added 126 μL of phenethylamine and the mixture was refluxed for 5 h. The resulting yellow solution was concentrated in vacuo to give a yellow oil. The yellow oil was diluted with 10 mL of methylene chloride, washed with 1 N HCl, and dried over $MgSO_4$. Evaporation of the solvent under reduced pressure gave succinic acid *N*-phenethylamide **5**, which was then dissolved in acetic anhydride and heated to reflux in the presence of DMAP. The solvent was removed in vacuo and the gummy residue was dissolved in saturated $NaHCO_3$, extracted with CH_2Cl_2, washed with 1 N HCl, and dried over $MgSO_4$. Concentration of the yellow solution yielded a yellow oil which was purified by flash chromatography (1.25 cm × 15 cm silica gel, eluted with 50:50 ethyl acetate/hexanes) to give the title compound as a white solid in 80% yield: mp = 133 °C; ^{1}H NMR ($CDCl_3$) δ 2.65 (s, 4 H), 2.88 (t, 2 H, J = 7.5 Hz), 3.75 (t, 3 H, J = 7.6 Hz), 7.19–7.33 (m, 5 H). IR 2973–2919, 1684, 1410, 1311, 1216, 1093, 991, 927, 793 cm^{-1}. Anal Calcd for $C_{12}H_{13}NO_2$: C, 70.90; H, 6.40; N, 6.70. Found: C, 70.67; H, 6.46, N, 6.91. HRMS calcd for $C_{12}H_{13}NO_2$ 203.0970, found 203.0939.

[^{14}C]AZT–[^{3}H]OX-26. [^{14}C]AZT succinate NHS ester was synthesized using the methods described for **3**, starting with [^{14}C]AZT (specific act. = 50 mCi/mmol). TLC analysis of the final NHS derivative of AZT succinate indicated that the final product contained ~20% unreacted AZT succinate. As AZT succinate was unreactive in the conjugation procedure, the above material was used without further purification to prepare radiolabeled AZT–OX-26 conjugates. Following the conjugation and purification, the specific activity of the conjugate was determined to be 78 mCi/mmol, which corresponds to a 1.6:1 drug to protein ratio. In order to obtain a dual-labeled sample, [^{14}C]AZT–OX-26, was tritiated using *N*-succinimidyl propionate (*13*) (100 Ci/mmol) to generate [^{14}C]-AZT–[^{3}H]OX-26 with the final specific activity of 800 mCi/mmol with respect to ^{3}H and 78 mCi/mmol with respect to ^{14}C.

Kinetic Studies. The in vitro release of AZT from the protein conjugates was assessed using an HPLC-based assay. Separations were achieved using a Vydac C_{18} column (catalog no. 218TP54) by applying a linear acetonitrile gradient (0% to 40% over 40 min) in 0.1% trifluoroacetic acid. The conjugates were incubated at 37 °C with various buffers spanning the pH range of 1.1–9.7. Kinetic time courses were developed by time programmed injection/analysis of the conjugate incubations. For the model compounds, the disappearance of the starting material ($-dS/dt$) as well as the appearance of the product (dP/dt) could be monitored. For the protein conjugates, only the appearance of the product could be accurately measured. Area integration of the AZT eluate (dP/dt) was converted to AZT concentration using the calculated linear regression line derived from the data in Figure 1a. A column wash at the end of the HPLC gradient served to elute bound protein and conjugates.

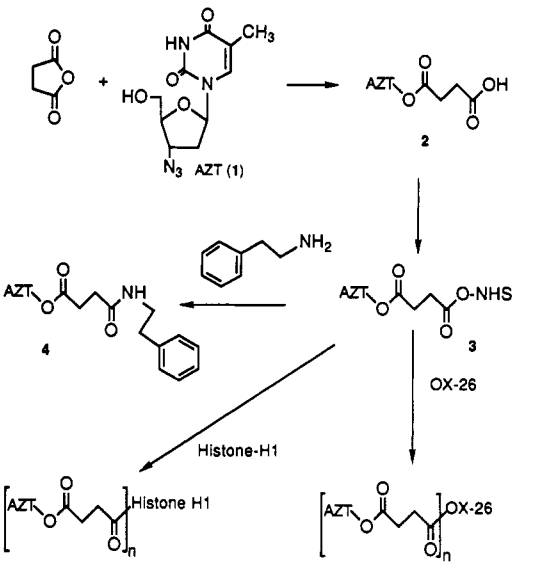
Immunohistochemistry. Immunohistochemical studies were performed essentially as described (*6*). Female Sprague–Dawley rats (125–150 g) were anesthetized with halothane prior to injection of conjugate via the tail vein. At sacrifice, the animals were perfused with either ice-cold phosphate-buffered saline (DPBS), pH 7.4, or 50 mM sodium acetate, pH 5.0, to wash blood from the vasculature. The brains were removed and frozen in liquid nitrogen. Thirty-micron sections were cut on a cryostat and placed on gelatin-coated slides. The slides were fixed in acetone (10 min, 23 °C) and stored at −20 °C. OX-26 was detected immunohistochemically using a biotinylated horse anti-mouse IgG/horseradish peroxidase Vectastain ABC kit from Vector Labs following the manufacturer's protocol. AZT was detected using a rabbit anti-thymidine antisera which cross reacts with AZT (A gift from Dr. D. Stollar, Tufts University) and a biotinylated goat anti-rabbit antisera from Vector Labs. Controls included sections from uninjected animals as well as animals injected with OX-26 alone or AZT alone. Additional controls included the omission of either primary or secondary antibody in the detection on sections from conjugate-injected animals.

Capillary Depletion. The procedure of Triguero et al. (*15*) was followed as described previously (*6*). The entire capillary pellet and aliquots of the unfractionated homogenate and the parenchyma supernatant fraction were solubilized in Soluene 350 (Packard) at room temperature overnight prior to liquid scintillation counting. All data were collected as dpms using a Beckman TD5000 liquid scintillation counter with quench correction. Data are expressed as percent of the injected dose of radioactivity in either the parenchyma or capillary fractions derived per rat brain. The amount of radioactivity in the brain due to blood contamination was subtracted in all cases.

RESULTS AND DISCUSSION

Synthesis of AZT Derivatives. The esterification of the 3′-hydroxyl group of 5′ protected nucleotides with a succinate group is a well-documented reaction most commonly applied as the attachment point of nucleic acids for automated synthesis on a solid support (*18*). As AZT bears only a single hydroxyl group at the 5′ position, the attachment of a succinate group to the 5′ position appeared feasible. It was envisioned that this linkage would be stable for preparation of drug conjugates, yet allow for sensitivity to esterases or nucleases in vivo (*11*). Prior to conjugate synthesis, succinic anhydride in the presence of pyridine was used to acylate the 5′-hydroxyl of AZT, thus forming 5′-AZT succinate, **2**. Succinate **2** was then activated at the carboxyl group using equimolar amounts of *N*-hydroxysuccinimide and dicyclohexylcarbodiimide to form the *N*-hydroxysuccinimido (NHS) ester **3**. The synthesis of the AZT derivatives and conjugates is outlined in Scheme I.

Scheme I



Synthesis of Conjugates. The resulting NHS ester **3** was used to acylate amine groups on the carrier proteins histone H1 and OX-26, at 4 °C. Using highly purified active ester, the acylation of protein amino groups typically occurred in 70–75% yield.

Conjugation Ratio. A combination of several methods was used to determine the drug loading on each carrier. Drug loading on histone H1 was estimated spectrophotometrically (AZT, $\epsilon_{266} = 8000$, Histone, $\epsilon_{266} \sim 3000$). At drug to protein ratios >5:1, the contribution of histone to the total absorbance at 266 nm approached zero. The absorbance of pooled fractions from gel filtration chromatography was therefore measured at 266 nm. Subsequently, the contribution to A_{280} from AZT ($A_{266}/A_{280} = 1.67$) was calculated from the estimated drug loading to yield the net absorbance at 280 nm, which was then used to calculate the histone concentration ($\epsilon_{280} \sim 5200$). Typically, 85–90% of the histone was recovered in the conjugate fraction. Histone concentration in the conjugate pool was also determined by the method of Lowry (*13*) and agreed to within 10% of the value estimated by the above spectrophotometric method. Drug loadings up to 15:1 were achieved by this procedure. Having determined the drug and protein concentration in unknown conjugate samples, a calibration table for AZT concentration versus area percent intergrated at 266 nm was established by HPLC. The integrated area of AZT was linear with respect to AZT concentration in the range of 0.1–4 nmol and is illustrated in Figure 1a ($r = 0.999$).

The drug loading on the OX-26 carrier could not be determined using the spectrophotometric technique described above due to the strong absorbance of OX-26 at 280 nm (OX-26 $\epsilon_{280} = 210\,000$) and lower drug loading levels. Using a combination of HPLC analysis of fully hydrolyzed conjugate (see In Vitro Release Kinetics; 2 h at pH >9.0) and Lowry protein determination, drug and protein concentrations were determined. For OX-26, drug loading ranged from 1:1 to 7:1.

In Vitro Release Kinetics. The detailed HPLC kinetic studies described below were performed on highly drug-loaded AZT–histone conjugates as these conjugates yielded superior signal to noise ratios. Using the calibration table

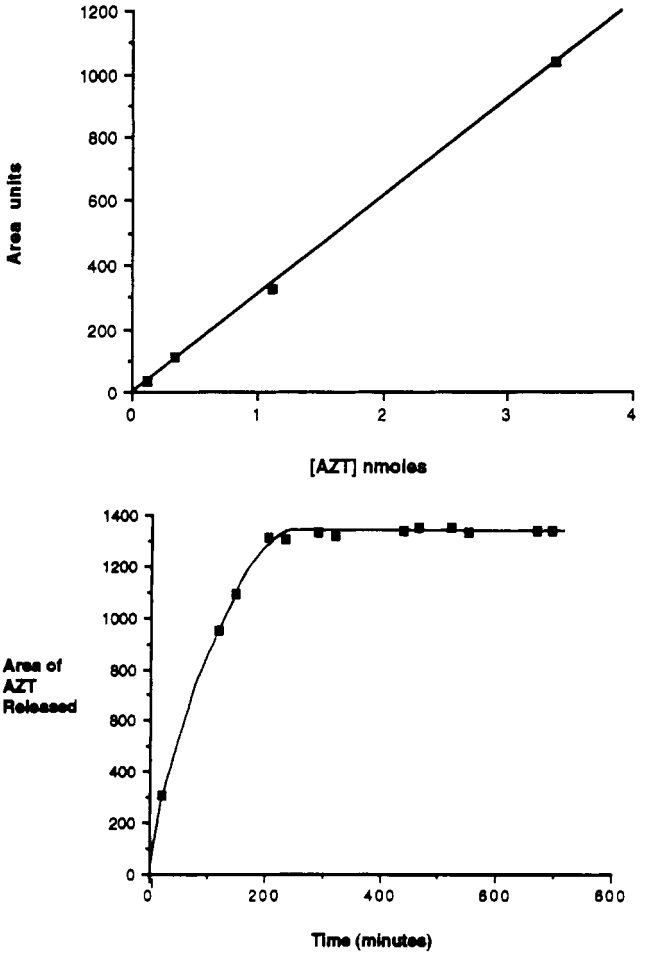


Figure 1. (a) AZT standard curve. A plot of AZT concentration versus area percent integration using HPLC reveals a linear correlation. These data were then used to calculate the concentration of AZT released from the conjugate during the HPLC kinetic analysis of the conjugates. (b) Release of AZT from an AZT–H1 conjugate at pH 8.4 at 37 °C. A plot of integrated area vs time demonstrates that AZT is rapidly released from the conjugate at pH 8.4. Using the standard curve derived in Figure 1a, all of the conjugated AZT appears released by 200 min.

Table I. Chemical Models To Study the Hydrolysis of AZT Conjugates

substrate	buffer	pH	K_{obs} (min^{-1})	$t_{1/2}$ (min)
AZT–histone	HEPES	7.4	7.80×10^{-4}	888
AZT succinate	HEPES	7.4	1.25×10^{-4}	5544
4	HEPES	7.4	10.20×10^{-4}	679

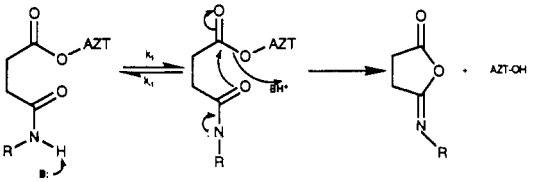
derived for AZT, the kinetic time course of AZT release from a histone conjugate (15 AZT:histone, AZT S_o = 0.190 mM, histone S_o = 0.0125 mM) was first measured at pH 8.4 at 37 °C as shown in Figure 1b. The data show that the release of AZT from the conjugate was rapid at pH 8.4, appeared to be first-order, and leveled off within 2 h. Furthermore, the amount of AZT released from the conjugate correlated to 100% of the amount of AZT spectrophotometrically determined to be on the conjugate, suggesting that the reaction had gone to completion. Next, the release of AZT from the histone conjugate and a model system, AZT succinate, was evaluated at pH 7.4. This data, as shown in Table I, indicated that the rate of AZT release from the conjugate is significantly faster than that of the control, AZT succinate. This observation suggests that the majority of the drug is released from the conjugate via a mechanism other than simple ester hydrolysis.

To understand the mechanistic pathway by which AZT is released from the conjugates, a model system was designed with a simple amine to mimic the ϵ-amino group of protein lysines. Phenethylamine served as good model because it forms an aliphatic amide with active esters and contributes an identifiable UV absorbance (phenyl) to aid in the interpretation of HPLC kinetic analysis. The synthesis of this compound starting from the active ester of AZT succinate is also outlined in Scheme I.

Table II. Kinetics of Hydrolyses of AZT Conjugates

substrate	buffer	pH	$K_{obs} \times 10^5$ (min^{-1})	$t_{1/2}$ (min)
AZT–histone	0.1 N HCl	1.1	6.30	11 000
AZT–histone	citrate	3.1	0.47	147 446
AZT–histone	citrate	4.1	1.30	53 307
AZT–histone	citrate	4.9	1.20	57 720
AZT–histone	MOPS	5.9	3.20	21 656
AZT–OX-26	MOPS	6.5	5.70	12 158
AZT–histone	HEPES	7.4	78.0	888
AZT–OX-26	HEPES	7.5	37.0	1 925
AZT–histone	phosphate	7.7	180.0	385
AZT–histone	HEPES	7.9	330.0	210
AZT–histone	HEPES	8.4	930.0	74
AZT–OX-26	HEPES	8.5	670.0	103
AZT–histone	borate	9.7	13000	5
AZT–histone	50% rat serum		310.0	233

Scheme II



A kinetic study of the this model conjugate, **4**, yielded rates of AZT release comparable to the histone conjugate as documented in Table I. Analysis of the products from this reaction, separated by HPLC, showed that **4** hydrolyzed into two major compounds at equivalent rates. These products were identified as AZT and a phenyl derivative eluting later than the nucleotide or starting material. In order to identify the other reaction product, the two possible derivatives of phenethylamine were synthesized, phenethylamido succinate **5**, and *N*-phenethylsuccinimide **6**. The HPLC elution characteristics of phenethylamine **5** and **6** indicated that the observed major product in the hydrolysis reaction was indeed imide **6**. Diode-array analysis of the reaction product and authentic imide eluted by HPLC confirmed the assignment of this product to the reaction pathway.

Next, the experimental measurement of the complete pH–rate profile was determined using the 15:1 AZT:histone conjugate and the HPLC kinetic assay. After appropriate pH adjustment, the starting concentration of conjugate solutions was measured by UV spectroscopy. Kinetic analysis was also performed on the OX-26–AZT conjugate at pH 6.4, 7.4, and 8.4 and yielded rates comparable to the histone conjugate. The kinetic data from both the histone conjugate and the OX-26 conjugate are summarized in Table II. The pH–rate profile for the histone conjugate is graphically depicted in Figure 2.

The experimental results at pH values surrounding neutrality (6–9) document a 10-fold increase in K_{obs} with each pH unit increase. This trend is characteristic of a specific base catalysis. Generally, the neutral amide is too weakly nucleophilic toward simple esters to effect catalysis. However, intramolecular acyl transfer, involving the anion of an amide group is a common reaction of suitable substituted esters (*16*). The reaction involves specific base catalysis followed by intramolecular nucleophilic attack by equilibrated amide anions as depicted in Scheme II. Under these conditions, the overall first-order

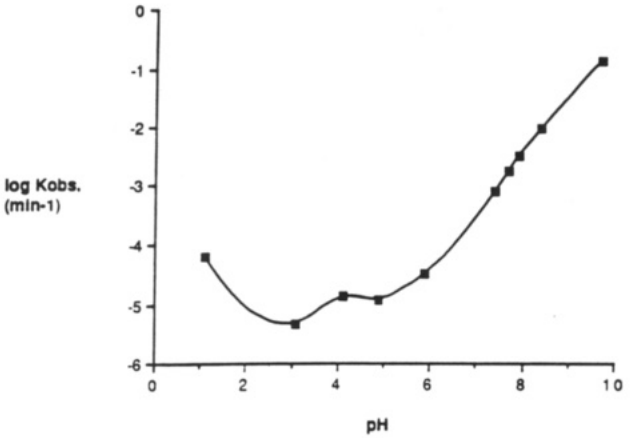


Figure 2. Dependence on pH of the rate of hydrolysis AZT–H1 at 37 °C in aqueous buffer. The profile illustrates the linear relationship between drug release and pH above pH 6.0 which is indicative of a specific base catalysis mechanism. The general shape of the pH profile is reflective of succinate esters.

rate constant, K_{obs}, can be described by eq 1, wherein k_{intra}

$$\text{AZT–H1} \begin{cases} \xrightarrow{\text{intramolecular}} \text{AZT} \\ \xrightarrow{\text{intermolecular}} \text{AZT} \end{cases} \quad (1)$$

$$v = \frac{-\text{d[AZT–H1]}}{dt} = \frac{\text{d[AZT]}}{dt} = k_{inter}[\text{AZT}] + k_{intra}[\text{AZT}]$$

$$K_{obs} = \frac{v}{[\text{AZT}]} = k_{inter} + k_{intra}$$

refers to the intramolecular imide formation and k_{inter} refers to the saponification of the ester in the reaction medium. Further analysis of the HPLC data derived from the hydrolysis of the model compound **6** reveals that $k_{intra} \sim k_{inter} \times 10$ for this reaction. This suggests that the simple ester hydrolysis mechanism accounts for only about 10% of the total reaction pathway. Overall, the kinetic pH profile is reminiscent of that described for the hydrolysis of succinate ester prodrugs (*17*); however, the rates are 10-fold faster. Succinates have been used in a variety of prodrugs, linkers, and supports over the years. Generally, it was thought that this attachment strategy would provide a bond which could be liberated by either an enzymatic process or saponification. The data here suggest that amide esters of succinates liberate the ester portion via an alternative mechanism and under mild conditions. This observation potentially impacts a number of commonly employed chemical reactions that have used this bond. These include solid-phase nucleic acid chemistry where an amide–ester bond on a succinate linker serves to tether the growing oligonucleotide to the controlled pore glass support (*18*) and some commercially available protein cross-linking agents (*19*). Our data not only indicate that the linkage can be cleaved under mild conditions but also indicate that added nucleophiles are unnecessary (*18*). The potential lability of this linkage at neutral pH would warrant a cautionary note about the use of amide esters of succinates in procedures involving extended exposure to neutral or basic aqueous conditions.

Localization of Conjugates in the Brain Vasculature. The anti-rat transferrin receptor antibody OX-26 has been shown to bind to brain capillary endothelial cells and to traverse the blood–brain barrier following iv administration into rats via the tail vein (*4*, *6*). The antibody also can function as a carrier for the delivery of methotrexate to the brain (*5*, *6*). Similar studies with AZT–histone H1 conjugates were unable to detect either component on the brain capillary endothelial cells nor in the brain (*20*). Therefore, the histone conjugates were not studied further in vivo.

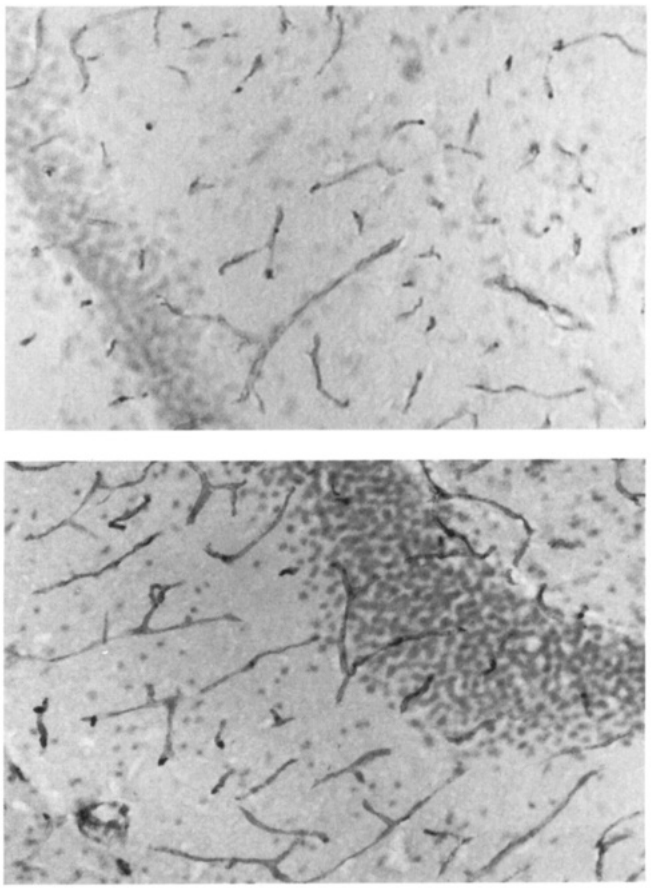


Figure 3. Immunohistochemical detection of an AZT–OX-26 conjugate in brain sections. Horse anti-mouse IgG (a) and rabbit anti-thymidine (b) antisera were used to detect the carrier antibody and the passenger drug, respectively, in the brain vasculature afer iv administration of 0.2 mg of AZT–OX-26 conjugate (×100).

Immunohistochemistry was used to determine if, following conjugation with AZT, OX-26 retained the ability to target and bind to brain capillary endothelial cells in vivo. At 1 h postinjection of the conjugate, both the antibody carrier and the AZT "passenger" were visualized in the brain using either anti-mouse IgG antisera or anti-thymidine antisera, respectively. A staining pattern similar to that reported for OX-26 alone (*6*) was revealed when sections from the conjugate-injected animals were stained for the carrier antibody (Figure 3a). A similar pattern of immunolocalization was obtained when sections were stained with the anti-thymidine antisera (Figure 3b), indicating colocalization of OX-26 and AZT in the brain vasculature. Control experiments indicated that the observed immunostaining was specific for either OX-26 or AZT and that the localization of the drug to the brain vasculature was dependent on the attachment of the drug to the anti-transferrin receptor antibody (data not shown).

Distribution of AZT–OX-26 in Brain Parenchyma and Capillaries. The results of the experiments described above showed qualitatively that the AZT–OX-26 conjugate binds to brain capillary endothelial cells following iv administration. To quantitate the amount of conjugate that reaches the brain as well as assess the vascular and parenchymal distribution, capillary depletion studies were performed using radiolabeled conjugate. This technique

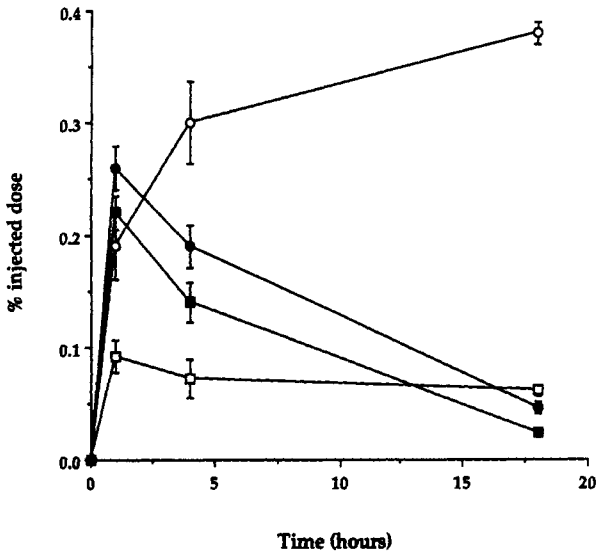


Figure 4. Delivery of AZT to the brain using the OX-26 carrier. Capillary deletion data on the AZT–OX-26 conjugate using double-labeled material. The data are expressed as percentage of the injected dose in the parechyma fraction and capillary pellet as a function of time. The values are means ± SEM (n = 3 rats per time point). Legend: parenchyma fraction, OX-26 (○), AZT (□); capillary pellet, OX-26 (●), AZT (■).

separates the brain into parenchyma and capillary fractions (*6*, *15*). Comparison of the relative amounts of radioactivity in the two fractions as a function of time determines whether the conjugate crosses the BBB. These studies employed a dual-labeled conjugate in which the AZT was ^{14}C-labeled and the antibody carrier was ^{3}H-labeled. This configuration allowed independent measurement of the disposition of both the carrier and the drug within the brain.

Throughout the time course studied (24 h), very similar levels of OX-26 and AZT were seen in the capillary fraction of the brain. These capillary levels decreased over time, suggesting that the drug and antibody were not being retained by the capillary endothelial cells (Figure 4). As the levels of OX-26 in the capillary fraction decreased, the levels in the parenchyma fraction increased, indicating that the antibody was migrating from the capillaries to the parenchyma in a time-dependent manner. In contrast, the levels of AZT in the brain parenchyma did not rise significantly, suggesting that the majority of the drug was released in the endothelial cells and was not transported across the BBB. Alternatively, the AZT could have been released to the parenchyma, but was rapidly cleared into the cerebrospinal fluid. On the basis of our findings in the in vitro studies, intramolecular hydrolysis of AZT from the conjugate ($t_{1/2}$ < 4 h, 50% rat serum) could be responsible for the time-dependent loss of AZT seen in these studies.

SUMMARY

The results presented here demonstrate first that AZT can be conjugated to protein carriers to serve as delivery agents using a succinate linkage. Second, that a prominent intramolecular pathway exists for release of ester-linked compound based on the kinetic and mechanistic studies of these conjugates. Third, that drugs linked to macromolecular carriers via a succinate linkage can be used to target compounds to a specific location, such as the brain capillaries with OX-26, with the added advantage of a relatively fast release of drug. We are currently employing this strategy to prepare antibody carrier–drug conjugates with other drugs offering greater therapeutic potential.

ACKNOWLEDGMENT

We would like to thank Dr. John Kozarich and Prof. Julius Rebek, Jr. for helpful discussions. We would also like to thank Fariba Tehrani and Joseph Eckman for their technical support. The gift of anti-thymidine and anti-histone antisera from Dr. David Stollar, Dept. of Biochemistry, Tufts University, is greatly appreciated. We thank Dr. Ruth Starzyk, Alkermes, Inc., for her data on the in vivo properties of histones.

LITERATURE CITED

(1) Kumagai, A. K., Eisenberg, J., and Pardridge, W. M. (1987) Absorptive Mediated Endocytosis of Cationized Albumin and a β-Endorphin-Cationized Albumin Chimeric Peptide by Isolated Brain Capillaries: Model System of Blood–Brain Barrier Transport. *J. Biol. Chem. 262*, 15214–15219.

(2) Goldstein, G. W., and Betz, A. L. (1986) The Blood-Brain Barrier. *Sci. Am. 255*, 70–79.

(3) Rodwell, J. D., Ed. (1988) *Antibody-Mediated Delivery Systems*, Marcel Dekker, Inc., New York, NY.

(4) Jefferies, W. A., Brandon, M. R., Hunt, S. V. Williams, A. F., Gatter, K. C., and Mason, D. Y. (1984) *Nature 312*, 162–163.

(5) Musso, G., Abelleira, S. M., and Morrow, A. R. Manuscript in preparation.

(6) Friden, P. M., Walus, L., Musso, G., Taylor, M., Malfroy, B., and Starzyk, R. (1991) Anti-Transferrin Receptor Antibody and Antibody-Drug Conjugates Cross the Blood-Brain Barrier. *Proc. Natl. Acad. Sci. U.S.A. 88*, 4771–4775.

(7) Pardridge, W. M., Triguero, D., and Buciak, J. (1989) Transport of Histone Through the Blood–Brain Barrier. *J. Pharmacol. Exp. Ther. 251*, 821–826.

(8) Zimmerman, T. P., Mahony, W. B., and Prus, K. L. (1987) 3′-Azido-3′-deoxythymidine, an Unusual Nucleoside Analogue that Permeates the Membrane of Human Erythrocytes and Lymphocytes by Nonfascilitated Difussion. *J. Biol. Chem. 262*, 5748–5754.

(9) Klecker, R. W., Jr., Collins, J. M., Thomas, R., Jenkins, J. F., Broder, S., and Myers, C. E. (1987) Plasma and Cerebrospinal Fluid Pharmacokinetics of 3′-Azido-3′-Deoxythymidine: A Novel Pyrimidine Analogue with Potential Application for the Treatment of Patients with AIDS and Related Diseases. *Clin. Pharmacol. Ther. 41*, 407–412.

(10) Terasaki, T., Pardridge, W. M. (1988) Restricted Transport of 3′-Azido-3′-Deoxythymidine and Dideoxynucleosides Through the Blood–Brain Barrier. *J. Infect. Dis. 158*, 630–632.

(11) Lidinsky, W. A., and Drewes, L. R. (1983) Characterization of the Blood–Brain-Barrier Protein Composition of the Capillary Endothelial Cell Membrane. *J. Neurochem. 41*, 1341–1345.

(12) Ey, P. L., Prowse, S. J., Jenkin, J. R. (1978) Isolation of Pure IgG_1, IgG_{2a}, and IgG_{2b} Immunoglobulins from Mouse Serum Using Protein A-Sepharose. *Immunochem. 15*, 429–436.

(13) Lowry, O. H., Rosebrough, N. J., Farr, A. L., and Randall, R. J. (1951) Protein Measurement with the Folin Phenol Reagent. *J. Biol. Chem. 193*, 265–275.

(14) Kummer, U. (1986) Tritium Radiolabeling of Antibodies to High Specific Activity with N-Succinimidyl (2,3-^{3}H)-propionate: Use in Detecting and Analyzing Monoclonal Antibodies. *Methods Enzymol. 121*, 670–678.

(15) Triguero, D., Buciak, J., and Pardridge, W. M. (1990) Capillary Depletion Method for quantification of Blood-Brain Barrier Transport of Circulating Peptides and Plasma Proteins. *J. Neurochem. 89–275*, 1–7.

(16) Bernhard, S. A., Berger, A., Carter, J. H., Katchalski, M., Sela, M., and Shalitin, Y. (1961) Co-operative Effects of Functional Groups in Peptides. I. Aspartyl-Serine Derivatives. *J. Am. Chem. Soc. 84*, 2421–2434.

(17) Anderson, B. D., Conradi, R. A., and Lambert, W. J. (1984) Carboxyl Group Catalysis of Acyl Transfer Reactions in Corticosteroid 17- and 21-Moonoesters. *J. Pharm. Sci. 73*, 604–611.
(18) Matteucci, M. D., and Caruthers, M. H. (1980) The Synthesis of Oligodeoxypyrimidines on a Polymer Support *Tetrahedron Lett. 21*, 719–722.
(19) Abdella, R. M., Smith, P. K., and Royer, G. P. (1979) *Biochem. Biophys. Res. Commun. 87*, 734–742.
(20) Ruth Starzyk, personal communication.

Ricin A-Chain Cytotoxicity Depends on Its Presentation to the Cell Membrane

P. Carayon,*,† A. Bord,† J. P. Gaillard,† H. Vidal,† P. Gros,† and F. K. Jansen‡

Sanofi Recherche, Centre de Montpellier, Montpellier, France. Received September 29, 1992

Anti-ricin-A-chain monoclonal antibodies (mAbs) were raised in order to study epitopes of the A-chain involved in the initiation of its transmembrane passage. Five nonoverlapping epitopes were selected by cluster formation using a cross-inhibition assay of mAbs from 172 specific hybridomas. For each cluster, representative high affinity mAbs were selected. These mAbs were disulfide-linked to $F(ab')_2$ fragments of a mAb directed against the CD5 antigen. The cytotoxicity of ricin A-chain bound by affinity through different epitopes to these hybrid mAbs was explored on the CD5-positive CEM cells. Without any enhancer, the hybrids displayed cytotoxicity varying in IC_{50} within a range of 1–10; in the presence of the enhancer NH_4Cl, this variation of activity was maintained ranging from 1 to 20; with the enhancer monensin, the variation of cytotoxicity of hybrids extended over a 1–80-fold range. These differences of cytotoxicity were not correlated with mAb properties such as the inhibition of A-chain enzymatic activity, the A-chain binding affinity, the capacity for releasing A-chain at low pH, or the capacity of hybrids for delivering A-chain on the cell surface. This lack of correlation strongly suggests that the different presentations of A-chain epitopes to the cell membrane may be the essential reason for cytotoxicity variations.

INTRODUCTION

The enzymatically active subunit of the potent polypeptide toxin ricin, its A-chain, is often used for the assembly of immunotoxins (ITs) by conjugating it to monoclonal antibodies (mAbs) or other specific ligands. ITs have become promising new drugs in cancer therapy, since they are able to induce partial remissions in B-lymphoma patients (*1*). Although part of their biological mechanism is already known in detail, i.e. their binding to cells, their endocytosis and intracellular pathway, and, at the end stage, their enzymatic activity on ribosomes (*2–4*), the passage of the toxic moiety, the A-chain, into the cytosol, in order to reach the final substrate, the ribosomes, is far from being fully understood.

In native ricin, A- and B-chain are associated together with an affinity of 5.6×10^6 M^{-1} (*5*). This association is probably due to hydrophobic interactions at the A-chain/B-chain interface as revealed by the crystallographic data (*6–8*). The role of the disulfide bond between the two subunits may be to maintain the linkage between A-chain and B-chain at low concentration of ricin. Studies about the interaction of A-chain or whole ricin with artificial membranes or vesicles (*9–12*) showed that only free A-chain was able to interact with lipid bilayers at neutral pH. These data suggest that the presentation of ricin A-chain to the membrane of target cells may be of considerable importance for its translocation.

We have already reported cytotoxicity variations between ITs in which mAb was attached to A-chain using linkages involving different amino acids of the toxin (*13*). In order to know if these variations were linked to the A-chain epitopes initiating the transmembrane passage, special hybrid molecules were constructed, in which A-chain was presented to cell membrane in different ways. Anti-A-chain mAbs directed against five different A-chain epitopes were chemically linked to ST1 mAb recognizing the CD5 antigen on human lymphocytes or leukemic cell lines.

The cytotoxicity of these hybrids varied to a considerable extent, especially in the presence of the enhancer monensin, although the ranking of cytotoxic potency was similar and independent of the enhancer used.

EXPERIMENTAL PROCEDURES

Reagents and Chemicals. Ricin-A-chain was purified from ricin (extracted from seeds of *Ricinus communis sanguineus*) as previously described (*14*). Anti-ricin A-chain serum was obtained from a rabbit immunized with ricin A-chain mixed with Freund's complete adjuvant. Rabbit anti-A-chain mAbs were purified by precipitation with ammonium sulfate. Anti-ricin A-chain immunoglobulins were modified with fluorescein isothiocyanate (FITC) (Molecular Probes), by reacting 1 mg of Abs with 100 μg of FITC in 1 mL of borate buffer, pH 8.5, for 2 h at room temperature and then dialyzing.

Anti-CD5 ST1 mAb (F111.98; IgG1 isotype) was prepared as described (*15*). Whole IgG mAb was digested with pepsin to produce divalent $F(ab')_2$ molecules (*16*). These mAb fragments were purified by gel filtration. Analysis of $F(ab')_2$ fragments by SDS–PAGE revealed less than 0.5% contamination by Fc fragments, whereas whole antibody traces were undetectable.

Classical IT was prepared by using the heterobifunctional *N*-succinimidyl 3-(2-pyridyldithio)propionate (SPDP) reagent according to a method previously described (*14*). An average value of 2 A-chain molecules linked per mAb fragment was obtained.

Ammonium chloride was purchased from Merck. Monensin, HEPES, and MES were obtained from Calbiochem Behring.

Cells. The human leukemic T-cell line CEM has been frequently cloned to ensure a homogeneous cell population. It expresses $3 \cdot 10^4$ determinants of CD5 antigen per cell (*17*). Cells were cultured at 37 °C in a 5% CO_2 atmosphere

* Author to whom correspondence should be addressed: P. Carayon, Sanofi Recherche, 371, rue du Professeur Joseph-Blayac, 34084 Montpellier Cedex 04, France. Telephone: 67.40.01.33 (Ext. 3634). Fax: 67.75.63.21.

† Sanofi Recherche.

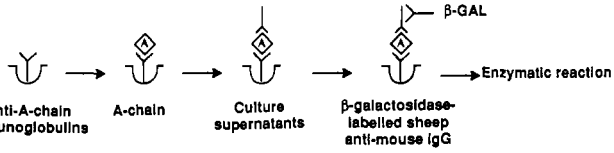
‡ Present address: Laboratoire Immunociblage, ORSTOM, Montpellier, France

1043-1802/93/2904-0146$04.00/0 © 1993 American Chemical Society

in RPMI 1640 medium (Flow Laboratories) supplemented with 10% heat-inactivated fetal calf serum and antibiotics (0.1 mg/mL streptomycin and 100 UI/mL penicillin).

Isolation of Monoclonal Antibodies. Anti-A-chain mAbs were prepared in our laboratory. BIOZZI mice were injected with A-chain following a protocol eliciting high frequency hybridoma production (*18*). A-chain was injected intraperitoneally without Freund's complete adjuvant at the doses of 50 μg/mouse at days -15 and -8 before cell fusion. At days -3, -2, and -1, the mice received 2.5 μg of A-chain by both intraperitoneal and intravenous routes. Spleen cells (10^8) were fused with X-653 myeloma cells ($2 \cdot 10^7$) using 40% (w/v) polyethylene glycol 4000 (Merck). After fusion, the cells were seeded in 96-well tissue culture plates and cultured in HAT medium (54 μg/mL hypoxanthine, 0.7 μg/mL aminopterin, and 15.6 μg/mL thymidine from SERVA).

Specific hybridomas were selected using an immunoenzymatic assay:



Rabbit anti-A-chain immunoglobulins were adsorbed on microtiter plates overnight at 4 °C (200 μL at 30 μg/mL). Following three washes in PBS, wells were incubated with 200 μL of 1% bovine serum albumin for 30 min. They were washed three times with PBS, and 200 μL of 200 ng/mL A-chain was added for 1 h at room temperature. After two washes, hybridoma culture supernatants (100 μL) were incubated for another hour. Following two washes, 100 μL of β-galactosidase-labeled sheep anti-mouse IgG $F(ab')_2$ at the dilution of 1/250 (Amersham) was added for 1 h. After the washes, 200 μL of 0.2 mg/mL 4-methylumbelliferyl β-D-galactopyranoside (Sigma) was used as substrate. Following addition of 100 μL of 100 mM glycine–NaOH buffer, pH 10.3, the fluorescence intensity of the reaction was measured using a Fluoroscan device (Flow Laboratories).

Cells secreting the desired mAbs were cultured in 24-well tissue culture plates. Cells were frozen and culture supernatants were used for the competitive inhibition assay.

Selected hybridomas were thawed and cloned by the limiting dilution method using macrophages as feeder cells. Cloned hybridoma cells were injected ($2 \cdot 10^6$) into the peritoneum of irradiated BALB/c mice that had been injected intraperitoneally with 0.5 mL of pristane two weeks previously. After 10–12 days, ascite fluids containing mAbs were obtained from the mice. Monoclonal antibodies were purified on protein A-Sepharose (Pharmacia). The resulting preparations were more than 95% pure by PAGE–SDS. All the final selected hybridomas used for this study secreted immunoglobulins of IgG1 isotype.

Competitive Inhibition Assay. One milligram of anti-A-chain purified mAbs was biotinylated with 20 μg of biotin *N*-hydroxysuccinimide ester (Calbiochem) during 15 min in 1 mL of borate buffer, pH 8.5. After dialysis, binding was determined by the immunoenzymatic method described above. Biotinylated mAbs were detected using 100 μL of streptavidin–β-galactosidase conjugate at a 1/4000 dilution (Amersham). In order to cluster mAbs recognizing close epitopes of ricin A-chain, 100 μL of the 172 hybridoma culture supernatants were mixed with each biotinylated mAb for binding inhibition evaluation.

Apparent Dissociation Constants (K_D) of the mAbs. K_D values of mAbs were determined by studying their binding at different concentrations on A-chain linked by affinity on polyclonal anti-A-chain immunoglobulins coated on microtiter plates. The binding of mAbs was tested using the immunoenzymatic assay described above. For each selected mAb, maximal binding was determined at a concentration of 10 μg/mL. The values of binding obtained at this concentration were taken as 100% binding. Saturation curves were established using a range of concentrations from 0.78 to 100 ng/mL in triplicate. Analysis of saturation data utilizing the iterative curve-fitting program BINDING (Millet and Caumel, Sanofi Recherche) allowed the determination of mAb concentrations giving 50% binding. These concentrations correspond to $1/K_D$.

Release of Ricin A-Chain in Acidic Media. Selected anti-A-chain mAbs were absorbed overnight at 4 °C on microtiter plates (200 μL at 50 μg/mL). Following washings in PBS, 100 μL of A-chain was introduced at 1 μg/mL for 1 h at room temperature. After washing in PBS, 200 μL of RPMI buffered with 30 mM HEPES and adjusted at pH 7.5, or buffered with 30 mM MES and adjusted at pH 6.5 or 4.5 with HCl, was added for 1 h. After washing, the remaining A-chain was determined with β-galactosidase-conjugated rabbit anti-A-chain immunoglobulins incubated for 1 h in neutral pH medium, using the immunoenzymatic assay already described.

Binding of Anti-A-Chain mAbs on Whole Ricin. Binding of mAbs on whole ricin was tested using the immunoenzymatic assay used for the screening of hybridoma culture supernatants. Ricin was introduced at a molar concentration of 3.3×10^{-9} M corresponding to the molar concentration of free A-chain tested in parallel.

Inhibition of Anti-A-Chain mAb Binding by N- and C-Terminal Peptides. N- or C-terminal peptides (10 amino acid residues) of ricin A-chain (Neosystem Laboratories) were preincubated at 10 mg/mL with mAbs (0.2 μg/mL) under 200 μL for 1 h at room temperature. The mixture was then introduced into wells of microtiter plates containing A-chain linked by affinity to coated rabbit anti-A-chain immunoglobulins. Binding of preincubated mAbs was evaluated in comparison with mAbs preincubated without added peptides, using the immunoenzymatic assay already described.

Hybrid AntibodiesFormation. Thiol groups were introduced into purified anti-A-chain mAbs by reacting 19.1 mg of *S*-acetyl mercaptosuccinic anhydride (Aldrich) with 5 mg of anti-A-chain mAb in 1 mL of KH_2PO_4 buffer (125 mM, pH 7.5) for 10 min at room temperature. In parallel, activated disulfide groups were introduced into the anti-CD5 $F(ab')_2$ fragment by reacting 0.1 μg of SPDP (Pharmacia) with 5 mg of anti-CD5 fragment in 1 mL of KH_2PO_4 buffer (125 mM, pH 7.5) for 10 min at room temperature. After dialysis of the different products, hybrids were prepared by mixing equimolar amounts of each of the modified mAbs in the presence of 50 mM hydroxylamine overnigh at pH 7. The elimination of unconjugated mAbs was carried out on a Sephacryl S200HR column (Pharmacia). Following the selection of the fractions corresponding to the molecular weight of hybrid molecules, the antibody concentrations were determined by optical density with $\epsilon = 1.4$ mg^{-1} mL cm^{-1}.

Binding Activity of Hybrid Molecules. Fifty microliters of PBS containing 10^6 cells was incubated with 50 μL of 10 μg/mL hybrid molecule at 4 °C for 1 h, washed twice, resuspended for 1 h in 100 μL of various concentrations of A-chain (10^{-10}–10^{-7} M), washed again twice,

Table I. Properties of the Selected mAbs

	cluster 1: 13G6	cluster 2: 1B5	cluster 3: 3C2	cluster 4: 14E2	cluster 5: 1D7	cluster 5: 4E9
			A. Inhibition of A-Chain Enzymatic Activity[a]			
	96.6	78.2	45.0	11.8	23.4	59.5
			B. K_D[b] ($\times 10^{-11}$)			
	4.2	7.1	11.0	5.8	5.8	6.7
			C. pH-Dependent Binding[c]			
pH 6.5/pH 7.5	0.99	0.84	0.99	0.98	0.96	0.93
pH 4.5/pH 7.5	0.78	0.52	0.99	0.99	0.83	0.70
			D. Binding Ratio[d]			
ricin/A-chain	0.98	0.97	0.97	0.20	0.15	0.13
			E. % Inhibition by Peptides[e]			
C-terminal	0	30.2	0	0	0	0
N-terminal	0	0	0	0	0	0

[a] Inhibition of the enzymatic activity of ricin A-chain was obtained by incubating the anti-A-chain mAbs with the A-chain before testing its enzymatic activity in a cell-free protein synthesis assay using rat liver fractions. The results are the percentage of inhibition calculated using the A-chain preincubated with a nonrelevant anti-trinitrophenyl mAb as a control. [b] The apparent dissociation constants K_D were determined by incubating the selected mAbs at various concentrations with ricin A-chain coated onto the wells of microtiter plates through rabbit anti-A-chain immunoglobulins. The concentrations giving 50% binding were used to determine K_D values. [c] The dissociation of the A-chain/mAb complex into free A-chain + free mAb was evaluated at pH 6.5 and 4.5. Coated anti-A-chain mAbs were incubated at pH 7.5 with A-chain, and after washing further incubated for 1 h with buffers at various pH. The results are the ratio between signals obtained at pH 6.5 or pH 4.5 and those obtained at pH 7.5. [d] The binding of anti-A-chain mAbs was assayed on free ricin A-chain or whole ricin at similar A-chain molar concentrations using an immunoenzymatic method. The binding activities on whole ricin are represented as a percent of maximal binding obtained on free A-chain. [e] The N- and C-terminal peptides were independently preincubated with anti-ricin A-chain mAbs. The binding of preincubated mAbs was evaluated on ricin-A-chain in comparison with mAbs preincubated without added peptides using the immunoenzymatic assay described in Experimental Procedures.

and incubated for 1 h with fluorescein-conjugated rabbit anti-A-chain immunoglobulins. Cells were submitted to flow cytometric analysis using a FACS IV instrument (Becton Dickinson). Propidium iodide-positive dead cells were excluded from the analysis.

Cytotoxicity of Hybrid Molecules in Vitro. Five hundred microliters of RPMI 1640 medium containing 10^7 cells was incubated at 4 °C with 500 μL of 10 μg/mL hybrid molecule. After two washes, 100-μL aliquots containing $4 \cdot 10^4$ cells, resuspended in RPMI 1640 medium with 10% heat-inactivated fetal calf serum and antibiotics, were dispensed in microtiter plates on ice. A-Chain was added in the same buffer at final concentrations varying over the range from 10^{-14} to 10^{-6} M. One hour later, enhancers such as NH_4Cl or monensin were added to a final concentration of 10 mM or 50 nM, respectively. The microtiter plates were incubated for 20 h at 37 °C and then for another 4 h in the presence of 1 μCi (^{14}C)-L-leucine. Finally, cells were collected using an automated cell harvester (Skatron Flow Laboratories), and cell-associated radioactivity was measured in a scintillation counter.

Enzymatic Activity Inhibition. A-Chain $2 \cdot 10^{-9}$ (50 μL) was mixed with $2 \cdot 10^{-6}$ M purified anti-A-chain mAbs (50 μL) overnight at 4 °C, in 0.05 M Tris buffer containing 0.1% bovine serum albumin and then introduced in a cell-free protein synthesis assay with rat liver microsomes as already described (*14*). Negative controls consisted of anti-trinitrophenyl mAbs. Incorporation of (^{14}C)phenylalanine into peptide chains was measured in the presence of the artificial messenger poly-U.

Calculation of Correlation Coefficients. Correlation coefficients were calculated using the IC_{50} values obtained for each hybrid in the cytotoxicity assay on CEM cells versus the values obtained for each studied parameter of the anti-A-chain mAbs. A multiple correlation study was carried out comparing IC_{50} values with two or three associated mAb parameters.

RESULTS

Selection of High-Affinity mAbs. Monoclonal antibodies were obtained after hyperimmunization of BIOZZI mice with purified ricin A-chain according to a protocol eliciting high-frequency production of hybridomas for soluble antigens (*18*). Immunization was carried out without the use of complete Freund's adjuvant in order to avoid the possible denaturation of hydrophobic epitopes. mAb activity was detected in an assay consisting of a double-layer system, in which ricin A-chain was bound to polyclonal rabbit anti-A-chain immunoglobulins coated on microtiter plates. This assay allowed the detection of mAbs exhibiting a better affinity for ricin A-chain than those detected using a screening assay in which ricin A-chain was directly coated on microtiter plates (data not shown). Out of 172 hybridomas with anti-A-chain activity, 13 were preselected for their strong binding to A-chain. After cloning, mAbs were produced in ascites and purified on protein-A Sepharose.

Antibody Cluster Formation by Competitive Inhibition. The selected mAbs were biotinylated and tested for binding inhibition after preincubation with the various culture supernatants. The supernatants blocking the binding of biotinylated mAbs by more than 50% were considered to form a cluster and to recognize one major epitope. Clusters inhibiting each other by less than 15% indicated independent, nonoverlapping epitopes. Competition of the 14 selected mAbs with the 172 culture supernatants allowed definition of five main, nonoverlapping clusters or epitopes. The mAbs with the highest affinity within each cluster were choosen to represent their cluster in later experiments. The apparent dissociation constants (K_D) of mAbs were determined from the concentrations of mAbs giving 50% binding following incubation with ricin A-chain linked by affinity to rabbit anti-A-chain immunoglobulins coated on microtiter plates. This assay, which is described in detail in Experimental Procedures, gave a good evaluation of the K_D of the mAbs and allowed comparison among them. The selected mAbs were found to possess K_D values ranging between 1.1×10^{-10} M (3C2) and 4.2×10^{-11} M (13G6) (Table I, part B).

Epitopes Recognized by Selected mAbs. In order to partially localize A-chain epitopes, mAbs were evaluated for their binding to synthetic peptides corresponding to

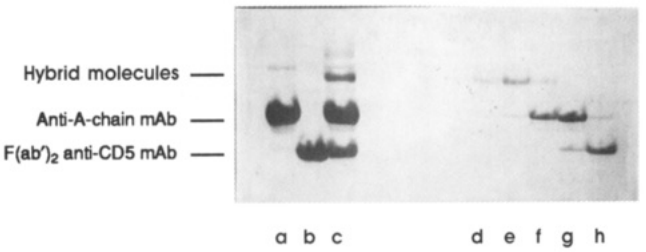


Figure 1. PAGE–SDS electrophoresis after fractionation of hybrid molecules on an ACA 34 Ultrogel column. Before fractionation: a, anti-A-chain mAb; b, $F(ab')_2$ anti-CD5 mAb; c, reaction mixture. After fractionation: d, fraction 105; e, fraction 110; f, fraction 125; g, fraction 150; h, fraction 170.

the last 10 amino acids of the N- or C-terminal parts of ricin A-chain. Peptides and mAbs were preincubated in a molar ratio of $10^4/1$, respectively. In a second step, the mAbs were incubated with A-chain using the immunoenzymatic binding assay. The N-terminal peptide had no effect on mAb binding. With the C-terminal peptide, only 1B5 mAb was slightly inhibited (Table I, part E), suggesting that it may bind near the C-terminus part of the A-chain. When comparing the binding of anti-A-chain mAbs to free A-chain or to whole ricin using the immunoenzymatic assay (Table I, part D), some mAbs did not recognize A-chain in whole ricin (14E2 from cluster 4, 4E9 and 1D7 from cluster 5). They should therefore be directed against either epitopes located at the A-chain/B-chain interface or epitopes whose conformation was changed by the dissociation of A-chain from B-chain. mAbs from groups 1–3 recognized free A-chain and ricin to the same extent, indicating that, in ricin, they recognize accessible epitopes. Moreover, binding of mAbs was evaluated on the A-chain of a classical disulfide, IT. All the anti-A-chain mAbs were able to recognize the A-chain of IT as well as free A-chain (data not shown).

Assembly of Hybrid Molecules by Conjugating Anti-A-Chain and Anti-CD5 mAbs. $F(ab')_2$ fragments of anti-CD5 ST1 mAb were coupled via a disulfide bridge to the different selected anti-A-chain mAbs as described in Experimental Procedures. PAGE–SDS electrophoresis (Figure 1) showed that fractions D and E contained a high proportion of hybrid molecules. These fractions did not show any detectable contaminations of the conjugates by neither polymers of mAbs nor free anti-CD5 mAbs. Under these conditions, however, the conjugation yields did not exceed 10% for all the hybrid preparations.

In Vitro Cytotoxicity of Hybrid mAbs. The cytotoxicity levels of the various hybrids on CEM cells were compared taking as reference a classical disulfide IT where A-chain is directly linked to the same $F(ab')_2$ fragment of anti-CD5 mAb. IC_{50} values obtained with the six selected A-chain-carrying hybrid mAbs were about 1 log higher than those of the disulfide-linked IT and varied from each other by a factor of 10 from 10^{-8} M to 10^{-7} M (Figure 2). In the presence of 10 mM NH_4Cl, IC_{50} values were found to be 100 times higher than with reference IT, indicating a lower enhancing effect of NH_4Cl on hybrid molecules. The variation of IC_{50} values between hybrids increased, ranging from 1.6×10^{-10} M to 3×10^{-9} M. Only with 50 nM monensin, two hybrids (4E9 and 1D7 mAbs) reached the IC_{50} value of 10^{-13} M of the reference IT. The other hybrids displayed higher IC_{50}s (up to 80 times higher), the worst hybrid (3C2 mAb) showing an IC_{50} of 8×10^{-12} M. IC_{50} values shown in Figure 2 are the mean of two separate experiments. In order to evaluate the technical variations when determining IC_{50} values of hybrid molecules, the 4E9 hybrid was tested in five different experiments. Without enhancer, the highest IC_{50} obtained on CEM cells was three times the lowest. In the presence of NH_4Cl or monensin, variations of 6- and 4-fold were observed, respectively. These variations cannot explain the variations observed among the different hybrids.

Relationship between Cytotoxicity and Inhibition of A-Chain Activity. The variation of the cytotoxicity of hybrids could be due to a different capacity of mAbs to inhibit the enzymatic activity of A-chain. The enzymatic A-chain activity measured on ribosomes in a rat liver acellular system of protein synthesis was unequally inhibited by the six representative mAbs. Under the experimental conditions used, an almost complete inhibition of 97% was found with the 13G6 mAb, whereas the lowest inhibition of 12% was obtained with the 14E2 mAb (Table I, part A).

However, no significant correlation could be found between enzymatic inhibition activity and cytotoxicity on whole cells (correlation coefficient $r = 0.54$). The best inhibiting mAb led only to an intermediate cytotoxicity on whole cells. On the other hand, the two most potent hybrids, built with the 4E9 and 1D7 mAbs, displayed identical cytotoxicity, although their capacities to inhibit acellular A-chain activity were highly different (60% versus 23%).

Relationship between Cytotoxicity and Cell Association Parameters in A-Chain–Antibody Complexes. No significant correlation was found between cytotoxicity and apparent dissociation constants (K_D) of mAbs ($r = 0.61$). Furthermore, the hybrid with the highest cytotoxicity (1D7 mAb) showed the same K_D as the hybrid 14E2 which had a 50 times lower cytotoxicity (Table I, part B). In order to exclude potential damage to hybrids during conjugation, the capacity of hybrids to deliver A-chain on the cell surface of CEM cells was evaluated by an indirect immunofluorescence assay using flow cytometry. Under conditions where hybrids saturated the CD5 antigen at the cell surface of CEM cells, the quantities of A-chain recognized by rabbit anti-A-chain immunoglobulins linked to FITC varied by a factor 3 among the different hybrids (Figure 3). The fluorescence intensities found when evaluating hybrid molecules were always lower than those obtained with classical IT. This may be due to a greater steric hindrance by the whole mAb–A-chain complex. Nevertheless, no correlation could be found between A-chain density and cytotoxicity ($r = -0.22$).

Another explanation of cytotoxicity variation could be a different dissociation of A-chain in an acidic environment following endocytosis. The binding capacities of the mAbs to A-chain at pH 6.5, which corresponds to an endosomal/lysosomal environment in the presence of 10 mM NH_4Cl, were almost identical (Table I, part C). No correlation was found between cytotoxicity of hybrids in the presence of NH_4Cl and dissociation at pH 6.5 ($r = 0.37$). But at pH 4.5, a value slightly lower than the pH found in lysosomes, dissociation values varied to a great extent (Table I, part C). The highest, but nevertheless not significant, correlations were found between cytotoxicity of hybrids without enhancer ($r = 0.72$) or with monensin ($r = 0.65$) and dissociation at pH 4.5. However, NH_4Cl, which increases pH in lysosomes to 6.5 (data not shown) and thereby inhibits A-chain dissociation at acidic pH, induced a variation of IC_{50} values identical to that observed without enhancer or in the presence of monensin (Figure 2). These data suggest that dissociation of A-chain in acidic compartments might not be the main reason for the variation of cytotoxicity.

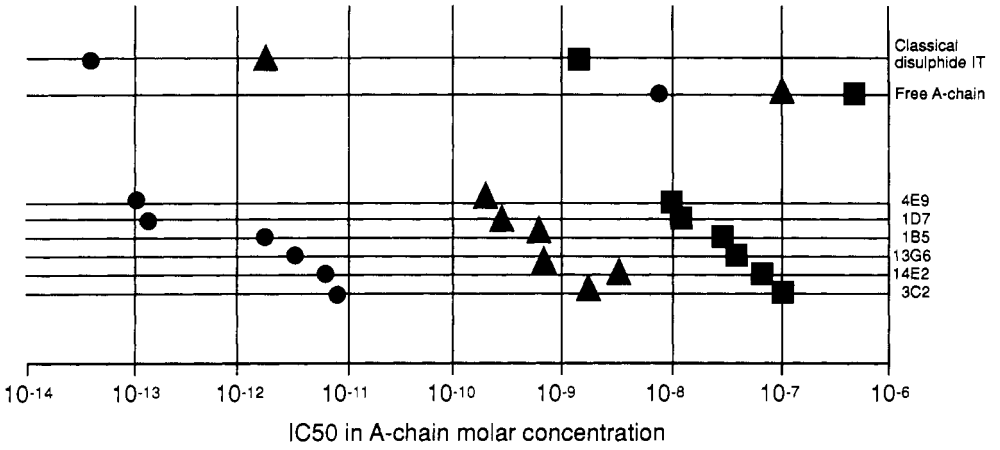


Figure 2. Cytotoxicity of hybrid molecules on CEM cells in vitro. CEM cells were incubated at 4 °C with 10 μg/mL hybrid molecules, washed, and dispensed into microtiter plates with ricin A-chain at concentrations varying over a range from 10^{-14} to 10^{-6} M. Enhancers were added 1 h later, and the cells were incubated for 20 h at 37 °C and then for another 4 h in the presence of (^{14}C)-L-leucine, allowing the determination of A-chain molar concentrations necessary to inhibit 50% of leucine incorporation (IC_{50}). Squares signify the absence of enhancer; triangles, the presence of 10 mM NH_4Cl; and circles, the presence of 50 nM monensin.

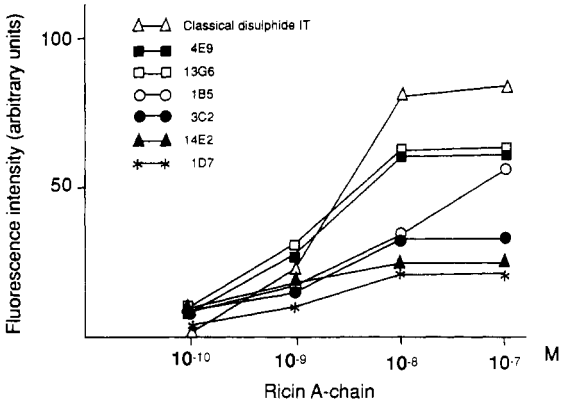


Figure 3. Immunofluorescence analysis of the capacity of hybrid molecules to deliver ricin A-chain to the cells. CEM cells were incubated with saturating concentrations of hybrid molecules, washed, incubated with various ricin A-chain concentrations, washed, and finally incubated with fluorescein-conjugated rabbit anti-A-chain immunoglobulins. A cytofluorometric analysis allowed the determination of the relative quantity of A-chain trapped by the hybrid molecules on the surface of CEM cells.

Multiple Correlation Study. All these parameters suspected of interfering with the efficacy of hybrids were associated in a multiple correlation test in order to evaluate if the association of two or three of them could be responsible for the cytotoxicity of hybrids. These multiple correlation coefficients were not higher than those obtained with the classical dual-correlation studies previously mentioned.

DISCUSSION

The presentation of ricin A-chain to cell membrane could be one among other different factors influencing its cytotoxicity. In native ricin, the toxic subunit is probably always presented to the cell membrane in the same manner. As a consequence, the C-terminal polypeptide of A-chain containing the free thiol used as anchoring group to bind the B-chain is partially hidden by the proximity of the carrier protein.

In order to know if the presentation of A-chain to the cell membrane has an incidence on its cytotoxicity, ricin A-chain was delivered to CEM cells linked by affinity to anti-A-chain mAbs through different epitopes. The disulfide bridge of the classical IT is now replaced by an anti-A-chain mAb which binds A-chain by affinity and which is itself chemically linked to the ST1 anti-CD5 mAb. In order to reduce the size of these hybrid molecules, the $F(ab')_2$ fragment of the ST1 mAb was used. Since the tested anti-A-chain mAbs were directed against different epitopes on the surface of the A-chain molecule, they presented A-chain to the cell from different sides. Such constructions were already reported to be specifically cytotoxic (*19*), but they were not very potent compared to classical ITs. Moreover, no information was given in the literature with respect to the presentation of A-chain by its different epitopes to cell membrane.

Among 172 anti-A-chain clones, six producing mAbs representative of five nonoverlapping epitopes were selected for high affinity. The intrinsic enzymatic A-chain activity could be blocked to a variable extent by the six mAbs. The best hybrid reduced A-chain activity by 97% and the worst by only 12%. However, the acellular test system does not involve a transmembrane passage of A-chain which could allow A-chain to recover its enzymatic activity.

Selected anti-A-chain mAbs linked to $F(ab')_2$ fragments of the ST1 anti-CD5 mAb were tested on intact CEM cells for their capacity for delivering a cytotoxic A-chain. Without enhancers their cytotoxicitic potency was decreased by 1–2 log with respect to the classical disulfide-linked IT. These results indicate that transmembrane passage of A-chain, including A-chain dissociation from its carrier in endosomes, is more easily obtained when A-chain is linked to the mAb by a disulfide bridge than by affinity. The decrease of cytotoxicity of hybrids versus classical ITs cannot be explained by different intracellular pathways. Contradictory results about the intracellular routing of anti-CD5 classical ITs have been reported. When adsorbed on colloidal gold, IT reached lysosomes (*20*) whereas a nonadsorbed ^{125}I-labeled anti-CD5 IT was not degraded into CEM cells (*21*). However, in hybrids as well as in classical ITs, the $F(ab')_2$ fragment of anti-CD5 mAb should direct the routing of ricin A-chain in the same manner. The sensitivity of conventional ITs to enhancement by the lysosomotropic amine NH_4Cl or by the carboxylic ionophore monensin has been previously evaluated (*22, 23*). When compared to the classical IT, hybrid molecules were considerably less enhanced by NH_4Cl (Figure 2). In contrast, enhancement by monensin produced similar cytotoxicity levels when comparing the best hybrid and the classical disulfide IT. So, neutralization of pH in endosomes by NH_4Cl seems to be less important

for hybrid molecules where A-chain is linked by affinity than for disulfide-linked A-chain molecules. Enhancement by monensin, which does not increase endosomal pH at the low doses used, is highly effective with both kinds of conjugates, suggesting a different mechanism of enhancement by carboxylic ionophores compared to lysosomotropic agents.

Another important result is that the different tested hybrids did not display the same efficacy. Their IC_{50}s (expressed as A-chain concentrations) varied over a 1–10 range without enhancers, a 1–20 range in the presence of NH_4Cl, and a 1–80 range in the presence of monensin (Figure 2). Moreover, the ranking of cytotoxicity values obtained with these hybrids was always the same whether or not enhancers were present.

The difference could not be explained by the inhibition by mAbs of intrinsic enzymatic A-chain activity. In fact, no correlation was observed between the cytotoxic potential of the hybrids on intact cells and the inhibition of enzymatic activity evaluated using an acellular assay. It could not be due to the different affinity constants of anti-A-chain mAbs, which can lead to a different concentration of A-chain on the cell surface. No correlation was found between cytotoxicity and either apparent dissociation constants or quantities of A-chain carried by hybrids on the cell surface of CEM cells. Furthermore, when comparing the two best hybrids, one delivered the highest and the other the lowest quantity of A-chain (4E9 and 1D7, respectively). This clearly indicates that the cytotoxic effect is not correlated to A-chain density at the cell surface (Figure 3).

The difference in the dissociation of A-chain from mAbs in endosomes at lower pH was also excluded. NH_4Cl known to increase pH of endosomes to a near neutral pH of about 6.5, was unable to decrease the variation of cytotoxicity of hybrids. Furthermore, the dissociation of A-chain at pH 6.5 was almost identical for all tested mAbs.

The different presentations of A-chain to cell membrane by the mAbs, with more or less favorable epitopes for the initiation of its transmembrane passage, may be the main reason for variations of hybrid cytotoxicity. The 1D7 and 4E9 mAbs, which recognize the same epitope, showed very close IC_{50} in the absence as well as in the presence of enhancers.

These results lead to investigating the identification of the A-chain epitopes more or less favorable for A-chain presentation. Preliminary results showed that one cluster was partially inhibited by the C-terminal peptide of A-chain. This cluster, represented by the 1B5 mAb, displayed an intermediate activity level, suggesting that this portion of the toxin does not seem strongly critical for the intrinsic activity of A-chain. This result may be compared to the ones obtained with ITs, in which A-chain was chemically linked to mAb using carboxyl groups instead of the natural thiol of A-chain. Such constructions were as active as classical disulfide ITs, indicating that this linkage is not critical for the intrinsic activity of A-chain. In contrast, ITs built using phenol groups were 30-fold less active than classical ITs, and ITs constructed using amino groups were slightly less active (*13*). Two other clusters of mAbs failed to recognize A-chain in whole ricin. However, these two clusters displayed opposite cytotoxicity levels. It is not known if these mAbs recognize epitopes hidden at the A-chain/B-chain interface of ricin or epitopes that have been modified following the dissociation of A-chain from B-chain. It is interesting to note that 4E9 or 1D7 mAbs, which do not recognize whole ricin, are as efficient as the classical disulfide-linked IT in the presence of monensin. The precise location of all these epitopes, including the one recognized by the 3C2 mAb, which is the less efficient for the A-chain cytotoxicity, must be investigated in order to understand the mechanism by which A-chain translocates through cell membrane.

LITERATURE CITED

(1) Ghetie, M. A., May, R. D., Till, M., Uhr, J. W., Ghetie, V., Knowles, P. P., Relf, M., Brown, A., Wallace, P. M., Janossy, G., Amiot, P., Vitetta, E. S., and Thorpe, P. E. (1988) Evaluation of ricin A chain-containing immunotoxins directed against CD19 and CD22 antigens on normal and malignant human B-cells as potential reagents for in vivo therapy. *Cancer Res. 48*, 2610–2617.

(2) Olsnes, S., Refsnes, K., and Pihl, A. (1974) Mechanism of action of the toxic lectins abrin and ricin. *Nature 249*, 627.

(3) Endo, Y., Mitsui, K., Motizuki, M., and Tsurugi, K. (1987) The mechanism of action of ricin and related toxic lectins on eukaryotic ribosomes. The site and the characteristics of the modification in 28 S ribosomal RNA caused by the toxins. *J. Biol. Chem. 262*, 5908–5912.

(4) Endo, Y., and Tsurugi, K. (1987) RNA N-glycosidase activity of ricin A-chain. Mechanism of action of the toxic lectin ricin on eukaryotic ribosomes. *J. Biol. Chem. 262*, 8128–8130.

(5) Lewis, M. S., and Youle, R. J. (1986) Ricin subunit association. Thermodynamics and the role of the disulfide bond in toxicity. *J. Biol. Chem. 261*, 11571–11577.

(6) Funatsu, G., Yoshitake, S., and Funatsu, M. (1978) Primary structure of isoleucine chain of ricin D. *Agric. Biol. Chem. 42*, 501–504.

(7) Funatsu, G., Kimura, M., and Funatsu, M. (1979) Primary structure of alanine chain of ricin D. *Agric. Biol. Chem. 43*, 2221–2224.

(8) Montfort, W., Villafranca, J. E., Monzingo, A. F., Ernst, S. R., Katzin, B., Rutenberg, E., Xuong, N. H., Hamlin, R., and Robertus, J. D. (1987) The three-dimensional structure of ricin at 2.8 Å. *J. Biol. Chem. 262*, 5398–5403.

(9) Beugnier, N., Falmagne, P., Zanen, J., and Jansen, F. K. (1982) Interaction of ricin and its two chains with model membranes. *Arch. Int. Physiol. Bioch. 90*, B93–B94.

(10) Ishida, B., Cawley, D. B., Reue, K., and Wisnieski, B. J. (1983) Lipid-protein interactions during ricin toxin insertion into membranes. Evidence for A and B chain penetration. *J. Biol. Chem. 258*, 5933–5937.

(11) Utsumi, T., Aizono, Y., and Funatsu, G. (1984) Interaction of ricin and its constituent polypeptides with dipalmitoylphosphatidylcholine vesicles. *Biochim. Biophys. Acta 772*, 202–208.

(12) Utsumi, T., Aizono, Y., and Funatsu, G. (1987) Receptor-mediated interaction of ricin with the lipid bilayer of ganglioside GM1-liposomes. *FEBS Lett. 216*, 99–103.

(13) Jansen, F. K., Bourrié, B., Casellas, P., Dussossoy, D., Gros, O., Vic, P., Vidal, H., and Gros, P. (1988) Toxin selection and modification: utilization of the A-chain of ricin. In *Immunotoxins* (A.E. Frankel, Ed.) pp 97–111, Kluwer Academic Publishers, Boston.

(14) Vidal, H., Casellas, P., Gros, P., and Jansen, F. K. (1985) Studies on components of immunotoxins: Purification of ricin and its subunits and influence of unreacted antibodies. *Int. J. Cancer 36*, 705–711.

(15) Carrière, D., Fontaine, C., Benoit, J. M., Thurneyssen, O., and Carrel, S. (1989) Four epitopes of the CD5 (67 kDa) molecule are defined by the mAb of the Workshop CD5 panel. In *"Leukocyte Typing IV, White Cell Differentiation Antigens"* (W. Knapp, Ed.) pp 335–336, Oxford University Press, Oxford.

(16) Stanworth, D. R., and Turner, M. W. (1973) Immunochemical analysis of immunoglobulins and their subunits. In *Handbook of Experimental Immunology* (D. M. Weir, Ed.) Vol. I, pp 1, Blackwell Scientific, London.

(17) Poncelet, P., and Carayon, P. (1985) Cytofluorometric quantification of cell-surface antigens by indirect immuno-

fluorescence using monoclonal antibodies. *J. Immunol. Methods 85*, 65–74.
(18) Cianfriglia, M., Armellini, D., Massone, A., and Mariani, M. (1983) Simple immunization protocol for high frequency production of soluble antigen-specific hybridomas. *Hybridoma 2*, 451–457.
(19) Raso, V., and Griffin, T. (1981) Hybrid antibodies with dual specificity for the delivery of ricin to immunoglobulin-bearing target cells. *Cancer Res. 41*, 2073–2078.
(20) Carrière, D., Ancier, J. M., Derocq, J. M., Fontaine, C., and Richer, G. (1989) Antigenic modulation induced by four monoclonal antibodies adsorbed on gold particles (specificity anti-CD4, anti-CD5, anti-CD7, and anti-150 kDA antigen): Relationship between modulation and cytotoxicity activity of immunotoxins. *Exp. Cell Res. 182*, 114–128.
(21) Ravel, S., and Casellas, P. (1990) Internalizations of the cytotoxic molecules of T101 F(ab')$_2$-(ricin-A-chain) immunotoxin into human T-leukemic cells. *Eur. J. Biochem. 192*, 469–473.
(22) Casellas, P., Bourrié, B. J. P., Gros, P., and Jansen, F. K. (1984) Kinetics of cytotoxicity induced by immunotoxins. Enhancement by lysosomotropic amines and carboxylic ionophores. *J. Biol. Chem. 259*, 9359–9364.
(23) Raso, V., and Lawrence, J. (1984) Carboxylic ionophores enhance the cytotoxic potency of ligand- and antibody-delivered ricin A chain. *J. Exp. Med. 160*, 1234–1240.

Preparation, Characterization, and in Vivo Biodistribution Properties of Synthetically Cross-Linked Multivalent Antitumor Antibody Fragments

Margaret E. Schott,* Kevin A. Frazier, Douglas K. Pollock, and Kathryn M. Verbanac†

Bioproducts Laboratory, The Dow Chemical Company, Midland, Michigan 48674. Received September 30, 1992

Two new antibody forms of the general structure $F(ab')_n$ (n = 3 or 4) were prepared and tested in vivo as part of an ongoing search for antibody candidates with improved biodistribution properties for cancer immunotargeting applications. The novel multivalent antibody forms, called $F(ab')_3$-x (tribody, 150 kDa, x = cross-linker) and $F(ab')_4$-x (tetrabody, 200 kDa), were constructed through chemical cross-linking of Fab' subunits derived from murine CC49 IgG, a monoclonal antibody which recognizes the tumor-associated antigen TAG-72. Two new chemical reagents (trismaleimide 1 and tetramaleimide 2) were synthesized for use in cross-linking cysteine sulfhydryl groups present on the hinge region of Fab'. Homogeneous Fab' was prepared by mild reduction of $F(ab')_2$ followed by selective reoxidation of interchain disulfide bonds, leaving a single hinge-region cysteine sulfhydryl group available for modification. For biodistribution studies, the parent $F(ab')_2$ fragment was first radiolabeled via lysine amine modification using the isothiocyanate derivative of the ^{105}Rh(BA-2,3,2-tet)Cl_2 complex. Both new fragment forms were shown to retain antigen binding ability in vitro using a solid-phase immunoassay. Although isolated yields for $F(ab')_3$-x and $F(ab')_4$-x were low (18 and 4%, respectively), sufficient quantities were prepared for preliminary biodistribution studies in Balb/c mice and, in the case of $F(ab')_3$-x, for a 5-day biodistribution study in tumor-bearing nude mice. A large proportion of the ^{105}Rh-labeled $F(ab')_4$-x was found to accumulate in the liver, possibly indicating an upper size limit for the in vivo use of cross-linked fragments. The biodistribution behavior of ^{105}Rh-labeled $F(ab')_3$-x in both Balb/c and nude mice was intermediate between that of IgG and $F(ab')_2$ for all organs studied. Kidney localization was reduced, while blood circulation time and tumor accumulation were slightly increased, for the trivalent species compared with $F(ab')_2$. The unique biodistribution profile of $F(ab')_3$-x suggests the possible use of this multivalent fragment for in vivo tumor targeting applications.

INTRODUCTION

The development of antibodies and antibody-like species with improved biodistribution properties for cancer immunotargeting applications is an area of intense current interest (for recent reviews, see Waldmann, 1991; Koppel, 1990). To date the most thoroughly studied antibody forms include IgG and its proteolytic fragments, $F(ab')_2$ and Fab. Although the smaller fragments have been shown to penetrate tumor tissue more readily than the parent immunoglobulin (Fujimori et al., 1989), both fragments localize extensively to the kidneys, limiting their usefulness particularly when conjugated to radiometals (Sharkey et al., 1990). And while genetically engineered single-chain antigen binding proteins offer the potential advantages of rapid plasma clearance, enhanced tumor penetrance (Milenic et al., 1991; Yokota et al., 1992), and reduced immunogenicity, the amount of sFv actually delivered to tumor sites is low in comparison with the slower clearing IgG. It is evident that no single immunoglobulin form will possess properties that match the requirements of all cancer diagnosis and therapeutic applicatons. The investigation of alternative structural forms should lead to a better understanding of the role of structure as it relates to biodistribution and may aid in the design of useful immunotargeting agents.

Various chemical cross-linking methods have been employed in the preparation of antibody forms possessing two or more antigen binding arms. One method involves the formation of chemical cross-links between lysine amine residues on whole antibodies and/or antibody fragments. This approach is considered nonspecific with respect to location of the chemical bonds formed on the protein surface and can result in heterogeneous product mixtures (Perez et al., 1985). Hetero-cross-linked IgG and Fab fragments have been constructed for the purpose of retargeting cytotoxic cells in vivo (Segal and Wunderlich, 1988). These authors note that since chemically linked heteroaggregates clear more rapidly from the circulation than monomeric IgG, their use may be limited to in vitro screening applications.

Hetero-cross-linked bivalent and multivalent antibody forms have also been constructed through site-specific reactions involving cysteine sulfhydryl groups obtained through mild reduction of disulfide bonds in the parent immunoglobulins or fragments. Several reports have appeared concerning the preparation of heterobifunctional $F(ab')_2$ species using bismaleimide cross-linkers (Glennie et al., 1987; French et al., 1991; Stickney et al., 1988). These novel fragments were formed through the chemical cross-linking of hinge-region sulfhydryl groups. Heterobifunctional fragments have also been prepared through reformation of hinge-region disulfide bonds via leaving-group chemistry (Brennan et al., 1985) or using a two-step reduction/reoxidation procedure (Staerz and Bevan, 1986). However, thioether bonds may be preferable to disulfide bonds based on evidence of their enhanced stability in vivo (Meares et al., 1988; Stevenson et al., 1989). In a recent study of the relative in vivo stability of radiolabeled $F(ab')_2$ versus bismaleimide-cross-linked $F(ab')_2$, the latter fragments (constructed with three different cross-linkers) showed significantly longer plasma circulation times

* Present address and to whom correspondence should be addressed: Laboratory of Tumor Immunology and Biology, National Cancer Institute, National Institutes of Health, 9000 Rockville Pike, Bldg 10, Room 8B07, Bethesda, MD 20892.

† Present address: Department of Surgery, East Carolina University School of Medicine, Greenville, NC 27858.

1043-1802/93/2904-0153$04.00/0 © 1993 American Chemical Society

compared with the native form (Quadri et al., 1992). Whether the plasma half-life of native $F(ab')_2$ is influenced by the number of hinge-region disulfide bonds was not reported.

Bismaleimide cross-linking has also been employed for the preparation of a "chimeric univalent" Fab-IgG (Stevenson et al., 1985). These authors also observed the putative IgG-$(Fab')_2$ species as a byproduct. Fab-IgG (200 kDa), which is univalent and thus capable of evading antigenic modulation on tumor surfaces, appeared to be "catabolized at the slow rate characteristic of autologous IgG". Bismaleimides reagents have also been used to construct the univalent FabFc species (100 kDa), possessing one antigen binding arm and an Fc region, and its bivalent counterpart, bisFabFc (200 kDa; Stevenson et al., 1989). Biodistribution data for these antibody forms were not reported. However, biodistribution studies for a structurally similar fragment called Fab/c, generated by the limited enzymatic digestion of IgG, were recently carried out (Demignot et al., 1990). In Balb/c mice, the half-lives of the catabolic (β) phase of plasma clearance for radioiodinated Fab/c and the parent IgG were identical, as was whole-body clearance. The distribution (α) phase of plasma clearance for Fab/c was steeper than that for IgG, suggesting a more rapid extravasation into tissues. A slightly greater kidney to blood ratio was observed for the Fab/c fragment compared with IgG. In tumor-bearing nude mice, Fab/c localized to tumor tissue but did so to a lesser extent than whole antibody, presumably due to the lower immunoreactivity of the univalent fragment.

The major pathway by which proteins enter the kidney is through glomerular filtration, a process which depends upon several factors including molecular size, shape, and charge (Sumpio, 1981). Proteins smaller than 50 kDa generally cross the glomerulus while intermediate and high molecular weight proteins greater than 60–70 kDa generally do not (Strober and Waldmann, 1974; Demignot et al., 1990). Anionic proteins are hindered to a greater extent than are charge-neutral or cationic proteins, particularly at sizes greater than 25 Å. Charge is less important for small proteins (Maack et al., 1979). The overall charge of a protein (as well as the distribution of charges on the molecule) are also known to influence uptake by the proximal tubules, with cationic proteins being taken up to a greater degree than anionic proteins of the same molecular weight (Christensen et al., 1983; Sumpio, 1981). The low isoelectric point of the immunoglobulin Fc piece (Goding, 1986) probably accounts for its relatively long circulation time compared with the Fab fragment (Waldmann and Strober, 1969), despite the similarity in molecular weight for Fc and Fab. Additionally, the similarity of the biodistribution patterns observed for IgG and its Fab/c fragment (see above), in striking contrast to the biodistribution observed for $F(ab')_2$ (also 100 kDa), suggests a role for Fc in keeping the Fab/c in circulation and out of the kidneys.

On the basis of the known literature concerning kidney handling of macromolecules, the extent of kidney localization for $F(ab')_2$ is surprising. In order to further investigate the role of fragment size on biodistribution, particularly kidney localization and blood-residence lifetime, we prepared two new homologues of the $F(ab')_n$ series, where $n = 3$ (tribody) and $n = 4$ (tetrabody). Because of their higher molecular weights, the tribody (150 kDa) and tetrabody (200 kDa) species would be expected to show decreased kidney localization compared with $F(ab')_2$ or Fab. Additionally, $F(ab')_3$-x seemed an interesting target because it has the same molecular weight as IgG but lacks the Fc region. Although a putative $F(ab')_3$ species was observed previously as a byproduct of Fab' chemical cross-linking (Glennie et al., 1987), its in vivo properties were not reported. The semisynthetic fragments $F(ab')_3$-x (x = cross-linker) and $F(ab')_4$-x were constructed from univalent Fab' subunits derived from CC49 $F(ab')_2$ using the newly designed and synthesized tri- and tetrafunctional maleimide cross-linking reagents **1** and **2** (Figure 1). The murine monoclonal antibody CC49 is an IgG1 that recognizes the tumor-associated antigen TAG-72 and reacts with a high percentage of tumor cells in a wide range of human carcinomas (Muraro et al., 1988). Radiolabeled CC49 efficiently localizes human carcinoma xenografts in vivo in athymic mice (Colcher et al., 1988). We report here the biodistribution patterns of radiolabeled CC49 $F(ab')_3$-x and $F(ab')_4$-x in Balb/c mice and the tumor localization of $F(ab')_3$-x in nude mice bearing LS-174T human tumor xenografts.

EXPERIMENTAL PROCEDURES

General Procedures. All phosphate buffer solutions were 0.1 M sodium phosphate adjusted to the desired pH, except PBS[1] (pH 7.4), which was prepared by reconstitution of a powder obtained from Sigma (St. Louis, MO). Iodoacetamide and DTT were prepared as 0.1 M solutions in pH 7.0 phosphate buffer. Sure/Seal dimethylformamide was obtained from Aldrich (Milwaukee, WI) and stored under a blanket of nitrogen. Centricon-30 concentrator units (30 000 MW cutoff) from Amicon (Beverly, MA) were used on a Du Pont Sorvall RT-6000B centrifuge equipped with an A-384 rotor at 5000–6000 rpm, 16 °C. Protein assays were performed according to the Pierce (Rockford, IL) Coomassie method, with bovine plasma γ-globulin from Bio-Rad (Richmond, CA) as a quantitation standard.

Monoclonal Antibodies. mAb CC49 is a murine IgG1 which was obtained by immunizing mice with purified TAG-72 (Muraro et al., 1988). For the present studies, CC49 IgG was harvested from bioreactor cultures and purified using an AbX column (Bio-Rad) followed by a Superose 12 gel filtration column (Pharmacia, Piscataway, NJ). CC49 $F(ab')_2$ fragments were prepared via enzymatic digestion of the parent IgG using either thiol-activated papain (neutral pH, nonreducing conditions) or using pepsin (pH 3.5) as described by Goding (1986). The progress of the digestion reactions was monitored by GF-250 HPLC until none of the parent IgG remained. The fragments were purified by gel filtration chromatography using a Superose 12 column and stored at −70 °C in 50 mM pH 6.8 phosphate buffer at approximately 5–10 mg/mL.

High Performance Liquid Chromatography. Analytical HPLC was used both for monitoring the progress of reactions and for checking the quality of final preparations. Preparative HPLC was used for the isolation of cross-linked fragment species and was performed on the same columns as the analytical work. HPLC for nonra-

[1] Abbreviations used: BA-2,3,2-tet, 6-[(4-aminophenyl)methyl]-1,4,8,11-tetraazaundecane; PBS, phosphate-buffered saline; TAG-72, tumor associated glycoprotein-72; DMF, dimethylformamide; THF, tetrahydrofuran; DMSO, dimethyl sulfoxide; EDTA, ethylenediaminetetraacetic acid; DTT, dithiothreitol; NEM, *N*-ethylmaleimide; DTNB, 5,5′-dithiobis(2-nitrobenzoic acid); TNB^{2-}, 5-mercapto-2-nitrobenzoic acid anion; BSA, bovine serum albumin; SDS–PAGE, sodium dodecyl sulfate–polyacrylamide gel electrophoresis; ELISA, enzyme-linked immunosorbent assay; IEF, isoelectric focusing; H′ and L, antibody fragment heavy and light chains (H′ is the same as Fd and is used here for clarity).

dioactive samples was performed on a Du Pont GF-250 column at a flow rate of 1.0 mL/min unless otherwise indicated. The mobile phase was 0.2 M pH 7.0 sodium phosphate containing 1 mM EDTA, which was included to slow oxidation of free thiol groups. For isolation and analysis of radiolabeled samples, both a Berthold LB 506A radioisotope flow-through radioisotope detector and a UV detector were employed, and the flow rate was slowed to 0.5 mL/min for $F(ab')_3$-x and 0.3 mL/min for $F(ab')_4$-x.

SDS–PAGE. Discontinuous SDS–PAGE was performed according to the method of Laemmli (1970) using a Bio-Rad Protean II apparatus (Richmond, CA). Nonreducing and reducing (5% β-mercaptoethanol) 10% polyacrylamide gels were run following denaturation of samples at 80 °C for 2 min. Permanent images of Coomassie Blue-stained polyacrylamide gels were obtained using the Electrophoresis Duplicating Paper system from Kodak (Rochester, NY). Autoradiography was performed on dried gels using Kodak X-Omatic cassettes and film. The progress of disulfide bond reduction, disulfide bond formation, and fragment cross-linking could be monitored by nonreducing SDS–PAGE following treatment of an aliquot (10–20 μL) with an equal volume of 0.1 M iodoacetamide for 15 min at room temperature. Use of nonreducing conditions allowed separation of the CC49 fragment H′ and L chains on 10% polyacrylamide gels. Under reducing conditions, H′ and L typically migrated together. In some experiments, cross-linked antibody fragments were subjected to reduction and alkylation prior to SDS–PAGE analysis on nonreducing gels. This procedure allowed visualization of the fragment H′ and L chains as well as cross-linked H′ chains. For example, an aliquot (18 μL) containing the fragment of interest was first treated with 0.2 M DTT (2 μL) in pH 7.0 phosphate buffer for 10–15 min at room temperature and then with an equal volume (20 μL) of 0.1 M iodoacetamide in pH 7.0 phosphate buffer for 30 min.

Immunoreactivity Assay. ELISA antigen binding assays were performed using 96-well polystyrene microtiter plates, which were precoated with TAG-72 prepared from LS-174T human colorectal carcinoma xenografts using a modification of a reported procedure (Johnson et al., 1986). Briefly, xenograft tumors were minced, homogenized in PBS in the presence of protease inhibitors, and centrifuged in two stages to yield a supernatant containing the tumor extract. The filtered homogenate was further purified by gel filtration chromatography on Sepharose CL-4B or CL-6B (Pharmacia) equilibrated with PBS. Fractions containing TAG-72 were identified by a direct-binding assay using radioiodinated antigen-specific antibody. Microtiter plates for ELISA were prepared by coating with TAG-72-enriched fractions (~10% of total protein) followed by blocking with 1% BSA in PBS. For ELISA, antibody fragment samples (50 μL/well) were incubated on precoated microtiter plates at starting concentrations of 10 μg/mL in 1% BSA. Dilutions (1:2) and transfers were performed using a Cetus Pro/Pette (Emeryville, CA). Plates were incubated for 2–3 h at 37 °C or overnight at 4 °C and washed with 0.025% Tween 20 using a Flow Laboratories plate washer, followed by incubation with a 1:200 solution of alkaline phosphatase-conjugated goat anti-mouse κ antibody (Southern Biotech, Birmingham, AL) in 1% BSA (50 μL) for 2–3 h at 37 °C. After washing, plates were treated with a freshly prepared solution of p-nitrophenol phosphate in diethanolamine buffer (100 μL/ Kirkegaard and Perry Laboratories, Gaithersburg, MD). Color development was monitored using a Dynatech MR600 microplate reader, and the reactions were stopped with 2 N NaOH (100 μL) when the absorbance readings were 1.0–1.2.

Preparation of Trismaleimide 1. Trimethyl 1,3,5-benzenetricarboxylate (10.08 g, 40 mmol) was stirred with ethylenediamine (60 mL) at room temperature under a constant stream of nitrogen. The reaction was monitored by TLC (2:2:1 $CHCl_3$/MeOH/concentrated NH_4OH). After 24 h the reaction appeared to be complete. Excess ethylenediamine was removed under reduced pressure on a rotary evaporator. A viscous oil was obtained which was dissolved in methanol (25–30 mL). The solution was then slowly poured into p-dioxane (350–400 mL). A white powder formed as the methanolic solution was added and the solid was collected by filtration. A tan powder (11 g, 32.7 mmol, 82%) was obtained and identified as the tris(amido amine). An additional amount (2.7 g) of impure material was obtained as a thick oil when the p-dioxane/ethanol solution was evaporated. ^{1}H NMR (d_6-DMSO) ppm: 1.90 (br s, 2 H, NH_2), 2.75 (br t, 2 H), 3.33 (br t, 2 H), 8.40 (s, 1 H), 8.63 (br s, 1 H). ^{13}C NMR (d_6-DMSO) ppm: 41.178, 43.120, 66.310, 79.079, 128.390, 134.975, 165.667.

Maleic anhydride (2.00 g, 20.4 mmol) was added all at once to a vigorously stirred solution of the tris(amido amine) (2.29 g, 6.8 mmol) dissolved in DMF (10 mL). The mixture warmed slightly as the material gradually dissolved. After 2 h a solid began to form again and eventually stirring was impeded. The reaction was left overnight and THF (200 mL) was added and the mixture was stirred rapidly. The white powder (3.2 g) obtained upon filtering the THF/DMF solution was identified as the trismaleamate. ^{1}H NMR (d_6-DMSO) ppm: 3.25–3.65 (m, 4 H), 6.26 (d, 1 H), 6.46 (d, 1 H), 7.97 (s, 1 H), 8.48 (s, 1 H), 8.80 (br s, 1 H), 9.23 (br s, 1 H). ^{13}C NMR (d_6-DMSO) ppm: 38.510, 38.851, 128.613, 131.962, 132.563, 134.776, 165.360, 165.646, 165.744.

Trismaleamate (1.54 g), anhydrous sodium acetate (1.54 g), and acetic anhydride (5 mL) were heated at 80 °C with stirring for 24 h. The mixture was then poured into ice water and stirred vigorously for 1 h. The solid was collected by filtration and was washed successively with water, anhydrous ethanol, and anhydrous ether. A tan solid (0.40 g) was obtained after drying under vacuum. Proton and carbon spectra confirm the structure as trismaleimide 1. ^{1}H NMR (d_6-DMSO) ppm: 3.34 (m, 2 H), 3.59 (m, 2 H), 6.95 (s, 2 H), 8.23 (s, 1 H), 8.79 (br s, 1 H). ^{13}C NMR (d_6-DMSO) ppm: 36.970, 37.721, 128.300, 134.442, 134.672, 165.556, 170.912.

Preparation of Tetramaleimide 2. Maleic anhydride (9.8 g, 100 mmol) was added in portions to a stirred mixture of 3,5-diaminobenzoic acid (7.6 g, 50 mmol) and acetic acid (250 mL) at room temperature. Cooling was necessary as the addition proved to be exothermic. The mixture was stirred for 72 h at room temperature and eventually became too thick to stir. Anhydrous ether (500 mL) was added and the mixture was filtered and the solid washed repeatedly with ether. The bismaelamic acid (18.2 g) was obtained as a yellow-green powder and was used directly for the next reaction.

Sodium acetate (15 g) and bismaleamic acid (15 g) were stirred at 80 °C in acetic anhydride (100 mL) and after 0.5 h the mixture set up as a firm solid. Another portion of acetic anhydride (100 mL) was added and the temperature was raised to 100 °C. After 2 h the reaction mixture was cooled, poured into ice water (300 mL), and left stirring overnight. The mixture was filtered and the solid was washed with absolute ethanol followed by anhydrous ether. The off-white powder (9.50 g, 61%) was identified as the

bismaleimide acid by NMR. ^{1}H NMR (d_6-DMSO) ppm: 7.21 (s, 4 H), 7.67 (t, 1 H), 8.00 (d, 2 H), COOH was not observed. ^{13}C NMR (d_6-DMSO) ppm: 126.310, 128.212, 132.238, 132.811, 134.774, 166.033, 169.533.

The bismaleimide acid (0.25 g) was stirred as a slurry in thionyl chloride (5 mL). The mixture was heated to reflux and gas evolution was monitored with a gas bubbler. The reaction mixture was heated overnight, allowing the solid to dissolve gradually. Excess thionyl chloride was removed under reduced pressure and then CCl_4 was added and the solvents were stripped again, yielding a tan solid. The acid chloride was used without further purification. ^{1}H NMR (d_6-DMSO) ppm: 7.24 (s, 4 H), 7.64 (s, 1 H), 8.01 (s, 2 H). ^{13}C (d_6-DMSO) ppm: 126.248, 128.462, 131.920, 132.330, 134.781, 165.745, 169.484.

The acid chloride (130 mg, 0.39 mmol) was added all at once to a room temperature solution of *p*-phenylenediamine (21 mg, 0.19 mmol) and triethylamine (65 μL, 0.45 mmol) in acetonitrile (5 mL). A small amount of heat was generated and a solid quickly formed. The reaction was stirred for 0.5 h and filtered. The solid was washed with water followed by acetonitrile again to yield a tan powder (65 mg). ^{1}H NMR (d_6-DMSO) ppm: 7.23 (s, 4 H), 7.64 (s, 1 H), 7.83 (s, 2 H), 8.08 (s, 2 H), 10.45 (s, 1 H). ^{13}C (d_6-DMSO) ppm: 120.757, 125.080, 127.584, 132.085, 134.723, 136.137, 163.415, 169.387; one aromatic signal was not detected.

Preparation of Fab′. Fab′ was prepared from F(ab′)$_2$ by mild reduction followed by selective reoxidation of H′–L interchain disulfide bonds. In a typical preparation, 2.0 mg of F(ab′)$_2$ in 0.9 mL of pH 7.0 phosphate buffer was treated with 0.2 M DTT (0.1 mL) for 15 min at room temperature. Interchain disulfide bonds were completely reduced under these conditions (Figure 2a). Sephadex G-25 QS-2B "mini-spin" columns from Isolab (Akron, OH) were equilibrated with 0.1 M pH 8.0 sodium phosphate buffer (10 mL) and spun to dryness in a refrigerated RT-6000B centrifuge before use (16 °C, A-384 rotor). Sample aliquots (100 μL) were applied to the tops of the columns, and following a 5-min equilibration period, the columns were spun for 10 min and the eluents collected into snugly fitting capless 1.5-mL Eppendorf tubes (Sarstedt, Princeton, NJ). Samples were left at room temperature for 3 h to allow H′–L disulfide bonds to reform. Pooled samples were treated with the appropriate volume of 0.1 M EDTA in pH 8.0 phosphate buffer to give a final concentration of 1 mM EDTA; samples prepared in this manner were used immediately for cross-linking experiments. Although actual yields of antibody fragments from mini-spin columns were ~80%, theoretical (100%) yields were used for calculating the cross-linker concentrations indicated below. Variations in the above procedure were also tested in order to evaluate the effects of pH, temperature, protein concentration, and mini-spin loading volume on the preparation of Fab′.

Quantitation of Fab′ Sulfhydryl Groups. Analyses were performed in order to quantitate the number of free sulfhydryl groups in the hinge region of Fab′. In one method, a sample of F(ab′)$_2$ (0.8 mg; from pepsin-digested IgG) was subjected to mild reduction and reoxidation of H′–L disulfide bonds as above and then treated with an equal volume of 20 mM DTNB (Ellman, 1964) to generate the Fab′–TNB adduct. After a few minutes at room temperature, the sample was concentrated on a Centricon-30 unit and residual reagent was removed by the addition of pH 7.0 phosphate buffer (2 × 2 mL) followed by respinning. The sample was then diluted to 1.0 mL with the same buffer and treated with 0.1 M β-mercaptoethanol (10 μL; in pH 7.0 buffer). The yellow color was quantitated by visible absorbance at 412 nm and the concentration of TNB^{2-} anion was determined using an extinction coefficient of 14 150 and applying a correction for the absorbance of the protein (Riddles et al., 1979). The antibody fragment concentration was calculated using the conversion factor of 1.48 per mg/mL at 280 nm (Mandy and Nisonoff, 1963).

Free sulfhydryl groups were also quantitatively evaluated using a modification of a previously reported isoelectric focusing method (Feinstein and Scott, 1972). Fab′ prepared as described above (150 μL) was treated for 30 min at room temperature with 0.2 M of 4-iodoacetamidosalicylic acid (Molecular Probes, Eugene, OR) in DMF (3.75 μL) to give a 5 mM final concentration of the alkylating reagent. A control sample was prepared in a similar manner using iodoacetamide. Following alkylation, the samples were diluted to 2.0 mL with pH 7.0 phosphate buffer, concentrated, and respun with additional buffer (2 × 2 mL) on Centricon-30 units. Analysis of the concentrated samples was performed on a pH 3–10 agarose isoelectric focusing gel obtained from FMC (Rockland, ME). Conditions were as follows: 11 °C, 1500 V, 20 mA, 1 W for 10 min followed by 25 W for 25 min on a Bio-Rad apparatus. The gel was fixed and stained using Coomassie Blue according to the manufacturer's protocol. The total number of interchain cysteines for mildly reduced (but not reoxidized) F(ab′)$_2$ was evaluated by a modified procedure in which mini-spin columns were pre-equilibrated in pH 7.0 phosphate buffer containing 1 mM EDTA, conditions developed to preserve free sulfhydryl groups during the elution step.

Fluorescence tagging was used to determine the location (H′ or L chain) of the Fab′ cysteine. An aliquot of Fab′ prepared as above (50 μL) was treated with 1 mM 5-fluorescein–maleimide (Molecular Probes) in DMF (5 μL) for 30 min at room temperature. SDS–PAGE was performed under nonreducing conditions and the gel was photographed under long-wavelength UV light prior to staining.

General Procedure for Fab′ Cross-Linking. Chemical cross-linking of Fab′ with **1** or **2** was performed as follows. A sample of Fab′ was prepared as described above, yielding approximately 2 mg (4 × 10^{-5} mmol based on MW 50 kDa) in pH 8.0 phosphate buffer containing 1 mM EDTA. Next, a solution of 0.33 mM trismaleimide **1** or 0.25 mM tetramaleimide **2** in DMF was added in four aliquots (10 μL each) over a 1-h period to give a final Fab′ to cross-linker molar ratio of 3:1 for tribody or 4:1 for tetrabody, the theoretical ratio for complete formation of the respective cross-linked fragments. Analytical GF-250 HPLC was used to monitor progress of the reactions, with or without prior alkylation of sample aliquots using excess iodoacetamide. Small aliquots were also removed periodically and quenched with iodoacetamide prior to SDS–PAGE analysis. Following the 1 h reaction period, 0.1 M NEM in DMF (10 μL) was added to give a final concentration of 1 mM. NEM serves to alkylate unreacted sulfhydryl groups; alternatively, excess iodoacetamide can be used. After 15 min at room temperature the entire sample was concentrated on a Centricon-30 unit and injected onto a GF-250 HPLC column using a slow flow rate (0.5 mL/min for tribody, 0.3 mL/min for tetrabody) to allow isolation of the peak of interest.

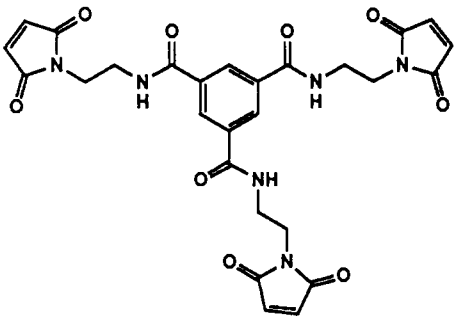
Preparation of Radiolabeled Tribody and Tetrabody. Radiolabeled tribody was prepared as described above, except that ^{105}Rh-labeled F(ab′)$_2$ (pepsin-digested) was used for generation of the Fab′ subunit. Labeling of F(ab′)$_2$ was performed according to a published procedure

(Kruper et al., 1988) in which lysing residues were conjugated by reaction with the isothiocyanate derivative of the radiometal complex ^{105}Rh(BA-2,3,2-tet)Cl_2. Previous studies had demonstrated the non-site-specific nature of conjugation using this complex in that both the heavy and light chains of IgG are radiolabeled. For preparation of radiolabeled tribody, two identical 2.0-mg samples of ^{105}Rh-labeled F(ab')$_2$ (specific activity ~0.1 mCi/mg) were used to prepare Fab' for cross-linking. Following the cross-linking and NEM alkylation steps, the samples were pooled, concentrated, and diluted to 200 μL with pH 7.0 phosphate buffer. GF-250 HPLC isolation was performed using four separate injections. Pooled fractions corresponding to the tribody were concentrated on a Centricon-30 unit, respun twice with PBS (2 × 2 mL), and diluted to 2.0 mL. The overall yield of tribody from F(ab')$_2$ was 18%, based on the Pierce Coomassie assay. Separate preparations of HPLC-isolated tribody were used for blood clearance and biodistribution studies in Balb/c mice, and for a 5-day study in tumor-bearing nude mice.

Radiolabeled tetrabody was prepared by a similar procedure except that two identical samples of ^{105}Rh-labeled Fab' were treated with four additions of 0.25 mM tetramaleimide in DMF (10 μL each), one aliquot every 15 min. Following the 1 h cross-linking step, samples were treated and isolated as described above for the tribody. The overall yield of tetrabody from F(ab')$_2$ was 4% based on the Pierce Coomassie assay. HPLC-isolated tetrabody was used for a 4-h blood-clearance study in Balb/c mice; the same animals were sacrificed at 24 h to obtain biodistribution data (Table II).

Biodistribution Studies. Female athymic nude mice (nu/nu, CD1 background) were obtained from Charles River (Wilmington, MA) at 5–8 weeks of age. Mice were housed on laminar flow racks in cages with filter bonnets and fed autoclaved rodent diet and sterilized tap water ad libitum. Balb/c female mice were obtained from Charles River (Portage, MI) at 4–5 weeks of age. All animals were acclimated at least 1 week prior to experimental use. LS-174T human colorectal carcinoma cell line (ATCC CL-188) was maintained in tissue culture in minimal essential media supplemented with 1% nonessential amino acids, 2 mM glutamine, and 10% fetal bovine serum. Cultures were harvested weekly with trypsin-EDTA and cell density and viability determined by trypan blue dye exclusion. Athymic nude mice were injected sc with 1 × 10^{-6} LS-174T cells/0.1 mL culture media and screened for tumor growth 11–13 days later. Mice bearing tumor xenografts in the range of 100–300 mg were selected for biodistribution studies and sorted into five groups. Prior to injection, four syringes of radioimmunoconjugate were randomly selected and expelled into counting tubes to serve as injection standards. Animals were lightly anesthetized with Metofane (Pittman Moore, Mundelein, IL) and the radioconjugate of interest (1–2 μCi/50 μL) injected into the tail vein. For early time point blood-clearance studies, mice were anesthetized with ketamine hydrochloride (Ketaset, Fort Dodge Laboratories, Fort Dodge, IA) to enable repeated sampling from the same animals. Blood samples for these studies were obtained by retroorbital puncture using heparinized capillary tubes. At 5, 24, 48, and 120 h postinjection, five animals were anesthetized and exsanguinated. The blood was placed in counting tubes and weighed. The liver, spleen, kidneys, and tumor, when present, were removed, rinsed in PBS, blotted dry, and weighed. These tissues were then placed in counting tubes. The GI tract, remaining carcass, and tail were placed directly in counting tubes. Radioactivity was determined using a "well-type" NaI scintillation detector coupled to a ND66 (Nuclear Data, Schaumberg, IL) γ-ray spectrometer and a Searle Model 1185 automatic sample changer (TM Analytic, Elk Grove Village, IL). Statistical outliers were identified and removed from the data set using the ANOVA program (SAS Institute Inc., Cary, NC).

Trismaleimide, 1



Tetramaleimide, 2

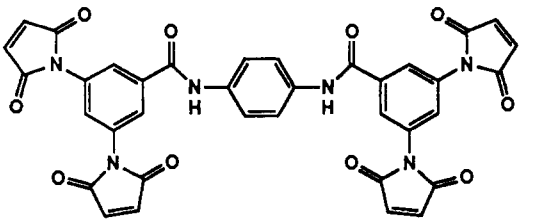


Figure 1. Structures of compounds used for cross-linking Fab' antibody subunits.

RESULTS AND DISCUSSION

Design of Cross-Linkers. A variety of cysteine sulfhydryl modification agents are known from the literature (for a review, see Means and Feeney, 1990). For the present work, we chose the maleimide functionality because of its excellent properties for use in protein covalent modification. These advantages include (a) rapid reactions in the neutral pH range using low, stoichiometric concentrations of protein and reagent, (b) specificity for cysteine sulfhydryl moieties, (c) synthetic accessibility of compounds of interest, and (d) stability of resulting thioether bonds to physiological buffer conditions. Although bromoacetamides are frequently used for modifying sulfhydryl groups on proteins, they are generally less reactive than maleimides (Goldberg et al., 1991) and therefore a greater stoichiometric excess is required. For the cross-linking applications described here, rapid stoichiometric reactions were desirable for obtaining the target immunoconjugates in a straightforward "one-pot" reaction.

Two new compounds, trismaleimide 1 and tetramaleimide 2 (Figure 1), were synthesized as Fab' cross-linking reagents. These multifunctional compounds represent an extension of the series beginning with the bismaleimide reagents previously reported for the preparation of "stabilized" F(ab')$_2$ (Quadri et al., 1992) and bispecific F(ab')$_2$ (Stickney et al., 1988; Glennie et al., 1987). The design of 1 and 2 was influenced by the notion of keeping the structures relatively simple and also taking advantage of known synthetic routes and available starting materials. Compounds 1 and 2 represent a starting point for the preparation of multifunctional antibody fragments; future modifications may be necessary in order to optimize the

structures for Fab′ cross-linking applications. At least one report has appeared on the use of a trifunctional alkylating agent for cross-linking protein subunits (Hiratsuka, 1988). The mustard compound tris(2-chloroethyl)-amine was shown to react with both cysteine sulfhydryl and lysine amine groups in the heavy chain domains of myosin adenosinetriphosphatase. The trifunctional and tetrafunctional reagents described in the present work were expected to be specific for cysteine sulfhydryl groups.

Preparation of **1** was achieved through a multistep procedure involving reaction of the trimethyl ester of 1,3,5-benzenetricarboxylic acid with an excess of ethylene diamine, followed by reaction with maleic anhydride to form a trismaleamate. Reaction of the trismaleamate with sodium acetate in acetic anhydride resulted in cyclization to the symmetrical trismaleimide. Tetramaleimide **2** was prepared using a slightly different approach involving attachment of preformed bismaleimide segments onto a central phenylenediamine moiety. Thus, 3,5-diaminobenzoic acid was converted in two steps to the bismaleimide acid intermediate, followed by formation of the acid chloride, and, finally, reaction with *p*-phenylenediamine to give **2**.

Preparation and Characterization of Fab′. The literature contains numerous methods for the preparation of Fab′ from $F(ab')_2$. In many of the reported procedures, however, the quality of Fab′ produced is less than optimal in that polyacrylamide gel analysis shows the presence of small amounts of H′ and L chains remaining after mild reduction of the parent fragment (Glennie et al., 1987). In the present work, a modification of an older method was used for the preparation of Fab′. The original procedure was developed for the preparation of bispecific $F(ab')_2$ (Nisonoff and Rivers, 1961) and involved reduction of interchain disulfides followed by reoxidation of both H′–L and H′–H′ bonds using a stream of oxygen at pH 8. Under these conditions, Fab′ is a likely intermediate since "intramolecular" (H′–L) disulfide bonds within the Fab′ subunit would be expected to form more rapidly than "intermolecular" (H′–H′) disulfide bonds between the Fab′ subunits.

We report here the preparation of Fab′ from the $F(ab')_2$ fragment of monoclonal antibody CC49 (murine IgG1 subclass). A multistep procedure was developed which involved mild reduction of $F(ab')_2$ followed by selective reoxidation of H′–L disulfide bonds. Preparations typically were carried out on a small scale (2 mg per batch). $F(ab')_2$ was first treated with excess dithiothreitol (20 mM) at neutral pH to effect reduction of all interchain disulfide bonds. Preliminary experiments were conducted to examine the influence of pH on the rate of disulfide bond reduction. As expected, reduction proceeded faster with increasing pH over the range of pH 6–8 (data not shown). Use of phosphate buffer at pH 7 allowed complete reduction of fragment interchain disulfides in less than 15 min (Figure 2a).

Following the mild reduction step, excess reducing agent was removed from reaction mixtures by a rapid gel filtration procedure (Meares et al., 1984), performed here using commercially available "mini-spin" columns. This procedure served both to aerate the elution buffer and to exchange the buffered solution to pH 8, conditions which allowed selective reoxidation of H′–L disulfide bonds (Figure 2b). The results show that formation of disulfide bonds between H′ and L chains was virtually complete following a 3-h incubation period at room temperature. Minimal H′–H′ bond formation was observed over the same time period, although incubation for longer periods did lead to significant formation of the unwanted $F(ab')_2$ dimer. These results are consistent with a relatively fast rate of disulfide bond formation between H′ and L chains compared with the rate of disulfide bond formation between Fab′ subunits.

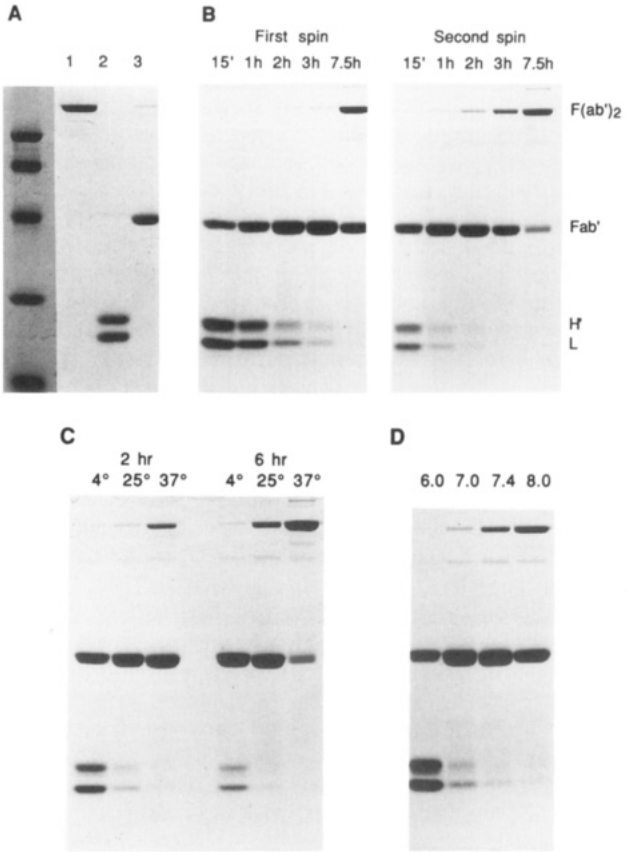


Figure 2. Studies on the preparation of CC49 Fab′ from $F(ab')_2$ by a process of disulfide bond reduction followed by selective reoxidation. In all panels, CC49 $F(ab')_2$ at 2 mg/mL was subjected to mild reduction using dithiothreitol, processed over mini-spin columns and incubated at room temperature (unless otherwise indicated) prior to quenching with excess iodoacetamide (for details see Experimental Procedures). SDS–PAGE analysis was performed on 10% polyacrylamide gels under nonreducing conditions. Molecular weight markers were phosphorylase B (95 kDa), serum albumin (66 kDa), ovalbumin (45 kDa), carbonic anhydrase (31 kDa), and trypsin inhibitor (21.5 kDa). Panel A: Antibody fragment reference standards for reoxidation studies. Lane 1, CC49 $F(ab')_2$; lane 2, $F(ab')_2$ treated with 20 mM DTT for 15 min at room temperature and quenched with iodoacetamide; lane 3, Fab′–pyridyl formed by treatment of mildly reduced fragments with 2,2′-dithiopyridine. Panel B: Time-dependence of disulfide bond reformation following mini-spin processing. $F(ab')_2$ was mildly reduced and aliquots were processed over mini-spin columns at pH 8. Lanes represent aliquots incubated at room temperature for the time periods indicated following one or two mini-spin processing steps. Panel C: Effect of incubation temperature on the rate of disulfide bond formation. $F(ab')_2$ was mildly reduced and processed over mini-spin columns at pH 8, and samples were incubated at various temperatures. Aliquots were quenched with iodoacetamide at postspin times of 2 and 6 h. Panel D: Effect of buffer pH on the rate of disulfide bond formation. $F(ab')_2$ was mildly reduced and processed over mini-spin columns using phosphate buffer adjusted to pH 6.0, 7.0, 7.4, or 8.0. Aliquots were quenched with iodoacetamide following a 6-h incubation time at room temperature.

Evidence pointing to the importance of buffer aeration was obtained from the following two experiments. In the first, mildly reduced $F(ab')_2$ was processed sequentially over two mini-spin columns, both at pH 8. Analysis by SDS–PAGE (Figure 2b) revealed that reoxidation of H′ and L chains to Fab′ was completed in approximately half

the time normally required for reoxidation using a single column. In the second experiment, $F(ab')_2$ was subjected to mild reduction using commercially available DTT beads. Samples were then processed over empty mini-spin columns (no resin, filter only) and left at ambient temperature for several hours. SDS–PAGE analysis revealed that disulfide bond formation was slowly significantly in comparison with the results seen with the usual protocol (data not shown).

Examination of the rate of disulfide bond formation as a function of temperature was carried out over the range 4–37 °C at pH 8 (Figure 2c). The results illustrate that disulfide bond formation is speeded up as the temperature is increased, and that nearly complete reformation of disulfide bonds between H′–L and H′–H′ chain pairs is possible when long incubation times and/or elevated temperatures are used (6 h at 37 °C, for example). Examination of the rate of disulfide bond formation as a function of pH was carried out at room temperature using mini-spin processing conditions ranging from pH 6 to 8 (Figure 2d). Not unexpectedly, the rate of disulfide bond formation was enhanced with increasing pH. It was also evident that a range of pH conditions could be used to produce Fab′, with appropriate adjustments in the incubation time.

Additional observations on the rate of disulfide bond formation were as follows. An increase in the protein concentration was observed to result in a higher proportion of the unwanted dimer form of the fragment when reoxidation was carried out at room temperature. Increasing the mini-spin column loading volume was found to slow reoxidation, presumably due to an increase in amount of DTT which eluted along with the protein fraction. When 1 mM EDTA was included in the mini-spin column elution buffer, disulfide bond formation was slowed dramatically over the pH range 6–8. (This procedure, when carried out at pH 6–7, is useful for the preparation of noncovalently associated H′L pairs). The above results suggest that various combinations of the reoxidation reaction parameters can be used to successfully prepare Fab′ subunits. Conditions selected for the routine preparation of Fab′ were as follows: 2 mg/mL initial concentration of $F(ab')_2$, with pH 8 processing over a mini-spin column (no EDTA present), and a 3-h incubation period at room temperature. Over the course of many experiments, some batch-to-batch variability was noted with respect to the incubation time required for complete H′–L disulfide bond formation, but 3 h appeared to be the average time required.

When EDTA was added to solutions containing Fab′ following the incubation period, subsequent disulfide bond formation was slowed dramatically at pH 8 and to a lesser extent at pH 7 (Figure 3). Therefore, Fab′-containing solutions were routinely made to 1 mM in EDTA following the oxidation step in order to slow dimerization. The presence of a small amount of dimer was not of concern, however, because the dimer could be separated from the higher molecular weight tribody or tetrabody product at a later time by gel filtration chromatography. If desired, the pH of the final solution containing Fab′ could be adjusted to a lower value to further slow dimerization while still allowing rapid reaction of the Fab′ sulfhydryl with the cross-linking reagent. However, the use of a pH 8 buffer was found to be convenient for both the Fab′ reoxidation and for the subsequent cross-linking step.

Following confirmation of the desired 50-kDa species by SDS–PAGE analysis, characterization of Fab′ also involved quantitation of hinge-region sulfhydryl groups.

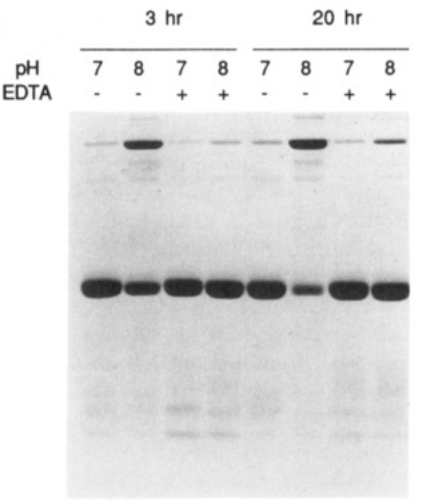


Figure 3. Effect of EDTA on the stability of Fab′. CC49 Fab′ was prepared by the standard protocol, and following the usual 3-h incubation period, the buffer was either adjusted to pH 7 or left at pH 8 in the presence or absence of 1 mM EDTA. The final concentration of Fab′ was approximately 1 mg/mL. Sample aliquots were quenched with iodoacetamide after 3 or 20 h at room temperature.

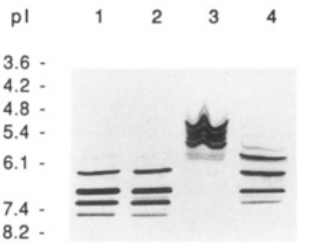


Figure 4. Isoelectric focusing analysis of charge-modified CC49 Fab′ and H′–L pairs. $F(ab')_2$ was mildly reduced and processed over mini-spin columns in one of two ways: At pH 7.0 in the presence of EDTA, to yield the H′L pair (lanes 1 and 3), or at pH 8.0 in the absence of EDTA, to yield Fab′ after the usual 3-h incubation period (lanes 2 and 4). Aliquots were then quenched either with iodoacetamide (lanes 1, 2) or with 4-iodoacetamidosalicylic acid (lanes 3, 4).

Murine IgG is known to possess three disulfide bonds in the hinge region. In published works, determination of free cysteines on Fab′ (prepared by the mild reduction of $F(ab')_2$ from pepsin-digested IgG1) reportedly gave close to the expected value using the colorimetric reagents 2,2′-dithiopyridine (Glennie et al., 1987) and DTNB (Brennan et al., 1985). Quantitation of free sulfhydryl groups on CC49 Fab′ by the latter method gave a TNB^{2-} to Fab′ molar ratio of 1.1:1. That the ratio was approximately 1:1 and not 3:1 suggests that two of the three hinge region sulfhydryl groups were reoxidized to form an intrachain disulfide bond, leaving one free sulfhydryl group available for subsequent modification.

Sulfhydryl groups on Fab′ were also quantitatively evaluated using a modification of a method reported by Feinstein and Stott (1972). The procedure involves chemical modification of a protein with a negatively charged alkylation reagent such as iodoacetic acid followed by isoelectric focusing analysis. In the present work, a single charge shift was observed by IEF analysis following alkylation of Fab′ with 4-iodoacetamidosalicylic acid (Figure 4, lane 4), indicating the presence of a single hinge-region cysteine. An advantage of using iodoacetamidosalicylic acid compared with iodoacetic acid was its reduced tendency to generate contaminating iodine (a sulfhydryl oxidant) upon storage. Also, iodoacetamidosalicylic acid was found to react more rapidly with Fab′ cysteine sulfhydryl groups (data not shown). In a variation of the

IEF analysis, mini-spin processing was carried out at pH 7 in the presence of 1 mM EDTA. Under these conditions, the newly generated cysteine sulfhydryls were preserved in their reduced state. IEF analysis of charge-modified Fab′ prepared in this manner (actually the noncovalently associated H′L pair) showed a striking shift toward the cathode, indicating charge modification at several cysteine residues (Figure 4, lane 3). This result is consistent with the expected number of sulfhydryls (five) for mildly reduced murine IgG1-derived Fab′. Control samples of Fab′ or the H′L pair which were alkylated with neutral reagents (NEM, iodoacetamide) showed no charge shifts by this analysis. Comparative IEF analysis showed that Fab′ prepared from both papain- and pepsin-digested $F(ab')_2$ gave virtually identical charge shifts following mild reduction and alkylation with 4-iodoacetamidosalicylic acid.

In a qualitative test to further define the location of the free cysteine, Fab′ was treated with an excess of 5-fluorescein–maleimide and analyzed by SDS–PAGE (data not shown). Under nonreducing conditions, a single fluorescent band was observed near 50 kDa. When a sample of fluorescein-modified Fab′ was subjected to mild reduction and alkylation prior to gel analysis, a fluorescent band corresponding to the migration of the H′ chain was observed, consistent with a pattern hinge-region modification.

The air-oxidation procedure described here for the preparation of Fab′ has several advantages over known methods. First, Fab′ is produced as a homogeneous product, with minimal dimer formation and lacking contamination from noncovalently bonded H′ and L chains (which would remain associated under neutral aqueous conditions). The fact that virtually all H′ and L chains are reconnected through disulfide bonds is significant in that no unwanted chemical cross-linking can occur at these sites. For some applications involving "intramolecular" cross-linking of cysteines in mildly reduced IgG, it may be desirable to effect covalent attachment of antibody heavy and light chains with sulfhydryl-specific modification reagents (Packard and Ededin, 1986; Liberatore et al., 1990; Goldberg et al., 1991). However, the successful preparation of $F(ab')_3$-x and $F(ab')_4$-x depends upon selective cross-linking at hinge-region sulfhydryl groups, and not between H′ and L chains.

A second advantage is that preparation of Fab′ is straightforward and does not involve time-consuming dialysis steps, and the entire procedure is completed in under 4 h. The resulting Fab′-containing solution is ready for use in subsequent chemical modification reactions or can be stored frozen for future use. Fab′ can also be prepared by a procedure proposed recently by Glennie and co-workers (1987). In this method, use of 2,2′-dithiopyridine apparently leads both to H′–L disulfide formation and to formation of a mixed disulfide at the hinge region to yield Fab′–pyridyl. The pyridyl group is then selectively removed by treatment with a reducing agent at low pH. In our hands, this method was found to yield a homogeneous preparation of Fab′–pyridyl (Figure 2a) and its reduced counterpart, Fab′ (not shown). However, the method involves additional steps compared with the air-oxidation protocol. Although not explored here, an alternative procedure for Fab′ preparation would be the controlled delivery of air or oxygen to a solution containing the mildly reduced fragment, in the manner reported previously for the preparation of $F(ab')_2$ heterodimers (Nisonoff and Rivers, 1961; Staerz and Bevan, 1986).

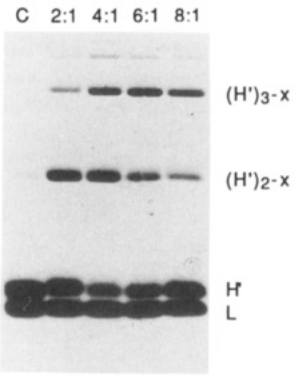


Figure 5. SDS–PAGE analysis of $F(ab')_3$-x preparation trials. CC49 $F(ab')_2$ was subjected to mild reduction, reoxidation, and incubation at pH 8 as described. Aliquots of Fab′ solution were then treated with trismaleimide 1 using the molar ratios indicated (given as 1:Fab′). Following a 1-h reaction period at room temperature, samples were subjected to mild reduction with dithiothreitol and alkylation with excess iodoacetamide to permit visualization of H′ and L chains as distinct bands under nonreducing conditions. Lane C represents control Fab′ with no cross-linker added.

Preparation of Multivalent Cross-Linked Antibody Fragments. Trismaleimide 1 was used for the development of suitable reaction conditions for joining Fab′ subunits. For these experiments, Fab′ was used as a 4×10^{-5} M solution (2 mg/mL) in pH 8 phosphate buffer. The results of a study designed to determine the optimal fragment to cross-linker ratio are shown in Figure 5. In this experiment, individual aliquots of freshly prepared Fab′ were treated with varying concentrations of 1 for 30 min at ambient temperature. Reaction mixtures were analyzed by SDS–PAGE under nonreducing conditions following mild reduction and alkylation, a treatment which allowed separation of the H′ and L bands. The data revealed that a Fab′ to 1 ratio of approximately 4:1 to 6:1 was optimal for tribody formation, as evidenced by an increase in intensity of the band corresponding to the cross-linked H′ chain (H'_3-x, 75 kDa). The observed decrease in the intensity of the H′ band (25 kDa) indicated that nearly all hinge-region sulfhydryl groups were reacted with the cross-linking reagent. Analysis of reaction mixtures by gel filtration HPLC yielded similar results (data not shown). In theory, a Fab′ to 1 ratio of 3:1 should be optimal for complete cross-linking. The discrepancy may be due in part to the loss of protein incurred during the mini-spin elution step (recoveries were ~80%).

One possible explanation for the incomplete formation of $F(ab')_3$-x from Fab′ is that side reactions may occur on non-cysteine residues, leading to the loss of one or more reactive maleimide functionalities (Glennie et al., 1987). This possibility also may explain the presence of small amounts of high molecular weight species that were often observed by SDS–PAGE or gel filtration HPLC. Also, the presence of more than one free cysteine in the hinge region of some Fab′ molecules could lead to unwanted multimeric species. While our analytical results suggested the presence of a single sulfhydryl group on average, the possibility exists that some of the Fab′ molecules were heterogeneous in this respect.

Various other observations from tribody preparation trials are noteworthy. Use of either pepsin or papain-derived fragments gave similar results in small-scale cross-linking reactions. (Due to availability, the former were used for most of the early analytical studies, and the latter were used for preparation of radiolabeled tribody and tetrabody for in vivo studies.) Cross-linking was observed to proceed faster with increasing pH (over the range pH

6–8), although similar product profiles were observed upon completion of the reaction. When a shorter incubation period than 3 h was used for Fab′ formation, the yield of $F(ab')_3$-x was decreased. A likely explanation is that disulfide formation within Fab′ subunits was incomplete, allowing "extra" cysteines on H′ and L chains to participate in cross-linking reactions. Alternatively, a low concentration of unoxidized DTT may have been present following the shorter incubation period, leading to rapid consumption of the cross-linking reagent.

$F(ab')_3$-x was found to be stable over a 6-h period at room temperature when exposed to buffer conditions in the pH range 7.0–8.8. Stability was monitored by SDS–PAGE under nonreducing conditions (data not shown). In contrast, $F(ab')_3$-x was slowly degraded at pH 9.6, as evidenced by the appearance of two new bands near 50 and 100 kDa, presumably the monomeric and dimeric forms of Fab′. (We also observed a pH-related instability for the bismaleimidooctane cross-linked fragment, $F(ab')_2$-x, which was approximately 50% degraded to a 50-kDa product after 24 h at pH 9.6.) Although the maleimide-derived thioether bond is considered to be stable to physiological conditions, it appears to be unstable at high pH, as has been noted previously for maleimide adducts of cysteine (Smyth et al., 1960).

Preparation of Radiolabeled Tribody and Tetrabody. Because of the observed instability of maleimide-cross-linked fragments at high pH, we decided to prepare radiolabeled $F(ab')_3$-x and $F(ab')_4$-x for animal studies using Fab′ generated from prelabeled $F(ab')_2$. This strategy avoided subjecting the unlabeled cross-linked products to the basic conditions (pH ≥ 9) typically required for attachment of the radiometal chelate to lysine residues. Radiolabeled $F(ab')_2$ was prepared via conjugation of lysine amines with the isothiocyanate derivative of the radiometal complex ^{105}Rh(BA-2,3,2-tet)Cl_2 (Kruper et al., 1988). As it possesses both γ- and β-emissions, ^{105}Rh is a candidate for use in cancer immunotargeting applications (Volkert et al., 1991). The stable radiometal chelate complex was favored for biodistribution studies over radioiodine due to the apparent tendency of the latter to dehalogenate in organs (Carrasquillo et al., 1984). Furthermore, it was expected that conjugation of the ^{105}Rh(BA-2,3,2-tet)Cl_2 complex onto lysine residues would lead to no net charge change, since the complex itself was believed to possess an overall charge of +1. This expectation was confirmed by isoelectric focusing analysis.

Radiolabeled $F(ab')_3$-x was prepared by addition of trismaleimide **1** to a freshly prepared sample of ^{105}Rh-labeled Fab′. A final Fab′ to **1** molar ratio of 3:1 was achieved by the addition of several small aliquots of the cross-linking reagent. This procedure was used for the preparative reactions in order to maximize formation of the desired product without risking local high concentrations of the cross-linker, and to prevent overaddition of the reagent. The composition of reaction mixtures was assessed by analytical SDS–PAGE with autoradiographic detection (Figure 6a). Under nonreducing conditions, a band corresponding to $F(ab')_3$-x was observed (150 kDa) along with bands corresponding to dimer and Fab′ monomer (100 and 50 kDa, respectively). Under reducing conditions, a band corresponding to cross-linked H′ chains (75 kDa) was observed, along with a lower molecular weight band presumably corresponding to H'_2-x. Following a brief alkylation step with *N*-ethylmaleimide, ^{105}Rh-labeled $F(ab')_3$-x was isolated by gel filtration chromatography (Figure 7a). HPLC analysis of the isolated product gave a single peak by both UV and radioactivity detection

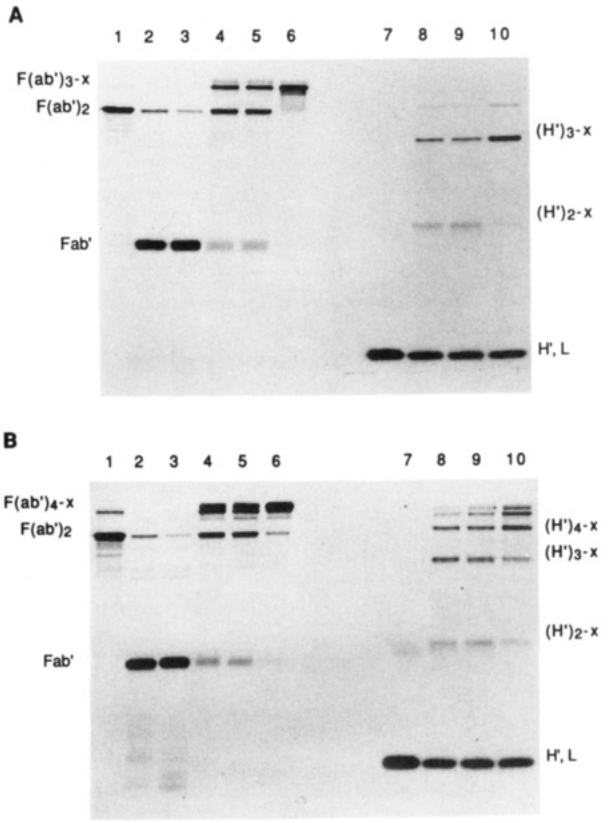


Figure 6. SDS–PAGE autoradiographic visualization of radiolabeled CC49 $F(ab')_3$-x and $F(ab')_4$-x preparations. For the cross-linking reactions, freshly prepared ^{105}Rh(BA-2,3,2-tet)-labeled Fab′ was treated with the theoretical molar excess of either trismaleimide **1** (panel A) or tetramaleimide **2** (panel B) as detailed in Experimental Procedures. Samples were run under nonreducing conditions (lanes 1–6) or reducing conditions (lanes 7–10). Lanes 1 and 7, radiolabeled $F(ab')_2$ starting material; lanes 2 and 3, Fab′ (identical samples in separate reaction vials); lanes 4, 5, 8, and 9, crude reaction mixtures following addition of cross-linker; lanes 6 and 10, GF-250 HPLC-isolated product.

(Figure 7a). The results of SDS–PAGE/autoradiography (Figure 6a) confirmed the purity of the isolated product, and revealed the presence of bands corresponding to H_3-x and L under reducing conditions.

Radiolabeled $F(ab')_4$-x was prepared in a similar manner, except that the final molar ratio of Fab′ to tetramaleimide **2** was 4:1. By SDS–PAGE/autoradiographic analysis, only a small fraction of protein in the reaction mixture corresponded to the desired 200-kDa product (Figure 6b). Other gel bands corresponded to lower molecular weight species including the trimeric, dimeric, and monomeric forms of Fab′. As shown in Figure 7b, HPLC-isolated ^{105}Rh-labeled $F(ab')_4$-x remained contaminated with tribody and unidentified high molecular weight forms. The low isolated yield of tetrabody permitted only a preliminary biodistribution study to be carried out in Balb/c mice. As it is possible that the characteristics of the cross-linking reagent (e.g. hydrophobicity, linker length) may play a role in its ability to react with sulfhydryl groups on Fab′, tetramaleimide **2** may not be an optimal reagent.

Immunoreactivity of the radiolabeled cross-linked fragments was assessed by ELISA (Figure 8). Unconjugated and ^{105}Rh-labeled $F(ab')_2$ showed similar profiles, while both the radiolabeled $F(ab')_3$-x and $F(ab')_4$-x forms showed enhanced binding compared to $F(ab')_2$. A possible explanation for the higher absorbance values observed at low dilution is that the second antibody may be capable of binding to more sites on the cross-linked fragments compared with $F(ab')_2$. Since both ^{105}Rh-labeled $F(ab')_3$-x

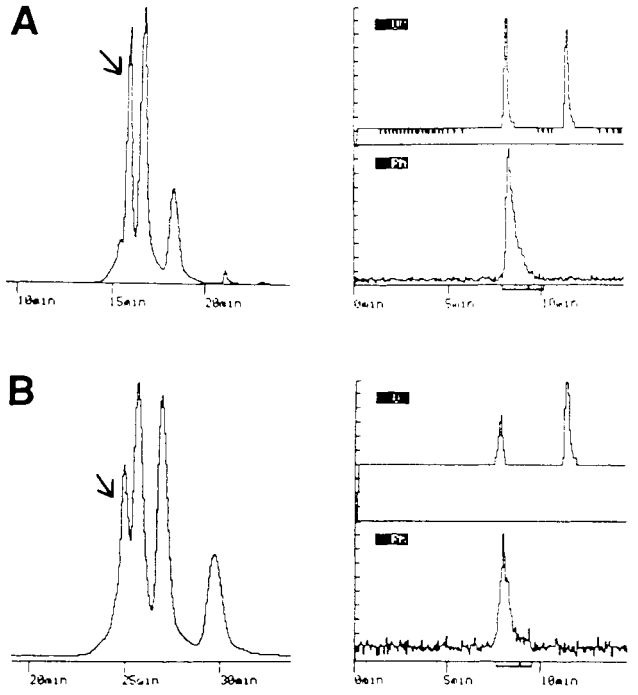


Figure 7. Gel filtration HPLC analysis of radiolabeled $F(ab')_3$-x and $F(ab')_4$-x reaction mixtures and isolated products. ^{105}Rh-labeled CC49 $F(ab')_3$-x (panel A) and $F(ab')_4$-x (panel B) were prepared as described, and product mixtures were subjected to GF-250 isolation. Preparative HPLC profiles with UV detection are shown on the left (note different windows of time shown for the two samples). Arrows indicate the peaks collected. Analytical profiles of the isolated $F(ab')_3$-x and $F(ab')_4$-x products are shown at right, with both UV detection (top) and radioactivity (bottom) detection shown. Flow rates for the isolation of $F(ab')_3$-x and $F(ab')_4$-x were 0.5 and 0.3 mL/min, respectively; the flow rate for analytical runs was 1.0 mL/min. The UV peak near 12 min was probably due to buffer salts.

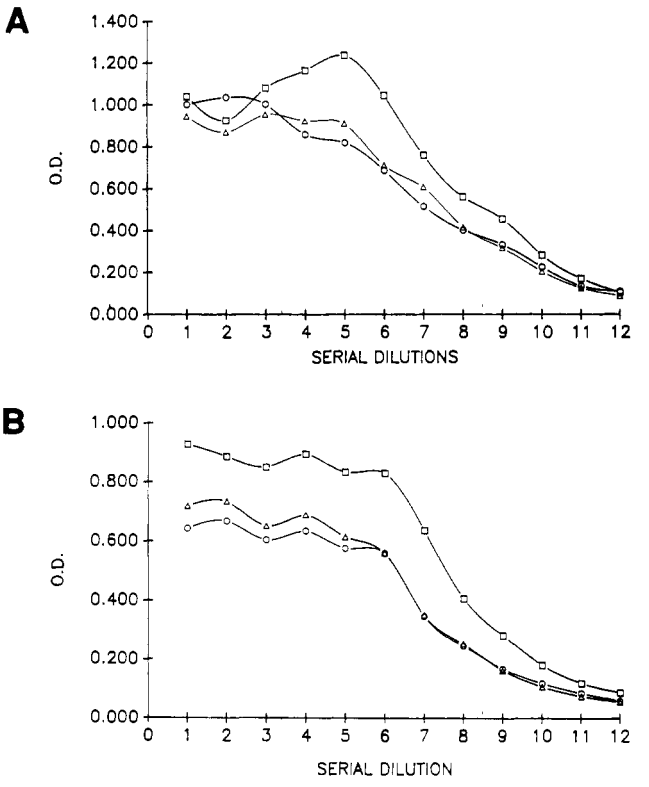


Figure 8. ELISA immunoreactivity analysis of ^{105}Rh-labeled CC49 $F(ab')_3$-x and $F(ab')_4$-x. HPLC-isolated tribody (panel A, squares) and tetrabody (panel B, □) were assessed for immunoreactivity by ELISA and compared in the same assay with unconjugated $F(ab')_2$ (○) and ^{105}Rh-labeled $F(ab')_2$ (△). Starting concentrations for all antibody forms were 10 μg/mL, and partially purified TAG-72 was used as antigen as detailed in Experimental Procedures.

and $F(ab')_4$-x were immunoreactive, it appeared that the cross-linking procedures did not compromise the ability of these forms to bind antigen in a solid-phase assay. (In previous studies, the bismaleimide-cross-linked $F(ab')_2$-x was found to retain full immunoreactivity compared with unmodified $F(ab')_2$).

Animal Biodistribution Studies. A preliminary biodistribution study comparing ^{105}Rh-labeled $F(ab')_2$ and $F(ab')_3$-x was carried out in Balb/c mice. Figure 9a shows early blood values and Table I lists biodistribution data for the same animals at 24 h postinjection. Compared with $F(ab')_2$, $F(ab')_3$-x showed a longer blood residence time and decreased kidney localization. Significantly higher liver, spleen, carcass, and whole-body retention levels were observed for $F(ab')_3$-x. The fact that both $F(ab')_2$ and $F(ab')_3$-x lack the Fc region may correlate with their relatively rapid blood clearance, since this segment is believed to be responsible for the long circulation time of the intact immunoglobin molecule (Waldmann and Strober, 1969).

The biodistribution of ^{105}Rh-labeled $F(ab')_4$-x in Balb/c mice was also studied. Results of a blood sampling study (Figure 9b) indicated that clearance of $F(ab')_4$-x from the circulation was similar to that of $F(ab')_2$ at early time points. Biodistribution data obtained for the same animals at 24 h (Table II) showed significantly greater localization of the radiolabel in the liver for $F(ab')_4$-x compared with $F(ab')_2$. Kidney localization was decreased, while spleen and whole-body retention were increased for the $F(ab')_4$-x. It seems plausible that the extensive accumulation of radiolabel in the liver for $F(ab')_4$-x may account for the relatively low accumulation in other organs. No further animal work was performed with $F(ab')_4$-x due to its high liver localization. Rapid localization of high molecular weight antibody complexes to liver has previously been reported by Goodwin and co-workers (1988).

The results of a 5-day biodistribution study in tumor-bearing nude mice with ^{105}Rh-labeled $F(ab')_3$-x are shown in Figure 10. For purposes of comparison, animal data for radiolabeled IgG and $F(ab')_2$ are also plotted, although these data were obtained in separate experiments (unpublished results). Blood- and whole-body clearance curves for $F(ab')_3$-x were more similar to those of $F(ab')_2$ than IgG, while kidney clearance more closely resembled that of IgG, consistent with the Balb/c result. Tumor accumulation of $F(ab')_3$-x appeared to be greater than that of $F(ab')_2$, although only the final time point was significantly different. Enhanced tumor uptake likely correlates with the longer blood residence time observed for $F(ab')_3$-x (W. Goeckeler, unpublished observations). The liver and spleen data were intermediate between those of IgG and $F(ab')_2$. Tumor to tissue ratios for radiolabeled $F(ab')_3$-x, $F(ab')_2$ and IgG are compared in Table III. At 120 h, the radiolabeled $F(ab')_3$-x gave radiolocation index (RI) values in between those of $F(ab')_2$ and IgG for liver, spleen, and kidney, with the kidney RI value more closely resembling that of $F(ab')_2$. However, the high blood RI value (65.3) achieved for $F(ab')_3$-x at 120 h was higher than for the other two antibody forms.

The kidney results for $F(ab')_3$-x are perhaps not surprising when molecular weight is considered. A species as large as 150 kDa would not be expected to pass through the kidney glomerulus. The fact that $F(ab')_2$ (100 kDa) enters the kidney supports the concept that other properties such as shape may influence the filtration process

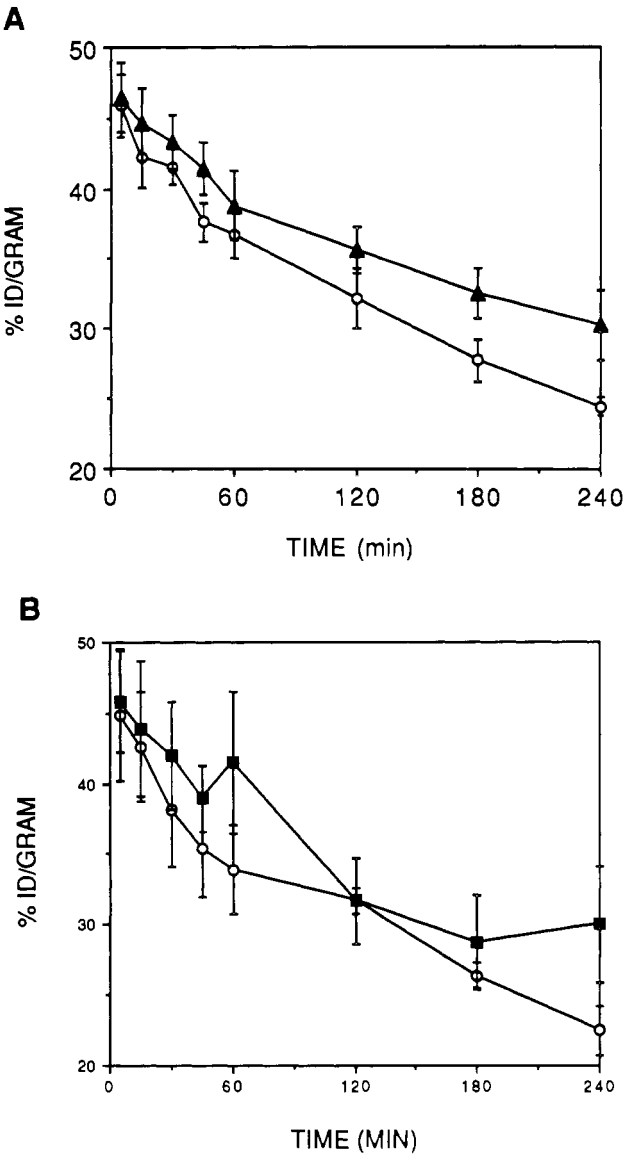


Figure 9. Comparison of blood-clearance curves for ^{105}Rh-labeled CC49 F(ab')$_3$-x and F(ab')$_4$-x Balb/c mice. Panel A shows F(ab')$_2$ (○) and F(ab')$_3$-x (▲). Panel B shows F(ab')$_2$ (○) and F(ab')$_4$-x (■). Blood samples were obtained at various times after iv injection of radiolabeled antibody (four or five animals per group).

Table I. Comparison of Biodistribution Data for ^{105}Rh-Labeled F(ab')$_2$ and F(ab')$_3$-x in Balb/c Mice[a]

	% injected dose/g		% injected dose/organ	
tissue	F(ab')$_2$ avg ± SD[b,e]	F(ab')$_3$-x avg ± SD[c,e]	F(ab')$_2$ avg ± SD[b,e]	F(ab')$_3$-x avg ± SD[c,e]
blood	3.07 ± 0.88	10.74 ± 1.53	4.06 ± 1.10	13.47 ± 1.26
liver	8.93 ± 0.19	16.08 ± 1.91	9.30 ± 0.17	15.22 ± 0.56
spleen	5.36 ± 0.42	10.37 ± 1.01	0.60 ± 0.03	1.04 ± 0.17
kidney	63.49 ± 3.97	12.14 ± 1.57	15.47 ± 0.77	2.93 ± 0.23
GI tract	nd[d]	nd	3.84 ± 0.38	5.57 ± 0.67
carcass	nd	nd	21.81 ± 1.01	32.66 ± 2.44
whole-body retention	nd	nd	53.16 ± 1.98	64.32 ± 3.86

[a] Radiolabeled antibody was administered intravenously, and animals were sacrificed at 24 h. [b] n = 5. [c] n = 5, except for blood value where n = 4. [d] nd = no data obtained. [e] SD = standard deviation.

(Sumpio, 1981). A recent investigation (Takakura et al., 1990) of the biodistribution of large and small macromolecules showed that while small species (<10 kDa) generally clear rapidly into the urine, positively charged species are taken up by the liver, and large and negatively charged species exhibit prolonged retention in the circulation. Similar overall results were also reported for synthetic branched polypeptides which differed in size, charge, and side-chain structure (Clegg et al., 1990). The biodistribution results for F(ab')$_3$-x appear to be consistent with these findings. Additionally, since the pI ranges of both the tribody and tetrabody remained unchanged from that of the parent F(ab')$_2$ fragment (pI = 6.5–7.0), it seems unlikely that charge alone played a significant role in the observed biodistribution patterns.

Table II. Comparison of Biodistribution Data for ^{105}Rh-Labeled F(ab')$_2$ and F(ab')$_4$-x in Balb/c Mice[a]

	% injected dose/g		% injected dose/organ	
tissue	F(ab')$_2$ avg ± SD[b,e]	F(ab')$_4$-x avg ± SD[c,e]	F(ab')$_2$ avg ± SD[b,e]	F(ab')$_4$-x avg ± SD[c,e]
blood	4.30 ± 1.23	6.12 ± 1.98	4.86 ± 0.92	7.08 ± 2.11
liver	6.68 ± 0.87	29.58 ± 2.28	7.10 ± 0.46	30.09 ± 1.81
spleen	6.08 ± 0.83	16.62 ± 1.46	0.40 ± 0.04	1.16 ± 0.08
kidney	65.37 ± 7.78	9.88 ± 1.02	15.49 ± 0.24	2.40 ± 0.26
GI tract	nd	nd	3.48 ± 0.50	2.81 ± 0.22
carcass	nd	nd	19.50 ± 0.96	17.92 ± 1.50
whole-body retention	nd	nd	48.11 ± 1.97	57.23 ± 3.33

[a] Radiolabeled antibody was administered intravenously, and animals were sacrificed at 24 h. [b] n = 5. [c] n = 4. [d] nd = no data obtained. [e] SD = standard deviation.

Table III. Comparison of Tumor to Tissue Ratios for ^{105}Rh-Labeled CC49 F(ab')$_3$-x, F(ab')$_2$, and IgG in Athymic Nude Mice Bearing LS-174T Tumor Xenografts[a]

	RI Values			
organ	5 h	24 h	48 h	120 h
		^{105}Rh-F(ab')$_3$-x		
blood	0.6	3.8	24.3	65.3
liver	1.5	3.3	5.7	6.4
spleen	2.0	4.8	11.1	13.3
kidney	0.8	2.8	6.5	7.1
		^{105}Rh-F(ab')$_2$		
blood	0.9	7.4	31.0	30.0
liver	1.9	4.2	5.3	4.0
spleen	2.9	5.9	8.6	7.5
kidney	0.4	0.6	1.2	1.5
		^{105}Rh-IgG		
blood	0.4	3.7	4.8	8.1
liver	0.8	6.8	9.0	15.2
spleen	1.4	10.1	13.0	21.1
kidney	1.5	18.0	26.7	42.2

[a] Radiolocalization Indices (RI) were calculated as the ratio of %ID/g for tumor divided by %ID/g for normal tissues.

In comparative biodistribution studies carried out previously, we found that native CC49 F(ab')$_2$ and bismaleimide-cross-linked F(ab')$_2$-x showed virtually identical behaviors in tumor-bearing athymic mice. This result contrasts with the observations of Quadri et al. (1992), who observed significantly longer plasma circulation times and enhanced tumor uptake for three different bismaleimide-cross-linked fragments compared with native F(ab')$_2$. One possible explanation for this discrepancy is that the circulation time may be influenced by the number of hinge-region disulfide bonds in the particular F(ab')$_2$ under study.

Overall, the in vivo behavior of F(ab')$_3$-x reveals a combination of relatively fast blood clearance, low kidney accumulation, and low to moderate tumor uptake when compared with intact IgG, F(ab')$_2$, and Fab (data not shown). These results suggest possible uses for F(ab')$_3$-x in immunotargeting applications where the long blood-residence time of IgG, and the high level of kidney accumulation of F(ab')$_2$ or Fab, are preferably avoided. Additionally, antibody species lacking the Fc region might

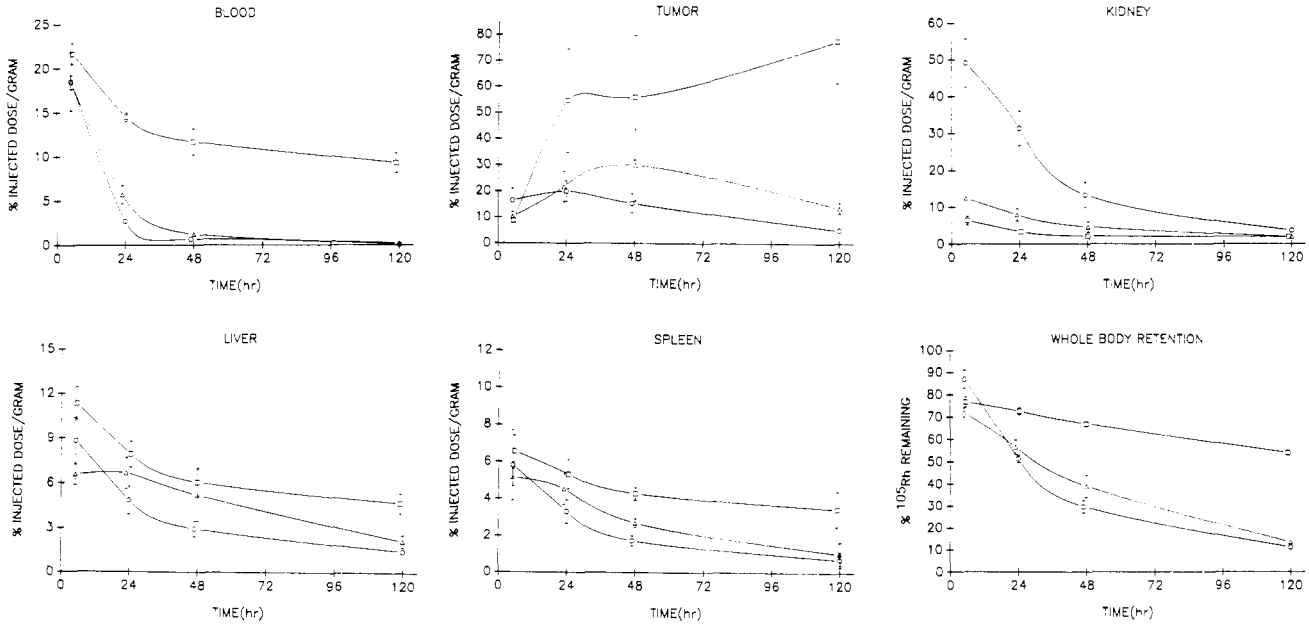


Figure 10. Biodistribution of ^{105}Rh-labeled CC49 F(ab')$_3$-x and other antibody forms in athymic mice bearing LS-174T tumor xenografts. Radiolabeled ^{105}Rh-labeled CC49 IgG (□), F(ab')$_2$ (○), and F(ab')$_3$-x (△) were injected iv in separate but otherwise identical experiments, and five animals were sacrificed at each time point as described in Experimental Procedures.

be expected to show decreased immunogenicity compared with the whole antibody.

SUMMARY AND CONCLUSION

Two new antibody fragment forms, F(ab')$_3$-x and F(ab')$_4$-x, were constructed from Fab' subunits using multifunctional cross-linking reagents. These two species can be considered an extension of the fragment series beginning with Fab' and bismaleimide-cross-linked F(ab')$_2$. Sufficient quantities of the radiolabeled target fragments were prepared for preliminary studies in Balb/c mice, and in the case of F(ab')$_3$-x, for a 5-day study in tumor-bearing nude mice. A large fraction of the radiolabeled tetrabody was found to accumulate in the liver, possibly indicating an upper size limit for the in vivo use of fragments constructed from Fab'. The in vivo behavior of F(ab')$_3$-x in both Balb/c and tumor-bearing nude mice was intermediate between that of IgG and F(ab')$_2$ for all organs studied. Kidney localization was significantly reduced, and blood circulation time and tumor accumulation were slightly increased for the trivalent species compared with F(ab')$_2$. These results are consistent with previous observations that immunoglobulin forms lacking the Fc region clear relatively rapidly from the circulation and that large macromolecules cannot penetrate the kidney glomerulus. On the basis of these results, F(ab')$_3$-x appears to be an interesting new antibody form with potentially useful properties for immunotargeting applications. The methodology developed for the preparation and cross-linking of Fab' subunits should also be applicable to small genetically designed antibody forms bearing a free cysteine moiety. This concept was recently demonstrated by Cumber and co-workers (1992), who introduced a carboxyl-terminal cysteine onto Fv and then used a bismaleimide cross-linker to form the bivalent Fv. Molecules possessing several antigen binding moieties would be expected to show enhanced antigen binding relative to the monovalent and divalent forms. It may also be possible to construct hetero-multivalent molecules possessing two or more different antigen-binding specificities.

ACKNOWLEDGMENT

The authors are grateful to W. J. Kruper for providing BA-2,3,2-tet, J. Coleman for providing antibody fragments, V. Treppa for performing antigen binding analysis, and G. Spittka and W. Goeckeler for providing technical assistance during the animal biodistribution experiments. We thank J. Schlom for providing the CC49 producing cell lines.

Note added in proof: A research article concerning a similar subject matter has been published and has just now come to our attention: Tutt, A., Stevenson, G. T., and Glennie, M. J. (1991) Trispecific F(ab')$_3$ derivatives that use cooperative signaling via the TCR/CD3 complex and CD2 to activate and redirect resting cytotoxic T cells. *J. Immunol. 147*, 60–69. While no in vivo biodistribution data was reported in this paper, and different cross-linking compounds were employed, the antibody products were similar to those we described.

LITERATURE CITED

Brennan, M., Davison, P. F., and Paulus, H. (1985) Preparation of bispecific antibodies by chemical recombination of monoclonal immunoglobulin G1 fragments. *Science 229*, 81.

Carrasquillo, J. A., Krohn, K. A., Beaumier, P., McGuffin, R. W., Brown, J. P., Hellstrom, K. E., Hellstrom, I., and Larson, S. M. (1984) Diagnosis of and therapy for solid tumors with radiolabeled antibodies and immune fragments. *Cancer Treat. Rep. 68*, 317.

Christensen, E. I., Rennke, H. G., and Carone, F. A. (1983) Renal tubular uptake of protein: effect of molecular charge. *Renal Fluid Electrolyte Physiol. 13*, F436.

Clegg, J. A., Hudecz, G., Pimm, M. V., Szekerke, M., and Baldwin, R. W. (1990) Carrier design: biodistribution of branched polypeptides with a poly(L-lysine) backbone. *Bioconjugate Chem. 1*, 425.

Colcher, D., Filomena, M. F., Roselli, M., Muraro, R., Simpson-Milenic, D., and Schlom, J. (1988) Radioimmunolocalization of human carcinoma xenografts with B72.3 second generation monoclonal antibodies. *Cancer Res. 48*, 4597.

Cumber, A. J., Ward, S. E., Winter, G., Parnell, G. D., and Warwrzynczak, E. J. (1992) Comparative stabilities in vitro and in vivo of a recombinant mouse antibody FvCys fragment and a bisFvCys conjugate. *J. Immunol. 149*, 120.

Demignot, S., Pimm, M. V., and Baldwin, R. W. (1990) Comparison of biodistribution of 791T/36 monoclonal antibody and its Fab/c fragment in balb/c mice and nude mice bearing human tumor xenographs. *Cancer Res. 50*, 2936.

Ellman, G. (1959) Tissue sulfhydryl groups. *Arch. Biochem. Biophys. 82*, 70.

Feinstein, A., and Stott, D. I. (1972) An electrofocusing technique for the analysis of thiol proteins applied to a mixture of intracellular plasmacytoma proteins. *J. Physiol. 226*, 34.

French, R. R., Courtenay, A. E., Ingamells, S., Stevenson, G. T., and Glennie, M. J. (1991) Cooperative mixtures of bispecific $F(ab')_2$ antibodies for delivering saporin to lymphoma in vitro and in vivo. *Cancer Res. 51*, 2353.

Fujimori, K., Covell, D. G., Fletcher, J. E., and Weinstein, J. N. (1989) A modeling analysis of monoclonal antibody percolation through solid tumors. *J. Nucl. Med. 30*, 903.

Glennie, M. J., McBride, H. M., Worth, A. T., and Stevenson, G. T. (1987) Preparation and performance of bispecific $F(ab')_2$ antibody containing thioether linked Fab' fragments. *J. Immunol. 139*, 2367.

Goding, J. W. (1986) Fragmentation of monoclonal antibodies. In *Monoclonal antibodies: Principles and practice, 2nd ed.*, Section 4.5, Academic Press, New York.

Goldberg, M., Knudsen, K. L., Platt, D., Kohen, F., Bayer, E. F., and Wilchek, M. (1991) Specific interchain cross-linking of antibodies using bismaleimides. Repression of ligand leakage in immunoaffinity chromatography. *Bioconjugate Chem. 2*, 275.

Goodwin, D. A., Meares, C. F., McCall, M. J., McTigue, M., and Chaovapong, W. (1988) Pre-targeted immunoscintigraphy with indium-111-labeled bifunctional haptens. *J. Nucl. Med. 29*, 226.

Hiratsuka, T. (1988) Cross-linking of three heavy-chain domains of myosin adenosinetriphosphatase with a trifunctional alkylating agent. *Biochemistry 27*, 4110.

Johnson, V. G., Schlom, J., Paterson, A. J., Bennett, J., Magnani, J. L., and Colcher, D. (1986) Analysis of a human tumor-associated glycoprotein (TAG-72) identified by monoclonal antibody B72.3. *Cancer Res. 46*, 850.

Koppel, G. A. (1990) Recent advances with monoclonal antibody drug targeting for the treatment of human cancer. *Bioconjugate Chem. 1*, 13.

Kruper, W. J., Jr., Pollock, D. K., Fordyce, W. A., Fazio, M. J., and Inbasekaran, M. N. (1988) Functionalized polyamine chelants and rhodium complexes thereof and process for their preparation. Eur. Pat. Appl. No. 88109799.2.

Laemmli, U. K. (1970) Cleavage of structural proteins during the assembly of the head of bacteriophage T4. *Nature (London) 227*, 680.

Liberatore, F. A., Comeau, R. D., McKearin, J. M., Pearson, D. A., Belonga, B. Q., III, Brocchini, S. J., Kath, J., Phillips, T., Oswell, K., and Lawton, R. G. (1990) Site-directed chemical modification and cross-linking of a monoclonal antibody using equilibrium transfer alkylating cross-link reagents. *Bioconjugate Chem. 1*, 36 (and accompanying paper).

Maack, T., Johnson, V., Kau, S. T., Figueiredo, J., and Sigulem, D. (1979) Renal filtration, transport, and metabolism of low-molecular weight proteins: A review. *Kidney Int. 167*, 251.

Mandy, W. J., and Nisonoff, A. (1963) Effect of reduction of several disulfide bonds on the properties and recombination of univalent fragments of rabbit antibody. *J. Biol. Chem. 238*, 206.

Means, G. E., and Feeney, R. E. (1990) Chemical modification of proteins: History and applications. *Bioconjugate Chem. 1*, 2.

Meares, C. F., McCall, M. J., Reardan, D. T., Goodwin, D. A., Diamanti, C. I., and McTigue, M. (1984) Conjugation of antibodies with bifunctional chelating agents: Isothiocyanate and bromoacetamide reagents, methods of analysis, and subsequent addition of metal ions. *Anal. Biochem. 142*, 68.

Meares, C. F., McCall, M. J., Deshpande, S. V., DeNardo, S. J., and Goodwin, D. A. (1988) Chelate radiochemistry: Cleavable linkers lead to altered levels of radioactivity in the liver. *Int. J. Cancer Suppl. 2*, 99.

Milenic, D. E., Yokota, T., Filpula, D. R., Finkelman, M. A. J., Dodd, S. W., Wood, J. F., Whitlow, M., Snoy, P., and Schlom, J. (1991) Construction, binding properties, metabolism, and tumor targeting of a single chain Fv derived from the pancarcinoma monoclonal antibody CC49. *Cancer Res. 51*, 6363.

Muraro, R., Kuroki, M., Wunderlich, D., Poole, D. J., Colcher, D., Thor, A., Greiner, J. W., Simpson, J. F., Molinolo, A., Noguchi, P., and Schlom, J. (1988) Generation and characterization of B72.3 second generation (CC) monoclonal antibodies reactive with the TAG-72 antigen. *J. Cancer Res. 48*, 4588.

Nisonoff, A., and Rivers, M. M. (1961) Recombination of a mixture of univalent antibody fragments of different specificity. *Arch. Biochem. Biophys. Acta 93*, 460.

Packard, B., and Edidin, M. (1986) Site-directed labeling of a monoclonal antibody: Targeting to a disulfide bond. *Biochemistry 25*, 3548.

Perez, P. R., Hoffman, W., Shaw, S., Bluestone, J. A., and Segal, D. M. (1985) Specific targeting of cytotoxic T cells by anti-T3 linked to anti-target cell antibody. *Nature 316*, 354.

Quadri, S. M., Lai, J., Vriesendorp, H. M., and Williams, J. R. (1992) Evaluation of stabilized F(ab')2 fragments of monoclonal antiferritin antibody in nude mouse model. *Antibody Immunoconjugate Radiopharm. 5*, 125 (abstract).

Riddles, P. W., Blakeley, R. C., and Zerner, B. (1979) Ellman's reagent: 5,5'-Dithiobis(2-nitrobenzoic acid)—A reexamination. *Anal. Biochem. 94*, 75.

Segal, D. M., and Wunderlich, J. R. (1988) Targeting of cytotoxic cells with heterocrosslinked antibodies. *Cancer Invest. 6*, 83.

Sharkey, R. M., Motta-Hennessy, C., Pawlyk, D., Siegel, J. A., and Goldenberg, D. M. (1990) Biodistribution and radiation dose estimates for yttrium- and iodine-labeled monoclonal antibody IgG and fragments in nude mice bearing human colonic tumor xenografts. *Cancer Res. 50*, 2330.

Smyth, D. G., Nagamatsu, A., and Fruton, J. S. (1960) Some reactions of N-ethylmaleimide. *J. Am. Chem. Soc. 82*, 4600.

Staerz, U. D., and Bevan, M. J. (1986) Hybrid hybridoma producing a bispecific monoclonal antibody that can focus effector T-cell activity. *Proc. Natl. Acad. Sci. U.S.A. 83*, 1453.

Stevenson, G. T., Glennie, M. J., Paul, F. E., Stevenson, F. K., Watts, H. F., and Wyeth, P. (1985) Preparation and properties of FabIgG, a chimeric univalent antibody designed to attack tumour cells. *Biosci. Rep. 119*, 991.

Stevenson, G. T., Pindar, A., and Slade, C. J. (1989) A chimeric antibody with dual Fc regions (bisFabFc) prepared by manipulations at the IgG hinge. *Anti-Cancer Drug Des. 3*, 219.

Stickney, D. R., Frincke, J. M., Slater, J. B., Ahlem, C. N., Merchant, B., and Slater, J. M. (1988) Bifunctional antibody technology: Clinical applications for CEA expressing tumors. Third International Conference on Monoclonal Antibody Immunoconjugates for Cancer, Feb. 4–6 (San Diego).

Strober, W., and Waldmann, T. A. (1974) The role of the kidney in the metabolism of plasma proteins. *Nephron 13*, 35.

Sumpio, B. E. (1981) Tubular absorption and catabolism of low molecular weight proteins. Ph.D. Dissertation.

Takakura, Y., Fujita, T., Hashide, M., and Sezaki, H. (1990) Disposition characteristics of macromolecules in tumor-bearing mice. *Pharm. Res. 7*, 339.

Volkert, W. A., Goeckeler, W. F., Ehrhardt, G. J., and Ketring, A. R. (1991) Therapeutic radionuclides: Production and decay property considerations. *J. Nuc. Med. 32*, 174.

Waldmann, T. A. (1991) Monoclonal antibodies in diagnosis and therapy. *Science 252*, 1657.

Waldmann, T. A., and Strober, W. (1969) Metabolism of immunoglobulins. *Prog. Allergy 13*, 1.

Yokota, T., Milenic, D. E., Whitlow, M., and Schlom, J. (1992) Rapid tumor penetrance of a single-chain Fv and comparison with other immunoglobulin forms. *Cancer Res. 52*, 3402.

New Application of Silane Coupling Agents for Covalently Binding Antibodies to Glass and Cellulose Solid Supports

Niedre M. Pope, David L. Kulcinski, Alan Hardwick, and Yu-An Chang*

Baxter Healthcare Corporation, Biotech Group–Immunotherapy Division, 3015 South Daimler Street, Santa Ana, California 92705. Received October 2, 1992

Bifunctional silane reagents (3-iodopropyl)trimethoxysilane (1), (γ-glycidoxypropyl)trimethoxysilane (2), and [1-(trimethoxysilyl)-2-(*m*-(or *p*-)chloromethyl)phenyl]ethane (3) were used to covalently link goat anti-mouse (GAM) antibodies (Ab) to glass microbeads and cuprammonium rayon hollow-fiber dialyzers. An average of 0.79 and 0.83 μg of GAM Ab/cm^2 was immobilized on the hollow-fiber dialyzers and the glass beads, respectively. The antibodies immobilized on glass microbeads or on hollow-fiber dialyzers were then used to selectively deplete CD34+ cells or CD4+ peripheral blood mononuclear cells (PBMC), respectively. Glass microbeads depleted 80% CD34+ cells with good selectivity, and the hollow-fiber dialyzers depleted an average of 81% CD4+ PBMC.

INTRODUCTION

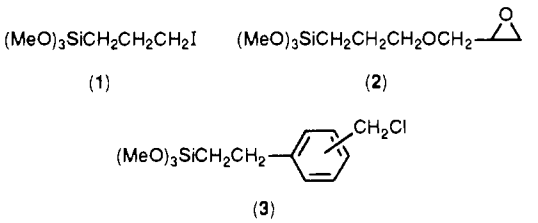
Immobilization of biologicals had its beginning in 1916 with work done by Nelson and Griffin (*1*) when they immobilized invertase onto charcoal and alumina. Since then, the immobilization of biologicals to a variety of solid supports has become a widely used technology.

Bifunctional silanes of the structure $(MeO)_3Si(CH_2)_nX$ (Scheme I) were used extensively in the 1970s as coupling agents to link enzymes to inorganic solid supports (*2*), such as minerals, including sand, diatomaceous earth, and hornblende, or fabricated materials, such as controlled-pore glass and ceramics, nickel oxides, and iron oxides (*3–6*). Since that time, technology has shifted to the method of directly coupling biologicals to chemically modified organic solid supports, such as derivatized vinyl polymers, polyamides, and polysaccharides (agarose, cellulose, Sepharose, Sephadex, etc.) (*7*). This shift to the use of organic solid supports occurred because these supports can be derivatized under mild conditions, and because a wide variety of functional groups can be put on organic solid supports (*8*).

Until recently, reaction conditions used to silanize inorganic solid supports were relatively harsh. For example, Weetall (*9*) activated glass by refluxing in a 10% solution of (γ-aminopropyl)triethoxysilane in toluene for 24 h. Toluene, with a boiling point of 110.6 °C, would destroy many organic solid supports. Frequently after silanization, further derivatization of the organic functionality on the silane was necessary prior to immobilization of a biological. Derivatization methods for silane-activated inorganic solid supports were limited and equally as harsh as those for silanization. Greenfield and Lawrence (*10*) used thiophosgene in chloroform to form a thiocyanate derivative which could then be coupled with the enzyme. Weetall and Filbert (*11*) used *p*-nitrobenzyl chloride in chloroform to form an aminoacyl derivative. The nitro group was then reduced with dithionite. After forming a diazo group with nitrous acid, the enzyme could be coupled to the solid supports.

In this study, we have used bifunctional silane coupling agents to immobilize antibodies onto low-density-glass microbeads and onto acetylated cellulose hollow-fiber dialyzers. Reaction conditions for silanizing the solid supports were mild and silane reagents were chosen such that further derivatization was not necessary. The immobilized antibodies were then tested for their ability to selectively deplete target cells.

Scheme I. Bifunctional Silane Reagents



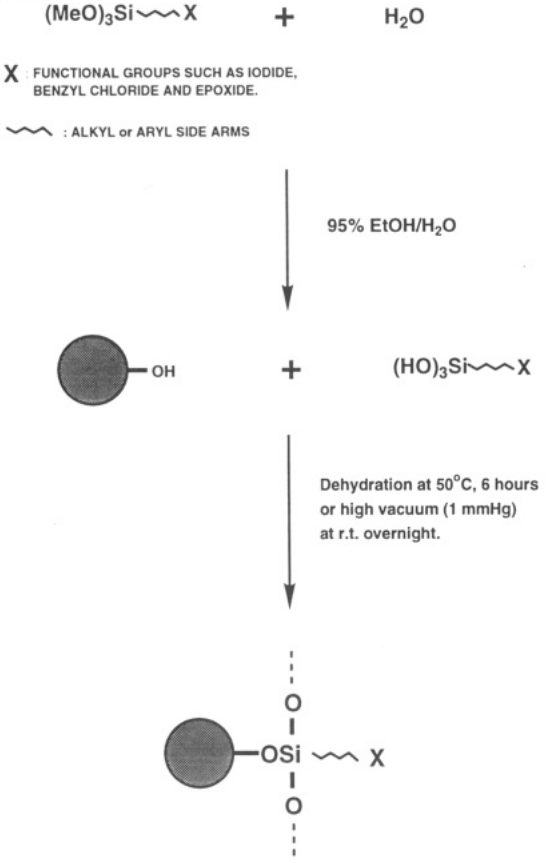
EXPERIMENTAL PROCEDURES

Reagents. (3-Iodopropyl)trimethoxysilane, (γ-glycidoxypropyl)trimethoxysilane, and [1-(trimethoxysilyl)-2-(*m*-(or *p*-)chloromethyl)phenyl]ethane were all purchased from Hüls American Corp., Bristol, PA. Cupraphan hollow fiber dialyzers were obtained from Baxter Healthcare Corp., Membrane and Materials Technology Group, Round Lake, IL. Low density floating glass Scotchlite microbeads (catalog no. H50/1000) were obtained from 3M, St. Paul, MN, boric acid and ethanol reagent alcohol were purchased from Baxter Healthcare Corporation, Scientific Products Division, McGaw Park, IL, and goat anti-mouse (cat. no. 115-005-071) and mouse IgG/HRPO were purchased from Jackson ImmunoResearch Labs, Inc., West Grove, PA. Anti-CD4 FITC, GAM FITC, GAM PE, Simultest control, mouse anti-Leu 3a (anti-CD4) Ab, and mouse anti-HPCA-1 (anti-CD34) Ab were purchased from Becton-Dickinson, Mountain View, CA; ABTS substrates A and B, from Kirkegaard and Perry; and Ficoll Histopaque 1077, Dulbecco's phosphate-buffered saline (dPBS), Hank's balanced salt saline (HBSS), Tween 20, RPMI, and fetal bovine serum (FBS), from Sigma Chemical Co., St. Louis, MO. ^{125}I-labeled GAM Ab was prepared using Boulton–Hunter Reagent from Du Pont.

Paraformaldehyde fixative was prepared by dissolving cacodylic acid (10.7 g) into 900 mL of deionized water. The pH was adjusted to 7 with 1 M HCl. The solution was heated to 70 °C with a water bath. Then paraformaldehyde (10 g) was added and the solution was returned to the 70 °C water bath with occasional stirring until all the paraformaldehyde was dissolved. The solution was then cooled to ambient temperature and the pH adjusted to 7.2 using 1 N NaOH. Next, the volume was adjusted to 1 L

1043-1802/93/2904-0166$04.00/0 © 1993 American Chemical Society

Scheme II. Activation of Glass Beads by Silane Reagents



and the solution filtered through a Corning 0.22-μm cellulose acetate membrane filter unit. The paraformaldehyde fixative was stored at 4 °C.

Preparation of the Microbeads. Floating glass microbeads were washed in concentrated HCl for 2 h followed by concentrated nitric acid at ambient temperature overnight to remove any coatings or contaminates on the microbeads. The microbeads were washed with deionized water until all traces of acid were removed. The microbeads were then centrifuged in 100 mL of deionized water for 5 min at 1000 rpm to remove any cracked or broken microbeads, which tended to sediment. This was done until no broken microbeads sedimented. Then the microbeads were washed with 100 mL of ethanol, filtered, and dried under reduced pressure.

Silane Activation of Microbeads. Silane solutions (40 mL, 10% solution in 95% ethanol/deionized water) were prepared from the three silanes (Scheme II). Each of them was added to 4 g of microbeads. The mixture was rotated end-over-end at ambient temperature for 1 h. The excess silane solution was filtered off and the microbeads were dried at 50 °C for 6 h, or under high vacuum (1 mmHg) overnight. Excess silane and aggregated microbeads were washed away by filtering microbeads through a metal screen (100 mesh) with ethanol. The microbeads were filtered and dried at 50 °C. These microbeads can be stored up to 6 months without loss of activity.

Coupling of GAM Ab to Silane-Activated Microbeads. Goat anti-mouse antibody was added to the microbeads in borate buffer (0.05 M, pH 9.6). The mixture was rotated end-over-end at ambient temperature overnight. The borate buffer was filtered off under reduced pressure, and the microbeads were washed with dPBS. Microbeads were then weighed out and stored in borate buffer for use in either functional protein binding or cell binding studies (Scheme III).

Analysis of Functional GAM Ab Content on Microbeads. HRPO-conjugated mouse IgG (mouse IgG/HRPO) was used to determine the quantity of functional GAM Ab bound to the microbeads. The ELISA was performed using 2 mg of silane-activated, GAM Ab coupled microbeads, and 2 mL of a 50× dilution of mouse IgG/HRPO (1 μg/mL) in 0.05% Tween 20/dPBS. The microbeads and mouse IgG/HRPO were incubated by end-over-end rotation at ambient temperature for 30 min. A set of standards was prepared (50 μL of diluted mouse IgG/HRPO + 950 μL dPBS) by serial dilution with dPBS. Three to five washes were done just prior to, and after, incubation using 1% Tween 20/PBS (2 mL), to remove nonbound antibody. Microbeads were filtered, weighed, and placed in dry test tubes. ABTS substrates A and B were mixed in a 1:1 ratio and then added to the microbeads (2 mL) in 5-s intervals and incubated at room temperature for 20 min. The reaction was quenched with oxalic acid (1 mL, 0.25 M). Concentrations of mouse IgG/HRPO bound were determined by comparison with a standard curve read at 405 nm (Scheme IV).

Preparation of KG1a Cells for Cell-Depletion Experiments. A flask of about 1×10^8 fluorochromed (100 μL) KG1a cells, which possess CD34 antigen on their surface, was spun down for 7 min at 1400 rpm and 4 °C. Cells were resuspended in a solution of 2% FBS/RPMI (40 mL) and were centrifuged as above. This procedure was repeated three times. Mouse anti-CD34 Ab was added to the cells (1 μg/1×10^6 cells), after which the cells were incubated at 4 °C for 30 min. Cells were washed three times in 2% FBS/RPMI, centrifuged as above between washes and counted using a hemocytometer. Cells were resuspended in 5 mL 2% FBS/RPMI and stored on ice until added to the glass microbeads.

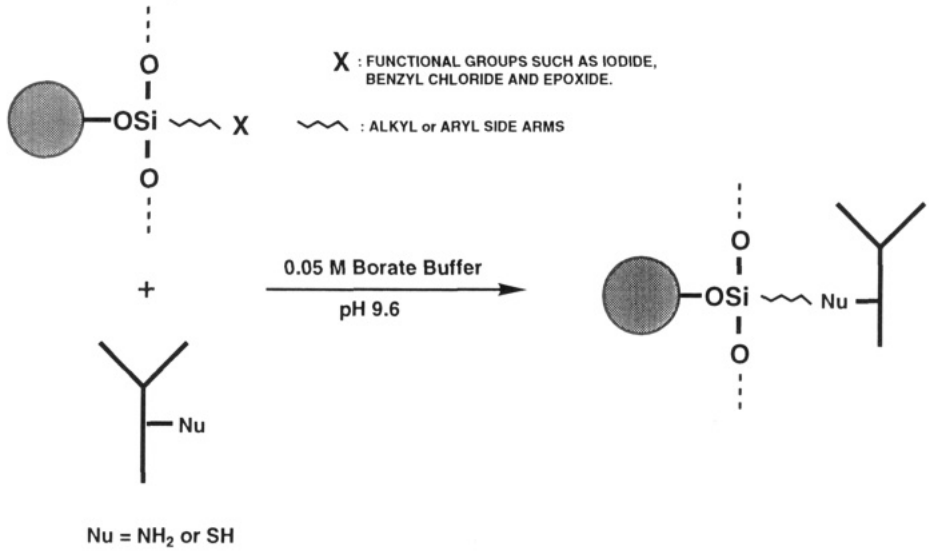
Depletion of KG1a Cells by the Glass Microbeads. KG1a cells were added to the glass microbeads in the ratio of 1×10^4 cells/mg bead. The volume was adjusted to 20 mL, and the microbeads and cells were incubated end-over-end at 10 rpm for 1 h at 4 °C. After incubation, microbeads were allowed to float to the top of the suspension and the underlying fluid (effluent) was drawn off. Cells in the effluent were counted with a hemocytometer (Scheme V).

Silane Activation of Hollow-Fiber Dialyzers. Activation solution [10% (γ-glycidoxypropyl)trimethoxysilane in 95% ethanol/water] was pumped via a peristaltic pump through a flow loop containing a small-scale hollow-fiber dialyzer for 20–22 h at a flow rate of 0.4 mL/min. The hollow-fiber dialyzer was dried under reduced pressure at ambient temperature. Hollow-fiber dialyzers were used within 3 days to a week (Figure 1).

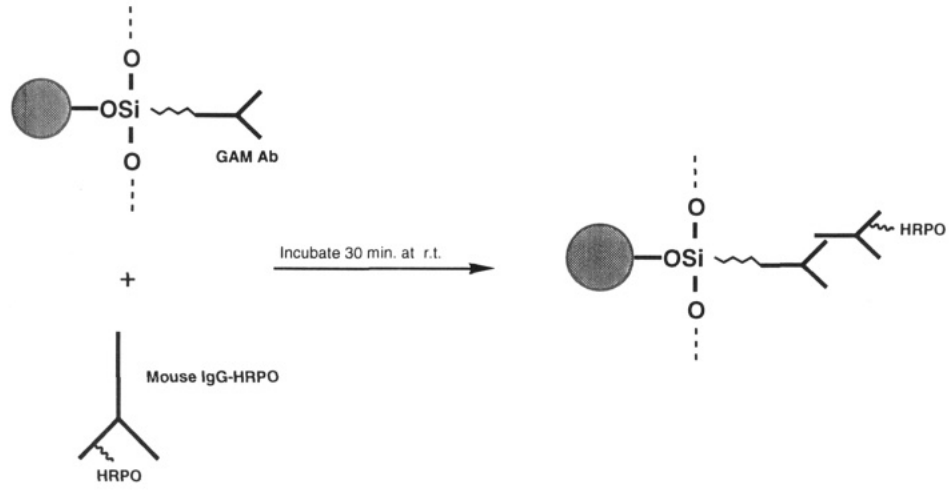
Coupling of GAM Ab to Hollow-Fiber Dialyzers. A solution of 1.67 mg GAM Ab/mL dPBS was pumped and recycled through the loop and hollow-fiber dialyzer for 20–22 h at a flow rate of 0.4 mL/min. Hollow-fiber dialyzers were then used for either ^{125}I-labeled GAM Ab binding or for cell binding studies.

Analysis of Antibody Content on Hollow-Fiber Dialyzers. ^{125}I-labeled GAM Ab buffer (3 mg GAM Ab + 0.16 mg ^{125}I–GAM Ab in 5 mL of dPBS) at a radiation level of 1×10^6 counts per minute (cpm) was recycled through the flow loop and hollow-fiber dialyzer for 20–22 h at a flow rate of 0.4 mL/min. After recycling, the hollow-fiber dialyzer was washed by flushing 35 mL of dPBS through the flow loop, followed by washing with 25 mL of 2% Tween 20/dPBS, to remove nonbound antibody. The

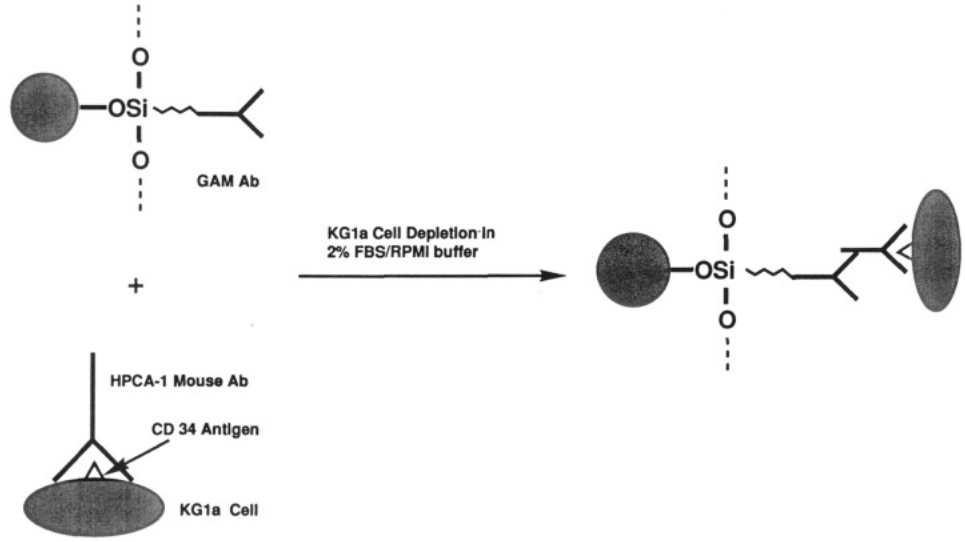
Scheme III. GAM Ab Coupling to the Activated Glass Beads



Scheme IV. HRPO Assay for Quantification of Functional GAM Ab



Scheme V. KG1a Cell Depletion by GAM Ab Immobilized Glass Beads



hollow-fiber dialyzer was immediately taken out of the flow loop, and the fibers were cut into 1-cm pieces with a razor blade. The fiber bundles were placed in sequentially numbered test tubes and assayed in a γ-counter for radioactivity. The amount of GAM Ab bound to a fiber bundle was calculated as follows: bound GAM Ab (mg) = measured cpm × (3.16 mg GAM Ab/1 × 10^6 cpm).

Preparation of Cells for PBMC Depletion Experiments. Fresh human blood (approximately 50 mL) was collected and heparinized. The blood was aliquoted such that 15 mL was added to a 50-mL centrifuge tube containing Ficoll Histopaque 1077 (10 mL). Each centrifuge tube was then filled to 40 mL with Hank's buffered-saline solution (HBSS). The tubes were centrifuged at

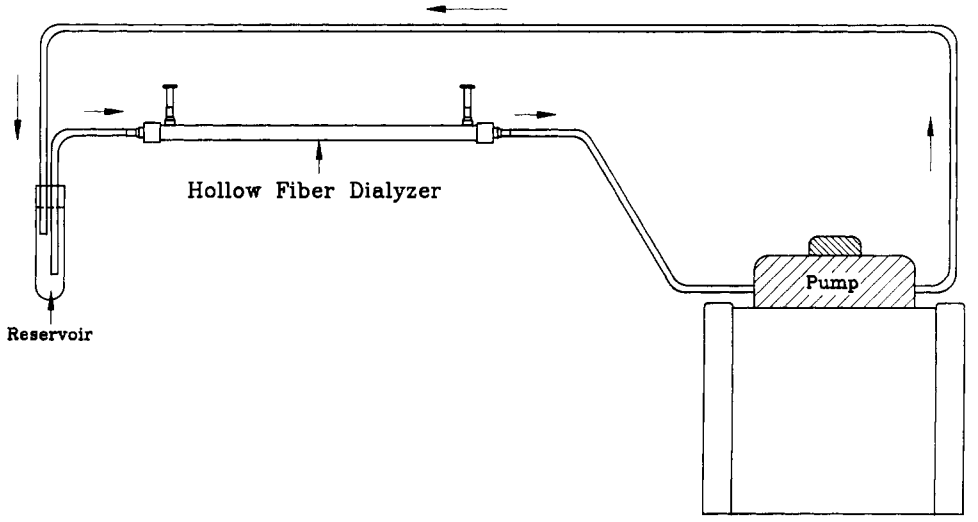


Figure 1. Flow loop for hollow-fiber dialyzer.

Table I. Preparation of Cell Samples for FACScan Analysis

sample number	sample prep.	first antibody	second antibody	third antibody
1	after 1st pass	anti-CD4	Simultest control	none
2	after 1st pass	anti-CD4	GAM-PE	anti-CD4-FITC
3	after 2nd pass	anti-CD4	Simultest control	none
4	after 2nd pass	anti-CD4	GAM-PE	anti-CD4-FITC
5	after 3rd pass	anti-CD4	Simultest control	none
6	after 3rd pass	anti-CD4	GAM-PE	anti-CD4-FITC

2000 rpm for 15 min at room temperature. The resulting layer of peripheral blood mononuclear cells (PBMC), some of which possess the CD4 surface antigen, was removed from each tube and pooled. The PBMC were washed twice in HBSS (centrifuged at 1000 rpm for 10 min) and were then resuspended in 2% FBS/RPMI (10 mL), yielding approximately 6×10^7 PBMC as determined by a Coulter counter.

Anti-CD4 antibody was then added to 4×10^7 PBMC in 2% FBS/RPMI (5 mL) and mixed for 30 min at 4 °C. Unbound antibody was removed by washing the cells in 2% FBS/RPMI twice (centrifuged at 1000 rpm for 10 min). The PBMC were then resuspended in 5 mL 2% FBS/RPMI and kept on ice until needed.

Depletion of PBMC Cells by the Hollow-Fiber Dialyzers. The starting PBMC suspension, which consisted of approximately 3×10^7 PBMC in 5 mL, was pumped once through the GAM Ab-coupled hollow-fiber dialyzer at a flow rate of 0.4 mL/min. Fresh 2% FBS/RPMI (2 mL) was then pumped through the hollow-fiber dialyzer to flush out unbound cells. All effluent was collected into a test tube. An effluent aliquot was removed for counting cells with a Coulter counter and for later FACScan analysis. The remaining effluent was then pumped through the hollow-fiber dialyzer a second time at a flow rate of 0.4 mL/min, followed by a 2-mL flush with 2% FBS/RPMI. Effluent from this second pass through the hollow-fiber dialyzer was also collected in a test tube, and aliquots were taken for cell counts and FACScan analysis. After a third and final pass of effluent through the hollow-fiber dialyzer, samples were prepared for FACScan analysis.

Preparation of Cell Samples for FACScan Analysis. After passage through the hollow-fiber dialyzer, cell samples were washed in 2% FBS/0.02% NaN_3/PBS buffer, and a second antibody, GAM Ab/FITC or -/PE, was added (Table I). Samples were incubated with a second antibody (20 μL) for 30 min at 4 °C. Samples to be incubated with a third antibody, anti-CD4 Ab/FITC, were first washed with 2% FBS/0.02% NaN_3/PBS buffer and then were incubated with the antibody (20 μL) for 30 min at 4 °C. All samples were washed once more and then resuspended in 500 μL of paraformaldehyde fixative solution. Samples were stored in the dark at 4 °C overnight until analyzed.

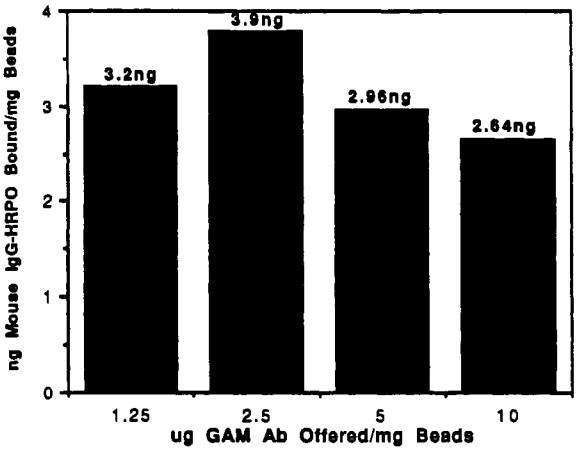


Figure 2. Optimum GAM Ab to bead ratio.

RESULTS

Functional GAM Ab Binding Assay. ELISA was used to determine the optimum functional GAM Ab coupled to glass microbeads activated with the benzyl chloride silane by varying the amount of GAM Ab offered per milligram of microbeads (Figure 2). The optimum GAM Ab to bead ratio was found to be 2.5 μg GAM Ab/mg of microbeads for this particular system. Next, the ability of microbeads activated with the three silane reagents to bind GAM Ab functionality at a 2.5 μg GAM Ab/mg microbead ratio (Figure 3) was compared. The iodide (1) and benzyl chloride (3) silanes performed better than the epoxide silane (2), perhaps due to instability of the epoxide under the basic (pH 9.6) conditions used to couple GAM Ab onto the silane-activated beads.

KG1a Cell Depletion. Control experiments were done using KG1a cells to compare the effects that the following conditions have on KG1a cell depletion: (A) nonactivated microbeads with and without GAM Ab incubation, (B) silane-activated microbeads with and without GAM Ab incubation, or (C) the use of KG1a cells which have not been sensitized by mouse IgG anti-CD34 Ab with silane-activated, GAM Ab-coupled microbeads (Figure 4). There

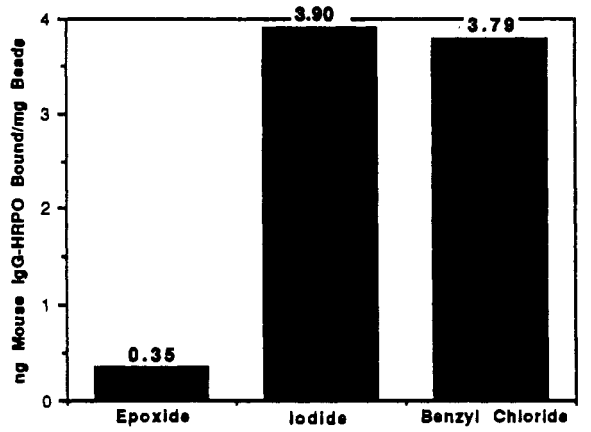


Figure 3. Comparison of three silane reagents.

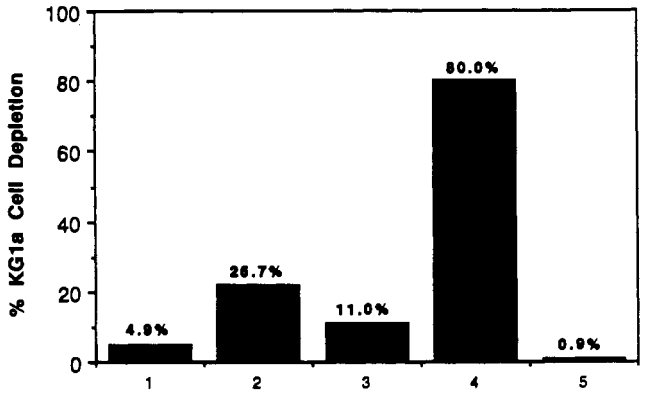


Figure 4. KG1a cell-depletion control experiments: unactivated beads (1) without GAM Ab and (2) with GAM Ab; activated beads (3) without GAM Ab and (4) with GAM Ab; (5) unsensitized KG1a cells using activated, GAM Ab-coupled beads.

was essentially no cell depletion observed for microbeads which were not incubated with GAM Ab. In addition, no cell depletion was obtained using nonsensitized KG1a cells. Silane-activated, GAM Ab-coupled microbeads showed significant cell depletion, although a small amount of depletion was seen with nonactivated microbeads which had been incubated with GAM Ab. These results indicate that the silane-activated glass bead system can efficiently deplete target cells without nonspecific trapping of the cells.

Additionally, 2% fluorochromed KG1a cells were mixed with nontarget cells (HL60 cells). These nontarget cells do not contain the CD34 antigen and were not fluorochromed. The GAM Ab-immobilized glass microbeads were incubated with this cell mixture. Percent KG1a cell depletion was essentially the same as those experiments done without HL60 cells. Further, no nonfluorochromed cells were depleted by the microbeads. This indicates that GAM Ab-immobilized glass microbeads can selectively deplete target cells (KG1a cells) from a large quantity of nontarget cells (98% HL60 cells) without sacrificing depletion purity and efficiency (Figure 5).

^{125}I–GAM Ab Binding Assay. GAM Ab was offered to the hollow-fiber dialyzers at a concentration of 1.66 mg/mL. Table II, which is a mass balance for the radiolabeled Ab, shows the final location of the radiolabeled antibody. Most of the ^{125}I-labeled GAM Ab ended up in the recycle solution or in the PBS wash. A Tween 20 detergent wash was done to remove any noncovalently bound protein. However, since the hollow-fiber dialyzers were saturated with GAM Ab for maximum immobilization, it is possible that even with a 2% Tween 20/PBS

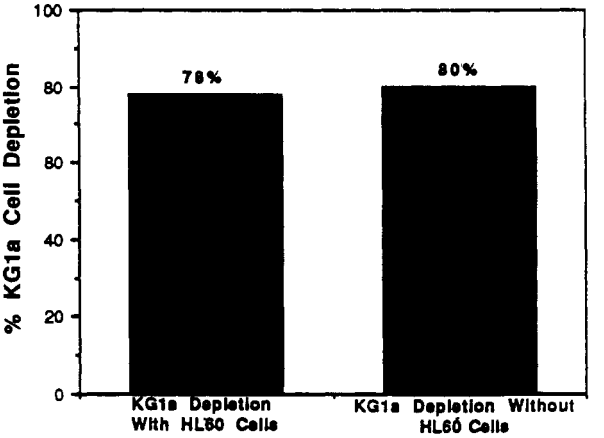


Figure 5. KG1a cell depletion with and without the presence of nontarget HL60 cells.

Table II. Location of ^{125}I-Labeled GAM Ab

dialyzer description	% bound to fibers	% in recycle solution	% in PBS wash	% in Tween wash	% recovery
untreated dialyzer	2	75	10	6	93
silane-activated dialyzer #1	3	84	10	5	102
silane-activated dialyzer #2	7	25	58	1	91

Table III. Amount of GAM Ab Bound to the Hollow-Fiber Dialyzers

dialyzer description	bound Ab (μg)	bound Ab/surface area (μg/cm^2)
untreated dialyzer	69	0.34[a]
silane-activated dialyzer #1	104	0.51
silane-activated dialyzer #2	217	1.07
GAM Ab-saturated glass beads	171	0.83[b]
GAM Ab-optimized glass beads	33	0.16[c]

[a] The surface area of the hollow fiber dialyzers is 203.5 cm^2. [b] The surface area of the glass microspheres is 1.029 m^2/g. The micrograms of GAM Ab bound was determined indirectly by a Pierce protein assay of the GAM Ab left in the supernatent after incubation with 20 mg of silane-activated glass beads. [c] The micrograms of GAM Ab bound under optimized conditions (0.0025 mg of GAM Ab/mg glass microsphere) was also determined by Pierce protein assay.

Table IV. Results of the CD4+ Cell Depletions

	cummulative % cell depletion		
	after 1st pass	after 2nd pass	after 3rd pass
	Control Experiment		
CD4+ cells			13[a]
non-CD4+ cells			3[a]
	Experiment 1		
CD4+ cells	39	50	63
non-CD4+ cells	18	20	36
	Experiment 2		
CD4+ cells	99.70	99.90	99.90
non-CD4+ cells	49	50	53

[a] Represent cells nonspecifically trapped in the hollow-fiber dialyzers.

wash, some noncovalently bound GAM Ab remained (Table III). The radiolabeled Ab binding studies also enabled the determination of the absolute amount of antibody bound to the hollow-fiber dialyzers, as shown in Table III.

CD4+ Cell Depletion. Three CD4+ cell depletions from peripheral blood mononuclear cells were carried out. Results from the Coulter counter and FACScan analysis are shown in Table IV. The control experiment differed from experiments 1 and 2 in that the hollow-fiber dialyzer was neither silane-activated, nor GAM Ab-coupled. Of

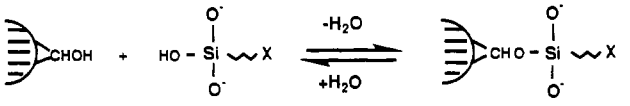
the 1.37×10^8 starting PBMC, 60% were CD4+. In experiment 1, the starting cell population consisted of 2×10^7 PBMC, of which 59% were CD4+ cells. In experiment 2, the starting cell population consisted of 3.4×10^7 PBMC, of which 29% were CD4+ cells. After passing these PBMC through the hollow-fiber dialyzers, the CD4 positive cells were depleted 13% (control), 63% (experiment 1), and 99% (experiment 2), respectively. In addition to the CD4+ cells that were depleted, 3%, 36%, and 53% of the CD4- cell population was also depleted. This indicates that there was a certain degree of nonspecific trapping of PBMC by the hollow-fiber dialyzers.

DISCUSSION

In this study we have developed a simple and versatile method to activate both organic and inorganic solid supports, under mild conditions, for subsequent immobilization of biologicals using bifunctional silane-coupling reagents. We have shown that silane-activated glass microbeads and acetylated cellulose hollow-fiber solid supports will indeed bind biological agents without loss of biological activity, so that specific target cells can then be captured.

The solid supports used in this work were chosen because they are inexpensive relative to many now on the market, and they provide a large surface area for bioselective separation.

One interesting observation made of the hollow fibers requires discussion. For covalent attachment of silane to take place with acetylated cellulose, the following reaction takes place:



thus forming a C–O–Si bond, which has been generally observed to be labile. In the liquid phase, lability is expected due to rapid hydrolysis of the C–O–Si bond. In the case of hollow-fiber solid supports, the C–O–Si linkages were formed under mild dehydration conditions. In terms of kinetics, two-phase reactions are usually slow. Since the C–O–Si linkages were made on the solid phase, when the activated hollow-fiber dialyzer was subjected to an aqueous environment, hydrolysis of these bonds was relatively slow. The ^{125}I-labeled-GAM Ab study and the CD4+ cell depletion data both indicate that the C–O–Si bonds on the solid support were stable during the bioassay time frame.

ACKNOWLEDGMENT

We wish to thank Ms. Virginia H. Mansour for providing KG1a cells, Mr. Dan Boggs for providing the hollow-fiber dialyzers, Dr. Bonnie Mills for aid with FASCan analysis, and Dr. William Lake for useful advice.

LITERATURE CITED

(1) Nelson, J. M., and Griffin, E. G. (1916) *J. Am. Chem. Soc. 38*, 1109.
(2) Plueddeman, E. P. (1982) Silane Coupling Agents, Chapter 8, pp 207–232, Plenum Press, New York.
(3) Cabral, J. M. S., and Kennedy, J. F. (1991) Covalent and Coordination Immobilization of Proteins. In *Protein Immobilization Fundamentals and Applications* (R. F. Taylor, Ed.) pp 73–138, Marcel Dekkar, New York.
(4) Kent, C., Rosevear, A., and Thomson, A. R. (1978) Enzymes Immobilized on Inorganic Supports. In *Topics in Enzyme and Fermentation Biotechnology*
(5) Scouten, W. H. (1981) *Chemical Analysis. Affinity Chromatography* (P. J. Elving, and J. D. Winefordner, Eds.) Vol. 59, John Wiley & Sons, New York.
(6) Scouten, W. H. (1983) *Chemical Analysis. Solid Phase Biochemistry* (P. J. Elving, and J. D. Winefordner, Eds.) Vol. 66, John Wiley & Sons, New York.
(7) Kinner, K. J. (1975) *Chem. Eng. News* Aug 8, 22–41.
(8) Wingard, L. B., Katchalski-Katzir, E., and Goldstein, L. (1976) *Applied Biochemistry and Bioengineering. Immobilized Enzyme Principles*, Vol. 1, Academic Press, New York.
(9) Weetall, H. H. (1969) *Nature 223*, 959.
(10) Greenfield, P. F., and Laurence, R. L. (1975) *J. Food Sci. 40*, 906.
(11) Weetall, H. H., and Filbert, A. M. (1974) *Methods Enzymol. 34*, 59–72.

Exploratory Photochemistry of Fluorinated Aryl Azides. Implications for the Design of Photoaffinity Labeling Reagents

Karlyn A. Schnapp, Russell Poe, Elisa Leyva, N. Soundararajan, and Matthew S. Platz*

Department of Chemistry, The Ohio State University, 120 West 18th Avenue, Columbus, Ohio 43210.
Received October 13, 1992

A series of fluorinated aryl azides and fluorinated azidobenzoates were studied by laser flash photolysis techniques. Using the pyridine ylide probe method it was possible to determine whether a singlet nitrene or ring-expanded ketenimine ylide is the trappable intermediate that is generated at ambient temperature. It was determined that two fluorine substituents, ortho and ortho' substituted relative to the azide group, are required to retard ring expansion and allow bimolecular capture of the singlet nitrene. LFP of ortho, ortho' difluorinated aryl azides in methanol produces the ground triplet state of the nitrene. The results are consistent with chemical analysis of reaction mixtures. The implications of this data for the design of photoaffinity labeling reagents are discussed.

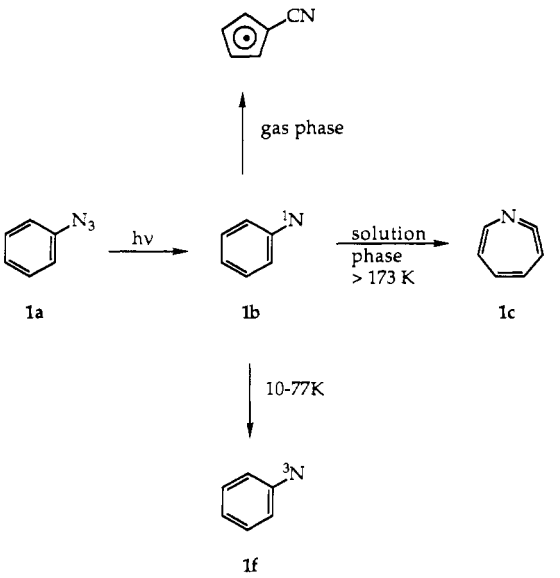
I. INTRODUCTION

The photochemistry of phenyl azide (**1a**) has been described as wonderfully complex (*1*). Over the last decade the complexity of this system has been reduced to that of Scheme I. Photolysis of phenyl azide **1a** produces singlet phenylnitrene (**1b**) which ring expands to ketenimine **1c** within 10–100 ps (*2*). The rate of rearrangement is sufficiently rapid to prevent bimolecular trapping of **1b**. The barrier to ring expansion is about 3 kcal/mol, which means that the rate of this process slows dramatically at cryogenic temperatures (*3*). Between 10 and 77 K, singlet phenylnitrene decays by intersystem crossing to triplet **1f**, which is the ground state of the nitrene (*4*, *5*). When the singlet nitrene is generated in the gas phase, it is formed in a vibrationally excited state which rearranges to cyanocyclopentadiene and ultimately forms the cyanocyclopentadienyl radical, which has been observed by absorption and emission spectroscopy (*6*).

Aromatic azides are widely used in photoaffinity labeling (PAL) experiments (*7*). PAL is a biochemical technique invented by Westheimer that is used to identify amino acid residues present in the binding sites of biological receptors (*8*). In this experiment, a light-sensitive moiety is appended to a natural substrate of an enzyme. Photolysis of the enzyme–substrate complex releases a reactive intermediate which in an ideal experiment will react with the first bond of the protein it encounters to form a robust new linkage between the reactive intermediate and the target biomolecule. The experiment will be defeated if the photogenerated intermediate is chemically discriminating because it can exit the binding site and react aspecifically with the protein.

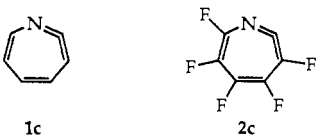
Unfortunately, the trappable intermediate produced from phenyl azide and most of its derivatives are ketenimines (**1c**) (*1*, *2*). These species are not ideal labeling reagents because they react rather sluggishly (*9*) ($\tau \gg 10$ μs) and only with nucleophiles. This laboratory (*10*), Keana's group (*11*), and Bayley (*7*) have proposed polyfluorinated azides as superior reagents for PAL studies. The research groups of Watt (*13*) and Katzenellenbogen and Pinney (*14*) have since used fluorinated aryl azides as PAL reagents with interesting results.

Scheme I



Predictions of a fluorine effect were based on Banks' findings that pyrolysis of polyfluorinated aryl azides in hydrocarbons leads to products from formal CH insertion of the nitrene in modest yields (*12*).

Recently we have demonstrated that singlet (pentafluorophenyl)nitrene (**2b**) ring expands at least 170 times more slowly than does singlet phenylnitrene (**1b**) at ambient temperature (*15*). This gives singlet nitrene **2b** sufficient time to react with alkanes, alkenes, aromatics, amines, ethers, sulfides, and sulfoxides to form adducts in reasonable yields. Furthermore, we found that pentafluoro ketenimine **2c** reacts with pyridine by nucleophilic

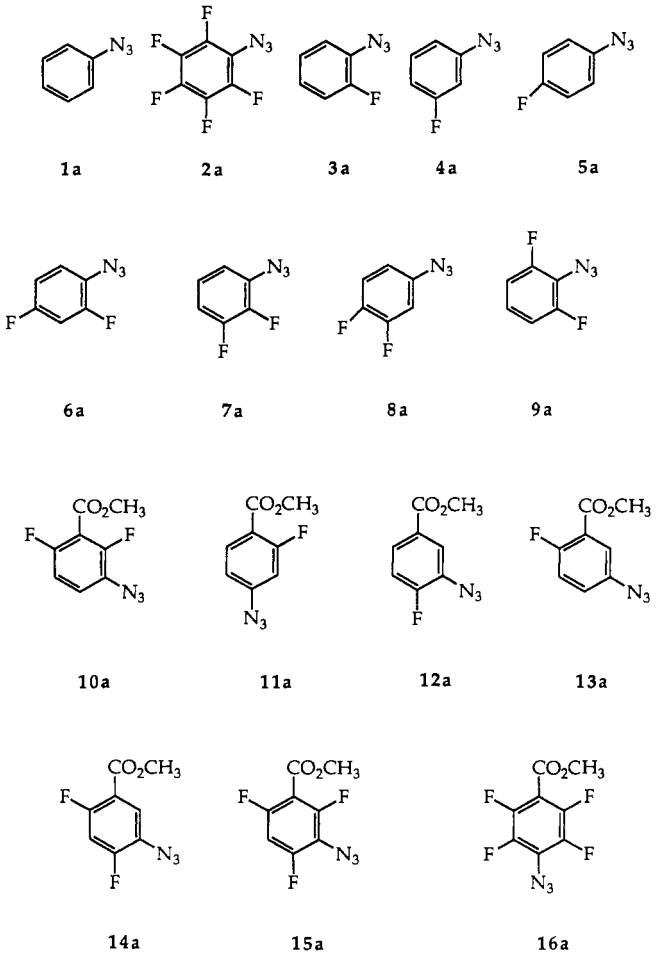


1c 2c

addition almost 10^4 times more rapidly than its nonfluorinated counterpart **1c**.

1043-1802/93/2904-0172$04.00/0 © 1993 American Chemical Society

Chart I



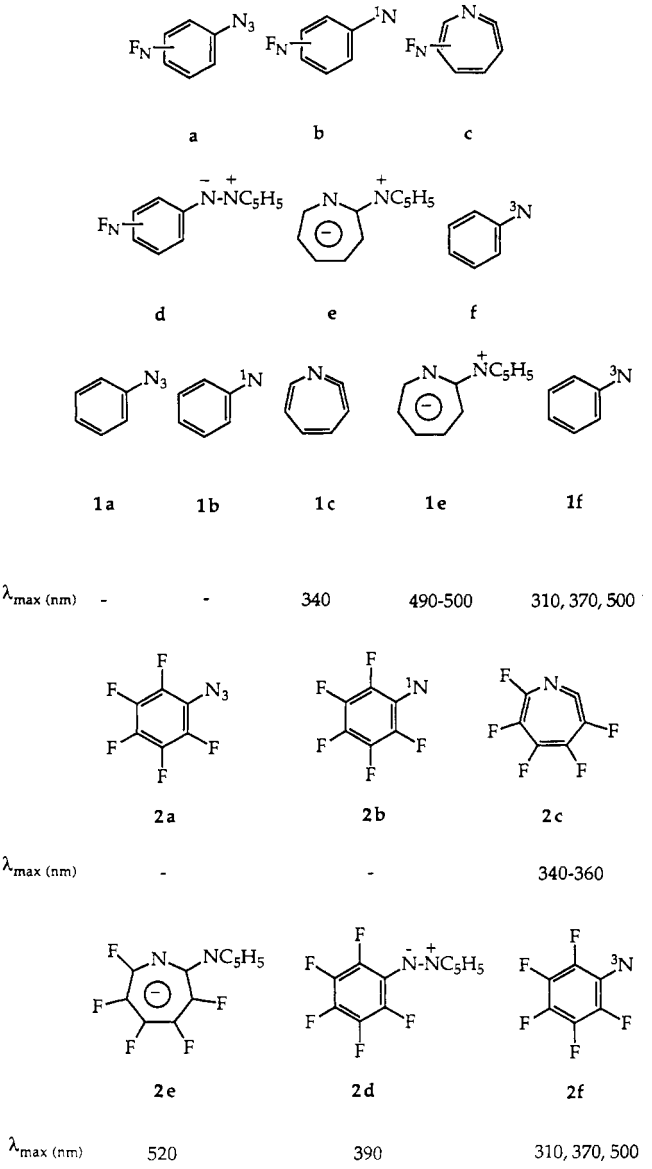
Thus two *extremely* reactive, but trappable, intermediates are produced upon photolysis of pentafluorophenyl azide (**2a**). Since the potential of using **2a** itself in PAL work is quite limited, it is important to determine the number of fluorine atoms as well as their positions relative to the azide moiety that is required to retard ring expansion and to achieve bimolecular trapping of the nitrene. In this regard we have prepared azides **1a**–**16a** and have studied these compounds by laser flash photolysis (LFP) techniques. We have also studied fluorinated azidobenzoates (*15*) by LFP techniques since many PAL reagents can be elaborated through the ester functional group. The results indicate that at ambient temperature two fluorine atom substituents positioned ortho and ortho′, or less effectively ortho and para to the azide moiety are sufficient to achieve the desired reactivity properties.

II. RESULTS

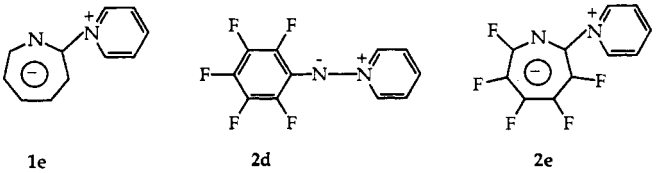
LFP Studies in CH_2Cl_2. Azides **1a**–**16a** (Chart I) were studied by LFP (XeCl excimer laser, 308 nm, 150 mJ, 17 ns) in CH_2Cl_2. Our earlier studies with **2a** have identified CH_2Cl_2 as an inert solvent toward singlet (pentafluorophenyl)nitrene (*15*). The results with azide **4a** (Chart II) are typical. The transient intermediate produced in this solvent is ketenimine **4c**, which is clearly identified by its transient absorption spectrum (Figure 1) and by comparison with that of **1c** produced by LFP of phenyl azide (*1*, *3*, *13*).

LFP Studies in Neat Pyridine. As reported elsewhere, LFP of phenyl azide (**1a**) and pentafluorophenyl azide (**2a**) in neat pyridine produce very different transient spectra (Chart II). In the perfluorinated system nitrene

Chart II



ylide **2d** is formed (λ_{max} = 390 nm) whereas with the parent azide **1a** it is ketenimine ylide **1e** that is formed with λ_{max} = 520 nm. It is possible to trap perfluorinated ketenimine **2c** with pyridine to form ylide **2e**, but dilute pyridine must



be used to allow singlet nitrene **2b** sufficient time to ring expand (Scheme II). Ylide **2d** is sufficiently stable to be isolated and its structure has been determined by X-ray crystallography (*15*). Ylides **1e** and **2e** could not be isolated.

Representative transient spectra are given in Figures 2 and 3 which are derived from LFP of two difluorinated aryl azides, **7a** and **9a** (Scheme II), in neat pyridine. The 2,3 difluorinated azide produces the ketenimine **7c** (or **7c′**) upon photolysis which is trapped in neat pyridine; the 2,6 isomer produces the nitrene **9b** which is trapped in pyridine. The results for azides **1a**–**16a** are summarized in Table I. LFP of **9a** in the presence of dilute pyridine

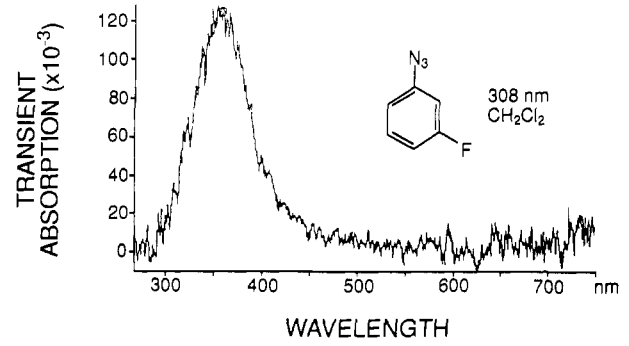


Figure 1. The transient spectrum of **4c** produced by LFP of **4a** in CH_2Cl_2 at ambient temperature.

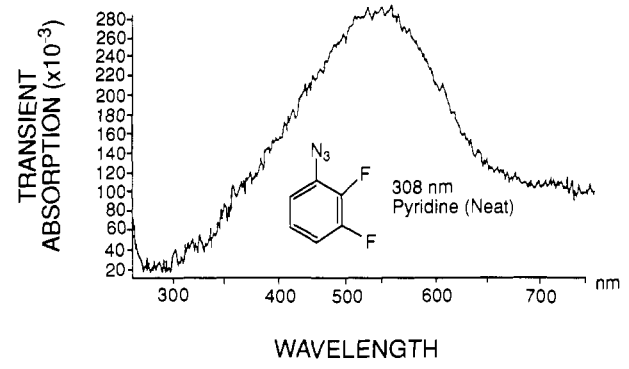
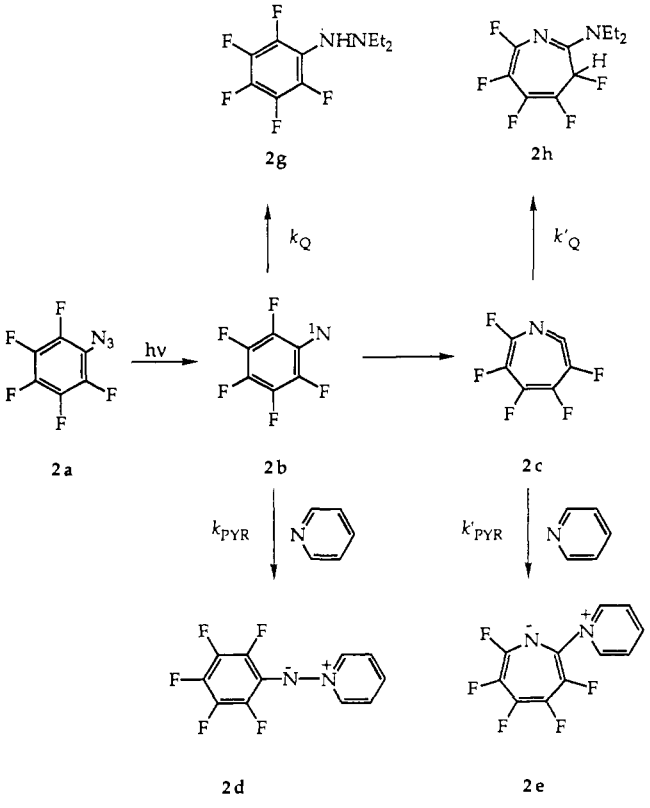
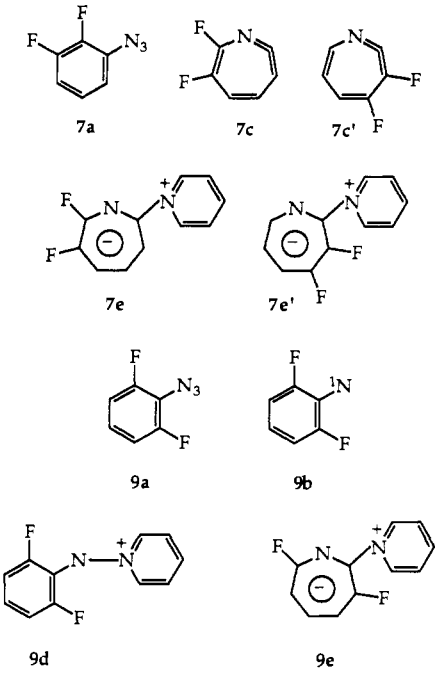


Figure 2. The transient spectrum of ketenimine **7c** (or **7c'**) derived ylide **7e** (or **7e'**) produced by LFP of **7a** in neat pyridine at ambient temperature.

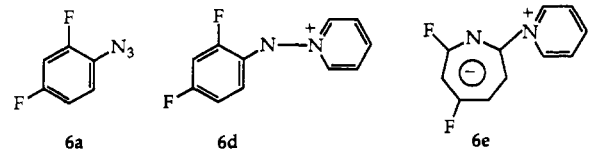
Scheme II



produces ketenimine-derived ylide **9e**. The ratio of nitrene ylide **9d**/**9e** is a linear function of pyridine concentration as predicted by Scheme II (Figure 4). It was not possible to use transient UV–vis spectroscopy to determine whether ketenimine **7c** or **7c'**, or both species, were trapped with pyridine to form either ylide **7e** or **7e'** or a mixture of both species.



In contrast to **7a** and **9a**, LFP of 2,4-difluorophenyl azide (**6a**) in neat pyridine produces the transient spectra of both the ketenimine **6e** and nitrene-derived ylide **6d** (Figure 5).

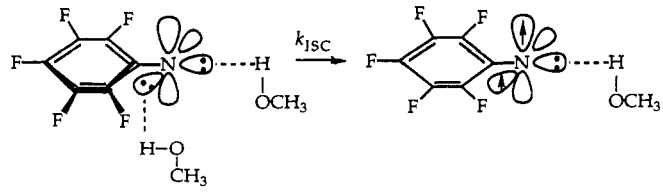


It was possible to resolve the rate of formation of the ketenimine-derived ylides (**1–16e**) by nanosecond spectroscopy. The rates were exponential and could be fit by the Marquardt[17] algorithm to yield an observed rate constant, k_{obs}. Scheme I predicts eq 1, where τ is the

$$k_{obs} = 1/\tau + k'_{PYR}[PYR] \quad (1)$$

lifetime of the ketenimine in the *absence* of pyridine and k'_{PYR} is the second-order rate constant for the reaction of ketenimines with pyridine (*18*). Indeed, plots of k'_{obs} versus [PYR] are linear (Figure 6) and the data are summarized in Table II. It is clear that increasing fluorine substitution dramatically increases the rate of nucleophilic attack on the ketenimine. This is in accord with earlier studies of Li (*9b*).

LFP Studies in Methanol. We have previously reported that LFP of pentafluorophenyl azide (**2a**) in methanol produces the triplet nitrene **2d** (*15*). Methanol



apparently catalyzes the rate constant (k_{ISC}) of singlet **2b** to triplet **2f** intersystem crossing. This has been attributed to differential hydrogen bonding, which lowers the energy of **2b** relative to that of **2f** thereby increasing the rate constant of the radiationless transition.

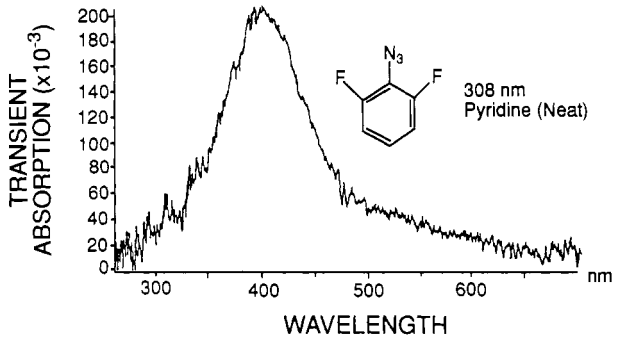


Figure 3. The transient spectrum of nitrene (**9b**) derived ylide **9d** produced by LFP of **9a** in neat pyridine at ambient temperature.

Table I. Reactive Intermediate Trapped upon LFP of the Azide at 25 °C

azide	intermediate trapped in neat pyridine	intermediate detected in CH_3OH
1a	ketenimine **1c**	ketenimine **1c**
2a	nitrene **2b**	triplet nitrene **2f**
3a	ketenimine **3c**	ketenimine **3c**
4a	ketenimine **4c**	ketenimine **4c**
5a	ketenimine **5c**	ketenimine **5c**
6a	nitrene **6b**, ketenimine **6c**	ketenimine **6c**[a]
7a	ketenimine **7c**	ketenimine **7c**
8a	ketenimine **8c**	ketenimine **8c**
9a	nitrene **9b**	triplet nitrene **9f**
10a	ketenimine **10c**	ketenimine **10c**
11a	ketenimine **11c**	ketenimine **11c**
12a	ketenimine **12c**	ketenimine **12c**[a]
13a	ketenimine **13c**	ketenimine **13c**
14a	nitrene **14c**	ketenimine **14c**
15a	nitrene **15b**	triplet nitrene **15f**
16a	nitrene **16b**	triplet nitrene **16f**

[a] A small amount of triplet nitrene is observed.

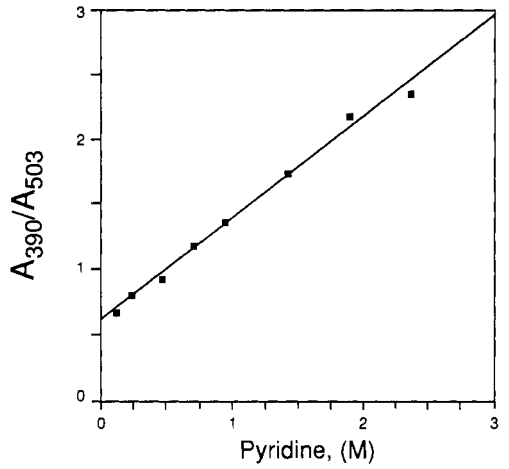


Figure 4. The ratio of transient absorption of nitrene ylide **9d** (A_{390}) to ketenimine ylide **9e** (A_{503}) produced by LFP of azide **9a** in CH_2Cl_2 as a function of pyridine concentration.

Thus, azides **3a–16a** were studied by LFP techniques in methanol. The results are summarized in Table I. It was found that the singlet nitrenes **2b**, **6b**, and **9b**, which are sufficiently long lived to be trapped by neat pyridine at ambient temperature, show methanol-catalyzed ISC. Figures 7 and 8 are representative. LFP of 2,6-difluorophenyl azide (**9a**) in methanol produces the transient spectrum of the triplet nitrene (Figure 7), but LFP of the 2,3 isomer **7a** in methanol again gives a ketenimine. The methanol catalysis of ISC is not universal but is restricted to singlet aryl nitrenes, which do not ring expand more rapidly than they react with pyridine.

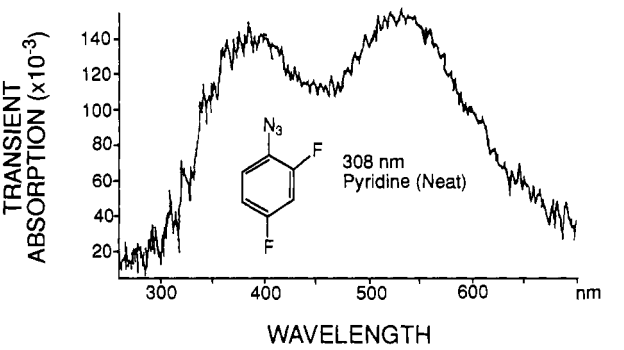


Figure 5. The transient spectra of ketenimine–pyridine ylide **6e** and nitrene–pyridine ylide **6d** produced by LFP of **6a** in neat pyridine at ambient temperature.

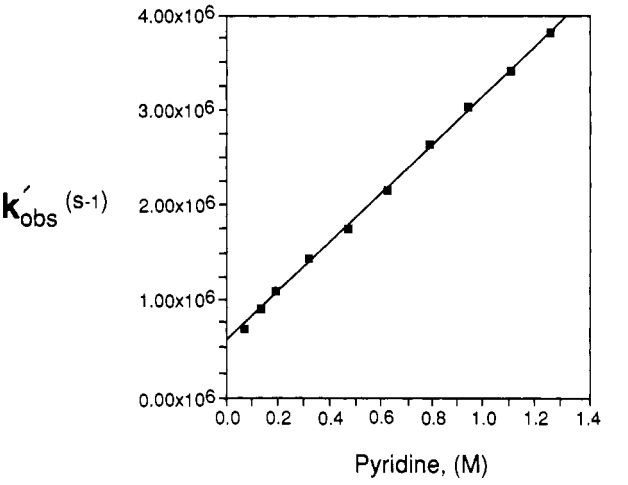


Figure 6. A plot of k'_{obs} versus pyridine concentration obtained by LFP of **4a** in CH_2Cl_2 at ambient temperature.

Table II. Absolute Rate Constants of Reaction of Ketenimines with Pyridine in CH_2Cl_2 at Ambient Temperature

azide	ketenimine	k'_{PYR} (M^{-1} s^{-1})	ylide λ_{max} (nm)
1a	**1c**	4.8×10^5 [a]	490–500
2a	**2c**	3.1×10^9 [a]	520
3a	**3c**	6.2×10^6	490
4a	**4c**	3.3×10^6	550
5a	**5c**	4.7×10^6	520
6a	**6c**	5.6×10^7	535
9a	**9c**	2.2×10^8	505
10a	**10c**	5.5×10^8	490

[a] Reference 14.

Product Studies in Methanol and Benzene. Azides **2a–16a** were photolyzed in methanol and the products analyzed. The study was repeated using a relatively inert solvent, benzene, as a point of comparison. Only singlet (2,6-difluorophenyl)nitrene (**9b**) reacts with benzene to give an adduct, in 9% yield. The principal products are anilines and azo compounds and tar. The data are summarized in Table III. As expected from the LFP experiments the yield of triplet nitrene-derived products (anilines and azo compounds) is larger in methanol than in benzene for those systems (azides **2a**, **6a**, and **9a**) which demonstrated methanol-catalyzed ISC by transient spectroscopy.

III. IMPLICATIONS FOR PHOTOAFFINITY LABELING

Photolysis of 2,6-difluoro-substituted aryl azides in hydrophobic environments generates *trappable* singlet nitrene intermediates. The singlet nitrenes react at near diffusion controlled rates with amines, sulfides, sulfoxides, and alkenes, and less efficiently with aromatic rings and

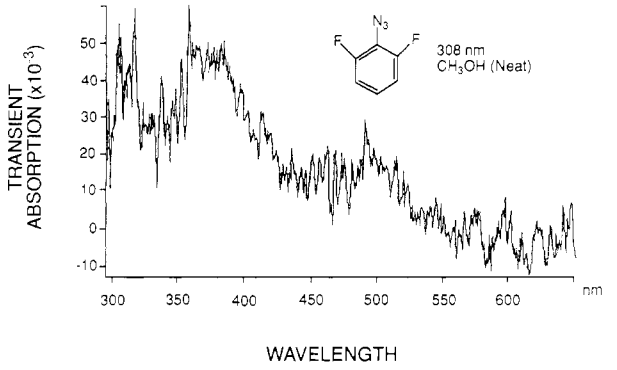


Figure 7. The transient spectrum of triplet nitrene **9f** produced by LFP of **9a** in methanol at ambient temperature.

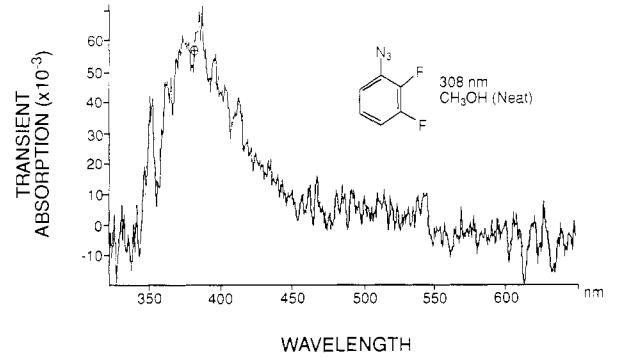


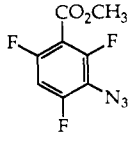
Figure 8. The transient spectrum of ketenimine **7c** produced by LFP of **7a** in methanol at ambient temperature.

Table III. The Combined Yield of Azo Compound (and Aniline) Type Products Formed on Photolysis of Fluorinated Aryl Azides in Benzene and Methonol at Ambient Temperature[a,b]

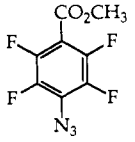
	solvent			solvent	
azide	benzene	methanol	azide	benzene	methanol
2a	5[d]	0[f]	**6a**	58	72
3a	58	65	**7a**	8	8
4a	0	0[e]	**8a**	0	0[e]
5a	0	0[e]	**9a**	9[d]	46[g]

[a] Samples were photolyzed in a Rayonet photoreactor with a 350-nm light source for 2 h. [b] Azide concentration: 0.01 M. Diphenylmethane (internal standard) concentration: 0.005 M. [c] Percent yields are absolute. [d] A benzene insertion product is the major product observed. [e] Large amounts of ketenimine–methanol adducts were detected by GC–MS. [f] A 56% yield of pentafluoroaniline was observed. [g] A 20% yield of 2,6-difluoroaniline was observed.

unactivated CH bonds. Thus they should be effective reagents for photoaffinity labeling of amino acids in *hydrophobic* environments. It is proposed that azides **15a**



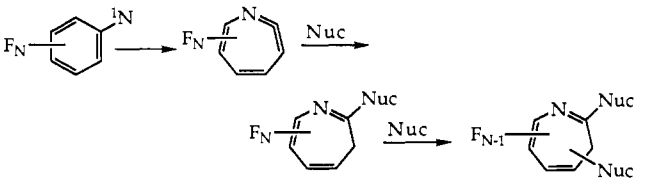
15a



16a

and **16a** will be useful synthons for the development of new PAL labels. Photolysis of 2,6-difluoro-substituted aryl azides in *hydrophilic* environments will generate triplet nitrene intermediates by hydrogen-bonding catalysis of intersystem crossing. The triplet nitrenes will undergo free-radical-like reactions with amino acids which are predicted to lead to cleavage rather than to labeling of biomolecules.

Photolysis of polyfluorinated aryl azides which lack the 2,6 substitution pattern leads to ring expansion to ketenimines rather than chemical trapping of the singlet nitrenes. The more fluorines that are present in the aryl azide the larger the rate constant of reaction of the corresponding ketenimine with the nucleophile and the greater the chance of the addition of a second nucleophile (Nuc) to the initial adduct, and cross-linking.



IV. EXPERIMENTAL PROCEDURES

General Methods. Melting points were recorded on an electrochemical capillary melting point apparatus and are uncorrected. ^{1}H NMR spectra were recorded on a Bruker AM-250 (250-MHz) spectrometer. All ^{1}H chemical shifts are reported relative to TMS as an internal standard. ^{19}F NMR spectra were recorded on a Bruker AM-250 (250-MHz) instrument and were proton decoupled. ^{19}F chemical shifts are reported relative to hexafluorobenzene (162.9 ppm as an internal standard). The ^{19}F NMR spectra were recorded on a Varian EM-360 (56.60 MHz) and the ^{19}F chemical shifts are reported relative to hexafluorobenzene (96 ppm) as an internal standard. Infrared spectra were recorded on a Perkin-Elmer Model 1710 infrared Fourier transform spectrometer. Mass spectra and exact masses were obtained on a V6 70-2S0S or a Kratos MS-30 mass spectrometer. GC–MS spectra were obtained with a Hewlett-Packard S890 gas chromatograph equipped with a Hewlett-Packard 5970B mass spectrometer detector and a 30 m x 0.254 nm J&W Scientific fused silica capillary column (DB-1, 0.25 μm).

Materials. Benzene, cyclohexene, hexane, ethyl acetate, diethylamine, 2-fluoroaniline, 3-fluoroaniline, 4-fluoroaniline, 2,3-difluoroaniline, 2,4-difluoroaniline, 2,5-difluoroaniline, and 3,4-difluoroaniline were purchased from Aldrich and were used without further purification.

Preparation of Compounds. The substituted aryl azides of this work were described previously (*11b*, *15*) and prepared from the appropriate corresponding anilines. All azo compounds used in this study were prepared by the method of Birchall (*18*) and Leyva (*11b*). The crude product was purified by passage through a neutral alumina column using a 9:1 mixture of hexane/ethyl acetate as described.

Product Studies. Solutions of azides (10^{-2} M) in the corresponding solvent were prepared. Samples were prepared by putting 0.5 mL of the azide solution in 6-mm Pyrex tubes which were prewashed with ammonium hydroxide and oven dried. The solutions were degassed using three freeze–pump–thaw cycles and then sealed under vacuum. Samples were photolyzed with a 350-nm light using Southern New England RPR 3500-Å lamps for 2 h. The product mixtures were analyzed by GC–mass spectrometry. The yields and identities of the products were determined by coinjection of authentic samples and by GC–mass spectrometry.

Laser Flash Photolysis. The laser flash photolysis system in use at The Ohio State University has been described (*20*) and standard protocols (*15*) were employed.

ACKNOWLEDGMENT

Support of this work by the NIH (GM34823) is gratefully acknowledged. One of us (K.A.S.) is grateful to The Ohio

State University for an Ohio State University College of Arts and Sciences postdoctoral fellowship.

LITERATURE CITED

(1) Shrock, A. K., and Schuster, G. B. (1984) Photochemistry of Phenyl Azide: Chemical Properties of the Transient Intermediates. *J. Am. Chem. Soc. 106*, 5228.

(2) Schuster, G. B., and Platz, M. S. (1992) Photochemistry of Phenyl Azide. *Adv. Photochem. 17*, 69.

(3) Leyva, E., Platz, M. S., Persy, G., and Wirz, J. (1986) Photochemistry of Phenyl Azide: The Role of Singlet and Triplet Phenyl Nitrene as Transient Intermediates. *J. Am. Chem. Soc. 108*, 3783.

(4) Wasserman, E. (1971) Electron Spin Resonance of Nitrenes. *Prog. Phys. Org. Chem. 8*, 319–335.

(5) Hayes, J. C., and Sheridan, R. S. (1990) Infrared Spectrum of Triplet Phenyl Nitrene on the Origin of Didehydroazepine in Low Temperature Matrices. *J. Am. Chem. Soc. 112*, 5879–5881.

(6) (a) Wentrup, C. (1984) Gas Phase and Matrix Studies. In *Azides and Nitrenes* (E. F. V. Scriven, Ed.) p 395–430, Academic, New York. (b) Cullin, D. W., Soundararajan, N., Platz, M. S., and Miller, T. A. (1990) Reinvestigation of the Electronic Spectrum of the Phenyl Nitrene Radical. *J. Phys. Chem. 94*, 8890. (c) Cullin, D. W., Yu, L., Williamson, J., Platz, M. S., and Miller, T. A. (1990) Laser-Induced Fluorescence Spectrum of the Cyanocyclopentadienyl Radical. A Band System Long Attributed to Triplet Phenyl Nitrene. *J. Phys. Chem. 94*, 3387.

(7) Bayley, H. (1983) *Photogenerated Reagents in Biochemistry and Molecular Biology*, Elsevier, Amsterdam.

(8) (a) Singh, A., Thornton, E. R., and Westheimer, F. H. (1962) The Photolysis of Diazo-acetylchymotrypsin. *J. Biol. Chem. 237*, PC 3006. (b) Fleet, G. W. J., Porter, R. R., and Knowles, J. R. (1969) Affinity Labelling of Antibodies with Aryl Nitrene as Reactive Group *Nature 224*, 511.

(9) (a) DeGraff, B. A., Gillespie, D. W., and Sundberg, R. J. (1974) Phenyl Nitrene. Flash Photolytic Investigation of the Reactin with Secondary Amines. *J. Am. Chem. Soc. 96*, 7491. (b) Li, Y.-Z., Kirby, J. P., George, M. W., Poliakof, M., and Schuster, G. B. (1988) 1,2-Didehydroazepines from the Photolysis of Substituted Aryl Azides: Analysis of Their Chemical and Physical Properties by Time-Resolved Spectroscopic Methods. *J. Am. Chem. Soc. 110*, 8092.

(10) (a) Leyva, E., Young, M. J. T., and Platz, M. S. (1986) High Yields of Formal CH Insertion Products in the Reactions of Polyfluorinated Aromatic Nitrenes. *J. Am. Chem. Soc. 108*, 8307. (b) Leyva, E., Munoz, D., and Platz, M. S. (1989) Photochemistry of Fluorinated Aryl Azides in Toluene Solution and in Frozen Polycrystals. *J. Org. Chem. 54*, 5938. (c) Young, M. J. T., and Platz, M. S. (1989) Polyfluorinated Aryl Azides as Photoaffinity Labelling Reagents; The Room Temperature CH Insertion Reactions of Singlet Pentafluorophenyl Nitrene with Alkanes. *Tetrahedron Lett. 30*, 2199. (d) Young, M. J. T., and Platz, M. S. (1991) Mechanistic Analysis of the Reactions of (Pentafluorophenyl)nitrene in Alkanes. *J. Org. Chem. 56*, 6403. (e) Poe, R., Grayzar, J., Young, M. J. T., Leyva, E., Schnapp, K. A., and Platz, M. S. (1991) Remarkable Catalysis of Intersystem Crossing of Single (Pentafluorophenyl)nitrene. *J. Am. Chem. Soc. 113*, 3209.

(11) (a) Keana, J. F. W., and Cai, S. X. (1990) New Reagents for Photoaffinity Labelling: Synthesis and Photolysis of Functionalized Perfluorophenyl Azides. *J. Org. Chem. 55*, 3640. (b) Keana, J. F. W., and Cai, S. X. (1989) Functionalized Perfluorophenyl Azides: New Reagents for Photoaffinity Labelling. *J. Fluorine Chem. 43*, 151. (c) Cai, S. X., and Keana, J. F. W. (1989) 4-Azido-7-Iodo-3,5,6-Trifluorophenyl Carbonyl Derivatives. A New Class of Functionalized and Iodinated Perfluorophenyl Azide Photolabels. *Tetrahedron Lett. 30*, 5409. (d) Cai, S. X., Glenn, D. J., and Keana, J. F. W. (1992) Toward the Development of Radiolabelled Fluorophenyl Azide-Based Photolabelling Reagents: Synthesis and Photolysis of Iodinated 4-Azidoperfluorobenzoates and 5-Azido-3,5,6-trifluorobenzoates. *J. Org. Chem. 57*, 1299–1304. (e) Cai, S. X., and Keana, J. F. W. (1991) Dizo and Azido-Functionalized Glutaraldehydes as Cross Linking Reagents and Potentail Fixatives for Electron Microscopy. *Bioconjugate Chem. 2*, 38–43.

(12) (a) Banks, R. E., and Sparkes, G. R. (1972) Studies in Azide Chemistry. Part V. Synthesis of 4-Azido-2,3,5,6-tetrafluoro,4-Azido-3-chloro-2,5,6-trifluoro-, and 4-Azido-3,5-dichloro-2,6-difluoro-pyridine, and Some Thermal Reactions of the Tetrafluorocompound. *J. Chem. Soc., Perkin Trans. 1* 2964–2970. (b) Banks, R. E., and Prakash, A. (1974) Studies in Azide Chemistry. Part VI. Some Reactions of Perfluoroazidobenzene and Perfluoro-4-azidotoluene. *J. Chem. Soc., Perkin Trans. 1* 1365–1371. (c) Banks, R. E., and Prakash, A. (1973) New Reactions of Azidopentafluorobenzene; Intermolecular Insertions into the N-H Bonds. *Tetrahedron Lett.* 99–102. (d) Banks, R. E., and Medany, I. M. (1990) Studies in Azide Chemistry. Part 14. Thermolysis of Perfluoro-4-azidopyridine and Perfluoro-4-azidotoluene in the Presence of Penta- and Hexa-Methylbenzene. *J. Fluorine Chem. 47*, 527–532. (e) Banks, R. E., and Venayak, N. D. Studies in Azide Chemistry. Part 13. Intermolecular Insertion of Azido-derived Polyfluorinated Aryl- and Heteroaryl-Nitrenes into Ring C-H Bonds of 1,3,5-Trimethyl and 1,3,5-Trimethoxybenzene. *J. Chem. Soc., Chem. Commun.* 900–901. (f) Banks, R. E., and Madany, I. M. (1985) Decisive Evidence for the Occurrence of Ring-expansion During Pyrolisis of Azidopentafluorobenzxene: X-Ray Crystallographic Analysis of Pentafluorophenyl-nitrene Dimer. *J. Fluorine Chem. 30*, 211–226.

(13) (a) Crocker, P. J., Imai, N., Rajogopalen, K., Boggess, M. A., Kwiatkowski, S., Dwyer, L. D., Vanaman, T. C., and Watt, D. (1990) Heterobifunctional Cross-Linking Agents Incorporating Perfluorinated Aryl Azides. *Bioconjugate Chem. 3*, 419. (b) Drake, R. R., Slam, J., Wall, K., Abramove, M., D'Souza, C., Elbein, A. D., Crocker, P. J., and Watt, D. S. (1992) Application of an N-(4-Azido-2,3,5,6-tetrafluorobenzoyl)tyrosine Substituted Peptide as a Heterobifunctional Cross-linking Agent in a Study of Protein O-Glycosylation in Yeast. *Bioconjugate Chem. 3*, 69–73.

(14) (a) Pinney, K. C., and Katzenellenbogen, J. A. (1991) Synthesis of a Tetrafluoro-substituted Aryl Azide and Its Protio Analogue as Photoaffinity Labelling Reagents for the Estrogen Receptor. *J. Org. Chem. 56*, 3125–3133. (b) Pinney, K. C., Carlson, K. E., Katzenellenbogen, B. S., and Katzenellenbogen, J. A. (1991) Efficient and Selective Photoaffinity Labelling of the Estrogen Receptor Using Two Nonsteroidal Ligands that Embody Aryl Azide or Tetrafluoroaryl Azide Photoreactive Functions. *Biochemistry 30*, 2421.

(15) Poe, R., Schnapp, K., Young, M. J. T., Grayzar, J., and Platz, M. S. (1992) Chemistry and Kinetics of Singlet (Pentafluorophenyl)Nitrene. *J. Am. Chem. Soc. 114*, 5054.

(16) Soundararajan, N., and Platz, M. S. (1990) Descriptive Photochemistry of Polyfluorinated Azide Derivatives of Methyl Benzoate. *J. Org. Chem. 55*, 2034.

(17) The Marquardt algorithm is described: Bevington, P. R. (1983) *Data Reduction and Error Analysis for the Physical Sciences*, McGraw-Hill, New York. We utilized a program based on the Marquardt algorithm written by Shamim Ahmed.

(18) The pyridine probe method is based upon models developed by Scaiano to probe free-radical reactions. For examples, see: (a) Small, R. D., Jr., and Scaiano, J. C. (1977) Reaction of Type II Biradicals with Paraquat Ions Measurement of a Biradical Lifetime. *J. Phys. Chem. 81*, 828. (b) Small, R. D., Jr., and Scaiano, J. C. (1977) Direct Detection of the Biradicals Generated in the Norrish Type II Reaction. *Chem. Phys. Lett. 50*, 431. (c) *Ibid.* (1978) *59*, 246.

(19) Birchall, J. M., Hazeldine, R. N., and Kemm, J. E. G. (1970) Polyfluoroarenes. Part X. Polyfluoroaromatic Azo-compounds. *J. Chem. Soc.* 449.

(20) Soundararajan, N., Platz, M. S., Jackson, J. E., Doyle, M. P., Oon, S.-M., Liu, M. T. H., and Anand, S. M. (1988) Addition of Arylchlorocarbenes to α,β-Unsaturated Esters. Absolute Rates, Substituent Effects and Variable Reactivities. *J. Am. Chem. Soc. 110*, 7143.

A Laser Flash Photolysis Study of Di-, Tri- and Tetrafluorinated Phenylnitrenes; Implications for Photoaffinity Labeling

Karlyn A. Schnapp and Matthew S. Platz*

Department of Chemistry, The Ohio State University, 120 West 18th Avenue, Columbus, Ohio 43210. Received November 6, 1992

Several fluorinated aryl azides (2,6 and 2,4-difluorophenyl azide, 2,4,6-trifluorophenyl azide, and methyl 4-azido-2,3,5,6-tetrafluorobenzoate) were studied by laser flash photolysis techniques. In each case, the azides form singlet nitrenes which can be intercepted with pyridine to form ylides. This allowed determination of the rate constant for ring expansion of the singlet nitrene to the dehydroazepine and measurement of the absolute rate constants for reaction of the singlet nitrenes with typical quenchers.

I. INTRODUCTION

The cascade of reactive intermediates formed upon photolysis of phenyl azide **1** has been previously discussed (*1*). It is clear that photolysis of phenyl azide and its simple derivatives release singlet aryl nitrenes. Singlet phenylnitrene **2S** ring expands to ketenimine **3** more rapidly than it can be captured by external trapping agents such as pyridine (PYR) or diethylamine ($k_{EXP} >> k_{PYR}$[PYR], Scheme I). The lifetime of **2S** at 25 °C is 10–100 ps. The effect of perfluorination on the photochemistry of phenyl azide is dramatic (*2*). Singlet (pentafluorophenyl)nitrene can be captured by pyridine and diethylamine to give adducts in respectable yields. Perfluorination results in a more favorable ratio of k_{PYR}[PYR] to k_{EXP} by retarding the rate of ring expansion. The lifetime of (perfluorophenyl)nitrene is 1–10 ns in solution at ambient temperature.

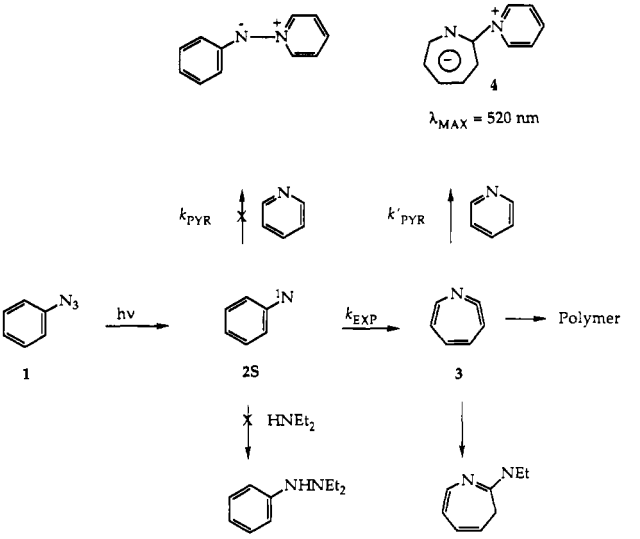
The impetus behind these studies was the development of new reagents for photoaffinity labeling (PAL) (*3*). In a PAL experiment, a light-sensitive moiety is appended to a substrate of a biological macromolecule (*4*). In an ideal experiment, photolysis of the modified ligand will release an extremely reactive intermediate which will combine immediately with unactivated bonds of the biological target to form a new linkage between the labeling reagent and the biological macromolecule. Perfluoro singlet nitrene **6S** reacts with a much wider range of substrates and with much larger rate constants than does ketenimine **3**, which is derived from phenyl azide. To effectively design new PAL reagents, it becomes necessary to determine the position and amount of fluorine substituents required to retard ring expansion.

In a companion paper we report the photochemistry of 16 fluorinated aryl azides (*5*). It was demonstrated that two fluorine substituents placed either 2,6 or, less effectively, 2,4 to the azide moiety are required to trap singlet nitrenes. Without this substitution pattern, the photogenerated nitrenes ring expand so rapidly to ketenimines that intermolecular capture of the nitrene is precluded.

In this paper we demonstrate that 2,6-difluorophenyl azide and a carboxy ester derivative of this azide recapitulate the desirable properties of pentafluorophenyl azide. The ester derivative of 2,6-difluorophenyl azide is proposed as a building block of new PAL reagents. It will also be demonstrated that 2,4-difluorophenyl azide and its derivatives are not expected to perform as well as the 2,6-difluoro isomers as photoaffinity labels at ambient temperature.

It is important to note that both Watt et al. and Katzenellenbogen et al. (*6*) have successfully used polyfluorinated aryl azide reagents in photoaffinity labeling experiments.

Scheme I



II. RESULTS FROM LASER FLASH PHOTOLYSIS STUDIES OF FLUORINATED ARYL AZIDES

2,6-Difluorophenyl Azide. Laser flash photolysis (LFP) studies in solution and low-temperature spectroscopy of samples immobilized in rigid matrices have revealed the EPR, UV–vis, and IR signatures of triplet nitrenes and ketenimines (*1*, *7*). Singlet aryl nitrenes have not yet been detected by spectroscopic methods. As with carbenic species, it is easier to detect the pyridine ylides derived from singlet nitrenes and ketenimines than the reactive intermediates themselves by LFP in solution (*2*, *8*). The pyridinium ylides have intense absorptions and long lifetimes which make them ideal probes of transient phenomena. Fortunately, the ylides derived from singlet nitrenes (λ_{max} = 390 nm) and ketenimines (λ_{max} = 520 nm) absorb in very different spectral regions and their spectra do not vary substantially with fluorine substituent.

LFP (Lambda Physik XeCl, excimer laser, 308 nm, 17 ns, 150 mJ) of 2,6-difluorophenyl azide (**10**) in the inert solvent CH_2Cl_2 produces the transient spectrum of ketenimine **13** (Figure 1). However, upon LFP of **10** containing >1 M pyridine, the absorption spectrum of nitrene ylide **12** is observed (Figure 2). The rate of growth of this transient absorption was faster than the time resolution of the apparatus (17 ns) when [PYR] ≥ 0.5 M. The yield

1043-1802/93/2904-0178$04.00/0 © 1993 American Chemical Society

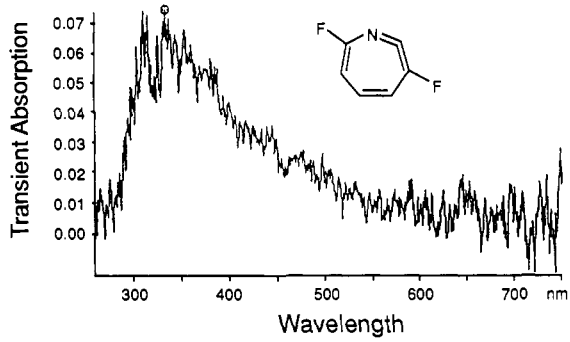


Figure 1. The transient spectrum of ketenimine **13** produced by LFP of 2,6-difluorophenyl azide in CH_2Cl_2.

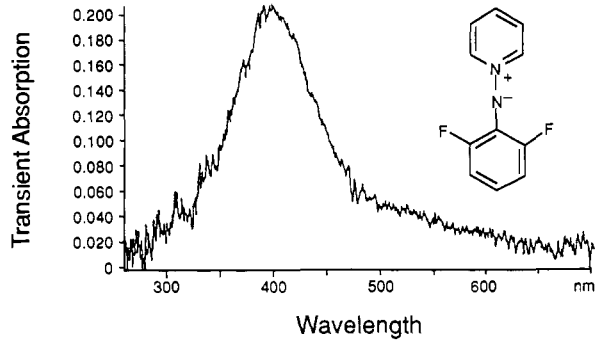
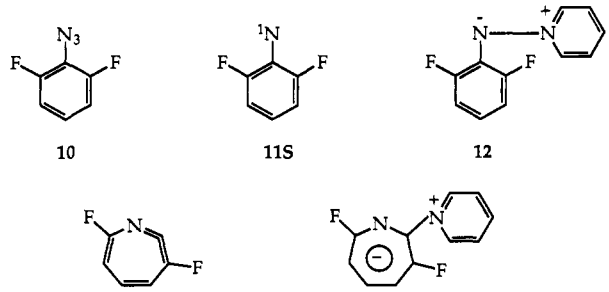


Figure 2. The transient spectrum of nitrene ylide **12** produced by LFP of 2,6-difluorophenyl azide in CH_2Cl_2/pyridine.



(A_{390}) of ylide in CH_2Cl_2 is zero when [PYR] = 0 and increases steadily as the pyridine concentration increases (Figure 3). However the optical yield of ylide (A_{390}) is saturated (A_{390}^{∞}) when [PYR] > 3 M (Figure 3). When [PYR] > 3 M, every singlet nitrene produced in a laser pulse is captured by pyridine to form ylide **12**. At the pyridine concentration which corresponds to $A_{390} = {}^1/_2A_{390}^{\infty}$, eq 1 is valid in CH_2Cl_2, a chemically inert solvent.

$$k_{PYR}[PYR] = k_{EXP} \quad \text{at [PYR] where } A_{390} = A_{390}^{\infty} \quad (1)$$

The magnitude of k_{PYR} must be less than that of a diffusion controlled rate constant (10^{10} M^{-1} s^{-1}) and must exceed 10^8 M^{-1} s^{-1}, as we cannot resolve the absolute rate of formation of **12** when [PYR] = 0.5 M. A reasonable estimate of k_{PYR} is 10^9 M^{-1} s^{-1}, which is commonly observed with carbenes (*8*). As [PYR] = 0.21 M when $A_{390} = {}^1/_2A_{390}^{\infty}$, we estimate $k_{EXP} = 2.1 \times 10^8$ M^{-1} s^{-1} or that the lifetime of singlet (2,6-difluorophenyl)nitrene is 5 ns in CH_2Cl_2 at room temperature. From this type of analysis, the lifetime of pentafluorophenyl singlet nitrene **6S** in CH_2Cl_2 was determined to be 17 ns, just slightly longer than that of **11S** (*2l*).

The yield of ylide was also measured in a more reactive solvent, tetrahydrofuran. In this solvent, eq 2 is valid when $A_{390} = {}^1/_2A_{390}^{\infty}$, where k_{THF} is the absolute rate

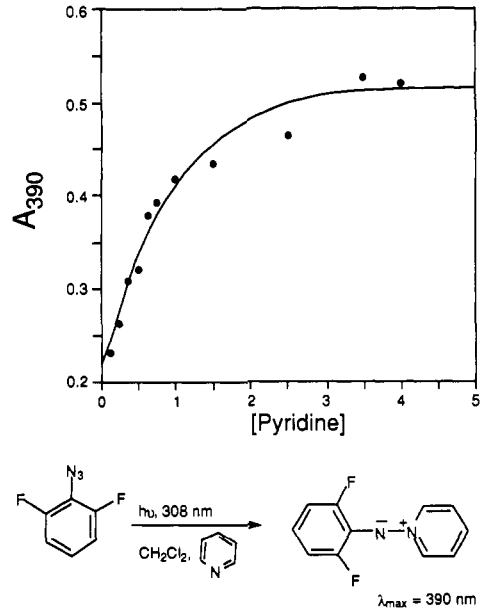
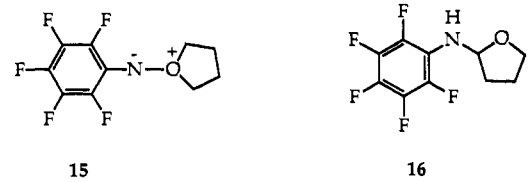


Figure 3. The yield (A_{390}) of nitrene ylide **12** produced by LFP of 2,6-difluorophenyl azide as a function of pyridine concentration.

$$k_{PYR}[PYR] = k_{EXP} + k_{THF}[THF] \quad (2)$$

constant of reaction of nitrene **11S** with THF. Assuming that k_{EXP} is solvent independent indicates that $k_{THF}[THF] = 5 \times 10^8$ s^{-1}. (Perfluorophenyl)nitrene reacts with THF to form ylide **15** and ultimately CH insertion product **16**, with $k_{THF}[THF] = 2.8 \times 10^8$ s^{-1} (see Table I) (*2l*).



The yield of ylide **12** is reduced in the presence of a competitive quencher of the singlet nitrene **11S** (e.g. diethylamine). Under these conditions, a Stern–Volmer plot of A^0_{390}/A_{390} versus quencher (Q) concentration at constant pyridine concentration will be linear (Figure 4), where A^0_{390} is the yield of ylide **12** when [Q] = 0. The slopes of these plots yield $k_Q/(k_{PYR}[PYR])$, where k_Q is the absolute rate constant of reaction of nitrene **11S** with the quencher, when the concentration of pyridine ([PYR] ≥ 3 M) is sufficient to capture all singlet nitrene generated in a single laser pulse (when [Q] = 0). Diethylamine, dimethyl sulfide, dimethyl sulfoxide, and tetramethylethylene form adducts with pentafluorophenyl singlet nitrene and quench the yield of ylide **12** (Table II), presumably through adduct formation.

We have reported that methanol catalyzes intersystem crossing of singlet to triplet (pentafluorophenyl)nitrene (*2k*). This effect is also observed for 2,6-difluorophenyl singlet nitrene. The Stern–Volmer quenching values are listed in Table II. For the sake of comparison, values for singlet (pentafluorophenyl)nitrene are reported as well.

LFP of **10** in CH_2Cl_2 containing dilute pyridine produces a new transient absorption band identified as ketenimine ylide **14** (Figure 5). As predicted by the mechanism of Scheme II, the ratio of nitrene to ketenimine-derived pyridine ylide increases linearly with pyridine concentration (Figure 6).

Table I. Approximate Values of k_{EXP} and Singlet Nitrene Lifetime τ in CH_2Cl_2 and k_{THF}[THF] at Ambient Temperature for Various Fluorinated Arylnitrenes Deduced by Assuming That $k_{PYR} = 1 \times 10^9$ M^{-1} s^{-1}

azide	singlet nitrene	k_{EXP}[a] (s^{-1})	τ_{ns}[a,b]	k_{THF}[THF] (s^{-1})
5[d]	6S	5.8×10^7	17	2.8×10^8
10	11S	2.1×10^8	5	5×10^8
17	18S	3.3×10^9	0.3	c
23	24S	4.5×10^7	22	1.19×10^9
26	27S	2.0×10^8	5	6×10^7

[a] Obtained by assuming that $k_{PYR} = 1 \times 10^9$ M^{-1} s^{-1}. [b] [PYR] = 0. [c] Could not be determined; see the text. [d] Reference 21.

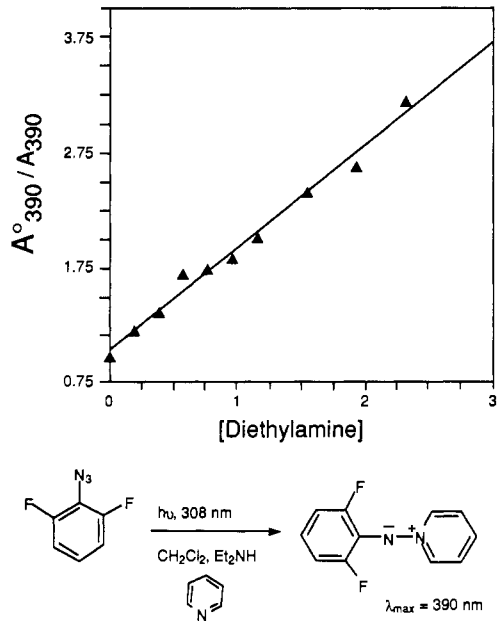
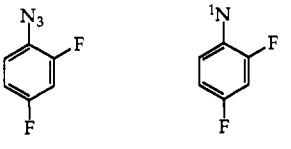


Figure 4. Stern–Volmer treatment of the quenching of the yield of nitrene ylide **12**, by diethylamine; see the text.

Table II. Stern–Volmer Quenching of Fluorinated Singlet Arylnitrenes Obtained by Monitoring Nitrene–Pyridine Ylide Yields (A_{390}) as a Function of Quencher

		quenching (k_Q/k_{PYR})				
azide	nitrene	CH_3-OH	CH_3-SCH_3	$CH_3S(O)$-CH_3	$(CH_3CH_2)_2$-NH	$(CH_3)_2$-C=C$(CH_3)_2$
5	6S	0.32	9.74	4.02	5.99	2.88
10	11S	0.77	31.5	4.19	3.45	4.1
23	24S	1.11	5.53	3.84	5.02	4.38
26	27S	0.43	47.6	7.21	45	4.29

2,4-Difluorophenyl Azide. The results with 2,4-difluorophenyl azide (**17**) are qualitatively different than those obtained with 2,6-difluorophenyl azide (**10**).



17 18S

LFP of **17** in neat pyridine (12.4 M) produces the transient spectra of both nitrene and ketenimine-derived pyridine ylides (Figure 7) in a nearly 1:1 ratio of transient absorption intensities. In contrast, a 1:1 ratio of ylide absorptions is produced from 2,6-difluorophenyl azide when [PYR] is only 0.8 M. This indicates that k_{EXP} with 2,4-difluoro singlet nitrene **18S** is ≈15.5 times as large as that of the 2,6-difluoro isomer at ambient temperature, or that $k_{EXP} = 3.3 \times 10^9$ s^{-1} for nitrene **18S**.

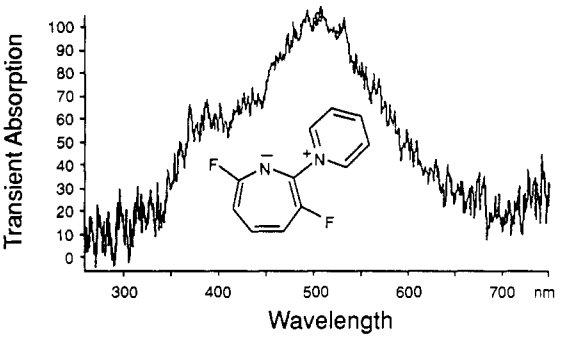


Figure 5. The transient spectrum of ketenimine ylide **14** formed by LFP of 2,6-difluorophenyl azide in CH_2Cl_2 containing dilute pyridine.

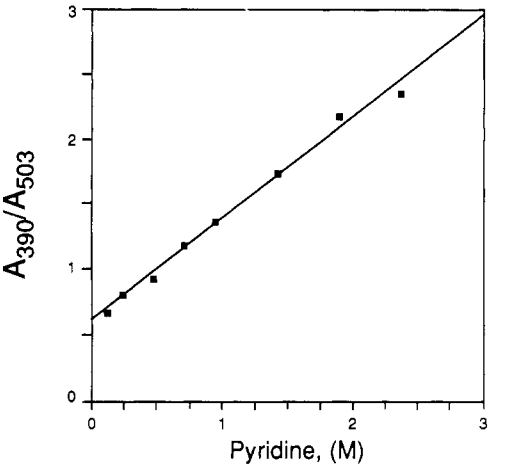
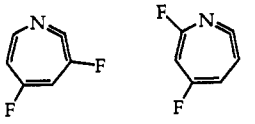


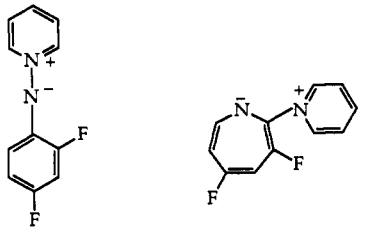
Figure 6. The ratio of nitrene ylide **12** (A_{390}) to ketenimine ylide **14** (A_{503}) formed as a function of pyridine upon LFP of 2,6-difluorophenyl azide.

It is not clear whether nitrene **18S** ring expands to form either **19** or **20** regioselectively, or as a mixture of ketenimines.



19 20

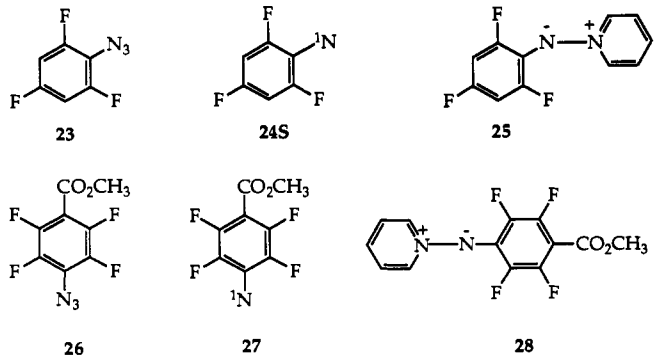
Due to the relatively low yield of nitrene ylide **21** in neat pyridine at ambient temperature, further LFP studies, as per those performed with the 2,6 isomer were not attempted.



21 22

2,4,6-Trifluorophenyl Azide and 4-Azido-2,3,5,6-tetrafluorobenzoate. Azides **23** and **26** were also studied by LFP techniques. The products formed on photolysis of **26** have previously been studied in some detail (*9*).

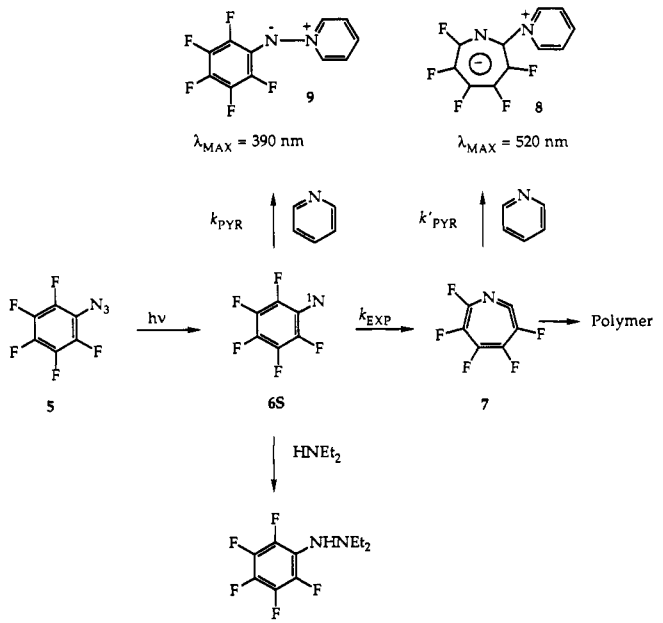
LFP of **23** and **26** gives a pattern of results similar to those obtained with 2,6-difluorophenyl azide (**10**) and perfluorophenyl azide (**5**). These results are summarized



23 24S 25

26 27 28

Scheme II

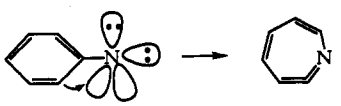


in Tables I and II. It is clear that **26** is a useful building block for new reagents for photoaffinity labeling.

III. DISCUSSION

The results presented herein demonstrate that 2,6-difluoro substitution relative to the azide moiety is required to achieve nitrene rather than ketenimine chemistry at ambient temperature. The 2,4-difluoro substitution relative to the azide group is not as effective as 2,6 disubstitution at achieving nitrene chemistry at ambient temperature.

The origin of the differences associated with the 2,6 versus the 2,4 substitution pattern is not entirely clear. Ring expansion most likely proceeds from the π^2 configuration of the singlet nitrene, despite the fact that it is not the lowest energy singlet configuration (*10*). We have



argued that the "perfluoro" effect in nitrenes is due to differential stabilization of the σ^2 configuration of the singlet nitrene, relative to the π^2 configuration due to π back-bonding of fluorine with the empty p–π orbital on nitrogen and also to fluorine stabilization of the σ–p orbital by hyperconjugation (*1*, *21*). We speculate that π back-bonding in the 2,4 and 2,6 isomers are identical but that the fluorine stabilization of the σ-p orbital is more significant in the 2,6 isomer than in the 2,4 compound.

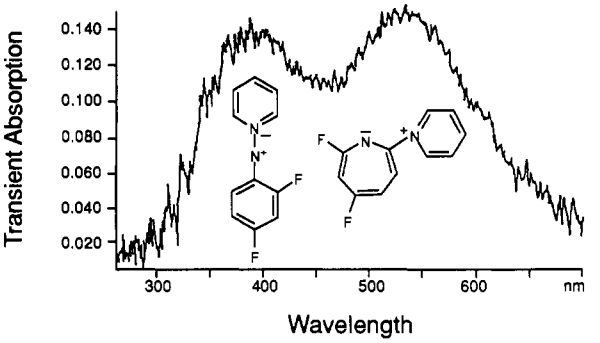


Figure 7. The transient spectra of nitrene ylide **29** and ketenimine-derived ylide **22** produced by LFP of 2,4-difluorophenyl azide (**17**) in neat pyridine at ambient temperature.

One can also speculate that fluorine substitution destabilizes ketenimines when positioned on the cumulene double bonds and thus retards the rate of ring expansion. These speculations underscore the need for high quality ab initio molecular orbital calculations on the fluorinated aryl nitrene systems, as per parent phenyl nitrene, (*10*) to interpret the data.

All of the 2,6 difluorinated aryl azides undergo ring expansion more slowly than singlet (2,4-difluorophenyl)nitrene. However, the variation in k_{EXP} between the different 2,6 difluorinated aryl azides (**5**, **10**, **23**, and **26**, reported in Table I) is less than a factor of 5. However, it is important to remember that these values are derived quantities which are based on the assumption that k_{PYR} is constant throughout these series of compounds. Small variations in k_{PYR} among **5**, **10**, **23**, and **26** may make these differences in k_{EXP} disappear.

The data of Table II demonstrates that nitrenes **11S**, **24S**, and **27S** can be captured with typical traps of singlet (pentafluorophenyl)nitrene and we predict will react efficiently with cystine, cysteine, methionine, phenylalanine, tyrosine, tryptophan, and lysine residues in proteins.

All four 2,6 difluorinated singlet aryl nitrenes apparently react with methanol. On the basis of our work with (pentafluorophenyl)nitrene, however, we believe that methanol catalyzes the intersystem crossing of the singlet nitrene to its triplet ground state. Thus, in hydrophilic environments these reagents are expected to generate triplet rather than singlet nitrenes.

IV. CONCLUSIONS

Laser flash photolysis of 2,6-difluorophenyl azide, 2,4-difluorophenyl azide, 2,4,6-trifluorophenyl azide, and methyl 4-azido-2,3,5,6-tetrafluorobenzoate in nonhydroxylic solvents generates singlet nitrenes which can be trapped with pyridine to form easily detected ylides ($\lambda_{max} \approx 390$ nm). Singlet 2,4 difluorinated arylnitrenes ring expand more rapidly than their 2,6-difluoro isomeric counterparts and are consequently less useful as photoaffinity labeling reagents. The 2,6 difluorinated nitrenes react rapidly with dimethyl sulfide, dimethyl sulfoxide, diethylamine, tetrahydrofuran, and tetramethylethylene. Singlet to triplet nitrene intersystem crossing is catalyzed by methanol. Thus, photolysis of 2,6 difluorinated aryl azides in hydrophobic media generates highly reactive, electrophilic singlet nitrenes useful for photoaffinity labeling. Photolysis of these azides in hydrophilic media generates triplet nitrenes which have free radical-like properties and are more likely to cut rather than to label biomolecules.

V. EXPERIMENTAL PROCEDURES

The synthesis of all azides used in this study (*2*, *9*) and the laser flash photolysis protocols (*2*, *5*, *11*) have been described previously.

General Procedures. Tetrahydrofuran was dried by distillation over sodium–benzophenone ketyl. Dimethyl sulfide, dimethyl sulfoxide, pyridine, diethylamine, and dichloromethane were purified by distillation over either barium hydroxide or molecular sieves. Pyridine was stored over KOH. Tetramethylethylene was passed through activated alumina prior to use.

Stern–Volmer Quenching Studies. General Procedures. In a typical Stern–Volmer quenching experiment, a stock solution of the azide in dichloromethane was prepared, having an optical density at 308 nm of ca. 0.5. An exact volume of the stock solution was then syringed into several cells followed by an exact volume of neat pyridine. To all but one cell, quencher was added in exact and increasing volume. The single cell without quencher therefore represented a standard ylide signal. All cells were degassed with argon and then subjected to three laser pulses and the resulting signals recorded.

Stern–Volmer Quenching Studies of 2,6-Difluorophenyl Azide (10). (*a*) *Methanol quenching study*: [PYR] = 4.3 M; [CH_3OH] = 0.43, 0.86, 1.34, 2.15, 2.68, 3.22, 3.76, 4.29, 5.37, 6.44 M.

(*b*) *Dimethyl sulfide quenching study*: [PYR] = 4.95 M; [CH_3SCH_3] = 0.03, 0.07, 0.17, 0.27, 0.34, 0.44, 0.51, 0.68, 1.02 M.

(*c*) *Dimethyl sulfoxide quenching study*: [PYR] = 3.96 M; [$CH_3S(O)SCH_3$] = 0.14, 0.28, 0.42, 0.56, 0.70, 0.85, 1.13, 1.69, 2.25 M.

(*d*) *Diethylamine quenching study*: [PYR] = 3.96 M; [$(CH_3CH_2)_2NH$] = 0.19, 0.39, 0.58, 0.77, 0.97, 1.16, 1.55, 1.93, 2.32, 2.71 M.

(*e*) *Tetramethylethylene quenching study*: [PYR] = 4.5 M; [$(CH_3)_2C{=}C(CH_3)_2$] = 0.19, 0.38, 0.57, 0.76, 0.96, 1.15, 1.53 M.

Stern–Volmer Quenching Studies of 2,4,6-Trifluorophenyl Azide (23). (*a*) *Methanol quenching study*: [PYR] = 4.3 M; [CH_3OH] = 0.27, 0.54, 1.07, 1.61, 2.15, 2.68, 5.37, 6.44 M.

(*b*) *Dimethyl sulfide quenching study*: [PYR] = 4.9 M; [CH_3SCH_3] = 0.07, 0.10, 0.17, 0.27, 0.34, 0.44, 0.51, 0.68, 1.02 M.

(*c*) *Dimethyl sulfoxide quenching study*: [PYR] = 4.3 M; [$CH_3S(O)CH_3$] = 0.15, 0.31, 0.61, 0.92, 1.22, 1.53, 1.84 M.

(*d*) *Diethylamine quenching study*: [PYR] = 4.3 M; [$(CH_3CH_2)_2NH$] = 0.21, 0.42, 0.84, 1.26, 1.68, 2.10, 2.52 M.

Stern–Volmer Quenching Studies of Methyl 4-Azido-2,3,5,6-tetrafluorobenzoate (26). (*a*) *Methanol quenching study*: [PYR] = 3.1 M; [CH_3OH] = 0.12, 0.31, 0.95, 1.85, 2.47, 3.70, 4.9 M.

(*b*) *Dimethyl sulfide quenching study*: [PYR] = 3.1 M; [CH_3SCH_3] = 0.07, 0.17, 0.24, 0.34, 0.41, 0.51, 0.68, 0.85 M.

(*c*) *Dimethyl sulfoxide quenching study*: [PYR] = 3.1 M; [$CH_3S(O)CH_3$] = 0.81, 0.35, 0.53, 0.70, 0.88, 1.06, 1.41, 2.1 M.

(*d*) *Tetramethylethylene quenching study*: [PYR] = 2.9 M; [$(CH_3)_2C{=}C(CH_3)_2$] = 0.2, 0.4, 0.6, 0.8, 1.0, 1.20, 1.6 M.

Laser Flash Photolysis. General Procedure. All laser flash photolysis experiments utilized one or more 308-nm laser pulses generated by a Lumonics TE-860-4 or Lambda Physik excimer laser (maximum pulse energy, 110 mJ; pulse duration, 8–10 ns) which contained a fill mixture comprised of HCl, helium, and xenon. Details of the LFP system have been reported previously (*2*, *5*, *10*). All transient absorbence spectra were obtained using the previously described excimer lase in conjunction with an E, G & G Princeton Applied Research Model 1460 optical multichannel analyzer. All samples were capped with a septum and degassed with dry argon for 3–4 min prior to photolysis. All laser flash photolysis experiments utilized quartz cells and were performed at ambient temperature.

Yield of Nitrene Ylide 12 and Ketenimine Ylide 14 Produced by LFP of 1,6-Difluorophenyl Azide as a Function of Pyridine Concentration. A stock solution of the azide **10** in dichloromethane was prepared having an optical density at 308 nm of ca. 0.5. An exact volume of the stock solution was then syringed into several cells. Increasing amounts of pyridine were added to each cell ([PYR] = 0.15, 0.29, 0.59, 0.88, 1.18, 1.77, 2.36, 2.94, 3.53 M) accompanied by the addition of dichloromethane to maintain a constant volume in each cell. All cells were degassed with argon and then subjected to three laser pulses, with monitoring at 390 nm for the formation of the nitrene ylide **12**. This same experiment was then repeated with monitoring at 503 nm for the formation of the ketenimine ylide **14**.

ACKNOWLEDGMENT

Support of this work by the National Institutes of Health (GM34823) is gratefully acknowledged. One of us (K.A.S.) is grateful for an Ohio State University College of Mathematics and Physical Sciences postdoctoral fellowship.

LITERATURE CITED

(1) Schuster, G. B., and Platz, M. S. (1992) Photochemistry of Phenyl Azide. *Adv. Photochem. 17*, 69.

(2) (a) Banks, R. E., and Sparkes, G. R. (1972) Studies in Azide Chemistry. Part V. Synthesis of 4-Azido-2,3,5,6-tetrafluoro, 4-azido-3-chloro-2,5,6-trifluoro, and 4-azido-3,5-dichloro-2, 6 difluoropyridine, and Some Thermal Reactions of the Tetrafluoro compound, *J. Chem. Soc., Perkin Trans. I* 2964–2970. (b) Banks, R. E., and Prakash, A. (1974) Studies in Azide Chemistry. Part VI. Some Reactions of Perfluoroazidobenzene and Perfluoro-4-azidotoluene, *J. Chem. Soc., Perkin Trans. I* 1365–1371. (c) Banks, R. E., and Prakash, A. (1973) New Reactions of Azidopentafluorobenzene; Intermolecular Insertions into the N–H Bonds, *Tetrahedron Lett.* 99–102. (d) Banks, R. E., and Medany, I. M. (1990) Studies in Azide Chemistry. Part 14. Thermolysis of Perfluoro-4-azidopyridine and Perfluoro-4-azidotoluene in the Presence of Penta- and Hexa-Methylbenzene, *J. Fluorine Chem. 47*, 527–532. (e) Banks, R. E., and Venayak, N. D. Studies in Azide Chemistry. Part 13. Intermolecular Insertion of Azido-derived Polyfluorinated Aryl- and Heteroaryl-Nitrenes into Ring C-H Bonds of 1,3,5-Trimethyl and 1,3,5-Trimethoxybenzene, *J. Chem. Soc., Chem. Commun.* 900–901. (f) Banks, R. E., and Madany, I. M. (1985) Decisive Evidence for the Occurrence of Ring-expansion During Pyrolisis of Azidopentafluorobenzene: X-Ray Crystallographic Analysis of Pentafluorophenyl-nitrene Dimer, *J. Fluorine Chem. 30*, 211–226. (g) Leyva, E., Young, M. J. T.; and Platz, M. S. (1986) High Yields of Formal CH Insertion Products in the Reactions of Polyfluorinated Aromatic Nitrenes, *J. Am. Chem. Soc. 108*, 8307. (h) Leyva, E., Munoz, D., and Platz, M. S. (1989) Photochemistry of Fluorinated Aryl Azides in Toluene Solution and in Frozen Polycrystals, *J. Org. Chem. 54*, 5938. (i) Young, M. J. T., and Platz, M. S. (1989) Polyfluorinated Aryl Azides as Photoaffinity Labelling Reagents; The Room Temperature CH Insertion Reactions of Singlet Pentafluorophenyl Nitrene with Alkanes, *Tetrahedron Lett. 30*, 2199. (j) Young, M. J. T., and Platz, M. S. (1991) Mechanistic Analysis of the Reactions of (Pentafluorophenyl)nitrene in Alkanes, *J. Org. Chem. 56*, 6403.

(k) Poe, R.; Grayzar, J., Young, M. J. T., Leyva, E., Schnapp, K. A., and Platz, M. S. (1991) Remarkable Catalysis of Intersystem Crossing of Single (Pentafluorophenyl)nitrene, *J. Am. Chem. Soc. 113*, 3209. (l) Poe, R., Schnapp, K., Young, M. J. T., Grayzar, J., and Platz, M. S. (1992) Chemistry and Kinetics of Singlet (Pentafluorophenyl)Nitrene, *J. Am. Chem. Soc. 114*, 5054. (m) Keana, J. F. W., and Cai, S. X. (1990) New Reagents for Photoaffinity Labeling: Synthesis and Photolysis of Functionalized Perfluorophenyl Azides, *J. Org. Chem. 55*, 3640. (n) Keana, J. F. W., and Cai, S. X. (1989) Functionalized Perfluorophenyl Azides: New Reagents for Photoaffinity Labeling, *J. Fluorine Chem. 43*, 151. (o) Cai, S. X., and Keana, J. F. W. 4-Azido-7-Iodo-3,5,6-Trifluorophenyl Carbonyl Derivatives. A New Class of Functionalized and Iodinated Perfluorophenyl Azide Photolabels, *Tetrahedron Lett. 30*, 5409. (p) Cai, S. X., Glenn, D. J., and Keana, J. F. W. (1992) Toward the Development of Radiolabeled Fluorophenyl Azide-Based Photolabeling Reagents: Synthesis and Photolysis of Iodinated 4-Azidoperfluorobenzoates and 5-Azido-3,5,6-trifluorobenzoates, *J. Org. Chem. 57*, 1299–1304. (q) Cai, S. X., and Keana, J. F. W. (1991) Diazo and Azido-Functionalized Glutaraldehydes as Cross Linking Reagents and Potential Fixatives for Electron Microscopy, *Bioconjugate Chem. 2*, 38–43.

(3) (a) Singh, A., Thornton, E. R., and Westheimer, F. H. (1962) The Photolysis of Diazo-acetylchymotrypsin, *J. Biol. Chem. 237*, PC 3006. (b) Fleet, G. W. J., Porter, R. R., and Knowles, J. R. (1969) Affinity Labeling of Antibodies with Aryl Nitrene as Reactive Group, *Nature, 224*, 511.

(4) Bayley, H. (1983) *Photogenerated Reagents in Biochemistry and Molecular Biology*, Elsevier, Amsterdam.

(5) Schnapp, K. A., Poe, R.; Leyva, E., Soundararajan, N., and Platz, M. S. Exploratory Photochemistry of Fluorinated Aryl Azides. Implications for the Design of Photoaffinity Labeling Reagents. *Bioconjugate Chem.*, preceding paper in this issue.

(6) (a) Crocker, P. J., Imai, N., Rajogopalen, K., Boggess, M. A., Kwiatkowski, S., Dwyer, L. D., Vanaman, T. C., and Watt, D. (1990) Heterobifunctional Cross-Linking Agents Incorporating Perfluorinated Aryl Azides, *Bioconjugate Chem. 3*, 419. (b) Drake, R. R., Slam, J., Wall, K., Abramove, M., D'Souza, C., Elbein, A. D., Crocker, P. J., and Watt, D. S. (1992) Application of an N-(4-Azido-2,3,5,6-tetrafluorobenzoyl)tyrosine Substituted Peptide as a Heterobifunctional Cross-linking Agent in a Study of Protein O-Glycosylation in Yeast, *Bioconjugate Chem. 3*, 69–73. (c) Pinney, K. C., and Katzenellenbogen, J. A. (1991) Synthesis of a Tetrafluoro-substituted Aryl Azide and its Protio Analogue as Photoaffinity Labeling Reagents for the Estrogen Receptor, *J. Org. Chem. 56*, 3125–3133. (d) Pinney, K. C., Carlson, K. E., Katzenellenbogen, S. B., and Katzenellenbogen, J. A. (1991) Efficient and Selective Photoaffinity Labeling of the Estrogen Receptor Using Two Nonsteroidal Ligands that Embody Aryl Azide or Tetrafluoroaryl Azide Photoreactive Functions, *Biochemistry 30*, 2421.

(7) (a) Leyva, E., Platz, M. S., Persy, G., and Wirz, J. (1986) Photochemistry of Phenyl Azide: The Role of Singlet and Triplet Phenyl Nitrene as Transient Intermediates, *J. Am. Chem. Soc. 108*, 3783. (b) Wasserman, E. (1971) Electron Spin Resonance of Nitrenes, *Prog. Phys. Org. Chem. 8*, 319–335. (c) Hayes, J. C., and Sheridan, R. S. (1990) Infrared Spectrum of Triplet Phenyl Nitrene, on the Origin of Didehydroazepine in Low Temperature Matrices, *J. Am. Chem. Soc. 112*, 5879–5881. (d) Wentrup, C. (1984) Gas Phase and Matrix Studies. In *Azides and Nitrenes* (E. F. V. Ed.) Scriven, pp 395–430, Academic Press, New York. (e) Cullin, D. W., Soundararajan, N., Platz, M. S., and Miller, T. A. (1990) Reinvestigation of the Electronic Spectrum of the Phenyl Nitrene Radical, *J. Phys. Chem. 94*, 8890. (f) Cullin, D. W., Yu, L., Willamson, J., Platz, M. S., and Miller, T. A. (1990) Laser-Induced Fluorescence Spectrum of the Cyanocyclopentadienyl Radical. A Band System Long Attributed to Triplet Phenyl Nitrene, *J. Phys. Chem. 94*, 3387. (g) Shrock, A. K., and Schuster, G. B. (1984) Photochemistry of Phenyl Azide: Chemical Properties of the Transient Intermediates, *J. Am. Chem. Soc. 106*, 5228. (h) DeGraff, B. A., Gillespie, D. W., and Sundberg, R. J. (1974) Phenyl Nitrene. Flash Photolytic Investigation of the Reaction with Secondary Amines, *J. Am. Chem. Soc. 96*, 7491. (i) Li, Y.-Z., Kirby, J. P., George, M. W., Poliakof, M., and Schuster, G. B. (1988) 1,2-Didehydroazepines from the Photolysis of Substituted Aryl Azides: Analysis of Their Chemical and Physical Properties by Time-Resolved Spectroscopic Methods, *J. Am. Chem. Soc. 110*, 8092. (j) Chapman, O. L., and LeRoux, J.-P. (1978) 1-Aza-1,2,4,6-cycloheptatetraene *J. Am. Chem. Soc. 100*, 282–285. (k) Nielsen, P. E., and Buchardt, O. (1982) Aryl Azides as Photoaffinity Labels. A Photochemical Study of Some 4-Substituted Aryl Azides *Photochem. Photobiol. 35*, 317–323.

(8) (a) Jackson, J. E., and Platz, M. S. (1993) Laser Flash Photolysis Studies of Ylide Forming Reactions of Carbenes. *Advances in Carbene Chemistry* (U. Brinker, Ed.) Vol. I, JAI Press, in press. The pyridine probe method is based upon models developed by Scaiano to probe free-radical reactions. For examples, see: (b) Small, R. D., Jr., and Scaiano, J. C. (1977) Reaction of Type II Biradicals with Paraquat Ions Measurement of a Biradical Lifetime, *J. Phys. Chem. 81*, 828. (c) Small, R. D., Jr., and Scaiano, J. C. (1977) Direct Detection of the Biradicals Generated in the Norrish Type II Reaction, *Chem. Phys. Lett. 50*, 431.

(9) Soundararajan, N., and Platz, M. S. (1990) Descriptive Photochemistry of Polyfluorinated Azide Derivatives of Methyl Benzoate, *J. Org. Chem. 55*, 2034.

(10) (a) Kim, S.-J., Hamilton, T. P., and Schaefer, H. F. III (1992) Phenylnitrene: Energetics, Vibrational Frequencies, and Molecular Structures, *J. Am. Chem. Soc. 114*, 5349. (b) Hrovat, D. A., Walli, E. and Borden, W. T. (1992) Ab Initio Calculations of the Singlet-Triplet Energy Difference in Phenylnitrene, *J. Am. Chem. Soc., 114*, 8698.

(11) Soundararajan, N., Platz, M. S., Jackson, J. E., Doyle, M. P., Oon, S.-M., Liu, M. T. H., and Anand, S. M. (1988) Addition of Arylchlorocarbenes to α,β-Unsaturated Esters. Absolute Rates, Substituent Effects and Variable Reactivities, *J. Am. Chem. Soc. 110*, 7143.

TECHNICAL NOTES

Detection of Psoralen Cross-Link Sites in DNA Modified by Psoralen-Conjugated Oligodeoxyribonucleoside Methylphosphonates

Joanne M. Kean and Paul S. Miller*

Department of Biochemistry, School of Hygiene and Public Health, The Johns Hopkins University, 615 North Wolfe Street, Baltimore, Maryland 21205. Received September 14, 1992

Oligodeoxyribonucleoside methylphosphonates conjugated with derivatives of psoralen cross-link with complementary single-stranded RNA and DNA and with duplex DNA targets when irradiated with long wavelength (365 nm) ultraviolet light. The position of cross-linking between pyranone-side adducts of psoralen-conjugated oligonucleoside methylphosphonates and DNA can be easily detected by treating the photoadduct with 1 M aqueous piperidine at 90 °C for 30 min, followed by analysis on a polyacrylamide gel run under denaturing conditions. This treatment results in hydrolysis of the methylphosphonate linkages and cleavage of the phosphodiester backbone at the cross-link site. Multiple cross-linking sites were detected with a single-stranded DNA target which contains four contiguous T residues. This may result from looping out of one or two of the T residues.

INTRODUCTION

Psoralen conjugates of oligodeoxyribonucleotides or oligonucleoside methylphosphonates, when hybridized to a complementary nucleic acid, can be triggered to form a photoadduct upon irradiation with long-wavelength ultraviolet light. Various types of psoralen-conjugated oligomers have been prepared and shown to cross-link in vitro with both single-stranded RNA and DNA and with duplex DNA targets (*1–17*). In addition, psoralen-conjugated oligomers have displayed highly selective antisense and antigene activity in a number of biochemical and biological experiments (*15*, *18–22*).

Psoralen cross-linking sites in RNA can be located using a combination of selective enzymatic and chemical cleavage reactions followed by 2-dimensional gel electrophoresis (*23*, *24*) or by using an oligodeoxyribonucleotide primer and reverse transcriptase (*12*, *25*). A method employing borohydride and aniline to cleave psoralen-thymidine photoadducts formed as a result of cross-linking psoralen-conjugated oligodeoxyribonucleotides to single-stranded DNA has been described recently (*16*). In this Note we describe a simple procedure for locating the site of cross-linking between psoralen-conjugated oligodeoxyribonucleoside methylphosphonates and DNA targets which employs piperidine-mediated cleavage of the phosphodiester backbone at the cross-link site.

EXPERIMENTAL PROCEDURES

Reagent-grade piperidine was distilled under an argon atmosphere and stored under argon at −80 °C. Solutions containing 1.0 or 1.25 M distilled piperidine in deionized water were freshly prepared just prior to use. Protected deoxyribonucleotide 3'-[β-cyanoethyl *N,N*-diisopropylphosphoramidites] were purchased from Glen Research Inc. and the protected deoxyribonucleoside 3'-[methyl *N,N*-diisopropylphosphonamidites] were a gift from JBL Scientific, San Luis Obispo, CA. Polyacrylamide gels were run using a gel buffer which contained 0.045 M Tris, 0.045 M boric acid, and 0.05 mM ethylenediamine tetracetate buffered at pH 8.0. All reagents used were reagent-grade or better. The sequences of the oligodeoxyribonucleotides and psoralen-derivatized oligonucleoside methylphosphonates are shown in Figure 1.

Syntheses of Oligodeoxyribonucleotides and Oligodeoxyribonucleoside Methylphosphonates. The oligodeoxyribonucleotide targets I and III were prepared on controlled pore glass supports in a Biosearch Model 8700 DNA synthesizer using standard phosphoramidite chemistry (*26*). The 5'-terminal dimethoxytrityl group of the protected oligomer was removed by the synthesizer, and the oligomer was then deprotected and removed from the support by heating with concentrated ammonium hydroxide in pyridine (1:1 v/v) at 55 °C for 5 h. The oligomers were phosphorylated using polynucleotide kinase and [γ-^{32}P]ATP (*27*), and the phosphorylated oligomers were purified by gel electrophoresis on a 30 cm × 40 cm, 20% polyacrylamide gel which contained 7 M urea run at 1800 V for 5 h. The oligomers were extracted from the gel at 37 °C with a solution containing 0.3 M sodium acetate and 10 mM Tris, pH 7.6, and the oligomers were desalted on a C-18 reversed-phase Sep Pak cartridge (*27*).

The oligodeoxyribonucleoside methylphosphonates were prepared on controlled pore glass supports in a Biosearch Model 8700 DNA synthesizer using standard methylphosphonamidite chemistry (*27*). The synthesizer was programmed to remove the 5'-terminal dimethoxytrityl group from the protected oligomer at the end of the syntheses, and the oligomer was deprotected and removed from the support by sequential treatment with a solution containing 85% hydrazine hydrate, pyridine, and glacial acetic acid (1:24:6 v/v) for 16 h at room temperature, followed by treatment with a solution of 50% ethylenediamine in ethanol (v/v) for 6 h at room temperature (*27*). The oligomers were purified by DEAE cellulose chromatography and then by preparative C-18 reversed-phase chromatography on a 1.0 cm × 25 cm Ranin Microsorb

1043-1802/93/2904-0184$04.00/0 © 1993 American Chemical Society

column using a gradient of 2% to 30% acetonitrile in 0.05 M sodium phosphate, pH 5.8. The oligomers were desalted on a C-18 Sep Pak cartridge (*27*).

The psoralen-derivatized oligodeoxyribonucleoside methylphosphonates II and IV were prepared according to literature procedures (*14*, *28*). The steps include (1) phosphorylating the oligomer using ATP and polynucleotide kinase, (2) converting the phosphorylated oligomer to its imidazolide derivative by treatment with 1-ethyl-3-[3-(dimethylamino)propyl]carbodiimide in 0.1 M imidazole buffer at pH 6.0, and (3) reaction of the imidazolide with 4'-[[*N*-(2-aminoethyl)amino]methyl]-4,5',8-trimethylpsoralen in 0.25 M lutidine hydrochloride buffer at pH 7.5. The psoralen-derivatized oligomers were purified by HPLC on a C-18 reversed-phase column using a 2% to 30% gradient of acetonitrile in 0.05 M sodium phosphate buffered at pH 5.8.

Preparation of the Photoadducts. A solution containing 0.1 μM 5'-[^{32}P]-end-labeled target DNA I or III and 5 μM psoralen-conjugated oligomer II or IV in 10 μL of 0.1 M sodium chloride, 50 mM Tris, pH 7.6, was irradiated in a borosilicate glass test tube for 15 min at 4 °C as previously described (*7*, *14*). For each photoadduct, a total of 16 reactions were run and then combined prior to purification. The photoadduct I–II or III–IV was purified by electrophoresis on a 14 cm × 16 cm, 20% polyacrylamide gel, which contained 7 M urea, run at 800 V for 2 h. The photoadduct was located by autoradiography and extracted from the gel as described above.

Characterization of the Photoadducts. The target DNA and the photoadduct (1–2.5 × 10^4 dpm) were each treated in separate reactions under the following conditions: (1) 50 μL of 1 M aqueous piperidine at 90 °C for 30 min; (2) 10 μL of a solution containing 70 μM potassium permanganate, 0.1 M sodium chloride, 50 mM Tris, pH 7.6 (I and I–II), or 70 μM potassium permanganate, 8 M urea (III and III–IV) for 30 min at 20 °C, after which the solution was treated with 2.5 μL of allyl alcohol and then treated with 40 μL of 1.25 M piperidine at 90 °C for 30 min; or (3) 10 μL of 88% formic acid for 5 min at 22 °C, after which the sample was precipitated with ethanol and the pellet treated with 50 μL of 1 M piperidine at 90 °C for 30 min. When each reaction was completed, the piperidine was lyophilized, and the residue was lyophilized twice from 10 μL of water. The residue was dissolved in 6 μL of 90% formamide and the sample was electrophoresed on a 30 cm × 40 cm, 20% acrylamide sequencing gel containing 7 M urea run at 1800 V for 2 h. The gel was autoradiographed at −80 °C using intensifying screens.

RESULTS AND DISCUSSION

The sequences of the oligodeoxyribonucleotide targets and their complementary oligodeoxyribonucleoside methylphosphonates which are conjugated with 4'-[[*N*-(2-aminoethyl)amino]methyl]-4,5',8-trimethylpsoralen, (ae)-AMT, are shown in Figure 1. Target oligomer I contains a single thymidine at position 16 which can serve as a site for reaction with the (ae)AMT group of II. Irradiation of a solution of 5'-[^{32}P]-I and II gives a cross-linked adduct (I–II) whose gel electrophoretic mobility is less than that of I as is shown in lanes 4 and 5 of Figure 2A. This photoadduct most likely results from a 2 + 2 cycloaddition reaction between the pyranone ring of the (ae)AMT group and the 5,6-double bond of a T-16 in the target. Because of steric constraints, it appears highly unlikely that photocycloaddition occurs through the furan ring of (ae)-AMT.

We found that piperidine hydrolysis could be used to locate psoralen cross-linking sites. Previous experiments

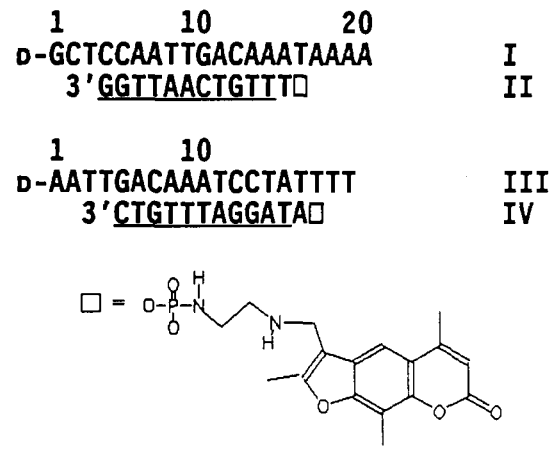


Figure 1. Psoralen-conjugated oligonucleoside methylphosphonates and their oligo DNA targets. The underline indicates methylphosphonate linkages.

have shown that methylphosphonate linkages are readily hydrolyzed in aqueous piperidine solution, even at 37 °C (*29*). Thus, treatment of photoadduct I–II with piperidine at 90 °C (lane 7) completely cleaves the methylphosphonate portion of the photoadduct to give a "truncated" photoadduct which contains only phosphodiester linkages and whose mobility is slightly less than that of strand I. In addition, a single 5'-[^{32}P]-labeled oligonucleotide is released whose mobility is consistent with cleavage at T-16, the psoralen cross-link site. In these experiments, we found it important to use freshly prepared [^{32}P]-end-labeled oligonucleotide in order to minimize nonspecific cleavage of the phosphodiester linkages. This and piperidine treatment conditions of 90 °C for 30 min resulted in a high signal to noise ratio, although the level of cleavage at the psoralen cross-link site was relatively low.

The photoadduct was also treated with potassium permanganate, which oxidizes the 5,6-double bonds of pyrimidines. When I–II was treated with potassium permanganate and then by piperidine (lane 8), cleavage occurred at T-16 and at C-2, T-3, and C-4, pyrimidines which are located outside or at the end of the methylphosphonate binding site. Cleavage was not observed at T-8 or T-9, residues which are base paired with the oligodeoxyribonucleoside methylphosphonate and therefore are not subject to potassium permanganate oxidation (*30*). Comparison of lanes 1 and 8 shows that sequential treatment with potassium permanganate followed by piperidine provides a footprint of the oligomer binding site as well as the location of the cross-link site. Treatment of I–II with formic acid under conditions which cause depurination, followed by treatment with piperidine, resulted in cleavage at purine residues and cleavage at T-16. No cleavage was observed at T-16 when I is treated with formic acid/piperidine although the same purine cleavage products were observed in both I and I–II at sites 5' to the cross-link site (lanes 3 and 6). Cleavage of purines 3' to the cross-link site in I–II appeared to be reduced relative to that which occurred in I.

The utility of this method was further demonstrated when applied to the characterization of the photoadducts formed by DNA target III and psoralen-conjugated oligodeoxyribonucleoside methylphosphonate IV. Although a single new slower moving product, III–IV, was observed after irradiation of III and IV, treatment of the photoadduct with piperidine resulted in cleavage at T-18 and T-19 in addition to the expected cleavage at T-17, as shown in lane 5 of Figure 2B. No cleavage of C-7, T-11, C-12, C-13, or T-14 was observed when III–IV was treated

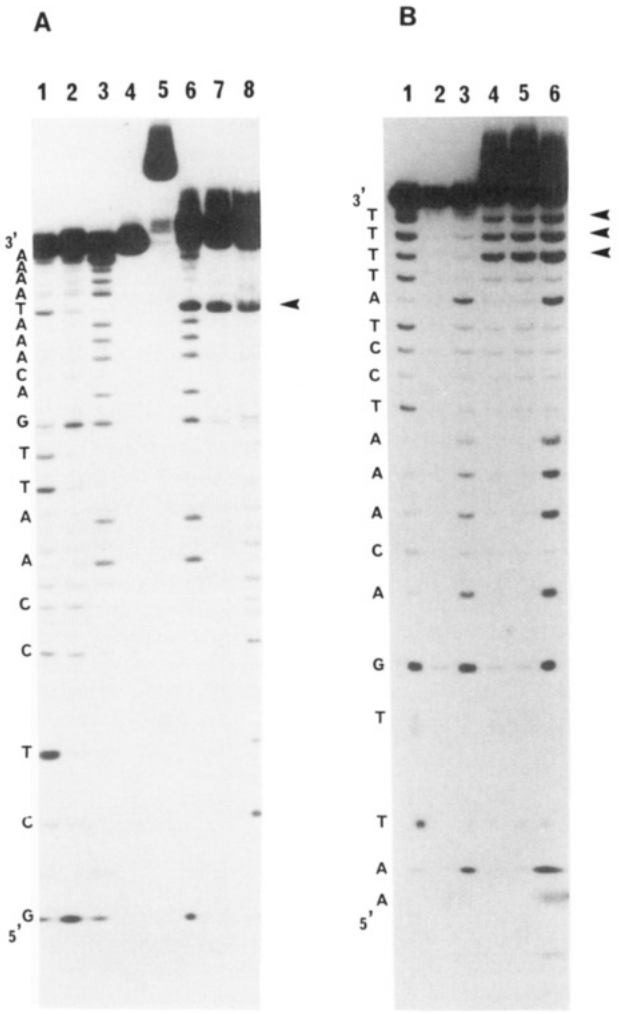


Figure 2. Characterization of psoralen cross-link sites. Panel A: I + potassium permanganate/piperidine (lane 1); I + piperidine (lane 2); I + formic acid/piperidine (lane 3); I with no treatment (lane 4); I–II with no treatment (lane 5); I–II + formic acid/piperidine (lane 6); I–II + piperidine (lane 7); and I–II + potassium permanganate/piperidine (lane 8). Panel B: III + potassium permanganate/piperidine (lane 1); III + piperidine (lane 2); III + formic acid/piperidine (lane 3); III–IV + potassium permanganate/piperidine (lane 4); III–IV + piperidine (lane 5); and III–IV + formic acid/piperidine (lane 6). The reaction conditions and gel electrophoresis conditions are given in the Experimental Procedures section. The arrowheads indicate the psoralen cross-linking site(s) and the nucleotide sequences of the DNA targets are shown along the left side of each autoradiogram.

with potassium permanganate/piperidine, consistent with the expected binding site of the oligomer. This can be seen by comparing lanes 1 and 4. Formic acid/piperidine treatment of the adduct gave the expected purine cleavage products in addition to cleavage at T-17, T-18, and T-19, as shown by comparing lanes 3 and 6. Cross-linking to T-17 is expected if the psoralen stacks on the last base pair formed between the oligomer/target and partially intercalates between T-16 and T-17 (*14*). A similar binding mode could occur between psoralen and T-18, if T-17 loops out, and between psoralen and T-19, if both T-17 and T-18 loop out. The apparent lack of cross-linking at T-16 suggests that photocycloaddition does not readily occur to the 3'-face of the T-16 nor does the psoralen intercalate between the last two base pairs of the duplex and react with the 5'-face of T-16. This behavior is in contrast to that seen in other systems, where cross-linking to the T of a terminal base pair was observed and probably reflects the effect of the sequence at the psoralen binding site on the position and extent of the cross-linking reaction (*14*).

Previous studies have shown that base treatment of psoralen cross-links results in cleavage of the cyclobutane ring and subsequent reversal of furan-side photoadducts, whereas pyranone-side cyclobutane adducts do not appear to be cleaved by this treatment (*17*, *31*). The strand scission at pyranone-side T photoadducts observed in our study may result from increased lability of the *N*-glycosyl bond caused by saturation of the 5,6-double bond of T. This increased lability would produce an abasic site which is subject to piperidine-catalyzed β-elimination. The observation that identical cleavage products are formed by potassium permanganate/piperidine treatment of the target is consistent with this argument.

The procedure described above provides a simple means to locate psoralen–thymidine photoadducts in DNA targets. Although we have used piperidine to characterize cross-links between psoralen-conjugated oligodeoxyribonucleoside methylphosphonates and single-stranded DNA targets, this method should also be applicable to detecting pyrone side adduct formed between other psoralen-derivatized oligonucleotides or oligonucleotide analogs and DNA targets.

ACKNOWLEDGMENT

This work was supported by a grant from the National Cancer Institute (CA 42762). We wish to thank Ms. Cynthia Cushman for assistance in preparing the oligomers and Dr. Bok L. Lee for helpful discussions.

LITERATURE CITED

(1) Gamper, H., Piette, J., and Hearst, J. E. (1984) Efficient formation of a crosslinkable HMT monoadduct at the Kpn I recognition site. *Photochem. Photobiol. 40*, 29–30.
(2) Houten, B. V., Gamper, H., Hearst, J. E., and Sancar, A. (1986) Construction of DNA substrates modified with psoralen at a unique site and study of the action mechanism of ABC exonuclease on these uniformly modified substrates. *J. Biol. Chem. 261*, 14135–14141.
(3) Houten, B. V., Gamper, H., Holbrook, S. R., Hearst, J. E., and Sancar, A. (1986) Action mechanism of ABC excision nuclease on a DNA substrate containing a psoralen crosslink at a defined position. *Procd. Natl. Acad. Sci. (U.S.A) 83*, 8077–8081.
(4) Gamper, H. B., Cimino, G. D., and Hearst, J. E. (1987) Solution hybridization of crosslinkable DNA oligonucleotides to bacteriophage M13 DNA. Effect of secondary structure on hybridization kinetics and equilibria. *J. Mol. Biol. 197*, 349–382.
(5) Shi, Y-B., and Hearst, J. E. (1987) Wavelength dependence for photoreactions of DNA-psoralen monoadducts. 1. Photoreversal of monoadducts. *Biochemistry 26*, 3786–3792.
(6) Cheng, A., Houten, B. V., Gamper, H. B., Sancar, A., and Hearst, J. E. (1988) Use of psoralen-modified oligonucleotides to trap three-stranded Rec A-DNA complexes and repair of these cross-linked complexes by ABC exonuclease. *J. Biol. Chem. 263*, 15110–15117.
(7) Lee, B. L., Murakami, A., Blake, K. R., Lin, S-B. and Miller, P. S. (1988) Interaction of psoralen-derivatized oligonucleoside methylphosphonates with single-stranded DNA. *Biochemistry 27*, 3197–3203.
(8) Lee, B. L., Blake, K. R., and Miller, P. S. (1988) Interaction of psoralen-derivatized oligodeoxyribonucleoside methylphosphonates with synthetic DNA containing a promoter for T7 RNA polymerase. *Nucleic Acids Res. 16*, 10681–10697.
(9) Kean, J. M., Murakami, A., Blake, K. R., Cushman, C. D., and Miller, P. S. (1988) Photochemical cross-linking of psoralen-derivatized oligonucleoside methylphosphonates to rabbit globin messenger RNA. *Biochemistry 27*, 9113–9121.
(10) Pieles, U., and Englisch, U. (1989) Psoralen covalently linked to oligodeoxyribonucleotides: Synthesis, sequence specific recognition of DNA and photo-cross-linking to pyrimidine residues of DNA. *Nucleic Acids Res. 17*, 285–298.

(11) Pieles, U., Sproat, B., Neuner, P., and Cramer, F. (1989) Preparation of a novel psoralen containing deoxyadenosine building block for the facile solid phase synthesis of psoralen-modified oligonucleotides for a sequence specific cross-link to a given target sequence. *Nucleic Acids Res. 17*, 8967–8978.
(12) Teare, J., and Wollenzien, P. (1989) Specificity of the site directed psoralen addition to RNA. *Nucleic Acids Res. 17*, 3359–3372.
(13) Teare, J., and Wollenzien, P. (1990) The structure of a pre-mRNA molecule in solution determined with a site directed cross-linking reagent. *Nucleic Acids Res. 18*, 855–864.
(14) Bhan, P., and Miller, P. S. (1990) Photo cross-linking of psoralen-derivatized oligonucleoside methylphosphonates to single-stranded DNA. *Bioconjugate Chemistry 1*, 82–88.
(15) Miller, P. S., Bhan, P., Cushman, C. D., Kean, J. M., and Levis, J. T. (1991) Antisense oligonucleoside methylphosphonates and their derivatives. *Nucleosides and Nucleotides 10*, 37–46.
(16) Woo, J., and Hopkins, P. B. (1991) Template-directed modification of single-stranded DNA by psoralen-tethered oligonucleotides—Sites of photoadduct formation analyzed by sequence-specific and sequence-random cleavage. *J. Am. Chem. Soc. 113*, 5457–5459.
(17) Takasugi, M., Guendouz, A., Chassignol, M., Decout, J. L., L'Homme, J., Thuong, N. T., and Helene, C. (1991) Sequence-specific photo-induced cross-linking of the two strands of double-helical DNA by a psoralen covalently linked to a triple helix-forming oligonucleotide. *Proc. Natl. Acad. Sci. U.S.A. 88*, 5602–5606.
(18) Kulka, M., Smith, C., Aurelian, L., Fishelvich, R., Meade, K., Miller, P., and Ts'o, P. O. P. (1989) Site specificity of the inhibitory effects of oligo(nucleoside methylphosphonate)s complementary to the acceptor splice junction of herpes simplex virus type 1 immediate early mRNA 4. *Proc. Natl. Acad. U.S.A. 86*, 6868–6872.
(19) Chang, E. H., Miller, P. S., Cushman, C. D., Devadas, K., Pirollo, K. F., and Ts'o, P. O. P. (1991) Antisense inhibition of *ras* p21 expression that is sensitive to a point mutation. *Biochemistry 30*, 8283–8286.
(20) Gasparro, F. P., Edelson, R. L., O'Malley, M. E., Ugent, S. J., and Wong, H. H. Photoactivatable antisense DNA: Suppression of ampicillin resistance in normally resistant *Escherichia coli*. *Antisense Res. Dev. 1*, 117–140.
(21) Duval-Valentin, G., Thuong, N. T., and Helene, C. (1992) Specific inhibition of transcription by triple helix-forming oligonucleotides. *Proc. Natl. Acad. Sci. U.S.A. 89*, 504–508.
(22) Miller, P. S. (1992) Psoralen-derivatized antisense oligonucleoside methylphosphonates. In *Gene Regulation: Biology of Antisense RNA and DNA* (R. P. Erickson, and J. G. Izant, Eds.) pp 83–93, Raven Press, Ltd, New York.
(23) Turner, S., Thompson, J. F., Hearst, J. E., and Noller, H. F. (1982) Identification of a site of psoralen crosslinking in *E. coli* ribosomal RNA. *Nucleic Acids Res. 10*, 2839–2849.
(24) Bachellerie, J.-P., and Hearst, J. E. (1982) Specificity of photoreaction of 4'-(hydroxymethyl)-4,5',8-trimethylpsoralen with ribonucleic acid. Identification of reactive sites in *Escherichia coli* phenylalanine-accepting transfer ribonucleic acid. *Biochemistry 21*, 1357–1363.
(25) Youvan, D. C., and Hearst, J. E. (1982) Sequencing psoralen photochemically reactive sites in *Escherichia coli* 16 S rRNA. *Anal. Biochem. 119*, 86–89.
(26) Brown, T., and Brown, J. S. (1991) Modern machine-aided methods of oligodeoxyribonucleotide synthesis. In *Oligonucleotides and Analogues. A Practical Approach* (F. Eckstein, Ed.) pp 1–24, IRL Press, Oxford.
(27) Miller, P. S., Cushman, C. D., and Levis, J. T. (1991) Synthesis of oligo-2'-deoxyribonucleoside methylphosphonates. In *Oligonucleotides and Analogues. A Practical Approach* (F. Eckstein, Ed.) pp 137–154, IRL Press, Oxford.
(28) Miller, P. S. (1992) Preparation of psoralen-derivatized oligodeoxyribonucleoside methylphosphonates. In *Methods in Enzymology* (D. M. J. Lilley, and J. E. Dahlberg, Eds.) Vol. 211, pp 54–64, Academic Press, New York.
(29) Murakami, A., Blake, K. R., and Miller, P. S. (1985) Characterization of sequence-specific oligodeoxyribonucleoside methylphosphonates and their interaction with rabbit globin mRNA. *Biochemistry 24*, 4041–4046.
(30) Hayatsu, H., and Ukita, T. (1967) The selective degradation of pyrimidines in nucleic acids by permanganate oxidation. *Biochem. Biophys. Res. Commun. 29*, 556–561.
(31) Shi, Y-b., Spielmann, H. P., and Hearst, J. E. (1988) Base-catalyzed reversal of a psoralen-DNA cross-link. *Biochemistry 27*, 5174–5178.

Bioconjugate Chemistry

MAY/JUNE 1993
Volume 4, Number 3

© Copyright 1993 by the American Chemical Society

ARTICLES

Synthesis of Bleomycin A_5 Oligonucleotide Derivatives and Site-Specific Cleavage of the DNA Target

Valentina F. Zarytova,* Dmitrij S. Sergeyev, and Tatjana S. Godovikova

Institute of Bioorganic Chemistry, Siberian Division of the Russian Academy of Sciences, Novosibirsk 630090, Russia. Received May 18, 1992

A method for coupling bleomycin A_5 to oligonucleotides is proposed. The reaction was carried out between an amino group of a spermidine residue of the Cu(II) complex of bleomycin A_5 (Cu(II)Blm-RH) and a 5′-phosphate group of the oligonucleotides d(pCCAAACA) (I), d(pCGTCCTC) (II), $d(pT)_{16}$ (III), d(pCAAACA) (IV), and d(pGCCAAACA) (V) activated with a mixture of triphenylphosphine and 2,2′-dipyridyl disulfide in the presence of 4-(*N*,*N*-dimethylamino)pyridine 1-oxide. The yields of the products Cu(II)Blm-R-d(pCCAAACA) (Ia), Cu(II)Blm-R-d(pCGTCCTC) (IIa), Cu(II)Blm-R-$d(pT)_{16}$ (IIIa), Cu(II)Blm-R-d(pCAAACA) (IVa), and Cu(II)Blm-R-d(pGCCAAACA) (Va) were 60–80%. After removal of the Cu(II) ion from the bleomycin A_5 oligonucleotide derivatives Ia–IIIa, compounds Ib–IIIb were obtained. Compounds Ia, IVa, Va, and Ib–IIIb were further used for modification of the target d(pTGTTTGGCGAAGGA) in the presence of Fe(II) ions and 2-mercaptoethanol. Site-specific cleavage of the target by Blm coupled to complementary oligonucleotides was demonstrated. It was shown that efficiency and position of cleavage of the complementary reagents Ia, Ib, IVa, and Va are determined by their oligonucleotide part while the action of the noncomplementary reagents IIb and IIIb was similar to that of the free antibiotic.

INTRODUCTION

Reactive oligonucleotide derivatives are widely used for site-specific modification of nucleic acids (*1–5*). They form complementary complexes with definite sequences of target nucleic acids and direct reactive groups to a certain nucleotide residue in the vicinity of these sequences. A number of oligonucleotides, bearing EDTA (*1–3*), 1,10-phenanthroline, or porphyrin (*4*, *5*), with chelated transition metal ions were prepared and used for sequence-specific oxidative cleavage of nucleic acids. One of the reagents for DNA oxidative cleavage is the antitumor antibiotic bleomycin (Blm). It is a clinically important agent, which is generally thought to disrupt cell proliferation by causing DNA strand scission (*6*). Blm has the following structural characteristics: a bithiazole terminal residue that is believed to contribute to the binding to DNA, β-aminoalanine, pyrimidine, and β-hydroxyhistidine moieties that can form metal-binding centers generating reduced oxygen to damage DNA (*7*), a dissaccharide moiety, and a linker moiety which connects each part of Blm at an appropriate distance and in desired orientation (Figure 1). The metal-binding center was reported to participate in recognition of nucleotide sequences (*8*). It has been well-documented that Blm cleaves DNA preferentially at the GT and GC sequences in the presence of

* Correspondence address: Institute of Bioorganic Chemistry, Siberian Division of the Russian Academy of Sciences, Lavrentjev pr.8, Novosibirsk 630090, Russia. Phone: 007-3832-35-45-19. Fax: 007-3832-35-34-59.

1043-1802/93/2904-0189$04.00/0 © 1993 American Chemical Society

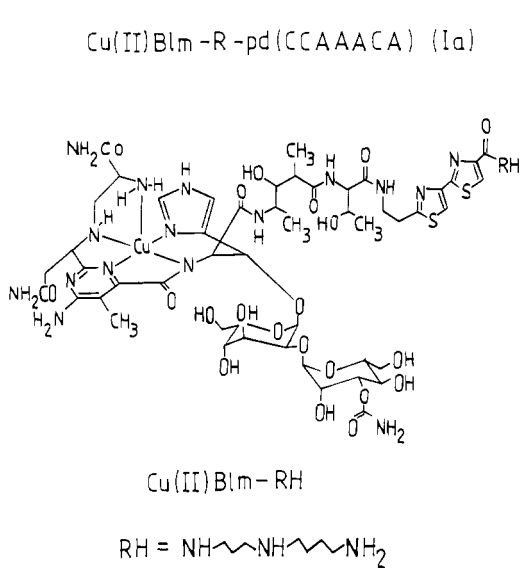


Figure 1. Structure of bleomycin A_5 oligonucleotide derivative Ia.

Fe(II) ions and molecular oxygen (*9*). Blm itself is not a specific agent because all DNA, be it a target nucleic acid in cancer cell or a specific sequence of a viral genome in infected cell, have GT and GC sequences. To achieve specificity, Blm may be coupled to oligonucleotides which bind only to those nucleic acids that have complementary nucleotide sequences. In this respect Blm-conjugated oligonucleotide derivatives may be accurate weapons affecting unique target nucleotide sequences.

However there are problems: the structure of bleomycin is complicated, having numerous nucleophilic groups able to react with activated phosphates of oligonucleotides, and there is a danger of affecting the metal-binding center of the antibiotic. Therefore the methods for designing bleomycin oligonucleotide derivatives have to be very special.

Earlier we have reported the synthesis of a bleomycin derivative of an oligonucleotide and effective scission by this reagent of DNA (*10*).

We describe here in detail a method for conjugation of bleomycin A_5 to oligonucleotides and prove that site-specific cleavage of a DNA target by the obtained bleomycin derivatives does take place. The results suggest that the bleomycin oligonucleotide derivatives could be important therapeutic drugs of the future.

EXPERIMENTAL PROCEDURES

General Procedures. All the oligonucleotides I–VII and the target d(pTGTTTGGCGAAGGA) were synthesized by the phosphotriester method (*11*). Ph_3P[1] and $(PyS)_2$ were from Fluka AG (Switzerland). DMAPO was prepared as described in ref 12. Bleomycin A_5 was purchased from the Pilot Plant of the Institute of Organic Synthesis, Latvian Academy of Sciences. UV/vis absorption spectra were recorded on a Specord M40 spectrophotometer (Carl Zeiss Jena) in the buffer 0.2 M NaCl, 0.01 M Tris-HCl (pH 7.5). T_m values of the oligonucleotide complexes were measured using equipment for thermal denaturing based on a Milichrom spectrophotometer (*13*). Molar extinction coefficients were estimated at $\lambda = 260$ nm for oligonucleotides I–VII and the target according to ref 14 and for their derivatives Ia–Va and Ib–IIIb as a sum of the oligonucleotide and the bleomycin molar extinction coefficients.

Synthesis of Bleomycin A_5 Oligonucleotide Derivatives Ia–Va. A cetyltrimethylammonium salt of oligonucleotide ($1 \cdot 10^{-7}$ mol) was dissolved in 40 mL of DMSO; 3.5 mg of Ph_3P, 3 mg of $(PyS)_2$, and 1.5 mg of DMAPO were added. After 10 min of incubation the zwitterionic oligonucleotide formed (Scheme I) was precipitated with 2% $LiClO_4$ in acetone. The Cu(II) complex of bleomycin A_5 hydrochloride ($1 \cdot 10^{-6}$ mol or 1.5 mg) in 40 mL of 0.2 M $NaHCO_3$ (pH 8.5) was added to the precipitate and the solution was incubated for 6 h. The bleomycin oligonucleotide derivatives formed were isolated by reversed-phase liquid chromatography (Figure 2) on a 4.6 × 250 mm Lichrosorb PR-18 10-μm column (Merck, Germany) using a 0–30% linear gradient of acetonitrile in 0.05 M $LiClO_4$ using an Altex-332 chromatograph. The yield was 60–80%. UV/vis absorption spectra of the compounds revealed an oligonucleotide moiety and a bleomycin residue (Figure 3). The effect of the antibiotic on the T_m of the complementary complex with Ia was studied (Figure 4). The phosphoramide bond in bleomycin oligonucleotide Ia was hydrolyzed in 1 M CHOONa (pH 3.5) at 37 °C for 16 h; the oligonucleotide I formed was subject to ion-exchange chromatography. To remove Cu(II) ions from the antibiotic residues of oligonucleotide derivatives Ia–IIIa, the latter ($1 \cdot 10^{-8}$ mol) were absorbed on to a 1 × 50 mm 10-μm Lichrosorb RP-18 column and washed with 7.5 mL of 0.1 M EDTA (pH 6.3) at a rate of 0.05 mL/min. The compounds Ib–IIIb so obtained were eluted by 0.4 mL of 20% acetonitrile in 0.05 M aqueous $LiClO_4$. The copper content of compounds Ib–IIIb was measured spectrophotometrically at $\lambda = 612$ nm and shown to be less than 10% of the original.

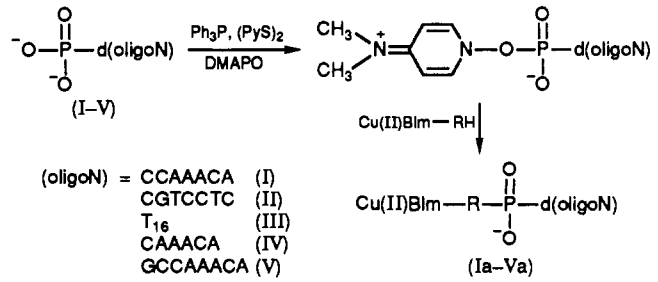
Target Degradation. The target d(pTGTTTGGCGAAGGA) was labeled at the 5′-end using [γ-^{32}P]ATP and T4 polynucleotide kinase (*15*) and isolated in a 20% denaturing gel. DNA degradation reaction (total volume 20 mL) was performed in 0.2 M LiCl, 0.01 M Tris-HCl (pH 7.5) at 0 or 20 °C. The concentrations were as follows: target and reagents, $1 \cdot 10^{-5}$ M; $Fe(NH_4)_2(SO_4)_2$, $1 \cdot 10^{-4}$ M; 2-mercaptoethanol, 0.05 M. The reactions were initiated by addition of Fe(II) ions. After the reaction, the oligonucleotide material was precipitated by addition of a 2% $LiClO_4$ solution in acetone. The reaction mixtures with or without piperidine treatment (45 min, 95 °C) were electrophoresed in a 20% polyacrylamide gel under denaturing conditions (Figures 5 and 6). The gels were visualized by autoradiography. Extents of modification were estimated in an Ultroscan laser densitometer (LKB).

RESULTS AND DISCUSSION

For the bleomycin oligonucleotide derivatives to be able to site-specifically damage a DNA target, it is necessary to preserve the cleaving capacity of bleomycin and not to lose the ability of the oligonucleotide tail to form complexes with complementary oligonucleotides. With this aim in view, the antibiotic was attached to the 5′-phosphate group of the oligonucleotide which had been activated with a mixture of triphenylphosphine and 2,2′-dipyridyl disulfide in the presence of 4-(*N*,*N*-dimethylamino)pyridine 1-oxide (Scheme I). These reagents activate exclusively terminal phosphate groups of oligonucleotides without interacting with internucleotide phosphate groups and deblocked heterocyclic bases. In this way the terminal phosphate is converted to a zwitterionic group readily reacting with aliphatic amino groups (*16*). Bleomycin A_5 has two regions containing amino groups (Figure 1): the terminal sper-

[1] Abbreviations: Ph_3P, triphenylphosphine; $(PyS)_2$, 2,2′-dipyridyl disulfide; DMAPO, 4-(*N*,*N*-dimethylamino)pyridine 1-oxide; Cu(II)Blm-RH, Cu(II) complex of bleomycin A_5.

Scheme I



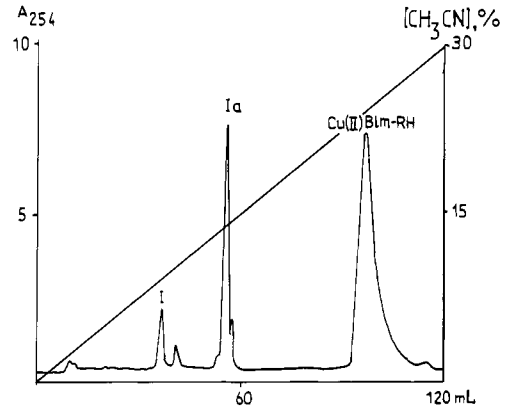


Figure 2. Profile of reversed-phase chromatography of the reaction mixture for synthesis of bleomycin A_5 oligonucleotide derivative Ia. A 4.6 × 250 mm column was used with Lichrosorb RP-18 10-μm, 0–30% gradient of acetonitrile in 0.05 M $LiClO_4$, flow rate 2 mL/min.

midine residue (RH) and a metal-binding domain. To preserve reactivity of the antibiotic, the reagent must be able to discriminate between these amino groups and not to react with the metal-binding center. A similar task was fulfilled by Umezawa (*17*) to obtain semisynthetic derivatives of a Cu(II) complex of the antibiotic. Thus the Cu(II) complex of bleomicin A_5 was chosen for the reaction with the activated zwitterionic 5′-terminal phosphates of oligonucleotides I–V (Scheme I).

A 10-fold excess of the antibiotic was used to stave off coupling of two or more molecules of an oligonucleotide to bleomycin. The obtained products Ia–Va were isolated by reversed-phase chromatography (Figure 2). They were eluted after the initial oligonucleotides and before the antibiotic. The isolated compounds were homogeneous by ion-exchange chromatography. Cu(II) complexes Ia–Va were eluted as compounds having two or three charges less than parent oligonucleotides I–V. The yields of Ia–Va were at least 60%.

UV/vis absorption spectra of the obtained compounds Ia–Va had maximal characteristics of both the oligonucleotide component (260 nm) and bleomycin (shoulder at 290–320 nm and band at 612 nm, $\epsilon = 1 \cdot 10^2 M^{-1} cm^{-1}$) (Figure 3). This proves that the Cu(II)–bleomycin complex was attached to the oligonucleotides. The experimental ratios $\epsilon_{600}/\epsilon_{260}$ were quite similar to the theoretical ones estimted for the case when equal molar amounts of the oligonucleotide and antibiotic were coupled.

The oligonucleotides and antibiotic were connected by a phosphoramide bond which was hydrolyzed at pH 3.5, 37 °C, during 16 h. There is not detectable depurination of the oligonucleotide part in these conditions. Data of ion-exchange and reversed-phase chromatographies showed that derivatives Ia–Va have been completely converted into compounds with chromatographic behavior equivalent to that of parent oligonucleotides. This and the ability of

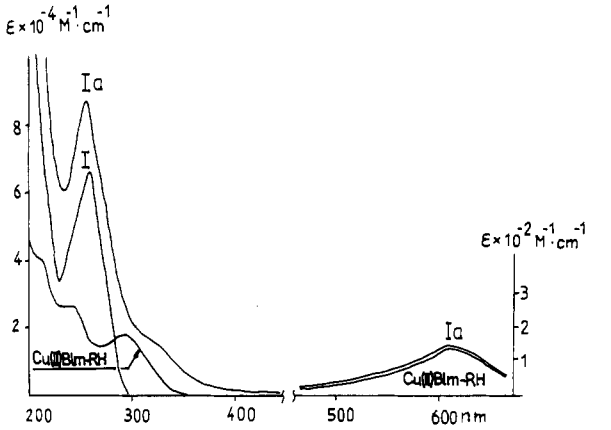


Figure 3. UV/vis absorption spectra of oligonucleotide I, its bleomycin derivative Ia, and Cu(II) complex of bleomycin A_5 (Cu(II)Blm-RH).

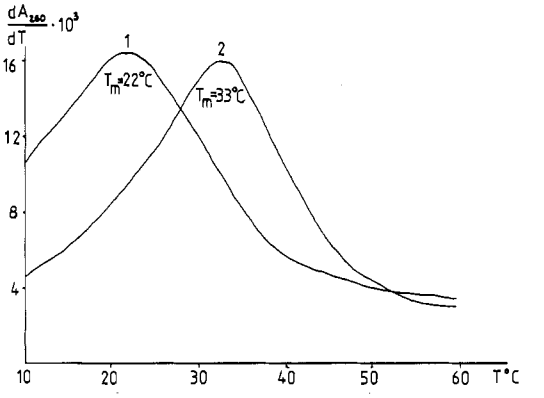


Figure 4. Differential curves of thermal denaturing of complementary complexes I + target (1) and Ia + target (2). Complex concentration was $2.5 \cdot 10^{-5}$ M in 0.16 M NaCl, 0.02 M Na_2HPO_4, 0.1 mM EDTA (pH 7.4).

bleomycin oligonucleotide derivatives to cleave DNA (see below) favor the oligonucleotide's attachment to a spermidine residue and not to the metal-binding center. However, to be sure which nitrogen of the spermidine residue is involved, we needed some additional data which can be obtained using NMR spectroscopy. This study is in progress now.

Bleomycin oligonucleotide derivatives Ia–Va are stable: their $3 \cdot 10^{-5}$ M aqueous solutions can be stored for a month at −10 °C without degradation.

It is known that the efficiency of site-specific modification of DNA by oligonucleotide reagents depends very much on stability of complementary complexes formed. We investigated the effect of a bulky antibiotic (Blm) covalently attached to an oligonucleotide (Ia) on complex formation. It was found that the T_m of the duplex formed by the target d(pTGTTTGGCGAAGGA) with Ia was 11 °C higher than that of its duplex with parent oligonucleotide I (Figure 4). This suggests that, due to a stabilizing effect of the antibiotic, bleomycin oligonucleotide derivatives should destroy functions of nucleic acids more effectively than parent oligonucleotides without bleomycin. It was important to check this ability of the antibiotic covalently attached to an oligonucleotide.

Earlier we demonstrated (*10*) that, after removal of the Cu(II) ion from Ia, Ib without metal ion was obtained. Further it was used for modification of the DNA target in the presence of Fe(II) ions and 2-mercaptoethanol (Scheme II). A 14-meric oligonucleotide was used as a target. The reaction of the reagent and the target was carried out in the presence of additional 7-meric oligo-

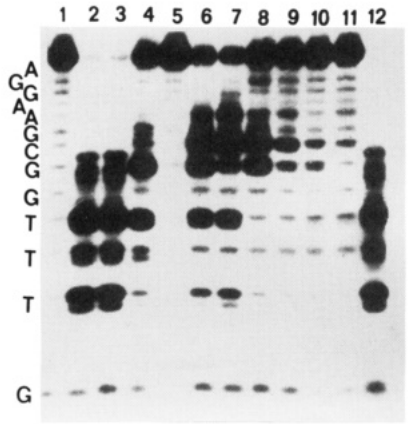
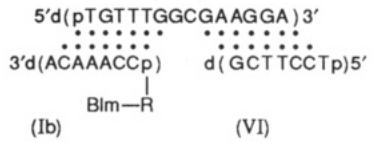


Figure 5. Autoradiogram of the DNA target cleavage. Lane 1, the target without reagents under reaction conditions ($1 \cdot 10^{-4}$ M Fe(II) ions, 0.05 M 2-mercaptoethanol in 0.2 M LiCl, 0.01 M Tris-HCl, pH 7.5); lanes 2–12, the target under reaction conditions in the presence of the following oligonucleotides and reagents: 2, Ib + VI; 3, Ib; 4, Ib + VI ($1 \cdot 10^{-5}$ M Fe(II) ions); 5, Ia + VI without Fe(II) ions; 6, I + VI + Blm-RH; 7, VII + Blm-RH; 8, I + VI + IIb; 9, VII + IIb; 10, I + VI + IIIb; 11, VII + IIIb; 12, Ia + VI. Concentrations of the reagents (Ia, Ib–IIIb, Blm-RH), target, and complementary oligonucleotides (VI, VII) were $1 \cdot 10^{-5}$ M. Reaction mixtures were incubated at 20 °C during 6 h and analyzed after piperidine treatment (30 min, 95 °C).

Scheme II



nucleotide VI complementary to the 3′-end of the target to imitate double-stranded DNA (*10*).

Reagent Ib cleaved the target effectively both in the presence and absence of oligonucleotide VI (Figure 5, lanes 2 and 3, respectively). What is really important here are Fe ions: at 10-fold excess of Fe(II) over reagent Ib, the target is degraded almost completely while at the equimolar ratio Fe(II)/Ib, a considerable part of the target remains intact (Figure 5, lanes 2 and 4, respectively). We have already mentioned that bleomycin derivatives of oligonucleotides are obtained in the form of copper complexes. It seems attractive to use such complexes for DNA degradation without removing the Cu(II) ions. It is reported that the Cu(II) complex of Blm is nearly as effective in vivo as the free Blm (*18*) and is able to degrade DNA in vitro (*19*). To demonstrate the possibility to use the Cu(II) complexes of bleomycin oligonucleotide derivatives for effective DNA cleavage, it is necessary to compare its reactivity with that of analogous compounds without Cu(II) ions. The latter were obtained by washing out the copper ions from Ia–IIIa absorbed on a reversed-phase sorbent with a solution of strong chelating agent such as EDTA which has an association constant not lower than that of bleomycin (*10,20*). Decreased copper content in Ia–IIIa leads to decreased absorption at $\lambda = 612$ nm, which makes it possible to control the process. We show that the Cu(II) complex of Blm coupled to oligonucleotide Ia does not damage DNA in the absence of the Fe(II) ions (Figure 5, lane 5). In contrast, in the presence of Fe ions, the same complex attached to the same oligonucleotide does modify the DNA (Figure 5, lane 12) under conditions employed. The combination of the antibiotic with Fe ions is likely to be the key factor for degradation in this case. Since, in the presence of Fe(II) ions and 2-mercaptoethanol, efficient degradation may be achieved by both the copper

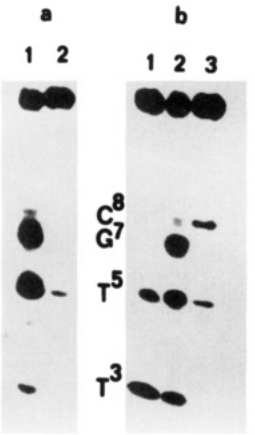
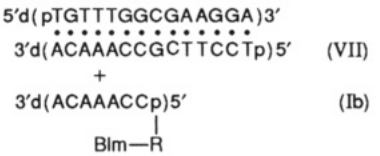


Figure 6. Autoradiogram of DNA target degradation: (a) lane 1, the target with reagent Ib; lane 2, the target with VII and reagent Ib; reaction mixtures were incubated at 20 °C for 2 h and analyzed; (b) the target was degraded by IVa (lane 1), Ia (lane 2), and Va (lane 3); reaction mixtures were incubated at 0 °C for 4 h and analyzed.

Scheme III



complex and free reagents, we used both these types of reagents in our experiments.

The products of degradation by free and tethered Blm were different for all cases investigated. As shown in Figure 5 (lane 2) and Figure 6a (lane 1) treatment of the target with reagent Ib having a complementary oligonucleotide part caused substantial cleavages of the target sites T^3-T^4-T^5 and G^7 without affecting C^8, which is characteristic of free bleomycin (Figure 5, lanes 6, 7). These results are identical with those described in ref 10. On the other hand, reagent Ib was almost inactive in the presence of oligonucleotide VII, which is complementary to the target (Scheme III) (Figure 6a, lane 2).

These results clearly show that reagent Ib is active only in a complementary complex formed with the DNA target. Oligonucleotide VII is a competitive inhibitor of modification because it is longer than Ib and its duplex with the target is more stable. Furthermore noncomplementary reagents IIb and IIIb failed to affect the target sites T^3-T^4-T^5 under conditions similar to those used for the cleavage with reagent Ib (Scheme III). They cleaved the target at the same sites as free Blm but less efficiently (Figure 5, lanes 7, 9, and 11). Similar results were obtained when oligonucleotide VII was replaced by I + VI, as shown by Scheme II (Figure 5, lanes 6, 8, and 10). It is suggested that both bleomycin coupled with uncomplementary oligonucleotides (compound IIb and IIIb) and free bleomycin damage the same sites of the target that are different from those cleaved by Blm coupled with the complementary oligonucleotide (compound Ib). A reason for the decrease of the cleavage efficiency of IIb and IIIb as compared with free Blm (Figure 5, lanes 7, 9, and 11) may be a result of addition of the negatively charged phosphate groups of the oligonucleotide to the positively charged C-terminal side chain of free Blm. Previous studies have demonstrated strong dependence of the DNA cleavage (*21*) and the unwinding of plasmid DNA (*22*) on the presence of positively charged groups in the Blm molecules. Thus Cu(II)-demethyl-Blm A_2 was found to be a much

Scheme IV [a]



[a] Sites of cleavage are indicated by arrows.

less effective unwinding and cleavage agent than Cu(II)-Blm A_2, though it differs from Blm A_2 only in that it lacks a methyl group and an associated positive charge at the C-terminus (*21*, *22*). Sequence-specificity is changed only if the oligonucleotide is complementary to the template. In this case it is just oligonucleotide that delivers the Blm "warhead" to the nucleosides of the target that are adjacent to the oligonucleotide binding site (Figure 5, lanes 2–4 and Figure 6b, lanes 1–3). Scheme IV shows that the target was cleaved at different sites by the reagents with different length (also Figure 6, lanes 1–3). The principal sites of cleavage were deoxyriboses of C^8 and T^5 for octanucleotide reagent Va, G^7, T^5, and partially T^3 for heptanucleotide Ia, and T^5 and T^3 for hexanucleotide IVa.

It is worth mentioning that 7- and 8-meric reagents Ia and Va attack target bases that are complementary to their last base carrying Blm at the 5'-phosphate (G^7 and C^8, respectively). On the contrary, 6-mer reagent IVa modifies T^5 and T^3 but not the last target base G^6, which is involved in complex formation with the reagent. Bases G^6 and T^4 did not react with any of the three reagents under study. The oligonucleotide moiety of the latter may target Blm to a definite complementary site of the DNA in the vicinity of which the Blm cleaves the nucleotide sequences in preference. In summary, the obtained results prove that the Blm linked to oligonucleotides cleaves the DNA target site-specifically and can be further used as site-directed agent in molecular biology studies. Also it can be considered as a candidate for future therapeutic use.

ACKNOWLEDGMENT

We are thankful to Dr. S. G. Lokhov, for measurements of melting temperatures of the duplexes, and Drs. V. V. Vlassov and N. N. Lomakina for helpful discussion.

LITERATURE CITED

(1) Boutorin, A. S., Vlassov, V. V., Kazakov, S. A., Kutyavin, I. V., and Podyminogin, M. A. (1984) Complementary addressed reagents carrying EDTA-Fe(II) groups for directed cleavage of single-stranded nucleic acids. *FEBS Lett. 172*, 43–46.

(2) Chu, B. C. F., and Orgel, L. E. (1985) Nonenzymatic sequence-specific cleavage of single-stranded DNA. *Proc. Natl. Acad. Sci. U.S.A. 82*, 963–967.

(3) Dreyer, G. B., and Dervan, P. B. (1985) Sequence specific cleavage of single stranded DNA. Oligodeoxynucleotide–EDTA·Fe(II). *Proc. Natl. Acad. Sci. U.S.A. 82*, 968–972.

(4) Chen, C. B., and Sigman, D. S. (1986) Nuclease activity of 1,10-phenanthroline-copper: Sequence-specific targeting. *Proc. Natl. Acad. Sci. U.S.A. 83*, 747–7151.

(5) Le Doan, T., Perrouault, L., Helene, C., Chassignol, M., and Thuong, N. T. (1986) Targeted cleavage of polynucleotides by complementary oligonucleotides covalently linked to iron-porphyrins. *Biochemistry 25*, 6736–6739.

(6) Suzuki, H., Nagai, K., Yamaki, H., Tanaka, N., and Umezawa, H. (1969) On the mechanism of action of bleomycin: Scission of DNA strands in vitro and in vivo. *J. Antibiot. 22*, 446–448.

(7) Petering, D. H., Byrnes, R. W., and Antholine, W. E. (1990) The role of redox-active metals in the mechanism of action of bleomycin. *Chem.-Biol. Interact. 73*, 133–182.

(8) Carter, B. J., Reddy, K. S., and Hecht, S. M. (1991) Polynucleotide recognition and strand scission by Fe-bleomycin. *Tetrahedron 47*, 2463–2474.

(9) Stubbe, J., and Kozarich, J. W. (1987) Mechanism of bleomycin-induced DNA degradation. *Chem. Rev. 87*, 1107–1136.

(10) Sergeyev, D. S., Godovikova, T. S., and Zarytova, V. F. (1991) Direct cleavage of a DNA fragment by a bleomycin-oligonucleotide derivative. *FEBS Lett. 280*, 271–273.

(11) Zarytova, V. F., Ivanova, E. M., and Romanenko, V. D. (1983) Synthesis of oligonucleotides by phosphotriester approach in chloroform. *Bioorg. Khim. 9*, 516–521.

(12) Katritzky, A. R. (1956) The preparation of some substituted pyridine 1-oxide. *J. Chem. Soc. 7*, 2404–2408.

(13) Zarytova, V. F., Kutyavin, I. V., Silnikov, V. M., and Shishkin, G. V. (1986) Modification of nucleic acids in stabilized complementary complexes. I. Synthesis of alkylating derivatives of oligodeoxyribonucleotides having a 5'-terminal N-(2-oxyethyl)-phenazinium residue. *Bioorg. Khim. 12*, 911–920.

(14) Cantor, C. R., and Tinoco, I. (1965) Absorption and optical rotatory dispersion of seven trinucleoside diphosphates. *J. Mol. Biol. 13*, 65–77.

(15) Berkner, K. L., and Folk, W. R. (1977) Polynucleotide kinase exchange reaction. *J. Biol. Chem. 252*, 3176–3184.

(16) Godovikova, T. S., Zarytova, V. F., Maltseva, T. V., and Khalimskaya, L. M. (1989) Reactive oligonucleotide derivatives with a zwitter-ionic terminal phosphate group for affinity reagents and probe construction. *Bioorg. Khim. 15*, 1246–1252.

(17) Takita, T., Fujii, A., Fukuoka, T., and Umezawa, H. (1973) Chemical cleavage of bleomycin to bleomycinic acid and synthesis of new bleomycins. *J. Antibiot. 26*, 252–254.

(18) Nakayama, Y., Kunishima, M., Omoto, S., Takita, T., and Umezawa, H. (1973) Chemistry of bleomycin. XII Isobleomycin A_2, a product of carbamoyl group migration. *J. Antibiot. 29*, 400–402.

(19) Ehrenfeld, G. M., Shipley, J. B., Heimbrook, D. S., Sugiyama, H., Long, E. C., van Boom, J. H., van der Marel, G. A., Oppenheimer, N. J., and Hecht, S. M. (1987) Copper-dependent cleavage of DNA by bleomycin. *Biochemistry 26*, 931–942.

(20) Solaiman, D., Rao, E. A., Antholine, W. E., and Petering, D. H. (1980) Properties of the binding of copper by bleomycin. *J. Inorg. Biochem. 12*, 201–220.

(21) Berry, D. E., Chang, L.-H., and Hecht, S. M. (1985) DNA damage and grouth inhibition in cultured human cells by bleomycin congeners. *Biochemistry 24*, 3207–3214.

(22) Levy, M. J., and Hecht, S. M. (1988) Copper(II) facilitates bleomycin-mediated unwinding of plasmid DNA. *Biochemistry 27*, 2647–2650.

Synthesis of *N*-[Tris[2-[[*N*-(benzyloxy)amino]carbonyl]ethyl]methyl]succinamic Acid, Trisuccin. Hydroxamic Acid Derivatives as a New Class of Bifunctional Chelating Agents[1]

Ahmad Safavy,*,† Donald J. Buchsbaum,† and M. B. Khazaeli‡

Departments of Radiation Oncology and Medicine and Comprehensive Cancer Center, University of Alabama at Birmingham, Birmingham, Alabama 35233. Received August 21, 1992

In an effort to generate bifunctional chelating agents (BCAs) with improved labeling, conjugation, and biodistribution properties, the synthesis of *trisuccin* is reported. This new hydroxamate BCA, after synthesis and characterization, was used for conjugation and radiolabeling of monoclonal antibodies with ^{99m}Tc. This new class of synthetic BCAs may be useful in the radioimmunodiagnosis and radioimmunotherapy of cancer.

INTRODUCTION

Due to their high antigen specificity, monoclonal antibodies (mAbs) constitute an increasingly important class of agents in both diagnosis and therapy of cancer (*1*). One of the main strategies in the treatment of cancer is the preparation of radiolabeled mAbs (*2, 3*). Both direct and indirect techniques have been used for radiolabeling of these proteins. The direct method involves the attachment of the radioactive element onto an appropriate amino acid side chain of the polypeptide backbone or the reduced disulfide bond(s) of the antibody; examples of these methods are radioiodination of antibodies through their tyrosine residues (*4*) and technetium-99m labeling through reduced S–S bonds (*5, 6*). It should also be noted that the term *direct*, in some reports, may refer to the radiolabeling of the BCA prior to its conjugation to the antibody (*7*), an approach also known as "preformed chelate" by Fritzberg et al. (*8*). In the indirect method, on the other hand, the radionuclide is attached to the protein through a linking molecule (*9*). In recent years, the latter method has gained more attention due to, particularly, a number of problems involved with directly radioiodinated mAbs (*8, 10*) and growing interest in radioactive metals. Moreover, the bifunctional chelating agents (BCAs) are molecules possessing a group capable of binding to a radioactive element (the chelating function) and one which binds to the protein (the conjugating function) (*11*).

A number of BCAs, with different types of functionalities, have been synthesized and used in the labeling of mAbs. More well-known and frequently used examples are diethylenetriaminepentaacetic acid, DTPA, and its derivatives (*12*) and *N*-(mercaptoacetyl)glycylglycyl-γ-aminobutyrate, MAG_2-GABA (*13*) for radiolabeling of mAbs. Although promising results have been achieved with some of these compounds, the field is still open to more elaborate designs.

Hydroxamic acids have been known for some time, for their chelating ability toward metallic nuclides (*14–16*), and their application in medicinal chemistry covers a broad range of activities. Natural and synthetic hydroxamic acid derivatives have shown interesting properties as antibiotics, antitumor, antifungal, and antiinflammatory agents (*17*) and have been studied in the development of enzyme inhibitors (*18, 19*). In nature, hydroxamic acids have been used by microorganisms for solubilization of iron. The metal exists in the biosphere mainly in the form of water-insoluble ferric hydroxide. To utilize iron, these species synthesize low molecular weight and specific organic molecules (siderophores) which form stable complexes with ferric cations (*20*). The soluble complex is then ingested by the organism. A large number of siderophores have hydroxamic acid functions incorporated into their structures (*21*). Furthermore, derivatives of hydroxamic acids have been reported for radiolabeling with ^{99m}Tc for imaging studies (*22, 23*). None of these synthetic compounds, however, had been designed for use as a BCA. So far the only hydroxamate derivative that has been used as a heterobifunctional radiolabeling agent is the natural siderophore desferrioxamine (*24*), a linear trihydroxamic acid compound produced by *Streptomyces pilosus*. This compound has been used extensively for radiolabeling of proteins with ^{67}Ga (*25, 26*) and, to some extent, ^{111}In (*27*).

As part of a program aimed at the design and development of BCAs for radiometal labeling of mAbs, we have developed a number of hydroxamic acid derivatives as a new class of BCAs. In this report, the synthesis of the first member of this family of compounds, *N*-[tris[2-[[*N*-(benzyloxy)amino]carbonyl]ethyl]methyl]succinamic acid, *trisuccin* (1, Scheme I), its conjugation to mAbs, and radiolabeling of the resulting conjugates and also the unconjugated free ligand (6, Scheme I) with ^{99m}Tc are described.

Although the potential of monohydroxamic acids as chelating agents for metals had been reported (*15, 18*), polyfunctional hydroxamates may result in higher ligand–metal complex stabilities. Raymond et al. reported the failure in uptake of iron(III) and gallium(III), by *Rhodotorula pilimanae*, from iron and gallium complexes of trihydroxamate siderophores such as ferrioxamine B,

* Address correspondence to A. Safavy, Ph.D., Department of Radiation Oncology, University of Alabama at Birmingham, 1824 6th Avenue South, Birmingham, AL 35233.

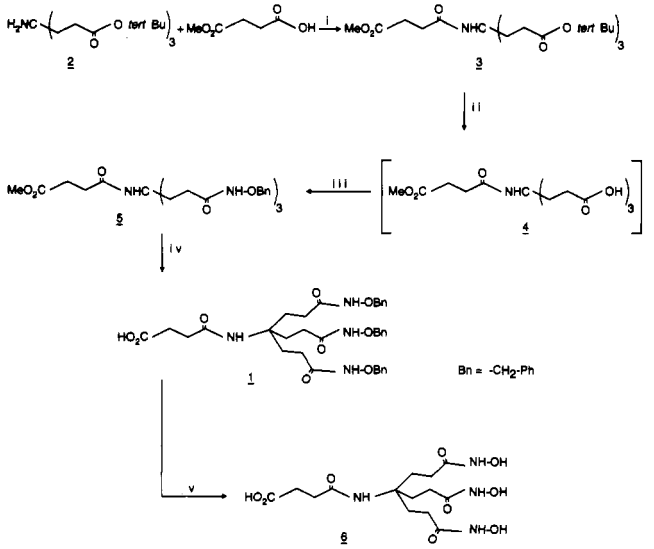
† Department of Radiation Oncology.

‡ Department of Medicine.

[1] Abbreviations: DCC, dicyclohexylcarbodiimide; DIEA, diisopropylethylamine; DMSO, dimethyl sulfoxide; DPBS, Dulbecco's phosphate-buffered saline; HOBT, 1-hydroxybenzotriazole; ITLC, instant thin-layer chromatography; NP-HPLC, normal-phase high-performance liquid chromatography; TFA, trifluoroacetic acid; TFP-OH, 2,3,5,6-tetrafluorophenol; THF, tetrahydrofuran; TLC, thin-layer chromatography.

1043-1802/93/2904-0194$04.00/0 © 1993 American Chemical Society

Scheme I.[a] Synthesis of Trisuccin



[a] (i) DCC, HOBT, THF, $CHCl_3$; (ii) TFA; (iii) $HCl \cdot H_2N$-OBn, DIEA, DCC, HOBT, THF, $CHCl_3$; (iv) $LiOH \cdot H_2O$, THF/H_2O, H_3O^+ workup; (v) H_2,Pd/C (10%).

coprogen, and ferricrocin (*28*). This observation was interpreted by these researchers as a result of much higher stabilities of the complexes of the metal with trihydroxamate derivatives. The same number of hydroxamate functions (three) was, therefore, considered for our compound. Also, we anticipated that an array of a number of hydroxamate groups positioned around a central carbon atom would create a cage-like assembly, capable of encapsulating a metallic nuclide, while maintaining some degree of flexibility due to their existence as open-end chains. This flexibility, coupled with the expected high stabilities of the ligand–cation complex, may impart to the molecule the potential of binding to different types of metallic nuclides. Taking into account all that this information suggests, one of several possibilities is a structure such as **1** in which three hydroxamate functions are attached to a quaternary central carbon. The sp^3 hybridization of this carbon may arrange the hydroxamate units in a suitable array for inclusion of a cation. The "inclusive" space in the center of this arrangement may further be expanded by the length of each *N*-hydroxypropanamide arm in the deblocked ligand structure (vide infra). The conjugating function, on the other hand, would strategically be placed at the opposite end of the molecule to minimize any interference in the independent functioning of each group. Therefore, the synthesis of the target compound was started with the amino triester **2** (*29*) as shown in Scheme I. This amine was coupled to monomethyl succinate through a reaction with DCC (*30*) and HOBT (*31*). The *tert*-butyl ester groups of the resulting amide **3** were removed with TFA to afford the tricarboxylic acid **4**. The latter compound, upon complete removal of the solvent,[2] was coupled to 3 equiv of *O*-benzylhydroxylamine in a DCC/HOBT reaction to form **5**. Base hydrolysis of the methyl ester **5** deblocked the carboxyl terminus (the protein-conjugating function) of the molecule.

Compound **1** was conjugated to three different mAbs, i.e., antimelanoma 14G2a and anticolon carcinoma antibodies D612 and CC49. The conjugation was carried out by activation of the carboxylic acid function of **1** with TFP-OH and DCC (*32*) in DMSO. The active ester was then added to a solution of the mAb in carbonate buffer. After purification and buffer change through dialysis, the benzyl protecting groups of the hydroxamate functions were removed by catalytic hydrogenation.

Although our main interest lies with radioisotopes with therapeutic potential, due to its availability, ease of handling, and chemistry, we decided to evaluate the labeling abilities of our conjugates with ^{99m}Tc. This was accomplished by in situ reduction of [^{99m}Tc]-pertechnetate with stannous chloride in the presence of hydroxyisobutyric acid and its subsequent transchelation by the mAb conjugate. High yields (up to 95%) of radiolabeled antibodies were obtained. To evaluate the integrity of the conjugates and their ability to survive the conjugation, hydrogenation, and radiolabeling conditions, the labeled products were subjected to size-exclusion chromatography and cell-binding assays (*33*). Both tests proved the preservation of the mAbs' structure and immunoreactivities of the conjugates.

To further evaluate the complexing ability of this ligand system, the radiolabeling of the nonconjugated ligand was examined. Thus compound **1** was deprotected by catalytic hydrogenation. All three benzyl protecting groups could be readily removed, within 75 min at room temperature, as proved by ^1H NMR and TLC of the product **6**. A positive test with ferric chloride, with the development of a deep burgundy color (*15*), also showed the presence of the hydroxamic functions. The mass spectrum of this compound showed the proper molecular weight. Technetium-99m radiolabeling of this product was carried out under the same conditions as for the antibody conjugates. The radiolabeling was analyzed by ITLC (*34*), which resulted in an average estimated yield of 80%. Furthermore, radiolabeling of the unconjugated mAbs, again under the same conditions as for the conjugates, showed only negligible yields (2.4%). These findings, i.e., radiolabeling of the conjugates and the unconjugated ligand and inability of the unconjugated antibody to radiolabel to the same extent, point to the fact that *trisuccin* is conjugated to antibodies, deprotected, and radiolabeled (with ^{99m}Tc in this case) after conjugation in a manner which preserves the immunoreactivity of the antibody.

EXPERIMENTAL PROCEDURES

All reagents and solvents were used as received without further purification. Dry solvents were purchased from Aldrich (Milwaukee, WI). All other solvents were HPLC grade and were used as received. Amino triester **2** (*29*) was a gift from Dr. G. R. Newkome, University of South Florida, Tampa, FL.

Melting points are uncorrected and were measured in open-end capillaries on an Electrothermal Model 9100 apparatus. ^1H NMR spectra were recorded on a Bruker WH400 at 400 MHz. Chemical shifts are relative to tetramethylsilane. Infrared spectra were recorded on a Perkin Elmer-1600 FTIR spectrometer. Mass spectra were determined by both a Varian MAT-311A (FAB mode) in a nitrobenzyl alcohol matrix and a Finnigan TSQ-700/ESI (electrospray ionization mode). HPLC for radiolabeled antibodies was performed on a system consisting of a Bio-Rad Model 1330 pump, a multichannel analyzer (Canberra, Series 35 Plus), and a sodium iodide crystal radiodetector (Gamma Products, Plos Hills, IL). A Bio-Sil SEC-250 (Bio-Rad) column (300 × 7.8 mm) was used for size-exclusion chromatography. For nonradioactive

[2] The presence of three free carboxylic acid functions in the same molecule resulted in possibilities of hygroscopicity and other difficulties in purification. Therefore, compound **4** was not isolated for further analysis.

compounds, the HPLC analyses were carried out with a Bio-Rad HRLC system equipped with Model 2700 pumps, a Model 7125T injector, a Model 1790 UV/vis monitor, and an HRLC system interface connected to an AST (Bravo/386SX) IBM-compatible computer. For the normal-phase analyses, an Adsorbosphere silica 10U (250 × 4.6 mm) column (Alltech, Deerfield, IL) was used. Column chromatography was carried out using silica gel 60 (EM Science, Gibbstown, NJ) and HPLC-grade solvents. Thin-layer chromatography was done on Whatman glass-backed silica gel plates (2.5 cm × 7.5 cm, coating thickness 250 μm, 60A, 254 nm). Instant thin-layer chromatography was performed on silica gel-impregnated glass-fiber sheets (Gelman Sciences, Ann Arbor, MI). The radioactivities were measured using an Auto-Gamma Series 5000 (Packard Instrument Co., Meriden, CT). Purified water was obtained through a Milli-QF Plus water-purification system (Millipore, Bedford, MA). The water and DPBS buffers were further purified through Chelex 100, sodium form, 50–100 mesh (Bio-Rad, Richmond, CA). Dialyses were carried out in Spectra/Por cellulose membranes (Spectrum, Houston, TX). Solvents for TLC and NP-HPLC were mixed on a v/v scale and are defined as follows: (A) 2-propanol/hexane/chloroform, 5:30:65, (B) ethyl acetate/chloroform, 25:75, (C) methanol/chloroform, 10:90; (D) acetic acid/methanol/chloroform, 3:20:77; (E) 2-propanol/chloroform, 15:85; (F) TFA/methanol/chloroform, 1.5:15:85; (G) C + 0.1% TFA; (H) acetic acid/methanol/chloroform, 5:25:70; (J) 1-butanol/acetic acid/water/pyridine, 15:3:8:10; (K) pyridine/acetic acid/water, 5:3:2. The ferric chloride reagent was a 5 mM solution of $FeCl_3$ in purified water. Microanalyses were performed by Atlantic Microlab Inc. (Norcross, GA). The NP-HPLC analyses reported below for compounds **5** and **1** show the solvent system (letter) as well as the retention times (min) and percent purity as the first and second numbers, respectively.

Conjugation Procedure. The solution of the mAb (7 mg/mL) was dialyzed, in a 1000-Da molecular weight cutoff (MWCO) membrane, against 0.1 M carbonate buffer (pH 9.5) at 4 °C. To the solution of **1** (1.86 mg, 2.80×10^{-3} mmol) in dry DMSO (0.15 mL) were added, successively, 0.01 mL each of 0.3 M solutions of TFP-OH and DCC in dry DMSO. The resulting mixture was incubated at room temperature for 2.5 h. The solution of mAb (2 mL) was cooled to −3 °C and the active ester solution was added dropwise with gentle stirring. This mixture was then allowed to stir with gradual warming to 10 °C within 2 h. The reaction was quenched with the addition of 0.01 mL of a 1 M solution of glycine in carbonate buffer, followed by dialysis (1000 Da MWCO) against DPBS. Protein recovery yields of at least 75% were estimated, by Lowry protein assay (*35*), for the conjugation step.

Ligand Deblocking Procedure. To a 1–2-mL solution of the conjugate in DPBS were added palladium on carbon (10%, 12 mg) and platinum on sulfide carbon (5%, 4 mg), and the mixture was hydrogenated, with slow shaking, at 10 psi for 3 h. Size-exclusion HPLC showed a single peak with the same retention time as the original mAb.

^{99m}Tc Labeling Procedure. ^{99m}Tc (2.3 mCi) in the form of sodium pertechnetate in saline was reduced with stannous chloride in the presence of hydroxyisobutyric acid (*36*) and was exchanged onto the conjugate with incubation at 25 °C. An aliquot of the reaction mixture was withdrawn after 15 min and tested by HPLC. Peak integration showed radiolabeling yields of up to 95%. No further improvements in these yields were observed after longer incubation times. The same procedure, used on unmodified, hydrogenated antibodies, resulted in only 2.4% nonspecific radiolabeling. The immunoreactivities of the radiolabeled conjugates were determined by the method of Lindmo (*33*). Values from 65% to 80% were observed.

The unconjugated, free hydroxamic acid **6** was radiolabeled with ^{99m}Tc under the same condition as for the conjugates. The reaction mixture (1–2 μL) was spotted on an ITLC plate (2 × 7 cm) and developed. Two solvent systems (G and H) were used independently. The solvent front was selected as 6 cm from the origin. The developed plates were sprayed with the ferric chloride reagent, to visualize the location of the ligand, cut into 8-mm pieces, and counted. In solvent G, the ligand–technetium complex remained on the origin while the free technetium moved with the solvent. In solvent H, the complex was observed at fraction 5. The average radiolabeling yield from these runs was estimated to be 80%.

Methyl *N*-[Tris[2-(*tert*-butyloxycarbonyl)ethyl]-methyl]succinamate, 3. To a solution of monomethyl succinate (0.414 g, 3.14 mmol) in THF (8 mL), at 0 °C and under argon, was added a solution of HOBT (0.42 g, 3.12 mmol) followed by the addition of the amino triester **2** (1.3 g, 3.12 mmol) in $CHCl_3$ (10 mL). The solution of DCC (0.68 g, 3.3 mmol) was added dropwise and within 10 min. The flask was then sealed and the reaction was allowed to stir under argon overnight, with gradual warming from 0 °C to room temperature. The solid precipitate was separated by vacuum filtration and the filtrate was concentrated to an oil in vacuum. The oil was redissolved in ethyl acetate (60 mL) and more precipitate was filtered off. The filtrate was washed, successively, with 15 mL each of water (1×), 10% citric acid solution (3×), water (2×), 10% sodium bicarbonate (3×), water (2×), and brine (1×) and dried over anhydrous magnesium sulfate powder. Distillation of the solvent afforded a solid which was purified by column chromatography on silica gel with hexane/chloroform, 50:50 (v/v), as the eluting solvent. A white solid powder (1.6 g, 96%) was obtained: mp 93.7–95.5 °C; TLC (I_2) R_f 0.50 (A), 0.74 (B); FTIR ($CHCl_3$) 3345 (s, br), 3019 (s), 2950 (s), 1724 (s), 1662 (s); ^{1}H NMR ($CDCl_3$) δ 1.45 (s, 27 H), 1.95 (t, J = 8.32 Hz, 6 H), 2.20 (t, J = 8.32, 6 H), 2.40 (t, J = 7.28 Hz, 2 H), 2.64 (t, J = 7.28 Hz, 2 H), 3.69 (s, 3 H), 5.96 (s, 1 H); MS m/e 530 $(M + H)^+$; MS/MS m/e 530 $(M + H)^+$. Anal. Calcd for $C_{27}H_{47}NO_9$: C, 61.22; H, 8.94; N, 2.64. Found, 61.18; 8.99; 2.66.

Methyl *N*-[Tris[2-[[*N*-(benzyloxy)amino]carbonyl]ethyl]methyl]succinamate, 5. Trifluoroacetic acid (15 mL) was added to **3** (1.5 g, 2.8 mmol) under argon and at room temperature. The solution was allowed to stand at room temperature for 5 h and at 4 °C overnight. The solvent was distilled under vacuum, and 15 mL each of chloroform, benzene, methanol, and dry THF were successively distilled from the residue. The oily product was titurated with anhydrous ether and used directly in the next step.

To the mixture of the tricarboxylic acid **4** (0.97 g, 2.7 mmol), HOBT (1.1 g, 8.1 mmol), and *O*-benzylhydroxylamine hydrochloride (1.31 g, 8.2 mmol) in THF (25 mL), at 0 °C and under argon, was added a solution of DCC (1.84 g, 8.9 mmol) within 3 min. A solution of DIEA (1.1 g, 8.5 mmol) in 5 mL of THF was immediately added. The reaction mixture was stirred under argon for 48 h and filtered through a plug of Celite. Distillation of the solvent under vacuum afforded a light brown oil, which was redissolved in chloroform and washed with citric acid/sodium bicarbonate solutions, as described in the previous

procedure, followed by flash chromatography on silica gel (25 g, 2 cm × 15 cm column) using chloroform and a 0–5% methanol/$CHCl_3$ gradient to yield 0.74 g (41%) of **5** as a glassy semisolid. TLC, R_f (A) 0.17, (C) 0.28; NP-HPLC (C) 4.65, 89.3%; FTIR ($CHCl_3$) 3289 (s, br), 3225 (s, br), 3018 (s), 1750 (s), 1670 (s); ^1H NMR ($CDCl_3$) δ 1.85 (t, J = 5.0 Hz, 6 H), 2.00 (t, J = 5.0 Hz, 6 H), 2.32 (t, J = 5.0 Hz, 2 H), 2.50 (t, J = 5.0 Hz, 2 H), 3.44 (s, 3 H), 4.78 (s, 6 H), 6.73 (s, 1 H), 7.32 (s, 15 H), 9.80 (s, 3 H); MS m/e 677 $(M + H)^+$.

***N*-[Tris[2-[[*N*-(benzyloxy)amino]carbonyl]ethyl]-methyl]succinamic Acid, 1.** To the solution of the methyl ester **5** (0.61 g, 0.9 mmol) in THF (5 mL) was added, under an argon atmosphere, a solution of $LiOH·H_2O$ (0.042 g, 1 mmol) in water (1 mL). A second portion of lithium hydroxide (0.084 g, 2 mmol) in 1.2 mL of water was added after 2 h and the reaction mixture was incubated at room temperature overnight. A TLC of the reaction showed no starting ester. The solvent was distilled under vacuum at slightly below room temperature. Water (20 mL) was added and the solution was extracted with 15 mL of ether, followed by addition of HCl to pH 1.5–2, at 5 °C. The precipitated product was extracted with ethyl acetate. The combined extracts were washed with water (2×) and brine (1×) and were dried over anhydrous magnesium sulfate. Distillation of the solvent afforded 0.42 g (70%) of the product as fine crystalline needles: TLC, R_f 0.62 (D), 0.11 (E); NP-HPLC (F) 4.57, 91.3%; FTIR ($CHCl_3$) 3475 (s, br), 3019 (s), 1675 (s), 1660 (s); ^1H NMR (DMSO-d_6) δ 1.77 (m, 6 H), 1.89 (m, 6 H), 2.33 (m, 2 H), 2.40 (m, 2 H), 4.76 (s, 6 H), 7.25 (s, 1 H), 7.38 (m, 15 H), 10.97 (s, 3 H); MS m/e 663 $(M + H)^+$; MS/MS m/e 663 $(M + H)^+$.

***N*-[Tris[2-[(*N*-hydroxyamino)carbonyl]ethyl]-methyl]succinamic Acid, 6.** The protected hydroxamic derivative 1 (0.20 g, 0.3 mmol) in 95% ethanol (5 mL) was hydrogenated with 0.2 g of palladium on carbon (10%) at 20 psi and room temperature. The reaction progress was followed by TLC, which showed no starting material after 75 min. After an additional 45 min, the catalyst was separated by filtration through a plug of Celite and the solution was concentrated to 0.5 mL. The product was precipitated from petroleum ether, filtered, and dried under argon. The solid product was redissolved in 1 mL of methanol and precipitated one more time from petroleum ether. Drying the white powder under argon afforded 0.08 g (67.6%) of the hydroxamic acid: TLC (I_2, $FeCl_3$) R_f 0.26 (J), 0.84 (K); FTIR (KBr) 3214 (br, 3446), 1655 (br, s, shoulders 1723, 1711); ^1H NMR (DMSO-d_6) δ 1.79 (m, 6 H), 1.86 (m, 6 H), 2.27 (m, 2 H), 2.85 (m, 2 H), 3.60 (br multiabsorption peak in the 2.6–4.3 range), 7.32 (s, 1 H); MS m/e 393 $(M + H)^+$.

ACKNOWLEDGMENT

The authors gratefully acknowledge the contribution by Dr. George R. Newkome (University of South Florida) in the form of a generous supply of compound **2**. We thank Drs. Raymond Furner (Neuropsychiatry, UAB) and James Riordan (Southern Research Institute) for obtaining the mass spectra. Assistance of the NMR Core Facility at UAB in obtaining the NMR spectra is further acknowledged. We also thank Sharon Garrison for preparing the manuscript.

LITERATURE CITED

(1) Waldmann, T. A. (1991) Monoclonal antibodies in diagnosis and therapy. *Science 252*, 1657.
(2) Schlom, J. (1986) Basic principles and applications of monoclonal antibodies in the management of carcinomas. *Cancer Res. 46*, 3225.
(3) Buchsbaum, D. J., and Lawrence, T. S. (1991) Tumor therapy with radiolabeled monoclonal antibodies. *Antib. Immunoconjug. Radiopharm. 4*, 245.
(4) Regoeczi, E. (1984) Methods of Protein Iodination. *Iodine Labeled Plasma Proteins*; pp 35–102, CRC Press, Inc., Boca Raton, FL.
(5) Mather, S. J., and Ellison, D. (1990) Reduction-mediated technetium-99m labeling of monoclonal antibodies. *J. Nucl. Med. 31*, 692.
(6) Hnatowich, D. J., Mardirossian, G., Rusckowski, M., Fogarasi, M., Virzi, F., and Winnard, Jr., P. (1993) Directly and indirectly technetium-99m-labeled antibodies—A comparison of in vitro and animal in vivo properties. *J. Nucl. Med. 34*, 109.
(7) Parker, D. (1990) Tumor targeting with radiolabeled macrocycle–antibody conjugates. *Chem. Soc. Rev. 19*, 271.
(8) Kasina, S., Rao, T. N., Srinivasan, A., Sanderson, J. A., Fitzner, J. N., Reno, J. M., Beaumier, P. L., and Fritzberg, A. R. (1991) Development and biologic evaluation of a kit for preformed chelate technetium-99m radiolabeling of an antibody Fab fragment using a diamide dimercaptide chelating agent. *J. Nucl. Med. 32*, 1445.
(9) Meares, C. F. (1986) Chelating agents for the binding of metal ions to antibodies. *Nucl. Med. Biol. 13*, 311.
(10) Engler, D., and Burger, A. G. (1984) The deiodination of the iodotyrosines and of their derivatives in man. *Endocr. Rev. 5*, 151.
(11) Sunberg, N. W., Meares, C. F., Goodwin, D. A., and Diamantic, C. I. (1974) Chelating agents for binding of metal ions to macromolecules. *Nature (London) 250*, 587.
(12) Brechbiel, M. W., Gansow, O. A., Atcher, R. W., Schlom, J., Esteban, J., Simpson, D. E., and Colcher, D. (1986) Synthesis of 1-(p-isothiocyanatobenzyl) derivatives of DTPA and EDTA. Antibody labeling and tumor-imaging studies. *Inorg. Chem. 25*, 2772.
(13) Fritzberg, A. R., Abrams, P. G., Beaumier, P. L., Kasina, S.; Morgan, A. C., Rao, T. N., Reno, J. M., Sanderson, J. A., Srinivasan, A., and Wilbur, D. S. (1988) Specific and stable labeling of antibodies with technetium-99m with a diamide-dithiolate chelating agent. *Proc. Natl. Acad. Sci. USA, 85*, 4025.
(14) Gagliardi, E., and Raber, H. (1962) Hydroxamsäuren als analytische reagentien. *Monatsh. Chem. 93*, 360.
(15) Buckles, R. E., and Thelen, C. J. (1950) Qualitative determination of carboxylic esters. *Anal. Chem. 22*, 676.
(16) King, T. J., and Harrison, P. G. (1972) Crystal and molecular structure of triphenyltin N-benzoyl-N-phenylhydroxamate. *J. Chem. Soc. Chem. Commun.* 815.
(17) Bauer, L., and Exner, O. (1974) The chemistry of hydroxamic acids and hydroxyimides. *Angew. Chem. Int. Ed. Engl. 13*, 376, and references cited therein.
(18) Fournié-Zaluski, M.-C., Coulaud, A., Bouboutou, R., Chaillet, P., Devin, J., Waksman, G., Costentin, J., and Roques, P. (1985) New bidentates as full inhibitors of enkephalin-degrading enzymes: Synthesis and analgesic properties. *J. Med. Chem. 28*, 1158.
(19) Nishino, N., and Powers, J. (1978) Peptide hydroxamic acids as inhibitors of thermolysin. *Biochemistry 17*, 2846.
(20) Winkelmann, G., van der Helm, D., and Neilands, J. B., Eds. (1987) *Iron Transport in Microbes, Plants and Animals*, VCH, Weinheim, New York.
(21) Bergeron, R. J. (1984) Synthesis and solution structures of microbial siderophores. *Chem. Rev. 84*, 587.
(22) Bhargava, K. K., Chervu, L. R., Chun, S. B., and Blaufox, M. D. (1987) Hydroxamic acid derviatives as ligands for technetium-99m labeled radiopharmaceuticals. 194th National Meeting of the American Chemical Society, Division of Nuclear Chemistry and Technology, New Orleans, LA., Abstract.
(23) Nakayama, M., Sawamura, H., Hasegawa, S., Harada, K., Sugii, A., Hara, M., Kinoshita, R., Ohyama, Y., Kojima, A., Tomiguchi, S., and Takahashi, M. (1992) Evaluation of Tc-99m-hydroxamic acids as tumor imaging agents. *J. Nucl. Med. 33*, 988, Abstract.
(24) Anderegg, G., L'Eplattenier, F., and Schwarzenbach, G. (1963) *Helv. Chim. Acta 46*, 1400.

(25) Yokoyama, A., Ohmono, Y., Horiuchi, K., Saji, H., Tanaka, H., Yamamoto, K., Ishii, Y., and Torizuka, K. (1982) Deferoxamine, a promising bifunctional chelating agent for labeling with gallium. *J. Nucl. Med. 23*, 909.

(26) Ryser, J. E., Jones, R. M. L., Egeli, R., Pelegrin, A., Rose, K., Kurt, A. M., Perin, M., Broquet, P. E., Ambrosetti, P., Fisch, I., Pochon, S., Donath, A., Mach, J-P., and Offord, R. E. (1992) Colon carcinoma immunoscintigraphy by monoclonal anti-CEA antibody labeled with gallium-67 aminooxyacetyldeferoxamine. *J. Nucl. Med. 33*, 1766.

(27) Ward, M. C., Roberts, K. R., Westwood, J. H., Coombes, R. C. C., and McCready, V. R. (1986) The effect of chelating agents on the distribution of monoclonal antibodies in mice. *J. Nucl. Med. 27*, 1746.

(28) Müller, G., Barclay, S. J., Raymond, K. N. (1985) The mechanism and specificity of iron transport in *Rhadotorula pilimanae* probed by synthetic analogs of rhodotorulic acid. *J. Biol. Chem. 260*, 13976.

(29) Newkome, G. R., Behera, R. K., Moorefield, C. N., and Baker, G. R. (1991) Cascade polymers: Synthesis and characterization of one-directional arborols based on adamantane. *J. Org. Chem. 56*, 7162.

(30) Sheehan, J. C., and Hess, G. P. (1955) A new method for forming peptide bonds. *J. Am. Chem. Soc. 77*, 1067.

(31) König, W., and Geiger, R. (1970). *Chem. Ber. 103*, 2024.

(32) Kisfaludy, J. K., and Ceprini, M. Q. (1967) On the optical purity of peptide active esters prepared by N,N′-dicyclohexylcarbodiimide and "complexes" of N,N′-dicyclohexylcarbodiimide pentachlorophenol and N,N′-dicyclohexylcarbodiimide pentafluorophenol. *J. Am. Chem. Soc.* **89**, 183.

(33) Lindmo, T., Boven, E., Cuttita, F., Fedorko, J., and Bunn, P. A., Jr. (1984) Determination of the immunoreactivity fraction of radiolabeled monoclonal antibodies by linear extrapolation to binding at infinite antigen excess. *J. Immunol. Methods 72*, 77.

(34) Kazikiewicz, J. M., Zimmer, A. M., Spies, S. M., and Rosen, S. T. (1986) Rapid miniaturized chromatography procedures for iodinated monoclonal antibodies: Comparison to gel exclusion chromatography. *J. Nucl. Med. Technol. 14*, 6, abstract.

(35) Lowry, O. H., Rosebrough, N. J., Farr, A. L., and Randall, R. J. (1951) Protein measurement with the folin phenol reagent. *J. Biol. Chem. 193*, 265.

(36) Colombo, F., Matarrese, M., Bugaj, J., Gerundini, P., Fazio, F., and Deutsch, E. (1988) Tc-99m complexes of α,α-disubstituted, α-hydroxycarboxylic acids. *J. Nucl. Med. (Suppl.) 29*, 934.

Contact-Dependent, Immunecomplex-Mediated Lysis of Hapten-Sensitized Liposomes

Bruce Babbitt,[†,‡] Lisa Burtis,[†] Patrick Dentinger,[†] Panayiotis Constantinides,[†,§] Larry Hillis,[†] Barbara McGirl,[∥] and Leaf Huang*[,∥,⊥]

LipoGen, Inc., 10515 Research Drive, Knoxville, Tennessee 37932, and Department of Biochemistry, University of Tennessee, Knoxville, Tennessee 37996-0840. Received October 26, 1992

Large unilamellar liposomes ($d \sim 160$ nm) composed of dioleoylphosphatidylethanolamine (DOPE) (80–90%), a negatively charged phospholipid stabilizer (10–20%), and a small amount (0.1–1%) of a haptenated lipid are unusually stable in divalent cation-free isotonic buffer at pH 7.4. The liposomes can be stored under this condition at 4 °C for at least 6 months without any detectable leakage of the entrapped fluorescent dye calcein. However, the liposomes undergo a rapid (1 h) aggregation and lysis reaction in the presence of free bivalent anti-hapten antibody. The liposome destabilization was immunospecific in that it did not occur with the normal IgG or in the presence of excess free hapten. Liposome lysis was always accompanied by liposome aggregation. Aggregation and lysis of the liposomes was completed in 5 min if the incubation temperature was raised to 70–80 °C. Replacing DOPE with dioleoylphosphatidylcholine in the liposomes did not abolish the liposome aggregation, but no liposome lysis was observed even at 80 °C. Since liposome aggregation appeared to be a necessary (but not sufficient) prerequisite for liposome lysis, we have named this new class of liposome "contact-sensitive liposomes". The immunodiagnostic potential of the contact-sensitive liposome was demonstrated with liposomes containing theophylline-DOPE. The aggregation and lysis of the liposomes induced by a monoclonal anti-theophylline antibody could be inhibited by free theophylline at concentrations of therapeutic significance. The observation could be the basis of a homogeneous assay for theophylline.

INTRODUCTION

The equilibrium state of an unsaturated phosphatidylethanolamine (PE)[1] such as dioleoyl-PE (DOPE) at physiological pH and temperature is the reverse hexagonal (H_{II}) phase (reviewed by Gruner et al., 1985). This is because the phosphorylethanolamine head group is relatively poor in attracting bound water (Cevc and Marsh, 1985; Sen and Hui, 1988) and the hydrophobic, cis-unsaturated acyl chains are relatively bulky in size (Gruner et al., 1985). However, stable bilayer liposomes can be prepared by mixing DOPE with appropriate amounts of other amphiphiles which can increase the interfacial hydration. Amphiphiles, termed "liposome stabilizers", used for this purpose include fatty acids (Düzgünes et al., 1985; Collins et al., 1990), fatty acyl amino acid (Connor et al., 1984), gangliosides (Tsao and Huang, 1985; Pinnaduwage and Huang, 1988), acidic phospholipids (Tari and Huang, 1989; Nayar and Schroit, 1985; Wang and Huang, 1984), acidic (Leventis et al., 1987; Collins et al., 1990) and basic (Felgner et al., 1987) double-chain amphiphiles, and amphipathic proteins (Taraschi et al., 1982; Pinnaduwage and Huang, 1989). Particularly interesting is the DOPE liposomes stabilized by amphiphiles which are capable of forming an immune complex. For example, liposomes comprising DOPE and *N*-[(dinitrophenyl)caproyl]-PE rapidly lyse in the presence of anti-dinitrophenol antibody which has been immobilized on a solid support (Ho and Huang, 1985). DOPE liposomes stabilized with glycophorin A also lyse when the liposomes come into contact with a glass surface coated with anti-glycophorin antibody (Ho and Huang, 1985). Similarly, liposomes containing DOPE and palmitoyl antibody against the gD glycoprotein of the herpes simplex virus also rapidly lyse in the presence of intact virus particles (Ho et al., 1986a,b, 1987b, 1988), cell membranes containing viral glycoproteins (Ho et al., 1986a, 1987a), or latex beads covalently coated with purified gD (Ho et al., 1988). In all cases, multivalent binding between the liposome and the immobilized antigen or antibody is required for lysis. This is probably because the stabilizer molecules are laterally aggregated in the liposome membrane which triggers a bilayer-to-H_{II} phase transition, leading to the destabilization of the liposomes (Ho and Huang, 1985; Ho et al., 1986a). This unusual type of liposome has been named "target-sensitive liposomes" (Ho et al., 1986a), and their potential uses in immunodiagnosis (Ho et al., 1986b, 1987b) and therapeutic drug delivery (Ho et al., 1987a) have been demonstrated.

We now report a related but different observation that DOPE liposomes, stabilized by an amphiphile and additionally containing a haptenated lipid, aggregate and lyse in the presence of free anti-hapten antibody. There is no requirement for immobilizing the antibody on any solid support. We have shown that the liposome lysis is immunospecific and can be accelerated by incubation at

* Corresponding author.
† LipoGen, Inc.
‡ Present address: Cellcor Therapeutics, Inc., 200 Wells Ave., Newton, MA 02159.
§ Present address: SmithKline Beecham Pharmaceuticals, Drug Delivery Department, P.O. Box 1539, King of Prussia, PA 19406-0939.
∥ University of Tennessee.
⊥ Present address: Department of Pharmacology, University of Pittsburgh School of Medicine, Pittsburgh, PA 15261.

[1] Abbreviations used: biotin-PE, *N*-biotinylphosphatidylethanolamine; CE, hexadecyl cholestanyl ether; DMPG, dimyristoylphosphatidylglycerol; DOPA, dioleoylphosphatidic acid; DOPC, dioleoylphosphatidylcholine; DOPE, dioleoylphosphatidylethanolamine; DOPG, dioleoylphosphatidylglycerol; DOPS, dioleoylphosphatidylserine; LUVET, large unilamellar vesicles prepared by extrusion; MPB-PE, *N*-[4-(*p*-maleimidophenyl)-butyryl]phosphatidylethanolamine; PE, phosphatidylethanolamine.

1043-1802/93/2904-0199$04.00/0 © 1993 American Chemical Society

a high temperature such as 80 °C. Liposome aggregation is a prerequisite for lysis, because if the aggregation is inhibited by free hapten no liposome lysis occurs even at 80 °C. Furthermore, the inhibition of liposome aggregation and lysis by free hapten depends on the hapten concentration. This last observation is the basis of using this novel type liposomes as a reagent in the homogeneous immunoassays, such as the one demonstrated in this report for theophylline.

EXPERIMENTAL PROCEDURES

Materials. DOPE, DOPS, DOPA, DOPC, DMPG, DOPG, MPB-PE, and biotin-PE were obtained from Avanti Polar Lipids, Inc. Theophylline-DOPE was prepared by the condensation of 8-(2-carboxyethyl)theophylline and DOPE (Hashimoto et al., 1985). The theophylline derivative was prepared by the general method of Cook et al. (1976). The theophylline-PE gave the same physical data as previously reported (Haga et al., 1981). The goat anti-biotin antibody, calcein, and protein A-agarose were supplied by Sigma Chemical Co. The mouse monoclonal (IgG1) anti-theophylline antibody was purchased from Immunoresearch, Inc. Liquid scintillation cocktail, Scintiverse, was purchased from Fisher Scientific. Biogel A15m was obtained from Bio-Rad Laboratories. The [^{3}H]CE was synthesized as previously described (Pool et al., 1982). The [^{3}H]cholesteryl oleate was supplied by New England Nuclear. The goat anti-biotin antibody was dialyzed against PBS for approximately 48 h and then filtered through a 0.2-μm Gelman Sciences Acrodisc filter to a final concentration of approximately 2 mg/mL.

Preparation of Liposomes. Lipid preparations were made of either DOPC or DOPE as the bulk phospholipid (80–90 mol %), a stabilizer (10–20 mol % of biotin-PE, MPB-PE, DOPS, etc.), and a haptenated lipid (0.1–1.0 mol % of biotin-PE or theophylline-DOPE). In some samples [^{3}H]CE was added to the lipid as a tracer. Lipid films were obtained by evaporation of the solvent from a chloroform–lipid mixture using a stream of N_2 gas and then placing the lipids in a desiccator at reduced pressure for a minimum of 4 h. Lipids were hydrated at room temperature for at least 30 min in 50 mM calcein in PBS at a lipid concentration of 10 mM. Calcein, 2′,7′-bis-[[(carboxymethyl)amino]methyl]fluorescein is a self-quenching dye that, at concentrations greater than 5 mM, undergoes progressive collisional fluorescence quenching (Allen, 1983). It has been widely used for analysis of liposome stability and/or leakage since it is not necessary to separate the liposomes from released dye in order to quantitate lysis. The calcein solution was prepared at 50 mM in distilled H_2O and the pH adjusted to 7.4 with 10 N NaOH. The osmolarity of the calcein was adjusted with 10× PBS to that of human serum, approximately 330 mosM. The lipid suspensions were formed by rigorous vortexing and sized by extrusion 10 times at 200 psi with a Lipex extruder through Nuclepore polycarbonate membranes (0.2-μm pore size). If small unilamellar liposomes were needed, the suspension was sonicated with a bath-type sonicator from Laboratory Supplies, Inc., for 7 min. Suspensions were left at room temperature for 1–2 h to allow for bilayer annealing before being fractionated by column chromatography. The size of the liposomes was determined by laser light scattering using the Coulter N4SD submicron particle analyzer. Free, unentrapped calcein was removed from liposomes by gel filtration utilizing a 10 mL Bio-Gel A15m column, preequilibrated, and eluted with PBS, pH 7.4. This gave a working lipid concentration of 7 mM. Initial calcein fluorescence was measured by adding a 5-μL liposome sample to 3 mL of PBS in a quartz cuvette and reading light-emission intensity on a Perkin-Elmer LS-5B luminescence spectrometer at an excitation wavelength of 490 nm and an emission wavelength of 520 nm. Total calcein fluorescence was monitored after the addition of 10 μL of 10% Triton X-100 to lyse the vesicles and release the entrapped dye. Percent fluorescence quenching of the entrapped calcein in the liposomes was calculated using the following equation:

$$\% \text{ quenching} = \frac{F_t - F_i}{F_t} \times 100$$

where F_i is the total fluorescence of the liposomes without detergent and F_t is the total fluorescence after Triton had been added to release all of the entrapped calcein. Freshly prepared, unlysed liposomes usually showed about 80% fluorescence quenching.

Antibody-Mediated Liposome Lysis. Three to 10 μL (21–70 nmol of lipid) of liposomes containing entrapped calcein were added to 200 μL of PBS, pH 7.4. Various concentrations of antibody were added, and incubation was carried out at various temperatures for different periods of time as specified in Table I or the figure captions. At the end of incubation the entire sample was diluted to 3 mL with PBS and the calcein fluorescence was measured as described above. The percent liposome lysis was calculated using the following equation:

$$\% \text{ lysis} = \frac{F - F_i}{F_t - F_i} \times 100$$

where F_i and F are the fluorescence of the liposomes before and after incubation, respectively. F_t is the total fluorescence after Triton had been added to release all of the entrapped calcein.

Nonspecific Liposome Lysis by Osmotic Pressure. Five microliters (35 nmol) of liposomes with 50 mM entrapped calcein, containing either 85 mol % of DOPE and 15 mol % of DMPG as stabilizer and 1 mol % of biotin-PE or 80 mol % of DOPE and 20 mol % of DOPG as stabilizer and 1 mol % of biotin-PE, were incubated in a final volume of 205 μL for 15 min at room temperature, 22 °C, at various aqueous dilutions of a stock PBS buffer, pH 7.4. The dilutions resulted in a range of osmotic strengths of the buffer from 45 mosM/kg of H_2O to approximately 3360 mosmol/kg of H_2O. Calcein fluorescence of the liposomes was measured as above.

Nonspecific Lysis of Liposomes by Divalent Cations. Five microliters (35 nmol) of liposomes containing 50 mM entrapped calcein, composed of 90 mol % of DOPE and 10 mol % of MPB-PE as stabilizer and 1 mol % of biotin-PE as the ligand, were mixed with various amounts of divalent cations (chloride salt) in a final volume of 205 μL of PBS, pH 7.4. The samples were incubated at room temperature, 22 °C, for 15 min before the liposome lysis was measured as described above, except that the diluted PBS contained 1 mM EDTA.

Electron Microscopy. LUVET of DOPE:MPB-PE: biotin-PE (90:10:1) (about 50 nmol of total lipid) were incubated for 1 h at 37 °C with 2.5 μg of anti-biotin antibody in a total volume of 15 μL. The liposomes were negatively stained with 1% uranyl acetate and viewed in a Hitachi 600 electron microscope operated at 75 kV.

RESULTS

We and others have previously shown that a number of amphiphiles, especially the charged ones, can stabilize the

Table I. Phospholipid Stabilizers for DOPE Liposomes

stabilizer	minimum mole % required to form stable liposomes[a]	stabilizer	minimum mole % required to form stable liposomes[a]
biotin-PE	10	DMPG	15
MPB-PE	10	DOPA	20
DOPS	15	DOPG	20
DPPG	15		

[a] Stable liposomes are defined as those showing no loss of entrapped calcein after storage at 4 °C for 30 days.

small unilamellar vesicles of DOPE (Düzgünes et al., 1985; Connor et al., 1984; Tsao and Huang, 1985; Tari and Huang, 1989; Wang and Huang, 1984; Collins et al., 1990). Table I shows that various synthetic phospholipids can also stabilize DOPE liposomes of larger size, i.e. average diameter of 162 ± 33 nm prepared by an extrusion method. These liposomes have been named LUVET (Hope et al., 1985). Also shown in the table are the minimum amounts of these phospholipid stabilizers which are required for the formation of stable liposomes. Stable liposomes are defined as those which have no loss of entrapped calcein after storage of the liposomes at 4 °C for at least 30 days. As can be seen from the table, two N-modified PE's, i.e. biotin-PE and MPB-PE, had the highest stabilization activity; only 10 mol % was required to form stable liposomes. The stabilization activity of the phospholipid stabilizer does not seem to correlate with the charge content of the molecule, since the doubly negatively charged DOPA was not as active as other singly negatively charged phospholipids such as DOPS. Furthermore, disaturated PG (DPPG and DMPG) were more active than the unsaturated PG (DOPG). This is in agreement with our previous results using small unilamellar vesicles (Tari and Huang, 1989). The unsaturated chains tend to favor the H_{II} phase more than the saturated chains, due to the larger molecular volumes occupied by the unsaturated chains (Gruner et al., 1985).

LUVET composed of DOPE and a phospholipid stabilizer could additionally contain 0.1–1 mol % of a haptenated lipid, such as biotin-PE or theophylline-DOPE, without affecting their size distribution, calcein-entrapment efficiency, and stability. These liposomes remained lysable by antibody (see below) even after a prolonged storage time (at least 6 months at 4 °C). However, the stability of the liposomes was dependent on the osmolarity of the storage medium. Data in Figure 1 show that the liposomes were most stable in the iso-osmotic medium. Both hypo- and hyperosmotic conditions promoted the leakage of the entrapped calcein even after a 15-min incubation at room temperature. Large liposomes are known to be osmotically sensitive (Bangham et al., 1967). Our data agrees with this conclusion.

The stability of the liposomes was also dependent on the divalent-cation content of the medium. Figure 2 shows the result of an experiment in which different amounts of three different divalent cations, i.e. Ca^{2+}, Mg^{2+}, and Mn^{2+}, were added to the medium. It is clear that Mn^{2+} was the most potent one to induce the liposome lysis; greater than 80% lysis was observed at concentrations as low as 1 mM. Ca^{2+} had the second highest activity, requiring more than 3 mM to induce a significant liposome lysis. Mg^{2+} was fairly ineffective, requiring much higher concentrations to achieve the same level of liposome lysis. The relative potency of divalent cations to induce the bilayer destabilization is probably related to their differential activities to dehydrate the bilayer, which leads to bilayer aggregation

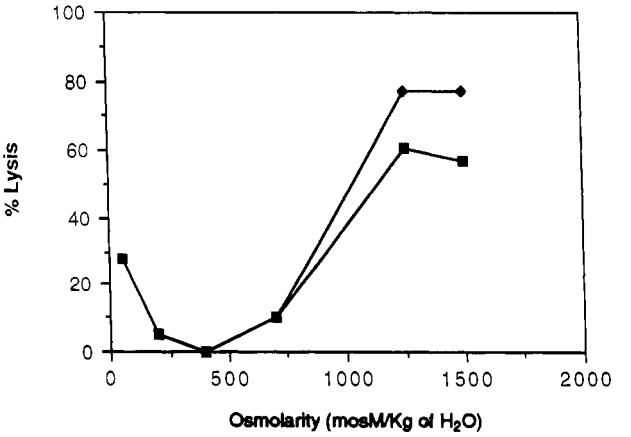


Figure 1. Stability of liposomes under osmotic stress. LUVET composed of DOPE:DMPG:biotin-PE (85:15:1) (■) or DOPE:DOPG:biotin-PE (80:20:1) (◆) were incubated for 15 min at 22 °C in phosphate buffers of various osmolarity. Liposome lysis was measured as release of the entrapped calcein as described in Experimental Procedures. Approximately 400 mosM/kg of H_2O was the iso-osmotic condition.

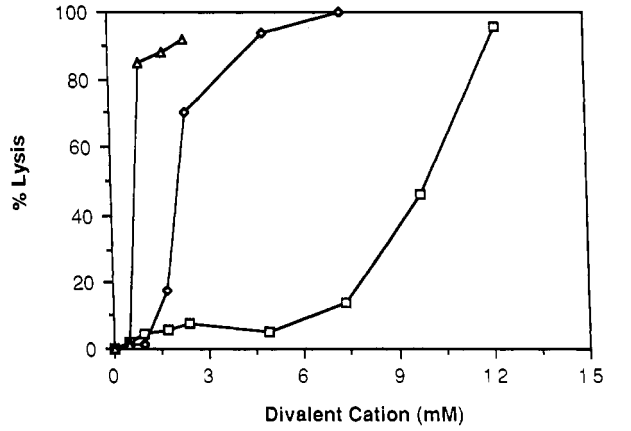


Figure 2. Stability of liposomes in solutions containing divalent cations. LUVET composed of DOPE:MPB-PE:biotin-PE (90:10:1) were incubated for 15 min at 22 °C in PBS buffer containing various amounts of Mg^{2+} (□), Ca^{2+} (◇), or Mn^{2+} (△). Liposome lysis was measured as release of the entrapped calcein.

and fusion (Portis et al., 1979). We routinely use divalent-cation-free PBS for the preparation and storage of the liposomes.

LUVET composed of DOPE:MPB-PE (9:1) containing either 0.1 or 1% biotin-PE as a ligand were tested for the effect of antibody on the stability of liposome. Various amounts of a purified goat anti-biotin antibody were mixed with the liposomes and incubated at 37 °C for 1 h. As can be seen in Figure 3, there was a concentration-dependent lysis of the liposomes. The lysis was immunospecific, because it could be blocked by the addition of an excess of free hapten, i.e. biotin. Liposome lysis also did not occur when normal goat IgG was used instead of the antibody (data not shown). The extent of liposome lysis depended on the surface density of the ligand; liposomes containing 1% biotin-PE could be lysed with lower concentrations of anti-biotin than those containing 0.1% biotin-PE. Liposomes containing no biotin-PE could not be lysed by the antibody (data not shown). We have noticed that liposome lysis mediated by the anti-biotin antibody was always associated with liposome aggregation as evidenced by the cloudiness or turbidity of the incubation mixture. Turbidity did not occur when excess biotin was present in the incubation mixture, or when the normal goat IgG was used. The appearance of the incubation

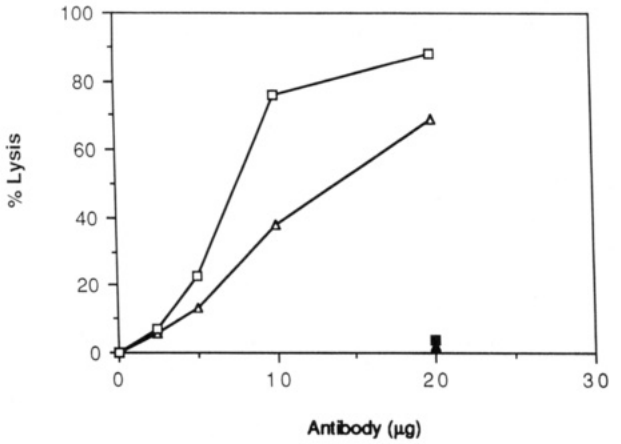


Figure 3. Antibody-mediated liposome lysis. LUVET composed of DOPE:MPB-PE (90:10), additionally containing either 1% (□) or 0.1% (△) biotin-PE, were incubated with goat anti-biotin antibody for 1 h at 37 °C. In parallel experiments, 0.2 μmol of free biotin was added to the antibody before mixing with the liposomes (▲, ■). Liposome lysis was measured as release of the entrapped calcein.

mixture after incubation was of uniform cloudiness with a background of yellowish-green color (due to the leaked calcein). Figure 4 shows the morphology of the aggregated liposomes.

The temperature dependence of the antibody-mediated liposome lysis was examined. LUVET composed of DOPE: DOPS:biotin-PE (85:15:1) were mixed with 10 μg of anti-biotin antibody and incubated for 5 min at various temperatures ranging from 22 to 80 °C. The extent of liposome lysis increased with increasing incubation temperature (Figure 5). At 80 °C, greater than 80% of the entrapped calcein was released after only a 5-min incubation with the antibody. Extensive liposome aggregation was also observed. In the absence of the antibody, there was no liposome aggregation nor significant lysis even at 80 °C. Also shown in Figure 5 is the effect of the phospholipid composition on the antibody-mediated lysis of the liposomes. LUVET composed of DOPC:DOPS: biotin-PE (85:15:1) did not lyse up to 80 °C incubation either in the presence or absence of the antibody, despite the fact that these liposomes could be aggregated by the antibody. Note the difference in the experimental conditions between the experiments described in Figures 3 and 5. The experiment described in Figure 3 was done with an incubation at 37 °C for 1 h; whereas the experiment described in Figure 5 was done with only a 5-min incubation. Therefore, the antibody-mediated lysis was greatly accelerated at the elevated temperatures.

Under the condition of shorter incubation at an elevated temperature, the effect of antibody concentration on the liposome lysis was examined over a wide range of antibody concentration. LUVET composed of DOPE:DOPS:biotin-PE (85:15:1) were incubated at 70 °C for 5 min in the presence of anti-biotin antibody up to 200 μg in 210-μL incubation volume (Figure 6). With increasing concentration of the antibody, there was an increasing level of liposome aggregation and lysis which plateaued at an antibody concentration of 20–40 μg. At higher antibody concentrations, the extent of liposomee aggregation and lysis progressively decreased such that less than 20% dye release was observed at the 200 μg antibody concentration. The overall dose–response curve is bell-shaped. This result indicated that there was an optimal antibody concentration for the aggregation and lysis of the liposomes.

We have examined in more detail the inhibition of the antibody-mediated lysis of liposomes by the free hapten.

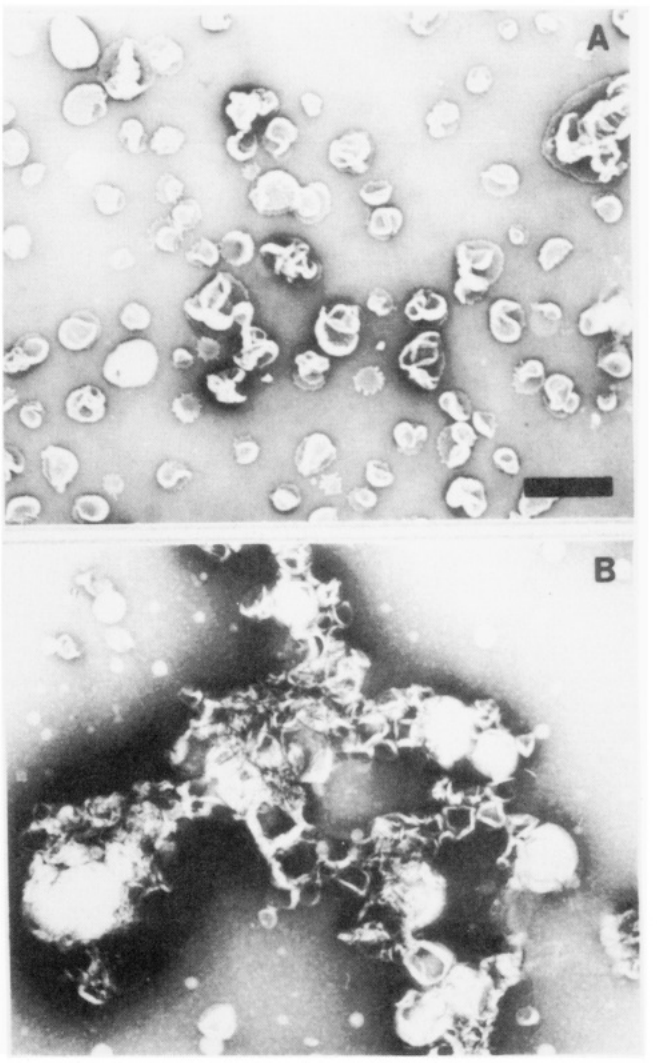


Figure 4. Aggregation of liposomes by antibody. LUVET composed of DOPE:MPB-PE:biotin-PE (90:10:1) were incubated for 1 h at 37 °C in PBS: (a) in the presence of 2.5 μg of goat anti-biotin antibody and (b) before addition of antibody, viewed with negative-stain electron microscopy. Magnification is 17 000X. Bar is 0.5 μm.

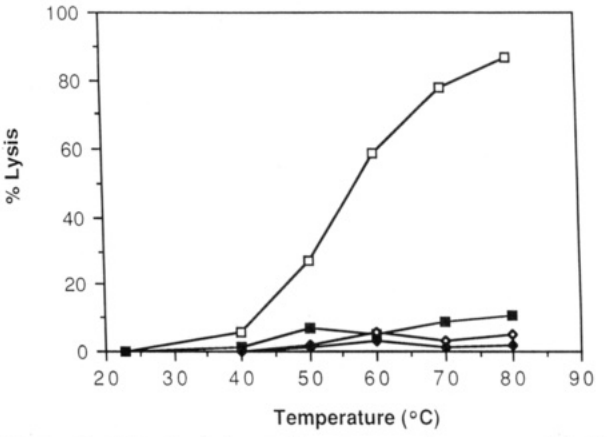


Figure 5. Effect of incubation temperature on antibody-mediated liposome lysis. LUVET composed of DOPE:DOPS: biotin-PE (85:15:1) (◇, ◆) were mixed with (open symbols) or without (solid symbols) 10 μg of goat anti-biotin antibody and incubated for 5 min at different temperatures. Liposome lysis was measured as release of the entrapped calcein.

In this experiment, LUVET composed of DOPE:DOPS: theophylline-DOPE = 85:15:1 were incubated with a mouse monoclonal anti-theophylline antibody at the optimal

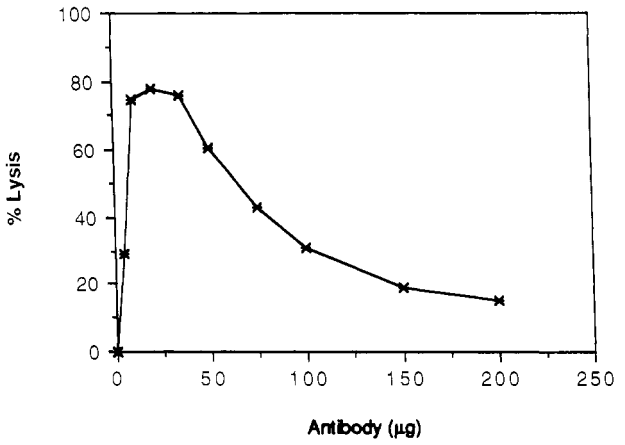


Figure 6. Effect of antibody concentration on the antibody-mediated liposome lysis at a high-incubation temperature. LUVET composed of DOPE:DOPS:biotin-PE (85:15:1) were incubated with various amounts of goat anti-biotin antibody for 5 min at 70 °C. Liposome lysis was measured as release of the entrapped calcein.

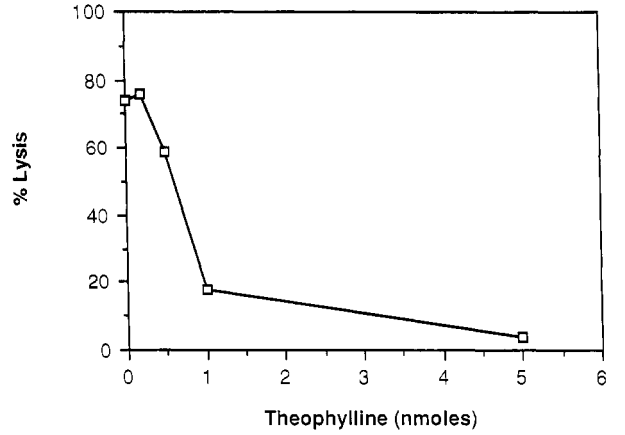


Figure 7. Effect of free ligand on the antibody-mediated liposome lysis. Various amounts of free theophylline were incubated with a mouse monoclonal anti-theophylline antibody (0.5 μg) for 5 min at 22 °C, followed by the addition of LUVET composed of DOPE:DOPS:theophylline-DOPE (85:15:1). The mixtures were then incubated for 5 min at 70 °C before the liposome lysis was measured as release of the entrapped calcein.

concentration for 5 min at 70 °C. Approximately 80% of liposome lysis was measured. However, if the anti-theophylline antibody had been preincubated with various amounts of free theophylline for 5 min at room temperature, there was an inhibition of the liposome lysis which was theophylline-concentration dependent (Figure 7). The liposomal theophylline-DOPE used in this experiment was 0.32 nmol. Fifty percent inhibition of the liposome lysis occurred at the free theophylline dose of approximately 0.7 nmol. Thus, it took a comparable amount of free hapten to inhibit the binding of the antibody to the liposomal hapten which presumably is a prerequisite of the liposome lysis. This result indicated that the binding affinity of the liposomal hapten to the antibody was similar to that of the free hapten.

DISCUSSION

The principal difference between the liposomes described in this report and those described by Ho and Huang (1985) is in the lipid composition of the liposomes. Although DOPE is the common major phospholipid used in both liposome formulations, Ho and Huang's liposomes contain at least 12% antigenic or haptenated lipid as a bilayer stabilizer (Ho and Huang, 1985) and the liposomes described here contain a phospholipid stabilizer which is itself not an antigen or hapten. An additional antigenic or haptenated lipid is added to the liposomes described here only at very low concentrations (1% or lower). The lysis of Ho and Huang's liposomes require the contact with a multivalent antibody, i.e. antibodies immobilized on a solid support such as a glass coverslip; free, bivalent antibody in solution does not lyse the liposomes (Ho and Huang, 1985). In contrast, our liposomes readily lyse in the presence of free IgG antibodies (Figures 3 and 5–7). Thus, the liposomes described in this report represent a new class of liposomes which can be lysed by the formation of the immune complex. Since the liposome lysis requires the aggregation of liposomes, we have named them the "contact-sensitive liposomes". One of the outstanding features of the "contact-sensitive liposome" is their stability in the absence of liposome aggregation. The liposomes can be stored at 4 °C in a divalent-cation-free, iso-osmotic buffer for prolonged periods of time (Table I, Figures 1 and 2). In the absence of the antibody-mediated liposome contact, either as a result of the absence of antibody or the presence of excess free hapten, liposome lysis was not observed even at elevated incubation temperatures (Figures 3 and 5). Such an extraordinary stability can be attributed to the proper choice of the liposome stabilizer. Data in Table I indicate that a number of synthetic, negatively charged phospholipids exhibit strong liposome-stabilization activities. Among them are biotin-PE, which is also a haptenated lipid, and MPB-PE, which is widely used as a sulfhydryl-reactive lipid for antibody conjugation to liposomes (Martin and Papahadjopoulous, 1982). In addition to the negatively charged phosphodiester bond, both lipids contain a relatively bulky, hydrophilic head group which presumably helps attract interfacial H_2O for the stability of the bilayer. Other synthetic phospholipids are less potent in activity, but they are more available commercially and resemble the naturally occurring phospholipids.

Free IgG antibody, polyclonal or monoclonal, mediates a liposome lysis which leads to the release of the entrapped fluorescent dye (Figures 3 and 5–7). That such lysis is immunospecific is supported by the facts that it can be blocked by the free hapten (Figures 3 and 7) and that it does not occur in the absence of the specific antibody (Figures 3 and 5). Furthermore, liposome lysis is closely correlated with liposome aggregation (Figure 4). When the aggregation is prevented by the saturation of the antibody to free hapten, no lysis of the liposomes occurs even with an 80 °C incubation (Figure 5). Evidently, the role of the IgG antibody is simply to cross-link the hapten-containing liposomes and to allow a close contact between the aggregated liposomes. This mechanism is supported by the bell-shaped antibody dose–response curve shown in Figure 6. It is well-known that immune complex formation exhibits an optimal antibody concentration as well as an optimal antigen concentration (Bellanti, 1985). Increasing amounts of antibody lead to increasing levels of liposome aggregation, until the antibody is present in excess, at which time only monovalent antibody binding to the hapten, instead of a bivalent cross-linking of haptens between the neighboring liposomes, occurs. Antibody-mediated liposome lysis is dependent on the hapten density of the liposomes; liposomes with a higher hapten density require lower antibody concentrations for aggregation and lysis and vice versa (Figure 3). This result is consistent with the mechanism of liposome cross-linking by the bivalent antibody. Higher hapten density of the liposomes would facilitate a greater chance of antibody-mediated

cross-linking of the liposomes and result in a higher level of liposome lysis.

It is easily understood that liposome–liposome contact (via aggregation) is a prerequisite of the liposome lysis. Destabilization of DOPE bilayer involves a bilayer-to-H_{II} phase transition which requires the close contact of the neighboring bilayers (Siegel, 1984, 1986). Such a requirement is most conveniently demonstrated by the second-order kinetics of liposome lysis reaction (Pinnaduwage and Huang, 1988). DOPE lipids at the contact region spontaneously reorganize into the so-called "intermembrane intermediate" (IMI) structures which eventually leads to the extensive H_{II} phase structure (Siegel, 1984). Although we have not yet studied the kinetic aspect of liposome lysis, our data are consistent with this mechanism. Furthermore, the data in Figure 5 indicate that liposomes mainly composed of DOPC, instead of DOPE, did not lyse despite the fact that extensive liposome aggregation had occurred. DOPC does not exhibit the capability of H_{II} phase formation (Gruner et al., 1985). Aggregated DOPC bilayers do not undergo bilayer destabilization as the DOPE bilayers do. Thus, a H_{II} phase forming lipid is a necessary ingredient of the "contact-sensitive liposomes".

The potential application of these liposomes in immunodiagnosis is demonstrated by the data in Figure 7. Lysis of liposomes containing a theophylline hapten can be progressively inhibited by the presence of free theophylline at the concentrations of therapeutic significance. Therefore, an inhibitory, competitive assay for the free theophylline can be theoretically established. The assay would not require any washing, centrifugation, or separation steps and would thus be a homogeneous assay. It would be significantly different from the other liposome homogeneous assays in which a lysis molecule such as complement (Haxby et al., 1969) or cytolysin (Litchfield et al., 1984) is required for liposome lysis. The fact that the "contact-sensitive liposomes" are extraordinarily stable makes such an application very attractive. Furthermore, the incubation time is only 5 min, which greatly facilitates the speed of the assay. The immunodiagnostic aspects of the "contact-sensitive liposomes" deserves further exploration.

The haptenated lipid of the "contact-sensitive liposomes" can be substituted with lipid–antibody conjugates. Aggregation of the immunoliposomes in the presence of a multivalent antigen such as virus particles leads to rapid liposome lysis. Such a design of an immunoliposome has recently been reported (Pinnaduwage and Huang, 1992).

ACKNOWLEDGMENT

We thank Carolyn Drake and Christine A. Hallahan for excellent help in word processing.

LITERATURE CITED

Allen, T. M. (1983) Calcein as a tool in liposome methodology. In *Liposome Technology* (G. Gregoriadis, Ed.) Vol. 3, p 177, CRC Press, Boca Raton.

Bangham, A. D., de Gier, J., and Greville, G. D. (1967) Osmotic properties and water permeability of phospholipid liquid crystals. *Chem. Phys. Lipids 1*, 225.

Bellanti, J. A. (1985) Immunology III, W. B. Saunders Co., Philadelphia.

Cevc, G., and Marsh, D. (1985) Hydration of noncharged lipid bilayer membranes: theory and experiments with phosphatidylethanolamine. *Biophys. J. 47*, 21.

Collins, D., Connor, J., Ting-Beall, H. P., and Huang, L. (1990a) Protons and divalent cations induce synergistic but mechanistically different destabilization of pH-sensitive liposomes composed of phosphatidylethanolamine and oleic acid. *Chem. Phys. Lipids 55*, 339.

Collins, D., Litzinger, D. C., and Huang, L. (1990b) Structure and function comparisons of pH-sensitive liposomes composed of phosphatidylethanolamine and three different diacylsuccinylglycerols. *Biochim. Biophys. Acta 1025*, 234.

Connor, J., Yatvin, M. B., and Huang, L. (1984) pH-sensitive liposomes: Acid induced liposome fusion. *Proc. Natl. Acad. Sci. U.S.A. 81*, 1715.

Cook, C. E., Twine, M. E., Myers, M., Amerson, E., Kepler, J. A., and Taylor, G. F. (1976) Theophylline radioimmunoassay: Synthesis of antigen and characterization of antiserum. *Res. Commun. Chem. Pathol. Pharmacol. 13*, 497–505.

Düzgünes, N., Straubinger, R. M., Baldwin, P. A., Friend, D. S., and Papahadjopoulos, D. (1985) Proton-induced fusion of oleic acid–phosphatidylethanolamine liposomes. *Biochemistry 24*, 3091.

Felgner, P. L., Gadek, T. R., Holm, M., Roman, R., Chan, H. W., Wenz, M., Northrop, J. P., Rongold, G. M., and Danielsen, M. (1987) Lipofection: A highly efficient, lipid-mediated DNA-transfection procedure. *Proc. Natl. Acad. Sci. U.S.A. 84*, 7413.

Gruner, S. M., Cullis, P. R., Hope, M. J., and Tilcock, C. P. S. (1985) Lipid polymorphism: The molecular basis of nonbilayer phases. *Annu. Rev. Biophys. Biophys. Chem. 14*, 211.

Haga, M., Sugawara, S., and Itagaki, H. (1981) Drug sensor: Liposome immunosensor for theophylline. *Anal. Biochem. 118*, 286–293.

Hashimoto, K., Loader, J. E., and Kinsky, S. C. (1985) Synthesis and characterization of methotrexate–dimyristoylphosphatidylethanolamine derivatives and the glycerophosphorylethanolamine analogs. *Biochim. Biophys. Acta 186*, 163.

Haxby, J. A., Gotze, O., Muller-Eberhard, H. J., and Kinsky, S. C. (1969) Release of trapped marker from liposomes by the action of purified complement components. *Proc. Natl. Acad. Sci. U.S.A. 64*, 290.

Ho, R. J. Y., and Huang, L. (1985) Interactions of antigen sensitized liposomes with immobilized antibody: A homogeneous solid-phase immunoliposome assay. *J. Immunol. 134*, 4035.

Ho, R. J. Y., Rouse, B. T., and Huang, L. (1986a) Target-sensitive immunoliposomes: Preparation and characterization. *Biochemistry 25*, 5500.

Ho, R. J. Y., Rouse, B. T., and Huang, L. (1986b) Destabilization of phosphatidylethanolamine immunoliposomes by antigen binding—A valuable approach for rapid virus detection. *Biochem. Biophys. Res. Commun. 138*, 931.

Ho, R. J. Y., Rouse, B. T., and Huang, L. (1987a) Target-sensitive immunoliposomes as an efficient drug carrier for antiviral activity. *J. Biol. Chem. 262*, 13973.

Ho, R. J. Y., Rouse, B. T., and Huang, L. (1987b) Interactions of target-sensitive immunoliposomes with herpes simplex virus: The foundation of a sensitive immunoliposome assay for the virus. *J. Biol. Chem. 262*, 13979.

Ho, R. J. Y., Ting-Beall, H. P., Rouse, B. T., and Huang, L. (1988) Kinetic and ultrastructural studies of interactions of target-sensitive immunoliposomes with herpes simplex virus. *Biochemistry 27*, 500.

Hope, M. J., Bally, M. B., Webb, G., and Cullis, P. R. (1985) Production of large unilamellar vesicles by a rapid extrusion procedure: characterization of size distribution, trapped volume and ability to maintain a membrane potential. *Biochim. Biophys. Acta 812*, 55.

Leventis, R., Diacovo, T., and Silvius, J. R. (1987) pH-dependent stability and fusion of liposomes combining protonable double-chain amphiphiles with phosphatidylethanolamine. *Biochemistry 26*, 3267.

Litchfield, W. J., Freytag, J. W., and Adamich, M. (1984) Highly sensitive immunoassay based on use of liposomes without complement. *Clin. Chem. 30*, 1441.

Martin, F. J., and Papahadjopoulos, D. (1982) Irreversible coupling of immunoglobulin fragments to preformed vesicles. *J. Biol. Chem. 10*, 286.

Nayar, R., and Schroit, A. J. (1985) Generation of pH-sensitive liposomes: use of large unilamellar vesicles containing N-succinyldioleoylphosphatidylethanolamine. *Biochemistry 24*, 5967.

Pinnaduwage, P., and Huang, L. (1988) β-Galactosidase induced destabilization of liposome composed of phosphatidylethanolamine and ganglioside GM_1. *Biochim. Biophys. Acta 939*, 375.

Pinnaduwage, P., and Huang, L. (1989) The role of protein-linked oligosaccharide in the bilayer stabilization activity of glycophorin A for dioleoyl phosphatidylethanolamine liposomes. *Biochim. Biophys. Acta 986*, 106.

Pinnaduwage, P., and Huang, L. (1992) Stable target-sensitive immunoliposomes. *Biochemistry 31*, 2850.

Pool, G. L., French, M. E., Edwards, R. A., Huang, L., and Lumb, R. H. (1982) Use of radiolabelled hexadecyl cholesteryl ether as a liposome marker. *Lipids 17*, 448.

Portis, A., Newton, C., Pangborn, W., and Papahadjopoulos, D. (1979) Studies on the mechanism of membrane fusion: evidence for an intermembrane Ca-phospholipid complex, synergism with Mg, and inhibition by spectrin. *Biochemistry 18*, 780.

Sen, A., and Hui, S. W. (1988) Direct measurement of headgroup hydration of polar lipids in inverted micelles. *Chem. Phys. Lipids 49*, 179.

Siegel, D. P. (1984) Inverted micellar structures in bilayer membranes: formation rates and half-lives. *Biophys. J. 45*, 399.

Siegel, D. P. (1986) Inverted micellar intermediates and the transitions between lamellar, cubic, and inverted hexagonal lipid phases. I. Mechanisms of the $L_\alpha \leftrightarrow H_{II}$ phase transition. *Biophys. J. 49*, 1155.

Taraschi, T. F., van der Steen, T. M., deKruijff, B., Tellier, C., and Verkleij, A. J. (1982) Lectin-receptor interactions in liposomes: evidence that binding of wheat germ agglutinin to glycophorin–phosphatidylethanolamine vesicles induces non-bilayer structure. *Biochemistry 21*, 5756.

Tari, A., and Huang, L. (1989) Structure and function relationship of phosphatidylglycerol in the stabilization of phosphatidylethanolamine bilayer. *Biochemistry 28*, 7708.

Tsao, Y. S., and Huang, L. (1985) Sendai virus-induced leakage of liposomes containing gangliosides. *Biochemistry 24*, 1092.

Wang, C. Y., and Huang, L. (1984) Polyhistidine meadiates an acid dependent fusion of negatively charged liposomes. *Biochemistry 23*, 4409.

Oligo-α-Thymidylates Covalently Linked to Intercalating Agents: Circular Dichroism Studies of Their Interaction with Complementary Sequences

Maurice Durand, Jean Claude Maurizot,* Ulysse Asseline, Nguyen Thanh Thuong, and Claude Hélène†

Centre de Biophysique Moléculaire, 1A, Avenue de la Recherche Scientifique, 45071 Orléans cedex 2, France, and Laboratoire de Biophysique, Museum National d'Histoire Naturelle, INSERM U201, CNRS, UA 481, 43 rue Cuvier, 75231 Paris 05, France. Received November 24, 1992

The interaction between oligo-α-thymidylates covalently linked to an intercalating agent (an acridine derivative) and their complementary sequences containing β-nucleosides (poly(rA), poly(dA), r(Ap)$_7$rA, p(dA)$_8$) has been studied using circular dichroism spectroscopy. Binding to poly(rA) and to poly(dA) of the modified oligonucleotides led to large changes in the induced circular dichroism signal of the acridine ring. These changes depend on whether the dye is linked to the 3′- or to the 5′-end of the oligonucleotide. Interaction with poly(rA) as well as interaction with an octadeoxyriboadenylate led to the formation of a 1A:1T complex. With poly(dA), in addition to the 1A:1T complex, a 1A:2T complex was observed when the acridine derivative was linked to the 3′-end of the octa-α-thymidylate. The double-stranded structures formed with poly(rA) and poly(dA) were characterized by different environments of the acridine dye. Binding to poly(rA) gave much stronger complexes than binding to poly(dA). With poly(rA) the complex was more stable when the dye was bound at the 5′-end of the oligonucleotide. Comparison between the circular dichroism changes observed upon binding at the level of polymers [poly(rA) or poly(dA)] and those obtained at the level of oligomers [r(Ap)$_7$rA or pd(A)$_8$] gave information relative to the position of the acridine ring in the helix.

INTRODUCTION

Synthesis of modified oligodeoxyribonucleotides which could be used to control gene expression has been the subject of active research during the past few years. It has been shown that the stability of the complexes formed by oligodeoxyribonucleotides with their complementary sequence could be increased without loss of specificity by covalent attachment of an intercalating agent to the 3′- or 5′-end of the oligonucleotide (*1–5*). Such conjugates have been used to selectively inhibit mRNA translation (*6, 7*). An oligonucleotide–intercalator conjugate targeted to the 3′-end of influenza virus (−)RNAs inhibited the cytopathic effect of the virus (*8*). DNA replication of simian virus SV40 in CV-1 cells in culture was inhibited by an oligonucleotide–intercalator conjugate (*9*).

The use of oligonucleotides synthesized with the α-anomeric nucleotide units, instead of the natural β-anomers, has been previously reported (*10–25*). These compounds are more resistant than their natural analogues in a number of different biological environments, which makes them very interesting tools for in vivo studies (*19*). An α-oligodeoxyribonucleotide, complementary to the region adjacent to the cap site, was shown to prevent the translation of rabbit β-globin mRNA (*24*). Further, the binding affinity of the α-oligodeoxyribonucleotides was reinforced by the covalent linking of an intercalating agent: acridine (*11, 12, 23*) and oxazolopyridocarbozole derivatives (*21, 22*). Recently, it has been shown that only the α-oligodeoxyribonucleotide linked to the acridine derivative complementary to the cap region displayed significant antisense properties in *Xenopus oocytes* (*25*).

A few years ago, we used circular dichroism spectroscopy to characterize the complexes formed by an α-octathymidylate with complementary sequences containing β-nucleosides: poly(rA), poly(dA), and octaribo- and deoxyriboadenylates (*15, 16*). We demonstrated that the α-octathymidylate is able to form complexes with its ribose- or deoxyribose-containing complementary β-strands and that binding is stronger than that of a β-octathymidylate. When an intercalating dye is covalently attached to an oligonucleotide, it becomes optically active and an induced circular dichroism spectrum can be observed in the visible and near-ultraviolet wavelength range where only the dye absorbs (*4, 26*). We have used such induced circular dichroism to study the interaction between α-octathymidylates covalently linked via their 3-′ or 5′-end to an acridine derivative (2-methoxy-6-chloro-9-aminoacridine) with their complementary sequences containing β-nucleosides, poly(rA), poly(dA), β-r(Ap)$_7$A, and β-d(pA)$_8$.

EXPERIMENTAL PROCEDURES

The α-octathymidylates bearing the acridine derivative linked via a pentamethylene chain to the 5′- or 3′-phosphate [hereafter abbreviated as α-Acrm$_5$(pT)$_8$ and α-(Tp)$_8$m$_5$Acr] were prepared and purified by the procedure previously described (*11*).

The oligonucleotides r(Ap)$_7$rA and d(pA)$_8$ and the polynucleotides poly(rA) and poly(dA) were purchased from P.L. Biochemicals and used without further purification. All measurements were performed in a buffer containing 0.1 M NaCl and 10 mM sodium cacodylate at pH 7.0.

Circular dichroism measurements were carried out with a Jobin-Yvon Mark III dichrograph in cells with pathlength ranging from 0.1 to 1 cm. Each CD spectrum was run at least twice and we checked for possible base line shifts. The temperature of the cell was adjusted with a circulating water bath and held constant to ±0.5 °C. Binding was followed by adding small amounts of a concentrated polyadenylate or oligoadenylate solution to a solution of oligothymidylate derivative of fixed concentration. The

* Address correspondance to J.C. Maurizot, Centre de Biophysique Moleculaire, 1A Avenue de la recherche scientifique, 45071 Orléans cedex 2, France. Fax (033) 38 63 15 17.
† Museum National d'Histoire Naturelle.

1043-1802/93/2904-0206$04.00/0 © 1993 American Chemical Society

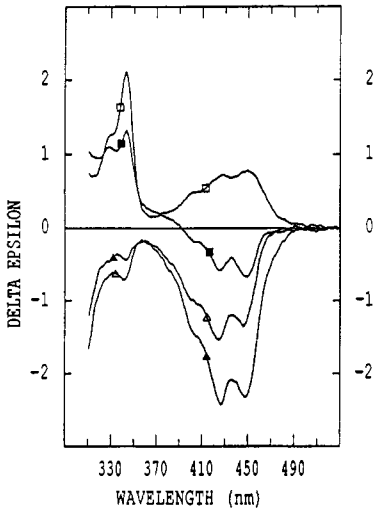


Figure 1. Circular dichroism spectra at 0 °C of β-$(Tp)_8m_5Acr$ (□); β-$Acrm_5(pT)_8$ (■); α-$(Tp)_8m_5Acr$ (▲); α-$Acrm_5(pT)_8$ (△) in a buffer containing 10 mM sodium cacodylate and 0.1 M NaCl at pH 7.0. The molar concentration in oligonucleotide was $6 \cdot 10^{-5}$ M.

concentration used to calculate the CD amplitude is that of the α-oligodeoxyribonucleotide. It was obtained by absorption measurement using the extinction coefficients previously determined (*11*).

RESULTS

Circular Dichroism of the α-Oligothymidylates. The CD behavior of the modified α-oligonucleotides alone was investigated as a prelude to the study of interactions with the complementary sequences. In Figure 1 are shown the CD spectra of α-$(Tp)_8m_5Acr$ and of α-$Acrm_5(pT)_8$ at 0 °C in the visible and near-ultraviolet region of the spectrum where only the acridine absorbs. For comparison the figure also includes the spectra of β-$(Tp)_8m_5Acr$ and β-$Acrm_5(pT)_8$. For both α-oligodeoxyribonucleotides the spectra are composed of several negative bands, which are more intense in the wavelength range 490–360 nm than in the 360–320-nm region. This is in contrast with the CD spectra of their β-analogues where the bands in the wavelength range 490–360 nm are smaller than those located in the 360–320 nm region (Figure 1). The CD spectra of the α-oligomers resemble the absorption spectra in shape and relative intensity of the different bands. In the range of concentration used (about $6 \cdot 10^{-5}$ M in oligonucleotide units) the CD signal did not depend on concentration reflecting the lack of acridine–acridine interaction under our experimental conditions. The presence of a CD signal in the visible and near-UV range reflects the existence of an asymmetric perturbation of the planar acridine ring by the oligonucleotide. The general shape of the CD spectra of α-$(Tp)_8m_5Acr$ and α-$Acrm_5(pT)_8$ are similar (the various bands are centered around the same wavelengths). However, we can observe in the 490–360 wavelength range that the bands of α-$(Tp)_8m_5Acr$ are larger than those of α-$Acrm_5(pT)_8$ and that is the contrary to what is seen for the bands located around 340 nm. These observations indicate that at 0 °C the environments of the acridine dye in the two compounds exhibit some similarity. This is in contrast with the behavior of their β-analogues where the environment of the dye is clearly dependent on its position (3′- or 5′-phosphate): in the visible range the CD is positive when Acr is attached to the 3′-end whereas it is negative when attached to the 5′-end (Figure 1).

Upon increasing the temperature of α-oligothymidylates, we observed a regular decrease of the CD signal without

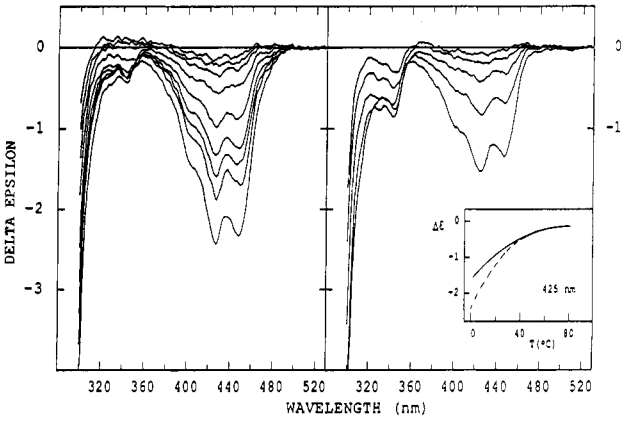


Figure 2. Circular dichroism spectra of α-$(Tp)_8m_5Acr$ (left) and α-$Acrm_5(pT)_8$ (right) as a function of temperature. For both compounds the spectra correspond, in order of decreasing intensity, to temperatures ranging from 0 to 80 °C. Other conditions are those of Figure 1. Inset: temperature dependence of CD amplitude at 425 nm of α-$Acrm_5(pT)_8$ (- -) and α-$(Tp)_8m_5Acr$ (—).

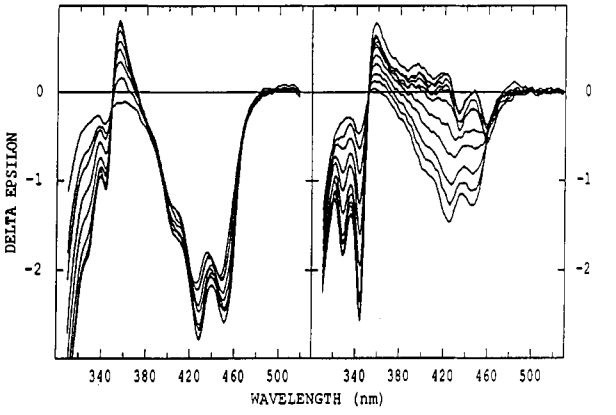


Figure 3. Circular dichroism spectra of α-$(Tp)_8m_5Acr$ (left) and α-$Acrm_5(pT)_8$ (right) in the presence of increasing concentrations of poly(rA). The ratio X of adenine to thymine concentration varied from 0 to 1.5. For α-$(Tp)_8m_5Acr$ the intensities at 340 and 450 nm increased with X, while for α-$Acrm_5(pT)_8$ it decreased at 450 nm and increased at 340 nm. The experimental conditions are those of Figure 1.

cooperative transition (Figure 2). At the highest temperature reached during the experiment (80 °C) the signal disappeared almost completely, indicating that at this temperature the interaction between the acridine chromophore and the rest of the α-oligonucleotide was very weak.

Interaction between α-Oligothymidylate–Acridine Conjugates and poly(rA). When poly(rA) was added to the modified α-oligothymidylates the CD spectra changed, reflecting an interaction between the oligomers and the polymer (Figure 3). The observed changes of the CD spectra were dependent on the position of the attachment site of the acridine derivative (3′- or 5′-phosphate). In the 490–380-nm wavelength range, when the acridine ring was linked to the 3′-phosphate end of the oligonucleotide, we observed a weak increase of the CD signal with a slight shift to the longer wavelengths. When the acridine residue was linked to the 5′-phosphate, we noted a large decrease of the CD signal with an important red-shift leading to the appearance of two new bands respectively centered at 460 and 435 nm. With both oligonucleotides we noted the formation of a positive band around 358 nm. Below 350 nm, the increase of the band located around 340 nm was larger with α-$Acrm_5(pT)_8$ than with α-$(Tp)_8m_5Acr$, and a

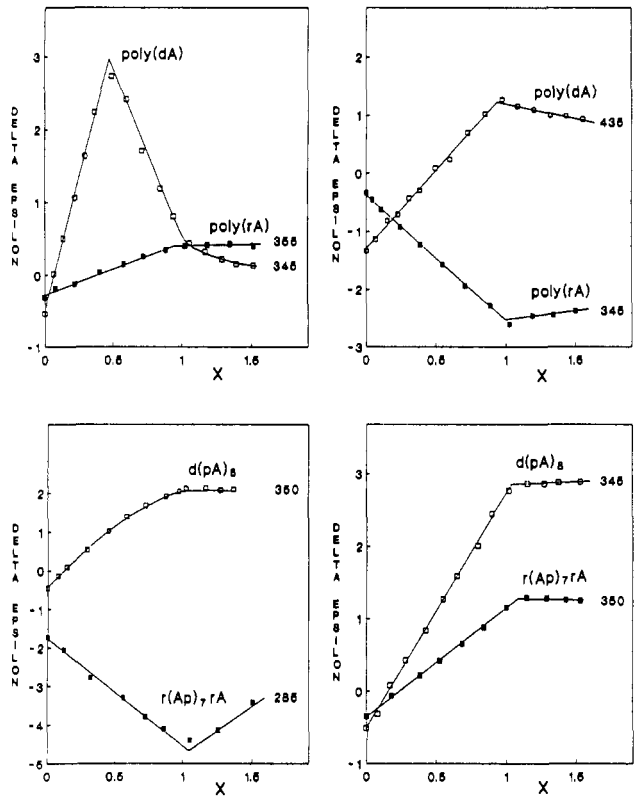


Figure 4. Titration curves of α-Acrm$_5$(pT)$_8$ (right) and of α-(Tp)$_8$m$_5$Acr (left) by the various adenylates compounds: poly(rA), poly(dA), r(Ap)$_7$rA, and d(pA)$_8$.

new band appeared around 330 nm with α-Acrm$_5$(pT)$_8$ whereas only a shoulder was seen with α-(Tp)$_8$m$_5$Acr.

We used the CD changes around 350 nm to follow the interactions between the α-oligomers and poly(rA). For both α- oligodeoxyribonucleotides the binding curves presented a linear variation of the amplitude of the CD signal with a sharp break when the ratio of adenine to thymine concentration reached a value close to one as shown on Figure 4. This demonstrated that the interaction between α-oligothymidylate–acridine conjugates and poly(rA) led to the formation of double-stranded helices.

An increase in temperature led to a reversal of the spectroscopic effects observed upon complex formation (Figure 5, left panel). At the highest temperatures reached during the experiments the CD signal in the visible region reached the values observed for the α-octathymidylate-acridine conjugates alone. When the melting phenomenon was followed in the visible range a decrease of the CD intensity was observed before complex dissociation indicating a premelting phenomenon (Figure 5, left panel). At 295 nm where the CD signal of poly(rA) alone is very small the CD variation was very large with a sigmoidal shape allowing an accurate determination of the melting temperature of complexes (inset of Figure 5). In our experimental conditions the α-Acrm$_5$(pT)$_8$-poly(rA) complex was slightly more stable (T_m = 49 °C) than the α-(Tp)$_8$-m$_5$Acr-poly(rA) complex (T_m = 45 °C).

Interaction between α-Oligothymidylate–Acridine Conjugates and poly(dA). As observed with poly(rA), the interaction between poly(dA) and the modified α-oligothymidylates induced drastic CD changes which were dependent on the position of attachment of the acridine dye (Figure 6).

During the titration we noticed three steps with α-(Tp)$_8$m$_5$Acr and two steps with α-Acrm$_5$(pT)$_8$. With α-(Tp)$_8$m$_5$Acr, up to an A/T ratio of 0.5, an inversion of

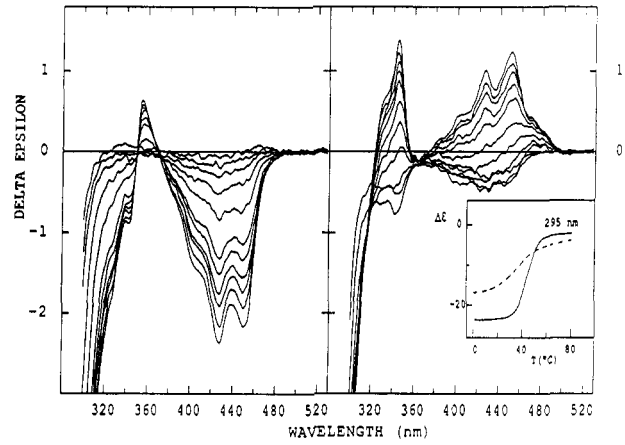


Figure 5. Circular dichroism spectra of the 1A:1T complexes between α-(Tp)$_8$m$_5$Acr and poly(rA) (left) and α-Acrm$_5$(pT)$_8$ and poly(dA) (right) as a function of temperature. In order of decreasing curve intensities the temperature varied from 0 to 80 °C. Inset: Melting curves followed at 295 nm for the α-(Tp)$_8$-m$_5$Acr-poly(rA) complex (—) and α-Acrm$_5$(pT)$_8$-poly(dA) complex (- -).

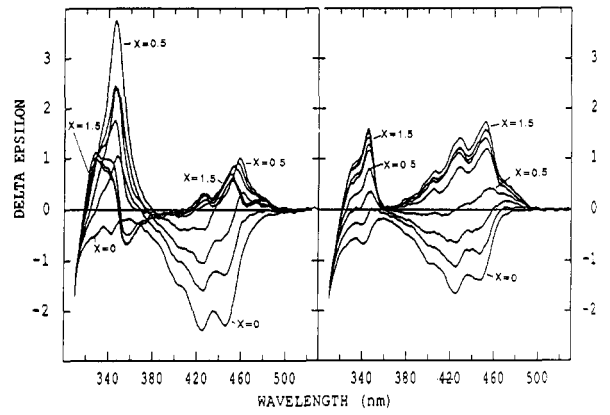


Figure 6. Circular dichroism spectra of α-(Tp)$_8$m$_5$Acr (left) and α-Acrm$_5$(pT)$_8$ (right) in the presence of increasing concentrations of poly(dA). The ratio X of adenine to thymine concentrations varied from 0 to 1.5. For α-(Tp)$_8$m$_5$Acr, as X varied from 0 to 0.5, the signal was inverted at 460 nm and a strong positive band appeared at 350 nm. As X further increased to 1.5, these bands were shifted to lower wavelengths with decreasing intensities. For α-Acrm$_5$(pT)$_8$, the signal was progressivelly inverted as X increased. Experimental conditions are those of Figure 1.

the spectrum was observed in the 480–380-nm wavelength range, giving rise to a positive band at 460 nm, whereas in the 380–320-nm region a positive band appeared around 350 nm. Upon further addition of poly(dA), up to an A/T ratio of 1, the intensity of the bands respectively centered around 460 and 350 nm decreased and shifted to lower wavelengths and a negative band appeared at 355 nm. For higher A/T ratios no changes of the CD spectrum were observed. When the CD signal was plotted versus A/T ratio, in the case of α-(Tp)$_8$m$_5$Acr a sharp break was observed at 0.5 and a change of the slope of the curve occurred around 1, indicating the formation of two types of complexes: one with a 1A:2T stoichiometry and another one with 1A:1T stoichiometry (Figure 4). With α-Acrm$_5$-(pT)$_8$, up to an A/T ratio of 1, we noted a progressive and linear inversion of the spectrum with a red-shift (Figure 6). When the ratio was close to 1 the mixing curve presented a sharp break (Figure 4). This result showed that the interaction between poly(dA) and α-Acrm$_5$(pT)$_8$ led to the formation of only one type of complex: a double-stranded helix.

An increase of temperature of the 1A:1T complexes induced reversal of the spectroscopic effects (Figure 5,

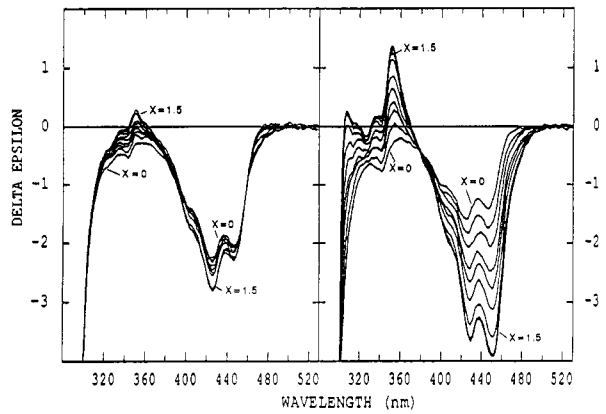


Figure 7. Circular dichroism spectra of α-$(Tp)_8m_5Acr$ (left) and α-$Acrm_5(pT)_8$ (right) in the presence of increasing concentrations of $r(Ap)_7rA$. The ratio of adenine to thymine concentration varied from 0 to 1.5. In both cases the negative intensity around 450 nm increased with X. Experimental conditions are those of Figure 1.

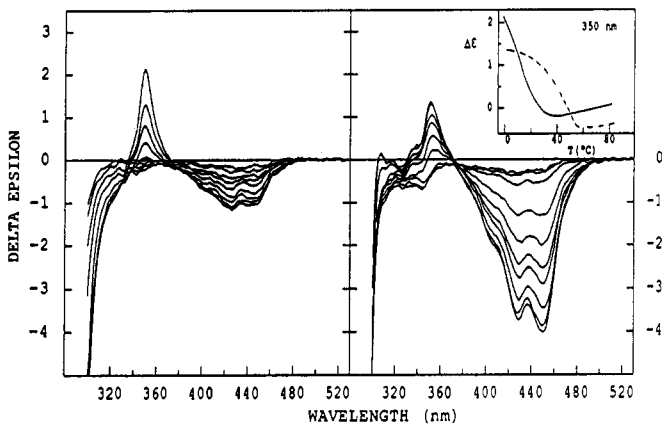


Figure 8. Circular dichroism as a function of temperature of the complexes α-$(Tp)_8m_5Acr$-$d(pA)_8$ (left) and α-$Acrm_5(pT)_8$-$r(Ap)_7rA$ (right). In order of decreasing curve intensities; the temperature varied from 0 to 80 °C. Inset: Melting profiles at 350 nm of α-$(Tp)_8m_5Acr$-$d(pA)_8$ (—) and α-$Acrm_5(pT)_8$-$r(Ap)_7rA$ (- -).

right panel). Using the CD signal to follow the melting process we noted for both complexes the same melting temperature (38 °C), reflecting identical thermal stabilities. We did not obtain any evidence of 1A:1T to 1A:2T transition with α-$(Tp)_8m_5Acr$-poly(dA) complex.

Interaction between α-Oligothymidylate–Acridine Conjugates and $r(Ap)_7rA$. When $r(Ap)_7rA$ was added to the modified α-oligothymidylates CD changes indicated the formation of complexes. With α-$(Tp)_8m_5Acr$ we observed CD changes smaller than those obtained with poly(rA) but of similar shape (Figure 7). To increase the precision, the titration curve was followed in the ultraviolet wavelength range at 285 nm. Clearly only a 1A:1T complex was formed.

When the dye was attached to the 5′-end of the α-oligodeoxyribonucleotide the CD titration curve also indicated the formation of a 1A:1T complex, but the CD spectrum of the complex was drastically different from that observed with poly(rA) showing a large negative band in the 380–500-nm wavelength range and a positive peak at 350 nm (Figure 7).

For both α-oligothymidylates an increase of temperature of the 1A:1T complexes induced reversal of the spectroscopic effects (Figure 8) and led to cooperative melting transition curves with a T_m lower for α-$(Tp)_8m_5Acr$ (35 °C) than for α-$Acrm_5(pT)_8$ (40 °C).

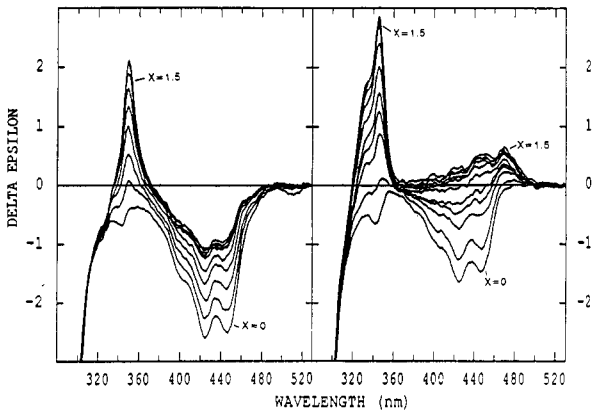


Figure 9. Circular dichroism spectra of α-$(Tp)_8m_5Acr$ (left) and α-$Acrm_5(pT)_8$ (right) in the presence of increasing concentrations of $d(pA)_8$. The ratio of adenine to thymine concentration varied from 0 to 1.5. For α-$Acrm_5(pT)_8$, when X increased, the signal intensity around 450 nm decreased and then became slightly positive. For α-$(Tp)_8m_5Acr$, the intensity around 450 nm decreased with X. In both cases a large positive band at about 350 nm appeared when X increased. Other experimental conditions are those of Figure 1.

Interaction between α-Oligothymidylate–Acridine Conjugates and $d(pA)_8$. A behavior similar to that observed with poly(dA) was observed upon addition of $d(pA)_8$ to α-$Acrm_5(pT)_8$: inversion of the CD signal in the wavelength range 320–480 nm and appearance of a sharp band centered at 345 nm (Figure 9). Only a 1A:1T complex was formed (Figure 4).

When $d(pA)_8$ was added to the α-octathymidylate with the acridine derivative linked to the 3′-phosphate, a behavior different from that obtained with poly(dA) was observed. The intensity of the negative band in the wavelength range 360–480 nm decreased and a sharp positive band appeared at 345 nm (Figure 9). The titration curve did not show a break for A/T ratio of 0.5 but instead a nonlinear increase followed by a plateau for A/T values larger than 1 (Figure 4).

The melting profile of the complex formed with α-$Acrm_5(pT)_8$ presented a wide transition, the T_m was 35 °C (data not shown). In the case of α-$(Tp)_8m_5Acr$-$d(pA)_8$ complex we noted a CD change starting from 0 °C (Figure 8), indicating that even at 0 °C the complex formed between α-$(Tp)_8m_5Acr$ and $d(pA)_8$ was in part dissociated. The T_m could not be determined accurately but in any case was lower than 15 °C.

Ionic Effects on Oligothymidylate–Oligoadenylate Complexes. To the final mixtures of oligothymidylate with oligodeoxyriboadenylates (A/T ratio between 1.35 and 1.5) NaCl was added to increase the salt concentration from 0.1 to 1 M. In three cases only minor changes—if any—were observed in the CD spectra. The only exception was for the mixture of $d(pA)_8$ and α-$(Tp)_8m_5Acr$. We noted that the final CD spectrum in 1 M NaCl was very similar to that observed when the same α-oligodeoxyribonucleotide was mixed with poly(dA) at an A/T ratio of 0.5. This clearly indicated that under these experimental conditions a 1A:2T complex was formed between the two oligonucleotides.

As expected, addition of 1 M NaCl led to an increase of the melting temperature of all the complexes studied. Depending on the complex, this increase varied from 10 to 12 °C (Table I).

DISCUSSION

2-Methoxy-6-chloro-9-aminoacridine is an achiral molecule which exhibits no intrinsic optical activity. However,

Table I. Melting Temperatures of 1A:1T Complexes in a Buffer Containing 0.1 M NaCl

	T_m,[a] °C			
compound	poly(rA)	poly(dA)	r(Ap)$_7$rA	d(pA)$_8$
α-(tp)$_8$	29	17	29(35)	18(31)
α-(Tp)$_8$m$_5$Acr	45	38	35(45)	(27)
α-Acrm$_5$(pT)$_8$	49	38	40(52)	35(47)

[a] The values in parentheses correspond to experiments in 1 M NaCl. The molar concentration expressed in oligonucleotide units was $1.2 \cdot 10^{-4}$ M.

when the dye is covalently linked to an oligonucleotide, optical activity is induced in the absorption band of the acridine ring. This reveals an asymmetric interaction of the acridine derivative with other groups of the oligonucleotide. The fact that the induced CD signal for α-oligothymidylate derivatives is different from that observed with β-analogues is in agreement with our previous conclusion that the main interaction is with the bases of the oligonucleotide. The CD spectra are of similar shape for the α-oligomers with acridine derivative linked to the 5′- and 3′-end, indicating that the stereochemistry of interacting species are similar and consequently more dependent on the oligonucleotide conformation than on the linkage of the dye. The lack of dependence of the CD signal on oligonucleotide concentration shows that these interactions are intra- and not intermolecular. As with their β-analogues an increase of temperature decreases the interaction between the dye and the bases.

The drastic CD change observed upon addition of a complementary adenylate sequence reflects the modification of the environment of the dye upon complex formation. The more likely explanation for this change is that the acridine dye is stacked with base pairs and that dye–base pair interactions make a strong contribution to the CD signal. An intercalation process is in agreement with the stabilization of the complex formed by the compounds with the dye as compared to their unsubstituted analogues (*11*).

The α-oligothymidylate with the dye linked to the 5′-end of the oligonucleotide α-Acrm$_5$(pT)$_8$ forms 1A:1T complexes with all the investigated adenylates (ribo or deoxyribo) and polymers as well as oligomers. This behavior is similar to that previously observed with the parent α-oligothymidylate unsubstituted by the acridine derivative (*15*).

When the dye is located at the 3′ end of the α-octathymidylate 1A:1T complexes are clearly formed with poly(rA) and r(Ap)$_7$rA. With poly(dA) the titration curve indicates that a 1A:2T complex is formed, followed by the formation of a 1A:1T complex, although some curvature is observed in the titration curve (Figure 4), indicating that 1A:1T and 1A:2T complexes still coexist. With d(pA)$_8$ the titration curve does not exhibit a sharp break indicative of a clear stoichiometry. The melting behavior of the equimolar mixture showed that even at 0 °C less than 100% of the molecules were engaged in a 1A:1T complex. The shape of the CD spectrum of the equimolar mixture of α-(Tp)$_8$m$_5$Acr and d(pA)$_8$ showed some similarity with that of the 1A:2T complex obtained between α-(Tp)$_8$m$_5$Acr and poly(dA). The similarity was even more marked when the CD spectrum of this mixture was taken in presence of 1 M NaCl. We therefore conclude that a mixture of 1A:2T and uncomplexed oligonucleotides or a mixture of 1A:2T and 1A:1T complexes is present in the mixture of α-(Tp)$_8$m$_5$Acr and d(pA)$_8$.

With the unsubstituted α-octathymidylate we did not observe any triple-helix formation (*15*). It is therefore the presence of the dye linked at the 3′-end of the oligonucleotide which stabilizes the triplex structure.

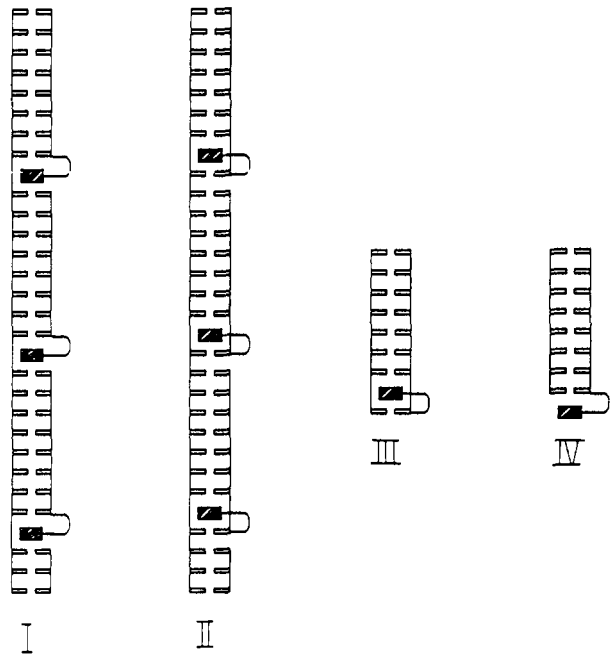


Figure 10. Schematic drawing of alternative complex structures showing either the dye stacked at one end of its carrier oligonucleotide (models I and IV) or intercalated "inside" its oligonucleotide carrier (models I and III). The hatched rectangle corresponds to the acridine ring.

Comparison between the CD complex spectra obtained with the polymers and those obtained with the oligomers provides information on the position of the dye in the complex. For example the CD spectrum of α-(Tp)$_8$m$_5$Acr complexed with poly(rA) is very similar to that obtained when it is complexed with r(Ap)$_7$rA. This indicates that in both complexes the dye is in the same environment. In contrast, when the acridine is located at the 5′-end of the oligonucleotide drastic differences are observed between the CD spectrum of the complexes formed with the oligomer and with the polymer.

A similitude between the CD spectra at the polymer and at the oligomer level suggests that the dye is intercalated "inside" the oligonucleotide as schematically shown in models II and III of Figure 10. A difference suggests that the dye is intercalated between adjacent oligonucleotides along the polymer (model I of Figure 10). In the oligomer–oligomer system this corresponds to model IV of Figure 10 with obviously a different CD signal due to a different environment of the dye. Alternatively an equilibrium between structures III and IV at the oligomer level might be shifted to structure I at the polymer level. In this case also the CD signal should be different because the dye–base geometries are different in models I and III or IV.

For the complexes with poly(rA) and r(Ap)$_7$rA, our data favour models II and III with the dye "inside" when the acridine is linked at the 3′-end of the α-octathymidylate and models I and IV with the dye "outside" when it is attached to the 5′-end of the oligonucleotide.

In the case of the complexes formed by α-Acrm$_5$(pT)$_8$ with poly(dA) and d(pA)$_8$, the general shapes of the CD spectrum are similar, but the relative intensities of the two groups of band are changed. This suggests that the complexes are of the same type (II and III), although some differences occur in the dye–base geometry.

Binding of oligothymidylate–acridine conjugates to polymeric matrices is cooperative (*2*). Interactions be-

tween contiguous oligonucleotides involve the acridine ring in structures of type I whereas in type II structures cooperativity arises from stacking between AT base pairs at the junctions between two successive oligomers.

Covalent attachment of an acridine derivative to the 5′- or 3′-end of the α-oligothymidylate strongly stabilizes the complexes with the complementary sequence. For example, the melting temperature of the parent α-octathymidylate complexed with poly(rA) at similar concentration was 29 °C (*15*) whereas it is 45 °C when the dye is linked to the 3′-end and 49 °C for the dye linked to the 5′-end. Our results demonstrate that the attachment of the dye at the 5′-end of the α-oligonucleotide leads to stronger stabilization than attachment at the 3′-end. As for the unsubstituted α-thymidylate, stabilization with poly(rA) is larger than with poly(dA). This makes α-oligothymidylate covalently linked to an acridine derivative very attractive for the development of selective targeting to mRNAs.

LITERATURE CITED

(1) Asseline, U., Thuong, N. T., and Helene, C. (1983) New substances with high and specific affinity toward nucleic acid sequences: Intercalating agent covalently linked to an oligodeoxynucleotide. *C. R. Acad. Sci. Paris 297*, 369–372.

(2) Asseline, U., Delarue, M., Lancelot, G., Toulme, F., Thuong, N. T., Montenay-Garestier, T., and Helene, C. (1984) Nucleic acid-binding molecules with high affinity and base sequence specificity: Intercalating agents covalently linked to oligodeoxynucleotides. *Proc. Natl. Acad. Sci. U.S.A. 81*, 3297–3301.

(3) Asseline, U., Toulme, F., Thuong, N. T., Montenay-Garestier, T., and Helene, C. (1984) Oligodeoxynucleotides covalently linked to intercalating dyes as base sequence-specific ligands. Influence of dye attachment site. *EMBO J. 3*, 795–800.

(4) Helene, C., Montenay-Garestier, T., Saison, T., Takasugi, M., Toulme, J. J., Asseline, U., Lancelot, G., Maurizot, J. C., Toulme, F., and Thuong, N.T. (1985) Oligodeoxynucleotides covalently linked to intercalating agents: a new class of gene regulatory substances. *Biochimie 67*, 777–783.

(5) Lancelot, G., Asseline, U., Thuong, N. T., and Helene, C. (1985) Proton and phosphorus nuclear magnetic resonance studies of an oligothymidylate covalently linked to an acridine derivative and of its binding to complementary sequences. *Biochemistry 24*, 2521–2529.

(6) Toulme, J. J., Krisch, H. M., Loreau, N., Thuong, N. T., and Helene, C. (1986) Specific Inhibition of mRNA Translation by Complementary Oligonucleotides Covalently linked to Intercalating Agents. *Proc. Natl. Acad. Sci. U.S.A. 83*, 1227–1231.

(7) Cazenave, C., Loreau, N., Thuong, N. T., Toulme, J. J., and Helene, C. (1987) Enzymatic amplification of translation inhibition of rabbit β-globin mRNA mediated by antimessenger oligodeoxynucleotides covalently linked to intercalating agents. *Nucleic Acids Res. 15*, 4717–4736.

(8) Zerial, A., Thuong, N. T., and Helene, C. (1987) Selective inhibition of the cytopathic effect of type A influenza viruses by oligodeoxynucleotides covalently linked to an intercalating agent. *Nucleic Acids Res. 15*, 9909–9919.

(9) Birg, F., Praseuth, D., Zerial, A., Thuong, N. T., Asseline, U., LeDoan, T., and Helene, C. (1990) Inhibition of Simian virus 40 DNA replication in CV-1 cells by an oligodeoxynucleotide covalently linked to an intercalating agent. *Nucleic Acids Res. 18*, 2901–2908.

(10) Morvan, F., Rayner, B., Imbach, J. L., Chang, D. K., and Lown, J. W. (1986) α-DNA I. Synthesis, characterization by high field ^{1}NMR, and base-pairing properties of the unnatural hexadeoxyribonucleotide α-[d(CpCpTpTpCpC)] with its complement β-[d(GpGpApApGpG)]. *Nucleic Acids Res. 14*, 5019–5035.

(11) Thuong, N. T., Asseline, U., Roig, V., Takasugi, M., and Helene, C. (1987) Oligo(α-deoxynucleotides) covalently linked to intercalating agent: Differential binding to ribo- and deoxyribopolynucleotides and stability towards nuclease digestion. *Proc. Natl. Acad. Sci. USA 84*, 5129–5133.

(12) Sun, J. S., Asseline, U., Rouzaud, D., Montenay-Garestier, T., Thuong, N. T., and Helene, C. (1987) Oligo-[α]-deoxynucleotides covalently linked to an intercalating agent. Double helices with parallel strands are formed with complementary oligo-[β]-deoxynucleotides. *Nucleic Acids Res. 15*, 6149–6158.

(13) Morvan, F., Rayner, B., Imbach, J. L., Thenet, S., Bertrand, J. R., Paoletti, J., Malvy, C., and Paoletti, C. (1987) α-DNA II. Synthesis of unnatural α-anomeric oligodeoxyribonucleotides containing the four usual bases and study of their substrate activities for nucleases. *Nucleic Acids Res. 15*, 3421–3437.

(14) Morvan, F., Rayner, B., Imbach, J. L., Lee, M., Hartley, J. A., Chang, D. K., and Lown, J. W. (1987) α-DNA-V. Parallel annealing, handedness and conformation of duplex of the unnatural α-hexadeoxyribonucleotide α-[d(GpApTpGpCpG)] with its β-complement β-[d(GpTpApCpGpC)] deduced from high field ^{1}H-NMR. *Nucleic Acids Res. 15*, 7027–7044.

(15) Durand, M., Maurizot, J. C., Thuong, N. T., and Helene, C. (1988) Circular dichroism studies of an oligo-α-thymidylate and of its interactions with complementary sequences. *Nucleic Acids Res. 16*, 5039–5053.

(16) Durand, M., Thuong, N. T., and Maurizot, J. C. (1989) Thermodynamic parameters of the binding of an oligo-α-thymidylate to its complementary oligo-β-adenylate sequences. *Biochem. Biophys. Res. Commun. 162*, 505–510.

(17) Arai, H., Emson, P. C., Agrawal, S., Christodoulou, C., and Gait, M. J. (1988) In situ hybridization histochemistry: localisation of vasopressin mRNA in rat brain using a biotinylate oligonucleotide probe. *Mol. Brain Res. 4*, 63–69.

(18) Holy, A. (1973) Nucleic acide components and their analogues. CLIV. Nucleoside and nucleotide derivatives of α-uridine, 2′-deoxy-α-uridine and 2′-deoxy-α-cytidine, and their affinity towards nucleolytic enzymes. *Collect. Czech. Chem. Commun. 38*, 100–114.

(19) Cazenave, L., Chevrier, M., Thuong, N. T., and Helene, C. (1987) Rate of degradation of [α]-and [β]-oligodeoxynucleotide in Xenopus oocytes. Implications for anti-messenger strategies. *Nucleic Acids Res. 15*, 10507–10521.

(20) Bacon, T. A., Morvan, F., Rayner, B., Imbach, J. L., and Wickstrom, E. (1988) α-Oligodeoxynucleotide stability in serum, subcellular extracts and culture medium. *J. Biochem. Biophys. Methods 16*, 311–318.

(21) Gautier, C., Morvan, F., Rayner, B., Huynh-Dinh, T., Igolen, J., Imbach, J. L., Paoletti, C., and Paoletti, J. (1987) α-DNA IV: α-anomeric and β-anomeric tetrathymidylate covalently linked to intercalating oxazolopyridocarbazole. Synthesis, physicochemical properties and poly(rA) binding. *Nucleic Acids Res. 15*, 6625–6641.

(22) Bazile, D., Gautier, C., Rayner, B., Imbach, J. L., Paoletti, C., and Paoletti, J. (1989) α and β tetrathymidylates covalently linked to oxazolopyridocarbazolium (OPC): comparative stabilization of oligo β-[dT]:oligo β-[dA] and oligo α-[dT]: oligo β-[dA] duplexes by the intercalating agent. *Nucleic Acids Res. 17*, 7749–7759.

(23) Praseuth, D., Chassignol, M., Takasugi, M., Le Doan, T., Thuong, N. T., and Helene, C. (1987) Double helices with parallel strands are formed by nuclease-resistant oligo-[α]-deoxynucleotides and oligo-[α]-deoxynucleotides covalently linked to an intercalating agent with complementary oligo-[β]-deoxynucleotides. *J. Mol. Biol. 196*, 939–942.

(24) Bertrand, J. R., Imbach, J. L., Paoletti, C., and Malvy, C. (1989) Comparative activity of α- and β-anomeric oligonucleotides on rabbit β globin synthesis: inhibitory effect of cap targeted α-oligonucleotides. *Biochem. Biophys. Res. Commun. 164*, 311–318.

(25) Boiziau, C., Kurfurst, R., Cazenave, C., Roig, V., Thuong, N. T., and Toulme, J. J. (1991) Inhibition of translation initiation by antisense oligonucleotides via an RNase-H independent mechanism. *Nucleic Acids Res. 19*, 1113–1119.

(26) Helene, C., Toulme, F., Delarue, M., Asseline, U., Takasugi, M., Maurizot, J. C., Montenay-Garestier, T., and Thuong, N. T. (1986) *Biomolecular Stereodynamics III* (R. H. Sarma, and M. H. Sarma, Eds.) pp 119–130, Adenine Press, New York.

p-Maleimidophenyl Isocyanate: A Novel Heterobifunctional Linker for Hydroxyl to Thiol Coupling

Michael E. Annunziato, Usha S. Patel, Madhuri Ranade, and Paul S. Palumbo*

PB Diagnostic Systems, Inc., 151 University Avenue, Westwood, Massachusetts 02090. Received December 7, 1992

p-Maleimidophenyl isocyanate (PMPI, 1) is a heterobifunctional cross-linking agent useful for thiol to hydroxyl coupling. Several maleimide-activated compounds were prepared and characterized and then shown to be reactive with thiol-containing proteins. Examples include activation of vitamin B_{12}, digoxigenin, digitoxigenin, estradiol, progesterone, and some serine-containing peptides.

Progress in immunochemistry has required the preparation of numerous protein–protein or protein–hapten conjugates (*1*). The attachment of cytotoxic drugs and toxins to tumor-localizing monoclonal antibodies is an approach to chemotherapy which has received much attention over the years (*2*). Stable, active enzyme–antigen and enzyme–antibody conjugates are of paramount importance in immunoassays (*3*). The successful immobilization of proteins or haptens onto a solid phase through the use of chemical agents is also a prerequisite for successful ELISA techniques. As a result, many reagents for the preparation of these conjugates have been reported (*4*). The so-called chemical cross-linking reagents, an outgrowth of protein modification chemistry, are designed to have specific reactivity with functional groups contained in each reactant. Both homo- and heterobifunctional reagents are available, with the latter having more utility. Since heteroreagents possess two selectively reactive groups that allow coupling to be carried out in a stepwise manner, better control of the conjugation chemistry is attainable. For instance, component A may be activated, purified, and characterized, before combining with component B.

By far the most popularly used heterobifunctional agents contain an amine reactive group (i.e., an *N*-hydroxysuccinimide ester) and a sulfhydryl reactive group (i.e., a maleimide) connected by a spacer (*5*) (see, for example, the commercially available GMBS[1] and SMCC). Most proteins and polypeptides contain one or more ε-aminolysine and/or cysteine residues which serve as convenient linking points via these agents. The spacer group serves several functions, not the least of which is its effect on steric hindrances; linear bridging between protein and/or hapten moieties with minimal steric interaction is often a requirement for maintaining proper immunoreactivity or enzyme activity. Careful selection of the linking group is essential for probing proximity and folding within biomolecules as well as in determining the interactions of biomolecules in complex systems. As a result, cross-linking agents are available in a host of linker types (*4b*).

Small molecules or haptens often do not possess one of the conventional functional groups, and so the task of linking becomes increasingly more difficult. One is usually faced with the need to chemically modify the material by more rigorous and formal chemistries. Often total synthesis of a drug analog is necessary in order to incorporate a reactive group. The efficacy and/or immunoreactivity of the resulting drug is then in question. Many haptens do, however, contain hydroxyl functionalities (consider for example the digitalis cardiac glycosides, adrenal hormones, rhodosaminylanthracyclinone-type anthracyclines, and serine-containing peptides, just to name a few). While linking via ester formation may be a tempting approach in those cases, the resulting ester-linked conjugate may often have only limited stability (*6*). There is a general need for a hydroxyl-reactive cross-linker which will lead to a stable product.

The isocyanate group is a highly reactive, sterically unencumbered functionality which will react with amines to form ureas and with alcohols to form carbamates (*7*); the resulting products display reasonable stability (*8*, *9*). We report the use of *p*-maleimidophenyl isocyanate (PMPI) for joining hydroxyl-containing compounds such as haptens and peptides to sulfhydryl-containing compounds such as proteins, most notably for us in the preparation of alkaline phosphatase conjugates of vitamin B_{12}, progesterone, estradiol, digitoxigenin, digoxigenin, and some serine-enriched peptides (Chart I). This heterobifunctional agent constitutes a net hydroxyl-to-thiol coupling.

EXPERIMENTAL PROCEDURES

Materials. Alkaline phosphatase was obtained from Boehringer Mannheim (enzyme immunoassay grade from calf intestine, ~3000 IU/mg). Chicken γ-globulin was obtained from Jackson Immuno Research Labs, Inc. Cyanocobalamin, digoxigenin, digitoxigenin, progesterone, β-estradiol, *N*-CBZ-Gly-Gly-Ser, and *N*-CBZ-Tyr-Ser methyl ester were obtained from Sigma. Maleic anhydride, *p*-aminobenzoic acid, DPPA, and TEA, were obtained from Aldrich. PD-10 columns were obtained from Pharmacia. 2-IT and DTNB were obtained from Pierce. DMSO (J.T. Baker) was stored over 3-Å molecular sieves in a sealed container. Toluene (J.T. Baker) was dried by distillation from sodium metal and stored over 3-Å molecular sieves in a sealed flask. TSMZ refers to a buffer containing 30 mM triethanolamine, 150 mM sodium chloride, 1 mM magnesium chloride, and 0.1 mM zinc chloride, with the pH adjusted to 7.3.

Melting Points. Melting points (mp) were obtained on an Electrothermal melting point apparatus and are uncorrected.

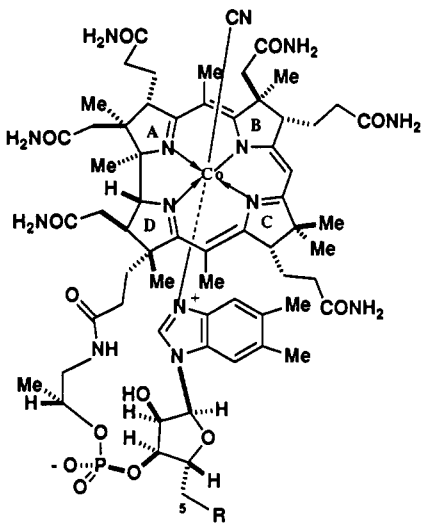
NMR Spectroscopy. Proton NMR spectra were

* Author to whom correspondence should be addressed.

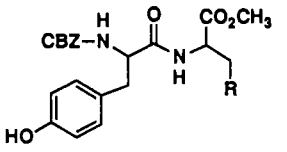
[1] Abbreviations used: PMPC = *N*-(*p*-maleimidophenyl)carbamate; GMBS = *N*-[(γ-maleimidobutyryl)oxy]succinimide; SMCC = succinimidyl 4-(*N*-maleimidomethyl)cyclohexane-1-carboxylate; 2-IT = 2-iminothiolane (Traut's reagent); DTNB = 5,5′-dithiobis(2-nitrobenzoic acid) (Ellman's reagent); DPPA = diphenyl phosphorazidate; CBZ = carbobenzyloxy; AP = alkaline phosphatase; B_{12} = vitamin B_{12}; TEA = triethylamine; Gly = glycine; Ser = serine; Tyr = tyrosine.

1043-1802/93/2904-0212$04.00/0 © 1993 American Chemical Society

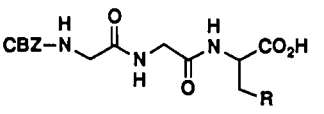
Chart I



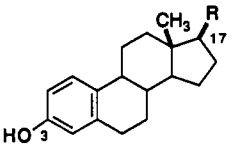
Vitamin B_{12}: R= -OH
2a: R= -O-PMPC



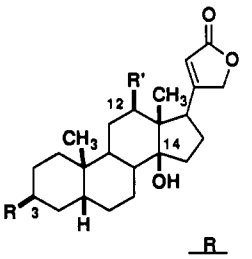
N-CBZ-TYR-SER, methyl ester: R= -OH
2i: R= -O-PMPC



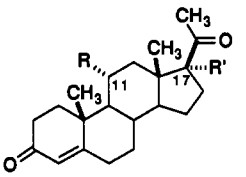
N-CBZ-GLY-GLY-SER: R= -OH
2d: R= -O-PMPC



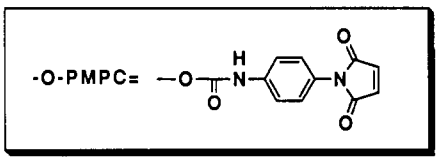
β-Estradiol: R= -OH
2f: R= -O-PMPC



	R	R'
Digoxigenin:	-OH	-OH
Digitoxigenin:	-OH	-H
2b:	-O-PMPC	-OH
2c:	-O-PMPC	-H



	R	R'
Progesterone:	-H	-H
11α-Hydroxyprogesterone:	-OH	-H
17α-Hydroxyprogesterone:	-H	-OH
2e:	-O-PMPC	-H
2h:	-H	-O-PMPC



obtained using either a Bruker AC300 (300 MHz), Varian XL 300 (300 MHz), or Varian EM390 (90 MHz) NMR spectrometer. The samples were dissolved in DMSO-d_6 (2.50 ppm), D_2O (4.80 ppm), or $CDCl_3$ (7.25 ppm) and the chemical shifts reported in ppm on the δ scale using the residual proton absorptions of these solvents as references. Proton assignments and structural determinations were made by analogy to published spectra for digitoxigenin and digoxigenin (*10*) and cyanocobalamin (*11*).

Infrared Spectroscopy. IR spectra were obtained on a Nicolet 20DXC FTIR spectrometer as KBr pellets.

Mass Spectroscopy. Mass spectral analyses were run on a Hewlett-Packard 5985 spectrometer. Both FAB (M^+ + 1) and EI (M^+) techniques were used, and the results are listed as such.

Ultraviolet Spectroscopy. UV absorbance spectra of aqueous solutions were measured using a Beckman DU-7 instrument.

Analyses. Elemental analyses (C, H, N) were performed by Galbraith Laboratories, Inc. (Knoxville, TN).

Thin-Layer Chromatography. Reactions were monitored on TLC using normal-phase, glass-backed silica plates (HLF, 0.25-mm thickness) and reversed-phase, glass-backed silica plates (RPS-F, 0.25-mm thickness) obtained from AnalTech. Spots were visualized under a 254-nm UV lamp (Model UVG-11 from UVP, Inc.) or by treatment with iodine vapors.

Gel Permeation Chromatography. PD-10 columns (Sephadex G-25) were equilibrated with the eluting buffer by passing five column volumes of the buffer through the column prior to sample application. Fractions (0.5–1.0 mL) were collected and the absorbance at 280 nm read for each. When plotted (OD_{280nm} vs fraction number), the chromatograms displayed complete baseline separation of the protein and small molecule components in all cases.

Silica Chromatography. Reversed-phase silica (C_{18} bonded, 35–75-μm particle size, 150-Å pore size) and normal phase silica (35–75-μm particle size, 60-Å pore size) was obtained in bulk from AnalTech. All silica purifications utilize flash techniques (*12*) unless otherwise noted.

Fractions were collected (0.5–2 mL) and products identified by TLC.

p-Maleimidobenzoic Acid (5). This benzoic acid derivative was synthesized according to the procedure of Yoshitake et al. (*13*). Thus, 4-aminobenzoic acid (4.26 g, 31 mmol) was suspended in 30 mL of acetone and solublized by the addition of 5 mL of methanol. A solution of maleic anhydride (3.66 g, 37 mmol) in 10 mL of acetone was added dropwise and the resulting precipitate stirred for 20 min. The material was suction filtered, washed with acetone, and vacuum-dried to afford a yellow powder (6.36 g). This material was dissolved in acetic anhydride (13 mL), treated with sodium acetate (1.08 g), and then heated with stirring at 50 °C for 2 h. The volatiles were then removed in vacuo, and the resulting residue was taken up in 150 mL of water and heated at 70 °C for 2.5 h. The resulting white precipitate was suction filtered, washed with water, and vacuum-dried overnight to afford compound **5** (4.7 g, 70%). Analysis by silica TLC (10% methanol in methylene chloride as eluent, visualized by UV absorption and/or iodine vapor staining) showed one spot at R_f 0.8. It was used without further purification. ^{1}H NMR ($CDCl_3$ + DMSO-d_6): δ 10.0–8.5 (br s, 1 H, CO_2H), 7.95 (d, J = 9 Hz, 2 H, Ar-H ortho to maleimide), 7.32 (d, J = 9 Hz, 2 H, Ar-H ortho to carboxylic acid), 6.8 (s, 2 H, maleimide vinyl). MS (FAB, 3-nitrobenzyl alcohol): m/e 218 (M^+ + 1).

p-Maleimidobenzoyl Azide (6). A stirred suspension of compound **5** (4.3 g, 20 mmol) in 150 mL of dry toluene was treated with triethylamine (3.04 mL, 22 mmol) and then DPPA (4.7 mL, 22 mmol). After stirring at room temperature for 2 days, the volatiles were removed in vacuo, and the resulting residue was chromatographed on silica with methylene chloride as eluent. The product, **6**, elutes as a pale yellow band and is isolated upon evaporation of solvent to afford a pale yellow crystalline mass (3.9 g, 91%). A recrystallized sample from methylene chloride showed the following behavior in a melting point apparatus: 115–120 °C, sample appears to "pop"; 125–130 °C dec with vigorous gas evolution [mp 131–132 °C (*14*)]. ^{1}H NMR ($CDCl_3$): δ 8.0 (d, J = 8 Hz, 2 H, Ar-H ortho to maleimide), 7.45 (d, J = 8 Hz, 2 H, Ar-H ortho to acyl azide), 6.75 (s, 2 H, maleimide vinyl). IR (KBr): 3110, 2160, 1720, 1690, 1600, 1510, 1400, 1380, 1310, 1275, 1210, 1180, 1150, 1120, 1070, 1040, 1010, 850, 830, 690 cm^{-1}. MS (FAB, 3-nitrobenzyl alcohol): m/e 215 (M^+ + 1).

p-Maleimidophenyl Isocyanate, PMPI (1). A solution of compound **6** (3.4 g, 14 mmol) in dry toluene (150 mL) is refluxed under nitrogen for 1 h and 20 min and then evaporated in vacuo. This quantitatively affords compound **1** as yellow micro needles (3 g). Mp 121–123 °C [mp 115–117 °C (*14*)]. This compound should be stored in a sealed vial, protected from light and moisture, in a freezer. ^{1}H NMR ($CDCl_3$): δ 7.2 (d, J = 9 Hz, 2 H, Ar-H ortho to maleimide), 7.02 (d, J = 9 Hz, 2 H, Ar-H ortho to isocyanate), 6.7 (s, 2 H, maleimide vinyl). IR (KBr): 3380, 3360, 3120, 3080, 2310, 1720, 1690 shoulder, 1520, 1390, 1150, 830, 690 cm^{-1}.

A small sample (38 mg) was dissolved in 1 mL of methylene chloride and treated with excess methanol (0.15 mL). After 1 h the volatiles were removed in vacuo to quantitatively afford methyl *N*-(*p*-maleimidophenyl)carbamate (**2g**). ^{1}H NMR ($CDCl_3$ + CD_3OD): δ 8.45 (br s, 1 H, amide), 7.45 (d, J = 9 Hz, 2 H, Ar-H ortho to maleimide), 7.1 (d, J = 9 Hz, 2 H, Ar-H ortho to carbamate), 6.7 (s, 2 H, maleimide vinyl), 3.67 (s, 3 H, OCH_3). MS (EI) m/e 246 (M^+).

***N,N'*-Bis(*p*-maleimidophenyl)urea (8).** A stirred, room temperature solution of PMPI (100 mg, 0.47 mmol) in DMSO (2 mL) was treated dropwise with 100 μL water. After 5 min, excess water was added (10 mL) to precipitate the product, which was isolated by suction filtration. After vacuum-drying, compound **8** was obtained as a yellow powder (175 g, 93% yield). ^{1}H NMR (DMSO-d_6): δ 8.8 (br s, 1 H, amide H), 7.5 (d, J = 9 Hz, 2 H, Ar-H ortho to maleimide), 7.15 (d, J = 9 Hz, 2 H, Ar-H ortho to urea), 7.1 (s, 2 H, maleimide vinyl). MS (EI) m/e 402 (M^+). Anal. Calcd for $C_{21}H_{14}N_4O_5 \cdot 0.3H_2O$: C, 61.85; H, 3.61; N, 13.74. Found: C, 62.05; H, 3.77; N, 13.61.

PMPI-Activated Vitamin B_{12} (2a). A solution of cyanocobalamin (54 mg, 0.04 mmol) in 0.5 mL of DMSO was treated with PMPI (97.3 mg, 0.45 mmol) and the resultant red solution stirred under argon, at room temperature, protected from light, overnight. The mixture was treated with ether (10 mL) and stirred vigorously to extract the DMSO. After decanting, the residue was stirred in ether (10 mL). After decanting again, the red oil was then triturated with methylene chloride to afford a red powder which was suction filtered, washed with excess methylene chloride, and vacuum-dried. The product was purified via flash chromatography on C-18 silica using methanol–water (2:3) as eluent. The product elutes as a red band and is isolated upon evaporation of solvent in vacuo, affording **2a** (41 mg, 66%) as a red powder. partial ^{1}H NMR (D_2O): δ 7.5 (d, 2 H, Ar-H ortho to maleimide), 7.26 (d, 2 H, Ar-H ortho to carbamate), 7.2 (s, 1 H, benzimidazole C-4 H), 7.1 (s, 1 H, benzimidazole C-2 H), 7.0 (s, 2 H, maleimide vinyl), 6.48 (s, 1 H, benzimidazole C-7 H), 6.3 (br s, 1 H, ribose C-1 H), 6.02 (s, 1 H, C-10 H), 4.3 (m, 4 H, ribose C-5, C-5', C-4, and C-2 H's), 4.18 (d, 1 H), 4.1 (d, 1 H), 3.6 (d, 1 H, propanolamine C-1 H), 3.4 (m, 1 H, C-8 H), 3.3 (d, 1 H, C-13 H), 3.01 (m, 1 H, propanolamine C-1' H), 2.5 (s, 3 H, C-35 CH_3), 2.48 (s, 3 H, C-53 CH_3), 2.2 (s, 3 H, benzimidazole CH_3), 2.18 (s, 3 H, benzimidazole CH_3), 1.8 (s, 3 H, C-25 CH_3), 1.34 (br s, 9 H, C-47 CH_3, C-54 CH_3, C-36 CH_3), 1.22 (d, 3 H, propanolamine CH_3), 1.24 (s, 3 H, C-46 CH_3), 1.0 (m, 2 H, C-41 H, C-60 H), 0.42 (s, 3 H, C-20 CH_3). MS (FAB): m/e 1570 (M^+ + 1). UV (H_2O): λ 280 (ϵ 16 626), 361 (ϵ 26 410), 548 nm (ϵ 7950).

3β-Digoxigenin *N*-(*p*-Maleimidophenyl)carbamate (2b). A solution of digoxigenin (53 mg, 0.136 mmol) in DMSO (1 mL) was treated with PMPI (29 mg, 0.136 mmol), and the resultant yellow solution was stirred at room temperature, under argon, and protected from light for 4 h. Dropwise addition of water (6 mL) affords a precipitate which was suction filtered, washed with excess water, and vacuum-dried. This crude residue was chromatographed on silica with 3% methanol in methylene chloride as eluent. The product elutes as a pale yellow band after two impurity bands. Evaporation of solvent in vacuo affords the product as a pale yellow precipitate (25 mg, 30%). Analysis by 300-MHz proton NMR suggests that the point of attachment is through the 3β-hydroxyl group (the equatorial C3-H is shifted downfield to δ 5.1; the axial C12-H remains at δ 3.4). ^{1}H NMR ($CDCl_3$): δ 7.5 (d, 2 H, Ar-H ortho to maleimide), 7.27 (d, 2 H, Ar-H ortho to carbamate), 6.84 (s, 2 H, maleimide vinyl), 6.7 (br s, 1 H, amide H), 5.93 (br s, 1 H, C-22 H), 5.10 (br s, 1 H, C-3 H), 4.9 (d, 1 H, C-21 H), 4.8 (d, 1 H, C-21' H), 3.4 (dd, 1 H, C-12 H), 3.3 (dd, 1 H, C-17 H), 2.15 (m, 1 H, C-16β H), 2.0–1.0 (complex m, 18 H), 0.98 (s, 3 H, C-19 CH_3), 0.8 (s, 3 H, C-18 CH_3). MS (FAB, 3-nitrobenzyl alcohol): m/e 606 (M^+ + 1). UV (TSMZ, pH 7.3, + 1% DMF): λ_{max} 246 nm (ϵ 16 680).

3β-Digitoxigenin *N*-(*p*-Maleimidophenyl)carbamate (2c) was prepared as in **2b** from digitoxigenin (77.39 mg, 0.2066 mmol). Progress of the reaction was followed

by normal phase TLC (2% CH_3OH in CH_2Cl_2 eluent: **2c** R_f 0.48, digitoxigenin R_f 0.31). The product was purified on silica (2% CH_3OH in CH_2Cl_2) to afford 46 mg (38%) of compound **2c** as a pale yellow solid. ^1H NMR ($CDCl_3$): δ 7.43 (d, 2 H, Ar-H ortho to maleimide), 7.2 (d, 2 H, Ar-H ortho to carbamate), 6.8 (s, 2 H, maleimide vinyl), 6.7 (s, 1 H, amide H), 5.8 (s, 1 H, C-22 H), 5.07 (br s, 1 H, C-3 H), 4.9 (d, 1 H, C-21 H), 4.74 (d, 1 H, C-21′ H), 2.7 (m, 1 H, C-17 H), 2.1 (m, 2 H, C-15α H, C-16β H), 1.82 (m, 3 H, C-6α H, C-4β H, C-16α H), 1.7–1.05 (complex m, 16 H), 0.9 (s, 3 H, C-19 CH_3), 0.8 (s, 3 H, C-18 CH_3). MS (FAB, 3-nitrobenzyl alcohol): m/e 590 ($M^+ + 1$), 611 ($M^+ + Na$). UV (TSMZ, pH 7.3, + 1% DMF): λ 246 nm (ϵ 16 000).

***N*-CBZ-Gly-Gly-Ser *N*-(*p*-Maleimidophenyl)carbamate (2d)** was prepared as in **2b** from *N*-CBZ-Gly-Gly-Ser (218 mg, 0.62 mmol). The resulting residue was chromatographed on silica with acetic acid–methanol–methylene chloride (1:10:89, by volume) to afford the pure product **2d** as a pale yellow solid (246 mg, 70%). ^1H NMR (DMSO-d_6): δ 8.32 (d, 1 H, amide H), 8.1 (br t, 1 H, amide H), 7.55 (d, 2 H, Ar-H ortho to maleimide), 7.5 (t, 1 H, amide H), 7.34 (br s, 6 H, benzyl-Ar + amide H), 7.2 (d, 2 H, Ar-H ortho to carbamate), 7.12 (s, 2 H, maleimide vinyl), 5.0 (s, 2 H, benzyl-CH_2), 4.6 (m, 1 H, Ser methine H), 4.45 (dd, 1 H, Ser methylene H), 4.25 (dd, 1 H, Ser methylene H′), 3.8 (s, 2 H), 3.66 (s, 2 H). MS (FAB, 3-nitrobenzyl alcohol): m/e 568 ($M^+ + 1$).

11α-Progesterone *N*-(*p*-maleimidophenyl)carbamate (2e) was prepared as in **2b** from 11α-hydroxyprogesterone (94 mg, 0.28 mmol). The product was purified by chromatography on silica using 2% methanol in methylene chloride as eluent, with isolation of the major highest R_f material to afford 90 mg (58% yield) as a pale yellow crystalline solid. ^1H NMR ($CDCl_3$): δ 7.74 (br s, 1 H, amide H), 7.47 (d, 2 H, Ar-H ortho to maleimide), 7.2 (d, 2H, Ar-H ortho to carbamate), 6.75 (s, 2 H, maleimide vinyl), 5.7 (s, 1 H, C-4 H), 5.2 (m, 1 H, C-11 H), 2.5–1.0 (complex m, 18 H), 2.07 (s, 3 H, C-21 CH_3), 1.25 (s, 3 H, C-18 CH_3), 0.7 (s, 3 H, C-19 CH_3). MS (FAB, 3-nitrobenzyl alcohol): m/e 546 ($M^+ + 1$).

17β-Estradiol *N*-(*p*-maleimidophenyl)carbamate (2f) was prepared as in **2b** from β-estradiol (35 mg, 0.13 mmol). The crude residue was chromatographed on silica with 1% methanol in methylene chloride as eluent to afford the purified product, **2f** (29 mg, 46%). Analysis by 300-MHz proton NMR suggests that the point of attachment is through the 17β-hydroxyl group (the 17α-H is shifted downfield to δ 4.65). ^1H NMR ($CDCl_3$): δ 7.46 (d, 2 H, Ar-H ortho to maleimide), 7.22 (d, 2 H, Ar-H ortho to carbamate), 7.1 (d, 1 H, C-1 H), 6.73 (s, 2 H, maleimide vinyl), 6.62 (s, 1 H, amide), 6.54 (dd, 1 H, C-2 H), 6.50 (d, 1 H, C-4 H), 4.70 (t, 1 H, αC-17 H), 2.75 (m, 2 H), 2.3–1.2 (complex m, 13 H), 0.8 (s, 3 H, CH_3). MS (FAB, 3-nitrobenzyl alcohol): m/e 486 ($M^+ + 1$).

***N*-CBZ-Tyr-Ser-OMe *N*-(*p*-Maleimidophenyl)carbamate, (2i)** was prepared as in **2b** from *N*-CBZ-Tyr-Ser methyl ester (220 mg, 0.53 mmol). The resulting crude yellow precipitate was stirred vigorously in absolute methanol (50 mL) and suction filtered and the filter cake washed with excess methanol. The filtrate was evaporated in vacuo and the resulting residue chromatographed on silica (3% methanol in methylene chloride as eluent) to afford the pure product, **2i**, as a pale yellow solid (227 mg, 68%). ^1H NMR ($CDCl_3$ and DMSO-d_6): δ 7.36 (d, J = 9 Hz, 2 H, Ar-H ortho to maleimide), 7.14 (s, 5 H, CBZ phenyl), 7.07 (d, J = 9 Hz, 2 H, Ar-H ortho to carbamate), 6.87 (d, J = 7 Hz, 2 H, Tyr Ar-H meta to OH), 6.74 (s, 2 H, maleimide vinyl), 6.57 (d, J = 7 Hz, 2 H, Tyr Ar-H ortho to OH), 4.9 (s, 2 H, CBZ methylene), 4.67 (t, 1 H, Ser methine), 4.3 (m, 3 H, Tyr methine and Ser methylene), 3.67 (s, 3 H, Ser OCH_3), 2.90 (t, 2 H, Tyr methylene). MS (FAB, 3-nitrobenzyl alcohol): m/e 631 ($M^+ + 1$).

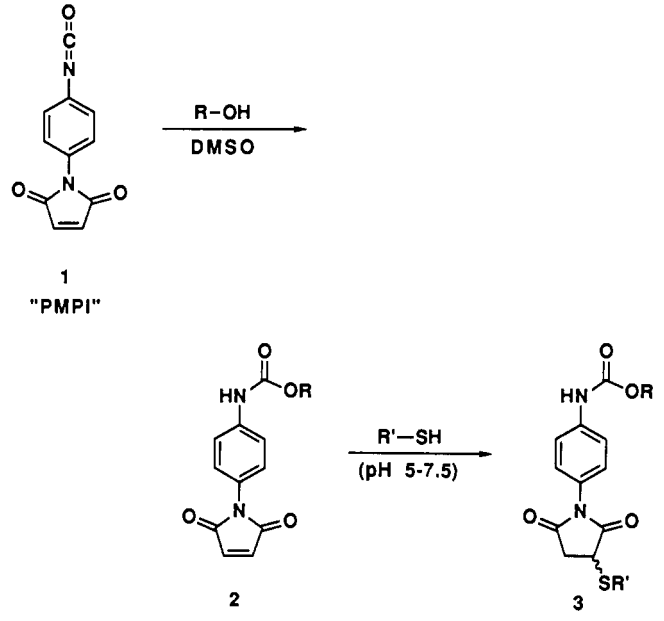
Maleimide Stability Study. According to the procedure of Kitagawa (*4a*), a 20 μL-aliquot of a 10 mM solution of **2d** in DMF was incubated in 0.5 mL of 0.05 M phosphate buffer (pH 6, 7, or 8) or 0.05 M acetate buffer (pH 5) for 30 min at 30 °C (run in duplicate). Next, 200 μL of 1 mM mercaptoethanol in 0.05 M phosphate (pH 6) was added, mixed well for 1–2 min, and then treated with 1.1 mL 0.2 M Tris-HCl buffer (pH 8.2) containing 0.02 M EDTA·Na_4, and then 0.2 mL of 10 mM methanolic DTNB was added. After 10 min the absorbance values at 412 nm of each test sample (A), a zero blank (B) (without the incubation), and the sample blank value (C) (20 μL of DMF instead of the sample solution, incubated at 30 °C/30 min) were obtained. The percent decomposition of the maleimide residue is calculated as $[(A-B)/(C-B)] \times 100$. The results are presented in Table II.

Preparation of a Vitamin B_{12}–Alkaline Phosphatase Conjugate (3a). The general procedure for alkaline phosphatase conjugation is illustrated below for vitamin B_{12}. Alkaline phosphatase is thiolated with 5 mM Traut's reagent for 20 min in a preliminary step and then treated with 30 equiv of the maleimido-activated compound of interest (dissolved in either buffer or a minimum amount of DMF). Thus the thiolation of alkaline phosphatase was carried out by treating alkaline phosphatase (1 mg, 7.1 nmol) in 1 mL TSMZ buffer (pH 7.3) with 2-iminothiolane hydrochloride (50.0 μL of a 100 mM solution in distilled water) and incubating for 20 min at room temperature. After treating with 10 μL of 1 M glycine, the excess reagents were removed using a PD-10 column, eluting with TSMZ buffer (pH 7.3). The fractions containing the activated alkaline phosphatase [analysis for free thiol groups using DTNB reagent (*15*) reveals 6–7 thiols/AP] were pooled (absorbance reading at 280 nm) and then treated immediately with compound **2a** (5-fold excess/mol of thiol). The solution was stored at room temperature for 1 h and then at 4 °C overnight. Gel filtration in a PD-10 column using TSMZ (pH 7.3) as an eluent separated the conjugate from the low molecular weight reactants. The UV spectrum of the conjugate showed the following absorbances: λ 277.4 (OD = 0.418), 361 (OD = 0.30), and 548.3 nm (OD = 0.097).

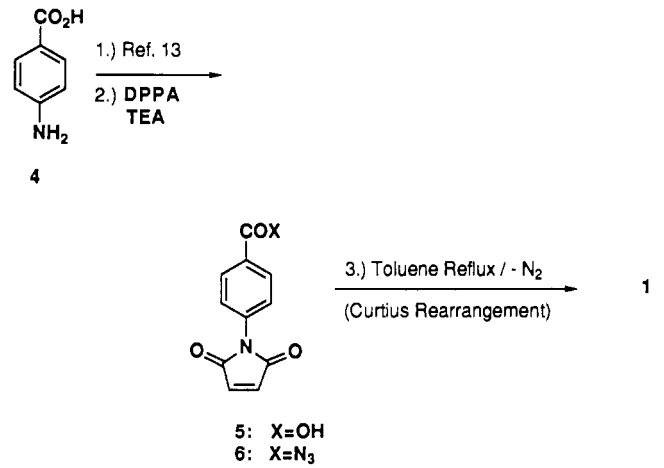
UV Determination of B_{12} Incorporation into AP. The extent of incorporation of B_{12} (conjugation ratio) was determined via spectral analysis of the resulting conjugate. Thus, relating absorbance at 361 and 280 nm for the conjugate relative to each component's respective absorbance at 361 and 280 nm gives a calculated B_{12} : protein ratio of 6.9:1 (a 1 mg/mL solution of AP gives an OD = 1.0 at λ 280 nm and an OD = 0 at λ 361 nm). This ratio agrees reasonably well with the DTNB results above and confirms the success of conjugation.

Preparation of a Panel of Digoxigenin–Alkaline Phosphatase Conjugates (3b). Alkaline phosphatase in TSMZ (pH 7.3) was adjusted to 5 mg/mL and reacted with 3 mM 2-IT at 28 °C. At 10, 20, and 120 min, aliquots were removed and quenched with a 1/100 volume of 1 M glycine (pH 7.3). Gel filtration chromatography over a PD-10 column equilibrated with TSMZ (pH 7.3) separated the thiolated protein from residual reagents. The thiol groups were quantified as in **3a** and gave thiol:protein values of 1.2:1, 1.9:1, and 6.0:1, respectively. The thiolated AP aliquots were then each reacted with **2b** at a mole ratio of 3:1 (mol of **2b**/mol of thiol). The conjugates were

Scheme I. Hydroxyl to Thiol Cross-Linking Using PMPI



Scheme II. Synthesis of PMPI



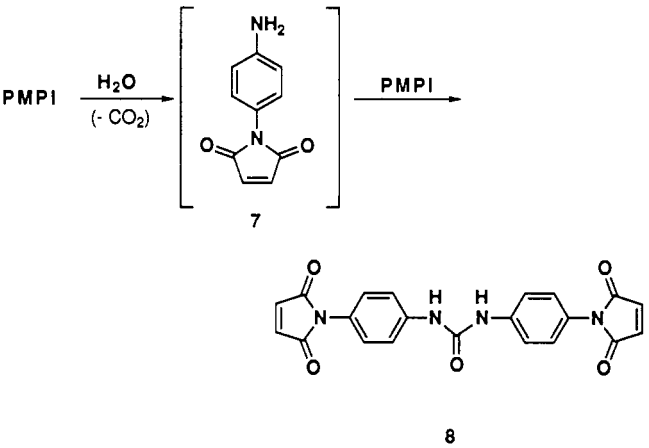
incubated for 18 h at 4 °C and then purified over PD-10 columns equilibrated with TSMZ (pH 7.3). The conjugation ratio was determined spectrally for each case and gave 1.1:1, 2.0:1, and 7.4:1, respectively.

A panel of digitoxigenin–antibody conjugates (3c) was prepared as in **3b** from chicken IgG, diluted to 4 mg/mL in TSMZ (pH 7.3). The thiol groups were quantified as in **3a** and gave thiol:protein values of 1.3:1, 3.8:1, and 6.6:1. Thiolated chicken IgG was reacted with **2c** at a ratio of 3:1 (mol of **2c**/mol of thiol). The conjugates were incubated for 18 h at 4 °C and then purified over PD-10 columns equilibrated with TSMZ (pH 7.3). The conjugation ratio was determined spectrally for each case and gave 0.6:1, 3.1:1, and 7.8:1, respectively.

RESULTS AND DISCUSSION

The preparation of PMPI involves the three-step sequence shown in Scheme II. Thus, *p*-maleimidobenzoic acid, **5**, prepared as described elsewhere (*13*), is treated at room temperature in toluene with 1 equiv of triethylamine followed by 1 equiv of DPPA. The resulting acyl azide, **6**, is isolated and purified on silica to afford yellow crystals, in 91% yield. This product undergoes a Curtius rearrangement with smooth release of nitrogen gas upon heating at reflux in dry toluene. The resulting isocyanate

Scheme III



(PMPI) is obtained in quantitative yield upon evaporation of solvent in vacuo. The use of DPPA alleviates the need for intermediate acid chloride formation as reported by Rao (*14*). PMPI is stable for months when stored dessicated and protected from light at <0 °C.

For the reaction of PMPI with hydroxyl-containing haptens, we have found DMSO to be the solvent of choice, especially in light of its catalytic effect on isocyanate reactivity (*16*). The hydroxyl compound is thus combined with 1 equiv of PMPI and stirred at room temperature in DMSO, under dry nitrogen, until TLC confirms the quantitative conversion to product.

Isocyanates are extremely unstable in water and therefore PMPI activation of alcohols must only be performed in dry organic solvents. In those cases where water might be present in the reaction mixture (either surreptitiously present or in the form of hydrated reactants), excess PMPI must be added. Water reacts quickly and quantitatively with PMPI to afford *N,N'*-bis(*p*-maleimidophenyl)urea, 8, a novel homobifunctional cross-linking reagent in its own right, presumably by the route shown in Scheme III. Once all water is consumed in this way, the additional PMPI is then free to react with the alcohol moiety present in the reactant. Because of this solvent limitation, PMPI will be mostly useful for activation of small molecules.

The carbamates formed, **2**, are conveniently purified by flash chromatography on either normal or reversed-phase silica. In this way the activated hapten can be characterized (MS, NMR, UV/vis, etc.) and stored as a purified material for later use. When ready, these products are coupled to sulfhydryl-containing proteins in the appropriate buffers (pH 5–7.5). Where water solubility is a problem, a DMF stock solution of the activated hapten is first prepared and added to the protein–buffer solution. At the end of the conjugation reaction, residual uncoupled material is conveniently removed by Sephadex G-25 chromatography.

We have found PMPI to undergo a wide scope of reactivity with various alcohol types (see Table I). In general, reaction with primary and secondary alcohols is facile, while tertiary alcohols are often incomplete or unsuccessful. Phenols also react with isocyanates; however, the hydrolytic stability of the resulting aryl carbamates may not be suitable for all applications (*17*). Two phenol examples that were tried (β-estradiol and *N*-CBZ-Tyr-Ser methyl ester) failed to afford any identifiable phenyl carbamate product, possibly due to instability in the chromatography. We have successfully reacted the secondary alcohol groups of digoxigenin (to give **2b**), digitoxigenin (to give **2c**), β-estradiol (to give **2f**), and 11α-

Table I. Reaction of Various Hydroxylic Compounds with PMPI and ^{1}H NMR Shift Data of Corresponding Products

reactant	product	isolated yield (%)	maleimide ^{1}H NMR data: δ (ppm), solvent
water	8	93	7.1, DMSO-d_6
methanol	**2g**	100	6.7, $CDCl_3/CD_3OD$
vitamin B_{12}	**2a**	66	7.0, D_2O
digoxigenin	**2b**	30	6.84, $CDCl_3$
digitoxigenin	**2c**	38	6.8, $CDCl_3$
N-CBZ-Gly-Gly-Ser	**2d**	70	7.12, DMSO-d_6
11α-hydroxyprogesterone	**2e**	58	6.75, $CDCl_3$
17β-estradiol	**2f**	46	6.73, $CDCl_3$
N-CBZ-Tyr-Ser, methyl ester	**2i**	68	6.74, $CDCl_3$/ DMSO-d_6

Table II.[a] Percent Decomposition of Maleimide Groups in Related Cross-Linkers after 30 min at 30 °C in pH 5.0, 6.0, 7.0, and 8.0 Buffers

sample[b]	pH 5.0	pH 6.0[e]	pH 7.0[e]	pH 8.0[e]
OBS	3.1[c]	6.2	21.4	69.0
MBS	2.9[c]	2.5	7.1	43.8
PBS	3.8[c]	6.6	32.0	52.0
2 d	0[d]	2.3	14.0	56.0

[a] Data for OBS, MBS, and PBS taken from ref 4a. [b] OBS, MBS, and PBS are *O*-(*o*-, -(*m*-, and -(*p*-maleimidobenzoyl)-*N*-hydroxysuccinimide, respectively. [c] Citrate Buffer. [d] 0.05 M acetate buffer. [e] 0.05 M phosphate.

hydroxyprogesterone (to give **2e**) and the primary alcohol groups of serine peptides (to give **2d** and **2i**) and vitamin B_{12} (to give **2a**). Several tertiary alcohol examples, including 17α-hydroxyprogesterone, failed to give any appreciable product (i.e., **2h**).

The aqueous stability of the model compound **2d** was studied and shown to be comparable to similar compounds (*4a*). The results, shown in Table II, indicate that the stability of the maleimide moiety decreases at pH >7. Maleimides, of course, undergo a facile Michael addition with free thiol groups under slightly acidic to neutral conditions (*18*). When activated haptens are dissolved in the appropriate buffers just prior to reaction, no significant decomposition is observed. The desired conjugation chemistry is obtained even when near stoichiometric reactant mole ratios are used.

PMPI methodology provides a stable, well-defined, vitamin B_{12}–alkaline phosphatase conjugate. Previous workers had shown that mild acid hydrolysis of cyanocobalamin yields a mixture of mono- and dicarboxylic acids and one tricarboxylic acid that is derived from the propionamide side chains (*19*). We felt that this approach to a B_{12} conjugate would certainly suffer from an obvious isomer problem and therefore require a tedious purification scheme. Yields are low and the product characterizations ambiguous (*20*). We instead chose to pursue the lone primary hydroxyl group located in the ribose ring as a potential point of attachment since we knew that this C-5 hydroxyl group was reported to react with anhydrides (*21*). Reaction with PMPI, indeed, afforded a single isomer, **2a**, in >60% yield after purification. Characterization by high-field NMR confirmed that we had successfully targeted the primary hydroxyl group [a 0.5 ppm downfield shift in the ribose C-5 methylene protons was observed (*11*)]; no reaction with the sterically hindered secondary alcohol group (ribose C-2 H) was seen, even under excess conditions (10 equiv of PMPI). Fortunately, attachment through the C-5 hydroxyl group provides maximal distance between the linking point and the porphyrin ring [3D models show that the activating group points down and away from the main body of the molecule (*22*)].

Table III. Comparison of Conjugation Ratio (Spectrophotometrically Determined) to Thiols Introduced for Alkaline Phosphatase (AP) and Chicken Antibody (IgG)

conjugation components	thiolation method/time (min)[a]	thiols/mol (titration)[b]	conjugation ratio (spectroscopic)[c]
AP/2a	A/20	6–7	6.9
AP/2b	B/10	1.2	1.1
AP/2b	B/20	1.9	2.0
AP/2b	B/120	6.0	7.4
IgG/2c	B/10	1.3	0.6
IgG/2c	B/20	3.8	3.1
IgG/2c	B/120	6.6	7.8

[a] Refer to Experimental Section for details; see example 3a for method A and example 3b and 3c for method B. [b] See ref 15. [c] See ref 1c.

Thiol groups were introduced into alkaline phosphatase via the use of 2-IT (*23*). In one example, alkaline phosphatase, adjusted to 1 mg/mL in TSMZ (pH 7.3), was treated with 5 mM 2-IT for 20 min. The resulting thiolated enzyme was purified by gel filtration chromatography on PD-10 and the number of thiols per AP molecule determined to be 6–7 [quantitated by the DTNB method (*15*)]. The resulting thiolated protein in TSMZ was then treated with a slight excess of compound **2a** (~5 mol/mol of thiol) and the conjugation reaction allowed to proceed overnight at 4 °C. Gel filtration on Sephadex G-25 (PD-10) with TSMZ separates the conjugate, **3a**, from residual reactants. Spectral analysis (*1c*), relating the absorbances at 361 and 280 nm, confirmed the success of conjugation.

Digoxigenin, the aglycon of digoxin, presented us with yet another regioselectivity challenge, since we wished to link this molecule to alkaline phosphatase through the 3-position. [Classical digoxin linking methodology targets the terminal digitoxose residue (*24*), but we had experienced unacceptable variability and low conjugation ratios using that chemistry.] From earlier work with digitoxigenin we knew that the tertiary hydroxyl group in the 14-position was essentially nonreactive with PMPI and would pose no threat to the activation selectivity. For example, digitoxigenin activation leads exclusively to the 3β-carbamate derivative, **2c**. Competitive reaction with the secondary hydroxyl group in the 12-position, however, was perceived as a real threat. To our delight, the major product obtained from the reaction of PMPI and digoxigenin was the desired 3-isomer, **2b**. While a small side product was observed on TLC, the 12-isomer was never isolated.

A panel of digoxigenin–AP conjugates (**3b** with varying conjugation ratios) were prepared. Similarly, we prepared a set of digitoxigenin–antibody conjugates (**3c**). At 3 mM 2-IT we found it convenient to quench aliquots at 10, 20, and 120 min and thereby introduce 1–7 mol of thiol/mol of protein from the same thiol activation vessel. In most cases the spectrally determined conjugation ratio values agree reasonably well with the thiol values obtained by titration with DTNB (see Table III). However, at the high end of the panels, conjugation appears to go further than theoretically possible.

Conjugation ratios can indeed be higher than the degree of thiolation if there are other reactive groups present in the macromolecule (i.e. amino groups). More than likely, however, the apparent inconsistency between the thiols introduced and the conjugation ratio is probably due to the inherent error present in both methods of determination (we have seen variability in both determinations to be as high as ±10%). In cases where the absorbance maxima of the reagent is close to or overlaps with the absorbance maxima of the macromolecule (examples **3b**

and **3c**), the UV determination of the conjugation ratio is not reliable and we tend to trust in the thiol titration value more. Indeed, in the vitamin B12 example, the absorbances are further removed from each other and the agreement between methods is better. Also, in the cases of the more hydrophobic examples (**2b** and **2c**), there is always a chance that residual reactant may bind noncovalently to the protein. When this is the case, more careful chromatography should be performed.

Protein conjugates that we have obtained by the methodology described above were found to be useful as elements in immunoassays. For example, the digoxigenin–AP conjugate (**3b**) is used in the OPUS digoxin assay (*25*).

ACKNOWLEDGMENT

We wish to thank Catherine M. Palumbo (Polaroid Corp.) for high-field NMR Spectroscopy and Dr. Gerald Dudek (Polaroid Corp.) for Mass Spectrometry.

LITERATURE CITED

(1) (a) Means, G. E., and Feeney, R.E. (1990) Chemical Modifications of Proteins: History and Applications. *Bioconjugate Chem. 1*, 2–12. (b) Means, G. E., and Feeney, R. E. (1971) *Chemical Modification of Proteins.* Holden-Day, San Francisco, CA. (c) Brinkley, M. (1992) A Brief Survey of Methods for Preparing Protein Conjugates with Dyes, Haptens, and Cross-Linking Reagents. *Bioconjugate Chem. 3*, 2–13.

(2) (a) Koppel, G. A. (1990) Recent Advances with Monoclonal Antibody Drug Targeting for the Treatment of Human Cancer. *Bioconjugate Chem., 1*, 13–23. (b) Ghose, T., and Blair, A. H. (1987) *CRC Crit. Rev. Ther. Drug Carrier Syst. 3*, 300–301. (c) Mueller, B. M., Wrasidlo, W. A., and Reisfeld, R. A. (1990) Antibody Conjugates with Morpholinodoxorubicin and Acid-Cleavable Linkers. *Bioconjugate Chem. 1*, 325–330. (d) Imai, N., Kometani, T., Crocker, P. J., Bowdan, J. B., Demir, A., Dwyer, L. D., Mann, D. M., Vanaman, T. C., and Watt, D. S. (1990) Photoaffinity Heterobifunctional Cross-Linking Reagents Based on N-(Azidobenzoyl)tyrosines. *Bioconjugate Chem. 1*, 138–143.

(3) (a) Kricka, L. J. (1985) *Ligand-Binder Assays. Labels and Analytical Strategies,* Marcel Dekker, New York. (b) Ngo, T. T., Ed. (1988) *Nonisotopic Immunoassay,* Plenum Press, New York. (c) Maggio, E. T., Ed. (1980) *Enzyme-Immunoassay,* CRC Press, Boca Raton, FL. (d) Kurstak, E. (1986) *Enzyme Immunodiagnosis,* Academic Press, New York. (e) Ngo, T. T., and Lenhoff, H. M., Eds. (1985) *Enzyme-Mediated Immunoassay,* Plenum Press, New York. (f) Engvall, E., and Pesce, A.J., Eds. (1978) *Quantitative Enzyme Immunoassays,* Blackwell Scientific, London, Great Britain.

(4) (a) Kitagawa, T., Shimozono, T., Aikawa, T., Yoshida, T., and Nashimura, H. (1981) Preparation and Characterization of Heterobifunctional Cross-Linking Reagents for Protein Modifications. *Chem. Pharm. Bull. 29* (4) 1130–1135 and references within. (b) Wong, S. S. (1991) *Chemistry of Protein Conjugation and Cross-Linking,* CRC Press, Boca Raton, FL.

(5) Haugland, R. P. (1992) Handbook of Fluorescent Probes and Research Chemicals, p54, Molecular Probes, Inc., Eugene, OR.

(6) Hermentin, P., Doenges, R., Gronski, P., Bosslet, K., Kraemer, H. P., Hoffmann, D., Zilg, H., Steinstraesser, A., Scharwz, A., Kuhlmann, L., Luben, G., and Seiler, F. R. (1990) Attachment of Rhodosaminylanthracyclinone-Type Anthracyclines to the Hinge Region of Monoclonal Antibodies. *Bioconjugate Chem. 1*, 100–107.

(7) For a review of the mechanisms of reactions of isocyanates with various nucleophiles, see: Satchell, D. P. N., and Satchell, R. S. (1975) Acylation by Ketenes and Isocyanates. Mechanistic Comparison. *Chem. Soc. Rev., 4*, 231–250.

(8) Lynn, K. R. (1965) Kinetics of Base-Catalyzed Hydrolysis of Urea. *J. Phys. Chem. 69*, 687–689.

(9) Adams, P., and Baron, F.A. (1965) Esters of Carbamic Acid. *Chem. Rev. 65*, 567–602.

(10) Drakenberg, T., Brodelius, P., McIntyre, D. D., and Vogel, H. J. (1989) Structural Studies of Digitoxin and Related Cardenolides by Two-Dimentional NMR. *Can. J. Chem. 68*, 272–277.

(11) Kurumaya, K., and Kajiwara, M. (1989) Proton Nuclear Magnetic Resonance (^{1}H-NMR) Signal Assignment of Vitamin B_{12} Based on Normal Two-Dimensional NMR and Feeding Experiments. *Chem. Pharm. Bull. 37* (1) 9–12.

(12) Still, W. C., Kahn, M., and Mitra, A. (1978) Rapid Chromatographic Technique for Preparative Separations with Moderate Resolution. *J. Org. Chem. 43*, 2923–2925.

(13) Yoshitake, S., Yamada, Y., Ishikawa, E., and Masseyeff, R. (1979) Conjugation of Glucose Oxidase from Aspergillus Niger and Rabbit Antibodies Using N-Hydroxysuccinimide Ester of N-(4-Carboxycyclohexylmethyl)-Maleimide. *Eur. J. Biochem. 101*, 395–399.

(14) Rao, B. S. (1989) Synthesis, Characterization, and Thermal Stability of Bismaleimides Derived from Maleimido Benzoic Acid. *J. Polym. Sci.: Part A: Polym. Chem. 27*, 2509–2518.

(15) Ellman, G. L. (1959) Tissue Sulfhydryl Groups. *Arch. Biochem. Biophys. 82*, 70–77.

(16) Dimethyl Sulfoxide Technical Bulletin, p 106, Crown Zellerbach, Chemical Products Division, Vancouver (Orchards), WA.

(17) Williams, A. (1973) Participation of an Elimination Mechanism in Alkaline Hydrolyses of Alkyl N-Phenylcarbamates. *J. Chem. Soc., Perkin Trans. 2* 1244–1247.

(18) Partis, M. D., Griffiths, D. G., Roberts, G. C., and Beechey, R. B. (1983) Cross-Linking of Protein by ω-Maleimido Alkanoyl N-Hydroxysuccinimido Esters. *J. Protein. Chem. 2*, 263–277.

(19) Bernhauer, K., Wagner, F., Beisbarth, H., Rietz, P., and Vogelmann, H. (1966) *Biochem. Z. 344*, 289–309.

(20) Anton, D. L., Hogenkamp, H. P. C., Walker, T. E., and Matwiyoff, N. A. (1980) Carbon-13 Nuclear Magnetic Resonance Studies of the Monocarboxylic Acids of Cyanocobalamin. Assignments of the *b*-, *d*-, and *e*-Monocarboxylic Acids. *J. Am. Chem. Soc. 102*, (7) 2215–2219.

(21) Bernstein, J., Varma, R. K., Vogt, B. R., and Weisenborn, F. L. (1980) Vitamin B_{12} Derivative Suitable for Radiolabeling. U.S. Patent 4,209,614.

(22) Golding, B. T. (1979) Vitamin B12. *Comprehensive Organic Chemistry* (Sir Derek Barton, F. R. S. and W. David Ollis, F. R. S., Eds.) Section 24.4, pp 549–584, Pergamon Press, New York.

(23) Jue, R, Lambert, J. M., Pierce, L. R., and Traut, R. R. (1978) Addition of Sulfhydryl Groups of Escherichia Coli Ribosomes by Protein Modification With 2-Iminothiolane (Methyl 4-Mercaptobutyrimidate). *Biochemistry 17*, 5399–5406.

(24) Butler, V. P., Jr., Schmidt, D. H., Watson, J. F., and Gardner, J. D. (1974) Production and Properties of Digoxin-Specific Antibodies. *Ann. N. Y. Acad. Sci. 242*, 717–730.

(25) Olive, C. (1991) PB Diagnostics' OPUS Immunoassay System. *J. Clin. Immunoassay 14*, 126–132.

N-(Iodoacetyl)-p-phenylenediamine–EDTA: A Reagent for High-Efficiency Incorporation of an EDTA-Metal Complex at a Rationally Selected Site within a Protein

Yon W. Ebright,† Yan Chen,† Richard D. Ludescher,‡ and Richard H. Ebright*,†

Department of Chemistry and Waksman Institute, and Department of Food Science, Rutgers University, New Brunswick, New Jersey 08855. Received December 10, 1992

We have developed a highly efficient procedure to incorporate an EDTA:metal complex at a rationally selected site within a full-length protein. Our procedure has two steps: In step one, we use site-directed mutagenesis to introduce a unique solvent-accessible cysteine residue at the site of interest. In step two, we derivatize the resulting protein with N-(iodoacetyl)-p-phenylenediamine–EDTA:metal, a novel haloacetyl derivative of EDTA:metal. We have used this procedure to incorporate each of three EDTA:metal complexes at amino acid 2 of the helix–turn–helix motif of the sequence-specific DNA binding protein Cro: a radioactive and nucleolytic EDTA:metal complex (EDTA:^{55}Fe), a radioactive EDTA:metal complex (EDTA:^{63}Ni), and a fluorescent and heavy-atom EDTA:metal complex (EDTA:Eu). Incorporation of EDTA:metal was highly efficient (>80% for EDTA:^{55}Fe and EDTA:^{63}Ni; 60% for EDTA:Eu) and highly site-specific (>99%). We have analyzed DNA affinity cleaving by the Cro derivative having EDTA:^{55}Fe at amino acid 2 of the helix–turn–helix motif. The Cro derivative cleaves DNA at base pairs −4 to 6 of the DNA half site in the protein–DNA complex, indicating that amino acid 2 of the helix–turn–helix motif of Cro is close to base pairs −4 to 6 of the DNA half site in the Cro–DNA complex in solution. The results are in agreement with the crystallographic structure of the Cro–DNA complex [Brennan, R., Roderick, S., Takeda, Y., and Matthews, B. (1990) *Proc. Natl. Acad. Sci. U.S.A. 87*, 8165] and with a previous DNA affinity cleaving analysis of the Cro–DNA complex [Ebright, Y., Chen, Y., Pendergrast, P. S., and Ebright, R. (1992) *Biochem. 31*, 10664]. The procedure of this report has potential applications in DNA affinity cleaving with sequence-specific DNA binding proteins, site-specific radioactive labeling of protein, site-specific fluorescent labeling of protein, and site-specific heavy-atom labeling of protein.

EDTA forms complexes with a wide range of metal ions, including radioactive, fluorescent, and reactive metal ions (*1*, *2*). EDTA:metal complexes can be conjugated to proteins having specificity for target biomolecules [e.g., monoclonal antibodies, sequence-specific DNA binding proteins, etc. (*3–27*)]. The resulting (EDTA:metal)–protein conjugates have applications as radiodiagnostics, radiotherapeutics, and affinity cleaving reagents.

For certain applications, it is essential to incorporate an EDTA:metal complex at a rationally selected site within a protein. One such application is EDTA:Fe DNA affinity cleaving to determine the location and orientation of the DNA site for a sequence-specific DNA binding protein (*14*, *16–18*, *23*, *24*, *26*). In EDTA:Fe DNA affinity cleaving, one incorporates EDTA:Fe at an amino acid not critical for protein–DNA complex formation but nevertheless close to DNA in the protein–DNA complex, forms the derivatized protein–DNA complex, initiates EDTA:Fe-mediated DNA cleavage by addition of reducing agent, and determines the nucleotide(s) at which EDTA:Fe-mediated DNA cleavage occurs.

Previously, incorporation of an EDTA:metal complex at a rationally selected site within a protein has been possible only by (i) total synthesis of the protein (*14–18*, *23–25*) or (ii) site-directed mutagenesis to introduce a unique solvent-accessible cysteine residue at the site of interest followed by derivatization of the resulting protein with S-(2-pyridylthio)cysteamine–EDTA:metal, an aromatic disulfide derivative of EDTA:metal (*26*; cf. ref 27). Procedure i is limited to small proteins (typically <60 amino acids). Procedure ii can yield low efficiencies of incorporation of EDTA:metal [0.1–0.4 mol EDTA:metal incorporated/mol protein subunit (*26*)] and yields a reduction-sensitive disulfide linkage between EDTA:metal and protein. *In this report, we describe a procedure to incorporate an EDTA:metal complex at a rationally selected site within any protein not having a preexisting essential solvent-accessible cysteine residue with high efficiency and with a reduction-insensitive thioether linkage between the EDTA:metal and protein.* Our procedure has two steps: In step one, we use site-directed mutagenesis (*28*) to introduce a unique solvent-accessible cysteine residue at the site of interest. In step two, we derivatize the resulting protein with N-(iodoacetyl)-p-phenylenediamine-EDTA:metal, a novel haloacetyl derivative of EDTA:metal (Figure 1). In addition, in this report, we describe application of our procedure to incorporate EDTA:^{55}Fe, EDTA:^{63}Ni, and EDTA:Eu complexes at a rationally selected site within bacteriophage λ Cro, and application of our procedure to EDTA:Fe affinity DNA cleaving with bacteriophage λ Cro.

EXPERIMENTAL PROCEDURES

EDTA Monoanhydride. In this and subsequent steps, glassware was acid-washed, and water and aqueous solutions were treated with Chelex-100 (Bio-Rad), in order to avoid trace metal contamination. EDTA monoanhydride was prepared by a modification of the procedure of ref 29. EDTA dianhydride (Aldrich; 5.00 g; 19.5 mmol) was suspended in 32 mL of anhydrous dimethylformamide

* Author to whom correspondence should be addressed. Telephone: (908) 932-5179. Telefax: (908) 932-5735.
† Department of Chemistry and Waksman Institute.
‡ Department of Food Science.

1043-1802/93/2904-0219$04.00/0 © 1993 American Chemical Society

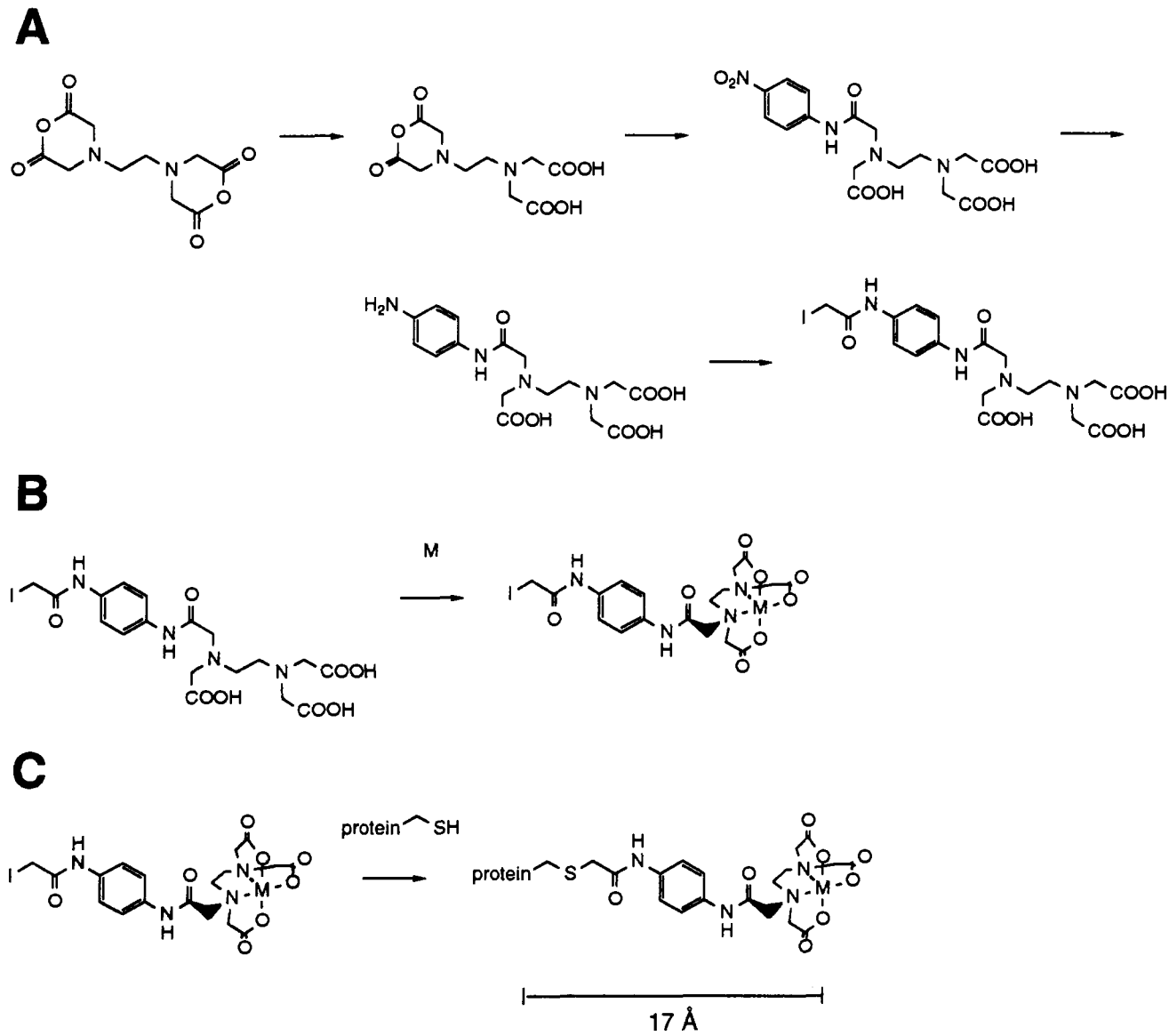


Figure 1. (A) Synthesis of *N*-(iodoacetyl)-*p*-phenylenediamine–EDTA. (B) Reaction of *N*-(iodoacetyl)-*p*-phenylenediamine–EDTA with a metal ion ("M"), yielding *N*-(iodoacetyl)-*p*-phenylenediamine–EDTA:metal. (C) Reaction of *N*-(iodoacetyl)-*p*-phenylenediamine–EDTA:metal with a protein having a unique solvent-accessible cysteine residue, yielding a conjugate of the form [(*N*-acetyl-*p*-phenylenediamine–EDTA:metal)-Cys]protein. If fully extended, the linker arm between the α carbon of the cysteine residue and the metal ion is 17 Å.

and was heated to 100 °C. The resulting solution was cooled to 75 °C. Into this solution, was added dropwise over a period of 1 h deionized water (0.350 mL; 19.4 mmol). The reaction mixture was stirred for an additional 2 h at 75 °C, after which the heat was removed, and the reaction mixture was stirred overnight to allow the product to precipitate. The product was collected by vacuum filtration and was dried under high vacuum. Yield: 4.09 g, 77%.

***p*-Nitroaniline–EDTA.** EDTA monoanhydride (2.00 g; 7.30 mmol) and triethylamine (2.02 mL; 14.5 mmol) were dissolved in 50 mL of anhydrous dimethylformamide. Into this solution, was added *p*-nitroaniline (Aldrich; 1.00 g; 7.25 mmol). The reaction mixture was stirred overnight, after which 10 mL deionized water was added, and the reaction mixture was stirred for an additional 2 h. The reaction mixture was evaporated under high vacuum to a yellow-orange semisolid. The product was purified by flash chromatography (150 mL dry silica gel, 230–400 mesh; ammonium hydroxide/ethanol, 1:3, v/v). Yield: 1.95 g, 63%. TLC (silica gel; ammonium hydroxide/ethanol, 1:3, v/v): R_f = 0.3. NMR (D_2O): 3.21 (2 H, br t), 3.39 (2 H, s), 3.51 (2 H, br t), 3.65 (2 H, s), 3.95 (4 H, s), 7.75 (2 H, d, J = 8.5 Hz), 8.20 (2 H, d, J = 8.5 Hz). MS: *m/e* 413 $(M + H)^+$.

***p*-Phenylenediamine–EDTA, Monotriethylammonium Salt.** *p*-Nitroaniline–EDTA (0.215 g; 0.501 mmol) and triethylamine (0.344 mL; 2.47 mmol) were dissolved in 10 mL anhydrous ethanol. Into this solution was added 0.060 g 10% Pd–charcoal (Aldrich). The reaction vessel was evacuated and purged with N_2 three times, and the reaction mixture was hydrogenated under 1 atm of H_2 overnight. The reaction mixture then was filtered through acid-washed Celite and was evaporated to a yellow oil. The product was purified by flash chromatography (silica gel, 230–400 mesh; triethylamine/water/ethanol, 1:2:15, v/v). Yield: 0.200 g, 83%. TLC (silica gel; ammonium hydroxide/ethanol, 1:3, v/v): R_f = 0.2. NMR (D_2O): 1.24 (9 H, t, J = 7.3; triethylammonium protons), 3.16 (2 H, s), 3.22 (2 H, br t), 3.27 (6 H, q, J = 7.3; triethylammonium protons), 3.39 (2 H, s), 3.52 (2 H, br t), 3.62 (2 H, s), 3.95 (2 H, s), 6.92 (2 H, d, J = 8.2 Hz), 7.37 (2 H, d, J = 8.2 Hz). MS: *m/e* 383 $(M + H)^+$.

N-(Iodoacetyl)-p-phenylenediamine–EDTA. p-Phenylenediamine–EDTA (0.0500 g; 0.104 mmol) and triethylamine (0.0125 mL; 0.0899 mmol) were dissolved in 2 mL of anhydrous methanol. Into this solution, was added iodoacetic anhydride (Aldrich; 0.067 g; 0.189 mmol). The reaction mixture was stirred for 2 h in the dark, after which additional iodoacetic anhydride (0.034 g; 0.095 mmol) was added and the reaction was stirred for an additional 1 h in the dark. The volume of the solution was reduced to 0.2 mL by evaporation, and the product was precipitated by addition of 5 mL of ethyl acetate. The precipitate was redissolved in 2 mL of anhydrous methanol and was reprecipitated by addition of 6 mL of ethyl acetate; this cycle was repeated three times. The product was washed twice with 0.4 mL of acetonitrile and was dried under high vacuum. Yield: 0.0216 g, 38%. TLC (silica gel; ammonium hydroxide/ethanol, 1:3, v/v): R_f = 0.3. MS: *m/e* 551 $(M + H)^+$.

N-(Iodoacetyl)-p-phenylenediamine–EDTA:metal. Reaction mixtures (100 μL) contained 32 mM *N*-(iodoacetyl)-*p*-phenylenediamine–EDTA, 37 mM $^{55}Fe(III)(NH_4)(SO_4)_2$ (50 Bq/nmol) or $^{63}Ni(II)Cl_2$ (60 Bq/nmol) or $Eu(III)Cl_3$, 50 mM potassium citrate (pH 5.6), and 200 mM KCl. Reactions were carried out in the dark and proceeded for 30 min at 23 °C.

Wild-Type Cro and [Cys17]Cro. Plasmid pAP119 encodes wild-type Cro under control of the *tac* promoter (30; gift of Dr. Robert Sauer, Massachusetts Institute of Technology, Cambridge, MA). Plasmid pYCCRO-17C encodes [Cys17]Cro under control of the *tac* promoter (*26*).

Wild-type Cro and [Cys17]Cro were purified by ion-exchange chromatography on P11 phosphocellulose (Whatman) followed by gel-filtration chromatography on Sephadex G-75 (Pharmacia), according to the procedure of ref 31, and were stored in aliquots at −70 °C in 20 mM Tris-HCl (pH 8.0), 200 mM KCl, 0.1 mM EDTA, 5% glycerol. After storage of [Cys17]Cro for several months, intermolecular disulfide bond formation was observed (≈20%). Prior to use of [Cys17]Cro in subsequent steps, intermolecular disulfide bonds were reduced by reaction with 1 mM dithiothreitol for 30 min at 23 °C followed by gel filtration chromatography on Bio-Gel P-6DG (Bio-Rad) in 20 mM Tris-HCl (pH 8.0), 200 mM KCl, 0.1 mM EDTA, 5% glycerol.

[(N-Acetyl-p-phenylenediamine–EDTA:metal)–Cys17]Cro. Reaction mixtures (500 μL) contained 0.008 mM [Cys17]Cro, 0.6 mM *N*-(iodoacetyl)-*p*-phenylenediamine-EDTA:$^{55}Fe(III)$ or *N*-(iodoacetyl)-*p*-phenylenediamine–EDTA:$^{63}Ni(II)$ or *N*-(iodoacetyl)-*p*-phenylenediamine–EDTA:Eu(III), 0.1 mM $^{55}Fe(III)NH_4(SO_4)_2$ or $^{63}Ni(II)Cl_2$ or $Eu(III)Cl_3$, 20 mM Tris-HCl (pH 8.0), 200 mM KCl, 1 mM potassium citrate, 0.1 mM EDTA, and 5% glycerol. Reactions were carried out in the dark and proceeded for 3 h at 23 °C followed by 15 h at 4 °C. The product was purified by gel filtration chromatography at 4 °C on Bio-Gel P-6DG (Bio-Rad), and the product was stored at −70 °C in a solution of 20 mM Tris-HCl (pH 8.0), 200 mM KCl, and 5% glycerol.

Efficiencies of incorporation of EDTA:^{55}Fe and EDTA:^{63}Ni were determined by liquid scintillation counting in ScintiVerse II (Fisher). Efficiencies of incorporation of EDTA:Eu were determined by time-resolved fluorescence spectroscopy in Delfia enhancement solution (Wallac) (cf. refs 12, 32). Time-resolved fluorescence spectroscopy was performed using a SPEX Industries F1T11i spectrofluorimeter equipped with a SPEX Industries 1934d phosphorescence accessory consisting of a pulsed xenon lamp and a gated delay amplifier. Excitation was performed at 338 nm, and emission was monitored at 614 nm for 3 ms after a delay of 70 μs; 30 pulse cycles were analyzed. Standards were prepared by dilution of a fresh stock solution of 10 mM $EuCl_3$ in 0.1 N HCl.

Efficiencies of incorporation also were determined by quantitation of solvent-accessible cysteine (*33*, *34*). Efficiencies of incorporation as determined by liquid scintillation counting agreed with efficiencies of incorporation as determined by quantitation of solvent-accessible cysteine within 20%.

DNA Affinity Cleaving: [(N-Acetyl-p-phenylenediamine–EDTA:^{55}Fe)–Cys17]Cro. Reactions were carried out using DNA fragment IλCRO (5′-GCAACGCAATTCTATCACCGCCGGTGATAAATAGGCACCC-3′/5′-GGGGTGCCTATTTATCACCGGCGGTGATAGAATTGCGTTG-3′; prepared according to the procedure of ref 35). Reaction mixtures (100 μL) contained: 0.1 nM [^{32}P]-labeled DNA fragment (30 Bq/fmol), 100 nM [(*N*-acetyl-*p*-phenylenediamine–EDTA:^{55}Fe)–Cys17]Cro, 1 mM ascorbic acid, 10 mM MOPS-NaOH (pH 7.3), 200 mM NaCl, and 50 μg/mL bovine serum albumin. Reactions proceeded for 3 h at 23 °C. Reactions were phenol extracted, chloroform extracted, and ethanol precipitated. Products were analyzed by denaturing gel electrophoresis through 20% polyacrylamide, 8.3 M urea slab gels (*36*). Following electrophoresis, gels were dried and were autoradiographed using Kodak X-Omat XAR5 film. Fragment lengths were determined by comparison to a Maxam-Gilbert G>A sequencing reaction (*36*) of the same DNA fragment.

Molecular Modeling. Coordinates for the crystallographic structure of the Cro–DNA complex (*37*) were obtained from R. Brennan, S. Roderick, and B. Matthews (University of Oregon, Eugene, OR). The positions of Cro backbone atoms and the positions of DNA backbone atoms have estimated uncertainties of ≈1 Å. The crystallographic structure of the Cro–DNA complex does not include base pairs −4 to −1 of the DNA half site. Model coordinates for base pairs −4 to −1 of the DNA half site were generated using the program DNA FIT MAN (*38*) assuming that base pairs −4 to −1 of the DNA half site exhibit canonical B-DNA conformation (cf. ref 26). Distances were measured using the program INSIGHT (BIOSYM). Diagrams were prepared using the program MOLSCRIPT (*39*).

RESULTS AND DISCUSSION

N-(Iodoacetyl)-p-phenylenediamine–EDTA:metal. *N*-(Iodoacetyl)-*p*-phenylenediamine was prepared in four steps: (i) reaction of EDTA dianhydride with water, yielding EDTA monoanhydride, (ii) reaction of EDTA monoanhydride with *p*-nitroaniline, yielding *p*-nitroaniline–EDTA, (iii) reduction of *p*-nitroaniline–EDTA, yielding *p*-phenylenediamine–EDTA, and (iv) reaction of *p*-phenylenediamine–EDTA with iodoacetic anhydride (Figure 1A). The overall yield was 15%. *N*-(Iodoacetyl)-*p*-phenylenediamine–EDTA:metal was prepared by incubation of *N*-(iodoacetyl)-*p*-phenylenediamine–EDTA with a 1.2-fold molar excess of the appropriate metal salt in citrate buffer at pH 5.6 (Figure 1B).

Cro Derivatives Having EDTA:Metal Complexes at Amino Acid 2 of the Helix–Turn–Helix Motif: [(N-Acetyl-p-phenylenediamine–EDTA:^{55}Fe)–Cys17]-Cro, [(N-Acetyl-p-phenylenediamine–EDTA:^{63}Ni)–Cys17]Cro, and [(N-Acetyl-p-phenylenediamine–EDTA:Eu)–Cys17]Cro. Cro is a helix–turn–helix motif sequence-specific DNA binding protein (review of Cro in ref 37; reviews of helix–turn–helix motif in refs 40–42).

Table I. Efficiencies of Incorporation of EDTA:Metal Complexes

EDTA:metal[a]	mol EDTA:metal incorporated/mol protein subunit	
	[Cys17]Cro	wild-type Cro
EDTA:^{55}Fe	0.81	<0.01
EDTA:^{63}Ni	0.84	<0.01
EDTA:Eu	0.60	<0.01

[a] Efficiencies of incorporation of EDTA:^{55}Fe and EDTA:^{63}Ni were determined by liquid scintillation counting. Efficiencies of incorporation of EDTA:Eu were determined by time-resolved fluorescence spectroscopy (cf. refs 12, 31). See Experimental Procedures.

Cro binds to a 17 base pair 2-fold-symmetric DNA site: 5′-TATCACCGCCGGTGATA-3′ (*43*, *44*). The crystallographic structure of Cro has been determined to 2.8 Å resolution (*45*), and the crystallographic structure of the Cro–DNA complex has been determined to 3.9 Å resolution (*37*).

Inspection of the structure of the Cro–DNA complex suggested that covalent incorporation of EDTA:metal with an *N*-acetyl-*p*-phenylenediamine linker at amino acid 2 of the helix–turn–helix motif of Cro (i.e., at amino acid 17 of Cro) would not prevent protein–DNA complex formation and would place the EDTA:metal moiety close to the DNA backbone in the protein–DNA complex. We have constructed and analyzed Cro derivatives having each of three EDTA:metal complexes at amino acid 2 of the helix–turn–helix motif of Cro: i.e., EDTA:^{55}Fe, a radioactive and nucleolytic EDTA:metal complex; EDTA:^{63}Ni, a radioactive EDTA:metal complex; and EDTA:Eu, a fluorescent and heavy-atom EDTA:metal complex.

Wild-type Cro has no pre-existing cysteine residues (*46*, *47*). To construct the Cro derivatives of interest, we used site-directed mutagenesis to introduce a unique solvent-accessible cysteine residue at amino acid 2 of the helix–turn–helix motif [by replacement of Thr17 by cysteine, constructing [Cys17]Cro (*26*)]. We then reacted [Cys17]-Cro with *N*-(iodoacetyl)-*p*-phenylenediamine–EDTA:metal.

The results are presented in Table I. For the EDTA:^{55}Fe and EDTA:^{63}Ni complexes, ≈0.8 mol of EDTA:metal was incorporated per mol of [Cys17]Cro subunit; for the EDTA:Eu complex, ≈0.6 mol of EDTA:metal was incorporated per mol of [Cys17]Cro subunit. Control experiments indicate that for each EDTA:metal complex, ≈0 mol of EDTA:metal was incorporated per mol wild-type Cro subunit. We conclude that incorporation of EDTA:metal by the method of this report is highly efficient. We conclude further that incorporation of EDTA:metal by the method of this report is highly site-specific, with incorporation occurring exclusively, or nearly exclusively, at the introduced cysteine residue at amino acid 2 of the helix–turn–helix motif.

DNA Affinity Cleaving by the Cro Derivative Having EDTA:^{55}Fe at Amino Acid 2 of the Helix–Turn–Helix Motif: [(*N*-Acetyl-*p*-phenylenediamine–EDTA:^{55}Fe)–Cys17]Cro. To assay DNA affinity cleaving by the Cro derivative having EDTA:^{55}Fe at amino acid 2 of the helix–turn–helix motif, we used a 40-base pair DNA fragment containing the consensus DNA site for Cro (*43*, *44*). We reacted [^{32}P]-end-labeled DNA fragment with the Cro derivative and ascorbic acid, and we analyzed the reaction products by denaturing polyacrylamide gel electrophoresis followed by autoradiography. The results are presented in Figure 2. The results indicate that DNA cleavage occurs at two sets of three adjacent nucleotides on each DNA strand. The nucleotides at which DNA cleavage occurs occupy 2-fold-symmetry-related positions

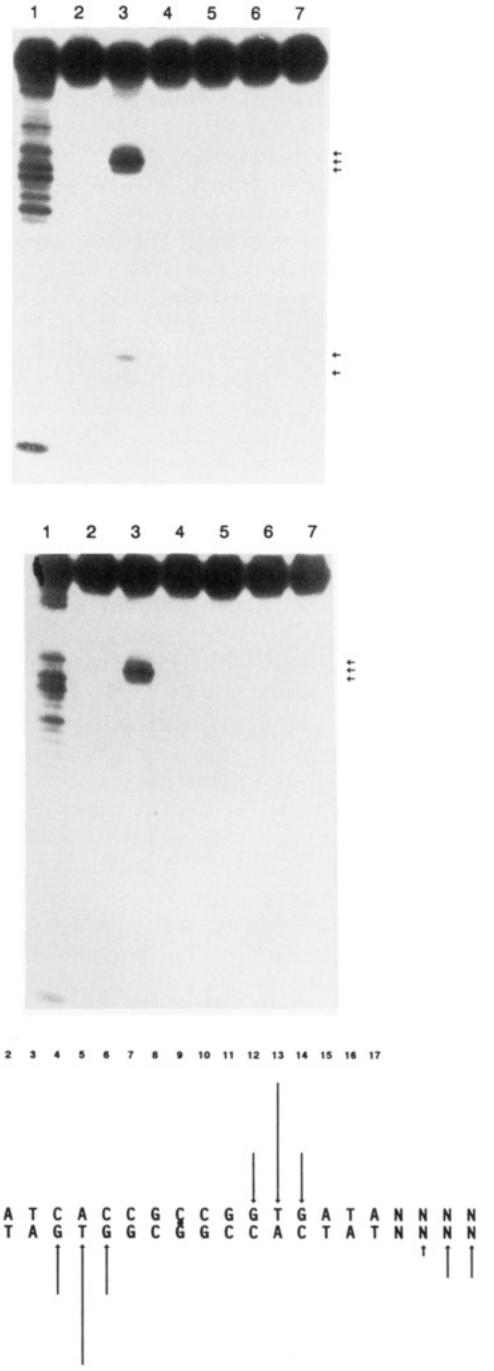


Figure 2. DNA affinity cleaving by the Cro derivative having EDTA:^{55}Fe at amino acid 2 of the helix–turn–helix motif: [(*N*-acetyl-*p*-phenylenediamine–EDTA:^{55}Fe)–Cys17]Cro. (A, top) Data for DNA fragment ^{32}P-5′-end-labeled on the bottom DNA strand. Lane 1, Maxam-Gilbert G>A sequencing reaction (*36*); lane 2, uncleaved DNA fragment; lane 3, DNA affinity cleaving reaction; lane 4, control reaction omitting the Cro derivative; lane 5, control reaction omitting ascorbic acid; lane 6, control reaction substituting underivatized Cro for the Cro derivative; lane 7, control reaction substituting underivatized Cro plus equimolar EDTA:Fe for the Cro derivative. Arrows indicate DNA cleavage products. In longer autoradiographic exposures, one additional DNA cleavage product is visible. (B, middle) Data for DNA fragment ^{32}P-5′-end-labeled on the top DNA strand. Lanes as in A. In longer autoradiographic exposures, three additional DNA cleavage products are visible. (C, bottom) Summary of DNA affinity cleaving by the Cro derivative. The figure illustrates the 17 base pair 2-fold-symmetric consensus DNA site for Cro (*43*, *44*). Arrows indicate the nucleotides at which DNA cleavage occurs; the lengths of the arrows indicate the relative extents of cleavage.

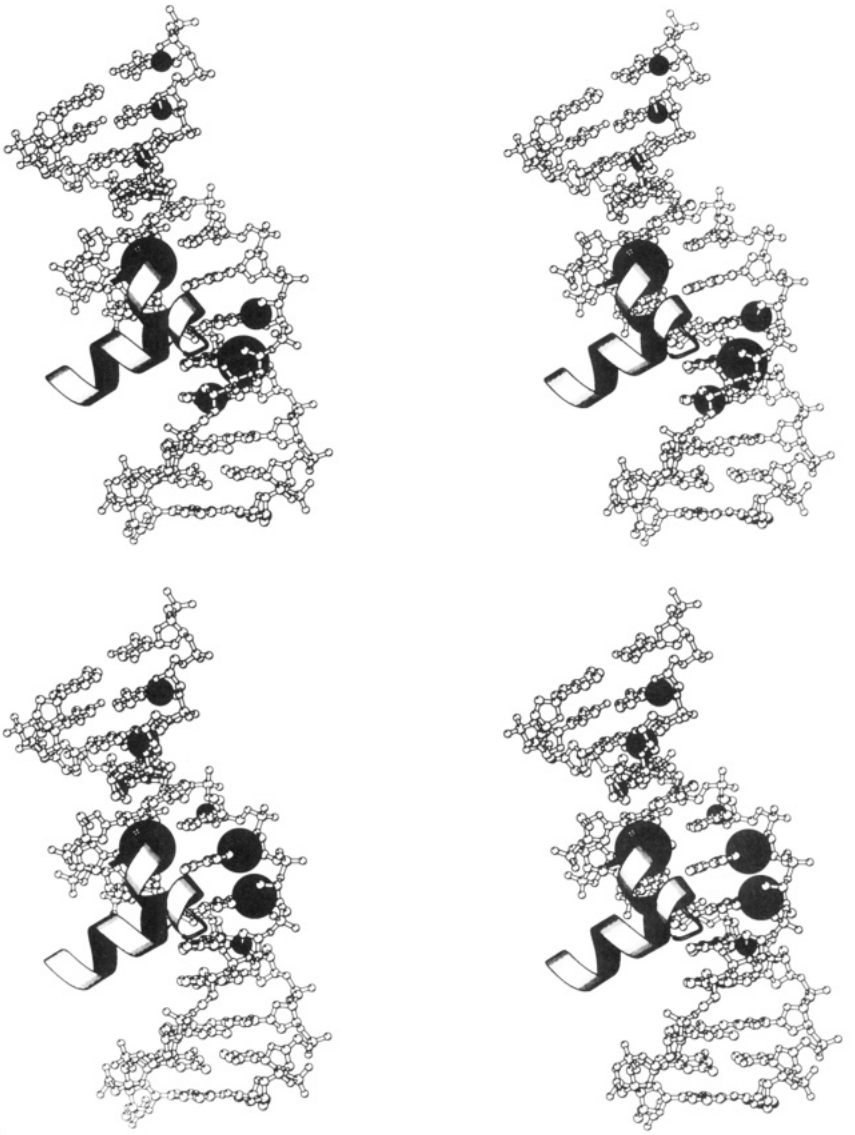


Figure 3. (A, top) Summary of DNA affinity cleaving by the Cro derivative having EDTA:^{55}Fe at amino acid 2 of the helix–turn–helix motif: [(*N*-acetyl-*p*-phenylenediamine-EDTA:^{55}Fe)–Cys17]Cro. The figure is a stereodiagram of the crystallographic structure of the Cro–DNA complex (*37*); for clarity, the figure illustrates only the helix–turn–helix motif of one subunit of Cro and the DNA of one DNA half site. The gray sphere indicates the α carbon of amino acid 2 of the helix–turn–helix motif of Cro. The black spheres indicate the C1′ atoms of nucleotides at which DNA cleavage occurs; the radii of the black spheres indicate the relative extents of cleavage. The mean distance between the α carbon of amino acid 2 of the helix–turn–helix motif of Cro and the C1′ atoms of nucleotides at which DNA cleavage occurs is 15 ± 1 Å (mean ± 1 SEM; 10–20 Å). (B, bottom) Summary of DNA affinity cleaving by the Cro derivative of ref 26 having EDTA:^{55}Fe at amino acid 2 of the helix–turn–helix motif: [(cysteamine–EDTA:^{55}Fe)–Cys17]Cro. The mean distance between the α carbon of amino acid 2 of the helix–turn–helix motif of Cro and the C1′ atoms of nucleotides at which DNA cleavage occurs is 13 ± 1 Å (mean ± 1 SEM; 7–16 Å). The greater mean distance in the case of [(*N*-acetyl-*p*-phenylenediamine–EDTA:^{55}Fe)–Cys17]Cro than in the case of [(cysteamine–EDTA:^{55}Fe)–Cys17]Cro (15 Å vs 13 Å) presumably is due to the greater length of the linker arm between the α carbon and the iron atom (17 Å vs 14 Å).

within the DNA site for Cro; i.e., DNA cleavage occurs at the top-strand nucleotides of base pairs −4 to −2 and the bottom-strand nucleotides of base pairs 4 to 6 of the DNA half site. Control experiments establish that DNA cleavage requires the Cro derivative and requires ascorbic acid. Additional control experiments establish that neither underivatized Cro nor underivatized Cro plus equimolar EDTA:Fe is able to substitute for the Cro derivative.

The DNA affinity cleaving results establish that amino acid 2 of the helix–turn–helix motif of Cro is close to the top-strand nucleotides of base pairs −4 to −2 and the bottom-strand nucleotides of base pairs 4 to 6 of the DNA half site in the Cro–DNA complex in solution. On the basis of the DNA affinity cleaving results together with the three-dimensional structure of canonical B-DNA (cf. ref 24), we infer that amino acid 2 of the helix–turn–helix motif of Cro approaches the DNA major groove and approaches most closely base pairs 1 to 2 of the DNA half site in the Cro-DNA complex in solution. We infer further that the helix–turn–helix motif of Cro is oriented such that its N-terminus is far from, and its C-terminus is close to, the 2-fold axis of the DNA site in the Cro–DNA complex in solution. These inferences are in agreement with the crystallographic structure of the Cro–DNA complex (*37*) and with a previous DNA affinity cleaving analysis of the Cro–DNA complex (*26*) (Figure 3). In the crystallographic structure of the Cro–DNA complex, the α carbon of amino acid 2 of the helix–turn–helix motif of Cro is an average of 15 ± 1 Å (10–20 Å) from the C1′ atoms of the top-strand nucleotides of base pairs −4 to −2 and the bottom-strand nucleotides of base pairs 4 to 6 of the DNA half site, approaches the DNA major groove, and approaches most closely base pair 1 of the DNA half site (*37*; R. Brennan, S. Roderick and B. Matthews, personal communication).

Prospect. In this report, we describe the use of a novel haloacetyl derivative of EDTA to incorporate each of three EDTA:metal complexes at a rationally selected site within a full-length protein. The haloacetyl derivative of EDTA of this report yields high efficiencies of incorporation and yields a reduction-insensitive thioether linkage between EDTA:metal and protein. Meares and coworkers (*48–50*) have reported three other haloacetyl derivatives of EDTA: i.e., 1-[*p*-(bromoacetamido)phenyl]-EDTA, 1-[*p*-(bromoacetamido)benzyl]-EDTA, and 1-[*p*-[[(bromoacetyl)alaninylleucylalaninylleucyl]amino]benzyl]-EDTA. However, synthesis of the haloacetyl derivatives of EDTA of refs 48–50 is more complex (6–11 steps with <5% overall yield), and use of the haloacetyl derivatives of refs 48–50 for incorporation of an EDTA:metal complex at a rationally selected site within a protein has not been demonstrated.

The haloacetyl derivative and procedures of this report have potential applications in EDTA:Fe-mediated DNA affinity cleaving with sequence-specific DNA binding proteins, site-specific radioactive labeling of protein, site-specific fluorescent labeling of protein, and site-specific heavy-atom labeling of protein.

ACKNOWLEDGMENT

We thank Drs. R. Brennan, S. Roderick, and B. Matthews for the coordinates for the crystallographic structure of the Cro–DNA complex. This work was supported by grants to R.H.E. from the Searle Scholar Program (89-G-106) and the Johnson & Johnson Discovery Research Fund.

LITERATURE CITED

(1) Bjerrum, J., Schwarzenbach, G., and Sillen, L. (1957) *Stability constants of metal-ion complexes, with solubility products of inorganic substances*, The Chemical Society, London.
(2) Bell, C. (1977) *Principles and applications of metal chelation*, Clarendon Press, Oxford.
(3) Sundberg, M., Meares, C., Goodwin, D., and Diamanti, C. (1974) Selective binding of metal ions to macromolecules using bifunctional analogs of EDTA. *J. Med. Chem. 17*, 1304–1307.
(4) Leung, C., and Meares, C. (1977) Attachment of fluorescent metal chelates to macromolecules using 'bifunctional' chelating agents. *Biochem. Biophys. Res. Commun. 75*, 149–155.
(5) Leung, C., Meares, C., and Goodwin, D. (1978) The attachment of metal-chelating groups to proteins: Tagging of albumin by diazonium coupling and use of the products as radiopharmaceuticals. *Int. J. Appl. Radiat. Isot. 29*, 687–692.
(6) Yeh, S., Meares, C., and Goodwin, D. (1979) Decomposition rates of radiopharmaceutical indium chelates in serum. *J. Radioanal. Chem. 53*, 327–336.
(7) Yeh, S., Sherman, D., and Meares, C. (1979) A new route to 'bifunctional' chelating agents: Conversion of amino acids to analogs of ethylenedinitrilotetraacetic acid. *Anal. Biochem. 100*, 152–159.
(8) Scheinberg, D., Strand, M., and Gansow, O. (1982) Tumor imaging with radioactive metal chelates conjugated to monoclonal antibodies. *Science 215*, 1511–1513.
(9) Wensel, T., and Meares, C. (1983) 'Bifunctional' chelating agents for binding metal ions to proteins. *Radioimmunoimaging and Radioimmunotherapy* (Burchiel, S. and Rhodes, B., Eds.) pp 185–196, Elsevier, Amsterdam.
(10) Meares, C., and Wensel, T. (1984) Metal chelates as probes of biological systems. *Acc. Chem. Res. 17*, 202–209.
(11) Meares, C., McCall, M., Rearden, D., Goodwin, D., Diamanti, C., and McTigue, M. (1984) Conjugation of antibodies with bifunctional chelating agents: Isothiocyanate and bromoacetamide reagents, methods of analysis, and subsequent addition of metal ions. *Anal. Biochem. 142*, 68–78.
(12) Hemmilä, I., Dakubu, S., Mukkala, V.-M., Siitari, H., and Lovgren, T. (1984) Europium as a label in time-resolved immunofluorometric assays. *Anal. Biochem. 137*, 335–343.
(13) Brechbiel, M., Ganslow, O., Atcher, R., Schlom, J., Esteban, J., Simpson, D., and Colcher, D. (1986) Synthesis of 1-(*p*-isothiocyanatobenzyl) derivatives of DTPA and EDTA. Antibody labeling and tumor-imaging studies. *Inorg. Chem. 25*, 2772–2781.
(14) Sluka, J., Horvath, S., Bruist, M., Simon, M., and Dervan, P. (1987) Synthesis of a sequence-specific DNA-cleaving peptide. *Science 238*, 1129–1132.
(15) Sluka, J., Griffin, J., Mack, D., and Dervan, P. (1990) Reagents and methods for the solid-phase synthesis of protein–EDTA for use in affinity cleaving. *J. Am. Chem. Soc. 112*, 6369–6374.
(16) Mack, D., Sluka, J., Shin, J., Griffin, J., Simon, M., and Dervan, P. (1990) Orientation of the putative recognition helix in the DNA-binding domain of Hin recombinase complexed with the Hix site. *Biochemistry 29*, 6561–6567.
(17) Graham, K., and Dervan, P. (1990) Structural motif of the DNA binding domain of gamma-delta resolvase characterized by affinity cleaving. *J. Biol. Chem. 27*, 16534–16540.
(18) Oakley, M., and Dervan, P. (1990) Structural motif of the GCN4 DNA binding domain characterized by affinity cleaving. *Science 248*, 847–850.
(19) Diamandis, E., and Christopoulos, T. (1990) Europium chelate labels in time-resolved fluorescence immunoassays and DNA hybridization assays. *Anal. Chem. 62*, 1149–1157.
(20) Rana, T., and Meares, C. (1990) N-terminal modification of immunoglobulin polypeptide chains tagged with isothiocyanato chelates. *Bioconjugate Chem. 1*, 357–362.
(21) Rana, T., and Meares, C. (1990) Specific cleavage of a protein by an attached iron chelate. *J. Am. Chem. Soc. 112*, 2457–2458.
(22) Rana, T., and Meares, C. (1991) Iron chelate mediated proteolysis: Protein structure dependence. *J. Am. Chem. Soc. 113*, 1859–1861.
(23) Shin, J., Ebright, R., and Dervan, P. (1991) Orientation of the Lac repressor DNA binding domain in complex with the left *lac* operator half site characterized by affinity cleaving. *Nucl. Acids Res. 19*, 5233–5236.
(24) Dervan, P. (1991) Characterization of protein–DNA complexes by affinity cleaving. *Methods Enzymol. 208*, 497–515.
(25) Arya, R., and Gariépy, J. (1991) Rapid synthesis and introduction of a protected EDTA-like group during the solid-phase assembly of peptides. *Bioconjugate Chem. 2*, 323–326.
(26) Ebright, Y., Chen, Y., Pendergrast, P.S., and Ebright, R. (1992) Incorporation of an EDTA–metal complex at a rationally selected site within a protein: application to EDTA–iron DNA affinity cleaving with catabolite gene activator protein (CAP) and Cro. *Biochemistry 31*, 10664–10670.
(27) Ermácora, M., Delfino, J., Cuenoud, B., Schepartz, A., and Fox, R. (1992) Conformation-dependent cleavage of staphylococcal nuclease with a disulfide-linked iron chelate. *Proc. Natl. Acad. Sci. U.S.A. 89*, 6383–6387.
(28) Kunkel, T., Bebenek, K., and McClary, J. (1991) Efficient site-directed mutagenesis using uracil-containing DNA. *Methods Enzymol. 204*, 125–138.
(29) Takeshita, T., Shimohara, T.-A., and Maeda, S. (1982) Synthesis of EDTA-monoalkylamide chelates and evaluation of the surface-active properties. *J. Am. Oil Chem. Soc. 59*, 104–107.
(30) Pakula, A., and Sauer, R. (1989) Amino acid substitutions that increase the thermal stability of the lambda cro protein. *Proteins 5*, 202–210.
(31) Leighton, P., and Lu, P. (1987) Lambda cro repressor complex with OR3 DNA: 15N NMR observations. *Biochemistry 26*, 7262–7271.
(32) Hartikka, M., Vihko, P., Södervall, M., Hakalahti, L., Torniainen, P., and Vihko, R. (1989) Radiolabelling of monoclonal antibodies: Optimization of conjugation of DTPA to $F(ab')_2$-fragments and a novel measurement of the degree of conjugation using Eu(III) labelling. *Eur. J. Nucl. Med. 15*, 157–161.
(33) Ellman, G. (1959) Tissue sulfhydryl groups. *Arch. Biochem. Biophys. 82*, 70–77.
(34) Zhang, X., Gunasekera, A., Ebright, Y., and Ebright, R. (1991) Derivatives of CAP having no solvent-accessible cysteine residues, or having a unique solvent-accessible cysteine residue at amino acid 2 of the helix-turn-helix motif. *J. Biomol. Struct. Dyn. 9*, 463–473.

(35) Ebright, R., Ebright, Y., and Gunasekera, A. (1989) Consensus DNA site for the *Escherichia coli* catabolite gene activator protein (CAP): CAP exhibits a 450-fold higher affinity for the consensus DNA site than for the *E. coli lac* DNA site. *Nucl. Acids Res. 17*, 10295–10305.
(36) Maxam, A., and Gilbert, W. (1980) Sequencing end-labeled DNA with base-specific chemical cleavages. *Methods Enzymol. 65*, 499–560.
(37) Brennan, R., Roderick, S., Takeda, Y., and Matthews, B. (1990) Protein-DNA conformational changes in the crystal structure of a lambda cro-operator complex. *Proc. Natl. Acad. Sci. U.S.A. 87*, 8165–8169.
(38) Warwicker, J., Engelman, B., and Steitz, T. (1987) Electrostatic calculations and model-building suggest that DNA bound to CAP is sharply bent. *Proteins 2*, 283–289.
(39) Kraulis, P. (1991) *MOLSCRIPT*: a program to produce both detailed and schematic plots of protein structure. *J. Appl. Crystallogr. 24*, 946–950.
(40) Brennan, R. (1991) Interactions of the helix–turn–helix binding domain. *Curr. Opin. Struct. Biol. 1*, 80–88.
(41) Brennan, R. (1992) DNA recognition by the helix–turn–helix motif. *Curr. Opin. Struct. Biol. 2*, 100–108.
(42) Pabo, C., and Sauer, R. (1992) Transcription factors: structural families and principles of DNA recognition. *Annu. Rev Biochem. 61*, 1053–1095.
(43) Kim, J., Takeda, Y., Matthews, B., and Anderson, W. (1987) Kinetic studies on Cro repressor-operator DNA interaction. *J. Mol. Biol. 196*, 149–158.
(44) Takeda, Y., Sarai, A., and Rivera, V. (1989) Analysis of the sequence-specific interactions between cro repressor and operator DNA by systematic base substitution experiments. *Proc. Natl. Acad. Sci. U.S.A. 86*, 439–443.
(45) Anderson, W., Ohlendorf, D., Takeda, Y., and Matthews, B. (1981) Structure of the cro repressor from bacteriophage lambda and its interaction with DNA. *Nature 290*, 754–758.
(46) Hsiang, M., Cole, R. D., Takeda, Y., and Echols, H. (1977) Sequence of *cro* gene of bacteriophage lambda. *Nature 270*, 274–277.
(47) Schwarz, E., Scherer, G., Hobom, G., and Kossel, H. (1978) Nucleotide sequence of *cro*, *cII*, and part of the *O* gene in phage lambda DNA. *Nature 272*, 410–414.
(48) DeRiemer, L., and Meares, C. (1979) BLEDTA: Tumor localization by a bleomycin analogue containing a metal-chelating group. *J. Med. Chem. 22*, 1019–1023.
(49) DeRiemer, L., and Meares, C. (1981) BLEDTA II: Synthesis of a new tumor-visualizing derivative of Co(III)-bleomycin. *J. Labelled Compd. Radiopharm. 18*, 1517–1534.
(50) Studer, M., and Meares, C. (1992) A convenient and flexible approach for introducing linkers on bifunctional chelating agents. *Bioconjugate Chem. 3*, 420–423.

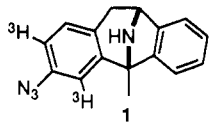
N-(3-Azidophenyl)-*N*-methyl-*N'*-([4-^{1}H]- and [4-^{3}H]-1-naphthyl)guanidine. A Potent and Selective Ligand Designed as a Photoaffinity Label for the Phencyclidine Site of the *N*-Methyl-D-aspartate Receptor

Kyle R. Gee,† Graham J. Durant,‡ Darren L. Holmes,† Sharad S. Magar,‡ Eckard Weber,*,§ Scott T. Wong,† and John F.W. Keana*,†

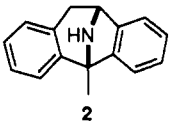
Department of Chemistry, University of Oregon, Eugene, Oregon 97403, Medicinal and Biological Chemistry Department, Cambridge NeuroScience, Inc., Cambridge, Massachusetts 02139, and Department of Pharmacology, University of California, Irvine, California 92717. Received December 22, 1992

A novel radiolabeled photoaffinity ligand has been synthesized for the phencyclidine (PCP) site of the *N*-methyl-D-asparatate (NMDA) receptor. *N*-(3-Azidophenyl)-*N*-methyl-*N'*-([4-^{3}H]-1-naphthyl)guanidine (**13**) was prepared with a specific activity of 25 Ci/mmol by diazotization of *N*-(3-aminophenyl)-*N*-methyl-*N'*-([4-^{3}H]-1-naphthyl)guanidine (**12**) followed by treatment with sodium azide. Guanidine **12** was obtained by catalytic tritiation of *N*-(4-bromo-1-naphthyl)-*N'*-methyl-*N'*-(3-nitrophenyl)guanidine (**11**). The nontritiated analog **5** of **13** was prepared beginning with *N*-methyl-*N'*-1-naphthyl-*N*-(3-nitrophenyl)guanidine (**9**). The guanidines **9** and **11** were prepared in moderate yield by the aluminum chloride-catalyzed reaction of *N*-methyl-3-nitroaniline hydrochloride with 1-naphthylcyanamide and 4-bromo-1-naphthylcyanamide, respectively. Azide **5** showed high selectivity and affinity (IC_{50} = 100 nM vs [^{3}H]MK801; 3000 nM vs [^{3}H]ditolylguanidine) for the PCP site of the NMDA receptor in guinea pig brain homogenate. Photolabeling experiments with **13**, however, failed to radiolabel a significant amount of receptor polypeptide.

The glutamate/NMDA receptor complex in the mammalian central nervous system has been strongly implicated in the mediation of nerve cell death in stroke and other ischemic events (*1*, *2*). The receptor complex also may provide a site of action for the administration of neuroprotective and anticonvulsant medicinal agents (*1*, *2*). The rat NMDA receptor nucleotide sequence was recently obtained via molecular cloning, and the predicted polypeptide has a calculated relative molecular mass of 105 500 (*3*). The phencyclidine (PCP) site lies within an ion channel associated with the NMDA receptor (*4–6*). The PCP site has been the target of photoaffinity labeling studies (*7–10*). For example, we recently developed the radiolabeled photoaffinity ligand **1** based on the potent PCP site ligand MK-801 (**2**) (*11*) and used **1** to label a M_r 115K polypeptide (*10*).



1



2

During the course of the development of diarylguanidine-based ligands for the mammalian brain sigma receptor (*12*, *13*), we discovered that certain diarylguanidines showed cross reactivity with the PCP site (*14*). Remarkably, the addition of a methyl group on one of the guanidine nitrogen atoms already bearing an aryl group resulted in a significant decrease in σ receptor affinity while the affinity for the PCP site was preserved or enhanced (*15*). We also noted from our earlier data that meta substitution on the phenyl ring was necessary for good PCP site affinity as seen by a comparison of **3** versus **4**. Reasoning that the meta position of the phenyl ring in the N-1-naphthyl-N'-methyl-N'-(3-substituted phenyl)guanidine ligands is important for PCP site binding, we undertook the development of azide **5** with the aim of using **5** to further probe the PCP site through photoaffinity labeling experiments.

EXPERIMENTAL PROCEDURES

General. All reactions were run under a nitrogen atmosphere. Chlorobenzene was freshly distilled from calcium hydride. Ether was freshly distilled from sodium benzophenone ketyl. Other reagents were used as received. Melting points are uncorrected. NMR spectra were recorded on a 300-MHz General Electric QE-300; chemical shifts are reported in δ units referenced to residual proton signals of the deuterated solvents. Infrared spectra were obtained on a Nicolet 5DXB FT-IR spectrometer, with the absorptions recorded in wavenumbers (cm^{-1}). Mass spectra were obtained on a VG ZAB-2-HF mass spectrometer with a VG-11-250 data system, in the electron ionization mode. Microanalyses were performed by Desert Analytics of Tuscon, AZ. 1-Naphthylcyanamide (*16*) was prepared (*17*) from 1-naphthylamine and BrCN (*caution, toxic*). *N*-Methyl-3-nitroaniline (*18*) was prepared using the methodology of Katrizky and Akutagawa (*19*).

***N*-Methyl-*N'*-1-naphthyl-N-(3-nitrophenyl)guanidine (9).** To a solution of 1-naphthylcyanamide (*16*, *17*) (**6**, 200 mg, 1.19 mmol) in chlorobenzene (5.0 mL) were added *N*-methyl-3-nitroaniline (*18*, *19*) hydrochloride (**7**, 224 mg, 1.19 mmol) and aluminum chloride (100 mg, 0.75 mmol). The resulting yellow mixture was stirred at 95 °C for 64 h, and the solvent was removed in vacuo. The residue was partitioned between 10% NaOH and methylene chloride (1:1, 25 mL). The layers were separated and the aqueous portion was extracted with methylene chloride (1 × 10 mL). The combined organic portions were washed with brine (1×) and dried (K_2CO_3). Concentration in vacuo

† University of Oregon.
‡ Cambridge NeuroScience, Inc.
§ University of California.

1043-1802/93/2904-0226$04.00/0 © 1993 American Chemical Society

afforded an amber oil, which was purified by flash chromatoghraphy using $CHCl_3$–MeOH–NH_4OH (1:0:0 to 50:1:0.01) as eluant. Guanidine **9** was obtained as 248 mg of a golden immobile oil (65% yield): ^1H NMR ($CDCl_3$) 3.61 (s, 3 H), 4.08 (br s, 2 H), 7.03 (d, J = 6.6 Hz, 1 H), 7.40–7.59 (m, 5 H), 7.73 (d, J = 8.2 Hz, 1 H), 7.84 (m, 1 H), 8.04 (dd, J = 8.0, 1.1 Hz, 1 H), 8.10 (m, 1 H), 8.24 (br s, 1 H); ^{13}C NMR ($CDCl_3$) 39.0, 117.5, 120.1, 120.6, 122.9, 124.3, 125.6, 126.4, 126.7, 128.3, 129.0, 130.4, 131.7, 135.2, 146.3, 146.9, 149.4, 150.4; HRMS 320.1256 (320.1273 calcd for $C_{18}H_{16}N_4O_2$).

The hydrochloride salt was prepared with hydrogen chloride in ether to give a white powder: mp 134–135.5 °C dec; IR (KBr) 1531, 1344 (NO_2). Anal. Calcd for $C_{18}H_{17}N_4O_2Cl$: C, 60.59; H, 4.80; N, 15.70. Found: C, 60.90; H, 5.12; N, 15.74.

***N*-(3-Aminophenyl)-*N*-methyl-*N'*-1-naphthylguanidine (10).** The method of Bellamy and Ou was adapted (*20*). A solution of **9** (98 mg, 0.31 mmol) and stannous chloride dihydrate (345 mg, 1.53 mmol) in ethyl acetate (3 mL) and ethanol (2 mL) was refluxed for 30 min. Ice was added, followed by saturated $NaHCO_3$. The resulting cloudy mixture was extracted with ethyl acetate (2 × 10 mL). The extract was washed with brine (1×) and dried ($MgSO_4$). Filtration and concentration in vacuo afforded **10** as 89 mg of a clear pale brown oil (100% yield): ^1H NMR ($CDCl_3$) 3.51 (s, 3 H), 3.75 (br s, 2 H), 3.99 (br s, 2 H), 6.55 (dd, J = 8.0, 1.4 Hz, 1 H), 6.66 (s, 1 H), 6.74 (d, J = 7.7 Hz, 1 H), 7.04 (d, J = 7.2 Hz, 1 H), 7.17 (t, J = 7.9 Hz, 1 H), 7.38–7.52 (m, 4 H), 7.82 (m, 1 H), 8.19 (m, 1 H); ^{13}C NMR ($CDCl_3$) 39.2, 113.70, 113.73, 116.9, 118.4, 122.6, 124.5, 125.4, 126.3, 126.7, 128.3, 129.6, 130.8, 135.2, 146.0, 146.3, 148.3, 151.5; MS m/e (rel intensity) 290 (M^+, 100), 289 (40); HRMS 290.1534 (290.1531 calcd for $C_{18}H_{18}N_4$).

The dihydrochloride salt was prepared with hydrogen chloride in ether to give a white powder: mp 235–238 °C dec.

***N*-(3-Azidophenyl)-*N*-methyl-*N'*-1-naphthylguanidine (5).** All manipulations were carried out under subdued light. To a stirred solution of **10**·2HCl (30 mg, 0.083 mmol)) in 3 N HCl (4 mL) that was cooled in a brine–ice bath was added sodium nitrite (29 mg, 0.42 mmol). The resulting yellow solution was stirred with cooling for 75 min. Sodium azide (22 mg, 0.33 mmol) was carefully added. The resulting mixture was allowed to warm to room temperature with the bath and stirred overnight. It was cooled again in an ice bath and basified to pH > 10 by adding 10% NaOH. The resulting cloudy yellow mixture was extracted with methylene chloride (3 × 4 mL). The extract was washed with brine (1×), dried (Na_2SO_4), and concentrated in vacuo to give **5** as 24 mg of a clear pale brown oil (92% yield): ^1H NMR ($CDCl_3$) 3.55 (s, 3 H), 4.01 (br s, 2 H), 6.92 (dd, J = 8.0, 1.5 Hz, 1 H), 7.04 (m, 2 H), 7.15 (d, J = 8.1 Hz, 1 H), 7.36–7.54 (m, 5 H), 7.82 (m, 1 H), 8.14 (m, 1 H); ^{13}C NMR ($CDCl_3$) 39.3, 117.1, 117.7, 118.1, 122.8, 123.3, 124.3, 125.5, 126.3, 126.6, 128.3, 129.3, 131.1, 135.2, 142.0, 146.1, 146.9, 150.9; HRMS 316.1422 (316.1436 calcd for $C_{18}H_{16}N_6$).

The hydrochloride salt was prepared with hydrogen chloride in ether to give a hygroscopic white powder which was crystallized from EtOAc/hexane: mp 72–74 °C dec; IR (KBr) 2102 (N_3); HPLC analysis (reverse phase, CH_3CN, UV detection) indicated a purity of >99.5%.

(4-Bromo-1-naphthyl)cyanamide (8). To a solution of 4-bromo-1-naphthylamine (145 mg, 0.653 mmol) in ether (3 mL) at 25 °C was added cyanogen bromide (130 mg, 1.23 mmol). The resulting mixture was stirred for 48 h and filtered. The lavender precipitate was collected (94 mg); NMR analysis indicated it to be a 3:1 mixture of 4-bromo-1-naphthylamine hydrobromide and **8**, respectively. The filtrate was concentrated in vacuo to give the title compound as 49 mg of a pale lavender-brown powder (89% total yield): mp 178–181 °C; IR (KBr) 2232; ^1H NMR (CD_3OD) 7.20 (d, J = 8.1 Hz, 1 H), 7.65 (m, 2 H), 7.79 (d, J = 7.9 Hz, 1 H), 7.99 (d, J = 8.1 Hz, 1 H), 8.22 (d, J = 8.2 Hz, 1 H); MS m/e (rel intensity) 248 (M^+, 100), 246 (M^+, 99), 167 (13), 140 (49). Anal. Calcd for $C_{11}H_7BrN_2$: C, 53.47; H, 2.86, N, 11.34. Found: C, 53.64; H, 2.80; N, 11.24.

***N*-(4-Bromo-1-naphthyl)-*N'*-methyl-*N'*-(3-nitrophenyl)guanidine (11).** A mixture of **8** (42 mg, 0.17 mmol), **7** (32 mg, 0.17 mmol), and aluminum chloride (14 mg, 0.11 mmol) in chlorobenzene (2.0 mL) was stirred at 110 °C for 22 h. The cloudy yellow reaction mixture was worked up as for **9** to give an amber oil, which was purified by preparative TLC (silica gel, 1000 μm) using $CHCl_3$–MeOH–NH_4OH (30:1:0.01) as eluant to give **11** as 37 mg of a clear golden oil (54% yield): ^1H NMR ($CDCl_3$) 3.60 (s, 3 H), 4.04 (br s, 2 H), 6.90 (d, J = 7.9 Hz, 1 H), 7.50–7.63 (m, 3 H), 7.71 (m, 2 H), 8.08 (d, J = 8.0 Hz, 1 H), 8.12 (d, J = 8.1 Hz, 1 H), 8.20 (d, J = 8.4 Hz, 1 H), 8.24 (t, J = 2.0 Hz, 1 H); MS m/e (rel intensity) 401 (M^+ + 1, 73), 358 (15), 248 (61), 168 (100).

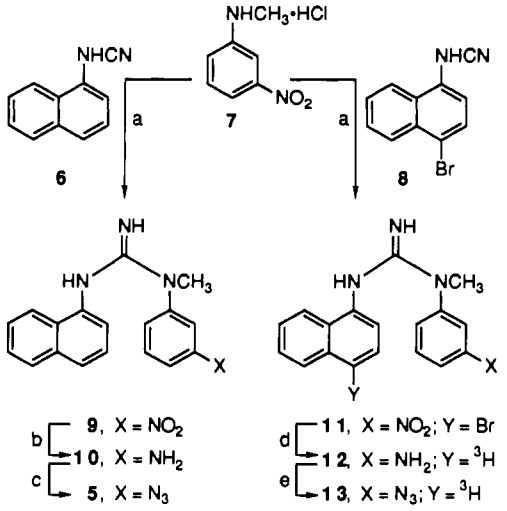
The hydrochloride salt was prepared with hydrogen chloride in ether to give a white powder: mp 152–154 °C dec; IR (KBr) 1532, 1349 (NO_2); ^{13}C NMR (CD_3OD) 40.0, 122.9, 123.7, 123.8, 126.6, 127.8, 128.4, 128.5, 130.1, 131.4, 131.8, 133.2, 133.7, 142.5, 149.8, 157.6. Anal. Calcd for $C_{18}H_{16}BrClN_4O_2$: C, 49.62; H, 3.70; N, 12.86. Found: C, 49.31; H, 3.42; N, 12.56.

***N*-(3-Aminophenyl)-*N*-methyl-*N'*-([4-^{3}H]-1-naphthyl)guanidine (12).** The tritiation reaction was performed by Amersham Corp. A mixture of **11**·HCl (8.5 mg, 0.020 mmol) and 10% Pd/C (10 mg) in ethanol (2 mL) and triethylamine (0.100 mL) was treated with 20 Ci of tritium gas. The catalyst was filtered off through a Millex SR filter and washed with ethanol. The combined filtrates were evaporated to dryness, and the labile tritium was removed by repeated rotary evaporation of an ethanol solution of the filtrate, leaving crude **12**. The total activity obtained was 475 mCi. A portion of **12** was purified by HPLC analysis as previously described for **1** (*10*) and used immediately for the next experiment.

***N*-(3-Azidophenyl)-*N*-methyl-*N'*-([4-^{3}H]-1-naphthyl)guanidine (13).** The title compound was prepared from **12** by diazotization with a molar excess of $NaNO_2$ (10 mg/mL in 3 N acetic acid) for 15 min on ice in darkness followed by addition of a molar excess of NaN_3 (10 mg/mL in 3 N acetic acid). After 15 min, the mixture was diluted with 0.1% trifluoroacetic acid and purified by reverse-phase HPLC as previously described for **1** (*10*). The major radioactive peak eluted at the same position as **5**. The specific activity of **13** was estimated to be 25 Ci/mmol by measuring the radioactivity associated with the ultraviolet peaks and interpolating the mass of these peaks from calibration curves generated from coeluting standards.

Pharmacology and Photoaffinity Labeling. The binding assay protocol and photoaffinity labeling experiments began with frozen guinea pig brains (Biotrol, Indianapolis, IN) and were performed as previously described for **1** (*10*). Azide **13** (200 000 cpm) was incubated for 30 min–2 h with rat or guinea pig membrane suspension (0.2–1.0 mg/mL) in 0.05 M Tris·HCl buffer at pH 7.4. After incubation, membrane-bound tracer was separated from free tracer by rapid filtration of the membrane suspension

Scheme I[a]



[a] (a) $AlCl_3$, PhCl; (b) $SnCl_2 \cdot 2H_2O$, EtOAc, EtOH; (c) (i) HCl, $NaNO_2$, (ii) NaN_3; (d) ^3H, cat.; (e) (i) AcOH, $NaNO_2$, (ii) NaN_3.

over glass-fiber filters. Membrane-bound radioactivity was determined by dissolving the filters in liquid scintillation cocktail followed by counting of the liquid in a liquid scintillation counter. It was found that under these conditions >90% of the radioactivity bound to the brain membranes was nonspecific, i.e. could not be displaced by adding an excess (10 μM) of the PCP receptor ligands MK801 or phencyclidine. Photolysis of the bound tracer was done by exposing the membranes on the filter to UV light (260 nm) on ice for 30 min. Extraction of the filters with SDS sample buffer and electrophoretic separation of the sample followed by fluorography of the SDS gels did not result in a detectable specific incorporation of radioactivity into a protein band.

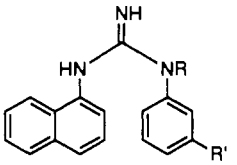
RESULTS AND DISCUSSION

The synthesis of cold *N*-(3-azidophenyl)-*N*-methyl-*N'*-naphthylguanidine (**5**, Scheme I) began with the preparation of the 3-nitro analogue **9** by reaction of 1-naphthylcyanamide (*16*, *17*) (**6**) with N-methyl-3-nitroaniline (*18*, *19*) hydrochloride (**7**). Heating the reagents either in chlorobenzene or without solvent (*12*) afforded **9** in less than 10% yield. However, when **6** and **7** were heated together in chlorobenzene in the presence of a catalytic amount of $AlCl_3$, the yields of **9** improved to better than 60%. The use of $AlCl_3$ to facilitate coupling of cyanamides and amine hydrohalides to give guanidines in good yield has recently been developed by Durant and Magar.[1] Reduction of **9** with stannous chloride dihydrate (*20*) quantitatively afforded amine **10**, which was diazotized and treated with sodium azide to give **5**. Cold azide **5** showed high selectivity and affinity for the PCP site (Table I), and binding was saturable and reversible.

In view of the favorable binding characteristics, we went on to synthesize a tritiated version of azide **5**. The [^{3}H]-labeled version **13** was synthesized by reaction of 4-bromo-1-naphthylcyanamide (**8**) with **7** in the presence of $AlCl_3$ to give **11**. Guanidine **11** was catalytically reduced in the presence of tritium gas to give the radiolabeled amine **12**. A sample of **12** was purified by HPLC analysis and then subjected to microdiazotization and reaction with sodium azide to give the radiolabeled photoaffinity label **13** with a specific activity of 25 Ci/mmol. Radiochemical purity was estimated to be greater than 95% based on HPLC analysis. Unfortunately, the radiolabeled compound showed high nonspecific binding (>90%) in radioligand binding assays using guinea pig and rat brain membrane homogenates. Furthermore, in contrast to our results with [^{3}H]-3-azido-MK801 (**1**) (*10*), no specific incorporation of radiolabel into a protein band was observed using the previously successful PCP site photolabeling protocol (*10*). Apparently the transiently formed nitrene was not suitably disposed for covalent insertion into the receptor protein. Another possible explanation for the low radiolabeling efficiency may be that the arylnitrene derived from **13** underwent ring expansion to the corresponding much less reactive dehydroazepine (*21*, *22*).

[1] A manuscript describing the scope and other applications of the $AlCl_3$ method for guanidine synthesis is in preparation by two of us (G.J.D. and S.S.M).

Table I. Binding Affinities for the PCP and σ Sites of Some *N*-Naphthyl-*N'*-phenyl Derivatives



	site affinity[a]	
	PCP[b]	σ[c]
3, R = Me; R' = Me	85	1860
4, R = Me, R' = H	1260	2950
5, R = Me; R' = N_3	100	3000

[a] IC_{50} values, nM. [b] Versus [^{3}H]-**2**. [c] Versus [^{3}H]-*N,N'*-ditolylguanidine (DTG).

ACKNOWLEDGMENT

We thank the National Institute on Drug Abuse (Grant DA 06726) and Cambridge NeuroScience, Inc. for support of this research.

Supplementary Material Available: ^{1}H NMR spectra for **5** and **10** (2 pages). Ordering information is given on any current masthead page.

LITERATURE CITED

(1) Greenamyre, J. T. (1986) The Role of Glutamate in Neurotransmission and in Neurologic Disease. *Arch. Neurol. 43*, 1058–1063.
(2) Wieloch, T. (1985) Hypoglocemia-Induced Neuronal Damage Prevented by an N-Methyl-D-Aspartate Antagonist. *Science 230*, 681–683.
(3) Moriyoshi, K., Masu, M., Ishii, T., Shigemoto, R., Mizuno, N., and Nakanishi, S. (1991) Molecular Cloning and Characterization of the Rat NMDA Receptor. *Nature 354*, 31–37.
(4) Sonders, M. S., Keana, J. F. W., and Weber, E. (1988) Phencyclidine and Psychotomimetic Opiates: Recent Insights into their Biochemical and Physiological Sites of Action. *Trends Neurosci. 11*, 37–40.
(5) Cotman, C. W., and Iversen L. L. (1987) Excitatory Amino Acids in the Brain—Focus on NMDA Receptors. *Trends Neurosci. 10*, 263–302.
(6) Anis, N. A., Berry, S. C., Burton, N. R., and Lodge, D. (1983) The Dissociative Anaesthetics, Ketamine and Phencyclidine, Selectively Reduce Excitation of Central Mammalian Neurons by N-Methyl-aspartate. *Br. J. Pharmacol. 79*, 565–575.
(7) Haring, R., Kloog, Y., and Sokolovsky, M. (1986) Identification of the Phencyclidine Receptor of Rat Hippocampus by Photoaffinity Labeling with [^{3}H]Azidophencyclidine. *Biochemistry 25*, 612–620.
(8) Haring, R., Kloog, Y., Kalir, A., and Sokolovsky, M. (1987) Binding Studies and Photoaffinity Labeling Identify Two Classes of Phencyclidine Receptors in Rat Brain. *Biochemistry 26*, 5854–5861.

(9) Sorensen, R. G., and Blaustein, M. P. (1986) M-Azido-Phencyclidine Covalently Labels the Rat Brain PCP Receptor, a Putative K Channel. *J. Neurosci. 6*, 3676–3681.
(10) Sonders, M. S., Barmettler, P., Lee, J. A., Kitahara, Y., Keana, J. F. W., and Weber, E. (1990) A Novel Photoaffinity Ligand for the PCP Site of the NMDA Receptor Labels A Mr 115,000 Polypeptide. *J. Biol. Chem. 265*, 6776–6781.
(11) Wong, E. H. F., Kemp, J. A., Priestly, T., Knight, A. R., Woodruff, G. N., and Iversen, L.L. (1986) The Anticonvulsant MK-801 is a Potent N-Methyl-D-aspartate Antagonist. *Proc. Natl. Acad. Sci. U.S.A. 83*, 7104–7108.
(12) Scherz, M. W., Fialeix, M., Fischer, J. B., Reddy, N. L., Server, A. C., Sonders, M. S., Tester, B. C., Weber, E., Wong, S. T., and Keana, J. F. W. (1990) Synthesis and Structure-Activity Relationships of N,N′-Di-*ortho*-Tolylguanidine Analogs; High Affinity Ligands for the Haloperidol-Sensitive Sigma (σ) Receptor and the PCP/MK-801 Receptor. *J. Med. Chem. 33*, 2421–2429.
(13) Weber, E., Sonders, M., Quarum, M., McLean, S., Pou, S., and Keana, J. F. W. (1986) [^{3}H]-1,3-Di-ortho-tolyl-guanidine: A Selective Ligand for Sigma Receptors to Psychotomimetic Opiates and Antipsychotic Drugs. *Proc. Natl. Acad. Sci. U.S.A. 83*, 8784–8788.
(14) Keana, J. F. W., McBurney. R. N., Scherz, M. W., Fischer, J. B., Hamilton, P. N., Smith, S. M., Server, A. C., Finkbeiner, S., Stevens, C. F., Jahr, C., and Weber, E. (1989) Synthesis and Characterization of a Series of Diarylguanidines that are Noncompetitive *N*-Methyl-D-aspartate Receptor Antagonists with Neuroprotective Properties. *Proc. Natl. Acad. Sci. U.S.A. 86*, 5631–5635.
(15) Reddy, N. L., Hu, L.-Y., Fischer, J. B., McBurney, R. N., Weber, E., Holmes, D. L., Wong, S. T., Prasad, R., and Keana, J. F. W. Synthesis and Structure-Activity Relationships of N-Alkyl and N,N′-Dialkyl Substituted N,N′-Diaryguanidines as Non-Competitive NMDA Antagonists. American Chemical Society 202nd National Meeting, New York, NY, August 1991.
(16) Kurzer, F. (1950) Cyanimides IV. The Interaction of Arylthioureas and Aromatic Sulfonyl Chlorides. *J. Chem. Soc.* 3269–3276.
(17) Geluk, H. W., Schut, J., and Schlatmann, J. L. M. A. (1969) Synthesis and Antiviral Properties of 1-Adamantylguanidine. A Modified Method for Preparing t-Alkylguanidines. *J. Med. Chem. 12*, 712–715.
(18) Pristera, F., Halick, M., Castelli, A., and Fredericks, W. (1960) Analysis of Explosives Using Infrared Spectroscopy. *Anal. Chem. 32*, 495–508.
(19) Katrizky, A. R., and Akutagawa, K. (1989) A Practical Synthetic Method for N-Methyl-*o*-toluidine. *Org. Prep. Proced. Int. Briefs 21*, No. 3, 340–341.
(20) Bellamy, F. D., and Ou, K. (1984) Selective Reduction of Aromatic Nitro Compounds with Stannous Chloride in Non Acidic and Non Aqueous Medium. *Tetrahedron Lett. 25*, 839–842.
(21) Shields, C. J., Chrisope, D. R., Schuster, G. B., Dixon, A. J., Poliakoff, M., and Turner, J. J. (1987) Photochemistry of Aryl Azides: Detection and Characterization of a Dehydroazepine by Time-Resolved Infrared Spectroscopy and Flash Photolysis at Room Temperature. *J. Am. Chem. Soc. 109*, 4723–4726.
(22) Li, Y. -Z., Kirby, J. P., George, M. W., Poliakoff, M., and Schuster, G. B. (1988) 1,2-Didehydroazepines from the Photolysis of Substituted Aryl Azides: Analysis of Their Chemical and Physical Properties by Time-Resolved Spectroscopic Methods. *J. Am. Chem. Soc. 110*, 8092–8098.

Biological Activity and in Vivo Clearance of Antitumor Antibody/Cytokine Fusion Proteins

Stephen D. Gillies,*,† Delano Young,†,§ Kin-Ming Lo,†,‖ and Stanley Roberts‡

Abbott Biotech, Inc., 119 Fourth Avenue, Needham Heights, Massachusetts 02194, and Pharmaceutical Products Division, Abbott Laboratories, Abbott Park, Illinois 60064. Received December 30, 1992

Several human cytokines including IL-2, GM-CSF, and tumor necrosis factors α and β were engineered as fusion proteins to the carboxyl terminus of a chimeric anti-ganglioside antibody, ch14.18, and expressed in transfected hybridoma cells. All of the fusion proteins were expressed at high levels and were easily purified by affinity or ion-exchange chromatography from culture supernatants. The effect of fusion on antigen binding activity was tested and found to vary with the particular cytokine. No significant decreases in antigen binding were observed, and fusion of IL-2 had the greatest positive effect in a direct antigen binding assay. All fusion proteins maintained normal levels of biological activity except for GM-CSF, which was approximately 20% active, compared to recombinant GM-CSF produced in bacteria. The clearance of the fusion proteins was examined in normal Balb/c mice after intraperitoneal injection or in athymic (nu/nu) mice after intravenous injection and was generally quite rapid, relative to ch14.18. This was mainly due to a very rapid initial clearance rate (α phase) since the half-lives of the β phase of the fusion proteins (about 30 h) were comparable to that of the free antibody (about 58 h). These results demonstrate that biologically active antibody/cytokine fusion proteins can be constructed by genetic engineering. Their relatively rapid clearance may require constant infusion rather than bolus injection in order to achieve clinical efficacy.

INTRODUCTION

The ability of many cytokines to elicit cellular immune responses to tumor cells has stimulated a renewed interest in cancer vaccines. Many groups have shown that tumor cells transfected with genes encoding various cytokines are rejected upon transplantation in syngeneic animal systems and that tumor-specific cellular immunity can be demonstrated (*1–4*). The clinical application of such an approach would involve the isolation, transfection, and readministration of a patient's tumor cells—a process that would be both time consuming and costly.

An alternative approach would be to target cytokines to tumor sites using the binding specificity of a tumor-specific antibody. Such an approach would not be patient-specific and would involve a simple injection or infusion of the Ig–cytokine fusion protein. Successful therapy might be achieved with only a small percentage of the tumor mass being targeted by the fusion protein since this would serve as the immunogen that would generate a specific, and hopefully long-lasting, cellular response.

We have already demonstrated (*5, 6*) that the human cytokines lymphotoxin (TNFβ) and IL-2 can be engineered as fusion proteins to chimeric mouse/human antibody 14.18 (ch14.18), which is reactive with the ganglioside GD2 expressed on most neuroblastoma and many melanoma tumors (*7, 8*). In both cases the antigen binding and cytokine functions were maintained. Such proteins do not have direct cytotoxic effects on GD2-positive tumor cells in vitro but may serve to elicit cellular responses through their various inflammatory and proliferative activities in vivo.

As a first step in evaluating these compounds as potential antitumor agents, we have examined their pharmacokinetic properties in normal Balb/c and athymic (nu/nu) mice. Two additional Ig–cytokine fusion proteins have also been constructed and tested for both function and blood clearance. These include fusion of the ch14.18 Ig to either human GM-CSF[1] or TNFα. Results indicate that most of these fusion proteins are cleared quite rapidly from the circulation with the exception of the GM-CSF construct. The potential role of altered antibody structure in determining the rate of clearance is discussed.

EXPERIMENTAL PROCEDURES

Plasmid Construction. The Ig–TNFβ and Ig–IL-2 fusion protein expression plasmids have been described (*5, 6*). The TNFα sequence was cloned from IFγ-treated U937 cells using PCR. The 5′ sense primer contained a *Sma*I site for fusion of the mature TNFα sequence to the *Sma*I site at the end of the human Cγ1 gene. The carboxyl terminal Lys residue of the H chain (which follows the Pro, Gly encoded by the *Sma*I site) was also encoded in the primer and immediately preceded the first residue of TNFα. The 3′ antisense primer places an *Xho*I site just after the translation stop codon. The PCR product was subcloned, sequenced, and ligated as a *Sma*I–*Xho*I fragment to a *Hin*dIII–*Sma*I fragment of the Cγ1 gene and cloned as a *Hin*dIII–*Xho*I insert. The GM-CSF sequence was chemically synthesized utilizing a coding bias for high GC content. Again the mature sequence was fused directly to the terminal Lys residue of the Cγ1 gene using the *Sma*I site and subcloned with the Cγ1 gene fragment as

* Address correspondence to Dr. Stephen D. Gillies at his present address: Fuji ImmunoPharmaceuticals, Corp. 125 Hartwell Avenue, Lexington, MA 02173.

† Abbott Biotech. Inc.

‡ Abbott Laboratories.

§ Present address: Transkaryotic Therapies Inc., 195 Albany St., Cambridge, MA 02139.

‖ Present address: Fuji ImmunoPharmaceuticals, Corp. 125 Hartwell Avenue, Lexington, MA 02173.

[1] Abbreviations used: ADCC, antibody-dependent cellular cytotoxicity; CDC, complement-dependent cytotoxicity; GM-CSF, granulocyte-monocyte colony stimulating factor; ip, intraperitoneal; iv, intravenous; MTX, methotrexate; PCR, polymerase chain reaction.

1043-1802/93/2904-0230$04.00/0 © 1993 American Chemical Society

a *Hin*dIII–*Xho*I insert. These inserts were subsequently excised and inserted into the antibody expression vector pdHL2 containing the V regions of the anti-GD2 antibody 14.18 (*9*).

Cell Culture and Transfection. Sp2/0 Ag14 mouse hybridoma cells were maintained and transfected as described (*10*). Drug selection in methotrexate (MTX) was at an initial concentration of 0.1 μM. Transfectants secreting fusion proteins were detected by ELISA (*10*) and adapted to growth in medium containing higher levels of MTX (1 μM).

Purification and Analysis of Fusion Proteins. Fusion proteins were purified from spent culture medium using either protein A Sepharose (Repligen, Cambridge, MA) or ABx Bakerbond (J.T. Baker, Phillipsburg, NJ) ion-exchange chromatography as described (*5*). The latter method was used for the LT fusion protein in order to prevent loss of biological activity during elution from protein A at low pH. Purified proteins were analyzed by SDS gel electrophoresis in the absence or presence of 5% 2-mercaptoethanol as indicated. In some cases the proteins (50 μg/mL) were first incubated with plasmin (0.1 casein units/mL) at 37 °C for 1 h in PBS containing 50 mM Tris, pH 8. The digestion products were concentrated by adsorption to protein A Sepharose and elution into gel sample buffer. The ch14.18, as well as the IL-2 and GM-CSF fusion proteins, were examined by FPLC size exclusion chromatography and no significant aggregation was detected (data not shown).

Antigen Binding Assay. A direct antigen binding assay was performed on GD2-coated microtiter plates as described (*9*), except that the GD2 was prepared from M21 human melanoma cells, which express high levels of the antigen. As a result, the assay was more sensitive than previously reported (*6*).

Biological Activity Assays. The cytostatic assay for TNFβ and TNFα has been described (*5*). IL-2 activity was measured in a mouse T cell proliferation assay (*11*). GM-CSF activity was measured in a proliferation assay using the GM-CSF-dependent acute myelogenous leukemia cell line, AML-193 (obtained from D. Santoli, Wistar Institute). After 2 days of growth in serum-free medium containing insulin and transferrin, dilutions of the test sample or recombinant GM-CSF standard (Collaborative Research, Lexington, MA) were added to the wells. After an additional 5 days, 5 μCi of [^{3}H]thymidine was added, and after 16 h, the radioactivity precipitated in 10% trichloroacetic acid was collected on GF/C filters and counted by liquid scintillation.

In Vivo Clearance Studies. Chimeric 14.18 antibody and cytokine fusion proteins were diluted to 50 μg/mL in sterile PBS and injected (0.5 mL/animal, two animals per sample) ip into normal Balb/C mice (Taconic Farms, Germantown, NY). Samples were collected from the tail vein at 2 and 24 h and refrigerated overnight. After spinning for 10 min in a microcentrifuge to remove clotted material, sera were assayed by ELISA for human Ig determinants (*10*). The IL-2 and GM-CSF fusion proteins (and control ch14.18) were studied further by iv injection (1 mg/kg in the tail vein) of athymic (nu/nu) mice using three mice per group. Samples were collected from the orbital sinus using microcapillary tubes and were stored at −20 °C prior to analysis as described above.

RESULTS

Expression of Cytokine Fusion Proteins. The fusion proteins between the anti-GD2 chimeric antibody ch14.18 and human TNFβ and IL-2 have already been described (*5*, *6*). The mature TNFβ or IL-2 protein sequences were directly fused to the carboxyl terminus of the CH3 exon of the human Cγ1 gene. The proteins secreted by transfectants, obtained with these constructs, were shown to be assembled into complete antibody molecules with the cytokines peptide-linked to the Ig H chains. In both cases the cytokines retained their biological activities.

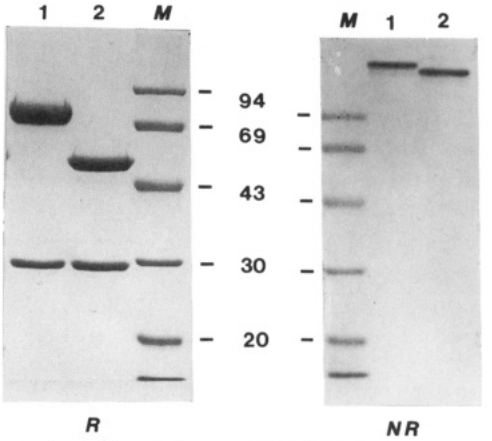


Figure 1. Analysis of ch14.18–GM-CSF fusion protein chain assembly. Proteins were diluted in gel sample buffer and boiled without (NR) or with (R) reduction (5% 2-mercaptoethanol) and analyzed on an 8% polyacrylamide gel containing SDS. Purified ch14.18 antibody (lanes 2) was compared to ch14.18–GM-CSF fusion protein (lanes 1).

Two more antibody/cytokine fusion proteins were constructed for potential use in targeting cytokines to solid tumors. In the first case, a TNFα fusion protein was made so that its effect in vivo could be compared to that of the TNFβ construct. TNFα has similar biological activities to TNFβ but has a more potent inflammatory effect (*12*). The second construct was a fusion with GM-CSF, a protein that is very different, structurally, from either IL-2 or the TNFs and has been shown to enhance the effector activity (ADCC) mediated by antibodies including ch14.18 (*13*). Both H chain gene fusions were expressed together with the 14.18 V regions and human Cκ using plasmid pdHL2 (*9*). Transfectants of the hybridoma line Sp2/0 Ag14 were selected and tested for secretion of human antibody determinants by ELISA.

The expression levels of the transfectants were comparable to those obtained for the ch14.18 antibody at the initial concentration of MTX used for selection. These levels were increased further by growing cells in increasing concentrations of MTX. Cell cultures growing in media containing intermediate levels of MTX (1 μM) were used for fusion protein purification by adsorption to and elution from protein A Sepharose.

Characterization of Fusion Proteins. Purified fusion proteins were analyzed for chain composition and assembly by SDS–PAGE in the presence or absence of reducing agent. As seen in Figure 1, the unreduced GM-CSF fusion protein migrated as a single molecular species with a higher apparent molecular weight than the ch14.18 antibody. Upon reduction, this structure dissociated into the normal L chain and a fusion H chain with an apparent molecular weight consistent with the fusion of GM-CSF (~75 kDa). A similar result was obtained with the TNFα construct (not shown). The assembly of IL-2 and TNFβ fusion proteins was reported earlier (*5*, *6*).

Next we tested the effect that the fusion of cytokines might have on the antigen binding activity of the antibody. Direct binding assays using GD2-coated plates were used to compare the fusion proteins to ch14.18 (Figure 2). As

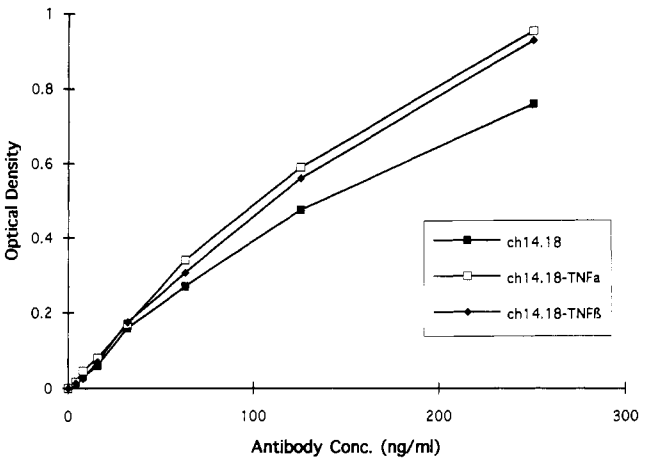


Figure 2. Antigen binding activities of Ig–cytokine fusion proteins. Serial dilutions of purified Ig–cytokine fusion proteins were compared to ch14.18 in a direct antigen binding ELISA using GD2-coated plates for capture and HRP-conjugated anti-human κ antiserum for detection.

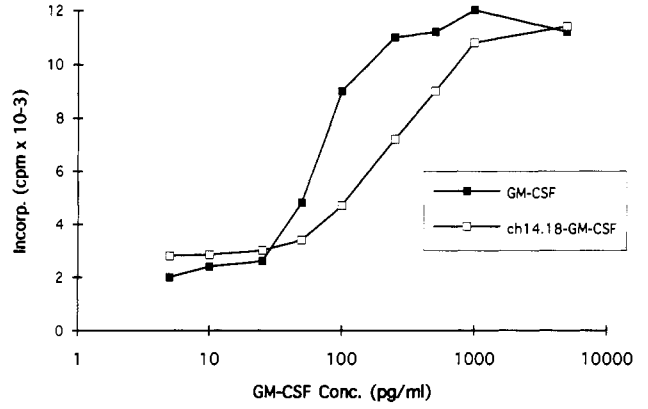


Figure 3. Proliferation activity assay of GM-CSF and ch14.18–GM-CSF fusion protein. Dilutions of purified Ig–GM-CSF fusion protein and recombinant GM-CSF were compared in a proliferation assay using a human GM-CSF-dependent acute myelogenous leukemia cell line. Values were normalized to the content of GM-CSF in the fusion protein.

reported earlier, the fusion of IL-2 resulted in a marked increase in antigen binding, and the fusion of TNFβ caused a small increase, as measured by both direct and competitive binding (*5*, *6*). The fusion of TNFα caused, as in the case of TNFβ, a slight but reproducible increase in binding while the fusion of GM-CSF caused a slight reduction.

Biological Activities of Fusion Proteins. The GM-CSF activity of the Ig–GM-CSF construct was tested in a proliferation assay using a GM-CSF-dependent acute myelogenous leukemic cell line (Figure 3). When compared to recombinant GM-CSF (produced in bacteria) on a molar basis, the fusion protein required approximately 5 times the concentration to achieve the same level of proliferation when assayed in the range of 100–800 pg/mL. At around 1 ng/mL, however, the activity of the Ig–GM-CSF approached that of the recombinant GM-CSF. Very little difference was seen between the activity of the GM-CSF fusion protein in the transfected cell culture media and that purified on protein A Sepharose, indicating that the low pH used for elution does not significantly reduce activity (not shown).

The TNFα activity of the Ig–TNFα construct was tested in a standard cytostatic assay using a mouse L cell line. The fusion protein was found to be as active as the TNFα standard and to be somewhat more active at the higher

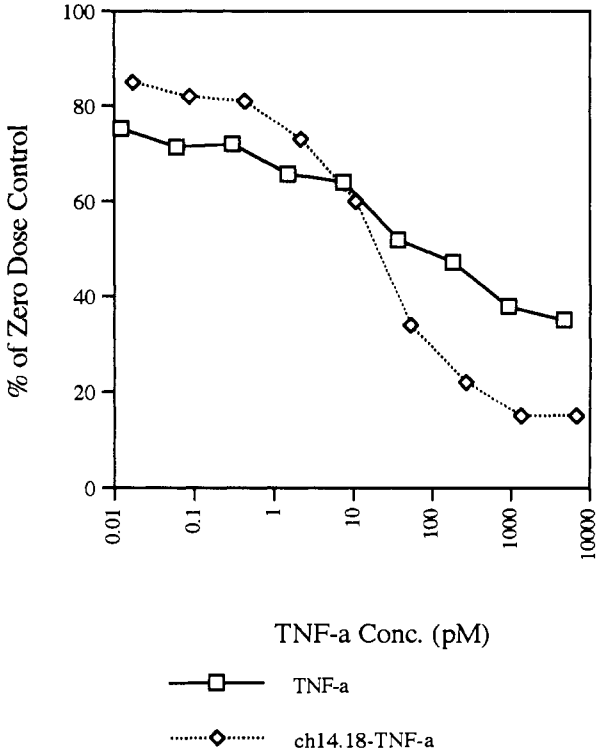


Figure 4. Activity of ch14.18–TNFα in a mouse L cell cytostatic assay. Dilutions of purified ch14.18–TNFα and recombinant TNFα were tested in a 2-day cytostatic assay using a TNF-sensitive mouse L 929 cell line. Monolayers were stained with crystal violet and the amount of stain retained by each well was measured and compared to cells not receiving any sample (zero-dose control).

concentrations (Figure 4). Unlike the Ig–TNFβ fusion protein (*5*), the activity of the Ig–TNFα fusion protein was not reduced by the acidic pH used for elution from protein A.

In Vivo Clearance of Cytokine Fusion Proteins. We initially used ip injection to estimate the rate of clearance in vivo. Purified fusion proteins were injected ip into Balb/c mice. No adverse effects were seen for any of the constructs. Most of the fusion proteins were rapidly cleared to approximately 10% of the serum concentration of the control 14.18 antibody by 2 h. The one exception was the GM-CSF fusion protein, which appeared to be intermediate in its rate of clearance and even at 24 h was found at concentrations that were 3–5 times those of the other constructs (data not shown).

We then examined the clearance of the IL-2 and GM-CSF fusion proteins more rigorously using iv injection of athymic nu/nu mice. This eliminates the time required for the proteins to enter the bloodstream from the peritoneum and, since nude mice were used, likely reduces the number of IL-2 receptor-bearing cells in the circulation. In this case three mice were used per group and each serum was assayed separately so that a range between different mice could be established. The results (Figure 5) show that the IL-2 fusion protein, despite its very large size (200 kDa), was rapidly removed from serum. In contrast, the GM-CSF fusion protein had an intermediate clearance rate (Figure 5). A comparison of the half-life ($t_{1/2}$) of the α and β phases (Table I) showed that the β phase (elimination phase) $t_{1/2}$ values of the free antibody and the two fusion proteins are very similar; the large difference in their catabolic rates are mainly due to the α phase (distribution phase) $t_{1/2}$. This suggests that an intravascular event, which removed the bulk of the fusion proteins

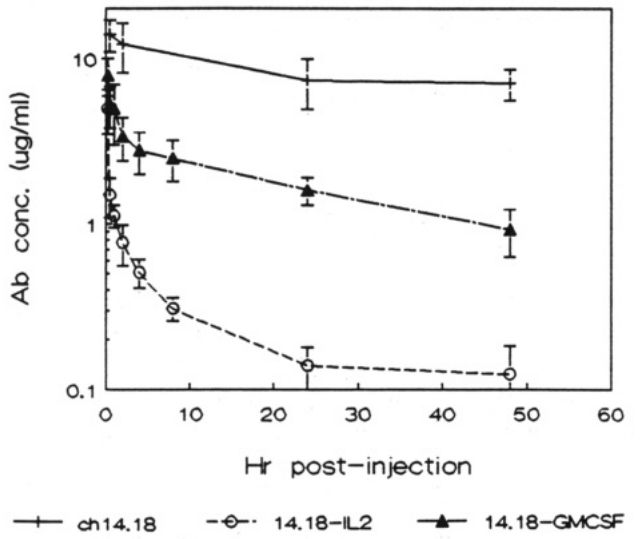


Figure 5. Clearance of ch14.18–IL2 and ch14.18–GM-CSF following iv injection of athymic (nu/nu) mice. Mice were injected in the tail vein (1 mg/kg) with the indicated protein (three mice per group) and blood samples were taken at 15 and 30 min and 1, 2, 4, 8, 24, and 48 h and assayed by ELISA.

Table I. Half-Lives of the α and β Phases of the Free Antibody and the Cytokine Fusion Proteins

	$t_{1/2}$, h	
	α	β
ch14.18	7.5	59
ch14.18–IL2	0.3	30
ch14.18–GM-CSF	1.4	28

into the extravascular space, may be responsible for the rapid clearance of the fusion proteins. As mentioned in Experimental Procedures, we found that these fusion proteins did not aggregate even after long-term storage. Thus we do not expect aggregation to be the cause of this rapid clearance.

Protease Sensitivity of the Antibody–Cytokine Junctions. One possible explanation for the rapid clearance of the cytokine fusion proteins (with the exception of the Ig–GM-CSF construct) is that the added domains alter the overall structure of the antibody resulting in recognition by some type of clearance receptor. The fact that fusion of the same cytokines (IL2, TNFβ, and TNFα) led to both enhanced antigen binding and rapid clearance suggests that both altered properties are related to structural differences that are not present in the GM-CSF construct. We demonstrated earlier that the peptide bond between the carboxyl terminus of the ch14.18 antibody and IL-2 is susceptible to cleavage with plasmin and that this cleavage restores normal antigen binding (*6*). This result suggests that IL-2 actively changes the antibody conformation, resulting in the accessibility to proteolysis of what was originally the carboxyl terminal tail of the antibody. When we probed the plasmin-sensitivity of the GM-CSF fusion protein (Figure 6) we found that the junction was resistant to cleavage. All of the other fusion proteins were cleaved near the junction to generate a normal H chain. This finding suggests that the fusion of GM-CSF to the ch14.18 antibody has a different effect on the protein structure than the other cytokines.

DISCUSSION

The recent widespread application of recombinant DNA technology to the study of protein structure and function has often involved the fusion of unrelated proteins or the

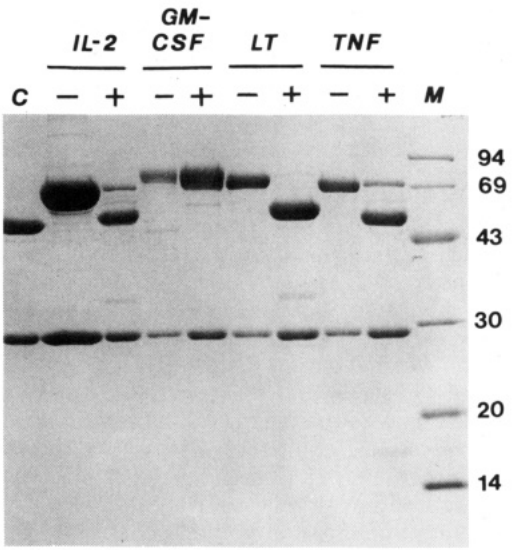


Figure 6. Protease sensitivity of Ig–cytokine fusion proteins. Samples (50 μg/mL, 0.5 mL) were incubated with or without plasmin, concentrated into gel sample buffer by adsorption to and elution from protein A Sepharose, and analyzed by SDS–PAGE. Proteins were visualized by Coomassie Blue staining.

shuffling of functional domains. Antibody fusion proteins usually are designed for the purpose of combining the targeting ability of the antigen binding domains with functional domains of other proteins such as enzymes, toxins, growth factors, etc. (*14–17*). In another application, the binding ability of non-antibody-binding proteins are joined to the Fc portion of an antibody H chain, replacing the antigen binding function of Fab. Such proteins, or "immunoadhesins" rely on the antibody portion either for effector function (ADCC, CDC, placental transfer in the case of IgG) or for conferring a longer in vivo half-life on the ligand binding domain (*18*).

Very few antibody fusion proteins have been examined in animal systems in terms of their pharmacokinetic properties. In the case of the CD4 immunoadhesins, the addition of antibody H chain domains results in an extended circulating half-life compared to CD4 alone but it is still shorter than that of a normal IgG (*18*). These proteins contain an intact H chain CH2 exon which has been shown to play a major role in the catabolism of antibodies (*19*). In the present study we have made fusion proteins in which the cytokine is peptide linked to the carboxyl terminus of an intact antibody. In this way we hoped to achieve complete assembly of the L and fusion H chains and to obtain a molecule with a long circulating half-life.

Only the fusion protein between the ch14.18 antibody and GM-CSF had a long half-life, although most of the others had half-lives longer than the native cytokines. For example, ch14.18–GM-CSF had a β half-life in nude mice of about 28 h (Figure 6) whereas that of native GM-CSF, following bolus injection in humans, has been reported to be from 50 to 85 min. (*20, 21*). It is important to point out, however, that human GM-CSF has low affinity (and activity) for the mouse GM-CSF receptor (*22*). This lack of binding to mouse cells may explain the long circulating half-life of ch14.18–GM-CSF. The ch14.18–IL2 construct, on the other hand, had a very rapid initial clearance rate followed by a β half-life of about 30 h. Thus the initial clearance may be due, in part, to the binding of the fusion protein to IL2 receptor-bearing cells. These cells would be lost when the blood was clotted, prior to preparation of the serum samples, together with the immunoreactive material being measured by ELISA. However, experi-

ments with iodinated ch14.18–IL2, in which total labeled fusion protein was measured directly, showed the same rapid clearance in nude mice (B. Mueller and R. Reisfeld, personal communication). This finding would argue against the idea that rapid clearance is due to receptor binding on circulating cells, especially since nude mice (which have greatly reduced numbers of mature T cells) were used.

An alternative explanation for the rapid initial (α) clearance of many of the cytokine fusion proteins is that structural changes in the antibody itself lead to recognition by some clearance mechanism and removal from the circulation. We have shown that the fusion of TNFβ, TNFα, and especially IL2 to the ch14.18 antibody significantly enhances its antigen binding activity (*5*, *6*) and that removal of IL2, for example, by proteolytic cleavage restores normal binding. These results strongly suggest that the fusion of the cytokines actively alters the structure of the antibody domains and results in changes in antigen/antibody interactions. The same process that alters binding may also increase the rate of clearance. In this regard it is noteworthy that the GM-CSF fusion protein had the least effect on antigen binding and had the longest half-life.

The common link between the two activities may be the CH2 domain. As discussed earlier (*23*), the CH2 domain interacts with Fab and may reduce antigen binding in some systems (e.g. the 14.18 anti-GD2 system) by reducing the flexibility of the Fab arm. Removal of the CH2 domain in the ch14.18 antibody was found to greatly enhance GD2 binding, presumably by increasing Fab flexibility. How the fusion of cytokines to the carboxyl terminus of an intact Ig molecule can achieve the same effect is more speculative, but it is possible that cytokine/CH2 interactions are strong enough to disrupt CH2/Fab interactions and free the Fab arm for antigen binding. This same CH2/cytokine interaction would then be responsible for the distortion of the Ig structure that results in rapid clearance, since this domain is critical in determining Ig half-life (*19*).

The interaction between the carboxyl-terminal cytokine and the CH2 domain would vary with differences in surface charge interactions, but when such an interaction takes place, it would likely involve a looping back around the CH3 domain. Such a structure might be susceptible to proteolytic cleavage, whereas a fusion protein in which the cytokine does not interact with CH2 would be more resistant. This explanation would account for the differences seen between ch14.18–GM-CSF and the other fusion proteins (Figure 6).

We have also demonstrated that it is possible to make biologically active antibody/cytokine fusion proteins with little or no loss of activity of either function. All of the constructs had full biological activity except for ch14.18–GM-CSF, which was approximately 20% active. It should be noted, however, that the recombinant GM-CSF standard that was used for comparison was produced in bacteria while the fusion protein was expressed in mammalian cells. Such preparations of recombinant GM-CSF, as well as those that are produced in mammalian cells and enzymatically treated to remove carbohydrate, have much higher (~20-fold) specific activities than the fully glycosylated forms (*24*). Thus, the fusion protein may be as active as native glycosylated GM-CSF.

The more important question is whether or not these fusion proteins are useful in targeting the various cytokines to tumors in vivo. One potential problem, in addition to rapid clearance, is that the fusion proteins will bind to the effector cells prior to reaching the tumor. It is also hard to predict what effect cytokine bivalency (since each H chain has a cytokine attached) will have on receptor internalization and subsequent signal transduction. We have already shown that GD2-positive melanoma cells coated with ch14.18–IL2 are much more readily killed by their autologous CTLs than are uncoated cells in the presence of free IL2 (*6*). This suggests that the fusion protein may serve a bridging function between the effector and target as an additional adhesion molecule.

Experiments to test the efficacy of these fusion proteins in tumor-bearing mice are currently underway and should determine whether of not their relatively short half-life is a serious problem. The construction of a ch14.18 fusion protein using mouse GM-CSF would also make the analysis in a syngeneic mouse tumor model possible and at the same time make it possible to test whether the long half-life of the 14.18–GM-CSF fusion protein is due to a lack of GM-CSF receptor binding.

ACKNOWLEDGMENT

We thank Ed Reilly for in vivo studies and Sue Foley, Joyce Coll, and Jing Sun for expert technical assistance.

LITERATURE CITED

(1) Tepper, R. I., Pattengale, P. K., and Leder, P. (1989) Murine interleukin-4 displays potent anti-tumor activity *in vivo*. *Cell 57*, 503.

(2) Fearon, E. R., Pardoll, D. M., Itaya, T., Golumbek, P., Levitsky, H. I., Simons, J. W., Karasuyama, H., Volgelstein, B., and Frost, P. (1990) Interleukin-2 production by tumor cells bypasses T helper function in the generation of an antitumor response. *Cell 60*, 397.

(3) Colombo, M. P., Ferrari, G., Stoppacciaro, A., Parenza, M., Rodolfo, M., Mavillo, F., and Parmiani, G. (1991) Granulocyte colony-stimulating factor gene transfer suppresses tumorigenicity of a murine adenocarcinoma *in vivo*. *J. Exp. Med. 173*, 889.

(4) Asher, A. L., Mule, J. J., Kasid, A., Restifo, N. P., Salo, J. C., Reichert, C. M., Jaffe, G., Fendly, B., Kriegler, M., and Rosenberg, S. (1991) Murine tumor cells transduced with the gene for tumor necrosis factor-α: evidence for paracrine immune effects of tumor necrosis factor against tumors. *J. Immunol. 146*, 3227.

(5) Gillies, S. D., Young, D., Lo, K.-M., Foley, S. F., and Reisfeld, R. (1991) Expression of genetically engineered immunoconjugates of lymphotoxin and a chimeric anti-ganglioside GD2 antibody. *Hybridoma 10*, 347.

(6) Gillies, S. D., Reilly, E. B., Lo, K.-M., and Reisfeld, R. (1992) Antibody-targeted interleukin 2 stimulates T-cell killing of autologous tumor cells. *Proc. Natl. Acad. Sci. U.S.A. 89*, 1428.

(7) Mueller, B. M., Romerdahl, C. A., Gillies, S. D., and Reisfeld, R. (1990) Enhancement of antibody-dependent cytotoxicity with a chimeric anti-GD2 antibody. *J. Immunol. 144*, 1382.

(8) Mujoo, K., Cheresh, D. A., Yang, H. M., and Reisfeld, R. (1986) Disialoganglioside GD2 on neuroblastoma: Target antigen for monoclonal antibody-mediated cytolysis and suppression of tumor growth. *Cancer Res. 47*, 1098.

(9) Gillies, S. D., Lo, K.-M., and Wesolowski, J. (1989) High-level expression of chimeric antibodies using adapted cDNA variable region cassettes. *J. Immunol. Methods 125*, 191.

(10) Gillies, S. D., Dorai, H., Wesolowski, J., Majeau, G., Young, D., Boyd, J., Gardner, J., and James, K. (1989) Expression of anti-tetanus toxoid antibody in transfected murine myeloma cells. *Biotechnology 7*, 799.

(11) Gillis, S., Ferm, M. M., Ou, W., and Smith, K. A. (1978) T-cell growth factor: Parameters of production and a quantitative microassay for activity. *J. Immunol. 120*, 2027.

(12) Goeddel, D. V., Aggarwal, B. B., Gray, P. W., Leung, D. W., Nedwin, G. E., Palladino, M. A., Patton, J. S., Pennica, D., Shepard, H. M., Sugarman, B. J., and Wong, G. H. (1986)

Tumor necrosis factors: gene structure and biological activities. *Cold Spring Harbor Sym. Quant. Biol. 51*, 597.
(13) Barker, E., Mueller, B. M., Handgretinger, R., Herter, M., Yu, A. L., and Reisfeld, R. A. (1991) Effect of a chimeric anti-ganglioside GD2 antibody on cell-mediated lysis of human neuroblastoma cells. *Cancer Res. 51*, 144.
(14) Neuberger, M. S., Williams, G. T., and Fox, R. O. (1984) Recombinant antibodies possessing novel effector functions. *Nature 312*, 604.
(15) Chaudhary, V. K., Queen, C., Junghans, R. P., Waldman, T. A., Fitzgerald, D. J., and Pastan, I. (1989) A recombinant immunotoxin consisting of two antibody variable domains fused to *Pseudomonas* exotoxin. *Nature 339*, 394.
(16) Shin, S.-U., and Morrison, S. L. (1990) Expression and characterization of an antibody binding specificity joined to insulin-like growth factor 1: Potential applications for cellular targeting. *Proc. Natl. Acad. Sci. U.S.A. 87*, 5322.
(17) Gillies, S. D., Wesolowski, J. S., and Lo, K.-M. (1990) Targeting human cytotoxic T lymphocytes to kill heterologous epidermal growth factor receptor-bearing tumor cells. *J. Immunol. 146*, 1067.
(18) Capon, D. J., Shaw, S. M., Mordenti, J., Marsters, S. A., Gregory, T., Mitsuya, H., Byrn, R. A., Lucas, C., Wurm, F. M., Groopman, J. E., Broder, S., and Smith, D. H. (1989) Designing CD4 immunoadhesins for AIDS therapy. *Nature 337*, 525.
(19) Mueller, B. M., Reisfeld, R. A., and Gillies, S. D. (1990) Serum half-life and tumor localization of a chimeric antibody deleted of the CH2 domain and directed against the disialoganglioside GD2. *Proc. Natl. Acad. Sci. U.S.A. 87*, 5702.
(20) Cebron, J., Dempsey, P., Fox, R. R., Kanomakis, G., Bonnem, E., Burgess, A. W., and Morstyn, G. (1988) Pharmacokinetics of human granulocyte-macrophage colony stimulating factor using a sensitive immunoassay. *Blood 72*, 1340.
(21) Herrmann, F., Schulz, G., Lindemann, A., Meyenburg, W., Oster, W., Krumwieh, D., and Mertelsmann, R. (1989) Hematopoietic responses in patients with advanced malignancy treated with recombinant granulocyte-macrophage colony-stimulating factor. *J. Clin. Oncol. 7*, 159.
(22) Kaushansky, K., Shoemaker, S. G., Alfaro, S., and Brown, C. (1989) Hematopoietic activity of granulocyte/macrophage colony-stimulating factor is dependent upon two distinct regions of the molecule: Functional analysis based upon the activities of interspecies hybrid growth factors. *Proc. Natl. Acad. Sci. U.S.A. 86*, 1213.
(23) Gillies, S. D., and Wesolowski, J. (1990) Antigen binding and biological activities of engineered mutant chimeric antibodies with human tumor specificities. *Hum. Antibod. Hybridomas 1*, 47.
(24) Moonen, P., Mermod, J.-J., Ernst, J. F., Herschi, M., and DeLamarter, J. F. (1987) Increased biological activity of deglycosylated recombinant human granulocyte/macrophage colony-stimulating factor produced by yeast or animal cells. *Proc. Natl. Acad. Sci. U.S.A. 84*, 4428.

Synthesis of 2-(*p*-Thiocyanatobenzyl)-1,4,7-triazacyclononane-1,4,7-triacetic Acid: Application of the 4-Methoxy-2,3,6-trimethylbenzenesulfonamide Protecting Group in the Synthesis of Macrocyclic Polyamines

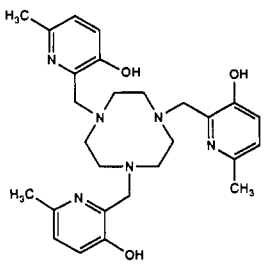
Thomas J. McMurry,* Martin Brechbiel, Chuanchu Wu, and Otto A. Gansow

Radiation Oncology Branch, National Cancer Institute, National Institutes of Health, Building 10, Room B3-B69, Bethesda, Maryland 20892. Received December 30, 1992

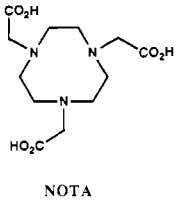
A synthesis of the bifunctional chelator 2-(*p*-thiocyanatobenzyl)-1,4,7-triazacyclononane-1,4,7-triacetic acid [2-(*p*-NCS-Bz)-NOTA] is described which illustrates the especial utility of the (4-methoxy-2,3,6-trimethylphenyl)sulfonyl (Mtr) protecting group as an alternative to the *p*-tolylsulfonyl (Ts) moiety commonly used for Richman–Atkins type cyclizations. Reaction of *N,N'*- bis(*p*-tolylsulfonyl)-1-(*p*-benzamidobenzyl)ethylenediamine with *N,N*-bis[2-[(*p*-tolylsulfonyl)oxy]ethyl]-*p*-toluenesulfonamide gave 2-(*p*-benzamidobenzyl)-1,4,7-tris(*p*-tolylsulfonyl)-1,4,7-triazacyclononane in 55% yield, whereas the analogous reaction using the Mtr-protected starting materials gave the corresponding Mtr-protected macrocycle in 34% yield. However, deprotection of the Ts- and Mtr-protected macrocycles (H_2SO_4, 90 °C) afforded 2-(*p*-benzamidobenzyl)-1,4,7-triazacyclononane in 23% and 60% yield, respectively, illustrating the relatively facile cleavage of the Mtr moiety. A modest improvement in overall percent conversion of (*p*-nitrobenzyl)ethylenediamine into substituted macrocyclic polyamine was observed when comparing the Mtr vs Ts protection (12.6 vs 10.6%). The macrocyclic triamine was converted to 2-(*p*-NCS-Bz)-NOTA by alkylation with bromoacetic acid (pH 9, 73%) followed by hydrolysis of the benzamide protecting group (6 M HCl, 70 °C, 87%) and reaction with thiophosgene (90%). The serum stability of the ^{67}Cu complexes of 1,4,7-triazacyclononane (**I**), 2-(*p*-nitrobenzyl)-1,4,7,10-tetraazacyclododecane (**II**), 2-(*p*-nitrobenzyl)-1,4,8,11-tetraazacyclotetradecane (**III**), 2-(*p*-PhCONH-Bz)-NOTA (**IV**), 2-(*p*-nitrobenzyl)-1,4,7,10-tetraazadodecane-1,4,7,10-tetraacetic acid (**V**), 2-(*p*-nitrobenzyl)-1,4,8,11-tetraazatetradecane-1,4,8,11-tetraacetic acid (**VI**), and the acyclic ligand 1-(*p*-nitrobenzyl)-4-methyldiethylenetriamine-*N,N,N',N'',N''*-pentaacetic acid (**VII**) was measured at 37 °C (5% CO_2) and showed the following order of relative stability: **I < VII ≪ VI ≪ IV < V ≅ II ≅ III.**

INTRODUCTION

The tridentate ligand 1,4,7-triazacyclononane forms an array of metal complexes, many of which exhibit rich chemistry as a consequence of the small macrocyclic ring N_3 donor set (*1*). Numerous N-alkylated derivatives, including acetates (*2*), amides (*3*), phenols (*4*), mercaptans (*5*), phosphinic acids (*6*), and tertiary amines (*7*), have been synthesized in order to investigate the properties of hexadentate N_3X_3 donor ligands. When modified with acetate or phenolic donor groups, the resulting macrocycles are unusually well-suited to the sequestering of metals with a high charge to ionic radius ratio, such as Fe(III) and Ga(III). Particularly noteworthy are the triphenolic derivative 1 prepared by Martell and co-workers (*8*), which



1



NOTA

2

sequesters the ferric ion more efficiently at pH 7.4 than the siderophore enterobactin, and the gallium(III) complex of triacetate ligand 1,4,7-triazanonane-1,4,7-triacetic acid (NOTA, **2**), which was shown to be remarkably stable to acid-catalyzed dissociation (*9*). NOTA has also been shown to stabilize unusual oxidation states of metals, such as Ni(III), by virtue of the efficient packing of the acetates around the small trivalent nickel ion (*10*).

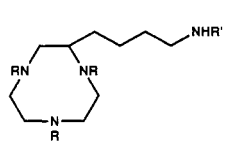
Our interest in the derivatives of 1,4,7-triazacyclononane lies in the need to sequester particle-emitting radioisotopes for use with monoclonal antibody in radioimmunodiagnosis and radioimmunotherapy, applications which place strict requirements on the need to prevent release of the radioactive metal in vivo (*11*). These conditions necessitate kinetic inertness and high thermodynamic stability of the metal complexes and are typically best fullfilled by a ligand which can completely satisfy the coordination requirements of the selected radiometal. X-ray crystallography of the [Cu(NOTA)] anion (*12*) and the neutral [Ga(NOTA)] complex (*13*) demonstrated full N_3O_3 coordination and suggested that NOTA warranted investigation as a ligand for mAb-mediated delivery of the particle emitters ^{67}Cu (β^-, $t_{1/2}$ 61.5 h) or ^{66}Ga (β^+, $t_{1/2}$ 9.45 h) to tumor cells. Subsequent kinetic studies from our laboratory confirmed that, in accordance with established tenets, the coordinatively saturated Cu(II) complex of NOTA was more resistant to acid-catalyzed dissociation than the analogous complexes of the tetraazamacrocyclic poly(amino carboxylates) 1,4,7,10-tetraazadodecane-1,4,7,10-tetraacetic acid (DOTA) and 1,4,8,11-tetraazatetradecane-1,4,8,11-tetraacetic acid (TETA) (*14*). These results prompted us to prepare a C-functionalized NOTA

* Address correspondence to Dr. Thomas J. McMurry, Metasyn, Inc., 71 Rogers St., Cambridge, MA 02142.

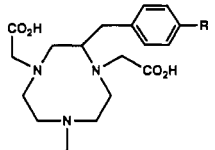
Not subject to U.S. Copyright. Published 1993 by American Chemical Society

which could be used to covalently modify tumor-seeking monoclonal antibody.

Two syntheses of such "bifunctional" NOTA derivatives have been reported. Using (*S*)-lysine as the starting material, Parker and co-workers prepared an ϵ-benzoyl-protected tritosylamide which was reacted with ethylene glycol ditosylate using classical Richman–Atkins cyclization conditions (Cs_2CO_3, DMF, 65 °C) to give a 71% yield of the macrocycle **3a** (*15*). Deprotection with H_2SO_4 (98%, 115 °C, 36 h) gave the triamine in 41% yield, which was converted to the aminobutyl-substituted poly(amino carboxylate) **3b** by alkylation ($BrCH_2CO_2R$, R = *t*-Bu, Et, or H) and subsequent cleavage of the benzoyl protecting group. Studer and Meares recently reported the preparation of C-functionalized 2-(*p*-NO_2-Bz)-NOTA (**4a**) start-



3a R=Ts, R'=COPh
3b R=CH_2CO_2H, R'=H



4a R=NO_2
4b R=NCS

ing from *p*-NO_2-Phe-Gly-Gly and employing an intramolecular tosylamide cyclization strategy as the key step (*16*). The incompatibility of an aryl nitro group to the conditions of a bimolecular Richman–Atkins cyclization (anhydrous DMF, deprotonated tosylamide, 65–80 °C) led us to develop high-dilution amide cyclizations for the preparation of 12- and 14-membered ring tetraaza macrocycles (*17*). However, these cyclizations could not be applied to the preparation of the 9-membered triazacyclononane ring due to the competing formation of a fused ring 5,6-acylamidine, thus necessitating a new synthetic approach.

Herein we report our preparation of C-functionalized NOTA **4b** and introduce the amine-protecting group (4-methoxy-2,3,6-trimethylphenyl)sulfonyl (Mtr) as a useful alternative to the ubiquitous *p*-toluenesulfonamide (Ts) for the preparation of macrocyclic polyamines via Richman–Atkins type cyclizations. In addition, an evaluation of the serum stability of the ^{67}Cu chelates of carbon-functionalized NOTA, DOTA, TETA and the ^{67}Cu complexes of their precursor bifunctional macrocyclic polyamines 1,4,7-triazacyclononane, 1,4,7,10-tetrazacyclododecane, and 1,4,8,11-teraazacyclotetradecane is presented.

EXPERIMENTAL PROCEDURES

General. Anhydrous THF and DMF were obtained from Aldrich. Triethylamine was distilled from CaH_2. Diborane·THF was used as received (Aldrich). (*p*-Nitrobenzyl)ethylenediamine dihydrochloride (**5**) was prepared as described previously (*18*). MtrCl (4-methoxy-2,3,6-trimethylbenzenesulfonyl chloride) was prepared by the literature procedure (*19*). Dimethyl iminodiacetate hydrochloride (**10**) was prepared by a literature procedure (*20*). Silica used for flash chromatography (*21*) was purchased from Fluka (silica gel 60, 230–400 mesh). Fetal bovine serum was purchased from Hyclone Lab, Inc. (Logan, UT) and stored at −20 °C. High-purity deionized water (Hydroservices Picosystem, >18 Ω cm) was used for all experiments.

Proton and ^{13}C NMR were obtained using a Varian 300XL or Gemini instrument. Chemical shifts are reported in ppm on the δ scale relative to TMS, TSP, or the following internal references (noted in text): CD_3CN (^1H, 1.93; ^{13}C, 1.30); CD_3CN (^{13}C, 118.2), dmso-d_6 solvent (^1H, 2.49; ^{13}C, 39.5), $CDCl_3$ solvent (^{13}C, 76.9). Proton chemical shifts are annotated as follows: ppm (multiplicity, integral, coupling constant (Hz)). Chemical ionization mass spectra (CI-MS) were obtained on a Finnegan 3000 instrument. Fast atom bombardment (FAB-MS) mass spectra were recorded on a JEOL JMS-SX102 instrument. Elemental analyses were performed by Atlantic Microlabs (Atlanta, GA). Due to the possibility of radioactive contamination, ^{14}C-labeled compounds were not submitted for elemental analysis, exact mass measurement, or NMR. However, the chromatographic behavior (HPLC) of the labeled compounds was identical to that observed for the non-radioactive analogs.

Analytical HPLC utilized to monitor purity of the synthesized compounds was performed by using a Beckman gradient system equipped with Model 114M pumps controlled by System Gold software and a Model 165 dual-wavelength detector operating at 254 and 280 nm. A Waters C-18 reverse-phase column (15-μm particles, 100-Å pore size, 3.9 × 300 mm) and a binary gradient of 0–100% B/25 min (solvent A = 0.05 M AcOH/Et_3N, pH 5.5, solvent B = MeOH) at 1.0 mL/min were used for all analyses.

For serum stability studies, FPLC was performed at room temperature on a Superose 12 gel filtration column (1 × 30 cm, Pharmacia) eluted with MES/Cl^- buffer (0.02 M in MES; 0.15 M in NaCl; 0.05% NaN_3; pH 6.5). The flow rate was maintained at 0.75 mL/min, and UV-absorbing substances were monitored in the eluent by a flow-through detector operating with a 280-nm filter. Fractions of ca. 0.33 mL (7 drops) were collected and then counted in an off-line γ counter. An aliquot of each injectate was also counted so that the recovery during FPLC analysis could be determined.

Serum Stability. The chemical structures of the ligands tested in the experiments are shown in Figure 1. Ligand **I** was obtained from Aldrich, whereas ligands **II**, **III**, and **V–VII** were prepared as described previously (*17*, *22*). The preparation of ligand **IV** is described below. To prepare stock solutions of the ligands, ca. 2 mg of the compounds were weighed into clean polypropylene vials and dissolved in deionized H_2O (1 mL). The concentration of ligands **I–III** was then determined by spectrophotometric titration with a standardized $Cu(ClO_4)_2$ solution, while the concentration of ^{14}C-labeled ligands **IV–VII** was determined by liquid scintillation counting. Stock ligand solutions (4.0×10^{-4} M) were prepared by dilution with chelexed H_2O and stored at 4 °C.

Copper-67 was obtained from Los Alamos National Laboratory and was purified by anion-exchange chromatography (Bio-Rad 1X-8, 2 M HCl). Typically, ligand stock solutions (25 μL of the 4.0×10^{-4} M) were mixed with ^{67}Cu (200 μCi), and the pH was adjusted to 6 with NaOAc (1 M). The reaction mixture was incubated at 60 °C for 10 min, and then loaded onto a column of Chelex-100 resin (3 mm × 40 mm, equilibrated with MES/Cl^- buffer). The complexes were eluted from the resin with MES/Cl^- buffer (0.5 mL). Dilution of the collected eluent to 1.0 mL gave the 1.0×10^{-5} M stock solutions of the ^{67}Cu labeled ligands. In every case, the labeling efficiency exceeded 90%. Analysis by paper chromatography (mobile phase, 0.2 M NH_4OAc, pH 6.8) confirmed that the unbound radioactivity was less than 0.5%.

Copper-67-labeled ligand (100 μL) was added to bovine serum (9.9 mL, Hyclone Lab., Inc.) to give a final ligand concentration of 0.1 μM. The mixture was then passed through a sterile 0.22-μm filter (Millipore, MA) and apportioned into 10 sterile culture tubes. The serum samples were maintained at 37 °C (pH 7.3 ± 0.1) in an incubator in a CO_2-enriched atmosphere (5% CO_2). On

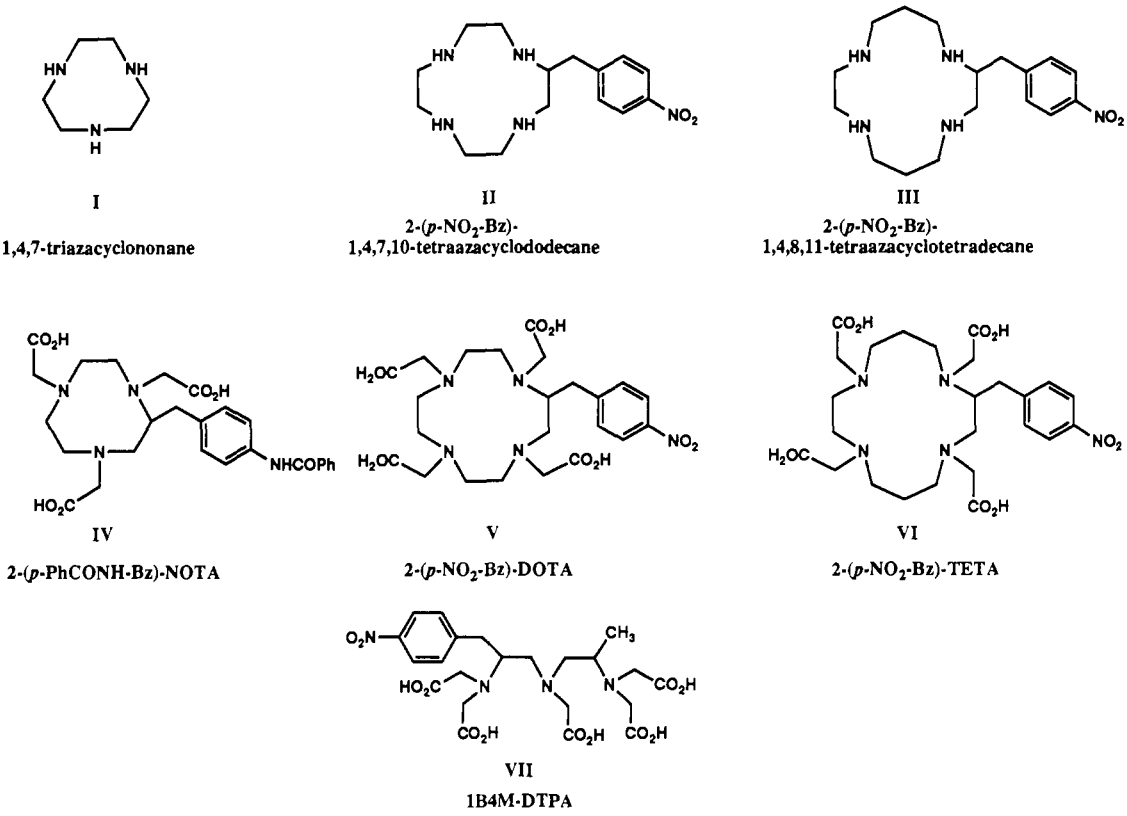


Figure 1. Chemical structures of bifunctional chelating agents tested for stability with ^{67}Cu in serum (37 °C, 6% CO_2).

days 0, 1, 3, 6, and 9, one tube of each complex was taken out from the incubator. A portion of the serum sample (400 μL) was filtered through a 0.45-μm centrifuge tube filter (Millipore Co. MA) and then analyzed by FPLC. The filter was washed with 3 × 200 μL of 0.05 M PBS buffer, pH 7.4 and then counted in the γ counter. The percentages of the precipitated radioactivity were calculated. As controls, free ^{67}Cu (acetate, pH 5.0) was added to bovine serum and BSA, and subsequently incubated and analyzed as described above.

Synthesis. *N,N'*-Bis(*p*-tolylsulfonyl)-1-(*p*-nitrobenzyl)ethylenediamine (6a). (*p*-Nitrobenzyl)ethylenediamine dihydrochloride (10 g, 0.037 mol) was suspended in CH_2Cl_2 (300 mL) blanketed with argon. Triethylamine (15.9 g, 21.8 mL, 0.157 mol) and *p*-toluenesulfonyl chloride (14.22 g, 0.074 mol) were added, and the solution was stirred for 14 h (room temperature). TLC (5% CH_3OH/CH_2Cl_2) showed clean product at R_f 0.52. The reaction was extracted with water (2 × 100 mL), 0.1 M HCl (3 × 100 mL), and H_2O (100 mL), and the organic layer dried (Na_2SO_4). The solvent was evaporated to dryness to give a pale yellow solid which was recrystallized from MeOH (18.0g, 96%): ^1H NMR ($CDCl_3$) δ 7.847 (d, 2 H, *J* = 8.66), 7.738 (d, 2 H, *J* = 8.61), 7.419 (d, 2 H, *J* = 8.20), 7.298 (d, 2 H, *J* = 8.18), 7.057 (d, 2 H, *J* = 7.7) 7.038 (d,2 H, *J* = 7.7), 5.539 (t, 1 H, *J* = 6.56), 5.403 (d, 1 H, *J* = 7.90), 3.490 (m, 1 H), 3.110 (m, 2 H), 2.940 (dd, 1 H, *J* = 5.23, 14.00), 2.752 (dd, 1 H, *J* = 9.30, 14.00), 2.427 (s, 3 H), 2.362 (s, 3 H); ^{13}C NMR (dmso-d_6) δ 146.22, 145.72, 142.74, 142.02, 137.87, 137.39, 130.11, 129.62, 128.97, 126.49, 125.89, 122.78, 54.37, 47.28, 36.74, 20.89, 20.60; MS (CI-NH_3) *m/e* 504 (M + H)$^+$, 521 (M + NH_4)$^+$. Anal. Calcd for $C_{23}H_{25}N_3O_6S_2$ (503.61): C, 54.86; H, 5.00; N, 8.34. Found: C, 54.95; H, 5.15; N, 8.05.

***N,N'*-Bis[(4-methoxy-2,3,6-trimethylphenyl)sulfonyl]-1-(*p*-nitrobenzyl)ethylenediamine (6b).** As described above for **6a**, (*p*-nitrobenzyl)ethylenediamine dihydrochloride (9.38 g, 0.035 mol) was suspended in CH_2Cl_2 (300 mL). Triethylamine (16.3 g, 22.5 mL, 0.16 mol) and 4-methoxy-2,3,6-trimethylbenzenesulfonyl chloride (MtrCl) (23.18 g, 0.093 mol) were added, and the mixture was stirred at room temperature for 14 h. The solution was extracted with H_2O (3 × 50 mL), 0.1 M HCl (2 × 50 mL), and saturated NaCl (50 mL). Following drying ($MgSO_4$), the CH_2Cl_2 was evaporated to give a brown solid. Recrystallization from acetone/methanol gave a white powder (17.1 g, 0.028 mol, 79%): ^1H NMR ($CDCl_3$) δ 7.832 (d, 2 H, *J* = 8.64), 7.049 (d, 2 H, *J* = 8.67), 6.576 (s, 1 H), 6.393 (s, 1 H), 5.516 (t, 1 H, *J* = 6.41), 5.31 (d, 1 H, *J* = 6.7), 3.859 (s, 3 H), 3.809 (s, 3 H), 3.600 (m, 1 H), 3.077 (m, 2 H), 2.929 (dd, 1 H, *J* = 5.2, 14.1), 2.778 (dd, 1 H, *J* = 9.3, 14.0), 2.642 (s, 3 H), 2.566 (s, 3 H), 2.501 (s, 3 H), 2.260 (s, 3 H), 2.141 (s, 3 H), 1.963 (s, 3 H); ^{13}C NMR ($CDCl_3$) δ 159.48, 159.41, 146.47, 144.81, 138.83, 138.60, 138.40, 138.11, 129.45, 128.78, 128.34, 125.49, 125.28, 123.19, 123.10, 112.13, 111.70, 55.45, 55.34, 54.88, 46.65, 38.66, 24.23, 24.14, 17.89, 17.81, 11.91, 11.70; MS (CI-NH_3): *m/e* 620(M + H)$^+$, 637(M+NH_4)$^+$. Anal. Calcd for $C_{29}H_{37}N_3O_8S_2$ (619.77): C, 56.20; H, 6.02; N, 6.78. Found: C, 56.28; H, 6.01; N, 6.80.

***N,N'*-Bis(*p*-tolylsulfonyl)-1-(*p*-aminobenzyl)ethylenediamine (7a).** *N,N'*-Bis(*p*-tolylsulfonyl)-1-(*p*-nitrobenzyl)ethylenediamine (**6a**) (11.6 g, 0.023 mol) was dissolved in DMF (100 mL) in a Parr hydrogenation flask. Catalyst (0.75 g, 10% Pd–C) was added and the solution was hydrogenated at 20 psi for 1.5 h. The resulting suspension was filtered through a pad of Celite 577 on a medium frit. The clear filtrate was evaporated to an oil to which MeOH (150 mL) was added. The solution was heated briefly to boiling and allowed to cool to room temperature. The white crystalline product was collected and vacuum dried to give 8.6 g of product. Following evaporation of the filtrate, a second crystallization from MeOH gave an additional 1.7 g of product, giving a total yield of 10.3 g (0.022 mol, 95%): ^1H NMR (dmso-d_6) δ 7.569 (d, 2 H, *J* = 8.27), 7.406 (d, 2 H, *J* = 8.3), 7.361 (d,

2 H, J = 8.15), 7.209 (d, 2 H, J = 8.18), 6.569 (d, 2 H, J = 8.30), 6.341 (d, 2 H, J = 8.30), 4.843 (s, 2 H), 3.167 (m, 1 H), 2.70–2.48 (m, 3 H), 2.394 (s, 3 H), 2.360 (s, 3 H), 2.183 (dd, 1 H, J = 7.84, 13.91); ^{13}C (dmso-d_6) δ 146.71, 142.50, 142.03, 138.37, 137.32, 129.47, 129.37, 129.16, 126.41, 126.10, 124.36, 113.67, 54.70, 45.85, 36.52, 20.88; MS (CI-NH_3) m/e 474 (M + H)$^+$, 491 (M + NH_4)$^+$. Anal. Calcd for $C_{23}H_{27}N_3O_4S_2$ (473.62): C, 58.33; H, 5.75; N, 8.87. Found: C, 58.42; H, 5.78; N, 8.93.

N,N'-Bis[(4-methoxy-2,3,6-trimethylphenyl)sulfonyl]-1-(p-aminobenzyl)ethylenediamine (7b). Compound **7b** was prepared as described for **7a** by hydrogenating N,N'-bis[(4-methoxy-2,3,6-trimethylphenyl)-sulfonyl]-1-(p-nitrobenzyl)ethylenediamine (14.75 g, 23.8 mmol) over 10% Pd–C catalyst (0.75 g) at 20 psi in DMF (100 mL) for 1.5 h. The product was recrystallized from MeOH to give a white crystalline solid (12.8 g, 21.7 mmol, 91%): ^{1}H NMR ($CDCl_3$) δ 6.640 (d, 2 H, J = 8.30), 6.564 (s, 1 H), 6.525 (s, 1 H), 6.537 (d, 2 H, J = 8.28), 5.12 (t, 1 H, J = 6.5), 4.616 (d, 1 H, J = 5.92), 3.850 (s, 6 H), 3.65 (br, 2 H), 3.349 (m, 1 H), 3.015 (m, 1 H), 2.882 (m, 1 H), 2.62 (s, 3 H), 2.61 (m, 1 H, partially obscured by singlet at 2.62), 2.549 (s, 6 H), 2.55 (m, 1 H, partially obscured by singlet at 2.549), 2.218 (s, 3 H), 2.143 (s, 3 H), 2.064 (s, 3 H); ^{13}C NMR (dmso-d_6) δ 158.46, 158.30, 146.39, 138.04, 137.85, 137.28, 129.43, 128.86, 128.78, 124.44, 124.01, 123.90, 113.42, 112.22, 111.91, 55.53, 55.46, 54.07, 45.51, 36.45, 23.79, 23.57, 17.44, 17.39, 11.66, 11.56; MS (CI-NH_3) m/e 590(M + H)$^+$ 607(M + NH_4)$^+$. Anal. Calcd for $C_{29}H_{39}N_3O_6S_2$ (589.78): C, 59.06; H, 6.67; N, 7.12. Found: C, 58.84; H, 6.76; N, 7.07.

N,N'-Bis(p-tolylsulfonyl)-1-(p-benzamidobenzyl)ethylenediamine (8a). N,N'-Bis(p-tolylsulfonyl)-1-(p-aminobenzyl)ethylenediamine (**7a**) (8.67 g, 0.018 mol), benzoic anhydride (0.019 mol, 4.35 g), and Et_3N (2.65 mL, 0.019 mol) were reacted in DMF (50 mL) at room temperature for 14 h. The DMF solution was poured into water (200 mL), and the resulting precipitate was collected and air-dried. The product was recrystallized from DMF/MeOH and isolated as a white solid (9.70 g, 92%): ^{1}H NMR (dmso-d_6) δ 10.149 (s, 1 H), 7.971 (d, 2 H, J = 6.57), 7.719 (t, 1 H, J = 6.11), 7.62–7.58 (m, 4 H), 7.558 (d, 2 H, J = 7.45), 7.505 (d, 2 H, J = 8.42), 7.399 (d, 2 H, J = 8.16), 7.337 (2 H, d, J = 8.18), 7.140 (d, 2 H, J = 8.18), 6.848 (d, 2 H, J = 8.42), 3.25 (m, 1 H), 2.81–2.74 (m, 2 H), 2.63 (m, 1 H), 2.412 (s, 3 H), 2.329 (partially obscured dd, 1 H, J = 5.1, ≅13); ^{13}C NMR (dmso-d_6) δ 165.20, 142.53, 141.84, 138.14, 137.43, 137.21, 135.05, 132.76, 131.28, 129.50, 129.07, 128.95, 128.22, 127.43, 126.40, 125.94, 119.74, 54.51, 46.45, 36.57, 20.84, 20.75; MS (CI-NH_3) m/e 578(M + H)$^+$, 595 (M + NH_4)$^+$. Anal. Calcd for $C_{30}H_{31}N_3O_5S_2$ (577.74): C, 62.37; H, 5.41; N, 7.27. Found: C, 62.28; H, 5.40; N, 7.34.

N,N'-Bis[(4-methoxy-2,3,6-trimethylphenyl)sulfonyl]-1-(p-benzamidobenzyl)ethylenediamine (8b). Compound **8b** was prepared by reacting **7b** (11.78 g, 0.020 mol), benzoic anhydride (4.76 g, 0.021 mol), and triethylamine (2.12 g, 2.93 mL, 0.021 mol) in anhydrous DMF (60 mL) for 12 h at room temperature. The reaction was poured into H_2O (200 mL) and the resulting precipitate collected on a medium frit. The solid was dissolved in CH_2Cl_2 (150 mL), extracted with H_2O (3 × 30 mL), dried ($MgSO_4$), and evaporated to an oil which solidified upon standing. The solid was recrystallized by slow evaporation of a MeOH solution (11.9 g, 86%): ^{1}H NMR ($CDCl_3$) δ 7.89–7.86 (m, 2 H), 7.818 (s, 1 H), 7.56–7.47 (m, 3 H), 7.392 (d, 2 H, J = 8.40), 6.871 (d, 2 H, J = 8.32), 6.573 (s, 1 H), 6.516 (s, 1 H), 5.195 (t, 1 H, J = 6.5), 4.813 (d, 1 H, J = 7.06), 3.851 (s, 3 H), 3.811 (s, 3 H), 3.394 (m, 1 H), 3.00–3.40 (m, 1 H), 2.86 (m, 1 H), 2.764 (dd, 1 H, J = 6.3, 14.0), 2.619 (s, 3 H), 2.60 (m, 1 H, partially obscured by resonance at 2.619), 2.552 (s, 3 H), 2.283 (s, 3 H), 2.144 (s, 3 H), 2.047 (s, 3 H); MS (CI-NH_3) m/e 694 (M + H)$^+$, 711 (M + NH_4)$^+$. Anal. Calcd for $C_{36}H_{43}N_3O_7S_2$ (693.90): C, 62.32; H, 6.25; N, 6.06. Found: C, 62.30; H, 6.30; N, 6.02.

N,N-Bis[2-[(p-tolylsulfonyl)oxy]ethyl]-p-toluenesulfonamide (9) (*23*). A solution of p-tolylsulfonyl chloride (229 g, 1.2 mol) in CH_2Cl_2 (200 mL) was cooled to 0 °C. Diethanolamine (40.4 g, 0.4 mol) dissolved in CH_2Cl_2 (170 mL) and Et_3N (170 mL) was added over 1 h. The solution was warmed to room temperature and stirred for 12 h. The solid Et_3N·HCl was filtered off, and the filtrate extracted with H_2O (100 mL), 0.5 M HCl (3 × 100 mL), and H_2O (100 mL). The CH_2Cl_2 was dried (Na_2SO_4) and evaporated to a yellow oil which crystallized upon standing. Pure product was obtained after washing with EtOAc and drying (159 g, 70%): ^{1}H NMR (dmso-d_6) δ 7.729 (d, 4 H, J = 8.30), 7.571 (d, 2 H, J = 8.30), 7.478 (d, 4 H, J = 8.30), 7.356 (d, 2 H, J = 8.1), 3.999 (t, 4 H, J = 5.83), 3.287 (t, 4 H, J = 5.77), 2.425 (s, 6 H), 2.374 (s, 3 H); ^{13}C NMR (dmso-d_6) δ 145.04, 143.64, 131.99, 130.19, 130.11, 129.82, 127.46, 126.87, 68.04, 47.21, 21.01, 20.86; MS (CI-NH_3) m/e 568 (M + H)$^+$, 585(M + NH_4)$^+$.

Dimethyl N-[(4-Methoxy-2,3,6-trimethylphenyl)sulfonyl]iminodiacetate (11). Dimethyl iminodiacetate hydrochloride (**10**) (10 g, 51 mmol) was suspended in CH_2Cl_2 (200 mL). Triethylamine (15.3 mL, 111 mmol) was added and the flask was cooled to 0 °C. MtrCl (12.18 g, 49 mmol) in $CHCl_3$ (60 mL) was added dropwise over ca. 2 h and the solution stirred at room temperature for 16 h. The solution was extracted with H_2O (100 mL), 1 M HCl (2 × 100 mL), and brine (100 mL). The organic phase was dried over $MgSO_4$, filtered, and rotary evaporated to a thick oil. The product was purified by column chromatography on silica gel 60 (Merck, 70-230 mesh, ASTM) eluting with $CHCl_3$. The fractions containing the product were combined and concentrated to an oil which crystallized on standing at room temperature (16.7 g, 91%): TLC on silica (Merck) with 5% MeOH in $CHCl_3$, R_f 0.64; ^{1}H NMR ($CDCl_3$) δ 6.504 (s, 1 H), 4.122 (s, 4 H), 3.780 (s, 3 H), 3.509 (s, 6 H), 2.594 (s, 3 H), 2.437 (s, 3 H), 2.069 (s, 3 H); ^{13}C NMR ($CDCl_3$) δ 169.34, 159.83, 140.61, 140.46, 126.97, 125.35, 112.07, 55.47, 52.05, 47.22, 24.34, 17.49, 11.94; MS (CI-NH_3) m/e 374 (M + 1)$^+$, 391 (M + 18)$^+$. Anal. Calcd for $C_{16}H_{23}N_1O_7S_1$ (373.44): C, 51.46; H, 6.21; N, 3.75. Found: C, 51.29; H, 6.22; N, 3.74.

N-[(4-Methoxy-2,3,6-trimethylphenyl)sulfonyl]diethanolamine (12). A solution of diester **11** (8.0 g, 21.4 mmol) in THF (75 mL) was added dropwise to LAH (1.46 g, 43 mmol) in THF (100 mL) under argon. After the addition was completed, the mixture was heated to mild reflux for 18 h. After cooling in an ice bath, 1 M NaOH (20 mL) was added carefully along with THF (75 mL). The suspension was filtered and the filtrate combined with Et_2O (200 mL) and then extracted with brine (3 × 100 mL). The organic phase was dried over $MgSO_4$, filtered, and rotary evaporated to an off-white solid (5.9 g, 87%): TLC on silica (Merck) with 10% MeOH in $CHCl_3$, R_f 0.34; ^{1}H NMR ($CDCl_3$) δ 6.594 (s, 1 H), 3.855 (s, 3 H), 3.732 (t, 4 H, J = 5.0), 3.554 (br s, 2 H), 3.343 (t, 4 H, J = 5.0), 2.662 (s, 3 H), 2.541 (s, 3 H), 2.144 (s, 3 H); ^{13}C NMR ($CDCl_3$) δ 159.81, 140.26, 140.16, 126.85, 125.48, 112.18, 61.04, 55.45, 50.56, 24.25, 17.52, 11.95; MS (CI-NH_3) m/e 318 (M + 1)$^+$, 335 (M + 18)$^+$. Anal. Calcd for $C_{14}H_{23}N_1O_5S_1$ (317.48): C, 52.97; H, 7.32; N, 4.41. Found: C, 52.95; H, 7.31; N, 4.46.

N,N-Bis[2-[(p-tolylsulfonyl)oxy]ethyl]-4-methoxy-2,3,6-trimethylbenzenesulfonamide (13). Diol 12 (5.0 g, 15.8 mmol) was dissolved in CH_2Cl_2 (100 mL), and triethylamine (4.4 mL, 31.5 mmol) was added. The solution was cooled to 0 °C while p-toluenesulfonyl choride (6.0 g, 31.5 mmol) in CH_2Cl_2 (50 mL) was added dropwise over 1 h. After the addition was complete the reaction was stirred at room temperature for 18 h. The solution was then extracted with H_2O (3 × 100 mL) and brine (100 mL). The CH_2Cl_2 solution was dried over $MgSO_4$, filtered, and rotary evaporated to a thick oil. The oil was taken up in MeOH (ca. 50 mL) and acetone was added to clarify the solution. The product crystallized upon standing (8.42 g, 85%): TLC on silica (Merck) with 1% MeOH in $CHCl_3$, R_f 0.42; ^1H NMR ($CDCl_3$) δ 7.639 (d, 4 H, J = 9.0), 7.265 (d, 4 H, J = 9.0), 6.487 (s, 1 H), 3.927 (t, 4 H, J = 5.0), 3.785 (s, 3 H), 3.372 (t, 4 H, J = 5.0), 2.497 (s, 3 H), 2.376 (s, 6 H), 2.034 (s, 3 H); ^{13}C NMR ($CDCl_3$) δ 160.02, 145.10, 140.33, 132.40, 129.93, 127.84, 126.22, 125.73, 112.20, 67.43, 55.49, 46.16, 24.16, 21.58, 17.47, 11.88; MS (CI-NH_3) m/e 626 $(M + 1)^+$, 643 $(M + 18)^+$. Anal. Calcd for $C_{28}H_{35}N_1O_9S_3$ (625.80): C, 52.74; H, 5.64; N, 2.24. Found: C, 52.26; H, 5.61; N, 2.28.

2-(p-Benzamidobenzyl)-1,4,7-tris(p-tolylsulfonyl)-1,4,7-triazacyclononane (14a). N,N'-Bis(p-tolylsulfonyl)-1-(p-benzamidobenzyl)ethylenediamine (**8a**) (5.22 g, 9.05 mmol) and N,N-bis[2-[(p-tolylsulfonyl)oxy]ethyl]-p-toluenesulfonamide (**9**) (5.13 g, 9.05 mmol) were dissolved in DMF (300 mL) under argon. Cesium carbonate (6.19g, 0.019 mol) was added and the reaction heated to 75 °C for 14 h. The reaction was cooled to room temperature, filtered, and evaporated to give to an oil which was dissolved in CH_2Cl_2 (200 mL) and extracted with H_2O (2 × 50 mL), 10% NaOH (2 × 50 mL), 0.1 M HCl (50 mL), and H_2O (50 mL). The CH_2Cl_2 was dried (Na_2SO_4) and evaporated to a solid which was recrystallized from DMF/CH_3OH (4.0 g, 5.0 mmol, 55%): ^1H NMR (dmso-d_6): δ 10.331 (s, 1 H), 8.010 (d, 2 H, J = 8.03), 7.818 (d, 2 H, J = 8.09), 7.755 (d, 2 H, J = 8.36), 7.714 (d, 2 H, J = 8.21), 7.62–7.53 (m, 3 H), 7.47–7.43 (m, 4 H), 7.341 (d, 2 H, J = 8.06), 7.155 (d, 2 H, J = 7.45), 7.095 (d, 2 H, J = 8.37), 4.435 (m, 1 H), 3.71–3.63 (m, 4 H), 3.28 (m, 1 H), 3.10–2.90 (m, 5 H), 2.420 (s, 3 H), 2.387 (s, 3 H), 2.378 (s, 3 H), 2.4–2.3 (obscured m, 1 H), 2.20 (m, 1 H); ^{13}C (dmso-d_6) δ 165.46, 143.74, 143.47, 143.38, 137.60, 136.48, 134.96, 134.02, 133.36, 133.29, 132.27, 131.45, 129.92, 129.68, 129.25, 128.32, 127.55, 127.18, 127.06, 120.04, 60.25, 53.21, 52.44, 49.98, 49.72, 45.55, 34.27, 20.92; MS (CI-NH_3) m/e 801 $(M + H)^+$, 818 $(M + NH_4)^+$. Anal. Calcd for $C_{41}H_{44}N_4O_7S_3$ (801.02): C, 61.48; H, 5.54; N, 6.99. Found: C, 61.32; H, 5.53; N, 7.00.

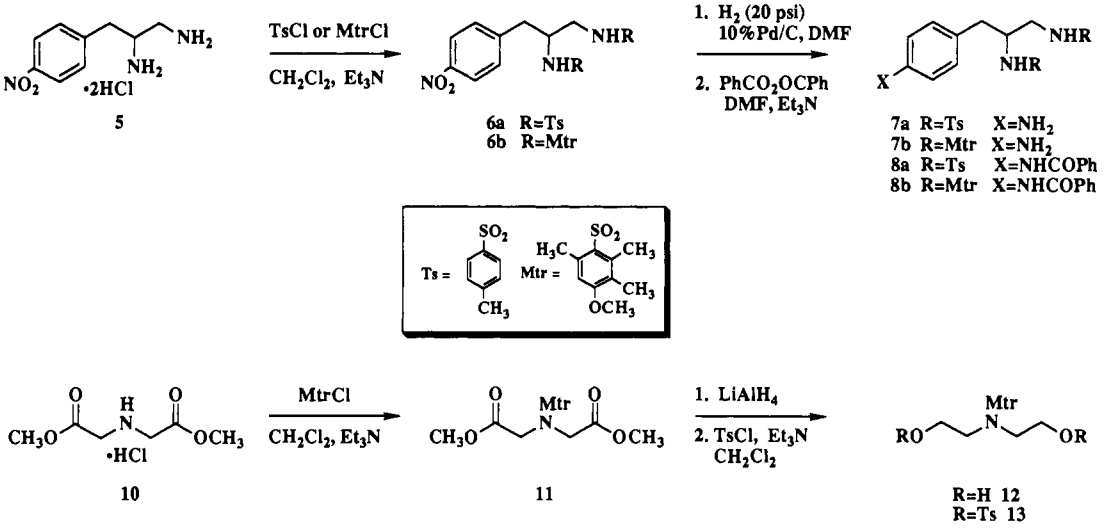
2-(p-Benzamidobenzyl)-1,4,7-tris[(4-methoxy-2,3,6-trimethylphenyl)sulfonyl]-1,4,7-triazacyclononane (14b). Compound **14b** was prepared as described for **14a** by reacting N,N'-bis[(4-methoxy-2,3,6-trimethylphenyl)sulfonyl]-1-(p-benzamidobenzyl)ethylenediamine (**8b**) (3.75 g, 5.4 mmol) with N,N-bis[2-[[(4-methoxy-2,3,6-trimethylphenyl)sulfonyl]oxy]ethyl]-p-toluenesulfonamide (**13**) (3.38 g, 5.4 mmol), and Cs_2CO_3 (3.91 g, 12 mmol) in DMF (75 mL) at 90 °C for 14 h. Following workup, the residue was flash chromatographed (silica, 41 × 200 mm, CH_2Cl_2 to 0.75% MeOH/CH_2Cl_2) and recrystallized from EtOAc/acetone to give a pale yellow solid (1.8g, 34%): ^1H NMR (dmso-d_6) δ 7.90–7.86 (m, 2 H), 7.831 (s, 1 H), 7.57–7.47 (m, 3 H), 7.331 (d, 2 H, J = 8.42), 6.651 (s, 1 H), 6.612 (s, 1 H), 6.411 (d, 2 H, J = 8.4), 6.396 (s, 1 H), 4.330 (dd, 1 H, J = 11.7, 14.8), 4.17–4.10 (m, 1 H), 4.024 (dd, 1 H, J = 10.2, 15.7), 3.95–3.80 (m, 3 H, obscured by s at 3.866 and 3.857), 3.866 (s, 3 H), 3.857 (s, 3 H), 3.796 (s, 3 H), 3.72–3.62 (m, 1 H), 3.526 (dd, 1 H, J = 9.9, 16.2), 3.21–3.10 (m, 2 H), 2.83–2.78 (m, 2 H), 2.713 (s, 3 H), 2.672 (s, 3 H), 2.544 (s, 3 H), 2.496 (s, 3 H), 2.355 (s, 3 H), 2.33 (m, 1 H, partially obscured by singlet at 2.355), 2.269 (s, 3 H), 2.153 (s, 3 H), 2.131 (s, 3 H), 2.070 (s, 3 H), 2.08–1.96 (m, 1 H); ^{13}C NMR ($CDCl_3$) δ 165.27, 159.65, 159.53, 159.27, 140.02, 139.83, 139.64, 139.38, 139.16, 136.39, 134.75, 132.72, 131.83, 129.40, 129.04, 128.77, 127.41, 127.18, 126.89, 125.81, 125.52, 124.85, 119.70, 112.49, 112.40, 112.23, 58.21, 55.53, 55.44, 50.40, 49.70, 46.45, 45.06, 41.64, 36.31, 25.11, 24.89, 23.91, 18.47, 17.99, 17.42, 12.09, 11.98, 11.88; MS (positive ion FAB) m/e 975 $(M + H)^+$. Anal. Calcd for $C_{50}H_{62}N_4O_{10}S_3$ (975.29): C, 61.58; H, 6.41; N, 5.74. Found: C, 61.07; H, 6.48; N, 5.69.

2-(p-Benzamidobenzyl)-1,4,7-triazacyclononane (15). 2-(p-Benzamidobenzyl)-1,4,7-tris(p-tolylsulfonyl)-1,4,7-triazacyclononane (**14a**) (4.0 g, 5 mmol) was dissolved in concentrated H_2SO_4 (20 mL) and heated to 95 °C for 22 h under argon. The resulting solution was cooled to room temperature and added in portions to Et_2O (200 mL, cooled to ca. −40 °C). The resulting hygroscopic precipitate was collected on a medium frit and vacuum-dried prior to dissolving in aqueous TFA (0.1%, 50 mL). The pH was adjusted to 2 with NaOH (1 M), and the solution diluted to 120 mL. Purification was achieved by HPLC chromatography (ca. 5 mL/run) using a Waters DeltaPak C-18 column (19 × 300 mm), a flow rate of 12.0 mL/min, and a gradient of 0-100% B/10 min (A = 0.1% TFA, B = 0.1% TFA/CH_3CN). The desired product eluted at 8.88 min. The combined fractions were evaporated to dryness and the resulting glass recrystallized from H_2O (4 mL) and 48% HBr (4 mL). The tan trihydrobromide salt was collected on a medium frit, washed with 2-propanol, and dried at 70 °C (0.1 mmHg) to give 0.67 g (23%): ^1H NMR (D_2O, pH 1, CD_3CN ref) δ 7.720 (d, 2 H, J = 7.47), 7.53–7.50 (m, 1 H), 7.447 (d, 2 H, J = 7.75), 7.392 (d, 2 H, J = 8.49), 7.247 (d, 2 H, J = 8.33), 3.54–3.26 (m, 5 H), 3.193 (dd, 1 H, J = 4.3, 13.5), 3.15–3.07 (m, 3 H), 2.971 (dd, 1 H, J = 4.2, 13.5), 2.828 (m, 1 H), 2.78-2.73 (m, 2 H); ^{13}C (D_2O, pH 1, CD_3CN) δ 170.10, 136.85, 134.65, 133.27, 130.75, 129.68, 128.21, 123.68, 55.21, 47.46, 44.67, 42.72, 40.14, 37.84; MS (CI-NH_3) m/e 339 $(M + H)^+$. Anal. Calcd for $C_{20}H_{26}N_4O{\cdot}3HBr$ (581.20): C, 41.33; H, 5.03; N, 9.64; Br, 41.24. Found: C, 41.15; H, 5.05; N, 9.58; Br, 41.09.

Via **14b.** 2-(p-Benzamidobenzyl)-1,4,7-tris[(4-methoxy-2,3,6-trimethylphenyl)sulfonyl]-1,4,7-triazacyclononane (**14b**) (1.17 g, 1.2 mmol) was dissolved in concentrated H_2SO_4 (10 mL) and heated to 90 °C under argon for 90 min. The solution was cooled to room temperature and added in portions to Et_2O (150 mL) which had been cooled to ca. −40 °C. The resulting hygroscopic precipitate was collected on a medium frit, washed with Et_2O, and immediately dissolved in H_2O. The aqueous solution was extracted once with Et_2O and concentrated to approximately 2 mL. To effect crystallization, an equal volume of 48% HBr was added and the solution set aside at room temperature. The hydrobromide salt was collected and vacuum-dried to give 0.42 g (60%). Physical properties were identical to the material isolated above.

2-(p-Benzamidobenzyl)-1,4,7-triazacyclononane-N,N',N''-triacetic Acid (16) (IV in Figure 1). 2-(p-Benzamidobenzyl)-1,4,7-triazacyclononane trihydrobromide (0.58 g, 1.0 mmol) was dissolved in H_2O (15 mL), heated to 45 °C, and neutralized with 5 M NaOH (0.4 mL). Bromoacetic acid (0.56 g, 4 mmol) was added, NaOH (5 M) was also added to maintain the pH at 9.0 (pH stat). After 24 h, additional $BrCH_2CO_2H$ (0.56 g, 4 mmol) was added and the reaction continued for another 24 h. The

Scheme I. Synthesis of Sulfonamide-Protected Cyclization Precursors



pH was reduced to 3.0 with concentrated HBr. The clear solution was left to stand at room temperature for 72 h. The white precipitate was collected and vacuum-dried (0.38 g, 0.73 mmol, 73%): ^{1}H NMR (dmso-d_6): δ 10.74 (s, 1 H), 7.948 (d, 2 H, J = 8.37), 7.719 (d, 2 H, J = 8.42), 7.59–7.49 (m, 3 H), 7.232 (d, 2 H, J = 7.63), 3.540 (dd, 2 H, J = 14, 35), 3.44–3.26 (m, 6 H), 3.18–2.70 (m, 10 H), 2.643 (unresolved dd, 1 H, J_{AB} = 12); ^{1}H NMR (D_2O, pH 12, CD_3CN ref) δ 7.706 (d, 2 H, J = 7.20), 7.51–7.30 (m, 3 H), 7.289 (d, 2 H, J = 8.30), 7.017 (d, 2 H, J = 8.23), 3.402 (br d, 1 H, J = 15.9), 3.172 (d, 1 H, J = 16.4), 3.09–3.00 (m, 4 H), 2.91–2.70 (m, 6 H), 2.58–2.38 (m, 3 H), 2.156 (unresolved dd, 1 H, J_{AB} = 12.9), 2.08–1.96 (m, 4 H); ^{13}C (dmso-d_6) 171.45, 170.58, 169.74, 165.37, 137.44, 134.98, 133.32, 131.38, 129.10, 128.26, 127.53, 120.40, 60.0 (v br), 59.36, 56.01, 51.0 (br), 46.0 (br), 43.5 (br), 33.04; ^{13}C (D_2O, pH 12, CD_3CN) δ 181.12, 180.73, 180.64, 169.75, 138.22, 136.18, 134.95, 133.19, 130.53, 129.72, 128.26, 123.20, 120.19, 63.17, 63.04, 61.71, 61.64, 59.02, 54.38, 53.73, 49.29, 45.69, 31.66; MS (positive ion FAB) m/e 513 (M + H)$^+$, 535 (M + Na)$^+$; HPLC t_R 16.35 min. Anal. Calcd for $C_{26}H_{32}N_4O_7 \cdot 0.5H_2O$ (521.58): C, 59.88; H, 6.38; N, 10.74. Found: C, 59.54; H, 6.18; N, 10.40.

2-(*p*-Benzamidobenzyl)-1,4,7-triazacyclononane-*N,N',N''*-tri(2-^{14}C)acetic Acid (16-^{14}C). The synthesis of ^{14}C-labeled **16** was performed as described above for nonradioactive **16** by alkylating **15** (1.74 g, 3 mmol) with 2-bromo[2-^{14}C]acetic acid (3.0 mCi, Chemsyn Science Labs) prior to adding nonradioactive bromoacetic acid (4.87 g, 0.035 mol, pH 9.0). The product was precipitated at pH 3 and dried: HPLC t_R 16.34 min.

The specific activity was determined by dissolving a known weight of ligand in a vial, determining the exact concentration by spectrophotometry (ϵ_{269nm} =12 950 L mol^{-1} cm^{-1}, pH 6.2, 0.01 M MesCl, determined for analytically pure **16**) and averaging the counts of four 50-μL aliquots: 1.01 mCi/mmol.

2-(*p*-Aminobenzyl)-1,4,7-triazacyclononane-*N,N',N''*-triacetic Acid (17). Benzamide **16** (0.34 g, 0.65 mmol) was dissolved in 6 M HCl (10 mL) and heated to 70 °C for 18 h. The solution was cooled to room temperature and filtered through a medium frit to remove benzoic acid. The filtrate was extracted with CH_2Cl_2 (5 × 5 mL) and lyophilized to give a pale yellow-green solid (0.32 g, 87%): ^{1}H NMR (D_2O, pH 1) δ 7.321 (d, 2 H, J = 8.2), 7.240 (d, 2 H, J = 8.3), 3.869 (dd, 4 H, J = 17.5, 32.3, obscures 1 H m, 3.9), 3.40–3.20 (br m, 8 H), 3.18–3.00 (m, 3 H), 2.898 (dd, 1 H, J = 7.3, 13.7), 2.79–2.59 (m, 2 H); MS (+FAB, noba) m/e 409 (M + H)$^+$, 431 (M + Na)$^+$; HPLC t_R 9.88 min. Anal. Calcd for $C_{19}H_{28}N_4O_6 \cdot 3HCl \cdot 2.5H_2O$ (562.89): C, 40.45; H, 6.45; N, 9.95. Found: C, 40.36; H, 6.11; N, 9.69.

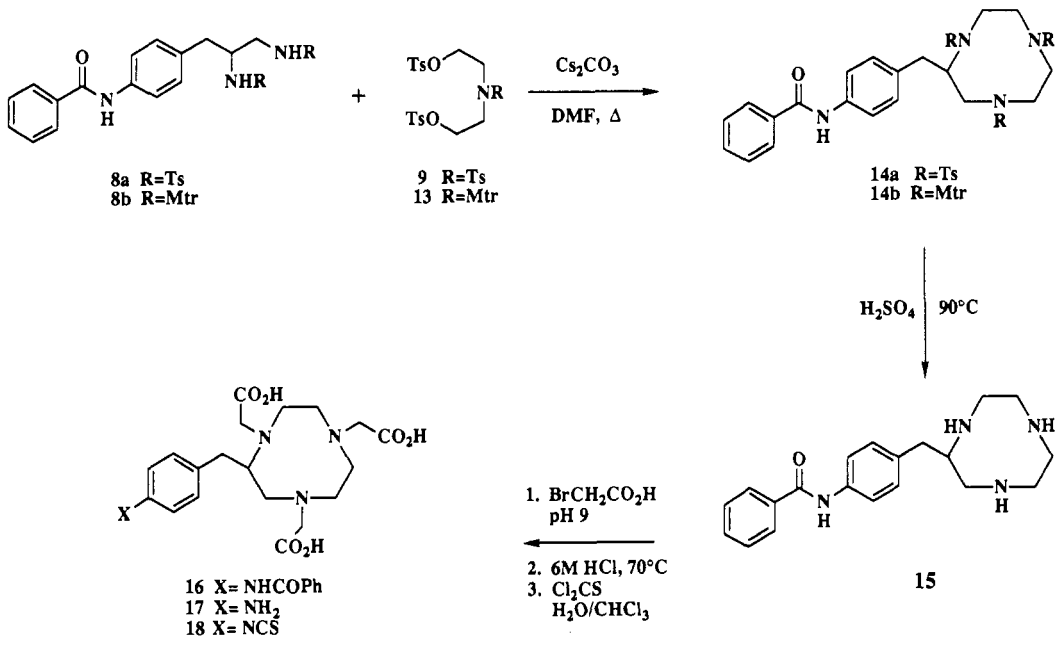
2-(*p*-Isothiocyanatobenzyl)-1,4,7-triazacyclononane-*N,N',N''*-triacetic Acid (4b). Aniline derivative **17** (0.103 g, 0.2 mmol) was dissolved in H_2O (0.40 mL) in an acid-washed Reacti-Vial. Thiophosgene (0.32 mL, 0.32 mmol, 1 M in $CHCl_3$) was added and the solution vigorously stirred for 2 h at room temperature. The aqueous layer was washed with $CHCl_3$ (4 × 0.1 mL) and then lyophilized to give 0.1 g (0.18 mmol, 90%): ^{1}H NMR (D_2O, pH 1) δ 7.319 (m, 4 H), 3.897 (dd, 4 H, J = 17.7, 34.4), 3.55–3.26 (m, 7 H), 3.24–3.34 (m, 4 H), 2.990 (dd, 2 H, J = 7.1, 14.0), 2.92–2.68 (m, 2 H); MS (+FAB, noba) m/e 451 (M + H)$^+$; IR 2080 cm^{-1}; HPLC t_R 18.44 min. Anal. Calcd for $C_{20}H_{20}N_4O_6S \cdot 3HCl \cdot 4H_2O$ (625.92): C,38.38; H, 4.99; N, 8.95; Cl, 16.99. Found: C, 38.66; H, 4.85; N, 8.86; Cl, 17.17.

RESULTS

Synthesis. The versatile (*p*-nitrobenzyl)ethylenediamine (**5**), readily prepared in three steps from the commercially available (*p*-nitrophenyl)alanine (*18*), was cleanly converted to the *N,N'*-tosylamide derivative by reaction with *p*-TsCl in anhydrous CH_2Cl_2 using Et_3N as a base (Scheme I). Reduction of the nitro group, performed in DMF due to the relative insolubility of the tosylamides in other solvents, followed by acylation of the amine with benzoic anhydride, gave the benzamide-protected substituted *N,N'*-(ditolylsulfonyl)ethylenediamine as a crystalline product. The analogous reactions using the Mtr protecting group proceeded uneventfully to give products which were more soluble in a variety of solvents than the corresponding Ts analogs, and were also able to be purified by recrystallization. The overall yield for the three-step transformation was 62%, as compared with 84% for the sequence involving tosylamide protection.

Reaction of the carbon-substituted tosylamide **8** with ditosylate **9** in the presence of 2.5 equiv of Cs_2CO_3 in DMF at 80 °C for 14 h yielded, upon evaporation of the DMF and aqueous workup, one major spot by TLC (Scheme II). Purification of this material was acheived by flash chromatography and subsequent recrystallization from ethanol to give pure macrocyclic tritosylamide **14** in 55% yield. Substitution of the Mtr protecting group for the Ts group in the cyclization components **8a** and **13** gave the mac-

Scheme II. Synthesis of 2-(*p*-NCS-Bz)-NOTA



rocycle **14a** in 34% yield after purification by flash chromatography and recrystallization from EtOAc/acetone.

Deprotection of the Ts derivative 14 was found to proceed more cleanly using H_2SO_4 instead of HBr/AcOH; *however, appreciable debenzoylation was noted in all cases.* If the reaction temperature exceeded 100 °C for several hours, the *p*-NH_2-Bz substituted macrocyclic triamine was the only observable product. Acceptable conditions were found to be deprotection at 90 °C for 22 h, which resulted in a mixture of the desired benzamide-protected macrocyclic triamine **15** and the debenzoylated impurity. Pure macrocycle **15** was separated from the mixture by HPLC and recrystallized from aqueous HBr to give analytically pure trihydrobromide salt in 23% yield. In contrast, when the Mtr-protected triamine was subjected to the same deprotection conditions (H_2SO_4, 90 °C), complete removal of the Mtr functionality was achieved in *90 min without competing debenzoylation.* Consequently, HPLC purification of the resulting triamine was not required and the product was directly recrystallized to give the hydrobromide salt in 60% yield.

Alkylation of the macrocyclic triamine using bromoacetic acid at pH 9.0 (pH stat) and subsequent precipitation at pH 3.0 gave a 73% yield of analytically pure poly(amino carboxylate) **16** (**IV** in Figure 1). In order to eventually permit accurate measurement of the number of chelating agents attached to antibody, a ^{14}C-labeled version of **16** was conveniently prepared at this stage in the synthesis by using bromo-(2-^{14}C) acetic acid. Purification and further reactions of the labeled material was performed in a manner identical to that described herein for the ^{12}C compounds. With the acetate functionality in place, the benzamide was hydrolyzed (6 M HCl, 70 °C) and the resulting aniline derivative **17** converted to the isothiocyanate **18** by reaction with thiophosgene. The identity and absolute purity of all compounds was demonstrated unequivocally by NMR, FAB-MS, and analysis.

Serum Stability. Representative FPLC radiochromatograms of the ^{67}Cu complexes of ligands acetate, **IV**, **V**, and **VI** sampled on days 1, 3, and 9 following incubation in bovine serum are shown in Figure 2. Copper-67 which dissociated from the complexes was transferred to serum proteins eluting primarily in fractions 35–42. Support for this interpretation comes from incubation of the weakly complexed ^{67}Cu acetate in serum (or with BSA), which resulted in rapid transfer of the Cu(II) ion to proteins which eluted in fractions 35–42. A minor component of free ^{67}Cu (ca. 2–3%) was complexed by an unidentified low molecular weight species which eluted in fraction 55. The percentage of this low molecular weight species decreased with increasing incubation time. The percentage of precipitated activity observed was <0.5% in all experiments, roughly equivalent to the binding of the copper complexes to the filter paper.

The percentage of ^{67}Cu released from the chelates as a function of time is shown in Figure 3. The complex of macrocyclic triamine **I** dissociated right after mixing with serum, and no further data are presented. Both the acyclic ligand 1B4M-DTPA (**VII**) and the 14-membered ring poly(amino carboxylate) ligand 2-(*p*-NO_2-Bz)-TETA (**VI**) formed significantly less stable complexes than ligands **II**–**V**. The copper-67 complex of 2-(*p*-PhCONH-Bz)-NOTA (**IV**) lost less than 2% of activity over the 9-day incubation period and is thus quite inert. However, the most stable copper complexes were formed by the ligands 2-(*p*-nitrobenzyl)-1,4,7,10-tetraazacyclododecane (**II**), 2-(*p*-nitrobenzyl)-1,4,8,11-tetraazacyclotetradecane (**III**) and 2-(*p*-NO_2-Bz)-DOTA (**V**), as evidenced by the fact that less than 1% of the ^{67}Cu activity dissociated over the 9-day incubation period.

DISCUSSION

Synthesis. The key step of our synthetic strategy to prepare C-functionalized NOTA relied upon the well-established Richman–Atkins tosylamide cyclization procedure to generate the *p*-tolylsulfonamide-protected macrocyclic triamine ring system. Utilization of the *p*-PhCONH-Bz-substituted ethylenediamine p-tolyl sulfonamide **8a** as a reactant with **9** allowed the preparation of the C-functionalized macrocycle **14a** in good yield without resorting to high-dilution cyclization conditions. However, in contrast to the results of Parker et al. (*14*), who observed little debenzoylation in the deprotection of **3a** using H_2SO_4 at 110 °C for 36 h, hydrolysis of the benzamide protecting group of **14a** eventually competed with detosylation at 90 °C and predominated if the

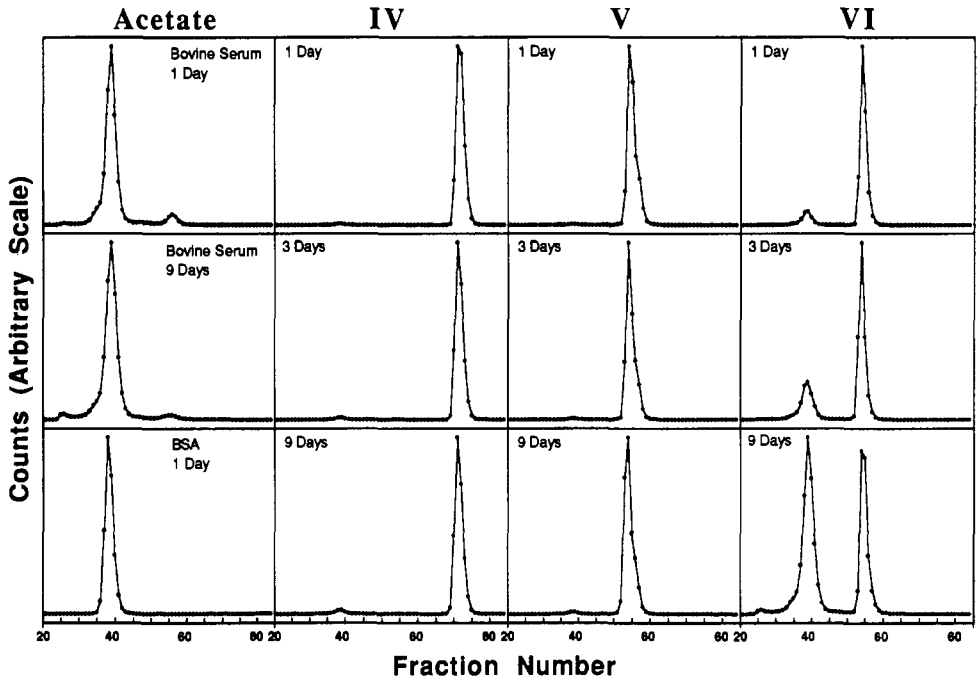


Figure 2. FPLC radiochromatograms (0.33 mL/fraction) observed following 1-, 3-, and 9-day incubation periods in serum of the ^{67}Cu complexes of the ligands acetate, 2-(*p*-PhCONH-Bz)-NOTA (**IV**), 2-(*p*-NO_2-Bz)-DOTA (**V**) and 2-(*p*-NO_2-Bz)-TETA (**VI**).

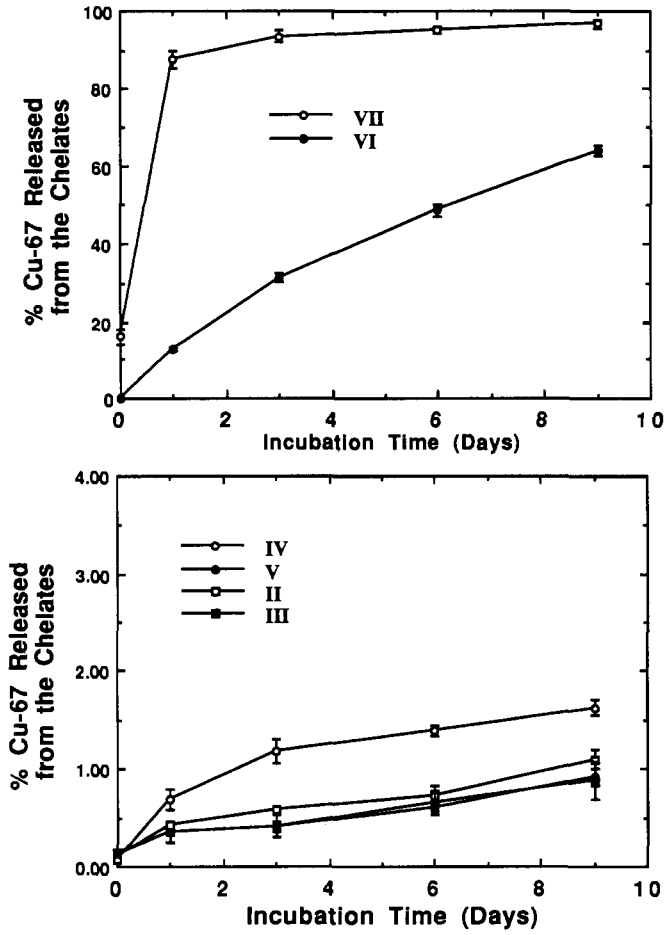


Figure 3. Percent loss of activity as a function of time for ^{67}Cu complexes of the ligands shown in Figure 1.

temperature exceeded 100 °C. Therefore, an alternative sulfonamide protecting group was sought which could function in the Richman–Atkins cyclization, yet might be removed under milder conditions. Fujino and co-workers evaluated a series of functionalized arylsulfonamides for use in peptide synthesis and concluded that the Mtr group was the most acid labile among those tested (*24*). Accordingly, we prepared the Mtr-protected precursors **8b** and **13** and cyclized them to form product **14b** in 34% yield. The decrease in yield as compared with that observed for the tosylamide-protected route (55%) was gratifyingly small considering the potential steric constraints imposed by the introduction of two ortho methyls in the Mtr sulfonamide. It is noteworthy that compound **8b** failed to react with the tris(Mtr) analog of **9**, suggesting that the Mtr group was a poor leaving group for nucleophilic substitution, necessitating the three-step preparation of **13**. The pure macrocycle was free of higher molecular weight peaks in the positive ion FAB MS and characterized by unique singlets for each of the Mtr methyl, methoxy, and ArH resonances in the 300-MHz ^1H NMR.

While Parker and co-workers have noted that (*p-methoxyphenylsulfonyl*-protected amines offered little advantage in the synthesis of the aminobutyl-substituted 1,4,7-triazacyclononane ring system (*15*), our results demonstrated a *significant improvement in yield for the H_2SO_4 deprotection step* using the (2,3,6-trimethyl-4-methoxyphenylsulfonyl (Mtr) protecting group (60% vs 23% for the Ts derivative). Although this increase was somewhat offset by the lower cyclization yield found for the Mtr system, a modest improvement in overall percent conversion of (*p*-nitrobenzyl)ethylenediamine into substituted macrocyclic polyamine was observed when comparing the Mtr vs Ts protection (12.6% vs 10.6%). More importantly, *no aniline production was observed* during the relatively facile deprotection (H_2SO_4, 90 °C, 1.5 h) of the Mtr moiety, rendering HPLC purification of the resulting amine unnecessary and contributing to an overall more attractive preparation of the triamine by the Mtr route. The overall efficiency for the synthesis of analytically pure p-PhCONH-Bz-NOTA (**6**) by the Mtr route from commerically available *p*-nitrophenylalanine was 6.4%, as compared with 7.7% (from (*S*)-lysine) for the preparation of Parker's benzamide protected, C-functionalized NOTA (*15*) and 1.34% (from *N*-(*tert*-butoxycarbonyl)-*p*-nitrophenylalanine) for the preparation of

p-NO_2-Bz-NOTA by a peptide route (*16*). These results suggest that the Mtr group may be useful for the preparation of other macrocyclic polyamines and their derivatives.

Serum Stability. Recognition of the kinetic lability of copper complexes of acyclic poly(amino carboxylates) EDTA or DTPA has led to application of macrocyclic 6-p-NO_2-Bz-TETA derivatives (*25*) to the problems of sequestering copper isotopes in vivo (*26*). However, with the notable exception of the 1,4,7-triazacyclononane/NOTA pair, 12–14-membered ring macrocyclic *polyamines* generally form copper complexes which are more thermodynamically stable than their amino carboxylate derivatives, as reflected by the stability constants of the 1,4,7,10-tetraazacyclododecane (log K_{CuL} = 24.8) and 1,4,8,11 tetraazacyclotetradecane (log K_{CuL} = 27.2) as compared with the corresponding poly(amino carboxylate) derivatives DOTA (log K_{CuL} = 22.2) and TETA (log K_{CuL} = 21.6) (*27*). Cationic macrocyclic tetraamine copper(II) complexes are also known to be kinetically inert toward acid-catalyzed dissociation of copper (*28*). Several groups have exploited the latter to advantage in the preparation and evaluation of several bifunctional macrocyclic tetraamines specifically designed for use with iostopes of copper (*29*). The bifunctional NOTA ligand provides *exactly* the number of donor atoms needed to satisfy the coordination sphere of the Cu(II) ion, and thus provides an interesting comparison to the N_4 donor macrocyclic tetraamines and the N_4O_4 donor macrocyles DOTA and TETA. As part of our initial screening of potential copper(II) sequestering agents, we evaluated the serum stability of 2-(*p*-PhCONH-Bz)-substituted NOTA (**IV**) and 1,4,7-triazacyclononane (**I**), as well as other potential candidates including 2-(*p*-NO_2-Bz)-DOTA (**V**), 2-(*p*-NO_2-Bz)-TETA (**VI**), 2-(*p*-NO_2-Bz)-1,4,7,10-tetraazacyclododecane (**II**), 2-(*p*-NO_2-Bz)-1,4,8,11 tetraazacyclotetradecane (**III**), and the acyclic 1B4M-DTPA (**VII**) (Figure 1).

The results clearly demonstrate the rate of loss of ^{67}Cu from 1,4,7-triazacyclononane (**I**), 1B4M-DTPA (**VII**), and 2-(*p*-NO_2-Bz)-TETA (**VI**) was significantly greater than that observed for any of the other complexes. The instability of the triazacyclononane complex was anticipated as the 1,4,7-triazacyclononane N_3 donor set is incapable of occupying four equatorial sites of a pseudooctahedral Cu(II) ion and is reflected in the relatively low thermodynamic stability of [Cu(1,4,7-triazacyclononane)]$^{2+}$ (log K_{ML} = 15.5). The observation that 2-(*p*-NO_2-Bz)-TETA lost Cu(II) at a significant rate in serum may be a consequence of the relatively large cavity size of the 1,4,8,11-tetraazacyclotetradecane ring system combined with the fact all eight (N_4O_4) donors cannot be simultaneously coordinated to one Cu(II) ion. Consistent with that notion, binuclear Cu(II) complexes of TETA have been crystallized, suggesting a mechanism for replacement of Cu(II) with a competing metal (*30*). However, it is important to note that the *position of the carbon substitution* affects the stability of the resulting copper complex, as evidenced by the fact that the copper complex of 6-(*p*-NO_2-Bz)-TETA was reported to be significantly more stable in serum than the complex of the 2-(*p*-NO_2-Bz) isomer in a direct comparison (*31*, *32*). While the serum studies reported herein were performed in *bovine* serum instead of human serum, qualitatively the results of the two reports are in excellent agreement. Our results also showed that 2-(*p*-NO_2-Bz)-DOTA (**V**) formed a kinetically stable complex with copper in serum, this despite the fact it might also have been expected to form a binuclear Cu(II) complex (*30*). Thus, the carbon-substituted DOTA ligand apparently retained the well-known kinetic stability of the divalent and trivalent metal complexes of the parent macrocycle DOTA (*33*). The copper complexes of ligands **II** and **III** were also remarkably stable in serum and could not be differentiated from the results observed for 2-(*p*-NO_2-Bz)-DOTA (**V**) within the error limits of the experiment. Interestingly, the Cu(II) complex of 2-(*p*-PhCONH-Bz)-NOTA was somewhat less stable in serum, suggesting that molecules with four equatorial N donors may be superior in vivo. However, although it has been reported that administration of weakly complexed copper will accumulate in the liver or kidney of laboratory animals (*29a*), it may be difficult to determine the fate of a small amount of copper isotope dissociating from chelate linked mAb due to the efficient trafficking of this ion in vivo (*34*). We anticipate careful in vivo studies will be required to ultimately select the optimal chelating agent for linkage of copper isotopes to mAb.

LITERATURE CITED

(1) Chaudhuri, P., and Wieghardt, K. (1987) The Chemistry of 1,4,7-Triazacyclononane and Related Tridentate Macrocyclic Compounds. *Prog. Inorg. Chem. 35*, 329.

(2) Takahashi, M., and Takamoto, S. (1977) The Preparation of Trivalent Metal Chelates with Some N_3O_3-Type Ligands. *Bull. Chem. Soc. Jpn. 50*, 3413–3414.

(3) Kataky, R., Matthes, K. E., Nicholson, P. E., Parker, D., and Buschmann, H.-J. (1990) Synthesis and Binding Properties of Amide-functionalised Polyaza Macrocycles. *J. Chem. Soc. Perkin Trans. 2* 1425–1432.

(4) Auerbach, U., Eckert, U., Wieghardt, K., Nuber, B., and Weiss, J. (1990) Synthesis and Coordination Chemistry of the Hexadentate Ligands 1,4,7-Tris(2-hydroxybenzyl)-1,4,7-triazacyclononane (H_3L) and 1,4,7-Tris(3-*tert*-butyl-2-hydroxybenzyl)-1,4,7-triazacyclononane (H_3L_2). Crystal Structures of [HL_1Cu^{II}] and [L_2Fe^{III}]acacH. *Inorg. Chem. 29*, 938–944.

(5) Moore, D. A., Fanwick, P. E., and Welch, M. J. (1989) Synthesis, Characterization and Solid-State Structure of a New Hexachelating Ligand and its Complex with Gallium(III). *Inorg. Chem. 28*, 1504–1506.

(6) Broan, C. J., Jankowski, K. J., Kataky, R., and Parker, D. (1990) Synthesis and Complex Stability of Parent and C-Functionalised Derivatives of 1,4,7-Triazacyclononane-1,4,7-tris[methylene(methylphosphinic acid)]: An Effective New Complexing Agent. *J. Chem. Soc., Chem. Commun.* 1738–1739.

(7) (a) Sessler, J. L., Hugdhal, J., Kurosaki, H., Sasaki, Y. (1988) Synthesis and Binding of a Triazamacrocyclic Ligand Bearing Pendant Pyridyl Groups. *J. Coord. Chem. 18*, 93–98. (b) Norante, G. d. M., Di Vaira, M., Mani, F., Mazzi, S., and Stoppioni, P. (1992) Transition Metal Complexes of a Functionalized Triazamacrocycle. *J. Chem. Soc., Dalton Trans.* 361–365.

(8) (a) Martell, A. E., Motekaitis, R. J., and Welch, M. J. (1990) N,N′,N″-Tris(3-hydroxy-6-methyl-2-pyridylmethyl)-1,4,7-triazacyclononane, a New Effective Ligand for Iron(III). *J. Chem. Soc., Chem. Commun.* 1748–1749. (b) Motekaitis, R. J., Sun, Y., and Martell, A. E. (1992) New synthetic, selective, high-affinity ligands for effective trivalent metal ion binding and transport. *Inorg. Chim. Acta 198–200*, 421–428.

(9) Broan, C. J., Cox, J. P. L., Craig, A. S., Kataky, R., Parker, D., Harrison, A., Randall, A. M., and Ferguson, G. (1991) Structure and Solution Stability of Indium and Gallium Complexes of 1,4,7-Triazacyclononanetriacetate and of Yttrium Complexes of 1,4,7,10-Tetraazacyclododecanetetraacetate and Related Ligands: Kinetically Stable Complexes for Use in Imaging and Radioimmunotherapy. X-Ray Molecular Structure of the Indium and Gallium Complexes of 1,4,7-Triazacyclononane-1,4,7-triacetic Acid. *J. Chem. Soc. Perkin Trans. 2* 87–99.

(10) van der Merwe, M., Boeyens, J. C. A., and Hancock, R. D. (1983) Optimum Ligand Hole Sizes for Stabilizing Nickel(III).

Structure of the Nickel(III) Complexes of 1,4,7-Triazacyclononane-N,N′,N″-triacetate. *Inorg. Chem. 22*, 3489–3490.
(11) Parker, D. (1990) Tumour Targeting with Radiolabelled Macrocycle-Antibody Conjugates. *Chem. Soc. Rev. 19*, 271–291.
(12) Wieghardt, K., Bossek, U., Chaudhuri, P., Herrmann, W., Menke, B. C., and Weiss, J. (1982) 1,4,7-Triazacyclononane-N,N′,N″-triacetate (TCTA), a Hexadentate Ligand for Divalent and Trivalent Metal Ions. Crystal Structures of [Cr^{III}(TCTA)], [Fe^{III}(TCTA)], and Na[Cu^{II}(TCTA)]·2NaBr·8H_2O. *Inorg. Chem. 21*, 4308–4314.
(13) Craig, A. S., Parker, D., Adams, H., and Bailey, N. A. (1989) Stability, ^{71}Ga NMR, and Crystal Structure of a Neutral Gallium(III) Complex of 1,4,7-Triazacyclononanetriacetate: a Potential Radiopharmaceutical? *J. Chem. Soc., Chem. Commun.* 1793–1794.
(14) Pippin, C. G., Kumar, K., and Gansow, O. A. Manuscript in preparation.
(15) Cox, J. P. L., Craig, A. S., Helps, I. M., Jankowski, K. J., Parker, D., Eaton, M. A. W., Millican, A. T., Millar, K., Beeley, N. R. A., and Boyce, B. A. (1990) Synthesis of C- and N-Functionalized Derivatives of 1,4,7-Triazacyclononane-1,4,7-triyltriacetic acid (NOTA), 1,4,7,10-Tetra-azacyclododecane-1,4,7,10-tetrayltetraacetic Acid (DOTA), and Diethylenetriaminepenta-acetic Acid (DPTA): Bifunctional Complexing Agents for the Derivatisation of Antibodies. *J. Chem. Soc. 1*, 2567–2576.
(16) Studer, M., and Meares, C. F. (1992) Synthesis of Novel 1,4,7-Triazacyclononane-N,N′,N″-triacetic Acid Derivatives Suitable for Protein Labeling. *Bioconjugate Chem. 3*, 338–341.
(17) McMurry, T. J., Brechbiel, M. W., Kumar, K., and Gansow, O. A. (1992) Convenient Synthesis of Bifunctional Tetraaza Macrocycles. *Bioconjugate Chem. 3*, 108–117.
(18) Brechbiel, M. W., Gansow, O. A., Atcher, R. W., Schlom, J., Esteban, J., Simpson, D. E., and Colcher, D. (1986) Synthesis of 1-(p-isothiocyanatobenzyl) derivatives of DTPA and EDTA. Antibody labeling and tumor-imaging studies. *Inorg. Chem. 25*, 2772–2781.
(19) Fujino, M., Wakimasu, M., and Kitada, C. (1981) Further Studies on the Use of Multi-substituted Benzenesulfonyl Groups for Protection of the Guanidino Function of Arginine. *Chem. Pharm. Bull. 29*, 2825–2831.
(20) Vaughn, S. R., and Eichler, J. A. (1953) The Preparation of Optically-Active Peptides Using Mixed Carbonic-Carboxylic Acid Anhydrides. *J. Am. Chem. Soc. 75*, 5556–5560.
(21) Still, W. C., Kahn, M., Mitra, A. (1978) Rapid Chromatographic Technique for Preparative Separations with Moderate Resolution. *J. Org. Chem. 43*, 2923–2925.
(22) Brechbiel, M. W., and Gansow, O. A. (1991) Backbone-Substituted DTPA Ligands for ^{90}Y Radioimmunotherapy. *Bioconjugate Chem. 2*, 187–194.
(23) Peacock, D. H., and Dutta, D. C. (1934) 281. ββ′-Diaminoethylamine. *J. Chem. Soc.*, 1303–1305.
(24) Wakimasu, M., Kitada, C., and Fujino, M. (1982) 4-Methoxy-2,3,6-trimethylbenzenesulfonyl (Mtr): A New Amino and Imidazole Protecting Group in Peptide Synthesis. *Chem. Pharm. Bull. 30*, 2766–2779.
(25) (a) Moi, M. K., Meares, C. F., McCall, M. J., Cole, W. C., and DeNardo, S. J. (1985) Copper Chelates as Probes of Biological Systems: Stable Copper Complexes with a Macrocyclic Bifunctional Chelating Agent. *Anal. Biochem. 148*, 249–253. (b) Moi, M. K., Yanuck, M., Deshpande, S. V., Hope, H., DeNardo, S. J., and Meares, C. F. (1987) X-Ray Crystal Structure of a Macrocyclic Copper Chelate Stable Enough for Use in Living Systems: Copper(II) Dihydrogen 6-(p-Nitrobenzyl)-1,4,8,11-tetraazacyclotetradecane-1,4,8,11-tetraacetate. *Inorg. Chem. 26*, 3458–3463.
(26) (a) Mathias, C. J., Welch, M. J., Green, M. A., Diril, H., Meares, C. F., Gropler, R. J., and Bergmann, S. R. (1991) In Vivo Comparison of Copper Blood-Pool Agents: Potential Radiopharmaceuticals for Use with Copper-62. *J. Nucl. Med. 32*, 475–480. (b) Deshpande, S. V., DeNardo, S. J., Meares, C. F., McCall, M. J., Adams, G. P., Moi, M. K., and DeNardo, G. L. (1988) Copper-67-Labeled Monoclonal Antibody Lym-1, a Potential Radiopharmaceutical for Cancer Therapy: Labeling and Biodistribution in RAJI Tumored Mice. *J. Nucl. Med. 29*, 217–225.
(27) K_{CuL} = [CuL]/[Cu][L]. Data from: Martell, A. E., and Smith, R. M. (1974) *Critical Stability Constants*, Plenum Press, New York.
(28) For example, see Curtis, N. F., and Osvath, S. R. (1988) Kinetics of Acid-Promoted Dissociation of Diamine-Diimine Macrocycle Complex Cations With Nickel (II) and Copper (II). *Inorg. Chem. 27*, 305.
(29) (a) Morphy, J. R., Parker, D., Kataky, R., Eaton, M. A. W., Milllican, A. T., Alexandere, R., Harrison, A., and Walker, C. (1990) Towards Tumor Targeting with Copper-radiolabelled Macrocycle-Antibody Conjugates: Synthesis, Antibody Linkage, and Complexation Behaviour. *J. Chem. Soc., Perkin Trans 2*, 573–585. (b) Smith-Jones, P. M., Fridrich, R., Kaden, T. A., Novak-Hofer, I., Siebold, K., Tschudin, D. A., and Maecke, H. R. (1991) Antibody Labeling with Copper-67 Using the Bifunctional Macrocycle 4-[(1,4,8,11-Tetraazacyclotetradec-1-yl)methyl]benzoic Acid. *Bioconjugate Chem. 2*, 415–421.
(30) Riesen, A., Zehnder, M., and Kaden, T. A. (1986) 219. Metal Complexes of Macrocyclic Ligands. Part XXIV. Binuclear Complexes with Tetraazamacrocycle-N,N′,N″,N‴-tetraacetic Acids. *Helv. Chim. Acta 69*, 2074–2080.
(31) Cole, W. C., DeNardo, S. J., Meares, C. F., McCall, M. J., DeNardo, G. L., Epstein, A. L., O'Brein, H. A., and Moi, M. K. (1986) Serum Stability of ^{67}Cu Chelates: Comparison with ^{111}In and ^{57}Co. *Nucl. Med. Biol. 13*, 363–368.
(32) Meares, C. F., Studer, M., Diril, H., Kukis, D. L. (1992) Preparation and Characterization of New Bifunctional Chelating Agents For Copper-67. *J. Nucl. Med. 33*, 942.
(33) Kasprzyk, S. P., and Wilkins, R. G. (1982) Kinetics of Interaction of Metal Ions with Two Tetraaza Tetraacetate Macrocycles. *Inorg. Chem. 21*, 3349–3352.
(34) (a) Earl, C. J., Moulton, J., and Selverstone, B. (1954) Metabolism of Copper in Wilson's Disease and in Normal Subjects. Studies with Cu-64. *Am. J. Med.* 205–213. (b) Bearn, A. G., and Kunkel, H. G. (1955) Metabolic Studies in Wilson's Disease Using Cu-64. *J. Lab. Clin. Med.* 623–631. (c) Neumann, P. Z., and Sass-Kortsak, A. (1967) The State of Copper in Human Serum: Evidence for an Amino Acid-bound Fraction. *J. Clin. Invest. 46*, 646–658.

TECHNICAL NOTES

Synthesis of Glycoconjugates by Covalent Coupling of *O*-Glycopyranosyl-*N*-hydroxysuccinimide Derivatives of Lactose to Proteins and Lipids and Polymerization of Their Parent Acryloyl Derivatives into Acrylamide Polymers

Mats Andersson* and Stefan Oscarson

Department of Organic Chemistry, Arrhenius Laboratory, Stockholm University, S-106 91, Stockholm.
Received August 31, 1992

Glycosides of *N*-hydroxysuccinimide have been synthesized and the succinimide moieties have been opened by amines to give glycolipids or spacer–glycosides. The latter have been coupled to proteins and, after acryloylation, copolymerized into acrylamide polymers. A ^{13}C-NMR study of the stability of the anomeric O–N–C(O) linkage showed the linkage to be stable under conditions used in most biological experiments.

INTRODUCTION

Oligosaccharides linked through a spacer unit to proteins, lipids, and synthetic polymers are frequently used as antigens in diagnostic tests or as immunogens (*1*). Another use of immobilized oligosaccharides is purification by affinity chromatography of antibodies and lectins. Synthetic oligosaccharides are coupled to a carrier using a variety of spacers introduced during some stage of the synthesis (*1*). Another approach, used, for example, by Dahmén et al. (*2*), is to introduce a group at the reducing end, which allows the introduction of various spacers to the same oligosaccharide and the subsequent formation of glycoconjugates.

We have described (*3*) a similar approach in which *N*-hydroxysuccinimide is reacted with a peracetylated saccharide (or a bromo or thioglycoside sugar) to give *O*-glycopyranosyl-*N*-hydroxysuccinimides, which are preactivated spacer glycosides in which the hydroxysuccinimide not only activates the reducing end but also eventually constitutes part of the spacer. In this paper we show the use of these derivatives in the formation of glycoconjugates.

EXPERIMENTAL PROCEDURES

General Methods. Concentrations were performed at <40 °C bath temperature. For optical rotations, a Perkin-Elmer 241 polarimeter was used, and measurements were performed at room temperatures. NMR spectra were recorded at 30 °C with a JEOL GSX-270 instrument. The following reference signals were used: ^{13}C, Me_4Si (δ 0.00) in $CDCl_3$ and dioxane (δ 67.40) in D_2O; ^{1}H, sodium [$^2H_4$]-3-(trimethylsilyl)propanoate (δ 0.00) in D_2O. Gel filtrations were performed on a column (2.6 × 90 cm) of Bio-Gel P-2 eluted with water (1% 1-butanol), unless otherwise stated, and a differential refractometer was used for monitoring the column effluents. Molecular weight determination was made on three consecutively-linked gel columns (Toyo Soda K PWH 5000 + 4000 + 3000) connected in series, using 0.25 M NaCl as eluent and dextran as standard. Silica gel 60 F-254 (Merck, Darmstadt, Germany) was used for TLC, and the spots were detected by charring with 8% sulfuric acid. Column chromatography was performed on Matrex silica gel 60 (0.035–0.070 mm, Amicon Corp.). Predried powdered molecular sieves (4 Å, Union Carbide) were used. Dialysis tubing from Spectrum Medical Industries, Inc. (Spectra/Por; mw cutoff, 12 000–14 000) was used. SDS–PAGE (10–15%) was run on a Pharmacia Phast System according to the manufacturer's instructions. A Pharmacia LMW (low molecular weight) kit of range 14.4–94 kDa together with BSA and mercaptoethanol-reduced BSA (*4*) were used as reference, and the gel was stained by the standard Coomassie technique.

Elemental analyses of the compounds were determined by use of the accurate mass technique (*5*, *6*) and in the positive ionization FAB mode (*7*) with a B-linear scan and detection in the centroid position mode. A JEOL SX102 mass spectrometer with a xenon gun, nitrobenzyl alcohol as matrix, and a mixture of polyethylene glycol 400/polyethylene glycol 600 1:1 as standard were used (*7*). A resolution of 3000, an acceleration voltage of 10 kV, a cycle time of 15 s, a scan slope of 20 s, and a mass range of m/z 100–800 were used. In all experiments the masses obtained deviated <5 mmu. When more than one possible composition was suggested, the incorrect alternatives were excluded by NMR data.

A standard TLC probe equipped with a dual-well target was used, and spectra were accumulated by altering every second scan between the standard and the sample to be determined (*8*).

***N*-(4-Hydroxysuccinyl)-*O*-β-D-lactosylhydroxylamine (2).** *O*-(2,2′,3,3′,4′,6,6′-Hepta-*O*-acetyl-β-lactopyranosyl)-*N*-hydroxysuccinimide (*3*) (1) (2.5 g, 3.41 mmol) in 0.25 M sodium hydroxide/ethanol 1:1 (500 mL) was stirred at room temperature for 1 h. Neutralization with Dowex H^+ resin, filtration, concentration, and freeze-drying gave **2** (1.55 g, 99%). $[\alpha]_D$ −8° (*c* 1.0, water). ^{13}C-NMR data (D_2O, pD 2): δ 28.0, 29.6 (CH_2), 60.8, 61.7 (C-6,6′), 69.4–78.7, (C-2,3,4,5,2′,3′,4′,5′), 103.7, 106.0 (C-1,1′), 172.7, 177.2 (carbonyl C). Mass deviation found: 1.5 mmu.

***N*-[4-(Pentamino)succinyl]-*O*-β-D-lactosylhydroxylamine (3). Route A.** *N*-Pentylamine (60 μL, 0.50

1043-1802/93/2904-0246$04.00/0 © 1993 American Chemical Society

mmol) was added to a stirred solution of 1 (74 mg, 0.10 mmol) in tetrahydrofuran (5 mL) containing molecular sieves (4 Å). The reaction mixture was kept at room temperature for 24 h and then concentrated to dryness. The remaining syrup was dissolved in a mixture of 0.25 M sodium hydroxide (aqueous)/ethanol 1:1 (15 mL) and stirred for 1 h. Neutralization with Dowex H^+ resin followed by filtration, concentration, and freeze-drying gave **3** (53 mg, 99%). $[\alpha]_D$ −12° (*c* 0.98, water). ^{13}C-NMR data (D_2O): δ 14.2 (CH_3), 22.5, 28.8, 29.0, 29.2, 31.5, 40.2 (CH_2), 60.8, 61.9 (C-6,6′), 69.4-78.7 (C-2,3,4,5,2′,3′,4′,5′), 103.8, 106.0 (C-1,1′), 172.5, 174.7 (carbonyl C). An accurate mass determination could not be performed on this sample due to overlap with the standards used.

***N*-[4-(Dodecamino)succinyl]-*O*-β-D-lactosylhydroxylamine (4). Route A.** A solution of **1** (103 mg, 0.14 mmol) and dodecylamine (137 mg, 0.74 mmol) in tetrahydrofuran (5 mL) containing molecular sieves (4 Å) was stirred at 60 °C for 30 h. The reaction mixture was then filtered through Celite and concentrated to dryness. Deacetylation in 0.25 M sodium hydroxide/methanol 1:4 (6 mL) for 1 h followed by neutralization with Dowex H^+ resin, filtration, evaporation with air, and then freeze-drying gave the slightly impure **4** (103 mg). Silica gel column chromatography (ethyl acetate/methanol/acetic acid/water 12:3:3:2) gave after concentration and freeze-drying **4** (83 mg, 95%). $[\alpha]_D$ −13° (*c* 1.0, methanol). ^{13}C-NMR data (methanol-d_4): δ 14.5 (CH_3), 23.8–40.6 (13 × CH_2), 62.0, 62.5 (C-6,6′), 70.4–80.1 (C-2,3,4,5,2′,3′,4′,5′), 105.1, 107.6 (C-1,1′), 172.4, 174.0 (carbonyl C). Mass deviation found: 1.4 mmu.

***N*-[4-(Dodecamino)succinyl]-*O*-β-D-lactosylhydroxylamine (4). Route B.** To a stirred solution of **2** (53 mg, 0.116 mmol) and dodecylamine (28.2 mg, 0.152 mmol) in dioxane/water 4:1 (2.5 mL) was added *N*-[3-(dimethylamino)propyl]-*N*′-ethylcarbodiimide hydrochloride (EDC) (33.8 mg, 0.176 mmol). The reaction was kept at room temperature for 3 h and then filtered through Dowex H^+ resins (prewashed in dioxane/water). Concentration and freeze-drying gave a mixture (83 mg) that was further purified on silica gel, as described above to give **4** (59 mg, 81%).

***N*-[4-[[2-(4-Nitrophenyl)ethyl]amino]succinyl]-*O*-β-D-lactosylhydroxylamine (5). Route A.** A solution of **1** (103 mg, 0.14 mmol), 2-(4-nitrophenyl)ethylamine hydrochloride (160 mg, 0.74 mmol), and triethylamine (206 mL, 1.53 mmol) in a mixture of tetrahydrofuran/*N*,*N*-dimethylformamide (10:1, 11 mL) containing molecular sieves (4 Å) was stirred at 60 °C for 96 h. The reaction mixture was filtered and concentrated to dryness. Deacetylation in 0.1 M sodium methoxide in methanol (10 mL) followed by neutralization with Dowex H^+ resins, filtration, and concentration gave a syrup (74 mg). Further purification on Bio-Gel P-2 gave, after concentration and freeze-drying, **5** (26 mg, 33%). $[\alpha]_D$ −10° (*c* 0.88, water). NMR data (D_2O): ^{13}C δ 28.7, 31.2, 35.5, 40.7 (CH_2), 60.8, 61.8 (C-6,6′), 69.4–78.7 (C-2,3,4,5,2′,3′,4′,5′), 103.8, 106.0 (C-1,1′), 124.4, 130.7, 147.0, 148.6 (aromatic C), 172.4, 174.8 (carbonyl C); ^{1}H (selected) δ 6.82 (d, 2 H), 7.10 (d, 2 H). Mass deviation found: 3.2 mmu.

***N*-[4-[[2-(4-Nitrophenyl)ethyl]amino]succinyl]-*O*-β-D-lactosylhydroxylamine (5). Route B.** To a stirred solution of **2** (69 mg, 0.15 mmol) and 2-(4-nitrophenyl)-ethylamine hydrochloride (38.9 mg, 0.193 mmol) in water (1 mL) was added EDC (39.2 mg, 0.204 mmol) and triethylamine (21 μL, 0.151 mmol). The reaction was kept at room temperature for 3 h and then added to the top of a Bio-Gel P-2 column. The desired product **5** and the cyclized byproduct **9** was obtained, after freeze-drying, in 55% (50 mg) and 16% (10.6 mg) yield, respectively. In a similar experiment, **2** (70.4 mg, 0.154 mmol) and 2-(4-nitrophenyl)ethylamine hydrochloride (43 mg, 0.212 mmol) were dissolved in *N*,*N*-dimethylformamide/dioxane/water (1:1:0.5, 2.5 mL), whereafter dicyclohexyl carbodiimide (DCC) (47.7 mg, 0.232 mmol) and triethylamine (25 μL, 0.184 mmol) were added. After 3 days, when no starting material could be detected by TLC (ethyl acetate/methanol/acetic acid/water 12:3:3:2), the reaction was diluted with water (10 mL). Filtration first through Celite and then through Dowex H^+ resins followed by concentration and freeze-drying gave a syrup that was further purified on a Bio-Gel P-2 column (40 cm, irrigated with 25% ethanol in water). Concentration and freeze-drying gave **5** (69 mg, 78%).

***N*-[4-[[2-(4-Aminophenyl)ethyl]amino]succinyl]-*O*-β-D-lactosylhydroxylamine (6) Route A.** A solution of **1** (310 mg, 0.42 mmol) and 2-(4-aminophenyl)ethylamine (287 mg, 2.10 mmol) in tetrahydrofuran (15 mL) was stirred at 60 °C for 17 h, whereafter the solvent was evaporated and methanol (10 mL) was added. Deacetylation by addition of 0.1 M sodium methoxide in methanol (2 mL) was performed at room temperature until TLC (chloroform/methanol/25% ammonia (aqueous), 65:40:14) showed one product (ca. 2 h). Neutralization (acetic acid) and concentration to dryness followed by purification, first on a Bio-Gel P-2 column and then on a short silica gel column (chloroform/methanol/25% ammonia (aqueous), 65:40:14), gave, after concentration and freeze-drying, **6** (214 mg, 88%). $[\alpha]_D$ −11° (*c* 0.89, water). ^{13}C-NMR data (D_2O): δ 29.0, 31.7, 34.6, 41.7 (CH_2), 60.8, 61.8 (C-6,6′), 69.4–78.8 (C-2,3,4,5,2′,3′,4′,5′), 103.8, 105.7 (C-1,1′), 117.5, 130.6, 140.0, 145.1 (aromatic C), 172.4, 174.9 (carbonyl C). Mass deviation found: 3.4 mmu.

***N*-[4-[[2-(4-Aminophenyl)ethylamino]succinyl]-*O*-β-D-lactosylhydroxylamine (6) from Hydrogenoylsis of 5.** **5** (112 mg, 0.185 mmol) in methanol (5 mL) and a catalytic amount of Pd/CC (10%) were subjected to hydrogenolysis for 3 h at atmospheric pressure. Filtration through Celite, concentration, and gel filtration on a Bio-Gel P-2 column gave, after freeze-drying, **6** (103 mg, 96%).

***N*-[4-[[2-(4-Acrylamidophenyl)ethyl]amino]succinyl]-*O*-β-D-lactosylhydroxylamine (7).** Compound **6** (18.2 mg, 0.032 mmol) was dissolved in a cooled (ice bath), stirred mixture of deaerated 0.5 M sodium borate (aqueous) (0.8 mL, pH 8.5) and methanol (2.4 mL), whereafter acroyl chloride (4 μL, 0.040 mmol) was added. When TLC (ethyl acetate/methanol/water, 10:6:2) showed that all the starting material was consumed (10 min), the reaction mixture was concentrated at room temperature to about one-third of its original volume. Purification on a Bio-Gel P-2 column and freeze-drying gave **7** (19.4 mg, 98%). $[\alpha]_D$ −10° (*c* 1.0, water). ^{13}C-NMR data (D_2O): δ 28.8, 31.3, 34.9, 41.3 (CH_2), 60.8, 61.8 (C-6,6′), 69.4–78.7 (C-2,3,4,5,2′,3′,4′,5′), 103.8, 106.0 (C-1,1′), 122.4, 129.1, 130.3, 131.3, 136.0, 137.3 (aromatic C, olefinic C), 167.4, 172.5, 174.8 (carbonyl C). Mass deviation found: 2.5 mmu.

Copolymerization of *N*-[4-[[2-(4-Acrylamidophenyl)ethyl]amino]succinyl]-*O*-β-D-lactosylhydroxylamine (7) and Acrylamide. To a solution of **7** (16.7 mg, 0.027 mmol) and acrylamide (22 mg, 0.31 mmol) in deaerated water (1 mL) were added first *N*,*N*,*N*′,*N*′-tetramethylendiamine (6 μL) and then ammounium persulfate (3.3 mg, in 300 μL of deaerated water). The mixture was stirred at room temperature overnight. TLC (ethyl acetate/methanol/water, 10:6:2) showed that almost all the **7** was consumed and that a charring baseline product

had been formed. The polymer was purified by gel chromatography on a Bio-Gel P-2 column eluted with 0.1 M pyridinium acetate (aqueous) (pH 5.4). The polymeric fraction, eluted in the void volume, was concentrated to dryness and dissolved in water (2 mL). A ^{1}H-NMR spectrum of the product, obtained after freeze-drying (30.2 mg), showed an average incorporation of 1 oligosaccharide/11 acrylamide units (Figure 2). The molecular weight distribution of the copolymer, as determined by gel filtration, was 2–1000 kDa. The average molecular weight was 327 kDa, with a standard deviation of 535 kDa.

Coupling of *N*-[4-[[2-(4-Aminophenyl)ethyl]amino]-succinyl]-*O*-β-D-lactosylhydroxylamine (6) to Bovine Serum Albumin (BSA). To a stirred, cooled (ice bath) solution of thiophosgene (17 μL, 0.17 mmol) in dry tetrahydrofuran (1 mL) was added the amino derivative **2** (10.3 mg, 18 mmol) in 0.85 M sodium borate buffer (2 mL, pH 8.5). The reaction was stirred for 10 min at room temperature and then extracted with diethyl ether (3 × 1.5 mL). The ether phases were discarded, and the water phase containing the isothiocyanate derivative **8** was added to a stirred solution of BSA (14 mg) in the same buffer system (0.5 mL). The pH was adjusted (from ca. 7.5 to 8.5) with 0.25 M sodium hydroxide (aqueous) (ca. 10 drops) and the coupling reaction was stirred at room temperature for 48 h. Dialysis against distilled water (4 × 1 L) and freeze-drying gave the lactose–BSA conjugate (17 mg).

Stability of the C–O–N–C Linkage (NMR). To five 5-mm NMR tubes each containing *N*-[4-(pentylamino)-succinyl]-*O*-β-D-glucopyranosylhydroxylamine (*3*) (50 mg, 137 μmol) was added (1) 1 M aqueous glycine buffer (270 μL, pH 2.5, HCl), dioxane (30 μL), and D_2O (30 μL), (2) 0.5 M aqueous sodium acetate (270 μL, pH 5.0) dioxane (30 μL), and D_2O (30 μL), (3) 50 mM aqueous sodium phosphate containing 0.14 M sodium chloride (270 μL), pH 7.4) and an inner tube containing dioxane/D_2O (30 μL), (4) 0.5 M aqueous sodium borate (270 μL, pH 8.5) and an inner tube containing dioxane/D_2O (30 μL), or (5) 1 M aqueous sodium hydroxide (270 μL) and an inner tube containing dioxane/D_2O (30 μL). The tubes were stored at 18 °C and the ^{13}C spectra obtained were recorded at room temperature using a standard pulse sequence.

RESULTS

Treatment of *O*-(2,2′,3,3′,4′,6,6′-hepta-*O*-acetyl-β-lactopyranosyl)-*N*-hydroxysuccinimide (*3*) (**1**) with sodium hydroxide in ethanol/water caused deacetylation and hydroxide opening of the imide to give quantitatively the carboxylate **2**. Carbodiimide-mediated coupling of **2** with dodecylamine or 2-(4-nitrophenyl)ethylamine then gave the glycolipid **4** (81%) and the spacer glycoside **5** (78%).

Treatment of the protected *N*-hydroxysuccinimide derivative **1** directly with pentylamine or dodecylamine also gave the derivatives **3** and **4** in almost quantitative yield (99 and 95%, respectively). The use of 2-(4-nitrophenyl)ethylamine in this direct approach gave low yields of **5** (33%), but if instead 2-(4-aminophenyl)ethylamine was used as nucleophile, a high yield (88%) of the expected product **6**, in which the more nucleophilic nonaromatic primary amine had opened the imide, was once more obtained. Compound **6** was also obtained from **5** by catalytic hydrogenolysis of the nitro group.

Compound **6** was further processed to give glycoconjugates. Treatment of **6** with acroyl chloride gave quantitatively the acrylamido derivative **7**, which was copolymerized with acrylamide to give an oligosaccharide–acrylamide polymer (*9*). An average incorporation of 1 oligosaccharide/11 acrylamide units was observed on the basis of integration of the ^{1}H-NMR spectrum. The average molecular weight of the polymer was determined by gel chromatography, using dextran as standard, to be 327 kDa, with a standard deviation of 520 kDa.

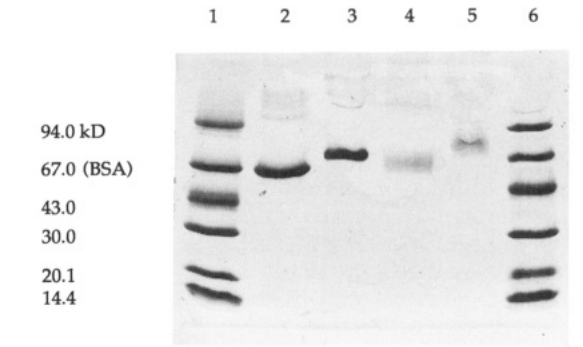


Figure 1. Coomassie-stained SDS–PAGE gel of BSA and the oligosaccharide conjugate of BSA. Lanes: (1) LMW kit, (2) BSA, (3) BSA (reduced), (4) OLS–BSA, (5) OLS–BSA (reduced), (6) LMW kit (reduced).

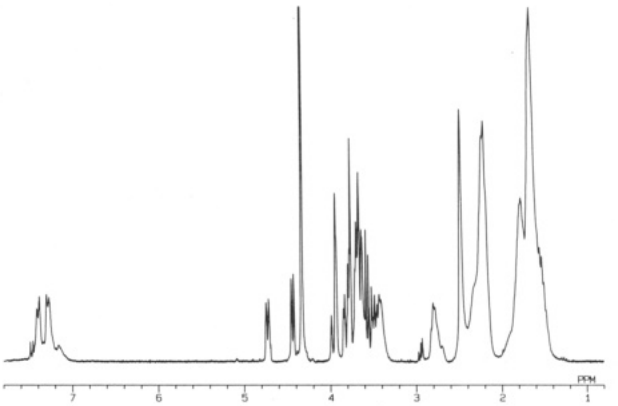


Figure 2. ^{1}H NMR in D_2O of the polyacrylamide polymer of *N*-[4-[2-(4-acrylamidophenyl)ethanamido]succinyl]-*O*-β-D-lactosylhydroxylamine.

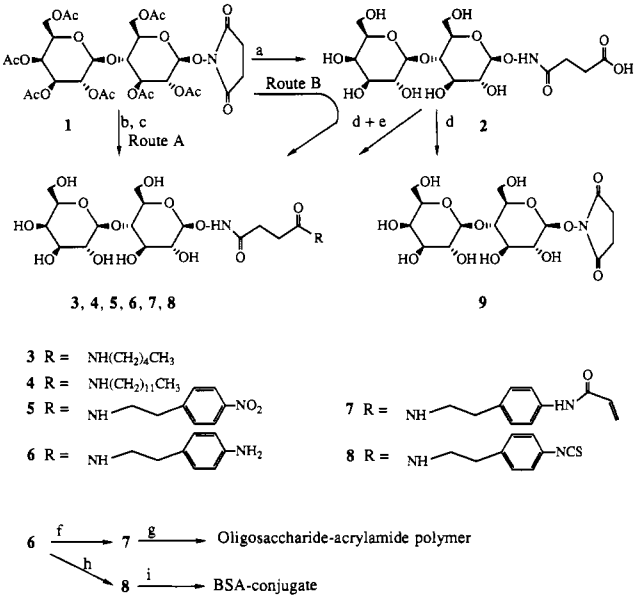
Compound **6** was also converted, by treatment with thiophosgene, to an isothiocyanate derivative (**8**), which was coupled to BSA to give a glycoprotein conjugate (*10*). The isothiocyanate derivative **8** is used in the coupling reaction directly without purification or characterization, but a ^{1}H NMR of the concentrated water phase containing **8** showed an aromatic singlet at 7.29 ppm, in contrast to the precursor **6**, which showed two aromatic doublets, thereby showing the change of substitution on the aromatic ring. The phenol–sulfuric test (*11*) showed the incorporation to be about 30 oligosaccharide units/mol protein. The incorporation was also indicated by running an SDS gel on which the BSA conjugate was shown to have different mobility compared to BSA itself both in the reduced and in the oxidized form (Figure 1).

Stability tests were performed on *N*-[4-(pentylamino)-succinyl]-*O*-β-D-glucopyranosylhydroxylamine, which was dissolved in five different solutions with pH ranging from 2.5 to 14, and ^{13}C-NMR spectra were run on the different samples after 1, 7, 14, 30, and 60 days. All samples were found to be stable for 7 days and only under basic conditions (4 and 5, see Experimental Section) some decomposition (less than 10%) was found after 14 days. Under physiological conditions, the compound was found to be stable even after 2 months.

DISCUSSION

Treatment of derivative **1** with different amines gave glycolipids (**3** and **4**) in almost quantitative yield. First

Scheme I



[a] (a) $OH^-/EtOH/H_2O$; (b) $R\text{-}NH_2$; (c) $MeO^-/MeOH$; (d) EDC; (e) $R\text{-}NH_2$; (f) $CH_2CHCOCl$; (g) $CH_2CHCONH_2$; (h) $CS(Cl)_2$; (i) BSA.

the amine opened up the succinimide ring to give the amide derivative, whereafter deacetylation occurred. The latter process was rather slow, subsequent deacetylation using sodium hydroxide gave a faster and cleaner reaction.

The glycolipids could also be obtained via a two-step procedure from **1** as described above (route **B** in Scheme I). In the carbodiimide-mediated formation of the carboxamide a slight shadow of the ring-closed succinimide derivative **9** could be detected on TLC. If this reaction was carried out in the absence of amine, the ring-closed compound was the main product and could easily be isolated. As a rule, the formation of glycolipids directly from **1** was simpler and gave higher yields of product, but in one case [with 2-(4-nitrophenyl)ethylamine] the two-step-procedure was preferable.

Attempts to make glycoproteins directly by mixing BSA with the derivatives **1** and **9** failed. In experiments where **1** and **9** were mixed with BSA in water solutions, only starting materials could be detected on TLC. This is probably due to lower reactivity of the BSA N^{ϵ}-amino groups of lysine residues. Furthermore, for the making of acrylamide polymers we needed to introduce an amino group into the oligosaccharide molecule. Therefore, compound **1** was treated with 2-(4-aminophenyl)ethylamine to give derivative **6**, suitable for attachment to proteins and for making acrylamide polymers. In reductive amination of oligosaccharides with 2-(4-aminophenyl)-ethylamine, either the aromatic amine or the aliphatic amine can react, depending on the experimental conditions used (*12*). Here only the aliphatic amine reacted to give derivative **6**, wherefore use of the 4-nitro compound followed by hydrogenolysis or selective protection of one of the amino groups was not necessary.

Formation of the acrylamide compound **7** and subsequent polymerization using standard techniques (*9*) proceeded smoothly and gave polymers in around 60% yield. The size of the copolymers was mainly in the range of 60–600 kDa, and the ratio of oligosaccharide to CH_2CH_2 groups in the polymer was in accordance with the ratio in the prepolymerization mixture, as found earlier (*12*).

Coupling of derivative **6** to BSA via a thiourea linkage (*10*) was also straightforward. Stability testing of the C–O–N–C linkage showed that these compounds are stable under basic, neutral, and acidic conditions for over 1 week.

Thus, *O*-glycopyranosyl-*N*-hydroxysuccinimide derivatives are shown to be good precursors for making glycoconjugates. They can be made in a number of ways, preferably through Lewis acid catalyzed reaction with the peracetylated oligosaccharide and *N*-hydroxysuccinimide (*3*). Both synthetic oligosaccharides or oligosaccharides extracted from nature should be possible to use, the latter after peracetylation. When treated with aliphatic amines, they give glycolipids in high yields, and when treated with 2-(4-aminophenyl)ethylamine, they give derivatives which be be transformed into glycoproteins or acrylamide polymers. The glycogonjugates synthesized are shown to be stable enough to be used in most biological experiments.

ACKNOWLEDGMENT

We thank Mr. Göran Lundin for recording the high-resolution FAB-MS spectra, Mr. Hans Grönlund, Kabi-Pharmacia Diagnostics AB, for running the SDS-PAGE gels, Prof. Per J. Garegg for his interest, and the Swedish Natural Science Research Council and the Swedish National Board for Technical Development for financial support.

LITERATURE CITED

(1) Reviews: Garegg, P. J., and Lindberg, A. A. (1988) The synthesis of oligosaccharides for biological and medical applications. In *Carbohydrate Chemistry*, (J. F. Kennedy, ed.) pp 500–559. Clarendon Press, Oxford. Kallin, E. (1990) New methods for the preparation of neoglycoconjugates. Thesis, University of Lund, Sweden.

(2) Dahmén, J., Frejd, T., Grönberg, G., Lave, T., Magnusson, G., and Noori, G. (1983) 2-Bromoethyl glycosides: applications in the synthesis of spacer-arm glycosides. *Carbohydr. Res. 118*, 292–301.

(3) Andersson, M., and Oscarson, S. (1992) Synthesis of *O*-glycopyranosyl-*N*-hydroxysuccinimides of glucose and lactose and their opening by nucleophiles into prespacer glycosides. *Glycoconjugate J. 9*, 122–125.

(4) Laemmli, U. K. (1970) Cleavage of structural proteins during the assembly of the head of bacteriophage T4. *Nature 227*, 680–685.

(5) Kimble, B. J. In *High Performance Mass Spectrometry: Chemical Applications*, (M. L. Gross, Ed.) American Chemical Society, Washington, DC, 1978.

(6) Biemann, K. (1990) Utility of exact mass measurements. *Methods Enzymol. 193*, 295–305.

(7) Gilliam, J. M., Landis, P. W., and Occolowitz, J. L. (1984) On-line accurate mass measurement in fast atom bombardment mass spectrometry. *Anal. Chem. 56*, 2285–2288.

(8) JEOL application note. Accurate mass measurement using a newly developed dual target introduction probe for FAB-MS.

(9) Horejs, V., Smolek, P., and Kocourek, J. (1978) XXXV. Water-soluble *O*-glycosyl polyacrylamide derivatives for specific precipitation of lectins. *Biochim. Biophys. Acta 538*, 293–298.

(10) Smith, D. F., Zopf, D. A., and Ginsburg, V. (1978) Carbohydrate antigens: Coupling of oligosaccharide phenylethylamine-isothiocyanate derivatives to bovine serum albumine. *Method Enzymol. 50*, 169–175.

(11) Hodge, J. E., and Hofreiter, B. T. (1962) Determination of reducing sugars and carbohydrates. *Methods Carbohydr. Chem.* (R. L. Whistler, and M. L. Wolfrom, Ed.) Academic Press, pp 388–389.

(12) Kallin, E., Lönn, H., Norberg, T., and Elofsson, M. (1989) Derivatization procedures for reducing oligosaccharides, Part 3: Preparation of oligosaccharide glycosylamines and their conversion into oligosaccharide–acrylamide copolymers. *J. Carbohydr. Chem. 8*, 597–611.

Bioconjugate Chemistry

JULY/AUGUST 1993
Volume 4, Number 4

© Copyright 1993 by the American Chemical Society

ARTICLES

Chemically Optimized Antimyosin Fab Conjugates with Chelating Polymers: Importance of the Nature of the Protein–Polymer Single Site Covalent Bond for Biodistribution and Infarction Localization

Vladimir S. Trubetskoy,*,† Jagat Narula,‡ Ban An Khaw,‡ and Vladimir P. Torchilin†

Center for Imaging and Pharmaceutical Research, Massachusetts General Hospital, Bldg 149, 13th Street, Charlestown, Massachusetts 02129, Bouve College of Pharmacy and Health Sciences, Center for Drug Targeting and Analysis, Northeastern University, Boston, Massachusetts 02115. Received November 13, 1992

Murine antimyosin Fab fragment was conjugated with ^{111}In-labeled N-terminal-modified DTPA–polylysine using three bifunctional reagents: *N*-hydroxysuccinimide esters of 3-(2-pyridyldithio)propionic acid (SPDP conjugate), 4-(maleimidomethyl)cyclohexanecarboxylic acid (SMCC conjugate) and bromoacetic acid (BrAc conjugate) for potential localization of experimental myocardial infarction. Using various antibody preparations and a rabbit acute myocardial infarction model the following parameters were observed: (1) an in vitro antigen binding activity of SPDP conjugate = SMCC conjugate > BrAc conjugate, (2) a blood clearance rate of SPDP conjugate > BrAc conjugate > SMCC conjugate, (3) a liver and splenic accumulation of SPDP conjugate > BrAc conjugate > SMCC conjugate, and (4) the infarcted tissue activity showed an accumulation of SMCC conjugate > SPDP conjugate > BrAc conjugate This study exemplifies the importance of rational chemical design of antimyosin Fab-chelating polymer conjugate for improved target tissue localization in vivo.

INTRODUCTION

The modification of monoclonal antibodies and their fragments with polylysine-based negatively charged chelating polymers has been recently shown to be effective in achieving improved immunoimaging of target tissues and reduced nontarget organ activities (*1*). This approach has been demonstrated with monoclonal antimyosin Fab coupled with DTPA–PLL[1] or deferroxamine–PLL (*2*, *3*) for radioimmunoscintigraphic localization of myocardial infarction.

The use of chelating polymers relative to low molecular weight chelates (like DTPA cyclic anhydride or isothiocyanatobenzyl-DTPA) to modify proteins is preferred due to a dramatic increase in labeling efficiency and the possibility of linking antibody and the corresponding chelating polymer (carrying multiple radioactive metal atoms) via a single covalent bond which should prevent loss of immunoreactivity usually observed with modification with multiple low molecular weight chelators (*4*).

Recently, a new coupling technique has been introduced which enabled a substantial increase in the isotope loading

* Corresponding author. Telephone No.: (617) 726-7834. FAX No.: (617) 726-7830.
† Massachusetts General Hospital.
‡ Northeastern University.

[1] Abbreviations used: DTPA, diethylenetriaminepentaacetic acid; PLL, poly-L-lysine; NPL, N-terminal modified polylysine; AMFab, antimyosin Fab fragment; SPDP, succinimidyl 3-(2-pyridyldithio)propionate; PDP, 3-(2-pyridyldithio)propionate; SMCC, succinimidyl 4-(maleimidomethyl)cyclohexyl carboxylate; BrAc-NHS, *N*-hydroxysuccinimide ester of bromoacetic acid; HBS, HEPES-buffered saline, pH 7.4.

1043-1802/93/2904-0251$04.00/0 © 1993 American Chemical Society

of the immunoconjugate with minimal loss in immunoreactivity. According to this procedure, a reactive group on the N-terminal of DTPA–polylysine is covalently conjugated to a monoclonal Fab fragment via a single covalent bond (*5*, *6*). The polymer is linked to the antibody like a 'tail', thus avoiding multipoint binding and protein cross-linking. Since the nature of this single chemical bond between antibody and polymer may influence the biodistribution and target accumulation of the conjugate, we undertook this study to demonstrate the in vivo properties of AMFab modified with DTPA–NPL via different single point cross-linkers and to determine the optimal chemical design of the AMFab–DTPA–NPL conjugate for the best myocardial infarction localization.

EXPERIMENTAL PROCEDURES

Monoclonal AMFab (R11D10) was prepared as previously described (*7*). DTPA–NPL bearing a PDP group on its N-terminal was synthesized as described by Slinkin et al. (*5*). Briefly, ε,*N*-carbobenzoxy-protected poly-D,L-lysine (Sigma; Mw 10 kDa, 15 mg), SPDP (Pharmacia, 2,5 mg), and triethylamine (0.5 μL) were mixed in 0.5 mL of dry dimethylformamide and incubated overnight at room temperature. The water-washed and lyophilized precipitate was deprotected with a 30% solution of HBr in glacial acetic acid (Aldrich, 2 mL). The deprotected polymer was washed with dry diethyl ether and lyophilized. Chelating residues were introduced into the polymer using DTPA bicyclic anhydride in 0.1 M bicarbonate, pH 8.0 (1.5 mg of anhydride/mg of NPL). Using trinitrobenzenesulfonic acid assay (*8*), DTPA residues were found to modify 95% of ε-amino groups of the polymer. The unmodified lysine ε-amino groups were blocked with succinic anhydride (15 mg/mg of dry polymer).

Preparation of SPDP-, SMCC-, and BrAc-NHS-Modified AMFab. SPDP, SMCC (Sigma), and BrAc-NHS (Sigma) were used as bifunctional modifiers to react with amino groups of AMFab. The reaction mixture typically consisted of 200 μg of AMFab and 10 μg of bifunctional reagent in 100 μL of HBS. The reaction was allowed to proceed for 1 h at room temperature and then was terminated by dialysis against HBS at 4 °C.

Conjugation of DTPA–NPL to AMFab. The homogeneity of AMFab and DTPA–NPL was confirmed by HPLC chromatography using Waters Protein-Pak 300SW column. Just prior to the reaction with modified AMFab, PDP-containing DTPA–NPL was activated by the treatment with 2.5 mM dithiotreithol in HBS for 20 min at 37 °C. Dithiotreithol was separated from the polymer using a Sephadex G-25 spin column equilibrated with HBS. Modified AMFab was mixed with reduced DTPA–NPL in a 1:1 weight ratio and this reaction mixture was incubated overnight at 4 °C in HBS. The conjugate was separated from unmodified Fab and free polymer using a DEAE Sephadex A-25 ion-exchange process (*2*). The fraction eluted with 0.35 M NaCl, 0.05 M phosphate, pH 6.0, was used for ^{111}In labeling.

Immunoreactivity in Vitro. Immunoreactivity of resultant conjugates as well as AMFab modified with the cross-linkers was determined by standard double-antibody ELISA using human heart myosin as the homologous antigen and peroxidase-labeled goat anti mouse IgG (Sigma) as the second antibody. All samples were run in duplicate and the highest average absorbance value on each plate was taken as 100% binding.

Labeling and in Vivo Studies. ^{111}In labeling was performed using the citrate transchelation method described in ref 2 except that a Sephadex G-100 column was used instead of a G-25 column as in original protocol. Along with the conjugates, we used DTPA–PLL (Mw = 12 000) as a control polychelator for in vivo experiments. For biodistribution studies New Zealand white rabbits were used. The animals were anesthetized with ketamine/xylazine (40 and 5 mg/kg, respectively) and further maintained on mechanical ventilation. A left thoracotomy was performed and the mid left anterior descending coronary artery was occluded with suture. After 40 min the suture was removed. At 1 h after reperfusion 100-300 μCi of ^{111}In-labeled AMFab–DTPA–NPL conjugate or DTPA–PLL were injected via the ear vein. Blood samples were taken starting at 1 min after conjugate administration up till 5 h to assess the clearance of the various preparations. After 5 h the animals were sacrificed by an overdose of pentobarbital. The hearts were excised and cut onto 0.5-cm slices. The slices were stained with 2% triphenyltetrazolium chloride solution for histochemical confirmation of myocardium necrosis. Then the heart slices were cut into 50–150-mg pieces (normal and infarcted heart tissue) and, along with samples of the major organs, were weighed and counted for ^{111}In radioactivity using a γ-counter (Compugamma, LKB). The number of animals in each group ranged from three to five.

RESULTS AND DISCUSSION

The aim of this study was to investigate the influence of the chemical bond between the AMFab and the chelating polymer on the biodistribution and infarct localization using ^{111}In-labeled DTPA–NPL conjugated to the antibody fragment via three different cross-linkers. The original procedure of conjugation using the disulfide bond was expanded to include SMCC- and BrAc-NHS-based conjugates. These latter conjugates utilized the stable C–S single thioether bond between Fab and the polymer (Figure 1). The choice of bifunctional reagents for the polymer coupling was determined by the following factors. Originally, the single-site Fab modification was developed for SPDP reagent only, so we needed to have a reagent introducing a stable C–S thioether bond for comparison. Among different maleimido-containing bifunctional reagents, SMCC has the most stable maleimido group (*9*). BrAc-NHS was chosen because it is not maleimido-containing reagent and possesses a less bulky spacer than the cyclohexyl carboxylate moiety in SMCC (Figure 1). This reagent also has demonstrated elevated conjugation yields in earlier studies with conventional multipoint bound DTPA–PLL–AMFab conjugates (*10*).

Specific Activity of Conjugates. The specific activity of DTPA–NPL itself was found to be approximately 70 μCi/μg of polymer by ^{111}In-labeling assessment. Average specific activities for conjugates (two or three preparations in each group) were found to be 145, 144, and 166 mCi/10 mg of protein for SPDP-, SMCC-, and BrAc-based conjugates, respectively. Since the labeling procedure of any of the three conjugates involved usually resulted in average of 150 μCi of ^{111}In/10 μg of protein, it was concluded that the Fab/polymer molar ratio in all conjugates is close to 1:1 assuming that the molecular weights of the Fab and the polymer are 50 and 10 kDa, respectively. This finding was quite expectable since the DEAE Sephadex A-25 anion-exchange purification process used for isolation of the conjugates allows separation of the total conjugation mixture onto several fractions which differ in polymer/protein ratio. Only one fraction of all three conjugates which has eluted at 0.35 M NaCl was used for labeling.

Immunoreactivity in Vitro. After separation of the conjugates from unmodified AMFab and unreacted poly-

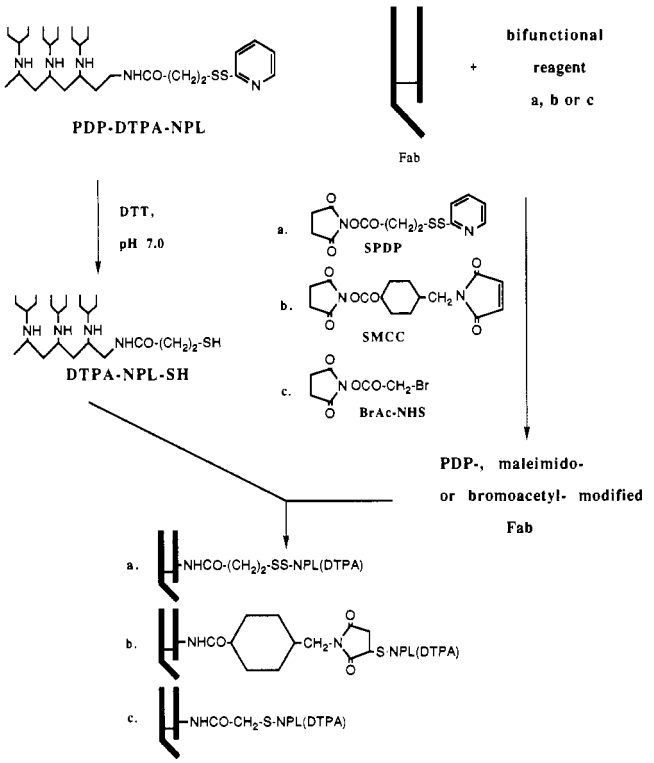


Figure 1. Synthesis of AMFab–DTPA–NPL conjugates.

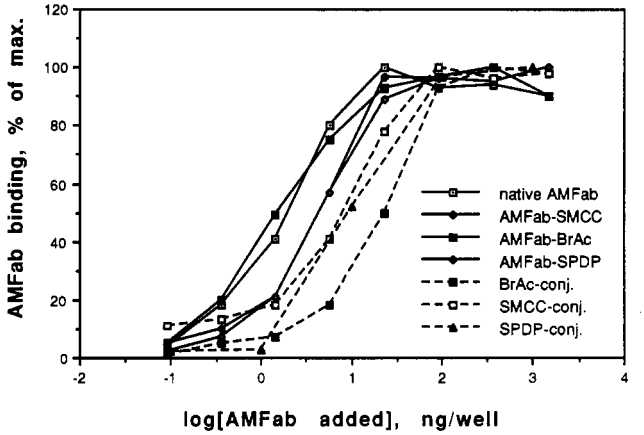


Figure 2. Antigen binding activity assay (ELISA) for the native AMFab, bifunctional reagent-modified AMFabs, and different AMFab–DTPA–NPL conjugates.

mer using Sephadex A-25 ion-exchange chromatography, the immunoreactivity of the modified antibodies was tested in vitro using an ELISA (Figure 2). For comparison purposes the data on the immunoreactivity of bifunctional reagent-modified AMFabs are also included in the figure. As one can see, the introduction of the bifunctional reagent itself does not significantly alter the immunoreactivity of AMFab while having bulky polymer attached to the antibody fragment leads to more severe damage (Figure 2, dotted lines). BrAc-NHS-based conjugate demonstrated the most considerable loss of binding relative to both SPDP- and SMCC-based conjugates. Since the AMFab/DTPA–NPL molar ratio was found to be the same in all three conjugates, the maximal loss of immunoreactivity in the BrAc-NHS-based conjugate might be explained by the fact that the BrAc modification site probably lies more closely to the antigen-binding region on the Fab protein globule which, in turn, leads to the impairment of antigen binding by the attached polymer.

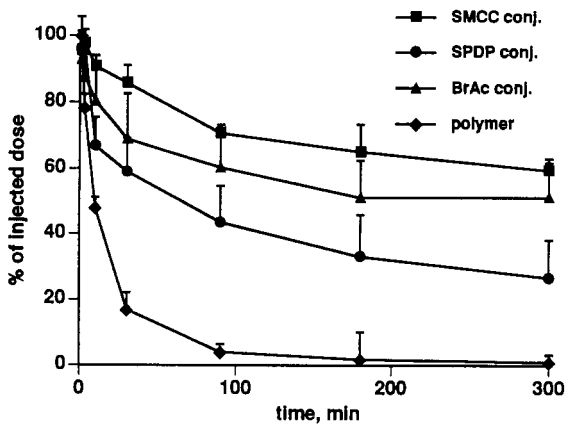


Figure 3. Blood clearance of ^{111}In–DTPA–PLL and ^{111}In–AMFab–DTPA–NPL conjugates in rabbit. Mean values are plotted (three to five animals per group).

Blood Clearance. These immunoconjugates were then tested in the rabbit acute myocardial infarction model for target accumulation, clearance, and label biodistribution. Figure 3 shows the blood clearance patterns for ^{111}In-labeled DTPA–PLL (a polymer without any reactive group) and all three ^{111}In-labeled immunoconjugates. The disulfide-containing SPDP conjugate cleared from the circulation the most rapidly, while the SMCC-based conjugate remained in the circulation for the longest period. The behavior of the BrAc-based conjugate is more or less close to that for the SMCC-based conjugate. Quite expectable for a small polymer, ^{111}In-labeled DTPA–PLL itself rapidly cleared from the circulation.

Thorpe et al. reported that the half-life of the disulfide bond containing immunotoxins in blood was approximately 6 h (*11*). Similarly, the immunoconjugate with a S–S bond used in our study had cleared maximally within the 5-h period, presumably due to the instability of the disulfides in vivo. Assuming that the radioactive polymer moiety of the conjugate is separated from the antibody, it should have a more rapid clearance from the blood, since it has a smaller molecular weight. Besides disulfide-linked immunotoxins, similar studies have also been performed where low molecular weight chelators have been conjugated to antibodies via different types of the covalent bond. Perala et al. has demonstrated the difference in blood clearance as well as in kidney and tumor activities of anti-prostate acid phosphatase IgG conjugated with DTPA directly, and via oxidized carbohydrate chains (*12*, *13*). Deshpande et al. found that the clearance rate of conjugates with a reducible S–S bond of benzyl-EDTA and murine IgG was faster than conventional benzyl-EDTA-linked antibody. Interestingly, this group found the accumulation of the S–S bond containing conjugate in the liver to be lower than stable thioether bond IgG–benzyl-EDTA conjugate (*14*).

Biodistribution and Infarct Accumulation. Conjugates used in our investigation exhibited not only dissimilarities in blood clearance rates but also substantial differences in the biodistribution patterns (Figure 4). Disulfide-containing SPDP-linked conjugate at 5-h postinjection time demonstrated high liver and splenic activities (up to 1% of injected dose/g of tissue in spleen). Stable thioether bond containing conjugates showed low radioactivity accumulation in the liver and spleen. Localization for S–S containing conjugate was remarkably lower in the infarct than thioether SMCC-based conjugate, perhaps due to the splitting of the polymer–Fab S–S bond in the blood or just due to increased blood clearance. Therefore, there is less intact conjugate to interact with the antigen.

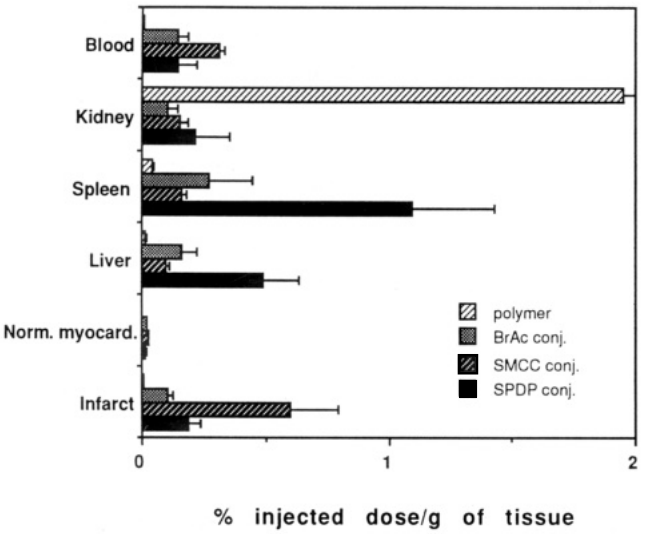


Figure 4. Biodistribution of ^{111}In–DTPA–PLL and ^{111}In–AMFab–DTPA–NPL conjugates in rabbits (5-h postinjection time, n = 3-5 animals per group).

BrAc-NHS-based conjugate demonstrated intermediate infarct accumulation. This may reflect the consequence of lower antigen binding activity found in the in vitro ELISA tests. For control polymer, DTPA–PLL, rapid clearance was followed by kidney accumulation without discrimination between infarcted and normal heart tissues (Figure 4). Unlike ^{111}In–DTPA–PLL, the DTPA–NPL accumulates mainly in liver and spleen as it can be concluded from the SPDP-based AMFab–DTPA–NPL biodistribution data. This phenomenon presumably takes place due to the following two-step process: (1) reduction of the SPDP-based conjugate in the blood with release of free sulfhydryl-containing ^{111}In–DTPA–NPL and (2) "secondary" binding of the polymer to the certain plasma proteins via sulfhydryl/disulfide exchange in a manner described in ref 15 for α_2-macroglobulin. These "secondary"-labeled products leave circulation relatively fast with subsequent accumulation of radioactivity in the liver and spleen.

It is interesting to observe that differences in radioactivity accumulation for all three conjugates leveled off in normal myocardium and are statistically insignificant for kidney. Only "actively" absorbing organs (like target infarct area and RES organs) exhibited differences in the uptake of the conjugates. Target/nontarget accumulation ratio (which may be as high as 25 for the SMCC-based conjugate) is determined exclusively by high infarct tissue uptake.

The SMCC-based conjugate showed the highest target area accumulation and the lowest liver and splenic activities. There is no polymer–Fab bond reduction and no drastic loss of immunoreactivity in this case. Unfortunately, the target/nontarget ratio of the SMCC-based conjugate was to some extent compromised due to the relatively high blood radiolabel content. Nevertheless, the infarcted tissue had maximal accumulation of this conjugate.

CONCLUSION

Our data clearly demonstrated that the specific chemical design of single site linked AMFab–DTPA–NPL conjugates might be useful in the development of new myocardial infarct localization probes for radioimmunoscintigraphy. Together with the data of other researchers (*11*, *12*) these results indicate that the nature of the chemical bond of the linkage between the antibody fragment and the chelating polymer is very important for the optimal performance of the immunoconjugates in vivo. Since the ideal properties of the ^{111}In-labeled immunoconjugate suitable for radioimmunoscintigraphy should be (1) long enough circulation time to provide sufficient contact with exposed antigen, (2) rapid removal from the circulation of nonbound conjugate after accumulation in the target area in order to increase target to blood activity ratios, and (3) insignificant accumulation of the conjugate in organs other than the target, we conclude that by varying the nature of the single covalent bond between antibody and chelating polymer one can influence and optimize the in vivo properties of the conjugate (such as circulation time and biodistribution) in order to make them closer to the properties of the ideal conjugate. Future studies should definitely focus on the Fab–polymer bonds of intermediate lability which allow rapid accumulation of the conjugate in the target area during the first phase after injection and rapid clearance of nonbound label during the second phase.

ACKNOWLEDGMENT

The work was partially supported by funding from Sterling Winthrop Pharmaceutical Research Division, Inc. and NCI Grant #CA 50505.

LITERATURE CITED

(1) Torchilin, V. P., and Klibanov, A. L. (1991) The antibody-linked chelating polymers for nuclear therapy and diagnosis. *CRC Crit. Rev. Ther. Drug Carrier Systems 7*, 275–308.

(2) Khaw, B. A., Klibanov, A. L., O'Donnel, S. M., Saito, T., Nossiff, N., Slinkin, M. A., Newell, J. B., Strauss, H. W., and Torchilin, V. P. (1991) Gamma imaging with negatively charge-modified monoclonal antibody: modification with synthetic polymers. *J. Nucl. Med. 32*, 1742–1751.

(3) Slinkin, M. A., Klibanov, A. L., Khaw, B. A., and Torchilin, V. P. (1990) Succinylated polylysine as a possible link between the antibody molecule and deferoxamine. *Bioconjugate Chem. 1*, 291–295.

(4) Yin, O., Narula, J., Nossif, N., and Khaw, B. A. (1991) Correlation of immunoreactivity and polymer formation to DTPA modification of monoclonal antibody. *Nucl. Med. Biol. 18*, 859–864.

(5) Slinkin, M. A., Klibanov, A. L., and Torchilin, V. P. (1991) Terminal modified polylysine-based chelating polymers: highly efficient coupling to antibody with minimal loss in immunoreactivity. *Bioconjugate Chem. 2*, 342–348.

(6) Trubetskoy, V. S., Torchilin, V. P., Kennel, S. J., and Huang, L. (1992) Use of N-terminal modified poly(L-lysine)–antibody conjugate as a carrier for targeted gene delivery in mouse lung endothelial cells. *Bioconjugate Chem. 3*, 323–327.

(7) Khaw, B. A., Mattis, J. A., Melincoff, G., Strauss, H. W., Gold, H. K., and Haber, E. (1984) Monoclonal antibody to cardiac myosin: Imaging of experimental infarction. *Hybridoma 3*, 11–23.

(8) Habeeb, A. F. S. A. (1966) Determination of free amino groups in proteins by trinitrobenzenesulfonic acid. *Anal. Biochem. 14*, 328–336.

(9) Yoshitake, S., Imagawa, M., Ishikawa, E., Niitsu, Y., Urushizaki, I., Nishiura, M., Kanazawa, R., Kurosaki, H., Tachibana, S., Nakazawa, N., and Ogawa, H. (1982) Mild and efficient conjugation of rabbit Fab' and horseradish peroxidase using a maleimide compound and its use for enzyme immunoassay. *J. Biochem. 92*, 1413–1424.

(10) Narula, J., Trubetskoy, V. S., O'Donnell, S. M., Strauss, H. W., Torchilin, V. P., and Khaw, B. A. (1992) Negatively charge polymer-modified antimyosin for infarct imaging: effects of different cross-linkers. *J. Nucl. Med. 33* (No 567), 959.

(11) Thorpe, P. E., Wallace, P. M., Knowles, P. P., Relf, M. G., Brown, A. N. F., Watson, G. J., Knyba, R. E., Wawrzynczak,

E. J., and Blakey, D. C. (1987) New coupling agents for the synthesis of immunotoxins containing a hindered disulfide bond with improved stability in vivo. *Cancer Res. 47*, 5924–5931.

(12) Perala, M., Vihko, P., Sodervall, M., Hekkila, J., and Vihko, R. (1990) Biodistribution in normal mice ^{111}In-labeled prostatic phosphatase-specific antibody and its F(ab)$_2$ fragments derivatized site-specifically or via bicyclic diethylenetriaminepentaacetic acid anhydride. *Eur. J. Nucl. Med. 16*, 621–626.

(13) Perala-Heape, M., Vihko, P., Pelkonen, I., Laine, A., and Vihko, R. (1991) Effect of conjugation on the biodistributionof ^{111}In-labeled anti-PAP and anti-PSA monoclonal antibodies examined in nude mice with PC-82 human tumor xenografts. *In vivo 5*, 159–166.

(14) Deshpande, S. V., DeNardo, S. J., Meares, C. F., McCall, M. J., Adams, G. P., and DeNardo, G. L. (1989) Effect of different linkages between chelates and monoclonal antibodies on levels of radioactivity in liver. *Nucl. Med. Biol. 16*, 587–597.

(15) Ghetie, M.-A., Uhr, J. W., and Vitetta, E. S. (1991) Covalent binding of human α_2-macroglobulin to deglycosylated ricin A chain and its immunotoxins. *Cancer Res. 51*, 1482–1487.

Synthesis and Binding of New Polyfluorinated Aryl Azides to α-Chymotrypsin. New Reagents for Photoaffinity Labeling

N. Soundararajan, Shwu Huey Liu, S. Soundararajan, and M. S. Platz*

Department of Chemistry, The Ohio State University,
120 West 18th Avenue, Columbus, Ohio 43210. Received November 23, 1992

The preparation of several new, water-soluble, polyfluorinated aryl azide reagents for use in photoaffinity labeling studies is described. The ability of some of these reagents and their nonfluorinated controls to noncovalently bind to α-chrymotrypsin is reported. It is found that polyfluorination does not interfere with ligand binding.

I. INTRODUCTION

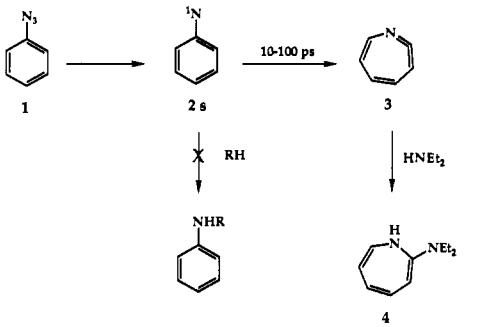
Photoaffinity labeling (PAL) is a technique for marking the binding sites of proteins (*1*). It was invented by Westheimer and co-workers in 1962 (*2*). In the seminal experiment the Westheimer group successfully labeled α-chymotrypsin, a serine-based protease with a diazo ester labeling reagent. As noted by the original workers, several diazo ester reagents suffer from photochemical Wolff rearrangement and the carbene intermediate which is generated by the action of light reacts rapidly with water. These two factors resulted in a low labeling efficiency.

In 1969 Knowles and Fleet introduced aryl azide reagents for PAL (*3*). Azides are more easily synthesized than their diazo counterparts and can better tolerate physiologically relevant pH's. It has been widely assumed by practitioners of the PAL technique that heat- and light-initiated decomposition of aryl azides efficiently generates aryl nitrenes which react rapidly and indiscriminately with a large variety of organic functional groups to give robust adducts in good yields. Unfortunately, the yields of the desired intermolecular adducts formed from aryl azides are generally either poor or zero (*4*). Recent work from these and other laboratories has demonstrated that the first trappable intermediate formed on photolysis of phenyl azide **1** is dehydroazepine **3** (Scheme I) (*4*). The dehydroazepine **3** reacts with amines to give azepines (e.g. **4**) in good yield (*5*). However, in the absence of amines, dehydroazepine **3** reacts with phenyl azide, or another ketenimine to eventually produce polymeric tar. The rate of ring expansion of singlet phenylnitrene at ambient temperature is so rapid as to preclude external trapping of the singlet nitrene (*4*).

In 1972 Banks reported that pyrolysis of polyfluorinated aryl azides generates nitrenes which can be intercepted in good yield (*6*). It was recognized (*1*) that this might lead to an attractive new type of PAL reagent because the small size of the fluorine substituent might not interfere with ligand binding, and furthermore that fluorine provides an NMR probe of the labeling process. This encouraged ourselves (*7*) and Keana's laboratory (*8*) to study azides of this type. We note that Watt (*9*), Katzenellenbogen (*10*), and Capaldi (*11*) and co-workers have recently employed fluorinated aryl azides in PAL experiments, albeit with mixed results.

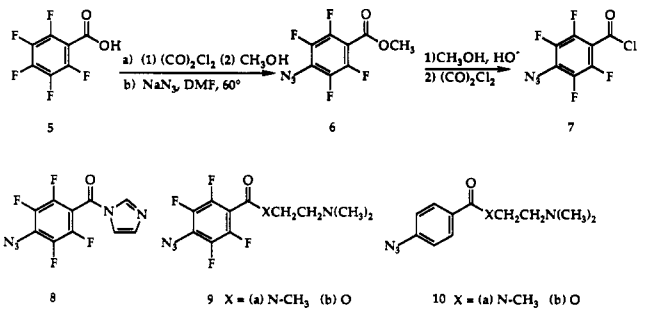
It is now amply demonstrated that polyfluorination retards ring expansion of singlet nitrenes by many orders of magnitude (*7*), which in turn allows efficient trapping of the nitrene intermediate. In this paper we are pleased to report the preparation of new water-soluble polyfluorinated aryl azides and to compare their binding to

Scheme I



1 2s 3 4

Scheme II



5 6 7 8 9 X = (a) N-CH3 (b) O 10 X = (a) N-CH3 (b) O

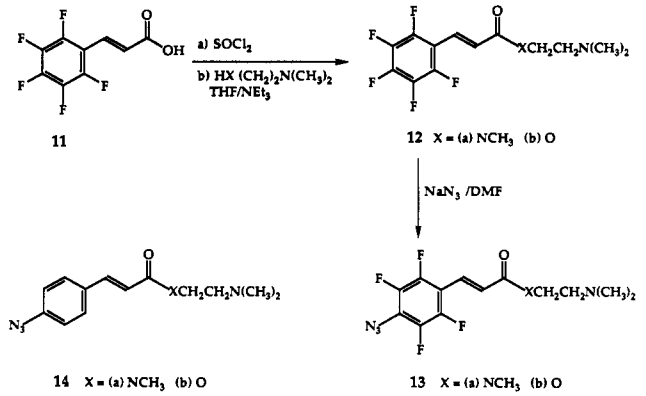
α-chymotrypsin with that of their nonfluorinated control compounds. We have found that polyfluorination of aryl azides does not interfere with binding of the substrate and thus these reagents should be valuable new tools for PAL experiments.

II. SYNTHESIS

Commercially available pentafluorobenzoic acid (**5**) is readily converted to pentafluorobenzoyl chloride and then to its methyl ester. The azide moiety can be introduced by heating the methyl ester with sodium azide in DMF to give **6**. The ester **6** can be converted to 4-azido-2,3,5,6-tetrafluorobenzoic acid by gentle hydrolysis and converted to the acid chloride **7** by treatment with oxalyl chloride (Scheme II). Compounds **8**, **9a**, and **9b** are prepared by treatment of the acid chloride with imidazole, *N,N*-dimethylaminoethanol or *N,N,N*-trimethylethylenediamine, respectively. Compounds **9a** and **9b** noncovalently bind α-chymotrypsin (*vide infra*) whereas **8**, first prepared by Keana (*8a*) et al., is expected to be useful for *covalent* labeling of α-chymotrypsin at serine-195 in the aromatic binding pocket (*12*). The nonfluorinated control compounds **10a,b** were prepared from 4-azidobenzoyl chloride (*13*).

1043-1802/93/2904-0256$04.00/0 © 1993 American Chemical Society

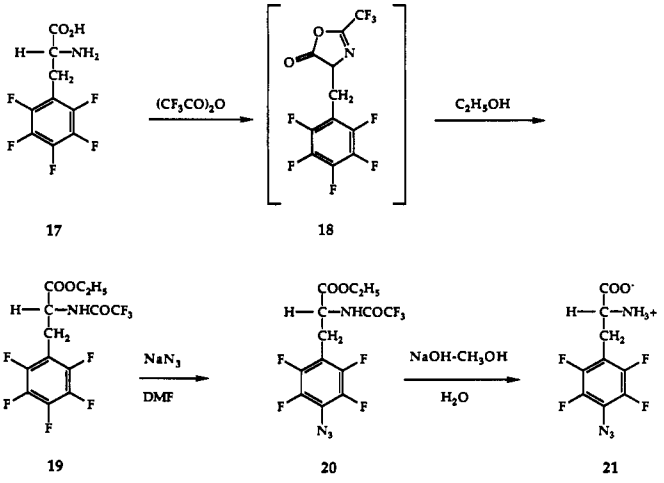
Scheme III



11 12 X = (a) NCH_3 (b) O

14 X = (a) NCH_3 (b) O 13 X = (a) NCH_3 (b) O

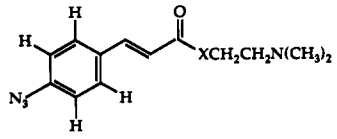
Scheme IV



17 18 19 20 21

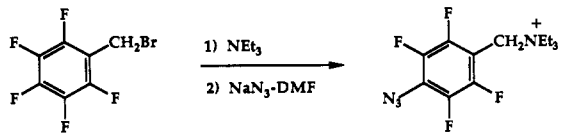
Cinnamic acid derivatives are known to bind strongly to α-chymotrypsin (*14*, *15*). Commercially available pentafluorocinnamic acid **11** was converted to water-soluble (HCl/H_2O, pH 3) compounds **13a** and **13b** (Scheme III) using the same strategy described previously.

For the sake of comparison, the nonfluorinated cinnamoyl azides **14a**,**4b** were also prepared.



14 X = (a) NCH_3 (b) O

Pentafluorobenzyl bromide **15** was converted to a water-soluble ammonium azide **16**.



15 16

A racemic tetrafluoroazide analog of phenylalanine **21** was prepared by the sequence shown in Scheme IV.

III. DETERMINATION OF DISSOCIATION CONSTANTS WITH α-CHYMOTRYPSIN

In order for a PAL experiment to be successful, the labeling reagent must bind tightly to the target biomolecule. Thus the effect of polyfluorination on the noncovalent binding of aryl azides to α-chymotrypsin was investigated.

Table I. Dissociation Contrants of Various PAL Reagents and α-Chymotrypsin Determined at pH 5 at Ambient Temperature

reagent	K_I (mM)	reagent	K_I (mM)
9a	0.15	**13b**	0.11
9b	0.32	**14a**	0.12
10a	0.40	**14b**	0.10
10b	0.014	**16**	0.33
13a	0.14		

Indole Inhibition Study. The competitive inhibition constant (K_I) of indole (I) determined against the hydrolysis of acetyltyrosine ethyl ester (ATEE) catalyzed by α-chymotrypsin has been reported to be 0.8 ± 0.2 mM at pH 8 (*16*). For the sake of comparison, we repeated this work at pH 8 and found K_I to be 0.88 mM, in good agreement with previously published work (*16*). Indole inhibition of acetyltyrosine ethyl ester (ATEE) (*17*) hydrolysis was also studied at pH 5, where α-chymotrypsin will bind aryl azides, but this is a pH where the enzyme activity is minimal and there will be little enzyme-catalyzed hydrolysis of benzoate esters and amides (*12*).

The reaction rates of ATEE hydrolysis catalyzed by α-chymotrypsin at pH 5 in the presence of inhibitor were determined. A first-order relationship was found between reaction velocity and ATEE concentration. The first-order catalytic constant and Michaelis constant are obtained by applying the Michaelis–Menten equation to the experimental data. In this manner, the catalytic constant $k_{cat,app}$ and Michaelis constant $K_{m,app}$ with varying indole concentration were obtained (*18*). From the linear plot of $(K_m/k_{cat})_{app}$ versus [I] the K_I of indole is obtained where $K_m/k_{cat} = 4.12 \times 10^{-3}$ mM s and $(K_m/k_{cat}) \times (1/K_I) = 2.37 \times 10^{-3}$ s^{-1}, thus K_I = intercept/slope = 1.7 mM, of indole, at pH 5.

Determinations of K_I in the PAL/α-Chymotrypsin Complexes. All of the PAL reagents of this work behave as competitive inhibitors of ATEE hydrolysis when they bind to α-chymotrypsin. The dissociation constants (K_d or K_I) of a PAL reagent with α-chymotrypsin are then calculated from the competitive inhibition equation (*18*):

$$\frac{1}{V} = \frac{K_m}{V_m} \times \left\{1 + \frac{[I]}{K_d}\right\} \times \frac{1}{[S]} + \frac{1}{V_m}$$

where K_m = 5.45 mM, $k_{cat} = 1.39 \times 10^3$ s^{-1}, [S] = 1 mM ATEE at pH 5, [I] = concentration of PAL in the sample solution, $[E_T]$ = concentration of α-chymotrypsin in the sample solution, and $V_m = k_{cat}[E_T]$.

The binding constants of the PAL reagents synthesized in this work are given in Table I.

The data indicates that all of the reagents bind α-chymotrypsin with almost equal affinity, with the exception of nonfluorinated ester **10b**. The origin of the unusual affinity of **10b** for α-chymotrypsin is unclear. However it is clear that the ability of fluorine substitution to enhance the desirable reactivity patterns of arylnitrenes, in particular the yield of bimolecular trapping products, does not interfere with noncovalent binding with a model enzyme, α-chymotrypsin. It is concluded that these new reagents will be useful tools for PAL experiments.

EXPERIMENTAL PROCEDURES

A. Materials. *General.* Melting points are uncorrected and were recorded on an Electrothermal apparatus, infrared spectra were obtained on a Beckman IR 4250 or a Perkin-Elmer 1710 infrared Fourier transform spectro-

photometer, UV spectra were recorded on a Perkin-Elmer Lambda 3B UV/VIS spectrophotometer, and high resolution mass spectra were obtained with a VG 70-250 S or Kratos MS-30 mass spectrometer. Elemental analyses were performed by M-H-W Laboratories. ^{1}H NMR ($CDCl_3$) and ^{19}F NMR ($CDCl_3$) were recorded using a Bruker AM-250 spectrometer. ^{1}H NMR are reported in ppm from internal standard tetramethylsilane (TMS) on the δ scale with splitting patterns, coupling constants, and relative integrated areas. The letter designates the multiplicity of the signal: s, singlet; bs, broad singlet; d, doublet; d,d, doublet of doublet; t, triplet, q, quartet; m, multiplet. ^{19}F NMR chemical shifts are obtained from the proton decoupled spectra and are reported in ppm relative to internal hexafluorobenzene (−162.9 relative to $CFCl_3$ = 0).

The solvents and reagents used were dried and purified prior to use. Dimethylformamide was distilled from NaH. Benzene, toluene, and tetrahydrofuran were distilled from sodium metal and benzophenone, methanol, and ethanol were distilled from their corresponding magnesium alkoxides. Column chromatography was performed, depending on the nature of the compound to be purified over either Brockman Activity 1 Basic or Neutral (80–200 mesh) alumina or silica gel. In places where essentially identical procedures for the synthesis and workup are involved, a general procedure is described and spectral and analytical data are given under each compound. Indole, pentafluorobenzoic acid, pentafluorocinnamic acid, *N,N*-dimethylethanolamine were obtained from Aldrich Chemical Co. *N*-Acetyl-L-tyrosine ethyl ester (ATEE), was purchased from Sigma. *N,N,N'*-Trimethylethylenediamine was purchased from Morton Thiokol, Inc. TLC aluminum plates were purchased from EM Science. All the other chemicals were reagent grade and were commercially available.

α-Chymotrypsin (92–97% protein, salt free, three times recrystallized) was purchased from Worthington Biochemical Corp. All enzyme activity assays were performed either on a Perkin-Elmer Lambda 3B UV/VIS or a Hewlett-Packard 8452A diode-array spectrophotometer. Lyophilizations were carried out with a Virtis Freeze mobile-6 lyophilizer. All kinetic data were calculated by the "Enzfitter" program purchased from Elsevier-Biosoft (68 Hills Road, Cambridge CB2, 1LA, United Kingdom).

B. Methods. *1. Determination of α-Chymotrypsin Concentration.* The concentration of α-chymotrypsin was determined by the UV absorbance of the protein at λ = 280 nm with a value of ϵ determined from Beer's law to be 5×10^4 M^{-1} cm^{-1}. Generally, the purity of the α-chymotrypsin was close to the value given on the label.

2. Enzyme Activity Assay. Enzyme activity was measured by the hydrolysis of ATEE (*17*) at pH 5. The ATEE substrate solution (1 mM) was prepared by dissolving 26.9 mg of ATEE in 1 mL of acetone and 99 mL of 0.1 M sodium acetate buffer, pH 5. Into both the sample and reference cuvettes was separately pipetted 3 mL of ATEE solution. Ten microliters of native or modified enzyme solution (32 mg/mL) was added into the sample cell. The decrease in absorbance at 237 nm with time followed a straight line and was recorded for 3 min. The slope of this line indicated the activity of the enzyme.

3. Inhibition by Indole. Solutions of different concentrations of indole/ATEE (0–1.2 mM, pH 5) were prepared. Three milliliters of these solutions were pipetted out into both the sample and the reference cells of a UV cuvette. One hundred microliters of α-chymotrypsin stock solution (8.9×10^{-5} M) was then added to the sample cell. The activities of enzyme solutions containing inhibitor were obtained by the decrease in absorbance at 237 nm over 3 min. The first-order catalytic constant ($k_{cat,app}$) and Michaelis constant ($K_{m,app}$) were obtained using the Michaelis–Menten equation:

$$\frac{V}{[E_T]} = \frac{k_{cat}[S]}{\{K_m + [S]\}} \quad (1)$$

In addition, competitive inhibition behavior was found by plotting $1/V$ versus [S]. The dissociation constant of inhibitor was then obtained by the Lineweaver–Burk equation (*18*):

$$\frac{[E_T]}{V} = \frac{K_m}{k_{cat}} \times \frac{1}{[S]} \times \left[1 + \frac{[I]}{K_I}\right] + \frac{1}{k_{cat}} = ([K_m/k_{cat}]_{app})(1/[S]) + 1/k \quad (2)$$

where $[K_m/k_{cat}]_{app} = K_m/k_{cat}\{1 + [I]/K_I\}$, [I] = [concentration of indole], [S] = [concentration of ATEE], and $[E_T]$ = concentration of α-chymotrypsin, thus, K_I = intercept/slope.

4. Binding Constant (K_I) Determination of Various PAL's and α-Chymotrypsin. Solutions with different concentrations of ATEE substrate (0.5–2 mM in pH 5 acetate buffer) were prepared. The PAL α-chymotrypsin complex was formed by dissolving 4×10^{-6} mol (100 mg) of α-chymotrypsin in 3 mL of water (pH 3, HCl) followed by addition of 8.5×10^{-5} mol of PAL reagent in 125 μL of acetonitrile and incubation in the dark for 1 h. Three milliliters of ATEE solution of various concentration was pipetted into both the sample and reference cuvettes, separately. Ten microliters of enzyme complex solution (32 mg/mL) was added to the sample cell. The enzyme activity was recorded using standard procedures as previously described. The binding constants for the PAL/α-chymotrypsin complex were calculated by the same procedure as the indole inhibition constant.

C. Synthesis. 4-Azidobenzoic acid (*13*, *19*), 4-azidobenzoyl chloride (*19*), methyl pentafluorobenzoate (*7g*, *20*), ethyl 4-azido-2,3,5,6-tetrafluorocinnamate (*20*), 4-azido-2,3,5,6-tetrafluorobenzoic acid (*8a*), methyl 4-azido-2,3,5,6-tetrafluorobenzoate (**6**) (*7g*, *8a*), and ethyl pentafluorocinnamate (*20*) have been described in the literature.

N-(4-Azidobenzoyl)-N,N',N'-trimethylethylenediamine (***10a***). *N,N,N'*-Trimethylethylenediamine (1.4 g, 13.5 mmol) was dissolved in dry THF (50 mL). K_2CO_3 (3 g) was added at room temperature followed by a solution of 4-azidobenzoyl chloride (*13*) (15 mL, 12.25 mmol) dropwise with stirring at room temperature. After 1 h of stirring at room temperature, the solvent was evaporated and the residue was taken up in water. The ethyl acetate extract of the aqueous solution was concentrated and passed through a column of neutral alumina in ethyl acetate. The product was obtained as a yellow oil: yield, 99%; ^{1}H NMR δ 1.9 (s, 6H, $N(CH_3)_2$ protons), 2.42 (t, J = 7 Hz, 2H methylene protons), 3.0 and 3.1 (s, 3H, NCH_3 protons), 3.3–3.5 (m, methylene protons), 7.0 (d, J = 6 Hz, 2H, aromatic protons), 7.4 (d, J = 6 Hz, 2H, aromatic protons); IR (neat) 2129, 2096, 1625, 1607 cm^{-1}.

2-(N,N-Dimethylamino)ethyl 4-Azidobenzoate (***10b***). Compound **10b** was prepared following the procedure described for **10a**, but substituting *N,N*-dimethylethanolamine in the place of *N,N,N'*-trimethylethylenediamine. The product was obtained as a yellow oil: yield, 70%; ^{1}H NMR δ 2.3 (s, 6H, $N(CH_3)_2$ protons), 2.7 (t, J = 7 Hz, 2H, methylene protons), 4.4 (t, J = 7 Hz, 2H, methylene protons), 7.0 (d, J = 6 Hz, 2H, aromatic protons), 8.0 (d, J = 6 Hz, 2H, aromatic protons); IR (neat) 2125, 1705, 1605 cm^{-1}.

General Procedure for the Nucleophilic Displacement of Fluorine by Azide. A solution of the pentafluoro compound (0.01052 mol) in dry dimethylformamide (15 mL) and powdered sodium azide (0.01157 mol) was stirred under nitrogen at 55–60 °C in an oil bath for 18 h. The solvent was removed by distillation below 60 °C under reduced pressure. The residue was dissolved in ethyl acetate (10 mL) and purified by passing through a column of neutral alumina in hexane/ethyl acetate (1:1).

General Procedure for the Synthesis of the Fluorinated Azides 8, 9a, and 9b from 6. A solution of the azidofluorobenzoic acid **6** (0.01 mol) in fresh oxalyl chloride (10 mL) was heated under reflux for 8 h. Excess oxalyl chloride was removed by distillation under reduced pressure and 10 mL of benzene was added to the cooled residue. Benzene was distilled under reduced pressure, leaving the azidofluorobenzoyl chloride. The acid chloride was used immediately without further purification and characterization in the next step.

Imidazole, amino alcohol, or diamine (0.01 mol) was dissolved in freshly distilled THF (50 mL) in a 100-mL round-bottomed flask. Distilled triethylamine (0.011 mol) was then added via syringe to the clear solution. The azidofluoro acid chloride dissolved in THF (5 mL) was then added dropwise to the contents of the flask with stirring at 0–5 °C. The reaction mixture was allowed to stir for 2 h at room temperature. Triethylamine hydrochloride precipitated and was filtered with suction and washed with fresh THF (10 mL) and the solvent distilled off under reduced pressure. The residue obtained was further purified by recrystallization from appropriate solvent(s).

N-(4-Azido-2,3,5,6-tetrafluorobenzoyl)imidazole (8) (*8a*): colorless crystalline solid; mp 61–63 °C (benzene/hexane) (lit. (*8a*) mp 63–64 °C); yield, 87%; ^{1}H NMR δ 7.98 (s, 1H, imidazole H), 7.46 (s, 1H, imidazole H), 7.18 (m, 1H, imidazole.H); ^{19}F NMR −139.71 (m, 2F), −149.72 (m, 2F); IR ($CHCl_3$) 2130, 1705, 1690, 1620, 1500, 1420, 1380, 1120 cm^{-1}; exact mass calculated for $C_{10}H_3F_4N_5O$ *m/e* 285.027, found 285.024. Anal. Calcd for $C_{10}H_3F_4N_5O$: C, 42.10; H, 1.06; N, 24.56. Found: C, 42.36; H, 1.08; N, 24.87.

N-(4-Azido-2,3,5,6-tetrafluorobenzoyl)-N,N′,N′-trimethylethylenediamine (9a): colorless crystals; mp 32–33 °C (hexane); yield, 87%; ^{1}H NMR δ 2.13 and 2.23 (s, 6H, $N(CH_3)_2$ protons), 2.40 and 2.57 (t, *J* = 6 Hz, 2H, methylene protons), 2.98 and 3.15 (s, 3H, N-CH_3 protons), 3.27 and 3.65 (t, *J* = 6 Hz, 2H, methylene protons); ^{19}F NMR −151.52 (m, 2F), −142.54 (m, 2F); IR ($CHCl_3$) 2940, 2860, 2830, 2780, 2130, 1710, 1460, 1400, 1520, 1310, 1120, 990 cm^{-1}; exact mass calculated for $C_{12}H_{13}F_4N_5O$ *m/e* 319.107, found 319.109. Anal. Calcd for $C_{12}H_{13}F_4N_5O$: C, 45.13; H, 4.11; N, 21.94. Found: C, 45.22; H, 4.18; N, 21.87.

2-(N,N-Dimethylamino)ethyl 4-azido-2,3,5,6-tetrafluorobenzoate (9b): pale amber colored oil at room temperature; yield, 92%; ^{1}H NMR δ 2.30 (s, 6H, CH_3 protons), 2.67 (t, *J* = 6 Hz, 2H, methylene protons), 4.45 (t, *J* = 6 Hz, 2H, methylene protons); ^{19}F NMR −139.77 (m, 2F), −152.21 (m, 2F); IR (neat) 2960, 2120, 1740, 1645, 1490, 160 cm^{-1}; exact mass calculated for $C_{11}H_{10}F_4N_4O_2$ *m/e* 306.073, found 306.075. Anal. Calcd for $C_{11}H_{10}F_4N_4O_2$: C, 43.13; H, 3.29; N, 18.30. Found: C, 43.28; H, 3.17; N, 18.38.

N-(2,3,4,5,6-Pentafluorocinnamoyl)-N,N′,N′-trimethylethylenediamine (12a). Compound **12a** was prepared from 2,3,4,5,6-pentafluorocinnamic acid following the general procedure described for **8–10**: pale yellowish oil at room temperature; yield, 95%; ^{1}H NMR δ 2.25 (s, 6H, $N(CH_3)_2$ protons), 2.47 (t, *J* = 6.6 Hz, 2H, methylene protons), 3.04 and 3.14 (s, 3H, NCH_3 protons), 3.47 and 3.54 (t, *J* = 6.6 Hz, 2H, methylene protons), 7.23 (d, *J* = 16 Hz, 1H, methine proton), 7.57 (d, *J* = 16 Hz, 1H, methine proton); ^{19}F NMR −141.45 (m, 2F), −154.09 (m, 1F), −163.29 (m, 2F); exact mass calculated for $C_{14}H_{15}F_6N_2O$ m/e 341.109, found 341.113. Anal. Calcd for $C_{14}H_{15}F_6N_2O$: C, 49.25; H, 4.43; N, 8.21. Found: C, 49.37; H, 4.38; N, 8.16.

2-(N,N-Dimethylamino)ethyl 2,3,4,5,6-Pentafluorocinnamate (12b). Compound **12b** was prepared from 2,3,4,5,6-pentafluorocinnamic acid following the general procedure described for **3–5**: pale brownish oil at room temperature; yield, 92%; ^{1}H NMR δ 2.33 (s, 6H, $N(CH_3)_2$ protons), 2.66 (t, *J* = 6.6 Hz, 2H, methylene protons), 4.33 (t, *J* = 6.6 Hz, 2H, methylene protons), 6.78 (d, *J* = 16.5 Hz, 1H, methine proton), 7.66 (d, *J* = 16.5 Hz, 1H, methine proton); ^{19}F NMR −162.74 (m, 2F), −152.29 (m, 1F), −140.53 (m, 2F); exact mass calculated for $C_{13}H_{12}F_6NO_2$ *m/e* 328.077, found 328.091. Anal. Calcd for $C_{13}H_{12}F_6NO_2$: C, 47.55; H, 3.69; N, 4.27. Found: C, 47.46; H, 3.58; N, 4.38.

N-(4-Azido-2,3,5,6-tetrafluorocinnamoyl)-N,N′,N′-trimethylethylenediamine (13a): pale yellowish oil at room temperature; yield, 84%; ^{1}H NMR δ 2.25 (s, 6H, $N(CH_3)_2$ protons), 2.47 (t, *J* = 6.6 Hz, 2H, methylene protons), 3.04 and 3.14 (s, 3H, NCH_3 protons), 3.47 and 3.54 (t, *J* = 6.6 Hz, 2H, methylene protons), 7.23 (d, *J* = 16 Hz, 1H, methine proton), 7.57 (d, *J* = 16 Hz, 1H, methine proton); ^{19}F NMR 163.29 (m, 2F), −154.09 (m, 1F), −141.45 (m, 2F); exact mass calculated for $C_{14}H_{15}F_4N_5O$ *m/e* 364.116, found 364.12. Anal. Calcd for $C_{14}H_{15}F_4N_5O$: C, 46.14; H, 4.15; N, 19.23. Found: C, 46.11; H, 4.18; N, 19.32.

2-(N,N-Dimethylamino)ethyl 4-azido-2,3,5,6-tetrafluorocinnamate (13b): pale brownish oil at room temperature; yield, 78%; ^{1}H NMR δ 2.30 (s, 6H, methyl protons), 2.63 (t, *J* = 6.6 Hz, 2H, methylene protons), 4.32 (t, *J* = 6.6 Hz, 2H, methylene protons), 6.76 (d, *J* = 16.5 Hz, 1H, methine proton), 7.65 (d, *J* = 16.5 Hz, 1H, methine proton); ^{19}F NMR −159.19 (m, 2F), −141.09 (m, 2F); exact mass calculated for $C_{13}H_{12}F_4N_4O_2$ *m/e* 332.089, found 332.097. Anal. Calcd for $C_{13}H_{12}F_4N_4O_2$: C, 46.98; H, 3.64; N, 16.87. Found: C, 46.92; H, 3.78; N, 16.94.

N-(4-Azidocinnamoyl)-N,N′,N′-trimethylethylenediamine (14a). This compound was prepared from 4-azidocinnamic acid following the general procedure described for **10a**: pale yellowish oil at room temperature; yield, 86%; ^{1}H NMR δ 2.28 (s, 6H, $N(CH_3)_2$ protons), 2.48 (t, *J* = 7 Hz, 2H, methylene protons), 3.07 and 3.18 (s, 3H, NCH_3 protons), 3.53–3.60 (m, methylene protons), 6.87 (d, *J* = 15 Hz, 1H, methine proton), 7.36 (d, *J* = 6 Hz, 2H, aromatic protons), 7.48 (d, *J* = 6 Hz, 2H, aromatic protons), 7.61 (d, *J* = 15 Hz, 1H, methine proton); exact mass calculated for $C_{14}H_{19}N_5O$ *m/e* 273.159, found 273.148. Anal. Calcd for $C_{14}H_{19}N_5O$: C, 61.50; H, 7.01; N, 25.63. Found: C, 61.43; H, 6.89; N, 25.69.

2-(N,N-dimethylamino)ethyl 4-Azidocinnamate (14b). This compound was prepared from 4-azidocinnamic acid following the general procedure described for **10b**: pale brownish oil at room temperature; yield, 82%; ^{1}H NMR δ 2.31 (s, 6H, methyl protons), 2.63 (t, *J* = 7 Hz, 2H, methylene protons), 4.30 (t, *J* = 7 Hz, 2H, methylene protons), 7.62 (d, *J* = 16 Hz, 1H, methine proton), 7.37 (d, *J* = 6 Hz, 2H, aromatic protons), 7.752 (d, *J* = 6 Hz, 2H, aromatic protons), 7.62 (d, *J* = 16 Hz, 1H, methine proton); exact mass calculated for $C_{13}H_{16}N_4O_2$ *m/e* 260.298, found 260.22. Anal. Calcd for $C_{13}H_{16}N_4O_2$: C, 61.74; H, 5.93; N, 20.58. Found: C, 61.65; H, 5.78; N, 20.52.

(4-Azido-2,3,5,6-tetrafluorobenzyl)triethylammonium Bromide (16). 2,3,4,5,6-Pentafluorobenzyl bromide (15) was heated under reflux with a 10% molar excess of triethylamine in THF. The precipitated salt was filtered, washed with THF, and dried under vacuu.: colorless crystals; mp 89–91 °C; yield, 100%; ^{1}H NMR δ 1.28 (t, J = 7 Hz, 9H, methyl protons), 3.25 (q, 6H, methylene protons), 4.51 (s, 2H, benzylic protons); ^{19}F NMR −137.00 (m, 2F), −149.61 (m, 2F), −161.53 (m, 1F); exact mass calculated for $C_{13}H_{17}F_5NBr$ m/e 361.046, found 181.064 [$M^+ - (C_2H_5)_3NHBr$]. Anal. Calcd for $C_{13}H_{17}F_5NBr$: C, 43.21; H, 3.88; N, 3.88. Found: C, 43.71; H, 3.68; N, 3.72. (4-Azido-2,3,5,6-tetrafluorobenzyl)triethylammonium bromide (16) was synthesized using the general procedure described for the displacement of fluorine by azide. After the distillation of the residual DMF, the residue was triturated with benzene and the resulting solid recrystallized from ethanol/water, yielding colorless powdery white crystals which started decomposing at 156–158 °C: yield, 94%; ^{1}H NMR δ 1.29 (t, J = 7 Hz, 9H, methyl protons), 3.34 (q, 6H, methylene protons), 4.68 (s, 2H, benzylic protons); ^{19}F NMR −133.83 (m, 2F), −158.53 (m, 2F). Anal. Calcd for $C_{13}H_{17}F_4N_4Br$: C, 40.62; H, 4.46; N, 14.58. Found: C, 40.74; H, 4.54; N, 14.64.

dl-2,3,4,5,6-Pentafluoro-N-(trifluoroacetyl)phenylalanine Ethyl Ester (19). dl-2,3,4,5,6-Pentafluorophenylalanine (17)[21] (12.76g, 0.05 mol) suspended in dry benzene (50 mL) was treated with trifluoroacetic anhydride (14g, 0.075 mol) in drops with stirring under nitrogen at 15–20 °C during 15 min. The reaction mixture, which was originally a slurry, became a clear solution. The clear solution was heated under reflux under nitrogen on a steam bath for 45 min. The solvent and excess trifluroacetic anhydride were distilled off at reduced pressure. The residue was treated with dry ethanol (75 mL) and refluxed on a steam bath for 45 min. Ethanol was distilled off at reduced pressure and the pasty residue obtained was recrystallized from ethyl acetate to give 16.15 g (yield, 87%) of a colorless cryatalline solid, 19: mp 90–91 °C; ^{1}H NMR δ 1.32 (t, J = 7 Hz, 3H, ester CH_3), 3.16–3.47 (m, 2H, benzylic protons), 4.22–4.35 (m, 2H, ester CH_2), 4.86 (q, J = 7 Hz, 1H, methine proton), 6.94 (bs, 1H, NH proton); ^{19}F NMR −162.49 (m, 2F), −154.82 (m, 1F), −143.40 (m, 2F), −77.20 (s, 3F); IR ($CHCl_3$) 3380, 1720, 1650, 1270, 1150, 1110, 980, 960 cm^{-1}; exact mass calculated for $C_{13}H_9F_8NO_3$ m/e 379.045, found 379.015. Anal. Calcd for $C_{13}H_9F_8NO_3$: C, 41.16; H, 2.39; N, 3.69. Found: C, 41.22; H, 2.28; N, 3.71.

4-Azido-dl-2,3,5,6-tetrafluoro-N-(trifluoroacetyl)phenylalanine Ethyl Ester (20). Colorless crystals were obtained by treatment of 19 with NaN_3 as described in the general procedure: mp 106–107 °C; yield, 77%; ^{1}H NMR δ 1.32 (t, J = 7 Hz, 3H, ester CH_3), 3.15–3.46 (m, 2H, benzylic protons), 4.20–4.34 (m, 2H, ester CH_2), 4.85 (q, J = 7 Hz, 1H, CH proton), 6.97 (bs, 1H, NH proton); ^{19}F NMR −152.66 (m, 2F), −143.88 (m, 2F), −77.23 (s, 3F); IR ($CHCl_3$) 3390, 2120, 1725, 1650, 1465, 1280, 1150, 965 cm^{-1}; exact mass calculated for $C_{13}H_9N_4O_3F_7$ m/e 402.056, found 402.015. Anal. Calcd for $C_{13}H_9N_4O_3F_7$: C, 38.80; H, 2.26; N, 13.93. Found: C, 38.91; H, 2.18; N, 13.72.

4-Azido-dl-2,3,5,6-tetrafluorophenylalanine (21). The azido amide ester 20 was hydrolyzed following the procedure described for the preparation of methyl 4-azido-2,3,5,6-tetrafluorobenzoate (6). The aqueous solution obtained after hydrolysis and extraction with methylene chloride was cooled to 0 °C and neutralized to pH 7.00. The precipitated solids were filtered, redissolved in the minimum amount of 10% hydrochloric acid, and neutralized to pH 7.00 using dilute ammonium hydroxide solution. The reprecipitated solid was filtered, washed with ice water and dried in a vacuum desicator over phosphorus pentoxide: colorless powder; mp 190–195 °C dec; yield, 76%; ^{1}H NMR (CD_3OD) δ 3.34–3.57 (m, 2H, benzylic protons), 4.42–4.47 (m, 1H, CH proton), 7.62 (bs, 2H, NH_2 proton), 12.09 (bs, 1H, acid proton); ^{19}F NMR (CD_3OD) −144.04 (m, 2F), −151.69 (m, 2F). Anal. Calcd for $C_9H_6F_4N_4O_2$: C, 38.84; H, 2.17; N, 20.17. Found: C, 38.71; H, 2.24; N, 20.14.

ACKNOWLEDGMENT

Support of this work by the National Institutes of Health (GM 34823) is gratefully acknowledged.

LITERATURE CITED

(1) Bayley, H. (1983) *Photogenerated Reagents in Biochemistry and Molecular Biology*; Elsevier, Amsterdam.

(2) Singh, A., Thornton, E. R., and Westheimer, F. H. (1962) The Photolysis of Diazoacetylchymotrypsin. *J. Biol. Chem. 237*, 3006.

(3) Fleet, G. W. J., Porter, R. R., and Knowles, J. R. (1969) Affinity Labelling of Antibodies with Aryl Nitrene as Reactive Group. *Nature, 224*, 511.

(4) Schuster, G. B., and Platz, M. S. (1992) Photochemistry of Phenyl Azide. *Adv. Photochem. 17*, 69.

(5) Doering, W. Von, and Odum, R. A. (1966) Ring Enlargement in the Photolysis of Phenyl Azide. *Tetrahedron, 22*, 81.

(6) (a) Banks, R. E., and Sparkes, G. R. (1972) Studies in Azide Chemistry. Part V. Synthesis of 4-Azido-2,3,5,6-tetrafluoro,4-Azido-3-chloro-2,5,6-trifluoro-, and 4-Azido-3,5-dichloro-2,6-difluoro pyridine, and Some Thermal Reactions of the Tetrafluorocompound. *J. Chem. Soc., Perkin Trans. I*, 2964. (b) Banks, R. E., and Prakash, A. (1974) Studies in Azide Chemistry. Part VI. Some Reaction of Perfluoroazidobenzene and Perfluoro-4-azidotoluene. *J. Chem. Soc., Perkin trans. I.*, 1365. (c) Banks, R. E., and Prakash, A. (1973) New Reactions of Azidopentafluorobenzene; Intermolecular Insertions into the N-H Bonds. *Tetrahedron Lett.*, 99. (d) Banks, R. E., and Medany, I. M. (1990) Studies in Azide Chemistry. Part 14. Thermolysis of Perfluoro-4-azidopyridine and Perfluoro-4-azidotoluene in the Presence of Penta- and Hexa-Methylbenzene. *J. Fluorine Chem. 47*, 527. (e) Banks, R. E., and Venayak, N. D. (1980) Studies in Azide Chemistry. Part 13. Intermolecular Insertion of Azido-derived Polyfluorinated Aryl- and Heteroaryl-Nitrenes into Ring C-H Bonds of 1,3,5-Trimethyl and 1,3,5-Trimethoxybenzene. *J. Chem. Soc., Chem. Commun.*, 900. (f) Banks, R. E., and Madany, I. M. (1985) Decisive Evidence for the Occurrence of Ring-expansion During Pyrolysis of Azidopentafluorobenzene: X-Ray Crystallographic Analysis of 'Pentafluorophenyl-nitrene. *J. Fluorine Chem. 30*, 211.

(7) (a) Leyva, E., Young, M. J. T., and Platz, M. S. (1986) High Yields of Formal CH Insertion Products in the Reactions of Polyfluorinated Aromatic Nitrenes. *J. Am. Chem. Soc. 108*, 8307. (b) Leyva, E., Munoz, D., and Platz, M. S. (1989) Photochemistry of Fluorinated Aryl Azides in Toluene Solution and in Frozen Polycrystals. *J. Org. Chem. 54*, 5938. (c) Young, M. J. T., and Platz, M. S. (1989) Polyfluorinated Aryl Azides as Photoaffinity Labelling Reagents; The Room Temperature CH Insertion Reactions of Singlet Pentafluorophenyl Nitrene with Alkanes. *Tetrahedron Lett. 30*, 2199. (d) Young, M. J. T., and Platz, M. S. (1991) Mechanistic Analysis of the Reactions of (Pentafluorophenyl)nitrene in Alkanes. *J. Org. Chem. 56*, 6403. (e) Poe, R., Grayzar, J., Young, M. J. T., Leyva, E., Schnapp, K. A., and Platz, M. S. (1991) Remarkable Catalysis of Intersystem Crossing of Single (Pentafluorophenyl)nitrene. *J. Am. Chem. Soc. 113*, 3209. (f) Poe, R., Schnapp, K., Young, M. J. T., Grayzar, J., and Platz, M. S. (1992) Chemistry and Kinetics of Singlet (Pentafluorophenyl)nitrene. *J. Am. Chem. Soc. 114*, 5054. (g) Soundararajan, N., and Platz, M. S. (1990) Descriptive Photochemistry of Polyfluorinated Azide Derivatives of Methyl Benzoate. *J. Org. Chem. 55*, 2034.

(8) (a) Keana, J. F. W., and Cai, S. X. (1990) New Reagents for Photoaffinity Labelling: Synthesis and Photolysis of Functionalized Perfluorophenyl Azides. *J. Org. Chem. 55*, 3640. (b) Keana, J. F. W., and Cai, S. X. (1989) Functionalized Perfluorophenyl Azides: New Reagents for Photoaffinity Labelling. *J. Fluorine Chem. 43*, 151. (c) Cai, S. X., and Keana, J. F. W. (1989) 4-Azido-7-Iodo-3,5,6-Trifluorophenyl Carbonyl Derivatives. A New Class of Functionalized and Iodinated Perfluorophenyl Azide Photolabels. *Tetrahedron Lett. 30*, 5409. (d) Cai, S. X., Glenn, D. J., and Keana, J. F. W. (1992) Toward the Development of Radiolabelled Fluorophenyl Azide-Based Photolabelling Reagents: Synthesis and Photolysis of Iodinated 4-Azidoperfluorobenzoates and 5-Azido-3,5,6-trifluorobenzoates. *J. Org. Chem. 57*, 1299. (e) Cai, S. X., and Keana, J. F. W. (1991) Diazo and Azido-Functionalized Glutaraldehydes as Cros Linking reagents and Potential Fixatives for Electron Microscopy. *Bioconjugate Chem. 2*, 38.

(9) (a) Crocker, P. J., Imai, N., Rajogopalen, K., Boggess, M. A., Kwiatkiwski, S., Dwyer, L. D., Vanaman, T. C., and Watt, D. (1990) Heterobifunctional Cross Linking Agents Incorporating Perfluorinated Aryl Azides. *Bioconjugate Chem. 3*, 419. (b) Drake, R. R., Slam, J., Wall, K., Abramove, M., D'Douza, C., Elbein, A. D., Crocker, P. J., and Watt, D. S. (1992) Application of an N-(4-Azido-2,3,5,6-tetrafluorobenzoyl)tyrosine Substituted Peptide as a Heterobifunctional Cross-linking Agent in a Study of Proteino-Glycosylation of Yeast. *Bioconjugate Chem. 3*, 69.

(10) (a) Pinney, K. C., and Katzenellenbogen, J. A. (1991) Synthesis of a Tetrafluoro-substituted Aryl Azide and Its Protio Analogue as Photoaffinity Labelling Reagents for the Estrogen Receptor. *J. Org. Chem. 56*, 3125. (b) Pinney, K. C., Carlson, K. E., Katzenellenbogen, B. S., and Katzenellenbogen, J. A. (1991) Efficient and Selective Photoaffinity Labelling of the Estrogen Receptor Using Two Nonsteroidal Ligands that Embody Aryl Azide or Tetrafluoroaryl Azide Photoreactive Functions. *Biochemistry 30*, 2421.

(11) (a) Aggeler, E., Cruz, K. C., Cai, S. X., Keana, J. F. W., and Capaldi, R. A. (1992) Introduction of Reactive Cysteine Residues in the ϵ Subunit of *Escherichia coli* F1 ATPase, Modification of These Sites with Tetrafluorophenyl Azide-Malemides, and Examination of Changes in the Binding of the ϵ Subunit When Different Nucleotides Are in Catalytic Sites. *J. Biol. Chem. 31*, 2956. (b) Aggeler, R., and Capaldi, R. A. (1992) Cross-Linking of the Gamma-Subunit of the *Escherichia coli* ATPase ECF(1) via Cysteines Introduced by Site- Directed Mutagenesis. *J. Biol. Chem. 267*, 21355.

(12) Walsh, C. (1979) *Enzymatic Reaction Mechanisms*; W. H. Freeman, San Francisco, CA, pp 49–108.

(13) Kanakarajan, K., Goodrich, R., Young, M. J. T., Soundararajan, S., and Platz, M. S. (1988) EPR Spectroscopy of Triplet Aryl Nitrenes Covalently Bound to α-Chymotrypsin. Application of Low-Temperature Methods to Photoaffinity Labelling. *J. Am. Chem. Soc. 110*, 6536.

(14) Bender, M. L., and Kezdy, F. J. (1961) The Spectrophotometric Determination of the Operational Normality of an α-Chymotrypsin Solution. *J. Biol. Chem. 236*, 2930.

(15) Bridges, A. J., and Knowles, J. R. (1974) An Examination of the Utility of Photogenerated Reagents by Using α-Chymotrypsin. *Biochem. J. 143*, 663.

(16) Kozdy, F. J., Feder, J., and Bender, M. L. (1967) The Catalytic Activity of Methionine-S-(N-2-Carboxy(sopropyl)-carbamylmethylsulfonium Bromide-192-α-Chymotrypsin. *J. Am. Chem. Soc. 89*, 1009.

(17) Schwert, G. W., and Takenaka, Y. (1955) A Spectrophotometric Determination of Trypsin and Chymotrypsin. *Biochim. Biophys. Acta 16*, 570.

(18) Segel, I. H. (1975) *Biochemical Calculations*, 2d ed., Wiley, New York.

(19) Nielsen, P. E., and Burchardt, O. (1982) Aryl Azides as Photoaffinity Labels. A Photochemical Study of Some 4-Substituted Aryl Azides. *Photochem. Photobiol. 35*, 317.

(20) Kanakarajan, K., Haider, K., and Czarnik, A. W. (1988) Nitrosations in Anhydrous Trifluroacetic Acid Media: A Modification for Insoluble or Deactivated Amine and Amide Precursors. *Synthesis*, 566.

(21) Filler, R., Ayyangar, N. R., Gustowski, W., and Kang, H. H. (1969) New Reactions of Polyfluoroaromatic Compounds. Pentafluorophenylalanine and Tetrafluorotyrosine. *J. Org. Chem. 34*, 534.

Functional Peptide–Polyurethane Conjugates with Extended Circulatory Half-Lives

James A. Braatz,*,† Yoshiaki Yasuda,‡ Kenneth Olden,§ Kenneth M. Yamada,∥ and Aaron H. Heifetz†

W. R. Grace & Company—Conn., Research Division, Department of Mammalian Cell Research, 7379 Route 32, Columbia, Maryland 21044, Department of Anatomy, School of Medicine, Kumamoto University, Kumamoto 880, Japan, National Institute of Environmental Health Sciences, P.O. Box 12233, Research Triangle Park, North Carolina 27709-2233, and Laboratory of Developmental Biology, National Institute of Dental Research, National Institutes of Health, Bethesda, Maryland 20892. Received January 12, 1993

Peptides containing the RGD sequence were covalently attached to an isocyanate-containing polyurethane prepolymer and the biological properties of the complexes were evaluated. For the pentapeptide H_2N-Tyr-Arg-Gly-Asp-Ser-OH (single-letter code, YRGDS), polymer conjugation lead to an increased half-life in the blood circulation of mice to >10 h. The effect of covalent attachment of polymer on biological activity was examined in a related peptide, H_2N-Gly-Arg-Gly-Asp-Ser-Pro-Ala-Cys-OH (GRGDSPAC). Inhibition of B16-F10 melanoma cell attachment and spreading on plates coated with fibronectin by an RGD-containing peptide and polymer-conjugated GRGDSPAC was observed to occur at similar concentrations. We conclude that the conjugation of peptides containing the Arg-Gly-Asp motif to this polymer resolves previous problems of their rapid loss from the circulation, while still allowing retention of full biological inhibitory activity.

INTRODUCTION

Synthetic polymers can be covalently attached to biological molecules, leading to an alteration of their biological properties which could render them useful for a variety of applications. For example, polymer conjugates with drugs have been described that retain activity at lower doses (Bamford et al., 1987). Deferoxamine (DFO), which is used clinically to chelate iron and aluminum, but with known toxic effects, has been coupled to dextran and starch (Hallaway et al., 1989). The DFO–polymer was shown to retain metal binding capacity while displaying an extended plasma half-life and lower toxicity.

This lowering of drug toxicity while potency is maintained would be of great benefit for cancer chemotherapeutic agents. In one such study, daunomycin linked to acrylamide copolymers through a degradable linkage was more effective than the native drug in extending mean survival times in mice inoculated with L1210 leukemia cells (Duncan et al., 1988). Similar conjugation with adriamycin decreased its toxicity against hematopoietic precursors in bone marrow while generating a negligible antibody response to the conjugates (Rihova et al., 1989). The antitumor activity of 5-fluorouracil conjugates with chitin and chitosan was demonstrated against P388 lymphocytic leukemia in mice at doses which were not acutely toxic (Ouchi et al., 1989).

The effect of polymer coupling to larger molecules has been examined. Polyethylene glycol (PEG) chains attached to enzymes modulate their activities in proportion to the extent of substitution, and the effect is also dependent on the molecular weight and functionality of the PEG used (Yoshinaga et al., 1987). The coupling chemistry also affected the activity of the conjugates (Yoshinaga et al., 1989). Modification of enzymes with PEG has also been found to render certain enzymes soluble and active in a variety of organic solvents (Takahashi et al., 1985, 1986, Kodera et al., 1986).

In addition, conjugation of water-soluble polymers, primarily polyethylene glycols, to proteins leads to alterations of their immunological properties (Abuchowski et al., 1977; Davis et al., 1979). There are numerous reports showing the effects of polymer conjugation on the clearance, immunogenicity, and activity of a variety of other proteins including immunoglobulins (Torchilin et al., 1987; Andersen et al., 1988), superoxide dismutase (Tamura et al., 1988; Beckman et al., 1988; Galcia-Alves et al., 1989), hemoglobin (Iwasaki et al., 1986), uricase (Tsuji et al., 1985; Fujita et al., 1990), and interleukin-2 (Katre et al., 1987; Knauf et al., 1988). Clinical trials using polyethylene glycol-modified therapeutic enzymes including asparaginase, superoxide dismutase, adenosine deaminase, and uricase are currently under evaluation (Fuertes and Abuchowski, 1990). This technology may prove useful in providing more effective treatment for a number of diseases while at the same time reducing the adverse side effects associated with these therapies.

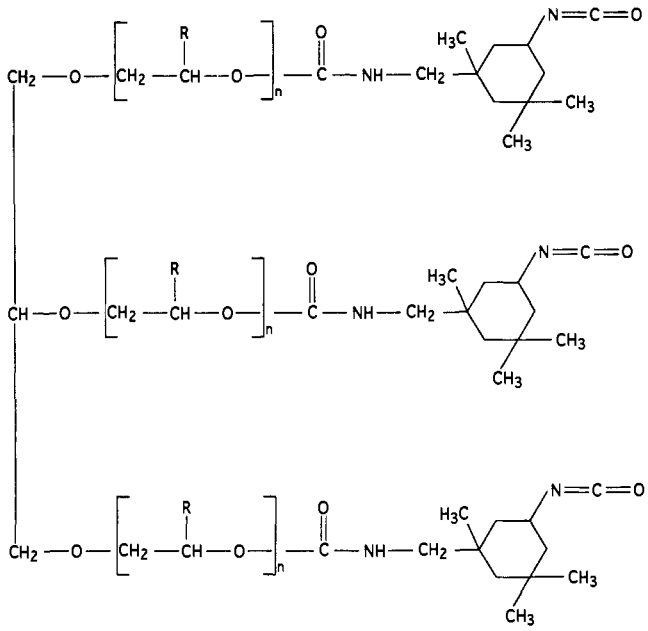
The successful use of polyethylene glycols prompted us to evaluate a series of isocyanate-based poly(ether urethane) prepolymers for their effects on certain properties of RGD-containing peptides. It was previously demonstrated that RGD-containing peptides could inhibit pulmonary metastasis of B15-F10 melanoma cells when administered simultaneously with the tumor cells in the tail veins of mice (Humphries et al., 1986, 1988). The simultaneous administration was required, at least in part, because of the rapid rate of clearance of the small peptide from the circulation. Studies with radiolabeled peptides showed that 75% of the peptide GRGDS was eliminated from the circulation within 2 min after injection, while the remainder was cleared with a half-life of 8 min. It would clearly be advantageous to have a more extended window in which to conduct studies such as these. The possible therapeutic potential of these peptides would also be improved considerably.

The prepolymers used here have a polyether backbone and a branched structure terminating in multiple isocy-

† W. R. Grace & Co.—Conn.
‡ Kumamoto University.
§ National Institute of Environmental Health Science.
∥ National Institute of Dental Research.

1043-1802/93/2904-0262$04.00/0 © 1993 American Chemical Society

Chart I



anate groups, having an active group (NCO)[1] functionality of ≥3. These trifunctional prepolymers appeared worthwhile to investigate in this context, as it has been shown that, in certain cases, enzymes retain more of their activity when modified with bifunctional as opposed to monofunctional PEGs (Bamford et al., 1987). These prepolymers could be used directly for modification of peptides, proteins, drugs, or other molecules which have an accessible group capable of reacting with isocyanates. We have found interesting effects on the properties of small peptides using these prepolymers in relatively straightforward coupling reactions. These effects are the subject of this report.

EXPERIMENTAL PROCEDURES

Materials. HYPOL XP-5 (formerly BIOPOL XP-5, from Hampshire Chemical Co., Lexington, MA) is a member of a family of poly(ether urethane) prepolymers prepared by end capping a branched polyether polyol with a diisocyanate (Braatz et al., 1992). A representative structure for these prepolymers is given in Chart I. In this structure, R can be H or CH_3. When R is H, the bracketed unit is ethylene oxide (EO), when R is CH_3, it is propylene oxide (PO). The number average molecular weight of the polyether triol component of the prepolymer is approximately 7000, and is composed of 75% EO and 25% PO units. Capping of the terminal hydroxyl groups of the polyether triol with isophorone diisocyanate (IPDI) produces the isocyanate-terminated prepolymer. However, during the capping reaction the isocyanate-terminated prepolymers can form dimer and higher oligomeric forms, producing a heterogenous prepolymer composition which is evident when analyzed by size-exclusion HPLC with dry organic solvent as mobile phase. The profile would appear nearly identical to that shown in Figure 1, panel A, between 12 and 22 min.

The prepolymer is soluble in aqueous solution and reacts with water to form a hydrogel after a period of time that depends on the amount of polymer dissolved. The reaction with water proceeds as follows:

$$R_1NCO + H_2O \rightarrow R_1NH_2 + CO_2 \text{ (slow)} \quad (1)$$

$$R_1NH_2 + R_2NCO \rightarrow R_1\text{-urea-}R_2 \text{ (very fast)} \quad (2)$$

The first reaction, conversion of isocyanate to a primary amine, is relatively slow. However, once the amine is formed, it reacts rapidly with an isocyanate group to form a urea cross-link. As this reaction proceeds, a three-dimensional cross-linked hydrogel structure will form. If, however, an amine-containing compound such as a peptide is included in the aqueous mixture, the following reaction can also occur:

$$R_1NCO + \text{peptide-}NH_2 \rightarrow R_1NHCONH\text{-peptide} \quad (3)$$

in which the peptide forms a urea linkage to the polymer. Since the amines react with isocyanate much faster than water, peptide can preferentially react with polymer to cap the termini of the prepolymer and prevent polymer–polymer cross-linking. This is evident from Figure 1, panel A, since, as mentioned above, the profile of the reaction product between prepolymer and peptide/water resembles the prepolymer in composition.

Peptides were obtained from Bachem Inc., Torrance, CA (YRGDS) and Peninsula Laboratories, Inc., Belmont, CA (GRGDSPAC). Iodine-125 (low pH) was obtained from New England Nuclear, Boston, MA. Disposable, prepacked Sephadex PD-10 columns were from Pharmacia LKB Biotechnology, Piscataway, NJ. Spectrapor dialysis tubing, 6000–8000 MW cutoff, was from Spectrum Medical Industries, Inc., Los Angeles CA. All chemicals used were the best grades available commercially.

Methods. *Preparation and Radiolabeling of Polymer–Tyramine.* To 5.0 g of Hypol XP-5 dissolved in 5.0 g of tetrahydrofuran (THF) was added 0.51 g of tyramine base (2 mol/equiv of NCO) dissolved in 5.0 g of THF + 30 mL of 2-propanol. After 17 h at room temperature, approximately 43% of the added tyramine became associated with the polymer, as determined by size-exclusion HPLC analysis. A portion of this reaction mixture was prepared for radioiodination by diluting 0.1 mL of this solution with 1 mL of 0.01 M sodium phosphate, filtering through a 0.45-μm filter, evaporating to dryness under a stream of nitrogen, and then redissolving in 0.05 mL of water. This conjugate was radioiodinated using $Na^{125}I$ (Hunter and Greenwood, 1962) and the free and bound iodine were separated using a PD-10 column with PBS as the eluant. In a separate experiment the iodination reaction was repeated using nonradioactive iodine in order to characterize the product. Size-exclusion HPLC analysis of the iodination product demonstrated that no significant alteration of the product's composition resulted from iodination.

Preparation and Radiolabeling of YRGDS–Polymer. A 5 mg/mL solution of YRGDS was prepared in PBS. To 0.3 mL of this solution (1.5 mg, 2.5×10^{-6} mol) was added 0.3 mL of 200 mg/mL HYPOL XP-5 (6.0 mg, 2.4×10^{-6} equiv of NCO) in 2-propanol. Product formation was monitored by size-exclusion high-performance liquid chromatography on a system which included a 9.5 mm × 25 cm Zorbax GF-250 column, a Hewlett-Packard 1050 quaternary pump and a Waters 990 photodiode-array detector. The mobile phase was 0.05 M sodium phosphate, pH 7.0, containing 0.3 M NaCl, which was run at 30 °C and 0.5 mL/min. Conjugates were detected by their absorption at 210 nm. Iodination of the YRGDS–polymer and separation of free and bound iodine were performed as described above for the tyramine–polymer conjugate. Iodination of YRGDS was performed as described above,

[1] Abbreviations used: NCO, isocyanate; PEG, poly(ethylene glycol); PBS, 0.01 M sodium phosphate, pH 7.4, containing 0.15 M NaCl; THF, tetrahydrofuran.

but the separation of free from bound iodine was done over a PD-10 column using water in place of PBS as the eluant.

Clearance of Peptide–Polymer from the Circulation. C57BL6 mice were injected with 0.2 mL of labeled polymer conjugates and the rate of clearance from the circulation was determined as previously described (Humphries et al., 1988), but with frequent sampling of blood during the first distribution phase. The percent remaining at each time point was based on the injected dose.

Preparation and Testing of GRGDSPAC–Polymer. To 80 mg of GRGDSPAC (1.05×10^{-4} mol) in 4.0 mL water were added 0.025 mL of 0.35 g/mL *N*-methylimidazole (1.05×10^{-4} mol) and 2.0 mL of 115 mg/mL HYPOL XP-5 (230 mg, 1.0×10^{-4} equiv NCO) in 2-propanol. This solution was incubated for 6 h at room temperature then 17 h at 4 °C. The solution was dialyzed for 24 h at 4 °C vs 1 L of water with four changes. Ellman analysis was performed to measure free thiol before and after the conjugation reaction (Riddles et al., 1979). The activity of this conjugate was determined by measuring inhibition of B16-F10 melanoma cell spreading on fibronectin as previously described (Yamada and Kennedy, 1984, 1987).

RESULTS

The conjugation of small peptides with an isocyanate-containing polyurethane prepolymer can proceed in a buffered aqueous solution since nucleophilic groups on the peptide react much faster than water. However, since water is present at a much higher concentration, substantial side reaction with the solvent will occur. Figure 1, panel A, is an HPLC profile of the product of the reaction between YRGDS and prepolymer. The major peak at 24 min corresponds to free YRGDS peptide. The complex series of peaks between 14 and 20 min is a typical profile for the prepolymer, which consists of a monomeric species eluting at about 19 min preceded by several smaller peaks at earlier retention times that correspond to higher oligomeric forms of the polymer. This profile demonstrates the distribution of polymer–peptide conjugate and unreacted peptide in a reaction mixture which contained approximately equimolar amounts of reactive groups. From the relative areas of these peaks, the yield of the reaction was estimated to be 46%. The contaminating free peptide was removed by gel permeation on a PD-10 column. The HPLC profile of the partially purified conjugate is shown in panel B of Figure 1. In this case the free peptide at 24 min has been essentially eliminated. This conjugate was radioiodinated and the labeled free and polymer-conjugated peptides were separated on a PD-10 column, as shown in panel C of Figure 1. The material excluded from the PD-10 column, fractions 3–5, Figure 1C, was used as the labeled conjugate for subsequent experiments.

The radiolabeled polymer–peptide conjugate was compared to the unmodified pentapeptide for their rates of clearance from the circulation. When injected iv into a mouse, YRGDS was cleared with a half-life of approximately 30 s in the first phase and 2.7 h in the second phase. The first- and second-phase clearance half-times for the polymer conjugate, on the other hand, were 0.5 and 11.3 h, respectively, as shown in Figure 2.

In addition to the above clearance study, the behavior of the polymer labeled with a simpler reporter molecule was examined. Excess tyramine was reacted with the isocyanate groups of the prepolymer to provide a labeling center. The radioiodinated form of this product when injected iv into mice had a half-life of approximately 7 h. This clearance pattern is also shown in Figure 2.

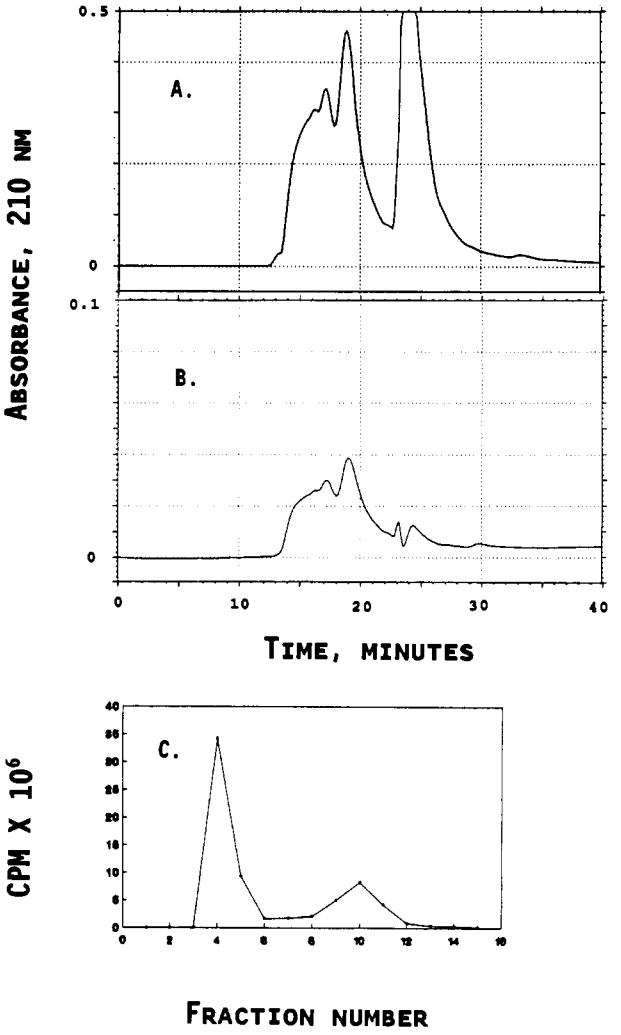


Figure 1. High-performance size-exclusion chromatography of YRGDS–HYPOL XP-5 conjugate: (A) HPLC of product before dialysis, (B) HPLC of product after dialysis, (C) PD-10 column fractionation after radioiodination of material from panel B.

The coupling reaction with YRGDS likely occurred with the primary amine of the peptide. With another peptide, GRGDSPAC, reaction with isocyanate may likewise occur at sites other than the terminal amine. For this peptide it was desired to link the polymer on the carboxyl terminal end in order to preserve the structure around the RGD sequence for subsequent activity analysis. To accomplish this, *N*-methylimidazole was added to the reaction to facilitate attachment to the sulfhydryl group. An indication that this in fact occurred is given in Table I, which shows the loss of a sulfhydryl group after conjugation. As with the pentapeptide, HPLC analysis demonstrated incomplete conjugation of peptide (Figure 3, panel A, free peptide) to polymer (Figure 3, panel B, unreacted peptide at 24 min, peptide–polymer conjugate at 14–20 min). The estimated yield for this reaction based on relative area in the HPLC profile was 35%. However, as shown in Figure 3, panel C, the free peptide in this case could be removed effectively by dialysis.

The effect of coupling of this polymer on the biological activity of this peptide is shown in Figure 4. The GRGDSPAC–polymer conjugate was found to be as effective, on a molar basis (see Discussion), as the unconjugated octapeptide in blocking peptide-mediated attachment of B16-F10 melanoma cells to a surface.

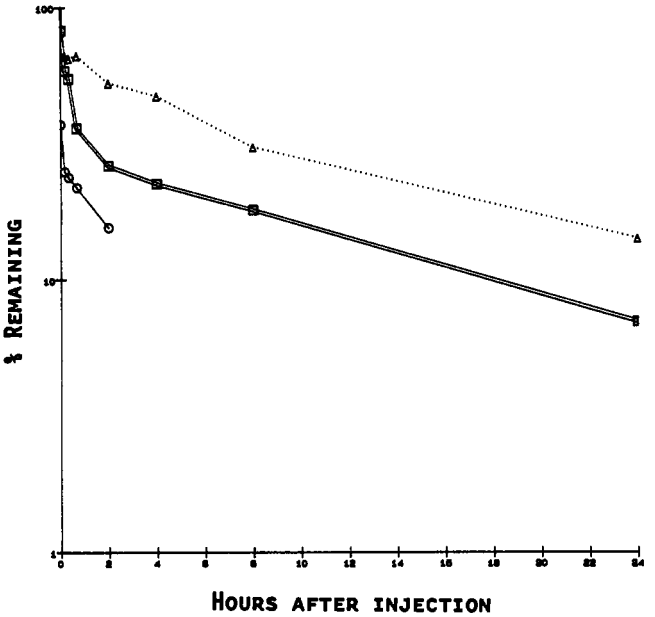


Figure 2. Circulatory clearance rates of native and polymer-linked pentapeptide: (○) [^{125}I]YRGDS, (□) [^{125}I]YRGDS–polymer, (△) [^{125}I]tyramine–polymer.

Table I. Peptide Sulfhydryl Content before and after Attachment to Polymer

sample	SH content, mol/mol of peptide
GRGDSPAC	0.66
GRGDSPAC–polymer	<0.03

DISCUSSION

The coupling reactions performed here were generally conducted at equimolar concentrations of peptide and polymer based on the molar content of isocyanate groups. Under these conditions, approximately 40% of the peptide became attached to the polymer. The unbound peptide could be removed from the conjugate by dialysis or gel filtration. The remaining peptide–polymer conjugate was not further characterized in terms of the relative number of peptides linked per unit of prepolymer, but it is probable that no cross-linking of polymer chains by the peptide occurred. This conclusion is inferred from the size-exclusion HPLC profiles which showed a distribution of product eluting between 14 and 20 min. The size-exclusion chromatographic pattern of the prepolymer is conserved after attachment of small peptides, suggesting that the polymer chains were not cross-linked by the peptides. Any cross-linking event of this type would produce a significant increase in the molecular weight of the components of the polymer and would be readily apparent in the chromatogram. If extensive cross-linking occurred, the product conjugate would have eluted more toward the void volume of the column (i.e., around 14 min). This result has in fact been observed with other larger and multifunctional molecules, which when reacted with the prepolymer gave product eluting primarily in the void volume with trailing into the working volume of the column.

In the coupling reaction between isocyanate–prepolymer and either YRGDS or GRGDSPAC, there are multiple functional groups on the peptides capable of reacting with isocyanate. In addition to the primary N-terminal amine, there are guanido, carboxylate, hydroxyl, and sulfhydryl groups available for reaction. Furthermore, since these reactions are conducted in aqueous solvent, water will compete for reaction with isocyanate. It seems clear that

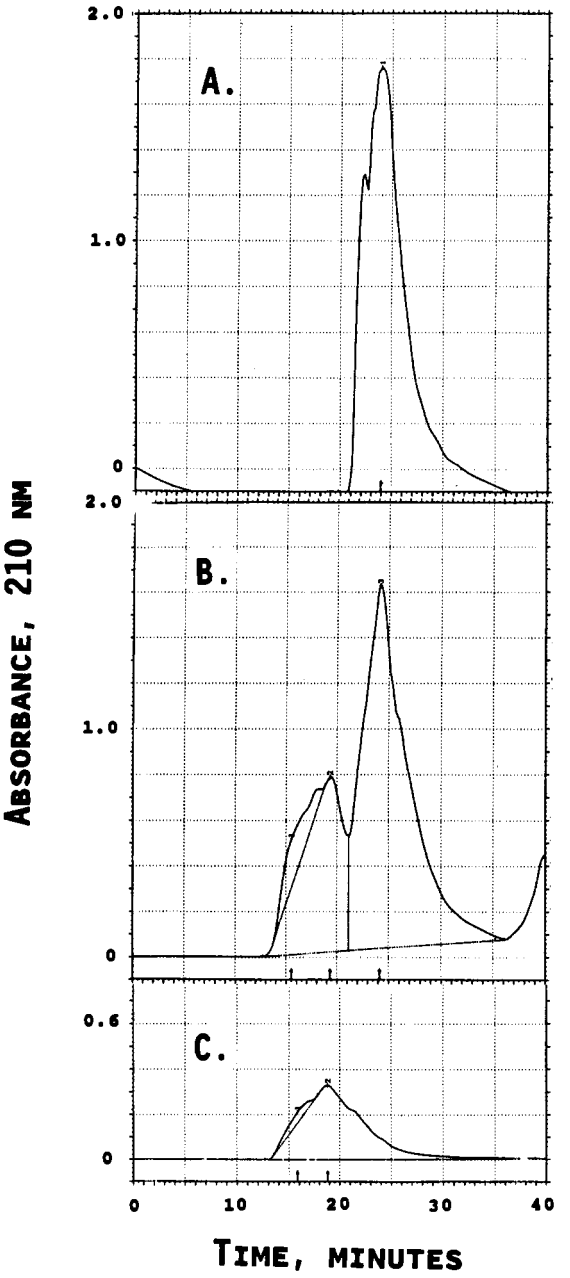


Figure 3. High-performance size-exclusion chromatography of native and polymer-linked GRGDSPAC: (A) native GRGDSPAC, (B) product of the GRGDSPAC reaction with HYPOL XP-5 before dialysis. (C) Product of the GRGDSPAC reaction with HYPOL XP-5 after dialysis.

water does effectively compete, since not all the peptide couples to the polymer in these studies. However, the reaction that does occur with unmodified peptide is most likely with primary amine, as the reactivity with this group is kinetically favored over the other possibilities. A more reactive center toward isocyanate than primary amine is the thiolate anion (Heifetz et al., 1990). This compound can be formed in the presence of *N*-methylimidazole and will react with isocyanate to form a thiourethane linkage. The loss of the free sulfhydryl group in the coupling experiment with GRGDSPAC suggests that this was the route taken in this reaction.

The effect the polymer imparts on the clearance rate of a small peptide is most likely due to the increased effective molecular size and, consequently, decreased glomerular filtration. As in other studies, the clearance curve is biphasic, with the initial phase accounting for the removal

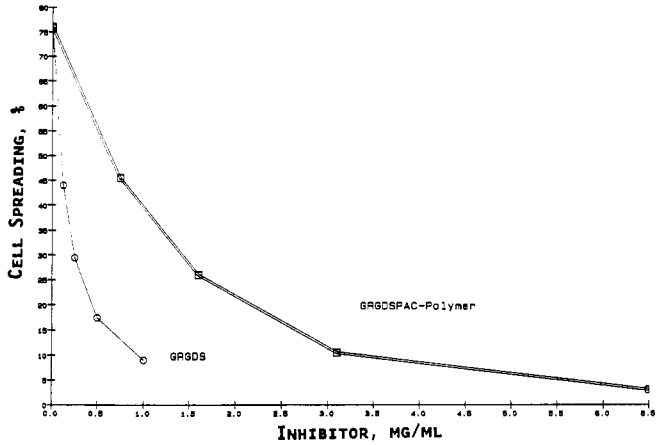


Figure 4. Inhibition of B16 melanoma cell spreading on fibronectin-coated plates by native and polymer-linked peptides: (○) native GRGDS, (□) GRGDSPAC–polymer.

of 65–75% of the injected label, probably as a result of rapid equilibration with interstitial fluids (Humphries et al., 1988). Small proteins and peptides of the size used here have been observed to have clearance half-lives of 10–15 min (Humphries et al., 1988; Beauchamp et al., 1983; Rajagopalan et al., 1985), although in this study the second-phase clearance half-life for the control peptide was about 2.7 h. This unexpected longer half-life may in part be due to the hydrophobic tyrosine residue and/or the bulky iodine substituent, which might slow clearance due to decreased hydrophilicity and increased size. The initial rapid and extensive clearance, however, made this evaluation difficult, as little label remained for these final measurements. Nevertheless, the peptide–polymer conjugate retained more label in the circulation at later times, and its half-life was significantly extended to more than 11 h. In a similar set of experiments, a tyramine–polymer conjugate was evaluated and found to have a half-life of about 7 h.

The effect of covalently attaching the polymer used in these studies on the activity of a biologically active peptide was evaluated for two different peptides. In one case the RGD-containing peptide GRGDSPAC was used for this purpose. The RGD-mediated cell adhesion phenomenon has been well-documented and standard *in vitro* assays are available for its quantitation. In the assay used here, B16-F10 melanoma cells adhere to fibronectin immobilized on a dish via the RGD sequence, and their adhesion can be inhibited by RGD-containing peptides. As shown in Figure 4, the octapeptide–polymer conjugate exhibits 50% inhibition at a concentration of 1.1 mg/mL. From the conjugation experiment it was calculated that this amount of peptide–polymer product comprises 0.26 mg of peptide. Thus, based on the molecular weight of this peptide, the concentration for half-maximal inhibition of cell attachment occurs at 0.34 mM. Similarly, the half-maximal response for the control peptide GRGDS was found to occur at 0.175 mg/mL, or 0.34 mM. Therefore, on a molar basis, the peptide was equally active in the free and the bound forms.

We previously described a different conjugate with this polymer which had an enhancement effect on cell growth (Heifetz et al., 1991). In those studies, a simple amino thiol conjugated through the amine group to the isocyanate of the prepolymer produced an adduct with terminal sulfhydryl groups. This conjugate was capable of stimulating growth of murine hybridoma cells and bovine aortic endothelial cells. Other polymer conjugates have been described in which the activity of the substance linked to the polymer was greatly enhanced (Bamford et al., 1986, 1987).

Finally, preliminary toxicological studies have been performed on the base polymer used in these studies after end capping to eliminate isocyanate groups (Braatz et al., 1992). In those studies, direct intravenous injection of the polymer caused no adverse effect on mice. Likewise, the sensitive chicken chorioallantoic membrane exhibited no inflammatory response to these materials. These evaluations, and others in progress, suggest the safety of the polymers used in this study for *in vivo* conjugated peptide use.

LITERATURE CITED

Abuchowski, A., van Es, T., Palczuk, N. C., and Davis, F. F. (1977) *J. Biol. Chem. 252*, 3578–3581.

Andersen, W. L., and Tomasi, T. B. (1988) *J. Immunol. Methods 109*, 37–42.

Bamford, C. H., Middleton, I. P., and Al-Lamee, K. G. (1986). *Biochim. Biophys. Acta 886*, 109–118.

Bamford, C. H., Middleton, I. P., and Al-Lamee, K. G. (1987) *Biochim. Biophys. Acta 924*, 38–44.

Beauchamp, C. O., Gonias, S. L., Menapace, D. P., and Pizzo, S. V. (1983) *Anal. Biochem. 131*, 25–33.

Beckman, J. S., Minor, R. L., White, C. W., Repine, J. R., Rosen, G. M., and Freeman, B. A. (1988) *J. Biol. Chem. 263*, 6884–6892.

Braatz, J. A., Heifetz, A. H., and Kehr, C. L. (1992) *J. Biomater. Sci. Polym. Ed. 3*, 451–462.

Davis, F. F., van Es, T., and Palczuk, N. C. (1979) U.S. Patent Number 4,179,337.

Duncan, R., Kopeckova, P., Stroholm, J., Hume, I. C., Lloyd, J. B., and Kopecek, J. (1988) *Br. J. Cancer 57*, 147–156.

Fuertges, F., and Abuchowski, A. (1990) *J. Controlled Release 11*, 139–148.

Fujita, T., Yasuda, Y., Takakura, Y., Hasida, M., and Sezaki, H. (1990) *J. Controlled Release 11*, 149–156.

Galcia-Alves, M., Kodowaki, Y., Iwashita, Y., and Nishi, K. (1989) *Jpn. J. Pharmacol. 51*, 199–209.

Hallaway, P. E., Eaton, J. W., Panter, S. S., and Hedlund, B. E. (1989) *Proc. Natl. Acad. Sci. U.S.A. 86*, 10108–10112.

Heifetz, A. H., Wolfe, R. A., Braatz, J. A., and Luthra, N. P. (1990) U.S. Patent Number 4,929,706.

Heifetz, A. H., Barry, R. M., Miller, D. A., Yang, K., and Braatz, J. A. (1991) *Clin. Biotechnol. 3*, 163–167.

Humphries, M. J., Olden, K., and Yamada, K. M. (1986) *Science 233*, 467–470.

Humphries, M. J., Yamada, K. M., and Olden, K. (1988) *J. Clin. Invest. 81*, 782–790.

Hunter, W. M., and Greenwood, F. C. (1962) *Nature 194*, 495–496.

Iwasaki, K., Iwashita, Y., Ikeda, K., and Uematsu, T. (1986) *Artif. Organs 10*, 470–474.

Katre, N. V., Knauf, M. J., and Laird, W. J. (1987) *Proc. Natl. Acad. Sci. U.S.A. 84*, 1487–1491.

Knauf, M. J., Bell, D. P.; Hirtzer, P., Luo, Z.-P., Young, J. D., and Katre, N. V. (1988) *J. Biol. Chem. 263*, 15064–15070.

Kodera, Y., Takahashi, K.; Nishimura, H., Matsushima, A., Saito, Y., and Inada, Y. (1986) *Biotechnol. Lett. 8*, 881–884.

Ouchi, T., Banba, T., Matsumoto, T., Suzuki, S., and Suzuki, M. (1989) *J. Bioact. Compat. Polym. 4*, 362–371.

Rajagopalan, S., Gonias, S. L., and Pizzo, S. V. (1985) *J. Clin. Invest. 75*, 413–419.

Riddles, P. W., Blakely, R. L., and Zebner, B. (1979) *Anal. Biochem. 94*, 74–81.

Rihova, B., Bilej, M., Vetvicka, V., Ulbrich, K., Strolham, J., Kopecek, J., and Duncan, R. (1989) *Biomaterials 10*, 335–341.

Takahashi, K., Ajima, A., Yoshimoto, T., Okada, M., Matsushima, A., Tamaura, Y., and Inada, Y. (1985) *J. Org. Chem. 50*, 3414–3415.

Takahashi, K., Matsushima, A., Saito, Y., and Inada, Y. (1986) *Biochem. Biophys. Res. Commun. 138*, 283–288.

Tamura, Y., Chi, L., Driscoll, E. M., Hoff, P. T., Freeman, B. A., Gallagher, K. P., and Lucchesi, B. R. (1988) *Circ. Res. 63*, 944–959.

Torchilin, V. P., Klibanov, A. L., Nossiff, N. D., Slinkin, M. A., Strauss, H. W., Haber, E., Smirnov, V. N., and Khaw, B. A. (1987) *Hybridoma 6*, 229–240.

Tsuji, J.-I., Hirose, K., Kasahara, E., Naitoh, M., and Yamamoto, I. (1985) *Int. J. Immunopharmacol. 7*, 725–730.

Yamada, K. M., and Kennedy, D. W. (1984) *J. Cell Biol. 99*, 29–36.

Yamada, K. M., and Kennedy, D. W. (1987) *J. Cell Physiol. 130*, 21–28.

Yoshinaga, K., Shafer, S., and Harris, J. M. (1987) *J. Bioact. Compat. Polym. 2*, 49–56.

Yoshinaga, K., and Harris, J. M. (1989) *J. Bioact. Compat. Polym. 4*, 17–24.

Forskolin Photoaffinity Probes for the Evaluation of Tubulin Binding Sites

Ashok J. Chavan,† Stewart K. Richardson,‡ Hyuntae Kim,† Boyd E. Haley,*,† and David S. Watt*,‡

Division of Medicinal Chemistry and Pharmaceutics, College of Pharmacy, and Department of Chemistry, College of Arts and Sciences, University of Kentucky, Lexington, Kentucky 40506. Received March 8, 1993

A photoactive C-7 derivative of forskolin, [^{125}I]-7-forskolinyl 2-(3-azido-5-hydroxy-4-iodophenoxy)acetate, enhanced GTP-promoted tubulin polymerization, preferentially bound the β-subunit, exhibited competition with the noniodinated version of the probe, and displayed saturation of labeling consistent with the presence of a forskolin binding site or sites on tubulin.

INTRODUCTION

Forskolin, a diterpene isolated from *Coleus forskohlii* exerts a positive inotropic effect on the heart, lowers blood pressure (*1*, *2*), and holds some potential as an antithrombic agent (*3*) or an antitumor agent (*4*). These intriguing effects of forskolin led to biochemical studies that indicated this compound, and certain analogs, were potent activators of most mammalian adenylate cyclases (*5*–*7*) and speculation that this stimulation was at the heart of its macroscopic effects. The discovery that forskolin, like other natural products including taxol and colchicine, had an effect on the polymerization of tubulin[1] led to the search for biologically active, photoaffinity probes of forskolin for the delineating of the specific forskolin binding domain-(s) on tubulin.[1,2]

EXPERIMENTAL PROCEDURES

General Chemical Procedures. Chemicals were purchased from Aldrich or Sigma and sodium [^{125}I]iodide was purchased from Amersham. Infrared spectra were determined on a Perkin-Elmer 337 spectrometer. The abbreviation TF denotes thin film. NMR spectra were determined on a Varian 400-MHz or Gemini 200-MHz spectrometer. Mass spectra were determined on a VG ZAB mass spectrometer. Elemental analyses were performed by Atlantic Microlabs, Atlanta, GA. Column chromatography using Macherey Nagel silica gel 60 is referred to as "chromatography on silica gel", preparative-layer chromatography on Macherey Nagel silica gel F254 is referred to as "chromatography on a silica gel plate", and the drying of an organic phase over anhydrous magnesium sulfate is simply indicated by the phrase "dried". 2-(3-Azido-5-methoxyphenoxy)acetic acid (**4a**) and 4-(3-azido-5-methoxyphenoxy)butyric acid (**4b**) were prepared as described previously (*9*).

1-(*tert*-Butyldimethylsilyl)forskolin (2). To a solution of 10 mg (0.024 mmol, 1.1 equiv) of forskolin (1) in 0.4 mL of anhydrous CH_2Cl_2 was added 6.2 μL (5.7 mg, 0.054 mmol, 2.2 equiv) of 2,6-lutidine and 6.1 μL (7 mg, 0.027 mmol, 1.1 equiv) of TBSOTf[3] (*8*). The mixture was stirred at 25 °C for 5 h, and the product was chromatographed on a silica gel plate using 3:7 EtOAc–hexane to give 10.8 mg (84%) of **2**: mp 58–61 °C; IR (KBr) 3480, 2960, 2870, 1700 cm^{-1}; ^{1}H NMR ($CDCl_3$) δ 0.14 (s, 3, $SiCH_3$), 0.87 (s, 9, $SiC(CH_3)_3$), 1.04, 1.25, 1.33, 1.46, 1.65 (5 s, 15, CH_3), 2.17 (s, 3, $OCOCH_3$), 2.35 (d, J_{gem} = 15 Hz, 1, C-12 H), 3.28 (d, J_{gem} = 15 Hz, 1, C-12 H), 4.44–4.50 (br m, 1, C-6α H), 4.56–4.63 (br m, 1, C-1β H), 4.91 (dd, J = 1 and 10 Hz, 1, C-15E vinylic H), 5.16 (dd, J = 17 and 1 Hz, 1, C-15Z vinylic H), 5.56 (d, J = 4 Hz, 1, C-7α H), 6.02 (dd, J = 10 and 17 Hz, 1, C-14 vinylic H). Anal. Calcd for $C_{28}H_{48}O_7Si$: C, 64.08; H, 9.22. Found: C, 64.08; H, 9.25.

1-(*tert*-Butyldimethylsilyl)-7-deacetylforskolin (3). To a solution of 10.8 mg (0.02 mmol, 1 equiv) of **2** in 0.8 mL of MeOH and 0.2 mL of water was added 4 mg (0.1 mmol, 5 equiv) of NaOH. The mixture was stirred for 5 h at 25 °C, and the solution was diluted with EtOAc. The solution was washed with brine and dried. The residue was chromatographed on a silica gel plate using 1:1 EtOAc–hexane to give 9.6 mg (97%) of **3**: IR (TF) 3500, 3220, 2960, 1705 cm^{-1}; ^{1}H NMR ($CDCl_3$) δ 0.04 and 0.16 (2 s, 6, $SiCH_3$), 0.97 (s, 9, $SiC(CH_3)_3$), 1.06, 1.25, 1.41, 1.43, 1.61 (5 s, 15, CH_3), 2.42 (d, J_{gem} = 16 Hz, 1, C-12 H), 3.22 (d, J_{gem} = 16 Hz, 1, C-12 H), 4.15–4.21 (br m, 1, C-7α H), 4.46–4.56 (br m, 1, C-6α H), 4.60–4.66 (br m, 1, C-1β H), 4.95 (d, J = 10 Hz, 1, C-15E vinylic H), 5.12 (d, J = 17 Hz, 1, C-15Z vinylic H), 6.18 (dd, J = 10 and 17 Hz, 1, C-14

* Authors to whom correspondence should be addressed: David S. Watt, Department of Chemistry, University of Kentucky, Lexington, KY 40506. Telephone: (606)-257-5294. FAX: (606)-257-4000. Boyd E. Haley, 058 Markey Cancer Center, University of Kentucky, Lexington, KY 40536. Telephone: (606)-257-4481. FAX: (606)-258-2074.

† Division of Medicinal Chemistry and Pharmaceutics.

‡ Department of Chemistry.

[1] Part of this work was disclosed at the 40th Southeast Regional Meeting of the American Chemical Society, Atlanta, GA, November 1988 (Synthesis and Application of a Forskolin Photoaffinity Probe to a Tubulin Binding Site. H.-W. Lee, D. S. Watt, H. Kim, and B. E. Haley).

[2] Part of this work was disclosed at the Joint Meeting of the American Society for Cell Biology and the American Society for Biochemistry and Molecular Biology, San Francisco, CA, January 1989 (Detection of a Forskolin Binding Site Using a Photoaffinity Probe. D. S. Watt, H.-W. Lee, H. Kim, and B. E. Haley).

[3] Abbreviations used: AD, Alzheimer's disease; buffer A, 100 mM MES, 1 mM magnesium chloride, 1 mM EGTA (pH 6.7); buffer B, 10 mM sodium phosphate, 1 mM magnesium chloride, 1 mM EGTA (pH 6.7); DCC, *N*,*N*′-dicyclohexylcarbodiimide; DMSO, dimethyl sulfoxide; EGTA, ethylene glycol bis(β-aminoethyl ether) *N*,*N*,*N*′,*N*′-tetraacetic acid; EtOAc, ethyl acetate; EtOH, ethanol; [^{125}I]APTG, monoanhydride of guanosine 5′-(trihydrogen diphosphate) tris(triethylammonium) salt and [^{125}I]-*N*-(4-azidophenyl)-2-phosphoramido-3-(4-hydroxy-3-iodophenyl)-propionamide; MeOH, methanol; MES, 2-(*N*-morpholino)-ethanesulfonic acid; NaOAc, sodium acetate; 8-N_3GTP, 8-azidoguanosine 5′-triphosphate tris(triethylammonium) salt; SDS, sodium dodecyl sulfate; TBSOTf, *tert*-butyldimethylsilyl triflate; THF, tetrahydrofuran; TLC, thin-layer chromatography; TRIS, tris(hydroxymethyl)aminomethane.

1043-1802/93/2904-0268$04.00/0 © 1993 American Chemical Society

vinylic H). Anal. Calcd for $C_{26}H_{46}O_6Si$: C, 64.69; H, 9.61. Found: C, 64.64; H, 9.65.

6-(3-Azido-5-methoxyphenoxy)caproic Acid (4c). Phloroglucinol (Aldrich) was converted to 5-aminoresorcinol, and 5-aminoresorcinol was diazotized and treated with sodium azide to afford 5-azidoresorcinol according to the procedure of Richardson (*9*). The alkylation of 5-azidoresorcinol with methyl 6-bromocaproate and saponification of the resulting ester according to the procedure of Richardson (*9*) afforded **4c**: IR (KBr) 3360 (br), 3050, 2200 (weak), 2110, 1715, 1600 cm^{-1}; ^1H NMR ($CDCl_3$) δ 1.45–1.95 (m, 6, CH_2), 2.40 (t, J = 8 Hz, 2, CH_2CO), 3.75 (s, 3, OCH_3), 3.95 (t, J = 8 Hz, 2, CH_2OAr), 6.12–6.30 (m, 3, ArH); exact mass spectrum calcd for $C_{13}H_{17}N_3O_4$ 279.1220, found 279.1220.

2-(3-Azido-4-iodo-5-methoxyphenoxy)acetic Acid (4d). To 200 mg (0.84 mmol) of methyl 2-(3-azido-5-methoxyphenoxy)acetate (*9*), 265 mg (1.77 mmol, 2.1 equiv) of NaI in 5 mL of acetonitrile, and 1 mL of water was added 200 μL (1.77 mmol, 2.1 equiv) of *tert*-butyl hypochlorite (*10*). The mixture was stirred at 25 °C for 8 h and quenched with 10% sodium thiosulfate solution. The product was extracted with EtOAc and dried. The product was chromatographed on silica gel using 1:4 EtOAc–hexane to afford 40 mg (13%) of methyl 2-(3-azido-4-iodo-5-methoxyphenoxy)acetate: ^1H NMR ($CDCl_3$) δ 3.79 (s, 3, $ArOCH_3$), 3.87 (s, 3, CO_2CH_3), 4.68 (s, 2, OCH_2CO), 6.10 (m, 1, ArH), 6.25 (d, J = 2 Hz, 1, ArH); exact mass spectrum calcd for $C_{10}H_{10}O_4N_3I$ 362.9716, found 362.9715. To a solution of 53 mg (0.16 mmol) of methyl 2-(3-azido-4-iodo-5-methoxyphenoxy)acetate in 1.8 mL of EtOH and 0.3 mL of water was added 24.3 mg (0.434 mmol, 2.8 equiv) of KOH. The mixture was stirred at 25 °C for 2 h, acidified to pH = 1 with 2 M HCl solution, and extracted with EtOAc. The organic layers were dried and concentrated to give 37 mg (74%) of **4d**: IR (KBr) 3450, 2920, 2110, 1730, 1580 cm^{-1}; ^1H NMR (CD_3OD) δ 3.90 (s, 3, OCH_3), 4.73 (s, 2, OCH_2CO), 6.17–6.20 (m, 1, ArH), 6.28–6.30 (m, 1, ArH); exact mass spectrum calcd for $C_9H_8O_4N_3I$ 348.9560, found 348.9560.

1-(*tert*-Butyldimethylsilyl)-7-forskolinyl-2-(3-Azido-5-methoxyphenoxy)acetate (5). To a solution of 8 mg (0.017 mmol, 1 equiv) of **3** and 3.9 mg (0.018 mmol, 1.1 equiv) of 2-(3-azido-5-methoxyphenoxy)acetic acid (**4a**) (*9*) in 0.15 mL of anhydrous THF at 25 °C under a N_2 atmosphere was added a mixture of 4 mg (0.019 mmol, 1.15 equiv) of DCC and 0.52 mg (0.0035 mmol, 0.2 equiv) of 4-pyrrolidinopyridine in 0.1 mL of anhydrous THF. The solution was stirred for 2 h at 25 °C, and the product was chromatographed on a silica gel plate using 1:3 EtOAc–hexane to give 7.4 mg (65%) of **5**: IR (TF) 3550, 3320, 2980, 2120, 1740, 1700, 1595 cm^{-1}; ^1H NMR ($CDCl_3$) δ –0.02 and 0.14 (2 s, 6, $SiCH_3$), 0.86 (s, 9, $SiC(CH_3)_3$), 1.02, 1.22, 1.27, 1.42, 1.54 (5 s, 15, CH_3), 2.32 (d, J_{gem} = 16 Hz, 1, C-12 H), 3.26 (d, J_{gem} = 16 Hz, 1, C-12 H), 3.77 (s, 3, OCH_3), 4.40–4.48 (br m, 1, C-6α H), 4.55–4.66 (br m, 1, C-1β H), 4.72 (s, 2, OCH_2CO), 4.89 (dd, J = 1 and 10 Hz, 1, C-15E vinylic H), 5.14 (dd, J = 1 and 17 Hz, 1, C-15Z vinylic H), 5.64 (d, J = 4 Hz, 1, C-7α H), 6.01 (dd, J = 10 and 17 Hz, 1, C-14 vinylic H), 6.20–6.36 (m, 3, ArH). Anal. Calcd for $C_{35}H_{53}O_9N_3Si$: C, 61.11; H, 7.77. Found: C, 61.04; H, 7.82.

7-Forskolinyl 2-(3-Azido-5-methoxyphenoxy)acetate (7) from 5. To a solution of 7.4 mg (0.011 mmol, 1 equiv) of **5** in 0.5 mL of anhydrous THF was added 11 μL of 1 M (0.011 mmol, 1 equiv) tetra-*n*-butylammonium fluoride solution (*8*) in THF. The solution was stirred at 25 °C for 15 min and chromatographed on a silica gel plate using 1:1 EtOAc–hexane to give a 2:1 ratio of C-7 to C-6 isomers from which **7** (yield not determined) was separated: IR (TF) 3440, 3000, 2940, 2860, 2110, 1730, 1695, 1590 cm^{-1}; ^1H NMR ($CDCl_3$) δ 1.04, 1.25, 1.31, 1.42, 1.63 (5 s, 15, CH_3), 2.47 (d, J_{gem} = 17 Hz, 1, C-12 H), 3.23 (d, J_{gem} = 17 Hz, 1, C-12 H), 3.79 (s, 3, OCH_3), 4.38–4.48 (br m, 1, C-6α H), 4.54–4.62 (br m, 1, C-1β H), 4.64 (s, 2, OCH_2CO), 4.99 (d, J = 10 Hz, 1, C-15E vinylic H), 5.29 (d, J = 16 Hz, 1, C-15Z vinylic H), 5.61 (d, J = 4 Hz, 1, C-7α H), 5.95 (dd, J = 16 and 10 Hz, 1, C-14 vinylic H), 6.10–6.36 (m, 3, ArH).

7-Forskolinyl 2-(3-Azido-5-methoxyphenoxy)acetate (7) from 6. The procedure described for the preparation of **5** was repeated using 10.6 mg (0.029 mmol) of desacetylforskolin (**6**) (*11*), 6.4 mg (0.029 mmol, 1 equiv) of **4a** (*9*), 6.8 mg (0.033 mmol, 1.15 equiv) of DCC, and 0.8 mg (0.005 mmol, 0.2 equiv) of 4-pyrrolidinopyridine in 0.4 mL of CH_2Cl_2 to afford, after chromatography on a silica gel plate using 1:1 EtOAc–hexane, 9.3 mg (57%) of **7** having spectral data identical to that described above.

7-Forskolinyl 4-(3-Azido-5-methoxyphenoxy)butyrate (8). The procedure described for the preparation of **5** was repeated using 10 mg (0.027 mmol) of desacetylforskolin (**6**) (*11*), 6.8 mg (0.027 mmol, 1 equiv) of **4b** (*9*), 6.4 mg (0.031 mmol, 1.15 equiv) of DCC, and 0.8 mg (0.005 mmol, 0.2 equiv) of 4-pyrrolidinopyridine in 0.55 mL of CH_2Cl_2 to afford, after chromatography on a silica gel plate using 1:3 EtOAc–hexane, 9.4 mg (57%) of **8**: IR (TF) 3460, 3020, 2960, 2890, 2130, 1710, 1595 cm^{-1}; ^1H NMR ($CDCl_3$) δ 1.04, 1.26, 1.30, 1.45, 1.72 (5 s, 15, CH_3), 2.46 (d, J_{gem} = 17 Hz, 1, C-12 H), 2.64 (t, J = 6 Hz, 2, CH_2CO), 2.95 (br s, 1, OH), 3.21 (d, J_{gem} = 17 Hz, 1, C-12 H), 3.79 (s, 3, OCH_3), 4.03 (t, J = 6 Hz, 2, CH_2OAr), 4.44–4.52 (br m, 1, C-6α H), 4.56–4.64 (br m, 1, C-1β H), 4.97 (d, J = 10 Hz, 1, C-15E vinylic H), 5.29 (d, J = 17 Hz, 1, C-15Z vinylic H), 5.54 (d, J = 4 Hz, 1, C-7α H), 5.94 (dd, J = 10 and 17 Hz, 1, C-14 vinylic CH), 6.10–6.32 (m, 3, ArH).

7-Forskolinyl 5-(3-Azido-5-methoxyphenoxy)caproate (9). The procedure described for the preparation of **5** was repeated using 10.5 mg (0.028 mmol) of desacetylforskolin (**6**) (*11*), 8 mg (0.028 mmol, 1 equiv) of **4c**, 6.8 mg (0.033 mmol, 1.15 equiv) of DCC, and 1.0 mg (0.007 mmol, 0.24 equiv) of 4-pyrrolidinopyridine in 0.6 mL of CH_2Cl_2 to afford, after chromatography on a silica gel plate using 1:3 EtOAc–hexane, 8.1 mg (45%) of **9**: IR (TF) 3480, 3300, 2120, 1720, 1600 cm^{-1}; ^1H NMR ($CDCl_3$) δ 1.05, 1.25, 1.33, 1.43, 1.70 (5 s, 15, CH_3), 1.68–1.86 (m, 6, CH_2), 2.60 (d, J_{gem} = 17 Hz, 1, C-12 H), 2.60 (t, J = 8 Hz, 2, CH_2CO), 3.22 (d, J_{gem} = 17 Hz, 1, C-12 H), 3.78 (s, 3, OCH_3), 3.90 (t, J = 8 Hz, 2, CH_2OAr), 4.25–4.50 (m, 1, C-6α H), 4.52–4.60 (m, 1, C-1β H), 4.97 (d, J = 10 Hz, 1, C-15E vinylic H), 5.30 (d, J = 17 Hz, 1, C-15Z vinylic H), 5.52 (d, J = 4 Hz, 1, C-7α H), 5.93 (dd, 1, J = 10 and 17 Hz, 1, C-14 vinylic H), 6.05–6.27 (m, 3, ArH).

7-Forskolinyl 2-(3-Azido-4-iodo-5-methoxyphenoxy)acetate (10). The procedure described for the preparation of **5** was repeated using 30 mg (0.081 mmol) of desacetylforskolin (**6**) (*11*), 28.5 mg (0.081 mmol, 1 equiv) of **4d**, 19.3 mg (0.094 mmol, 1.15 equiv) of DCC, and 2.4 mg (0.016 mmol, 0.2 equiv) of 4-pyrrolidinopyridine in 2 mL of CH_2Cl_2 to afford, after chromatography on silica gel plates using 3:7 EtOAc–hexane, 22 mg (81%) of **10**: IR (TF) 3550, 3010, 2960, 2880, 2130, 1730, 1700, 1580 cm^{-1}; ^1H NMR ($CDCl_3$) δ 1.03, 1.24, 1.25, 1.42, 1.56 (5 s, 15, CH_3), 2.44 (d, J_{gem} = 17 Hz, 1, C-12 H), 2.84 (br s, 1, OH), 3.22 (d, J_{gem} = 17 Hz, 1, C-12 H), 3.90 (s, 3, OCH_3), 4.41–4.50 (br m, 1, C-6α H), 4.55–4.65 (br m, 1, C-1β H), 4.83 (d, J = 2 Hz, 2, OCH_2CO), 4.98 (d, J = 10 Hz, 1, C-15E vinylic

H), 5.29 (d, J = 17 Hz, 1, C-15Z vinylic H), 5.62 (d, J = 4 Hz, 1, C-7α H), 5.90–6.04 (m, 1, C-14 vinylic H), 6.13–6.35 (m, 2, ArH). Anal. Calcd for $C_{29}H_{38}O_9N_3I$: C, 49.72; H, 5.61. Found: C, 49.66; H, 5.66.

7-Forskolinyl 2-(3-Azido-5-hydroxyphenoxy)acetate (12). The procedure described for the preparation of **5** was repeated using 48.9 mg (0.133 mmol) of desacetylforskolin (**6**) (*11*), 36.9 mg (0.266 mmol, 2 equiv) of bromoacetic acid, 31.5 mg (0.266 mmol, 2 equiv) of DCC, and 3.9 mg (0.027 mmol, 0.2 equiv) of 4-pyrrolidinopyridine in 1 mL of CH_2Cl_2 to afford, after chromatography on silica gel plates using 1:3 EtOAc–hexane, 7-forskolinyl 2-bromoacetate (yield not determined): IR (KBr) 3450, 3300, 1720 cm^{-1}; ^{1}H NMR ($CDCl_3$) δ 1.04, 1.26, 1.35, 1.45, 1.75 (5 s, 15, CH_3), 2.48 (d, J_{gem} = 17 Hz, 1, C-12 H), 3.22 (d, J_{gem} = 17 Hz, 1, C-12 H), 3.94 (d, J = 2 Hz, 2, CH_2Br), 4.45–4.55 (m, 1, C-6α H), 4.55–4.65 (m, 1, C-1β H), 4.99 (d, J = 10 Hz, 1, C-15E vinylic H), 5.28 (d, J = 17 Hz, 1, C-15Z vinylic H), 5.53 (d, J = 4 Hz, 1, C-7α H), 5.95 (d, J = 10 and 17 Hz, 1, C-14 vinylic H). To 14.7 mg (0.030 mmol) of 7-forskolinyl 2-bromoacetate in 0.25 mL of anhydrous acetone under a N_2 atmosphere were added 21.4 mg (0.142 mmol, 4.7 equiv) of 5-azidoresorcinol (*9*) and 20.7 mg (0.150 mmol, 5 equiv) of K_2CO_3. The mixture was stirred for 0.5 h at 60 °C. The solution was evaporated and chromatographed on a silica gel plate in 1:9 EtOAc–CH_2Cl_2 to afford 9.5 mg (57%) of **12**: IR (KBr) 3400 (br), 2920, 1735, 1710, 1595 cm^{-1}; ^{1}H NMR ($CDCl_3$) δ 0.97, 1.07, 1.23, 1.35, 1.37 (5 s, 15, CH_3), 2.53 (d, J_{gem} = 17 Hz, 1, C-12 H), 2.82 (br s, 1, OH), 3.18 (d, J_{gem} = 17 Hz, 1, C-12 H), 4.34–4.40 (m, 1, C-6α H), 4.62 (s, 2, CH_2OAr), 4.65–4.75 (m, 1, C-1β H), 5.01 (d, J = 10 Hz, 1, C-15E vinylic H), 5.21 (d, J = 17 Hz, 1, C-15Z vinylic H), 5.95–6.55 (m, 5, C-7α, C-14 H and ArH).

7-Forskolinyl 2-(3-Azido-5-hydroxy-4-iodophenoxy)acetate (13). To 12.1 mg (0.022 mmol) of **12** and 6.5 mg (0.043 mmol, 2 equiv) of NaI in 150 μL of acetonitrile and 38 μL of water was added 5.2 μL (0.043 mmol, 2 equiv) of *tert*-butyl hypochlorite (*10*). The mixture was stirred at 25 °C for 2.5 h and quenched with 10% sodium thiosulfate solution. The product was extracted with EtOAc and dried. The product was chromatographed on silica gel using 1:1 EtOAc–hexane to afford 3.3 mg (27%) of unreacted **12** and 3.2 mg (22%) of **13**: ^{1}H NMR ($CDCl_3$) δ 0.95, 1.07, 1.23, 1.37, 1.39 (5 s, 15, CH_3), 2.49 (d, J_{gem} = 17 Hz, 1, C-12 H), 2.94 (br s, 1, OH), 3.16 (d, J_{gem} = 17 Hz, 1, C-12 H), 4.30–4.33 (m, 1, C-6α H), 4.60 (s, 2, CH_2OAr), 4.65–4.69 (m, 1, C-1β H), 4.92 (d, J = 10 Hz, 1, C-15E vinylic H), 5.17 (d, J = 17 Hz, 1, C-15Z vinylic H), 5.95–6.55 (m, 4, C-7α, C-14 H and ArH).

[^{125}I]-7-Forskolinyl 2-(3-Azido-5-hydroxy-4-iodophenoxy)acetate (14). *The following procedure was performed exclusively in a fume hood with all appropriate precautions to minimize exposure to the investigator.* To a vial containing 18 μL (9 mCi) of [^{125}I]NaI was added in succession 20 μL of 1 M NaOAc buffer (pH 3.9), 5.2 μL of 8.6 mM 7-forskolinyl 2-(3-azido-5-hydroxyphenoxy)acetate (**12**) in acetonitrile, 15 μL of acetonitrile, and 5.3 μL of *tert*-butyl hypochlorite. The mixture was vortexed briefly and allowed to stand for 2.5 h at 25 °C. The reaction was quenched by adding 20 μL of 5% sodium thiosulfate solution. The mixture was applied to an analytical, glass-backed Merck silica gel F254 plate (10 cm × 20 cm) that had been predeveloped in EtOAc and dried. The plate was eluted with 1:1 EtOAc–hexane, and the location of the product was determined by autoradiography. The silica gel was carefully scraped from the plate (in fume hood) and loaded into a disposable glass pipet with a glass wool plug. The product **14** was eluted from the silica gel with EtOAc and evaporated under a stream of dry N_2. The product was characterized by TLC comparison with nonradioactive, iodinated forskolin derivative **13**. The product was stored in absolute MeOH at –20 °C and had a specific activity of 25 mCi/μmol. Although the anticipated specific activity based upon using carrier-free [^{125}I]-NaI was expected to be higher than this value, the low activity obtained was presumably due to our inability to separate the small amounts of the radioiodinated product **14** from small amounts of starting material **12** that contaminated the product.

Tubulin Preparations. Microtubule protein was isolated from fresh bovine or ovine brain by two cycles of the reversible assembly method of Shelanski (*12*). Microtubules obtained from the second cycle of polymerization were stored at –70 °C until needed. Prior to use, pellets were thawed and purified by gel filtration on Sephadex G-25 (medium) using either buffer A for the polymerization assay or buffer B for the photolabeling experiments.

Human Brain Homogenate. Normal and AD brain homogenates were prepared from 400–600-mg pieces of respective brain tissue collected on autopsy by the Sanders–Brown Center for Aging at the University of Kentucky. The samples were collected as soon as possible after death and immediately frozen. Homogenized samples (20% w/v) were prepared using a Potter–Elvehjem all-glass homogenizer.

Polymerization Assay. Microtubule formation was followed by the light-scattering assay using a Beckman Model 25 spectrophotometer equipped with a cuvette chamber heated to 37 °C (*13*). The change in absorbance was monitored at 350 nm.

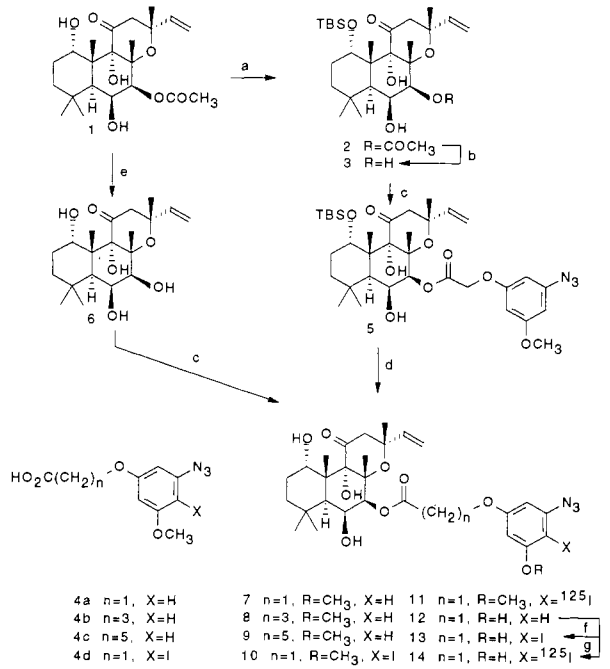
Photoaffinity Labeling. Photolabeling of tubulin was optimized for irradiation time, preincubation time, concentration of DMSO, protein concentration, salt concentration, type of buffer, and pH of the solution. Tubulin solutions (5 μg) in buffer B in Eppendorf tubes were incubated with the radioiodinated forskolin derivative **14** in 30 μL of the final volume for 2 min at 4 °C, photolyzed for 2 min at 4 °C with a hand-held UV lamp with the glass face removed (4600 μW/cm^2, Model UVS-11, Ultra-Violet Products, Inc.) at a distance of 4 cm. Upon completion of photolabeling, the samples were denatured by the addition of a "protein-solubilizing mixture" containing 25% sucrose, 2.5% SDS,[1] 0.25 mg/mL pyronin Y, 25 mM TRIS-HCl (pH 8.0), and 15.4 mg/mL dithiothreitol. The α- and β-tubulin monomers were separated on 10% SDS–PAGE. Protein bands were stained with Coomassie Brilliant Blue, destained, dried on a slab gel dryer, subjected to autoradiography, and cut from the gel to determine the radioactivity in Minaxi Gamma Counter 5000 series (Packard Instruments Co.).

Photolabeling of denatured tubulin was performed as described in Figure 4. The results in Figure 4 differ from the above experiment in that the tubulin was denatured (heat, 1% SDS, or 8 M urea) prior to photolabeling.

RESULTS

Chemical Synthesis. The route shown in Scheme I, in which the C-1 hydroxyl of forskolin (**1**) was protected as a TBS ether (**2**), was designed to avoid initial concerns about the competitive acylation of the C-1 and C-7 positions in **1**. The saponification of the C-7 acetate in **2** and the acylation of the C-7 hydroxyl group in **3** with 2-(3-azido-5-methoxyphenoxy)acetic acid (**4a**) (*9*) provided the TBS-protected derivative **5**. However, removal of the

Scheme I. Synthetic Routes[a]



[a] Reagents: (a) TBSOTf, 2,6-lutidine; (b) NaOH, aqueous MeOH; (c) **4a**, **4b**, **4c**, or **4d**, DCC, 4-(pyrrolidino)pyridine; (d) $(n\text{-Bu})_4$NF, THF; (e) see refs 11, 14; (f) NaI, *t*-BuOCl; (g) [^{125}I]NaI, *t*-BuOCl.

TBS group in **5** using tetra-*n*-butylammonium fluoride (*8*) led to scrambling of the aryl azide-containing acyl group (*11*), and a separable 2:1 mixture of the C-6 and C-7 esters was obtained. A similar acyl scrambling occurred in forskolin (**1**) itself when exposed to basic alumina (*11*) or tetra-*n*-butylammonium fluoride. The direct C-7 acylation of desacetylforskolin (**6**) with 2-(3-azido-5-methoxyphenoxy)acetic acid (**4a**) provided a mixture of the C-6 and C-7 analogs in which the desired C-7 derivative **7** was the principal product. Acylation at C-1 was not observed. The C-7 derivatives **8** and **9** with longer "spacers" between the aryl azide and forskolin subunits were also prepared using 4-(3-azido-5-methoxyphenoxy)butyric acid (**4b**) (*9*) and 6-(3-azido-5-methoxyphenoxy)caproic acid (**4c**), respectively. The direct iodination of the forskolin derivative **7** failed to provide the iodinated derivative **10**, presumably as a consequence of the deactivating influence of the azide group. A marginally useful synthesis of **10** involved the iodination of **4a** in order to obtain **4d** and the subsequent coupling of **4d** and desacetylforskolin (**6**) in order to obtain **10** in low yield. Efforts, however, to adapt this procedure to the preparation of a radioiodinated analog **11** led to a probe with low specific activity (10 mCi/mmol). Since a hydroxyl group on the aryl azide moiety would facilitate the iodination reaction better than a methoxy group, desacetylforskolin (**6**) was converted first to the 7-bromoacetyl derivative and then subjected to an S_N2 reaction with 3-azidoresorcinol (*9*) to furnish the resorcinol derivative **12**. The iodination or radioiodination of **12** provided the forskolin photoaffinity probes **13** and **14**, respectively, having, in the case of the latter derivative, the necessary high specific activity (25 mCi/μmol).

Polymerization Assay. Microtubule formation was followed by the light-scattering assay described by Gaskin (*13*) using a Beckman Model 25 spectrophotometer equipped with a cuvette chamber heated to 37 °C. The change in absorbance was monitored at 350 nm and indicated that forskolin (**1**) and the derivative **12** enhanced the GTP-promoted polymerization of tubulin as indicated in Figure 1.

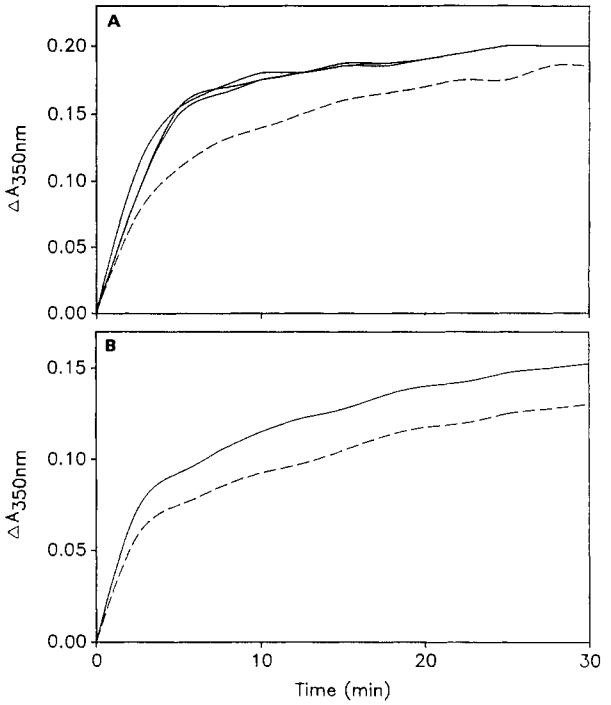


Figure 1. Effect of forskolin (**1**) and probe **12** on GTP-promoted tubulin polymerization: (A) tubulin (1 mg) was incubated at 37 °C in a 1-mL final volume of 10% DMSO in buffer A in the presence of either 1 mM GTP alone (- -) or in the presence of 1 mM GTP and 10 μM, 100 μM, or 1 mM forskolin (**1**) (—). The change in absorbance was monitored at 350 nm; (B) same as A using 1 mM GTP alone (- -) or 1 mM GTP and 100 μM probe (**12**) (—).

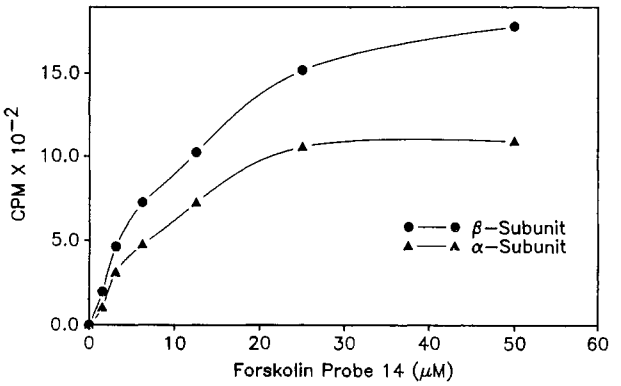


Figure 2. Saturation of photolabeling. Tubulin (5 μg) was exposed to varying concentrations of probe **14** in buffer B (final volume 30 μL), incubated (2 min, 4 °C), irradiated (2 min, 4 °C), and analyzed on 10% SDS–PAGE gels that were subsequently sliced and radioactivity determined using a Minaxi γ-counter.

Saturation Experiments. The tubulin solutions were incubated with increasing concentrations of forskolin probe **14** and photolyzed to produce the results shown in Figure 2. The β-tubulin showed saturation of labeling at a concentration of approximately 25 μM of forskolin probe **14** with an apparent K_d of 8–10 μM. The α-subunit was also labeled with approximately the same saturation concentration and apparent K_d; however, the labeling in the α-subunit was 35% less than that in the β-subunit at the saturation concentration.

Competition Experiments. Tubulin solutions (5 μg) in buffer B in an Eppendorf tube were incubated successively with various concentrations of non-iodinated probe **12** (10 min, 4 °C) and 5 μM radioiodinated probe

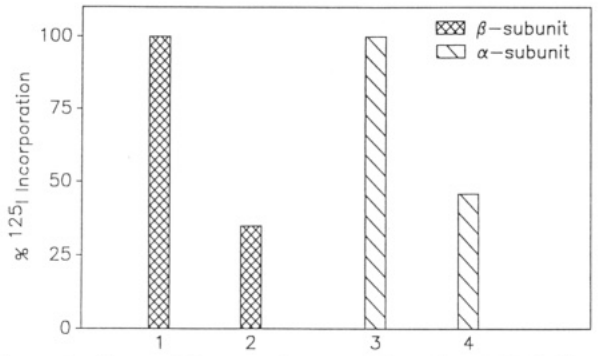


Figure 3. Competition experiments with probe **14**. Tubulin (5 μg) was exposed to 1000 μM of probe **12** in buffer B (final volume 30 μL), incubated (10 min, 4 °C), exposed to probe **14**, incubated (2 min, 4 °C), irradiated (2 min, 4 °C), and analyzed on 10% SDS–PAGE gels as in Figure 2: column 1, photolabeling of α-tubulin in the absence of probe **12**; column 2, photolabeling of α-tubulin in the presence of probe **12**; column 3, photolabeling of β-tubulin in the absence of probe **12**; and column 4, photolabeling of β-tubulin in the presence of probe **12**.

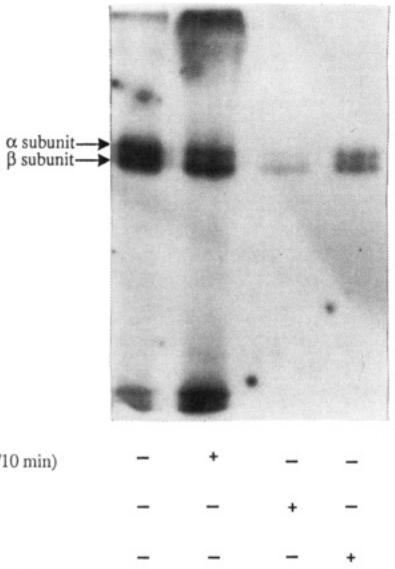


Figure 4. Effect of denaturation. Tubulin (5 μg) was denatured in various ways and exposed to 10 μM of probe **14**, incubated (2 min, 4 °C), irradiated (2 min, 4 °C), and analyzed on 10% SDS–PAGE gels. Autoradiography was performed for 8 h.

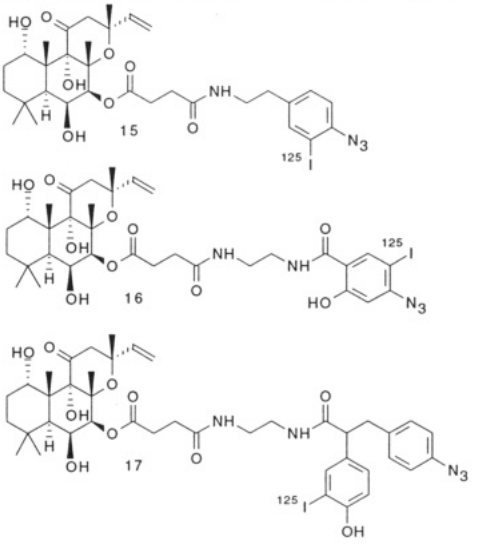
14 (2 min, 4 °C) in 30 μL of the final volume, photolyzed, and analyzed to give the results shown in Figure 3. Relatively high concentrations of the noniodinated probe were required to afford protection of labeling. At 1000 μM concentration of the competing noniodinated probe, approximately 65% of labeling in the β-subunit was protected whereas 54% of labeling in the α-subunit was protected.

Specificity. Denatured tubulin failed to bind the radioiodinated analog **14** as indicated by the autoradiogram of the SDS–PAGE gels in Figure 4. Human brain homogenate (10 μL of 20% from either normal or AD brains) in buffer B in an Eppendorf tube was incubated with 10 μM of probe **14** either alone or with 100 μM of various competitors for 2 min at 0 °C, photolyzed, and analyzed to give the autoradiogram of the SDS–PAGE gels shown in Figure 5. Five major protein bands were labeled. In addition to α- and β-tubulin, a band with M_r of 25 kDa was also labeled.

DISCUSSION

The development of a suitable forskolin photoaffinity probe required a balance between the biological activity

Scheme II. Selected Forskolin Photoaffinity Probes



necessary to guarantee that the probe would mimic forskolin itself and the chemical properties necessary to achieve reasonable levels of cross-linking and detection. Although many modifications of forskolin (**1**) led to diminished activity (*11*) with respect to the stimulation of adenylate cyclase (AC), the C-7 forskolin analogs **7–9** possessed significant potency (*15*). Ruoho (*16*) and Pfeuffer (*17*) also reported C-7 forskolin derivatives **15** and **16**, respectively, (Scheme II) that possessed a phenyl azide attached to forskolin through a different connecting arm. The most significant difference in these probes was the presence of an activating hydroxyl group on the phenyl azide in the latter probe (**16**) that facilitated radioiodination. These forskolin derivatives bound the glucose transporter but did not activate adenylate cyclase. Shanahan (*18*) used [^{3}H]forskolin in a direct photoaffinity labeling study of the glucose transporter. Finally, Mende and Ho (*15*) described another C-7 derivative (**17**) that also possessed a phenyl azide but included a tyrosine group, again to facilitate radiolabeling, as part of the connecting arm. The forskolin probe **17** activated adenylate cyclase but not at the same level as the C-7 forskolin derivatives **7–9**. On this basis, these latter derivatives seemed the most reasonable candidates for the tubulin binding study, and after studying the problem of incorporating a radiolabel of high specific activity, the iodinated probes **10** and **13** as well as [^{125}I]-labeled probe **14** were prepared. Forskolin (**1**) and the derivative **12** enhanced the GTP-promoted polymerization of tubulin as shown in Figure 1. The increase in the extent of polymerization was saturated at 1 μM of forskolin (**1**). The chemically denatured tubulin (using either 1% SDS or 8 M urea) showed, as expected, minimal or no forskolin-binding ability, as shown in Figure 4. Heat denaturation (Figure 4) produced diminished binding, presumably as a consequence of incomplete denaturation or the exposure of some hydrophobic domains for which the forskolin probe had some affinity. Since the chemical denaturants were not removed prior to photolabeling, these specific or nonspecific hydrophobic binding domains were not accessible to the probe as in the case of heat denaturation.

Necessary studies validated the attributes of **14** as a forskolin photoaffinity probe: the demonstration of saturation effects; the prevention of photoinsertion by the natural compound (*i.e.*, the probe is a mimic at concentrations that agree with the known K_d of the natural compound); and the selectivity of labeling (*i.e.*, the probe only photoinserts into proteins that are known to bind the

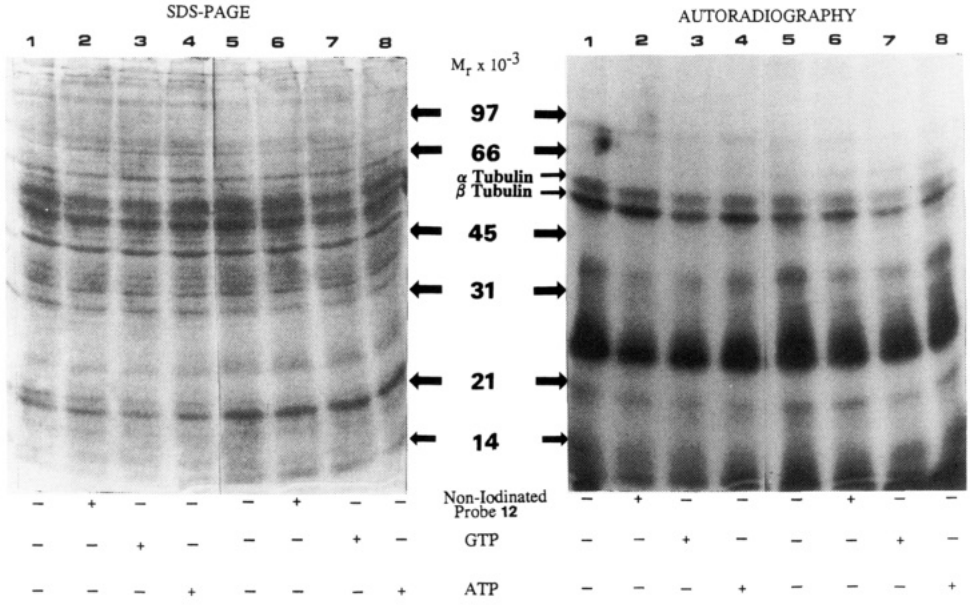


Figure 5. Photolabeling of human control (lanes 1–4) and AD brain homogenate (lanes 5–8) with probe **14**. Homogenates (7 μL of 20%) was exposed either to 10 μM of probe **14** alone or 10 μM of probe **14** and 100 μM of various competitors in buffer B (final volume 30 μL), incubated (2 min, 4 °C), irradiated (2 min, 4 °C), and analyzed on 10% SDS–PAGE gels. Autoradiography was performed for 12 h.

native compound). Preliminary photolabeling studies indicated that maximal incorporation of the probe **14** into tubulin subunits occurred within 5 min of irradiation, was unaffected by long incubation times, and was maximized at a 12% DMSO–buffer B concentration. Using tubulin prepared from bovine or ovine brain (*12*), it was demonstrated that the forskolin probe **14** exhibited saturation of the binding sites on both the α- and β-subunit of tubulin as shown in Figure 2. Significant amounts of binding to both subunits was noted, although under the optimal conditions developed for the photolabeling experiments using a 10 mM sodium phosphate buffer with 1 mM magnesium chloride and 1 mM EGTA, the β-subunit was preferentially labeled.

Competition for the binding of the radioiodinated forskolin probe **14** was demonstrated using the noniodinated probe **12**. Consistent with the observations of Ruoho, relatively high concentrations of **12** were required to achieve the results in Figure 3. These observations are consistent with a low K_d value for forskolin and rapid binding of forskolin or the probes **12** and **14** to the binding site. Consistent with these suggestions, the order in which the probes were added to the tubulin preparation had a dramatic effect on the competition experiments.

However, the efficiency of cross-linking in photolabeling experiments was judged to be too low to permit isolation of the cross-linked peptide and sequencing efforts. The photolabeling efficiency using forskolin probe **14** ranged from 0.07 to 2% in four separate experiments. This result should be contrasted with literature reports using other forskolin probes shown in Scheme II, in which the efficiency was suggested to be "high" (*16*), was not reported (*17*), or was comparable (0.09%) (*18*). The low efficiency in the particular case of forskolin probe **14** was ascribed to the electron-rich nature of hydroxy- or alkoxy-substituted dehydroazepine intermediate (*19*, *20*) generated in the photolysis of the alkoxy-substituted aryl azide and to a photodeiodination process (*21*) that competes effectively with the photolysis of the aryl azide. In the normal brain homogenate, forskolin probe **14** photolabeled three protein bands including α- and β-tubulin as well as a 25 kDa M_r protein. It was interesting that α- and β-tubulin photolabeling could be protected to some extent by GTP, suggesting a conformation change in the presence of GTP that altered forskolin binding or perhaps the prevention of nonspecific labeling by forskolin in the presence of GTP.

The forskolin probe **14** photolabeled α- and β-tubulins in AD brain homogenates in addition to three other principal bands. In comparison to photolabeling experiments with purified tubulin, it was of interest that the forskolin probe **14** exhibited slightly more selectivity for β-tubulin than α-tubulin in AD brain homogenates. It was also of interest that photolabeling of the β-tubulin from AD brains was observed using the forskolin probe **14** but was not observed using "GTP" probes, [γ-^{32}P]-8-N_3-GTP (*22*) and [^{125}I]APTG (*23*). These results suggested that there is a differential binding of the forskolin probe **14** on tubulin from AD and normal brains and raised the possibility that a forskolin-modified affinity resin might permit the isolation of tubulin from AD brains reported to have aberrant polymerization properties (*24*). In summary, the demonstration that the forskolin **14** photolabeled tubulin and activated adenylate cyclase augured well for future plans to engineer a more successful probe that incorporates a photoactive group capable of cross-linking with higher efficiency than the phenyl azide probe in **14**.

ACKNOWLEDGMENT

We thank the National Institutes of Health (HL 20780) for their generous financial support.

LITERATURE CITED

(1) Lindner, E., Dohadwalla, A. N., and Bhattacharya, B. K. (1978) Positive inotropic and blood pressure lowering activity of diterpene derivatives isolated from *Coleus forskohlii*: forskolin. *Arzneim. Forsch. 28*, 284–289.

(2) Seamon, K. B., Padgett, W., and Daly, J. W. (1981) Forskolin: unique diterpene activator of adenylate cyclase in membranes and in intact cells. *Proc. Natl. Acad. Sci. U.S.A. 78*, 3363–3367.

(3) Siegel, A. M., Daly, J. W., and Smith, J. B. (1982) Inhibition of aggregation and stimulation of cyclic AMP generation in intact human platelets by the diterpene forskolin. *Mol. Pharmacol. 21*, 680–687

(4) Agarwal, K. C., and Parks, R. E., Jr. (1983) Forskolin: A potential antimetastatic agent. *Int. J. Cancer 32*, 801–804.
(5) Metzger, H., and Linder, E. (1981) The positive inotropic-acting forskolin, a potent adenylate cyclase activator. *Arzneim. Forsch. 31*, 1248–1250.
(6) de Souza, N. J., Dohadwalla, A. N., and Reden, J. (1983) Forskolin: A labdane diterpenoid with antihypertensive, positive inotropic, platelet aggregation inhibitory, and adenylate cyclase activating properties. *Med. Res. Rev. 3*, 201–219.
(7) Daly, J. W. (1984) Forskolin, adenylate cyclase, and cell physiology: An overview. *Adv. Cyclic Nucleotide Protein Phosphorylation Res. 17*, 81–89.
(8) Corey, E. J., and Venkateswarlu, A. (1972) Protection of hydroxyl groups as tert-butyldimethylsilyl derivatives. *J. Am. Chem. Soc. 94*, 6190–6191.
(9) Richardson, S. K., Jeganathan, A., Mani, R. S., Haley, B. E., Watt, D. S., and Trusal, L. R. (1987) Synthesis and biological activity of C-4 and C-15 aryl azide derivatives of anguidine. *Tetrahedron 43*, 2925–2934.
(10) Kometani, T., Watt, D. S., Ji, T., and Fitz, T. (1985) An improved procedure for the iodination of phenols using sodium iodide and tert-butyl hypochlorite. *J. Org. Chem. 50*, 5384–5387.
(11) Bhat, S. V., Bajwa, B. S., Dornauer, H., and de Souza, N. J. (1982) Reactions of forskolin, a biologically active diterpenoid from *Coleus forskohlii*. *J. Chem. Soc., Perkin Trans. 1* 767–771.
(12) Shelanski, M. L., Gaskin, F., and Cantor, C. R. (1973) Microtubule assembly in the absence of added nucleotides. *Proc. Nat. Acad. Sci. U.S.A. 70*, 765–768.
(13) Gaskin, F., Cantor, C. R., and Shelanski, M. L. (1974) Turbidimetric studies of the in vitro assembly and disassembly of porcine neurotubules. *J. Mol. Biol. 89*, 737–758.
(14) Seamon, K. B., Daly, J. W., Metzger, H., de Souza, N. J., and Reden, J. (1983) Structure-activity relationships for activation of adenylate cyclase by the diterpene forskolin and its derivatives. *J. Med. Chem. 26*, 436–439.
(15) Ho, L. T., Nie, Z. M., Mende, T. J., Richardson, S., Chavan, A., Kolaczkowska, E., Watt, D. S., Haley, B. E., and Ho, R.-J. (1988–89) Modification of adenylate cyclase by photoaffinity analogs of forskolin. *Second Mess. Phosphoprot. 12*, 209–233.
(16) Wadzinski, B. E., Shanahan, M. F., and Ruoho, A. E. (1987) Derivatization of the human erytrocyte glucose transporter using a novel forskolin photoaffinity label. *J. Biol. Chem. 262*, 17683–17689.
(17) Pfeuffer, E., and Pfeuffer, T. (1989) Affinity labeling of forskolin-binding proteins. Comparison between glucose carrier and adenylate cyclase. *FEBS Lett. 248*, 13–17.
(18) Shanahan, M. F., Morris, D. P., and Edwards, B. M. (1987) [^{3H}]-Forskolin. Direct Photoaffinity labeling of the erythrocyte D-glucose transporter. *J. Biol. Chem. 262*, 5978–5984.
(19) Torres, M. J., Zayas, J., and Platz, M. S. (1986) A formal CH insertion reaction of an aryl nitrene into an alkyl CH bond. Implications for photoaffinity labelling. *Tetrahedron Lett. 27*, 791–794.
(20) Shields, C. J., Chrisope, D. R., Schuster, G. B., Dixon, A. J., Poliakoff, M., and Turner, J. J. (1987) Photochemistry of aryl azides: detection and characterization of a dehydroazepine by time-resolved infrared spectroscopy and flash photolysis at room temperature. *J. Am. Chem. Soc. 109*, 4723–4726.
(21) Watt, D. S., Kawada, K., Leyva, E., and Platz, M. S. (1989) Exploratory photochemistry of iodinated aromatic azides. *Tetrahedron Lett. 30*, 899–902.
(22) Kim, H., Ponstingl, H., and Haley, B. E. (1987) Identification of the guanosine interacting peptide of the GTP binding site of β-tubulin using $8N_3GTP$. *Fed. Proc. 46*, 2229.
(23) Chavan, A. J., Kim, H., Haley, B. E., and Watt, D. S. (1990) A photoactive phosphonamide derivative of GTP for the identification of the GTP binding domain in β-tubulin. *Bioconjugate Chem. 1*, 337–344.
(24) Iqbal, K., Zaidi, T., Wen, G. Y., Grundke-Iqbal, I., Merz, P. A., Shaikh, S. S., Wisniewski, H. M., Alafuzoff, I., and Winblad, B. (1986) Defective brain microtubule assembly in Alzheimer's disease. *Lancet* 421–426.

Synthesis, Metal Chelate Stability Studies, and Enzyme Digestion of a Peptide-Linked DOTA Derivative and Its Corresponding Radiolabeled Immunoconjugates

Min Li and Claude F. Meares*

Department of Chemistry, University of California, Davis, California 95616-0935. Received March 22, 1993

By directly coupling a tetrapeptide to DOTA through an amide bond, we synthesized a novel DOTA derivative, DOTA-glycylglycylglycyl-L-*p*-nitrophenylalanine amide. We converted this new precursor bifunctional chelating agent to DOTA-glycylglycylglycyl-L-*p*-isothiocyanatophenylalanine and conjugated it to monoclonal antibody Lym-1. Serum stability studies show that the radiolabeled conjugates are kinetically inert under physiological conditions. The rates of loss of radiometals in human serum are 0.1 ± 0.1% per day for In^{III}, 0.02 ± 0.15% per day for Y^{III}, and 0.3 ± 0.2% per day for Cu^{II} labeled immunoconjugates. In the presence of the liver enzyme cathepsin B, an *in vitro* digestion of ^{114m}In-labeled conjugate yields a small fragment containing ^{114m}In. Characterization of the cleavage products shows that this liver enzyme hydrolyzes the peptide linkage before the phenylalanine residue, freeing the In–DOTA–triglycine complex from the conjugate. However, the liver enzyme cathepsin D does not cleave the linkage over the span of 7 days.

INTRODUCTION

Bifunctional chelating agents (BCAs[1]) which contain a chemically reactive functional group for binding to proteins and a strong metal chelating group have been used to label monoclonal antibodies (mAbs) with radiometals for cancer diagnosis and therapy (*1–5*). Metallic radioisotopes such as ^{111}In, ^{99m}Tc, ^{67}Cu, ^{90}Y, and ^{68}Ga are primary candidates for labeling mAbs due to their favorable physical properties (*4, 6*). BCAs in which the chelating moiety can hold radiometals with high stability under physiological conditions are essential to avoid excessive radiation damage to nontarget cells (*7*). In recent years, macrocyclic poly(amino carboxylate) BCAs have gained considerable attention (*8–13*). One of the most promising agents studied so far is DOTA; its derivatives form extraordinarily stable complexes with a variety of metal ions under physiological conditions (*9, 12, 14*). Several DOTA derivatives have been synthesized, each synthesis involving multiple steps (*9, 10, 15, 16*).

Another major detriment to the use of radiometal-labeled mAbs for radiopharmaceutical applications is the high accumulation of radioactivity in the normal organs, particularly the liver (*17–20*). One approach to reducing the liver uptake of radioactivity is to attach the chelate to the antibody through a readily metabolizable chemical linker (*21–23*). This may accelerate the cleavage of the chelate from the antibody when the antibody–chelate conjugate is endocytosed into an enzyme-rich intracellular compartment (*21, 24*). Once cleaved, the chelated radiometal may be returned to the circulation and rapidly excreted through the kidney.

This paper describes the chemical and biochemical properties of a novel DOTA derivative containing a cleavable linker. This new BCA does not contain a carbon-linked side chain; the linker is attached through an amide bond to a DOTA carboxyl group (see Scheme I).

EXPERIMENTAL PROCEDURES

Chemicals. Triglycine, cathepsin B (EC 3.4.22.1), cathepsin D (EC 3.4.23.5), and dithiothreitol were purchased from Sigma Chemical Co. 2-[[(*tert*-Butoxycarbonyl)oxy]imino]-2-phenylacetonitrile, *p*-nitrophenol, isobutyl chloroformate, palladium on charcoal (10%), thiophosgene, and DTPA were obtained from Aldrich. DOTA (sodium salt) was bought from Parish Chemical Co. and its purity (87.2%) was determined by a Cobalt-57 binding assay (*25*). Disodium EDTA and CF_3COOH were obtained from Fisher Scientific. DTPA anhydride was purchased from Pierce. Peptide substrate for cathepsin D, BOC-Phe-Ala-Ala-(*p*-NO_2)Phe-Phe-Val-Leu-4-(hydroxymethyl)pyridine was bought from Research Plus, Inc. Lym-1, an anti B cell lymphoma IgG_{2a} mAb (*26*), was obtained from Damon Biotech (Needham Heights, MA; Encapcel murine mAb, lot #3-171-860813). Lym-1 was further purified by protein A affinity column chromatography prior to use. $^{57}CoCl_2$, $^{67}CuCl_2$, $^{114m}InCl_3$, and $^{88}YCl_3$ were purchased from ICN, Brookhaven, Du Pont, and Los Alamos, respectively. Pure water (18 MΩ cm^{-1}) was used throughout. All glass labware was washed with a mixed acid solution and thoroughly rinsed with deionized, distilled water (*27*). All plastic labware was washed with 3 M HCl and thoroughly rinsed. All other chemicals were the purest grade available.

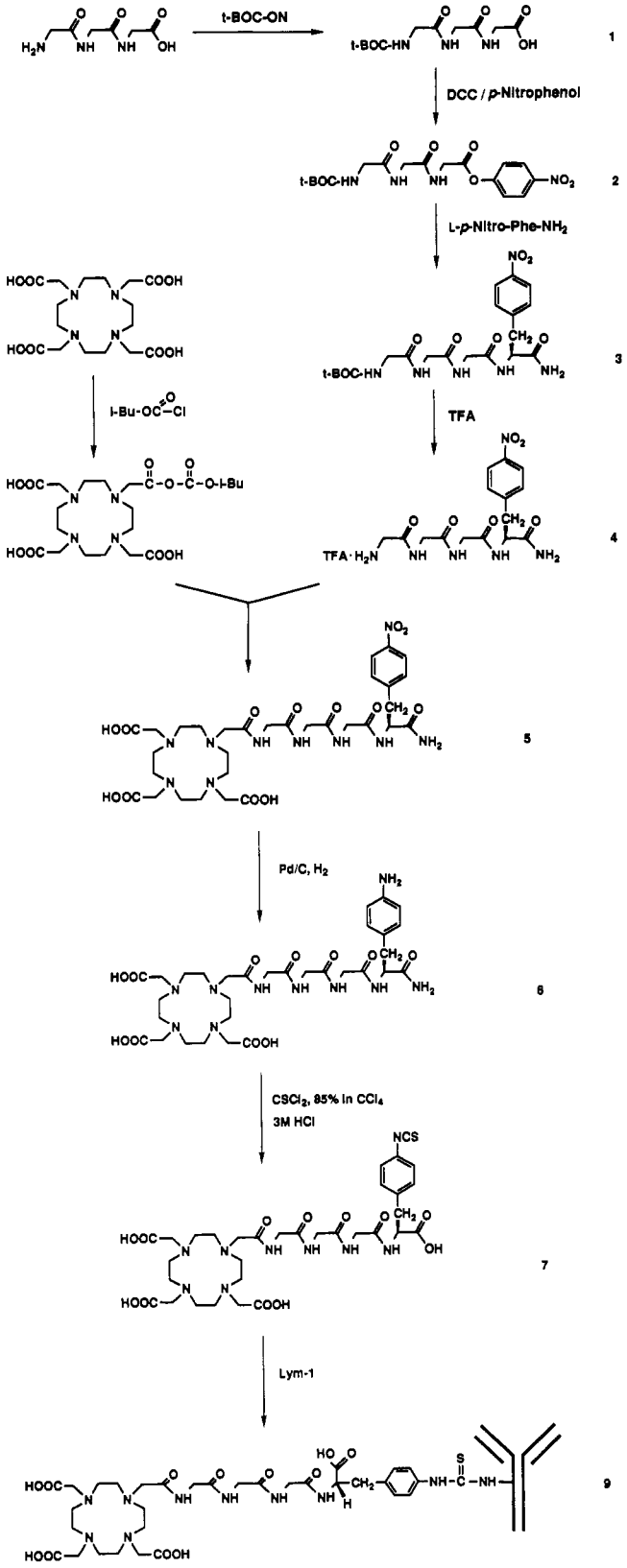
Thin-Layer Chromatography. TLC was run on plastic-backed silica gel plates (Kieselgel 60 F_{254}, EM Science) using various solvents as described below. For the metal-binding assays, a solution containing equal volumes of 10% (w/v) aqueous ammonium acetate and methanol was used as the eluent.

High-Performance Liquid Chromatography. HPLC was performed at room temperature on a Rainin HPXL system or a Waters HPLC instrument (pump model M-45, controller model 660). The columns, gradients, and solvent systems are described below. The UV-absorbing fractions were detected either at 254 nm or at 280 nm using an ISCO UA-5 detector.

[1] Abbreviations used: BAT, 6-(*p*-(bromoacetamido)benzyl)-1,4,8,11-tetraazacyclotetradecane-*N,N′,N″,N‴*-tetraacetic acid; BCA, bifunctional chelating agent; DOTA, 1,4,7,10-tetraazacyclododecane-*N,N′,N″,N‴*-tetraacetic acid; DTPA, diethylenetriaminepentaacetic acid; EDTA, ethylenediaminetetraacetic acid; 2IT, 2-iminothiolane; PBS, phosphate-buffered saline. TMSP, 3-(trimethysilyl)propionic-*2,2,3,3,-d*$_4$ acid, sodium salt.

1043-1802/93/2904-0275$04.00/0 © 1993 American Chemical Society

Scheme I



Radiation Counting. γ-counting was done with a Beckman Model 310 counter. TLC plates and protein gels containing radiolabeled materials were visualized with an AMBIS Radioanalytical Imaging System. The HPLC effluent was monitored by a Beckman 170 flow-through radioisotope detector.

Spectroscopy. NMR spectra were recorded on a General Electric QE 300 spectrometer at 300 MHz for ^1H and at 75 MHz for ^{13}C. The chemical shifts are relative to the monoprotonated solvents (HOD, 4.80 ppm; CD_3OH, 3.30 ppm; $CD_3(SO)CD_2H$, 2.49 ppm) and TMSP as an external reference. Reported pH meter readings are not corrected for the deuterium isotope effect.

Mass spectra and exact mass measurements were obtained on a ZAB-HS-2F mass spectrometer (VG Analytical, Wythenshawe, UK). During mass spectroscopic measurements, either 3-nitrobenzyl alcohol or dithiothreitol/dithioerythritol (3:1 w/w) was used as a matrix along with small amounts of *p*-toluenesulfonic acid.

IR spectra were performed on an IBM 32 FTIR spectrophotometer.

Concentrations of antibody (MW 155 kDa) were determined by absorbance at 280 nm ($E^{1\%}_{280}$ = 13.5 (*28*)). The measurements were recorded on a Gilford Model 250 spectrophotometer using a 1-cm pathlength microcell.

The cathepsin D enzyme activity assay was performed on an HP 8450A UV/vis spectrophotometer.

Bifunctional Chelating Agent Synthesis. *N*-(*tert*-Butoxycarbonyl)glycylglycylglycine (1). Triglycine (29.25 g, 154.8 mmol) and triethylamine (32.3 mL, 154.8 × 1.5 mmol) in 100 mL of water was mixed with 2-[[(*tert*-butoxycarbonyl)oxy]imino]-2-phenylacetonitrile (42.47 g, 154.8 × 1.1 mmol) in 100 mL of dioxane at room temperature under N_2. After stirring for 6 h, 100 mL of water and 100 mL of ethyl acetate were added. The aqueous phase was washed with ethyl acetate (5 × 200 mL) and then acidified to pH 1 using 6 M HCl and extracted with ethyl acetate (10 × 200 mL). The extracts were taken to dryness under reduced pressure. The residue was washed with ethyl ether and allowed to air dry at room temperature to yield 1 as a white solid: yield, 32.8 g, 73%; ^1H NMR (D_2O) δ 1.35 (s, 9H), 3.75 (s, 2H), 3.95 (s, 4H); FAB-MS *m/e* = 290 ($M + H^+$).

***N*-(*tert*-Butoxycarbonyl)glycylglycylglycine *p*-Nitrophenyl Ester (2).** *p*-Nitrophenol (0.865 g, 5.51 × 1.2 mmol) was added to a solution of 1 (1.50 g, 5.15 mmol) in 25 mL of pyridine. Then 1,3-dicyclohexylcarbodiimide (1.4 g, 5.15 × 1.2 mmol) was added at 0 °C under N_2. The reaction temperature was kept at 0 °C for 30 min, then at room temperature for 4.5 h. The precipitate was filtered off and the filtrate was evaporated to dryness under reduced pressure. The residue was taken up in hot 2-propanol and upon cooling, 2 crystallized as a white solid: yield, 1.68 g, 79%; TLC (eluent, $CHCl_3$/ethyl acetate/CH_3OH 5:5:1 v/v/v) R_f = 0.24; ^1H NMR (CD_3OD) δ 1.35 (s, 9H), 3.75 (s, 2H), 3.95 (s, 2H), 4.25 (s, 2H), 7.45 (d, 2H), 8.30 (d, 2H); FAB-MS *m/e* = 411 ($M + H^+$).

***N*-(*tert*-Butoxycarbonyl)glycylglycylglycyl-L-*p*-nitrophenylalanine Amide (3).** L-*p*-Nitrophenylalanine amide (112 mg, 0.488 × 1.1 mmol), prepared according to Yeh *et al.* (*29*), was added to a solution of 2 (200 mg, 0.488 mmol) in 5 mL of *N*,*N*-dimethylformamide at room temperature. After stirring for 5 h, the solvent was evaporated to dryness under reduced pressure and the resulting yellow residue was washed with CH_3OH five times to give 3 as a white precipitate: yield, 120 mg, 51%; TLC (eluent, $CHCl_3/CH_3OH$ 1:1 v/v) R_f = 0.60; ^1H NMR (dimethyl sulfoxide-d_6/D_2O 1:1) δ 1.35 (s, 9H), 2.90 (m, 1H), 3.15 (m, 1H), 3.6–3.8 (m, 6H), 4.40 (m, 1H), 7.45 (d, 2H), 8.10 (d, 2H); FAB-MS *m/e* = 481 ($M + H^+$).

Glycylglycylglycyl-L-*p*-nitrophenylalanine amide–Trifluoroacetic Acid (4). Compound 3 (94 mg, 0.196 mmol) was dissolved in 5 mL of neat CF_3COOH at 0 °C and the solvent was removed after 1 h under reduced pressure. The residue was lyophilized twice from water to give 4 as a white solid in quantitative yield: ^1H NMR

Table I. Radiolabeling Immunoconjugates

conjugate	chelates per mAb	radioisotope	starting radioactivity, μCi	labeling buffer	labeling conditions	challenge chelate stock solution	conjugate final conc, mg/mL	specific activity, mCi/mg
DOTA-Gly_3-L-Phe-thiourea-Lym-1	1.2 ± 0.1	^{114m}In	26	0.1 M NH_4OAc, pH = 5.5	2 h RT	100 mM EDTA in 2 M $(NH_4)_3$citrate	0.94	0.018
		^{88}Y	24	2.0 M NH_4OAc, pH = 7.0	3 h RT	50 mM DTPA in 0.2 M $(NH_4)_3$citrate	0.94	0.026
		^{67}Cu	250	0.1 M $(NH_4)_3$citrate, pH = 5.0	0.5 h RT	100 mM EDTA in 2 M $(NH_4)_3$citrtae	0.73	0.65
DTPA-Lym-1	3.5 ± 0.1	^{114m}In	33	0.5 M NH_4OAc, pH = 5.5	1 h RT	100 mM EDTA in 2 M $(NH_4)_3$citrate	0.63	0.14
		^{88}Y	26	0.1 M $(NH_4)_3$citrate, pH = 6.5	1 h RT	50 mM DTPA in 0.2 M $(NH_4)_3$citrate	0.39	0.031
BAT-2IT-Lym-1	2.2 ± 0.1	^{67}Cu	131	0.1 M $(NH_4)_3$citrate, pH = 5.0	0.5 h RT	100 mM EDTA in 2 M $(NH_4)_3$citrate	0.23	0.61

(D_2O) δ 3.15 (m, 1H), 3.35 (m, 1H), 3.8–4.1 (m, 6H), 4.65 (m, 1H), 7.45 (d, 2H), 8.20 (d, 2H); FAB-MS *m/e* = 381 (M + H^+). Anal. Calcd for $C_{15}H_{20}N_6O_6 \cdot {}^4/_3CF_3COOH \cdot H_2O$: C, 38.55; H, 4.27; N, 15.27; F, 13.81. Found: C, 38.63; H, 4.28; N, 15.23; F, 14.04.

DOTA-Glycylglycylglycyl-L-*p*-nitrophenylalanine Amide (5). DOTA sodium salt (81 mg, 0.20 mmol) was dissolved in 10 mL of a *N,N*-dimethylformamide and triethylamine mixture (4:1 v/v) overnight at room temperature. Isobutyl chloroformate (26.5 μL, 0.20 mmol) was added dropwise at 0 °C to the mixture. After 15 min, **4** (98 mg, 0.20 mmol) was added and the reaction was kept at room temperature for 5 h. The reaction mixture was purified by reversed-phase HPLC using a 21.4 × 250 mm C_{18} column (Dynamax 60 Å) with a flow rate of 12.5 mL/min. A 20-min linear gradient, from 15% to 100% solvent B (solvent A, 0.1 M aqueous ammonium acetate, pH 6.0; solvent B, CH_3OH) was used. The major peak at retention time 10.5 min was collected and dried to give **5** as a light yellow solid: yield, 68 mg, 45% by weight; purity, 96.2% by ^{57}Co binding assay (*25*); ^1H NMR (D_2O, pH 6.0) δ 3.6–4.1 (m, 32H), 4.65 (m, 1H), 7.45 (d, 2H), 8.20 (d, 2H); ^{13}C NMR (D_2O, pH 6.0) δ 37.52, 43.42, 43.58, 49.18, 49.51, 51.65, 57.72, 54.88, 55.41, 57.13, 57.56, 124.56, 131.10, 146.06, 147.51, 170.45, 172.10, 173.05, 173.29, 173.60, 175.78, 176.82; FAB-MS *m/e* for $C_{31}H_{47}N_{10}O_{13}$ (M + H^+) = 767.3324, found 767.3352. Anal. Calcd for $C_{31}H_{46}N_{13}O_{13}$: C, 48.56; H, 6.05; N, 18.27. Found: C, 48.64; H, 6.16; N, 18.15.

DOTA-Glycylglycylglycyl-L-*p*-aminophenylalanine Amide (6). Compound **5** (50 mg, 65 μmol) was dissolved in 15 mL of water and the pH was adjusted to 11.5 with 0.2 M NaOH. The reaction was placed in an ice bath and 1 mg of 10% Pd/C was added to the cold solution. The mixture was stirred under 1 atm of H_2 for 8 h at 0 °C. The reaction solution was neutralized with 1 M HCl and then filtered through a 0.45-μm syringe filter (Nylon-66, Rainin) to remove the Pd/C catalyst. The filtrate was lyophilized to give **6** as a white solid in quantitative yield: ^1H NMR (D_2O, pH 5.7) δ 2.7–4.1 (m, 32H), 4.50 (m, 1H), 6.90 (d, 2H), 7.10 (d, 2H); FAB-MS *m/e* = 737 (M + H^+), 759 (M + Na^+), and 781 (M + $2Na^+$).

DOTA-Glycylglycylglycyl-L-*p*-isothiocyanatophenylalanine (7) and DOTA-Glycylglycylglycyl-L-*p*-isothiocyanatophenylalanine Amide (8). Compound **6** (48 mg, 65 μmol) in 5 mL of 3 M HCl was added to 3 mL of $CSCl_2$ (85% in CCl_4) at room temperature. The reaction was stirred vigorously for 6 h. The aqueous phase was washed with chloroform (4 × 3 mL) to remove excess $CSCl_2$ and then purified by reversed-phase HPLC using a 21.4 × 250 mm C_{18} column (Dynamax 60 Å) with a flow rate of 12.5 mL/min. A 40-min linear gradient, from 15% to 100% solvent B (solvent A, 0.1% CF_3COOH in H_2O; solvent B, 0.1% CF_3COOH in CH_3OH), was used. Two major peaks were collected, at retention times 25.0 and 27.0 min. The second major peak at 27.0 min was dried to give **7** as a white solid: yield, 8.6 mg, 17% by ^{57}Co binding assay; ^1H NMR (D_2O, pH 1.4) δ 2.8–4.3 (m, 32H), 4.60 (m, 1H), 7.20 (d, 4H); FAB-MS *m/e* for $C_{32}H_{46}N_9O_{12}S$ (M + H^+) = 780.2987, found 780.2997; IR (KBr) 2118 cm^{-1} ($\nu_{N=C=S}$). Anal. Calcd for $C_{32}H_{45}N_9O_{12}S \cdot 1.42CF_3COOH$: C, 44.44; H, 4.97; N, 13.39; F, 8.58; S, 3.41. Found: C, 44.73; H, 4.90; N, 13.72; F, 9.01; S, 3.60. The first peak was dried to give DOTA-glycylglycylglycyl-L-*p*-isothiocyanatophenylalanine amide (**8**) as a white solid: yield, 19.8 mg, 39% by ^{57}Co binding assay; ^1H NMR (D_2O, pH 1.4) δ 2.8–4.3 (m, 32H), 4.50 (m, 1H), 7.20 (d, 4H); FAB-MS *m/e* for $C_{32}H_{47}N_{10}O_{11}S$ (M + H^+) = 779.3147, found 779.3150; IR (KBr) 2116 cm^{-1} ($\nu_{N=C=S}$). Calcd for $C_{32}H_{46}N_{10}O_{11}S \cdot {}^4/_3CF_3COOH$: C, 44.73; H, 5.13; N, 15.05; F, 8.16; S, 3.44. Found: C, 45.00; H, 5.22; N, 14.93; F, 9.88; S, 3.05. Both products were reinjected on an HPLC using a 10 × 250 mm C_{18} column (Dynamax 60 Å) with a flow rate of 3.0 mL/min. A 30-min linear gradient, from 15% to 100% solvent B (solvent A, 0.1% CF_3COOH in H_2O; solvent B, 0.1% CF_3COOH in CH_3OH), was used. A single peak was observed for both cases. The retention times for product **7** and **8** were 24 and 23 min.

Preparation of DOTA-Gly-Gly-Gly-L-Phe-Thiourea-Lym-1 conjugate (9). An aqueous solution of **7** (50 μL, 15.14 mM) was added to 1.5 mL of Lym-1 antibody solution (16 mg/mL) in 0.1 M tetramethylammonium phosphate buffer, pH 8.0. The Lym-1 antibody solution had been prepared by exchanging the phosphate-buffered saline with storage buffer using a Sephadex G-50 centrifuged gel-filtration column (*25*, *30*). After mixing of the reactants, the pH was adjusted to 8.89 with 2 M triethanolamine and the reaction mixture was incubated at 37 °C for 2.5 h. The conjugate **9** was then purified using another centrifuged gel-filtration column. The degree of aggregation of the conjugate was determined by TSK 3000 gel filtration HPLC (solvent, 0.1 M aqueous ammonium acetate, pH 6.0; flow rate, 1.0 mL/min). The immunoconjugate peak (150 kDa) appeared at retention time 9.0 min and no aggregate was observed.

Radiolabeling of DOTA-Gly-Gly-Gly-L-Phe-Thiourea-Lym-1. The radionuclides ^{114m}In, ^{88}Y, and ^{67}Cu were used for labeling the conjugate. Labeling conditions are listed in Table I. Radiometal solutions (^{114m}In and ^{67}Cu were in 0.5 M HCl, ^{88}Y was in 6 M HCl) were dried under a heat lamp and dissolved in 2 μL of labeling buffer. To each of these solutions was added 18 μL of **9** (12.8 mg/mL) in the same labeling buffer and the mixture incubated at room temperature for a certain period (see Table I). The

solutions were then diluted with 115 μL of labeling buffer, and 15 μL of challenge chelate stock solution was added to give a final concentration of 10 mM EDTA (or 5 mM DTPA). The solutions were incubated for another hour at room temperature, followed by purification and solvent exchange into H_2O using a centrifuged gel-filtration column. An aliquot of each final solution was mixed with the same volume of challenge chelate solution. This mixture was incubated for 1 h and examined by TLC (eluent, 10% (w/v) NH_4OAc/CH_3OH 1:1 v/v; R_f = 0.0 for all the metal-conjugates, R_f = 0.70 for In–EDTA and Cu–EDTA, and R_f = 0.60 for Y-DTPA). The TLCs showed that the conjugate chelated each radioisotope quantitatively.

Preparation and Radiolabeling of DTPA–Lym-1. The conjugate was prepared by the method of Hnatowich *et al.* (*31*). An aqueous solution of Lym-1 (24 mg) was dried under reduced pressure and then mixed with solid DTPA anhydride (1 mg, 2.79 mmol). One mL of 0.1 M tetramethylammonium phosphate buffer, pH 7.0, was added. The reaction mixture was incubated at room temperature for 1 h. The DTPA–Lym-1 conjugate was then purified using a centrifuged gel-filtration column.

The conditions for radiolabeling the DTPA–Lym-1 conjugate with ^{114m}In and ^{88}Y are listed in Table I. Radiometal solutions (^{114m}In was in 0.5 M HCl, ^{88}Y was in 6 M HCl) were dried under a heat lamp and dissolved in 5 μL of labeling buffer. To each of these solutions was added 15 μL of DTPA–Lym-1 (8.2 mg/mL) in the same labeling buffer and the mixture incubated for 1 h at room temperature. The procedures for purification and characterization of radiolabeled conjugates were the same as described above for conjugate **9**.

Preparation and Radiolabeling of BAT–2IT–Lym-1. This conjugate was prepared according to the method of Deshpande *et al.* (*32*).

The conditions for ^{67}Cu labeling are listed in Table I. The ^{67}Cu solution (in 0.5 M HCl) was dried under a heat lamp and dissolved in 2 μL of labeling buffer. Then 4.6 μL of BAT–2IT–Lym-1 (10.8 mg/mL) in the same labeling buffer was added and the mixture was incubated at room temperature for 0.5 h. The procedures for purification and characterization of ^{67}Cu–BAT–2IT–Lym-1 were the same as described above for conjugate **9**.

Immunoreactivity Assay. Conjugate **9** was labeled with ^{111}In using the same labeling method as labeling with ^{114m}In. ^{111}In-labeled conjugate **9** and ^{67}Cu–BAT–2IT–Lym-1 were assayed for immunoreactivity by the solid-phase radioimmunoassay method using ^{125}I-labeled Lym-1 as a standard (*33*). The immunoreactivities of conjugate **9** and BAT–2IT–Lym-1 were 89.9% and 85.5% relative to ^{125}I-labeled antibody.

Serum Stability Studies. Blood was collected from a healthy volunteer, allowed to clot for 1 h at room temperature in a closed tube, and then centrifuged. The supernatant serum was transferred to sterile plastic culture tubes and incubated at 37 °C in a humidified carbon dioxide incubator (Equatherm CO_2 incubator, Model 330). The pH of the serum was measured as 7.4 before aliquoting into separate sterile vials for the addition of radiolabeled Lym-1 conjugates.

A 10–40-μL aliquot of radiolabeled conjugate was added to 1–2 mL of serum. The final concentrations of chelating agent are listed in Table II. The samples were maintained at 37.0 ± 0.2 °C and at pH 7.4 ± 0.1 (air:CO_2 was approximately 95:5 by volume) throughout the experiment. The stability of each conjugate in human serum was determined by analyzing small samples of serum at daily intervals for 2 weeks. Eight percent polyacrylamide native protein slab gels (*34*) were used to resolve the different proteins in the serum samples. Bromophenol blue solution in adjacent lanes marked the dye front. The gels were dried, visualized on the AMBIS, cut into slices, and quantified using a γ-counter.

Table II. Results of Human Serum Stability Studies

conjugate	chelating agent final conc, nM	% loss/day[a]
In–DOTA–Gly_3-L-Phe–thiourea–Lym-1	123	0.05 ± 0.07
	184	0.18 ± 0.21
In–DTPA–Lym-1	157	0.76 ± 0.42
Y–DOTA–Gly_3-L-Phe–thiourea–Lym-1	121	0.02 ± 0.22
	182	0.01 ± 0.08
Y–DTPA–Lym-1	97	1.06 ± 0.60
Cu–DOTA–Gly_3-L-Phe–thiourea–Lym-1	95	0.38 ± 0.19
	95	0.19 ± 0.14
Cu–BAT–2IT–Lym-1	69	0.85 ± 0.92

[a] Errors are 95% confidence limits.

***In Vitro* Enzyme Digestion of ^{114m}In-Labeled Lym-1 Conjugate 9 with Cathepsin B and Cathepsin D.** Five microliters of 75 mM dithiothreitol and 12.5 μL of 0.3 M tetramethylammonium acetate, pH 4.8, were mixed with 2.5 μL of either cathepsin B (activity = 22 units/mL (*35*)) or cathepsin D (activity = 2.2 units/mL (*36*)). After 15 min at room temperature, 30 μL of ^{114m}In-labeled conjugate **9** in 0.1 M ammonium acetate, pH 4.8, was added to give a final concentration of 0.55 μM. The final activities of cathepsin B and cathepsin D were 1.1 and 0.11 units/mL. After incubation at room temperature for 0.25, 1, 12, 18, 24, 36, 48, 72, 96, and 165 h, aliquots of the solutions were analyzed by TLC (eluent, 10% (w/v) NH_4OAc/CH_3OH 2:1 v/v).

After 165 h of incubation, each digest solution was analyzed by reversed-phase HPLC to identify the cleavage products. A 4.6 × 250 mm C_{18} column (Dynamax 300 Å) with a flow rate of 0.7 mL/min and a 30-min linear gradient from 5% to 100% solvent B (solvent A, 0.1% CF_3COOH in H_2O; solvent B, 0.1% CF_3COOH in CH_3OH) was used. The cleaved products were monitored by both a UV detector and a flow-through radioisotope detector. Unsubstituted ^{114m}In–DOTA was independently prepared and used as a standard.

Cathepsin D Activity Assay. Because this enzyme showed no activity against the DOTA peptide linker, it was assayed to confirm that it was active against a standard substrate. The assay followed the method described by Agarwal *et al.* (*37*). Phe-Ala-Ala-(*p*-NO_2)Phe-Phe-Val-Leu-4-(hydroxymethyl)pyridine was used as a peptide substrate. The rate of cleavage of the peptide was followed spectrophotometrically at 310 nm in 0.01 M sodium formate buffer, pH 3.5, at room temperature. The concentrations of the substrate and enzyme were 0.047 mM and approximately 0.005 μM.

By comparison of the concentrations of enzyme found by weight and by assay, the enzyme activity assay shows that cathepsin D is 60% active.

RESULTS

Synthesis. The synthesis of DOTA–glycylglycylglycyl-L-*p*-nitrophenylalanine amide (**5**) is shown in Scheme I. Because of its solubility in *N*,*N*-dimethylformamide, L-*p*-nitrophenylalanine amide was used as a starting material instead of L-*p*-nitrophenylalanine methyl ester. In the preparation of **5**, a side product detected by HPLC, retention time 15 min, was also collected and identified

by mass spectroscopy as DOTA conjugated to two peptides. Treatment of **6** with $CSCl_2$ not only converts the aromatic amine to the isothiocyanate but also partially hydrolyzes the primary amide. DOTA–glycylglycylglycyl-L-*p*-isothiocyanatophenylalanine (**7**) was found to have an HPLC retention time of 27.0 min (17% yield). Another major peak detected at 25.0 min was identified as DOTA–glycylglycylglycyl-L-*p*-isothiocyanatophenylalanine amide (**8**) (39% yield).

Conjugation and Radiolabeling. The ratios of chelate to Lym-1 for DOTA–Gly_3-L-Phe–thiourea–Lym-1, DTPA–Lym-1, and BAT–2IT–Lym-1 are listed in Table I. The results were determined by UV absorbance and ^{57}Co binding assay (*25*). The final concentration of Lym-1 conjugates and the specific activity after radiolabeling are also listed in Table I.

Serum Stability Studies. Serum mixtures of ^{114m}In–, ^{88}Y–, and ^{67}Cu–DOTA–Gly_3-L-Phe–thiourea–Lym-1 at different times of incubation under physiological conditions were analyzed by electrophoresis. The relative mobility (R_m) of the labeled antibody, transferrin, and albumin was found to be 0.22, 0.40, and 0.60, respectively. The gel electrophoresis profiles showed that there were negligible counts in the R_m 0.35–0.45 region throughout the experiment period for all three different radiometal-labeled Lym-1 peptide–DOTA conjugates. However, some counts were found in the R_m 0.95–1.05 region, which were most likely due to free chelates cleaved from the antibody by hydrolysis. Deshpande *et al.* (*14*) reported a similar observation for Lym–2IT–2-(*p*-(bromoacetamido)benzyl)DOTA–^{88}Y. For comparison, ^{114m}In–DTPA–Lym-1, ^{88}Y–DTPA–Lym-1 and ^{67}Cu–BAT–2IT–Lym-1 were prepared as described above and studied under the same conditions. The gel electrophoresis profiles for these radiolabeled conjugates showed that the counts in the transferrin R_m 0.35–0.45 (for ^{114m}In and ^{88}Y) or albumin R_m 0.50–0.65 (for ^{67}Cu) and R_m 0.9–1.1 regions increased to varying degrees with time.

The sum of counts in R_m 0–0.35 and 0.9–1.1 regions were divided by total counts to determine the percentage of intact metal chelates as a function of time. The results are plotted in Figure 1. Since the metals were present in trace amounts, the initial loss of metal from the chelate to serum proteins should follow pseudo-first-order kinetics (*12*). Table II lists the apparent rate constants corresponding to the curves shown in Figure 1. The plots in Figure 1 should be fit by exponential functions as $\exp(-k_i t)$, where k_i is a pseudo-first-order rate constant and t is time. Since the rates of loss of metal from the chelates are quite slow, only a small fraction of the metal was lost during each experiment. Thus, the plots can be expressed by straight lines [when $k_i t \ll 1$, $\exp(-k_i t) \approx 1 - k_i t$].

Enzyme Digestion of the Conjugate with Cathepsins. A typical scan profile of a TLC plate is shown in Figure 2. With the chosen TLC system, the products cleaved from the antibody (small molecules containing chelated ^{114m}In) have R_f 0.20, while the conjugate remains at the origin. The counts at the origin were compared with the counts at R_f 0.20 to determine the percentage of protein-bound ^{114m}In. The results are plotted in Figure 3. A small molecule containing ^{114m}In was cleaved from the conjugate by cathepsin B with a half-life ($T_{1/2}$) of 20 h. However, no cleaved radioactive products were observed in either the cathepsin D solution or the control solution.

An HPLC profile of the cathepsin B digestion, recorded by a flow-through radioisotope detector, can be seen in Figure 4A. By comparison to a standard sample, the cleaved product (t_R 9.5 min) had a different retention time

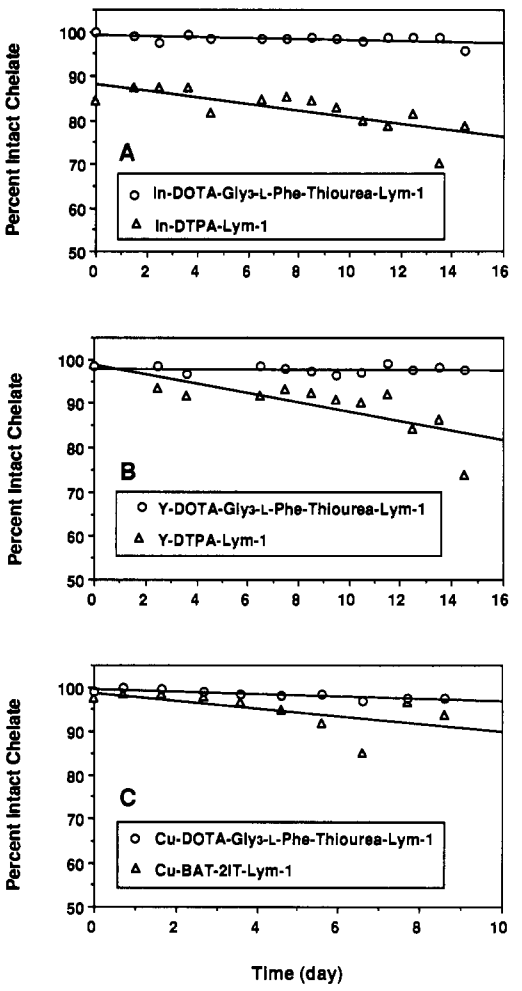


Figure 1. Percentage of intact metal chelates as a function of time of incubation in serum under physiological conditions, determined from polyacrylamide native protein slab gel electrophoresis. (A) indium; (B) yttrium; (C) copper. Lines are least-squares fits.

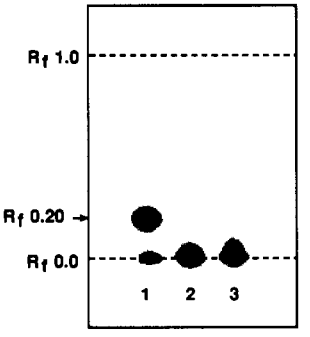


Figure 2. AMBIS scan profile of a TLC plate of *in vitro* enzyme digestions of ^{114m}In-labeled Lym-1 conjugate **9** with cathepsins at 165-h incubation time: small molecules, R_f 0.20; protein, R_f 0.0; lane 1, cathepsin B solution; lane 2, cathepsin D solution; lane 3, control solution (same conditions, no enzymes added).

from unsubstituted ^{114m}In–DOTA (t_R 8.0 min). Since no peaks could be found by the UV detector (Figure 4A), the cleaved product did not contain an aromatic group.

In order to identify the cleavage products, a parallel experiment was performed. Under the same experimental conditions, ^{114m}In-labeled DOTA–Gly_3-L-(*p*-NO_2)Phe-NH_2 was mixed with a cathepsin B solution. After a 70-h incubation at room temperature, an aliquot of the mixture was analyzed by HPLC. The HPLC profiles recorded by the radioisotope and the UV detectors are shown in Figure

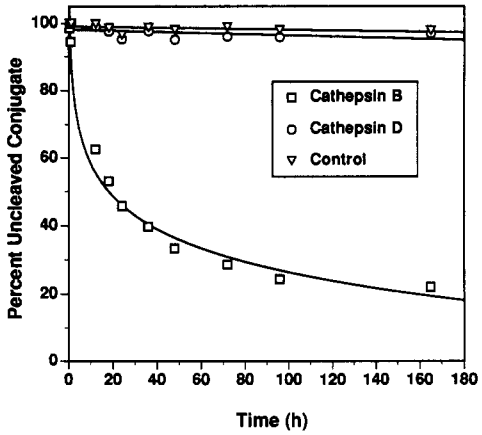


Figure 3. Percentage of uncleaved conjugate as a function of time of *in vitro* enzyme digestions of ^{114m}In-labeled Lym-1 conjugate **9** with cathepsins.

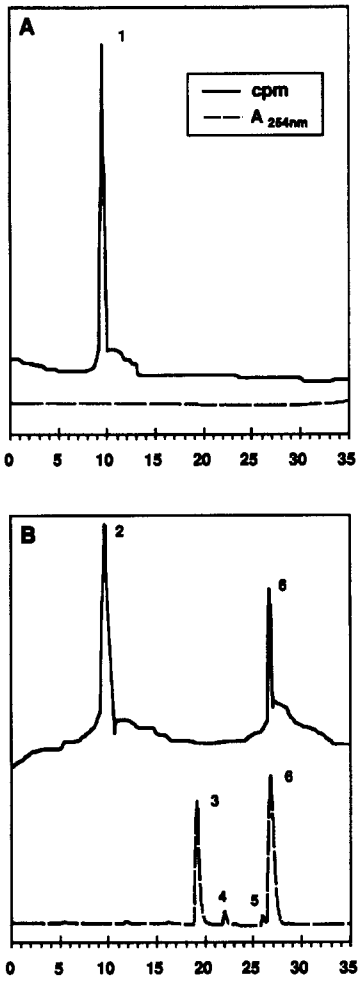


Figure 4. Radio- and UV-HPLC profiles of cathepsin B digestions of (**A**) ^{114m}In-labeled Lym-1 conjugate **9** after a 165-h incubation and (**B**) ^{114m}In-labeled DOTA-Gly$_3$-L-*p*-NO_3Phe-NH_2 after a 70-h incubation. Peaks 1–3 are cleaved products; peak 6 is the starting material; the small peaks 4 and 5 are unidentified.

4B. The peak of the peptide cleavage product with ^{114m}In observed at t_R 9.5 min (peak 2) by the radioisotope detector had the same retention time as the ^{114m}In complex cleaved from ^{114m}In-labeled conjugate **9** (peak 1, Figure 4A). Another cleavage product from the peptide digest was found by the UV detector at t_R 19 min (peak 3). This product had the same retention time as L-(*p*-NO_2)Phe-NH_2. The peptide cleavage product was further identified by the mass spectrum. DOTA-Gly$_3$-L-(*p*-NO_2)Phe-NH_2 was labeled with ^{115}In and then incubated with cathepsin B over 5 days. The eluent at t_R 7.5–11.5 was collected and characterized by mass spectrometry as ^{115}In–DOTA–glycylglycylglycine + H^+ (m/e = 688). Other species, such as ^{115}In–DOTA–glycylglycine + H^+ (m/e = 631), ^{115}In–DOTA–glycine + H^+ (m/e = 574), or ^{115}In–DOTA + H^+ (m/e = 517), were not found in the mass spectrum.

DISCUSSION

Since DOTA has a remarkable stability with many useful radionuclides, DOTA derivatives have been extensively investigated in recent years. Several C-functional and N-functional derivatives have been reported (*9*, *10*, *15*, *16*). However, multiple synthetic steps are usually involved. For example, a minimum of 10 steps is required to synthesize 2-(*p*-nitrobenzyl)DOTA (*9*, *38*). Direct attachment of a functional moiety, which can be attached to proteins, to a carboxyl group of DOTA via an amide bond (amide attachment) is a simple alternative. In addition, DOTA is commercially available or can be synthesized easily from the macrocyclic amine cyclen (*39*). The mixed anhydride method is well-known for coupling an amine to a carboxyl group (*40*). By using this attachment method, any desirable functional side chain with an amino group (or other suitable nucleophile) can be attached to DOTA or the other poly(amino carboxylates). This provides a novel option to make linkers of different types and sizes between the chelate and the protein without complicated syntheses.

The direct attachment of DOTA to lysine side chains by acylation of ε-amino groups has been investigated by Sieving *et al.* (*41*). Wu *et al.* (*42*) also used the same method to link DOTA to biotin. We chose a simple system to study the effects of adding a linker between DOTA and antibody. The easily synthesized tetrapeptide Gly$_3$-L-(*p*-NO_2)Phe-NH_2 was used as a functional arm. This new BCA, **5**, serves as a model of amide-attached DOTA derivatives with a cleavable linker. *In vitro* kinetic stability studies and digestions with liver enzymes were used to characterize its metal-binding stability and susceptibility to protease cleavage.

The kinetic stability of its metal complexes, a key property of a BCA, depends strongly on the structure of the chelator (*43*). When a DOTA carboxyl group is converted to an amide, a weaker metal coordinating group results. According to the crystal structure of Cu–DOTA (*44*), two carboxyl groups and four tertiary amino nitrogens of DOTA coordinate to Cu^{II}. Thus the conversion of one of the four carboxyl groups to an amide group might not influence the stability of Cu^{II}–DOTA.

For In^{III}, higher coordination numbers (>6) have been reported (*45*), including a coordination number of 8 in In–DTPA crystals (*46*). Since the crystal structure of In–DOTA has not been determined, the fourth carboxyl group may or may not coordinate to In^{III}. However, Riesen *et al.* (*45*) have reported that the fourth carboxyl group of DOTA contributes little to the serum stability of In^{III}–DOTA. Therefore, chemical modifications on the fourth carboxyl group of In^{III}–DOTA may not change its kinetic stability.

Y^{III}–DOTA may lose some degree of stability by this modification due to the high coordination number of Y^{III}. By studying the related Gd(III)–DOTA–propylamide complexes, Sherry *et al.* (*47*) have found that the conversion of a carboxylic group into an amide does not result in an increase in the number of inner-sphere water

molecules. This suggests that the amide occupies a site in the Gd(III) coordination sphere and, although weakly bound, interacts well enough to preclude the entrance of additional water molecules into the inner coordination sphere. Aime *et al.* (*48*) also observed that the bond distances between carboxylate oxygen and carboxamide oxygen to Gd(III) are quite similar on the basis of the X-ray structure of a related Gd(III)–DOTA–monoamide complex. Because the properties of Y^{III} are similar to those of lanthanide(III) ions, it is reasonable to expect that Y^{III} and Gd(III) have similar strengths of interaction with amide. Thus, the influence on the stability of Y^{III}–DOTA due to introduction of an amide is expected to be limited.

The kinetic stability of metal chelates under physiological conditions can be estimated by study of their behavior in serum. In this study, metal chelates at extreme dilution (≤200 nM) are surrounding by metal-binding proteins, such as transferrin and albumin (*49*). If there are any metals lost from the chelator, they are not likely to return (*50,51*). The gel electrophoresis profiles obtained here show that the transcomplexation of ^{114m}In, ^{88}Y, or ^{67}Cu from the DOTA–peptide to transferrin or albumin can nearly be ignored. The very low rate constants for loss of ^{114m}In–, ^{88}Y–, and ^{67}Cu–DOTA–Gly_3-L-Phe–thiourea–Lym-1 listed in Table II suggest that amide-attached DOTA derivatives are comparable to the C-functional or N-functional derivatives (*9, 12, 14*) and therefore they are excellent prospects for *in vivo* use.

It also has been noted that carbon backbone-substituted EDTA or DTPA derivatives form In or Y-radiolabeled complexes or immunoconjugates which have higher serum stability than the N-attached (including amide-attached) derivatives such as the amides (*9, 52–54*). These results may be explained by the increase in steric rigidity which helps to keep the metal in the chelator (*55*). However, this may be less important for DOTA derivatives since DOTA itself possesses a sterically rigid structure (*44, 56*).

Using a cleavable linker between the chelating agent and the antibody is one approach to decrease the accumulation of radioactivity in the liver. Several different linkers have been investigated (*21–23*). The results of those experiments have shown that the liver clearance indeed depends upon the linkers, although the observed effects were relatively small. Little is known about the mechanism of the liver metabolism of radiolabeled antibodies; however, several trends have been found. In studying the metabolism of Lym-1–benzyl-EDTA–^{111}In, Deshpande *et al.* (*52*) have shown that the radioactivity excreted in the urine is still practically completely bound by the chelator. For the uptake and metabolism of ^{111}In-labeled mAb B6.2 (labeled using the cyclic DTPA anhydride method) by the rat liver, Jones *et al.* (*24*) found that ^{111}In seems to be trapped in the form of low molecular weight In complexes (<1000 Da). These complexes have been hypothesized to be unaltered In chelates with one or more amino acids attached, but no identification of the main products has been made.

In order to examine the features of the cleavable linker, *in vitro* digestions of ^{114m}In-labeled conjugate **9** with liver enzymes were performed. The cathepsins, acid proteases present within hepatic lysosomes (*57*) were chosen for *in vitro* digestions. Cathepsin B and cathepsin D, which are believed to be responsible for the greatest part of the protein turnover in the liver (*58*), were used as models of liver proteases. Both cathepsins are endopeptidases (*59*). However, cathepsin B also exhibits exopeptidase (carboxypeptidase) activity under certain conditions (*60*). In the enzyme digestions, the experimental conditions were designed to approximate the lysosomal environment found in the human liver (pH 4.8–5.0, thiols present, and activities of cathepsin B and cathepsin D 1.1–2.1 (*58*) and 0.18 units/mL (*36*)).

Figure 3 shows that cathepsin B efficiently cleaves the chelate from the protein, with an apparent half-life ($T_{1/2}$) of approximately 20 h. However, cathepsin D does not show any proteolytic activity to the conjugate over the span of 7 days. From both TLC and HPLC profiles (Figures 2 and 4A) of the cathepsin B digestion, a single cleaved product was observed. This cleaved product had the same HPLC retention time as the one cleaved from ^{114m}In–DOTA–Gly_3-L-(*p*-NO_2)Phe-NH_2 by cathepsin B (peak 1 and peak 2 in Figure 4). This suggests that both cleavage products are identical and that the cleaved product from the conjugate does not contain any fragments of the protein. According to the mass spectrum, the cleaved product is In–DOTA–glycylglycylglycine and the site of cleavage is between glycine and phenylalanine. Neither the di- nor the monoglycyl derivatives were observed.

Since the simple linker Gly-Gly-Gly-Phe used in this study is not an optimal substrate for the cathepsins, future studies will include both sequence-specific linkers that exhibit high cathepsin activity and *in vivo* biodistribution studies. The excellent metal-binding properties of amide-attached DOTA derivatives have shown that this new type of BCA may offer practical advantages over other DOTA derivatives.

Acknowledgment. We thank Douglas P. Greiner, David L. Kukis, and Anil K. Mishra, for their technical advice and helpful discussions, and Daniel Jones and Kei Miyano, for running the FAB-MS. This work was supported by Research Grant CA16861 from the National Cancer Institute, NIH.

LITERATURE CITED

(1) Meares, C. F. (1986) Chelating Agents for the Binding of Metal Ions to Antibodies. *Nucl. Med. Biol. 13*, 311–318.

(2) Otsuka, F. L., and Welch, M. J. (1987) Methods to Label Monoclonal Antibodies for Use in Tumor Imaging. *Nucl. Med. Biol. 14*, 243–249.

(3) Hnatowich, D. J. (1990) Antibody Radiolabeling, Problems and Promises. *Nucl. Med. Biol. 17*, 49–55.

(4) Liu, Y., and Wu, C. (1991) Radiolabeling of Monoclonal Antibodies with Metal Chelates. *Pure Appl. Chem. 63*, 427–463.

(5) Subramanian, R., and Meares, C. F. (1991) Bifunctional Chelating Agents for Radiometal-Labeled Monoclonal Antibodies. *Cancer Imaging with Radiolabeled Antibodies* (D. M. Goldenberg, Ed.) pp 183–199, Kluwer Academic Pubs., Boston.

(6) Wessels, B. W., and Rogus, R. D. (1984) Radionuclide Selection and Model Absorbed Dose Calculations for Radiolabeled Tumor Associated Antibodies. *Med. Phys. 11*, 638–645.

(7) Klein, J. L., Leichner, P. L., Callahan, K. M., Kopher, K. A., and Order, S. E. (1988) Effects of Anti-antibodies on Radiolabeled Antibody Therapy. *Antibody, Immunoconjugates Radiopharm. 1*, 55–64.

(8) Moi, M. K., Meares, C. F., McCall M. J., Cole, W. C., and DeNardo, S. J. (1985) Copper Chelates as Probes of Biological Systems: Stable Copper Complexes with a Macrocyclic Bifunctional Chelating Agent. *Anal. Biochem. 148*, 249–253.

(9) Moi, M. K., Meares, C. F., and DeNardo, S. J. (1988) The Peptide Way to Macrocyclic Bifunctional Chelating Agents: Synthesis of 2-(*p*-Nitrobenzyl)-1,4,7,10-tetraazacyclododecane-*N*,*N*′,*N*″,*N*‴-tetraacetic Acid and Study of Its Yttrium(III) Complex. *J. Am. Chem. Soc. 110*, 6266–6267.

(10) Cox, J. P. L., Craig, Andrew S., Helps, L. M., Jandowski, K. J., Parker, D., Eaton, M. A. W., Millican, A. T., Millar, K., Beeley, N. R. A., and Boyce, B. A. (1990) Synthesis of C-and

N-Functionalised Derivatives of 1,4,7-Triazacyclononane-1,4,7-triyltriacetic acid (NOTA), 1,4,7,10-Tetra-azacyclododecane-1,4,7,10-tetrayltetra-acetic Acid (DOTA), and Diethylenetriaminepenta-acetic Acid (DTPA): Bifunctional Complexing Agents for the Derivatisation of Antibodies. *J. Chem. Soc. Perkin Trans. 1* 2567–2576.

(11) Parker, D (1990) Tumer Targeting with Radiolabeled Macrocycle-Antibody Conjugates. *Chem. Soc. Rev. 19*, 271–291.

(12) Meares, C. F., Moi. M. K., Diril, H., Kukis, D. L., McCall, M. J., Deshpande, S. V., DeNarso, S. J., Snook, D., and Epenetos, A. A. (1990) Macrocyclic Chelates of Radiometals for Diagnosis and Therapy. *Br. J. Cancer, Suppl. 10*, 21–26.

(13) Gansow, O. A. (1991) Newer Approaches to the Radiolabeling of Monoclonal Antibodies by Use of Metal Chelates. *Nucl. Med. Biol. 18*, 369–381.

(14) Deshpande, S. V., DeNardo, S. J., Kukis, D. L., Moi, M. K., McCall, M. J., DeNardo, G. L., and Meares, C. F. (1990) Yttrium-90-Labeled Monoclonal Antibody for Therapy: Labeling by a New Macrocyclic Bifunctional Chelating Agent. *J. Nucl. Med. 31*, 473–479.

(15) Kline, S. J., Betebenner, D. A., and Johnson, D. K. (1991) Carboxymethyl-Substituted Bifunctional Chelators: Preparation of Aryl Isothiocyanate Derivatives of 3-(Carbozymethyl-3-azapentanedioic Acid, 3, 12-Bis(carbozymethyl-6,9-dioxa-3,12-diazatetradecanedioic Acid, and 1,4,7,10-Tetraazacyclododecane-*N*,*N*′,*N*″,*N*‴-Tetraacetic Acid for Use as Protein Labels. *Bioconjugate Chem. 2*, 26–31.

(16) McMurry, T. J., Brechbiel, M., Kumar, K., and Gansow, O. A. (1992) Convenient Synthesis of Bifunctional Tetraaza Macrocycles. *Bioconjugate Chem. 3*, 108–117.

(17) Halpern, S. E., Hagan, P. L., Garver, P. R., Kozol, J. A., Chen, A. W. N., Frincke, J. M., Bartholomew, R. M., David, G. S., and Adams, T. H. (1983) Stability, Characterization, and Kinetics of ^{111}In Labeled Monoclonal Antitumor Antibodies in Normal Animals and Nude-mouse Human Tumor Models. *Cancer Res. 43*, 5347–5355.

(18) Pimm, M. V., Perkins, A. C., and Baldwin, R. W. (1985) Differences in Tumor and Normal Tissue Concentrations of Iodine and Indium Labeled Monoclonal Antibody. II. Biodistribution studies in Mice with Human Tumor Xenografts. *Eur. J. Nucl. Med. 11*, 300–304.

(19) Larson, S. M., and Carrasquillo, J. A. (1988) Advantages of Radioiodine over Radioindium Labeled Monoclonal Antibodies for Imaging Solid Tumors. *Nucl. Med. Biol. 15*, 231–233.

(20) DeNardo, S. J., DeNardo, G. L., Deshpande, S. V., Adams, G. P., Macey, D. J., Mills, S. L., Epstein, A. L., and Meares, C. F. (1988) The Design of a Radiolabeled Monoclonal Antibody for Radioimmunodiagnosis and Radioimmunotherapy. *Radiolabeled Monoclonal Antibodies for Imaging and Therapy-Potential, Problems and Prospects* (S. C. Srivastava, Ed.) pp 111–121, Plenum, New York.

(21) Haseman, M. K., Goodwin, D. A., Meares, C. F., Kaminski, M. S., Wensel, T. G., McCall, M. J., and Levy, R. (1986) Metabolizable ^{111}In-chelate Conjugated Anti-idiotype Monoclonal Antibody for Radioimmunodetection of Lymphoma in Mice. *Eur. J. Nucl. Med. 12*, 455–460.

(22) Paik, C. H., Quadri, S. M., and Reba, R. C. (1989) Interposition of Different Chemical Linkages between Antibody and ^{111}In-DTPA to Accelerate Clearance from Non-target Organs and Blood. *Nucl. Med. Biol. 16*, 475–481.

(23) Deshpande, S. V., DeNardo, S. J., Meares, C. F., McCall, M. J., Adams, G. P., and DeNardo, G. L. (1989) Effect of Different Linkage Between Chelates and Monoclonal Antibodies on Levels of Radioactivity in the Liver. *Nucl. Med. Biol. 16*, 587–597.

(24) Jones, P. L., Brown, B. A., and Sands, H. (1990) Uptake and Metabolism of ^{111}In-labeled Monoclonal Antibody B6.2 by the Rat Liver. *Cancer Res. Suppl. 50*, 825s–856s.

(25) Meares, C. F., McCall, M. J., Reardan, D. T., Goodwin, D. A., Diamanti, C. I., and McTigue, M. (1984) Conjugation of Antibodies with Bifunctional Chelating Agents: Isothiocyanate and Bromoacetamide Reagents, Methods of Analysis, and Subsequent Addition of Metal Ions. *Anal. Biochem. 142*, 68–78.

(26) Epstein, A. L., Zimmer, A. M., and Spies, S. M. (1985) Radioimmunodetection of Human B-cell Lymphomas with a Radiolabeled Tumor specific Monoclonal Antibody (Lym-1). *Malignant Lymphomas and Hodgkin's Disease: Experimental and Therapeutic Advance* (F. Cavalli,G. Bonadonna, and M. Rozencweig, Eds.) pp 569–577, Martinus Nijhoff Publishing Co., Boston.

(27) Thiers, R. C. (1957) Contamination in Trace Element Analysis and Its Control. *Methods Biochem. Anal. 5*, 273–335.

(28) Harlow, E., and Lane, D. (1988) *Antibodies: A Laboratory Manual*, pp 673, Cold Spring Harbor Laboratory, Cold Spring Harbor, New York.

(29) Yeh, S. M., Sherman, D. G., and Meares, C. F. (1979) A New Route to "Bifunctional Chelating Agents". *Anal. Biochem. 100*, 68–78.

(30) Penefsky, H. S. (1979) A Centrifuged-Column Procedure for the Measurement of Ligand Binding by Beef Heart F_1. *Methods Enzymol. 56*, Part G, 527–530.

(31) Hnatowich, D. J., Layne, W. W., and Childs, R. L. (1982) The Preparation and Labeling of DTPA-Coupled Albumin. *Int. J. Appl. Radiat. Isot. 33*, 327–332.

(32) Deshpande, S. V., DeNardo, S. J., Meares, C. F., McCall, M. J., Adams, G. P., and DeNardo, G. L. (1988) Copper-67-Labeled Monoclonal Antibody Lym-1, A Potential Radiopharmaceutical for Cancer Therapy: Labeling and Biodistribution in RAJI Tumored Mice. *J. Nucl. Med. 29*, 217–225.

(33) DeNardo, S. J., Peng, J.-S., DeNardo, G. L., Mills, S. L., and Epstein, A. L. (1986) Immunochemical Aspects of Monoclonal Antibodies Important for Radiopharmaceutical Development. *Nucl. Med. Biol. 13*, 303–310.

(34) Davis B. J. (1964) Disc Electrophoresis II. Method and Application to Human Serum Proteins. *Ann. NY Acad. Sci. 121*, 404–427.

(35) Bajkowsky, A. S., and Frankfater, A. S. (1975) Specific Spectrophotometric Assay for Cathepsin B_1. *Anal. Biochem. 68*, 119–127.

(36) Barrett, A. J. (1970) Purification of Isoenzymes from Human and Chicken Liver. *Biochem. J. 117*, 601–607.

(37) Agarwal, N., and Rich, D. H. (1983) An Improved Cathepsin-D Substrate and Assay Procedure. *Anal. Biochem. 130*, 158–165.

(38) Renn, O., and Meares, C. F. (1992) Large Scale Synthesis of the Bifunctional Chelating Agent 2-*p*-Nitrobenzyl-1,4,7,10-tetraazacyclododecane-*N*,*N*′,*N*″,*N*‴-tetraacetic Acid and the Determination of Its Enantiomeric Purity by Chiral Chromatography. *Bioconjugate Chem. 3*, 563–569.

(39) Desreux, J. F. (1980) Nuclear Magnetic Resonance Spectroscopy of Lanthanide Complexes with a Tetraacetic Tetraaza Macrocycle. Unusual Conformation Properties. *Inorg. Chem. 19*, 1319–1324.

(40) Krejcarek, G. E., and Tucker, K. L. (1977) Covalent Attachment of Chelating Groups to Macromolecules. *Biochem. Biophys. Res. Commun. 77*, 581–585.

(41) Sieving, P. F., Watson, A. D., and Rocklage, S. M. (1990) Preparation and Characterization of Paramagnetic Polychelates and Their Protein Conjugates. *Bioconjugate Chem. 1*, 65–71.

(42) Wu, C., Virzi, F., and Hnatowich, D. J. (1992) Investigations of N-linked Macrocycles for ^{111}In and ^{90}Y Labeling of Proteins. *Int. Med. Biol. 19*, 239–244.

(43) Margerum, D. W., Cayley, G. R., Weatherburn, D. C., and Pagenkopf, G. K. (1978) Kinetics and Mechanisms of Complex Formation and Ligand Exchange. *Coordination Chemistry* (A. E. Martell, Ed.) Vol. 2, Chapter 1, ACS Monograph 174, American Chemical Society, Washington, DC.

(44) Riesen, A., Zehnder, M., and Kaden, T. A. (1986) Synthesis, Properties, and Structures of Mononuclear Complexes with 12- and 14-Membered Tetraazamacrocycle-*N*,*N*′,*N*″,*N*‴-tetraacetic Acids. *Helv. Chim. Acta 69*, 2067–2073.

(45) Riesen, A., Kaden, T. A., Ritter, W., and Mäcke, H. R. (1989) Synthesis and X-Ray structural Characterization of Seven Coordinate Macrocyclic In^{3+} Complexes with Relevance to Radiopharmaceutical Applications. *J. Chem. Soc., Chem. Commun.* 460–462.

(46) Mäcke, H. R., Riesen, A., and Ritter, W. (1989) The Molecular Structure of Indium-DTPA. *J. Nucl. Med. 30*, 1235–1239.

(47) Sherry, A. D., Brown, R. D., III, Geraldes, C. F. C., Koeng, S. H., and Kuan, K.-T. (1989) Synthesis and Characterization of the Gadolinium(3+) Complex of DOTA-Propylamide: A Model DOTA–protein Conjugate. *Inorg. Chem. 28*, 620–622.

(48) Aime, S., Anelli, P. L., Botta, M., Fedeli, F., Grandi, M., Paoli, P., and Uggeri, F. (1992) Synthesis, Characterization, and $1/T_1$ NMRD Profiles of Gadolinium(III) Complexes of Monoamide Derivatives of DOTA-like Ligands. X-ray Structure of the 10-[2-[[2-Hydroxy-1-(hydroxymethyl)ethyl]amino]-1-[(phenylmethoxy)methyl]-2-oxo-ethyl]-1,4,7,10-tetraazacyclododecane-1,4,7-triacetic Acid–Gadolinium(III) Complex. *Inorg. Chem. 31*, 2422–2428.

(49) Ritzmann, S. E., and Daniels, J. C. (1982) Serum electrophoresis and Total Serum Proteins. *Serum Protein Abnormalities: Diagnostic and Clinical Aspects* (S. E. Ritzmann, and J. C. Daniels, Eds.) pp 3–26, Alan R. Liss, New York.

(50) Hosain, F., McIntyre, P. A., Poulose, K., Stein, R. S., and Wagner, H. N., Jr. (1969) Binding of Trace Amounts of Ionic Indium-113m to Plasma Transferrin. *Clin. Chim. Acta 24*, 69–75.

(51) Sarkar, B., Laussac, J.-P., and Lau, S. (1983) Transport Forms of Copper in Human Serum. *Biological Aspects of Metals and Metal Telated Diseases* (B. Sarkar, Ed.) pp 23–40, Raven Press, New York.

(52) Deshpande, S. V., Subramanian, R., McCall, M. J., DeNardo, S. J., DeNardo, G. L., and Meares, C. F. (1990) Metabolism of Indium Chelates Attached to Monoclonal Antibody: Minimal Transchelation of Indium from Benzyl-EDTA Chelate In Vivo. *J Nucl. Med. 31*, 218–224.

(53) Cole, W. C., DeNardo, S. J., Meares, C. F., McCall, M. J., DeNardo, G. L., Epstein, A. L., O'Brien, H. A., and Moi, M. K. (1987) Comparative Serum Stability of Radiochelates for Antibody Radiopharmaceuticals. *J. Nucl. Med. 28*, 83–90.

(54) Washburn, L. C., Sun, T. T. H., Lee, Y-C. C., Byrd, B. L., Holloway, E. C., Crook, J. E., Stubbs, J. B., Stabin, M. G., Brechbiel, M. W., Gansow, O. A., and Steplewski, Z. (1991) Comparison of Five Bifunctional Chelate Techniques for ^{90}Y-Labeled Monoclonal Antibody CO17-1A. *Nucl. Med. Biol. 18*, 313–321.

(55) Yeh, S. M., Meares, C. F., and Goodwin, D. A. (1979) Decomposition Rates of Radiopharmaceutical Indium Chelates in Serum. *J. Radioanal. Chem. 53*, 327–336.

(56) Loncin, M. F., Desreux, J. F., and Merciny, D. (1985) Coordination of Lanthanides by Two Polyamino Polycarboxylic Macrocycles: Formation of Highly Stable Lanthanide Complexes. *Inorg. Chem. 25*, 2646–2648.

(57) Barrett, A. J. (1967) Lysosomal Acid Proteinase of Rabbit Liver. *Biochem. J. 104*, 601–608.

(58) Barrett, A. J., and Kirschke, H. (1981) Cathepsin B, Cathepsin H, Cathepsin L. *Methods Enzymol. 80*, 535–561.

(59) Taylor, S. L., and Tappel, A. L. (1974) Identification and Separation of Lysosomal Carboxypeptidases. *Biochim. Biophys. Acta 341*, 99–111.

(60) Koga, H., Yamada, H., Nishimura, Y., Kato, K., and Imoto, T. (1991) Multiple Proteolytic Action of Rat Liver Cathepsin B: Specificities and pH-Dependences of the Endo- and Exopeptidase Activities. *J. Biochem. 110*, 179–188.

A Fluorescent Probe and a Photoaffinity Labeling Reagent To Study the Binding Site of Maytansine and Rhizoxin on Tubulin

Takayuki Sawada,† Yuzo Kato,† Hisayoshi Kobayashi,† Yuichi Hashimoto,† Tohru Watanabe,‡ Yuichi Sugiyama,‡ and Shigeo Iwasaki*,†

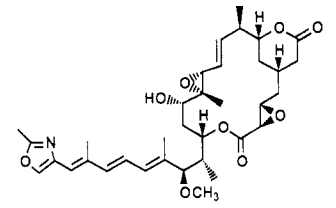
Institute of Molecular and Cellular Biosciences, The University of Tokyo, Bunkyo-ku, Yayoi 1-1-1, Tokyo 113, Japan, and Faculty of Pharmaceutical Sciences, The University of Tokyo, Bunkyo-ku, Hongo 7-3-1, Tokyo 113, Japan. Received February 26, 1993

A fluorescent probe (20-demethoxy-20-[3-[[[5-(dimethylamino)naphthalen-1-yl]sulfonyl]amino]propyl]maytansinol 3-isobutyrate, Dan-PDM-3) and a photoaffinity labeling reagent (20-demethoxy-20-[(*p*-azidobenzoyl)oxy]maytansinol 3-isobutyrate, DABMI) were prepared by derivatization of ansamitocin P-3 (ASMP-3), a maytansinoid. Dan-PDM-3 consists of a tethered dansyl moiety and a maytansinoid moiety. DABMI contains a *p*-azidobenzoyl group instead of the tethered dansyl moiety of Dan-PDM-3. These compounds were synthesized by reacting 20-demethoxy-20-hydroxymaytansinol-3 isobutyrate (PDM-3) with the corresponding alkyl halide or benzoic acid. Both inhibit tubulin polymerization as potently as ASMP-3 and compete with ASMP-3 for binding to tubulin. The inhibition constants (K_i) of DABMI for the binding to tubulin of rhizoxin and ASMP-3 were 0.54 and 0.36 μM, respectively, which were nearly equal to the dissociation constant (K_d = 0.43 μM) of DABMI measured by the use of [^{14}C]DABMI. The results suggest that Dan-PDM-3 and DABMI interacted with tubulin at the same site as rhizoxin and maytansine. DABMI is irreversibly bound to tubulin upon irradiation. Dan-PDM-3 and DABMI should be useful probes for studying the binding site.

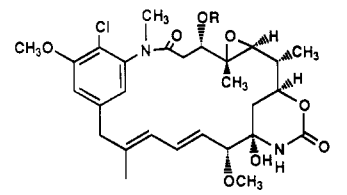
INTRODUCTION

Maytansine (MAY; Figure 1) is an antimitotic antitumor drug, which acts through binding to tubulin, an essential protein at mitosis (*1*). Tubulin consists of alternating globular subunits of α- and β-tubulin, which have similar molecular weights of about 50 000, similar amino acid composition, and similar overall molecular shapes. Most antimitotic drugs, including maytansine, colchicine (CLC), benzimidazole, vinblastine (VLB), and rhizoxin (RZX), inhibit tubulin polymerization by binding to tubulin, but the mechanism of action and the location of the binding sites on the three-dimensional structure of tubulin are obscure.

It had been claimed that tubulin has two distinct drug-binding sites, the CLC site and the VLB/MAY site (*2*). Our previous study revealed that RZX binds in a competitive manner with MAY, while the binding of VLB only partially competes with that of RZX. This result suggests that the VLB/MAY site might be differentiated into two sites: a VLB site to which VLB binds and an RZX/MAY site to which RZX and MAY bind (*3*). Another drug, phomopsin-A, was recently found to bind at the RZX/MAY site on porcine brain tubulin (*4*). Elucidation of the nature of the RZX/MAY site has, therefore, become important for the design of new antimitotic drugs.



Rhizoxin



Maytansin: R=COCH(CH$_3$)N(CH$_3$)COCH$_3$

Ansamitocin P-3: R=COCH(CH$_3$)$_2$

Figure 1. Structures of rhizoxin and maytansinoids (maytansine and ansamitocin P-3).

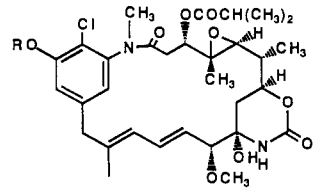
We previously showed that RZX binding to tubulin is determined by the nature of the 100th amino acid residue of β-tubulin. In the rhizoxin-resistant mutant of *Aspergillus nidulans*, the AAC codon for Asn-100 of the wild type (rhizoxin sensitive) β-tubulin gene was altered to ATC, coding for Ile (*5*). *Schizosaccharomyces pombe* and *Saccahromyces cerevisiae* are naturally resistant to rhizoxin, and the 100th amino acid residue of their tubulin is Ile or Val, respectively. The point mutation of Ile-100 of *S. pombe* and the Val-100 of *S. cerevisiae* to Asn resulted in mutants sensitive to rhizoxin (*6*).

Fluorescent and photoaffinity probes are useful for studying the binding sites of drugs (*7*, *8*). We recently

* Author to whom correspondence should be addressed.
† Institute of Molecular and Cellular Biosciences.
‡ Faculty of Pharmaceutical Science.

[1] Abbreviations used: Dan-PDM-3, 20-demethoxy-20-[3-[[[5-(dimethylamino)naphthalen-1-yl]sulfonyl]amino]propyl]maytansinol 3-isobutyrate; DABMI, 20-demethoxy-20-[(*p*-azidobenzoyl)oxy]maytansinol 3-isobutyrate; ASMP-3, ansamitocin P-3; K_i, inhibition constant; K_d, dissociation constant; MAY, maytansine; CLC, colchicine; VLB, vinblastine; RZX, rhizoxin; PDM-3, 20-demethoxy-20-hydroxymaytansinol 3-isobutyrate; DMAP, (dimethylamino)pyridine; FTNB, 1-fluoro-2,4,6-trinitrobenzene; MES, 4-morpholineethanesulfonic acid; EGTA, 1,2-bis(2-aminoethoxy)ethane-*N,N,N',N'*-tetraacetic acid; SDS, sodium dodecyl sulfate.

1043-1802/93/2904-0284$04.00/0 © 1993 American Chemical Society



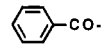
R=

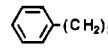
1 (PDM-3): H-

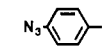
2 : CH_3CO-

3 : $CH_3(CH_2)_2CO$-

4 : $CH_3(CH_2)_6CO$-

5 : 

6 : 

7 (DABMI): 

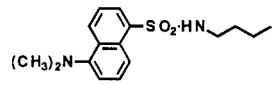
8 (Dan-PDM-3): 

Figure 2. Structures of C(20) derivatives of ansamitocin P-3.

reported that Dan-RZX and Adan-RZX, derivatives of rhizoxin, are useful fluorescent and photoaffinity probes for studying the RZX/MAY site (*9*). UV irradiation led to the irreversible binding of Adan-RZX to tubulin at the RZX/MAY site, and the location of this irreversibly labeled site was identified as Met-363–Lys-379 on β-tubulin (*10*).

In this paper we describe (i) the design, by the derivatization of 20-demethoxy-20-hydroxymaytansinol 3-isobutyrate (PDM-3), of two other fluorescent and photoaffinity probes, Dan-PDM-3 and DABMI (maytansine analog; Figure 2), based on the observed biological activities of a series of C(20) acylated derivatives of PDM-3, and (ii) their application for the further study of the RZX/MAY site.

EXPERIMENTAL PROCEDURES

General. The derivatives **2**–**7** were homogeneous by both TLC and HPLC; the derivative **8** was homogeneous by TLC. The ^{14}C-labeled compounds were homogeneous by HPLC. IR spectra were measured on a Japan Spectroscopic Apparatus (Model A-102) and recorded in cm^{-1}. Mass spectra were measured on JEOL JMS-HX110 and recorded in *m/z*. ^1H NMR were measured on JEOL GX-400 (400 MHz) and GX-500 (500 MHz) instruments; chemical shifts are given in ppm (in δ) relative to TMS as an internal standard; s = singlet, d = doublet, dd = double doublet, t = triplet, m = multiplet; coupling constants are given in hertz. HPLC was performed on a Shimadzu apparatus (Model LC-7A), with an ODS column unless otherwise stated. Fluorescence intensity was measured with a spectrofluorometer (812-FP, Japan Spectroscopic Co. Ltd.).

Chemicals. Ansamitocin P-3 and PDM-3 were generous gifts from Takeda Chemical Industry. [*carbonyl*-^{14}C]-*p*-Aminobenzoic acid (specific activity 20 mCi/mmol) and [^{14}C]methyl iodide (specific activity 30 mCi/mmol) were purchased from Amersham.

Strains. *S. pombe* strain JY266 (h^-, leu1) was kind gift from Dr. M. Yamamoto (University of Tokyo). *S. pombe* transformant strain 266-107 was described previously (*6*).

Determination of Drug Sensitivity. The drug sensitivity of *S. pombe* was determined in YPD (1% yeast extract, 2% bacto-peptone, 2% glucose, and 1.5% agar) containing different concentrations of DABMI.

Synthesis of 20-Demethoxy-20-[3-[[[5-(dimethylamino)naphthalen-1-yl]sulfonyl]amino]propyl]maytansinol 3-Isobutyrate (Dan-PDM-3) (8). Triethylamine (140 μL; 1.0 mmol) was added to a mixture of 5-(dimethylamino)naphthalene-1-sulfonyl chloride (100 mg; 0.42 mmol) and 3-bromo-1-propylamine hydrobromide (101 mg; 0.46 mmol) in $CHCl_3$ (1 mL) at room temperature. After evaporation, the residue was redissolved in ethyl acetate (50 mL), then the solution was washed with 2 N $NaHCO_3$ (50 mL) and brine (100 mL). The organic layer was evaporated to give the corresponding alkyl halide (141 mg; 0.38 mmol; 90.3% yield). This product (60 mg; 0.162 mmol) was dissolved in acetonitrile (1 mL) and added to a solution of PDM-3 (90 mg; 0.144 mmol) in acetonitrile (9 mL) containing KF–Al_2O_3 (240 mg; 1.65 mmol) (*11*). The mixture was stirred for 4 days at room temperature, then ethyl acetate was added, and the solution was filtered to remove Al_2O_3. The filtrate was washed with water, and the organic layer was evaporated. The residue was subjected to preparative thin-layer chromatography (benzene–acetone = 1:1) to give Dan-PDM-3 (50 mg; 0.055 mmol; 55.9% yield) with recovery of PDM-3 (29 mg; 0.047 mmol). FAB MS: *m/z* 911 $(M + H)^+$, 933 $(M + Na)^+$. high-resolution FAB MS: calcd for $C_{46}H_{60}O_{11}N_4ClS$, *m/z* 911.3668, found 911.3620. ^1H NMR ($CDCl_3$): 0.82 (3H, s, 4-CH_3), 1.20 (3H, d, J = 6.7, 6-CH_3), 1.25–1.30 (6H, m, $OCOCH(CH_3)_2$), 1.40–1.60 (3H, m, 6 and 8-H), 1.68 (3H, s, 14-CH_3), 2.04 (2H, m, 23-H), 2.20 (1H, dd, J = 3.5 and 14, 2-H), 2.58 (2H, m, 2-H and $OCOCH(CH_3)_2$), 2.88 (6H, s, $N(CH_3)_2$), 2.94 (1H, d, J = 5, 5-H), 3.16 (3H, s, NCH_3), 3.20 (4H, m, 24 and 15-H), 3.35 (3H, s, OCH_3), 3.48 (1H, d, J = 4, 10-H), 3.52 (1H, s, OH), 4.16 (2H, m, 22-H), 4.26 (1H, m, 7-H), 4.80 (1H, dd, J = 3 and 12, 3-H), 5.26 (1H, t, J = 6, -$NHSO_2$-), 5.46 (1H, dd, J = 9 and 15, 11-H), 6.15 (1H, d, J = 11, 13-H), 6.25 (1H, s, –NH–), 6.44 (1H, dd, J = 11 and 15.5, 12-H), 6.77 (1H, d, J = 1.5, 17-H), 6.89 (1H, d, J = 1.5, 21-H), 7.18 (1H, d, J = 7.5, 2′-, 4′-, 6′- or 8′-H), 7.51 (2H, m, 3′- and 7′-H), 8.25 (1H, d, J = 8, 2′-, 4′-, 6′- or 8′-H), 8.3 (1H, d, J = 9, 2′-, 4′-, 6′- or 8′-H), 8.55 (1H, d, J = 8, 2′-, 4′-, 6′- or 8′-H).

Acylation of 20-Demethoxy-20-hydroxymaytansinol 3-Isobutyrate (PDM-3). (1) 20-Demethoxy-20-acetoxymaytansinol 3-Isobutyrate (2). A solution of 1-fluoro-2,4,6-trinitrobenzene (FTNB) (12 mg; 0.05 mmol) and acetic acid (3 mg; 0.05 mmol) in acetonitrile (1 mL) was added to a solution of PDM-3 (10 mg; 0.016 mmol) in acetonitrile (1 mL) containing 4-(dimethylamino)pyridine (DMAP) (10 mg; 0.083 mmol) (*12*). The whole was stirred for 30 min at room temperature. After evaporation of the solvent, the product was purified by PTLC developed with $CHCl_3$–CH_3OH (10:1) to give 9.6 mg of **2** (90% yield) as a colorless powder: $C_{33}H_{43}N_2O_{10}Cl$. FAB MS: *m/z* 663 $(M + H)^+$. IR (KBr): 3450, 1750, 1740, 1715, 1670. ^1H NMR ($CDCl_3$): 0.81 (3H, s, 4a-H), 0.85–1.55 (6H, m), 1.21 (3H, d, J = 7, $COCH(CH_3)_2$), 1.27 (3H, d, J = 7, $COCH(CH_3)_2$), 1.69 (3H, s, 14a-H), 2.20–2.65 (3H, m), 2.39 (3H, s, $COCH_3$), 2.94 (1H, d, J = 9.5, 5-H), 3.00–3.55 (4H, m), 3.18 (3H, s, OCH_3), 3.35 (3H, s, NCH_3), 4.27 (1H, dd, J = 3.0 and 11.0, 7-H), 4.80 (1H, dd, J = 3.0 and 11.0, 3-H), 5.48 (1H, dd, J = 10.0 and 15.0, 11-H), 6.15 (1H, d, J = 11.0, 13-H), 6.18 (1H, s, –NH–), 6.43 (1H, dd, J = 11.0 and 15.0, 12-H), 7.11 (1H, d, J = 2.0, 17-H), 7.16 (1H, d, J = 2.0, 21-H).

The other acyl derivatives, **3**–**7**, were similarly prepared with the corresponding carboxylic acids in more than 90% yield and purified by TLC to yield powders.

(2) 20-Demethoxy-20-butyroxymaytansinol 3-isobutyrate (3): $C_{35}H_{47}N_2O_{10}Cl$. FAB MS: *m/z* 691 $(M + H)^+$. IR (KBr): 3450, 1770, 1745, 1725, 1675. ^1H NMR ($CDCl_3$): 0.81 (3H, s, 4a-H), 0.87–1.90 (10H, m), 1.09 (3H, t, J = 7.0, $CO(CH_2)_2CH_3$), 1.20 (3H, d, J = 7.0, $COCH(CH_3)_2$), 1.29 (3H, d, J = 7.0, $COCH(CH_3)_2$), 1.70 (3H, s, 14a-H), 2.20–2.60 (3H, m), 2.64 (2H, t, J = 6.0, $COCH_2CH_2CH_3$), 2.95 (1H, d, J = 9.5, 5-H), 3.00–3.50 (4H, m), 3.18 (3H, s, OCH_3), 3.35 (3H, s, NCH_3), 4.26 (1H, dd, J = 11.0 and 11.0, 7-H), 4.79 (1H, dd, J = 3.0 and 11.0, 3-H), 5.46 (1H, dd, J = 10.0 and 15.0, 11-H), 6.15 (1H, d, J = 11.0, 13-H), 6.19 (1H, s, NH), 6.44 (1H, dd, J = 11.0 and 15.0, 12-H), 7.10 (1H, d, J = 2.0, 17-H), 7.15 (1H, d, J = 2.0, 21-H).

(3) 20-Demethoxy-20-(octanoyloxy)maytansinol 3-isobutyrate (4): $C_{39}H_{55}N_2O_{10}Cl$. FAB MS: *m/z* 747 $(M + H)^+$. IR (KBr): 3450, 1775, 1750, 1725, 1670. ^1H NMR ($CDCl_3$): 0.81 (3H, s, 4a-H), 0.85–1.80 (16H, m), 0.90 (3H, t, J = 6.0, $CO(CH_2)_6CH_3$), 1.20 (3H, d, J = 7.0, $-COCH(CH_3)_2$), 1.28 (3H, t, J = 7.0, $COCH(CH_3)_2$), 1.68 (3H, s, 14a-H), 2.20–2.60 (3H, m), 2.65 (2H, t, J = 7.0, $COCH_2(CH_2)_5CH_3$), 2.94 (1H, d, J = 9.5, 5-H), 3.00–3.50 (4H, m), 3.18 (3H, s, OCH_3), 3.35 (3H, s, NCH_3), 4.27 (1H, dd, J = 3.0 and 11.0, 7-H), 4.80 (1H, dd, J = 3.0 and 11.0, 3-H), 5.46 (1H, dd, J = 10.0 and 15.0, 11-H), 6.16 (1H, d, J = 11.0, 13-H), 6.19 (1H, s, –NH–), 6.43 (1H, dd, J = 11.0 and 15.0, 12-H), 7.09 (1H, d, J = 2.0, 17-H), 7.15 (1H, d, J = 2.0, 21-H).

(4) 20-Demethoxy-20-(benzoyloxy)maytansinol 3-isobutyrate (5): $C_{38}H_{45}N_2O_{10}Cl$. FAB MS: *m/z* 725 $(M + H)^+$. IR (KBr): 3450, 1745, 1725, 1670. ^1H NMR ($CDCl_3$): 0.85 (3H, s, 4a-H), 0.87–1.65 (6H, m), 1.21 (3H, d, J = 7, $COCH(CH_3)_2$), 1.29 (3H, d, J = 7, $COCH(CH_3)_2$), 1.71 (3H, s, 14a-H), 2.25–2.70 (3H, m), 2.95 (1H, d, J = 9.5, 5-H), 3.00–3.50 (4H, m), 3.20 (3H, s, OCH_3), 3.36 (3H, s, NCH_3), 4.27 (1H, dd, J = 3.0 and 11.0, 7-H), 4.82 (1H, dd, J = 3.0 and 11.0, 3-H), 5.48 (1H, dd, J = 10.0 and 15.0, 12-H), 7.21 (1H, d, J = 2.0, 17-H), 7.29 (1H, d, J = 2.0, 21-H), 7.57 (2H, m, Ph), 7.71 (1H, m, Ph), 8.25 (2H, d, J = 6.0, Ph).

(5) 20-Demethoxy-20-[(3-phenylpropionyl)oxy]maytansinol 3-isobutyrate (6): $C_{40}H_{49}N_2O_{10}Cl$. FAB MS: *m/z* 753 $(M + H)^+$. IR (KBr): 3440, 1770, 1745, 1725, 1670. ^1H NMR ($CDCl_3$): 0.80 (3H, s, 4a-H), 0.85–1.65 (6H, m), 1.20 (3H, d, J = 7.0, $COCH(CH_3)_2$), 1.28 (3H, d, J = 7.0, $COCH(CH_3)_2$), 1.66 (3H, s, 14a-H), 2.20–2.65 (3H, m), 2.94 (1H, d, J = 9.5, 5-H), 2.96–3.40 (4H, m), 2.98 (2H, t, J = 10.0, CH_2CH_2Ph), 3.14 (2H, t, J = 10.0, CH_2CH_2Ph), 3.16 (3H, s, OCH_3), 3.35 (3H, s, NCH_3), 4.27 (1H, dd, J = 3.0 and 11.0, 7-H), 4.78 (1H, dd, J = 3.0 and 11.0, 3-H), 5.45 (1H, dd, J = 10.0 and 15.0, 11-H), 6.15 (1H, d, J = 11.0, 13-H), 6.20 (1H, s, NH), 6.43 (1H, dd, J = 11.0 and 15.0, 12-H), 6.99 (1H, d, J = 2, 17-H), 7.14 (1H, d, J = 2, 21-H), 7.30 (5H, m, Ph).

(6) 20-Demethoxy-20-[(*p*-azidobenzoyl)oxy]maytansinol 3-isobutyrate (DABMI) (7): $C_{38}H_{44}N_5O_{10}Cl$. High-resolution FAB MS: calcd for $C_{38}H_{45}N_5O_{10}Cl$, *m/z* 766.2856, found 766.2899. IR (KBr): 3450, 2140, 1745, 1710, 1675. ^1H NMR ($CDCl_3$): 0.84 (3H, s, 4a-H), 0.85–1.55 (6H, m), 1.22 (3H, d, J = 7, $COCH(CH_3)_2$), 1.71 (3H, s, 14a-H), 2.25–2.65 (3H, m), 2.95 (1H, d, J = 9.5, 5-H), 3.10–3.55 (4H, m), 3.20 (3H, s, OCH_3), 3.36 (3H, s, NCH_3), 4.28 (1H, dd, J = 3.0 and 11.0, 7-H), 4.83 (1H, dd, J = 3.0 and 11.0, 3-H), 5.45 (1H, dd, J = 10.0 and 15.0, 11-H), 6.18 (1H, d, J = 11.0, 13-H), 6.21 (1H, s, NH), 6.48 (1H, dd, 12-H), 7.18 (2H, d, J = 9.0, Ph), 7.21 (1H, d, J = 2.0, 17-H), 7.26 (1H, d, J = 2.0, 21-H), 8.23 (2H, d, J = 9.0, Ph).

Preparation of [^{14}C]DABMI. Concentrated HCl (50 μL) was added through a syringe to a suspension of [^{14}C]-*p*-aminobenzoic acid (50 μCi) in water (100 μL) at 0 °C in a microtube sealed with a Teflon cap, and the whole was stirred for 10 min. To the mixture was added aqueous sodium nitrite (500 μg in 50 μL) and, after 10 min of stirring, aqueous sodium azide (500 μg in 50 μL) (*13*). The reaction mixture was further stirred for 20 min at 0 °C and then extracted with ethyl acetate. The separated organic layer was evaporated to dryness. To the residue dissolved in acetonitrile (100 μL) was added FTNB (1 mg; 4.3 μmol) and a solution of PDM-3 (3 mg; 4.8 μmol) and DMAP (1 mg; 8.2 μmol) in acetonitrile (100 μL) (*12*). The whole was stirred for 3 h at room temperature. After evaporation of the solvent, the resulting mixture was separated by TLC to give a crude product, which was further purified by HPLC on a Senshu-Pak ODS-H-2151 column eluted with acetonitrile–water (65:35) to give 240 μg of [^{14}C]DABMI (specific activity 17 mCi/mmol).

Preparation of [^{14}C]Ansamitocin P-3. A solution of PDM-3 (3 mg; 4.8 μmol) and KF-Al_2O_3 (2 mg; 12.5 μmol) in acetonitrile (500 μL) was placed in a microtube sealed with a Teflon cap, and [^{14}C]CH_3I (100 μCi) in acetonitrile (500 μL) was added through a syringe (*11*). The mixture was stirred for 20 h at room temperature and then filtered to remove insoluble materials. The residue after evaporation of the filtrate was separated by PTLC developed with acetonitrile–methanol (10:1) to give a crude product which was further purified by HPLC on a Senshu-Pak ODS-H-2151 column eluted with acetonitrile–water (45:51) to give 375 μg of [^{14}C]ansamitocin P-3 (specific activity; 15 mCi/mmol).

Purification of Microtubule Protein and Polymerization Assay. Microtubule protein was prepared from porcine brain tubulin as described previously (*14*). Polymerization of tubulin was followed by turbidity measurement at 37 °C in MES buffer solution containing 2 mg of protein/mL of solution. The turbidity was measured at 400 nm on a Shimadzu UV-300 photospectrometer. The compounds tested were added as DMSO solutions. The experiments for determining IC_{50} values (Table I) were reproducible with error of less than 20% of the value. The values from one typical set of the experiments were shown in Table I.

Purification of Tubulin. Tubulin was purified from microtubule proteins by phosphocellulose chromatography (*15*). Its purity was assayed by polyacrylamide gel electrophoresis (*16*).

Binding of Dan-PDM-3 to Tubulin. The amounts of Dan-PDM-3 bound to tubulin were measured by a gel filtration method using a Sephadex G25 column (*9*). The tubulin preparation [0.2 mg/0.25 mL MES buffer (100 mM MES–1 mM EGTA–0.5 mM $MgSO_4$–1 mM GTP–1 mM 2-mercaptoethanol)] was incubated at 37 °C for 1 h in the presence of various concentrations of test compound(s). The mixture was subjected to Sephadex G25 gel column chromatography (bed volume 1.0 mL), and eluted with MES buffer. The first 0.45 mL of eluate was discarded, and the next 0.4 mL was collected for measurement of its fluorescence intensity (excitation at 350 nm, emission at 520 nm). The experiments were reproducible with the errors of less than 15%. The results from one typical set of experiments were shown in Figure 3.

Binding of DABMI to Tubulin. The amounts of drugs bound to tubulin were measured by the charcoal method (*17, 18*). The tubulin preparation (0.2 mL; 0.5 μM) was incubated at 30 °C for 15 min in the presence of various concentrations of drugs including ^{14}C-labeled compounds. To this solution was added a 0.12% charcoal

Table I. Inhibitory Activity against Tubulin Assembly of Ansamitocin P-3 and C(20) Derivatives of Ansamitocin P-3 (2~8)

compounds	IC50 (μM)
ansamitocin P-3	2.5
2	2.2
3	1.8
4	2.0
5	4.5
6	3.0
7 (DABMI)	1.5
8 (Dan-PDM-3)	5.0

suspension (0.2 mL). After 30 s at 0 °C, the mixture was centrifuged for 30 s at 10000*g*. Then 0.3 mL of supernatant was collected and its radioactivity was measured with a liquid scintillation counter.

Photoaffinity Labeling of DABMI. Tubulin (0.3 mL; 10 μM) was incubated in the presence of [^{14}C]DABMI (5 μM) for 15 min at 25 °C. Then the mixture was irradiated with a high-pressure mercury lamp for 15 min at 25 °C. To the 0.1 mL of the reaction mixture was added 0.1 mL of sample buffer (0.25 M Tris-HCl, pH 6.8, 2% SDS, 30% glycerol, 10% 2-mercaptoethanol, 0.5% bromophenol blue) and the whole was boiled for 2 min at 100 °C. The mixture was electrophoresed on SDS polyacrylamide gels. The gels was dried and sliced into 1-mm segments, which were solubilized in gel-dissolving solution, and the radioactivity was measured with a liquid scintillation counter.

RESULTS

Design of Fluorescent and Photoaffinity Labeling Analogs of Maytansine. In order to probe the RZX/MAY binding site on tubulin, we planned to synthesize fluorescent and photoaffinity derivatives of ansamitocin P-3. Studies on the structure–activity relationships of maytansinoids have demonstrated that various O-alkyl substituents at C(20) cause no significant change in the biological activity (*19*). Therefore we planned to introduce a fluorescent group and a photoreactive group at C(20). The dansyl group and [^{14}C]-*p*-azidobenzyl group were selected as fluorescent and photoreactive groups, respectively.

The dansyl group was introduced by alkylation with a C-3 spacer (Figure 2; compound **8**, Dan-PDM-3). On the other hand, *p*-azidobenzoate at C(20) of ASMP-3 was designed as a photoaffinity labeling reagent for tubulin (Figure 2, compound **7**, DABMI). Since this compound does not have a spacer between the ASMP-3 moiety and the photolabel functional group, it might be expected that photoaffinity labeling would take place near the binding site. The O-acylated derivatives at C(20) of ASMP-3 have not yet been examined for biological activity. To begin with, we looked at the inhibition of tubulin polymerization by various C(20) acylated derivatives, **2–6** (Figure 2).

A series of C(20) acylated derivatives were prepared by acylation of PDM-3 with corresponding carboxylic acids in the presence of 4-(dimethylamino)pyridine (DMAP) and 1-fluoro-2,4,6-trinitrobenzene (FTNB). The IC_{50} values of the derivatives **2–6** for *in vitro* polymerization of tubulin were determined and the results are summarized in Table I. All these derivatives showed activity comparable to that of ASMP-3. This result suggested that acylation at C(20) with aliphatic or aromatic carboxylic acids has no significant effect on the biological activity.

Fluorescent Probe, Dan-PDM-3, for the RZX/MAY Binding Site of Tubulin. Dan-PDM-3, designed as a fluorescent probe for the RZX/MAY site, consists of an ASMP-3 skeleton and a tethered dansyl moiety. We prepared it by alkylation of PDM-3 with the corresponding alkyl halide in the presence of KF–Al_2O_3 (Figure 2; compound **8**). Dan-PDM-3 inhibited tubulin polymerization as potently as did ASMP-3; the IC_{50} value of Dan-PDM-3 was estimated to be 5 μM under the experimental conditions used (Table I). This activity was considered to be due to its binding to tubulin. In fact, Dan-PDM-3 binding to tubulin was saturated at the concentration of 10 μM under the experimental conditions used. The binding site was analyzed by binding competition analysis with other typical antimitotic agents such as colchicine (CLC; it binds at a different site from the RZX/ MAY site), rhizoxin (RZX), and ansamitocin P-3 (ASMP-3). The amounts of Dan-PDM-3 were calculated from its fluorescence intensity; Dan-PDM-3 competed with RZX and ASMP-3, but not with CLC (Figure 3; since the presence of RZX and ASMP-3 alone did not cause change in the fluorescense intensity of Dan-PDM-3, we concluded that the reduction of fluorescense intensity in binding competition assay was attributed to the reduction of the amounts of Dan-PDM-3 bound to RZX/MAY site.) The results suggested that Dan-PDM-3 binds specifically to the RZX/MAY site.

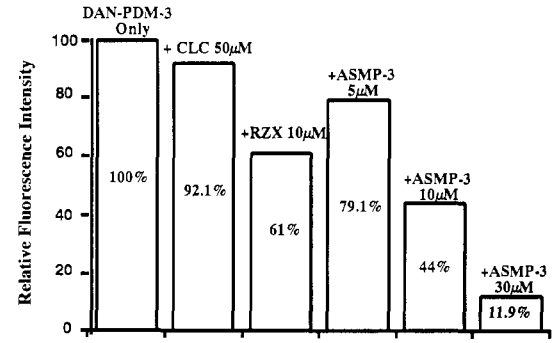


Figure 3. Binding competition of Dan-PDM-3 with colchicine, rhizoxin, or ansamitocin P-3. The amounts of Dan-PDM-3 bound to tubulin were calculated from the fluorescence intensity, and the amount in the absence of other drugs was defined as 100% (concentration of Dan-PDM-3, 10 μM).

Photoaffinity Labeling Reagent, DABMI, for the RZX/MAY Site. We designed DABMI, in which an ansamitocin P-3 derivative is acylated with *p*-azidobenzoic acid (Figure 2), as a photoaffinity labeling reagent for the RZX/MAY site. DABMI was prepared by reacting PDM-3 with *p*-azidobenzoic acid in the presence of DMAP and FTNB in the same way as used for derivatives **2–6**. As shown in Table I, DABMI exhibited potent anti-tubulin activity comparable to those of derivatives **2–6**.

The growth of a rhizoxin-resistant wild type strain (JY266) of *Schizosaccharomyces pombe* was not inhibited at all in the presence of DABMI at 30 μM, whereas the rhizoxin-sensitive transformant (266-107) was also very sensitive to this compound, and its growth was completely inhibited by DABMI even at 1 μM (data not shown). This result suggested that DABMI interact with tubulin at the same site as maytansine. A binding competition assay with [^{14}C]ansamitocin P-3 and [^{14}C]rhizoxin was carried out to confirm that DABMI binds to the RZX/MAY site. [^{14}C]Ansamitocin P-3 was prepared by reacting PDM-3 with [^{14}C]methyl iodide. As shown in Figure 4a,b, DABMI competed with ansamitocin P-3 and rhizoxin; the inhibition constants (K_i) were 0.36 and 0.54 μM, respectively. From these results, we concluded that DABMI does indeed bind to the RZX/MAY site.

[^{14}C]DABMI was prepared as a photo-/radioactive analog of maytansine by reacting PDM-3 with [*carbonyl-*

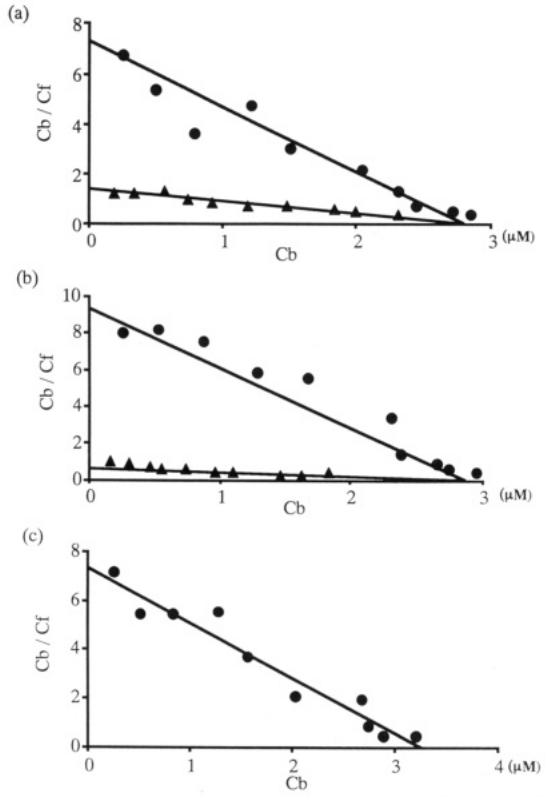


Figure 4. Scatchard analysis of the binding of [^{14}C]rhizoxin, [^{14}C]ansamitocin P-3, or [^{14}C]DABMI: (a) the amounts of rhizoxin bound to tubulin were measured in the absence (●) or presence (▲) of DABMI (5 μM); (b) the amounts of ansamitocin P-3 bound to tubulin in the absence (●) or presence (▲) of DABMI (5 μM) were measured; (c) the amounts of DABMI bound to tubulin were measured at various concentrations of DABMI; Cb, concentration of bound ^{14}C compounds; Cf, concentration of unbound ^{14}C compounds.

^{14}C]-*p*-azidobenzoic acid, which was derived from [*carbonyl*-^{14}C]-*p*-aminobenzoic acid. We directly determined its dissociation constant (K_d) by Scatchard analysis. The K_d value was 0.43 μM and there was only one binding site (Figure 4c). This K_d value is nearly equal to the K_i values of DABMI in competitive binding with [^{14}C]ASMP-3 and [^{14}C]RZX; this fact again strongly supports the conclusion that DABMI binds to the RZX/MAY site.

Irradiation-Induced Covalent Binding of DABMI to Tubulin. The tubulin preparation (10 μM) was incubated with [^{14}C]DABMI (5 μM) at 25 °C for 15 min; then the mixture was irradiated with a high-pressure mercury lamp for 15 min at 25 °C. To determine whether a covalent reaction had occurred between tubulin and DABMI, the tubulin in the reaction mixture was denatured in the sample buffer (see Experimental Procedures), and electrophoresed on SDS polyacrylamide gel. The gel was stained with Coomassie Blue, destained, and then subjected to autoradiography. The electrophoretic patterns of photolabeled tubulin as detected autoradiographically and by protein staining are shown in Figure 5. [^{14}C]-DABMI was still incorporated into tubulin after denaturation, that is, DABMI was irreversibly bound to tubulin by irradiation.

Furthermore, binding assay with photolabeled tubulin provided evidence for the specificity of photolabeling of DABMI to the RZX/MAY site on tubulin. Tubulin was photolabeled with nonradiolabeled DABMI. One of two control tubulin preparations was intact tubulin, and the other was obtained by irradiation without DABMI. The capacity of each tubulin preparation to bind [^{14}C]ASMP-3 was measured. Tubulin that had been prephotolabeled

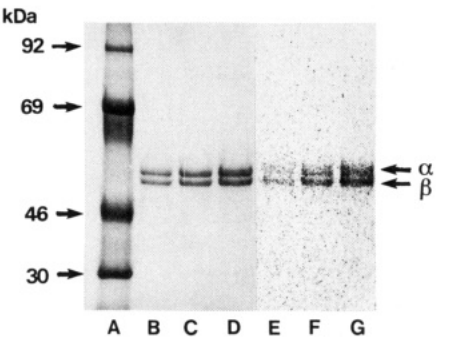


Figure 5. Electrophoretic and fluorographic analysis of tubulin photolabeled with DABMI: protein stained with Coomassie Brilliant Blue; lane A, phosphorylase b (92 kDa), bovine serum albumin (69 kDa), ovalbumin (46 kDa), carbonic anhydrase (30 kDa); lanes B, C, D, 2.5, 5.5, and 7.5 μg of photolabeled tubulin, respectively; lanes E, F, and G are fluorographic representations of lanes B, C, D.

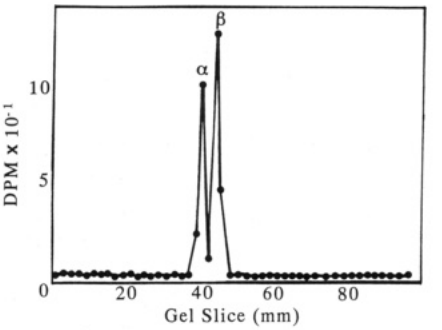


Figure 6. Radioactivity incorporation of [^{14}C]DABMI into both α- and β-subunits.

Table II. Specific Incorporation of [^{14}C]DABMI to Tubulin by Irradiation

proteins	incorporation of [^{14}C]DABMI (dpm/500 μM proteins)
tubulin	4560
bovine serum albumin[a]	586

[a] Photolabeling of bovine serum albumin (BSA) was carried out under the conditions described in Experimental Procedures, using BSA instead of tubulin.

with DABMI had only one-third of the [^{14}C]ASMP-3 binding capacity of intact tubulin preparation. In addition, irradiated tubulin without DABMI showed an unaltered [^{14}C]ASMP-3 binding capacity (data not shown). Thus, covalently bound DABMI inhibits [^{14}C]ASMP-3 binding. This result suggested that irradiation-induced covalent binding of DABMI occurred specifically at the RZX/MAY site.

As shown in Figure 5, [^{14}C]DABMI was covalently incorporated into both α- and β-subunits of tubulin. To analyze the distribution of radioactivity of DABMI between α- and β-subunits, the photolabeling profile was obtained by measuring the radioactivity in 1-mm gel slices (Figure 6). Under these conditions, DABMI was incorporated into both α- and β-subunits of tubulin in a ratio of 4:5. On the other hand, the amounts of nonspecifically bound DABMI were less than 15% of the total bound DABMI (Table II). This suggested that specific binding is more than 85%, as shown in Figures 5 and 6. From these results, we concluded that DABMI was covalently bound by irradiation into both α- and β-subunits of tubulin.

DISCUSSION

Dan-PDM-3 has been synthesized as a useful fluorescent probe for the RZX/MAY site. It inhibits *in vitro* micro-

tubule assembly and binds to tubulin in a mutually competitive manner with respect to ansamitocin P-3 and rhizoxin. Dan-PDM-3 does not inhibit tubulin binding of colchicine, which binds at a different site from the RZX/MAY site. These results suggest that Dan-PDM-3 binds specifically at the RZX/MAY site on tubulin. Therefore, we concluded that Dan-PDM-3 is a useful fluorescent probe for studies of the RZX/MAY site. Generally, the fluorescent properties of the dansyl moiety offer a valuable and safe alternative to radiolabeling and, moreover, a fluorescent probe has greater potential for studying binding sites than a radiolabeled probe (*10, 20*). We expect that Dan-PDM-3 will be useful for a variety of studies of the RZX/MAY site.

A series of C(20) acylated derivatives of ansamitocin P-3 has also been synthesized in order to study the effect of C(20) acylation on the biological activity. As can be seen in Table I, the C(20) acylated derivatives inhibit tubulin polymerization as potently as ASMP-3. From this relationship, we predicted that DABMI, designed as the photoaffinity probe, would bind to the RZX/MAY site. In fact, DABMI competed with ASMP-3 and RZX, and its K_i values for [^{14}C]ASMP-3 and [^{14}C]RZX binding were nearly equal to its K_d value measured directly (Figure 4). Therefore, we concluded that DABMI does bind to the RZX/MAY site on tubulin.

UV irradiation led to irreversible binding of DABMI to tubulin. Nonradiolabeled DABMI covalently bound to tubulin by irradiation decreased the [^{14}C]ASMP-3 binding capacity of tubulin. This fact suggested that the covalent binding of DABMI induced by irradiation occurred specifically at the RZX/MAY site. We concluded that DABMI is a useful photoaffinity labeling reagent to study the RZX/MAY binding site on tubulin.

The distribution of radioactivity of DABMI between α- and β-subunit of tubulin was analyzed after SDS polyacrylamide gel electrophoresis, both by counting the radioactivity in gel slices and by autoradiography. The total covalent incorporation of DABMI into both subunits of tubulin did not show apparent selectivity between α- and β-subunits. Though observed radioactivity is that of total binding, our negative control experiments suggest that more than 85% of the total binding is specific (*vide supra*). Considering these fact, we concluded that DABMI photochemically labeled both α- and β-subunits to almost same extent through specific binding to the RZX/MAY site. The azido function of DABMI produces a highly reactive nitrene upon irradiation, and this nitrene would react with amino acid residues in the vicinity of the binding site. Therefore, the lack of reaction selectivity of DABMI between α- and β-subunits suggests that the RZX/MAY binding site may be located close to the interface between the two subunits.

ACKNOWLEDGMENT

The authors thank the Central Research Institute of Takeda Chemical Industry for the supply of ansamitocin P-3 and PDM-3. Thanks are also due to Dr. M. Yamamoto (University of Tokyo) for providing the microorganisms. This work was supported in part by a Grant-in-Aid for Cancer Research from the Japanese Ministry of Education, Science and Culture.

LITERATURE CITED

(1) Remillard, S., Rehbun, L. I., Howie, G.A., and Kupchan, S. M. (1975) Antimitotic activity of the potent tumor inhibitor maytansine. *Science 189*, 1002–1005.
(2) Mandelbaum-Shavit, F., Wolpert-DeFilippes, M. K., and Johns, D. G. (1976) Binding of maytansine to rat brain tubulin. *Biochem. Biophys. Res. Commun. 72*, 47–54.
(3) Takahashi, M., Iwasaki, S., Kobayashi, H., Okuda, S., Murai, T., and Sato, Y. (1987) Rhizoxin binding to tubulin at the maytansin-binding site. *Biochem. Biophys. Acta. 926*, 215–223.
(4) Li, Y., Kobayashi, H., Tokiwa, Y., Hashimoto, Y., and Iwasaki, S. (1992) Interaction of phomopsin A with porcine brain tubulin. *Biochem. Pharmacol. 43*, 219–224.
(5) Takahashi, M., Kobayashi, H., and Iwasaki, S. (1989) Rhizoxin resistant mutants with an altered β-tubulin gene in *Aspergillus nidulans*. *Mol. Gen. Genet. 220*, 53–59.
(6) Takahashi, M., Matsumoto, S., Iwasaki, S., and Yahara, I. (1990) Molecular basis for determining the sensitivity of eukaryotes to the antimitotic drug rhizoxin. *Mol. Gen. Genet. 222*, 169–175.
(7) Baley, H., and Knowels, J. R. (1977) Photoaffinity labeling. *Methods in Enzymol. 46*, 69–114.
(8) Chowdhry, V., and Westheimer, F. H. (1979) Photoaffinity labeling of biological systems. *Annu. Rev. Biochem. 48*, 293–325.
(9) Sawada, T., Hashimoto, Y., Li, Y., Kobayashi, Y., and Iwasaki, S. (1991) Fluorescent and photoaffinity labeling derivatives of rhizoxin. *Biochem. Biophys. Res. Commun. 178*, 558–562.
(10) Sawada, T., Kobayashi, H., Hashimoto, Y., and Iwasaki, S. Identification of the Fragment Photoaffinity-Labeled with Azidodansyl-Rhizoxin as Met-363–Lys-379 on β-Tubulin. *Biochem. Pharmacol. 45*, 1387–1394.
(11) Ando, T., Yamazaki, J., Kawate, T., Sumi, S., and Hanafusa, T. (1982) Fluoride salts on alumina as reagents for alkylation of phenols and alcohols. *Bull. Chem. Soc. Jpn. 55*, 2504–2507.
(12) Kim, S., and Yang, S. (1981) Direct, high-yield esterification of carboxylic acids. *Synth. Commun. 11*, 121–124.
(13) For azido preparation see; Neilsen, P. E., and Buchard, O. (1982) Alkyl azide as photoaffinity labels. A photochemical study of some 4-substituted aryl azido. *Photochem. Photobiol. 35*, 317–323.
(14) Takahashi, M., Iwasaki, S., Kobayashi, H., Okuda, S., Murai, T., Sato, Y., Haraguchi-Hiraoka, T., and Nagano, H. (1987) Studies on macrocyclic lactone antibiotics XI. Antimitotic and antitubulin activity of new antitumor antibiotics, rhizoxin and its homologues. *J. Antibiotics 40*, 66–72.
(15) Williams, R. C., and Lee, J. C. (1982) Preparation of Tubulin from Brain. *Methods Enzymol. 85*, 376–385.
(16) Laemmli, U. K. (1970) Cleavage of structural proteins during the assembly of the head of bacteriophage T4. *Nature 227*, 680–685.
(17) Sherline, P., Bodwin, C. K., and Kipnis, D. M. (1974) A new colchicine binding assay for tubulin. *Anal. Biochem. 62*, 400–407.
(18) Hashimoto, Y., and Shudo, K. Cytosolic-nuclear tumor promoter-specific binding protein: association with the 90kDa heat shock protein and translocation into nuclei by treatment with 12-O-tetradecanoylphorbol 13-acetate. *Jap. J. Cancer Res.* 82: 665–675, 1991.
(19) Hashimoto, N., Shimadzu, H., and Akimoto, H. (1981) Ansa-azacyclophanes and their preparation. Jpn. Kokai 193479, May 22.
(20) Shimazawa, R., Hibino, S., Mizoguchi, H., Hashimoto, Y., Iwasaki, S., Kagechika, H., and Shudo, K. (1991) fluorescent probes for retinoic acid receptors: molecular measures for the ligand binding pocket. *Biochem. Biophys. Res. Commun. 180*, 249–254.

Enzymatic Activity of Chymotrypsin and Its Poly(ethylene glycol) Conjugates toward Low and High Molecular Weight Substrates

Hsin-Cheng Chiu, Samuel Zalipsky,*,† Pavla Kopečková, and Jindřich Kopeček*

Departments of Pharmaceutics and Pharmaceutical Chemistry/CCCD and Bioengineering, University of Utah, Salt Lake City, Utah 84112, and Department of Chemistry, Rutgers—The State University of New Jersey, Piscataway, New Jersey 08855. Received December 28, 1992

Native chymotrypsin and its polyethylene glycol (PEG) conjugates, obtained using the succinimidyl carbonate of methoxy-PEG (SC-PEG) as the amino group modifying reagent, were tested for their activity toward several low and high molecular weight substrates. Tripeptide and tetrapeptide *p*-nitroanilides either as N^{α}-benzyloxycarbonyl derivatives or attached via their N-terminals to *N*-(2-hydroxypropyl)methacrylamide (HPMA) copolymers or to PEG, as well as the proteins albumin and azoalbumin, were used as substrates. Extensively modified chymotrypsin bearing on average of 14 PEG chains per chymotrypsin molecule ($PEG_{14}CHT$) and a moderately modified one containing 10 PEG chains ($PEG_{10}CHT$) both degraded the low molecular weight *p*-nitroanilides at rates comparable to, and in the case of $PEG_{10}CHT$, greater than, the rates exhibited by the native enzyme. Synthetic high molecular weight substrates and azoalbumin were also degraded by the PEG-modified enzymes. However, rates of such enzymatic reactions were lower for the PEG–enzymes than for the native one. Native albumin, as compared to azoalbumin, resisted degradation by both PEGCHTs yet was readily digested by the native chymotrypsin. The results obtained indicate that substrate-size-dependent specificity of PEG-modified enzymes cannot be explained *solely* by steric hindrance considerations. The decreased activity of PEG–enzymes toward protein substrates is consistent with the well-documented ability of PEG to exclude proteins from its surroundings and with the influence of protein unfolding on the susceptibility to degradation.

INTRODUCTION

Enzymes modified by covalent attachment of polyethylene glycol (PEG)[1] have found uses in several different fields. Due to the increased amphipatic nature of such modified enzymes they become soluble in organic solvents and can act as catalysts for numerous organic reactions (*1*). The affinity of PEG–enzymes to the upper phase of PEG/dextran or PEG/salt two-phase aqueous systems makes these conjugates useful in diagnostic (*2*) and bioreactor applications (*3*). Various PEG–enzyme conjugates were developed as new therapeutics, taking advantage of their decreased immunogenicity, resistance to proteolytic degradation, and persistence in the bloodstream (*4–7*).

Usually, PEG–enzymes are prepared by reaction between methoxypolyethylene glycol (mPEG) carrying a reactive electrophile group ("activated PEG") with nucleophilic residues on the surface of a protein (for a comprehensive review see ref 8). In some cases the preservation of enzymatic activity of PEG–enzyme conjugates was dependent on the chemistry of PEG activation and subsequent attachment to enzymes, as well as on the extent of modification (*7, 8*). Use of PEG-based acylating reagents, which react selectively with amino groups of proteins under very mild conditions, often led to good preservation of enzymatic activity of the conjugates. This was particularly general occurrence for enzymes acting on low molecular weight substrates.

Preparation of functionally active, yet extensively modified PEG conjugates derived from proteins having large size substrates, proved more difficult. For example, several PEG-tissue plasminogen activator conjugates were prepared using succinimidyl succinate and imidazolyl formate derivatives of mPEG (*6*). Regardless of the activated PEG employed, the fibrinolytic activity of the conjugates decreased substantially with the increase in the extent of modification. Similar decrease in fibrinolytic activities was exhibited by PEG-modified acyl–plasmin–streptokinase complexes (*9*). Elastase modified with mPEG–dichloro-*s*-triazine partially preserved its ability to act on its small synthetic substrate, yet completely lost elastin hydrolysing activity (*10*). Proteolytic activity of PEG-modified trypsin was also essentially lost in contrast to the well preserved and in some cases even enhanced activity toward low-molecular weight substrates (*11, 12*).

It does not appear that significant conformational changes occur as a result of covalent attachment of PEG to proteins and thus cannot be used as an explanation for the substrate-size-dependent specificity changes. For example, using far-ultraviolet circular dichroism and intrinsic protein fluorescence, Pasta et al. (*13*) showed that a PEG-modified serine protease, subtilisin, maintains its native secondary structure and the integrity of its catalytic site. Similarly, no conformational changes, as judged by CD spectra, were detected in PEG–ribonuclease

† Rutgers. Present address: Liposome Technology, Inc., 1050 Hamilton Ct., Menlo Park, CA 94025.

[1] Abbreviations: Amino acids abbreviations are those recommended by IUPAC–IUB, cf., *J. Biol. Chem.* (1972) *247*, 977. AIBN, 2,2′-azobisisobutyronitrile; Boc, *tert*-butyloxycarbonyl; BSA, bovine serum albumin; CHT, chymotrypsin; DCC, dicyclohexylcarbodiimide; DMSO, dimethyl sulfoxide; DMF, dimethylformamide; EDC, 1-ethyl-3-[3-(dimethylamino)propyl]carbodiimide; GF-HPLC, gel filtration high-performance liquid chromatography; HONb, *N*-hydroxy-5-norbornene-2,3-dicarboximide; HPMA, *N*-(2-hydroxypropyl)methacrylamide; MA, methacryloyl; mPEG, methoxypolyethylene glycol; ONp, *p*-nitrophenoxy; NAp, *p*-nitroanilide; P, HPMA polymeric backbone; $PEG_{10}CHT$ and $PEG_{14}CHT$, conjugates of chymotrypsin with 10 or 14 PEG chains bound; SC-PEG, succinimidyl carbonate of mPEG; TNBS, 2,4,6-trinitrobenzenesulfonic acid; Tris, 2-amino-2-(hydroxymethyl)-1,3-propanediol; Z, benzyloxycarbonyl.

1043-1802/93/2904-0290$04.00/0 © 1993 American Chemical Society

conjugates (*14*), which showed clear dependence of activity on the size of the substrate. While good preservation of activity toward low molecular weight cytidine 2′,3′-cyclic monophosphate was obtained even for extensively modified RNase, large enzymatic activity losses were observed when ribonucleic acid was used as a substrate.

The substrate-size-dependent specificity changes of PEG–enzymes are usually explained on the basis of steric hindrance, which limits the access of large substrates to PEG-modified proteins. While this explanation seems reasonable, is it possible that other properties of the conjugates are also contributing. Understanding these phenomena undoubtedly would have important theoretical as well as practical implications.

In this paper we report the results of the first series of experiments aimed toward gaining an understanding of the substrate-size-dependent specificity of PEG–enzymes. For our study we chose α-chymotrypsin as a convenient model enzyme. This readily available enzyme has a well-defined specificity. It cleaves peptides at carboxyls of hydrophobic amino acid residues of L-configuration (Trp, Tyr, Phe) and naturally accepts substrate molecules of various sizes from polypeptides of hundreds of kilodaltons to simple amino acid derivatives. Although, chymotrypsin was previously modified with PEG and used as a reagent for peptide synthesis in organic solvents (*15–22*), heretofore no studies describing the relationship between size of a substrate and activity of PEG–chymotrypsin have appeared. Our choice of chymotrypsin was also prompted by the fact that derivatives of L-phenylalanine *p*-nitroanilide constitute readily accessible synthetic targets. Thus we prepared several low molecular weight and polymeric substrates and examined their activity with native and PEG-modified chymotrypsins. The ability of these chymotrypsin derivatives to digest bovine serum albumin (BSA) and a chromogen-containing protein (azoalbumin) was also evaluated.

EXPERIMENTAL PROCEDURES

Chemicals. Phe and Leu were of L-configuration. Z-Gly-Gly-OH, Z-Gly-Leu-OH, Boc-Leu-OH, H-Phe-NAp, BSA, and azoalbumin were purchased from Sigma, St. Louis, MO; α-chymotrypsin from bovine pancreas was purchased from Worthington Corp., Freehold, NJ. mPEG-OH of molecular weight 5000 was a gift from Dr. S. Verma of Union Carbide Corp., S. Charleston, WV. It was converted into a reactive succinimidyl carbonate derivative (SC-PEG) using previously published procedures (*12, 23*). *N*-(2-Hydroxypropyl)methacrylamide (*24*), *p*-nitrophenyl esters of N-methacryloylated oligopeptides, MA-Gly-Gly-ONp (*25*) and MA-Gly-Leu-ONp (*26*), were prepared as described previously.

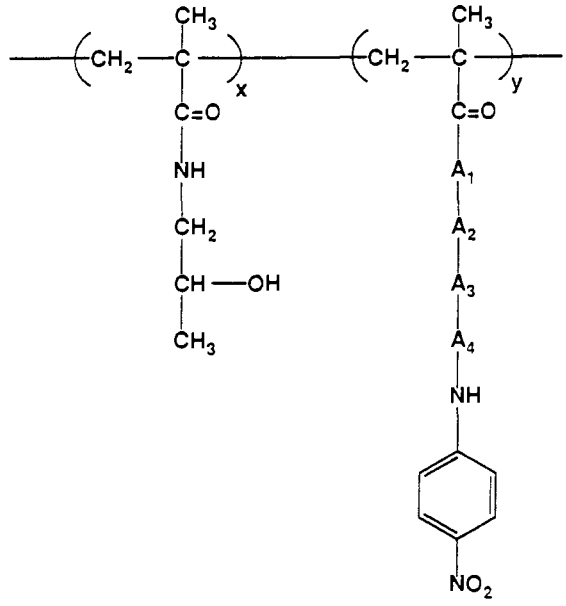
Preparations of PEG-Modified Chymotrypsin. Solid SC-PEG (1 g, ≈0.2 mmol) was added to a stirred solution of chymotrypsin (100 mg, ≈4×10^{-6} mol) in 20 mM $CaCl_2$ solution (20 mL) adjusted to pH 6. After all of the polymer went into solution (≈2 min), the pH was raised to 8.5 and maintained at this level for 30 min by automatic titration with sodium hydroxide (0.5 N). The solution was acidified to pH 3 with hydrochloric acid (0.1 N) and diafiltered against 1 mM HCl containing 20 mM $CaCl_2$ until no more free PEG was detected in the filtrate (*27*). Trinitrobenzenesulfonic acid-based assay (*28*) showed that 84% of the amino groups originally present on chymotrypsin were substituted. This corresponds to an average attachment of 14.3 mPEG chains per molecule of the conjugate. Fluorescamine-based assay (*29*) of the conjugate showed 79% substitution of the amino groups, which corresponds to 13.4 mPEG chains per molecule. This conjugate is refered to here as $PEG_{14}CHT$. The second PEG–chymotrypsin conjugate was prepared by the same procedure using only half the amount of SC-PEG. This conjugate contained on average 10.7 mPEG chains per molecule (63% of amines modified) by TNBS assay and 9.2 mPEGs per molecule (54% of amines modified) by fluorescamine assay. It is refered to here as $PEG_{10}CHT$. GF-HPLC analysis (Zorbax GF-450) showed good homogeneity of the PEG–protein conjugates and substantially increased molecular weight as compared to the parent protein.

Oligopeptide *p*-Nitroanilides. H-Leu-Phe-NAp was synthesized by reaction of Boc-Leu-OH with H-Phe-NAp in ethyl acetate using dicyclohexylcarbodiimide (DCC) as the coupling agent. Deprotection was carried out in 15% methanolic HCl. Mp: (base) 157–158 °C (from AcOEt/Et_2O). TLC: R_f = 0.59 ($CHCl_3$/MeOH 5:1), ϵ = 14 700 M^{-1} cm^{-1} (330 nm; DMSO). Z-Gly-Gly-Phe-NAp (**1**) and Z-Gly-Leu-Phe-NAp (**2**) were prepared by reaction of Z-protected dipeptides and H-Phe-NAp in the presence of equimolar amount of 1-hydroxybenzotriazole using the DCC method in DMF. Z-Gly-Gly-Phe-NAp was obtained in 60% yield. Mp: 191 °C (EtOH/AcOEt). ϵ = 11 700 M^{-1} cm^{-1} (318 nm; EtOH). TLC: acetone, single spot (UV detection), R_f = 0.58, free of H-Phe-NAp (R_f = 0.45) and original dipeptide (R_f = 0.09). IR (KBr): 3320 (NH, urethane, amide), 1710 (C=O, urethane), 1650 (amide I), 1520 (amide II), 1345 (NO_2). Z-Gly-Leu-Phe-NAp was obtained in 64% yield. Mp: 189 °C (EtOH), ϵ = 12 000 M^{-1} cm^{-1} (318 nm; EtOH). TLC: acetone, R_f = 0.60. IR (KBr): 3300 (NH, urethane, amide), 1700 (C=O, urethane), 1645 (amide I), 1520 (amide II), 1385 (isobutyl, binding vibration), 1345 (NO_2).

Oligopeptide *p*-Nitroanilides Attached to HPMA Copolymers. Polymeric substrates with HPMA backbone and oligopeptidyl *p*-nitroanilides in the side chains were prepared by a two-step procedure: (a) first polymeric precursors were prepared, as previously described (*30*), from HPMA and *p*-nitrophenyl esters of methacryloylated diglycine or glycylleucine (molar ratio of HPMA:ONp comonomer = 95:5) by radical precipitation polymerization in acetone at 50 °C (12.5 wt % of monomers, 0.6 wt % of AIBN, 24 h). After polymerization, the precipitated polymer was isolated and reprecipitated from methanolic solution into an excess of acetone. The contents of ONp groups in polymeric precursors, as determined spectrophotometrically (ϵ = 9500 M^{-1} cm^{-1}, 274 nm, DMSO), were 4.6 (P-Gly-Gly-ONp) and 3.8 (P-Gly-Leu-ONp) mol %. The weight and number average molecular weights were determined using the FPLC Pharmacia system on a Superose 6 column (buffer 0.05 M Tris + 0.5 M NaCl, pH 8.0) calibrated with polyHPMA fractions. M_w of polymeric precursors (after aminolysis of ONp groups with 1-amino-2-propanol) are shown in Table I; (b) in the second step the reaction of polymeric precursors (15 wt %) with H-Phe-NAp or H-Leu-Phe-NAp (20% molar excess with respect to the reactive ONp groups) was carried out in DMSO for 12 h. The polymeric *p*-nitroanilides P-Gly-Gly-Phe-NAp (**3**), P-Gly-Leu-Phe-NAp (**4**) and P-Gly-Gly-Leu-Phe-NAp (**5**) were precipitated into acetone and reprecipitated again from methanolic solution. The purity of the polymer (the absence of unbound *p*-nitroanilide) was checked using a Sephadex G-15 column. The content of NAp groups (see Table I) was determined spectrophotometrically in water (ϵ = 12 500, 315 nm). The structure of oligopeptide *p*-nitroanilides attached to HPMA copolymer is shown in Scheme I.

mPEG-O(C=O)-Gly-Gly-Phe-NAp (6): SC-PEG (10 g, 2 mmol) was added to a stirred aqueous solution of

Scheme I. Structure of HPMA Copolymer-Bound Oligopeptide *p*-Nitroanilide



Oligopeptide spacer	Polymer No. (3)	(4)	(5)
A1	Gly	Gly	Gly
A2	Gly	Leu	Gly
A3	Phe	Phe	Leu
A4			Phe

H-GlyGly-OH (1.05 g, 8 mmol in 40 mL) while pH 8.5 was maintained. After 20 min of reaction, solid sodium chloride (10 g) was dissolved in the solution (another 15 min) and it was acidified to pH 3.4 with 12 N HCl. The polymer was extracted from the aqueous phase with dichloromethane (3 × 60 mL). After drying ($MgSO_4$) the solvent was rotary evaporated and the remaining polymer recrystallized twice from 2-propanol and dried in vacuo. The yield was 9.5 g (92%). IR (film on NaCl, cm^{-1}): 3330 (NH, urethane, amide), 1725 (C=O, urethane), 1684 (C=O, amide) cm^{-1}. The carboxyl group content of the product was 1.96×10^{-4} mol/g [101% of the theoretical value calculated for mPEG-O(C=O)GlyGly-OH], as determined by a titration with sodium methoxide (*31*).

An aqueous solution (35 mL) of mPEG-O(C=O)GlyGly-OH (5.2 g, 1 mmol), H-Phe-NAp (1 g, 3.6 mmol), and *N*-hydroxynorbornenedicarboxyimide (0.19 g, 1 mmol) was treated with EDC (2 g, 10 mmol) for 3 h, while the pH was in the range 4.6–5.5. The solution was brought to pH 8, filtered, and washed with ethyl acetate (2 × 75 mL). After acidification to pH 2.5 with concentrated HCl, the product was extracted from the aqueous phase with dichloromethane (2 × 100 mL). The organic solution was dried ($MgSO_4$) and evaporated to dryness. The product was crystallized three times from 2-propanol and dried *in vacuo* to yield 4.8 g (92%) of white powder. TLC (CH_2Cl_2/MeOH 5:1) showed that the product gave a single UV-absorbing spot (R_f = 0.6) and it was free of H-Phe-NAp (R_f = 0.8). GF-HPLC (Zorbax GF-450) showed single peak. UV (λ_{max} = 315 nm, ϵ = 13 000 M^{-1} cm^{-1}) of the product showed that 1 g of material contained 1.9×10^{-4} mol of *p*-nitroanilide.

Table I. Characterization of Polymeric Substrates

substrate no.	structure	M_W	NAp content mol %	NAp content mmol/g
3	P-Gly-Gly-Phe-NAp	21 000	4.1	0.262
4	P-Gly-Leu-Phe-NAp	22 500	3.4	0.218
5	P-Gly-Gly-Leu-Phe-NAp	21 000	3.9	0.243
6	mPEG-O(C=O)-Gly-Gly-Phe-NAp	5 480	0.9[a]	0.182

[a] Calculated considering Gly-Gly-Phe-NAp a monomer unit. One PEG chain (degree of polymerization ~114) contains one oligopeptide *p*-nitroanilide moiety.

Amino acid analysis of a hydrolyzed sample of the product gave a Gly:Phe ratio of 1.99:1.

Chymotryptic Activity: General. The stock solutions of native and modified chymotrypsins were prepared in 1 mM HCl with 20 mM $CaCl_2$. Their concentrations were determined spectroscopically using $\epsilon = 5.2 \times 10^4$ for chymotrypsin. By titration of active sites (*32*) it was determined that chymotrypsin contained 62% active molecules. For the measurement of enzymatic activity, stock solutions of low molecular weight substrates (**1**, **2**) in DMSO were diluted in Tris buffer (0.08 M Tris + 0.01 M $CaCl_2$, pH 8.0), so that the final concentration of DMSO in the incubation mixtures was ≤5% (v/v). The polymeric substrate solutions were prepared directly in the Tris buffer.

Cleavage of *p*-Nitroanilide Substrates. The release of *p*-nitroaniline was monitored at 410 nm using Lambda 9 Perkin-Elmer spectrophotometer at 37 °C and initial rates calculated using ϵ = 8800 M^{-1} cm^{-1}. The concentrations of incubation mixtures were as follows: 2×10^{-7} M enzyme and 4×10^{-6}–8×10^{-5} M low molecular weight substrates or 1.5×10^{-4}–4×10^{-3} M for polymeric substrates. Each set of kinetic measurement was repeated twice with eight different substrate concentrations. The kinetic parameters were calculated from Lineweaver–Burk and Hofstee plots of the initial rates of the appearance of *p*-nitroaniline.

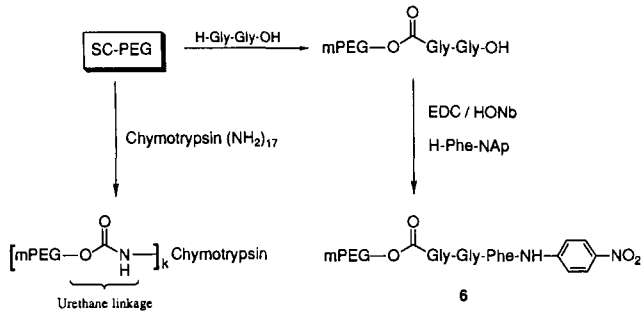
Cleavage of Protein Substrates. The extent of cleavage was followed by size exclusion chromatography. The incubation mixture contained 5 mg/mL of albumin or azoalbumin and the appropriate chymotrypsin derivative (7×10^{-6} M). At time intervals of 0, 2, 4, 8, 12, 24 h, the samples were withdrawn, diluted four times with eluent buffer (Tris 0.05 M + NaCl 0.5 M), and applied on a Superose 12 column (Fast Protein Liquid Chromatography System, Pharmacia). The degradation was monitored by the decrease in the peak area of the appropriate protein substrate with time, using UV and refractometric detection.

RESULTS AND DISCUSSION

The succinimidyl carbonate of methoxypolyethylene glycol (SC-PEG), a recently introduced polymeric reagent (*12*, *23*), was used for attachment of PEG to chymotrypsin (Scheme II). The conditions used in the modification reactions were similar to those reported previously for trypsin (*12*). The conjugates were purified by diafiltration, which was continued until the filtrate gave a negative test for the presence of PEG (*27*). The extent of the modifications was determined by measuring the number of amino groups consumed by the reactions with SC-PEG. An extensively modified chymotrypsin, bearing on average 14 mPEG-5000 residues per chymotrypsin molecule (PEG_{14}CHT), as well as a moderately modified one containing 10 mPEG chains (PEG_{10}CHT), were prepared by using the appropriate amounts of SC-PEG.

We prepared two low molecular weight substrates Z-Gly-Gly-Phe-NAp (**1**) and Z-Gly-Leu-Phe-NAp (**2**) by DCC-

Scheme II. Preparation of PEG–Chymotrypsin Conjugates ($k \approx 10, 14$) and PEG–Chymotryptic Substrate



mediated coupling of Z-protected dipeptides with the *p*-nitroanilide of phenylalanine. Polymeric substrates based on water-soluble *N*-(2-hydroxypropyl)methacrylamide copolymers (structures **3-5**) were prepared by reacting phenylalanine *p*-nitroanilide or dipeptide *p*-nitroanilides with the appropriate polymeric precursors, i.e., HPMA copolymers containing dipeptide side chains terminating in *p*-nitrophenyl esters using previously published procedures (*30*). The PEG-based substrate (**6**) was prepared by a two-step synthesis in water (Scheme II). First, SC-PEG was reacted with excess H-Gly-Gly-OH at pH 8.5. Then, the recovered mPEG-oxycarbonyl-Gly-Gly-OH at pH 5 was coupled with H-Phe-NAp in presence of EDC and HONb. The product contained the theoretical amount of NAp, comparable to the other polymeric nitroanilides (≈0.2 mmol/g). The summary of the polymeric *p*-nitroanilide substates and their characteristics are presented in Table I.

Michaelis–Menten kinetic constants of all the synthetic nitroanilide substrates were determined (Table II). The native enzyme and its PEG conjugates exhibited activity toward all the nitroanilide substrates examined. The PEG-modified enzymes had well preserved and in the case of $PEG_{10}CHT$ even elevated activity toward low molecular weight substrates. For the substrate, Z-Gly-Gly-Phe-NAp, which, due to unfavorable S_2–P_2 interactions (*33*), is the slower of the two substrates (1 and 2), an almost 2-fold increase in activity of the enzyme was observed. This result, although somewhat surprising, is consistent with the results obtained using N^{α}-benzoyl-L-tyrosine ethyl ester and *p*-nitroanilide substrates, toward which SC-PEG-modified chymotrypsins had a higher specific activity than the native enzyme (*23*). Even more dramatic increases in enzymatic activity toward low molecular weight substrates were recently reported for PEG-modified trypsins (*12, 34, 35*). Since the PEG modification of CHT does not apparently cause a dramatic change in the specificity of the enzyme, the increase in the activities of PEG-modified CHT toward low molecular weight substrates may be due to either a slight change in conformation, which results in a better fit of the low molecular weight substrates with the active site; a change in the pH–activity profile; and/or a change of the microenvironment around the chymotrypsin molecule as a result of PEG chains attachment. However, further investigation is necessary to determine the exact mechanism by which PEG enhances the activity of CHT toward low-molecular weight substrates.

The activity of the native and the PEG-modified CHT toward HPMA polymeric substrates (**3–5**) was essentially governed by the steric and structure effects of the substrates. In agreement with the previous reports (*30, 36*), the longer the oligopeptidyl sequence which is available to interact with the active site of the enzyme, the higher the values of k_{cat} and k_{cat}/K_M. Substrate **5**, which contains four amino acid residues in the oligopeptide sequence was cleaved 5–10 times faster by the native and the PEG-modified CHT than substrates **3** and **4**, which contain three amino acids in the oligopeptidyl sequence. This result is not surprising, since it is well-known that chymotrypsin can accomodate in its active site four amino acid residues toward the NH_2 end of the substrate. Consequently, the steric hindrance of the HPMA copolymer chain on the formation of the enzyme–substrate complex is considerably lower for substrate **5** when compared with substrates **3** and **4** (*37*).

Both HPMA- and oxyethylene-based polymeric substrates were cleaved 2–9 times more readily by the native than by the PEG-modified CHT derivatives. This apparent decrease of activity was mainly due to decrease in k_{cat} values. Interestingly, for the polymeric tripeptide-containing substrates (**3**, **4**, and **6**), K_M values were lower for the more extensively modified $PEG_{14}CHT$ than for the moderately modified chymotrypsin, indicating improved substrate–enzyme complex formation. This result clearly contradicts the conventional "steric hindrance" explanation of interactions between macromolecular substrates and PEG–enzymes. The relative reactivity ratios for **3**, **4**, and **5** remained approximately the same for each chymotrypsin derivative. Similar results were obtained when chymotrypsin was modified with HPMA copolymers (*30*). Among the three enzymes, $PEG_{14}CHT$ presented the lowest activity toward HPMA polymeric substrates.

Each chymotrypsin derivative hydrolyzed the PEG-based substrate (**6**) 2–3 times faster than the substrate **3**, even though each substrate contains an identical peptide sequence, Gly-Gly-Phe. These differences in the reactivity were substantially due to the contribution of the K_M values. This indicates that the PEG-based substrate has higher affinity than **3** toward native and PEG-modified chymotrypsins. In contrast to HPMA copolymer-based substrates bearing chymotrypsin-cleavable oligopeptide *p*-nitroanilide residues fixed as pendant groups, the substrate **6** contains the enzymatically cleavable residue as an end group. The differences between these two types of substrates were previously discussed in the literature (*36, 38*). Our results are in agreement with the previously made observation that the end-group type of substrate is expected to be the more reactive one (*36*). The effect of the different molecular weight of the substrates **3** and **6** on the rate of *p*-nitroaniline release should not be important, since it was shown that the influence of molecular weight on the rate of cleavage of polymer-bound oligopeptide *p*-nitroanilides is small (*39*).

The third type of substrates examined in this work were protein-based substrates. The enzymatic degradation of both azoalbumin and albumin was followed by size exclusion chromatography, in which the decrease in the peak area of the appropriate protein substrate was monitored. The results of these experiments are shown in Figures 1 and 2. Azoalbumin was degraded readily ($t_{1/2}$ ≈25 min) by the native chymotrypsin, somewhat slower by $PEG_{10}CHT$ ($t_{1/2}$ ≈2 h), and substantially slower by $PEG_{14}CHT$ (Figure 1). Native albumin, in contrast to azoalbumin, was accepted as a substrate only by the native enzyme (Figure 2). We feel that the different behavior of the two protein-based substrates is due to the partial unfolding and denaturation of azoalbumin, which is obtained by extensive modification of native albumin with hydrophobic chromophore residues (*40*). Indirectly, evidence of azoalbumin unfolding was obtained from an observed 2-fold increase in its hydrodynamic radius as

Table II. Kinetic Parameters of the Cleavage of Low Molecular Weight and Polymeric *p*-Nitroanilides by Native and PEG-Modified Chymotrypsins[a]

		native CHT			$PEG_{10}CHT$			$PEG_{14}CHT$		
substrate no.	structure	k_{cat} (s^{-1})	K_M (M)	k_{cat}/K_M (M^{-1} s^{-1})	k_{cat} (s^{-1})	K_M (M)	k_{cat}/K_M (M^{-1} s^{-1})	k_{cat} (s^{-1})	K_M (M)	k_{cat}/K_M (M^{-1} s^{-1})
1	Z-GlyGlyPheNAp	0.145	4.33×10^{-5}	3400	0.180	2.98×10^{-5}	6040	0.154	4.42×10^{-5}	3480
2	Z-GlyLeuPheNAp	0.226	4.53×10^{-5}	5000	0.324	4.56×10^{-5}	7100	0.182	3.35×10^{-5}	5400
3	P-GlyGlyPheNAp	0.577	2.77×10^{-3}	210	0.325	5.90×10^{-3}	55	0.164	4.60×10^{-3}	36
4	P-GlyLeuPheNAp	3.80	7.50×10^{-3}	510	2.90	1.16×10^{-2}	250	1.20	8.43×10^{-3}	140
5	P-GlyGlyLeuPheNAp	25.90	1.90×10^{-3}	13600	16.70	3.10×10^{-3}	5390	9.70	3.70×10^{-3}	2640
6	PEG-GlyGlyPheNAp	0.68	1.10×10^{-3}	618	0.58	3.60×10^{-3}	161	0.14	2.02×10^{-3}	69

[a] Each set of kinetic measurement was repeated twice with eight different substrate concentrations. The standard error was typically less than 10% of the mean.

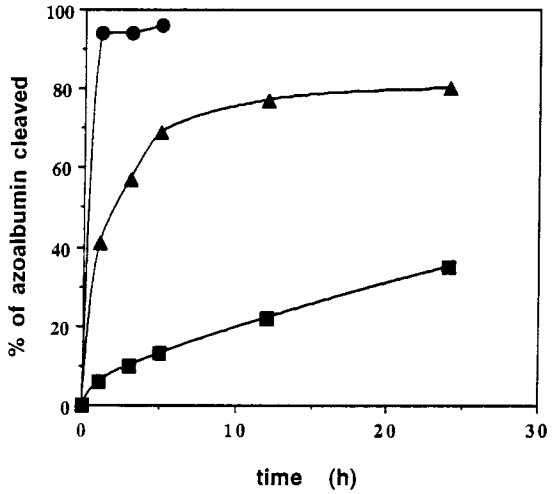


Figure 1. Cleavage of azoalbumin by native chymotrypsin (●), $PEG_{10}CHT$ (▲), and $PEG_{14}CHT$ (■). Incubation mixture contained 7×10^{-6} M native or modified chymotrypsin and 5 mg/mL of azoalbumin.

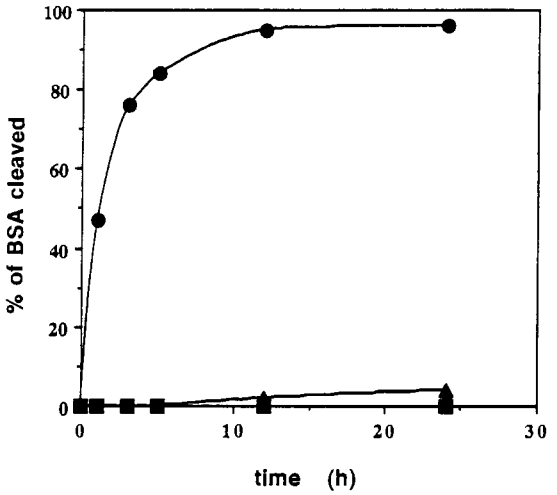


Figure 2. Cleavage of BSA by native chymotrypsin (●), $PEG_{10}CHT$ (▲), and $PEG_{14}CHT$ (■). Incubation mixture contained 7×10^{-6} M native or modified chymotrypsin and 5 mg/mL of BSA in Tris buffer pH 8.0.

compared to that of BSA on a Superose 12 column (results not shown). The decreased activity of PEG-modified chymotrypsins toward protein substrates is consistent with the ability of PEG to exclude proteins from its surroundings (*41–43*) and with the protein repulsion properties of PEG-modified surfaces (*44–46*). The rapid movement of hydrated PEG chains on the chymotrypsin surface probably influences the microthermodynamic properties at the interface and renders the interaction with a protein substrate more difficult. Apparently, a repulsive force develops due to a loss of configurational entropy of the PEG chains, when a protein approaches the PEG-modified surface (*46*). Consequently, the tightly "packed" globular native proteins, such as BSA, are not degraded by PEG-modified chymotrypsin. On the other hand, the (partially) denaturated azoalbumin, despite its larger hydrodynamic volume, can be cleaved. Apparently, the unfolding of the azoalbumin molecules increases the probability that they will be able to penetrate the PEG layer on the enzyme surface.

The results of this study indicate that the susceptibility of low molecular weight chymotrypsin substrates to degradation by PEG–chymotrypsins is well-preserved and in some cases even enhanced. The degradation depends upon the structure of the oligopeptide residue used in a particular substrate and upon the extent of chymotrypsin modification with PEG. We demonstrated that synthetic high molecular weight substrates, including azoalbumin, are degraded by the PEG-modified enzymes, and in some instances (e.g. **5**) even at rates comparable to low molecular weight substrates. However, such enzymatic reactions are slower for PEG-modified than for the native enzyme.

As found with other protease–PEG conjugates (*6, 9–12*), PEG–chymotrypsin conjugates showed a drastically reduced ability to degrade proteins or a complete lack thereof. The rate of degradation was inversely dependent on the PEG-chain density (degree of substitution) on the enzyme surface and increased with unfolding of the protein substrate. The results are in agreement with the repulsion properties of PEG chains, probably due to PEG's low interfacial free energy with water, unique solution properties and molecular conformation in aqueous solution, hydrophilicity, high surface mobility, and steric stabilization effects (*45*). However, examination of the degradation of a series of PEG- and protein-based substrates of various molecular weights by chymotrypsin and its PEG derivatives, as well as experiments with relatively high polymer concentrations, might provide additional insights into the mechanism of the substrate-size-specificity of PEG–enzymes.

LITERATURE CITED

(1) Inada, Y., Takahashi, K., Yoshimoto, T., Ajima, A., Matsushima, A., and Saito, Y. (1986) Application of polyethylene glycol-modified enzymes in biotechnological processes: Organic solvent-soluble enzymes. *Trends Biotechnol. 4,* 190–194.

(2) Mattiasson, B. (1983) Partition affinity ligand assay (PALA) for quantifying haptens, macromolecules and whole cells. *Methods Enzymol. 92,* 498–522.

(3) Pollak, A., and Whitesides, G. M. (1976) Organic synthesis using enzymes in two-phase aqueous ternary system. *J. Am. Chem. Soc. 98,* 289–291.

(4) Knauf, M. J., Bell, D. P., Hirtzer, P., Luo, Z.-P., Young, J. D., and Katre, N. V. (1988) Relationship of effective molecular size to systemic clearance in rats of recombinant interleukin-2 chemically modified with water-soluble polymers. *J.Biol. Chem. 263,* 15064–15070.

(5) Davis, F. F., Van Es, T., and Palczuk, N. C. (1979) Non-immunogenic polypeptides. U.S. Patent 4,179,337.
(6) Berger, H., and Pizzo, S. V. (1988) Preparation of polyethylene glycol-tissue plasminogen activator adducts that retain functional activity: Characteristics and behavior in three different species. *Blood 71,* 1641–1647.
(7) Delgado, C., Francis, G. F., and Fisher, D. (1992) The uses and properties of PEG-linked proteins. *CRC Crit. Rev. Ther. Drug Carrier Syst. 9,* 249–304.
(8) Zalipsky, S., and Lee, C. (1992) Use of functionalized polyethylene glycols for modification of polypeptides. *Poly(ethylene glycol) Chemistry: Biotechnical and Biomedical Applications* (J. M. Harris, Ed.) pp 347–370, Plenum Press, New York.
(9) Tomiya, N., Watanabe, K., Awaya, J., Kurono, M., and Fujii, S. (1985) Modification of acyl-plasmin-streptokinase complex with polyethylene glycol: Reduction of sensitivity to neutralizing antibody. *FEBS Lett. 193,* 44–48.
(10) Kiode, A., and Kobayashi, S. (1983) Modification of amino groups in porcine pancreatic elastase with polyethylene glycol in relation to binding activity towards anti-serum and to enzymatic activity. *Biochem. Biophys. Res. Commun. 111,* 659–667.
(11) Abuchowski, A., and Davis, F. F. (1979) Preparation and properties of polyethylene glycol-trypsin adducts. *Biochim. Biophys. Acta 578,* 41–46.
(12) Zalipsky, S., Seltzer, R., and Menon-Rudolph, S. (1992) Evaluation of a new reagent for covalent attachment of polyethylene glycol to proteins. *Biotechnol. Appl. Biochem. 15,* 100–114.
(13) Pasta, P., Riva, S., and Carrea, G. (1988) Circular dichroism and fluorescence of polyethylene glycol-subtilisin in organic solvents. *FEBS Lett. 236,* 329–332.
(14) Caliceti, P., Schiavon, O., Veronese, F. M., and Chaiken, I. M. (1990) Effects of monomethoxypoly(ethylene glycol) modification of ribonuclease on antibody recognition, substrate accessibility and conformational stability. *J. Mol. Recognit. 3,* 89–93.
(15) Fulcrand, V., Jacquier, R., Lazaro, R., and Viallefont, P. (1991) Enzymatic peptide synthesis in organic solvent mediated by gels of copolymerized acrylic derivatives of α-chymotrypsin and polyoxyethylene. *Int. J. Pept. Protein Res. 38,* 273–277.
(16) Babonneau, M.-T., Jacquier, R., Lazaro, R., and Viallefont, P. (1989) Enzymatic peptide synthesis in organic solvent mediated by α-chymotrypsin. *Tetrahedron Lett. 30,* 2787–2790.
(17) Gaertner, H., and Puigserver, A. J. (1988) Peptide synthesis catalyzed by polyethylene glycol-modified chymotrypsin in organic solvents. *Proteins 3,* 130–137.
(18) Gaertner, H., and Puigserver, A. (1989) Kinetics and specificity of serine proteases in peptide synthesis catalyzed in organic solvents. *Eur. J. Biochem. 181,* 207–213.
(19) Gaetner, H., Watanabe, T., Sinisterra, J. V., and Puigserver, A. (1991) Peptide synthesis catalyzed by modified α-chymotrypsin in low-water organic media. *J. Org. Chem. 56,* 3149–3153.
(20) Matsushima, A., Okada, M., and Inada, Y. (1984) Chymotrypsin modified with polyethylene glycol catalyzes peptide synthesis reaction in benzene. *FEBS Lett. 178,* 275–277.
(21) Pina, C., Clark, D., and Blanch, H. (1989) The activity of PEG-modified chymotrypsin in aqueous and organic media. *Biotechnol. Techniq. 3,* 333–338.
(22) Takahashi, K., Ajima, A., Yoshimoto, T., Okada, M., Matsushima, A., Tamaura, Y., and Inada, Y. (1985) Chemical reactions by polyethylene glycol modified enzymes in chlorinated hydrocarbons. *J. Org. Chem. 50,* 3414–3415.
(23) Zalipsky, S., Seltzer, R., and Nho, K. (1991) Succinimidyl carbonates of polyethylene glycol: Useful reactive polymers for preparation of protein conjugates. *Polymeric Drugs and Drug Delivery Systems* (R. L. Dunn, and R. M. Ottenbrite, Eds.) pp 91–100, American Chemical Society, Washington, DC.
(24) Kopeček, J., and Bažilová, H. (1973) Poly[N-(2-hydroxypropyl)methacrylamide]. I. Radical polymerization and copolymerization. *Eur. Polym. J. 9,* 7–14.
(25) Rejmanová, P., Labský, J., and Kopeček, J. (1979) Aminolyses of monomeric and polymeric *p*-nitrophenyl esters of methacryloylated amino acids. *Makromol. Chem. 178,* 2159–2168.
(26) Kopeček, J. (1979) Reactive copolymers of N-(2-hydroxypropyl)methacrylamide with N-methacryloylated derivatives of L-leucine and L-phenylalanine. I. Preparation, characterization and reaction with diamines. *Makromol. Chem. 178,* 2169–2183.
(27) Zalipsky, S., and Barany, G. (1990) Facile synthesis of α-hydroxy-ω-carboxymethylpolyethylene oxide. *J. Bioact. Compat. Polym. 5,* 227–231.
(28) Habeeb, A. F. S. A. (1966) Determination of free amino groups in proteins by trinitrobenzenesulfonic acid. *Anal. Biochem. 14,* 328–336.
(29) Stocks, S. J., Jones, A. J. M., Ramey, C. W., and Brooks, D. E. (1986) A fluorometric assay of the degree of modification of protein primary amines with polyethylene glycol. *Anal. Biochem. 154,* 232–234.
(30) Kopeček, J., Rejmanová, P., and Chytrý, V. (1981) Polymers containing enzymatically degradable bonds, 1: Chymotrypsin catalyzed hydrolysis of *p*-nitroanilides of phenylalanine and tyrosine attached to side-chains of copolymers of N-(2-hydroxypropyl)methacrylamide. *Makromol. Chem. 182,* 799–809.
(31) Patchornik, A., and Rogozinski, S. E. (1959) Nonaqueous titration of organic acids, anhydrides, acyl halides, strong inorganic acids and reactive alkyl halides in various mixtures. *Anal. Chem. 31,* 985–989.
(32) Kezdy, F. J., and Kaiser, E. T. (1970) Principles of active site tiration of proteolytic enzymes. *Methods Enzymol. 19,* 3–20.
(33) Kurachi, K., Powers, J. C., and Wilcox, P. E. (1971) Kinetics of the reaction of chymotrypsin A_α with peptide chloromethyl ketones in relation to its subsite specificity. *Biochemistry 12,* 771–777.
(34) Gaertner, H. F., and Puigserver, A. J. (1992) Increased activity and stability of poly(ethylene glycol)-modified trypsin. *Enzyme Microb. Technol. 14,* 150–155.
(35) Munch, O., Tritsch, D., and Biellmann, J.-F. (1991) Polyethylene glycol modified trypsin kinetics in buffer and in benzene: Dipeptide synthesis. *Biocatalysis 5,* 35–47.
(36) Ulbrich, K., Strohalm, J., and Kopeček, J. (1986) Poly(ethylene glycol)s containing enzymatically degradable bonds. *Makromol. Chem. 187,* 1131–1144.
(37) Kopeček, J., and Rejmanová, P. (1983) Enzymatically degradable bonds in synthetic polymers. *Controlled Drug Delivery* (S. D. Bruck, Ed.) *Vol. I,* pp 81–124, CRC Press, Boca Raton, Florida.
(38) Ouchi, T., and Azuma, T. (1984) Enzyme and nonenzyme hydrolyses of end ester group in polyethylene glycol esters. *J. Macromol. Sci. Chem. A21,* 583–591.
(39) Fu, T. Y., and Morawetz, H. (1976) Enzymatic attack on side chains of synthetic polymers. Chymotrypsin catalyzed hydrolysis of specific substrate groups attached to acrylamide or acrylic acid copolymers. *J. Biol. Chem. 251,* 2083–2086.
(40) Tomarelli, R. M., Charney, J., and Harding, M. L. (1949) The use of azoalbumin as a substrate in the colorimetric determination of peptic and tryptic activity. *J. Lab. Clin. Med. 34,* 428–433.
(41) Ingham, K. C. (1984) Protein precipitation with polyethylene glycol. *Methods Enzymol. 104,* 351–356.
(42) Arakawa, T. (1985) The mechanism of increased elution volume of proteins by polyethylene glycol. *Anal. Biochem. 144,* 267–268.
(43) Topchieva, I. N. (1980) Biochemical applications of poly(ethylene glycol). *Russ. Chem. Rev. 49,* 260–517.
(44) Andrade, J. D., Nagaoka, S., Cooper, S., Okano, T, and Kim, S. W. (1987) Surfaces and blood compatibility: current hypotheses. *ASAIO J. 10,* 75–84.
(45) Lee, J.-H., Kopeček, J., and Andrade, J. D. (1989) Protein-resistant surfaces prepared by PEO-containing copolymer surfactants. *J. Biomed. Mater. Res. 23,* 351–368.
(46) Lee, J.-H., Kopečková, P., Kopeček, J., and Andrade, J. D. (1990) Surface properties of copolymers of alkyl methacrylates with methoxy (polyethylene oxide) methacrylates. *Biomaterials 11,* 455–464.

TECHNICAL NOTES

Synthesis of an End-Group Functionalized Polyethylene Glycol–Lipid Conjugate for Preparation of Polymer-Grafted Liposomes

Samuel Zalipsky

Liposome Technology, Inc., 1050 Hamilton Court, Menlo Park, California 94025. Received March 9, 1993

Synthesis of a distearoylphosphatidylethanolamine–polyethylene glycol (DSPE–PEG) conjugate, bearing a hydrazide group at the unattached end of the polymer chain, was achieved using a new heterobifunctional polymeric reagent. The heterobifunctional PEG derivative carrying on one end a reactive succinimidyl carbonate (SC) group and at the other terminal a *tert*-butyloxycarbonyl (Boc) protected hydrazide group was prepared by an efficient four step process from readily available PEG-2000. The SC-end group of the polymer reacted readily with the amino group of DSPE forming a stable urethane attachment between lipid and PEG. Acidolytic removal of the Boc group yielded a hydrazide–PEG–lipid conjugate suitable for preparation of polymer-grafted liposomes. Taking advantage of the well-documented chemical versatility of hydrazide groups, various biologically relevant ligands can be linked to this type of functionalized liposomes.

INTRODUCTION

Lack of toxicity, excellent solubility, and superb biocompatibility made polyethylene glycol (PEG[1]) one of the most popular modifiers of biologicals (*1*). Examples of PEG conjugates range from low molecular weight drugs prepared to alter pharmacokinetics, biodistribution, or toxicity (*2, 3*) to surfaces of biomaterials used to reduce protein adsorption and thrombogenicity (*4*). PEG has been used extensively to alter *in vivo* properties of biological macromolecules, particularly proteins (5–7). More recently, liposomes carrying PEG chains on their exterior were discovered to have extended half-lifes in bloodstream (up to $t_{1/2}$ = 48 h in humans). With this, one of the most important limitations of liposomal drug delivery was overcome (*8–12*). Such liposomes were named Stealth[2] liposomes for their ability to avoid uptake by reticuloendothelial system. In the scientific literature they have been referred to as sterically stabilized liposomes on the basis of a proposed mechanism where protein adsorption is inhibited by a steric barrier created by the polymeric "brush" (for a comprehensive review see ref 9).

Now that long-circulating liposomes are within our reach, the next frontier is to use them as carriers for various ligands. One can envisage use of such conjugates for targeting and immunomodulation. Ligands of potential interest can be directly linked to polar groups of conventional lipids coincorporated into liposomes with PEG-PE. Not surprisingly, this approach has a drawback in that PEG chains interfere with the interaction between a ligand and its target (*12*). The polymer would also be expected to interfere with chemical reactions between reactive groups on the surface of a liposome and a potential ligand. Thus, for numerous applications it seems attractive to link potential ligands to the far end of PEG chains. In light of the fact that all the PEG–lipids used to date for preparation of liposomes have been derived from commercially available methoxy-PEG (mPEG) and thus carry unreactive methoxy end groups, it is essential to develop a new approach toward functionalized PEG-lipid conjugates.

In this paper I am presenting an efficient method for synthesis of a new type of functionalized PEG–lipid conjugate, namely DSPE–PEG–hydrazide (1), suitable for preparation of PEG–liposomes with reactive hydrazide groups positioned on the exterior.

RESULTS AND DISCUSSION

DSPE was previously shown to be the starting material of choice for preparation of modified lipids suitable for incorporation into liposomes. For example, urethane-linked mPEG–DSPE incorporated into liposomes performed well by improving pharmacokinetics and biodistribution (*9*). The functionalized conjugate sought as the target of this study in its simplest form is an analog of mPEG–DSPE in which the inert methoxy group is replaced by hydrazide. It is apparent that efficient preparation of such a material is dependent on the availability of a heterobifunctional derivative of PEG having a reactive acyl group on one terminal and a hydrazide group on the other. The hydrazide group has to be in a protected form to prevent undesirable reaction between the two terminal groups of the polymer.

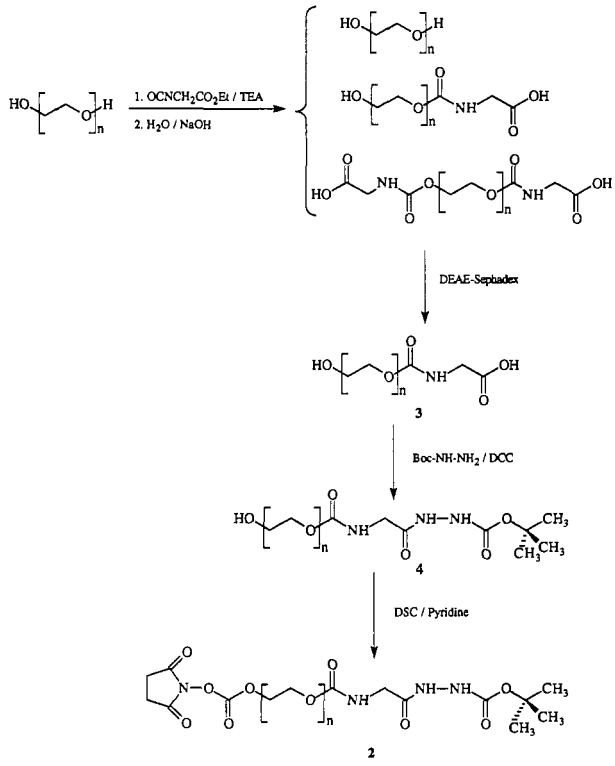
Succinimidyl carbonate (SC) derivatives of PEG were recently introduced for modification and cross-linking of proteins (*13, 14*) and preparation of high molecular weight polymers (*15, 16*). Both applications were successful due to very efficient urethane formation reactions of SC groups with amino-containing molecules. Preliminary experiments showed that SC–PEG reacted within minutes with DSPE, producing a product identical to the mPEG–DSPE obtained by the previously published procedure (*10*). Given this result, the SC group was chosen as the active acyl

[1]Abbreviations used: PEG, polyethylene glycol; mPEG, methoxy-PEG; PMA, polymethacrylic acid; PE, phosphatidylethanolamine; DSPE, distearoyl-PE; Boc, *tert*-butyloxycarbonyl; DCC, dicyclohexylcarbodiimide; DSC, disuccinimidyl carbonate; SC, succinimidyl carbonate.

[2]Stealth is a registered trademark of Liposome Technology, Inc.

1043-1802/93/2904-0296$04.00/0 © 1993 American Chemical Society

Scheme I

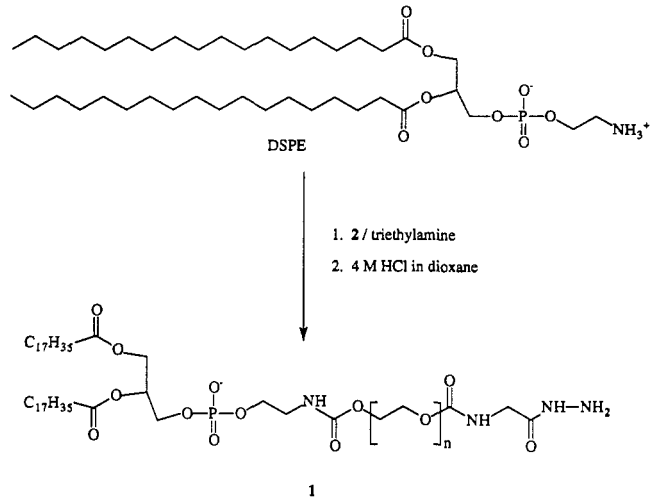


group for the heterobifunctional PEG. The choice of the hydrazido-protecting group (*tert*-butyloxycarbonyl, Boc) was governed by the stability of the mPEG–DSPE under acydolytic deprotection conditions.

Scheme I illustrates the sequence of reactions used to obtain Boc-protected hydrazido PEG having a reactive SC group at the opposite terminal (**2**). First, the ω-hydroxy acid derivative of PEG (**3**) was prepared using a modification of the previously published procedure (*17*). Ethyl isocyanatoacetate was employed for partial introduction of carboxyl groups onto PEG of molecular weight 2000 forming a mixture of dicarboxylated PEG, ω-hydroxy acid derivative, and unreacted starting polymer (*18*). The ω-hydroxy acid derivative (**3**) purified by ion exchange chromatography was coupled with *tert*-butyl carbazate in the presence of dicyclohexylcarbodiimide, thus introducing a protected hydrazide group on one end of the polymer (derivative **4**). Activation of the hydroxy end group with disuccinimidyl carbonate in the presence of pyridine was performed by a modification of the published procedure for Sepharose activation (*19*). This deviation from the original protocol, requiring treatment of the polymer with phosgene as the first step (*13*, *14*), was necessary due to the instability of both the Boc and hydrazide groups under these conditions. However, incorporation of the SC groups under the new set of conditions proceeded quantitatively, as was confirmed by NMR and titration of the active acyl groups.

A slight excess of **2** reacted with chloroform-suspended DSPE in the presence of triethylamine (Scheme II). The lipid derivative was quickly solubilized during this reaction. Taking advantage of its very low critical micelle concentration, the product was purified by dialysis using a 300 000 molecular weight cutoff (MWCO) membrane and then lyophilized. The structure of the Boc-protected conjugate was confirmed by NMR, and it was shown to be pure by TLC analysis. Deprotection with 4 M HCl in dioxane produced the target DSPE–PEG–hydrazide (**1**), as was ascertained by comparison of its NMR spectra with those

Scheme II



of the Boc-protected starting material, urethane-linked mPEG–DSPE, and mPEG-oxycarbonyl–glycine hydrazide. The last material was obtained by hydrazinolysis of the corresponding ethyl ester (*20*). Treatment of **1** in borate buffer solution with trinitrobenzene sulfonate produced the red-maroon color (λ_{max} = 500 nm) characteristic to hydrazides. This color reaction failed when **1** was preincubated with an excess of valeraldehyde or 4-carboxybenzaldehyde. These observations are consistent with the known hydrazide–aldehyde reactivity leading to hydrazone formation and indicate that the conjugate **1** is functionally reactive.

The conjugate **1** can be formulated with lecithin and cholesterol into a liposomal preparation containing reactive hydrazide groups. Preliminary experiments demonstrated that such PEG–hydrazide liposomes showed pharmacokinetic profiles similar to the more conventional mPEG–DSPE counterparts. The chemical versatility of hydrazide group, its use as a starting material for introduction of other functional groups, and its ability to participate in numerous types of conjugation schemes is well-documented in literature (*21*). Particularly useful is its reactivity toward various glycoproteins, e.g. immunoglobulins (*22*). Studies of hydrazide-containing PEG–liposomal conjugates are currently underway and will be reported in the future.

This paper presents a facile and an efficient procedure for a new heterobifunctional PEG derivative (**2**), employing readily available and inexpensive PEG-diol as a starting material. Unlike alternative procedures for synthesis of PEGs with two different end groups (see for example, Yokoyama *et al.* (*23*) and references cited therein), this method does not involve polymerization of toxic and explosive ethylene oxide. The scope of potential applications of the heterobifunctional polymer **2** goes beyond the synthesis of the lipid conjugate shown in Scheme II. For example, it is suitable for attachment of ligands to surfaces, linking cofactors to enzymes, and preparation of various other macromolecular conjugates. One can take advantage of the presence of 1 equiv of glycine in the reagent for characterization of such conjugates by amino acid analysis of their hydrolysates (*20*).

EXPERIMENTAL PROCEDURES

Preparation of 3. PEG-diol of molecular weight 2000 (42 g, 42 mequiv of OH) was dissolved in toluene (200 mL), azeotropically dried, and then treated with ethyl isocyanatoacetate (2.3 mL, 21 mmol) and triethylamine

(1.5 mL, 10 mmol). After overnight reaction at 25 °C the solution was evaporated to dryness. The residue was dissolved in 0.2 M NaOH (100 mL), a trace of toluene was evaporated, and pH 12 was maintained with periodic dropwise additions of 4 M NaOH. When the pH stopped dropping, the solution was acidified to pH 3.0 and the product extracted with methylene chloride (100 mL × 2). TLC on silica gel G (iPrOH/H_2O/concentrated ammonia 10:2:1) gave the typical chromatogram of partially carboxylated PEG (*17*, *18*) consisting of unreacted PEG (R_f = 0.67) and monocarboxylated (R_f = 0.55) and dicarboxylated (R_f = 0.47) derivatives of the polymer. This solution was dried ($MgSO_4$), filtered, and evaporated to dryness. The remaining PEG mixture was dissolved in water (50 mL). One third of this solution (30 mL, ≈14 g of derivatized PEG) was loaded onto DEAE-Sephadex A-25 (115 mL of gel in borate form). After the underivatized PEG was washed off the column with water (confirmed by a negative PMA test (*17*)), a gradient of ammonium bicarbonate (2–20 mM at increments of 1–2 mM every 200 mL) was applied, and 50-mL fractions were collected. It was determined by the PMA test and TLC that fractions 1–25 contained only PEG monoacid. These fractions were pooled together, concentrated to ≈70 mL, acidified to pH 2, and extracted with methylene chloride (50 mL × 2). The CH_2Cl_2 solution was dried ($MgSO_4$), concentrated, and poured into cold stirring ether. The precipitated product was dried *in vacuo*. Yield: 7 g. Titration of carboxyl groups gave $4.6 \cdot 10^{-4}$ mequiv/g (97% of theoretical value).

Preparation of 4. The ω-hydroxy acid derivative of PEG (**3**, 5 g, 2.38 mmol) and *tert*-butyl carbazate (0.91 g, 6.9 mmol) were dissolved in CH_2Cl_2–ethyl acetate (1:1, 7 mL). The solution was cooled on ice and treated with DCC (0.6 g, 2.9 mmol) predissolved in the same solvent mixture. After 30 min the ice bath was removed and the reaction was allowed to proceed for an additional 3 h. The reaction mixture was filtered from dicyclohexylurea and evaporated. The product was recovered and purified by two precipitations from ethyl acetate–ether (1:1) and dried *in vacuo* over P_2O_5. Yield: 5.2 g, 98%. TLC of the product gave one spot (R_f = 0.68) different from the starting material (R_f = 0.55). H NMR ($CDCl_3$): δ 1.46 (s, tBu, 9H), 3.64 (s, PEG, 178H), 3.93 (br d, J = 4.5 Hz, $HNCH_2$-CO, 2H), 4.24 (t, $J \approx$ 4.5 Hz, CH_2OCONH, 2H) ppm. ^{13}C NMR ($CDCl_3$): δ 28.1 (tBu), 43.4 (CH_2 of Gly), 61.6 (CH_2-OH), 64.3 (CH_2OCONH), 69.3 (CH_2CH_2OCONH), 70.5 (PEG), 72.4 (CH_2CH_2OH), 81.0 (CMe_3), 155.1 (C=O of Boc), 156.4 (C=O of urethane), 168.7 (C=O of Gly hydrazide) ppm.

Preparation of 2. The ω-hydroxy Boc-hydrazide derivative of PEG (**4**, 5 g, 2.26 mmol) was dissolved in pyridine (1.1 mL), CH_2Cl_2 (5 mL), and CH_3CN (2 mL) and treated with DSC (1.4 g, 5.5 mmol) at 25 °C overnight. The solution was filtered and gradually added to cold ethyl ether (100 mL). The precipitated product was dissolved in warm ethyl acetate (45 mL), chilled, and mixed with an equal volume of ethyl ether. The precipitate was collected by filtration and dried *in vacuo* over P_2O_5. Yield: 4.8 g 90%. SC groups content $4.15 \cdot 10^{-4}$ mequiv/g (98% of theoretical value) was determined by titration (*13*). H NMR ($CDCl_3$): δ 1.46 (s, tBu, 9H), 2.83 (s, succinimide), 3.64 (s, PEG, 178H), 3.79 (t, J = 4.7 Hz, $CH_2CH_2OCO_2$, 2H), 3.93 (br d, J = 4.5 Hz, CH_2 of Gly, 2H), 4.24 (t, J = 4.5 Hz, CH_2OCONH, 2H), 4.46 (t, J = 4.7 Hz, CH_2OCO_2, 2H) ppm. ^{13}C NMR: δ 25.5 (succinimide), 28.2 ($(CH_3)_3C$), 43.3 ($NHCH_2CO$), 64.3 (CH_2OCONH), 68.3 (CH_2OCO_2), 69.4 ($CH_2CH_2OCO_2$), 70.6 (PEG), 80.9 ($(CH_3)_3C$), 151.6 (OCO_2), 155.3 (C=O of Boc), 156.7 (C=O of urethane), 168.6 (C=O of succinimide), 169.1 (C=O of Gly) ppm.

Preparation of 1. Boc-hydrazide–PEG–SC (**2**, 693 mg, 0.29 mmol) was dissolved in chloroform (4 mL) and treated with solid DSPE (200 mg, 0.27 mmol) and triethylamine (0.1 mL, 0.72 mmol). The suspension was vigorously mixed and maintained at 45 °C for ≈10 min. During this time a clear solution was formed. TLC (chloroform–methanol–water 90:18:2) showed complete disappearance of ninhydrin-positive DSPE (R_f = 0.22) and formation of a new product (R_f = 0.55, I_2 vapor visualized) in addition to a weak spot due to the unreacted PEG reagent (R_f = 0.73). Acetic acid (42 mL, 0.73 mmol) was added to the reaction mixture and it was evaporated to dryness. The solid residue was slowly dissolved in water (5 mL) and the trace of remaining chloroform evaporated. The solution (pH ≈ 6) was transferred into Spectrapor CE dialysis tubing (MWCO 300,000) and dialyzed against saline solution (≈50 mM) at 4 °C until the dialysis solution became negative to the PMA test for PEG (*17*) (3 × 1000 mL, 8–16 h per period). The conjugate solution was further dialysed against deionized water, filtered through a 0.2-μm sterile filter, and lyophilized, producing white solid Boc-hydrazide–PEG–DSPE (520 mg, 65%). H NMR ($CDCl_3$): δ 0.88 (t, J = 6.8 Hz, CH_3, 6H), 1.26 (s, CH_2, 56H), 1.46 (s, tBu, 9H), 1.58 (br, t, J = 7.3 Hz, 4H), 2.28 (2 overlapping t, $J \approx$ 7.3 Hz, CH_2C=O, 4H), 3.36 (br, m, OCH_2CH_2NH, 2H), 3.64 (s, PEG, ≈180H), 3.94 (br m, CH_2 of Gly and CH_2CH_2O-P, 4H), 4.17 (dd, J = 7.0, 12 Hz, glycerol CH_2O-P, 2H), 4.19–4.25 (br m, CH_2-O of both urethanes, 4H), 4.39 (dd, J = 3.2, 12 Hz, glycerol CH_2O-C=O, 2 H), 5.20 (m, CH glycerol, IH) ppm. ^{13}C NMR ($CDCl_3$): δ 14.1 (CH_3), 22.7 (CH_2CH_3), 25.0 (CH_2CH_2C=O), 28.3 (CH_3 of tBu), 29.7 (polyCH_2), 31.9 ($CH_2CH_2CH_3$), 34.2 and 34.4 (two CH_2C=O), 42.4 ($HNCH_2C$=O), 43.4 ($HNCH_2CH_2$), 62.8 (CH_2OC=O), 63.4 and 63.5 (CH_2O-P), 64.3 and 64.4 (CH_2OCONH), 69.5 (CHOC=O), 70.6 (PEG), 81.0 (Cq of tBu), 155.4 (C=O of Boc), 156.6 (urethane C=O), 169.2 (C=O of Gly), 173.0 and 173.4 (C=O of 2 esters) ppm. Deprotection was carried out in 4 M HCl in dioxane for 60 min. The product was recovered as a white solid after removal of the volatiles and thorough drying *in vacuo*. Yield: 98%. Disappearance of the *tert*-butyl peak at 1.46 ppm of the H-NMR spectra and 28.3, 81.1, and 155.4 ppm peaks from the ^{13}C-NMR spectra confirmed the complete removal of the Boc group. The remainder of the NMR spectra of **1** were essentially the same as those of the protected conjugate.

ACKNOWLEDGMENT

I wish to thank Dr. Virginia W. Miner of Acorn NMR for her skillful acquisition of NMR spectra, Dr. Aleksander L. Klibanov of the University of Pittsburgh for his helpful suggestion on the purification of PEG-lipids; and Liposome Technology, Inc., for support and for publication of this work.

LITERATURE CITED

(1) Topchieva, I. N. (1990) Synthesis of biologically active polyethylene glycol derivatives. A review. *Polymer Sci. USSR 32*, 833–851.

(2) Ouchi, T., Yuyama, H., and Vogl, O. (1987) Synthesis of 5-Fluorouracil-terminated monomethoxypoly(ethylene glycol)s, their hydrolysis behavior, and their antitumor activities. *J. Macromol. Sci.-Chem., A24*, 1011–1032.

(3) Zalipsky, S., Gilon, C., and Zilkha, A. (1983) Attachment of drugs to polyethylene glycols. *Eur. Polym. J. 19*, 1177–1183.

(4) Merrill, E. W. (1992) Poly(ethylene oxide) and blood contact: A chronicle of one laboratory. *Poly(Ethylene Glycol)*

Chemistry: *Biotechnical and Biomedical Applications* (J. M. Harris, Eds.) pp 199–220, Plenum Press, New York.
(5) Veronese, F. M., Caliceti, P., Schiavon, O., and Sartore, L. (1992) Preparation and properties of monomethoxypoly-(ethylene glycol)-modified enzymes for therapeutic applications. *Poly(Ethylene Glycol) Chemistry*: *Biotechnical and Biomedical Applications* (J. M. Harris, Eds.) pp 127–137, Plenum Press, New York.
(6) Zalipsky, S., and Lee, C. (1992) Use of functionalized polyethylene glycols for modification of polypeptides. *Poly(ethylene glycol) Chemistry*: *Biotechnical and Biomedical Applications* (J. M. Harris, Eds.) pp 347–370, Plenum Press, New York.
(7) Dreborg, S., and Akerblom, E. B. (1990) Immunotherapy with monomethoxypolyethylene glycol modified allergens. *Crit. Rev. Ther. Drug Carrier Syst. 6*, 315–365.
(8) Papahadjopoulos, D., Allen, T. M., Gabizon, A., Mayhew, E., Matthay, K., Huang, S. K., Lee, K.-D., Woodle, M. C., Lasic, D. D., Redemann, C., and Martin, F. J. (1991) Sterically stabilized liposomes: Improvements in pharmacokinetics and antitumor therapeutic efficacy. *Proc. Natl. Acad. Sci. U.S.A. 88*, 11460–11464.
(9) Woodle, M. C., and Lasic, D. D. (1992) Sterically stabilized liposomes. *Biochim. Biophys. Acta 1113*, 171–199.
(10) Woodle, M. C., Matthay, K. K., Newman, M. S., Hidayat, J. E., Collins, L. R., Redemann, C., Martin, F. J., and Paphadjopoulos, D. (1992) Versatility in lipid compositions showing prolonged circulation with sterically stabilized liposomes. *Biochim. Biophys. Acta 1105*, 193–200.
(11) Senior, J., Delgado, C., Fisher, D., Tilcock, C., and Gregoriadis, G. (1991) Influence of surface hydrophilicity of liposomes on their interaction with plasma protein and clearance from the circulation: Studies with poly(ethylene glycol)-coated vesicles. *Biochim. Biophys. Acta 1062*, 77–82.
(12) Klibanov, A. L., Maruyama, K., Beckerleg, A. M., Torchilin, V. P., and Huang, L. (1991) Activity of amphiphathic poly-(ethylene glycol) 5000 to prolong the circulation time of liposomes depends on the liposome size and is unfavorable for immunoliposome binding to target. *Biochim. Biophys. Acta 1062*, 142–148.
(13) Zalipsky, S., Seltzer, R., and Nho, K. (1991) Succinimidyl carbonates of polyethylene glycol: Useful reactive polymers for preparation of protein conjugates. *Polymeric Drugs and Drug Delivery Systems* (R. L. Dunn, and R. M. Ottenbrite, Eds.) pp 91–100, American Chemical Society, Washington, DC.
(14) Zalipsky, S., Seltzer, R., and Menon-Rudolph, S. (1992) Evaluation of a new reagent for covalent attachment of polyethylene glycol to proteins. *Biotechnol. Appl. Biochem. 15*, 100–114.
(15) Nathan, A., Zalipsky, S., Erthel, S. I., Agathos, S. N., Yarmush, M. L., and Kohn, J. (1993) Copolymers of lysine and polyethylene glycol: A new family of functionalized drug carriers. *Bioconjugate Chem. 4*, 54–62.
(16) Nathan, A., Bolikal, D., Vyavahare, N., Zalipsky, S., and Kohn, J. (1992) Hydrogels based on water-soluble poly(ether urethane) derived from L-lysine and poly(ethylene glycol). *Macromolecules 25*, 4476–4484.
(17) Zalipsky, S., and Barany, G. (1990) Facile synthesis of α-hydroxy-ω-carboxymethylpolyethylene oxide. *J. Bioact. Compatible Polym. 5*, 227–231.
(18) Zalipsky, S., and Barany, G. (1986) Preparation of polyethylene glycol derivatives with two different groups at the termini. *Polym. Prepr. Am. Chem. Soc. Div. Polym. Chem. 27(1)*, 1–2.
(19) Wilchek, M., and Miron, T. (1985) Activation of sepharose with N,N′-disuccinimidyl carbonate. *Appl. Biochem. Biotechnol. 11*, 191–193.
(20) Zalipsky, S., Albericio, F., Slomczynska, U., and Barany, G. (1987) A convenient general method for synthesis of N^{α}- or N^{ω}-dithiasuccinoyl (Dts) amino acids and dipeptides: Application of polyethylene glycol as a carrier for functional purification. *Int. J. Pept. Protein Res. 30*, 740–783.
(21) Inman, J. K. (1974) Covalent linkage of functional groups, ligands and proteins to polyacrylamide beads. *Methods Enzymol. 34*, 30–58.
(22) Wilchek, M., and Bayer, E. A. (1987) Labeling glycoconjugates with hydrazide reagents. *Methods Enzymol. 138*, 429–442.
(23) Yokoyama, M., Okano, T., Sakurai, Y., Kikuchi, A., Ohsako, N., Nagasaki, Y., and Kataoka, K. (1992) Synthesis of poly-(ethylene oxide) with heterobifunctional reactive groups at its terminals by an anionic initiator. *Bioconjugate Chem. 3*, 275–276.

Labeling of Immunoglobulins with Bifunctional, Sulfhydryl-Selective, and Photoreactive Coumarins

Janina Baranowska-Kortylewicz and Amin I. Kassis*

Department of Radiology, Nuclear Medicine Division, Harvard Medical School, Shields Warren Radiation Laboratory, 50 Binney Street, Boston, Massachusetts 02115. Received October 27, 1992

4-(Bromomethyl)-6,7-dimethoxy-2-oxo-2*H*-benzopyran (**1a**) and 4-(bromomethyl)-7-methoxy-2-oxo-2*H*-benzopyran (**1b**) and their iodo analogs (**2**) reacted selectively with the sulfhydryl groups generated in a limited reduction of the hinge disulfide bonds of an immunoglobulin G (IgG) giving proteins labeled with a fluorescent and/or radioactive moiety. Quantitative alkylation of free thiol groups was obtained with **1** and $^{125/127}$I-**2**. Photodimerization of these adducts produced IgG with covalently joined heavy chains.

Photoreactive reagents for modification of proteins usually carry two distinct reactive moieties, one photosensitive, such as an azide, and the second conventional, such as an active ester, imidate, or active halogen. The covalent bond formation between side chains of the amino acid backbone of proteins and these modifying reagents relies predominantly on the nucleophilicity of the ϵ-amino group of lysine. The modification at more specific sites involves sulfhydryl groups of cysteine residues obtained by the reduction of either intra- or interchain disulfide bridges and, in glycoproteins, oxidized carbohydrate chains (*1*). Only a few classes of photosensitive groups are currently available in protein-modifying compounds such as azides, diazo derivatives, and benzophenones. Nitrenes and carbenes generated from these compounds upon photolysis react indiscriminately with proteins and solvents. The reaction is nonselective and does not require any specific functional groups. This broad reactivity may not be desirable, however, when a precise reaction site is needed. This is particularly evident in the case of antibodies and enzymes where random covalent modification of protein always involves the risk of reacting amino acid residues in or near the binding site (*2*).

Immunoglobulins in their monomeric form consist of four polypeptide chains, two identical heavy chains (H)[1] and two identical light chains (L), per macromolecule. Each heavy chain is covalently connected to one light chain (HL), and in turn these two HL halves are linked to each other by disulfide bonds. Cysteine residues of immunoglobulins, particularly those that link the two heavy chains, offer a potential site for modification in areas of an antibody remote from the antigen-binding site. The access to these cysteine sulfhydryls requires breaking of the intramolecular disulfide bridges, thus producing two halves of the protein now monofunctional and with an altered structure. The commonly applied sulfhydryl-reactive reagents are based on maleimide derivatives or employ active halides. None of these is capable of rejoining the two HL portions to produce intact IgG. Except for the elegant approach developed by Mitra and Lawton (*3*), which utilizes equilibrium transfer alkylating cross-linking reagents, there are no compounds that can modify IgG at the hinge sulfhydryls and then connect two heavy chains together at the same site.

In an attempt to develop site-selective bifunctional reagents for modification of sulfhydryl groups of cysteine at the hinge of immunoglobulins, we have considered 4-(bromomethyl)coumarins as thiol-alkylating and photoreactive reagents. This class of compounds offers a combination of an active halide, the 4-(bromomethylene) substituent, as a conventional group reactive toward thiols, and a photosensitive moiety, the 3,4-bond of the coumarin ring, known to produce photodimers upon irradiation with incident light of 340–400-nm wavelength. This is a region of the electromagnetic spectrum to which proteins are transparent, so the radiation damage to the target can be minimized. A special feature of these reagents is that the cross-linking can take place only when two coumarins are in the immediate vicinity of each other, i.e., during the reestablishment of the conformational folding of a protein.

EXPERIMENTAL PROCEDURES

All chemicals were reagent grade. Sodium [^{125}I]iodide (specific activity 2200 Ci/mmol) in 10^{-5} M NaOH was purchased from NEN (Du Pont, Billerica, MA). HPLC analyses were conducted on either a C_{18} reverse-phase column using CH_3CN/H_2O (1/1, v/v) as solvent at a flow rate of 1 mL/min or a Maxisil5 silica column (250 × 10 mm; Phenomenex, Rancho Palos Verdes, CA) with CH_2Cl_2/hexane (80/20, v/v) as solvent at a flow rate of 1 mL/min with detection at 280 nm. The radioactive species were detected with a NaI(Tl) 3-in. crystal detector. TLC was done on silica gel plates $60F_{254}$ in $CHCl_3/CH_3OH$ (100/1, v/v) unless otherwise indicated. ITLC of labeled proteins was performed on silica gel impregnated fiber sheets in 80% aqueous methanol (Gelman Sciences Inc., Ann Arbor, MI). ^{1}HNMR spectra were recorded on a Varian T60 spectrometer and UV spectra on a Cary 17 spectrophotometer. SDS-PAGE gels (5–12% gradient) were run according to the standard Laemmli procedure (*4*). Gels of proteins labeled with a fluorescent moiety were photographed using illumination with a hand-held Model UVGL-25 Mineralight lamp at 366 nm (UVP, Inc., San Gabriel, CA). Melting points were taken on a Fisher-Johns melting point apparatus and are uncorrected. Elemental analyses were performed by Galbraith Laboratories (Knoxville, TN).

* Author to whom correspondence should be addressed.

[1] Abbreviations: H, heavy chain of IgG; L, light chain of IgG; HL, half IgG obtained during limited reduction of disulfide bonds; IgG, immunoglobulin G; BSA, bovine serum albumin; ITLC, instant thin-layer chromatography; SDS-PAGE, sodium dodecyl sulfate-polyacrylamide gel electrophoresis; PBS, phosphate-buffered saline, pH 7.4; DTT, dithiothreitol; EDTA, ethylenediaminetetraacetic acid; DMF, *N,N*-dimethylformamide.

1043-1802/93/2904-0300$04.00/0 © 1993 American Chemical Society

Iodination of Coumarin Derivatives (Scheme I). The iodination of both coumarin derivatives has been accomplished using a published procedure without modifications (5). To a shielded-from-light, stirred mixture of 3.34 mmol of coumarin **1a** or **1b** and silver trifluoroacetate (3.34 mmol) in 75 mL of anhydrous $CHCl_3$ was added, over a 30-min period, a solution of an equimolar amount of iodine (6.68 mmol) in 25 mL of $CHCl_3$. This was followed by additional I_2 solution (0.1 g/mL) until no decolorization was observed. The mixture was stirred for 4 h at room temperature or sonicated for 20–60 min. After the substitution was complete, as indicated by TLC, the precipitated AgI was removed by filtration. The filtrate was washed with 0.01% aqueous $NaHSO_3$ and water and was dried over anhydrous $MgSO_4$. The residue obtained after evaporation of $CHCl_3$ was chromatographed on a flash silica gel column in $CHCl_3/CH_3OH$ (200/1, v/v) for **2a** or $CHCl_3$ for **2b,c**.

Radioiodination of Coumarin Derivatives. In a tightly stoppered vial a mixture of 1 mg of Chloramine-T and 0.1–1.0 mCi of $Na^{125}I$ (specific activity 2200 Ci/mmol for no-carrier-added and 1 Ci/mmol for carrier-added preparations in 10^{-5} M NaOH neutralized with equimolar amounts of 10^{-5} M CH_3COOH) in 0.1 mL of water was stirred for 30 min. Chloroform (0.5 mL) was added to this mixture and the stirring continued for up to 30 min until most of the radioactivity was recovered in the chloroform. The organic layer was separated, dried over anhydrous $MgSO_4$, and transferred to a vial containing a stirred mixture of 3.34 μmol of 1 and 4.0 μmol of CF_3COOAg in 0.1 mL of $CHCl_3$. The mixture was allowed to react at room temperature with or without sonication and filtered to remove AgCl and the unreacted CF_3COOAg, and the solvent was evaporated to dryness under nitrogen. The residue was dissolved in either 0.1 mL CH_3CN/H_2O (1/1, v/v) (**2a**) or $CHCl_3$ (**2b,c**) and filtered through a 0.22-μm Millipore filter. Compound **2a** was purified on an HPLC C_{18} reverse-phase column, and compounds **2b** and **2c** on an HPLC silica column. The identity of these compounds was verified by comparing their HPLC and TLC properties with those of **^{127}I-2**.

Limited Reduction of Proteins (Scheme II). Immunoglobulin G (IgG, mouse or rabbit) at a concentration of 5 mg/mL (3.33×10^{-5} M) was dissolved in 0.01 M PBS (2.7 mmol KCl, 120 mmol NaCl), pH 7.6. The solution also contained 0, 10, 20, 50, or 100 molar equiv of DTT and 0.002 M EDTA to chelate any metals that might catalyze the oxidation of free sulfhydryl groups (*6*). The reaction was allowed to proceed at room temperature for 1–2 h, depending on the required degree of reduction. Initially the extent of the reduction in the partially reduced IgG was quantitated with 2,2′-dithiodipyridine (*7*, *8*). Once the selectivity of 1 and 2 was established, these were used to measure the number of free sulfhydryl groups. Partially reduced, not alkylated HL was separated on a Sephadex G-100 column, with 0.1 M propionic acid containing 0.002 M DTT as eluent.

Labeling of Proteins with Radioiodinated Coumarins. To the solution of partially reduced IgG (HL) isolated from a Sephadex G-100 column was added an equal volume of 0.1 M carbonate buffer, pH 8, saturated with argon, and the mixture was concentrated by size-exclusion filtration on Centricon microconcentrators (Amicon Corporation, Danvers, MA). Buffer exchange was repeated three times. After the final filtration the protein content was adjusted to 1 mg/mL, and variable amounts of **^{125}I-2** (0.1–1 mCi) in 10 μL of DMF were added to 0.1 mg of protein depending on the degree of substitution desired. The reaction was continued for 30 min at room temperature. Radiolabeled proteins were chromatographed on a Sephadex G-25 column with PBS as the eluent. The protein fraction collected in the void volume was concentrated on a Centricon filter and the incorporation of radioiodine was determined by trichloroacetic acid precipitation or ITLC in CH_3OH/H_2O (80/20, v/v). Over 98% of ^{125}I was associated with protein. The average conjugation yield was 12%.

Labeling of Proteins with Fluorescent Coumarins. To the crude reaction mixture obtained after the limited reduction of IgG was added 1 either absorbed on Celite (see below) or dissolved in DMF (1 mg/mL) (the reagent was used in sufficient molar excess to remove DTT still present in the reaction mixture and to allow at least an additional 2 molar equiv to react with the protein). The mixture was stirred for 1 h and transferred to a Sephadex G-25 column, and the labeled protein was eluted with PBS. Alternatively, when purified HL fragments were used, the reaction mixture was filtered through 0.2/0.8-μm Acrodisc PF filters (Gelman Sciences, Ann Arbor, MI). Satisfactory labeling was achieved in all cases 10 min after the initiation of the reaction (the visibility of fluorescence of a 1-μg protein band on polyacrylamide gels was used as the criterion). Reaction times of 60 min or longer resulted in complete alkylation of free sulfhydryl groups.

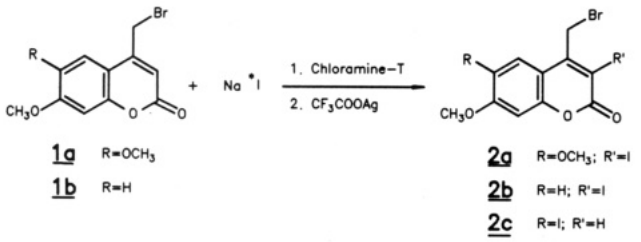
Adsorption of 1 on Celite. To 100 mg of 1 dissolved in 100 mL of chloroform was added 400 mg of Celite which had been dried at 300 °C for 10 min. The chloroform was evaporated to dryness, and the residual powder was dried *in vacuo* overnight and stored shielded from light in a desiccator at room temperature (*9*). The reagent is stable and reactive toward thiols even after 6 months of storage.

Photodimerization (Scheme III). A solution of coumarin-*S*-alkylated HL fragments (3) in PBS (1 mg/mL) was placed in quartz cuvettes and irradiated from a distance of 20 cm with a General Electric long-wave UV plant light at 0–4 °C for 0–180 min. Aliquots of the reaction mixture were analyzed on a reducing 5–12% gradient SDS–PAGE. Typically after 120 min, H fragments were not detectable on gels either with Coumassie Blue staining or by fluorescence. HL labeled with more than six molecules of 1 or **$^{125/127}$I-2** produced the covalently cross-linked HH as a major product, but the presence of protein fragments of molecular mass greater than 100 000 Da on SDS–PAGE run under reducing conditions and the quenching of fluorescence associated with L indicated, in addition, production of covalently cross-linked HL and LHHL molecules.

RESULTS

The iodination of 4-(bromomethyl)-6,7-dimethoxy-2-oxo-2*H*-benzopyran (**1a**) and 4-(bromomethyl)-7-methoxy-2-oxo-2*H*-benzopyran (**1b**) was accomplished in the modified Prévost reaction as described previously (*5*, *10–12*). Trifluoroacetyl hypoiodite generated *in situ* from I_2 or ICl, the latter obtained by oxidation of NaI with *N*-chlorosuccinimide or Chloramine-T, substituted the 3-position of the lactone portion of the coumarin **1a**, producing 3-iodo-4-(bromomethyl)-6,7-dimethoxy-2-oxo-2*H*-benzopyran (**2a**), and the 3- or 6-position of **1b**, giving a mixture of 3-iodo and 6-iodo regioisomers (Scheme I). When the reaction mixture was sonicated, the time required to achieve quantitative substitution was substantially reduced from about 4 h to 20 min. The radioiodinations were conducted under identical conditions. Attempts to iodinate 1 in the absence of silver salt using I_2, ICl, or NaI with a variety of oxidants traditionally used in radioiodinations resulted in the recovery of the unchanged starting material.

Scheme I



The reductive cleavage of the exposed disulfide bonds in IgG was carried out with DTT in PBS (*6*). The reducing agent was used in 10–100 molar excess compared to the moles of protein. The disulfide bridge in rabbit IgG was reduced quantitatively with 10–50 molar equiv of DTT and reaction times not extending beyond 2 h. The reaction with interchain disulfide bonds in the vicinity of the hinge region went to completion with minimal reduction of H–S–S–L bridges, as indicated by gel electrophoresis under nonreducing conditions and by free sulfhydryl determination. For mouse IgG, 100 molar equiv of DTT and longer reaction times were required to generate HL halves of the IgG molecule since this protein contains several hinge disulfide bonds. The number of free sulfhydryl groups in the reduced proteins was estimated with 2,2′-dithiodipyridine using the extinction coefficient of 7600 cm^{-1} M^{-1} at 343 nm in PBS (*7*, *8*). When the selectivity of **1** for thiol groups in proteins was confirmed, the degree of protein alkylation was measured at 350 nm (ϵ 10 120 cm^{-1} M^{-1} for **1a** and ϵ 9600 cm^{-1} M^{-1} for **1b**). Under these conditions, 2–6 thiol groups on average were generated per molecule of rabbit IgG and 8–10 per molecule of mouse IgG. Extinction coefficients (ϵ) used to measure the degree of thiol substitution were determined for model compounds 4-[*S*-(2′-aminoethyl)thio]-6,7-dimethoxy-2-oxo-2*H*-benzopyran and its 7-methoxy analog.

The conjugation of coumarins **1** to reduced IgG was carried out either in a heterogeneous mixture using **1** adsorbed on Celite or in a homogeneous solution by adding the reagent dissolved in DMF to the solution of protein in PBS (Scheme II). The reactions proceeded at approximately the same rate. The use of solid **1** allowed for a simple purification using only filtration through a 0.2-μm filter. For homogeneous reactions it was necessary to use gel filtration chromatography on a Sephadex G-25 column (1 × 15 cm) to remove the unreacted reagent (some precipitation of coumarin occurred at higher coumarin to protein ratios). The removal of excess DTT proved unnecessary in either case since, with the amounts of **1** equal to the molar excess of DTT plus 2 molar equiv for each free SH, quantitative alkylation was achieved (the alkylation product of DTT with **1** is insoluble in buffers and most organic solvents). The labeling of protein with

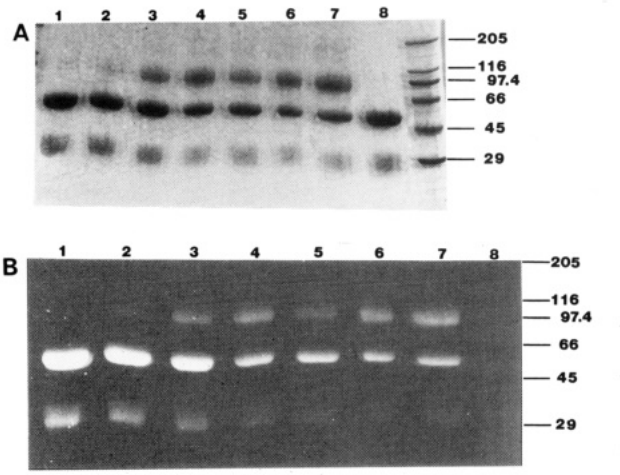
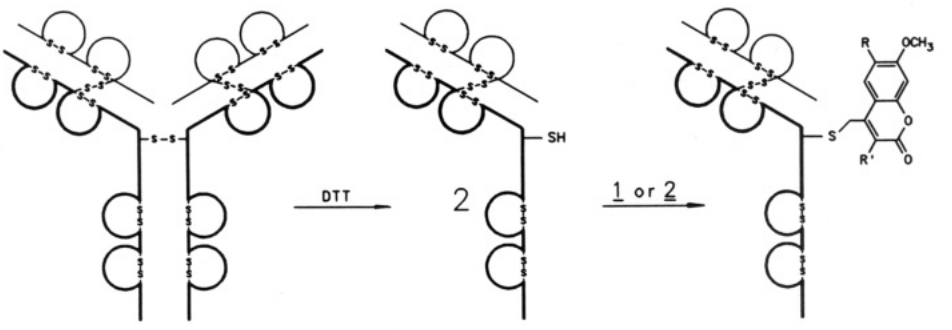


Figure 1. Reducing 5–12% SDS–polyacrylamide electrophoresis of partially reduced rabbit IgG (HL) conjugated to **1a**, irradiated with UV light at 0–4 °C in PBS, and treated at 95 °C with mercaptoethanol-containing buffer. (A) Gel stained with Coomassie Brilliant Blue following irradiation of **3** for 0 (lane 1), 5 (lane 2), 10 (lane 5), 20 (lane 3), 40 (lane 4), 60 (lane 6), and 80 (lane 7) min. In lane 8: intact IgG exposed to a 500 molar excess of **1a**, passed through Sephadex column, irradiated for 120 min, and heated at 95 °C with reducing buffer. In the unmarked lane are SDS–PAGE molecular mass markers: myosin, 205 kDa; β-galactosidase, 116 kDa; phosphorylase b, 97 kDa; BSA, 66 kDa; ovalbumin, 45 kDa; and carbonic anhydrase, 29 kDa. (B) Same gel photographed under illumination with a hand-held UV light.

high specific activity ^{125}**I-2** required the separation of HL chains on a Sephadex column to avoid wasting the radioiodinated reagent in the alkylation of unreacted DTT. The incorporation of radioiodocoumarin into the protein was not as efficient for no-carrier-added preparations as it was for either **1** or carrier-labeled **2**. This is probably attributable to the dilution effect. Trichloroacetic acid precipitation and ITLC indicated that typically about 12% of the total added radioiodinated **2** was covalently bound to HL.

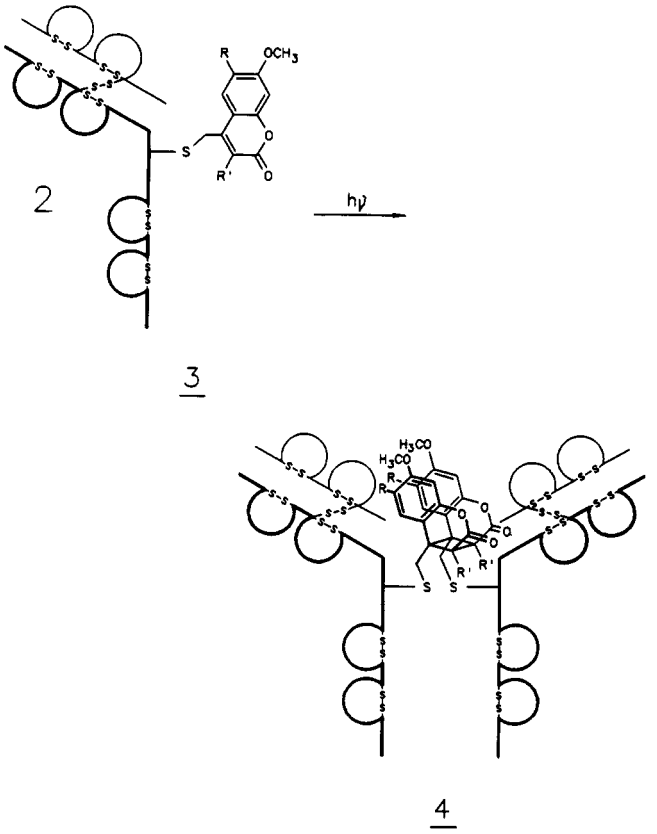
Photodimerization of the adduct **3** or $^{125/127}$**I-3** gave IgG with covalently joined heavy chains (Figure 1A,B; Scheme III). The reaction proceeded without sensitization at 0–4 °C and approached completion after 120 min. For proteins alkylated with six or more coumarin residues, the fluorescence of covalently linked chains persisted even after 120 min. SDS–PAGE of aliquots of the reaction mixture treated with mercaptoethanol at 95 °C was used to determine the progress of photodimerization (Figure 1A,B). Under these conditions all disulfide bridges are reduced; therefore the appearance of new bands with molecular masses other than those of the light and heavy chains is a good measure of the extent of the formation of new covalent bonds not reduced with mercaptoethanol,

Scheme II



3

Scheme III



e.g. photodimers. The individual heavy chains were not detectable after approximately 2 h of irradiation. The major product was two covalently linked heavy chains (molecular mass of about about 100 000 Da), but the quenching of the fluorescence associated with the light chain and the appearance of faint bands with molecular masses over 100 000 Da on reducing SDS gels indicated production of covalently cross-linked HHL (about 125 000 Da) and LHHL (about 150 000 Da) fragments. There were no isolated HL fragments (molecular mass about 75 000 Da) present, indicating that the heavy chains reacted preferentially. The control sample of protein was not reduced with DTT but was directly exposed to 500 molar equiv of 1, then passed through the Sephadex column and irradiated for 120 min. There was neither fluorescence associated with thus treated protein nor any detectable cross-links formed (lane 8 in Figure 1A,B). The photodimerization of $^{125/127}$I-3 resulted in considerable loss of iodine (about 20%–40%) but produced products identical to those observed for 3.

DISCUSSION

Various maleimide and iodoacetamide derivatives of coumarin have been applied as fluorescent probes in histochemistry (*13*, *14*), to measure thiol levels in viable cells in flow cytometry (*15*, *16*), as energy transfer donors or acceptors (*17*, *18*), and to prepare fluorescent enzyme substrates (*19*). Of the two derivatives of coumarin used in this study, 4-(bromomethyl)-7-methoxycoumarin has been reported to S-label thiouridine of tRNA in aqueous solution (*20*, *21*) and to react with pyrimidines found in serum (*22*). The 6,7-dimethoxy analog has been used as a sensitive fluorescent label for chromatographic detection of carboxylic acids in organic solvents (*23*). Nevertheless, the bromine in 4-(bromomethylene)-substituted coumarins is relatively inert. Evidently, it is not replaced by phenols, alcohols, or amines, but it easily reacts with thiols (*21*). Owing to their reactivity toward sulfhydryls, 1 and 2 provide an alternative to the maleimides typically used to label cysteine residues in proteins. Both compounds can be radioiodinated (*5*). The mixture of the original compound and its radiolabeled analog can be used to label proteins, permitting a sensitive, dual detection. The efficiency of sulfhydryl labeling is quantitative when a slight excess of coumarin is used, and we have successfully used this method to determine the number of free thiols on several proteins. This has been tested with DTT-treated human and bovine serum albumins, avidin, and several immunoglobulins. Detection with either UV light at 350 nm or fluorescence is possible. With a quantum yield of over 0.6 in phosphate buffer for 4-substituted, noniodinated 1 (*23*), these compounds may be useful in rapid assays of the immunointegrity of partially reduced antibodies tagged at a site remote from the antigen-binding domain.

A special feature of these reagents is their ability to form photodimers. The chemistry resembles that of psoralen–DNA interactions (*24*). Comparison of the behavior of BSA and half-IgG, both labeled with either **1a** or **1b**, suggests that noteworthy photodimerization can be achieved only when two reacting coumarins are in close vicinity to each other. Labeled albumin, when irradiated with the UV light, reacted slowly and reducing gel electrophoresis on polyacrylamide of samples irradiated for 8 h showed only a small amount of high molecular mass aggregates (data not shown). On the other hand, the photoreaction of 3 gave after 10 min detectable cross-linking of two heavy chains (Figure 1). The effect of distance on the efficiency of photodimerization is presently being tested in our laboratory on model compounds and denatured HL fragments.

The contrasting behavior of free coumarin and 3 gives a good indication of the importance of the ideal arrangement of two photoreacting benzopyran rings. When an aqueous solution of 2-oxo-2*H*-benzopyran was irradiated for 4 weeks, only about 1% of the photodimer was produced (*25*). A similar outcome was observed when the reaction was carried out in ethanol (*26*). These two reports (*25*, *26*) also give some information on the stereochemistry of 4. The only observed product in protic solvents was the *cis*-head-to-head dimer. The reactions run in benzene gave modest yield of *trans*-head-to-head along with traces of *trans*-head-to-tail dimers. Our reactions are conducted in aqueous solution without sensitizers. Therefore the *cis*-head-to-head-dimer seems to be the most probable stereoisomer. It is unlikely that the protein environment is sufficiently hydrophobic [the hinge region of immunoglobulins is proline- and cysteine-rich (*27*)] and that coincidentally a tryptophan residue is located close enough to allow for the energy transfers required to produce the *trans* isomer. Although the precise knowledge of the isomer formed has no bearing on the fact of the formation of photodimer 4, this issue is also being studied with model compounds.

ACKNOWLEDGMENT

This research was supported by DOE Grant DE-FG02-86ER60460 and NIH Grant RO1 CA 15523. The authors wish to thank Dr. Zbigniew P. Kortylewicz for helpful discussions and Mr. Robert M. Berman for excellent technical assistance.

LITERATURE CITED

(1) Brinkley, M. (1992) A brief survey of methods for preparing protein conjugates with dyes, haptens, and cross-linking reagents. *Bioconjugate Chem. 3*, 2–13.
(2) Embleton, M. J., and Garnett, M. C. (1985) *Monoclonal Antibodies for Cancer Detection and Therapy* (R. W. Baldwin, and V. S. Byers, Eds.) pp 317–335, Academic Press Inc., London.
(3) Mitra, S., and Lawton, R. G. (1979) Reagents for the cross-linking of proteins by equilibrium transfer alkylation. *J. Am. Chem. Soc. 101*, 3097–3110.
(4) Laemmli, U. K. (1970) Cleavage of structural proteins during the assembly of the head of bacteriophage T4. *Nature 227*, 680–685.
(5) Baranowska-Kortylewicz, J., and Kortylewicz, Z. P. (1991) Radioiodination of 7-methoxy- and 6,7-dimethoxy-4-bromomethylcoumarins. *J. Labeled Compds. Radiopharm. 29*, 1301–1307.
(6) Konigsberg, W. (1972) Reduction of disulfide bonds in proteins with dithiothreitol. *Methods Enzymol. 25B*, 185–188.
(7) Grassetti, D. R., and Murray, J. F. (1967) Determination of sulfhydryl groups with 2,2′- or 4,4′-dithiodipyridine. *Arch. Biochem. Biophys. 119*, 41–49.
(8) Pedersen, A. O., and Jacobsen, J. (1980) Reactivity of the thiol group in human and bovine albumin at pH 3–9, as measured by exchange with 2,2′-dithiodipyridine. *Eur. J. Biochem. 106*, 291–295.
(9) Rinderknecht, H. (1960) A new technique for the fluorescent labelling of proteins. *Experientia 16*, 430–431.
(10) Wilson, C. V. (1957) The reaction of halogens with silver salts of carboxylic acids. *Org. Reactions 9*, 332–387.
(11) Chen, E. M., Keefer, R. M., and Andrews, L. J. (1967) Acetyl hypoiodite as an aromatic iodinating agent. *J. Am. Chem. Soc. 89*, 428–430.
(12) Barnett, J. R., Andrews, L. J., and Keefer, R. M. (1972) Trifluoroacetyl hypohalites as aromatic halogenating agents. *J. Am. Chem. Soc. 94*, 6129–6134.
(13) Sippel, T. O. (1981) New fluorochromes for thiols: Maleimide and iodoacetamide derivatives of a 3-phenylcoumarin fluorophore. *J. Histochem. Cytochem. 29*, 314–316.
(14) Sippel, T. O. (1981) Microfluorometric analysis of protein thiol groups with a coumarinylphenylmaleimide. *J. Histochem. Cytochem. 29*, 1377–1381.
(15) Olive, P. L., Biaglow, J. E., Varnes, M. E., and Durand, R. E. (1983) Characterization of the uptake and toxicity of a fluorescent thiol reagent. *Cytometry 3*, 349–353.
(16) Durand, R. E., and Olive, P. L. (1983) Flow cytometry techniques for studying cellular thiols. *Radiat. Res. 95*, 456–470.
(17) Holowka, D., and Baird, B. (1983) Structural studies on the membrane-bound immunoglobulin E-receptor complex. 2. Mapping of distances between sites on IgE and the membrane surface. *Biochemistry (Washington) 22*, 3475–3484.
(18) Odom, O. W., Dabbs, E. R., Dionne, C., Müller, M., and Hardesty, B. (1984) The distance between S1, S21, and the 3′ end of 16S RNA in 30S ribosomal subunits. The effect of poly(uridylic acid) and 50S subunits on these distances. *Eur. J. Biochem. 142*, 261–267.
(19) Knight, C. G. (1991) A quenched fluorescent substrate for thimet peptidase containing a new fluorescent amino acid, DL-2-amino-3-(7-methoxy-4-coumaryl)propionic acid. *Biochem. J. 274*, 45–48.
(20) Yang, C.-H., and Söll, D. (1974) Covalent attachment of fluorescent groups to transfer ribonucleic acid. Reactions of 4-bromomethyl-7-methoxy-2-oxo-2*H*-benzopyran. *Biochemistry (Washington) 13*, 3615–3621.
(21) Secrist, J. A., III, Barrio, J. R., and Leonard, N. J. (1971) Attachment of a fluorescent label to 4-thiouracil and 4-thiouridine. *Biochem. Biophys. Res. Commun. 45*, 1262–1270.
(22) Yoshida, S., Hirose, S., and Iwamoto, M. (1986) Use of 4-bromomethyl-7-methoxycoumarin for derivatization of pyrimidine compounds in serum analysed by high-performance liquid chromatography with fluorimetric detection. *J. Chromatogr. 383*, 61–68.
(23) Farinotti, R., Siard, P., Bourson, J., Kirkiacharian, S., Valeur, B., and Mahuzier, G. (1983) 4-Bromomethyl-6,7-dimethoxycoumarin as a fluorescent label for carboxylic acids in chromatographic detection. *J. Chromatogr. 269*, 81–90.
(24) Cimino, G. D., Gamper, H. B., Isaacs, S. T., and Hearst, J. E. (1985) Psoralens as photoactive probes of nucleic acid structure and function: organic chemistry, photochemistry, and biochemistry. *Annu. Rev. Biochem. 54*, 1151–1193.
(25) Anet, R. (1962) The photodimers of coumarin and related compounds. *Can. J. Chem. 40*, 1249–1257.
(26) Hammond, G. S., Stout, C. A., and Lamola, A. A. (1964) Mechanisms of photochemical reactions in solution. XXV. The photodimerization of coumarin. *J. Am. Chem. Soc. 86*, 3103–3106.
(27) Jeske, D. J., and Capra, J. D. (1986) Immunoglobulins: structure and function. *Fundamental Immunology* (W. P. Paul, Ed.) pp 136–137, Raven Press, New York.

Labeling of Sulfhydryl Groups in Intact Mammalian Cells with Coumarins

Janina Baranowska-Kortylewicz and Amin I. Kassis*

Department of Radiology, Nuclear Medicine Division, Harvard Medical School, Shields Warren Radiation Laboratory, 50 Binney Street, Boston, Massachusetts 02115. Received October 27, 1992

4-(Bromomethyl)-6,7-dimethoxy-2-oxo-2*H*-benzopyran (1) and its 3-[^{125}I]iodo derivative (2) were reacted with sulfhydryl groups of proteins in viable Chinese hamster V79 lung fibroblasts. Pretreatment of cells with dithiothreitol (DTT) as the reducing agent was necessary to give detectable levels of fluorescence. In the absence of DTT, V79 cells incorporated about 1×10^{-3} pCi/cell of the radioiodinated, no-carrier-added derivative; following incubation of cells with 320 μM DTT the uptake was nearly doubled (1.87×10^{-3} pCi/cell).

Several derivatives of coumarin have been used in histopathology as fluorescent probes to label thiol groups in tissue sections (*1, 2*). Some of these reagents have also been examined for their ability to bind to living cells (*3*). Only 3-(4-maleimidylphenyl)-4-methyl-7-(dimethylamino)coumarin stained viable cells (*3, 4*). Since we have found that 4-(bromomethyl)-6,7-dimethoxycoumarin (1) selectively reacts with free sulfhydryl groups in soluble proteins, it was of interest to determine whether this reactivity would also be expressed toward sulfhydryl groups in intact mammalian cells. Such an agent could also be useful in examining the radiotoxic effects of Auger-electron-emitting radioisotopes, such as ^{125}I, when localized on the cell surface. Chinese hamster V79 lung fibroblasts were incubated with fluorescent compound 1 or the no-carrier-added, radioiodinated derivative 2, and the ability of these compounds to label thiol groups in intact cells was examined.

EXPERIMENTAL PROCEDURES

All chemicals were reagent grade. Sodium [^{125}I]iodide (specific activity 2200 Ci/mmol) in 10^{-5} M NaOH was purchased from NEN (Du Pont, Billerica, MA). Radioiodination of coumarin has been described previously (*5*).

Direct Coupling of 3-[^{125}I]Iodo-4-(bromomethyl)-6,7-dimethoxy-2-oxo-2*H*-benzopyran (2) to Sulfhydryl Groups on Cell Membranes. Exponentially growing monolayers of Chinese hamster V79 fibroblasts were released from plates by 0.1% trypsin, washed with Ca^{+2}- and Mg^{+2}-free PBS,[1] and suspended in the same buffer (1×10^7 cells/mL). A solution of DTT (0.1 M) in Ca^{+2}- and Mg^{+2}-free PBS was added to the cell suspension in a final concentration of 0, 3.2, 32, or 320 μM. After a 1-h incubation at 0–4 °C on a hematological roller shaker, the cells were washed three times with PBS by pelleting (900*g*, 10 min) and resuspended in PBS containing 0.1 μCi of 2 (2200 Ci/mmol) per 10^7 cells. The reaction was continued at 0–4 °C for 1 h on a rotating mixer. The cells were pelleted at 600*g* for 10 min. Aliquots of supernatant were counted in a γ counter. Cell pellets were washed three times in Dulbecco's Modified Eagle Medium containing 10% fetal calf serum and their radioactive content was determined. The viability of radiolabeled cells was checked by the trypan blue dye exclusion assay. Routinely about 70% of the cells were viable.

For determination of membrane-bound ^{125}I, cell pellets were suspended in 0.001 M potassium phosphate buffer, pH 7.0, containing 0.25 M sucrose and 0.001 M EDTA, allowed to swell for about 10 min, and disrupted in a Dounce homogenizer with a loosely fitting Teflon pestle. The slurry was centrifuged at 2000*g* for 20 min to remove unbroken cells and nuclei. The pellet was then homogenized and centrifuged a second time. The supernatants from the two centrifugations were combined and centrifuged at 10000*g* for 30 min to collect cell membranes (*6*). The radioactivity associated with membrane pellets was determined in a γ counter. Control cells were first treated with 320 μM DTT and then incubated with 0.01% L-cysteine in PBS for 20 min. After washing with medium and PBS, cells were resuspended in Ca^{+2}- and Mg^{+2}-free PBS and reacted with 2 at 0–4 °C for 1 h. Following this treatment cells were processed as described above.

Coupling of 3-[^{125}I]Iodo-4-(bromomethyl)-6,7-dimethoxy-2-oxo-2*H*-benzopyran (2) to V79 Lung Fibroblasts through *N*-Succinimidyl 3-(2-Pyridyldithio)propionate (SPDP). The cell-surface amino groups of V79 cells were reacted with 25 μmol SPDP/10^7 cells per mL of PBS at 0–4 °C for 20 min on a rotating mixer. Cells were washed twice with medium containing 10% fetal calf serum to remove any free SPDP and twice with PBS by pelleting (900*g*, 10 min). They were then suspended in PBS (10^7 cells/mL) and reacted with 0, 3.2, 32, or 320 μM DTT (see above). The optical density of supernatants at 343 nm was used as an approximate measure of the total number of free sulfhydryl groups on the cell surface (*7, 8*). For 0 and 3.2 μM DTT the change in absorbance was below 0.005 AU and thus outside the limits of experimental error. Cells washed with PBS were then reacted with 2 and treated as described above.

Fluorescence Microscopy. V79 cells grown overnight as monolayers on glass slides were incubated with 320 μM DTT in Ca^{+2}- and Mg^{+2}-free PBS, washed with the same buffer, incubated with 0.1 μM 1 in saline for 5–10 min, washed with medium and PBS, and then examined under the fluorescence microscope.

RESULTS AND DISCUSSION

The labeling of sulfhydryl groups on the cell membrane was examined to determine the potential value of 1 and 2 as fluorescent probes in flow cytometry, in assessing the cell-membrane thiol content, and as carriers of Auger-

* Author to whom correspondence should be addressed.

[1] Abbreviations: PBS, phosphate-buffered saline, pH 7.4; DTT, dithiothreitol; EDTA, ethylenediaminetetraacetic acid; SPDP, *N*-succinimidyl 3-(2-pyridyldithio)propionate.

1043-1802/93/2904-0305$04.00/0 © 1993 American Chemical Society

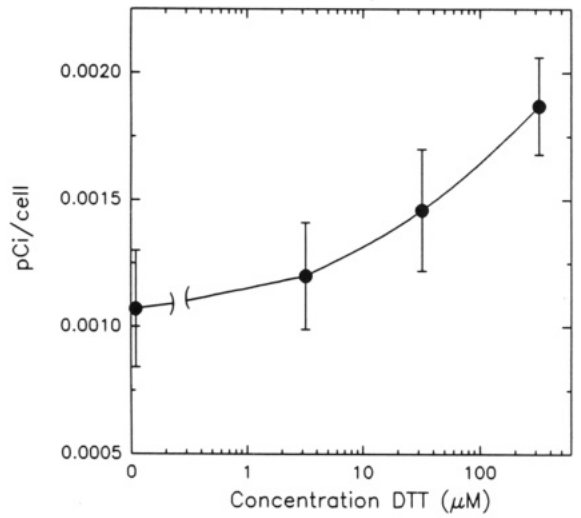


Figure 1. Uptake of no-carrier-added radioiodinated coumarin **2** in Chinese hamster V79 lung fibroblasts exposed to variable concentrations of DTT (mean and standard error of mean are shown; $n = 3$). Cells were treated with DTT, washed with PBS, and reacted with 0.1 μCi/10^7 cells.

electron-emitting radionuclides for examining their cellular radiotoxicity. Both coumarins were found to label the sulfhydryl groups of intact mammalian cells. The incorporation of radioiodide as measured in disrupted and fractionated cells indicated that about 1×10^{-3} pCi/cell reacted with the proteins of the V79 lung fibroblast membranes in the absence of DTT; when cells pretreated with 320 μM DTT were exposed to **2** the incorporation was nearly doubled (1.8×10^{-3} pCi/cell) (Figure 1). The average labeling of the cell surface was 1.07×10^{-3} [standard deviation (SD) 0.40×10^{-3}] pCi/cell for cells not treated with DTT and 1.20×10^{-3} (SD 0.36×10^{-3}), 1.46×10^{-3} (SD 0.42×10^{-3}), and 1.87×10^{-3} (SD 0.34×10^{-3}) pCi/cell for cells treated with 3.2, 32, and 320 μM DTT, respectively (mean and standard deviation were determined from data obtained in three experiments). All of the ^{125}I was found to be associated with cell membranes. Control cells that were first treated with 320 μM DTT and then incubated in PBS containing 0.01% L-cysteine incorporated only 2.73% (SD 1.05) of the total added **2**. The radioactivity associated with cell membranes was 4×10^{-4} pCi/cell (SD 1×10^{-4}), about 50% less that in untreated cells, indicating that there are free sulfhydryl groups on the cell surface even prior to DTT treatment. Since the labeling with the no-carrier-added material resulted in a relatively low degree of substitution, surface proteins of viable V79 cells were derivatized with SPDP to increase the number of available thiol groups. V79 cells that were first reacted with SPDP and then reduced with DTT incorporated over 30% of the total added radioactivity (3.5×10^{-3} pCi/cell; SD 0.5×10^{-3}) but only 40% of this ^{125}I was bound to the cell membranes. The average incorporation into SPDP-treated cells without DTT was about 1×10^{-3} pCi/cell, 20% of which was located on the cell surface. A no-carrier-added reagent was used in all experiments involving DTT reduction as well as in these with SPDP/DTT; therefore the labeling of intracellular proteins in cells derivatized with SPDP cannot be attributed to the concentration of the tracer. A more likely explanation seems to be the damaging effect of SPDP/DTT treatment on cell membranes.

Fluorescence microscopy confirmed binding of **1** to V79 cells (Figure 2) and demonstrated that pretreatment of the cell surface with excess DTT was necessary to achieve detectable labeling levels. Cysteine, which also reacts with

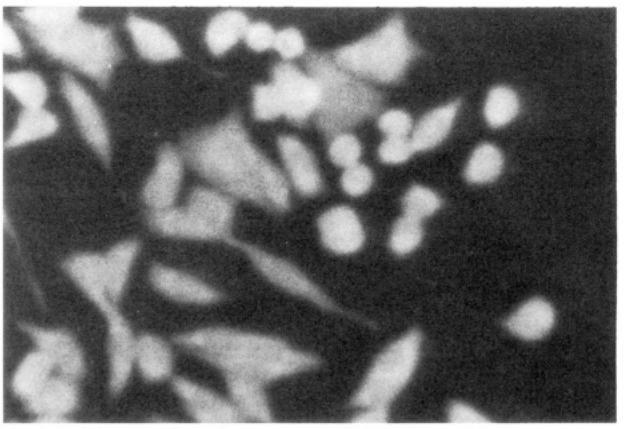


Figure 2. Fluorescent staining of cell membranes; UV excitation, original magnification ×40. Live Chinese hamster V79 lung fibroblasts were treated with 320 μM DTT and exposed to 0.1 μM **1** for 10 min. Cells incubated with **1** alone were invisible under fluorescence microscopy (data not shown).

free sulfhydryl groups on the cell surface (*9*), effectively blocked binding of radiolabeled coumarin and its fluorescent analog, indicating that only sulfhydryl groups were derivatized.

The viability of V79 fibroblasts following treatment with DTT and **1** or **2** was reduced from over 95% to 70%, as indicated by the trypan blue dye exclusion estimate. The coumarin derivative tested by Olive *et al.* (*3*) had a mean lethal dose (MLD; approximate concentration required to reduce survival to 37%) of 8 μg/mL; the concentration of no-carrier-added **2** was several orders of magnitude lower than the MLD. Similarly the concentration of **1** was about 200 times lower than the MLD. Therefore it appears that the reduction of the viability of fibroblasts to 70% resulted from the overall handling of cells (reaction with DTT, repeated washing, etc.).

The estimated number of sulfhydryl groups radiolabeled with **2** is about 300/cell; the DTT pretreatment increases this value to 600. Earlier estimates put the number of sulfhydryl groups at 2.75×10^5, 19×10^5, and 370×10^5/cell in platelets, lymphocytes, and Ehrlich ascites tumor, respectively (*9*). Since it is unlikely that V79 cells have an extremely small number of sulfhydryl groups on the cell surface, it appears that our method may have grossly underestimated the total expected number of cellular thiols. It is also possible that since cellular binding is reported to be directly dependent on the coumarin:cell ratio (*3*), only the most accessible sulfhydryl groups are radiolabeled at the trace levels of **2**.

ACKNOWLEDGMENT

This research was supported by DOE Grant DE-FG02-86ER60460 and NIH Grant RO1 CA 15523. The authors wish to thank Dr. Zbigniew P. Kortylewicz for helpful discussions and Mr. Robert M. Berman for his excellent technical assistance.

LITERATURE CITED

(1) Sippel, T. O. (1981) New fluorochromes for thiols: maleimide and iodoacetamide derivatives of 3-phenylcoumarin. *J. Histochem. Cytochem. 29*, 314–316.

(2) Sippel, T. O. (1981) Microfluorometric analysis of protein thiol groups with coumarinylphenylmaleimide. *J. Histochem. Cytochem. 29*, 1377–1381.

(3) Olive, P. L., Biaglow, J. E., Varnes, M. E., and Durand, R. E. (1983) Characterization of the uptake and toxicity of a fluorescent thiol reagent. *Cytometry 3*, 349–353.

(4) Durand, R. E., and Olive, P. E. (1983) Flow cytometry techniques for studying cellular thiols. *Radiat. Res. 95*, 456–470.
(5) Baranowska-Kortylewicz, J., and Kortylewicz, Z. P. (1991) Radioiodination of 7-methoxy and 6,7-dimethoxy-4-bromomethylcoumarins. *J. Labelled Compds. Radiopharm. 29*, 1301–1307.
(6) Morre, D. J., and Morre, D. M. (1989) Preparation of mammalian plasma membranes by aqueous two-phase partition. *Biotechniques 7*, 946–958.
(7) Grassetti, D. R., and Murray, J. F. (1967) Determination of sulfhydryl groups with 2,2′- and 4,4′-dithiodipyridine. *Arch. Biochem. Biophys. 119*, 41–49.
(8) Pedersen, A. O., and Jacobsen, J. (1980) Reactivity of the thiol group in human and bovine albumin at pH 3–9, as measured by exchange with 2,2′-dithiodipyridine. *Eur. J. Biochem. 106*, 291–295.
(9) Mehrishi, J. N., and Grassetti, D. R. (1969) Sulfhydryl groups on the surface of intact Ehrlich ascites tumour cells, human blood platelets and lymphocytes. *Nature 224*, 563–564.

Bioconjugate Chemistry

SEPTEMBER/OCTOBER 1993
Volume 4, Number 5

© Copyright 1993 by the American Chemical Society

ARTICLES

Synthesis and Characterization of a Penicillin–Poly(L-Lysine) Which Recognizes Human IgE Anti-Penicillin Antibodies

Enrico Caneva, Patrizia Di Gennaro, Francesca Farina, Marco Orlandi, and Bruno Rindone*

Dipartimento di Chimica Organica e Industriale, Universitá di Milano, and CNR Center, Via Venezian 21, I-20133 Milano, Italy

Paolo Falagiani

Lofarma Allergeni S.R.L., Viale Cassala 40, I-20143 Milano, Italy. Received August 5, 1992

Conjugates of poly(L-lysine) containing a penicillin or a penicilloyl residue were prepared and characterized by ^1H NMR and by size-exclusion HPLC. These conjugates and conjugates with human serum albumin were used in radioallergosorbent tests (RAST) for the determination of allergy toward penicillins.

INTRODUCTION

In spite of a recent claim suggesting the overestimation of allergy to penicillin (*1*), most research groups agree with the importance of this pathology (*2*), which may cause severe health problems (*3*). Penicillins are low molecular weight substances which are not themselves antigenic but give rise to a number of different antigenic determinants either by metabolism in vivo or by breakdown in vitro before administration (*4*). The major antigenic determinant is the penicilloyl group derived from the cleavage of the β-lactam ring of penicillin (*5*), and many allergic reactions to penicillin are due to antibodies specific to this group (*6*). Other β-lactam cleavage products may also act as haptens and are known as "minor determinants" (*7*). These are associated with the majority of the severe immediate reactions to penicillin G (*8*). Allergy to penicillin itself is not clearly documented.

Skin tests are often used for the diagnosis of penicillin allergy (*9–12*). The materials used for these tests are essentially penicillin-protein conjugates (*13*). Several "in vitro" tests for the determination of allergy to penicillin derivatives are also based on penicillin–protein conjugates (*14*). These conjugates are not generally chemically well-characterized, and this has a consequence in the uncertainty about the structure of the determinant(s).

A chemical characterization of these compounds is also necessary since penicillin conjugates with tissue macromolecules (proteins, carbohydrates, lipids) are the compounds which elicit antibody formation (*15,16*). Moreover, knowledge of the structure of the antigenic determinants of penicillin conjugates may allow the preparation of monovalent derivatives which could be used to desensitize patients prior to administration of the drug (*17*).

EXPERIMENTAL PROCEDURES

Instrumentation. NMR spectra were measured in D_2O using a Varian AC300 instrument. HPLC analyses were performed with a Waters 600E HPLC. The detector was a Hewlett-Packard 1040 diode-array detector. Electrophoresis was performed with a LKB 2117 Multiphor II instrument. The γ-counter was a Packard Cobra instrument.

Reagents. Poly(L-lysine) (L-PLL) hydrobromide ($n \approx$ 145 and 54) and human serum albumin (HSA) were

1043-1802/93/2904-0309$04.00/0 © 1993 American Chemical Society

purchased from Sigma Chemicals; *N*-[3-(dimethylamino)-propyl]-*N'*-ethylcarbodiimide (ECDI), *tert*-butylamine, and isobutyl chlorocarbonate were Aldrich products; penicillin G and V were Farmitalia Carlo Erba products. Membranes for dialysis were Spectra/Por products. Polystyrene beads were activated with glutaraldehyde according to the Italian Patent No. 1,218,348. Labeled, affinity-purified anti-human IgE from goat was a Lofarma product.

Preparation of Penicillin G–Poly(L-lysine) (PG-L-PLL). (*a*) *Using the Carbodiimide 3 as Coupling Reagent.* Penicillin G (**2**) (33 mg, 0.09 mmol) was added to a solution of L-PLL (**1**) (13 mg, 0.0007 mmol) in 5 mL of 0.2 M aqueous buffer, pH 7.1 (K_2HPO_4/KH_2PO_4), and the resulting solution was stirred at 4 °C. After 5 min, 17 mg (0.09 mmol) of the carbodiimide **3** was added and this solution was stirred at 4 °C for 12 h. Low molecular weight reagents and byproducts were removed by dialysis for 120 h at 4 °C with a 3500 Da cutoff membrane. The product **4** (10 mg) was then obtained by lyophilization.

(*b*) *Using the Method via Mixed Anhydride.* *tert*-Butylamine (12 μL, 0.115 mmol) and 15 μL of isobutyl chlorocarbonate (0.115 mmol) were added to a solution of 30 mg (0.0898 mmol) of penicillin G (**2**) in 2 mL of pyridine and the resulting solution was stirred at 4 °C for 30 min and then poured into a solution of 15 mg of L-PLL (**1**) (0.00075 mmol) in 3.8 mL of a 0.2 M aqueous phosphate buffer, pH 8 (K_2HPO_4/KH_2PO_4), maintained at 4 °C. After 4 h at the same temperature, the solution was dialyzed at 0 °C for 7 days with a 3500 Da cutoff membrane. The product (15 mg) was then obtained by lyophilization.

Preparation of L-PLL Conjugates. L-PLL conjugates at different pH's were prepared using the carbodiimide **3** as coupling reagent in 0.2 M aqueous phosphate buffer of the required pH.

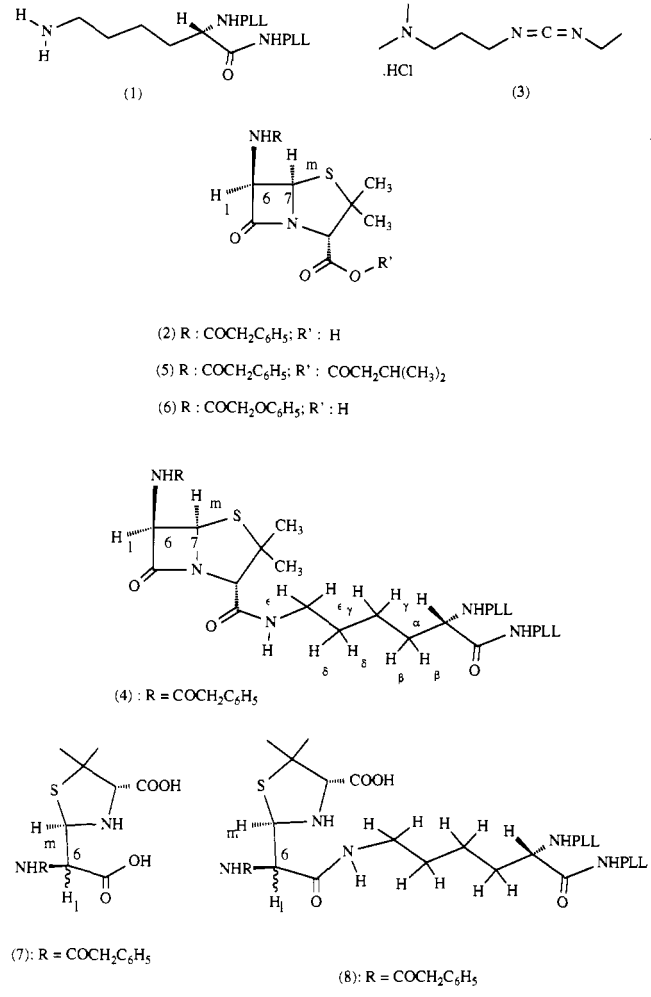
Preparation of HSA Conjugates. Penicillin G (**2**) (100 mg, 0.174 mmol) was added to a solution of HSA (100 mg, 0.00147 mmol) in 15 mL of 0.2 M aqueous buffer at the required pH (K_2HPO_4/KH_2PO_4) and the resulting solution was stirred at 4 °C. After 5 min, 67 mg (0.36 mmol) of the carbodiimide **3** was added and this solution was stirred at 4 °C for 12 h. Low molecular weight reagents and byproducts were removed by dialysis for 120 at 4 °C with a 3500 Da cutoff membrane. The product (80 mg) was then obtained by lyophilization.

Conjugates at pH 11. The conjugates at pH 11 were prepared using a 0.2 M phosphate buffer alkalinized with sodium hydroxide.

HPLC Analyses. SE-HPLC was performed by dissolving 2 mg of the sample in 0.03 M phosphate buffer (K_2HPO_4/KH_2PO_4 pH = 6.8)–0.1 M potassium chloride and injecting through a Rheodyne 100-μL loop. The instrument was equipped with a Synchropak GPC 100 (30 cm × 7.8 mm i.d.) SE column. The separation was achieved under isocratic conditions; the elution solvent was 0.03 M phosphate buffer (K_2HPO_4/KH_2PO_4, pH 6.8)–potassium chloride 0.1 M at a flow rate of 0.8 mL/min.

Radioallergosorbent Test (RAST). A solution of the conjugate (0.1 mg/mL) was treated for 12 h at 25 °C with glutaraldehyde-activated polystyrene beads. Human serum (50 μL) were incubated with the solid phase for 3 h at 25 °C in a horizontal shaker. After three washing cycles with 0.15 M phosphate buffer, pH 7.2, containing 0.15% BSA and 0.4% Tween 20, each solid phase was incubated with 50 μL of anti-human goat IgE antibody labeled with ^{125}I (4 μCi/100 tubes) for 12 h at 25 °C in a horizontal shaker. After three further washing cycles as above, the solid phases were counted with a γ-counter. The results are expressed as percent bound radioactivity.

Chart I



RESULTS AND DISCUSSION

The reaction of poly(L-lysine) (L-PLL-NH_2, **1**, Chart I), average MW 20 kDa (*18*), with excess penicillin G (PG, **2**), at pH 7.1, in the presence of the water-soluble carbodiimide **3** (ECDI) (*19*) gave, after extensive dialysis at 0 °C, the conjugate **4**. This was constituted of a family of poly(L-lysines) derivatized at the primary amino group at C_ϵ with a penicillin fragment. This conclusion resulted from the ^1H NMR spectrum in D_2O. H_l and H_m appeared at δ 5.45 and 5.53 with a J = 4 Hz. Hence, they were in the same position and had the same multiplicity as the corresponding protons in PG. In particular, the coupling constant showed also that the chirality at C_6 and C_7 had been retained. The aromatic hydrogens of the penicillin residue appeared at δ 7.75 as a multiplet. The hydrogens H_α, H_β, H_γ, H_δ, and H_ϵ of the poly(L-lysine) residue resonated as multiplets at δ 4.29, 1.77, 1.45, 1.77, and 3.00, respectively. These attributions were confirmed by a ^1H-COSY experiment (Figure 1).

The integration of the aromatic protons and H_α suggested that the family of derivatized poly(L-lysine) molecules constituting the conjugate contained, on average, 10% penicillin residues. This value indicates that an average amount of 14.1 molecules of PG were attached to each poly(L-lysine) molecule. Hence, the conjugate consisted of an average distribution of one residue of PG for 11.0 L-lysines in L-PLL.

This evaluation of percent haptenization of a polypeptide or a protein turned out to be by far more precise that the spectrophotometric determination which was per-

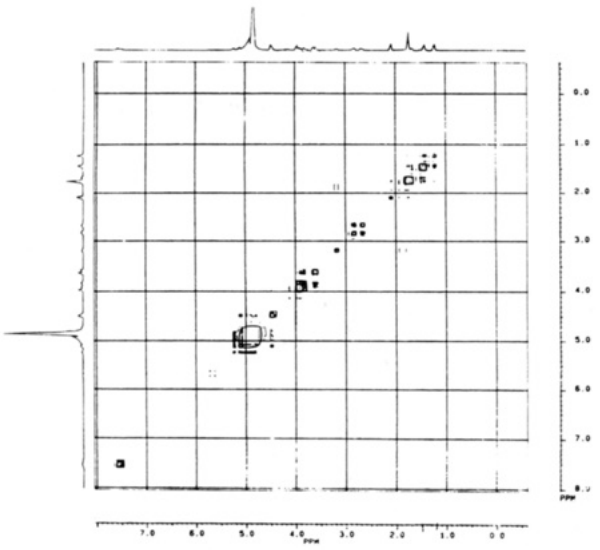


Figure 1. ^{1}H-COSY spectrum of PG-L-PLL (prepared at pH 7.1) in D_2O.

formed by monitoring the absorbance at 260 nm. At this wavelength the penicillin residue has its maximum, and L-PLL does not absorb. For the quantitative evaluation of percent haptenization the molar extinction coefficient (ϵ) of PG (2) was used, and this introduced an approximation to the measure since the value of ϵ for PG is expected to be different from that of PG-L-PLL. In fact, a 5.5% haptenization resulted from this method.

The high percent haptenization of L-PLL obtained with this synthetic method is of value. It has been pointed out that a too low percent haptenization of the protein carrier lowers the effectiveness of the conjugate in eliciting wheal and flare in penicillin-sensitized human subjects (*20*). Using penicilloylated BSA as the immunizing antigen in mice, it was found that an epitope number higher than 11 penicilloyl residues per protein molecule induces significant antibody formation after a single injection, whereas 0.6 penicilloyl residues per BSA molecule do not induce penicilloyl-specific antibodies (*21*).

A further indication of the presence of the intact penicillin residue in the conjugate was obtained by putting a gel containing a culture of *Bacillus subtilis* (*22*) over the plate which had been used in an electrophoretic analysis of **4**. The growth of the microorganism was inhibited in the area to which **4** had migrated, showing that **4** had retained the antibacterial property typical of intact penicillin G[23] (Figure 2).

Size-exclusion HPLC (SE-HPLC) analysis of the conjugate was performed monitoring the eluate at 220 nm (the absorption maximum of PLL) and at 260 nm (the absorption maximum of PG). A peak absorbing at 220 nm appeared at the elution time of L-PLL, and in its tail there appeared the absorption at 260 nm due to where the penicillin residue was concentrated (Figure 3a).

Other authors have prepared penicillin–poly(L-lysine) conjugates. An alkaline pH was generally used. In particular, a recent synthetic method (*24*) forms a benzylpenicilloyl–poly(L-lysine) (BPO-L-PLL), and this conjugate has been used in the determination of IgE antibodies to the BPO determinant (*25*). We repeated this preparation at pH 9.5 in the scope of giving a structure to this conjugate by ^{1}H NMR spectroscopy. A blank experiment showed that penicillin G is transformed at pH 9.5 into a 2:1 mixture of two diastereoisomers of penicilloic acid (**7**) as shown by the ^{1}H NMR spectrum (Figure 4). In fact, the two methyl groups of the major stereoisomer resonated



Figure 2. Electrophoretic analysis of PG-L-PLL (prepared at pH 7.1). The plate was incubated with *B. subtilis*. Growth was inhibited in the positions where PG-PLL had migrated.

at δ 1.27 and 1.55 as singlets. Those of the minor diastereoisomer resonated at δ 1.09 and 1.63. H_l and H_m resonated at δ 4.26 and 5.10 as multiplets. Hence, a downfield shift occurred with both protons, indicating the cleavage of the β-lactam ring. The presence of two diastereoisomers could be attributed to the racemization of the chiral center at C_6 in alkaline conditions. Hence, the conjugate of PG and L-PLL prepared at alkaline pH was likely to consist in two diastereoisomeric families of compounds. In fact performing the reaction at pH 11 gave a conjugate whose ^{1}H-NMR spectrum showed a 16% haptenization. The signals of H_l and H_m in the ^{1}H-COSY spectrum (Figure 5) suggested a benzylpenicilloyl–poly(L-lysine) structure (**8**) for this conjugate. In fact, a multiplet at δ 5.10 attributable to the diastereoisomeric H_m was observed in this spectrum. H_l resonated in the same region of H_α of L-PLL and could not be observed. The SE-HPLC analysis (Figure 3b) confirmed that this conjugate was different from that prepared at pH 7.1.

An alternative procedure for the preparation of PG-L-PLL consisted in the formation of the mixed anhydride **5** by reaction of **2** with isobutyl chlorocarbonate in pyridine. The reaction of **5** with L-PLL at pH 8.5 gave a conjugate which showed a 16% haptenization of L-PLL. The SE-HPLC analysis is shown in Figure 3c. Three peaks containing the aromatic chromophore were present. The SE-HPLC retention time and the ^{1}H-NMR analysis of the mixture showed that one of them was PG-L-PLL. Hence, this procedure was not suitable for the preparation of chemically defined conjugates.

The use of L-PLL of lower molecular weight (5-10 kDa) gave results very similar to those reported above.

The fact that different penicillin derivatives were present in the conjugates independent of the conjugation procedure stimulated us to prepare conjugates of human serum albumin (HSA) and PG or PV. These are in fact used is solid-phase assays (*26*) and BPO-HSA conjugates were found in sera of penicillin-treated patients (*27*).

A reaction performed at pH 7, where a prevalence of unchanged penicillin molecules should be attached to HSA, gave a conjugate which was analyzed by SE-HPLC (Figure 3d). PG-HSA had the main peak at 8.8 min and two further peaks at 11.1 and 11.7 min. A blank experiments showed that HSA is eluted at 7.8 min in the same conditions. Hence, haptenization of HSA resulted in a longer elution time. This chromatographic behavior suggests that PG-HSA fits the pores of the SE-HPLC material more efficiently than HSA. This occurs generally either when the molecular size is decreased (e.g. by a fragmentation reaction) or when folding of the polypeptide chain has

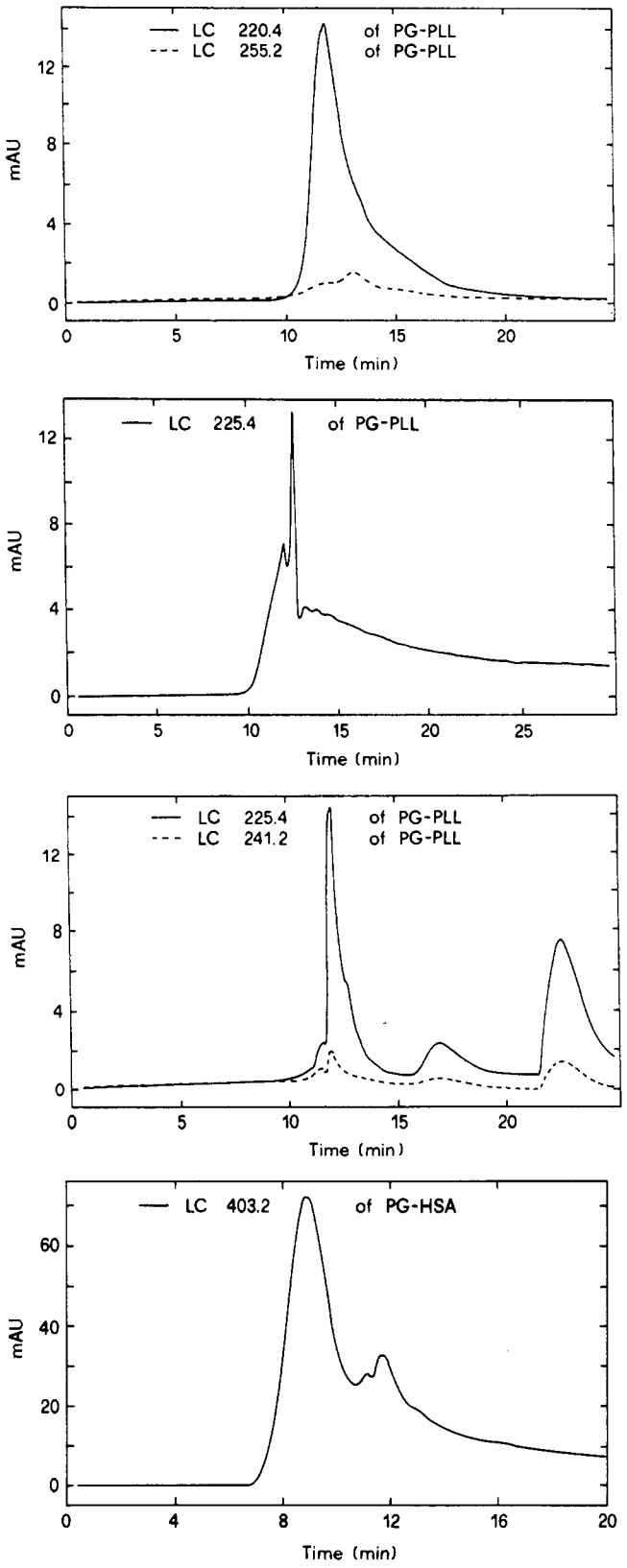


Figure 3. SE-HPLC analysis (eluent, 0.1 M phosphate buffer, pH 6.8; column, Synchropack GPC 100 at a flow of 0.8 mL/min) of crude PG-L-PLL (a) prepared at pH 7.1 with ECDI, (b) prepared at pH 11 with ECDI, and (c) prepared via mixed anhydride, (d) SE-HPLC analysis (eluent, 0.1 M phosphate buffer pH 6.8; column, Synchropack GPC 100 at a flow of 0.8 mL/min) of crude PG-HSA prepared at pH 7.1 with ECDI.

occurred. Folding of the HSA structure upon haptenization may be the reason of this behavior. These data indicated that a conformational change had occurred on

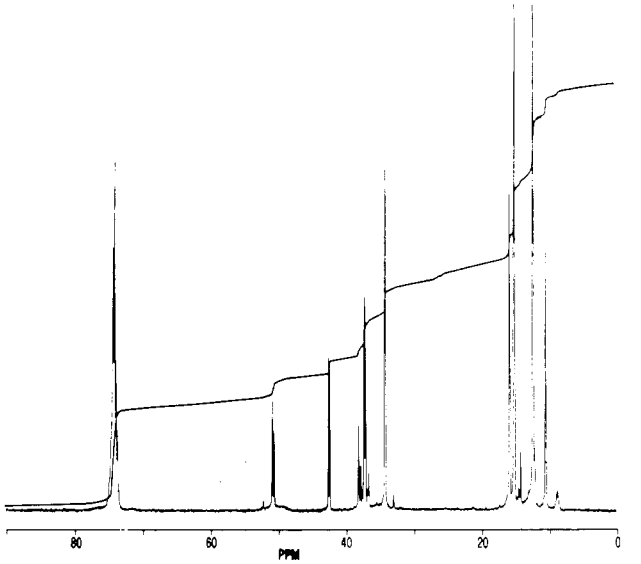


Figure 4. ^{1}H-NMR spectrum of BPO (prepared at pH 9.5) in D_2O.

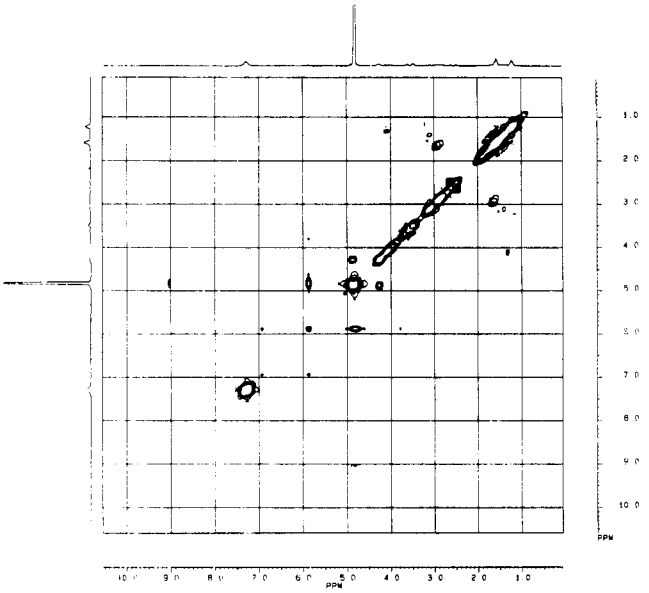


Figure 5. ^{1}H-COSY spectrum of PG-L-PLL (prepared at pH 11) in D_2O.

HSA upon haptenization. Interestingly, this change was not noticed in PG-L-PLL.

All these conjugates and the analogues prepared using penicillin V (**6**, PV) were then used in a radioallergosorbent test (RAST) (*28*). The conjugates were immobilized in polystyrene beads and used to test the presence of human IgE antibodies in the sera of some patients known to be allergic to penicillin. They were workers professionally exposed to penicillins and having a clinical anamnesis of allergy to penicillins. The results are shown in Table I. First of all, RAST positivity was obtained using conjugates prepared by reaction of PG or PV with HSA or PLL at pH 11 without any conjugation agent. This suggests that the penicilloyl–poly(L-lysine) determinant thus formed was recognized by IgE's of patients. A blank experiment performed in the same conditions at pH 7 did not give any RAST positivity.

The second point is the difference in RAST positivity independent of the pH of the conjugation reaction. This difference was noted in patient MC but not in patient AG. The RAST positivity at neutral pH 7, where the penicillin

Table I. RAST Activity Observed after Incubating Sera of Allergic Patients with PG and PV Conjugates of HSA and PLL Prepared under Different Conditions

patient	protein	hapten[a]	pH of conj	conj reagent	% RAST activity
AG	HSA	PG	11		12.5
	HSA	PV	11		10.3
	HSA	PG	7	ECDI	7.1
	HSA	PG	8	ECDI	5.9
	HSA	PG	9	ECDI	5.7
	HSA	PG	10	ECDI	8.9
	HSA	PV	7	ECDI	6.0
	HSA	PV	8	ECDI	8.4
	HSA	PV	10	ECDI	9.5
	PLL	PG	7	ECDI	9.6
	PLL	PV	7	ECDI	7.8
MC	HSA	PG	11		17.8
	HSA	PV	11		16.7
	PLL	PG	11		15.7
	PLL	PV	11		14.2
	HSA	PG	7	ECDI	1.2
	HSA	PG	8	ECDI	
	HSA	PG	9	ECDI	
	HSA	PG	10	ECDI	21.0
	HSA	PV	7	ECDI	2.6
	HSA	PV	8	ECDI	5.9
	HSA	PV	9	ECDI	15.1
	HSA	PV	11	ECDI	2.8
	PLL	PV	7	ECDI	1.8
F	HSA	PG	11		14.8
	HSA	PV	11		15.0
L	HSA	PG	11		1.1
	HSA	PV	11		0.9
S	HSA	PV	11		2.1
	HSA	PG	11		1.7

[a] Background bound radioactivity = 0.2%.

nucleus is present in the conjugate, suggests that anti-penicillin IgE antibodies are present in the serum of the patient.

In conclusion, ^{1}H NMR and SE-HPLC analysis of penicillin–protein conjugates allowed the percent haptenization and structure of the conjugate to be obtained. This is especially useful when the hapten may undergo modifications during the haptenization procedure.

ACKNOWLEDGMENT

This work was supported by a CNR grant (Piano Finalizzato Chimica Fine). We thank our students Ezio Bolzacchini, Anna Brocca, and Monica Odiardo for their collaboration in the experimental work.

LITERATURE CITED

(1) Surtees, S. J., Stockton, M. G., and Gietzen, T. W. (1991) Allergy to penicillin, fable or fact? *Br. Med. J. 302*, 105–106.

(2) Pearson, C. R. (1991) Allergy to penicillin. *Br. Med. J. 302*, 1462. Walley, T., and Coleman, J. (1991) *Br. Med. J. 302*, 1462–1463. McSharry, C., Lewis, C., and Kirkwood, E. (1991) *Br. Med. J. 302*, 1463. Surtees, S. J., Stockton, M. G., Gietzen. T. W. (1991) *Br. Med. J. 302*, 1463.

(3) Sogon, D. D. (1984) Penicillin Allergy. *J. Allergy Clin. Immunol. 74*, 589–593.

(4) De Weck, A. L. (1974) Low Molecular Weight Antigens, in Sela. *The Antigens*, Vol. 2, pp 141–248, Academic Press, New York.

(5) Beeley, L. (1984) Allergy to Penicillin. *Br. Med. J. 288*, 511–512.

(6) Erffmeyer, J. E. (1981) Adverse reactions to penicillin. *Ann. Allergy 47*, 288–300.

(7) Levine, B. B., and Redmond, A. P. (1969) Minor Haptenic Determinant-Specific Reagents of Penicillin Hypersensitivity in Man. *Int. Arch. Allergy Appl. Immunol. 35*, 445–455.

(8) Levine, B. B., Redmond, A. P., and Fellner, A. J. (1966) Penicillin Allergy and the Heterogeneous Immune Response of Man to Benzylpenicillin. *J. Clinical Invest. 45*, 1895–1906.

(9) Ressler, C., and Mendelson, L. M. (1987) Skin Test for Diagnosis of Penicillin Allergy. Current Status. *Ann. Allergy 59*, 167–170.

(10) Van Dellen, R. D. (1981) Skin Testing for Penicillin Allergy. *J. Allergy Clin Immunol. 68*, 169–180.

(11) Van Arsdel, P. P., Jr. (1978) Adverse Drug Reactions. In *Allergy, Principles and Practice* (E. Middleton, Jr., C. E. Reed, and F. F. Ellis, Eds.) pp 1153–1154.

(12) Sullivan, T. J., Wedner, H. J., Shatz, G. S., Yecies, L. D., and Parker, C. W. (1981) Skin testing to detect penicillin allergy. *J. Allergy Clin. Immunol. 68*, 171–180.

(13) Parker, C. W. (1967) Conjugation of penicillin and its derivatives. In *Methods in Immunology and Immunochemistry* (C. A. Williams, and M. W. Chase, Eds.) Vol. 1, pp 133–143.

(14) Wide, L., Bennich, H., and Johansson, S. G. O. (1967) Diagnosis of allergy by an in vitro test for allergen antibodies. *Lancet 2*, 1105–1107.

(15) Kristoffersson, A., Ahlstedt, S., Petterson, E., and Svärd, P. O. (1977) A radioimmunoassay for Detection of Penicilloylated Protein Contaminants in Penicillin Preparations. *Int. Arch. Allergy Appl. Immunol. 55*, 13–22.

(16) Landsteiner, K. (1962) In *The Specificity of Serological Reactions*, Dover, New York. Eisen, H. N. (1959) In *Cellular and Humoral Aspects of the Hypersensitive State* (H. S. Lawrence, Ed) Haeber, New York.

(17) Schwartz, M. A. (1969) Chemical Aspects of Penicillin Allergy. *J. Pharm. Sci. 58*, 643–661.

(18) Wakana, H., Shigaki, T., and Saito, N. (1982) Intramolecular alpha helix-beta structure-random coil Transitions in Polypeptides. *Biochem. Chem. 16*, 275–285.

(19) Khorana, H. G. (1953) The Chemistry of Carbodiimides. *Chem. Rev. 53*, 145–166.

(20) Levine, B., and Redmond, A. P. (1968) The Nature of the Antigen-Antibody Complexes Initiating the Specific Wheal-and-Flare Reaction in Sensitized Man. *J. Clin. Invest. 47*, 556–567.

(21) Kristofferson, A., Ahlsted, S., and Svärd, P. O. (1977) Antigens in Penicillin Allergy. *Int. Arch. Allergy Applied Immunol. 55*, 23–28.

(22) Jackson, G. E. D., and Strominger, J. L. (1984) Synthesis of Peptidoglycan by High Molecular Weight Penicillin Binding of Bacillus Subtilis and Bacillus Stearothermophilus. *J. Biol. Chem. 259*, 1483–1490.

(23) Stanier, R. Y., Ingraham, J. L., Wheels M. L., and Painter, P. R. (1988) *The Microbial World*, Prentice Hall: Englewood Cliffs, NJ, pp 158–166.

(24) Edwards, R. G., Speckman, D. A., and Dewdney, J. M. (1982) Development and use of three radioallergosorbent tests in the diagnosis of penicillin allergy. *Int. Arch. Allergy Appl. Immunol. 68*, 352–357.

(25) Blanca, M., Mayorga, C., Perez, M., Suau, R., Juarez, C., Vega, J. M., Carmona, M. J., Perez Estrada, M., and Garcia, J. (1992) Determination of IgE antibodies to the benzyl penicilloyl determinant. A comparison between poly-L-lysine and human serum albumin as carriers. *J. Immunol. Methods 153*, 99–105.

(26) Lafaye, P., and Lapresle, C. (1988) Fixation of penicilloyl groups to albumin and appearance of anti-penicilloyl antibodies in penicillin-treated patients. *J. Clin. Invest. 82*, 7–12.

(27) Lapresle, C., and Wal, J.-M. (1979) The binding of penicillin to albumin molecules in bisalbuminemia induced by penicillin therapy. *Biochim. Biophys. Acta 586*, 106–111.

(28) Ceska, M., Eriksson, R., and Varga, J. M. (1972) Radioimmunosorbent assay of allergens. *J. Allergy Clin. Immunol. 49*, 1–9.

Protected Thiol–Polyethylene Glycol: A New Activated Polymer for Reversible Protein Modification

Clement Woghiren,*,† Basant Sharma,‡ and Stanley Stein†

Center for Advanced Biotechnology and Medicine, 679 Hoes Lane, Piscataway, New Jersey 08854.
Received February 17, 1993

Monomethoxypolyethylene glycol (mPEG) of average molecular weight 5000 was transformed in a series of synthetic steps to a new activated form of PEG, a stable thiol-protected intermediary, for reaction with cysteine residues in proteins under mild conditions to produce PEG–protein conjugates as possible candidates for therapeutics. The modified protein has PEG polymer molecules attached to the backbone by the newly formed disulfide bonds, which are readily cleaved to regenerate the native protein under mild reducing conditions. The model protein papain, which has seven cysteine residues including a lone cysteine in its active site, was modified through the free available thiol. The resulting PEG–papain was characterized by matrix-assisted laser desorption mass spectrometry, SDS-PAGE, and high performance gel filtration chromatography. The major modified PEG–papain variant was demonstrated to be 5000 Da larger than the unreacted papain.

INTRODUCTION

Polyethylene glycol (PEG) has been used to modify enzymes and other proteins for the purpose of preparing improved therapeutic agents (*1*). The conjugated protein acquires longer circulatory life in the body due to increased resistance to proteolytic digestion (*2–5*). Generally, succinimidyl succinate-activated PEG is allowed to react with amino groups on the protein. Other studies have been based on alternative activation chemistries for PEG (*6, 7*), but they share a similar mode of attachment to the protein, through amino groups. In many instances, this is undesirable, such as when derivatization of a specific lysine residue may inactivate the protein. For example, although many enzymes have been shown to retain activity after PEG modification (*8*), other proteins such as monoclonal antibodies may become inactivated (*9*). Furthermore, more controlled and specific modification of a protein by PEG may be achievable by using another target amino acid, such as cysteine, which in the reduced form is typically less abundant than lysine in proteins.

In our studies, we have prepared a new activated form of PEG that is a stable reagent, but readily reacts with the thiol group of cysteine to form a disulfide-linked PEG adduct. The usefulness of this reagent has been demonstrated by modification of papain.

EXPERIMENTAL PROCEDURES

Materials. mPEG 5000 and potassium thioacetate were obtained from Fluka Chemicals, Ronkonkoma, NY. Tosyl chloride, 4,4-dipyridyl disulfide, dry methanol, dry pyridine, and sodium methoxide (methanolic 25%) were the products of Aldrich Chemical, Milwaukee, WI. Dithiothreitol (DTT), Ellman's reagent [5,5′- dithiobis(2-nitrobenzoic acid)], bovine pancreatic trypsin inhibitor (BPTI), papain (from papaya latex), and cysteine were obtained from Sigma Chemicals, St. Louis, MO. Sephadex G-25 (coarse) was from Pharmacia LKB Biotechnology, Piscataway, NJ. Triethylamine (sequenal grade) was obtained from Pierce Chemicals, Rockford, IL. Polymethacrylate (25%) was obtained from Polysciences, Warrington, PA, and precast polyacrylamide gels (10–20%) were purchased from Intergrated Separations Systems Inc., Natick, MA. All aqueous solutions were made with deionized water (Milli-Q, Millipore, Bedford, MA).

General Procedures. Gel Filtration. The products obtained after each synthetic step were purified through G-25 coarse material. Elution was with degassed 0.1 N acetic acid.

PEG Detection. To each 50-μL aliquot of the gel filtration fractions was added 1 mL of 0.02% polymethacrylate (PMA) in 0.02 N HCl (*10*). The intensity of light scattering at 412 nm was directly proportional to the amount of PEG. (Data not shown).

Free Thiol Detection. The standard Ellman method (*11*) was adapted. To each 150-μL aliquot of the gel filtration fractions was added 1 mL of 0.1 M potassium phosphate buffer, pH 8, and 40 μL of 5,5′-dithiobis(2-nitrobenzoic acid) at 5 mg/mL in the phosphate buffer. The solution was mixed and assayed at 412 nm.

Determination of the 4-Thiopyridone Content in PEG–SS–4TP. A varying amount of PEG–SS–4TP (100, 200, and 400 μL of 2 μmol/mL in water) was reacted separately with an excess of cysteine (200 μL of 91 μmol/mL in water) and diluted to a final volume of 1.4 mL with 0.1 M potassium phosphate buffer, pH 7. The amount of 4-thiopyridone liberated was quantitated using a molar extinction coefficient of 1.98×10^4 (*12*) at 323 nm.

HPLC. A Hitachi liquid chromatography system equipped with an L-6200 pump and L-4200 variable detector was used. A TSK 3000 SW_{XL} gel permeation column was used with a mobile phase of 0.12 M potassium phosphate/0.2 M sodium chloride, pH 6.6. A Supelco C-4 reverse-phase column was used for desalting, with water and acetonitrile as mobile phases. A HEMA CM cation exchage column (15 cm × 4.6 mm) from Alltech (Deerfield, IL) was used with 20 mM sodium acetate, pH 5.8, and 50 mM sodium acetate/0.5 M sodium chloride/1 M potassium chloride, pH 6.2, as mobile phases A and B, respectively.

Preparation of Tosyl–PEG. Methoxypolyethylene glycol of molecular weight 5000 (5 g, 1 mmol) was dissolved in 26 mL of dry pyridine and treated with tosyl chloride

* To whom correspondence should be addressed. Phone: (908) 235-5320. Fax: (908) 235-4850.

† Department of Chemistry, Rutgers—The State University of New Jersey, Piscataway, NJ 08854.

‡ R.W. Johnson PRI, Rt 202, Raritan, NJ 08869.

1043-1802/93/2904-0314$04.00/0 © 1993 American Chemical Society

(9 g, 50 mmol). The solution was stirred and brought to 65 °C in a hot water bath. It was allowed to react for 3 h and left under ambient conditions overnight. The pyridine was evaporated under vacuum to dryness. The tosyl–PEG was purified from tosyl chloride by passage through Sephadex G-25 (coarse, 50 cm × 3 cm), with 0.1 N acetic acid as eluant. The void volume, positive to the PMA test (see above), was collected, frozen, and evaporated to dryness using a vacuum concentrator. PEG recovery was 80%.

Preparation of PEG–Thioacetate. The tosyl–PEG was taken up in 6 mL of dry pyridine with extensive mixing using a vortex mixer. In a separate flask, 1.2 g (10.5 mmol) of potassium thioacetate was dissolved in 15 mL of pyridine/methanol (2:1) mixture. The tosyl–PEG solution was then added to the thioacetate mixture with stirring and 500 μL of triethylamine was added. The flask was then layered with N_2, capped, and left to react overnight. It was evaporated to dryness under vacuum. The PEG–thioacetate was then purified using Sephadex G-25 as above. The void volume, positive to PMA (see above), was collected, frozen, and evaporated to dryness in the vacuum concentrator. PEG recovery was 70%.

The product was brown to dark purple, with a UV maximum at 260 nm.

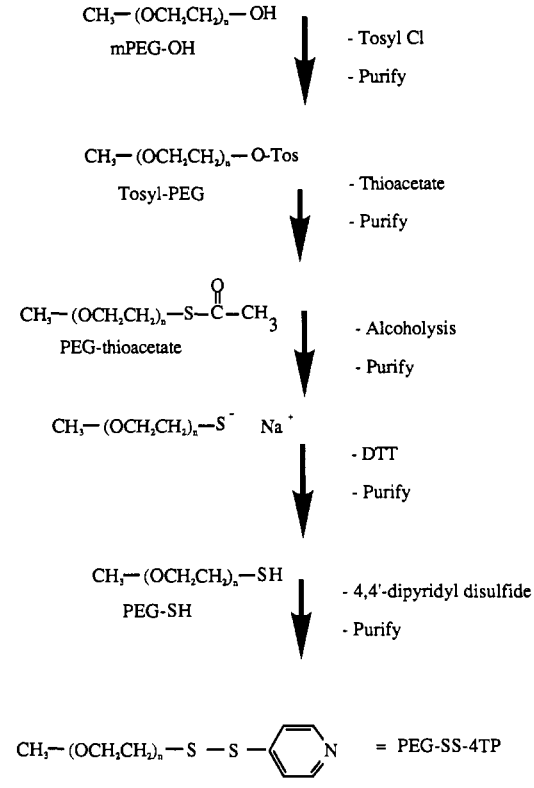
Alcoholysis of the PEG–Thioacetate. PEG–thioacetate (480 mg) was dissolved in 16 mL of dry methanol. Hydroxylamine (1.5 g) was added to form a saturated solution. Sodium methoxide, 25% in methanol (3.64 mL), was also added to make a 1 M solution. It was heated in a water bath with stirring at 60 °C for 1 h and then left under ambient conditions overnight (24 h). The solution was neutralized with 9 mL of 5 N acetic acid, frozen, and evaporated to dryness using a vacuum concentrator. The product obtained after purification through the Sephadex column was negative to the Ellman reagent. The product was then reduced by dissolving in 4.2 mL of 0.1 M potassium phosphate buffer, pH 8.4, and adding 155 mg of dithiothreitol (DTT). It was incubated at 65 °C for 40 min and purified through Sephadex G-25, as before. The void volume was positive to PMA, indicating the presence of PEG, and also positive to the Ellman reagent, indicating the presence of a free thiol on the PEG. The recovery of PEG was about 70% by weight.

Protection of the Free Thiol. PEG–SH (284 mg, 56 μmol) in 800 μL water was mixed with 245 mg (1.1 mmol) of 4,4′-dipyridyl disulfide in 700 μL of methanol. Then 1 mL of 0.1 M Tris/0.3 M NaCl, pH 10, was added and the reaction mixed. This was incubated at 65 °C for 30 min with intermittent mixing. The solution was cooled and separated by Sephadex G-25, as before. The void volume was collected, frozen, and evaporated to dryness using a vacuum concentrator.

Anal. Calcd for $C_{234}H_{463}O_{114}NS_2$: C, 54.28; H, 8.98; N, 0.27; S, 1.24. Found: C, 53.97; H, 9.10; N, 0.26; S, 1.04.

Preparation of PEG–Papain. Papain (15.5 mg, 674 nmol) was dissolved in 0.5 mL of water (degassed) and added dropwise to a 15-fold excess of PEG–SS–4TP (10.4 μmol) in 0.075 M MOPS buffer, pH 7.5, while being gently mixed. The reaction mixture was kept under ambient conditions and constantly mixed on a rotator for 2 h. It was then diluted to 12 mL with water and chromatographed using weak cation-exchange HPLC. Excess PEG–SS–4TP was not retained, while the PEG–papain was slightly less retained than unreacted papain. PEG–papain was then purified using high performance gel filtration chromatography. The peaks of modified protein were collected and desalted on a reverse-phase C-4 column before application to SDS–PAGE.

Scheme I



Formation of PEG–BPTI at Varying pH. BPTI, a protein known to contain 18 Cys residues, all disulfide linked, was reduced and reacted with PEG–SS–4TP as follows: 113 mg of trypsin inhibitor and 4.8 mg of DTT were dissolved in 5 mL of 0.1 M potassium phosphate, pH 8.4, and incubated at 65 °C for 35 min. A 3-mL fraction was applied to a gel filtration column, 50 cm × 0.7 cm, packed with Sephadex G-25 (coarse) and eluted with 0.2 N acetic acid. The void volume containing the protein (monitored at 280 nm) was pooled and lyophilized. The three reactant solutions were prepared in separate containers as follows: (1) 2.6 mg of the reduced BPTI in 0.5 mL of 0.2 N acetic acid, (2) 3.6 mg of the native (unreduced) BPTI (control) in 0.5 mL of 0.2 N acetic acid, and (3) 19.3 mg of the PEG–SS–4TP in 1 mL of water. The conjugation experiment was then carried out in five separate reaction buffers of varying pH: (a) 0.1 M Tris HCl/0.3 M NaCl, pH 10; (b) 0.025 M Tris HCl/0.1 M NaCl, pH 7.6; (c) 0.1 M Tris HCl/0.3 M NaCl, pH 6.5; (d) 0.1 M potassium phosphate, pH 4.7; (e) 0.2 N acetic acid (pH = 2.7). Reagent 1 or 2 (100 μL) was mixed with 100 μL of reagent 3 and 800 μL of the particular buffer and reacted for 10 min at room temperature. A scan was taken from 400 to 220 nm.

RESULTS AND DISCUSSION

The transformation of monomethoxypolyethylene glycol to the thiol-protected PEG–SS–4TP was carried out according to Scheme I. The lone relatively unreactive hydroxyl group on the mPEG was activated by tosylation in dry pyridine (*13, 14*). The resultant tosyl–PEG was partially purified by Sephadex G-25 and reacted with potassium thioacetate (*15, 16*) to produce the PEG–thioacetate. This was also partially purified by Sephadex G-25 and subsequently treated in basic alcoholysis (*17*) to give the PEG-SH. The reactive free thiol was then protected using 4,4′-dipyridyl disulfide (*12, 18*).

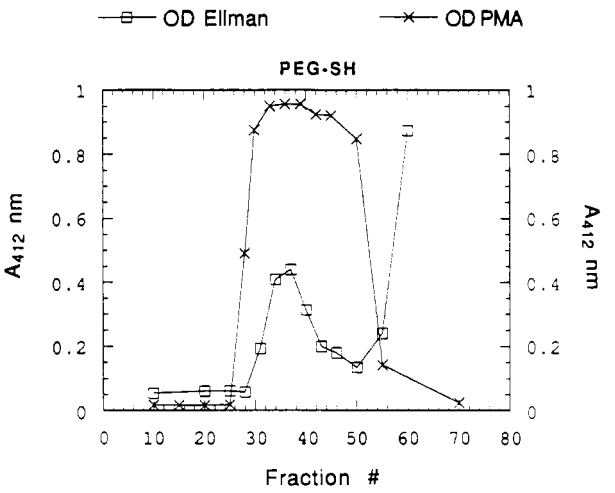


Figure 1. Gel filtration chromatography of reduced thiol–PEG: 1.8 g of thiol–PEG/byproducts from the basic alcoholysis was reduced with 148 mg DTT and separated on Sephadex G-25 (coarse packed in a 50 × 1.5 cm column) with 0.1 N acetic acid as eluent. Eluent was collected per 0.5 min (2.5 mL). The presence of PEG was detected by taking 50-μL aliquot of the gel filtration collect fractions and adding to 1 mL of 0.02% PMA in 0.02 N HCl. The intensity of light scattering at 412 nm is directly proportional to the amount of PEG. A modified Ellman method was used to detect free thiols: A 150-μL aliquot of the fraction was added to 1 mL of 0.1 M potassium phosphate buffer, pH 8, and 40 μL of Ellman's reagent (5 mg/mL in the phosphate buffer) was subsequently added. The solution was mixed and detected at 412 nm.

Characterization of the Thiol–PEG. The tosylation reaction of the mPEG was accomplished in a few hours (*14, 15*) and the excess tosyl chloride was conveniently eliminated from the product in the gel filtration purification step. The PEG adduct eluted in the void volume, as identified by its characteristic turbidity in acidified 0.02% polymethacrylate solution in the PEG detection assay. The thiol–PEG resulting from the basic alcoholysis of the PEG–thioacetate was not initially positive to the Ellman test, but after reduction with DTT and separation by gel filtration, the product became positive to the Ellman test (Figure 1). This initial product (before reduction) may have been a disulfide-linked PEG dimer. On prolonged storage in solution, the unprotected thiol–PEG was found to be oxidized, according to Ellman's assay. Analysis of the final product, thiol-protected PEG (PEG–SS–4TP), by matrix-assisted laser desorption mass spectrometry (LDMS) using sinampinic acid as sample matrix gave a single peak with an average mass of 5199 Da (Figure 2A).

A value of 15% was determined as the amount of reactive species in this PEG–SS–4TP preparation. This was estimated from the amount of 4-thiopyridone liberated from PEG–SS–4TP with an excess of cysteine (20–90-fold, see above), representing the PEG–thiolating capacity of this particular PEG–SS–4TP preparation. The inactive species may contain unreacted PEG accumulated from each previous synthetic step. Also contributing may be PEG molecules containing two thiol groups intramolecularly connected in a disulfide bridge which can form from reaction of contaminating PEG diols. The content of dimethoxypolyethylene glycol in the monomethoxypolyethylene glycol starting material can be as high as 30%, depending on the supplier.

Conjugation of the PEG–SS–4TP with Free Thiols. The PEG–SS–4TP was found to react readily in the presence of small molecular free thiols, such as cysteine or cysteine-containing peptides, under mild conditions at neutral pH (data not shown). The reaction can be

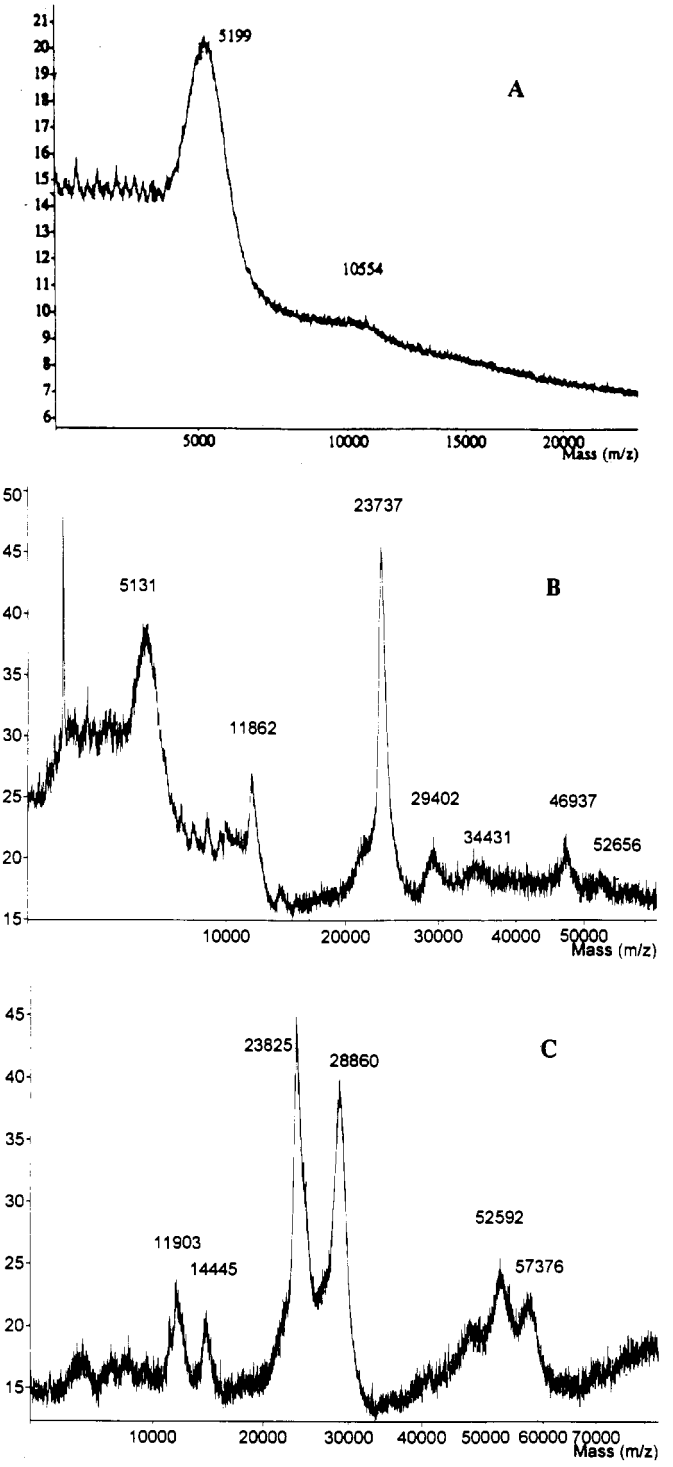


Figure 2. (A) LDMS spectrograph of PEG–SS–4TP. (B) LDMS of a papain/PEG–SS–4TP reaction mixture. Unreacted PEG–SS–4TP and papain are observed at *m/z* 5131 and 23 737, respectively. Papain–$(PEG)_n$ can be seen at 29 402 (n = 1) and 34 431 (n = 2). Laser-induced dimeric papain and doubly charged papain are detected at *m/z* 46 937 and 11 862, respectively. (C) LDMS of the partially purified PEG–papain major product. The unreacted protein is seen at *m/z* 23 835, while the PEG–papain is at *m/z* 28 860. Their laser-induced dimer molecular ions are observed at *m/z* 52 292 and 57 376; while their doubly charged ions are detected at *m/z* 11 903 and 14 445, respectively. They were run on a Finnigan MAT LaserMAT. Calibration was done using native papain (MW = 23 426). Sinnampic acid was used as the sample matrix. Settings: positive polarity; laser power = 30; laser shots = 10; gain = 31 mV. Note: Inherent mass accuracy is no better than 0.1% of the expected value.

monitored by the new absorbance maximun at 323 nm, corresponding to the 4-thiopyridone leaving group (Figure

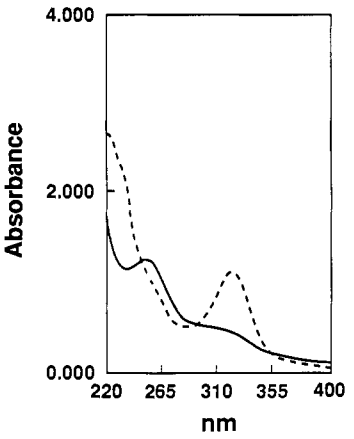


Figure 3. UV–VIS spectra scan of the PEG–SS–4TP reaction with cysteine (between 400 and 220 nm): (—) PEG–SS–4TP only, at 2.5 mg/mL (1 mL, 0.49 μmol) in 0.1 M potassium phosphate, pH 8.4; (--) 112 μL of cysteine solution at 5 mg/mL (4.6 μmol) was reacted with PEG–SS–4TP for 3 min.

3). The reaction with free cysteine was found to be complete within 3 min, but additional time was allowed for proteins due to potential steric hindrance.

After reaction with papain, partial purification of the PEG–papain from unreacted protein and complete separation from excess PEG–SS–4TP was achieved using cation-exchange HPLC separation. The PEG–papain was found to be enriched in the earlier fractions, even though none of the ionic sites was expected to be modified. This difference in characteristics may be due to the masking of positively charged regions on the protein surface by the PEG molecule. The PEG–papain from the ion-exchange column was then characterized using high-performance gel filtration chromatography (Figure 4). Two new peaks eluting 5.1 (minor) and 3.2 min (major) before the unreacted papain peak (22.71 min) were collected and desalted using reverse-phase HPLC. LDMS of the partially purified PEG–papain major product (19.47 min) showed a new mass ion 5000 Da higher than that of native papain (Figure 2C). The minor PEG–papain variant was detected at m/z 33 688 (data not shown). These PEG–papain variants may be characterized as papain-$(PEG)_n$, where $n = 1$ in the major product and $n = 2$ in the minor product. Correspondingly, two new bands of higher molecular weight (about 29 000 and 34 000 Da) were observed in the SDS–PAGE analysis (Figure 5, lanes 9 and 10). Reduction of these PEG–papain variants with DTT before SDS–PAGE caused these bands to revert to the lower mass of the native papain (Figure 5, lanes 5 and 6). Electrophoretic analysis (not shown) indicated that the newly formed disulfide bond between the thiol–PEG and the papain can be selectively broken under very mild reducing conditions (6.6 mmol of cysteine) equivalent to that recommended (*19*) for activating papain from its inactive zymogen state. Approximately 10% of the starting papain was converted to the PEG–papain product, according to peak areas from the LDMS of the reaction mixture (Figure 2B).

Nevertheless, the final yield of PEG–papain was not extensively determined, because commercially available preparations contain varying amounts of papain with the reactive and free SH group (*18*). The three types of the protein present in the mixture are (i) an active papain with an available SH on cysteine-25, (ii) an inactive papain-L-cysteine mixed disulfide, and (iii) an inactive protein which may have a sulfonic acid function instead of the SH. Only type i, which typically constitutes about 25%, may react with PEG–SS–4TP.

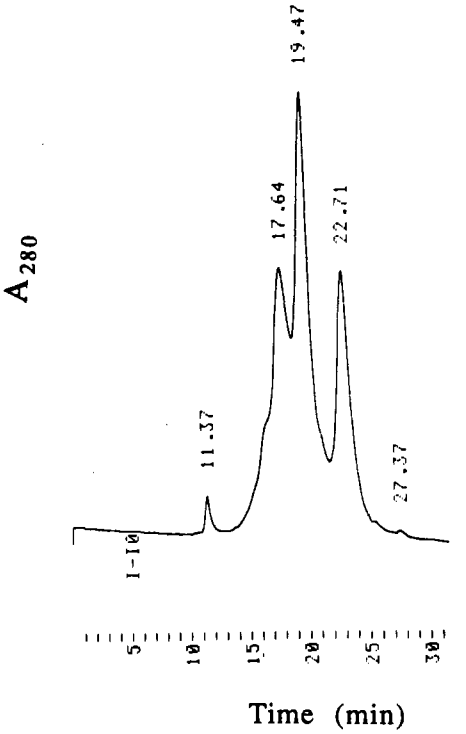


Figure 4. High-performance gel filtration chromatography (HP-GPC) of PEG–papain. Partial purification from unreacted papain and complete separation from excess PEG–SS–4TP was previously done by cation exchange. The collected product was concentrated, and 60 μL of the concentrate (unknown protein content) was injected unto the GPC column. Three fractions collected at retention times 17.6, 19.5, and 22.7 min were again desalted and analyzed by SDS–PAGE (see below). Native papain, run the same day, eluted under similar conditions at 22.8 min. They were run on a Hitachi HPLC system equipped with an L-6200 pump and L-4200 variable detector set at 280 nm. The column used was a TSK 3000SW_{XL}, 30 cm × 7.6 mm, 5 μm, eluted with 0.12 M potassium phosphate/0.2 M potassium chloride, pH 6.8, at a flow rate of 0.5 mL/min.

Reaction of reduced BPTI, to determine the reactivity of PEG–SS–4TP with proteins in different buffer conditions, was monitored by the characteristic 4-thiopyridone absorption maximum at 323 nm. The extent of reaction at 10 min was the same at pH 7.6, 6.5, and 4.7. The reaction at pH 2.7 was slow, but the signal at 323 nm continued to increase until the 1-h reaction time, reaching the same level as the others. No reaction was observed in the control unreduced BPTI at each pH value, nor was there any evidence of spontaneous hydrolysis of the 4-thiopyridone group from the PEG–SS–4TP in the above reaction conditions.

In all the PEG conjugation steps for proteins in this study, it was observed that when PEG–SS–4TP reagent solution (in any molar ratio) was added dropwise to peptide or protein solution and the mixture allowed to react for a few hours or overnight, the recovered product did not contain any detectable amount of the expected conjugated PEG–protein. This is apparently related to protein dimerization. This may occur because the initially formed PEG–protein is still reactive toward the excess reactive protein present, to form the more stable protein dimer. However, when protein was added to a molar excess of PEG–SS–4TP, the prefered PEG–protein conjugate was obtained. In general, to obtain the desired PEG–protein conjugate, the PEG–SS–4TP should be in molar excess at all times so that the protein–protein dimer byproduct is minimized in the newly formed disulfide bonds. This is achievable when protein is added to the PEG–SS–4TP and not in the reverse order.

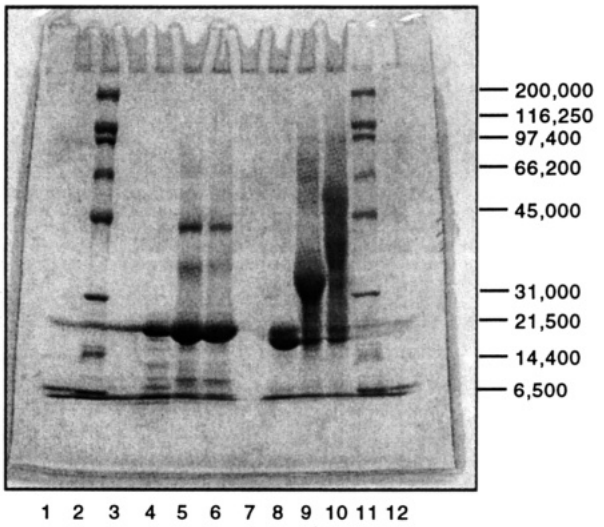


Figure 5. SDS–PAGE of PEG–papain: Lanes 2 and 11 have molecular weight markers (200 000, 116 250, 97 400, 66 200, 45 000, 31 000, 21 500, 14 400, and 6500 Da); lane 8 contains native papain; lane 9 has the PEG–papain variant eluting 3 min earlier than native on the high performance gel filtration chromatography, while lane 10 contains the other PEG–papain variant eluting 5 min earlier than native; lanes 4, 5, and 6 contain the same samples as in 8, 9, and 10, respectively, except they were treated with reducing buffer prior to running on gel. SDS–PAGE electrophoresis was run using an LKB 200 system on a 10–20% gradient precast minigel. Detection was by coomassie stain. I

CONCLUSION

We have synthesized a novel thiol-protected activated PEG for conjugation to cysteine-containing proteins, such as enzymes. The amount of PEG conjugated to the protein depends on the number of available free thiol groups on the protein. The low yield of conversion of the native protein to its PEG derivative may be due to steric hindrance of access by the single active group on the PEG polymer to the lone cysteine residue. Or, the availability of the reactive (reduced) thiol may determine the yield. This can vary with the target protein and must be addressed on a case by case basis. The attached PEG can be conveniently removed under mild reducing conditions, making it the first readily reversible PEG conjugate reported. This is a possible approach for modification of therapeutic proteins either as enhancer of longer circulatory life or in a long-acting drug-delivery mode, whereby the active protein may be released from its PEG conjugate under physiological reducing conditions.

LITERATURE CITED

(1) Davis, S., Abuchowski, A., Park, Y. K., and Davis, F. F. (1981) Alteration of the circulating life and antigenic properties of bovine adenosine deaminase in mice by attachment of polyethylene glycol. *Clin. Exp. Immunol. 46*, 649–652.

(2) Abuchowski, A., McCoy, J. R., Palczuk, N. C., van Es, T., and Davis, F. (1977) Effect of covalent attachment of polyethylene glycol on immunogenicity and circulating life of bovine liver catalase. *J. Biol. Chem. 252*, 3582–3586.

(3) Beauchamp, C. O., Gonias, S. L., Menapace, D. P., and Pizzo, S. V. (1983) A new procedure for the synthesis of polyethylene glycol-protein adducts; effects on function, receptor recognition, and clearance of superoxide dismutase, lactoferrin, and alpha2-macroglobulin. *Anal. Biochem. 131*, 25–33.

(4) Abuchowski, A., Van ES, T., Palczuk, N. C., and Davis, F. F. (1977) Alterations of immunological properties of bovine serum albumin by covalent attachment of PEG. *J. Biol. Chem. 252*, 3578–3581.

(5) Sada, E., Katoh, S., Yamanaka, K., and Itakura, Y. (1991) Resistance to proteolysis of antibody ligands modified with PEG. *J. Ferment. Bioeng., 71*, 2, 137–139.

(6) Sartore, L., Caliceti, P., Schiavon, O., and Veronese, F. M. (1991) Enzyme modification by MPEG with an amino acid or peptide as spacer arms. *Appl. Biochem. Biotechnol., 27*, 45–54.

(7) Boccu, E., Largajolli, R., and Veronese, F. M. (1982) Coupling of monomethoxypolyethyleneglycols to proteins via active esters. *Z. fur Naturforsch. 38c*, 94–99.

(8) Somack, R., Saifer, M. G. P., and Williams, D. L. (1991) Preparation of long acting superoxide dismutase using high molecular weight polyethylene glycol (41 000–72 000 daltons) *Free Rad. Res. Commun. 12–13*, 553–562.

(9) Suzuki, T., Kambara, K., Tomono, T., Hayashi, N., and Shinohara, I. (1984) Physicochemical and Biological Properties of Poly(ethylene glycol)-Coupled Immunoglobulin G. *Biochimica et Biophisica Acta 788*, 248–255.

(10) Smith, K. L., Winslow, A. E., and Peterson, D. E. (1959) Poly(alkylene Oxides) and Polymeric Poly(carboxylic Acids) *Ind. Eng. Chem. 51*, 11, 1361–1364.

(11) Riddles, P. W., Blakely, R. L., and Zerner, B. (1979) Ellman's Reagent: 5,5′-Dithiobis(2-nitrobenzoic Acid)- a Reexamination. *Anal. Biochem. 94*, 75–81.

(12) Grassetti, D. R. and Murray Jr, J. F. (1967) Determination of sulfhydryl groups with 2,2′- or 4,4′-dithiopyridine. *Arch. Biochem. Biophys. 119*, 41–49.

(13) Polgar, L., and Bender, M. L. (1966) A new enzyme containing a synthetically formed active site. *J. Am. Chem. Soc. 88*, 3153–3154.

(14) Strumeyer, D. H., White, W. N., and Koshland Jr, D. E. (1963) Role of serine in chymotrypsin action. Conversion of the active serine to dehydroalanine. *Biochemistry 50*, 931–935.

(15) Photaki, I., and Bardakos, V. (1965) Transformation of L-serine peptides to L-cysteine peptides. *J. Am. Chem. Soc. 87*, 3489–3492.

(16) Weiner, H., White, W. N., Hoare, D. G., and Koshland Jr., D. E. (1966) The formation of anhydrochymotrypsin by removing the elements of water from the serine at the active site. *J. Am. Chem. Soc. 88*, 3851–3859.

(17) Zioudrou, C., Wilchek, M., and Patchornik, A. (1965) Conversion of the L-serine residue to an L-cysteine residue in peptides. *Biochemistry 4*, 1811–1822.

(18) Brocklehurst, K., Carlsson, J., Kierstan, M. P. J., and Crook, E. M. (1973) Preparation of fully active papain from dried papaya latex. *Biochem. J. 133*, 573–584.

(19) Brocklehurst, K., and Kierstan, M. P. J. (1973) Propapain and its conversion to papain: a new type of zymogen activation mechanism involving intramolecular thiol-disulfide interchange. *Nature New Biol. 242*, 167–170.

Oligonucleotide Derivatives Bearing Reactive and Stabilizing Groups Attached to C5 of Deoxyuridine[1]

Asya S. Levina, David R. Tabatadse, Ludmila M. Khalimskaya, Tatjana A. Prichodko, Gennadii V. Shishkin, Ludmila A. Alexandrova,† and Valentina P. Zarytova*

Institute of Bioorganic Chemistry, Siberian Division of the Russian Academy of Sciences, Prospect Lavrentjeva, 8 Novosibirsk 630090, Russia, and Institute of Molecular Biology, Russian Academy of Sciences, Vavilova, 32, Moskow, Russia. Received March 1, 1993

Oligonucleotides bearing an aliphatic amino group at the C5-position of deoxyuridine ($U^{LNH_2}TCCCA$, $TU^{LNH_2}CCCA$, $U^{LNH_2}CCACTT$, where L = $-CH_2-$, $-CH_2OCH_2CH_2-$ or $-CH_2NHCOCH_2CH_2-$) have been synthesized. The photoactive (*p*-azidotetrafluorobenzamido, 2-nitro-5-azidobenzamido, or *p*-azidobenzamido), alkylating [4-[*N*-(2-chloroethyl)-*N*-methylamino]benzyl], or intercalating [*N*-(2-hydroxyethyl)phenazinium] groups were attached to the amino linker of oligonucleotides. The T_m values were determined for the duplexes formed by the above oligonucleotide derivatives. The alkylating group does not change the melting temperature of the corresponding duplex. The duplex stability is increased a little in the case of photoactive groups. The influence of the phenazinium residue on the duplex stability strongly depends on its location in the oligonucleotide. The spacer length between the C5 atom of deoxyuridine and the photoactive or phenazinium group was shown to influence the complementary duplex stability.

INTRODUCTION

The oligonucleotide derivatives bearing different reactive groups and labels are widely used in molecular biology, biotechnology, and medicine. The common practice is to introduce chemical groups at the 5′-terminal phosphate of oligonucleotides (*1*). Over the last few years oligonucleotides bearing different labels (fluorescent, biotin, complexes with metals) and reactive groups in heterocyclic bases have been reported (*2–7*). If these derivatives have reactive groups, they may be used for site-specific modification of nucleic acid targets on the condition that these groups are at positions that do not take part in complex formation. The oligonucleotides bearing reactive groups at heterocyclic bases have some advantages. These groups can be introduced anywhere on the oligonucleotides; they can be brought closer to the complementary chain and have a stronger influence on it (or on the whole duplex), and the local site of their action on the targets may be more accurate. It has been shown that an alkylating group coupled to the C5-position of deoxyuridine disposed in the middle of oligonucleotide alkylates the complementary chain in only one base (*4–6*). Furthermore, introduction of any groups in the heterocyclic base of one of the nucleosides allows other groups to be attached to terminal phosphates. In all cases, amino spacers or SH groups were preliminarily introduced into the oligonucleotides.

There are several ways of synthesis of oligonucleotide derivatives with different groups at the C5-position of deoxyuridine. The most common approach is the introduction of an alkene or alkyne having amino groups into the heterocyclic bases of oligonucleotides by using palladium catalysts (*8–10*).

In this paper we suggest a simple and convenient method for the synthesis of oligonucleotide derivatives bearing an aliphatic amino group at the C5-position of deoxyuridine. We used this method to prepare the oligonucleotide derivatives bearing reactive (alkylating or photoreactive) and intercalating groups. The ability of the compounds obtained for complex formation has been investigated.

EXPERIMENTAL PROCEDURES

Chemicals. In the present work the following chemicals were used. N,5′-Protected nucleosides and dimethoxytrityl chloride were from Olaine. *N*-(2-Hydroxyethyl)-phenazinium chloride (*11*), *N*-(trifluoroacetyl)aminoethanol (11), *N*-hydroxysuccinimide ester of *N*-(trifluoroacetyl)-β-alanine (12), 4-[*N*-(2-chloroethyl)-*N*-methylamino]benzaldehyde (*13*), and 3′,5′-diacetyl-5-bromomethyldeoxyuridine)-*N*-methylamino]benzaldehyde (*13*), and 3′,5′-diacetyl-5-bromomethyldeoxyuridine (*14*) were synthesized according to the referenced methods. 3′-H-Phosphonates of protected nucleosides were prepared according to ref 15. Oligonucleotides were synthesized by the H-phosphonate method (*16*). The amino linker was incorporated into the terminal phosphates of oligonucleotides as described in ref 17; *p*-azidotetrafluorobenzoic acid and *N*-hydroxysuccinimide esters of all azidobenzoic acids used were prepared as described in ref 18. The mixture of phosphodiesterase and 5′-nucleotidase from snake venom was a gift of Dr. V. I. Yamkovoi from Novosibirsk State University (Russia).

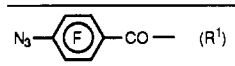
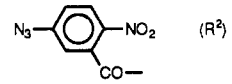
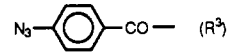
Chromatography. Isolation and purification of unprotected oligonucleotides and their derivatives were performed by HPLC on a Waters system with Polisil SA (10 μm) anion exchange (a gift of Dr. S. I. Yastrebov from the Institute of Molecular Biology, Novosibirsk, Russia) and Lichrosorb RP 18 (5 μm) (Merck) reverse-phase columns. After enzymatic digestion, the oligonucleotide hydrolyzate was chromatographed on a Milichrom liquid chromatograph with Lichrosorb RP 18 (5 μm) using the

* Author to whom correspondence should be addressed.
† Institute of Molecule Biology, Russian Academy of Science.

[1] Abbreviations used: Phn, *N*-(2-hydroxyethyl)phenazinium residue; TFA-β-Ala-OSuc, *N*-hydroxysuccinimide ester of *N*-(trifluoroacetyl)-β-alanine; DMTr, dimethoxytrityl group; dRib, deoxyribose residue; T_m, melting temperature of an oligonucleotide duplex determined at the point of curve bending. Only deoxyderivatives are used in this report, therefore the prefix "d" in the symbols of deoxyribonucleosides and oligonucleotides is omitted.

1043-1802/93/2904-0319$04.00/0 © 1993 American Chemical Society

Table I. Absorption Spectral Data of Azidoarylamides $RNH(CH_2)_3OH$ in a 1:9 Ethanol–Water Mixture

R	λ_{min}, nm (ϵ, $M^{-1}\cdot cm^{-1}$)	λ_{max}, nm (ϵ, $M^{-1}\cdot cm^{-1}$)	ϵ_{260}, $M^{-1}\cdot cm^{-1}$
 (R^1)	229 (5800)	258 (23600)	23300
 (R^2)	286 (6500)	318 (8800)	6700
 (R^3)	233 (2100)	269 (14600)	12400

gradient of methanol in water. The products of the reaction of derivatives **XIV** with $Na_2S_2O_3$ were analyzed in the same manner (*19*).

Physical Measurements. UV–visible absorption spectra of oligonucleotide derivatives in water were recorded in the 200–600-nm range on a Specord M-40 instrument (Carl Zeiss, Jena, Germany). ^1H NMR spectra of the C5-modified derivatives of deoxyuridine were run on a Bruker WP-200 spectrometer; chemical shifts are reported in ppm downfield from Me_4Si. T_m values of the oligonucleotide complexes ($2\cdot10^{-5}$ M) were measured in a buffer 0.16 M NaCl–0.02 M Na_2HPO_4–0.1 mM EDTA (pH 7.5), using the equipment for thermal denaturing based on a Milichrom spectrophotometer (*20*). Molar extinction coefficients (ϵ) were estimated at 260 nm for oligonucleotides according to ref 21. For the oligonucleotide derivatives, they were calculated as a sum of ϵ values for the unmodified oligonucleotide and the conjugated group. For 4-[*N*-(2-chloroethyl)-*N*-methylamino]benzyl and 2-(alkylamino)-10-(2-hydroxyethyl)phenazinium groups the values of ϵ_{260} $14.7\cdot10^3$ $M^{-1}\cdot cm^{-1}$ (*22*) and $10\cdot10^3$ $M^{-1}\cdot cm^{-1}$ (*11*) were used, respectively. The spectral data for the azidoarylamido groups are represented in Table I.

To estimate the ϵ values of the azidoarylamido groups, the *N*-hydroxysuccinimide esters of the azidobenzoic acids used were dissolved in a 1:9 ethanol–water mixture with 3 equiv of propanolamine, and the absorption spectra were recorded after 2 min (by that time the reaction was completed). The ϵ values of the *N*-hydroxysuccinimide formed in these reactions was taken into account. The spectral data are represented in Table I.

5-(Azidomethyl)deoxyuridine, $U^{CH_2N_3}$ (IVa). 3′,5′-Diacetyl-5-(bromomethyl)deoxyuridine (**I**) prepared from 3 mmol (Ac)T(Ac) (*14*) was dissolved in 5 mL of dry dimethylformamide; 200 mg of LiN_3 was added. The reaction was monitored by TLC in ethyl acetate–hexane (8:2). After storage for 16 h, the reaction mixture was diluted with chloroform (30 mL) and washed with water (2 × 10 mL), the organic extracts were collected and evaporated in vacuo, and concentrated NH_4OH (10 mL) and ethanol (2 mL) were added. The reaction mixture was stirred for 3 h at 20 °C,[2] then it was evaporated and 5-(azidomethyl)deoxyuridine was isolated by silica gel chromatography. After evaporation, the desired product (**IVa**) was crystallized from ethanol with a yield of 80% (0.68 g, 2.4 mmol), relative to (Ac)T(Ac). The ^1H NMR spectral data of **IVa** are presented in Table II. Compound **IVa** has a band at 2130 cm^{-1} in the IR spectrum (spectrometer Perkin-Elmer 180).

Synthesis of $U^{CH_2OCH_2CH_2NHCOCF_3}$ (IVb). 3′,5′-Diacetyl-5-(bromomethyl)deoxyuridine (**I**) prepared from 1 mmol of (Ac)T(Ac) (*14*) was dissolved in 5 mL of dry dimethylformamide; 0.9 mL (5.4 mmol) of *N*-(trifluoroacetyl)aminoethanol was added. The reaction was monitored by TLC with chloroform–ethanol (95:5). After storage for 16 h the reaction mixture was evaporated and treated with concentrated NH_4OH (16 h, 20 °C) for 5′3′-deblocking. The intermediate compound $U^{CH_2OCH_2CH_2NH_2}$ (**II**) was isolated by reverse-phase chromatography on a 30 × 350 mm Silasorb C8 column (Chemapol) using gradient of ethanol (0–50%) in water with a yield of 40% (0.4 mmol) (monitoring by TLC in ethanol–concentrated NH_4OH, 8:2; the presence of an amino group in the product was confirmed by the ninhydrine reaction). Compound **II** was dissolved in 7 mL of methanol, and 0.6 mL (5 mmol) of ethyl trifluoroacetate was added. After 16 h (monitoring by TLC with chloroform–ethanol, 1:1), the desired product (**IVb**) was isolated by silica gel chromatography in 70% yield. The ^1H NMR spectral data of **IVb** are presented in Table II.

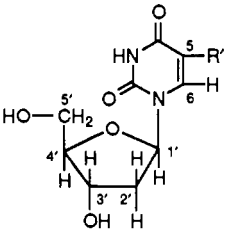
Synthesis of $U^{CH_2NHCOCH_2CH_2NHCOCF_3}$ (IVc). 3′5′-Diacetyl-5-(bromomethyl)deoxyuridine **I** prepared from 4 mmol of (Ac)T(Ac) (*14*) was dissolved in 20 mL of concentrated NH_4OH. After 30 min (monitoring by TLC with chloroform–ethanol, 8:2) 5-(aminomethyl)deoxyuridine (**III**) was isolated by chromatography on Dowex-50×2 (H^+) with a 55% yield (2.16 mmol). A 890-μmol portion of this compound was dissolved in 2 mL of dry dimethylformamide, and 282 mg (1 mmol) of TFA-β-Ala-OSuc was added. After storage for 2 h (monitoring by TLC with chloroform–methanol, 8:2), the desired product (**IVc**) was isolated by silica gel chromatography in 65% yield (565 μmol). The ^1H NMR spectral data are given in Table II.

Synthesis of (DMTr)$U^{CH_2NHCOCH_2CH_2NHCOCF_3}$ (Vc). A 582-mg (1 mmol) portion of 5′-*O*-(dimethoxytrityl)-5-(azidomethyl)deoxyuridine was prepared from derivative **IVa** by the reaction with dimethoxytrityl chloride in 70% yield and dissolved in a 2-mL mixture of pyridine–water–triethylamine (15:5:1), and H_2S was passed through during 1 h. The reaction was monitored by TLC with chloroform–ethanol (9:1). The presence of an amino group in product **VII** was confirmed by the ninhydrine reaction. Compound **VII** was isolated by silica gel chromatography in a yield of 80% (0.8 mmol). It was dissolved in 5 mL of dry dimethylformamide, and 300 mg (1 mmol) of TFA-β-Ala-OSuc was added. After 3 h (monitoring by TLC with chloroform–ethanol, 9:1), the desired product **Vc**) was isolated by gel filtration on LH-20 (column, 50 mL; eluent, chloroform–ethanol, 1:1) in 56% yield (0.45 mmol). The structure of the compound prepared was confirmed after deblocking. A DMTr group was removed by 1% CF_3COOH in dry methylene chloride (1 min) followed by product isolation by gel chromatography on LH-20. After removal of the trifluoroacetyl protecting group (concentrated NH_4OH in a water–ethanol mixture, 1:3, 1 h, 50 °C) the product, 5-(*N*-(β-aminopropionyl)aminomethyl)deoxyuridine, was isolated by chromatography on Dowex-50×2 (H^+). Its ^1H NMR spectrum was recorded (Table II).

Synthesis of Oligonucleotides with the C5-Modified Derivatives of Deoxyuridine (VIII-X). C5-modified compounds **IV** were converted by a standard method (*15*) to the corresponding 5′-*O*-(dimethoxytrityl) 3′-H-phosphonates **VI** by the reaction with PCl_3 and imidazole described in ref 15. H-Phosphonates were isolated by silica gel chromatography using a gradient of ethanol in chloroform in a yield of 80–90%. They were used for the synthesis of oligonucleotides according to ref 16 on a polymer support (CPG-500, Sigma) with a capacity for DMTr-nucleoside about 50 μmol/g. The synthesis in-

[2] Long treatment with ammonia or the heating of the reaction mixture at 50 °C causes substitution of an azido by an amino group.

Table II. ^{1}H-NMR Data (δ, ppm) for 5-Substituted Derivatives of Deoxyuridine



R′	CH(6) s	CH(1′) t (J = 7 Hz)	CH(3′) m	CH(4′) m	CH_2(5′) m	CH_2(2′) m	CH_2(a)	CH_2(b)	CH_2(c)	NH(3) br s	NH(e) br s	NH(d) br s
CH_3[a]	7.65	6.25	4.46	4.02	3.82	2.37	1.87 s[d]					
CH_2N_3[a] (**IVa**) a b c d	8.00	6.25	4.46	4.05	3.82	2.40	2.40 s					
$CH_2OCH_2CH_2NHCOCF_3$[b] (**IVb**)	8.39	6.74	4.85	4.24	4.04	2.54	4.32 s		3.57m	13.07		10.37
$CH_2OCH_2CH_2NHCOCF_3$[c] (**IVb**) a e b c d	8.26	6.59	4.80	4.25	3.99	2.45	4.25 s		3.60 m			
$CH_2NHCOCH_2CH_2NH(COCF_3)$[b] (**IVc**)	8.45	6.86	4.89	4.39	4.08	2.53	4.30 d (J = 5 Hz)	2.77 t (J = 7 Hz)	3.81 m	13.16	9.24	10.59
$CH_2NHCOCH_2CH_2NH(COCF_3)$[c] (**IVc**)	8.22	6.64	4.82	4.32	4.02	2.47	4.21 s	2.76 t (J = 7 Hz)	3.75 t (J = 7 Hz)			
$CH_2NHCOCH_2CH_2NH_2$[c]	8.36	6.80	4.82	4.30	4.00	2.53	4.30 s	2.53 t (J = 7 Hz)	3.06 t (J = 7 Hz)			

[a] D_2O, [b] C_5D_5N, and [c] C_5D_5N/D_2O (9:1) were solvents. [d] Signals of the 5-CH_3 group of thymidine.

Table III. Molar Ratio of Products after Enzymatic Digestion of Oligonucleotides XCCACTT and YZCCCA Determined by HPLC Data

X in XCCACTT	compd	T	X	C	A
$U^{CH_2OCH_2CH_2NH_2}$	**VIIIb**	2.0	1.0	3.0	0.8
$U^{CH_2NHCOCH_2CH_2NH_2}$	**VIIIc**	2.1	1.0	3.0	1.1
$U^{CH_2NHR^1}$ [a]	**XIa**	2.0	0.9	3.2	1.0
$U^{CH_2OCH_2CH_2NHR^1}$	**XIb**	2.0	0.9	3.0	0.8
$U^{CH_2NHCOCH_2CH_2NHR^1}$	**XIc**	2.0	0.9	3.1	1.1
T		3.0		3.2	1.1

YZ in YZCCCA	compd	T	YZ	Y	C	A
$U^{CH_2NH_2}T$	**IXa**	1.0		0.8	2.6	1.0
$TU^{CH_2NH_2}$	**Xa**		0.9		3.0	1.0
$U^{CH_2NHCOCH_2CH_2NH_2}T$	**IXc**	1.0		0.9	2.9	0.9
$TU^{CH_2NHCOCH_2CH_2NH_2}$	**Xc**		1.1		2.4	1.0
$U^{CH_2NHPhn}T$	**XVa**	1.1		1.0	2.9	1.2
$U^{CH_2NHCOCH_2NHPhn}T$	**XVc**	1.3		1.0	2.8	1.2
$TU^{CH_2NHCOCH_2CH_2NHPhn}$	**XVIc**		1.1		2.7	1.5

[a] R^1 as in Table I.

cluded repeating the following stages: 5′-deprotection with 2% trifluoroacetic acid in methylene dichloride and the coupling reaction in the presence of pivaloyl chloride. The concentrations of H-phosphonate synthones and the condensing agent in the pyridine–acetonitrile mixture (1:1) were 0.05 and 0.25 M, respectively. We used a 5-fold excess of H-phosphonates to the 5′-hydroxy group on the polymer support. The coupling efficiency and the average yield in each stage were the same as for standard monomers (more than 95% by DMTr cation and 60–80% according to the isolated oligonucleotide). The oligonucleotides containing $U^{CH_2N_3}$ were converted to compounds **VIII–X,a** by passing H_2S through the oligonucleotide solution in a mixture of pyridine–water (1:1) for 1 h (the azido group was partially substituted by the amino group on treatment with concentrated NH_4OH for 16 h at 50 °C). The oligonucleotides bearing the modified deoxyuridine residue were isolated by ion-exchange and reverse-phase chromatography. Their composition was confirmed by enzymatic digestion (Table III).

Synthesis of Arylazido Derivatives of Oligonucleotides XIa–d, XIIb, XIIIb. The amino derivatives of heptanucleotide **VIIIa–c** and $NH_2(CH_2)_3NH$pTCCACTT ($1\cdot10^{-7}$ mol) were dissolved in 15 μL of a water–dimethylformamide mixture (1:2); 6 μmol of the *N*-hydroxysuccinimide ester of the corresponding azidobenzoic acid in 20 μL of dimethylformamide was added in 10-, 5-, and 5-μL portions at 30-min intervals. After 1.5 h, the reaction products were precipitated with 2% $LiClO_4$ in acetone, washed with acetone, and isolated by reverse-phase chromatography (Figure 1A,B). The yields of acylation products were 70–80%. The UV spectra of *p*-azidotetrafluorobenzamido and 2-nitro-5-azidobenzamido derivatives XIb and XIIb are presented in Figure 2. The enzymatic digestion data for compounds **XIa–c** are given in Table III.

Synthesis of the Alkylating Derivatives of Oligonucleotides XIVa–c. The heptanucleotide dU^{LNH_2}-CCACTT (**VIIIa–c**) (0.1–0.2 μmol) was dissolved in 4 μL of water; 3 μL (21 μmol) of triethylamine, 1 mg (5 μmol) of 4-[*N*-(2-chloroethyl)-*N*-methylamino]benzaldehyde in 8 mL of ethanol, and in 15–25 min 1.5 mg (40 μmol) of $NaBH_4$ were added. After 30 min the products were precipitated with 2% $LiClO_4$ in acetone and isolated by reverse-phase chromatography (Figure 1C) with a yield of 20–50%, as follows from chromatographic data.

Synthesis of Phn-Containing Oligonucleotides XV-XVII. The Phn residue was attached to the amino linker of oligonucleotides **IXa,c**, **Xa,c**, and $NH_2(CH_2)_3NH$-pTTCCCA according to ref 11. A 0.2–0.5 μmol portion of an amino-containing oligonucleotide was dissolved in 80 μL of 0.05 M *N*-(2-hydroxyethyl)phenazinium chloride in 0.2 M aqueous Na_2CO_3. After 10 min of incubation, the product was precipitated and isolated by reverse-phase chromatography with a yield of 80–90%. The typical elution profile is shown in Figure 1D. The absorption spectrum of compound **XVc** is presented in Figure 2. The enzymatic digestion data for compounds **XVa,c** and **XVIc** are shown in Table III.

Enzymatic Hydrolysis of Modified Oligonucleotides. Modified oligonucleotides ($1\cdot10^{-2}$ μmol) were treated with a mixture of phosphodiesterase at 5′-nucleotidase from snake venom in the buffer 0.5 M Tris-HCl, 0.025 M $MgCl_2$, pH 8.5, during 16 h, then the reaction mixture was heated for 10 min at 100 °C and analyzed by reverse-phase chromatography. The digestion data are presented in Table III. The hydrolysis of oligonucleotides results in a mixture of A, C, T, and U^{LNHR} monomers for the compounds bearing the modified deoxyuridine residue

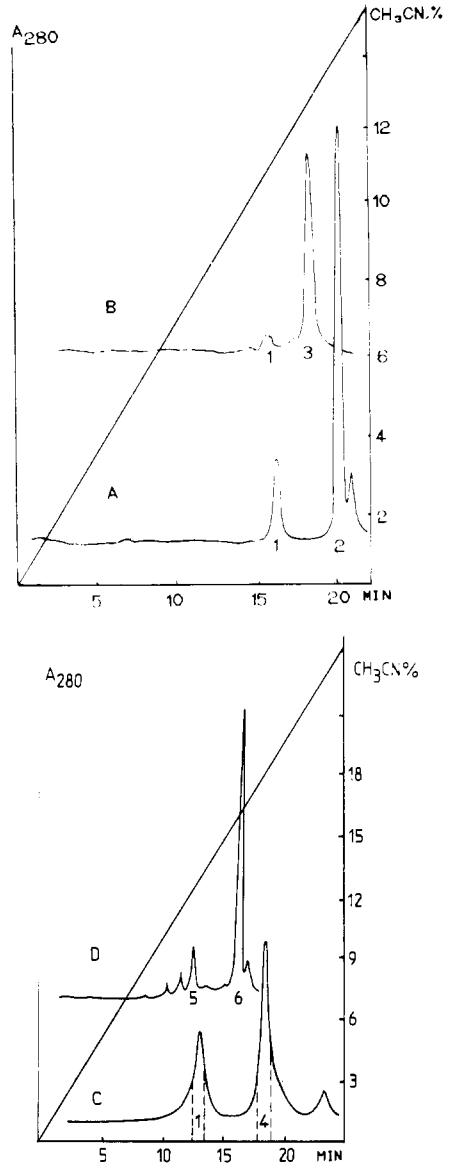


Figure 1. Results of isolation of modified oligonucleotides from the reaction mixture by a Lichrosorb RP 18 HPLC column (4 × 250 mm): (A) U^{LNHR^1} CCACTT (XIb), (B) U^{LNHR^2} CCACTT (XIIb), (C) U^{LNHR^4} CCACTT (XIVc), and (D) U^{LNHPhn}TCCCA (XVc). R^1, R^2, and R^4 are the same as in Tables I and IV. Phn is the *N*-(2-hydroxyethyl)phenazinium residue. (1) U^{LNH_2}CCACTT, (2) XIb, (3) XIIb, (4) XIVc, (5) U^{LNH_2}TCCCA, (6) U^{LNHPhn}TCCCA (XVc). The flow rate was 2 mL/min with a linear gradient of acetonitrile in 0.05 M $LiClO_4$.

at the 5′-end (**VIII, IX, XI, XV**) and dimers TU^{LNHR} and A and C nucleosides for the compounds TU^{LNHR}CCCA (**X and XVI**). The chromatographic mobility of U^{LNH_2} is higher than that of T and is the same as that of control samples $U^{CH_2NH_2}$ (**III**), $U^{CH_2OCH_2CH_2NH_2}$, and $U^{CH_2NHCOCH_2CH_2NH_2}$. The last two were obtained after removing the protecting group from compounds **IVb** and **IVc**. U^{LNHPhn} and U^{LNHR^1} are eluted after all nucleosides due to the high hydrophobicity of the aromatic residues. TU^{LNHPhn} has the maximum retention time. The ϵ values for U^{LNHR} were considered to be the same for T in the case of R = H or as a sum of spectra for T and Phn or R^1 if R was the corresponding residue.

RESULTS AND DISCUSSION

The oligonucleotides containing an amino linker at the C5-position of deoxyuridine have been synthesized. For this purpose, the following deoxyuridine derivatives were preliminary obtained according to Scheme I.

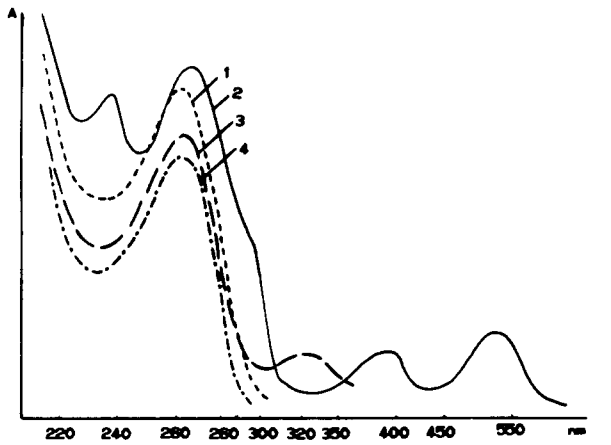
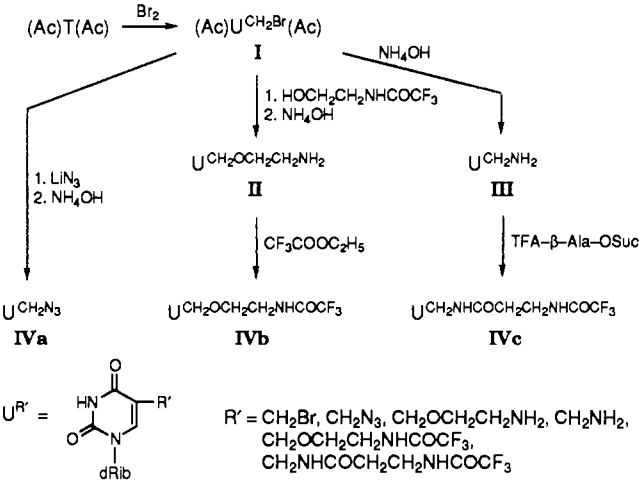


Figure 2. Electron absorption spectra of TTCCCA (1), U^{LNHPhn}TCCCA (XVc) (2), U^{LNHR^2} CCACTT (XIIb) (3), and U^{LNHR^1} CCACTT (XIb) (4) in water (10^{-5}–10^{-6} M). R^1 and R^2 are the same as in Table I; Phn is the *N*-(2-hydroxyethyl)phenazinium residue.

Scheme I



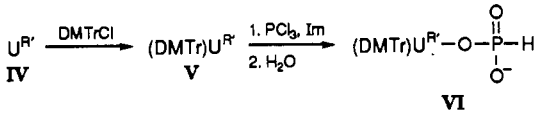
5′,3′-Diacetylthymidine was brominated (*14*) and 5′,3′-diacetyl-5-(bromomethyl)deoxyuridine (**I**) was used for the preparation of the modified derivatives of deoxyuridine (**IVa–c**). To prepare 5-(azidomethyl)deoxyuridine (**IVa**), compound **I** was sequentially treated with lithium azide and ammonia. In another experiment, the brominated product **I** reacted with *N*-(trifluoroacetyl)aminoethanol, ammonia, and the ethyl ester of trifluoroacetic acid, giving the derivative **IVb**. Compound **IVc** was synthesized via the formation of intermediate **III**, which was converted to the desired product by reaction with the *N*-hydroxysuccinimide ester of (trifluoroacetyl)-β-alanine.

The structures of the compounds obtained were confirmed by the IR and ^1H NMR spectra. In the NMR spectra of derivatives **IVb,c**, the signals of deoxyuridine and amino linker protons (R′) (Table II) are recorded.

In the NMR spectrum of product **IVa**, the displacement of signals of the 5-CH_2 protons (2.40 ppm) is observed downfield compared to the 5-CH_3 protons of thymidine (1.87 ppm) (Table II). This indicates that the proton in the CH_3 group is substituted by an electron-accepting group. In the IR spectrum of this compound, there is a line at 2130 cm^{-1} corresponding to the antisymmetric valency oscillation of the azido group (*23*).

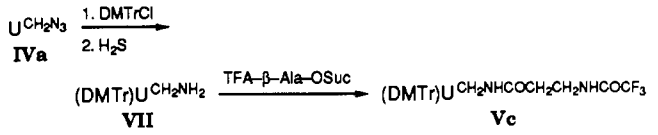
Derivatives **IVa–c** were converted to the corresponding

Scheme II



a: R′ = CH_2N_3
b: R′ = $CH_2OCH_2CH_2NHCOCF_3$
c: R′ = $CH_2NHCOCH_2CH_2NHCOCF_3$
Im = imidazole

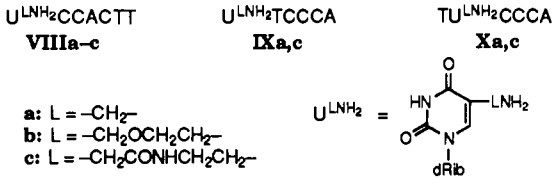
Scheme III



H-phosphonate synthones (**VIa–c**) by a standard procedure (*15*, *16*) (Scheme II).

Compound **Vc** can also be prepared in an alternative manner, by using the 5-(azidomethyl)deoxyuridine (**IVa**) and passing H_2S through for the reduction of the N_3 group to the NH_2 group (Scheme III).

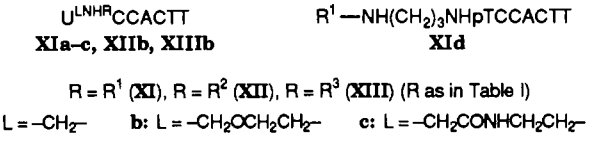
The modified and unmodified H-phosphonate synthones were used for the synthesis of amino-containing oligonucleotides **VIII–X**.



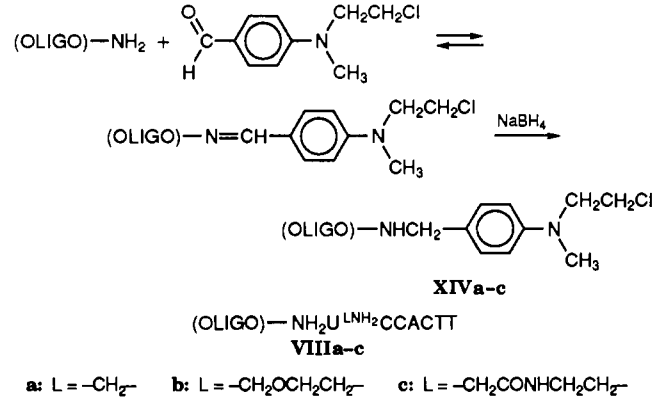
The composition of the modified oligonucleotides prepared was confirmed by enzymatic digestion with phosphodiesterase and 5′-nucleotidase from snake venom (Table III).

The presence of an amino group in oligonucleotides makes it possible to join them with different labels. We have synthesized oligonucleotides with the alkylating, photoreactive, and intercalating groups at the 5′-terminal phosphate or at the C5-position of deoxyuridine.

The photoactive derivatives of heptanucleotides **XI–XIII** were synthesized by the reaction of the amino group



Scheme IV

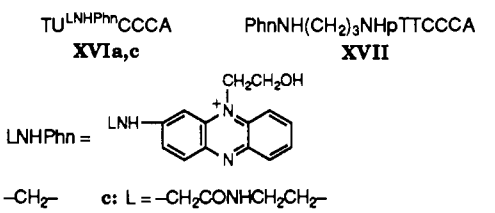


of compounds **VIIIa–c** and $NH_2(CH_2)_3NHpTCCACTT$ with *N*-hydroxysuccinimide esters of *p*-azidotetrafluorobenzoic, 2-nitro-5-azidobenzoic, or *p*-azidobenzoic acids.

The alkylating 4-[*N*-(2-chloroethyl)-*N*-methylamino]-benzyl group was attached to the amino spacer of an oligonucleotide by the reaction of an amino group with 4-[*N*-(2-chloroethyl)-*N*-methylamino]benzaldehyde followed by the reduction of the Schiff base with sodium borohydride (Scheme IV).

The covalent chlorine amount (80–90%) was estimated by the reaction of compounds **XIV** with $Na_2S_2O_3$ and subsequent reverse-phase chromatography of the reaction products (*19*).

The residue *N*-(2-hydroxyethyl)phenazinium (Phn) which stabilizes the complementary complexes, was attached to the amino group of oligonucleotide derivatives **IXa,c**, **Xa,c** and $NH_2(CH_2)_3NHpTTCCCA$ according to ref 11. The following Phn derivatives were obtained:



The oligonucleotide derivatives **XI–XVII** were isolated by reverse-phase HPLC in a yield of 70–80% for compounds carrying the photoreactive groups (**XIa–c**, **XIIb**, and **XIIIb**), 20–50% for alkylating derivatives (**XIVa–c**), and 80–90% for Phn-containing oligonucleotides (**XVa,c**, **XVIa,c**, and **XVII**). Figure 1 shows typical chromatography elution profiles for reagents **XIb**, **XIIb**, **XIVc**, and **XVc**. The products bearing the groups mentioned above were eluted at a higher concentration of acetonitrile than the parent amino derivatives of oligonucleotides, which indicates hydrophobic residue coupling.

The composition of some of the derivatives obtained was confirmed by the enzymatic digestion (see Table III).

As follows from Figure 2, the absorption spectra of compounds **XI–XVII** were the combination of the spectra of the oligonucleotide moiety and the corresponding attached group. In the case of the oligonucleotide derivative **XIIb** bearing the 2-nitro-5-azidobenzamide group, which has an absorption at 318 nm (Table I), there are two absorption bands in the spectrum. The spectra of compounds **XIa–c** and **XIIIb** are close to the spectrum of the parent oligonucleotide TCCACTT. In the electron spectra of compounds **XV–XVII** with the phenazinium residue, we have observed absorption at 237, 268, 290 (sh), 390, and 530 nm, in agreement with literature data (*11*). When the aromatic group and the oligonucleotide residue have absorption at different wavelengths, they are in a 1:1 ratio.

The interaction of oligonucleotides carrying different groups with nucleic acids depends on their ability to form the complementary complexes. Therefore the influence of the attached groups on complex formation was estimated using the oligonucleotide derivatives prepared (Table IV). To compare the properties of oligonucleotide derivatives bearing some group at the C5-position and at the terminal phosphate (the most well-investigated ones), we have synthesized compounds **XId** and **XVII**.

It is shown that the alkylating group does not change the melting temperature of the corresponding duplex. The duplex stability does not decrease but, on the contrary, increases a little in the case of the reagents bearing photoactive groups; the effect of the incorporated residue depends on the spacer length (it is minimal for L = $-CH_2-$)

Table IV. Melting Temperatures (T_m, °C) of Duplexes A and B[a]

$^{5'}$TAAGTGGAGTTTGGC$^{3'}$
- - - - - - - -
- - - - - - - -
$^{3'}$TTCACCX$^{5'}$ (duplex A)

X	compd	T_m, °C
T		25
pT		25
$U^{CH_2NH_2}$	**VIIIa**	25
$U^{CH_2OCH_2CH_2NH_2}$	**VIIIb**	27
$U^{CH_2NHCOCH_2CH_2NH_2}$	**VIIIc**	27
$R^1NH(CH_2)_3NHpT$	**XId**	30
$U^{CH_2NHR^1}$	**XIa**	26
$U^{CH_2OCH_2CH_2NHR^1}$	**XIb**	29
$U^{CH_2NHCOCH_2CH_2NHR^1}$	**XIc**	29
$U^{CH_2NHCOCH_2CH_2NHR^2}$	**XIIc**	29
$U^{CH_2NHCOCH_2CH_2NHR^3}$	**XIIIc**	29
$U^{CH_2NHCOCH_2CH_1NHR^4}$	**XIVc**[b]	26

$^{5'}$TGAATGGGAACA$^{3'}$
- - - - - -
- - - - - -
$^{3'}$ACCCZY$^{5'}$ (duplex B)

YZ	compd	T_m, °C
TT		16
$U^{CH_2NHPhn}T$	XVa	18
TU^{CH_2NHPhn}	**XVIa**	<3
$U^{CH_2NHCOCH_2CH_2NHPhn}T$	**XVc**	25
$TU^{CH_2NHCOCH_2CH_2NHPhn}$	**XVIc**	22
PhnNH$(CH_2)_2$NHpTT	**XVII**	34

[a] Concentration of the oligonucleotide complexes was $2 \cdot 10^{-5}$ M in 0.16 M NaCl–0.02 M Na_2HPO_4–0.1 mM EDTA, pH 7.5, buffer. [b] Before the melting experiments compound **XIVc** was kept during 48 h for the active chlorine hydrolysis (*24*). $R^4 = CH_2C_6H_4N(CH_3)(CH_2CH_2OH)$.

and does not depend on the site where the photoactive group is attached (C5 of deoxyuridine or 5′-terminal phosphate).

Interesting results have been observed for the Phn-containing derivatives. The Phn residue at the 5′-phosphate was shown in ref 11 to stabilize the duplexes. The influence of the Phn residue on duplex stability strongly depended on its location in the oligonucleotide.

The maximum ΔT_m value (18 °C) was observed when the Phn residue was attached to the 5′-terminal phosphate. When the Phn residue is located in the heterocyclic base of the first 5′-terminal nucleoside (compounds **XVa,c**), the T_m value increases by 9 or 2 °C, depending on the spacer length (L = $-CH_2NHCOCH_2CH_2-$ or $-CH_2-$, respectively). The attachment of the Phn residue to the second nucleoside from the 5′-end (compounds **XVIa,c**) yields ΔT_m = 6 °C in the case of a longer spacer (L = $-CH_2NHCOCH_2CH_2-$), but the duplex is not detected at all in the case of a short spacer (L = $-CH_2-$).

Thus the maximum stabilizing effect of the Phn residue is observed when it is connected with the terminal phosphate. If it is necessary, the Phn residue may also be attached to the heterocycle of the terminal nucleoside unit through a flexible spacer.

So, flexible spacers with a five- or six-atom chain are more favorable for attachment of any groups.

The results obtained show that the method suggested for the synthesis of oligonucleotide amino derivatives can be applied for introduction of different groups. The groups used in this work do not interfere with duplex formation, and in some cases even increase duplex stability and therefore the reactive oligonucleotide derivatives can be used for modification of nucleic acids in complementary complexes.

ACKNOWLEDGMENT

We are indebted to N. I. Komarova for fulfilling the chromatography of the enzymatic oligonucleotides hydrolysates, to S. V. Lochov for the T_m measurements, and to T. M. Ivanova for the synthesis of 3′,5′-diacetyl-5-(bromomethyl)deoxyuridine. The work was supported by a grant from the state program "The New Methods of Bioengineering".

LITERATURE CITED

(1) Knorre, D. G., and Zarytova, V. F. (1991) Novel antisense derivatives: Antisense DNA intercalators, cleavers, and alkylators. *Prospects for Antisense Nucleic Acid Therapy of Cancer and AIDS* (E. Wickstrom, Ed.) pp 195–218, Wiley & Sons, Inc., New York.

(2) Tesler, J., Cruicshank, K. A., Morrison, L. E., and Netzel, T. L. (1989) Synthesis and characterization of DNA oligomers and duplexes containing covalently attached molecular labels by thermodinamic and optical spectroscopic measurements. *J. Am. Chem. Soc. 111*, 6966–6976.

(3) Tesler, J., Cruicshank, K. A., Schanze, K. S., and Netzel, T. L. (1989) DNA oligomers and duplexes containing a covalently attached derivative of tris(2,2′-bipyridyl)ruthenium (II): Synthesis and characterization by thermodinamic and optical spectroscopic measurements. *J. Am. Chem. Soc. 111*, 7221–7226.

(4) Beyer, R. B., Tabone, J. C., Jr., Hurst, G. D., Smith, T. M., and Gamper, H. (1989) Efficient, specific cross-linking and cleavage of DNA by stable, synthetic complementary oligonucleotides. *J. Am. Chem. Soc. 111*, 8517–8519.

(5) Iverson, B. L., and Dervan, P. B. (1987) Nonenzymatic sequence-specific cleavage of single-stranded DNA to nucleotide resolution. DNA methyl thioether probes. *J. Am. Chem. Soc. 109*, 1241–1243.

(6) Povsic, T. J., and Dervan, P. B. (1990) Sequence-specific alkylation of double-helical DNA by oligonucleotide-directed triple-helix formation. *J. Am. Chem. Soc. 112*, 9428–9430.

(7) Casale, R., and Mc Laughlin, L. W. (1990) Synthesis and properties of an oligonucleotides containing a polycyclic aromatic hydrocarbon site specifically bound to the N^2-amino group of a 2′-deoxyguanosine residue. *J. Am. Chem. Soc. 112*, 5264–5271.

(8) Hobbs, F. W. (1989) Palladium-catalyzed synthesis of alkynyl amino-nucleosides. *J. Org. Chem. 54*, 3420–3422.

(9) Cruickshank, K. A., and Stockwell, D. L. (1988) Oligonucleotide labeling: A concise synthesis of a modified thymidine phosphoroamidite. *Tetrahedron Lett. 29*, 5221–5224.

(10) Haralambidis, J., Chai, M., and Tregear, G. W. (1987) Preparation of base-modified suitable for non-radioactive label attachment and their incorporation into synthetic oligonucleotides. *Nucl. Acids Res. 15*, 4857–4876.

(11) Lokhov, S. G., Podyminogin, M. A., Sergeev, D. S., Silnikov, V. N., Kutyavin, I. V., Shishkin, G. V., and Zarytova, V. F. (1992) Synthesis and high stability of complementary complexes of N-(2-hydroxyethyl)phenazinium derivatives of oligonucleotides. *Bioconjugate Chem. 3*, 414–419.

(12) Anderson, G. W., Zimmerman, J. E., and Callahan, F. M. (1964) The use of esters of N-hydroxysuccinimide in peptide synthesis. *J. Am. Chem. Soc. 86*, 1839–1842.

(13) Popp, F. D. (1964) Synthesis of potential antineoplastic agents. X. Preparation and reactions of aldehydes related to benzaldehyde mustard.

(14) Bärwolff, D., and Langer, P. (1978) 2′-deoxy-5(hydroxymethyl)uridine and 2′-deoxy-5-formyluridine selective promination of the 5-methyl group of 5-methylpyrimidine nucleosides. *Nucleic Acid Chemistry* (L. B. Townsend, and R. S. Tipson, Eds.) Vol. 1, pp 359–366, Wiley & Sons, Inc., New York.

(15) Garegg, P. J., Regberg, T., Stawinski, J., and Stromberg, R. (1984) Nucleoside hydrogen phosphonates in oligonucleotide synthesis. *Chem. Scr. 26*, 59–62.

(16) Froekler, B. C., Ng, P. G., and Matteucci, M. D. (1986) Synthesis of DNA via deoxynucleoside H-phosphonate intermediates. *Nucl. Acids Res. 14*, 5399–5407.

(17) Zarytova, V. F., Godovikova, T. S., Kutyavin, I. V., and Khalimskaya, L. M. (1987) Reactive oligonucleotide derivatives as affinity reagents and probes in molecular biology. *Biophosphates and the Analogues, Synthesis, Structure, Metabolism and Activity* (K. S. Bruzik, and W. J. Stec, Eds.) pp 149–164, Elsevier, Amsterdam.

(18) Dobrikov, M. I., Prichodko, T. A., Safronov, I. V., and Shishkin, G. V. (1992) Synthesis of photosensitive kapron membranes. Photoimmobilization of DNA. *Sibir. Khim. J. 13*, 65–77.

(19) Zarytova, V. F., Kutyavin, I. V., Silnikov, V. N., and Shishkin, G. V. (1986) Modification of nucleic acids in stabilized complementary complexes. I. Synthesis of alkylating derivatives of oligodeoxyribonucleotides having a 5′-terminal N-(2-oxyethyl)phenazinium residue. *Bioorg. Khim. 12*, 911–920.

(20) Grachev, M. A., and Perelroyzen, M. P. (1978) Measurement of the differential melting profile of promotor containing fragment of T7 DNA by means of microspectrophotometer. *Nucl. Acids Res. 5*, 2557–2564.

(21) Cantor, C. R., and Tinoko, I. (1965) Absorption and optical rotatory dispersion of seven trinucleoside diphosphates. *J. Mol. Biol. 13*, 65–77.

(22) Baram, G. I., Buneva, V. N., Dobrikova, E. Yu., and Petrov, V. N. (1986) Plurality of RNase affinity modification on its alkylation with 5′-deoxyribonucleotide reactive derivatives. *Bioorg. Khim. 12*, 613–620.

(23) Boyer, J. (1951) Addition of hydrazoic acid to conjugated systems. *J. Amer. Chem. Soc. 73*, 5248–5252.

(24) Graifer, D. M., Zenkova, M. A., Malygin, A. A., Mamaev, S. V., Mundus, D. A., and Karpova, G. G. (1990) Identification of a site on 18S rRNA of human placenta ribosomes in the region of the mRNA binding center. *J. Mol. Biol. 214*, 121–128.

Synthesis, Characterization, and *in Vitro* Evaluation of Nitroimidazole–BATO Complexes: New Technetium Compounds Designed for Imaging Hypoxic Tissue

K. E. Linder, Y. W. Chan, J. E. Cyr, D. P. Nowotnik,* W. C. Eckelman, and A. D. Nunn

Bristol-Myers Squibb Pharmaceutical Research Institute, P.O. Box 4000, Princeton, New Jersey 08543-4000.
Received March 9, 1993

Several technetium-99 BATO (*b*oronic acid *a*dduct of *t*echnetium dioximes) complexes $TcX(dioxime)_3BR$ (X = Cl) that contain a boron cap R which bears a 2- or 4-nitroimidazole moiety have been prepared from either $TcCl(dioxime)_3$ or from $Tc(dioxime)_3(\mu\text{-}OH)SnCl_3$ [dioxime = dimethyl glyoxime (DMG) or cyclohexanedione dioxime (CDO)]. Two hydroxy analogs (X = OH) were isolated by treatment of the corresponding chloro complexes with aqueous NaOH. The complexes have been characterized by elemental analysis, mass spectrometry, NMR, UV/vis spectroscopy, and high-performance liquid chromatography. These complexes have the potential for selective retention in hypoxic tissue, by a mechanism believed to be the result of nitro reduction. The electrochemistry and enzymatic reduction of these complexes was studied to assess the potential for reduction *in vivo*. The nitroreductase enzyme xanthine oxidase was shown to reduce the nitroimidazole group on the complexes $^{99}TcOH(DMG)_3BBNO_2$ and $^{99}TcOH(DMG)_3BprenNO_2$ under anaerobic conditions in the presence of hypoxanthine. However, the results indicated that the rate of reduction might be slow *in vivo*, limiting the suitability of these compounds for imaging of regions of hypoxia.

INTRODUCTION

Recently, there has been considerable interest in the concept of imaging hypoxia (areas of low oxygen tension) with radiolabeled derivatives of nitroimidazoles. Other groups have reported the binding of ^{14}C- (*1-4*), ^{3}H- (*5, 6*), ^{82}Br- (*7, 8*), and ^{18}F-labeled (*9-12*) 2-nitroimidazole derivatives to hypoxic cells or tissues in cerebral ischemia (*13*), myocardial infarction (*6, 10, 11, 14*), and malignant tumors or tumor spheroids (*1-5, 12, 15*). Reports of iodine-labeled nitroimidazole derivatives (*14, 16-19*) have also been published recently. It was apparent to us that the development of a technetium-based hypoxia-localizing nitroimidazole would be a useful contribution to the field of nuclear medicine, as it would make hypoxia imaging available to the majority of nuclear medicine centers. One class of technetium compounds that we have studied are nitroimidazole–BATO complexes $TcX(dioxime)_3BR$ (X = Cl, OH; R = a nitroimidazole derivative, BATO = *b*oronic *a*cid adduct of *t*echnetium di*o*xime (*20, 21*); see Figure 1). Technetium BATO compounds have already proved to be useful for perfusion imaging of the heart and brain (*22*), and BATOs derivatized with an isothiocyanato functionality have been used to radiolabel antibodies (*23, 24*). It seemed reasonable to incorporate a nitroimidazole functionality into the boron cap of one of these molecules, as one approach to the design of a technetium-based hypoxia imaging agent. The syntheses of the nitroimidazole boronic acids appear in a separate report (*25*). The structures of these compounds are shown in Figure 2. In this report we describe the syntheses, characterization, and electrochemistry of the BATO complexes derived from nitroimidazole boronic acids, and their initial evaluation *in vitro* using an assay which evaluates their ability to be reduced by the nitroreductase enzyme xanthine oxidase. As the uptake of ^{18}F-labeled misonidazole *in vivo* was found to be dependent on the degree of hypoxia, whereas the uptake of labeled metronidazole was less selective (*26*), the reduction properties of the nitroimidazole boronic acids and nitroimidazole–BATOs were compared to those of misonidazole and metronidazole.

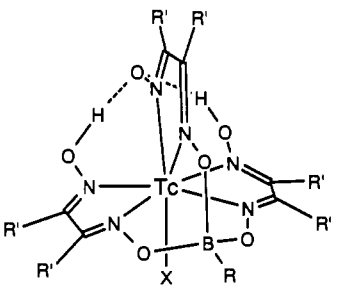


Figure 1. The general structure of BATOs [$TcX(dioxime)_3BR$ (dioxime = DMG, CDO)]. The R′ groups represent methyl, in DMG. Alternatively, two R′ groups combined represent $CH_2CH_2CH_2CH_2$, in CDO. X = Cl or OH. R is the substituent containing the nitroimidazole moiety.

EXPERIMENTAL PROCEDURES

Materials and Reagents. Dimethylglyoxime (DMG, Eastern Chemicals) and cyclohexanedione dioxime (CDO, Fluka) were used as received. The syntheses of the nitroimidazole boronic acids are described elsewhere (*25*). Misonidazole was obtained as a gift from Prof. K. Krohn, University of Washington. Metronidazole (Aldrich), 2-nitroimidazole (Aldrich), tris(hydroxymethyl)aminoethane (Fisher Scientific), $Ru(acac)_3$ (Strem), and $CdSO_4$ (Johnson Mathey Puratronic) were used as received. Bu_4NBF_4 (Aldrich), a supporting electrolyte, was recrystallized twice from $MeOH/H_2O$ or acetone/ether, dried, and stored under vacuum. The complexes $Tc(DMG)_3(\mu\text{-}OH)SnCl_3{\cdot}3H_2O$, $Tc(CDO)_3(\mu\text{-}OH)SnCl_3$, $TcCl(DMG)_3$, and $TcCl(CDO)_3$ were prepared as described previously (*21*). All solvents were reagent grade or better and used as received. Water was purified using a Millipore MilliQ system.

HPLC measurements were made on either a 15-cm Hamilton PRP-1 10-μm column (Alltech Associates), using a mobile phase of acetonitrile/0.1 M NH_4OAc (pH 4.6) at

1043-1802/93/2904-0326$04.00/0 © 1993 American Chemical Society

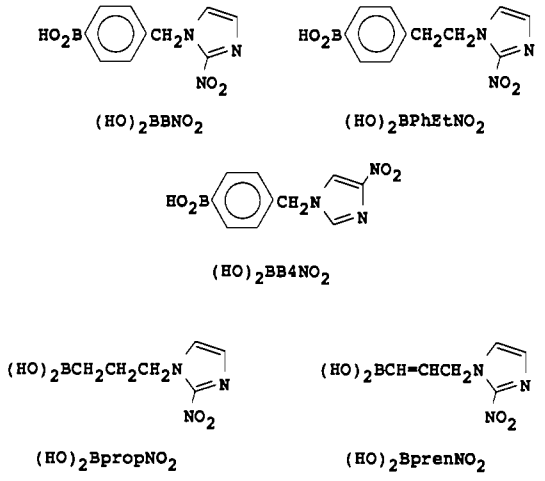


Figure 2. The structures of the nitroimidazole boronic acids ($(HO)_2BR$).

a flow rate of 2.0 mL/min, or on a 4.6 × 300 mm Nucleosil C-8 column (Alltech Associates) using a mobile phase of acetonitrile/0.1 M citric acid (pH 2.3) at a flow rate of 1.5 mL/min.

Infrared measurements were recorded as KBr pellets on a Sirius 100 FT-IR instrument. UV/visible spectra were recorded using a Hewlett-Packard HP 8451A photodiode-array spectrophotometer. Air-sensitive reduced solutions were analyzed under nitrogen by carefully transferring them *via* syringe into a spectroscopy cell sealed with a rubber septum (flushed with N_2). Fast atom bombardment mass spectra were obtained on a VG-ZAB-2F spectrometer. ^1H NMR spectra were recorded on a JEOL GX-270 instrument. Elemental analyses were performed in-house by the Microanalytical Department.

Xanthine oxidase (XOD, xanthine:oxygen Oxidoreductase, EC 1.1.3.22; isolated from cow milk) was obtained from Boeringer Mannheim as a suspension in ammonium sulfate solution (3.2 mol/L in $(NH_4)_2SO_4$, pH ~8, [EDTA] = 10 mmol/L). The solution had a specific activity of about 1 unit/mg of protein and contained 20 units/mL. The enzyme was stored at 4 °C until use. Xanthine (20 mg/L) and hypoxanthine (0.01 M) solutions were prepared by stirring the purines (Sigma) in water or phosphate buffer at near boil until dissolved. All pH 7.4 phosphate buffer (0.025 or 0.1 M) contained 20 mg/L of $Na_2EDTA{\cdot}2H_2O$. Solutions were freshly prepared for each assay.

Synthesis and Characterization of Technetium Complexes. *Synthesis of $^{99}TcCl(CDO)_3BBNO_2$.* To $Tc(CDO)_3(\mu\text{-}OH)SnCl_3{\cdot}3H_2O$ (90.3 mg, 0.11 mmol) in 10 mL of warm acetonitrile was added $(OH)_2BBNO_2$ (31 mg, 0.129 mmol), followed by 1.5 mL of 3 N HCl. The solution was heated gently for 30 min., 10 mL of 1 M HCl was added, and the solution was cooled to room temperature. The resulting orange solid was isolated by suction filtration, washed with 5 mL of 1 N HCl and 5 mL of H_2O, and dried *in vacuo* to give 61 mg (78%) of crude product. The product was dissolved in 10 mL of warm acetonitrile and filtered, and an equal volume of 1 N HCl was added dropwise. Analytically pure microcrystals precipitated on cooling. Anal. Calcd for $C_{28}H_{34}N_9BClO_8Tc$: C, 43.68; H, 4.45; N, 16.37. Found: C, 43.59; H, 4.43; N, 16.20.

Synthesis of $^{99}TcCl(DMG)_3BBNO_2$. To $Tc(DMG)_3(\mu\text{-}OH)SnCl_3{\cdot}3H_2O$ (55 mg, 0.074 mmol) in 10 mL of warm acetonitrile was added $(OH)_2BBNO_2$ (25 mg, 0.10 mmol), followed by 1 mL of 3 N HCl. The solution was heated gently for 30 min, 10 mL of 1 N HCl was added, and the solution was cooled to room temperature. After a slight delay, red-orange crystals precipitated. These were isolated by suction filtration, washed with 2 × 5 mL of 1 N HCl, and dried *in vacuo*. A second crop was isolated after 6 h. The overall crude yield was 41 mg (80.5%). The product was partially purified by recrystallization from 10 mL of boiling acetonitrile, to which was added 2 mL of 1 N HCl and 15 mL of water. Further recrystallization from 2 mL of boiling acetonitrile, 1 mL of CH_2Cl_2, and 1 drop of 1 N HCl yielded pure product on slow evaporation. Anal. Calcd for $TcCl(DMG)_3BBNO_2{\cdot}0.5H_2O$ ($C_{22}H_{29}N_9BClO_{8.5}Tc$): C, 37.71, H, 4.17; N, 17.99. Found: C, 37.62; H, 4.33; N, 17.63.

Synthesis of $^{99}TcOH(DMG)_3BBNO_2$. To $TcCl(DMG)_3BBNO_2$ (45 mg, 0.065 mmol) in 2 mL of warm acetonitrile were added 3 drops of 2 N NaOH and 2 mL of H_2O. The resulting suspension was stirred with gentle heating for 15 min. During this time, all starting material dissolved and was converted to desired product, as determined by HPLC (Nucleosil C-8, 50/50 CH_3CN/0.1 M NH_4OAc, 1.5 mL/min; t_R of $TcCl(DMG)_3BBNO_2$ = 5.83, t_R of $TcOH(DMG)_3BBNO_2$ = 4.88 min). Water (2 mL) was added, and the solution was heated until precipitation of product began. Orange microcrystals (30.5 mg) were isolated after the solution was cooled to room temperature. A second crop (6 mg, 80% yield overall) was isolated after 4 h. The product was washed with water and dried *in vacuo* for 1 h.

Synthesis of $^{99}TcCl(DMG)_3BPhEtNO_2$. To $Tc(DMG)_3(\mu\text{-}OH)SnCl_3{\cdot}3H_2O$ (77.1 mg, 0.104 mmol) in 5 mL of acetonitrile was added $(OH)_2BPhEtNO_2$ (28.8 mg, 0.11 mmol), followed by 2 drops of concentrated HCl. The solution was heated at a boil for 30 min, during which time an orange solid precipitated (68 mg, 93% yield). Product was washed well with acetonitrile and dried *in vacuo*. This crude solid (identity unknown, not $TcCl(DMG)_3BPhEtNO_2$) was dissolved in 1 mL of DMF, 2 mL of acetonitrile, and 1 mL of 1 M HCl and boiled for 30 min. HPLC analysis (PRP-1, 70/30 CH_3CN/0.1 M NH_4OAc, 2 mL/min) demonstrated that starting material (t_R = 1.17 min) was slowly converted to desired product (t_R = 2.35 min) over this time. Crystals (31 mg, 40% overall yield) formed upon cooling overnight. Anal. Calcd for $TcCl(DMG)_3BPhEtNO_2{\cdot}0.5DMF$ ($C_{24.5}H_{33}N_{9.5}BClO_{8.5}Tc$): C, 39.64; H, 4.81; N, 17.92. Found: C, 39.80, H, 4.60; N, 17.55.

Synthesis of $^{99}TcCl(DMG)_3BpropNO_2$. To $Tc(DMG)_3(\mu\text{-}OH)SnCl_3{\cdot}3H_2O$ (143 mg, 0.193 mmol) in 10 mL of acetonitrile was added $(OH)_2BpropNO_2$ (41.8 mg, 0.21 mmol), followed by 3 mL of 2 N HCl. The reaction mixture was heated gently for 30 min, 50 mL of 1 N HCl was added, and the solution was cooled to room temperature. The resultant flocculant orange solid was isolated by suction filtration, washed with 1 M HCl and H_2O, and dried *in vacuo* to yield 97 mg (78%) of crude product. This was dissolved in 1 mL of $CHCl_3$ and chromatographed on a 1 × 10 cm silica gel column that was conditioned and eluted with $CHCl_3$. The major orange band was evaporated to dryness, redissolved in 3 mL of CH_2Cl_2, and treated with 30 mL of hexane. Analytically pure solid was isolated in 57% yield overall. Anal. Calcd for $C_{18}H_{28}N_9BClO_8Tc$: C, 33.58; H, 4.38; N, 19.58. Found: C, 33.66; H, 4.20; N, 19.28.

Synthesis of $^{99}TcCl(DMG)_3BprenNO_2$. To $Tc(DMG)_3(\mu\text{-}OH)SnCl_3{\cdot}3H_2O$ (135.5 mg, 0.183 mmol) in 10 mL of acetonitrile was added $(OH)_2BprenNO_2$ (39.4 mg, 0.20 mmol), followed by 3 mL of 2 N HCl. The reaction mixture was heated gently with stirring for 30 min, 15 mL of 1 N HCl was added, and the solution was cooled to room temperature. An orange oil formed, which was stirred with scratching until the product solidified. The crude

solid (85 mg, 73%) was isolated by suction filtration, washed with H_2O, and dried *in vacuo*. It was then dissolved in a minimal volume of $CHCl_3$ and chromatographed on a 2.5 × 8 cm silica gel column that was conditioned and eluted with 10% ethyl acetate/90% $CHCl_3$. The major orange band was collected as four fractions, the first of which was discarded after analysis by HPLC demonstrated the presence of a lipophilic impurity. The other fractions were pooled and rotary evaporated to an oil, and the oil was redissolved in 5 mL of acetonitrile. Treatment with 15 mL of 0.5 N HCl caused precipitation of an orange microcrystalline solid.

Synthesis of $^{99}TcOH(DMG)_3BprenNO_2$. To $TcCl(DMG)_3BprenNO_2$ (100 mg, 0.156 mmol) in 2 mL of warm acetonitrile were added 3 drops of 2 N NaOH and 2 mL of H_2O. The solution was heated with stirring for 1 h, the volume was reduced using an N_2 stream, 2 mL of H_2O was added, and the product was extracted into 3 × 4 mL of CH_2Cl_2. The organic layer was washed with water (3 × 4 mL), and 5 mL of acetonitrile was added to the organic phase. The solvent was removed by rotary evaporation to yield an orange oil. Addition of water (2 mL) caused precipitation of an oily solid, which was stirred, with scratching, until completely solid. The product was isolated by suction filtration, washed with water, and air-dried to yield 99 mg of orange brown product.

Synthesis of $^{99}TcCl(DMG)_3BB4NO_2$. A mixture of $TcCl(DMG)_3$ (32.7 mg, 0.068 mmol) and $(OH)_2BB4NO_2$ (17.7 mg, 0.073 mmol) in 5 mL of acetonitrile and 0.5 mL of 2 N HCl was heated with stirring for 15 min. Solvents were then removed by evaporation. The product was purified on a silica gel column eluted with 40/60 ACN/CH_2Cl_2. The major orange band was evaporated to dryness and recrystallized from ether (61% yield). Anal. Calcd for $TcCl(DMG)_3BB4NO_2 \cdot 0.2C_4H_{10}O$ ($C_{22}H_8N_9O_8BClTc \cdot 0.2C_4H_{10}O$): C, 38.75; H, 4.28; N, 17.84. Found: C, 38.39; H, 4.21; N, 17.44.

Synthesis of $^{99}TcCl(CDO)_3BB4NO_2$. A mixture of $TcCl(CDO)_3$ (25.07 mg, 0.046 mmol) and $(OH)_2BB4NO_2$ (11.6 mg, 0.048 mmol) was dissolved in 5 mL of ACN and 0.5 mL of 3 M HCl and heated with stirring for 30 min. An orange solid was precipitated by adding 5 mL of 1 M HCl, collected by filtration (crude yield, 83%), and recrystallized from ether. Anal. Calcd for $C_{28}H_{34}N_9O_8ClBTc \cdot 0.5C_4H_{10}O$: C, 44.65; H, 4.87; N, 15.62. Found: C, 44.81; H, 4.95; N, 16.05.

Synthesis of ^{99m}Tc Complexes. ^{99m}Tc–BATO nitroimidazoles were prepared by methods similar to those reported previously (*23*) involving addition of the boronic acid derivative to freeze-dried tris-dioxime kits. The radiochemical purities (RCPs) of these complexes were determined using reversed-phase high-performance liquid chromatography (using the PRP-1 and Nucleosil C_8 systems, described above). RCPs were typically >90%.

Electrochemical Studies. Instrumentation and experimental conditions for electrochemical studies in DMF were as described elsewhere (*27*). The CV of $Ru(acac)_3$ was determined on a daily basis to compensate for variations in the reference potential. All measured potentials were corrected to an absolute peak reduction potential for $Ru(acac)_3$ of −1.210 V vs $Ag/AgNO_3$ (acetonitrile) at Hg (−0.790 V vs SCE at Pt).

Determination of Rate of Reduction by Xanthine Oxidase Catalysis. *Standardization of Enzyme Solutions.* The specific activity (units/mL) of the xanthine oxidase solutions was assayed by measuring the rate of XOD-catalyzed formation of uric acid from xanthine, following the procedure of Bray (*28*). Based upon the assay results, 0.5 units of enzyme was added per study.

Effect of 5% DMF on the activity of XOD. A xanthine oxidase suspension (10 μL) was diluted to 1 mL with 990 μL of pH 7.4 phosphate/EDTA buffer. To a quartz cuvette was added 1.0 mL of xanthine solution (20 mg/L of water) followed by 1.75 mL of phosphate buffer and 150 μL of DMF. The reaction was initiated by adding 100 μL of diluted enzyme solution. Absorbance at 292 nm was monitored for 10 min, and data were converted to "change in absorbance units/min" relative to a comparable reaction in the absence of DMF (Table VI). Similar studies were performed with 0 and 10% DMF. Appropriate UV/vis blanks contained water in place of xanthine solution.

XOD-Catalyzed Reduction of Nitroimidazole Boronic Acids and Nitro Compounds. To a 3-mL quartz cuvette was added solutions of hypoxanthine (10 μmol) and nitro compound (0.25 μmol) dissolved in sufficient pH 7.6 phosphosaline (PBS; 0.025 M phosphate in saline) or pH 7.4 phosphate buffer (0.025 M) to bring the total volume to 2 mL. The cuvette was sealed with a rubber septum and purged of oxygen by passage of a stream of ultra high purity argon through the solution. Meanwhile, to a 5-mL siliconized vial was added 1.05 mL of PBS or phosphate buffer followed by about 150 μL of XOD suspension. The vial was crimp sealed and deoxygenated by passing a flow of argon over the surface of the enzyme solution for exactly 15 min.

To initiate the reaction, 500 μL of the deoxygenated enzyme solution (0.5 units) was added to the degassed nitro solution *via* a gas-tight noncoring syringe. The final assay solution (2.5 mL) was 0.2 units/mL in XOD, 100 μM in nitro compound, and 4 mM in hypoxanthine. The cuvette was inverted to mix and then monitored by UV-vis (vs PBS buffer blank) to follow the disappearance of the nitro group absorbance. Both the spectrum of the solution from 280 to 450 nm and absorbance at 326 nm were recorded every 5 min. Data were automatically stored to disk for later retrieval and analysis. The absorbance at 326 nm was converted to concentration, and plots of log[concentration] vs time were prepared using Excel software. All of the 2-nitroimidazole boronic acids, misonidazole, and metronidazole were tested as described above. Data for the 4-nitroimidazole compound $(OH)_2BB4NO_2$ was obtained in the same fashion, except that the absorbance was monitored at 310 nm instead of 326 nm.

XOD-Catalyzed Reduction of $^{99}TcOH(DMG)_3R$ (R = $BBNO_2$, $BprenNO_2$). To a 3-mL quartz cuvette was added 0.2 μmol of the $^{99}TcOH(DMG)_3R$ complex in 125 μL of DMF, 1.0 mL of 0.01 M hypoxanthine solution in 0.1 M phosphate/EDTA buffer (pH 7.4), and 0.875 mL of 0.1 M sodium phosphate buffer. The cuvette was sealed with a rubber septum and was purged of oxygen by passage of a stream of ultra high purity argon through the solution. Meanwhile, to a 5-mL siliconized vial was added 1.05 mL of pH 7.4 phosphate buffer (0.1 M) and approximately 150 μL of XOD suspension. The vial was crimp sealed and deoxygenated by passing a flow of argon over the surface of the enzyme solution for exactly 15 minutes.

To initiate the reaction, 500 μL of enzyme solution (0.5 units) was added to the degassed nitro solution *via* a gas-tight noncoring syringe. The final assay solution (2.5 mL) was 0.2 units/mL in XOD, 80–100 μM in nitro compound, 4 mM in hypoxanthine, and 5% in DMF. The spectrum of the resulting solution was recorded from 280 to 600 nm every 15 min for 10 h. Data were stored to disk for later retrieval and analysis as above. Similar assays were

conducted with $(OH)_2BBNO_2$ and $(OH)_2BprenNO_2$ to allow direct comparison of boronic acid and Tc complex data in 5% DMF.

Control reactions (in the absence of enzyme or in the absence of hypoxanthine) were also carried out, substituting phosphate buffer for reagents not added. In addition, a control reaction substituting the non-nitro compound $^{99}TcCl(DMG)_3BPh$ was carried out.

RESULTS AND DISCUSSION

Syntheses and Characterization of Nitroimidazole–BATOs. Synthesis of the ^{99}Tc–BATO nitroimidazoles from either $Tc(dioxime)_3(\mu\text{-}OH)SnCl_3$ or $TcCl(dioxime)_3$ (dioxime = DMG or CDO) usually proved to be straightforward, following procedures described previously (*21*) for the synthesis of non-nitroimidazole BATOs (the exception was $TcCl(DMG)_3BPhEtNO_2$, which gave an unidentified polar product, which converted to the required BATO on recrystallization from HCl-acidified DMF). Isolated yields of 70–80% could be obtained after heating the Tc starting material with a nitroimidazole boronic acid in HCl-acidified acetonitrile. The structures of the nitroimidazole boronic acids used are shown in Figure 2.

Two BATO–nitroimidazole compounds, in which the axial X ligand (Figure 1) was hydroxyl, were also prepared. On treatment of the chloro compounds $TcCl(DMG)_3BBNO_2$ and $TcCl(DMG)_3BprenNO_2$ with NaOH, chloro to hydroxy exchange to form $TcOH(DMG)_3BBNO_2$ and $TcOH(DMG)_3BprenNO_2$ was observed, as has been noted for other BATO compounds (*29*). These hydroxy compounds must not be vacuum-dried after isolation, or the material will turn deep brown, as observed for other BATOs with an axial hydroxyl ligand (*30*). A sample of $TcOH(DMG)_3BprenNO_2$ that was vacuum-dried overnight yielded a molecular ion corresponding to the mass of the dimer:

$$RB(DMG)_3Tc\text{–}O\text{–}Tc(DMG)_3BR$$

After recrystallization, satisfactory analyses could be obtained on all chloro nitroimidazole BATO compounds, as determined by NMR, mass spectrometry, IR, and elemental analysis.[1]

The infrared spectra of the isolated products all showed two strong nitro bands (ν_{as} and ν_{sym}) (*31, 32*) in the range 1535–1546 and 1360–1400 cm^{-1}, respectively, indicating that the nitroimidazole moiety had survived the reaction conditions required for the synthesis of the BATOs.

All compounds showed similar UV/visible spectra. All of the absorption bands found in a normal BATO are also present in the nitroimidazole BATOs. However, the peak at 320 also contains a significant contribution from a $\pi \rightarrow \pi^*$ transition (*33*) from the nitroimidazole cap.

In the ^1H NMR spectra of all nitro BATO complexes, the DMG protons are found as a multiplet (18H) at δ 2.35–2.45 ppm, and the CDO protons are found at δ 1.8 (12H) and 3.0 (12H) ppm. These chemical shifts are not significantly different from those observed for other BATOs (*20, 21*). The dioxime protons, if observed, fall at about δ 14.8 ppm. In $CDCl_3$, these protons appear as a sharp singlet, but in CD_2Cl_2, this peak is quite broad. The phenyl protons of both the $BBNO_2$ and $BB4NO_2$ complexes appear as a pair of doublets at δ 7.2 and 7.8 ppm, consistent with para substitution. The benzyl protons (s, 2H) fall at δ 5.2 ppm for both the CDO and DMG $BB4NO_2$ complexes and at δ 5.6 for the corresponding $BBNO_2$ complexes.

[1] There was insufficent material to obtain an elemental analysis on $^{99}TcCl(DMG)_3BprenNO_2$.

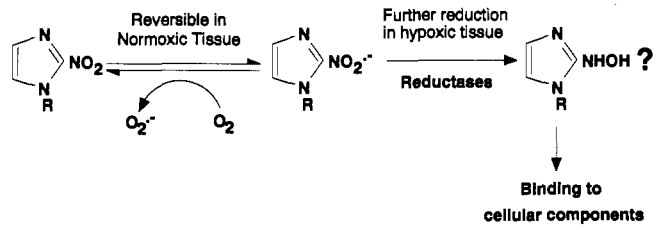


Figure 3. Proposed mechanism for the preferential entrapment of nitroimidazoles in hypoxic tissue.

The imidazole protons of both the CDO and DMG $BB4NO_2$ compounds appear as a pair of singlets at δ 7.4–7.5 and 7.7 ppm (1H each). In the $TcCl(DMG)_3BpropNO_2$ and $TcCl(DMG)_3PhEtNO_2$ complexes, where the protons of the 2-nitroimidazole group are adjacent to one another, the protons also appear as two singlets (1H each) (δ 7.1, 7.2, and 6.9, 7.05 ppm respectively). In the spectrum of both $TcCl(DMG)_3BBNO_2$ and $TcCl(CDO)_3BBNO_2$, the imidazole protons appear to be coincidentally equivalent and fall as a singlet at δ 7.15 (2H) in both compounds.

Fast atom bombardment mass spectral (FAB-MS) fragmentation patterns for the nitroimidazole BATOs were similar to those observed for other BATOs (*34*). A molecular ion and protonated molecular ion were seen for all of the chloro compounds in the positive mode. Loss of the axial ligand (as HCl) was also observed. All of the benzyl compounds (CDO and DMG complexes with $BBNO_2$ and $BB4NO_2$ caps) also showed loss of the 2-nitroimidazole group under positive FAB conditions. In the negative mode, ions corresponding to a mass of $[M - H]^-$ and $[M - HCl]^-$ were noted for all of the chloro compounds.

FAB-MS of the hydroxyl complex $TcOH(DMG)_3BBNO_2$ showed only a very weak molecular ion, as has been observed previously for other BATO hydroxy complexes (*21*). The base peak in the spectrum of this complex corresponded to $[M + H - H_2O]^+$ or $[M - H_2O]^-$ under FAB positive and negative conditions, respectively. Like the chlorobenzyl complexes, loss of the 2-nitroimidazole group was noted in the positive mode, for the $BBNO_2$ cap only. A molecular ion was noted in the spectrum of the propene analog $TcOH(DMG)_3BprenNO_2$, as well as fragment ions due to loss of water, as noted above for the $BBNO_2$ complex.

Electrochemical Studies. *In vivo* reduction of the nitro group to a reactive hydroxylamine species, followed by binding to cellular components (Figure 3), has been proposed as the mechanism by which nitroimidazoles are selectively retained in hypoxic tissue (*35*). As the reduction potential of nitroaromatic compounds appears to be an important determinant of a compound's ability to progress along this pathway, we decided to study the electrochemistry of the nitroimidazole BATOs and their boronic acid precusors.

Ideally, the electrochemical behavior of these complexes should be studied under conditions which mimic those *in vivo*; i.e. under aqueous conditions at pH 7.4. However, the majority of the nitroimidazole–BATOs are not sufficently soluble in water to achieve a concentration level suitable for normal electrochemical studies (ca. 0.2 mM) (*27*). As a result, the nitroimidazole–BATOs were examined in DMF. Although the observed electrochemical reductive processes for nitroimidazoles are different in DMF and water (in DMF, a one-electron reduction of the nitro group has been reported (*36*), while in aqueous media, a single irreversible four-electron process was observed (*37*)), Breccia et al. (*36*) demonstrated good correlation

Table I. Cyclic Voltammetry Data for Nitroimidazole Compounds in DMF[a]

compound	nitro-centered reduction	BATO-centered reduction
BATO–Nitroimidazoles		
^{99}Tc(Cl)(DMG)$_3$BBNO$_2$	−1.58	−1.31
^{99}Tc(Cl)(DMG)$_3$BB4NO$_2$	−1.84	−1.30
^{99}Tc(Cl)(DMG)$_3$BPhEtNO$_2$	−1.56	−1.29
^{99}Tc(Cl)(DMG)$_3$BpropNO$_2$	−1.64	−1.34
^{99}Tc(Cl)(DMG)$_3$BprenNO$_2$	−1.60	−1.32
^{99}Tc(Cl)(CDO)$_3$BBNO$_2$	−1.56	−1.22
^{99}Tc(Cl)(CDO)$_3$BB4NO$_2$	−1.84	−1.23
^{99}Tc(OH)(DMG)$_3$BBNO$_2$	−1.56	−1.83
^{99}Tc(OH)(DMG)$_3$BprenNO$_2$	−1.58	−1.83
"Simple" BATOs[b]		
^{99}Tc(Cl)(DMG)$_3$Ph		−1.30
^{99}Tc(Cl)(DMG)$_3$Bu		−1.35
^{99}Tc(Cl)(CDO)$_3$Ph		−1.24
^{99}Tc(OH)(DMG)$_3$Bu		−1.84, −2.56

[a] Scan rate = 100 mV/s. All solutions were 0.2–0.7 mM in sample and 0.1 M in tetrabutylammonium tetrafluoroborate. Hanging mercury drop working electrode vs Ag/AgNO$_3$ reference. [b] From ref 27.

between reduction potentials of nitroimidazoles determined in DMF and water.

Cyclic voltammetry at Hg in DMF of the N-substituted nitroimidazoles showed a reduction/oxidation couple which can be ascribed to reduction of the nitro substituent (*37*). Peak potential values for nitro and BATO core reduction are tabulated in Table I. Note that, in DMF, the reduction potentials for the BATO "core" occur at a less negative value than those of the nitro group, indicating that, in DMF, the BATO "core" may be easier to reduce than the nitro group. The reduction potentials for the BATO "core" in DMF are similar to those observed for "simple" BATOs (*27*). The nitro reduction potentials of the 2-nitroimidazole–BATOs (and the boronic acids) fall between those of misonidazole and metronidazole. On the basis of these data we cannot predict whether the BATO–nitroimidazoles will be reduced in hypoxic tissue. The order of ease of reduction of DMG–BATO complexes in DMF is $BBNO_2 \gg BPhEtNO_2 > BpropNO_2 \gg BprenNO_2$, with $BBNO_2$ being closest to misonidazole. More detail on the electrochemistry of BATO nitroimidazole derivatives will appear in a separate report.

Reduction of Nitroimidazole–BATOs by Xanthine Oxidase. As the electrochemistry studies demonstrated that the reduction potentials of the 2-nitroimidazole–BATOs were similar to those of misonidazole (providing the first indication of potential for imaging of hypoxic tissue), it was necessary to demonstrate that these nitroimidazole–BATO complexes could be reduced by nitroreductase enzymes. The rates of reduction relative to misonidazole (*38*) would provide some additional indication of the potential of these new technetium complexes for imaging hypoxia *in vivo*. Xanthine oxidase (XOD) is a convenient model nitroreductase to use with these Tc–nitroimidazole–BATO compounds, as it is a readily available enzyme that has already been shown to reduce a variety of nitro heterocyclic compounds (*39*). *In vivo*, XOD catalyzes the oxidation of hypoxanthine to xanthine and of xanthine to uric acid:

$$\text{xanthine} + O_2 + H_2O \rightarrow \text{urate} + H_2O_2$$

XOD shows very broad specificity for both oxidant and reductant. Reducing substrates include purines, such as xanthine and hypoxanthine, aldehydes, and NADH (*28*). Oxidizing substrates include O_2, pyrimidines (*40*), and nitro

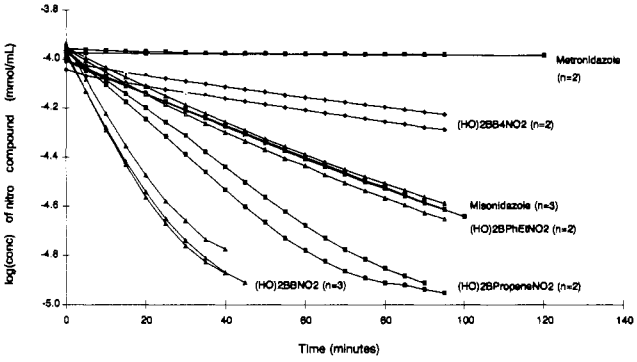


Figure 4. Reduction of nitroimidazole boronic acids by xanthine oxidase.

compounds such as misonidazole (*41, 42*) and fluoromisonidazole (*43*). Therefore, even in the absence of oxygen, a substrate will be reduced, provided some other suitable source of oxidant is added. The XOD assay described here is based on methods previously reported (for example, see ref 43). It provides a measure of the effectiveness of a nitroimidazole derivative (as the oxidizing agent) in the XOD-catalyzed reduction of hypoxanthine in the absence of oxygen.

Reduction of Nitroimidazole Boronic Acids. In a typical reaction of the boronic acid $(OH)_2BBNO_2$ with xanthine oxidase and hypoxanthine under anaerobic conditions, hypoxanthine is first oxidized to xanthine and then to uric acid, as determined by HPLC (data not shown). At the same time, the UV absorbance peak at 326 nm (which is attributable to the nitro group) disappears. Figure 4 shows a comparison of the rate of decrease of the nitro absorbances of $(OH)_2BBNO_2$, $(OH)_2PhEtNO_2$, $(OH)_2BB4NO_2$, $(OH)_2BprenNO_2$, misonidazole, and metronidazole under identical assay conditions. Under the conditions tested, all of the 2-nitroimidazole boronic acids reacted with XOD at a rate that was equal to or faster than that observed for the 2-nitroimidazole compound misonidazole. The nitro group of the 4-nitroimidazole boronic acid $(OH)_2BB4NO_2$ was consumed at a much slower rate, and metronidazole (a 5-nitroimidazole) was found to be almost unreactive in this assay.

XOD-Catalyzed Reduction of ^{99}Tc–BATO–Nitroimidazoles. As DMF was added to help solubilize the Tc complexes, the effect of DMF on xanthine oxidase was tested. Enzyme activity in the standard assay drops as the concentration of DMF is increased. At 5% DMF, activity was 76% of that observed in the absence of DMF. This was deemed significant but tolerable.

Unfortunately, the ^{99}Tc–chloro–BATO–nitroimidazole compounds were not sufficiently water-soluble, even if 5% DMF was added to help solubilize the Tc complex. Therefore, enzyme studies on Tc–BATO–nitroimidazoles were conducted with the more soluble hydroxy analogs ^{99}TcOH(DMG)$_3$BR (*29*).

A plot showing the reaction between TcOH-(DMG)$_3$BprenNO$_2$ and hypoxanthine in the presence of XOD under anaerobic conditions is shown in Figure 5. A slow but significant drop in absorbance at 326 nm is seen, consistent with loss of the nitro group. Only minor changes are noted in other portions of the BATO spectrum. After the reaction is complete, the final spectrum of the reaction mixture is very similar to that of non-nitro imidazole–BATO compounds (*21*). In control experiments performed in the absence of XOD or the absence of hypoxanthine, no reaction was seen over 16 h. When the non-nitro containing BATO TcCl(DMG)$_3$BPh was used, no reaction

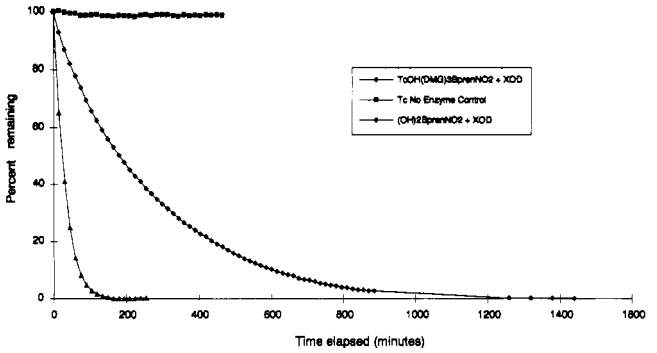


Figure 5. Comparison of rate of reduction of ^{99}Tc(OH)-(DMG)$_3$prenNO$_2$ and its boronic acid precursor.

occurred. These results suggest that only the nitroimidazole group is reduced in the presence of XOD, without dramatically affecting the rest of the BATO core. This is of interest because, in electrochemical reduction of BATO nitro compounds at mercury electrodes in DMF, BATO core reduction preceeds nitro reduction. These results demonstrate the importance of enzyme specificity in this reaction.

Similar spectral results were obtained in the reaction of XOD with TcOH(DMG)$_3$BBNO$_2$. In the presence of enzyme, significant changes occurred in the nitro absorption region, with little change in the other peaks in the UV/vis spectrum. In the no enzyme control, only a 1% decrease in absorbance was noted at all wavelengths (indicative of minor precipitation) over 8 h.

Comparison to Boronic Acids. To allow a direct comparison of the rate of reduction of a nitroimidazole boronic acid to its Tc complex, the enzymatic reduction of (HO)$_2$BprenNO$_2$ was also studied in 5% DMF. Figure 5 displays data from that study, comparing the rate of disappearance of the nitro group in TcOH(DMG)$_3$-BprenNO$_2$ to its boronic acid precusor. These results show that the unchelated boronic acid was reduced by XOD at a much faster rate than was the corresponding BATO compound. A similar result was obtained when TcOH-(DMG)$_3$BBNO$_2$ was compared to (HO)$_2$BBNO$_2$ (data not shown). This may be due in part to changes in the reduction potential of the nitro group. On coordination to technetium, the boron changes from three- to four-coordinate, which appears to decrease the reduction potential of the nitro group. It may also be that high lipophilicity of BATOs (*44*) relative to misonidazole (*45*) and/or steric hindrance from the rather bulky Tc complex hinder(s) binding of the nitro group at the active site of the enzyme.

Comparison with Results from the Literature. The rates that we observed for the XOD-catalyzed reduction of misonidazole (initial rate of 6.2 nmol/min/unit of XOD) were comparable to initial rates reported by Josephy *et al.* (*42*) (6 nmol/min/unit), Clarke *et al.* (*46*) (8 ± 2 nmol/min/unit) and Prekeges (5.7 + 0.7 nmol/min/unit) (*43*). Clarke *et al.* (*46*) have also reported that XOD reduced metronidazole very slowly; this is consistent with our observed half-life of ≫20 hours. As expected from previous studies that show 4- and 5-substituted nitroimidazoles to be harder to reduce (*47*) than are 2-nitro compounds, both the 4-nitro-substituted boronic acid and the Tc-BB4NO$_2$ compound were reduced at a significantly slower rate than any of the 2-nitro compounds.

A study by Clarke *et al.* (*46*) indicated that the redox potential ($E_{1/2}$) and the rate of XOD-catalyzed nitroreduction show good correlation in a series of 15 nitroimidazoles, using xanthine as the electron donator. Based on Clarke's results, the predicted order of rate of enzyme reduction in our nitroimidazole boronic acids should be miso > (OH)$_2$BBNO$_2$ = (OH)$_2$BPhEtNO$_2$ > (OH)$_2$-BprenNO$_2$ > metronidazole ≫ (OH)$_2$BB4NO$_2$. However, the observed order (Table II) for these compounds was, in fact, (OH)$_2$BBNO$_2$ > (OH)$_2$BprenNO$_2$ > miso = (OH)$_2$BPhEtNO$_2$ > (OH)$_2$BB4NO$_2$ ≫ metronidazole. There was no correlation between the rate of enzymatic reduction and redox potential (using data on the 2-nitroimidazole derivatives shown in Table II; r^2 = 0.134, n = 4). The reaction of (OH)$_2$BPhEtNO$_2$ with XOD was considerably slower ($T_{1/2}$ = 40 min) than that of the methylene analog (OH)$_2$BBNO$_2$, ($T_{1/2}$ = 13 min) despite the fact that the one- electron reduction potential of the BPhEt ligand indicates that it should be slightly easier to reduce. These data suggest that some factor other than redox potential is affecting the rate of reduction in these boronic acids (a finding that is not unexpected for an enzyme-catalyzed reaction). A similar result was reported recently by O'Connor *et al.* (*48*), who found, in a series of nitroacridines, that xanthine oxidase exhibited significant substrate specificity beyond that imposed by redox potential.

Table II. Comparison of Enzyme Assay Data and Redox Potentials for Nitroimidazole Boronic Acids and Standards

	$T_{1/2}$ for nitro group loss (n)	E_{pc} (volts) for NO_2 reduction[a]
(OH)$_2$BBNO$_2$	13.0 ± 2.8 min (6)	−1.52
(OH)$_2$BprenNO$_2$	21.6 ± 1.7 min (5)	−1.56
(OH)$_2$BPhEtNO$_2$	39.0 ± 1.4 min (4)	−1.53
(OH)$_2$BB4NO$_2$	~120 min (2)	−1.80
misonidazole	36.5 ± 1.7 min (4)	−1.49
metronidazole	>20 h (2)	−1.62

[a] In DMF at mercury working electrode (0.1 M in TBA BF_4) vs Ag/$AgNO_3$ (ACN) reference. Scan rate = 100 mV/s. In DMF this is a quasi-reversible one-electron process.

CONCLUSIONS

We have synthesized and characterized a series of BATO–nitroimidazole complexes and conducted a preliminary assessment of their potential as radiopharmaceuticals for imaging of hypoxic tissue by studying their electrochemical and enzymic reduction.

In DMF the nitro reduction potentials of the 2-nitroimidazole–BATOs (and the boronic acids) fall between those of misonidazole and metronidazole, indicating that these compounds may possess slightly suboptimal reduction potentials. Overall, these data would indicate that the 2-nitroimidazole-substituted BATOs have reduction potentials in the range that might be anticipated as promising for compounds which are expected to bind in hypoxic tissue.

The 4-substituted nitroimidazoles are more difficult to reduce than metronidazole, suggesting that these compounds will probably not be as useful as the 2-nitroimidazoles for imaging hypoxia.

Under anaerobic conditions, xanthine oxidase rapidly reduces nitroimidazole boronic acids at a rate that is, unexpectedly, faster than that observed for misonidazole. The enzyme also reduces the nitro group of BATO–nitroimidazoles, although the initial rate is slower than that of the corresponding boronic acid by at least a factor of 10. This may, in part, be due to a negative shift in redox potential upon coordination to Tc, or it may be due to the relatively high steric bulk and/or lipophilicity of the technetium BATO complexes examined in this study. These results suggest that the BATO–nitroimidazoles have some of the properties required for a hypoxia imaging

agent, but that reduction *in vivo* could be slower than desired. However, BATO–nitroimidazoles and their boronic acid precursors are clearly recognized as substrates for xanthine oxidase. This is of note because technetium is not a naturally occuring element, and literature examples where technetium complexes are recognized by enzymes are rare. A technetium-labeled ribonucleoside was shown to be an inhibitor of ribonuclease U2 (*49*), and technetium-labeled progestin derivatives displayed *in vitro* binding to the progesterone receptor (*50*). Previous reported examples of technetium complexes which are believed to be metabolized by enzyme catalysis are TcO(ECD) (*51*), an ester derivative of Tc-(4-MeO-SAL_3TAME)$^+$ (*52*), and Tc-$(CNC(CH^3)_2(COOCH_3)_6^+$ (*53*). All of these complexes are de-esterified in serum or tissue homogenate. While *in vivo* reduction has been proposed to explain the behavior of certain technetium cationic complexes (*54*), we believe that the BATO–nitroimidazoles are the first example of a series of technetium complexes in which enzymatic reduction has been demonstrated. These promising results lead us to examine a nitroimidazole derivative of another technetium complex (PnAO) (*55*), which has demonstrated promise as an imaging agent for hypoxia in an *in vivo* model (*56*).

ACKNOWLEDGMENT

We thank K. Krohn for providing misonidazole, K. Ramalingam and N. Raju for the syntheses of the nitroimidazole boronic acids, and Al Bauer for writing the Basic program for the automatic data collection from the UV/vis spectrometer.

Supplementary Material Available: Details of the 270-MHz ^{1}H-NMR spectra, FAB mass spectra (positive and negative ion modes), and IR spectra (4 pages). Ordering information is given on any current masthead page.

LITERATURE CITED

(1) Varghese, A. J., Gulyas, S., and Mohindra, J. K. (1976) Hypoxia-dependant reduction of 1-(2-nitro-1-imidazoyl)-3-methoxy-2-propanol by Chinese hamster ovary cells and KHT tumor cells in-vitro and in-vivo. *Cancer Res. 36*, 3761–3765.

(2) Garrecht, B. M., and Chapman, J. D. (1983) The labeling of EMT-6 tumors in BALB/C mice with [C-14]-misonidazole. *Br. J. Radiol. 26*, 745–753.

(3) Horowitz, M., Blasberg, R., Molnar, P., Strong, J., Kornblith, P., Pleasants, R., and Fenstermacher, J. (1983) Regional [^{14}C]misonidazole distribution in experimental RT-9 brain tumors. *Cancer Res. 43*, 3800–3807.

(4) Koch, C. J., Stobbe, C. C., and Baer, K. A. (1984) Metabolism induced binding of ^{14}C-misonidazole to hypoxic cells: Kinetic dependence on oxygen concentration and misonidazole concentration. *Int. J. Radiat. Oncology Biol. Phys. 10*, 1327–1331.

(5) Urtasun, R. C., Chapman, J. D., Raleigh, J. A., Franko, A. J., and Koch, C. J. (1986) Binding of ^{3}H-misonidazole to solid human tumors as a measure of tumor hypoxia. *Int. J. Radiat. Oncol. Biol. Phys. 12*, 1263–1267.

(6) Martin, G. V., Caldwell, J. H., Rasey, J. S., Grunbaum, Z., Cerqueira, M., and Krohn, K. A. (1989) Enhanced binding of the hypoxic cell marker [^{3}H]fluoromisonidazole in ischaemic myocardium. *J. Nucl. Med. 30*, 194–201.

(7) Olive, P. L., Rasey, J. S., and Durand, R. E. (1986) Comparison between the binding of [^{3}H]misonidazole and AF-2 in Chinese hamster V79 spheroids. *Radiat. Res. 105*, 105–114.

(8) Jette, D. C., Weibe, L. I., and Chapman, J. D. (1983) Synthesis and in vivo studies of the radiosensitizer 4-[^{82}Br]bromomisonidazole. *Nucl. Med. Biol. 10*, 205–210.

(9) Jerabek, P. A., Patrick, T. B., Kilbourn, M. R., Dischino, D. D., and Welch, M. J. (1986) Synthesis and biodistribution of ^{18}F-labeled fluronitroimidazoles: Potential in vivo markers of hypoxic tissue. *Int. J. Appl. Radiat. Isotop. 37*, 599–605.

(10) Martin, G. V., Rasey, J. S., Caldwell, J. C., Grunbaum, Z., and Krohn, K. A. (1987) Fluoromisonidazole uptake in ischemic canine myocardium. *J. Nucl. Med. 28*, 668.

(11) Shelton, M. E., Dence, C. S., Hwang, D.-R, Welch, M. J., and Bergmann, S. R. (1989) Myocardial kinetics of fluorine-18 misonidazole: A marker of hypoxic myocardium. *J. Nucl. Med. 30*, 351–358.

(12) Rasey, J. S., Nelson, N. J., Chin, L., Evans, M. L., and Grunbaum, Z. (1990) Characteristics of the binding of labeled fluoromisonidazole in cells in vitro. *Radiat. Res. 122*, 301–308.

(13) Hoffman, J. M., Rasey, J. S., Spence, A. M., Shaw, D. W., and Krohn, K. A. (1987) Binding of the hypoxic tracer [^{3}H]misonidazole in cerebral ischaemia. *Stroke 18*, 168–176.

(14) Martin, G. V., Biskupiak, J. H., Caldwell, J. H., Grierson, J. R., and Krohn, K. A. (1990) Iodovinylmisonidazole: A metabolic marker for myocardial ischemia. *J. Nucl. Med. 31*, 833.

(15) Koh, W. J., Rasey, J. S., Evans, M. L., Grierson, J. R., Krohn, K. A., and Lewellan, T. K. (1990) Imaging of hypoxia in human tumors with [F-18]fluoromisonidazole. *J. Nucl. Med. 31*, 756.

(16) Jette, D. C., Wiebe, L. I., Flanagan, R. J., et al. (1986) Iodoazomycin riboside, a hypoxic cell marker. Synthesis and in vivo characterization. *Radiat. Res. 105*, 169–179.

(17) Biskupiak, J. E., Grierson, J. R., Rasey, J. S., Martin, G. V., and Krohn, K. A. (1991) Synthesis of an (Iodovinyl)misonidazole Derivative for Hypoxia Imaging. *J. Med. Chem. 34*, 2165–2168.

(18) Mannan, R. H., Somayaji, V. V., Lee, J., Mercer, J. R., Chapman, J. D., and Wiebe, L. I. (1991) Radioiodinated 1-(5-iodo-5-deoxy-β-D-arabinofurnaosyl)-2-nitroimidazole (Iodoazomycin arabinoside: IAZA): A novel marker of tissue hypoxia. *J. Nucl. Med. 32*, 1764–1770.

(19) Moore, R. B., Chapman, J. D., Mercer, J. R., Mannan, R. H., Wiebe, L. I., McEwan, A. J., and McPhee, M. S. (1993) Measurement of PDT-Induced Hypoxia in Dunning Prostate Tumors by Iodine-123-Iodoazomycin Arabinoside. *J. Nucl. Med. 34*, 405–411.

(20) Treher, E. N., Francesconi, L. C., Gougoutas, J. Z., Malley, M. F., and Nunn, A. D. (1989) Monocapped tris(dioxime) complexes of technetium(III): Synthesis and structural characterization of TcX(dioxime)$_3$B-R (X = Cl, Br; dioxime = dimethylglyoxime, cyclohexanedione dioxime; R = CH_3, C_4H_9). *Inorg. Chem. 28*, 3411–3416.

(21) Linder, K. E., Malley, M. F., Gougoutas, J. Z., Unger, S. E., and Nunn, A. D. (1990) Neutral, seven-coordinate dioxime complexes of technetium(III): Synthesis and characterization. *Inorg. Chem. 29*, 2428–2434.

(22) Nowotnik, D. P., and Nunn, A. D. (1992) Technetium compounds for imaging myocardial and cerebral perfusion. *Drug News Perspectives 5*, 174–183.

(23) Linder, K. E., Wen, M. D., Nowotnik, D. P., Malley, M. F., Gougoutas, J. Z., Nunn, A. D., and Eckelman, W. C. (1991) Technetium-labeling of monoclonal antibodies with functionalized BATOs: 1. TcCl(DMG)$_3$PITC (PITC = phenylisothiocyanate). *Bioconjugate Chem. 2*, 160–170.

(24) Linder, K. E., Wen, M. D., Nowotnik, D. P., Ramalingam, K., Sharkey, R. M., Yost, F., Narra, R. K., Nunn, A. D., and Eckelman, W. C. (1991) Technetium-labeling of monoclonal antibodies with functionalized BATOs: 2. TcCl(DMG)$_3$CPITC (CPITC = carboxyphenylisothiocyanate) labeling of B72.3 and NP-4 whole antibodies and NP-4 F(ab')$_2$. *Bioconjugate Chem. 2*, 407–414.

(25) Raju, N., Ramalingam, K., and Nowotnik, D. P. (1993) Syntheses of some nitroimidazole boronic acids: Precursors to technetium-99m complexes with potential for imaging hypoxic tissue. *Tetrahedron 48*, 10233–10238.

(26) Mathias, C. J., Welch, M. J., Kilbourn, M. R., Jerabek, P. A., Patrick, T. B., Raichle, M. E., Krohn, K., Rasey, J. S., and Shaw, D. W. (1987) Radiolabeled hypoxic cell sensitizers: tracers for assessment of ischemia. *Life Sci. 41*, 199–206.

(27) Cyr, J. E., Linder, K. E., and Nowotnik, D. P. (1993) Electrochemistry of boron-capped ^{99}Tc dioxime complexes. *Inorg. Chim. Acta. 206*, 97–104.

(28) Bray, R. C. (1975) Molybdenum iron-sulfur flavin hydroxylases and related enzymes. *The Enzymes* (P. D. Boyer, Ed.) pp 300–419, Academic Press, New York.
(29) Jurisson, S., Hirth, W., Linder, K., Di Rocco, R. J., Narra, R. K., Nowotnik, D. P., and Nunn, A. D. (1991) Chloro→hydroxy substitution on technetium BATO ($TcCl(dioxime)_3BR$) complexes. *Nucl. Med. Biol. 18*, 735–744.
(30) Linder, K., unreported data.
(31) Nakamoto, K. (1978) *Infrared and Raman Spectra of Inorganic and Coordination Compounds*, J. Wiley and Sons, New York.
(32) Stambaugh, J. E., and Manthei, R. W. (1968) The infrared and nuclear magnetic resonance spectra of some 5-nitroimidazoles. *Canadian Spectr. 13*, 134–138.
(33) Nagarajan, K., Sudarsanam, V., Parthasarathy, P. C., Arya, V. P., and Shenoy, S. J. (1982) Nitroimidazoles: Part X - Spectral studies on isomeric 1-substituted 4- and 5-nitroimidazoles and some 2-nitroimidazoles. *Indian. J. Chem. Sect. B. 21B*, 1006–1021.
(34) Unger, S. E., McCormick, T. J., Treher, E. N., and Nunn, A. D. (1987) Comparison of desorption ionization methods for the analysis of neutral seven-coordinate technetium radiopharmaceuticals. *Anal. Chem. 59*, 1145–1149.
(35) Varghese, A. J., and Whitmore, G. F. (1980) Binding of nitroreduction products of misonidazole to nucleic acids and proteins. *Radiosensitizers: Their use in Clinical Management of Cancer* (L. W. Brady, Ed.) pp 57–60, Masson USA, New York.
(36) Breccia, A., Berrilli, G., and Roffia, S. (1979) Chemical radiosensitization of hypoxic cells and redox potentials. Correlation of voltammetric results with pulse radiolysis data of nitro-compounds and radiosensitizers. *Int. J. Radiat. Biol. 36*, 85–89.
(37) Tocher, J. H., and Edwards, D. I. (1988) Electrochemical characteristics of nitroheterocyclic compounds of biological interest. I. The influence of solvent. *Free Radical. Res. Commun. 4*, 269–276.
(38) Franko, A. J. (1986) Misonidazole and other hypoxia markers: metabolism and applications. *Int. J. Radiat. Oncology Biol. Phys. 11*, 1195–1202.
(39) Kedderis, G. L., and Miwa, G. T. (1988) The metabolic activation of nitroheterocyclic therapeutic agents. *Drug Metab. Rev. 19*, 33–62.
(40) Krenitsky, T. A., Neil, S. M., Elion, G. B., and Hitchings, G. H. (1972) A comparison of the specificities of xanthine oxidase and aldehyde oxidase. *Arch. Biochem. Biophys. 150*, 585–599.
(41) Clarke, E. D., Wardman, P., and Goulding, K. H. (1980) Anaerobic reduction of nitroimidazoles by reduced flavin mononucleotide and by xanthine oxidase. *Biochem. Pharmacol. 29*, 2684–2687.
(42) Josephy, P. D., Palcic, B., and Skarsgard, L. D. (1981) Reduction of misonidazole and its derivatives by xanthine oxidase. *Biochem. Pharmacol. 30*, 849–853.
(43) Prekeges, J. L., Rasey, J. S., Grunbaum, Z., and Krohn, K. A. (1991) Reduction of Fluoromisonidazole, a New Imaging Agent for Hypoxia. *Biochem. Pharmacol. 42*, 2387–2395.
(44) Nunn, A. D., Feld, T., and Narra, R. K. (1990) Quantitative structure distribution relationships (QSDRs) of BATOs. *Technetium and Rhenium in Chemistry and Nuclear Medicine 3* (M. Nicolini, G. Bandoli, and U. Mazzi, Eds.) pp 399–404, Cortina International, Verona, Italy.
(45) Chapman, J. D., Lee, J., and Meeker, B. E. (1989) Cellular reduction of nitroimidazole drugs: Potential for selective chemotherapy and diagnosis of hypoxic cells. *Int. J. Radiat. Oncology Biol. Phys. 16*, 911–917.
(46) Clarke, E. D., Goulding, K. H., and Wardman, P. (1982) Nitroimidazoles as anaerobic electron acceptors for xanthine oxidase. *Biochem. Pharmacol. 31*, 3237–3242.
(47) Greenstock, C. L., Ruddock, G. W., and Neta, R. (1976) Pulse radiolysis and ESR studies of the electron affinic properties of nitroheterocyclic radiosenstizers. *Radiat. Res. 667*, 472.
(48) O'Connor, C. J., McLennan, D. J., Sutton, B. M., Denny, W. A., and Wilson, W. R. (1991) Effect of reduction potential on the rate of reduction of nitroacridine by xanthine oxidase and by dihydro-flavin mononucleotide. *J. Chem. Soc., Perkin Trans. 2*, 951.
(49) Chen, Y. C. J., and Janda, K. D. (1992) A New Approach Toward the Inhibition of Ribonucleases—A Water-Stable Ribonucleoside Technetium Chelate. *J. Am. Chem. Soc. 114*, 1488–1489.
(50) DiZio, J. P., Fiaschi, R., Davison, A., Jones, A. G., and Katzenellenbogen, J. A. (1991) Progestin-rhenium complexes: Metal-labeled steroids with high receptor affinity, potential receptor-directed agents for diagnostic imaging or therapy. *Bioconjugate Chem. 2*, 353–366.
(51) Edwards, D. S., Cheesman, E. H., Watson, M. W., Maheu, L. J., Nguyen, S. A., Dimitre, L., Nason, T., Watson, A. D., and Walovitch, R. (1990) Synthesis and characterization of technetium and rhenium complexes of N,N′-1,2-diethylenediylbis-L-cysteine. Neurolite and its metabolites. *Technetium and Rhenium in Chemistry and Nuclear Medicine 3* (M. Nicolini, G. Bandoli, and U. Mazzi, Eds.) pp 433–444, Cortina International, Verona, Italy.
(52) Pilcher, G. D., Coveney, J. R., Marmion, M. E., Nosco, D. L., and Strubel, T. W. (1989) Biological characteristics of Tc-99m complexes with ester analogues of 1,1,1-tris(4-methoxysalicylaldimino-methyl)ethane (4-MeO-SAL_3TAME). *J. Nucl. Med. 30*, 937.
(53) Kronauge, J. F., Noska, M. A., Davison, A., Holman, B. L., and Jones, A. G. (1992) Interspecies variation in biodistribution of technetium (2-carbomethoxy-2-methyl isocyanopropane)$_6^+$. *J. Nucl. Med. 33*, 1357–1365.
(54) Deutsch, E. A., Vanderheyden, J.-L., Gerundini, P., Libson, K., Hirth, W. W., Colombo, F., Savi, A., and Fazio, F. (1987) Development of non-reducible technetium-99m(III) cations as myocardial perfusion imaging agents: Initial experience in humans. *J. Nucl. Med. 28*, 1870–1880.
(55) Linder, K. E., Cyr, J. E., Chan, Y. W., Raju, N., Ramalingam, K., Nowotnik, D. P., and Nunn, A. D. (1992) Chemistry of a Tc-PnAO-nitroimidazole complex that localizes in hypoxic tissue. *J. Nucl. Med. 33*, 919.
(56) Di Rocco, R. J., Bauer, A., Kuczynski, B. L., Pirro, J. P., Linder, K. E., Narra, R. K., and Nunn, A. D. (1992) Imaging regional hypoxia with a new technetium-labeled imaging agent in rabbit myocardium after occlusion of the left anterior descending coronary artery. *J. Nucl. Med. 33*, 865.

Antitumor Activities of a Cephalosporin Prodrug in Combination with Monoclonal Antibody–β-Lactamase Conjugates

Vivekananda M. Vrudhula, Håkan P. Svensson, Karen A. Kennedy, Peter D. Senter,* and Philip M. Wallace*

Bristol-Myers Squibb Pharmaceutical Research Institute, 3005 First Avenue, Seattle, Washington 98121.
Received March 11, 1993

7-(Phenylacetamido)cephalosporin mustard (CM) and 7-(4-carboxybutanamido)cepahalosporin mustard (CCM) were developed as anticancer prodrugs that could be activated site selectively by monoclonal antibody–β-lactamase conjugates targeted to antigens present on tumor cell surfaces. Both CM and CCM were hydrolyzed by purified β-lactamases from *Escherichia coli* (ECβL), *Bacillus cereus* (BCβL), and *Enterobacter cloacae* (EClβL). This resulted in the release of phenylenediamine mustard (PDM), a potent cytotoxic drug. The K_m and k_{cat} values of the reactions were determined, and it was found that EClβL effected the hydrolysis of CM and CCM more rapidly than the other enzymes. Conjugates of EClβL were prepared by reacting maleimide-substituted F(ab')$_2$ fragments of the monoclonal antibodies L6 and P1.17 to EClβL that had been modified with sulfhydryl groups. In vitro experiments indicated that CCM (IC_{50} = 25–45 μM) was less toxic than PDM (IC_{50} = 1.5 μM) to H2981 lung adenocarcinoma cells (L6 antigen positive, P1.17 antigen negative) and that immunologically specific prodrug activation took place when the cells were treated with L6–EClβL. In vivo experiments in nude mice demonstrated that CCM was less toxic than CM, and that both prodrugs were much less toxic than PDM. Neither CCM nor PDM exerted antitumor activity on subcutaneous H2981 tumors in vivo. However, a significant antitumor effect was obtained in mice that received L6–EClβL 96 h prior to the administration of CCM. The effect was immunologically specific ($P < 0.05$), since a smaller degree of antitumor activity was obtained in mice that received the nonbinding control conjugate P1.17–EClβL prior to CCM. These studies demonstrate the potential therapeutic utility of monoclonal antibody–β-lactamase conjugates for the activation of cephalosporin-containing prodrugs.

INTRODUCTION

Several recent reports have described the use of monoclonal antibodies (mAbs)[1] as delivery agents for enzymes that are capable of generating anticancer drugs from relatively noncytotoxic precursors (reviewed in ref 1). By introducing a high level of an enzyme activity within a tumor mass, it should be possible to convert a suitable prodrug substrate into an active anticancer agent and obtain a level of selectivity that cannot be achieved by systemic administration of the corresponding released drug. A considerable amount of evidence has accumulated indicating that substantial levels of in vitro and in vivo antitumor activities can be obtained using mAb–enzyme conjugates for prodrug activation (*1*).

There are a number of factors that must be taken into account in selecting appropriate enzyme/prodrug combinations for this targeting strategy. Ideally, the prodrug should be stable, nontoxic, and converted to active drug only by the targeted enzyme. This suggests the use of nonendogenous enzymes that catalyze reactions not ordinarily occurring within the body. In addition, it would be advantageous for a single mAb–enzyme conjugate to activate a panel of prodrugs into anticancer drugs that can act synergistically in combination chemotherapy. Therefore, the targeted enzyme should have broad substrate specificity. β-Lactamases are enzymes that might meet these criteria. These enzymes cleave the β-lactams of a variety of penicillins and cephalosporins—many of which have been shown to possess considerable stability in the human body (*2*). Thus, for the approach described here, prodrugs that are activated as a result of β-lactam cleavage would be expected to be stable when administered in vivo until they contact the targeted mAb–β-lactamase conjugate.

Promising in vitro data have been obtained with several β-lactamase/prodrug combinations (*3–5*). We have previously demonstrated that 7-(phenylacetamido)cephalosporin mustard (CM) could be formed by linking the drug phenylenediamine mustard (PDM) to the 3′-position of a cephalosporin (*5*). CM was at least 50 times less toxic than PDM on H2981 human lung adenocarcinoma cells, but could be fully activated by a mAb–β-lactamase conjugate that bound to cell surface antigens. The β-lactamases used for the activation of CM were obtained from *Escherichia coli* and *Bacillus cereus*. Here, we extend these findings to include 7-(4-carboxybutanamido)cephalosporin mustard (CCM), which is less toxic and easier to administer in vivo than CM. Activation of CCM is mediated both in vitro and in vivo in an immunologically specific manner by a β-lactamase from *Enterobacter cloacae* (EClβL) conjugated to a mAb that binds to tumor-associated antigens.

EXPERIMENTAL PROCEDURES

Materials. Crude *B. cereus* and *E. cloacae* β-lactamases were obtained from Sigma Chemical Co. *B. cereus* β-lactamase (II) (BCβL) was purified according to a

* Authors to whom correspondence should be addressed.

[1] Abbreviations used: BCβL, *Bacillus cereus* β-lactamase (II); CCM, 7-(4-carboxybutanamido)cephalosporin mustard; CM, 7-(phenylacetamido)cephalosporin mustard; ECβL, *Escherichia coli* TEM-2 β-lactamase; EClβL, *Enterobacter cloacae* P99 β-lactamase; mAb, monoclonal antibody; IC_{50}, concentration that gives 50% cell kill; MTD, maximum tolerated dose; PDM, phenylenediamine mustard.

1043-1802/93/2904-0334$04.00/0 © 1993 American Chemical Society

previously described procedure, which involved heat precipitation followed by cation-exchange chromatography (5). *E. coli* TEM-2 β-lactamase (ECβL) was purified on an affinity column as previously described (5). CM (5), 1 (6), and PDM (5, 7) were prepared according to literature methods (structures shown in Figures 1 and 2). The mAb L6 binds to antigens on many human carcinomas including the H2981 human lung adenocarcinoma (8). P1.17 shows no detectable binding to H2981 cells. Both mAbs are of the IgG_{2a} isotype. The $F(ab')_2$ fragments of the mAbs were prepared by digestion with pepsinogen as previously described (5).

Preparation of 7-(4-Carboxybutanamido)cephalosporin Mustard (CCM). The known cephalosporin alcohol, 2, was prepared through modifications of a literature method (6). A mixture of the monopotassium salt of 1 (4.73 g, 11.2 mmol) (6) and immobilized esterase (4.73 g, Bristol-Myers Squibb Industrial Division, Syracuse, NY) in 50 mL of 0.1 M bicarbonate (pH 9.0) was stirred overnight at room temperature. Analysis by TLC (SiO_2, ethyl acetate–methanol–acetic acid, 8:1:1) revealed that the reaction was complete, and that a more polar product was formed. The reaction mixture was filtered, partially concentrated, and applied to a C-18 column (100 g, 3 × 24 cm), which was washed with H_2O. Fractions that eluted between 150 and 220 mL contained the desired product. The H_2O was removed by lyophilization, and the resulting pale yellow powder was triturated with methanol and filtered. The filtrate was evaporated to give 2 as the sodium salt. ^1H NMR (DMSO-d_6) indicated loss of the acetate methyl resonance and a new signal at δ 4.3 for the 3′-CH_2. Formation of the bis(triethylammonium) salt of 2 was achieved by dissolving the compound in 0.1 M triethylammonium acetate buffer and applying the solution to a C-18 column (3 × 24 cm) equilbrated in the same buffer. Fractions containing 2 as the triethylammonium salt were combined and evaporated, and the residue was dried over P_2O_5 to give 4.27 g (70% yield) of a pale yellow gum that was used without further purification.

To an ice-cold, stirred suspension of the HCl salt of PDM (969 mg, 3.6 mmol) (7) in dry THF (40 mL) under an N_2 atmosphere was added diisopropylethyl amine (0.63 mL, 3.6 mmol). After 10 min, a solution of phosgene in toluene (1.95 mL, 1.9 M) was added dropwise. TLC analysis (SiO_2, ethyl acetate–hexane, 1:4) indicated completion of the reaction after 1 h with the formation of a less polar product. The isocyanate solution was introduced via a canula and N_2 pressure into an ice-cold solution of the bis(triethylammonium) salt of 2 (1.64 g) in anhydrous DMF (10 mL) containing diisopropylethyl amine (1.6 mL, 9.2 mmol) under N_2. The resulting orange solution was stirred on an ice bath for 3 h. Acetonitrile (30 mL) was added, followed by the addition of 10 g of C-18 silica gel. Volatiles were removed, and the residue was applied to a C-18 column (2 × 12 cm), which was equilibrated with 30% acetonitrile in 1% aqueous acetic acid. The column was washed with 200 mL of the above solvent, and then with 500 mL each of 40% and 50% acetonitrile in 1% aqueous acetic acid. The first 75 mL were discarded, and then 15-mL fractions were collected. Fractions 25–30 (containing CCM) were combined and evaporated to give 500 mg of a pale yellow gum. Addition of ethyl acetate (6 mL) resulted in the formation of a yellow solution from which CCM crystallized as a white fluffy solid (350 mg, 20% yield). HRMS: M^+ 602.1022 (calcd, 602.1005). ^1H NMR (DMSO-d_6, 300 MHz): δ 9.42 (s, 1 H, NH), 8.83 (d, 1 H, NH, J = 8.1 Hz), 7.26 (d, 2 H, ArH, J = 9.3 Hz), 6.68 (d, 2 H, ArH, J = 9.3 Hz), 5.66 (dd, 2 H, 7-H, J = 4.1 and 8.1 Hz), 5.10 (d, 1 H, 6-H, J = 4.8 Hz), 5.02 (d, 1 H, 3-CH_2O, J = 12.6 Hz), 4.72 (d, 1 H, 3-CH_2O, J = 12.6 Hz), 3.67 (s, 8 H, $(NCH_2CH_2Cl)_2$), 3.64 (d, 1 H, 2-H, J = 18.0 Hz), 3.52 (d, 1H, 2-H, J = 18.0 Hz), 2.21 (m, 4 H, 2′- and 4′-CH_2), 1.71 (m, 2 H, 3′-CH_2). Anal.: Found C, 47.51; H, 4.66; N, 9.37; Cl, 11.36; S, 5.30. Theory: C, 47.77; H, 4.68; N, 9.28; Cl, 11.75; S, 5.31.

Enzymatic Activity Assays. The activities of the β-lactamases were measured using spectrophotometric assays with nitrocefin, CM, and CCM as substrates. Δε values were established by measuring the maximum change in absorbance of nitrocefin (ΔA_{490nm}), CM (ΔA_{266nm}), and CCM (ΔA_{266nm}) of standard solutions that were treated with BCβL (10 μg/mL) as described below.

(A) Nitrocefin Assay. The enzymatic activities of the β-lactamases were determined using nitrocefin as a substrate (5, 9). Solutions containing ECIβL (5.0 ng of enzyme/mL for the ECIβL-containing conjugates, and 4.75 ng/mL for unconjugated ECIβL) were incubated at room temperature with nitrocefin (50 μM) in phosphate-buffered saline, pH 7.4 (PBS), containing 12.5 μg/mL bovine serum albumin in a quartz cuvette. The absorbance at 490 nm was determined every 30 s for 5 min starting 30 s after the reaction was initiated. Under these conditions, the increase of absorbance at 490 nm ($\Delta\epsilon_{490nm}$ = 19 500 M^{-1} cm^{-1}) was linear.

(B) Assays with CM and CCM. The kinetic parameters for the hydrolyses of CM and CCM (in PBS containing 12.5 μg/mL bovine serum albumin) with the β-lactamases were obtained spectrophotometrically by determination of the initial velocities of the reactions as a function of substrate concentration. Lineweaver–Burk plots of the data were used to estimate the K_m and V_{max} values. Cleavage of the β-lactam ring resulted in a loss of absorbance at 266 nm for both CM ($\Delta\epsilon_{266nm}$ = 1.8 × 10^4 M^{-1} cm^{-1}) and CCM ($\Delta\epsilon_{266nm}$ = 2.1 × $10^4 M^{-1}$ cm^{-1}). The enzyme and substrate concentrations were as follows: ECβL (1 μg/mL) with CM (5.7–86 μM) or CCM (10.6–79.5 μM); BCβL (50 ng/mL) with CM (3.5–25.9 μM); BCβL (25 ng/mL) with CCM (4.7–78.7 μM); ECIβL (100 ng/mL) with CM (3.3–100.2 μM) or CCM (3.5–69.7 μM). The reactions were monitored at room temperature in a cuvette by reading A_{266nm} every 0.1 min for 1.05 min starting at 0.15 min after the addition of enzyme. All assays were run in duplicate, and the experiments were repeated up to three times. Between experiments, the kinetic parameters differed by less than 10%.

Purification of ECIβL. All manipulations during the enzyme purification were carried out at 4 °C. Crude ECIβL (Sigma Chemical Co.) was taken up in ice-cold H_2O and centrifuged for 30 min at 900*g*. The supernatant was applied to a boronic acid affinity column (hydrophilic-L type, 10) which was equilibrated in 20 mM triethanolamine hydrochloride containing 0.5 M NaCl (pH 7.0). The column was washed with this buffer until A_{280nm} was zero, and the enzyme was eluted with 0.5 M sodium borate containing 0.5 M NaCl (pH 7.0). Fractions that contained β-lactamase activity (using nitrocefin as a substrate) were pooled and dialyzed against PBS. The purified enzyme (>95% pure by SDS–PAGE) was concentrated by ultrafiltration, sterile filtered (0.2-μm filter), and stored at 4 °C.

HPLC Analysis of the Hydrolysis of CCM by ECIβL. To 99.5 μL of CCM (1 mM) in PBS was added ECIβL (13 μg in 5 μL PBS). Under these conditions, complete conversion of CCM to PDM occurred within 1 min. The course of reaction was monitored by HPLC on an IBM

5-μm ODS C-18 column (4.6 mm × 250 mm) with a linear gradient (20 min) of 40–100% CH_3CN in 0.1 M NH_4OAc. The eluent was monitored at 260 nm, and the flow rate was 0.5 mL/min. PDM and CCM eluted at 13.2 and 4.6 min, respectively.

Conjugate Preparation. The conjugates were prepared as described earlier for the preparation of mAb–BCβL conjugates (*5*) with modifications in the method used for conjugate purification. Briefly, the $F(ab')_2$ mAbs (5–10 mg/mL) were modified with maleimide groups by the reaction with *N*-succinimidyl 4-(maleimidomethyl)cyclohexane-1-carboxylate (SMCC, Pierce Chemical Co., final concentration 0.25 mM) and then combined with ECIβL (1:1 molar ratio) that had been modified with 2-iminothiolane (1.7 mM). After 50 min at room temperature, the reaction was terminated by the addition of 2-aminoethanethiol (0.1 mM final concentration) followed by N-ethylmaleimide (0.2 mM final concentration) in rapid succession. The mixture was concentrated by ultrafiltration and applied to a Sephacryl S-300 column equilibrated with 20 mM triethanolamine hydrochloride containing 0.5 M NaCl (pH 7.0) in order to remove aggregates and unbound enzyme. Fractions containing monomeric mAb–ECIβL adducts (determined by SDS–PAGE and enzymatic activity) were pooled and applied to a boronic acid affinity column (hydrophilic-L type, *10*). The column was washed with the above buffer until A_{280nm} was zero to remove unconjugated mAb. mAb–ECIβL conjugates were eluted with 0.5 M borate containing 0.5 M NaCl (pH 7.0). Fractions were analyzed by SDS–PAGE and relative enzyme activity. Conjugate containing fractions were pooled, dialyzed into PBS, concentrated by ultrafiltration, sterile filtered, and stored at −70 °C. Concentrations of mAb and ECIβL were determined spectrophotometrically at 280 nm using $E^{1\%}$ values of 14 and 15.3, respectively (obtained with the BCA protein assay from Pierce Chemical Co. using bovine serum albumin to obtain a standard curve). The purity of the conjugates (>95%) was assessed by SDS–PAGE, and enzyme activities were measured using nitrocefin as a substrate. The ability of the L6–ECIβL conjugate to bind to antigens on the H2981 human lung adenocarcinoma cell line was determined using a previously described method (*5*). The yield of the purified conjugates ranged from 16 to 18% in three separate experiments.

In Vitro Cytotoxicity. H2981 cells (5×10^5) were suspended in 0.4 mL of Roswell Park Memorial Institute 1640 media containing 10% (v/v) fetal bovine serum with or without the mAb–ECIβL conjugates at 0.316 μg/mL. Blocking experiments were performed by preincubating the cells with unconjugated L6 (1 mg/mL) for 10 min prior to the addition of L6–ECIβL in the above medium. The cells were incubated for 30 min at 4 °C, rinsed three times with media, resuspended, and plated into 96-well tissue culture plates at 10^4 cells/well (0.1 mL volume). CCM and PDM (freshly diluted in media) were added to the wells (0.1 mL volume). After 1 h at 37 °C, the cells were washed three times with Iscove's modified Dulbecco's medium with 10% (v/v) fetal bovine serum, 200 units/mL penicillin, 0.1 mg/mL streptomycin, and 2 mM glutamine (IMDM) and then incubated overnight in IMDM (0.1 mL/well). The media was removed, and the cells were pulsed with [^{3}H]thymidine (1 μCi in 0.1 mL media) for 24 h. The cells were then washed with PBS, trypsinized, and harvested onto glass-fiber filters. The filters were counted on an LKB Beta plate cell harvester.

In Vivo Experiments. Female athymic nude mice (8-weeks-old from Harlan–Sprague Dawley, Indianapolis, IN) were implanted subcutaneously in the flank with H2981 tumors (ca. 32 mm sections from in vivo passaging). Treatment was initiated on day 20, when the tumors were established and growing. Conjugates (1 mg mAb component/kg in PBS containing 0.1% bovine serum albumin) were injected iv. After 96 h, CCM (46.7 mg/kg/injection in PBS containing 10% DMSO) was administered in 3 equal doses spaced 4 h apart. Other groups were treated with CCM (62.2 mg/kg/injection), PDM (1.4 mg/kg/injection in saline), or PBS containing 10% DMSO according to the same schedule, but without having received prior conjugate treatment. Tumor volumes were estimated by the formula: longest length × (perpendicular width)^2/2. Each treatment group consisted of eight mice. No premature deaths resulting from the tumor implants or therapeutic regimen occurred during the course of the experiment. Toxicity experiments were performed as indicated in Table II using three to six mice/dose. Maximum tolerated doses (MTDs) resulted in no deaths, and were within 30% or less of doses where drug-related deaths occurred. Statistical analyses were performed using the Student *t*-test, and *P* values that were less than 0.05 were deemed as being statistically significant.

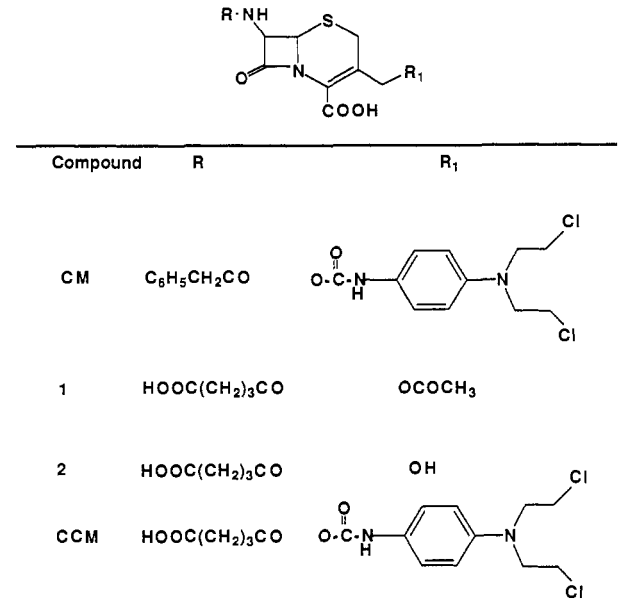


Figure 1. Structures of the cephalosporin derivatives used in this study.

RESULTS

Preparation of CM and CCM. Hydrolysis by β-Lactamases. The preparation of CM (Figure 1) was carried out as previously described (*5*). CCM was prepared from the monopotassium salt of 1 (*6*) by enzymatic removal of the acetoxy group, followed by condensation of the resulting 3-(hydroxymethyl)-containing product (**2**) with the isocyanate derivative of PDM (*5*, *7*). The structure of CCM was confirmed by 300-MHz ^{1}H NMR, high-resolution mass spectrometry, and elemental analysis.

Enzymatic hydrolyses of CM and CCM were investigated using β-lactamases isolated from *B. cereus*, *E. coli*, and *E. cloacae*. The enzymes from *B. cereus* (BCβL) and *E. coli* (ECβL) were purified from crude extracts as previously described (*5*). *E. cloacae* β-lactamase (ECIβL) was purified from a commercially available crude preparation using a boronic acid affinity column (*10*). The purified enzymes appeared as single bands on SDS–PAGE gels, and had the following apparent molecular weights: BCβL, 25 kDa; ECβL, 30 kDa; ECIβL, 43 kDa (data not shown). This is consistent with the literature values (*11–13*).

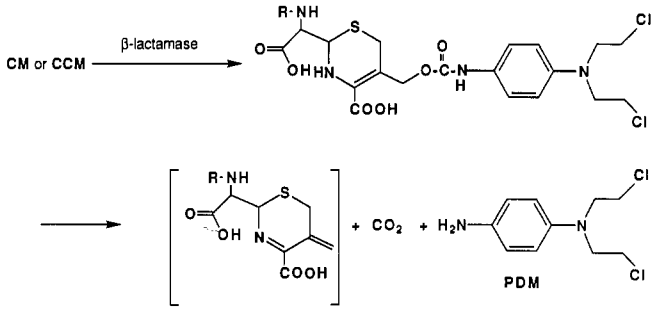


Figure 2. Mechanism of drug release catalyzed by β-lactamase.

Table I. Kinetic Constants for β-Lactamases

	CM		CCM	
enzyme	K_m (μM)	k_{cat} (s^{-1})	K_m (μM)	k_{cat} (s^{-1})
ECβL	25.6	8.3	61.2	1.6
BCβL	6.2	63	31.1	116
ECIβL	7.0	119	43.2	337

A spectrophotometric method was used to quantify the rate of β-lactam hydrolysis of CM and CCM catalyzed by each of the three enzymes. This involved determination of the loss of absorbance at 266 nm, which is most likely associated with the migration of the conjugated double bond when the β-lactam ring is hydrolyzed (*5*, *14*). The kinetic constants, derived from Lineweaver–Burk plots, indicated that CM had higher affinity for the enzymes than CCM (Table I). ECIβL displayed the highest k_{cat}/K_m ratios and absolute turnover numbers with both substrates. The proposed reaction mechanism (Figure 2) is based on HPLC identification of PDM as the released product (see Experimental Procedures and ref 5), and on detailed mechanistic studies reported elsewhere with related molecules (*14*, *15*).

mAb–β-Lactamase Conjugates. On the basis of the kinetic properties shown in Table I, mAb conjugates of ECIβL were prepared for further evaluation. The $F(ab')_2$ fragments of the IgG_{2a} mAbs L6 (anticarcinoma, *8*) and P1.17 (nonbinding control) were modified with maleimide groups through the reaction with SMCC. These were combined with ECIβL that contained free sulfhydryl groups as a result of the reaction with 2-iminothiolane. The thioether-linked conjugates thus formed were subjected to a two-step purification procedure. Gel filtration served to remove unconjugated enzyme and high molecular weight aggregates. A boronic acid affinity column (*10*) was then used to remove the unconjugated mAbs from the mAb–ECIβL conjugates. The principle products consisted of monomeric adducts of the mAbs to ECIβL having molecular weights of approximately 140 kDa (data not shown).

Binding studies were performed using a competitive binding assay as previously reported for L6–BCβL conjugates (*5*). Briefly, the L6 conjugates were allowed to compete with a L6–fluorescein isothiocyanate adduct (L6–FITC) for binding to antigens on the H2981 human lung adenocarcinoma cell line (L6 antigen positive). Fluorescence-activated cell sorter (FACS) analysis was used to determine the extent to which L6–FITC bound to the H2981 cells, and from this, conjugate binding data was obtained. L6–ECIβL was able to compete with L6–FITC for binding to H2981 cells, but was less effective in doing so compared to L6–BCβL (Figure 3). FACS analysis indicated that P1.17 and P1.17–ECIβL showed no measurable specific binding to H2981 cells (data not shown).

The β-lactamase activities of the conjugates were determined using nitrocefin as a substrate (*5*, *9*). Figure

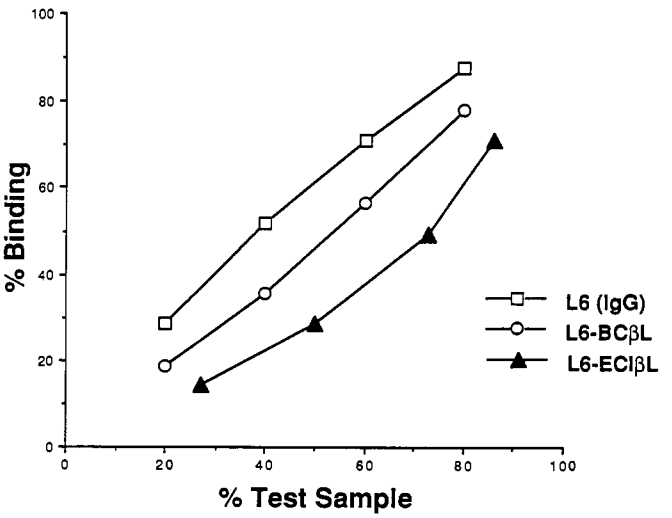


Figure 3. Competitive binding assay. H2981 cells were incubated with various concentrations of the test samples (L6 (IgG_{2a}), L6–BCβL, and L6–ECIβL) mixed with L6(IgG_{2a})–fluorescein isothiocyanate. Fluorescence activated cell sorter analysis was used to determine H2981 fluorescence intensity.

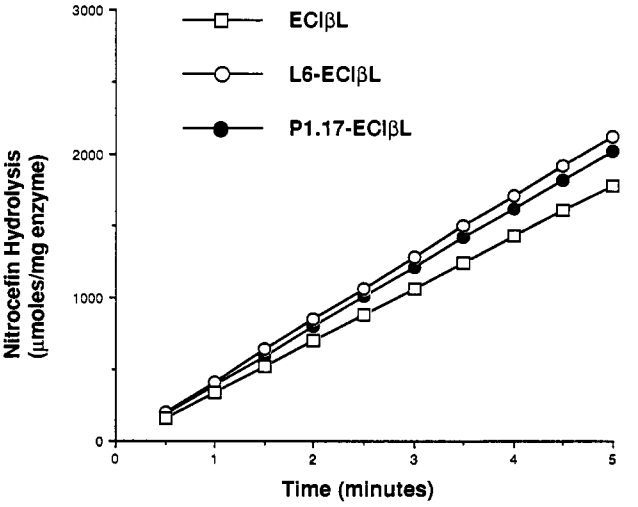


Figure 4. Enzymatic activities of ECIβL (4.75 ng/mL) and mAb–ECIβL conjugates (5 ng/mL ECIβL component) using nitrocefin (50 μM) as a substrate.

4 shows that the enzyme activities of the mAb–ECIβL conjugates were approximately the same as unmodified ECIβL. Thus, the procedures used for the preparation and purification of the conjugates had little effect on enzyme activity. This is consistent with what was previously observed with mAb–BCβL conjugates (*5*).

In Vitro Cytotoxicity. The cytotoxic effects of CCM, PDM, and combinations of the mAb–ECIβL conjugates with CCM were determined on the H2981 cell line (L6 antigen positive, P1.17 antigen negative). Cells were exposed to CCM or PDM for 1 h, washed, and incubated for a total of 48 h. Viability was determined by measuring the incorporation of [^{3}H]thymidine into DNA. The cytotoxic activity of CCM (IC_{50} = 25–45 μM) was much lower than that of PDM (IC_{50} = 1.5 μM, Figure 5). A significant increase in the cytotoxic activity of CCM was obtained on cells that were pretreated with L6–ECIβL. The activity of this combination (IC_{50} = 3.2 μM) was comparable to that for PDM.

Prodrug activation occurred in an immunologically specific manner as evidenced by the fact that P1.17–ECIβL did not increase the cytotoxic activity of CCM. A second method to show immunological specificity involved sat-

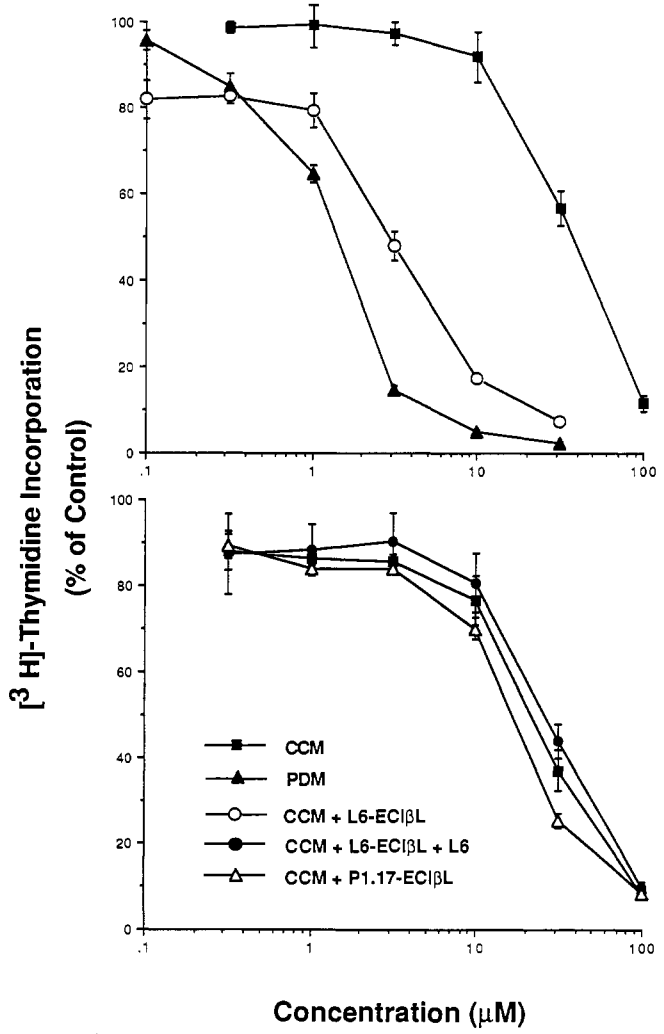


Figure 5. In vitro cytotoxicity. H2981 cells (L6 antigen positive, P1.17 antigen negative) were treated with L6–ECIβL or P1.17–ECIβL (0.316 μg/mL), washed, and then treated with CCM. Antigen blocking was achieved by treating the cells with saturating amounts of L6 (1 mg/mL) prior to treatment with L6–ECIβL.

urating H2981 cells with unmodified L6 prior to exposure to L6–ECIβL. Again, there was no enhancement in the cytotoxic activity of CCM (IC_{50} = 30 μM). These experiments establish that CCM is a prodrug and that prodrug activation is mediated in an immunologically specific manner by conjugate that binds to cell-surface antigens.

In Vivo Studies. Initial experiments in H2981 tumor bearing mice that were treated with mAb–β-lactamase conjugates indicated that the antitumor activities of CM and CCM were significantly higher when the prodrugs were administered intravenously (iv) compared to intraperitoneally (data not shown). Therefore iv administration was used to establish maximum tolerated doses (MTDs) of CM, CCM, and PDM. The toxicities of CM, CCM, and PDM in nude mice were determined by injecting the agents at a variety of doses using two different dosing schedules. The MTD is defined as the dose that resulted in no deaths, and where drug-related deaths occurred with dose increases of 30% or less.

Table II shows the MTDs for the various agents. It was found that both CM and CCM had significantly higher MTDs than PDM. When administered in three doses spaced 12 h apart, the MTDs of CM and CCM were 3.6 and >9.9 times greater than PDM on a molar basis. However, CM caused extensive necrosis at the site of injection, which limited subsequent prodrug administration. In contrast, no apparent necrosis was associated with the administration of CCM. Consequently, therapy experiments with CCM in combination with the mAb–ECIβL conjugates were the subject of subsequent investigation.

Table II. Maximum Tolerated Doses of CM, CCM, and PDM in Nude Mice[a]

compd	schedule	dose (mg/kg/injection)
CM	3 doses, 12 h apart	23
CCM	3 doses, 12 h apart	>62[b]
CCM	3 doses, 4 h apart	62
PDM	3 doses, 12 h apart	2.8
PDM	3 doses, 4 h apart	1.4

[a] The agents listed were administered iv (tail vein) in female athymic nude mice (3 to 6 animals/group). [b] Highest dose tested.

In vivo therapy experiments were performed on mice that had established subcutaneous H2981 tumors. The mice were randomized just before the initiation of therapy so that there were no significant differences in tumor sizes between any of the groups. Treatment was initiated 20 days after implantation, at which time the tumors were established (approximately 180 mm^3 in volume) and growing. The mAb–ECIβL conjugates were administered iv at 1 mg mAb component/kg, which corresponds to approximately 25 μg/mouse. After 96 h, the prodrug CCM (46.7 mg/kg/injection) was then administered in three separate doses spaced 4 h apart. This dosing schedule was selected since at 96 h after conjugate administration the blood levels of enzymatic activity were low. In addition, it was possible to administer more CCM cumulatively in three separate doses compared to a single bolus injection. Other groups were treated with CCM (62 mg/kg/injection) or PDM (1.4 mg/kg/injection) without prior conjugate treatment. In these experiments, the drug and prodrug doses used were at or very near to the MTDs. The MTD of CCM in conjugate-treated mice (46.7 mg/kg/injection) was lower than when CCM was given alone (62 mg/kg/injection), owing most likely to the formation of PDM by the mAb–enzyme conjugate. There were no treatment or tumor related toxicities during the entire course of the experiment.

The prodrug, CCM, and drug, PDM, had little to no effect on tumor growth (Figure 6). In contrast, a significant level of antitumor activity was obtained in mice treated with L6–ECIβL prior to the administration of CCM. The antitumor effect appeared to be immunologically specific, since a lower level of antitumor activity was obtained when CCM was administered to animals that had previously been treated with the nonbinding control conjugate P1.17–ECIβL. Statistical analysis of the data from day 34 onward indicated that the tumors in L6–ECIβL/CCM treated mice were smaller than in any of the other treatment groups ($P < 0.05$).

DISCUSSION

Previously, it was demonstrated that CM was a prodrug that released PDM upon treatment with β-lactamases from *E. coli* and *B. cereus* (5). In vitro cytotoxicity experiments indicated that CM was approximately 50 times less cytotoxic to H2981 cells than PDM, and that L6–BCβL could activate CM in an immunologically specific manner. These results prompted us to investigate the in vivo activities of CM in combination with mAb–β-lactamase conjugates.

In vivo experiments indicated that CM was significantly less toxic to mice than PDM (Table II). However, treatment with CM was hampered by severe tail necrosis following iv injection. We reasoned that the necrosis might

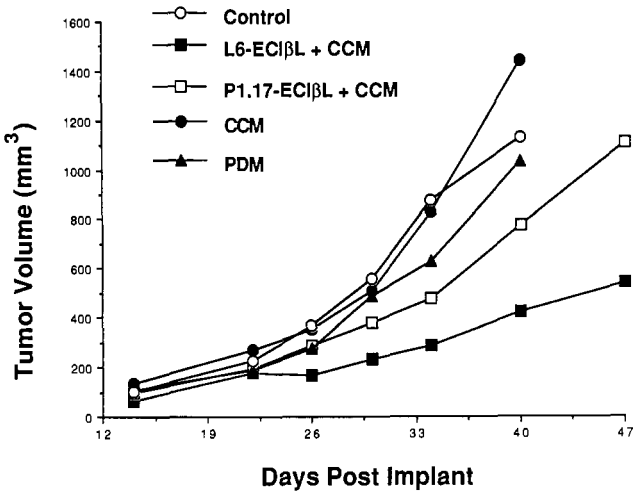


Figure 6. Effects of PDM, CCM, and mAb–ECIβL conjugates in combination with CCM on subcutaneous H2981 tumors in nude mice (eight mice/group). Conjugates (1 mg/kg) were administered on day 20. This was followed 96 h later by CCM (46.7 mg/kg/injection). The therapeutic effects were compared to those of CCM (62.2 mg/kg/injection) and PDM (1.4 mg/kg/injection) in mice that did not receive prior conjugate treatment. All drugs were administered in three doses spaced 4 h apart.

be due to in vivo precipitation of the prodrug, and that precipitation would not occur with more water-soluble analogues. This provided the rationale for the synthesis of CCM, which has a carboxylic acid containing side chain appended to the 7-position of the cephalosporin. In CM, this position is substituted with a hydrophobic phenylacetyl group. CCM was shown to be less cytotoxic than PDM on H2981 cells (Figure 5). This was anticipated, since previous studies have demonstrated that electron-withdrawing or highly polar substituents appended to the aromatic rings on nitrogen mustards lead to reductions in cytotoxic activity (*5, 16–19*). ECβL, BCβL, and ECIβL were all able to catalyze β-lactam hydrolysis of CCM.

On the basis of the kinetic data shown in Table I, mAb–ECIβL conjugates were prepared and tested for their abilities to activate CCM. In vitro studies indicated that L6–ECIβL effected the activation of CCM on L6 antigen positive H2981 cells (Figure 5). Prodrug activation occurred in an immunologically specific manner, since no such enhancement took place on P1.17–ECIβL treated cells. Thus, while the binding of L6–ECIβL is impaired compared to L6 (Figure 3), enough binding activity is retained by the conjugate to selectively convert CCM to PDM. The reduced binding of L6–ECIβL compared to L6–BCβL was reproducibly found in three separate experiments. We believe that this is due to steric interaction between ECIβL with one of the L6 antigen binding sites. Efforts are currently underway to explore the effects that other conjugation strategies have on the antigen binding and prodrug activation characteristics of L6–ECIβL.

The approach of using targeted enzymes for prodrug activation will be therapeutically useful only if it clearly has advantages over conventional cytotoxic chemotherapy. One way to establish such an advantage is to compare the activities on subcutaneous tumor xenografts, even though such tumor models bear little resemblance to actual tumors that grow and metastasize in humans. With this limitation in mind, it is encouraging that L6–ECIβL in combination with CCM was superior in activity to PDM in vivo (Figure 6). This is noteworthy, since H2981 tumor xenografts were well-established and unresponsive to therapy with MTDs of PDM or CCM without prior conjugate administration. These results are consistent with other mAb–enzyme/prodrug combinations that have also demonstrated superior in vivo activities compared to conventional drug therapy (*1, 16, 17, 20–22*). The fact that some degree of antitumor activity was mediated by P1.17–ECIβL in combination with CCM (Figure 6) may be due to residual levels of systemic and tumor-associated enzyme activity when the prodrug was administered. Previous in vivo studies with conjugates of alkaline phosphatase in combination with mitomycin phosphate have given similar results (*20*).

Even though the in vivo therapeutic effects of the L6–ECIβL/CCM combination are superior to systemic drug administration, it is apparent from the data shown in Figure 6 that continued efforts to enhance the activities yet further are required. It should be noted that the effects of conjugate dose and timing of prodrug administration have not been extensively explored. Parameters such as these will likely have strong influences on antitumor activity (22) and immunological specificity. Also, in vivo experiments with other cephalosporin-containing prodrugs, such as cephalosporin doxorubicin (*15*), are currently the subject of investigation, since the nature of the released drug will undoubtedly play an important role in therapeutic efficacy.

ACKNOWLEDGMENT

The authors are grateful to Steven Klohr for analytical data, Clay Siegall for comments on the manuscript, and David Lowe, Karl Erik Hellström, and Ingegerd Hellström for their support during the course of this work.

LITERATURE CITED

(1) Senter, P. D., Wallace, P. M., Svensson, H. P., Vrudhula, V. M., Kerr, D. E., Hellström, I, and Hellström, K. E. (1993) Generation of cytotoxic agents by targeted enzymes. *Bioconjugate Chem. 4*, 3–9.

(2) Neuhaus, F. C., and Georgopapadakou, N. H. (1992) Strategies in β-lactam design. *Emerging Targets in Antibacterial and Antifungal Chemotherapy* (J. A. Sutcliffe, and N. H. Georgopapadakou, Eds.) pp 205–273, Chapman and Hall, New York.

(3) Meyer, D. L., Jungheim, L. N., Mikolajczak, S. D., Shepherd, T. A., Starling, J. J., and Ahlem, C. (1992) Preparation and characterization of β-lactamase-Fab′ conjugates for the site specific activation of oncolytic agents. *Bioconjugate Chem. 3*, 42–48.

(4) Alexander, R. P., Beeley, N. R. A., O'Driscoll, M., O'Neill, F. P., Millican, T. A., Pratt, A., J., and Willenbrock, F. W. (1991) Cephalosporin nitrogen mustard carbamate prodrugs for "ADEPT". *Tetrahedron Lett. 32*, 3269–3272.

(5) Svensson, H. P., Kadow, J. F., Vrudhula, V. M., Wallace, P. M., and Senter, P. D. (1992) Monoclonal antibody–β-lactamase conjugates for the activation of a cephalosporin mustard prodrug. *Bioconjugate Chem. 3*, 176–181.

(6) Suzuki, N., Sowa. T., and Murakami, M. (1978) Process for preparing 7-aminocephalosporanic acid derivatives. U.S. Patent 4,079,180, March 14, 1978.

(7) Everett, J., L., and Ross, W. C. J. (1949) Aryl-2-halogenoalkylamines. Part II. *J. Chem. Soc. 1949*, 1972–1983.

(8) Hellström, I., Horn, D., Linsley, P. S., Brown, J. P., Brankovan, V., and Hellström, K. E. (1986) Monoclonal antibodies raised against human lung carcinoma. *Cancer Res. 46*, 3917–3923.

(9) Madgwick, P. J., and Waley, S. G. (1987) β-Lactamase I from *Bacillus cereus*. *Biochem. J. 248*, 657–662.

(10) Cartwright, S. J., and Waley, S. G. (1984) Purification of β-lactamases by affinity chromatography on phenylboronic acid-agarose. *Biochem. J. 221*, 505–512.

(11) Bush, K. (1989) Characterization of β-lactamases: Groups 1,2a,2b, and 2b′. *Antimicrob. Agents Chemother. 33*, 264–270.

(12) Davies, R. B., and Abraham, E. P. (1974) Separation, purification and properties of β-lactamase I and β-lactamase II from *Bacililus cereus* 569/H/9. *Biochem. J. 143*, 115–127.

(13) Galleni, M., Lindberg, S., Normark, S., Cole, S., Honare, N., Joris, B., and Frere, J. M. (1988) Sequence and comparative analysis of three *Enterobacter cloacae* ampC β-lactamase genes and their products. *Biochem. J. 250*, 753–760.

(14) Boyd, D. B. (1984) Electronic structures of cephalosporins and penicillins. 15. Inductive effect of the 3-position side chain in cephalosporins. *J. Med. Chem. 27*, 63–66.

(15) Hudyma, T. W., Bush, K., Colson, K. L., Firestone, R. A., and King, H. D. (1993) Synthesis and release of doxorubicin from a cephalosporin based prodrug by a β-lactamase-immunoconjugate. *Bioorg. Med. Chem. Letts. 3*, 323–328.

(16) Bagshawe, K. D., Springer, C. J., Searle, F., Antoniw, P., Sharma, S. K., Melton, R. G., and Sherwood, R. F. (1988) A cytotoxic agent can be generated selectively at cancer sites. *Br. J. Cancer 58*, 700–703.

(17) Wallace, P. M., and Senter, P. D. (1991) In vitro and in vivo activities of monoclonal antibody-alkaline phosphatase conjugates in combination with phenol mustard phosphate. *Bioconjugate Chem. 2*, 349–352.

(18) Palmer, B. D., Wilson, W. R., Pullen, S. M., and Denny, W. (1990) Hypoxia-selective antitumor agents 3. Relationships between structure and cytotoxicity against cultured tumor cells for substituted N,N-bis(2-chloroethyl)anilines. *J. Med. Chem. 33*, 112–121.

(19) Chakravarty, P. K., Carl, P. L., Weber, M. J., and Katzenellenbogen, J. A. (1983) Plasmin-activated prodrugs for cancer therapy. 1. Synthesis and biological activity of peptidylacivicin and peptidylphenylenediamine mustard. *J. Med. Chem. 26*, 633–638.

(20) Senter, P. D., Schreiber, G. J., Hirschberg, D. L., Ashe, S. A., Hellström, K. E., and Hellström, I. (1989) Enhancement of the in vitro and in vivo antitumor activities of phosphorylated mitomycin C and etoposide derivatives by monoclonal antibody-alkaline phosphatase conjugates. *Cancer Res. 49*, 5789–5792.

(21) Senter, P. D., Saulnier, M. G., Schreiber, G. J., Hirschberg, D. L., Brown, J. P., Hellström, I., and Hellström K. E. (1988) Anti-tumor effects of antibody-alkaline phosphatase conjugates in combination with etoposide phosphate. *Proc. Natl. Acad. Sci.* U.S.A. *85*, 4842–4846.

(22) Springer, C. J., Bagshawe, K. D., Sharma, S. K., Searle, F., Boden, J. A., Antoniw, P., Burke, P. J., Rogers, G. T., Sherwood. R. F., and Melton, R. G. (1991) Ablation of human choriocarcinoma xenografts in nude mice by antibody-directed enzyme prodrug therapy (ADEPT) with three novel compounds. *Eur. J. Cancer 27*, 1361–1366.

Temperature-Responsive Bioconjugates. 2. Molecular Design for Temperature-Modulated Bioseparations†

Yoshiyuki G. Takei, Takashi Aoki, Kohei Sanui, Naoya Ogata, Teruo Okano,*,‡ and Yasuhisa Sakurai‡

Department of Chemistry, Faculty of Science and Technology, Sophia University, 7-1 Kioi-cho, Chiyoda, Tokyo 102, Japan, and Institute of Biomedical Engineering, Tokyo Women's Medical College, 8-1 Kawada-cho, Shinjuku, Tokyo 162, Japan. Received March 15, 1993®

We have synthesized carboxyl semitelechelic oligo(*N*-isopropylacrylamide) (OIPAAm) using radical telomerization with 3-mercaptopropionic acid. This telomerization is also effective for the synthesis of carboxyl semitelechelic co-oligomers of IPAAm with butyl methacrylate (BMA) as hydrophobic or *N*,*N*-dimethylacrylamide (DMAAm) as hydrophilic comonomers. All co-oligomers are highly water-soluble at lower temperatures and exhibit phase separation with increasing temperature. Pure OIPAAm exhibits a lower critical solution temperature (LCST) at 32 °C, and the LCST for co-oligomers can be controlled to increase over 32 °C with increasing DMAAm composition and to decrease below 32 °C with increasing BMA composition. OIPAAm was grafted to bovine serum albumin (BSA) and bovine plasma fibrinogen (BPF) by activated ester–amine coupling. These OIPAAm–biomolecule conjugates maintain their temperature responses, are soluble in cold water, and precipitate over a range of temperatures related to oligomer content. Conjugates could be selectively precipitated and independently separated from conjugate solution mixtures with increasing temperature. In this case, the number of OIPAAm molecules attached to a conjugate affects the aggregate sizes of precipitated conjugates in mixtures. Both conjugate mixture ratios and solution concentrations influence the contamination of oligo(IPAAm–*co*-DMAAm)–BSA conjugates in precipitated oligo(IPAAm–*co*-BMA)–BPF conjugates. Furthermore, precipitated conjugates separated using centrifugation and filtration redissolve in water and maintain their biofunctionality, indicating the potential of strategy in reversible bioreactors and protein separations.

INTRODUCTION

Poly(*N*-isopropylacrylamide) (PIPAAm)[1] is a water-soluble polymer exhibiting remarkable hydration–dehydration changes in aqueous media in response to changes in temperature, resulting in a lower critical solution temperature (LCST) (*1*). These networks have been investigated for molecular separation (*2*), sorption–desorption of solutes (*3*), control of enzyme activity (*4*), and release of solutes (*5*). Temperature-responsive PIPAAm hydrogels are capable of controlling drug release rates by temperature change, demonstrating a potential to achieve an intelligent drug-delivery system (*6*). Random copolymer hydrogels composed of IPAAm and alkyl methacrylates as comonomers are used to control the LCST and subsequent "on–off" regulation of drug permeation (*7–9*). PIPAAm-grafted polystyrene is used as cell culture substrates and controls cell attachment–detachment using the hydration–dehydration phenomena of these polymer chains (*10*).

Chen et al. have reported polymer–protein conjugates using PIPAAm (*11*, *12*). IPAAm copolymers with comonomers containing reactive groups were synthesized and conjugated with proteins. It was unclear if protein is coupled with polymer chains by single or multiple attachments, which might significantly influence the activity and properties of the conjugated protein. Moreover, conjugation of copolymer with proteins may affect the bioactivity of proteins through the steric hindrance of polymers as well as promoting formation of protein aggregates. We previously reported the synthesis of oligo-IPAAm (OIPAAm) with reactive end groups by the telomerization of IPAAm using 3-mercaptopropyonic acid as telogen (*13*). We also reported control of chain length, introduction of end-standing carboxyl groups, and temperature-responsive phase-transition phenomena of these oligomers. Oligomers with reactive end groups allow facile synthesis not only of block and graft copolymers but also of oligomer-modified biomolecules. Semitelechelic oligomers would be expected not only to maintain high protein bioactivity by reduced steric hindrance arising from conjugated oligomers but also to import high temperature sensitivity due to the inherently high mobile nature of oligomer free end groups. These system avoids nonsepcific problems associated with the process of biomolecule conjugation because they posses one reactive end group per oligomer. OIPAAm-grafted collagen conjugates, a model for OIPAAm–biomolecule conjugates, dissolved in water regardless of isotonic conditions and demonstrated an LCST near 34 °C (*13*).

As the phase transition of PIPAAm corresponds to the stability of hydrophobic groups in polymer chain in aqueous media, OIPAAms copolymerized with another hydrophobic or hydrophilic comonomers show different LCSTs compared to homogeneous PIPAAm. Moreover, bioconjugates coupled with OIPAAms of different LCSTs should maintain these different LCSTs attributable to

† For Part 1, see ref. 13.

* Author to whom correspondence should be addressed.

‡ Tokyo Women's Medical College.

® Abstract published in *Advance ACS Abstracts*, September 1, 1993.

[1] Abbreviations used: IPAAm, *N*-isopropylacrylamide; PIPAAm, poly-IPAAm; OIPAAm, oligo-IPAAm; BMA, butyl methacrylate; DMAAm, *N*,*N*-dimethylacrylamide; MPA, 3-mercaptopropionic acid; AIBN, *N*,*N*′-azobisisobutylonitrile; DMF, *N*,*N*-dimethylformamide; IBc, oligo(IPAAm–*co*-BMA) with carboxyl end group; IDc, oligo(IPAAm–*co*-DMAAm) with carboxyl end group; BSA, bovine serum albumin; BPF, bovine plasma fibrinogen; F-B3/30, BPF–IBc conjugate; A-D5/5, BSA–IDc conjugate.

1043-1802/93/2904-0341$04.00/0 © 1993 American Chemical Society

Table I. Preparation of IPAAm Oligomers[a]

oligo(IPAAm-co-BMA)				oligo(IPAAm-co-DMAAm)			
code	IPAAm (10^{-2} mol)	BMA (10^{-4} mol)	MPA (10^{-4} mol)	code	IPAAm (10^{-2} mol)	DMAAm (10^{-4} mol)	MPA (10^{-4} mol)
IBc-1	4.29	6.79	8.36	IDc-5	4.10	2.24	8.75
IBc-3	4.18	13.25	8.31	IDc-7	4.00	3.07	8.33
IBc-5	4.07	21.81	8.42	IDc-10	3.85	4.35	8.57
				IDc-15	3.62	6.43	8.37

[a] IPAAm, *N*-isopropylacrylamide; DMAAm, *N,N*-dimethylacrylamide; MPA, 3-mercaptopropionic acid, solvent, *N,N*-dimethylformamide (50 mL); initiator, *N,N'*-azobisisobutyronitrile (2 mmol/L); synthesized at 70 ± 1 °C for 300 min; $[S]/[M]_{total} = 0.022$; [S], concentration of chain transfer agent; $[M]_{total}$, total monomer concentration.

the respective conjugated OIPAAms (*11*). These conjugates are expected to be bioactive in aqueous solution with an intrinsic ability to be conveniently separated from reactive products with small temperature increases. In bioseparation processes and clinical diagnosis, these compounds should prove valuable for assay and subsequent separation and recovery. This strategy introduces temperature-responsive activities into biomolecules, a first step toward the development of "intelligent bioconjugates".

We now report the synthesis of semitelechelic OIPAAms with reactive carboxyl end groups which show different LCST values on the basis of radical telomerization. Moreover, we discuss temperature-modulated phase-separation systems using OIPAAm–biomolecule conjugates.

EXPERIMENTAL PROCEDURES

Materials. *N*-Isopropylacrylamide (IPAAm) and *N,N*-dimethylacrylamide (DMAAm) were provided by Kojin (Tokyo, Japan). IPAAm was purified by recrystallization from toluene/petroleum ether and dried at room temperature in vacuo (*1*). DMAAm was dried at room temperature in vacuo. Butyl methacrylate (BMA) was obtained from Wako Pure Chemicals (Tokyo, Japan). BMA was distilled under reduced pressure and the fraction of bp 61 °C/4 mmHg was used. 3-Mercaptopropionic acid (MPA) was purchased from Aldrich Chemical Co. (Milwaukee, WI) and was distilled under reduced pressure and the fraction of bp 95 °C/5 mmHg was used. *N,N*-azobisisobutyronitrile (AIBN), *N,N'*-dimethylformamide (DMF), and ethyl acetate were obtained from Wako Pure Chemicals and purified by conventional methods. Ultrapure water used for sample solutions was provided by a commercial water-purification device (Toray, Model LV-10T). Other chemicals used in the synthesis of oligo(IPAAm-*co*-BMA) and oligo(IPAAm-*co*-DMAAm) are the same as those described in previous work (*13*).

Preparation of Biomolecules. Bovine serum albumin (BSA, A3350) and bovine plasma fibrinogen (BPF, F8630) were obtained from Sigma Chemical Co. (St. Louis, MO), and were dialyzed against 0.15 M phosphate buffer solution (PBS, pH 7.3) and then lyophilized. Albumin concentration was determined by formation of a color complex (λ_{max} = 630 nm) with bromocresol green (Merck) (*14*). Fibrinogen concentration was determined by clotting with thrombin (Sigma, T4648) digestion of the clot and biuret analysis of the resulting solution (*15*).

Co-Oligomerization Procedure. Semitelechelic IPAAm co-oligomers (IBc-X; X denotes the mole fraction of comonomer in feed) were prepared by radical oligomerization of IPAAm and BMA with MPA using AIBN as an initiator in DMF. The reaction mixture was subjected to freeze–thaw cycles, in order to remove oxygen. The ampules were degassed and sealed under reduced pressure. The reaction was performed in sealed ampules at 70 ± 1 °C for 5 h (*16*). The preparation of co-oligomers is summarized in Table I. OIPAAms of molecular weight near 6000 g/mol were prepared in this study. After evaporation, the products were dissolved in DMF and poured into diethyl ether to precipitate the oligomers. Oligomers were further purified by repeated precipitation from DMF into diethyl ether. Radical oligomerization of IPAAm with DMAAm (IDc-X) was carried out by the same method.

Characterization of Co-Oligomers. Proton NMR spectra were recorded for $CDCl_3$ solutions of the oligomers at ambient temperature on a spectrometer operating at 270-MHz frequency (JEOL, NJ-270E, Tokyo, Japan). Oligomer molecular weights were determined by gel-permeation chromatography (GPC, Shimadzu; C-R4AX, Shodex; KF-80M × 2) in tetrahydrofran at 40 °C (polystyrene standard; Polyscience Inc., Warrington, PA). The molecular weight of oligomers was also determined by end-group titration using 0.01 M NaOH and phenolphthalein at 4 °C, which detects the carboxyl group at the end of oligomer molecules.

Transmittance Measurements. Optical transmittance of oligomer solutions (10 mg/mL) at various temperatures was carried out by monitoring transmittance at 500 nm using a spectrophotometer (Shimadzu, UV-240). The observation cell was thermostatted by a circular water jacket (Iuchi, HT-01C).

Modification of Biomolecules with Co-Oligomers. Oligomers were activated by *N*-hydroxysuccinimide with dicyclohexylcarbodiimide in dry ethyl acetate at 4 °C for 16 h in a molecular ratio of 1:1.2:1.2, respectively. After evaporation, the residue was dissolved in ethyl acetate and poured into diethyl ether to precipitate activated OIPAAm. Activated ester groups were confirmed by infrared and ultraviolet spectroscopy (*17*). Bioconjugates of OIPAAm with protein were synthesized by following the protocol of Bückman et al. with a weight feed ratio of OIPAAm to biomolecule of 10 and 50 (*18*). The reaction solution was adjusted to and maintained at pH 8.5 during the course of the reaction and all steps were carried out at 4 °C. Activated OIPAAm was dissolved in 4 mL of dry DMF and added to 100 mg of biomolecule in 50 mL of PBS. This process was repeated four more times at 30-min intervals. The total reaction time was 8 h with gentle stirring at 4 °C. The solution was dialyzed (cellulose, 10 000 molecular weight cutoff) against PBS, pH 7.4, and lyophilized. The resulting biomolecule–OIPAAm conjugate molecular weights were measured by high-performance size-exclusion chromatography (HPSEC; HLC-802, equipped with TSK-G4000SW, Toso, Tokyo, Japan). A calibration curve for globular proteins was determined by the retention of standard proteins, obtained from Boehringer Mannheim Biochemica, including β-galactosidase (Mr = 465 000), IgG (Mr = 150 000), IgG Fab fragment (Mr = 50 000), myoglobin (Mr = 17 000) and Gly-Tyr (Mr = 238). Transmittance changes of purified conjugates in

Table II. Analysis of Oligo(IPAAm-*co*-BMA)[a]

code	mole fraction of BMA (mol %) in feed	mole fraction of BMA (mol %) observed[b]	molecular weight from analysis of end group[d]	$\overline{Mn}$[c]	$\overline{Mw}$[c]	number of COOH in one molecules[d]	LCST (°C)
IBc-1	1	0.92	6200	5800	6300	0.97	31.0
IBc-3	3	2.81	6300	6050	6500	1.05	28.0
IBc-5	5	4.80	5900	5800	5900	1.07	26.0

[a] Oligo(IPAAm-*co*-BMA), in DMF (1.0 mol/L) at 70 ± 1 °C, AIBN, 2 mmol/L; reaction time, 300 min. [b] ^{1}H NMR. [c] GPC in THF at 40 °C. [d] Average (n = 3).

Table III. Analysis of Oligo(IPAAm-*co*-DMAAm)[a]

code	mole fraction of DMAAm (mol %) in feed	mole fraction of DMAAm (mol %) observed[b]	molecular weight from analysis of end group[d]	$\overline{Mn}$[c]	$\overline{Mw}$[c]	number of COOH in one molecules[d]	LCST (°C)
IDc-5	5	6.44	5900	5600	6200	1.02	35.0
IDc-7	7	8.12	6200	5700	5900	0.97	36.0
IDc-10	10	11.93	6300	6600	7100	1.09	38.0
IDc-15	15	17.21	5900	5500	6100	1.02	42.0

[a] Oligo(IPAAm-*co*-DMAAm), in DMF (1.0 mol/L) at 70 ± 1 °C; AIBN, 2 mmol/L; reaction time, 300 min. [b] ^{1}H NMR. [c] GPC in THF at 40 °C. [d] Average (n = 3).

aqueous solution (10 mg/mL) were also recorded as a function of temperature as described above.

Separation by Temperature-Modulated Precipitation. Optical transmittance for the mixtures of bioconjugate (10 mg/mL total) was measured by spectrophotometry at various temperatures. Contamination by BSA conjugates in aggregated BPF conjugates was calculated from the data of BSA solution concentration after BPF precipitation as a function of BSA conjugate ratios. Furthermore, effects of solution concentration on contamination by BSA conjugate in aggregated BPF conjugates were calculated.

RESULTS AND DISCUSSION

Synthesis of IPAAm Co-Oligomers. Carboxyl semitelechelic co-oligomers of IPAAm with BMA or DMAAm were synthesized by telomerization using MPA as telogen at 70 °C in DMF. Compositions of oligo(IPAAm-*co*-BMA) and oligo(IPAAm-*co*-DMAAm) were determined, from an analysis of the ^{1}H NMR spectra in $CDCl_3$ solutions. The mole fraction of BMA in oligo(IPAAm-*co*-BMA) was calculated from the area of the singlet at 0.9 ppm due to the terminal methyl protons of the alkyl chains and the area of the singlet at 4.01 ppm, attributed to the resonance of the C-2 proton of the isopropyl groups. The mole fraction of DMAAm in oligo(IPAAm-*co*-DMAAm) was also calculated from the area of the triplet centered at 2.79 ppm attributed to the methyl protons of the *N*-substituted methyl groups and the area of the singlet at 4.01 ppm, attributed to the resonance of the C-2 proton of the isopropyl groups. Results obtained in the co-oligomerization of IPAAm with DMAAm or BMA are summarized in Table II and III, respectively. NMR confirms copolymer formation as shown by these data. Yields of co-oligomers were 20–30% for 300-min reaction time. Considering the small amounts of comonomer fed in these reactions, the copolymerizability of DMAAm with IPAAm is better than that of BMA with IPAAm. Monomer reactivity ratios evaluated according to the Fineman–Ross method (*19*) were r_1 = 0.341 and r_2 = 1.937 (M_1 = BMA, M_2 = IPAAm) and r_1 = 0.977 and r_2 = 0.820 (M_1 = DMAAm, M_2 = IPAAm), respectively. A value of r_1r_2 reported previously for copolymerization of *N*-alkyl-substituted acrylamides (*20*) is consistent with formation of random copolymers. Our evidence supports this.

As mentioned in the introduction, control of OIPAAm molecular weight is possible by adjusting the relative concentration of monomers to MPA in the starting mixture for the telomerization. OIPAAm molecular weights near 6000 are readily achieved by this strategy, and copolymerization of IPAAm with BMA or DMAAm using MPA via telomerization is confirmed. Molecular weights calculated from the carboxy group analysis assuming one carboxyl group per OIPAAm molecular were approximately equivalent to those determined from GPC data. All data were consistent with one OIPAAm molecule averaging one carboxyl end group per polymer chain.

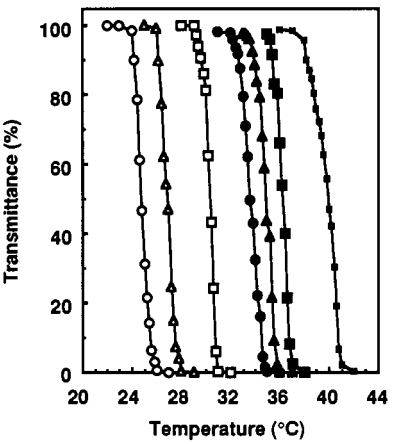


Figure 1. Temperature dependence of optical transmittance for aqueous solutions (○, IBc-5, △; IBc-3, □; IBc-1, ●; IDc-5, ▲; IDc-7, ■; IDc-10, ∗; IDc-15, 10 mg/mL solution, λ = 500 nm).

Phase Transitions of IPAAm Co-Oligomers. All oligomers were soluble in water at room temperature. The series of OIPAAm samples in aqueous solution was examined for optical transmittance changes at various temperatures as shown in Figure 1. All OIPAAms obtained by the copolymerization demonstrated their LCST in the range 26–42 °C. Taylor and Cerankowski proposed as a general rule that the LCST should decrease with increasing polymer hydrophobicity (*21*). The LCST change of IBc and IDc aqueous solutions is shown in Figure 2. IBc oligomers exhibited LCST values below 32 °C and transmittance of IBc oligomer solutions collapsed sharply corresponding to dehydration. Upon increasing the mole fraction of BMA as hydrophobic comonomer, the LCSTs shift to lower temperatures. On the other hand, as hydrophilic components in polymer chains demand larger dehydration energy, IDc oligomers exhibit LCST values

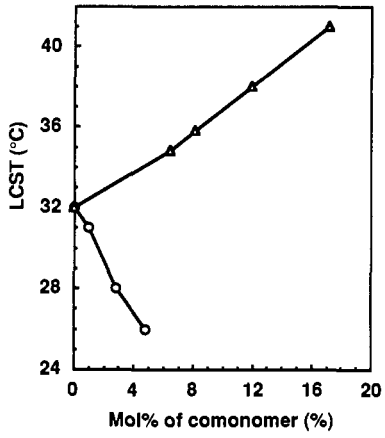


Figure 2. LCST changes of co-oligomer aqueous solutions as a function of mole fraction of comonomers in co-oligomers (○; IBc, △; IDc, 10 mg/mL, λ = 500 nm).

above 32 °C and transmittance changes of IDc oligomer solutions are broader. Increasing the mole fraction of DMAAm as hydrophilic comonomer, shifts LCSTs to higher temperatures. Phase-transition behavior of OIPAAm depends on OIPAAm molecular weight and solution concentration. For low molecular weight OIPAAm precipitated from low-concentration solution, microaggregates of precipitated OIPAAm disperse in aqueous media and are unable to be recovered by centrifugation (*6*, *22*). We have recovered higher molecular weight OIPAAms (Mw = 6100) from precipitated OIPAAm solutions (10 mg/mL). From these results, we show the regulation of LCST values in OIPAAms with carboxyl end groups by telomer mediated copolymerization with hydrophobic or hydrophilic comonomers.

Temperature-Responsive Bioconjugates. Table IV describes the preparation and analysis of these bioconjugates. OIPAAm–biomolecule conjugates were prepared by coupling activated esters of OIPAAm with free amines in biomolecules. Two biomolecules were modified by different temperature-responsive oligomers. BPF was conjugated with IBc oligomer exhibiting an LCST below 32 °C. BSA was conjugated with IDc oligomer exhibiting a higher LCST above 32 °C. OIPAAm–biomolecule conjugates are described by a three sequence code, such as F-B3/7, where F refers to BPF, B3 to IBc-3 oligomer, and 7 to the number of IBc-3 molecules grafted per conjugate. The number of grafted OIPAAm molecules was estimated by the molecular weight of conjugates from HPSEC data. The obtained conjugates are soluble in water at room temperature regardless of isotonic conditions. Also, these conjugates become soluble in organic solvents such as ethanol and DMF.

Transmittance changes in aqueous solutions of OIPAAm–biomolecule conjugates are shown in Figure 3. Unconjugated biomolecule solutions were transparent at temperatures up to and over 50 °C. OIPAAm–biomolecule conjugates, however, precipitated with increasing temperature. Grafting of semitelechelic OIPAAms to biomolecules in this experiment yields the advantages of high polymer chain mobility and rapid response to small temperature changes compared to multiple-point conjugation. Precipitates grafted by increasing temperature were identified as either BPF-IBc conjugates or BSA-IDc conjugates by their molecular weight from HPSEC data. The A-D5/29 bioconjugate exhibited an LCST near 37 °C, the obvious physiologically relevant temperature. Although IBc-3 oligomers showed an LCST at 28 °C in aqueous systems, the F-B3/7 conjugates exhibited a temperature response at 29.4 °C. The LCST for the conjugate system is shifted to a higher temperature range than the LCST of original temperature-responsive polymers. The conjugate constructed by water-soluble biomolecules and temperature-responsive polymers would disturb the OIPAAm dehydration and increase the energy needed for precipitation. The LCST of the F-B3/30 conjugate at 28.8 °C is slightly lower than that of F-B3/7, at 29.4 °C. Also, the LCST of A-D5/29 at 37.2 °C is obviously higher than that for A-D5/5, at 36.2 °C. Increasing the hydrophobic component in IPAAm copolymer chains facilitates polymer chain dehydration. As F-B3/30 conjugates contain more grafted IBc-3 molecules than F-B3/7 conjugates, less thermal energy is required for the precipitation of the F-B3/30 conjugates, providing a lower LCST than that for F-B3/7. By contrast, as A-D5/29 conjugates contain more grafted IDc-5 molecules than the A-D5/5 conjugate, A-D5/29 conjugates require a significantly higher hydrophobic driving force. Therefore, the LCST of A-D5/29 is shifted to a higher temperature range than A-D5/5, reflecting the energy change required for sufficient dehydration of the former conjugate.

We have also estimated the biofunction of conjugated biomolecules by the dye binding for albumin and the fibrin clot formation for finrinogen as described in the Experimental Procedures. It was apparant that all the bioconjugates exhibited the similar biofunctionality as the original proteins, with the exception of A-D5/29, in the assay. Although A-D5/29 conjugates indicate phase-transition phenomena, A-D5/29 conjugates may be deprived of the properties of BSA through conjugation. A-D5/29 contained an average of 29 molecules of IDc-5 oligomer per protein, and the amount of OIPAAm was 72.5 wt % of conjugate as shown in Table IV. The F-B3/30 conjugate included 30 molecules of IBc oligomer per protein molecule. By contrast with A-D5/29, the amount of OIPAAm in F-B3/30 was, however, only 27.5 wt % of the conjugate as shown in Table IV. We propose that expanded and hydrated polymer chains with highly mobile free end groups contribute not only to effective steric hindrance of the biomolecule active site but also import large structural hydration–dehydration changes with small temperature changes.

Temperature-Modulated Bioseparations. Selective precipitation of bioconjugates from mixtures was investigated to assess the ability to separate active proteins. F-B3/30 conjugates (50 mg) and A-D5/5 conjugates (50 mg) were dissolved in water at 4 °C. The mixture was heated from 27 °C, and transmittance changes in the mixture were measured at 0.2 °C intervals. Transmittance changes of mixtures are shown in Figure 4. Precipitation was first observed at 30.4 °C. The mixture was then filtered at 32 °C. When the supernatant was subsequently heated from 32 °C to higher temperatures, another precipitation was observed at 36.4 °C. The first precipitate was redissolved in PBS and confirmed to consist of BPF, as the F-B3/30 conjugate. The second precipitate was redissolved in PBS and determined to be BSA, as the A-D5/5 conjugate. We conclude that different bioconjugates having different LCST values precipitate in the sequential order of LCST temperatures from mixtures with temperature increases.

Purity of the precipitated F-B3/30 at lower temperatures was also investigated, particularly with regard to contamination by A-D5/5 conjugates in the precipitate (shown in Figure 5). When A-D5/5 conjugate ratios become higher than 0.5, A-D5/5 content is generally very low in the F-B3/30 precipitate. At a conjugate ratio of 0.2, contamination

Table IV. Preparation and Analysis of Biomolecule–OIPAAm Conjugates

code	biomolecule ($\bar{M} \times 10^3$)	OIPAAm ($\bar{M}w^a$)	activated OIPAAm in feed (mol/mol biomolecule)	molecular weight of conjugates[b] ($\times 10^3$)	amount of OIPAAm coupled: mol/mol biomolecule	amount of OIPAAm coupled: wt %[c]	LCST (°C)
F-0			0	340	0	0	
F-B3/7	BPF	IBc-3	10	380	6.6	10.5	29.4
F-B3/30	(340)	(6500)	50	524	30.2	27.5	28.8
A-0			0	66	0	0	
A-D5/5	BSA	IDc-5	10	99	5.4	33.3	36.2
A-D5/29	(66)	(6200)	50	240	28.6	72.5	37.2

[a] GPC in THF at 40 °C. [b] Determined by HPSEC. [c] (wt OIPAAm/wt conjugates).

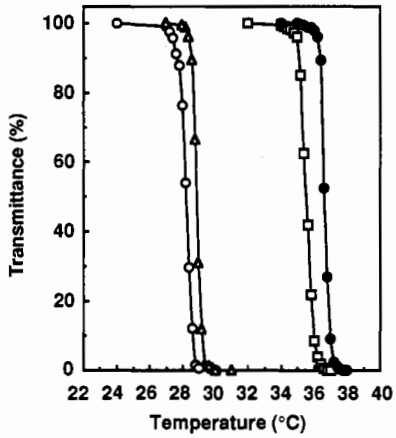


Figure 3. Temperature dependence of optical transmittance for OIPAAm–biomolecule conjugate aqueous solutions (○; F-B3/30, △; F-B3/7, □; A-D5/5, ●; A-D5/29, 10 mg/mL solution, λ = 500 nm).

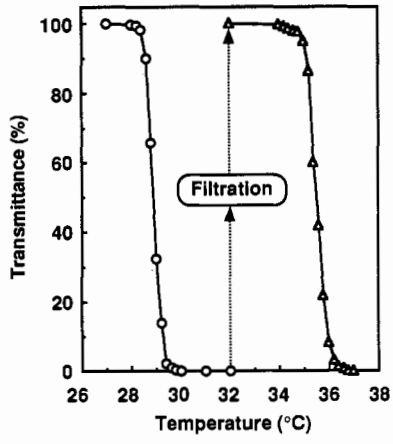


Figure 4. Temperature dependence of optical transmittance for OIPAAm–biomolecule conjugate solution mixtures (○; F-B3/30, △; A-D5/5, 10 mg/mL solution, bioconjugates ratio = 1:1, λ = 500 nm).

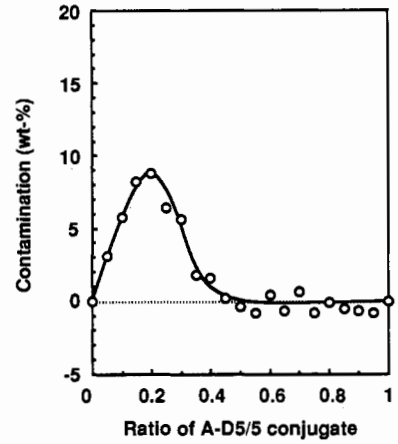


Figure 5. Effect of A-D5/5 ratio on the entrapment of A-D5/5 into temperature-induced F-B3/30 precipitates from OIPAAm–biomolecule conjugate solution mixtures (total concentration = 10 mg/mL, precipitated at 32 °C).

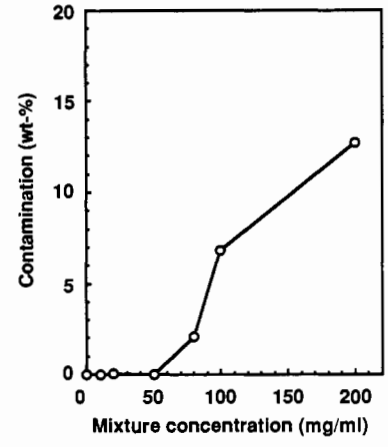


Figure 6. Effect of mixture concentration on contamination of A-D5/5 into F-B3/30 precipitates from OIPAAm–biomolecule conjugate solution mixtures (conjugate ratio = 1:1 by weight).

reached a maximum (8.7 wt %). Alternatively, when F-B3/30 conjugate ratios are higher than 0.5, F-B3/30 contamination of A-D5/5 precipitates is barely detectable. At low A-D5/5 conjugate ratios, F-B3/30 is proposed to enfold A-D5/5 molecules in mixtures, resulting in A-D5/5 entrainment into the resulting F-B3/30 precipitate. As the F-B3/30 conjugate had 5 times greater molecular weight than the A-D5/5 conjugate, F-B3/30 molecules would readily distribute around A-D5/5 molecules at lower A-D5/5 conjugate ratios. Molecules of each conjugate would be phase-separated in mixtures at higher conjugate ratios. The concentration of A-D5/5 entrapped in precipitated F-B3/30 would be minimized, therefore, at A-D5/5 conjugate ratios higher than 0.5, where phase separation would inhibit interaction.

The influence of solution concentration on A-D5/5 contamination into F-B3/30 precipitates is shown in Figure 6. Mixtures of equivalent conjugate ratios were used. At concentrations greater than 100 mg/mL, A-D5/5 contamination in F-B3/30 precipitates ranges from 5 to 15 wt %. Since mixtures had high viscosities at concentrations higher than 100 mg/mL, we believe that F-B3/30 molecules interact and enfold molecules of A-D5/5 and then precipitate. Altering mixture concentration can be used to optimize the contamination of A-D5/5 conjugates into precipitated F-B3/30 conjugates. From these results, both the conjugate ratios and mixture concentrations optimize the contamination of the solute in the precipitate in temperature-modulated phase separation. Polymer mixtures usually exhibit simple coacervation. As bioconjugate water-solubility corresponds to the phase-transition behavior of the OIPAAms, the chain mobility and hydration of grafted OIPAAm mediates the temperature-modulated

phase separation and the biofunction of conjugated biomolecules.

CONCLUSIONS

(i) Temperature-responsive semitelechelic co-oligomers with carboxyl end-groups were synthesized by the radical telomerization of IPAAm with BMA or DMAAm using MPA as a telogen.

(ii) Oligo(IPAAm-*co*-BMA) demonstrated an LCST below 32 °C corresponding to an increase in polymer chain hydrophobicity. Oligo(IPAAm-*co*-DMAAm) demonstrated an LCST above 32 °C, attributed to increases in the hydrophilic nature of the polymer chain.

(iii) OIPAAm-biomolecule conjugates demonstrate LCST values ranging from 28 to 42 °C, depending upon the chemistry and molecular weight of the grafted OIPAAms.

(iv) Large, highly temperature sensitive structural hydration-dehydration changes for bioconjugates are demonstrated due to the inherently high mobile nature of oligomer free end groups.

(v) OIPAAm-biomolecule conjugates can be separated from mixtures by temperature-modulated precipitation with temperature increases.

(vi) Both the conjugate mixture ratios and mixture concentration can modulate the entrapment and contamination of solute into conjugate precipitate in temperature-modulated phase separation.

ACKNOWLEDGMENT

The authors are grateful to Dr. David W. Grainger, Oregon Graduate Institute of Science and Technology, and Dr. Glen S. Kwon, International Center for Biomaterial Science, Tokyo Women's Medical College, for their valuable comments and discussions.

LITERATURE CITED

(1) Heskins, M., Guillet, J. E., and James, E. (1968) Solution properties of poly(*N*-isopropylacrylamide). *J. Macromol. Sci. Chem. A2*, 1441–1455.

(2) Freitas, R. F. S., and Cussler, E. L. (1987) Temperature sensitive gels as extraction solvents. *Chem. Eng. Sci. 42*, 97–103.

(3) Hoffman, A. S., Afrassiabi, A., and Dong, L. C. (1986) Thermally reversible hydrogels; II. Delivery and selective removal of substances from aqueous solutions. *J. Controlled Release 4*, 213–222.

(4) Dong, L. C. and Hoffman, A. S. (1986) Thermally reversible hydrogels; III. Immobilization of enzymes for feedback reaction control. *J. Controlled Release 4*, 223–227.

(5) Bae, Y. H., Okano, T., Hsu, R, and Kim, S. W. (1987) Thermosensitive polymer as on-off switches for drug release. *Makromol. Chem., Rapid Commun. 8*, 481–485.

(6) Bae, Y. H., Okano, T., and Kim, S. W. (1990) Temperature dependence of swelling of crosslinked poly(*N,N'*-alkyl substituted acrylamides) in water. *J. Polym. Sci. Polym. Phys. 28*, 923–936.

(7) Okano, T., Bae, Y. H., Jacobs, H., and Kim, S. W. (1990) Thermally on-off switching polymers for drug permeation and release. *J. Controlled Release 11*, 255–265.

(8) Yoshida, R., Sakai, K., Okano, T., Sakurai, Y., Bae, Y. H., and Kim, S. W. (1991) Surface-modulated skin layers of thermal responsive hydrogels as on-off switches; I. Drug release. *J. Biomater. Sci., Polym. Ed. 3*, 155–162.

(9) Yoshida, R., Sakai, K., Okano, T., Sakurai, Y. (1992) Surface-modulated skin layers of thermal responsive hydrogels as on-off switches: II. Drug permeation. *J. Biomater. Sci., Polym. Ed. 3*, 243–252.

(10) Yamada, N., Okano, T., Sakai, H., Karikusa, F., Sawasaki, Y., and Sakurai, Y. (1990) Thermo-sensitive polymeric surfaces; control of attachment and detachment of cultured cells. *Makromol. Chem., Rapid Commun. 11*, 571–576.

(11) Chen, J. P., Yang, H. J., and Hoffman, A. S. (1990) Polymer-protein conjugates I. Effect of protein conjugation on the cloud point of poly(*N*-isopropylacrylamide). *Biomaterials 11*, 625–630.

(12) Chen, J. P., and Hoffman, A. S. (1990) Polymer-protein conjugates II. Affinity precipitation separation of human immunogammaglobulin by a poly(*N*-isopropylacrylamide)-protein A conjugates. *Biomaterials 11*, 631–634.

(13) Takei, Y. G., Aoki, T., Sanui, K., Ogata, N., Okano, T., and Sakurai, Y. (1993) Temperature-responsive bioconjugates I. Synthesis of temperature-responsive oligomers with reactive end groups and their coupling to biomolecules. *Bioconjugate Chem. 4*, 42–46.

(14) Cooper, R. G., Ed. (1972) *Standard method of clinical chemistry* vol. 7, pp 175, Academic Press, New York.

(15) Horbett, T. A. (1981) Adsorption of proteins from plasma to a series of hydrophilic-hydrophobic copolymers. II. Compositional analysis with the prelabeled protein technique. *J. Biomed. Mater. Res. 15*, 673–695.

(16) Okano, T., Katayama, M., and Shinohara, I. (1978) The influence of hydrophilic and hydrophobic domains on water wettability of 2-hydroxyethyl methacrylate-styrene copolymers. *J. Appl. Polym. Sci. 22*, 369–377.

(17) Miron, T., and Wilchek, M. (1982) A spectrophotometric assay for soluble and immobilized *N*-hydroxysuccinimide esters. *Anal. Biochem. 126*, 433–435.

(18) Bückmann, A. F., and Morr, M. (1981) Functionalization of poly(ethylene glycol) and monomethoxy-poly(ethylene glycol). *Makromol. Chem. 182*, 1379–1384.

(19) (a) Fineman, M., and Ross, S. D. (1950) Linear method for determinating monomer reactivity ratios in copolymerization. *J. Polym. Sci. 5*, 259–265. (b) Ito, K. and Yamashita, Y. (1965) NMR study of styrene-methyl methacrylate copolymer obtained by radical polymerization. *J. Polym. Sci. B3*, 625–630.

(20) Braudrup, J., and Immergut, E. H., Eds. Polymer Handbook pp 111–114, John Wiley & Sons., New York.

(21) Taylor, L. D., and Cerankowski, L. D. (1975) Preparation of films exhibiting a balanced temperature dependence to permeation by aqueous solutions. *J. Polym. Sci., Polym. Chem. 13*, 2551–2570.

(22) Kubota, K., Ando, I., and Fujishige, S. (1990) Solution properties of poly(*N*-isopropylacrylamide) in water. *Polym. J. 22*, 15–21.

Antibody–Magnetite Nanoparticles: *In Vitro* Characterization of a Potential Tumor-Specific Contrast Agent for Magnetic Resonance Imaging

Louis X. Tiefenauer,* Guido Kühne, and Roger Y. Andres

Paul Scherrer Institute, CH-5232 Villigen PSI, Switzerland. Received March 16, 1993®

Target-specific superparamagnetic contrast agents may allow the localization of specific tissues such as tumors by magnetic resonance imaging (MRI). In this report the preparation and *in vitro* characterization of tumor-specific superparamagnetic particles (SMP) are described. Particles of uniform size (9.6 ± 0.8 nm) were prepared from an alkaline solution of ferric and ferrous ions and isolated by differential centrifugation. The resulting nanoparticle suspension is stabilized in buffer using a polypeptide coat to which a monoclonal antibody, specific to carcinoembryonic antigen (CEA), was covalently attached at the hinge region. The resulting anti-CEA SMP have a hydrodynamic radius of less than 50 nm, and specifically bind to CEA *in vitro*. The visualization of epitopes, present on a cell surface in very low density as expected for tumor antigens or receptors, may be achieved due to the high R_2 relaxivity of 300 L mmol^{-1} s^{-1} of the contrast agent described here. Furthermore, the polypeptide coat chosen provides an ideal platform for the attachment of biological modifiers needed for the reduction of the antigenicity and blood clearance rate of anti-CEA SMP.

INTRODUCTION

The potential of superparamagnetic particles (SMP), in particular magnetite, as contrast agents in magnetic resonance imaging (MRI) has been recognized early (*1–3*). If SMP can be endowed with the capability of specific recognition of cell types, a precise localization of selected cells, e.g. tumor cells, may be achieved. Such a material may be considered a "magnetic tracer" giving to MRI diagnostic capabilities equal or superior to those of nuclear medical methods without the use of ionizing radiation.

Recently, SMP have been used to improve the diagnostic quality of MRI investigations of liver, bone marrow, splenic lymphomas, and lymph nodes (*4–8*). In these instances, the inherent capacity of phagocytotic cells of the reticuloendothelial system (RES) has been utilized to trap SMP. Therefore, no biological vector on the contrast agent was needed to induce homing of the contrast agent. Genuine receptor-directed targeting of biologically derivatized SMP has been reported: Asialoglycoprotein covered magnetite for normal liver tissue (*9, 10*) and antimyosin–magnetite was used for infarcted heart muscle (*11*). In both of these cases the number of target molecules (receptors or antigens) per volume is very high. Tumor antigens, however, may be present on a cell in a limited number only and the corresponding targeting task may be substantially more difficult. In fact only one report describing a tumor-specific superparamagnetic contrast agent is known to us (*12*). Independent corroboration of those results is still lacking.

Essentially, functional particles have to escape the elimination by phagocytotic cells and to accumulate in the target tissue. Liposomes are used as carriers of drugs for systemic applications and it is known that size, surface charge, and surface chemistry are critical parameters (*13*). Target-specific nanoparticles have to meet analogous requirements. To prevent fast elimination by the RES, a small particle size is advantageous. Furthermore, particles of a diameter larger than 50 nm can hardly pass trough the pore of the capillary walls and reach the tumor antigens (*14*).

The design of an appropriate surface is not less important. A biological vector, e.g. a monoclonal antibody (mAb), has to be attached covalently to the inorganic surface in order to achieve sufficient stability and in doing so the binding capacity must be preserved. Aggregation of the particles can be prevented by a negative net charge present on the surface. The fast elimination from circulation is induced by binding of specific serum proteins, e.g. complement factors, to the surface (opsonization) as known from erythroid cells (*15*). Thus, the coating material and chemical procedure must be carefully selected. Finally, coated superparamagnetic particles should exhibit a high "magnetic" capacity (expressed as relaxivity) in order to be detectable at low concentration. In this report the preparation and *in vitro* characterization of a superparamagnetic contrast agent specific for the carcinoembryonic antigen (CEA) that closely approximates the above requirements and provides a maximum of flexibility for further surface modifications are described.

EXPERIMENTAL PROCEDURES

Preparation of SMP. Solutions of 200 mL of H_2O, 200 mL of 10 mmol $Fe^{II}Cl_2$, and 200 mL of 5.5 mmol $Fe^{III}Cl_3$ were mixed and 400 mL of 25% ammonium hydroxide was added (*16*). The resulting black suspension was precipitated by centrifugation (2300*g*) and resuspended. The pH was adjusted to 2.1 with 1 mol/L HCl, the glass vessel with the suspension put in a water bath of 47 °C and exposed to a strong ultrasonic field (Branson 450 sonifier, position 4, 10 min; Branson Ultrasonics Corp., Danbury, CT). After centrifugation (100 min, 2200*g*) the pellet was resuspended in 10 mmol/L hydrochloric acid by ultrasonification (Branson, 1 min, position 4). Large particles were removed from this suspension by centrifugation (100 min, 30000*g*). By further centrifugation (100 min, 100000*g*), small magnetite particles of nearly uniform size (see Results) were isolated and they were stored at 4

* Corresponding author. Tel.: 0041 56 99 21 11. Fax: 0041 56 98 26 35.

® Abstract published in *Advance ACS Abstracts*, August 15, 1993.

1043-1802/93/2904-0347$04.00/0 © 1993 American Chemical Society

°C in 10 mmol/L hydrochloric acid until further use. The overall yield ranged from 2 to 10%. SMP are not stable at pH 7 unless they are coated with a polypeptide (see below).

Determination of SMP Concentrations. The amount of particles was determined by measuring their iron concentration by atomic absorption analysis. The reliability of this method was confirmed by neutron activation experiments carried out using the Saphir reactor at our institute (PSI). More simply, concentrations of SMP can be estimated by measuring the light absorption at 405 nm using a multichannel spectrophotometer (EAR 400 FW, SLT Laboratories, Salzburg, Austria). In this case the absorption of samples were compared to SMP calibration solutions of known iron concentrations.

Coating of the SMP. The magnetite particles were coated using the following procedure: To 100 μg of magnetite suspension in 50 μL of 10 mM hydrochloric acid was added 50 μg of poly(glutamic acid, lysine, tyrosine) 6:3:1 (PEKY, Sigma, St. Louis, MO). The sample was stirred for 2 min and then neutralized by the addition of 6.8 μL of 100 mmol 4-(2-hydroxyethyl)-1-piperazineethanesulfonic acid (HEPES) ammonium buffer, pH 6.8 (buffer 1), and 200 μL of 10 mM HEPES ammonium buffer, pH 7.3 (buffer 2). After mild sonification, excess PEKY was removed by washing with buffer 2. In addition to a stabilization effect, the PEKY coat provides the necessary reactive amino groups used in the subsequent modification steps.

Cross-Linking and Chemical Functionalization. In order to stabilize the polypeptide coat, lysine residues of the PEKY molecules were cross-linked. In addition, a chemically reactive group is needed for covalent coupling of antibodies. Stabilization and functionalization was achieved in a single incubation step: To a concentrated suspension of PEKY-coated magnetite (150 μL of 13 mg Fe/mL) was added 53 μL of dimethyl sulfoxide containing 5 mg/mL of each ethylene glycol bis(succinimidyl succinate) (EGS; Pierce, Rockford, IL; cross-linker (*17*)) and *m*-maleimidobenzoic acid *N*-hydroxysulfosuccinimide ester (Sulfo-MBS, Pierce; reactive towards free sulfhydryl groups (*18*)). After a 2 h incubation at room temperature, the particles were washed three times using buffer 2 as described above. The stability of the coating was tested using iodinated PEKY and >95% of the radioactivity was found to be associated to the particles after 50 days. The particles remain in suspension for months, if stored at 4 °C in HEPES buffer. The expected negative net charge was confirmed by their observed electrophoretical migration toward the cathode. In addition, PEKY coated particles of a known Fe content were lyophilized in a volatile buffer (ammonium acetate) and their dry weight was determined. The amount of iron oxide used for a coating process can be varied in a range from 0.5 mg to 10 mg Fe. However, the crosslinker concentration was kept constant.

Oriented Immobilization of Anti-CEA to SMP. The preservation of the binding capacity of antibodies upon coupling to SMP is achieved by using the SH groups of reduced Cys-Cys residues in the hinge region (*19*). Affinity purified murine anti-CEA mAb (mAb 35) (*20*) was partly reduced by the addition of 1.3 mg of solid DL-dithiothreitol to the protein solution (320 μL, 1.3 mg in 10 mM buffer 1). After an incubation of 1 h at room temperature the excess of the reducing agent was removed by gel chromatography (PD-10; Pharmacia, Uppsala, Sweden). To 33 μL (20 μg) of the reduced antibody was added 100 μg (1 mg/mL) of PEKY-coated particles prepared as described above. All solutions used were flushed with nitrogen. After an overnight incubation at 4 °C, the resulting anti-CEA SMP were washed free of excess reactants by two centrifugations in buffer 2 and stored at 4 °C. The coupling yield was approx. 65%, determined using iodinated antibody.

^{59}Fe Labeling of Anti-CEA SMP and Radioactivity Measurements. To 700 μg of anti-CEA SMP in 500 μL of sodium acetate (100 mM, pH 4.5) was added $^{59}Fe^{III}Cl$ (0.75 MBq, IFS-1, Amersham International, Amersham, England). After incubation overnight at room temperature, excess radioactivity was removed by washing the particles using buffer 2. Complete resuspension was assured by gentle sonification of the final product. The antibody binding capacity was not affected by this treatment as tested using iodinated CEA antigen (see below). Radioactivity of ^{59}Fe and/or ^{125}I was measured using a highly shielded γ-counter (Cobra, Model 5002, Packard Instrument Group, Downers Grove, IL).

^{125}I Labeling. CEA, anti-CEA, PEKY, and human thyroglobuline were labeled with ^{125}I by the use of Iodogen (*21*).

Size Determinations. *Size-exclusion chromatography* was performed on Sephacryl S-1000 sf columns (0.9 × 28 cm, Pharmacia) in 100 mM tris(hydroxymethyl)-aminomethane (Tris) hydrochloride, pH 7.2, containing 100 mM sodium chloride, 1 mg/mL human serum albumin (HSA), 5 mg/mL sodium azide, and 10% (w/v) Synperonic F-108 (Serva, Heidelberg, Germany). The column was calibrated using latex particles (120, 51, 48 nm; Polyscience, Warrington, PA), ^{125}I-labeled human thyroglobuline (JBC Chemical Co. Inc., San Luis Obispo, CA), and phenol red. The mobile phase was added using a peristaltic pump with a flow rate of 10 mL/h.

Laser-light scattering was used for size determinations and performed on a Nicomp 370 submicron particle sizer (*22*). Samples of anti-CEA SMP (200 μg/mL) were suspended in buffer 2.

Electron Microscopy. Images of particles were taken without staining at ETH Zürich (see Acknowledgements). From five different, enlarged prints the diameters of 180 SMP were measured, and the mean diameter was determined.

Electrophoresis. The net charge of anti-CEA SMP was determined by electrophoresis in dilute agarose gels (0.22% w/v) at neutral pH (in buffer 2). Samples were spotted on filter paper and stuck into the gel. Electrophoresis was performed at 50 mA/80 V for 5 h at room temperature.

Determination of Relaxivity. Suspensions of anti-CEA SMP (0.5-20 μg/mL) in water were placed in a NMR imaging spectrometer (4.7 T SISCO-200/330, Varian Instruments, Palo Alto, CA), T_2 relaxation times were measured using a CPMG sequence ($\tau \approx 1$ ms), and the relaxivity R_2 ($1/T_2$ per mM Fe) was calculated.

Bioassays. *Liquid System.* The binding capacity of antibody coupled to SMP was determined using an iodinated CEA tracer. The tracer was diluted in incubation buffer 3 (10 mM HEPES, 0.9% NaCl, 0.2% BSA, 0.1% Tween 20, pH 7.3) and incubated with ^{59}Fe-labeled mAb–SMP in the presence of mAb 35 at known concentrations. After an overnight incubation at room temperature on a shaker, the particles were separated from the supernatant by centrifugation. The percentage of tracer bound to anti-CEA SMP (^{125}I) and particle concentrations (^{59}Fe) were determined simultaneously in the γ-counter.

Solid-Phase System. To imitate more closely the situation at the cell surfaces of a tumor, a solid-phase system was developed on the basis of microtiter plates

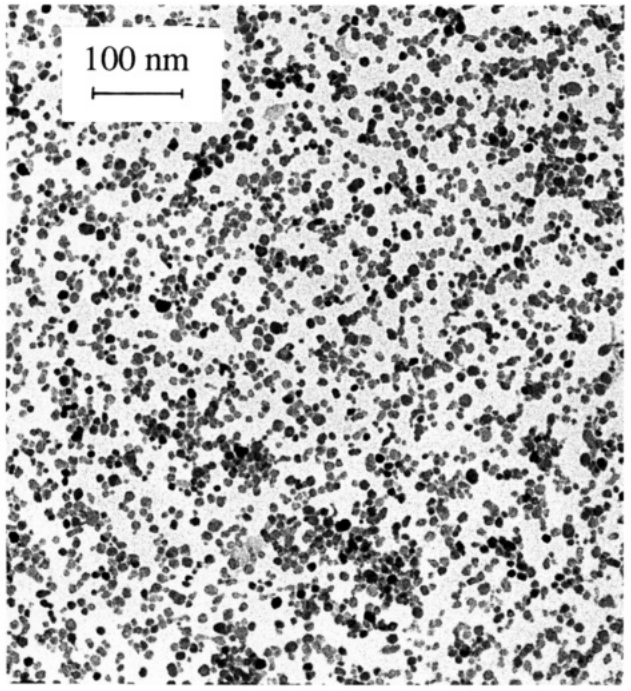


Figure 1. Electron micrograph of uncoated magnetite nanoparticles. Fractionation of the crude precipitate by centrifugation results in a preparation of spherical particles of uniform size.

(Break-apart module maxisorb 1, Nunc, Roskilde, Denmark) which have been coated with avidin as previously described (*23*). The CEA antigen (DA2 ×556 form DAKO A/S Glostrup) was biotinylated using ϵ-biotinamidocaproate *N*-hydroxy-3-sulfosuccinimide ester (Pierce) as described (*24*). Biotinyl-CEA (200 mL of 500 ng/mL per well), dissolved in buffer 4 (10 mM HEPES, 0.9% NaCl, 0.2% BSA, pH 7.3), was added to the avidin-coated microtiter plates and after an incubation of 30 min at room temperature the plates were washed with buffer 4. ^{59}Fe-labeled mAb–SMP was suspended in buffer 4 and added to the wells. After an overnight incubation at room temperature on a shaker, the wells were washed once with incubation buffer 4, broken apart, and put into plastic test tubes, and the radioactivity was determined.

RESULTS

Physical and Chemical Characterization of Anti-CEA SMP. Electron microscopy (Figure 1) reveals the magnetite cores to be nearly spherical, small, and of uniform size (9.6 ± 0.8 nm).

Various attempts to identify the electron-transparent coat of organic material by negative staining have failed. This may indicate an essentially unhindered penetration of staining salts, such as uranylacetate, into the organic coat. This hypothesis is supported by the ease of exchange labeling of anti-CEA SMP (see Experimental Procedures) that also necessitates the penetration of $^{59}Fe^{III}$ through the organic layer.

Using size-exclusion chromatography (Figure 2), a hydrodynamic radius between 30 and 50 nm was found. This result indicates that a major part of the particle consists of PEKY, antibody, and associated water. The coat may also include chromatographic carrier material (detergents, albumin) needed to prevent adsorption of the anti-CEA magnetite to the chromatographic column, and the size range given above may represent an overestimation. Laser-light scattering indicates a minimal mean size (number weighted) of 26 ± 19 nm. The two methods used

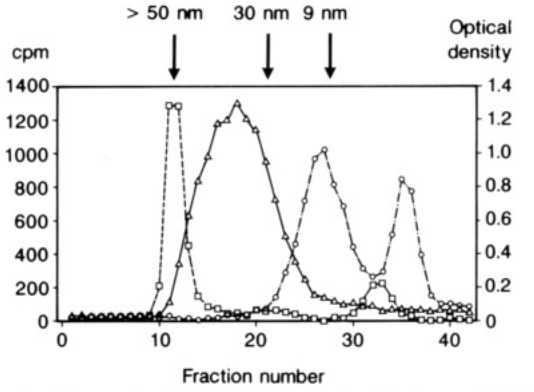


Figure 2. Size-exclusion chromatography (Sephacryl S-1000 sf) of anti-CEA ^{59}Fe–SMP. Markers were latex particles (□ and arrows, see Experimental Procedures), ^{125}I-labeled human thyroglobulin and [^{125}I]iodine (○). Anti-CEA ^{59}Fe–SMP (△) are eluted between 30 and 50 nm.

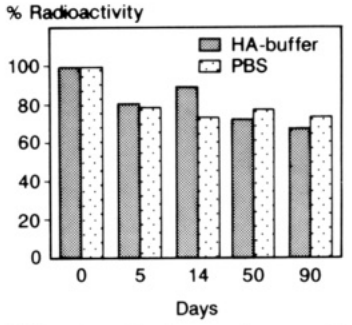


Figure 3. Stability of antibody attachment. Samples of ^{125}I–anti-CEA SMP were stored at 4 °C for the time indicated. After centrifugation of the particulate material, the radioactivity in the supernatant was determined and decay time corrected. HA buffer, 10 mM HEPES ammonium, pH 7.3 (buffer 2); PBS, 10 mM phosphate, pH 7.2, containing 0.15 M NaCl.

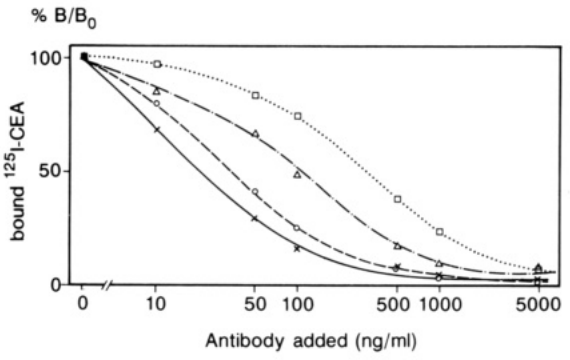
for the determination of the total hydrodynamic radius therefore give compatible results. From the specific radioactivity of the components ([^{59}Fe]-magnetite, ^{125}I-PEKY, ^{125}I–anti-CEA) the relative mass ratios of these materials in the final product may be estimated: magnetite/PEKY/antibody = 10:17:1. Assuming a density of 1 g/cm^3 for biological material and 5.5 g/cm^3 for magnetite, a single anti-CEA magnetite particle theoretically consist of a magnetite core of 9.6-nm diameter with a shell of 5.5 nm of organic material resulting in a particle approx. 20 nm in diameter, which is similar to the hydrodynamic radius found in gel-permeation chromatography and laser-light scattering.

Electrophoresis in agarose gels indicates a net negative charge of the anti-CEA SMP. Particles form a small spot (1 mm) at the end of their migration in agarose which is an indication of a high uniformity. The distance of migration was reduced from 12 to 3 mm, if antibody was coupled in various amounts.

From the transversal relaxation time (T_2) measurements a relaxivity (R_2) of 305 L mmol^{-1} s^{-1} was calculated.

The stability of the antibody immobilization was tested by storing ^{125}I–anti-CEA SMP in two buffer systems at 4 °C. The results are summarized in Figure 3. After an initial loss (5 days), only very little radioactivity is detached from the inorganic core within 90 days, indicating a stable linkage. No systematic difference was found for the two buffers, phosphate and HEPES. If the PEKY coat was not cross-linked with EGS, the washout was in the range of 80%, in particular in phosphate buffer (data not shown).

Biological Activity of Anti-CEA SMP. The capability of anti-CEA SMP to bind to the antigen was



	2000 ng Fe	500 ng Fe	100 ng Fe	20 ng Fe
B_0/T	21.4%	13.3%	5.5%	2.3%
50% IC	300 ng/ml	90 ng/ml	40 ng/ml	25 ng/ml

Figure 4. Binding of ^{125}I–CEA to anti-CEA SMP. Anti-CEA SMP were incubated overnight with ^{125}I–CEA–tracer and neat CEA in various proportions at room temperature in buffer 3 (total volume 210 μL). Particle-bound ^{125}I–CEA–tracer was separated from unbound radioactivity by centrifugation. The binding (B) is expressed as a fraction of maximal binding in the absence of free antibody (B_0). B_0 and 50% intercept (IC) are dependent on the amount of anti-CEA SMP present (B_0/T, fraction of ^{125}I–CEA bound in the absence of free antibody; 50% IC represents the amount of free antibody needed to reduce tracer binding to 50%).

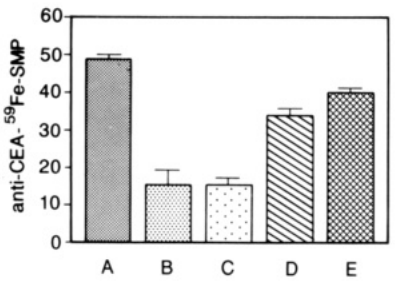


Figure 5. Binding of anti-CEA ^{59}Fe–SMP to surface-immobilized CEA. Biotinylated CEA was immobilized on avidin-coated module microtiter plates. Anti-CEA ^{59}Fe–SMP and various amounts of free CEA were added in buffer 4 (total volume 200 μL). After incubation and washing, the radioactivity was measured. Data are expressed as the fraction of bound to the total amount of anti-CEA ^{59}Fe–SMP; error bars represent one standard deviation (n = 8). (A) No free antibody added; (B) no CEA on the plate (= nonspecific binding); (C, D, E) Displacement of anti-CEA ^{59}Fe–SMP from immobilized CEA by the addition of free antibody (500, 10, and 5 ng/well, respectively).

demonstrated in two different assay formats: using ^{125}I–CEA as a tracer in a liquid-phase assay and using immobilized CEA in a solid-phase assay. The binding of ^{125}I–CEA tracer to anti-CEA SMP was studied using various proportions of the reactants, and in the presence of various amounts of unlabeled CEA. As expected, the resulting competition curves (Figure 4) indicate an antigen/antibody binding process: ^{125}I–CEA can be displaced from anti-CEA SMP in a manner that depends on the dose of both the anti-CEA SMP and unlabeled CEA. An estimation of the affinity indicates that immobilized antibody retained almost its full binding capacity.

As expected, the binding of labeled anti-CEA SMP to immobilized CEA is specific and displaceable (Figure 5); binding to plates without antigen is significantly lower, and free CEA competes in a dose-dependent manner with immobilized CEA. Nonspecific binding was relatively high (approximately 15% of the ^{59}Fe–anti-CEA SMP added) in spite of the addition of a carrier protein (HSA). Recently we found that nonspecific binding can be reduced below 5% if BSA in incubation buffer 4 is replaced by dry milk powder.

DISCUSSION

The development of a tumor-specific contrast agent for MRI represents a challenge, mainly due to the limited number of target sites and their relative inaccessibility. The ideal contrast agent consists of a moiety of maximal "magnetic activity" (relaxivity) bound to a biological vector of maximal targeting capabilities. More precisely, maximal targeting requires adequate circulation time of the nanoparticles and sufficient, specific binding capacity to achieve an accumulation in the target tissue required to generate an image contrast. The concepts underlying the development of the anti-CEA SMP presented in this paper may be summarized as follows: (1) The magnetite core must have a diameter of some nanometers and a very high relaxivity. (2) The hydrodynamic diameter of the final anti-CEA SMP should not exceed 50 nm. (3) A coat has to stabilize the inorganic magnetite core in an aqueous environment and allow covalent coupling of molecules. (4) The conjugation of antibody molecules to the coat must be done carefully and with high yield. (5) The final anti-CEA SMP should escape the RES in order to achieve a sufficiently long circulation time. The *in vitro* results reported above will now be discussed in light of these five requirements.

Size and Relaxivity. *Magnetite Core Size.* The procedure chosen for the preparation of magnetite nanoparticles takes advantage of the difference in sedimentation velocities as a function of size. Particles of larger sizes can easily be prepared by changing the centrifugation procedure (*25*). The particle size range used here corresponds to the size considered to be optimal for tumor targeting. The lower size limit is defined by the number of binding sites on the cell surface and the minimal magnetite concentration needed to achieve an image contrast. Assuming 5×10^4 antigenic sites per cell, of which 2% can be targeted, and a minimal magnetite concentration of 2 μg of Fe/mL for contrast generation, the required diameter of the magnetite particle is calculated to be 9 nm (Fe_3O_4 of 5.4 g/mL). In addition, relaxivity decreases if particles are smaller than approx. 10 nm (*26*). Thus, a core size of about 10 nm seems to be optimal.

Size of Anti-CEA SMP. The upper size limit is given by pore size of the capillary walls. Binding of a contrast agent to tumor cells must be preceded by its crossing of the capillary wall (extravascularization). The maximum particle diameter is therefore limited by the size of the capillary pores with a maximum diameter of approximately 50 nm (*14*, *27*). Such pores are particularly abundant in developing capillary beds, e.g. a growing tumor. The relevant size in these considerations is the hydrodynamic radius of a target-specific SMP, that includes any associated material such as the biological vector or bound water. In addition to higher extravascularization rates, a smaller size of the SMP also reduces the chance of entrapment by the RES (*28*), thereby increasing the circulation time. The size of anti-CEA SMP is within the range that a partial extravascularization through the pores of the capillaries can be expected (*14*, *27*).

Relaxivity. The transversal relaxivity (R_2) found for anti-CEA SMP is among the highest reported for superparamagnetic particles (*29*) and is much higher than for ultrasmall particles (*28*), even if taking into account that different media are used which may have a strong influence

on the R_2 value (*30*). This is true also at lower field strengths for which a direct comparison with commercially available material has been performed (data not shown). These results indicate a virtually pure magnetite preparation. The relaxivity of particles is in average 3 times higher if coated as well using HSA as PEKY (*30*). Therefore, no significant change of the reported relaxivity is expected by further surface modifications.

Stabilization and Chemical Functionalization. Various substances (proteins, polysaccharides, etc.) were tested for stabilization and functionalization of SMP. PEKY was finally chosen for three main reasons: net negative charge, simple chemical reactions via the amino groups in the lysine residues, and the lowest ratio of coat material to SMP (less "magnetic dead weight"). The procedure as described above presumably results in a stable network encapsulating the magnetite core, and provides a framework for simple conjugation of biological vectors. Recently we found that PEKY can be replaced by a analogue polypeptide (PEK) lacking the tyrosine (Y) residue. The absence of the hydrophobic Tyr residue may be advantageous to prevent opsonization (see below).

Conjugation of Antibody to SMP. The method chosen here takes advantage of the differential sensitivity of sulfhydryl groups in an IgG antibody molecule towards reduction. Under the conditions specified above, free sulfhydryls are generated in the hinge region (*19*). These groups, being distal to the binding domain, provide a location for coupling that does not interfere with the biologically active site. In addition, the reaction of the maleimido moiety with sulfhydryl groups allows unidirectional conjugation avoiding the formation of antibody or SMP dimers. The gain in antibody binding capacity using an oriented immobilization procedure is a factor of 2 compared to a random immobilization as expected from theoretical considerations (*31*).

Circulation Time. The major factor limiting the targeting efficiency is the circulation time. Particles are very efficiently trapped by the phagocytotic cells of RES. Strategies must therefore be devised to avoid the scavenging of anti-CEA SMP by the cells of the RES. In addition to keeping the size as small as possible, a negative charge may be helpful in increasing circulation time and, through mutual repulsion, aggregation of particles. The material described in this work has a net negative charge under physiological conditions. However, a negative charge may be an important factor, but is not sufficient as recent results suggest. When compared to other target-specific contrast agents, such as asialoglycoprotein–magnetite (*9*, *10*) or anti-myosin–magnetite (*11*), the expected circulation time of anti-CEA SMP is shorter, due to their larger diameter. However, the magnetite cores used in those preparation are probably too small to achieve a contrast-enhancing concentration of magnetite in a tumor. Strategies other than reduction of size must therefore be followed in order to increase circulation time. Such a possible strategy involves the conjugation of modifiers on the particles, hiding them from the action of the RES. Such modifiers may be polyethylene glycol (*32*), glycophorin (*33*), gangliosides (*34*), other sialic acid compounds or simple succinic acid (*35*). In addition, such hiding strategies may mitigate the problem of human-anti-mouse antibodies (HAMA), resulting from an immune reaction toward the target-specific contrast agent. HAMA, a clearly recognized hazard when applying non human antibodies to patients (*36*), may preclude the repeated administration of antibody–magnetite, unless sufficient precautions are taken. The PEKY-coated SMP as described above are an ideal platform for the simple introduction of biological modifiers. Work is under way to both test the currently available material in an *in vivo* model (nude mice, human CEA-producing tumor) and to improve the targeting efficiency by introducing biological modifiers.

ACKNOWLEDGMENT

The technical skills of Mr. J. J. Hefti, Mr. J. P. Dobler and Mr. A. Schuler have greatly contributed to this work. Laser size determinations were performed by Prof. H.-G. Weder and electron micrographs were done by Dr. E. Wehrli, both from ETH-Zürich. Their contributions are gratefully acknowledged.

LITERATURE CITED

(1) Mendonca, M. H., and Lauterbur, P. C. (1987) Contrast agents for nuclear magnetic resonance imaging. *Biol. Trace Elem. Res. 13*, 229–39.
(2) Renshaw, P. F., Owen, C. S., and McLaughlin, A. C. (1986) Ferromagnetic contrast agents: A new approach. *Magn. Reson. Med. 3*, 217–25.
(3) Widder, D. J., Greif, W. L., Widder, K. J., Edelman, R. R., and Brady, T. J. (1987) Magnetite albumin microspheres: A new MR contrast material. *Am. J. Roentgenol. 148*, 399–404.
(4) Saini, S., Stark, D. D., Hahn, P. F., Bousquet, J. C., Introcasso, J., Wittenberg, J., Brady, T. J., and Ferrucci, J. T. (1987) Ferrite particles: A superparamagnetic MR contrast agent for enhanced detection of liver carcinoma. *Radiology 162*, 217–222.
(5) Stark, D. D., Weissleder, R., Elizondo, G., Hahn, P. F., Saini, S., Todd, L. E., Wittenberg, J., and Ferrucci, J. T. (1988) Superparamagnetic iron oxide: Clinical application as a contrast agent for MR imaging of the liver. *Radiology 168*, 297–301.
(6) Weissleder, R., Elizondo, G., Wittenberg, J., Rabiato, C. A., Bengele, H. H., and Josephson, L. (1990) Ultrasmall superparamagnetic iron oxide: An intravenous contrast agent for assessing lymph nodes with MR imaging. *Radiology 175*, 494–498.
(7) Senéterre, E., Weissleder, R., Jaramillo, D., Reimer, P., Lee, A. S., Brady, T. J., and Wittenberg, J. (1991) Bone marrow: Ultrasmall superparamagnetic iron oxide for MR imaging. *Radiology 179*, 529–533.
(8) Weissleder, R., Stark, D. D., Rummeny, E. J., Compton, C. C., and Ferrucci, J. T. (1988) Splenic lymphoma: Ferrite-enhanced MR imaging in rats. *Radiology 166*, 423–430.
(9) Josephson, L., Groman, E. V., Menz, E., Lewis, J. M., and Bengele, H. H. (1990) A functionalized superparamagnetic iron oxide colloid as a receptor directed MR contrast agent. *Magn. Reson. Imag. 8*, 637–646.
(10) Reimer, P., Weissleder, R., Wittenberg, J., Brady, T. J. (1992) Receptor-directed contast agents for MR imaging: Preclinical evaluation with affinity assays. *Radiology 182*, 565–569.
(11) Weissleder, R., Lee, A. S., Khaw, B. A., Shen, T., and Brady, T. J. (1992) Antimyosin-labeled monocrystalline iron oxide allows detection of myocardial infarct: MR antibody imaging. *Radiology 182*, 381–385.
(12) Cerdan, S., Lötscher, H. R., Künnecke, B., and Seelig, J. (1989) Monoclonal antibody-coated magnetite particles as contrast agents in magnetic resonance imaging of tumors. *Magn. Reson. Med. 12*, 151–163.
(13) Allen, T. M., Austin, G. A., Chonn, A., Lin, L., and Lee, K. C. (1991) Uptake of liposoms by cultured mouse bone marrow macrophages: Influence of liposome composition and size. *Biochim. Biophys. Acta 1016*, 56–64.
(14) Schoefl, G. I. (1963) Studies on inflammation. III. Growing capillaries: Their structure and permeability. *Virchow's Arch. Path. Anat. 337*, 97–141.
(15) Lutz, H. U. (1990) Erytrocyte Clearance. *Blood Cell Biochemistry* (J. R. Harris., Ed.) Vol. 1, Erythroid cells, Chapter 4 pp 81–120, Plenum Press, New York.
(16) Buske, N., Sonntag, H., and Götze, T. (1984) Magnetic fluids—Their preparation, stabilisation and application in colloid science. *Colloids Surfaces 12*, 195–202.

(17) Abdella, P. M., Smith, P. K., and Royer, G. P. A new cleavable reagent for cross-linking and reversible immobilization of proteins (1979). *Biochem. Biophys. Res. Commun. 87*, 734–742.
(18) O'Sullivan, M. J., Gnemmi, E., Morris, D., Chieregatti, G., Simmonds, A. D., Bridges, J. M., and Marks, V. (1979) Comparison of two methods of preparing enzyme-antibody conjugates: Application of these conjugates for enzyme immunoassay. *Anal. Biochem. 100*, 100–108.
(19) Hermentin, P., Doenges, R., Franssen, U., Bieva, C., Vander Brugghen, F. J., Strycksmans, P., Friesen, H.-J., Otaczy, B., Schneider, S., Ax, W., Enssle, K. H., Kurrle, R., and Seiler, F. R. (1990) Hinge-thiol coupling of monoclonal antibody to silanized iron oxide particles and evaluation of magnetic cell depletion. *Bioconjugate Chem. 1*, 411–418.
(20) Haskell, C. M., Buchegger, F., Schreyer, M., Carrel, S., and Mach, J.-P. (1983) Monoclonal antibodies to carcinoembryonic antigen: Ionic strength as a factor in the selection of antibodies for immunoscintigraphy. *Cancer Res. 43*, 3857–3864.
(21) Andres, R. Y., Schubiger, P. A., Tiefenauer, L., Seybold, K., Locher, J. T., Mach, J.-P., and Buchegger, F. (1988) Immunoscintigraphic localization of inflammatory lesions: Concept, radiolabeling and in vitro testing of a granulocyte specific antibody. *Eur. J. Nucl. Med. 13*, 582–586.
(22) Elings, V. B., and Nicoli, D. F. (1984) A recent advance in submicron particle sizing by dynamic light scattering. *Am. Lab. 16*, 34–39.
(23) Bodmer, D. M., Tiefenauer, L. X., and Andres, R. Y. (1989) Antigen- versus antibody immobilized ELISA procedures using a biotin-estradiol conugate. *J. Steroid Biochem. 33*, 1161–1166.
(24) Tiefenauer, L. X., and Bodmer, D. M. (1988) Antibody coating using various avidin-biotin complexes employed to an enzyme immunoassay for estradiol. *Fresen. Z. Anal. Chem. 330*, 342.
(25) Andres, R. Y., and Kühne, G. (1990) Towards extravascular superparamagnetic contrast agents: Spin-spin relaxivity as a function of particle size. 9th Annual Meeting of the Society of Magnetic Resonance in Medicine, New York, Abstract No. 1192.
(26) Moiny, F., Gillis, P., Roch, A., and Muller, R. N. (1992) Transverse relaxation of superparamagnetic contrast agents: A numerical analysis. 11th Annual Meeting of the Society of Magnetic Resonance, in Medicine, Berlin, Abstract No. 1431.
(27) Renkin, E., and Curry, F. (1982) Endothelial permeability: Pathways and modulations. *Ann. N.Y. Acad. Sci. 401*, 248–59.
(28) Weissleder, R., Elizondo, G., Wittenberg, J., Rabiato, C. A., Bengele, H. H., and Josephson, L. (1990) Ultrasmall superparamagnetic iron oxide: Characterization of a new class of contrast agents for MR imaging. *Radiology 175*, 489–493.
(29) Pouliquen, D., Perroud, H., Calza, F., Jallet, P., and LeJeune, J. J. (1992) Investigation of the magnetic properties of iron oxide nanoparticles used as contrast agent for MRI. *Magn. Reson. Med. 24*, 75–84.
(30) Kühne, G., Tiefenauer, L., Schuler, A., and Andres, R. (1992) Superparamagnetic nanoparticles: Influence of coating and medium on the T_2 relaxivity. 11th Annual Meeting of the Society of Magnetic Resonance in Medicine, Berlin, Abstract No. 1415.
(31) Tiefenauer, L. X., and Hintermann, T. (1993) Oriented immobilization of antibody molecules to magnetite nanoparticles used as a target specific contrast agent in MRI. 22nd FEBS Meeting, Stockholm, Abstract C25-307.
(32) Abuchowski, A., McCoy, J. R., and Palczuk, N. C. (1977) Effect of covalent attachment of polyethylene glycol on immunogenicity and circulating life of bovine liver catalase. *J. Biol. Chem. 252*, 3582–3586.
(33) Gabizon, A., and Papahadjopoulos, D. (1988) Liposome formulations with prolonged circulation time in blood and enhanced uptake by tumors. *Proc. Natl. Acad. Sci. U.S.A. 85*, 6949–6953.
(34) Allen, T. M., Hansen, C., and Rutledge, J. (1989) Liposomes with prolonged circulation times: Factors affecting uptake by reticuloendothelial and other tissues. *Biochim. Biophys. Acta 981*, 27–35.
(35) Papisov, M. I., Schaffer, B., Weissleder, R., Bogdanov, A., Nossiff, N., Shen, T., and Brady, T. J. (1992) 11th Annual Meeting of the Society of Magnetic Resonance in Medicine, Berlin, Abstract No. 1403.
(36) Chatenoud, L. (1986) The immune response against therapeutic monoclonal antibodies. *Immunol. Today 7*, 367–368.

Application of Monoclonal Antibodies against Cytosine Deaminase for the in Vivo Clearance of a Cytosine Deaminase Immunoconjugate

David E. Kerr,* Ursula S. Garrigues, Philip M. Wallace, Karl Erik Hellström, Ingegerd Hellström, and Peter D. Senter

Bristol-Myers Squibb Pharmaceutical Research Institute, 3005 First Avenue, Seattle, Washington 98121. Received April 12, 1993

The selective delivery of anticancer drugs to tumors vs normal tissue using targeted antibody–enzyme conjugates for prodrug activation is limited by the amount of drug generated by blood-borne enzyme. Clearance of non-tumor-associated conjugate would increase the tumor/blood conjugate ratio, and enable larger amounts of prodrugs to be administered. A method for clearing the monoclonal antibody (mAb) conjugate L6–cytosine deaminase (L6–CD) was established by using an antibody raised against CD. The mAb 102–26 was obtained by immunizing BALB/C mice with CD conjugated to keyhole limpet hemocyanin. 102–26 was able to precipitate purified CD from solution as assessed by radioimmune precipitation and recognized CD in Western blot analyses. Similar studies were used to establish that 102–26 also recognized CD when conjugated to the L6 and 1F5 mAbs. Selective removal of L6–CD from the circulation of nude mice bearing H2981 human lung adenocarcinoma (L6-antigen positive) was achieved by injecting 102–26 24 h after L6–CD administration. High T/B ratios were obtained by clearance of a L6–CD (38:1 compared to 1.3:1 without clearance).

INTRODUCTION

Although 5-fluorouracil (5-FU)[1] is the drug most commonly used for treating colon cancer (*1*), it is rarely curative, and a great deal of research has been directed toward the improvement of 5-FU therapy. These methods include direct injections of 5-FU into the affected area (*2*), coadministration of the folate analog, leucovorin (*3*), and the immunostimulant, levamisole (*4*), inhibition of *de novo* pyrimidine synthesis with (phosphonoacetyl)-*l*-aspartate (*5*), implantation of CD-containing capsules for the generation of 5-FU at the tumor (*6*), and transfecting tumor cells with the gene for CD to render cells sensitive to 5-FC (*7*). These treatment modalities are aimed at increasing the local concentration of 5-FU, the effectiveness of the drug, or the protection of nontarget tissues from toxic side effects.

We have previously demonstrated that a chemical conjugate of the anticarcinoma mAb L6 and the enzyme CD yields a molecule capable of binding to L6-positive tumor cells and enzymatically converting 5-FC to 5-FU (*8*). This provides a method for delivering 5-FU to areas where the conjugate is present. A problem recognized early in in vivo studies was that blood-borne L6–CD can convert 5-FC to 5-FU in the circulation and contribute significantly to generalized toxicity. mAb–enzyme conjugates are frequently retained in the circulation for extended periods of time, which can lead to low T/B conjugate ratios (*9*). Though the use of mAb fragments (e.g. $F(ab')_2$, Fab', or sFv) conjugated to enzymes can improve T/B ratios (*10*, *11*), the absolute amounts of conjugate delivered to tumors with fragments is reduced compared to whole mAbs.

In order to optimize therapy with mAb–CD conjugates in vivo, it is necessary to achieve high conjugate levels at the tumor site while low enzyme levels are maintained in the blood. This could be accomplished using a clearance mechanism to selectively remove conjugate from the systemic system. This paper describes the isolation of a mAb against CD and the use of this anti-CD mAb for the clearance of L6–CD from the circulation of nude mice bearing human tumor xenografts. A dramatic increase in the T/B ratio of L6–CD is obtained via the administration of the anti-CD mAb.

EXPERIMENTAL PROCEDURES

CD was purchased from Calzyme Laboratories (San Luis Obispo, CA). The mAbs used are L6 (IgG_{2a}), selective for an antigen on human carcinomas (*12*); 1F5 (IgG_{2a}), which binds to CD-20 (*13*); and ME-20 (IgG_1), selective for a melanoma antigen (*14*); all the mAbs are murine. The cell line H2981 is a human lung adenocarcinoma to which L6 binds strongly (*12*). SMCC, 2-iminothiolane hydrochloride, and ε-biotinamidocaproate *N*-hydroxysuccinimide ester were purchased from Pierce (Rockford, IL).

Preparation of KLH-CD. To a solution of CD in 50 mM sodium borate, pH 8.0, was added 2-iminothiolane hydrochloride (final concentration = 2 mM). After 90 min at 4 °C, the protein was separated from the salts on a G-25 Sephadex column (Pharmacia, Piscataway, NJ). KLH in 25 mM potassium phosphate, pH 8.0 was modified with sulfo-SMCC (final concentration = 21 mM). After 1 h at room temperature the reaction was centrifuged and the supernatant applied to a G-25 Sephadex column to remove unreacted sulfo-SMCC. The modified proteins were combined (5 mg of CD plus 100 mg of KLH) and after 2 h at room temperature the reaction mixture was purified on G-75 Sephadex (using 0.1 M ammonium bicarbonate, pH 7.0, as eluant) to remove unreacted CD. KLH–CD was lyophilized and reconstituted with PBS for injections.

* Author to whom correspondence should be addressed. Telephone: 206-727-3523. Fax: 206-727-3603.

[1] Abbreviations used: 5-FC, 5-fluorocytosine; 5-FU 5-fluorouracil; CD, cytosine deaminase; DEAE, (diethylamino)ethyl; ELISA, enzyme-linked immunosorbent assay; HRP, horseradish peroxidase; ID, injected dose; KLH, keyhole limpet hemocyanin; mAb, monoclonal antibody; PBS, phosphate-buffered saline (10 mM sodium phosphate, 150 mM NaCl at pH 7.2); SDS–PAGE, sodium dodecyl sulfate–polyacrylamide gel electrophoresis; SMCC, succinimidyl 4-(2-maleimidylethyl)cyclohexane-1-carboxylate; T/B, tumor to blood.

1043-1802/93/2904-0353$04.00/0 © 1993 American Chemical Society

Conjugation of CD to mAbs. CD was conjugated to L6 and 1F5 as previously described for penicillin-G amidase (*15*). Briefly, CD was modified with SMCC to yield 1–2 maleimide groups per enzyme. The mAbs were treated with dithiothreitol to reduce approximately one disulfide per antibody. The two proteins were mixed, purged with nitrogen, and reacted at 4 °C overnight. *N*-Ethylmaleimide (0.1 mM) was then added and the conjugate was applied to an S-300 Sephacryl gel filtration column (Pharmacia, eluted with 20 mM Tris, 60 mM NaCl, pH 7.5) to remove aggregates and unconjugated CD. Ion-exchange chromatography on DEAE Sephadex (Pharmacia) was used to remove unconjugated mAb. The DEAE Sephadex column was washed with the above Tris buffer until the absorbance at 280 nm was close to zero. Conjugate was eluted with 20 mM Tris, 1 M NaCl, pH 7.5. SDS–PAGE indicated that the conjugate consisted of primarily 1:1 mAb:CD adducts.

mAbs to CD. BALB/C mice were immunized with 100 μg per injection of KLH–CD in Ribi adjuvant system prepared with an equal volume of Montanide ISA 50 oil (Seppic, Paris, France). The first injection of antigen/adjuvant mixture was given either intraperitoneally or subcutaneously, followed by two consecutive intraperitoneal injections of KLH–CD in oil at 3–4 week intervals. A final boost of KLH–CD in saline was performed 3 days before the mice were sacrificed. Spleen cells of immunized mice were hybridized with Px63-Ag8.653 (ATCC) mouse myeloma cells (*16*).

The initial selection of hybridomas was based on the reactivity of cell supernatants with purified CD using ELISA assays. Hybridoma cell lines 64–25 and 102–26, which produced mAb specific for CD, were obtained by this procedure, cloned, and expanded in vitro. Culture supernatants were purified by affinity chromatography on immobilized anti-κ light-chain column (*17*). An ELISA isotyping assay was utilized to determine the class of each mAb produced (Fisher Biotech, Pittsburgh, PA).

Radioimmune Precipitation of CD. CD was iodinated with iodogen and Na[^{125}I] as described (*18*) resulting in a specific activity of 2.2 μCi/mg of protein. Incubations were performed in precipitation buffer (20 mM phosphate, 0.5 M sodium chloride, 0.5% NP-40, pH 7.5) with ^{125}I-labeled CD (2.5 μg/mL) and 100 μg/mL of either 64–26, 102–26, or ME-20 (control). Immune complexes were precipitated with anti-κ-chain mAb immobilized on Sepharose 4B gel and washed four times with precipitation buffer. Samples were heated in nonreducing sample buffer (0.125 M Tris, 20% glycerol, 4% SDS, 0.02% bromophenol blue, pH 6.8) and separated on a 16% SDS–PAGE gel (Novex, Encinitas, CA). Bands were detected by autoradiography.

Biotinylation of mAbs. To 0.9 mL of 64–25, 102–26, or ME-20 (control) (all at 1 mg/mL) in PBS was added 0.1 mL of 0.5 M sodium borate, pH 8.5. To each was added ε-biotinamidocaproate *N*-hydroxysuccinimide ester (final concentration = 0.4 mM). After 1 h, unreacted biotin was removed by gel filtration on a G-25 column (PD-10, Pharmacia) with PBS/0.02% sodium azide as eluant.

Western Blot Analysis of 64–25 and 102–26. CD was separated on a 16% SDS–PAGE gel and transferred to nitrocellulose at 25 mA for 18 h in 12 mM Tris, 96 mM glycine, pH 8.3 with 20% methanol. The filter was placed in blocking buffer (2% powdered milk in PBS) for 1 h; incubated at 4 °C with 0.5 μg/mL biotinylated 102–26, 64–25, or ME-20 (control) for 18 h; and washed 4 × 10 min with PBS/0.1% Tween. The blot was then incubated for 1 h in avidin–HRP (Vector Laboratories, Burlingame, CA) (1:1000), washed as above, and developed with 4-chloro-1-naphthol.

ELISA Assay for Anti-CD mAbs. L6–CD (1 μg/mL in 50 mM carbonate buffer, pH 9.6) was plated in 96-well Immulon plates (Dynatech Labs, Chantilly, VA). After storage overnight at 4 °C, the plates were blocked with specimen diluent (Genetic Systems, Redmond, WA) for 1 h. Serial dilutions of biotinylated mAb were added to the plates, incubated for 1 h at room temperature, washed 5 times with PBS/0.1% Tween, and then incubated for 30 min with avidin–HRP. The plates were washed five times with PBS/Tween, and 3,3′,5,5′-tetramethylbenzidine in buffered substrate (Genetic Systems) was added. The reaction was stopped after 15 min by adding 3 N H_2SO_4. The absorbance was then measured at 450 nm on a Biotek Instruments EL 312 microplate reader (Winooski, VT).

1F5–CD (0.06–60 μg/mL) was incubated for 4 h with 0.6 μg/mL biotinylated 102–26. These mixtures were then added to plates coated with L6–CD as before. After 1 h, the wells were washed as before, incubated with the avidin–HRP reagent, and developed as before. This was repeated with L6–CD at concentrations of 0.06–60 μg/mL, biotinylated 102–26 at 0.6 μg/mL, and plates coated with 1F5–CD.

Activity of CD in the Presence of 102–26. CD (1.4 μg/mL, 42 nM) or L6–CD (6.7 μg/mL L6, 44 nM) were incubated for 30 min at room temperature with 350 nM, 1.18 μM, or 3.5 μM 102–26 in a total volume of 0.9 mL. 5-FC (0.1 mL at 30 mM in H_2O) was then added and the reaction was incubated at 37 °C. Aliquots (50 μL) were removed at various times and quenched in 0.1 N HCl (1 mL) and the concentrations of 5-FC to 5-FU were determined as previously described (*8*).

Clearance of L6–CD Using 102–26. Groups of nude mice bearing subcutaneous H2981 tumor xenografts (three mice per group) were injected intravenously with 100 μg of L6–CD. After 24 h, 102–26 (25, 50, or 100 μg) was injected, also intravenously. After an additional 24 h, blood was removed from the orbital plexus into a heparinized tube and centrifuged, and the plasma was frozen at −70 °C until used. To determine intratumoral enzyme concentrations, mice were sacrificed at 24 and 48 h and tumors were removed.

The presence of L6–CD in tumors and blood was quantified by measuring CD activity levels. To 1 mL of 5-FC in PBS (3 mM at 37 °C) was added 50 μL of plasma. At various times, 50-μL aliquots were removed, and the concentrations of 5-FC and 5-FU were determined as described before (*8*). Enzyme levels in tumors were measured by mincing and homogenizing the tumors in 0.45 mL PBS containing 1 μg/mL aprotinin, 30 μg/mL phenylmethyl sulfonyl fluoride, and 5 mM ethylenediaminetetraacetic acid. To this was added 50 μL of 30 mM [^{3}H]-5-FC (2 μCi/sample), and the reactions were incubated at 37 °C with periodic mixing. At various time intervals 50 μL of each mixture were removed and quenched in 0.5 mL of methanol. The samples were evaporated to dryness, and the residue suspended in 20 μL of methanol. After centrifugation, 5 μL of supernatant was applied to Baker-Flex IB-F TLC plates (J. T. Baker, Philipsburg, NJ), which were developed in 6:1 $CHCl_3$/MeOH (R_f 5-FC = 0.2, R_f 5-FU = 0.7). The sections containing 5-FC and 5-FU were cut out and placed into scintillation vials. The radioactivity was measured on a Beckman 3801 scintillation counter in Optifluor (Packard Instruments, Downers Grove, IL) and the amount of 5-FU generated per gram of tumor tissue was determined. All

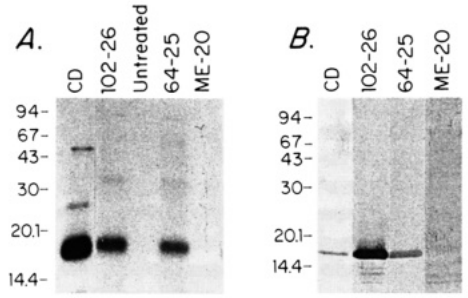


Figure 1. Radioimmunoprecipitation and Western analyses of 102–26 and 64–25. (A) ^{125}I-labeled CD was immunoprecipitated with 102–26 (lane 2), an antibody-free solution (lane 3), 64–26 (lane 4), or ME-20 (lane 5). The pellets were heated in sample buffer, centrifuged, and applied to a 16% SDS–PAGE gel. Lane 1 is ^{125}I-labeled CD (100 ng) alone. (B) CD was run on a 16% SDS–PAGE gel, transferred to nitrocellulose, and probed with biotinylated 102–26 (lane 2), 64–26 (lane 3), and ME-20 (lane 4). Avidin–HRP was added, and the bands were visualized with 4-chloro-1-naphthol. Lane 1 is a Coomassie Blue stain of purified CD.

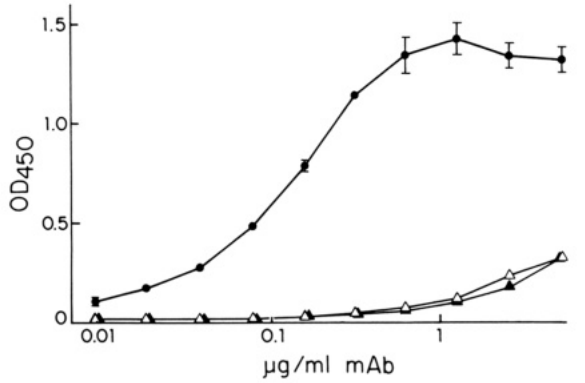


Figure 2. ELISA assays of the binding of 102–26 and 64–25 to CD: 102–26 (●), 64–25 (△), ME-20 (▲). CD was plated on immulon 96-well microtiter plates at 1 μg/mL. Biotinylated mAb's at varying concentrations were added, incubated 1 h, and washed, and avidin–HRP was added for 30 min and washed. Color was visualized with 3,3′,5,5′-tetramethylbenzidine.

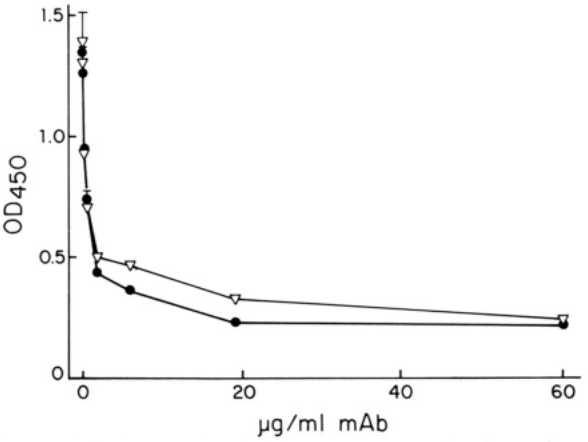


Figure 3. Blocking of the binding of 102–26 to L6–CD and IF5–CD. L6–CD was plated on Immulon 96-well microtiter plates at 1 μg/mL. 1F5–CD (▽) at varying concentrations was mixed with biotinylated 102–26 at 0.6 μg/mL. These mixtures were added 4 h later to the microtiter wells. After 1 h, the plate was washed with PBS/Tween, and incubated with avidin–HRP for 30 min and washed. Color was visualized with the 3,3′,5,5′-tetramethylbenzidine. L6–CD (●) was incubated with biotinylated 102–26 for 4 h and added to a 96-well plate coated with IF5–CD at 1 μg/mL. The plate was washed and treated with avidin–HRP and 3,3′,5,5′-tetramethylbenzidine.

reactions were linear for the time required to consume 1 μmol of 5-FC.

RESULTS

mAb–CD Conjugates. The enzyme CD was conjugated to the mAbs L6 and 1F5 as previously described for the preparation of L6–penicillin-G amidase conjugates (*15*). This involved partial reduction of the mAb disulfides with dithiotheitol and reaction with maleimidyl-substituted CD to yield thioether-linked conjugates. After purification, the conjugates were devoid of unconjugated mAb or CD, and consisted primarily of 1:1 mAb:CD adducts. The conjugates retained enzymatic and binding activities according to assays as previously described (*8*).

mAbs to CD. In preliminary experiments, it was determined that unconjugated CD was not an adequate immunogen to generate specific antibodies. As a result, CD was attached to KLH to render it more immunogenic. Conjugation of CD to KLH yielded a high molecular weight molecule free of unbound CD which could hydrolyze 5-FC to 5-FU. This was used with adjuvant to immunize BALB/C mice using the treatment schedule outlined in the Experimental Procedures section. Hybridization of spleen cells from treated mice with mouse myeloma cells and subsequent selection and cloning yielded two positive hybridomas secreting mAbs which recognized CD. These were designated 64–25 (IgG_1) and 102–26 (IgG_{2b}). The mAbs were purified using an affinity column with immobilized anti-κ-chain mAb (*17*).

The anti-CD mAbs were tested for their specificities and abilities to precipitate the enzyme in radioimmune precipitation studies. Figure 1A shows that both 64–25 and 102–26 were able to precipitate CD from solution, whereas ME-20 was not. This shows that both mAbs recognize CD in solution. Western blot analysis of the binding of these mAbs to purified CD (Figure 1B) shows that both 64–25 and 102–26 bind to CD, but do not recognize the minor impurities present in the CD preparation (Figure 1A, lane 1). This provides evidence that these antibodies are specific for CD.

The ability of 102–26 and 64–25 to bind to CD was also measured in an ELISA assay. CD (1 μg/mL) was plated in 96-well plates and biotinylated 102–26, 64–25, or ME-20 (control) was titrated into the wells. As can be seen in Figure 2, 102–26 was specific for CD, whereas 64–25 was no better than ME-20 at binding to CD. The reduced binding of 64–25 is consistent with the data shown in Figure 1, indicating that 64–25 immunoprecipitated less CD from solution than 102–26 (Figure 1A, lane 4 vs lane 2) and displayed weaker binding in a Western blot (Figure 1B, lane 3 vs lane 2). Subsequent experiments were, therefore, performed using 102–26. The ability of 102–26 to recognize CD bound covalently to mAbs was tested by incubating L6–CD (0.06–60 μg/mL) for 4 h with biotinylated 102–26 (0.6 μg/mL) and the binding of 102–26 to 1F5–CD in an ELISA format was measured. This was repeated with 1F5–CD (0.06–60 μg/mL) incubated with biotinylated 102–26 at 0.6 μg/mL, and the binding of 102–26 to L6–CD was assessed. Figure 3 shows that 102–26 did bind to both L6–CD and 1F5–CD and that the binding could be blocked by the opposite immunoconjugate.

Effect of 102–26 on CD Activity. The effects of 102–26 on the enzymatic activity of free CD or L6–CD was determined. CD and L6–CD were each incubated with an 8-, 24-, and 75-fold molar excess of 102–26. The ability of CD to facilitate the conversion of 5-FC to 5-FU was then measured. There was virtually no decrease in activity of CD in the presence of 8 times as much mAb, while the

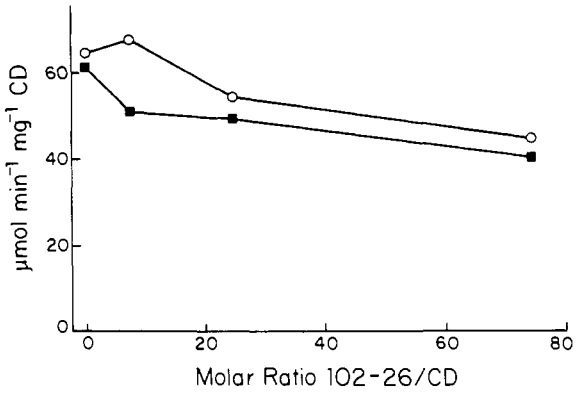


Figure 4. Effect of 102–26 on CD activity. CD (○) or L6–CD (■) at 42 and 44 nM, respectively, were incubated for 30 min with 102–26 at 8-, 24-, and 75-fold molar excess. CD activity was then assessed as outlined in Experimental Procedures. Points are the average of duplicate determinations which differ by less than 5%.

Table I. Clearance of L6–CD by 102–26[a]

time postinjection of L6–CD (h)	102–26 (μg)	% ID/g of tumor	% ID/mL of blood	tumor/ blood ratio
24	0	4.3 ± 0.8	5.4 ± 0.2	0.8
48	0	3.9 ± 1.1	2.9 ± 0.6	1.3
48	25	3.9 ± 2.8	1.5 ± 0.3	2.6
48	50	2.7 ± 0.5	0.3 ± 0.1	9.0
48	100	1.9 ± 1.0	<0.05[b]	>38

[a] Mice (three per group) were injected with 100 μg per mouse of L6–CD. 24 h later, 102–26 was administered. At 48 h, blood and tumors were taken and CD activity was measured. [b] Below the limit of detection.

activity of L6–CD was reduced 20%. At a 75-fold excess of 102–26, the reduction of either CD or L6–CD was 30% (Figure 4).

Clearance of L6–CD by 102–26. The ability of 102–26 to reduce the levels of blood-borne CD activity in mice treated with L6–CD was tested in nude mice bearing subcutaneous H2981 tumors. The levels of L6–CD in the tumors and blood of mice that received 100 μg of L6–CD did not undergo dramatic change between 24 and 48 h (Table I). At 24 h the T/B ratio was 0.8, while after 48 h this ratio had only increased to 1.3. To test the ability of 102–26 to increase T/B ratios, mice were injected with L6–CD, followed 24 h later by varying amounts of 102–26. The T/B ratios of L6–CD were determined 24 h after the administration of 102–26. As shown in Table I, 102–26 was able to increase the T/B ratio of L6–CD in a dose-dependent manner. Administration of 25 μg of 102–26 increased the T/B ratio to 2.6, which was twice as high as in untreated mice. By increasing the dose of 102–26 to 100 μg, the T/B ratio was raised to >38. At this dose, the level of CD activity in the blood was below the limit of detection. The increase in the T/B ratio after 102–26 administration was not accompanied by corresponding decreases in the levels of tumor-associated conjugate. Treatment of mice with 100 μg of 102–26 resulted in a 2.1-fold decrease in enzymatically active L6–CD (from 3.9 to 1.9% ID/g), whereas blood levels were reduced greater than 58-fold. The individual mice that received 100 μg of 102–26 retained 3.0, 1.2, and 1.4% ID/g intratumoral CD activity. The reduced amount of CD activity measured in the tumors may actually reflect the clearance of L6–CD from the tumor vascular bed and not removal of antigen-bound conjugate. Thus, we have shown that 102–26 dramatically reduces the levels of CD activity in the blood without severely affecting tumor levels.

DISCUSSION

mAbs are currently the subject of a great deal of research for the delivery of drugs, toxins, and radionuclides to tumor cell populations (*19, 20*). While some promising preclinical data have been obtained (*21–23*), there is a number of limitations to this form of cancer therapy, particularly for the treatment of solid tumors. These include the limited amount of drug that can be attached to the mAb, the heterogeneity of antigen expression in tumors (*24, 25*), and the fact that macromolecules cannot easily penetrate into solid tumors (*24, 26*).

We have worked on an approach that is designed to address these limitations (*27*). Briefly, a mAb–enzyme conjugate is administered and allowed to bind to tumor cells and clear from the circulation, at which time a relatively nontoxic prodrug is given systemically. The targeted enzyme is selected for its ability to convert the prodrug into a potent anticancer drug. This approach amplifies the number of drugs delivered to the tumor because of the catalytic conversion of prodrug to drug. Drugs that are released on the outside of antigen-expressing cells should be able to enter into antigen-negative cells and penetrate to interior portions of the tumor, otherwise inaccessible to the conjugate. Many example of this approach have been described recently (*27–29*). It is apparent that optimal therapy using mAb–enzyme for prodrug activation will require high T/B ratios of conjugate. In this study we have addressed this issue by isolating a mAb that can bind to the enzyme component of a mAb–enzyme conjugate and showing that the antienzyme mAb accelerates the clearance of the conjugate in the systemic circulation. The mAb 102–26 recognizes both free and conjugate-bound CD. Upon binding to CD, 102–26 leads to minimal loss in enzyme activity (Figure 4). The use of such a clearance mechanism was necessitated by the observation that L6–CD is not rapidly cleared, and has a very modest T/B ratio (Table I). 102–26 was able to dramatically increase the T/B ratio of L6–CD from 1.3 to >38. This was achieved mainly by reducing the blood level of conjugates by a factor of at least 58. The finding that the tumor level was reduced 2.1-fold may be due to both loss of the conjugate from the tumor vascular bed, and to some loss of antigen-bound conjugate. The amount remaining in the tumor (1.9% ID/g) is comparable to that obtained with other targeting strategies (*30*), and may be sufficiently high to generate cytotoxic quantities of 5-FU intratumorally.

The approach described here is related to a recently published report by Sharma and co-workers, who have shown that the anti-carboxypeptidase G2 (CPG-2) mAb SB43 can accelerate the clearance of a mAb–CPG-2 conjugate (*9*). However, SB43 inactivated CPG-2 such that there was approximately 95% inactivation with a 6-fold excess of SB43. As a result, it was necessary to modify SB43 with galactose to accelerate its clearance, in order to avoid the inactivation of tumor-associated CPG-2. With the mAb against CD described here, this was not necessary.

The use of an antienzyme mAb for conjugate clearance complements other recently described clearance mechanisms which include modification of conjugates with sugars (*30*), use of anti-idiotypes (*28, 31, 32*), plasmapheresis (*33*), and clearance of biotinylated mAbs with avidin (*28, 34*). The advantages of the approach described here is that potentially any enzyme conjugate can be cleared; and free enzyme that may either contaminate the conjugate preparation or results from conjugate fragmentation can be cleared as well. By lowering the level of non-tumor-

associated conjugate it should be possible to increase the amount of prodrug that can be administered. Such studies are now underway.

ACKNOWLEDGMENT

We would like to thank George Schreiber for valuable discussions and Ana Wieman for preparation of the manuscript.

LITERATURE CITED

(1) Kemeny, N., Lokich, J. J., Anderson, N., and Ahlgren, J. D. (1993) Recent advances in the treatment of advanced colorectal cancer. *Cancer 71*, 9–18.
(2) Speyer, J. L., Collins, J. M., Dedrick, R. L., Brennan, M. F., Buckpitt, A. R., Londer, H., DeVita Jr., V. T., and Myers, C. E. (1980) Phase I and pharmacological studies of 5-fluorouracil administered intraperitoneally. *Cancer Res. 40*, 567–572.
(3) Leichman, C. G., Leichman, L., Spears, C. P., Rosen, P. J., Jeffers, S., and Groshen, S. (1993) Prolonged continuous infusion of fluorouracil with weekly bolus of leucovorin: a phase II study in patients with disseminated colorectal cancer. *J. Natl. Cancer Inst. 85*, 41–44.
(4) Grem, J. L. (1990) Levamisole as a therapeutic agent for colorectal carcinoma. *Cancer Cells 2*, 131–137.
(5) Morrell, L. M., Bach, A., Richman, S. P., Goodman, P., Fleming, T. R., and MacDonald, J. S. (1991) A phase II multi-institutional trial of low-dose N-(phosphonoacetyl)-*l*-aspartate and high-dose 5-fluorouracil as a short-term infusion in the treatment of adenocarcinoma of the pancreas. *Cancer 67*, 363–366.
(6) Nishiyama, T., Kawamura, Y., Kawamoto, K., Matsumura, H., Yamamoto, N., Ito, T., Ohyama, A., Katsuragi, T., and Sakai, T. (1985) Antineoplastic effects in rats of 5-fluorocytosine in combination with cytosine deaminase capsules. *Cancer Res. 45*, 1753–1761.
(7) Mullen, C. A., Kilstrup, M., and Blaese, R. M. (1992) Transfer of the bacterial gene for cytosine deaminase to mammalian cells confers lethal sensitivity to 5-fluorocytosine: A negative selection system. *Proc. Natl. Acad. Sci. U.S.A. 89*, 33–37.
(8) Senter, P. D., Su, P. C., Katsuragi, T., Sakai, T., Cosand, W. L., Hellström, I., and Hellström, K. E. (1991) Generation of 5-fluorouracil from 5-fluorocytosine by monoclonal antibody-cytosine deaminase conjugates. *Bioconjugate Chem. 2*, 447–451.
(9) Sharma, S. K., Bagshawe, K. D., Burke, P. J., Boden, R. W., and Rogers, G. T. (1990) Inactivation and clearance of an anti-CEA carboxypeptidase G2 conjugate in blood after localisation in a xenograft model. *Br. J. Cancer 61*, 659–662.
(10) Yokota, T., Milenic, D. E., Whitlow, M., and Schlom, J. (1992) Rapid tumor penetration of a single-chain Fv and comparison with other immunoglobulin forms. *Cancer Res. 52*, 3402–3408.
(11) King, D. J., Mountain, A., Adair, J. R., Owens, R. J., Harvey, A., Weir, N., Proudfoot, K. A., Phipps, A., Lawson, A., Rhind, S. K., Pedley, B., Boden, J., Boden, R., Begent, R. H. J., and Yarronton, G. T. (1992) Tumor localization of engineered antibody fragments. *Antibody, Immunoconjugates, Radiopharm. 5*, 159–170.
(12) Hellström, I., Horn, D., Linsley, P., Brown, J. P., Brankovan, V., and Hellström, K. E. (1986) Monoclonal mouse antibodies raised against human lung carcinoma. *Cancer Res. 46*, 3917–3923.
(13) Clark, E. A., Shu, G., and Ledbetter, J. A. (1985) Role of the Bp35 cell surface polypeptide in human B-cell activation. *Proc. Natl. Acad. Sci. U.S.A. 82*, 1766–1770.
(14) Hellström, I., Marquardt, H., Maresh, G., Wan, H., Anderson, J., and Hellström, K. E. An internalizing murine monoclonal antibody (ME20) binds to an antigen with high specificity for human melanoma. In preparation.
(15) Bignami, G. S., Senter, P. D., Grothaus, P. G., Fischer, K. J., Humphreys, T., and Wallace, P. M. (1992) N-(4′-hydroxyphenyacetyl)palytoxin: A palytoxin prodrug that can be activated by a monoclonal antibody-penicillin-G amidase conjugate. *Cancer Res. 52*, 5749–5764.
(16) Köhler, G. and Milstein, C. (1975) Continuous cultures of fused cells secreting antibody of predefined specificity. *Nature 256*, 495–497.
(17) Yelton, D. E., Desaymard, C., and Scharff, M. D. (1981) The use of monoclonal anti-mouse immunoglobulin to detect mouse antibodies. *Hybridoma 1*, 5–11.
(18) Markwell, M. A. K. and Fox, C. F. (1978) Surface-specific iodination of membrane proteins of viruses and eucaryotic cells using 1,3,4,6-tetrachloro-3α,6α-diphenylgycouril. *Biochemistry 17*, 4807–4817.
(19) Pimm, M. V. (1988) Drug-monoclonal antibody conjugates for cancer therapy: potentials and limitations. *Crit. Rev. Ther. Drug Carrier Syst. 5*, 189–227.
(20) Pietersz, G. A. and McKenzie, I. F. C. (1992) Antibody conjugates for the treatment of cancer. *Immunol. Rev. 129*, 57–81.
(21) Johnson, D. A., Baker, A. L., Laguzza, B. C., Fix, D. V., and Gutowski, M. C. (1990) Antitumor activity of L/1C2-4-desacetylvinblastine-3-carboxyhydrazide immunoconjugate in xenografts. *Cancer Res. 50*, 1790–1794.
(22) Beaumier, P. L., Venkatesan, P., Vanderheyden, J.-L., Burgua, W. D., Kunz, L. L., Fritzberg, A. R., Abrams, P. G., and Morgan, A. C., Jr. (1991) ^{186}Re radioimmunotherapy of small cell lung carcinoma xenografts in nude mice. *Cancer Res. 51*, 676–681.
(23) Friedman, P. N., Mcandrew, S. J., Gawlak, S. L., Chace, D., Trail, P. A., Brown, J. P., and Siegall, C. B. (1993) BR96 sFv-PE40, A potent single-chain immunotoxin that selectively kills carcinoma cells. *Cancer Res. 53*, 334–339.
(24) Weinstein, J. N. and van Osdol, W. (1992) Early intervention in cancer using monoclonal antibodies and other biological ligands: Micropharmacology and the "binding site barrier". *Cancer Res. 52*, 2747s–2751s.
(25) Cobb, P. W., and LeMaistre, C. F. (1992) Therapeutic use of immunotoxins. *Semin. Oncol. 29*, 6–13.
(26) Jain, R. K. (1991) Haemodynamic and transport barriers to the treatment of solid tumours. *Int. J. Radiat. Biol. 60*, 85–100.
(27) Senter, P. D., Wallace, P. M., Svensson, H. P., Vrudhula, V. M., Kerr, D. E., Hellström, I., and Hellström, K. E. (1993) Generation of cytotoxic agents by targeted enzymes. *Bioconjugate Chem. 4*, 3–9.
(28) Bamias, A. and Epenetos, A. A. (1992) 2-Step strategies for the diagnosis and treatment of cancer with bioconjugates. *Antibody Immunoconjugates, Radiopharm. 5*, 385–395.
(29) Bagshawe, K. D. (1990) Antibody-directed enzyme/prodrug therapy (ADEPT). *Biochem. Soc. Trans. 18*, 750–752.
(30) Mattes, M. J., Sharkey, R. M., Goldenberg, D. M., and Ong, G. L. (1991) Manipulation of Blood Clearance of Antibodies by Galactose Conjugation. *Antibody, Immunoconjugates, Radiopharm. 4*, 877–884.
(31) Sharkey, R. M., Boerman, O. C., Natale, A., Pawlyk, D., Monestier, M., Losman, M. J., and Goldenberg, D. M. (1992) Enhanced clearance of radiolabeled murine monoclonal antibody by a syngeneic anti-idiotype antibody in tumor-bearing nude mice. *Int. J. Cancer 51*, 266–273.
(32) Pedley, R. B., Dale, R., Boden, J. A., Begent, R. H., Keep, P. A., and Green, A. J. (1989) The effect of second antibody clearance on the distribution and dosimetry of radiolabeled anti-CEA antibody in a human colonic tumor xenograft model. *Int. J. Cancer 43*, 713–718.
(33) Henry, C. A., Clavo, A. C., and Wahl, R. L. (1991) Improved monoclonal antibody tumor/background ratios with exchange transfusions. *Int. J. Radiat. Appl. Instrum. [B] 18*, 565–567.
(34) Paganelli, G., Malcovati, M., and Fazio, F. (1991) Monoclonal antibody pretargeting techniques for tumour localization: The avidin-biotin system. *Nucl. Med. Commun. 12*, 211–234.

Trypsin Modification by Vinyl Polymers with Variable Solubilities in Response to External Signals

Yoshihiro Ito,* Masaaki Kotoura, Dong-June Chung, and Yukio Imanishi

Department of Polymer Chemistry, Faculty of Engineering, Kyoto University, Yoshida Honmachi, Sakyo-ku, Kyoto, Japan 606-01. Received April 12, 1993®

Trypsin was modified with various vinyl polymers by the graft polymerization of vinyl monomers using a trypsin derivative containing aliphatic azo groups as the initiator. The graft polymers were chosen to be sensitive to external signals, e.g., a redox-sensitive poly[3-carbamoyl-1-(*p*-vinylbenzyl)pyridinium chloride] and a pH-sensitive poly(methacrylic acid–*co*-methyl methacrylate). The trypsin modified with the redox-sensitive polymer became insoluble in water in the presence of $Na_2S_2O_4$, and redissolved when H_2O_2 was added. However, the enzymatic activity of the homogeneous solution was not proportional to the concentration of the modified trypsin remaining in the solution. The trypsin modified with the pH-sensitive polymer was insoluble and soluble in acidic and neutral solutions, respectively. The enzymatic activity of the homogeneous solution changed reversibly with pH in proportion to the concentration of the modified trypsin remaining in the solution.

INTRODUCTION

Immobilization is useful in the stabilization and repeated use of enzymes. On the other hand, soluble state is necessary when the enzymes are used to digest insoluble substrates such as cellulose, and when the diffusion-determining reaction speed in the homogeneous state is higher than that in the heterogeneous state. Therefore, an enzyme modification that enables an efficient catalysis in solution during the reaction and easy recovery by subsequent insolubilization has been desired. Toward this goal, several attempts have been made including modifying enzymes with polyelectrolytes carrying carboxylic acid groups to control the solubility according to pH or the ionic strength of the solution (*1–3*) and magnetic recovery of an enzyme hybrid (*4*).

In this study, we considered a redox reaction as well as the variation of pH or ionic strength as external signals. Poly[3-carbamoyl-1-(*p*-vinylbenzyl)pyridinium chloride] (PCVPC)[1] (*5*) and poly(methacrylic acid–*co*-methyl methacrylate) [P(MA-MMA)] (*1–3*) were chosen a redox-responsive and pH-responsive polymers, respectively. We reported a novel method for grafting a wide range of vinyl polymers to enzymes (*6–8*). According to this, aliphatic azo groups were connected to trypsin. The azo-containing trypsin was used as an initiator for graft polymerization of monomers for signal-responsive graft chains. The solubility change of the modified enzyme and the consequent catalytic activity of the homogeneous solution in response to external signals was investigated.

EXPERIMENTAL PROCEDURES

Reagents. Trypsin was of bovine pancreas origin (type 1, T-8003, Mw 23 000) and purchased from Sigma Chemical Co. (St. Louis, MO). 4,4′-Azobis(4-cyanovaleric acid) was purchased from Aldrich Chemical Co. (Milwaukee, WI). 4-Morpholineethanesulfonic acid was purchased from Dojin Chemical Institute (Kumamoto, Japan). 2,4,6-Trinitrobenzenesulfonic acid and 1-ethyl-3-[3-(dimethylamino)propyl]carbodiimide hydrochloride, which is water-soluble, were purchased from Wako Pure Chemical Ind. Co. (Osaka, Japan). *p*-(Chloromethyl)styrene was a product of Tokyo Kasei Co. (Tokyo, Japan). Nicotinamide, methacrylic acid, and methyl methacrylate were purchased from Nacalai Tesque Inc. (Kyoto, Japan). Nicotinamide was recrystallized from acetone. Monomers were used after purification as described below. Sodium hydrosulfite and N^{α}-benzoyl-DL-arginine *p*-nitroanilide hydrochloride were purchased from Nacalai Tesque Inc. and used without further purification.

Synthesis and Purification of Monomers. 3-Carbamoyl-1-(*p*-vinylbenzyl)pyridinium chloride was synthesized as reported previously (*9*). *p*-(Chloromethyl)-styrene (11.9 g, 78.2 mmol) and nicotinamide (15 g, 123 mmol) were mixed in *N*,*N*-dimethylformamide (250 mL) and the solution was stirred for 24 h at 4 °C. A white precipitate was recovered by centrifugation and crystallization from ethanol. Anal. Calcd of 3-carbamoyl-1-(*p*-vinylbenzyl)pyridinium chloride ($C_{15}H_{15}N_2OCl$): calculated to be C, 65.58; H, 5.50; N, 10.20, Cl, 12.90. Found: C, 65.65; H, 5.49; N, 10.23; Cl, 12.97. Mp 228–229 °C [lit. (*9*) mp 228 °C].

Methacrylic acid was purified by distillation under reduced pressure (63 °C, 12 mmHg). Methyl methacrylate was washed with 5% NaOH and double-distilled water, dehydrated with anhydrous sodium sulfate overnight, and then distilled under reduced pressure (50 °C, 160 mmHg).

Trypsin Modification with Vinyl Polymers. The synthetic scheme of trypsin modification with vinyl polymers is shown in Figure 1. First, aliphatic azo groups were connected to trypsin by the following method. 4,4′-Azobis(4-cyanovaleric acid) (73 mg) and water-soluble carbodiimide (50 mg) were added to an aqueous solution (20 mL) buffered to a specific pH value with 0.05 M 4-morpholineethanesulfonate buffer (pH 5.5), 0.05 M phosphate buffer (pH 6.7), 0.05 M phosphate buffer (pH 7.2), or 0.05 M borate buffer (pH 8.7). The solution was incubated for 2 h at 4 °C, and trypsin (10 mg) was added. The mixture was further incubated for 24 h at 4 °C. Unreacted chemicals were removed by dialysis for 2 days,

® Abstract published in *Advance ACS Abstracts*, August 15, 1993.

[1] Abbreviations used: PCVPC, poly[3-carbamoyl-1-(*p*-vinylbenzyl)pyridinium chloride]; [P(MA-MMA)], poly(methacrylic acid–*co*-methyl methacrylate).

1043-1802/93/2904-0358$04.00/0 © 1993 American Chemical Society

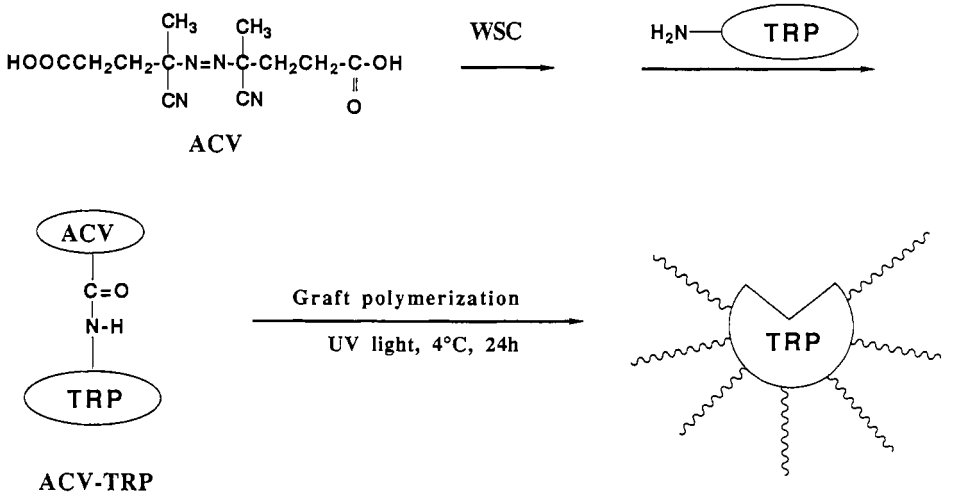


Figure 1. Synthetic scheme of azo-modified trypsin and vinyl polymer-modified trypsin. WSC, water-soluble carbodiimide; TRP, trypsin.

and the trypsin attached to 4,4′-azobis(4-cyanovaleric acid) was freeze-dried.

The graft polymerization of vinyl monomers to trypsin was carried out as follows. Azo-containing trypsin (5 mg) was added to aqueous 3-carbamoyl-1-(*p*-vinylbenzyl)-pyridinium chloride (20 wt %, 2.5 mL) or a mixture of methacrylic acid (3.18 mL) and methyl methacrylate (1.34 mL) (3/1 mol/mol), and the mixtures were irradiated with a 120-W mercury lamp for 24 h under a nitrogen atmosphere.

The polymerization solution was poured into acetone to precipitate the graft-polymerized 3-carbamoyl-1-(*p*-vinylbenzyl)pyridinium chloride. The precipitate was redissolved in 0.05 M phosphate-buffered saline (pH 7.0), and the grafted trypsin was purified by fractionation through a column packed with Sephadex G-200.

Graft copolymerization of methacrylic acid and methyl methacrylate was achieved by pouring the polymerization solution into methanol containing hydrochloric acid to precipitate the product. The precipitate was redissolved in a 0.05 M phosphate buffer (pH 7.0), and the solution was fractionated through a column packed with Sephadex G-200 to separate trypsin grafted with poly(methacrylic acid–*co*-methyl methacrylate) [P(MA-MMA)].

The molecular weight of polymer-modified trypsin was calculated from the retention volume in a Sephadex G-200 column fractionation by using a calibration curve, which was obtained by using proteins of known molecular weight, namely, ribonuclease A, chymotrypsinogen A, ovalbumin, and albumin.

Determination of the Azo Content in Trypsin Containing Azo Groups. The level was determined as follows (*10*). Three solutions were prepared: (A) an aqueous trypsin (0.5 mg/mL), (B) aqueous $NaHCO_3$ (4%, pH 8.5), (C) aqueous 2,4,6-trinitrobenzenesulfonic acid (0.1%). Portions of each solution (1 mL of each) were mixed and incubated in the dark for 2 h at 37 °C. The mixtures were 10-fold diluted with solution B, and the absorption intensity at 350 nm due to amine-substituted 2,4,6-trinitrobenzenesulfonic acid was measured. The amount of unreacted amino groups in the azo-containing trypsin is proportional to 350-nm absorption; thus, the content of the azo group in the azo-modified trypsin was determined.

Measurement of Enzymatic Activity. N^{α}-benzoyl-DL-arginine *p*-nitroanilide hydrochloride was used as the substrate for trypsin. A 1.2 mM substrate solution in a 0.05 M phosphate buffer (pH 7.0) was prepared. The enzyme activity was estimated by measuring the intensity of absorption at 410 nm due to *p*-nitroaniline, which is a hydrolysis product of the substrate at 35 °C. The enzyme activity was represented as the amount of *p*-nitroaniline produced per unit time per unit weight of trypsin at pH 7.0 (*11*).

The solubility of the polymer-modified trypsin was determined by measuring the dry weight of the precipitate produced on adding a reducing reagent or on lowering the pH of the solution.

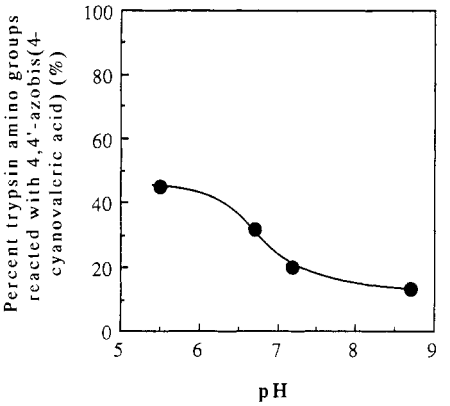


Figure 2. Content of azo groups coupled with trypsin at various pH values.

RESULTS AND DISCUSSION

Synthesis of Azo-Containing Trypsin. It is shown in Figure 2 that the number of azo groups in the azo-modified trypsin is higher under more acidic conditions. This should have been caused by the faster activation of carboxy groups in the 4,4′-azobis(4-cyanovaleric acid) with water-soluble carbodiimide under more acidic solutions. A similar observation has been reported elsewhere (*12*). In this investigation, azo-containing trypsin at pH 5.5 was used to initiate graft polymerization. About 6–7 azo groups were connected to amino groups in trypsin, which possesses 15 amino groups.

Graft Polymerization of 3-Carbamoyl-1-(*p*-vinylbenzyl)pyridinium Chloride. The elution patterns of the native and grafted trypsins through a Sephadex G-200 column are shown in Figure 3. The crude product of graft polymerization, which was obtained by pouring the reaction solution into acetone, should contain a homopolymer PCVPC (curve b), and therefore the enzymatic

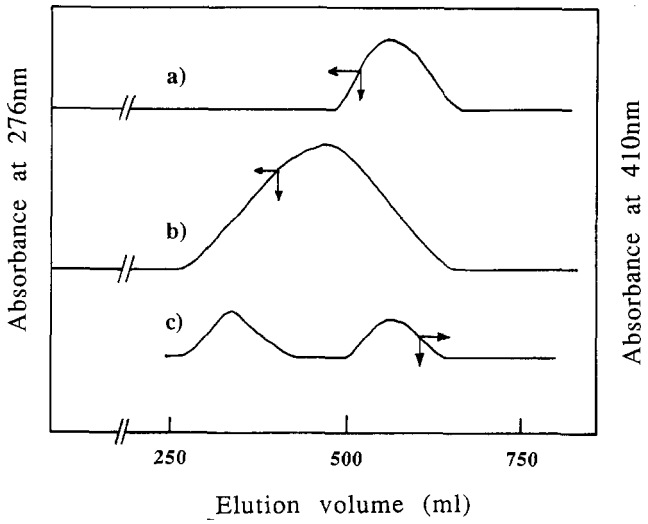


Figure 3. Elution patterns of native and modified trypsin: (a) native trypsin, (b) PCVPC–trypsin as polymerized, (c) enzymatic activity of fractionated PCVPC–trypsin [separation column, Sephadex G-200 (diameter, 3.3 cm; length, 87 cm); eluent, 0.05 M phosphate buffer (pH 7.0); detection, UV absorption at 276 nm in a and b and 410 nm (*p*-nitroaniline of substrate) in c].

Table I. Effect on Enzymatic Activity of Trypsin by Polymer Modification and by Addition of Redox Reagents

sample	amount of *p*-nitroaniline produced by the reaction of trypsin and BANA[a] at 35 °C (μmol/min mg of trypsin)	Relative enzymatic activity (%)
trypsin	4.80	100
azo-modified trypsin	2.51	52
PCVPC–trypsin	0.81	17
trypsin + $Na_2S_2O_4$[b]	4.36	91
trypsin + H_2O_2[b]	1.50	31

[a] N^{α}-Benzoyl-DL-arginine *p*-nitroanilide hydrochloride. [b] Reaction conditions are the same as those for Figure 5.

activity of each fraction was measured (curve c). Consequently, the high molecular weight component, which appeared after the graft polymerization, was considered to be the PCVPC–trypsin. The molecular weight of the PCVPC–trypsin was calculated to be 143 000. This value indicates that the molecular weight of the graft chain is 18 000, on the assumption that all azo groups in the azo-modified trypsin were used in the initiation of graft polymerization.

The effects of the introduction of azo groups to trypsin and the graft polymerization on the enzymatic activity of trypsin were estimated by measuring the catalytic activities of the modified trypsin during hydrolysis. As is shown in Table I, the catalytic activity of azo-containing trypsin decreased to about half that of the original and that of PCVPC–trypsin to about 16% of the native. The drastic decrease in the activity of the graft polymerized enzyme should be due to a conformational change induced by the graft polymerization or to coverage of the catalytic site of trypsin with graft chains.

Figure 4a shows that the water solubility of the modified trypsin (PCVPC–trypsin) as well as the graft chain (PCVPC) decreases with increasing concentration of reducing reagent. The solubility decrease should be due to the loss of electric charges by the reduction of PCVPC chains. The solubility decrease of PCVPC was faster than that of PCVPC–trypsin. This could be explained by taking into consideration the heightened water solubility of PCVPC–trypsin due to the presence of trypsin.

It was anticipated that the enzyme activity of the homogeneous solution would be lowered on adding reducing reagent because of the decreased enzyme concentration resulting from precipitation of reduced PCVPC–trypsin. As shown in Figure 4b, a small amount of $Na_2S_2O_4$ decreased the enzyme activity of the homogeneous solution. However, the extent of the activity decrease was more than that of solubility decrease. This may be due to the obstruction of substrate access to the partially reduced PCVPC–trypsin, which might form microaggregates in aqueous solution or might be blocked by adsorption of hydrophobic reduced graft chains. Table I shows that the reducing reagent $Na_2S_2O_4$ does not seriously deteriorate the enzymatic activity of trypsin.

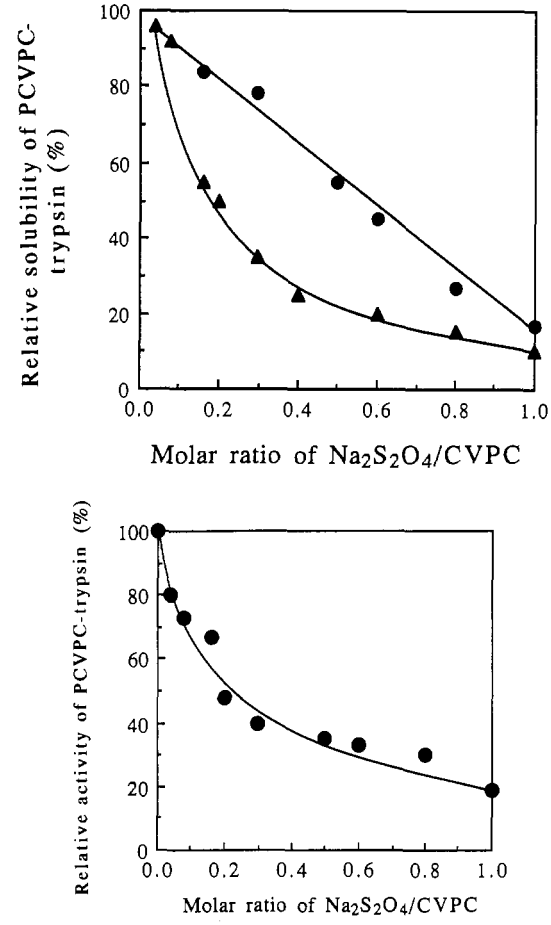


Figure 4. The change of the water solubility on PCVPC–trypsin (a) and the enzymatic activity remaining in a homogeneous solution (b) at various molar ratios of $Na_2S_2O_4$/CVPC: (●) PCVPC–trypsin (1.25 mg/mL phosphate buffer; concentration of CVPC, 3.6 mM), (▲) PCVPC (1.0 mg/mL phosphate buffer;3.6 mM).

The solubility of PCVPC–trypsin and the enzyme activity remaining in the homogeneous solution by alternate reductions and oxidations were investigated, and the results are shown in Figure 5. The water solubility of PCVPC–trypsin in an oxidized state, which carries positive charges and is highly soluble in water, decreased on adding $Na_2S_2O_4$, and was precipitated. Finally the enzyme activity of the homogeneous solution totally disappeared. After adding H_2O_2, PCVPC–trypsin recovered total water solubility. However, the enzyme activity of the homogeneous solution was not fully restored by the oxidation. As shown in Table I, under the same conditions, the catalytic activity of the native trypsin decreased to one-third of the original activity upon addition of H_2O_2. These results show that the absence of activity reversibility after redox reactions are due to the damage sustained by trypsin during oxidation.

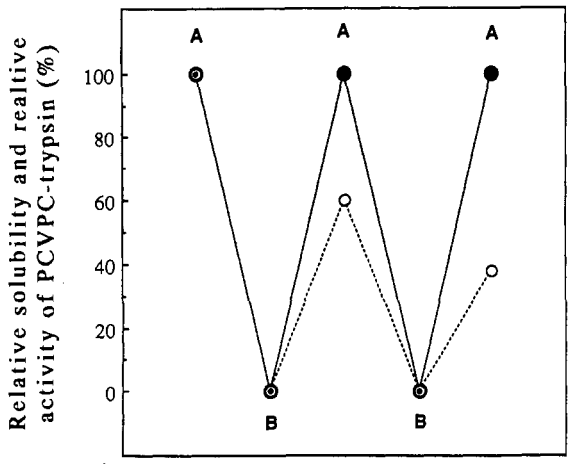


Figure 5. The change of water solubility of PCVPC–trypsin (1.25 mg/mL phosphate buffer; concentration of CVPC, 3.6 mM) and the enzymatic activity remaining in a homogeneous solution in response to repeated redox reactions by adding H_2O_2 (0.02 mM, A) and $Na_2S_2O_4$ (0.2 mM, B): (●) solubility, (○) activity.

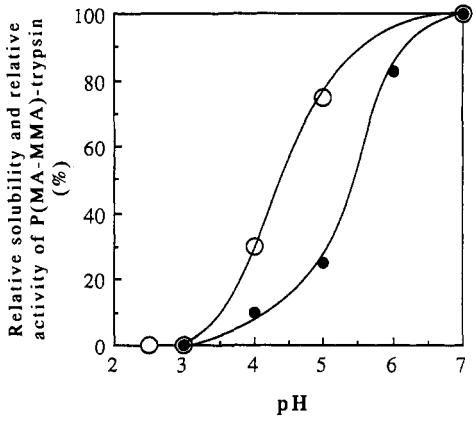


Figure 6. The solubility of P(MA-MMA)–trypsin (1 mg/mL phosphate buffer; concentration of trypsin, 17 μM) and the enzymatic activity remaining in a homogeneous solution at various pH values: (○) solubility, (●) activity.

pH-Dependent Solubility and Activity of P(MA-MMA)–Trypsin. The water solubility of P(MA-MMA), which was prepared from a methacrylic acid/methyl methacrylate mixture at a molar ratio of 2/1 [$r_{\text{methacrylic acid}}$ = 0.63 and $r_{\text{methyl methacrylate}}$ = 1.18 as previously reported (*14*)], changed drastically at pH 5. P(MA-MMA) was not soluble in water below pH 4, but soluble above pH 6. The molecular weight of P(MA-MMA)–trypsin was 80 000, corresponding to the molecular weight of the graft chain being 8500. The enzyme activity of P(MA-MMA)–trypsin was about 14% of native trypsin, which is nearly the same as PCVPC–trypsin. As shown in Figure 6, the water solubility of P(MA-MMA)–trypsin was low under acidic conditions. The enzyme activity remaining in the homogeneous solution also decreased with decreasing pH values. A slight decrease of the solubility in water was accompanied by a sudden decrease of the enzyme activity remaining in the homogeneous solution. This phenomenon occurred with PCVPC–trypsin, too.

The changes of the solubility of P(MA-MMA)–trypsin in water and the enzyme activity remaining in the homogeneous solution at various pH values ranging from 3 to 7 were investigated, and the results are shown in Figure 7. Either solubility or enzyme activity changed almost reversibly with the pH variation. These results show the absence of an irreversible trypsin transformation in the range of pH values studied.

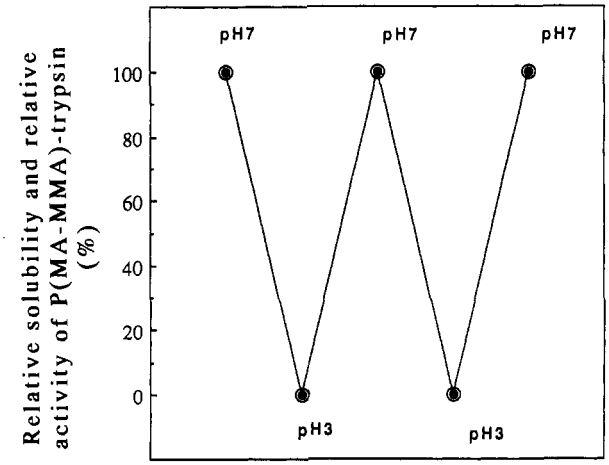


Figure 7. Reversible change of the solubility in water of P(MA-MMA)–trypsin (1 mg/mL phosphate buffer; concentration of trypsin, 17 μM) and the enzymatic activity remaining in a homogeneous solution in response to repeated pH changes: (○) solubility, (●) activity.

In summary, modified trypsins were synthesized, the solubilities of which varied in response to external signals such as redox reactions and pH variations. More useful devices can be synthesized by choosing suitable external signal/sensoring polymer combinations, in which possible damage to the enzyme can be minimized.

LITERATURE CITED

(1) Fuijimura, M., Mori, T., and Tosa, T. (1987) Preparation and properties of soluble-insoluble immobilized proteases. *Biotechnol. Bioeng. 29*, 747–752.

(2) Taniguchi, M., Tanahashi, S., and Fujii, M. (1990) Properties and repeated use of a reversibly soluble-insoluble yeast lytic enzyme. *Appl. Microbiol. Biotechnol. 33*, 629–635.

(3) Fujii, M., and Taniguchi, M. (1991) Application of reversibly soluble polymers in bioprocessing. *TIBTECH. 9*, 191–196.

(4) Yoshimoto, T., Mihama, T., Takahashi, K., Saito, Y., Tamura, Y., and Inada, Y. (1987) Chemical modification of enzymes with activated magnet modifier. *Biochim. Biophys. Res. Commun. 145*, 908–914.

(5) Eismer, U., and Kuthan, J. (1972) The chemistry of dihydropyridines. *Chem. Rev. 72*, 1–42.

(6) Ito, Y., Fujii, H., and Imanishi, Y. (1992) Enzyme hybridization with synthetic polymers for use in organic media. *Makromol. Chem. Rapid Commun. 13*, 315–319.

(7) Ito, Y., Fujii, H., and Imanishi, Y. (1992) Lipase modification by various synthetic polymers for use in chloroform. *Biotech. Lett. 14*, 1149–1152.

(8) Ito, Y., Fujii, H., and Imanishi, Y. (1993) Catalytic peptide synthesis by trypsin hybridized with polystyrene in chloroform. *Biotech. Prog. 9*, 128–130.

(9) Endo, T., and Okawara, M. (1979) Preparation of polymers containing 1,4-dihydronicotinamide structure and their use in the reduction of vicinal tricarbonyl compounds. *J. Polym. Sci., Polym. Chem. Ed. 17*, 3667–3674.

(10) Habeeb, A. F. S. A. (1966) Determination of free amino groups in proteins by trinitrobenzene-sulfonic acid. *Anal. Biochem. 14*, 328–383.

(11) Mole, J. E., and Horton, H. R. (1973) Kinetics of papain-catalyzed hydrolysis of α-*N*-benzyl-L-arginine-*p*-nitroanilide. *Biochemistry 12*, 816–825.

(12) Papisov, M. I., Maksimenko, A. V., and Torchilin, V. P. (1985) Optimization of reaction conditions during enzyme immobilization on soluble carboxyl-containing carriers. *Enzyme Microb. Technol. 7*, 11–20.

(13) Ryabov, A. V., Smimova, L. A., and Panova, G. D., and Tsareva, L. V. (1970) Effect of water on the copolymerization on methyl methacrylate with methacrylic acid. *Tr. Khim. Khim. Tekhno. 2*, 221–229.

Bisulfite Ion-Catalyzed Transamination of Cytosine Residues with α,ω-Alkanediamines: The Effect of Chain Length on the Reaction Kinetics

John Molander,[†] Pertti Hurskainen,[‡] Jari Hovinen,[†] Marjo Lahti,[†] and Harri Lönnberg*,[†]

Department of Chemistry, University of Turku, FIN-20500 Turku, Finland, and Wallac Oy, P.O. Box 10, FIN-20101 Turku, Finland. Received May 17, 1993[⊗]

Pseudo-first-order rate constants for the bisulfite ion-catalyzed transamination of cytidine with 1,2-ethanediamine, 1,3-propanediamine, 1,4-butanediamine, and 1,6-hexanediamine have been determined. Hydrolytic deamination has been shown to compete with transamination under acidic conditions, but is of minor importance at pH > 5.3 when the total concentration of diamine is greater than 0.2 mol dm^{-3}. The dependence of the transamination rate on pH and the concentration of diamine and bisulfite ion indicates that the major reaction involves nucleophilic attack of the diamine monocation on the N3 protonated bisulfite adduct of cytidine. The effect of the chain length of the diamine on the rate of transamination is discussed, and the results are compared with those obtained by reacting single-stranded DNA with the same diamines and labeling the transaminated product with a europium chelate.

INTRODUCTION

The bisulfite ion-catalyzed displacement of the C4 amino group of cytosine residues with 1,2-ethanediamine is a reaction used widely for the introduction of aliphatic amino groups into polynucleotides (*1–6*). These amino functions then serve as reaction centers and enable further derivatization of the polynucleotide *via* attachment of various reporter groups, including immunoreactive groups, fluorescent or spin labels, photochemical cross-linking agents, intercalators, alkylating groups, and catalytically active metal chelates. The transamination reaction proceeds by a rapid initial addition of bisulfite ion to the 5,6-double bond of the cytosine ring, followed by displacement of the 4-amino group with the entering amine (Scheme I) (*7*). Elimination of the bisulfite ion from the C5–C6 site then completes the reaction sequence. Hydrolytic deamination to uracil derivatives, which also proceeds *via* the same bisulfite adduct, competes with transamination at low pH (*7–10*).

Both the formation of the bisulfite adduct (*11–14*) and its deamination (*13–16*) have been studied in detail, whereas quantitative results on the transamination reaction are scanty. The kinetically relevant data are limited to the pH and temperature dependence of the reaction of cytosine, cytidine, and cytidine 5′-monophosphate with amino acids and dipeptides (*8, 9*) and the rate constants of transamination of poly(C) with 1,2-ethanediamine and 1,3-propanediamine at a fixed pH and bisulfite concentration (*9*). Moreover, semiquantitative data on the preparation of several N^4-alkyl- and N^4-arylcytosine nucleosides by transamination have been reported (*7, 10*). The present paper is aimed at giving a more clearcut picture of the kinetics of transamination of a cytosine residue with alkanediamines and the competition between transamination and deamination under various conditions. Since for some purposes transamination of polynucleotides with α,ω-alkanediamines longer than 1,2-ethanediamine is advantagenous, comparative kinetic studies of transamination of cytidine with four different alkanediamines, *viz.* 1,2-ethanediamine, 1,3-propanediamine, 1,4-butanediamine, and 1,6-hexanediamine, have been performed. The results of these studies are compared with those obtained by treating single-stranded DNA with the same diamines in the presence of bisulfite ion and labeling the transaminated product with a europium chelate.

EXPERIMENTAL PROCEDURES

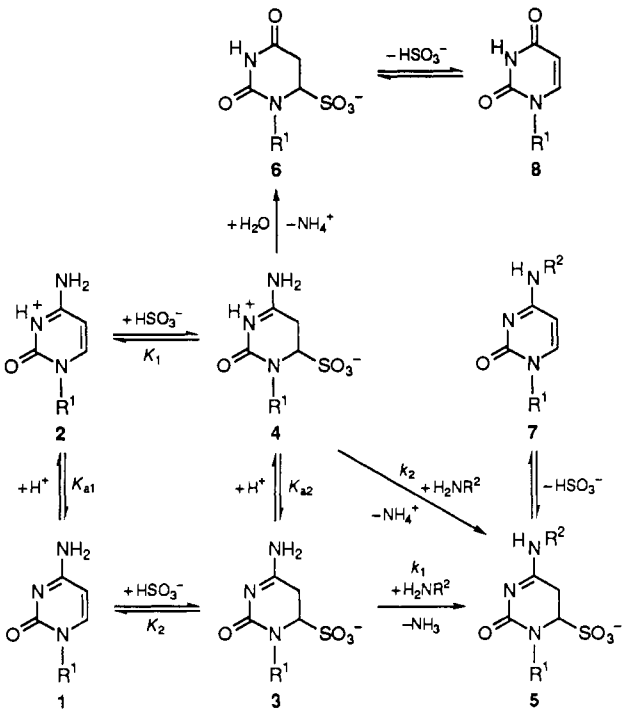
Materials. The nucleosides, *viz.* cytidine and uridine, were commercial products of Sigma. They were used as received after checking of the purity by HPLC. Of the alkanediamines employed, 1,2-ethanediamine was a product of Fluka (puriss. p.a.), and 1,3-propanediamine, 1,4-butanediamine, and 1,6-hexanediamine were products of Merck (>99 %). Sodium bisulfite (Mallinckrodt) was of reagent grade (AnalR). Standard hydrogen chloride and sodium hydroxide solutions of Baker were used to adjust the hydrogen ion concentration of the reaction solutions. The ionic strength was adjusted with sodium chloride (Merck, p.a.). All solutions were prepared in degassed ice cold distilled water to minimize the decomposition of bisulfite ion.

Kinetic Measurements. Reactions were initiated by dissolving 0.04 mmol of cytidine in 50 cm^3 of a prethermostated reaction mixture. Aliquots (1 cm^3) withdrawn at appropriate intervals were cooled in an ice bath, and their pH was adjusted to 8 with sodium hydroxide to stop the reaction and to decompose the bisulfite adducts. The compositions of the aliquots were determined by HPLC on a Hypersil ODS column (4.6 × 250 mm, 5 μm) using UV detection (270 nm) and aqueous ammonium acetate (0.025 mol dm^{-3}, flow rate of 1 cm^3 min^{-1}) as eluant. The areas of the cytidine and uridine signals were converted to concentrations by comparing them to those of calibration samples of known concentrations. First-order rate constants for the disappearance of the starting material were calculated from the integrated first-order rate law. These rate constants were bisected to the rate constants of the parallel transamination and deamination reactions with the aid of the mole fraction of uridine formed during the first half-life of the disappearance of cytidine. Since N^4-alkylated cytidines are known to undergo deamination

[†] University of Turku.
[‡] Wallac Oy.
[⊗] Abstract published in *Advance ACS Abstracts*, September 1, 1993.

1043-1802/93/2904-0362$04.00/0 © 1993 American Chemical Society

Scheme I



less readily than cytidine (*17*), uridine is formed almost entirely from cytidine and not *via* its transamination products. The sulfite ion concentration was determined before and after each kinetic run by iodometric titration.

The first-order rate constant for the release of cytidine from its bisulfite adduct was determined spectrophotometrically under the conditions employed in HPLC analyses. Accordingly, 30 mm^3 of a solution of cytidine (5×10^{-3} mol dm^{-3}) in a HSO_3^-/SO_3^{2-} buffer (0.125/0.125 mol dm^{-3}) was diluted with 3 cm^3 of ammonium acetate solution (0.025 mol dm^{-3}) in a spectrophotometer cell, and the decomposition of the bisulfite adduct was followed at 270 nm. The first-order rate constant was calculated by the method of Guggenheim.

Determination of the Stability Constant of the Bisulfite Adduct of Cytidine. The stability constant of the bisulfite adduct of cytidine was determined by measuring the concentration of free cytidine as a function of bisulfite ion concentration in HSO_3^-/SO_3^{2-} buffers having a fixed buffer ratio ($[HSO_3^-]/[SO_3^{2-}]$ 4/1, 1/1, 1/3, or 1/5). The measurements were carried out at 293 K by the HPLC technique described above. The total concentration of cytidine was kept constant (5×10^{-4} mol dm^{-3}) within each series of measurements. Since the retention time of the bisulfite adduct was about 2 min, the adduct did not markedly decompose during the chromatographic separation (half-life ~ 30 min). The stability constant, K, was obtained as the slope of eq 1

$$[\mathrm{Ctd}]_{\mathrm{tot.}}/[\mathrm{Ctd}]_{\mathrm{free}} = K[HSO_3^-] + 1 \qquad (1)$$

where $[\mathrm{Ctd}]_{\mathrm{tot.}}$ and $[\mathrm{Ctd}]_{\mathrm{free}}$ stand for total concentration of cytidine and the concentration of free cytidine, respectively.

Transamination of DNA. Herring sperm DNA (Sigma) was dissolved in water (1 mg cm^{-3}) and denaturated by heating an aliquot (100 mm^3) of the resulting solution for 10 min at 98 °C. After cooling on ice, the freshly prepared transamination solution (900 mm^3, pH 6.1), containing sodium bisulfite (0.25 mol dm^{-3}) and the appropriate diamine (0.5 mol dm^{-3}), was added, and the reaction was allowed to proceed for 6 h at 60 °C. Transaminated DNAs were purified by dialysis against two exchanges of water, concentrated, and precipitated with ethanol. The precipitates were dissolved in aqueous sodium carbonate (100 mm^3, 0.05 mol dm^{-3}) containing 5×10^{-4} mol dm^{-3} EDTA. The solutions were pipeted on 1.3 mg of the europium(III) chelate of 4-[2-(4-isothiocyanatophenyl)ethyl]-2,6-bis[*N*,*N*-bis(carboxymethyl)aminoethyl]pyridine (*18*) and kept at room temperature overnight. Eu-labeled DNAs were purified on a Sephacryl S-400 column (7 × 460 mm) using a Tris/Tris·HC -buffer (0.010 mol dm^{-3}, pH 8.5) containing sodium chloride (0.1 mol dm^{-3}) as eluent. The extent of labeling was determined by releasing the europium(III) ion in solution with the fluorescence enhancement solution and measuring the fluorescence on a time-resolved fluorometer (1234 DELFIA Research fluorometer) against a europium(III) chloride standard solution (*19*). The total amount of DNA in each sample was estimated by measuring the UV absorbance at 260 nm and subtracting the contribution of the DNA bound chelate.

RESULTS AND DISCUSSION

It has been shown previously (*14*) that protonation of cytidine (**1**) at *N*3 moderately favors the addition of bisulfite ion across the 5,6 double bond, the logarithmic stability constants of the adducts derived from neutral cytidine and its *N*3 monocation (**3** and **4**) being $\log(K_1/\mathrm{dm^3\,mol^{-1}}) = 1.0$ and $\log(K_2/\mathrm{dm^3\,mol^{-1}}) = 0.6$ at $T = 298.2$ K and $I = 2.0$ mol dm^{-3} (Scheme I). Since the pK_{a1} value of cytidine monocation **2** is 4.2 under the same conditions (*14*), the pK_{a2} value of the *N*3-protonated adduct must be 4.7. In other words, **3** predominates over **4** in the pH range (pH 5.3–6.8) employed in the present investigation. In spite of this, transamination may take place *via* the *N*3 protonated adduct **4**, since it is known that this species undergoes hydrolytic deamination at least 2 orders of magnitude more readily than its unprotonated analogue (**3**). Bearing this in mind, the pseudo-first-order rate constant, k_{obs}, observed for the transamination of cytidine may be expressed by eq 2, where the rate and equilibrium

$$k_{obs} = \frac{\{k_1K_2 + k_2(K_1/K_{a1})[H^+]\}(K_{aA}/[H^+])[\mathrm{amine}]_{\mathrm{tot.}}[HSO_3^-]_{\mathrm{tot.}}}{1 + [H^+]/K_{a1} + K_2[HSO_3^-]_{\mathrm{tot.}} + (K_1/K_{a1})[H^+][HSO_3^-]_{\mathrm{tot.}}} \qquad (2)$$

constants are those indicated in Scheme I. The derivation of this equation is based on the assumption that only the monoprotonated forms of the alkanediamines react with cytidine; the diprotonated forms are unable to act as nucleophiles, while the concentration of the neutral species is at pH < 7 from 1 to 3 orders of magnitude smaller than that of the monoprotonated species (*20–22*). Since the diprotonated diamines overwhelmingly prevail under the experimental conditions, the concentration of the monoprotonated species is directly proportional to the total concentration of the amine ($(K_{aA}/[H^+])[\mathrm{amine}]_{\mathrm{tot.}}$, where K_{aA} is the acidity constant of the diprotonated form). Since the measurements were carried out at $[\mathrm{Ctd}]_{\mathrm{tot.}} \ll [\mathrm{amine}]_{\mathrm{tot.}}$ and $[HSO_3^-]_{\mathrm{tot.}}$, the equilibrium concentrations of amine and bisulfite ion may be replaced by the total concentrations of these species.

Table I records the rate constants, k_{obs}, obtained under different conditions for the transamination of cytidine with the α,ω-alkanediamines studied. The values listed have been corrected with respect to the deamination that

Table I. Pseudo-First-Order Rate Constants for the Bisulfite Ion-Catalyzed Transamination of Cytidine with Various α,ω-Alkanediamines at 333.2 K[a]

pH	[amine]/mol dm^{-3}	[HSO_3^-]/mol dm^{-3}	$k_{obs}/10^{-5}$ s^{-1} 1,2-EDA	1,3-PDA	1,4-BDA	1,6-HDA
5.3	0.30	0.25	13.0 ± 0.4	4.2 ± 0.1	2.7 ± 0.1	
5.7	0.50	0.20	12.6 ± 0.2	4.4 ± 0.1		
	0.10	0.20	4.6 ± 0.1	2.8 ± 0.1		
6.0	0.30	0.25	11.4 ± 0.2	3.9 ± 0.1	2.7 ± 0.1	2.0 ± 0.1
6.3	0.50	0.125	8.8 ± 0.1	2.1 ± 0.1	0.95 ± 0.03	0.73 ± 0.03
	0.30	0.125	5.7 ± 0.1	1.5 ± 0.1		0.51 ± 0.08
	0.20	0.125	4.1 ± 0.1	1.2 ± 0.1		
	0.10	0.125	2.2 ± 0.1	0.77 ± 0.01		
	0.50	0.075	1.2 ± 0.1			
	0.50	0.050	0.82 ± 0.02			
6.8	0.30	0.10	3.3 ± 0.1	1.12 ± 0.02	0.58 ± 0.02	0.39 ± 0.01

[a] The ionic strength was adjusted to 2 mol dm^{-3} with sodium chloride. 1,2-EDA, 1,3-PDA, 1,4-BDA, and 1,6-HDA refer to 1,2-ethanediamine, 1,3-propanediamine, 1,4-butanediamine and 1,6-hexanediamine, respectively.

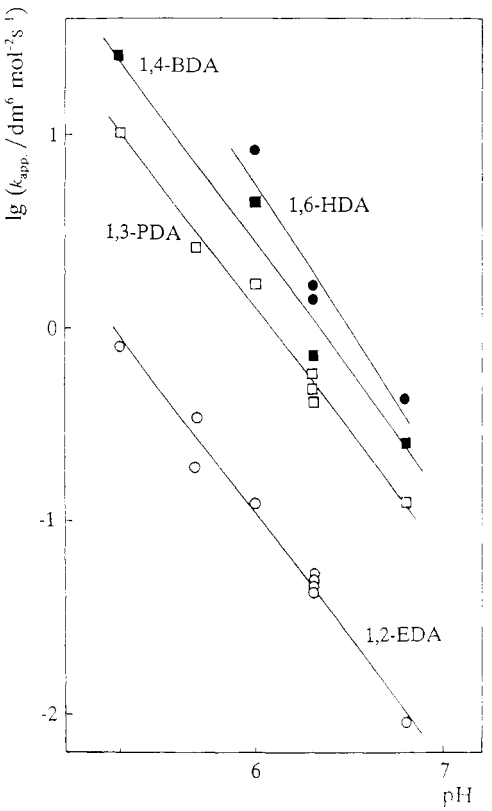


Figure 1. Transamination of cytidine with α,ω-alkanediamines at I = 2.0 mol dm^{-3} (adjusted with NaCl) and T = 333.2 K: the dependence of the values of $k_{app.} = k_1K_2 + k_2(K_1/K_{a1})[H^+]$ on the hydronium ion concentration of the reaction mixture. For the partial rate and equilibrium constants see Scheme I. The abbreviations of the alkanediamines are those in the footnote of

took place as a minor side reaction under the experimental conditions employed. The proportion of the latter reaction was always less than 5% of the total rate of disappearance of cytidine. The rate constants, k_{obs}, of transamination enable, together with the equilibrium constants of bisulfite adduct formation (*14*) and the acidity constants of diprotonated alkanediamines (*20–22*), calculation of the values of $k_{app} = k_1K_2 + k_2(K_1/K_{a1})[H^+]$ at different hydronium ion concentrations. The logarithms of these values are presented in Figure 1 as a function of pH. With each of the diamines studied the plot of log (k_{app}/dm^6 mol^{-2} s^{-1}) *vs* pH is a descending straight line having a slope on the order of −1. In other words, the term $k_2(K_1/K_{a1})[H^+]$ determines the magnitude of k_{app}, which means that the transamination proceeds *via* the *N*3-protonated bisulfite adduct **4**, and not via the unprotonated form **3**. For this

Table II. Pseudo-First-Order Rate Constants, k_{obs}, of the Transamination of Cytidine with α,ω-Alkanediamines ([amine]$_{tot.}$ = 0.5 mol dm^{-3}) at pH 6.3 and 333.2 K and Second-Order Rate Constants, k_2, of the Reaction of *N*3-Protonated Bisulfite Adduct of Cytidine 4 with the Alkanediamine Monocations (see Scheme I)[a]

α,ω-alkanediamine	$k_{obs}/10^{-5}$ s^{-1}	k_2/dm^3 mol^{-1} s^{-1}
1,2-ethanediamine	8.8	0.042
1,3-propanediamine	2.1	0.40
1,4-butanediamine	0.95	0.72
1,6-hexanediamine	0.73	1.40

[a] [HSO_3^-]/[SO_3^{2-}] = 0.125/0.125 mol dm^{-3}; the ionic strength was adjusted to 2 mol dm^{-3} with sodium chloride.

reason, the transamination is inevitably rather slow; increasing the concentration of the reactive form of alkanediamine by increasing the pH decreases the concentration of the reactive form of the bisulfite adduct.

Table II summarizes the pseudo-first-order rate constants, k_{obs}, of transamination at a fixed concentration of amine (0.5 mol dm^{-3}) and hydronium ion (pH 6.3; refers to 298 K) and the second-order rate constant, k_2, of the reaction between the protonated bisulfite adduct (**4**) and the diamine monocations. The latter values clearly indicate that the reactivity of the diamine monocation is markedly increased with the increasing chain length. This is expected, since the protonated amino function inductively lowers the nucleophilicity of the attacking neutral amino group, and this effect is the stronger the shorter the distance is between the two amino groups. However, as the values of k_{obs} reveal, the rate-accelerating effect of the increasing chain length is overcompensated by the opposite influence on the preequilibrium concentration of the reactive species, *i.e.*, the diamine monocation: the longer the alkyl chain is the higher the pK_a value of the diprotonated diamine (pK_{aA} in eq 1) is, and hence the lower the concentration of the monoprotonated species is at a fixed pH lower than the pK_{aA}. Consequently, transamination with 1,2-diaminoethane appears to be preferable to the usage of longer alkanediamines. The transamination rates with the latter compounds are from 10 to 30% of those obtained with 1,2-ethanediamine, and this reactivity difference is large enough to increase the risk of appearance of deamination as an undesirable side reaction.

As mentioned above, the values of k_2 listed in Table II are calculated with the aid of the equilibrium constants determined spectrophotometrically by Shapiro *et al.* (*14*) at 298 K. Our HPLC approach gave somewhat lower values for K_2 at the same temperature, *viz.* 2.5 mol dm^{-3} instead of 3.9 mol dm^{-3}. This difference, nor the fact that the equilibrium constants refer to a lower temperature than

the values of k_{obs}, does not question the conclusions drawn, although the absolute values of k_2 might experience a systematic change. When denaturated herring sperm DNA was transaminated with the diamines discussed above and then labeled with a europium(III) chelate, the extent of labeling was observed to correlate with the rates of transamination of monomeric cytidine. The results obtained at $[amine]_{tot}$ = 0.5 mol dm^{-3} and $[HSO_3^-]_{tot}$ = 0.25 mol dm^{-3} (pH 6.1; 6 h; 333 K) were as follows: 1,2-ethanediamine, 8.1%; 1,3-propanediamine, 2.2%; 1,4-butanediamine, 1.2%; and 1,6-hexanediamine, 0.9%. Since the labeling was carried out in a large excess of the europium chelate, the extent of labeling may be expected to be determined by the extent of transamination. Accordingly, the results obtained at monomeric level appear to be valid at polymeric level.

LITERATURE CITED

(1) Draper, D. E., and Gold, L. (1980) A Method for Linking Fluorescent Labels to Polynucleotides: Application to Studies of Ribosome-Ribonucleic Acid Interactions. *Biochemistry 19*, 1774–1781.

(2) Viscidi, R. P., Connelly, C. J., and Yolken, R. H. (1986) Novel Chemical Method for the Preparation of Nucleic Acids for Nonisotopic Hybridization. *J. Clin. Microbiol. 23*, 311–317.

(3) Turchinskii, M. F., Ainbinder, E. I., and Sverdlov, E. D. (1988) Multiple Hybridization in Genome Analysis. I. Reaction of Diamines and Bisulfite with Cytosine for Introduction of Nonradioactive Labels into DNA. *Mol. Biol. (Engl. Transl.) 22*, 1229–1235.

(4) Karpyshev, N. N., Bondarenko, T. Y., Vtorushina, I. A., and Kipriyanov, S. M. (1991) Introduction of Aminoalkyl Functions into Synthesized Oligodeoxyribonucleotides via Transamination of Cytosine Residues. *Bioorg. Khim. 17*, 809–812.

(5) Avignolo, C., Roner, R., Cai, S., and Bignone, F. A. (1991) Biotinylation of Denaturated Double-stranded DNA after Transamination of Cytidines: Molecular Biology Applications. *J. Biochem. Biophys. Methods 23*, 193–202.

(6) Avignolo, C., Pizzorno, G., Cai, S., and Biogne, F. (1991) HPLC Analysis of DNA upon Cytidine Transamination at 100 °C. *J. Biochem. Biophys. Methods 23*, 202–205.

(7) Shapiro, R., and Weisgras, J. M. (1970) Bisulfite-catalyzed Transamination of Cytosine and Cytidine. *Biochem. Biophys. Res. Commun. 40*, 839–843.

(8) Boni, I. V., and Budowsky, E. I. (1973) Transformation of Non-covalent Interactions in Nucleoproteins into Covalent Bond Induced by Nucleophilic Reagents. *J. Biochem. (Tokyo) 73*, 821–830.

(9) Draper, D. E. (1984) Attachment of Reporter Groups to Specific, Selected Cytidine Residues in RNA using a Bisulfite-catalyzed Transamination Reaction. *Nucleic Acids Res. 12*, 989–1002.

(10) Miller, P. S., and Cushman, C. D. (1992) Selective Modification of Cytosines in Oligodeoxyribonucleotides. *Bioconjugate Chem. 3*, 74–79.

(11) Hayatsu, H., Wataya, Y., Kai, K., and Iida, S. (1970) Reaction of Sodium Bisulfite with Uracil, Cytosine and Their Derivatives. *Biochemistry 9*, 2858–2865.

(12) Hayatsu, H., Wataya, Y., and Kai, K. (1970) The Addition of Sodium Bisulfite to Uracil and to Cytosine. *J. Am. Chem. Soc. 92*, 724–726.

(13) Shapiro, R., Servis, R. E., and Welcher, M. (1970) Reactions of Uracil and Cytosine Derivatives with Sodium Bisulfite. A Specific Deamination Method. *J. Am. Chem. Soc. 92*, 422–424.

(14) Shapiro, R., DiFate, V., and Welcher, M. (1974) Deamination of Cytosine Derivatives by Bisulfite. Mechanism of the Reaction. *J. Am. Chem. Soc. 96*, 906–912.

(15) Hayatsu, H., and Sono, M. (1971) Dual Role of Bisulphite in the Deamination of Cytidine 5′-Phosphate. *J. Chem. Soc. Chem. Commun.* 1178–1179.

(16) Sono, M., Wataya, Y., and Hayatsu, H. (1973) Role of Bisulfite in the Deamination and the Hydrogen Isotope Exchange of Cytidylic Acid. *J. Am. Chem. Soc. 95*, 4745–4749.

(17) Kusmierek, J., Käppi, R., Neuvonen, K., Shugar, D., and Lönnberg, H. (1989) Kinetics and Mechanisms of Hydrolytic Reactions of Methylated Cytidines under Acidic and Neutral Conditions. *Acta Chem. Scand. 43*, 196–202.

(18) Hurskainen, P., Dahlen, P., Ylikoski, J., Kwiatkowski, M., Siitari, H., and Lövgren, T. (1991) Preparation of Europium-labelled DNA Probes and Their Properties. *Nucleic Acids Res. 19*, 1057–1061.

(19) Hemmilä, I., Dakubu, S., Mukkala, V.-M., Siitari, H., and Lövgren, T. (1984) Europium as a Label in Time-resolved Immunofluorometric Assays. *Anal. Biochem. 137*, 335–343.

(20) Sigel, H., Huber, P. R., and Pasternack, R. F. (1971) Ternary Complexes in Solution. X. The Influence of the Size of the Chelate Rings on the Stability of Mixed-Ligand Copper(II) Complexes. *Inorg. Chem. 10*, 2226–2228.

(21) Schwarzenbach, G., Maissen, B., and Ackermann, H. (1952) Metallkomplexe mit Polyaminen VII: Diamine und Silber(I). *Helv. Chim. Acta 35*, 2333–2336.

(22) Labadi, I., Jenei, E., Lahti, R., and Lönnberg, H. (1991) Interaction of Pyrophosphate Ion with Di-, Tri- and Tetraamines in Aqueous Solution: A Potentiometric and Calorimetric Study. *Acta Chem. Scand. 45*, 1055–1059.

Preparation of Hybrid "DNA Cleaver-Oligonucleotide" Molecules Based on a Metallotris(methylpyridiniumyl)porphyrin Motif

Christiane Casas, C. Jeffrey Lacey, and Bernard Meunier*

Laboratoire de Chimie de Coordination du CNRS, 205 route de Narbonne, 31077 Toulouse cedex, France.
Received February 17, 1993®

Methods are reported for conjugating a cationic tris(methylpyridiniumyl)porphyrin-manganese(III) complex to oligonucleotides. The DNA cleaver motif used in the present work is related to Mn-TMPyP, a highly efficient artificial endonuclease able to hydroxylate C-H bonds of DNA sugars at nanomolar concentrations. A general coupling method has been developed by using porphyrin precursors having a linker attached at the *para* position of the *meso* phenyl group of the macrocycle and terminating with an activated ester of 1-hydroxybenzotriazole. Coupling reactions were monitored by HPLC. Purification of metalloporphyrin-oligonucleotide conjugates was performed by HPLC and desalting on Bio-Gel P-2. The purity of conjugates was always above 95%.

INTRODUCTION

Besides antisense RNAs (*1*) and ribozymes (*2*), chemically modified oligonucleotides (*3*, *4*) are among the possible approaches for the regulation of gene expression of specified targets on DNA or RNA. Preliminary data indicate that oligonucleotides modified by a DNA cleaver and ribozymes might be considered both as possible selective antiviral therapeutic agents, targeted against various viruses, including HIV (*5-11*), and also as anti-oncogenes (*11*, *12*). Current efforts have been being made to improve cell penetration of antisense oligonucleotides and to enhance their nuclease resistance, two important limiting factors for the pharmacological development of these molecules.

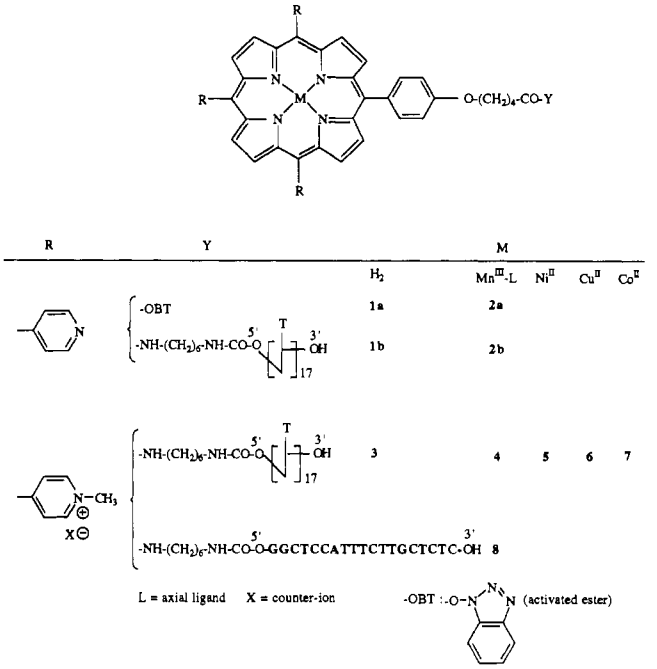
However, another limitation is the rather high concentration (0.1-1 μM) which is required to observe significant biological activity (*13*). In order to overcome this limitation, we decided to link an efficient DNA cleaver, the manganese derivative of *meso*-tetrakis(4-*N*-methylpyridiniumyl)porphyrin, Mn-TMPyP, to oligonucleotides via a 5'-amino link. We recently reported that the affinity of a DNA cleaver is a key factor for the nuclease activity of these cationic metalloporphyrins (*14*, *15*).

In addition, these cationic manganese porphyrin derivatives exhibit an anti-HIV activity at micromolar concentrations (*16*). These recent data lend an additional support for the preparation of hybrid "metal-tris-MPyP-oligonucleotide" molecules which are reported in the present article. Previously, noncationic porphyrin derivatives have been linked to oligonucleotides (*17*, *18*), but these hybrid molecules have a rather weak nuclease activity because of the absence of DNA affinity of the cleaver moiety.

RESULTS AND DISCUSSION

In the present work several hybrid molecules have been prepared: (i) the nonmetalated and the manganese(III) noncationic trispyridylporphyrin derivatives of a T_{17}-mer, **1b** and **2b** respectively; (ii) the nonmetalated and the manganese(III), nickel(II), copper(II), and cobalt(II) cationic tris(methylpyridiniumyl)porphyrin derivatives of the same T_{17}-mer, **3**, **4**, **5**, **6**, and **7**, respectively; and finally (iii) the manganese(III) tris(methylpyridiniumyl)porphyrin derivative **8** of a 19-mer complementary to a region containing the AUG initiation codon of the HIV-1 TAT gene (5360-5394, according to the numbering from ref *19*) (see Scheme I for structures of these hybrid molecules and Tables I and II for HPLC and UV-vis data). Because only cationic manganese porphyrins are efficient DNA cleavers, conjugates **1b**, **2b**, and **5** were not isolated for actual DNA cleavage experiments. In these cases just the conversion of starting oligonucleotide into conjugate was given based upon HPLC analysis. Conjugate **3**, based on a nonmetalated porphyrin moiety, was prepared and purified before metalation by manganese, copper, and cobalt. Corresponding metalated conjugates **4**, **6**, and **7** were analyzed by HPLC.

Scheme I.[a] Structures of Hybrid "Cationic Metalloporphyrin-Oligonucleotide" Molecules



[a] For manganese derivatives, the axial ligand Y is a water molecule at pH < 7 and a hydroxo ligand at basic pH values. The counterion X^- of the tris(methylpyridiniumyl)porphyrin used for coupling is I^-.

* Author to whom correspondence should be addressed.

® Abstract published in *Advance ACS Abstracts*, September 1, 1993.

1043-1802/93/2904-0366$04.00/0 © 1993 American Chemical Society

Table I. HPLC Data (Retention Time) for Oligonucleotides and Conjugates

compound	retention time[a]
oligonucleotide 5′-NH_2-T_{17}	23.6
1b	26.8
2b	21.2
4	17.6
5	18.3
5	18.3
6	17.9
7	18.1
oligonucleotide 19-mer	22.6
8	20.1

[a] Gen-Pak Fax column, A, Tris-HCl, 25 mM, pH 8.5; B, A + 1 M NaCl; linear gradient from 10% B to 90% B in 45 minutes at 0.7 mL/min.

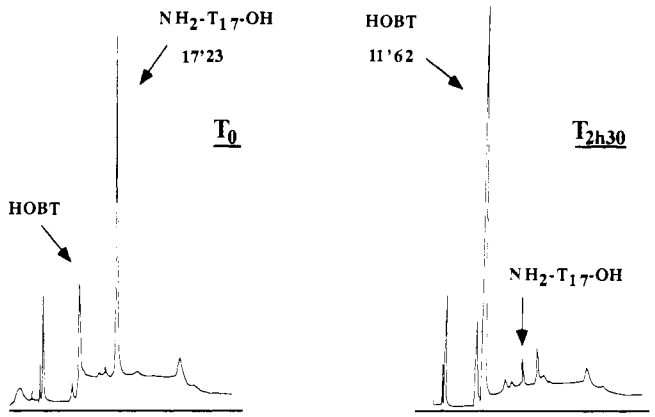


Figure 1. Conversion of 5′-NH_2-T_{17}-OH in the coupling reaction with **1a** monitored by HPLC (C18 nucleosil column, linear gradient for 40 min, detection at 254 nm, see Experimental Procedures for details).

Starting from trispyridyl- or tris(methylpyridiniumyl)-porphyrin having an acid function at the *para* position of the *meso*-phenyl group (*20*), we have used a common strategy for the coupling reaction, which allowed the preparation of diverse porphyrin conjugates. Hydrophobic as well as water-soluble porphyrins, metalated or non-metalated, can be covalently tethered to an oligonucleotide via a 5′-amino link by a carbonyldiimidazole activation of the acid function, followed by conversion of the imidazolide to the more stable and selective HOBT ester. The coupling reaction, for hydrophobic porphyrins, can be monitored indirectly by reverse-phase HPLC on a C_{18} column by observing the disappearance of starting oligonucleotide and the appearance of liberated HOBT (see Figure 1). The ability to extractively remove excess HOBT and imidazole (see Experimental Procedures) from the reaction mixture permits one to monitor the reaction as described. In the case of cationic porphyrins, such a simple preliminary procedure is not possible, and the reaction is carried out without removal of excess HOBT and imidazole, the latter being produced when excess CDI is destroyed by addition of buffer. Here, and in the above case as well, formation of product can be observed by direct injection of the reaction mixture on an anion-exchange column (Gen-Pak Fax). At the end of the reaction the solvents can be removed under vacuum and the residue redissolved in water, or the mixture may be diluted with water and the resulting solution applied to a column of Sephadex G25 (DNA grade) or Bio-Gel P-2. This procedure allows one to nicely separate the reaction products as well as starting material from the excess porphyrin and, in the case of cationic porphyrin conjugates, the HOBT and imidazole. When the oligonucleotide is composed of bases other than T (*e.g.* **8**) we observed during desalting of the chromatographically purified conjugate on Sephadex a loss of material by an unexplained decomposition, as evidenced by formation of brown material which remained on the Sephadex column. For these reasons, Bio-Gel P-2 was used for preliminary purification and desalting for heterobase conjugates. In our case the use of Bio-Gel is also superior because it allows one to recover the hydrolyzed cationic porphyrin, which can be regenerated.

The UV–visible data of the porphyrin precursors, amino-linked oligonucleotides, and conjugates are reported in Table II. The absorbance ratios A_{vis}/A_{UV} of conjugates (A_{vis} was the Soret band of the porphyrin entity and A_{UV} was taken at the usual maximum for oligonucleotides), measured directly by a diode-array detector from the HPLC peak of the purified conjugate, indicate that only one molecule of porphyrin derivative is covalently attached to the oligonucleotide vector. These A_{vis}/A_{UV} values are slightly different from the calculated $\epsilon_{vis}/\epsilon_{UV}$ ratios (for

Table II. UV–Visible Data Concerning Oligonucleotides, Porphyrins, and Conjugates

			ratio vis/UV	
compounds[h]	UV: λ_{max} (nm), ϵ (M^{-1} cm^{-1})	visible: λ_{max} (nm), ϵ (M^{-1} cm^{-1})	calcd $\epsilon_{vis}/\epsilon_{UV}$	meas A_{vis}/A_{UV}
oligonucleotide 5′-NH_2-T_{17}	260, 1.4×10^5 [a]			
porphyrin precursor of **1b**	260, 2.6×10^4 [b]	420, 3.7×10^5 [b]		
1b	265[d]	422[d]	2.2,[c] 2.6[f]	2.4[d]
porphyrin precursor of **2b**	260, 2.8×10^4 [b]	465, 1.0×10^5 [b]		
2b	260[d]	470[d]	0.59,[c] 0.71[f]	0.64[d]
porphyrin precursor of **3, 4, 6, 7**	260, 1.4×10^4 [b]	428, 2.0×10^5 [b]		
3	265[d]	435[d]	1.3,[c] 1.4[f]	1.3[d]
4	270[d]	468[d]	0.85[g]	0.81[d]
6	265[d]	435[d]		0.82[d]
7	265[d]	432[d]		0.84[d]
porphyrin precursor of **5**	260, 3.6×10^4 [b]	424, 1.3×10^5 [b]		
5	270[d]	435[d]	0.72,[c] 0.90,[e] 0.93[f]	0.95[d]
oligonucleotide 5′-NH_2-19-mer	260, 1.6×10^5 [a]			
porphyrin precursor of **8**	260, 2.7×10^4 [b]	466, 0.98×10^5 [b]		
8	264[d]	468[d]	0.51,[c] 0.64,[e] 0.61[f]	0.63[d]

[a] Calculated from ref 23. [b] Measured values for porphyrin precursors in Milli-Q water. [c] Calculated $\epsilon_{vis}/\epsilon_{UV\ ratio}$ for conjugates with conjugate ϵ_{UV} = oligonucleotide ϵ_{UV} + porphyrin ϵ_{UV} and conjugate ϵ_{vis} = porphyrin ϵ_{vis}. [d] Measured values for conjugates from HPLC peak by diode-array detector. [e] Calculated value for conjugates based on the following ratio: (porphyrin ϵ_{vis}) × 1.25/conjugate ϵ_{UV}. This correcting factor (1.25) is due to the 25% hyperchromicity of cationic metalloporphyrin when interacting to oligonucleotides (see Results and Discussion). [f] This ratio corresponds to porphyrin ϵ_{vis}/oligonucleotide ϵ_{UV}. By coincidence, and because of the hyperchromicity of cationic metalloporphyrin when interacting with oligonucleotide (see note *e* and Discussion) this value is close to the measured value. The UV contribution of the porphyrin is compensated by the hyperchromicity of the Soret band. [g] See Results and Discussion. [h] For all porphyrin precursors, the UV–visible data indicated in the present table correspond to the porphyrin with the free acid function, not the OBT ester.

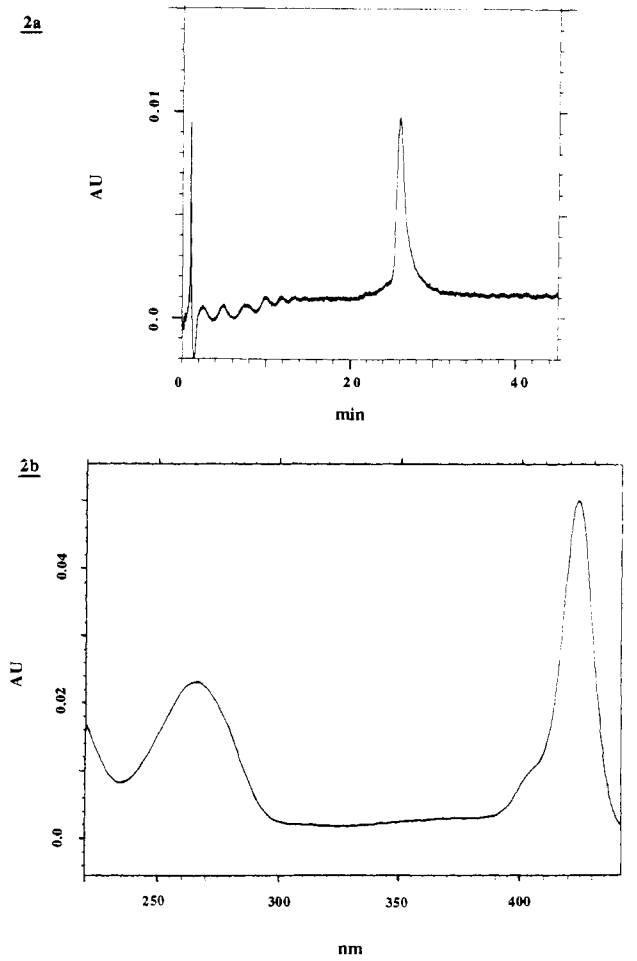


Figure 2. (a) HPLC profile of the porphyrin conjugate **1b** on Gen-Pak Fax column (linear gradient for 45 min, detection at 422 nm, see Experimental Procedures for details) and (b) UV–visible spectrum of **1b** peak obtained with a diode-array detector (measured A_{422}/A_{265} ratio = 2.4).

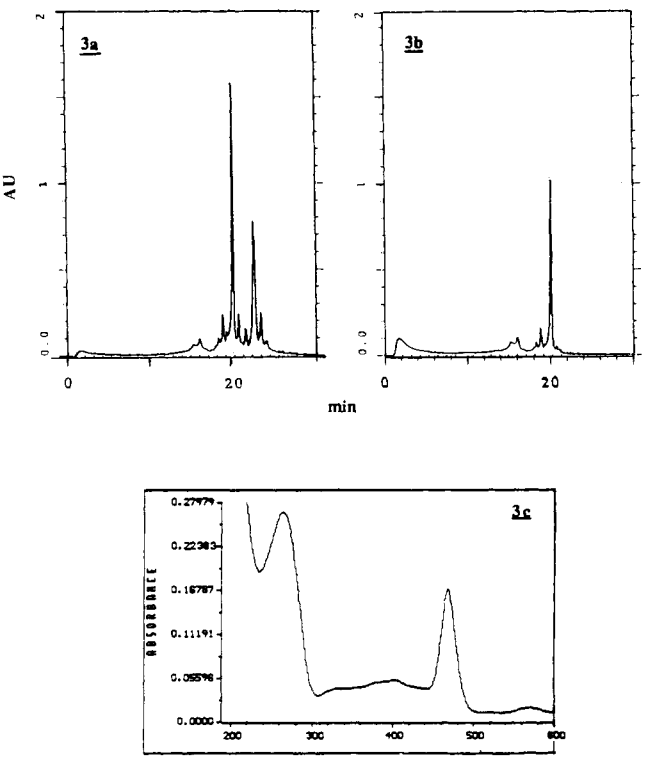


Figure 3. (a and b) HPLC profiles of the coupling reaction mixture with manganese porphyrin conjugate **8** (t_R = 20.1 min) and the starting amino-linked oligonucleotide (t_R = 22.6 min) on a Gen-Pak Fax column [linear gradient for 45 min, detection at 264 (a) and 468 nm (b), see Experimental Procedures for details] and (c) UV–visible spectrum of **8** after purification (concentrated in water = 0.27 OD/mL, measured A_{468}/A_{264} ratio = 0.63).

instance, see conjugates **5** and **8** data from Table II and footnotes *c*, *e*, and *f* of this table for different modes of calculations), because of the interactions of cationic metalloporphyrins with oligonucleotides. These interactions have an influence on both chromicity and shift of the Soret band of the porphyrin moiety. The hyperchromicity is usually 25 to 30% (25% in the case of the porphyrin precursors of conjugates **5** and **8**) according to data obtained with cationic manganese porphyrins and single-stranded oligonucleotides (data not shown). Such high Soret band hyperchromicity is well established in the case of cationic manganese porphyrins interacting with double-stranded DNA (*14*). In the case of conjugate **8** (see Table II), the calculated $\epsilon_{vis}/\epsilon_{UV}$ ratio is 0.51 and has to be compared to the measured value 0.63. When taking into consideration the hyperchromicity contribution of the metalloporphyrin Soret band in conjugate **8**, a new calculated $\epsilon_{vis}/\epsilon_{UV}$ ratio is obtained: 0.64. This value is closer to the measured value of 0.63. Finally, it should be noted that 0.63 is also very close to 0.61, the third calculated $\epsilon_{vis}/\epsilon_{UV}$ value, which is just the ratio of the ϵ_{vis} of the porphyrin precursor versus the ϵ_{UV} of the oligonucleotide. By coincidence, the UV contribution of the porphyrin moiety (28% of the Soret band absorbance) is compensated by the Soret band hyperchromicity due to the metalloporphyrin–oligonucleotide interactions. For hydrophobic nonmetalated porphyrins (case of **1b** precursor) the UV contribution is 7 ± 2% of the Soret band (the ϵ value of the Soret band of free porphyrins is usually 4 times that of the corresponding metalated derivatives). In the case of cationic nonmetalated porphyrins (see porphyrin precursor of **3**) the ϵ value of the free porphyrin is only 2 times that of the corresponding metalated porphyrin (ϵ values of cationic nonmetalated porphyrins are usually 2.0 ± 0.1 × 10^5). The measured A_{vis}/A_{UV} ratio of conjugate **3** (a nonmetalated cationic porphyrin attached to a T_{17} oligonucleotide) is 1.3 and compares well to the calculated value 1.3 (see footnote *c* for the mode of calculation). After metalation by manganese, the measured A_{vis}/A_{UV} ratio is 0.81, which can be compared to a calculated value (0.85), taking in consideration the decrease of the Soret band after metalation (divided by 2) and the hyperchromicity effect (25%).

A remarkable feature of the water-soluble free porphyrin–T_{17} conjugate **3** is the possibility to metalate it with various metal ions: manganese, copper, or cobalt. The metalation step requires only 1 h at 100 °C, and no conjugate degradation is detected under these rather drastic conditions. However, for oligonucleotides containing purine bases (like the 19-mer used for the synthesis of conjugate **8**), it was necessary in this case to perform the metalation of the water-soluble porphyrin precursor before the coupling reaction to overcome degradation problems during metalation of conjugates.

Preliminary experiments (*21*) indicate that the vectorized cationic manganese porphyrin **8** is able to recognize its complementary sequence incorporated in a 35-mer, even in the presence of a large excess of salmon sperm DNA, and to cleave the target at very low concentrations (5–50 nM) when activated by potassium monopersulfate, an oxygen atom donor that we used to mimic bleomycin activity (*15*, *22*). Work is in progress to develop these vectorized cationic manganese porphyrins having an

efficient nuclease activity with a low cleaver/target ratio (1 to 5/1) as antiviral agents or antioncogens.

EXPERIMENTAL PROCEDURES

Materials. Oligonucleotides were synthetized on a Cyclone Plus DNA Syntheziser by an automated phosphoramidite method (using all commercially available precursors), functionalized at the 5′ position by the method of Wachter *et al.* (*24*), and purified by reverse-phase HPLC. ϵ values of the oligonucleotides were calculated from ref *23*. Porphyrin precursors were prepared according to ref *20*. The different mode of calculation of the $\epsilon_{vis}/\epsilon_{UV}$ ratios of conjugates are indicated in Table II footnotes.

Synthesis of Conjugate 1b. A 25-mL flask equipped with a magnetic stirring bar was charged with the porphyrin (R = pyridyl and Y = OH) (5 mg, 6.8 μmol) (*20*). The solid was covered with 1.5 mL of dry dichloromethane and 1,1′-carbonyldiimidazole (CDI) (11 mg, 68 μmol) was added. The mixture was stirred at room temperature for 3.5 h, then to one-half of the solution was added 9.2 mg of HOBT (68 μmol) and the reaction mixture was stirred overnight. Formation of the imidazolide and the active ester **1a** was monitored by TLC (silica gel, CH_2Cl_2/EtOH; 9/1, v/v; R_f = 0.55), and as the reaction progressed, a deep purple solution formed. The reaction solution was diluted to 30 mL with dichloromethane (synthesis grade), washed with deionized water (2 × 20 mL), dried over sodium sulfate, filtered, and concentrated to dryness. The active ester was used immediately without further purification. **1a** (2.5 mg, 3 μmol, 250 equiv) was dissolved in 90 μL of dry DMF and the resulting red solution added to 2 OD_{260} units (12 nmol, 1 equiv) of 5′-NH_2-T_{17} oligonucleotide dissolved in 10 μL of HEPES buffer (0.2 M, pH = 8). The mixture was heated at 60 °C for 3 h. The progress of the coupling reaction was followed indirectly by reverse-phase HPLC (Nucleosil column 10 μm, C_{18}, 250 × 4.6 mm; A = triethylammonium acetate, 0.1 M, pH = 6.5, B = CH_3CN; linear gradient, 10% B to 20% B over 20 min; flow rate = 0.7 mL/min) by monitoring the disappearance of starting oligonucleotide (t_R = 17.2 min) and the appearance of free HOBT (t_R = 11.6 min) (Figure 1). The reaction mixture was concentrated to dryness with a Speed-Vac, the residue was taken up in 0.5 mL of H_2O, the solution was applied to a column of G-25 (F) Sephadex (gel volume = 10 mL) equilibrated with water, and the crude product was eluted with water. The conjugate was purified further by HPLC (Gen-Pak Fax column from Waters; A = Tris·HCl, 0.025 M, pH = 8.5; B = A + 1 M NaCl; linear gradient, 10% B to 90% B over 45 min; flow rate = 0.7 mL/min). The chromatogram was observed using a 2-channel diode-array detector (265 and 422 nm). The retention time of the conjugate was 26.8 min compared to 23.6 min for the starting oligonucleotide. A sample of the conjugate was subjected to PAGE (15%, non-denaturating gel). The product migrated as a discrete orange-red band slower than the free oligonucleotide. The colored band was excised and the product extracted into water at 4 °C overnight. Its HPLC analysis revealed the same profile as the pure product obtained after HPLC purification. Oligonucleotide ϵ_{260} = 1.4 × 10^5 M^{-1} cm^{-1}, free porphyrin ϵ_{260} = 2.6 × 10^4 M^{-1} cm^{-1}, free porphyrin ϵ_{420} = 3.7 × 10^5 M^{-1} cm^{-1}; observed A_{422}/A_{265} = 2.4 (Figure 2). 60% of the starting oligonucleotide was converted to the conjugate according to HPLC profiles.

Synthesis of 2b. The metalloporphyrin (M = Mn^{III}, Y = OH) (7 mg, 9.5 μmol) was covered with dry dichloromethane (2.5 mL) and 19 mg (117 μmol, 12.3 equiv) of CDI was added. After 20 h of stirring at room temperature, HOBT (44 mg, 326 μmol, 34 equiv) was added and stirring continued for 2.5 h. Formation of the active ester **2a** was monitored by TLC (silica gel, CH_2Cl_2/MeOH; 8/2, v/v; R_f = 0.63). The green-brown solution was diluted to 60 mL with CH_2Cl_2 and washed with 2 × 30 mL of water. The organic layer was dried over sodium sulfate, filtered, and concentrated to dryness. The active ester (2 mg, 2.2 μmol, 244 equiv) was immediately dissolved in 90 μL of dry DMF, the solution added to 1.5 OD_{260} of NH_2-T_{17} oligonucleotide (9 nmol, 1 equiv) in 10 μL of HEPES buffer, and the mixture heated at 60 °C for 3 h. Workup was as described for **1b**. The product displayed t_R = 21.2 min. Desalting was carried out using G-25(F) Sephadex (gel volume = 10 mL). Oligonucleotide ϵ_{260} = 1.4 × 10^5 M^{-1} cm^{-1}, Mn-porphyrin ϵ_{260} = 2.8 × 10^4 M^{-1} cm^{-1}, Mn-porphyrin ϵ_{465} = 1.0 × 10^5 M^{-1} cm^{-1}; measured A_{470}/A_{260} = 0.64. 95% of starting oligonucleotide is converted into conjugate.

Synthesis of 3. The cationic free porphyrin (R = methylpyridiniumyl, Y = OH) (13.6 mg, 11.7 μmol) was dissolved in 300 μL of dry DMF followed by addition of CDI (16.4 mg, 101 μmol, 8.6 equiv), and the solution was stirred at room temperature for 13 h. HOBT (27.3 mg, 202 μmol, 172 equiv) was then added and stirring continued for 2.5 h. The unreacted CDI was quenched by the addition of 30 μL of HEPES buffer for 30 min. One-half of the resulting active ester solution was added to 13 OD_{260} of NH_2-T_{17} oligonucleotide (78 nmol) in 20 μL of HEPES buffer. The solution was heated at 60 °C for 5 h, and then solvents were removed with a Speed-Vac. A crude purification was carried out by passing an aqueous solution of the residue through G-25(F) Sephadex equilibrated with water. Purification by HPLC (Gen-Pak Fax column, t_R = 17.9 min) followed by desalting on a bed of G-25(F) Sephadex rendered the pure conjugate. Oligonucleotide ϵ_{260} = 1.4 × 10^5 M^{-1} cm^{-1}, free porphyrin ϵ_{260} = 1.4 × 10^4 M^{-1} cm^{-1}, free porphyrin ϵ_{428} = 2.0 × 10^5 M^{-1} cm^{-1}; measured A_{435}/A_{265} = 1.3. $Yield_{265}$ = 45% after final purification and desalting. Yield was measured by UV–visible at 265 nm in 1 mL of pure water.

Synthesis of 4, 6, and 7. The hybrid molecule **3** (1.5 OD_{265}) was dissolved in 150 μL of a solution of Mn(OAc)$_2$·4H_2O (5 mg/mL). After heating for 1 h at 100 °C, HPLC analysis revealed quantitative conversion (without detectable degradation) to the metalated species as evidenced by the shift of the Soret band from 435 to 467 nm. The axial ligand of this water-soluble manganese porphyrin is a hydroxo above neutral pH and a water molecule in acidic medium. The copper(II) and cobalt(II) complexes, **6** and **7**, were prepared in same fashion using $CuCl_2$ and $CoCl_2$·6H_2O, respectively. Again, the conversion was quantitative and degradation negligible. Because the difference of the position of the Soret band between the nonmetalated and the copper porphyrin is small, in order to prove that metalation did occur, the Cu(II) conjugate was subjected to treatment with Mn(OAc)$_2$ under the same conditions. No Soret shift to 465 nm was observed, indicating that the Cu(II) was already inserted in the porphyrin core and a single product was observed by HPLC. A short G-25(F) column (gel volume = 1 mL) is necessary to remove the excess of salts. The observed A_{vis}/A_{UV} ratios and t_R values were respectively 0.81 and 17.6 min for the Mn conjugate **4**, 0.82 and 17.9 min for the Cu conjugate **6**, and 0.84 and 18.1 min for the Co conjugate **7**.

Synthesis of 5. In a 25-mL flask was added 5.65 mg (6.0 μmol) of the cationic nickel(II) porphyrin precursor (M = Ni, R = methylpyridiniumyl, Y = OH) followed by 250 μL of dry DMF and CDI (10 mg, 60 μmol, 10 equiv).

After 2 h of stirring at room temperature, HOBT (16.4 mg, 120 μmol, 20 equiv) was added and stirring continued for 1 h. The excess of CDI was destroyed by addition of 20 μL of HEPES buffer with stirring for 15 min. To 135 μL of active ester solution was added 3 OD_{260} of NH_2-T_{17} oligonucleotide (18 nmol) in 10 μL of HEPES buffer and the resulting solution heated at 60 °C for 3 h. Removal of solvents under vacuum, crude purification on G-25(F) Sephadex, and final purification by HPLC (t_R = 18.3 min) rendered pure conjugate **5**, which was desalted as previously described. Oligonucleotide $\epsilon_{260} = 1.4 \times 10^5\ M^{-1}\ cm^{-1}$, Ni(II)porphyrin $\epsilon_{260} = 3.6 \times 10^4\ M^{-1}\ cm^{-1}$, Ni(II)porphyrin $\epsilon_{424} = 1.3 \times 10^5\ M^{-1}\ cm^{-1}$; observed $A_{435}/A_{270} = 0.95$. 78% of starting oligonucleotide is converted into conjugate.

Synthesis of 8. The cationic functionalized porphyrin (R = methylpyridiniumyl, Y = OH) was metalated by partially dissolving 5 mg (4.06 μmol) of it in 600 μL of a solution of $MnCl_2 \cdot 4H_2O$ (10.3 mg, 52 μmol, 13 equiv) and heating in a sealed screw-cap Eppendorf tube for 4.5 h. The solution was evaporated to near dryness (Speed-Vac), the residue dissolved in dry DMF, the solution filtered, and the product precipitated by addition of THF (in the last stage of this work, we have observed that some demetalation occurs to various extents using this procedure. Now the preferred method is to dilute the aqueous solution with 3.5 volumes of DMF and then carry out the precipitation with THF. Under these conditions no loss of metal occurs; see also ref 20). The mixture was centrifuged (8000 rpm, 25 min), the supernatant drawn off, the pellet triturated with THF, and the mixture centrifuged a second time. The product was dried under vacuum. The metalated cationic porphyrin (2.87 mg, 2.3 μmol) was dissolved in 150 μL of dry DMF, and addition of CDI (7.11 mg, 44 μmol, 19 equiv) followed. Formation of the imidazolide was allowed to take place over 13 h. HOBT (12 mg, 88 μmol, 38 equiv) was added and after 4 h at room temperature the excess of CDI was quenched by addition of 20 μL of HEPES buffer. After 30 min the solution was added to 2.1 OD_{260} of NH_2-19-mer oligonucleotide (13.4 nmol) in 20 μL of buffer. The solution was incubated at 37 °C for 20 h. The solvents were removed under vacuum (Speed-Vac), the residue was taken up in 500 μL of water, and the solution was applied to a column (2.5 g, 10 mL) of Bio-Gel P-2(F) from Bio-Rad equilibrated with water. The crude product was purified by HPLC on Gen-Pak Fax column (Figure 3a,b) and desalted using the same gel (2 g, water). In fact, we strongly recommend Bio-Gel over Sephadex gels for the purification of all these metalloporphyrin conjugates. A comparison of the UV–vis spectra before and after desalting revealed no loss of product. Oligonucleotide $\epsilon_{260} = 1.6 \times 10^5\ M^{-1}\ cm^{-1}$, Mn(III)porphyrin $\epsilon_{260} = 2.7 \times 10^4\ M^{-1}\ cm^{-1}$, Mn(III)porphyrin $\epsilon_{466} = 0.98 \times 10^5\ M^{-1}\ cm^{-1}$; observed $A_{468}/A_{264} = 0.63$ (cf. Figure 3c). $Yield_{264}$ = 25% after final purification and desalting. t_R values = 20.1 and 22.6 min for the conjugate **8** and the starting oligonucleotide, respectively (Figure 3a).

ACKNOWLEDGMENT

This work was supported by ANRS (french agency for research on AIDS), ARC (Villejuif), Genset (Paris), Pierre Fabre Médicaments (Castres), and Région Midi-Pyrénées. One of us (J.L.) is indebted to CNRS and Genset for fellowships. One reviewer is gratefully acknowledged for several constructive comments.

LITERATURE CITED

(1) Inouye, M. (1988) Antisense RNA: Its functions and applications in gene regulation—A review. *Gene 72*, 25–34.

(2) Cech, T. R., and Bass, B. (1986) Biological catalysis by RNA. *Ann. Rev. Biochem. 55*, 599–629.

(3) Goodchild, J. (1990) Conjugates of oligonucleotides and modified oligonucleotides: A review of their synthesis and properties. *Bioconjugate Chem. 1*, 165–187.

(4) Englisch, U., Gauss, D. H. (1991) Chemically modified oligonucleotides as probes and inhibitors. *Angew. Chem. Int. Engl. Ed. 30*, 613–722.

(5) Sarver, N., Cantin, E. M., Chang, P. S., Zaia, J. A., Ladne, P. A., Stephens, D. A., and Rossi, J. J. (1990) Ribozymes as potential anti-HIV-1 therapeutic agents. *Science 247*, 1222–1225.

(6) Zamecnik, P. C., and Stephenson, M. L. (1978) Inhibition of Rous sarcoma virus replication and cell transformation by a specific oligodeoxynucleotide. *Proc. Natl. Acad. Sci. U.S.A. 75*, 280–284.

(7) Lemaitre, M., Bayard, B., and Lebleu, B. (1978) Specific antiviral activity of a poly(L-lysine)-conjugated oligodeoxyribonucleotide sequence complementary to vesicular stomatitis virus N protein mRNA initiation site. *Proc. Natl. Acad. Sci. U.S.A. 84*, 648–652.

(8) Matsukura, M., Shinozuka, K., Zon, G., Mitsuya, H., Reitz, M., Cohen, J. S., and Broder, S. (1987) Phosphorothioate analogs of oligodeoxynucleotides: Inhibitors of replication and cytopathic effects of human immunodeficiency virus. *Proc. Natl. Acad. Sci. U.S.A. 84*, 7706–7710.

(9) Hélène, C., and Toulmé, J. J. (1990) Specific regulation of gene expression by antisense, sense and antigene nucleic acids. *Biochem. Biophys. Acta 1049*, 99–125.

(10) Rayner, B., Matsukura, M., Morvan, F., Cohen, J. S., and Imbach, J. L. (1990) *C. R. Acad. Sci. Paris 310 III.*, 61–64.

(11) Agrawal, S. (1991) Antisense oligonucleotides: A possible approach for chemiotherapy of AIDS. *Prospects for Antisense Nucleic Acid Therapy of Cancer and AIDS* (E. Wickstrom, Ed.), pp 143–158, Wiley-Liss, New York.

(12) Wickstrom, E. L., Bacon, T. A., Gonzalez, A., Freeman, D. L., Lyman, G. H., and Wickstrom, E. (1988) Human promyelocytic leukemia HL-60 cell proliferation and c-*myc* protein expression are inhibited by an antisense pentadecadeoxynucleotide targeted against c-*myc* mRNA. *Proc. Natl. Acad. Sci. U.S.A. 85*, 1028–1032.

(13) Vlassov, V., and Yakubov, L. A. (1991) Oligonucleotides in cell and in organisms: Pharmacological considerations. *Prospects for Antisense Nucleic Acid Therapy of Cancer and AIDS* (E. Wickstrom, Ed.), pp 243–266, Wiley-Liss, New York.

(14) Ding, L., Bernadou, J., and Meunier, B. (1991) Oxydative degradation of cationic metalloporphyrins in the presence of nucleic acids: A way to binding constants? *Bioconjugate Chem. 2*, 201–206.

(15) Pitié, M., Pratviel, G., Bernadou, J., and Meunier, B. (1992) Preferential hydroxylation by the chemical nuclease *meso*-tetrakis-(4-*N*-methylpyridiniumyl)porphyrinatomanganese^{III} pentaacetate/$KHSO_5$ at the 5′ carbon of deoxyriboses on both 3′ sides of three contiguous A.T base pairs in short double-stranded oligonucleotides. *Proc. Natl. Acad. Sci. U.S.A. 89*, 3967–3971.

(16) Ding, L., Balzarini, J., Schols, D., Meunier, B., and De Clercq, E. (1992) Anti-human immunodeficiency virus effects of cationic metalloporphyrin–ellipticine complexes. *Biochem. Pharmacol. 44*, 1675–1679.

(17) Le Doan, T., Praseuth, D., Perrouault, L., Chassignol, M., Thuong, N. T., and Hélène, C. (1990) Sequence-targeted photochemical modifications of nucleic acids by complementary oligonucleotides covalently linked to porphyrins. *Bioconjugate Chem. 1*, 108–113.

(18) Frolova, E. I., Ivanova, E. M., Zarytova, V. F., Abramova, T. V., and Vlassov, V. V. (1990) Porphyrin-linked oligonucleotides. Synthesis and sequence-specific modification of ssDNA. *FEBS Lett. 269*, 101–104.

(19) Wain-Hobson, S., Sonigo, P., Danos, O., Cole, S., and Alizon, M. (1985) Nucleotide sequence of the AIDS virus, LAV. *Cell 40*, 9–17.

(20) Casas, C., Saint-Jalmes, B., Loup, C., Lacey, C. J., and Meunier, B. (1993) Synthesis of cationic metalloporphyrin

precursors related to the design of DNA cleavers. *J. Org. Chem. 58*, 2913–2917.
(21) Pitié, M., Casas, C., Lacey, J., Pratviel, G., Bernadou, J., and Meunier, B. (1993) Efficient cleavage of a 35-mer single-stranded DNA containing the initiation codon of the TAT gene of HIV-1 by a targeted cationic manganese porphyrin. *Angew. Chem. Int. Engl. Ed. 32*, 557–559.
(22) Pratviel, G., Bernadou, J., and Meunier, B. (1988) Evidence for high-valent iron-oxo species active in the DNA breaks mediated by iron bleomycin. *Biochem. Pharmacol. 38*, 133–140.
(23) G. Fasman, Ed. *Handbook of Biochemistry and Molecular Biology—Nucleic Acids*, 3rd ed. (1975), CRC Press, Cleveland, p 175.
(24) Wachter, L., Jablonski, J. A., and Ramachandran, K. L. (1986) A simple and efficient procedure for the synthesis of 5′-aminoalkyl oligodeoxynucleotides. *Nucleic Acids Res. 14*, 7985–7994.

Polyamidoamine Cascade Polymers Mediate Efficient Transfection of Cells in Culture†

Jean Haensler and Francis C. Szoka, Jr.*

School of Pharmacy, University of California, San Francisco, California 94143-0446. Received May 7, 1993®

Cascade polymers also known as Starburst dendrimers are spheroidal polycations that can be synthesized with a well-defined diameter and a precise number of terminal amines per dendrimer. We show, using luciferase and beta-galactosidase containing plasmids, that dendrimers mediate high efficiency transfection of a variety of suspension and adherent cultured mammalian cells. Dendrimer-mediated transfection is a function both of the dendrimer/DNA ratio and the diameter of the dendrimer. Maximal transfection of luciferase are obtained using a diameter of 68 Å and a dendrimer to DNA charge ratio of 6/1 (terminal amine to phosphate). Expression is unaffected by lysomotrophic agents such as chloroquine and only modestly affected (2-fold decrease) by the presence of 10% serum in the medium. Cell viability, as assessed by dye reduction assays, decreases by only 30% at 150 μg dendrimer/mL in the absence of DNA and about 75% in the presence of DNA. Under similar conditions polylysine causes a complete loss of viability. Gene expression decreased by 3 orders of magnitude when the charge ratio is reduced to 1:1. When GALA, a water soluble, membrane-destabilizing peptide, is covalently attached to the dendrimer via a disulfide linkage, transfection efficiency of the 1:1 complex is increased by 2–3 orders of magnitude. The high transfection efficiency of the dendrimers may not only be due to their diameter and shape but may also be caused by the pK_a's (3.9 and 6.9) of the amines in the polymer. The low pK_a's permit the dendrimer to buffer the pH change in the endosomal compartment. The characteristics of precise control of structure, favorable pK_a's, and low toxicity make the dendrimers suitable for gene-transfer vehicles.

INTRODUCTION

Molecular biologists have identified the chromosomal defects in a large number of human hereditary diseases, raising the prospects for cures using gene therapy. This emerging branch of medicine aims to correct genetic defects by transferring cloned and functionally active genes into the afflicted cells. At present, viruses are the most efficient vectors for gene transfer (*1*, *2*), but potential risks associated with viruses have catalyzed a search for synthetic DNA-delivery systems (*3*). Early work showed that polycations such as polylysine and DEAE–dextran promote the uptake of proteins (*4*) and single- and double-stranded polynucleotides into animal cells (*5*, *6*), and since then, polylysine-based vectors for gene transfer have been extensively studied (*7*). However, the linear polycations are relatively cytotoxic and by themselves not very efficient, which limits their usefulness for transfection of cells in culture.

In spite of these drawbacks, polylysines have a number of advantages: they help to assemble DNA into a compact structure, destabilize cell membranes, and provide a handle for the attachment of other effectors to the nucleic acid. Neutralization and condensation of DNA by polylysines into small (ca. 100 nm) toroid-like structures promotes the endocytosis of the nucleic acid into cells *in vitro* (*8*). The endocytic process can be further stimulated by the covalent attachment to the polycation of specific ligands like transferrin (*9*), asialoorosomucoid (*10*), or insulin (*11*). When polycation transfection procedures are based upon receptor-mediated or fluid-phase endocytosis, a large fraction of the endocytosed DNA becomes trapped in intracellular vesicles and is ultimately degraded in the lysosomes. Lysosomal degradation can be partially bypassed by the addition of lysomotrophic agents such as chloroquine during the transfection (*12*) or by the attachment of endosome disrupting agents to the polylysine, such as inactivated viruses (*13*) or viral fusogenic peptides (*14*). The ability of polylysine–DNA complexes to transfect cells is strongly dependent upon the presence of these effectors.

As an alternative to polylysine for transfection, we describe a nonlinear polycationic cascade polymer which combines the DNA-binding and delivery properties of polylysine and the lysomotrophic effects of weak bases (*15*). We show that polyamidoamine (PAMAM) cascade polymers, a well-defined class of dendritic polymers synthesized from methyl acrylate and ethylenediamine (*16*), are well-tolerated by cells and when complexed to plasmids encoding reporter genes mediate highly efficient transfection of a wide variety of cells in culture. In addition, the covalent attachment of the amphipathic peptide GALA (*17*) to the cascade polymer can significantly enhance transfection efficiency in both primary cells and cell lines.

EXPERIMENTAL PROCEDURES

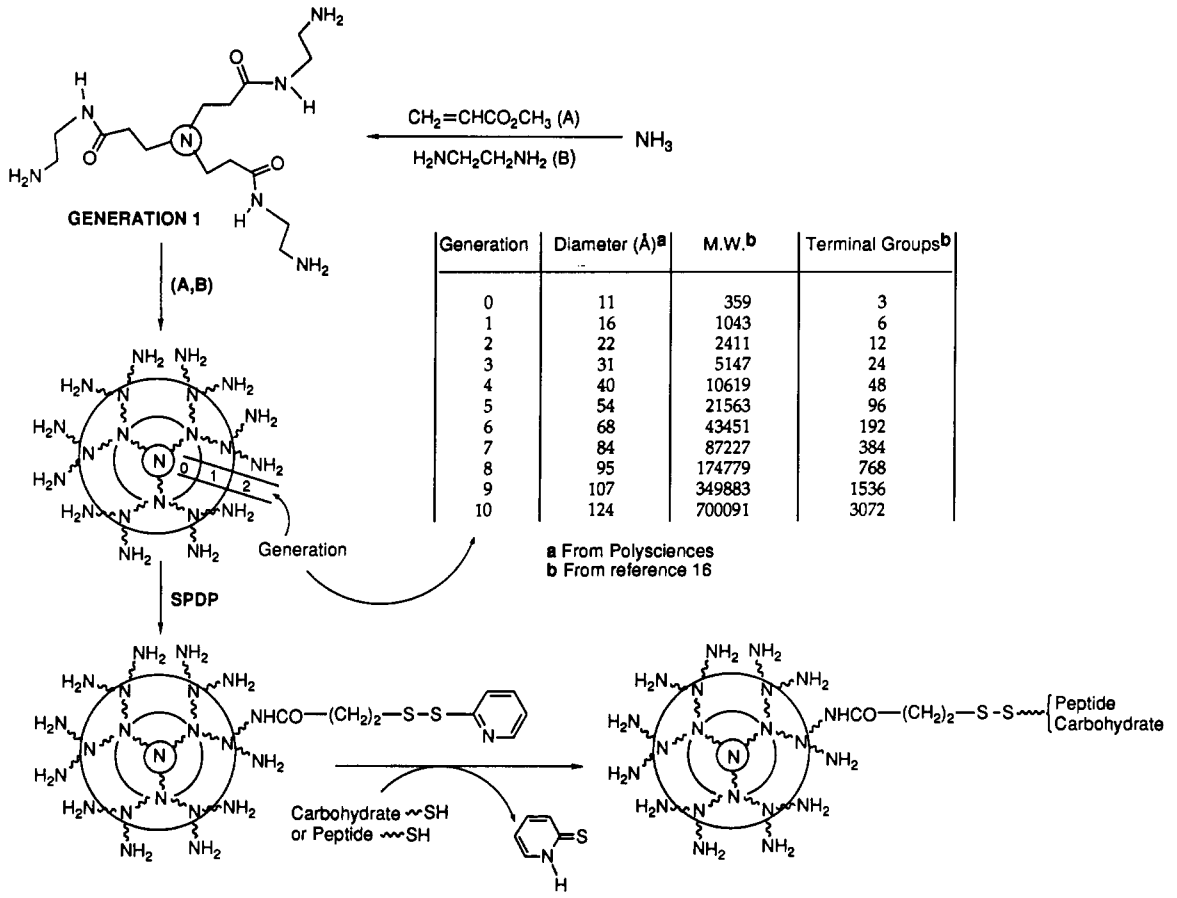
Materials. PAMAM cascade polymers synthesized from an ammonia initiator core (generation 2–10) were obtained from Polysciences, Inc. (Warrington, PA) and are designated as Starburst dendrimers. When needed, dendrimer solutions were concentrated using a Savant

* Address correspondence to this author.

† Abbreviations used: DME, Dulbecco's modified Eagle's medium; EDTA, ethylenediaminetetraacetic acid; FCS, fetal calf serum; HBS, Hepes buffered saline (10 mM Hepes; 150 mM NaCl, pH 7.3); Hepes, *N*-(2-hydroxyethyl)piperazine-*N*'-(2-ethanesulfonic acid); MEM, minimal essential Eagle's medium; MTT, 3-(4,5-dimethylthiazol-2-yl)-2,5-diphenyltetrazolium bromide; Tris, tris(hydroxymethyl)aminomethane; PAMAM SD54 and SD68, polyamidoamine Starburst dendrimer 54 and 68 Å in diameter; pLys115, poly(L-lysine) with an average chain lengh of 115 monomers.

® Abstract published in *Advance ACS Abstracts*, September 1, 1993.

1043-1802/93/2904-0372$04.00/0 © 1993 American Chemical Society



Generation	Diameter (Å)[a]	M.W.[b]	Terminal Groups[b]
0	11	359	3
1	16	1043	6
2	22	2411	12
3	31	5147	24
4	40	10619	48
5	54	21563	96
6	68	43451	192
7	84	87227	384
8	95	174779	768
9	107	349883	1536
10	124	700091	3072

a From Polysciences
b From reference 16

Figure 1. Synthesis, physical characteristics, and functionalization of PAMAM cascade polymers (modified from ref 16).

SC110 Sped Vac system. Similar results to those reported here are obtained when the cascade polymer was synthesized in our laboratory using the published method (*16*) but starting from tris(2-aminoethyl)amine (unpublished results, C. Redemann, J. Haensler, and F. Szoka). The commercially available dendrimers should be analyzed on a calibrated gel permeation column to insure that the material conforms to the specified diameter, since we have received a few lots that did not conform to specifications. Poly(L-lysine) hydrobromide with an average chain length of 115 lysine residues (pLys115) was obtained from Sigma Chemical Co. (St. Louis, MO). *N*-Succinimidyl 3-(2-pyridyldithio)propionate (SPDP) was obtained from Pierce (Rockford, IL). GALAcys (WEAALAEALAE-ALAEHLAEALAEALEACAA) a cysteine-containing analog of the amphipathic peptide GALA was synthesized at the UCSF Bioresources Center, purified, and analyzed essentially as previously described for GALA (*17*).

Modification of SD54 with GALAcys. The PAMAM dendrimer of the fifth generation (54 Å in diameter, SD54) was modified following the scheme in Figure 1.

Functionalization of SD54 with SPDP. The dendrimer (66 μmol terminal amines, 15 mg) in 0.5 mL of water was diluted with 0.75 mL of 0.1 M phosphate buffer (pH 8.0), and 0.75 mL of a 15 mM solution of SPDP in ethanol was added dropwise. The reaction mixture was stirred for 1 h under argon and fractionated on a Biogel P2 column (2.8 × 20 cm) eluted with 0.1M phosphate buffer (pH 7.4). The fractions containing 3-(2-pyridyldithio)propionate-modified dendrimers (PDP-SD54 with an average of 16 dithiopyridine groups per particle) were pooled together and concentrated to a final volume of 3 mL.

Reaction of PDP-SD54 with GALAcys. One milliliter of a 10 mM solution of GALAcys in a 0.1 M phosphate buffer (pH 7.2) was added dropwise to 1 mL of the concentrated PDP-SD54 solution. The mixture was stirred overnight under argon, then the GALA conjugate was purified by fractionating the reaction mixture on a calibrated Sephade G75-120 column (2 × 90 cm) [calibration kit: Sigma MW-GF-70 containing aprotinin (6500), cytochrome C (12 400), carbonic anhydrase (29 000), albumin (66 000), and blue dextran (2 000 000)]. The column was eluted with 0.1M phosphate buffer (pH 7.4). The fractions containing the conjugate, which eluted with an apparent molecular weight of about 50 000, were pooled, concentrated, and dialyzed against HBS (10 mM Hepes; 150 mM NaCl, pH 7.3). The dialyzed material was diluted with HBS to 1 mg of dendrimer/mL and sterile filtered through a 0.45-μm Millipore membrane.

Expression Vectors. The plasmids pCLUC4 (18) encoding firefly luciferase and pCMV-βGal (*19*) encoding β-galactosidase were generous gifts from Dr. M. Cotten (Institute of Molecular Pathology, Vienna, Austria) and Dr. G. McGregor (Howard Hughes Medical Institute, Houston, TX), respectively. Plasmids were grown in *Escherichia coli*, extracted by the alkali lysis technique, and purified by centrifugation in equilibrum CsCl gradients. The purity of the plasmids was checked by electrophoresis on a 0.8% agarose gel and the DNA concentration was determined by absorbance at 260 nm.

Preparation of Complex. A typical complex was made by diluting 6 μg of plasmid DNA into 330 μL of HBS in a polystyrene tube. The polycation and/or its GALA-functionalized derivative (2–160 μg) were diluted in 170 μL of HBS and added dropwise to the DNA. When the addition was completed the solution was gently mixed. The formation of the polycation–DNA complex was shown by a gel retardation assay; samples (30 μL) were electro-

phoresed through a 0.8% agarose gel using a Tris-acetate–EDTA buffer system (pH 8.0) and DNA was visualized using ethidium bromide staining.

Cells and Transfection Protocol. The adherent cell lines CV-1 (monkey fibroblast), HeLa (human carcinoma), and HepG2 (human hepatoma) were provided by the UCSF cell culture facility. Cells were plated at a density of about 5×10^5 cells per 60 mm culture dish (Falcon) in 3 mL of DME-H21 containing 10% FCS and antibiotics (100 units/mL penicillin, and 100 units/mL Streptomycin). The cells were grown to half confluency at 37 °C in a humidified atmosphere containing 5% CO_2. In a typical experiment, cells were transfected in 1.5 mL of medium without serum by addition of 0.5 mL of HBS containing 6 μg of plasmid complexed with the indicated amount of polycation. Five hours later the medium was removed and replaced by fresh medium containing 10% FCS. The cells were cultured for an additional 24- or 48-h period and tested for reporter gene expression.

The suspension cell lines K-562 (human erythroleukemia), EL-4 (mouse lymphoma), and Jurkat (human T-cells) were obtained from the UCSF cell culture facility and grown in RPMI 1640 containing 10% FCS and antibiotics. For the transfection experiment, 1.2×10^6 cells in 1.5 mL of RPMI 1640 containing 7.5% FCS were introduced into each well of a 6-well plate or rotated in polypropylene tubes and transfected with 6 μg of DNA as described above. Five hours later the cells were transferred to fresh medium containing 10% FCS. This was accomplished after centrifugation of the plate or tubes (1200 rpm for 5 min) and by removing 90% of the transfection medium and replacing it with fresh prewarmed medium. The cells were cultured for an additional 24- or 48-h period and tested for reporter gene expression.

Freshly isolated rat hepatocytes were obtained from Dr. M. Bissel (Liver center, UCSF) and plated at a density of 2×10^6 cells per 60-mm culture dish in 3 mL of a medium (hepatocyte medium) composed of 75% MEM and 25% Waymouths and containing 10% FCS, insulin (10 μg/mL), transferrin (10 μg/mL), dexamethasone (1 μM), and antibiotics (100 units/mL penicillin, 100 μg/mL streptomycin, and 25 μg/mL gentamycin). Cells were grown at 37 °C in a humidified atmosphere containing 5% CO_2. The cells were transfected 5–6 h later as described above with 6 μg of plasmid in 2 mL of the hepatocyte medium containing 2% FCS. After an overnight incubation period, the transfection medium was removed and replaced with 3 mL of fresh hepatocyte medium containing 2% FCS. The cells were further cultured for 24 h and tested for reporter gene expression.

β-Galactosidase gene expression was detected 24 h after transfection by histochemical staining of the cells using X-Gal (*20*). Luciferase reporter gene expression was quantitated 48 h after transfection on cell lysates by measuring the light emission with a bioluminometer (Analytical bioluminescence, San Diego, CA) in the presence of luciferin and ATP (*21*).

The effect of chloroquine on transfection efficiency was studied by performing the transfection in medium containing 100 μM of this lysomotrophic agent. When hepatocytes were transfected in the presence of chloroquine, the transfection step was reduced to 5 h to avoid acute cytotoxicity.

Toxicity Assay. The effects of the cascade polymers on cell growth were assessed by measuring total protein content after transfection as well as by using a colorimetric dye reduction assay (*22*). The effect of the sixth generation dendrimer (68 Å in diameter, SD68) was compared to the effect of polylysine (pLys115). The polycations were added to the cells with or without plasmid DNA at a ratio of 10 terminal amines of the polycation per nucleotide. Cells were plated at a density of about 5×10^4 cells per well in 300 μL of DME H-21 in 96-well trays. After an overnight culture at 37 °C in a 5% CO_2 humidified atmosphere, the cells were incubated in triplicates with 200 μL of serum-free medium containing 0–60 μg of pLys115 or SD68. After 5 h the media were replaced with 200 μL of fresh DME H-21 containing 10% FCS, and the cells were cultured for an additional 48 h. Then, 10 μL of 3-(4,5-dimethylthiazol-2-yl)-2,5-diphenyltetrazolium bromide (MTT, 5 mg/mL) was added per well and allowed to react for 2 h at 37 °C. Solubilizing solution (0.4 N HCl in 2-propanol, 200 μL) was added and the plate incubated for 30 min at room temperature. Absorbance at 570 nm was measured using an automatic ELISA plate reader (MR 700, Dynatech Laboratories Inc.) and corrected for background absorbance obtained on cells treated with 6M guanidinium hydrochloride (100% death). Results are expressed as percent reduction in cell viability = $\{1 - [OD_{570}(\text{treated cells}) - \text{background}]/[OD_{570}(\text{untreated cells}) - \text{background}]\} \times 100$.

RESULTS

Synthesis and Characterization of Modified Cascade Polymers. One goal of this work was to use the dendrimer as a platform to attach functional groups to polynucleotides such as DNA to create gene delivery vehicles. The fifth generation PAMAM dendrimer was linked to GALAcys, a cysteine-containing analog of the amphipathic peptide GALA, by using standard SPDP coupling chemistry (*23*) (Figure 1). The fifth generation dendrimer has a hydrodynamic radius of 54 Å, a molecular weight of 21 563 and contains 96 terminal amines. The dendrimer was successively functionalized with the heterobifunctional reagent SPDP and reacted with an excess of GALAcys. The resulting conjugate eluted from a calibrated Sephade G75-120 column with an apparent molecular weight of about 50 000 Da. This suggests the presence of about 10 GALA residues per dendrimer. An average of 13 GALA residues were found to be conjugated to one dendrimer when GALA was quantified by using a molar extinction coefficient for tryptophan of $\epsilon_{280nm} = 5570$ M^{-1} cm^{-1} (pH 7.5). Since GALA contains eight negative charges per peptide, most of the unmodified amines on the conjugates are probably neutralized at pH 7.4, a supposition that is supported by the weak binding of the GALA conjugate to DNA (vide infra).

Binding of Cascade Polymers to DNA. PAMAM dendrimers bind to DNA as demonstrated by retention of the complex at the point of application on an agarose electrophoresis gel (Figure 2). Both the polylysine (lanes 2 and 3) and the cascade polymer (lanes 4 and 5) were able to retard and immobilize the DNA on the gel. Gel retardation is a result of electrostatic and steric effects and suggests the formation of a charge complex between the positively-charged dendrimers and the anionic DNA. Because dendrimer terminal amines have lower pK_a than lysine $\epsilon NH2$ (see Discussion), the dendrimer was slightly less effective in inducing gel retardation than polylysine (Figure 2). With polylysine, total retention of the plasmid was observed at a 1:1 ϵNH_2 to nucleotide ratio (lane 3); with the dendrimer total retention occurred at about 1.5:1 terminal NH_2 to nucleotide ratio (lane 5). The exact ratio of total retention varied by one dilution factor among experiments. The GALA–dendrimer conjugate did not immobilize the DNA and affected only slightly the

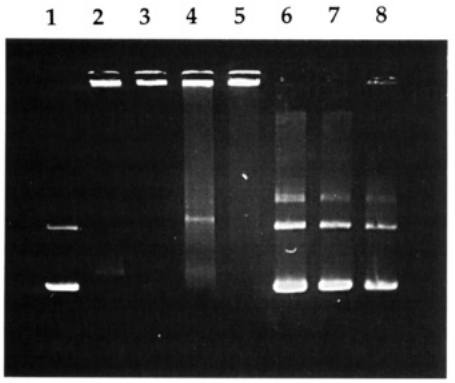


Figure 2. Effect of pLys115, SD68, SD54, and GALA–SD54 on the electrophoretic mobility of plasmid DNA. Samples (30 μL) of polycation–pCMV-βGal complexes were incubated for 20 min and electrophoresed through a 0.8% agarose gel using a Tris-acetate–EDTA buffer system (pH 8.0). The complexes were formed as described in Experimental Procedures by mixing 6 μg of pCMV-βGal plasmid diluted in 330 μL of HBS with the following agents in 170 μL of HBS: lane 1, pCMV-βGal alone; lane 2, 2 μg of pLys115; lane 3, 4 μg of pLys115; lane 4, 4 μg of SD68; lane 5, 6 μg of SD68; lane 6, 4 μg of SD54 provided by the GALA–SD54 conjugate; lane 7, 160 μg of SD54 provided by the GALA–SD54 conjugate; lane 8, 4 μg of SD54 provided by an equimolar mixture of SD54 and GALA–SD54. After the electrophoresis was completed the gel was stained with ethidium bromide to visualize DNA.

migration of the plasmid even when used in large excess over the DNA (lanes 6 and 7). A combination of GALA–dendrimer conjugate and unmodified dendrimer (1:1 ratio, as used in the transfection assays) partially retained the plasmid (lane 8).

Optimization of the Complex for Transfection. An unexpected finding of this work is that PAMAM cascade polymers alone could transfect DNA (e.g. plasmids encoding reporter genes) into cells in culture (Table I; Figures 3–5). The transfection activity was particularly high when an excess of terminal amines to nucleotide was used. To define the parameters controlling gene delivery and expression by the dendrimers, CV-1 cells were transfected with pCLUC4–dendrimer complexes and luciferase expression measured as a function of the diameter and amount of the dendrimer in the complex (TableI). Transfection was sensitive to both factors. High luciferase expression required an excess of polycation; at a low dendrimer input ([dendrimer primary amines] ≤ [nucleotides]) cells were only poorly transfected by the complexes.

In the concentration range studied, large diameter dendrimers ($\phi \geq 40$ nm), mediated better transfection efficiencies than the smaller ones. Luciferase expression increased by 2–3 orders of magnitude when the diameter of the complex-forming dendrimer was increased from 40 (generation 4) to 54 Å (generation 5). This can be best appreciated from examining the data on a three-dimensional plot (Figure 3). Maximal levels of transfection were obtained ($\geq 10^{10}$ light units (LU)/mg cell protein) with the dendrimer of the sixth generation. The sixth generation dendrimer, designated SD68, has a hydrodynamic radius of 68 Å and a molecular weight of 43 451 and contains 192 terminal amines. Using SD68 at a ratio of six primary amines per nucleotide, luciferase expression in CV-1 cells was about a 1000-fold greater than that obtained with an equivalent amount of polylysine 115 (Table I) and a 100-fold greater than that obtained with the cationic lipid DOTMA (*24, 25*). The optimized conditions were tested in 10 separate experiments in CV-1 cells; luciferase activities between 2×10^9 and 3×10^{10} LU/mg of cell proteins were obtained. When CV-1 cells were transfected with dendrimer in medium containing 10% FCS, the luciferase expression was decreased by about 2-fold, whereas expression decreased by 50-fold in the case of DOTMA (25).

A dose response of luciferase activity versus DNA input at a constant terminal amines/nucleotide ratio of 6/1 was constructed using SD-68 (Figure 4). When the complex was first formed and then diluted to the stated amount of pCLUC4 plasmid, a linear decrease in expression of luciferase was observed (Figure 4). If non-luciferase-containing plasmid was used to dillute the luciferase plasmid and the dendrimer added, the transfecting activity also decreased in a linear fashion. When the plasmid was first diluted and a constant amount of dendrimer was added (in this case dendrimer/plasmid ratio increases with the dilution of the pCLUC4 plasmid), transfection activity decreased to a greater extent (Figure 4).

Transfection of Mammalian Cells with SD68–DNA Complexes at Low Terminal Amines/Nucleotide Ratios. Every cell type examined in this study could be transfected under conditions of excess terminal amines over nucleotides, with PAMAM dendrimer–luciferase plasmid. The cells examined included adherent and suspension cells and both primary cultures and established lines (Figure 5A). Transfection efficiency of the optimized complex was also examined using the pCMV-βGal plasmid as the reporter gene. β-Galactosidase activity was detected by a histochemical stain 24 h after transfection and transfected cells counted. The percentage of transfected cells in the population detected by the histochemical stain is indicated at the end of the bar on the graph (Figure 5A). The cell types studied differed in their ability to undergo transfection (up to 80% transfection in CV-1, less than 1% transfection in EL-4 and Jurkat). This variability is a general property shared by all gene delivery systems; the reason for such variable transfection among cell types is not understood yet.

At the lower dendrimer input, the transfection efficiency of the dendrimer–DNA complexes was dramatically reduced (Figure 5A,B). Reduced transfection activity with lower terminal amines/nucleotide ratios is similar to results seen with polylysines. Thus we examined whether or not treatments that can increase transfection mediated by linear polycations could increase the dendrimer-mediated transfection. Interestingly, transfection was essentially insensitive to chloroquine (not shown) but increased significatively when the fusogenic peptide GALA was attached to the dendrimer.

Enhancement of Transfection by Covalent Attachment of the Amphipathic Peptide GALAcys to the Cascade Polymer. The endosome disruptive effects of inactivated viral particles and of viral fusogenic peptides have been exploited to trigger or enhance polylysine-mediated gene transfer (*13, 14*). The 30 amino acid peptide GALA was designed to destabilize lipid bilayers in a pH-sensitive manner to mimic the properties of viral fusogenic proteins (*17*). We attached GALA to the dendrimer to learn if it could increase transfection as do the viral particles or the viral fusogenic peptides. At a low terminal amines to nucleotide ratio, the transfection efficiency of dendrimer–DNA complexes was low; however, transfection was significantly improved when 50% of the dendrimer in the complex was replaced for its GALA conjugate (Figure 5B). Under these conditions the conjugate can function at a low dendrimer/plasmid ratio (about 50:1 in these experiments). In the case of some cell types, such as K562, the GALA conjugate was as effective as using the 6-fold

Table I. Influence of the Amount and Size of PAMAM Cascade Polymer Complexed to pCLUC4 Plasmid on Luciferase Reporter Gene Expression in CV-1 Cells

generation	diameter, Å	luciferase activity[a] 0.5[b]	1	3	6	10	16	25
				Starburst Dendrimer				
2	22	$(8.9 \pm 0.8)10^4$	$(1.6 \pm 0.01)10^5$	$(1.9 \pm 0.2)10^5$	$(4.1 \pm 0.06)10^5$	$(3.7 \pm 0.7)10^5$	$(4.3 \pm 0.4)10^5$	$(5.7 \pm 0.9)10^5$
3	31	$(7.5 \pm 0.1)10^3$	$(7.7 \pm 4.5)10^4$	$(1.0 \pm 0.3)10^5$	$(3.9 \pm 0.3)10^5$	$(7.5 \pm 0.05)10^5$	$(1.5 \pm 0.5)10^6$	$(1.1 \pm 0.08)10^6$
4	40	$(2.7 \pm 0.2)10^3$	$(2.9 \pm 0.2)10^3$	$(2.7 \pm 1.8)10^5$	$(9.8 \pm 4.0)10^5$	$(1.2 \pm 0.3)10^6$	$(3.4 \pm 0.4)10^6$	$(7.7 \pm 1.1)10^6$
5	54	$(3.1 \pm 1.8)10^4$	$(6.1 \pm 0.5)10^5$	$(1.1 \pm 0.03)10^8$	$(1.5 \pm 0.2)10^8$ [92%]	$(2.6 \pm 0.3)10^8$ [88%]	$(6.1 \pm 0.4)10^8$ [74%]	$(5.9 \pm 1.1)10^8$ [72%]
6	68	$(7.5 \pm 5.8)10^4$	$(2.7 \pm 0.05)10^5$	$(4.0 \pm 0.5)10^8$	$(1.0 \pm 0.1)10^{10}$ [64%]	$(1.3 \pm 0.4)10^{10}$ [56%]	$(1.2 \pm 0.3)10^9$ [53%]	$(4.8 \pm 0.6)10^8$ [45%]
7	84	$(1.9 \pm 0.3)10^4$	$(4.8 \pm 0.1)10^5$	$(4.9 \pm 0.5)10^7$ [93%]	$(2.3 \pm 0.5)10^8$ [60%]	$(5.1 \pm 0.7)10^8$ [56%]	$(2.5 \pm 0.4)10^8$ [43%]	$(7.3 \pm 0.6)10^7$ [26%]
8	95	$(1.9 \pm 0.4)10^4$	$(5.7 \pm 0.6)10^5$ [90%]	$(2.8 \pm 0.9)10^7$ [82%]	$(1.8 \pm 0.5)10^7$ [77%]	$(3.5 \pm 0.3)10^7$ [60%]	$(7.4 \pm 2.0)10^7$ [38%]	$(1.1 \pm 0.3)10^8$ [25%]
9	107	$(3.2 \pm 2.6)10^4$	$(7.7 \pm 1.2)10^4$	$(3.9 \pm 0.3)10^7$	$(1.9 \pm 0.2)10^8$ [90%]	$(1.9 \pm 0.4)10^8$ [68%]	$(1.8 \pm 0.06)10^8$ [61%]	$(1.7 \pm 0.03)10^8$ [44%]
10	124	$(2.4 \pm 0.3)10^3$	$(2.8 \pm 0.2)10^3$	$(7.7 \pm 0.6)10^6$	$(1.4 \pm 0.07)10^7$ [91%][c]	$(8.4 \pm 0.6)10^6$ [76%]	$(1.0 \pm 0.03)10^7$ [65%]	$(4.4 \pm 0.02)10^6$ [60%]
				$pLys_{115}$				
		$(1.6 \pm 0.5)10^4$	$(1.7 \pm 0.6)10^5$	$(1.9 \pm 0.1)10^6$ [88%][c]	$(7.3 \pm 2.3)10^6$ [57%]	$(1.7 \pm 0.2)10^7$ [37%]	$(1.9 \pm 0.6)10^7$ [11%]	[0%][c]

[a] Luciferase activity in the transfected cells (light units per mg of cell protein) is shown as the mean ± range of duplicates. [b] Primary amines/nucleotides. [c] When the transfection procedure was toxic, the percentage recovery of cell protein in transfected cells compared to nontransfected cells is indicated in brackets.

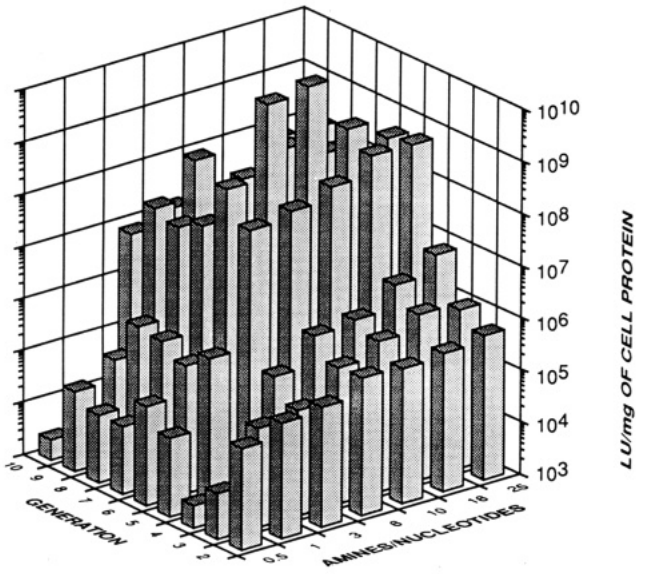


Figure 3. Effect of dendrimer diameter and amount in mediating transfection in CV-1 cells (data from Table I).

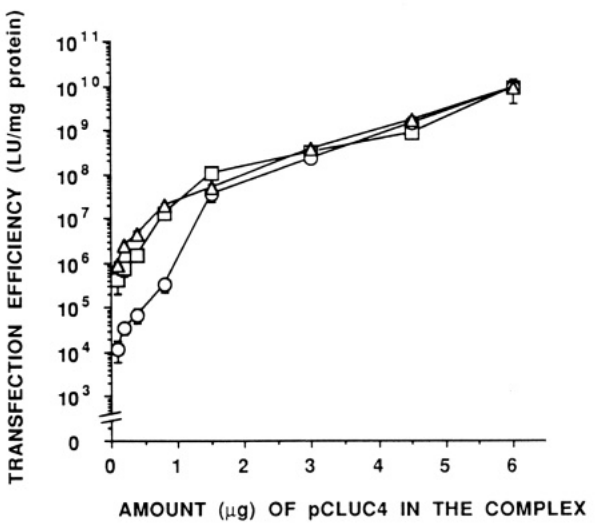


Figure 4. Dose–response of luciferase activity versus the amount of pCLUC4 plasmid used for the transfection. CV-1 cells (500 000 cells per 60-mm dish) were transfected in duplicate with increasing amounts of pCLUC4 (0.1–6 μg) complexed to SD68. The complexes were formed as described in Experimental Procedures by adding the dendrimer dissolved in 170 μL of HBS to the DNA in 330 μL of HBS; □, complexes were first formed by adding 25 μg of SD68 on 6 μg of pCLUC4 and then diluted in HBS to the stated amount of DNA; ○, the plasmid was first diluted in HBS and 25 μg of SD68 was added; △, a non-luciferase-containing plasmid was added to the diluted pCLUC4 plasmid to keep the total amount of DNA constant at 6 μg/330 μL and then 25 μg of SD68 was added. Luciferase expression was measured 48 h post-transfection as described in Table I. Each value is the mean ± range of duplicate determinations.

excess of dendrimer for transfection (Figure 5A,B). These results indicate that GALA is a transfection-enhancing agent probably by catalyzing endosome leakage. At a dendrimer input where transfection was maximal, expression was not enhanced further by GALA. This may be because dendrimers display lysosomotrophic effects (see Discussion).

Comparison of Cytotoxicity of PAMAM Cascade Polymer to pLys 115. One index of the toxicity of the transfection procedure is the amount of cell protein obtained from the cultures following transfection. Treatments that resulted in a decrease in the yield of cell protein when compared to nontreated cells are indicated in brackets in Table I. Dendrimer–DNA-induced cytotoxicity seemed to be controlled by three main parameters: the diameter of the dendrimer, the amount added, and whether or not DNA was present.

The last factor can be better appreciated when the toxicity of the dendrimer SD68 was compared to polylysine 115 on CV-1 cells in the presence and the absence of plasmid DNA (Figure 6). The overall cytotoxicity of SD68 was low when compared to that of pLys115. In the absence of DNA, the LD_{50} of pLys115 for CV-1 cells was 25 μg/mL and the LD_{50} of SD68 was greater than 300 μg/mL. In the presence of plasmid DNA (ratio of 10:1 primary amines of polycation to nucleotide), the cytotoxicity of pLys115 was not affected while that of SD68 was increased (LD_{50} of SD68–DNA = 100 μg/mL) but still was significantly less than that of pLys115.

Under the optimized transfection conditions, the concentration of SD68 was 12.5 μg/mL, a level of dendrimer that induced about a 35% decrease in dye reduction (Figure

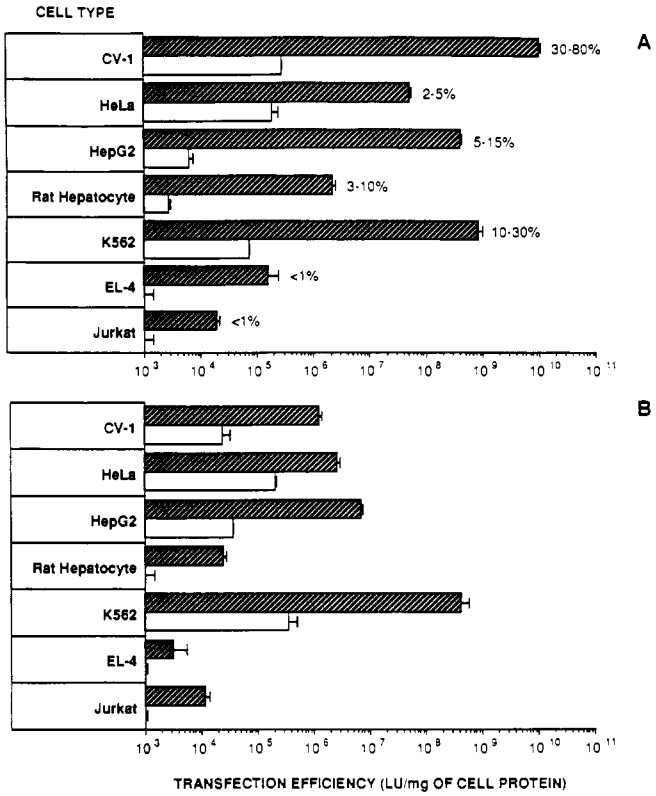


Figure 5. PAMAM cascade polymer mediated transfection of mammalian cells. (A)Cells were transfected in duplicates as described in Experimental Procedures with 6 μg of plasmid complexed to SD68. The transfection efficiency of the optimized complex (25 μg of SD68/6 μg of plasmid, hatched bar) was compared to that obtained with complexes formed with 4 μg of SD68/6 μg of plasmid ([terminal amines] = [nucleotides], □). Luciferase activity in the pCLUC4-transfected cells was measured 48 h post-transfection as described in Table I or 24 h post-transfection in the case of primary hepatocytes. Each value is the mean ± range of duplicate determinations. The percentage of transfected cells in the optimized conditions was estimated with the pCMV-βGal plasmid. Transfected cells were detected by histochemical staining using X-Gal, 24 h post-transfection (20). Results are shown as percentages on the histogram. (B)Cells were transfected as above with 6 μg of pCLUC4 complexed to 4 μg of dendrimer provided by unmodified SD54 (□) or by an equimolar mixture of unmodified SD54 and GALA-SD54 (hatched bar).

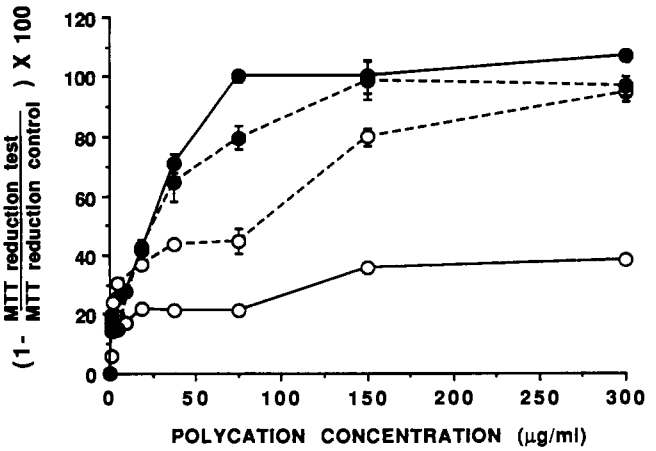


Figure 6. Comparison of the toxicity of pLys115 and SD68 on CV-1 cells. CV-1 cells in a 96-well plate were treated for 5 h in serum-free DME H-21 with increasing amounts of polycation [pLys115 (●) or SD68 (○)] complexed (- -) or not (—) to plasmid DNA and cultured for an additional 48-h period in DME H-21 containig 10% FCS. After this period, toxicity of the treatments was estimated by the MTT dye reduction assay. Formazan was quantified after lysis of the cells by its absorbance at 570 nm. Background absorbance was obtained by running the assay on cells treated with 6 M guanidinium hydrochloride. Percent reduction in cell viability = {1 − [OD_{570}(treated cells) − background]/[OD_{570}(untreated cells) − background]} × 100. Each value is the mean ± SD of triplicate determinations.

6) as well as in cell protein recovery (Table I). According to the cell protein recovered at the end of the assay, the transfection with SD68–DNA complexes was reasonably well-tolerated by all of the different cell types tested (protein recovery ≥ 60%).

DISCUSSION

Polycationic polymers such as polylysines have been extensively used for gene transfer into animal cells (*7*). Polylysine-based vectors have a high delivery capacity but efficient transfection of target cells occurs only in the presence of endosome disrupting or lysomotrophic agents (*12, 26*). Our goal was to identify a polycationic polymer which would combine the delivery capacity of polylysines and the transfection capacity of a virus.

We thought that functionalized PAMAM cascade polymers (*16*) also known as Starburst dendrimers might be ideal for this purpose. The PAMAM cascade polymers used in this study are derived from an ammonia core and $CH_2CH_2CONHCH_2CH_2N$ units resulting from successive additions of methyl acrylate and ethylenediamine (Figure 1). The controlled step-growth propagation of this structure produces increasingly higher generations of polymers with dimensionally precise surfaces and with a defined number of surface groups (*16*). The diameter of the higher generation dendrimers is similar to the diameter of the histone core of chromatin (ca. 70 Å) (*27*) and might act as a scaffold to condense the DNA. PAMAM dendrimers differ from polylysines due to their well-characterized formula and structure, their branching, and the low pK_a of their terminal amines (pK_a = 6.9, ref 16) and internal amines (pK_a = 3.9, ref 16).

The efficient internalization of DNA when associated with polycations may be due to a zipper-like association of the excess positive charges of the polycation–DNA complex with negatively charged cell-surface groups. This interaction may result in adsorptive endocytosis and membrane destabilization, such as has been proposed by Behr for cationic liposomes–DNA complexes (*28*). Indeed, the DNA binding abilities of polylysine and the dendrimer, studied by gel retardation, are similar (Figure 2). To increase membrane destabilization after endocytosis we have attached the membrane destabilizing peptide GALA to the dendrimer.

When tested for plasmid delivery and transfection, the unmodified PAMAM dendrimers displayed interesting activities. The transfection efficiency was dependent on the size and amount of the dendrimer in the DNA–dendrimer complex. Most notably, a dramatic increase in transfection was observed when the diameter of the dendrimer was increased from 40 (generation 4) to 54 Å (generation 5). The reason for this threshold effect is still unclear but may be related to the diameter and structure of the polymer. Upon going from generation 3 to generation 5, a structural change occurs in the polymer; through generation 3, PAMAM dendrimers resemble a starfish, by generation 5 they have a spheroidal form of about 54 Å in diameter (*16*). This spherical shape might serve as a highly structured core to favorably constrain the DNA, such as occurs in chromatin (*27*). Alternatively, the spherical form may be more efficient at destabilizing

membranes than either the lower generation dendrimers or the linear polycations.

PAMAM cascade polymers also differ from polylysines by the pK_a of their primary and interior amino groups (pK_a's = 6.9, 3.9). We think that this property is also important for transfection. At physiologic pH, the PAMAM dendrimers are only partially protonated and should display lysosomotrophic effects similar to weak bases (*15*). In addition, the interior tertiary amino groups, which constitute the branching of the dendrimer, have a pK_a of 3.9 and might also contribute to the lysomotrophic effect. Thus, the dendrimer should buffer endosomal acidification after endocytosis of the complex. The putative lysomotrophic properties of the PAMAM dendrimers would explain why an excess of dendrimers are required for high transfection whereas an excess of polylysines does not increase transfection (Table I). In the case of polylysine, the side chain amino groups (pK_a = 9–10) are strongly charged at neutral pH and cannot buffer acidification of the endosome. This conjecture is supported by the observation that transfection efficiency of the dendrimer–DNA complex is not enhanced by chloroquine (not shown); whereas the transfection efficiency of polylysine–DNA complexes is usually dramatically enhanced in the presence of chloroquine (*12*).

The complex composed of plasmid DNA and SD68 at a ratio of six terminal amines of SD68 per nucleotide displayed the best transfection activity. In these optimal conditions, there are about 320 SD68 particles per pCLUC4 plasmid; however all the dendrimer particles may not be in complexes with DNA; as suggested above the excess dendrimer might act as a lysomotrophic agent. Above this optimal ratio, the system becomes less efficient. Increasing the amount of SD68 may decrease transfection because of toxicity associated with the complex. Alternatively, an increase in the amount of noncomplexed dendrimer may compete with the DNA–dendrimer for putative binding sites on the cell surface. This would decrease the level of cell associated DNA and in this fashion decrease transfection.

Increasing the diameter of the dendrimer, while the 6/1 ratio is maintained, did not increase toxicity, but transfection efficiency was reduced. Observation of cells in the optical microscope that were exposed to dendrimer–DNA complexes formed from greater than the sixth generation dendrimer revealed the presence of large intracytoplasmic vacuoles in the treated cells. Large vacuoles are not observed in cells treated with complexes formed from dendrimers of the sixth or lower generations. Whether the vacuoles are related to the reduced transfection rates requires further study.

Toxicity was further examined by using the MTT dye reduction assay. The SD68 dendrimer is very well-tolerated by cells, much better than equivalent amounts of pLys115. The marked difference in toxicity between pLys115 and SD68 is probably due to the difference in the ionization state of the particles. At physiological pH, polylysines bear more positive charges than dendrimers and should have a stronger interaction with cell membranes. The toxicity of the dendrimer was significantly increased in presence of plasmid DNA but remained less than that of the corresponding polylysine–DNA complexes. As can be stated for all synthetic DNA delivery systems, the exact extent of interaction and fate of dendrimer–DNA complexes when interacting with cells will require considerably more study before their mechanisms of DNA delivery are understood.

It is particularly encouraging that the GALA peptide was able to significantly increase the transfection activity of the complex when the GALA was covalently attached to the dendrimer (Figure 5B). GALA was designed to be a water-soluble membrane destabilizer (*17*) and its pH-dependent interaction with membranes has been well studied (*29* and references therein). Peptides with the GALA motif have been attached to antibodies to increase their tumor cell retention and internalization (*30*). The fact that dendrimer–GALA conjugates mixed with unmodified dendrimers at a 1:1 ratio could enhance transfection is an indication that the dendrimer may be an excellent platform for the synthesis and assembly of highly efficicent transfection systems.

Starburst PAMAM dendrimers based transfection procedures constitute simple and efficient methods for gene transfer into animal cells. The good results obtained on a wide variety of cells (Figure 5) are encouraging and, by themselves, PAMAM dendrimers may be ideally suited for the direct application of genes into animals by delivery via the airways or intramuscular. The dendrimers are also able to increase the cellular uptake and nuclear localization of other polynucleotides such as oligonucleotides (G. Green and F. Szoka, unpublished observation). Furthermore, the promising transfection levels obtained with the GALAcys peptide suggest to us that the selectivity and transfection efficiency of the system can be improved by attaching targeting ligands, fusogenic peptides, and/or nuclear localization peptides to the cascade polymer. This approach has already been tried with polylysines (*14, 31*), and because of their structure, pK_a properties, and defined molecular weights, the PAMAM cascade polymers may be ideally suited to form the basis for such a modular DNA delivery system.

ACKNOWLEDGMENT

We are grateful to Robert Stull, Mary Tang, and other members of the Szoka group and Kun Bee Chang for helpful discussions and technical assistance. Thanks are also extended to the UCSF mass spectrometry facility supported by RR01614 and the UCSF Liver Center (POAM26743A). This work was partially supported by the National Institute of Health. The GALA aspect was supported by GM-30163 and the dendrimer aspect by DK-46052.

LITERATURE CITED

(1) Gilboa, E., Eglitis, M. A., Kantoff, P. W., and Anderson, W. F. (1986) Transfer and expression of cloned genes using retroviral vectors. *Biotechniques 4*, 504–512.
(2) Felgner, P. L., and Rhodes, G. (1991) Gene therapeutics. *Nature 349*, 351–352.
(3) Rosenfeld, M. A., Siegfried, W., Yoshimura, K., Yonehama, K., Fukayama, M., Stier, L. E., Paakko, P. K., Gilardi, P., Stratford-Perricaudet, L. D., Perricaudet, M., Jallat, S., Pavirani, A., Lecocq, J. P., and Crystal, R. G. (1991) Adenovirus mediated transfer of a recombinant alpha-1 anti trypsin gene to the lung epithelium in vivo. *Science 252*, 431–434.
(4) Ryser, H. P. (1968) Uptake of protein by mammalian cells: An underdeveloped area. *Science 159*, 390–396.
(5) Juliano, R., and Mayhew, E. (1972) Interaction of polynucleotides with cultured mammalian cells. I. Uptake of RNA by Ehrlich ascites carcinoma cells. *Exp. Cell. Res. 73*, 3–12.
(6) Mayhew, E., and Juliano R. (1973) Interaction of polynucleotides with cultured mammalian cells. II. Effect of cell surface charge on RNA uptake. *Exp. Cell. Res. 77*, 409–414.
(7) Felgner, P. L. (1990) Particulate systems and polymers for in vitro and in vivo delivery of polynucleotides. *Adv. Drug Delivery Rev. 5*, 163–187.
(8) Wagner, E., Cotten, M., Foisner, R., and Birnstiel, M. L. (1991) Transferrin–polycation DNA complexes: The effect of

polycation on the structure of the complex and DNA delivery to cells. *Proc. Natl. Acad. Sci. U.S.A. 88*, 4255–4259.
(9) Zenke, M., Steinlein, P., Wagner, E., Cotten, M., Beug, H., and Birnstiel, M.L.(1990) Receptor-mediated endocytosis of transferrin-polycation conjugates: An efficient way to introduce DNA into hematopoietic cells. *Proc. Natl. Acad. Sci. U.S.A. 87*, 3655–3659.
(10) Wu, G. Y., and Wu, C. H. (1988) Evidence for targeted gene delivery to HepG2 hepatoma cells in vitro. *Biochemistry 27*, 887–892.
(11) Huckett, B., Ariatti, M., and Hawtrey, A. O. (1990) Evidence for targeted gene transfer by receptor-mediated endocytosis: Stable expression following insulin-directed entry of neo into HepG2 cells. *Biochem. Pharmacol. 40*, 253–263.
(12) Cotten, M., Langle-Rouault, F., Kirlappos, H., Wagner, E., Mechtler, K., Zenke, M., Beug, H., and Birnstiel, M. L. (1990) Transferrin–polycation-mediated introduction of DNA into human leukemic cells: Stimulation by agents that affect the survival of transfected DNA or modulate transferrin receptor levels. *Proc. Natl. Acad. Sci. U.S.A. 87*, 4033–4037.
(13) Wagner, E., Zatloukal, K., Cotten, M., Kirlapos, H., Mechtler, K., Curiel, D.T., and Birnstiel, M. L. (1992) Coupling of adenovirus to transferrin–polylysine/DNA complexes greatly enhances receptor-mediated gene delivery and expression of transfected genes. *Proc. Natl. Acad. Sci. U.S.A. 89*, 6099–6103.
(14) Wagner, E., Plank,C., Zatloukal, K., Cotten, M., and Birnstiel, M. L. (1992) Influenza virus hemagglutinin HA-2 N-terminal fusogenic peptides augment gene transfer by transferrin–polylysine–DNA complexes: Toward a synthetic virus-like gene-transfer vehicle. *Proc. Natl. Acad. Sci. U.S.A. 89*, 7934–7938.
(15) Stenseth, K., and Thyberg, J. (1989) Monensin and chloroquine inhibit transfer to lysosomes of endocytosed macromolecules in cultured mouse peritoneal macrophages. *Eur. J. Cell. Biol. 49*, 326–333.
(16) Tomalia, D. A., Naylor, A. M., and Goddard, W. A., III (1990) Starburst cascade polymers: Molecular-level control of size, shape, surface chemistry, topology, and flexibility from atoms to macroscopic matter. *Angew. Chem. Int. Ed. Engl. 29*, 138–175.
(17) Subbarao, N. K., Parente, R. A., Szoka, F. C., Nadasdi, L., and Pongracz, K. (1987) pH-dependent bilayer destabilization by an amphipathic peptide. *J. Biol. Chem. 26*, 2964–2972.
(18) De Wet, J. R., Wood, K. V., De Luca, M., Helinsky, D. R., and Subramani, S. (1987) Firefly luciferase gene: Structure and expression in mammalian cells. *Mol. Cell Biol. 7*, 725–737.
(19) Mc Gregor, G. R., and Caskey, C. T. (1989) Construction of plasmids that express E. coli β-galactosidase in mammalian cell lines. *Biotechniques 7*, 1116–1122.
(20) Lim, K., and Chae, C-B. (1989) A simple assay for DNA transfection by incubation of the cells in culture dishes with substrates for beta-galactosidase. *Biotechniques 7*, 576–579.
(21) Brasier, A. R., Tate, J. E., and Habener, J. F. (1989) Optimized use of the firefly luciferase assay as a reporter gene in mammalian cell lines. *Biotechniques 7*, 1116–1122.
(22) Mosmann, T. R. (1983) Rapid colorimetric assay for cellular growth and survival: Application to proliferation and cytotoxycity assays. *J. Immunol. Methods 65*, 55–63.
(23) Carlsson, J., Drevin, H., and Axén, R. (1978) Protein thiolation and reversible protein-protein conjugation. N-succinimidyl 3-(2-pyridyldithio) propionate, a new heterobifunctional reagent. *Biochem. J., 173*, 723–737.
(24) Felgner, P. L., Gadek, T., Holm, M., Roman, R., Chan, H. W., Wentz, M., Northrop, J. P., Ringold, G. M., and Danielsen, M. (1987) Lipofection: A highly efficient, lipid-mediated DNA-transfection procedure. *Proc. Natl. Acad. Sci. U.S.A. 84*, 7413–7417.
(25) Legendre, J. Y., and Szoka, F. C. (1992) Delivery of plasmid DNA into mammalian cell lines using pH-sensitive liposomes: Comparison with cationic liposomes. *Pharm. Res. 9*, 1235–1242.
(26) Cotten, M., Wagner, E., Zatloukal, K., Phillips, S., Curiel, D. T., and Birnstiel, M. L. (1992) High efficiency receptor-mediated delivery of small and large (48Kb) gene constructs using the endosome disruption activity of defective or chemically-inactivated adenovirus particles. *Proc. Natl. Acad. Sci. U.S.A. 89*, 6094–6098.
(27) Richmond, T. J., Fink, J. T., Rushton, B., Rhodes, D., and Klug, A. (1984) Structure of the nucleosome core particle at a 7 Å resolution. *Nature 311*, 532–537.
(28) Behr, J.-P. (1993) Synthetic gene-transfer vectors. *Acc. Chem. Res. 26*, 274–278.
(29) Parente, R. A., Nadasdi, L., Subbarao, N., and Szoka, F. C., Jr. (1990) Association of a pH-sensitive peptide with membrane vesicles: Role of amino acid sequence. *Biochemistry 29*, 8713–8719.
(30) Anderson, D. C., Manger, R., Schroeder, J., Woodle, D., Barry, M., Morgan, A. C., and Fritzberg, A. R. (1993) Enhanced in vitro tumor cell retention and internalization of antibody derivatized with synthetic peptides. *Bioconjugate Chem. 4*, 10–18.
(31) Plank, C., Zatloukal, K., Cotten, M., Mechtler, K., and Wagner, E. (1992) Gene transfer into hepatocytes using asialoglycoprotein receptor mediated endocytosis of DNA complexed with an artificial tetra-antennary galactose ligand. *Bioconjugate Chem. 3*, 533–539.

End Attachment of Phenol–Oligonucleotide Conjugates to Diazotized Cellulose

Marie-laurence Fontanel,† Hervé Bazin,‡ and Robert Téoule*,†

Laboratoire de Radiobiochimie, Centre d' Etudes Nucléaires de Grenoble, DRFMC/SESAM, 85X, 38041 Grenoble Cedex, France, and Laboratoire des Sondes Moléculaires, CIS Bio International, BP32-91192 Gif-Sur-Yvette, Cedex, France. Received April 2, 1993®

The synthesis of a novel phosphoramidite reagent with a hexanediol backbone is described. This reagent has been used to incorporate a phenol moiety on an oligonucleotide (ODN) directly in the course of its automated synthesis. Multiple phenol attachments can be achieved by repetitive coupling cycles. A simple and rapid immobilization method is described where phenol-modified ODNs are covalently attached to diazotized cellulose. The binding capacity of the membrane can be modulated, depending on the ODN concentration used, to ca. 180 pmol/cm^2. There is at least 80% end attachment of the ODN through the phenol group. In addition, the phenol residue can be used as a carrier for the radiolabeling with ^{125}I. The non-nucleosidic hexanediol derivative incorporated at the 5′-end of the ODN is recognized as a substrate by the T4 polynucleotide kinase and the terminal hydroxyl group is successfully phosphorylated allowing its ^{32}P labeling.

INTRODUCTION

One of the most common methods for the detection of specific nucleic acid sequences typically involves the immobilization of the target nucleic acid on solid supports such as nitrocellulose or nylon membranes followed by hybridization with an appropriate labeled signal probe. The immobilization methods such as the "baking procedure" or UV irradiation suffer from a low retention efficiency and proceed by random attachment along the polynucleotide. Another approach involves the coupling of DNA to cyanogen bromide activated supports (*1, 2*) and to Sephadex, Sephacryl and cellulose via diazotized aromatic amines (*3–5*). Multiple attachments through base residue (mostly guanine) inhibit hybridization. All these methods are restricted to the immobilization of long DNA (>400 bp), but for ODNs (14–30 mers), the hybridization process can be disrupted. This led to the development of chemical covalent methods in which there is generation of a specific and stable linkage preferentially between the 5′-end of the ODN and the support.

Procedures for the modification of ODNs have been reviewed (*6*). One of the methods is based on carbodiimide-mediated end attachment of nucleic acids to polysaccharide matrix such as cellulose (*7*), Sephadex (*3*), or Sephacryl (*8*) and to hydroxyl polystyrene beads through ODN 5′-phosphate group (*9*). Attachments of 5′-amino alkyl ODNs to carboxyl polystyrene beads (*9*) or controlled pore glass (CPG) derivatized with long-chain alkylamine or carboxylic Sephacryl have been reported (*10*). For most of these reported methods the 5′-terminal attachment efficiency is low even with long reaction times and the nonspecific binding to the support is high.

The development of the automated synthesis of short ODN probes makes them readily available. They show better hybridization kinetics and high sensitivity in the detection of mutations. They have become a powerful tool either in the PCR technology and in the reverse dot hybridization format (*11*), where the target nucleic acid probe is hybridized to a capture ODN probe. Numerous 5′-modifications of ODNs based on the phosphoramidite approach for the introduction of 5′-NH_2 or 5′-SH have been investigated. The reaction time required for the attachment to the support has been considerably decreased from 20 to 3 h (*12*). Further improvements allowed a reaction time of 1 min (*13*), but the coupling efficiency was still too low.

More recently, more specific reactions were used at the 5′-end of the ODN (*14*). The systems showed stable and efficient attachment at one end of the ODN (*15–18*) on different solid supports: nylon beads (*17*), membranes (*15*), magnetic beads (*18*), and polyacrylamide (*19*).

In this work we describe a simple and rapid method for covalent attachment of ODNs modified by a phenol group on a diazotized cellulose matrix. The phenol groups were incorporated into the ODNs by using a phenylphosphoramidite derivative according to the direct labeling procedure described by Roget *et al.* (*20*). Other authors reported the synthesis of simple non-nucleosidic phosphoramidite units: Misiura *et al.* (*21*) expanded the use of 1,2-ethanediol phosphoramidite reagents derived from a glycerol intermediate. Nelson's reagent (*22*) is based on a 1,3-propanediol backbone. Both provide multiple incorporation and 3′-labeling. The use of the present 1,2-ethanediol backbone is not only restricted to the immobilization but it can be used for the radiolabeling (either ^{125}I (*26*) or ^{32}P). When the modification is introduced at the 5′-end of the ODN, it is still recognized as a substrate by the T_4 polynucleotide kinase (PNK).

EXPERIMENTAL PROCEDURES

Iodine-125 S4 (200 mCi/mL) was a product of Cis Bio International. Adenosine 5′-triphosphate (ATP) was purchased from Boehringer (100 mM) and [γ-^{32}P]ATP (10 mCi/mL) came from Amersham. Cellulose membranes (APT Cellulose) came from Schleicher and Schull. T_4 polynucleotide kinase was obtained from Pharmacia. Analytical grade solvents were used, and dichloromethane stabilized with 2-methyl-2-butene was used for synthesis. The ^{1}H NMR and ^{31}P-NMR spectra were recorded respectively on AC 200 and WM 250 Bruker spectrometers. The *J* values are reported in hertz. The mass spectra were recorded on a Fisons-VG type ZAB2-SEQ spectrom-

* To whom correspondence should be addressed.
† Centre d'Etudes Nucleaires de Grenoble.
‡ CIS Bio International.
® Abstract published in *Advance ACS Abstracts*, September 1, 1993.

1043-1802/93/2904-0380$04.00/0 © 1993 American Chemical Society

eter using a cesium gun. Short-column chromatography was run on silica G60 (Merck) and TLC analysis was performed on plastic sheets (60F(254), 0.2 mm layer, Merck). The HPLC analysis were performed on a Varian 5000 equipped with a Lichrospher RP-18 (5 μm) column (Merck) working at a flow rate of 1 mL/min (gradient 1,10% to 50% B in 20 min and then 50% to 100% B in 30 min, where A = 5% CH_3CN in 25mM triethylammonium acetate (TEAAc) and B = 50% CH_3CN in 25mM TEAAc) and on a Mono Q HR 5/5 anion-exchange column (Pharmacia), working at a flow rate of 1 mL/min (gradient 2, 0–2 min 0% B, 5 min 20% B, 40 min 40% B, where A = 20% CH_3CN in 40 mM sodium acetate, pH 5.5, and B = 20% CH_3CN in 40 mM sodium acetate, 1.5 M lithium chloride).

1,2-*O*-Isopropylidene-1,2,6-hexanetriol (2). A solution of 1,2,6-hexanetriol (20 g, 149 mmol) in a mixture of acetone (45 mL) and petroleum ether (45 mL) containing 4-toluenesulfonic acid was heated in a round-bottom flask fitted with a Vigreux column, a Dean–Stark apparatus, and a condenser (Drierite guard). After 22 h under reflux the cooled reaction mixture was neutralized with saturated aqueous $NaHCO_3$ (25 mL) and concentrated in vacuo. The residue was taken up in dichloromethane (100 mL) and washed with saturated $NaHCO_3$ (3 × 100 mL) and water (100 mL). The organic phase was evaporated and coevaporated with carbon tetrachloride. Compound **2** was obtained as an oil. Yield: 21.5 g (83%). R_f = 0.46 in chloroform/methanol (90/10, v/v). ^1H NMR ($CDCl_3$): 4.06 (psq, J = 6.33 , 1H, H-2), 4.03 (pst, J= 7.35 and 6.33, 1H, H-1), 3.63 (pst, J = 6.39 and 6.48, 2H, H-6,6′), 3.51 (pst, J= 7.33 and 7.35, 1H, H-1′), 1.74–1.20 (*m*, 6H, 3 × CH_2, 1.38 (*s*, 3H) and 1.32 (*s*, 3H) (2 × isopropylidene CH_3).

1,2-*O*-Isopropylidene-6-*O*-(4-toluenesulfonyl)hexanetriol (3). Compound **2** (13 g, 74.7 mmol) was coevaporated with dry pyridine (2 × 50 mL) and dissolved in dichloromethane (100 mL) containing diisopropylethylamine (9.65 g, 74.7mmol) and 4-(dimethylamino)pyridine (122 mg, 1 mmol). A solution of 4-toluenesulfonyl chloride (15.6 g, 87.2 mmol) in dichloromethane (40 mL) was added dropwise at 0 °C with stirring. After 7 h at 0 °C the reaction mixture was extracted with water (3 × 150 mL) and evaporated to dryness. The residue was purified over a short silica gel column using a gradient of dichloromethane in petroleum ether (from 30 to 100%). The compound **3** is obtained as an oil. Yield: 23.4 g (96%). R_f = 0.67 in ethyl acetate/hexane (1/1, v/v). ^1H NMR ($CDCl_3$): 7.84 (*d*, J = 8 , 2H) and 7.32 (*d*, 2H) (tosyl H), (4.15–3.70 (*m*, 4H, H-1, H-2 and H-6,6′), 3.43 (pst, J = 10, 1H, H-1′), 2.45 (*s*, 3H) (tosyl CH_3), 2.0–1.1 (*m*, 6H) 3 × CH_2, 1.45 (*s*, 3H) and 1.39 (s, 3H) 2-(isopropylidene × CH_3).

1,2-*O*-Isopropylidene-6-azido-1,2-hexanediol (4). To a solution of **3** (25 g , 76 mmol) in dimethylformamide (450 mL) were added sodium azide (6 g, 92 mmol) and ammonium chloride (5.3 g, 100 mmol). The reaction mixture was kept at 120 °C for 2 h with stirring. The solvent was distilled off (oil pump). The residue dissolved in dichloromethane (400 mL) was washed with saturated $NaHCO_3$ (3 × 300 mL) and water (400 mL). The crude compound was purified on a silica gel column with a gradient of dichloromethane in petroleum ether (30–100%). Yield: (64%). R_f = 0.6 in ethyl acetate/hexane (3/7, v/v). ^1H NMR ($CDCl_3$): 4.10–4.01 (*m*, 1H, H-2), 4.0 (pst, J = 7.0 and 6.0, 1H, H-1), 3.44 (pst, J = 8 and 7, 1H, H-1′), 3.23 (pst, J = 6.0 and 7.0, 2H, H-6,6′), 1.68–1.10 (*m*, 6H) 3 × CH_2, 1.39 (*s*, 3H) and 1.26 (*s*, 3H) (2 × isopropylidene CH_3).

1,2-*O*-Isopropylidene-6-amino-1,2-hexanediol (5). Lithium aluminium hydride (366 mg, 37.9 mmol) in 10 mL of THF) was added dropwise to a cooled (0 °C) solution of **4** (640 mg, 3.2 mmol) in THF (15 mL) with stirring. After 15 min at 0 °C and then 4 h at 25 °C, the reaction mixture was treated with water (0.4 mL), 15% aqueous NaOH (0.4 mL), and water (1.2 mL). The white precipitate was filtered over celite and washed with THF (2 × 10 mL). The combined fitrates were evaporated and the residue was purified with a gradient of methanol in dichloromethane (5–50%). The title compound was obtained as an oil. Yield: 481 mg (87%). R_f = 0.16 in methanol/dichloromethane (2/8, v/v). ^1H NMR ($CDCl_3$): 4.2–3.9 (*m*, 2H, H-1 and H-2), 3.5 (*t*, J = 6.4 , 1H, H-1′), 2.7 (*t*, J = 6.2 , 2H, H-6,6′), 1.72 (*s*, 2H, NH_2), 1.7–1.1 (*m*, 6H, 3 × CH_2), 1.4 (*s*, 3H) and 1.32 (*s*, 3H) (2 × isopropylidene CH_3).

1,2-*O*-Isopropylidene-*N*-[3-(4-hydroxyphenyl)propanoyl]-6-amino-1,2-hexanediol (6): Compound **5** (2.5 g, 14.5 mmol) dissolved in a mixture of acetonitrile (10 mL) and dichloromethane (20 mL) was reacted with *N*-succinimidyl 3-(4-hydroxyphenyl)propanoate (5.2 g, 19.7 mmol) in the presence of diisopropylethylamine (1.87 g, 14.5 mmol). After 3 h of stirring, the reaction mixture was diluted with dichloromethane and washed with saturated $NaHCO_3$ solution (2 × 100 mL) and water (100 mL), and the organic layer was dried over Na_2SO_4 and evaporated. The crude compound was loaded onto a silica gel column packed in a dichloromethane petroleum ether mixture (8/2) and eluted with a stepwise gradient to dichloromethane and then to 5% methanol in dichloromethane. Yield: 4.08 g (88%). R_f = 0.63 in dichloromethane/methanol (9/1, v/v). ^1H NMR ($CDCl_3$): 7.0 (*d*, J = 8.4 , 2H, H-2,6 arom), 6.76 (*d*, 2H, H-3,5 arom), 4.1–3.8 (*m*, 2H, H-1,2), 3.5–3.3 (*m*, J = 5.2 , 1H, H-1′), 3.3–3.0 (*m*, 2H, H-6,6′), 2.85 (*t*, J = 7.4, 2H, H-2,2′, propanoyl), 2.38 (*t*, 2H, CH-3,3′, propanoyl), 1.7–1.0 (*m*, 6H, 3 × CH_2), 1.39 (*s*, 3H) and 1.34 (*s*, 3H) (2 × isopropylidene CH_3).

***N*-[3-(4-Hydroxyphenyl)propanoyl]-6-amino-1,2-hexanediol (7).** Compound **6** (2.9 g, 30 mmol) was treated with Dowex 50 W-X12 (100–200 mesh, H^+ form) in a dioxane-water mixture (1/1, 50 mL) for 45 min at 100 °C. The ion-exchanger was filtered off and washed with a dioxane/methanol mixture (1/1, 10 mL). The filtrate was evaporated and the residue was dried under vacuum over P_2O_5. Yield: 2.12 g (83%). R_f = 0.8 in dichloromethane/methanol (8/2, v/v). ^1H NMR ($CDCl_3$): 7.0 (*d*, J = 8.4, 2H, H-2,6 arom), 6.76 (*d*, 2H, H-3,5 arom), 3.72–3.27 (*m*, 3H, H-1,1′ and H-2), 3.25–2.97 (*m*, 2H, H-6,6′), 2.78 (*t*, J = 7.3, 2H, H-2,2′, propanoyl), 2.35 (*t*, 2H, H-3,3′, propanoyl), 1.6–1.1 (*m*, 6H, 3 × CH_2).

***N*-[3-[4-(Ethoxycarbonyl)oxy]phenyl]propanoyl]-6-amino-1,2-hexanediol (8).** To a cold (0 °C) solution of **7** (2.1 g, 5.4 mmol) in THF (60 mL) containing triethylamine (1.2 mL, 8.4 mmol) was added a solution of ethyl chloroformate (1.09 g, 9.8 mmol) in THF (4 mL) dropwise. After 1 h at room temperature the reaction mixture was evaporated to dryness, dissolved in ethyl acetate (10 mL), and precipitated from hexane (100 mL) as a powder. Yield: 1.53 g (58%). R_f = 0.47 in dichloromethane/methanol (8/2, v/v). ^1H NMR ($CDCl_3$): 7.3–6.8 (*m*, 4H, arom), 4.28 (*q*, J = 7.1, 2H, CH_2CH_3), 3.6–3.45 (*m*, 2H, H-1 and H-2), 3.4–3.27 (*m*, 1H, H-1′), 3.25–3.0 (*m*, 2H, H-6,6′), 2.88 (*t*, J =7.5, 2H, H-2,2′, propanoyl), 2.38 (*t*, 2H, H-3,3′, propanoyl), 1.55–1.10 (*m*, 9H, 3 × CH_2 and CH_3). MS (FAB^+): *m/e* (MH^+) = 354.4, (MNa^+) = 376.

1-*O*-(4,4′-Dimethoxytrityl)-N-[3-[4-[(ethoxycarbonyl)oxy]phenyl]propanoyl]-6-amino-1,2-hexane diol (9). Compound **8** (1.4 g, 4 mmol) was coevaporated with

dry pyridine (2 × 20 mL), dissolved again in pyridine (35 mL), and 4,4′-dimethoxytrityl chloride (1.7 g, 5 mmol) in pyridine (10 mL) was added at 0 °C. After 4 h at 0 °C, water (20 mL) was added and the reaction mixture was partitioned between dichloromethane (100 mL) and saturated $NaHCO_3$ solution (100 mL). The organic layer was washed with $NaHCO_3$ (100 mL) and water (2 × 100 mL). After evaporation and coevaporation with toluene the residue was purified on a short silica gel column packed in a petroleum ether/dichloromethane mixture (6/4) containing 5% of triethylamine, eluting successively with a gradient of dichloromethane in petroleum ether and then 1% methanol in dichloromethane. Yield: 2.24 g (86%). R_f = 0.28 in dichloromethane/methanol (9/1). ^{1}H NMR ($CDCl_3$): 7.6–7.0 (*m*, 13H, arom DMT), 6.82 (*d*, *J* = 8.6, 4H, DMT), 4.28 (*q*, *J* = 7.1, 2H, CH_2CH_3), 3.95–3.60 (*m*, 1H, H-2), 3.8 (*s*, 6H, 2 × CH_3O, DMT), 3.35–2.90 (*m*, 6H, H-1,1′, H-2,2′, H-6′6′, and H-2,2′, propanoyl), 2.4 (*t*, *J* = 7.35, 2H, H-3,3′, propanoyl), 1.65–1.10 (*m*, 9H, 3 × CH_2 and 3 × CH_3). MS (FAB^+): (MNa^+) = 678.7.

1-*O*-(4,4′-Dimethoxytrityl)-2-*O*-[[(2-cyanoethyl)oxy]-(*N*,*N*-diisopropylamino)phosphino]-*N*-[3-[4-[(ethoxycarbonyl)oxy]phenyl]propanoyl]-6-amino-1,2-hexanediol (10). Compound **9** (1.7 g, 2.6 mmol) was coevaporated with dry acetonitrile and taken up in dichloromethane (22 mL) under argon. Diisopropylammonium tetrazolide (263 mg, 1.5 mmol) and 2-cyanoethyl-*N*,*N*,*N*′,*N*′-tetraisopropylphosphorodiamidite (1.07 mL, 3.4 mmol) were added. After 3 h the reaction mixture was diluted with dichloromethane (50 mL) and washed with saturated $NaHCO_3$ (2 × 20 mL) and brine (2 × 100 mL). The organic layer was dried over Na_2SO_4 and evaporated. The residue was loaded onto a short silica gel column eluting with a gradient from hexane/dichloromethane/triethylamine (90/9/1) to hexane/dichloromethane/triethylamine (50/49/1). The relevant fractions were evaporated, coevaporated with toluene and lyophilized from benzene in several serum flasks fitting on the DNA synthesizer. Yield: 1.55 g (70%). R_f = 0.6 and 0.54 in hexane/dichloromethane/triethylamine (45/45/10). ^{1}H NMR (CD_3COCD_3): 7.6–7.1 (*m*, 9H, DMT, 7.28 (*d*, *J* = 8.0, 2H, H-2,6, arom), 7.1 (*d*, 2H) H-3,5 (arom), 6.90 (2*d*, *J* = 9.0, 4H, DMT, 4.28 (*q*, *J* = 7.1, 2H, CH_2CH_3), 3.9–3.5 (*m*, 5H, 2 × $CH(CH_3)_2$, H-2, CH_2CH_2CN), 3.80 (2*s*, 6H, 2 × CH_3O, DMT), 3.3–3.1 (*m*, 2H, H-1,1′), 3.0–2.85 (*m*, 4H, H-6,6′ and H-2,2′, propanoyl), 2.58 (*t*, *J* = 6.2, 2H, CH_2CH_2CN), 2.55–2.35 (*m*, 2H, H-3,3′, propanoyl), 1.5–1.1 (*m*, 21H, 3 × CH_2 and 5 × CH_3).

General Protocol for the Attachment of Oligonucleotides. Disks (0.5 cm^2) were cut out of the APT–cellulose membrane with a punch. They were activated as follows (volumes given for each square centimeter).

Activation. The disks were soaked for 5 min in 1 mL of cold 1.2 M HCl solution (0 °C). A solution of sodium nitrite (freshly prepared) was added (30 μL at 10 mg/mL) and the disks (bright yellow color) were incubated for 30 min at 0 °C with gentle shaking.

Washings. The membranes were washed with ice cold sodium acetate buffer 50 mM, pH 4 (2 × 1 min) and with ice-cold water (1 min).

Fixation. The disks were immediately transferred and incubated in the fixation solution (50 mM phosphate buffer, pH 7) containing the phenol–ODN conjugate at a concentration of 0.5 OD units/mL. For the determination of the binding capacity, the corresponding 5′-^{32}P-labeled oligonucleotide was added (ca. 10^5 cpm/sample, 700 cpm/pmol).

Inactivation of the Remaining Diazonium Groups. The membranes were washed with 0.1 N NaOH (3 × 1 mL) and water (1 mL).

General Protocol for Hybridization. The disks (0.5 cm^2) of cellulose-bound ODNs were incubated for 2.5 h at 50 °C in 150 μL of 5× SSPE solution (NaCl 750 mM, NaH_2PO_4 50 mM, EDTA 5 mM, pH 7.4) containing the complementary ODN (ca. 2 × 10^5 cpm, specific activity: 3 × 10^4–10^5 cpm/pmol).

Iodination of the Phenol-Modified ODN. An 11-pmol portion of ODN **12** (Scheme II) in 10 μL of 0.25 mM phosphate buffer pH 8.5 was added to 1 μL of iodine (200 μCi) in 10 μL of phosphate buffer. Then 10 μL of freshly prepared chloramine T (5 mg/mL of phosphate buffer) was added and after 1 min the reaction was quenched with 65 μL of aqueous sodium metabisulfite (2.4 mg/mL phosphate buffer). This iodinated ODN was purified by gel filtration on a NAP 10 column (Pharmacia) equilibrated in water. After the void volume, the fraction (900 μL) containing the labeled ODN was collected.

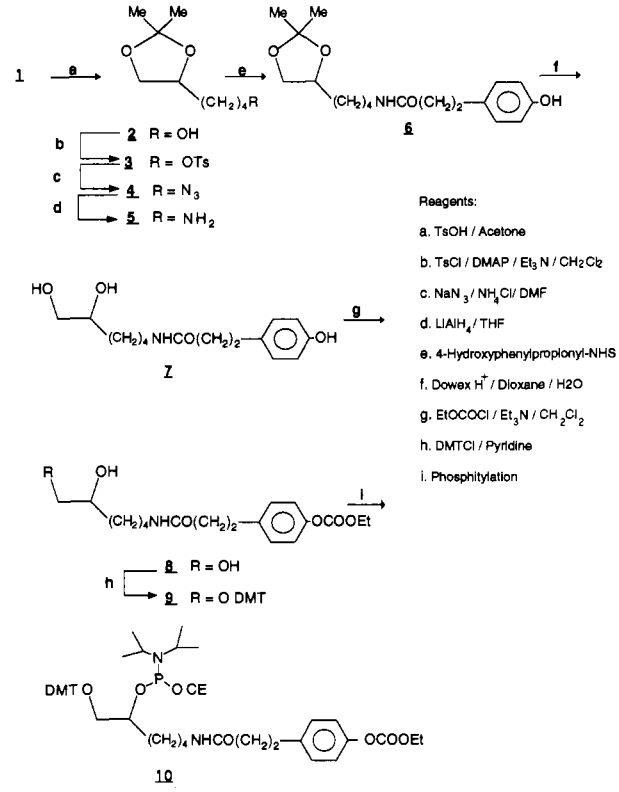
Action of the T4 Polynucleotide Kinase (PNK) on Modified ODN with 1,2-Ethanediol Moiety. Each reaction mixture (20 μL) contained kinase buffer (50 mM Tris-HCl, pH 7.5, 5 mM dithiothreitol, 10 mM $MgCl_2$), 450 pmol of ODN, 6800 pmol of ATP, and 10 units of polynucleotide kinase. The samples were incubated at 37 °C for 30 min and then analyzed by reverse phase HPLC. For the radiolabeling of the ODN, the incubation previously described was realized in the presence of 0.6 pmol of [γ-^{32}P]ATP (5000 mCi/mmol).

RESULTS AND DISCUSSION

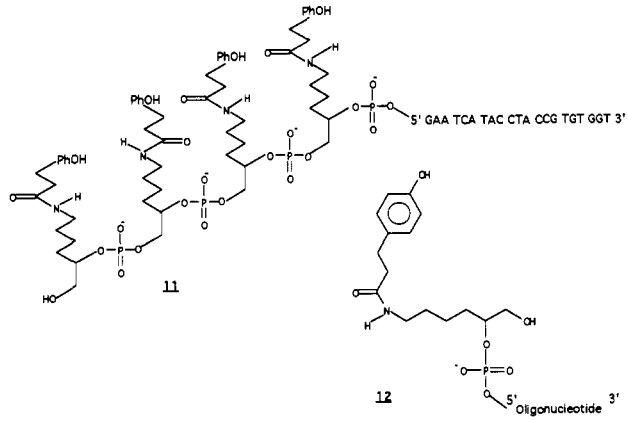
Synthesis of the Phenol Phosphoramidite 10. The 1,2-diol system of **1** was protected as its isopropylidene derivative by reaction with acetone in the presence of toluenesulfonic acid as catalyst in 83% yield (Scheme I). The isopropylidene **2** was treated with toluene sulfonyl chloride giving **3** with 95% yield. The azido derivatives **4** was prepared in 64% yield by nucleophilic displacement of the tosylate **3** with sodium azide in DMF. The azide **4** was reduced with lithium aluminium hydride (LAH) to give the amino derivative **5** (87% yield) which was treated with the *N*-succinimidyl 3-(4-hydroxyphenyl)propanoate to give the amide **6** with 81% yield. The isopropylidene group on **6** was removed by treatment with Dowex H^+ resin in dioxane-water mixture, the diol **7** was isolated in 84% yield. The phenol functions are reactive toward phosphitylation reagents and toward the iodine oxidation mixture used on the DNA synthesizer, therefore the phenol group must be masked. After some preliminary studies, the ethoxycarbonyl group was selected as being stable throughout the synthetic cycle and readily cleaved during the final ODN deprotection in aqueous ammonia. The phenolic hydroxyl of **7** was protected by reaction with ethyl chloroformate in the presence of triethylamine in dichloromethane, giving the ethoxy carbonate **8** in 58% yield. The primary hydroxyl of **8** was selectively protected by reaction with dimethoxytrityl chloride in anhydrous pyridine (85% yield). The resulting dimethoxytrityl ether was phosphitylated with bis(diisopropylamino)[(2-cyanoethyl)oxy]phosphine in the presence of diisopropylammonium tetrazolide to give the fully protected phosphoramidite **10** in 70% yield, which upon freeze-drying from benzene was obtained as an oil.

Synthesis of an Oligonucleotide–Phenol Conjugate and Its Complementary Sequence. The phosphoramidite **10** in 0.1 M acetonitrile solution was coupled four times on a CPG support bearing the ODN **11** (Scheme II)

Scheme I. Synthesis of Phosphoramidite Reagent Bearing a Phenol Residue



Scheme II. Oligonucleotides Modified with a Phenol Residue



(sequence = 5′GAA TCA TAC CTA CCG TGT GGT3′) according to the phosphoramidite procedure. The 5′-terminal dimethoxytrityl (DMT) group was not removed, in order to act as a lipophilic "handle" on reverse-phase HPLC. In a separate experiment, the coupling efficiencies for **10** were higher than 95%, as determined photometrically (498 nm) from the release of dimethoxytrityl cation (0.1 M toluenesulfonic acid in acetonitrile). After deprotection in 25% aqueous ammonia and evaporation, the crude compound ODN **11** was purified over HPLC using gradient 1. The main peak (t_R = 22 min) was collected and the corresponding compound was detritylated (acetic acid/water 8/2). The fully deprotected ODN **11** showed a single peak (t_R = 15 min) on HPLC (gradient 1). The complementary ODN **13** (sequence = 5′ACC ACA CGG TAG GTA TGA TTC3′) and ODN **14** (sequence = 5′TGT ACC TGA ATC GTC CGC CAT3′) were synthesized and deprotected in ammonia as described above and purified on HPLC giving a main peak at t_R = 17 min (gradient: from 25% to 50% B in 30 min).

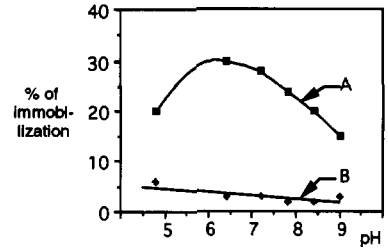


Figure 1. Effect of the pH on the immobilization in sodium phosphate buffer 50 mM, pH 5–8, and citrate, borate, phosphate buffer, pH 9: (A) ODN 11 modified with a phenol residue, (B) unmodified ODN with the sequence of ODN 11, negative control.

Diazotized Cellulose Filter as Oligonucleotide Support. A suitable immobilization support should have a high capacity, should be adequately rigid and durable and should not interfere with hybridization of DNA. For solid phase type, hybridization membranes are a suitable substrate. Cellulose membranes are easy to handle, reasonably resistant, and convenient for both hybridization and detection procedures. Cellulose membrane functionalized with amino phenyl thioether groups (APT paper) are commercially available. This aryl amine substituted cellulose is stable, can be stored at 4 °C, and is activated just before use in ice cold sodium nitrite hydrochloric acid mixture.

The immobilization described herein is based on the general method used for coupling DNA to activated supports bearing diazotized aromatic amines (*3–5*). Such a method applied to a short ODN would strongly affect its hybridization properties. The introduction at one end (3′ or 5′) of the ODN of a group more reactive than guanosine should favorize the end attachment rather than random binding. The ODN are functionalized by introducing a phenol group at their 3′ or 5′ end during automated synthesis by mean of the phosphoramidite **10** described in Scheme I.

Optimized Immobilization Conditions. We gained optimal immobilization in phosphate buffer, pH 6–7 (25 to 50 mM), within 15–30 min (Figure 1). We have observed an additional 10% fixation by the pretreatment of the buffer with diazo paper. Following the activation the paper should be washed in sodium acetate buffer, pH 4, and then with cold H_2O (2 × 1 min) in order to keep the diazonium reactivity.

Effect of the Number of Phenol Residue. The capacity of covalent binding has been improved by increasing the number of phenol residues introduced on the ODN: 2–5 times with 4–10 phenol residues. Not only the higher number of potential site of attachment can explain this increase but probably the phenol linkers themselves can act as a spacer between the binding site and the ODN chain.

Specificity of the Attachment. It is well-known that the diazonium salts react mainly with the electron-rich center at the C-8 position of the guanine residues and to a lesser extent with adenine residues which gives rise to unstable products (*24*). The phenol group incorporated at the 3′- or 5′-end of the ODN is a better center for electrophilic attack than the purine bases and should develop faster kinetics. Moreover the linker attached to the phenol favors its accessibility and should allow a selective reaction. The amount of immobilized ODN was determined by ^{32}P-labeling of the same ODN (*17*).

The quantity of covalently immobilized ODN is proportional to the quantity of ODN reacted to the activated cellulose support (Figure 2).

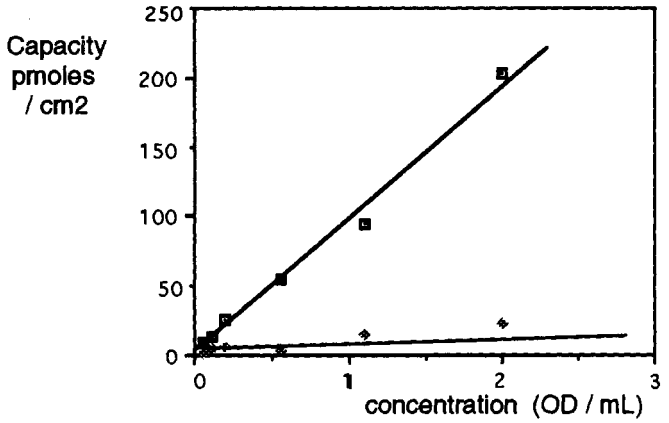


Figure 2. Immobilization capacity of the cellulose.

A covalent binding efficiency of 20–30% was achieved after 15–30 min of immobilization. The percentage of end attachment through the phenol linker was calculated taking into account the extent of binding of an unmodified ODN. We obtained about 87% specific end attachment.

The extent of passive adsorption was evaluated using a phenol modified ODN and inactivated (NaOH treatment) diazoaryl cellulose.

A capacity of 200 pmol/cm^2 for 2 OD units/mL loaded was evaluated (Figure 2). This binding capacity was of the same order as those previously reported for the hybridization formats involving the use of a membrane. Zhang (*15*) immobilized ODNs tethered at their 5′-end with aminopolyethylene glycol linker on carboxylic nylon membrane at more than 50 pmol/cm^2 and 90% end attachment. 5′-NH_2 ODNs were attached to carboxylic nylon membrane at 200 pmol/cm^2 (*16*). An original format with miniaturized matrix was successfully applied to DNA sequencing and automated. Polyacrylamide gel on a glass plate is derivatized with hydrazide groups that react with ODN 3′-uridine treated with $NaIO_4$ (*19*). However it failed as concerns the criteria of durability and easy handling. Other types of formats (nylon (*17*), magnetic latex (*18*), and glass (*25*) beads) have been developed for the hybridization of target nucleic acids. In the case of Van Ness nylon beads (*17*) coated with PEI, the non-immobilized activated triazinyl-ODN cannot be recycled. Solid phase synthesis has been proposed as a way for definitive immobilization: the ODN remains tethered to the glass beads after ammonia deprotection (*25*).

Hybridization Assay Performance of the Cellulose Matrix. Our work is based on a simple model using a capture probe (21 mers) immobilized on a cellulose matrix. Hybridizations were carried out with the complementary labeled probe. A non complementary labeled ODN 14 was used as a negative control. The melting temperature was first evaluated in solution by a spectroscopic method and confirmed by monitoring the hybridization on the support. Maximum rate of hybridization occurs at 25 °C below the T_m. Reactions were carried out at 20 °C below the T_m at low stringency (*26*). Washes were performed at increasing stringency (low salt) until the cpm values of the negative control attained lower values than those of the target. In a reported hybridization study of Sephacryl-bound ODN with a purified target nucleic acid, hybridization was complete after 1–2 h (*27*). Our experiment showed similar results: the extent of hybridization was sufficient within 2 h (Figure 3). Hybridization efficiency has been estimated to 60% with a non specific binding less than 0.5%. Hybridization with Denhart's reagent (BSA, volume exclusion reagents, Ficoll, and PVP) showed

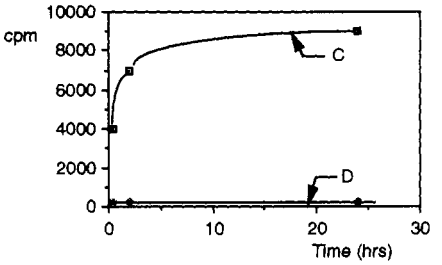


Figure 3. Kinetics of hybridization: ODN 11 immobilized on the cellulose: (C) complementary ODN 13, (D) noncomplementary ODN 14.

no significant effect whereas prehybridization with this reagent for 1.5 h at 50 °C improved the hybridization efficiency 2-fold. This is consistent with the fact that dextran sulfate could displace from the surface adsorbed ODN probes covalently attached at their 5′-ends by disrupting the adsorbtion forces holding the ODN to the surface of the support. This adsorption could interfere with their ability to hybridize target DNA from the solution (*27*). Higher capture yields were observed with increasing amounts of ODNs.

Iodination of the Phenol Moiety of the Modified ODN. Radioiodination of ODN can be done through a two step procedure where ODNs bearing a free amino group are reacted in a postsynthetic step with a 4-methoxyphenyl isothiocyanate (*28*) or a *N*-succinimidyl 3-(4-hydroxyphenyl)propanoate (*23*). Sauvaigo et al. (*23*) developed a simple method where a tyramine residue was incorporated into the ODN during the automated synthesis. The conjugated ODN is able to be radioiodinated with 200 μCi of [^{125}I]NaI according to the reported chloramine-T oxidation procedure. This method was tested for the phenol modified ODN 12 (Scheme II). The yield of iodine incorporation was 20% and the specific activity was 3.4 Ci/μmol.

Synthesis of Oligonucleotide Models. $(dT)_{10}$, X-$(dT)_{10}$, and pX$(dT)_{10}$ (phosphorylation was carried out with Phostel, a phosphoramidite purchased from American Bionetics, Inc. that allowed chemical phosphorylation) were synthesized and purified as described above. 5′-DMT $(dT)_{10}$ and X$(dT)_{10}$ ODNs were purified by reverse phase HPLC. X$(dT)_{10}$: Rt = 26.7 min (gradient 1) and t_R = 12.2 min after detritylation (gradient: from 10% to 40% B in 20 min). pX$(dT)_{10}$ was purified by an anion exchange column HPLC. The main peak, t_R = 11.5 min, was collected (gradient 2). LiCl was eliminated by precipitation with 5 volumes of ethanol and acetone mixture (1/1).

Action of the T_4 Polynucleotide Kinase (PNK) on Modified ODN with 1,2-Ethanediol Moiety. One or four 1,2-ethanediol units were incorporated at the 5′-end of $(dT)_{10}$ (X and $X_4(dT)_{10}$) (Scheme II). Both labeled ODNs were tested for their substrate capacity toward the phosphorylating activity of PNK. HPLC showed clearly that, within 30 min, XdT_{10} incorporated a phosphate group; pX$(dT)_{10}$, being more hydrophilic than its precursor, has a shorter retention time on the reverse-phase column (19.7 vs 10.8 min). The same trend was observed for $X_4(dT)_{10}$ (19.7 vs 21.7 min). pX$(dT)_{10}$ coelutes with authentic material obtained by chemical phosphorylation. In the case of the use of [γ-^{32}P]ATP and PNK, pX$(dT)_{10}$ was found to be radioactive. Both the incorporated radioactivity and the peak areas calculated from HPLC indicated a 50% yield of phosphorylation within 30 min at 37 °C. The unreacted X$(dT)_{10}$ from HPLC was again allowed to react with ATP in the presence of PNK without any success.

The results reported here show that a $(dT)_{10}$ modified on the 5′-position with one or more non-nucleosidic

ethanediol moieties is still recognized as a substrate by the PNK. The ethanediol derivative includes a 4-[3-(4-hydroxyphenyl)propionamido]butyl chain in the C-2 position. The stereochemistry of the conjugates (2*R* or 2*S*) determines two diastereoisomers after the incorporation in dT_{10}. We determined the extent of phosphorylation to be 50%, which led us to think that only one of the two diastereoisomers is recognized as a substrate by the enzyme. This supports the hypothesis of a steric hindrance that would prevent the enzyme to bind to the first internucleotide phosphate group (*29*).

Concluding Remarks. In this study we propose the synthesis of a novel phosphoramidite reagent based on a unique 1,2-ethanediol backbone that possesses many advantageous features. It can conveniently be used in automated DNA synthesis for the direct incorporation of conjugates in oligonucleotide chains even internally at any position of the ODN. The conjugate is the substrate of choice for either radiolabeling (both iodination (*26*) and 5′-end phosphorylation with [γ-^{32}P]ATP and T_4 PNK) or immobilization on a diazotized cellulose matrix.

The immobilization is site specific rather than a random attachment in photochemical cross-linkings (UV). The immobilization process is short (less than 30 min), the azo linkage is stable. Moreover, the ODN in excess during the immobilization procedure can be recycled. The capacity is higher than that previously described for the membrane attachment methods. This type of support is not compatible with colorimetric detection systems but a chemiluminescent detection can be performed.

With the reverse dot procedure it may be applied in the screening of different sequences or the detection of point mutations (*ras*, *c-myc* genes).

LITERATURE CITED

(1) Siddell, S. G. (1978) RNA hybridization to DNA coupled with cyanogen-bromide-activated sephadex. *Eur. J. Biochem. 92*, 621–629.

(2) Arndt-Jovin, D. J., Jovin, T. M., Bähr, W., Frischauf, A-M., and Marquardt, M. (1975) Covalent attachment of DNA to agarose. *Eur. J. Biochem. 54*, 411–418.

(3) Bünemann, H., Westhoff, P., and Herrmann, R. G. (1982) Immobilization of denatured DNA to macroporous supports: I. Efficiency of different coupling procedures. *Nucleic Acids Res. 10*, 7163–7180.

(4) Noyes, B. E., and Stark, G. R. (1975) Nucleic acid hybridization using DNA covalently coupled to cellulose. *Cell, 5*, 301–310.

(5) Seed, B. (1982) Diazotizable arylamine cellulose papers for the coupling and hybridization of nucleic acids. *Nucleic Acids Res. 10*, 1799–1810.

(6) Goodchild, J. (1990) Conjugates of oligonucleotides and modified oligonucleotides: A review of their synthesis and properties. *Bioconjugate Chem. 1*, 165–187.

(7) Gilham P. T. (1971) The covalent binding of nucleotides, polynucleotides, and nucleic acids to cellulose. *Method Enzymol. 21*, 191–197.

(8) Langdale, J. A., and Malcolm, A. D. B. (1985) A rapid method of gene detection using DNA bound to sephacryl. *Gene, 36*, 201–210.

(9) Lund, V., Schmid, R., Rickwood, D., and Hornes, E. (1988) Assessment of methods for covalent binding of nucleic acids to magnetic beads, Dynabeads™, and the characteristics of the bound nucleic acids in hybridization reactions. *Nucleic Acids Res. 16*, 10861–10880.

(10) Ghosh, S. S., and Musso, G. F. (1987) Covalent attachment of oligonucleotides to solid supports. *Nucleic Acids Res. 15*, 5353–5372.

(11) Saiki, R. K., Walsh, P. S., Levenson, C. H., and Ehrlich, H. A. (1989) Genetic analysis of amplified DNA with immobilized sequence-specific oligonucleotide probes. *Proc. Natl. Acad. Sci. U.S.A. 86*, 6230–6234.

(12) Kremsky, J. N., Wooters, J. L., Dougherty, J. P., Meyers, R. E., Collins, M., and Brown, E. L. (1987) Immobilization of DNA via oligonucleotides containing an aldehyde or carboxylic acid group at the 5′ terminus. *Nucleic Acids Res. 15*, 2891–2909.

(13) Bischoff, R., Coull, J. M., and Regnier, F. E. (1987) Introduction of 5′-terminal functional groups into synthetic oligonucleotides for selective immobilization. *Anal. Biochem. 164*, 336–344.

(14) Rasmussen, S. R., Larsen, M. R., and Rassmusen, S. E. (1991) Covalent immobilization of DNA onto polystyrene microwells: the molecules are only bound at the 5′ end. *Anal. Biochem. 198*, 138–142.

(15) Zhang, Y., Coyne, M. Y., Will, S. G., Levenson, C. H., and Kawasaki, E. S. (1991) Single-base mutational analysis of cancer and genetic diseases using membrane bound modified oligonucleotides. *Nucleic Acids Res. 19*, 3929–3933.

(16) Weiss, J A. J., McEhlhinney S. A., and Larry A. B. (1989) The catalysis of protein and nucleic acid coupling to an affinity membrane substrate. *BioTech 7*, 1012–1016.

(17) Van Ness, J., Kalbfleisch, S., Petrie, C. R., Reed, M. W., Tabone, J. C., and Vermeulen, M. J. (1991) A versatile solid support system for oligonucleotide probe-based hybridization assays. *Nucleic Acids Res. 19*, 3345–3350.

(18) Albretsen, C., Kalland, K-H., Haukanes, B-I., Havarstein, L-S., and Kleppe, K. (1990) Applications of magnetic beads with covalently attached oligonucleotides in hybridization: Isolation and detection of specific measles virus mRNA from a crude cell lysate. *Anal. Biochem. 189*, 40–50.

(19) Khrapko, K. R., Lysov, Y. P., Khorlin, A., Ivanov, I. B., Yershow, G. M., Vasilenko, S. K., Florentiev, V. L., and Mirzabekov, A. D. (1991) A method for DNA dequencing by hybidization with oligonucleotide matrix. *DNA Sequence—J. DNA Sequencing Mapping, 1*, 375–388.

(20) Roget, A., Bazin, H. and Téoule, R. (1989) Synthesis and use of labelled nucleotide phosphoramidite building blocks bearing a reporter group: Biotinyl, dinitrophenyl, pyrenyl and dansyl. *Nucleic Acids Res. 19*, 7643–7651.

(21) Misiura, K., Durrant, I., Evans, M. R., and Gait, M. (1990) Biotinyl phosphoramidite derivatives useful in the incorporation of multiple reporter groups on synthetic oligonucleotides. *Nucleic Acids Res. 18*, 4345–4354.

(22) Nelson, P. S., Kent, M., and Muthini, S. (1992) Oligonucleotide labelling methods 3. Direct labelling of oligonucleotides employing a novel, non nucleosidic, 2-aminobutyl-1,3 propanediol backbone. *Nucleic Acids Res. 20*, 4355–4360.

(23) Sauvaigo, S., Fouqué, B., Livache, T., Bazin, H., Chypre, C., and Téoule, R. (1990) Fast solid support detection of PCR amplified viral DNA sequences using radioiodinated or hapten labelled primers. *Nucleic Acids Res. 18*, 3175–3183.

(24) Kochetkov, N. K., Budovskii, E. I., Sverdlov, N. A., Simuka, M. F., Turchinskii, M. F., and Shibaev, V. N. (1972) Reactions at the nitrogen atom of an exocyclic amino group, Substitution and addition reaction reactions in heterocyclic rings. *Organic Chemistry of Nucleic Acids* (N. K. Kochetkov, and E. I. Budovskii, Eds.), Part B, pp 280–281 and 367–370, Plenum Press, London.

(25) Maskos, U., and Southern, E. M. (1992) Oligonucleotide hybidizations on glass supports: A novel linker for oligonucleotide synthesis and hybridization properties of oligonucleotides synthesised *in situ*. *Nucleic Acids Res. 20*, 1679–1684.

(26) Wetmur, J. G. (1991) DNA probes: Applications of the principles of nucleic acid hybridization. *Crit. Rev. Biochem. Mol. Biol. 26* (3/4), 227–259.

(27) Gingeras, T. R., Kwoh D. Y., and Davis, G. R. (1987) Hybridization properties of immobilized nucleic acids. *Nucleic Acids Res. 15*, 5373–5390.

(28) Dewanjee, M. K., Ghafouripour, A. K., Werner, R. K., Serafini, A. N., and Sfakianakis, G. N. (1991) Development of sensitive radioiodinated anti-sense oligonucleotide probes by conjugation technique. *Bioconjugate Chem. 2*, 195–200.

(29) Richardson, C. C. (1965) Phosphorylation of nucleic acid by an enzyme from T4 bacteriophage-infected Escherichia coli. *Proc. Natl. Acad. Sci. U.S.A. 54*, 158–165.

Photoaffinity Behavior of a Conjugate of Oligonucleoside Methylphosphonate, Rhodamine, and Psoralen in the Presence of Complementary Oligonucleotides

John Thaden and Paul S. Miller*

Department of Biochemistry, The Johns Hopkins University School of Hygiene and Public Health, 615 North Wolfe Street, Baltimore, Maryland 21205. Received March 30, 1993®

A 3′-[[2-[*N*-(3-aminopropyl)-*N*-(2-hydroxyethyl)amino]ethylphosphoryl]oligodeoxyribonucleoside methylphosphonate 12-mer was synthesized using the Aha-CPG solid support [Thaden, J. and Miller, P. S. (1993) *Bioconjugate Chem.*, companion paper in this issue]. The oligomer was conjugated at the 3′ primary aliphatic amine with tetramethylrhodamine 5-isothiocyanate. The rhodamine linker/spacer was stable in 10% fetal calf serum. After enzymatic phosphorylation, the molecule was conjugated at the 5′ phosphate with 4′-[*N*-(2-aminoethyl)aminomethyl]-4,5′,8-trimethylpsoralen [(ae(AMT)]. The rhodamine/psoralen doubly-conjugated oligomer formed photoadducts with complementary single-stranded DNA and RNA oligonucleotides when irradiated with long-wavelength ultraviolet light. The efficiency of UV cross-linking slightly exceeded that of a colinear, psoralen-derivatized oligonucleoside methylphosphonate, and exhibited relationships with UV fluence and temperature that are characteristic for psoralen-conjugated methylphosphonates. The 1:1 complex formed with the oligodeoxyribonucleotide target could be detected by its red fluorescence. Mouse L_{949} cells grown in the presence of the double conjugate were shown by means of computer-assisted epifluorescence microscopy to have internalized it. There was an accumulation of intensely fluorescent points and spots in a juxtanuclear region of the cytoplasm, and a faint, diffuse signal in the entire cell area.

Previous reports from our laboratory and elsewhere have demonstrated that psoralen-conjugated oligonucleoside methylphosphonates can effectively cross-link to single-stranded DNA targets and to mRNA *in vitro* upon activation with long-wavelength UV light (Lee *et al.*, 1988a,b; Kean *et al.*, 1988; Bhan and Miller 1990; Isaacs *et al.*, 1989; Levis, 1993). Psoralen-conjugated oligomers were also shown to be effective, sequence-specific inhibitors of herpes simplex virus replication in infected cells (Kulka *et al.*, 1989) and of p21 synthesis in *ras* oncogene transformed NIH 3T3 cells (Chang *et al.*, 1991).

For mechanistic studies in cell culture, the utility of psoralen-derivatized oligonucleoside methylphosphonates could be considerably enhanced if they were conjugated to an easily detectable fluorescent label. The tetramethylrhodamine fluorophore is strongly excited by the 546 nm emission of a mercury arc lamp, resists photobleaching, is not readily obscured by cellular autofluorescence (Simon and Taylor, 1986; Benson *et al.*, 1979), is insensitive to pH in the physiological range (Geisow, 1984), and has little spectral overlap with the photoactivation and emission spectra of psoralen compounds.

In this paper we describe the synthesis of a psoralen/rhodamine doubly-conjugated oligonucleoside methylphosphonate. We demonstrate that the linkage to rhodamine is stable under cell culture conditions, that the oligomer efficiently cross-links with single-stranded RNA and DNA targets when irradiated with near UV light, that the rhodamine fluorescence survives UV irradiation and cross-linking to a target, and that the oligomer is readily taken up by cells in culture.

* Author to whom correspondence should be addressed.

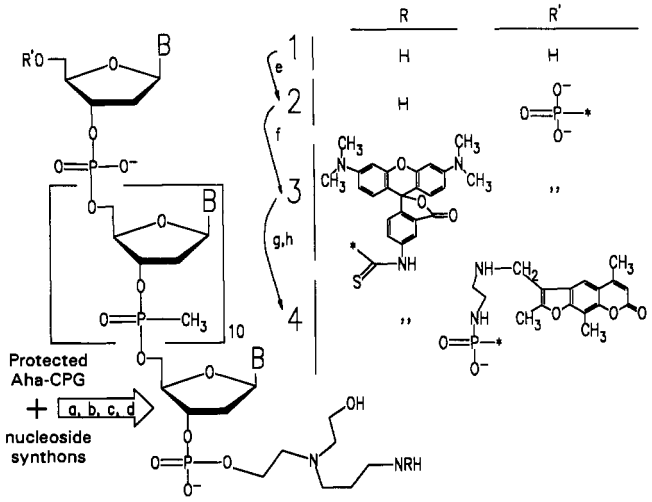
® Abstract published in *Advance ACS Abstracts*, September 1, 1993.

EXPERIMENTAL PROCEDURES

Reversed-phase HPLC was performed as described (Bhan and Miller, 1990), on either Rainin Microsorb C18 80–215-C5 or Whatman ODS-3 RAC II columns for analytical purposes and on Whatman ODS-3 RAC columns for preparative work. These were eluted at rates of 1, 1.5, and 4 mL min^{-1}, respectively, using linear acetonitrile gradients of slope 1.5% min^{-1} for analytical runs and 0.75% min^{-1} for preparative runs. For HPLC with multiple-wavelength detection, a RAC II column was mounted on a Waters 600E system with a Model 990 photodiode-array detector. Two denaturing PAGE procedures were used: (I) 15 or 20% polyacrylamide gels (acrylamide/bisacrylamide 19:1, 0.75 × 170 mm) containing 7 M urea and TBE (Maniatis *et al.*, 1982) were electrophoresed at 35 V cm^{-1}; (II) gels were formulated as described except TBE was replaced by TPE buffer (0.089 M Tris base, 0.089 N phosphoric acid, 0.1 mM EDTA) and 33 mM dithiothreitol. The presence of dithiothreitol greatly retards fluorescence fading (Picciolo and Kaplan, 1984). TPE-buffered gels were electrophoresed at 20 V cm^{-1}. Rhodamine fluorescence in gels was detected either under room light or, for faint bands, with the gel on a short-wavelength UV transilluminator. The latter was used during fluorophotography with Polaroid 665 film and a deep yellow filter (e.g. Wratten #9, Eastman, Inc.), as for photography of ethidium bromide gels. Autoradiography was done with XAR-5 film (Eastman) at −20 °C. Solvent removal was by evaporation *in vacuo* (oil pump) at not more than 40 °C. Desalting of oligomers was accomplished with Sep-Pak C_{18} cartridges (Waters) prewashed with acetonitrile (10 mL) followed by 50% acetonitrile (5 mL) and, unless noted, 5% acetonitrile in 0.1 M sodium phosphate (pH 5.8, 10 mL). Samples were loaded as solutions in more of the final prewash buffer. Loaded cartridges were washed with water (20 mL). Desalted products were eluted with 50% acetonitrile (4 mL), and solvents were removed. All

1043-1802/93/2904-0386$04.00/0 © 1993 American Chemical Society

Scheme I. Synthesis of a Rhodamine/Psoralen Doubly-Conjugated Oligonucleoside Methylphosphonate[a]



[a] (a) Automated synthesis on support 6; (b) hydrazine hydrate/HOAc/pyr; (c) ethylenediamine/95% EtOH; (d) 80% HOAc; (e) ATP/T^4 polynucleotide kinase/kinase buffer/MeCN; (f) TRITC isomer G/bicine–NaOH buffer, pH 9/EtOH; (g) EDAC/imidazole–HCl buffer, pH 6/MeCN; (h) (ae)AMT/2,6-lutidine–HCl buffer, pH 7.5/MeCN.

operations with substances containing rhodamine and/or psoralen were conducted under red or subdued light. Rhodamine-modified oligomers were stored dry at −20 °C. Operations involving RNA were done using diethylpyrocarbonate-treated liquids (Maniatis *et al.*, 1982) and oven-baked labware.

Synthesis of Substances Illustrated in Scheme I. 3′-(Aha[1]-phosphoryl)oligodeoxyribonucleoside Methylphosphonate 1 (Scheme I). Substance 1 was prepared upon the Aha-CPG support as described in a companion paper in this issue (Thaden and Miller, 1993) using nucleoside 2-cyanoethyl phosphoramidite synthons for the first and last couplings and methylphosphonamidite synthons for all others.

5′-Phosphoryl-3′-(Aha-phosphoryl)oligodeoxyribonucleoside methylphosphonate 2 (Scheme I). This kinase reaction was done first because the presence of a 5′-phosphate facilitated later HPLC purification. To a solution of oligomer 1 (1 μmol) in 50% acetonitrile (0.6 mL) were added 0.5 M Tris-HCl buffer 0.05 M $MgCl_2$ (pH 7.6, 0.3 mL), 0.1 M ATP (0.1 mL), 50 mM dithiothreitol (0.3 mL), and water (1.7 mL) and, after swirling, T_4-polynucleotide kinase (10 μL, 300 units). The reaction solution was incubated at 37 °C, with swirling gently every 15 min. More kinase (5 μL) was added at 30 and 60 min, the last bolus preceded by dropwise addition of acetonitrile (180 μL). At 90 min, the reaction solution was diluted with 0.2 M sodium phosphate (pH 5.8, 1 vol) and desalted. Phosphorylation went to completion as assayed by HPLC.

[1] Abbreviations used: (ae)AMT, 4′-[[*N*-(2-aminoethyl)amino]methyl]-4,5′,8-trimethylpsoralen; Aha, *N*-(3-aminoprop-1-yl)-*N*-(2-hydroxyethyl)-2-aminoethyl; CCD, charge-coupled device; DIC, differential interference contrast (Nomarski) optics; EDAC, 1-ethyl-3-[3-(dimethylamino)propyl]carbodiimide; EDTA, ethylenediaminetetraacetic acid, 0.8 M stock, pH 8.0; EMEM, minimal essential medium with Earle's salts; FBS, fetal bovine serum, not heat-treated; HBSS, Hank's buffered saline solution; phosphate buffer, 0.1 M sodium phosphate buffer, pH 5.8; T_c, temperature at which nucleic acid cross-linking by psoralen-conjugated oligomers is half-maximal; TPE buffer, 0.089 M Tris base, 0.089 N phosphoric acid, 0.1 mM EDTA; TRITC isomer G, *N,N′*-tetramethylrhodamine 5-isothiocyanate.

5′-Phosphoryl-3′-[[*N*-[3-[[(*N,N,N′,N′*-tetramethylrhodaminyl-5-yl)thiocarbamoyl]amino]prop-1-yl)-*N*-(2-hydroxyethyl)-2-aminoethyl]phosphoryl]oligodeoxyribonucleoside Methylphosphonate 3 (Scheme I). TRITC isomer G (Molecular Probes, Inc., 5 mg, 10.4 μmol) was vortexed and sonicated with reagent alcohol (0.6 mL, Fisher Scientific) until dissolved. The dye solution was immediately added to a solution of oligomer 2 (1 μmol) in bicine–sodium hydroxide buffer (0.2 M, pH 9.0, 1 mL) and reagent alcohol (0.4 mL). The reaction was stirred in the dark for 18 h. Solvents were evaporated, and the residue was dissolved in a minimal volume of 0.1 M sodium phosphate buffer (pH 5.8) containing 25% acetonitrile. The solution was loaded onto a Sephadex G-15 column (1.6 × 20 cm). Products were eluted with the same buffer. The first red peak was collected and freed of acetonitrile under vacuum. Product 3 was separated from unreacted oligomer 2 by preparative HPLC and both fractions were desalted. Conjugation yield was typically 85% as determined by HPLC peak area.

5′-(ae)AMT-3′-[[*N*-[3-[[(N,N,*N′,N′*-tetramethylrhodamin-5-yl)thiocarbamoyl]amino]prop-1-yl]-*N*-(2-hydroxyethyl)-2-aminoethyl]phosphoryl]oligodeoxyribonucleoside Methylphosphonate 4 (Scheme I). Following the adaptation of Bhan and Miller (1991) of the two-step procedure of Chu *et al.* (1983), substance 3 (40 A_{254} units, 0.3 μmol) was dissolved with acetonitrile (120 μL) and 0.1 M imidazole–hydrochloride buffer (pH 6.0, 0.6 mL). Freshly made 1 M EDAC (80 μL) was added. The reaction was allowed to proceed at 22 °C in the dark for 3 h. A Sep-Pak cartridge was prepared, but using 0.2 M bicine–sodium hydroxide (pH 9.0) containing 10% (*v/v*) acetonitrile for the final prewash solvent. The reaction solution was diluted with 0.8 mL of the same solvent, loaded onto the column, and desalted. The dried, crude imidazolide was dissolved with acetonitrile (66 μL) and 0.25 M 2,6-lutidine hydrochloride (pH 7.6, 280 μL) and reacted with 0.05 M (ae)AMT (70 μL) in the dark for 3 d at 22 °C. After desalting by the normal protocol, products were separated by denaturing PAGE and visualized under subdued room light.

To identify compound 4 among several red bands, all but extremely minor bands were excised from the gel. Gel pieces were macerated. The pastes were steeped in 25% acetonitrile (3 mL, 2 h). After low-speed centrifugation, supernatants were sampled for the following test: Samples were treated with 0.1 N hydrochloric acid (1 h, 37 °C). The acid was removed by coevaporation with water. Products were resolved by denaturing PAGE alongside a lane of authentic compound 3 and visualized by fluorophotography. Acid converted only the most abundant psoralen conjugation product (R_f = 0.65 relative to compound 3) to a species that comigrated with 3 on gels. The macerated gel piece containing the R_f 0.65 species was eluted twice more as above. The pooled eluate was diluted with 0.35 M sodium phosphate buffer (pH 5.8, 2.5 vol). The entire volume was loaded onto a Sep-Pak cartridge for desalting.

Other Synthetic Oligomers. The 5′-(ae)AMT-oligonucleoside methylphosphonate 5, (Scheme I), oligodeoxyribonucleotide 6 (Chart I), and oligoribonucleotide 7 (Chart I) were generously donated by Dr. J. M. Kean. The nucleic acid targets were enzymatically phosphorylated using [γ-^{32}P]ATP and polynucleotide kinase as described (Miller *et al.*, 1991). 5′-[^{32}P]-labeled compound 3 was prepared by sequential reactions with calf intestinal phosphatase and polynucleotide kinase (Chaconas and van de Sande, 1980, method 3).

***In Vitro* Cross-Linking.** Two procedures were used, both adapted from the assay of Lee *et al.* (1988b).

Probe in Excess. The reactions were done in borosilicate glass tubes (10 x 75 mm, Corning). Each tube contained cross-linking buffer (50 mM Tris, 0.1 M sodium chloride pH 7.6, 10 μL) in which had been dissolved either probe 4 or probe 5 (5 μM, 50 pmol) and radiolabeled oligonucleotide target 6 or 7 (0.1 μM, 1 pmol). The conjugate probe 5, not pictured, is identical with probe 4 in both base sequence and 5′-psoralen/linker structure, but it lacks the 3′-rhodamine/linker modification of 4. The stoppered tubes were equilibrated to a chosen temperature, then some of them were irradiated with a Blak-Ray Longwave UV lamp (UVP, San Gabriel) for 15 min as follows: The tubes were mounted on a rotator such that the center of the bulb face was parallel to the tubes' sides, and at a distance varying with rotation from 6 to 10 cm measured to the bottom, center, of each tube. Rotation carried tubes through a water bath set at the pre-equilibration temperature, and also through the most intense spot of the lamp. Wavelengths shorter than 300 nm are absorbed by the borosilicate glass tubes. This geometry has been reported to deliver long-wave UV light to the solutions at a fluence rate of 8.3 kJ m^{-2} min^{-1} (Lee *et al.*, 1988b). The samples were then analyzed by PAGE procedure I and autoradiography of the wet gels. Isotopic bands were quantified by excision from the gel and scintillation counting. Equivalent regions from dummy lanes were likewise measured to determine background levels. Cross-linking was calculated as the percentage of the total counts above background that resided in gel-shifted bands.

Target in Excess. Tubes contained cross-linking buffer (20 μL) in which was dissolved probe 4 (120 pmol or 160 pmol as specified) and radiolabeled DNA target 6 at twice the concentration of the probe. A 10-min pre-equilibration was followed by UV irradiation for 10 min or for the interval specified. Samples were resolved by PAGE. After autoradiography and fluorophotography of the gels, isotopic bands were quantified. Percentage of cross-linking was calculated. Fluorophotograph negatives were laser-scanned (LKB Ultroscan XL, x width = 4) to produced density plots of each lane. Plots were copied to 20 lb xerographic paper. Baselines were fitted using plots of empty lanes, and peaks were cut out with scissors and weighed.

Cell Culture and Treatment with Oligomer. Mouse L_{929} fibroblasts (L cells) were maintained in 25 cm^2 culture flasks with 1:10 splits done twice weekly. The close distance between objective and condenser lenses on the microscope used to view living cells dictated the design of chambered slides upon which cells were grown and viewed. A hole (1.9 cm diam) was drilled in each of several stainless steel plates (7.6 cm × 5.1 cm × 1 mm). Cover glasses (#$1^1/_2$, 22 mm square) were soaked in 6 N nitric acid, rinsed with deionized water, soaked in 0.1 mM EDTA, and again rinsed with deionized water. A cover glass was mounted over one side of the hole in each plate using silicone stopcock grease. Cylinders (1.2 cm high) were cut from a clear acrylic pipe (1.9 cm i.d., 2.6 cm o.d.) and the cut surfaces were sanded smooth. A cylinder was affixed to the upper side of each hole using stopcock grease. The resulting chambers were placed in Petri dishes and autoclaved. Subconfluent L cells were trypsinized and seeded at one-fourth density into chamber assemblies each containing EMEM (0.5 mL) supplemented with 10% FBS. When the cells were again subconfluent (48 h), the medium was changed to EMEM containing 1% FBS and 10 μM of 4, prepared as follows: Compound 4 was sterilized in 70% ethanol, dried *in vacuo*, and dissolved in filtered EMEM lacking FBS. The solution was sonicated for 2 min, supplemented with FBS (to 1%), and used immediately. Control medium was prepared likewise, but omitting oligomer. The cells were incubated for 9 h.

Fluoromicroscopy. The acrylic cylinder was detached. Cells were rinsed several times with HBSS. A cover glass was pressed into the grease which had secured the cylinder, forming a 1 mm thick chamber filled with HBSS (≈0.3 mL). Cells exhibited no morphological changes for at least 40 min in these chambers during microscopy at ambient temperature without buffer refreshment. The chambered slide was placed on the stage of an inverted microscope outfitted with both epifluorescence and differential interference contrast (DIC) optics, a CCD camera (Callahan *et al.*, 1992), and a dedicated image processing system (Perceptics Corp., Knoxville, TN, Model 9210-VI).[2] Cells viewed through a 100× oil immersion objective were located and brought into focus using transmitted light and DIC optics. To limit bleaching, a gray filter (0.03, 97% attenuation) and a deep yellow filter (Wratten #9, Eastman) were inserted in the light path, illumination was limited by the field diaphragm to the central two-thirds of the viewed area, and exposures were kept brief. The microscope was switched to epifluorescence optics using a filter set designed for rhodamine fluorescence. Without altering the focus, the camera was activated and the portion of the view framed by the camera was excited for 5 s by incident illumination from a 100-W mercury arc light, which was 90% attenuated by a gray filter (0.1). The microscope was switched back to DIC optics and a second digital image was captured during 2 s of transillumination by white tungsten filament light, 97% filter-attenuated. The stage was moved to a new field of cells located at least five field-diameters from the prior one, and the process was repeated. Ten to 40 different optical fields were imaged in this manner from cell lawns originally grown in each chamber.

Image Processing. Algorithms for processing images of cells were implemented on a Macintosh computer using HyperScope (Perceptics, Inc.), an extension to the HyperCard programming language. Each image was an array of 512 × 384 pixels. Pixels collected photons from contiguous square areas (0.23 μm per side with the 100× lens) on the surface of the chambered slide. After mathematical application of a shading correction (Aikens *et al.*, 1989) to images, the CCD camera pixels were seen be linear throughout a dynamic range of over 2.5 log units of fluorescence intensity (Callahan *et al.*, 1992). The following shading correction formula was used[3]

$$I' = \frac{I - (\sum^{10} D/10)}{\bar{L} - (\sum^{10} D/10)}$$

where I is the raw image, I' is the corrected image, L is a *luminous field mean image* formed by averaging ten images of various optical fields on a chambered slide loaded with a solution of rhodamine B (A_{557} = 0.005) and 33 mM

[2] Additional details of the microscope, optics, light sources, CCD camera, image processor, and processor-related software are described in a manuscript in preparation [Callahan, D. E., Ts'o, P. O. P., and Lesko, S. A. (1993) *Exp. Cell Res.*].

[3] Image shading correction was necessitated by a "hot spot" of epi-illumination caused by imperfect diffusion of the arc image, and "vignetting" introduced by the microscope optics. It also removes interpixel differences in camera performance.

Chart I. Base Sequence of Methylphosphonate 1–5 and Phosphodiester 6, 7 Oligomers[a]

D-5′AATTGACAAATCCTATTTT3′ **6**

3′CTGTTTAGGATA5′-D **1-5**

R-5′AAUUGACAAAUCCUAUUUU3′ **7**

[a] Underlined letters represent nucleosides with 3′-methylphosphonate linkages.

dithiothreitol, and *D* is each of ten *dark current images*, captured with the camera shielded from light.[4] These calibration images were captured during the same session and at the same shutter speed as the experimental images of cells.

Each DIC image was scaled so its brightest pixel was white, sharpened by spatial masking methods (Gonzalez and Wintz, 1987), and registered in the x–y plane to the matching fluorescence image by the alignment of features, typically cell processes and edges of nuclei, which were visible in both images. Registration usually involved horizontal or vertical motion of the DIC image by less than 3 pixels.

For color photographs, fluorescence images were displayed in red while the corresponding DIC images were overlaid at one-third intensity in both green and blue. The computer monitor screen was photographed.

RESULTS AND DISCUSSION

Synthesis of the Fluorescent Oligomer. Using a special controlled pore glass solid support (Aha-CPG) described elsewhere in this issue (Thaden and Miller, 1993), we synthesized an oligonucleoside methylphosphonate which had a base sequence (Chart I) complementary to nucleotides 165-176 of vesicular stomatitis virus matrix protein mRNA (Rose and Gallione, 1981) and a 2-(*tert*-aminoethyl)phosphoryl structure at its 3′ end.

The 3′ modification provided a primary aliphatic amine for subsequent conjugation with an amine-reactive fluorophore. We enzymatically phosphorylated the oligomer's 5′ end and then reacted the oligomer with excess tetramethylrhodamine 5-isothiocyanate. It was necessary to alter the buffer used in this reaction because standard isothiocyanate reaction buffers (sodium bicarbonate, borate, or phosphate at pH 8.5–9.5) produced ladders of oligomer degradation products on PAGE gels. In bicine buffer (pH 9), the result was an intact oligomer, joined at its 3′ end to tetramethylrhodamine by a linker/spacer containing thiocarbamoyl and phosphodiester linkages.[5]

Stability of the 3′ End Modifications. To see if the conjugate was stable under cell culture conditions, a solution of compound **3** in growth medium containing 10% fetal bovine serum was incubated at 37 °C and sampled at 3.5 and 24 h. HPLC with multiple wavelength detection was performed on these samples, on untreated conjugate **3**, and on the medium alone (Figure 1). The chromatographic profile for untreated conjugate **3** (Figure 1a) revealed a species which absorbed at both 254 and 540 nm

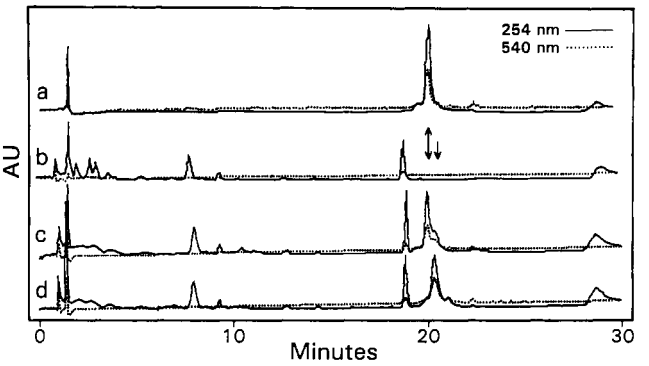


Figure 1. Reversed-phase HPLC study with detection at both 254 (—) and 540 nm (· ·) of (a) 5′-phosphorylated, 3′-rhodamine-conjugated oligonucleoside methylphosphonate (**3**); (b) EMEM cell culture medium containing 10% fetal bovine serum, and (c) 3.5-h and (d) 24-h incubations of a solution of compound **3** in like medium, at 37 °C. Arrows point to eluted species which change in amount during incubation in the presence of serum. HPLC: 45 mL linear 1–46% acetonitrile gradient in 0.1 M sodium phosphate, pH 5.8, 1.5 mL min^{-1}.

and which eluted 20 min after the start of the gradient (upward arrow). A chromatogram of the medium alone (Figure 1b) revealed several A_{254} components of the serum eluting during the first 10 min of the gradient, and the phenol red indicator dye eluting at 18.5 min, which absorbed weakly at 540 nm also. When compound **3** was incubated with serum-containing medium for 3.5 h (Figure 1c), the single conjugate **3** peak eluting at 20 min developed a shoulder on its trailing edge (downward arrows). The peak and its shoulder were evident at both 254 and 540 nm, and the area ratio between them appeared the same at both wavelengths. When incubation had proceeded for 24 h (Figure 1d), the conjugate **3** peak eluting at 20 min appeared to have been replaced by a peak of equal size eluting 40 s later, at the position where the shoulder had been. No other peaks were found at either incubation time which were not also found in medium alone.

The 40-s delay in HPLC elution time was identical with that produced during removal of the 5′-phosphate from conjugate **3** by reaction with calf intestinal phosphatase (not shown). In separate experiments, we and others have shown that ^{32}P-labeled oligonucleoside methylphosphonates are dephosphorylated in serum-containing medium (unpublished; Akhtar *et al.*, 1991), with a rate that is slower than for phosphodiester oligomers and variable, depending on serum lot and media storage conditions.[6]

We did not see evidence of degradation other than 5′-dephosphorylation: One would expect exo- or endonucleolytic cleavage of the methylphosphonate backbone to give a mélange of earlier-eluting species at the expense of the major peak. This result was not seen nor was it expected, since nuclease resistance of the methylphosphonate linkage has been established (Agrawal and Goodchild, 1987; Akhtar *et al.*, 1991). One would expect a scission at any bond in the linker/spacer to uncouple the elution of the major A_{254} and A_{540} components of conjugate **3** during HPLC. This also was not seen. If, by chance, a linker/spacer scission were to generate decay product with chromatographic elutions identical to the starting compound, then such a scission might elude detection. Since 5′-dephosphorylation shifted the coincident peaks of 254 and 540 nm absorbance without unmasking a chance coelution of decay products, a more reasonable conclusion

[4] Unlike bright-field images, dark-current images were dim, i.e. used few of the 65 536 gray levels. Hence, they were low in precision and high in noise. These problems were minimized by the summation of ten dark-field images. The gain in precision was preserved by relocating the averaging step (division by ten) to the flat-fielding formula, which could be implemented using floating point arithmetic.

[5] In attempts to conjugate *N*-hydroxysuccinimides and other active esters of a xanthine dye to an oligomer with the same 3′ modification as compound **3**, we were thwarted by the appearance of a nonfluorescent major product.

[6] Medium for this experiment had been sterility-tested overnight at 37 °C and then stored at 4 °C for 2 weeks.

is that the linkage between the oligomer and the rhodamine dye was resistant to nucleases and other degradative enzymes present in the medium containing 10% fetal bovine serum.

Attachment of the Psoralen. In two steps, the 5′-phosphate of conjugate **3** was reacted with the amino-modified psoralen (ae)AMT, in order to furnish the oligomer with a photoreactive cross-linking capability. This modification also protects the 5′ terminus from nuclease-catalyzed hydrolysis. To identify substance **4** among several fluorescent products resolved by denaturing PAGE, advantage was taken of the fact that phosphoramidate linkages like that in compound **4** are cleaved by acid to the corresponding phosphate, which in this case would be the starting compound **3**, whereas side products with unusual linkages, modified bases, altered 3′ structures, etc., would not be expected to revert to starting material. Only the most abundant product reverted to a species with electrophoretic behavior like that of substance **3** (not shown). On this evidence, it was isolated and used in further experiments as conjugate **4**.

A colleague has shown that this linkage of (ae)AMT to oligomers is stable in medium containing 10% serum during incubation at 37 °C for 24 h (Levis, 1993). When administered to cells in culture for various times, ^{32}P-labeled, 5′-psoralen-conjugated methylphosphonates can be recovered largely intact from cell lysates at 4 h (unpublished). The majority is intact in both lysates and the overlying medium at 12 h; however, there is significant degradation at 24 h (Levis, 1993).

Effect of the 3′ End Modification upon Cross-Linking (Probe in Excess). Buffered salt solutions were prepared which contained either the 3′-rhodamine/5′-psoralen doubly conjugated methylphosphonate **4** or the colinear 5′-psoralen conjugated methylphosphonate **5** in excess over either end-labeled DNA (**6**) or an analogous RNA single-stranded 19-mer target (**7**). Each solution was apportioned to four tubes. After equilibration in ice water for 1 h, two of the four tubes in each set were UV irradiated at 4 °C. The sixteen samples were analyzed by PAGE, followed by autoradiography (Figure 2a).

The radiolabeled, single-stranded DNA and RNA targets are boldly evident in the nonirradiated sample lanes (1, 2, 7, 8) of the left and right illustrations, respectively. The RNA target ran slightly slower than the DNA relative to xylene cyanol dye. In all samples that had been UV-irradiated (lanes 3–6), the target band was greatly reduced and a new isotopic species was resolved as a single, gel-retarded band. Its position depended upon which conjugated methylphosphonate species the irradiated sample contained. With the double conjugate **4** (lanes 5–8), the photoadduct ran slower than that produced with conjugate **5** (lanes 1–4). These observations are consistent with the new species being urea-stable complexes formed of probe and target. One would expect such photoadducts to electrophorese more slowly if tetramethylrhodamine and the *tert*-amine linker/spacer were attached. In the past, psoralen-conjugated oligonucleoside methylphosphonates such as control **5** have been shown to efficiently cross-link to complementary single-stranded nucleic acid targets when conjugate/target mixtures are irradiated with near-UV light (Lee *et al.*, 1988a,b; Kean *et al.*, 1988; Bhan and Miller, 1990; Levis, 1993). The rhodamine on conjugate **4** does not prevent cross-linking from occurring.

Cross-linking percentages are shown beneath the autoradiographs in Figure 2a, averaged for each pair of duplicate tubes/lanes. Duplicate irradiated tubes differed from each other by at most 1.8%. Lane 6 on the RNA gel

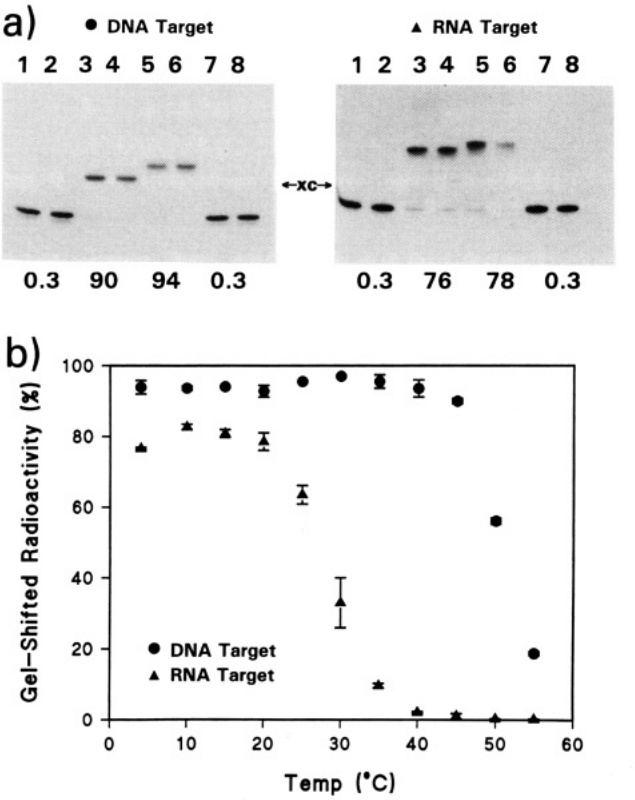


Figure 2. Denaturing 20% PAGE studies of cross-linking by an excess of psoralen/rhodamine doubly-conjugated dodecanucleoside methylphosphonate probe, to complementary, single-stranded, ^{32}P-labeled DNA (▲) and RNA (●) targets. Cross-linking was quantified by scintillation counting of excised gel bands. See the text for details. (a) Effect of the 3′-rhodamine and amino linker (Rh±) and UV irradiation (UV±) on cross-linking at 4 °C. Numbers below gels are cross-linking percentages (mean of duplicate tubes). Lanes: (1, 2) Rh–, UV–, (3, 4) Rh–, UV+, (5, 6) Rh+, UV+, (7, 8) Rh+, UV–. (b) Effect of temperature on cross-linking (triplicate tubes, duplicate lanes of each; brackets show ±1 sd; data from three tubes were discarded due to nuclease degradation of RNA target, one tube each at 20, 45, and 55 °C).

was apparently underloaded by about half, but because cross-linking is a ratio expression, that lane could still be used for quantitation. The mean cross-linking in all irradiated tubes (lanes 3–6, both gels) was 84% (standard deviation, 8). Lanes containing nonirradiated samples had negligible isotope (0.3%) at the position of the cross-linked complex in the other lanes.

The effectiveness of UV-induced cross-linking at 4 °C was sensitive to both variables tested in this experiment. When the backbone ribose sugars in the nucleic acid target were replaced by 2′-deoxyribose (and uracil by thymine), the mean cross-linking increased from 77% to 92% ($P < 0.0001$[7]). Differences in DNA and RNA cross-linking by psoralen-conjugated methylphosphonates have been observed previously.[8]

When the 3′ terminal group of the psoralen-conjugated methylphosphonate probe was changed from a hydroxyl to a group which includes a tetramethylrhodamine, a tertiary amine, and a phosphodiester, the mean cross-linking showed a small but significant increase (83% to 86%, $P < 0.004$). Therefore, there occurred neither an adverse interaction between the rhodamine and psoralen

[7] A two-factor analysis of variance was performed on all data from irradiated samples in order to test for statistical significance of probe effects, target effects, and interaction effects.

[8] Kean, J. M., and Miller, P. S., unpublished results.

chromophores, nor significant interference by the 3′ modification with base-pairing.

An interaction between the two variables (probe choice and target choice) was not detected ($P > 0.5$); the 3′ modification did not detectably prejudice cross-linking in favor of either the RNA or the DNA target during cross-linking at 4 °C.

Effect of Temperature upon Cross-Linking (Probe in Excess). Temperature has proven to be an important variable in sequence-selective cross-linking (e.g. Lee *et al.*, 1988b). Conjugate **4** was incubated at 11 different temperatures in solutions containing either DNA (**6**) or RNA (**7**) radiolabeled targets, and the solutions were irradiated at those temperatures. Cross-linking was calculated and plotted as a function of temperature (Figure 2b). Three different temperature zones could be described: a *permissive zone* at low temperatures within which cross-linking was efficient, a *critical zone* spanning 10–15 °C within which cross-linking was extremely sensitive to temperature and inversely related to it; and a *prohibitory zone* at high temperatures within which cross-linking to RNA was not seen and cross-linking to DNA was not measured. The temperature where half-maximal cross-linking was observed (T_C) fell roughly in the middle of the critical zone. Both the DNA and RNA series showed this quasisigmoidal response to temperature.

The advantage enjoyed by DNA in cross-linking with conjugates **4** and **5** at 4 °C (above) was reproduced in this temperature study for conjugate **4** at 4 °C (94% vs 76%; Figure 2a,lanes 5–6), at the temperature of maximum cross-linking (97% vs 82%), and throughout the permissive zone. The most striking difference between DNA and RNA cross-linking was the temperature range of the critical zone. The permissive zone for DNA cross-linking persisted to much higher temperatures before the critical zone was reached, a fact best conveyed by the much higher T_C for DNA versus RNA (51 °C vs 29 °C).

RNA cross-linking by conjugate **4** exhibited a temperature of half-maximal cross-linking of 29 °C. This is 6 °C higher than any reported to date for RNA cross-linking by a psoralen-derivatized methylphosphonate. As indicated in the 4 °C cross-linking experiment (Figure 2), the presence of the 3′ terminal modifications on conjugate **4** may facilitate cross-linking. At higher temperatures, the 3′ modification may preferentially aid RNA cross-linking.

For both DNA and RNA cross-linking, the initial response to an increase in temperature was a shallow rise in cross-linking, peaking at approximately 20 °C below the T_C. This trend was less obvious with DNA (3%) than with RNA (6%). Neither target was 100% cross-linked at the temperature of maximal cross-linking. Since the psoralen-derivatized probe was in 50-fold excess over the target, failure to convert 100% of the target to the cross-linked complex was probably not due to incomplete duplex formation during pre-equilibration in the dark, but rather to competing photodegradation of the psoralen moiety (Hearst, 1981).

Since the 3′ modification is at maximal distance from the psoralen on compound **4**, it is likely that the enhanced cross-linking observed at 4 °C (and possibly at higher temperatures with the RNA target) was due to helix stabilization rather than direct action of the rhodamine upon the psoralen. How this occurs is unknown. Possible mechanisms include (a) intercalation or (b) end-stacking by the tetramethylrhodamine, (c) zwitterion formation or (d) reversible ionic cross-linking by the *tert*-alkylamine in the 3′ linker after its quaternization, (e) concerted action by the rhodamine and the amine, and (f) some effect of the amine in its uncharged, tertiary state. Discussing these in order, conjugation of acridine derivatives at the 3′ end of oligonucleotides is known to enhance binding to polynucleotides (Hélène *et al.*, 1986). The planar, heterocyclic conformation of acridine and other intercalators is a feature also of tetramethylrhodamine in its ground state. We found no reports in the literature, however, of intercalation by rhodamines, nor did tetramethylrhodamin-5-amine or rhodamine B stain the chromatin of cells (not shown). Failure to observe interactions of rhodamine with conventional duplexes does not rule out unique interactions with methylphosphonate heteroduplexes. Melting studies are planned to explore this further. Bauman *et al.* (1981) saw no difference in the melting temperatures of rhodamine 3′ labeled and unlabeled poly(U) when assayed by poly(A)–Sepharose columns, but did see a marginal positive effect of a terminal rhodamine upon hybridization of RNA heteropolymers to complementary DNA–Sepharose. Cardullo *et al.* (1991) reported an average increase in T_m of 4 °C when oligodeoxyribonucleotides of length 6 to 20 were end-linked to rhodamine with an ethyl spacer. Whether by mechanism c or d, a quaternary 3′ amine would act to reduce the local charge density of the helix. Concerted stabilization by a 3′-acridine derivative and various positively-charged 3′ substituents has been described (Asseline *et al.* 1985). In a recent report, the stability of duplexes of oligonucleoside methylphosphonates and oligodeoxyribonucleotides was enhanced if the normal oligomer had a 3′-amino group (Gryaznov and Letsinger, 1992). The effect was thought not to be due to the positive charge of the amine.

Fluorescence Detection of Cross-Linking (Target in Excess). In the probe-in-excess assays discussed above, unreacted probe was easily visible on gels transilluminated by short-wave UV light (not shown). It appeared as a red-fluorescent, nonisotopic band running well above the photoadduct band. The 1:1 complex, present in less than $^1/_{50}$ the amount, was scarcely visible. To increase the yield of the photoadduct, the amount of 2′-deoxy target **6** was increased 320-fold and conjugate **4** was approximately tripled (160 pmol), resulting in a 2:1 mole ratio. Solutions were pre-equilibrated and UV-irradiated at 25 °C and then assayed on PAGE gels containing an antifading agent. Figure 3a illustrates autoradiographs (left) and red-emission fluorophotographs (right) of parts of four gels from four cross-linking trials. Control lanes from one of the experiments are included: the control in lane 1 was masked during UV irradiation; that in lane 2 was irradiated normally, but lacked the DNA 19-mer target; that in lane 3 was irradiated at 55 °C. Lanes 4–4c were loaded with complete reaction solutions which had been UV-irradiated at 25 °C.

All samples were supplemented with a noncomplementary, radiolabeled oligodeoxyribonucleotide 11-mer prior to gel loading as an internal control of loading efficiency (band v). Complementary DNA 19-mer **6** was present in all but control lane 2 and appears as a strongly radioactive, nonfluorescent band (iv). The double conjugate **4** was not radiolabeled and is seen only on the fluorophotographs (band ii). Though shorter than oligonucleotide **6**, conjugate **4** ran slower because nine of its 11 internucleoside linkages were nonionic methylphosphonates. Band ii appears blurred and split in all but lane 1, the only lane loaded with nonirradiated reaction solution. Band ii is markedly attenuated in lanes 4–4c. Those lanes contain a new species (band iii) are discussed below. A fraction of the radioactive material in each lane remained at or near the wells (band i). This phenomenon occurred

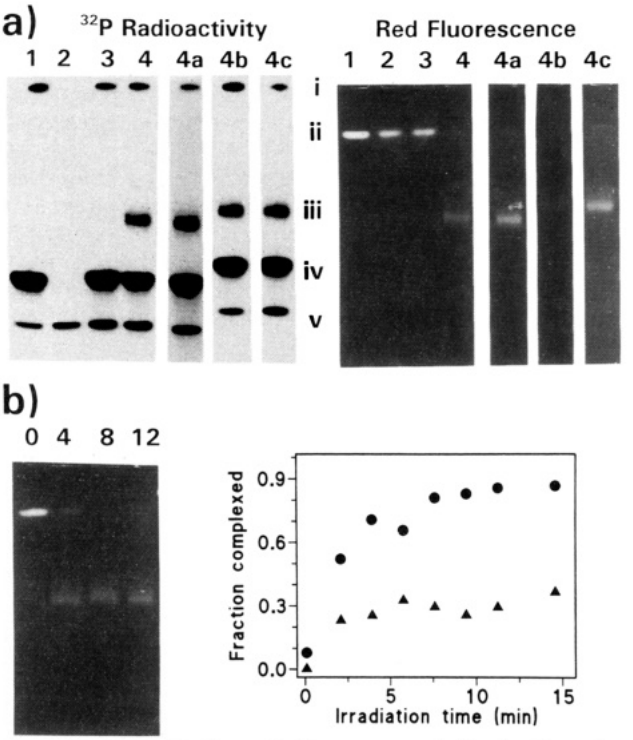


Figure 3. Cross-linking of a fluorescent, rhodamine/psoralen doubly-conjugated oligodeoxyribonucleoside methylphosphonate to excess, ^{32}P-labeled, complementary single-stranded DNA. Photoadducts iii were resolved by denaturing PAGE. See text for details. (a) Autoradiograph (left) and fluorophotograph (right) of portions of four gels from four replicate experiments. Lanes: Abolition of cross-linking by (1) protection from UV light, (2) omission of DNA target, and (3) elevated temperature (55 °C), compared with (4, 4a-4c) UV irradiated, DNA-containing solutions treated at 25 °C. (b) Fluorophotograph (left) and plot (right) illustrating dependence of photo-cross-linking upon UV fluence. Lane numbers represent minutes of UV exposure. Fraction of fluorescence (●) and of radioactivity (▲) found in photoadduct iii is plotted as a function of irradiation time.

regardless of treatment. Its cause is unknown. The wells also appear bright on the fluorophotographs, but upon close inspection, this appears to be due to light having been scattered from or concentrated by the gels' edges.

Band iii, the photoadduct, shows up on both the autoradiograph and the fluorophotograph in a position midway between the radioactive band of DNA 19-mer **6** (iv), and the fluorescent band of methylphosphonate conjugate **4** (ii). It is strong in lanes 4–4c, the only lanes loaded with complete reaction solutions that were irradiated at a permissive temperature. On the original films, an extremely faint band was visible at the same position in lanes 1 and 3. Some cross-linking may have occurred during gel loading, since room lighting was subdued but not absent.

Taken together, these observations establish that cross-linking by the doubly-conjugated oligomer **4** can also occur under the condition of target excess, and that the photoadduct product of its cross-linking (band iii) is a readily detectable, fluorescent species. As in the probe-in-excess experiments, cross-linking stopped short of 100% usage of the less abundant species. Other psoralen photoreactions are known to occur during long-wave UV irradiation besides nucleic acid cycloadduct formation, and these include photodestruction of the psoralen (Hearst, 1981). In lane 2, and in prior studies (discussed in Kean *et al.*, 1988), near-UV irradiation of psoralen-conjugated oligomers generates small amounts of electrophoretically discernable products even in the absence of a nucleic acid target. For (ae)AMT conjugates such as **4**, these were not photoreversible (Lee *et al.*, 1988b). With excess target and pre-equilibration at 25 °C, nearly all of conjugate **4** would be expected to be duplexed at the time of irradiation. The blurring and splitting of conjugate **4** (lanes 4–4c) suggest, therefore, that duplex formation does not entirely protect the psoralen moiety from photobreakdown, and that a significant portion of photoproducts in the blurred region were incompetent to covalently cross-link the DNA strand. This would explain the less-than-100% cross-linking observed under both assay conditions and suggests that duplexed, photodamaged conjugate **4** may act as a competitive inhibitor of cross-linking.

In a second target-in-excess cross-linking experiment, solutions contained 240 pmol of oligodeoxyribonucleotide **6** and 120 pmol of conjugate **4**. They were UV-irradiated at 25 °C for periods ranging from 0 to 15 min and then analyzed by PAGE. The fluorophotograph of one of the two gels is reproduced in Figure 3b. The fluorescent (and isotopic) photoadduct was formed in all tubes except the zero-time tube, and could be seen to increase in intensity with longer UV irradiations. The radioactivity and fluorescence of the photoadduct band were quantified by scintillation counting and densitometry respectively, and expressed as fractions of the total signal in the lane. The plot in Figure 3b confirms the pattern of increasing cross-linking seen on the fluorophotograph and shows that radioactivity associated with the photoadduct increases in a concerted fashion. Because the radioactive species was in excess, the fraction complexed was lower. The shape of these curves is similar to those published previously for various psoralen-conjugated methylphosphonates (Lee *et al.*, 1988b; Bhan and Miller, 1990).

Interaction with Mouse L Cells. Fluorescence microscopy of living fibroblasts which had been grown for 9 h in medium containing conjugate **4** showed strong rhodamine fluorescence associated with the cells (Figure 4). Treated cells had a mean brightness 2.5-fold higher than that due to back-scatter and autofluorescence in untreated cells and had a maximum brightness 7.4-fold that of the brightest point in untreated cells. The cells pictured in Figure 4 exemplify the predominant fluorescence distribution pattern seen with both conjugate **4** and conjugate **3** under a wide range of treatment times and concentrations. The most intense signal was found in points or speckles in the cytoplasm, most of which were less than 1 μm in diameter. In the majority of cells, the bright points were particularly concentrated and coalesced next to, over, or under the nucleus. This pattern differs markedly from the generalized cytoplasmic fluorescence gotten when the free rhodamine dye, tetramethylrhodamin-5-amine, was administered to L cells (not shown).

A number of laboratories have reported punctate, perinuclear patterns of fluorescence in cells in culture treated with a variety of fluorescent oligonucleotides and oligonucleotide analogues (Jaroszewski and Cohen, 1991; Bennett *et al.*, 1992; Iversen *et al.*, 1992; Marti *et al.*, 1992; Shoji *et al.*, 1991; Thierry and Dritschilo, 1992). Some nuclear localization has also been noted. The juxtanuclear pattern of spots is generally attributed to confinement of the reagents to vesicles, particularly endosomes, and cycling of the endosomes between the plasma membrane and the Golgi area. Endosomal containment could potentially limit the bioavailability of antisense and antigene reagents at their presumed sites of action.

While the vesicular pattern is strikingly bright due to local concentration, a significant amount of the total cellular fluorescence was distributed diffusely over the

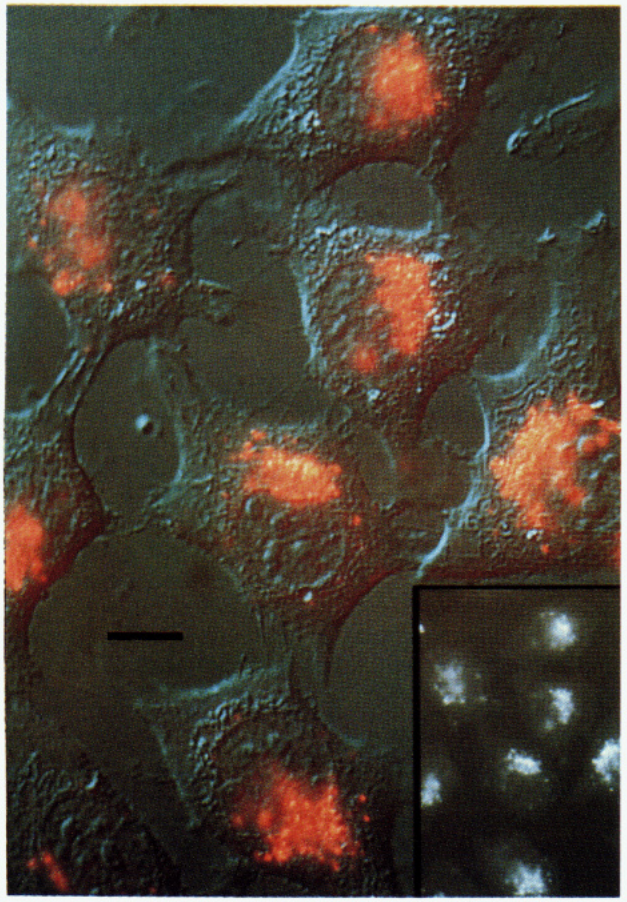


Figure 4. Cellular distribution of a fluorescent, psoralen/rhodamine doubly-conjugated oligodeoxyribonucleoside methylphosphonate. Color composite image formed by alignment of a Nomarski differential interference contrast image (blue-green) and an epifluorescence image (red) of live mouse L_{929} fibroblasts cultured for 9 h in medium containing 5 μM of the oligomer conjugate (see the text for details). Length of bar is 10 μm. Inset: Black-and-white epifluorescence image of the same cells, but with fluorescence intensity displayed on a logarithmic scale to emphasize less intensely fluorescent areas.

entire cell area. This is apparent if one displays the same cells with fluorescence brightness displayed on a logarithmic scale in order to de-emphasize areas of extraordinary intensity (Figure 4, inset).

Finally, an "outline" effect was sometimes also seen, where part or all of a cell boundary appeared bright. This is a feature observed when fluorescent probes react with elements of the plasma membrane (Willingham and Pastan, 1985). Also characteristic of a membranal distribution is a vesicular, cytoplasmic pattern focused in the Golgi area, due to membrane recycling, and a weak fluorescence over the entire cell due to overlying and underlying cell membrane. The distribution illustrated in Figure 4 differs from a purely membranal one in that the outline effect is not very striking and not visible on every cell.

Diffuse brightness over the cell area could be due to Rayleigh scattering of the intense emission from vesicularized probe, or it could be due to presence of conjugate **4** in the cytosol. If conjugate **4** was free in the cytosol, then its behavior in these mouse fibroblasts is not as one might predict from studies where fluoresceinated methylphosphonates and rhodamine-labeled oligodeoxyribonucleotides were microinjected into the cytoplasm of human and mouse fibroblasts respectively (Chin *et al.*, 1990; Leonetti *et al.*, 1991). These conjugates were reported to become rapidly sequestered in the nucleus. Liposomally encapsulated, phosphorothioate-capped oligonucleotides eventually migrated to the nucleus also (Thierry and Dritschilo, 1992).

In this article, we have detailed the synthesis of a conjugate formed of three well-characterized molecules: oligonucleoside methylphosphonate, tetramethylrhodamine, and 4′-[*N*-(aminoethyl)aminomethyl]-4,5′,8-trimethylpsoralen. We have demonstrated that the linkage between the methylphosphonate and the rhodamine is stable in serum-containing medium. The linkage to psoralen has previously been shown to meet that test. We have demonstrated the capacity of the conjugate to cross-link to single-stranded, complementary oligoribo- and oligodeoxyribonucleotides *in vitro*. Finally, we have demonstrated that the conjugate can be taken up by fibroblastic cells growing in monolayer culture and have given some indication of its distribution in these cells. The stability, fluorescence, and cell penetrability of the psoralen/rhodamine doubly-conjugated oligonucleoside methylphosphonate **4** are properties required if one is to use it for microscopic studies of antisense behavior in living cells and tissues. The photoaffinity it shows for complementary single-stranded DNA and RNA *in vitro* affords an opportunity to directly assay for antisense interaction of an antisense reagent with messenger RNA in living cells.

ACKNOWLEDGMENT

Financial support for this work was provided through grants from the National Cancer Institute (CA42762), the National Institutes of Health (ES03841 and CA09110), and the Department of Energy (DEFG02-88ER60636). We gratefully acknowledge the expert advice of J. M. Kean, who also generously provided us with oligomers **5**–**7**. S. A. Lesko and D. E. Callahan provided invaluable training and advice on microscopy and image processing. (ae)AMT was synthesized by P. Bhan. HPLC with diode-array detection was done with the assistance of S. D. Morrow.

LITERATURE CITED

Agrawal, S., and Goodchild, J. (1987) Oligonucleoside methylphosphonates: Synthesis and enzymatic degradation. *Tetrahedron Lett. 28*, 3539–3542.

Aikens, R. S., Agard, D. A., and Sedat, J. W. (1989) Solid-state imagers for microscopy. *Meth. Cell Biol. 29*, 291–313.

Akhtar, S., Kole, R., and Juliano, R. L. (1991) Stability of antisense DNA oligonucleotide analogues in cellular extracts and sera. *Life Sci. 49*, 1793–1801.

Asseline, U., Nguyen, T. T., and Hélène, C. (1985) Oligonucleotides covalently linked to intercalating agents. Influence of positively charged substituents on binding to complementary sequences. *J. Biol. Chem. 260*, 8936–41.

Bauman, J. G. J., Wiegant, J., and Van Duijn, P. (1981) Cytochemical hybridization with fluorochrome-labeled RNA. I. Development of a method using nucleic acids bound to agarose beads as a model. *J. Histochem. Cytochem. 29*, 227–237.

Bennett, C. F., Chiang, M. Y., Chan, H. D., Shoemaker, J. E. E., and Mirabelli, C. K. (1992) Cationic lipids enhance cellular uptake and activity of phosphorothioate antisense oligonucleotides. *Mol. Pharmacol. 41*, 1023–1033.

Benson, R. C., Meyer, R. A., Zaruba, M. E., and McKhann, G. M. (1979) Cellular autofluorescence--Is it due to flavins? *J. Biochem. Cytochem. 27*, 44–48.

Bhan, P., and Miller, P. S. (1990) Photo-cross-linking of psoralen-derivatized oligonucleoside methylphosphonates to single-stranded DNA. *Bioconjugate Chem. 1*, 82–88.

Bonfils, E., Depierreux, C., Midoux, P., Thuong, N. T., Monsigny, M., and Roche, A. C. (1992) Drug targeting: synthesis and endocytosis of oligonucleotide-neoglycoprotein conjugates. *Nucleic Acids Res. 20*, 4621–29.

Callahan, D. E., Karim, A., Zheng, G., Ts'o, P. O. P., and Lesko, S. A. (1992) Quantitation and mapping of integrated human papillomavirus on human metaphase chromosomes using a fluorescence microscope imaging system. *Cytometry 13*, 453–461.

Cardullo, R. A., Agrawal, S., Yoder, J., and Wolf, D. E. (1991) Structure of duplex oligodeoxynucleotides using non-radiative fluorescence resonance energy transfer. *Biophys. J. 59*, 414a.

Chaconas, G., and van de Sande, J. H. 5′-^{32}P labeling of RNA and DNA restriction fragments. *Methods Enzymol. 65*, 75–85.

Chang, E. H., Miller, P. S., Cushman, C., Devadas, K., Pirollo, K. F., Ts'o, P. O. P., and Yu, Z. P. (1991) Antisense inhibition of *ras* p21 expression that is sensitive to a point mutation. *Biochemistry 30*, 8283–8286.

Chin, D. J., Green, G. A., Zon, G., Szoka, F. C., Jr., and Straubinger, R. M. (1990) Rapid nuclear accumulation of injected oligodeoxyribonucleotides. *New Biol. 2*, 1091–1100.

Chu, B. C. F., Wahl, G. M., and Orgel, L. E. (1983) Derivatization of unprotected polynucleotides. *Nucleic Acids Res. 11*, 6513–6529.

Geisow, M. J. (1984) Fluorescein conjugates as indicators of subcellular pH. *Exp. Cell Res. 150*, 29–35.

Gonzalez, R. C., and Wintz, P. (1987) *Digital Image Processing, 2nd ed.*, pp 140–143, Wiley, New York.

Goodchild, J. (1990) Conjugates of oligonucleotides and modified oligonucleotides: a Review of their synthesis and properties. *Bioconjugate Chem. 1*, 165–187.

Gryaznov, S. M., and Letsinger, R. L. (1992) Synthesis and properties of oligonucleotides containing aminodeoxythymidine units. *Nucleic Acids Res. 20*, 3403–3409.

Hearst, J. E. (1981) Psoralen photochemistry. *Annu. Rev. Biophys. Bioeng. 10*, 69–86.

Hélène, C., Toulmé, F., Delarue, M., Asseline, U., Takasubi, M., Maurizot, J. C., Montenay-Garestier, T., and Thuong, N. T. (1986) Oligonucleotides covalently linked to an intercalating agent. Structural and thermodynamic studies of a dodecathymidylate and its binding to polynucleotides. *Biomolecular Stereodynamics* (R. H. Sarma and M. H. Sarma, Eds.) Vol. III,pp 119–130, Adenine Press, Guilderland, New York.

Isaacs, S. T., Tessman, J. W., and Levenson, C. H. (1989) Synthesis and characterization of photocrosslinkable oligonucleotide probes. *Photochem. Photobiol. 49 (Suppl)*, 10S.

Iversen, P. L., Zhu, S., Meyer, A., and Zon, G. (1992) Cellular uptake and subcellular distribution of phosphorothioate oligonucleotides into cultured cells. *Antisense Res. Dev. 2*, 211–222.

Jaroszewski, J. W., and Cohen, J. S. (1991) Cellular uptake of antisense oligodeoxynucleotides. *Adv. Drug Deliv. Rev. 6*, 235–50.

Kean, J. M., Murakami, A., Blake, K. R., Cushman, C. D., and Miller, P. S. (1988) Photochemical cross-linking of psoralen-derivatized oligonucleoside methylphosphonates to rabbit globin messenger RNA. *Biochemistry 27*, 9113–9121.

Kulka, M. , Smith, C. C., Aurelian, L., Fishelevich, R., Meade, K., Miller, P., and Ts'o, P. O. P. (1989) Site specificity of the inhibitory effects of oligo(nucleoside methylphosphonate)s complementary to the acceptor splice junction of herpes simplex virus type 1 immediate early mRNA 4. *Proc. Natl. Acad. Sci. U.S.A. 86*, 6868–6872.

Lee, B. L., Blake, K. R., and Miller, P. S. (1988a) Interaction of psoralen-derivatized oligodeoxyribonucleoside methylphosphonates with synthetic DNA containing a promoter for T7 RNA polymerase. *Nucleic Acids Res. 16*, 10681–10697.

Lee, B. L., Murakami, A., Blake, K. R., Lin, S.-B., and Miller, P. S. (1988b) Interaction of psoralen-derivatized oligodeoxyribonucleoside methylphosphonates with single-stranded DNA. *Biochemistry 27*, 3197–3203.

Leonetti, J. P., Mechti, N., Degols, G, Gagnor, C., and Lebleu, B. (1991) Intracellular distribution of microinjected antisense oligonucleotides. *Proc. Natl. Acad. Sci. U.S.A. 88*, 2702–6.

Levis, J. T. (1993) A mechanistic study of psoralen-derivatized oligonucleotide analogues: interaction with VSV mRNA *in vitro* and behavior in cell culture. Ph.D. Dissertation, The Johns Hopkins University.

Lin, S-B (1988) Studies of oligodeoxyribonucleoside methylphosphonate-nucleic acid interaction. Ph.D. Dissertation, The Johns Hopkins University.

Maniatis, T., Fritsch, E. F., and Sambrook, J. (1982) *Molecular Cloning, A Laboratory Manual*, pp 156, 190, Cold Spring Harbor Laboratory, Cold Spring Harbor, NY.

Marti, G., Egan, W., Noguchi, P., Zon, G., Matsakura, M., and Broder, S. (1992) Oligo-deoxyribonucleotide phosphorothioate fluxes and localization in hematopoietic cells. *Antisense Res. Dev. 2*, 27–39.

Miller, P. S., Cushman, C. D., and Levis, J. T. (1991) Synthesis of oligo-2′-deoxyribonucleoside methylphosphonates. In: *Oligonucleotides and Analogues. A Practical Approach.* (F. Eckstein, Ed.) pp 137–154, IRL Press Limited, Oxford, England.

Picciolo, G. L., and Kaplan, D. S. (1984) Reduction of fading of fluorescent reaction product for microphotometric quantitation. *Adv. Appl. Microbiol 30*, 197–233.

Rose, J. K., and Gallione, C. J. (1981) Nucleotide sequences of the mRNA's encoding the vesicular stomatitis virus G and M proteins determined from cDNA clones containing the complete coding regions. *J. Virol. 39*, 519–528.

Shoji, Y., Akhtar, S., Periasamy, A., Herman, B., and Juliano, R. L. (1991) Mechanism of cellular uptake of modified oligodeoxynucleotides containing methylphosphonate linkages. *Nucleic Acids Res. 19*, 5543–50.

Simon, J. R., and Taylor, D. L. (1986) Preparation of a fluorescent analog: acetamidofluoresceinyl-labeled *Dictyostelium discoideum* α-actinin. *Methods Enzymology 134*, 487–507.

Thaden, J.,and Miller, P. S. (1993) Automated synthesis of oligodeoxyribonucleoside methylphosphonates having [*N*-(3-aminoprop-1-yl)-*N*-(2-hydroxyethyl)-2-aminoethyl]phosphate or methylphosphonic acid at the 3′ end using a modified controlled pore glass support. *Bioconjugate Chem.*, following paper in this issue.

Thierry, A. R., and Dritschilo, A. (1992) Intracellular availability of unmodified, phosphorothioated and liposomally encapsulated oligodeoxynucleotides for antisense activity. *Nucl. Acids Res. 20*, 5691–5698.

Ti, G. S., B. L. Gaffney, and R. A. Jones (1982) Transient protection: Efficient one-flask synthesis of protected deoxynucleosides. *J. Am. Chem Soc. 104*, 1316–1319.

Willingham, M. C., and Pastan, I. (1985) *An Atlas of Immunofluorescence in Cultured Cells.* Academic Press, Inc., Orlando, FL.

TECHNICAL NOTES

Automated Synthesis of Oligodeoxyribonucleoside Methylphosphonates Having [*N*-(3-Aminoprop-1-yl)-*N*-(2-hydroxyethyl)-2-aminoethyl] Phosphate or Methylphosphonic Acid at the 3′ End Using a Modified Controlled Pore Glass Support

John Thaden and Paul S. Miller*

Department of Biochemistry, The Johns Hopkins University School of Hygiene and Public Health, 615 North Wolfe Street, Baltimore, Maryland 21205. Received March 30, 1993 ●

To provide a solid support for automated synthesis of 3′-(aminoalkyl)-modified oligonucleoside methylphosphonates, controlled pore glass beads were functionalized with a protected *N*-(3-aminoprop-1-yl)-*N*-(2-hydroxyethyl)-2-aminoethyl ester of succinic acid. This "Aha-CPG" was used for automated synthesis of oligo-2′-deoxyribonucleoside methylphosphonates having either of two distinct 3′ terminal modifications. If the first coupling to the beads was of a base-protected 5′-(dimethoxytrityl)-2′-deoxyribonucleoside 3′-(β-cyanoethyl *N,N*-diisopropylphosphoramidite) synthon, then, upon completion of methylphosphonate oligomer synthesis and deprotection, the 3′-[*N*-(3-aminoprop-1-yl)-*N*-(2-hydroxyethyl)-2-aminoethyl] phosphate] derivative of an oligonucleoside methylphosphonate was produced and was shown to be a stable structure which affords a primary alkylamine group suitable as a site for further conjugations. If the first coupling was of a 5′-(dimethoxytrityl)-2′-deoxyribonucleoside 3′-(*N,N*-diisopropylmethylphosphonamidite) synthon, the initial product of synthesis and deprotection underwent a spontaneous, regiospecific ester cleavage in aqueous solution to produce an oligonucleoside methylphosphonate 3′-(methylphosphonate). An application of the Aha-CPG to the synthesis of rhodamine-conjugated oligonucleoside methylphosphonates is described in a companion paper [Thaden, J. and Miller, P. S. (1993) *Bioconjugate Chem.*, preceding paper in this issue].

As the development of nonisotopic oligonucleotide probes and bioactive "antisense" and triplex synthetic oligonucleotide reagents continues, so too does the demand for chemically modified oligomers (reviewed by Goodchild, 1990; Uhlmann and Peyman, 1990) having new properties such as resistance to nucleases. If modification introduces a primary aliphatic amine, then oligomers may be selectively conjugated with a variety of substituents including fluorophores, enzymes, biotin, intercalators, cross-linkers, nucleic acid cleaving reagents, and modifiers of cellular uptake. Commonly, the 5′ end of the oligomer has been the site of conjugation. However methods for modifying the 3′ end are also of interest because this provides an additional site for conjugation.

For our continuing studies on nuclease resistant oligonucleoside methylphosphonates (Miller, 1989; Miller and Ts'o, 1988), we required the ability to selectively introduce a single fluorescent label to the 3′-end of the oligomer (Thaden and Miller, 1993). This could be most readily achieved by using a specifically functionalized solid support for the automated synthesis of oligomers. The moderate base sensitivity of the methylphosphonate linkage necessitated the use of a support which would allow release and deprotection of oligomers under mild conditions. Upon review, available supports failed to meet this criterion, or presented other complications. In this Technical Note we describe the preparation of Aha-CPG, a controlled pore glass support functionalized with a protected *N*-(3-aminoprop-1-yl)-*N*-(2-hydroxyethyl)-2-aminoethyl ester of succinic acid. This support is compatible with oligonucleoside methylphosphonate synthesis and provides an aliphatic amine linker arm at the 3′ end of the oligomer. In addition, this support allows the synthesis of oligomers which terminate with a 3′-(methylphosphonate) group.

EXPERIMENTAL PROCEDURES

Silica gel TLC was carried out on plastic-backed Merck 60 F_{254} silica using the following solvent systems: I, 9:1 dichloromethane–methanol; II, 184:15:1 dichloromethane–methanol–triethylamine; III, 20:4:1 dichloromethane–methanol–ammonia (aqueous). Compounds were visualized by UV shadowing, and, in the case of compounds containing DMT[1] groups, by exposure to hydrochloric acid fumes. Silica gel for column chromatography was 230–400 mesh (Merck). Diethanolamine was distilled under low-pressure argon using an air-cooled condenser. Pyridine was refluxed with and distilled from chlorosulfonic acid followed by further reflux and distillation from sodium hydroxide pellets. Triethylamine, EDA, piperidine and 1,2-dichloroethane were each distilled from calcium hydride. Other reagents were used without further purification unless otherwise noted.

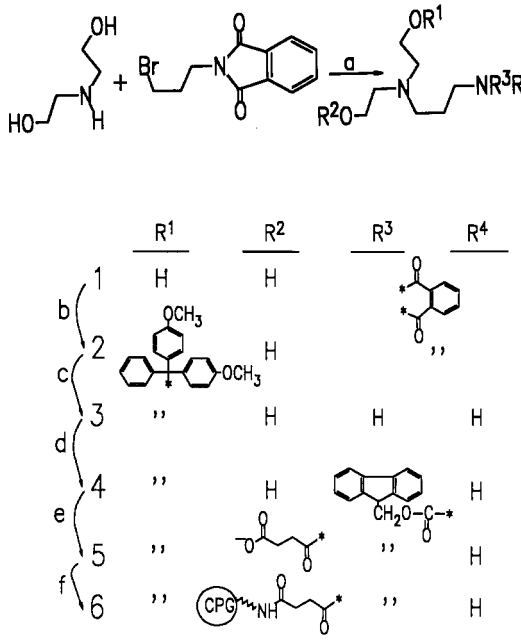
* Author to whom correspondence should be addressed.

● Abstract published in *Advance ACS Abstracts*, October 1, 1993.

[1]Abbreviations: CPG, controlled pore glass modified with long-chain alkylamine; DMAP, 4-(dimethylamino)pyridine; DMT, 4,4′-dimethoxytrityl; EDA, ethylenediamine; EDAC, 1-ethyl-3-[3-(dimethylamino)propyl]carbodiimide; Fmoc, 9-fluorenylmethoxycarbonyl.

1043-1802/93/2904-0395$04.00/0 © 1993 American Chemical Society

Scheme I. Construction of a CPG Solid Support for Automated Synthesis of 3′ Modified Oligonucleitide Analogs[a]



[a] (a) excess amine, neat; (b) DMT-Cl/pyr; (c) hydrazine hydrate/MeOH; (d) $MeCl_2/(Et)_3N/(Me)_3SiCl$; (e) Fmoc-Cl/$(Et)_3N$; (f) pyr/$H_2O$; (g) succinic anhydride/pyr/DMAP; (h) TCA-pretreated CPG/pyr/DMAP/EDAC/$(Et)_3N$.

Synthesis of Components of the Solid Support (Scheme I). Care was taken during workup of compounds **2**–**6** to not exceed pH limitations of the DMT and Fmoc protecting groups.

***N*-[*N*-Phthaloyl-3-aminoprop-1-yl]-*N*,*N*-bis(2-hydroxyethyl)amine (1, Scheme I).** A solution of *N*-(3-bromopropyl)phthalimide (24 g, 90 mmol) in melted diethanolamine (78 mL, 0.81 mol) was stirred in a stoppered 250-mL flask submerged in a water bath set to 63 °C. At 12 h, the bath temperature had risen to 72 °C and no *N*-(3-bromopropyl)phthalimide was detected by TLC. Unreacted amine was removed by high-vacuum distillation, under conditions where the liquor temperature did not exceed 190 °C. A suspension of the remaining syrup in 5% sodium carbonate (300 mL) was extracted twice with chloroform (2 × 150 mL). The chloroform solution, which contained one major (R_f 0.54) and five minor (R_f < 0.01, 0.34, 0.39 0.69, 0.74) components as assayed by TLC (solvent I), was dried over anhydrous sodium sulfate and then decanted into a flask containing dry silica gel (24 g). The mixture was evaporated to a free-flowing solid. This solid was added to the top of a column (4.9 cm i.d.) packed with silica (315 g). The column was eluted with 1 L each of 3%, 5%, 10% and 15% methanol in chloroform containing ammonia (0.2%). Pooled R_f 0.54 fractions were evaporated to a colorless oil (7.6 g, 26 mmol, 29%). ^{1}H NMR: (300 MHz, $CDCl_3$, δ) 1.89 (quin, 2 H, J = 6.9 Hz, $CH_2CH_2CH_2$), 2.58 (t, 2 H, J = 6.8 Hz, $CH_2N(EtOH)_2$), 2.64 (t, 4 H, J = 5.4 Hz, $N(CH_2CH_2OH)_2$), 2.9 (br, 2 H, O*H*), 3.61 (t, 4 H, J = 5.2 Hz, CH_2OH), 3.78 (t, 2 H, J = 7.1 Hz, phthal-NCH_2), 7.70–7.85 (m, 4 H, phthal).

***N*-[*O*-(4,4′-Dimethoxytrityl)-2-oxyethyl]-*N*-[*N*-phthaloyl-3-aminoprop-1-yl]-*N*-(2-hydroxyethyl)amine (2, Scheme I).** A solution of 4,4′-dimethoxytrityl chloride (9.1 g, 27 mmol) in pyridine (88 mL) was added dropwise to a solution of substance 1 (7.13 g, 24 mmol) in pyridine (80 mL). After 17 h, the reaction mixture was diluted with water (1 L) and the solution extracted with dichloromethane (4 × 200 mL). The dichloromethane solution was washed with 10% sodium carbonate (200 mL) and evaporated. The residual syrup was coevaporated with toluene (100 mL total) and kept at reduced pressure for 16 h to yield an amber resin (14.7 g). This was purified on three serial silica columns, using either dichloromethane or alumina-treated chloroform containing 0–5% of 9:1 (v/v) methanol–triethylamine. Fractions containing a component with R_f 0.55 (TLC solvent II) were pooled and evaporated to give an amber foam (3.93 g, 6.6 mmol, 27%). ^{1}H NMR (300 MHz, $CDCl_3$, δ) 1.8–2.0 (m, 2 H, $CH_2CH_2CH_2$), 2.6–2.8 (m, 6 H, $CH_2N(CH_2CH_2OH)_2$), 3.2–3.25 (m, 2 H, CH_2O-DMT), 3.57 (t, 2 H, J = 5 Hz, CH_2OH), 3.67 (t, 2 H, J = 7.1 Hz, phthal-NCH_2), 3.79 (s, 6 H, CH_3O-Ph), 6.8 (d, J = 8.6 Hz, 4 H, DMT aryl), 7.2–7.43 (m, 9 H, DMT aryl), 7.70–7.84 (m, 4 H, phthal).

***N*-(3-aminoprop-1-yl)-*N*-[*O*-(4,4′-dimethoxytrityl)-2-oxyethyl]-*N*-(2-hydroxyethyl)amine (3, Scheme I).** A solution of compound **2** (3.8 g, 6.4 mmol) dissolved in methanol (55 mL) was refluxed for 3.3 h with 85% hydrazine hydrate (0.83 mL, 14.0 mmol), after which only a trace of the phthalimide remained (TLC, solvent II). Solvents were evaporated, and the remaining white solid was suspended in 95% ethanol (50 mL) and 0.1 M potassium hydroxide (5 mL). The solvents were again evaporated, and the residue was coevaporated with 95% ethanol (120 mL total) and then with water (50 mL total). The solid was refluxed in chloroform (200 mL) and 0.1 M potassium hydroxide (54 mL) for 20 min. The chloroform layer was replaced with fresh chloroform (200 mL) and refluxing was repeated. The pooled chloroform extracts were dried over granular potassium carbonate and evaporated to give an amorphous solid (2.55 g) with major (R_f 0.30) and minor (R_f 0.88) dimethoxytrityl-containing components on TLC (solvent III). The product was purified on a column (4.9 × 15 cm) using a stepwise increasing gradient (0%, 5%, 10%, 15%, 20%) of methanol–ammonia (4:1 v/v) in dichloromethane. Pooled fractions containing product were dried over potassium carbonate and evaporated to give a colorless glass (1.24 g, 2.6 mmol, 41%).

***N*-[*N*-[(9-Fluorenylmethoxy)carbonyl]-3-aminoprop-1-yl]-*N*-[*O*-(4,4′-dimethoxytrityl)-2-oxyethyl]-*N*-(2-hydroxyethyl)amine (4, Scheme I).** The silyl-protected urethane synthesis of Ti *et al.* (1982) was adapted: a solution of compound **3** (0.7 g, 1.4 mmol) in dry dichloromethane (4.3 mL) and triethylamine (588 μL, 4.2 mmol) was chilled in ice water while chlorotrimethylsilane (0.50 mL, 3.9 mmol) was slowly added. After stirring for 15 min at 22 °C, the solution was refluxed for 40 min, during which compound **3** was converted to a substance with an R_f of 0.18 (TLC, solvent I). The solution was cooled to 4 °C and was treated with dry triethylamine (0.20 mL, 1.4 mmol) and Fmoc chloride (389 mg, 1.5 mmol). The reaction mixture was removed from the ice water bath and stirred for 30 min. Major (R_f 0.65) and minor (R_f 0.46) dimethoxytrityl-containing components resulted (TLC solvent I). The reaction mixture was incubated (37 °C, 48 h) with pyridine (25 mL) and water (12.5 mL), after which the R_f 0.46 substance predominated. The volume was reduced to 15 mL by rotary evaporation, and coevaporation was done with toluene (30 mL). A solution of the residue in dichloromethane (50 mL) was washed with 5% sodium dihydrogen phosphate (50 mL), dried over anhydrous sodium sulfate, and evaporated to give an amber foam which contained some white solid and traces

of pyridine. The pyridine was removed by coevaporation with toluene (25 mL). The remaining solids were triturated with 3% methanol in dichloromethane (5 mL) and filtered. The filtrate was chromatographed on a 3.65 × 12.5 cm column using the same solvent, followed by 6% methanol in dichloromethane. Fractions containing the product were pooled and evaporated to give a light yellow foam (0.34 g, 0.5 mmol, 35%).

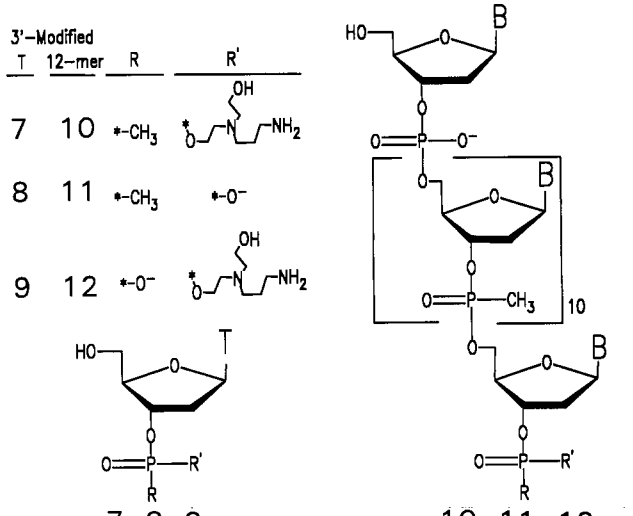
***N*-[*N*-[(9-Fluorenylmethoxy)carbonyl]-3-aminoprop-1-yl]-*N*-[*O*-(4,4′-dimethoxytrityl)-2-oxyethyl]-*N*-[(*O*-(3-carboxylatopropionyl)-2-oxyethyl]amine (5, Scheme I).** Succinylation was by the method of Pon *et al.* (1988). A solution of compound 4 (0.32 g, 0.47 mmol) in pyridine (3 mL) was treated with succinic anhydride (0.14 g, 1.4 mmol) and DMAP (30 mg, 0.24 mmol) for 18 h at 22 °C, after which nearly all dimethoxytrityl-containing material had an R_f of 0.29 (TLC solvent I). The same material was also observed in an earlier, half-scaled reaction (0.15 g, 0.22 mmol of compound 4). The two reaction solutions were pooled, and evaporated to an amber oil (1.5 mL). This was coevaporated with toluene (2 mL) and diluted with ethyl acetate (15 mL). The solution was washed repeatedly with brine (6 × 10 mL), and the brine washes were extracted with fresh ethyl acetate (15 mL). The pooled ethyl acetate solution was dried over anhydrous sodium sulfate and evaporated to a foam. The product was further purified on a silica gel column (2.85 × 10 cm) which was eluted sequentially with 3% and 8% methanol in dichloromethane. After extensive evaporation (oil pump), a pale yellow glass remained (0.50 g, 0.64 mmol, 90%). MS (+FAB, thioglycerol, **5** = $C_{47}H_{50}N_2O_9$): *m/z* calcd 786.89; found 787.2.

5-Derivatized Controlled Pore Glass (6 Scheme I). Long-chain alkylamine controlled pore glass (Pierce Chemical Co., 3.5 g) was pretreated for 2 h with trichloroacetic acid (1.5 g) in 1,2-dichloroethane (50 mL), washed with aliquots of dichloromethane (100 mL total) and anhydrous ether (100 mL total), and dried *in vacuo*. This acid pretreatment has been reported by Pon *et al.* (1988) to reduce anomalously high coupling yields often seen during the first one or two cycles of oligonucleotide synthesis on CPG supports. To each dry gram of CPG was added pyridine (10 mL), DMAP (12 mg, 98 μmol), EDAC (382 mg, 2 mmol), triethylamine (80 μL), and compound **5** (146 μg, 200 μmol). After shaking for 18 h, the beads were given multiple washes of pyridine (5 × 5 mL), methanol (3 × 10 mL), and chloroform (3 × 10 mL) and then dried *in vacuo*. Loading was quantified by (a) measurement of the A_{500} of DMT cation released by acid treatment and (b) ninhydrin assay following the procedure of Sarin *et al.* (1981), but omitting the tetrabutylammonium chloride wash. Typical loading was 30–40 μmol of compound **5** per gram. Support **6** was stored desiccated at −20 °C.

Capping. Unreacted primary amines and other reactive sites were eliminated by reaction with acetic anhydride just prior to oligomer synthesis, as recommended by Pon *et al.* (1988). Synthesis columns (1 μmol scale) were filled with support **6** and mounted on a Biosearch Model 8700 synthesizer. A program was run which percolated first a solution of 0.2 M DMAP in pyridine through the columns for 0.5 s followed by a 4.5-s pause, then 2:3 acetic anhydride–THF on the same schedule. This cycle was repeated for 10 min, after which the support was washed with acetonitrile. In one experiment, a commercial support was likewise treated.

Synthesis and Purification of 3′ Modified Oligomers and Monomers (Chart I). Automated synthesis was performed according to published methods for the preparation of oligodeoxyribonucleoside methylphosphonates (Miller *et al.*, 1991), wherein synthesis and coupling programs differ from standard oligodeoxyribonucleotide programs only in that an additional capping cycle is inserted before the oxidation step. Properties of the 3′ modifier supports dictated the following alterations: When specifying the sequence to be synthesized, keystrokes were made corresponding to the 12-mer sequence common to oligomers **10** and **12** (**Chart I**), followed by the entry of any single letter. The 13th letter functions as a placeholder and is needed because the synthesizer is designed for use with monomer supports, which contribute the first (3′) monomer to the oligomer. The 3′modifier supports do not. For oligomer **10**, the five synthon bottles were filled with the base-protected 5′-(dimethoxytrityl)-2′-deoxyribonucleoside 3′-(methyl *N,N*-diisopropylphosphonamidite) synthons of A, G, T, and C, and the base-protected 5′-(dimethoxytrityl)-2′-deoxyribonucleoside 3′-(β-cyanoethyl *N,N*-diisopropylphosphoramidite) synthon of A. For oligomer **12**, the methyl phosphonamidite of C was substituted by the phosphoramidite of C.[2] After oligomer synthesis was complete, the last 5′-(dimethoxytrityl) group was left on. Monomer syntheses were detritylated on the machine, unless noted. Coupling efficiency was determined by comparing the absorbance at 500 nm of dimethoxytrityl alcohol released at each detritylation step.

Chart I. Oligomers and Monomers Synthesized on Support 6[a]



[a] The base sequence for **10**, **11**, and **12** is 5′ATAGGATTTCTC3′.

Deprotection by the EDA Procedure. The method of Miller *et al.* (1991) was scaled up and modified to permit back-washing. The oligomer-bearing support was removed from the four synthesis columns and pooled in a back-washing device comprising a 5-mL polypropylene chromatography column with a porous frit, a 5-mL polypropylene syringe for introducing fluids, and an interconnecting length of silicone tubing (0.8 mm i.d., 0.8 mm wall, 4–6 cm) terminated with adaptors (0.8 mm hose barb to female luer). The syringe was filled with a solution

[2] For a second sequence that contained all four 3′-methylphosphonates and two different 3′-phosphodiesters, synthesis was halted briefly while one of the five bottles which had expended its monomer was washed under manual control, filled with the sixth synthon, and manually primed. Coupling yield was not affected.

containing pyridine (4.8 mL), glacial acetic acid (1.2 mL), and 85% hydrazine hydrate (0.2 mL). The solution was introduced to the support in two or three injections over 24 h. Between injections, a polypropylene cap with a sealable pin-hole was used to close the column top. The pin-hole prevented sudden pressure changes, which can induce buffer crystallization. After treatment, excess solution was decanted from the support. The support was back-washed with 95% ethanol followed by acetonitrile (20 mL each). The column was detached from the tubing, loosely covered, and dried *in vacuo* with moderate centrifugation for 10 min. A solution of 95% ethanol–EDA (1:1 v/v, 2 mL) and a small bubble of air was drawn into the syringe, and the device was reassembled. All but 0.2 mL of the solution was injected and the column was stored, capped, for 6 h at room temperature. After removal of cap, the remaining solution and enough air to clear the column tip was injected. The adaptor/tubing assembly was removed from the column tip, and the solution in the column was collected. The support was washed with pyridine–95% ethanol (1:1 v/v, 2 mL) and back-washed with two like portions, pooling the wash solutions with the first eluate. Solvents were evaporated. Traces of pyridine were removed by coevaporation with four 2-mL portions of 95% ethanol. Some browning of the residue occurred unless evaporations were stopped short of total dryness. The residue was dissolved in 1.5 mL of a solution containing 100 mM sodium dihydrogen phosphate and 30% acetonitrile. Final adjustment of the pH to 6–7.5 was made with microliter additions of acetic acid. In this pH range, most but not all of the residual solids were redissolved. Single-cycle test syntheses of 3′-modified thymidines were deprotected in like manner, but omitting the back-wash device, the hydrazine reaction, and ensuing washes. Hydrazine pretreatment is required only if cytosines are present (Miller *et al.*, 1991). Deprotection efficiency was calculated by dividing the actual mole yield of full-lengthed product, as determined by reversed-phase HPLC peak area analysis relative to co-injected standards, by the predicted yield, as estimated by the product of CPG loading and overall coupling efficiency.

Purification of Crude 3′-Modified Oligomers. Insoluble material, believed to be Fmoc hydrolyzates, was pelleted by low-speed centrifugation and a portion of the supernatant containing not more than 125 A_{254} units was drawn into an HPLC injection syringe. One-half volume of water was drawn into the syringe, mixed by inverting once, and immediately injected onto a preparative reversed-phase HPLC column (Thaden and Miller, 1993). The broad HPLC peak eluting during the last half of the gradient (16–38% acetonitrile, linear, 30 min) was collected, concentrated by rotary evaporation, and desalted. The residue was dissolved in acetic acid (80%, 1 mL) and incubated (30 min, 22 °C) to remove the 5′-dimethoxytrityl group. Acid was removed by evaporation and by coevaporation with water (3 × 1 mL). Dimethoxytrityl alcohol was extracted from the residue with ether. At this stage, oligomer **12** was sufficiently pure for use in conjugation reactions (Thaden and Miller, 1993), or could be purified further by PAGE or HPLC.

Monomer products of single-cycle synthesis were analyzed and purified by reversed-phase HPLC (Thaden and Miller, 1993; 2–12% acetonitrile, 16 min). HPLC-purified products were desalted, but omitting acetonitrile from final prewash and loading buffers.

RESULTS AND DISCUSSION

Existing 3′ Modifier Supports. Methods which can produce end modifications during automated oligonucleotide synthesis eliminate the risk of side reactions with bases, which are blocked, and greatly simplify workup of intermediates, which are support-bound. Since oligomers are usually synthesized in the 3′-to-5′ direction, an advantage unique to 3′ end modification during automated synthesis is the certainty that 100% of full-lengthed products will be modified. But because the 3′ terminus is covalently bound to a solid support, specialized solid supports are required. Those described to date that are compatible with automated synthesis by the standard phosphoramidite chemistry have been designed to produce, upon deprotection, oligodeoxynucleotides modified at the 3′ terminus either with phosphate (Felder *et al.*, 1984; Lohrmann *et al.*, 1984; Markiewicz and Wyrzykiewicz, 1989; Kumar *et al.*, 1991; Gryaznov and Letsinger, 1992) or with phosphoesters of 3-aminopropane-1,2-diol (Nelson *et al.*, 1989), 6-amino-*n*-hexan-1-ol (Asseline and Thuong, 1990; Petrie *et al.*, 1992), *n*-hexadecane-1,16-diol (MacKellar *et al.*, 1992), cholesterol (MacKellar *et al.*, 1992; Reed *et al.* 1991), modified acridine (Reed *et al.*, 1991), or polyamides (Haralambidis *et al.*, 1990).

A common feature of existing 3′ modifier supports is the use of a strong ammoniacal reagent at some point during deprotection and release of support-bound oligonucleotides. The moderate base-sensitivity of methylphosphonate linkages precludes the use of high concentrations of ammonia. Instead, a milder procedure involving buffered hydrazine followed by ethanolic EDA has been used to release methylphosphonates from standard, nucleoside-esterified supports (Miller *et al.*, 1983). These conditions might also be expected to work on 3′ modifier supports which utilize the same succinate ester linkage (Reed *et al.*, 1991; MacKellar *et al.*, 1992; Nelson *et al.*, 1989) or other carboester bonds (Haralambidis *et al.*, 1990). Indeed Chin and co-workers reported synthesis of 3′ modified oligonucleoside methylphosphonates using the support of Nelson *et al.* (1989) although no experimental details were provided. A strong base would appear to be obligatory for some supports (Asseline and Thuong, 1990; Felder *et al.*, 1984; Kumar *et al.*, 1991; support 1 of Markiewicz and Wyrzykiewicz, 1989; Petrie *et al.*, 1992; Gryaznov and Letsinger, 1992). The remaining supports use conditions that are of untested compatibility with methylphosphonates (support 2 of Markiewicz and Wyrzykiewicz, 1989; Lohrmann *et al.*, 1984).

In our hands, attempts to synthesize oligonucleoside methylphosphonates on a commercial solid support ("3′-amino-modifier CPG", Glen Research) of the succinate-linked, 3-aminopropane-1,2-diol design (Nelson *et al.* 1988) were not wholly successful. Our attempts fell into two classes, depending upon whether the first nucleoside was coupled to the support via a methylphosphonate or a phosphodiester linkage. Coupling of the 3′-(*N,N*-diisopropylmethylphosphonamidite) 5′-(dimethoxytrityl)thymidine to the support to form a methylphosphonate linkage was successful (99%). But upon deprotection with EDA, only thymidine was detected, as determined by HPLC using two different gradient systems. The desired aminopropanediol 3′-methylphosphonate of thymidine apparently did not survive deprotection conditions. This behavior is consistent with previous studies which showed that methylphosphonate diester linkages are readily hydrolyzed if one of the ester carbons is adjacent to a carbon bearing a hydroxyl group (Miller *et al.*, 1983).

In experiments of the latter class, a phosphoramidite synthon was used for the first round of coupling. In order to synthesize 3′ modified, 5′-DMT oligonucleoside methylphosphonates, this initial phosphodiester linkage was

followed by multiple couplings of methylphosphonamidite synthons and a final phosphoramidite coupling. The synthesis was efficient (mean coupling 95%), but deprotection and cleavage from the support by the EDA procedure was not. In two trials, 59% and 38% of the dimethoxytrityl groups remained on the support after the standard EDA treatment. The small amount of crude oligomer which had been released was detritylated and subjected to reversed-phase HPLC analysis. There was a major peak, preceded by a series of very minor peaks. The minor peaks were the "failure" fragments typical of crude oligomers and were present in unexceptional amounts. The major peak appeared to be heterogeneous, however, with prominent shoulders on its trailing edge.

A sample of the 5′-OH crude oligomer was phosphorylated using T_4 polynucleotide kinase and [^{32}P]ATP. When this crude oligomer was electrophoresed on denaturing PAGE gels, two major bands were observed atop a ladder of very minor ones. The minor bands were typical of a crude oligomer, but the presence of two major bands was not.

The HPLC and PAGE results suggest that the full-lengthed oligomer contained different modifications at its 3′ end. Similar electrophoretic behavior has previously been reported for an oligodeoxyribonucleotide 11-mer prepared on this support and deprotected with ammonia (Reed *et al.*, 1991; Petrie *et al.*, 1992). These authors suggested that the multiple products, and failure of this oligomer to react completely with an activated ester, could be due to isomerization of the oligomer's 3′-phosphate, from the primary alcohol of the 3-aminopropane-1,2-diol linker, to its secondary alcohol, and ultimately to its amine.

The 3′-(2-cyanoethyl phosphoramidite) of 5′-(dimethoxytrityl)thymidine was coupled by a single round of synthesis to the aminopropyl diol support, and to the support after having acetylated it afresh using a proven capping method (see Capping, above). The products were deprotected with EDA. This experiment was designed to confirm that the particular lot of support we used was properly capped. If not, deprotection could appear inefficient, since chains initiating upon nonacetylated silyl or amino groups on the support will show up in trityl assays but will not be freed by standard deprotection methods. The coupling efficiency was 108% and 100%, but the deprotection efficiency was only 10% and 7%, respectively, for the once-capped and twice-capped aliquots. Reacetylation did not improve the deprotection efficiency of the support. By this test, the succinate-linked aminopropyl diol support appears to have been properly capped as received from the manufacturer, and one must look elsewhere for an explanation of deprotection failure. One possibility is that a competing reaction to succinate ester cleavage is occurring during EDA treatment, namely, succinate ester aminolysis by the primary amine on the support after it has lost its Fmoc protecting group. The resulting succinamide would resist cleavage in EDA.

We conclude that a commercial support of the succinate-linked 3-aminopropane-1,2-diol design is, in our hands, incompatible with oligonucleoside methylphosphonate synthetic chemistry. The problems encountered depended upon whether the first coupling to the support was a phosphodiester or a methylphosphonate, but in either case, the problems were consistent with isomerizations having occurred.

Aha-CPG. The resistance of an aminoalkyl diol support to such intramolecular rearrangements might be significantly enhanced if, unlike the support discussed above, the three functional groups did not reside on adjacent carbons. We set out to make such a support (compound **6** in Scheme I). The linker functionality of the support is *N*-(3-aminopropyl)diethanolamine. The primary amine of this linker is protected with Fmoc. One of the hydroxyls is protected with dimethyoxytrityl, and the other hydroxyl is esterified *via* a succinyl group to the support.

The synthesis of the support is outlined in Scheme I. Diethanolamine was converted to **1** by reaction with *N*-(3-bromopropyl)phthalimide. Compound **1** was reacted with limiting 4,4-dimethoxytrityl chloride to give the monotritylated derivative **2**. The phthalimide group was then removed with hydrazine and the resulting compound, **3**, was treated with Fmoc chloride to give **4**. Compound **4** was treated with succinic anhydride. Support **6** was obtained by reacting the succinate ester, **5**, with CPG.

3′-(Methylphosphonate). We studied the synthesis of oligonucleoside methylphosphonates on support **6**. As with the commercial support, we looked at compounds coupled to the support's linker functionality by either a methylphosphonate or a phosphate diester. When the 3′-(methylphosphonamidite) of 5′-(dimethoxytrityl)thymidine was reacted with support **6** and subsequently deblocked, three peaks having the thymine chromophore were detected by HPLC. During incubation of an aqueous solution of these products at 37 °C, the earliest-eluting peak increased in size at the expense of the remaining two, closely-spaced peaks until, after 16 h, the early peak was the only product observed. This compound coeluted with an authentic sample of thymidine 3′-(methylphosphonate). No thymidine was observed. This result suggests that the two diastereoisomers of **7** shown in Chart I were slowly converted to thymidine 3′-(methylphosphonate), **8**.

Similar behavior was observed when oligomer **10** was prepared on support **6**. The 5′-dimethoxytritylated oligomer was deprotected using the standard EDA procedure and was purified by reversed-phase HPLC. The 5′-(dimethoxytrityl) group was then removed and the product was purified to homogeneity by reversed-phase HPLC. A sample of the oligomer prepared in this manner was phosphorylated with polynucleotide kinase and [^{32}P]ATP and analyzed by PAGE. In addition to the expected 5′-^{32}P derivative of **10**, a new product with faster electrophoretic mobility was observed. When radiolabeled **10** was incubated in 25% ethanol solution at 37 °C, it was converted to this new product. The disappearance of **10** was exponential, with a half-life of 6 h. The increased electrophoretic mobility of the new product is consistent with it being oligomer **11**, the 3′-(methylphosphonate) derivative of an oligonucleoside methylphosphonate.

These results and the analogous observations with thymidine derivative **7** suggest that when the support-derived linker/spacer moiety is esterified through a methylphosphonate to a nucleic compound, it can act upon the linkage to bring about an unusual regioselective cleavage, of only the nearest of the two ester bonds. Our failure to detect any 3′-hydroxyl products of cleavage argues that the regioselectivity is the same regardless of the stereoconfiguration (*R* or *S*) at the phosphorus. Such cleavage could occur if the tertiary nitrogen of the linker were to attack the carbon linked to the methylphosphonate group, resulting in formation of an aziridinium intermediate and elimination of the methylphosphonate. This elimination reaction would be analogous to that which occurs in nitrogen mustards.

To see if the resulting 3′-(methylphosphonate) group could be further derivatized, compound **11** was subjected to water-soluble carbodiimide in imidazole buffer in the

manner used by Chu *et al.* (1983) to derivatize the 5′-phosphate on unprotected polynucleotides. The 3′-(methylphosphonate) of compound 11 was not reactive under these conditions.

Oligonucleotide 3′-methylphosphonic acids are isosteric with naturally occurring 3′-phosphorylated nucleic acids. Unlike 3′-phosphates, 3′-(methylphosphonates) of oligodeoxyribonucleotides were found to be considerably resistant to alkaline phosphatase and to nucleases in fetal bovine serum and to be totally resistant to snake venom phosphodiesterase (Tidd and Warenius, 1989). Thus, the 3′-(methylphosphonate) group may find utility in the preparation of nuclease resistant oligonucleotides.

3′-[[*N*-(3-Aminoprop-1-yl)-*N*-(2-hydroxyethyl)-2-aminoethyl] phosphates]. When the 3′-(2-cyanoethyl phosphorodiamidite) of 5′-(dimethoxytrityl)thymidine was reacted with support 6 and subsequently deblocked, the crude product (9) was free of thymidine or 3′-thymidine monophosphate as determined by reversed-phase HPLC. There was no change in the HPLC profile after incubation in 28% acetonitrile for 24 h at 37 °C.

Monomeric compound 9 was again prepared on support 6, in parallel with an analogous coupling to the commercial, succinate-linked, 3-aminopropane-1,2-diol support discussed previously. The coupling efficiencies were 65% and 104%, and the deprotection efficiencies were 92% and 10%, respectively, for support 6 and the commercial support. The lower coupling efficiency to 6 may be due to greater steric hindrance in areas of dense loading, since it is functionalized with a bulkier group than is the commercial support. The much higher deprotection efficiency implies that the mechanism which subverts deprotection of the commercial support does not act on support 6. All else being equal, support 6 is predicted to yield 5–6 times more product than the commercial support.

We proceeded with synthesis of oligomer 12 on support 6 (initial coupling, 70%, mean of subsequent couplings, 95%). The 5′-dimethoxytritylated oligomer was deprotected using the standard EDA procedure and was purified by reversed-phase HPLC. After the 5′-(dimethoxytrityl) group was removed, a single peak was observed on reversed-phase HPLC. A sample of 12 prepared in this manner was phosphorylated with polynucleotide kinase and [^{32}P]ATP. Radiolabeled 12 was analyzed by PAGE. We observed one major band, and traces of shorter products. The chromatographic and electrophoretic behaviors of 12 were changed neither by storage for up to 6 months in 30% acetonitrile at −20 °C, nor by storage for 4 days at 22 °C.

Oligomer 12 gave a positive ninhydrin test consistent with the presence of a primary amino group. In addition, the oligomer can be conjugated readily to an amine-reactive dye, tetramethylrhodamine 5-isothiocyanate, with 85% yield (Thaden and Miller, 1993). These results demonstrate the utility of the Aha-CPG support (6) in the preparation of oligonucleoside methylphosphonates which terminate with an addressable primary amine function.

In this Technical Note, we have detailed the six-step synthesis of a modified controlled pore glass, Aha-CPG (6). We have provided chromatographic and spectroscopic evidence of its identity. We have demonstrated that the beads can be used as an effective solid support for automated synthesis of 3′ modified oligonucleoside methylphosphonates. The modification is a stable, (2-*tert*-aminoethyl)phosphoryl group, one arm of which is a primary aliphatic amine suitable for conjugation with fluorophores and related agents. Normal oligodeoxyribonucleotides should also be 3′ modifiable using this support, since their synthesis is comparable to (if less exacting than) methylphosphonate synthesis. Because the 3′ modification preserves base contiguity and is distant from 5′ modifications, oligomers built upon the Aha-CPG support are excellent candidates from which to make doubly-conjugated oligomers.

In addition, we report the finding that Aha-CPG can be used to cap oligonucleoside methylphosphonates with a methylphosphonic acid group. 3′ Terminal methylphosphonate is known to render oligodeoxyribonucleotides resistant to nucleases and phosphatases.

ACKNOWLEDGMENT

Financial support for this work was provided through grants from the National Cancer Institute (CA42762), the National Institutes of Health (ES03841 and CA09110), and the Department of Energy (DEFG02-88ER60636). We gratefully acknowledge the technical advice of P. Bhan, J. Cormier and T. E. Leonard and the assistance of L-S. Kan and T. L. Trapane, for NMR spectral analyses, and R. T. Streeper and R. J. Cotter of the Middle Atlantic Mass Spectrometry Laboratory (an NSF Regional Instrumentation Facility), for FAB positive ion MS analysis.

LITERATURE CITED

Asseline, U., and Thuong, N. T. (1990) New solid-phase for automated synthesis of oligonucleotides containing an aminoalkyl linker at their 3′ end. *Tetrahedron Lett. 31*, 81–84.

Chin, D. J., Green, G. A., Zon, G., Szoka F. C., and Straubinger, R. M. (1990) Rapid nuclear accumulation of injected oligodeoxyribonucleotides. *New Biologist 2*, 1091–1100.

Felder, E., Schwyzer, R., Charubala, R., Pfleiderer, W., and Schulz, B. (1984) A new solid phase approach for rapid syntheses of oligonucleotides bearing a 3′-terminal phosphate group. *Tetrahedron Lett. 25*, 3967–3970.

Goodchild, J. (1990) Conjugates of oligonucleotides and modified oligonucleotides: A review of their synthesis and properties. *Bioconjugate Chem. 1*, 165–187.

Gryaznov, S. M., and Letsinger, R. L. (1992) A new approach to synthesis of oligonucleotides with 3′phosphoryl groups. *Tetrahedron Lett. 33*, 4127–4128.

Haralambidis, J., Duncan, L., Angus, K., and Tregear, G. W. (1990) The synthesis of polyamide-oligonucleotide conjugate molecules. *Nucleic Acids Res. 18*, 493–499.

Kumar, P., Bose, N. K., and Gupta, K. C. (1991) A versatile solid phase method for the synthesis of oligonucleotide-3′-phosphates. *Tetrahedron Lett. 32*, 967–970.

Lohrmann, R., Arnold, L., Jr., and Ruth, J. (1984) New solid supports for DNA synthesis. *DNA 3*, 122.

MacKellar, C., Graham, D., Will, D. W., Burgess, S., and Brown, T. (1992) Synthesis and physical properties of anti-HIV antisense oligonucleotides bearing terminal lipophilic groups. *Nucl. Acids Res. 20*, 3411–3417.

Markiewicz, W. T., and Wyrzykiewicz, T. K. (1989) Universal solid supports for the synthesis of oligonucleotides with terminal 3′-phosphates. *Nucleic Acids Res. 17*, 7149–58.

Miller, P. S. (1989) Non-ionic antisense oligonucleotides. *Topics Mol. Biol. 12*, 79–95.

Miller, P. S., Agris, C. H., Murakami, A., Reddy, P. M., Spitz, S. A. and Ts'o, P. O. P. (1983) Preparation of oligodeoxyribonucleoside methylphosphonates on a polystyrene support. *Nucleic Acids Res. 11*, 6225–42.

Miller, P. S., Cushman, C. D., and Levis, J. T. (1991) Synthesis of Oligo-2′-deoxyribonucleoside Methylphosphonates. *Oligonucleotides and Analogues. A Practical Approach* (F. Eckstein, Ed.) pp 137–154, IRL Press, Oxford.

Miller, P. S., and Ts'o, P. O. P. (1988) Oligonucleotide inhibitors of gene expression in living cells: new opportunities in drug design. *Annu. Rep. Med. Chem. 23*, 295–304.

Nelson, P. S., Frye, R. A., and Liu, E. (1989) Bifunctional oligonucleotide probes synthesized using a novel CPG support are able to detect single base pair mutations. *Nucleic Acids Res. 17*, 7187–7194.

Petrie, C. R., Reed, M. W., Adams, A. D., and Meyer, R. B., Jr. (1992) An improved CPG support for the synthesis of 3′-amine-tailed oligonucleotides. *Bioconjugate Chem. 3*, 85–87.

Pon, R. T., Usman, N., and Ogilvie, K. K. (1988) Derivatization of controlled pore glass beads for solid phase oligonucleotide synthesis. *Biotechniques 6*, 768–775.

Reed, M. W., Adams, A. D., Nelson, J. S., and Meyer, R. B., Jr. (1991) Acridine- and cholesterol-derivatized solid supports for improved synthesis of 3′-modified oligonucleotides. *Bioconjugate Chem. 2*, 217–225.

Sarin, V. K., Kent, S. B. H., Tam, J. P., and Merrifield, R. B. (1981) Quantitative monitoring of solid-phase peptide synthesis by the ninhydrin reaction. *Anal. Biochem. 117*, 147–157.

Ti, G. S., Gaffney, B. L., and Jones, R. A. (1982) Transient protection: efficient one-flask synthesis of protected deoxynucleosides. *J. Am. Chem. Soc. 104*, 1316–1319.

Tidd, D. M., and Warenius, H. M. (1989) Partial protection of oncogene, anti-sense oligodeoxynucleotides against serum nuclease degradation using terminal methylphosphonate groups. *Br. J. Cancer 60*, 343–350.

Thaden, J., and Miller, P. S. (1993) Photoaffinity behavior of a conjugate of oligonucleoside methylphosphonate, rhodamine, and psoralen in the presence of complementary oligonucleotides. *Bioconjugate Chem.*, preceding paper in this issue.

Uhlmann, E., and Peyman, A. (1990) Antisense oligonucleotides: A new therapeutic principle. *Chem. Rev. 90*, 543–584.

Synthesis of Dextran Derivatives with Thiol-Specific Reactive Groups for the Preparation of Dextran–Protein Conjugates

Sabine Herman,† Geertrui Persijn,† Joel Vandekerckhove,‡ and Etienne Schacht*,†

Department of Organic Chemistry, Biomaterials Research Group, and Laboratory of Physiological Chemistry, University of Ghent, Krijgslaan 281, B-9000 Ghent, Belgium. Received December 7, 1992

A novel strategy is described for the preparation of dextran–protein conjugates containing disulfide linkages. "Dormant" protected thiol groups are introduced as side chains on dextran. These can, in a later stage, be converted into thiol-specific reactive disulfides by reaction with (alkoxycarbonyl)sulfenyl chloride. A dextran-protein conjugate is then easily formed by reaction with a thiol group of a cysteine side chain. The disulfide linkage between dextran and the model tripeptides reduced glutathion and *N*-Ac-L-Cys-L-Ala-L-Lys remains intact, even after 24 h of incubation at 37 °C in blood.

INTRODUCTION

The clinical efficiency of many peptides and proteins with potentially interesting pharmacological qualities is often limited because of degradation by proteolytic enzymes, thermal instability, or immunogenicity.

Over the last few years, there has been a great incentive to develop new protein delivery systems, by covalent attachment of proteins to soluble polymers such as poly(vinyl alcohol) (*1*), carboxymethylcellulose (*2*), methoxypolyethylene glycols (*3–5*), dextran (*6–8*). As an example, Marshall (*6–8*) and Vegarud (*9*) have demonstrated that linkage of enzyme analogs to dextran results in a longer *in vivo* half-life and a reduced immunogenicity.

Most methods for the covalent attachment of polymers to proteins are based on the acylation of amino side groups of lysine residues. However, in cases where the active site of the protein is modified in a way that the biological activity is reduced or even lost, it is necessary to seek a different strategy for the preparation of polymer–protein conjugates.

The thiol function of the cysteine side chain offers an alternative opportunity for synthetizing protein–polymer conjugates. This requires a strategy whereby cysteine thiol functions react quantitatively and selectively with a polymer, containing thiol-reactive groups, to create well-defined conjugates. *N*-Succinimidyl 3-(2-pyridyldithio)-propionate (SPDP[1]) is a bivalent reagent that is being used for the preparation of asymmetrical disulfides, including polymer–protein conjugates (*10*).

An attractive alternative for coupling thiol derivatives was developed by Brois et al. (*11*) using alkoxycarbonyl disulfides as the thiol-specific reactive groups. The latter can be prepared by reacting trityl-, *tert*-butyl-, or acetamidomethyl-protected thiol groups with (alkoxycarbonyl)sulfenyl chloride.

In this work we have exploited this chemistry, which has the advantage over others that, along a dextran chain, "dormant" protected thiol groups can be introduced which in a later stage can be converted into thiol specific reactive disulfides by reaction with an (alkoxycarbonyl)sulfenyl chloride.

This approach is particularly attractive for the preparation of macromolecular drug derivatives whereby a polymer serves as carrier for both drug moieties and antibody fragments (*13*). In the strategy for preparing such conjugates it is preferable that the fragile antibody fragment is introduced in the last step of the reaction sequence. The "dormant" thiol group has the advantage over the SPDP derivatization method that it is more stable in the steps prior to coupling of the Fab' fragments.

The feasibility of this strategy for introducing "dormant" protected thiol side groups, their subsequent activation, and coupling with thiols was investigated using reduced glutathion and the tripeptide *N*-Ac-L-Cys-L-Ala-L-Lys as model peptides.

Furthermore, the stability of the polymer–peptide disulfide linkage in blood was evaluated. The disulfide stability in blood has been questioned before (*12*). Hence this information is most valuable because blood instability would imply that the conjugate is not suitable for intravenous administration because of premature polymer–peptide cleavage. For these in vitro studies, the peptides were labeled with fluorescein isothiocyanate (FITC).

EXPERIMENTAL PROCEDURES

Materials and Methods. 2-Aminoethanol hydrochloride (**1**), reduced glutathion (**7**), and fluorescein isothiocyanate (**15**) were obtained from Janssen Chimica (Beerse, Belgium). Triphenylmethanol (**2**) and (methoxycarbonyl)sulfenyl chloride (**5**) were obtained from Fluka (Buchs, Switzerland). 4-nitrophenyl chloroformate (**4**) was obtained from Merck (Darmstadt, Germany). *N*-Ac-L-Cys-L-Ala-L-Lys was prepared according to standard procedures of peptide chemistry. Methanol and ethanol were dried over calcium oxide. All other solvents were dried over calcium hydride. ^{1}H NMR spectra were recorded on a Bruker WH-360 or a Bruker WH-500 spectrometer. Preparative gel permeation chromatography was performed on a Pharmacia column (K2670), packed with Sephadex G 25 (Pharmacia; Upsalla, Sweden). Double-distilled water was used as eluent (3 mL/min). Eluting components were detected via refractive index. For the stability studies, PD10 columns (Sephadex G 25, Pharmacia; Sweden) were used. The UV absorbance during

† Department of Organic Chemistry.

‡ Laboratory of Physiological Chemistry.

[1] Abreviations used: GPC, gel permeation chromatography; trityl, triphenylmethyl; SPDP, N-succinimidyl 3-(2-pyridyldithio)propionate; DMAP, 4-(dimethylamino)pyridine; DMSO, dimethyl sulfoxide; OPA, *o*-phtalaldehyde; FITC, fluorescein isothiocyanate; DTT, dithiothreitol; Tris, tris(hydroxymethyl)aminomethane.

1043-1802/93/2904-0402$04.00/0 © 1993 American Chemical Society

GPC fractionations were monitored by a Uvikon 810 UV spectrometer (Kontron, Switzerland).

S-Trityl-2-mercaptoethylamine (3). 2-Aminoethanethiol (1) (3 g, 26.5 mmol) and 7 g (26.9 mmol) of triphenylmethyl alcohol (2) are dissolved in 20 mL of trifluoroacetic acid. After stirring at room temperature for 20 min, the solvent is removed under reduced pressure at 60 °C. The oily residue is treated with 400 mL of ether and stored overnight at −18 °C to allow crystallization. The product is isolated, washed with ether and water at 0 °C. A concentrated ammonia solution (30 mL) is added and the aqueous phase is washed four times with 100 mL of ether. The pooled ether phase is dried over $MgSO_4$. The solvent is removed under reduced pressure and the product is dried under vacuum.

^{1}H NMR (500 MHz, MeOD d_3): δ 2.33 (t, 2H, methylene function α of the protected thiol), 2.41 (t, 2H, methylene function α of the ammonium), 7.21 (m, 3H, the para protons of the trityl group), 7.28 (m, 6H, meta protons of the trityl group), 7.41 ppm (m, 6H, ortho protons of the trityl group).

Activation of Dextran with 4-Nitrophenyl Chloroformate (4). Dextran (9) (Mw = 30950, Mw/Mn = 1.19) (dried over P_2O_5) 2.5 g, 15 mmol glucose units) is dissolved in 150 mL of DMSO/pyridine (1/1, v/v) at 0 °C, and 0.25 g (1.24 mmol) of 4-nitrophenyl chloroformate (4) is added. A 10 mol % (vs 4) portion of DMAP is added as a catalyst. The reaction mixture is stirred under N_2 for 4 h at 0 °C. The reaction product is isolated by precipitation in 500 mL of ether/ethanol (1/1, v/v). The precipitate is isolated by filtration and washed with ethanol/ether (1/1, v/v) and then with ether.

The carbonate content is determined as described by Vandoorne (*13*). The total carbonate content was 6.9% (defined as the amount of carbonates on 100 glucose units)

Preparation of Dextran with 2-Aminoethyl Trityl Sulfide Side Groups (11). The 4-nitrophenyl-activated dextran (10) is dissolved in 150 mL of DMSO/pyridine (2/1, v/v) and a 2-fold excess (compared to the number of carbonates) of 2-aminoethyl trityl sulfide (3) is added. The mixture is stirred under N_2 for 48 h. After precipitation in 600 mL of ether/ethanol (1/1, v/v), the reaction product is isolated by centrifugation and filtration. The product is dissolved in 10 mL of H_2O and purified by preparative gel permeation chromatography on Sephadex G-25 (eluent double distilled water) followed by freeze-drying of the collected fraction.

^{1}H NMR (360 MHz, DMSO-d_6): δ 2.2 (br, methylene function α of the protected thiol), 3.1–3.9 (polysaccharide protons and methylene function α of the urethane), 4.35 (acetal function of dextran), 4.48, 4.87, and 4.95 ppm (hydroxyl functions of dextran). Degree of substitution: 2.90% (defined as the amount of 2-aminoethyl trityl sulfide side groups on 100 glucose units).

Reaction of 2-Aminoethyl Trityl Sulfide Modified Dextran with (Methoxycarbonyl)sulfenyl Chloride. 2-Aminoethyl trityl sulfide modified dextran (11) (1.5 g, 8.7 mmol) is dissolved in 15 mL of formamide/2 mL of methanol and stirred under N_2 for 15 h with 1 mL of (methoxycarbonyl)sulfenyl chloride. The reaction product is precipitated in 100 mL of ether/methanol (1/1, v/v), centrifuged, and filtered. The precipitate is washed with ether/methanol (1/1, v/v) and then with ether.

Finally the polymer is dissolved in 10 mL of H_2O and purified by preparative GPC on Sephadex G25 (eluent, double distilled water) and freeze-drying.

^{1}H NMR (360 MHz, DMSO-d_6): 2.2 (br, methylene function α of the protected thiol), 3.1–3.9 (polysaccharide protons and methylene function α of the urethane), 4.35 (acetal function of dextran), 4.48, 4.87, and 4.95 ppm (hydroxyl functions of dextran). No aromatic signals are observed.

Reaction of Methoxycarbonyl Disulfide Substituted Dextran (12) with Model Thiols. As an example is given the reaction with reduced glutathion (7). A 200-mg portion of methoxycarbonyl disulfide substituted dextran (12) is dissolved in 10 mL of oxygen-free sodium phosphate buffer (0.1 M, pH = 7). A 40-mg sample of reduced glutathion (7) is added and the mixture is stirred under argon for 1 h at room temperature. The conjugate is isolated by preparative GPC on Sephadex G-25 (eluent, double distilled water), followed by freeze-drying.

The reaction with *N*-Ac-L-Cys-L-Ala-L-Lys (pept-SH) (8) occurs under the same reaction conditions as described above for reduced glutathion.

Determination of the Degree of Substitution. The degree of substitution was determined by measuring the content of free amine groups belonging to the tripeptides, using OPA as an amine-specific reagent. The measurements were performed as described by the following standard procedure.

A 250-μL sample (~1 mg/mL) was taken; 750-μL of double distilled water, 1.5 mL of 0.05% mercaptoethanol solution (in borax buffer, pH = 10), and 500 μL of an OPA solution (20 mg in 10 mL of EtOH and 40 mL of double distilled water) were added. After 10 min the fluorescence is measured at 334.5 nm.

Bovine serum albumin, which contains 60 available primary amine groups, was used as a reference.

The degree of substitution of the dextran–glutathion conjugate (13): 3.2% (defined as the amount of glutathion units on 100 glucose units). Degree of substitution of the dextran-peptide conjugate (14): 1.5%

Reaction of the Dextran-Glutathion Conjugate (13) with FITC (15). A 50-mg portion of dextran-glutathion conjugate (13) is dissolved in 10 mL of Na_2CO_3 buffer (0.1 N; pH = 9.6). FITC (15) (10.5 mg) dissolved in a minimum amount of acetone is added. The reaction mixture is stirred in the dark for 1 h. The fluorescent labeled conjugate 16 is purified by preparative GPC on Sephadex G-25 (eluent, double distilled water) followed by freeze-drying of the collected fraction.

The reaction of the dextran-peptide conjugate (14) with FITC (15) occurs under the same reaction conditions as described above for the dextran-glutathion conjugate.

Stability Study of the Disulfide Bond in the Dextran-Peptide Conjugates. The stability of the dextran-peptide conjugates is analyzed by gel permeation chromatography using a PD-10 column (Sephadex G-25). The reliability of this method was first explored by dissolving the conjugate in Tris buffer (pH = 7.5) at a concentration of 6 mg/mL. The intact conjugate is collected in fractions 2–9 (each fraction containing 30 droplets).

After treatment of the solution with DTT, to reduce the disulfide bonds, 200 μL of the solution is put on the column. In fractions 2–9, no absorbance at 499 nm is observed. The low molecular weight FITC derivatives are now strongly adsorbed on the Sephadex column. After 11 fractions, the eluent is replaced by a 2-propanol/Tris (45/55, v/v) mixture and the low molecular weight derivatives are collected in fractions 16–32.

All further experiments are performed following the same procedure: The conjugate is dissolved in human blood plasma, in a concentration of 6 mg/mL. The solution is incubated at 37 °C. After 24 hours, 200 μL of this solution is put on a PD-10 column (Sephadex G 25) and

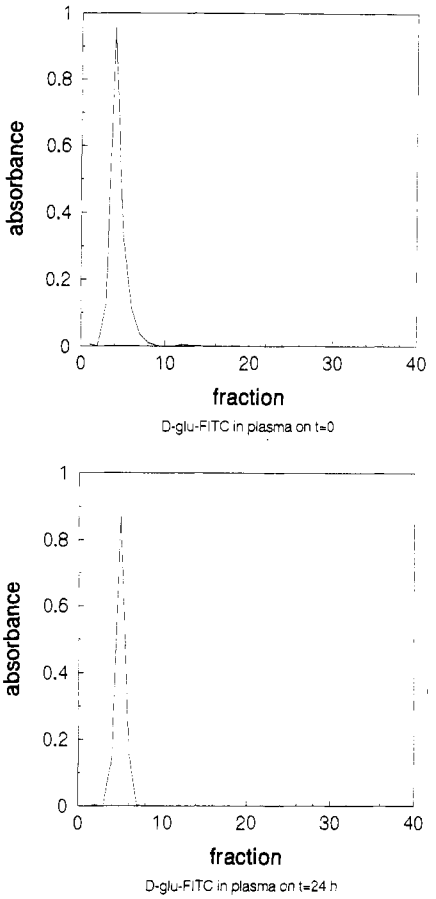
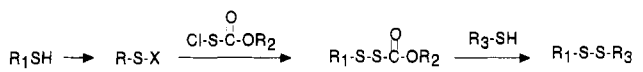


Figure 1. GPC analysis of the FITC-labeled dextran-glutathion (**13**) conjugate incubated in human blood plasma at 37 °C for t = 0 (1a) and t = 24 h (1b).

eluated with Tris buffer (pH=7.5). The eluated solution is collected in fractions of 30 droplets. After 11 fractions, the eluent is displaced by a 2-propanol/Tris (45/55, v/v) mixture to collect possible low molecular weight FITC derivatives. The absorbance of each fraction is measured at 499 nm.

RESULTS AND DISCUSSION

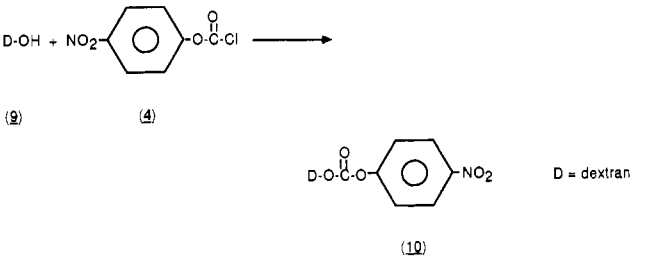
A strategy has been worked out for the preparation of disulfide linked polymer–protein conjugates. In this work we have exploited the chemistry described by Brois et al. (*11*), using alkoxycarbonyl disulfides as the thiol specific reactive groups. The latter can be prepared by reacting trityl-, *tert*-butyl- or acetamidomethyl-protected thiol groups with (alkoxycarbonyl)sulfenyl chloride.



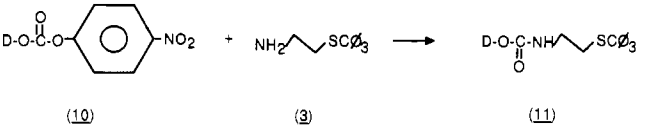
The feasibility of this strategy for introducing "dormant" protected thiol side groups, their subsequent activation, and coupling with thiols was investigated using reduced glutathion and the tripeptide *N*-Ac-L-Cys-L-Ala-L-Lys as model peptides.

Both polymer-protein conjugates were well-characterized and evaluated on their stability in blood.

1. Preparation of Disulfide Coupled Dextran-Peptide Conjugates. S-trityl-protected thiol side groups are introduced in dextran by coupling of *S*-trityl-2-mercaptoethylamine with activated dextran. Dextran (Mw = 30950, Mw/Mn = 1.19) is activated by reaction with 4-nitrophenyl chloroformate.

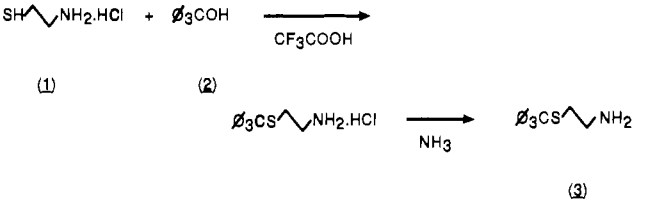


The degree of activation can be adjusted by the amount of chloroformate added and the duration of the reaction (Vandoorne) (*14*). The activated polymer contains both

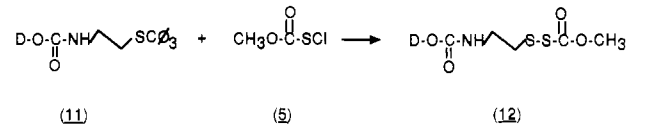


4-nitrophenyl carbonate and 5-membered cyclic carbonate structures which both can react with amines leading to urethane derivatives.

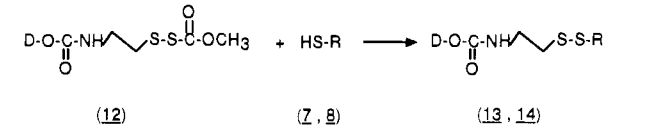
S-trityl-2-mercaptoethylamine was prepared by selective tritylation of the thiol group of cysteamine with triphenylmethyl alcohol in trifluoro acetic acid and subsequent conversion into its free base by treatment with concentrated ammonia.



The *S*-trityl side groups in the dextran derivative can subsequently be converted into thiol-specific reactive groups by reaction with (methoxycarbonyl)sulfenyl chloride (**5**).



The polymer derivative is now available for reaction with peptides and proteins carrying thiol groups.



In this study reduced glutathion (**7**) and the tripeptide *N*-Ac-L-Cys-L-Ala-L-Lys (**8**) are used as model thiols. Both tripeptides are suitable models since they contain, in addition to acidic and amino groups, a thiol function.

The degree of substitution was determined by analyzing the amino groups in the coupled peptide via the OPA method (*15*).

2. Stability of Disulfide-Coupled Dextran-Peptide Conjugates in Blood Plasma. In order to evaluate the

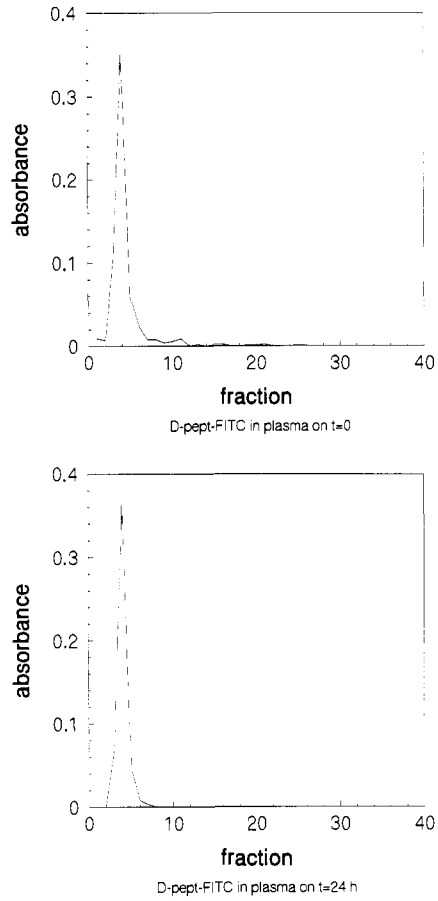
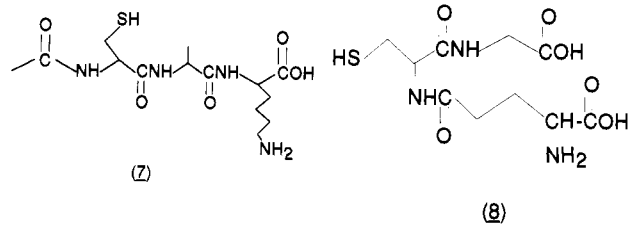
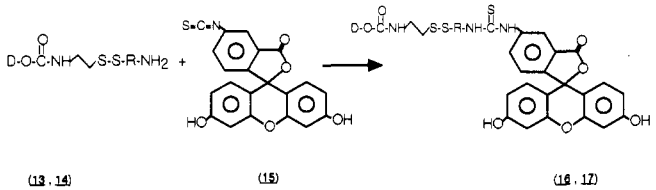


Figure 2. GPC analysis of the FITC labeled dextran-peptide **(14)** conjugate incubated in human blood plasma at 37 °C for t = 0 (2a) and t = 24 h (2b).



(7) (8)

plasma stability of the dextran-peptide conjugates, in particular the S–S bond, dextran-peptide conjugates were marked with FITC **(15)**.



(13, 14) (15) (16, 17)

Fluorescent labeling of the conjugates allows monitoring of the stability of the disulfide linkage in the conjugate in blood plasma. The polymer conjugates were incubated in human blood plasma at 37 °C for 24 h. Cleavage of the disulfide and release of low molecular weight FITC derivatives was checked by gel permeation chromatography analysis. As indicated in Figures 1 and 2, the absorbance at 499 nm of the polymer fractions remains the same and no low molecular weight fragments are observed in fractions 16–32, corresponding with the low molecular weight fractions. This indicates that cleavage of S–S bonds is negligible over a 24-h time period.

ACKNOWLEDGMENT

The authors wish to thank the "National Fund for Scientific Research (Belgium)" for providing a research assistantship to Sabine Herman.

LITERATURE CITED

(1) Hixson, H. F. (1973) Water-soluble enzyme-polymer grafts: Thermal stabilization of glucose oxidase. *Biotechnol. Bioeng. 15*, 1011–1016.

(2) Mitz, M. A., and Summaria, L. J. (1961) Synthesis of biologically active cellulose derivatives of enzymes. *Nature 189*, 576–577.

(3) Abuchowski, A., van Es, T., Palczuk, N. C., and Davis, F. F. (1977) Alteration of immunological properties of bovine serum albumin by covalent attachment of polyethylene glycol. *J. Biol. Chem. 252* (11), 3578–3581.

(4) Abuchowski, A., McCoy, J., Palczuk, N., van Es, T., and Davis, F. (1977) Effect of covalent attachment of polyethylene glycol on immunogenecity and circulating life of bovine liver catalase. *J. Biol. Chem. 252* (11), 3582–3586.

(5) Lisli, P. J., van Es, T., Abuchowski, A., Palczuk, N. C., and Davis, F. F. (1982) Enzyme therapy: I. Polyethylene glycol: β-glucuronidase conjugates as potential therapeutic agents in acid mucopolysaccharidosis. *J. Appl. Biochem. 4*, 19–33.

(6) Marshall, J. (1978) Manipulation of the properties of enzymes by covalent attachment of carbohydrate. *Trends Biol. Sci.* 79–83.

(7) Marshall, J., and Rabinowitz, M. (1976) Preparation and charachterization of a dextran-trypsin conjugate. *J. Biol. Chem. 254* (4) 1081–1087.

(8) Marshall, J., Humphreys, J. D., and Abramson, L. (1977) Attachment of carbohydrate to enzymes increases their circulatory lifetimes. *FEBS. Lett. 83* (2) 249–251.

(9) Vegarud, G., and Christensen, T. (1975) Glycosylation of proteins: A new method of enzyme stabilization. *Biotechn. Bioeng. 17*, 1391.

(10) Carlsson, J., Drevin, H., and Axen, R. (1978) Protein thiolation and reversible protein–protein conjugation. N-succinimidyl 3-(2-pyridyldithio)propionate a new heterobifunctional reagent. *Biochem. J. 173*, 723–737.

(11) Brois, S. J., Pilot, J. F., and Barnum, H. W. (1970) A new pathway to unsymmetrical disulfides. The thiol-induced fragmentation of sulfenyl thiocarbonates. *J. Am. Chem. Soc. 92* (26), 7629–7631.

(12) Cumber, A. J., Westwood, J. H., Henry, R. V., Parnell, G. D., Coles, B. F., and Wawrzynczak, E. J. (1992) Structural Features of the Antibody-A Chain Linkage that Influence the Activity and Stability of Ricin A Chain Immunotoxins. *Bioconjugate Chem. 3*, 397–401.

(13) Ringsdorf, H. (1975) Structure and properties of pharmacologically active polymers. *J. Polymer Sci.: Symp. 51*, 135.

(14) Vandoorne, F., Vercauteren, R., Permentier, D., and Schacht, E. (1985) Reinvestigation of the 4-nitrophenyl chloroformate activation of dextran. Evidence for the formation of different types of carbonate moieties. *Makromol. Chem. 186*, 2455–2460.

(15) Roth, M. (1971) Fluorescence reaction for amino acids. *Anal. Chem., 43* (7) 880–882.

Synthesis of 3-(Triethylstannyl)propanoic Acid: An Organotin Mass Label for DNA†

Frederick V. Sloop,‡ Gilbert M. Brown,§ Robert S. Foote,‡ K. Bruce Jacobson,‡ and Richard A. Sachleben*,§

Biology and Chemistry Divisions, Oak Ridge National Laboratory, Oak Ridge, Tennessee 37831.
Received March 25, 1993

The synthesis of 3-(triethylstannyl)propanoic acid (TESPA), an organometallic reporter group that enables the mass labeling of oligonucleotides with stable isotopes of tin, is described. Synthesized from commercially available isotopically-enriched SnO_2 in a five step process, the NHS ester of TESPA is produced with an overall yield of 40%. This simplification of the standard synthetic scheme, with two less synthetic steps and a coincident 60% yield increase, is accomplished through the use of the reagent *N*-(acryloxy)succinimide and the free radical initiator AMPN. The conditions for the attachment of the reporter group to priming oligonucleotides and the subsequent HPLC isolation of the labeled primers are also detailed.

INTRODUCTION

To perform current DNA sequencing and mapping procedures we rely on the sensitive detection of a label that is either incorporated into the target DNA or into a probe that specifically binds to the target DNA. Traditionally, the radioisotopes ^{32}P and ^{35}S have been used for this purpose. These labels present problems in terms of handling and disposing of radioactive materials and by the fact that the label is lost at the rate of the half-life of the isotope. To circumvent these and other shortcomings, additional labels have been developed for DNA, including fluorescent (*1–4*), chemiluminescent (*5*) and bioactive reporter groups (*6, 7*).

Recently, we have proposed the use of stable isotopes of iron, tin (*8*) and the rare earths (*9, 10*) as labels for DNA. This labeling scheme is feasible due to the unique masses of individual stable isotopes of given elements and the ability of mass spectrometers to differentiate one unique mass label from another. The use of stable isotopes as DNA labels is attendant with a number of advantages including (1) their stability, (2) the large number of chemically identical, individually distinguishable labels, (3) the detection sensitivity potential using RIS/MS[1] and (4) the high rate at which RIS/MS can analyze sequencing gels (*10*).

Our initial work involved the attachment of [^{57}Fe]ferrocene to DNA and its subsequent detection by RIS/MS (*8, 11*). Efforts to expand the utility of the stable isotopes method led to the selection of tin since it forms stable organometallic compounds (*12–15*) and has 10 isotopes (Table I), eight of which are commercially available (Table II). With modifications for scale, adaptations of the synthetic schemes of Van der Kerk et al. (*12–15*) and Anderson, et al. (*16*) for the production of the NHS ester of the organotin compound TESPA (NHS–TESPA) resulted in a seven step synthesis (Figure 1A), including two chromatographic purification operations, with a 20–25% overall yield from tin oxide (*17*). To provide a multispectral–multiplexing capability for DNA sequencing, mapping, and diagnostic procedures, TESPA has been synthesized from all eight commercially available isotopic forms of tin. These eight labels make possible the simultaneous analysis of eight different DNAs, twice the current maximum of any other labeling approach. After the reporter groups were attached to DNA oligonucleotides via an aminohexyl linker arm (*18*), their stability to the

Table I. Natural Abundance of Tin Isotopes

isotope	mass	% natural abundance
^{112}Sn	111.90	0.96
^{114}Sn	113.90	0.66
^{115}Sn	114.90	0.35
^{116}Sn	115.90	14.30
^{117}Sn	116.90	7.61
^{118}Sn	117.90	24.03
^{119}Sn	118.90	8.58
^{120}Sn	119.90	4.72
^{122}Sn	121.90	4.72
^{124}Sn	123.91	5.94

Table II. Composition of Enriched Tin Isotopes[a]

	% composition of isotope							
isotope	^{112}Sn	^{116}Sn	^{117}Sn	^{118}Sn	^{119}Sn	^{120}Sn	^{122}Sn	^{124}Sn
^{112}Sn	**98.93**	<0.02	0.08	<0.01	<0.02	<0.02	<0.03	0.04
^{114}Sn	1.04	<0.02	0.04	<0.01	<0.02	<0.02	<0.03	0.04
^{115}Sn	0.05	0.07	0.06	<0.02	<0.02	<0.02	<0.03	0.02
^{116}Sn		**96.68**	2.34	0.37	0.40	0.13	0.86	0.21
^{117}Sn		1.23	**89.2**	0.79	0.85	0.11	0.46	0.17
^{118}Sn		1.18	4.5	**95.75**	3.63	0.61	1.64	0.43
^{119}Sn		0.22	1.12	1.22	**84.48**	0.66	0.71	0.31
^{120}Sn		0.52	2.16	1.61	9.98	**98.05**	3.91	1.07
^{122}Sn		0.05	0.26	0.15	0.44	0.34	**91.24**	1.00
^{124}Sn		0.05	0.28	0.07	0.20	0.10	1.18	**96.71**

[a] Our source for ^{112}Sn with ISOTEC, Inc. All other isotopes as obtained from ORNL.

† Research supported by the ORNL Exploratory Studies Program and the Office of Health and Environmental Research, U.S. Department of Energy, under contract DE-AC05-85OR21400 with Martin Marietta Energy Systems, Inc.

* Address for correspondence: Dr. Richard A. Sachleben, Chemistry Division, Oak Ridge National Laboratory, Building 4500S/Mailstop 6119, Oak Ridge, TN 37831.

‡ Biology Division.

§ Chemistry Division.

[1] Abbreviations used: RIS/MS, resonance ionization spectroscopy/mass spectrometry; NHS, *N*-hydroxysuccinimide; TESPA, 3-(triethylstannyl)propanoic acid; NHS–TESPA, *N*-succinimidyl 3-(triethylstannyl)propanoate; PCR, polymerase chain reaction; THF, tetrahydrofuran; AMPN, 2,2′-azobis(2-methylpropionitrile); TEAA, triethylamine acetate; DMF, dimethylformamide.

1043-1802/93/2904-0406$04.00/0 © 1993 American Chemical Society

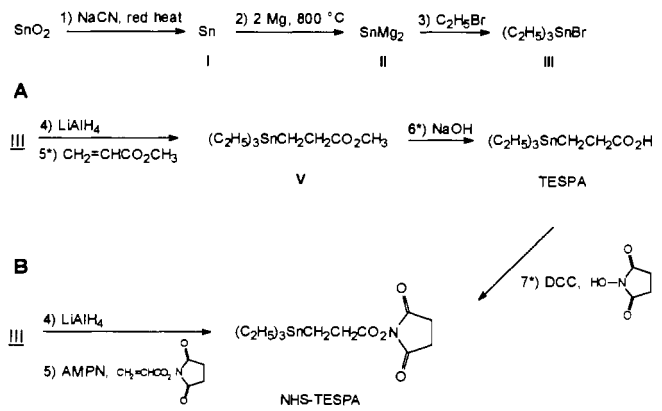


Figure 1. Synthesis of NHS-TESPA. Reactions 1–4, leading to the synthesis of triethylstannane [$(C_2H_5)_3SnH$], are common to both the standard synthetic route to NHS–TESPA synthesis and the newly described method presented in the text. Following the formation of $(C_2H_5)_3SnH$ (product IV) as a consequence of reaction 4, part A represents the original standard synthetic method, with individual reaction steps designated as 5*–7*, while part B illustrates the new synthetic route. All isolated reaction products are designated by numerals (**I, II, III, V**) or by acronyms described in the text. Product **IV** is not isolated, therefore it is not shown in this figure.

conditions encountered in standard molecular biology manipulations was confirmed (*11, 17, 19–21*). TESPA-labeled priming oligomers and the DNA fragments arising from PCR and Sanger reactions so primed have been electrophoretically separated in polyacrylamide gels, and then successfully detected by RIS/MS (*11, 17,19–21*) by virtue of their isotopic tin signatures. A number of isotopic forms of TESPA have been used in these demonstrations of the utility of the stable isotopes method.

Once TESPA's usefulness as a mass label for DNA was established, subsequent efforts were directed at improving the synthesis of the compound. Here we describe the results of that effort, a simplification of the procedure (Figure 1B) with two less synthetic steps, a single chromatographic operation, the avoidance of a troublesome side reaction, and a final overall yield increase of 60%. Reaction conditions necessary for attaching NHS–TESPA to the terminal amine group of priming oligonucleotides are also described.

EXPERIMENTAL PROCEDURES

General. Preparative column chromatography was performed using silica gel 60, 60–200 mesh. Gas chromatography was accomplished with a Hewlett-Packard 5890 Series II equipped with a 30 m × 0.25 mm DB1 capillary column and flame ionization detector. NMR spectra were obtained on a Bruker MSL-400 FT-NMR in $CDCl_3$ using residual $CHCl_3$ as the internal standard. Chemical shifts (in ppm) were reported for intermediates enriched in ^{118}Sn in order to avoid spin-coupling between protons and non-zero-spin tin isotopes. IR spectra were run on a Digilab FTS-60 FTIR. Mass spectral analyses were performed by the Organic Spectroscopy Group, Analytical Chemistry Division, Oak Ridge National Laboratory. Oligonucleotides were synthesized on an Applied Biosystems PCR-MATE Model 391 DNA synthesizer using standard phosphoramidite chemistry (22). The 5′ terminus of each oligomer was derivatized with an aminohexyl group[2] in a final automated step. Following deprotection and HPLC purification, the $H_2N(CH_2)_6PO_4$

[2]5′ Amino Modifier C_6, Glen Research Corp., 44901 Falcon Place, Sterling, VA 22170.



Figure 2. Derivitization of hexylamine oligonucleotide with TESPA.

oligonucleotides were reacted with the NHS–TESPA to provide tin-labeled primers (Figure 2). The presence of the tin reporter groups on the oligonucleotides was certified by RIS/MS analysis utilizing instrumentation as previously described (*11, 19*). Reported yields for given reactions are typical and represent values averaged from >10 repeats carried out for each reaction step. Test reactions were performed utilizing both natural abundance and isotopically-enriched tin reagents.

Reagents. Isotopes were obtained as SnO_2 from the Oak Ridge Isotope Distribution Office[3] with isotopic compositions as listed in Table II, except for ^{112}Sn, which was obtained as the metal from ISOTEC, Inc.[4] Grignard-grade magnesium turnings were used to prepare the Mg_2Sn alloy. THF was distilled from sodium benzophenone ketyl. Anhydrous dioxane was passed over alumina before use. Diethyl ether was distilled to remove the free radical scavenger di-*tert* butyl-*p*-cresol. *N*-(Acryloxy)succinimide, 99%, and AMPN were purchased from Eastman Fine Chemicals. All other reagents were used as obtained from commercial sources.

HPLC. HPLC analyses and separations were performed on a Waters HPLC using a Sepralyte C-18 (5 μm, 4.6 x 250 mm) reverse phase column and a 40 min 0–80% linear gradient of 95% acetonitrile/0.1 M TEAA in 5% acetonitrile/0.1 M TEAA. Elution buffers were passed through a 0.2-μm filter and utilized pure water (18 MΩ). UV monitoring was performed at 260 nm.

Reduction of Tin Oxide to Tin (I). Tin oxide (635 mg, 4.25 mmol) was placed in a single layer between two layers of sodium cyanide (2.54 g, 39.0 mmol) in a 12 mm i.d. × 15 mm o.d. × 16 cm L quartz tube. The mixture was heated over a burner to glowing orange heat for 0.5 h. After cooling, water (5 mL) was added, and the mixture was heated to boiling for several minutes. Upon cooling the ingot of tin metal was removed with tweezers, rinsed with water, and air-dried to obtain 480 mg (4.0 mmol, 94%).

Preparation of Tin/Magnesium Alloy (II). Magnesium turnings (200 mg, 8.2 mmol) and the tin ingot (480 mg, 4.0 mmol) were heated in a quartz tube under a purge of argon until melted and then allowed to cool. The tube was broken, and the brittle, metallic-blue alloy was removed from the glass fragments with tweezers to obtain 660 mg (3.9 mmol, 97%), which was pulverized in a mortar for subsequent reaction.

Synthesis of Bromotriethylstannane (III). Finely ground Mg_2Sn (400 mg, 2.4 mmol), bromoethane (1.2 mL, 15.8 mmol), and cyclohexane (3.5 mL) were placed in a thick-walled Pyrex tube which was frozen in dry ice/acetone, flame sealed under vacuum, and heated at 160 °C in a tube furnace for 18 h. The tube was allowed to cool, frozen in ice/water, and carefully opened. Care should be taken when opening the tube as residual pressure was occasionally observed at this point. The supernatant was decanted, and the residue was thoroughly washed with cyclohexane. The combined organic solution was filtered,

[3]Isotope Distribution Office, Oak Ridge National Laboratory, P. O. Box 2003, Oak Ridge, TN 37831.

[4]ISOTEC, Inc., 3858 Benner Road, Miamisburg, OH 45342.

then the solvent was removed by distillation through a 7-cm Teflon helices-packed column. The product was analyzed by capillary GC. Typically, the mixture consisted of 85% bromotriethylstannane and 10% tetraethylstannane, with the remainder being trace impurities. Processing through the next two synthetic steps was performed without further purification. Occasionally, significant quantities of dibromodiethylstannane were obtained, whereupon the mixture was purified by fractional vacuum distillation. Vacuum distillation was performed in a bulb to bulb apparatus, heated in an oil bath to 90 °C at 1 Torr. Distillate consisting of >85% bromotriethylstannane (containing <1% dibromodiethylstannane by GC) was collected at 0°C. Product stannanes were characterized by mass spectrometry. Bromotriethylstannane (^{118}Sn): MS *m/e* 282/284 (M^+), 253/255 ($M^+ - C_2H_5$), 224/226 ($M^+ - C_4H_{10}$), 145 (C_2H_5Sn).

Synthesis of Triethylstannane (IV). Bromotriethylstannane (600 mg, 2.0 mmol) was refluxed with lithium tetrahydridoaluminate (230 mg, 6.0 mmol) in 10 mL of distilled diethyl ether for 6 h. Excess hydride was destroyed by careful addition of water (2–3 drops) followed successively by 1 N NaOH (4 drops) and water (4 drops). The mixture was filtered through a bed of Celite, which was washed with an additional 10 mL of ether. This solution was used in the subsequent reaction.

Synthesis of *N*-Succinimidyl 3-(Triethylstannyl)propanoate (NHS–TESPA). One-half of the ether solution of triethylstannane was added to 8 mL of cyclohexane. The combined solution was purged with argon for 15 min and then heated at 60 °C for 30 min in a flask equipped with a 10-cm helices-packed column to allow removal of the ether by distillation. *N*-(Acryloxy)succinimide (169 mg, 1.0 mmol) and 1.64 mg (10 μmol) of the free radical initiator AMPN were then added to the reaction vessel. This mixture was refluxed at 60 °C, under argon purge, for 17 h. Solvent was then removed *in vacuo* and the product isolated by chromatography on silica gel [20 g, 0–20% acetone in benzene (**Caution**: benzene is a known carcinogen), 5% increments of 50 mL each] to yield 193 mg (0.51 mmol, 51%) of NHS–TESPA. NMR (400 MHz, $CDCl_3$) δ 2.82 (4H, s, NHS), 2.78 (2H, tr, J = 8.4, $-CH_2CO_2-$), 1.18 (9H, t, J = 8.0, $SnCH_2CH_3$), 1.10 (2H, tr, J = 8.4, $SnCH_2CH_2$), 0.86 (6H, q, J = 8.0, $SnCH_2CH_3$); IR (CCL_4) 1814, 1719 (ester C=O), 1646 (imide C=O).

Attachment of TESPA to Oligonucleotides. A solution of triethylamine (5 μL), 5′-aminohexyl oligonucleotide (10 μL at 2.0 nmol/μL in water, 20 nmol), and NHS–TESPA (20 μL at 20 nmol/μL in DMF, 400 nmol) in DMF (65 μL) was reacted with occasional agitation for 80 min at room temperature (Figure 2). When the reaction was deemed complete by HPLC analysis (typically 1.0–1.5 h), *N*-propylamine (1 μL, 12 μmol) was added to quench excess NHS–TESPA. After 10 min the TESPA-labeled oligonucleotide was isolated by C-18 reversed-phase HPLC and then ethanol precipitated from 0.5 M ammonium acetate. The presence of the attached reporter group was established using RIS/MS analysis to certify that the isotope distribution pattern was consistent for the tin isotope incorporated in the TESPA. Typical recovery of labeled oligonucleotide was 10–12 nmol (50–60%) as determined by UV absorption.

DISCUSSION

Our original synthetic scheme (*17*) for the production of NHS-TESPA revolved around adaptations of literature methods (*12–16*) that were required for the comparatively small reaction scales (millimolar) necessitated when using costly, isotopically enriched starting materials. The 20–25% overall yield achieved via this seven-step synthetic procedure was satisfactory for early experimental work, but a simplification of the synthesis and an increase in yield were desirable for routine reporter production.

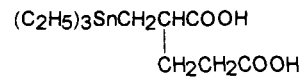


Figure 3. Polymerization byproduct of reaction 5*, 2-[(triethylstannyl)methyl]glutaric acid.

In our original procedure (*17*) (Figure 1A) methyl acrylate was added in 10-fold excess (reaction 5*) to triethylstannane (**IV**), producing methyl 3-(triethylstannyl)propanoate (**V**) in 50% yield, following product isolation by silica gel chromatography. The methyl group was then removed hydrolytically by reflux in 1 N sodium hydroxide. Following solvent removal *in vacuo* the product, triethylstannane (**IV**), was dissolved in water, acidified to pH 2.0, and extracted with ether. Evaporating the dried ether extract produced 3-(triethylstannyl)propanoic acid (TESPA) in a 78% yield. This compound was coupled, using dicyclohexylcarbodiimide, with *N*-hydroxysuccinimide in anhydrous THF to produce the labeling reagent NHS-TESPA in a 76% yield following silica gel chromatography.

The large molar excess of methyl acrylate, necessary to drive the addition reaction (reaction 5*) to completion in a reasonable amount of time (~18 h), also favored the formation of an unwanted polymerization product, 2-[(triethylstannyl)methyl]glutaric acid. (Figure 3; the structure and identity of the bifunctional byproduct were determined by NMR following hydrolysis of methyl groups and acidification.) This undesired byproduct incorporated 53% as much isotopic tin as was found in the monofunctional methyl 3-(triethylstannyl)propanoate. This represented a major loss from the pool of isotopic tin available for TESPA production. Elimination or reduction of the bifunctional product was considered vital before a significant increase in the yield of NHS–TESPA could be realized. Our best efforts in the seven-step synthetic procedure achieved only a slight reduction in the polymerization product in favor of the monoester.

In order to minimize the polymerization product and realize a two step reduction in the synthetic scheme yielding NHS–TESPA, we replaced methyl acrylate in the coupling step with *N*-(acryloxy)succinimide. Reaction of an equimolar amount of this reagent with triethylstannane (**IV**), in the presence of the radical initiator AMPN, resulted in a 51% yield of NHS–TESPA following silica gel chromatography. To prevent the destruction of the AMPN, the reaction (reaction 5) was conducted under an argon atmosphere in ether purified by distillation to remove the free radical scavenger di-*tert*-butyl-*p*-cresol. The final result was a simplified synthetic scheme (five steps), incorporating a single chromatographic procedure (for final product isolation), in which the overall yield of the final product increased to 40% from tin oxide, a 60% improvement over the 20–25% yield achieved via the seven-step synthesis.

NHS–TESPA serves as a DNA reporter group when attached to priming oligonucleotides used in Sanger sequencing and PCR reactions. The reporter's attachment is rapidly accomplished when performed under somewhat alkaline conditions in a solvent system containing a small amount of water (10% by volume). TESPA's presence on the oligonucleotide increases the oligomer's hydrophobicity. The resulting increase in retention time on a C-18

reversed-phase column permits the ready isolation of the derivatized primer by HPLC.

ACKNOWLEDGMENT

We thank Philip Britt for helpful discussions and suggestions. This work was supported by the Exploratory Studies Program of the Oak Ridge National Laboratory and by the Office of Health and Environmental Research, U. S. Department of Energy, under contract DE-AC05-84OR21400 with Martin Marietta Energy Systems, Inc. We wish to acknowledge the contributions of our colleagues at Oak Ridge National Laboratory and Atom Sciences, Inc., whose efforts provided much of the supporting research referenced in this paper.

LITERATURE CITED

(1) Ansorge, W., Sproat, B. S., Stegemann, J., and Schwager, C. (1986) A nonradioactive automated method for DNA sequence determination. *J. Biochem. Biophys. Methods 13,* 315–323.

(2) Ansorge, W., Sproat, B. S., Stegemann, J., Schwager, C., and Zenke, M. (1987) Automated DNA sequencing: ultrasensitive detection of fluorescent bands during electrophoresis. *Nucleic Acids Res. 15,* 4593–4602.

(3) Smith, L. M., Fung, S., Hunkapiller, T. J., and Hood, L. E. (1985) The synthesis of oligonucleotides containing an aliphatic amino group at the 5′ terminus: Synthesis of fluorescent DNA primers for use in DNA sequence analysis. *Nucleic Acids Res. 13,* 2399–2412.

(4) Smith, L. M., Sanders, J. Z., Kaiser, R. J., Hughes, P., Dodd, C., Connell, C.R., Heiner, C., Kent, S.B.H., and Hood, L. E. (1986) Fluorescence detection in automated DNA sequence analysis. *Nature 321,* 674–679.

(5) Beck, S., O'Keeffe, T., Coull, J. M., and Köster, H. (1989) Chemiluminescent detection of DNA: Application for DNA sequencing and hybridization. *Nucleic Acids Res. 17,* 5115–5123.

(6) Langer, P. R., Waldrop, A. A., and Ward, D. C. (1981) Enzymatic synthesis of biotin-labeled polynucleotides: Novel nucleic acid affinity probes. *Proc. Natl. Acad. Sci. U. S. A. 78,* 6633–6637.

(7) Shimkus, M., Levy, J., and Herman, T. (1985) A chemically cleavable biotinylated nucleotide: Usefulness in the recovery of protein–DNA complexes from avidin affinity columns. *Proc. Natl. Acad. Sci. U. S. A. 82,* 2593–2597.

(8) Jacobson, K. B., Arlinghaus, H. F., Schmitt, H. W., Sachleben, R. A., Brown, G. M., Thonnard, N., Sloop, F. V., Foote, R. S., Larimer, F. W., Woychik, R. P., England, M.W., Burchett, K. L., and Jacobson, D.A. (1991) An approach to the use of stable isotopes for DNA sequencing. *Genomics 9,* 51–59.

(9) Jacobson, K. B., Arlinghaus, H. F., Buchanan, M. V., Chen, C-H., Glish, G.L., Hettich, R. L., and McLuckey, S. A. (1991) Applications of mass spectrometry to DNA sequencing. *Genet. Anal. Tech. Appl. 8,* 223–229.

(10) Jacobson, K. B. and Arlinghaus, H .F. (1992) Development of resonance ionization spectroscopy for DNA sequencing and genome mapping. *Anal. Chem. 64,* 315A-328A.

(11) Arlinghaus, H. F., Thonnard, N., Spaar, M. T., Sachleben, R. A., Larimer, F. W., Foote, R. S., Woychik, R.P., Brown, G. M., Sloop, F. V., and Jacobson, K. B. (1991) Potential application of sputter-initiated resonance ionization spectroscopy for DNA sequencing. *Anal. Chem. 63,* 402–407.

(12) Van der Kerk, G. J. M., and Luijten, J. G. A. (1954) Investigations of organo-tin compounds II. The preparation of ethyltin compounds from tin–magnesium alloy. *J. Appl. Chem. 4,* 307–313.

(13) Van der Kerk, G. J. M., Noltes, J. G., and Luijten, J. G. A. (1957) Investigations of organo-tin compounds VII. The addition of organo-tin hydrides to olefinic double bonds. *J. Appl. Chem. 7,* 356- 365.

(14) Van der Kerk, G. J. M., Noltes, J. G., and Luijten, J. G. A. (1957) Investigations of organo-tin compounds VIII. Preparation of some organo-tin hydrides. *J. Appl. Chem. 7,* 366–369.

(15) Van der Kerk, G. J. M., and Noltes, J. G. (1959) Investigations of organo-tin compounds XI. The alkaline hydrolysis of organo-tin esters and nitriles. *J. Appl. Chem. 9,* 113–120.

(16) Anderson, G. W., Zimmerman, J. E., and Callahan, F. M. (1964) The use of esters of N-hydroxysuccinimide in peptide synthesis. *J. Am. Chem. Soc. 86,* 1839–1842.

(17) Sachleben, R. A., Brown, G. M., Sloop, F. V., Arlinghaus, H. F., England, M. W., Foote, R. S., Larimer, F.W., Woychik, R. P., Thonnard, N., and Jacobson, K. B. (1991) Resonance ionization spectroscopy for multiplex sequencing of tin-labeled DNA. *Genet. Anal. Tech. Appl. 8,* 167–170.

(18) Connolly, B. A. (1987) The synthesis of oligonucleotides containing a primary amino group at the 5′-terminus. *Nucleic Acids Res. 15,* 3131–3139.

(19) Arlinghaus, H. F., Thonnard, N., Spaar, M. T., Sachleben, R. A., Brown, G.M., Foote, R. S., Sloop, F. V., Peterson, J. R., and Jacobson, K. B. (1991) Comparison of sputter-initiated resonance ionization spectroscopy and laser atomization resonance ionization spectroscopy to localize tin-labeled deoxyribose nucleic acid. *J. Vac. Sci. Technol. A9,* 1312–1319.

(20) Doktycz, M. J., Arlinghaus, H. F., Allen, R. C., and Jacobson, K. B. (1992) Electrophoresis and detection of tin-labeled DNAs on open-faced gels. *Electrophoresis 13,* 521–528.

(21) Doktycz, M. J., Gibson, W. A., Arlinghaus, H. F., Allen, R. C., and Jacobson, K. B. (1993) Use of resonance ionization spectroscopy to detect DNA bands on ultra-thin spin-coated gels. *Appl. Theor. Electrophoresis* (in press).

(22) Beaucage, S. L., and Caruthers, M. H. (1981) Deoxynucleoside phosphoramidites—A new class of key intermediates for deoxypolynucleotide synthesis. *Tetrahedron Lett. 22,* 1859–1862.

Bioconjugate Chemistry

NOVEMBER/DECEMBER 1993
Volume 4, Number 6

© Copyright 1993 by the American Chemical Society

REVIEWS

Nucleic Acid-Incorporated Azidonucleotides: Probes for Studying the Interaction of RNA or DNA with Proteins and Other Nucleic Acids

Lee A. Sylvers[†,*] and Jacek Wower[‡]

Department of Molecular Biophysics and Biochemistry, Yale University, New Haven, Connecticut 06511, and Department of Biochemistry and Molecular Biology, University of Massachusetts, Amherst, Massachusetts 01003.
Received July 12, 1993

TABLE OF CONTENTS

1. Introduction 411
2. Azidonucleotides: Synthesis and Photochemistry 412
   A. Synthesis 412
   B. Photochemistry 413
3. Incorporation of Azidonucleotides into Polynucleotides 413
   A. Specific Incorporation 413
      (i) "Cut and Paste" Approach 414
      (ii) Chemical Synthesis Approach 415
   B. Random Incorporation 415
4. Reported Applications 415
5. Conclusions and Future Prospects 416

1. INTRODUCTION

Nucleic acid–protein interactions are central to many cellular processes including replication, transcription, and translation. Additionally, nucleic acid–nucleic acid interactions are critical in translation (Noller, 1991) and RNA processing (Mattaj et al., 1993; Fournier and Maxwell, 1993). Attaining a detailed molecular understanding of these processes requires tools for studying the structural topography of nucleic acid–protein and nucleic acid–nucleic acid interactions. Cross-linking provides one such tool. When used appropriately, cross-linking can yield detailed information about what parts of each interacting molecules are in close proximity. The use of photochemical cross-linking reagents allow for more tightly regulated cross-linking experiments than attainable with chemical cross-linkers, and have thus become increasingly popular over the years.

Irradiation with far-UV light (~254 nm) has been frequently used to induce covalent cross-links within nucleic acid–protein complexes. However, since far-UV light is structurally damaging to both nucleic acids and proteins, this approach may lead to cross-links which lack biological relevance. Many RNAs, particularly tRNAs, possess a variety of naturally-occurring modified bases which are inherently photoreactive with near-UV light (300–360 nm). However, their utility in photochemical cross-linking is limited by the scarcity and preordained sequence location of these bases in RNA, their lack of appearance in DNA, and their generally low yields and/or high specificity of cross-linking. Some of these shortcomings can be alleviated by derivatization with cross-linking reagents at either modified bases found in RNA or the termini of either DNA or RNA.

Most photo-cross-linking reagents used for base- or termini-derivatization are composed of an aryl azide compound in which the azido group is positioned 10–30 Å away from the derivatized base (Reiser and Wagner, 1971; Bayley and Knowles, 1977; Bayley, 1983). One of the better reagents of this type is the 11-Å-long cross-linking reagent *p*-azidophenacyl bromide (Hixson and Hixson, 1975), which has been used for derivatization at thiolated bases (Chen et al., 1985; Stade et al., 1989) and 5′-terminal thiols (Burgin and Pace, 1990). While, to our

* Correspondence to Dr. Lee A. Sylvers, Ambion, Inc., 2130 Woodward St., Austin, TX 78744-1832. Tel: (512) 445-6979. Fax: (512) 445-7139.
† Yale University.
‡ University of Massachusetts.

1043-1802/93/2904-0411$04.00/0 © 1993 American Chemical Society

knowledge, the latter method has only been used on RNA, its ease of application to DNA is obvious. As is the case for most aryl azides, *p*-azidophenacyl bromide is highly photoreactive and has the ability to form a broad range of covalent bonds upon generation of the reactive nitrene species in response to near-UV light. Additionally, this reagent can be cleaved from the derivatized base with a reducing agent, thus facilitating analysis of cross-links (Burgin and Pace, 1990). Unfortunately, the cross-links which are formed are necessarily 11 Å away from the base, and therefore do not reflect the most immediate environment of the base. While many labs still use this and other comparable *long-range* cross-linkers, the development of methods which allow for very *short-range* cross-links from defined positions in RNA or DNA molecules is a recent advance which should be capitalized on. Although the approaches which we will discuss are general enough to be applied to virtually any photoreactive nucleotide, we concentrate on azidonucleotides. These aryl azides have the unique advantage that they generally produce high-yield cross-links with a low degree of specificity (Bayley and Staros, 1984).

This review focuses first on the array of available or readily synthesized azidonucleotides and their photochemical properties and then surveys the wide variety of approaches available for their incorporation into polynucleotide chains. The recently attained ability to incorporate azidonucleotides virtually anywhere in an RNA or DNA molecule broadens the potential use of azidonucleotides for studies of nucleic acid–protein and nucleic acid–nucleic acid interactions.

2. AZIDONUCLEOTIDES: SYNTHESIS AND PHOTOCHEMISTRY

Azidonucleotides have long been used for the study of nucleotide binding sites on proteins (for review, see Haley, 1983). Most of these studies have utilized 8-azidoadensine ($8N_3A$)[1] nucleotides, with a more limited use of 8-azidoguanosine ($8N_3G$) and 2-azidoadenosine ($2N_3A$) phosphates. The azidoadenosines and, more recently, 5-azidouridine ($5N_3U$) and 2,6-diazidopurine ($2,6diN_3R$) nucleotides, have all been used for incorporation into RNA (Cartwright and Hutchinson, 1980; Wower et al., 1988, 1989, 1990, 1993a,b; Sylvers et al., 1989, 1992; Dontsova et al., 1992b). Similarly, $5N_3dUTP$ and $8N_3dATP$ have been synthesized and incorporated into DNA (Evans et al., 1986; Evans and Haley, 1987; Lee et al., 1991; Meffert and Dose, 1988; Meffert et al., 1990).

The azidonucleosides or bases that are available through reported synthetic routes are shown in Figure 1. They are all classified as aryl azides and consequently can be photolyzed with near-UV light. Another category of azidonucleotides, containing azide residues attached to a saturated carbon of the ribose ring, is reactive only with far-UV light. Since common nucleosides are also photolyzed with far-UV light, the aryl azide group of azidonucleotides is preferable for photo-cross-linking studies.

A. Synthesis. 8-Azidoadenosine has been synthesized in various states of phosphorylation by many groups (Cartwright et al., 1976; Haley, 1975; Houstek and Smrt, 1979; Koberstein, 1976; Koberstein et al., 1976; Schäfer and Penades, 1977; Schäfer et al., 1976) and are the only azidonucleotides that are widely available. However, the 3′,5′-bisphosphate of $8N_3A$, which is required for incorporation of the nucleotide into RNA using T4 RNA ligase, and all other azidonucleotides, with the exception of [α-^{32}P]$8N_3GTP$, are not. The synthesis of these azidonucleotides is, however, remarkably straightforward and easily carried out. From halogenated nucleosides, nucleophilic substitution with either sodium azide or hydrazine followed by diazotization with nitrous acid (Schaeffer and Thomas, 1958) will lead to azides in good yields. Alternatively, exocyclic amino groups of purines and pyrimidines can be diazotized followed by addition of sodium azide (Smith, 1984). Additionally, azidoadenosines and azidoguanosines are readily converted to azidoinosines and azidoxanthosines, respectively, by deamination with nitrous acid (Cartwright and Hutchinson, 1980; Wower et al., 1993b). The structural formulas of azido-substituted bases, nucleosides, and nucleotides reported in the literature are depicted in Figure 1.

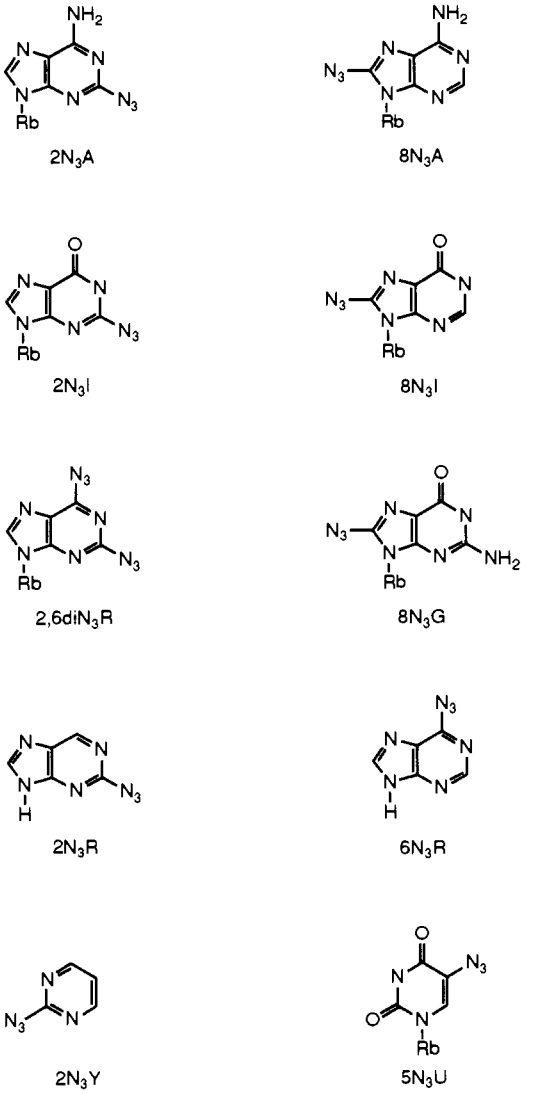


Figure 1. Azidonucleosides and bases available or easily prepared for incorporation into polynucleotides. References for those compounds not discussed in the text are as follows: $2N_3R$, Johnson et al., 1966; $6N_3R$, Temple and Montgomery, 1965; and $2N_3Y$, Bendich et al., 1957.

To function as substrates for nucleic acid synthesizing enzymes, azidonucleosides have to be prepared either as 5′-diphosphates, 3′,5′-bisphosphates, or 5′-triphosphates. Numerous methods for nucleoside phosphorylation have

[1] Abbreviations used: $2N_3A$, 2-azidoadenosine; $8N_3A$, 8-azidoadenosine; $8N_3dA$, 8-azidodeoxyadenosine; $2N_3I$, 2-azidoinosine; $8N_3I$, 8-azidoinosine; $2N_3R$, 2-azidopurine; $6N_3R$, 6-azidopurine; $2,6diN_3R$, 2,6-diazidopurine; $2N_3Y$, 2-azidopyrimidine; $8N_3G$, 8-azidoguanosine; $5N_3U$, 5-azidouridine; $5N_3dU$, 5-azidodeoxyuridine; NDP, nucleoside diphosphate; NTP, nucleoside triphosphate; Rb, ribose.

been described. However, the simplest method involves the utilization of pyrophosphoryl chloride, which, under specific conditions, produces an isomeric mixture of 2′,5′- and 3′,5′-bisphosphates (Barrio et al., 1978). This mixture can be used in conjunction with RNA ligase for labeling nucleic acids at their 3′ ends. Separation of the isomers is not necessary, as the high stereospecificity of RNA ligase insures that only the 3′,5′-bisphosphate isomer is incorporated into the polynucleotide (England and Uhlenbeck, 1978). When treated with nuclease P1, 3′,5′-bisphosphates are converted to 5′-monophosphates which can then be phosphorylated to form 5′-diphosphates or 5′-triphosphates using nucleoside monophosphate and nucleoside diphosphate kinases (Symons, 1974; Walseth and Johnson, 1979). 5′-^{32}P-Labeled 3′,5′-bisphosphates can be prepared *via* exchange of the 5′-phosphate of a 3′,5′-bisphosphate nucleoside with the γ phosphate from [γ-^{32}P]ATP using 3′-phosphatase-free T4 polynucleotide kinase (Sylvers et al., 1989). Subsequent ligation of the ^{32}P-labeled azidonucleoside 3′,5′-bisphosphate into RNA positions a radioactive label in close proximity to the base which would be directly involved in a cross-link. This allows for greater flexibility in cross-link identification and characterization. In addition, 5′-^{32}P-labeled 3′,5′-bisphosphates can be used for the production of α-^{32}P-labeled NDPs and NTPs using the route described above. For preparation of larger quantities of nonradioactive 5′-triphosphates from 5′-monophosphates, a chemical method employing a pyrophosphate coupling procedure is recommended (Michelson, 1964).

Azido-substituted nucleotides can also be incorporated into polynucleotides by chemical synthesis. However, phosphoramidite synthons, the most commonly used nucleotide units in chemical synthesis, are incompatible with azides due to reactivity with the trivalent phosphorus (Staudinger and Meyer, 1919; Staudinger and Hauser, 1921; Abramovitch and Kyba, 1971). Therefore, phosphotriester or H-phosphonate azidonucleotide synthons are required and can be prepared by standard methods starting with the desired azidonucleoside (Fritz et al., 1982; Gait et al., 1982; Froehler et al., 1986). While the prospect for using azidonucleotides in a chemical synthesis approach is promising, it should be emphasized that there has been no report of its application in the literature.

B. Photochemistry. Azidonucleotides are rapidly photolyzed by irradiation with UV light to form highly reactive nitrene species. The mechanisms of photoreaction for azidonucleotides are assumed to be similar to that of better-characterized aryl azides. These compounds can react to form nitrenes through either photolysis or thermolysis (Smith, 1984). Arylnitrene half-lives may vary by nearly 2 orders of magnitude, depending upon substitution of the aromatic ring. Initially, the newly formed nitrene exists in a short-lived (nano- to microsecond) singlet state which is then followed by generation of the triplet (Reiser and Wagner, 1971; Bayley, 1983). Both species are highly unstable and will react quite rapidly with molecular constituents in their immediate environment (Bayley, 1983; Bayley and Staros, 1984). This may lead directly to bond insertion (*i.e.* cross-link) or the formation of a reactive intermediate. Possibilities for the latter include rearrangement of the singlet to form fully bonded electrophiles, such as benzazirines and cycloheptatetraenes, or hydrogen atom abstraction by the triplet to form an anilinyl radical. These electrophilic intermediates are highly reactive with the nucleophiles abundant in biological macromolecules, and thus also may lead to cross-link formation.

Studies concerning the photoreactivity of azidonucleosides are complicated by the propensity of these nucleosides to undergo a pH-dependent tautomeric rearrangement to tetrazoles, which are considered to be nonphotoreactive (MacFarlane et al., 1982). If the presence of tetrazoles is great enough to adversely affect binding and cross-linking reactions, preincubation of the azidonucleotide-containing nucleic acid at low pH will allow the azide form to predominate and should alleviate any problems (L. A. Sylvers, unpublished data). Since the tautomerization is a relatively slow process (MacFarlane et al., 1982), cross-linking reactions can generally be performed quickly enough so that the azide is still the main tautomer present. Of the compounds listed in Figure 1, only 5-substituted pyrimidines and 8-substituted purines do not form tetrazole tautomers.

UV spectroscopy provides a reliable and easy method for determining the progress of the photoreaction. The azidonucleotides have different absorption spectra and higher λ_{max} values than their corresponding photolysis (or thermolysis) products. For example, $8N_3$ATP has a λ_{max} of 281 nm, whereas its photolysis product has a λ_{max} of 274 nm (Potter and Haley, 1983). Irradiation of $5N_3$dUTP results in the loss of absorbance in the 260–320-nm range (Evans and Haley, 1987). This suggests destruction of the conjugated ring system, probably due to an intramolecular rearrangement caused by formation of the nitrene (Bayley and Knowles, 1977). Photolysis of $2N_3$A leads to an abolition of λ_{max} at 271 nm but does not affect the tetrazole bands at 309 and 321 nm (MacFarlane et al., 1982; J. Wower and L. A. Sylvers, unpublished observations).

Detailed analysis of the photoproducts produced by irradiation of $2N_3$A in alcohols led to the discovery that not only reduction of the nitrene at the 2-position occurs but, in certain alcohols, an appreciable amount of 8-substituted purines are formed as well (Xing et al., 1990). While the reaction mechanism that leads to the 8-substituted products remains unclear, and may be unique to photoreaction in alcohols, this study highlights the point that the photochemistry of azidonucleosides is quite complex.

3. INCORPORATION OF AZIDONUCLEOTIDES INTO POLYNUCLEOTIDES

Methods for the incorporation of azidonucleotides into RNA include "cut and paste" approaches, alternatively referred to as "recombinant RNA" (for review, see Cedergren and Grosjean, 1987), chemical synthesis, and *in vitro* transcription. While the former two approaches allow for site-specific replacement of nucleotides, the latter leads to either total or random nucleotide substitution.

To date, the incorporation of azidodeoxynucleotides into DNA has been accomplished exclusively by enzymatic polymerization with DNA polymerase I (Evans et al., 1986; Evans and Haley, 1987; Lee et al., 1991; Meffert and Dose, 1988; Meffert et al., 1990). However, since DNA fragments and deoxynucleotide 3′,5′-bisphosphates can be used as unconventional substrates for T4 RNA ligase (Brennan et al., 1983), products of enzymatic or chemical DNA synthesis can be used in a "synthesize and paste" approach to generate site-specific azidonucleotide-substituted DNA molecules.

A. Specific Incorporation. Analysis of cross-linked complexes is greatly facilitated when the site of adduct formation on one of the two covalently joined molecules is already known. Therefore, it is often preferrable to carry out a photochemical cross-linking experiment with

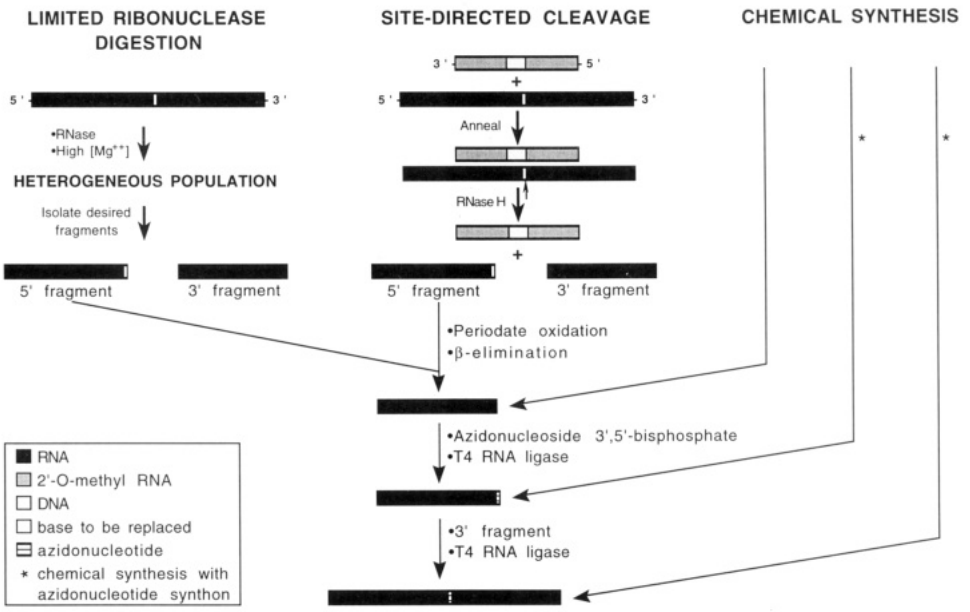


Figure 2. Strategies for site-specific incorporation of azidonucleotides. Although recombinant RNA is the theme of this figure, site-directed cleavage, ligation, and chemical synthesis approaches are available for DNA and are discussed in the text.

an RNA or DNA molecule which has been specifically substituted at a known location with an azidonucleotide. However, it should be noted that there is an element of risk associated with this approach as the nucleotide chosen for substitution might not be in contact with the target molecule. Therefore, when little is known about the interacting molecules, one may opt for random incorporation of azidonucleotides (discussed in section 3.B).

(*i*) "*Cut and Paste*" *Approach.* Recombinant RNA technology can be used to make sequence variants of RNA including specific base substitutions and deletions. The approach, in general, involves the *cutting* of RNA by controlled nucleolytic and/or chemical cleavage, followed by the *pasting* together of some of the products with other mono- and/or oligoribonucleotides using T4 RNA ligase (Figure 2). Kaufmann and Littauer (1974) were the first to utilize such an approach. The acid lability of the Y base in the anticodon loop of yeast $tRNA^{Phe}$ provided an avenue for the specific deletion of this base followed by ligation with RNA ligase to create a unique six-base anticodon loop. In the early 1980s, Uhlenbeck's group brought this methodology to the forefront, with the addition of partial nuclease digestion, to create anticodon sequence variants of $tRNA^{Phe}$ for assessing the role of the anticodon in recognition of its cognate aminoacyl-tRNA synthetase (Bruce and Uhlenbeck, 1982a,b). Other groups quickly used this and similar strategies to study a variety of tRNA species (Fournier et al., 1983; Ohtsuka et al., 1983; Schulman and Pelka, 1983; Bare and Uhlenbeck, 1985; Carbon and Ebel, 1987). Recombinant RNA approaches have recently been adopted for the site-specific incorporation of azidonucleotides within the 3′ terminal ACCA sequence (Wower et al., 1988, 1989, 1993a; Sylvers et al., 1989), the anticodon loop (Sylvers et al., 1992; Wower et al., 1993a), and the anticodon arm (Wower et al., 1990) of tRNA.

It is important to note that the pasting steps of a recombinant RNA approach are not limited to the use of T4 RNA ligase. Moore and Sharp (1992) have recently made use of a neglected property of T4 DNA ligase to create novel RNA substrates for studying the mammalian spliceosome. In 1970, Khorana and co-workers found that two RNA oligomers can be ligated with T4 DNA ligase if they are in a heteroduplex with DNA (Kleppe et al., 1970). The use of DNA ligase in this approach circumvents some of the problems associated with ligating two pieces of RNA with RNA ligase. When the two RNA oligomers to be ligated do not form a structure which maximizes a close approach of the desired ends to be ligated, yield is greatly sacrificed and, in the absence of protection of 3′-hydroxyls, circular and concatemeric structures are easily formed. These problems can be avoided, as described above, by the use of a complementary DNA, which acts as a "splint" to bring the 5′ and 3′ termini of two RNA molecules in close juxtaposition for ligation with T4 DNA ligase. Another advantage of using T4 DNA ligase is that its K_m for the substrate is many orders of magnitude lower than that of T4 RNA ligase, thus allowing the use of smaller amounts of RNA. Additionally, since single-stranded RNA is not a substrate for DNA ligase, circular and concatemeric products cannot be formed. Ligation yields with this approach can be nearly quantitative (Moore and Sharp, 1992).

A facile and universal method has recently been developed for the site-directed cleavage of RNA. This method involves the use of RNase H, which degrades the RNA component within an RNA/DNA duplex (Donis-Keller, 1979). Ohtsuka and co-workers demonstrated that RNA can be specifically cleaved at a single location of choice by annealing a chimeric oligonucleotide, containing a tetradeoxynucleotide flanked on either side with a 2′-*O*-methyloligoribonucleotide (a more stable analogue of RNA), to a defined RNA sequence followed by incubation with RNase H (Inoue et al., 1987; Shibahara et al. 1987; Shibahara et al., 1987; Hayase et al., 1990). This allows for a targeted cleavage by RNase H to the phosphodiester bond in the RNA at the site complementary to the 5′ junction of the chimeric oligonucleotide (Figure 2). This site-directed cleavage approach has been linked to the "pasting" part of a recombinant RNA strategy to create inosine-substituted derivatives of $tRNA^{Gln}$ (Hayase et al., 1992) and variants of $tRNA^{Glu}$ with specific base modification deficiencies (Sylvers et al., 1993) to study the recognition of these substrates by their cognate aminoacyl-tRNA synthetase. More recently this approach has been used to construct a derivative of $tRNA^{Glu}$ with 2-azidoadenosine placed at position 37 in the anticodon loop (L. A. Sylvers and D. Söll, unpublished results). The general scheme for this recombinant RNA approach is outlined in Figure 2.

The recent discovery that eubacterial DNA polymerases can act as structure-specific endonucleases with oligodeoxynucleotides directing single-site cleavages in DNA or RNA (Lyamichev et al., 1993) provides an alternative for the RNase H approach described above, and allows for the use of single-stranded DNA as a substrate in "cut and paste" strategies.

(*ii*) *Chemical Synthesis Approach.* Solid-support synthesis of DNA and RNA can be readily carried out using a variety of nucleoside synthons. By far the most popular and efficient approach utilizes phosphoramidite chemistry (McBride and Caruthers, 1983). There has been a recent surge in research utilizing phosphoramidite chemistry to create and insert modified bases throughout chemically synthesized DNA (Connolly and Newman, 1989; Nikiforov and Connolly, 1992) or RNA (for review, see Usman and Cedergren, 1992). Presently, only a limited number of photoreactive phosphoramidite nucleoside analogues have been synthesized. These include 5-bromouridine (Slim et al., 1991), 2- and 4-thiothymidine (Connolly and Newman, 1989) and 6-thiodeoxyguanosine (Nikiforov and Connolly, 1992). Although, as explained earlier, azidonucleotides cannot be prepared as phosphoramidites, there are apparently no barriers to the synthesis of any desired H-phosphonate or phosphotriester azidonucleoside synthon. Chemical synthesis of nucleic acids using H-phosphonates is considerably more rapid than with phosphotriesters and is therefore the method of choice. H-Phosphonate synthons have been effectively used for both DNA and RNA synthesis (Froehler and Matteucci, 1986; Garegg et al., 1986). The main limitation associated with the H-phosphonate approach is chain length. Due to decreases in yield and competing hydrolysis during the final oxidation step, 100 nucleotides is the practical size limit for oligonucleotides synthesized in this manner (B. C. Froehler, personal communication). Using this approach, azidonucleotides can be incorporated, with precision, into any position of a nucleic acid molecule. If longer polynucleotides are required than chemical synthesis allows, two or more shorter oligonucleotides can subsequently be ligated.

In the chemical synthesis of functional RNA there may be some limitations with respect to the length of the polynucleotide. Early attempts to synthesize $tRNA^{fMet}$ (77 nucleotides in length) produced a tRNA molecule exhibiting only 10% of the aminoacyl-acceptor activity of the native tRNA (Ogilvie et al., 1988). The low acceptor activity was originally attributed to either the lack of modified bases normally present in the native tRNA or incomplete deprotection. It has since been demonstrated that the *in vitro* transcript of $tRNA^{fMet}$ has comparable activity to the native tRNA (Schulman and Pelka, 1988); therefore, the dramatic loss of activity was most likely due to poor deprotection. However, with the latest advances in solid-support RNA synthesis, it is now quite reasonable to synthesize fully deprotected RNAs with chain-lengths of 50–100 nucleotides (Vinayak et al., 1992). Nevertheless, as RNA length is increased, yield decreases. This, in addition to the obvious desire to have a number of variants with azidonucleotides placed in different positions, makes it preferable to synthesize short synthetic azidonucleotide-substituted oligoribonucleotides to be ligated to natural RNA fragments produced by the methods described in the previous section. This strategy, which is depicted in Figure 2, would allow for the generation of several distinct RNA populations with single azidonucleotide substitutions throughout a limited region of the molecule. This would provide the means for a very detailed study mapping the RNA–protein or RNA–nucleic acid contacts along a specified stretch of RNA.

B. Random Incorporation. Since 1988, when Uhlenbeck and co-workers successfully used T7 RNA polymerase to produce $tRNA^{Phe}$ transcripts for functional studies (Sampson and Uhlenbeck, 1988), other groups studying RNA–protein interactions quickly took advantage of this method. The cornerstone of *in vitro* transcription is the ability to rapidly produce large amounts of high quality RNA for biochemical and/or biophysical studies of RNA structure and function. The usefulness of *in vitro* transcription is further broadened by the ability to incorporate modified nucleotides randomly throughout an RNA chain. Examples include the use of phosphorothioates to modify the phosphodiester backbone by total or random replacement of phosphoryl oxygen atoms with sulfur (Griffiths et al., 1977; Ruffner and Uhlenbeck, 1990). This has been useful for the identification of phosphates important in RNA–RNA interactions (Ruffner and Uhlenbeck, 1990; Suh and Waring, 1992) and RNA–protein interactions *via* a novel footprinting approach which takes advantage of iodine-induced scission of exposed sulfur residues in the backbone (Schatz et al., 1991). Others have incorporated halogenated nucleotides for use in cross-linking (Tanner et al., 1988; Gott et al., 1991) and NMR studies (for examples see Chu et al., 1992). Additionally, 4-thiouridine has been incorporated into model mRNAs and tRNAs for use in cross-linking (Stade et al., 1989; Rinke-Appel et al., 1991; Dontsova et al., 1991, 1992a; Rosen et al., 1993; Zimmerly et al., 1993). Recently, Dontsova et al. (1992b) used T7 RNA polymerase to generate $5N_3U$-substituted transcripts for use in cross-linking experiments to help define the path of mRNA on the translating ribosome. Although Evans and Haley (1987) had previously demonstrated that $5N_3UTP$ is a substrate for *E. coli* RNA polymerase, the work of Dontsova et al. (1992b) represents the first, and so far only, use of azidonucleotide-substituted RNA transcripts for cross-linking studies.

The main limitation in template-directed incorporation of modified nucleotides into RNA is the inability of many derivatives to form canonical Watson–Crick base pairs, which thus prevents their incorporation. While 5-substituted pyrimidines "read" the complementary purine during transcription, 2- and 8-substituted purines are prevented from proper pairing by steric hindrance or altered nucleotide conformation, respectively (Knoll et al., 1992; J. Wower, unpublished). Other modifications may lead to promiscuous incorporation as indicated by Piccirilli et al. (1990). Therefore, at the present time it appears that the only suitable azidonucleotide for template-directed incorporation into RNA is $5N_3UTP$.

The limitations that pertain to template-directed incorporation of azidonucleotides into RNA do not seem to apply to DNA. While the azido-modified purines are not substrates for RNA polymerases, $8N_3dATP$ is a substrate for DNA polymerase I and has been successully incorporated into DNA (Meffert and Dose, 1988; Meffert et al., 1990). Although $8N_3dATP$ is the only azidopurine nucleotide to be incorporated into DNA in a template-directed manner to date, it is expected that others might also prove to be acceptable substrates. Finally, as previously mentioned, $5N_3dUTP$ has been demonstrated to be a good substrate for DNA polymerase (Evans et al., 1986).

4. REPORTED APPLICATIONS

Azidopurine nucleotides have frequently been used for the study of nucleotide binding sites on proteins (Haley, 1983). However, the use of azidonucleotide-substituted nucleic acids has been limited. Polynucleotides containing $8N_3A$ and $8N_3I$ residues have been prepared from mixtures

of nucleoside diphosphates using polynucleotide phosphorylase and used as photoaffinity probes to explore the subunit topography of RNA polymerase from *E. coli* (Cartwright and Hutchinson, 1980). The discovery that RNA ligase has a high tolerance for the use of modified bases as ligation donors (Barrio et al., 1978), opened the possibility for using 2- and 8-azidoadenosines, which are not substrates for template-dependent RNA polymerases, as photoreactive probes in a site-directed cross-linking approach. These azidoadenosines have been incorporated into specific positions in tRNA molecules and then used to delineate the topography of tRNA binding sites on the *E. coli* ribosome (Wower et al., 1988, 1989, 1990, 1993a,b; Sylvers et al., 1989, 1992).

The synthesis of $5N_3$UTP, $5N_3$dUTP (Evans et al., 1986), and $8N_3$dATP greatly expanded the utility of azidonucleosides for studying nucleic acid–protein interactions. The use of $5N_3$U-substituted nucleic acids has been adopted for studying mRNA–ribosome (Dontsova et al., 1992b), 5S DNA–TFIIIA (Lee et al., 1991), and *lac* operator–repressor (Evans et al., 1986) complexes. Also, 2- and $8N_3$dATP were used to synthesize 2′-5′ oligoadenylate 5′-triphosphates (2-5A) by 2-5A synthetase from rabbit reticulocyte lysates (Suhadolnik et al., 1988). This 2-5A photoaffinity probe was then used to study the nucleotide binding domain of RNase L (Suhadolnik et al., 1988). Finally, $8N_3$dATP has been demonstrated to be a substrate for DNA polymerase I and has been incorporated into pBR322 for studying DNA–histone interactions (Meffert and Dose, 1988) and into a DNA fragment containing the *tet* operator sequence to explore complexes with the tet repressor protein (Meffert et al., 1990).

5. CONCLUSIONS AND FUTURE PROSPECTS

Azidonucleotides meet the requirements for being effective photo-cross-linking reagents. They can be readily synthesized, are reasonably stable, display close structural similarity to their parent nucleotides, and are chemically inert except when irradiated with UV light or exposed to extreme heat (>130 °C). The nitrenes generated upon irradiation display little specificity with regard to bond insertion and generally produce high-yield cross-links to molecular constituents in its immediate environment. Finally, since azidonucleotides absorb at longer wavelengths than nucleic acids and proteins, they can be selectively photolyzed without damage to these macromolecules.

Despite the long history of the use of azidonucleotides for labeling nucleotide binding proteins, the photochemistry of these aryl azides is still poorly understood. It has been the general expectation that the photochemistry of azidonucleotides would be, in large part, similar to that of better-characterized aryl azides. However, aside from the propensity of aryl azides to yield reactive nitrenes upon exposure to UV light or heat, the reaction pathways utilized by the generated nitrene vary according to the composition and environment of the aryl group. Additionally, the pH-dependent tautomerization of some azidonucleotides to tetrazoles has only been addressed in a few studies. Detailed studies of azidonucleotide photochemistry and tautomerization may lead to an even more effective use of these photo-cross-linking reagents, allowing for prediction of adduct structures formed in a given cross-link and conditions for long-term stabilization of azide tautomers.

Recent developments in molecular biology and chemistry have greatly expanded the possibilities for incorporation of azidonucleotides into nucleic acids. A number of procedures that allow for the preparation of nucleic acid probes substituted with photoreactive nucleotides either randomly or in a site-specific fashion have been devised. These photoreactive probes have been used to detect the sites of contact within stable nucleic acid–protein complexes and, in a few cases, nucleic acid–nucleic acid complexes. However, it is expected that azidonucleotide-substituted nucleic acids will also be used effectively to study transient nucleic acid–protein and nucleic acid–nucleic acid interactions. Similarly, the potential use of azidonucleotides for studying the folding and conformational changes of RNA has yet to be exploited. The full potential of these probes for studying macromolecular interactions is only now being recognized. We hope that the methodological information provided here will make this photo-cross-linking approach more accessible to researchers studying the structure and function of nucleic acids.

ACKNOWLEDGMENT

This review was written while L.A.S. and J.W. were under the support of NIH grants to Dieter Söll and Robert A. Zimmermann, respectively.

LITERATURE CITED

Abramovitch, R. A., and Kyba, E. P. (1971) Decomposition of organic azides. In *The Chemistry of the Azido Group* (S. Patai, Ed.) pp 221–329, Interscience, New York.

Bare, L., and Uhlenbeck, O. C. (1985) Aminoacylation of anticodon loop substituted yeast tyrosine transfer RNA. *Biochemistry 24*, 2354–2360.

Barrio, J. R.; Barrio, M. C. G., Leonard, N. J., England, T. E., and Uhlenbeck, O. C. (1978) Synthesis of modified nucleoside 3′,5′-bisphosphates and their incorporation into oligoribonucleotides with T4 RNA ligase. *Biochemistry 17*, 2077–2081.

Bayley, H. (1983) Photogenerated reagents in biochemistry and molecular biology. In *Laboratory techniques in biochemistry and molecular biology, vol. 12* (T. S. Work, and R. H. Burdon, Eds.) pp 1–187, Elsevier, New York.

Bayley, H., and Knowles, J. R. (1977) Photoaffinity labeling. *Methods Enzymol. 46*, 69–114.

Bayley, H., and Staros, J. V. (1984) Photoaffinity labeling and related techniques. In *Azides and Nitrenes: Reactivity and Utility* (E. F. V. Scriven, Ed.) pp 433–490, Academic Press, Orlando, FL.

Bendich, A., Giner-Sorolla, A., and Fox, J. J. (1957) In *CIBA foundation symposium on the chemistry and biology of purines* (G. E. W. Wolstenholme, and C. M. O'Connor, Eds.) p 10, J. and A. Churchill, Ltd., London.

Brennan, C. A., Manthey, A. E., and Gumport, R. I. (1983) Using T4 RNA ligase with DNA substrates. *Methods Enzymol. 100*, 38–52.

Bruce, A. G., and Uhlenbeck, O. C. (1982a) Enzymatic replacement of the anticodon of yeast phenylalanine transfer ribonucleic acid. *Biochemistry 21*, 855–861.

Bruce, A. G., and Uhlenbeck, O. C. (1982b) Specific interaction of anticodon loop residues with yeast phenylalanyl-tRNA synthetase. *Biochemistry 21*, 3921–3926.

Burgin, A. B., and Pace, N. R. (1990) Mapping the active site of ribonuclease P RNA using a substrate containing a photoaffinity agent. *EMBO J. 9*, 4111–4118.

Carbon, P., and Ebel, J.-P. (1987) *In vitro* construction of yeast $tRNA^{Asp}$ variants: nucleotide substitutions and additions in T-stem and T-loop. *Nucleic Acids Res. 15*, 1933–1950.

Cartwright, I. L., and Hutchinson, D. W. (1980) Azidopolynucleotides as photoaffinity reagents. *Nucleic Acids Res. 8*, 1675–1691.

Cartwright, I. L., Hutchinson, D. W., and Armstrong, V. W. (1976) The reaction between thiols and 8-azidoadenosine derivatives. *Nucleic Acids Res. 3*, 2331–2339.

Cedergren, R., and Grosjean, H. (1987) RNA design by *in vitro* RNA recombination and synthesis. *Biochem. Cell. Biol. 65*, 677–692.

Chen, J.-K., Franke, L. A., Hixson, S. S., and Zimmermann, R. A. (1985) Photochemical cross-linking of $tRNA^{Arg}_{1}$ to the 30S ribosomal subunit using aryl azide reagents attached to the anticodon loop. *Biochemistry 24*, 4777–4784.

Chu, W. C., Feiz, V., Derrick, W. B., and Horowitz, J. (1992) Fluorine-19 nuclear magnetic resonance as a probe of the solution structure of mutants of 5-fluorouracil-substituted *Escherichia coli* valine tRNA. *J. Mol. Biol. 227*, 1164–1172.

Connolly, B. A., and Newman, P. C. (1989) Synthesis and properties of oligonucleotides containing 4-thiothymidine, 5-methyl-2-pyrimidinone-1-beta-D(2′-deoxyriboside) and 2-thiothymidine. *Nucleic Acids Res. 17*, 4957–4974.

Donis-Keller, H. (1979) Site-specific enzymatic cleavage of RNA. *Nucleic Acids Res. 7*, 179–192.

Dontsova, O., Kopylov, A., and Brimacombe, R. (1991) The location of mRNA in the ribosomal 30S initiation complex; site-directed cross-linking of mRNA analogues carrying several photo-reactive labels simultaneously on either side of the AUG start codon. *EMBO J. 10*, 2613–2620.

Dontsova, O., Dokudovskaya, S., Kopylov, A., Bogdanov, A., Rinke-Appel, J., Jünke, N., and Brimacombe, R. (1992a) Three widely separated positions in the 16S rRNA lie in or close to the ribosomal decoding region; a site-directed cross-linking study with mRNA analogues. *EMBO J. 11*, 3105–3116.

Dontsova, O., Rosen, K. V., Bogdanova, S. L., Skripkin, E. A., Kopylov, A. M., and Bogdanov, A. A. (1992b) Identification of the *Escherichia coli* 30S ribosomal subunit protein neighboring mRNA during initiation of translation. *Biochimie 74*, 363–371.

England, T. E., and Uhlenbeck, O. C. (1978) Enzymatic oligoribonucleotide synthesis with T4 RNA ligase. *Biochemistry 17*, 2069–2076.

Evans, R. K., and Haley, B. E. (1987) Synthesis and biological properties of 5-azido-2′-deoxyuridine 5′-triphosphate, a photoactive nucleotide suitable for making light-sensitive DNA. *Biochemistry 26*, 269–276.

Evans, R. K., Johnson, J. D., and Haley, B. E. (1986) 5-azido-2′-deoxyuridine 5′-triphosphate: a photoaffinity labeling reagent and tool for the enzymatic synthesis of photoactive DNA. *Proc. Natl. Acad. Sci. U.S.A. 83*, 5382–5386.

Fournier, M. J., and Maxwell, E. S. (1993) The nucleolar snRNAs: Catching up with the spliceosomal snRNAs. *TIBS 18*, 131–135.

Fournier, M., Haumont, E., de Henau, S.; Gangloff, J., and Grosjean, H. (1983) Post-transcriptional modification of the wobble nucleotide in anticodon-substituted yeast $tRNA^{Arg}_{II}$ after microinjection into *Xenopus laevis* oocytes. *Nucleic Acids Res. 11*, 707–718.

Fritz, H.-J., Frommer, W.-B., Kramer, W. Jr., and Werr, W. (1982) Simplified preparations of blocked 2-deoxyribonucleotides as starting materials for chemical oligonucleotide synthesis. In *Chemical and enzymatic synthesis of gene fragments: A laboratory manual* (H. G. Gassen, and A. Lang, Eds.) pp. 43–52, Verlag Chemie, Weinheim.

Froehler, B. C., and Matteucci, M. D. (1986) Nucleotide H-phosphonates: Valuable intermediates in the synthesis of deoxyoligonucleotides. *Tetrahedron Lett. 27*, 469–472.

Froehler, B. C., Ng, P. G. and Matteucci, M. D. (1986) Synthesis of DNA *via* deoxynucleoside H-phosphonate intermediates. *Nucleic Acids Res. 14*, 5399–5407.

Gait, M. J., Matthes, H. W. D., Singh, M., Sproat, B. S., and Titmes, R. C. (1982) Synthesis of oligodeoxyribonucleotides by a continuous flow phosphotriester method on a kieselguhr/polyamide support. In *Chemical and enzymatic synthesis of gene fragments: A laboratory manual* (H. G. Gassen, and A. Lang, Eds.) pp. 1–42, Verlag Chemie, Weinheim.

Garegg, P. J., Lindh, I., Regbert, T., Stawinski, J., and Strömberg, R. (1986) Nucleoside H-phosphonates. IV. Automated solid phase synthesis of oligoribonucleotides by the hydrogen phosphonate approach. *Tetrahedron Lett. 27*, 4055–4058.

Gott, J. M., Willis, M. C., Koch, T. H., and Uhlenbeck, O. C. (1991) A specific, UV-induced RNA-protein cross-link using 5-bromouridine-substituted RNA. *Biochemistry 30*, 6290–6295.

Griffiths, A. D., Potter, B. V. L., and Eperon, I. C. (1987) Stereospecificity of nucleases towards phosphorothioate-substituted RNA: stereochemistry of transcription by T7 RNA polymerase. *Nucleic Acids Res. 15*, 4145–4162.

Haley, B. E. (1975) Photoaffinity labeling of adenosine 3′,5′-cyclic monophosphate binding sites of human red cell membranes. *Biochemistry 14*, 3852–3857.

Haley, B. E. (1983) Development and utilization of 8-azidopurine nucleotide photoaffinity probes. *Fed. Proc. 42*, 2831–2836.

Hayase, Y., Inoue, H., and Ohtsuka, E. (1990) Secondary structure in formylmethionine tRNA influences the site-directed cleavage of ribonuclease H using chimeric 2′-*O*-methyl oligodeoxyribonucleotides. *Biochemistry 29*, 8793–8797.

Hayase, Y., Jahn, M., Rogers, M. J., Sylvers, L. A., Koizumi, K., Inoue, H., Ohtsuka, E., and Söll, D. (1992) Recognition of bases in *E. coli* $tRNA^{Gln}$ by glutaminyl-tRNA synthetase: a complete identity set. *EMBO J. 11*, 4159–4165.

Hixson, S. H., and Hixson, S. S. (1975) *p*-Azidophenacyl bromide, a versatile photolabile bifunctional reagent. *Biochemistry 14*, 4251–4254.

Houstek, J., and Smrt, J. (1979) Synthesis of 8-azidoadenosine 5′-phosphate. *Collection Czechoslov. Chem. Commun. 44*, 976–980.

Inoue, H., Hayase, I.; Imura, A., Iwai, S., and Ohtsuka, E. (1987) Sequence-dependent hydrolysis of RNA using modified oligonucleotide splints and RNase H. *FEBS Lett. 215*, 327–330.

Johnson, J. A., Jr., Thomas, H. J., and Schaeffer, H. J. (1966) Synthesis of potential anticancer agents. XIII. Ribosides of 6-substituted purines. *J. Org. Chem. 341*, 699–701.

Kaufmann, G., and Littauer, U. Z. (1974) Covalent joining of phenylalanine transfer ribonucleic acid half-molecules by T4 RNA ligase. *Proc. Natl. Acad. Sci. U.S.A. 71*, 3741–3745.

Kleppe, K., van de Sande, J. H., and Khorana, H. G. (1970) Polynucleotide ligase-catalyzed joining of deoxyribo-oligonucleotides on ribonucleotide templates and of ribo-oligonucleotides on deoxyribonucleotide templates. *Proc. Natl. Acad. Sci. U.S.A. 67*, 68–73.

Knoll, D. A., Woody, R. W., and Woody, A. Y. (1992) Mapping of the active site of T7 RNA polymerase with 8-azidoATP. *Biochim. Biophys. Acta 1121*, 252–260.

Koberstein, R. (1976) 8-Azidoadenine analogs of NAD^+ and FAD. Synthesis and coenzyme properties with NAD^+ dependent and FAD-dependent enzymes. *Eur. J. Biochem. 67*, 223–229.

Koberstein, R., Cobianchi, L., and Sund, H. (1976) Interaction of the photoaffinity label 8-azido-ATP with glutamate dehydrogenase. *FEBS Lett. 64*, 176–180.

Lee, D. K., Evans, R. K., Blanco, J., Gottesfeld, J., and Johnson, J. D. (1991) Contacts between 5S DNA and *Xenopus* TFIIIA identified using 5-azido-2′-deoxyuridine-substituted DNA. *J. Biol. Chem. 266*, 16478–16784.

Lyamichev, V., Brow, M. A. D., Dahlberg, J. E. (1993) Structure-specific endonucleolytic cleavage of nucleic acids by eubacterial DNA polymerases. *Science 260*, 778–783.

MacFarlane, D. E., Mills, D. C. B., and Srivastava, P. C. (1982) Photoaffinity labeling of red blood cell platelets with 2-azidoadenosine triphosphate. *Biochemistry 21*, 544–549.

Mattaj, I. W., Tollervey, D., Seraphin, B. (1993) Small nuclear RNAs in messenger RNA and ribosomal RNA processing. *FASEB J. 7*, 47–53.

McBride, L. J., and Caruthers, M. H. (1983) An investigation of several deoxynucleoside phosphoramidites useful for synthesizing deoxyoligonucleotides. *Tetrahedron Lett. 24*, 245–248.

Meffert, R., and Dose, K. (1988) UV-induced cross-linking of proteins to plasmid pBR322 containing 8-azidoadenosine 2′-deoxyribonucleotides. *FEBS Lett. 239*, 190–194.

Meffert, R., Rathgeber, G., Schäfer, H.-J., and Dose, K. (1990) UV-induced cross-linking of tet repressor to DNA containing tet operator sequences and 8-azidoadenines. *Nucleic Acids Res. 18*, 6633–6636.

Michelson, A. M. (1964) Synthesis of nucleotide anhydrides by anionic exchange. *Biochim. Biophys. Acta 91*, 1–13.

Moore, M., and Sharp, P. A. (1992) Site-specific modification of pre-mRNA: The 2′-hydroxyl groups at the splice sites. *Science 256*, 992–997.

Nikiforov, T. T., and Connolly, B. A. (1992) Oligodeoxynucleotides containing 4-thiothymidine and 6-thiodeoxyguanosine as affinity labels for the Eco RV restriction endonuclease and modification methylase. *Nucleic Acids Res. 20*, 1209–1214.

Noller, H. F. (1991) Ribosomal RNA and translation. *Annu. Rev. Biochem. 60*, 191–227.

Ogilvie, K. K., Usman, N., Nicoghosian, K., and Cedergren, R. J. (1988) Total chemical synthesis of a 77-nucleotide-long RNA sequence having methionine-acceptance activity. *Proc. Natl. Acad. Sci. USA 85*, 5764–5768.

Ohtsuka, E., Doi, T., Fukumoto, R., Matsugi, J., and Ikehara, M. (1983) Modification of the anticodon triplet of *E. coli* $tRNA^{fMet}$ by replacement with trimers complementary to non-sense codons UAG and UAA. *Nucleic Acids Res. 11*, 3863-3872.

Piccirilli, J. A., Krauch, T., Moroney, S. E., and Benner, S. A. (1990) Enzymatic incorporation of a new base pair into DNA and RNA extends the genetic alphabet. *Nature 343*, 33–37.

Potter, R. L., and Haley, B. E. (1983) photoaffinity labeling of nucleotide binding sites with 8-azidopurine analogs: techniques and applications. *Methods Enzymol. 91*, 613–633.

Reiser, A., and Wagner, H. M. (1971) Photochemistry of the azido group. In *The Chemistry of the Azido Group* (S. Patai, Ed.) pp 441–501, Interscience, New York.

Rinke-Appel, J., Jünke, N., Stade, K., and Brimacombe, R. (1991) The path of mRNA through the *Escherichia coli* ribosome; site-directed cross-linking of mRNA analogues carrying a photo-reactive label at various points 3′ to the decoding site. *EMBO J. 10*, 2195–2202.

Rosen, K. V., Alexander, R. W., Wower, J., and Zimmermann, R. A. (1993) Mapping the central fold of $tRNA_2^{fMet}$ in the P site of the *Escherichia coli* ribosome. *Biochemistry*. In press.

Ruffner, D. E., and Uhlenbeck, O. C. (1990) Thiophosphate interference experiments locate phosphates important for the hammerhand self-cleavage reaction. *Nucleic Acids Res. 18*, 6025–6029.

Sampson, J. R., and Uhlenbeck, O. C. (1988) Biochemical and physical characterization of an unmodified yeast phenylalanine transfer RNA transcribed *in vitro*. *Proc. Natl. Acad. Sci. U.S.A. 85*, 1033–1037.

Schaeffer, J. H., Thomas, J. H. (1958) Modified nucleosides: Synthesis of 2-substituted adenosine derivatives. *J. Am. Chem. Soc. 80*, 3738–3742.

Schäfer, G., and Penades, S. (1977) Photolabeling of the adenine nucleotide carrier by 8-azido-ATP. *Biochem. Biophys. Res. Commun. 78*, 811–818.

Schäfer, H.-J., Scheurich, P., and Dose, K. (1976) Synthesis of 8-azido derivatives of ATP, ADP and AMP from ATP and first application of characterization of metal(II)-ion-adenosinetriphosphatases. *Hoppe-Seyler's Z. Physiol. Chem. 357*, 278.

Schatz, D., Leberman, R., and Eckstein, F. (1991) Interaction of *Escherichia coli* $tRNA^{Ser}$ with its cognate aminoacyl-tRNA synthetase as determined by footprinting with phosphorothioate-containing tRNA transcripts. *Proc. Natl. Acad. Sci. U.S.A. 88*, 6132–6136.

Schulman, L. H. and Pelka, H. (1983) Anticodon loop size and sequence requirements for recognition of formylmethionine tRNA by methionyl-tRNA synthetase. *Proc. Natl. Acad. Sci. U.S.A. 80*, 6755–6759.

Schulman, L. H., and Pelka, H. (1988) Anticodon switching changes the identity of methionine and valine transfer RNAs. *Science 242*, 765–768.

Shibahara, S., and Mukai, S., Hishihara, T., Inoue, H., Ohtsuka, E., Morisawa, H. (1987) Site-directed cleavage of RNA. *Nucleic Acids Res. 15*, 4403–4415.

Slim, G., Pritchard, C., Biala, E., Asseline, U., and Gait, M. J. (1991) Synthesis of site-specifically modified oligoribonucleotides for studies of the recognition of TAR RNA by HIV-1 tat protein and studies of hammerhead ribozymes. *Nucleic Acids Symp. Ser. 24*, 55–58.

Smith, P. A. S. (1984) Aryl and heteroaryl azides and nitrenes. In *Azides and Nitrenes*: Reactivity and Utility (E. F. V. Scriven, Ed.) pp 95–204, Academic Press, Orlando, Fla.

Stade, K., Rinke-Appel, J., and Brimacombe, R. (1989) Site-directed cross-linking of mRNA analogues to the *Escherichia coli* ribosome; identification of 30S ribosomal components that can be cross-linked to the mRNA at various points 5′ with respect to the decoding site. *Nucleic Acids Res. 17*, 9889–9908.

Staudinger, H., and Hauser, E. (1921) Über neue organische phosphorverbindungen IV. *Helv. Chim. Acta 4*, 861–886.

Staudinger, H., and Meyer, J. (1919) Über neue organische phosphorverbindungen III. Phosphinmethylenderivate und phosphinimine. *Helv. Chim. Acta 2*, 635–646.

Suh, E., and Waring, R. B. (1992) A phosphorothioate at the 3′ splice-site inhibits the second splicing step in a group intron. *Nucleic Acids Res. 20*, 6303–6309.

Suhadolnik, R. J., Kariko, K., Sobol, R. W. Jr., Li, S. W., Reichenbach, N. L., and Haley, B. E., (1988) 2- and 8-azido photoaffinity probes. 1. Enzymatic synthesis, characterization, and biological properties of 2- and 8-azido photoaffinity probes of 2-5A and photoaffinity labeling of 2-5A binding proteins. *Biochemistry 27*, 8840–8846.

Sylvers, L. A., Wower, J., Hixson, S. S., and Zimmermann, R. A. (1989) Preparation of 2-azidoadenosine 3′,5′-[5′-^{32}P]bisphosphate for incorporation into transfer RNA: Photoaffinity labeling of Escherichia coli ribosomes. *FEBS Lett. 245*, 9–13.

Sylvers, L. A., Kopylov, A. M., Wower, J., Hixson, S. S., and Zimmerman, R. A. (1992) Photochemical cross-linking of the anticodon loop of yeast $tRNA^{Phe}$ to 30S-subunit protein S7 at the ribosomal A and P sites. *Biochimie 74*, 381–389.

Sylvers, L. A., Rogers, K. C., Shimizu, M., Ohtsuka, E., and Söll, D. (1993) A 2-thiouridine derivative in $tRNA^{Glu}$ is a positive determinant for aminoacylation by *Escherichia coli* glutamyl-tRNA synthetase. *Biochemistry 32*, 3836–3841.

Symons, R. H. (1974) Synthesis (alpha-^{32}P) ribo- and deoxyribonucleoside 5′-triphosphates. *Methods Enzymol. 29*, 102–115.

Tanner, N. K., Hanna, M. M., and Abelson, J. (1988) Binding interactions between yeast tRNA ligase and a precursor transfer ribonucleic acid containing two photoreactive uridine analogues. *Biochemistry 27*, 8852–8861.

Temple, C., Jr., and Montgomery, J. A. (1965) Studies on azidoazomethine–tetrazole equilibrium. *J. Org. Chem. 30*, 826–829.

Usman, N., and Cedergren, R. (1992) Exploiting the chemical synthesis of RNA. *TIBS 17*, 334–339.

Vinayek, R., Anderson, P., McCollum, C., and Hampel, A. (1992) Chemical synthesis of RNA using fast oligonucleotide deprotection chemistry. *Nucleic Acids Res. 20*, 1265–1269.

Walseth, T. F., and Johnson, R. A. (1979) The enzymatic preparation of [alpha-^{32}P]nucleoside triphosphates, cyclic [^{32}P] AMP, and cyclic [^{32}P] GMP. *Biochim. Biophys. Acta 526*, 11–31.

Wower, J., Hixson, S. S., and Zimmermann, R. A. (1988) Photochemical cross-linking of yeast $tRNA^{Phe}$ containing 8-azidoadenosine at positions 73 and 76 to the *Escherichia coli* ribosome. *Biochemistry 27*, 8114–8121.

Wower, J., Hixson, S. S., and Zimmermann, R. A. (1989) Labeling of the peptidyl trnasferase center of the *Escherichia coli* ribosome with photoreactive tRNA derivatives containing azidoadenosine at the 3′ endo of the acceptor arm: A model of the tRNA-ribosome complex. *Proc. Natl. Acad. Sci. U.S.A. 86*, 5232–5236.

Wower, J., Malloy, T. A. IV, Hixson, S. S., and Zimmermann, R. A. (1990) Probing tRNA binding sites on the *Escherichia coli* 30S ribosomal subunit with photoreactive analogs of the anticodon arm. *Biochim. Biophys. Acta* **1050**, 38–44.

Wower, J., Scheffer, P., Sylvers, L. A., Wintermeyer, W., and Zimmermann, R. A. (1993a) Topography of the E site on the *Escherichia coli* ribosome. *EMBO J. 12*, 617–623.

Wower, J., Sylvers, L. A., Rosen, K., and Zimmermann, R. A. (1992b) A model of tRNA binding sites on the *Escherichia coli* ribosome. In *The Translational Apparatus* (K. H. Nierhaus, F. Franceschi, A. R. Subramanian, V. A. Erdmann, and B. Wittmann-Liebold, Eds.) pp 455–464, Plenum Press, New York.

Xing, Y., Hixson, S. S., and Zimmermann, R. A. (1990) Photochemistry of 2-azidoadenine in alcohols. *Tetrahedron Lett. 31*, 5849–5850.

Zimmerly, S., Drainas, D., Sylvers, L. A., and Söll, D. (1993) Identification of a 100 kilodalton protein associated with nuclear RNase P activity in *Schizosaccharomyces pombe*. *Eur. J. Biochem. 217*, 501–507.

ARTICLES

Synthesis of Cobalt Carbonyl Complexes of Cortisol and Testosterone. Study of Their Recognition by Specific Polyclonal Antibodies

Valérie Philomin, Anne Vessiéres, Michel Gruselle, and Gérard Jaouen*

Ecole Nationale Supérieure de Chimie de Paris, URA CNRS 403, 11 rue Pierre et Marie Curie, 75231 Paris Cedex05, France. Received February 10, 1993®

We have synthesized organometallic complexes of steroids (cortisol, testosterone, dihydrotestosterone) for potential use as tracers in nonisotopic carbonyl-metal immunoassays (CMIA). An ethynyl/$Co_2(CO)_6$ fragment at the end of a five-atom spacer was coupled to position 3 of the steroid skeleton. In the case of cortisol, we exploited the difference in reactivity of the ketone and enone functions toward amines in order to form an enamine which was then made to react with carboxymethylamine to yield 3-[(carboxymethyl)oxime] steroid. Activation of the carboxylic acid function with *N,N'*-dicyclohexylcarbodiimide in the presence of propargylamine introduced an acetylenic function at the end of the spacer. The triple bond was then complexed by $Co_2(CO)_8$ to form complexes **5a–c**. Complexes for use in CMIA should be stable in biologic media and effectively recognize specific antibodies. Complexes **5a–c** were stable in the buffers we use in biochemical tests. Their cross reactivities for anti-cortisol and anti-testosterone antibodies ranged from 50 to 110% according to batch, indicating, first, that the addition of an organometallic complex in position 3 of the steroid skeleton does not hinder recognition between the organometallic steroid and antibody and, second, that their individual behavior differs substantially according to antibody batch. Although all of these complexes could be used as tracers in CMIA, it is necessary, in each case, to establish which tracer–antibody duo gives rise to the most sensitive immunoassay.

INTRODUCTION

In the context of our general studies on the use of organometallic complexes for the study of protein–ligand molecular recognition, we recently focused on the specific case of the interaction between organometallic-substituted steroids and steroid hormone receptors (*1*, *2*). To prepare steroids with affinity for specific receptors, it is necessary to meet strict criteria. For example, it is essential to keep the 3- and 17β-OH functions of estradiol or the 3-enone function of testosterone whereas cumbersome substituents are often acceptable in position 17α (*3*). With these constraints in mind, we have in the past synthesized various metal (Cr, Co, Mo, Os, Ru, Rh) complexes of estradiol (*4*, *5*), some with high affinity for the estrogen receptor, and have, moreover, shown that complexation of the α-face of the aromatic ring with a π organometallic moiety leads to compounds with acceptable affinity for the receptor whereas complexation of the β-face results in a near total loss in receptor recognition. This discrimination between the α and β faces of estradiol is a unique advantage offered by organometallic chemistry. Some of the organometallic steroids we prepared are affinity labeling agents, *i.e.*, bind covalently to the estrogen receptor, and have enabled the putative identification of amino acids within the binding site (*6*).

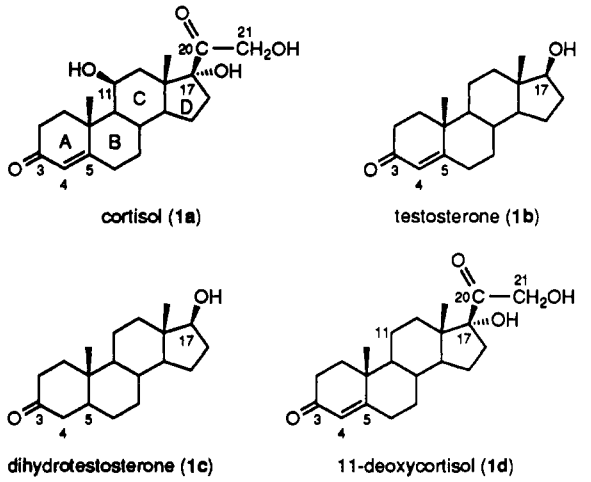
In the present paper we describe the synthesis of organometallic complexes with potential for use as tracers in a nonisotopic immunoassay (CMIA)[1] such as the one we have already developed for the assay of an antiepileptic drug, phenobarbital (*7*). The first two steps involved are the preparation of the antibodies and the preparation of the tracer. Specific polyclonal antibodies for steroid assays are prepared by injection of an antigen, obtained by coupling a derivative of the steroid (hapten) to a carrier protein, *e.g.*, BSA, to animals. In the case of antibody–steroid interactions, the possible modification sites of the steroids are very different from those discussed above for receptor interaction. Indeed, the functional 3, 17, or 21 positions that are preserved for receptor interaction are the ones that are most often used to couple a carboxylic acid function which is then linked to the carrier protein (*8*). The same strategy is employed to synthesize organometallic tracers that recognize these specific antibodies of the hormone and will be illustrated in the present paper by the preparation of cortisol and testosterone derivatives substituted at C3 with an organocobalt moiety. The cross reactivities (CR) of these derivatives for several polyclonal anti-cortisol and anti-testosterone antibodies have been determined and we show that although steroid complexation does not hinder antibody recognition, there is great variation in the extent of this recognition.

® Abstract published in *Advance ACS Abstracts*, September 1, 1993.

[1] Abbreviations used: CMIA, carbonyl–metal immunoassay; BSA, bovine serum albumin; DCC, dextran-coated charcoal; testosterone, 17-β-hydroxy-4-androsten-3-one; dihydrotestosterone, 17-β-hydroxy-5α-androstan-3-one; cortisol, 11β,17α,21-trihydroxypregn-4-ene-3,20-dione; 11-deoxycortisol, 17α,21-dihydroxypregn-4-ene-3,20-dione; CR (%), cross reactivity; CMO, (carboxymethyl)oxime.

1043-1802/93/2904-0419$04.00/0 © 1993 American Chemical Society

Scheme I



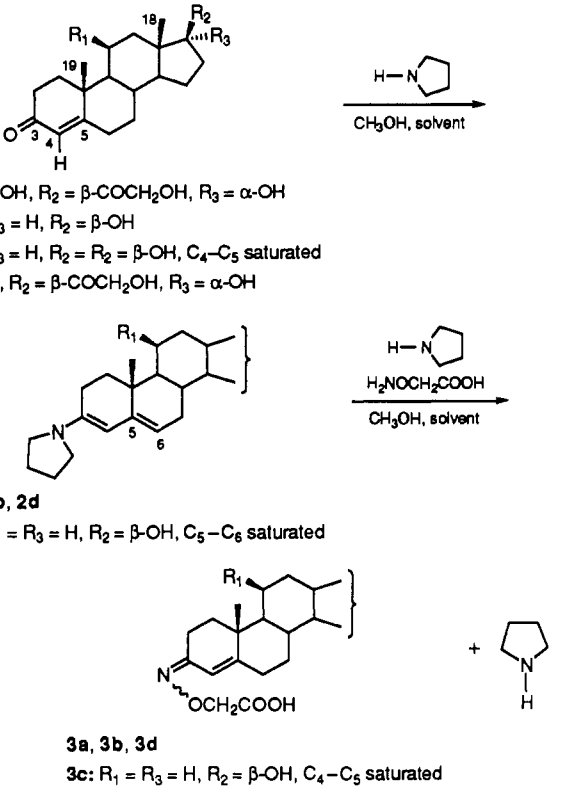
RESULTS AND DISCUSSION

Synthesis and Characterization of the Organometallic Hormones. The aim was to synthesize organometallic complexes of cortisol, testosterone, and dihydrotestosterone (Scheme I) for use as tracers in a CMIA. Both the position of the steroid skeleton to which the organometallic moiety is coupled and the nature of the moiety have to be considered. The steroids we chose to assay have in common a 3-keto group on ring A but differ otherwise: testosterone has a 17β-OH function whereas cortisol has three hydroxy groups (11β, 17α, 21) and a 20-one function. Dihydrotestosterone lacks the C4–C5 double bond of testosterone, and 11-deoxycortisol the 11β-hydroxy group of cortisol. To assay these steroids within a mixture, it is necessary to use antibodies that will distinguish them, *i.e.*, that will recognize their specific features. It is generally accepted that the antibodies formed on injection of an antigen to an animal recognize preferentially that part of the molecule that is furthest from the carrier protein (*9*). For example, previous studies have shown that coupling of 11-deoxycortisol to BSA via the 3-ketone yields antibodies that specifically recognize epitopes (regions of the hapten recognized by the antibody) corresponding to the C and/or D rings of the steroid [10]. Thus, to obtain antibodies specific of the D ring, it is preferable to keep the functions at C17 intact and to modify the more distant 3-ketone.

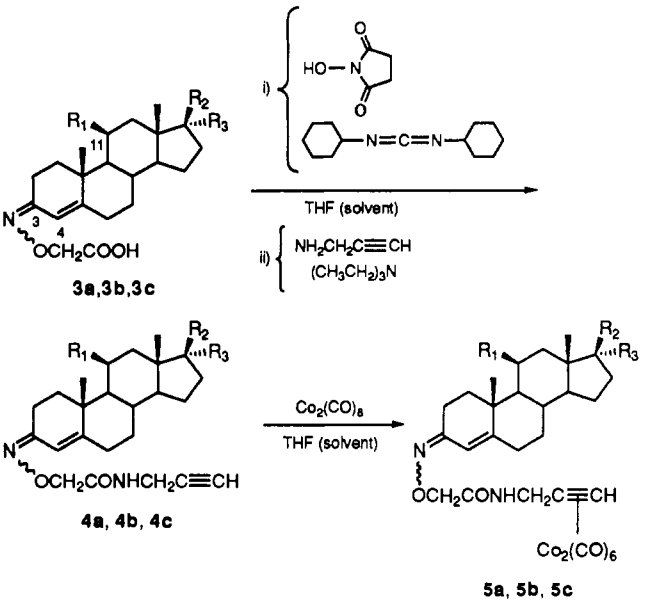
In CMIA the quantitative analysis of the organometallic tracer is based on the measurement of the intensity of the ν(CO) bands of their IR spectra (*7*). The tracer must therefore be characterized not only by stability in the usual buffer systems but also by very high intensity ν(CO) bands. Previous studies on estradiol organometallic complexes have shown that $Co_2(CO)_6$ coordinated to a triple bond gives rise to stable complexes and to intense ν(CO)bands in the 2000–2100 cm^{-1} region(*11*). Other work on organometallic complexes of the mycotoxin zearalenone has established that the antibodies recognized best are often those in which the organometallic complex is linked by a five-atom spacer (*12*). The most promising option therefore seemed to be to link an alkyne/$Co_2(CO)_6$ moiety to the end of a five-atom spacer.

In the case of cortisol (**1a**) with two keto functions, one in the 3 and the other in the 20 position, the organometallic moiety has to be selectively guided to position 3. This was done by exploiting the differing reactivities of the 3-enone and 20-ketone functions toward amines previously described by Janosky (*13*). Pyrrolidine reacted selectively with the 3-enone function to yield the dienamine **2a**, which

Scheme II



Scheme III



was made to react with carboxymethoxylamine to give cortisol 3-[*O*-(carboxymethyl)oxime] (**3a**) (Scheme II). The carboxylic acid function was then activated to form a peptide-type bond between the activated acid and the amine function of propargylamine (*14*) yielding compound **4a**, which has an acetylenic function at the end of a $-OCH_2CONHCH_2-$ spacer (Scheme III). Complexation of the triple bond with $Co_2(CO)_8$ in CH_2Cl_2 solution (*15*) gave a mixture of two isomers **5a** (*Z*+*E*) with an overall yield of 30%. In the case of testosterone and dihydrotestosterone, which lack a carbonyl in position 20, compounds **3b** and **3c** can be prepared directly without prior activation by pyrrolidine (Scheme II) and the isomer mixtures **5b** and **5c** (*Z*+*E*) were obtained as above (Scheme III). The mixtures were separated by thin-layer chromatography.

Scheme IV

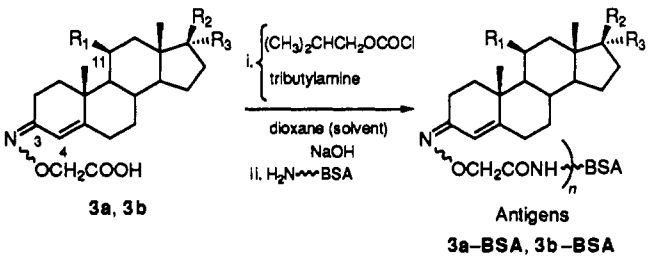


Table I. Chemical Shifts of the *Z* and *E* Isomers

compound	3d	5a	5b
δ 4-H (ppm) for isomer *Z*	6.50[a]	6.32[b]	6.40[c]
δ 4-H (ppm) for isomer *E*	5.76[a]	5.66[b]	5.65[c]

[a] Value from ref 15. [b] ^{1}H NMR (250 MHz, in acetone-d_6). [c] ^{1}H NMR (250 MHz, in $CDCl_3$).

The attribution of *Z* and *E* isomery was made by analogy with 11-deoxycortisol acid 3-CMO **3d** (*16*) and was based on the difference in chemical shift of the 4-H proton. For this compound the 4-H proton of the Z isomer exhibits an anisotropic effect from the CO group of the carboxylic function leading to a shift toward low fields (δ = 6.50 ppm for **3d**-*Z*) whereas the 4-H proton of the *E* isomer resonates in stronger fields (δ = 5.76 ppm for **3d**-*E*). Similar chemical shift differences are observed in other isomer mixtures; the 4-H proton of isomer *Z* also undergoes an anisotropic effect from the CO group of the amide and resonates in stronger fields than that of isomer *E* (Table I). Isomer *E* is the major isomer (73.5% for the cortisol derivative, 60% for the testosterone derivative) probably because of lesser steric hindrance between position 4 of the steroid and the OCH_2CO_2H substituent in 3 for the *E* configuration.

Synthesis of the Antigens. Frozen polyclonal anti-testosterone antisera from sheep were supplied by Société Medgenix (Fleurus, Belgium) and lyophilized anti-cortisol antibodies from rabbits by Professor J. Fiet (Hôpital St Louis, Paris, France). We tested three batches of anti-testosterone antisera from three different sheep (anti-testosterone 1–3) and two batches of anti-cortisol antibodies (anti-cortisol 1 and 2) obtained at a three monthly interval from the same rabbit. In both cases, the injected antigens were 3-CMO steroids (**3a**–BSA, **3b**–BSA, Scheme IV) synthesized by the method of Erlanger (*17*) which consists of creating a peptide-type bond between the carboxylic acid function of the cortisol or testosterone derivatives (**3a,b**) and the amine groups of the lysine residues of BSA. The antigens and our organometallic complexes are analogous in that they are both modified in position 3 and both have a $NOCH_2CONH$ arm that is bound to the carrier protein (BSA) in the case of the antigen and to the [ethynyl/$Co_2(CO)_6$] fragment in the organometallic complex.

Study of the Recognition between Antibodies and Organometallic Hormones. We determined the cross reactivities (CR) of dihydrotestosterone 1c and complexes **5b** and **5c** for anti-testosterone antibodies 1–3 (Table II) and of 11-deoxycortisol **1d** and complexes **5a**-*E* and **5a**-*Z* for anti-cortisol antibodies 1 and 2 (Table III). These CRs are calculated from competition curves (see illustrative example in Figure 1) which give the quantities of non-radioactive compound that displace by 50% the binding of a radioactive tracer ([^{3}H]cortisol or [^{3}H]testosterone according to antibody). The CR (%) is equal to the ratio (×100) of test compound which displaces by 50% the binding of the corresponding radioligand over the quantity of cortisol or testosterone also giving a 50% displacement. By definition the CR for the reference compounds cortisol and testosterone are equal to 100%. A high CR indicates that the test compound recognizes the antibody well.

Table II. Cross-Reactivity (%) of the Testosterone Derivatives for Anti-Testosterone Antibodies[a]

antibody	1b	5b	1c	5c
anti-testosterone 1[b]	100[e]	110 ± 9.1	96 ± 3.5	108 ± 8.5
anti-testosterone 2[c]	100	80 ± 5.6	78 ± 9.2	56 ± 2.8
anti-testosterone 3[d]	100	62 ± 1.4	89 ± 0.5	85 ± 6.4

[a] Cross-reactions were performed in presence of 0.16 pmol of [1,2,6,7-^{3}H]testosterone. Separation of the free and bound fractions was performed by using DCC (1.25 mg/mL of charcoal, 0.125 mg/mL of dextran). CR_{50}(%) = pmol of tested compounds displacing 50% of [^{3}H]testosterone/pmol of testosterone displacing 50% of [^{3}H]testosterone. Each value is the mean of two experiments. [b] Used at a final dilution of 1/100. [c] Used at a final dilution of 1/5000. [d] Used at a final dilution of 1/1000. [e] Value equal to 100 by definition.

Table III. Cross-Reactivity (%) of the Cortisol Derivatives for Anti-Cortisol Antibodies[a]

antibody	1a	1d	5a-*Z*	5a-*E*
anti-cortisol 1[b]	100[d]	46 ± 3.7[e]	58 ± 1.75[e]	84 ± 0.5[e]
anti-cortisol 2[c]	100[d]	59 ± 2.6[f]	67 ± 1.2[f]	68 ± 1.4[f]

[a] Cross-reactions were performed in presence of 0.17 pmol of [1,2,6,7-^{3}H]cortisol. Separation of the free and bound fractions was performed by using DCC (1.25 mg/mL of charcoal, 0.125 mg/mL of dextran). CR_{50}(%) = pmol of tested compounds displacing 50% of [^{3}H]cortisol/pmol of cortisol displacing 50% of [^{3}H]cortisol. [b] Used at a final dilution of 1/300. [c] Used at a final dilution of 1/600. [d] Value equal to 100 by definition. [e] Means of three experiments. [f] Means of two experiments.

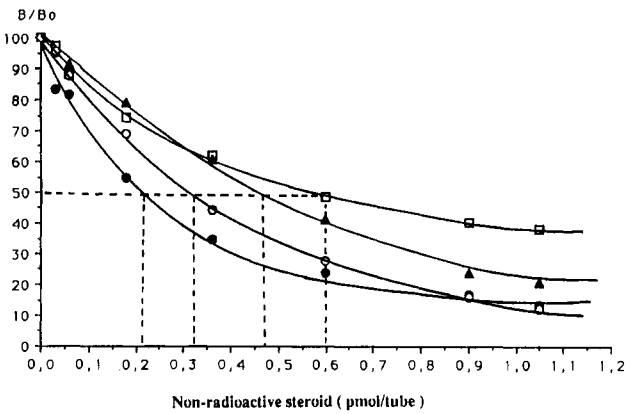


Figure 1. Competition curves by radioimmunoassay between 0.17 pmol of [1,2,6,7-^{3}H]cortisol and increasing amounts of nonradioactive steroids: cortisol (●), deoxycortisol (□), **5a**-*E* (○), **5a**-*Z* (▲) (antibody, anti-cortisol 2; dilution, 1/300).

In Tables II and III the CRs are high, from 56 to 110%, indicating that the introduction of an organometallic moiety in position 3 does not substantially modify antigen–antibody recognition. These values are much higher than those obtained for the interaction between organometallic steroids and receptors, which rarely exceed 15–20%. Moreover, although all the antibody batches were prepared with steroid 3-CMO-BSA, the CRs varied substantially according to batch.

The antibody anti-testosterone 1 (Table II) gave CRs above 100% for the organometallic complexes **5b** and **5c** (CRs = 110 and 108% respectively), which were higher than the CRs of the reference steroids **1b** and **1c** (CRs = 100 and 96% respectively). This suggests that the antibodies recognize the complexes better than the reference steroids, *i.e.*, that the complexes are closer to the hapten used to produce the antibodies than are the reference steroids. Analogous results have been recorded

for organometallic complexes of cymantrene (7). The CRs of complexes **5b** and **5c** for antibody anti-testosterone 2 were about 20% lower than those of the parent compounds (CRs = 100 and 80 for **1b** and **5b**; CRs = 78 and 56 for **1c** and **5c**). Results with the third antibody anti-testosterone 3 were different: complexation of dihydrotestosterone hardly modified its CR (CRs = 89 and 85% for **1c** and **5c**) whereas complexation of testosterone decreased CR by about 40% (CRs = 100 and 62% for **1b** and **5b**). Furthermore, this antibody recognized the dihydrotestosterone complex **5c** better than the testosterone complex **5b** (CRs = 85 and 62% respectively).

Both anti-cortisol antibodies (Table III) recognized 11-deoxycortisol (**1d**) least well (CR = 49 and 59%)[2]. The antibody anti-cortisol 1 distinguished isomers **5a**-*E* and **5a**-*Z* relatively well since the CRs differed by 25% (83 and 58% respectively), unlike antibody anti-cortisol 2 which gave virtually identical CRs (67 and 68%) for these isomers. The anti-cortisol 2 antibody, which recognizes both isomers to the same extent, is therefore probably specifically directed toward that part of the molecule that is common to both isomers whereas anti-cortisol 1 antibody, which distinguishes isomers *Z* and *E*, may be more specific of the geometry of the arm in relation to the C=N double bond.

These results emphasize the diversity in behavior of the complexes according to antibody batch and are not unexpected since we used polyclonal antibodies that are a mixture of subsets of antibodies, each specifically recognizing only a part of the test molecule. However, as the antibody–tracer interactions are also dependent on the concentration of tracer used, the cross-reactivity values must be determined using the same tracer quantities as were used in CMIA.

The possibility of using these organometallic complexes of cortisol as tracers in a CMIA of blood cortisol will be explored in a forthcoming paper.

CONCLUDING REMARKS

The above results show that the introduction of an organometallic moiety at position 3 of the steroid skeleton and the use of a five-atom spacer lead to organometallic complexes that are recognized by antibodies and that have a potential application as tracers in a nonisotopic CMIA. However, the CRs can vary from 50 to 100% according to antibody batch, demonstrating clearly that, for each immunoassay, it is necessary to carefully test different antibody–tracer pairs before selecting the antibody–tracer duo most suitable for a reliable CMIA.

EXPERIMENTAL SECTION

A. Chemistry. Chemicals, Materials, and Methods. 17-β-Hydroxy-4-androsten-3-one (testosterone), 17-β-hydroxy-5α-androstan-3-one (dihydrotestosterone), and 11β,17α,21-trihydroxypregn-4-ene-3,20-dione (cortisol) were purchased from Sigma Chemical Co., $Co_2(CO)_8$ was purchased from Strem Co., and *N*,*N*′-dicyclohexylcarbodiimide, carboxymethylamine, *N*-hydroxysuccinimide, and propargylamine were purchased from Aldrich. [**Caution**: propargylamine is highly toxic by inhalation and by contact with skin and must be handled under a well-ventilated hood.] Solvents (pentane, THF, CH_2Cl_2) were purchased from S. D. S, France. Analytical thin-layer chromatography was performed on 0.2-mm silica gel plates (Merck 60F 254) and spots were visualized by 254-nm ultraviolet light. Preparative thin-layer chromatography was carried out on 1-mm silica gel plates (Merck 7730). Syntheses of organometallic complexes were carried out under a dry argon atmosphere. THF was dried by distillation from benzophenone–sodium, pentane on sodium, and CH_2Cl_2 on CaH_2. Melting points were determined on a Kofler apparatus and are uncorrected. IR spectra were recorded on a FT Bomem Michelson 100 spectrometer as KBr pellets. UV spectra were recorded on a Kontron-Uvikon 860 in ethanol solutions. ^1H NMR spectra were recorded on a Bruker AM 250 spectrometer and chemical shifts are reported relative to TMS. Mass spectra were recorded on a Ribermag R-10–10 spectrometer coupled with a PDP computer. Elemental analyses were performed by the microanalysis department of the CNRS, Vernaison, France.

11β,17α,21-Trihydroxypregn-4-en-20-one 3-[*O*-(Carboxymethyl)oxime] (3a). Cortisol (**1a**) (0.543 g, 1.5 mmol) and pyrrolidine (0.25 mL, 3 mmol) were added in the dark at 0 °C in a Schlenk tube containing 25 mL of methanol. After 5 min a yellow precipitate of **2a** appeared. The mixture was heated at 50 °C, then pyrrolidine (0.25 mL, 3 mmol) was added followed by carboxymethylamine (0.325 g, 1.5 mmol). The mixture become clear within 5 min. After evaporation of the solvent, the dry residue was dissolved in 50 mL of water and then adjusted to pH 2, leading to a white precipitate. This precipitate was made soluble in 3 × 50 mL of ethyl acetate. The organic phase was then extracted by 3 × 50 mL of NaOH (4%) and the alkaline fraction washed with 100 mL of ethyl acetate, acidified to pH 2, extracted by 3 × 100 mL of ethyl acetate, washed with water until neutral pH, and then dried on $MgSO_4$. The white solid obtained after evaporation of the solvent was identified as **3a** (0.594 g, 91%). Mass spectrum *m*/*z* 436 $[M + H]^+$, 418 $[M + H - H_2O]^+$; IR (KBr) 1629, 1720, 2928, 3441 cm^{-1}.

11β,17α,21-Trihydroxypregn-4-en-20-one 3-[*O*-[(*N*-Propargylcarbamoyl)methyl]oxime] (4a). Compound **3a** (0.180 g, 0.4 mmol), prepared as described above was stirred for 15 min at 4 °C in 20 mL of THF, and *N*-hydroxysuccinimide (0.575 g, 0.5 mmol) and *N*,*N*′- dicyclohexylcarbodiimide (0.126 g, 0.65 mmol) in 10 mL of THF were then added. The mixture was stirred for 4 h at 4 °C and 20 h at room temperature. The white precipitate of *N*,*N*′-dicyclohexylurea obtained was then eliminated by filtration. Propargylamine (54 μL, 0.8 mmol) and triethylamine (416 μL, 2.8 mmol) were added to the remaining organic solution. The mixture was stirred for 4 h at 4 °C and 20 h at room temperature. The solvent was then evaporated and the dry residue was dissolved in 20 mL of CH_2Cl_2, washed three times with water and dried over $MgSO_4$. The white solid obtained after evaporation of the solvent was identified as **4a** (0.176 g, 90%). Mass spectrum *m*/*z* 473 $[M + H]^+$, 455 $[M + H - H_2O]^+$. Anal. Calcd for $C_{26}H_{34}O_6N$: C, 66.1; H, 7.63; O, 20.34; N, 5.93. Found: C, 65.28; H, 7.98; O, 20.02; N, 5.20.

11β,17α,21-Trihydropregn-4-en-20-one 3-[*O*-[(*N*-Propargylcarbamoyl)methyl]oxime] Hexacarbonyldicobalt (5a-*E* and 5a-*Z*). Dicobaltoctacarbonyl (0.342 g, 1 mmol) dissolved in 10 mL of THF was added to **4a** (0.446 g, 0.95 mmol) prepared as described above and dissolved in 50 mL of THF. The mixture was allowed to stir for 30 min at room temperature. The red solid (**5a**-(*Z* + *E*), yield 30%) obtained after evaporation of the solvent was chromatographed on silica gel plates using pentane/ethyl acetate (2/8) as eluent. The red solids collected were identified as **5a**-*E* (0.16 g, 73.5%) and **5a**-*Z* (0.057 g, 26.5%). **5a**-*E*: mp 92 °C dec; ^1H NMR (250 MHz, $CDCl_3$, δ ppm) 4.55 (s, 2H, $-OCH_2CO-$), 5.66 (s, 1H, H-4), 6.06 (s, 1H, $-C{\equiv}CH$), 6.7 (m, 1H, CONH); IR (KBr) 1529, 1665, 1709, 2023, 2056, 2097, 2925, 3436 cm^{-1}; UV (ethanol): λ_{max} = 348 nm with ε = 2012 L mol^{-1} cm^{-1}; λ_{max} = 247 nm with ε = 14716 L mol^{-1} cm^{-1}. **5a**-*Z*: mp 92 °C dec; ^1H NMR (250 MHz, $CDCl_3$, δ ppm) 4.55 (s, 2H, $-OCH_2-CO-$), 6.07 (s, 1H, μ-$[Co_2(CO)_6]C{\equiv}CH$), 6.32 (s, 1H, H-4), 6.7 (m, 1H, CONH); IR (KBr) 1523, 1664, 1709, 2023, 2055, 2097, 2927, 3430 cm^{-1}. UV (ethanol): λ_{max} = 348 nm; ε = 3111 L mol^{-1} cm^{-1}; λ_{max} = 247 nm; ε = 15340 L mol^{-1} cm^{-1}.

4-Androsten-17β-ol 3-[*O*-(Carboxymethyl)oxime] [3b (*Z* + *E*)]. The experimental procedure was the same as described above for **3a**. Starting from testosterone **1b** (0.288g, 1 mmol) and using 2 × 2 mmol (0.17 mL) of pyrrolidine and 1 mmol (0.219 g) of carboxymethylamine we obtained 0.325 g of **3b** (yield 90%).

[2] Since the aim is generally of assaying cortisol without a simultaneous assay of 11-deoxycortisol, it is necessary for a real immunoassay to use antibodies with a minimum of cross reactivity for 11-deoxycortisol. With a CR value of about 50%, the antibodies used here are not convenient for this practical test but are very well suited for studying the feasability of the organometallic approach.

3b: mp 182 °C; mass spectrum m/z 362 $[M + H]^+$; ^1H NMR(250 MHz, $CDCl_3$ δ ppm) 0.84 (s, 3H, Me-18), 0.99 and 1.03 [2s, 2 × 3H, 2 Me-19($Z + E$)], 4.51 (s, 2H, $-OCH_2CO-$), 5.68 and 6.37 [2s, 2 × 1H, H-4 ($Z + E$)], 6.65 (s, 1H, COOH); IR (KBr) 1631, 1738, 2934, 3390 cm^{-1}.

4-Androsten-17β-ol 3-[*O*-[(*N*-Ppropargy)carbamoyl)-methyl]oxime] [4b (*Z*+*E*)]. The experimental procedure was the same as described above for **4a**. Starting from **3b** (0.260 g, 0.72 mmol) and using 0.104 g (0.9 mmol) of *N*-hydroxysuccinimide, 0.233 g (1.2 mmol) of *N,N'*-dicyclohexylcarbodiimide, 96 μL (1.44 mmol) of propargylamine, and 760 μL (5.14 mmol) of triethylamine we obtained 0.230 g of **4b** (yield 80%): mass spectrum m/z 399 $[M + H]^+$; NMR ^1H (250 MHz, acetone-d_6, δ ppm) 0.82 (s, 3H, Me-18), 1.09 and 1.14 [2s, 2 × 3H, 2 Me-19($Z + E$)], 2.62 (t, 1H, C≡C-H), 3.99 and 4.01 [m, 2 x 2H, 2 $CONHCH_2$-($Z + E$)], 4.40 and 4.43 [2s, 2H, 2 OCH_2CO-($Z + E$)], 5.71 and 6.43 [2s, 2 x 1H, H-4-($Z + E$)], 7.38 (s, 1H, NH).

4-Androsten-17β-ol 3-[*O*-[(*N*-propargylcarbamoyl)methyl]oxime] Hexacarbonyldicobalt (5b-*E* and 5b-*Z*). The experimental procedure was the same as described above for **5a**-*E* and **5a**-*Z*. Starting from 0.2 g (0.5 mmol) of **4b** and 0.205 g (0.6 mmol) of octacarbonyldicobalt, we obtained 0.103 g (yield 30%) of **5b**. The red solid obtained was then chromatographed on silica gel plates using pentane/ethyl acetate (4/6) as eluant. The red solids collected were identified as **5a**-*E* (0.57 g, 60%) and **5b**-*Z* (0.385 g, 40%). **5b**-*E*: ^1H NMR (250 MHz, acetone-d_6, δ ppm) 0.77 (s, 3H, Me-18), 1.14 (s, 3H, Me-19), 4.46 (s, 2H, $-OCH_2CONH-$), 4.67 (d, 2H, $CONHCH_2$), 5.70 (s, 1H, H-4), 6.40 (s, 1H, μ-$[Co_2(CO)_6]C{\equiv}CH$), 7.74 (m, 1H, NH). **5b**-*Z*: ^1H NMR (250 MHz, acetone-d_6, δ ppm), 0.77 (s, 3H, Me-18), 1.14 (s, 3H, Me-19), 4.43 (s, 2H, $-OCH_2CO-$), 4.68 (d, 2H, $CONHCH_2$), 6.40 (s, 1H, H-4 plus s, 1H, μ-$[Co_2(CO)_6]C{\equiv}CH$), 7.75 (m, 1H, NH); IR (KBr of **5b**) 1520, 1669, 2021, 2053, 2093, 2931, 3424 cm^{-1}.

5α-Androstan-17β-ol 3-[*O*-(Carboxymethyl)oxime] (3c). The experimental procedure was the same as described above for **3a**. Starting from dihydrotestosterone 1c (0.29 g, 1 mmol) and using 2 × 2 mmol (0.17 mL) of pyrrolidine, 1 mmol (0.219 g) of carboxymethylamine we obtained 0.26 g of **3c** (yield 90%): mp 150 °C; mass spectrum m/z 364 $[M + H]^+$; ^1H NMR (250 MHz, $CDCl_3$, δ ppm) ; 0.74 (s, 3H, Me-18), 0.91 (3H, s, Me-19); 4.58 (s, 2H, OCH_2CO); IR (KBr) 1659, 2911, 2990, 3326 cm^{-1}.

5α-Androstan-17β-ol 3-[*O*-[(*N*-Propargylcarbamoyl)-methyl]oxime] (4c). The experimental procedure was the same as described above for **4a**. Starting from **3c** (0.260 g, 0.72 mmol) and using 0.104 g (0.9 mmol) of *N*-hydroxysuccinimide, 0.233 g (1.2 mmol) of *N,N'*-dicyclohexylcarbodiimide, 96 μL (1.44 mmol) of propargylamine, and 760 μL (5.14 mmol) of triethylamine we obtained 0.258 g of **4c** (yield 90%): mass spectrum m/z 401 $[M + H]^+$; ^1H NMR (250 MHz, $CDCl_3$, δ ppm), 0.75 (s, 3H, Me-18), 0.92 (s, 3H, Me-19), 2.33 (t, 1H, C≡CH), 4.16 (m, 2H, $CONHCH_2$), 4.33 (s, 2H, s, OCH_2CO), 4.99 (s, 1H, NH).

5α-Androstan-17β-ol 3-[*O*-[(*N*-Propargylcarbamoyl)-methyl]oxime] Hexacarbonyldicobalt (5c). The experimental procedure was the same as described above for **5a**. Starting from 0.2 g (0.5 mmol) of **5c** and 0.205 g (0.6 mmol) of octacarbonyldicobalt, we obtained 0.105 g (yield 30%) of **5c**: ^1H NMR (250 MHz, $CDCl_3$, δ ppm), 0.72 (s, 3H, Me-18), 0.90 (s, 3H, Me-19), 4.46 (s, 2H, OCH_2CO), 4.46 (2H, d, $CONHCH_2$), 6.20 (s, 1H, μ-$[Co_2(CO)_6]C{\equiv}CH$), 6.7 (m, 1H, NH); IR (KBr) 1672, 1725, 2022, 2054, 2093, 2934, 3392 cm^{-1}.

B. Biochemical Materials and Methods. Charcoal (Norit A) and dextran T70 were purchased from Sigma Chemical Co. [1,2,6,7-^3H]Cortisol (specific activity 97 Ci/mmol) and [1,2,6,7-^3H]testosterone (specific activity 90 Ci/mmol) were supplied by the Radiochemical Centre, Amersham.

The metal carbonyl-labeled derivatives (**5a–c**) were synthesized as described in the chemical section. Stock solutions (1×10^{-3}M in absolute ethanol) of these complexes were prepared. These solutions were stable for several months provided they were stored in the dark at about −20 °C prior to use. Successive dilutions were performed just before biochemicals experiments.

Competion Curves by Radioimmunoassay. Fractions (500 μL) containing 50 μL of antibody (final dilution equal to inverse of the titer value), 100 μL of the [^3H]steroid (0.17 pmol of [^3H]cortisol or 0.16 pmol of [^3H]testosterone), and increasing amounts of the steroid to be tested (0.03 to 1.0 pmol) in 350 μL of buffer (phosphate 3 mM, 1% glycerol) were incubated for 1 h at room temperature. At the end of the incubation the free and bound fractions were separated by DCC treatment (1.25% of charcoal; 0.125% of dextran T70). The supernatant liquids, containing the bound fractions, were transferred into vials and the radioactivity was counted on a LKB-1211 Rackbeta counter using ACS (Amersham) scintillation liquid.

ACKNOWLEDGMENT

We wish to thank Pr J. Fiet and the "Société Medgenix" for the gift of antibodies, Annie Cordaville for technical assistance, and Tiiu Ojasoo for helpful discussions.

LITERATURE CITED

(1) Vessières, A., Top, S., Ismail, A. A., Butler, I. S., Louer, M., and Jaouen, G. (1988) Organometallic estrogens. Synthesis, interaction with uterine estrogen receptor, and detection by infrared spectroscopy. *Biochemistry 27*, 6659–6666.

(2) Jaouen, G., and Vessières, A. (1989) The use of high affinity binding bioligands modified by transition metal carbonyl moieties. *Pure Appl. Chem. 61*, 565–572.

(3) Raynaud, J. P., Ojasoo, T., Bouton, M. M., Bignon, E., Pons, M., and Crastes de Paulet, A. (1985) In *Estrogens in the Environment*; McLachlan, J. A., Ed.; Elsevier: Amsterdam, pp 24–42.

(4) Vessières, A., Jaouen, G., Gruselle, M., Rossignol, J. L., Savignac, M., Top, S., and Greenfield, S. (1988) Synthesis and receptor binding of polynuclear organometallic estradiol derivatives. *J. Steroid Biochem. 30*, 301–305.

(5) El Amouri, H., Vessières, A., Vichard, M., Top, S., Gruselle, M., and Jaouen, G. (1992) Synthesis and affinities of novel organometallic labeled estradiol derivatives: A structure-affinity relationship. *J. Med. Chem. 35*, 3130–3135.

(6) Vessières, A., Top, S., Vaillant, C., Osella, D., Mornon, J. P., and Jaouen, G. (1992) Transition metal carbonyl clusters in the design of suicide substrates for the study of target proteins. Application to the estradiol receptor. *Angew. Chem., Int. Ed. Engl. 31*, 753–755.

(7) Salmain, M., Vessières, A., Brossier, P., Butler, I. S., and Jaouen, G. (1992) Carbonylmetalloimmunoassay (CMIA), a new type of non-radioisotopic immunoassay. Principles and application to phenobarbital assay. *J. Immunol. Methods 148*, 65–75.

(8) See, for example: (a) Perry, L. A., Al-Dujaili E. A. S., and Edwards, C. R. W. (1982) A direct radioimmunoassay for 11-deoxycortisol. *Steroids 39*, 115–128. (b) Erlanger, B. F., Borek, F., Beiser, S. M., and Lieberman, S. (1957) Steroid-protein conjugates. Preparation and characterization of conjugates of bovine serum albumine with testosterone and with cortisone. *J. Biol Chem. 228*, 713–727.

(9) Erlanger, B. F. (1980) The preparation of antigenic hapten-carrier conjugates : a survey. *Methods Enzymol. 70*, 85–104.

(10) Fiet, J., Galons, H., Villette, J. M., Boudou, P., Guechot, J., Gueux, B., Gourmel, B., Julien, R., Brerault, J. L., Vexiau, P., and Dreux, C. (1990) *Immunoanal. Biol. Spec. 22*, 41–52.

(11) Jaouen, G., Vessières, A., Top, S., Savignac, M., Ismail, A. A., and Butler, I. S. (1987) Transition metal carbonyl clusters as novel infrared markers for estradiol. *Organometallics 6*, 1985–1987.

(12) Gruselle, M., Deprez, P., Vessières, A., Greenfield, S., Jaouen, G., Larue, J. P., and Thouvenot, D. (1989) Cobalt and Molybdenum carbonyl clusters in immunology. Synthesis and binding properties of mycotoxin derivatives of zearalenone. *J. Organometal. Chem. 359*, C53-C56.

(13) Janosky, A. H., Shulman, F. C., and Wright, G. E. (1974) Selective 3-(O-carboxymethyl) oxime formation in steroidal 3,2-diones for hapten immunospecificity. *Steroids 23*, 49–64.

(14) Anderson, G. W., Zimmerman, J. E., and Callahan, F. M. (1964) The use of esters of N-hydroxysuccinimide in peptides synthesis. *J. Am. Chem. Soc. 86*, 1839–1842.

(15) Greenfield, H., Sternberg H. W., Friedel, R. A., Wotiz, J. H., Markby R., and Wender, I. Acetylenic dicobalt hexacar-

bonyls. (1956) Organometallic compounds derivated from alkynes and dicobalt octacarbonyl. *J. Am. Chem. Soc. 78*, 120–124.
(16) Galons, H., Fiet, J., Gueux, B., Bonette, R., Villette, J. M., Julien, R., Miocque, M., and Dreux. C. (1987) *C. R. Acad. Sc. Paris, Série II t 304*, 75–77.
(17) Erlanger, B. F., Borek, F., Beiser, S. M., and Lieberman, S. (1957) Steroid–protein conjugates. Preparation and characterization of conjugates of bovine serum albumine with testosterone and with cortisone. *J. Biol. Chem. 228*, 713–727.
(18) Vessières, A., Salmain, M., Philomin, V., and Jaouen, G. (1992) *Immunoanal Biol. Spec. 31*, 9–17.

Labeling of Proteins by Organometallic Complexes of Rhenium(I). Synthesis and Biological Activity of the Conjugates

Michèle Salmain, Michèle Gunn, Abdellaziz Gorfti, Siden Top, and Gérard Jaouen*

Laboratoire de Chimie Organométallique, URA 403, Ecole Nationale Supérieure de Chimie de Paris, 11 rue Pierre et Marie Curie, F-75231 Paris Cedex 05, France. Received February 17, 1993®

We describe herein a totally new pathway for the introduction of rhenium in the form of low oxidation state organometallic complexes covalently attached to various proteins. The synthesis of several rhenium conjugates takes advantage of the specificity of *N*-succinimidyl esters for amino residues. Conjugation experiments were carried out under various conditions, and analysis of the conjugates was performed by FT-IR spectroscopy. Yields were optimized and reached 50%. Furthermore, the conjugate resulting from the coupling of *N*-succinimidyl 4-[η^5-cyclopentadienylrhenium tricarbonyl] 4-oxobutanoate to an anti-hTSH monoclonal antibody retained a satisfactory immunoreactivity. Finally, IR detection of conjugates adsorbed onto nitrocellulose membranes was achieved and response was found to be related to the coupling extent of the conjugate.

INTRODUCTION

The main concern of our research is to provide new "cold" biological probes, mainly organometallic, suitable for quantitative and qualitative analysis of ligand/receptor interactions. Thus our early purpose was the synthesis of steroid hormones modified by an organometallic moiety, and affinity measurements for the natural receptor protein (*1*). This approach was extended to the labeling of haptens for the purpose of designing a new immunological assay method that we called CMIA[1] for "*c*arbonyl*m*etallo*i*m-muno*a*ssay" which associates metal–carbonyl probes and FT-IR spectroscopy as a detection technique (*2*). More recently, we developed a method of introduction of cobalt–carbonyl fragments into proteins in order to extend the field of CMIA to antigen assays (*3*).

The introduction of metals into biologicals has been the subject of numerous publications reflecting the various applications (*4*). Among them, radiolabeling with the aim of radioimmunodetection of cancer tumors shows great promise at the moment. This technique requires the use of specific monoclonal antibodies labeled with a γ-emitting radioisotope. Among these, ^{99m}Tc is particularly interesting because of its ideal properties (*5*). On the other hand, monoclonal antibodies labeled with an adequate radioisotope (β-emittor this time) could be used in radioimmunotherapy procedures. For this purpose, isotopes ^{188}Re and ^{186}Re are valuable (*5*).

The synthesis of labeled antibodies proceeds either from direct introduction onto the protein (with prior reduction of generator-produced $^{99m}TcO_4^-$ or $^{186}ReO_4^-$ (*6*) to lower oxidation state forms) or indirect introduction by prior coupling of strong chelating agents followed by complexation of the conjugate by $^{99m}Tc^V$ (*7*). However, both of these labeling techniques suffer from possible nonspecific binding that can induce leaching of the radioisotope and high background levels *in vivo*. On the other hand, the indirect introduction of ^{99m}Tc (*8*) or ^{186}Re (*9*) as preformed coordination complexes may prevent this phenomenon. Organometallic complexes can also serve this purpose very well. Moreover, they have the advantage of being highly stable in biological media because of the very strong linkage between the metal and some well-chosen surrounding ligands (*10*).

In the field of protein labeling, we have explored the organometallic chemistry of Re with a double aim in mind: first, the synthesis of new metal-carbonyl markers for CMIA assays and, second, the introduction of strongly bound Re into proteins as a model for radiolabeling with ^{99m}Tc, ^{186}Re or ^{188}Re. Our experience in the conjugation of organometallic entities of cobalt to proteins was based on the indirect introduction of the metal in its *coordinated* form (*3*). Moreover, the use of *N*-succinimidyl esters which are specific for amino residues allows for the very strong attachment of the metal to the protein. This finding, and the absence of low-affinity binding of these markers, could make them very useful for *in vivo* studies. This was applied to rhenium and we describe in this article the synthesis of three rhenium carbonyl *N*-succinimidyl esters and their reactivity toward proteins like BSA and a monoclonal antibody anti-hTSH coded JOSS 2-2. Results of biological activity of the conjugate are also reported.

EXPERIMENTAL PROCEDURES

General. $Re_2(CO)_{10}$ was purchased from Strem Chemical Inc. (Newburyport, MO). Cyclopentadienylrhenium tricarbonyl ($CpRe(CO)_3$) was synthesized in one step from $Re_2(CO)_{10}$ (yield = 90%) according to Tam et al. (*11*). Other chemicals were purchased from Aldrich (St. Louis, MO) or Janssen (Geel, Belgium). Solvents were purchased from Prolabo (Paris, France) or SDS (Peypin, France). Tetrahydrofuran was distilled under argon from a sodium/benzophenone mixture before use. Bovine serum albumin (BSA) fraction V was obtained from Sigma (St. Quentin Fallavier, France) and the monoclonal antibody anti-hTSH coded JOSS 2-2 (3.2 mg/mL solution in PBS) was generously donated by Clonatec (Paris, France). The following buffers were prepared: phosphate buffered saline (PBS, 0.01 M, 0.15 M NaCl, pH = 7.1), carbonate buffer (0.1 M, pH = 9.5), borate buffer A (0.1 M, pH = 8.0),

* Author to whom correspondence should be addressed.

® Abstract published in *Advance ACS Abstracts,* October 1, 1993.

[1] Abbreviations used: CMIA, carbonylmetalloimmunoassay; FT-IR, Fourier transform infrared; NHS, *N*-hydroxysuccinimide; DCC, dicyclohexylcarbodiimide; DTGS, deuteriotriglycine sulfate; BSA, bovine serum albumin; hTSH, human thyroid stimulating hormone; PBS, phosphate-buffered saline; mAb, monoclonal antibody; CE, coupling extent; CY, coupling yield; PR, protein recovery.

1043-1802/93/2904-0425$04.00/0 © 1993 American Chemical Society

borate buffer B (0.1 M, pH = 8.6), and borate buffer C (0.1 M, pH = 9.0).

Analytical and preparative thin-layer chromatography (TLC) were performed on silica gel glass plates (F60 Merck, thickness 0.25 and 1 mm respectively), with UV visualization. Melting points were measured on a Köfler apparatus (Reichert, Model 184321).

IR spectra were recorded on a Bomem (Quebec, Canada) Michelson 100 FT-spectrometer using a conventional DTGS detector for qualitative analysis and a liquid-nitrogen-cooled InSb detector for quantitative analysis.

^{1}H NMR data were obtained with a Bruker AM-250 or -200 spectrometer (250 and 200 MHz, respectively). Mass spectra were recorded on a Nermag R 10-10C spectrometer controlled by a digital PDP 11 system using electronic impact EI (70 eV) or desorption chemical ionization (DCI) with NH_3 as the reactant gas as indicated below. UV–visible spectra were recorded on a Kontron Uvikon 860 (Zurick, Switzerland). Elemental analyses (C, H, N) were performed at the SIAR of Jussieu (Paris, France).

Synthesis of Rhenium Carbonyl Markers. All the experiments were performed under dry argon atmosphere, using standard Schlenk techniques.

β-Alanine Chloroacetamide Ethyl Ester **2.** Chloroacetic acid (0.01 mol, 1 g) in THF was treated with equimolar quantities of NHS and DCC. After a night, the white precipitate of dicyclohexylurea was removed by filtration and the solvent was evaporated to dryness. The residue was redissolved in dry CH_2Cl_2 and dry pentane was added to precipitate *N*-succinimidyl chloroacetate **1** (1.3 g, 68%): mp 120 °C; ^{1}H NMR ($CDCl_3$) δ 4.4 (s, 2H, CH_2), 2.89 (s, 4H, NHS); IR (CH_2Cl_2) ν_{CO} 1837w, 1790w, 1746m.

To β-alanine ethyl ester hydrochloride (1 g, 6.5 mmol) dissolved in THF was added triethylamine (0.66 g, 6.6 mmol). A white precipitate was formed. *N*-Succinimidyl chloroacetate (1.5 g, 6.3 mmol) was added and the mixture was stirred at room temperature for 4 h. After filtration and evaporation of the solvent, an oily residue was obtained which was washed with 0.1 M HCl and water. The organic fraction was evaporated and β-alanine chloroacetamide ethyl ester **2** (1.2 g, 72%) was obtained as a yellow oil: IR (CH_2Cl_2) ν_{CO} 1729 m, 1677 m, 1530 m; MS (EI) *m/z* 194 $[M]^{\bullet+}$, 158 $[M - Cl]^{\bullet+}$, 148 $[M - OEt]^{\bullet+}$, 116 $[H_2NCH_2CH_2COOEt]^{\bullet+}$, 77 $[ClCH_2CO]^{\bullet+}$; ^{1}H NMR ($CDCl_3$) δ 7.25 (s, 1H, NH), 4.18 (q, 2H, J = 7 Hz, $COOCH_2CH_3$), 4.05 (s, 2H, $ClCH_2$), 3.58 (q, 2H, J = 6 Hz, NCH_2), 2.59 (t, 2H, J = 6 Hz, CH_2CO), 1.29 (t, 2H, J = 7 Hz, $COOCH_2CH_3$). Anal. Calcd for $C_7H_{12}O_3NCl$: C, 43.31; H, 6.20; N, 7.20. Found: C, 43.77; H, 6.20; N, 7.52.

β-Alanine [Rhenium pentacarbonyl]acetamide Ethyl Ester **3.** $Re_2(CO)_{10}$ (0.50 g, 0.76 mmol) was allowed to react with a 1% Na/Hg amalgam (0.05 g of Na, 5 g of Hg) in THF. The colorless solution turned yellow and then red. The reaction was followed by IR upon the disappearance of the 2069-cm^{-1} ν_{CO} band of $Re_2(CO)_{10}$ and was completed in 3 h. $NaRe(CO)_5$ formed *in situ* was then allowed to react with β-alanine chloroacetamide ethyl ester **2** (0.3 g, 1.5 mmol). The mixture returned immediately to colorless. After 30 min, the mixture was filtered and the solvent evaporated. The residue was redissolved in ethyl ether and purified by TLC (eluent ethyl ether/THF 2/1). A 0.58-g (80%) portion of **3** was obtained as a white solid after recrystallization from an ethyl ether/pentane mixture: mp 90 °C; ^{1}H NMR ($CDCl_3$) δ 5.84 (s, 1H, NH), 4.13 (q, 2H, J = 7 Hz, $COOCH_2CH_3$), 3.49 (q, 2H, J = 6 Hz, NCH_2), 2.52 (t, 2H, J = 6 Hz, CH_2COO); 1.68 (s, 2H, $ReCH_2$), 1.26 (t, 3H, J = 7 Hz, $COOCH_2CH_3$); IR (CH_2Cl_2) ν_{CO} 2133w, 2063sh, 2016vs, 1978m, 1778m, 1735w, 1642w, 1518w; MS (EI) *m/z* (Re = 187) 485 $[M]^{\bullet+}$, 457 $[M - CO]^{\bullet+}$, 429 $[M - 2CO]^{\bullet+}$.

β-Alanine[rhenium pentacarbonyl]acetamide **4.** $(CO)_5ReCH_2CONHCH_2CH_2COOEt$ **3** (0.5 g, 1 mmol) was saponified by 0.03 M NaOH in ethanol/water 2/1. After 4 h, the solution was acidified by HCl and the solvent evaporated under reduced pressure. The residue was washed with ethyl ether to eliminate the unreacted ester. A 0.34 g (73%) portion of a white powder was obtained after recrystallization from an acetone/pentane mixture: mp 150 °C; ^{1}H NMR (DMSO-d_6) δ 12.06 (s, 1H, COOH), 7.50 (t, 1H, NH), 3.20 (q, 2H, NCH_2), 2.30 (t, 2H, CH_2CO), 1.60 (s, 2H, $ReCH_2$); ^{13}C NMR (DMSO-d_6) δ 184.24 (4 CO, Re(CO)), 181.67, 181.31, 173.27 (3 CO, Re(CO), CONH, COOH), 34.82, 34.75 (CH_2–CH_2), −4.23 ($ReCH_2$); IR (THF) ν_{CO} 2133w, 2063w, 2016vs, 1977m, 1733w, 1642w, 1517w; MS (EI) *m/z* (Re = 187) 457 $[M]^{\bullet+}$, 429 $[M - CO]^{\bullet+}$, 401 $[M - 2CO]^{\bullet+}$.

4-[Rhenium tricarbonyl(η^5-cyclopentadienyl)] 4-Oxobutanoic Acid **6.** To a suspension of $AlCl_3$ (0.347 g, 1.3 mmol) in dichloromethane was added dropwise a solution containing equimolar amounts of succinic anhydride and $CpRe(CO)_3$ in CH_2Cl_2. The mixture was then heated to reflux for 24 h. It was cooled to room temperature and hydrolyzed with crushed ice and 0.3 mL of concentrated HCl. The mixture was treated with 20% sodium carbonate (w/v). The aqueous phase was acidified to pH 2 and extracted with ethyl ether. Then evaporation of the organic phase gave 0.29 g (42%) of a white solid which was recrystallized in an ethyl acetate/hexane mixture; 0.2 g of unreacted $CpRe(CO)_3$ was also recovered: mp 134 °C; ^{1}H NMR ($CDCl_3$) δ 6.03 (t, 2H, J = 2.4 Hz, Cp), 5.41 (t, 2H, J = 2.4 Hz, Cp), 2.91 (m, 2H, $COCH_2$), 2.75 (m, 2H, CH_2-COOH); IR (CH_2Cl_2) ν_{CO} 2032s, 1939s, 1714w, 1689w; MS (EI) *m/z* (Re = 187) 436 $[M]^{\bullet+}$, 408 $[M - CO]^{\bullet+}$, 322 $[M - 2CO]^{\bullet+}$. Anal. Calcd for $C_{12}H_9O_6Re$: C, 33.10; H, 2.06. Found: C, 33.14; H, 2.18.

[η^5-Cyclopentadienyl carboxylic acid] Rhenium Tricarbonyl **8.** To $CpRe(CO)_3$ (0.5 g, 1.5 mmol) in THF at −78 °C was added sec-BuLi (1.7 mL, 2.1 mmol, 1.4 M solution in hexane). After 45 min, solid CO_2 (2 g) was added to the mixture, which was kept at −78 °C for 10 min. The cooling bath was removed, and after 5 min the mixture was diluted with CH_2Cl_2 and aqueous HCl was added. The organic compounds were extracted with CH_2Cl_2. After evaporation of the organic phase, the crude product was washed with pentane and 0.46 g of a white powder was obtained. After crystallization from a CH_2Cl_2/pentane mixture, 0.38 g of **8** was collected as white crystals (67%): mp 210 °C (lit. (*12*) mp 206–208 °C); ^{1}H NMR (acetone-d_6) δ 6.21 (t, 2H, J = 2.2 Hz, Cp), 5.71 (t, 2H, J = 2.2 Hz, Cp); IR (CH_2Cl_2) ν_{CO} 2033s, 1939s, 1738w, 1653w; MS (EI) *m/z* (Re = 187) 380 $[M]^{\bullet+}$, 352 $[M - CO]^{\bullet+}$, 324 $[M - 2CO]^{\bullet+}$, 296 $[M - 3CO]^{\bullet+}$.

Synthesis of the *N*-Succinimidyl Esters of 4, 6, and 8. *Activation of* **4.** To **4** (0.2 g, 0.56 mmol) in 15 mL of THF were added NHS (0.07 g, 0.61 mmol) and DCC (0.126 g, 0.61 mmol). After one night at room temperature, dicyclohexylurea was filtered out and the solvent evaporated under reduced pressure. The resulting white powder was identified to compound **5** by IR (see Table I) and used in labeling trials with no further purification.

Activation of **6.** **6** (0.1 g, 0.23 mmol) was activated into its *N*-succinimidyl ester in a similar way in 10 mL of THF by addition of NHS (0.031 g, 0.26 mmol) and DCC (0.054 g, 0.26 mmol). The resulting white powder was identified to **7** by IR analysis (see Table I).

Activation of 8. 8 (0.1 g, 0.26 mmol) was activated into its *N*-succinimidyl ester in a similar way in 8 mL of THF by addition of NHS (0.031 g, 0.26 mmol) and DCC (0.054 g, 0.26 mmol). The remaining white powder was washed with dry pentane and dried under vacuum. It was identified to compound 9 by IR analysis (see Table I).

Labeling Studies of Amino Acids with 7'. *In THF.* Complete studies were carried out with the manganese equivalent of 7 called 7', which was synthesized in the same manner according to the procedure described by Le Plouzennec and Dabard (*13*). In a typical experiment, equimolar amounts of 7', the C-protected amino acid hydrochloride, and triethylamine in THF were allowed to react at room temperature for 3 h. The main compounds were purified by TLC and characterized by classical spectroscopic methods. The results are reported in Table II.

In a Water/THF Mixture. Equimolar quantities of β-alanine and $NaHCO_3$ were dissolved in water and allowed to react with 7' in THF (final mixture, water/THF 1/3). The mixture was stirred for 3 h at room temperature. It was then acidified to pH = 2 and extracted with ethyl ether. After evaporation of the organic phase, 0.08 g (32%) of a yellow solid was obtained: mp 156 °C; IR (KBr pellet) ν_{CO} 2023s, 1938s, 1679m, 1626m, 1560m; ^1H NMR (acetone-d_6) δ 10.70 (s, 1H, COOH) 7.22 (s, 1H, NH), 5.72, 5.13 (s, s, 2H, 2H, 2Cp) 3.42 (s, 2H, $NHCH_2$), 2.96 (s, 2H, $COCH_2$), 2.51 (s, 4H, CH_2COOH and CH_2CO). Anal. Calcd for $C_{15}H_{14}O_7NMn$: C, 48.00; H, 3.73; N, 3.73. Found: C, 48.09; H, 3.88; N, 3.63.

Labeling Studies of BSA with 5 and 7. All experiments were performed on 21 nmol (1.5 mg; final protein concentration 0.75 mg/mL) of BSA following the same general protocol and using 60 molar equiv of the *N*-succinimidyl markers. Solutions (1.5×10^{-3} M) of the markers in THF were prepared just before use. A 1.5 mg/mL solution of protein was prepared in carbonate buffer (0.1 M, pH = 9.5). To 1 mL of protein solution was added 1 mL of 5 or 7. Mixtures were incubated for 15 h at 4 °C.

Labeling Studies of BSA with 9. All labeling experiments were performed from a 1 mg/mL stock solution of BSA in the incubation buffer (final protein concentration, 0.5 mg/mL) and from a 1×10^{-2} M stock solution of 9 in ethanol or DMF (60 molar equiv; final concentration 5.1 mM).

Effect of Reaction Time on the Labeling Ratio. To 6 mL of BSA in carbonate buffer, pH = 9.5, were added 600 μL of the ethanolic solution of 9 and 5.4 mL of ethanol (ethanol/water 1/1) or 600 μL of the DMF solution of 9, 600 μL of DMF and 4.8 mL of buffer (DMF/water 1/9). The mixtures were incubated at 4 °C and periodically assayed for $(CO)_3Re$ binding.

Effect of pH on the Labeling Ratio. To 1 mL of BSA in PBS (pH = 7.1) or borate buffer A (pH = 8.0) borate buffer B (pH = 8.6), or borate buffer C (pH = 9.0) or carbonate buffer (pH = 9.5) were added 100 μL of 9 in DMF, 100 μL of DMF, and 800 μL of buffer (DMF/water 1/9). The mixtures were incubated for 24 h at 4 °C.

Effect of Percent Solvent on the Labeling Ratio. Two-milliliter solutions containing BSA and 9 were incubated in ethanol/water or DMF/water (pH = 9.5) mixtures for 24 h at 4 °C.

Stability of BSA–$Re(CO)_3$ Conjugates. A PBS solution of conjugate was incubated for 24 h at 37 °C. Protein and marker concentrations were assayed as described below and the results were compared to non-treated conjugate.

Labeling of JOSS 2-2 with 7. A monoclonal antibody anti-hTSH called JOSS 2-2 (IgG form, 99% purity) available as a PBS stock solution (3.2 mg/mL) constituted the source of protein. To 312.5 μL of stock solution (1 mg, 6.7 nmol) was added 100 μL of a 2×10^{-3} M solution of 7 in acetonitrile (i.e. 30-fold molar excess, 201 nmol, final concentration 100 μM). The volume was completed to 2 mL with carbonate buffer (0.1 M, pH = 9.5). The mixture was stirred at 4 °C for 2 h.

Purification of the Rhenium Carbonyl Conjugates. All conjugates (BSA and JOSS 2-2) were purified on a gel filtration column (5 cm × 2 cm; Sephadex G-25, ready to use PD10 column, Pharmacia). The incubation mixtures were completed to 2.5 mL, filtered on Millex-GV (0.22 μm), and poured onto the top of the column previously equilibrated with PBS. The elution was performed with PBS. Ten 1-mL fractions were collected. Each fraction was assayed for a metal–carbonyl fragment by IR and protein by the Coomassie Blue method as previously described (*3*). Fractions containing protein were combined and coupling extent (CE), coupling yield (CY), and protein recovery (PR) were calculated from the following formulas:

$$CE = \frac{\text{nmol of bound metal–carbonyl fragments}}{\text{nmol of protein}} \quad (1)$$

$$CY = \frac{\text{nmol of bound marker}}{\text{initial nmol of marker}} \quad (2)$$

$$PR = \frac{\text{nmol of recovered protein}}{\text{initial nmol of protein}} \times 100 \quad (3)$$

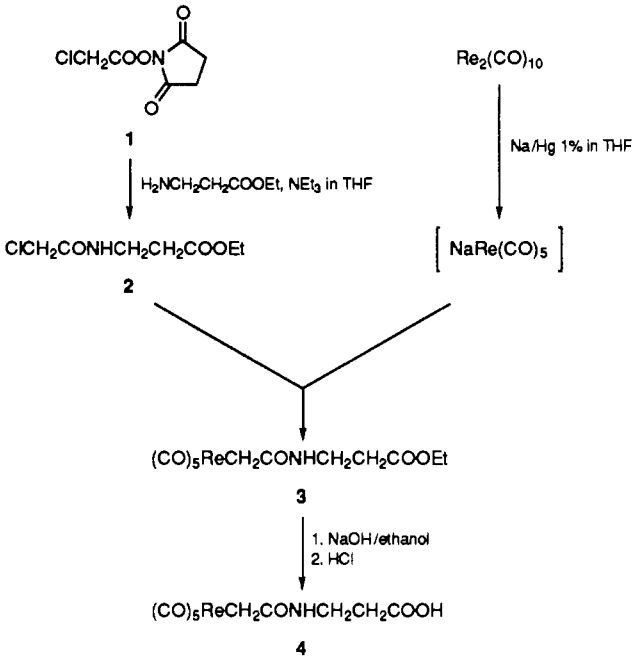
Immunoreactivity Assay. Dilutions (1/2 to 1/20 000) of $(CO)_3Re$-labeled or native JOSS 2-2 (initial concentration 0.2 mg/mL in PBS) were incubated for 3 h at room temperature with a constant amount of ^{125}I-hTSH (10 000 cpm; NEN). After equilibration, bound antibody fractions were separated by immunoprecipitation by addition of a 1/50 dilution of a goat anti-mouse IgG antibody (Calbiochem) in PBS-Tween 20 0.1% containing 5% of PEG (incubation for 30 min at room temperature). Suspensions were centrifuged at 3000 rpm and precipitates counted for radioactivity.

Detection of BSA–$Re(CO)_3$ Conjugates by FT-IR Spectroscopy. Various dilutions of two conjugates with CE of 17 and 21 in a PBS solution were prepared. A 9-mm nitrocellulose membrane filter (0.45-μm porosity, Alltech, Templeuve, France) was dipped into each tube and incubated for 1 or 1.5 h at room temperature. The filters were then removed, washed with PBS, and dried under vacuum for 30 min. The FT-IR spectrum was then recorded with a measurement time of 1 min (20 scans) taking a filter incubated in PBS as the reference. The absorbance of the 2030 cm^{-1} carbonyl band was serially measured and plotted versus the protein concentration.

RESULTS

Synthesis of the Rhenium–Carbonyl Carboxylic Acids. Two families of low oxidation state organometallic complexes of rhenium have been synthesized from commercial available $Re_2(CO)_{10}$ during this work. The first family has the general structure $R–Re(CO)_5$, where Re is attached to a carbon *via* a σ bond and R bears a carboxylic function at the end of a linear bridge arm. This first type of marker has been chosen because it is readily accessible by condensation of sodium pentacarbonylrhenate which is strongly nucleophilic, with alkyl halides RCl, in which R possesses an ester group. This ester can be then hydrolyzed to the carboxylic acid which is condensed with a protein. This family of complexes presents a typical

Scheme I. Synthesis of Rhenium Pentacarbonyl Acid 4

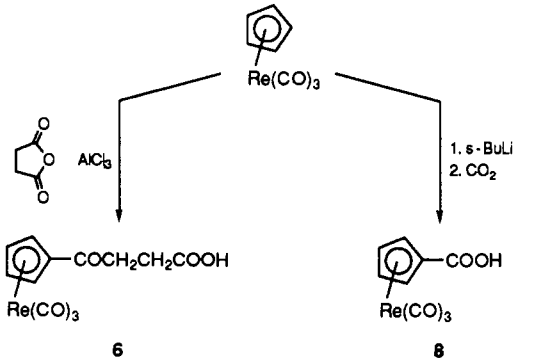


infrared ν_{CO} spectrum consisting of a sharp and intense band at about 2020 cm^{-1} and a weaker band at about 1980 cm^{-1}. The parent compound of this series, $(CO)_5ReCH_2COOH$, was first prepared in this manner (*14*). However its activation into an *N*-succinimidyl ester failed. This nonactivation is the consequence of the $Re(CO)_5$ effect, which causes a dramatic decrease of the acidity of the carboxylic function. In fact a pK_a of 8.5 has been found for this acid, proving its weakness (*14*). One might think about using the acid $(CO)_5ReCH_2CH_2COOH$, where the effect of the metal–carbonyl entity on the acid function is diminished by addition of another CH_2 radical, but we also failed to activate this acid. This lack of success may be attributed to the β-elimination process which is commonly observed in organometallic systems (*15*). As a consequence, we oriented our research toward derivatives possessing a bridge with a long arm and no hydrogen in the β-position of the $Re(CO)_5$ group. The carboxylic acid **4** was synthesized as shown in Scheme I in four steps, the last one being the saponification of the ester to form the acid. The bridge was obtained separately by condensation of chloroacetic acid with β-alanine ethyl ester. The manganese analog of **4** was obtained in the same manner (data not shown).

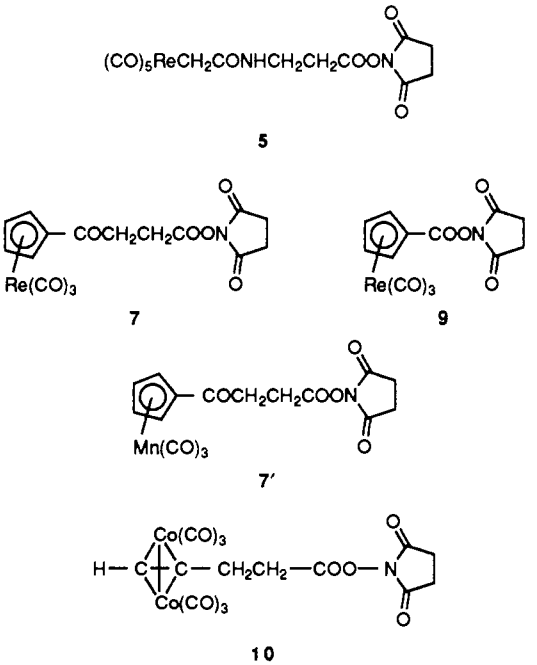
The second family can be represented by $(RC_5H_4)Re(CO)_3$, where R bears a carboxylic function and is attached to the cyclopentadienyl ligand (Cp), which is very strongly π-coordinated to the metal. Like its homolog cymantrene, cyclopentadienylrhenium tricarbonyl reacts with succinic anhydride in the presence of $AlCl_3$ according to the Friedel–Crafts reaction (Scheme II). Compound **6** was thus directly obtained by this method with its carboxylic function removed to the γ-position from the cyclopentadienyl ring. From $Re_2(CO)_{10}$, which is the starting material, an overall yield of 38% was obtained. The cyclopentadienylrhenium tricarbonyl carboxylic acid **8** was prepared in one step by reaction of dry ice with the salt $(CO)_3Re(C_5H_4Li)$ (Scheme II) (overall yield from $Re_2(CO)_{10}$, 60%). All the compounds were characterized by classical spectroscopic methods and the results were in accordance with the expected structures.

Activation of the Acids by *N*-Hydroxysuccinimide (NHS). The acids **4**, **6**, and **8** were activated into the corresponding esters **5**, **7**, and **9** (Scheme III). The

Scheme II. Synthesis of Rhenium Tricarbonyl Acids 6 and 8



Scheme III. *N*-Succinimidyl Re, Mn, and Co Carbonyl Esters



formation of the *N*-succinimidyl ester function was confirmed by its typical IR features in the ν_{CO} region. Yields were quantitative in all cases. Three bands are typically observed for the three carbonyls of *N*-succinimidyl esters (see Table I). All the activated esters are stable under a dry atmosphere.

Reactivity of Activated Ester 7′ with a Series of Amino Acids. The reactivity of **7′** was evaluated on a series of amino acids in THF (Table II) and in a water/THF mixture. In THF, expected condensation products were obtained with good yields (60% for β-alanine and cysteine, 40% for lysine). One can notice that in the case of lysine, the product of dicondensation was the only one separated, which explains the lower yield. In a water/THF mixture, the expected condensation product of **7′** with unprotected β-alanine was obtained with a yield of 32%. Side compounds observed were different, depending on the reaction medium. In THF, unreacted **7′** was the only compound observed. In the THF/water mixture, a mixture of **7′** and its corresponding carboxylic acid were observed but were not quantified.

We have checked that **5**, **7**, and **9** had a behavior very similar to that of **7′** in the reaction with β-alanine ethyl ester. Yields in rhenium carbonyl amides were on the same order of magnitude (50–60%).

Labeling Studies of BSA with 5, 7, and 9. Labeling

Table I. IR Spectroscopic Data of Rhenium Carbonyl *N*-Succinimidyl Esters

marker	ν_{CO} (cm^{-1})	assignment
$(CO)_5ReCH_2CONHCH_2CH_2COO-$ (N-succinimidyl)	1816w 1785w 1741m	COON
5		
	2134w 2063w 2019s 1988s	$(CO)_5Re$
	in CH_2Cl_2	
$Re(CO)_3$-(C$_5$H$_4$)-$COCH_2CH_2COO-$ (N-succinimidyl)	1816w 1787w 1745m	COON
7		
	2028s 1936s	$(CO)_3Re$
	in THF	
$Mn(CO)_3$-(C$_5$H$_4$)-$COCH_2CH_2COO-$ (N-succinimidyl)	1818w (lit. 1825) 1784w (lit. 1784) 1739m (lit. 1739) (*13b*)	COON
7′		
	2027s (lit. 2021) 1945s (lit. 1937)	$(CO)_3Mn$
	in CH_2Cl_2	
$Re(CO)_3$-(C$_5$H$_4$)-$COO-$ (N-succinimidyl)	1805w 1773w 1742m	COON
9		
	2030s 1959s 1934s	$(CO)_3Re$
	in KBr	

studies of BSA with rhenium carbonyl markers **5** and **7** were performed within the conditions previously described for the dicobalt hexacarbonyl marker **10** (*3*), except that ethanol was replaced by THF as the organic cosolvent (i.e. 15-h incubation time, % solvent = 50, pH = 9.5). An initial 60-fold molar excess of marker was chosen because it corresponds to the number of potentially reactive amino functions of BSA (59 lysine residues + 1 N-terminal residue). Purification of the conjugates was performed by gel-filtration chromatography. Calculation of the coupling extent, coupling yield, and protein recovery was carried out from IR measurements on KBr micropellets (for the quantitation of bound and free metal–carbonyl markers) and spectrophotometric measurements (for protein quantitation, Coomassie Blue method). The Coomassie Blue reagent is known to react mostly with arginine residues and can then be used to quantify the conjugates as well as the native protein (*16*). On the other hand, the intensity of the infrared signals of the bound marker is proportional to the number of metal–carbonyl entities. As a consequence, the sensitivity of a CMIA assay including a metal–carbonyl conjugate should increase with its CE. The results are reported in Table III. Coupling extents of 43 and 27 were measured for reagents **5** and **7**, respectively. Protein recovery was found equal to 80%. As observed during our previous work with marker **10** (*3*), not all the amino functions are labeled and it seems that only approximately 40 lysines are accessible in the presence of an excess of reagent.

Several parameters were studied in the course of labeling of BSA with **9**, including the reaction time, the percent cosolvent (and the type of solvent), and the pH of the reaction mixture. Concentrations of protein (0.5 mg/mL) and marker (5.1 mM) and temperature (4 °C) were kept constant.

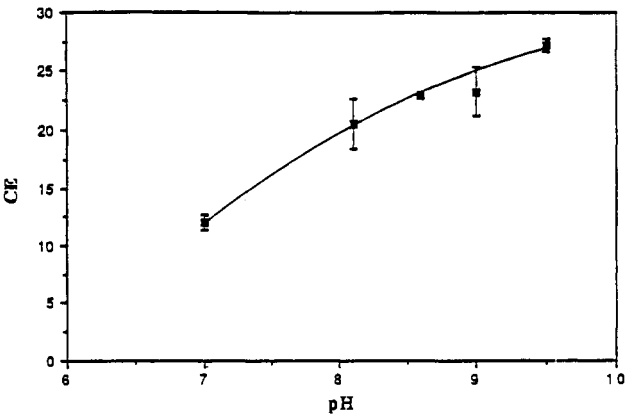


Figure 1. Effect of pH on the extent of labeling of BSA with **9** (mean of two experiments).

The kinetics of labeling of BSA at pH 9.5 was performed in ethanol/water 50/50 and DMF/water 10/90 media. In the first case, the coupling extent is found nearly constant (average value, 18 ± 2; n = 9). In the second case, the average CE is slightly higher (24 ± 2; n = 4).

The influence of percent cosolvent on the final coupling extent was studied for ethanol and DMF mixtures. A percentage of cosolvent ranging from 5 to 50% (v/v) was added to the mixture, which was incubated for 24 h at pH 9.5. When the cosolvent was ethanol, the maximum labeling was obtained for 25% and a slight decrease was observed with a higher percentage (18 ± 2; n = 9). When the solvent was DMF, the coupling extent was nearly constant and led to overall better results than ethanol (average value 27 ± 2; n = 7).

We finally studied the influence of pH of the incubation mixture on the coupling extent of marker **9** to BSA. The results are presented in Figure 1. This figure clearly indicates that the coupling extent of **9** to BSA increases with the pH in the range 7.1–9.5. Protein recovery remained constant and was almost quantitative. Surprisingly, the labeling of BSA occurs at neutral pH but to a lesser extent.

In conclusion, the best conditions are pH = 9.5 and use of DMF as the cosolvent (10%). As for the reaction time, 1 h seems sufficient. The average coupling extent with 60 equiv of **9** is then 24.

Labeling of JOSS 2-2 with 7. The mAb JOSS 2-2 labeled with horseradish peroxidase is included as the second antibody in the ELISA kit for the assay of hTSH commercialized by Clonatec. Its immunological features have been reported (*17*). The labeling of native JOSS 2-2 with **7** was performed using conditions precedently described for the cobalt carbonyl marker **10** (*3*) and using a 30-fold initial excess of marker. This initial ratio of 30 to 1 was chosen because we had previously demonstrated that maximum CY was obtained within these conditions and that the resulting conjugate kept an unchanged immunoreactivity toward its antigen. The percentage of acetonitrile was decreased to 5% in order to limit denaturation processes which had been noticed. The results are reported in Table III. The coupling yield is comparable to that reported for BSA (CY = 50%).

Immunoreactivity Study. The immunoreactivity of $Re(CO)_3$-labeled JOSS 2-2 (CE = 15) was evaluated by a classical dilution assay using a ^{125}I-radiotracer. The binding of ^{125}I-hTSH to $Re(CO)_3$–JOSS 2-2 was measured and compared to that of native JOSS 2-2. For an antibody

Table II. Condensation of Some C-Protected Amino Acids with 7′ in THF

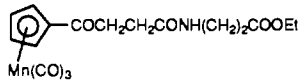
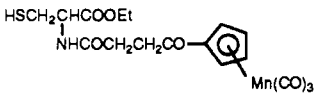
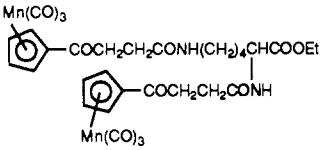
amino acid	main compound	yield	IR ν_{CO} (cm^{-1})	^1H NMR δ (ppm)	MS m/z	anal.
$H_2NCH_2CH_2COOEt$		60%	2030s 1953sh 1944s 1730w 1681 m 1522w in CH_2Cl_2	6.24 (s, 1H, NH) 5.47, 4.66 (s, s, 4H, Cp) 4.16 (q, 2H, $COOCH_2CH_3$) 3.55 (m, 2H, $NHCH_2$) 2.96 (t, 2H, $COCH_2$) 2.53 (m, 4H, CH_2CONH and CH_2COO) 1.27 (t, 3H, $COOCH_2CH_3$) in $CDCl_3$	EI 404 $[MH]^{\cdot+}$ 319 $[M-3CO]^{\cdot+}$	Calcd for $C_{17}H_{19}NO_7Mn$ C, 50.62 H, 4.46 N, 3.47 Found C, 50.93 H, 4.91 N, 3.77
$HSCH_2CH(NH_2)COOEt$		60%	2031s 1947s 1738w 1679m 1515w in CH_2Cl_2	6.97 (s, 1H, NH) 5.50, 4.85 (s, s, 4H, Cp) 4.85 (CH) 4.20 (q, 2H, $COOCH_2CH_3$) 3.18 (s,2H, CH_2SH) 2.99 (m, 2H, CH_2CO) 2.68 (t, 2H, CH_2CONH) 1.28 (t, 3H, $COOCH_2CH_3$) in $CDCl_3$	DCI 436 $[MH]^+$	
$H_2N(CH_2)_4CH(NH_2)COOEt$		40%	2030s 1948s 1772w 1725w 1675w in CH_2Cl_2	7.46 (d, 1H, NHCH) 7.19 (s, 1H, NH) 5.73, 5.12 (t, t, 8H, 2Cp) 4.32 (m, 1H, CH) 4.11 (q, 2H, $COOCH_2CH_3$) 3.17, 2.98 (m, m, 10H, $COCH_2CH_2CO$, $NHCH_2$) 2.53, 1.76, 1.44 (m, m, m, 2H, 2H, 2H, $CH_2CH_2CH_2$) 1.22 (t, 3H, $COOCH_2CH_3$) in acetone-d_6	DCI 747 $[M]^+$ 543 $[M-CpMn(CO)_3]^+$	

Table III. Labeling of BSA and JOSS 2-2 with 5 and 7[a]

protein	marker	CE[b]	CY,[c] %	PR,[d] %	ν_{CO} (cm^{-1}, KBr pellet)
BSA	7	27[e]	45	80	2020 1978
BSA	5	43[f]		80	2025 1931
JOSS 2-2	7	15[g]	50	50	2025 1931

[a] BSA concentration = 0.4 mg/mL; THF/water mixture 1/1; pH = 9.5; reaction time = 15 h. JOSS 2-2 concentration = 0.75 mg/mL; acetonitrile/water mixture 5/95; pH = 9.5; reaction time = 2 h. [b] Coupling extent. [c] Coupling yield. [d] Protein recovery. [e] 60-Fold molar excess of reagent. [f] 1650-Fold molar excess of reagent. [g] 30-Fold molar excess of reagent.

dilution of 1/20, the percentage of binding of ^{125}I-hTSH was 33% for native JOSS 2-2 and 21% for $Re(CO)_3$–JOSS 2-2.

Detection of $(CO)_3Re$-Labeled BSA by FT-IR Spectroscopy on Nitrocellulose Filters. The choice of an adequate solid support is primordial for the design of a new immunoassay system based on IR detection. We had previously tested classical polystyrene microtiter wells (*3*), but they soon revealed themselves inadequate because of their lack of transparency in the mid-IR region and their low protein binding capacity. Nitrocellulose membranes are high protein binding capacity solid supports. Furthermore, they prove to be quite transparent in the 1800–2200-cm^{-1} region, giving a very low noise level. The adsorption of $(CO)_3Re$-labeled BSA onto nitrocellulose filters was achieved from various dilutions of protein in buffer and the IR detection of the carbonyl bands of the probes was performed. A typical spectrum of adsorbed BSA–$Re(CO)_3$ is shown in Figure 2. The two conjugates tested led to two adsorption curves that could be fitted at first approximation to a linear regression (Figure 3).

DISCUSSION

The common source of Re for both families of markers ($Re(CO)_5$ and $CpRe(CO)_3$) is the commercial compound

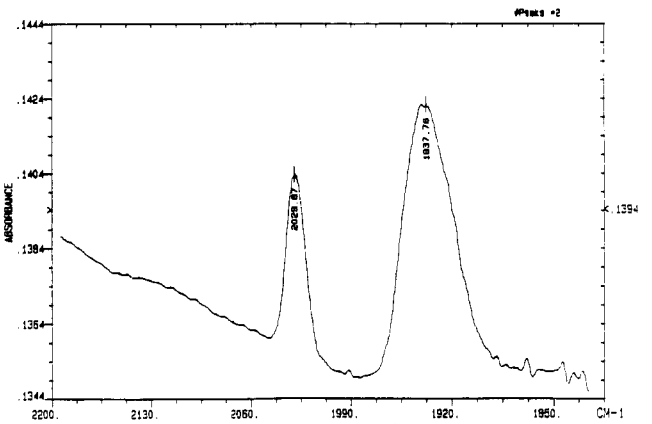


Figure 2. FT-IR spectrum (1800–2200-cm^{-1} region) of BSA–$Re(CO)_3$ adsorbed onto a nitrocellulose membrane. Adsorption from a 290 μg/mL PBS solution of conjugate after 1 h at room temperature.

$Re_2(CO)_{10}$. In the perspective of synthesizing radioactive equivalents of our low oxidation state markers, generator-produced $NaTcO_4$ (^{99m}Tc) or $NaReO_4$ (^{186}Re or ^{188}Re) should be first converted to $Tc_2(CO)_{10}$ or $Re_2(CO)_{10}$. This synthesis has already been described for both metals and was performed under CO pressure (*18*, *19*). Both R–$CpRe(CO)_3$ and R–$Re(CO)_5$ products are very stable, non-light-sensitive compounds readily obtained for the former, reasonably for the latter and have remarkable IR features in terms of position and intensity of ν_{CO} bands. Quantitative spectral data of compounds **5** and **7** in CH_2Cl_2 solution are reported in Table IV and are compared to IR data of RC≡CR′ [$Co_2(CO)_6$] recorded under the same conditions. Compound **5** presents a very strong and sharp band at 2020 cm^{-1} and another weaker and wider one around 1990 cm^{-1}. Compound **7** shows two bands at 2031 and 1936 cm^{-1}. Therefore, both compounds have bands above 2020 cm^{-1}, a region most appropriate for sensitive IR analysis (*20*). Moreover the 2020-cm^{-1} band of com-

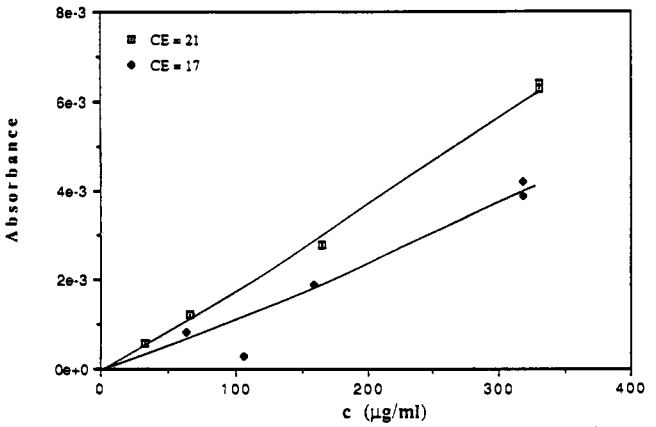


Figure 3. Adsorption curves of two BSA–$Re(CO)_3$ conjugates on nitrocellulose membrane filters. Incubation as indicated for Figure 2. Detection by FT-IR spectroscopy (absorbance read at 2030 cm^{-1}) using an InSb detector. Scan time, 1 min.

Table IV. IR Quantitative Data for Rhenium Carbonyl Complexes 4 and 6 Compared with a Cobalt Carbonyl Complex

compound[a]	ν_{CO} (cm^{-1})	ϵ ($M^{-1}\cdot cm^{-1}$)
4	2020	5800
	1988	nonquantifiable
6	2031	2900
	1939	3300
[RC≡CR']$Co_2(CO)_6$	2087	480
	2048	2800
	2024	3200

[a] In solution in CH_2Cl_2; pathlength = 1 mm.

pound **5** has the highest intensity measured, which makes $Re(CO)_5$ derivatives very good candidates for CMIA.

On the other hand, R–$CpRe(CO)_3$ compounds, which are more easily obtained but have less intense IR bands, could be a good basis for new side-chain-specific radioactive labels for proteins with the view of imaging tumors, for example.

Reactivity of the manganese analog of **7** was tested for a series of C-protected amino acids. In THF, markers **5**, **7**, **7'**, and **9** reacted with β-alanine ethyl ester and led to the expected compounds with 60% yields. With cysteine, which has two potentially reactive sites (SH, NH_2), only the compound resulting from the reaction with NH_2 was separated. With lysine, which has also two potential reacting sites α-NH_2 and ε-NH_2 the main compound resulted from the double condensation of **7'**, indicating an identical reactivity of both amino functions on lysine. In a THF/water mixture, reaction of **7'** with β-alanine easily occurred to produce the expected product, but a lower yield was observed because of competitive hydrolysis of **7'**.

The labeling of BSA and JOSS 2-2 with markers **5** and **7** was carried out under the conditions previously described for marker **10** (*3*). With a 60-fold molar excess of **7**, 27 out of the 60 available amino functions were labeled whereas the CE is 36 with the manganese equivalent **7'** under the same conditions. The latter seems to be slightly more reactive and the result is approaching the one obtained with compound **10** (CE of 40). When a large excess of marker **5** was used, the coupling extent was found to be around 40. Among the 60 potentially reacting amino groups of BSA, only a constant fraction is actually labeled. This fraction is constituted with the residues accessible to the solvent and reagents.

Protein recovery is different for BSA and JOSS 2-2, 50% of protein being lost in the second case. In the case of the mAb, the use of organic solvent and/or basic pH may be the causes of partial loss of protein. It should be interesting to perform the conjugation of the marker at a neutral pH since we demonstrated it to be possible with BSA.

A careful study of several parameters influencing the final coupling yield was performed for marker **9**. For all experiments, an initial ratio of 60 markers per molecule of protein was chosen because it corresponds to the number of potentially reactive sites on BSA (59 lysine residues + 1 N-terminal residue). A temperature of 4 °C was chosen because it usually favors reaction of *N*-succinimidyl esters (*21*). The kinetics of coupling was measured in an ethanol/water 1/1 medium or a DMF/water 10/90 medium. In both cases, the coupling reaction is completed in 1 h. *N*-Succinimidyl esters are very reactive compounds and competitive hydrolysis is slower than reaction with amines (*22*).

As noted earlier, BSA is soluble in media containing high percentages of organic solvent. This behavior is unusual among proteins, which are generally much more sensitive to solvents than BSA and undergo denaturation and/or precipitation upon disruption of folding (*23*). On the other hand, *N*-succinimidyl esters are insoluble in buffers. A compromise should then be found. The influence of percent cosolvent on the final coupling extent was studied for both ethanol and DMF. In the case of ethanol, the maximum coupling extent was obtained for 25% cosolvent. In the case of DMF, the maximum labeling was obtained for 10% and the same CE was found with higher percentages. For 5% of solvent the coupling extent is a little lower. These results can be interpreted from the solubility of marker **9** in the considered solvent. Since **9** is much more soluble in DMF, coupling extents are higher.

The influence of pH was also suspected because of the mechanism of labeling. *N*-Succinimidyl esters react with amino groups in the free form and not in the protonated form. Theoretically, pH should be placed at a value above 10.5 which is the pK_a of the ε-NH_2 of lysine. In practice, use of such a basic medium is very likely to induce denaturation of most proteins and we have limited our study to pH values less than 9.5. We have observed that the final coupling extent increases with pH. This result is in accordance with those reported for the coupling of antibodies with *N*-succinimidyl ester reagents (*9*, *24*). When the pH is increased, more lysine residues become available for the reaction with the *N*-succinimidyl esters. The value of CE = 10 for pH = 7.1 signifies that a few lysines are reactive at this pH because of their particular environment. The fact that BSA is an acidic protein (p*I* = 4.8) (*22*) may provide another explanation because at neutral pH it already bears a negative charge, leaving at least a part of the primary amino groups in the free form.

The stability of the $Re(CO)_3$ conjugates is remarkable at 37 °C. No loss of the organometallic entities has been observed after 24 h in a physiological buffer when assayed by IR spectroscopy. As the IR features of the $CpRe(CO)_3$ conjugate are specific of the complex and not only the metal, a decomplexation would result in a total disappearance of the signals. FT-IR spectroscopy is therefore the best tool to ensure a correct checking of the conjugates.

Coupling of marker **7** was performed with a monoclonal anti-hTSH antibody coded JOSS 2-2. We synthesized a conjugate with a CE of 15. Its biological activity, evaluated in terms of binding capacity to ^{125}I hTSH, was found to be significantly lower (21% of binding compared to 33% for the native protein at a concentration of 0.1 µg/mL). But this conjugate could still be usable in a two-site

immunoassay of hTSH on a solid phase as the second antibody with final quantitation by FT-IR spectroscopy. It is worth noticing that high coupling extents of metal are still compatible with the conservation of good immunoreactivity. This result differs markedly from labeling of antibodies with radioactive iodine, where only two atoms are tolerated without loss of immunoreactivity (*25*), and is very favorable for obtaining an adequate sensitivity of CMIA assays including these labeled antibodies.

Finally, IR detection of BSA labeled with $Re(CO)_3$ groups adsorbed onto nitrocellulose surfaces was achieved. The IR absorption is shown to be proportional to the initial protein concentration and the slope of the response depends on the coupling extent of the conjugate. With a CE of 17 the slope value was found to be 1.3×10^{-5} while it is equal to 2.0×10^{-5} for the conjugate with CE = 21. This result clearly confirms that sensitivity will be a function of the extent of conjugation of metal–carbonyl probes on proteins (antibody or antigen). A compromise has then to be found to optimize IR response without too much loss of immunoreactivity.

As pointed out in the introduction, coupling of such Re entities with ^{186}Re or ^{188}Re to anti-tumor antibodies for radioimmunodiagnostic and/or therapy purposes could be an alternative application of these reagents. In this case, high derivatization of the antibodies is not usually researched. On the contrary, high coupling extents are regarded as unfavorable as a rapid decrease of immunoreactivity with the antigen occurs with the increase of the number of metals bound. Therefore, optimal conditions still have to be found if the conjugates are to be included in radiodiagnostic procedures.

CONCLUSION

The low oxidation state organorhenium complexes described here were successfully coupled to proteins. These compounds are particularly stable in biological media. Coupling yields are fairly good (50%) and the IR features of the conjugates, especially the rhenium pentacarbonyl derivative, are noteworthy. They can be easily detected on nitrocellulose membranes which appear to be ideal solid supports fully compatible with IR detection. Rhenium tricarbonyl compounds in a radioactive form (^{186}Re or ^{188}Re) may be interesting alternatives to existing markers for the labeling of anti-tumor antibodies, provided their synthesis is adapted to the manipulation of short-lifetime, high specific activity radioisotopes.

ACKNOWLEDGMENT

We wish to thank Dr. C. Brisson from Clonatec (Paris, France) for performing the immunological studies.

LITERATURE CITED

(1) (a) Jaouen, G., Vessières, A., Top, S., Ismail, A. A., and Butler, I. S. (1985) Metal carbonyl fragments as a new class of markers in molecular biology. *J. Am. Chem. Soc. 107*, 4778–4780. (b) Vessières, A., Top, S., Ismail, A. A., Butler, I. S., Louer, M., and Jaouen, G. (1988) Organometallic estrogens: Synthesis, interaction with lamb uterine estrogen receptor, and detection by infrared spectroscopy. *Biochemistry 27*, 6659–6666.

(2) Salmain, M., Vessières, A., Brossier, P., Butler, I. S., and Jaouen, G. (1992) Carbonylmetalloimmunoassay (CMIA) a new type of non-isotopic immunoassay. Principles and applications to phenobarbital assay. *J. Immunol. Methods 148*, 65–75.

(3) Varenne, A., Salmain, M., Brisson, C., and Jaouen, G. (1992) Transition metal carbonyl labeling of proteins. A novel approach to a solid phase two-site immunoassay using Fourier transform Infrared spectroscopy. *Bioconjugate Chem. 3*, 471–476.

(4) (a) Petsko, G. H. (1985) Preparation of heavy-metal derivatives. *Methods Enzymol. 114*, 147–156. (b) Kostic, N. M. (1988) Selective labeling, cross-linking and cleavage of proteins with transition-metal complexes. *Comments Inorg. Chem. 8*, 137–162.

(5) Griffiths, G. L., Goldenberg, D. M., Jones, A. L., and Hansen, H. J. (1992) Radiolabeling of monoclonal antibodies and fragments with Technetium and Rhenium. *Bioconjugate Chem. 3*, 91–99.

(6) John, E., Thakur, M. L., McDevitt, M. R., and Damjanov I. (1993) Rhenium-186-labeled monoclonal antibodies for radioimmunotherapy: Preparation and evaluation. *J. Nucl. Med. 34*, 260–267.

(7) (a) Nicolotti, R. A., and Dean, R. T. (1987) Coupling agents for radiolabeling proteins. Eur. Pat. Appl. 87304716.1. (b) Koch, P., and Mäcke, H. R. (1992) ^{99m}Tc labeled biotin conjugate in a tumor "pretargeting" approach with monoclonal antibodies. *Angew. Chem. Int. Ed. Engl. 31*, 1507–1509.

(8) (a) Linder, K. E., Wen, M. D., Nowotnik, D. P., Malley, M. F., Gougoutas, J. Z., Nunn, A. D., and Eckelmann, W. C. (1991) Technetium labeling of monoclonal antibodies with functionalized BATOs. 1. $TcCl(DMG)_3PITC$. *Bioconjugate Chem. 2*, 160–170. (b) Fritzberg, A. R., Adams, P. G., Beaumier, P. L., Kasina, S., Morgan, C., Ras, T. N., Reno, J. M., Sanderson, J. A., Srinivasan, A., and Wilbur, D. S. (1988) Specific and stable labeling of antibodies with technetium-99m with a diamine dithiolate chelating agent. *Proc. Natl. Acad. Sci. U.S.A. 85*, 4025–4029. (c) Kasina, S., Rao, T. N., Srinivasan, A., Sanderson, J. A., Fitzner, J. N., Reno, J. M., Beaumier, P. L., and Fritzberg, A. R. (1991) Development and biological evaluation of a kit for preformed chelate technetium-99m radiolabeling of an antibody Fab fragment using a diamide dimercaptide chelating agent. *J. Nucl. Med. 32*, 1445–1451.

(9) Goldrosen, M. H., Biddle, W. C., Pancook, J., Bakshi, S., Vanderheyden, J.-L., Fritzberg, A. R., Morgan, A. C., Jr., and Foon, K. A. (1990) Biodistribution pharmacokinetic and imaging studies with Re-labeled NR-Lu-10 whole antibody in LS174T colonic tumor-bearing mice. *Cancer Res. 50*, 7973–7978.

(10) (a) Top, S., Gunn, M., Jaouen, G., Vaissermann, J., Daran, J. C., and Thornback, J. R. (1991) Reactions of *eq,eq*-$Re_2(CO)_8(MeCN)_2$ with phenylacetylene and α-ethynylestradiol. A new synthesis of acetylide complexes. *J. Organometal. Chem. 414*, C22–C27. (b) Top, S., Gunn, M., Jaouen, G., Vaissermann, J., Duran, J. C., and McGlinchey, M. J. (1992) Synthetic, structural and reactivity studies of dirhenium carbonyl complexes of 17α-ethynylestradiol and phenylacetylene: Variable temperature ^{13}C NMR spectra and X-ray crystal structure of $(\mu\text{-H})(\mu\text{-C}\equiv\text{C-R})Re_2(CO)_7(MeCN)$. *Organometallics 11*, 1201–1209. (c) Top, S., Vessières, A., Jaouen, G., and Quivy, J. (1992) French patent no. 92 04411.

(11) Tam, W., Lin, G.-Y., Wong, W.-K., Kiel, W. A., Wong, V. K., and Gladysz, J. A. (1982) Synthesis and electrophile-induced disproportionation of the neutral formyl $(\eta\text{-}C_5H_5)$-$Re(NO)(PPh_3)(CHO)$. *J. Am. Chem. Soc. 104*, 141–152.

(12) Kolobova, N. E., and Makarov, Y. B. (1968) Two types of reaction of cyclopentadienylmanganese–(Rhenium)–tricarbonyl with metalling agents. *Izv. Akad. Nauk SSSR, Ser. Khim. 11*, 2529–2531.

(13) (a) Le Plouzennec, M., and Dabard, R. (1972) *Bull. Soc. Chim. Fr.*, 3594–3599. (b) Lavastre, I., Besançon, J., Brossier, P., and Moise, C. (1991) The use of metallocenic esters of N-Hydroxysuccinimide for metallohapten synthesis. *Appl. Organometal. Chem. 5*, 143–149.

(14) Ariyaratne, J. P. K., Bierrum, A. M., Green, M. L. H., Ishaq, M., and Prout, C. K. (1969) Evidence for near-neighbour interactions in some substituted methyl derivatives of transition metals including the molecular crystal structure determination of $(\pi\text{-}C_5H_5)Fe(CO)_2CH_2COOH$ and $(\pi\text{-}C_5H_5)Mo(CO)_3$-$CH_2COOH$. *J. Chem. Soc. (A)* 1309–1321.

(15) Green, M. L. H., and Nagy, P. L. I. (1963) Studies on some alkyl and olefin complexes of iron and manganese. *J. Organometal. Chem. 1*, 58–69.
(16) Compton, S. J., and Jones, C. G. (1985) Mechanism of dye response and interference in the Bradford protein assay. *Anal. Biochem. 151*, 369–374.
(17) Braun, J. M., and Charreire, J. (1990) Production and characterization of monoclonal antibodies directed against epitopes of human thyroid stimulating hormone. *J. Immunol. Methods 132*, 197–203.
(18) Calderazzo, F., and Poli, R. (1985) Reduction of ammonium perrhenate by CO: A convenient method for preparing $Re_2(CO)_{10}$. *Gazz. Chim. Ital. 115*, 573–574.
(19) Hileman, J. C., Huggins, D. K., and Kaesz, H. D. (1961) Technetium carbonyl. *J. Am. Chem. Soc. 83*, 2953–2954.
(20) Salmain, M., Vessières, A., Jaouen, G., and Butler, I. S. (1991) Fourier Transform infrared spectroscopic method for the quantitative trace analysis of transition metal carbonyl-labeled bioligands. *Anal. Chem. 63*, 2323–2329.
(21) Brinkley, M. (1992) A brief survey of methods for preparing protein conjugates with dyes, haptens and cross-linking reagents. *Bioconjugate Chem. 3*, 2–13.
(22) Lomant, A. J., and Fairbanks, G. (1976) Chemical probes of extended biological structures: Synthesis and properties of the cleavable protein cross-linking reagent [^{35}S]Dithiobis-(succinimidyl propionate). *J. Mol. Biol. 104*, 243–261.
(23) Peters, T., Jr. (1985) Serum Albumin. *Advances in protein chemistry vol. 37* (C. B. Anfinsen, and J. T. Edsall, Eds.) pp 161–245, Academic Press New York.
(24) Vaidyanathan, G., and Zalutsky, M. R. (1990) Protein radiohalogenation: Observations on the design of N-succinimidyl ester acylation agents. *Bioconjugate Chem. 1*, 269–273.
(25) Johnson, D. A., Day, E. D., and Pressman, D. (1960) The effect of iodination on antibody activity. *J. Immunol. 84*, 213–220.

Synthesis of Bulky β-Lactams for Inhibition of Cell Surface β-Lactamase Activity†

D. Nedra Karunaratne, Susan Farmer, and Robert E. W. Hancock*

Department of Microbiology, University of British Columbia, 6174 University Boulevard, Vancouver, British Columbia, Canada V6T 1Z3. Received April 6, 1993®

Procedures are described for the preparation of a series of compounds consisting of methicillin linked to β-cyclodextrin through variable hydrophilic linkers. β-Cyclodextrin was coupled to the antibiotic methicillin to prevent the antibiotic from permeating the outer membranes of bacteria. Stoichiometric oxidation of the β-cyclodextrin with sodium metaperiodate provided a functional group for coupling to the linker. Methicillin was coupled to the linker via its carboxyl group. These compounds were tested for activity toward purified β-lactamase. The length of the spacer arm between β-cyclodextrin and methicillin was crucial in binding β-lactamase and inhibiting activity. Compounds with longer spacers were effective inhibitors of β-lactamase. We have deduced that the length of the spacer should be greater than 16 Å for optimum inhibition of β-lactamase.

INTRODUCTION

The biochemical targets of β-lactam molecules (the penicillin-binding proteins) are located on the cytoplasmic membrane. In Gram-negative bacteria the antibiotic molecules must first permeate the barrier formed by the outer membrane. The penetration of the bacterial surface by β-lactam molecules occurs by diffusion through the water-filled channels of porins (Hancock and Bell, 1988). These channels are just a little larger than the β-lactams themselves, and uptake is influenced by frictional, steric, and charge interactions (Yoshimura and Nikaido, 1985). The permeability of the outer membrane is known to affect the antibacterial effectiveness (MIC value). An accurate method for the measurement of diffusion rates of β-lactams across the outer membrane has been developed utilizing a periplasmic β-lactamase (Bellido et al., 1991). As long as the cells are not "leaky" and the β-lactamase molecules remain in the periplasmic space, the in vivo rate of hydrolysis of various β-lactams at equilibrium is diffusion limited and thus may be used to calculate the rate of diffusion of these molecules through the outer membrane (Zimmermann and Rosselet, 1977). This assay is not accurate when the cells are leaky (Lei et al., 1991), or when the bacterial strains express surface β-lactamase activity (Liu and Nikaido, 1991). Therefore the synthesis of a β-lactamase inhibitor which could not penetrate the outer membrane and interfere with periplasmic β-lactamase was attempted. It was necessary that the inhibitor was water-soluble to permit free access to surface-bound β-lactamase. The bulky water soluble carbohydrate β-cyclodextrin was used as the soluble support to which the antibiotic methicillin was linked through varying lengths of spacers.

EXPERIMENTAL PROCEDURES

Chemicals. Methicillin, ethylenediamine, diethylenetriamine, triethylenetetraamine, β-cyclodextrin, and sodium metaperiodate were purchased from Sigma; succinic anhydride was purchased from Aldrich; 1-ethyl-3-[3-(dimethylamino)propyl]carbodiimide hydrochloride was purchased from Bio-Rad; sodium borohydride, and DMSO were purchased from BDH. Pyridine was dried over molecular seives. HPLC-grade methanol was purchased from Fisher Scientific. Nitrocefin was kindly provided by C. O'Callaghan (Glaxo Research Groups Ltd., Middlesex, England).

Chromatography and Spectrometric Techniques. Gel-permeation chromatography was performed on a Bio-Gel P4 -400 mesh column (1.5 × 27 cm) irrigated with 0.02% sodium azide in water or a Bio-Gel P30 column (2.5 × 100 cm) irrigated with 1 M acetic acid adjusted to pH 5.0 with pyridine.

HPLC was performed on a Beckman System Gold instrument with a dual-pump programmable solvent module 126 and programmable UV-detector module 166. An Ultrasphere C_{18} ion-pair reverse-phase analytical column (5 μm, 4.6 mm (i.d.) × 15 cm) was used. The solvents used were as follows: (A) 10 mM sodium dihydrogen phosphate buffer, pH 2.5, and (B) methanol. Samples were run isocratically in 65% buffer A and 35% B or a solvent gradient programmed at 15% B for 5 min, increasing from 15 to 50% (B) in 20 min, then 50% B for 5 min, and back to 15% B in 5 min. Elution of sample was monitored at a wavelength of 225 nm. The flow rate was 1 mL/min, at a pressure of 1.8 kpsi.

Ion-exchange chromatography was performed on a column (1.2 × 20 cm) of Amberlite IR-120 (H^+) analytical-grade resin in the H^+ form in water. Samples were loaded and eluted by washing continuously with water, until two bed volumes were collected (approximately 40 mL) and then lyophilized.

Thin-layer chromatography was performed on silica gel 60 F_{254} precoated aluminium sheets (layer thickness, 0.2 mm) from E. Merck, Darmstadt, Germany. The plates were developed in 2-propanol (30%)/methanol (70%) solvent. The compounds were visualized by UV light (254 nm).

^{1}H-NMR spectra were recorded at 400 MHz on a Brucker WH 400 spectrometer. Compounds were dissolved in deuterated water. TMS was used as the external standard.

* Author to whom correspondence should be addressed.

† Abbreviations used: DMSO = dimethyl sulfoxide. EDC = 1-ethyl-3-[3-(dimethylamino)propyl]carbodiimide hydrochloride. HPLC = high-pressure liquid chromatography. LSIMS = liquid secondary ion mass spectrometry. MIC = minimum inhibitory concentration. NMR = nuclear magnetic resonance spectroscopy. TMS = tetramethylsilane

® Abstract published in *Advance ACS Abstracts,* November 1, 1993.

1043-1802/93/2904-0434$04.00/0 © 1993 American Chemical Society

Liquid secondary ion mass spectrometry (LSIMS) was performed on a Kratos concept II HQ mass spectrometer using a Cs^+ ion gun of 12 kV.

Synthetic Methodology. Oxidation of β-Cyclodextrin. To β-cyclodextrin (2.0 g,1.76 mmol) was added 0.05 M $NaIO_4$ at pH 6.0 (7.0 mL, 3.5 mmol). The solution was mixed and left at 4 °C in the dark. The optical density was measured at 223 nm to monitor uptake of periodate (Hay et al., 1965). The reaction was allowed to run for 60 h and then quenched with ethylene glycol (0.5 mL), and the products were dialyzed and lyophilized to yield 2.150 g of the oxidized product. ^1H NMR (D_2O) δ 9.3 (s, 0.7H), 5.4 (br signal 2.4H), 5.0 (d, 6H, $J = 4$ Hz anomeric), 3.5–4.0 (series of m, 43H, ring protons).

Refer to Scheme I for the general reaction pathways of the following reactions.

Coupling Ethylenediamine to Oxidized β-Cyclodextrin To Synthesize Compound 1. To the oxidized β-cyclodextrin (60 mg, 0.05 mmol) in 5 mL of water was added ethylenediamine (33 μL, 0.5 mmol) and the mixture stirred for 15 h at 4 °C in a sealed vial (Jeffrey et al., 1975). Subsequently sodium borohydride (12 mg, 0.33 mmol) was added and the mixture stirred for 16 h in a vented flask. It was then diluted with 4 mL of water, and glacial acetic acid was added dropwise until there was no more evolution of gas. Borate was removed by coevaporation with methanol.

Coupling of Methicillin to Diamino Compounds: Synthesis of Compounds 2–4 and P1. To methicillin in water (4 mL) were added an equimolar proportion of the corresponding amine-containing compound and an equimolar amount of EDC [1-ethyl-3-[3-(dimethyl amino)-propyl]carbodiimide hydrochloride] as follows: (i) methicillin (201 mg, 0.5 mmol), ethylenediamine (33 μL, 0.5 mmol), EDC (96 mg, 0.5 mmol); (ii) methicillin (201 mg, 0.5 mmol), diethylenetriamine (60 μL, 0.5 mmol), EDC (96 mg, 0.5 mmol); (iii) methicillin (201 mg, 0.5 mmol), triethylenetetraamine (70 mg, 0.5 mmol), EDC (96 mg, 0.5 mmol); (iv) methicillin (40 mg, 0.1 mmol), compound 1 (70 mg, 0.05 mmol), EDC (42 mg, 0.22 mmol). The pH was maintained at 6.0 with 2 M HCl for a period of 4 h in an ice bath. The reaction was allowed to proceed overnight at 4 °C. The final reaction products **2–4** and **P1** were lyophilized. The compounds **2–4** and P1 were run isocratically on HPLC. Their retention times were 2.9, 2.64, 2.8, and 1.99 min, respectively. The retention times of methicillin, oxidized β-cyclodextrin, compound **2**, ethylenediamine, diethylenetriamine, and triethylenetetraamine were 26.44, 1.77, 2.92, 2.2, 2.46, and 1.69 min, respectively. All compounds did not contain free methicillin or any unreacted reactants. **P1** (in 2 mL water) was loaded on Bio-Gel P30. **P1** eluted as a sharp peak (elution volume of 80 mL) very close to, but before, the elution volume of free β-cyclodextrin (90 mL). A second broad peak (which did not inhibit β-lactamase) eluted immediately thereafter. The yield of **P1** was 68 mg. R_f values of 0.56, 0.56, and 0.40 were obtained for TLC of compounds **2**, **3**, and **4**, while methicillin had a R_f value of 0.60. The three compounds **2**, **3**, and **4** were not purified further. Their crude yields were 337, 342, and 335 mg, respectively.

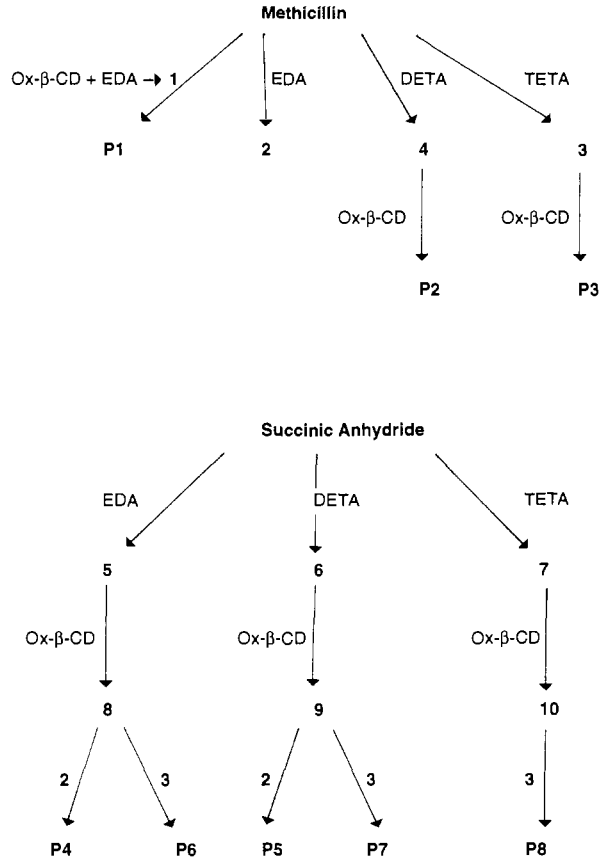
Formation of *N*-(Aminoethyl)succinamic Acid Compounds 5–7. To succinic anhydride (100 mg, 1 mmol) in dry pyridine (5 mL) was added either ethylenediamine (67 μL, 1 mmol), diethylenetriamine (100 μL, 1 mmol), or triethylenetetraamine (146 mg, 1 mmol) and the mixture stirred for 22 h. Pyridine was removed by repeated coevaporation with water, and the product **5**, **6**, or **7** were respectively lyophilized. The crude yields of the compounds were 178, 182, and 240 mg, respectively.

Linking of *N*-(Aminoethyl)succinamic Acid to Oxidized β-Cyclodextrin: Synthesis of 8–10. To oxidized β-cyclodextrin (500 mg, 0.44 mmol) in 8 mL water was added *N*-(aminoethyl)succinamic acid [69 mg (0.44 mmol) of compound **5**] and the pH adjusted to 10.0 with 2 M NaOH. Similarly, to oxidized β-cyclodextrin (425 mg, 0.37 mmol) was added either 75 mg (0.37 mmol) of compound **6** or 91 mg (0.37 mmol) of compound **7** and the pH was increased to pH 10 by the addition of 6 or 7 drops of 2 M NaOH. The solutions were stirred for 18 h at 4 °C. Sodium borohydride was added to the former (60 mg, 1.5 mmol) and to the two latter vessels (40 mg, 1 mmol) and allowed to react at room temperature for 24 h. Excess borohydride was neutralized with 2 N HCl and the entire sample passed through a column of IR-120 (H^+) cation-exchange resin. The resulting yellow solution was concentrated by rotary evaporation and coevaporated with acidified methanol to remove borate. The products obtained were lyophilized to yield **8** (603 mg), **9** (530 mg), or **10** (544 mg), respectively.

Synthesis of β-Cyclodextrin Coupled Methicillin Derivatives. (a) Synthesis of P2 and P3. To the amino-spacer-linked methicillin compounds [0.05 mmol of **4** (23 mg) or **3** (25 mg)] in water was added oxidized β-cyclodextrin (56 mg, 0.05 mmol) and the pH was adjusted to 10 with 3 drops of 2 M NaOH. After allowing the reaction to proceed at room temperature for 24 h, sodium borohydride (10 mg, 0.25 mmol) was added and stirring continued at room temperature for a further 20 h. The solution was neutralized with 2 M HCl and passed through a column of IR-120 (H^+) resin. The eluate was concentrated and coevaporated with acidified methanol to remove borate and yield compound **P2** (83 mg) or **P3** (89 mg). **P2** appeared as a sharp peak at a retention time of 1.91 min and **P3** at 1.84 min when subjected to HPLC. Peaks due to free β-cyclodextrin, compound **4**, or compound **3** at retention times of 1.77, 2.8, or 2.64 min, respectively, were absent.

(b) Synthesis of P4-P8. To an aqueous solution (10 mL) of β-cyclodextrin linked to *N*-(aminoethyl)succinamide (**8**, **9**, or **10**) was added an amino-spacer-linked methicillin compound (**2** or **3**) as follows: (i) compound **8** (102 mg, 0.08 mmol) and compound **2** (34 mg, 0.08 mmol); (ii) compound **9** (200 mg, 0.15 mmol) and compound **2** (63 mg, 0.15 mmol); (iii) compound **8** (255 mg, 0.20 mmol) and compound **3** (101 mg, 0.20 mmol); (iv) compound **9** (200 mg, 0.15 mmol) and compound **3** (76 mg, 0.15 mmol); (v) compound **10** (215 mg, 0.15 mmol) and compound **3** (76 mg, 0.15 mmol). The solutions were kept in an ice bath and the pH was adjusted to 6 with 1 M NaOH where necessary. After addition of EDC (equimolar amounts to each) the pH was maintained at 5.5–6.0 with the addition of 0.1 M HCl over a period of 4h and thereafter stirred at 4 °C for a further 20 h. The solutions were lyophilized to yield **P4**, **P5**, **P6**, **P7**, and **P8**, respectively. All products [**P4-P8** in a and b above] were purified on a Bio-Gel P4 –400 mesh column in 0.02% sodium azide. The eluates were monitored by the phenol sulfuric method for carbohydrates (Dubois et al., 1956). The modified compounds eluted before unmodified β-cyclodextrin and were well-resolved from free methicillin. The major peak appearing in the elution region of 30–40 mL was pooled and lyophilized to give **P4** (41 mg), **P5** (210 mg), **P6** (335 mg), **P7** (244 mg), or **P8** (143 mg). Minor peaks observed after this peak were also pooled and tested for β-lactamase inhibitory activity. Only the major peak was an active

Scheme I



General reaction pathways—see text for details. Abbreviations: EDA = ethylenediamine, DETA = diethylenetriamine, TETA = triethylenetetraamine, Ox-β-CD = oxidized β-cyclodextrin.

inhibitor. Therefore the later-eluting minor peaks were not characterized further. P4 was observed at 1.99 min by isocratic elution on HPLC. Alternatively, purification of P4 was also performed by HPLC by repeated injection of 50 μL of a 15 mg/mL soluton at each run and collection of eluant between the retention times of 1.8 and 2.5 min. Since this method was not suitable for large-scale purification, Bio-Gel P4 chromatography was utilized to purify **P4** successfully. **P5** and **P6** were observed at retention times of 1.89 and 1.85 min, respectively, when HPLC was performed using the solvent gradient program. Methicillin eluted at 25.8 min on this program.

P7 ^{1}H NMR (D_2O): δ 7.4 (t, 1H, J = 6 Hz, aromatic H-4), 6.7 (d, 2H, J = 6 Hz, aromatic H-3,5), 5.4 (d, 1H, J = 4 Hz, anomeric), 5.0 (d, 6H, J = 4 Hz, anomeric), 3.5 - 4.0 (series of m, 51H, ring protons, aromatic OCH_3, methicillin ring), 3.2 (m, 12H, spacer), 2.9 (m, 12H, spacer), 1.6 (s, 3H, methicillin CH_3), 1.5 (s, 3H, methicillin CH_3). Mass spectrum (thioglycerol): m/z 1780 $(M - OMe)^+$. **P8** ^{1}H NMR (D_2O): δ 7.4 (t, 1H, J = 6 Hz, aromatic H-4), 6.7 (d, 2H, J = 6 Hz, aromatic H-3,5), 5.4 (d, 1H, J = 4 Hz, anomeric), 5.0 (d, 6H, J = 4 Hz, anomeric), 3.5–4.0 (series of m, 51H, ring protons, aromatic OCH_3, methicillin ring), 3.2 (m, 16H, spacer), 2.9 (m, 12H, spacer), 1.6 (s, 3H, methicillin CH_3), 1.5 (s, 3H, methicillin CH_3). Mass spectrum (thioglycerol); m/z 1805 $(M - H_2O - OCH_3)^+$. Biological assays demonstrated that these compounds were stable in lyophilized state for more than 6–8 weeks; however, in solution their ability to inhibit β-lactamase deteriorated within days.

Biological Methods. β-Lactamase Assays. β-Lactamase assays were performed (Angus et al., 1982) using

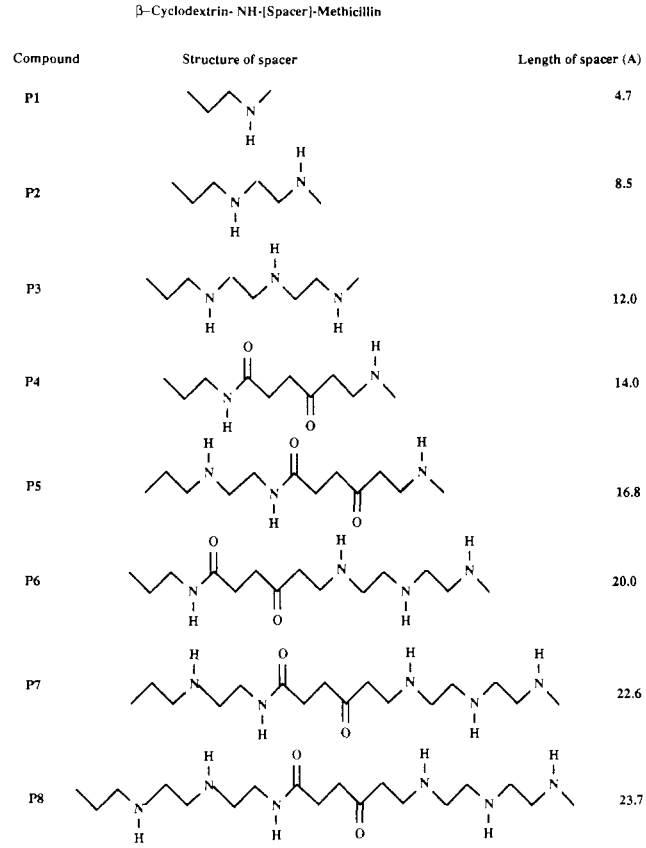


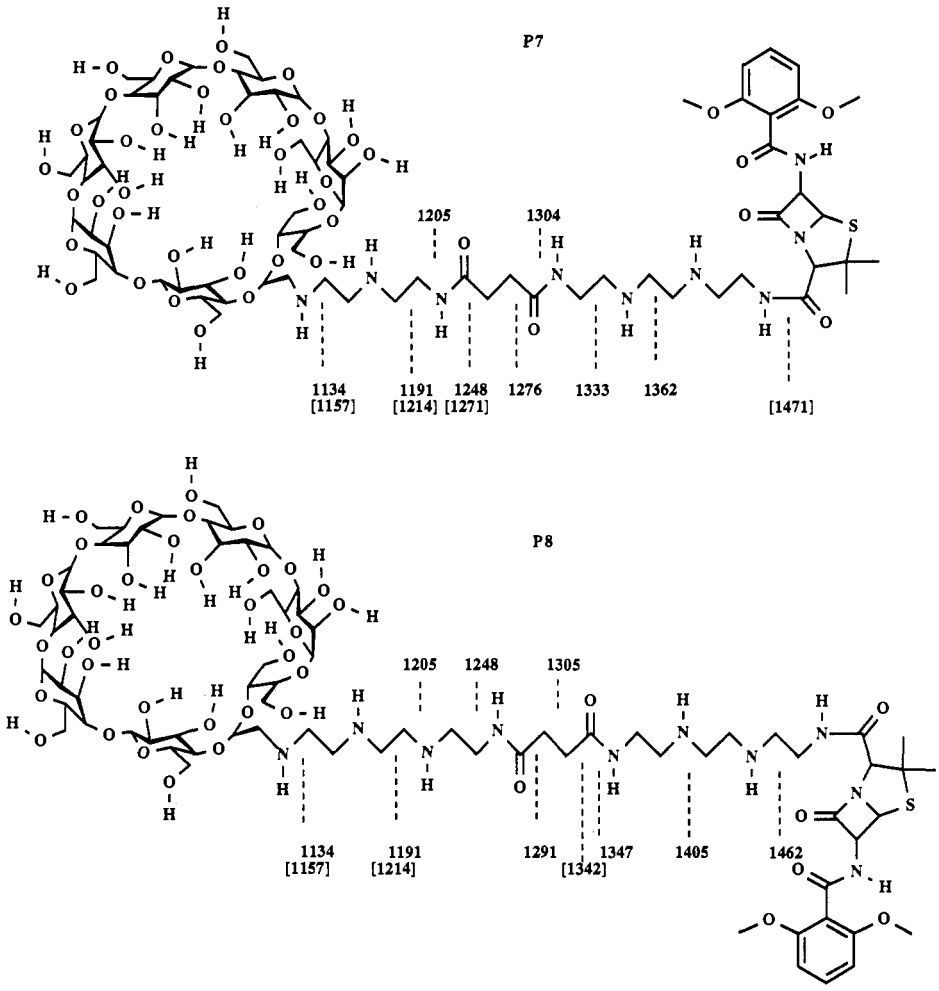
Figure 1. The structures of the different spacers in the compounds **P1-P8** formed between β-cyclodextrin and methicillin are shown here. The spacer consists of two amino termini, one of which is linked to the aldehyde generated in β-cyclodextrin (not drawn in the model), the other to the carboxyl group of methicillin. The lengths of the spacers were calculated from molecular models generated by using the Alchemy program.

the chromogenic cephalosporin nitrocefin (O'Callaghan et al., 1972). *Pseudomonas aeruginosa* PAO1 strain H103 containing the TEM-2 β-lactamase encoded by plasmid RP1 was grown to an optical density at 660 nm (OD_{660}) of 0.5–0.8 in Luria broth. The cells were then centrifuged and washed and resuspended in 5 mM sodium Hepes, pH 7.2, to OD_{600} = 0.5. Assays were performed on whole cells which were left at 23 °C, or incubated on ice for 10 min to release high levels of β-lactamase. Cells were then preincubated with the test compounds for 10 min before performing a nitrocefin hydrolysis assay. One hundred microliters of cells was added to 0.65 ml of nitrocefin solution (0.1 mg/ml in 5 mM Hepes) in a semimicrocuvette, and the kinetics of nitrocefin hydrolysis was monitored at OD_{495} using a Perkin-Elmer (lambda 3) dual-beam spectrophotometer coupled to a Perkin-Elmer 561 chart recorder. Initially compounds were tested for inhibition of activity of a crude extract of β-lactamase from *Enterobacter cloacae* rather than whole cells. Compounds **P1** and **P2** were found to be inactive and therefore discontinued in the study of the effect of the compounds on whole cells.

RESULTS AND DISCUSSION

Outer membrane permeability in intact cells is usually measured by the Zimmermann–Rosselet (1977) approach in which an equilibrium is established between the rate of diffusion across the outer membrane and the rate of hydrolysis of β-lactams by intact cells. Thus the rate of diffusion can be estimated as the rate of cleavage of the β-lactam ring by a β-lactamase enzyme present in the

Scheme II



Fragmentation pattern obtained for the compounds **P7** and **P8** and the *m/z* values for major fragments observed in the negative LSIMS spectra are indicated. The fragments observed in the positive LSIMS spectra showing the addition of Na^+ are indicated in square brackets. Ions due to sequential loss of sugar units (162 mass units) were also observed. Mass ions at *m/z* 1287 and 1229 are due to loss of a water molecule from the fragments of mass 1305 and 1247 in **P8**. **P7** shows an ion at *m/z* 1285 due to loss of water and H from the fragment of mass 1304. The peak at *m/z* 1169 in both spectra arises from the loss of two water molecules from the fragment of mass 1205.

periplasm (the cellular compartment that is immediately internal to the outer membrane) (Liu and Nikaido, 1991) or the rate of disappearance of β-lactam from the extracellular space (Bellido et al., 1991). Since the rate of hydrolysis of β-lactam by β-lactamase sequestered in the periplasm is often only 1–5% of the rate of hydrolysis that would be observed if this β-lactamase was in free solution, any leakage of β-lactamase into the supernatant (Angus et al., 1982) or to the cell surface (Liu and Nikaido, 1991) can result in considerable errors in estimations of diffusion rate.

Therefore we sought here to produce a class of high molecular weight inhibitors that could not cross the outer membrane, but instead inhibited only external β-lactamase. We chose to investigate compounds that had previously been conjugated to beads as a means of purifying β-lactamases. Preliminary experiments, utilizing aminoboronic acid or 6-aminopenicillanic acid as the conjugated compound, revealed a complete absence of inhibition in the former case and, in the latter case, inhibition of a cephalosporinase-type β-lactamase (the chromosomal β-lactamase of *Enterobacter cloacae*; Bellido et al., 1991) but no inhibition of the penicillinase-type β-lactamase TEM-2. Therefore, we concentrated these studies on methicillin as the conjugated compound since preliminary studies demonstrated that conjugates inhibited both classes of enzymes. Since TEM-2 β-lactamase is expressed from the plasmid RP1, which is a broad host range plasmid capable of being delivered by conjugation to virtually any Gram-negative bacterium, the methicillin conjugates would be broadly useful in outer membrane permeability studies.

Methicillin has been previously demonstrated to act as a β-lactamase inhibitor (Sutherland and Batchelor, 1964). In addition it has been coupled to ethylenediamine and 1,6 diaminohexane bound to Sepharose and used effectively as a matrix for purification of penicillinase (Coombe and George, 1976). The method used by these authors for coupling methicillin was similar to that reported in this paper, in that carbodiimide was utilized for linking the carboxyl group of methicillin to the free amino group of the matrix-bound diaminoalkane. Therefore a series of compounds were synthesized using β-cyclodextrin (oxidized to introduce an aldehyde functional group) as the soluble matrix and the antibiotic methicillin (Scheme I). The carboxyl group on methicillin was linked to form an amide bond with one amino end of diamino alkyl derivatives, leaving the other end free to link to oxidized β-cyclodextrin. The length of the spacer was gradually increased by coupling the free amino group to succinic anhydride and then to a second diamino alkyl derivative

to produce hydrophilic spacers. The compounds synthesized contained spacers ranging from 4 to 24 Å (Figure 1).

The final products were pure as judged by HPLC, TLC, and, in selected instances, NMR. The active compounds with the longest spacers (**P7** and **P8**) were characterized by NMR and cesium ion ionization mass spectrometry. Proton NMR spectra indicated that only a single spacer and a single methicillin moeity were attached to one oxidized β-cyclodextrin molecule. The ion obtained by cleavage of the side arm was prominent in negative-ion LSIMS (oxidized β-cyclodextrin with loss of a proton, m/z 1133) and in positive-ion LSIMS (oxidized β-cyclodextrin + Na^+, m/z 1157]). Ions due to fragmentation as shown in Scheme II were also observed.

β-Cyclodextrin was chosen as the bulky group in these studies because of its solubility in water and the ease of modification of its sugars. The bulky cyclic nature of the molecule would prevent its entry across any channels in the bacterial outer membrane (Hancock and Bell, 1988). β-Lactamase has a binding site for β-lactams which is located below its surface, and therefore when the spacer arm between β-cyclodextrin and the β-lactam is not long enough, the bulky β-cyclodextrin would not allow the antibiotic to fit into the binding site on the β-lactamase molecule. The activity of β-lactamase was measured by using the nitrocefin assay (Angus et al., 1982). When β-lactamase was inhibited by the compound, nitrocefin hydrolysis did not occur. Initially the inhibitory activity was measured using intact washed *P. aeruginosa* cells that had been kept at 23 °C. Although the amount of β-lactamase activity was low, it was suppressed nearly 3-fold by compounds **P4-P8** at a concentration of 1 mM (Figure 2A). In contrast, **P3** had virtually no inhibitory activity, whereas free methicillin suppressed both excreted and periplasmic (cell-associated) β-lactamase activity. A control experiment to show that cyclodextrin and linker without methicillin would not inhibit β-lactamase was not performed. However, lack of inhibitory activity of **P1-P3** are an equivalent negative control. All compounds with methicillin and spacer alone were effective inhibitors of the enzyme. Methicillin inhibited β-lactamase at 0.1 and 1.0 mM concentrations, but did not inhibit at 0.01 mM concentration. Therefore our compounds were tested at concentrations between 0.1 and 1.0 mM. There was no inhibition at concentrations below 0.5 mM, and therefore the tests were performed at 1.0 mM concentration. To improve the sensitivity of this assay, cells were incubated for 10 min at 4 °C. This led to a 7.6-fold increase in β-lactamase leakage (Figure 2B), consistent with the observations of Lei et al. (1991). Under these more extreme conditions, the extent of inhibition of external β-lactamase activity varied with the length of the cross-linker when all compounds were present at concentrations of 1 mM. Thus, the extents of inhibition of surface and secreted β-lactamase were 6% using **P3**, 20% using **P4**, 43% using **P5**, 77% using **P6**, 91% using **P7**, and 100% using **P8** (see Figure 2 legend for actual rates of hydrolysis) at a nitrocefin substrate concentration of 71 μg/mL. Therefore we consider both **P7** and **P8** to be adequate for suppressing external β-lactamase activity, with the latter being more reliable under extreme conditions. As expected, methicillin at 1 mM concentration completely suppressed whole cell β-lactamase activity, suppressing surface-associated and periplasmic β-lactamase. By performing similar experiments at different concentrations of compounds, it was determined that free methicillin was about 10-fold more effective (on a molar basis) at inhibiting β-lactamase than, for example, **P8**, presumably due to the influence of

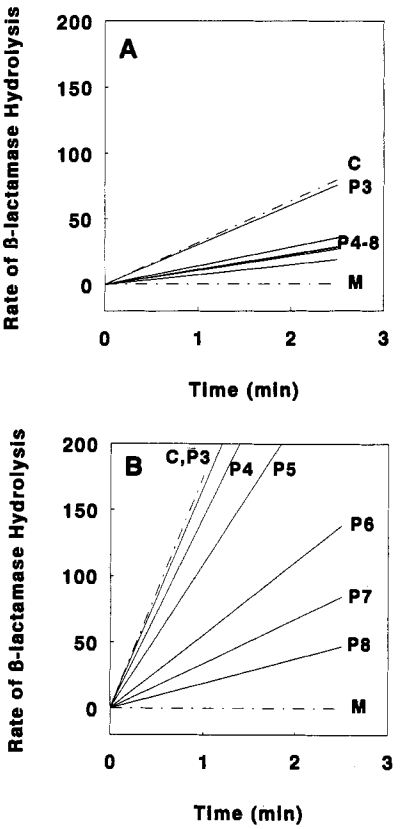


Figure 2. Inhibition of β-lactamase activity on whole cells preincubated with test compounds. (A) Cells at 23 °C. Dashed lines represent the controls with buffer only (C; β-lactamase activity 17.1 pmol of nitrocefin hydrolyzed/mg of cells per min) and using free methicillin as an inhibitor (M; 0 pmol/mg of cells per min). Solid lines represent β-lactamase activity in the presence of **P3**, **P4**, **P5**, **P6**, **P7**, and **P8** (respectively 16.25, 7.6, 6.0, 6.2, 4.0, and 6.0 pmol/mg of cells per min). (B) Cells pretreated 10 min at 4 °C. See 2A for legend. β-Lactamase activities were (in pmol of nitrocefin hydrolyzed/mg of cells per min) C = 94.5, M = 0, **P3** = 89.8, **P4** = 77.5, **P5** = 58.3, **P6** = 29.7, **P7** = 18.1, P8 = 10.0.

derivatization of the carboxyl group. Nevertheless, **P8** (under ice treatment conditions) and **P4-P8** (at room temperature) were able to suppress surface-associated and secreted β-lactamase. The residual unsuppressed β-lactamase activity provided an estimate of the actual rate of diffusion of nitrocefin into *P. aeruginosa* cells. At this substrate concentration, it was estimated as 6.6 ± 2.0 pmol of nitrocefin/mg of cells per min. Since it is well-known that the β-lactams do not bind to the interior of nonspecific porin channels (Bellido et al., 1991; Yoshimura and Nikaido, 1985), we are confident that, even at 1.0 mM compound concentration, porin diffusion would not be affected. We conclude therefore that the described compounds will be useful for measuring outer membrane permeability in diverse Gram-negative bacteria, to prevent substantial errors introduced by leakage of β-lactamase out of cells (Bellido et al., 1991; Lei et al., 1991; Liu and Nikaido, 1991).

From these data it appears that the minimum length of the spacer should be at least 16 Å (Figure 1) to provide maximum interaction between the β-lactam (methicillin) and its binding site within the β-lactamase molecule. This does not imply that the binding site is 16 Å below the surface of the β-lactamase molecule, because X-ray studies conducted with antibiotics bound to these enzymes showed that the β-lactam is oriented such that the carboxyl group is directed partially into the interior of the binding cavity (Ghuysen, 1991). Since these compounds all contain

spacers linked to the carboxyl group, the spacer may span the entire length of the binding cavity.

ACKNOWLEDGMENT

The authors are grateful to the Canadian Bacterial Diseases Network for funding this project.

LITERATURE CITED

Angus, B. L., Carey, A. M., Caron, D. A., Kropinski, A. M. B., and Hancock, R. E. W. (1982) Outer membrane permeability in *Pseudomonas aeruginosa*: Comparison of a wild type with an antibiotic supersceptible mutant. *Antimicrob. Agents Chemother. 21*, 299–309.

Bellido, F., Pechere, J.-C., and Hancock, R. E. W. (1991) Novel method for measurement of outer membrane permeability to new β-lactams in intact *Enterobacter cloacae* cells. *Antimicrob. Agents Chemother. 35*, 68–72.

Coombe, R. G., and George, A. M. (1976) An alternative coupling procedure for preparing activated Sepharose for affinity chromatography of Penicillinase. *Aust. J. Biol. Sci. 29*, 305–316.

Dubois, M., Gilles, K. A., Hamilton, J. K., Rebers, P. A., and Smith, F. (1956) Colorimetric method for determination of sugars and related substances. *Anal. Chem. 28*, 350–356.

Ghuysen, J.-M. (1991) Serine β-lactamases and penicillin-binding proteins. *Annu. Rev. Microbiol. 45*, 37–67.

Hancock, R. E. W., and Bell, A. (1988) Antibiotic uptake into Gram-negative bacteria. *Eur. J. Clin. Microbiol. Infect. Dis. 7*, 713–720.

Hay, G. W., Lewis, B. A., and Smith, F. (1965) Periodate oxidation of polysaccharides: General polysaccharides. *Methods Carbohydr. Chem. Vol. V. General Polysaccharides.* (R. L. Whistler, J. N. Be Miller, and M. L. Wolfrom, Eds.) pp 358–360, Academic Press, New York.

Jeffrey, A. M., Zopf, D. A., and Ginsburg, V. (1975) Affinity chromatography of carbohydrate specific immunoglobulins: coupling of oligosaccharides to sepharose. *Biochem. Biophys. Res. Commun. 62*, 608–613.

Lei, Y., Satake, S., Ishii, J., and Nakae, T. (1991) Factors that influence the permeability assay of the outer membrane of *Pseudomonas aeruginosa*. *FEMS Microbiol. Lett. 80*, 337–340.

Liu, W., and Nikaido, H. (1991) Contribution of the cell-surface-associated enzyme in the Zimmermann-Rosselet assay of outer membrane permeability to β-lactam antibiotics. *Antimicrob. Agents Chemother. 35*, 177–179.

O'Callaghan, C. H., Morris, A., Kirby, S. M., and Shingler, A. N. (1972) Novel method for detection of β-lactamases by using a chromogenic cephalosporin substrate. *Antimicrob. Agents Chemother. 1*, 283–288.

Sutherland, R., and Batchelor, F. R. (1964) Synergistic activity of penicillins against penicillinase-producing Gram negative bacteria. *Nature. 201*, 868–869.

Yoshimura, F., and Nikaido, H. (1985) Diffusion of β-lactam antibiotics through the porin channels of *Escherichia coli* K-12. *Antimicrob. Agents Chemother. 27*, 84–92

Zimmermann, W., and Rosselet, A. (1977) Function of the outer membrane of *Escherichia coli* as a permeability barrier to β-lactam antibiotics. *Antimicrob. Agents Chemother. 12*, 368–372.

Biologically Active Interleukin 2–Ricin A Chain Fusion Proteins May Require Intracellular Proteolytic Cleavage To Exhibit a Cytotoxic Effect

Jonathan P. Cook, Philip M. Savage,† J. Michael Lord, and Lynne M. Roberts*

Department of Biological Sciences, University of Warwick, Coventry CV4 7AL, UK, and the Imperial Cancer Research Fund, Clinical Oncology Group, Hammersmith Hospital, London W12 OHS, UK. Received April 9, 1993®

DNA fusions encoding chimeric proteins in which human interleukin 2 (IL2) was fused to the A subunit of the plant cytotoxin ricin (RA) have been expressed in *Xenopus* oocytes. The constructs contained N-terminal IL2 and C-terminal RA, or N-terminal RA and C-terminal IL2. In the expressed chimeric proteins, the IL2 and RA moieties were joined by a peptide sequence containing a proteolytic cleavage site. Two proteolytically-sensitive peptide sequences were utilized; a peptide that forms the trypsin-sensitive disulfide-bonded loop in diphtheria toxin (DT) or a synthetic peptide containing the factor Xa recognition site in a sequence flanked by two cysteine residues. In an *in vitro* cell free system the RA component was biologically active in all chimeric proteins produced since it specifically depurinated 28S ribosomal RNA. Proteolytic cleavage of the chimeras with either trypsin or factor Xa as appropriate separated the IL2 and RA moieties, but they did not remain covalently linked by a disulfide bond. Because of this, the cytotoxicity of protease-treated chimeras could not be assessed. Chimeras not pretreated with factor Xa but which contained the factor Xa target sequence were not cytotoxic to CTLL-2 cells. Rather, these molecules had a stimulatory effect that was ascribed to the IL2 moiety. In contrast, recombinant chimeric toxins containing the DT loop sequence were cytotoxic to CTLL-2 cells. Taken together the data suggest that RA-containing chimeras require intracellular proteolytic cleavage to release the RA moiety to render them cytotoxic to target cells.

INTRODUCTION

Bacterial toxins such as diphtheria toxin (DT) or *Pseudomonas* exotoxin A (PE) possess three functional domains: a cell-binding domain responsible for binding the toxin to specific protein receptors present on the surface of target cells, a translocating domain which allows a toxic fragment to cross an intracellular membrane during endocytosis and thereby reach the cell cytosol, and a catalytically active domain responsible for the ADP-ribosylation of elongation factor-2 in the cytosol (*1*, *2*). The toxic fragment containing the ADP-ribosylating domain is generated during endocytic uptake by a proteolytic cleavage step which is catalyzed by host cell protease(s). After proteolytic processing, but prior to the membrane translocation step, the toxic fragment remains covalently linked to the translocating and the cell binding domains through a single disulfide bond (*3*).

Recombinant chimeric bacterial toxins with novel cell binding specificities have been generated by deleting the portion of the toxin gene encoding the cell binding domain and replacing it with DNA encoding an alternative cell binding peptide such as a growth factor (*4*, *5*), lymphokine (*6*, *7*), or single chain antibody (*8*, *9*). Such gene fusions have been expressed in *Escherichia coli*, purified, and, if appropriate, renatured. Provided that the new cell-binding domain and the toxin's translocating domain are linked to the ADP-ribosylating domains of the toxin via the disulfide-bonded loop containing the protease-sensitive site, the chimeric proteins are potently cytotoxic, although their target cell recognition has been altered (*10*).

It has not proved possible to extend this approach for making single chain chimeric cytotoxins containing toxic plant proteins such as ricin. Ricin consists of a translocationally-competent toxic polypeptide, the A chain (RA) (in this case a 28S rRNA *N*-glycosidase (*11*)), and a cell binding polypeptide, the B chain, both of which initially occur together within the plant cell as a single proprotein (*12*). The proteolytic processing step that separates the two polypeptides occurs during toxin biogenesis within the plant (*13*). Processing does not involve cleavage at a serine protease-sensitive site, as is the case with the bacterial toxins, but rather involves the removal of a short linker peptide from within a disulfide-bonded loop (*12*). The endoprotease responsible for this processing, which requires cleavage after asparagine residues, is commonly found in plant cells but is apparently not present in mammalian cells (*14*). Intoxication of mammalian cells with mature plant cytotoxins, such as ricin, does not therefore require target cell proteolytic activity to release the toxic (RA) polypeptide for subsequent translocation into the cytosol.

In the present paper we describe the construction of recombinant chimeric toxins in which interleukin (IL) 2, which has been successfully utilized as the cell-binding component in chimeric toxins based on both DT (*5*) and PE (*6*), has been joined to ricin A chain. However, recombinant fusion proteins containing RA are not normally cytotoxic, even when their component parts are biologically active *in vitro*, since proteolytic release of a translocationally-competent RA does not occur (*15*). To overcome this limitation we have engineered proteolytic cleavage sites into the RA-IL2 fusions to allow them to be processed either before or after cell entry in order to confer cytotoxicity. The proteolytic cleavage sites were present either in a peptide sequence that forms a naturally occurring disulfide bonded loop (from DT with a trypsin-

† Corresponding author: Lynne M. Roberts, Department of Biological Sciences, University of Warwick, Coventry CV4 7AL, UK. Telephone: 0203 523558. Fax: 0203 523701.

† Imperial Cancer Research Fund.

® Abstract published in *Advance ACS Abstracts*, October 1, 1993.

1043-1802/93/2904-0440$04.00/0 © 1993 American Chemical Society

sensitive site) or in a synthetic peptide that contained the factor Xa (FXa) recognition site in a sequence flanked by two cysteine residues. The data presented show that while both these protease-sensitive sites were readily cleaved by the appropriate protease, the cysteine residues flanking the cleavage sites did not form a disulfide bond. In the case of the chimeric proteins containing the diphtheria toxin linker sequence, this limitation did not prevent these molecules from exhibiting a cytotoxic effect since proteolytic release of the RA component could apparently occur within target cells. The RA-IL2 fusion protein is therefore a potential cytotoxic agent for cells bearing IL2 receptors and may be developed as a useful therapeutic agent in the treatment of diseases where IL2 receptor-positive cells are involved (*16*).

EXPERIMENTAL PROCEDURES

Materials. Restriction and DNA modification enzymes were from Gibco BRL Ltd., Paisley, UK, or Amersham International plc, Aylesbury, UK. RPMI 1640 culture medium was purchased from Gibco and [^{35}S]methionine (1000 Ci/mmol) was from Amersham. DNA encoding human IL2 and goat anti-IL2 antibodies were from British Biotechnology Ltd, Oxon, UK. Recombinant IL2 and soybean trypsin inhibitor were from Boehringer Mannheim UK Ltd., Lewes, UK. Trypsin, ricin, phenylmethanesulfonyl fluoride and aprotinin were purchased from Sigma Chemical Company Ltd., Poole, UK, and Bio-Beads SM2 were from BioRad Laboratories Ltd., Hemel Hempstead, UK. Aniline was from BDH Chemicals Ltd., Lutterworth, UK. Oligonucleotides encoding the factor Xa loop were produced on an Applied Biosystems DNA synthesizer, Model 380B, and those encoding the diphtheria toxin loop were provided by Greg Winter, MRC, Cambridge, UK. The oocytes were provided by H. Woodland, University of Warwick.

Plasmid Construction. Oligonucleotides encoding the diphtheria toxin loop (DTL) (Figure 1A) were annealed and cloned into pUC18 to give pJK100. An *Nde*I (blunted with S_1 nuclease)/*Hin*dIII fragment encoding human interleukin 2 was ligated to the 3′ side of DTL in pJK100 to give pJK200. A *Sal*I/*Sma*I fragment encoding ricin A chain (*12*) was ligated with the *Sma*I/*Hin*dIII fragment from pJK200 into pUC9 (*Sal*I/*Hin*dIII) to give pJK314. An *Eco*RI/*Hin*dIII fragment (blunted with T_4 DNA polymerase) was ligated into pSP64ΔBam (*17*) to provide an ATG start codon. The new plasmid pJK401 was used for transcription reactions utilizing the SP6 promoter and encoded ricin A chain–DTL–IL2 (RADIL). An *Eco*RI/*Cla*I fragment encoding the full ricin signal sequence and part of RA (*18*) was inserted into the pJK314 similarily digested. An *Eco*RI/*Hin*dIII fragment encoding preRADIL (where the prefix "pre" refers to the presence of DNA encoding the ricin signal sequence) was then ligated into pGEM1 and pSPJC1 (below) to give pJC914G and pJC914X, respectively. Transcripts from the latter (encoding preRADIL) were used in *Xenopus* oocyte translocations. pSPJC1 is a modified version of pSP64T (*19*). The multiple cloning site (MCS) and upstream *Hin*dIII site were removed from pSP64T by blunting and religation. Annealed oligonucleotides containing a new MCS of *Eco*RI/*Nde*I/*Sal*I/*Hin*dIII were introduced into the *Bgl*II site to give pSPJC1. The region encoding the DTL was replaced in three constructs with annealed oligonucleotides (with overhangs of *Kpn*I/*Xho*I), encoding the factor Xa (FXa) recognition sequence within an unstructured loop (GlyAlaGlyAlaGly) and bounded by cysteine residues (Figure 1B). This was performed in the following plasmids: pJK401, pJC914G, and pJC914X to give pJC688, pJC934G, and pJC934X respectively. pJC688 encodes RA–FXa loop–IL2 (RAXIL), and pJC934G and pJC934X encode preRAXIL.

In constructing fusions carrying IL2 preceding RA DNA, a *Xho*I (blunted with T_4 DNA polymerase)/*Hin*dIII fragment encoding RA was ligated to the 3′ side of DTL in pJK100. The *Bam*HI (blunted with S_1 nuclease)/*Hin*dIII fragment from this plasmid was ligated into pGEMIL2 (*Hpa*I/*Hin*dIII) to give pJC371. This plasmid encodes IL2–DTL–RA (ILDRA). Annealed oligonucleotides (with overhangs of *Eco*RI/*Xho*I) encoding the FXa loop were ligated to the 5′ side of RA. The *Hpa*I/*Hin*dIII fragment from this plasmid was ligated into pGEMIL2 to give pJC812, which encodes IL2–FXa loop–RA (ILXRA). The *Eco*RI/*Hin*dIII fragments (blunted with S_1 nuclease) from pJC371 and pJC812 were ligated to the 3′ side of the full ricin signal sequence in pGEM1 to give pJC971G and pJC982G, respectively. These plasmids encode preILDRA and preILXRA, respectively. *Eco*RI/*Sal*I fragments from these plasmids were ligated into pSPJC1 to give pJC971X and pJC982X for oocyte translation experiments. Clones encoding preIL2 were constructed in a similar manner.

DNA Manipulations. Standard methods for DNA manipulation were used as described (*20*).

In vitro Transcription/Translation. Approximately 2 μg of linearized DNA was incubated in a final volume of 20 μL with 40 mM Hepes–KOH, pH 7.5, 6.5 mM magnesium acetate, 2 mM spermidine, 10 mM dithiotreitol, 100 μg/mL bovine serum albumin, 0.5 mM each of ATP, CTP, and UTP, 0.1 mM GTP, 0.25 mM 7 mG(5′)ppp(5′)G, 20 units RNasin, and 15 units of SP6 or T7 RNA polymerase. The mixture was incubated at 40 °C for 30 min and GTP in 20 mM Hepes–KOH, pH 7.5, was then added to a final concentration of 0.4 mM and the reaction continued for 30 min. Transcript RNA (1 μL) was translated in a wheat germ lysate system and labeled with [^{35}S]methionine as described (*21*).

Samples (typically 12 μL) from an *in vitro* translation reaction were digested with trypsin or factor Xa (described below), immunoprecipitated (*22*) with either rabbit anti-RA or goat anti-IL2 antibodies, and analyzed by sodium dodecyl sulfate–polyacrylamide gel electrophoresis (SDS–PAGE) (*23*).

Trypsin Digestion. Samples were digested with 10 μg/mL trypsin in 50 mM Tris-HCl, pH 7.0, at 37 °C and stopped with 50 μg/mL soybean trypsin inhibitor.

Factor Xa Digestion. Samples were digested with 24 μg/mL factor Xa (FXa) in 10 mM Tris-HCl, pH 7.6, 140 mM NaCl, and 1 mM EDTA for 1 h at 25 °C.

Ribosome Depurination Assay. The action of ricin A chain on rRNA is to remove an adenine base. The site of this depurination is susceptible to cleavage by aniline, releasing a 390 base RNA fragment which is indicative of RA activity. 2 μL of transcript RNA was translated in a non-nucleased reticulocyte lysate (provides the maximum amount of substrate for RA). Proteins were solubilized by the addition of 1% (w/v) SDS and then extracted with phenol/chloroform. The RNA was then precipitated with ethanol. A 4-μg portion of RNA was incubated, in the dark, with 20 μL of 1 M aniline/acetic acid, pH 4.8 (*24*) at 60 °C for 2 min. The treated RNA was precipitated and resuspended in 60% (v/v) deionized formamide, 3.6 mM Tris, 3 mM sodium dihydrogen orthophosphate, and 0.2 mM EDTA. Aniline-treated and untreated RNA samples were denatured at 65 °C and analyzed on an 1.2% agarose–50% formamide gel.

***Xenopus* Oocyte Translation.** Transcripts were

translated in oocytes as described by Colman (22). A 50-nL sample of transcript RNA (1 mg/mL) was injected into each of approximately 30 oocytes. The oocytes were incubated overnight at 15 °C, half of them with 45 μCi [^{35}S]methionine. The oocytes were homogenized in a buffer of 20 mM Tris-HCl, pH 7.6, 0.1 M NaCl, and 1% (v/v) Triton X-100 (25 μL per oocyte). The homogenate was treated with Bio-Beads SM2 to remove the Triton. Unlabeled samples were normalized for total protein content (measured at A_{280}). Two-thirds of each of the labeled homogenates was digested with trypsin or factor Xa, immunoprecipitated (22) with rabbit anti-RA and goat anti-IL2 antibodies, and analyzed by reducing/nonreducing SDS-PAGE.

Cytotoxicity Assays. CTLL-2 cells (25) were maintained in RPMI 1640 medium supplemented with 10% fetal calf serum, 2 mM glutamine, 50 IU penicillin, and 50 μg/mL streptomycin plus 10 units/mL recombinant interleukin 2. Before use the cells were washed three times with fresh media and incubated for 18 h without IL2. For ricin cytotoxicity measurements cells were plated at 2 × 10^5 cells/mL and supplemented with 10 units/mL IL2. Doubling dilutions of whole ricin (0.05–100 ng/mL) were then added to the cells. For cytotoxicity measurements with oocyte homogenates, cells were plated at a final density of 2 × 10^5 cells/mL supplemented with 5 units/mL IL2 with various dilutions of homogenates. The cells were then incubated overnight at 37 °C and 5% CO_2 in air. Cells were labeled with 1 μCi [^{35}S]methionine for 2 h followed by harvesting and counting. Samples were analyzed in quadruplicates and expressed as a percentage of cells with no additions.

RESULTS

Construction of Transcription Vectors. DNA fusions between the coding sequence of human IL2 and that of ricin A chain (RA), separated by DNA encoding a linker peptide with a protease-sensitive site, were constructed in the transcription vectors pSP64 and pGEM1 as described in Experimental Procedures. The chimeric molecules encoded by these DNA fusions consisted of N-terminal RA and C-terminal IL2 or N-terminal IL2 and C-terminal RA. In each case the toxin and cytokine domains were separated by either a short amino acid sequence containing the disulfide-linked peptide loop with a trypsin-sensitive cleavage site from diphtheria toxin or a synthetic disulfide-linked peptide loop with a factor Xa-specific cleavage site (Figure 1).

In a further series of constructs each fusion was preceded in frame by DNA encoding the N-terminal leader sequence (which includes the endoplasmic reticulum (ER) targeting signal sequence) from preproricin (18). Since transcripts encoding the signal sequence were to be expressed in *Xenopus* oocytes, they were cloned into the transcription vector pSP64T, modified as described in Experimental Procedures. In this vector, the constructs were flanked by the 5′ and 3′ untranslated regions of *Xenopus* B-globin cDNA which, upon transcription, provided stability to the RNA when injected into oocytes. DNA encoding human IL2, with or without that encoding the ricin signal sequence, was also cloned into the transcription vectors. A schematic illustration of the chimeric proteins possessing a signal sequence is shown in Figure 2.

***In Vitro* Transcription and Translation.** Transcripts were prepared for RADIL, ILDRA, RAXIL, and ILXRA in an *in vitro* system using the SP6 or T7 promoter and driven by SP6 or T7 RNA polymerase, respectively. Transcripts were translated in a wheat germ cell-free lysate

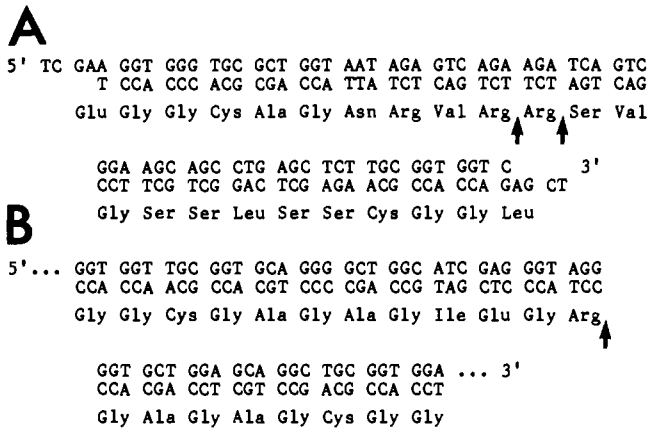


Figure 1. Oligonucleotides encoding the protease sensitive loops. (A) diphtheria toxin loop; (B) 'factor Xa loop'. Two versions of the FXa loop were made with (i) *KpnI*/*XhoI* and (ii) *HpaI*/*XhoI* compatable ends. The arrows indicate the expected site of proteolytic cleavage.

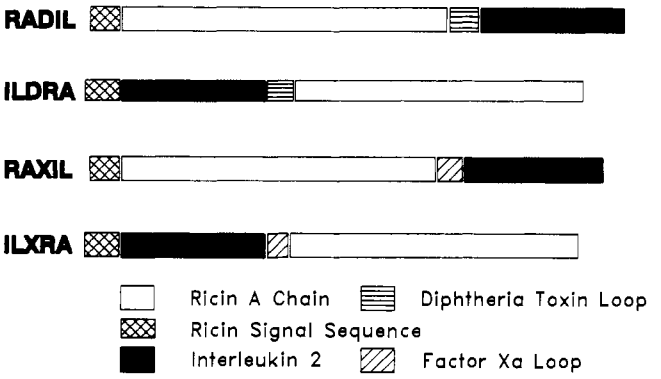


Figure 2. Schematic Representation of the Fusion Proteins Employed. Fusions were made with (as shown) and without the ricin signal sequence. Proteins made with an N-terminal signal sequence were prefixed 'pre'.

in the presence of [^{35}S]methionine. The translation products were separated by SDS-PAGE and visualized by fluorography. All four transcripts gave polypeptide products of the expected molecular mass (Figure 3A, lanes 1, RADIL, 51.5 kDa; Figure 3B, Lanes 1, ILDRA, 47.5 kDa; Figure 3C, lanes 1, RAXIL, 49.5 kDa and ILXRA, 46.5 kDa).

Proteolytic Cleavage and Identification of the Cleavage Products. The RADIL and ILDRA translation products were incubated with trypsin. At various times, samples were removed and further proteolysis was prevented by adding soybean trypsin inhibitor. ILDRA digestion was found to be more specific than was the case with RADIL, therefore the former was allowed to proceed for longer times. Each sample was divided into three. Material in one-third was immunoprecipitated using antibodies raised against RA, another third with antibodies against IL2, and the final third was not immunoprecipitated. Trypsin digestion produced fragments of the expected size containing either RA (~30 kDa) (Figure 3A,B, lanes RA 2–4) or IL2 (~15.5 kDa) (Figure 3A,B, lanes IL2 2–4).

The RAXIL and ILXRA translation products were incubated for 60 min with factor Xa and then treated as above. Once again factor Xa digestion produced fragments of the appropriate size: RA (~30 kDa) (Figure 3C, lanes RA 2) or IL2 (~15.5 kDa) (Figure 3C, lanes IL2 2).

The small amounts of fragments produced did not permit purification and N-terminal microsequence anal-

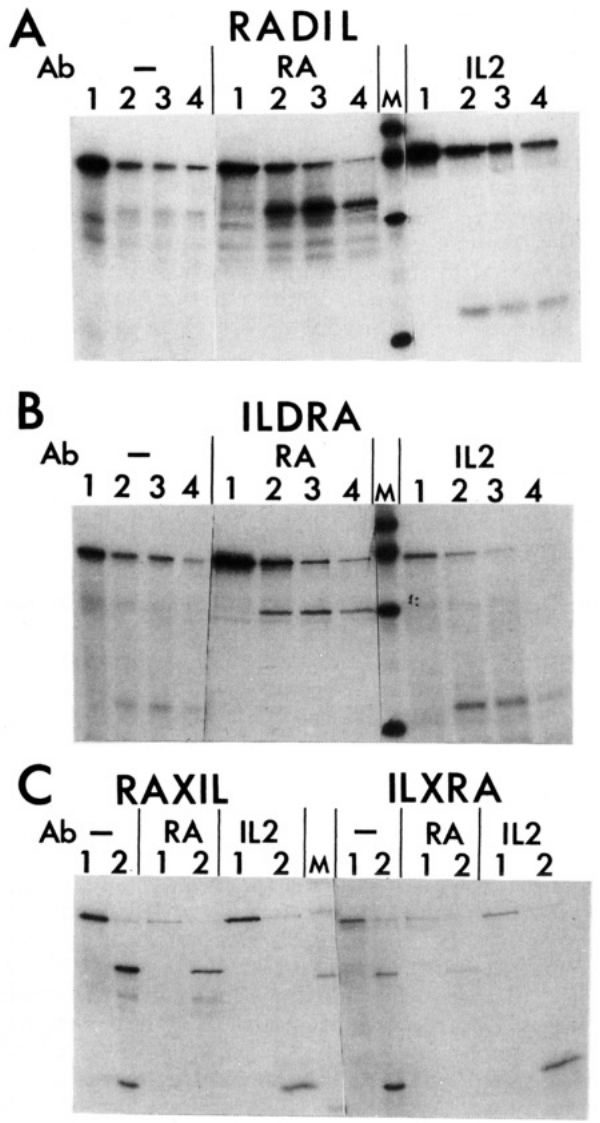


Figure 3. Protease sensitivity of fusion proteins. Samples from a wheat germ lysate translation were digested with protease for various times and immunoprecipitated with anti-RA (RA) or anti-IL2 (IL2) antibodies (Ab) or not immunoprecipitated (–) (see Experimental Procedures) and analyzed by SDS–PAGE: (A) RADIL digested with trypsin for 0 (lane 1), 4 (lane 2), 8 (lane 3), and 12 min (lane 4); (B) ILDRA digested with trypsin for 0 (lane 1), 8 (lane 2), 16 (lane 3), and 32 min (lane 4); and (C) RAXIL and ILXRA digested with factor Xa for 0 (lane 1) and 60 min (lane 2). Lane M, molecular mass markers increasing in sizes of 14.3, 30, 46 and 69 kDa.

ysis, so it is only assumed from sizing and antibody reactivities that cleavage occurs at the expected sites.

The Chimeric Molecules Catalytically Inactivate Ribosomes. RA kills cells by depurinating 28S rRNA at a specific site close to the 3′ end of the molecule (*11*). Ribosomes containing the modified 28S rRNA can no longer carry out protein synthesis. Depurination renders isolated 28S rRNA susceptible to amine-catalyzed hydrolysis of the phosphodiester bonds on either side of the modification site. This cleavage generates a small RNA fragment of approximately 390 ribonucleotides from rabbit reticulocyte 28S rRNA. This fragment is therefore diagnostic of RA-catalyzed depurination.

A variety of transcripts were translated in a rabbit reticulocyte lysate system. The products of RA transcripts (Figure 4A, lane 2; Figure 4B, lane 1) or of preRA transcripts (Figure 4A, lane 3) released the characteristic RNA fragment (arrowed) upon aniline treatment of

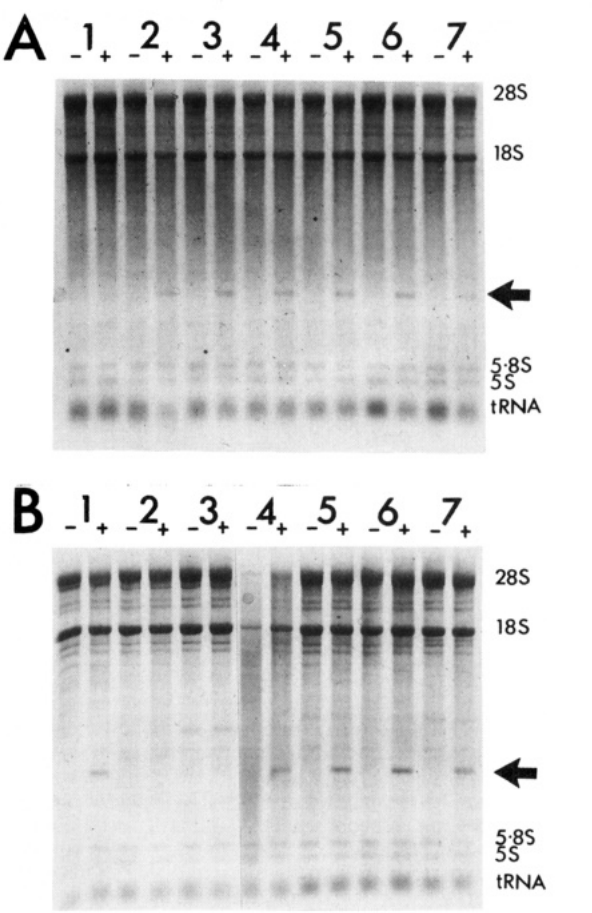


Figure 4. Ribosomal modification by the fusion proteins. Transcripts were translated in a rabbit reticulocyte lysate system. The rRNA was extracted and briefly treated with acetic–acid aniline. A treated sample (+) was run next to an untreated sample (–) on a formamide–agarose gel. The arrow indicates the RNA fragment released by aniline treatment of modified rRNA: (A) lane 1, transcript encoding yeast prepro-α factor; 2, mature ricin A chain (RA); 3, preRA; 4, RADIL; 5, preRADIL; 6, RAXIL, and 7, preRAXIL, (B) lane 1, RA; 2, interleukin 2 (IL2); 3, preIL2; 4, ILDRA; 5, preILDRA; 6, ILXRA; and 7, preILXRA.

isolated rRNA; the products of preproalpha factor (Figure 4A, lane 1), IL2 (Figure 4B, lane 2), and preIL2 (Figure 4B, lane 3) transcripts did not. All of the products from the RA–IL2 fusion transcripts prepared in the present study, with or without an N-terminal signal sequence, produced the diagnostic fragment (Figure 4A, lanes 4–7; Figure 4B, lanes 4–7). These data clearly show that the RA component of the fusion proteins was catalytically active, regardless of its position within the chimeric molecule.

Expression in *Xenopus* Oocytes. Recombinant proteins were produced by microinjecting transcripts into *Xenopus* oocytes. In this case the transcripts, which also encoded an N-terminal signal sequence, were used so that the protein products would be directed to the lumen of the oocyte ER to facilitate folding and disulfide bond formation. The microinjected oocytes were incubated with [^{35}S]methionine and the recombinant products were recovered by immunoprecipitation.

Figure 5A (lane 1) shows the total [^{35}S]-labeled products synthesized by oocytes which had been microinjected with preIL2 transcripts. Immunoprecipitation with anti-human IL2 antibodies recovered a product which, after reduction, ran on the gel with an apparent molecular mass of 16.5 kDa (Figure 5A, lane 2R) and was not present in homogenate from control oocytes that had been mock injected with water (data not shown). When the immu-

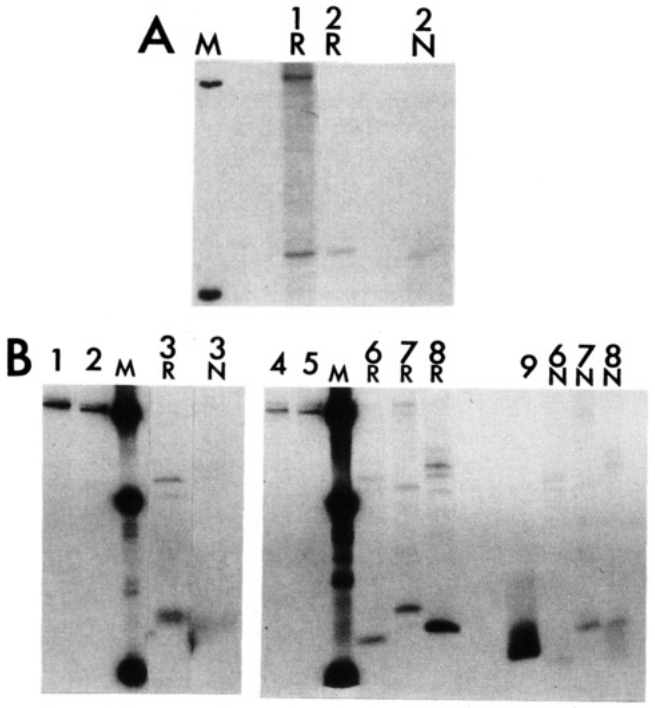


Figure 5. Translation in *Xenopus* oocytes and protease sensitivities. Transcripts were microinjected into oocytes. After incubation the oocytes were homogenized, samples were immunoprecipitated and analyzed by SDS–PAGE under reducing (R) and nonreducing (N) conditions: (A) lane 1, total homogenate from oocytes expressing IL2; 2, equivalent sample immunoprecipitated with anti-IL2 antibodies; and M, molecular mass markers increasing in sizes of 14.3 and 30 kDa; (B) Lane 1, RADIL; 2, ILDRA; 3, ILDRA digested with trypsin; 4, RAXIL; 5, ILXRA; 6, RAXIL digested with factor Xa; 7, ILXRA digested with factor Xa; 8, RADIL digested with trypsin; 9, IL2; and M, molecular mass markers increasing in sizes of 14.3, 30 and 46 kDa.

noprecipitated product was run under nonreducing conditions, it had an increased mobility on the gel (Figure 5A, lane 2N), suggesting that the intrachain disulfide bond, essential for IL2 activity (*26*), was present in the recombinant IL2 molecule.

Homogenates prepared from oocytes which had been microinjected with transcripts encoding preRADIL (Figure 5B, lane 1), preILDRA (Figure 5B, lane 2), preRAXIL (Figure 5B, lane 4), or preILXRA (Figure 5B, lane 5) all contained recombinant products of the expected molecular size (46–51 kDa) which were recovered by immunoprecipitation using a mixture of anti-RA and anti-IL2 antibodies. The unnicked fusions migrate in an identical fashion in the presence (shown) or absence (not shown) of reducing agent. When these products were treated with the appropriate protease, immunoprecipitated with the same antibody mixture, and run on the gels under reducing conditions, cleavage products representing both RA and IL2 components of the recombinant molecules were seen (Figure 5B, lanes 3R, 6R, 7R, and 8R). When the protease cleavage products were electrophoresed under nonreducing conditions, the same faint fragments were also seen (Figure 5B, lanes 3N, 6N, 7N and 8N). What is quite clear in the nonreducing lanes is that a product of the size of the noncleaved fusion protein is absent (compare lanes 1 and 8N, 2 and 3N, 4 and 6N, and 5 and 7N). This clearly indicates that the cleaved fragments did not remain covalently associated as disulfide-linked heterodimers. Apparently the two cysteine residues present in the linker peptides from either diphtheria toxin or the synthetic peptide with the factor Xa target sequence were not amenable to disulfide bond formation as the chimeric proteins folded in the lumen of the oocyte ER.

Biological Activity of the Chimeric Proteins. The recombinant fusion proteins produced in *Xenopus* oocytes were assayed through their effect on the proliferation of the IL2-dependent murine cell line CTLL-2. In order that the stimulatory effects of IL2 and the inhibitory effects of RA could be compared directly, we measured [^{35}S]-methionine incorporation into protein as an indication of proliferation. The proliferation seen with IL2 and certain of the chimeric proteins was more pronounced when measured as [^{3}H]thymidine incorporation into DNA (data not shown). The rates of protein synthesis with the recombinant oocyte products were expressed as a percentage of that for cells treated with an equivalent volume of homogenate from control oocytes. As shown in Figure 6A, homogenates from oocytes expressing IL2 stimulated the proliferation of CTLL-2 cells, whereas whole ricin was potently cytotoxic. Homogenates from oocytes expressing either RAXIL or ILXRA were stimulatory (Figure 6B), the former to the level seen with equivalent dilutions of the IL2-containing homogenate. Presumably the cells were not able to proteolytically process these chimeric molecules which in this form were not cytotoxic since they were unable to reach the cytosol for the RA component to exert its effects. The stimulation seen therefore, reflects a positive effect from the IL2 component. In contrast, oocyte homogenates containing either RADIL or ILDRA inhibited cellular protein synthesis. This is ascribed to the liberation of an active RA component due to cleavage of the fusion protein by cellular protease(s). Such cleavage must generate a translocation-competent form of RA which is able to reach its ribosomal substrates in the cytosol. The inhibitory effect of RA was apparently sufficient to overcome any stimulatory effect of the IL2 component. None of the IL2-containing fusion proteins had any effect on Vero cells when compared with an oocyte homogenate control (data not shown). Since the cleavage fragments generated by proteolytic pretreatment of the recombinant chimeric molecules were not linked by a disulfide bond, their effect on CTLL-2 cells was not determined. The fragments would predictably give a stimulatory effect due to the action of the released IL2 component.

DISCUSSION

We have constructed fusion proteins which contain the catalytically active subunit of the plant cytotoxin ricin (RA) and human IL2. The chimeric proteins consisted of either N-terminal RA and C-terminal IL2 or N-terminal IL2 and C-terminal RA. Previously IL2 has been fused to bacterial toxins to produce chimeric proteins in which IL2 was at the N-terminus of a fusion with PE (IL2–PE40 (*6*)) or at the C-terminus of a fusion with DT (DAB_{486}–IL2 (*5*)). Both the bacterial toxin fusions were cytotoxic to cells bearing IL2 receptors (*5*, *6*).

In IL2–PE40 and DAB_{486}–IL2 the toxin and IL2 moieties were separated by the protease-sensitive disulfide-bonded loop of the native cytotoxins. During endocytic uptake of bacterial toxins by mammalian cells, this loop is the site of cleavage of the toxin polypeptide by host cell protease(s). This releases the toxic domain from the cell-binding domain although they remain covalently linked via a disulfide bond.

This type of target cell proteolytic processing does not occur with plant toxins such as ricin, since the cleavage step which separates the enzymatic/translocation-competent and cell binding domains of ricin occurs during toxin biosynthesis (*13*) and is catalyzed by a plant protease with a target-site specificity not found for mammalian proteases (*14*). The RA–IL2 fusions produced in the

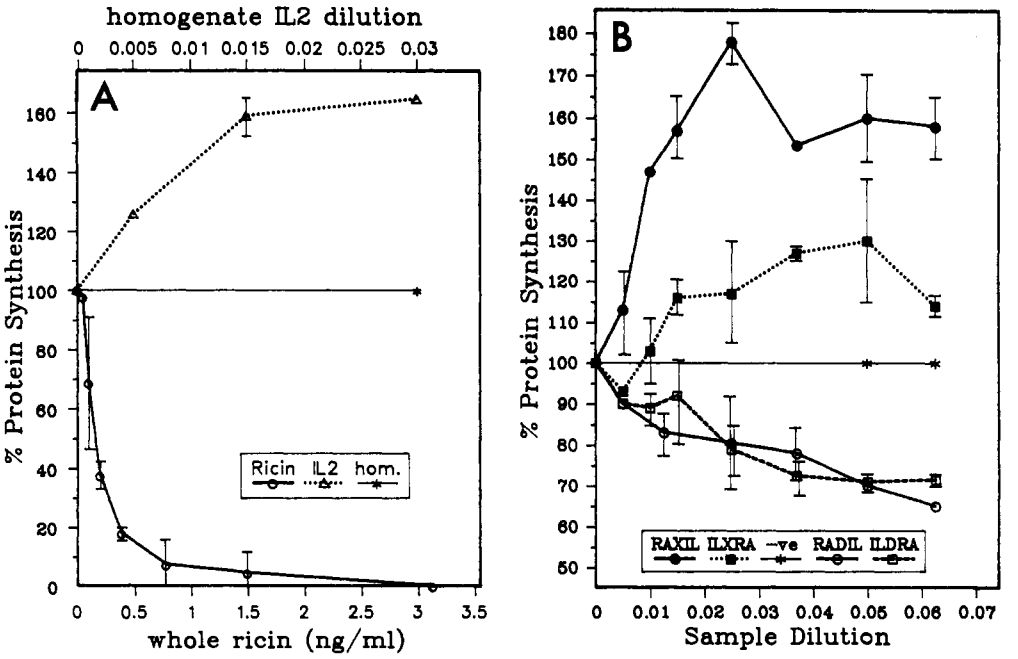


Figure 6. Cytotoxicity of fusion proteins. CTLL-2 cells (2×10^5 cells/mL) were incubated with (A) doubling dilutions of whole ricin and various dilutions of oocyte homogenate containing IL2 (where 1.0 represents neat homogenate and 0.01 represents a 100-fold dilution) and (B) various dilutions of oocyte homogenate containing a fusion protein. Culture details can be found in Experimental Procedures. Figures were normalized to give homogenate only control (hom, –ve) as 100%.

present study were therefore modified to allow proteolytic separation of the RA and IL2 components either before or during uptake by mammalian cells. This was achieved by including peptide sequences containing either a trypsin-sensitive cleavage site within a naturally occurring disulfide loop (from DT (*15*)), or a synthetic sequence containing the factor Xa recognition site flanked by two cysteine residues potentially capable of forming a disulfide bond (Figure 1). Factor X is a serine protease of the blood clotting cascade and is normally synthesized and secreted only by liver cells. Activated factor X (Xa) is involved in the activation of prothrombin and has the target site IEGR↓.

Recombinant proteins were produced by translating *in vitro* transcripts in a wheat germ cell-free system or, after microinjection, *Xenopus* oocytes. In all cases protein products of the expected size were obtained (Figures 3 and 5). Cleavage of the recombinant proteins with the appropriate protease also generated two polypeptide fragments of the expected size. The uncleaved proteins were immunoprecipitated by antibodies raised against either RA and IL2, whereas the cleavage fragments reacted with either anti-RA or anti-IL2 antibodies. The RA component of the chimeric proteins was catalytically active regardless of the position of RA within the chimeric molecules and regardless of whether such proteins possessed an uncleaved N-terminal signal sequence (Figure 4).

The protein products of transcripts microinjected into *Xenopus* oocytes were directed to the ER lumen to faciliate protein folding and correct disulfide bond formation. PreIL2 transcripts produced a recombinant product which we assume contained the correct IL2 intrachain disulfide bond (between Cys58 and Cys105). Immunoprecipitated IL2 ran with an increased mobility on gels when electrophoresed under nonreducing conditions as compared to reducing conditions (Figure 5A, lanes 2N and 2R), indicating the presence of a disulfide bond. Since this recombinant IL2 was biologically active (Figure 6A) and since the intrachain C_{58}–C_{105} disulfide is essential for biological activity (*26*), we assume that it had been correctly formed. A similar change in gel mobility was observed when comparing reduced and nonreduced IL2 derived from the chimeric molecules after proteolytic cleavage. This suggested that the intrachain disulfide bond of IL2 was correctly formed in the chimeric proteins (Figure 5B, lanes 3, 6, 7, and 8). In contrast, a disulfide bond between the cysteine residues flanking the linker sequence containing the proteolytic cleavage sites was not apparently formed, since electrophoresis of proteolytically-cleaved chimeric molecules resulted in separate RA and IL2 bands under both reducing and nonreducing conditions. Previous studies in our laboratory have shown that the signal sequence of preproricin effectively delivers protein into the oocyte ER lumen (*27*), where the oxidizing environment and the presence of protein disulfide isomerase facilitate disulfide bond formation. The reason why the putative disulfide bond did not form in the chimeric molecules is unclear, particularly as the DT-derived disulfide loop allowed correct disulfide bond formation when it was included in RA–staphylococcal protein A fusions that were expressed in the periplasmic space of *E. coli* (*15*) and a factor Xa-site containing linker allowed disulfide bond formation when included in the central proricin linker (*28*). We assume that the folding patterns of the chimeric molecules produced in this system in the present work precluded formation of the anticipated disulfide bond.

The IL2-dependent cell line CTLL-2 was stimulated by recombinant IL2 produced in oocytes and was intoxicated by whole ricin (Figure 6A). For the chimeric molecules, RAXIL and ILXRA were both stimulatory to CTLL-2 cells, presumably reflecting the biological activity of the IL2 component. Although RA is catalytically active in these chimeric molecules, we assume that the lack of an observed cytotoxic effect in CTLL-2 cells was because the RA component was not released from the chimeric molecule and as such was not able to cross an intracellular membrane in order to reach its ribosomal substrate. These fusions carrying the factor Xa specific site are not likely to encounter a protease with factor Xa specificity within CTLL-2 cells. Both RADIL and ILDRA were cytotoxic to CTLL-2 cells (Figure 6B) but were not cytotoxic to

Vero cells, which lack the IL2 receptor (data not shown). We assume that the cytotoxicity resulted from intracellular cleavage at the trypsin-sensitive site. This is consistent with our findings in an earlier study in which a biologically active recombinant RA–staphylococcal protein A fusion protein was not cytotoxic to antibody-coated cells (*15*). Cytotoxicity was conferred by including the DT loop in the RA–protein A fusions which permitted intracellular release of the RA component (*15*). In this case the desired disulfide bond was formed between RA and protein A, allowing the fusions to be cleaved by trypsin treatment before cell application, an approach that was not feasible in the present study because of the failure to produce the disulfide bond.

The cytotoxic effect we observed with RADIL and ILDRA was not very pronounced (a Student's *t*-test indicated that, for RADIL, the dilution points 0.037, 0.05, and 0.0625 were significantly different ($p < 0.05$) from the negative control and that the dilution point 0.037 was significantly different ($p < 0.05$) from the points 0.05 and 0.0625. For ILDRA, the test indicated that the dilution points 0.025, 0.037, 0.05, and 0.0625 were significantly different ($p < 0.05$) from the negative control and that the first three of these points were significantly different ($p < 0.05$) from each other and the dilution points 0.005, 0.01, and 0.015 (data not shown). This may be due to a compensatory stimulatory effect caused by the IL2 component together with the low levels of chimeric molecules produced in the oocyte system used here (approximately 1 ng per 10 oocytes). Use of a serine protease inhibitor (phenylmethanesulfonyl fluoride) and aprotinin did not improve the apparent yields upon oocyte homogenization (data not shown). Although the amounts of the toxic fusion proteins were too low to be quantified accurately, the relative amounts of each fusion used in the dilution series (shown in Figure 6) are comparable. This comparability was achieved for each fusion by assessing the amounts of [^{35}S]methionine-labeled immunoprecipitates from a small number of radiolabeled oocytes taken from a larger unlabeled batch. The crude homogenate volumes were then adjusted to take account of product yield variability prior to dilution and use in the cytotoxicity assessment. However, the extremely low levels of recombinant molecules produced in this expression system is clearly a serious limitation which prevented a more complete characterization of the proteolytic fragments. Because of this, we are currently reexpressing the constructs in a bacterial host. The results presented here do clearly show, however, that potentially useful chimeric toxins containing RA can be made where both the cell binding and toxic components retain biological activity, but they emphasize that the RA component must be proteolytically released within the target cell for such molecules to be cytotoxic. The intracellular compartment where proteolytic processing takes place has not been identified, but the endosome seems to be a likely site, since processing of trypsin-sensitive sequences in PE and DT has been shown to occur in this organelle.

ACKNOWLEDGMENT

We wish to thank Dr. Robert Spooner for his helpful discussions and Dr. Ken Flint for performing the Student's *t*-test. The factor Xa was a gift from P. Esnouf, Radcliffe Hospital, Oxford, UK. This work was supported by UK SERC grant No. GR/G/00877 and a UK SERC studentship to J.P.C.

LITERATURE CITED

(1) Hwang, J., FitzGerald, D. J., Adhya, S., and Pastan, I. (1987) Functional domains of *Pseudomonas* exotoxin identified by deletion analysis of the gene expressed in *E. coli*. *Cell 48*, 129–136.

(2) Olsnes, S., Kozlov, J. V., van Deurs, B., and Sandvig, K. (1991) Bacterial protein toxins acting on intracellular targets. *Sem. Cell Biol. 2*, 7–14.

(3) Ogata, M., Chaudhary, V. K., Pastan, I., and FitzGerald, D. J. (1990) Processing of *Pseudomonas* exotoxin by a cellular protease results in the generation of a 37,000-Da toxin fragment that is translocated to the cytosol. *J. Biol. Chem. 265*, 20678–20685.

(4) Chaudhary, V. K., FitzGerald, D. J., Adhya, S., and Pastan, I. (1987) Activity of a recombinant fusion protein between transforming growth factor type alpha and *Pseudomonas* exotoxin. *Proc. Natl. Acad. Sci. U.S.A. 84*, 4538–4542.

(5) Wen, Z., Tao, X., Lakkis, F., Kiyokawa, T., and Murphy, J. R. (1991) Diphtheria toxin-related alpha-melanocyte-stimulating hormone fusion toxin. *J. Biol. Chem. 266*, 12289–12293.

(6) Lorberboum-Galski, H., FitzGerald, D. J., Chaudhary, V. K., Adhya, S., and Pastan, I. (1988) Cytotoxic activity of an interleukin 2-*Pseudomonas* exotoxin chimeric protein produced in *Escherichia coli*. *Proc. Natl. Acad. Sci. U.S.A. 85*, 1922–1926.

(7) Williams, D. P., Parker, K., Bacha, P., Bishai, W., Borowski, M., Genbauffe, F., Strom, T. B., and Murphy, J. R. (1987) Diphtheria toxin receptor binding domain substitution with interleukin-2: Genetic construction and properties of a diphtheria toxin-related interleukin-2 fusion protein. *Protein Eng. 1*, 493–498.

(8) Chaudhary, V. K., Queen, C., Junghans, R. P., Waldmann, T. A., FitzGerald, D. J., and Pastan, I. (1989) A recombinant immunotoxin consisting of two antibody variable domains fused to *Pseudomonas* exotoxin. *Nature 339*, 394–397.

(9) Batra, J. K., FitzGerald, D. J., Chaudhary, V. K., and Pastan, I. (1991) Single chain immunotoxins directed at the human transferrin receptor containing *Pseudomonas* exotoxin A or diphtheria toxin: Anti-TFR(Fv)-PE40 and DT388-Anti-TFR-(Fv). *Mol. Cell. Biol. 11*, 2200–2205.

(10) Pastan, I., and FitzGerald, D. J. (1991) Recombinant toxins for cancer treatment. *Science 254*, 1173–1177.

(11) Endo, Y., and Tsurugi, K. (1987) RNA N-glycosidase activity of ricin A chain. Mechanism of action of the toxic lectin ricin on eukaryotic ribosomes. *J. Biol. Chem. 262*, 8128–8130.

(12) Lamb, I., Roberts, L. M., and Lord, J. M. (1985) Nucleotide sequence of cloned cDNA coding for preproricin. *Eur. J. Biochem. 148*, 265–270.

(13) Lord, J. M. (1985) Precursors of ricin and *Ricinus communis* agglutinin. *Eur. J. Biochem. 146*, 403–409.

(14) Harley, S. M., and Lord, J. M. (1985) *In vitro* endoproteolytic cleavage of castor bean lectin precursors. *Plant Sci. 41*, 111–116.

(15) O'Hare, M., Brown, A. N., Hussain, K., Gerhardt, A., Watson, G., Roberts, L. M., Vitetta, E. S., Torpe, P. E., and Lord, J. M. (1990) Recombinant Staphylococcal protein-A ricin A chain fusion proteins containing a proteolytically cleavable spacer are cytotoxic to antibody-coated cells. *FEBS Lett. 273*, 200–204.

(16) Waldmann, T. A. (1989) Multichain interleukin 2 receptor: A target for immunotherapy in lymphoma. *J. Natl. Cancer Inst. 81*, 914–923.

(17) May, M. J., Hartley, M. R., Roberts, L. M., Kreig, P. A., Osborn, R. W., and Lord, J. M. (1989) Ribosome inactivation by ricin A chain: a sensitive method to assess the activity of wild-type and mutant polypeptides. *EMBO. J. 8*, 301–308.

(18) Richardson, P. T., Westby, M., Roberts, L. M., Gould, J. H., Colman, A., and Lord, J. M. (1989) Recombinant proricin binds galactose but does not depurinate 28S ribosomal RNA. *FEBS Lett. 255*, 15–20.

(19) Krieg, P. A., and Melton, D. A. (1984) Functional messenger RNAs are produced by SP6 *in vitro* transcription of cloned cDNAs. *Nucleic Acid Res. 12*, 7057–7070.

(20) Sambrook, J., Fritsch, E. F., and Maniatis, T. (1989) *Molecular cloning: a laboratory manual*, 2nd ed., Cold Spring Harbor Laboratory, Cold Spring Harbor, NY.

(21) Anderson, C. W., Strauss, J. W., and Dudock, B. S. (1983) Preparation of a cell free protein synthesizing system from wheat germ. *Methods Enzymol. 101*, 635–644.

(22) Colman, A. (1984) Translation of eukaryotic messenger RNA in *Xenopus* oocytes. *Transcription and translation—A practical approach* (D. Hames, and S. Higgins, Eds.) pp 271–302, IRL Press, Oxford.

(23) Laemmli, U. K. (1970) Cleavage of structural proteins during assembly of the head bacteriophage T_4. *Nature 227*, 680–685.

(24) d'Alessio, J. D. (1982) RNA sequencing. *Gel electrophoresis of nucleis acids* (D. Rickwood and B. D. Hames, Eds.) pp 173–179, IRL Press, Oxford.

(25) Gillis, S. and Smith, K. (1977) Long term culture of tumor-specific cytotoxic T cells. *Nature 268*, 154–156.

(26) Robb, R. J., Kutny, R. M., Panico, M., Morris, H. R., and Chowdry, V. (1984) Amino acid sequence and post-translational modification of human interleukin 2. *Proc. Natl. Acad. Sci. U.S.A. 81*, 6486–6490.

(27) Richardson, P. T., Gilmartin, P., Colman, A., Roberts, L. M., and Lord, J. M. (1988) Expression of functional ricin B chain in *Xenopus* oocytes. *Bio/Technol. 6*, 565–570.

(28) Westby, M., Argent, R. H., Pitcher, C., Lord, J. M., and Roberts, L. M. (1992) Preparation and characterization of recombinant proricin containing an alternative protease-sensitive linker sequence. *Bioconjugate Chem. 3*, 375–381.

Efficient Transformation of Mammalian Cells Using DNA Interpolyelectrolyte Complexes with Carbon Chain Polycations

Alexander V. Kabanov,* Irina V. Astafieva, Irina V. Maksimova,† Eugenii M. Lukanidin,†,‡ Georgii P. Georgiev,† and Victor A. Kabanov§

Moscow Institute of Biotechnology, Inc., and Department of Biopolymer Chemistry, Russian Research Center of Molecular Diagnostics and Therapy, Simpheropolsky Boulevard 8, Moscow 113149, Russia, Institute of Gene Biology, ul. Vavilova 34/5, Moscow 117334 GSP-1, Russia, and Department of Polymer Chemistry, Faculty of Chemistry, M. V. Lomonosov Moscow State University, Vorobievi Gory, Moscow 119899 GSP, Russia. Received April 26, 1993®

A new method for mammalian cell transformation is proposed which is based on incorporation of plasmids into interpolyelectrolyte complexes (IPECs) with carbon chain polycations. The method is illustrated by examples of pRSV CAT and pβ-Gal plasmid IPECs with poly(*N*-ethyl-4-vinylpyridinium bromide) (C_2PVP) and poly(*N*-ethyl-4-vinylpyridinium)–poly(*N*-cetyl-4-vinylpyridinium) bromides random copolymer (C_{16}PVP). These IPECs are produced spontaneously due to formation of a cooperative system of interchain electrostatic bonds after mixing DNA and polycation solutions. The interaction of IPEC with normal mouse fibroblasts NIH 3T3, human T-lymphoma "Jurkat", and Mardin Darby canine kidney cells has been studied. The data obtained has revealed that plasmid incorporation into IPECs significantly enhances both DNA adsorption on the plasma membrane and DNA uptake into a cell. The *in vitro* transformation of NIH 3T3 cells was monitored by a standard cloramphenicol acetyltransferase (CAT) assay (pRSV CAT plasmid) and by detection of β-galactosidase (β-Gal) expression using 4-methylumbeliferril β-D-galactopyranoside as a substrate (pβ-Gal plasmid). In both cases it has been proved that IPEC-incorporated plasmids possess an ability for efficient cell transformation. The transforming activity of IPECs depends on their composition and polycation chemical structure. Under optimal conditions the efficiency of cell transformation with IPECs is several fold higher than that observed during standard calcium phosphate precipitation. The mechanism of the phenomenon observed is discussed. According to this mechanism polycations form positively charged loops fixed on DNA molecules. These loops interact with negatively charged lipids on plasma membranes, which probably induces effective endocytosis and subsequent cell transformation.

INTRODUCTION

Targeting of foreign nucleic acids into intact cells is the basis of many key genetic engineering methods (*1*). At present there exist several methods for introducing DNA into cells, the most common of them being precipitation with calcium phosphate (*2*) or with DEAE-dextran[1] (*3*), electroporation (*4*), microinjection (*5*), and incorporation of DNA into reconstructed virus coats (*6*) or liposomes (*7*).

Despite the great variety of these methods, the search for new ways of transforming animal, plant, and prokaryotic cells continues. On the one hand, there is need to enhance the efficiency of transformation in comparison with that achieved by using traditional approaches, and that can be applied only to a limited number of cell lines (*8*). On the other hand, traditional approaches seem to be ineffective for introducing RNA molecules into cells (*9*). And finally, most of these approaches cannot be used for genetic transformation *in vivo* (*10*).

Recently, a new approach has been suggested based on incorporation of nucleic acids into soluble interpolyelectrolyte complexes (IPECs) with polycations (*11–13*). In particular, Wu *et al.* (*11*) suggested conjugation of a polycation with a molecule ("vector") capable of receptor-mediated endocytosis into a cell. The mixing of this conjugate with DNA polyanion resulted in formation of IPEC carrying a ligand which provided for receptor-mediated uptake of IPEC and cell transformation. Wu *et al.* used asialoglycoprotein–poly(L-lysine) conjugate for transformation of receptor-positive HepG2 hepatoma cells (11) as well as for DNA-targeted delivery into liver and hepatocyte transformation *in vivo* (*10, 14*). In further studies transferrin (*8, 15, 16*) and insulin (*17*) were used as vectors instead of asialoglycoprotein for transforming various eukariotic cells *in vitro*. On the basis of the works by Wu *et al.* (*10, 14*), Trubetskoy *et al.* (*18*) developed a system for gene targeting in mouse lung endothelian cells

* Address all correspondence to A. V. Kabanov, Moscow Institute of Biotechnology, 550 Rue Sherbrooke Quest, Bureau 1205, Montreal, QC, Canada, H3A1B9.

† Institute of Gene Biology.

‡ Present address: The Fibiger Institute, Strandboulevarden 49, opg. 7.1, 3,s. DK-2100 Copenhagen, Denmark.

§ Moscow State Univeristy.

® Abstract published in *Advance ACS Abstracts,* October 1, 1993.

[1] Abbreviations used: β-Gal, β-galactosidase; C_2PVP, poly(*N*-ethyl-4-vinylpyridinium bromide); C_{16}PVP, poly(*N*-ethyl-4-vinylpyridinium)–poly(*N*-cetyl-4-vinylpyridinium) bromides random copolymer; CAT, chloramphenicol acetyltransferase; Con A, concanavalin A; DEAE-dextran, [2-(diethylamino)ethyl]-dextran; DMEM, Dulbecco's modified Eagle's medium; FACS, fluorescence-activated cell sorter; φ, IPEC composition, namely the basic mole ratio [polycation]/[DNA] in the system; HBS, HEPES-buffered saline; HEPES, *N*-(2-hydroxyethyl)piperazine-*N'*-(2-ethanesulfonic acid); IPEC; interpolyelectrolyte complex; MDCK, Mardin Darby canine kidney (cells); P_w, weight-average degree of polymerization; PANa, sodium poly(acrylate); PBS, phosphate-buffered saline; PVP, poly(vinylpyridine); TLC, thin-layer chromatography; Tris, 2-amino-2-(hydroxymethyl)-1,3-propanediol; Triton X-100, α-[4-(1,1,3,3-tetramethylbutyl)-phenyl]-ω-hydroxypoly(oxy-1,2-ethanediyl).

1043-1802/93/2904-0448$04.00/0 © 1993 American Chemical Society

using a poly(L-lysine) conjugate with mAb to lung-surface antigens as a DNA carrier.

Meanwhile, we demonstrated that DNA incorporation into IPEC with vector-free carbochain polycations (namely quaternized PVPs) significantly enhanced the efficiency of transformation of *Bacillus subtilis* cells (*12, 19*). This phenomenon was explained (*19*) by hydrophobization of DNA molecules upon their incorporation in IPEC, which intensified interaction of the latter with the cellular membrane. A similar approach based on DNA complexion with lipospermines was used by Behr *et al.* for transforming mammalian cells (*13*). In this work we study transformation of mammalian cells using DNA IPECs with quaternized PVPs.

EXPERIMENTAL PROCEDURES

Synthetic Polymers. PVP was obtained by radical polymerization of freshly rectified 4-vinylpyridine (boiling temperature of 65 °C at 15 mmHg, n^{20}_D = 1.5520) using the modified method (*20*). The polymerization reaction in 25% monomer solution in methanol was initiated by the azodinitrile of bisisobutiric acid and conducted under an argon atmosphere at 65 °C during 40 h. The polymer obtained was precipitated into ether and dried under vacuum. The break up fractionation of PVP was performed by precipitation of 1–5% methanol solution of the polymer into ethyl acetate. The obtained liquid PVP layer was separated, washed, dissolved in methanol, and precipitated into ether. The molecular mass of the high molecular PVP fractions was determined using quasielastic light scattering. The molecular mass of low molecular (oligomeric) PVP fractions was determined by ebulioscopy in chloroform.

C_2PVPs (P_w = 18 and 500) and C_{16}PVP (P_w = 400) were obtained by alkylation of corresponding PVP fractions with cetyl and/or ethyl bromides according to the procedure previously described (*21*). The degree of PVP alkylation was determined by IR spectroscopy (*21*). According to these data, C_2PVPs contained from 90 to 95% alkylated units and C_{16}PVP contained 3% and 90% cetylated and ethylated units, respectively.

The polymers obtained were purified by dialysis and gel filtration on Biogel P2, lyophilized, and then dissolved in doubly distilled water with a partial conductivity of 0.06 μs/cm (purified by a "Milli-Q" device, Millipore). The concentrated (from 1 to 3 basic mmol/L) stock solutions of C_2PVPs and C_{16}PVP were sterilized in an autoclave for 30 min (0.5 atm, 100 °C) and stored under sterile conditions. The polymers concentration in the solutions obtained were controlled spectrophotometrically by measuring the absorbency of *N*-alkylpyridinium bromide units at 280 nm (the coefficient of molar absorption of the unit equals 3500 opt units/mol).

Cell Lines and Culture Conditions. NIH 3T3 cells were grown at 37 °C, under a 5% CO_2 atmosphere as a monolayer stationary culture in DMEM, containing 2 mM glutamine and 10% fetal calf serum. To obtain the cell suspension the exponentially growing NIH 3T3 cells were harvested by trypsin treatment and then grown for at least three passages (37 °C, 5% CO_2). Mardin Darby canine kidney (MDCK) cells were grown (37 °C, 5% CO_2) as a monolayer stationary culture in 199 medium containing 10 mM HEPES, 0.075% sodium bicarbonate, 10% fetal calf serum, and 200 μg/mL gentamycin. Jurkat cells were grown (37 °C, 5% CO_2) as a suspension culture in RPMI-1640 medium containing 2 mM glutamine and 10% fetal calf serum.

Cell Viability. The cells were incubated in serum-free medium for 1 h at 37 °C with the polycations or IPECs. The cells were then washed and incubated for 48 h in the fresh medium containing 10% fetal calf serum at 37 °C. In the course of incubation (24 h), the medium was substituted for the fresh one. The amount of living cells was determined via FACS analysis using the propidium iodide fluorescein diacetate staining (*22*).

Plasmids. pRSV CAT and pβ-Gal plasmids were kindly presented by Dr. E. Tulchinsky (V.A. Engelgardt Institute of Molecular Biology, Russian Academy of Sciences). They were propagated and purified by standard techniques (*23*). Plasmid pRSV CAT (*24*) was composed of the ampicillin-resistant cistron and the origin of replication was from plasmid pBR322 by joining to a hybrid eukaryotic transcription unit. The transcription unit in this plasmid was composed of the Rous sarcoma virus long terminal repeat (Rous LTR) promoter, the driving expression of *Escherichia coli* CAT encoding sequence, and the simian virus 40 (SV40) mRNA processing signals (including the small-t intron and early region polyadenilation site). Plasmid pβ-Gal was composed of the ampicillin-resistant cistron and the origin of replication from plasmid pUC19 by joining to a hybrid eukaryotic transcription unit, which contained the *E. coli* β-Gal encoding sequence.

DNA Radiolabeling. DNA was labeled with [α-^{32}P]-dCTP according to a standard protocol for nick translation reactions using an Amersham nick translation kit. The specific radioactivity of labeled DNA equaled 3.7·10^6 cpm/μg.

Polycomplex Formation. The IPECs were obtained by simple mixing of polycation and DNA solutions. To this end, from 0.5 to 50 μL of polycation stock solution was added to 5 μL of 0.2 μg/μL DNA solution in PBS or HBS (pH 7.4). According to the data previously reported (*19*), rapid (minutes) IPEC formation took place under these conditions. The system obtained was incubated for 1 h at room temperature, filtered using 0.22-μm filters, and then used in further experiments. An independent experiment revealed that IPEC filtration did not result in the loss of polycomplex components. The basic molar [polycation]/[DNA] ratio is conditionally termed below as IPEC composition (φ).

DNA Binding and Internalization in Cells. Suspended Jurkat (2·10^6) and 3T3 (5·10^5) cells or monolayers of 3T3 and MDCK cells in 90-mm plates were washed with cold (4 °C) serum-free medium and then placed in 1 mL of serum-free medium containing 20 mM HEPES (pH 7.4). From 0.02 to 0.6 μg of radiolabeled DNA or its IPECs with C_2PVP in PBS (pH 7.4) or HBS (pH 7.4) were added to the cells. After 1.5-h incubation at 4 or 37 °C, the cells were washed from three to four times with cold (4 °C) PBS and then treated according to one of the following procedures for determination of the amounts of bound (A) or internalized DNA (B-D).

(A) The cells were lysed at 0 °C using 0.1% Triton X-100 solution in 1 mM Tris-HCl buffer (pH 7.4), and [^{32}P] radioactivity in the lysate was measured in a toluene scincillator using a Rackbeta-II β-counter. The concentration of cell protein in the lysate samples was determined by the Bradford method (*25*).

(B) The cells were placed in 1 mL of 50 mM Tris-HCl buffer (pH 5.0) containing 4.2 mM MgCl, 0.1% DTT, and 6 μL of 1 mg/mL DNAse I solution. After 1 hour incubation at 4 °C, the cells were carefully washed and lysed. The DNA radioactivity and concentration of cell protein were determined as described in A.

(C) The cells were incubated for 1 h in 1 mL of cold (4 °C) PBS (pH 7.8) containing from 20 to 30 μL of 10 mM

PANa solution and then washed and treated according to the procedure described in B.

(D) The cells were treated for 6 min at 4 °C with 0.2 M acetic acid (pH 2.5) containing 0.15 M NaCl and then washed and lysed. The DNA radioactivity and concentration of cell protein in the lysate were determined as described in A.

For comparison, the binding and internalization of the same amounts of DNA during calcium phosphate precipitation were also studied using the protocol described below.

Cell Transformation Using IPECs. In order to produce cell monolayers, suspended NIH 3T3 cells were seeded at $5 \cdot 10^5$ per 90-mm plate and incubated overnight in 10 mL of growth medium. Twenty-four hours before the transformation the serum-containing medium was substituted for the serum-free one. One hour before the transformation the suspended NIH 3T3 cells ($2 \cdot 10^5$ to 10^6) were washed and resuspended in 0.5 mL of the serum-free medium.

Two to 5 mL (cell monolayers) or 0.5 mL (cell suspension) of the serum-free medium containing 2–16 μg of DNA or its IPECs of varying composition was added dropwise to the plate of cells or 0.5 mL of the cell suspension. The mixtures were gently agitated and incubated for 2 h at 37 °C under 5% CO_2. Then the cells were washed five or six times with the fresh media (cells in suspension were replated to dishes) and incubated in DMEM containing 10% fetal calf serum for 48 h at 37 °C under 5% CO_2. In the course of incubation (16 h) the medium was substituted for the fresh one. After incubation, the cells were washed twice in PBS, trypsinized, and washed twice in PBS, and CAT or β-Gal activities were determined.

Cell Transformation Using Calcium Phosphate Precipitation. The calcium phosphate transformation was performed using the optimized protocol described in ref 26. To this end 2–16 μg of plasmid DNA was mixed with 0.5 mL of 0.25 M $CaCl_2$. This mixture was slowly added dropwise to 0.5 mL of 2×HBS (pH 7.1) with continuous vortexing (22–25 °C). The obtained slightly opaque solution was incubated for 10 min at room temperature and then added dropwise to the plate of cells or to the suspended cells. The mixture was swirled gently and incubated for 24 h at 37 °C under 5% CO_2. The medium was removed, and the cells were rinsed twice with growth medium (cells in suspension were replated to dishes) and incubated in DMEM containing 10% fetal calf serum for an additional 24 h at 37 °C under 5% CO_2. After incubation, the cells were washed and trypsinized, and CAT or β-Gal activities were determined. The above protocol is optimized (pH, sample volumes, temperature) for NIH 3T3 cell transformation with pβ-Gal plasmid.

CAT Assay. The CAT activity in the transformed cells was determined by the method of Gorman *et al.* (27). Briefly, the cells were suspended in 100 μL of 0.2 M Tris-HCl (pH 7.4), lysed by several freeze/thaw cycles, incubated for 10 min at 65 °C for inactivation of diacetylases, and centrifuged in an Eppendorf centrifuge at 3000 rpm. A 50-μL portion of supernatant was then mixed with 50 μL of Tris-HCl buffer containing 20 μCi/mL [^{14}C]chloramphenicol (53 mCi/mmol). The reaction was initiated by adding 20 μL of 4 mM Con A solution. After 1-h incubation, cloramphenicol and the products of its enzymatic hydrolysis were extracted with ethyl acetate, analyzed by TLC, and autoradiographed. Each transformation experiment using pRSV CAT plasmid (IPEC or calcium phosphate precipitation) was performed in duplicate (two samples for each experimental point) and repeated independently at least four times. The results of the typical experiments are presented below.

Table I. Effect of Polycations on NIH 3T3 Cell Viability

polycation	polycation concentration (basic mmol/L)	viability after incubation[a] (%)
control (without polycation)		75.0
C_2PVP (P_w = 18)	75	80.4
C_2PVP (P_w = 500)	16	80.7
C_{16}PVP (P_w = 400)	850	47.9
	50	75.6

[a] 3T3 NIH cell suspension was incubated with polycations for 1 h at 37 °C. The cells were then washed and incubated for 48 h at 37 °C as described in Experimental Procedures.

β-Gal Assay. The cells were suspended and lysed by several freeze/thaw cycles as described above for determination of CAT activity. However, in this case the extract was not incubated at 65 °C. After the extract centrifugation, 50 μL of supernatant were mixed with 50 μL of 1 mM 4-methylumbeliferril β-D-galactopyranoside solution in 0.1 M phosphate buffer (pH 7.4) and then incubated for 20 min at 37 °C. The reaction was terminated by adding 50 μL of 0.4 M glycine buffer (pH 10.5). The formation of methylbelliferon (λ_{ex} = 365; λ_{em} = 450) was monitored at 37 °C by a Hitachi F 4000 spectrofluorimeter.

RESULTS

Effect of Polycations on Cell Viability. The effects of C_2PVP and C_{16}PVP on cell viability were studied. Briefly the cells were incubated with the polycations, washed, and then incubated again in the fresh media under conditions similar to those used in the transfection experiments. After incubation the cell viability was determined by a standard FACS technique (22). Table I shows that, in the case of NIH 3T3 cells, the polycations did not affect cell viability at concentrations that exceeded by manifold those used during transfection. A similar result was obtained when corresponding IPECs were used instead of free polycations (data not presented in the table). Therefore, unlike calcium phosphate treatment, which usually leads to a loss of from 50 to 90% of the cells, the transfection procedure proposed in this paper does not possess a cytotoxic effect.

A Method for Separate Determination of DNA Binding and Uptake. The interaction of free and IPEC-incorporated plasmids with the cells was studied. To this end, the cells (3T3, MDCK, Jurkat) were incubated with [^{32}P]-labeled pRSV CAT plasmid (or its IPEC with C_2-PVP) at 4 or 37 °C, washed, and then treated according to one of the procedures (A–D) (described in Experimental Procedures), permitting separate determination of DNA binding and uptake. Here we illustrate this approach by examples of plasmid (or IPEC) interaction with NIH 3T3 suspension (Table II).

The total amount of the cell-bound DNA was determined by measuring DNA radioactivity in the cell lysate (procedure A). In order to remove DNA molecules adsorbed on the cell surface and thus to determine the amount of internalized nucleic acid, the cells were first treated with DNAse I and then lysed (procedure B). Such treatment resulted in complete removal of cell-bound DNA in cases when the cells were incubated with the free plasmid (Table II). This indicates that the free DNA adsorbs on the cell surface only but does not internalize within the cells.

After calcium phosphate precipitation, a significant part of cell-bound DNA was not accessible to DNAse digestion. This part corresponded to DNA internalized into the cells during the precipitation procedure. The part of DNA

Table II. Interaction of Free or IPEC-Incorporated pRSV CAT Plasmid with NIH 3T3 Cell Suspension

system studied[a]	temp (°C)	cell-bound DNA (ng/mg cell protein)[b] A	B	C	D
free DNA	37	7(±2)	2(±1)	<1	2(±1)
calcium phosphate precipitation	37	20(±2)	11(±3)	10(±1)	11(±2)
IPEC	4	56(±8)	40(±9)	6(±2)	8(±4)
	37	153(±16)	143(±19)	50(±5)	56(±7)

[a] Free DNA was incubated with the cells at 37 °C or precipitated using the calcium phosphate method. DNA/C_2PVP (P_w = 500) IPEC (φ = 10) was incubated with the cells at 4 or 37 °C. The amount of DNA and the number of cells in suspension equaled 0.25 μg and 5 × 10^5, respectively. [b] After incubation with DNA or IPEC, the cells were treated according to procedures A–D described in Experimental Procedures: (A) washed with buffer; (B) incubated with DNAse I; (C) incubated with PANa and then with DNAse I; (D) washed with acetic acid. Values are means ± SD ($P < 0.05$, $n = 6$).

which was cleaved during DNAse treatment related to the nucleic acid adsorbed on the plasma membrane. In this case, the amount of adsorbed nucleic acid was determined as a difference between DNA total binding and uptake.

However, this method was unsuitable for the study of IPEC-incorporated DNA uptake. As is shown in Table II, DNAse did not remove the major part of cell-bound nucleic acid even when the cells were preincubated with IPEC at 4 °C. Meanwhile, under these conditions, endocytosis was abolished and all cell-bound DNA (IPEC) should have been localized outside the cells. Therefore unlike free DNA, the IPEC-incorporated one was not accessible to DNAse I on the cell surface. This result was in good agreement with the previously obtained data (*19*), demonstrating that DNA incorporation into IPEC prevented DNA cleavage with nucleases.

In order to study the endocytosis of IPEC-incorporated plasmid, we suggest use of procedure C or D. According to procedure C, the cells, preincubated with IPEC, were first treated with a molar excess (with respect to the polycation) of PANa and then with DNAse. We had previously demonstrated that polycarbonic acid anions replaced DNA in the complex with polycation (*19*). This resulted in formation of free DNA, which becomes accessible to DNAse and therefore was removed from the cell surface.

An alternative method for removal of adsorbed IPEC (procedure D) consisted of cell treatment with acetic acid. Such treatment usually extracts macromolecules that are noncovalently bound with the cell membrane (*28*). As is shown in Table II, both procedures C and D led to a complete removal of DNA in the case when the cells were preincubated with IPEC at 4 °C. This proves that under the given conditions the polycomplex did not penetrate into the cells. Meanwhile at 37 °C a significant amount of DNA remained in the cells after the treatment according to C or D. Therefore, at 37 °C the uptake of IPEC-incorporated DNA takes place.

Whereas both procedures C and D gave the same results (Table II), they are equivalently accessible for determination of the IPEC-incorporated DNA uptake. Below we present data on DNA adsorption and uptake (free DNA, IPECs, calcium phosphate precipitation) which were obtained using procedure C. It should also be emphasized that procedures C and D gave the same result as procedure B in the case when free DNA was precipitated by the calcium phosphate method (Table II).

Effect of DNA Incorporation into IPEC on Binding and Uptake. This effect was studied using DNA IPEC with C_2PVP (P_w = 500). The data on free DNA and IPEC

Table III. Interaction of the Free or IPEC-Incorporated pRSV CAT Plasmid with Mammalian Cells

cells[a]	system studied	temp (°C)	cell-bound DNA (ng/mg cell protein)[b] total binding	adsorption	uptake
NIH 3T3 (suspension)	free DNA	37	7(±2)	7(±2)	<1
	calcium phosphate precipitation	37	20(±2)	10(±3)	10(±1)
	IPEC	4	70(±8)	64(±10)	6(±2)
		37	153(±16)	103(±21)	50(±5)
MDCK	free DNA	37	1.0(±0.5)	1.0(±0.5)	0
	calcium phosphate precipitation	37	25(±4)	9(±7)	16(±3)
	IPEC	4	100(±10)	78(±13)	22(±3)
		37	165(±14)	97(±20)	68(±6)
Jurkat	free DNA	37	30(±5)	30(±5)	<1
	calcium phosphate precipitation	4	50(±6)	25(±10)	25(±4)
	IPEC	4	80(±7)	35(±11)	45(±4)
		37	360(±32)	228(±44)	132(±12)

[a] The cells were treated using calcium phosphate precipitation or incubated as described in Experimental Procedures with free DNA or DNA/C_2PVP (P_w = 500) IPEC (φ = 10). DNA amounts added to cells equaled 0.25 μg (3T3 NIH), 0.5 μg (MDCK), or 0.2 μg (Jurkat). [b] The total amount of cell-bound DNA was determined in the cell lysate after cell washing with buffer (procedure A); the amount of the internalized DNA was determined after cell treatment with PANa and DNAse I (procedure C); the amount of the DNA adsorbed on the cell surface was determined as a difference between DNA total binding and uptake. Values are means ± SD ($P < 0.05$, $n = 6$).

interaction with NIH 3T3, MDCK, and Jurkat cells are summarized in Table III. These data demonstrate that free DNA internalized into the cells neither at 4 °C nor at 37 °C. Meanwhile, in the case of calcium phosphate precipitation alongside with DNA adsorbtion, a significant amount of internalized nucleic acid was also registered.

Incorporation into IPEC resulted in the enhancement of plasmid total binding with the cells. Under these conditions, DNA adsorbtion on the plasma membrane as well as DNA uptake was considerably increased. In particular, the adsorbtion of IPEC-incorporated plasmid was from 8-fold (3T3, Jurkat) to 100-fold (MDCK) stronger than that of free nucleic acid and approximately 8-fold stronger than that observed after calcium phosphate precipitation. The adsorbtion of IPEC-incorporated DNA is a temperature-dependent process. The temperature dependence of adsorbtion in the range of from 4 to 37 °C was observed at least in the cases of NIH 3T3 and Jurkat cells (Table III).

Figure 1 represents concentration dependencies of DNA uptake in NIH 3T3 cells obtained during IPEC incubation with the cells or calcium phosphate precipitation. The uptake increased linearly with the increase of DNA concentration in the culture medium. In the concentration range studied (from 0.02 to 0.4 μg/mL) the uptake of IPEC-incorporated plasmid was several fold higher than that achieved during calcium phosphate precipitation. A similar picture was observed for all three cell lines studied: the plasmid incorporation into IPEC led to a significant increase of the uptake if compared with calcium phosphate precipitation (Table III).

The uptake of IPEC-incorporated DNA represented a temperature-dependent process, which was significantly suppressed at 4 °C (Figure 1 and Table III). However, some difference among various cell lines was observed here. After precincubation of NIH 3T3 cell suspension with IPEC at 4 °C, practically the whole cell-bound nucleic acid (more than 90% of its total amount) was localized on

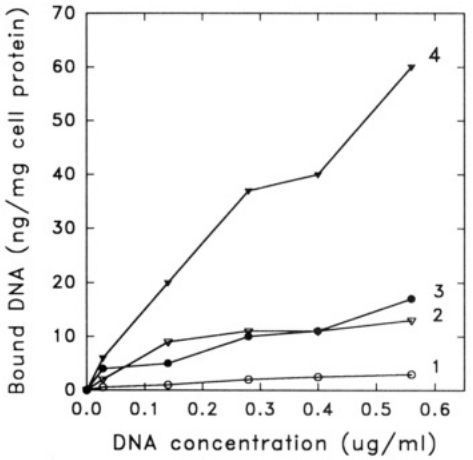


Figure 1. The uptake of free or IPEC-incorporated pRSV CAT plasmid in a NIH 3T3 cell monolayer. The cells were incubated with free plasmid at 37 °C (curve 1); the plasmid was precipitated using the calcium phosphate procedure (curve 2); the cells were incubated with DNA/C_2PVP (P_w = 500) IPEC (φ = 10) at 4 °C (curve 3) or 37 °C (curve 4). After incubation with DNA, the cells were treated with PANa and DNAse according to procedure C as described in Experimental Procedures. The dependence of uptake on DNA concentration is presented.

the external side of the plasma membrane and was removed by DNAse I treatment (procedure C). Meanwhile, in the case of Jurkat cells, almost 50% of the cell-bound DNA was not cleaved by the nuclease under the same conditions.

Cell Transformation with DNA–IPECs. The transformation of NIH 3T3 cells with DNA–IPECs was studied using pRSV CAT and pβ-Gal plasmids, which contained CAT and β-Gal encoding genes, respectively. IPECs of varying compositions were formed by mixing plasmid and polycation (C_2PVP or C_{16}PVP) solutions and then incubated with cell suspensions or monolayers for 2 h as described in Experimental Procedures. The data on cell transformation by calcium phosphate precipitation using the same amounts of DNA are presented for comparison.

Figure 2 represents the results of cell transformation with pRSV CAT plasmid (calcium phosphate precipitation) and its IPECs. Both DNA/C_2PVP and DNA/C_{16}PVP IPECs revealed an ability for cell transformation. The transformation efficiency of IPECs was comparable or even higher (cells in suspension) than that achieved by calcium phosphate precipitation. It depended on several factors, namely on the polycation chemical structure, its length (weight-average degree of polymerization), and IPEC composition (the basic mole ratio φ = [polycation]/[DNA]). In particular, the plasmid complex with C_{16}PVP was less effective than that with C_2PVP (Figure 2A). DNA IPEC with C_2PVP (P_w = 500) possessed a significantly higher transforming activity than the complex with a shorter polycation (P_w = 18) (Figure 2A,B). The maximal activity was observed for DNA/C_2PVP (P_w = 500) IPEC with φ = 10: a shift from this optimal value (φ = 5 and 15) caused a decrease in cell transformation.

pβ-Gal plasmid was used for quantitative estimation of DNA and IPEC transforming activities. In this case, cell transformation was registered by measuring *E. coli* β-Gal activity by a spectrofluorimetric assay. Since the cell lysates possessed an endogenous β-Gal activity, the reaction was carried out at pH 7.4 under conditions when the endogenous enzyme was practically inactive (data not shown). The results of transfection experiments are presented in Table IV. DNA IPECs with C_2PVP and C_{16}PVP showed the transforming activity under conditions

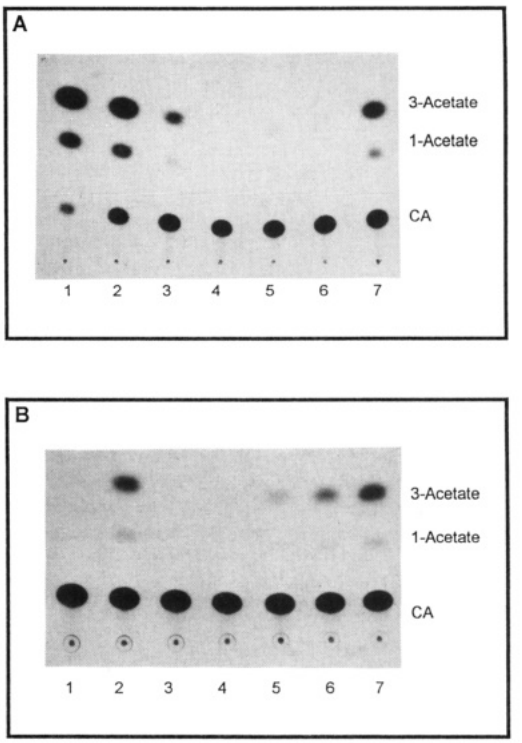


Figure 2. Assay of gene transformation in NIH 3T3 cells. The cells were transformed in (A) suspension ($7{\cdot}10^5$ cells/mL) or (B) monolayer as described in Experimental Procedures. (A) Lanes 1–6, cells transformed with 8 μg of polycomplex-incorporated pRSV CAT plasmid: lane 1, DNA/C_2PVP (P_w = 500; φ = 10); lane 2, DNA/C_2PVP (P_w = 500; φ = 15); lane 3, DNA/C_{16}PVP (P_w = 400; φ = 10); lane 4, DNA/C_{16}PVP (P_w = 400; φ = 15); lane 5, DNA/C_2PVP (P_w = 18; φ = 10); lane 6, DNA/C_2PVP (P_w = 18; φ = 15). Lane 7, cells transformed by calcium phosphate precipitation using the same amounts of DNA. (B) Lanes 1 and 3 contain [^{14}C]chloramphenicol alone. Lane 2, cells transformed by calcium phosphate precipitation using 5 μg DNA. Lanes 4–7, cells transformed with 5 μg of polycomplex-incorporated pRSV CAT plasmid: lane 4, DNA/C_2PVP (P_w = 18; φ = 5); lane 5, DNA/C_2PVP (P_w = 500; φ = 5); lane 6, DNA/C_2PVP (P_w = 18; φ = 10); lane 7, DNA/C_2PVP (P_w = 500; φ = 10).

Table IV. Gene Transformation in NIH 3T3 Cells Using pβ-Gal Plasmid

transformation conditions[a]	φ (for IPEC)	β-Gal activity per mg cell protein (arb units)[b]	
		suspension	monolayer
calcium phosphate precipitation		17(±5)	15(±5)
DNA/C_2PVP[c] IPEC	1.0	1.5(±1.5)	1.0(±1.0)
	3.0	17(±5)	13(±4)
	5.0	62(±11)	56(±10)
	10.0	104(±16)	110(±15)
	15.0	100(±15)	100(±14)
DNA/C_{16}PVP IPEC	1.0	2.5(±2.0)	
	3.0	22(±4)	
	5.0	42(±6)	
	7.5	55(±4)	
	10.0	49(±7)	

[a] Cell suspension or monolayer was transformed as described in Experimental Procedures by calcium phosphate precipitation or using DNA IPECs of varying composition. DNA amounts used for transformation equaled 1 (suspension) or 4 μg (monolayer). [b] The β-Gal activity was determined as a difference between the rates of methylbelliferon formation in the lysates of transformed and nontransformed cells. Values are means ± SD ($P < 0.05$, $n = 5$). [c] P_w = 500.

when the polycomplex composition was higher than 1. At lower φ, the transformation did not proceed (data not presented). At $\varphi > 1$, the transformation efficiency monotonously increased with increasing φ and reached

the maximum at φ = 10 (C_2PVP) or φ = 7.5 (C_{16}PVP). Under these optimal conditions, the transformation efficiency was from 4- to 7-fold higher than that achieved by calcium phosphate precipitation. In general, the data obtained using pβ-Gal plasmid were in good agreement with those observed for pRSV CAT plasmid.

DISCUSSION

The main information gained from this work is that DNA incorporation into polycomplexes with carbon chain polycations (quaternized PVPs) significantly enhances nucleic acid adsorbtion on cell plasma membranes and its uptake into cells and finally provides for its ability to efficiently transformation mammalian cells *in vitro*. This phenomenon seems to be of significant importance not only due to the possibility of using IPECs for cell transformation during molecular and cell biology studies but also because some serious efforts have been made over the last few years to develop nucleic acid delivery systems on the basis of DNA polyelectrolyte complexes (*10*, *14*, *18*).

When an aqueous solution of a nucleic acid is mixed with that of a linear polycation, there follows cooperative binding of oppositely charged polyions resulting in formation of an IPEC (*29*). The general regularities of formation of such complexes have been described elsewhere (*30*). If the polycation chain has a hydrophobic backbone, its "sticking" to the nucleic acid chain, accompanied by compensation of the phosphate group charges, results in formation of a hydrophobic site. The length and number of such sites is determined by the length (degree of polymerization) of the polycation and by IPEC composition. Therefore, physicochemical properties of IPECs strongly depend on their composition (*31*). In solutions with rather high ionic strengths (I = 1.0–1.5) soluble IPECs of DNA and quaternized PVP are formed at low φ values (C_2PVP, $\varphi < 0.5$; C_{16}PVP, $\varphi < 0.2$ (*31*)). Under these conditions, polycation chains are uniformly distributed among DNA molecules (the contour length of PVP is at least 1 order of magnitude smaller the that of DNA). Further addition of PVP causes a typical disproportionation phenomenon: in parallel with soluble IPEC, the insoluble complex is formed (*31*). A similar behavior is typical for IPECs of synthetic polyions (*31*). At $\varphi = 1.0$, the polyion charges are fully compensated and IPECs are insoluble. However when the polycation base mole concentration exceeds that of the polyanion, the complex dissolution ($\varphi > 1.0$) may be observed, as a result of formation of positively charged polycation loops bound on the polyanion chain (*32*).

According to our data, neither soluble IPECs with $\varphi <$ 1 nor insoluble ones (φ close to 1) possess the transforming activity with respect to mammalian cells. The transformation is observed only in the case of the complexes with $\varphi \gg 1$, which presumably are positively charged. In this respect it is probable that the first stage of cell transformation is conditioned by cooperative interaction of IPEC-incorporated polycation loops with negatively charged phospholipids of the plasma membrane. Such interaction provides for the enhancement of DNA adsorbtion on the cell surface observed in our experiments.

Meanwhile, the polycation interaction with the plasma membrane can result in significant changes of the properties of the latter (its structure, ion permeability, etc. (*33–38*)) which in its turn may serve as a "signal"-inducing endocytosis. The phenomenon of polycation-induced endocytosis is well-described in literature (*39–42*). We believe that it may be the reason causing effective uptake of IPEC-incorporated DNA into cells. The additional factor which can probably facilitate such uptake is a significant condensation of DNA after its incorporation into IPECs, which was observed during ultracentrifugation (*19*) and electron microscopy (*16*) studies. Such condensation can facilitate DNA (IPEC) entrapment into endocytic vesicles, the diameter of which is about 30–100 nm (*43*).

Therefore we believe that the polycation role in cell transformation consists of directing IPEC-incorporated DNA along the endocytic pathway. It is likely that normal endocytosis is involved here since the uptake is strongly dependent on temperature.

In this respect, the described phenomenon is similar to cell transfection using DNA IPECs with poly(L-lysine) conjugates (*8*, *11*, *17*). However, unlike other authors (*8*, *11*, *17*), who achieved transfection via receptor-mediated endocytosis, we probably deal here with a receptor-independent process that is realized due to DNA incorporation into IPECs with membrane-active polycations.

The polycation chemical structure seems to influence significantly the uptake and transfection efficiencies. In particular, according to previously reported data (*16*), no cell transformation was observed when free poly(lysine) was used instead of its conjugate with a vector molecule. The difference between our data and the results described in ref 16 may well be due to some differences between the structure and properties of DNA IPECs formed by quaternized PVPs and polypeptides. Meanwhile, it can also result from the difference in different polycations interaction with the plasma membrane. In any case, it is evident that further analysis of physicochemical regularities of IPEC formation and membrane interaction is required to better understand of the mechanism of cell transformation with IPECs.

The next stage of cell transfection must evidently involve DNA elaboration from endocytic vesicles into the cytoplasm. Since the efficiency of this process is low, this will evidently create a serious obstacle for transformation. Therefore further efforts in development of cell transformation systems should be focused on the search for some tools to facilitate passing over the endocytic barrier.

ACKNOWLEDGMENT

The authors would like to thank Drs. Valery Alakhov, Nikolai Melik-Nubarov, and Vladimir Slepnev for stimulating discussions and valuable comments concerning the described study. We are also grateful to Dr. Alexey Psheszhetsky for the help in determination of the β-Gal activity.

LITERATURE CITED

(1) Glover, D. M. (Ed.) (1985) *DNA Cloning. A Practical Approach*, Vols. I, II. IRL Press, Oxford.

(2) Graham, F., and van der Eb, A. (1973) A new technique for the assay of infectivity of human adenovirus 5 DNA. *Virology 52*, 456–467.

(3) Sompayrac, L., and Danna, K. (1981) Efficient infection of monkey cells with DNA of simian virus 40. *Proc. Natl. Acad. Sci. U.S.A. 12*, 7575.

(4) Potter, H., Weir, L., and Leder, P. (1984) Enhancer-dependent expression of human immunoglobulin genes introduced into mouse pre-B lymphocytes by electroporation. *Proc. Natl. Acad. Sci. U.S.A. 81*, 7161–7165.

(5) Capecchi, M. R. (1980) High efficiency transformation by direct microinjection of DNA into cultured mammalian cells. *Cell 22*, 479.

(6) Gitman, A. G., Graessmann, A., and Loyter, A. (1985) Targeting of loaded Sendai virus envelopes by covalently

attached insulin molecules to virus receptor-depleted cells: Fusion-mediated microinjection of ricin A and simian virus 40 DNA. *Proc. Natl. Acad. Sci. U.S.A. 82*, 7309–7313.

(7) Wang, C.-Y., and Huang, L. (1987) pH-sensitive immunoliposomes mediate target-cell-specific delivery and controlled expression of a foreign gene in mouse. *Proc. Natl. Acad. Sci. U.S.A. 87*, 3410–3414.

(8) Zenke, M., Steinlein, P., Wagner, E., Cotten, M., and Beug, H. (1990) Receptor-mediated endocytosis of transferrin-polycation conjugates: An efficient way to introduce DNA into hematopoetic cells. *Proc. Natl. Acad. Sci. U.S.A. 87*, 3655–3659.

(9) Malone, R. W., Felgner, P. L., and Verma, I. M. (1989) Cationic liposome-mediated RNA transfection. *Proc. Natl. Acad. Sci. U.S.A. 86*, 6077–6081.

(10) Wu, G. Y., and Wu, C. H. (1988) Receptor-mediated gene deliver and expression *in vivo*. *J. Biol. Chem. 263*, 14621–14624.

(11) Wu, G. Y., and Wu, C. H. (1988) Evidence for targeted gene delivery to Hep G2 hepatoma cells *in vitro*. *Biochemistry 27*, 887–892.

(12) Kabanov, A. V., Kiselev, V. I., Chikindas, M. L., Astafieva, I. V., Glukhov, A. I., Gordeev, S. A., Izumrudov, V. A., Zezin, A. B., Levashov, A. V., Severin, E. S., and Kabanov, V. A. (1989) Increasing of transforming activity of plasmid DNA by incorporating it into interpolyelectrolyte complex with a carbon chain polycation. *Dokl. Acad. Nauk SSSR 306*, 226–229 (Engl. edn.: 133–136).

(13) Behr, J.-P., Demeneix, B., Loeffler, J.-P., and Perez-Mutcel, J. (1989) Efficient gene transfer into mammalian primary endocrine cells with lipopolyamine-coated DNA. *Proc. Natl. Acad. Sci. U.S.A. 86*, 6982–6986.

(14) Wu, G. Y., Wilson, J. M., Shalaby, F., Grossmann, M., Shafritz, D. A., and Wu, C. H. (1991) Receptor-mediated gene delivery in vivo. Partial correction of genetic analbuminemia in nagase rats. *J. Biol. Chem. 266*, 14338–14342.

(15) Cotten, M., Lungle-Rouault, Kirlappos, H., Wagner, E., Mechtler, K., Zenke, M., Beug, H., and Birnstiel, M. L. (1990) Transferrin-polycation-mediated introduction of DNA into human leukemic cells: stimulation by agents that affect the survival of transfected DNA or modulate transferrin receptor levels. *Proc. Natl. Acad. Sci. U.S.A. 87*, 4033–4037.

(16) Wagner, E., Cotten, M., Foisner, R., and Birnsteil, M. L. (1991) Transferrin-polycation-DNA complexes: the effect of polycations on the structure of the complex and DNA delivery to cells. *Proc. Natl. Acad. Sci. U.S.A. 88*, 4255–4259.

(17) Rozenkrants, A. A., Yachmenev, S. V., and Sobolev, A. S. (1990) Using of artificial constructions for selective transfer of genetic material into human cells via receptor-mediated endocytosis. *Dokl. Acad. Nauk SSSR* (in Russian) *312*, 493–494.

(18) Trubetskoy, V. S., Torchilin, V. P., Kennel, S. J., and Huang, L. (1992) Use of N-terminal modified poly(L-lysine)-antibody conjugate as a carrier for targeted gene delivery in mouse lung endothelian cells. *Bioconjugate Chem. 3*, 323–327.

(19) Kabanov, A. V., Astafieva, I. V., Chikindas, M. L., Rosenblat, G. F., Kiselev, V. I., Severin, E. S., and Kabanov, V. A. (1991) DNA interpolyelectrolyte complexes as a tool for efficient cell transformation. *Biopolymers 31*, 1437–1443.

(20) Fuoss, R. M., and Strauss, U. P. (1948) Polyelectrolytes. II. Poly-4-vinylpyridinium chloride and poly-4-vinylpyridinium bromide. *J. Polym. Sci. 2*, 246–263.

(21) Starodubtzev, S. G., Kirsh, Yu. E., and Kabanov, V. A. (1987) Solvation effects and reactivity of free pyridine residues in macromolecules of poly-4-vinylpyridine. *Eur. Polym. J. 10*, 739–745.

(22) Jones, K. H., and Senft, J. A. (1985) An improved method to determine cell viability by simultaneous staining with fluorescein diacetate-propidium iodide. *J. Histochem. Cytochem. 33*, 77–79.

(23) Maniatis, T., Fritsch, E. F., and Sambrook, J. (1982) *Molecular cloning: A laboratory manual.* Cold Spring Harbor, New York.

(24) Gorman, C. M., Merlino, G. T., Willingham, M. C., Pastan, I., and Howard, B. H. (1982) The Rous sarcoma virus long terminal repeat is a strong promoter when introduced into a variety of eukariotic cells by DNA-mediated transfection. *Proc. Natl. Acad. Sci. U.S.A. 79*, 6777–6781.

(25) Bradford, M. M. (1976) A rapid and sensitive method for the quantitation of microgram quantities of protein utilizing the principle of protein-dye binding. *Anal. Biochem. 72*, 248–254.

(26) ProFection Mammalian Transfection Systems. Technical Manual (1990) pp. 2–9. Promega, Madison.

(27) Gorman, C. M., Moffat, L. F., and Howard, B. H. (1982) Recombinant genomes which express chloramphenicol acetyltransferase in mammalian cells. *Mol. Cell. Biol. 2*, 1044–1051.

(28) Haigler, H. T. (1983) Receptor-mediated endocytosis of epidermal growth factors. In: *Methods of Enzymology, vol. 98, Biomembranes, Part L. Membrane Biogenesis: Processing and Recycling.* (S. Fleishner and B. Fleishner, Ed.) pp 283–290. Academic Press, New York.

(29) Miller, I. R., and Bach, D. (1968) Interaction of DNA with heavy metal ions and polybases: cooperative phenomena. *Biopolymers 6*, 169–179.

(30) Kabanov, V. A., and Zezin, A. B. (1984) Water-soluble nonstoichiometric polyelectrolyte complexes: a new class of synthetic polyelectrolytes. In: *Soviet Scientific Reviews. B. Chemistry Reviews* (M. E. Volpin, Ed.) vol. 4, pp 207–282.

(31) Kabanov, V. A., Kabanov, A. V., and Astafieva, I. V. (1991) Complexes of DNA with synthetic polycations for cell transformation, *Polym. Prep. 32*, 592–593.

(32) Izumrudov, V. A., Zezin, A. B., and Kabanov, V. A. (1991) The equilibrium of interpolyelectrolyte reactions and the phenomenon of molecular recognition in the solutions of interpolyelectrolyte complexes, *Uspekhi Khim. 60*, 1510–1595.

(33) Petrukhina, O. O., Ivanov, N. N., Feldstein, M. H., Vasilev, A. E., Plate, N. A., and Torchilin, V. P. (1986) The regulation of liposome permeability by polyelectrolyte. *J. Contr. Release 3*, 137–141.

(34) Walter, A., Steer, C. J., and Blumental, R. (1986) Polylysine induces pH-dependent fusion of acidic phospholipid vesicles: a model for polycation-induced fusion *Biochim. Biophys. Acta 861*, 319–330.

(35) Ohki, S., and Duax, J. (1986) Effect of cations and polyamines on the aggregation and fusion of phosphatidylserine membranes. *Biochim. Biophys. Acta 861*, 177–186.

(36) Schroeder, U. K. O., and Tirrel, D. A. (1989) Structural reorganization of phosphatidylcholine vesicle membranes by poly(2-ethylacrylic acid). Influence of the molecular weight of the polymer. *Macromolecules 22*, 765–769.

(37) Takahashi, H., Matuoka, S., Kato, S., Okhi, K., and Hatta, I. (1991) Electrostatic interaction of poly(L-lysine) with dipalmitoylphosphatidic acid studied by X-ray difraction. *Biochim. Biophys. Acta 1069*, 229–234.

(38) Brashford, C. L., Alder, G. M., Menestrina, G., Miklem, K. L., Murphu, J. J., and Pasternak, C. A. (1986) Membrane damage by hemolytic viruses, toxins complement and other cytotoxic agents. *J. Biol. Chem. 261*, 9300–9308.

(39) Shen, W. G., and Ryser, H. J.-P. (1978) Conjugation of poly-L-lysine to albumin and horseradish peroxidase: A novel method for enhancing the cellular uptake of the protein. *Proc. Natl. Acad. Sci. U.S.A. 75*, 1872–8176.

(40) Ryser, H. J.-P., and Shen, W. C. (1978) Conjugation of methotrexate to poly(L-lysine) increases drug transport and overcome drug resistance in cultured cells. *Proc. Natl. Acad. Sci. U.S.A. 75*, 3867–3870.

(41) Ryser, H. J.-P., and Shen, W. C. (1986) Drug-poly(lysine) conjugates: their potential for chemiotherapy and for the study of endocytosis. In: Targeting of drugs and synthetic systems (G. Gregoriadis, J. Senior and G. Poste, Eds.) pp 103–121, Plenum Press, New York.

(42) Leonetti, J.-P., Degals, S., and Lebleu, B. (1990) Biological activity of oligonucleotide–poly(L-lysine) conjugates: Mechanism of cell uptake. *Bioconjugate Chem. 1*, 149–153.

(43) Steinman, R. M., Mollman, I. S., Muller, W. A., and Cohn, Z. A. (1983) Endocytosis and recycling of plasma membrane. *J. Cell. Biol. 96*, 1–27.

Preparation and Characterization of Conjugates of Monoclonal Antibodies and Staphylococcal Enterotoxin A using a New Hydrophilic Cross-Linker

Eva Akerblom,*,† Mikael Dohlsten,‡,§ Charlotte Brynö,† Maria Mastej,† Ingrid Steringer,† Gunnar Hedlund,‡,§ Peter Lando,‡ and Terje Kalland‡,§

Kabi Pharmacia AB, S-751 82 Uppsala, Sweden. Received April 27, 1993®

Conjugates between monoclonal antibodies recognizing human cancer cells and the superantigen staphylococcal enterotoxin A (mAb–SEA) represent a potential novel approach to tumor therapy. Such mAb–SEA conjugates direct T-cells to lyse colon carcinoma cells in vitro. The synthesis of mAb–SEA conjugates which were prepared by introducing thiol groups on SEA and iodoacetyl or maleimide groups on mAb forming a stable thioether linkage between SEA and mAb is described. A hydrophilic spacer, composed of repeated ethylene oxide units, was constructed to increase the distance between SEA and mAb, preserving biological activity of both proteins. The degree of modification of mAb with SEA was determined with SDS–PAGE. Variables influencing the composition of the conjugates and their effect on the tumor-cell cytotoxicity were studied and optimal conditions for the synthesis were established. Functionally active mAb–SEA conjugates were prepared from a panel of different mAb and T-cell-dependent cytotoxicity against several human cancer types including colon, ovarial, breast, and renal cancer was obtained. This suggests that mAb–SEA conjugates may be of value in the treatment of human neoplastic disease.

1. INTRODUCTION

Monoclonal antibodies (mAb) have been developed against a variety of tumor types and utilized for experimental as well as clinical studies (*1*). The use of mAb in the therapy of solid tumors has however met with limited success (*2*) and a number of critical factors determining the therapeutic outcome have been identified. The amount of mAb accumulating in the tumor area is generally low (*3*) and the effector mechanisms responsible for tumor-cell destruction, e.g. Fc-receptor cell mediated cytotoxicity or complement dependent lysis, seem to be insufficient. To overcome these limitations various mAb conjugates have been developed to increase the therapeutic efficacy. They include mAb conjugated to cytotoxic plant or bacterial toxins, radioactive isotopes, and cytotoxic agents as well as heteroconjugates simultaneously binding to the tumor cell and to activation structures on cytotoxic lymphocytes (*4*).

Staphylococcal enterotoxin A (SEA) belongs to a family of bacterial and viral superantigens that at picomolar concentrations activate a large frequency of T-cells (*5*). Superantigens bind with high affinity to MHC class II molecules and subsequently interact with subgroups of T-cells based on their β-chain variable region expressed within their T-cell receptor (TCR). We recently described that conjugates of mAb against colon carcinomas and SEA bind to tumor cells expressing the relevant antigen and subsequently direct cytotoxic T-cells to lyse the tumor cells irrespective of the MHC class II expression (*6*). This suggests that the TCR might be directly trigged by tumor-bound mAb–SEA proteins.

This paper describes the synthesis of such mAb–SEA conjugates and the variables which influence the composition of the conjugates and their capacity to induce T-cell-mediated tumor cytotoxicity. A thioether linkage which is stable and resistant to metabolic degradation was used to couple SEA to mAb to minimize the potential degradation of mAb–SEA conjugates in vivo (*7*). The mAb–SEA conjugates were prepared by introducing thiol groups on SEA and iodoacetyl groups or maleimide groups on mAb.

The efficacy of antibody–ricin conjugates has been shown to be increased by the introduction of a flexible peptide spacer in the conjugates (*8*). We have constructed a hydrophilic spacer, composed of repeated ethylene oxide units, in order to examine if such a spacer might facilitate the interaction of mAb–SEA conjugates with the membranes of colon cancer cells and CTLs, and thus increase the activity of the conjugates. Such hydrophilic spacers are likely to be useful in any system where it is desirable to increase the distance between two active constituents of a conjugate or when an active compound is coupled to a solid phase (*9*).

2. EXPERIMENTAL PROCEDURES

Material. SEA prepared with a recombinant technique (rSEA) was expressed in *Escherichia coli* strain W 3110 and secreted to the periplasmic space.[1] Frozen cells were diluted with buffer, thawed, and centrifuged. The supernatant was applied to a Q-Sepharose column. The eluted crude rSEA fraction was after concentration fractionated on a Sephadex G-75 column and the final purification was performed on a Q-Sepharose column. The different mAbs used were obtained from the following sources and were reported to have the specificities listed in Chart I.

* Author for correspondence.
† Department of Bioorganic Chemistry, Kabi Pharmacia AB, Uppsala.
‡ Department of Immunology, Kabi Pharmacia AB, Lund.
§ Department of Tumor Immunology, The Wallenberg Laboratory, University of Lund.
® Abstract published in *Advance ACS Abstracts*, September 15, 1993.

[1] Abrahamsén et al. To be published.

1043-1802/93/2904-0455$04.00/0 © 1993 American Chemical Society

Chart I

mAb	source	subclass	reported reactivity	ref
E11	Claes Juhlin, University Hospital, Uppsala, Sweden	IgG 1	parathyroid tumors	10
G250	Centocor, Leyden, The Netherlands	IgG 1	renal cell carcinoma	11
D612	J. Schlom, Bethesda, MD	IgG 2a	colon carcinoma	12
B3	Ira Pastan, Bethesda, MD	IgG1	pancarcinoma	13
SM-3	ICRF, London	IgG 1	breast cancer	14
Ma642	Kabi Pharmacia AB, Uppsala, Sweden	IgG 1	breast cancer	
Ma710	Kabi Pharmacia AB, Uppsala, Sweden	IgG 1	breast cancer	
IB16-6	R. Barth, Columbus, OH	IgG 2a	mouse melanoma	15
MOv-18	Centocor, Leyden, The Netherlands	IgG 1	ovarian carcinoma	16
C215	Kabi Pharmacia AB, Uppsala, Sweden	IgG 2a	colon carcinoma	
C242	Kabi Pharmacia AB, Uppsala, Sweden	IgG 1	colon carcinoma	
Anti-Thy-1.2	Sigma, St. Louis, MO	IgG 2a	mouse T-cells	17

17-(Iodoacetylamino)-3,6,9,12,15-pentaoxaheptadecanoic Acid (3a). Isopropyl 17-amino-3,6,9,12,15-pentaoxaheptadecanoate (1.1 g, 3.2 mmol) (*18*) was hydrolyzed in 3 mL of 1 M NaOH for 30 min. 1.5 mL of 6 M HCl was added and the mixture was evaporated to dryness. The product was taken up in dichloromethane. A 545-mg portion of 17-amino-3,6,9,12,15-pentaoxaheptadecanoic acid hydrochloride (1) was obtained after evaporation of the solvent. Compound 1 (460 mg, 1.39 mmol) was dissolved in 10 mL of 1 M borate buffer, pH 8.4. A solution of 432 mg (1.52 mmol) of *N*-succinimidyl 2-iodoacetate (**2a**) (Sigma) in 5 mL of dioxane was added and the pH was kept at 8.4 by addition of 5 M NaOH. The reaction was run in an N_2 atmosphere and was completed in 15 min. The pH of the reaction solution was then adjusted to 3 and the solution was fractionated on a reversed-phase PEP-RPC HR 30/26 (Pharmacia Biotech AB) column using a gradient of 0–13% acetonitrile with 0.1% trifluoroacetic acid (TFA) followed by isocratic separation at 13% acetonitrile, 0.1% TFA. Fractions were pooled and lyophilized, giving 351 mg (76%) of **3a**: ^{1}H NMR (D_2O) 4.23 (s, OCH_2COOH), 3.76 (s, ICH_2), 3.71–3.76 (m, OCH_2CH_2O), 3.65 (t, $NHCH_2CH_2O$), 3.41 (t, $NHCH_2CH_2O$).

17-[[3-(2-Pyridyldithio)propionyl]amino]-3,6,9,12,15-pentaoxaheptadecanoic Acid (3b). Compound 1 (183 mg, 0.55 mmol) was dissolved in 5 mL of 1 M borate buffer, pH 8.4. *N*-Succinimidyl 3-(2-pyridyldithio)propionate (SPDP, Pharmacia Biotech AB) (190 mg, 0.61 mmol) dissolved in 1.5 mL of dioxane was added and pH was adjusted to 8 with 5 M NaOH. After 30 min of reaction, the pH was adjusted to 4.6 with 5 M HCl and the reaction solution was filtered and lyophilized. The reaction mixture was fractionated on a reverse-phase PEP RPC HR 30/26 column using a gradient of 0.17% acetonitrile with 0.1% TFA followed by isocratic separation at 17% acetonitrile with 0.1% TFA. Fractions were pooled and lyophilized giving 152 mg (88%) of **3b**: ^{1}H NMR (D_2O) 8.5 (6 H, pyridine), 8.0 (3 and 5 H, pyridine), 7.4 (4 H, pyridine), 4.15 (s, OCH_2COOH), 3.68–3.72 (m, $-OCH_2CH_2O-$), 3.62 (t, $NHCH_2CH_2O$), 3.37 (t, $-NHCH_2CH_2O-$), 3.12 (t, $-SCH_2CH_2-$), 2.7 (t, $-SCH_2CH_2-$).

17-[(3-Maleimidopropionyl)amino]-3,6,9,12,15-pentaoxaheptadecanoic Acid (3c). Compound 1 (225 mg, 0.68 mmol) was dissolved in 5 mL of 1 M borate buffer, pH 8.0, and the pH was adjusted with NaOH to pH 8.0. *N*-Succinimidyl 3-maleimidopropionate (190 mg, 0.71 mmol) was dissolved in 3 mL of warm acetonitrile and added dropwise to the above solution. pH decreased and was adjusted to 8.0 with NaOH. The reaction was finished in 15 min and pH was adjusted to 4.4 with 5 M HCl. The reaction solution was partly evaporated and then lyophilized. The crude product was fractionated on a PEP-RPC HR 30/26 column using a gradient of 0–10% acetonitrile with 0.1% TFA followed by isocratic separation at 10% acetonitrile with 0.1% TFA. Fractions were pooled and lyophilized giving 112 mg (37%) **3c**. ^{1}H NMR ($CDCl_3$) 6.7 (s, HC=CH), 4.18 (s, CH_2COOH), 3.82 (t, NCH_2), 3.4–3.8 (m, $-CH_2CH_2O-$), 2.58 (t, $-CH_2CONH-$).

Preparation of the *N*-Hydroxysuccinimide Ester of 3a, 3b, and 3c (10, 6, and 12). **3a**, **3b**, or **3c** (25 μmol) was dissolved in 0.6 mL of dry dioxane and added to 2.9 mg (25 μmol) of hydroxysuccinimide in a reaction vial. A 107-μL sample of a dioxane solution with dicyclohexylcarbodiimide (37.5 μmol) was added and the reaction vial was closed. After 4 h the reaction mixture was filtered and analyzed with NMR for content of **10**, **6**, and **12**, respectively. Moisture was excluded to obtain a high yield.

Preparation of [3-(2-Pyridyldithio)propionyl]amino–rSEA (4) and (3-Mercaptopropionyl)amino–rSEA (5). SPDP (0.31 mg, 0.98 μmol) dissolved in 54 μL of dioxane was added to a solution of rSEA (13.7 mg, 0.49 μmol) in 2.4 mL of 0.1 M borate buffer, pH 8.0. The reaction was completed in 30 min. A 100-μL portion of the reaction solution was added to a Sephadex G25 NAP5 column (Pharmacia Biotech AB) to remove excess SPDP and the protein fraction was analyzed for content of coupled SPDP groups on rSEA by the method described in ref 19. The pH of the reaction solution was adjusted to 4.8 with 2 M acetic acid and then 7.4 mg of dithiotreitol dissolved in 100 μL of 0.9% sodium chloride was added to reduce the disulfide bond. The reaction was run for 20 min and thereafter the reaction solution was separated on a Sephadex G25M PD 10 column (Pharmacia Biotech AB). The protein was eluted with 3.3 mL of 0.1 M phosphate buffer the pH (7.5, 6.0 or 5.4) of which was depending on the pH used in the following coupling reaction to mAb. The protein content was determined by amino acid analysis. The solution was stored under a nitrogen atmosphere and used within 3 h.

Preparation of [17-[[3-(2-Pyridyldithio)propionyl]amino]-3,6,9,12,15-pentaoxaheptadecanoyl]amino–rSEA (7) and [17-[(3-Mercaptopropionyl)amino]-3,6,9,12,15-pentaoxaheptadecanoyl]amino–rSEA (8). The procedure was the same as for preparation of the compound **5**, except that the reduction was performed at pH 2.5 to avoid precipitation.

Preparation of (Iodoacetyl)amino–mAb (9). A solution of 0.58 mg (2.05 μmol) of *N*-succinimidyl 2-iodoacetate **2a** in 11 μL of dioxane was added to a solution of 20 mg (0.13 μmol) of mAb C215 in 10 mL of 0.1 M borate buffer, pH 8.0. The reaction was run for 30 min and thereafter the reaction solution was fractionated on a Superdex 75 HR 16/50 column (Pharmacia Biotech AB) using 0.1 M phosphate buffer, pH 7.5, with 0.9% NaCl as eluent. The protein fraction was collected and concentrated in an Amicon cell through a YM 30 filter to 3.9 mL. The protein content was determined by amino acid analysis to be 4.0 mg/mL. The number of iodoacetyl groups per mAb was determined by iodine analysis to be 10.

Table I. Synthesis of mAb(rSEA)$_p$ Conjugates According to Method 1 (Scheme IV)

		starting materials			reaction conditions[b]			products						
								% yield[c]		% composition of monomer mAb(rSEA)$_p$[d]				
mAb	synthesis no.	molar ratio of 2a or 10/mAb	n for mAb (spacer)$_n$[a]	m for rSEA (SH)$_m$	mAb (spacer)$_n$ concn, mg/mL	molar ratio of rSEA(SH)$_m$/ mAb(spacer)$_n$	reaction time, h	mono-mer	dimer + polymer	$p = 0$	$p = 1$	$p = 2$	$p = 3$	$p = 4$ ($p = 5$)
C215	1	27	19	1.5	2.3	3.4	19	52	41	33	31	21	12	
	2	16	10	1.7	2.3	4.3	17	51	49	40	27	17	8	
C215	3	28	16.6	1.9	2.6	1.8	16	56	48	30	36	22	11	
	4	28	16.6	1.9	2.2	2.7	45	43	41	14	43	34	9	
	5	28	16.6	1.9	1.8	3.6	43	49	78	3	22	34	23	17 (6)
	6	15	7.7	1.4	2.9	3.4	22	88	36	42	32	17	9	
	7	10	5.1	1.6	1.9	5.3	19	76	45	30	36	26	10	
	8	15	9.0	1.6	2.6	4.1	20	74	49	21	28	30	14	1
	9	15	8.4	1.6	2.6	3.8	15	94	37	33	33	26	7	1
C242	10	15	8.5	1.6	1.4	3.1	18	88	12	47	39	14	1	
	11	22	13.9	1.6	2.3	3.2	20	89	37	24	38	30	19	
anti-Thy-1,2	12	23	11.5	1.6	1.3	3.2	18	75	32	22	40	27	8	
	13	18	7.1	1.9	1.9	4.4	20	68	32	11	25	30	21	11
E11	14	20	7.7	1.6	1.3	4	17	85	17	48	35	14	3	
B3	15	15	9.6	1.6	2.2	3.3	17	104	21	41	34	19	6	
IB16-6	16	17	7.6	1.6	1.6	5.7	21	58	28	28	31	25	16	

[a] Compound 9, syntheses 1 and 2; compound 11, syntheses 3–16. [b] Coupling was performed at pH 7.5. [c] The yield of monomer and dimer + polymer respectively was counted as percent protein obtained regardless of that the molecular weight of mAb(rSEA)$_p$ was higher than that for the starting material mAb. [d] Composition of monomer mAb(rSEA)$_p$ in the reaction mixture including unconjugated mAb.

When using a 27 times molar excess of **2a**, the number iodoacetyl groups per mAb was 19.

Preparation of [17-[(Iodoacetyl)amino]-3,6,9,12,15-pentaoxaheptadecanoyl]amino–mAb (11). mAb was reacted with reagent **10** and the reaction conditions and the purification procedure was the same as described in the proceeding example for **9**. The molar excess of reagent **10** per mAb used for different synthesis is given in Table I. The number of iodoacetyl spacers substituted to mAb was determined by amino acid analysis using compound 1 as reference, and the values are given in Table I.

Preparation of [17-[(3-Maleimidopropionyl)amino]-3,6,9,12,15-pentaoxaheptadecanoyl]amino–mAb (13). Reagent **12** was reacted with mAb under the following different conditions.

(a) Reagent **12** was reacted with mAb at pH 8.0 for 30 min and then the reaction solution was fractionated on a Superdex 75 HR 16/50 column using 0.1 M phosphate buffer, pH 7.5, as eluent. The protein fractions were pooled and concentrated in an Amicon cell through a YM 30 filter. The purification procedure was completed in 4–6 h (syntheses 17–20, Table II).

(b) Reagent **12** was reacted with mAb at pH 8.0 or 7.5 for 15 min and then fractionated on a Superdex 75 column using as eluent phosphate buffer, pH 7.0, 6.5, or 6.0, or acetate buffer, pH 5.4 (syntheses 21–38, Table II).

The molar excess of reagent **12** per mAb used for the different synthesis is given in Table II. The number of maleimido spacers substituted on to mAb was determined by amino acid analysis and the values are given in Table II.

General Procedure for Preparing Conjugate 14, 15, and 17. (3-Mercaptopropionyl)amino–rSEA (**5**) was added to a solution of (iodoacetyl)amino–mAb (**9**), [17-(iodoacetyl)amino-3,6,9,12,15-pentaoxaheptadecanoyl]amino–mAb (**11**), and [17-[(3-maleimidopropionyl)amino]-3,6,9,12,15-pentaoxaheptadecanoyl]amino–mAb (**13**), respectively, and the reaction was run under an N_2 atmosphere at room temperature. Details of the individual syntheses are given in Tables I and II. After the reported reaction time the reaction solution was analyzed with SDS–PAGE and then fractionated on a Superdex 200 HR 16/60 column (Pharmacia Biotech AB) (Figure 2). Fractions containing the monomer conjugate were pooled in different ways, giving conjugates of different composition. Syntheses 1–16 (Table I) were, before fractionation, treated for 1 h with a 2 times molar excess of mercaptoethanol based on the number of iodoacetyl groups on mAb for reaction with unsubstituted iodine groups.

Preparation of Conjugate 16 with a 42-Atom-Long Spacer Arm. [17-[(3-Mercaptopropionyl)amino]-3,6,9,-12,15-pentaoxaheptadecanoyl]amino–rSEA (2.6 mg, 0.095 μmol) (**8**) was added to 7.0 mg (0.045 μmol) of iodoacetyl spacer modified mAb (**11**). The reaction vessel was filled with N_2 and closed. After 18 h, 0.74 μmol of mercaptoethanol was added to react with an excess of iodine groups for 1 h. The reaction solution was then fractionated on a Superdex 200 HR 16/60 column. The monomer peak was divided into two parts. The high molecular weight part gave conjugate **16a** (Figure 6d).

Removal of Unconjugated mAb from mAb(rSEA)$_p$ Conjugates. Affinity Chromatography on a Sepharose 4B–anti-r-SEA Column followed by Size-Exclusion Chromatography on Superdex 200. Rabbit antibodies against SEA were coupled to CNBr-activated Sepharose 4B according to the instructions supplied by the manufacturer (Pharmacia Biotech AB). A Sepharose 4B–anti-r-SEA column (16 × 30 mm) was packed and equilibrated with 0.1 M phosphate, pH 7.5, containing 0.5 M NaCl at a flow rate of 60 mL/h. Purified mAb(rSEA)$_p$ conjugate also containing unconjugated mAb (in 0.1 M phosphate buffer, pH 7.5, 0.5 M NaCl) was applied to the column. The effluent volume was continuously monitored at 280 nm using a UV detector. Unspecific binding to the adsorbent was prevented by adding extra salt (0.5 M NaCl) to the buffer. After careful washing of the column, the mAb(rSEA)$_p$ conjugate was eluted backward with 0.2 M glycine, pH 2.8, at a flow rate of 30 mL/h. The fractions collected were immediately neutralized to pH 7.5 with 1 M Tris-HCl, pH 8.5. The fractions containing mAb-(rSEA)$_p$ were pooled.

A Superdex 200 column (50 × 100 mm) (Pharmacia Biotech AB) was prepared for gel filtration of the mAb-(rSEA)$_p$ conjugate. The column was equilibrated with 20

Table II. Synthesis of mAb(rSEA)$_p$ Conjugates According to Method 2 (Scheme V)

		starting materials							reaction conditions				products						
		reaction mAb + 12											% yield[a]		% composition of monomer mAb(rSEA)$_p$[b]				
			reaction condn		purification condn														
mAb	synthesis no.	molar ratio 12/mAb	pH	h	pH	h	n for mAb (spacer)$_n$ (13)	m for rSEA (SH)$_m$	mAb (spacer)$_n$ concn, mg/mL	molar ratio rSEA(SH)$_m$/ mAb(spacer)$_n$	coupling pH	reaction time, h	monomer	dimer + polymer	$p = 0$	$p = 1$	$p = 2$	$p = 3$	$p = 4$
C215	17	10	8.0	0.5	7.5	4.25	3.7	1.6	3.0	2.1	7.5	<1	35	38	43	36	20	1	
	18	10	8.0	0.5	7.5	4.25	3.7	1.6	2.4	3.7	7.5	<1	50	39	40	40	20	1	
	19	16	8.0	0.5	7.5	5.75	5.9	1.6	4.4	1.2	7.5	<1	42	54	40	35	24		
	20	16	8.0	0.5	7.5	5.75	5.9	1.6	3.4	2.3	7.5	<1	30	25	44	38	22		
	21	10	8.0	0.25	7.0	2	3.9	1.6	1.2	2.1	7.0	1	33	33	24	38	29	9	
	22	10	8.0	0.25	7.0	2	3.9	1.6	1.1	3.2	7.0	1	36	43	22	38	29	14	
	23	14	7.5	0.25	6.5	2	4.9	1.5	0.8	2.6	6.5	20	37	35	47	20	17	11	2
	24	20	7.5	0.25	6.0	2	5.6	1.7	0.8	3.2	6.0	20	41	44	20	34	30	14	2
	25	10	8.0	0.25	5.4	2	3.9	1.6	1.4	1.5	5.4	20	34	38	37	39	19	4	
	26	10	8.0	0.25	5.4	2	3.9	1.6	1.3	2.2	5.4	20	48	57	27	42	22	7	
	27	7	8.0	0.25	5.4	2	2.3	0.86	1.2	3.4	5.4	23	53	42	43	26	18	10	2
	28	7	8.0	0.25	5.4	2	2.3	0.86	1.1	4.5	5.4	23	53	45	41	24	18	10	5
C242	29	8	8.0	0.25	5.4	2	4.0	0.86	1.2	3.3	5.4	20	81	43	25	39	25	9	2
	30	8	8.0	0.25	5.4	2	4.0	0.86	1.1	4.5	5.4	20	72	33	19	37	28	13	3
	31	8	8.0	0.25	5.4	2	4.0	0.86	1.0	5.6	5.4	20	65	29	17	36	30	14	3
SM-3	32	16	7.5	0.25	6.0	2	6.8	1.5	1.1	4.4	6.0	23	84	45	8	34	36	18	4
Mov18	34	14	7.5	0.25	6.0	0.5	8.6	1.5	1.2	3.1	6.0	20	53	62	17	31	29	16	5
G250	35	17	7.5	0.25	5.4	0.5	5.8	1.5	1.2	2.8	5.4	18	83	33	23	32	27	16	3
MA710	36	15	7.5	0.25	6.0	0.5	4.1	1.5	1.3	3.0	6.0	18	71	38	31	31	20	12	4
MA642	37	15	7.5	0.25	6.0	0.5	4.9	1.5	1.2	3.2	6.0	18	71	41	26	31	22	14	5
D612	38	12	7.5	0.25	5.4	0.5	4.7	1.5	1.2	2.8	5.4	17	62	39	23	32	27	16	3

[a] The yield of monomer and dimer + polymer respectively was counted as percent protein obtained regardless of that the molecular weight of mAb(rSEA)$_p$ was higher than that for the starting material mAb. [b] Composition of the monomer mAb(rSEA)$_p$ in the reaction mixture including unconjugated mAb.

mM phosphate buffer, pH 7.5, 0.9% NaCl at a flow rate of 300 mL/h. Pooled material was applied to the column and eluted with the same buffer. Separation of the monomer and dimer form of mAb(rSEA)$_p$ was obtained and the fractions with monomer mAb(rSEA)$_p$ were pooled and further concentrated by membrane filtration.

Determination of Dimer and Polymer by Size-Exclusion Chromatography (SEC). The content of dimers and polymers in mAb(rSEA)$_p$ conjugates was determined by SEC using a Superdex 200 HR 16/60 column. A 150-μg sample of protein was applied to the column. 20 mM phosphate, 0.9% NaCl, pH 7.5 was used as an eluent and a UV detector at 280 nm was used for monitoring. The dimer, polymer, and monomer form of the mAb(rSEA)$_p$ conjugate were determined gravimetric and the dimer and polymer form calculated as percent of the total content.

Phast Analysis of the Composition of mAb(rSEA)$_p$ Conjugates. SDS-PAGE. Phast System from Pharmacia Biotech AB was used for electrophoretic separation of the mAb(rSEA)$_p$, staining, and destaining. PhastGel gradient 4–15 was used for analysis under non-reducing conditions in the presence of 2.5% SDS. Each sample was boiled for 3 min. Separation and staining procedures were carried out according to the instructions given in file no. 130, 200, and 210 supplied by the manufacturer. Some modifications were made by running the electrophoresis for 80 V h and using an extra washing step in the CBB staining. One microliter of mAb(rSEA)$_p$ conjugate containing 1–4 mg of protein/mL for CBB staining and 0.1–0.2 mg of protein/mL for silver staining was subjected to electrophoresis. Pharmacia calibration kit proteins for high molecular weight measurements, with molecular weights between 14 400 and 94 000 Da, were used as standards.

Evaluation with PhastImage. PhastImage (Pharmacia Biotech AB) was used for the evaluation of the PhastGel media. A 613-nm filter was used when scanning CBB-stained gels and a 546-nm filter for silver stained gels in the gel analyzer.

An Olivetti personal computer with PhastImage software controlled the gel analyzer and also evaluated the one-dimensional separations. PhastImage defined contours around the bands and transferred them into a peak data curve which was possible to integrate.

The distribution of mAb(rSEA)$_p$ (p = 0, 1, 2...) was calculated. Each area was compared with the total area for all peaks/bands.

Cell Lines. The colon carcinoma lines SW620, COLO 205, and LoVo and the ovarian carcinoma line HeLa were obtained from the American Type Culture Collection and cultured in R medium [RPMI 1640 medium (GIBCO) supplemented with 10% fetal calf serum, 1 mM nonessential amino acids, 50 μM 2-mercaptoethanol, and 1 mM pyruvate (Flow Laboratories)]. The mammary carcinoma line MDA-MB 361 was obtained from CanAg and cultured as described above. T-cell lines were established by stimulation of human peripheral blood lymphocytes with SEA (1 ng/mL) as detailed earlier (*20*). These T-cell lines were all >99% CD3$^+$ as determined by flow-cytometric analysis.

Cytotoxicity Assay. Cytotoxicity was measured at an effector/target cell ratio of 30:1 in a standard 4-h ^{51}Cr-release assay as described (*20*). SEA, mAb, or conjugates were added at various concentrations directly into the assay. The percentage specific cytotoxicity was computed according to the formula: % specific cytotoxicity = 100 × [experimental release (cpm) − spontaneous release (cpm)/maximum release (cpm) − spontaneous release (cpm)].

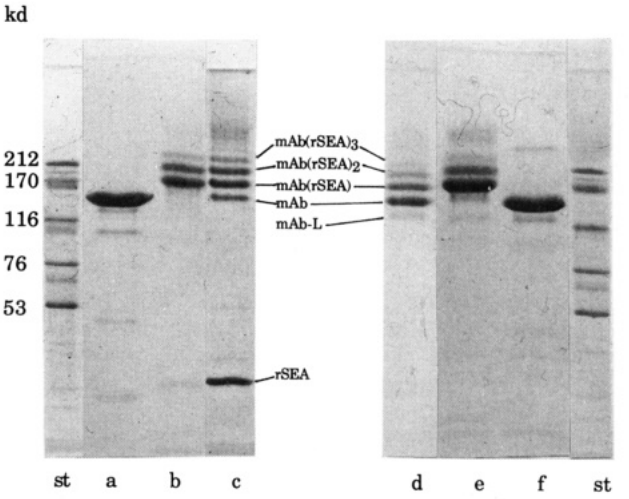


Figure 1. SDS–PAGE of mAb(rSEA)$_p$ conjugates and their protein components: (a) mAb C242, (b) C242(rSEA)$_p$ purified from unconjugated mAb with affinity chromatography, (c) reaction mixture of C242(rSEA)$_p$ synthesis, (d) C215(rSEA)$_p$, (e) C215(rSEA)$_p$ purified from unconjugated mAb with affinity chromatography, (f) mAb C215, (st) molecular weight standard.

3. CHEMICAL RESULTS

3.1. Composition of the mAb(rSEA)$_p$ Conjugates. The composition of the mAb(rSEA)$_p$ conjugates was determined with SDS–PAGE analysis and is presented in Tables I and II. SDS–PAGE analysis under nonreducing conditions gave separate bands for mAb and mAb(rSEA)$_p$ with 1–5 rSEA and a broad band for the corresponding dimer forms (Figure 1).

Scanning the bands with PhastImage gel analyzer gave good reproducibility for the composition of the monomer conjugate when staining with CBB. However, concentrations > 1 mg/mL were required. The limited availability of material made it therefore often necessary to use silver nitrate staining. This method has not been documented for quantitative use. However, we found reproducible results and good conformity with CBB staining when concentrations of 0.1–0.2 mg/mL were analyzed (data not shown). Scanning of the broad dimer band gave too low values. Quantification of dimer was therefore performed with SEC analysis.

Separation of the bands on SDS–PAGE required heating of the sample solution. This caused some dissociation of light chain in mAb and mAb(rSEA)$_p$ conjugates. The values in Tables I and II were corrected for loss of light chains.

3.2. Purification of mAb(rSEA)$_p$ Conjugates. A good separation of the mAb(rSEA)$_p$ conjugate and the monomer and dimer form of rSEA(SH)$_m$ (*5*) was obtained by SEC on a Superdex 200 column (Figure 2, peaks 2, 3, and 4, respectively). There was also a fairly good separation between the monomer conjugate peak 2 and peak 1 representing material with high molecular weight including complexes of two molecules of antibody or more, together with an unknown number of rSEA molecules.

Peak 2 with the monomer mAb(rSEA)$_p$ conjugate was divided in fractions. However, each fraction showed overlapping species with 1–4 rSEA substituted on to the mAb and also unconjugated mAb. Fractions in the beginning of the peak were enriched in highly substituted

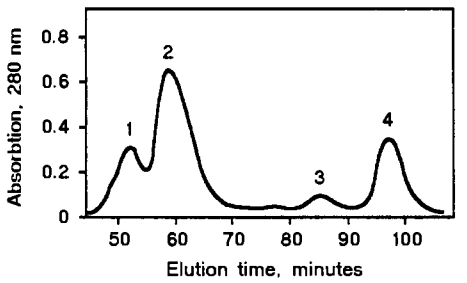
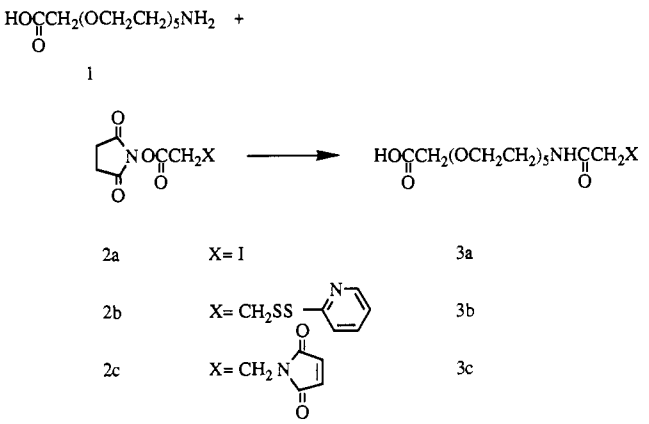


Figure 2. Purification of mAb(rSEA)$_p$ conjugate on Superdex 200 column: peak 1, aggregated mAb(rSEA)$_p$; peak 2, monomer mAb(rSEA)$_p$; peak 3, dimer of rSEA(SH)$_m$; peak 4, monomer of rSEA(SH)$_m$.

Scheme I



mAb and in the end of the peak low-substituted and unconjugated mAb was found.

Unconjugated mAb was removed effectively from mAb-(rSEA) conjugates on a rabbit IgG anti-rSEA–Sepharose 6B column (Figure 1). However, due to the high efficiency of the column, only 50% of the conjugate was recovered. Three conjugates were purified from unconjugated mAb whereas the other conjugates were tested for cytotoxic activity without removal of free mAb since presence of the latter showed no interference with the in vitro test results (compare Figure 6a,b). Attempts to remove unconjugated mAb on Red A gel (Amicon Ltd.), Red Sepharose Cl-6B (Pharmacia Biotech AB) or hydroxyapatite were unsuccessful (data not shown).

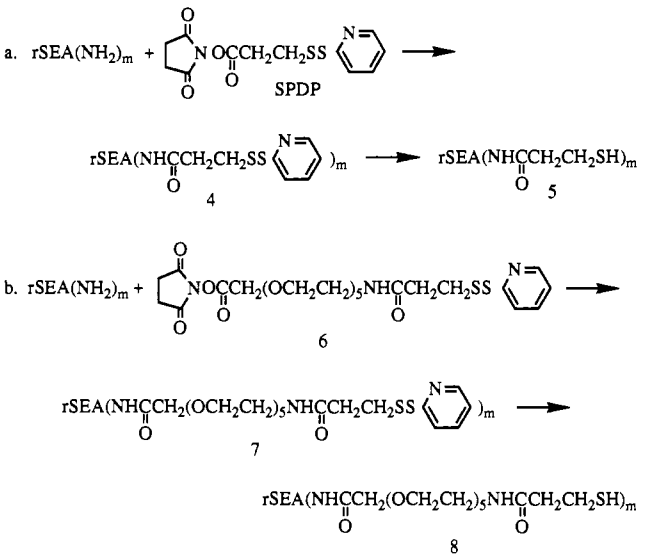
3.3. Coupling Procedure. Two methods were used for coupling rSEA via a thioether linkage to mAb (Schemes IV and V). In both cases thiol groups were introduced on the lysines of rSEA either with the SPDP reagent or the spacer reagent **6** (Scheme II).

A 2-fold molar excess of SPDP per rSEA and a concentration of rSEA around 6 mg/mL and pH 8.0 gave 1.5–1.7 SH groups per rSEA. A 1.25 molar excess of SPDP gave 0.9 SH groups per rSEA. A 4.5 molar excess of reagent **6** per rSEA gave 2.9 SH groups.

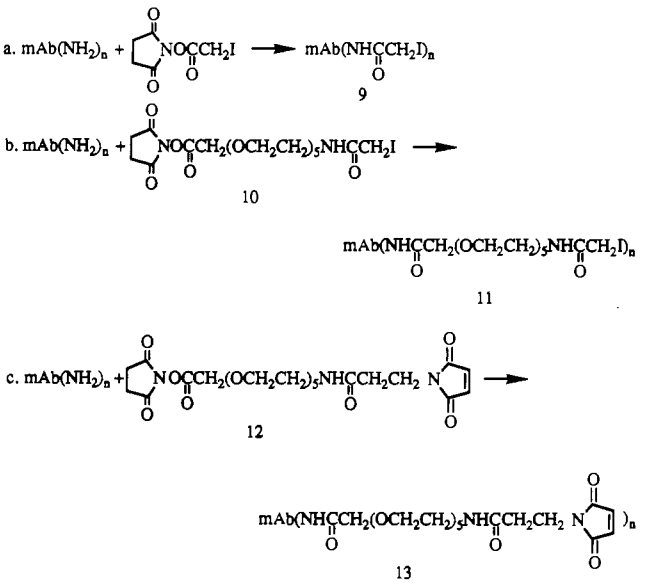
In method 1 iodoacetyl groups were introduced on the lysines of mAb and in method 2 maleimide groups were introduced (Schemes IV and V, respectively). Both methods gave a stable thioether linkage between rSEA and mAb. The mAb(rSEA)$_p$ conjugates formed were a heterogenous mixture of conjugates with 1–4 rSEA and unconjugated mAb (Tables I and II).

3.3.1. Method 1. Coupling with Iodoacetyl Groups. Iodoacetyl groups were coupled to mAb at pH 8.0 using a concentration of mAb around 2 mg/mL. By using different excessive amounts of *N*-succinimidyl iodoacetate **2a** and iodoacetyl reagent **10**, respectively, a different number of spacers was coupled to mAb. The valid

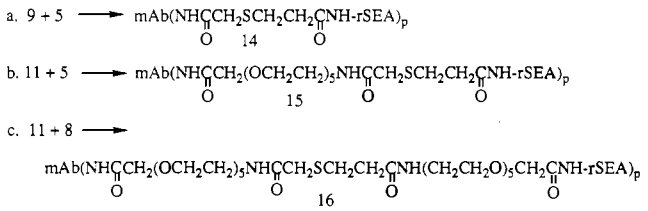
Scheme II



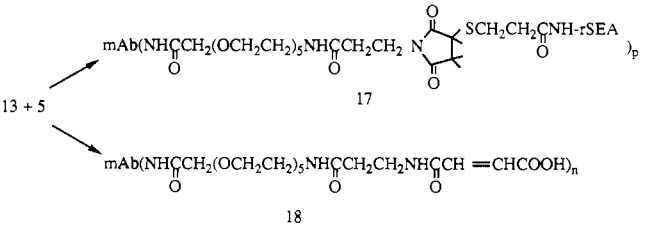
Scheme III



Scheme IV



Scheme V



correlation had to be determined for each mAb. Figure 3 shows the correlation found for mAb C215. The iodoacetylated mAb products **9** and **11** could not be stored frozen, as they were found to aggregate.

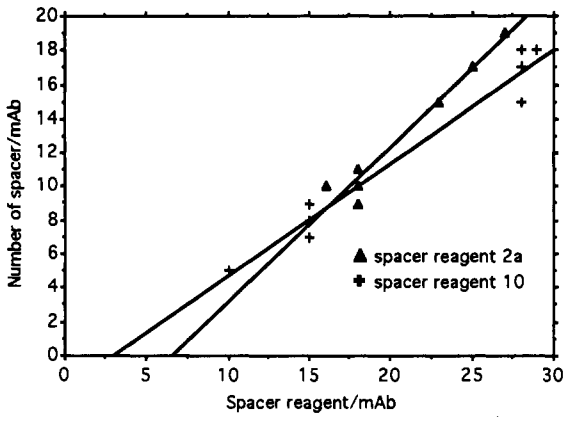


Figure 3. Linear correlation between excess of spacer reagent **2a** and **10**, respectively, per C215 and degree of substitution of C215(spacer)$_n$ (**9** and **11**, respectively). Correlation coefficients squared for both lines were 0.96.

pH 7.5 was used for coupling thiol-substituted rSEAs **5** and **8** to iodoacetylated mAbs **9** and **11**. This pH was chosen to avoid reoxidation of the thiol groups on rSEA to a disulfide dimer of rSEA which occurred if coupling was performed at a higher pH (data not shown). A total of 1.6 thiol groups on rSEA were chosen to avoid excessive cross-linking to high molecular weight conjugates.

To optimize the coupling reaction conditions a different number of iodoacetyl spacers on mAb was used and the molar excess of rSEA(SH)$_m$ **5** was varied (Table I). The reaction rate was studied for synthesis 6 with eight spacers on mAb C215 and a 3.4 molar excess of rSEA(SH)$_m$ **5**. The composition of the formed monomer conjugate was analyzed after 1, 4.5, and 21 h with SDS–PAGE (Figure 4a). There was still 42% unconjugated mAb in the monomer after 21 h. Increasing the reaction time further up to 40 h gave as a rule a lower yield of monomer conjugate as more high molecular material was formed.

A more complete reaction was obtained either by increasing the molar excess of rSEA(SH)$_m$ as in synthesis 8 or increasing the number of spacers as in synthesis **4**. Optimal conjugates with mainly one and two rSEA substituted on to the mAb were obtained by using 8–10 iodoacetyl spacers on the mAb and a 4 molar excess of rSEA(SH)$_m$ **5**.

The excess of iodoacetyl groups on the mAb(rSEA)$_p$ conjugate was reacted with mercaptoethanol. Certain mAbs, e.g. C215, were sensitive to treatment with a large molecular excess of mercaptoethanol. SDS–PAGE analysis showed loss of the light chain, indicating that disulfide bands in the mAb had been reduced.

3.3.2. Method 2. Coupling with Maleimide Groups. Maleimide groups were coupled to mAb by reacting different molar excesses of spacer reagent **12** with mAb at pH 7.5 and 8.0. When the coupling reaction was run for 0.5 h at pH 8.0 and purification took 4–6 h at pH 7.5, the following reactions with rSEA(SH)$_m$ gave incomplete coupling, indicating hydrolysis of the maleimide ring (syntheses 17–20, Table II). To avoid this side reaction, coupling of **12** to mAb is recommended to be performed at pH 7.5 for 15 min and with a purification time of less than 2 h.

To optimize the coupling reaction between **13** and **5** (Scheme V) the number of maleimide spacers on mAb was varied and different amounts of molar excess of rSEA-(SH)$_m$ **5** were used as well as changes of the coupling pH (Table II).

The reaction rate was studied for syntheses 17–28 by analyzing with SDS–PAGE the composition of the formed

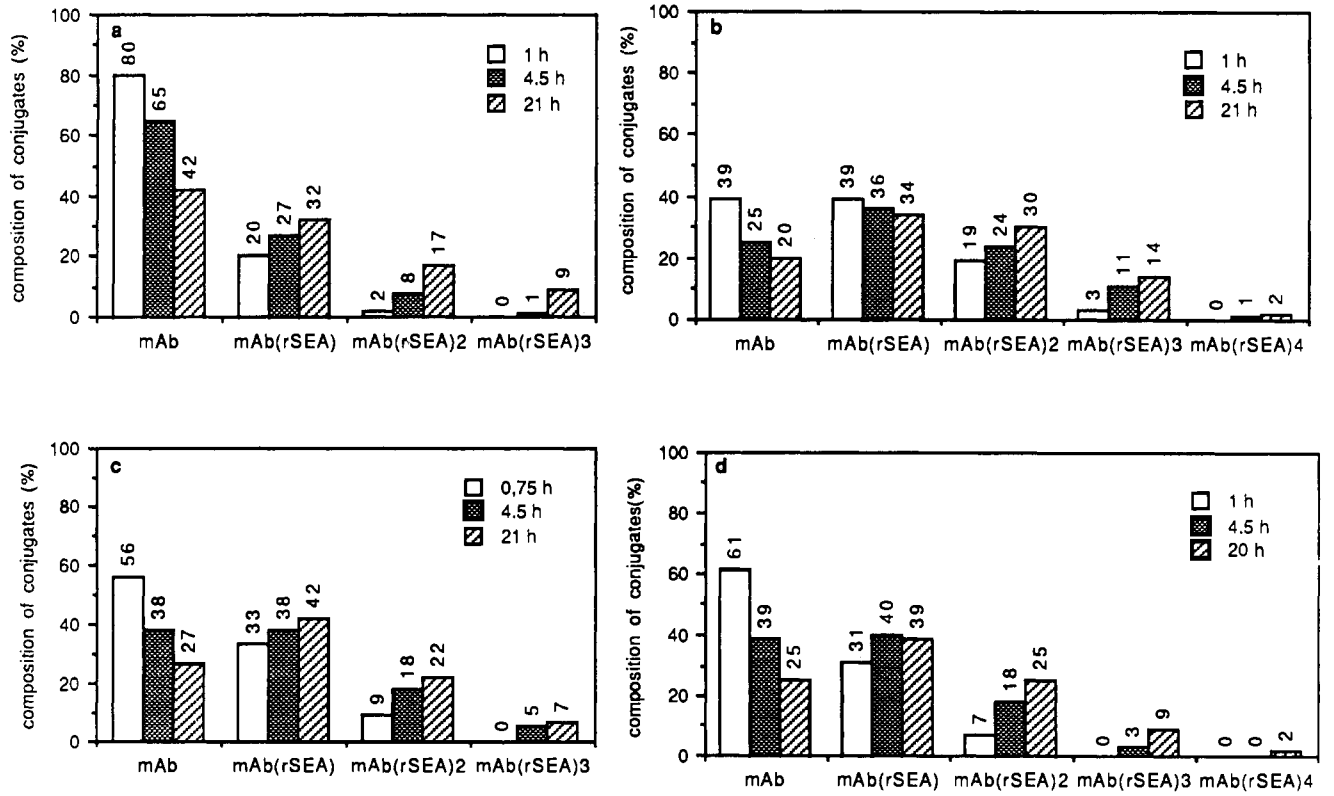


Figure 4. The composition of formed monomer mAb(rSEA)$_p$ conjugates measured with SDS–PAGE after different reaction times: (a) synthesis 6 (Table I) reaction between C215 with iodoacetyl spacer (**11**) and rSEA(SH)$_m$, (b) synthesis 24 (Table II) reaction between C215 with maleimide spacer (**13**) and rSEA(SH) at pH 6.0, (c) synthesis 26 (Table II) reaction between C215 with maleimide spacer (**13**) and rSEA(SH)$_m$ at pH 5.4, (d) synthesis 29 (Table II) reaction between C242 with maleimide spacer (**13**) and rSEA(SH)$_m$ at pH 5.4.

Table III. Stability of mAb(rSEA)$_p$ Conjugates

conjugate from synthesis	storage temp, °C	time, months	dimer or polymer[a] %
3	−20	11	25
4 (**15c**)	−20	10	16
5 (**15f**)	−20	10	traces
6 (**15b**)	−20	0	0.5
		1	18
		3	15
7 (**15a**)	−20	0	10
		1	23
		3	23
8 (**15e**)	−70	1	traces
		12	1
9 (**15h**)	−70	3	12
		10	10
17	−70	1	9
		3.5	9
25	−70	0.3	6
		4	5
		6	5

[a] Determined by size-exclusion chromatography.

monomer conjugate after 1, 4.5, and 20–21 h. The reaction was rapid at pH 7.0 and 7.5 and completed in 1 h (syntheses 17–20) (Data not shown). The reaction was slower at 5.4, 6.0, and 6.5 and needed more than 4 h. Data for syntheses 24, 26, and 29 are given in Figure 4, parts b, c, and d, respectively.

Reaction at pH 6.5 and 7.0 is not recommended since rSEA(SH)$_m$ **5** had limited solubility at these pH and precipitations were observed.

The coupling reaction gave significant dimer and polymer products. An effort to minimize these products by using only 0.86 thiol groups on rSEA(SH)$_m$ was not successful (syntheses 27–31). The amount of dimer and polymer products formed was dependent on the individual mAb used as earlier found for method 1.

The optimal coupling conditions for obtaining conjugates with mainly one or two rSEA with method 2 were when coupling occurred at a pH interval of 5.4–6.0 and 4–8 spacers on the mAb were used together with 1.6 SH groups on rSEA and 3 times excess of rSEA(SH)$_m$ (Table II).

3.4. The Stability of mAb(rSEA)$_p$ Conjugates. The stability of mAb(rSEA)$_p$ conjugates prepared with both method 1 and 2 and stored in 20 mM PBS, pH 7.5, 0.9% NaCl at −20 or −70 °C is presented in Table III. The freezing–thawing process gave traces of dimer + polymer (all data not presented). Storage at −20 °C gave between 15 and 25% dimer + polymer on storage up to 11 months. Storage at −70 °C was preferable as the dimer + polymer formed was only 1–12%. There was no difference in stability between conjugates prepared with the two different methods.

4. RESULTS OF BIOLOGICAL ACTIVITY

4.1. Cytotoxicity. The C215(rSEA)$_p$ conjugates induced strong T-cell-dependent tumor cell lysis at 10 ng/mL and significant lysis at 1 ng/mL, whereas unconjugated mAb and SEA itself had a marginal effect even at concentrations of 1000 ng/mL. The coefficient of analytical variation, calculated from the measurements carried out in triplicate, was routinely less than 15%. A difference in activity is significant when the concentration of two conjugates, giving similar cytotoxicity, differs 4-fold or more. Variation in the maximal level of cytotoxicity recorded in the different experiments most likely depends on variation in activity from one T-cell line to another and to changes in the T-cell line during the in vitro cultivation time.

The cytotoxicity of rSEA seen in the different experiments may be due to low expression of the SE receptor distinct from the MHC class II receptor (*21*). A high concentration of the relevant but not of an irrelevant antibody blocks SADCC induced by the mAb(rSEA)$_p$ conjugates, suggesting an antigen-specific effect (*6*). Cell lines expressing the relevant target antigen were sensitive to SADCC while cell lines lacking the antigen were resistant (unpublished data). Studies of binding were performed on tumor cells expressing the mAb-defined antigen and demonstrated that the C215(rSEA)$_p$ conjugates displayed target cell binding in a similar range as the native mAb C215 ($K_d = 2 \times 10^{-9}$ M) (data not shown).

4.1.1. Cytotoxicity of Conjugates with a Different Number of Spacers. The cytotoxicity of C215(rSEA)$_p$ conjugates (**15**) with 5, 7, and 17 spacers (**15a–c**) prepared with method 1 was compared (Figure 5a,b). All conjugates (**15a–c**) mediated strong lysis and only marginal differences could be recorded. Thus, mAb C215 allowed substitution with 17 spacers without loss of activity, whereas other mAbs (C242 and anti-Thy 1.2) lost activity at high rates of substitution (data not shown). It is therefore recommended to substitute mAbs with not more than 8–10 spacers when preparing new mAb(rSEA)$_p$ conjugates with method 1.

4.1.2. Cytotoxicity of Conjugates with a Different Number of rSEA Substituents. We were not able to identify effective separation conditions to isolate mAb-(rSEA)$_p$ conjugate with 1, 2, or 3 rSEA per mAb. We have therefore compared the activity of C215(rSEA)$_p$ conjugates with different composition (**15d–f**) (Figure 5c,d). Conjugate **15d** was composed mainly of mAb with one rSEA whereas **15e** was a mixture of mAb with 1, 2, and 3 rSEA. Conjugate **15f** was a highly substituted conjugate. The different conjugates mediated similar cytotoxic activity.

4.1.3. Cytotoxicity of Conjugates Prepared with Different Methods. Conjugates **15h** and **17a** with similar composition but prepared with method 1 and 2, respectively, showed similar cytotoxicity (Figure 6a). Furthermore, conjugates **15h** and **17a**, with unconjugated mAb removed, showed essentially the same cytotoxic activity as conjugate **15g**, where 17% mAb was present.

4.1.4. Cytotoxicity of Conjugates with Different Lengths of Spacers. Conjugates were prepared with 6-, 24-, and 42-atom-long spacer arms (**14**, **15**, and **16**, respectively) (Scheme IV), and their cytotoxicity was compared (Figure 6b). There was no difference in activity between conjugates prepared with 6- or 24-atom spacer (**14a** and **15f,h**, respectively). The difference in activity of conjugate with a 42-atom spacer (**16a**) was within the variability of the test method. Conjugates with the short 6-atom spacer gave about the same activity as those with 10- and 19-atom spacers (data not shown).

4.1.5. Cytotoxicity Using a Panel of mAb–SEA Conjugates with Different Tumor Selectivity. To analyze whether active mAb–SEA conjugates could be developed with several different mAb, we conjugated a panel of mAb reactive with different tumor types, i.e. colon cancer, ovarial cancer, breast cancer, and lung cancer. The mAbs C215, C242, and D612 reactive with colon carcinomas induced T-cells to mediate strong lysis of SW620, LoVo, and Colo205 cells, whereas unconjugated mAb or SEA alone had marginal effects (Figure 7a,b). The HeLa cell line was strongly lysed by T-cells in the presence of MOv18-(rSEA)$_p$ and C215(rSEA)$_p$ conjugates, while no lysis was seen by unconjugated mAb and SEA. Similarly MA642-(rSEA)$_p$, MA710(rSEA)$_p$, and C215(rSEA)$_p$ conjugates mediated strong lysis of the breast cancer cell line MDA-

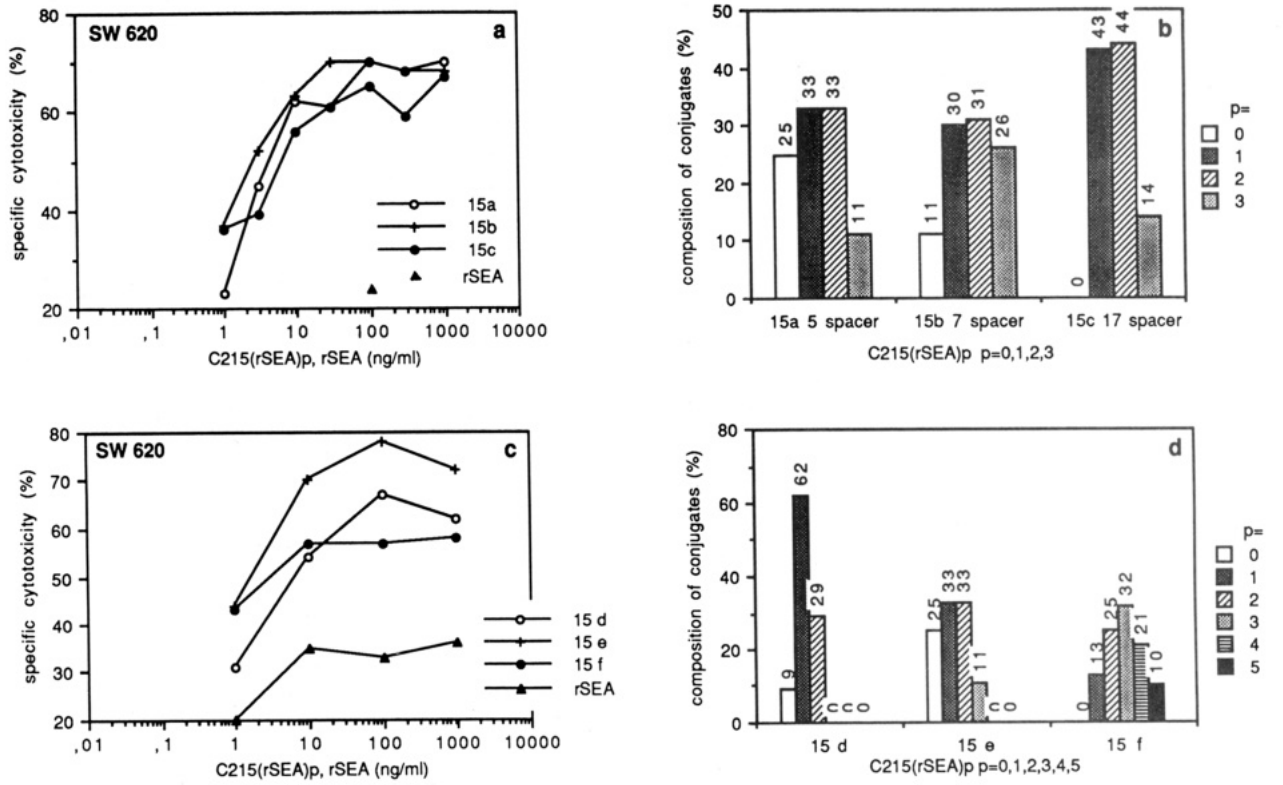


Figure 5. The capacity of C215(rSEA)$_p$ conjugates and rSEA to target SEA-responsive CTLs against the C215$^+$MHC class II$^-$ colon carcinoma cell lines SW 620: (a) C215(rSEA)$_p$ conjugates prepared with different number of iodoacetyl spacers on mAb 11 (n = 5, 7, 17 Scheme 3) and (b) their chemical composition; (c) C215(rSEA)$_p$ conjugates with different degree of substitution of rSEA and (d) their chemical composition. All conjugates were prepared with iodoacetyl spacer **11** method 1.

MD361 (Figure 7d), whereas the tumor cells remained resistant to unconjugated mAb and SEA alone.

5. DISCUSSION

mAb(rSEA)$_p$ conjugates act by binding of the mAb moiety to the membrane of the tumor cell. The rSEA displayed on the tumor cell surface is recognized by a high frequency of T-cells and the tumor cell is subsequently lysed by the T-cells (*6*) (Figure 8). Thus, the mAb(rSEA)$_p$ conjugates work with a mechanism distinct from that of immunotoxins (*22*) and do not require internalization.

The coupling strategy is therefore different from that of the immunotoxins, which usually require a cleavable bond between mAb and toxin to be cytotoxic. The mAb-(rSEA)$_p$ conjugates did not need to be processed to activate T-cells and should have a stable linkage between the mAb and rSEA to minimize the side effects of free rSEA. A stable thioether linkage was therefore chosen instead of the often used disulfide bond. The new hydrophilic spacer reagents **6**, **10**, and **12** are composed of five repeated ethylene oxide units. Polymers with ethylene oxide units, polyethylene glycols, have several advantages compared to other spacers. They do not interfere with the conformation of peptides or proteins to which they are attached and they have amphiphilic characteristics enhancing solubility in both water and polar organic solvents (*23*). In aqueous solution they appear to exist as a freely permeable coil.

One thiol group per rSEA is ideal to prevent cross-linking of mAb to high molecular weight material. However chemical coupling always results in a mixture of rSEA-(SH)$_m$ products with different number of thiol groups. An average substitution of 1.5–1.7 thiol groups per rSEA was chosen. Most rSEA molecules are expected to have one or two thiol groups and a lesser fraction no or more than two thiol groups.

The amount of high molecular weight material formed was rather high (20–50%) and was found to be dependent on the individual mAb used rather than on the number of thiol groups on rSEA. rSEA with 0.89 thiol groups per mAb gave a similar amount of high molecular weight material as rSEA with 1.6 groups (syntheses 27 and 28 compared with syntheses 17–26, Table II).

The number of spacers on the mAb was varied from 2 to 19. The reaction between thiol groups and maleimide groups was more rapid than the corresponding reaction with iodoacetyl groups. A lower number of maleimide spacers than iodoacetyl spacers was therefore needed to obtain satisfactory coupling results. Four maleimide spacers on the mAb and a 3 times excess of rSEA(SH)$_m$ gave a similar composition of the mAb(rSEA)$_p$ conjugate as 8–9 iodoacetyl spacers on the mAb and a 4 times excess of rSEA(SH)$_m$ (synthesis 22, Table II, and syntheses 8 and 9, Table I, respectively). It should also be noted that the concentration of mAb(spacer)$_n$ was only 1.1 mg/mL in synthesis 22 compared with 2.6 mg/mL in the syntheses 8 and 9. In general it is advantageous to use as few spacers as possible to avoid possible interference with antibody binding.

The maleimide group is sensitive to hydrolysis (*24*). Coupling of the spacer to the mAb during 0.5 h at pH 8.0 followed by purification for 6 h at pH 7.5 gave 40% unmodified mAb in the product (syntheses 17–20) independent of the number of spacers and the amount of rSEA-(SH)$_m$ used. This indicates that the maleimide spacer was partly hydrolyzed before coupling to rSEA(SH)$_m$. Coupling of the latter to the maleimide spacer at pH 7.0 and 7.5 was very rapid but carries the risk of hydrolysis at pH 7.5. At pH 6.5–7.0 the rSEA(SH)$_m$ had limited solubility, which was most obvious in synthesis 23 with 47% unconjugated mAb in the mAb(rSEA)$_p$ conjugate. Coupling at pH 5.4–6.0 worked well for a series of different

mAb (Table II). Coupling at a pH value near the p*I* value of the mAb should in general be avoided since there is risk for precipitation.

Method 2 using maleimide spacer was more convenient than method 1 using iodoacetyl spacer but gave a lower yield. The stability at −70 °C of mAb(rSEA)$_p$ conjugates coupled with the two methods was about the same (Table III).

Most experiments were performed with the hydrophilic spacers **3a** and **3c** but for comparison some couplings were made with iodoacetylated mAb and rSEA(SH)$_m$, (Scheme IV, part a). The latter reaction was slower than the corresponding reaction with iodoacetylhydrophilic spacer (Scheme IV, part 6). Synthesis 2 gave a much lower substitution than synthesis 8 and the same was found for synthesis 1 if compared with syntheses 3 and 5. The yield was also lower for synthesis 2 compared with syntheses 6–9 (Table I). These results show that the 21-atom spacer arm on mAb facilitates coupling to thiol groups on rSEA.

The high amount of unconjugated mAb in all mAb-(rSEA)$_p$ conjugates after completed reaction (Table I and II) was unexpected. The reaction stopped despite the iodine groups left on the mAb and the excess of rSEA-(SH)$_m$. Prolongation of the reaction time from 20 to 45 h gave only slightly higher substitution. All attempts to get complete mAb conjugation resulted in conjugates with higher substitution.

We were interested in studying the variables involved in mAb(rSEA)$_p$ construction and their effect on the cytotoxicity. It has been reported that for ricin immunotoxins the biricin conjugates were 8 times more potent than the monoricin conjugates (*25*) and that a 29-residue flexible peptide spacer increased the potency 10 times (*8*). However, the structure–activity studies of the mAb conjugates were complicated by their heterogeneity. All mAb(rSEA)$_p$ conjugates prepared were a mixture of conjugates with different number of rSEA substituted. Moreover, the coupling site of rSEA to mAb could vary for conjugates with the same degree of substitution. Another complication was that the SADCC test used for analyzing cytotoxicity does not allow measurements of minor differences in activity. The differences must be 4-fold or greater to be detected.

It is reported that the number of spacers which can be coupled to an mAb without interfering with the affinity of the antibody is dependent on the individual mAb (*26*). mAb C215 allowed a very high number of spacers to be coupled with essentially unchanged antigen binding (*6*). No difference in cytotoxicity was seen for conjugates with 5, 7, or 17 spacers on C215 (Figure 5a). The maximal degree of substitution for the other mAbs was not examined, but the number of spacers was kept between 8 and 10 when using coupling method 1 and between 4 and 8 when using coupling method 2 to reduce interference with essential binding residues in the mAb CDR regions.

Further we found that increasing the number of SEA molecules in the mAb–SEA conjugates did not improve the efficacy compared to those with one SEA per mAb. This observation suggests no major beneficial effects of multivalency (Figure 5c). No difference in cytotoxicity was seen between conjugates prepared with methods 1 and 2 (Figure 6a) and no improvement in cytotoxic activity was seen when the length of the spacer arm was increased as reported for ricin mAb conjugates (Figure 6c).

A significant advantage of the hydrophilic spacer described in this report was that it increased the rate of

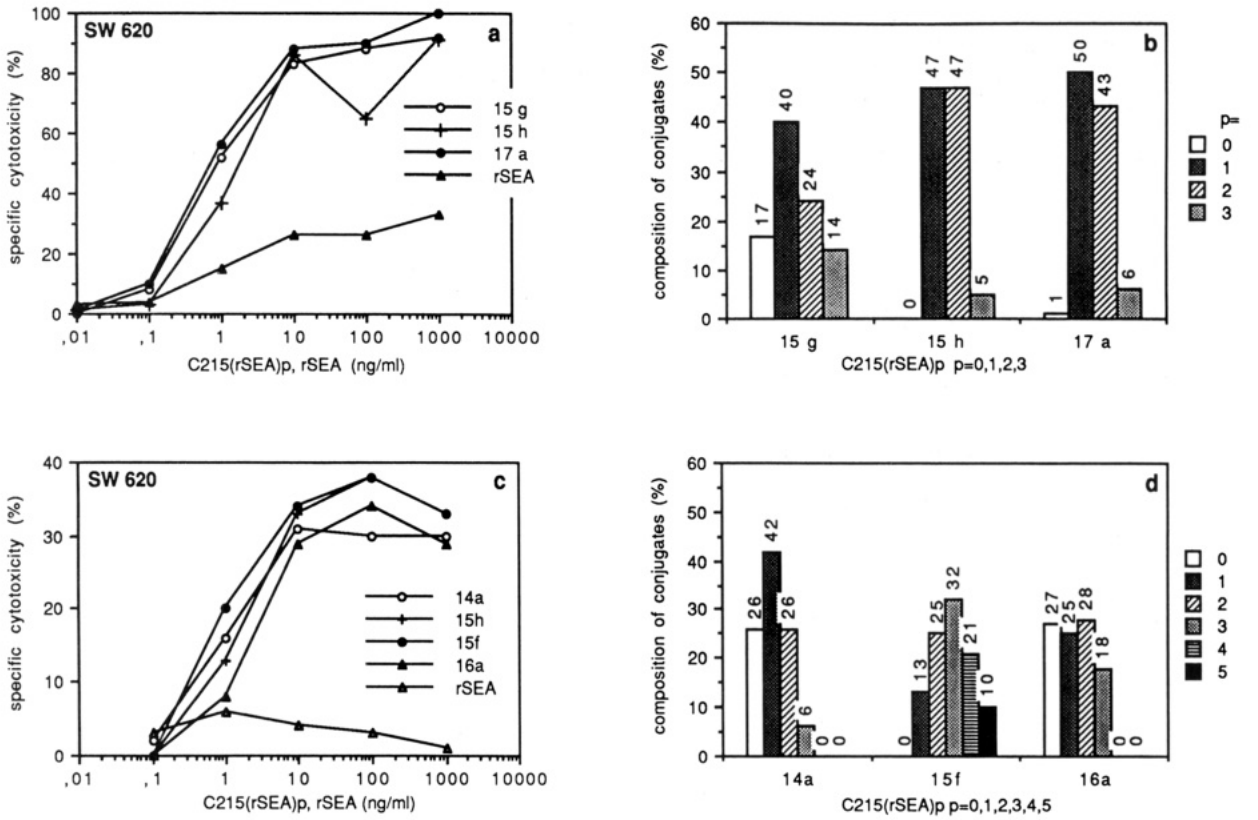


Figure 6. The capacity of C215 (rSEA)$_p$ conjugates and rSEA to target SEA-responsive CTCs against the C215$^+$MHC class II$^-$ colon carcinoma cell lines SW 620: (a) The cytotoxicity of C215(rSEA)$_p$ conjugates **15h** and **17a** prepared with method 1 and 2, respectively, and purified from unconjugated mAb and conjugate **15g** prepared with method 1 and containing 17% unconjugated mAb and (b) their chemical composition; (c) the cytotoxicity of C215(rSEA)$_p$ conjugates with different lengths of the spacer arm (**14a** with a 6-atom spacer, **15h** and **15f** with a 24-atom spacer, **16a** with a 42-atom spacer) and (d) their chemical composition. The chemical composition of **15f** is presented in Figure 5d.

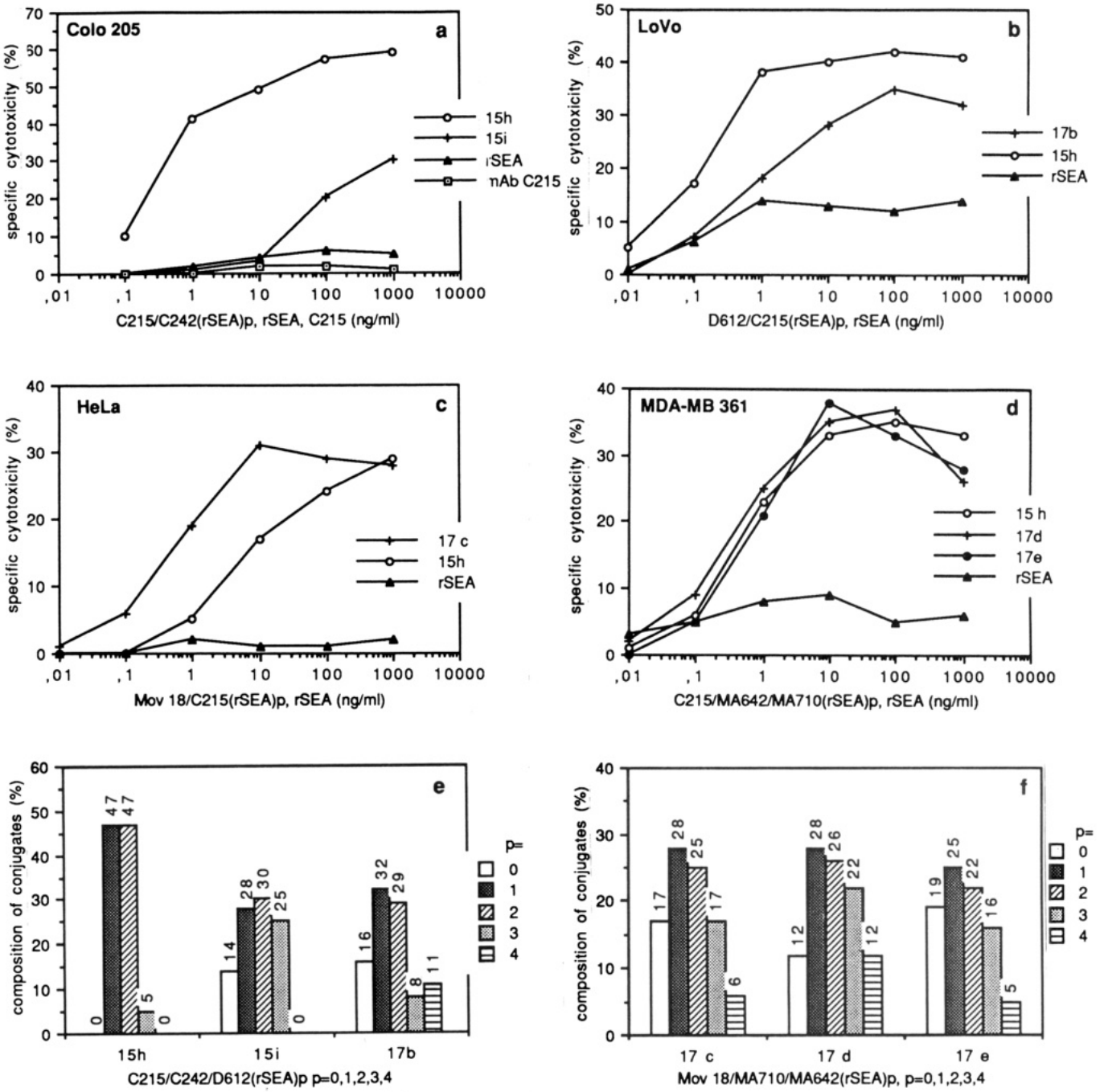


Figure 7. The cytotoxicity of a panel of mAb–SEA conjugates with different tumor selectivity: (a) The cytotoxicity of C215(rSEA)$_p$ **15h** and C242(rSEA)$_p$ **15i** against colon carcinoma cell line Colo 205, (b) the cytotoxicity of C215(rSEA)$_p$ **15h** and D612(rSEA)$_p$ **17b** against the colon carcinoma cell line LoVo, (c) the cytotoxicity of C215(rSEA)$_p$ **15h** and Mov18(rSEA)$_p$ **17c** against the ovarial carcinoma cell line HeLa, (d) the cytotoxicity of C215(rSEA)$_p$ **15h**, MA642(rSEA)$_p$ **17d**, and 710(rSEA)$_p$ **17e** against the breast cancer cell line MDA-MD361, (e and f) the chemical composition of **15h**, **15i**, **17b**, **17c**, **17d**, and **17e** measured with SDS–PAGE.

the reaction between rSEA(SH)$_m$ and iodoacetyl-modified mAb and probably also with maleimide modified mAb. Less rSEA(SH)$_m$ was therefore needed and the yield was better. The two methods developed for C215 and described in this paper have been shown to work very well for other mAbs examined (Tables I and II). Method 2 with maleimide-modified mAb is the method of choice as it is less laborious than method 1 and requires less rSEA.

mAb(rSEA)$_p$ conjugates represent a novel class of antitumor agents which has potential as new drugs for cancer therapy. We have conjugated about 15 different tumor-selective mAbs with SEA using the presently described methods. More than 50% of the mAb–SEA conjugates are potent antitumor agents in vitro. The tumor cell spectrum sensitive to mAb–SEA effects has included colon, ovarial, mammary (Figure 7) and renal cancer (data not shown). This suggests that mAb–SEA conjugates may be of therapeutic value against a broad range of tumors and warrant further investigation as anticancer agents in vivo.

ACKNOWLEDGMENT

We thank Ms. Elisabeth Hugosson, Ms. Ingegerd Andersson, Ms. Lill Ivarsson, and Mr. Per Anders Bertilsson for excellent technical assistant and Dr. Per Björk for purification of some of the antibodies, and Dr. D. Eaker for modification of the amino acid analysis to measure the 17-amino-3,6,9,12,15-pentaoxaheptadecanoic acid. Many thanks to Mr. Göran Forsberg and Ms. Eva Lagerholm for

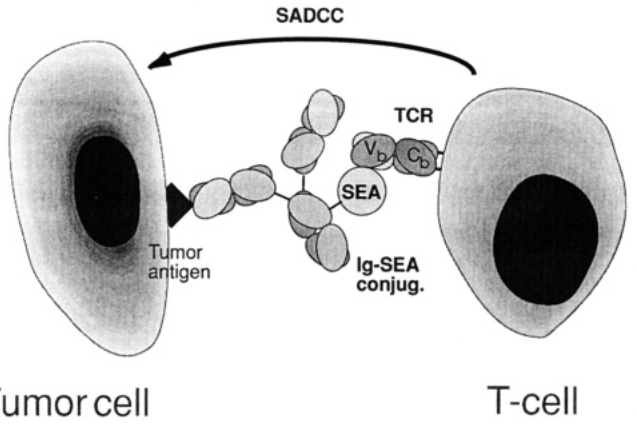


Figure 8. A cytotoxic T-cell with TCR expressing the appropriate TCR V_β sequence binds to the mAb(rSEA)$_p$ conjugate on a target. The lytic activity of the T-cell is activated and the tumor cell lysed (superantigen–antibody-dependent cell-mediated cytotoxicity, SADCC).

purification of rSEA and to Dr. Peter Lind for preparation of Figure 8.

LITERATURE CITED

(1) Houghton, A. N., and Scheinberg, D. S. (1991) Monoclonal antibodies. In *Comprehensive Textbook of Oncology* (A. K. Moosa, C. Schimpff, and M. C. Robson, Eds.) p 601, Williams & Wilkins, Baltimore.

(2) Harris, D. T., and Mastrangelo, M. J. (1989) Serotherapy of cancer. *Sem. Oncol. 16*, 180–198.

(3) Jain, R. K. (1987) Transport of molecules in the tumor interstitium: A review. *Cancer Res. 47*, 3039–3051.

(4) Foon, K. A. (1989) Biological response modifiers: The new immunotherapy. *Cancer Res. 49*, 1621–1639.

(5) Marrack, P., Kappler, J. (1990) The staphylococcal enterotoxins and their relatives. *Science 248*, 705–711.

(6) Dohlsten, M., Hedlund, G., Akerblom, E., Lando, P. A., and Kalland, T. (1991) Monoclonal antibody-targeted superantigens: A different class of anti-tumour agents. *Proc. Natl. Acad. Sci. U.S.A. 88*, 9287–9291.

(7) Wong, S. S. (1991) Chemistry of protein conjugation and cross-linking, pp 267–288, CRC Press, Inc., Boca Raton, FL.

(8) Marsh, J. W., and Neville, D. M., Jr. (1988) A flexible peptide spacer increases the efficacy of holoricin anti-T-cell immunotoxins. *J. Immunol. 140*, 3674–3678.

(9) von Kiederowski, G. (1991) Light-directed parallel synthesis of up to 250 000 different oligopeptides and oligonucleotides. *Angew. Chem. Int. Ed. Engl. 30*, 822–823.

(10) Juhlin, C., Lundgren, S., Johansson, H., Lorenzten, J., Rask, L., Larsson, E., Rastad, J., Akerström, G., and Klareskog, L. (1990) 500-Kilodalton calcium sensor regulating cytoplasmic Ca^{2+} in cytotrophoblast cells of human placenta. *J. Biol. Chem. 265*, 8275–8279.

(11) Oosterwijk, E., Ruiter, D. J., Hoedemaeker, Ph. J., Pauwels, E. K. J., Jonas, U., Zwartenduk, J., and Warnaar, S. O. (1986) Monoclonal antibody G250 recognizes a determinant present in renal-cell carcinoma and absent from normal kidney. *Int. J. Cancer 38*, 489–494.

(12) Muraro, R., Nuti, M., Natali, P. G., Bigotti, A., Simpson, J. F., Primus, F. J., Colcher, D., Greiner, J. W., and Schlom, J. (1989) A monoclonal antibody (D612) with selective reactivity for malignant and normal gastro-intestinal epithelium. *Int. J. Cancer 43*, 598–607.

(13) Pastan, I., Lovelace, E. T., Gallo, M. G., Rutherford, A. V., Magnani, J. L., and Willingham, M. C. (1991) Characterization of monoclonal antibodies B1 and B3 that react with mucinous adenocarcinomas. *Cancer Res. 51*, 3781–3787.

(14) Burchell, J., Gendler, S., Taylor-Papadimitriou, J., Girling, A., Lewis, A., Millis, R., and Lamport, D. (1987) Development and characterization of breast cancer reactive monoclonal antibodies directed to the core protein of the human milk mucin. *Cancer Res. 47*, 5476–5482.

(15) Tzeng, J. J., Barth, R. F., Johnson, C. W., and Adams, D. M. (1990) Distinct and non-crossreactive epitopes are recognized on B16 melanoma by LAK cells and anti-B16 monoclonal antibodies. *Biochim. Biophys. Acta 1026*, 69–79.

(16) Miotti, S., Canevari, S., Menard, S., Mezzanzanica, D., Porro, G., Pupa, S. M., Regazzoni, M., Tagliabue, E., and Colnaghi, M. I. (1987) Characterization of human ovarian carcinoma associated antigens defined by novel monoclonal antibodies with tumor-restricted specificity. *Int. J. Cancer 39*, 297–303.

(17) Opitz, H. G., Opitz, U., Hewlett, G., and Schlumberger, H. D. (1982) A new model for investigations of T-cell functions in mice: Differential immunosuppressive effects of two monoclonal anti-Thy-1.2 antibodies. *Immunobiol. 160*, 438–453.

(18) Agback, H., Ahrgren, L., Haraldsson, M., and Akerblom, E. (1991) A conjugate substance, a reagent and novel polyethers. International patent appl. PCT/SE91/00497 (Publication no WO92/01474).

(19) Carlsson, J., Drevin, H., and Axén, R. (1978) Protein thiolation and reversible protein-protein conjugation. N-succinimidyl 3-(2-pyridyldithio)propionate, a new heterobifunctional reagent. *Biochem. J. 173*, 723–737.

(20) Dohlsten, M., Lando, P. A., Hedlund, G., Trowsdale, I., and Kalland, T. (1990) Targeting of human cytotoxic T-lymphocytes to MHC class II expressing cells by staphylococcal enterotoxins. *Immunology 71*, 96–100.

(21) Dohlsten, M., Hedlund, G., Segren, S., Lando, P., Herrman, T., Kelly, A., and Kalland, T. (1991) Human major histocompatibility complex class II-negative colon carcinoma cells present staphylococcal superantigens to cytotoxic T-lymphocytes: Evidence for a novel enterotoxin receptor. *Eur. J. Immunol. 21*, 1229–1233.

(22) Cumber, A. J., Westwood, J. H., Henry, R. V., Parnell, G. D., Coles, B. F., and Wawrzynczak, E. J. (1992) Structural features of the antibody linkage that influence the activity and stability of ricin A chain immunotoxins. *Bioconjugate Chem. 3*, 397–401.

(23) Powers, S. P., Foo, I., Pinon, D., Klueppelberg, U. G., Hedstrom, J. F., and Miller, L. J. (1991) Use of photoaffinity probes containing poly(ethylene glycol) spacers for topographical mapping of cholecystokinin receptor complex. *Biochemistry 30*, 676–682.

(24) Kitagawa, T., Shimozono, T., Aikawa, T., Yoshida, T., and Nishimura, H. (1981) Preparation and characterization of hetero-bifunctional crosslinking reagents for protein modifications. *Chem. Pharm. Bull. 29*, 1130–1135.

(25) Marsh, J. W., and Neville Jr., D. M. (1986) Kinetic comparison of ricin immunotoxins: Biricin conjugates has potensiated cytotoxicity. *Biochemistry 25*, 4461–4467.

(26) Baldwin, R. W., and Byers, V. S. (1987) Monoclonal antibody targeting of cytotoxic agents for cancer therapy. In *Immunology of malignant diseases* (V. S. Byers, and R. W. Baldwin, Eds.) pp 44–54, MTP press, Lancaster.

2′,5′-Oligoadenylate:Antisense Chimeras—Synthesis and Properties

Krystyna Lesiak,† Shahrzad Khamnei, and Paul F. Torrence*

Section on Biomedical Chemistry, Laboratory of Medicinal Chemistry, Building 8, Room B2A02, National Institute of Diabetes and Digestive and Kidney Diseases, National Institutes of Health, Bethesda, Maryland 20892. Received May 17, 1993®

We have synthesized a novel bioconjugate which joins an antisense oligonucleotide to a unique and potent inhibitor of translation, $p_n5'A2'(p5'A2')_mp5'A$ (2–5A). Two residues of 4-hydroxybutyl phosphate were employed as linkers to attach the 2′,5′-oligoadenylate moiety through its 2′-terminus to the 5′-terminus of the chosen antisense sequence, $(dT)_{20}$. The syntheses were carried on a solid support according to the phosphite triester method of DNA synthesis (Letsinger, R. L., and Lunsford, W. B. (1976) *J. Am. Chem. Soc. 98*, 3655–3661; Beaucage, S. L., and Caruthers, M. H. (1981) *Tetrahedron Lett. 22*, 1859–1862). The generated 2-5A antisense chimeras retained both the ability of the 2-5A molecule to activate the 2-5A-dependent RNase as well as the ability of the oligo(dT) moiety to hybridize to the complementary poly(A). Moreover, the chimera, when annealed to its target nucleic acid sequence, was still effectively bound to the 2-5A-dependent nuclease. The methodology described represents a new approach to the selective modulation of mRNA expression.

INTRODUCTION

Regulation of the availability and/or stability of mRNA may be one avenue to the regulation of gene expression by exogenous agents which could find possible use in the therapy of cancer, cardiovascular diseases, and infection by parasites, viruses, and other microorganisms. Two very different approaches to such regulation at the translational level include modulation of RNA lability by the 2-5A system (*1–3*) and control of RNA availability and stability by antisense oligonucleotides (*4, 5*).

The small and unique 2′,5′-phosphodiester-bond-linked oligonucleotide referred to as 2-5A [$p_n5'A2'(p5'A2')_mp5'A$] has been shown to play an important role in the anti-encephalmyocarditis virus action of interferon (*6, 7*). 2-5A is biosynthesized by 2-5A synthetase [ATP:(2′-5′)oligo-(A) adenylyl transferase, EC 2.7.7.19] from ATP after the synthetase is activated by the double-stranded RNA presumably arising from initial viral replication (*1–3*). The synthesized 2-5A in turn activates a 2-5A-dependent endonuclease (RNase L) which is capable of degrading viral mRNA as well as cellular mRNA and rRNA (*1–3*). For this reason, the 2-5A molecule is a potent inhibitor of translation, blocking cell-free protein synthesis at nanomolar concentrations. 2-5A also can block translation and viral replication in intact cells, but only when any of a variety of manipulations (hypertonic salt treatment, calcium phosphate coprecipitation, liposome encapsulation, etc.) have been employed to enhance the uptake of this highly charged oligonucleotide (*2*). The poor uptake of the 2-5A molecule would have to be regarded as a liability in any effort to employ it as an exogenous regulator of mRNA stability. Another potential limitation of any attempt to capitalize on the 2-5A system to modulate the stability of a *specific* RNA would be the relatively nonspecific endonucleolytic action of its target RNase L, which cleaves RNA after UNp residues (*8, 9*).

Oligonucleotide antisense agents have been found to be highly specific inhibitors of mRNA expression through the mechanisms of passive hybridization or via degradation of the generated hybrid by RNase H (*4, 5*). However, certain modifications destined to enhance the potency of such antisense reagents abolish the RNase H degradation pathway since the corresponding hybrids are no longer substrates (*10*). To circumvent this problem and to enhance the versatility and potency of antisense oligonucleotides as potential therapeutic agents, a number of modified oligodeoxynucleotides have been prepared which would cause target nucleic acid chain scission through chemical, photochemical, or nuclease-induced cleavage (*11–19*).

Recently we have reported (*20*) on a new approach to the specific and targeted cleavage of RNA by combining the extreme specificity of the antisense concept with the potent RNA-degrading activity of the 2-5A-dependent endonuclease RNase L. Herein, we report on the synthesis, structure confirmation, and properties of such 2-5A–antisense chimeras. The structures of oligonucleotides prepared for this study and their corresponding abbreviations used throughout this report are presented in Scheme I.

EXPERIMENTAL PROCEDURES

Chemicals. Most reagents used in this study were from Aldrich (Milwaukee, WI), including anhydrous solvents (SureSeal packing). Snake venom phosphodiesterase used for characterization of synthesized oligonucleotides was obtained from Cooper Biomedical, and bacterial alkaline phosphatase was from US Biochemicals (Cleveland, OH). Long-chain alkylamino controlled-pore glass solid support (CPG-LCA, pore size 500A) and 5′-*O*-(4,4′-dimethoxytrityl)thymidine 3′-*O*-[2-cyanoethyl *N,N*-diisopropylphosphoramidite] were from Sigma (St. Louis, MO).

Physical Measurements. Concentrations of oligonucleotides were measured spectrophotometrically using extinction coefficients for adenosine and thymidine (and their oligomers) reported in the literature (*21*). UV absorption spectra were recorded on a Varian DMS-200 spectrophotometer. ^1H NMR and ^{31}P NMR spectra were recorded on either Varian XL-300 or GE GN-300 instruments in the solvents indicated below.

* Author to whom correspondence should be addressed.
† Present address: Laboratory of Biophysics, Division of Allergenic Products and Parasitology, Center for Biologics Evaluation and Research, FDA, Bethesda, MD 20892.
® Abstract published in *Advance ACS Abstracts*, September 1, 1993.

Not subject to U.S. Copyright. Published 1993 by American Chemical Society

Scheme I

p5'A2'(p5'A2')$_2$p5'A2'p1[OCH$_2$(CH$_2$)$_2$CH$_2$O]4p1[OCH$_2$(CH$_2$)$_2$CH$_2$O]4p5'dT3'(p5'dT3')$_{16}$p5'dT

pA$_4$:T$_{18}$

A2'(p5'A2')$_2$p5'A2'p1[OCH$_2$(CH$_2$)$_2$CH$_2$O]4p1[OCH$_2$(CH$_2$)$_2$CH$_2$O]4p5'dT3'(p5'dT3')$_{16}$p5'dT

A$_4$:T$_{18}$

p5'A2'(p5'A2')$_2$p5'A2'p1[OCH$_2$(CH$_2$)$_2$CH$_2$O]4p1[OCH$_2$(CH$_2$)$_2$CH$_2$O]4p5'dT3'(p5'dT3')$_2$p5'dT

pA$_4$:T$_4$

A2'p1[OCH$_2$(CH$_2$)$_2$CH$_2$O]4p1[OCH$_2$(CH$_2$)$_2$CH$_2$O]4p5'dT3'(p5'dT3')$_2$p5'dT

A:T$_4$

A2'p1[OCH$_2$(CH$_2$)$_2$CH$_2$O]4p1[OCH$_2$(CH$_2$)$_2$CH$_2$O]4p5'dT

A:T

HPLC Methods. Two HPLC systems were used throughout this study. The first (system A) included two Beckman 110B solvent delivery modules and a 167 UV/vis variable-wavelength detector (set to operate at 260 and 280 nm) controlled with Beckman System Gold software. The second system (system B) consisted of two Beckman 110B solvent-delivery modules (controlled by a NEC controller) and a Beckman 153 UV detector operating at 254 nm. The following HPLC columns were used: a semipreparative Ultrasphere ODS [Altex, reversed-phase C_{18}, 10 × 250 mm, flow rate of 2 mL/min, linear gradients of mobile phase B in buffer A, where A was 50 mM ammonium acetate, pH 7.0, and B consisted of 50% (v/v) methanol in water], an analytical Ultrasphere ODS column [Altex, reversed-phase C_{18}, 4.9 × 250 mm, flow rate of 1 mL/min, linear gradients of B (as defined above) in 20 mM ammonium phosphate, pH 7.0], a Vydac 304OL [Separations Group, 4.6 × 250 mm, DEAE ion exchange, flow rate of 1 mL/min, linear gradients of ammonium phosphate, pH 6.7, in 20% (v/v) aqueous acetonitrile], and a TSK-GEL DEAE-NPR (TosoHaas, nonporous ion exchange, 4.6 × 35 mm, flow rate of 1 mL/min, linear gradients of 0.5 M NaCl in 20 mM Tris, pH 8.0).

High-Performance Capillary Electrophoresis. Analyses were performed on an Applied Biosystems 270A-HT capillary electrophoresis instrument using MICRO-GEL$_{100}$ (Applied Biosystems Inc., Foster City, CA) gel-filled capillaries (50 μm i.d., effective length 27 cm; running buffer, 75 mM Tris phosphate, pH 7.6, 10% methanol). Detection was at 260 nm.

Synthesis of Oligonucleotides. Syntheses were performed manually on DNA synthesis columns (1.5 cm, American Bionetics, Inc.) loaded with approximately 1.5 μmol of CPG-bound 5'-*O*-(dimethoxytrityl)thymidine (*22*), using adaptors and gas-tight syringes (*23*). The procedure was based on the phosphite triester method of DNA/RNA synthesis (*24–28*) using for chain elongation 2-cyanoethyl phosphoramidite derivatives of 5'-*O*-(4,4'-dimethoxytrityl)thymidine, 4-*O*-(4,4'-dimethoxytrityl)-1,4-butanediol (as protected linker in the chain extension), or 5'-*O*-(4,4'-dimethoxytrityl)-3'-*O*-(*tert*-butyldimethylsilyl)-N^6-benzoyladenosine (*29*). The complete synthetic cycle is presented in Table I. When needed, oligonucleotides were 5'-end phosphorylated with bis(2-cyanoethoxy)(diisopropylamino)phosphine (*30*). Syntheses were monitored by quantitating spectrophotometrically the release of the dimethoxytrityl cation. The synthesized oligonucleotides were cleaved from the solid support with a mixture of concentrated (28%) aqueous ammonia and ethanol (3:1) by 2-h incubation at room temperature. N^6-Benzoyl groups, protection for adenosine residues, were removed by incubating the resulting solutions for 6 h at 55 °C. Finally, the 3'-*O*-(*tert*-butyldimethylsilyl) protecting groups were removed by treatment with 1 M tetrabutylammonium fluoride in THF for at least 12 h at room temperature.

Table I. Solid-Phase Synthesis of Oligonucleotides–Coupling Cycle

step	solvents/reagents	time	volume, mL
1. detrilylation	3% DCA in CH_2Cl_2	90 s	1
2. washing	2% Py in acetonitrile		1
3. washing	acetonitrile		3
4. drying	nitrogen	3 min	
5. coupling	0.2 M monomer in 0.5 M tetrazole/ acetonitrile	8 min for Ado, 3 min for Thd and 5'-end phosphitylation	0.15
6. washing	acetonitrile		3
7. drying	nitrogen	2 min	
8. capping	A + B, 1:1 A: 30% Ac_2O in THF B: 0.6 M DMAP in Py/THF (3:2 v/v)	2 min	1
9. washing	acetonitrile		3
10. drying	nitrogen	2 min	
11. oxidation	0.1 M I_2 in lutidine: THF:water, 20:80:1	45 s	1
12. washing	acetonitrile		3
13. drying	nitrogen	3 min	

Coupling efficiencies for oligonucleotide synthesis were as follows: for dT coupling, 99%; for butanediol linker coupling, 89–90%; for 2',5'-linkages, 89–95%. Final yields, after HPLC purification and desalting, were as follows: for A:T, 63%; for A:T$_4$, 50%; for pA$_4$:T$_4$, 25%; for pA$_4$:T$_{18}$, 23%.

4-O-(4,4'-Dimethoxytrityl)-1,4-butanediol. 1,4-Butanediol (9 g, 10 mmol) was dried by repeated coevaporation with anhydrous pyridine and then dissolved in 50 mL of the same solvent containing triethylamine (2 g, 20 mmol). 4,4'-Dimethoxytrityl chloride (3390 mg, 10 mmol) was added to this solution and the mixture was kept for 2 h at room temperature. The reaction was terminated by pouring the mixture into a beaker containing ice (100 g), and products were extracted with ethyl acetate. The extract was dried with magnesium sulfate, concentrated, and purified on a silica gel column, which then was eluted with methylene chloride containing 1% methanol. The yield was 870 mg (22%). ^{1}H NMR ($CDCl_3$, 1% deuteriopyridine) δ [ppm]: 1.68 (m, 4H, CH_2), 3.10 (t, J = 5.7 Hz, 2H, CH_2O), 3.62 (t, J = 5.8 Hz, 2H, CH_2OH), 3.76 (s, 6H, CH_3O), 6.79–7.46 (m, aromatic protons). High-resolution mass spectrum (electron impact: calculated for $C_{25}H_{28}O_4$

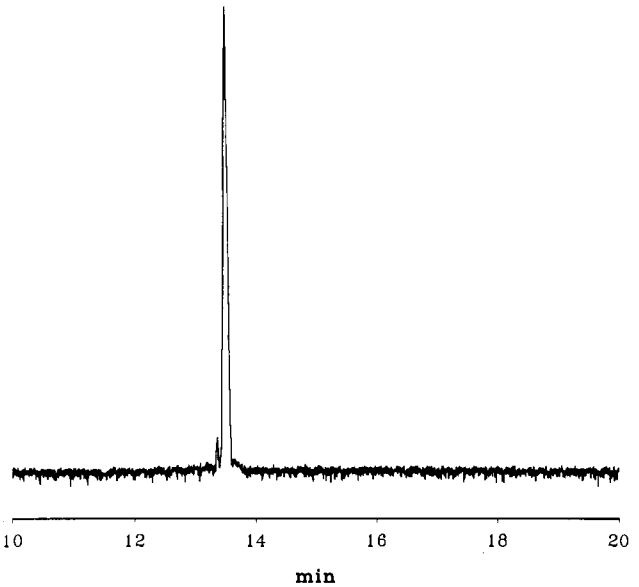


Figure 1. Electropherogram of $pA_4:T_{18}$. The region of the chromatogram from 0–10 min contained no peaks and is therefore not shown.

392.1988, found 392.1981. This product was converted to *2-cyanoethyl 4-(4,4'-dimethoxytrityl)butyl N,N-diisopropylphosphoramidite*. (2-Cyanoethyl)-*N,N*-diisopropylphophonamidic chloride (237 mg, 1 mmol) was added slowly to a solution of 4-*O*-(4,4'-dimethoxytrityl)-1,4-butanediol (390 mg, 1 mmol) and ethyldiisopropylamine (510 mg, 4 mmol) in anhydrous methylene chloride (3 mL) under anhydrous conditions with cooling (ice bath). The mixture was kept at room temperature for 1 h, the solvent was evaporated, and the product was purified on a silica gel column (1.8 × 14 cm, eluted with benzene–petroleum ether–triethylamine (6:3:1). The yield was 330 mg (90%). ^{1}H NMR ($CDCl_3$, 1% deuteriopyridine) δ [ppm]: 1.17 (t, J = 7.0 Hz, 12H, CH_3C), 1.70 (m, 4H, CH_2C), 2.60 (t, J = 6.5 Hz, 2H, CH_2CN), 3.08 (t, J = 5.7 Hz, 2H, CH_2O); 3.80 (m, 4H, CH_2OP), 3.78 (s, 6H, CH_3O), 3.80 (m, 2H, CH), 6.80–7.49 (m, aromatic protons). ^{31}P NMR ($CDCl_3$, 1% deuteriopyridine) δ [ppm]: 147.6. High-resolution mass spectrum (FAB): calculated for $C_{34}H_{46}N_2O_5P$ 593.3144, found 593.3112.

Preparation of Oligonucleotide $A_4:T_{18}$. This oligonucleotide was prepared by alkaline phosphatase digestion (2 units, 0.1 M Tris chloride, pH 8.0, 37 °C, overnight) of the crude $pA_4:T_{18}$ and was purified on a DEAE-NPR anion-exchange column.

Oligonucleotide Purification. Oligonucleotide $pA_4:T_{18}$ was purified on the Vydac column using HPLC system B with an elution gradient of 0.02 to 0.28 M ammonium phosphate, in 30 min. Approximately 80% of applied sample was recovered. The compound showed only one major peak when analyzed on the DEAE-NPR ion-exchange column (HPLC system A, with a 30-min gradient of 0.1 to 0.4 M NaCl, t_R = 28 min) and by capillary electrophoresis (Figure 1). Oligonucleotide $A_4:T_{18}$ was purified under similar conditions on the DEAE-NPR column. Oligonucleotides $pA_4:T_4$, $A:T_4$, and A:T were purified on the semipreparative Ultrasphere ODS column (system B, a 30-min gradient of 20 to 100% of B).

Oligonucleotide Characterization. The oligonucleotides were characterized by digestion with snake venom phosphodiesterase. Substrate (0.1–0.2 OD) was incubated with 0.05–0.1 unit of SVPD in 50 mM Tris chloride, pH 8.0, 0.5 mM $MgCl_2$, 1–3 h, 37 °C. When oligonucleotide $A:T_4$ was digested under these conditions, there resulted two products formed in a 4:1 ratio. The product appearing in greater quantity was 5'-TMP. The other product corresponded to adenosine coupled to the butanediol linkers (referred to hereafter as A_{linker}) since upon overnight reaction with 0.5 M KOH, it gave adenosine 2'(5')-monophosphate. Digestions of oligonucleotides $pA_4:T_{18}$, $A_4:T_{18}$, and $pA_4:T_4$ with snake venom phosphodiesterase under the above conditions gave the following products in the indicated ratios: 5'-TMP, 5'-AMP, $p5'A_{linker}$ (18:3:1); 5'-TMP, A, 5'-AMP, $p5'A_{linker}$ (18:1:2:1); and 5'-TMP, 5'-AMP, $p5'A_{linker}$ (4:3:1).

The structures of oligonucleotides $pA_4:T_4$, $A:T_4$, and A:T were corroborated further by proton NMR.

Oligonucleotide $pA_4:T_4$ ^{1}H NMR (D_2O) δ [ppm]: 1.84 and 1.87 (both s, total of 12 H, 4 thymidine CH_3's), 6.05–6.25 (m, 4 H, 4 adenosine H-1' protons), 6.45–6.55 (m, 4 H, 4 thymidine H-1' protons), 7.80–8.40 (m, 12 H, adenine H-2 and H-8, thymine H-6 protons).

Oligonucleotide $A:T_4$ ^{1}H NMR (D_2O) δ [ppm]: 1.83 and 1.85 (12 H, 4 thymidine CH_3's), 6.13 (d, J = 7.2 Hz, 1 H, adenosine H-1' proton), 6.22 (m, 4 H, thymidine H-1' protons), 7.63 to 7.65 (m, 4 H, thymine H-6 protons), 8.21 and 8.31 (both s, adenine H-2 and H-8).

Oligonucleotide A:T ^{1}H NMR (D_2O) δ [ppm]: 1.91 (s, 3H, thymidine CH_3), 6.29 (d, 1H, adenosine H-1', J = 6.6 Hz), 6.34 (t, 1H, thymidine H-1', J = 7.0 Hz), 7.74 (s, 1H, thymine H-6), 8.36 and 8.58 (s, 1H, adenine H-2 and H-8).

RESULTS AND DISCUSSION

Joining 2-5A in covalent linkage to an antisense 3',5'-linked oligonucleotide conceivably could produce a chimeric molecule with the advantages of both of the two distinct approaches to inhibition of mRNA expression. A high degree of specificity, apparently missing from RNase L-directed cleavages, could be imparted by the antisense domain of the chimera, whereas the 2-5A domain could provide a localized [by virtue of the 2',5'-phosphodiesterase (*31*)] activation of the potent 2-5A-dependent RNase L. The antisense partner in the cojoined molecule also may facilitate the uptake of the 2-5A since it is believed that antisense DNA oligomers are taken up by cells, perhaps, by a specific transport mechanism (*32*). For the design of a first-generation of 2-5A–antisense chimeras, we chose to prepare an oligo(dT) 18-mer to simplify both synthesis and characterization of this molecule. We added the tetrameric 2-5A derivative p5'A2'p5'A2'p5'A2'p5'A to the 5'-terminus of the antisense oligomer. Only a 5'-monophosphate was required at the terminus of the 2-5A component since the human RNase L from CEM and Daudi lymphoblastoid cells can be activated by the monophosphate and does not require a 5'-triphosphate, as does RNase L from most lines of mouse cells (*33, 34*). The two biologically active molecules were linked with two 1,4-butanediol units joined to each other and to the antisense and 2-5A by phosphodiester bonds. This allowed the synthesis of both components and the linkage reaction also to be carried out in one reaction sequence on a solid support using phosphoramidite oligonucleotide synthesis technology. Although we linked the 2'-terminus of the 2-5A domain through butanediol linkers to the 5'-end of the antisense oligonucleotide, other modes of linkage would be equally viable options. The only exception would be linkages that would incorporate the 5'-terminus of the 2-5A partner in the chimera. Previous studies (*35*) have shown that incorporation of this 5'-phosphate into an internucleotide linkage results in significantly decreased binding to RNase L.

Our choice of two butanediol units as linkers was somewhat arbitrary. Our chief reason to use linkers at all

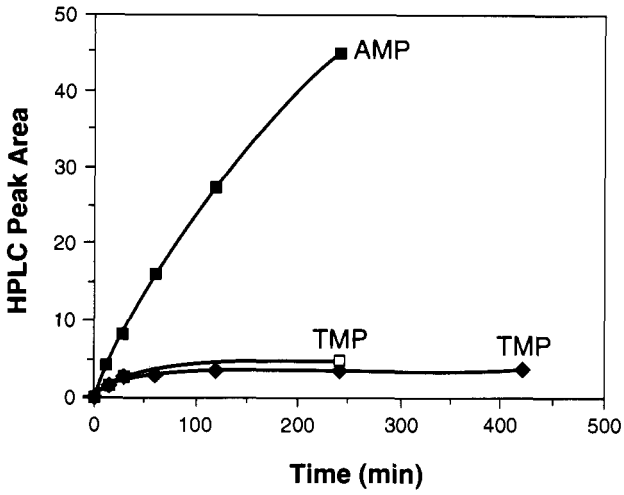


Figure 2. Kinetics of the hydrolysis of 2-5A monophosphate as compared to the 2-5A:AS chimeras. Oligonucleotides A:T_4 (□) and p5′A2′p5′A2′p5′A2′p5′A (■) were both evaluated at initial concentrations of 0.25 mM whereas the initial concentration of oligonucleotide pA_4:T_{18}(◆) was 0.13 mM. Reaction mixtures were constituted in 50 mM Tris HCl, pH 8.0, 1 mM $MgCl_2$, containing 2.5×10^{-3} units of snake venom phosphodiesterase (Cooper Biomedical). Incubation was at 37 °C. Aliquots were removed at the indicated times and analyzed by HPLC. In the case of 2-5A tetramer monophosphate, the formation of 5′AMP was used as a marker of degradation whereas, for the other two oligomers, 5′TMP formation was used to follow degradation since no AMP was released during the time of reaction. In addition, the parent (n) oligonucleotide peak could not be employed for exact quantitation during degradation since its integration was interfered with by the $n - 1$ peak formed by action of the phosphodiesterase. See the text for further details.

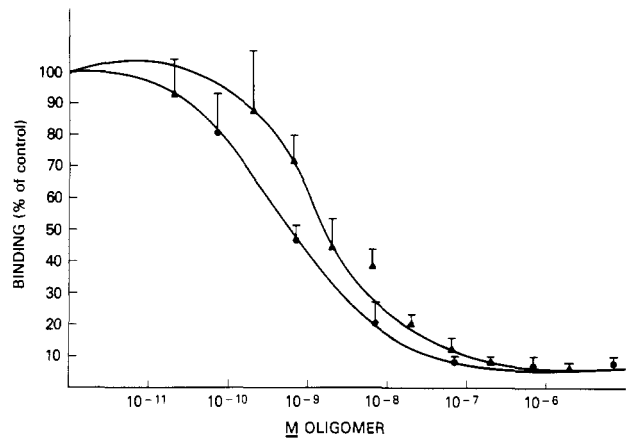


Figure 3. Radiobinding assays to determine the affinity of the chimera pA_4:T_{18} (▲) for the 2-5A-dependent RNase of mouse liver cytoplasmic extract as compared to 2-5A (ppp5′A2′p5′A2′-p5′A, ●) itself. This procedure employed the radiolabeled probe p5′A2′p5′A2′p5′A2′p5′A3′[^{32}P]p5′C3′p and a nitrocellulose filter binding assay (*39*) to determine the concentration of 2-5A or chimera required to displace a constant concentration of radiolabeled probe from the 2-5A-dependent RNase. 100% binding refers to the binding of radiolabeled probe in the absence of any other added oligonucleotide. The data for pA_4:T_{18} represent the means and standard deviations from six assays whereas the 2-5A data were gathered from seven determinations.

was governed by a concern that the 2-5A-dependent endonuclease might distrub hybrid helix formation if it were proximal to the antisense component, or that the resulting hybrid helix formation might interfere with binding of the 2-5A component to the 2-5A-dependent endonuclease. Current studies are addressing the effect, if any, of the nature and length of linker needed for optimal chimera activity.

The structures of the synthesized 2-5A:antisense chimeras were confirmed by the enzymatic digestion and NMR (vide supra). Snake venom phosphodiesterase digestion permitted determination of the ratio of adenylate residues to thymidylate residues and in the case of compounds pA_4:T_{18} and pA_4:T_4 allowed identification of the 5′-terminal residue. Proton NMR confirmed the presence of the requisite numbers of thymidine methyl groups and pyrimidine H6 and anomeric (H1′) protons as well as adenosine H2, H8, and anomeric protons.

The oligonucleotide, 2-5A, is subject to facile degradation by phosphodiesterases including one with specificity toward 2′,5′-linkages (*36*, *37*). We examined enzymic degradation of chimeric constructs by monitoring HPLC's of aliquots removed at various times during digestion by snake venom phosphodiesterase. Although, we monitored both the starting oligonucleotide peak and intermediate peaks ($n - 1$, etc.), as well as formation of product dTMP and/or AMP peaks, it was most descriptive to present the results of the degradation of 2-5A itself as AMP formation and the degradation of chimeric molecules by TMP formation, since in the latter instance no AMP was detectable during degradation (Figure 2). This is to be expected since snake venom phosphodiesterase acts from the 3′(2′)-terminus of the oligonucleotide. Addition of the oligothymidylate antisense component to the 2′-terminus of the 2′,5′-oligoadenylate completely protected the 2-5A moiety from degradation by snake venom phosphodiesterase under conditions that led to rapid degradation of unmodified 2-5A itself (Figure 2). Observation of this effect required the use of a 100-fold smaller concentration of enzyme than was employed for the enzyme characterization studies (vide supra). Presumably this antisense "tailing" (*38*) of 2-5A also would provide resistance to degradation by the 2′,5′-phosphodiesterase. Other chemical modifications at the 2′-terminus of 2-5A have been shown to impart considerable resistance to phosphodiesterases and to potentiate translational inhibition and antiviral activity (*2*).

The ability of the 2-5A:antisense constructs to bind to the 2-5A-dependent RNase L was evaluated using a radiobinding assay (*39*) which measures the ability of 2-5A or an analogue to compete with a ^{32}P-labeled probe, p5′A2′p5′A2′p5′A2′p5′A3′[^{32}P]p5′C3′p, for the endonuclease. Chimeric 2-5A:antisense congeners were undiminished in their ability to bind to the 2-5A-dependent RNase. Thus the tetramer-tetramer adduct pA_4:dT_4, when examined for its affinity for the 2-5A-dependent RNase of mouse liver, gave an IC_{50} (concentration needed to inhibit probe binding by 50%) of 1×10^{-9} M, not significantly different from the IC_{50} of 7×10^{-10} M obtained for 2-5A itself, in agreement with previous reports (*40*, *41*). The length of the antisense sequence of the chimera did not have any negative effect on endonuclease binding since as is clear from the data of Figure 3, there was very little, if any, significant decrease in the IC_{50} of 5′A2′p5′-A2′p5′A as compared to ppp5′A2′p5′A2′p5′A itself.

As noted earlier (*20*), UV absorbance–temperature profiles revealed that the 2-5A moiety of the pA_4:dT_{18} chimera did not prevent the ability of the T_{18} region to anneal with its complementary sequence as represented in poly(A) (Figure 4). When this pA_4:dT_{18}–poly(A) complex was denatured in such a melting experiment and the solution was allowed to cool down to room temperature, the complex reformed, thereby indicating that the complex formation was fully reversible and that no significant decomposition occurred during the melting process. Under the same conditions, the complex d(T)$_{20}$:poly(A) had a T_m

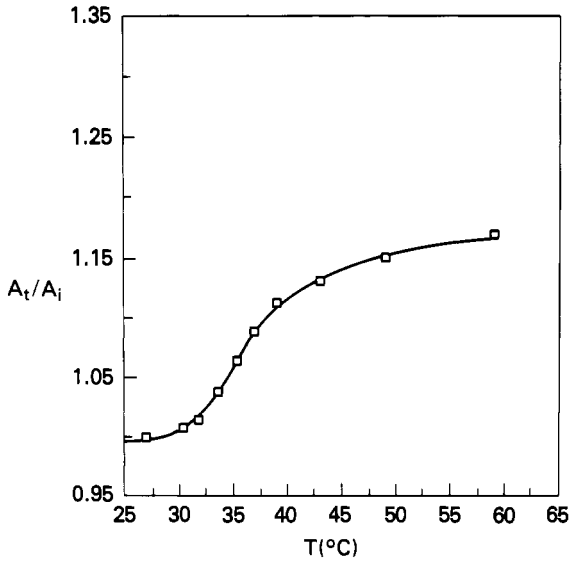


Figure 4. Absorbance–temperature profile of an equimolar mixture of poly(A) and pA_4:T_{18} as determined in KH_2PO_4 buffer (40 mM, pH 7.0). In this experiment, 1000 μL of 3.2×10^{-6} M poly(A) in KH_2PO_4 buffer (pH 7.0, 40 mM) was mixed with 1000 μL of 2.9×10^{-6} M pA_4:T_{18} in KH_2PO_4 buffer, and the resulting mixture was incubated at 4 °C overnight before determination of melting temperature. A_t/A_i refers to the ratio of absorbance (A_t) at a given temperature compared to the absorbance (A_i) at the initial temperature (25–30 °C). No attempt was made to determine complex stoichiometry (2- or 3-stranded). Under similar conditions, an equimolar mixture of poly(A) and oligo-$(dT)_{20}$ gave a complex with a T_m of 40 °C.

of 40 °C, in good agreement with literature values reported under similar conditions (*21*). To date, we have not determined whether or not the pA_4:dT_{18} possesses self-complementary structure.

When the antisense region of the chimera was annealed to its complementary sequence, there was no significant effect on the ability of the construct to bind to 2-5A-dependent RNase of mouse liver. For example, when pA_4:dT_{18} was mixed in various concentrations with excess poly(A), there was no significant change in the binding affinity as compared with the unannealed pA_4:dT_{18} or as compared to 2-5A itself (Figure 3). In addition, when a radiobinding assay was performed on an aliquot of the above solution that had been used to determine the T_m of the pA_4:T_{18} complex, an identical binding curve was obtained (data not shown).

We have prepared a novel bioconjugate; specifically, a chimera formed by the linkage of an antisense oligonucleotide to 2′,5′-oligoadenylate, thereby linking the antisense strategy for control of gene expression with the interferon-associated 2-5A system. Such conjugate molecules retained their ability to bind to both relevant receptors, i.e., the nucleic acid sequence complementary to the antisense sequence present in the conjugate as well as the binding of the 2-5A domain to the 2-5A-dependent RNase (*42*), which would be responsible for targer RNA degradation. Moreover, the hybrid complex between the 2-5A:antisense chimera and the target RNA also retained undiminished 2-5A-dependent RNase binding ability. We also have demonstrated that the antisense oligonucleotide component of the 2-5A:antisense conjugate targets a specific RNA sequence to which it binds while the accompanying 2-5A component activates the latent constitutive 2-5A-dependent RNase thereby causing the cleavage of the RNA (*20*). This strategy and methodology was demonstrated to produce specific cleavages proximal to an antisense-targeted sequence within a modified HIV-1 RNA in a cell-free system from human lymphoblastoid cells (*20*).

LITERATURE CITED

(1) Kerr, I., and Brown, R. E. (1978) pppA2′p5′A2′p5′A: An inhibitor of protein synthesis synthesized with an enzyme fraction from interferon treated cells. *Proc. Natl. Acad. Sci., U.S.A. 75*, 256–260.

(2) Johnson, M. I., and Torrence, P. F. (1984) The role of interferon-induced proteins, double-stranded RNA and 2′,5′-oligoadenylate on the interferon-mediated inhibition of viral translation. *Interferon* (R. M. Friedman, Ed.) Vol. 3 pp 189–298, Elsevier Science, New York.

(3) Sen, G. C., and Lengyel, P. (1992) The interferon system. A bird's eye view of its biochemistry. *J. Biol. Chem. 267*, 5019–5020.

(4) Cohen, J. (1989) *Oligonucleotides: Antisense Inhibitors of Gene Expression*, Macmillan Press, London.

(5) Uhlman, E., and Peyman, A. (1990) Antisense oligonucleotides: A new therapeutic principle. *Chem. Rev. 90*, 543–584.

(6) Gribaudo, G., Lembo, D., Cavallo, G., Landolfo, S., and Lengyel, P. (1991) Interferon action: Binding of viral RNA to the 40-kilodalton 2′,5′-oligoadenylate synthetase in interferon-treated HeLa cells infected with encephalomyocarditis virus. *J. Virol. 65*, 1748–1757.

(7) Chebath, J., Benech, P., Revel, M., and Vigneron, M. (1987) Constitutive expression of a 2′,5′-oligoadenylate synthetase confers resistance to picoravirus infection. *Nature 330*, 587–588.

(8) Wreschner, D. H., McCauley, J. W., Skehel, J. J., and Kerr, I. M. (1981) Interferon action-sequence specificity of the ppp-(A2′p)n A-dependent ribonuclease. *Nature 289*, 414–417.

(9) Floyd-Smith, G., Slattery, E., and Lengyel, P. (1981) Interferon action: RNA cleavage pattern of a (2′-5′)-oligoadenylate-dependent endonuclease. *Science 212*, 1030–1032.

(10) Gagnor, C., Bertrand, J. R., Thenet, S., Lemaitre, M., Morvan, F., Rayher, B., Malvey, C., Lebleu, B., Imbach, J.-L., and Paoletti, C. (1987) α-DNa VI. Comparative study of α- and β-anomeric oligodeoxynucleotides in hybridization to mRNA and in cell free translation. *Nucleic Acids Res. 15*, 10419–10436.

(11) Le Doan, T., Praseuth, D., Perrouault, L., Chassignol, M., Thuong, N. T. , and Helene, C. (1990) Sequence-targeted photochemical modifications of nucleic acids by complementary oligonucleotides covalently linked to porphyrins. *Bioconjugate Chem. 1*, 108–113.

(12) Francois, J.-C., Saison-Behmoaras, T., Chassignol, M., Thuong, N., and Helene, C. (1989) Sequence targeted cleavage of single- and double-stranded DNA by oligothymidylates covalently linked to 1,10-phenantroline. *J. Biol. Chem. 264*, 5891–5898.

(13) Chen, C. B., and Sigman, D. S. (1986) Nuclease activity of 1,10-phenantroline–copper: Sequence-specific targeting. *Proc. Natl. Acad. Sci., U.S.A. 83*, 7147–7151.

(14) English, U. and Gauss, D. H. (1991) Chemically modified oligonucleotides as probes and inhibitors. *Angew. Chem., Int. Ed. Eng. 30*, 613–722.

(15) Dreyer, G. B., and Dervan, P. B. (1985) Sequence-specific cleavage of single-stranded DNA: Oligodeoxynucleotide–EDTA–Fe(II). *Proc. Natl. Acad. Sci., U.S.A. 82*, 968–972.

(16) Li, Y., Guerrier-Takada, C., and Altman, S. (1992) Targeted cleavage of mRNA in vitro by RNase P from Escherichia coli. *Proc. Natl. Acad. Sci., U.S.A. 89*, 3185–3189.

(17) Corey, D. R., Pei, D. and Schultz, P. G. (1989) Sequence-selective hydrolysis of duplex DNA by an oligonucleotide-directed nuclease. *J. Am. Chem. Soc. 111*, 8523–8525.

(18) Corey, D. R., Pei, D., and Schultz, P. G. (1989) Generation of a sequence-specific hybrid DNase. *Biochemistry 28*, 8277–8286.

(19) Rossi, J. J., Cantin, E. M., Sarver, N., and Chang, P. F. (1991) The potential use of catalytic RNA's in therapy of HIV infection and other diseases. *Pharmac. Ther. 50*, 245–254.

(20) Torrence, P. F., Maitra, R. K., Lesiak, K., Khamnei, S., Zhou, A., and Silverman, R. H. (1993) Targeting RNA for degradation with a 2',5'-oligoadenylate-antisense chimera. *Proc. Natl. Acad. Sci., U.S.A. 90*, 1300–1304.

(21) Janik, B. (1971) *Physicochemical characteristics of oligonucleotides and polynucleotides*, IFI Plemun, New York.

(22) Pond, R. T., Usman, N., and Ogilvie, K. K. (1988) Derivatization of controlled pore glass beads for solid phase oligonucleotide synthesis. *Biotechniques 6*, 768–775.

(23) Uznanski, B., Koziolkiewicz, M., and Stec, W. J. (1986) New components for improved solid-phase synthesis of base and backbone-modified oligodeoxyribonucleotides. *Chem. Scr. 26*, 221–224.

(24) Letsinger, R. L., and Lunsford, W. B. (1976) Synthesis of thymidine oligonucleotides by phosphite triester intermediates. *J. Am. Chem. Soc. 98*, 3655–3661.

(25) Beaucage, S. L., and Caruthers, M. H. (1981) Deoxynucleoside phosphoramidites—A new class of key intermediates for deoxypolynucleotide synthesis. *Tetrahedron Lett. 22*, 1859–1862.

(26) Ogilvie, K. K., Usman, N., Nicoghosian, K., and Cedergren, R. J. (1988) Total chemical synthesis of a 77-nucleotide-long RNA sequence having methionine-acceptance activity. *Proc. Natl. Acad. Sci. U.S.A. 85*, 5764–5768.

(27) Usman, N., Ogilvie, K. K., Jiang, M.-Y., and Cedergren, R. J. (1987) Automated chemical synthesis of long oligoribonucleotides using 2'-O-silylated ribonucleoside 3'-O-phosphoramidites on a controlled-pore glass support: Synthesis of a 43-nucleotide sequence similar to the 3'-half molecule of *Escherichia coli* formylmethionine tRNA. *J. Am. Chem. Soc. 109*, 7845–7854.

(28) Scaringe, S. A., Franclyn, C., and Usman, N. (1990) Chemical synthesis of biologically active oligoribonucleotides using β-cyanoethyl protected ribonucleoside phosphoramidites. *Nucleic Acids Res. 18*, 5433–5441.

(29) Ogilvie, K. K., Beaucage, S. L., Schifman, A. L., Theriault, N. Y., and Sadana, K. L. (1978) The synthesis of oligoribonucleotides II. The use of silyl protecting groups in nucleoside and nucleotide chemistry VII. *Can. J. Chem. 56*, 2768–2780.

(30) Uhlman, E., and Engels, J. (1986) Chemical 5'-phosphorylation of oligonucleotides valuable in automated DNA synthesis. *Tetrahedron Lett. 27*, 1023–1026.

(31) Nielsen, T. W., and Baglioni, C. (1979) Mechanisms for discrimination between viral and host mRNA in interferon-treated cells. *Proc. Natl. Acad. Sci., U.S.A. 76*, 2600–2604.

(32) Loke, S. L., Stein, C. A., Zhang, X. H., Mori, K., Nakanishi, M., Subasinghe, C., Cohen, J. S., and Neckers, L. M. (1989) Characterization of oligonucleotide transport into living cells. *Proc. Natl. Acad. Sci., U.S.A. 86*, 3474–3478.

(33) Haugh, C. M., Cayley, P. J., Serafinowska, H., Norman, D. G., Reese, C. B., and Kerr, I. M. (1983) Analogues and analogue inhibitors of ppp(A2'p)n A: Their stability and biological activity. *Eur. J. Biochem. 132*, 77–84.

(34) Imai, J., Lesiak, K., and Torrence, P. F. (1985) Respective roles of each purine N6-amino groups of 5'-O-triphosphoryladenylyl(2'-5')adenylyl(2'-5')adenosine in binding to and activation of RNase L. *J. Biol. Chem. 260*, 1390–1393.

(35) Torrence, P. F., Imai, J., Lesiak, K., Jamoulle, J.-C., and Sawai, H. (1984) Oligonucleotide structural parameters that influence binding of 2-5A to the 2-5A-dependent endonuclease: Chain length, phosphorylation state and heterocyclic base. *J. Med. Chem. 27*, 726–733.

(36) Schmidt, A., Chernajovsky, Y., Shulman, L., Federman, P., Berissi, H., and Revel, M. (1979) An interferon-induced phosphodiesterase degraing (2'-5')oligoisoadenylate and the CCA terminus of tRNA. *Proc. Natl. Acad. Sci., U.S.A. 76*, 4788–4792.

(37) Johnson, M. I., and Hearl, W. G. (1987) Purification and characterization of a 2'-phosphodiesterase from bovine spleen. *J. Biol. Chem. 262*, 8377–8382.

(38) Imai, J., Johnston, M. I., and Torrence, P. F. (1982) Chemical modification potentiates the biological activities of 2-5A and its congeners. *J. Biol. Chem. 257*, 12739-12745.

(39) Silverman, R. H., and Krause, D. (1987) Analysis of antiviral mechanisms: Interferon regulated 2',5'-oligoadenylate and protein kinase systems. *Lymphokines and interferons: A practical approach* (M. J. Clemens, A. G. Morris, and A. J. H. Gearing, eds.) pp 149–193.

(40) Torrence, P. F., Brozda, D., Alster, D., Charubala, R., and Pfleiderer, W. (1988) Only one 3'-hydroxyl group of 2-5A is required for activation of the 2-5A-dependent endonuclease. *J. Biol. Chem.* 263, 1131–1139.

(41) Kitade, Y., Nakata, Y., Hirota, K., Maki, Y., Pabuccuoglu, A. and Torrence, P. F. (1991) 8-Methyladenosine-substituted analogues of 2-5A: Synthesis and their biological activities. *Nucleic Acids Res. 19*, 4102–4108.

(42) Zhou, A., Hassel, B. A., and Silverman, R. H. (1993) Expression cloning of 2-5A-dependent RNase: A uniquely regulated mediator of interferon action. *Cell 72*, 753–765.

Comparison of the Cytotoxic Effect of Hormonotoxins Prepared with the Use of Heterobifunctional Cross-Linking Agents *N*-Succinimidyl 3-(2-Pyridyldithio)propionate and *N*-Succinimidyl 6-[3-(2-Pyridyldithio)propionamido]hexanoate

Vinod Singh,*,† Anil K. Mavila,† and S. K. Kar‡

Institute of Self Organising Systems and Biophysics, North-Eastern Hill University, Shillong-793 022, Meghalaya, India, and Centre for Biotechnology, Jawaharlal Nehru University, New Delhi-110 067, India.
Received May 19, 1993®

With the aim of developing cytotoxic hybrid molecules which can be selectively targeted to specific cells in the gonads, a single chain ribosome-inactivating protein, gelonin, was conjugated to ovine luteinizing hormone (oLH) with the use of heterobifunctional cross-linking agents *N*-succinimidyl 3-(2-pyridyldithio)-propionate (SPDP) and long-chain SPDP. Four hormonotoxins were synthesized having a variable spacer arm between oLH and gelonin. The spacer arms in C200A, C210A, C220A, and C230A were 13.6, 22.4, 22.4, and 31.2 Å long, respectively. Extensive physicochemical and biochemical analysis revealed a 1:1 molar ratio of the ingredients in its oLH–S–S–gelonin conjugates. The linkage occurred through the ϵ-NH_2 group of the α-subunit of oLH as judged from RP-HPLC analysis. The hormonotoxins retained substantial receptor binding ability, steriodogenic activity, and immunoreactivity of oLH and gelonin to their respective antibodies. Hormonotoxins bind to Leydig tumor cells via oLH, leaving gelonin free as judged by competitive displacement analysis. The hormonotoxins internalized to a sufficient degree to effectively inhibit protein synthesis. Upon comparison, immunoreactivity, receptor binding steroidogenic activity, and cytotoxicity of oLH–S–S–gelonin conjugates prepared with the use of only LC-SPDP (C230A, 31.2-Å spacer arm) and by using both SPDP and LC-SPDP (C210A and C220A, 22.4-Å spacer arm) were found to be comparable with that of conjugate prepared with SPDP alone (C200A, 13.6-Å spacer arm). Therefore, it may be concluded that the cytotoxicity of oLH-based hormonotoxin remained unaffected with the use of long-chain spacer arms which are believed to be used generally to avoid steric hindrance.

INTRODUCTION

The selective destruction of tumor cells by using hybrid molecules possessing both the functions of specific recognition and cytotoxic ability has been under active investigation (for review, see refs 1–5). These novel antitumor agents called "immunotoxins" have been synthesized in several laboratories by covalently linking the bacterial or plant toxins to the antibodies directed against the tumor-associated antigens (*1–5*). The conjugates, after binding to the antigens on the target cell surface, are endocytosed, and the toxin irreversibly inactivates the protein synthesis machinery of the cells (*1–5*). Among plant toxins, the most widely used are ricin, from castor bean, and abrin, from jequerity bean. These toxins are glycoproteins comprised of two chains: the B-chain, which binds to galactose residues on the cell surface, and the A-chain, which translocates in the cell and arrests protein synthesis machinery by enzymatically inactivating the ribosomes (*6–9*). The nonspecific toxicity of these toxins due to B-chain was avoided either by using immunotoxins in the presence of excess galactose or by completely depleting B-chain from the ricin. Thus the isolated A-chain was directly linked to the antibody molecule and the immunotoxin thus constructed was effective in a variety of animal models (*1–5*). Similar to the ricin A-chain, single-chain RIP[1] such as PAP, gelonin, and saporin are nontoxic to the intact cell but can inactivate the eukaryotic ribosomes and inhibit protein synthesis once they gain entry into the cell by a receptor-mediated process (*6–9*).

Like immunoglobulins, several hormones or growth factors such as human placental lactogen (*10*), insulin (*11*), human chorionic gonadotropin (*12, 13*), thyrotropin-releasing hormone (*14*), ovine luteinizing hormone (*15*), and corticotropin-releasing factor (*16*) have been conjugated to selected toxins. Recently, with the aim of targeting such toxins to the selected cells in the gonads, we have designed bioeffective conjugates of ovine LH with a single chain RIP, gelonin, by using SPDP as a cross-linking agent (*15, 17–21*). In these studies, both proteins

* For correspondence: Vinod Singh, Ph.D., Institute of Self Organising Systems and Biophysics, North-Eastern Hill University, Permanent Campus, Shillong-793 022, Meghalaya, India.
† North-Eastern Hill University.
‡ Jawaharlal Nehru University.
® Abstract published in *Advance ACS Abstracts*, October 1, 1993.

[1] Abbreviations used: BSA, bovine serum albumin; DTT, dithiothreitol; RIP, ribosome-inactivating protein; oLH, ovine luteinizing hormone; PAP, pokeweed antiviral protein; FCA, Freund's complete adjuvant; IFA, incomplete Freund's adjuvant; SPDP, *N*-succinimidyl 3-(2-pyridyldithio)propionate; LC-SPDP, *N*-succinimidyl 6-[3-(2-pyridyldithio)propionamido]hexanoate; Iodogen, 1,3,4,6-tetrachloro-3a,6a-diphenylglycoluril; CMC, (carboxymethyl)cellulose, RP-HPLC, reverse-phase high-performance liquid chromatography, RPMI, Roswell Park Memorial Institute, SDS–PAGE, sodium dodecyl sulfate–polyacrylamide gel electrophoresis, TCA, trichloroacetic acid, TFA, trifluoroacetic acid, EDTA, ethylenediaminetetraacetic acid, RIA, radioimmunoassay, eCG, equine chorionic gonadotropin, hCG, human chorionic gonadotropin, BMV, Brome mosaic virus, mRNA, messenger ribonucleic acid, GnRH, gonadotropin releasing hormone, DMEM, Dulbecco's modified Eagle's medium, HEPES, *N*-(2-hydroxyethyl)piperazine-*N'*-(2-ethanesulfonic acid).

1043-1802/93/2904-0473$04.00/0 © 1993 American Chemical Society

were thiolated by SPDP and subsequently reacted under appropriate conditions to form an oLH-S-S-gelonin complex (*15*, *17–21*). SPDP modification introduces a 6.8-Å spacer arm, which may induce some steric hindrance in the conjugates for the receptor recognition. In order to limit such steric hindrance, recently a long-chain SPDP has been introduced which has a 15.6-Å spacer arm. The present paper describes a comparative study of the synthesis, characterization, and bioefficacy of oLH–gelonin conjugate by using SPDP and LC-SPDP as heterobifunctional cross-linking agents.

EXPERIMENTAL PROCEDURES

Heterobifunctional cross-linking reagents (SPDP and LC-SPDP) and DTT were obtained from Pierce, Rockford IL. Sephadex G-25, G-100 and CMC-52 were from Pharmacia Fine, Chemicals, Sweden. BSA (Cohn fraction IV), FCA, and IFA were obtained from Sigma, Chemicals, St. Louis, MO. Radioactive Iodine ($Na^{125}I$, IMS-30) was obtained from Amersham, Corp. L-(3,4,5-^{3}H)leucine of specific activity 143 Ci/mmol was purchased from Dupont–NEN. Dry seeds of *Gelonium multiflorum* were purchased from United Chemicals and Allied Products, Calcutta, India. All other chemicals were of highest purity available commercially.

oLH was purified from the sheep pituitary powder according to the procedure described earlier (*15*, *22*). The purified hormone was subjected to physicochemical, immunological, and biological characterization especially for receptor binding and steroidogenic activity prior to use for covalent coupling to gelonin. The hormone was stored as a dry powder at 4 °C.

Gelonin was isolated from the dry deshelled seeds of *G. multiflorum* using aqueous extraction, ammonium sulfate precipitation, cation-exchange, and finally gel-filtration chromatography (*23*, *24*). A recent comparative study (*25*) on three methods of purification of gelonin clearly revealed that the presently used method yields more purified preparation, devoid of nonproteinous materials which absorb at 280 nm (*25*). The purified protein was subjected to purity, homogeneity (by using RP-HPLC), and molecular weight determinations (by a SDS–PAGE technique). Gelonin used in the present investigation was judged to be over 98% pure, as analyzed by RP-HPLC, and retained its ability to inhibit protein synthesis in an *in vitro* cell-free translation system (*26*).

Polyclonal antibodies against oLH and gelonin were developed in rabbit by immunizing them following the protocol described earlier (*15*, *24*). Sera were collected after the appropriate booster injections, and the immunoglobulin fraction was obtained after ammonium sulfate precipitation (*15*, *24*). The immunoglobulin fractions were dialyzed extensively, lyophilized, and stored as powder at 4 °C.

Murine Leydig tumor cell line, MLTC-1, used in the present investigation was gifted by Dr. R. Victor Rebois, NIH, Bethesda, MD. The cells were propagated and maintained in culture according to the published procedure (*27*). The cells grown in 24-multiwell plates were used to determine steroidogenic and cytotoxic activity of the hormonotoxins.

Modification of ϵ-NH_2 Groups of oLH/Gelonin with SPDP or LC-SPDP. The ϵ-NH_2 groups of oLH or gelonin were modified by LC-SPDP according to the standard procedure described for SPDP (*28*). Briefly, the protein was allowed to react with cross-linking agents in an appropriate molar ratio to modify one ϵ-NH_2 group ($\sim$1:1.2 $\pm$ 0.3) in each protein. oLH/gelonin dissolved in sodium phosphate buffer (0.1 M, pH 7.5, containing 0.15 M NaCl) was activated with SPDP or LC-SPDP, dissolved in the minimal volume of ethanol. The reaction was carried out at 25 °C for 30 min and then passed through a G-25 column and eluted with 5 mM ammonium bicarbonate. The protein peak eluting in the void volume of the column was pooled, lyophilized, and stored at 4 °C for further analysis. The extent of amino group modification was determined on the basis of liberation of pyridine-2-thione upon DTT treatment. The reaction was followed by recording the UV–visible spectra. From the absorption at 343 nm, the number of pyridine-2-thione groups liberated was calculated using the extinction coefficient $\epsilon_{343} = 8.08 \times 10^{-3}\ M^{-1}$ (*29*). The absorption at 280 nm was corrected for pyridine-2-thione contribution (*29*).

To initiate conjugation, the SPDP- or LC-SPDP-modified gelonin in 0.1 M sodium phosphate buffer, pH 6.0, containing 0.15 M NaCl was treated with DTT to generate an SH group and then gelonin–SH was passed through a Sephadex G-25 column to remove small molecular weight reduced products. Prior to G-25 chromatography, the UV–visible spectra was recorded in order to determine the number of SH groups generated as described above. Gelonin–SH was then mixed with oLH-SPDP or -LC-SPDP in 0.1 M sodium phosphate buffer, pH 7.5, containing 0.15 M NaCl. The mixture was left at 25 °C for 24 h, later concentrated by Centriprep-10, and fractionated on a G-100 column at 4 °C using 0.05 M ammonium bicarbonate buffer. Prior to G-100 chromatography, the UV–visible spectra was recorded to determine the liberation of pyridine-2-thione during the conjugation reaction (see the Results and Discussion section). The contribution of pyridine-2-thione absorption at 280 nm was corrected in calculating its molar concentration and the hormone:gelonin molar ratio was determined. Appropriate conjugated fractions were pooled, dialyzed, and lyophilized.

Characterization of Hormonotoxins. The conjugates of oLH with gelonin as prepared above were subjected to extensive physicochemical, immunochemical, and biological characterization. SDS–PAGE and RP-HPLC analysis were carried out to establish the purity and molecular weight of the conjugate.

RP-HPLC analysis. RP-HPLC analysis was used to analyze the purity of the ingredients and hormonotoxins as described above. RP-HPLC was performed on a Water's μBondapak phenyl column (4 mm × 250 mm) using a continuous gradient as described (*15*, *17–19*, *24–28*). The samples dissolved in water containing 0.1% TFA (solvent A) were run on the above column pre-equilibrated in solvent A + 25% CH_3CN containing 0.1% TFA. A gradient of 25–50% was run over 30 min at a flow rate of 2 mL/min in a DuPont HPLC, and data were analyzed by a computer.

Immunoreactivity determination. The immunoreactivity of oLH, gelonin, their SPDP- and LC-SPDP-modified derivatives and hormonotoxins was determined by a competitive displacement analysis as described earlier (*15*, *17–19*, *24–28*). ^{125}I-oLH required for RIA was radioiodinated by the Iodogen method (*30*) essentially following the procedure described for GnRH (*31–33*). Free $Na^{125}I$ and ^{125}I-oLH (or ^{125}I-gelonin were separated by gel-filtration chromatography on a Sephadex G-25 (1.0 × 50 cm) column. The specific activity as determined by an autodisplacement method was in the range of 50–80 μCi/μg. The labeled hormone/gelonin was stored in aliquots at −70 °C and used within a month of preparation.

The competitive displacement assay of the hormone

was performed essentially following the procedure described earlier (*15, 17–19, 28*). Briefly, the test samples, labeled and unlabeled oLH, and anti-oLH antibody were diluted in assay buffer (0.05 M sodium phosphate, pH 7.5, containing 0.15 M NaCl and 0.1% each of BSA and sodium azide). One hundred microliter of diluted anti-oLH antibody giving 30–50% binding in the same buffer was incubated with 100 μL of different concentrations of test samples (competitors). After 12 h of incubation at 4 °C, 100 μL of ^{125}I–oLH was added and further incubation for 12 h at 4 °C was carried out. Bound and unbound ^{125}I–oLH were separated by addition of 0.2 mL of 1:5 diluted Pansorbin (Calibiochem). The tubes were incubated further at room temperature for 20–30 min and centrifuged at 3000*g* for 15 min. The supernatant containing unbound ^{125}I-oLH was removed by aspiration and the pellet was counted in a LKB-Rack mini γ counter. The inhibition lines were obtained by plotting $(B/B_0) \times 100$ against the log dose of the competitor (where B_0 represent the binding of ^{125}I–oLH in the absence of cold oLH and B in the presence of competitor). The extent of percentage cross-reactivity was expressed as $C = (L_{50}/U_{50}) \times 100$, where the L_{50} is the dose of the competitor which shows 50% inhibition and U_{50} is the dose of native oLH which shows the 50% inhibition (*15, 17–20*).

Immunoreactivity of gelonin was also determined by a competitive displacement assay as described earlier (*24, 25*) with minor modification. The radioiodination of gelonin was carried out by the Iodogen method as described for oLH. Five micrograms of gelonin was radioiodinated with 1 mCi of Na^{125}I, and iodinated gelonin was purified on a Bio-Gel P6DG disposable column. The specific activity of the ^{125}I–gelonin, calculated by the incorporation efficiency, was ~80 μCi/μg. The immunoreactivity of the labeled gelonin was estimated by measuring the binding ability (>80%) in the presence of excess of anti-gelonin antibody (*24, 25*).

Antibody binding and competitive binding assays were carried out following the methods described earlier (*24, 25*) with the difference that double antibody precipitation was used instead of precipitation by Pansorbin. The method of calculation of the extent of cross-reactivity was the same as described earlier (*24, 25*).

Receptor Binding Property. The receptor binding of oLH, SPDP-/LC-SPDP-modified oLH, and their conjugates with gelonin was determined by RRA using rat testicular homogenate as a source of gonadotropin receptors as described earlier (*15, 17–19*). In brief, 100 μL each of labeled oLH (~70 000 CPM/tube), test samples, unlabeled oLH, and assay buffer (25 mM, Tris-HCl, pH 7.5, containing 10 mM $MgCl_2$ and 1 mg/mL BSA) were incubated at 22–25 °C for 16–20 h. The reaction was terminated by addition of 2 mL of assay buffer and centrifugation in cold at 3000*g* for 30 min. Supernatant was aspirated and the pellet was counted in a γ counter as described above.

Steroidogenic Ability Determination. The progesterone induction ability of oLH, SPDP- or LC-SPDP-modified oLH, and their conjugates to gelonin was evaluated by incubation with ovarian granulosa cells of immature female rats as described earlier (*15, 17–19*). The immature female rats were primed with eCG and after 48-h incubation, the granulosa cells were collected and incubation with test samples in DMEM, containing 20 mM HEPES, pH 7.5, and 0.1% BSA at 37 °C under 95% oxygen and 5% carbon dioxide for 4 h. Progesterone secreted in the medium was estimated by a specific RIA as reported earlier (*15, 17–19*).

In-Vitro Cell Free Translation Assay. The inhibitory activity of gelonin and their SPDP-modified derivatives on cell-free protein synthesis was determined using a system consisting of nuclease-treated rabbit reticulocyte lysate (*34, 35*). The extent of protein synthesis was determined by measuring radioactive leucine incorporated into the TCA-insoluble protein fraction. Briefly, in a total of 15 μL of reaction mixture, 2 μL of test sample was incubated with 1 μL of BMV mRNA (0.5 μg/μL), 2 μL each amino acid mixture (minus leucine) and tritiated leucine, 0.5 μL each of 500mM potassium acetate and 200mM magnesium acetate, and 7 μL nuclease treated rabbit reticulocyte lysate. The positive control was incubated with mRNA (no test sample) while the negative control received an equal volume of RNAse-free water. After incubation at 30 °C for 60 min, 5 μL of reaction mixture was spotted at least 10–15 places on the 3-mm Whatman filter paper and dipped in cold 5% TCA containing 0.2% leucine. Three more washings of 2 min each were carried out with cold TCA. The paper was heated at 90 °C in 5% TCA for 2 min and then quickly washed with cold ethanol and dried in the air. The protein precipitated was counted in a scintillation counter (Beckman of ~70% efficiency) after adding 8 mL of scintillation cocktail. Percentage of protein synthesis was calculated on the basis of radioactivity incorporated in the precipitate. The protein synthesis inhibition = $(B/B_0) \times 100$ where B is the radioactivity incorporated in the TCA precipitate in the presence of inhibitor and B_0 is in the absence of any inhibitor. IC_{50} is the dose of inhibitor required for 50% inhibition of protein synthesis.

Binding and Cytotoxicity to Leydig Tumor Cells. The binding and cytotoxicity experiments were carried out as desribed earlier (*17–19*). Briefly, for binding experiments, MLTC-1 cells (~1.5×10^5 cells/well) were plated in 24-well plates (flat bottom, Flow laboratory) and grown for 24–48 h. When the cells occupied most of the space, the wells were washed two times with serum-free medium. The cells received different concentrations of hormonotoxins and appropriate concentration of gelonin as a control. The plates were incubated for 2–4 h at 37 °C in a humidified chamber containing 95% O_2 and 5% CO_2. After incubation, the wells were washed three times with serum-free medium and each well received 50 μg of gelonin antibody purified by 50% ammonium sulfate fractionation as described above. After 2-h incubation, the wells were again washed with serum-free medium and incubated with ^{125}I–protein-A (~200 000 CPM/well) for 2 h. The iodination of protein-A was carried out by the Iodogen method (*30*) essentially as described above for oLH. The wells were washed extensively, and the bound radioactivity was counted after solubilizing cells with 0.1 N NaOH. For competition experiments, 10 μg/well concentration of the conjugate was used. This was determined after preliminary binding experiments. Fifty micrograms/well of native oLH was added together with the conjugate. After 2-h incubation in the presence of native oLH, the wells were again washed with serum-free medium and the conjugate bound to the cells was estimated by addition of ^{125}I–protein-A as described above.

The test for cytotoxicity of the conjugate was carried out on MLTC-1 cells as described before (*17–19*). Briefly, the cells were plated in RPMI-1640 medium in 24-multiwell plates, and after 24-h culture, the medium was replaced with the fresh medium, different concentrations of test samples were added, and plate was left for 18–24 h more at 37 °C in a humidified chamber containing 95% O_2 and 5% CO_2. The cells were washed after 24 h with serum-

Table I. Conjugates Synthesized with the Use of SPDP and LC-SPDP

oLH–gelonin conjugate code	spacer arm (Å)	cross-linking agent used: activation of oLH with	cross-linking agent used: activation of gelonin with	structure
C200A	13.6	SPDP	SPDP	oLH-HNC(O)$(CH_2)_2SS(CH_2)_2$C(O)NH–gelonin
C210A	22.4	SPDP	LC-SPDP	oLH-HNC(O)$(CH_2)_2SS(CH_2)_2$C(O)NH$(CH_2)_5$C(O)NH–gelonin
C220A	22.4	LC-SPDP	SPDP	oLH-HNC(O)$(CH_2)_5$HNC(O)$(CH_2)_2SS(CH_2)_2$C(O)NH–gelonin
C230A	31.2	LC-SPDP	LC-SPDP	oLH-HNC(O)$(CH_2)_5$HNC(O)$(CH_2)_2SS(CH_2)_2$C(O)NH$(CH_2)_5$C(O)NH–gelonin

free medium and were pulsed for 2 h with [^{3}H]leucine (0.5 μCi/well) in leucine-free RPMI-1640 medium. After 4-h incubation, the cells were extensively washed with 5% TCA to remove nonspecifically bound radioactivity. The cells were solubilized with 0.5 mL of warm 0.1 N NaOH, and solubilized protein was mixed with 5 mL of scintillation fluid and counted in the scintillation counter as described above.

RESULTS

A careful titration to determine the necessary molar ratio of oLH/gelonin versus SPDP or LC-SPDP was carried out. Present and earlier experience with SPDP (*24*, *25*, *28*) revealed that a molar ratio of 1:2 for oLH/gelonin: SPDP thiolated 1.2 ± 0.2 amino groups. Similarly, our recent investigation on the effect of LC-SPDP modification of ε-NH_2 groups of oLH clearly revealed that a 1:2 molar ratio of oLH and LC-SPDP thiolated 1:1.3 ± 0.2 amino groups per molecule (*36*). The conjugation of oLH to gelonin was initiated following the protocol as described in the Experimental Procedures. The conjugation mixtures were fractionated on a Sephadex G-100 column and elution profiles of all the conjugates are shown in Figure 1. The upper portion of Figure 1A shows the elution positions of oLH, gelonin, and the void volume (V_0) of the column. The chemical structures of four different conjugates, C200A, C210A, C220A, and C230A are shown in Table I. This table also shows the activation of oLH and gelonin with SPDP and LC-SPDP. In all the cases, SPDP-/LC-SPDP-modified gelonin was only treated with DTT to generate SH groups which were subsequently used for conjugation with oLH/SPDP or LC-SPDP. In C200A conjugate both the ingredients were activated with SPDP and later the conjugation was initiated after mixing with the DTT-treated gelonin–SPDP as described earlier (*15*, *17–19*). C210A and C220A conjugates were prepared with the use of both SPDP and LC-SPDP while C230A was synthesized with the use of only LC-SPDP. Therefore the spacer arm in C200A conjugate was calculated to be 13.3 Å long, while in C230A the spacer arm was 31.2 Å long. The C210A and C220A conjugates had spacer arms of 22.4 Å in length (Table I). The protein peak appearing before oLH and gelonin was considered to be their conjugate and was pooled (designated as A peak). The unconjugated oLH or gelonin peaks were designated as B and C, respectively. In each conjugate, the pool A peak was concentrated and rerun on the same column (Figure 1). In the rechromatographic run, the major peak eluting before oLH was pooled (designated as ARA) and lyophilized directly. The unconjugated peaks of oLH and gelonin were lyophilized separately. Figure 1A shows the elution profile of C200 and C210 conjugate whereas Figure 1B recorded the profile of C220 and C230 conjugation mixture. A small peak appearing between fractions 110 and 140 was due to the release of pyridine-2-thione, which appart from its absorption at 343 nm also absorbs at 280 nm. Therefore, in order to determine the molar concentration, the molar extinction coefficient of pyridine-2-thione is used to apply a correction for its contribution at 280 nm (*29*).

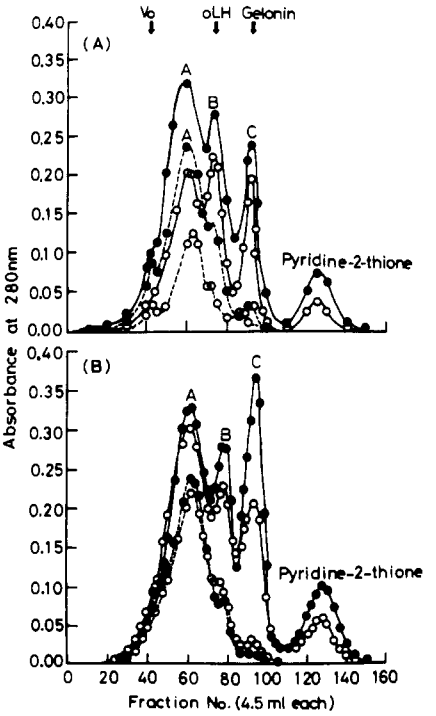


Figure 1. Gel-filtration chromatography of oLH–gelonin conjugation mixtures on a Sephades-G-100 column. The protein was eluted with 50 mM ammonium bicarbonate at a flow rate of 20 mL/h. Arrows in the upper portion of A indicate the void volume and elution positions of oLH and gelonin. (A) This shows gel-filtration chromatograms of the conjugation mixtures of C200 (●) and C210 (○). The major peak eluting before oLH and gelonin was their conjugate (designated as C200A and C210A). This peak was concentrated and rechromatographed on the same column. The dashed line (– –) chromatograms show the rechromatographed C200A and C210A. The peak A (designated as C200ARA and C210ARA) was pooled and lyophilized directly. The unconjugated peaks of oLH and gelonin were lyophilized separately. (B) Gel-filtration chromatograms of the conjugation mixtures of C220 (●—●) and C230 (○—○). The chromatograms shown by ●– –● and ○– –○ indicate rechromatography of peak A of peak C220 (as C220A) and C230 (as C230A). The major peaks of the rechromatography of C220A and C230A were designated as C220ARA and C230ARA, respectively. As described above, these portions of the peaks were directly lyophilized.

In SDS–PAGE analysis, the patterns of the conjugates were compared with those of the ingredients, oLH and gelonin. The samples analyzed on SDS–PAGE under reduced and unreduced conditions are shown in Figure 2. Under nonreduced conditions (Figure 2, left panel), the conjugates showed the absence of either free oLH or gelonin (lanes 3, 4, 7, 8, and 11). These conjugates showed the distinct presence of both oLH and gelonin once they are reduced (Figure 2, right panel). The native oLH appears as a diffused band between 31 and 45 kDa (Figure 2, left panel, lane 13) and gelonin appears as a sharp band at ~31 kDa (lane 12, left and right panel). The conjugates showed multiple bands of slower migrating component with apparent molecular weights of 55–116 kDa (lanes 3, 4, 7, 8, and 11). The conjugates showed the distinct

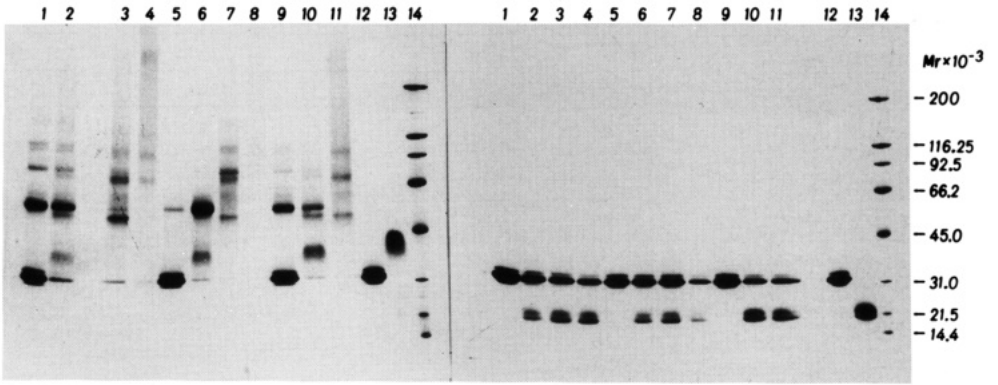


Figure 2. SDS–PAGE analysis of oLH–gelonin conjugate prepared by using SPDP and LC-SPDP. SDS–PAGE (reduced, right panel; nonreducing, left panel) analysis of the conjugate and other peaks. A gel consisting of 5–15% (w/v) acrylamide was used. The gel was fixed in methanol/acetic acid, stained with Commassie Blue and destained with methanol/acetic acid for 24 h. Lane 1, C210C-P85-100; lane 2, C210B-P72-80; lane 3, C210A-P50-65; lane 4, C210ARA-P50-67; lane 5, C220C-P87-100; lane 6, C220B-P72-80; lane 7, C220ARA-P50-66; lane 8, C200A-P35-46; lane 9, C230C-P87-100; lane 10, C230B-P75-80; lane 11, C230ARA-P45-65; lane 12, gelonin; lane 13, oLH; lane 14, molecular weight markers [myosin (200 kDa); β-galactosidase (116.25 kDa), phosphoamylase B (92.5 kDa), bovine serum albumin (66.2 kDa), ovalbumin (45 kDa), carbonic anhydrase (31 kDa), Soyabean trypsin inhibitor, (21.5 kDa), lysozyme, (14.4 kDa)]. A sample of 40 μg each was run under reduced (right) and unreduced (left) panel conditions on the gel. Densitometric scan and quantitation were done on the reduced gel in order to determine molar ratio of the conjugate.

presence of both oLH and gelonin once they are reduced. (Figure 2, right panel).

The conjugates synthesized above were further analyzed by RP-HPLC. Figure 3 shows the RP-HPLC chromatograms of native oLH, gelonin, and their SPDP- and LC-SPDP-modified derivatives. The analysis was carried out on the Water's μBondapak phenyl column, using a continuous gradient (as described in the legend of the Figure 3). A comparative study of oLH and SPDP- or LC-SPDP-modified oLH chromatograms clearly reveal that ϵ-NH_2 group modification primarily occurs in the α-subunit of the hormone as seen by the emergence of new prominent fractions at t_R = 8.2 and 9.4 min for SPDP–oLH and t_R = 8.98, 9.4, and 9.98 min for LC-SPDP–oLH (Figure 3A). In both cases, the pattern of LH-β peaks in the elution zone at 14–16 min remains essentially unaltered (Figure 3A). The appearance of more peaks at the higher retention time may be due to the increase in hydrophobicity of LC-SPDP compared to SPDP. The elution pattern of SPDP– or LC-SPDP–gelonin essentially remains the same at $t_R \sim 21.10$ min, except that its extinction coefficient is higher. RP-HPLC of different conjugates are also shown in Figure 3B–D. A comparison of RP-HPLC chromatograms clearly reveals the presence of the LHβ component in the expected zone, but there is a complete absence of the modified α-subunit, as this now remains covalently linked to gelonin in a disulfide bond. This further confirms that the conjugation selectively occurs through one of the amino groups of the α-oLH. The acidic conditions used in the RP-HPLC causes complete dissociation of the oLH subunits, which is distinctly separated by the gradient elution. The β-subunit eluting as a doublet in the t_R = 14–16 min zone was due to the αLH–S–S–gelonin complex. Due to the higher extinction coefficient of gelonin, the conjugate peak eluting at t_R = 21–23 min as a broad peak indicated a relatively higher concentration than for the β-subunit (Figure 3B–D). Furthermore, the conjugates do not have free hormone contamination (free SPDP- or LC-SPDP-modified oLH) because of the lack of α-subunit peaks, which if present would have been easily detectable under the conditions employed here. This observation further confirms the SDS–PAGE data in which the conjugates did not show the presence of either of the ingredients (Figure 2 left panel, lane 3, 4, 7, 8, and 11).

The molar ratio of oLH and gelonin in the conjugates

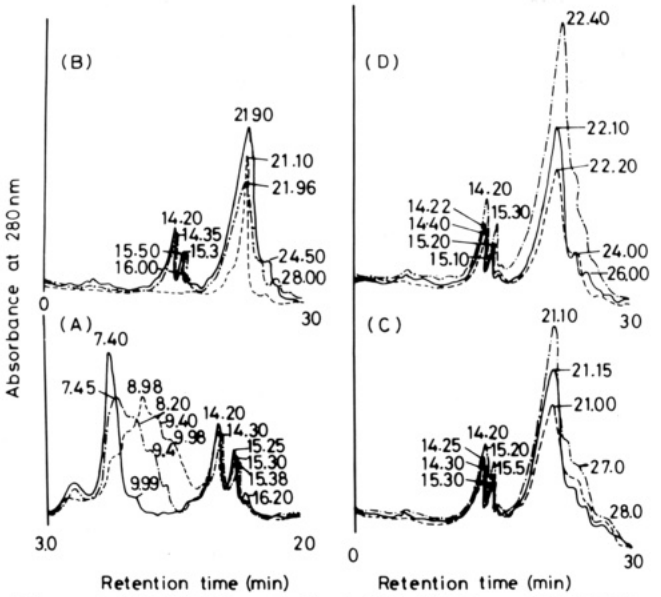


Figure 3. RP-HPLC analysis of oLH, SPDP- and LC-SPDP-modified oLH, gelonin, and the conjugates. The samples were dissolved in H_2O containing 0.1% TFA (solvent A) and the analysis was performed on a Water's μBondapak phenyl column (4 × 250mm) and equilibrated in solvent A + 25% CH_3CN and 0.1% TFA. A gradient of 25–50% was run over 30 min at a flow rate of 2 mL/min and monitored at 280 nm. In case of oLH, oLH–SPDP, and oLH–LC-SPDP, the chromatograms were analyzed between 3 and 20 min; however in case of gelonin, oLH–gelonin conjugates the chromatograms were analysed between 0 and 30 min. The RP-HPLC chromatograms of oLH (—), oLH–SPDP (-·-) and oLH–LC-SPDP (- -) are shown in pane A. Please note that the modification occurs in α-subunit (t_R = 7.4 min) while β-subunit (t_R = 14–16 min) remains unaltered. The RP-HPLC chromatograms of gelonin-SPDP (- -) and oLH-gelonin conjugates C200A (—) and C200ARA (-·-) are shown in panel B. The RP-HPLC chromatograms of C210A (—), C210ARA (- -) and C220A (-·-) are shown in panel C. The RP-HPLC chromatograms of C220ARA (—), C230A (- -) and C230ARA (-·-) are shown in panel D. The structure of C200, C210, C220, and C230 conjugates is shown in Table I. Note all the conjugates did not show the presence of α-subunit as it was covalently conjugated to gelonin. Under the acidic conditions, the β-subunit, which is associated noncovalently, was dissociated from the complex and eluted around t_R = 14–16 min.

was determined by spectrophotometric, SDS–PAGE, and amino acid analysis as described earlier (*15*, *17–19*). Spectrophotometrically, the molar concentration of py-

Table II. Amino Acid Composition of oLH, Gelonin, and Their Conjugates Prepared with the Use of SPDP and LC-SPDP[a]

amino acid	molar ratio oLH	molar ratio gelonin	for 1:1 adduct	experimental observation for the conjugates C200ARA	C210ARA	C220ARA	C230ARA
Lys	12	20	32	30.4	31.4	30.2	32.5
His	6	2	8	8	8	8	8
Arg	11	11	22	23.0	22.4	21.9	22.4
Asp	11	26	37	37.5	38.2	34.4	37.6
Thr	16	12	28	24.5	26.5	28.5	29.9
Ser	14	12	26	25.5	24.5	26.8	27.0
Glu	14	22	36	37.5	38.2	38.0	38.0
Pro	27	10	37	ND	ND	ND	ND
Gly	11	15	26	26.4	26.2	28.0	28.4
Ala	15	15	30	32.4	30.5	33.0	31.4
half Cys	22	2	24	ND	ND	ND	ND
Val	13	13	26	25.2	25.8	27.0	26.8
Met	7	2	9	ND	ND	ND	ND
Ile	7	14	21	20.4	21.5	19.8	21.9
Leu	14	20	34	31.5	35.8	36.0	34.5
Tyr	7	9	16	16.2	17.4	18.0	16.9
Phe	8	11	19	19.9	20.4	22.0	21.5
Trp	0	?	?	ND	ND	ND	ND
carbohydrate	+	+	+	+	+	+	+

[a] oLH values are from the structure of the α- and β-subunit. Gelonin composition was determined on the purified preparation used for the conjugation in the present investigation. ND, not determined.

Table III. Molar Ratio of oLH and Gelonin in the Conjugates As Determined by Different Methods

conjugate code	molar ratio (oLH:gelonin) spectrophotometric	gel electrophoresis	amino acid composition
C200ARA	1:1.30	1:1.20	1:1
C210ARA	1:1.40	1:1.32	1:1
C220ARA	1:1.20	1:1.20	1:1
C230ARA	1:1.30	1:1.25	1:1

ridine-2-thione liberated after DTT treatment of the SPDP-/LC-SPDP-gelonin followed by mixing with SPDP-/LC-SPDP-oLH was estimated (*15*, *17–19*). In order to determine the ratio in the conjugates by SDS-PAGE, different concentrations of oLH and gelonin were run under reducing conditions and a concentration dependence of the staining pattern was established by densitometry (*17*). A fixed amount (40 μg) of the conjugate was run in a parallel gel. The protein bands were stained with Coomassie Brilliant Blue stain and scanned for protein concentration. The amino acid composition of oLH, gelonin, and their conjugates was determined by the ninhydrin method as described (*15*, *18*) and are recorded in Table II. The experimentlly determined amino acid composition of the conjugates closely agrees with the theoretical prediction on the basis of a 1:1 ratio (Table III). The molar ratio of oLH and gelonin in the conjugate thus determined are recorded in Table III. Reactivity of oLH and gelonin with their specific antibodies in the different fractions of the conjugates was determined by competitive RIA as described in the Experimental Procedures. The competitive displacement curves of oLH is shown in Figure 4. The quantitative immunoreactivity data of oLH and gelonin are recorded in Table IV. The immunoreactivity of oLH was drastically reduced (>86% activity) after a single ϵ-NH_2 group modification by SPDP. In case of LC-SPDP-modified oLH, the activity was further reduced (>89%) (Figure 4, Table IV), which may be due to the increase in hydrophobicity of oLH-LC-SPDP. However, after conjugation, with gelonin, the oLH immunoreactivity was further affected by 3–5% (Table IV). When oLH-SPDP or oLH-LC-SPDP immunoreactivity was taken as 100%, the activity of the gelonin conjugates varied from 22 to 41% (Table IV). In a 1:1 molar ratio conjugate, the immunoreactivity was doubled (Table IV). Similarly, the gelonin immunoreactivity was reduced up

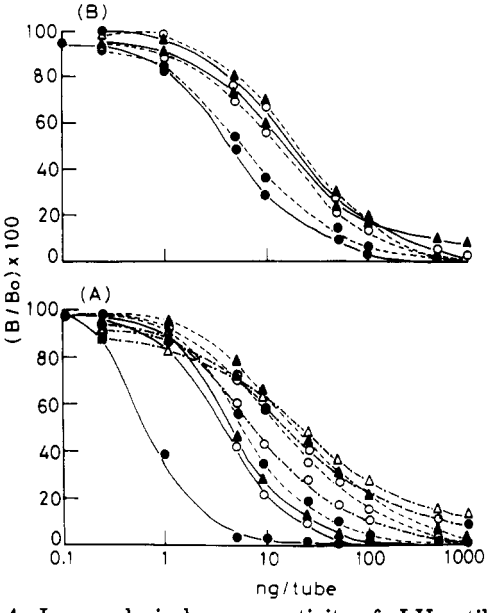


Figure 4. Immunological cross-reactivity of oLH antibody to oLH, its SPDP- and LC-SPDP-modified derivatives, and their conjugates to gelonin. The percent immunoreactivity was determined by competitive displacement analysis using specific RIA as described in the Experimental Procedures: Lower panel, A. The displacement cures are oLH (●—●), oLH-SPDP (○—○), oLH-LC-SPDP (△—△), C200A (▲- -▲), C200B (●- -●), C200ARA (○- -○), C230A (●- -●), C230B (○-·-○), C230ARA (△-·-△); upper panel, B, the displacement curves of C210A (○—○), C210B (●—●), C210ARA (▲—▲), C220A (○- -○), C220B (●- -●), and C220ARA (▲- -▲). The quantitative data based on these displacement curves are recorded in Table IV.

to 30–36% after a single ϵ-NH_2 group modification with SPDP or LC-SPDP. However, the activity was not further affected after conjugation with oLH (Table IV).

One of the primary requirements of biological activity of hormonotoxins are their binding to the hormone receptor. The receptor binding was determined by using rat testicular homogenate as a source of gonadotropin receptor. After a single NH_2 group modification with SPDP or LC-SPDP, the activity was reduced to 8.5% and 7.0%, respectively (Table V). This was further reduced upon conjugation to gelonin (Table V). As compared to SPDP-oLH or LC-SPDP-oLH with a single amino group modification and correction for increase in the molecular

Table IV. Immunoreactivity of oLH and Gelonin in the Conjugates[a]

hormone–cross-link–gelonin	hormone assay			gelonin assay		
		% cross-reactivity			% cross-reactivity	
	ED_{50} (ng)	A	B	ED_{50} (ng)	A	B
oLH	0.60	100	–			
oLH–SPDP	4.15	14.5	100			
oLH–LC-SPDP	5.45	11.0	100			
gelonin				0.90	100	
gelonin–SPDP				2.50	36.0	100
gelonin–LC-SPDP				3.00	30.0	100
oLH–S–S–gelonin						
C200A	18.70	3.2 (6.4)	22.10 (44.20)	5.45	16.50 (33.0)	45.80 (91.60)
C200B	3.75	16.0	110.6	18.00	5.00	13.90
C200C	ND	ND	ND	2.30	39.00	108.00
C200ARA	12.50	4.8	33.20 (66.40)	5.15	17.50	48.50 (97.00)
C210A-P50-65	51.80	3.8 (7.6)	26.26 (56.53)	5.00	18.00 (36.00)	60.00 (120.00)
C210B-P72-80	4.10	14.5	101.20	30.00	3.00	10.00
C210C-P85-100	ND	ND	ND	2.80	32.00	107.00
C210ARA-P50-67	14.30	4.20	29.00 (58.00)	5.50	16.50 (33.00)	54.54 (109.10)
C220A-P50-64	13.30	4.50 (9.00)	40.90 (81.80)	4.73	19.00 (38.00)	52.85 (105.70)
C220B-P72-80	6.00	10.00	90.83	30.00	3.00	8.33
C220C-P87-100	ND	ND	ND	2.25	40.00	111.11
C220ARA-P50-66	17.10	3.50 (7.00)	31.87 (63.74)	5.62	16.00 (32.00)	48.48 (88.96)
C230A-P52-65	15.80	3.80 (7.60)	34.50 (69.00)	5.62	16.00 (32.00)	53.40 (106.80)
C230B-P75-80	7.50	8.00	72.66	45.00	2.00	6.60
C230C-P87-100	ND	ND	ND	2.50	36.00	120.00
C230ARA-P45-65	18.75	3.20 (6.40)	29.06 (58.13)	5.60	16.00 (32.00)	53.60 (107.20)

[a] The immunoreactivity is expressed as a percentage with respect to native oLH or gelonin (column A) and oLH–SPDP/LC-SPDP or gelonin–SPDP or gelonin–LC-SPDP (column B), which were taken as 100%. The details of the experimental design are given in the Experimental Procedures. Numbers in parentheses for the hormone assay show values when corrected for molecular weight of the conjugate assuming 1:1 complex formation. In the gelonin assay similar correction also applies for the presence of hormone in the concerned fraction.

Table V. Receptor Binding Activity, Ribosome-Inactivating Property, and Steroidogenic Activity of oLH–S–S–Gelonin Conjugates[a]

hormone–cross-link–gelonin	receptor binding activity			protein-synthesis-inhibitor activity			steroidogenic activity (%)
		% activity			% activity		
	ED_{50} (ng)	A	B	IC_{50} (ng)	A	B	
oLH	0.95	100					100
oLH–SPDP	11.20	8.5	100				110–120
oLH–LC-SPDP	13.60	7.0	100				120–130
gelonin				0.25	100		
gelonin–SPDP				1.67	15.0	100	
gelonin–LC-SPDP				2.08	12.0	100	
oLH–S–S–gelonin							
C200A	79.10	1.20 (2.40)	14.16 (28.32)	5.43	4.6 (9.2)	30.75 (61.50)	3.4 (6.8)
C200ARA	59.40	1.60 (3.20)	18.85 (37.70)	4.80	5.2 (10.4)	34.80 (69.60)	3.2 (6.4)
C210A	68.00	1.40 (2.80)	16.48 (32.96)	6.25	4.0 (8.0)	33.30 (66.60)	4.0 (8.0)
C210ARA	61.00	1.56 (3.12)	18.36 (36.72)	5.70	4.4 (8.8)	36.50 (73.00)	3.6 (7.2)
C220A	105.00	0.90 (1.80)	12.95 (25.95)	4.50	5.5 (11.0)	37.10 (74.20)	3.0 (6.0)
C220ARA	79.20	1.20 (2.40)	17.20 (34.40)	5.00	5.0 (10.0)	33.40 (66.80)	2.6 (5.2)
C230A	79.20	1.20 (2.40)	17.20 (34.40)	5.20	4.8 (9.6)	40.00 (80.00)	3.5 (7.0)
C230ARA	63.40	1.50 (3.00)	21.45 (42.90)	6.25	4.0 (8.0)	33.30 (66.60)	2.5 (5.0)

[a] The receptor binding is expressed as a percentage with respect to native oLH (column A) and oLH–SPDP/LC-SPDP (column B) which were taken as 100%. Similarly the percentage protein synthesis was calculated on the basis of radioactivity incorporated in the precipitate as described in the Experimental Procedures. IC_{50} is the dose of inhibition required for 50% inhibition of protein synthesis. Numbers in parentheses show the value when corrected for the molecular weight of the conjugate assuming 1:1 complex formation.

weight, the relative activity of the conjugate varied from 25 to 43% (Table V). The chromatographically repurified conjugates (designated as C200ARA, C210ARA, C220ARA, and C230ARA) showed relatively higher receptor recognition than C200A, C210A, C220A, and C230A (Table V). As observed earlier (*15*, *17–19*), all the conjugates stimulated progesterone production in rat granulosa cells, with a tendency to enhance steroidogenesis to the same extent as native oLH (Figure 5). Their relative potencies, when corrected for the presence of gelonin in the complex, varied from 5 to 8% (Table V).

Cell-free translation experiments were carried out on native gelonin, SPDP- or LC-SPDP-modified gelonin, and their conjugates with oLH in order to determine their ability to inhibit protein synthesis, and the quantitative data are recorded in Table V. The percentage bioactivity was determined after measuring the IC_{50}. A single amino group modification resulted in more than an 85% loss in

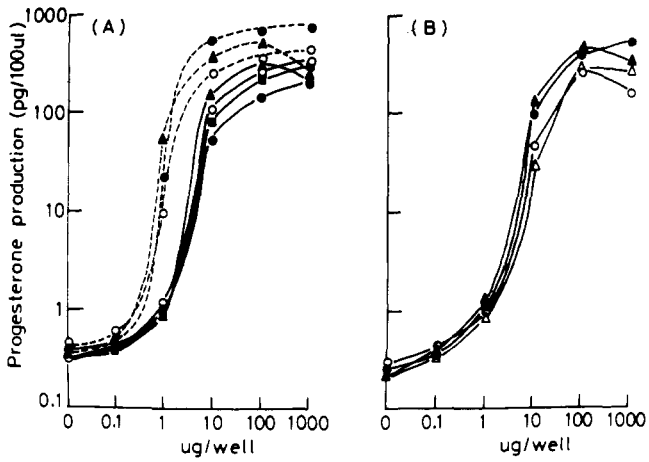


Figure 5. Steroidogenic activity of native oLH, SPDP- and LC-SPDP-modified oLH, and their conjugates with gelonin. The progesterone induction ability was determined in Leydig tumor cells as described in the Experimental Procedures: left panel, A, shows the progesterone induction ability of oLH (●- -●), oLH-SPDP (○- -○), oLH-LC-SPDP (▲- -▲), C200A (●—●), C-200ARA (○—○), C210A (▲—▲), and C220ARA (■—■); left panel, B, shows the profile of C220A (●—●), C220ARA (○—○), C230A (▲—▲), and C230ARA (△—△). Progesterone produced in 4-h incubation was quantitated by specific RIA by using specific anti-progesterone antibodies. The quantitative data are recorded in Table V.

the ribosome-inactivating property (Table V). Upon conjugation with oLH, the *in vitro* protein synthesis inhibition activity was further affected (Table V). By taking gelonin–SPDP or gelonin–LC-SPDP activity as 100%, and correcting for oLH contribution in a 1:1 molar ratio in the conjugate, the activity varied from 61 to 80% (Table V).

The binding of the conjugates to the Leydig tumor cells was demonstrated with the help of gelonin antibody and by using ^{125}I-protein-A as the probe. The binding of C200A, C200ARA, C210A, and C210ARA conjugates are shown in the left panel of Figure 6 whereas, C220A, C220ARA, C230A, and C230ARA conjugates are shown in right panel of Figure 6. The nonspecific binding was determined by incubation of the appropriate quantity of gelonin (as shown by the dotted line in Figure 6).

All the conjugates saturate the receptors at a concentration of ~10 μg/mL (Figure 6). The nonspecific binding was also increased in the presence of half of the concentration of gelonin used, but this was always less than 10%. This was in agreement with our earlier observations (*17–19*). On the basis of the present observation, a concentration of 10 μg/mL of the conjugate was used for a competitive displacement analysis. The binding and displacement experiments are shown in Figure 7. Open bars indicate the binding of untreated cells and cells treated with gelonin as well as with the conjugates (Figure 7). Binding and competition experiments of C200 and C210 are shown in the lower panel of Figure 7. The upper panel of this figure shows the data for C220 and C230 hormonotoxin. The solid bars show similar binding, except the last one, which indicates the competitive ability of the native oLH with the conjugates. It is evident from the data that the presence of native oLH in the binding reaction clearly inhibited the conjugates to bind to the gonadotropin receptors of the tumor cells.

The cytotoxicity of the hormonotoxins was evaluated using MLTC-1 cells which possess receptors for gonadotropin hormone, and their action is mediated by internalization. The cytotoxicity was determined by a leucine incorporation assay as described earlier (*15, 17–19*). All

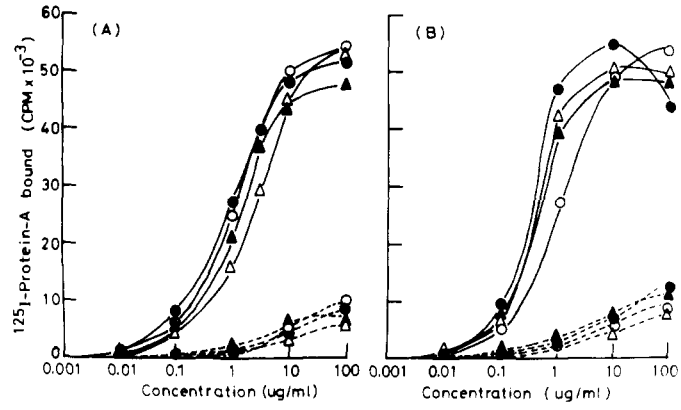


Figure 6. Saturation binding and competition ability of hormonotoxin to the Leydig tumor cells. Saturation binding, determined as described in the text, is shown by the solid line while the nonspecific binding is indicated by the dashed line. The cells were grown for 48 h and subsequently washed with serum-free medium and reacted with the indicated test materials. Following incubation and washing to remove unbound proteins, the cells were challenged with the anti-gelonin antibodies. The amount of antibody bound to the cells (via the gelonin in the conjugate) was quantitated in a subsequent reaction with ^{125}I-labeled protein-A. The number of counts (cpm) observed in each instance is a direct reflection of hormonotoxin binding via the LH receptor binding site in the conjugate and detected by the antibody directed against gelonin. The left panel shows the saturation analysis of C200A (●—●), C200ARA (○—○), C210A (△—△), and C210ARA (▲—▲). The right panel shows the analysis of C220A (●—●), C220ARA (○—○), C230A (△—△), and C230ARA (▲—▲). The radioactivity incorporated in each set is a direct reflection of hormonotoxin binding via the gonadotropin site of the conjugate as described by gelonin antibodies.

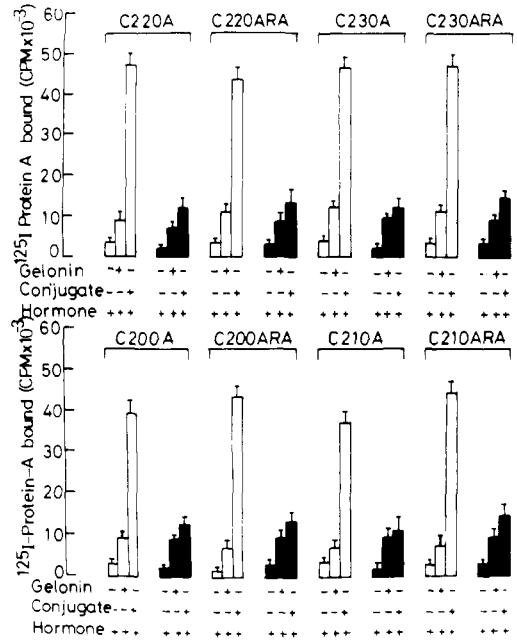


Figure 7. Competition ability of native oLH to the hormonotoxins for the binding to the Leydig tumor cells as described in the Experimental Procedures. The binding assay was performed as described in Figure 6. The binding ability of the hormonotoxin (as shown by open bar) was drastically inhibited (as shown by closed bar) in the presence of competitor (i.e., native oLH), indicating that the binding occurs via oLH.

the conjugates were toxic to the cells and the IC_{50} for C200A, C200ARA, C210A, C210ARA, C220A, C220ARA, C230A, and C230ARA was 8.2×10^{-11}, 1.2×10^{-10}, 5.5×10^{-11}, 7.5×10^{-11}, 8.0×10^{-11}, 1.0×10^{-10}, 1.7×10^{-10}, and 1.3×10^{-10} M, respectively. The cytotoxicity of the

conjugates gradually decreased in the order of C200A > C220A > C210A > C230A. After rechromatography the order was C210ARA > C220ARA > C200ARA > C230ARA. In the parallel set, the conjugates incubated in the presence of native oLH did not show cytotoxicity (data not shown).

DISCUSSION

Present investigation is in continuation of our earlier efforts to design a hormonotoxin which could be selectively targeted to appropriate cells in the gonads (*15*, *17–21*). The gonadotropins such as ovine LH or hCG have been covalently cross-linked to a ribosome-inactivating proteins, by using SPDP as a cross-linking agent (*13*, *15*, *17–21*). Ovine LH/hCG was chosen as a carrier because of the selective presence of its receptor(s) in the ovary and testis (*37*, *38*) and the hormone itself can be obtained in highly purified form with extensive information available on its structure and function (*39–42*). On the basis of the structure function data that revealed that the ϵ-NH_2 groups of the α-subunit are more sensitive to chemical modification while the amino groups of β-subunit are resistant to such modifications, an attempt was made to cross-link the β-subunit to the toxin, prior to recombination with the α-subunit (*43*, *44*). But the failure of recombination with the native α-subunit forced us to use native oLH cross-linked to the toxin by using SPDP as a cross-linking agent (*15*, *17–21*). oLH and gelonin have been modified by SPDP to introduce one potential site for conjugation. Later SPDP-modified gelonin was reduced with DTT to generate SH groups which were subsequently used to obtain an oLH–S–S–gelonin conjugate. Recently, similar to SPDP, a long-chain SPDP has been introduced as a heterobifunctional cross-linking agent by Pierce Chemicals Co. Long-chain SPDP introduces a 15.6-Å-long spacer arm while SPDP could attach an arm of 8.6 Å. The hypothesis was that the introduction of a long spacer arm can effectively overcome the steric hinderance of oLH, which may help increase receptor binding and cytotoxicity. Therefore, the hormonotoxins in this study were synthesized with the help of SPDP alone (C200A and C200ARA), LC-SPDP alone (C230A and C230ARA), and both SPDP and LC-SPDP (C210, C220, C210ARA, and C220ARA) to obtain conjugates with an intermediate spacer arm, and a comparative study on immunoreactivity, receptor binding, biological activity, and cytotoxicity was carried out. As observed in case of SPDP, the primary modification of the ϵ-NH_2 group occurs in the α-subunit of oLH. But RP-HPLC analysis clearly demonstrated that the LC-SPDP-modified α-oLH was more hydrophobic in nature compared to the SPDP-modified derivative (Figure 3). The α-subunit had 11 NH_2 groups (10 ϵ-NH_2 group and 1 α-NH_2) while β-oLH possessed only 3 NH_2 groups (2 ϵ-NH_2 and 1 α-NH_2). Data reported here and in greater detail in other communications (*36*) indicated that the amino groups of α-subunit are more accessible to LC-SPDP modification than those of the β-subunit. Similar observation was also made for SPDP modification (*28*). The molar ratio of oLH and gelonin in the conjugate is equimolar, as corroborated by three different methods of assessment (Table III).

The oLH–gelonin conjugates prepared with the use of LC-SPDP were subjected to SDS–PAGE and RP-HPLC analysis. SDS–PAGE clearly revealed that the conjugate did not contain unreacted SPDP–LC-SPDP–oLH or –gelonin as a contaminant. This measurement is important at this stage since oLH, if present as contaminant, will compete with the conjugated gelonin, which eventually will reduce the receptor binding and cytotoxicity of the conjugate. Immunoreactivity, receptor binding steroidogenic activity, and cytotoxicity of oLH–gelonin conjugate prepared with the use of LC-SPDP was comparable with that of SPDP (Table V). The present investigation further demonstrated that, in case of hormonotoxin, the cytotoxicity is not affected with the use of long chain spacer arm.

ACKNOWLEDGMENT

The financial support received from the Rockefeller Foundation, New York, New York, the Council of Scientific and Industrial Research, New Delhi, India, and the University Grants Commission, New Delhi, India, is gratefully acknowledged. A part of this work was carried out during the stay of V.S. at the Department of Biology, Washington University, St. Louis, MO. During the stay, the research support received from the State of Missouri, Centre for Plant Science and Biotechnology, Washington University, St. Louis, MO, is also gratefully acknowledged. Authors are extremely grateful to Prof. Roy Curtiss III, Chairman, Department of Biology, Washington University, for his constant encouragement and support. We are also thankful to Dr. Victor Rebois for his generous gift of mouse Leydig tumor cell (MLTC-1) line.

LITERATURE CITED

(1) Frankel, A. E., Ed. (1988) *Immunotoxins*, Kluwer Academic Publishers, Norwell MA.

(2) Vogel, C-W., Ed. (1987) *Immunoconjugates: Antibody Conjugates in Radioimaging and Therapy of Cancer*, Oxford University Press, New York.

(3) Moller, G., Ed. (1982) Antibody carriers of drug and toxins in tumor therapy, *Immunol. Rev. 62*, 5–216.

(4) Vitetta, E. S., Krolick, K. A., Miyama-Inaba, M., Cushely, W. and Uhr, J. W. (1984) Immunotoxins: a new approach to cancer therapy, *Science 219*, 644–650.

(5) Vitetta, E. S., Fulton, R. J., May, R. D., Till, M., and Uhr, J. W. (1987) Redesigning nature's poison to create anti-tumor reagents. *Science 238*, 1098–1104.

(6) Stripe, F., and Barbieri, L. (1986) Ribosome inactivating proteins upto date. *FEBS Lett. 195*, 1–8.

(7) Barbieri, L., and Stripe, F. (1982) Ribosome-inactivating proteins from plants: Properties and possible uses, *Cancer Surv. 1*, 489–520.

(8) Jiminez, A., and Vasquez, D. (1985) Plant and fungal protein and glycoprotein toxins inhibiting eukaryotic protein synthesis. *Annu. Rev. Microbiol. 39*, 649–672.

(9) Lord, J. M., Hartely, M. R., and Roberts, L. M. (1991) Ribosome inactivating proteins in plants. *Semin. Cell. Biol. 2*, 15–22.

(10) Chang, T., Dazord, A., and Neville, D. M., Jr. (1977) Artificial hybrid protein containing a toxin protein fragment and a cell membrane receptor binding moiety in a disulfide complex. *J. Biol. Chem. 252*, 1515–1522.

(11) Miskimins, W. K., and Shimizu, N. (1979) Synthesis of a cytotoxic insulin cross-linked to diphtheria toxin fragment A capable of recognising insulin receptors. *Biochem. Biophys. Res. Commun. 91*, 143–151.

(12) Oeltman, T. N., and Heath, E. C. (1979) A hybrid protein containing a toxic subunit of ricin and the cell-specific subunit of human chorionic gonadotropin. I. Synthesis and characterization. *J. Biol. Chem. 254*, 1022–1027.

(13) Oeltman, T. N. (1985) Synthesis and *in-vitro* activity of a hormone-diphtheria toxin fragment A hybrid. *Biochem. Biophys. Res. Commun. 133*, 430–435.

(14) Bacha, P., Murthy, J. R., and Reichlein, S. (1983) Thyrotropin releasing hormone-diphtheria toxin related polypeptide conjugates: Potential role of the hydrophobic domain in toxin entry. *J. Biol. Chem. 258*, 1565–1570.

(15) Singh, V., Sairam, M. R., Bhargavi, G. N., and Akhras, R. G. (1989) Hormonotoxins: Preparation and characterization

of ovine luteinizing hormone–gelonin conjugate. *J. Biol. Chem. 264*, 3089–3095.
(16) Schwartz, J., Penke, B., Rivier, J., and Vale, W. (1987) A new cytotoxin, specific for the target cells of the corticotropin releasing factor. *Endocrinology 121*, 1454–1460.
(17) Singh, V., and Sairam, M. R. (1989) Hormontoxins: Conjugation of chorionic gonadotropin with ribosome-inactivating protein, gelonin and comparison with a lutropin conjugate. *Mol. Cell. Endocrinol. 67*, 217–229.
(18) Singh, V. (1991) Hormonotoxins: Synthesis, Characterization, and bioefficacy of some defined disulfide conjugates of ovine luteinizing hormone with a ribosome-inactivating protein, gelonin. *Indian J. Exp. Biol. 29*, 916–925.
(19) Singh, V., and Das, C. (1991) *In-vitro* selective killing of gonadal tumor cells by hormonotoxins composed of ovine luteinizing hormone linked by a disulfide bond to a ribosome-inactivating protein, gelonin. *Biochem. Int. 24*, 689–699.
(20) Singh, V. (1991) Design and synthesis of bioeffective hormonotoxins for selective elimination of gonadal cells. In *Horizons in Endocrinology, Vol III* (M. Maggi and V. Geenen, Eds.) Serono Symposia Series, Vol 76, Raven Press, New York, pp 197–202.
(21) Singh, V. (1992) Hormonotoxins in *Recent Frontiers in Reproduction Research*, (C. Das and J. Sengupta, Eds.) In press.
(22) Sairam, M. R. (1976) Role of arginine residue in ovine lutropin: Reversible modification by 1,2-cyclohexanedione. *Arch. Biochem. Biophys. 176*, 197–203.
(23) Stripe, F., Olsnes, S., and Phil, A. (1980) Gelonin, a new inhibitor of protein synthesis, non-toxic to intact cell. Isolation, characterization and preparation of cytotoxic complexes with concanavalin A. *J. Biol. Chem. 255*, 6947–6953.
(24) Singh, V., and Sairam, M. R. (1989) Effect of thiolation on immunoreactivity of a ribosome-inactivating protein, gelonin. *Biochem. J. 263*, 417–423.
(25) Singh, V., and Kar, S. K. (1992) Properties of a ribosome-inactivating protein, gelonin purified from three different methods. *Indian. J. Biochem. Biophys. 29*, 31–41.
(26) Singh, V. (1991) Effect of thiolation of amino groups of gelonin on its protein biosynthesis inhibitor activity, *Biochem. Int. 24*, 677–688.
(27) Rebois, R. V. (1982) Establishment of gonadotropin-responsive murine leydig tumor cell line. *J. Cell. Biol. 94*, 70–76.
(28) Singh, V., and Sairam, M. R. (1989) Effect of thiolation of amino groups of ovine lutropin on immunoreactivity, receptor binding and bioactivity. *Mol. Cell. Endocrinol. 63*, 255–262.
(29) Carlsson, J., Drevin, M., and Axen, R. (1978) Protein thiolation and reversible protein-protein conjugation. N-succinimidyl 3-(2-pyridyl dithio)propionate, a new heterobifunctional reagent. *Biochem. J. 173*, 723–737.
(30) Fraker, P. J., and Speck, J. R. (1978) Protein and cell membrane iodinations with a sparingly soluble chloramide 1,3,4,4-tetrachloro 3α,6α-diphenylglycouril. *Biochem. Biophys. Res. Commun. 80*, 849–857.
(31) Singh, V. (1986) Structural requirement for the recognition of luteinizing hormone releasing hormone (LHRH) by monoclonal and conventional anti-LHRH antibodies. *Biochem. Cell. Biol. 64*, 1372–1177.
(32) Singh, V. (1987) Immunospecificity and affinity studies on the monoclonal anti-gonadotropin releasing hormone (GnRH) antibodies: Monoclonal produced by azotized GnRH preferentially recognize to native GnRH. *Biochem. Int. 15*, 153–162.
(33) Talwar, G. P., Gupta, S. K., Singh, V., Sahal, D., Iyer, K. S. N., and Singh, O. (1985) Bioeffective monoclonal antibody against the decapeptide gonadotropin releasing hormone: Reacting determinant and action on ovulation and estrus suppression. *Proc. Natl. Acad. Sci. U.S.A. 82*, 1128–1231.
(34) Singh, V., and Curtiss, R., III (1991) Abrogation of ribosome-inactivating property of gelonin in the disulfide linked ovine-luteinizing hormone-gelonin conjugates. *Biochem. Int.* 25, 531–536.
(35) Alam, A., Bhuri, S. K., Mavila, A. K., and Singh, V. (1992) Design of liposomes to improve encapsulation efficiency of gelonin and its effect of immunoreactivity and ribosome inactivating property. *Mol. Cell. Biochem. 112*, 97–107.
(36) Singh, V., and Curtiss, R., III (1993) Effect of amino group modification of ovine lutropin by LC-SPDP on immunological and biological properties: A comparative study with SPDP modified oLH. *Mol. Cell. Biochem.* In press.
(37) Strickland, T. D., Norland, T. D., and Puett, D. (1980) Gonadotropin testicular receptor interaction and subunit-subunit interactions. In *Functional Correlates of Hormone Receptors in Reproduction* (W. B. Mahesh, Ed.) Elsevier/North Holland, Amsterdam, pp 463–479.
(38) Strickland, T. W., and Puett, D. (1981) Contribution of subunits to the functions of the luteinizing hormone/human chorionic gonadotropin recombinants. *Endocrinology 109*, 1933–1942.
(39) Pierce, J. G., and Parson, T. F. (1981) Glycoprotein hormones: Structure and function. *Annu. Rev. Biochem. 50*, 465–495.
(40) Ward, D. N. (1978) Chemical approaches to the structure–function relations of the luteinizing hormone (lutropin). In *Structure function of gonadotropins*. (K. W. McKerns, Ed.) Plenum Publishing Corporation, New York, pp 31–45.
(41) Ryan, R. J., Charlesworth, M. C., McCromic, D. J., Milius, R. P., and Keutmann, H. T. (1988) The glycoprotein hormones: recent studies of structure-function relationship. *FASEB J. 2*, 2661–2669.
(42) Sairam, M. R. (1983) Gonadotropin hormones relationship between structure and function with emphasis on antagonists. In *Hormonal Proteins and Peptides* (C. H. Li, Ed.) Academic Press, New York, pp 1–79.
(43) Singh, V., and Sairam, M. R. (1989) Hormonotoxins: I. Strategy for synthesis of ovine luteinizing hormone-gelonin conjugate bearing toxin in the beta subunit. *Int. J. Pept. Protein Res. 33*, 22–28.
(44) Singh, V., Mavila, A. K., and Alam, A. (1992) Effect of lysine residue modification of ovine luteinizing hormone by heterobifunctional cross-linking agent SPDP on subunit-subunit association, receptor binding and biological activity. *Indian J. Exp. Biol. 30*, 1093–1100.

Basic Fibroblast Growth Factor–*Pseudomonas* Exotoxin Chimeric Proteins; Comparison with Acidic Fibroblast Growth Factor–*Pseudomonas* Exotoxin

Susan L. Gawlak, Ira Pastan,† and Clay B. Siegall*

Bristol-Myers Squibb, Pharmaceutical Research Institute, Molecular Immunology Department, 3005 First Avenue, Seattle, Washington 98121. Received May 19, 1993®

We have constructed growth factor–toxin chimeric molecules composed of basic fibroblast growth factor (bFGF) and two different binding mutant forms of *Pseudomonas* exotoxin termed bFGF–PE40 and bFGF–PE4E KDEL. The chimeric molecules were expressed in *Escherichia coli* and localized to both inclusion bodies and the spheroplast cytoplasm. The bFGF–toxin fusion protein that was isolated and purified from inclusion bodies was 3-fold more active in inhibiting protein synthesis than that purified from spheroplast cytoplasm. Immunoreactivity of purified bFGF–toxin fusion protein to anti-bFGF antibodies was similar to that of native bFGF, as determined by ELISA analysis. A variety of carcinoma cell lines were sensitive to bFGF–PE40 and bFGF–PE4E KDEL, including H3396 (breast), Hep G2 (hepatocellular), and A431 (epidermoid). The concentration of chimeric toxin that inhibited protein synthesis by 50% (EC_{50}) was 110, 70, and 18 ng/mL for bFGF–PE40 and 15, 1, and 18 ng/mL for bFGF–PE4E KDEL. In comparison with fusion-toxins composed of acidic fibroblast growth factor (aFGF) and either PE40 or PE4E KDEL, bFGF–PE40 and bFGF–PE4E KDEL were similarly cytotoxic on most cell lines tested. Human aortic smooth muscle cells were sensitive to both bFGF and aFGF toxin fusion proteins. However, human aortic endothelial cells were sensitive to the bFGF–toxins but were resistant to both aFGF–toxin forms. Time course studies showed that bFGF–PE40 needed a 4–6-h exposure to target cells for peak inhibition of protein synthesis on both MCF-7 and A431 cells, while aFGF–PE40 was almost fully active within a 2-h incubation. The addition of heparin competed for the cytotoxic activity of bFGF–PE40 but not for aFGF–PE40 on MCF-7 and A431 cells. Cytotoxic forms of bFGF and aFGF may be useful in eliminating populations of cells that express both or one of these FGF receptors.

INTRODUCTION

Basic fibroblast growth factor (bFGF, FGF-2) belongs to the family of FGF proteins which includes acidic fibroblast growth factor (aFGF, FGF-1), the oncogene products *int-2* (FGF-3), and *hst/K-fgf* (FGF-4), and FGF-5, FGF-6, and keratinocyte growth factor (KGF, FGF-7) (*1, 2*). Basic FGF has multiple activities, including stimulating some cell types to proliferate and others to differentiate (*3, 4*). Basic FGF has also been shown to be a potent angiogenic factor (*5*).

There are at least five different genes that encode high affinity bFGF receptors (bFGFR). The receptors are transmembrane and display two or three immunoglobulin-like domains extracellularly and a tyrosine kinase domain intracellularly (*6–11*). There is evidence for the involvement of bFGF and its receptor in certain human tumors (*12–17*). Actively growing vasculature that supports tumor growth is dependent on growth factors including bFGF (*18, 19*). Basic FGF binds to both high and low affinity receptors (heparan sulfate molecules found in the extracellular matrix of cells and on cell surfaces) (*20, 21*).

Several laboratories have used cell-specific reagents, including antibodies and growth factors, to deliver protein toxins to target cells (*22, 23*). These hybrid molecules bind to cells that display the receptor or antigen of choice and are cytotoxic through the action of the protein toxin. We have previously reported on aFGF–P*seudomonas* exotoxin molecules that are specifically toxic to tumor cells (*24*), smooth muscle cells (*25*), and endothelial cells (*26*) expressing aFGF receptors. Conjugates composed of bFGF and the plant protein toxin saporin (SAP) have been shown to kill many cell types including tumor cells (*27–29*), pancreatic islet cells (*30*), and vascular cells (*31, 32*).

Pseudomonas exotoxin (PE), an ADP-ribosyl transferase, has three distinct domains (*33, 34*). Domain I is responsible for the binding of PE to its cell surface receptor. Domain II is essential for the translocation of PE to the cytosol, and domain III contains the ADP-ribosylation activity of PE, which is responsible for its cytotoxic effect. The enzymatic activity of domain III inhibits protein synthesis by catalyzing the transfer of the ADP-ribosyl moiety of oxidized NAD onto elongation factor 2. Elongation factor 2 is required for the addition of amino acids onto developing protein chains and its inactivation results in cell death. Many growth factors and cytokines, including interleukin-2, insulin-like growth factor I, transforming growth factor α, and interleukin-6, have been fused to *Pseudomonas* exotoxin and shown to be cytotoxic to the specific target chosen (*35–39*).

In this report, chimeric proteins composed of bFGF and PE were made by fusing the cDNA encoding bFGF to both a gene fragment encoding a truncated form of PE, PE40 (devoid of domain I), and the gene encoding a binding mutant form of PE (containing mutations in domain I that destroy native receptor binding) and by expressing the gene fusions in *Escherichia coli*. The cytotoxic portion

* Author to whom correspondence should be addressed.
† Laboratory of Molecular Biology, National Cancer Institute, National Institutes of Health, 9000 Rockville Pike, Bldg 37, Room 4E16, Bethesda, MD 20892.
® Abstract published in *Advance ACS Abstracts*, October 1, 1993.

1043-1802/93/2904-0483$04.00/0 © 1993 American Chemical Society

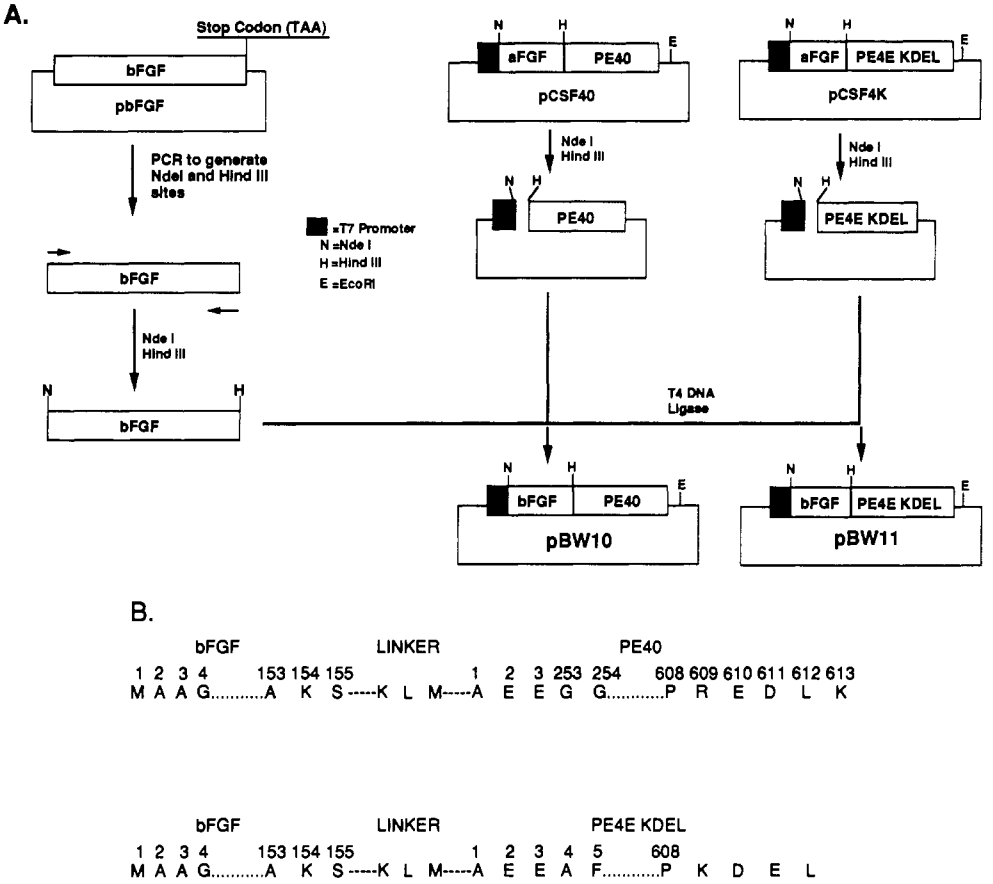


Figure 1. (A) Schematic diagram for the construction of plasmid pBW10, encoding the basic FGF–PE40 protein and plasmid pBW11 encoding the basic FGF–PE4E KDEL protein and (B) linear structure of the bFGF–PE40 and bFGF–PE4E KDEL fusion proteins. Details are shown at the junction between bFGF and PE. Mutated areas are also shown.

of the PE molecule was able to enter the cells through bFGF receptors and was cytotoxic to various cell types expressing the bFGF receptor. We compared the cytotoxic activities of the bFGF–toxin molecules to aFGF–toxin molecules and determined their differential cytotoxic activities toward a variety of human cancer and vascular cells.

EXPERIMENTAL PROCEDURES

Reagents. The human basic fibroblast growth factor gene encoded in plasmid pbFGF, bFGF protein, and rabbit anti-basic FGF neutralizing antibody were purchased from (R & D Systems, Minneapolis, MN). Q-Sepharose and heparin-Sepharose were purchased from Pharmacia (Uppsala, Sweden). Immunoblots were performed using rabbit anti-bovine basic FGF antibodies (Upstate Biotechnology, Inc., Lake Placid, NY). Rabbit polyclonal anti-PE antibody was kindly supplied by Dr. David FitzGerald, National Institutes of Health (Bethesda, MD). ABC immunoblot kits were purchased from Vector Laboratories (Burlingame, CA). IPTG (isopropyl 1-thio-β-D-galactopyranoside) was purchased from Strategene (La Jolla, CA). [^{3}H]leucine was purchased from New England Nuclear (Boston, MA).

Cell Culture. All tumor cells were from human carcinomas. MCF-7 (breast), A431 and KB (epidermoid), and Hep G2 (hepatocellular) cells were obtained from ATCC (Rockville, MD). RCA (colon) cells were obtained from M. Brattain, Baylor University, (Houston, TX), and L2987 (lung), H3606 (melanoma), H3396 (breast), and H3719 (colon) were obtained from I. Hellström, Bristol-Myers Squibb (Seattle, WA). The tumor cell lines were cultured in RPMI 1640 supplemented with 10% fetal bovine serum (FBS), 2 mM L-glutamine, and 50 units/mL penicillin/streptomycin at 37 °C with the exception of Hep G2 cells, which were cultured in DMEM. Human aortic smooth muscle cells and endothelial cells were purchased as primary cultures from Clonetics, Inc. (San Diego, CA) and cultured in smooth muscle growth medium (SMGM) or endothelial growth medium (EGM). SMGM is composed of modified MCDB 131 media, 10 ng/mL EGF, 2 ng/mL bFGF, 5% FBS, 1 μM dexamethasone, 0.05 mg/mL gentamycin, 0.05 μg/mL amphotericin-B. EGM is composed of modified MCDB 131 media, 10 ng/mL EGF, 1.0 μg/mL hydrocortisone, 2% FBS, 0.4% bovine brain extract, 0.05 mg/mL gentamycin, and 0.05 μg/mL amphotericin-B.

Construction of bFGF–PE40 and bFGF–PE4E KDEL. The expression plasmids encoding bFGF–PE40 and bFGF–PE4E KDEL were constructed as shown in Figure 1. The bFGF gene was amplified using PCR, resulting in a 500 bp DNA fragment. The 5′ PCR primer 5′-AGC-TTA-CCT-CAT-ATG-GCA-GCC-GGG-3′ incorporated an *Nde*I restriction site and the 3′ PCR primer 5′-GAA-TTC-GGA-TCC-AAG-CTT-GCT-CTT-AGC-AGA-3′ a *Hin*dIII site. The PCR-amplified DNA fragment was digested with *Nde*I and *Hin*dIII, followed by ligation into either a similarly digested plasmid encoding PE40 or PE4E KDEL. In this case, the PE40 and PE4E KDEL plasmids contained the aFGF gene (pCS F40 and pCS F4E KDEL, respectively), which was excised by the *Nde*I/*Hin*dIII digestion and replaced with the bFGF gene by ligation. The expression plasmids encoding bFGF–PE40 and bFGF–PE4E KDEL, were termed pBW 10 and pBW 11, respectively. PE4E KDEL encodes a PE gene in which the binding domain is mutated at four residues

(57, 246, 247, and 249) to glutamate, thereby abrogating normal PE binding. The KDEL portion of the mutant PE molecule encodes the endoplasmic reticulum retention sequence and has been shown to increase specific cytotoxicity toward certain target cells (*40*).

Expression and Isolation of Recombinant Proteins. Basic FGF-PE40 and bFGF-PE4E KDEL were expressed in *E. coli* BL21 (λDE3) by culturing in Superbroth (Digene, Inc., Silver Spring, MD) containing 75 μg/mL of ampicillin at 37 °C until A_{260} is approximately 1.3, followed by induction with isopropyl 1-thio-β-D-galactopyranoside (IPTG) to a final concentration of 1 mM. The cells were harvested after 90 min, washed in sucrose buffer (20% sucrose, 30 mM Tris-HCl (pH 7.4), 1 mM EDTA), and osmotically shocked in ice-cold H_2O. The cell pellet was resuspended in TE buffer (50 mM Tris, pH 8.0/1 mM EDTA), sonicated three times (30 s each), and centrifuged at 30 000 rpm (Beckman Ti45 rotor) for 45 min. The pellet (inclusion bodies) was denatured in 7 M guanidine hydrochloride, 20 mM Tris-HCl (pH 7.4), and 1 mM EDTA, sonicated as before, and refolded by rapid dilution in phosphate-buffered saline (PBS) supplemented with 0.4 M L-arginine. Alternatively, the supernatant (spheroplast cytoplasm) was used as the source of the protein. The bFGF-toxin proteins were extensively dialyzed against 0.02 M Tris-HCl (pH 7.4) and were purified by anion-exchange (Q-Sepharose) with a Pharmacia fast protein liquid chromatography (FPLC) system, as described previously (*24*).

Heparin-Affinity Chromatography. Fractions pooled from Q-Sepharose columns were further purified by heparin affinity chromatography. Heparin-Sepharose beads (Pharmacia) were washed extensively with 0.4 M NaCl/0.01 M Tris HCl, pH 7.4. The sample was adjusted to 0.4 M NaCl and batch adsorbed to the heparin-Sepharose (1.5 g dry weight/100 mg bFGF-toxin) for 18 h at 4 °C (with gentle rocking). The bFGF-toxin bound beads were washed stepwise with 0.4 M NaCl/0.01 M Tris-HCl (pH 7.4) and 0.6 M NaCl/0.01 M Tris HCl (pH 7.4). The bound bFGF-PE forms were eluted with 1.2-2.5 M NaCl/0.01 M Tris HCl (pH 7.4). Recovery of purified bFGF-PE40 after heparin affinity was 2.5% of the crude protein applied to the column. In comparison, the recovery of aFGF-PE40, was approximately 10% of the crude protein.

Inhibition of Protein Synthesis Assay. Tumor cells (10^5 cells/mL) in growth media were added to 96-well flat bottom tissue culture plates (0.1 mL/well) and incubated at 37 °C for 16 h. Dilutions of growth factor-toxins (bFGF-PE40, bFGF-PE4E KDEL, aFGF-PE40, and aFGF-PE4E KDEL) were made in leucine-free RPMI (assay media) and 0.1 mL was added to each well for 20 h at 37 °C. Each dilution was done in triplicate. The cells were pulsed with [^{3}H]leucine (1 μCi/well) for an additional 4 h at 37 °C. The cells were lysed by freezing-thawing and harvested using a Tomtec cell harvester (Orange, CT). Incorporation of [^{3}H]leucine into cellular protein was determined using an LKB Beta-Plate liquid scintillation counter. A time course study was also done in which the FGF-toxins were incubated with the cells for 1, 2, 4, and 6 h before removal and replacement with fresh growth media and further incubated for a total of 20 h prior to the measurement of cellular protein synthesis as described above.

The effects of the FGF-toxin proteins on protein synthesis of aortic endothelial cells and aortic smooth muscle cells were also studied. Primary human smooth muscle cells (SMC) and primary human endothelial cells (EC) were cultured in SMGM or EGM, respectively. The FGF-toxins dilutions were prepared in EGM or SMGM. The incorporation of [^{3}H]leucine into cellular protein was done exactly as described for the tumor cells.

bFGF ELISA. Two-fold dilutions of bFGF, bFGF-PE40, and bFGF-PE4E KDEL in PBS (50 μL/well) were incubated in Dynatech Immulon II 96 well plates for 2 h at 37 °C. Acidic FGF-PE40 and aFGF-PE4E KDEL were similarly prepared and used for comparison. The plates were washed five times in PBS, blocked with PBS, 3% gelatin for 2 h at 37 °C, and washed five times in PBS. Polyclonal rabbit anti-bFGF (human) antibody (Collaborative Research Inc., Bedford, MA), 1 μg/mL in PBS, 1% BSA (50 μL/well) was incubated for 1 h at 37 °C and washed in PBS, 0.2% Tween 20, 1% BSA (PTB buffer). Anti-rabbit IgG alkaline phosphatase conjugate (Pierce, Rockford, IL) was added to each well (50 μL of a 1:1000 dilution in PBS, 1% BSA) and incubated at 37 °C for 1 h. Plates were washed five times with PTB, three times with phosphatase buffer (PBS, 75 mM Tris, 0.1 M NaCl, 5 mM $MgCl_2$, pH 9.4), and reacted with *p*-nitrophenyl phosphate (Sigma, St. Louis, MO), freshly made in phosphatase buffer (100 μL), for 30 min at 37 °C. The reaction was stopped by the addition of 2 N NaOH (100 μL/well). The plates were analyzed at 405 nm using a microplate reader (Molecular Devices, Menlo Park, CA).

RESULTS

Construction of bFGF-*Pseudomonas* Exotoxin Gene Expression Plasmids. Plasmids containing synthetic DNA encoding the human bFGF gene and two mutated forms of the gene coding for *Pseudomonas* exotoxin were constructed as described in Experimental Procedures (Figure 1A). The plasmids pBW10 (bFGF-PE40) and pBW11 (bFGF-PE4E KDEL) were expressed under control of the bacteriophage T7 promoter (*41*). Both expression plasmids encode the mature bFGF gene (amino acids 1-155), followed by a three amino acid linker that added the residues lysine, leucine, and methionine (KLM), and one of two mutant PE forms. PE40 encodes amino acids 1, 2, 3, and 253-613 of the native PE protein sequence (*42*). PE4E KDEL encodes amino acids 1-608 with residues KDEL on the carboxyl terminus of the protein sequence and glutamate substitutions at codons encoding residues 57, 246, 247, and 249 (*43*). The carboxyl terminal KDEL sequence represents the endoplasmic reticulum retention sequence and is used in place of the native PE terminus, REDLK. The addition of the KDEL sequence has previously been shown to increase the cytotoxic activity of PE against target cell lines (*40*). The four-glutamate substitution (all in PE domain I) inactivates normal PE binding activity and makes this molecule analogous to the PE40 molecule in which domain I is deleted (*44*). A depiction of the linear protein structure of bFGF-PE40 and bFGF-PE4EKDEL, detailing the fusion protein junction and mutated PE regions, is shown in Figure 1B.

Expression and Purification of bFGF-Toxin Proteins. bFGF-PE40 and bFGF-PE4E KDEL fusion proteins were expressed in *E. coli* upon IPTG induction. The fusion proteins localized to the soluble (spheroplast cytoplasm) and insoluble fraction (inclusion bodies) of the spheroplast. The insoluble fraction was denatured in guanidine hydrochloride and renatured by rapid dilution in PBS containing L-arginine as described in Experimental Procedures. Both the soluble and renatured protein from the inclusion bodies were dialyzed against 20 mM Tris-HCl, pH 7.4, and initially purified using Q-Sepharose (anion-exchange) chromatography. The peak fractions

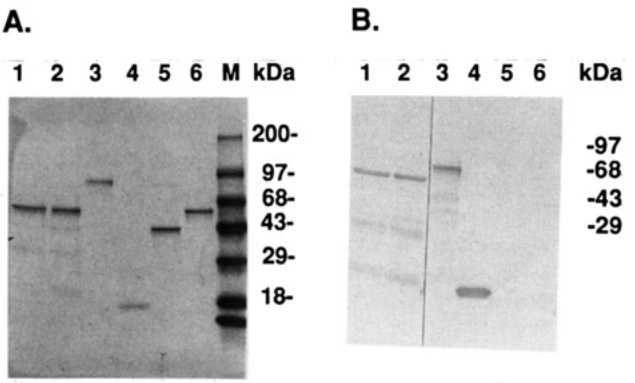


Figure 2. SDS–PAGE analysis of bFGF–PE forms following heparin-Sepharose purification, stained with Coomassie Blue: lane 1, bFGF–PE40 (insoluble-refolded fusion protein); lane 2, bFGF–PE40 (soluble); lane 3, bFGF–PE4E KDEL (insoluble-refolded fusion protein); lane 4, bFGF (native); lane 5, PE40; lane 6, aFGF–PE40 (insoluble-refolded fusion protein).

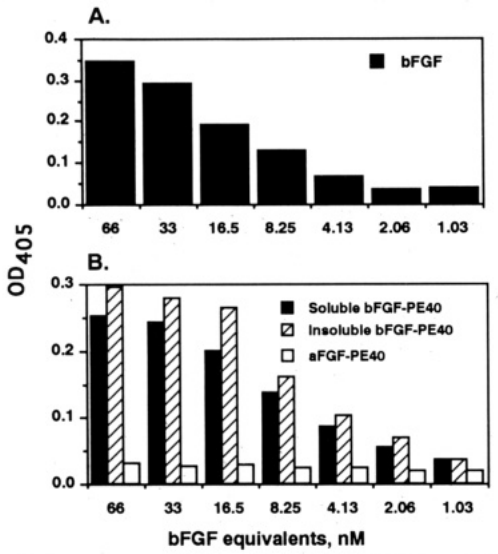


Figure 3. Immunoreactivity analysis of (A) bFGF and (B) soluble and insoluble–refolded bFGF–PE40 and aFGF–PE40, on ELISA plates coated with polyclonal rabbit anti-bFGF antibody and probed with anti-rabbit IgG antibody. Soluble bFGF–PE40 represents fusion protein that was isolated and purified from the soluble *E. coli* spheroplast cytosol. Insoluble–refolded bFGF–PE40 represents fusion protein that was isolated from the *E. coli* inclusion bodies, denatured, renatured, and purified.

were pooled and the proteins were further purified using heparin affinity chromatography. Purified bFGF–PE40 and bFGF–PE4E KDEL migrated at 55 and 81 kDa, respectively, equivalent to their predicted molecular sizes as visualized by Coomassie-stained SDS–PAGE (Figure 2). The majority of the bFGF–PE40 fusion protein eluted between 1.2 and 1.5 M NaCl. The fractions eluting at 1.2 and 1.5 M NaCl were pooled, concentrated, and quantitated by Bradford analysis (*45*).

bFGF ELISA. To determine that the bFGF fusion proteins were folded in the correct fashion, anti-bFGF antibody immunoreactivity assays were performed. Comparison of the same molar amounts of bFGF–PE40, bFGF–PE4E KDEL, and bFGF (native) were used in the assay. The bFGF domains of native bFGF (Figure 3A) and bFGF–PE40 from both soluble and insoluble preparations (Figure 3B) were functional, as determined by their immunoreactivity to anti-bFGF antibody in an ELISA experiment. The immunoreactivity of bFGF–PE40 that was renatured following guanidine hydrochloride treatment was increased relative to the fusion protein that was purified from the soluble fraction of the spheroplasts. The bFGF–toxin

Table I. Cytotoxic Activities of bFGF–PE40 and aFGF–PE40 Chimeric Proteins on Various Carcinoma Cell Lines

	EC_{50} (ng/mL)	
carcinoma line, type	bFGF–PE40	aFGF–PE40
MCF-7 (breast)	30	30
L2987 (lung)	250	150
KB (epidermoid)	350	75
A431 (epidermoid)	18	10
Hep G2 (hepatoma)	70	20
RCA (colon)	200	900
H3396 (breast)	110	200
H3719 (colon)	500	400

Table II. Cytotoxic Activities of bFGF–PE4E KDEL and aFGF–PE4E KDEL Chimeric Proteins on Various Cell Lines

	EC_{50} (ng/mL)	
carcinoma line, type	bFGF–PE4E KDEL	aFGF–PE4E KDEL
MCF-7 (breast)	70	25
KB (epidermoid)	150	50
A431 (epidermoid)	18	15
Hep G2 (hepatoma)	1	5
RCA (colon)	100	300
H3606 (melanoma)	40	200
H3396 (breast)	15	30
H3719 (colon)	35	40

fusion proteins were immunoreactive to anti-bFGF antibody as well as bFGF (native). bFGF–PE4E KDEL was also immunoreactive with the anti-bFGF antibody equivalent to both native bFGF and bFGF–PE40 (data not shown). The assay was specific for bFGF, since aFGF (native) and aFGF–PE40 were not immunoreactive with the bFGF antibody in the ELISA assay.

Cytotoxic Activity of bFGF–Toxin Fusion Proteins toward Cancer Cells. We compared the cytotoxic activity of bFGF–PE40 that was isolated from spheroplast cytoplasm and the inclusion bodies. Both proteins were purified with the same techniques (Q-Sepharose and heparin-Sepharose) and were equivalent in purity based on SDS–PAGE analysis (Figure 2). The fusion protein from inclusion bodies that was denatured with guanidine hydrochloride and refolded was 3-fold more potent in inhibiting protein synthesis in A431 cells than was the fusion toxin that was found in the soluble portion of the spheroplast compartment (10 ng/mL for refolded versus 30 ng/mL for soluble). Since renatured fusion protein was more active in both binding (Figure 3B) and cytotoxicity assays, all further experiments described in the paper use refolded material.

We assayed a variety of cancer cell lines to determine protein synthesis inhibition activity of bFGF–PE40 (Table I). A431 cells were the most sensitive carcinoma line tested with an EC_{50} value of 18 ng/mL. MCF-7 breast carcinoma cells were also quite sensitive to bFGF–PE40, with an EC_{50} value of 30 ng/mL. Hep G2 (hepatocellular), H3396 (breast), L2987 (lung), and KB (epidermoid) carcinoma cells were less sensitive, with EC_{50} values of 70, 110, 250, and 350 ng/mL, respectively. The cytotoxic activity of bFGF–PE40 was compared to that of aFGF–PE40 (Table I). While the protein synthesis inhibition activity of both bFGF–PE40 and aFGF–PE40 forms were equivalent for many lines, all were slightly more sensitive to aFGF–PE40 except for H3396 and MCF-7, both breast carcinoma lines, which were more sensitive to bFGF–PE40.

We also determined the cytotoxic activity of bFGF–PE4E KDEL against the same cell lines with the addition of the melanoma line H3606. As shown in Table II, bFGF–PE4E KDEL was active in inhibiting protein synthesis in

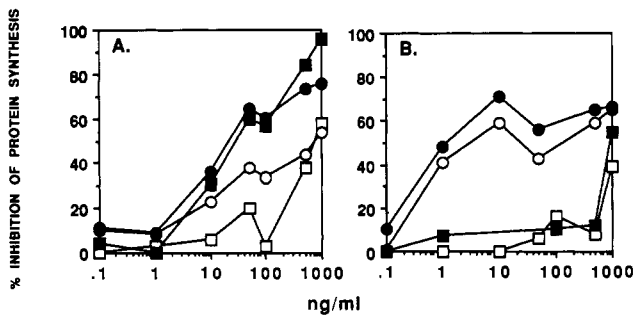


Figure 4. Sensitivity of vascular cells to FGF-toxin fusion proteins: (A) primary human aortic smooth muscle cells and (B) primary human aortic endothelial cells. Both vascular cell lines were used at passage 5. Legend: bFGF-PE40 (○), bFGF-PE4E KDEL (●), aFGF-PE40 (□), aFGF-PE4E KDEL (■).

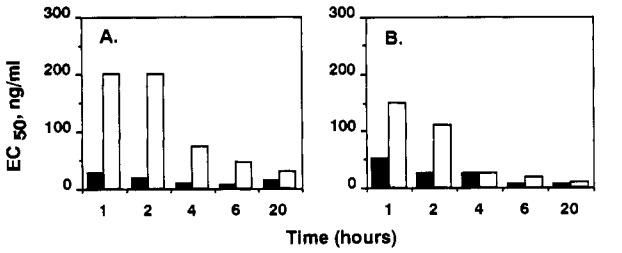


Figure 5. Cytotoxicity time course of bFGF-PE40 (□) and aFGF-PE40 (■) on (A) MCF-7 and (B) A431 cells. FGF-toxins were incubated with tumor cells for 1, 2, 4, and 6, and 20 h. For the 1–6 h time points, supernatants were removed, fresh media was added, and cells further incubated for a total of 20 hours. Cells were then pulse labeled for 4 h with [^{3}H]leucine to determine cellular protein synthesis.

all the cell lines tested. Hep G2 cells were the most sensitive line tested with an EC_{50} value of 1 ng/mL. A431, H3396, and MCF-7 cells were all sensitive to bFGF-PE4E KDEL at EC_{50} values less than 25 ng/mL. aFGF-PE4E KDEL was equally cytotoxic to Hep G2 cells and less toxic to H3396 breast carcinoma and H3606 melanoma cells than was bFGF-PE4E KDEL (Table II).

Sensitivity of Vascular Cells to FGF-Toxin Fusion Proteins. We also compared the sensitivity of primary human smooth muscle and endothelial cells to both bFGF- and aFGF-toxin forms. Human aortic smooth muscle cells (passage 5) were more sensitive to bFGF-PE40 than to aFGF-PE40, and equally sensitive to bFGF-PE4E KDEL and aFGF-PE4E KDEL (Figure 4A). The human endothelial cells were very sensitive to both bFGF-PE40 and bFGF-PE4E KDEL (EC_{50} values of 10 and 2 ng/mL, respectively). Alternatively, the human endothelial cells were quite resistant to both aFGF-PE40 and aFGF-PE4E KDEL (Figure 4B).

Exposure Time for Cytotoxic Activity. To determine the time of exposure necessary for cytotoxic activity of bFGF-PE40 on target cells, we performed a time course protein synthesis inhibition assay. A431 and MCF-7 cells were incubated with bFGF-toxin for various time periods, washed free of the toxin, replenished with fresh growth media, and incubated for a sum total of 20 h. MCF-7 cells, treated with bFGF-PE40 were relatively insensitive to the toxin at 1- or 2-h exposure times, and even a 6-h exposure time was still not as active as 20 h of exposure (Figure 5A). Alternatively, aFGF-PE40 was almost fully active in inhibiting protein synthesis in MCF-7 cells, with only a 1-h exposure time. With a 2-h exposure, protein synthesis was maximally inhibited.

Using A431 cells, bFGF-PE40 was near full activity with a 4-h exposure (Figure 5B), as compared to greater than 6 h against MCF-7 cells. Acidic FGF-PE40 was almost

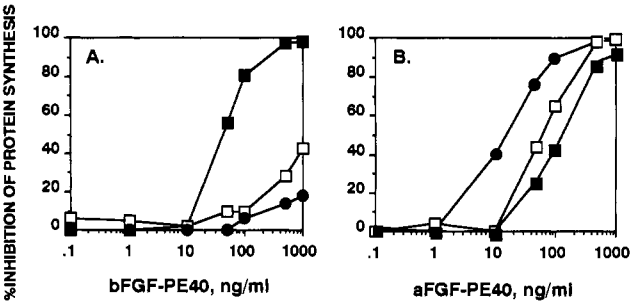


Figure 6. Effect of heparin on the cytotoxic activity of bFGF-PE40 versus aFGF-PE40 against MCF-7 cells. The cells were incubated with toxins in the presence of absence of heparin for 20 h followed by a 4-h incubation with [^{3}H]leucine: (A) bFGF-PE40 and (B) aFGF-PE40, with no heparin (■), 5 units/mL heparin (□), 50 units/mL heparin (●).

fully active with a 2 h exposure to the toxin, similar to the data obtained for activity in MCF-7 cells.

Effect of Heparin on FGF-Toxins. Since heparin has a biological effect on the FGF family of proteins, we assayed whether heparin would potentiate, block, or have no effect on the cytotoxic activity of the FGF-toxin proteins. Coincubation with heparin (50 units/mL) blocked the ability of bFGF-PE40 to inhibit protein synthesis in MCF-7 cells (Figure 6A). Heparin at 5 units/mL blocked the cytotoxic activity of bFGF-PE40 to a lesser degree than 50 units/mL. Alternatively, coincubation of heparin (at both 5 and 50 units/mL) and aFGF-PE40 produced a small increase in the inhibition of protein synthesis in the tumor cell line (Figure 6B).

DISCUSSION

We have constructed and characterized fusion proteins that are cytotoxic toward cells expressing bFGF receptors. These recombinant toxin molecules were produced by expressing gene fusions encoding bFGF and binding mutant forms of PE in *E. coli*. The hybrid bFGF-PE molecules accumulated intracellularly and were found in both soluble and insoluble forms. Both forms were purified by a two-step procedure using anion-exchange followed by heparin-affinity chromatography. The insoluble form was denatured and renatured prior to purification. Following purification, refolded bFGF-PE40 fusion protein was found to bind anti-bFGF antibody better than soluble bFGF-PE40 (Figure 3B), and to be more active in inhibiting protein synthesis than the intracellular, soluble form. The fusion protein isolated from the spheroplast cytoplasm may have contained mixed disulfides that reduced specific binding. With mixed disulfides in the fusion protein, the internalization ability of the growth factor may also have been affected. The heparin binding activity of the recombinant bFGF-toxin fusion proteins was retained, as evidenced by the heparin affinity of the material. However, retention of heparin affinity is no guarantee of bFGF receptor binding affinity.

The bFGF-toxin fusion proteins were immunoreactive with anti-bFGF antibodies in an ELISA based assay (Figure 3). From this analysis, the bFGF fusion proteins display the bFGF epitope necessary for interaction with the anti-bFGF antibody. Thus, in this respect the refolded protein is similar in immunoreactivity to native bFGF. Specificity for bFGF was demonstrated since aFGF-toxin fusion proteins were not immunoreactive with the anti-bFGF antibody.

Basic FGF-PE40 was effective at inhibiting protein synthesis in a variety of tumor cell lines. In comparison with aFGF-PE40, bFGF-PE40 was generally found to be

a less potent cytotoxic reagent toward cancer cells with the exception of breast carcinoma and melanoma cell lines (Tables I and II). This may be due to expression levels of the high-affinity receptors for the two FGF forms. The difference in activity may also be due to rates of internalization, as suggested by the time-course experiments (Figure 5A,B). The protein synthesis inhibition activity of aFGF–PE40 is near maximal within 2 h of exposure to target cells, as compared to 6 h for bFGF–PE40. Perhaps the molecular interaction of bFGF and the high-affinity bFGF receptor requires a longer time period to promote internalization than does the interaction of aFGF and its receptor.

Since bFGF has been shown to be a potent angiogenic agent and its receptor is expressed on vascular cells (*46, 47*), we investigated its ability to inhibit protein synthesis of endothelial and smooth muscle cells. Both vascular cell types were sensitive to bFGF–PE40 and bFGF–PE4E KDEL (Figure 4). Similar cytotoxic activities have also been reported for bFGF-SAP (*31, 32*). Alternatively, the two aFGF–toxin forms were active against smooth muscles cells but relatively inactive, as compared to the two bFGF–PE molecules, against human endothelial cells (Figure 4B).

Basic FGF can be internalized through both high and low affinity receptors (*20, 21*). The low affinity receptors can be blocked by the addition of heparin (*21*). We found that heparin was able to compete with much of the ability of bFGF–PE40 to inhibit protein synthesis in MCF-7 breast carcinoma cells (Figure 6A). This suggests that binding to low-affinity receptors is important to facilitate optimized internalization. Against the same MCF-7 cells, aFGF–toxin forms were more potent in inhibiting protein synthesis in the presence of heparin (Figure 6B). It has been previously shown that heparin enhances the binding of aFGF to its high-affinity receptor (*48*).

We conclude that bFGF linked to recombinant forms of PE are specifically cytotoxic to receptor-bearing target cells. We suggest that these chimeric toxins could be used to select cells deficient in FGF receptors to help identify the role of this receptor in controlling growth and differentiation.

ACKNOWLEDGMENT

We thank E. Kozlowski for oligonucleotide synthesis and Drs. P. Fell and K. E. Hellström for helpful suggestions and continued support.

LITERATURE CITED

(1) Burgess, W. H., and Maciag, T. (1989) The heparin-binding (fibroblast) growth factor family of proteins. *Annu. Rev. Biochem. 58*, 575–606.

(2) Basilico, C., and Moscatelli, D. (1992) The FGF family of growth factors and oncogenes. *Adv. Cancer Res. 59*, 115–165.

(3) Gospodarowicz, D. (1989) Fibroblast growth factor. Crit. *Rev. Ongogen. 1*, 1–26.

(4) Rifkin, D. B., and Moscatelli, D. (1989) Recent developments in the cell biology of basic fibroblast growth factor. *J. Cell Biol. 109*, 1–6.

(5) Folkman, J., and Klagsbrun, M. (1987) Angiogenic Factors. *Science 235*, 442–447.

(6) Lee, P. D., Johnson, D. E., Cousens, L. S., Fried, V. A., and Williams, L. T. (1989) Purification and complementary DNA cloning of a receptor for basic fibroblast growth factor. *Science 245*, 57–60.

(7) Dionne, C. A., Crumley, G., Bello, F., Kaplow, J. M., Searfoss, G., Ruta, M., Burgess, W. H., Jaye, M., and Schlessinger, J. (1990) Cloning and expression of two distinct high-affinity receptors cross-reacting with acidic and basic fibroblast growth factors. *EMBO J. 9*, 2685–2692.

(8) Keegan, K., Johnson, D. E., Williams, L. T., and Haymas, M. J. (1991) Isolation of an additional member of the fibroblast growth factor receptor family, FGFR3. *Proc. Natl. Acad. Sci. U.S.A. 88*, 1095–1099.

(9) Partanen, J., Makela, T. P., Eerola, E., Korhonen, J., Hirvonen, H., Claesson-Welsh, L., and Alitalo, K. (1991) FGFR-4, a novel acidic fibroblast growth factor receptor with a distinct expression pattern. *EMBO J. 10*, 1347–1354.

(10) Pasquale, E. B. (1990). A distinctive family of embryonic protein-tyrosine kinase receptors. *Proc. Natl. Acad. Sci. U.S.A. 87*, 5812–5816.

(11) Johnson, D. E., and Williams, L. T. (1993). Structural and functional diversity in the FGF receptor multigene family. *Adv. Can. Res. 60*, 1–41.

(12) Halaban, R., Kwon, B. S., Ghosh, S., Delli Bovi, P., and Baird, A. bFGF as an autocrine growth factor for human melanomas. (1988). *Oncogene Res. 3*, 177–186.

(13) Armstrong, E., Vainikka, S., Patanen, J., Korhonen, J., and Alitalo, R. (1992). Expression of fibroblast growth factor receptors in human leukemia cells. *Cancer Res. 52*, 2004–2007.

(14) Hattori, Y., Odagiri, H., Nakatani, H., Miyagawa, K., Naito, K., Sakamoto, H., Katoh, O., Yoshida, T., Sugimura, T., and Terada, M. (1990). K-sam, an amplified gene in stomach cancer, is a member of the heparin-binding growth factor receptor genes. *Proc. Natl. Acad. Sci. U.S.A. 87*, 5983–5987.

(15) Luqmani, Y. A., Graham, M., and Coombes R. C. (1992) Expression of basic fibroblast growth factor, FGFR1 and FGFR2 in normal and malignant human breast, and comparison with other normal tissues. *Br. J. Cancer. 66*, 273–280.

(16) Zagzag, D., Miller, D. C., Sato, Y., Rifkin, D. B., and Burstein, I. (1990) Immunohistochemical localization of basic fibroblast growth factor in astrocytomas. *Cancer Res. 50*, 7393–7398.

(17) New, B. A., and Yeoman, L. C. (1992) Identification of basic fibroblast growth factor sensitivity and receptor and ligand expression in human colon tumor cell lines. *J. Cell. Phys. 150*, 320–326.

(18) Folkman, J., Watson, K., Ingber, D., Hanahan, D. (1989). Induction of angiogenesis during the transition from hyperplasia to neoplasia. *Nature 3339*, 58–61.

(19) Weidner, N., Semple, J. P., Welch, W. R., and Folkman, J. (1991). Tumor angiogenesis and metastasis: correlation in invasive breast carcinoma. *N. Engl. J. Med. 324*, 1–8.

(20) Moscatelli, D. (1987) High and low affinity binding sites for basic fibroblast growth factor on cultured cells; absence of a role for low affinity binding in the stimulation of plasminogen activator production by bovine capillary endothelial cells. *J. Cell. Physiol. 131*, 123–130.

(21) Roghani, M., and Moscatelli, D. (1992) Basic fibroblast growth factor is internalized through both receptor-mediated and heparan sulfate-mediated mechanisms. *J. Biol. Chem. 267*, 22156–22162.

(22) Pastan, I., Chaudhary, V., and FitzGerald, D. J. (1992) Recombinant toxins as novel therapeutic agents. *Annu. Rev. Biochem. 61*, 331–354.

(23) Vitetta, E. S., and Thorpe, P. E. (1991) Immunotoxins containing ricin or its A chain. *Sem. Cell. Biol. 2*, 47–58.

(24) Siegall, C. B., Epstein, S., Speir, E., Hla, T., Forough, R., Maciag, T., FitzGerald, D. J., and Pastan, I. (1991) Cytotoxic activity of chimeric proteins composed of acidic fibroblast growth factor and *Pseudomonas* exotoxin on a variety of cell types. *FASEB J. 5*, 2843–2849.

(25) Biro, S., Siegall, C. B., Fu, Y-M., Speir, E., Pastan, I., and Epstein, S. E. (1992) *In vitro* effects of a recombinant toxin targeted to the fibroblast growth factor receptor on rat vascular smooth muscle and endothelial cells. *Circ. Res. 71*, 640–645.

(26) Merwin, J. R. , M. J. Lynch, J. A. Madri, I. Pastan, and C. B. Siegall. (1992) Acidic FGF–P*seudomonas* exotoxin chimeric protein elicits anti-angiogenic effects on endothelial cells. *Cancer Res. 52*, 4995–5001.

(27) Lappi, D. A. , D. Martineau, and A. Baird. (1989) Biological and chemical characterization of basic FGF-saporin mitotoxin. *Biochem. Biophys. Res. Comm. 160*, 917–923.

(28) Lappi, D., Maher, P. A., Martineau, D., and Baird, A. (1991) The basic fibroblast growth factor-saporin mitotoxin acts through the basic fibroblast growth factor receptor. *J. Cell. Phys. 147*, 17–26.

(29) Beitz, J. G., Davol, P., Clark, J. W., Kato, J., Medina, M., Frackelton, A. R., Jr., Lappi, D. A., Baird, A., and Calabresi, P. (1992) Antitumor activity of basic fibroblast growth factor-saporin mitotoxin *in vitro* and *in vivo*. *Cancer Res. 52*, 227–230.

(30) Beattie, G. M., Lappi, D. A., Baird, A., and Hayek, A. (1990) Selective elimination of fibroblasts from pancreatic islet monolayers by basic fibroblast growth factor-saporin mitotoxin. *Diabetes 39*, 1002–1005.

(31) Casscells, W., Lappi, D. A. Olwin, B. B., Wai, C., Siegman, M., Speir, E. H., Sasse, J., and Baird, A. (1992) Elimination of smooth muscle cells in experimental restenosis: Targeting of fibroblast growth factor receptors. *Proc. Natl. Acad. Sci. U.S.A. 89*, 7159–7163.

(32) Lindner, V., Lappi, D. A., Baird, A., Majack, R. A., and Reidy, M. A. (1991) Role of basic fibroblast growth factor in vascular lesion formation. *Circ. Res. 68*, 106–113.

(33) Pastan, I., and FitzGerald, D. (1991) Recombinant toxins for cancer treatment. *Science 254*, 1173–1177.

(34) FitzGerald, D., and Pastan, I. (1991) Redirecting *Pseudomonas* exotoxin. *Sem. Cell. Biol. 2*, 31–37.

(35) Chaudhary, V. K., FitzGerald, D. J., Adyha, S., and Pastan, I. (1987) Activity of a recombinant fusion protein between transforming growth factor alpha and *Pseudomonas* toxin. *Proc. Natl. Acad. Sci. U.S.A. 84*, 4538–4552.

(36) Lorberboum-Galski, H., FitzGerald, D. J. P., Chaudhary, V., Adhya, S., and Pastan, I. (1988) Cytotoxic activity of an interleukin 2-*Pseudomonas* exotoxin chimeric protein produced in *E. coli*. *Proc. Natl. Acad. Sci. U.S.A. 85*, 1922–1926.

(37) Siegall, C. B., Chaudhary, V. K., FitzGerald, D. J., and Pastan, I. (1988) Cytotoxic activity of an interleukin 6-*Pseudomonas* exotoxin fusion protein on myeloma cells. *Proc. Natl. Acad Sci. U.S.A. 85*, 9738–9742.

(38) Ogata, M., Chaudhary, V. K., FitzGerald, D. J. P., and Pastan, I. (1989) Cytotoxic activity of a recombinant fusion protein between interleukin 4 and *Pseudomonas* exotoxin. *Proc. Natl. Acad. Sci. U.S.A. 86*, 4215–4219.

(39) Prior, T. I., Hellman, L. J., FitzGerald, D. J., and Pastan, I. (1991) Cytotoxic activity of a recombinant fusion protein between insulin-like growth factor I and *Pseudomonas* exotoxin. *Cancer Res. 51*, 4215–4219.

(40) Seetharam, S. Chaudhary, V., FitzGerald, D., and Pastan, I. (1991) Increased cytotoxic activity of Pseudomonas exotoxin and two chimeric toxins ending in KDEL. *J. Biol. Chem. 266*, 17376–17381.

(41) Studier, F. W., and Moffat, B. A. (1986) Use of bacteriophage T7 RNA polymerase to direct selective high-level expression of cloned genes. *J. Mol. Biol. 189*, 113–130.

(42) Kondo, T., FitzGerald, D., Chaudhary, V. K., Adyha, S., and Pastan, I. (1988) Activity of immunotoxins constructed with modified *Pseudomonas* exotoxin A lacking the cell recognition domain. *J. Biol. Chem. 263*, 9470–9475.

(43) Chaudhary, V. K., Jinno, Y., Gallo, M. G., FitzGerald, D., and Pastan, I. (1990) Mutagenesis of *Pseudomonas* exotoxin in identification of sequences responsible for the animal toxicity. *J. Biol. Chem. 265*, 16306–16310.

(44) Chaudhary, V. K., Jinno, Y., FitzGerald, D. J., and Pastan, I. (1990) *Pseudomonas* exotoxin contains a specific sequence at the carboxyl terminus that is required for cytotoxicity. *Proc. Natl. Acad Sci. U.S.A. 87*, 308–312.

(45) Bradford, M. M. (1976) A rapid and sensitive method for the quantitation of microgram quantities of proteins utilizing the principle of protein-dye binding. *Anal. Biochem. 72*, 248–254.

(46) Lindner, V., Majack, R. A., and Reidy, M. A. (1990) Basic FGF stimulates endothelial regrowth and proliferation in denuded arteries. *J. Clin. Invest. 85*, 2004–2008.

(47) Neufeld, G., and Gospodarowicz, D. (1988) Identification of the fibroblast growth factor receptor in human vascular endothelial cells. *J. Cell. Phys. 136*, 537–542.

(48) Friesel, R., Burgess, W. H., Mehlman, T., and Maciag, T. (1986) The characterization of the receptor for endothelial cell growth factor by covalent ligand attachment. *J. Biol. Chem. 261*, 7581–7584.

Conjugation of Cu,Zn-Superoxide Dismutase with Succinylated Gelatin: Pharmacological Activity and Cell-Lubricating Function

Yuichiro Kojima,† Akihiko Haruta,‡ Teruko Imai,‡ Masaki Otagiri,‡ and Hiroshi Maeda*,†

Department of Microbiology, Kumamoto University School of Medicine, and Faculty of Pharmaceutical Sciences, Kumamoto University, Kumamoto 860, Japan. Received June 1, 1993®

Superoxide dismutase (SOD) and succinylated gelatin (succinyl gelatin) were conjugated to improve *in vivo* pharmacological activity of SOD. Lysyl residues of human recombinant Cu,Zn-SOD were cross-linked with carboxyl residues of succinyl gelatin using 1-ethyl-3-[3-(dimethylamino)propyl]carbodiimide. Various chemical and pharmacokinetic parameters of the conjugate were determined. Analysis by atomic absorption spectrometry and amino acid composition revealed that the conjugate was composed of about 2.9 mol of succinyl gelatin (with a mean molecular weight of 23 000) to 1 mol of SOD and exhibited an apparent mean molecular weight of 98 000. The conjugate retained almost 100% of its original activity on a molar basis. When the succinyl gelatin-conjugated Cu,Zn-SOD (Suc-gel-SOD) was administered intravenously to mice, its plasma half-life was prolonged to 29.7 min compared with 4.5 min for native SOD. Tissue distribution analysis revealed that intravenously administered Suc-gel-SOD showed a much greater accumulation than native SOD in the liver followed by in decreasing order the kidney, the lung, and the spleen; native SOD was excreted more rapidly into urine before it accumulated in tissues. Furthermore, Suc-gel-SOD exhibited lower antigenicity and immunogenicity than native SOD, and it had a better therapeutic effect against ischemic edema of the foot pad in mice. The conjugate was found to accumulate more than native SOD in the ischemic foot pad. A newly added property of the conjugate is cell-lubricating activity, which facilitated cell passage through micropores and reduced hemolysis during cell passage *in vitro*. Thus, Suc-gel-SOD appears to be a promising protein drug with greatly improved pharmacological properties *in vivo* while possessing the same enzyme activity as native SOD.

INTRODUCTION

Superoxide dismutase (SOD)[1] catalyzes the dismutation of highly reactive superoxide anion radical ($O_2^{\cdot-}$) to molecular oxygen and hydrogen peroxide, which are then converted to molecular oxygen and water by catalase. SOD has been suggested as a possible therapeutic agent for many diseases associated with $O_2^{\cdot-}$, such as allergy (*1*), ischemic myocardial damage (*2*), Crohn's disease (*3*) and virus infection (*4*). We previously showed in a model experiment that mice infected with influenza virus are cured to a greater extent with the use of divinyl ether-maleic anhydride [pyran] copolymer-conjugated SOD compared with native SOD, which indicates the importance of pharmacokinetic improvements (*4, 5*). Native Cu,Zn-SOD from bovine red blood cells (RBCs) appears to have little clinical applicability because of its poor pharmacokinetic and immunological properties. A tactic used to circumvent these problems is chemical conjugation with various polymers, on which we have been working for the past 15 years (*6-16*). Among these polymers, polyethylene glycol (PEG; polyethylene oxide) was most extensively studied, and conjugates of SOD with PEG had a prolonged half-life (*17, 18*). Conjugates with other polymers such as poly(styrene-*co*-maleic acid)anhydride (*11*), divinyl ether-maleic anhydride [pyran] copolymer (*4, 5*) and poly(vinyl alcohol) (*16*) showed a similarly prolonged *in vivo* half-life after intravenous (iv) injection, as a consequence of which there were improved therapeutic effects and an elimination of immunological reactivity. Although not described in this article, other critical advantages are removal of toxic Cu^{2+} liberated from Cu,Zn-SOD (*19*), stabilization of SOD itself, and protection from hydroxyl radical generation by Cu^{2+} (from SOD) via a Fenton-type reaction (ref 19 and unpublished data). In this study, we explored the highly biocompatible natural polymer gelatin for conjugation with SOD.

Gelatin is a biocompatible and biodegradable polymer that has been used for a long time in the food, pharmaceutical, and medical fields. It possesses low immunogenicity and thus is used also as a plasma expander (*20*). We have previously shown that gelatin has a lubricating effect on RBCs and reduces hemolysis when RBCs are passed through micropores (*21, 22*) under hydrostatic pressure. During ischemic reperfusion, tissue damage is thought to be associated with $O_2^{\cdot-}$ generation (*23*) and may result from increased vascular resistance at the capillary level. It may be possible to decrease the resistance of the capillary and facilitate plasma cell passage by lubrication

* Corresponding author: Professor Hiroshi Maeda,Department of Microbiology, Kumamoto University School of Medicine, Honjo 2-2-1, Kumamoto 860, Japan. Telephone: (81)-96-344-2111 ext. 6321. Fax: (81)-96-362-8362.

† Kumamoto University School of Medicine.

‡ Kumamoto University Faculty of Pharmaceutical Sciences.

® Abstract published in *Advance ACS Abstracts,* October 1, 1993.

[1] Abbreviations used: SOD, superoxide dismutase; $O_2^{\cdot-}$, superoxide anion radical; PEG, polyethylene glycol; iv, intravenous(ly); RBCs, red blood cells; succinyl gelatin, succinylated gelatin; Suc-gel-SOD, succinyl gelatin-conjugated Cu,Zn-SOD; DTPA, diethylenetriaminepentaacetic acid; EDCI, 1-ethyl-3-[3-(dimethylamino)propyl]carbodiimide; FITC, fluorescein isothiocyanate isomer I; SDS-PAGE, sodium dodecyl sulfate-polyacrylamide gel electrophoresis; TNBS, trinitrobenzenesulfonic acid; PAGE, polyacrylamide gel electrophoresis; SDS, sodium dodecyl sulfate; AUC, area under the plasma concentration vs time curve; PBS, 0.01 M sodium phosphate-buffered 0.15 M NaCl; F-native SOD, FITC-labeled native SOD; F-Suc-gel-SOD, FITC-labeled Suc-gel-SOD; FP value, fluorescence polarization value; PCA, passive cutaneous anaphylaxis; IgE, immunoglobulin E; IgG, immunoglobulin G.

1043-1802/93/2904-0490$04.00/0 © 1993 American Chemical Society

and to simultaneously remove $O_2^{\cdot-}$ by use of a gelatin–SOD conjugate.

Gelatin was converted to a more hydrophilic form by succinylation. The substrate-binding site (lysine) for serine proteases can be blocked, thus producing resistance to proteases. Furthermore, the chemistry of cross-linking is simplified because very few amino groups (0.1 mol per gelatin) are now available in succinylated gelatin (succinyl gelatin); thus only SOD provides most of amino group (24 free amino groups).

The purpose of this study was to explore the potential of succinylated gelatin for protein tailoring; to evaluate succinyl gelatin-conjugated Cu,Zn-SOD (Suc-gel–SOD) with regard to plasma half-life, immunogenic potential, and biological activity *in vivo*; and to characterize the chemical nature of the conjugate.

EXPERIMENTAL PROCEDURES

Animals. Male ddY and A/J mice and Wistar rats were obtained from SLC, Shizuoka, Japan.

Chemicals and Reagents. Xanthine and cytochrome *c* were purchased from Sigma Chemical Co., St. Louis, MO. Diethylenetriaminepentaacetic acid dianhydride (DTPA anhydride), 1-ethyl-3-[3-(dimethylamino)propyl]-carbodiimide (EDCI), and fluorescein isothiocyanate isomer I (FITC) were purchased from Dojindo Laboratories, Kumamoto, Japan. Xanthine oxidase was purchased from Boehringer Mannheim GmbH, Mannheim, Germany. $^{51}CrCl_3$ was purchased from ICN Biochemicals Inc., Costa Mesa, CA. Human recombinant Cu,Zn-SOD (molecular weight 31 800; specific activity, 4220 units/mg protein) with a purity of more than 99%, in which two free NH_2-terminal amino group were available, was a generous gift from Nippon Kayaku Co., Ltd., Tokyo, Japan. SOD is composed of a dimeric subunit and contains 22 free ϵ-amino groups of lysine and two free NH_2-terminal amino groups. Fragmented gelatin with a mean weight of 23 000 was obtained from Seiwa Kasei Co., Ltd., Osaka, Japan and is referred to as gelatin in this report. The molecular weight of gelatin was determined by sodium dodecyl sulfate–polyacrylamide gel electrophoresis (SDS–PAGE). All other chemicals were of analytical grade commercially available.

Preparation of Succinyl Gelatin. To block the free amino groups and increase solubility, gelatin (1.0 g) was succinylated with an excess amount of (500 mg) succinic anhydride at pH 8.3 as described previously (*24*). The reaction mixture was dialyzed under pressure with distilled water using an Amicon 8050 ultrafiltration system (YM-5 membrane; W. R. Grace & Co., Danvers, MA), and the final volume of 10 mL was lyophilized. This process gave 850 mg of succinyl gelatin, with 98.0% modification of the amino groups as estimated by quantification of the remaining free amino groups using trinitrobenzenesulfonic acid (TNBS) (*25*).

Conjugation of SOD with Succinyl Gelatin. Succinyl gelatin (160 mg) was dissolved in 5 mL of 0.1 M potassium phosphate buffer (pH 6.0) containing 50 mg of SOD, and then 100 mg of EDCI was added. The reaction continued for 1 h at room temperature and for 16 h at 4 °C with stirring. The sample was concentrated to about 2 mL using an Amicon system (YM-30 membrane) and was chromatographed on a column of Sephacryl S-200 (3.5 × 70 cm) (Pharmacia-LKB, Uppsala, Sweden) with 50 mM potassium phosphate buffer (pH 7.0). It was then eluted in 5-mL fractions. Fraction nos. 70–90 were pooled and used as Suc-gel–SOD. Fractions of the conjugates were washed repeatedly with distilled water by ultrafiltration, and the final volume of 5 mL was lyophilized and yielded 64.5 mg of Suc-gel–SOD.

Quantitation of the Degree of Conjugation of Succinyl Gelatin to SOD. The amount of succinyl gelatin in the conjugate was calculated on the basis of the content of hydroxyproline, copper, and zinc in comparison with native SOD as determined by amino acid analysis and atomic absorption spectrometry, respectively. The amount of free amino groups in SODs was determined by TNBS method.

Polyacrylamide Gel Electrophoresis (PAGE). PAGE with or without sodium dodecyl sulfate (SDS) at 0.1% was carried out to examine the purity of each preparation in a thin slab (1.0 mm) gel according to the method described by Laemmli (*26*). The concentration of acrylamide was 14% at pH 8.8 using 0.375 M Tris-HCl buffer.

Enzyme Activity. SOD activity was measured according to the procedure using cytochrome *c* (*27*). Briefly, in 3 mL of 50 mM potassium phosphate buffer at pH 7.8 containing 0.1 mM ethylenediaminetetraacetic acid, the reaction mixture was prepared to give final concentrations of 10 μM cytochrome *c*, 50 μM xanthine, and about 10 nM xanthine oxidase. One unit of SOD activity is defined as the amount of SOD required for 50% inhibition of the rate of reduction of cytochrome *c*, where the rate of reduction of cytochrome *c* is defined as a decrease of 0.025 absorbance unit per min at 550 nm.

Radiolabeling of Proteins. Succinyl gelatin and native SOD and Suc-gel–SOD were labeled with ^{51}Cr by attaching the chelating agent DTPA anhydride (*28–30*). Specifically, gelatin was reacted at first with 1 molar equivalent of DTPA over 1 mol gelatin followed by Shephadex G-25 column chromatography and lyophilization. Then, it was succinylated as described above. Chelation of chromium gives greater stability than iodination of tyrosine residues, which frequently yields unreliable values (*29*), and the association constant of DTPA is on the order of 10^{23} or higher.

Pharmacokinetic Experiments. The plasma half-life of the native and conjugated SODs was measured in ddY mice by administering SODs (15 000 units/kg) via iv injection, and SOD activity was assayed by the above method. The plasma level of native SOD and Suc-gel–SOD as a function of time was analyzed by a compartment model, and the plasma half-life was estimated by using the nonlinear least squares program MULTI described by Yamaoka et al. (*31*), in which the area under the plasma concentration vs time curve (AUC) was calculated using the trapezoidal rule and extrapolating to infinity. The total body clearance (CL) was calculated as

$$CL\ (mL/h) = \text{dose (units)}/AUC_{0-\infty}\ (\text{units}\cdot h/mL)$$

Tissue Distribution of ^{51}Cr-Labeled Gelatin, Succinyl Gelatin, Native SOD, and Suc-gel–SOD in Mice. ^{51}Cr-labeled proteins were injected into the tail vein of ddY mice at a dose of 12 mg/kg in 0.1 mL of saline. The mice were killed under ether anesthesia at different time intervals after iv injection; various tissues were removed, and radioactivity was counted with use of a γ-counter. Each DTPA-conjugated protein had the following specific radioactivity (dpm/mg) after labeling with ^{51}Cr: native gelatin, 8.6×10^6; succinyl gelatin, 9.2×10^5; native SOD, 3.0×10^6; and Suc-gel–SOD, 4.0×10^6.

Fluorescence Polarization. FITC labeling was described previously (*32*). Briefly, 10 mol of excess FITC over SODs was reacted for 2 h at pH 8.3, room temperature, and 0.63 and 1.16 mol of FITC were respectively coupled

per mol of native SOD and Suc-gel–SOD, which still retained about 21 mol of free amino groups. Measurements were carried out in 0.01 M sodium phosphate-buffered 0.15 M NaCl (PBS) (pH 7.3) by using a Model MAC-2 fluorescence spectropolarimeter (Japan Immunoresearch Laboratories, Ltd., Takasaki, Japan), under strict temperature control at 37.0 ± 0.05 °C. A cuvette containing FITC-labeled native SOD (F-native SOD) (2 μg/mL) or FITC-labeled Suc-gel–SOD (F-Suc-gel–SOD) (2 μg/mL, native SOD equivalent) in PBS, in a total volume of 2 mL, was placed in the polarizer. Then, after addition of anti-native SOD serum (100 μL) or normal rabbit serum (100 μL) to each cuvette, the fluorescence polarization value (FP value) was determined as described previously (*33*).

Immunological Experiments. The antigenicity of Suc-gel–SOD was examined by use of rabbit anti-native SOD serum. The quantitative precipitin reaction assay between SOD and anti-native SOD serum was performed as described (*34*). Anti-native SOD serum was obtained from rabbits after immunization three times with 2 mg of native SOD by subcutaneous injection with Freund's complete adjuvant.

Immunogenicity of native SOD and Suc-gel–SOD was evaluated by measuring anti-SOD production in rabbits, and in A/J and ddY mice. For the rabbit, anti-Suc-gel–SOD serum was obtained from rabbits after immunization as above using 2 mg of SOD equivalent of the conjugate. The quantitative precipitin reaction assay was performed between native SOD and anti-native SOD serum and Suc-gel–SOD and rabbit anti-Suc-gel–SOD serum.

A/J or ddY mice received an intraperitoneal injection of 0.1 or 1.0 mg of SOD equivalent of the conjugate with Freund's complete adjuvant on days 0 and 14, respectively. Serum samples were collected on day 21. The passive cutaneous anaphylaxis (PCA) reaction to test anti-SOD immunoglobulin E (IgE) in the serum was evaluated with Wistar rats as described (*35*). Three hours after subcutaneous injection of 4-fold-diluted mouse serum, the degree of the PCA reaction was quantified by measuring the diameter of Evans blue-bound albumin that had entered the skin from the vascular lumen.

Ischemic Paw Edema. Paw edema was induced by use of a commercial rubber band (1.8 mm^2 cut area of the band; ring diameter = 42 mm), which was tightened to induce ischemia in the leg of mice as described (*36*). Saline or SOD solutions (20 000 units/kg, 0.2 mL) were injected into the tail vein. The mouse was placed in a plastic cylinder with a slit opening at the right side where the right leg was allowed to come out. Thirty minutes after injection of saline or SOD solutions, the right hind leg was bound (12 turns) with a rubber band just above the articulation. The rubber band was removed after 20 min. The paw thickness was measured at 0, 0.33, 0.66, 1.0, 2.0, and 4.0 h after resuming reperfusion, the values were divided by the pretreatment value; and suppression of edema by SOD derivatives was recorded.

Vascular Permeability in Reperfused Paw. To determine the change in vascular permeability of the paw, 0.1 mL of Evans blue solution (1% in saline) was iv injected just before the removal of the rubber band. Twenty minutes after the injection, mice were killed by bleeding under ether anesthesia and then the paw was excised. The permeability values were determined spectrophotometrically at 600 nm after extraction of the tissue-associated Evans blue from various tissues immersed with formamide for 24 h at room temperature.

Heat-inactivated Suc-gel–SOD was prepared by incubation of 2.4 mg/mL in saline at 100 °C for 1 h. Enzyme activity that remained was less than 0.01% of unheated Suc-gel–SOD.

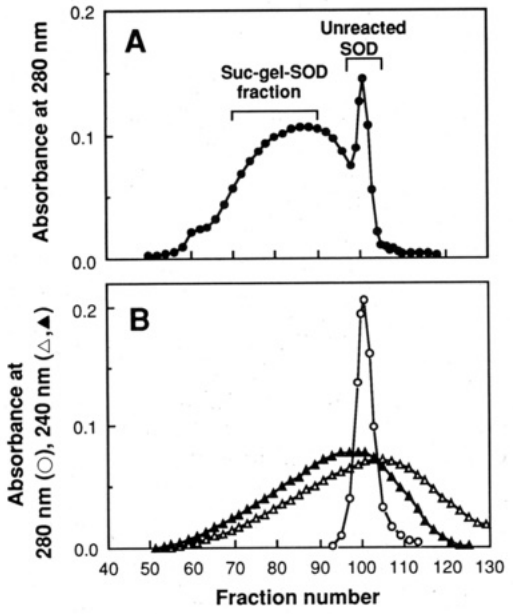
Lubricating Effect on Red Blood Cells. Human blood obtained from healthy volunteers was citrated at 0.1 mM, pH 7.8, and RBCs were separated after washing three times with Alserver's solution (2.26 mM citric acid, 27.2 mM sodium citrate, 71.8 mM NaCl, and 113.9 mM glucose, pH 6.7). A suspension of RBCs at 1% (v/v) was prepared by adding the appropriate volume of PBS (pH 7.3). The filtration apparatus was described by Maeda et al. (22). A cellulose nitrate membrane filter with average pore size of 3 μm was used (Sartorius Membrane Filter GmB., Goettingen, Germany). Each test material dissolved in PBS was added to the RBC suspension and incubated for 30 min at 37 °C. Subsequently, 1 mL of the suspension was taken into a plastic syringe that was connected to the filtration system. RBCs were allowed to pass through the membrane at 100 mmHg at 37 °C. Hemolyzed cells and membrane-filtered RBCs after centrifugation at 2000 rpm for 5 min and then lysing with a hypotonic solution were quantified by measuring absorbance at 420 nm. The ratios of the RBCs that passed through the micropores and the number of hemolyzed cells relative to the total number of RBCs applied were calculated.

RESULTS

The typical elution profile of Suc-gel–SOD, native gelatin, succinyl gelatin, and native SOD from a Sephacryl S-200 column is shown in Figure 1A,B. Suc-gel–SOD eluted earlier than native SOD, and its peak width was broadened, indicating that the conjugate has a broader molecular distribution than SOD. Fractions of the conjugates (fractions 70–90) were pooled and used as Suc-gel–SOD. About two-thirds of the succinyl gelatin added to the reaction mixture (4.4 molar excess vs SOD) was conjugated to SOD, and three membrane filtrations (cutoff of 30 000) eliminated unreacted succinyl gelatin. The elute from the Sephacryl column was concentrated and washed to $^1/_{20}$ volume using distilled water. Therefore, the contamination of Suc-gel–SOD with unreacted succinyl gelatin was negligible (<0.3%) as judged by absorption at 240 nm.

PAGE was carried out for these preparations with or without SDS, which are shown in Figure 1C. The Suc-gel–SOD conjugate showed contamination of neither free SOD, succinyl gelatin, or free gelatin (gel a). Succinyl gelatin also showed apparently larger molecular mass (Figure 1C, gel a, lane 4) than the native gelatin fragment (lane 3), perhaps because of a more expanded conformation. In the presence of 0.1% SDS, native recombinant SOD behaved like tetramer as reported (*37*), which became monomer plus dimer upon heating for 5 min before running SDS–PAGE (not shown). PAGE without SDS showed faster mobility of succinyl gelatin toward the cathode due to its more anionic character (Figure 1C, gel b, lane 4) than native gelatin (lane 3), as expected. The staining character with Coomassie Brilliant Blue became much weaker for succinyl gelatin (Figure 1C).

The chemical properties of native SOD, Suc-gel–SOD, and succinyl gelatin are summarized in Table I. The amount of copper and zinc remaining in Suc-gel–SOD decreased to 0.66 and 0.65 μg/mg of protein from the initial 1.99 and 2.05 μg/mg of protein in native SOD, respectively. Amino acid analysis showed increased hydroxyproline content compared with native SOD, which has no hydroxyproline, as a result of attaching succinyl gelatin. These results indicate that about 2.9 mol of succinyl



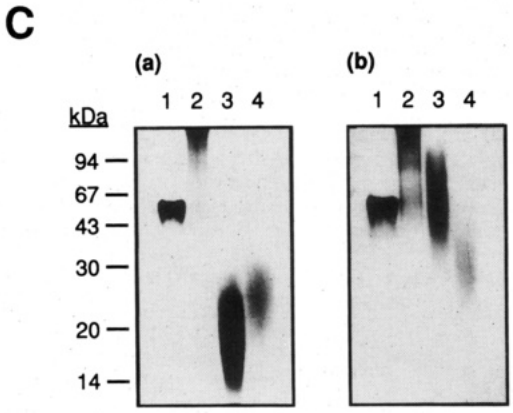


Figure 1. (A) Elution profile of the reactive mixture of native SOD with succinyl gelatin from a Sephacryl S-200 column. (B) Elution profile of native SOD (○), native gelatin (△), and succinyl gelatin (▲) from a Sephacryl S-200 column. SODs and gelatins were detected at 280 and 240 nm, respectively. Gel permeation chromatography was carried out on a Sephacryl S-200 column (3.5 × 70 cm) with 50 mM potassium phosphate buffer (pH 7.0) at 4°C. The flow rate was 50 mL/h and 5.0-mL fractions were collected. The amounts of applied samples were as follows: reactive mixture of native SOD with succinyl gelatin, 155 mg protein; native SOD, 14 mg; native gelatin, 50 mg; succinyl gelatin, 50 mg. (See the text for details.) (C) Polyacrylamide gel electrophoresis (acrylamide concentration, 14%) of SODs and gelatins. (a) Gel contained 0.1% sodium dodecyl sulfate (SDS). (b) Gel contained no SDS. Lane 1, human recombinant Cu,Zn-SOD (5 μg); lane 2, Suc-gel–SOD (7.5 μg); lane 3, native gelatin (50 μg); lane 4, succinyl gelatin (100 μg).

gelatin was attached to Suc-gel–SOD (Table I). Furthermore, the number of remaining amino groups in Suc-gel–SOD, determined by the TNBS method, decreased to 21.8 mol for Suc-gel–SOD from the initial 24 mol/mol of SOD. This result indicates that about 3.2 mol of succinyl gelatin was attached to Suc-gel–SOD. Therefore, all data appeared consistent. The enzymatic activity of SOD after modification with succinyl gelatin did not change from that of native SOD on a molar basis.

Figure 2 shows the plasma level of native SOD and Suc-gel–SOD injected iv into mice. Native SOD disappeared rapidly from the circulation with a half-life of 4.5 min, whereas Suc-gel–SOD did so more slowly (half-life of 29.7 min; Table II). The AUC of Suc-gel–SOD was about 6.2 times greater than that of native SOD.

Table I. Chemical Properties of Native SOD, Suc-gel-SOD, and Succinyl Gelatin

property	native SOD	Suc-gel-SOD	succinyl gelatin
Hyp content (w/w %)[a]	0	8.20	12.1
metal content (mol/mol of protein)[b]			
Cu	2.0	0.67	0
Zn	2.0	0.63	0
SOD content (w/w %)[c]			
based on Hyp	100.0	32.5	0
based on Cu	100.0	33.3	0
based on Zn	100.0	31.7	0
mean molecular weight[d]	31800	98000	23000
free amino group by TNBS (mol/mol of protein)[e]	24.0	21.8	0.1
enzymatic activity (SOD) (%)			
based on Hyp	100.0	100.0	0
based on Cu	100.0	97.9	0
based on Zn	100.0	102.8	0
numbers of succinyl gelatin attached[f]			
(metal)	0	2.9	–
(TNBS)	0	3.2	–

[a] Hydroxyproline (Hyp) was determined by amino acid analysis. [b] Copper and zinc were determined by atomic absorption analysis. [c] Content of SOD expressed as weight percent in the total preparation. [d] Mean molecular weight was determined by chemical composition, i.e., on the basis of the increase in hydroxyproline and the decrease in metals as a result of conjugation of succinyl gelatin. [e] Free amino groups were determined by the TNBS method. [f] Metal means the value obtained from the average value obtained from Cu and Zn analysis, and TNBS means the value obtained from decreased free amino groups in Suc-gel-SOD compared with native SOD.

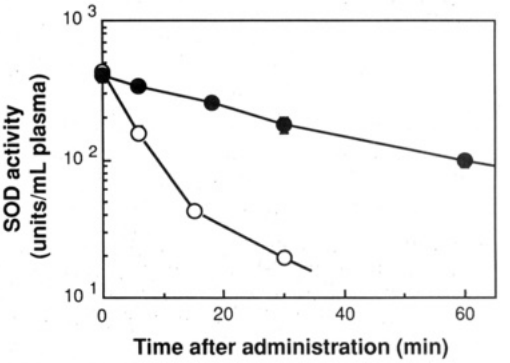


Figure 2. SOD activity in plasma after iv injection of native SOD (○) and Suc-gel–SOD (●) into mice. Male ddY mice were injected with 15 000 units of native SOD or the SOD derivative. Values represent the mean ± SE for four mice. (No deviation seen.)

Table II. Pharmacokinetic Parameters of Native SOD and Suc-gel-SOD in Mice

material	$t_{1/2}$[a] (min)	$AUC_{0-\infty}$[b] (units·min/mL)	CL[c] (mL/h)
native SOD	4.5 ± 0.2	2715 ± 107	10.0 ± 0.4
Suc-gel-SOD	29.7 ± 2.4	16752 ± 1637	1.7 ± 0.1

[a] Half-life ($t_{1/2}$) required to reach to half-concentration of time zero by interpolation. [b] Area under the plasma concentration vs time curve. [c] Total body clearance. Values represent the mean ± SE for four mice.

Tissue distributions of native SOD and Suc-gel–SOD at 1 h after iv administration are shown in Table III. Native gelatin was rapidly cleared from blood by either excretion into urine, proteolytic degradation, or entrapment in organs. However, the blood level of succinyl gelatin was higher than that of native gelatin. Accumulation of Suc-gel–SOD was greatest in the liver (24.6% injected dose) followed by urine (18.2%) and kidney (9.1%). Native SOD accumulated to the greatest extent in urine (43.0%)

Table III. Tissue Distribution of Radioactivity of ^{51}Cr-Labeled Gelatin, Succinyl Gelatin, Native SOD, and Suc-gel-SOD at 1 h after Intravenous Administration in Mice

organ/tissue	radioactivity (% dose/g of tissue)[a] gelatin	succinyl gelatin	native SOD	Suc-gel-SOD
brain	0.01 ± 0.01	0.13 ± 0.01	0.01 ± 0.01	0.17 ± 0.07
lung	0.41 ± 0.05	1.19 ± 0.27	0.16 ± 0.03	1.70 ± 0.62
heart	0.44 ± 0.02	1.17 ± 0.09	0.30 ± 0.06	1.40 ± 0.41
liver	3.83 ± 0.39	11.47 ± 0.98	1.03 ± 0.10	24.61 ± 2.22
kidney	10.38 ± 1.62	33.63 ± 4.30	20.57 ± 3.24	9.08 ± 2.73
spleen	0.73 ± 0.12	4.13 ± 0.13	0.14 ± 0.07	5.03 ± 1.26
stomach	0.68 ± 0.13	1.36 ± 0.05	0.13 ± 0.04	0.71 ± 0.15
small intestine	0.41 ± 0.12	0.82 ± 0.03	0.14 ± 0.02	0.68 ± 0.04
muscle	0.09 ± 0.01	0.40 ± 0.05	0.07 ± 0.01	0.16 ± 0.06
blood (1 mL)	0.69 ± 0.05	3.72 ± 0.05	0.67 ± 0.03	4.32 ± 1.38
urine (total)	38.39 ± 9.50	30.01 ± 5.32	43.04 ± 3.96	18.16 ± 4.72

[a] Values represent the mean ± SE for three mice.

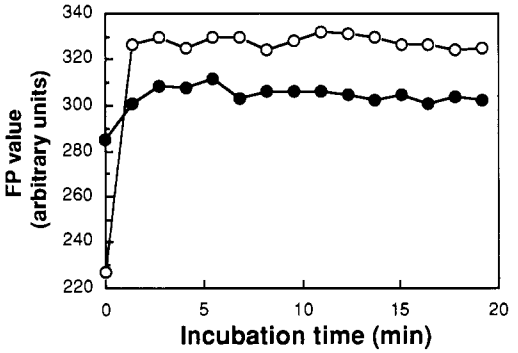


Figure 3. Time course of immunocomplex formation of F-native SOD (○) or F-Suc-gel-SOD (●) with anti-native SOD serum determined by the fluorescence polarization method (*32*). F-native SOD (2 μg/mL) or F-Suc-gel-SOD (2 μg/mL, native SOD equivalent) was incubated at 37 °C with 100 μL anti-native SOD rabbit serum or normal serum. The FP value was determined after different time intervals.

followed by kidney (20.6%) and liver (only 1.0%). In plasma, the Suc-gel-SOD level was about six times higher than native SOD at 1 h. Retention of native SOD in many other places, except kidney and urine, was much lower than that of the conjugate Suc-gel-SOD (Table III).

The kinetics of the immune complex formation of native SOD or Suc-gel-SOD with anti-native SOD serum were studied by fluorescence polarization (Figure 3). FP values increased rapidly and reached a plateau within 5 min when F-native SOD or F-Suc-gel-SOD was incubated with anti-native SOD serum in PBS. Values remained almost constant throughout an incubation period of 3 h (data not shown). Each FP value increased to about 44.1 or 5.6% above the value for free F-native SOD or free F-Suc-gel-SOD, respectively.

The antigenic epitope of Suc-gel-SOD was tested against anti-native SOD serum *in vitro* (Figure 4A). Results showed that the amount of immune precipitin formed increased markedly with the amount of native SOD added up to 15 μg; Suc-gel-SOD showed a slower increase in precipitin formation up to 40 μg (Figure 4A). Figure 4B shows the results of the precipitin reaction between each SOD and its respective rabbit antiserum. Suc-gel-SOD showed a weak immunogenicity in rabbits compared with native SOD because a small amount of the immune complex was formed.

Furthermore, in order to reveal Suc-gel-SOD-directed IgE-dependent local skin reaction we have undertaken PCA reaction using Suc-gel-SOD-sensitized mice sera (which may or may not contain IgE against SODs) (*35*).

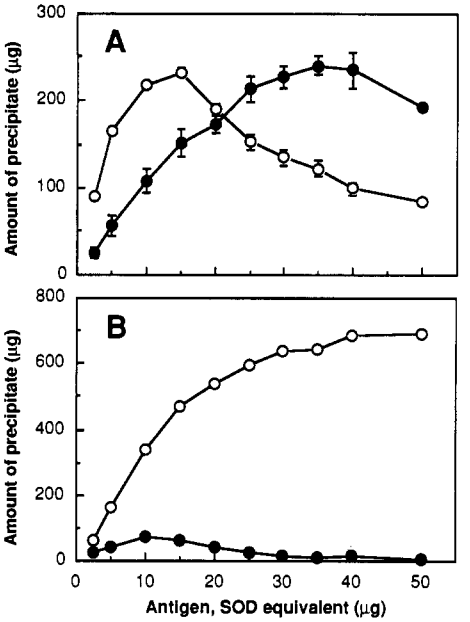


Figure 4. Antigenicity of native SOD and Suc-gel-SOD: (A) precipitin reaction curve of native SOD (○) and Suc-gel-SOD (●) against anti-native SOD rabbit serum (33 μL); (B) precipitin reaction curve of native SOD (●) against anti-native SOD rabbit serum (100 μL) and that of Suc-gel-SOD (●) against anti-Suc-gel-SOD rabbit serum (100 μL). Values (protein content) in A represent the mean ■ SE for three experiments, and values in B represent the mean of two experiments. The reaction mixture were allowed to stand at 4 °C for 24 h, after which precipitates were separated and quantified by Lowry's method.

Table IV. Passive Cutaneous Anaphylaxis (PCA) Reaction in Two Different Strains of Mice[a]

materials	mouse strain	degree of PCA reaction and positive percentage[b] −	+	++	+++
native SOD	A/J	0	0	0	100
	ddY	60	20	0	20
Suc-gel-SOD	A/J	25	25	0	50
	ddY	100	0	0	0

[a] The sensitization doses of each SOD derivative for A/J and ddY mice were 0.1 and 1.0 mg of SOD equivalent per animal on day 0 and day 14, respectively. The induction doses of each SOD derivative for Wistar rats were 1.0 mg of SOD equivalent per animal. Blood was withdrawn from sensitized mice after 21 days; 0.1 mL of a 4-fold-diluted antiserum was injected into Wistar rats subcutaneously. [b] Diameter of vascular permeability shown by Evans blue dye in the skin; −, <5 mm; +, 5–10 mm; ++, 10–15 mm; +++, 15–20 mm. Percentages indicate the results for a group of four or five mice.

As shown in Table IV, the PCA reaction induced by sera from both A/J and ddY mice at 7 days after the last sensitization with Suc-gel-SOD was lower than with native SOD. These SODs induced greatly different immunogenic responses in these mouse strains: the A/J strain showed stronger immunogenicity than the ddY strain. Suc-gel-SOD showed lower immunogenicity in both strains, which indicates a low potential for anaphylaxis (perhaps because of low IgE production).

The protective effect of both SODs on ischemic paw edema in mice is shown in Figure 5. Swelling of the paw in mice injected with saline alone increased by 37% of the initial thickness at 40 min after release from ischemia. No significant protective effect on the swelling was observed for native SOD. However, Suc-gel-SOD inhibited the swelling significantly up to 4 h after cessation of ischemia.

To test whether SODs affect a change in vascular permeability in the ischemic paw of mice, the amount of the Evans blue–albumin accumulated in the paw was

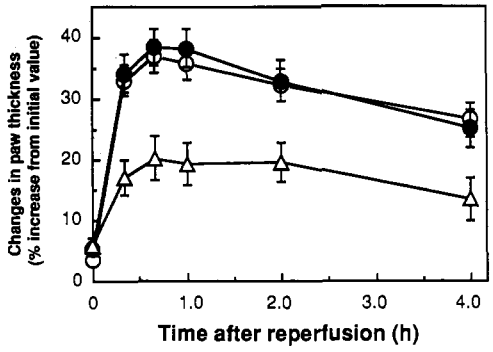


Figure 5. Time course of suppression of ischemic paw edema after iv injection of native SOD or Suc-gel–SOD 30 min before ischemia: ○, saline (control); ●, native SOD (2×10^4 units/kg); △, Suc-gel–SOD (2×10^4 units/kg). Values represent the mean ± SE for 12 mice.

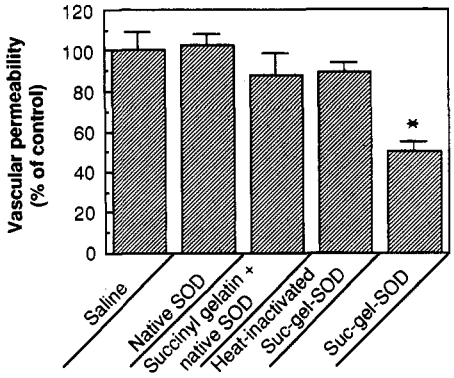


Figure 6. Suppression of vascular permeability by various SODs in the ischemic/reperfused mouse paw. Each mouse received an iv injection of saline (control), native SOD, succinyl gelatin plus native SOD, heat-inactivated Suc-gel–SOD, or Suc-gel–SOD at a dose of 4.74 mg SOD equivalent (20 000 units/kg) 30 min before ischemia. The dose of succinyl gelatin was 9.48 mg/kg, equivalent to Suc-gel–SOD. Data are expressed as the mean ± SE for five paws. An asterisk indicates that the value is significantly different from the control group as shown by Student's t test for $p < 0.01$.

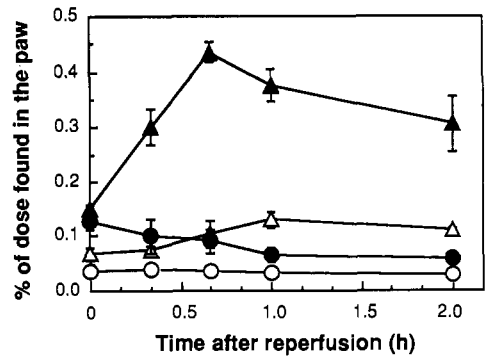


Figure 7. Accumulation of ^{51}Cr-labeled SODs in the ischemic and nonischemic mouse paw: ○, native SOD (nonischemic); ●, Suc-gel–SOD (nonischemic); △, native SOD (ischemia/reperfusion); ▲, Suc-gel–SOD (ischemia/reperfusion). Values represent the mean ± SE for three paws.

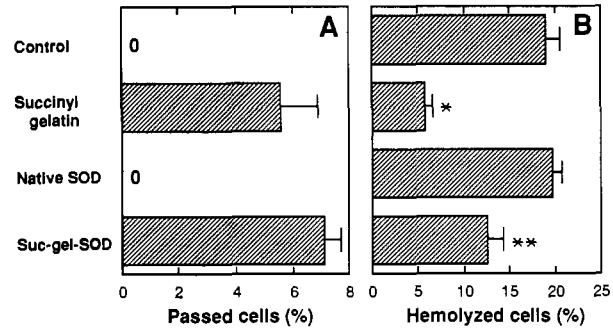


Figure 8. Lubricating effect of succinyl gelatin, native SOD, and Suc-gel–SOD on human RBCs on passage through a membrane filter with pore size of 3.0 μm (A) and on hemolyzed cells (B): control, 0.01 M sodium phosphate-buffered 0.15 M NaCl, pH 7.3 (PBS) alone; succinyl gelatin (1 mg/mL, PBS); native SOD (0.4 mg/mL, 17 000 units/mL, PBS); Suc-gel–SOD (1.4 mg/mL, 17 000 units/mL, PBS). Data are expressed as mean ± SE ($n = 5$): 0, not observed; *, significantly different from the control group as shown by Student's t test for $p < 0.001$; **, significantly different from native SOD group as shown by Student's t test for $p < 0.01$. (See the text for details.)

determined after iv administration of the SODs (Figure 6). Accumulation of the dye was inhibited significantly by Suc-gel–SOD; saline, native SOD, succinyl gelatin, and heat-inactivated Suc-gel–SOD did not produce significant suppression.

In the ischemic paw, the accumulated amounts of ^{51}Cr-labeled SODs were determined after iv SOD administration. Forty minutes after reperfusion from ischemia, about 0.44% and 0.09% of the dose of Suc-gel–SOD per paw had accumulated in the ischemic and nonischemic paws, respectively (Figure 7). About 5-fold greater targeting efficiency to the lesion site is seen with Suc-gel–SOD compared with native SOD, which accumulated in ischemic and nonischemic paws at a lower level: 0.04% and 0.10%, respectively. Thus there was 10 times more effective accumulation of Suc-gel–SOD in the lesioned paw.

Effects of Suc-gel–SOD on facilitated passage of human RBCs through membrane filters with 3-μm micropores were examined *in vitro* (Figure 8). RBCs suspended in PBS (control cells) did not pass through micropores and extensive hemolysis took place, whereas when Suc-gel–SOD was added at 1.4 mg/mL to an RBC suspension, about 7% of the cells penetrated the micropores and hemolysis was greatly reduced, from 19% to 6% (Figure 8B).

DISCUSSION

These results are part of our series of experiments on polymer–SOD conjugates using biocompatible polymers. We recently reported that Cu,Zn-SOD generates highly reactive hydroxyl radicals in the course of interaction between SOD and its enzymatic reaction product, hydrogen peroxide (*19*). $O_2^{\cdot-}$ is converted to hydrogen peroxide by SOD; thus, the inactivation of SOD just mentioned is itself a toxic metabolite-producing reaction. Hydroxyl radical is generated by Cu liberated from the ligand of SOD using hydrogen peroxide (*19*). It was found that α_1-protease inhibitor, a major endogenous elastase inhibitor and anti-inflammatory component, is readily degraded into inactive fragments by this reaction. As a consequence, inactivation of α_1-protease inhibitor in an inflammatory condition could be deleterious to the host. Therefore, fragile SOD molecules could be toxic rather than beneficial if not coexisting with catalase.

The purpose of the present study was to explore the possibility of preparing derivatives more resistant to oxidative stress with greater pharmacologically activity by polymer conjugation. In addition, the experiment was intended to confirm a second function for SOD: lubrication of RBCs. This paper focuses on the chemical and pharmacological characterization of a new conjugate, Suc-gel–SOD.

The gelatin used in this study was a fragmented gelatin with a mean molecular weight of 23 000 and containing about 3 mol % lysyl residues. We therefore prepared succinyl gelatin to block all the free amino groups, so that the carboxyl groups only became functional groups with

the amino groups of SOD, and consequently no cross-linking with gelatin would occur. Furthermore, succinylation would make gelatin more hydrophilic and anionic; the latter property makes the conjugates repulsive to each other and less likely to interact with vascular and cellular surfaces which are negatively charged (*38, 39*). PAGE analysis indeed showed the more acidic character of Suc-gel–SOD compared to native SOD. The reactivity of the amino groups in Suc-gel–SOD toward FITC was greater than that of native SOD (1.16 mol vs 0.63 mol), which may indicate that the conformational integrity of Suc-gel–SOD may be better expanded with succinylation, as observed with maleylation, due to repulsion of each negatively charged carboxyl group (*40, 41*).

The number of succinyl gelatin in Suc-gel–SOD was estimated at 3, based on the analysis of copper, zinc, and hydroxyproline (Table I). The molar enzymatic activity of Suc-gel–SOD remained almost 100% of that of native SOD after conjugation. Recently, Zanma et al. (*42*) reported conjugation of bovine erythrocyte Cu,Zn-SOD with the Fc fragment of immunoglobulin G (IgG). They showed that when the number of modifications of the lysyl residues in SOD was reduced to fewer than four using the bifunctional cross-linking agent *N*-succinimidyl 4-(*N*-maleimido)butyrate, about 90% of enzyme activity was retained with a plasma half-life of 42 h in mice. In the present study, only three amino groups in SOD were substituted by the succinyl gelatin, and the conjugate retained 100% of the initial enzymatic activity.

The half-lives of SOD activity in plasma were 4.5 and 29.7 min for native and Suc-gel–SOD, respectively (Table II). Suc-gel–SOD has a molecular weight of about 98 000, which is higher than the threshold for glomerular filtration (50 000) (*43*). However, the half-life of Suc-gel–SOD was not as long as that of other SOD polymer conjugates, e.g., the conjugate with PEG (20 h) depending on the number of PEG molecules (*18*), or the conjugate with poly(vinyl alcohol) (6.0 h) (*16*). Because of its peptide nature, the gelatin portion may be gradually degraded and the half-life may be shorter than that of the synthetic polymers.

Ikada and Tabata (*44*) showed that gelatin was opsonic during macrophage phagocytosis and that a gelatin–interferon conjugate was more effective than free interferon in potentiating *in vitro* and *in vivo* tumor growth inhibitory activity of macrophages. Greater accumulation of the gelatin–interferon conjugate than native interferon was observed in the liver and spleen of normal mice (*45*). Cosio and Bakaletz (*46*) showed that dinitrophenyl–gelatin formed a complex with plasma fibronectin *in vivo*, that the complex bound to specific fibronectin receptors in hepatic Kupffer cells and splenic macrophages, and that, as a result, dinitrophenyl–gelatin was phagocytosed. This process may apply in the present case because of relatively rapid clearance from the circulation. As shown in Table III, the tissue accumulation of succinyl gelatin and Suc-gel–SOD was much greater (10–24 times) in the liver, and much less so in the spleen, lung, and most other tissues compared with that of native gelatin and SOD. One explanation for this is that native SOD is cleared more than 10 times faster than Suc-gel–SOD (Table II), and thus the native SOD did not have time to accumulate. Another possibility is that Suc-gel–SOD was trapped by the Kupffer cells in the liver and macrophages in the spleen.

Fujita et al. (*47*) evaluated the potential of galactosylated SOD and mannosylated SOD for selective targeting to hepatic cells in mice. Both SOD derivatives accumulated in the liver (about 70% of dose), the cellular localization patterns were rather different. Galactosylated SOD accumulated predominantly in the parenchymal cells (about 5.0 times greater than in nonparenchymal cells) of the liver, whereas mannosylated SOD was recovered in the nonparenchymal cell fraction (about 9.6 times greater than in the other cells). Thus, similarly, Suc-gel–SOD may be delivered to Kupffer cells in the liver and macrophages in the spleen, although more studies are needed to confirm this possibility.

The use of SOD for treatment of various diseases including rheumatoid arthritis has been discussed for a long time (*48*), but little success has been reported in the clinical setting. However, the clinical application of bovine Cu,Zn-SOD has considerable limitations because of rapid clearance from the circulation and immunogenicity. To solve the immunological problem, human-type DNA recombinant Cu,Zn-SOD was prepared in bacteria, which was also cleared rapidly from mice: the plasma half-life in the circulation was about 5 min, resulting in a limited pharmacological effect. In contrast, Suc-gel–SOD conjugates showed almost 6 times larger AUC or 6 times prolonged plasma half-life (Figure 2, Table II). In our experiment with PEG-SOD and other polymer–SOD conjugates, prolonged half-life alone did not produce a therapeutic benefit, perhaps because of the aforementioned hydroxyl radical generation.

Immunogenicity is an important issue for protein drugs. As shown in Figure 3, Suc-gel–SOD showed a much weaker antibody-combining ability than did native SOD (*34*). Furthermore, when the precipitin reaction for Suc-gel–SOD against anti-native SOD antibody was tested *in vitro*, more Suc-gel–SOD was required to form the same amount of immune precipitin compared with native SOD (Figure 4A). Thus, modification of amino groups (up to 88%) with succinyl gelatin may reduce the effected formation of the immune complex. It is also known that antigen excess will frequently result in solubilization of the immune complex (*34*) which is consistent with present data (Figure 4A). To investigate further, rabbits and mice were immunized with native SOD or Suc-gel–SOD with Freund's complete adjuvant and antibody formation was examined. Suc-gel–SOD exhibited much lower antibody formation (Figure 4B).

In addition, antiserum from mice immunized with native SOD had detectable PCA reactivity 7 days after the last immunization, whereas Suc-gel–SOD produced a much lower PCA reaction (Table IV). A similar result was reported for a PEG-conjugated bacterial Mn-SOD (*49*). It was interesting to note that there was a difference in immune response among different strains of mice (Table IV): strain A/J showed much higher sensitivity than ddY. These results indicate that Suc-gel–SOD has remarkably low immunogenicity, if any at all, and hence stimulation of IgG and IgE antibody formation is minimal.

PEG-conjugated ovalbumin and PEG-conjugated ragweed pollen suppressed ongoing IgE antibody formation markedly in sensitized animals on subsequent injections of the shock-inducing dose equivalent of the respective antigens (*50*). Furthermore, specific suppressor T cells were induced by treatment of mice with PEG-conjugated ovalbumin or monomethoxy PEG-conjugated ovalbumin (*51*). This same mechanism may be operating with Suc-gel–SOD.

Ischemic reperfusion is known to involve $O_2^{\cdot-}$ generation (*26*), which results in edema and tissue damage in the case of artificially induced paw ischemia in mice (*36*). SOD may be a therapeutic candidate: the experiment with Suc-gel–SOD showed that it was significantly effective against paw edema in suppressing ischemic reperfusion (Figures

5 and 6), whereas native SOD was not suppressive. The pronounced therapeutic effects in this model may be explained by the high concentration of Suc-gel–SOD in plasma and tissues (Figures 2 and 7). In our separate experiment using type II collagen induced arthritis in mice this Suc-gel–SOD showed a significant effect while native SOD or pyran copolymer conjugated SOD had no therapuetic effect (*52*).

Experiments on the lubricating effect on PBCs by succinyl gelatin and Suc-gel–SOD confirmed facilitation of the passage of RBCs through micropores, as observed previously with gelatin and succinyl gelatin. The membrane filter used had a diameter of 3 μm, which is much smaller than the diameter of RBCs (6.5 μm). Suc-gel–SOD and gelatin also prevented hemolysis of cells during passage (Figure 8). The present *in vitro* findings imply that Suc-gel–SOD seems to be useful agent as a cellular lubricant in the peripheral microcirculation under both physiological and pathological conditions. In disease states, highly elevated coagulating activity and antigen–antibody complex formation or vascular permeability enhancement are known to occur, which would impede blood circulation by either physical obstruction or a decreased fluid phase and slugging at the capillary level. Under these conditions, facilitated passage of plasma cells would be accomplished by the presence of Suc-gel–SOD at the microcirculation level. These results showed that a second function can be added to the enzymatic action of SOD, and these two factors may be beneficial at the peripheral circulation level.

In conclusion, conjugation of succinyl gelatin to the enzyme SOD seems to improve pharmacological drawbacks and has provided some basic data for further pharmacological development. Also, stability of the conjugate against hydrogen peroxide because of a copper chelating effect, (not described in this report) would explain these improved pharmacological effects, in addition to the lubrication effect.

ACKNOWLEDGMENT

We thank Ms. Judith B. Gandy for editorial work, and a Research Grant from the Ministry of Education, Science, and Culture (Monbusho) of Japan to H. Maeda for 1992–1993.

LITERATURE CITED

(1) Brigham, K. L. (1986) Role of free radicals in lung injury. *Chest 6*, 859–863.

(2) Gardner, T. J., Stewart, J. R., Casale, A. S., Downey, J. M., and Chambers, D. E. (1983) Reduction of myocardial ischemic injury with oxygen-derived free radical scavengers. *Surgery 94*, 423–427.

(3) Suematsu, M., Suzuki, M., Kitahora, T., Miura, S., Suzuki, K., Hibi, T., Watanabe, M., Nagata, H., Asakura, H. and Tsuchiya, M. (1987) Increased respiratory burst of leukocytes in inflammatory bowel diseases-the analysis of free radical generation by using chemiluminescence probe. *J. Clin. Lab. Immunol. 24*, 125–128.

(4) Oda, T., Akaike, T., Hamamoto, T., Suzuki, F., Hirano T. and Maeda, H. (1989) Oxygen radicals in influenza-induced pathogenesis and treatment with pyran polymer-conjugated SOD. *Science (Washington, DC) 244*, 974–976.

(5) Akaike, T., Ando, M., Oda, T., Doi, T., Ijiri, S., Araki S. and Maeda, H. (1990) Dependence on O_2^- generation by xanthine oxidase of pathogenesis of influenza virus infection in mice. *J. Clin. Invest. 85*, 739–745.

(6) Maeda, H., Takeshita, J. and Kanamura, R. (1979) A lipophilic derivative of neocarzinostatin: A polymer conjugation of an antitumor protein antibiotic. *Int. J. Pept. Protein Res. 14*, 81–87.

(7) Maeda, H., Matsumoto, T., Konno, T., Iwai, K. and Ueda, M. (1984) Tailor-making of protein drugs by polymer conjugation for tumor targeting: A brief review on smancs. *J. Protein Chem. 3*, 181–193.

(8) Maeda, H., Ueda, M., Morinaga, T. and Matsumoto, T. (1985) Conjugation of poly(styrene-*co*-maleic acid) derivatives to the antitumor protein neocarzinostatin: Pronounced improvements in pharmacological properties. *J. Med. Chem. 28*, 455–461.

(9) Maeda, H., Matsumura, Y., Oda, T. and Sasamoto, K. (1986) Cancer selective macromolecular therapeutics: Tailoring of an antitumor protein drug. *Protein Tailoring for Food and Medical Uses* (R. E. Feeney and J. R. Whitaker, Eds.) pp 353–382, Marcel Dekker, Inc., New York-Basel.

(10) Maeda, H., Oda, T., Matsumura, Y. and Kimura, M. (1988) Improvement of pharmacological properties of protein-drugs by tailoring with synthetic polymers. *J. Bioact. Compat. Polym. 3*, 27–43.

(11) Ogino, T., Inoue, M., Ando, Y., Awai, M., Maeda, H. and Morino, Y. (1988) Chemical modification of superoxide dismutase: Extension of plasma half life of the enzyme through its reversible binding to the circulating albumin. *Int. J. Pept. Protein Res. 32*, 153–159.

(12) Maeda, H. and Mutsumura, Y. (1989) Tumoritropic and lymphotropic principles of macromolecular drugs. *Crit. Rev. Ther. Drug Carrier Syst. 6*, 193–210.

(13) Maeda, H. (1991) SMANCS and polymer-conjugated macromolecular drugs: Advantages in cancer chemotherapy. *Adv. Drug Delivery Rev. 6*, 181–202.

(14) Maeda, H., Seymour, L. W. and Miyamoto, Y. (1992) Conjugates of anticancer agents and polymers: Advantages of macromolecular therapeutics *in vivo*. *Bioconjugate Chem. 3*, 351–362.

(15) Maeda, H., Kimura, M., Sasaki, I., Hirose, Y. and Konno, T. (1992) Toxicity of bilirubin and detoxication by PEG-bilirubin oxidase conjugate: A new tactic for treatment of jaundice. *Biochemical Application of PEG Chemistry* (M. Harris, Ed.) pp 153–169, Plenum Pub. Corp., New York.

(16) Kojima, Y. and Maeda, H. (1993) Evaluation of polyvinyl alcohol for protein tailoring: Improvements in pharmacokinetic properties of superoxide dismutase. *J. Bioact. Compat. Polym. 8*, 115–131.

(17) Pyatak, P. S., Abuchowski, A. and Davis, F. F. (1980) Preparation of a polyethylene glycol: Superoxide dismutase adduct, and an explanation of its blood circulation life and anti-inflammatory activity. *Res. Commun. Chem. Pathol. Pharmacol. 29*, 113–127.

(18) Veronese, F. M., Boccu, E., Schiavon, O., Velo, G. P., Conforti, A., Franco, L. and Milanino, R. (1983) Anti-inflammatory and pharmacokinetic properties of superoxide dismutase derivatized with polyethyleneglycol via active esters. *J. Pharm. Pharmacol. 35*, 757–758.

(19) Sato, K., Akaike, T., Kohno, M., Ando, M. and Maeda, H. (1992) Hydroxyl radical production by H_2O_2 plus Cu,Zn-superoxide dismutase reflects the activity of free copper released from the oxidatively damaged enzyme. *J. Biol. Chem. 267*, 25371–25377.

(20) Zokorn, D. (1969) Modified gelatin as plasma substitutes. *Bibl. Haematol. 33*, 33–60.

(21) Maeda, H., Nishi, K. and Mori, I. (1980) Facilitating effects of alpha-1 acid glycoprotein on the passage of erythrocytes through the membrane-filter. *Life Sci. 27*, 156–161.

(22) Maeda, H., Morinaga, T., Mori ,I. and Nishi, K. (1984) Further characterization of the effects of alpha-1-acid glycoprotein on the passage of human erythrocytes through micropores. *Cell Struct. Funct. 9*, 279–290.

(23) Grisham, M. B., Hernandez, L. A. and Granger, D. N. (1986) Xanthine oxidase and neutrophil infiltration in intestinal ischemia. *Am. J. Physiol. 251*, G251-G267.

(24) Maeda, H. (1974) Chemical and biological characterization of succinyl neocarzinostatin. *J. Antibiot. 27*, 303–311.

(25) Fields, R. (1972) The rapid determination of amino groups with TNBS. *Methods Enzymol. 25*, 464–468.

(26) Laemmli, U. K. (1970) Cleavage of structural proteins during the assembly of the head of bacteriophage T4. *Nature 227*, 680–685.

(27) McCord, J. M. and Fridovich, I. (1969) Superoxide dismutase, an enzymic function for erythrocuprein (hemocuprein). *J. Biol. Chem. 244,* 6049–6055.
(28) Hnatowich, D. J., Layne, W. W. and Childs, R. L. (1982) The preparation and labeling of DTPA-coupled albumin. *Int. J. Appl. Radiat. Isot. 33,* 327–332.
(29) Halpern, S., Stern, P., Hagan, P., Chen, A., Frincke, J., Bartholomew, R., David, G. and Adams, T. (1983) Labeling of monoclonal antibodies with indium-111: Technique and advantages compared to radioiodine labeling. *Radioimmunoimaging and Radioimmunotheraphy* (S. W. Burchiel and B. A. Rhodes, Eds.) pp 197–205, Elsevier Science Publishing Co., Inc., New York.
(30) Matsumura, Y. and Maeda, H. (1986) A new concept for macromolecular therapeutics in cancer chemotherapy: Mechanism of tumoritropic accumulation of proteins and the antitumor agent smancs. *Cancer Res. 46,* 6387–6392.
(31) Yamaoka, K., Tanigawara, Y., Nakagawa, T. and Uno, T. (1981) A pharmacokinetic analysis program (MULTI) for microcomputer. *J. Pharmacobio-Dyn. 4,* 879–885.
(32) Maeda, H. (1979) Assay of proteolytic enzymes by the fluorescence polarization technique. *Anal. Biochem. 92,* 222–227.
(33) Maeda, H. (1978) Assay of an antitumor protein, neocarzinostatin, and its antibody by fluorescence polarization. *Clin. Chem. 24,* 2139-2144.
(34) Kabat, E. A. and Mayer, M. M. (1961) *Experimental Immunochemistry* (Second edition) pp 72–76, C. C. Thomas, Publisher, Springfield, Illinois, U. S. A.
(35) Garvey, J. S., Cremer, N. E.and Sussdorf, D. H. (1977) Passive cutaneous anaphylaxis. *Methods in Immunology* (Third edition) pp 455–458, W. A. Benjamin, Inc., Reading, MA.
(36) Õyanagui, Y., Sato, S. and Okajima,.T. (1988) Suppressions of ischemic paw oedema in mice, rats and guinea pigs by superoxide dismutases from different sources. *Free Radical Res. Commun. 4,* 385–396.
(37) Kajihara, J., Enomoto, M., Nishijima, K., Yabuuchi, M. and Katoh, K. (1988) Comparison of properties between human recombinant and placental copper-zinc SOD. *J. Biochem. 104,* 851–854.
(38) Simionescu, M., Simionescu, N., Santoro, F. and Palade, G. E. (1985) Differentiated microdomains of the luminal plasmalemma of murine muscle capillaries: Segmental variations in young and old animals. *J. Cell. Biol. 100,* 1396–1407.
(39) Simionescu, N. (1983) Cellular aspects of transcapillary exchange. *Physiol. Rev. 63,* 1536–1579.
(40) Habeeb, A. F. S.A., Cassidy, H. G. and Singer, S. J. (1958) Molecular structural effects produced in proteins by reaction with succinic anhydride. *Biochim. Biophys. Acta 29,* 587–593.
(41) Qasim, M. A. and Salahuddin, A. (1979) The conformational consequences of maleylation of amino groups in ovalbumin. *J. Biochem. 85,* 1029–1035.
(42) Zanma, A., Matsumoto, Y. and Masuho, Y. (1991) Conjugates of superoxide dismutase with the Fc fragment of immunoglobulin G. *J. Biochem. 110,* 868–872.
(43) Taylor, A. E. and Granger, N. D. (1984) Exchange of macromolecules across the microcirculation. *Handbook of Physiology: The Cardiovascular System IV* (E. M. Renkin and C. C. Michael, Eds.) pp 467–520, American Physiological Society, Bethesda, MD.
(44) Ikada, Y. and Tabata, Y. (1986) Phagocytosis of bioactive microspheres. *J. Bioact. Compat. Polym. 1,* 32–46.
(45) Tabata, Y., Uno, K., Yamaoka, T., Ikada, Y. and Muramatsu, S. (1991) Effects of recombinant α-interferon-gelatin conjugate on *in vivo* murine tumor cell growth. *Cancer Res. 51,* 5532–5538.
(46) Cosio, F. G. and Bakaletz, A. P. (1987) Role of fibronectin on the clearance and tissue uptake of antigen and immune complex in rats. *J. Clin. Invest. 80,* 1270–1279.
(47) Fujita, T., Nishikawa, M., Tamaki, C., Takakura, Y., Hashida, M. and Sezaki, H. (1993) Targeted delivery of human recombinant superoxide dismutase by chemical modification with mono- and polysaccharide derivatives. *J. Pharmacol. Exp. Ther. 263,* 971–978.
(48) Menander-Huber, K. B. and Huber, W. (1977) Orgotein, the drug version of bovine Cu-Zn superoxide dismutase. II. A summary of clinical trials in man and animals. *Superoxide and Superoxide Dismutase* (A. M. Michelson, J. M. McCord, and I. Fridovich, Eds.) pp 537–556, Academic Press, London.
(49) Miyata, K., Nakagawa, Y., Nakamura, M., Ito, T., Sugo, K., Fujita, T. and Tomoda, K. (1988) Altered properties of *Serratia* superoxide dismutase by chemical modification. *Agric. Biol. Chem. 52,* 1575–1581.
(50) Wie, S. I., Wie, C. W., Lee, W. Y., Filion, L. G., Sehon A. H. and Akerblom, E. (1981) Suppression of reaginic antibodies with modified allergens, III. Preparation of tolerogenic conjugates of common allergens with monomethoxypolyethylene glycols of different molecular weights by the mixed anhydride method. *Int. Arch. Allergy Appl. Immunol. 64,* 84–99.
(51) Lee, W. Y., Sehon, A. H. and Akerblom, E. (1981) Suppression of reaginic antibodies with modified allergens, IV. Induction of suppressor T cells by conjugates of polyethylene glycol (PEG) and monomethoxy PEG with ovalbumin. *Int. Arch. Allergy Appl. Immunol. 64,* 100–114.
(52) Kakimoto, K., Kojima, Y., Ishii, K., Onoue, K. and Maeda, H. (1993) The suppressive effect of gelatin-conjugated superoxide dismutase on disease development and severity of collagen-induced arthritis in mice. *Clin. Exp. Immunol.* In press.

Nucleosides and Nucleotides. 121. Synthesis of Oligonucleotides Carrying Linker Groups at the 1'-Position of Sugar Residues†

Akira Ono,‡ Akihito Dan, and Akira Matsuda*

Faculty of Pharmaceutical Sciences, Hokkaido University, Kita-12, Nishi-6, Kita-ku, Sapporo 060, Japan.
Received June 8, 1993®

Novel 2'-deoxyuridine analogues carrying aminoalkyl linkers at the 1'-position of the sugar residues were synthesized and incorporated into oligonucleotides, then intercalating groups such as an anthraquinone derivative and a pyrene derivative were attached to the amino groups. Duplexes consisting of the oligonucleotides carrying the linker groups and a complementary ribonucleotide were more stable than an unmodified parent duplex, but the duplexes consisting of the oligonucleotides and a complementary deoxyribonucleotide were less stable. The oligonucleotides carrying the linker groups were more resistant to nuclease P1 and venom phosphodiesterase than an unmodified oligonucleotide. Furthermore, a duplex formed by the oligonucleotide analogue and the complementary ribonucleotide was a substrate for ribonuclease H.

INTRODUCTION

Oligonucleotide analogues containing modified backbones or carrying various functional groups have been synthesized and used for biological and biophysical studies such as antisense studies (*1, 2*). From these studies, it is apparent that the potency of any given antisense oligonucleotide is highly dependent on its resistance to nucleolytic digestion. Therefore, oligonucleotides containing nuclease-resistant phosphodiester analogues, such as oligonucleotides with phosphorothioate and methylphosphonate linkages, have been synthesized (*1, 2*).

However, no complete oligonucleotide analogue for antisense study has been established. For instance, methylphosphonate and α-anomeric oligonucleotides with target RNAs form duplexes that are not substrates for RNase H. Thus, the oligonucleotide analogues need relatively high concentration for antisense activity since RNase H-mediated degradation is a major mechanism by which antisense oligonucleotides inactivate mRNA (*1, 3*). Phosphorothioate oligonucleotides are taken up into cells more slowly than normal oligonucleotides and have affinity for certain proteins (*4–6*). Also, the oligonucleotides with methylphosphonate and phosphrothioate linkages have been practically synthesized as mixtures of stereoisomers because of asymmetry about the phosphorus, so that only a small part of the isomers can form stable duplexes with target mRNAs (*7*).

Several studies have demonstrated that oligonucleotides modified at the 3' end are more resistant to nucleases than unmodified ones (*8, 9*). It suggested that oligonucleotides are largely degraded by 3'-exonucleases and that a single modification of the oligonucleotides at the 3'-end is sufficient to inhibit these enzymes. With target mRNAs, the 3'-modified oligonucleotides form more stable duplexes than the oligonucleotides modified at every phosphate, such as phosphorothioates and methylphosphonates, and the duplexes are substrates for RNase H. Therefore, the 3'-modified oligonucleotides have almost complete properties, except that the 3'-modified oligonucleotides could be degraded by endonucleases in cells.

In this report, we describe a new method for introducing functional groups into oligonucleotides to provide nuclease resistance, even if the oligonucleotides contain normal phosphodiester linkages. Many methods to attach the functional groups at several sites on the oligonucleotides, such as the 5'- and 3'-ends, the 5-position of uracil residues, the *N*-4 of cytosine residues, phosphate residues, and the 2-position of adenine residues, have been reported (*1, 2, 10*). On the other hand, few methods to attach the functional groups at the sugar moieties have been reported (*11, 12*). However, it can be supposed that the bulky functional group attached at sugar moieties may inhibit hydrolysis by nucleases since the functional groups are close to phosphodiester linkages.

Therefore, we introduced nucleosides carrying amino linkers at the 1'-position, **1** and **2** (Figure 1) (*13*), into oligonucleotides, then functional groups such as an anthraquinone derivative and a pyrene derivative were attached to the amino group to give oligonucleotides containing **3–6**.

On the other hand, the functional groups may not destabilize duplex formation as follows. The functional groups should be accommodated in the minor groove when the oligonucleotide analogues form duplexes with complementary strands. Since the 1'-position of the sugar moiety in a duplex is in the center of the minor groove, the linker groups may not sterically disorder the duplex formation, especially in the minor groove of RNA–DNA heteroduplexes since the minor grooves of the heteroduplexes are wider than those of DNA–DNA duplexes (*14*).

RNase H recognizes sugar puckering of duplexes distinctly so that duplexes formed by RNAs and oligonu-

* Author to whom all correspondence and reprint requests should be addressed.

† Part 120: Kakefuda, A., Yoshimura, Y., Sasaki, T., Matsuda, A. (1993) *Tetrahedron*. In press.

‡ Present address: Department of Chemistry, Faculty of Science, Tokyo Metropolitan University, Minamiosawa, Hachioji, Tokyo 192-03, Japan.

® Abstract published in *Advance ACS Abstracts*, October 1, 1993.

[1] Abbreviations used: AIBN, 2,2'-azobis(isobutyronitrile); Bu_3SnH, tributyltin hydride; Bu_4NF, tetrabutylammonium fluoride; DMTr, 4,4'-dimethoxytrityl; DMTrCl, 4,4'-dimethoxytrityl chloride; Fmoc, 9-fluorenylmethoxycarbonyl; FmocCl, 9-fluorenylmethyl chloroformate; HEPES, *N*-(2-hydroxyethyl)piperazine-*N*'-2-(ethanesulfonic acid); HPLC, high-pressure liquid chromatography; RNase H, ribonuclease H; TIPDS; 1,1,3,3-tetraisopropyldisiloxane-1,3-diyl; $TIPDSCl_2$, 1,3-Dichloro-1,1,3,3-tetraisopropyldisiloxane; TEAA, triethylammonium acetate.

1043-1802/93/2904-0499$04.00/0 © 1993 American Chemical Society

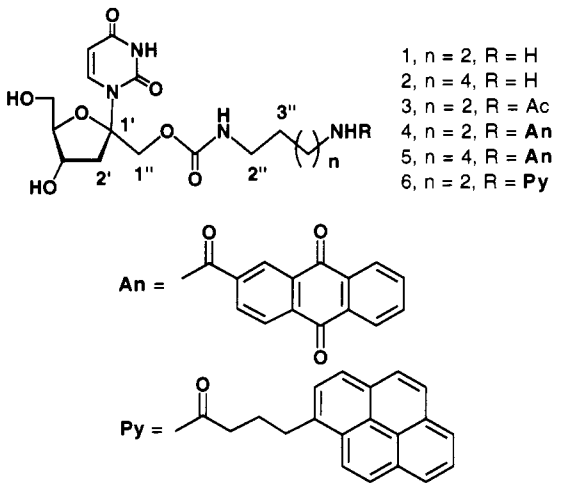


Figure 1. Structure and numbering of the nucleoside analogues.

cleotides containing 2′-modified sugar moieties are not substrates for the enzyme (*15, 16*). However, it is also known that "chimeric" oligonucleotides composed of regions containing modified sugar derivatives linked to an unmodified region can form duplexes with target RNAs and the duplexes are substrates for RNase H (*17*). Therefore, duplexes formed by RNAs and the oligonucleotides containing new nucleoside analogues, 1–6, could be substrates for the enzyme.

RESULTS AND DISCUSSION

The oligonucleotide analogues used in this study were synthesized by the phosphoramidite method on a commercially available DNA synthesizer. A scheme for a synthesis of 3′-phosphoramidite derivatives of the 2′-deoxyuridine analogues is shown in Figure 2. 1″,3′,5′-Tri-*O*-benzoyl-1′-(hydroxymethyl)-2′-deoxyuridine was synthesized by the reported method (*18*) with several modifications (Figure 2). The *O*,2′-anhydro linkage of **7** was hydrolyzed under acidic conditions to give **8**, then **8** was converted into (thiocarbonyl)imidazolide **9**, which was treated with Bu_3SnH (*19*) to give 2′-deoxy derivative **10** in good yield. After 3′- and 5′-hydroxyl groups were protected by a TIPDS group (*20*), diaminoalkanes were conjugated with the unprotected 1″-hydroxyl group of **11** to give deoxyuridine analogues carrying aminoalkyl linkers at the 1′-position, **12** and **13**, in good yields. After the amine function was protected with an Fmoc group, the TIPDS group was deprotected, then the nucleosides were converted into corresponding nucleoside 3′-phosphoramidites, **20** and **21**.

Table I. Synthesized Oligonucleotides

I-NH_2	$1(T)_{15}$	**III-An**	$(T)_7 5(T)_8$
I-Ac	$3(T)_{15}$	**IV-$(NH_2)_2$**	$(T)_5 1(T)_4 1(T)_5$
I-An	$4(T)_{15}$	**IV-$(An)_2$**	$(T)_5 4(T)_4 4(T)_5$
II-NH_2	$(T)_7 1(T)_8$	**IV-$(Py)_2$**	$(T)_5 6(T)_4 6(T)_5$
II-Ac	$(T)_7 3(T)_8$	**V-$(NH_2)_3$**	$(T)_3 1(T)_3 1(T)_3 1(T)_4$
II-An	$(T)_7 4(T)_8$	**V-$(An)_3$**	$(T)_3 4(T)_3 4(T)_3 4(T)_4$
II-Py	$(T)_7 6(T)_8$	**V-$(Py)_3$**	$(T)_3 6(T)_3 6(T)_3 6(T)_4$
III-NH_2	$(T)_7 2(T)_8$		

In this study, the nucleoside analogues were introduced into oligonucleotides with a model sequence, $(T)_n$. Oligonucleotides were synthesized on a DNA synthesizer by the phosphoramidite method (*21*). An average coupling yield of the nucleoside 3′-phosphoramidites **20** and **21** was about 85%. The yield was lower than that of the thymidine 3′-phosphoramidite probably due to a steric effect of the linkers at the 1′-position, and not due to a purity problem of the amidite samples since the purity of the nucleoside 3′-phosphoramidites measured by ^{31}P-NMR was more than 99% (data not shown). Fully protected oligonucleotides were deprotected and purified by the same procedure as for the purification of natural oligonucleotides. Then, the oligonucleotides were treated with acetic anhydride, *N*-[(anthraquinone-2-carbonyl)oxy]succinimide(**22**), or *N*-succinimidylpyrenebutanolate (*22*) to give the oligonucleotides containing **3**–**6**. The oligonucleotides synthesized in the study are listed in Table I.

Purity and nucleoside composition of the oligonucleotides in this preparation were analyzed by HPLC. The oligonucleotides had single peaks by HPLC analysis with the C-18 silica gel column. An example is shown in Figure 3a. Also, each oligonucleotide phosphorylated with ^{32}P at the 5′-end had a single spot by polyacrylamide gel

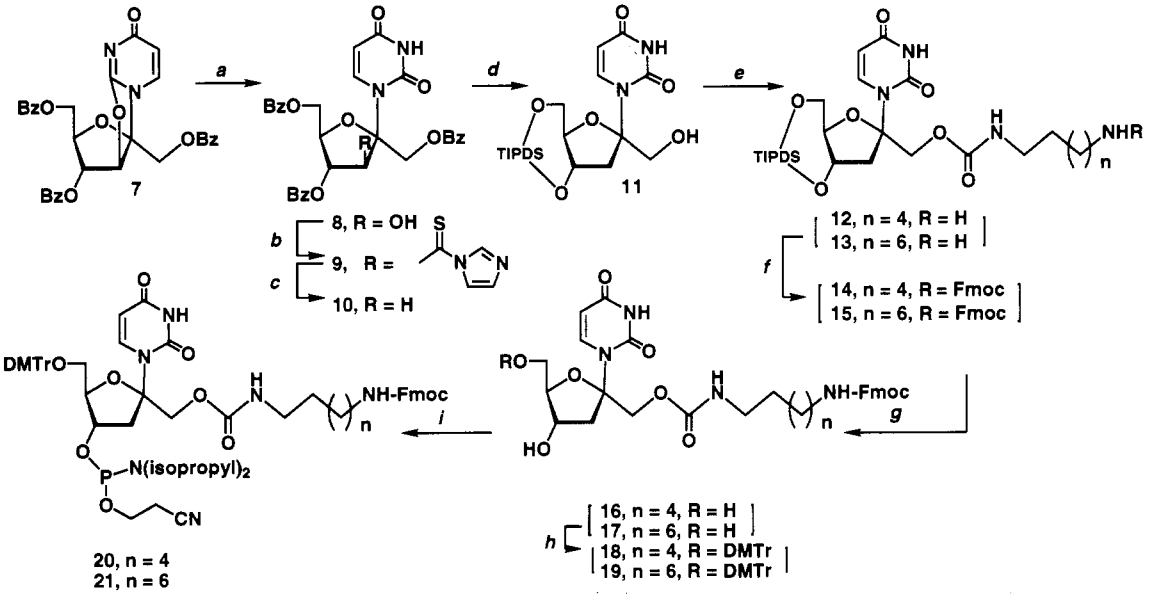


Figure 2. Synthesis of nucleoside 3′-phosphoramidites. (*a*) a mixture of 2 N HCl and DMF (2:5, v/v), rt, 95% yield; (*b*) *N*,*N*′-thiocarbonyldiimidazole, DMF; (*c*) Bu_3SnH, AIBN, toluene, 92% yield from **8**; (d) (1) NaOMe, MeOH, (2) $TIPDSCl_2$, 57% yield; (*e*) *N*,*N*′-carbonyldiimidazole, diaminoalkane, dioxane, 95% yield; (*f*) 9-fluorenylmethyl chloroformate, pyridine, 86% yield; (*g*) Bu_4NF, THF, 98% yield; (*h*) DMTrCl, pyridine, 83% yield; (*i*) 2-cyanoethyl *N*,*N*-diisopropylphosphoramidochlorite, *N*,*N*-diisopropylethylamine, CH_2Cl_2, 80% yield.

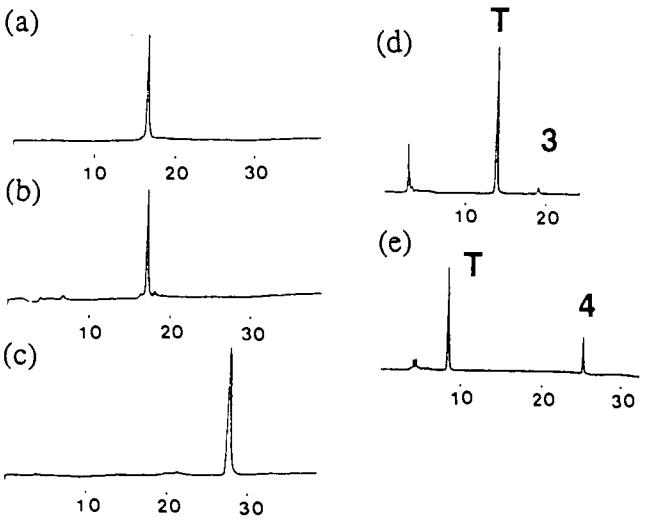


Figure 3. Examples of HPLC profiles of the oligonucleotides: (a) **II-NH_2**, a linear gradient of CH_3CN from 10 to 20% (20 min) in 0.1 M TEAA buffer pH 6.8; (b) **II-Ac**, 10 to 20%; (c) **II-An**, 20 to 33%; (d) the nucleoside mixture obtained by complete hydrolysis of **II-Ac**, a linear gradient of MeOH from 8 to 20% (20 min) in water; (e) the nucleoside mixture obtained by complete hydrolysis of **II-An**, 20 to 45% (10 min) to 80% (5 min) to 80% (15 min). The peaks were observed at 254 nm.

electrophoresis under denaturing conditions (*23*) (data not shown). Each oligonucleotide was completely hydrolyzed by venom phosphodiesterase and alkaline phosphatase to the corresponding nucleosides, then the nucleoside composition was confirmed by HPLC with the C-18 silica gel column; however, no sharp peak corresponding to **1** was observed (data not shown). Therefore, to certify the existence of the amino group, oligonucleotide **II-NH_2** was treated with acetic anhydride to give acetylated oligonucleotide **II-Ac**, the retention time of which was slightly longer than that of **II-NH_2** (Figure 3b). **II-Ac** was completely hydrolyzed and the nucleoside composition was analyzed by HPLC (Figure 3d). A peak corresponding to **3** was observed clearly and the nucleoside composition calculated from areas of the peaks (Figure 3d) was approximately T:**3** = 15:1. Also, the oligonucleotide carrying the anthraquinone derivative **II-An**, the retention time of which was longer than those of **II-NH_2** and **II-Ac** (Figure 3c), was hydrolyzed and the existence of the nucleoside analogue **4** was confirmed (Figure 3e). **4** had a longer retention time than that of **3**, owing to a hydrophobicity of the **An** group. The peaks for **3** and **4** were confirmed by coelution with authentic samples.

The applicability of antisense oligonucleotides as inhibitors of gene expression is limited by various factors. For instance, solubility in water, ability to hybridize to complementary targets, and resistance to nucleolitic hydrolysis are required for the antisense oligonucleotides. Furthermore, target RNAs forming duplexes with the antisense oligonucleotides must be substrates for RNase H in order to degrade the target RNAs.

The first key factor examined was the stability of duplexes consisting of the oligonucleotides carrying the functional groups and complementary strands. T_ms were measured by thermal denaturation. One-transition curves that were similar each other were observed for all melting profiles (data not shown). T_ms are shown in Tables II and III. The stability of the duplexes was examined by changing the kinds of the functional groups, their positions, and complementary strands (Table I). The stability of the duplexes depended upon the position of the functional groups and the complementary strands. With $(dA)_{16}$ as

Table II. T_ms of Duplexes[a]

	T_m (°C) complementary strands	
	poly(rA)	$(dA)_{16}$
$(T)_{16}$	31	33
I-NH_2	34	33
I-Ac	32	33
I-An	38	35
II-NH_2	30	25
II-Ac	30	24
II-An	35	29
II-Py	33	29
III-NH_2	31	25
III-An	34	27

[a] Experimental conditions are described in Experimental Procedures.

Table III. T_ms of Duplexes[a]

	T_m (°C) of complementary strands	
	poly(rA)	$(dA)_{16}$
$(T)_{16}$	31	33
II-NH_2	30	25
IV-$(NH_2)_2$	29	18
V-$(NH_2)_3$	28	7
II-An	35	29
IV-$(An)_2$	35	22
V-$(An)_3$	33	12
II-Py	35	29
IV-$(Py)_2$	32	26
V-$(Py)_3$	27	17

[a] Experimental conditions are described in Experimental Procedures.

the complementary strand, the T_ms of the duplexes carrying the linker groups in the center of them, **II-NH_2**–$(dA)_{16}$, **II-Ac**–$(dA)_{16}$, **II-An**–$(dA)_{16}$, and **II-Py**–$(dA)_{16}$, were lower than the T_m of the control duplex $(T)_{16}$–$(dA)_{16}$, but the T_ms of the duplexes carrying the linker groups at the 5′-end, **I-NH_2**–$(dA)_{16}$, **I-Ac**–$(dA)_{16}$, and **I-An**–$(dA)_{16}$, were similar to that of the control. On the other hand, when poly(rA) was used as the complementary strand, T_ms of the duplexes carrying the linker groups at their centers were similar to that of the control. Furthermore, T_ms of the duplexes carrying the linker groups at the 5′-ends were higher than that of the control.

The functional groups should be accommodated in the minor groove when the oligonucleotide analogues form duplexes with the complementary strands since the 1′-position of the sugar moiety in a duplex is in the minor groove. Since the minor groove of the B-type duplex (DNA–DNA duplexes) was narrower than that of the A-type duplex (DNA–RNA and RNA–RNA duplexes) (*14*), attachment of the bulky group at the 1′-position of the sugar in the center of the B-type duplexes may disturb the duplex conformation, but attachment at the 5′-end may not. In contrast, modification in the minor groove of the A-type duplexes did not destabilize the duplex formation. The phenomenon was supported by the CD spectroscopic study of the duplexes. The study indicated that the spectra of the duplexes containing poly(rA) as the complementary strand were almost identical to that of the control duplex $(T)_{16}$–poly(rA), but the spectra of the duplexes containing $(dA)_{16}$ were different in intensity from the spectra of $(T)_{16}$–$(dA)_{16}$ even though their splitting patterns are similar (data not shown).

Besides the minor-groove substitutions, another factor which might be considerred to estimate the stability of the duplex formation, is the lack of the methyl group at 5-position of the nucleoside analogues. Since it is well-known that the 5-methyl group of thymidine stabilizes the duplex formation (*24*), the stability of the duplexes

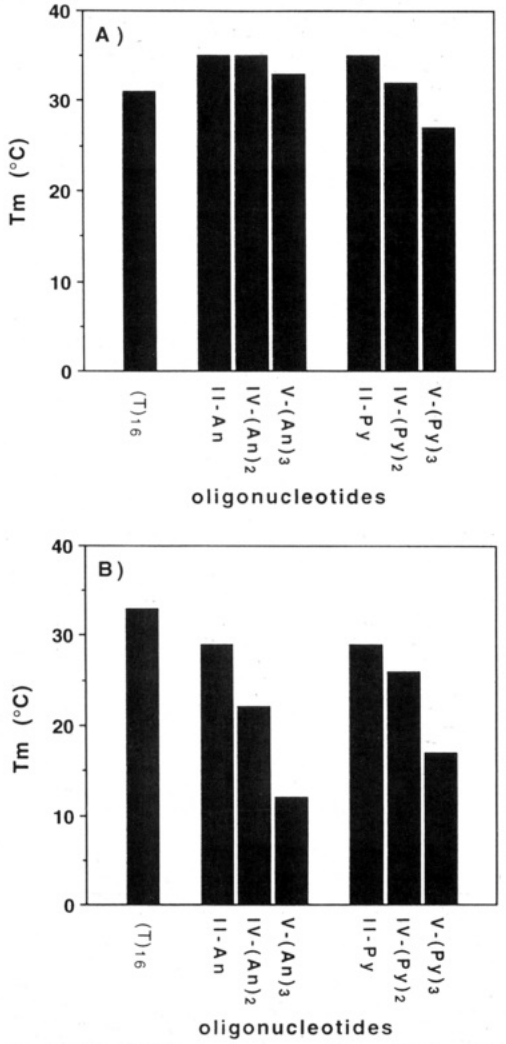


Figure 4. (a) T_ms of the duplexes consisting of the oligonucleotides and poly(rA). (b) T_ms of the duplexes consisting of the oligonucleotides and $(dA)_{16}$.

could be improved by alkyl substitution at the 5-position of the nucleoside analogues **1**–**6**.

Depending upon the kinds of the functional groups in the minor groove, the following orders of T_ms were observed: **I-An**–poly(rA) > **I-NH$_2$**–poly(rA) ≥ **I-Ac**–poly(rA) (in the duplexes modified at the 5′-end) and **II-An**–poly(rA) = **II-Py**–poly(rA) > **II-NH$_2$**–poly(rA) ≥ **II-Ac**–poly(rA) (in the duplexes modified at the center). The same order was observed for duplexes containing $(dA)_{16}$ as the complementary strand. The results are described as **An** and **Py**-conjugated duplexes > free aminobutyl duplex ≥ acetylated duplex, and the phenomenon can be interpreted as follows. A positive charge on the terminal amino group of the linker was expected to stabilize the duplex formation electrostatically. However, the acetylation (*i.e.* the erasure of the positive charge) did not destabilize the duplex formation much, probably because the effect of the positive charge was not crucial under the conditions used for the thermal denaturation study. In contrast to the acetylation, the **An** and **Py** derivatization efficiently stabilized the duplex formation even though these modifications, like the acetylation, erased the positive charge on the free amino group. Intercalation of **An** and **Py** into the base pairs or hydrophobic interaction between the functional groups and the surface of the minor groove could stabilize the duplex formation effectively.

There were no significant difference between T_ms of the duplexes carrying the diaminobutane linker (**II-NH$_2$**

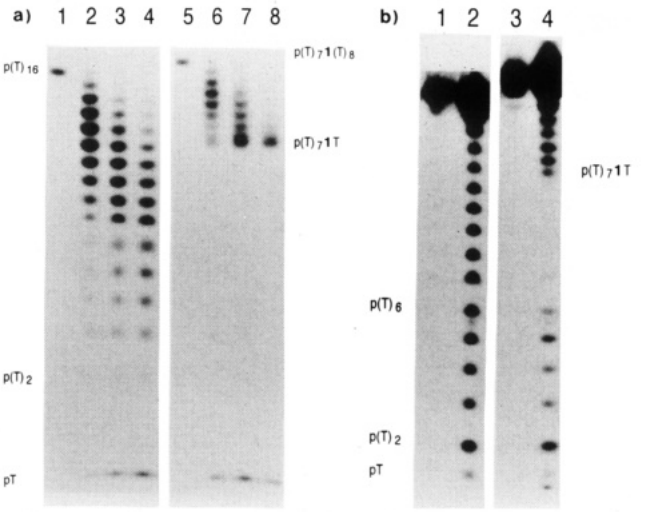


Figure 5. Polyacrylamide gel electrophoresis of oligonucleotides hydrolyzed by nucleases: (a) $(T)_{16}$ (lanes 1–4) and **II-NH$_2$** (lanes 5–8) were incubated with venom phosphodiesterase for 0 min (lanes 1 and 5), 10 min (lanes 2 and 6), 20 min (lanes 3 and 7), and 30 min (lanes 4 and 8); (b) $(T)_{16}$ (lanes 1 and 2) and **II-NH$_2$** (lanes 3 and 4) were incubated with nuclease P1 for 0 min (lanes 1 and 3) and 10 min (lanes 2 and 4). Experimental conditions are described in Experimental Procedures.

and its derivatives) and those of duplexes carrying the diaminohexane linker (**III-NH$_2$** and **III-An**). Therefore, we used the diaminobutane linker for further studies.

Then the stability of the duplexes depending upon the number of the functional groups attached to the oligonucleotides was examined. T_ms are summarized in Table III and Figure 4. As expected from above studies, the duplexes formed by $(dA)_{16}$ and the oligonucleotide analogues became less stable as the numbers of the functional groups attached to them increased (Figure 4B). In contrast, the duplexes formed by poly(rA) and the oligonucleotide analogues carrying two or three functional groups, **IV-(An)$_2$**–poly(rA), **V-(An)$_3$**–poly(rA), and **VI-(Py)$_2$**–poly(rA), were more stable than the control duplex $(T)_{16}$–poly(rA), except that the duplex carrying three **Py** groups, **V-(Py)$_3$**–poly(rA), was slightly less stable than the control (Figure 4A). Consequently, the attachment of one functional group stabilized the duplex formation with the complementary polyribonucleotide greatly and the increases of the number of the functional groups did not largely destabilize the duplex formation.

The second key factor examined was the stability of the oligonucleotides to nucleolytic degradation. Two kinds of nucleases, snake venom phosphodiesterase (a 3′-exonuclease) and nuclease P1 (an endonuclease), were used in this study. The oligonucleotides labeled at the 5′-end with ^{32}P (*23*) were incubated with an appropriate nuclease and the reaction was analyzed by polyacrylamide gel electrophoresis under denaturing conditions (*23*) (Figure 5). Although the control $(T)_{16}$ was hydrolyzed randomly by venom phosphodiesterase after 30 min (Figure 5a, lanes 2–4), **II-NH$_2$** was hydrolyzed only at the 3′-side from the nucleoside analogue (lanes 6–8). The phosphodiester linkage at the 3′-side of the nucleoside carrying the linker group was resistant to the nuclease. However, the linkage was not perfectly resistant to the nuclease and was hydrolyzed under the conditions for complete digestion (See Experimental Procedures; data not shown). Also, the phosphodiester linkages at the 3′- and 5′-sides of the nucleoside analogue were more resistant to nuclease P1 than the phosphodiester linkages beside thymidines (Figure 5b).

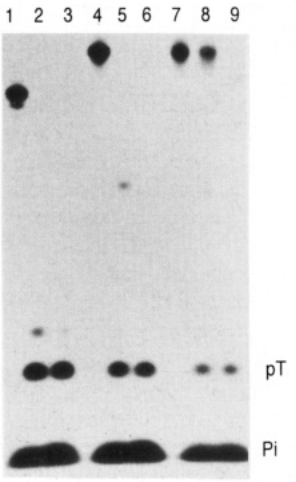


Figure 6. Polyacrylamide gel electrophoresis of oligonucleotides hydrolyzed by nuclease P1. T_{16} (lanes 1–3), **V-(NH$_2$)$_3$** (lanes 4–6), and **V-(An)$_3$** (lanes 7–9) were incubated with nuclease P1 for 0 h (lanes 1, 4, 7), 12 h (lanes 2, 5, 8), and 24 h (lanes 3, 6, 9). Experimental conditions are described in Experimental Procedures.

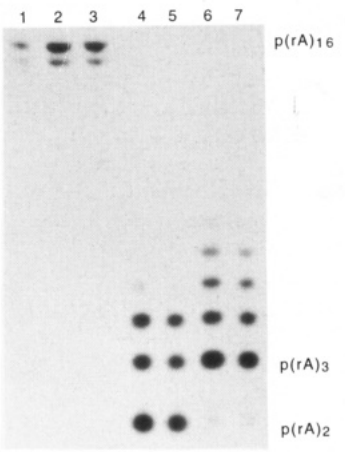


Figure 7. Polyacrylamide gel electrophoresis of $(rA)_{16}$ hydrolyzed by RNase H in the presence of complementary strands: Lane 1, $(rA)_{16}$; lane 2, $(rA)_{16}$ + enzyme; lane 3, $(rA)_{16}$ + $(T)_{16}$; lanes 4 and 5, $(rA)_{16}$ + $(T)_{16}$ + enzyme; lanes 6 and 7, $(rA)_{16}$ + **V-(An)$_3$** + enzyme. Same experiments were repeated in lanes 4 and 5 or lanes 6 and 7. Experimental conditions are described in Experimental Procedures.

To investigate the resistance of the phosphodiester linkages between the nucleoside analogues to the nuclease, the oligonucleotides carrying two or three functional groups were incubated with P1 (Figure 6). Under conditions in which the $(T)_{16}$ was hydrolyzed completely after 12 h (lane 2), the oligonucleotide carrying three aminobutane linkers, **V-(NH$_2$)$_3$**, was also hydrolyzed almost completely (lane 5). In contrast, a spot for intact **V-(An)$_3$**, the oligonucleotide carrying three **An** groups, was still observed (lane 8) under the same conditions. A bulky group, **An**, attached to the sugar moiety could increase resistance to the endonuclease. Interestingly, in lane 8, just three spots, corresponding to P_i (phosphoric acid), pT, and intact **V-(An)$_3$**, and a very faint spot for a fragment of the oligonucleotide hydrolyzed at the middle of it were observed. This lot of nuclease P1 seemed to contain a certain phosphatase activity that might hydrolyze the phosphomonoester at the 5′-end to release P_i. Therefore, it can be interpreted that the spot for intact **V-(An)$_3$** could be decreased by releasing $^{32}P_i$ from the 5′-end by a phosphatase activity, hydrolyzing the phosphodiester linkage at the 5′-end by the phosphodiesterase activity, but phosphodiester linkages inside the oligonucleotides were not hydrolyzed seriously. Several studies investigated how the oligonucleotides modified at the 3′-ends were resistant to 3′-exonucleases (*8*, *9*). Consequently, moderately and properly modified oligonucleotides containing the nucleoside analogues not only inside the oligonucleotide but also at the 3′- and 5′-ends could be highly resistant to the endonuclease.

The last key factor examined was degradation of the target RNA by RNase H. The duplexes consisting of **V-(An)$_3$** and $(rA)_{16}$ labeled with ^{32}P at the 5′-end was incubated with RNase H, and the products were analyzed by polyacrylamide gel electrophoresis (Figure 7). $(rA)_{16}$ in the **V-(An)$_3$**–$(rA)_{16}$ molecules duplex (lanes 4 and 5) and the $(T)_{16}$–$(rA)_{16}$ duplex (lanes 6 and 7) were similarly hydrolyzed by RNase H. It has been known that RNase H recognize sugar puckering distinctly so that duplexes formed by target RNAs and sugar-modified oligonucleotides were not substrates for RNase H (*15*). However, it has also been known that "chimeric" oligonucleotides composed of regions containing modified sugar derivatives linked to an unmodified region can form duplexes with target RNAs and the duplexes are substrates for RNase H (*17*). Furthermore, it was obvious from our results that RNase H can cleave the duplex carrying the bulky group at every fourth nucleoside.

In above study, we demonstrated that the duplexes formed by the oligonucleotide analogues and the ribonucleotide were substrates for RNase H since the oligonucleotides were substituted moderately so that the enzyme can recognize regions containing unmodified backbone as substrates. Furthermore, the moderate substitution could be enough for providing resistance to exo and endonucleases, even if the oligonucleotides contain unmodified nucleosides and phosphodiester linkages. Consequently, the results may indicate that the properly modified oligonucleotides containing the unmodified phosphodiester linkages can be applied for antisense study.

CONCLUSION

It has been shown in this study that the oligonucleotide analogues with normal phosphodiester linkages can be used as potential antisense agents. The duplexes formed by the oligonucleotides carrying the functional groups at the 1′-position of the sugar moiety and the complementary polyribonucleotide were more stable than the unmodified control duplex. Also, the oligonucleotide analogues were resistant to degradation by exo and endonuclease. Moreover, the duplexes formed by the oligonucleotide analogues and the ribonucleotides were substrates for RNase H. The results indicated that the moderately substituted oligonucleotides could be applicable to antisense studies.

EXPERIMENTAL PROCEDURES

General Experimental. Melting points were measured on a Yanagimoto MP-3 micromelting point apparatus (Yanagimoto, Japan) and are uncorrected. Mass spectra (MS) were measured on a JEOL JMX-DX303 spectrometer (JEOL, Japan) at an ionizing voltage of 70 eV. Field desorption mass spectra (FD-MS) and fast atom bombardment mass spectra (FAB-MS) were measured on a JEOL JMS-HX110 at an ionizing voltage of 70 eV. The ^1H NMR spectra were recorded on a JEOL JNM-FX 100FT (100-MHz) spectrometer or a JEOL JNM-GX 270 (270-MHz) spectrometer or a JEOL JNM-EX 400 (400-MHz) spectrometer with tetramethylsilane as an internal standard. Chemical shifts are reported in parts per million (δ), and signals are expressed as s (singlet), d (doublet),

t (triplet), m (multiplet), or br (broad). All exchangeable protons were detected by disappearance on the addition of D_2O. TLC was done on Merck Kieselgel F254 precoated plates (Merck). The silica gel, the neutralized silica gel, or the silanized silica gel used for column chromatography were YMC gel 60A (70-230 mesh) (YMC Co., Ltd.), or ICN silica 60A (ICN Biochemicals), or preparative C18 125Å (Waters), respectively. UV absorption spectra were recorded with a Shimadzu UV-240 spectrophotometer (Shimadzu Corp.).

1-(1,4,6-Tri-*O*-benzoyl-β-D-fructofuranosyl)uracil (8). 2,3′-*O*-Anhydro-1-(1,4,6-tri-*O*-benzoyl-β-D-fructofuranosyl)uracil (7) (*18*) (12.0 g, 21.1 mmol) was dissolved in a mixture of DMF (500 mL) and 2 N HCl (200 mL), and the mixture was stirred at room temperature for 2 days. The reaction mixture was neutralized by adding 4 N NaOH (100 mL), and precipitates were filtered off. The liquid layer was concentrated to dryness *in vacuo*, and the residue was dissolved in ethyl acetate. The solution was successively washed with water (three times) and then brine, dried over Na_2SO_4, and concentrated to about one-fourth. The resulting precipitates were collected to give 1 (11.2 g, 91%). The filtrate was chromatographed over a silica gel column (2.7 × 7 cm) with 30–70% ethyl acetate in *n*-hexane as eluents. Fractions were concentrated to give a further amount of 1 (0.6 g, 5%). The physical data were identical with those of an authentic sample previously reported (*25*).

1-(1,4,6-Tri-*O*-benzoyl-3-deoxy-β-D-psicofuranosyl)uracil (10). A mixture of 8 (14.8 g, 24.8 mmol) and *N,N′*-thiocarbonyldiimidazole (*19*) (14.1 g, 74.4 mmol) in DMF (130 mL) was stirred at room temperature for 3 days under an Ar atmosphere. The reaction mixture was diluted with ethyl acetate (500 mL) and the solution was successively washed with water (50 mL, 5 times) and then brine, dried over Na_2SO_4, and concentrated to give thiocarbonylimidazolide 9. After being dehydrated by coevaporation with toluene twice, 9 was dissolved in toluene (200 mL) containing AIBN (200 mg) and Bu_3SnH (*19*) (19 mL, 74.4 mmol). The mixture was heated under reflux for 40 min, then the solvent was removed by evaporation. The residue was directly crystallized from a mixture of MeOH and $CHCl_3$ to give 10 (12.2 g, 87%). The mother liquid was concentrated and chromatographed over a silica gel column (6 × 15 cm) with 10–50% ethyl acetate in *n*-hexane as eluents. Fractions were concentrated to give a further amount of 10 (0.7 g, 5%): ^1H NMR (270 MHz, $CDCl_3$) 8.21 (1 H, br s, 3-NH), 8.11–7.37 (16 H, m, Ph and H-6), 5.69 (1 H, m, H-4′), 5.54 (1 H, d, H-5, $J_{5,6}$ = 8.8 Hz), 4.92–4.78 (4 H, m, H-1′a, H-5′, and H-6′), 4.50 (1 H, d, H-1′b, $J_{1'gem}$ = 9.3 Hz), 3.12 (2 H, m, H-3′a,b).

1-[3-Deoxy-4,6-*O*-(1,1,3,3-tetraisopropyldisiloxane-1,3-diyl)-β-D-psicofuranosyl]uracil (11). (*20*) NaOMe (1 N, 15 mL) was added to a suspension of 10 (9.5 g, 16.7 mmol) in MeOH (140 mL) and the mixture was stirred at room temperature for 13 h. The reaction mixture was neutralized by addition of Dowex 50 (H^+ form) and the resin was filtered and washed with hot MeOH. The combined filtrate and washings were concentrated to dryness *in vacuo*. After it was successively coevaporated with benzene (three times) and then DMF (once), the deprotected compound was dissolved in DMF (100 mL). Imidazole (2.5 g, 36.8 mmol) was added to the solution and the mixture was stirred at −30 °C under an Ar atmosphere. $TIPDSCl_2$ (4.9 mL, 15.5 mmol) was added dropwise over 20 min to the solution and the mixture was stirred for 2 h at −30 °C, then overnight at room temperature. MeOH (5 mL) was added to the reaction mixture, and the solvents were concentrated. The residue was chromatographed over a silica gel column (5 × 12 cm) with 0–20% EtOH in $CHCl_3$ as eluents. Fractions were concentrated to give 11 (4.8 g, 57% as a white foam): EI-MS *m/z* 469 ($M^+ - CH_2OH$), 457 (M^+-isopropyl), 389 (M^+-base); ^1H NMR (270 MHz, $CDCl_3$) 8.26 (1 H, br s, 3-NH), 7.95 (1 H, d, H-6, $J_{5,6}$ = 8.1 Hz), 5.67 (1 H, dd, H-5, $J_{5,NH}$ = 2.4 Hz), 4.34 (1 H, ddd, H-4′, $J_{4',5'}$ = 8.1, $J_{3'a,4'}$ = 7.0, $J_{3'b,4'}$ = 10.6 Hz), 4.13–3.95 (4 H, m, H-6′a,b and H-1′a,b, $J_{6'gem}$ = 13.2, $J_{5',6'}$ = 2.6, $J_{1'gem}$ = 12.0 Hz), 3.84 (1 H, dt, H-5′, $J_{5',6'}$ = 2.6, $J_{4',5'}$ = 8.1 Hz), 2.93 (1 H, dd, H-3′a, $J_{3'gem}$ = 13.6, $J_{3'a,4'}$ = 7.0 Hz), 2.43 (1 H, dd, H-3′b, $J_{3'b,4'}$ = 10.6 Hz), 1.05 (28 H, m, isopropyl).

1′-[[[*N*-(4-Aminobutyl)carbamoyl]oxy]methyl]-3′,5′-*O*-(1,1,3,3-tetraisopropyldisiloxane-1,3-diyl)-2′-deoxyuridine (12). After it was dehydrated by coevaporation three times with toluene, 11 (300 mg, 0.6 mmol) was dissolved in dioxane (5 mL). *N,N′*-Carbonyldiimidazole (146 mg, 0.9 mmol) was added to the solution and the mixture was stirred for 2 h at room temperature, then a further amount of *N,N′*-carbonyldiimidazole (49 mg) was added to the mixture, which was stirred for a further 2 h. The reaction mixture was diluted with H_2O (30 mL) and the solution was extracted with ethyl acetate (40 mL, three times). The combined organic layers (about 100 mL) were added slowly to a solution of 1,4-diaminobutane (0.3 mL, 3.0 mmol) in ethyl acetate (30 mL). The reaction proceeded immediately. The solution was successively washed with water (five times) and then brine, dried over Na_2SO_4, and concentrated to give 12 (360 mg, 99% as a foam), which was used for the next reaction without further purification: EI-MS *m/z* 614 (M^+), 571 (M^+-isopropyl), 503 (M^+-base); ^1H NMR (270 MHz, $CDCl_3$) 10.70 (1 H, br s, 3-NH), 7.93 (1 H, d, H-6, $J_{5,6}$ = 8.3 Hz), 5.99 (1 H, br t, OCONH), 5.73 (1 H, d, H-5), 4.81 (1 H, d, H-1″a, $J_{1''gem}$ = 11.5 Hz), 4.38–4.25 (2 H, m, H-1″b and H-3′), 4.02 (2 H, m, H-5′a,b), 3.86 (1 H, m, H-4′), 3.05 (5 H, m, H-2′a, H-2″, and H-5″), 2.26 (1 H, dd, H-2′b), 1.75, 1.55 (each 2 H, m, H-3″a,b, or H-4″a,b), 1.00 (28 H, m, isopropyl).

1′-[[[*N*-[4-[(9-Fluorenylmethoxycarbonyl)amino]-butyl]carbamoyl]oxy]methyl]-3′,5′-*O*-(1,1,3,3-tetraisopropyldisiloxane-1,3-diyl)-2′-deoxyuridine (14). Pyridine (65 μL, 0.8 mmol) and 9-fluorenylmethyl chloroformate (FmocCl, 207 mg, 0.8 mmol) were added to a solution of 12 (326 mg, 0.53 mmol) in CH_2Cl_2 (5 mL). The reaction mixture was stirred for 2 h at room temperature. Ethyl acetate (50 mL) was added to the reaction mixture and the solution was successively washed with water (three times) and then brine, dried over Na_2SO_4, and concentrated. The residue was chromatographed over a silica gel column (1.7 × 8 cm) with 0–4% EtOH in $CHCl_3$ as eluents. Fractions were concentrated to give 13 (391 mg, 88% as a white foam): FD-MS *m/z* 836 (M^+); ^1H NMR (400 MHz, $CDCl_3$) 8.18 (1 H, br s, 3-NH), 7.90 (1 H, d, H-6, $J_{5,6}$ = 8.3 Hz), 7.76–7.30 (8 H, m, Fmoc), 5.66 (1 H, d, H-5), 4.75 (1 H, d, H-1″a, $J_{1''gem}$ = 11.3 Hz), 4.41 (2 H, d, Fmoc-CH_2, J_{vic} = 7.3 Hz), 4.36 (1 H, d, H-1″b), 4.35 (1 H, m, H-3′), 4.22 (1 H, t, H-9 of Fmoc, J_{vic} = 7.3 Hz), 4.20 (2 H, dd, H-5′a,b, $J_{5'gem}$ = 13.0, $J_{4',5'}$ = 3.0 Hz), 3.85 (1 H, dt, H-4′, $J_{3',4'}$ = 8.3 Hz), 3.19 (4 H, m, H-2″ and H-5″), 3.05 (1 H, dd, H-2′a, $J_{2'gem}$ = 13.7, $J_{2'a,3'}$ = 6.6 Hz), 2.34 (1 H, dd, H-2′, $J_{2'b,3'}$ = 9.9 Hz), 1.50 (4 H, m, H-3″ and 4″), 1.00 (28 H, m, isopropyl).

1′-[[[*N*-[4-[(9-Fluorenylmethoxycarbonyl)amino]-hexyl]carbamoyl]oxy]methyl]-3′,5′-*O*-(1,1,3,3-tetraisopropyldisiloxane-1,3-diyl)-2′-deoxyuridine (15). Compound 11 (860 mg, 1.7 mmol) was treated with *N,N*-carbonyldiimidazole (837 mg, 5.1 mmol) and 1,6-diaminohexane (3.6 g, 31 mmol) to give a nucleoside carrying a

hexylamine group (**13**), which was treated with FmocCl (480 mg, 1.9 mmol) as described above. The mixture was chromatographed over a silica gel column (2.2 × 12 cm) with 0–2% EtOH in $CHCl_3$ as eluents. Fractions were concentrated to give **15** (1.0 g, 68% from **11**, as a white foam): FAB-MS *m/z* 865 ($M^+ + 1$); ^1H NMR (270 MHz, $CDCl_3$) 8.21 (1 H, br s, 3-NH), 7.89 (1 H, d, H-6, $J_{5,6}$ = 8.2 Hz), 7.78–7.28 (8 H, m, Fmoc), 5.65 (1 H, d, H-5), 4.88 and 4.74 (each 1 H, br t, OCONH), 4.72 (1 H, d, H-1″a, $J_{1''gem}$ = 11.5 Hz), 4.45–4.30 (4 H, m, H-3′, H-1″b, and Fmoc-CH_2), 4.22 (1 H, t, H-9 of Fmoc), 4.08 (2 H, m, H-5′a,b), 3.84 (1 H, dt, H-4′, $J_{3',4'}$ = 8.2 Hz), 3.18 (4 H, m, H-2″ and H-7″), 3.04 (1 H, dd, H-2′a, $J_{2''gem}$ = 13.7, $J_{2'a,3'}$ = 7.1 Hz), 2.33 (1 H, dd, H-2′b, $J_{2'b,3'}$ = 10.0 Hz), 1.50 (4 H, m, H-3″ and H-6″), 1.30 (4 H, m, H-4″ and H-5″), 1.00 (28 H, m, isopropyl). Anal. Calcd for $C_{44}H_{64}N_4O_{10}Si_2$: C, 61.08; H, 7.46; N, 6.48. Found: C, 61.09; H, 7.36; N, 6.16.

1′-[[[*N*-[4-[(9-Fluorenylmethoxycarbonyl)amino]butyl]carbamoyl]oxy]methyl]-2′-deoxyuridine (16). Bu_4NF (1 M, 1.2 mL, THF solution) was added to a solution containing **14** (391 mg, 0.47 mmol) and acetic acid (150 μL) in THF (10 mL), and the whole was stirred overnight at room temperature. MeOH (1 mL) was added to the mixture and the solution was concentrated to dryness. The residue was chromatographed over a silica gel column (1.7 × 6 cm) with 0–10% EtOH in $CHCl_3$ as eluents. Fractions were concentrated to give **16** (273 mg, 98% as a white foam): FAB exact mass calcd for $C_{30}H_{35}O_9N_4$ 595.2403, found 595.2375; ^1H NMR (270 MHz, DMSO-d_6) 7.88 (1 H, d, H-6, $J_{5,6}$ = 7.7 Hz), 7.90–7.30 (8 H, m, Fmoc), 7.29 and 7.12 (each 1 H, br t, OCONH), 5.46 (1 H, d, H-5), 5.21 (1 H, d, 3′-OH, J = 5.3 Hz), 4.60 (1 H, d, H-1″a, $J_{1''gem}$ = 11.4 Hz), 4.31–3.99 (6 H, m, H-1″b, H-3′, H-4′, H-9 of Fmoc, and Fmoc-CH_2), 3.45 (2 H, m, H-5′a,b), 2.95 (4 H, m, H-2″ and H-5″), 2.65 (1 H, dd, H-2′a, $J_{2''gem}$ = 14.5, $J_{2'a,3'}$ = 6.5 Hz), 2.27 (1 H, dd, H-2′b, $J_{2'b,3'}$ = 3.5 Hz), 1.34 (4 H, m, H-3″ and H-4″).

1′-[[[*N*-[4-[(9-Fluorenylmethoxycarbonyl)amino]hexyl]carbamoyl]oxy]methyl]-2′-deoxyuridine (17). Compound **15** (980 mg, 1.1 mmol) was treated with Bu_4NF as described above. The product was purified by silica gel chromatography (2.8 × 10 cm) with 0–12% EtOH in $CHCl_3$ as eluents. Fractions were concentrated to give **17** (660 mg, quant. as a white foam): FAB exact mass calcd for $C_{32}H_{39}N_4O_9$ 623.2717, found 623.2719; ^1H NMR (270 MHz, $CDCl_3$) 9.41 (1 H, br s, 3-NH), 7.98 (1 H, d, H-6, $J_{5,6}$ = 8.2 Hz), 7.74–7.25 (8 H, m, Fmoc), 5.60 (1 H, d, H-5), 5.42 (1 H, br s, 3′-OH), 5.19 (1 H, br s, 5′-OH), 4.67 (1 H, d, H-1″a, $J_{1''gem}$ = 12.1 Hz), 4.45–4.16 (6 H, m, Fmoc-CH_2, H-9 of Fmoc, H-1″b, H-3′, and H4′), 3.28 (2 H, m, H-5′a,b), 3.09 (4 H, m, H-2″ and H-7″), 2.87 (1 H, m, H-2′a), 2.50 (1 H, m, H-2′b), 1.75–1.60 (8 H, m, H-3″, H-4″, H-5″, and H-6″).

1′-[[[*N*-[4-[(9-Fluorenylmethoxycarbonyl)amino]butyl]carbamoyl]oxy]methyl]-5′-*O*-(dimethoxytrityl)-2′-deoxyuridine (18). After it was dehydrated by coevaporation with pyridine (three times), **16** (279 mg, 0.47 mmol) was dissolved in pyridine (3 mL). DMTrCl (167 mg, 0.49 mmol) was added to the solution and the mixture was stirred at room temperature. After 3 h, 8 mg of DMTrCl was added and the reaction was stirred overnight. MeOH (1 mL) was added to the reaction mixture, the solvents were removed, and the residue was chromatographed over a silica gel column (1.7 × 7 cm) with 0–4% EtOH in $CHCl_3$ as eluents. Fractions were concentrated to give **18** (350 mg, 83% as a white foam): FAB exact mass calcd for $C_{51}H_{53}O_{11}N_4$ 897.3711, found 897.3738; ^1H NMR (270 MHz, $CDCl_3$) 8.25 (1 H, br s, 3-NH), 7.78 (1 H, d, H-6, $J_{5,6}$ = 8.2 Hz), 7.76–7.20 (8 H, m, Fmoc), 7.33–6.78 (13 H, m, DMTr), 5.49 (1 H, dd, H-5), 5.02 and 4.95 (each 1 H, br t, OCONH), 4.65 (1 H, d, H-1″a, $J_{1''gem}$ = 11.5 Hz), 4.42–4.20 (7 H, m, H-3′, 4′, 5′a,b, H-9 of Fmoc, and Fmoc-CH_2), 3.77 (6 H, s, OMe), 3.17 (4 H, m, H-2″ and H-5″), 2.84 (1 H, dd, H-2′a, $J_{2'gem}$ = 15.3, $J_{2'a,3'}$ = 5.8 Hz), 2.66 (1 H, br d, H-2′b), 2.47 (1 H, br s, 3′-OH), 1.48 (4 H, m, H-3″ and H-4″).

1′-[[[*N*-[4-[(9-Fluorenylmethoxycarbonyl)amino]hexyl]carbamoyl]oxy]methyl]-5′-*O*-(dimethoxytrityl)-2′-deoxyuridine (19). After it was dehydrated by coevaporation with pyridine (three times), **17** (365 mg, 0.59 mmol) was dissolved in pyridine (3 mL), then DMTrCl (208 mg, 0.62 mmol) was added to the solution. The mixture was stirred for 2.5 h at room temperature, then MeOH (1 mL) was added to the reaction and the solvents were removed. The residue was dissolved in ethyl acetate and the solution was washed with water, dried over Na_2SO_4, and concentrated. The residue was chromatographed over a neutralized silica gel column (2.7 × 6 cm) with 35–100% ethyl acetate in *n*-hexane as eluents. Fractions were concentrated to give **19** (445 mg, 82% as a white foam). FAB-MS *m/z* 926 ($M^+ + 1$); ^1H NMR (270 MHz, $CDCl_3$) 8.35 (1 H, br s, 3-NH), 7.77 (1 H, d, H-6, $J_{5,6}$ = 8.2 Hz), 7.77–7.20 (8 H, m, Fmoc), 7.29–6.81 (13 H, m, phenyl), 5.47 (1 H, dd, H-5), 4.90 (2 H, br s, OCONH), 4.62 (1 H, d, H-1″a, $J_{1''gem}$ = 11.7 Hz), 4.42–4.18 (7 H, m, Fmoc-CH_2, H-9 of Fmoc, H-1″b, H-3′, H-4′, and H-5′a,b), 3.77 (6 H, s, OMe), 3.18 (4 H, m, H-2″ and H-7″), 2.82 (1 H, m, H-2′a), 2.64 (1 H, m, H-2′b), 2.62 (1 H, br s, 3′-OH), 1.62 (8 H, m, H-3″, H-4″, H-5″, and H-6″).

β-Cyanoethyl [1′-[[[*N*-[4-[(9-Fluorenylmethoxycarbonyl)amino]butyl]carbamoyl]oxy]methyl]-5′-*O*-(dimethoxytrityl)-2′-deoxyuridin-3′-*O*-yl]-*N*,*N*-diisopropylphosponamidite (20). After it was dehydrated by coevaporation with pyridine twice, **18** (172 mg, 0.19 mmol) was dissolved in CH_2Cl_2 (5 mL) containing *N*,*N*-diisopropylethylamine (50 μL, 0.29 mmol). 2-Cyanoethyl *N*,*N*-diisopropylphosphoramidochloridite (*26*) (50 μL, 0.23 mmol) was added to the solution and the reaction mixture was stirred for 0.5 h at room temperature. $CHCl_3$ and aqueous saturated $NaHCO_3$ were added to the mixture, and the separated organic layer was washed with aqueous saturated $NaHCO_3$ (three times), dried over Na_2SO_4, and concentrated. The residue was chromatographed over a silica gel column (1.8 × 5.5 cm) with ethyl acetate as an eluent. Fractions were concentrated to give **19** (167 mg, 80% as a foam): FAB exact mass calcd for $C_{60}H_{70}N_6O_{12}P$ 1097.4789, found 1097.4860; ^{31}P NMR (270 MHz, $CDCl_3$) 149.32, 149.12 (diastereomers).

β-Cyanoethyl [1′-[[[*N*-[4-[(9-Fluorenylmethoxycarbonyl)amino]hexyl]carbamoyl]oxy]methyl]-5′-*O*-(dimethoxytrityl)-2′-deoxyuridin-3′-*O*-yl]-*N*,*N*-diisopropylphosphonamidite (21). Compound **19** (388 mg, 0.42 mmol) was phosphitylated as described above to give **21** (472 mg, 98% as a yellow foam).

1′-[[[*N*-(4-Aminobutyl)carbamoyl]oxy]methyl]-2′-deoxyuridine (1). Compound **16** (75 mg, 0.13 mmol) was dissolved in concentrated NH_4OH (28%, 4 mL) and the solution was kept overnight at room temperature. The mixture was concentrated to dryness and the residue was chromatographed over a silanized silica gel column (0.7 × 1.5 cm) with water as an eluent. Fractions were concentrated and the residue was successively coevaporated with EtOH and then toluene to give **1** (44 mg, 95% as a solid): FAB exact mass calcd for $C_{15}H_{25}N_4O_7$ 373.1723, found 373.1731; ^1H NMR (270 MHz, DMSO-d_6) 7.86 (1 H, d, H-6, $J_{5,6}$ = 8.3 Hz), 7.13 (1 H, br t, OCONH), 5.45 (1 H,

d, H-5), 4.61 (1 H, d, H-1″a, $J_{1''gem}$ = 11.0 Hz), 4.15–3.98 (3 H, m, H-1″b, H-3′, and H-4′), 3.50 (2 H, m, H-5′a,b), 2.90 (4 H, m, H-2″ and H-5″), 2.65 (1 H, dd, H-2′a), 2.27 (1 H, dd, H-2′b), 1.30 (4 H, m, H-3″ and H-4″).

1′-[[[*N*-(4-Acetamidobutyl)carbamoyl]oxy]methyl]-2′-deoxyuridine (3). Triethylamine (42 μL, 0.3 mmol) and acetic anhydride (23 μL, 0.24 mmol) were added to a solution of **12** (0.2 mmol) in CH_2Cl_2 (3 mL), and the reaction mixture was stirred for 20 min at room temperature. MeOH (1 mL) was added to the reaction, and the solvents were evaporated. The residue was chromatographed over a silica gel column (1.8 × 6 cm) with 0–4% EtOH in $CHCl_3$ as eluents. Fractions were concentrated and white crystals were collected to give the TIPDS derivative of **3** (111 mg, 85%). An analytical sample was recrystallized from a mixture of ethyl acetate and ethyl ether: mp 129.5–130.5 °C; FAB-MS *m/z* 657 ($M^+ + 1$); ^1H NMR (270 MHz, $CDCl_3$) 8.38 (1 H, br s, 3-NH), 7.90 (1 H, d, H-6, $J_{5,6}$ = 8.2 Hz), 5.88 (1 H, br s, OCON*H*), 5.66 (1 H, dd, H-5, $J_{NH,5}$ = 2.3 Hz), 4.87 (1 H, br t, NH of CH_3CONH), 4.83 (1 H, dd, H-1″a, $J_{1''gem}$ = 11.5 Hz), 4.35 (1 H, ddd, H-3′, $J_{2'a,3'}$ = 6.6, $J_{2'b,3'}$ = 9.9, $J_{3',4'}$ = 8.2 Hz), 4.30 (1 H, d, H-1″b), 4.03 (2 H, dd, H-5′a,b, $J_{5'gem}$ = 6.6, $J_{4',5'}$ = 2.8 Hz), 3.86 (1 H, dt, H-4′), 3.23 (4 H, m, H-2″ and H-5″), 3.08 (1 H, dd, H-2′a, $J_{2'gem}$ = 13.7 Hz), 2.35 (1 H, dd, H-2′b), 2.03 (3 H, s, Ac), 1.48 (4 H, m, H-3″ and H-4″), 1.00 (28 H, m, isopropyl). Anal. Calcd for $C_{29}H_{52}N_4O_9Si_2$: C, 53.02; H, 7.98; N, 8.53. Found: C, 53.03; H, 8.00; N, 8.62.

A 1 M Bu_4NF solution (THF, 0.3 mL) was added to the solution of the above nucleoside (92 mg, 0.14 mmol) in THF (2 mL). The whole was stirred for 10 min at room temperature, then MeOH (1 mL) was added to the reaction, and the solvents were evaporated. The residue was chromatographed over a silica gel column (1.8 × 6.5 cm) with 0–20% EtOH in $CHCl_3$ as eluents. Fractions were concentrated to give **3** (49 mg, 84% as a solid): FAB-MS *m/z* 415 ($M^+ + 1$); ^1H NMR (270 MHz, DMSO-d_6) 11.12 (1 H, br s, 3-NH), 7.86 (1 H, d, H-6, $J_{5,6}$ = 8.2 Hz), 7.76 and 7.14 (each 1 H, br t, CH_3CONH), 5.46 (1 H, d, H-5), 5.22 (1 H, d, 3′-OH, J = 3.8 Hz), 4.88 (1 H, t, 5′-OH, J = 5.5 Hz), 4.61 (1 H, d, H-1″a, $J_{1''gem}$ = 11.6 Hz), 4.12 (2 H, m, H-1″b and H-3′), 3.99 (1 H, m, H-4′), 3.42 (2 H, m, H-5′a,b), 2.91 (4 H, m, H-2″ and H-5″), 2.64 (1 H, dd, H-2′a, $J_{2'gem}$ = 14.8, $J_{2'a,3'}$ = 6.1 Hz), 2.27 (1 H, dd, H-2′b, $J_{2'b,3'}$ = 3.0 Hz), 1.77 (3 H, s, CH_3CO), 1.30 (4 H, m, H-3″ and H-4″).

1′-[[[*N*-[4-[(2-Anthraquinonylcarbonyl)amino]-butyl]carbamoyl]oxy]methyl]-2′-deoxyuridine (4). Thionyl chloride (0.5 mL) was added to a solution of anthraquinone-2-carboxylic acid (980 mg, 0.32 mmol) in DMF (1 mL) and the mixture was concentrated, then the residue was dissolved in pyridine (5 mL). The solution was added dropwise to a solution of **14** (105 mg, 0.17 mmol) in pyridine (5 mL) at 0 °C. The whole was stirred for 0.5 h at 0 °C, then the solvent was evaporated and the residue was dissolved in ethyl acetate. The solution was successively washed with water (three times) and then brine, dried over Na_2SO_4, and concentrated. The residue was chromatographed over a silica gel column (2.8 × 7 cm) with 0–3% EtOH in $CHCl_3$ as eluents. Fractions were concentrated to give TIPDS derivative of **4** (127 mg, 87% as a solid): mp 167.5–169 °C; FAB-MS *m/z* 849 (M^+). Anal. Calcd for $C_{42}H_{56}N_4O_{11}Si_2$: C, 59.41; H, 6.65; N, 6.60. Found: C, 59.27; H, 6.61; N, 6.61.

Bu_4NF (1 M, THF, 0.23 mL) was added to a solution of the above nucleoside (65 mg, 77 μmol) in THF (2 mL). After 15 min, the mixture was concentrated and the residue was chromatographed over a silica gel column (1.8 × 7 cm) with 0–12% EtOH in $CHCl_3$ as eluents. Fractions were concentrated to give **4** (37 mg, 79% as a gum): UV (MeOH) λ_{max} (nm) 257, 330; ^1H NMR (270 MHz, DMSO-d_6) 11.10 (1 H, br s, 3-NH), 8.91 and 7.15 (each 1 H, br t, OCON*H*), 8.63–7.91 (7 H, m, **An**), 7.85 (1 H, d, H-6, $J_{5,6}$ = 8.2 Hz), 5.45 (1 H, d, H-5), 5.20 (1 H, d, 3′-OH, J = 3.3 Hz), 4.85 (1 H, t, 5′-OH, J = 5.2 Hz), 4.59 (1 H, d, H-1″a, $J_{1''gem}$ = 11.0 Hz), 4.11 (2 H, m, H-1″b and H-3′), 3.98 (1 H, m, H-4′), 3.40 (2 H, m, H-5′a,b), 3.15 and 2.92 (each 2 H, m, H-2″ and H-5″), 2.65 (1 H, dd, H-2′a, $J_{2'gem}$ = 14.7, $J_{2'a,3'}$ = 5.9 Hz), 2.20 (1 H, m, H-2′b), 1.50 (4 H, m, H-3″ and H-4″).

***N*-[(Anthraquinone-2-carbonyl)oxy]succinimide (22).** 1-Ethyl-3-[(3-(dimethylamino)propyl]carbodiimide hydrochloride (976 mg, 0.4 mmol) and *N*-hydroxysuccinimide (45 mg, 0.4 mmol) were added to a solution of anthraquinone-2-carboxylic acid (51 mg, 0.2 mmol) in a mixture of THF and DMF (10:1, 5.5 mL), and the whole was stirred for 2 h at room temperature. The solvents were evaporated, the residue was dissolved in CH_2Cl_2, and the solution was successively washed with water, aqueous saturated $NaHCO_3$, and then brine, dried over Na_2SO_4, and concentrated. A mixture of ethyl acetate and acetone was added to the residue and the resulting precipitate was collected to give **22** (57 mg, 82%): EI-MS *m/z* 349 (M^+); ^1H NMR (100 MHz, $CDCl_3$) 9.08–7.24 (7 H, m, anthraquinone), 2.96 (4 H, m, $-CH_2CH_2-$). Anal. Calcd for $C_{19}H_{11}NO_6$: C, 65.33; H, 3.17; N, 4.01. Found: C, 65.04; H, 3.05; N, 3.97.

Synthesis of Oligonucleotides. Oligonucleotides were synthesized on a DNA synthesizer (Applied Biosystem Model 381A) by the phosphoramidite method (*21*). Synthesis was monitored by spectrophotometric measurement of released dimethoxytrityl cation at 500 nm on each addition. Then, fully protected oligonucleotides were deprotected and purified by the same procedure as for the purification of natural oligonucleotides. That is, each oligonucleotide linked on the resin was treated with concentrated NH_4OH for 5 h at 55 °C, then the released oligonucleotide was chromatographed over a C-18 silica gel column (1 ×10 cm, Waters) with a linear gradient of acetonitrile in 0.1 M TEAA buffer (pH 7.0). Fractions were concentrated and the residue was treated with 80% acetic acid for 20 min at room temperature. The solution was concentrated and the residue was coevaporated with water. The residue was dissolved in water and the solution was washed with ethyl ether, then the water layer was concentrated to give a deprotected oligonucleotide. The sample was purified by HPLC with the C-18 silica gel column (Inertsil ODS-2, GL Science Inc.) when necessary.

Acetylation of Oligonucleotides. A solution containing each oligonucleotide (1 OD unit at 254 nm) and acetic anhydride (2 μL) in 0.2 M HEPES buffer (500 μL, pH 7.8) was kept for 50 min at room temperature. The oligonucleotide was passed through a short C-18 column (Dispo SPE C-18, YMC) and was used for next studies without further purification.

Reaction of Oligonucleotides with *N*-[(Anthraquinone-2-carbonyl)oxy]succinimide. A solution of **22** (0.5 mg) in DMF (70 μL) was added to a solution of each oligonucleotide (1.5 OD units at 254 nm) in 50 mM $NaHCO_3$–Na_2CO_3 (70 μL, pH 10.3) and the mixture was kept overnight at room temperature. After the pH of the mixture was adjusted to 3 by adding 0.1 N HCl, the solution was washed with ethyl acetate (four times), then saturated $NaHCO_3$ was added to the water layer to neutralize it.

The reaction mixture was purified by HPLC to remove the reagents to give the oligonucleotide carrying **An**.

Pyrene Derivatization of Oligonucleotides. A solution of *N*-succinimidyl pyrenebutanoate (*22*) (0.5 mg) in DMF (50 μL) was added to a solution of each oligonucleotide (1.5 OD units at 254 nm) in 50 mM $NaHCO_3$–Na_2CO_3 (50 μL, pH 10.3) and the mixture was kept for 2 h at room temperature. Workup and purification procedure were done as described above to give the oligonucleotide carrying **Py**.

Complete Hydrolysis of Oligonucleotides. Each oligonucleotide (0.1–0.5 OD units at 254 nm) was incubated with venom phosphodiesterase (10 μg, Boehringer Mannheim) and alkaline phosphatase (0.4 units, Takara Shuzo Co., Ltd.) in a buffer containing 0.1 M Tris-HCl (pH 8.2) and 2 mM $MgCl_2$ (total 140 μL) for 24 h at 37 °C. The reaction mixture was heated for 5 min at 100 °C and cooled at 0 °C, then cold EtOH (0 °C, 320 μL) was added to the solution. The whole was kept for 1 h at −20 °C, then the solution was centrifuged for 20 min at 0 °C (12 000 rpm). A supernatant was separated and concentrated. The residue was analyzed by HPLC.

Thermal Denaturation. Each solution contained each oligonucleotide (84 μM/base) and poly(rA) (84 μM/base) in a buffer of 0.01 M sodium phosphate and 0.05 M NaCl (pH 7.0). The thermally induced transition of each mixture was monitored at 260 nm on a Gilford Response II.

Partial Hydrolysis of Oligonucleotide with Venom Phosphodiesterase. (*27*). Each oligonucleotide labeled with ^{32}P at the 5′-end (0.01 OD units) (*23*) was incubated with venom phosphodiesterase (0.4 μg) in the presence of Torula RNA (0.3 OD units at 260 nm) in a buffer containing 37.5 mM Tris-HCl (pH 8.0) and 7.5 mM $MgCl_2$ (total 20 μL) at 37 °C. At appropriate periods, aliquots of the reaction mixture were separated and added to a solution of EDTA (5 mM, 10 μL), then the mixtures were heated for 3 min at 100 °C. The solutions were analyzed by electrophoresis on 20% polyacrylamide gel containing 8 M urea (*23*).

Partial Hydrolysis of Oligonucleotides with Nuclease P1. (*28*). Each oligonucleotide labeled with ^{32}P at the 5′-end (0.01 OD units) was incubated with nuclease P1 (12 ng, Yamasa Shoyu Co., Ltd.) in the presence of Torula RNA (0.3 OD units) in a buffer containing 6.8 mM ammonium acetate (pH 5.3) and 0.1 mM $ZnCl_2$ (total 22 μL) at 10 °C. At appropriate periods, aliquots of the reaction mixture were separated and added to a solution of EDTA (5 mM, 10 μL), then the solutions were heated for 5 min at 100 °C. The solutions were analyzed by gel electrophoresis as described above.

Hydrolysis of Duplexes with RNase H. $(rA)_{16}$ labeled with ^{32}P at the 5′-end (50 pmol) was incubated with ribonuclease H (6 units) (Takara Shuzo Co., Ltd.) in the presence or in the absence of the complementary strand [$(T)_{16}$ or **V-(An)$_3$**] (50 pmol) in a buffer containing 40 mM Tris-HCl (pH 7.7), 4 mM $MgCl_2$, 1 mM DTT, 4% glycerol, and 0.003% bovine plasma albumin (total 10 μL) at 20 °C (*17*). After 20 min, reaction mixtures were heated for 1 min at 100 °C, then the reactions were analyzed by gel electrophoresis as described above.

ACKNOWLEDGMENT

This work was supported in part by a Grant-in-Aid for Scientific Research on Priority Areas from the Ministry of Education, Science, and Culture, Japan.

LITERATURE CITED

(1) Cohen, J. S. (Ed.) (1989) Oligodeoxynucleotides: *Antisense inhibitors of gene expression*, The Macmillan Press Ltd, London.

(2) Beaucage, S. L., and Iyer, R. P. (1993) The functionalization of oligonucleotides via phosphoramidite derivatives. *Tetrahedron 49*, 1925–1963.

(3) Gagnor, C., Bertrand, J.-R., Thenet, S., Lemaitre, M., Morvan, F., Rayner, B., Malvy, C., Lebleu, B., Imbach, J.-L., and Paoletti, C. (1987). α-DNA VI: comparative study of α- and β-anomeric oligodeoxynucleotides in hybridization to mRNA and in cell free translation inhibition. *Nucleic Acids Res. 15*, 10419–10436.

(4) Stein, C. A., Mori, K., Loke, S. L., Subasinghe, C., Shinozuka, K., Cohen, J. S., and Necker, L. M. (1988). Phosphorothioate and normal oligodeoxyribonucleotides with 5′-linked acridine: characterization and preliminary kinetics of cellular uptake. *Gene 72*, 333–341.

(5) Majumdar, C., Stin, C. A., Cohen, J. S., Broder, S., and Wilson, S. H. (1989) Stepwise Mechanism of HIV Reverse Transcriptase: primer function of phosphorothioate oligodeoxynucleotide. *Biochemistry 28*, 1340–1346.

(6) Murakami, A., Nagahara, S., Uematsu, H., Otoi, K., Haruna, T., Ide, H., and Makino, K. (1992) Interaction of antisense DNA with nucleic acids/proteins. *Nucleic Acids Res., Symp. Ser. 27*, 123–124.

(7) Murakami, A., Tamura, Y., Nishi, M., Morii, T., Ide, H., and Makino, K. 1992) Separation and characterization of diastereoisomeric oligonucleotide. *Nucleic Acids Res. Symp. Ser.* 27, 137–138.

(8) Shaw, J.-P., Kent, K., Bird, J., Fishback, J., and Froehler, B. (1991) Modified deoxyoligonucleotides stable to exonuclease degradation in serum. *Nucleic Acids Res. 19*, 747–750.

(9) Gamper, H. B., Reed, M. W., Cox, T., Virosco, J. S., Adams, A. D., Gall, A. A., Scholler, J. K., and Meyer, R. B. Jr. (1993) Facile preparation of nuclease resistant 3′ modified oligonucleotides. *Nucleic Acids Res. 21*, 145–150, and references therein.

(10) Kido, K., Inoue, H., and Ohtsuka, E. (1992) Sequence-dependent cleavage of DNA by alkylation with antisense oligodeoxyribonucleotides containing 2-(*N*-iodoacetylaminoethyl)thioadenine. *Nucleic Acids Res. 20*, 1339–1344.

(11) Yamana, K., Nishijima, Y., Ikeda, T., Gokota, T., Ozaki, H., Nakao, H., Sangen, O., and Shimidzu, T. (1990) Synthesis and interactive properties of an oligonucleotide with anthraquinone at the sugar fragment. *Bioconjugate Chem. 1*, 319–324.

(12) Dan, A., Yoshimura, Y., Ono, A., and Matsuda, A. (1993) Synthesis of oligonucleotides containing a novel 2′-deoxyuridine analogue that carries an aminoalkyl tether at 1′-position; stabilization of duplex formation by an intercalating group accommodated in the minor groove. *BioMed. Chem. Lett. 3*, 615–618.

(13) According to Holy (*18*), the nucleosides can be named as psicofuranosyluracil derivatives. In this report, for convenience, we named them as 2′-deoxyuridine derivatives.

(14) Saenger, W. (1984) *Principle of nucleic acid structure*; Springer-Verlag New York Inc., New York.

(15) Kawasaki, A. M., Casper, M. D., Freier, S. M., Lesnik, E. A., Zounes, M. C., Cummins, L. L., Gonzalez, C., and Cook, P. D. (1993) Uniformly modified 2′-deoxy-2′-fluoro phosphorothioate oligonucleotides as nuclease-resistant antisense compounds with high affinity and specificity for RNA targets. *J. Med. Chem. 36*, 831–841.

(16) Nakamura, H., Oda, Y., Iwai, S., Inoue, H., Ohtsuka, E., Kanaya, S., Kimura, S., Katsuda, C., Katayanagi, K. (1991) How dose RNase H recognize a DNA-RNA hybrid? *Proc. Natl. Acad. Sci. USA, 88*, 11535–11539.

(17) Hayase, Y., Inoue, H., and Ohtsuka, E. (1990) Secondary structure in formylmethionine tRNA influences the site-directed cleavage of ribonuclease H using chimeric 2′-*O*-methyl oligodeoxyribonucleotides. *Biochemistry 29*, 8793–8797.

(18) Holy, A. (1974) Synthesis of 1-[3-deoxy-β-D-psicofuranosyl]-uracil and related compounds. *Nucleic Acids Res. 1*, 289–298.

(19) Barton, D. H. R., and McCombie, S. W. (1975) A new method for the deoxygeneation of secondary alchols. *J. Chem. Soc. Perkin I.* 1974–1975.

(20) Tatsuoka, T., Imao, K., and Suzuki, K. (1986) Phosphono nucleoside. 1. Synthesis of 2,3′-anhydro-1′-deoxy-1′-phosphono-1-β-D-fructofuranosyluracil. *Heterocycles 24*, 617–620.

(21) Beaucage, S. L., Caruthers, M. H. (1981). Deoxynucleotide phosphoramidite—A new class of key intermediates for deoxypolynucleotide synthesis. *Tetrahedron Lett. 22*, 1859–1862.

(22) Telser, J., Cruickshank, K. A., Morrison, L. E., and Netzel, L. (1989) Synthesis and characterization of DNA oligomer and duplexes containing covalently attached molecular labels; comparison of biotin, fluorescein, and pyrene labels by thermodynamic and optical spectroscopic measurements. *J. Am. Chem. Soc. 111*, 6966–6976.

(23) Maniatis, T., Fritsch, E. F., and Sambrook, J. (1982) *Molecular cloning*; Cold Spring Harbor Laboratory, New York.

(24) Riley, M., Maling, B., and Chamberlin, M. J. (1966) Physical and chemical characterization of two- and three-stranded adenine–thymine and adenine–uracil homopolymer complexes. *J. Mol. Biol. 20*, 359–389.

(25) Yoshimura, Y., Otter, B., Ueda. T., and Matsuda, A. (1992) Synthesis and optical properties of *syn*-fixed carbon-bridged pyrimidine cyclonucleosides. *Chem. Pharm. Bull. 40*, 1761–1769.

(26) Sinha, N. D., Biernat, J., and Koster, H. (1983) β-Cyanoethyl *N,N*-dialkylamino/*N*-morpholinomonochloro phosphoamidites, new phosphitylating agents facilitating ease of deprotection and work-up of synthesized oligonucleotides. *Tetrahedron Lett. 24*, 5843–5846.

(27) Jay, E., Bambara, R., Padmanabhan, R., and Wu, R. (1974). DNA sequence analysis: a general, simple and rapid method for sequencing large oligonucleotide fragments for mapping. *Nucleic Acids Res. 1*, 331–353.

(28) Silberklang, M., Gillum, A. M., and RajBhndary, U. L. (1977) The use of nuclease P1 in sequence analysis of end group labeled RNA. *Nucleic Acids Res. 4*, 4091–4108.

Preparation and Properties of Thermoreversible, Phase-Separating Enzyme–Oligo(*N*-isopropylacrylamide) Conjugates

Guohua Chen and Allan S. Hoffman*

Center for Bioengineering, FL-20, University of Washington, Seattle, Washington 98195. Received June 10, 1993®

A thermoreversible *N*-isopropylacrylamide (NIPAAm) oligomer with an *N*-hydroxysuccinimide (NHS) ester functional end group has been prepared for coupling to an enzyme, β-D-glucosidase, to form a thermoreversible, phase-separating polymer–enzyme conjugate. This conjugate can be used for separation, recovery, and recycle of an enzyme simply by applying small temperature changes to the reaction medium. In contrast to the random polymer–enzyme conjugates previously reported by us and others in the literature, in this study the conjugate is formed by a single, end attachment of each oligomer chain to the enzyme. Preliminary studies show that the conjugated enzyme exhibits very high retention of activity, even higher than native enzyme, and shows improved thermal stability compared to native enzyme.

INTRODUCTION

Immobilized enzymes have been widely used in chromatographic columns (*1*). In addition, because of the ease of recovery and recycle as well as enhanced stability, immobilized enzymes on particulates have also been used in fluidized or packed-bed bioreactors (*2*, *3*). However, diffusion limitations of substrate into and/or product out of the solid carrier is a fundamental problem with insoluble enzyme conjugates, particularly when a macromolecular substrate is utilized. Furthermore, it is impractical for solid substrates to be used with immobilized enzyme catalysts.

To overcome these problems, soluble polymer–enzyme conjugates have received more attention since they exhibit many advantages over enzymes immobilized on or within porous solid carriers, especially when used for macromolecular or solid substrates (*4*). In particular, when enzymes are conjugated to reversible, phase-separating polymers, the enzymatic reaction can occur in solution, after which the enzyme can be recovered in an insoluble state by small changes of pH (*5–8*) or temperature (*9–12*). Our aim in this study is to prepare thermoreversible, phase-separating, polymer–enzyme conjugates and to apply them to reactions with macromolecular or solid substrates. One case would be the use of polymer-conjugated cellulase for conversion of cellulose into glucose.

It is well-known that poly(*N*-isopropylacrylamide) (PNIPAAm) is a thermoreversible water-soluble polymer and that aqueous solutions of this polymer exhibit a lower critical solution temperature (LCST) ca. 33 °C (*13*). The reversible phase-separation behavior of PNIPAAm has been utilized to reversibly precipitate and then redissolve a PNIPAAm–antibody conjugate (*9*) and other protein conjugates (*14*, *15*). However, in all of those studies, the polymers used have been random copolymers of NIPAAm with comonomers containing reactive groups for conjugation of the proteins. Since the copolymers may have more than one reactive group in each polymer chain, it is hard to know (a) if the enzyme is coupled to a polymer chain by a single or multiple attachment, (b) whether more than one enzyme is conjugated to one polymer chain, and also (c) at what point along the chain the conjugation occurs, all of which might significantly influence the activity and properties of the conjugated enzymes. In some cases, the conjugates were not completely water-soluble because a cross-linked network of enzyme and polymer may have formed (*11*).

In order both to simplify and to define more precisely the structure of the conjugated enzyme, we have previously synthesized a new type of NIPAAm oligomer having an end-capped carboxyl group and used this group for conjugation to β-D-glucosidase, one of the three enzymes comprising cellulase (*16*). In that preliminary study, the coupling reaction was run by mixing the oligomer and enzyme together with the activation reagent, a water-soluble carbodiimide, 1-ethyl-3-[3-(dimethylamino)propyl]carbodiimide (EDC). Therefore, it is possible that besides the polymer–enzyme conjugate, enzyme–enzyme conjugates, which could be either water-soluble or water-insoluble, might be formed during the coupling reaction. Although no insoluble aggregates were noted after reaction, soluble enzyme–enzyme conjugates could coexist in the end product since both carboxyl and amino groups are present in the enzyme and they might also be conjugated to each other along with the polymer, to form polymer–enzyme–enzyme conjugates. This could also yield poorly defined structures of the conjugates.

In order to overcome this problem, in this study the carboxylated NIPAAm oligomer was first separately activated by esterification with *N*-hydroxysuccinimide in methylene chloride in the presence of *N*,*N*-dicyclohexylcarbodiimide (DCC) (*17*) to obtain the NIPAAm oligomer with a functionally reactive NHS ester group at one end. It is well-known that the NHS ester is very reactive toward amino groups and has widely been used as a functional group for coupling reactions with proteins, ligands, etc. (*18*). This NHS-activated end group on the oligomer was coupled with β-D-glucosidase to form a thermoreversible, phase-separating PNIPAAm–β-D-glucosidase conjugate with the polymer chain uniquely attached to the enzyme by a single end attachment, and without formation of enzyme–enzyme conjugates. Properties of this unique polymer-conjugated enzyme are reported here.

EXPERIMENTAL PROCEDURES

Materials. β-D-Glucosidase (from almonds), *p*-nitrophenyl β-D-glucopyranoside (pNPG), dicyclohexylcarbodiimide (DCC), and *N*-hydroxysuccinimide (NHS) were

* Correspondence should be addressed to Allan S. Hoffman.

® Abstract published in *Advance ACS Abstracts*, October 1, 1993.

1043-1802/93/2904-0509$04.00/0 © 1993 American Chemical Society

purchased from Sigma, St. Louis, MO. PNIPAAm oligomer terminated with a carboxyl group at one end with a molecular weight of 4000 was prepared as described previously (*16*). All other reagents used were of analytical grade.

Preparation of *N*-Hydroxysuccinimide Esterified PNIPAAm Oligomer. A 4-g (1 mmol) sample of the carboxylated PNIPAAm oligomer was dissolved in 40 mL of anhydrous methylene chloride and cooled to 0 °C. NHS (2 mmol) and DCC (2 mmol) were added under stirring. The stirring was continued for 4 h, while the temperature was raised to 20 °C. After reaction, the insoluble dicyclohexylurea was removed from the reaction mixture by filtration and the polymer was isolated by precipitation into anhydrous diethyl ether. The degree of NHS esterification was evaluated spectrophotometrically by the release of *N*-hydroxysuccinimide in alkaline solution (*17*).

Conjugation of β-D-Glucosidase with PNIPAAm. The NHS-esterified PNIPAAm oligomer (40 mg) was dissolved in a solution of β-D-glucosidase in 0.05 M phosphate buffer (the enzyme concentration and the volume of the enzyme solution used are summarized in Table I) at 4 °C and resultant solution was gently shaken at 4 °C for 16 h. After reaction, 0.5 mL of a saturated ammonium sulfate solution (which reduces the precipitation temperature of PNIPAAm (12, 14)) was added and the mixture was diluted to ca. 8 mL with the same buffer and warmed up to 30 °C. The resulting precipitate was recovered by centrifugation (12000 rpm for 10 min at 30 °C). The precipitate was redissolved at 4 °C in 8 mL of 0.05 M citric acid + phosphate buffer (CP buffer having a pH of 5.0, which is the optimal pH for the native enzyme). To this solution 0.5 mL of saturated ammonium sulfate was added and the mixture was warmed up to 30 °C. The resulting precipitate was recovered again by centrifugation. This procedure was repeated another two times. The final precipitate was dissolved in 10 mL of buffer (pH 5.0) and stored at 4 °C for further study. The enzymatic activity of the solution was tested (see below). The amount of protein conjugated by PNIPAAm was determined by the BCA protein assay method (*19*).

Enzyme Assay. A 0.01-mg portion of the native or conjugated β-D-glucosidase was incubated in 3.0 mL of 0.05 M CP buffer and pNPG was added as a model substrate (0.45 mM, pH 5.0, 25 °C, unless otherwise indicated) for 5 min. The reaction was stopped by adding 1.0 mL of 0.25 M sodium carbonate solution to adjust the pH to around 9. The enzyme activity was determined by measuring the released *p*-nitrophenol spectrophotometrically at 405 nm. One unit of the enzyme activity was expressed as the production of 1 μM *p*-nitrophenol/min under the assay conditions (*20*).

Recycling Process of Solution Reaction—Phase Separation Recovery of the PNIPAAm-β-D-glucosidase Conjugate. In 6 mL of 0.45 mM substrate (pNPG)–buffer solution (pH 5.0), 0.02 mg of conjugated enzyme plus 3.0 mg of NIPAAm oligomer was added (the latter was added to enhance the precipitation and to aid complete recovery of the conjugate) (*14*). The mixture was incubated at 25 °C for 10 min. The reaction was stopped by addition of 2.0 mL of 0.25 M sodium carbonate solution to adjust the pH to ca. 9. Then 1.0 mL of saturated ammonium sulfate solution was added and the mixture was warmed up to 30 °C to precipitate the conjugate along with the added oligomer. The resulting precipitate was recovered by centrifugation (12000 rpm for 10 min at 30 °C). The enzyme activity was assayed by spectrophotometrically measuring the concentration of *p*-nitrophenol in the supernatant produced during the enzymatic reaction. The collected precipitate was redissolved in the same buffer as above at 25 °C for the next cyclic enzymatic reaction process, which was carried out under all the same conditions as before. Each cycle the enzyme activity was assayed by measuring the supernatant solution. A control was run using a physical mixture of β-D-glucosidase with free NIPAAm oligomer in the same buffer solution at similar enzyme and polymer concentrations, and following the same solution–precipitation cycles, i.e., dissolving at 25 °C and warming to 35 °C to precipitate the polymer (except in this case the enzyme activity was assayed by taking samples from the solution after each cycle, to run the enzymatic reaction at 25 °C).

Optimal pH. The activities of native enzyme, PNIPAAm-conjugated enzyme, and a physical mixture of native enzyme with free PNIPAAm were measured at different pHs (ranging from 3.5 to 8.5) at 25 °C with a pNPG concentration of 0.45 mM in 0.05 M buffer.

Kinetic Constants. The kinetic parameters for free, native β-D-glucosidase and PNIPAAm conjugated β-D-glucosidase were determined using pNPG as substrate in the concentration range of 0.11–0.68 mM at 25 °C, pH 5.0 and 7.0, respectively. K_m values were calculated from Lineweaver–Burke (double, double reciprocal) plots.

Optimal Temperature and Thermal Inactivation. The optimal temperature of hydrolysis of the substrate by native and polymer-conjugated β-D-glucosidase was tested over a range of temperatures. The enzyme was incubated with pNPG at a particular temperature for 15 min with gentle stirring, and the reaction was stopped by the addition of 0.25 M sodium carbonate solution to adjust the pH to ca. 9, at which the enzyme is inactivated. After cooling to room temperature, the *p*-nitrophenol concentration was measured (405 nm).

To examine thermal stability over time, native and PNIPAAm-conjugated β-D-glucosidase were incubated either at 60 °C for 45 min with sampling at 5 min intervals or at a variety of temperatures for 15 min each with gentle stirring. After incubation, the samples were cooled to room temperature and kept there for at least 2 h, assuring that all the samples were at the same temperature before the activity assays. The activities were then measured at 25 °C, pH 5.0. For comparison, controls were based on physical mixtures of native enzyme and free NIPAAm oligomer with the same amount of each as for the native or conjugated enzymes.

Storage Stability. Solutions with concentrations of ca. 0.1 mg/mL of native and polymer-conjugated β-D-glucosidase were stored at 4 °C in 0.05 M CP buffer at pH 5.0. The activities were measured at 25 °C, pH 5.0, as a function of storage time.

RESULTS AND DISCUSSION

Preparation of NHS End-Capped NIPAAm Oligomers and PNIPAAm-β-D-Glucosidase Conjugates. *N*-Isopropylacrylamide (NIPAAm) oligomer with a carboxyl group at one end of the chain was synthesized by radical polymerization using 2,2′-azoisobutyronitrile (AIBN) and β-mercaptopropionic acid (MPA) as initiator and chain-transfer reagent, respectively, as described previously (*16*) and also shown in Figure 1, step I. The polymer used in this work was prepared by solution polymerization using *tert*-butanyl alcohol as solvent, at 60 °C for 20 h, with the weight ratio of monomer to initiator to chain transfer reagent of 100:1:4. The polymer has a

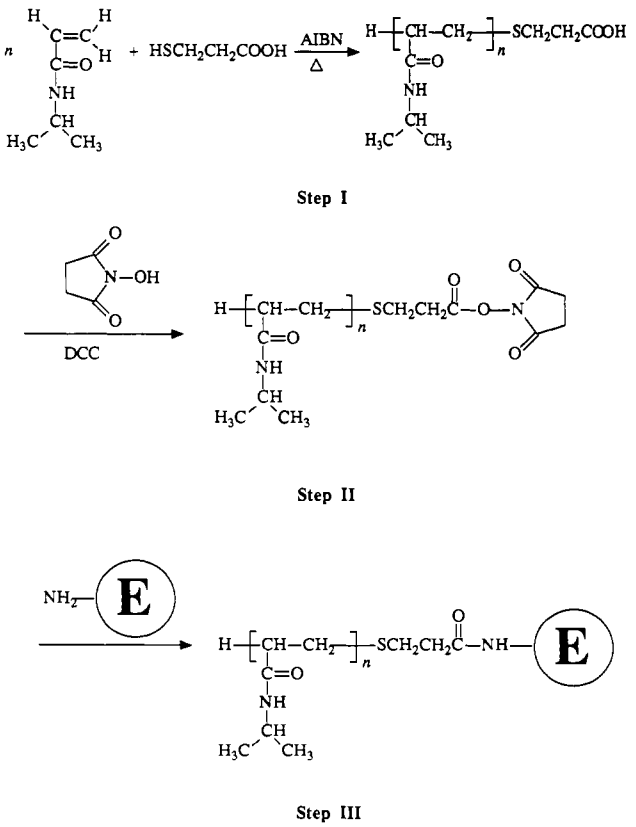


Figure 1. Scheme of synthesis of the NIPAAm oligomer with terminal functionality and its conjugation with enzyme.

molecular weight of 4000, evaluated by end-group titration, and shows an LCST of 34 °C, as expected for this polymer.

We wanted to avoid the formation of enzyme–enzyme conjugates, which may have occurred using our earlier protocol (*16*), where we simultaneously activated and coupled the carboxylated NIPAAm oligomer with β-D-glucosidase in the same solution using a water-soluble carbodiimide (WSC) as the activation reagent. Therefore, in the present study, the carboxylated NIPAAm oligomer was first esterified with *N*-hydroxysuccinimide using *N*,*N*-dicyclohexylcarbodiimide (DCC) (*17*) to activate the oligomer COOH, and then the activated NIPAAm oligomer was coupled with NHS (see Figure 1, step II). The activation reaction was carried out in anhydrous methylene chloride with molar ratios of polymer to NHS to DCC of 1:2:2. After activation, the polymer was recovered by precipitation into diethyl ether with a 91% yield and 81% conversion of the carboxyl to the ester group. This oligomer with the NHS-esterified terminal group was next used for the enzyme conjugation study.

The conjugation of the NHS-esterified NIPAAm oligomer with β-D-glucosidase was performed in 0.05 M phosphate buffer (pH 6–8) or Tris buffer (pH 9) at 4 °C for 16 h with gentle shaking (see Figure 1, step III). After coupling, the conjugated enzyme was easily isolated as a precipitate from the reaction medium by warming to a temperature above the LCST (32–33 °C) of the polymer and centrifuging to leave any unconjugated free enzyme in the supernatant. The oligoNIPAAm–β-D-glucosidase conjugates were found to be completely water soluble at temperatures below 32 °C and to precipitate above 32 °C, showing that the conjugated enzyme does not alter the LCST of the polymer.

Table I gives the coupling results under the different coupling conditions. In two control studies, neither any protein nor any enzymatic activity could be detected in

Table I. Effect of Polymer/Enzyme Concentration on the Conjugation and Resultant Enzyme Activity

	reaction medium			product	
exp	[P + E][a] (mg/mL)	pH	P/E (wt/wt)	mg E/g polymer (conjugated)	retention of activity[b] (%)
1	6.3	8.0	4:1	34.0 ± 1.1	83 ± 2
2	12.5	8.0	4:1	38.0 ± 1.4	85 ± 4
3	25.0	8.0	4:1	41.0 ± 1.1	89 ± 5
4	50.0	8.0	4:1	48.7 ± 4.8	96 ± 14
5[c]	50.0	8.0	4:1	negl	negl
6[d]	50.0	8.0	4:1	negl	negl
7	50.0	8.0	4:2	39.6 ± 5.6	107 ± 4
8	50.0	8.0	4:3	41.4 ± 5.6	105 ± 5
9	50.0	8.0	4:4	43.5 ± 1.7	106 ± 3
10	50.0	6.0	4:1	22.3 ± 2.5	104 ± 6
11	50.0	7.0	4:1	45.1 ± 5.0	101 ± 10
12	50.0	9.0	4:1	77.9 ± 10.9	117 ± 20

[a] P = PNIPAAm oligomer, E = β-D-glucosidase. [b] The retention of activity was calculated by dividing the specific activity of conjugated β-D-glucosidase by the specific activity of the same amount of native enzyme (the specific activity of native enzyme is taken as 100%). [c] This control was run with the mixture of β-D-glucosidase with the unactivated carboxyl-terminated NIPAAm oligomer (negl for negligible). [d] This control was run with the mixture of β-D-glucosidase with free PNIPAAm which had no functional group. [e] Conjugation was run in 0.05 M phosphate buffer at 4 °C for 16 h.

the precipitates recovered from physical mixtures of the enzyme with either the carboxylated NIPAAm oligomer or the PNIPAAm without a COOH end group. The mixtures were also treated under the same conditions as those used for coupling activated NIPAAm oligomer with the enzyme. These results indicate that the enzyme which is in the precipitate is covalently conjugated with the oligomer, not physically entrapped within the polymer (see control exp 5 and 6, Table I). The amount of enzyme conjugated with the polymer increases with increase of total (polymer + enzyme) (P + E) concentration, which is probably due to the increased reaction rates. The "retention of activity" for the conjugated enzyme (defined as the ratio of the specific activity of conjugated enzyme to the specific activity of the same amount of native enzyme and the specific activity of native enzyme as 100%, see also footnote in Table I) also increases with increase of the concentration (exp 1–4, Table I). The ratio of NIPAAm oligomer to β-D-glucosidase was found to have little effect on either the amount of PNIPAAm–β-D-glucosidase conjugate or its relative activity (exp 4, 7–9, Table I). The pH of the coupling medium, however, significantly affected the amount of conjugated enzyme. The amount of conjugated β-D-glucosidase increases with increase of pH (exp 4, 10–12, Table I), probably due to more free enzyme amino groups available for conjugation at higher pHs. As can be seen in Table I, the relative activity for the conjugated enzyme is little affected by either the pH of the coupling medium or the ratio of NIPAAm oligomer to β-D-glucosidase. Also, sometimes relative activity for the conjugated β-D-glucosidase was even higher than the native enzyme (exp 7–12, Table I). This may be due to a (favorable) modification in the microenvironment of the enzyme caused by the conjugated polymer. As discussed above, the NHS-esterified NIPAAm oligomer has only one NHS functional group at one end of each polymer chain. Therefore, the conjugation of PNIPAAm with the enzyme occurs via a single end linkage. This is quite similar to the way proteins have been conjugated with polyethylene oxide (PEO) (21). A few examples in the literature also show improvements in enzyme–PEO activities over that of the unconjugated enzyme, which may also result from modifications in the microenvironment of the enzyme active site (*22–24*). One example is the conjugation of

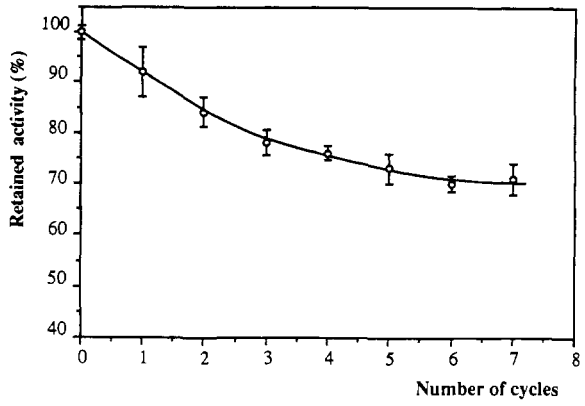


Figure 2. Retained activity of PNIPAAm-β-D-glucosidase conjugates as a function of successive solution reaction–precipitation cycles. Solution reaction was run at 25 °C using pNPG as substrate (0.45 mM) in 0.05 M CP buffer, pH 5.0; precipitation occurred by warming up to 30 °C in the presence of 0.5 M $(NH_4)_2SO_4$ (The retained activity of the conjugates before the recycling is defined as 100%).

trypsin with poly(ethylene glycol), which was recently found to increase trypsin activity (*24*). It is also possible that allosteric changes in the enzyme are caused in our case by the conjugated PNIPAAm (see below).

Thermal Recycling of the Conjugated β-D-Glucosidase. The enzymatic reaction of PNIPAAm–β-D-glucosidase conjugates with the model substrate (pNPG) was carried out in solution at 25 °C (below the LCST of PNIPAAm), and after reaction the conjugate was recovered in its insoluble form by precipitation and centrifugation at 30 °C in the presence of 0.5 M $(NH_4)_2SO_4$ (which lowers the LCST of PNIPAAm below 30 °C). The resultant precipitate was redissolved and used for repeat reaction–precipitation cycles. As shown in Figure 2, the retained activity of the conjugated β-D-glucosidase decreased after each cycle, with a smaller decrease as the number of cycles increased. After seven cycles, the conjugate still retained 70% of its original activity with an average of ≥95% recovery of activity for each cycle. A physical mixture of native β-D-glucosidase and free PNIPAAm had little loss in activity following a similar seven temperature cycles (data not shown), indicating that the ca. 30% loss of the conjugate activity after seven cycles is not because of thermal deactivation during the temperature cycles but probably due to the incomplete precipitation, recovery, and recycle of the enzyme conjugate in each step. Apparently the conjugates which are most difficult to precipitate are lost in the first few cycles.

Properties of the Conjugated β-D-Glucosidase. The effect of the pH of the reaction medium on the activity of native and conjugated β-D-glucosidase was investigated. The activities of both native and conjugated β-D-glucosidase are very sensitive to the pH of the reaction medium. The same activity–pH profiles were found for native β-D-glucosidase, the physical mixture of native β-D-glucosidase with free PNIPAAm, and the conjugated β-D-glucosidase. At pH >8.0, almost no activity could be detected for those enzymes, and therefore, in most cases of this study we stopped the enzymatic reaction by adjusting the pH to ca. 9.0.

Preparation and Properties of Thermosensitive Soluble–Insoluble Enzyme–PNIPAAm Conjugates. Conjugation of NIPAAm oligomer to β-D-glucosidase may cause a change in the affinity between enzyme and substrate, possibly leading to changes in the enzyme kinetics for the conjugated enzyme. Therefore, determination of the apparent Michaelis–Menten constants (K_m)

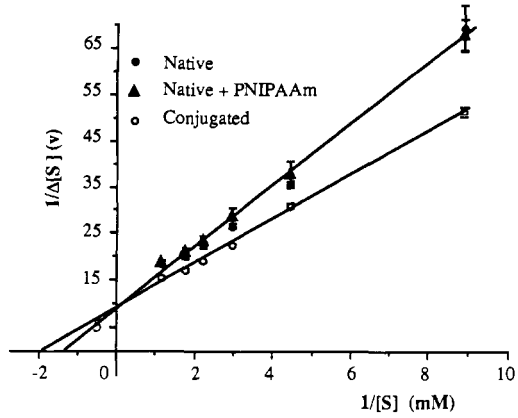


Figure 3. Lineweaver–Burk plot for native and conjugated β-D-glucosidase (pNPG as substrate at 25 °C in 0.05 M CP buffer, pH 5.0).

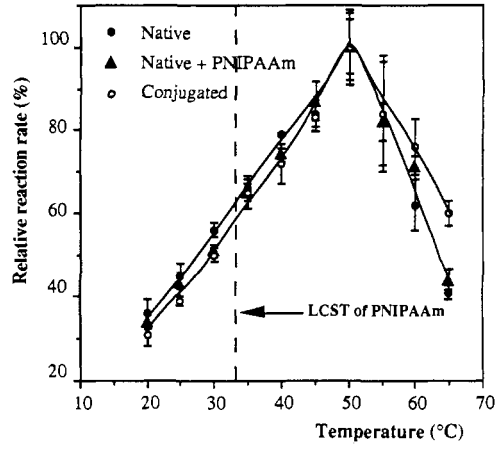


Figure 4. Effect of reaction temperature on the relative reaction rate of native and conjugated β-D-glucosidase using pNPG as substrate in 0.05 M CP buffer, pH 5.0. Enzyme activities were determined by incubating the enzyme with pNPG at a particular temperature for 15 min and measuring the production of *p*-nitrophenol at room temperature (The relative reaction rate of the enzymes at the optimal temperature is taken as 100%).

was done at 25 °C for the native β-D-glucosidase, the conjugate and the physical mixture of native β-D-glucosidase with free PNIPAAm, using pNPG as substrate at pH 5.0 and 7.0, respectively. As shown in Figure 3, free PNIPAAm had little effect on the kinetics of native β-D-glucosidase; however, when PNIPAAm was conjugated to β-D-glucosidase, the kinetics of the conjugated β-D-glucosidase were affected. From the Lineweaver–Burk plots obtained at various concentrations, the K_m values were calculated by least-squares evaluation. For native β-D-glucosidase, K_m was 1.66 mM at pH 5.0 and 1.42 mM at pH 7.0, respectively, while lower K_m values were found for the conjugated β-D-glucosidase, 1.19 mM at pH 5.0 and 1.25 mM at pH 7.0, respectively. This may mean that the conjugated enzyme has somewhat higher affinity for the substrate than the native enzyme. This increased affinity of the conjugated β-D-glucosidase for the substrate could be due to an allosteric conformational change of the enzyme active site. These may also be some undefined "microenvironmental" effect such as favorable partitioning of the substrate near the active site (*24*).

The effect of temperature on the rate of pNPG hydrolysis is shown in Figure 4 for the conjugated, native β-D-glucosidase, and the physical mixture of native β-D-glucosidase with free PNIPAAm. The reaction rate increased with increase of temperature until the optimal temperature was reached (50 °C for all three cases) and

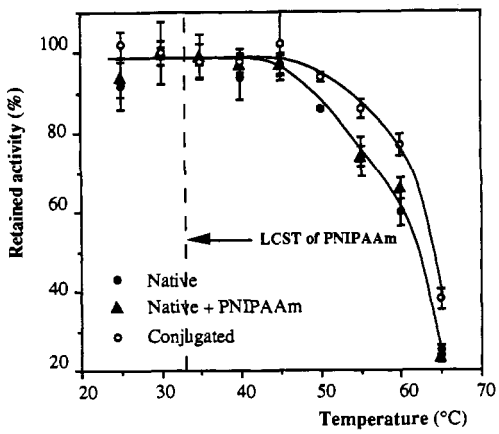


Figure 5. Effect of incubation at various temperatures at pH 5.0 (15 min) on the retained activity of native and conjugated β-D-glucosidase. The activity was measured for each sample at 25 °C using pNPG as substrate in 0.05 M CP buffer, pH 5.0, 120 min after incubation (The retained activity of the enzymes activated at 25 °C is taken as 100%).

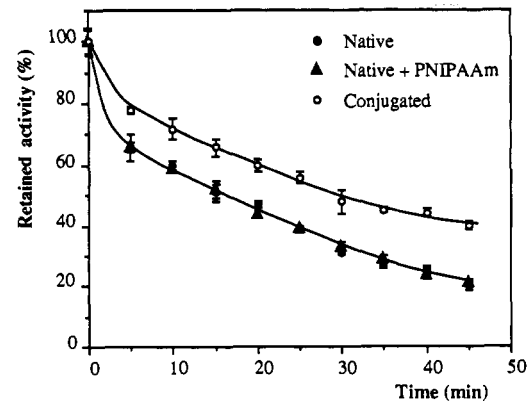


Figure 6. Effect of incubation time at 60 °C (pH 5.0) on the retained activity of native and conjugated β-D-glucosidase. The activity was measured for each sample at 25 °C using pNPG as substrate in 0.05 M CP buffer, pH 5.0, 120 min after incubation. (The retained activity of the original enzymes without incubation at 60 °C is taken as 100%.)

then decreased dramatically, which is mainly due to the predominant thermal inactivation. It should be noted that above the LCST of PNIPAAm (34 °C), the PNIPAAm–β-D-glucosidase conjugate precipitates, and although the enzymatic reaction continues, it occurs heterogeneously (where gentle stirring of reaction mixture was applied during the reaction). Despite this dramatic difference, the temperature dependence of the enzymatic reaction is essentially the same as for the native enzyme up to 45–50 °C. Above this temperature the conjugate loses activity less sharply than the native enzyme, perhaps due to the higher thermal stability of the conjugate (see below). For the conjugated β-D-glucosidase, it is curious that the increase of reaction rate with temperature continues smoothly above the LCST of PNIPAAm, where the conjugate precipitates and the reaction becomes heterogeneous. This may be related to the small molecular weights of substrate and product involved in the reaction, such that diffusion to and from the active site is unaffected by the solid phase, which is also generally found for the immobilized enzymes on solid carriers (*1*). Also, the low molecular weight PNIPAAm which was conjugated to the enzyme by one end is probably not large enough to interfere with the access of the substrate to the active side of the enzyme.

Figure 5 shows the effect of heat treatment at a variety of temperatures on the residual activities for native and conjugated β-D-glucosidase. It is evident that the conjugated β-D-glucosidase is more stable at higher temperature (>45 °C) than either the native enzyme or the physical mixture of native enzyme with free PNIPAAm.

Figure 6 shows the time course for the thermal inactivation of the enzymes at 60 °C. (The samples were incubated at 60 °C for various times, then cooled to 25 °C where activities were measured.) Free PNIPAAm does not protect the enzyme from the thermal inactivation. The native enzyme retains only ca. 20% of its initial activity by a heat treatment at 60 °C for 45 min, whereas the conjugated β-D-glucosidase still retains 40% of its original activity. It is clear that the conjugate is more thermally stable, indicating that the conjugation of β-D-glucosidase with NIPAAm oligomer provides protection against thermal inactivation of the enzyme at temperatures well above the LCST of the polymer. This is different from the well-known stabilization of proteins conjugated with PEO (*24*) or polysaccharides (*25*, *26*), since the PEO or polysaccharide chains remain soluble. The protection of PNIPAAm-conjugated enzyme against thermal inactivation may be due to the reduction in mobility for the precipitated conjugate above 34 °C. Many examples have been reported in the literature of the protection against thermal inactivation for immobilized enzymes on solid carriers, and this protection has been explained as due to the reduction of mobility of the enzyme after immobilization on the solid carriers (*27–29*). Nevertheless, it is interesting to note in our case (with a small substrate and product) that the kinetics up to the temperature at the maximum rate are the same for the conjugated or free enzyme (Figure 4).

Solutions of both native and conjugated β-D-glucosidase in 0.05 M CP buffer (ca. 0.1 mg/mL, pH 5.0) were stored at 4 °C, and the activities of these solutions were measured as function of storage time. After 2 months storage the PNIPAAm–β-D-glucosidase conjugate retains 85% of its initial activity, while the native enzyme only retains 70% of its original activity. The relatively high stability of the conjugates at 4 °C as compared to native β-D-glucosidase may be due to the expanded and hydrated PNIPAAm chain (*24*, *30*) to form a "protective colloid" surrounding the enzyme (*26*, *31*), which could protect the enzyme from slow deactivation in solution or on the vessel walls. This is similar to the proposed action of PEO–enzyme conjugates (*24*).

CONCLUSIONS

Thermally-reversible soluble–insoluble PNIPAAm–β-D-glucosidase conjugates have been successfully prepared via the reaction of a terminal active ester group on the NIPAAm oligomer with amino groups on the enzyme. The conjugated β-D-glucosidase retains a high percent of the free enzyme activity and can repeatedly undergo solution–precipitation cycles without significant loss of specific activity. Improved stability against activity loss at high temperature (60 °C) or after long storage at 4 °C was observed for the conjugated β-D-glucosidase compared to the native enzyme. More extensive study of its use with macromolecular or solid substrates in a recycle process is underway.

ACKNOWLEDGMENT

The National Science Foundation (NSF) (Grant No. BCS-9101716) and the Washington Technology Center (WTC) are gratefully acknowledged for their financial support of this project.

LITERATURE CITED

(1) Zaborsky, O. R. (1973) *Immobilized Enzymes*, C. R. C. Press, Cleveland.
(2) Chibata, I., Ed. (1978) *Immobilized Enzymes, Research and Development*, Halsted, New York.
(3) Rosevear, A., Kennedy, J. F., and Cabral, J. M. S. (1987) In *Immobilized Enzymes and Cells*, IOP Pub. Ltd., Adam Hilger, Brestol and Philadelphia.
(4) Epton, R., Marr, G., and Morgan, G. J. (1977) Soluble polymer–protein conjugates: 1. reactive N-(sym-trinitroaryl)-polyacrylamide/acrylhydrazide copolymers and derived carbonic anhydrase conjugates. *Polymer 18*, 319–323.
(5) Okamura, K., Ikura, K., Yoshikawa, M., Sakaki, R., and Chiba, H. (1984) Preparation of soluble-insoluble interconvertible enzymes. *Agri. Biol. Chem. 48*, 2435–2440.
(6) Margolin, A. L., Izumrudov, V. A., Svedas, V. K., and Zezin, A. B. (1982) Soluble-insoluble immobilized enzymes. *Biotechnol. Bioeng. 24*, 237–240.
(7) Taniguchi, M., Kobayashi, M., and Fujii, M. (1989) Properties of a reversible soluble-insoluble cellulase and its application to repeated hydrolysis of crystalline cellulose. *Biotechnol. Bioeng. 34*, 1092–1097.
(8) Taniguchi, M., Hoshino, K., Watanabe, K., Sugai, K., and Fujii, M. (1992) Production of soluble sugar from cellulosic materials by repeated use of a reversibly soluble-autoprecipitating cellulase. *Biotechnol. Bioeng. 39*, 287–292.
(9) Monji, N., and Hoffman, A. S., (1987) A novel immunoassay system and bioseparation process based on thermal phase separating polymers. *Appl. Biochem. Biotechnol. 14*, 107–120.
(10) Cole, C.-A., Schreiner, S. M., Priest, J. H., Monji, N., and Hoffman, A. S. (1987) N-Isopropylacrylamide and N-acryloxysuccinimide copolymer, a thermally reversible, water-soluble, activated polymer for protein conjugation. *ACS Symp. Series*, pp 245–254, Vol. *350*, American Chemical Society, Washington D.C.
(11) Steinke, K., and Vorlop, K. D. (1990) Precitable enzyme–polymer conjugates with high activity. *DECHEMA Biotechnol. Conf., 4* (Pt. B, Lect. DECHEMA Annu. Meet. Biotechnol. 8th), 889–892; *Chem. Abstr. 115*, 47742*b*.
(12) Nguyen, A. L., and Luong, J. H. T. (1989) Syntheses and applications of water-soluble reactive polymers for purification and immobilization of biomolecules. *Biotechnol. Bioeng. 34*, 1186–1190.
(13) Heskins, M., and Guillet, J. E. (1968) Solution properties of poly(N-isopropylacrylamide). *J. Macromol. Sci., Chem. A2*, 1441–1455.
(14) Chen, J. P., Yang, H. J., and Hoffman, A. S. (1990) Polymer-protein conjugates I. Effect of protein conjugation on the cloud point of poly(N-isopropylacrylamide). *Biomaterials 11*, 625–630. Chen, J. P., and Hoffman, A. S. (1990) Polymer-protein conjugates II. Affinity precipitation separation of human immunogammaglobulin by a poly(N-isopropylacrylamide)–protein A conjugate. *Biomaterials 11*, 631–634.
(15) Park, T. G., and Hoffman, A. S. (1993) Synthesis and characterization of a soluble, temperature-sensitive polymer-conjugated enzyme. *J. Biomater. Sci. Polym. Ed. 4*, 493–504.
(16) Chen, G. H., and Hoffman, A. S. (1992) Synthesis of carboxylated poly(NIPAAm) oligomers and their application to form thermo-reversible polymer–enzyme conjugates. *Polym. Prep. 33* (2), 468–469; *J. Biomater. Sci. Polym. Ed.*, in press.
(17) Sartore, L., Caliceti, P., Schiavon, O., and Veronese, F. M. (1991) Enzyme modification by MPEG with an amino acid or peptide as spacer arms. *Appl. Biochem. Biotechnol. 27*, 45–54.
(18) Scouten, W. H. (1981) In *Affinity Chromatography, Bioselective Adsorption on Inert Matrices*, pp 75–77, John Wiley & Sons, New York.
(19) Smith, P. K., Krohn, R. I., Hermanson, G. T., Mallia, A. K., Gartner, F. H., Provenzano, M. D., Fujimoto, E. K., Geoke, N. M., Olson, B. J., and Klenk, D. C. (1985) Measurement of protein using bicinchoninic acid. *Anal. Biochem. 150*, 76–85.
(20) Ong, E., Gilkes, N. R., Miller Jr., R. C., Warren, R. A. J., and Kilburn, D. G. (1991) Enzyme immobilization using a cellulose-binding domain: Properties of a β-glucosidase fusion protein. *Enzyme Microb. Technol. 13*, 59–65.
(21) Yoshinga, K., and Harris, J. M. (1989) Effects of coupling chemistry on the activity of poly(ethylene glycol)-modified alkaline phosphatase. *J. Bioact. Compat. Polym. 4*, 17–24.
(22) Remy, M. H., Bourdillon, C., and Thomas, D. (1985) Microenvironmental effects on enzyme catalysis. A kinetic study of hydrophobic derivatives of chymotrypsin. *Biochim. Biophys. Acta 829*, 69–75.
(23) Goldstein, L. C. (1972) Microenvironmental effects on enzyme catalysis. A kinetic study of polyanionic and polycationic derivatives of chymotrypsin. *Biochemistry 11*, 4072–4084.
(24) Gaertner, H. F., and Puigserver, A. J. (1992) Increased activity and stability of poly(ethylene glycol)-modified trypsin. *Enzyme Microb. Technol. 14*, 150–155.
(25) Lenders, J. P., and Crichton, R. R. (1984) Thermal stabilization of amylolytic enzymes by covalent coupling to soluble polysaccharides. *Biotechnol. Bioeng. 26*, 1343–1351.
(26) Srivastava, R. A. K. (1991) Studies on stabilization of amylase by covalent coupling to soluble polysaccharides. *Enzyme Microb. Technol. 13*, 164–170.
(27) Ulbrich, R., Schellenberger, A., and Damerau, W. (1986) Studies on the thermal inactivation of immobilized enzymes. *Biotechnol. Bioeng. 28*, 511–522.
(28) Emi, S., Murase, Y., Hayashi, T., and Nakajima, A. (1990) Protease immobilization onto copoly(ethylene/acrylic acid) fiber. *J. Appl. Polym. Sci. 41*, 2753–2767.
(29) Hayashi, T., and Ikada, Y. (1990) Lipoprotein lipase immobilization onto polyacrolein microspheres. *Biotechnol. Bioeng. 36*, 593–600.
(30) Blomhoff, H. K., and Christensen, T. B. (1983) Effect of dextran and dextran modifications on the thermal and proteolytic stability of conjugated bovine testis β-galactosidase and human serum albumin. *Biochim. Biophys. Acta 743*, 401–407.
(31) Perutz, M. F. (1978) Electrostatic effects in proteins. *Science 201*, 1187–1191.

Protein Conjugates of Defined Structure: Synthesis and Use of a New Carrier Molecule

L. Antonio Vilaseca,† Keith Rose,*,† Raymond Werlen,† Anne Meunier,† Robin E. Offord,† Cynthia L. Nichols,‡ and William L. Scott‡

Biochimie Médicale, Centre Médical Universitaire, CH 1211 Geneva 4, Switzerland, and Lilly Research Laboratories, Indianapolis, Indiana 46285. Received June 15, 1993®

A new carrier molecule, NH_2OCH_2CO-$(Gly)_3$-[Lys(H-Ser-)]$_5$-Gly-OH, has been synthesized to facilitate the preparation of protein conjugates of defined structure. Special features are as follows: (i) (aminooxy)-acetyl as a terminal group, which reacts specifically to form an oxime bond under very mild conditions with an aldehyde group placed on a protein in a prior step; (ii) a spacer group of three Gly residues; and (iii) a set of five Lys residues, each of which is acylated with a Ser residue. A second form of the carrier molecule, HCO-*m*-C_6H_4CH=$NOCH_2CO$-$(Gly)_3$-[Lys(H-Ser)]$_5$-Gly-OH, was also prepared. This form possesses a terminal aldehyde group which permits site-specific attachment by formation of a hydrazone bond to the carboxyl termini of polypeptide chains which have been modified enzymatically with carbohydrazide in a prior step. Once the carrier is linked to protein in one of the above ways, i.e. through formation of either an oxime or hydrazone bond, the Ser residues of the carrier (but not of the protein) may be oxidized by very mild periodate treatment to generate aldehyde groups. Drugs possessing a hydrazide group (e.g. methotrexate γ-hydrazide or desacetylvincaleukoblastine hydrazide) may then be conjugated via hydrazone formation to the aldehyde groups of the carrier. A cluster of five drug molecules may thus be attached to a single site on a protein, giving a relatively homogeneous product in spite of the high drug conjugation ratio. Synthesis of the carrier, formation of a pentadrug–protein conjugate, and wider implications of the chemistry are presented.

INTRODUCTION

In recent years it has become possible to modify the structure of unprotected polypeptides and proteins site specifically and under mild aqueous conditions. For example, oxidation of an N-terminal Ser or Thr residue to a glyoxylyl residue permits coupling reactions to be directed exclusively to this position in a second step (*1*, *2*); reverse proteolysis may be used to place a hydrazide (or other group having unique reactivity) specifically at the C-terminus of a polypeptide chain, further reaction is then directed to that position (*3*, *4*), and large unprotected synthetic fragments may be brought together using site-specific chemistry (*5*). Such site-specific operations lead to a more homogeneous product than is obtained by random attack on side chains, and a homogeneous product of defined structure is a great advantage if the conjugate is to be used for medical purposes: registration and quality control should be facilitated, modification of production procedures should become less problematic since it can be shown directly whether the product has been affected, and interpretation of biological results becomes more reliable than is possible when dealing with a mixture of regioisomers. However, if several molecules of interest (reporter group, drug, chelator, etc.) must be attached to each protein molecule and the advantages of single-site attachment to protein are to be preserved, then it is necessary to construct a carrier molecule. The carbohydrate moiety of a glycoprotein constitutes a natural carrier, oxidation of which permits attachment of various molecules to the aldehyde groups generated (*6*). Unfortunately, glycosylation may be heterogeneous or absent entirely from the protein of interest, or the harsh oxidation conditions may adversely affect protein function. Human serum albumin has been used as a carrier between drug molecules and an antibody (reviewed by Pietersz (*7*)), but linkage of drug to carrier and of carrier to antibody was not site-specific with respect to the antibody. In order to improve product homogeneity, several other types of carrier molecules have been developed.

Polyaldehyde dextran, amino dextran, and poly(amino acids) have mostly been used (*7*). Some of these polymers offer a uniquely reactive terminus for univalent attachment to biomolecules (e.g. refs *8–10*). So far, use of even these monovalent-attachment carrier molecules has been a source of product heterogeneity for some (or all) of the following reasons: the polymeric carrier is not monodisperse, attachment of drug to carrier is not quantitative, and attachment of carrier to protein does not proceed in a site-specific manner.

We are interested in the preparation of cytotoxic antitumor immunoconjugates for medical purposes. In an attempt to improve homogeneity of the final bioconjugate, we decided to synthesize a carrier of defined structure, thus removing the polydispersity problem. We chose carbonyl chemistry to link carrier to protein, since this is very mild, does not disturb disulfide bonds, and techniques exist which permit site-specific attachment either to the N-terminus (*1*, *2*) or to the C-terminus (*3*, *4*) of the protein. Drug release from final product was designed to occur through spontaneous hydrolysis of a hydrazone drug–carrier linkage, either upon internalization or within the tumor microenvironment (*11*). The carrier molecule was used to form a pentadrug conjugate of defined chemical structure with des-Ala^{B30}-insulin (DAI)[1] as a

† Centre Médical Universitaire.

‡ Lilly Research Laboratories.

® Abstract published in *Advance ACS Abstracts*, October 1, 1993.

[1] Abbreviations: DAI, des-Ala^{B30} porcine insulin; HPLC, high pressure liquid chromatography; ESMS, electrospray ionization mass spectrometry; TFA, trifluoroacetic acid; DMSO, dimethylsulfoxide; DMF, dimethylformamide; Fmoc, fluorenylmethyloxycarbonyl; DAVLB, des-acetyl vincaleukoblastine.

1043-1802/93/2904-0515$04.00/0 © 1993 American Chemical Society

model protein. DAI was used in order to be able to follow precisely, by reversed-phase HPLC and ESMS, the various steps involved. A brief description of this work was presented at the 1992 European Peptide Symposium (*12*). Experiments with antibodies will be described in detail elsewhere.

EXPERIMENTAL PROCEDURES

Unless otherwise specified, all solvents and reagents were obtained from commercial sources, were of analytical or higher grade, and were used without further purification. Temperature was room temperature (about 22 °C) except where indicated.

High-Pressure Liquid Chromatography. Analytical reversed-phase HPLC was performed using a 250 mm × 4 mm i.d. Nucleosil 300-Å 5-μm C_8 column; solvent A was 0.1% TFA; solvent B was 0.1% TFA in 90% acetonitrile prepared as previously described (*3*). Except where otherwise noted, the conditions were as follows: flow rate, 0.6 mL/min; 5 min isocratic at 100% solvent A followed by a linear gradient of 2% solvent B/min to 100% B. The analytical column was also used for small semipreparative separations. Where mentioned, preparative work was carried out using a column 250 mm × 21 mm i.d., packed with the same material and eluted at a flow rate of 10 mL/min. Components were collected manually at the detector outlet, frozen and lyophilized in a vacuum centrifuge (SpeedVac, Savant) without heating.

Mass Spectrometry. FABMS was performed in positive ion mode as previously described (*15*). For FABMS, masses found and calculated are the monoisotopic values of the protonated species, $M + H^+$. ESMS was performed in positive ion mode on a Trio 2000 machine (VG BioTech, Altrincham, England) equipped with a 3000 amu RF generator. Samples were introduced at 2 μL/min either directly (if in the TFA/acetonitrile HPLC solvent) or (if dried) in solution in water/MeOH/AcOH (49.5:49.5:1, by volume). For ESMS, masses found and calculated are average values based on the isotopic envelope and are expressed as molecular weights of uncharged species. Where multiple protonation led to a series of signals, the neutral mass is given ± the standard deviation of the measurements.

Preparation of H-Gly$_3$-[Lys(*t*-Boc-Ser(Bzl))]$_5$-Gly-OCH$_2$-PAM Resin. The resin-bound protected nonapeptide Fmoc-Gly$_3$-[Lys(*t*-Boc)]$_5$-Gly-OCH$_2$-PAM resin was synthesized by the standard fluorenylmethyloxycarbonyl (Fmoc) protocol using 0.5 mmol starting *t*-Boc-Gly-OCH$_2$-PAM resin [(phenylacetamido)methyl resin, ABI Inc., substitution of 0.825 mmol/g] on an ABI 430A automated peptide synthesizer. Each cycle was controlled by ninhydrin analysis (ABI protocol) and coupling was almost quantitative. The average yield was 1.26 g of resin. A pool of five batches of such resin (6.31 g) was treated with 63 mL of TFA for 2 h, filtered, washed with dichloromethane (2 × 40 mL), methanol (2 × 40 mL), dichloromethane (40 mL), and methanol (40 mL), and then dried.

t-Boc-Ser(Bzl)-OSu (9.81 g, 25 mmol, Bachem) was dissolved in 50 mL of dry DMSO and the apparent pH (damp pH paper) brought to 8–9 with 250 μL of *N*-methylmorpholine. The resin was added to this solution and the apparent pH readjusted to 8–9 with *N*-methylmorpholine. The mixture was agitated for 2 h in the dark. A portion of resin (approx. 5 mg) was removed, washed with methanol (2 × 2 mL) and dichloromethane (2 × 2 mL), and then dried in a vacuum centrifuge. The standard ninhydrin test showed that acylation was almost quantitative. The bulk of the acylated resin was then filtered, washed, and dried as described above for the TFA deprotection. To remove Fmoc protection, the resin was treated with a mixture of 20 mL of piperidine and 30 mL of DMF for 2 h with gentle mixing. The resin was then filtered, washed, and dried as before. Ninhydrin analysis showed that deprotection was successful.

Preparation of *t*-Boc-NHOCH$_2$CO-Gly$_3$-[Lys(*t*-Boc-Ser(Bzl))]$_5$-Gly-OCH$_2$-PAM Resin. To 1.91 g (10 mmol) of [[(*tert*-butyloxycarbonyl)amino]oxy]acetic acid (prepared according to ref *13*, except that crude product was extracted into ethyl acetate to remove KCl and then dried by rotary evaporation) in 30 mL of ethyl acetate was added a solution of 1.15 g (10 mmol) of *N*-hydroxysuccinimide in 30 mL of the same solvent. Under constant mixing, a solution of 2.06 g (10 mmol) of *N,N'*-dicyclohexylcarbodiimide in 3 mL of ethyl acetate was then added and mixing was continued at room temperature. Reaction was followed by TLC on silica gel 60 using chloroform/methanol (1:1 by vol) as eluent and spraying with a solution of *N,N*-dimethylbarbituric acid (50 mg/mL) in pyridine/water (9:1 by vol) to reveal remaining diimide (*14*). After 5 h, no diimide was detected, dicyclohexylurea was removed by filtration and the filtrate was dried by rotary evaporation to yield 2.0 g.

t-Boc-NHOCH$_2$COOSu (1.8 g 6.25 mmol), prepared as above, was dissolved in 50 mL dry DMSO and the apparent pH (estimated by spotting onto humidified pH paper) adjusted to 8–9 with N-methylmorpholine. The H-Gly$_3$-[Lys(*t*-Boc-Ser(Bzl))]$_5$-Gly-OCH$_2$-PAM resin (prepared above) was added to this solution and the apparent pH found to be 8–9. The mixture was stirred for 2 h, and a 5-mg portion of resin was removed, washed with methanol (2 × 2 mL) and dichloromethane (2 × 2 mL), and then dried in the vacuum centrifuge. The standard ninhydrin analysis revealed that acylation was almost quantitative. The bulk of the acylated resin was then filtered, washed, and dried as before to yield 5.8 g.

Preparation of NH$_2$OCH$_2$CO-Gly$_3$-[Lys(H-Ser)]$_5$-Gly-OH. One gram of t-Boc-NHOCH$_2$CO-Gly$_3$-[Lys(*t*-Boc-Ser(Bzl))]$_5$-Gly-OCH$_2$-PAM resin (prepared above) was treated with 10 mL of TFA for 30 min with gentle stirring. Trifluoromethanesulfonic acid (1 mL) was then added and stirring continued for 1.5 h. Dry ether (25 mL) was added, under vigorous stirring, and the mixture cooled to 0 °C for 15 min. The precipitate formed was recovered by centrifugation and decantation and washed with dry ether (3 × 20 mL). After drying under vacuum, the precipitate, still in the presence of cleaved resin, was taken up in water (2 × 40 mL) and filtered through a Chromafil filter (type 0-45/25, Machery Nagel) to remove resin particles. Analytical HPLC showed the presence of one major component (t_R = 20.7 min) and several minor components. The crude material was purified in portions on the preparative column, isocratically with 100% solvent A at 10 mL/min, and the major fraction, t_R = 23–41 min, was collected, frozen, and lyophilized in the vacuum centrifuge. The material was shown to be pure by analytical HPLC. Analysis by FABMS in positive ion mode showed a protonated molecular ion at *m/z* 1395.41 (calculated M + H = 1395.75), consistent with the expected structure NH$_2$OCH$_2$CO-Gly$_3$-[Lys(H-Ser)]$_5$-Gly-OH. Further confirmation of stucture was provided by reacting the compound with isophthalaldehyde (see below). The uncorrected yield (based on starting Gly resin) was 47% on a weight basis; the powder obtained was shown to be about 73% peptide by weight (the remainder presumably

being trifluoroacetate counterion and water, not at all unusual for peptides purified in this way).

Reaction of NH_2OCH_2CO-Gly_3-[Lys(H-Ser)]$_5$-Gly-OH with Isophthalaldehyde. A solution of NH_2OCH_2-CO-Gly_3-[Lys(H-Ser)]$_5$-Gly-OH (1.39 mg, 1 μmol, in 1 mL water) was added to a solution of isophthalaldehyde (1 mL, 5 mM in 0.1 M acetate buffer, sodium counterion, pH 4.65, containing 20 mL/L acetonitrile). After 2 h, analysis by HPLC showed that transformation to a more hydrophobic product (t_R = 28.8 min under standard conditions), later identified as the oxime, had occurred quantitatively. The new product, HCO-*m*-C_6H_4CH=$NOCH_2CO$-$(Gly)_3$-[Lys(H-Ser)]$_5$-Gly-OH, was purified by HPLC on the analytical column at 1 mL/min under the following conditions: after 5 min at 100% solvent A, a linear gradient of solvent B, 1.75%/min, was applied until 7% B, which was maintained for 10 min and followed by a linear gradient of 1%/min B to 50%. Excess isophthalaldehyde and product eluted at t_R = 21 and 31 min, respectively. The product was characterized by positive ion FABMS and showed a strong signal at *m/z* 1511.57 (calculated M + H = 1511.78), consistent with the expected structure HCO-*m*-C_6H_4CH=$NOCH_2CO$-$(Gly)_3$-[Lys(H-Ser)]$_5$-Gly-OH.

Preparation of H-Gly_3-[Lys(H-Ser)]$_5$-Gly-OH. H-Gly_3-[Lys(*t*-Boc-Ser(Bzl))]$_5$-Gly-OCH_2-PAM resin (100 mg, prepared as above) was cleaved with TFA/trifluoromethanesulfonic acid (as described above) and the peptide precipitated and washed with ether. Analysis by HPLC showed the presence of two components. The major component (earlier eluting, t_R = 17 min on the analytical column) was purified on the preparative column, eluted isocratically with solvent A at 10 mL/min (t_R = 12–13.5 min). Analysis by FABMS in the positive ion mode showed a strong signal at *m/z* 1322.85 (calculated M + H = 1322.74), consistent with the expected structure H-Gly_3-[Lys(H-Ser)]$_5$-Gly-OH. The later-eluting component (t_R = 17.5 min on the analytical column) was found by FABMS to be heavier than the first by one Ser residue (87 amu).

Oxidation of H-Gly_3-[Lys(H-Ser)]$_5$-Gly-OH and Oximation. Ten microliters of a solution of H-Gly_3-[Lys-(H-Ser)]$_5$-Gly-OH (0.5 mM in water) was added to 1 mL of imidazole buffer (1 mM, pH 6.95, chloride counterion), and then 20 μL of a solution of $NaIO_4$ (2.5 mM in water) was added. Final concentrations were thus approximately 5 μM peptide (25 μM Ser), 50 μM periodate, and 1 mM imidazole. At various times (5 min to 24 h), aliquots (15 μL) were analyzed by HPLC under standard conditions. Similar experiments were performed at higher final concentrations: 50 μM peptide, 500 μM periodate, 10 mM imidazole; 250 μM peptide, 2.5 mM periodate, and 50 mM imidazole. Product (t_R = 20 min) was collected and shown to be the expected oxidation product, H-Gly_3-[Lys-(HCOCO)]$_5$-Gly-OH, by ESMS (using the signal due to the diprotonated form, found 1167.42, calcd 1167.20).

Preparation of DAI-NHNHCONHN=CH-*m*-C_6H_4-CH=$NOCH_2CO$-$(Gly)_3$-[Lys(H-Ser)]$_5$-Gly-OH. DAI-$NHNHCONHNH_2$ was prepared as a solution (0.2 mM) in acetate buffer (0.1 M, pH 4.6) as previously described (*3*). This solution was used to dissolve 2 equiv of freshly lyophilized HCO-*m*-C_6H_4CH=$NOCH_2CO$-$(Gly)_3$-[Lys(H-Ser)]$_5$-Gly-OH, prepared as above, and the mixture was allowed to react for 17 h. Reaction progress was assessed by analytical HPLC under the following conditions: after 5 min at 100% solvent A, a linear gradient of 2% B/min was applied to 30% B, whereupon the slope was lowered to 0.5% B/min to 50% B. Small quantities (*ca.* 100 μg) of product were isolated on the analytical column. Larger quantities (milligram amounts) were purified on a C18 Sep-Pak cartridge, washing with 0.1% TFA in 20% acetonitrile to remove excess reagent and eluting with 0.1% TFA in 50% acetonitrile. After lyophilization, the product was characterized by ESMS: found 7271.06 ± 1.05, calcd 7272.23.

Preparation of DAI-NHNHCONHN=CH-*m*-C_6H_4CH=$NOCH_2CO$-$(Gly)_3$-[Lys(DAVLB-NHN=CHCO)]$_5$-Gly-OH. DAI-NHNHCONHN=CH-*m*-C_6H_4-CH=$NOCH_2CO$-$(Gly)_3$-[Lys(H-Ser)]$_5$-Gly-OH, prepared as above, was dissolved (final concentration 167 μM) in 50 mM imidazole buffer (chloride counterion, pH 6.95, uncorrected glass electrode), containing 50% acetonitrile. Twenty equivalents (4 equiv for each of the five Ser residues of the carrier) of periodic acid (0.1 M in the imidazole buffer) was added. After 15 min, the reaction was diluted with 3 volumes of 0.1% TFA and injected onto the analytical column equilibrated at 30% solvent B. After 5 min at 30% B, a linear gradient was applied to 40% B over 40 min. Oxidized product, which elutes slightly earlier than traces of remaining unoxidized material, was collected and lyophilized. The oxidized material was dissolved (100 μM) in a mixture of aqueous 0.1 M acetic acid/acetonitrile (2:1 v/v). DAVLB-$NHNH_2$ (desacetylvincaleukoblastine hydrazide hemisulfate; Eli Lilly, Inc.) was added as a concentrated solution (0.1 M in water) to obtain 30 mM as a final concentration, whereupon the pH was raised to an indicated (paper) value of between 4.3 and 5. After 22 h and 45 min, products were separated on the analytical column under the following conditions: after 5 min at 20% solvent B, a linear gradient of 1% B/min was applied to 60% B. The product, which eluted as the major peak following the excess DAVLB-$NHNH_2$, was characterized by ESMS.

RESULTS AND DISCUSSION

Preparation and Characterization of the Carrier Molecule. The preparation of the carrier molecule is shown in Figure 1. Standard solid-phase techniques were used and the desired product was purified by HPLC and characterized by mass spectrometry. It is important that the coupling of Boc-Ser(Bzl)OSu be carefully performed, using a mild base (*N*-methylmorpholine, not the more usual *N,N*-diisopropylethylamine), room temperature, and a reaction time of 2–3 h. Otherwise, partial loss of Fmoc protection occurs, such loss being followed by acylation of the exposed amino group. By careful attention to detail, we have repeated this synthesis more than 20 times without problem.

The aldehyde form of the carrier molecule was prepared by reaction of the aminooxy form with a 5-fold excess of isophthalaldehyde (Figure 1), a procedure used previously to convert an aminooxy chelator to an aldehyde form (*3*).

Oxidation of the Carrier Molecule. The high susceptibility of 1-amino-2-hydroxy compounds to periodate has been well studied for the case of one such site per polypeptide (*1, 2, 16, 17*). In order to optimize conditions for the oxidation of our carrier molecule, which contains five terminal Ser residues per molecule, we used the model compound H-Gly_3-[Lys(H-Ser)]$_5$-Gly-OH. At dilute concentration, approximately 5 μM peptide (25 μM Ser), 50 μM periodate, 1 mM imidazole, analysis by HPLC showed that after 5 min the starting peptide had disappeared and that a new compound, eluting later as a sharp peak, was formed. After 1.5-h reaction, there was no further change (not shown). When higher final concentrations were used (50 μM peptide, 500 μM periodate, 10 mM imidazole), a reaction time of 5 min led to a clean transformation (Figure 2a) whereas after 1.5 h (Figure 2b) there were signs of

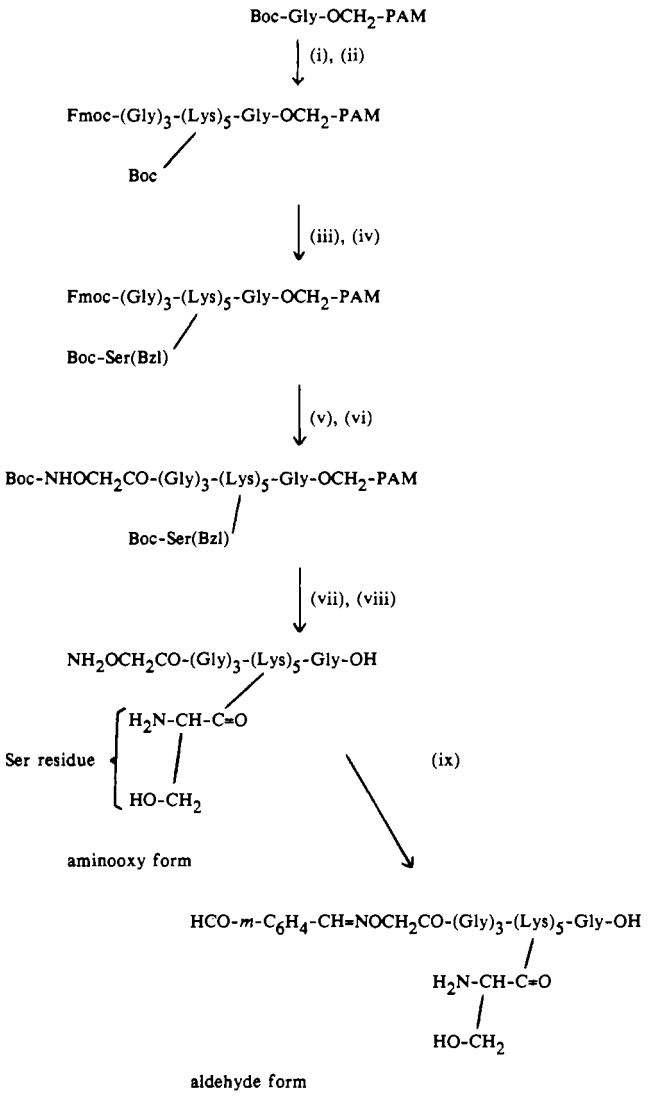


Figure 1. Synthesis of the carrier molecule in aminooxy and aldehyde forms: (i) TFA to remove Boc; (ii) standard Fmoc automated peptide synthesis; (iii) TFA; (iv) Boc-Ser(Bzl)-OSu; (v) piperidine/DMF; (vi) Boc-$NHOCH_2COOSu$; (vii) TFA; (viii) TFA/TFMSA; (ix) HCO-*m*-C_6H_4CHO.

overreaction. When even higher final concentrations were used (250 μM peptide, 2.5 mM periodate, 50 mM imidazole), a reaction time of 5 min led to a very slight overreaction whereas after 1.5 h extensive overreaction was observed and, after 20 h, the first-formed oxidation product was completely destroyed (not shown). Addition of ethylene glycol (2 equiv over periodate) after 5 min reaction was found to prevent the overreaction of peptide. The first-formed oxidation product, shown to be H-Gly_3-[Lys(HCO-CO)]$_5$-Gly-OH by ESMS, once isolated by HPLC, was stable as a lyophilized powder at −20 °C.

Preparation of DAI-NHNHCONHN=CH-*m*-C_6H_4CH=$NOCH_2$CO-(Gly)$_3$-[Lys(DVLB-NHN=CHCO)]$_5$-Gly-OH. Des-Ala^{B30}-insulin (DAI) was used as a model protein in order to be able to follow precisely, by reversed-phase HPLC and mass spectrometry, the various steps involved (Figure 3).

Step 1. A hydrazide function was introduced at the carboxyl terminus of DAI by reverse proteolysis using carbohydrazide as nucleophile (*3*). This mild enzymatic technique of site-specific protein modification is applicable to antibodies and their fragments and places the modification far from the antigen-binding region (*4*).

Step 2. The aldehyde form of the defined carrier was

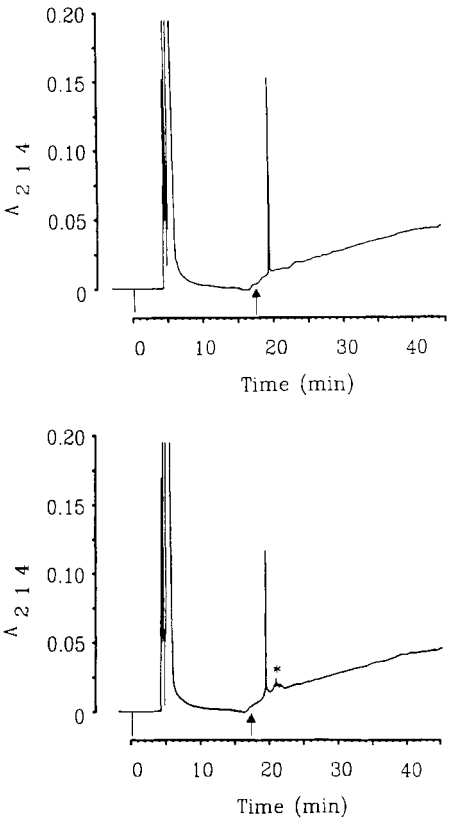


Figure 2. Oxidation of the model H-Gly_3-[Lys(H-Ser)]$_5$-Gly-OH with periodate. Analysis by HPLC of oxidation reactions involving (a) 50 μM peptide, 5 min; (b) 50 μM peptide, 1.5 h. The arrow and the asterisk indicate the elution positions of the unoxidized peptide and of overoxidized material, respectively.

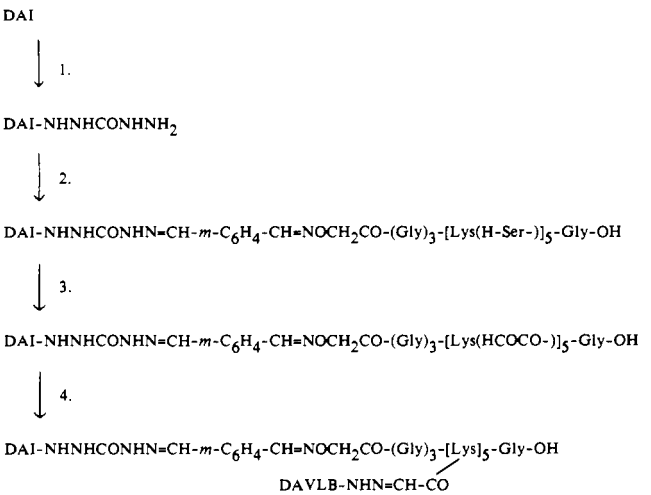


Figure 3. Synthesis of the site-specific pentadrug cluster of DAI: step 1, enzyme-catalyzed attachment of carbohydrazide specifically to residue B30; step 2, condensation with the aldehyde form of the carrier molecule; step 3, very mild periodate oxidation of the 1-amino-2-hydroxy function of the Ser residues; and step 4, hydrazone formation with the drug DAVLB-$NHNH_2$.

attached to the hydrazide group on the protein by hydrazone formation, a general reaction which is mild and perfectly specific (*3*). Figure 4 shows the result of analysis of the reaction mixture by HPLC. Very little DAI-carbohydrazide remains, and the product was identified as the desired hydrazone by ESMS.

Step 3. Ser residues of the carrier, which possess a 1-amino-2-hydroxy structure very susceptible to periodate, were oxidized under very mild conditions and the reaction followed by HPLC (Figure 5). The protein polyaldehyde

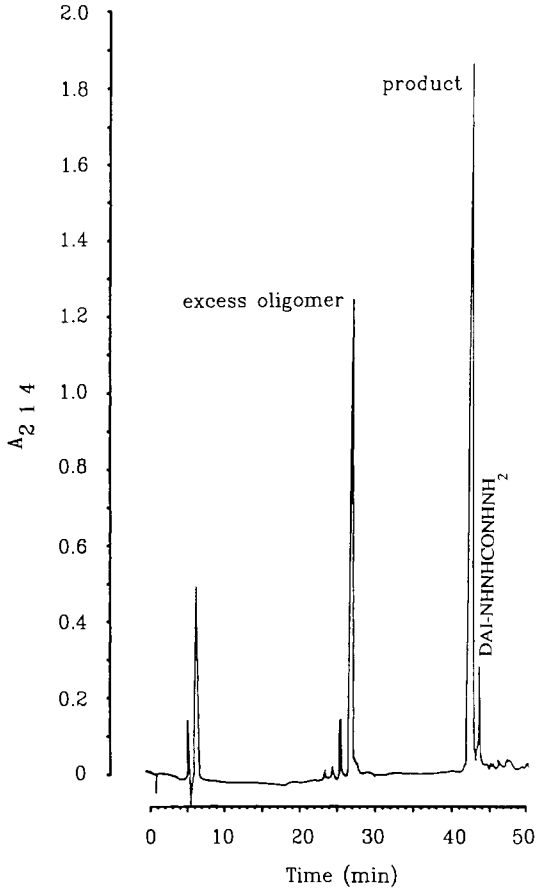


Figure 4. HPLC of the reaction between DAI-NHNHCONHNH$_2$ and the aldehyde form of the carrier molecule. Excess carrier elutes after 26 min; product DAI-NHNHCONHN=CH-*m*-C_6H_4CH=NOCH$_2$CO-(Gly)$_3$-[Lys(H-Ser)]$_5$-Gly-OH is responsible for the major peak at 42 min, and remaining DAI-NHNHCONHNH$_2$ elutes after 43 min.

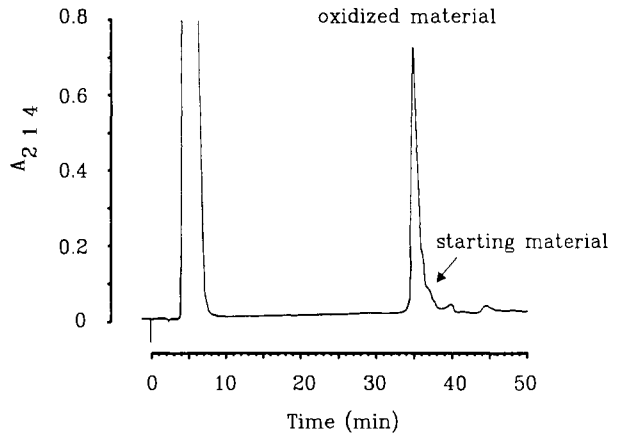


Figure 5. HPLC of the periodate oxidation of DAI-NHNHCONHN=CH-*m*-C_6H_4CH=NOCH$_2$CO-(Gly)$_3$-[Lys(H-Ser)]$_5$-Gly-OH. The major peak is due to oxidized material. Unoxidized material elutes slightly later and may be responsible for the slight tailing of the product peak.

did not give an interpretable mass spectrum, but must have been formed since the product of the oxidation went on to form the desired hydrazone (see below).

Step 4. The drug DAVLB-NHNH$_2$ was conjugated to the aldehyde groups of the carrier. Depending on the drug excess and reaction conditions used, a cluster of up to five drug molecules was formed. The reaction was followed by reversed-phase HPLC (Figure 6) and the products identified by electrospray ionization mass spectrometry.

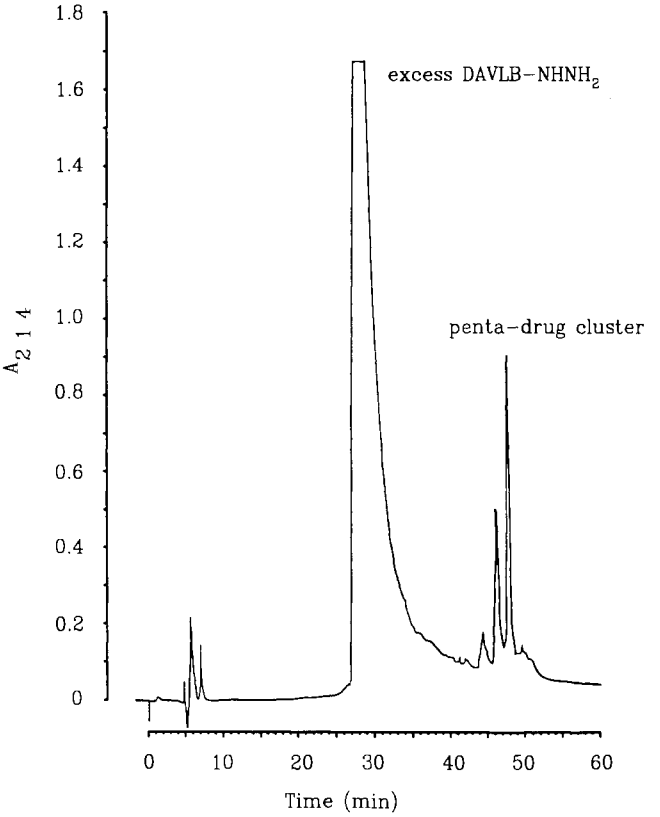


Figure 6. HPLC of the formation of DAI-NHNHCONHN=CH-*m*-C_6H_4CH=NOCH$_2$CO(Gly)$_3$-[Lys(X)]$_5$-Gly-OH, where X = DAVLB-NHN=CHCO. Approximate retention times are as follows: excess drug, 26 min; tridrug product, 44 min; tetradrug product, 46 min, and pentadrug product, 47 min.

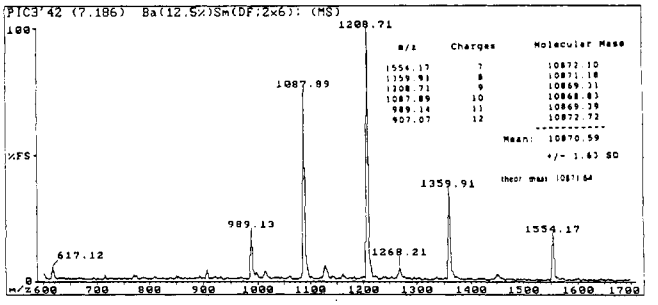


Figure 7. Electrospray ionization mass spectrum of the pentadrug conjugate DAI-NHNHCONHN=CH-*m*-C_6H_4CH=NOCH$_2$CO-(Gly)$_3$-[Lys(X)]$_5$-Gly-OH, where X = DAVLB-NHN=CHCO. The experimentally determined molecular weight is 10870.59 ± 1.63, very close to the calculated value of 10871.64.

Minor components visible in Figure 6 were thus shown to carry four and three drug molecules, whereas Figure 7 shows the electrospray mass spectrum of the major product, DAI-NHNHCONHN=CH-*m*-C_6H_4CH=NOCH$_2$CO-(Gly)$_3$-[Lys(DAVLB-NHN=CHCO)]$_5$-Gly-OH: found 10870.59 ± 1.63, calcd 10871.64. The five drug molecules are all attached to a single site on the protein: the C-terminus of the B chain of the model protein DAI. A hydrazide drug has thus been conjugated to the aldehyde groups of the oxidized carrier, producing a conjugate of defined chemical structure carrying 5 mol of drug/mol of protein. The pentadrug conjugate was found to be stable in 50 mM imidazole hydrochloride buffer at pH 7 for at least 24 h, whereas at pH 2 it became hydrolyzed, as expected, to a mixture of tetra-, tri-, and didrug forms and free drug, over a period of 5 h (not shown).

In other experiments (Scott, W. L., data not shown), the aminooxy version of the defined carrier has been used

to attach clusters of hydrazide drugs (DAVLB-$NHNH_2$ and methotrexate γ-hydrazide) to antitumor monoclonal antibodies, and the resulting immunoconjugates have exhibited promising effects in tumor xenograft studies in mice.

CONCLUSIONS

A defined carrier possessing a single reactive group (aminooxy or aldehyde), a spacer function (three Gly residues), and five potential aldehyde groups (in the form of Ser residues) has been prepared and characterized.

In its aldehyde form, this defined carrier was attached to a protein in good yield under very mild conditions at a specific site, i.e. the carboxyl terminus of a polypeptide chain to which carbohydrazide has been fixed by reverse proteolysis. Oxidation by periodate, under very mild conditions, of the pendant Ser residues of the carrier generated a cluster of new aldehyde groups. A hydrazide drug was conjugated to the generated aldehyde groups and produced a conjugate of defined chemical structure carrying up to 5 mol of drug/mol of protein. The conjugate was stable at neutral pH, and drug was released during incubation at low pH (not shown).

The aminooxy version of the defined carrier has been used to attach clusters of drugs to antitumor monoclonal antibodies. This aminooxy form may be attached to proteins which carry an aldehyde group specifically at the N- (*1*, *2*) or C-terminus (*16*), or on side chains (*11*) (not shown).

ACKNOWLEDGMENT

We thank Ms. Irène Rossitto and Mr. Pierre-Olivier Regamey for expert technical assistance, the Schmidheiny Foundation for some of the HPLC equipment used, and the Fonds National Suisse de la Recherche Scientifique and the Sandoz Stiftung for support of the Geneva mass spectrometry facility.

LITERATURE CITED

(1) Geoghegan, K. F., and Stroh, J. G. (1992) Site-directed conjugation of non-peptide groups to peptides and proteins via periodate oxidation of a 2-amino alcohol. *Bioconjugate Chem. 3*, 138–146.

(2) Gaertner, H. F., Rose, K., Cotton, R., Timms, D., Camble, R., and Offord, R.E. (1992) Construction of protein analogues by site-specific condensation of unprotected fragments. *Bioconjugate Chem. 3*, 262–268.

(3) Rose, K., Vilaseca, L. A., Werlen, R., Meunier, A., Fisch, I., Jones, R. M. L., and Offord, R. E. (1991) Preparation of well-defined protein conjugates using enzyme-assisted reverse proteolysis. *Bioconjugate Chem. 2*, 154–159.

(4) Fisch, I., Künzi, G., Rose, K., and Offord, R. E. (1992) Site-specific modification of a fragment of a chimeric monoclonal antibody using reverse proteolysis. *Bioconjugate Chem. 3*, 147–153.

(5) Schnölzer, M., and Kent, S. B. H. (1992) Constructing proteins by dovetailing unprotected synthetic peptides: backbone-engineered HIV protease. *Science 256*, 221–225.

(6) O'Shannessy, D. J., and Quarles, R. H. (1987) Labeling of the oligosaccharide moieties of immunoglobulins. *J. Immunol. Methods 99*, 153-161.

(7) Pietersz, G. A. (1991) The linkage of cytotoxic drugs to monoclonal antibodies for the treatment of cancer. *Bioconjugate Chem. 1*, 89–95.

(8) Kato, Y., Umemoto, N., Kayama, Y., Fukushima, H., Takeda, Y., Hara, T., and Tsukada, Y. (1984) A novel method of conjugation of daunomycin with antibody with a poly-L-glutamic acid derivative as intermediate drug carrier. An anti-alpha-fetoprotein antibody-daunomycin conjugate. *J. Med. Chem. 27*, 1602–1607.

(9) Slinkin, M. A., Klibanov, A. L., and Torchilin, V. P. (1991) Terminal-modified polylysine-based chelating polymers: highly efficient coupling to antibody with minimal loss in immunoreactivity. *Bioconjugate Chem. 2*, 342–348.

(10) Mann, J. S., Huang, J. C., and Keana, J. F. W. (1992) Molecular amplifiers: synthesis and functionalization of a poly(aminopropyl)dextran bearing a uniquely reactive terminus for univalent attachment to biomolecules. *Bioconjugate Chem. 3*, 154–159.

(11) Scott, W. L., Horvath, S., Nichols, C. L., Johnson, D. A., Starling, J. J., Vorndran-Jones, C., Baker, A. L., Owens, R., Cullinan, G., Laguzza, B. C., and Bumol, T. (1990) Drug releasability as a critical factor in the design of active immunoconjugates: an evolution to new, broadly applicable, lysine-based, drug-releasing linkers yielding active conjugates of antibodies and their fragments. *Antibody Immunoconjugate Radiopharm. 3*, 65.

(12) Vilaseca, L. A., Rose, K., Werlen, R., Meunier, A., Offord, R. E., Nichols, C.L., and Scott, W. L. (1993) Synthesis and use of a defined oligomer for targetted drug therapy. In *Peptides 1992* (C. H. Schneider, and A. N. Eberle, Eds.) pp 819–820, ESCOM, Leiden, The Netherlands.

(13) Pochon, S., Buchegger, F., Pélegrin, A., Mach, J.-P., Offord, R. E., Ryser, J. E., and Rose, K. (1989) A novel derivative of the chelon desferrioxamine for site-specific conjugation to antibodies. *Int. J. Cancer 43*, 1188–1194.

(14) Kohn, J., and Wilchek, M. (1982) Selective and highly sensitive spray reagent for detection of nanomolar quantities of carbodiimides on thin-layer plates. *J. Chromatogr. 240*, 262–263.

(15) Savoy, L.-A., Jones, R. M. L., Pochon, S., Davies, J. G., Muir, A. V., Offord, R. E., and Rose, K. (1988) Identification by fast atom bombardment mass spectrometry of insulin fragments produced by insulin proteinase. *Biochem. J. 249*, 215–222.

(16) Rose, K., Jones, R. M. L., Sundaram, G., and Offord, R. E. (1989) Attachment of linker groups to carboxyl termini using enzyme-assisted reverse proteolysis. In *Peptides 1988*, (G. Jung, and E. Bayer, Eds.) pp 274–276, W. de Gruyter, Berlin.

(17) Gaertner, H. F., Rose, K., Cotton, R., Timms, D., Camble, R., and Offord, R.E. (1993) Construction of protein analogues by site-specific condensation of unprotected fragments. In *Peptides 1992*, (C. H. Schneider, and A. N. Eberle, Eds.) pp 239–240, ESCOM, Leiden, The Netherlands.

(6-Maleimidocaproyl)hydrazone of Doxorubicin—A New Derivative for the Preparation of Immunoconjugates of Doxorubicin

David Willner,* Pamela A. Trail,† Sandra J. Hofstead, H. Dalton King, Shirley J. Lasch,†
Gary R. Braslawsky,‡ Robert S. Greenfield,§ Takushi Kaneko,⊥ and Raymond A. Firestone

Bristol-Myers Squibb Company, 5 Research Parkway, Wallingford, Connecticut 06492-7660. Received June 27, 1993®

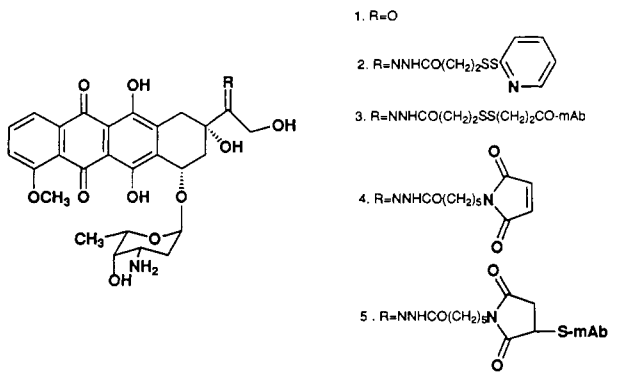
The (6-maleimidocaproyl)hydrazone of doxorubicin was synthesized and conjugated to several mAbs, including chimeric BR96, via a Michael addition reaction to thiol-containing mAbs. DTT reduction of disulfides present in the mAb was a reliable and general method for generating a consistent number of reactive SH groups. The conjugates, after purification by Bio-Beads, were free of unreacted linker and/or doxorubicin. All conjugates released doxorubicin under acidic conditions that mimic the lysosomal environment, while they were relatively stable at neutral pH. BR96 conjugates showed antigen-specific cytotoxicity.

The antitumor agent doxorubicin (DOX,[1] 1; Chart I) (and other antitumor anthracyclines) has been linked to monoclonal antibodies (mAb) to enhance its activity against solid tumors, and also to decrease its side effects of cardiac toxicity and myelosuppression (*1*). Of particular interest are immunoconjugates that release the chemotherapeutic agent due to the acid sensitivity of the linker (*2–6*). Thus, compound **2**, a hydrazone derivative of 1, has been shown to release DOX at pH 4.5–5.5, and furthermore, conjugates of this linker with several mAbs show good *in vitro* and *in vivo* activity (*3a,b, 5, 6*). Following antigen-specific binding, the conjugates are internalized into the acidic environment of the lysosomes where DOX is released from the acid-labile linker (*7*).

When compound **2** is conjugated to a thiol-containing mAb, the linkage formed includes a disulfide bridge (structure **3**), which is susceptible to cleavage by thiols (*3a, 8*). Conjugates of ricin A and other toxins with disulfide linkages are unstable when administered *in vivo* and this instability could be due to the slow splitting of the disulfide bond by reduced glutathione or to the action of a disulfide reductase (*9, 10*). In some cases (*11, 12*) no decomposition of the conjugate was found, and it was reasoned that the immunotoxins were cleared from the blood so fast that the slower breakdown reaction could not be detected (*9*). This instability of the disulfide bond was also proposed to explain the need for high therapeutic doses of DOX conjugates in certain carcinoma models (*6*).

A linker containing a thioether group should provide a much more stable conjugate (*8*). Such a thioether could be formed by reacting a thiol derivative of the therapeutic agent with either a haloacetyl (*13*) or a maleimide derivative of a mAb (*3c, 14, 15*) or, conversely, by reacting a haloacetyl or maleimide derivative of the drug with a thiol-containing antibody (*15*). Using the latter approach, we have synthesized the (6-maleimidocaproyl)hydrazone of DOX-(MC-DOXHZN), **4**, a new hydrazone, and covalently attached it to several mAbs that have free thiols generated by two methods. The resulting conjugates, **5**, were tested in vitro and showed antigen-specific cytotoxicity.

Chart I



EXPERIMENTAL PROCEDURES

General. Melting points were determined on a Fisher-Johns melting point apparatus and are uncorrected. NMR spectra were obtained on a Bruker AM 300 in various solvents (specified) and are reported as δ values downfield from tetramethylsilane. Multiplicities of resonances are described as broad (b), singlet (s), doublet (d), triplet (t), quartet (q), or multiplet (m). IR spectra were run as KBr pellets or $CHCl_3$ solutions on a Perkin-Elmer (PE) FTIR Model 1800. MS and HRMS were obtained with a Kratos MS25RFA and MS50TC instrument, respectively. Elemental analyses were performed by Oneida Research Services.

Flash chromatography was performed with Woelm silica gel (silica 32-63). TLC was carried out on Analtec silica gel GHLF plates, 250 μm. For HPLC, a PE QC-620 pump equipped with a PE ISS-200 injector and LKB Multitemp II Thermostatic controller was used. The detector was an HP 1046 fluorescent detector and the integrator a PE Nelson Turbochrome. HPLC was performed on a Jones column using a 70:30 mixture of methanol and 0.025 M

† Present address: Bristol-Myers Squibb Pharmaceutical Research Institute, P.O. Box 4000, Princeton, NJ 08543.
‡ Present address: 124 Heritage Drive, Glastonbury, CT 06033.
§ Present address: 10 Sieter Hill Rd, Wallingford, CT 06492.
⊥ Present address: Pfizer Central Research, Groton, CT 06430.
® Abstract published in *Advance ACS Abstracts,* October 1, 1993.

[1] The abbrevations used are as follows: DOX, doxorubicin; mAb, monoclonal antibody; HRMS, high-resolution mass spectrum; SEC, size-exclusion chromatography; THF, tetrahydrofuran; DMF, *N,N*-dimethylformamide; MC-DOXHZN, (6-maleimidocaproyl)hydrazone of doxorubicin; SPDP, *N*-succinimidyl 3-(2-pyridinyldithio)propionate; DTT, dithiothreitol; PBS, phosphate-buffered saline. MR, molar ratio; mAb–DOX, conjugate of doxorubicin (mAb specified when necessary); cpm, counts per minute.

1043-1802/93/2904-0521$04.00/0 © 1993 American Chemical Society

ammonium phosphate, pH 4.5, as a mobile phase, at a 1.5 mL/min flow rate. The eluted DOX was detected by excitation at ca. 233 nm and emission monitored at ca. 570 nm. Size-exclusion chromatography (SEC) was done on a TSK column, Model G3000SWXL, and respective guard column from Hewlett Packard. The mobile phase was 0.2 M KH_2PO_4 in saline adjusted to pH 6.8 with 4 N KOH, and detection was done by UV and visible light at 280 and 495 nm, respectively. Stirred cells for diafiltration and accessories were from Amicon, Inc. (Beverly, MA). Bio-Beads (SM-2) were from Bio-Rad Laboratories (Richmond, CA).

Antibodies. mAb BR96 is a mouse/human chimeric mAb which identifies a Le^y-related tumor-associated antigen expressed on the cell membrane of carcinomas of the lung, breast, colon, and ovary and is internalized following antigen-specific binding (*16*). The chimeric mAb (humanized IgG1 Fc portion) was produced from a murine mAb by a modification of the homologous recombination procedure as described previously (*17*). mAb BR 64 (*6*, *16*) was obtained from Brunswick BioTechnetics (San Diego, CA). mAb L6, an anticarcinoma mAb which does not internalize following antigen-specific binding (*18*) was obtained from CellTech Ltd. (Berkshire, U.K.). Conjugates prepared from this antibody were used for synthetic comparisons. Human IgG, obtained from Rockwell Inc. (Gilbertsville, PA), was used to produce control, non-binding immunoconjugates.

Tumor Cell Lines. L2987 is a human lung adenocarcinoma line which expresses the BR96 antigen and was obtained from I. Hellstrom (Bristol-Myers Squibb, Seattle, WA).

Chemicals. DOX hydrochloride was obtained from Sanraku, Inc. All other chemicals were obtained from commercial sources.

6-(2,5-Dihydro-2,5-dioxo-1*H*-pyrrolo)-1-hexanoic Acid (6-Maleimidocaproic Acid), 8 (*20*, *21*). Maleic anhydride (29.4 g, 0.3 mol) and 6-aminocaproic acid (39.35 g, 0.3 mol) were refluxed in glacial acetic acid (900 mL) for 16 h. Acetic anhydride (30.6 g, 0.3 mol) was added dropwise over a period of 2 h and reflux was continued for 1 h. The acetic acid was removed under vacuum at 70 °C to yield a yellow syrup which solidified. The material was chromatographed over silica using methylene chloride–methanol–acetic acid (100:5:1) affording a crystalline solid: mp 87–91 °C (27.8 g, 43%); NMR (DMSO) 6.95 (s, 2H), 3.35 (t, 2H), 2.15 (t, 2H), 1.45, 1.18 (2m, 6H).

6-(2,5-Dihydro-2,5-dioxo-1*H*-pyrrolo)-1-hexanoic Acid Hydrazide (6-Maleimidocaprohydrazide) and Its Trifluoroacetic Acid Salt, 10 (*20*). 6-Maleimidocaproic acid (2.11 g, 10 mmol) in dry THF (200 mL) was stirred under nitrogen at 4 °C with *N*-methylmorpholine (1.01 g, 10 mmol) followed by dropwise addition of isobutyl chloroformate (1.36 g, 10 mmol) in THF (10 mL). After 5 min, a solution of *tert*-butyl carbazate (1.32 g, 10 mmol) in THF (10 mL) was added dropwise. The reaction mixture was kept at 4 °C for 30 min and at room temperature for 1 h. The solvent was evaporated and the residue was partitioned between ethyl acetate and water. The organic layer was washed with dilute HCl solution, water, and dilute sodium bicarbonate and dried over anhydrous sodium sulfate, and the solvent was evaporated. The residual foam was chromatographed over silica using a gradient solvent system of methylene chloride–methanol (100:1-2). The protected hydrazide, **9**, was obtained in 70% yield (2.24 g).

Compound **9** (545 mg, 2.4 mmol) was dissolved in ice-cold trifluoroacetic acid (10 mL) and stirred in an ice bath for 8 min. The acid was removed under high vacuum at room temperature. The residue was triturated with ether to yield the crystalline trifluoroacetic acid salt of 6-maleimidocaprohydrazide (**10**) (384 mg, 70%). An analytical sample was prepared by crystallization from methanol–ether: mp 102–5 °C; NMR ($CDCl_3$–DMSO) 7.24 (broad peak superimposed on chloroform peak), 6.55 (s, 2H), 3.34 (t, 2H), 2.06, (t, 2H), 1.46 (m, 4H), 1.15 (m, 2H); MS $[MH]^+$ 226. Anal. Calcd for $C_{10}H_{15}N_3O_3 \cdot 0.8CF_3COOH$: C, 44.02; H, 4.99; N, 13.28. Found: C, 44.13; H, 5.00; N, 12.75.

The salt (220 mg) was converted to the free base by chromatography over silica using a methylene chloride–methanol–ammonium hydroxide (100:5:0.5) solvent system. The material obtained (124 mg, 80%) was crystallized from methylene chloride–ether: mp 92–93 °C. Anal. Calcd for $C_{10}H_{15}N_3O_3$: C, 53.33; H, 6.67; N, 18.67. Found: C, 53.12; H, 6.67; N, 18.44.

(6-Maleimidocaproyl)hydrazone of DOX, 4. DOX hydrochloride (5.2 g, 8.96 mmol) and 6-maleimidocaprohydrazide trifluoroacetate salt (**10**) (9.2 g, 27.1 mmol) were dissolved in 1750 mL of methanol. Trifluoroacetic acid (0.5 mL) was added and the solution was stirred at room temperature for 24 h while being protected from light. The methanolic solution was concentrated under reduced pressure at 31 °C to a volume of 250 mL. Acetonitrile (1250 mL) was added and the resulting suspension was allowed to stand at 4 °C for 48 h for crystallization of the product. The red solid hydrazone was isolated by centrifugation, washed with fresh methanol-acetonitrile (1:10), and dried under vacuum to yield the (6-maleimidocaproyl)hydrazone of DOX (5.78 g, 7.7 mmol, 86% yield): mp >200 °C dec; IR (KBr) 3430, 2936, 1704, 1666, 1616, 1582, 1446, 1410, 1378, 1284, 1208, 1014, 986, 824 cm^{-1}; NMR (CD_3OD) 7.94 (bd, 1H), 7.82 (t, 1H), 7.55 (d, 1H), 6.78 (s, 2H), 5.48 (s, 1H), 5.07 (t, 1H), 4.59 (d, 1H), 4.21 (m, 1H), 4.02 (s, 3H), 3.63–3.30 (m, 5H), 2.55-2.26 (m, 4H), 2.19–1.88 (m, 3H), 1.69-1.18 (m, 12 H including a doublet, 3H, at 1.26); MS $(M + H)^+$ 751; HRMS calcd for $C_{37}H_{43}N_4O_{13}$: 751.2827. Found: 751.2823. Anal. Calcd for $C_{37}H_{42}N_4O_{13} \cdot HCl$: C, 56.45; H, 5.73; N, 7.12, Cl, 4.50. Found: C, 56.73; H, 5.73; N, 6.89; Cl, 3.76.

Conjugation of mAb with MC-DOXHZN via SPDP Thiolation. The conjugation of hydrazones to mAbs was described previously (*3a*,*b*, *5*). The following conjugation of BR96 with MC-DOXHZN is typical for all mAb used in this study. A solution of BR96 in PBS buffer (27.5 mL, 12.53 mg/mL, 7.83×10^{-5} M, total of 2.15 μmol; the protein concentration was determined by UV absorption at 280 nm, 1 mg/mL = 1.4 AU) was treated with a 10 mM ethanolic solution of SPDP (1.7 mL, 5.3 mg, 17 μmol). The solution was incubated at 31 °C for 35 min, chilled in ice, and treated with a 50 mM solution of DTT (1.7 mL, 13.09 mg, 85 μmol) for 15 min at 4 °C. The solution was transferred to a dialysis tube (Spectrum Medical Industries, Los Angeles, CA) and dialyzed 4 × 8 h in PBS–0.1 M histidine buffer, pH 7.4 (4.5 L). The amount of mAb was determined as above (27.5 mL, 9.29 mg/mL, 5.8×10^{-5} M, total of 1.6 μmol) and the SH concentration was determined by the Ellman method (*19*) (2.06×10^{-4} M, 5.7 μmol total); MR SH/mAb = 3.6. The thiolated BR96 (17 mL, 0.99 μmol) was treated with an equivalent molar amount of MC-DOXHZN in DMF (5 mg/mL, 6.3×10^{-3} M; 0.59 mL, 3.7 μmol) and the reaction mixture was incubated overnight at 4 °C. The solution was centrifuged and transferred to a dialysis tube and dialyzed as above. The dialyzed solution was centrifuged and the supernatant shaken gently with Biobeads for a few hours at 4 °C. The solution (19 mL) was freed

from the Bio-Beads by centrifugation and the amount of DOX was determined by UV absorption at 495 nm (ϵ495 = 8030 cm^{-1} M^{-1}; 117 μM, 67.9 μg/mL). The amount of mAb was determined by absorbance at 280 nm according to the formula (*3a*)

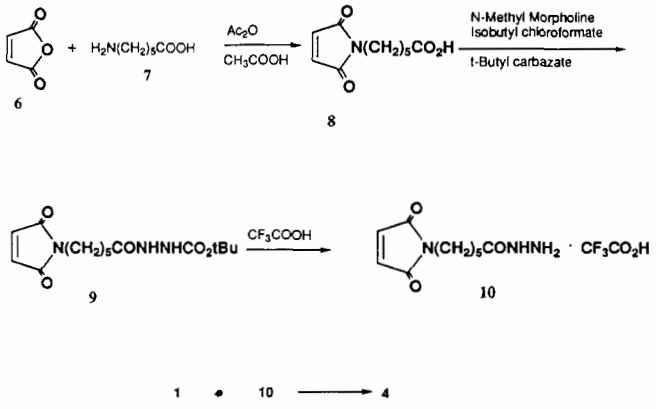
$$\text{mAb (mg/mL)} = \frac{A_{280} - (0.724 \times A_{495})}{1.4}$$

(*A* is the observed absorbance at noted wavelength) which includes a correction for the absorbance of DOX at the same wavelength (6.53 mg/mL, 4.08×10^{-5} M; yield 72%). The MR DOX/mAb was 2.9.

Conjugation of mAbs with MC-DOXHZN via DTT Thiolation. The following procedure for mAb BR96 was found applicable to other mAbs in this study. mAb BR96 in PBS buffer (500 mL, 10.49 mg/mL, 6.56×10^{-5} M determined as above, total of 32.8 μmol) was heated under nitrogen to 37 °C, stirred gently, and treated with DTT (10 mM solution in PBS, 23 mL, 230 μmol). The solution was kept under these conditions for 3 h and then transferred into 2 400-mL Amicon stirred ultrafiltration cells (Model #8400) each fitted with a YM 30 ultrafilter (molecular weight cutoff 30 000) and connected to a reservoir (Model #RC800) containing PBS solution. The mAb solution was diafiltered until no more thiol groups could be detected in the effluent by the Ellman method (*19*). The mAb solution (526 mL) was transferred from the cells to a sterile container and kept in ice under nitrogen. The concentration of protein and thiol was determined as above (9.91 mg/mL, 6.19×10^{-5} M, 32.6 μmol and 5.05×10^{-4} M, 265.6 μmol, respectively; MR of SH/protein was 8.16) and 1 molar equiv of MC-DOXHZN (50.6 mL of a 5 mg/mL, 6.3×10^{-3} M distilled water solution, 319.1 μmol) was added with stirring. The solution was kept at 4 °C for 30 min after which it was filtered through a 0.22-mm cellulose acetate membrane. A 2.5 × 50 cm column was packed with a slurry of 100 g of Bio-Beads in PBS buffer. The beads had been prepared by soaking in methanol and washing in succession with several volumes of distilled water and buffer. The filtered conjugate solution was percolated through this column at a rate of 2–2.5 mL/min. After that, the solution (530 mL) was filtered again through a cellulose acetate membrane and the concentration of mAb and DOX determined (9.45 mg/mL, 5.91×10^{-5} M; 232 mg/mL, 0.400×10^{-3} M, respectively). The mAb yield was 96% and the MR of DOX to mAb was 6.78. As shown in Table I the mAb yields for BR96 conjugates were 90–100%. The conjugates were frozen in liquid nitrogen and stored at −80 °C. Other mAbs were conjugated in a similar manner, and the data are given in Table I.

Relationship between DTT/mAb Ratio and the Number of Thiol Groups Generated. mAb BR96 or BR64 in PBS buffer, at a concentration of approximately 10 mg/mL, was treated for 3 h at 37 °C under an atmosphere of argon with 10–150 mM DTT in PBS to achieve the desired ratio of DTT to mAb (see Figure 1). The mAb sample was then passed through a Pharmacia PD-10 column with deoxygenated PBS buffer at pH 7.4. The protein fraction was collected in a sealed test tube under argon. SH groups were determined using Ellman's reagent (*19*). For large samples (≥100 mg mAb) the passage over a PD-10 column was substituted by ultrafiltration against PBS buffer, pH 7.4, in an Amicon stirred cell fitted with an Amicon YM-30 membrane and pressurized with argon at 40 psi. Dialysis was continued until the stirred cell eluant tested negative with Ellman's reagent (*19*), and the number of SH groups was determined in the same manner.

Scheme I



Relationship between SPDP/mAb and Number of Thiols Generated. This experiment was carried out similarly to the previous one, except that the thiolating agent was SPDP. BR64 and BR96 were treated with an ethanolic solution of SPDP for 30 min at 30 °C under argon, cooled to 0 °C, and treated with a 5-fold molar amount of DTT for 15 min. The solution was then purified by passing it through a PD-10 column with deoxygenated PBS, pH 7.4, and collected in a sealed test tube under argon. The SH titer was determined by the Ellman method (*19*). The results are plotted in Figure 2.

Air Reoxidation of DTT Reduced BR64. BR64 in PBS (10.72 mg/mL, 6.7×10^{-5} M, 1 mL) was treated with DTT solution in PBS (50 μL of 134 mM solution) and the reaction mixture was incubated at 37 °C for 1 h. The mAb was purified on a PD-10 column and 1.5 mL solution was collected in a 12 × 75 mm glass tube which was left open to atmosphere for 21 h. Aliquots were removed at the beginning (t = 0) and subsequent intervals and the SH concentration determined as above. The results are shown in Figure 3.

In Vitro Cytotoxicity Assays. The activity and specificity of BR96–DOX conjugates was evaluated as described previously (*6*). Briefly, monolayer cultures were harvested using trypsin–EDTA (GIBCO, Grand Island, NY), and the cells counted and resuspended to 1×10^5/mL in RPMI-1640 containing 10% heat-inactivated fetal calf serum (RPMI-10% FCS). Cells (0.1 mL/well) were added to each well of 96-well microtiter plates and incubated overnight at 37 °C in a humidified atmosphere of 5% CO_2. Media were removed from the plates and serial dilutions of DOX or mAb–DOX conjugates added to the wells. All dilutions were performed in quadruplicate. Cells were exposed to DOX or mAb–DOX conjugates for 2 h at 37 °C in a humidified atmosphere of 5% CO_2. The mAb-DOX conjugate or DOX was removed and the cells washed three times with RPMI–10% FCS and cultured in RPMI–10% FCS (37 °C, 5% CO_2) for an additional 48 h. At this time the cells were pulsed for 2 h with 1.0 mCi/well of [^{3}H]thymidine (New England Nuclear, Boston, MA). The cells were harvested onto glass-fiber mats (Skatron Instruments, Inc., Sterling, VA) and dried, and filter-bound [^{3}H]thymidine radioactivity was determined (β-Plate scintillation counter, Pharmacia LKB Biotechnology, Piscataway, NJ). Inhibition of [^{3}H]thymidine uptake was determined by comparing the mean cpm for treated samples with that of the untreated control.

RESULTS AND DISCUSSION

Preparation of Linker 4. 6-Maleimidocaproic acid (8) (Scheme I) was previously prepared from 6-aminocaproic acid and *N*-(methyoxycarbonyl)maleimide which in

Table I. Conjugates Prepared via DTT and SPDP Thiolation

	DTT			SPDP		
mAb	MR SH	MR DOX	yield of mAb (%)	MR SH	MR DOX	yield of mAb (%)
BR96	8.6	7.9	100	3.1	3.5	73
	6.4	5.8	100	3.6	2.9	72
	8.7	8.4	95	6.5	4.9	46
	8.2	7.6	100	7.8	5.6	30
	8.2	6.8	95	6.9	5.3	23
	8.6	7.2	93			
	7.9	7.0	94			
BR64	7.8	5.3	97	10.6	7.1	95
				7.3	6.0	77
				8.5	7.2	77
				5.7	4.8	99
				6.6	6.0	88
L6	9.8	7.4	100	8.9	7.3	54
	5.3	4.9	84			
IgG	8.8	7.2	96	7.9	6.23	82
	8.9	8.1	100			

turn was prepared from maleimide and methyl chloroformate (*20*). An alternate synthesis (*21*) started from the amino acid and maleic anhydride to form 6-[(3-carboxy-1-oxo-2-propenyl)amino]hexanoic acid, which was cyclized in toluene in the presence of triethylamine. Acid **8** (as well as its homologues) could be synthesized in a single step by heating maleic anhydride and 6-aminocaproic acid (or its homologue) in acetic acid followed by treatment with acetic anhydride.[2] It was converted to its hydrazide, **10**, via a mixed anhydride and *tert*-butyl carbazate followed by removing the *tert*-butoxycarbonyl group with trifluoroacetic acid. The hydrazone **4** was prepared by treating DOX hydrochloride and **10** in methanol overnight with catalytic trifluoroacetic acid (*5*). The final product still containdd 3–5% of unreacted **1** but this did not interfere with the conjugation and purification of the conjugate.

Generation of Reactive Thiol Groups on the mAb. Previous conjugations of DOX hydrazones to mAbs were done through thiolation of the mAb and reacting it with linker **2** to form a disulfide bridge between the mAb and the drug, e.g. **3** (*3, 5, 6*; however also see *4*). The thiolation of the mAb was achieved by reacting the lysine moieties of the mAb with SPDP and reducing the S–S bond with DTT. Initially, we used the same thiolation methodology for our four mAbs (see Table I). Although as the SPDP ratio to BR64 and BR96 rose to 50 and the MR of SH groups to these mAb increased smoothly up to 12 (see Figure 2), thiolated BR96 with MR above 8–9 suffered from reduced binding to the antigen,[3] presumably because of reaction on active-site lysines. An additional problem arose when we switched from mAb BR64 to chimeric BR96. Conjugates that were prepared via SPDP thiolation and had a MR of 8 were soluble in PBS buffer when BR64 was used, but not with BR96. Owing to precipitation, yields of conjugates plummeted when final MRs were raised above 3.5, which is too low for good antitumor activity (*6*). Adding L-histidine or mannitol to the buffer gave little benefit. The tendency to precipitate resided in the antibody, not the linker, because it persisted with either mono or dithio links, and with thiolation by either SPDP or iminothiolane (data not shown). The use of the latter reagent shows also that loss of positive charge, which occurs when lysine amino groups react with SPDP but not with

[2] We thank Dr. I. Monkovic for these procedures.

[3] Binding determinations were done according to ref 3a,b. We thank Ms. K. Kadow for performing these measurements.

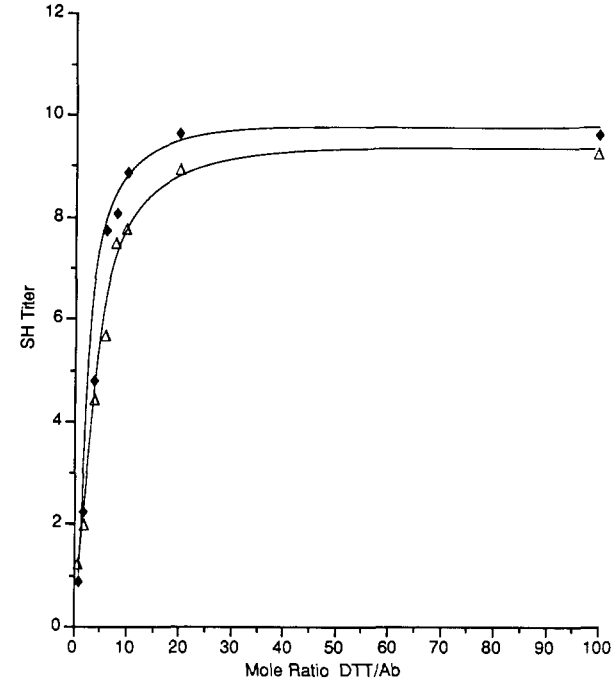


Figure 1. Number of thiol groups generated from mAb by treatment with DTT at 37 °C as a function of MR of DTT to mAb (BR64 ♦; BR96 △).

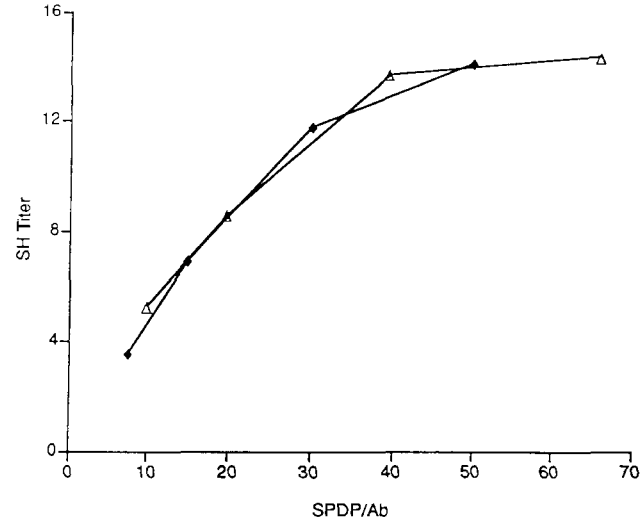


Figure 2. Number of thiol groups generated from mAb by treatment with SPDP at 30 °C as a function of MR of SPDP to mAb (BR64 ♦; BR96 △).

2-iminothiolane, was not responsible for the precipitation. Only when thiolation of lysines was abandoned altogether was the precipitation problem overcome (*vide infra*).

Another way to generate free SH groups in the mAb is by reduction of the mAb with DTT. The light and heavy chains of antibodies are held together through noncovalent interactions, with interchain disulfide bridges providing additional stability to the structure (*22*). These interchain disulfide bonds can be reduced in preference to the interchain disulfide in the absence of a denaturing reagent (Figure 4)(*23–25*). Under mild reduction conditions, the mAb remains intact, retaining its binding, while providing free SH groups for conjugation (*26*). Further, it was shown that when immune serum globulins (a mixture of isotypes with $\gamma 1$ predominating) were treated similarly with DTT only four disulfide linkages were reduced corresponding to the number of interchain linkages present in an IgG1 type (*27*). Very recently (*28*) mAb BR96 was subjected to

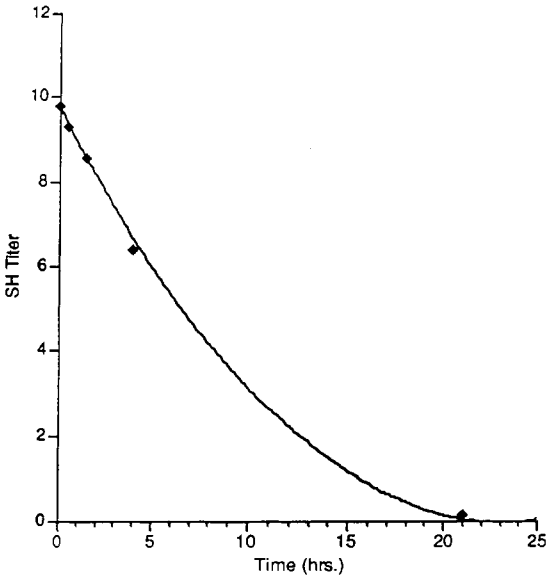


Figure 3. Reoxidation of DTT-reduced BR64 in open atmosphere.

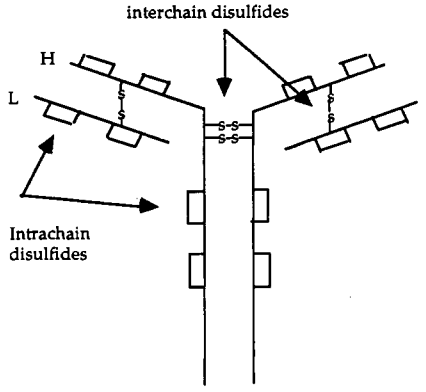


Figure 4. Schematic drawing of BR96 mAb. The heavy (H) and light (L) chain are held together through noncovalent interactions and the interchain disulfides provide additional stability to the molecule.

DTT reduction but with the generation of only four SH groups rather than the expected eight.

We investigated the DTT reduction of mAb BR96 by carrying out the reaction at 37 °C under nitrogen and using varied molar ratios of DTT to mAb. The data, given in Figure 1, clearly indicate that the number of SH groups levels off at eight no matter how much excess DTT is used. Thus, we were able to improve on the earlier procedure (*28*) and apply this thiolation method to the preparation of conjugates. In our best procedure, BR96 (and other mAbs; see Table I) is treated with 7 molar equiv of DTT at 37 °C for 3 h. This reaction and all subsequent steps through the final conjugation must be done with air excluded because reoxidation of thiols is facile (see Figure 3). Excess DTT is removed by diafiltration (which takes only hours, as opposed to dialysis, which takes days) and the thiol molar concentration is determined. This value is used to determine the amount of hydrazone needed for conjugation. The advantage of this method is that it yields consistently the same number of SH groups and hence a consistent MR of drug to mAb. Immunoconjugates made from BR96, in which thiols were generated in this way, do not precipitate, regardless of whether a mono or dithio linker is used, and high yields are always obtained. This method of producing thiols was then adopted for all subsequent conjugation, working equally well for mAb BR64, L6, and IgG (see Table I).

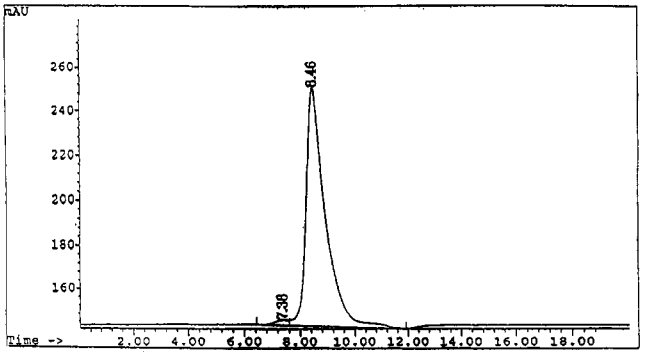


Figure 5. SEC-HPLC of BR96–DOX conjugate in saline–0.2M KH_2PO_4 buffer. Absorbance (mAU) was measured at 280 nm.

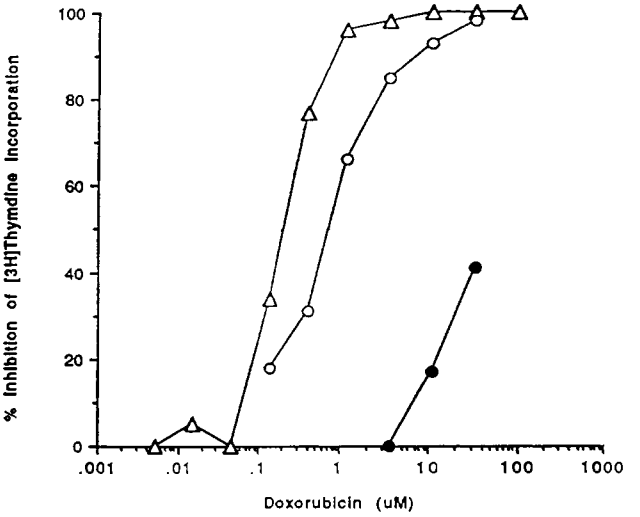


Figure 6. Cytotoxicity of BR96–DOX conjugates against the L2987 lung carcinoma line. Cells were exposed for 2 h at 37 °C to DOX or DOX conjugates, washed and cultured for an additional 48 h prior to the addition of [^{3}H]thymidine. Data are presented as percent inhibition of [^{3}H]thymidine uptake relative to control cells. Cells were treated with DOX (△), BR96-DOX, MR = 7.59 (○); or nonbinding IgG-DOX, MR = 8.11 (●).

Most importantly, these immunoconjugates maintain their molecular integrity despite the loss of bridging disulfide units, presumably owing to noncovalent forces between the chains. This was shown in four ways. (1) Size-exclusion chromatography finds a single entity of mw 150 000 (Figure 5). (2) Gel electrophoresis under nondenaturing conditions gives the same result (data not shown). (3) Binding is not significantly (<10%) lost after conjugation (*29*). (4) Antitumor activity is strong and antigen specific both in vitro (Figure 6) and in vivo (*30*).

That all or almost all interchain disulfides have been reduced in the immunoconjugate is shown by the fact that although SDS–PAGE without prior heating shows principally intact conjugate with only traces of separate heavy and light chains, pretreatment with SDS for 2 min at 100 °C causes virtually complete separation into heavy and light chains. DTT-reduced mAb BR96 is also completely dissociated in this way, but unreduced BR96 retains is integrity even after 2 min at 100 °C with SDS.[4] Further evidence is the fact that reduction of BR96, even with a great excess of DTT, stops after reaction of four disulfides, which is the number of interchain disulfides in this mAb (see Figure 1).

Another aspect of the thiolation method is the question of uniformity from molecule to molecule of the immu-

[4] Unpublished experiments by Drs. K. Leister, D. Kirkley, and associates.

noconjugate with respect to (1) which individual sites are derivatized and (2) how many DOX molecule are carried by each mAb molecule. Since there is apparently no preferred group of lysines that reacts faster than the others with SPDP (Figure 2), a different subset of lysines can be expected to be derivatized for each individual mAb molecule. Furthermore, at any given overall mole ratio there must be a wide spread of individual molecules with MRs higher and lower than the average. Thus immunoconjugate molecules made in this way are grossly nonuniform, both individually and collectively. In addition, those product molecules with highest MRs—the most valuable ones therapeutically—are just the ones that will bind most poorly to the target cell. As a result, the effective MR is less than the measured one, with the potentially most effective portion of the immunoconjugate wasted. In contrast, there does appear to be a preferred subset of disulfides that react fastest with DTT directly (see Figure 1) and therefore this method of thiolation leads to a product wherein all molecules are derivatized in the same location to about the same extent, and subsequently bind the same.

Conjugation of the mAb with Linker. Initially, DTT-thiolated BR96 was reacted with MC-DOXHZN overnight at 4 °C, but 30 min was found to be sufficient. The standard cleanup by dialysis was lengthy (4 days) and cumbersome, with loss of DOX from the conjugate through hydrolysis. It was replaced by column treatment with Bio-Beads (2–3 h) which removes unreacted linker **4** and DOX. The resulting product is virtually free of these contaminants. From start to finish a 3-g batch of conjugate now takes 15–17 h. The MR of DOX to mAb is six to eight groups, consistent with the number of SH groups generated by DTT. No loss of mAb due to precipitation occurs. Regardless of whether the conjugate is purified by dialysis or a Bio-Bead column, the mAb yield is consistently 95–100%, a vast improvement over SPDP thiolation.

Release Rate Data. The release of DOX from its conjugates at pH 5 and 7, at 37 °C, was monitored by HPLC in a similar manner to that described for other hydrazones (*3a,b*, *5*). The half-lives ($T_{1/2}$) of BR96 conjugates are 158 and 3.2 h at pH 7 (0.1 M phosphate buffer) and 5 (0.1 M acetate buffer), respectively. As expected, the conjugate releases DOX faster (almost 50 fold) under acidic conditions than under neutral conditions. The long $T_{1/2}$ of the conjugate at pH 7 allows us to predict good stability of the conjugate for *in vivo* testing. The precursor, linker **4**, was insoluble in phosphate buffer at pH 7. However, at pH 5, its $T_{1/2}$ is 2.9, similar to that of the conjugate. In comparison, the $T_{1/2}$ of linker **2** is 120 and 13.9 h at pH 7 and 5, respectively.[5] It has been established that the release rate of DOX from linker **2** and **4** at pH 5 is dependent on acetate buffer concentration (L. Padilla, unpublished results; *5*).

Antigen-Specific Cytotoxicity of BR96-DOX Conjugates *in Vitro*. Representative data for the *in vitro* cytotoxicity of mAb–DOX conjugates and unconjugated DOX are shown in Figure 6. The BR96–DOX conjugates demonstrated antigen-specific cytotoxicity *in vitro* when evaluated against the L2987 human carcinoma line. The BR96–DOX conjugate was approximately 50-fold more potent that the nonbinding IgG–DOX conjugate (IC_{50}'s = 0.7 and > 33 μM based on DOX content, respectively) and approximately 4-fold less potent than unconjugated DOX (IC_{50} = 0.2 μM). A detailed description of both *in vitro* and *in vivo* experiments will be published elsewhere (*30*).

In summary, the (6-maleimodocaproyl)hydrazone of DOX was synthesized and conjugated to several mAbs, including chimeric BR96. The conjugation was done via a Michael addition reaction to thiol containing mAbs. Generation of thiols on the mAb was done in three ways but best by DTT, and the procedure was developed into a reliable general method providing a consistent number of SH groups. All conjugates released DOX under conditions that mimic the lysosomal environment, but were relatively stable at neutral pH. The BR96 conjugates showed good specificity in *in vitro* studies, being much more active than a conjugate made from an irrelevant antibody. These findings suggest further studies *in vivo*.

[5] Unpublished results by L. Padilla and G. Dubowchik.

ACKNOWLEDGMENT

We wish to thank the Analytical Research Group for spectral and analytical data, in particular Mr. Ed Pack for the HPLC data. We thank also Dr. Kirk Leister and his group at Bristol-Myers Squibb AR&D, Syracuse, NY, for their help. Finally, we thank Drs. Terrence W. Doyle and Dinesh M. Vyas for their encouragement and support.

LITERATURE CITED

(1) Hermentin, P., and Seiler, E. R. (1988) Investigations with monoclonal antibody drug (anthracycline) conjugates. *Bhering Inst. Mitt. 82*, 197–215.

(2) (a) Shen, W. C., and Reiser, J. P. (1981) cis-Aconityl spacer between daunomycin and macromolecular carriers: a model of pH-sensitive linkage releasing drug from a lysosomotropic conjugate. *Biochem. Biophys. Res. Commun. 102*, 1048–1054. (b) Yang, H. M., and Reisfeld, R. A. (1988) Doxorubicin conjugates with a monoclonal antibody directed to a human melanoma-associated proteoglycan suppresses the growth of established tumor xenographs in nude mice. *Proc. Natl. Acad. Sci. U.S.A. 85*, 1189–1193.

(3) (a) Greenfield, R. S., Kaneko, T., Daues, A., Edson, M. A., Fitzgerald, K. A., Olech, L., Grattan, J. A., and Braslawsky, G. R. (1990) Evaluation in vitro of adriamycin–immunoconjugates synthesized using an acid sensitive hydrazone linker. *Cancer Res. 50*, 6600–6607. (b) Braslawsky, G. R., Edson, M. A., Pearce, W., Kaneko, T., and Greenfield, R. S., (1990) Antitumor activity of adriamycin (hydrazone linked) immunoconjugates compared to free adriamycin and specificity of tumor cell killing. *Cancer Res. 50*, 6608–6614. (c) Greenfield, R. S., Braslawsky, G. R., Olech, L. and Kaneko, T. (1989) Anthracycline protein conjugates having a novel linker and methods for their production. EP # 0 328 147. (d) Kato, Y., Endo, N., and Hara, K. (1988) Hydrazides and method for their preparation. J. P. Kokai No. 63-57569.

(4) Mueller, B. M., Wrasidlo, W. A., and Reisfeld, R. A. (1990) Antibody conjugates with morpholinodoxorubicin and acid cleavable linkers. *Bioconjugate Chem. 1*, 325–330.

(5) Kaneko, T., Willner, D., Monkovic, I., Knipe, J. O., Braslawsky, G. R., Greenfield, R. S., and Vyas, D. M. (1991) New hydrazone derivatives of adriamycin and their immunoconjugates—A correlation between acid stability and cytotoxicity. *Bioconjugate Chem. 2*, 133–141.

(6) Trail, P. A., Willner, D., Lasch, S. H., Henderson, A. J., Greenfield, R. S., King, D., Zoeckler, M. E., and Braslawsky, G. R. (1992) Antigen specific activity of carcinoma reactive BR64-adriamycin conjugates evaluated in vitro and in human tumor xenograft models. *Cancer Res. 52*, 5693–5700.

(7) Braslawsky, G. R., Kadow, K., Knipe, J., McGoff, K., Edson, M., Kaneko, T., and Greenfield, R. (1991) Adriamycin (hydrazone)–antibody conjugates require internalization, intracellular hydrolysis for antitumor activity. *Cancer Immunol. Immunother. 33*, 367–374.

(8) (a) Means, G. E., and Feeney, R. E. (1990) Chemical modification of protein: history and application. *Bioconjugate Chem. 1*, 2–12 (b) Koppel, G. A. (1990) Recent advances with monoclonal antibody drug targeting for the treatment of human cancer. *Bioconjugate Chem. 1*, 13–23.

(9) Thorpe, P. E., Wallace, P. M., Knowless, P. P., Relf, M. G., Brown, A. N. F., Watson, G. J., Knyba, R. E., Wawrzynczak, E. J., and Blakey, D. C. (1987) New coupling agents for the

synthesis of immunotoxins containing a hindered disulfide bond with improved stability in vivo. *Cancer Res. 47*, 5924–5931.

(10) Candiani, C., Franceschi, A., Chignola, R., Pasti, M., Anselmi, C., Benoni, G., Tridente, G., and Colombatti, M. (1992) Blocking effect of human serum but not of cerebrospinal fluid on ricin A chain immunotoxin potentiation of carrier protein-monensin conjugates. *Cancer Res. 52*, 623–630.

(11) Raso, V., and Basola, M. (1984) Monoclonal antibodies as cell targeted carriers of covalently and non-covalently attached toxins. *NATO Adv. Study Inst. Ser. A Life Sci. 82*, 119–138.

(12) Bourrie, B. J. P., Casellas, P., Blythman, H. E. and Jansen, F. K. (1986) Study of the plasma clearance of antibody-ricin-A-chain immunotoxins. Evidence for specific recognition site on the A – chain that mediate rapid clearance of the immunotoxin. *Eur. J. Biochem. 155*, 1–10.

(13) Li, P., Medon, P. P., Skingle, D. C., Lanser, J. A., and Symons, R. H. (1987) Enzyme linked synthetic oligonucleotides probes: non radioactive detection of enterotoxigenic Escherichia coli in faecal specimens. *Nucleic Acids Res. 15*, 5275–5287.

(14) Senter, P. D., Saunier, M. G., Schreiber, G. J., Hirschberg, D. L., Brown, J. P., Hellström, I., and Hellström, K. E. (1988) Antitumor effects of antibody–alkaline phosphatase conjugates in combination with etoposide phosphate. *Proc. Natl. Acad. Sci. U.S.A. 85*, 4842–4846.

(15) Ghosh, S. S., Kao, P. M., McCue, A. W., and Chappelle, H. L. (1990) Use of maleimidothiol chemistry for efficient synthesis of oligonucleotide–enzyme conjugates hybridization probes. *Bioconjugate Chem. 1*, 71–76.

(16) Hellström, I., Garrigues, H. J., Garrigues, U., and Hellström, K. E. (1990) Highly tumor-reactive, internalizing, mouse monoclonal antibodies to Le^y-related cell surface antigen. *Cancer Res. 50*, 2183–2190.

(17) Fell, H. P., Yarnold, S., Hellström, I., Hellström, K. E., and Folger, K. R. (1989) Homologous recombination in hybridoma cells: heavy chain chimeric antibody produced by gene targeting. *Proc. Natl. Acad. Sci. U.S.A. 86*, 8507–8511.

(18) Hellström, I., Beaumier, P. L., and Hellström, K. E. (1986) Antitumor effects of L6, an IgG2a antibody reacting with most human carcinomas. *Proc. Natl. Acad. Sci. U.S.A. 83*, 7059–7063.

(19) Riddles, P. W., Blakeley, R. L., and Zerner, B. (1979) Ellmans's reagent: 5,5′-Dithiobis(2-nitrobenzoic acid)—A reexamination. *Anal. Biochem. 94*, 75–81.

(20) Keller, O., and Rudinger, J. (1975) Preparation and some properties of maleimido acids and maleoyl derivatives of peptides. *Helv. Chim. Acta 58*, 531–541.

(21) Rich, D. H., Gesellchen, P. D., Tong, A., Cheung, A., and Buckner, C. K. (1975) Alkylating derivatives of amino acids and peptides. Synthesis of maleoylamino acids [1-(N-maleoylglycyl)cysteinyl]oxytocin and [1-(N-maleoyl-11-aminoundecanoyl)cysteinyl]oxytocin. Effect of vassopresin-stimulated water loss from isolated toad bladder. *J. Med. Chem. 15*, 1004–1010.

(22) Marquart, M., and Deisenhofer, J. (1982) The three dimensional structure of antibodies. *Immunol. Today 3*, 160–166.

(23) Nissonof, A. (1984) *Introduction to molecular immunology*, p 20. Sinauer Associates Inc., Sunderland, MA.

(24) Gunewardena, P., and Cook, K. B. (1966) 1,4-dithiothreitol as a reagent for reductive degradation of human J-G globulin. *Biochem. J. 99*, 8 p.

(25) Gorevic, P. D., Prelli, F. C., and Frangione, B. (1985) Immunoglobulin G. *Methods Enzymol. 116*, 3–25.

(26) Goldberg, M., Knudsen, K. L., Platt, D., Kohen, A., Bayer, E. A., and Wilchek, M. (1991) Specific interchain cross linking of antibodies using bis maleimide. Repression of ligand leakage in immunoaffinity chromatography. *Bioconjugate Chem. 2*, 275–280.

(27) Schroeder, D. D., Tankersly, D. L., and Lundblad, J. L. (1981) A new preparation of modified immune serum globulin (human) suitable for intravenous administration. *Vox Sang. 40*, 373–382.

(28) Siegall, C. B., Gawlak, S. L., Chin, J. L., Zoeckler, M. E., Kadow, K. F., Brown, J. P. and Braslawsky, G. R. (1992) Cytotoxicity of chimeric (human-murine) monoclonal antibody BR96, IgG, $F(ab')_2$, and Fab′ conjugated to *Pseudomonas* exotoxin. *Bioconjugate Chem. 3*, 302–307.

(29) Zhao, H., Willner, D., Cleveland, J. S., Braslawsky, G. R., and Brown, J. P. (1992) Determination of immunoreactivity of doxorubicin antibody immunoconjugates by a Le^y competitive RIA. *Bioconjugate Chem. 3*, 549–553.

(30) Trail, P. A., Willner, D., Lasch, S. J., Henderson, A. J., Hofstead, S. J., Casazza, A. M., Firestone, R. A., Hellström, I. and Hellström, K. E. (1993) Cure of xenografted human carcinomas by BR96–doxorubicin Immunoconjugates. *Science 261*, 212–215.

Oriented and Covalent Immobilization of Target Molecules to Solid Supports: Synthesis and Application of a Light-Activatable and Thiol-Reactive Cross-Linking Reagent†

André Collioud, Jean-François Clémence, Michael Sänger, and Hans Sigrist*

Institute of Biochemistry, University of Berne, Freiestrasse 3, CH-3012 Berne, Switzerland. Received June 27, 1993®

Light-dependent oriented and covalent immobilization of target molecules has been achieved by combining two modification procedures: light-dependent coupling of target molecules to inert surfaces and thiol-selective reactions occurring at macromolecule or substrate surfaces. For immobilization purposes the heterobifunctional reagent *N*-[*m*-[3-(trifluoromethyl)diazirin-3-yl]phenyl]-4-maleimidobutyramide was synthesized and chemically characterized. The photosensitivity of the carbene-generating reagent and its reactivity toward thiols were ascertained. Light-induced cross-linking properties of the reagent were documented (i) by reacting first the maleimide function with a thiolated surface, followed by carbene insertion into applied target molecules, (ii) by photochemical coupling of the reagent to an inert support followed by thermochemical reactions with thiol functions, and (iii) by thermochemical modification of target molecules prior to carbene-mediated insertion into surface materials. Procedures mentioned led to light-dependent covalent immobilization of target molecules including amino acids, a synthetic peptide, and antibody-derived F(ab') fragments. Topically selective, light-dependent immobilization was attained with the bifunctional reagent by irradiation of coated surfaces through patterned masks. Glass and polystyrene served as substrates. Molecular orientation is asserted by inherently available or selectively introduced terminal thiol functions in F(ab') fragments and synthetic polypeptides, respectively.

INTRODUCTION

Covalent immobilization of biomolecules to various substrate surfaces has yielded biosurfaces applicable for molecular analysis (Bhatia et al., 1992), separation (Brocklehurst et al.; 1984; Berry et al., 1991; O'Shannessy, 1990), targeting (Martin et al., 1982), synthesis (Fodor et al., 1992), and diagnosis (Ljungquist et al., 1989). Most procedures used to date for target molecule immobilization are based on thermochemical reactions: covalent bonds are formed between surface-exposed amino, carboxyl, or thiol functions or generated aldehydes and suitably modified solid supports, membrane surfaces, or macromolecular aggregates. For optimal performance of biosurfaces, full retention of biological activities (Fassina, 1992) and molecular orientation is attempted (Wimalasena and Wilson, 1991; Matson and Little, 1988). Approaches mentioned require functionalization of either the target molecules, the substrate surface, or both (Larsson et al., 1987). In addition, thermochemical reaction conditions may affect biological activities and multiple-site attachment of individual molecules may occur. To overcome drawbacks of thermochemical reactions, noninvasive coupling procedures and mild reaction conditions are necessary to retain native biomolecule structures. Brunner and Richards (1980) and others (Bayley, 1983; Brunner, 1989) have introduced (trifluoromethyl)aryl diazirines as hydrophobic (membrane) protein labels. On the basis of these investigations, new routes of biomolecule immobilization have been initiated (Sigrist et al., 1992; Sänger et al., 1992). Since photoactivatable reagents are topically addressable, photoimmobilization of biomolecules became a subject of intense research toward the development of resistant materials, biosensors, and biomaterials (Fodor et al., 1992; Rosznyai et al., 1992; Yan et al., 1993).

For topically addressable and oriented biomolecule immobilization, we designed a linking agent which fulfills the requirements for molecular orientation and noninvasive (light-dependent) activation. The reagent, *N*-[*m*-[3-(trifluoromethyl)diazirin-3-yl]phenyl]-4-maleimidobutyramide (Figure 1A), carries a maleimide function for thermochemical modification of cysteine thiols (Bhatia et al., 1989) and an aryldiazirine function for light-dependent, carbene-mediated binding to solid supports, biomimetic devices, or biological surfaces. Activation of a carbene-generating aryldiazirine with a 350-nm light source has been shown to lead to covalent coupling of proteins, enzymes, immunoreagents, carbohydrates, and nucleic acids (Sigrist et al., 1992; Klingler et al., 1991; Clémence, unpublished) under conditions such that biological activity is not impaired (Gao et al., unpublished; Küng et al., unpublished).

In this study the synthesis, chemical characterization, and reactivity of the new heterobifunctional cross-linking reagent are described. Selected applications of this cross-linker are depicted in Figure 1B-D, all of which lead to thermochemical/photochemical immobilization of target molecules. Basic immobilization procedures are elaborated with amino acids and a terminally thiolated peptide. With regard to future applications in diagnostic procedures, the versatility and applicability of the new bifunctional cross-linking agent are investigated with immu-

† Abbreviations used: TRIMID, 3-(trifluoromethyl)-3-(*m*-isothiocyanophenyl)diazirine; FEP-OH, Hydroxylated fluorinated ethylenepropylene; PPO, 2,5-diphenyloxazole; POPOP, 2,2'-*p*-phenylenebis(5-phenyloxazole); HEPES, 4-(2-hydroxyethyl)piperazine-1-ethanesulfonic acid; EDTA, ethylenediaminetetraacetic acid; PSA, prostate-specific antigen; DTNB, 5,5'-dithiobis(2-nitrobenzoic acid); TEA, triethylamine; TLC, thin-layer chromatography; DMF, dimethylformamide; BSA bovine serum albumin; MAD, *N*-[*m*-[3-(trifluoromethyl)diazirin-3-yl]-phenyl]-4-maleimidobutyramide; CDPGYIGSR, Cys-Asp-Pro-Gly-Tyr-Ile-Gly-Ser-Arg-NH_2.

® Abstract published in *Advance ACS Abstracts,* November 1, 1993.

1043-1802/93/2904-0528$04.00/0 © 1993 American Chemical Society

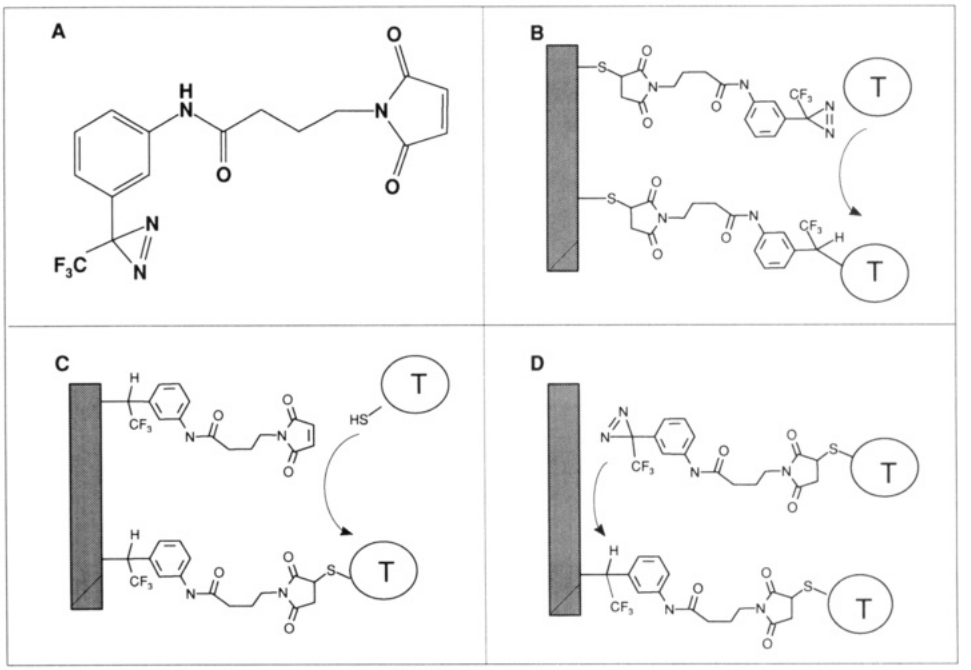


Figure 1. Chemical structure and reaction routes of MAD-mediated target-molecule immobilization: (A) Structure of MAD (N-(4-maleimidobutyryl)-*N*-[*m*-[3-(trifluoromethyl)diazirin-3-yl]phenyl amide); (B) reaction route 1, thermochemical coupling of MAD to thiolated surfaces is followed by photochemical target molecule coupling; (C) reaction route 2, photochemical coupling of the reagent to an inert surface is followed by thermochemical reactions with thiol functions; (D) reaction route 3, thermochemical modification of target molecules prior to carbene-mediated insertion to surface materials. T: target molecule.

noreagents. F(ab′) fragments of monoclonal anti-prostate-specific-antigen antibodies (anti-PSA antibodies) are covalently attached through photoimmoblization on polystyrene.

EXPERIMENTAL PROCEDURES

Materials. ^{1}H-NMR spectra were recorded on a Varian EM 360L and absorption measurements were carried out on an Uvicon 810 or a Beckmann DU 64 spectrophotometer. IR spectra were recorded on a Perkin-Elmer 782 infrared spectrophotometer. Melting points were determined with a Büchi 510 instrument and a CH 7A Varian MAT was used for mass spectroscopy. Radioactive disintegrations were measured in 5 mL of scintillation fluid (1080 mL of toluene, 5.4 g of PPO, 0.2 g of POPOP, 920 mL of Triton X-100, and 40 mL of acetic acid) on a Betamatic V liquid scintillation counter. Thin-layer chromatography (TLC) was performed with silica gel 60 F_{254} plates (Merck). Silica gel 60 (particle size 0.040–0.063 mm, 230–400 mesh ASTM) for flash chromatography was from Merck. Light sources for irradiation were either a HBO 350 mercury lamp from Osram (filtered with a Schott WG 320 and a 1-cm layer of saturated $CuSO_4$ in H_2O; transmission bandwidth 320–550 nm) or the Stratalinker UV 2400 (Stratagene) with five 365-nm bulbs. The SVX 1530 mercury lamp power supply (constant power output of 200 W) and the MU4 timer were from Mueller Electronics (Moosinning, Germany). Light intensities were measured with a Suss UV intensity meter Model 1000 (Hilpert AG). HPLC was performed with a wide-pore butyl (C_4) Bakerbond standard column (particle size, 5 μm; dimensions 4.6 × 250 mm; Baker Inc., Phillipsburg, NJ) on a Hewlett-Packard 1090 liquid chromatograph equipped with a Perkin-Elmer LC 75 detector (280 nm) and a Hewlett-Packard 3396A integrator. The UVmax ELISA microplate reader was from Molecular Device. FEP-OH membranes (3 cm in diameter) were a gift of Prof. Aebischer. The photomask with 300-μm slits separated by 500-μm spacings was purchased from Towne Laboratories Inc. Somerville, NJ.

Bovine serum albumin (BSA) was purchased from Fluka. F(ab′)$_2$ fragments of monoclonal anti-PSA antibodies were provided by Hoffmann-La Roche, Basel, Switzerland. 3-(Trifluoromethyl)-3-(*m*-aminophenyl)diazirine was synthesized according to Dolder et al. (1990). The peptide Cys-Asp-Pro-Gly-Tyr-Ile-Gly-Ser-Arg-NH_2 (CDPGYIGSR) was from Sigma. 4-Maleimidobutyric acid, ethylchloroformate (purum), TEA (puriss), DMF, (3-mercaptopropyl)trimethoxysilane (purum), and DTNB were from Fluka. Sodium cyanoborohydride and dithiothreithol (DTT) were from Merck. [^{14}C]Tyrosine (468 mCi/mmol), [^{14}C]formaldehyde (46.7 mCi/mmol), and [^{35}S]cysteine (20–150 mCi/mmol) were from Amersham. All other chemicals were reagent grade. PD-10 (Sephadex G-25, medium) columns were obtained from Pharmacia. For sandwich type ELISA, reagents provided with the Cobas Core PSA assay kit were used (Hoffmann-La Roche, Basel, Switzerland). Polystyrene MicroWell modules polysorb F8 and Immunowash 8 were from NUNC (Intermed). Microplate wells were coated with BSA prior to antibody photoimmobilization.

Methods. Synthesis and Chemical Characterization of *N*-[*m*-[3-(Trifluoromethyl)diazirin-3-yl]phenyl]-4-maleimidobutyramide. 4-Maleimidobutyric acid (40 mg, 0.22 mmol) was dissolved in 4 mL of DMF and cooled to −20 °C under nitrogen. Triethylamine (56 μL, 0.4 mmol) was added to the stirred solution followed by dropwise addition of ethyl chloroformate (37.8 μL, 0.4 mmol) in 500 μL of DMF. The reaction mixture was stirred for 15 min and freshly prepared 3-(trifluoromethyl)-3-(*m*-aminophenyl)diazirine (45.9 mg, 0.22 mmol) in 500 μL of DMF was slowly added. The solution was allowed to warm to ambient temperature and was stirred for 1.5 h. The reaction mixture was poured into 20 mL of 1 M NaCl on ice under vigorous stirring and extracted four times with 5-mL aliquots of ether. Ether extracts were washed twice with 1 M HCl (5 mL each) and four times with water

(5 mL each) and dried over anhydrous Na_2SO_4. Solvents were removed under reduced pressure, and the crude product was purified by flash chromatography on silica gel 60 with ethyl acetate/hexane 1/1 (v/v) as eluent. Product-containing fractions were pooled and organic solvents evaporated. The procedure described yielded 65.2 mg of MAD (0.17 mmol, 77%), which recrystallized as white needles. The cross-linking reagent was stored at −20 °C.

Chemical homogeneity and the molecular structure of the bifunctional reagent were confirmed as follows. TLC: R_f 0.34 in ethyl acetate/hexane, 1/1 (v/v). Mp: 96.5–98 °C. UV absorption spectrum (in ethanol): MAD shows a characteristic absorption shoulder at 360 nm constituted by both the diazirine (ϵ_{347} = 446 M^{-1} cm^{-1}; Dolder et al. 1990) and the maleimide absorption band (ϵ_{300} = 620 M^{-1} cm^{-1}; Roberts and Rouser, 1958). IR ($CHCl_3$): 3040 (C=CH), 1720 (C=O), 1605 cm^{-1} (N=N). MS (FAB): *m/e* (rel intensity) 366 (M + H, 3.19), 338 (26.28), 228 (29.58), 173 (100), 172 (58.95), 166 (49.03), 138 (45.97), 110 (61.14), 98 (15.32), 28 (16.49), 18 (28.49). HRMS (FAB): *m/e* calcd for ($C_{16}F_3H_{13}N_4O_3$ + H) 366.0939, found 366.0936. ^1H NMR ($CDCl_3$, chemical shifts (δ) in parts per million): 8.2 (s, 1H), 6.9–7.8 (m, 4H), 6.7 (s, 2H), 3.6 (t, 2H), 1.9–2.5 (m, 4H).

Preparation of Anti-PSA F(ab') Fragments. $F(ab')_2$ fragments of anti-PSA monoclonal antibodies (270 μg, 2.05 mg/mL) in 0.1 M sodium phosphate buffer, pH 6.8, were combined with DTT (final concentration 1 mM) and incubated for 50 min at 37 °C. F(ab') fragments were separated from excess reducing agent by chromatography on PD-10 in 0.1 M sodium acetate, 0.5 M NaCl, 1 mM EDTA, pH 5.0. Fractions (600 μL) were collected and protein contents were analyzed by measuring the 280-nm absorption ($A_{280}^{1\%}$ = 14.0). Generated fragments were used immediately after separation to avoid thiol oxidation.

Preparation of [^{14}C]-Methylated $F(ab')_2$ and F(ab') Fragments. $F(ab')_2$ fragments of F5 anti-PSA antibody (540 μg, 2.05 mg/mL) in 0.1 M sodium phosphate buffer pH 6.8 were transferred to 0.1 M HEPES buffer, pH 7.5, by chromatography on PD-10. [^{14}C]Formaldehyde (2 μmol, 100 μCi) and sodium cyanoborohydride (final concentration 24 mM) were added to the pooled protein fractions, and the reaction mixture was stirred for 4 h at ambient temperature. [^{14}C]-Methylated protein was purified on PD-10 (equilibrated with 0.1 M sodium phosphate buffer, pH 6.8) or by HPLC on Ultrapac TSK 3000 SW (7.6 × 300 mm; elution conditions, 1 mM EDTA, 0.1 mM sodium phosphate buffer, pH 6.8; flow, 0.75 mL/min; detection, 280-nm absorbance).

[^{14}C]-Methylated F(ab') was prepared by reduction of [^{14}C]-methylated $F(ab')_2$ with 1 mM DTT for 1 h at 37 °C before HPLC separation. Conditions for the thermochemical reaction of the [^{14}C]-methylated F(ab') with MAD or maleimide supports were identical to those described below for nonradiolabeled F(ab') fragments.

PSA Microplate ELISA Assay. The COBAS Core PSA solid-phase enzyme immunoassay was modified to the extent that F(ab') fragments of anti-PSA antibodies were photoimmobilized on the bottom of microplate wells. Samples were dried, placed 4 cm distant from the light source, and illuminated with an irradiance of 0.7 mW/cm^2. Titer plates were mounted on a reflecting mirror and agitated perpendicular to the light bulbs with a deflection of 4 cm and a frequency of 26 cycles/min. In all experimental protocols, wells were saturated with 1% (w/v) BSA in PBS, pH 7.4, for 2 h at 37 °C and washed three times with doubly distilled water before ELISA procedures were carried out. Aliquot samples of the PSA standard (10 μL, 0.6 ng/well) and 40 μL of anti-PSA-POD conjugate were added to coated wells. Following incubation for 15 min at 37 °C with permanent shaking, wells were washed with doubly distilled water (3 × 300 μL/well). Enzyme-catalyzed reactions were initiated with the addition of 50 μL of substrate solution (3,3',5,5'-tetramethylbenzidine) and terminated after 15 min at 37 °C with stop solution (4.9% sulfuric acid, 200 μL/well). Color development was monitored at 450 nm with the UVmax microplate reader.

Functionalization of Solid Supports with the Maleimide-Diazirine Bifunctional Reagent. (*a*) *Glass Supports with Terminal Diazirines (Preparation of MAD-Derivatized Glass-Fiber Disks).* GF-C Whatman glass-fiber disks (9 cm in diameter) were thiopropylated according to Aebersold and collaborators (1986) using (3-mercaptopropyl)trimethoxysilane instead of the corresponding (3-aminopropyl)trimethoxysilane. "Curing" of the support was omitted to avoid thiol oxidation. Surface thiolation yielded 12 ± 2 nmol of thiol groups per mg of glass fiber quantitated by the Ellman reagent (Riddles et al., 1983). Glassware was treated with chromic acid and DTNB-containing solutions were degassed and stored under nitrogen. Dried thiopropylated glass-fiber sheets were cut into disks (12 mm diameter) and incubated in acetone containing 0.1% TEA (v/v) for 1 h at room temperature with a 2-fold molar excess MAD (assuming a fiber volume of 25 μL). After removal of excess reagent with 20 mL of acetone, disks were dried under reduced pressure at ambient temperature. As quantitated by Ellman procedures, 95% of the SH groups were modified by MAD. MAD-functionalized glass fibers were stored at −20 °C in the dark.

(*b*) *Polystyrene with Terminal Maleimide Functions* (Preparation of MAD-Derivatized Polystyrene). MAD (30 μL, 79 μg, 216 nmol) dissolved in MeOH was placed in modular microplate wells. MeOH was removed by evaporation at 37 °C during 1 h followed by additional drying at room temperature for (1 h, 0.02 mbar). Wells were then irradiated in the Stratalinker for 20 min. Control samples were treated identically but omitting the irradiation step. Wells were then washed four times with 250 μL of methanol.

(*c*) *Preparation of BSA-Precoated Polystyrene with Terminal Maleimide Functions.* To form an adsorptive protein adlayer on polystyrene (Andrade and Hlady, 1986), modular microplate wells were precoated with BSA (2% solution (w/v) in PBS, pH 7.4). Aliquots (300 μL) were distributed to each well and incubated for 1.5 h at 37 °C. Excess solution was removed, and modules were dried at room temperature (1.5 h, 0.02 mbar). MAD was dissolved in 50 μl of 2% EtOH in 10 mM sodium phosphate buffer, pH 5.0 (v/v), and applied in indicated concentrations (Figure 6) to BSA-precoated wells. Liquids were removed under reduced pressure (0.02 mbar) at ambient temperature and wells were irradiated with the Stratalinker for various lengths of time. Noncovalently bound reagent was removed by washing the wells with 2% EtOH in 10 mM sodium phosphate buffer, pH 5.0 (v/v) (four times), and doubly distilled water (twice).

Thermochemical Functionalization of Cysteine, a Terminally Thiolated Peptide, and F(ab') Fragments with MAD. (*a*) *MAD Modification of [^{35}S]Cysteine.* MAD was reacted with [^{35}S]Cys in EtOH/20 mM citric acid, 35 mM Na_2HPO_4, 108 mM NaCl, 1 mM EDTA, pH 6.5 (1/1, v/v). [^{35}S]Cys (8 μL, 0.64 μmol) and Cys (6 μL, 0.35 μmol) were added to 500 μL of a stirred MAD solution

(256 μg , 0.7 μmol) and incubated for 30 min. Aliquot samples (50 μL) were withdrawn from the mixture and analyzed by HPLC on butyl (C_4) Bakerbond. Linear gradient elution protocols were followed replacing solvent A (0.1% v/v TFA in H_2O) with solvent B (0.1% v/v TFA in CH_3CN/H_2O, 3/1 by vol) from 0 to 100% in 30 min with a flow rate of 1.3 mL/min. After completion of the reaction, the product was purified by HPLC as detailed above, and solvents were removed under reduced pressure. The product (MAD–[^{35}S]Cys) was quantified by its diazirine UV adsorption (ϵ_{357} = 446 M^{-1} cm^{-1}) and stored at −20 °C in MeOH. The yield was 47.5% (0.33 μmol).

(b) *Modification of CDPGYIGSR with MAD.* The peptide (CDPGYIGSR, 1 mg, lyophilized with buffer salts and 2-mercaptoethanol) was dissolved in 1 mL of H_2O. The solution was stored at −20 °C until use. Aliquot samples (155 nmol peptide 200 μL) were brought to pH 6.5, and 187 μg (500 nmol) of MAD in 200 μL of EtOH was added. The mixture was incubated for 1 h at room temperature. Product formation was surveyed by HPLC under the same conditions as described for MAD–Cys. For quantitation purposes the synthetic peptide was radiolabeled by reductive methylation according to Jentoft and Dearborn (1979). To attain this, the following reagents were added to the above reaction mixture upon completion of the reaction with MAD: $NaCNBH_3$ (100 μL, 240 mM), 100 μL of 1M HEPES buffer, pH 7.5, and 20 μL of [^{14}C]-formaldehyde in water (4.6 μCi, 153 nmol). After incubation for 3 h at room temperature the product was isolated by HPLC as above. The radiolabeled product eluted with the same retention time as MAD–CDPGYIGSR. Solvents were evaporated under reduced pressure, and the product was dissolved in 1 mL of EtOH/H_2O 1/1 (v/v). Radiolabeled MAD–[^{14}C]CDPGYIGSR was quantitated by diazirine absorption (ϵ_{347} = 446 M^{-1} cm^{-1}) at 347 nm. These procedures yielded 69 nmol (45%) MAD–[^{14}C]-methylated-CDPGYIGSR with a specific radioactivity of 14.05 nCi/nmol and 48% methylated amino functions.

(c) *Thermochemical Coupling of MAD to F(ab′) Fragments.* Freshly prepared F(ab′) fragments (130 μg, 2.6 nmol) were dissolved in 950 μL of 0.1 M sodium acetate, 0.5 M NaCl, 1 mM EDTA, pH 5.0, and combined with the cross-linking reagent (19 μg, 52 nmol dissolved in 9.6 μL of EtOH). The reaction mixture was incubated at ambient temperature for 16 h in the dark. Excess MAD was removed by chromatography on PD 10 in 15 mM sodium phosphate buffer, pH 6.5. Fractions containing protein (A_{280}) were pooled and used immediately (MAD–F(ab′) fragments).

Photochemical Coupling of Target Molecules to MAD-Derivatized Supports. (Reaction Route 1, Figure 1B). *Photocoupling of [^{14}C]Tyrosine to MAD-Derived Glass Supports.* MAD-derived glass-fiber disks (see previous text for preparation) were soaked with 10 μL of EtOH before [^{14}C]Tyr (0.66 nmol, 305 nCi) was applied. Disks were then dried under vacuum (50 mbar) for 1 h at ambient temperature in the dark. Photolabeled glass disks were placed between two quartz slides under argon in a custom-made holder and mounted at a distance of 45 cm from the light source. Samples were photoactivated for 12 min (6 min each side) with the filtered light of the high pressure mercury lamp (150 mW/cm^2). Control samples were treated identically, but light exposure was omitted. Photoactivated and control disks were then washed extensively (Sigrist et al., 1990) and analyzed for radioactivity by liquid scintillation counting. Net light-dependent amino acid binding was determined by subtracting nonspecifically adsorbed reagent (control) from the radioactivity recovered on irradiated disks.

Thermochemical Immobilization of Target Molecules to Surfaces with Terminal Maleimides. (Reaction Route 2, Figure 1C). (a) *[^{35}S]Cysteine Coupling to Polystyrene.* MAD-derivatized polystyrene microplate wells (see previous text for preparation) were incubated with 5 nmol (112.5 nCi) of [^{35}S]Cys dissolved in MeOH/20 mM citric acid, 35 mM Na_2HPO_4, 108 mM NaCl, 1 mM EDTA buffer, pH 6.5 (1/1, v/v), for 2 h at ambient temperature. To remove free reagent, wells were washed four times with 250 μL of H_2O, four times with 250 μL of MeOH/H_2O (1/1, v/v), and four times with 250 μL of MeOH. Washed wells were analyzed for radioactivity by liquid scintillation counting, and coupling efficiencies were determined.

(b) *Thermochemical Coupling of F(ab′) Fragments to BSA-Precoated MAD-Derivatized Microplates.* Freshly prepared F(ab′) fragments were dissolved in 0.1 M sodium acetate, 0.5 M NaCl, 1 mM EDTA, pH 5.0, to a final concentration of 30 μg of F(ab′)/mL. Aliquot samples (50 μL, 1.5 μg F(ab′)) were applied to BSA-precoated, MAD-derivatized wells and microplates were incubated in the dark for 24 h under argon at 4 °C. After this thermochemical reaction, wells were washed twice with the coupling buffer, once with PBS pH 7.4, and once with doubly distilled water to remove free F(ab′) fragments. Immunological activity of the immobilized F(ab′) fragments was analyzed by sandwich type ELISA procedures, and binding efficiency was quantified by liquid scintillation counting.

Photochemical Coupling of MAD-Derivatized Target Molecules to Solid Supports. (Reaction route 3, Figure 1D). (a) *Photocoupling of MAD–[^{35}S]Cys to Polystyrene.* MAD–[^{35}S]Cys in MeOH (27.5 μL, 10 nmol, 19 140 dpm) was added to microplate wells and dried for 1 h at 50 mbar and ambient temperature. Coated wells were irradiated for 15 min in the Stratalinker (1.3 mW/cm^2, in this experiment the distance of the support surface to the light bulbs was 1 cm). Control samples were treated identically, but irradiation was omitted. Wells were washed four times with 250 μL of MeOH. Retained radioactivity was measured by liquid scintillation counting.

(b) *Photocoupling of MAD–[^{14}C]CDPGYIGSR to Polystyrene.* MAD–[^{14}C]CDPGYIGSR (30 μL, 1.8 nmol, 64 820 dpm) in EtOH/H_2O (1/1, v/v) was placed into microplate wells and dried for 1 h at 37 °C and 1 h at ambient temperature at 0.02 mbar. Wells were irradiated for 20 min in the Stratalinker (0.7 mW/cm^2). Wash procedures and determination of coupling yields were carried out as described for MAD–[^{35}S]Cys.

(c) *Photocoupling of MAD–F(ab′) Fragments onto BSA-Precoated Microplate Wells.* Various concentrations (0–1.0 μg/well) of MAD–F(ab′) fragments in 15 mM sodium phosphate buffer, pH 6.5, were applied to BSA-precoated microplate wells and adjusted to a final volume of 70 μL with the same buffer. Wells were dried at ambient temperature and 0.02 mbar. Photoactivation was carried out with the Stratalinker (0.7 mW/cm^2). Wells were then washed four times with doubly distilled water to remove buffer salts and noncovalently coupled protein. Control samples were treated identically except that irradiation was omitted.

Photocoupling of MAD–[^{35}S]Cys to Hydroxylated FEP Membranes through a Patterned Mask. MAD–[^{35}S]Cys (0.13 μmol, 3.4 μCi) was dissolved in 200 μL of EtOH and spread on a FEP-OH membrane. The solvent was evaporated (1 h at 40 °C followed by drying for 2 h

at 0.02 mbar and ambient temperature). Dried membranes were covered with the patterned mask and placed between two quartz glasses. Photoactivation for 10 min with the mercury lamp (lamp to sample distance of 47 cm, 11.6 mW/cm^2). Adsorbed MAD-[^{35}S]Cys was removed by sonication for 1 min in 60 mL of EtOH (three times), MeOH/H_2O (1/1, v/v), MeOH, H_2O, and MeOH (once each). Membranes were exposed for 2 days to an X-ray film (Hyperfilm MP, Amersham).

RESULTS

Synthesis and Characterization of MAD. Condensation of the amino function of 3-(trifluoromethyl)-3-(*m*-aminophenyl)diazirine with 4-maleimidobutyric acid required activation. Carboxyl group activation with dicyclohexylcarbodiimide and 4-(dimethylamino)pyridine was not successful. Synthesis of MAD was achieved via a mixed-anhydride intermediate. Chemical reactions were monitored by TLC. All methods including ^{1}H NMR used for chemical characterization of MAD confirmed the structure depicted in Figure 1A. Thiol groups reacted within minutes (Figure 2A) with the maleimide moiety of the heterobifunctional photo-cross-linker in aqueous media, leaving the diazirine function intact for light-dependent reactions. When irradiated with UV light (≥320 nm), diazirines decayed to highly reactive carbene intermediates and nitrogen (Figure 2B). Crystalline MAD was stored at −20 °C in the dark over a period of more than 8 months without appreciable deterioration. MAD is soluble in most organic solvents. In the experiments described, MAD was dissolved in ethanol before addition to aqueous solutions. Stock solutions in ethanol were stored at −20 °C and used within1 week. Exposure to intense sunlight and artificial light was avoided.

Thermochemical Functionalization of Cysteine and a Terminally Thiolated Peptide. *Modification of [^{35}S]Cysteine with MAD.* The reaction of substoichiometric amounts of MAD with cysteine was complete within minutes. Product formation was analyzed by HPLC. Under the conditions used for product separation, the retention times were 2.5 min for Cys, 17.1 min for MAD–Cys, and 20.5 min for MAD. Eluted products were identified by reference analysis (Cys, MAD) and on the basis of the radioactivity elution pattern ([^{35}S]Cys, MAD–[^{35}S]Cys). Pool fractions of MAD–Cys were further characterized by UV spectroscopy. MAD–Cys showed a characteristic diazirine absorption band at 357 nm, which disappeared after irradiation.

Since MAD–Cys mimics the thermochemical reaction product of MAD with any thiolated target molecule, the derivative was used to investigate the kinetics of the photoreaction. For kinetic studies, the concentration C_t of the diazirine at a defined irradiation time (t) was quantitated by the absorption difference $A_t - A_\infty$ at 357 nm, where A_∞ is the absorption under saturating light conditions (300-s irradiation). $\log \{[A_t - A_\infty]/[A_0 - A_\infty]\}$, expressed as a function of the irradiation time, yielded a straight line (Figure 3), consistent with the anticipated first-order kinetic process (Nassal, 1983).

Modification of CDPGYIGSR with MAD. Commercially available CDPGYIGSR was stabilized with salts and 2-mercaptoethanol. Initially, attempts were made to remove the stabilizing agents by HPLC procedures prior to the thermochemical reaction with MAD. It was noted that reactive thiol functions were modified—most probably oxidized—during this HPLC separation, and the HPLC-purified material failed to react with MAD. Therefore, educt purification was not carried out, and CDPGYIGSR was used as purchased. It was modified with a 3.2-fold molar excess of MAD. MAD–CDPGYIGSR was purified by HPLC. It eluted with a retention time of 16.6 min under the conditions described in the Experimental Procedures.

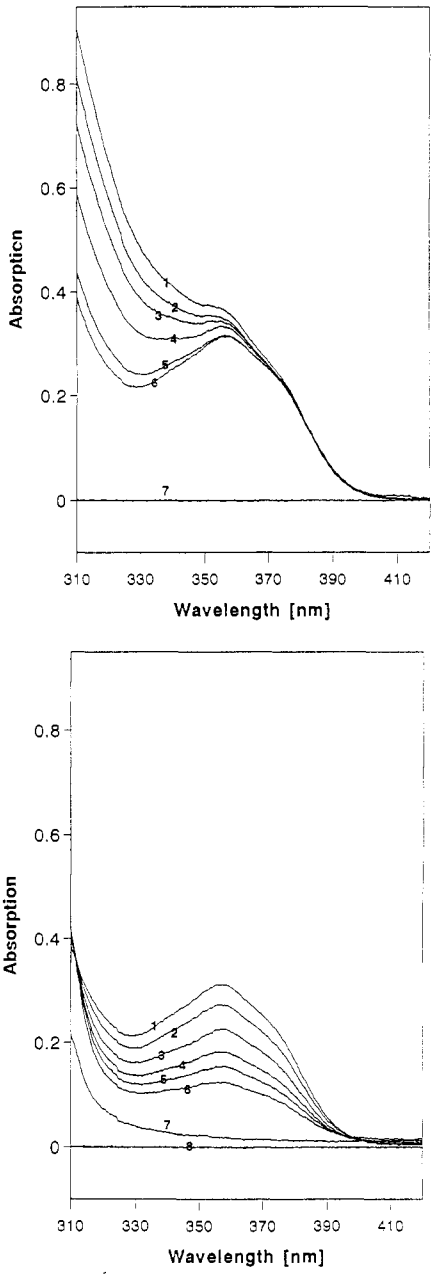


Figure 2. (A, top) Thermochemical reaction of the maleimide function of MAD. Spectroscopic analysis of MAD (0.9 μmol, 0.33 mg in 1 mL of EtOH/20 mM citric acid, 35 mM Na_2HPO_4, 108 mM NaCl, 1 mM EDTA, pH 6.5 (1/1, v/v)). Absorption spectra were recorded before (1) and after the addition of (2) 0.1 μmol, (3) 0.2 μmol, (4) 0.4 μmol, (5) 0.6 μmol, and (6) 0.9 μmol of cysteine; (trace 7, baseline (solvents only). (B, bottom), Spectroscopic analysis of the photoreaction of cysteine-modified MAD. After completion of the thermochemical reaction described in Figure 2A, sample 6 was irradiated for differing lengths of time: (1) 0 s, (2) 10 s, (3) 20 s, (4) 30 s, (5) 40 s, (6) 50 s, (7) 300 s, (8, baseline). A high-pressure mercury lamp with a constant 200-W output was used for irradiation. The irradiance was 150 mW/cm^2.

Thermochemical and Photochemical Coupling of Amino Acids and Peptides to Functionalized Supports. Before investigations of oriented F(ab') fragment immobilization were carried out, various routes of MAD-mediated target molecule immobilization were tested with

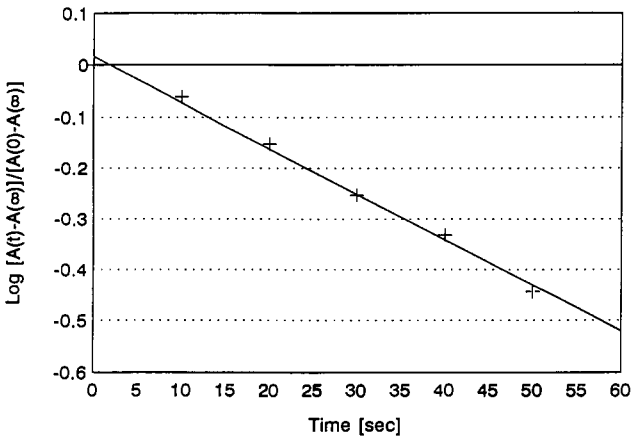


Figure 3. Kinetics of MAD photoactivation. MAD (0.9 μmol) was dissolved in 1 mL of EtOH/ 20 mM citric acid, 35 mM Na_2HPO_4, 108 mM NaCl, 1 mM EDTA, pH 6.5 (1/1, v/v), and irradiated for varous lengths of time under conditions described in Figure 2B.

low molecular weight reference substances, including radiolabeled [^{14}C]Tyr, [^{35}S]Cys, MAD–[^{35}S]Cys, and MAD–[^{14}C]CDPGYIGSR. Results obtained in these studies are summarized in Table I.

Preparation of MAD-Derived Glass Supports and Photochemical Coupling of [^{14}C]Tyr (Reaction Route 1, Figure 1B). Procedures for glass thiolation and determination of the coupling efficiency of route 1 reactions (Figure 1B) were necessary. Glass-surface thiolation was monitored analytically by measuring accessible thiol functions with the Ellman reagent. Surface thiolation of glass fibers yielded 12 ± 2 nmol of SH groups/mg of glass support. To avoid thiol oxidation, thiopropylated glass fibers were processed after preparation. Thermochemical functionalization of thiopropylated glass fibers was nearly quantitative: 95% of available thiol functions were blocked by MAD. The integrity and the amount of introduced diazirine functions could not be quantitated directly. Therefore, the photocoupling capacity was tested by analyzing the light-dependent binding of [^{14}C]Tyr. Coupling efficiency was 4%, and the extent of nonphotochemical, physically adsorbed [^{14}C]Tyr was 20-fold lower. Effective removal of this physically adsorbed amino acid was attained with washing procedures described earlier (Sigrist et al., 1990). Coupling efficiencies match those for light-dependent tyrosine binding to TRIMID–glass surfaces (Sigrist et al., 1990). Bochariov and Kogon (1992) reported 8% cross-linking of modified Phe-tRNA to ribosomes with an amino group specific, cleavable, carbene-generating, cross-linking reagent. In the latter system, molecular interactions among the constituents were enforced by the inherent bioaffinity.

Photoimmobilization of MAD to Polystyrene (Reaction Route 2, Figure 1C). Reaction route 2 procedures do not require functional groups on the support surface. Efficiency of photoimmobilization was assessed indirectly by thermochemical [^{35}S]Cys coupling via the maleimide function. The treatment yielded a target molecule density of approximately 60 pmol of [^{35}S]Cys/cm^2 (20 pmol/well). Functionalization of surfaces by reaction route 2 is advantageous for the immobilization of biomolecules in that the primary step is easily attained by photochemical procedures and thermochemical target molecule coupling is effected by thermochemical reactions in aqueous media. The procedure does not require target molecule dehydration.

Photocoupling of MAD–[^{35}S]Cys and MAD–[^{14}C]-CDPGYIGSR to Polystyrene. The reaction route 3 applied for photocoupling of MAD–[^{35}S]Cys and MAD–[^{14}C]CDPGYIGSR is depicted in Figure 1D. Target molecules were photolinked to microplate wells under slightly different, yet saturating, irradiation conditions: MAD–[^{35}S]Cys was irradiated for 15 min at 1.3 mW/cm^2, whereas MAD–[^{14}C]CDPGYIGSR was photocoupled for 20 min with 0.7 mW/cm^2. Coupling efficiencies were 7% and 2%, respectively, and the extent of removal of physically adsorbed target molecules was similar for both systems (Table I). It was noted that the efficiency of photoimmobilization depended on the inherent physicochemical properties of the target molecules and their molecular interaction with the surface material.

Topically Addressed Photoimmobilization of MAD–[^{35}S]Cys. Addressability by light is a genuine property of photoactivatable reagents. Topically selective, light-dependent activation of the radiolabeled target MAD–[^{35}S]Cys has been assessed to qualify the reagent for future multidomain-coating applications. Figure 4 depicts the 300-μm-sized slit pattern obtained after exposure of a MAD–[^{35}S]Cys-coated FEP-OH surface to activating light. Autoradiography of the washed support shows that the irradiated and nonirradiated areas are distinctly separated.

MAD-Mediated Immobilization of F(ab') Fragments. *Immunoreagent Immobilization via MAD–F(ab').*

Table I. MAD-Mediated Photoimmobilization[e]

reagent, target	support	route	analysis/detection method	% coupling efficiency[a]	light-dependent vs adsorptive binding[b]	target molecule density/activity
MAD	glass	1	photocoupled [^{14}C]-Tyr	4	20.6:1	20 pmol/mg
MAD	polystyrene	2	thermocoupled [^{35}S]-Cys	0.4	5.5:1	60 pmol/cm^2
MAD-[^{35}S]-Cys	polystyrene	3	radioactivity	7	13.1:1	2.1 nmol/cm^2
MAD-[^{14}C]-CDPGYIGSR	polystyrene	3	radioactivity	2	13.8:1	111 pmol/cm^2
MAD–F(ab')	BSA-precoated	3	ELISA procedures	50[d]	6:1[c]	0.82 E_{450}/well[c]
MAD–[^{14}C]-F(ab')	polystyrene		radioactivity[d]		(3:1)[d]	11.2 pmol/cm^2 [d]
SH–F(ab')	BSA-precoated, MAD-modified polystyrene	2	ELISA procedures	30–40[d]	6:1[c]	1.8 E_{450}/well[c]
SH–[^{14}C]-F(ab')	modified polystyrene		radioactivity[d]		(3:1)[d]	50 pmol/cm^2 [d]

[a] Coupling efficiency is defined as the amount of reagent which is retained due to light activation. The total amount of reagent applied is set to 100%. Coupling efficiency values do not include target-molecule immobilization due to physisorption. [b] Ratios given describe the quality of the coupling process. Net light-dependent immobilization is compared with the extent of immobilization recovered in nonirradiated control samples (physisorption), the latter being set to 1. [c] Immunoreagent immobilization is quantitated by the extent of immunocomplex formation. [d] Data obtained with [^{14}C]-methylated F5 anti-PSA F(ab') fragments. Methylation of lysines may lead to surface polarity change and affect the immunological activity of antibodies. [e] Reaction route 1: Thermochemical coupling of MAD to a thiolated surface is followed by photochemical target-molecule coupling. Reaction route 2: Photochemical coupling of the reagent to an inert surface is followed by thermochemical coupling to target thiol functions. Reaction route 3: Thermochemical target modification occurs prior to carbene-mediated insertion into surface materials.

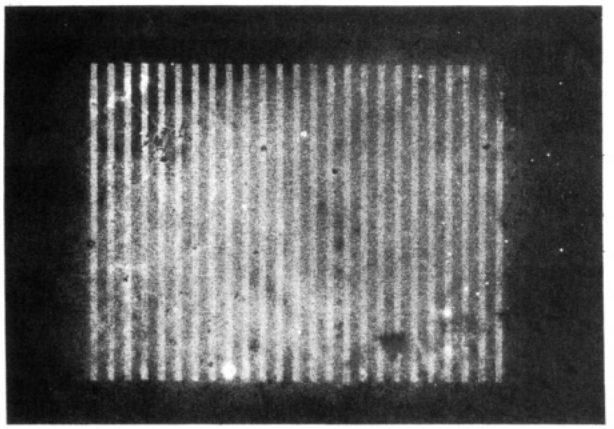


Figure 4. Topically immobilized MAD–[^{35}S]Cys on hydroxylated FEP membranes. Spreading of MAD–[^{35}S]Cys on hydroxylated FEP was carried out as described in the Methods section. The coated membrane was covered with a photomask (slit width, 300 μm; spacings, 500 μm) and irradiated for 10 min with a mercury lamp (11.6 mW/cm^2). Physically adsorbed MAD–[^{35}S]-Cys was removed and residual (photoimmobilized) label distribution was analyzed by autoradiography. White (radioactive) areas correspond to the slit openings (300 μm × 1.5 cm) of the mask.

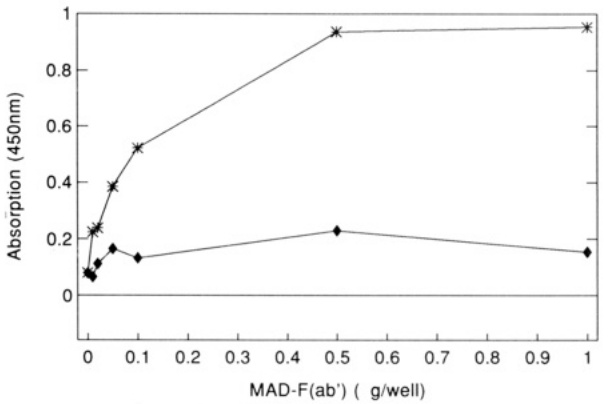


Figure 5. Immobilization of MAD–F(ab′) onto BSA precoated microwells (reaction route 3). Indicated amounts of MAD–F(ab′) fragments were applied to BSA-precoated wells and irradiated for 20 min (*). Analogous experiments were carried out with BSA-precoated wells and MAD–F(ab′), but the samples were not irradiated (■). Antibody binding was analyzed by sandwich-type ELISA procedures.

MAD was thermochemically linked to freshly prepared F(ab′) fragments following the conditions described by Prisyazhnoy and collaborators (1988). Since MAD is not soluble in water, it was dissolved in ethanol prior to addition to the protein. MAD was added in a 20-fold molar excess over available thiol functions, and excess reagent was removed by gel chromatography (PD-10). The photoreactivity of MAD–F(ab′) fragments was investigated by analyzing the light-dependent coupling to BSA-precoated microplates. Efficiency of photoimmobilization was measured by liquid scintillation counting using [^{14}C]-methylated F(ab′). Up to 50% of radiolabeled antibody was covalently linked to BSA-precoated polystyrene. Immunoreactions carried out in BSA-precoated wells yielded activities (450-nm absorption) which were 6 times higher (3 times for [^{14}C]-methylated F(ab′)) than nonirradiated control samples. Enzyme-linked immunoreactions saturated at 0.5–1.0 μg MAD–F(ab′)/well (Figure 5).

Immunoreagent Immobilization to BSA-Precoated and Subsequently MAD-Derivatized Surfaces. F(ab′) fragments were successfully coupled to MAD-derived BSA surfaces following reaction route 2. BSA-precoated microplate wells were modified with the indicated amounts

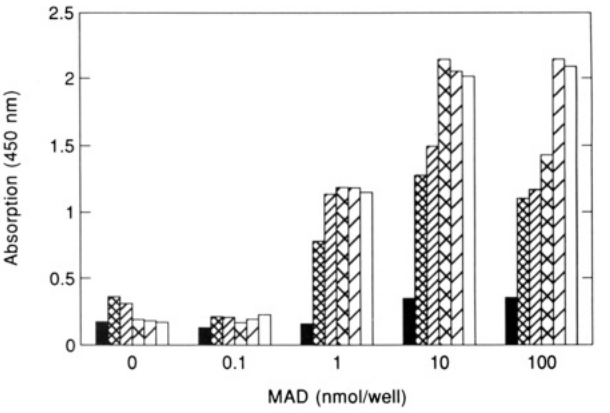


Figure 6. Photoimmobilization of MAD onto BSA-precoated microplates (reaction route 2). MAD immobilization procedures were optimized by varying the amount of applied cross-linker and the irradiation time. Indicated quantities of MAD were dried onto BSA-precoated microwells and irradiated for the following time lengths: 0, 5, 10, 15, 20 and 30 min (from dark to bright bars). Freshly prepared F(ab′) fragments (1.5 μg/well) were then thermochemically coupled to modified supports and antibody binding was analyzed by sandwich type ELISA procedures.

of MAD by photoimmobilization procedures. The light dependency of the process was evident. BSA-precoated wells, without MAD treatment, showed marginal F(ab′) retention. Both, irradiation time and MAD concentration were varied to delineate optimal conditions for F(ab′) binding to MAD–BSA. Generally, with increased quantities of MAD and longer irradiation times, higher immunoresponses were attained. This applies to samples which were modified with more than 0.1 nmol of MAD/well. With 1 nmol MAD/well, light exposure saturated after 10 min. Irradiation times of 15–20 min were required for samples which were modified with 10 and 100 nmol MAD/well (Figure 6). Quantitation of [^{14}C]-methylated F(ab′) binding by liquid scintillation counting yielded binding efficiencies of 30–40% (100 nmol MAD/well, irradiation time of 20 min).

Oriented Coupling. Binding differences between [^{14}C]-methylated and native F(ab′) fragments were ascribed to changes of surface polarity and possible modification of the binding domain of the antibody. Residual immunological activity of radiolabeled F(ab′) was analyzed with photoimmobilized [^{14}C]-methylated F(ab′). To delineate the oriented coupling capacity, the specific immunoactivity (absorbance 450 nm/mg of immobilized [^{14}C]-methylated F(ab′)) of immobilized samples was determined. Specific immunoactivity was 2–4 times higher with photoimmobilized [^{14}C]-methylated F(ab′) than with adsorbed (not photoactivated) [^{14}C]-methylated F(ab′). These results apply to both [^{14}C]-methylated F(ab′) binding to MAD–BSA and MAD–[^{14}C]-methylated-F(ab′) photocoupling to BSA-precoated wells.

DISCUSSION

Due to the specificity of biomolecules and macromolecular aggregates, there is no doubt that biocatalysts and biosensors will find increasing applications in analytical diagnostics, bioprocessing, control systems, medical and material sciences. Applications mentioned require, however, covalent attachment and molecular orientation. Orientation of biomolecules in vivo is crucial for cell survival. Living systems accomplish unique biomolecule orientation by concerted actions of topical molecular association, compartimentalization, and timed biosynthesis. These parameters are not easily reconstructed for the fabrication of biomimetic devices, and new regimes

are needed to establish molecular orientation. Light-dependent immobilization procedures were introduced to circumvent drawbacks imposed by thermochemical reactions and, at the same time, gain topical addressability (Sigrist et al., 1992; Rozsnyai et al., 1992). Photochemical reactions are advantageous in that covalent coupling is initiated by light and functionalization of the target molecules is not required if photoactivatable surfaces are provided (reaction route 1). Recent studies which compare physical adsorption and photoimmobilization of F(ab') fragments have shown that photolinker-polymer-mediated immobilization is superior to physical adsorption (Gao et al. unpublished) and photolinker-polymer-mediated immobilization of oligonucleotides is attained by light exposure of photolinker-polymer-coated surfaces (Küng et al., unpublished).

The heterobifunctional photo-cross-linker described in this study combines photoreactivity and the selectivity of reaction with thiols. Most biomolecules carry functional groups at the surface of their native folded structures. Reactive functional groups are asymmetrically distributed at the surface and bear individual chemical reaction characteristics. Site-specific orientation and immobilization is easy to obtain if uniquely reactive groups are available at the surface of biomolecules. However, selectively reactive functional groups, preferably located at a single site, are seldom. Multi-site attachment and random coupling of biomolecules is most probable by targeting at ubiquitous surface exposed amino functions (Domen et al., 1990). Reactive thiol groups located at the surface of proteins are relatively rare. They can be generated (bio)chemically, obtained through chemical synthesis of biopolymers, or constructed by genetic engineering. Examples are as follows: (i) $F(ab')_2$ fragments produced by pepsin treatment of antibodies, (subsequent reduction of disulfide bridges in the hinge region yields immunoreagents which provide a selectively reactive thiol function opposite to the binding domain of the antibody.), (ii) synthetic biopolymers designed for oriented coupling with reactive thiol functions at the N-terminal end of receptor binding peptides (Graf et al., 1987), and finally, (iii) unique thiol functions (T8C or T65C) introduced by site-directed mutagenesis into cytochrome b_5 (Stayton et al., 1992), a similar approach has been chosen by Aggeler and Capaldi (1992) to prepare the molecular basis for site-directed cross-linking of the ECF_1 γ-subunit.

In both biological and biomimetic systems, molecular interactions between biomolecules and material surfaces are initiated by physical contacts at chemical bond distances. These interactions ultimately lead to biomolecule immobilization which is either physical adsorption, protein (or receptor) binding mediated adsorption, or covalent immobilization. For biomolecule immobilization on material surfaces, it is of particular importance that noncovalent adsorption and random orientation are suppressed. Data presented in this study show that MAD-mediated immobilization of low molecular weight target molecules can be attained by various routes; all of them lead to the ultimate goal of covalent immobilization. The extent of physical adsorption is generally low, given by the target molecule's surface characteristics, the material surface properties, and the interfacial behavior of both system constituents.

Covalent, light-dependent, and oriented immobilization of F(ab') fragments using MAD as the cross-linking agent has been achieved by both reaction routes 2 and 3. Molecular orientation was attained with the thermochemical reaction of the maleimide with F(ab') sulfhydryl groups. Covalent binding to support materials was effected by carbene insertion. MAD-mediated target molecule immobilization can be controlled by selective irradiation of defined micron-sized areas. Thus, multiple-domain functionalization of surfaces with target (bio)molecules was feasible. Due to the unique molecular structure of antibodies, MAD-based immobilization procedures can be applied to any antibody derived F(ab') fragment. Through usage of MAD, any biomolecule (proteins, peptides, nucleotides) which contains reactive and accessible cysteine residues (thiol functions) at the surface can be immobilized photochemically. With the diazirine as the photoactivatable group, there are no restrictions with respect to the nature of the solid support except the availability of covalent chemical bonds.

ACKNOWLEDGMENT

The authors thank Prof. R. Scheffold for helpful discussions. This work was supported by grants from the Swiss National Science Foundation, the Swiss Priority Program on Materials, and the Central Laboratory, Blood Transfusion Service of the Swiss Red Cross.

LITERATURE CITED

Aebersold, R. H., Teplow, D. B., Hood, L. E., and Kent, S. B. H. (1986) Electroblotting onto activated glass. *J. Biol. Chem. 261*, 4229–4238.

Aggeler, R., and Capaldi, R. A. (1992) Cross-linking of the γ subunit of the Escherichia coli ATPase (ECF_1) via cysteines introduced by site-directed mutagenesis. *J. Biol. Chem. 267*, 21355–21359.

Andrade, J. D., and Hlady, V. (1986) Protein adsorption and material biocompatibility: A tutorial review and suggested hypotheses. *Adv. Polym. Sci. 79*, 3–58.

Bayley, H. (1983) *Photogenerated reagents in biochemistry and molecular biology*. Elsevier Science Publishers, Amsterdam.

Berry, M. J., Davies, J., Smith, C. G., and Smith, I. (1991) Immobilization of Fv antibody fragments on porous silica and their utility in affinity chromatography. *J. Chromatogr. 587*, 161–169.

Bhatia, S. K., Shriver-Lake, L. C., Prior, K. J., Georger, J. H., Calvert, J. M., Bredehorst, R., and Ligler, F. S. (1989) Use of thiol-terminal silanes and heterobifunctional crosslinkers for immobilization of antibodies on silica surfaces. *Anal. Biochem. 178*, 408–413.

Bhatia, S. K., Hickman, J. J., and Ligler F. S. (1992) New approach to producing patterned biomolecular assemblies. *J. Am. Chem. Soc. 114*, 4432–4433.

Bochariov, D. E., and Kogon, A. A. (1992) Application of 3-[3-(3-(triflouromethyl)diazirin-3-yl)phenyl]-2,3-dihydroxypropionic acid, carbene-generating cross-linking reagent for photoaffinity labeling. *Anal. Biochem. 204*, 90–95.

Brocklehurst, K., Carlsson, J., Kierstan, M. P. J., and Crook, E. M. (1984) Covalent chromatography by thiol-disulfide interchange. *Methods Enzymol. 34*, 531–545.

Brunner, J. (1989) Photochemical labeling of apolar phase of membranes. *Methods Enzymol. 172*, 628–687.

Brunner, J., and Richards, F. M. (1980) Analysis of membranes photolabeled with lipid analogues. *J. Biol. Chem. 255*, 3319–3329.

Dolder, M., Michel, H., and Sigrist, H. (1990) 3-(trifluoromethyl)-3-(m-Isothiocyanophenyl)diazirine: Synthesis and chemical characterization of a heterobifunctional carbene-generating cross-linking reagent. *J. Protein Chem. 9*, 407–415.

Domen, P. L., Nevens, J. R., Krishna Mallia, A., Hermanson, G. T., and Klenk, D. C. (1990) Site-directed immobilization of proteins. *J. Chromatogr. 510*, 293–302.

Fassina, G. (1992) Orientied immobilization of peptide ligands on solid supports. *J. Chromatogr. 591*, 99–106.

Fodor, S. P. A., Read, J. L., Pirrung, M. C., Stryer, L., Lu, A. T., and Solas, D. (1991) Light-directed, spatially addressable parallel chemical synthesis. *Science 251*, 767–773.

Graf, J., Ogle, R. C., Robey, F. A., Sasaki, M., Martin, G. R., Yamada, Y. and Kleinman, H. K. (1987) A pentapeptide from

the laminin B1 chain mediates cell adhesion and binds the 67000 laminin receptor. *Biochemistry 26*, 6896–6900.

Jentoft, N., and Dearborn, D. G. (1979) Labeling of proteins by reductive methylation using sodium cyanoborohydride. *J. Biol. Chem. 254*, 4359–4365.

Klingler-Dabral, V., Collioud, A., Schaller, J., Herbst, F., Forssmann, W. G., and Sigrist, H. (1991) Gas-phase sequencing of photoimmobilized peptides. *Chimia 45*, 43–45.

Larsson, P. H., Johansson, S. G. O., Hult, A., and Göthe, S. (1987) Covalent binding of proteins to grafted plastic surfaces suitable for immunoassays I. Binding capacity and characteristics of grafted polymers. *J. Immun. Methods 98*, 129–135.

Ljungquist, C., Jansson, B., Moks, T., and Uhlen, M. (1989) Thiol-directed immobilization of recombinant IgG-binding receptors. *Eur. J. Biochem. 186*, 557-561.

Martin, F. J., and Papahadjopoulos, D. (1982) Irreversible coupling of immunoglobulin fragments to preformed vesicles. *J. Biol. Chem. 257*, 286–288.

Matson, R. S., and Little, M. C. (1988) Strategy for the immobilization of monoclonal antibodies on solid-phase supports. *J. Chromatogr. 458*, 67–77.

Nassal, M. (1983) 4-(1-Azi-2,2,2-trifluoroethyl)benzoic acid, a highly photolabile carbene generating label readily fixable to biochemical agents. *Liebigs Ann. Chem.* 1510–1523.

O'Shannessy, D. J. (1990) Hydrazido-derivatized supports in affinity chromatography. *J. Chromatogr. 510*, 13–21.

Prisyazhnoy, V. S., Fusek, M., and Alakhov, Y. B. (1988) Synthesis of high-capacity immunoaffinity sorbents with oriented immobilized immunoglobulins or their Fab' fragments for isolation of proteins. *J. Chromatogr. 424*, 243–253.

Riddles, P. W., Blakeley, R. L., and Zerner, B. (1983) Reassessment of Ellmann's reagent. *Methods Enzymol. 91*, 49–60.

Roberts, E., and Rouser, G. (1958) Spectrophotometric assay for reaction of N-ethylmaleimide with sulfhdryl groups. *Anal. Chem. 30*, 1291–1292.

Rozsnyai, L. F., Benson, D. R., Fodor S. P. A., and Schultz, P. G. (1992) Photolithographische Immobilisierung von Biopolymeren auf festen Trägern. *Angew. Chem. 104*, 801–802.

Sänger, M., Borle, F., Heller, M., and Sigrist, H. (1992) Light-induced coupling of aqueous soluble protein to liposomes formed from carbene-generating phospholipids, *Bioconjugate Chem. 3*, 308–314.

Sigrist, H., Mühlemann, M., and Dolder, M. (1990) Philicity of amino acid site chains for photogenerated carbenes. *J. Photochem. Photobiol. 7*, 277–287.

Sigrist, H., Gao, H., and Wegmüller, B. (1992) Light-dependend, covalent immobilization of biomolecules on 'inert' surfaces. *Bio/Technology 10*, 1026–1028.

Stayton, P. S., Olinger, J. M., Jiang, M., Bohn, P. W., and Sligar, S. G. (1992) Genetic engineering of surface attachement sites yields oriented protein monolayers. *J. Am. Chem. Soc. 114*, 9298–9299.

Wimalasena, R. L., and Wilson, G. S. (1991) Factors affecting the specific activity of immobilized antibodies and their biologically active fragments. *J. Chromatogr. 572*, 85–102.

Yan, M., Cai, S. X., Wybourne, M. N., and Keana, J. F. W. (1993) Photochemical fuctionalization of polymer surfaces and the production of biomolecule-carrying micrometer-scale structures by deep-UV lithography using 4-substituted perfluorophenyl azides. *J. Am. Chem. Soc. 115, 814–816.*

Site-Directed Double Fluorescent Tagging of Human Renin and Collagenase (MMP-1) Substrate Peptides Using the Periodate Oxidation of N-Terminal Serine. An Apparently General Strategy for Provision of Energy-Transfer Substrates for Proteases

Kieran F. Geoghegan,* Michael J. Emery, William H. Martin, Alexander S. McColl, and Gaston O. Daumy

Central Research Division, Pfizer Inc., Eastern Point Road, Groton, Connecticut 06340. Received July 6, 1993®

Periodate in neutral aqueous solution rapidly converts N-terminal Ser or Thr to an α-*N*-glyoxylyl moiety that can serve as the locus for incorporation of a modifying group [Geoghegan, K. F., and Stroh, J. G. (1992) *Bioconjugate Chem. 3*, 138–146. Gaertner, H. F. et al. (1992) *Bioconjugate Chem. 3*, 262–268]. The usefulness of this procedure has been further illuminated in a route to "energy-transfer" substrates for endoproteases. Each such substrate is an oligopeptide cleavable by a proteinase, but modified (usually at its termini) with two chromophores that form an energy donor–acceptor pair. Production of these substrates is an exercise in double site-directed peptide modification. The new route is composed of three steps, beginning from an unprotected peptide in which a sequence recognized by the pertinent enzyme is placed between N-terminal Ser and C-terminal Lys. Lys may not occur elsewhere in the peptide. Periodate oxidation converts the N-terminal Ser to an α-*N*-glyoxylyl group, which is then allowed to form a hydrazone with the carbohydrazide derivative Lucifer Yellow CH, a hydrophilic fluor with a large Stokes shift (excitation maximum, 425 nm; emission maximum, 525 nm). Finally, the modified peptide is allowed to react with 5-carboxytetramethylrhodamine succinimidyl ester. This reaction selectively modifies the ε-amino group of C-terminal Lys, the only amino group remaining in the peptide. 5-Carboxytetramethylrhodamine strongly (>90%) quenches Lucifer Yellow fluorescence by resonance energy transfer in the intact substrate, but enzyme-catalyzed cleavage eliminates the quenching. The resulting increase in fluorescence may be used to follow the hydrolytic reaction. New substrates for human renin and fibroblast collagenase (matrix metalloproteinase-1) have been made to illustrate the procedure. Each was characterized by structural, spectroscopic, and kinetic methods and furnished a continuous fluorescence-based assay for its respective proteinase. It appears that the scheme can be applied to the preparation of comparable substrates for other proteinases.

INTRODUCTION

Site-directed modification is the delivery of a modifying group uniquely to a preselected site in a peptide.[1] Like classical chemical modification, it is effected using a reagent specific for a single type of functional group that may exist in a peptide (*1*), but consists of applying such a reagent to a peptide containing only one group of the target type. The result is that there can be only one modification event. This is sometimes achieved by designing or redesigning the molecule to harbor only a single instance of one of the reactive groups naturally found in peptides (for example, a cysteine thiol) and making this group the locus of site-directed modification (*2, 3*).

A complementary strategy is to direct the modification to a group that is *not* naturally present in peptides and whose reactivity distinguishes it from those which are. One approach exploits the very rapid and selective attack of periodate on N-terminal Ser or Thr (*4, 5*). This reaction converts the N-terminal residue to an α-*N*-glyoxylyl moiety, OHCCO-, providing an aldehyde function for follow-up chemistry that introduces a modifying group (*6–9*). This may be non-peptide or peptide-like in character, and work to date has centered on the use of hydrazide modifiers that form usefully stable hydrazones. Reduction of the hydrazone is a further option in some cases (*9*).

This method can be one element of a strategy for double site-directed modification. There are cases in which a peptide must be modified with two distinct groups at known sites, with the aim of supporting an application based on the interaction of the two modifying groups (*10, 11*). Alternatively, it may be necessary to introduce two unconnected non-native properties into a peptide by dual modification. We have applied this concept to the provision of "energy-transfer" fluorescent substrates for the continuous assay of proteinases (*12–21*).

In this type of substrate, two chromophoric groups that form a Forster energy donor–acceptor pair are placed at opposite ends of a peptide. The fluorescence emission spectrum of the donor overlaps the absorption spectrum of the acceptor, causing the fluorescence of the donor to be quenched while the substrate remains intact. When the intervening peptide region is cleaved by a proteinase, relief of the strongly distance-dependent quenching provides the means to follow this activity.

Here we describe the preparation of new energy-transfer substrates for human renin and fibroblast collagenase (matrix metalloproteinase-1). A peptide substrate of each enzyme was doubly modified with Lucifer Yellow CH and 5-carboxytetramethylrhodamine, and the resulting fluorogenic substrates were used in continuous assays of their

® Abstract published in *Advance ACS Abstracts*, October 1, 1993.

[1] Abbreviations: "peptide" is often used here in a broad sense meaning "peptide or protein"; PDMS, plasma desorption mass spectrometry; TFA, trifluoroacetic acid; LY– denotes Lucifer Yellow CH in hydrazone linkage with the α-*N*-glyoxylyl moiety at the N-terminus of a peptide following periodate oxidation; *CTMR*– denotes the 5-carboxytetramethylrhodamine moiety coupled to the C-terminal lysyl residue of the peptide.

1043-1802/93/2904-0537$04.00/0 © 1993 American Chemical Society

respective proteinases. This report draws most attention to the direct and, in our view, relatively simple process by which unprotected peptides were converted to doubly-modified derivatives ready for practical use. It appears that the process can be repeated in order to provide comparable substrates for other proteinases.

EXPERIMENTAL PROCEDURES

Reagents. Lucifer Yellow CH and 5-carboxytetramethylrhodamine succinimidyl ester were purchased from Molecular Probes, P.O. Box 22010, 4849 Pitchford Ave., Eugene, OR 97402. The optical properties of these reagents were taken to be those quoted in the supplier's catalog. The peptides SIHPFHLVIHTK (renin substrate) and SGPLGLRAK (collagenase substrate) were supplied as custom syntheses by Synthecell/Vega Biomolecules Corp., 7101 Riverwood Dr., Columbia, MD 21046. Sodium *m*-periodate was purchased from Aldrich, 1001 West Saint Paul Ave., Milwaukee, WI 53233. Periodate solutions were prepared freshly each day. Recombinant human renin (EC 3.4.23.15) was the highly purified material described (*22*) or a partly purified preparation derived from the same starting material. Recombinant human fibroblast procollagenase (EC 3.4.24.7) was produced in a baculovirus expression system, purified by immunoaffinity chromatography (*23*), and activated by treatment with bead-immobilized trypsin (Pierce).

Mass Spectrometry. PDMS was performed using a Bio-Ion 20 spectrometer (Applied Biosystems). Prefabricated nitrocellulose-coated targets were soaked with about 0.21 mL of 10% ethanol until the nitrocellulose was fully wet (15–30 s), spun briefly to leave only a thin layer of the wetting solution, and loaded with 15 μL of sample, which was usually dissolved in 0.1% TFA. The instrument was normally run in positive ion mode with the acceleration potential at 15 kV, but was also used in negative ion mode at −12 kV. Masses were estimated either by using the built-in search program or by placing the twin cursors on each side of the topmost segment of the peak and calculating a centroid. This procedure produced mass results within 0.1% of true values for standards.

Chromatography. HPLC was performed on a Hewlett-Packard 1090 Series II system equipped with a diode-array detector or on an LDC analytical gradient system using two spectroMonitor III variable single-wavelength detectors. Solvents in all cases were A, 0.1% (v/v) TFA; and B, 0.085% (v/v) TFA in 80% (v/v) CH_3CN. All preparative fractionations were performed using a Vydac C4 column (1.0 × 25 cm; type 214TP1010) operating at a flow rate of 4 mL/min with a linear gradient from 0 to 55% solvent B in 36 min beginning 4 min after injection. In experiments to characterize the products of enzyme-catalyzed hydrolysis of the new substrates, the column was either a Vydac C18 column (0.2 × 25 cm; type 218TP52) or an Aquapore ODS cartridge (0.2 × 10 cm) (Applied Biosystems). Each of these columns was used with a flow rate of 0.2 mL/min and a linear gradient from 0 to 55% of solvent B in 35 min beginning 4 min after injection. Peaks were collected by hand.

Fluorescence Spectroscopy. Fluorescence emission spectra were collected on a Perkin-Elmer LS 50 luminescence spectrometer. The excitation wavelength was 430 nm and both slits were set to a bandwidth of 4 nm. Conditions for kinetic studies are given below.

Preparation of *LY*-IHPFHLVIHTK-*CTMR* (Renin substrate). *Step 1: Oxidation of SIHPFHLVIHTK.* A 1.6-mg sample of SIHPFHLVIHTK (1.1 μmol) dissolved in 0.04 M sodium phosphate buffer, pH 7.0, at a concentration of 1.9 mg/mL was treated with 2.5 mM $NaIO_4$ for about 3 min at room temperature, after which the mixture was fractionated by HPLC. (The peptide had to be dissolved initially at 10 mg/mL in 0.01% aqueous TFA before being diluted into the phosphate buffer.) The single product peak, expected to be α-*N*-glyoxylyl-IHPFHLVIHTK, was collected and dried in a centrifugal concentrator.

Step 2: Coupling of Lucifer Yellow CH to α-N-glyoxylyl-IHPFHLVIHTK. A 200-μL portion of 25 mM Lucifer Yellow CH in sodium acetate buffer, pH 4.5, 25% CH_3CN was added to the dried α-*N*-glyoxylyl-IHPFHLVIHTK (1.5 mg) and the reaction was allowed to proceed at room temperature overnight, after which the presence of some precipitated material (presumed to be a reaction product) was noted. This was solubilized by adding 0.1% TFA in 25% CH_3CN to the incubate, which then was fractionated using the same HPLC procedure as before. The reaction product eluted at 29.2 min, expected to be *LY*-IHPFHLVIHTK, was collected and dried.

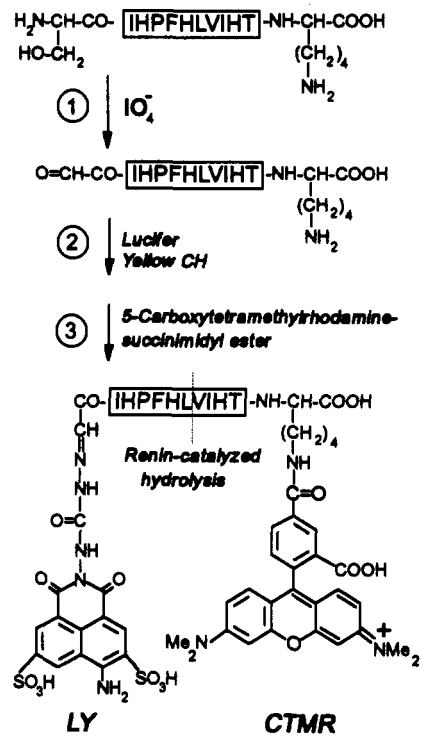
Step 3: Coupling of 5-Carboxytetramethylrhodamine to LY-IHPFHLVIHTK. The dried *LY*-IHPFHLVIHTK was redissolved in 300 μL of 133 mM $NaHCO_3$, pH 8.8, and treated with 75 μL of 20 mM 5-carboxytetramethylrhodamine succinimidyl ester in CH_3CN (final concentrations: 5-carboxytetramethylrhodamine succinimidyl ester, 4 mM; *LY*-IHPFHLVIHTK, 1 mM). After 1 h incubation at room temperature, the reaction mixture was injected onto the HPLC using the gradient program described above. The product peak, expected to be *LY*-IHPFHLVIHTK-*CTMR*, was collected at 34.5 min. As this procedure gave only about two-thirds conversion of *LY*-IHPFHLVIHTK to *LY*-IHPFHLVIHTK-*CTMR*, it was later repeated using a final concentration of 9 mM 5-carboxytetramethylrhodamine succinimidyl ester. This second experiment gave full conversion of *LY*-IHPFHLVIHTK to the doubly-tagged product, and is the one shown in Figure 3 (see Results).

Specificity of Renin-Catalyzed Hydrolysis of *LY*-IHPFHLVIHTK-*CTMR*. A 0.02-μg sample of renin was added to 40 μL of *LY*-IHPFHLVIHTK-*CTMR* solution (140 μM in 0.02 M Mes, pH 6.5, containing 5% DMSO). The reaction was incubated at 37 °C for 2 h, after which 15 μL was injected onto the HPLC (second of the two systems described above). Separate product peaks containing the Lucifer Yellow and 5-carboxytetramethylrhodamine chromophores, respectively, were eluted earlier than intact substrate, and fractions containing these products were dried and characterized by PDMS.

Continuous Fluorescence-Based Assay of Renin Using *LY*-IHPFHLVIHTK-*CTMR*. Renin activity was measured at 22 °C by monitoring the change in fluorescence of a sample containing various amounts of *LY*-IHPFHLVIHTK-*CTMR* and human renin dissolved in 0.05 M sodium phosphate buffer, pH 6.8, containing 0.1 M NaCl and 4% DMSO. The fluorescent substrate was excited at 430 nm and emission was read at 520 nm in a Perkin-Elmer LS-5B luminescence spectrometer. The excitation and emission slits were each set to a bandwidth of 10 nm.

As the concentration of *LY*-IHPFHLVIHTK-*CTMR* was increased, internal filtering of Lucifer Yellow fluorescence was also enhanced due to increasing absorbance by 5-carboxytetramethylrhodamine. A correction for this was applied by first collecting enough data to estimate the rate of fluorescence change, and then adding 2 μM CP-108,671 (a strong renin inhibitor) in order to suppress further renin-induced fluorescence changes. The extent

Scheme I



Optical Properties of Fluorescent Probes

Lucifer Yellow CH *(LY)*

λ_{ex} 420 nm; ϵ_{420} = 12,000 $M^{-1}cm^{-1}$;
λ_{em} 520-540 nm (maximum)

Reactivity: carbohydrazide derivative (forms hydrazone with α-*N*-glyoxylyl-peptide)

5-Carboxytetramethylrhodamine *(CTMR)*

λ_{ex} 540-560 nm; ϵ_{560} = 60,000 $M^{-1}cm^{-1}$;
λ_{em} 580 nm (maximum)

Reactivity: succinimidyl ester (modifies side chain of Lys)

Note overlap of LY emission spectrum with CTMR absorption spectrum

of the internal filtering effect was then gauged by adding Lucifer Yellow CH, so that its concentration was increased by 96 nM, and comparing the resulting fluorescence change to that caused by the same concentration of Lucifer Yellow in the absence of 5-carboxytetramethylrhodamine. Observed rates were then normalized on the basis of this estimate of quenching.

Preparation of *LY*-GPLGLRAK-*CTMR* (Collagenase Substrate). Preparation of the collagenase substrate closely followed the method described for the renin substrate, with the following differences. The starting material SGPLGLRAK was directly soluble in the phosphate reaction buffer for the first step, and did not require solubilization in 0.01% TFA; there was no need to add acetonitrile to the reaction mixture for the coupling of Lucifer Yellow CH to α-*N*-glyoxylyl-GPLGLRAK; there was no precipitate formed in this reaction; and the final product, *LY*-GPLGLRAK-*CTMR* was readily soluble at near millimolar concentration in its assay buffer of 0.05 M Tris, 0.2 M NaCl, 0.005 M $CaCl_2$, pH 7.7. Intermediates, the product itself, and the products of its collagenase-catalyzed cleavage were characterized by the methods used for the renin substrate, including PDMS.

Specificity of Collagenase-Catalyzed Hydrolysis of *LY*-GPLGLRAK-*CTMR*. To determine the site of cleavage catalyzed by recombinant collagenase, 200 μL of *LY*-GPLGLRAK-*CTMR* solution (20 μM) in 0.05 M Tris, 0.15 M NaCl, 0.005 M $CaCl_2$, pH 7.5, was treated with 10 μL of activated collagenase solution (nominally about 5 μg of enzyme, although this is probably an overestimate). After 4 h at 37 °C, the substrate initially present in the reaction mixture was shown by HPLC to be >90% cleaved. The two product peaks were collected, dried, and subjected to mass analysis.

Continuous Fluorescence-Based Assay of Collagenase Using *LY*-GPLGLRAK-*CTMR*. Fluorescence-based rate measurements of collagenase activity were taken at room temperature using a buffer of 0.05 M Tris, 0.15 M NaCl, 0.005 M $CaCl_2$, pH 7.7, in the Perkin-Elmer LS 50 luminescence spectrometer. The excitation wavelength was set to 430 nm (slit at 10-nm bandwidth), and fluorescence emission was recorded at 530 nm (5-nm slit).

RESULTS

Strategy for Double Site-Directed Tagging of a Renin Substrate Peptide. Human renin selectively liberates angiotensin I from the N-terminal region of angiotensinogen by hydrolyzing the peptide bond Leu^{10}-Val^{11}. It has no other known enzymatic activity, exerting an extreme specificity due to active center subsites that recognize the substrate at least across the P4–P1′ residues (and probably more extensively, as in mouse renin) (*24*). Synthetic substrates must match this extended structure, leaving little scope for the inclusion of a non-native chromophore and suggesting that continuous assays for renin are most easily designed using the energy-transfer principle. Two recent reports described such assays (*20, 21*).

Site-directed labeling requires a unique group that becomes the locus of modification. Double site-directed labeling requires the presence of two such groups with distinct reactivities. Design of the renin substrate consisted of taking a renin-sensitive core sequence, IHPF-HLVIH (residues 5–13 of human angiotensinogen), and flanking it with additional N-terminal and C-terminal residues selected to match the intended chemistry. The core was flanked N-terminally by Ser to provide the locus for the first round of modification, consisting of periodate oxidation and subsequent introduction of Lucifer Yellow CH at the resulting α-*N*-glyoxylyl group. It was flanked C-terminally by Thr-Lys to provide an extra residue of spacing and an amino group for targeted modification by reaction with 5-carboxytetramethylrhodamine succinimidyl ester. The complete reaction scheme is summarized in Scheme I.

Lucifer Yellow has a broad absorption band centered near 425 nm (ϵ_{425} of 12 000 M^{-1} cm^{-1}) and a fluorescence emission centered near 525 nm. Complementing this as energy acceptor was the strong chromophore 5-carboxy-

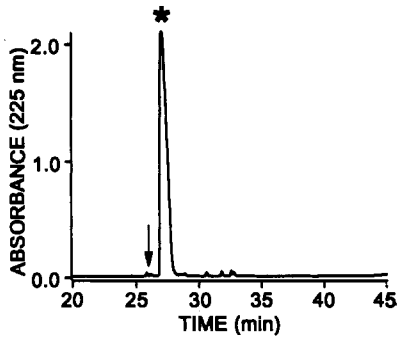


Figure 1. HPLC analysis of the periodate oxidation of SIHPFHLVIHTK. The arrow marks the retention time of SIHPFHLVIHTK prior to modification, and the oxidation product peak marked with an asterisk was collected for mass analysis (Table I).

Table I. Predicted and Observed Masses for Intermediates, Substrate, and Products of Renin-Catalyzed Hydrolysis of the Renin Substrate[a]

	MH+	
	theoretical	observed
SIHPFHLVIHTK	1429.7	1429.5
α-*N*-glyoxylyl-IHPFHLVIHTK	1398.7 (unhydrated)	1398.9
	1416.7 (hydrated)	1417.1
LY-IHPFHLVIHTK	1826.1	1825.2
LY-IHPFHLVIHTK-*CTMR*	2238.1	2238.9
LY-IHPFHL	1247.5	1247.3
VIHTK-*CTMR*	1009.7	1010.2

[a] Mass analyses were performed by PDMS (see Materials and Methods).

tetramethylrhodamine (ϵ_{546} of 63 000 M^{-1} cm^{-1}), whose absorption spectrum overlapped sufficiently well with the fluorescence of Lucifer Yellow (see below) to suggest that it could adequately quench Lucifer Yellow fluorescence prior to hydrolysis of the twice-fluorotagged peptide by renin.

Periodate Oxidation of SIHPFHLVIHTK. HPLC and PDMS (Table I) were used to verify the identity and purity of the starting material SIHPFHLVIHTK. Periodate oxidation of this peptide (see Experimental Procedures) gave quantitative conversion to a single product which was recovered by HPLC (Figure 1) and shown by PDMS to be the expected α-*N*-glyoxylyl-IHPFHLVIHTK (Table I). Characteristically (*8*), the α-*N*-glyoxylyl-peptide gave two peaks in PDMS, one corresponding to its unhydrated form and one corresponding to its hydrated form (Table I).

Conjugation of Lucifer Yellow CH to α-*N*-glyoxylyl-IHPFHLVIHTK. The α-*N*-glyoxylyl-IHPFHLVIHTK was dried and was then allowed to react with Lucifer Yellow CH in sodium acetate buffer, pH 4.5, containing 25% CH_3CN to aid in solubilizing the somewhat hydrophobic peptide. Material presumed to be a reaction product came out of solution during the overnight coupling and was resolubilized by acidifying the reaction mixture with 0.1% TFA in 25% CH_3CN. The reaction mixture was then fractionated using the same HPLC method as before, and the result (Figure 2a) again showed complete conversion of the starting material to a single product. The absorption spectrum of the product showed that the new material contained Lucifer Yellow (Figure 2b). PDMS showed that the product had a mass consistent with the hydrazone of Lucifer Yellow CH with α-*N*-glyoxylyl-IHPFHLVIHTK (Table I), denoted *LY*-IHPFHLVIHTK.

UV spectral analysis (not shown) of a comparable adduct (*LY*-IGSLAK) demonstrated the presence of an absorbance band centered at 262 nm (ϵ_{262} of 13 200 M^{-1} cm^{-1}) that does not exist in the spectrum of α-*N*-glyoxylyl-IGSLAK or free Lucifer Yellow CH, and therefore must be a property of the adduct. The position of this band supported the conclusion that Lucifer Yellow CH added to the peptide as a hydrazone (see Figure 8 of ref 8), and not as a Schiff base. This hydrazone can presumably be made in two isomeric forms (*syn* and *anti* configurations about the hydrazone bond), but the products have not so far been resolved into multiple forms by any of our preparative methods or analyzed (e.g. by NMR) to characterize their putative distribution between these two forms.

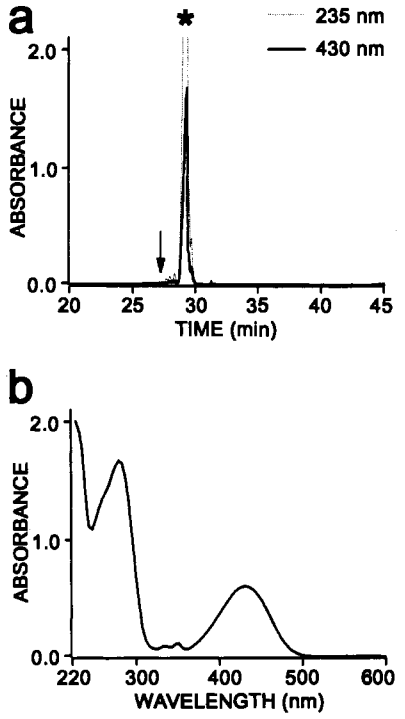


Figure 2. Conjugation of Lucifer Yellow CH to α-*N*-glyoxylyl-IHPFHLVIHTK. (a) HPLC analysis of the coupling reaction, showing absorption traces at (· ·) 235 and (–) 430 nm. The arrow marks the retention time of α-*N*-glyoxylyl-IHPFHLVIHTK prior to reaction, and the product peak marked with an asterisk was collected for mass analysis (Table I). (b) Absorption spectrum of the product, showing the presence of the Lucifer Yellow chromophore.

Conjugation of 5-Carboxytetramethylrhodamine to *LY*-IHPFHLVIHTK. *LY*-IHPFHLVIHTK was dried and then redissolved in 0.13 M $NaHCO_3$ for the third and final step of the preparation. For a first attempt, 5-carboxytetramethylrhodamine succinimidyl ester dissolved in CH_3CN (20 mM) was added to the peptide (final concentration 1 mM) at a final concentration of 4 mM. The desired product *LY*-IHPFHLVIHTK-*CTMR* formed in about 66% yield in 1 h and was recovered by HPLC. The incomplete conversion obtained in this trial was attributed to use of insufficient 5-carboxytetramethylrhodamine succinimidyl ester. A separate experiment using 9 mM 5-carboxytetramethylrhodamine succinimidyl ester resulted in complete conversion of *LY*-IHPFHLVIHTK to the desired product (Figure 3a). The product peak was distinguished from several peaks due to residual 5-carboxytetramethylrhodamine by its absorption spectrum (Figure 3b), showing local maxima due to Lucifer Yellow (ϵ_{425} 12 000 $M^{-1}cm^{-1}$) and 5-carboxytetramethylrhodamine (ϵ_{546} 63 ,000 $M^{-1}cm^{-1}$) in about a 1:5 ratio of intensity at the wavelengths of these absorptivities, consistent with their presence in 1:1 ratio, and then by

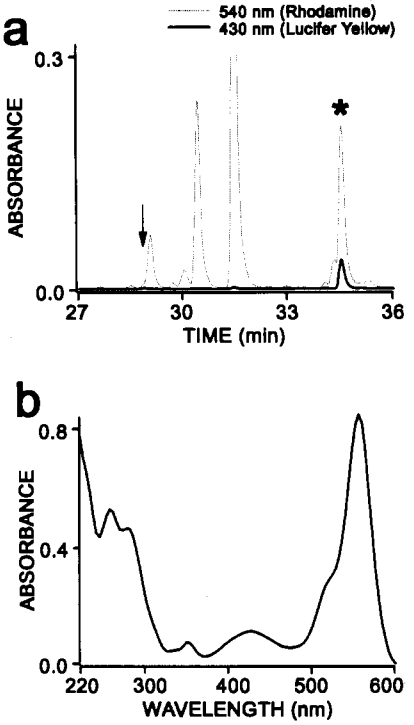


Figure 3. Conjugation of 5-carboxytetramethylrhodamine to *LY*-IHPFHLVIHTK. (a) HPLC analysis of the coupling reaction, showing absorption traces at (–) 430 and (· ·) 540 nm. The arrow marks the retention time of *LY*-IHPFHLVIHTK prior to reaction, and the product peak marked with an asterisk was collected for mass analysis (Table I). (b) Absorption spectrum of the product, showing the presence of the Lucifer Yellow and 5-carboxytetramethylrhodamine chromophores.

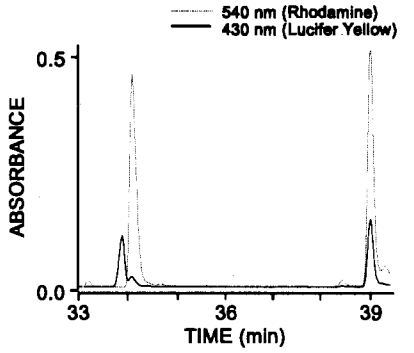


Figure 4. HPLC analysis of the products formed by renin-catalyzed hydrolysis of *LY*-IHPFHLVIHTK-*CTMR*. The substrate (peak at 39 min) was converted to two earlier-eluted product peaks. Absorption traces are shown at (–) 430 (Lucifer Yellow) and (· ·) 540 nm (5-carboxytetramethylrhodamine). See Table I for mass analysis results.

PDMS (Table I). The product was dried and stored at −20 °C. It was soluble in DMSO to at least 1.6 mM, and DMSO therefore was selected as the solvent used to deliver it into kinetic experiments.

Action of Renin on *LY*-IHPFHLVIHTK-*CTMR*. HPLC fractionation of an incubate of *LY*-IHPFHLVIHTK-*CTMR* with purified renin yielded two product peaks containing, respectively, Lucifer Yellow (detected at 430 nm) and 5-carboxytetramethylrhodamine (detected at 540 nm) (Figure 4). PDMS results for these products agreed with predicted MH^+ values for *LY*-IHPFHL and VIHTK-*CTMR* (Table I). These results showed that human renin cleaved the doubly fluorotagged substrate at the Leu-Val bond that it recognizes in angiotensinogen and set the stage for fluorescence-based studies of renin activity (see below).

Table II. Predicted and Observed Masses for Intermediates, Substrate, and Products of Collagenase-Catalyzed Hydrolysis of the Collagenase Substrate[a]

	MH^+	
	theoretical	observed
SGPLGLRAK	899.1	899.2
α-*N*-glyoxylyl-GPLGLRAK	868.1 (unhyrated)	868.1
	886.1 (hydrated)	886.2
LY-GPLGLRAK	1295.6	1294.9
LY-GPLGLRAK-*CTMR*	1707.5	1707.0
LY-GPLG[b]	$(M-H)^-$ theor 825.0	$(M-H)^-$ obs 824.9
LRAK-*CTMR*	900.6	899.9

[a] Methods are the same as those noted in Table I. [b] *LY*-GPLG could not be successfully analyzed by positive ion PDMS, but was detected without difficulty when the spectrometer was operated in negative ion mode.

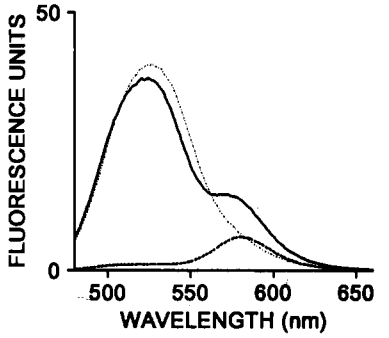


Figure 5. Fluorescence emission spectra showing the increase in detectable Lucifer Yellow fluorescence consequent to renin-catalyzed hydrolysis of *LY*-IHPFHLVIHTK-*CTMR*. Excitation wavelength was 430 nm. The emission spectra are shown for 4.5 μM solutions of (– –)*LY*-IHPFHLVIHTK-*CTMR* (intact substrate), (—) the products of renin-catalyzed hydrolysis of *LY*-IHPFHLVIHTK-*CTMR*, and (– ·) *LY*-IHPFHLVIHTK (the peptide tagged with only Lucifer Yellow CH, and therefore not fluorescence-quenched). Samples were dissolved in 0.04 M Mes, pH 6.5, with 10% DMSO.

Double Site-Directed Tagging of a Collagenase Substrate Peptide. Vertebrate collagenases are specialized zinc metalloenzymes that cleave strands of the collagen triple helix at Gly-Leu bonds. As this activity is significant in inflammatory disease (*25*), the enzymes are further important targets of drug-discovery efforts. A fluorogenic substrate was planned around a collagenase-sensitive sequence (*26*) which was flanked by N-terminal Ser and C-terminal Lys, to give SGPLGLRAK as the starting material. This was doubly tagged in the same way as the renin substrate, and the intermediates and final product were characterized likewise (Table II). Treating the new substrate, *LY*-GPLGLRAK-*CTMR*, with recombinant human collagenase yielded products whose absorption and mass spectra (Table II) led them to be identified as *LY*-GPLG and LRAK-*CTMR*, indicating that cleavage occurred at the Gly-Leu bond.

Fluorescence Changes Consequent to Substrate Hydrolysis. The fluorescence emission spectrum of 4.5 μM *LY*-IHPFHLVIHTK-*CTMR* was compared with that of the product mixture from its renin-catalyzed hydrolysis (Figure 5). The same experiment was performed for *LY*-GPLGLRAK-*CTMR* and the products of its collagenase-catalyzed hydrolysis (data not shown, as the result closely resembles that in Figure 5). For both substrates, Lucifer Yellow fluorescence increased by over 10-fold following cleavage, indicating their good potential for successful use in fluorescence-based assays (see below).

Excitation at 430 nm, while directed toward the Lucifer

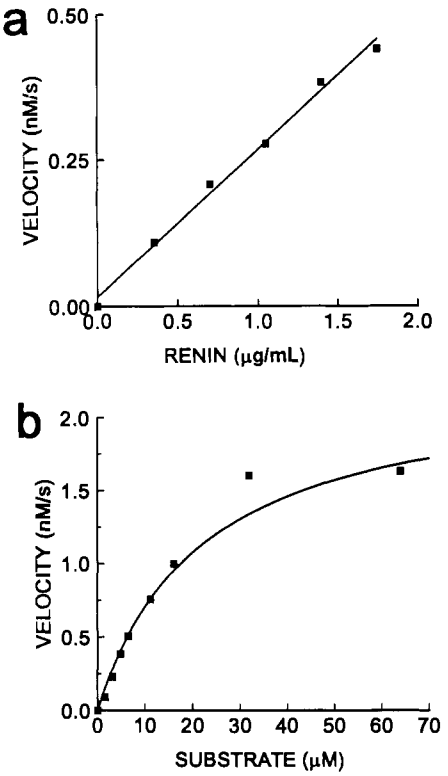


Figure 6. Data from fluorescence-based assays of renin activity using *LY*-IHPFHLVIHTK-*CTMR*. (a) Dependence of initial rate on enzyme concentration; data from experiments using 1 μM substrate. The line is a linear regression plot through the data points; its nonzero *y*-intercept was considered to reflect experimental error, as no rate was detected in the absence of enzyme. (b) The initial rate of hydrolysis of *LY*-IHPFHLVIHTK-*CTMR* was measured using 0.24 μg/mL renin and various substrate concentrations. Each point represents the mean of three observations. Data were fit to the Michaelis–Menten equation (curve), giving K_M of 20 μM.

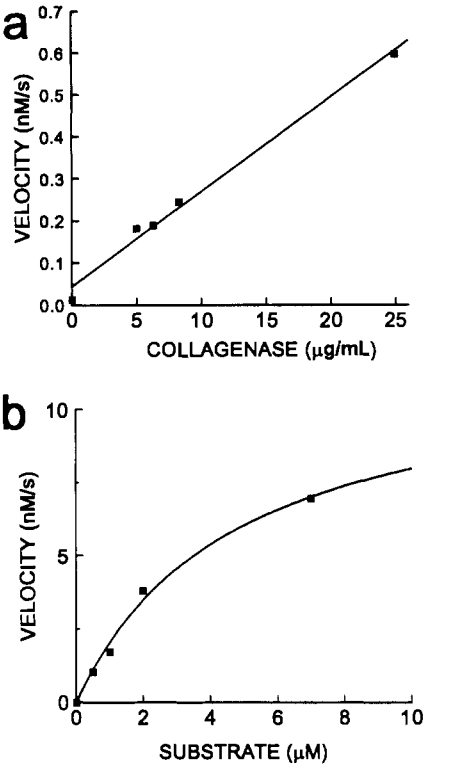


Figure 7. Data from fluorescence-based assays of collagenase activity using *LY*-GPLGLRAK-*CTMR*. Due to the complexity of the collagenase activation process, the concentration of active enzyme in these experiments was not accurately known. (a) Dependence of initial rate on enzyme concentration; data from experiments using 3.5 μM substrate. The line is a linear regression plot through the data points; its nonzero *y*-intercept was considered to reflect experimental error, as no rate was detected in the absence of enzyme. (b) Dependence of rate on substrate concentration. Each point represents a single observation. Data were fit to the Michaelis–Menten equation (curve), giving K_M of 3.9 μM.

Yellow chromophore, also caused some direct excitation of 5-carboxytetramethylrhodamine and generated a minor fluorescence signal centered at 580 nm (Figure 5). This did not interfere with the major signal change from Lucifer Yellow that followed hydrolysis of the peptide midsection.

Renin Activity Assay. The initial rate of cleavage of *LY*-IHPFHLVIHTK-*CTMR* showed linear dependence on the concentration of added renin (Figure 6a). Under the conditions described in the Experimental Procedures, the reaction followed saturation kinetics with K_M equal to 20 μM and V_{max} equal to 2.37 nM s^{-1} (Figure 6b). This value for K_M agreed with results reported elsewhere for the same peptide substrate sequence in its unmodified form (*27*).

Collagenase Activity Assay. In kinetic studies of *LY*-GPLGLRAK-*CTMR* with recombinant collagenase, the reaction rate exhibited linear dependence on the amount of enzyme added (Figure 7a). Inconsistent results were observed if the reaction buffer was not supplemented with 1 μM zinc(II), indicating the need to maintain full loading of the collagenase with the active site metal. Variation of the substrate concentration from 0.1 to 4 μM indicated that substrate binding began to be saturated in this range, with a calculated K_M of 3.9 μM (Figure 7b).

This result was in the same range as the K_M reported for another fluorescent substrate of collagenase, Dnp-PLGLWAdR-NH_2, for which a K_M of 7.1 μM was determined at 37 °C and pH 7.7 (*17*). This substrate has the same sequence as *LY*-GPLGLRAK-*CTMR* in positions P_3–P_1'. However, the specificity of collagenase is highly dependent on the substrate structure, and this was noted during selection of the core sequence of *LY*-GPLGLRAK-*CTMR*. The choice of Arg at P_2' was inspired by indications that it would strongly enhance substrate binding relative to many other amino acids that might be placed at that position (*26*), which seemed to be the case. However, the control experiment to show that Arg actually had this effect was not done.

DISCUSSION

Selective proteolytic action continues to be recognized as a central mechanism of biological control. Elucidation of its details has created a growing need for direct and continuous assays of highly specific proteinases, which is often best met with intramolecularly quenched "energy-transfer" substrates. The usual strategy, and the one followed here, is to place the fluorescence donor and acceptor groups on opposing sides of a peptide substrate sequence. A variation is to employ a chromophoric amino acid as both a specificity determinant and a component of the energy relay (*17, 28*).

As this application calls for adding different nonpeptide groups to opposite ends of a peptide, it is especially opportune to use chemistry with intrinsic specificity for the N-terminus. Periodate oxidation of N-terminal Ser or Thr is an exceptionally fast reaction that proceeds best at neutral pH (*5, 8*). It is also highly selective when a low molar excess of periodate over peptide is used, as the

desired oxidation is faster than a number of the potentially competing reactions (*8*). The N-terminal oxidations of both SIHPFHLVIHTK and SGPLGLRAK (Scheme I) were accomplished without complications because neither peptide contained any residue with periodate-sensitivity comparable to that of N-terminal Ser (*29*). HPLC analysis indicated quantitative formation of the desired products, as illustrated for the renin substrate SIHPFHLVIHTK (Figure 1).

Lucifer Yellow CH readily formed a hydrazone with α-*N*-glyoxylyl-IHPFHLVIHTK in the second step of this preparation (Figure 2), consistent with earlier experience of comparable reactions (*8*). The dye itself was freely soluble in water (0.25 M can be achieved using the dilithium salt), but the relative hydrophobicity of the renin substrate peptide necessitated the addition of acetonitrile to the coupling buffer. No organic cosolvent was required in the coupling reaction with the more hydrophilic collagenase substrate.

The third and final step was modification of the ε-amino group of C-terminal Lys with 5-carboxytetramethylrhodamine succinimidyl ester. When a mixture of 5- and 6-carboxytetramethylrhodamine was employed in trial experiments using the peptide SIGSLAK (not shown), products derived from the two dye isomers were separated via reversed-phase HPLC to give very complex chromatograms. Although the use of purified 5-carboxytetramethylrhodamine succinimidyl ester mostly eliminated this problem, different forms of the dye (presumably active ester and free acid) were retained by the HPLC column and gave multiple 540-nm peaks that could have complicated product identification (Figure 3a). However, judicious selection of detector wavelengths or, preferably, use of a diode-array detector allowed the desired product peak to be recognized by the presence of spectral features due to both Lucifer Yellow and 5-carboxytetramethylrhodamine (Figure 3b).

HPLC indicated >90% conversion of starting material to desired product in each of the three steps (Figures 1–3). Product identifications were based on the combination of mass spectrometry (Tables I and II) and absorption spectroscopy (Figures 2b and 3b). The same methods were used to show that renin cleaved *LY*–IHPFHLVIHTK–*CTMR* at the Leu-Val peptide bond (Figure 4, Table I), and that collagenase cleaved *LY*–GPLGLRAK–*CTMR* at the Gly-Leu bond (Table II). In each case, this was the expected cleavage site.

The present route to fluorogenic substrates (and other doubly-tagged peptides) may be broadly useful. One restriction is that the starting peptide must possess only two amino groups, one in the N-terminal Ser or Thr and the other in C-terminal Lys,[2] in order to preserve site specificity in the final step of modification. This is a problem only when Lys must occur in the sequence recognized by the proteinase. In such cases, enzyme-catalyzed fragment coupling (*7*) might represent an interesting route to the provision of a substrate with the required sequence.

In this preparation, the fluorescence donor was the first group of the energy-transfer pair to be coupled. As indicated by Wang et al. (*30*), this can be a significant point to consider in developing synthetic routes to fluorescent substrates. Assuming that the final product is more likely to be contaminated with a residue of the second reagent to be coupled than with the first, it is preferable that this second reagent be the fluorescence acceptor. This is because residual acceptor harms the assay only if it is present at sufficiently high levels to introduce internal optical filtering due to its absorbance, while residual fluorescence donor creates a background of unquenched fluorescence in the assay. This is especially true if a highly fluorescent donor with a superior quantum yield is used.

Lucifer Yellow does not meet this description, being a relatively weak chromophore (ϵ_{max} of 12 000 M^{-1} cm^{-1}) and fluorophore compared to excellent fluors such as fluorescein or 5-carboxytetramethylrhodamine (each with ϵ_{max} > 60 000 M^{-1} cm^{-1}). However, the present method could be adapted to allow use of other fluorophores and chromophores. The pair of Lucifer Yellow with 5-carboxytetramethylrhodamine was selected for the present work because both reagents were commercially available and had complementary optical and chemical properties. An added important benefit of this pair is the relatively hydrophilic character of its components, which may be less restrictive of substrate solubility in aqueous buffers than some alternatives. It was also important to find a donor–acceptor pair that operates in the visible region. High-wavelength donor–acceptor pairs are preferred in the screening of pharmaceutical sample banks for new inhibitors, because compound files may be rich in UV-absorbing compounds that interfere with assays based on energy-transfer in the ultraviolet.

A general problem in assays of this type is the effect known as internal or inner filtering, the blocking of fluorescent emission due to absorbance by the quenching chromophore. The extent of this effect is a function of the molar absorptivity of this chromophore at the relevant wavelength, its concentration, and the cuvette light path for emission. It is not connected to properties of the enzyme. With the present pair of chromophores under the present conditions of assay, internal filtering is significant even at a substrate concentration of 2 μM (where absorbance at 520 nm due to 5-carboxytetramethylrhodamine is 0.06), and so a correction for this was routinely applied to all rate measurements (see Experimental Procedures).

It may appear from Scheme I that the order of steps 2 and 3 could be reversed if desired. On trying this with the collagenase substrate, and treating α-*N*-glyoxylyl-GPLGLRAK with 5-carboxytetramethylrhodamine succinimidyl ester at pH 8.8, we detected oligomerized conjugates of 5-carboxytetramethylrhodamine with the oxidized peptide (data not shown). Condensation of the α-*N*-glyoxylyl moiety with the Arg residue, neither of which is involved in the reaction with 5-carboxytetramethylrhodamine succinimidyl ester, was suspected to be the basis of this result, but this was not clearly established. This limited venture suggested that the N-terminal chemistry, which creates but then suppresses the aldehyde function, should be completed before modification of C-terminal Lys is attempted at pH >8.

Hydrazones are potentially subject to hydrolysis when they are removed from the equilibrium conditions in which they are formed. This potential lability has not yet been quantified for the various types of hydrazone that can be formed after modifying N-terminal Ser, but should not be ignored when using this type of bioconjugate (*8*). In particular, such hydrazones are expected to exhibit an increased equilibrium degree of dissociation with decreas-

[2] The Lys residue need not be at the C-terminus of the peptide, but must be to the C-terminal side of the scissile peptide bond. It might be useful to increase the water solubility of substrates containing hydrophobic peptide sequences by placing an Arg residue (for example) C-terminal to the Lys intended for modification.

ing initial concentration. This matter requires more direct experimental evaluation in the future. In response to this concern, Gaertner et al. (*9*) showed that hydrazones formed by carboxylic hydrazides can be reduced with cyanoborohydride. We confirmed this result, also noting that borohydride gives faster reductions (K. Geoghegan and M. Emery, unpublished). The present substrates were used successfully to perform enzyme assays at and below the micromolar level, which is their intended function, but it remains important when using these and comparable conjugates to bear their potential pH-dependent (*8*) lability in mind and check it when possible.

While the provision of fluorogenic substrates is an interesting application of peptide modification chemistry, it has been used here principally as a test case. The question has been whether chemistry originating with the selective periodate oxidation of N-terminal Ser provides stable adducts that perform well in a significant biochemical application. While there continues to be incomplete knowledge regarding the stability of the hydrazones formed under the present reaction scheme, it has now been made clear that they are decidedly useful compounds. The impressively clean and simple nature of the process by which these compounds are made further recommends it for consideration in cases requiring N-terminal derivatization of peptides or proteins.

LITERATURE CITED

(1) Means, G. E., and Feeney, R. E. (1971) *Chemical Modification of Proteins*, Holden-Day, San Francisco.

(2) Wingfield, P., Graber, P., Shaw, A. R., Gronenborn, A. M., Clore, G. M., and MacDonald, H. R. (1989) Preparation, characterization and application of interleukin-1β mutant proteins with surface-accessible cysteine residues. *Eur. J. Biochem. 179*, 565–571.

(3) Chollet, A., Bonnefoy, J.-Y., and Odermatt, N. (1990) Preparation, application and biological characterization of interleukin-1β mutant protein biotinylated at a single site. *J. Immunol. Meth. 127*, 179–185.

(4) Nicolet, B. H., and Shinn, L. A. (1939) The Action of Periodic Acid on α-Amino Alcohols. *J. Am. Chem. Soc. 61*, 1615.

(5) Dixon, H. B. F., and Fields, R. (1972) Specific Modification of NH_2-Terminal Residues by Transamination. *Methods Enzymol. 25*, 409–419.

(6) Maassen, A., Thielen, T. P. G. M., and Moller, W. (1983) Synthesis and Application of Two Reagents for the Introduction of Sulfhydryl Groups into Proteins. *Eur. J. Biochem. 134*, 327–330.

(7) Offord, R. E. (1990) Chemical Approaches to Protein Engineering. *Protein Design and the Development of New Therapeutics and Vaccines.* (J. B. Hook and G. Poste, Eds.) pp 253–282, Plenum Publishing Corp., New York.

(8) Geoghegan, K. F., and Stroh, J. G. (1992) Site-Directed Conjugation of Nonpeptide Groups to Peptides and Proteins via Periodate Oxidation of a 2-Amino alcohol. Application to Modification at N-Terminal Serine. *Bioconjugate Chem. 3*, 138–146.

(9) Gaertner, H. F., Rose, K., Cotton, R., Timms, D., Camble, R., and Offord, R. E. (1992) Construction of Protein Analogues by Site-Specific Condensation of Unprotected Fragments. *Bioconjugate Chem. 3*, 262–268.

(10) Stryer, L., and Haugland, R. P. (1967) Energy Transfer: A Spectroscopic Ruler. *Proc. Natl. Acad. Sci. U.S.A. 58*, 719–726.

(11) Stryer, L. (1978) Fluorescence Energy Transfer as a Spectroscopic Ruler. *Annu. Rev. Biochem. 47*, 819–846

(12) Latt, S. A., Auld, D. S., and Vallee, B. L. (1972) Fluorescence Determination of Carboxypeptidase A Activity Based on Electronic Energy Transfer. *Anal. Biochem. 50*, 56–62.

(13) Carmel, A., Zur, M., Yaron, A., and Katchalski, E. (1973) Use of Substrates with Fluorescent Donor and Acceptor Chromophores for the Kinetic Assay of Hydrolases. *FEBS Lett. 30*, 11–14.

(14) Yaron, A., Carmel, A., and Katchalski-Katzir, E. (1979) Intramolecularly Quenched Substrates for Hydrolytic Enzymes. *Anal. Biochem. 95*, 228–235.

(15) Nishino, N., and Powers, J. C. (1980) *Pseudomonas aeruginosa* Elastase: Development of a New Substrate, Inhibitors, and an Affinity Ligand. *J. Biol. Chem. 255*, 3482–3486.

(16) Deyrup, C., and Dunn, B. M. (1983) A New Substrate for Porcine Pepsin Possessing Cryptic Fluorescence Properties. *Anal. Biochem. 129*, 502–512.

(17) Stack, M. S., and Gray, R. D. (1989) Comparison of Vertebrate Collagenase and Gelatinase Using a New Fluorogenic Substrate Peptide. *J. Biol. Chem. 264*, 4277–4281.

(18) Geoghegan, K. F., Spencer, R. W., Danley, D. E., Contillo, L. G., Jr., and Andrews, G. C. (1990) Fluorescence-based continuous assay for the aspartyl protease of human immunodeficiency virus-1. *FEBS Lett. 262*, 119–122.

(19) Matayoshi, E. D., Wang, G. T., Krafft, G. A., and Erickson, J. (1990) Novel Fluorogenic Substrates for Assaying Retroviral Proteases by Resonance Energy Transfer. *Science 247*, 954–957.

(20) Oliveira, M. C. F., Hirata, I. Y., Chagas, J. R., Boschcov, P., Gomes, R. A. S., Figueiredo, A. F. S., and Juliano, L. (1992) Intramolecularly Quenched Fluorogenic Peptide Substrates for Human Renin. *Anal. Biochem. 203*, 39–46.

(21) Wang, G. T., Chung, C. C., Holzman, T. F., and Krafft, G. A. (1993) A Continuous Fluorescence Assay of Renin Activity. *Anal. Biochem. 210*, 351–359.

(22) Geoghegan, K. F., Lanzetti, A. J., Ammirati, M. J., Danley, D. E., O'Connor, B. A., and Hobart, P. M. (1991) Simple Procedure for Recovery of Crystallizable Human Renin from Mammalian Cell-Conditioned Medium. *Structure and Function of the Aspartyl Proteases* (B. M. Dunn, Ed.) pp. 379–381, Plenum Press, New York.

(23) Birkedal-Hansen, B., Moore, W. I. G., Taylor, R. E., Bhown, A. S., and Birkedal-Hansen, H. (1988) Monoclonal Antibodies to Human Fibroblast Procollagenase. Inhibition of Enzymatic Activity, Affinity Purification of the Enzyme, and Evidence for Clustering of Epitopes in the NH_2-Terminal End of the Activated Enzyme. *Biochemistry 27*, 6751–6758.

(24) Dhanaraj, V., Dealwis, C., Frazao, C., Badasso, M., Sibanda, B. L., Tickle, I. J., Cooper, J. B., Driessen, H. P. C., Newman, M., Aguilar, C., Wood, S. P., Blundell, T. L., Hobart, P. M., Geoghegan, K. F., Ammirati, M. J., Lanzetti, A. J., Danley, D. E., O'Connor, B. A., and Hoover, D. J. (1992) X-Ray Analyses of Peptide Inhibitor Complexes Define the Structural Basis of Specificity for Human and Mouse Renins. *Nature 357*, 466–472.

(25) Nagase, H. and Woessner, J. F., Jr. (1993) Role of Endogenous Proteinases in the Degradation of Cartilage Matrix. *Joint Cartilage Degradation. Basic and Chemical Aspects* (J. F. Woessner and D. Howell, Eds.) pp 159–185, Marcel Dekker, New York.

(26) Netzel-Arnett, S., Fields, G., Birkedal-Hansen, H., and Van Wart, H. E. (1991) Sequence Specificities of Human Fibroblast and Neutrophil Collagenases. *J. Biol. Chem. 266*, 6747–6755.

(27) Cumin, F., Le-Nguyen, D., Castro, B., Menard, J., and Corvol, P. (1987) Comparative enzymatic studies of human renin acting on pure natural or synthetic substrates. *Biochim. Biophys. Acta 913*, 10–19.

(28) Pohl, J., Davinic, S., Blaha, I., Strop, P., and Kostka, V. (1987) Chromophoric and Fluorophoric Peptide Substrates Cleaved through the Dipeptidyl Carboxypeptidase Activity of Cathepsin B. *Anal. Biochem. 165*, 96–101.

(29) Clamp, J. R., and Hough, L. (1965) The Periodate Oxidation of Amino Acids with Reference to Studies on Glycoproteins. *Biochem. J. 94*, 17–24.

(30) Wang, G. T., Matayoshi, E., Huffaker, H. J., and Krafft, G. A. (1990) Design and Synthesis of New Fluorogenic HIV Protease Substrates Based on Resonance Energy Transfer. *Tetrahedron Lett. 31*, 6493–6496.

Chlorinated Phenyl Azides as Photolabeling Reagents. Synthesis of an ortho,ortho'-Dichlorinated Arylazido PCP Receptor Ligand

Sui Xiong Cai,[†,⊥] Denis J. Glenn,[†] Kyle R. Gee,[†,∥] Mingdi Yan,[†] Ronald E. Cotter,[‡] N. Laxma Reddy,[‡] Eckard Weber,[§] and John F. W. Keana*[,†]

Department of Chemistry, University of Oregon, Eugene, Oregon 97403, Cambridge NeuroScience, Inc., Cambridge, Massachusetts 02139, and Department of Pharmacology, University of California, Irvine, California 92717. Received July 14, 1993[•]

The enhanced photolabeling properties of chlorinated phenyl azides are demonstrated by the synthesis and photolysis of methyl 4-azido-2,3,5,6-tetrachlorobenzoate (**3**) and methyl 4-azido-3,5-dichlorobenzoate (**4**). Photolysis of azide **3** in 1 M diethylamine/cyclohexane as the trapping medium gave 34% NH-insertion product. Similar photolysis of azide **4** gave 35% NH insertion product. These results demonstrate that chlorinated phenyl azides are significantly better at undergoing NH insertion than nonhalogenated analogs and suggest that improvement of existing aryl azide-based photolabels might be achieved by introduction of chlorine atoms on either side of the azide group. As an application, 3-azido-2,4-dichloro-10,5-(iminomethano)-10,11-dihydro-5*H*-dibenzo[*a*,*d*]cycloheptene (**19**), an analog of the potent PCP receptor ligand IDDC (**14**), was synthesized and its affinity for the PCP receptor was determined to be 6.3 ± 0.7 μM (IC_{50} against [^{3}H]MK801).

INTRODUCTION

Photoaffinity labeling (PAL) is used to examine the spatial relationship between components in biological systems (*1–3*). Typically, the photolabel is a ligand modified with a photoreactive group which can form a stable covalent bond between the label and biological macromolecule of interest. The success of experiments using PAL reagents depends in part on the CH or NH bond insertion efficiency of the label upon photolysis. Aryl azides are often employed as the photoactive group in PAL reagents (*4*). These reagents form a highly reactive nitrene intermediate upon photolysis which can then undergo NH or CH insertion at the site of labeling with formation of a covalent bond. However, low levels of labeling are sometimes observed with aryl azides. These low labeling levels are attributed to ring expansion of the nitrene intermediate to the less reactive dehydroazepine intermediate. This intermediate is incapable of undergoing a bond insertion reaction (*5, 6*) and instead reacts with solvent or nearby nucleophiles.

We (*7–10*) and others (*11–15*) have been developing a series of functionalized perfluorophenyl azides (PFPAs) as a new class of PAL reagents. Fluorophenyl azide (FPA) based photolabeling reagents have shown significant improvement in both CH and NH insertion efficiency in organic solvents over nonfluorinated analogs. However, introduction of the FPA functionality into existing aryl azide-based photolabels or their amine precursors is complicated by the difficulty of fluorinating the aryl ring (*16*). We were therefore prompted to investigate the behavior of representative chlorophenyl azides (CPAs) for potential use as photoaffinity labels (*17*).

CPAs are more readily available than the FPAs owing to the variety of methods available for aromatic chlorination (*18*). Photolysis of *m*- or *p*-chlorophenyl azides in dimethylamine has been shown to give ring-expansion products (*19, 20*). Herein we report the synthesis and photochemical properties of the tetrasubstituted functionalized CPA methyl 4-azido-2,3,5,6-tetrachlorobenzoate (**3**), and the ortho,ortho'-disubstituted CPA methyl 4-azido-3,5-dichlorobenzoate (**4**). As an application of this technique, 3-azido-2,4-dichloro-10,5-(iminomethano)-10,11-dihydro-5*H*-dibenzo[*a*,*d*]cycloheptene (**19**), a ligand for the PCP receptor site (*21*) of the NMDA receptor in the mammalian central nervous system, was synthesized.

EXPERIMENTAL PROCEDURES

^{1}H NMR spectra were measured at 300 MHz in $CDCl_3$ unless otherwise noted. IR spectra were recorded in $CDCl_3$. Mass spectra were obtained in the electron ionization mode, and relative intensities are reported in parentheses after the *m/z* value. Solvents were reagent grade unless otherwise specified. $MgSO_4$ was used to dry organic solutions. All reactions involving azides were run under subdued light by wrapping flasks with aluminum foil. Analytical thin-layer chromatography was performed on Merck silica gel 60 F_{254} with a fluorescent indicator. Flash chromatography was performed using 200–425 mesh (Aldrich) silica gel. Preparative TLC was performed on Analtech GF precoated silica gel glass-backed plates (20 × 20 cm). Photolyses were carried out at ambient temperature in a Rayonet photochemical reactor with 350-nm lamps and the progress of photolysis was followed by IR at 2123 cm^{-1} (azide absorption). Solutions were purged with argon for 1 min before photolysis.

Methyl 4-Azido-2,3,5,6-tetrachlorobenzoate (3). To a stirred solution of 312 mg (1.08 mmol) of aniline **1** (*22*) in CF_3CO_2H (20 mL) at 0 °C was added 173 mg (2.51 mmol) of $NaNO_2$ at once. The solution was stirred at 0 °C for 1 h and then 187 mg (2.88 mmol) of NaN_3 was added. The solution was allowed to come to room temperature and stirred for 1 h. It was then added dropwise to ice water, forming a yellow precipitate. The suspension was filtered and washed with ice water to leave 97 mg (29%) of **3** as a yellow powder, which was purified by crystallization from $CHCl_3$/pentanes and then acetone/

† University of Oregon.
⊥ Present address: Acea Pharmaceuticals, Inc., Irvine, CA.
∥ Present address: Molecular Probes, Inc., Eugene, OR.
‡ Cambridge NeuroScience, Inc.
§ University of California, Irvine.
• Abstract published in *Advance ACS Abstracts*, October 1, 1993.

1043-1802/93/2904-0545$04.00/0 © 1993 American Chemical Society

H_2O to give a fine yellow powder: mp 137–139 °C; IR 2127, 1744 cm^{-1}; ^1H NMR 4.00 (s); MS *m/z* 315 (6, M^+), 301 (5), 287 (58), 282 (18), 272 (43), 256 (11), 244 (40), 228 (100), 194 (27), 156 (69), 121 (66), 86 (50), 58 (85); HRMS 312.8971 (312.8979 calcd for $C_8H_3{}^{35}Cl_4N_3O_2$).

Methyl 4-Azido-3,5-dichlorobenzoate (4). Ester **4** was prepared from aniline **2** (*23*) in a similar manner to ester **3** and was isolated as an off-white powder (68%). The sample was purified by sublimation (0.003 Torr, 40 °C) to give a white microcrystalline powder: mp 70–72 °C; IR 2130, 2112, 1728 cm^{-1}; ^1H NMR 3.92 (s, 3H), 7.95 (s, 2H); MS *m/z* 245 (M^+, 18), 217 (100), 202 (550), 174 (67), 158 (73); HRMS 244.9769 (244.9759 calcd for $C_8H_5{}^{35}Cl_2N_3O_2$).

Photolysis of Azide 3 in Diethylamine/Cyclohexane. A solution of 51 mg of **3** in 1 M diethylamine/cyclohexane (51 mL) was photolyzed for 2 h. The crude photolysis mixture was concentrated to dryness in vacuo, leaving an oily residue which was separated by preparative TLC (2:1 $CHCl_3$/hexanes) to give aniline **1** (*23*) as a white powder (35%, R_f = 0.53) and hydrazine **7** as a yellow oil (34%, R_f = 0.66). For hydrazine **7**: ^1H NMR 1.06 (t, *J* = 7.2 Hz, 6H), 2.81 (q, *J* = 7.2 Hz, 4H), 3.96 (s, 3H), 5.25 (s, 1H); MS *m/z* 360 (M^+, 100), 345 (43), 329 (29), 309 (30), 288 (30); HRMS 357.9809 (357.9809 calcd for $C_{12}H_{14}{}^{35}Cl_4N_2O_2$).

Photolysis of Azide 4 in Diethylamine/Cyclohexane. A solution of 50 mg of **4** in 1 M diethylamine/cyclohexane (50 mL) was photolyzed for 2 h. The crude photolysis mixture after evaporation of the solvent was separated by preparative TLC (1:4 ethyl acetate/hexanes) to give aniline **2** (*23*)as a white powder (45%, R_f = 0.60) and hydrazine **8** as an oily yellow solid (35%, R_f = 0.77). For hydrazine **8**: ^1H NMR 1.06 (t, *J* = 6.9 Hz, 6H), 2.79 (q, *J* = 6.9 Hz, 4H), 3.87 (s, 3H), 5.26 (s, 1H), 7.87 (s, 2H); MS *m/z* 291 (M^+, 100), 275 (45), 261 (23), 239 (60), 218 (95); HRMS 290.0561 (290.0585 calcd for $C_{14}H_{16}{}^{35}Cl_2N_2O_2$).

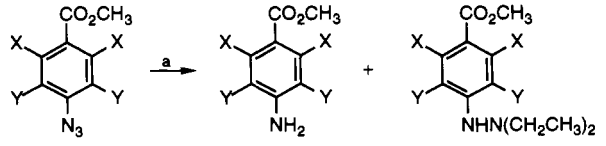
Photolysis of Azide 10 in Diethylamine/Cyclohexane. A solution of 45 mg of **10** in 1 M diethylamine/cyclohexane (45 mL) was photolyzed for 8 h. The crude mixture after evaporation of the solvent was separated by preparative TLC with ethyl acetate/chloroform/hexanes (1:1:1) as the developing solvent to give **11** as a yellow oil (21%, R_f = 0.75) with a NMR spectrum identical to that reported for **11** (*24*), and **12** as a yellow oil (16%, R_f = 0.58). The prep TLC plates were pre-eluted with the developing solvent containing 2% v/v of diisopropylamine followed by the developing solvent. For **12**: ^1H NMR (d_6-acetone) 1.00 (t, *J* = 7.2 Hz, 6H), 3.03 (q, *J* = 7.2 Hz, 4H), 3.70 (s, 3H), 5.72 (d, *J* = 3.6 Hz, 1 H), 7.09 (d, *J* = 3.6 Hz, 1 H), 7.16 (d, *J* = 7.2 Hz, 1 H), 7.21 (d, *J* = 7.2 Hz, 1 H), 7.43 (br, 1H); MS *m/z* 223 (20), 222 (M^+, 100), 207 (17), 193 (28), 161 (61), 105 (24); HRMS 222.1379 (222.1368 calcd for $C_{12}H_{18}N_2O_2$).

12-Acetyl-3-amino-10,5-(iminomethano)-10,11-dihydro-5*H*-dibenzo[*a,d*]cycloheptene (16). The method of Bellamy and Ou (*25*) was adapted. A mixture of **15** (*26*) (150 mg, 0.486 mmol), ethanol (2 mL), ethyl acetate (3 mL), and stannous chloride dihydrate (549 mg, 2.43 mmol) was refluxed for 3 h, and poured into 20 mL of ice water. Saturated $NaHCO_3$ (10 mL) was carefully added, and the resulting mixture was extracted with ethyl acetate (2 × 15 mL). The extract was dried and concentrated. The residue was dissolved in $CHCl_3$ and passed through a short plug of silica gel and the eluant concentrated in vacuo to give 136 mg (100%) of the title compound as a solid pale yellow foam. The NMR spectrum consisted of a 4:1 mixture of rotational isomers about the *N*-Ac group: mp 203–206 °C; ^1H NMR (major isomer) 2.05 (s, 3H), 2.92 (dd, *J* = 17.2, 2.3 Hz, 1H), 3.50 (dd, *J* = 17.2, 4.5 Hz, 1H), 3.58 (br s, 2H), 3.74 (dd, *J* = 10.4, 3.8 Hz, 1H), 3.86 (m, 1H), 4.03 (dd, *J* = 10.3, 1.3 Hz, 1H) 5.86 (dd, *J* = 4.3, 2.6 Hz, 1H), 6.52 (qd, *J* = 8, 2 Hz, 3H), 7.2 (m, 4H); ^1H NMR (minor isomer) 2.29 (s, 3H), 3.06 (dd, *J* = 16.9, 2.3 Hz, 1H), 3.42 (dd, *J* = 16.9, 4.4 Hz, 1H), 3.58 (br s, 2H), 3.61 (dd, *J* = 12.4, 4.1 Hz, 1H), 3.86 (m, 1H), 4.18 (d, *J* = 13.0 Hz, 1H), 6.80 (t, *J* = 7.2 Hz, 3H), 7.2 (m, 4H); ^{13}C NMR (major isomer) 22.4, 38.6, 47.6, 52.6, 52.9, 115.11, 115.17, 124.5, 125.2, 126.1, 127.8, 128.1, 132.8, 137.8, 141.0, 141.4, 145.0, 170.2; ^{13}C NMR (minor isomer) 22.0, 39.9, 46.8, 51.2, 57.5, 114.9, 115.1, 123.1, 125.4, 125.7, 127.5, 128.5, 132.5, 137.1, 141.4, 141.7, 145.3, 169.8; MS *m/z* 278 (M^+, 9), 207 (25), 206 (100), 130 (17); HRMS 278.1407 (278.1419 calcd for $C_{18}H_{18}N_2O$). Anal. Calcd for $C_{18}H_{18}N_2O{\cdot}0.5H_2O$: C, 75.23; H, 6.66; N, 9.75. Found: C, 75.47; H, 6.35; N, 9.90.

12-Acetyl-3-amino-2,4-dichloro-10,5-(iminomethano)-10,11-dihydro-5*H*-dibenzo[*a,d*]cycloheptene (17). To a solution of **16** (64 mg, 0.23 mmol) in DMF (1.0 mL, dried over molecular sieves) at room temperature was added NCS (64 mg, 0.48 mmol) in one portion. The resulting pale brown solution was stirred overnight and diluted with water (5 mL). The resulting mixture was extracted with dichloromethane (3 × 4 mL). The extract was washed with water (3 × 5 mL) and brine (1 × 7 mL) and dried (K_2CO_3). Evaporation of the solvent left 76 mg of a brown syrup, which was purified by preparative TLC (silica gel, 1000 μm, $CHCl_3$/MeOH/NH_4OH 50:1:0.01) to give the title compound as a colorless oil as a 4:1 mixture of *N*-Ac rotational isomers (44 mg, 55% yield): IR ($CDCl_3$) 1635, 1618, 1412 cm^{-1}; ^1H NMR (major isomer) 2.06 (s, 3H), 2.94 (dd, *J* = 17.3, 2.3 Hz, 1H), 3.50 (dd, *J* = 17.3, 4.3 Hz, 1H), 3.77 (dd, *J* = 10.8, 4.2 Hz, 1H), 3.96 (dd, *J* = 10.9, 1.2 Hz, 1H), 4.42 (br s, 2H), 4.99 (m, 1H), 5.84 (dd, *J* = 4.1, 2.8 Hz, 1H), 6.87 (s, 1H), 7.25 (m, 4H); ^1H NMR (minor isomer) 2.28 (s, 3H), 3.08 (dd, *J* = 17.1, 2.5 Hz, 1H), 3.42 (dd, *J* = 17.5, 4.2 Hz, 1H), 3.66 (dd, *J* = 13.1, 4.7 Hz, 1H), 4.10 (d, *J* = 10.2 Hz, 1H), 4.38 (br s, 2H), 5.07 (t, *J* = 3.4 Hz, 1H), 5.95 (t, *J* = 3.6 Hz, 1H), 6.85 (s, 1H), 7.25 (m, 4H); ^{13}C NMR (major isomer) 22.2, 39.3, 40.8, 50.0, 51.8, 118.2, 119.0, 125.3, 125.6, 126.1, 128.2, 128.3, 130.4, 136.6, 137.9, 138.7, 139.8, 170.1; ^{13}C NMR (minor isomer) 21.9, 30.0, 40.0, 40.5, 56.9, 118.3, 118.6, 124.4, 125.9, 126.2, 128.0, 128.7, 130.0, 137.3, 137.5, 138.9, 140.2, 169.4; *m/z* 346 (M^+, 7), 311 (9), 303 (11), 282 (11), 274 (68), 130 (57), 43 (100); HRMS 346.0647 (346.0640 calcd for $C_{18}H_{16}N_2O^{35}Cl_2$).

3-Amino-2,4-dichloro-10,5-(iminomethano)-10,11-dihydro-5*H*-dibenzo[*a,d*]cycloheptene (18). A mixture of **17** (34.5 mg, 0.099 mmol), ethylene glycol (1.25 mL, distilled from CaH_2), and hydrazine hydrate (1.25 mL, 85% solution) was heated at reflux with stirring for 1.5 h. The resulting pale yellow solution was cooled, and KOH (150 mg, 2.3 mmol) was added. Reflux was resumed for 18 h. After cooling, the reaction mixture was treated with 5% NaOH (5 mL), and the resulting mixture was extracted with dichloromethane (3 × 8 mL). The extract was washed with water (2 × 10 mL) and brine and dried (K_2CO_3). Filtration and concentration afforded the title compound as a pale yellow-brown oil (21.7 mg, 72%). An analytical sample was obtained by flash chromatography over silica gel using $CHCl_3$/MeOH (15:1) to give a colorless oil: ^1H NMR δ 1.90 (br s, 1H), 3.10 (dd, *J* = 17.3, 4.1 Hz, 1H), 3.34 (dd, *J* = 21.1, 5.8 Hz, 1H), 3.41 (dd, *J* = 17.4, 3.3 Hz, 1H), 3.55 (d, *J* = 12.2 Hz, 1H), 4.24 (t, *J* = 3.7 Hz, 1H), 4.36 (br s, 2H), 4.82 (d, *J* = 5.5 Hz, 1H), 6.87 (s, 1H), 7.15–7.29 (m, 4H); ^{13}C NMR 40.0, 41.2, 49.7, 54.9, 125.0, 126.4, 127.5, 127.7, 127.9, 128.1, 131.3, 132.2, 136.1, 139.8, 141.0, 141.7;

Table I.[a] Photolysis of Chloro- and Fluoro-Substituted Phenyl Azides



3,4,5 1,2,6 7,8,9

model	X	Y	isolated product (%) aniline	NH insertion
3	Cl	Cl	1 (35)	7 (34)
4	H	Cl	2 (45)	8 (35)
5[b]	F	F	6 (24)[b]	9 (65)[b]

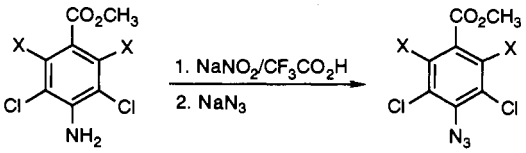
[a] Photolysis was carried out in 1 M diethylamine/cyclohexane for 2 h at 350 nm for azides 3 and 4. [b] Photolysis results with 5 are taken from Keana and Cai (8).

MS *m/z* 304 (M^+, 65), 275 (100), 240 (30), 204 (17), 130 (55); HRMS 304.0519 (304.0534 calcd for $C_{16}H_{14}N_2{}^{35}Cl_2$).

3-Azido-2,4-dichloro-10,5-(iminomethano)-10,11-dihydro-5*H*-dibenzo[*a*,*d*]cycloheptene (19). To a stirred mixture of 18 (25.3 mg, 0.0829 mmol) in 3 N HCl (4 mL) that was being cooled in a brine/ice bath was added sodium nitrite (28 mg, 0.41 mmol). The resulting yellow solution was stirred with cooling for 75 min, and sodium azide (40 mg, 0.62 mmol) was carefully added. The resulting mixture was allowed to warm to room temperature with the cooling bath, and then it was stirred for 16 h. The colorless mixture was cooled in an ice bath and basified to pH > 10 by addition of Na_2CO_3 (6 mL), and the resulting mixture was extracted with dichloromethane (3 × 5 mL). The extract was washed with brine, dried (Na_2SO_4), and concentrated to a pale yellow oil, which was purified by flash chromatography ($CHCl_3$/benzene 1:1 to 1:0) to give the title compound as a colorless oil (20.7 mg, 75%): IR ($CDCl_3$) 2127 (N_3) cm^{-1}; ^1H NMR δ 1.87 (br s, 1H), 3.16 (dd, J = 17.9, 4.1 Hz, 1H), 3.36 (dd, J = 12.2, 5.8 Hz, 1H), 3.48 (dd, J = 18.0, 3.0 Hz, 1H), 3.54 (d, J = 12.4 Hz, 1H), 4.26 (t, J = 3.7 Hz, 1H), 4.89 (d, J = 5.6 Hz, 1H), 6.99 (s, 1H), 7.16–7.30 (m, 4H); ^{13}C NMR δ 40.0, 41.2, 49.7, 54.9, 125.0, 126.4, 127.5, 127.7, 127.9, 128.1, 131.3, 132.2, 136.1, 139.8, 141.0, 141.7; MS *m/z* 330 (M^+,15), 302 ($M^+ - N_2$, 61), 273 (47), 267 (43), 238 (33), 130 (100); HRMS 330.0443 (330.0439 calcd for $C_{16}H_{12}N_4{}^{35}Cl_2$).

RESULTS AND DISCUSSION

Synthesis. Azide 3 was prepared by diazotization of amino ester 1 (22) followed by treatment with sodium azide (eq 1). Attempts to prepare 3 by reaction of sodium azide



(1)

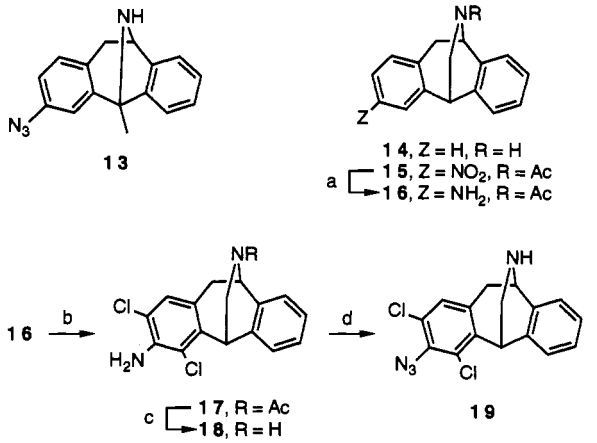
1, X = Cl
2, X = H

3, X = Cl
4, X = H

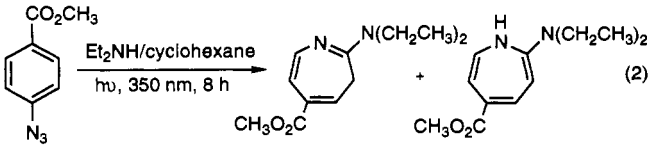
with methyl 2,3,4,5,6-pentachlorobenzoate were not successful. This latter reaction was patterned after that used for the preparation of 5 from methyl 2,3,4,5,6-pentafluorobenzoate. Methyl 4-azido-3,5-dichlorobenzoate (4) was prepared by diazotization of amino ester 2 (23) followed by treatment with sodium azide.

Photolysis. A solution of tetrachlorophenyl azide 3 in 1 M diethylamine/cyclohexane was photolyzed at 350 nm to give the NH insertion product hydrazine 7 (34%) and aniline 1 (35%) (Table I). Similar results were obtained for dichlorophenyl azide 4. In contrast, photolysis of the nonhalogenated analog methyl 4-azidobenzoate (10) in cyclohexane with diethylamine as the trapping agent gave 5-carbomethoxy-2-(diethylamino)-3*H*-azepine (11) (21%) (24) and 5-carbomethoxy-2-(diethylamino)-1*H*-azepine (12) (16%) as the major products (eq 2). Both 11 and 12

Scheme I[a]



[a] Key: (a)$SnCl_2{\cdot}2H_2O$, EtOAc, EtOH; (b) NCS, DMF; (c) KOH, $NH_2NH_2{\cdot}H_2O$, $(CH_2OH)_2$; (d) (i) HCl, $NaNO_2$, (ii) NaN_3.



10 11 12

21% 16%

resulted from ring expansion of the nitrene intermediate derived from 10 upon photolysis. Li *et al.* (5) reported that photolysis of 4-azidobenzoic acid and 4-azidoacetophenone in diethylamine/cyclohexane gave the corresponding anilines and 3*H*-azepines as the only isolated products. Thus, our results show that although CPAs are not as efficient at undergoing NH insertion as are the FPAs (Table I), the NH insertion yields derived from the CPAs are nevertheless significantly better relative to those seen for nonhalogenated phenyl azide analogs.

Synthesis of 3-Azido-2,4-dichloro-IDDC (19). The photoaffinity labeling and characterization of the PCP site in mammalian brain has been an ongoing project in our laboratory (26–29). A problem encountered which is common to receptor photoaffinity labeling approaches has been a low efficiency of nitrene insertion of the activated photoaffinity label into the receptor protein (27). Thus far photolabeling approaches have utilized aromatic azides such as 3-azido-MK801 (13) (27, 28) that do not have halogen atoms ortho to the azido group. It was therefore of interest to synthesize dichloroazide 19, a derivative of the potent PCP receptor ligand 10,5-(iminomethano)-10,11-dihydro-5*H*-dibenzo[*a*,*d*]cycloheptene (26) (IDDC, 14) (Scheme I) as a potentially efficient photolabel.

The nitro group of 3-nitro-*N*-acetyl-IDDC (15) (26) was reduced quantitatively to amine 16 using the method of Bellamy and Ou (25). Controlled ortho,ortho'-dichlorination to give 17 was achieved by reaction of 16 with 2.1 equiv of *N*-chlorosuccinimide (NCS) in *N*,*N*-dimethylformamide (DMF) at room temperature. Acidic hydrolysis (refluxing HCl or H_2SO_4) of amide 17 failed to provide the diamine 18 in adequate yield. However, under strongly

basic conditions (hydrazine, KOH, ethylene glycol, reflux), **18** was obtained in good yield. Diazotization followed by treatment with sodium azide afforded the azide **19**.

The affinity of **19** for the PCP receptor was assessed in terms of its ability to compete with [^{3}H]MK801, a ligand with high selectivity and affinity for the PCP receptor (*29*). For **19**, the IC_{50} value was determined to be 6.3 ± 0.7 μM (n = 3) whereas that of the corresponding nonchlorinated 3-azido-IDDC was 0.5 μM. Thus we find that in the specific case of **19** the presence of the chlorine atoms decreased the receptor binding affinity. Since in general it is not possible to predict the effect of adding *o*-chlorine atoms to other aryl azide-based receptor ligands, in other instances the chlorinated ligands may well show satisfactory receptor affinity. For example, Hawkinson *et al.* (*17*) report that 1-(4-azido-3,5-dichlorophenyl)-4-*tert*-butyl-2,6,7-trioxabicyclo[2.2.2]octane is a 16-fold more potent inhibitor of [^{3}H]TBOB binding than the corresponding nonhalogenated analog for the [^{3}H]TBOB binding site of the $GABA_A$ receptor complex.

In conclusion, we have developed the chlorinated phenyl azides **3** and **4** as models for a new class of photolabeling reagents. In photolysis experiments these models showed significant improvement in NH insertion in 1 M diethylamine/cyclohexane relative to the nonhalogenated analog **10**. In addition, the relative ease by which amine precursors of existing aryl azide-based photolabels may be chlorinated should make application convenient. By way of illustration, the dichloroazido analog **19** of the PCP receptor ligand IDDC (**14**) was synthesized and its affinity for the PCP receptor was determined.

ACKNOWLEDGMENT

This work was supported by NIH Grant GM-27137, by the National Institute on Drug Abuse (DA 06726), and by Cambridge NeuroScience, Inc.

LITERATURE CITED

(1) Bayley, H. (1983) *Photogenerated Reagents in Biochemistry and Molecular Biology* Elsevier, New York.

(2) Knorre, D. G., and Vlassov, V. V. (1989) *Affinity Modification of Biopolymers* CRC Press, Boca Raton, FL.

(3) Schuster, D. I., Probst, W. C., Ehrlich, G. K, and Singh, G. (1989) Photoaffinity Labeling. *Photochem. Photobiol. 49*, 785,

(4) Bayley, H., and Staros, J. (1984) *Azides and Nitrenes* (E. F. V. Scriven, Ed.) Chapter 9, Academic Press, San Diego, CA.

(5) Li, Y.-Z., Kirby, J. P., George, M. W., Poliakoff, M., and Schuster, G. B. (1988) 1,2-Didehydroazepines from the Photolysis of Substituted Aryl Azides: Analysis of Their Chemical and Physical Properties by Time-Resolved Spectroscopic Methods. *J. Am. Chem. Soc. 110*, 8092.

(6) Schuster, G. B., and Platz, M. S. (1992) Photochemistry of Phenyl Azide. *Adv. Photochem. 17*, 69.

(7) Keana, J. F. W., and Cai, S. X. (1989) Functionalized Perfluorophenyl Azides: New Reagents for Photoaffinity Labeling. *J. Fluorine Chem. 43*, 151.

(8) Keana, J. F. W., and Cai, S. X. (1990) New Reagents for Photoaffinity Labeling: Synthesis and Photolysis of Functionalized Perfluorophenyl Azides. *J. Org. Chem. 55*, 3640.

(9) Cai, S. X., Glenn, D. J., and Keana, J. F. W. (1992) Toward the Development of Radiolabeled Fluorophenyl Azide-Based Photolabeling Reagents: Synthesis and Photolysis of Iodinated 4-Azidoperfluorobenzoates and 4-Azido-3,5,6-trifluorobenzoates. *J. Org. Chem. 57*, 1299.

(10) Aggelar, R., Chicas-Cruz, K., Cai, S. X., Keana, J. F. W., and Capaldi, R. A. (1992) Introduction of Reactive Cysteine Residues in the ϵ Subunit of *Escherichia coli* F_1 ATPase, Modification of These Sites with Tetrafluorophenyl Azide-Maleimides, and Examination of Changes in the Binding of the ϵ Subunit When Different Nucleotides Are in Catalytic Sites. *Biochemistry. 31*, 2956.

(11) Leyva, E., Munoz, D., and Platz, M. S. (1989) Photochemistry of Fluorinated Aryl Azides in Toluene Solution and in Frozen Polycrystals. *J. Org. Chem. 54*, 5938.

(12) Soundararajan, N., and Platz, M. S. (1990) Descriptive Photochemistry of Polyfluorinated Azide Derivatives of Methyl Benzoate. *J. Org. Chem. 55*, 2034.

(13) Poe, R., Schnapp, K., Young, M. J. T., Grayzar, J., and Platz, M. S. (1992) Chemistry and Kinetics of Singlet (Pentafluorophenyl)nitrene. *J. Am Chem. Soc. 114*, 5054.

(14) Pinney, K. G., and Katzenellenbogen, J. R. (1991) Synthesis of a Tetrafluoro-Substituted Aryl Azide and Its Protio Analogue as Photoaffinity Labeling Reagents for the Estrogen Receptor. *J. Org. Chem. 56*, 3125.

(15) Crocker, P. J., Imai, N., Rajagopalan, K., Boggess, M. A., Kwiatkowski, S., Dwyer, L. D., Vanaman, T. C., and Watt, D. S. (1990) Heterobifunctional Cross-Linking Agents Incorporating Perfluorinated Aryl Azides. *Bioconjugate Chem. 1*, 419.

(16) Wilkinson, J. A. (1992) Recent Advances in the Selective Formation of the C-F Bond. *Chem. Rev. 92*, 505.

(17) Hawkinson, J. E., Goeldner, M. P., Palmer, C. J., and Casida, J. E. (1991) Photoaffinity Ligands for the [^{3}H]TBOB Binding Site of the $GABA_A$ Receptor. *J. Recept. Res. 11*, 391.

(18) Smith, J. R. L., McKeer, L. C., and Taylor, J. M. (1988) Highly Selective Aromatic Chlorinations. Part 2. The Chlorination of Substituted Phenols, Anisoles, Anilines, and Related Compounds with *N*-Chloroamines in Acidic Solution. *J. Chem Soc., Perkin Trans. 2* 385.

(19) Boer, T. de, Cadogan, J. I. G., McWilliam, H. M., and Rowley, A. G. (1975) Reduction of Nitro- and Nitroso-compounds by Tervalent Phosphorus Reagents. Part X. Ring Expansion to give 2-Diethylamino-3*H*-azepines. *J. Chem. Soc. Perkin Trans. 2* 554.

(20) Odum, R. A., and Aaronson, A. M. (1969) An Intramolecular Reaction of an Aryl Nitrene. *J. Am. Chem. Soc. 91*, 5680.

(21) Sonders, M. S., Keana, J. F. W., and Weber, E. (1988) Phencyclidine and psychotomimetic sigma opiates: recent insights into their biochemical and physiological sites of action. *Trends NeuroSci. 11*, 37.

(22) Weil, E. D., and Dorfman, E. (1970) 4-Amino-2,3,5,6-tetrachlorobenzoic Acid and Derivatives Thereof. United States Patent 3,505,389.

(23) van der Stelt, C., and Nauta, W. Th. (1959) The Chlorination of 4-Aminobenzoic Acid and its Methyl Ester. *Rec. Trav. Chim. 78*, 534.

(24) Nielsen, P. E., and Buchardt, O. (1982) Aryl Azides as Photoaffinity Labels. A Photochemical Study of Some 4-Substituted Aryl Azides. *Photochem. Photobiol. 35*, 317.

(25) Bellamy, F. D., and Ou, K. (1984) Selective Reduction of Aromatic Nitro Compounds with Stannous Chloride in Non Acidic and Non Aqueous Medium. *Tetrahedron Lett. 25*, 839.

(26) Gee, K. R., Barmettler, P., Rhodes, M. R., McBurney, R. N., Reddy, N. L., Hu, L.-Y., Cotter, R. E., Hamilton, P. N., Smith, S. M., Weber, E., and Keana, J. F. W. (1993) 10,5-(Iminomethano)-10,11-dihydro-5*H*-dibenzo[*a*,*d*]cycloheptene and Derivatives. Potent PCP Receptor Ligands. *J. Med. Chem.* **1993**, *36*, 1938-1946.

(27) Sonders, M. S., Barmettler, P., Lee, J. A., Kitahara, Y., Keana, J. F. W., and Weber, E. (1990) A Novel Photoaffinity Ligand for the Phencyclidine Site of the *N*-Methyl-D-aspartate Receptor Labels a M_r 120,000 Polypeptide. *J. Biol. Chem. 265*, 6776.

(28) Gee, K., Durant, G. J., Holmes, D. L., Magar, S. S., Weber, E., Wong, S. T., and Keana, J. F. W. (1993) *N*-(3-Azidophenyl)-*N*-methyl-*N'*-([4-^{1}H]- and [4-^{3}H]-1-naphthyl)guanidine. A Potent and Selective Ligand Designed as a Photoaffinity Label for the Phencyclidine Site of the *N*-Methyl-D-aspartate Receptor. *Bioconjugate Chem. 4*, 226.

(29) Keana, J. F. W., Scherz, M. W., Quarum, M., Sonders, M. S., and Weber, E. (1988) Synthesis and Characterization of a Radiolabelled Derivative of the Phencyclidine/N-Methyl-D-aspartate Receptor Ligand (+)MK-801 with High Specific Radioactivity. *Life Sci. 43*, 965.

Synthesis and Ribosome Binding Properties of Model mRNAs Modified with Undecagold Cluster

Eugene Skripkin,*,† Gulnara Yusupova,‡ Marat Yusupov,‡ Pascal Kessler,§ Chantal Ehresmann, and Bernard Ehresmann

UPR 9002 du CNRS, Institut de Biologie Moléculaire et Cellulaire, 15 rue René Descartes, 67084 Strasbourg Cedex, France, Institute of Protein Research, Russian Academy of Science, 142292 Pushino, Moscow Region, Russian Federation, and CEA, Centre d'Etudes de Saclay, DIEP, Batiment 152, 91191 Gif-sur-Yvette Cedex, France. Received July 20, 1993®

The synthesis and purification of short model messenger RNAs modified with undecagold cluster are described. A monoamino undecagold cluster was introduced on the oxidized 3′ *cis*-glycol group of the mRNA followed by reduction of the formed Schiff's base. The stability of the modified mRNA under the conditions used for *in vitro* messenger RNA translation is studied. The possibility of the formation of a specific translational initiation complex with bacterial ribosomes and modified mRNAs is shown. The results of these experiments indicate that the attachment of an undecagold cluster to a mRNA is a useful tool for electron microscopic and crystallographic studies.

INTRODUCTION

Heavy-metal-atom derivatives have successfully been used in protein crystallography and are undoubtedly good tools for structural determination of large particles, like ribosomes. Crystals of ribosome particles have already been obtained from different microorganisms, and X-ray analysis of these crystals are in progress (for reviews see *e.g.* refs 1 and 2). For correct phase determination of such large ribonucleoprotein complexes (molecular weight 2 700 000) it is necessary to place a compact heavy-atom cluster to one site on the ribosomal surface. Undecagold clusters (AuC)[1] containing 11 gold atoms in a central core surrounded by triarylphosphine ligands and coordinating counterions (Figure 1) are a suitable tool for this purpose (*3–6*). The peripheral amide groups provide the water solubility and the amino group raises the possibility to produce labeling reagent with different specificities.

One easy way to obtain heavy-atom derivatives of ribosomes is to soak them in a gold cluster solution, leading to their equilibrium binding to the crystalline molecule. However, such big particles have a large surface area, leading to the potential binding of a variable number of clusters to a single ribosome. A way to overcome this problem is to use heavy-atom derivatives of nonribosomal components such as tRNA or messenger RNA, which are able to form stable functional complexes with the ribosome. Such RNAs have the advantage that the aldehyde generated by oxidation from the free *cis*-glycol group of the 3′-terminal ribose can be readily coupled to the amino group of the gold cluster (*4*). Recently, two different functional ribosome/mRNA/tRNA complexes have been obtained in similar crystal forms (*7, 8*). It was also demonstrated that it is possible to selectively label a tRNA (yeast $tRNA^{Phe}$) by a gold cluster, although in this case by a different chemistry (*9*).

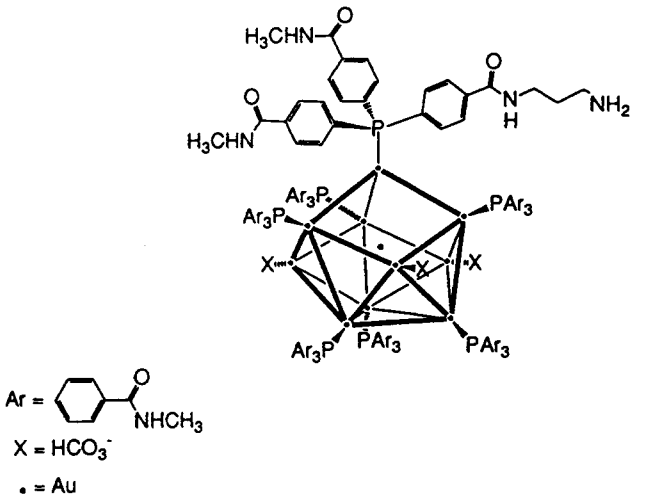


Figure 1. Monofunctional undecagold cluster with a dense core (0.8 nm in diameter) of 11 gold atoms surrounded by an organic shell.

In the present work, we describe the labeling procedure of a short mRNA by the undecagold cluster. The ability of AuC-modified mRNAs to form a translational initiation complex between the small ribosomal subunit from *Escherichia coli* and initiator $tRNA^{Met}f$ was tested and compared with that of natural mRNAs.

EXPERIMENTAL PROCEDURES

Materials. Restriction endonuclease *Bam*HI was from New England Biolabs. Taq DNA polymerase was from GIBCO BRL. Placental RNase inhibitor (RNasin) was from Promega Biotec. Phage T7 RNA polymerase was purified from the overproducing strain BL21/pAR1219, kindly supplied to us by F. W. Studier (Upton, NY). $tRNA^{Met}f$ was purchased from Boehringer Manheim. M13

* Author to whom correspondence should be sent. Present address: Institut de Biologie Moléculaire et Cellulaire, 15 rue René Descartes, 67084 Strasbourg Cedex, France. Tel.: 33.88.41.70.53. FAX: 33.88.61.06.80. E-mail: skripkin@IBMC.U-Strasbg.FR

† On leave from Moscow State University, Moscow, W-234, Russian Federation.

‡ Russian Academy of Science.

§ CEA.

® Abstract published in *Advance ACS Abstracts,* October 15, 1993.

[1] Abbreviations used (in order of appearence in the text): AuC, undecagold cluster; PCR, polymerase chain reaction; DTE, dithioerythritol, Cleland's other reagent; BSA, bovine serum albumin; SDS, sodium dodecyl sulfate; SD sequence, Shine–Dalgarno sequence; RBS, ribosome binding site.

1043-1802/93/2904-0549$04.00/0 © 1993 American Chemical Society

reverse-sequence primer dCAGGAAACAGCTATGAC and primer complementary to λ cro-mRNA dTGCGTTGTTCCATAC were synthesized on Applied Biosystems 392 DNA/RNA Synthesizer by A. Hoeft (Strasbourg, France). [α-^{32}P]ATP was from Amersham. 2-Mercaptoethanol, acrylamide, and *N,N'*-methylenebisacrylamide were from ROTH.

Plasmid Isolation and Purification. Construction of the plasmid pMZ31, containing the fragment of the coding part of the cro-mRNA of the bacteriophage λ under control of the T7 promoter, has been described previously in (*10*). *E. coli* strain XL1-Blue (Stratagene) was used for plasmid manipulation and preparation. Standard procedures were used for isolation and purification of the plasmid (*11*).

Amplification of DNA. A double-stranded DNA fragment was prepared by the polymerase chain reaction (PCR) technique from plasmid pMZ31 (*10*), using the M13 reverse-sequencing primer for coping the sense chain and the primer complementary to the coding region of cro-mRNA to position +13 (the A residue of the AUG codon being +1) for amplification of the antisense chain of the minigene. Fifty picomoles of the reverse M13 and mRNA-(+13) primers and 0.05 pmol of pMZ31 DNA were amplified up to 25 cycles in 70 μL of PCR buffer containing 10 mM Tris-HCl (pH 8.8), 2 mM $MgCl_2$, 50 mM NaCl, 0.05 mM of each dNTP, and 2.5 units Taq DNA polymerase, at 95 °C for 1.5 min, 48 °C for 1.5 min, 72 °C for 1 min and then extented at 70 °C for 5 min. Amplified DNA was purified by phenol–chloroform extraction and ethanol precipitation.

Preparation of Model mRNA. Two synthetic RNAs were used for modification by the amino undecagold cluster: mRNA (+26), pppGGCAAGGAGGUUGUAUGGAACAACGCAUAACCUUGGGAUC; mRNA (+13), pppGGCAAGGAGGUUGUAUGGAACAACGCA. mRNA-(+26) was obtained by T7 RNA polymerase directed transcription of plasmid pMZ31 DNA linearized by restriction endonuclease *Bam*HI. The only site of recognition of this endonuclease is located at position +26 of the coding part of the minigene (*10*). mRNA(+13) is a 27mer corresponding to a 13-nucleotide-shorter derivative of the same coding region of the above mRNA, obtained by T7 RNA polymerase directed transcription of the DNA fragment described in the previous section.

DNA (20 pmol) was incubated in 0.1 mL of T7 transcription buffer containing 40 mM Tris-HCl (pH 8.1 at 37 °C), 2.5 mM spermidine, 12.5 mM DTE, 0.03 mg/mL BSA, 5 mM UTP, CTP, and GTP, 50 μM ATP supplemented with 30 μCi of [α-^{32}P]ATP, 270 units of T7 RNA polymerase, and 200 units of RNasin, at 37 °C for 1 h. The concentration of ATP was then increased to 5 mM, 270 units of T7 RNA polymerase was added, and the mixture was incubated for 50 min at 37 °C. The solution was extracted with phenol, and the mRNA was precipitated with ethanol, dissolved in water, and purified by electrophoresis in a 12% polyacrylamide (19/1 bis)–7 M urea gel. After elution with 0.3 M sodium acetate, pH 7.0, 0.1% SDS and 1/4 v/v buffer-saturated phenol, the mRNA was precipitated with ethanol and the pellet was suspended in the water.

Synthesis of Monoamino Undecagold Cluster. The monoamino undecagold cluster was prepared as described (*5*) and stored as a 21 mM solution in ethanol at −20 °C.

Modification of the 3′ End of the mRNA or DNA by Monoamino Undecagold Cluster. The mRNA (5 μM) in 10 mM sodium acetate buffer (pH 4.5) containing 10 mM $NaIO_4$ was incubated for 1 h at 20 °C in the dark. The oxidized mRNA was precipitated by ethanol, dissolved in the same volume of 0.1% ethylene glycol and incubated for 30 min at 0 °C to remove the excess of $NaIO_4$. The mRNA was purified by reprecipitation with ethanol and dissolved in 50 mM sodium borate buffer (pH 9.0) to a final concentration of 25 μM. Monoamino undecagold cluster was added to a concentration of 1 mM. The reaction mixture was allowed to stand in the dark for 12–14 h at 4 °C. Then 1/20 (v/v) $NaBH_4$ (100 mg/mL) in 50 mM sodium borate buffer (pH 9.0) was added twice each time followed by 30-min incubation at 4 °C. The mRNA was precipitated with ethanol and purified by electrophoresis in 10% polyacrylamide gel (19/1 bis) 50 mM Tris–borate buffer (pH 8.3) without urea and EDTA. After elution with water at 4 °C, GC-modified mRNA was precipitated with ethanol and dissolved in water. Gold determination in the complex was performed by thermoelectric atomization in a graphite oven (HGA-500).

Formation and Analysis of 30S/mRNA/tRNA Complex. *E. coli* ribosomal 30S subunits were prepared from 70S ribosomes as described in ref 12 and generously provided for this work by Dr. C. Philippe (Strasbourg, France). Ribosomal 30S subunits were previously activated at a concentration of 4 mM by heating for 15 min at 37 °C. Then, 8 pmol of 30S subunits and a corresponding amount of mRNA were incubated for 5 min at 37 °C in 0.05 mL of 20 mM Tris acetate buffer (pH 7.5) containing 10 mM magnesium acetate, 60 mM ammonium acetate, 2 mM 2-mercaptoethanol (binding buffer). Four micrograms (160 pmol) of *E. coli* initiator $tRNA^{Met}f$ was added and incubated for 5 min at 37 °C. The incubation mixture was loaded on an FPLC TSK 400 gel-filtration column (Bio-Rad) equilibrated with the binding buffer. Elution was with the binding buffer. Fractions (300-μL) were collected and counted.

RESULTS AND DISCUSSION

Choice of the Model mRNA. To obtain a translational initiation complex very similar to the natural one, we synthesized a short-model mRNA containing the determinants crucial for the formation of a stable initiation complex between the mRNA and the ribosome (see for review ref 13): the translational initiation codon (usually AUG), the polypurine-rich Shine–Dalgarno (SD) sequence located upstream from the initiator codon, and the absence of strong secondary interactions between these two determinants and the rest of the polynucleotide chain. We decided to use the mini-cro-mRNA, a short message containing the intact ribosome binding site (RBS) of the bacteriophage λ *cro* gene (*14*). This RBS includes an extended (nine-nucleotides-long) SD sequence located only three nucleotides upstream from the initiator AUG codon. Also, this message becomes single-stranded after formation of the ternary complex with the initiator tRNA and the small ribosomal subunit (*14*). The natural cro-mRNA contains, besides the initiator AUG codon in the RBS, an additional AUG codon on the 5′ end. Balakin et al. (*15*) showed that at least *in vitro* this particular initiator codon can participate in the formation of aberrant initiation complexes. To avoid this, mRNAs were constructed in which this codon was eliminated. This could easily be done during replacing the original λ P_R promotor by the T7 promotor (*10*). Also, the size of the sequence downstream from the initiaton codon of mRNAs is essential. Indeed it has been shown that the region covering the first five codons is in tight contact with the ribosomal 30S subunit and is sufficient to allow stable ternary 30S/mRNA/initiator tRNA complex formation as shown by

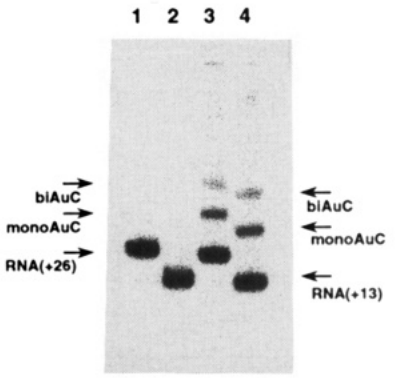


Figure 2. Nondenaturing gel electrophoresis of unmodified and undecagold cluster modified mini-cro-mRNAs: lane 1, unmodified mRNA(+26); lane 2, unmodified mRNA(+13); lane 3, AuC-modified mRNA(+26); lane 4, AuC-modified mRNA(+13). Position of unmodified mRNA(+13), mRNA(+26), the mono gold cluster adduct (monoAuC), and postulated dimeric gold cluster adduct (biAuC) are marked by arrows.

toeprinting experiments (*13*). As shown by cross-linking experiments, even region +18 to +22 of the mRNA was able to interact with such region of the ribosome as the 5′ end of 16S rRNA or ribosomal proteins S2/S3 (*10*; Bakin, A., Skripkin, E., and Shatsky, I., unpublished results). The first model mRNA contains 13 nucleotides downstream from the initiator AUG. It means that in this case we can expect the bulky AuC-constituent on the 3′ end of the model mRNA to be situated at the edge of the ribosomal subunit. To exclude any interference during complex formation between the modified polynucleotide chain and the mRNA binding site of the ribosome, the size of the second mRNA region downstream AUG was increased to 26 nucleotides.

Synthesis of mRNA Derivatives. The monoamino undecagold cluster (Figure 1), synthesized as described earlier (*5*), was linked to the 3′ end of the mini-cro-mRNAs by Schiff's base formation, which was then stabilized by reduction with sodium borohydride. To monitor all steps of the synthesis and next binding experiments, the mRNA was labeled during T7 transcription with radioactive [α-^{32}P]ATP. The oxidation–reduction conditions were used according to ref 17 with some modification. The yield of the reaction was estimated by counting radioactive bands after electrophoretic separation in 10% nondenaturing polyacrylamide gel (Figure 2) or by HPLC reverse-phase separation on a C18 column (data not shown). The degree of modification was 25–35% as calculated from the distribution of radioactivity either by direct counting of the radioactivity or by scanning of the gels with an image scanner (Fuji, Model BAS 2000). The bands marked as monoAuC on Figure 2 contain a near equimolar amount of the gold cluster per mRNA molecules, as was shown by atomic absorption analysis (Table III). Some amount of product with higher molecular weight was found (see bands marked as biAuC in lanes 3 and 4, Figure 2). The yield of these dimeric side products was not higher than 10%. Their appearance could be due to the interaction of monoamino undecagold cluster with the second aldehyde group derived from ribose *cis*-glycol. In all binding experiments only monoadducts of mRNAs were used.

Interaction of Undecagold Cluster Modified mRNA with the Ribosome. The binding of the mRNAs to the *E. coli* ribosomal 30S subunits was performed with unmodified mRNAs, mRNAs after oxidation and following reduction of the 3′ end *cis*-glycol, and mono undecagold cluster derivatives of the mRNA(+13) and mRNA(+26). To study initiation complex formation, binary mRNA-30S ribosomal subunit complex formation as the first step with subsequent initiator tRNA^{Met}f addition was used (*14*). After incubation with tRNA, the mixture was loaded on an FPLC TSK-400 gel-filtration column. Typical distributions of radioactivity for ribosomal complexes are shown in Figure 3. The major peak of radioactivity comigrates with the UV-detected peak of ribosomal subunits. Figure 4 expresses ternary 30S subunit/mRNA/tRNA^{Metf} complex formation as a function of the 30S:mRNA ratio. From these results we can conclude that the binding level of the AuC-modified and control mRNAs is very similar. The slightly lower yield reproducibly obtained in the case of AuC-modified mRNA(+13) compared to unmodified mRNA(+13) can easily be interpreted as due to some steric hindrance of the undecagold cluster at the 3′ end due to the shorter length of the AUG downstream region, as was mentioned above. However, the markedly lower yield of complex formation with both control and AuC-modified mRNAs(+26) compared to the mRNA(+13) should be noted. This mRNA contains in comparison with mRNA(+13) an additional nucleotide sequence. Part of this sequence (CCUUG) is able to interact with 5′ half of the SD sequence (CAAGG) and to compete with the anti-SD sequence of the ribosomal subunit.

The specificity of binding of the AuC-modified mRNA was checked in competition experiments with unmodified mRNA. In a control experiment, an 18 times dilution of ^{32}P-labeled mRNA(+13) with unlabeled mRNA(+13) increased the mRNA binding from 5% to 60% per ribosomal subunit. For gold cluster modified mRNA(+13), 14 times dilution with unmodified and nonradioactive sample also increased the binding from 7.5% (for 11 molar excess of ribosomal subunits) to 48% (in the case 1.5 molar excess of mixture of modified, radioactive, and nonlabeled mRNAs) (see Table I); from these data we can conclude that modified mRNA(+13) has very similar specificity and other binding parameters as the control.

Stability of Modified mRNA. To determine the stability of the AuC-modified mRNAs, an unpurified mixture of modified and nonmodified mRNA(+13) was used. RNA samples were incubated in the binding buffer with or without initiator tRNA^{Met}f and ribosomal subunits at 37 °C. Electrophoretic analysis of AuC-modified mRNA after incubation with ribosomes and tRNA shows that at least 76% of mRNA is stable in the binding buffer and the

Table I. Competition for Ribosome Binding between Undecagold Cluster Labeled and Control mRNAs(+13)

	control mRNA		AuC-modified mRNA	
^{32}P-labeled mRNA (cpm)	1402	1174	1143	1020
^{32}P-labeled mRNA (pmol)	0.37	0.31	0.45	0.43
cold mRNA (pmol)		5.4		5.4
mRNA (cpm) in the 30S fraction[a]	939	483	762	335
total mRNA (pmol) in the 30S fraction[a]	0.25	2.35	0.3	1.91

[a] Contains 4 pmol of 30S ribosomal subunits and 20 pmol of tRNA^{Met}f.

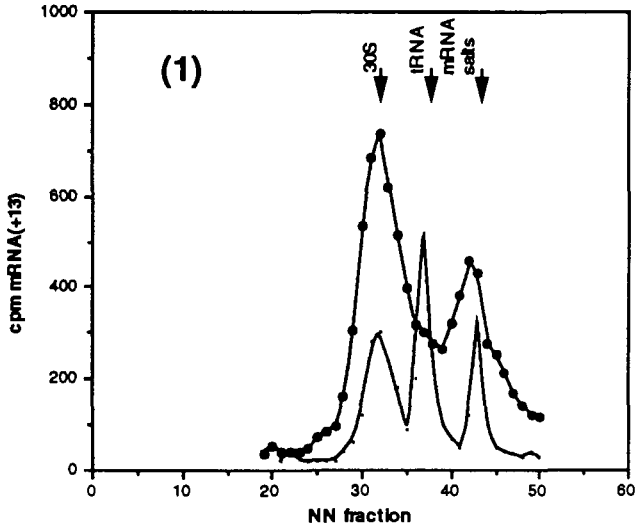
Table II. Stability of Undecagold Cluster Modified mRNA(+13)

	without treatment	incubation in the binding buffer	incubation with ribosomes and tRNA
% AuC-modified RNA in the mixture	23	17.5	18.6

Table III. Determination of Gold Atoms in Au-Modified mRNA(+26)

	concentration of Au (mg/L)	amount of AuC in the sample (pmol)	amount of mRNA (pmol)	% modification of mRNA(+26) by AuC
AuC-mRNA[a] (experiment 1)	37 ± 4	1.80	1.70	106 ± 11
AuC-mRNA (experiment 2)	29 ± 3	0.90	1.11	81 ± 8
30S/AuC-mRNA/tRNA^{Met}f[b] (experiment 1)	9.4 ± 1.5	0.43	0.85	51 ± 8
30S/AuC-mRNA/tRNA^{Met}f (experiment 2)	13.2 ± 1.5	0.60	1.30	46 ± 5

[a] mRNA(+26), modified by undecagold cluster. [b] Purified initiation complex, isolated by gel filtration.



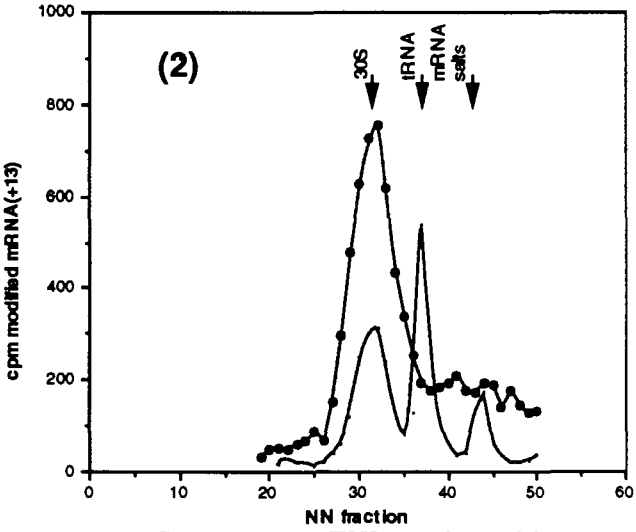


Figure 3. HPLC gel filtration on TSK-400 column of the ternary ribosomal 30S subunit/mRNA/tRNA^{Metf} complexes: panel 1, 30S subunit (4 pmol)/mini-cro-mRNA(+13) (0.6 pmol)/tRNA^{Metf} (20 pmol); panel 2, the similarly composed undecagold cluster modified mini-cro-mRNA(+13) (0.3 pmol). The UV profile is shown below the radioactivity profile; arrows indicate peaks of 30S ribosomes initiation complexes, tRNA^{Metf}, and low molecular weight compounds (mRNA and salts).

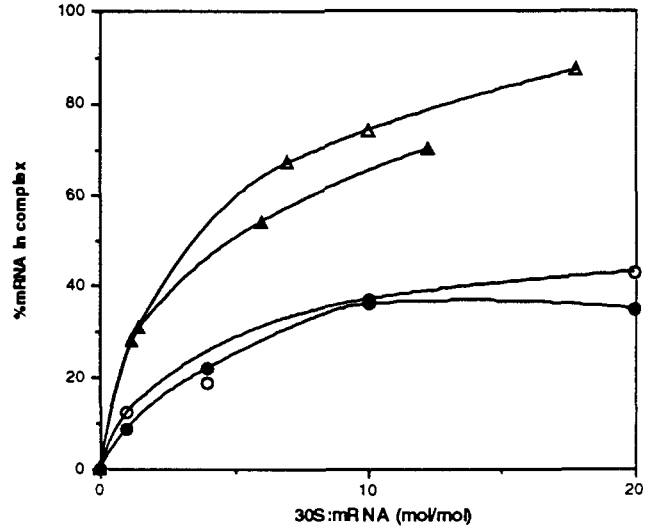


Figure 4. Ternary ribosomal 30S subunit/mRNA/tRNA^{Met}f complex formation as a function of the 30S:mRNA ratio: unmodified mRNA(+26) (○), AuC-modified mRNA(+26) (●), unmodified mRNA(+13) (△), AuC-modified mRNA(+13) (▲).

ternary complex formation does not destroy the modified mRNA (Table II).

The presence of gold atoms in the modified mRNA was verified by using the method of atomic absorption (Table III). These data showed that after modification and purification of the modified mRNA(+26) by gel electrophoresis at least 80% of the mRNA molecules contained the complete gold cluster. However, after formation and isolation of the complex with the 30S ribosomal subunit and tRNA, the AuC-modified mRNA had lost approximately half of its gold atoms.

Conclusion. In this work, we describe the synthesis and purification of a messenger RNA modified with undecagold cluster at its 3′ end. The AuC-modified mRNA is stable and active enough to form a ternary translational initiation complex in the presence of ribosomal 30S subunits and initiator tRNA^{Met}f.

Preliminary crystallographic experiments with ribosomes modified with a gold cluster showed that such undecagold clusters are suitable for the phasing of reflections from ribosomal crystals (*6, 18*). The low-resolution localization of the mRNA region downstream from the AUG codon by immune electron microscopy was already described on the small ribosomal subunit in the cleft region between head and body (*19–21*). This will obviously provide additional information for interpretation of the crystallographic signals.

Although only 30–40% of ribosomal complexes would carry a gold cluster, this yield should be suitable for phase determination, as already shown in the above mentioned crystallographic works (*6, 18*) in which partial decomposition of the AuC-modified ribosomes was also observed.

ACKNOWLEDGMENT

We wish to thank Dr. C. Philippe (Strasbourg, France) and Dr. S. Kirillov (St. Petersburg, Russia) for providing us samples of 30S ribosomal subunits. We are indebted to Dr. A. Bentz, Centre de Rech. Nucl. (Strasbourg, France), for help in the gold determination, Dr. V. Shirokov

(Pushino, Russia), Dr. M. Gottikh, and Dr. A. Yolov (Moscow, Russia) for helpful discussions, and Dr. J. Ofengand (Nutley, NJ) for critical reading of the manuscript. G.Y. and E.S. are working in the frames of a Russian–French scientific cooperation and were supported by grants from CNRS.

LITERATURE CITED

(1) Yonath, A., Bennett, W., Weinstein, S., and Wittmann, H. G. (1990) Crystallography and image reconstruction of ribosomes. In *The Ribosome: Structure, Function and Evolution* (W. E. Hill, A. E. Dalberg, R. A. Garret, O. B. Moore, D. Schlessinger, and J. R. Warner, Eds.) pp 134–147, American Society of Microbiology, Washington, DC.

(2) Yusupov, M. M., Garber, M. B., Vasiliev, V. D., and Spirin, A. S. (1991) *Thermus thermophilus* ribosomes for crystallographic studies. *Biochimie 73*, 887–897.

(3) Bartlett, P. A., and Bauer, S. J. (1978) Synthesis of water-soluble undecagold cluster compounds of potential importance in electron microscopic and other studies of biological systems. *J. Am. Chem. Soc. 100*, 5085–5089.

(4) Lipka, J. J., Hainfeld, J. F., and Wall, J. S. (1983) Undecagold labeling of a glycoprotein: STEM visualization of an undecagoldphosphine cluster labeling the carbohydrate sites of human haptoglobin-hemoglobin complex. *J. Ultrastructure Res. 84*, 120–129.

(5) Safer, D., Bolinger, L., and Leigh, J. S. (1986) Undecagold clusters for site-specific labeling of biological macromolecules: simplified preparation and model applications. *J. Inorg. Biochem. 26*, 77–91.

(6) Weinstein, S., Jahn, W., Hansen, H., Wittmann, H. G., and Yonath, A. (1989) Novel procedures for derivatization of ribosomes for crystallographic studies. *J. Biol. Chem. 264*, 19138–19142.

(7) Hansen, H. A. S., Volkmann, N., Piefke, J., Glotz, C., Weinstein, S., Makovski, I., Meyer, S., Wittmann, H. G., and Yonath, A. (1990) Crystals of complexes mimicking protein biosynthesis are suitable for crystallographic studies. *Biochim. Biophys. Acta 1050*, 1–7.

(8) Yusupova, G., Yusupov, M., Spirin, A., Ebel, J.-P., Moras, D., Ehresmann, C., and Ehresmann, B. (1991) Formation and crystallization of *Thermus thermophilus* 70S ribosome/tRNA complexes. *FEBS Lett. 290*, 69–72.

(9) Hainfeld, J. F., Sprinzl, M., Mandiyan, V., Tumminia, S. J., and Boublik, M. (1991) Localization of a specific nucleotide in yeast tRNA by scanning transmission electron microscopy using an undecagold cluster. *J. Struct. Biol. 107*, 1–5.

(10) Dontsova, O. A., Rosen, K. V., Bogdanova, S. L., Skripkin, E. A., Kopylov, A. M., and Bogdanov, A.A. (1992) Identification of the Escherichia coli 30S ribosomal subunit protein neighbouring mRNA during initiation of translation. *Biochimie 74*, 363–371.

(11) Maniatis, T., Fritsch, E. F., and Sambrook, J. (1983) *Molecular Cloning. A Laboratory Manual*, Cold Spring Harbor Laboratory Press, Cold Spring Harbor, NY.

(12) Makhno, V. I., Pechin, N. N., Semenkov, Y. P., and Kirillov, S. V. (1988) The modified procedure of preparation of "tight" 70S ribosomes highly active in definite stages of elongation of translation. *Mol. Biol. 22*, 670–679 (Russ.).

(13) Gold, L. (1988) Posttranscriptional regulatory mechanisms in *Escherichia coli*. *Annu. Rev. Biochem. 57*, 199–233.

(14) Balakin, A., Skripkin, E., Shatsky, I., and Bogdanov, A. (1990) Transition of the mRNA sequence downstream from the initiation codon into a single-stranded conformation is strongly promoted by binding of the initiator tRNA. *Biochim. Biophys. Acta 1050*, 119–123.

(15) Balakin, A. G., Skripkin, E. A., Shatsky, I. N., and Bogdanov, A. A. (1992) Unusual ribosome binding properties of mRNA encoding bacteriophage λ repressor. *Nucleic Acids Res. 20*, 563–571.

(16) Balakin, A. G., Bogdanova, S. L., and Skripkin, E. A. (1992) mRNA containing an extended Shine-Dalgarno sequence is translated independently of ribosomal protein S1. *Biochem. Int. 27*, 117–129.

(17) Shatsky, I. N., Mochalova, L. V., Kojouharova, M. S., Bogdanov, A. A., and Vasiliev, V. D. (1979) Localization of the 3′ end of *Escherichia coli* 16S RNA by electron microscopy of antibody-labelled subunits. *J. Mol. Biol. 133*, 501–515.

(18) Weinstein, S., Jahn, W., Laschever, M., Arad, T., Tichelaar, W., Haider, M., Glotz, C., Boeckh, T., Berkovitch-Yellin, Z., Franceschi, F., and Yonath, A. (1992) Derivatization of ribosomes and of tRNA with an undecagold cluster: Crystallographic and functional studies. *J. Cryst. Growth 122*, 286–292.

(19) Evstafieva, A. G., Shatsky, I. N., Bogdanov, A. A., Semenkov Y. P., and Vasiliev, V. D. (1983) Localization of 5′- and 3′-ends of the ribosome bound segment of template polynucleotides by immune electron microscopy. *EMBO J. 2*, 799–804.

(20) Stöffler, G., and Stöffler-Meilike, M. (1984) Immuno electron microscopy of ribosomes. *Annu. Rev. Biophys. Bioeng. 13*, 303–330.

(21) Olson, H. M., Lasater, L. S., Cann, P. A., and Glitz, D. G. (1988) Messenger RNA orientation on the ribosome. Placement by electron microscopy of antibody-complementary oligonucleotide complexes. *J. Biol. Chem. 263*, 15196–15204.

Chemical Modification of Silk Fibroin with Cyanuric Chloride-Activated Poly(ethylene glycol): Analyses of Reaction Site by ^{1}H-NMR Spectroscopy and Conformation of the Conjugates

Yohko Gotoh,* Masuhiro Tsukada, and Norihiko Minoura†

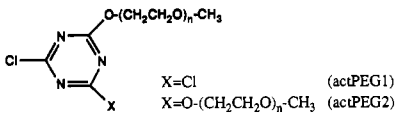
National Institute of Sericultural and Entomological Science, 1-2 Ohwashi, Tsukuba, Ibaraki 305, Japan, and National Institute of Materials and Chemical Research, 1-1 Higashi, Tsukuba, Ibaraki 305, Japan.
Received August 6, 1993®

Solubilized silk fibroin (SF) in 0.1 M borate buffer (pH 9.4) was modified with 2-*O*-[methoxy(polyethylene glycol)]-4,6-dichloro-*s*-triazine (actPEG1) at 4 °C. The weight of the modified SF (PEG1–SF) was at least 3.2 times that of the starting material SF. Amino acid analysis of PEG1–SF suggested that the nucleophilic ϵ-amino group of the lysine residue and the nucleophilic imidazole group of the histidine residue in SF reacted with actPEG1. The ^{1}H-NMR spectrum of PEG1–SF showed a downfield shift of the aromatic protons of the tyrosine residue from the corresponding protons of SF. The ^{1}H-NMR spectrum of the SF reacted with cyanuric fluoride (CyF), whose fluorine atoms are known to react with the phenolic hydroxyl group of the tyrosine residue, also showed the downfield shift. These results suggested that the reaction site of SF with actPEG1 was the phenolic hydroxyl group of the tyrosine residue in addition to the lysine and histidine residues. The conformation of PEG1–SF in a solid state was examined by means of IR and X-ray measurement. The IR spectrum of PEG1–SF revealed a change in secondary structure from random coil to β-sheet due to the coexistence of PEG molecules. The X-ray diffraction pattern of PEG1–SF indicated that the PEG molecules covalently bonding to SF narrowed the spacing of the interchain periodicity and promoted the formation of the interchain β-sheet.

INTRODUCTION

The conjugation of synthetic or natural macromolecules to proteins has been widely developed since the 1970s (*1–10*). The purpose of the conjugation is to stabilize the protein and to add new properties to the protein. Poly(ethylene glycol) (PEG)[1] is a nonimmunogenic and amphipathic polymer. The consequences of protein modification with PEG are the reductions of the immunoreactivity and immunogenicity of the antigenic protein (*3–6*). The protein modification with PEG makes the enzyme soluble and active in organic solvents (*3, 7*). Therefore, many kinds of activated PEG, whose hydroxyl end groups are converted into functional groups to attach covalently to proteins, have been developed as chemical modifiers (*3–9*). Cyanuric chloride is one of the most effective and widely applicable coupling agents to attach synthetic or natural polymers such as polysaccharides to proteins (*10*). Inada et al. developed cyanuric chloride-activated poly(ethylene glycol), for example 2-*O*-[methoxy(polyethylene glycol)]-4,6-dichloro-*s*-triazine (actPEG1) (*3, 4, 8*) and 2,4-bis[*O*-[methoxypoly(ethylene glycol)]]-6-chloro-*s*-triazine (actPEG2) (*3, 7*) (Scheme I). Nevertheless, the toxicity and excessive reactivity of the cyanuric chloride have been pointed out recently (*9*). Although the biochemical properties of the PEG–protein conjugate have been studied extensively, the reaction site and structural analysis of the conjugate with the aid of spectroscopy have not been reported.

Scheme I



In this paper, the PEG–silk fibroin (SF) conjugate (PEG1–SF) was prepared by reacting actPEG1 with the solubilized SF in order to obtain a new functional biopolymer. We chose SF as the protein of the PEG conjugate, because SF has recently been applied to biomaterials such as an enzyme-immobilization material (*11*) and a cell culture substrate (*12*). SF (molecular weight of 370 kDa estimated by Shimura et al. (*13*)) is a fibrous protein consisting mainly of the sequence Gly-Ala-Gly-Ala-Gly-X, where X is an alanine or serine residue (*14*). Its partial primary structure is currently determined by sequencing the cDNA of the *Bombyx mori* silkworm (*15*). Its conformational characteristics have been studied widely (*11, 14, 16*).

The purpose of this paper is to modify SF with cyanuric chloride-activated PEG and to clarify the reaction site and secondary structure of the modified SF. The reaction site of SF with actPEG1 was clarified by ^{1}H-NMR spectroscopy. The secondary structure of the modified SF was revealed by IR measurement and X-ray diffractometric measurement.

EXPERIMENTAL PROCEDURES

Materials. 2-*O*-[Methoxy(polyethylene glycol)]-4,6-dichloro-*s*-triazine (actPEG1, MW 5000) and methoxy-

* To whom correspondence should be addressed.
† National Institute of Materials and Chemical Research.
® Abstract published in *Advance ACS Abstracts,* October 15, 1993.

[1] Abbreviations used: SF, silk fibroin; actPEG1, 2-*O*-[methoxypoly(ethylene glycol)]-4,6-dichloro-*s*-triazine; PEG1–SF, the silk fibroin modified with actPEG1; ^{1}H-NMR, proton nuclear magnetic resonance; CyF, cyanuric fluoride; IR, infrared absorption; PEG, poly(ethylene glycol); actPEG2, 2,4-bis[*O*-[methoxypoly(ethylene glycol)]-6-chloro-*s*-triazine; PEG-OMe, methoxypoly(ethylene glycol); Tris, tris(hydroxymethyl)aminomethane; CyF–SF, the silk fibroin reacted with CyF; DSS, 3-(trimethylsilyl)propanesulfonic acid sodium salt.

1043-1802/93/2904-0554$04.00/0 © 1993 American Chemical Society

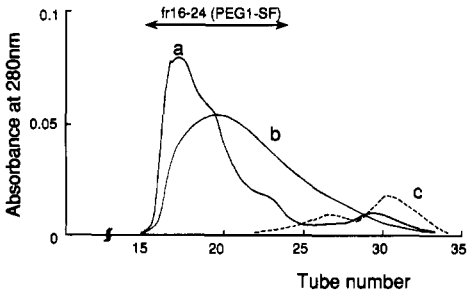


Figure 1. Gel filtration profiles of PEG1–SF (a), SF (b), and actPEG1 (c) using Sephacryl S-300 column (2.6 × 70 cm, each fraction = 6.0 mL). UV absorbance at 280 nm was used for the detection of each sample.

poly(ethylene glycol) (PEG-OMe, MW 5000) were purchased from Sigma Chemical Co. (St. Louis, MO). Sephacryl S-300 was purchased from Pharmacia Fine Chemicals (Sweden). Cyanuric fluoride (CyF) was obtained from Wako Pure Chemicals Industries Co. Ltd. (Osaka, Japan). All other chemicals were reagent-grade products obtained commercially. An ultrafiltration cell with an XM-50 membrane was purchased from the Amicon Division of W. R. Grace Co. (Danvers, MA).

Preparation of the PEG1–SF Conjugate. The shells of cocoons of *Bombyx mori* were cut into pieces, and 15 g of cut cocoons was degummed with aqueous boiling 0.5% (w/v) Na_2CO_3 solution for 30 min and rinsed with hot water. After drying in air, 11 g of degummed SF fiber was obtained. SF solution was prepared by dissolving 1.25 g of the degummed fiber in 25 mL of 9 M LiBr aqueous solution at 60 °C over 30 min (*11, 17, 18*).[2] The dissolved solution was dialyzed against water using a cellulose tube for a few days, and then 61 mL of 1.9% (w/v) silk fibroin solution was obtained.

To ionize the residues of SF under basic conditions and make the residues reactive, a solution of 5 mL of 0.12 M sodium borate buffer (pH 9.4) (*4, 8*) was added to 1 mL of 1.9% (w/v) SF aqueous solution. Then 6 mL of the 0.32% (w/v) SF–0.1 M sodium borate aqueous solution (pH 9.4) containing 19 mg of starting material SF was prepared. To this solution was added 100 mg of actPEG1 at 4 °C over 15 min. After the reaction mixture was kept at 4 °C for 1 h, the solution was dialyzed against cold 0.1 M phosphate buffer (pH 7.0) for several hours and subsequently 5 M urea–0.02 M Tris·HCl buffer (pH 8.0) overnight for gel filtration.

In order to remove the unreacted modifier (actPEG1), the dialyzed solution was applied to a column of Sephacryl S-300 (2.6 × 70 cm) preequilibrated with 5 M urea–0.02 M Tris·HCl (pH 8.0) and eluted with the same buffer (*13*) at a flow rate of 0.3 mL/min. Each fraction of 6.0 mL of the eluate was collected by a fraction collector. Its elution pattern obtained by measuring the absorbance at 280 nm is shown in Figure 1. The PEG1–SF conjugate was eluted first. The eluate (fractions 16–24) was collected and dialyzed against water overnight. Finally, the solution of PEG1–SF was concentrated by ultrafiltration using an XM-50 membrane. After the evaporation of the concentrated solution, 61 mg of PEG1–SF product was obtained.

Reaction of Silk Fibroin with CyF. To 2 mL of 2% (w/v) SF aqueous solution was added 6 mL of 1.0 M $NaHCO_3$ aqueous solution (pH 9.1). A mixture of 0.1 mL of CyF and 1 mL of 1,4-dioxane was added to this 8-mL solution of 0.5% (w/v) SF containing 0.75 M $NaHCO_3$ (pH 9.1) at 4 °C (*19, 20*). The reaction mixture was allowed to stand at 4 °C for 1.5 h. The solution was dialyzed against cold water overnight and concentrated by ultrafiltration. The concentrated solution gave 35 mg of the SF reacted with CyF (CyF–SF).

Amino Acid Analysis. Each sample (12 mg) of control SF, PEG1–SF, and CyF–SF was hydrolyzed under vacuum in 2 mL of 6 N HCl at 110 °C for 20 h. The hydrolyzed samples were dried in a rotary evaporator at 40 °C and dissolved in 10 mL of 0.02 N HCl. These sample solutions were filtered through a membrane filter to remove a small amount of the residues and were applied to an amino acid analyzer. Amino acid analysis was carried out using a Hitachi L-8500 type rapid amino acid analyzer.

^{1}H-NMR Measurement. Proton nuclear magnetic resonance (^{1}H-NMR) spectra were observed at 25 °C using a JEOL EX-90 NMR spectrometer operating at 90 MHz. The WEFT technique utilizing the difference in relaxation times of SF and HDO was applied as follows. The pulse angles used were 90° (23 μs) and 180° (46 μs). The pulse interval between 180° and 90° was set as a variable parameter for auto stacking more than 1 s in order to weaken the peak of HDO. The ^{1}H-NMR chemical shift is represented in parts per million downfield from internal 3-(trimethylsilyl)propanesulfonic acid sodium salt (DSS).

The films of SF and CyF–SF prepared according to the procedure described in the IR measurement section were soluble in water. Thus, NMR samples of CyF–SF and a mixture consisting of 71 wt % SF and 29 wt % PEG-OMe were prepared by dissolving these films in D_2O. Because the PEG1–SF film was insoluble in water, the aqueous solution of PEG1–SF was exchanged with D_2O by ultrafiltration, and the spectrum of PEG1–SF was measured in about 90% D_2O–10% H_2O. The concentrations of these samples were about 2% (w/v).

IR Measurement. The films of PEG1–SF and SF were obtained by casting each solution (0.5–1% (w/v)) onto thin polyethylene films as a casting substrate and drying at room temperature overnight (*11, 17*). The blended film (the weight ratio of actPEG1 to SF was 2.2) was prepared by casting a mixture of aqueous SF solution and aqueous actPEG1 solution. The infrared absorption (IR) spectra of these films were recorded using a Perkin-Elmer 1760X FT-IR spectrometer.

X-Ray Diffractometric Measurement. X-ray diffractometric measurement was performed with a diffractometer (Rigaku Denki Co., Ltd. Ru-200) with a scintillation counter using Cu Kα (λ = 1.54 Å) radiation. The voltage and current of the X-ray source were 25 kV and 10 mA, respectively. The diffraction intensity curves were measured with a scanning rate of 1 deg/min, a time constant of 1 s, and a scanning region of 5–35°. The films of SF and PEG1–SF prepared by the method described above were measured. The control specimen of SF having a β-sheet structure was prepared as follows. SF film was immersed in 50% (v/v) methanol–water mixture for 4 h at room temperature and dried in air overnight (*11, 17*).

RESULTS AND DISCUSSION

Synthesis of PEG1–SF Conjugate. Figure 1 shows that PEG1–SF eluted more rapidly than unmodified SF. This result suggests an increase in the molecular weight of PEG1–SF as a result of the modification. From 19 mg of starting material SF was prepared 61 mg of product PEG1–SF. Assuming that 100% of the starting material SF was recovered, the weight of the product PEG1–SF was 3.2 times that of the starting material SF. This means

[2] The dissolution of SF in a concentrated solution of a neutral salt induced depolymerization of SF and led to the heterogeneous molecular weight of SF from 50 to 200 kDa (*18*).

Table I. Results of Amino Acid Analyses of PEG1–SF, CyF–SF, and SF[a]

amino acid	PEG1–SF (mol %)	CyF–SF (mol %)	SF (mol %)	PEG1–SF/SF	CyF–SF/SF
Asp	1.45	1.51	1.43	1.0	1.1
Thr	0.88	0.89	0.85	1.0	1.0
Ser	11.1	10.9	10.7	1.0	1.0
Glu	0.93	1.18	0.96	0.97	1.2
Gly	45.5	45.6	45.6	1.0	1.0
Ala	29.6	29.3	29.8	0.99	0.98
Val	2.29	2.17	2.37	0.97	0.92
Met	0.13	0.11	0.11	1.2	1.0
Ile	0.63	0.60	0.62	1.1	0.97
Leu	0.46	0.45	0.55	0.84	0.82
Cys					
Tyr	4.99	5.21	5.00	1.0	1.0
Phe	0.72	0.67	0.70	1.0	0.96
Lys	0.22	0.24	0.32	0.69	0.75
His	0.11	0.15	0.18	0.61	0.83
Arg	0.41	0.45	0.44	0.93	1.0
Pro	0.55	0.53	0.48	1.1	1.1

[a] The errors inherent in the amino acid analyses of major components were within 5%, but the errors inherent in the analyses of minor components were about 20% because of their very small contents.

that PEG1–SF is composed of PEG and SF in the weight ratio of 2.2:1 and contains 32% SF. If the average molecular weights of the amino acid unit constituting SF and actPEG1 are supposed to be 75[3] and 5000, respectively, the mole ratio of amino acid residue to PEG is calculated to be 30 (=(1/75)/(2.2/5000)). This result implies that 3.3 mol % of amino acid residues in SF were modified with actPEG1. However, this value is only a minimum estimate based on the assumption of 100% recovery of SF. Thus, more than 3.3 mol % of the residues were modified.

Amino Acid Analysis. The results of the amino acid analyses of the SF before and after the modification are summarized in Table I. On the basis of these results, we noticed that the contents of the lysine and histidine residues in PEG1–SF were considerably decreased by the modification. King et al. reported that the amino acid analysis of the allergen modified with cyanuric chloride-activated PEG also showed a considerable decrease in the lysine residue, and the bond joining the ϵ-amino group of the lysine residue with the triazine nucleus was only partially stable under hydrolysis conditions (*6*). Thus, our result means that nucleophilic groups such as the ϵ-amino group of the lysine residue and the imidazole group of the histidine residue in SF reacted with actPEG1 but that some linkages between these groups and actPEG1 had a possibility of being broken in the hydrolysis step.

A slight decrease in the content of the arginine residue in PEG1–SF is considered to be due to some errors in the analysis. The methionine and leucine residues are considered not to react with actPEG1, because these residues have no reactive groups. Since more than 3.3 mol % of the residues in SF were modified, it is estimated that not only the lysine (0.32 mol %) and histidine (0.18 mol %) residues but also other residues reacted with actPEG1.

^{1}H-NMR Spectrum of PEG1–SF. In order to analyze the reaction sites, the ^{1}H-NMR spectrum of PEG1–SF

[3] The average molecular weight (W) of the amino acid unit constituting SF was calculated to be 75 by considering the amino acid composition of SF (Table I) (*17*, *18*). Namely, the average molecular weight was calculated using the following equation:

$$W = \Sigma w_i c_i$$

where w_i = molecular weight of each amino acid residue and c_i = mole content of each amino acid residue (Table I, column 3).

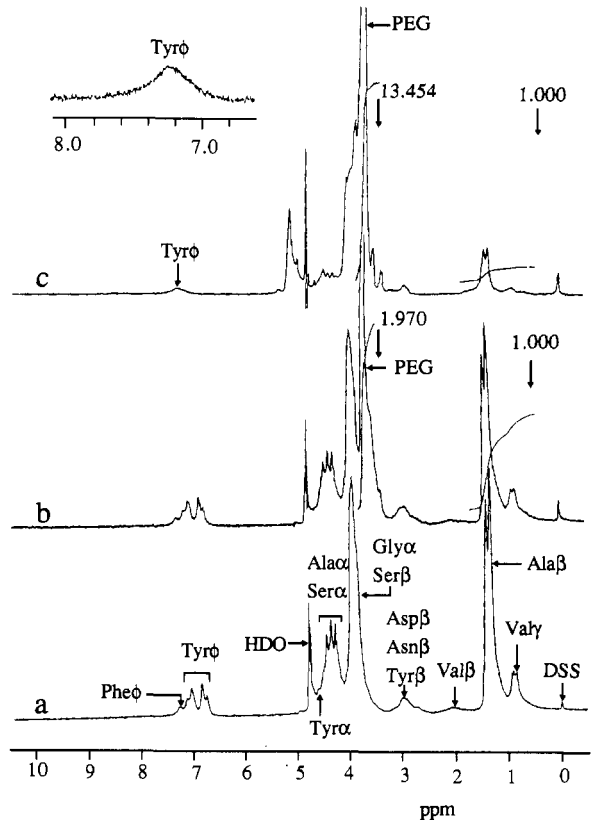


Figure 2. ^{1}H-NMR spectra of SF in D_2O (a), the mixture of SF and PEG-OMe in D_2O (b), and PEG1–SF in about 10% H_2O–90% D_2O (c).

was measured (Figure 2). Considering the amino acid composition of SF (Table I), the peaks of SF were assigned as follows (*21*). The γ-CH_3 and β-CH resonances of the valine residue were observed at 0.88 ppm (doublet, J = 7 Hz) and 2.1 ppm (broad singlet), respectively. The β-CH_3 resonance of the alanine residue appeared at 1.39 ppm (doublet, J = 7 Hz). The broad resonance at 3.0 ppm was assigned to the β-CH_2 of the tyrosine, asparagine, and aspartic acid residues. The α-CH_2 resonance of the glycine residue and the β-CH_2 resonance of the serine residue appeared at 3.94 ppm as an overlapped signal. The resonances at 4.29–4.45 ppm were assigned to the α-CH of the serine, alanine, and other residues. The shoulder at about 4.6 ppm was assigned to the α-CH of the tyrosine residue. The aromatic protons of the tyrosine residue appeared as doublet peaks (J = 7 Hz) at 6.79 and 7.09 ppm. The resonance at about 7.3 ppm was assigned to the aromatic protons of the phenylalanine residue.

The spectrum of PEG1–SF showed a singlet peak at 3.70 ppm. This peak was assigned to the methylene protons of the actPEG1 bonded to SF (*8*) because the spectrum of the mixture composed of SF and PEG-OMe showed the same spectrum as SF except for a singlet peak at 3.70 ppm assigned to the methylene protons of PEG-OMe. In the spectrum of PEG1–SF, the peaks at 6.79 and 7.09 ppm of the tyrosine residue disappeared, and a broad singlet peak at 7.25 ppm appeared. This downfield shift reveals the change in the molecular environment of the tyrosine residue caused by the modification, that is, the shift is derived from the shielding effect of the triazine ring on the tyrosine residue (*22*). Thus, the tyrosine residue of SF is thought to react with actPEG1.

In order to prove that the downfield shift of the tyrosine residue is the result of chemical bonding of the triazine ring in actPEG1 to the tyrosine residue, SF was reacted

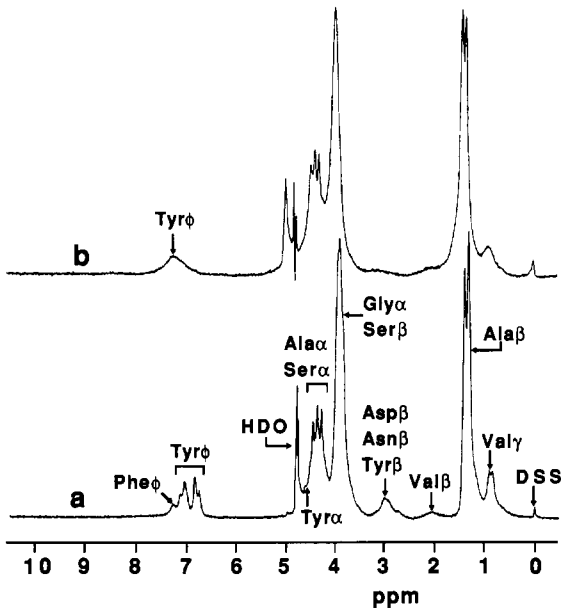
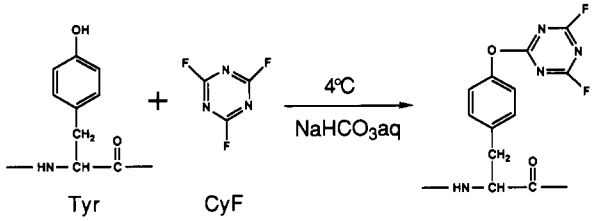


Figure 3. ^{1}H-NMR spectra of SF (a) and CyF–SF (b) in D_2O.

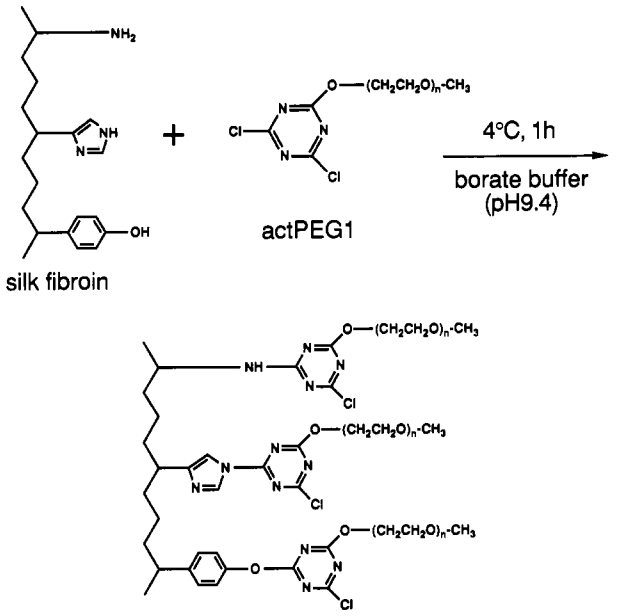
Scheme II



with CyF. CyF has the same triazine ring as act1PEG1, and the fluorine atoms in CyF are known to react with the phenolic hydroxyl group of the tyrosine residue of proteins (Scheme II) (*19*, *20*). In the ^{1}H-NMR spectrum of CyF–SF, a broad singlet peak assigned to the aromatic protons of the tyrosine residue appeared at 7.20 ppm (Figure 3). The downfield shift of the tyrosine residue in CyF–SF is similar to that in PEG1–SF. This result suggests that the phenolic hydroxyl group of the tyrosine residue in SF reacted with the chlorine atom of the triazine in actPEG1. Johnson et al. reported that cyanuric chloride (2,4,6-trichloro-*s*-triazine) reacted with nucleophilic groups such as amino, imino, and hydroxyl groups (*23*). Muijlwijk et al. reported that the chlorine atom of cyanuric chloride was substituted for phenolic hydroxyl groups (*24*). Thus, our NMR analysis results agree with their report.

Although the ^{1}H-NMR spectrum of PEG1–SF indicated the modification of the tyrosine residue, amino acid analysis of PEG1–SF did not show a reduction in the tyrosine content. In order to prove that the ether linkage between the triazine of actPEG1 and the hydroxyl group of the tyrosine residue was completely cleaved under hydrolysis conditions, amino acid analysis of the model compound CyF–SF was carried out. The result of the analysis of CyF–SF indicated a considerable decrease in lysine content and a slight decrease in histidine content but did not show any decrease in tyrosine content (Table I). Moreover, the ^{1}H-NMR spectrum of the hydrolyzed product of CyF–SF for amino acid analysis showed sharp doublet peaks at 6.90 and 7.22 ppm corresponding to the aromatic protons of the tyrosine. These peaks are similar to the peaks of the aromatic protons of the unmodified tyrosine residue. These results suggest that, since the ether bond between the triazine and the hydroxyl group of the tyrosine residue was weaker than the linkages between

Scheme III



the triazine and the amino or imidazole group, the ether bond was completely broken during the hydrolysis. Therefore, although the result of amino acid analysis of PEG1–SF did not show a reduction in the tyrosine content, the tyrosine residue was modified with actPEG1.

The aliphatic hydroxyl groups of the serine and threonine residues, which are much less reactive than the phenolic hydroxyl group of the tyrosine residue (*25*), could react with actPEG1. It was difficult to observe the shift in resonances of the serine and threonine residues in PEG1–SF. The peaks of the α-CH and β-CH_2 of the serine residue overlapped with the big PEG peak and the peaks of other residues. The peak of the threonine residue could not be detected because of its low content. Because the nucleophilicities of the amino group of the lysine residue and the imidazole group of the histidine residue compete with that of the phenolic hydroxyl group of the tyrosine residue (*8*, *25*, *26*), these residues should react with actPEG1. However, the peaks of these residues could not be detected by NMR measurement owing to their low contents.

From the results of our amino acid analysis and NMR measurement, the reaction sites are considered to be the ϵ-amino group of the lysine residue, the imidazole group of the histidine residue, and the phenolic hydroxyl group of the tyrosine residue (Scheme III). Taking into account the lysine (0.32 mol %), histidine (0.18 mol %), and tyrosine content (5 mol %) in SF, the minimum amounts of the modified residues (3.3 mol %) obtained by the weight measurement seem to be reasonable.

The content of PEG in PEG1–SF was also calculated from the integral of the NMR spectrum. The mixture composed of PEG-OMe and SF (the weight ratio of PEG-OMe to SF was 0.405) served as a standard. The integral value of the γ-CH_3 of the valine residue and the β-CH_3 of the alanine residue, which were not modified with act-PEG1, in the region of 0.8–1.5 ppm was used as the integration reference. The ratio of the integral value of PEG-OMe methylene protons as 3.70 ppm to that of the valine and alanine residues in the region of 0.8–1.5 ppm was 1.97 (Figure 2). In the spectrum of PEG1–SF, the ratio of the integral value of PEG methylene protons at 3.70 ppm to that of the reference valine and alanine

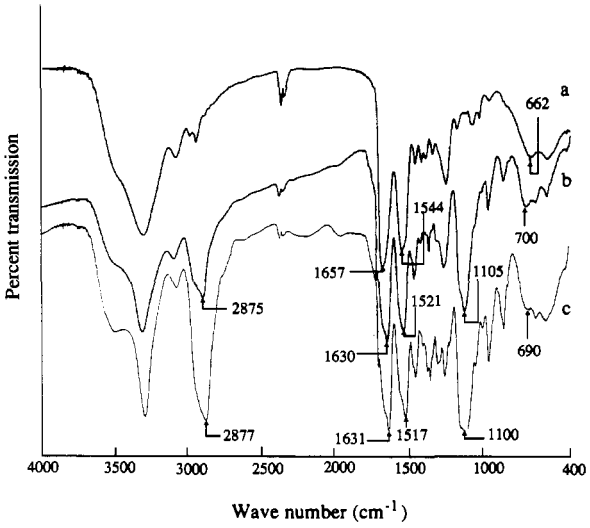


Figure 4. IR spectra of films of SF (a), the mixture of SF and actPEG1 (b), and PEG1–SF (c).

residues in the region of 0.8–1.5 ppm was 13.5. Thus, the weight ratio of PEG to SF in PEG1–SF is calculated to be 2.8 (=(13.5/1.97) × 0.405). By following the calculation described in the above section on synthesis of PEG1–SF conjugate, the mole ratio of the amino acid residue to PEG is calculated to be 24 (=(1/75)/(2.8/5000)), and 4.2 mol % of the residues in SF was modified with actPEG1. Therefore, the amount of the modified residues calculated from the integration is more reasonable than that obtained by the weight measurement.

IR Spectrum of PEG1–SF. Figure 4 shows IR spectra of the SF films before and after the modification with actPEG1. In the spectrum of PEG1–SF, two new bands appeared at 2877 and 1100 cm^{-1} compared with the spectrum of SF. The bands at 2877 and 1100 cm^{-1} are assigned to $-CH_2-$ stretching (*27*) and C–O–C stretching (*28*), respectively. Therefore, these new peaks are attributed to PEG. This means that the PEG chains were successfully introduced to SF.

The conformational characteristic of PEG1–SF in the solid state was examined. SF exhibited absorption bands at 1657 (amide I), 1544 (amide II), and 662 cm^{-1} (amide V), which are characteristic of a random-coil conformation (*11, 14, 16, 29*), while PEG1–SF exhibited absorption bands at 1631 (amide I), 1517 (amide II), and 690 cm^{-1} (amide V), which are characteristic of a β-sheet (*11, 14, 16, 29*). The IR spectrum of a mixture of SF and actPEG1 was also measured in comparison and is shown in Figure 4b. The absorption bands of amides I, II, and V appeared at 1630, 1521, and 700 cm^{-1}, respectively. These bands are characteristic of a β-sheet. These results suggested that the coexistence with the PEG molecule in SF caused the conformational change from random coil to β-sheet.

X-ray Diffraction Pattern of PEG1–SF. The solid-state structure of PEG1–SF was studied in detail by means of X-ray diffraction. In Figure 5, the original SF film showed a broad, weak peak which is attributed to a random-coil conformation with a low degree of molecular orientation. After immersion of the original SF film in 50% (v/v) methanolic aqueous solution, a peak appeared at 20.2° corresponding to the 4.39-Å spacing. This spacing for the 201 reflection was used as the interchain periodicity of the β-sheet crystal (*14, 16, 30*).

The PEG1–SF film showed the peak at 21.5° corresponding to the 4.13-Å spacing of the interchain β-sheet (Figure 5). The spacing of the interchain periodicity of PEG1–SF is narrower than that of SF. These results mean

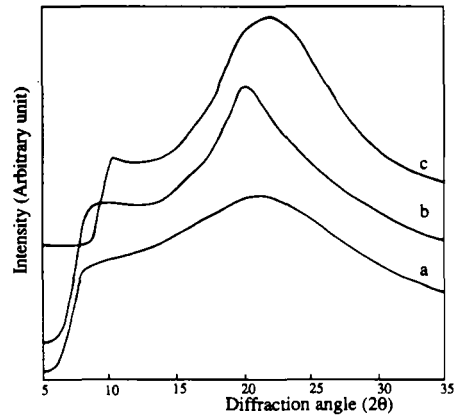


Figure 5. X-ray diffraction patterns of films of SF (a), SF treated with 50% (v/v) methanolic aqueous solution (b), and PEG1–SF (c).

that the PEG molecules covalently bonding to SF strengthened the hydrogen bondings between SF chains and promoted the formation of the interchain β-sheet. Nevertheless, the peak of PEG1–SF widened compared with that of the SF having the β-sheet conformation. Although the covalently bonded PEG molecules prompted the formation of the interchain β-sheet of SF molecules, they disordered the molecular orientation as a whole.

CONCLUSION

Solubilized SF was chemically modified with actPEG1. The reaction sites were the ε-amino group of the lysine residue, the imidazole group of the histidine residue, and the phenolic hydroxyl group of the tyrosine residue. The PEG molecules covalently bonding to SF narrowed the spacing of the interchain periodicity and promoted the formation of the interchain β-sheet in the solid state.

LITERATURE CITED

(1) Lui, F.-T. and Katz, D. H. (1979) Immunological tolerance to allergenic protein determinants: A therapeutic approach for selective inhibition of IgE antibody production, *Proc. Natl. Acad. Sci. U.S.A. 76*, 1430–1434.

(2) Maeda, H., Ueda, M., Morinaga, T., and Matsumoto, T. (1985) Conjugation of poly(styrene-*co*-maleic acid) derivatives to the antitumor protein neocarzinostatin: Pronounced improvements in pharmacological properties, *J. Med. Chem. 28*, 455–461.

(3) Inada, Y., Yoshimoto, T., Matsushima, A., and Saito, Y. (1986) Engineering physicochemical and biological properties of proteins by chemical modification, *Trends Biotechnol. 4*, 68–73.

(4) Abuchowski, A., van Es, T., Palczuk, N. C., and Davis, F. F. (1977) Alteration of immunological properties of bovine serum albumin by covalent attachment of polyethylene glycol, *J. Biol. Chem. 252*, 3578–3581.

(5) Abuchowski, A., Kazo, G. M., Verhoest, C. R., Jr., van Es, T., Kafkewitz, D., Nucci, M. L., Viau, A. T., and Davis, F. F. (1984) Cancer therapy with chemically modified enzymes. I. Antitumor properties of polyethylene glycol-asparaginase conjugates, *Cancer Biochem. Biophys. 7*, 175–186.

(6) King, T. P., Kochoumian, L., and Lichtenstein, L. M. (1977) Preparation and immunochemical properties of methoxypolyethylene glycol-coupled and N-carboxymethylated derivatives of ragweed pollen allergen, antigen E, *Arch. Biochem. Biophys. 178*, 442–450.

(7) Takahashi, K., Ajima, A., Yoshimoto, T., and Inada, Y. (1984) Polyethylene glycol-modified catalase exhibits unexpectedly high activity in benzene, *Biochem. Biophys. Res. Commun. 125*, 761–766.

(8) Jackson, C.-J. C., Charlton, J. L., Kuzminski, K., Lang, G. M., and Sehon, A. H. (1987) Synthesis, isolation, and characterization of conjugates of ovalbumin with monomethoxypolyethylene glycol using cyanuric chloride as the coupling agent, *Anal. Biochem. 165*, 114–127.
(9) Zalipsky, S., Seltzer, R., and Menon-Rudolph, S. (1992) Evaluation of a new reagent for covalent attachment of polyethylene glycol to proteins, *Biotechnol. Appl. Biochem. 15*, 100–114.
(10) Usui, M. and Matuhasi, T. (1979) IgE-selective and antigen-specific unresponsiveness in mice I. Induction of the unresponsiveness by administration of ovalbumin-pullulan conjugate, *J. Immunol. 122*, 1266–1272.
(11) Kuzuhara, A., Asakura, T., Tomoda, R., and Matsunaga, T. (1987) Use of silk fibroin for enzyme membrane, *J. Biotechnol. 5*, 199–207.
(12) Minoura, N., Aiba, S., Fujiwara, Y., Taguchi, K., and Tsukada, M. (1988) Cell attachment and growth on silk protein membranes, *Sen-i Gakkai (Soc. Fiber Sci. Tec., Jpn.) Symposia Preprints* A 29–31.
(13) Shimura, K., Kikuchi, A., Katagata, Y., and Ohotomo, K. (1982) The occurrence of small component proteins in the cocoon fibroin of *Bombyx mori. J. Seric. Sci. Jpn. 51*, 20–26.
(14) Fraser, R. D. B. and MacRae, T. P. (1973) Conformation in fibrous proteins, *Conformation in fibrous proteins and related synthetic polypeptides*, Chapter 13 Silks, pp 293–343, Academic Press, New York.
(15) Mita, K. and Ichimura, S. (1992) The primary structure and organization of silk fibroin gene, *19th International Congress of Entomology Abstracts*, pp 628.
(16) Ha, W. S., Oh, S. K., Kim, J. H., and Kim, K. Y. (1987) Effect of structural changes on the surface characteristics of regenerated and graft copolymerized silk fibroin films, *Sen-i Gakkaishi 43*, 587–594.
(17) Gotoh, Y., Tsukada, M., and Minoura, N. (1992) Chemical modification of arginyl residues in silk fibroin: 1. Reaction of 1,2-cyclohexanedione in borate buffer, *Int. J. Biol. Macromol. 14*, 198–200.
(18) Tsukada, N., Gotoh, Y., and Minoura, N. (1990) Characterization of the regenerated silk fibroin from *Bombyx mori*, *J. Seric. Sci. Jpn. 59*, 325–330.
(19) Kurihara, K., Horinishi, H., and Shibata, K. (1963) Reactions of cyanuric halides with proteins I. Bound tyrosine residues of insulin and lysozyme as identified with cyanuric fluoride, *Biochim. Biophys. Acta 74*, 678–687.
(20) Aoyama, M., Kurihara, K., and Shibata, K. (1965) States of amino acid residues in proteins VII. Hydrogen bonding of tyrosine residues in the insulin molecule, *Biochim. Biophys. Acta 107*, 257–265.
(21) Bundi, A. and Wüthrich, K. (1979) ^{1}H-NMR parameters of the common amino acid residues measured in aqueous solutions of the linear tetrapeptides H-Gly-Gly-X-L-Ala-OH, *Biopolymers 18*, 285–297.
(22) Jackman, L. M. and Sternhell, S. (1969) Theory of chemical shift, *Applications of Nuclear Magnetic Resonance Spectroscopy in Organic Chemistry* 2nd ed., pp 61–113, Pergamon Press, Oxford.
(23) Johnson, D., Mendicino, J., Cormier, M., and Travis, J. (1974) Cyanuric chloride: A new coupling reagent for affinity chromatography, *Fed. Proc. 33*, 1502.
(24) van Muijlwijk, A. W., Kieboom, A. P. G., and van Bekkum, H. (1974) Hydrogenolysis of 2,4,6-tris(aryloxy)-*s*-triazines over palladium: a new method for the replacement of phenolic hydroxyl groups by hydrogen, *Recl. Trav. Chim. Pay-Bas 93*, 204–206.
(25) Vallee, B. L. and Riordan, J. F. (1969) Chemical approaches to the properties of active sites of enzymes, *Annu. Rev. Biochem. 38*, 733–793.
(26) Tanford, C. and Hauenstein, J. D. (1956) Hydrogen ion equilibria of ribonuclease, *J. Am. Chem. Soc. 78*, 5287–5291.
(27) Nakanishi, K., Solomon, P. H., and Furutachi, N. (1990) *Infrared Absorption Spectroscopy* 25th ed., pp 17–20, Nankodo, Tokyo.
(28) Nakanishi, K., Solomon, P. H., and Furutachi, N. (1990) *Infrared Absorption Spectroscopy* 25th ed., pp 35–36, Nankodo, Tokyo.
(29) Miyazawa, T. and Blout, E. R. (1961) The infrared spectra of polypeptides in various conformations: Amide I and II bands, *J. Am. Chem. Soc. 83*, 712–719.
(30) Nagura, M. and Ishikawa, H. (1983) Molecular motion in poly(amino acid)s: 7. Molecular motion in the β-form crystal of silk fibre, *Polymer 24*, 820–822.

Biotinylated Isocoumarins, New Inhibitors and Reagents for Detection, Localization, and Isolation of Serine Proteases

Chih-Min Kam, Ahmed S. Abuelyaman, Zhaozhao Li, Dorothy Hudig,† and James C. Powers*

The School of Chemistry and Biochemistry, Georgia Institute of Technology, Atlanta, Georgia 30332-0400, and The School of Medicine and The College of Agriculture, Howard Building, University of Nevada, Reno, Nevada 89557-0046. Received July 29, 1993®

Eight new biotinylated, mechanism-based isocoumarin serine protease inhibitors have been designed and synthesized to detect, localize, and isolate serine proteases. Isocoumarins that contain a 4-chloro group, a biotinylated substituent at the 7-position, and different 3-alkoxy groups are inhibitors of various serine proteases including human leukocyte elastase (HLE), porcine pancreatic elastase (PPE), trypsin, human recombinant granzyme A, chymotrypsin, and cathepsin G. Insertion of spacers between the isocoumarin moiety and the biotin moiety enhanced enzyme inhibitory potency and may also promote binding of the enzyme–inhibitor complex to avidin. The 3-alkoxy groups conferred selectivity toward different serine proteases with chymotrypsin being inhibited effectively by compounds with 3-phenylethoxy groups while derivatives with 3-methoxy, ethoxy, or propoxy groups were potent inhibitors of HLE and moderate inhibitors of PPE. Full enzymatic activity was regained after the immediate addition of hydroxylamine to the inactivated chymotrypsin and PPE derivatives, which indicated that a simple acyl enzyme derivative is formed initially in the inhibition reaction. Egg avidin did not effect the rate of spontaneous enzyme reactivation rate while streptavidin accelerated the reactivation reaction. PPE inhibited by 7-[[6-(biotinylamino)caproyl]amino]-4-chloro-3-ethoxyisocoumarin (BIC 5) or 7-[[6-[[6-(biotinylamino)caproyl]amino]caproyl]amino]-4-chloro-3-methoxyisocoumarin (BIC 7) was bound to immobilized avidin columns. Most of inhibited PPE could be eluted from the monomeric or tetrameric avidin columns but only a portion (40–70%) of the enzyme was active due to the partial formation of a stable alkylated enzyme derivative during the isolation process. Under ideal circumstances and formation of a simple acyl enzyme derivative, BICs should be useful for the isolation of new active serine proteases. Biotinylated isocoumarins should also have wide applicability for the detection, quantitation, and histochemical localization of stable biotinylated serine protease derivatives in a variety of physiological situations.

INTRODUCTION

Serine proteases play important roles in a number of physiological processes including digestion, blood coagulation, complement activation, fibrinolysis, reproduction, development, and the release of physiologically active peptides (Neurath, 1984). Uncontrolled proteolysis by serine proteases is also related to diseases such as pulmonary emphysema, adult respiratory distress syndrome, and pancreatitis. Thus, there is considerable interest in characterizing new serine proteases, determining their sites of storage and biological activity, and studying their roles in various normal and abnormal biological processes.

Synthetic inhibitors tagged with biotin have frequently been utilized to detect, localize, and recover proteases from pathological tissues. For example, the chloromethyl ketone affinity label biotin–Arg–CH_2Cl has been utilized to detect trypsin and thrombin in electrophoretic gels using Western blotting and a streptavidin/alkaline phosphatase detecting system (Kay et al., 1992; Walker et al., 1992). The diazomethyl ketone cysteine protease inhibitor biotin–Phe–Ala–CHN_2 has been used to detect a cathepsin B-like precursor produced by breast-tumor cells in culture (Cullen et al., 1992). Biotin–Phe-Pro-Arg–CH_2Cl has been used as a specific probe for the detection of factor Xa and factor VIIa by blotting techniques and has also been used to remove traces of active enzymes from zymogen preparations in the coagulation and fibrinolytic pathways (Williams et al., 1989). Two biotinylated derivatives of the ACE[1] inhibitor lisinopril, have been synthesized (Berstein et al., 1990) and one derivative with a sizable spacer was used to isolate ACE from a crude mixture of proteins.

Biotin with its high affinity ($K_d = 10^{-15}$ M) toward avidin and streptavidin has been covalently linked to numerous peptides and proteins, and the complexes have been used for the detection of hormone–receptor complexes, the isolation of peptide and protein receptors, and the study of protein–protein interactions (Billingsley et al., 1987; Finn et al., 1984). Biotinylated antibodies, which are detected by avidin-linked chromogens or fluorophores, are commonly used for the immunolocalization of antigens (Towbin and Gordon, 1984). Thus, biotinylated serine proteases would also be expected to have numerous applications.

Effective inhibitors of serine proteases include both peptide derivatives and heterocyclic structures such as isocoumarins (Powers and Harper, 1986). 3,4-Dichloroisocoumarin is a general serine protease inhibitor and 3-alkoxy-4-chloro-7-substituted isocoumarins are potent and more specific inhibitors for serine proteases such as

* Author to whom correspondence should be addressed.
† University of Nevada.
® Abstract published in *Advance ACS Abstracts,* November 1, 1993.

[1] Aca, 6-aminocaproic acid; ACE, angiotensin-converting enzyme; BIC, biotinylated isocoumarin; Boc-Gly, *tert*-(butyloxycarbonyl)glycine; Cat G, cathepsin G; CDI, 1,1′-carbonyldiimidazole; DCC, *N,N′*-dicyclohexylcarbodiimide; DMF, dimethylformamide; Et_3N, triethylamine; Hepes, *N*-(2-hydroxyethyl)piperazine-*N′*-2-ethanesulfonic acid; HLE, human leukocyte elastase; HOBt, 1-hydroxybenzotriazole; HR granzyme A, human recombinant granzyme A; *p*NA, *p*-nitroanilide; PPE, porcine pancreatic elastase; SBzl, thiobenzyl ester; Suc, succinyl; Z, benzyloxycarbonyl.

1043-1802/93/2904-0560$04.00/0 © 1993 American Chemical Society

PPE, HLE, chymotrypsin, and the trypsin-like enzymes that initiate blood coagulation and the complement cascade (Harper and Powers, 1985; Kam et al., 1988; Powers et al., 1990; Kam et al., 1992). These reagents are mechanism-based or "suicide" inhibitors where the isocoumarin ring is opened by a serine protease to unmask a new, potent reactive structure which can further inactivate the enzyme by covalent bond formation. Isocoumarins have several potential advantages in the inhibition process due to the possible formation of either an acyl enzyme derivative or an alkylated enzyme derivative. The acyl enzyme can be reactivated by hydrolysis or treatment with a nucleophile, while the alkylated enzyme is stable and not reactivatable.

In this paper we report the synthesis and characterization of several isocoumarin-based serine protease inhibitors that incorporate a biotin tag. The biotin was attached to the isocoumarin either directly or through a spacer of different lengths. These derivatives have the ability to inhibit serine proteases with the inhibition specificity being controlled by the 3-substituent on the isocoumarin ring. After coupling to serine proteases, the biotin of the inhibitor is accessible to avidin. We have probed the structures of the enzyme–inhibitor complexes with nucleophile hydroxylamine to distinguish between reactivatable simple acyl enzyme derivatives and nonreactivatable alkylated enzyme derivatives. We also demonstrate with representative serine proteases that these biotinylated isocoumarins can be used to isolate and recover inactivated serine proteases.

EXPERIMENTAL PROCEDURES

Reagents. Biotin was obtained from Chemical Dynamics Corp., South Plainfield, NJ. Avidin, streptavidin, bovine trypsin, and bovine chymotrypsin were obtained from Sigma Chemical Co., St Louis, MO. Tetrameric avidin agarose was obtained from Vector Laboratories, Inc., Burlington, CA. Immobilized monomeric avidin was obtained from Pierce, Rockford, IL. Porcine pancreatic elastase (PPE) was obtained from United States Biochemical Corp., Cleveland, OH. Human leukocyte elastase (HLE) and cathepsin G (Cat G) were obtained from Athens Research and Technology, Inc., Athens, GA. Human recombinant granzyme A was obtained from Dr. Duke Virca at Immunex Corp., Seattle, WA. 6-Aminocaproic acid and *N*-hydroxysuccinimide were purchased from Aldrich Chemical Co., Inc., Milwaukee, WI. Hepes was purchased from Research Organics, Inc., Cleveland, OH. 7-Amino-4-chloro-3-(2-phenylethoxy)isocoumarin, 7-amino-4-chloro-3-ethoxyisocoumarin, 7-amino-4-chloro-3-methoxyisocoumarin (Harper and Powers, 1985), and 7-amino-4-chloro-3-propoxyisocoumarin (Powers et al., 1990) were prepared as previously described.

7-(Biotinylamino)-4-chloro-3-(2-phenylethoxy)isocoumarin (BIC 1). The acid chloride derived from biotin was prepared by incubating biotin (0.4 g, 1.6 mmol) in 6 mL of thionyl chloride at 25–35 °C for 1 h, followed by removal of excess thionyl chloride *in vacuo*. The residue was dissolved in a few milliliters of DMF, 7-amino-4-chloro-3-(2-phenylethoxy)isocoumarin (0.26 g, 0.8 mmol) and Et_3N (0.082 g, 0.8 mmol) were added and the reaction mixture was stirred at room temperature overnight. The product was purified by column chromatography and eluted with CH_2Cl_2/MeOH = 15:1: yield 34%; mp 182–185 °C; ^1H NMR (DMSO) δ 10.3 (s, 1H), 8.50 (d, 1H), 8.0 (dd, 1H), 7.65 (d, 1H), 7.20–7.40 (m, 5H), 6.30–6.50 (d, 2H), 4.55 (t, 2H), 4.15–4.13 (m, 2H), 3.0–3.20 (m, 3H), 2.80 (m, 1H), 2.60 (m, 1H), 2.30 (t, 2H), 1.30–1.70 (m, 6H); MS (FAB$^+$) *m/e* 542 ($M^+ + 1$). Anal. Calcd for $C_{27}H_{28}N_3O_5ClS \cdot 0.25H_2O$: C, 59.39; H, 5.22, N, 7.70. Found: C, 59.08; H, 5.37; N, 7.94.

7-(Biotinylamino)-4-chloro-3-propoxyisocoumarin (BIC 2). This compound was prepared from 7-amino-4-chloro-3-propoxyisocoumarin using the procedure described for BIC 1: yield 20%; mp 127–131 °C; ^1H NMR (DMSO) δ 10.3 (s, 1H), 8.50 (d, 1H), 8.0 (dd, 1H), 7.60 (d, 1H), 6.3–6.5 (d, 2H), 4.3 (t, 2H), 4.15, (m, 2H), 3.10 (m, 1H), 2.8 (m, 1H), 2.6 (m, 1H), 2.35 (m, 2H), 1.7–1.8 (m, 2H), 1.2–1.7 (m, 6H), 1.0 (t, 3H); MS (FAB$^+$) *m/e* 502 ($M^+ + Na + 1$). Anal. Calcd for $C_{22}H_{26}N_3O_5ClS \cdot H_2O$: C, 53.06; H, 5.67; N, 8.44; Cl, 7.12. Found: C, 53.30; H, 5.67; N, 8.49; Cl, 7.03.

7-[[6-(Biotinylamino)caproyl]amino]-4-chloro-3-(2-phenylethoxy)isocoumarin (BIC 3). 6-(Biotinylamino)caproic acid was prepared from the *N*-hydroxysuccinimide ester of biotin (Jasiewicz et al., 1976) and methyl 6-aminocaproate acid hydrochloride by a previously described method (Hofmann et al., 1984). 6-(Biotinylamino)-caproic acid chloride was prepared by incubating 6-(biotinylamino)caproic acid (0.36 g, 1 mmol) in 4 mL of thionyl chloride at 25–35 °C for 1 h and removing excess thionyl chloride *in vacuo*. The residue was dissolved in a few milliliters of DMF, 7-amino-4-chloro-3-(2-phenylethoxy)-isocoumarin (0.34 g, 1 mmol) and Et_3N (0.1 g, 1 mmol) were added, and the reaction mixture was stirred at room temperature overnight. The product was purified by column chromatography and eluted with CH_2Cl_2/MeOH = 10:1: yield 28%; mp 163–167 °C; ^1H NMR (DMSO) δ 10.3 (s, 1H), 8.50 (d, 1H), 8.0 (dd, 1H), 7.75 (m, 1H), 7.60 (d, 1H), 7.20–7.40 (m, 5H), 6.40 (d, 2H), 4.55 (t, 2H), 4.10–4.30 (m, 2H), 3.0–3.10 (m, 5H), 2.80 (m, 1H), 2.60 (m, 1H), 2.35 (t, 2H), 2.0 (m, 2H), 1.20–1.60 (m, 12H); MS (FAB$^+$) *m/e* 655 ($M^+ + 1$). Anal. Calcd for $C_{33}H_{39}N_4O_6ClS \cdot H_2O$: C, 58.87; H, 6.14; N, 8.32; Cl, 5.27. Found: C, 58.72; H, 6.22; N, 8.90; Cl, 5.50.

7-[[6-(Biotinylamino)caproyl]amino]-4-chloro-3-propoxyisocoumarin (BIC 4). This compound was prepared from 7-amino-4-chloro-3-propoxyisocoumarin using the procedure described for BIC 3: yield 25%; mp 141–145 °C; ^1H NMR (DMSO) δ 10.3 (s, 1H), 8.50 (d, 1H), 8.0 (dd, 1H), 7.75 (b, 1H), 7.65 (d, 1H), 6.3–6.4 (d, 2H), 4.3 (m, 3H), 4.1 (m, 1H), 2.95–3.15 (m, 3H), 2.8 (m, 1H), 2.6 (m, 1H), 2.3 (m, 2H), 2.0 (m, 2H), 1.9 (m, 2H), 1.2–1.7 (m, 12H), 1.0 (t, 3H); MS (FAB$^+$) *m/e* 593 (M^++1). Anal. Calcd for $C_{28}H_{37}N_4O_6ClS \cdot 0.5H_2O$: C, 55.14; H, 6.13; N, 9.53; Cl, 6.04. Found: C, 54.81; H, 6.26; N, 9.47; Cl, 5.93.

7-[[6-(Biotinylamino)caproyl]amino]-4-chloro-3-ethoxyisocoumarin (BIC 5). This compound was prepared from 7-amino-4-chloro-3-ethoxyisocoumarin using the procedure described for BIC 3: yield 15%; mp 156–162 °C; ^1H NMR (DMSO) δ 10.3 (s, 1H), 8.50 (d, 1H), 8.0 (dd, 1H), 7.75 (b, 1H), 7.65 (d, 1H), 6.3-6.45 (d, 2H), 4.4 (q, 2H), 4.2–4.3 (m, 2H), 2.95–3.15 (m, 3H), 2.8 (m, 1H), 2.6 (m, 1H), 2.3 (t, 2H), 2.0 (m, 2H), 1.2–1.7 (m, 15H); MS (FAB$^+$) *m/e* 601 ($M^+ + Na + 1$). Anal. Calcd for $C_{27}H_{35}N_4O_6ClS \cdot H_2O$: C, 55.03; H, 6.43; N, 9.17; Cl, 5.80. Found: C, 54.81; H, 6.26; N, 9.23; Cl, 5.69.

7-[[6-[[6-(Biotinylamino)caproyl]amino]caproyl]-amino]-4-chloro-3-(2-phenylethoxy)isocoumarin (BIC 6). 6-[[6-(Biotinylamino)caproyl]amino]caproic acid was prepared by coupling biotin sequentially to two units of 6-aminocaproic acid. Biotin (2.27 g, 9.3 mmol) was dissolved in 70 mL of DMF at 100 °C, and CDI (1.5 g, 9.3 mmol) was added with continuous stirring. After 0.5 h, heating was terminated and stirring was continued at room temperature for 2 h. Methyl 6-aminocaproate (1.6 g, 9.3 mmol) and Et_3N (1.3 mL, 9.3 mmol) were added, and the

reaction mixture was stirred overnight. Any solid that formed was removed by filtration and the solvent was evaporated *in vacuo*. A solution of 1 N NaOH (24 mL) was added, followed by a few drops of MeOH until a clear solution was obtained. The alkaline solution was stirred for 2 h. Most of the solvent was then removed *in vacuo*. The solution was cooled in ice and acidified with concentrated HCl. During the acidification, a white precipitate formed, was collected, and recrystallized from boiling water to give a white product, 6-(biotinylamino)caproic acid: yield 2.6 g, 79%; mp 221–222 °C; TLC R_f = 0.3 ($CHCl_3$/MeOH/H_2O = 8:3:1). This compound was then coupled to methyl 6-aminocaproate to give 6-[[6-(biotinylamino)caproyl]amino]caproic acid using the same procedure: yield 75%; mp 197–199 °C. The NMR spectra of the two intermediates are consistent with their proposed structures. 6-[[6-(Biotinylamino)caproyl]amino]caproic acid (0.5 g, 1.1 mmol) was dissolved in 15 mL of DMF at 70 °C and cooled to 40 °C, then 7-amino-4-chloro-3-(2-phenylethoxy)isocoumarin (0.4 g, 1.3 mmol) was added, followed by the addition of HOBt (0.172 g, 1.3 mmol) and diisopropylcarbodiimide (0.16 g, 1.3 mmol). The mixture was stirred at room temperature overnight and the solvent was removed by evaporation. The crude product was purified by silica gel chromatography using $CHCl_3$/MeOH/HOAc = 65:10:3 as an eluant. The eluted product contained HOBt, which was removed by washing several times with 1 N HCl. The final product was obtained as a yellow solid: yield 33%; mp 163–165 °C; ^{1}H NMR (DMSO) δ 10.30 (s, 1H), 8.50 (d, 1H), 8.00 (dd, 1H), 7.85–7.68 (bs, 2H), 7.63 (d, 1H), 7.35–7.15, (m, 5H), 6.35 (d, 2H), 4.55 (t, 2H), 4.35–4.25 and 4.15–4.05 (m and m, 2H), 3.13–2.90 (m, 7H), 2.85 and 2.75 (dd and d, 2H), 2.35 (t, 2H), 2.00 (q, 4H), 1.70–1.11 (m, 18H); MS (FAB$^+$) *m/e* 768 (M + 1). Anal. Calcd for $C_{39}H_{50}N_5O_7ClS$: C, 60.96; H, 6.56; N, 9.11; Cl, 4.60. Found: C, 60.72; H, 6.60; N, 9.04; Cl, 4.67.

7-[[6-[[6-(Biotinylamino)caproyl]amino]caproyl]amino]-4-chloro-3-methoxyisocoumarin (BIC 7). 6-[[6-(Biotinylamino)caproyl]amino]caproic acid (0.65 g, 1.4 mmol) was dissolved in 15 mL of DMF at 70 °C and cooled to 40 °C, then 7-amino-4-chloro-3-methoxyisocoumarin (0.37 g, 1.7 mmol) was added, followed by the addition of HOBt (0.22 g, 1.7 mmol) and DCC (0.34 g, 1.7 mmol). The mixture was stirred at room temperature overnight, and the solvent was removed by evaporation. The crude product was purified by silica gel chromatography using $CHCl_3$/MeOH/HOAc = 65:10:2 as an eluant. The eluted product contained HOBt which was removed by washing several times with 1 N HCl; ^{1}H NMR (DMSO) δ 10.30 (s, 1H), 8.55 (d, 1H), 8.00 (dd, 1H), 7.80–7.70 (bs, 2H), 7.65 (d, 1H), 6.40 (d, 2H), 4.35–4.25 and 4.15–4.08 (m and m, 2H), 4.03 (s, 3H), 3.15–2.95 (m, 5H), 2.80 and 2.55 (dd and d, 2H), 2.35 (t, 2H), 2.05 (q, 4H), 1.70–1.15 (m, 18H); MS (FAB) *m/e* 677 (M$^+$). Anal. Calcd for $C_{32}H_{44}N_5O_7ClS{\cdot}0.5H_2O$: C, 55.93; H, 6.59, N, 5.15; Cl, 10.19. Found: C, 55.55; H, 6.57; N, 5.15; Cl, 10.06.

7-[[[[[[2-(Biotinylamino)ethyl]amino]carbonyl]methyl]carbamoyl]amino]-4-chloro-3-(2-phenylethoxy)isocoumarin (BIC 8). Biotin (1 g, 4.1 mmol) was dissolved in 20 mL of DMF at 70 °C and cooled to 40 °C. CDI (0.97 g, 6 mmol) in 3 mL of DMF was then added and a white precipitate appeared. After stirring at room temperature for 2 h, ethylenediamine (1.34 mL, 20 mmol) in 10 mL of DMF was added and the reaction mixture was stirred for another 3 h. After the DMF was removed by evaporation, the semisolid residue was dissolved in 50 mL of refluxing methanol and the unreacted biotin was removed by filtration. The solution was evaporated to dryness, the residue was washed with $CHCl_3$ to remove imidazole, dissolved in 6 mL of water, acidified to pH 3.0 with 1 N HCl, and evaporated to dryness. The residue was crystallized from methanol to give 1.04 g of biotinylethylenediamine hydrochloride: yield 79 %; TLC R_f = 0.21 (butanol/acetic acid/H_2O = 4:1:1); mp 241–242 °C; ^{1}H NMR (DMSO) δ 8.05 (bs, 1H), 7.86 (bs, 3H), 6.42 (bd, 2H), 4.31 (t, 1H), 4.12 (t, 1H), 3.25 (m, 2H), 3.09 (m, 1H), 2.83 (m, 3H), 2.56 (d, 1H), 2.05 (t, 2H), 1.53–1.28 (m, 6H).

Biotinyl-NH$(CH_2)_2$NH-COCH$_2$NH-Boc was prepared by the reaction of biotinylethylenediamine hydrochloride, DCC, and Boc-Gly in the presence of triethylamine in DMF: yield 53%; TLC R_f = 0.55 (butanol/acetic acid/H_2O = 4:1:1), mp 136–139 °C; NMR is consistent with assigned structure; MS (FAB$^+$) *m/e* 444 (M + 1). Deblocking the Boc group from biotin-NH$(CH_2)_2$NH-COCH$_2$-NH-Boc with trifuoroacetic acid at 0 °C and the addition of saturated HCl in ethyl acetate to the residue gave biotinyl-NH$(CH_2)_2$NHCOCH$_2$NH·HCl: yield 81%; TLC R_f = 0.32 (butanol/acetic acid/H_2O = 4:1:1); mp 146–148 °C; ^{1}H NMR (DMSO) δ 8.43 (bs, 1H), 8.03 (bs, 3H), 7.90 (bs, 1H), 6.41 (bs, 2H), 4.30 (t, 1H), 4.13 (m, 1H), 3.49 (m, 2H), 3.14 (m, 5H), 2.79 (dd, 1H), 2.55 (d, 1H), 2.06 (t, 2H), 1.52–1.28 (m, 6H).

BIC 8 was synthesized by the reaction of 7-amino-4-chloro-3-(2-phenylethoxy)isocoumarin (0.43 g, 1.35 mmol) with CDI (0.24 g, 1.48 mmol) in 8 mL of DMF at 0 °C. After the isocoumarin solution was stirred at room temperature for 4 h, a solution of biotin-NH$(CH_2)_2$-NHCOCH$_2$NH·HCl (0.47 g, 1.23 mmol) and triethylamine (0.17 ml, 1.23 mmol) in DMF was added. The reaction mixture was stirred at room temperature for 24 h, decolorized, filtered, and evaporated to give a dark greenish residue. The residue was washed with water and 0.5 N HCl, and purified by silica gel chromatography using $CHCl_3$/MeOH = 5:1 as an eluant. The final product was obtained as yellowish green solid: yield 13%; TLC R_f = 0.46 ($CHCl_3$/MeOH = 5:1); mp 192–193 °C dec; ^{1}H NMR (DMSO) δ 9.28 (d, 1H), 8.31 (s, 1H), 8.03 (d, 2H), 7.80 and 7.54 (m, 3H), 7.31–7.20 (m, 5H), 6.39 (d, 2H), 4.52 and 4.39 (d of t, 2H), 4.28 (t, 1H), 4.11 (t, 1H), 3.72 (d, 2H), 3.10 (m, 4H), 3.04 (m, 2H), 2.93 (t, 1H), 2.78 (m, 1H), 2.55 (d, 1H), 2.03 (t, 2H), 1.60–1.22 (m, 6H); MS (FAB$^+$) *m/e* 686 (M+1). Anal. Calcd for $C_{32}H_{37}N_6O_7ClS$: C, 56.09; H, 5.44; N, 12.27. Found: C, 55.92; H, 5.46; N, 12.15.

Substrate Kinetics. Enzymatic hydrolysis rates of peptide *p*-nitroanilides catalyzed by chymotrypsin, PPE, HLE, Cat G, and trypsin were measured at 410 nm (ϵ_{410} = 8800 M^{-1} cm^{-1}; Erlanger et al., 1961). A 0.1 M Hepes, 0.5 M NaCl, pH 7.5 buffer containing 5–10% Me_2SO was used for all enzymes except for trypsin, where a 0.1 M Hepes, 0.01 M $CaCl_2$, pH 7.5 buffer was used. Stock solutions of the substrates were prepared in Me_2SO and stored at −20 °C. Chymotrypsin and Cat G were assayed with Suc-Val-Pro-Phe-*p*NA (0.48 mM; Tanaka et al., 1985). HLE and PPE were assayed with MeO-Suc-Ala-Ala-Pro-Val-*p*NA (0.24–0.47 mM; Nakajima et al., 1979) and Suc-Ala-Ala-Ala-*p*NA (0.29–0.48 mM; Bieth et al., 1974), respectively. Trypsin was assayed with Z-Glu-Phe-Arg-*p*NA (0.032 mM; Cho et al., 1984). The initial rates were measured at 410 nm using a Beckman 35 spectrophotometer when 10–25 μL of an enzyme stock solution was added to a cuvette containing 2.0 mL of buffer and 25 μL of substrate. HR granzyme A was assayed with Z-Arg-SBzl (0.120 mM; Odake et al., 1991) in the presence of 4,4′-dithiodipyridine (Grassetti and Murray, 1967). The initial rates of thiobenzyl ester hydrolysis were measured at 324 nm (ϵ_{324} = 19 800 M^{-1} cm^{-1}) when a 10–25 μL of an enzyme

Table I. Inhibition of Serine Proteases by Biotinyl Isocoumarin Derivatives[a]

	$k_{obs}/[I]$ (M^{-1} s^{-1})					
inhibitors	chymotrypsin[b]	Cat G[c]	HLE[d]	PPE[e]	trypsin[f]	HR granzyme A[g]
BIC 1	330	NI[h]	740	NI	1.1	
BIC 2	65	6.7	20,000	470	2.2	
BIC 3	1,100	13%[i]	670	NI	1.0	NI
BIC 4	260	3.3	77,000	350	10.6	NI
BIC 5	260	59	96,000	520	16.6	26%[i]
BIC 6	1,100	NI	230	NI		NI
BIC 7	170	2.2	38,000	7,100		5%[i]
BIC 8	640	19%[i]	6.6			18%[i]

[a] Inhibition was measured in 0.1 M Hepes, 0.5 M NaCl (or 0.01 M $CaCl_2$), pH 7.5 buffer, 5–10% Me_2SO and at 25 °C. Suc-Val-Pro-Phe-*p*NA (0.48 mM) was used as the substrate for chymotrypsin and Cat G. MeO-Suc-Ala-Ala-Pro-Val-*p*NA (0.24–0.47 mM) and Suc-Ala-Ala-Ala-*p*NA (0.29–0.48 mM) were used as the substrates for HLE and PPE, respectively. Z-Glu-Phe-Arg-*p*NA (0.032 mM) was the substrate for trypsin. Z-Arg-SBzl (0.120 mM) was a substrate for human recombinant (HR) granzyme A. [b] Inhibitor concentrations were 20–400 μM. [c] Inhibitor concentrations were 75–400 μM. [d] Inhibitor concentrations were 1.6–210 μM. [e] Inhibitor concentrations were 38–78 μM. [f] Inhibitor concentrations were 41–42 μM. [g] Inhibitor concentrations were 160–210 μM. [h] No inhibition after 10 min of incubation of inhibitor and enzyme. [i] Percent inhibition after incubation of inhibitor and enzyme for 10 min.

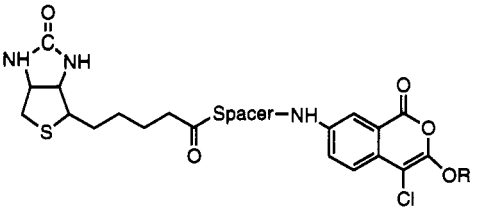
stock solution was added to a cuvette containing 2.0 mL of buffer, 150 μL of 5 mM 4,4′-dithiodipyridine, and 25 μL of substrate. The same volumes of substrate and 4,4′-dithiodipyridine were added to the reference cell in order to compensate for the background hydrolysis rate of the substrates.

Enzyme Inactivation—Incubation Method. An aliquot of inhibitor (15–25 μL) in Me_2SO was added to 0.5 mL of a buffered enzyme solution (0.06–2.3 μM) to initiate the inactivation. Aliquots (15–25 μL) were withdrawn at various intervals, and the residual enzymatic activity was measured as described above. Pseudo-first-order inactivation rate constants (k_{obs}) were obtained from plots of ln v_t/v_0 vs time, and the correlation coefficients were greater than 0.98.

Reactivation Kinetics. The reactivation of enzymes inhibited by substituted biotinylated isocoumarins was studied by monitoring the recovery of enzymatic activity upon standing of the inhibited solution at 25 °C after removal of excess inhibitor. Excess inhibitor was removed by two cycles of dilution and concentration by centrifugation at 0 °C with Amicon Centricon-10 microconcentrators. Enzymatic activity of the inhibited solution was assayed at varying time intervals as described above. Reactivation was also measured after the addition of 3–4 units of avidin or streptavidin (1 unit is the amount required to bind 1 μg of D-biotin) to 2 nmol of chymotrypsin or PPE which had been inhibited by a biotinylated isocoumarin. This amount of enzyme derivative contained 0.5 μg of biotin. Hydroxylamine-catalyzed reactivation was measured in the presence of excess inhibitor after the addition of buffered hydroxylamine (0.3–0.4 M).

RESULTS AND DISCUSSION

Synthesis. Eight biotinylated isocoumarins (BICs) that contained various 3-alkoxy substituents on the isocoumarin ring and various spacer groups were synthesized from the corresponding 7-aminoisocoumarins (Figure 1). The alkoxy groups on the isocoumarin ring including 3-methoxy, ethoxy, propoxy, and phenylethoxy groups are a major determinant of the specificity of the inhibitors. The biotin moiety was either directly attached to the isocoumarin or



BIC 1: Spacer = None, OR = $O(CH_2)_2$-Ph

BIC 2: Spacer = None, OR = $O(CH_2)_2CH_3$

BIC 3: Spacer = Aca, OR = $O(CH_2)_2$-Ph

BIC 4: Spacer = Aca , OR = $O(CH_2)_2CH_3$

BIC 5: Spacer = Aca , OR = OCH_2CH_3

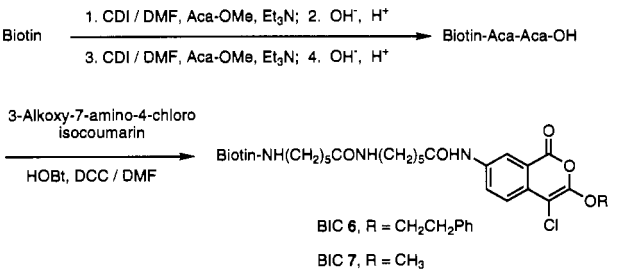
BIC 6: Spacer = Aca-Aca, OR = $O(CH_2)_2$-Ph

BIC 7: Spacer = Aca-Aca, OR = OCH_3

BIC 8: Spacer = $NH\text{-}(CH_2)_2NHCOCH_2NHCO$, OR = $O(CH_2)_2$-Ph

Figure 1. Structures of biotinylated isocoumarin serine protease inhibitors.

Scheme I. Synthesis of Biotinylated Isocoumarins

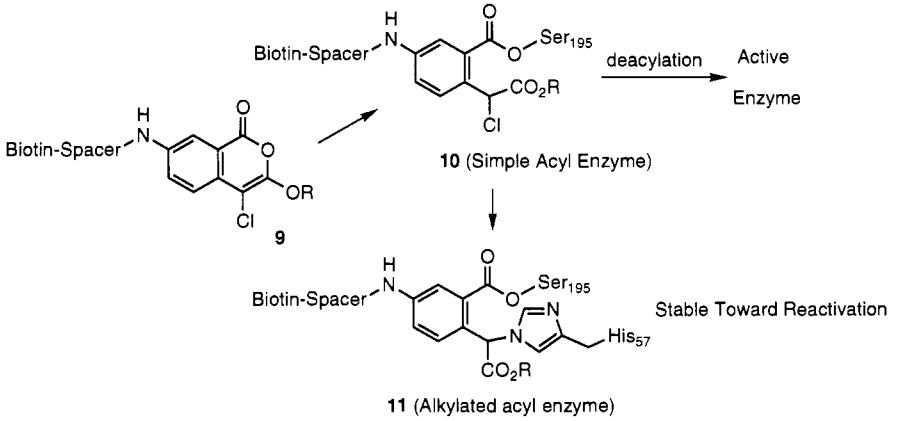


various spacer groups including one or two 6-aminocaproyl (Aca) groups or a $NHCH_2CH_2NHCOCH_2NHCO$ group separating the 7-aminoisocoumarin and biotin. BIC 1 and 2 were prepared from the acid chloride of biotin and the corresponding 3-alkoxy-7-amino-4-chloroisocoumarin in DMF using Et_3N as a base. BICs 3–5 were prepared from 6-(biotinylamino)caproyl chloride and the corresponding 3-alkoxy-7-amino-4-chloroisocoumarin. BICs 6 and 7 were prepared from 6-[[6-(biotinylamino)caproyl]amino]caproic acid and the corresponding 3-alkoxy-7-amino-4-chloroisocoumarin using the DCC/HOBt coupling method (the synthetic scheme is shown in Scheme I). BIC 8 was prepared by reaction of 7-amino-4-chloro-3-(2-phenylethoxy)isocoumarin and CDI to yield the isocyanate derivative which was then coupled to biotin-$NH(CH_2)_2NH$-$COCH_2$-NH_2·HCl in the presence of Et_3N. The final products were purified by column chromatography and characterized by NMR, mass spectra, and elemental analysis.

Inhibition Kinetics. The biotinylated isocoumarins were tested as irreversible inhibitors of representative serine proteases including chymotrypsin, cathepsin G (Cat G), porcine pancreatic elastase (PPE), human leukocyte elastase (HLE), trypsin, and HR granzyme A, and second order inhibition rates $k_{obs}/[I]$ are reported in Table I.

The substituents at both the 3- and 7-positions of the isocoumarin ring profoundly affected the reactivity and specificity of BICs toward the various serine proteases tested. The specificity of many isocoumarin inhibitors toward various serine proteases has previously been shown to be determined by the nature of the 3-alkoxy group which usually binds to the primary specificity pocket of serine proteases such as chymotrypsin and elastases (Harper and Powers, 1985). As expected, similar trends were observed with BICs. For example, BICs 3, 6, and 8, which contain

Scheme II. Mechanism of Inhibition of Serine Proteases by Biotinylated Isocoumarins and Mechanisms of Reactivation



a 3-phenylethoxy substituent, were good inhibitors for bovine chymotrypsin, which prefers aromatic amino acids at the P_1 site[2] in good substrates, but these BICs were poor inhibitors for PPE which prefers P_1 amino acid residues with short alkyl groups in good peptide substrates. Comparison of the inhibition rates of compounds with an Aca spacer and varying 3-alkoxy substituents illustrates the preference of chymotrypsin for the 3-phenylethoxy group. BIC **3** (with a 3-phenylethoxy group) effectively inhibited chymotrypsin, with a $k_{obs}/[I]$ of 1100 M^{-1} s^{-1}, which was 4-fold faster than the inhibition rates of BICs **4** and **5**, which had 3-ethoxy or 3-propoxy substituents, respectively. The reactivity of BIC **3** with chymotrypsin is consistent with the results observed in the inhibition of chymotrypsin by the non-biotin analog 7-amino-4-chloro-3-(phenylethoxy)isocoumarin, which had a $k_{obs}/[I]$ of 1200 M^{-1} s^{-1} (Harper and Powers, 1985).

BICs with longer spacer groups inhibited serine proteases more potently than comparable BICs that had no spacer or shorter spacers. For example, BICs **3**, **6**, and **8** were 2–3-fold better inhibitors for chymotrypsin than BIC **1** (no spacer). A similar effect was observed in the inactivation rates of HLE, where BIC **4** had a better inhibition rate constant than BIC **2**. However, there appeared to be little advantage to spacers longer than a single aminocaproyl group. The longer spacers with two repeated aminocaproyl groups (BIC **6**) or the $NHCH_2CH_2NHCOCH_2NHCO$ group (BIC **8**) afforded no increase in reactivity over BIC **3**, which had only a single aminocaproyl spacer. Thus a suitable spacer is needed for good reactivity, but extended spacers appear unwarranted.

The biotinylated inhibitors which contained spacers of varying lengths were as reactive or more reactive inhibitors than comparable nonbiotinylated isocoumarins. For example, BIC **5**, which had an aminocaproyl spacer, had an irreversible inhibition rate constant of 520 M^{-1} s^{-1} with PPE. This is similar to the rate constant for the nonbiotinylated derivative 7-amino-4-chloro-3-ethoxyisocoumarin, for which $k_{obs}/[I]$ = 700 M^{-1} s^{-1} with PPE. In another comparison, the 3-methoxy derivative BIC **7**, with a spacer of two 6-aminocaproyl groups, was actually more reactive than the nonbiotinylated 7-amino-4-chloro-3-methoxyisocoumarin with PPE. The rate constants were respectively 7100 vs 1000 M^{-1} s^{-1}. BICs **5** and **7** also inhibited HLE more effectively than the corresponding nonbiotinylated isocoumarin inhibitors by 10- and 4-fold respectively (96 000 vs 9400 M^{-1} s^{-1}; 38 000 vs 10 000 M^{-1} s^{-1}). The 3-phenylethoxy inhibitor BIC **3**, which also has an aminocaproyl spacer, inhibited chymotrypsin with a rate constant of 1100 M^{-1} s^{-1}, which is comparable to the rate constant for inhibition of chymotrypsin by 7-amino-4-chloro-3-(phenylethoxy)isocoumarin (1200 M^{-1} s^{-1}). Thus, the inhibitory reactivity of isocoumarins was maintained or even enhanced when there were spacer groups present. This indicates that the spacer group or the biotin moiety may be interacting with the extended substrate binding site of the enzyme.

Inhibition Mechanism and Reactivation Kinetics. The mechanism of inactivation of serine proteases by biotinylated isocoumarins is similar to the mechanism of inhibition by nonbiotinylated isocoumarin inhibitors (Scheme II; Harper and Powers, 1985; Kam et al., 1988). The mechanism involves the initial formation of an acyl enzyme (**10**) by reaction of the isocoumarin carbonyl group with the active site Ser-195. This reaction unmasks a 4-aminobenzyl chloride functional group, which can eliminate chloride to give a quinone imine methide intermediate. This intermediate can react further with an enzyme nucleophile such as His-57 to give an alkylated enzyme (**11**) or with a solvent molecule to produce a new acyl enzyme that can regenerate active enzyme upon deacylation. The alkylated enzyme is stable toward reactivation, while active enzyme can be regenerated from the simple acyl enzyme.

To assess the extent of alkylation of the active site histidine by BICs after the initial inhibition reaction and formation of the acyl enzyme derivative (**10**), we determined the extent of reactivation of the inhibited serine proteases by spontaneous deacylation of the inhibited enzyme during storage at room temperature after removal of excess inhibitors and the extent of reactivation after treatment with the strong nucleophile hydroxylamine. The results obtained with three serine proteases inhibited by five biotinylated isocoumarins are shown in Table II. Chymotrypsin inhibited by BICs **1** or **3** regained only 10–15% of activity after removal of excess inhibitor with Amicon Centricon-10 microconcentrators and storage at room temperature at pH 7.5 for 2 days. In contrast, PPE, which had been inhibited by BICs **2**, **4**, or **5**, regained 35–66% of the original enzyme activity during the same 2-day incubation period. This indicates that PPE is undergoing a slow spontaneous deacylation reaction, while chymotrypsin is forming a more stable acyl enzyme derivative.

Hydroxylamine was quite effective at regenerating active enzyme from the acyl enzyme derivatives (**10**). Chymotrypsin regained 100% activity if NH_2OH was added

[2] The nomenclature used for the individual amino acid residues (P_1, P_2, etc.) of a substrate and the subsites (S_1, S_2, etc.) of the enzyme is that Schecter and Berger (1967).

Table II. Reactivation of Inhibited PPE, Chymotrypsin, and Trypsin by Biotinyl Isocoumarins in Buffer or after Hydroxylamine Treatment[a]

	enzyme activity recovered (%)				
	PPE		chymotrypsin		trypsin
inhibitors	buffer	NH_2OH[b]	buffer	NH_2OH[b]	buffer
BIC 1			10	100	
BIC 2	35	98			
BIC 3			15	100	
BIC 4	37	90			33
BIC 5	66	93			92

[a] Enzyme (1.7 μM) was incubated with inhibitor (40 μM) in 0.1 M Hepes, 0.5 M NaCl, pH 7.5 buffer, 10% Me_2SO at 25 °C for 40–50 min. The residual enzyme activity was then less than 10%. Recovered enzyme activity was then measured after removal of excess inhibitor by two cycles of dilution and concentration by centrifugation at 0–5 °C with Centricon-10 microconcentrators and incubation at 25 °C for 2 days. [b] Recovered enzyme activity was determined 5–60 min after the addition of 0.4 M NH_2OH to the inhibited enzyme solution.

immediately after inhibition by BICs 1 or 3. Similarly, PPE regained >90% activity when NH_2OH was added immediately after inhibition with compounds 2, 4, or 5. Full recovery of enzyme activity with the addition of NH_2OH indicates the formation of a reactivatable acyl enzyme derivative (10) in the case of chymotrypsin and PPE, and not the alkylated derivative 11. We have some data to indicate that there may be a slow conversion of the acyl enzyme derivative (10) to the alkylated form (11). When NH_2OH was added after a few hours to an inhibited PPE derivative, less than the 90% of the potential enzyme activity was regained. These results are consistent with a slow conversion of 10 to 11.

Effects of Avidin and Streptavidin on the Reactivation Reaction. We next evaluated the potential for egg white avidin or bacterial streptavidin to affect the reactivation of the inhibited enzyme derivatives. Avidin and streptavidin differ considerably in their net charges, with p*I*s of ~10 and ~5, respectively. We were initially concerned that the interactions between the biotinylated, inhibited serine proteases and avidin or streptavidin might promote the deacylation reaction and thereby restrict the utility of the biotinylated protease derivatives for detection and/or recovery of biotinylated proteases. Reactivation of chymotrypsin and PPE inhibited by BICs 1-4 were measured in the presence of excess avidin or streptavidin (Table III).

The acidic bacterial protein streptavidin appeared to promote reactivation of chymotrypsin inactivated by BICs 1 and 3 and slightly increased reactivation of PPE inactivated by BICs 2 and 4. In contrast, interactions with an excess molar concentration of the basic protein egg white avidin caused no changes in enzyme recovery, even though both avidins have similar affinities for biotin. It is our conclusion that similar evaluations should be performed for each biotinylated, inactivated serine protease–avidin combination being considered for cytochemical use or for use in serine protease isolation.

The spacers between biotin and the isocoumarin ring serve the purpose of increasing accessibility of avidin to the biotin associated with enzyme–inhibitor complexes. The spacer could also affect the stability of the avidin–BIC–protease complex. For example, the insertion of a 6-aminocaproic acid spacer between the biotin and insulin exerted a stabilizing effect on the complexes with avidin, when biotinylated hormones were used as ligands to isolate the hormone receptors on avidin–Sepharose columns (Hofmann et al., 1984). With BICs, the lack of a spacer

Table III. Effect of Streptavidin and Avidin on Reactivation of Inhibited Chymotrypsin and PPE Derivatives[a]

	enzyme activity recovered (%)					
	chymotrypsin			PPE		
	buffer	streptavidin	avidin	buffer	streptavidin	avidin
BIC 1	10	27	10			
BIC 2				35	51	32
BIC 3	15	39	12			
BIC 4				37	43	32

[a] Enzyme (1.7 μM) was incubated with inhibitor (40 μM) in 0.1 M Hepes, 0.5 M NaCl, pH 7.5 buffer, 10% Me_2SO at 25 °C for 40–50 min. The residual enzyme activity was then less than 10%. Recovered enzyme activity was then measured after removal of excess inhibitor by two cycles of dilution and concentration by centrifugation at 0–5 °C with Centricon-10 microconcentrators. Then 3–4 units of avidin or streptavidin (6–8 μM) were added and enzymatic activity was monitored for 2 days.

decreased the reactivity of the inhibitors, but had little effect on the recovery of enzyme activity upon treatment with avidin or streptavidin. In the case of a BIC with no spacer, it is possible that the avidin is unable to interact with the biotin portion of the inhibited enzyme. However, in the case of enzyme derivatives with longer spacers, we have demonstrated interaction of the biotin with avidin by two methods. The first involves column chromatography (following section) and the second involves detection on protein blots. The biotin in chymotrypsin–inhibitor complexes and lymphocyte granzyme–inhibitor complexes formed with BICs 6 and 7 can be detected on protein blots developed with avidin–alkaline phosphatase (N. J. Allison and D. Hudig, unpublished results). Thus it is clear that the biotin in the complexes is accessible to avidin.

Isolation of BIC-Inhibited PPE via an Avidin Column. One use of biotinylated isocoumarins would be the isolation of new serine proteases using the strong binding of biotin to avidin in BIC–protease complexes. If the enzyme-inhibitor complex remains in the form of an acyl enzyme (10) for a period of several hours, the serine protease could be released from the isolated complex by deacylation with NH_2OH treatment or an increase of the pH to >8. We have used PPE as a model enzyme to evaluate the potential utility of BICs for serine protease isolation and recovery. Experimental results are shown in Table IV.

PPE was inhibited by BIC 5 or 7 in pH 7.5 Hepes buffer with effective loss of all enzyme activity (step 1). Excess inhibitors were removed by gel filtration on a Sephadex G-25 column in a pH 5 acetate buffer (step 2). A low pH buffer was used to avoid reactivation of inhibited enzyme. After gel filtration, the inhibited PPE solution regained a small amount of enzyme activity (<10%). The biotinylated enzyme was then immobilized on monomeric avidin coupled to an agarose matrix (step 3a) and subsequently eluted with PBS buffer (pH 7.2) containing an excess of free biotin (step 4a), which binds to monomeric avidin with a K_d of 10^{-8} M. For PPE inhibited by BIC 7, the most potent PPE inhibitor in the series, 80–90% of the protein was initially bound to the column and then eluted with biotin, as measured by absorbance at 280 nm. However, only 40–50% of the original enzyme activity could be recovered by subsequent hydroxylamine treatment. If a tetrameric avidin column was used instead of the monomeric avidin (step 3b), the affinity of the biotin for the column was so great ($K_d = 10^{-15}$ M) that free biotin would not displace the BIC–protease complex from the column. However, treatment of the column directly with hydroxylamine (step 4b) results in recovery of 70% of the

Table IV. Isolation of BIC-Inhibited PPE

procedures	enzyme activity (%)[a] [protein concentration[b]]		
	PPE	PPE + BIC 5	PPE + BIC 7
(1) Inhibition in pH 7.5 Hepes		0–3	3–5
(2) Sephadex G-25, elute with pH 5.0 buffer		3–6	5–9
(3a) Monomeric avidin–agarose column, wash with pH 5.0 acetate buffer	[100]	[14]	[7–8]
(4a) Elute with biotin-containing PBS pH 7.2 buffer, followed by NH_2OH treatment		10 [80]	40–50 [80–90]
(3b) Tetrameric avidin–agarose column, wash with pH 5.0 buffer	[90–100]	[15]	[11]
(4b) Elute with 0.5 M NH_2OH-containing pH 7.5 buffer		40–60 [40–50]	70 [70]

[a] Enzyme activity was measured with Suc-Ala-Ala-Ala-*p*NA (0.470 mM) in 0.1 M Hepes, 0.5 M NaCl, pH 7.5 solution, and the percent enzyme activity is relative to the original PPE solution. The results represent the range observed in three separate experiments. [b] Percent protein recovered was obtained by comparing the absorbance of the solution at 280 nm with that of the original PPE solution.

original enzyme activity. It is likely that the biotinylated inhibitor moiety remained associated with the column and the active enzyme was released by deacylation from the inhibitor structure. For PPE inhibited by BIC **5**, 80% of protein was bound and then eluted from the monomeric avidin column and only 10% of the original PPE activity was recovered (step 4a). If a tetrameric avidin column was used, 40–60% of the original active enzyme was recovered by hydroxylamine and eluted from the column (step 4b). Control experiments indicates that PPE alone does not bind to either monomeric or tetrameric avidin column. Thus, with both BICs **5** and **7**, more active PPE was recovered if tetrameric avidin was used and treated immediately with hydroxylamine than an alternate procedure involving binding the inactive enzyme–inhibitor complex first to monomeric avidin, followed by elution with biotin, and then treatment with hydroxylamine.

Elastase activity was only partially recovered upon hydroxylamine treatment of PPE inactivated by BIC **5** or **7** after isolation of the PPE from immobilized monomeric avidin (Table IV). For PPE inhibited by BIC **5** or **7**, between 10 and 70% of active enzyme was recovered under the various conditions used to retain and reactivate the elastase. Incomplete enzyme recovery occurred when treatment with the strong nucleophile hydroxylamine was delayed until several hours after the initial inhibition or acylation reaction. During this time, formation of quinone imine methide groups would produce a larger fraction of alkylated enzyme (11), where the enzyme activity cannot be restored by NH_2OH treatment. Thus conditions which prevent alkylation, such as low pH, are likely to increase the potential for active enzyme recovery during isolation of enzyme–biotinylated inhibitor complexes.

BIC derivatives of other serine proteases such as HLE, chymotrypsin, and other lymphocyte granzymes (Hudig et al., unpublished results) have also been tested on tetrameric avidin agarose columns. Chymotrypsin inhibited by BIC **3**, **6**, or **8** spontaneously reactivated so rapidly in the gel filtration process that it did not bind appreciably to the columns even in a pH 5.0 acetate buffer. HLE inhibited by BIC **5** or **7** lost some enzyme activity during the hydroxylamine-dependent elution process from the avidin columns which resulted in a lower yield of recovered active enzyme. Thus, there are two requirements for the use of BICs for isolation of active serine proteases from avidin columns. The first is the formation of a stable nonalkylated acyl enzyme. The second requirement is stability of the enzyme during NH_2OH treatment or under other conditions necessary to regenerate active enzyme.

For many applications, unlike active serine protease isolation, the formation of a stable alkylated enzyme derivative upon reaction with BICs would be the preferred reaction course. A stable BIC–protease derivative is almost a necessity for applications involving cytochemistry or protein blots since these procedures require hours if not days to complete. In one such technique, BICs **6** and **7** have been used to tag granule serine protease contents in lymphocytes expressing multiple granzymes so that the bound biotin could be subsequently detected with fluorescent avidin using confocal microscopy (S. L. Woodard and D. Hudig, unpublished results). BIC **7** has also been used to detect multiple biotinylated proteins in cytotoxic RNK-16 granules in which multiple granzyme serine protease activities were inactivated, using egg avidin-alkaline phosphatase to detect proteins blotted to nitrocellulose after SDS–PAGE separation at alkaline pH. Another potential use would involve the isolation of inactivated BIC derivatives of new serine proteases from physiological systems. Subsequently, sufficient sequence information could be obtained which would then allow the preparation of DNA probes for the new serine protease gene.

SUMMARY

Isocoumarins with biotinylated substituents at the 7-position and differing 3-alkoxy groups are good mechanism-based inhibitors for representative serine proteases including PPE, HLE, trypsin, and chymotrypsin. Increased reactivity was observed with BIC derivatives which contained a single aminocaproyl spacer group. The 3-alkoxy groups on the isocoumarin ring determined the selectivity of the isocoumarins toward the different serine proteases, with 3-phenylethoxy groups reacting best with chymotrypsin, and shorter 3-methoxy, ethoxy, and propoxy groups reacting primarily with the elastases HLE and PPE. Full enzymatic activity was regained after the addition of hydroxylamine immediately to inhibited chymotrypsin and PPE derivatives. This indicates that simple acyl enzymes are formed initially during the inhibition reaction. However, upon longer incubation of the inhibitor–enzyme complexes, alkylated enzyme derivatives were also formed. Egg avidin did not effect the reactivation of the acyl enzyme derivative, while streptavidin facilitated this process. PPE inhibited by BIC **5** or **7** was bound to avidin–agarose columns. Most of inhibited PPE protein could be eluted from monomeric avidin columns; however active enzyme was only partially recovered due to the formation of alkylated enzyme derivatives during the isolation process. We believe that BICs may be useful for the isolation of new serine proteases under ideal circumstance where the enzyme forms a stable nonalkylated acyl enzyme and is stable to the reactivation conditions. We also suggest that BIC–protease derivatives may have wider applications when stable alkylated derivatives are formed. Such applications would include cytochemical localization of serine proteases in cells, detection and analysis of serine proteases on protein blots, and determination of sequence information for new serine protease found in various physiological systems.

ACKNOWLEDGMENT

This research was supported by Grant R01 GM42212 (to D.H. and J.C.P.) from the National Institutes of Health.

LITERATURE CITED

Berstein, K. E., Welsh, S. L., and Inman, J. K. (1990) A Deeply Recessed Active Site in Angiotensin-Coverting Enzyme Is Indicated from the Binding Characteristics of Biotin–Spacer–Inhibitor Reagents. *Biochem. Biophys. Res. Commun. 167*, 310–316.

Bieth, J., Spiess, B., and Wermuth, C. G. (1974) Synthesis and Analytical Use of a Highly Sensitive and Convenient Substrate of Elastase. *Biochem. Med. 11*, 350–357.

Billingsley, M. L., Pennypacker, K. R., Hoover, C. G., and Kincaid, R. L. (1987) Biotinylated Proteins As Probes of Protein Structure and Protein-Protein Interactions. *BioTechniques 5*, 22–31.

Cho, K., Tanaka, T., Cook, R. R., Kiesiel, W., Fujikawa, K., Kurachi, K., and Powers, J. C. (1984) Active-Site Mapping of Bovine and Human Blood Coagulation Serine Proteases Using Synthetic Peptide 4-Nitroanilide and Thioester Substrates. *Biochemistry 23*, 644–650.

Cullen, B. M., Halliday, I. M., Kay, G., Nelson, J., and Walker, B. (1992) The Application of a Novel Biotinylated Affinity Label for the Detection of Cathepsin B-Like Precursor Produced by Breast-Tumor Cells in Culture. *Biochem. J. 283*, 461–465.

Erlanger, B. F., Kokowsky, N., and Cohen, W. (1961) Preparation and Properties of Two Chromogenic Substrates of Trypsin. *Arch. Biochem. Biophys. 95*, 271–278.

Finn, F. M., Titus, G., and Hofmann, K. (1984) Ligands for Insulin Receptor Isolation. *Biochemistry 23*, 2554–2558.

Grassetti, D. R., and Murray, J. F., Jr. (1967) Determination of Sulfhydryl Groups with 2,2′- or 4,4′-Dithiodipyridine. *Arch. Biochem. Biophys. 119*, 41–49.

Harper, J. W., and Powers, J. C. (1985) Reaction of Serine Proteases with Substituted 3-Alkoxy-4-chloroisocoumarins and 3-Alkoxy-7-amino-4-chloroisocoumarins: New Reactive Mechanism-Based Inhibitors. *Biochemistry 24*, 7200–7213.

Hofmann, K., Zhang, W. J., Romovacek, H., Finn, F., Bothner-By, A. A., and Mishra, P. K. (1984) Syntheses of Biotinylated and Dethiobiotinylated Insulins. *Biochemistry 23*, 2547–2553.

Jasiewicz, M. L., Schoenberg, D. R., and Muller, G. C. (1976) Selective Retrieval of Biotin-Labeled Cells Using Immobilized Avidin. *Exp. Cell Res. 100*, 213–217.

Kam, C.-M., Fujikawa, K., and Powers, J. C. (1988) Mechanism-Based Isocoumarin Inhibitors for Trypsin and Blood Coagulation Serine Proteases: New Anticoagulants. *Biochemistry 27*, 2547–2557.

Kam, C.-M., Oglesby, T. J., Pangburn, M. K., Volanakis, J. E., and Powers, J. C. (1992) Substituted Isocoumarins As Inhibitors of Complement Serine Proteases. *J. Immunology 149*, 163–168.

Kay, G., Ballie, J. R., Halliday, I. M., Nelson, J., and Walker, B. (1992) The Synthesis, Kinetic Characterization and Application of Biotinylated Aminoacylchloromethanes for the Detection of Chymotrypsin and Trypsin-Like Proteinases. *Biochemical J. 283*, 455–459.

Nakajima, K., Powers, J. C., Ashe, B. M., and Zimmerman, M. (1979) Mapping the Extended Substrate Binding Site of Cathepsin G and Human Leukocyte Elastases. Studies with Peptide Substrates Related to the α_1-Protease Inhibitor Reactive Site. *J. Biol. Chem. 254*, 4027–4032.

Neurath, H. (1984) Evolution of Proteolytic Enzymes. *Science 224*, 350–357.

Odake, S., Kam, C.-M., Narasimhan, L., Poe, M., Blake, J. T., Krahenbuhl, O., Tschopp, J., and Powers, J. C.(1991) Human and Murine Cytotoxic T Lymphocyte Serine Proteases: Subsite Mapping with Peptide Thioester Substrates and Inhibition of Enzyme Activity and Cytolysis by Isocoumarins. *Biochemistry 30*, 2217–2227.

Powers, J. C., and Harper, J. W. (1986) Inhibitors of Serine Proteinases. In *Proteinase Inhibitors* (A. J. Barrett and G. Salvesen, Eds.) Elsevier, Amsterdam, New York, Oxford, pp 55–152.

Powers, J. C., Oleksyszyn, J., Narasimhan, L., Kam, C.-M., Radhakrishnan, R., Meyer, E. F., Jr. (1990) Reaction of Porcine Pancreatic Elastase with 7-Substituted-3-alkoxy-4-chloroisocoumarins: Design of Potent Inhibitors Using the Crystal Structure of the Complex Formed with 4-Chloro-3-ethoxy-7-guanidinoisocoumarin. *Biochemistry 29*, 3108–3118.

Schecter, I., and Berger, I. (1967) On the Size of the Active Site in Protease. 1. Papain. *Biochem. Biophys. Res. Commun. 27*, 157–162.

Towbin, H., and Gordon, J. (1984) Immunoblotting and Dot Immunobinding-Current Status and Outlook. *J. Immunol. Methods 72*, 313–340.

Walker, B., Cullen, B. M., I. M., Kay, Halliday, G., MacGinty, A., and Nelson, J. (1992) The Synthesis, Kinetic Characterization and Application of a Novel Biotinylated Affinity Label for Cathepsin B. *Biochemical J. 283*, 449–453.

Williams, E. B., Krishnaswamy, S., and Mann, K. G. (1989) Zymogen/Enzyme Discrimination Using Peptide Chloromethyl Ketones. *Biol. Chem. 264*, 7536-7545.

TECHNICAL NOTES

A Simplified Method for the Preparation of Succinimidyl Carbonate Polyethylene Glycol for Coupling to Proteins

Talia Miron and Meir Wilchek*

Department of Biophysics, The Weizmann Institute of Science, Rehovot 76100, Israel. Received January 21, 1993®

An improved method for the activation of polyethylene glycol with commercially available succinimidyl carbonate is described. The activated polyethylene glycol was coupled to proteins in high yield.

INTRODUCTION

Proteins modified with polyethylene glycol have become very important due to their numerous applications in diagnostics (*1*), in medicine (*2–4*) and for the enzymatic synthesis in organic solvents (*5*, *6*).

Recently, it has been shown that succinimidyl carbonate polyethylene glycol (SC-PEG)[1] is the reagent of choice for covalent attachment to proteins (*7*). However, the described method for the preparation of this "activated PEG" is relatively time-consuming, laborious, and dangerous.

In the following we describe a simple, rapid method for the preparation of SC-PEG in high yield by using *N*-succinimidyl chloroformate (*8*) or a commercially available reagent, namely *N,N'*-disuccinimidyl carbonate (*9*).

These reagents have been used in our laboratory for the last 10 years for the activation of polyethylene glycol or monomethoxypolyethylene glycol, their coupling to proteins has been accomplished according to Scheme I and, the protocol is outlined below.

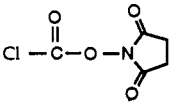
EXPERIMENTAL PROCEDURES

Reagents, all chemicals, solvents, polyethylene glycol (8000), and monomethoxypolyethylene glycol (2000 and 5000) were from Aldrich (Milwaukee, WI). Proteins were obtained from Sigma Chemical Co. (St. Louis, MO). *N*-Succinimidyl chloroformate was prepared according to the method of Gross and Bilk (*10*). *N,N'*-Disuccinimidyl carbonate and 4-(Dimethylamino)pyridine were from Fluka (Buchs, Switzerland). Prestained SDS–PAGE standards of low molecular weight was from Bio-Rad (Richmond, CA). Thin-layer chromatography (TLC) was carried out on aluminium sheets precoated with silica gel 60 F_{254} from Merck (Darmstadt, Germany).

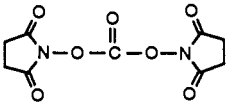
Preparation of SC-PEG. Polyethylene glycol or monomethoxypolyethylene glycol (1 mmol of powder) was dissolved in 5–25 mL of dry (molecular sieve) dioxane by heating in a water bath. The clear solution was brought to room temperature, and either *N*-succinimidyl chloroformate or *N,N'*-disuccinimidyl carbonate (5–7 mmol dissolved in 10 mL of dry acetone) was added.

4-(Dimethylamino)pyridine (5–7 mmol in 10 mL of dry acetone) was added slowly under magnetic stirring. Activation proceeded for 2 h for *N*-succinimidyl chloroformate and 6 h for *N,N'*-disuccinimidyl carbonate at room temperature. The activation mixture with *N*-succinimidyl chloroformate, contained a white precipitate of 4-(dimethylamino)pyridine hydrochloride, which was filtered through a fine sintered-glass funnel. The supernatant was collected, and the activated PEG was precipitated by diethyl ether until no more precipitation was observed (3–4 vol). In the activation mixture with *N,N'*-disuccinimidyl carbonate, the activated PEG was directly precipitated from the clear solution by diethyl ether. Several

Scheme I. Preparation of Succinimidyl Carbonate Polyethylene Glycol Methyl Ether (SC-PEG) (A) and PEG–Proteins (B)



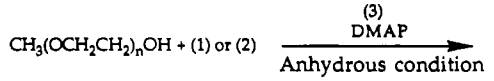
(1) N-Hydroxysuccinimidyl chloroformate



(2) N, N' Disuccinimidyl carbonate

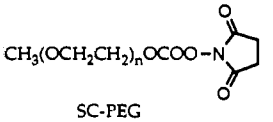
(3) 4-Dimethylaminopyridine (DMAP)

A. Activation:



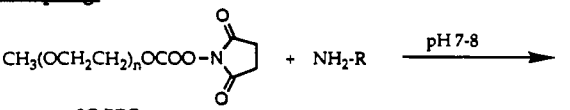
Poly(ethylene glycol) methyl ether

mPEG



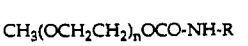
SC-PEG

B. Coupling:



SC-PEG

Protein



PEG-Protein

[®] Abstract published in *Advance ACS Abstracts*, October 1, 1993.

[1] Abbreviations used: PEG, polyethylene glycol; SC-PEG, succinimidyl carbonate polyethylene glycol.

1043-1802/93/2904-0568$04.00/0 © 1993 American Chemical Society

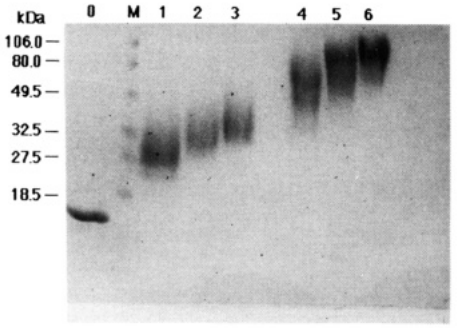


Figure 1. SDS-PAGE (12%) of non-pegylated (Lane 0) and pegylated hen egg white lysozyme (lanes 1–6) carried out at 4 °C for 16 h. Pegylation was done either with SC-PEG-2000 (lanes 1–3) or with SC-PEG-5000 (lanes 4–6). SC-PEG was used in ratio to lysine residues of 0.3:1 (lanes 1, 4), in excess of 2:1 (lanes 2, 5), and 8:1 (lanes 3, 6). M is prestained SDS–PAGE molecular weight markers [from top to bottom, in kDa]: phosphorylase B (106), bovine serum albumin (80), ovalbumin (49.5), carbonic anhydrase (32.5), soybean trypsin inhibitor (27.5) lysozyme (18.5). On each lane (0–6) 20 μg was loaded. The gel was stained with coomassie briliant blue G-250.

cycles of redissolving of the product in acetone and precipitation were carried out in both cases. Removal of the starting materials in the activated PEG were followed by chromatography on TLC in chloroform–methanol (5:1) system. The activated PEG was stored dry and desiccated at 4 °C and is stable for at least 1 year. The yield was over 95% as determined spectrophotometrically according to a previously published procedure (*11*). When the reactions were performed with triethylamine instead of 4-(dimethylamino)pyridine, the yield of the activated PEG was only around 40%. No efforts were made to remove unreacted PEG at this stage, since it does not disturb subsequent reaction with proteins.

Coupling of SC-PEG. Amino-containing ligands and proteins were derivatized with SC-PEG in 10–100 mM phosphate buffer, pH 6.5–7.5, at 4° C for 4–16 h. Nonreacting SC-PEG was removed by dialysis. An example for modulated modification of protein with activated monomethoxypolyethylene glycol is shown in Figure 1, where hen egg white lysozyme solutions (mg/mL) were modified with either SC-PEG-2000 or SC-PEG-5000.

LITERATURE CITED

(1) Sharp, K. A., Yalpani, M., Howard, S. J., and Brooks, D. E. (1986) Synthesis and application of a poly(ethylene glycol)-antibody affinity ligand for cell separation in aqueous polymer two-phase systems. *Anal. Biochem. 154*, 110–117.

(2) Abuchowski, A., Kazo, G. M., Verhoest, C. R., Jr., Van Es, T., Kafkewitz, D., Nucci, M. L., Viau, A. T., and Davis, F. F. (1984) Cancer therapy with chemically modified enzymes. I. Antitumor properties of polyethylene glycol asparaginase conjugates. *Cancer Biochem. Biophys. 7*, 175–186.

(3) Berger, H., Jr., and Pizzo, S. V. (1988) Preparation of polyethylene glycol-tissue plasminogen activator adducts that retain functional activity: characteristics and behavior in three animal species. *Blood 71*, 1641–1647.

(4) Katre, N. V., Knauf, M. J., and Laird, W. J. (1987) Chemical modification of recombinant interleukin 2 by polyethylene glycol increases its potency in the murine Meth A sarcoma model. *Proc. Natl. Acad. Sci. U.S.A. 84*, 1487–1491.

(5) Pina, C., Clark, D., and Blanch, H. (1989) The activity of PEG-modified chymotrypsin in aqueous and organic media. *Biotech. Tech. 3*, 333–338.

(6) Gaertner, H., Watanabe, T., Sinisterra, J. V., and Puigserver, A. (1991) Peptide synthesis catalyzed by modified α-chymotrypsin in low-water organic media. *J. Org. Chem. 56*, 3149–3153.

(7) Zalipsky, S., Seltzer, R., and Menon-Rudolph, S. (1992) Evaluation of a new reagent for covalent attachment of polyethylene glycol to proteins. *Biotech. Appl. Biochem. 15*, 100–114.

(8) Wilchek, M., and Miron, T. (1982) Immobilization of enzymes and affinity ligands onto agarose via stable and uncharged carbamate linkages. *Biochem. Internat. 4*, 629–635.

(9) Wilchek, M., and Miron, T. (1985) Activation of Sepharose with *N,N'*-disuccinimidyl carbonate. *Appl. Biochem. Biotech. 11*, 191–193.

(10) Gross, H., and Bilk, L. (1967). *Angew. Chem. 79*, 532–533.

(11) Miron, T., and Wilchek, M. (1982) A spectrophotometric assay for soluble and immobilized *N*-hydroxysuccinimide esters. *Anal. Biochem. 126*, 433–435.

Preparation of Sulfhydrylborane–Dextran Conjugates for Boron Neutron Capture Therapy

Anders Holmberg*,† and Lennart Meurling‡

Kabi Pharmacia Diagnostics AB, S-751 82 Uppsala, Sweden, and Mercodia AB, S-752 28 Uppsala, Sweden.
Received April 12, 1993®

This study presents a carrier system for boron, potentially useful in boron neutron capture therapy (BNCT). $Na_2B_{12}H_{11}SH$ (BSH) was covalently coupled to dextran derivatives. This was accomplished in two ways. The first method comprises activation of dextran with 1-cyano-4-(dimethylamino)pyridine (CDAP) with subsequent coupling of 2-aminoethyl pyridyl disulfide (method A). The thiolated dextran could then couple BSH in a disulfide exchange reaction. In the second procedure, dextran was derivatized to a multiallyl derivative (method B) which reacted with BSH in a free-radical-initiated addition reaction. The assessment of boron content of the conjugates was done by elemental analysis of sulfur and atomic spectroscopy of boron (ICP-AES). With method A, only limited numbers of boron cages could be coupled (10–20 cages per dextran chain). With method B, 100–125 boron cages per dextran chain was obtained, corresponding to 1200–1500 boron atoms per dextran chain. This result makes this derivative a promising template for use in the development of BNCT agents.

INTRODUCTION

The principle for boron neutron capture therapy (BNCT) for treatment of cancer is the nuclear reaction that occurs when ^{10}B is irradiated with thermal neutrons. This reaction yields an unstable intermediate, ^{11}B, which undergoes fission, yielding ^{7}Li and ^{4}He. One of the conditions for this therapy to be successful depends on the ability to transport sufficient concentrations of boron to the tumor tissue and preferably localize the boron into the cell. The induced radiation should then ultimately kill the tumor. The effects and medical possibilities of neutrons were described by Locher (Locher, 1936) and further by Bale (Bale, 1952). Clinical trials were first performed in the United States during the period 1951–1961, however with discouraging results.

In the last two decades treatment of brain tumors using BNCT has been performed in Japan (Hatanaka, 1990) using improved boron compounds and neutron irradiation techniques. Promising results have been obtained and the interest for BNCT is increasing. One of the main problems in BNCT is the delivery of boron to the target tissue.

Thus many workers are involved in the construction of carrier systems with capacity for enhanced loads of boron. A variety of compounds have been developed as boron carriers, for example antibodies (Bale and Spar, 1967; Hawthorne et al., 1976), amino acids (Ichihashi et al., 1982), porphyrins (Kahl et al., 1990), and low-density lipoproteins (Laster et al., 1991).

In the present study we have investigated the possibility to use dextran and BSH as a template for a BNCT agent. BSH is currently the best documented boron compound for BNCT, and dextran has previously been used in numerous studies as a microcarrier for both low and high molecular weight substances (De Belder, 1990; Foster, 1975; Hirai et al., 1989; Jost and Yaron, 1974; Melton et al., 1987) including tumor targeting applications (Bernstein et al., 1978; Hurwitz et al., 1980). Antibodies have been boronated via a dextran bridge (Pettersson et al., 1989). The activation methods employed have usually been periodate oxidation and conventional cyanogen bromide activation. Dextran is also well-known as a blood plasma volume expander. The preparation of BSH–dextran conjugates was done with two different methods, dextran activation with CDAP (Kohn and Wilchek, 1983) and subsequent thiolation with 2-aminoethyl pyridyl disulfide (method A) and reaction of BSH with allyl dextran (method B). The mechanism for the addition of mercaptans to double bonds in the presence of free-radical initiators has been described earlier (Stacey and Harris, 1963). The analysis of the boron content was made by elemental analysis of sulfur (Holmberg et al., 1992) and atomic spectroscopy of boron, ICP-AES, (Moore, 1990).

With method A, only moderate numbers of boron cages could be coupled, that is 10–20 boron cages per dextran chain. However with method B, 100–125 boron cages per dextran chain were coupled with retained solubility of the conjugate. This corresponds to 1200–1500 boron atoms per dextran chain. The high carrying capacity of this derivative makes it potentially useful as a BNCT agent.

EXPERIMENTAL PROCEDURES

Materials. Dextran T70 (Pharmacia Biotech AB, Sweden) with an average molecular weight of 70 kDa was used. 1-cyano-4-(dimethylamino)pyridinium salt (CDAP) for dextran activation and 2-aminoethyl pyridyl disulfide (AE-PDS) for thiolation were gifts from Kabi Pharmacia Diagnostics AB, Sweden. Triethylamine (TEA) from Rietel De Haen AG, Germany, was used. $Na_2B_{12}H_{11}SH$ (BSH) from Boron Biologicals was used as the boron compound. The separation and purification were carried out with gel filtration on NAP-5 G-25 and PD-10 G-25 disposable Sephadex G-25 columns from Pharmacia Biotech AB Sweden. The purity of the products was analyzed on a Sephadex G-25 1 × 10 cm column, Pharmacia Biotech AB, connected to a Shimadzu refractive index detector.

* The author to whom correspondence should be addressed. Telephone: 4618163587. Fax: 4618126419.
† Kabi Pharmacia Diagnostics AB.
‡ Mercodia AB.
® Abstract published in *Advance ACS Abstracts*, October 1, 1993.

1043-1802/93/2904-0570$04.00/0 © 1993 American Chemical Society

UV absorbance measurements were done with a Beckman UV spectrophotometer. ICP-AES was done with a Varian ICP-AES Liberty 200 instrument (Analytica AB, Sweden).

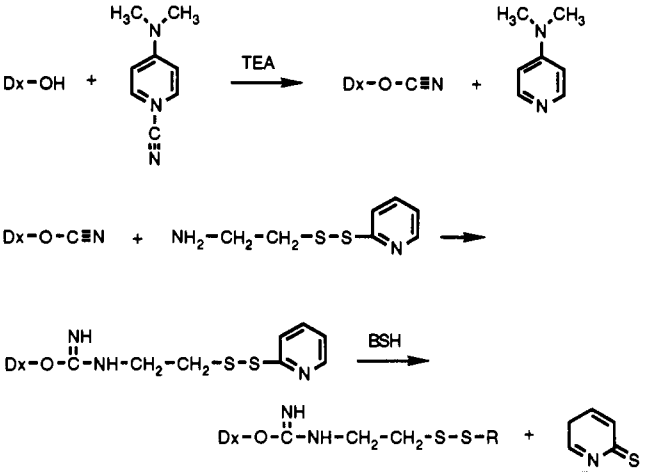
Methods. *CDAP Method (method A).* Dextran T70 (250 mg, 3.5 μmol) was dissolved in 25 mL of distilled water and mixed with 125 mg (0.55 mmol) of CDAP for 10 s. Triethylamine (75μL, 0.5 mmol) was added dropwise and the reaction mixture was stirred for 150 s at room temperature. A 250-μL sample of the reaction mixture was withdrawn and immediately mixed with the coupling solution containing 2.5 mg of AE-PDS in 250μL of 0.4 M Na_2HPO_4, pH 8.0. The conjugation was performed at room temperature for 120 min. After the conjugation low molecular weight residues were removed on a NAP-5 G-25 column equilibrated with 0.5 M NaCl. The sample was eluted with 0.2 M Na_2HPO_4, pH 8.0. A 75-μL sample of the thiolated dextran was then withdrawn and diluted to 3 mL in 0.2 M Na_2HPO_4,pH 8.0. Dithiothreitol (30 mg) was added and after incubation for 10 min the absorbance was recorded at 343 nm in a spectrophotometer. From the released thiopyridone (E 8080) the subtitution of AE-PDS could be calculated. The thiol dextran mixture was then added to a coupling solution containing 20 mg of BSH (0.14 mmol) in 0.5 mL of 0.2 M Na_2HPO_4,pH 8.0, and stirred at room temperature overnight. After the incubation a new 75-μL sample was taken and diluted to 3 mL in the same buffer as above. The released thiopyridone was measured at 343 nm and the efficiency of the reaction could be calculated. Finally, the conjugate was purified on a PD-10 G-25 column (equilibrated with 0.5 M NaCl) and eluted with distilled water. The purity of the product was confirmed by analytical chromatography on a 1 × 10 cm G-25 column. The eluate was analyzed with a refractive index detector and was found to be homogenous. Finally the product was lyophilized. The sulfur content was determined by elemental analysis (Kirsten and Nordenman, 1987). From the results obtained, the degree of substitution was calculated and hence the boron content, assuming two sulfur atoms per boron cage.

Allyl Bromide Method (Method B). Dextran T70 (20 g) was dissolved in 150 mL of distilled water together with 5 g of NaOH and 0.2 g of sodium borohydride. Allyl bromide (35 g, 0.30 mol) was added at 40°C. The mixture was stirred at 60 °C for 3 h and then neutralized with acetic acid. The product was purified by repeated precipitations in ethanol and dried to a constant weight under vacuum. The allyl content was determined by bromination of the dextran derivative in water, followed by potentiometric titration of released bromide with silver nitrate.

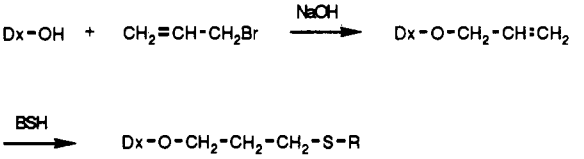
To a solution of 20 mg of allyl dextran in 0.2 mL of distilled water was added 30 mg of BSH (0.13 mmol) and 20 mg of ammonium persulfate. The solution was stirred for 2 h at 50°C. The reaction mixture was purified by gel filtration on a PD-10 G-25 column according to the manufacturers recommendations. The purity of the product was confirmed by analytical gel chromatography on a 1 × 10 cm G-25 column. The eluate was analysed with a refractive index monitor and was found to be homogenous. Finally the product was lyophilized.

The product was analysed for boron content by means of inductively coupled plasma atomic emission spectroscopy (ICP-AES). The sulfur content was determined by elemental analysis.

Scheme I



Scheme II



R = Boron cage

Dx = Dextran

RESULTS

The overall reaction of CDAP with dextran and coupling of BSH is shown in Scheme I.

With the CDAP method 10–20 boron cages per dextran chain was coupled. This is in agreement with the number of thiol groups introduced (12–20 AE-PDS per dextran chain) and the released thiopyridone after the BSH coupling. The reaction was quantitative. The elemental analysis gave figures from 0.5% to 0.9% sulfur corresponding to a boron content from 10 to 18 μg/mg of conjugate (assuming two sulfur atoms per boron cage), that is 10–20 boron cages. Attempts to raise the substitution level by increasing the activation invariably resulted in precipitation either during the activation or in the coupling of AE-PDS. The pH optimum for the coupling of AE-PDS was approximately pH 8. When the activation and the subsequent coupling of AE-PDS could be done without precipitation, the complex remained soluble during and after the disulfide exchange reaction with BSH. In order to increase the amount of boron bound we introduced the allyl bromide method, which is shown in Scheme II.

With method B, the substitution of boron was higher. The ICP-AES analysis gave 150 μg of boron/mg of conjugate. The sulfur content was 3.5–4%. This corresponds to a substitution of 100–125 boron cages per dextran chain or 1200–1500 boron atoms per dextran chain. Since the allyl content was determined to be 3.75 mmol/g of dextran derivative (70% of the glucose units had been substituted with an allyl group), approximately 50% of the allyl groups had been substituted with a boron cage. The complex remained soluble in all steps of the synthesis.

DISCUSSION

In this study we described two methods to couple boron cages to dextran. Method A is easy to perform and very

fast but has some disadvantages: first, low capacity and, second, the product sometimes precipitates. The precipitation occurring was probably due to cross-linking of the dextran. In the activation step the reactive species reacts further with adjacent hydroxyl groups, thus cross-linking the dextran. This side reaction increases with increasing degree of activation. In the coupling of the thiol compound the precipitation could be explained by S–S formation between dextran chains. The results indicate that the CDAP method as an activator of dextran does not provide enough carrying capacity for boron as required for BNCT. However, the CDAP method can be useful for the preparation of other targeting compounds using dextran and with lower requirements for carrying capacity. The CDAP method gives the same products as the cyanogen bromide reaction. It should always be preferred before the conventional toxic and inefficient cyanogen bromide method.

The B method proved to be very efficient as an activator of dextran, giving capacity to couple a high number of boron cages. The general carrying requirement for a BNCT compound (i.e. 1000 boron atoms/conjugate) was exceeded. We believe that the carrying capacity of this derivative can be even more improved by further optimization. The charge of the derivative is anionic, which can be of importance for in vivo localization (Maeda et al., 1992). It is possible to couple a targeting molecule to the boron–dextran, making it tumor-specific, for example epidermal growth factor (Andersson et al., 1991) or another tumor-specific molecule. BSH–dextran can thus be seen as a template for a potentially useful BNCT agent. The BSH–dextran derivative might by itself have a potential as a "passive" targeting BNCT agent. The concept of "passive" targeting has been extensively studied and described by Maeda (Maeda et al., 1992) and Seymour (Seymour, 1992). It is based on the increased permeability for macromolecules of tumor vasculature and the impaired or absent lymph drainage. This leads to prolonged retention of macromolecules in tumor tissue (the enhanced permeability and retention effect, EPR). EPR is seen in most solid tumors, and it is probable that EPR is of dominating importance for any tumor targeting compound, specific or passive. The most positive clinical results obtained with BNCT has been with BSH "passively" administered to the tumor even though the mechanism for the affinity of BSH for tumors remains still unclear.

The dimer of BSH has been shown to have even stronger tumor uptake than the monomer (Joel et al., 1990). The "poly BSH" derivative described here might show a similar affinity for tumor tissue. Another direct application of boron–dextran could be BNCT of arterio venous malformations (AVM). This treatment possibility has been proposed by Larsson (Larsson, 1988). Lately BNCT for AVM has been performed in Japan by Hatanaka (Hatanaka et al., 1992). The BSH–dextran derivative described here could be very suitable for this purpose. Experiments to evaluate the clinical relevance of the above mentioned boron dextran are in progress and will be reported elsewhere.

ACKNOWLEDGMENT

This work was supported by Kabi Pharmacia Diagnostics AB, S-751 82 Uppsala, Sweden. The author wants to thank Dr. Holmlund at MERCODIA AB for fruitful discussions and Dr. Weinreich at IMR, University of Zurich, for supporting the boron analysis.

LITERATURE CITED

Andersson, A., Holmberg, A., Carlsson, J., Carlsson, J., Ponten, J., and Westermark, B. (1991) Binding of epidermal growth factor-dextran conjugates to cultured glioma cells. *Int. J. Cancer 47*, 439–444.

Bale, W. F. (1952) Variation in effect of electromagnetic radiation with changes in quantum energy. *Proc. Natl. Cancer Conf. 2*, 967–976.

Bale, W. F., and Spar, I. L. (1967) Towards the use of antibodies as carriers of radioactivity for therapy. *Monogr. Adv. Biol. Med. Phys. 5*, 286–356.

Carlsson, J., Drevin, H., and Axen, R. (1977) Protein thiolation and reversible protein–protein conjugation. *Biochem. J. 173*, 723–737.

De Belder, A. N. (1990) *Dextran*, Pharmacia Leo Therapeutics, Uppsala, Sweden. Bernstein, A., Hurwitz, E., Maron, R., Arnon, R., Sela, M., and Wilchek, M. (1978) Higher antitumor efficacy of daunomycin when linked to dextran: In vivo and in vitro studies. *J. Natl. Cancer Inst. 60*, 379–384.

Foster, R. L. (1975) Preparation and properties of a soluble trypsin–dextran conjugate. *Experentia. 31*, 772–773.

Hatanaka, H. (1990) Clinical results of boron neutron capture therapy. In *Neutron Beam Design, Development and Performance for Neutron Capture Therapy* (O. K. Harling, J. A. Bernard, Jr., and R. G.Zamenhof, Eds.) pp 15–21, Plenum Press, New York.

Hatanaka, H., Nakagawa, Y., and Sakaki, S. (1992) Endovascular boron-neutron capture radiotherapy for giant arteriovenous malformations. *5th Int. Symp. Neutron Capture Ther. 122*, 62.

Hawthorne, M. F., Wiersema, R. J., and Takasugi, M. (1976) Preparation of tumour specific compounds: In vitro studies using boron labelled antibodies and elemental boron as neutron targets. *J. Med. Chem. 19*, 1290–1294.

Hirai, H., Nozomu, H., Shinzo, N., Tsukada, Y., Hurwitz, E., and Sela, M. (1989) Protein recognition of immobilized ligands. *Immobilization of antigens, antibodies and drugs on carbohydrate chains and their use in oncology.* pp 257–265. Alan R. Liss, Inc., New York.

Holmberg, A., Meurling, L., Wernli, B., and Weinreich, R. (1992) The analysis of boron in dextran-sulfhydrylborane conjugates. *5th International Symposium on Neutron Capture Ther. 122*,

Hurwitz, E., Wilchek, M., and Pitha, J. (1980) Soluble macromolecules as carriers for daunomycin. *J. Appl. Biochem. 2*, 25–35.

Ichihashi, M., Nakanishi, T., and Mishima, Y. (1982) Specific Killing effect of $^{10}B_1$-Para-borophenylalanin in thermal neutron capture therapy of malignant melanoma: In vitro radiobiological evaluation. *J. Invest. Dermatol. 78*, 215–218.

Joel, D. D., Fairchild, R. G., Laissue, J. A., Saraf, S. K., Kalef-Ezra, J. A., and Slatkin, D. N. (1990) Boron neutron capture therapy of intracerebral rat gliosarcomas. *Proc. Natl. Sci. U.S.A. 87*, 9808–9812.

Jost, R., and Yaron, A. (1974) Preparation of soluble and insoluble polysaccharide conjugates of peptides with a free alpha amino group. *Eur. J. Biochem. 48*, 119–129.

Kahl, S. B., Joel, D. D., Nawrocky, M. M., Micca, P. L., Tran, K. P., Finkel, G. C., and Slatkin, N. L. (1990) Uptake of a nido-carboranylporphyrin by human glioma xenografts in athymic nude mice and by syngenic ovarian carcinomas in immunocompetent mice. *Proc. Natl. Acad. Sci. U.S.A. 87*, 7265–7269.

Kirsten, W., and Nordenmark, B. (1987) Rapid, automatic, high-precision method for micro, ultramicro, and trace determinations of sulphur. *Anal. Chim. Acta 196*, 59–68.

Kohn, J., and Wilchek, M. (1983) 1-Cyano-4-dimethylamino pyridinium tetrafluoroborate as a cyanylating agent for the covalent attachment of ligand to polysaccharide resins. *FEBS Lett. 154*, 209–210.

Larsson, B. (1988) *Clinical Aspects of Neutron Capture Therapy* (R. G. Fairchild, V. P. Bond, and A. V. Woodhead, Eds.) pp 21–26 Plenum, New York.

Laster, B. H., Popenoe, E. A., Pate, D. W., and Fairchild, R. G. (1991) Biological efficacy of boronated low density lipoprotein for boron neutron capture therapy as measured in cell culture. *Cancer Res. 51,* 4588–4593.

Locher, G. L. (1936) Biological effects and therapeutic possibilities of neutrons. *Am. J. Roentgenol. Radium Ther. 36,* 1–13.

Maeda, H., Seymour, L. W., and Miyamoto, Y. (1992) Conjugates of anticancer agents and polymers: Advantages of macromolecular therapeutics in vivo. *Bioconjugate Chem. 3,* 351–362.

Melton, R. G., Wiblin, C. N., Foster, R. L., and Sherwood, R. F. (1987) Covalent linkage of carboxypeptidase G2 to soluble dextrans. *Biochem. Pharmacol. 36,* 105–112.

Moore, D. E. (1990) A review of techniques for the analysis of boron in the development of neutron capture therapy agents. *J. Pharm. Biomed. Anal.8,* 547–553.

Pettersson, M. L., Courel, M. N., Girard, N., Gabel, D., and Delpech, B. (1989) In vitro immunological activity of a dextran-boronated monoclonal antibody. *Strahlenther. Onkol. 165,* 151–152.

Seymour, L. W. (1992) Passive tumour targeting of soluble macromolecules and drug conjugates. *Crit. Rev. Ther. Drug Carrier Sys. 9,* 135–187.

Stacey, F. W., and Harris, J. F., Jr. (1963) In *Organic Reactions,* Vol 150.

Synthesis and Radioiodination of *N*-Boc-*p*-(tri-*n*-butylstannyl)-L-phenylalanine Tetrafluorophenyl Ester: Preparation of a Radiolabeled Phenylalanine Derivative for Peptide Synthesis

D. Scott Wilbur,*,† Donald K. Hamlin,† Rajiv R. Srivastava,† and H. Donald Burns‡

Department of Radiation Oncology, University of Washington, Seattle, Washington 98195, and Merck Research Laboratories, West Point, Pennsylvania 19486. Received June 2, 1993®

An investigation to prepare a phenylalanine derivative which could be radioiodinated and used directly in peptide synthesis was conducted. *N*-Boc-*p*-(tri-*n*-butylstannyl)-L-phenylalanine tetrafluorophenyl ester was targeted and synthesized from *N*-Boc-*p*-iodo-L-phenylalanine. The requisite aryl stannylation reaction was found to be best conducted using the phenylalanine methyl ester. Thus, *N*-Boc-*p*-iodo-L-phenylalanine methyl ester was prepared and stannylated using bis(tributyltin) and tetrakis-(triphenylphosphine)palladium(0) in refluxing toluene to prepare *N*-Boc-*p*-(tri-*n*-butylstannyl)-L-phenylalanine methyl ester. Demethylation with aqueous base was accomplished without racemization to yield *N*-Boc-*p*-(tri-*n*-butylstannyl)-L-phenylalanine. Preparation of the targeted stannylphenylalanine tetrafluorophenyl ester was then accomplished using 2,3,5,6-tetrafluorophenol and 1,3-dicyclohexylcarbodiimide in anhydrous THF. Iodination and radioiodination reactions of the targeted compound were conducted in MeOH/1% HOAc to yield 83–95% of the desired *N*-Boc-*p*-[*I]iodo-L-phenylalanine tetrafluorophenyl ester.

INTRODUCTION

Many biologically active peptides, such as growth factors (*1, 2*) and neuropeptides (*3, 4*), are being evaluated as potential new pharmaceuticals (*5, 6*). Modification and development of new synthetic versions of peptides are currently under study. Ultimately, the biological properties of new peptides must be evaluated *in vitro* (e.g. protein association and stability) and *in vivo* (biological half-life, pharmacokinetics, and biodistribution) for application in biological systems. However, new peptides cannot be readily assessed without labeling them with a marker such as fluorescent dyes (*7, 8*) or radioisotopes (*9, 10*). For many applications, the peptides might be intrinsically labeled with tritium ($t_{1/2}$ = 12.35 y), carbon-14 ($t_{1/2}$ = 5730 y) or sulfur-35 ($t_{1/2}$ = 87 d). However, for some applications labeling with these isotopes may not be practical. For instance, *in vivo* evaluation of some peptides might be severely limited when radiolabeled with tritium, sulfur-35, or carbon-14 because the serum half-life may be very short, and only minute quantities of the radiolabeled peptide may be administered due to the pharmacological response elicited. Further, external imaging of the peptide *in vivo* may be desired to study distribution and pharmacokinetics, but this cannot be accomplished with these radionuclides due to their emission properties.

An alternative to labeling with the β-emitting radionuclides tritium, carbon-14, or sulfur-35 is to label with γ-emitting radionuclides. There are a number of different radionuclides which can be used to radiolabel proteins and peptides (*11*). Radionuclides of iodine (e.g. iodine-125, $t_{1/2}$ = 60 d; iodine-131, $t_{1/2}$ = 8 d) are most often employed, where direct radioiodination of peptides has provided a method of labeling which routinely results in very high specific activity. However, incorporation of radioiodine into peptides also has its drawbacks. Importantly, the oxidizing conditions used in electrophilic radioiodinations can be deleterious to other functional groups in the peptide, causing reduced or complete loss of biological activity. Radioiodination can also change the pK_a of a phenolic hydroxyl group on tyrosine when it has reacted with that amino acid and can alter the steric environment of any amino acid which is labeled. Further, the radioiodine can be labile under some *in vitro* and *in vivo* evaluation conditions, adding questions about whether the results are reflective of the peptide or free radionuclide. Methods of radioiodination involving small molecule conjugates of proteins and peptides (*12*) can be used to stabilize the radioiodine, but this may alter the nature of the peptide significantly.

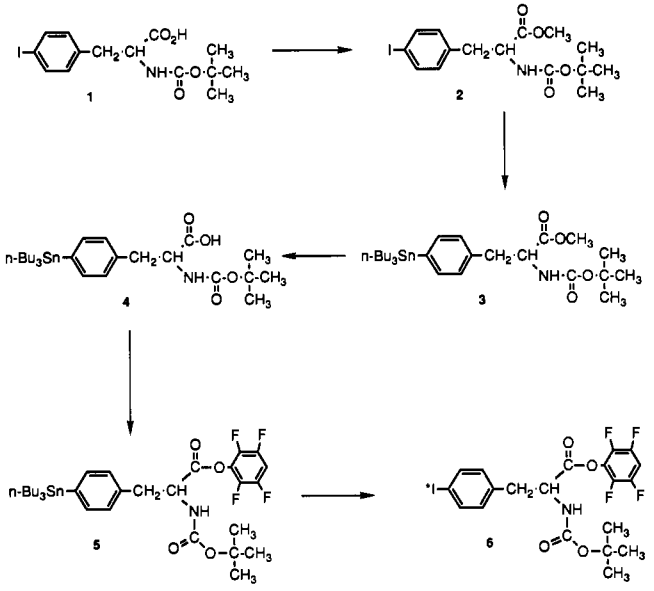
Another method of incorporating radioiodine into peptides is to prepare an amino acid analog that can be incorporated into the peptide. Using this method one could either incorporate a precursor molecule into a peptide and later radiolabel the peptide or radioiodinate the derivatized amino acid prior to its incorporation through peptide synthesis (*13–18*). While radioiodine could be incorporated into a number of different amino acids, incorporation into phenylalanine is particularly attractive, as the product should provide a stable radiolabel for both *in vitro* and *in vivo* evaluations. Additionally, although the incorporation of a *para*-iodinated phenylalanine in a peptide would be expected to alter its nature somewhat due to the increased steric nature and lipophilicity of the iodine, it might be expected to cause minimal alterations in many peptides.

Radioiodinated *p*-iodophenylalanine derivatives of peptides have been previously prepared (*19–21*), and the incorporation of the radioiodine has been found to be well tolerated. Indeed, in one case incorporation of iodine led

* Address reprint requests to D. Scott Wilbur, Department of Radiation Oncology, University of Washington, XD-48, 2121 N. 35th Street, Seattle, WA 98103-9103.
† University of Washington.
‡ Merck Research Laboratories.
® Abstract published in *Advance ACS Abstracts,* October 15, 1993.

1043-1802/93/2904-0574$04.00/0 © 1993 American Chemical Society

Scheme I. Synthesis and Iodination of Phenylalanine Derivatives



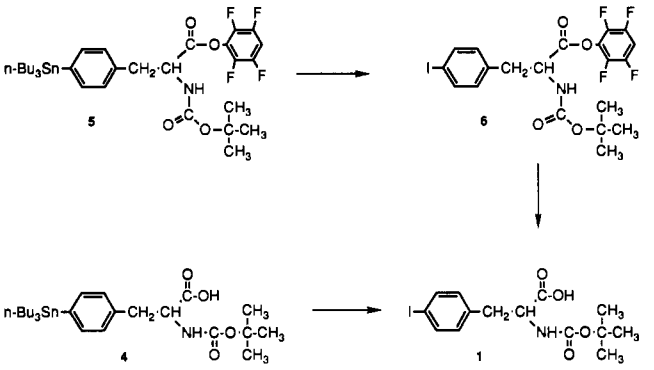
to an increased affinity and selectivity of an enkephalin for the δ-opioid receptor (*20*). The method for incorporation of radioiodine (^{125}I) in these studies was through preparation and decomposition of diazonium salt derivatives of phenylalanine residues in the peptides. Although the studies demonstrated the successful application of diazonium decompositions (i.e. Gatterman/Sandmeyer reactions) to prepare several radioiodinated peptides, this method of radioiodination requires that the corresponding aminophenylalanine derivative be prepared and that other functional groups in the peptide be stable to diazotization conditions. Further, low radiochemical yields (e.g. 1–25%) are often obtained.

We have focused our efforts on developing alternative methods for preparing radioiodinated *p*-iodophenylalanine-containing peptides utilizing organometallic intermediates. On the basis of our previous experiences with radioiodination of aryl compounds using organometallic intermediates (*12*), it was anticipated that peptides could be radioiodinated (with ^{123}I, ^{125}I, or ^{131}I) using a variety of organometallic phenylalanine derivatives under mild reaction conditions to yield high specific activity products in high radiochemical yields. Thus, we have begun our peptide radioiodination studies by investigating the synthesis of a phenylalanine derivative which could be readily radioiodinated and subsequently incorporated into a peptide through peptide synthesis. Herein, we report on the synthesis of *N*-Boc-*p*-(tri-*n*-butylstannyl)-L-phenylalanine tetrafluorophenyl ester, **5**, and its radioiodination reactions to form *N*-Boc-*p*-[^{125}I]iodo-L-phenylalanine tetrafluorophenyl ester, [^{125}I]-**6**, as depicted in Schemes I and II.

EXPERIMENTAL PROCEDURES

General. All chemicals purchased from commercial sources were analytical grade or better and were used without further purification unless noted. Halogenated L- and D,L-phenylalanine derivatives were obtained from Bachem (Bioscience, Inc. Philadelphia). THF was dried over Na/benzophenone prior to use. HPLC chiral columns used in evaluation of phenylalanine enantiomeric purity were a 25 cm × 4.6 mm Supelcosil LC-(*R*)-DNB-PG (Supelco, Inc., Bellefonte, PA) and a 25 cm × 4.6 mm β-cyclodextrin column, (*R,S*)-hydroxypropyl ether Cyclobond I RSP (Advanced Separation Technologies, Inc., Whippany, NJ).

Scheme II. Iodination of Phenylalanine Derivatives for Analysis of L-Enantiomeric Excess



^{1}H NMR were obtained on either a Varian VXR-300 (300 MHz) or a Bruker AC-200 (200 MHz) instrument. NMR data are referenced to tetramethylsilane as an internal standard (δ = 0.0 ppm). IR data were obtained on a Perkin-Elmer 1420 IR spectrophotometer and refer to absorptions of strong intensity unless otherwise noted for (m) medium intensity or (w) weak intensity. Mass spectral data (both low and high resolution) were obtained on a VG Analytical (Manchester, England) VG-70 SEQ mass spectrometer with associated 11250J Data System. FAB$^+$ mass spectral data were obtained at 8 kV using a matrix of sodium salt of 3-nitrobenzyl alcohol. Melting points were obtained on a Melt-Temp II and are uncorrected.

HPLC separations of the nonradioactive compounds were obtained on a Hewlett-Packard 1050 gradient pumping system with a multiple-wavelength UV detector (220, 254, and 280 nm) or a Hewlett-Packard 1050 isocratic pumping system with variable wavelength UV detector (220 or 254 nm) and a Hewlett-Packard 1047A refractive index detector. Analyses of the HPLC data were conducted on a Hewlett-Packard Vectra QS/16S computer employing Hewlett-Packard HPLC ChemStation software. Gradient HPLC separations were conducted at a flow rate of 1 mL/min on a 5 μm, 125 × 4 mm C-18 column (LiChrospher 100 RP-18) with an initial elution mixture of either 80% MeOH/20% of a 1% HOAc in H_2O mixture or a 80% MeOH/20% of a 5 mM tetrabutylammonium phosphate (TBAP) in H_2O mixture. The gradient was held at the initial elution mixture for 5 min, increased in percentage of MeOH to 98% for 10 min, and held at 98% MeOH for 10 min. Retention times for compounds are as follows: **1** = 1.0 min, **2** = 2.7 min, **3** = 10.9 min, **4** = 6.3 min, **5** = 12.3 min, **6** = 5.2 min, under the described conditions.

The radioiodination of **5** was analyzed by HPLC using a 5-μm C-18 column (PartiSphere C-18, Whatman) eluting with a gradient of MeOH and TBAP in H_2O as described above. The HPLC equipment used in this analysis consisted of two Beckman Model 110B pumps, a Beckman 420 controller, a Beckman Model 153 UV detector (254 nm), and a Beckman Model 170 radioisotope detector. Retention times on this system for the stannyl derivative **5** was 18.7 min and for the iodinated product **6** was 3.8 min.

Chiral HPLC analyses were conducted on the isocratic system described above at a solvent flow rate of 1 mL/min on a β-cyclodextrin column (Cyclobond I) eluting with 15% MeOH/85% of a 1% triethylamine solution (adjusted to pH 5 with HOAc). Samples of *N*-Boc-*p*-iodo-L-

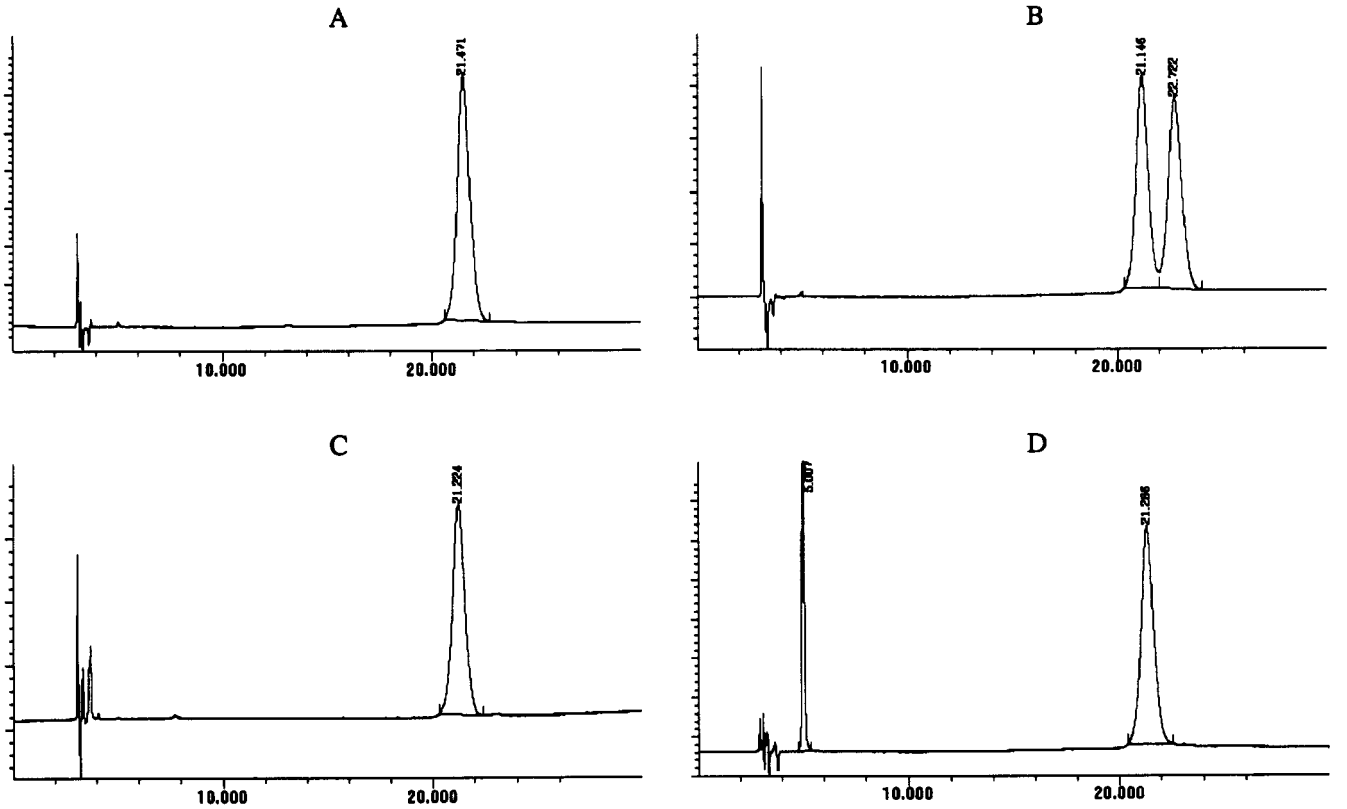


Figure 1. Chiral HPLC chromatograms of *N*-Boc-*p*-iodophenylalanine: A, *N*-Boc-*p*-iodo-L-phenylalanine standard (Bachem); B, *N*-Boc-*p*-iodo-D,L-phenylalanine standard (Bachem); C, product mixture from iodination of *N*-Boc-*p*-(tri-*n*-butylstannyl)-L-phenylalanine, **4**; D, product mixture from iodination of and de-esterification of *N*-Boc-*p*-(tri-*n*-butylstannyl)phenylalanine tetrafluorophenyl ester, **5**.

phenylalanine and *N*-Boc-*p*-iodo-D,L-phenylalanine for analysis were prepared as 1 mg/mL solutions in MeOH/1% HOAc. Analyses were conducted with 2-μL aliquots of the standard solutions (Figure 1A,B). Similar quantities of materials from the reaction mixtures were used in comparative analyses.

Synthesis of *N*-Boc-*p*-iodo-L-phenylalanine Methyl Ester, 2. To a solution of 5.02 g (12.8 mmol) of *N*-Boc-*p*-iodo-L-phenylalanine in 60 mL of dimethylformamide was added 1.42 g of $NaHCO_3$ (16.9 mmol) followed by 3.0 mL of methyl iodide (48.2 mmol). This mixture was stirred under argon for 40 h at room temperature. After this time, 150 mL of ethyl acetate was added and the mixture was washed with 3 × 100 mL of deionized water. The organic layer was separated, dried over $MgSO_4$, and concentrated under vacuum to yield 5.99 g of a yellow oily solid. This crude mixture was placed on a silica gel column (200 g, 4 × 34 cm, 60 Å) and eluted with 50/50 EtOAc/hexanes. Collection of 75-mL fractions yielded 4.72 g (91%) of a white solid when fractions 4–8 were combined and the solvent was removed: mp 78.5–80 °C; IR (Nujol, cm^{-1}) 3340, 1750, 1680, 1520, 1260, 830(m), 800(w); ^1H NMR ($CDCl_3$, δ) 7.61 (2H, d, J = 4.2 Hz), 6.87 (2H, d, J = 4.2 Hz), 4.97 (1H, d, J = 3.7 Hz), 4.56 (1H, m), 3.71 (3H, s), 3.02 (2H, m), 1.42 (9H, s); HRMS FAB$^+$ M + H, calcd for $C_{15}H_{21}NO_4I$ 406.0515, found 406.0525; M + Na, calcd for $C_{15}H_{20}NO_4INa$ 428.0335, found 428.0355.

Synthesis of *N*-Boc-*p*-(tri-*n*-butylstannyl)-L-phenylalanine Methyl Ester, 3. To a solution of 4.5 g (11 mmol) of **2** in 60 mL of dry toluene was added 23 mL (46 mmol) of bis(tributyltin) followed by 200 mg (0.17 mmol) of tetrakis(triphenylphosphine)palladium(0). The mixture was stirred under argon at room temperature for 10 min before heating to reflux (bath temperature, 120 °C) for 90 min. At that time the mixture changed from clear/light yellow to opaque/black. After cooling to room temperature, the solvent was removed under vacuum and the resulting black oil was dissolved in 20 mL of hexanes. To this solution was added 15 mL of triethylamine and the mixture stirred for 30 min. The precipitate was filtered and the filtrate was concentrated to a brown oil. This oil was placed on a silica gel column (200 g, 4 × 34 cm, 60 Å), eluting with 5% EtOAc in hexanes. Collection of 50-mL fractions yielded 5.16 g (81%) of a colorless oil when fractions 17–24 were combined and solvent was removed: IR (neat, cm^{-1}) 1740, 1715, 1490, 1360, 1165; ^1H NMR ($CDCl_3$, δ), 7.38 (2H, d, J = 3.9 Hz), 7.08 (2H, d, J = 3.9 Hz), 4.97 (1H, d, J = 3.7 Hz), 4.58 (1H, m), 3.71 (3H, s), 3.05 (2H, m), 1.52 (6H, m), 1.41 (9H, s), 1.33 (6H, m, J = 7.2 Hz), 1.03 (6H, m), 0.88 (9 H, m, J = 7.2 Hz).

Synthesis of *N*-Boc-*p*-(tri-*n*-butylstannyl)-L-phenylalanine, 4. To a solution of 4.5 g (7.9 mmol) of **3** in 27 mL of methanol was added 9 mL of 1 N sodium hydroxide. The solution clouded with the addition of the NaOH and then cleared over time. This solution was stirred for 4 h at room temperature then concentrated to 5 mL by rotary evaporation. The resulting oily solid was dissolved in EtOAc and washed with deionized water. The organic layer was separated, dried over $MgSO_4$, and concentrated to yield 4.23 g (96%) of sticky colorless solid. HPLC analysis indicated that the compound was 95+% pure, so it was used without further purification: IR (neat, cm^{-1}) 3350, 1750, 1595, 1530, 1275, 1250, 1170, 1050, 860(m), 790(m), 775(m), 760(m); ^1H NMR (acetone-d_6, δ), 7.33 (2H, d, J = 3.9 Hz), 7.23 (2H, d, J = 3.9 Hz), 4.27 (1H, m), 3.28 (1H, m), 2.97 (1H, m), 1.56 (6H, m), 1.33 (15H, m), 1.05 (6H, m), 0.88 (9 H, t, J = 7.2 Hz).

Synthesis of *N*-Boc-*p*-(tri-*n*-butylstannyl)-L-phenylalanine Tetrafluorophenyl Ester, 5. To a solution of 4.0 g (7.2 mmol) **4** in 60 mL anhydrous THF was added

4.5 g (22 mmol) 1,3-dicyclohexylcarbodiimide and 2.4 g (14 mmol) 2,3,5,6-tetrafluorophenol. This mixture was stirred for 2 days at room temperature. The THF was then removed by rotary evaporation and 30 mL of EtOAc was added to the flask. The solid that did not dissolve was removed by vacuum filtration and the filtrate was concentrated to a light yellow oil (11 g; theoretical 5.1 g). A total of 6 g (55%) of this oil was then placed on a silica gel column (200 g, 4 × 34 cm, 60 Å) and eluted with hexanes. After collection of 15 × 50 mL fractions, the solvent was changed to 5% EtOAc in hexanes. Continued collection of 50-mL fractions yielded 1.45 g of a colorless oily solid when fractions 21–26 were combined. The oily solid was dissolved in 20 mL of acetonitrile and filtered to remove insoluble solid material. The solution was then diluted to 40 mL with acetonitrile and 10 mL of deionized water was added. The precipitate was collected by gravity filtration and rinsed with 20 mL of water and allowed to dry to yield 932 mg of white solid (33% based on a theoretical yield of 2.1 g for chromatographed material): mp 80.5–81 °C; IR (Nujol, cm^{-1}) 3345, 1785, 1690, 950, 860, 805; ^1H NMR ($CDCl_3$, δ) 7.43 (2H, d, J = 3.9 Hz), 7.19 (2H, d, J = 3.9 Hz), 7.02 (1H, m), 4.95 (2H, m), 3.24 (2H, m), 1.53 (6H, m), 1.43 (9H, s), 1.32 (6H, m, J = 7.2 Hz), 1.04 (6H, m), 0.88 (9 H, t, J = 7.2 Hz); MS/EI [Sn – 10 isotopes] calculated mass 701 (75), 702 (49), 703 (100), 704 (35); no peaks found; M – nBu calculated mass 644 (75), 645 (46), 646 (100), 647 (31); mass found (% of base); 644 (7.5), 645 (4.9), 646 (9.6), 647 (4.3); HRMS FAB$^+$ M + Na, calcd for $C_{32}H_{45}F_4NO_4SnNa$ (^{120}Sn) 726.2204, found 726.2250.

Synthesis of *N*-Boc-*p*-iodo-L-phenylalanine Tetrafluorophenyl Ester, 6 (from 1). To a solution of 1.0 g (2.6 mmol) of 1 in 20 mL of anhydrous THF was added 800 mg (3.9 mmol) of 1,3-dicyclohexylcarbodiimide and 860 mg (5.2 mmol) of 2,3,5,6-tetrafluorophenol. This mixture was stirred for 22 h at room temperature. The THF was removed by rotary evaporation and the residue diluted with 15 mL of EtOAc. The insoluble solid was filtered and the filtrate was concentrated to yield 2.24 g of an off-white solid (theoretical yield, 1.4 g).

A 867-mg portion (39%) of the isolated solid was placed on a silica gel column (40 g, 2 × 26 cm, 60 Å) and eluted with 15% EtOAc in hexanes. Upon concentration of the fractions containing UV absorbing materials, 425 mg (78% based on theoretical yield) of a white solid was obtained: mp 110–112 °C; IR (Nujol, cm^{-1}) 3350(m), 1780(m), 1685, 1520, 1480, 955(m), 940(m); ^1H NMR ($CDCl_3$, δ) 7.67 (2H, d, J = 4.1 Hz), 7.06 (1H, m), 7.00 (2H, d, J = 4.1 Hz), 4.93 (2H, m), 3.21 (2H, m), 1.43 (9H, s); HRMS FAB$^+$ M + H, calcd for $C_{20}H_{19}NO_4F_4I$ 540.0295, found 540.0308; M + Na, calcd for $C_{20}H_{18}NO_4F_4INa$ 562.0114, found 562.0135.

Synthesis of *N*-Boc-*p*-iodo-L-phenylalanine Tetrafluorophenyl Ester, 6 (from 5). To a solution of 20 mg (0.028 mmol) of 5 in 1 mL of MeOH/1% HOAc in a 1-mL conical vial was added 5.1 mg (0.034 mmol) of NaI. After stirring for 2 min, 4.8 mg (0.028 mmol) of *N*-chlorosuccinimide (NCS) was added in one portion. The reaction mixture initially turned brown and then went colorless within 15 s. The reaction mixture was analyzed by HPLC to show a complete conversion to 6 (i.e. identical HPLC retention time as coinjected standard).

Synthesis of *N*-Boc-*p*-[^{125}I]iodo-L-phenylalanine tetrafluorophenyl Ester, [^{125}I]-6. *Carrier Added.* A 10-μL aliquot of a 1 mg/mL solution of NaI (10 μg; 0.067 μmol) and 2 μL of a 0.01 N NaOH solution of Na[^{125}I]I were mixed in a small vial. In a separate vial, 50 μL of a 1 mg/mL MeOH/1% HOAc solution of 5 (50 μg; 0.071 μmol) and 30 μL of a 1 mg/mL MeOH solution of NCS (30 μg, 0.22 μmol) were mixed. The two mixtures were combined to give a colorless solution within 3 min. The reaction was quenched after 3 min with 10 μL of a 0.72 mg/mL aqueous solution of $Na_2S_2O_5$. Radio-HPLC analysis indicated that 95% of the radioactivity was present as the desired product, [^{125}I]-6.

No Carrier Added. A 50 μL solution containing 1 mg/mL of 5 (50 μg) in MeOH/1% HOAc was added to a small (500 μL) vial. To this solution was added 10 μL of a 1 mg/mL MeOH solution of NCS (10 μg) and then 2 μL of a 0.01 N NaOH solution of Na[^{125}I]I (930 μCi). The reaction mixture was stirred for 3 min and was quenched with 10 μL of a 0.72 mg/mL solution of $Na_2S_2O_5$. HPLC analysis of the reaction mixture indicated that 83% of the radioactivity was present in the peak which corresponded to the desired product, [^{125}I]-6.

Synthesis of *N*-Boc-*p*-iodo-L-phenylalanine, 1 (from 4). A 10-mg (0.018 mmol) quantity of 4 was dissolved in 1 mL of a MeOH/1% HOAc solution. To this solution was added 2.6 mg (0.017 mmol) of NaI, followed by 3.1 mg (0.018 mmol) of NCS. The resultant dark brown mixture cleared within 15 s, and was stirred for 3 min before being analyzed by HPLC. HPLC of the reaction mixture indicated that a new product had been obtained which was less lipophilic, having the same retention time as the standard. The reaction solution (2 μL) was examined by chiral HPLC after a 1:10 dilution with MeOH/1% HOAc (Figure 1C). NMR and IR gave further confirmation that the desired product had been obtained.

Synthesis of *N*-Boc-*p*-iodo-L-phenylalanine, 1 (from 5). To a 10-mg (0.014 mmol) quantity of 5 dissolved in 1 mL of MeOH/1% HOAc was added 2.5 mg (0.017 mmol) of NaI, followed by 2.4 mg (0.014 mmol) of NCS. After 3 min (disappearance of color), 200 μL of this solution was added to 400 μL of a 1 N aqueous NaOH solution. After another 3 min, the reaction mixture was examined by HPLC and was found to have been completely converted from the stannyl-TFP ester 5 to the free acid 1. This solution was examined (1 μL) by chiral HPLC (Figure 1D).

RESULTS AND DISCUSSION

The object of this research effort was to obtain a L-phenylalanine derivative which could be readily radioiodinated and used directly in peptide synthesis. To accomplish this objective it was necessary to prepare a L-phenylalanine derivative which had the α-amino group protected and had a carboxylate activated ester for coupling to the growing peptide (*17,18*). Another requirement was to incorporate a method of radioiodination, which could be carried out in the presence of the active ester and amine protecting group, as the last chemical step prior to use in peptide synthesis. An important consideration in the design of the phenylalanine derivative was that none of the synthetic steps cause racemization of the L-isomer.

Although previous studies had shown that phenylalanine could be labeled with radioiodine through exchange reactions (*22, 23*), the reaction conditions employed would not be compatible with requisite amine protecting groups or activated esters. Another method of radioiodination that was considered was preparation through an aryldiazonium salt or aryltriazine derivative of an appropriately protected phenylalanine (*23*). This was of interest as iodination/radioiodination of aryl compounds using these functional groups had been studied previously (*24–27*), and the preparation of the requisite *p*-aminophenylalanine

had previously been described (28–31). In fact, examples of the use of diazonium salts for radioiodination of peptides have been described in the literature (19–21), where *p*-nitrophenylalanine or *p*-aminophenylalanine were incorporated via peptide synthesis and subsequently converted to the diazonium salts. Unfortunately, radiochemical yields obtained in iododediazoniation reactions are often low, and hydrolysis of the diazonium compound to form phenols is a competing reaction where high specific activity radioiodine is used (25, 27).

Other studies on radioiodination of aryl compounds had shown that aryl organometallic groups could be used as intermediates to provide high radiolabeling yields under mild reaction conditions (32). In fact, an iodination via an aryltrimethylsilyl derivative of phenylalanine had been reported (33). Although it was demonstrated that iodination could be accomplished using the arylsilane when methyl and ethyl esters were present, based on previous studies involving iodination of arylsilanes (34), radioiodination of a phenylalanine derivative which had an "activated ester" would be very difficult using this method. Thus, we chose to prepare a different organometallic intermediate, a *p*-tri-*n*-butylstannyl derivative of phenylalanine. A number of studies have demonstrated that radioiodinations of arylstannanes can be accomplished rapidly in high yields under very mild conditions (12, 32, 35).

Peptide synthesis is most often conducted with the α-amine protected as a carbamate, generally the *tert*-butyloxycarbonyl (Boc) (36) or 9-fluorenylmethyloxycarbonyl (Fmoc) (37), when employing the Merrifield synthesis method (13, 36, 38). On this basis, and the considerations listed above, *N*-Boc-*p*-(tri-*n*-butylstannyl)-L-phenylalanine, **4**, was targeted for synthesis. Synthesis of **4** was first attempted using readily obtained *N*-Boc-*p*-bromophenylalanine via palladium-catalyzed stannylation (39). As this reaction did not yield the desired product, the same reaction was attempted using commercially available *N*-Boc-*p*-iodo-L-phenylalanine, **1**. This reaction was also unsuccessful, and after analysis of the reaction products indicated that the Boc protecting group had come off in the reaction, the corresponding *N*-Fmoc-*p*-bromophenylalanine derivative was prepared and used in the stannylation reaction. Again, reaction conditions appeared to remove the amine protecting group.

Aryl compounds containing free carboxylic acid functionalities have been successfully stannylated using the palladium-catalyzed reaction; however, higher yields in the stannylation reaction have been obtained when the carboxylate was protected as an ester (40). Thus, the carboxylate group of the phenylalanine derivative was esterified using 2,3,5,6-tetrafluorophenyl ester (TFP) to prepare *N*-Boc-*p*-iodo-L-phenylalanine tetrafluorophenyl ester, **6**. Application of the TFP ester was investigated since, if successfully stannylated, a compound which could be employed directly in peptide synthesis would be obtained. The TFP "active ester" was chosen because this ester has previously been found to be quite stable under a number of conditions, yet undergoes aminolysis rapidly (41–43). Further, an example of a stannylation of a benzoic acid TFP ester had been reported (44). Upon subjecting **6** to the stannylation reaction conditions, the desired product, **5**, was obtained, but the yield was low, prompting continued investigation of other routes to the synthesis.

Following these initial experiences, the synthetic route to obtain *N*-Boc-*p*-(tri-*n*-butylstannyl)-L-phenylalanine tetrafluorophenyl ester, **5**, was changed to incorporate a methyl ester in the stannylation step as shown in Scheme I. The use of a methyl ester in the stannylation of aryl compounds had previously improved yields in the stannylation reaction (40). Thus, *N*-Boc-*p*-iodo-L-phenylalanine, **1** was converted to the methyl ester **2** using sodium bicarbonate and methyl iodide in DMF. The methyl ester **2** was stannylated using bis(tributyltin)/tetrakis(triphenylphosphine)palladium(0) to prepare *N*-Boc-*p*-(tri-*n*-butylstannyl)-L-phenylalanine, **3**, in high yield. Deprotection of the acid functionality was accomplished by base hydrolysis of the methyl ester to yield *N*-Boc-*p*-(tri-*n*-butylstannyl)-L-phenylalanine, **4** . The hydrolysis step was of concern as it was uncertain if racemization of the L-isomer would occur under the reaction conditions. Attempts to evaluate the base-hydrolyzed stannylphenylalanine product, **4**, on chiral HPLC columns were unsuccessful. However, a separation of enantiomers of *N*-Boc-*p*-iodophenylalanine, **1**, was obtained on a β-cyclodextrin column (Figure 1, chromatograms A and B). Thus, after the methyl ester had been hydrolyzed, the product **4** was iodinated to give **1** (Scheme II), and was analyzed by HPLC for racemization (Figure 1, chromatogram C). Only a trace of the D-isomer was detected by chiral HPLC. Re-esterification of the Boc-protected stannylphenylalanine **4**, using 2,3,5,6-tetrafluorophenol and dicyclohexylcarbodiimide (DCC) in anhydrous THF, provided a moderate yield of the targeted compound, *N*-Boc-*p*-(tri-*n*-butylstannyl)-L-phenylalanine, **5**.

Prior to conducting the iodination/radioiodination reactions with **5**, an iodinated standard was synthesized from the *N*-Boc-*p*-iodo-L-phenylalanine, **1**. *N*-Boc-*p*-iodo-L-phenylalanine tetrafluorophenyl ester, **6**, was prepared by reacting **1** with 2,3,5,6-tetrafluorophenol and DCC in anhydrous THF. Iodination of **5** was then conducted using *N*-chlorosuccinimide (NCS) and NaI in MeOH. However, it was found that although the iodination was very fast, methanolysis of the tetrafluorophenyl ester also occurred very rapidly, and after only 5 min, 17% of the iodophenylalanine methyl ester **2** was observed by HPLC analysis. The methyl ester was also obtained when a standard of **6** was diluted in MeOH. Following that experiment, all dilutions of samples of either **5** or **6** were made in CH_3CN or MeOH containing 1% HOAc.

The enantiomeric excess of the targeted product, **6**, was also examined. To accomplish this, stannylphenylalanine **5** was iodinated with NaI and NCS in MeOH/1% HOAc, and subsequently the tetrafluorophenyl ester of **6** was hydrolyzed using aqueous NaOH, as depicted in Scheme II. The chromatogram of the product mixture from the two synthetic steps (Figure 1, chromatogram D) was very similar to that obtained for the reaction mixture from iodination of **4**, with an additional tetrafluorophenol peak (5.0 min). The analysis indicated that only a trace of the D-isomer was present. As the quantity of D-isomer was not increased from that seen after hydrolysis of the methyl ester, it can be concluded that racemization does not occur in the formation of the TFP ester or under the iodination reaction conditions.

Radioiodinations of **5** were conducted using Na[^{125}I]I and NCS in MeOH/1% HOAc. A carrier-added radioiodination was conducted with slightly less than 1 equiv of Na[^{125}I]I / NaI, resulting in 95% of the activity being present in the product peak by HPLC analysis. It was estimated that this product had a specific activity of 18 mCi/mmol. A no-carrier-added radioiodination resulted in 83% of the radioactivity eluting on HPLC at a retention time equal to that of the desired iodophenylalanine, **6**. On the basis of limited HPLC data for **6**, the specific activity

of this product was estimated to be >200 mCi/mmol (probably much higher). Another carrier-added radioiodination was conducted after nearly 7 months of storage (at −20 °C) of **5**, and a radiochemical yield of 87% was obtained. Thus, the stability of **5** seems quite good under the storage conditions employed, but it should be noted that radioiodinated **6** decreased in purity by roughly 5% within the first hour at room temperature.

CONCLUSION

In conclusion, the radioiodinated iodophenylalanine TFP ester **6** should be a fairly versatile reagent, potentially being useful in peptide synthesis, or in derivatizing the terminal amino group of peptides. It seems reasonable that such a radiolabeled compound could be coupled using the manual or "tea-bag" method of peptide synthesis, such that the contaminated reaction vessels can be disposed of readily and inexpensively. The carrier-added product, [^{125}I]-**6**, appeared to be of sufficient purity to use directly in a peptide synthesis. Other applications of this reagent may include its reaction with biologically active peptides or proteins to radiolabel them, similar to the previously developed *N*-succinimidyl *p*-[*I]iodobenzoic acid (*40*) and *N*-succinimidyl *m*-[*I]iodobenzoic acid (*45*) reagents. The no-carrier-added radioiodinated product might be useful in such an application, as this would offer a minimal derivatization of the peptide or protein. In fact, a similar radioiodinated tyrosine derivative has been described (*46*). Such a reagent is of interest as conjugation with a peptide would result in retention of the peptide's positive charge after removal of the Boc protecting group.

ACKNOWLEDGMENT

The authors thank Dr. Ross Lawrence from the Department of Medicinal Chemistry, University of Washington, for his assistance in obtaining mass spectral data. We also thank Merck Research Laboratories (formerly Merck, Sharpe and Dohme) for funding this research.

LITERATURE CITED

(1) Barnes, D., and Sirbasku, D. A. (Eds.) (1987) Peptide Growth Factors, *Methods in Enzymology*, Vol. 146 (Part A) and Vol. 147 (Part B), Academic Press, Inc., New York.

(2) Barnes, D., Mather, J. P., and Sato, G. H. (Eds.) (1991) Peptide Growth Factors, *Methods in Enzymology*, Vol. 198 (Part C), Academic Press, Inc. New York.

(3) Gainer, H. (Ed.) (1977) *Peptides in Neurobiology*, Plenum Press, Clifton, NJ.

(4) Boulton, A. A., Baker, G. B., and Pittman, Q. J. (Eds.) (1987) *Peptides*, Humana Press, Clifton, NJ.

(5) Hruby, V. J., and Rich, D. H. (Eds.) (1983) *Peptides. Structure and Function*, Pierce Chemical Co., Rockford, IL.

(6) Ward, D. J. (Ed.) (1991) *Peptide Pharmaceuticals. Approaches to the Design of Novel Drugs*, Elsevier, New York.

(7) Brinkley, M. (1992) A Brief Survey of Methods for Preparing Protein Conjugates with Dyes, Haptens, and Cross-linking Reagents. *Bioconjugate Chem. 3*, 2–13.

(8) Anumula, K. R., Schulz, R. P., and Back, N. (1992) Fluorescent N-Methanthranilyl (Mantyl) Tag for Peptides: Its Application in Subpicomole Determinations of Kinins. *Peptides 13*, 663–669.

(9) Kienhuis, C. B. M., Heuvel, J. J. T. M., Ross, H. A., Swinkels, L. M. J. W., Foekens, J. A., and Benraad, T. J. (1991) Six Methods for Direct Radioiodination of Mouse Epidermal Growth Factor Compared: Effect of Nonequivalence in Binding Behavior between Labeled and Unlabeled Ligand. *Clin. Chem. 37*, 1749–1755.

(10) Bakker, W. H., Krenning, E. P., Breeman, W. A., Kooij, P. P. M., Reubi, J.-C., Koper, J. W., de Jong, M., Lameris, J. S., Visser, T. J., and Lamberts, S.W. (1991) In Vivo Use of a Radioiodinated Somatostatin Analogue: Dynamics, Metabolism, and Binding to Somatostatin Receptor-Positive Tumors in Man. *J. Nucl. Med. 32*, 1184–1189.

(11) Kas, J., and Rauch, P. (1983) Labeled Proteins, Their Preparation and Applications. *Topics in Current Chemistry* (F. L. Boschke, Ed.) Vol. 112, pp 163–230, Springer-Verlag, New York.

(12) Wilbur, D. S. (1992) Radiohalogenation of Proteins: An Overview of Radionuclides, Labeling Methods, and Reagents for Conjugate Labeling. *Bioconjugate Chem. 3*, 433–470.

(13) Merrifield, R. B. (1986) Solid Phase Synthesis. *Science 232*, 341–347.

(14) Bodanszky, M. (1984) *Principles of Peptide Synthesis*, Springer-Verlag, New York.

(15) Kent, S. B. H. (1988) Chemical Synthesis of Peptides and Proteins. *Annu. Rev. Biochem. 57*, 957–989.

(16) Bayer, E. (1991) Towards the Chemical Synthesis of Proteins. *Angew. Chem. Int. Ed. Engl. 30*, 113–129.

(17) Stewart, J. M., and Young, J. D. (1984) *Solid Phase Peptide Synthesis*, 2nd ed., Pierce Chemical Co., Rockford, IL.

(18) Bodanszky, M. (1984) *The Practice of Peptide Synthesis*, Springer-Verlag, New York.

(19) Bosse, R., Neugebauer, W., and Escher, E. (1989) Peptide Iodination on Phenylalanine Residues. *Synthesis and Applications of Isotopically Labelled Compounds 1988*, (T. A. Baillie, and J. R. Jones, Eds.) pp 761-766, Elsevier Science Publishers B. V., Amsterdam, The Netherlands.

(20) Sharma, S. D., Toth, G., and Hruby, V. J. (1991) A Simple General Method for (Radio)iodination of a Phenylalanine Residue in Peptides: Preparation of [D-Pen^2,4′-^{125}I-Phe,D-Pen^5]-Enkephalin, a Peptide with Extraordinary Selectivity for δ-Opioid Receptors. *J. Org. Chem. 56*, 4981–4983.

(21) Bosse, R., and Escher, E. (1991) Synthesis of radio-iodinated ligands with high affinity and selectivity for μ- and δ-opioid receptors. *Peptides 1990* (E. Giralt, and D. Andreu, Eds.) pp 632–634, ESCOM Science Publishers, Leiden, The Netherlands.

(22) Counsell, R. E., Smith, T. D., Diguilio, W., and Beierwaltes, W. H. (1968) Tumor Localizing Agents. VIII. Radioiodinated Phenylalanine Analogs. *J. Pharm. Sci. 57*, 1958–1961.

(23) Gielow, P. (1984) ^{123}I-Labeling of Iodophenylalanine Derivatives. *Int. J. Appl. Radiat. Isot. 35*, 1144–1145.

(24) Merkushev, E. B. (1988) Advances in the Synthesis of Iodoaromatic Compounds. *Synthesis* 923–937.

(25) Meyer, G.-J., Rossler, K., and Stocklin, G. (1979) Reaction of Aromatic Diazonium Salts with Carrier-Free Radioiodine and Astatine. Evidence for Complexation. *J. Am. Chem. Soc. 101*, 3121–3123.

(26) Foster, N. I., Dannals, R., Burns, H. D., and Heindel, N. D. (1981) A Condition Variation Study for Radioiodination via Triazene Intermediates. *J. Radioanal. Chem. 65*, 95–105.

(27) Satyamurthy, N., Barrio, J. R., Schmidt, D. G., Kammerer, C., Bida, G. T., and Phelps, M. E. (1990) Acid-Catalyzed Thermal Decomposition of 1-Aryl-3,3-dialkyltriazines in the Presence of Nucleophiles. *J. Org. Chem. 55*, 4560–4564.

(28) Okuda, V. T., and Tatsumi, S. (1957) *J. Biochem. 44*, 631–635.

(29) Burckhalter, J. H., and Stephens, V. C. (1951) Synthesis of Phenylalanine Analogs as Antimetabolites. *J. Am. Chem. Soc.* 73, 56–58.

(30) Bergmann, E. D. (1952) *p*-Amino and *p*-Fluoro-β-phenylalanine. *J. Am. Chem. Soc. 74*, 4947–4948.

(31) Bergel, F., and Stock, J. A. (1954) Cyto-Active Amino-acid and Peptide Derivatives. Part. I. Substituted Phenylalanine. *J. Chem. Soc.* 2409–2417.

(32) Coenen, H. H., Moerlein, S. M., and Stocklin, G. (1983) No-Carrier-Added Radiohalogenation Methods with Heavy Halogens. *Radiochimica Acta 34*, 47–68.

(33) Wilson, S. R., and Jacob, L. A. (1986) Iodination of Aryltrimethylsilanes: A Mild Approach to Iodophenylalanine. *J. Org. Chem. 51*, 4833–4836.

(34) Wilbur, D. S., Anderson, K. W., Stone, W. E., and O'Brien, H. A. (1982) Radiohalogenation of Non-Activated Aromatic

Compounds via Aryltrimethylsilyl Intermediates. *J. Labelled Compds. Radiopharm. 19*, 1171–1188.
(35) Hylarides, M. D., Wilbur, D. S., Hadley, S. H., and Fritzberg, A. R. (1989) Synthesis and Iodination of Methyl 4-Tri-*n*-Butylstannylbenzoate, 4-Carbomethoxyphenyl Mercuric Chloride and 4-Carbomethoxyphenyl Boronic Acid. *J. Organomet. Chem. 367*, 259–265.
(36) Merrifield, R. B. (1964) Solid-Phase Peptide Synthesis. III. An Improved Synthesis of Bradykinin. *Biochemistry 3*, 1385–1390.
(37) Carpino, L. A. (1987) The 9-Fluorenylmethyloxycarbonyl Family of Base-Sensitive Amino-Protecting Groups. *Acc. Chem. Res. 20*, 401–407.
(38) Merrifield, R. B. (1963) Solid Phase Peptide Synthesis. I. The Synthesis of a Tetrapeptide, *J. Am. Chem. Soc. 85*, 2149–2154.
(39) Kosugi, M., Shimizu, K., Ohtani, A., and Migita, T. (1981) Palladium Catalyzed Reaction of Hexabutylditin with Aryl Bromides: Preparation of Negatively Substituted Aryltributyltin *Chem. Lett.* 829–830.
(40) Wilbur, D. S., Hadley, S. W., Hylarides, M. D., Abrams, P. G., Beaumier, P.L., Morgan, A. C., Reno, J., and Fritzberg, A. R. (1989) Development of a Stable Radioiodinating Reagent to Label Monoclonal Antibodies For Radiotherapy of Cancer. *J. Nucl. Med. 30*, 216–226.
(41) Hui, K. Y., Holleran, E. M. and Kovacs, J. (1988) Protected amino acid tetrafluorophenyl esters for peptide synthesis. *Int. J. Peptide Protein Res. 31*, 205–211.
(42) Hadley, S. W., and Wilbur, D. S. (1990) Evaluation of Iodovinyl Antibody Conjugates: Comparison with a *p*-Iodobenzoyl Conjugate and Direct Radioiodination. *Bioconjugate Chem. 2*, 154–161.
(43) Fritzberg, A. R., Abrams, P. G., Beaumier, P. L., Kasina, S. , Morgan, A. C., Rao, T. N., Reno, J. M., Sanderson, J. A., Srinivasan, A., Wilbur, D. S., and Vanderheyden, J.-L. (1988) Specific and stable labeling of antibodies with technetium-99m with a diamide dithiolate chelating agent. *Proc. Natl. Acad. Sci. U.S.A. 85*, 4025–4029.
(44) Shen, X, Hanson, R. N., and Elmaleh, D. R. (1991) Synthesis and Evaluation of Radioiodinated Tetrafluorophenyl *m*-Iodobenzoate and Tetrafluorophenyl-5-Iodopentenoates as Conjugating Agents for Proteins and Antibodies. *J. Labelled Compds. Radiopharm. 30*, 222–223 (Abstract).
(45) Zalutsky, M. R., and Narula, A. S. (1987) A Method for the Radiohalogenation of Proteins Resulting in Decreased Thyroid Uptake of Radioiodine. *Appl. Radiat. Isot. 38*, 1051–1055.
(46) Assoian, R. K., Blix, P. M., Rubenstein, A. H., and Tager, H. S. (1980) Iodotyrosylation of Peptides Using *tertiary*-butyloxycarbonyl-L-[^{125}I]iodotyrosine N-hydroxysuccinimide ester. *Anal. Biochem. 103*, 70-76.

Purification and Characterization of IL6–PE^{4E}, a Recombinant Fusion of Interleukin 6 with *Pseudomonas* Exotoxin

Robert J. Kreitman and Ira Pastan*

Laboratory of Molecular Biology, Division of Cancer Biology, Diagnosis and Centers, National Cancer Institute, National Institutes of Health, 9000 Rockville Pike, Building 37, Room 4E16, Bethesda, Maryland 20892.
Received June 11, 1993®

We have developed a procedure to purify the recombinant fusion toxin IL6–PE^{4E} from *Escherichia coli* which results in a high yield of fully active monomeric protein of high purity and very low endotoxin content. The chimeric toxin is composed of human interleukin 6 (IL6) fused to a derivative of *Pseudomonas* exotoxin (PE) containing mutations in the binding domain which prevent binding to the PE receptor. In a typical preparation, 20 g of *E. coli* cells expressing the plasmid encoding IL6–PE^{4E} were treated with lysozyme and washed repeatedly with detergent (Triton X-100), to obtain 500 mg of inclusion bodies. The recombinant protein was denatured and reduced in guanidine hydrochloride solution containing dithioerythritol and refolded in a redox buffer containing oxidized glutathione and L-arginine. After purification of the dialyzed protein by anion-exchange, polymyxin B, and sizing chromatography, we obtained 100 mg (20% of recombinant protein) of purified monomer with 0.6–2.5 endotoxin units/mg of protein. Amino terminal sequencing confirmed the first 20 amino acids. IL6–PE^{4E} purified in this manner was fully cytotoxic toward human multiple myeloma, hepatoma, epidermoid carcinoma, and prostate carcinoma cell lines. After intravenous injection into mice, we found the dose-limiting toxicity to be to the liver, by measurement of serum transaminases and histologic evaluation of the liver. The LD_{50} was 450 μg/kg. We conclude that IL6–PE^{4E} can be purified efficiently for preclinical testing.

INTRODUCTION

Interleukin 6 (IL6) is a multifunctional cytokine important for the differentiation of human B cells, but is also involved in several disease states, such as rheumatoid arthritis, human T cell leukemia virus (HTLV-1) and HIV infection, and multiple myeloma (*1*). IL6 receptors (IL6R's) have been found not only on myeloma cells (*2*) but on hepatocellular carcinoma cells as well (*3*). While hepatoma is an important cause of cancer throughout the world, prostate cancer incidence is increasing in the United States, and such cells also express IL6R (*4*). Moreover, in a recent study 11 of 13 malignant prostates from patients contained high levels of IL6R mRNA (*5*). In 1989, it was shown that IL6R-bearing cells could be targeted using a recombinant fusion of IL6 with a derivative of *Pseudomonas* exotoxin (PE) (*6*).

PE is a 613 amino acid protein which kills normal animal cells by binding to the PE receptor, internalizing, translocating to the cytosol, and ADP-ribosylating elongation factor 2. Of the three structural domains, domain Ia (amino acids 1–252) binds to the PE receptor, domain II (amino acids 253–364) mediates translocation of the C-terminal portion of the toxin (amino acids 280–613) to the cytosol, and domain III (amino acids 400–613) contains the ADP-ribosylating activity (*7, 8*).

In our most effective IL6-toxin, IL6-PE66^{4Glu} (IL6–PE^{4E}), human IL6 is fused to the amino terminus of full length PE (*9*), but in domain Ia of PE, four basic residues (Lys57, His246, Arg247, and His249) have been replaced with Glu to prevent the toxin from binding to the PE receptor. IL6–PE^{4E} was selectively cytotoxic toward four groups of malignant cell lines: multiple myeloma, hepatoma, prostate carcinoma, and epidermoid carcinoma (*3, 4, 9*). IL6–PE^{4E} caused regression of PLC/PRF/5 human hepatoma cells growing as xenografts in nude mice (*10*). To assess its potential efficacy as a purging agent for autologous bone marrow transplantation in multiple myeloma, we tested fresh bone marrow specimens and over half of the patients had cells which were killed by the toxin (*11*). In contrast, normal hematopoietic precursor cells (BFU-E and CFU-GM) showed no sensitivity.

For our previous tissue culture and murine studies, unwashed inclusion bodies of IL6–PE^{4E} were dissolved in guanidine solution, diluted into PBS and purified by anion exchange and sizing chromatography (*9*). A typical yield was 1.5–7 mg of purified monomer from 5 g of cells producing ~100 mg of total recombinant protein (1.5–7% yield) (Siegall, Kreitman, and Pastan, unpublished data). For primate toxicity studies and clinical trials, we needed a more efficient protocol which would afford a higher yield and provide clinical-grade material with low endotoxin content. Currently, humans and other primates treated with recombinant protein should receive <10 endotoxin units/kg/day. In this study, we describe a procedure which satisfied both requirements. The purified protein was tested for cytotoxicity in tissue culture and tested for toxicity in mice.

EXPERIMENTAL PROCEDURES

Plasmid Expression. Plasmid pCS64G, encoding IL6–PE^{4E}, contains the T7 late promoter (*12*) and was published previously (*9*). Competent *E. coli* BL21 (λDE3) cells were transformed with the plasmid and grown overnight on LB agar plates containing ampicillin (100 μg/mL). Cells were resuspended in Superbroth (Diagene Inc., Gaithersburg, MD) containing ampicillin (100 μg/mL), extra glucose (5 g/L), and $MgSO_4$ (1.4 mM). The cells were shaken (330 mL/2-L shake flask) at 37 °C for 3 h and at an OD_{650} of 2.0 induced by the addition of isopropyl β-D-thiogalactopyranoside (United States Biochemical Corp., Cleveland,

* Author to whom correspondence should be addressed.
® Abstract published in *Advance ACS Abstracts*, November 1, 1993.

Not subject to U.S. Copyright. Published 1993 by American Chemical Society

OH) to a final concentration of 1 mM. After continued shaking at 37 °C for 90 min, each liter containing ~10 g of cells was harvested and resuspended in 75 mL of cold sucrose solution (sucrose 20%, 30 mM Tris, pH 7.4, 2 mM EDTA). The cells were centrifuged at 8000*g* for 10 min, resuspended in cold H_2O (75 mL/L of culture) for 10 min, and centrifuged at 16000*g* for 10 min. The spheroplast pellet from each liter of original culture was resuspended with a tissuemizer (Thomas Scientific, Swedesboro, NJ) in 160 mL of TE (50 mM Tris pH 7.4 + 2 mM EDTA). After 30 min, lysozyme was added to a final concentration of 0.25 mg/mL and the mixture shaken intermittently for 1 h. NaCl and then 25% Triton X-100 were added to final concentrations of 0.5 M and 2.5%, respectively. After shaking intermittently for 30 min, the mixture was centrifuged at 27000*g* for 50 min. The inclusion body pellet was washed four times by resuspension in TE containing 2.5% Triton X-100 (180 mL/L of original culture) with the tissuemizer and centrifugation at 27000*g* for 50 min. The pellet was then washed four times in the same volume of TE without Triton X-100.

The washed inclusion body pellet was mixed to a slurry with ~1 mL of TE and resuspended by sonication in 7 M guanidine hydrochloride containing 0.1 M Tris, pH 8, and 5 mM EDTA to a final concentration of 10 mg/mL, measured by the Pierce Coomassie Plus reaction using BSA as a standard. Dithioerythritol (Sigma, St. Louis, MO) was added to a final concentration of 10 mg/mL. The reduced protein solution was incubated at 22 °C for 24 h and after clarifying by centrifugation at 40000*g* for 15 min, the protein was diluted 100-fold into cold stirring refolding buffer containing 0.1 M Tris, pH 8.0, 0.5 M L-arginine hydrochloride, 0.9 mM oxidized glutathione (Sigma) and 2 mM EDTA. The clear refolding solution was incubated at 10 °C for 36 h and then concentrated 10-fold on a CH2 concentrator using hollow-fiber cartridges containing 30 kDa exclusion pores (Amicon, Beverly, MA). The cloudy concentrated protein was dialyzed by continuous dilution/ultrafiltration with dialysis buffer (0.02 M Tris, pH 7.4, containing 0.1 M urea). After removal of the protein from the concentrator and dilution with washings of dialysis buffer, the conductance of the mixture was 2.4 mMho. The protein was clarified by centrifugation at 27000*g* for 30 min and filtration through a 0.45-μm filter. The clear filtrate was loaded onto a Q-Sepharose (Pharmacia, Piscataway, NJ) column (~1 mL of resin/5 mg of protein) and washed with 0.02 M Tris, pH 7.4. The protein was eluted with 0.02 M Tris, pH 7.4, containing 0.3 M NaCl, diluted 5-fold with 0.02 M Tris, pH 7.4, and loaded on a MonoQ (Pharmacia) column. The MonoQ column was eluted with a linear gradient of 0.02 M Tris, pH 7.4, + (0 → 0.5 M) NaCl. The monomeric protein eluted between 0.18 and 0.23 M NaCl (Figure 1A). Aggregates had the appropriate molecular weight on reducing SDS–PAGE but behaved as high molecular weight proteins on non-reducing SDS–PAGE and sizing chromatography (data not shown). To remove endotoxin, the protein solution was circulated overnight through a polymyxin B column (Biorad, Melville, NY) (using 1 mL of resin/100 mg of protein). The protein solution was diluted 10-fold with 0.02 M Tris, pH 7.4, loaded onto a Q-Sepharose column (12 mg protein/mL resin), and eluted in a minimal volume with 0.02 M Tris, pH 7.4, containing 0.5 M NaCl. The protein was loaded on a Superdex 16/60 column (Pharmacia) and eluted from bottom to top with PBS. The single peak at 38–48 mL of elution volume (Figure 1B) was pooled. Endotoxin content was determined using limulus amebocyte lysate reagent and endotoxin standards obtained from Associates of Cape Cod, Woods Hole, MA. The first 20 amino acids were determined by protein sequencing (Protein Analysis Core Laboratory, Wake Forest University, Winston-Salem, NC).

Cytotoxicity Assays. Adherent cell lines LNCaP, HUH7, HEPG2, and A431 were plated at 1.5×10^4 cells/well in 96-well plates, 24 h before toxin addition. U266 cells, which grew in suspension, were plated at 4×10^4 cells/well immediately before toxin addition. The media was RPMI containing 10% FBS for U266 and LNCaP, and DMEM containing 5% FBS for HUH7, HEPG2, and A431. After toxin addition, cells (0.1-mL aliquots for U266, 0.2 mL for other lines) were incubated for 20–24 h and pulsed with 1 μCi [^{3}H]leucine/well for an additional 3–5 h. After freezing/thawing, the cells were harvested onto a glass-fiber filter and incorporated [^{3}H]leucine was counted. Medians of triplicate experiments, each of which usually varied from the mean by <10%, were used for data analysis.

Toxicity of IL6–PE^{4E} in Mice. Nude female mice, obtained from the National Cancer Institute at Frederick, MD, weighed 18–22 g and were 6 weeks old. IL6–PE^{4E} was diluted in PBS containing 0.2% human serum albumin (HSA–PBS) and 0.2 mL containing various amounts of IL6–PE^{4E} was injected iv via the tail vein. Four days later, serum was obtained from surviving mice via the orbital sinus. Chemistry tests were performed by Anylitics, Gaithersburg, MD. Several mice were sacrificed to observe internal organs for gross abnormalities and to obtain hepatic and renal tissue samples. Hematoxylin/eosin (H/E) stains were prepared by American Histolabs (Gaithersburg, MD).

RESULTS

IL6–PE^{4E}, a fusion protein containing human IL6 and a variant of PE containing mutations in the PE receptor binding domain, is currently being studied for the potential therapy of several disorders including multiple myeloma, hepatocellular carcinoma, and prostate carcinoma. A major technical problem in conducting clinical trails with such agents is in the production of sufficient amounts of protein with low endotoxin content from bacteria. To obtain large amounts of pure IL6–PE^{4E}, we developed a procedure utilizing extensive washing of insoluble recombinant protein with detergent, following by solubilization and refolding of the protein in a redox buffer.

To obtain pure insoluble protein, which in *E. coli* is produced in inclusion bodies, periplasm was removed from the spheroplast by osmotic lysis, and the bacterial membranes in the spheroplast were dissolved in 2.5% Triton X-100. The inclusion body pellet was extensively washed in detergent to remove as much endotoxin as possible prior to refolding. Because IL6–PE^{4E} contains a total of 12 cysteines which must correctly form six disulfide bonds, we reduced the solubilized protein with DTE and then allowed the disulfide bonds to oxidize slowly in a redox buffer containing the oxidizing agent GSSG. L-Arginine was present to prevent premature aggregation. The refolded protein could then be easily purified by ion-exchange (Q-Sepharose and MonoQ) and sizing (Superdex) chromatography. Typical chromatograms are depicted in Figure 1. In Figure 1A, the MonoQ profile indicates that the Q-Sepharose-purified protein contained significant amounts of aggregate eluting at >0.25 M NaCl. Monomeric protein eluted from 0.18 to 0.23 M NaCl. However, Figure 1B shows that the MonoQ-purified protein was essentially 100% monomer, with no left-

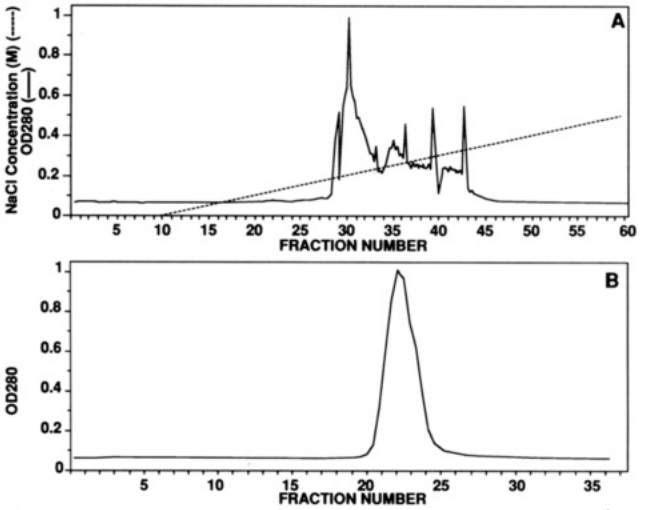


Figure 1. Chromatographs from purification of IL6–PE^{4E}. (A) Elution of IL6–PE^{4E} from an 8-mL MonoQ column. The column was eluted with 0.02 M Tris, pH 7.4, containing a 200-mL linear gradient of NaCl (0 → 0.5 M). Four-milliliter fractions were obtained. (B) Elution of Superdex 16/60 column loaded with 50 mg of IL6–PE^{4E} in 5 mL of PBS. The column was eluted with PBS and 2-mL fractions were obtained.

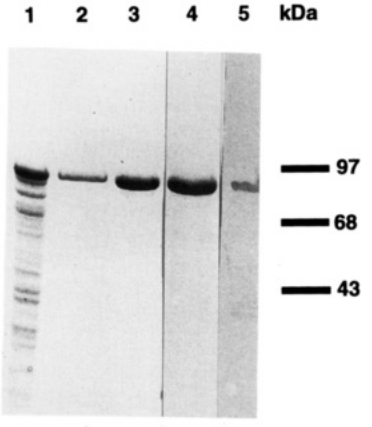


Figure 2. SDS-PAGE gel of IL6–PE^{4E}: lane 1, total cell pellet; lane 2, inclusion body protein; lane 3, purified IL6–PE^{4E} (4 μg) (Samples in lanes 1–3 were reduced with β-mercaptoethanol); lane 4, nonreduced purified IL6–PE^{4E} (4 μg); lane 5, immunoblot of 0.2 μg pure IL6–PE^{4E} using rabbit anti-PE polyclonal antibody.

handed shoulder evident on the Superdex elution profile. The center of the peak for the 86-kDa IL6–PE^{4E} was at 44 mL of elution volume (Figure 1B), compared to 42 mL for IgG (155 kDa) and 47 mL for HSA (68 kDa) (data not shown). The Coomassie Blue stained SDS–PAGE gel in Figure 2 shows that IL6–PE^{4E} comprised <50% of protein in the total cell pellet, but >95% in inclusion bodies and after the final sizing step. The final protein showed the same purity by nonreducing SDS-PAGE (Figure 2). An immunoblot using anti-PE antibodies was consistent with previous immunoblots of IL6–PE^{4E} using anti-PE and anti-IL6 antibodies (*13*).

To access the purity of the protein preparation at different stages of the procedure, we measured cytotoxic activity and endotoxin content after anion-exchange chromatography, polymyxin B endotoxin removal, and Superdex sizing chromatography. Table I shows the yield of protein after each purification step. Endotoxin content is also listed. From 20 g of the cell paste, we obtained 500 mg of recombinant inclusion body protein. The endotoxin content was only 2200–9000 EU/mg, indicating the importance of repeated detergent washes. The endotoxin content of non-detergent-washed inclusion bodies was 50–

Table I

purification steps	protein amount	endotoxin content[a] (EU/mg)
cell paste	20 g	not tested
inclusion bodies	500 mg	2200–9000
refolded–dialyzed	440 mg	5000–20000
Q-Sepharose	300 mg	430–1700
Mono-Q	105 mg	20–80
polymyxin B	103 mg	2.5–10
Superdex 16/60	100 mg	0.6–2.5

[a] Results are based on one of several representative preparations. Since exotoxin data are obtained from 2-fold dilutions of samples and standards, the results are expressed as 4-fold ranges.

1000-fold higher (data not shown). While the reducing gel in Figure 2 indicates the inclusion body protein is already >95% pure, cytotoxic activity was not yet significant due to the failure of *E. coli* to oxidize the correct disulfide bonds during expression (data not shown). After renaturation of the solubilized and reduced IL6–PE^{4E} in the redox buffer and dialysis against the dilute Tris buffer, endotoxin content was similar at 5000–20000 EU/mg (Table I), but the protein mixture had 8–12% of full cytotoxic activity against IL6R-bearing target cells (data not shown). DNA, incorrectly folded aggregates, and endotoxin were removed by the Q-Sepharose step, leaving 430–1700 EU/mg and 50% of maximum cytotoxic activity (Table I). Following the MonoQ step, the protein reached its maximum biologic purity and consisted of >95% monomer by nonreducing SDS-PAGE (Figure 2). The subsequent steps, polymyxin B exposure and Superdex sizing chromatography, were utilized to remove endotoxin. Table I shows the final endotoxin content was 0.6–2.5 EU/mg.

To compare the IL6–PE^{4E} made in this protocol from that made in the standard protocol, we determined biologic activity and endotoxin content of toxin from both preparations. Table II shows that IL6–PE^{4E} prepared by the new protocol was just as cytotoxic toward myeloma, hepatoma, prostate, and epidermoid carcinoma cell lines. However, material from the previous preparation had 30–500-fold higher endotoxin content. Thus, this new protocol afforded recombinant toxin with full biologic activity and much lower endotoxin content.

Toxicity of IL6–PE^{4E} in Mice. To determine the LD_{50} of IL6–PE^{4E} made in this protocol, we injected 4, 8, or 12 μg (200, 400, or 600 μg/kg, respectively) intravenously (iv) into mice. Table III indicates that one death in five mice was observed at the 400 μg/kg dose. The calculated LD_{50} was 450 μg/kg. To determine the dose-limiting toxicity in mice, we obtained serum on day 4 and examined renal and hepatic function. In the group receiving 400 μg/kg, the levels of hepatic enzymes SGPT, SGOT, and alkaline phosphatase were elevated to about twice that of untreated mice, while renal function, assessed by BUN and creatinine, was unchanged. Animals in the group receiving 400 μg/kg were sacrificed and had hemorrhagic liver necrosis without any other gross pathology (data not shown). Hepatic toxicity was dose dependent, with milder and less significant SGOT elevation and histopathologic abnormalities in the group receiving 200 μg/kg. Thus, the dose-limiting toxicity of IL6–PE^{4E} in mice was from hepatic toxicity.

DISCUSSION

Our goal in this study was to devise a protocol to obtain the recombinant fusion toxin IL6–PE^{4E} in sufficient quantity and with low enough endotoxin content for primate and human studies. We found that by extensively

Table II. Comparison of Activity of IL6-PE^{4E} Purified by New and Previous Protocols

	IC_{50} (ng/ml)					
	multiple myeloma U266	prostate carcinoma LNCaP	hepatoma HUH7	hepatoma HEPG2	epidermoid carcinoma A431	endotoxin content (EU/mg)
standard preparation	0.4	0.4	2.5	3	40	85–340
new protocol	0.4	0.35	2.5	3	32	0.6–2.5

Table III. Toxic Effect of Various Doses of IL6-PE^{4E} in Mice[a]

dose (μg/kg)	0	200	400	600
mortality/total mice	0/4	0/5	1/5	2/2
SGPT (U/L)	109 ± 69	118 ± 76	351 ± 238	
SGOT (U/L)	326 ± 294	420 ± 115	672 ± 405	
alkaline phosphatase (U/L)	127 ± 38	167 ± 55	212 ± 97	
bilirubin (U/L)	0.18 ± 0.1	0.12 ± 0.04	0.18 ± 0.15	
BUN (mg/dL)	17 ± 4	15 ± 2	19 ± 4	
creatinine (mg/dL)	0.5 ± 0.1	0.3 ± 0.15	0.3 ± 0.15	
weight change (%)	−0.01 ± 1.5	−1 ± 1.5	−5 ± 4	

[a] Nude female mice (20 g) were injected iv with vehical (0.2% human serum albumin in PBS) or the indicated doses of IL6-PE^{4E}. Four days later, the surviving mice were weighed and bled via the orbital sinus to obtain serum for chemistries. Serum chemistries are reported as means ± standard deviation.

washing insoluble inclusion bodies of recombinant toxin with detergent, and refolding the solubilized protein in a redox buffer, we could obtain a 20% yield of fully active monomer with endotoxin content only 0.6–2.5 EU/mg. This endotoxin content would allow us to administer up to 4 mg/kg/iv dose (9 times the mouse LD_{50}) without exceeding the limit of 10 EU/kg/dose.

IL6–PE^{4E} presents a challenge for high-yield renaturation due to its six disulfide bonds, which are most likely either wrongly paired or reduced in the bacterial inclusion bodies. We have recently found with the recombinant immunotoxin B3(Fv)–PE38KDEL that an adequate yield requires specific redox conditions during refolding (*14*). We utilized a similar redox buffer, except that, for practical reasons, our concentrations of DTE and GSSG were 0.65 and 0.9 mM, rather than 3 mM and 10 mM, respectively. Another modification was to wash inclusion bodies four times rather than once with detergent. It has recently been found that the first 3 or 4 washes with detergent, but not later washes, contain significant endotoxin levels (Wang and Pastan, unpublished data, 1992). Large scale refolding of B3(Fv)–PE38KDEL by the current modified protocol gives a 2–3% yield of monomer from total recombinant protein. The 20% yield for IL6–PE^{4E} is probably due to the presence of a natural ligand, IL6, which can fold more efficiently than a single chain Fv molecule held together by a polypeptide linker (*14*). Our yield of IL6–PE^{4E} using the current protocol was also several-fold higher than renaturing IL6–PE^{4E} without a redox refolding buffer (*9*).

We have used a slight modification of this procedure to purify a wide variety of other recombinant proteins. While we have not routinely tested endotoxin content of proteins purified for murine or tissue culture experiments, the improved yields of purified monomer from total recombinant protein indicate that this method has general utility. These preparations are all nearly identical to that described for IL6–PE^{4E} except that a TSK sizing column was used as a final step rather than polymyxin B and Superdex. For the anti-interleukin 2 receptor immunotoxin anti-Tac(Fv)–PE40 and several close derivatives (*15,16*), our yields have been 4–6%, compared to <1% using the standard protocol of diluting denatured inclusion bodies into PBS (*17*). In purifying fusions of interleukin 4 with truncated forms of PE (*18*), the yield was 12–20% with the current protocol compared to <1% with the standard method. In purifying fusions of interleukin 2 with the first 388 amino acids of diphtheria toxin (DT) (*19*), the yield was ~6% with the newer protocol compared to 0.8% with the standard. We have recently made DT388–anti-Tac(Fv)–PE40 containing both truncated PE and DT in one molecule and found a similar advantage (4.3% vs 0.9%) using the current protocol. Molecules without toxins, such as interleukin 4 and mutants of this 15-kDa protein, have been refolded using this protocol and purified on a cation exchange column. Yields of 0.8–2.4% have been reported previously using a standard protocol (*20*). Using the current protocol, we have consistently obtained yields of 20–30% of such proteins (data not shown). Thus, using the same redox conditions in the refolding buffer (0.65 mM DTE + 0.9 mM GSSG), we have been able to significantly improve the yields of many unrelated recombinant proteins.

We found that the single-dose LD_{50} of IL6–PE^{4E} in mice is 450 μg/kg iv. This value is very close to the LD_{50} of 500 μg/kg obtained previously by single-dose intraperitoneal injection (*10*). We found that the dose limiting toxicity in mice was from hemorrhagic hepatic necrosis. No evidence of renal toxicity was observed and hematologic toxicity was not found previously in mice (*10*). Also, IL6–PE^{4E} is not cytotoxic to normal human bone marrow cells and hematopoietic progenitor cells (*11*). It is unclear if the liver toxicity is due to targeting of IL6–PE^{4E} to IL6R-bearing hepatic cells (*21*) or simply from nonspecific internalization of the toxin into the hepatocyte. The LD_{50} of IL6–PE^{4E} is close to that of IL2-PE^{4E} (*22*), which targets IL2 receptors not present on hepatocytes, and much greater than that of TGFα–PE^{4E} (*23*), which targets EGF receptors which are abundant in the liver. Thus, the liver toxicity of IL6–PE^{4E} is probably due to nonspecific hepatocellular internalization, even though the liver has some IL6 receptors (*21*). Primate toxicity studies with IL6–PE^{4E} should be helpful in predicting the toxicity toward human liver and other tissues.

ACKNOWLEDGMENT

We thank Q. C. Wang for his work on refolding B3(Fv)–PE38 and C. Siegall for his previous work with IL6–PE^{4E}. We also thank G. Phil and K. O'Conner at Ares Sorono, Inc., for information regarding reproducing this protocol on an industrial scale. We thank B. Lovelace and A. Harris for assistance in cell culturing. We acknowledge A. Jackson for editorial assistance.

LITERATURE CITED

(1) Kishimoto, T., Akira, S., and Taga, T. (1992) Interleukin-6 and its receptor: A paradigm for cytokines. *Science 258*, 593–597.

(2) Kawano, M., Hirano, T., Matsuda, T., Taga, T., Horii, Y., Iwato, K., Asaoku, H., Tang, B., Tanabe, O., Tanaka, H., Kuramoto, A., and Kishimoto, T. (1988) Autocrine generation and requirement of BSF-2/IL-6 for human multiple myelomas. *Nature 332*, 83–85.

(3) Siegall, C. B., Nordan, R. P., FitzGerald, D. J., and Pastan, I. (1990) Cell-specific toxicity of a chimeric protein composed of interleukin-6 and *Pseudomonas* exotoxin (IL6-PE40) on tumor cells. *Mol. Cell. Biol. 10*, 2443–2447.

(4) Siegall, C. B., Schwab, G., Nordan, R. P., FitzGerald, D. J., and Pastan, I. (1990) Expression of the interleukin 6 receptor and interleukin 6 in prostate carcinoma cells. *Cancer Res. 50*, 7786–7788.
(5) Siegsmund, M. J., and Pastan, I. (1993) Interleukin 6 receptor mRNA in prostate carcinomas and benign prostate hyperplasia. *J. Urol.* (submitted).
(6) Siegall, C. B., Chaudhary, V. K., FitzGerald, D. J., and Pastan, I. (1988) Cytotoxic activity of an interleukin 6-*Pseudomonas* exotoxin fusion protein on human myeloma cells. *Proc. Natl. Acad. Sci. U.S.A. 85*, 9738-9742.
(7) Allured, V. S., Collier, R. J., Carroll, S. F., and McKay, D. B. (1986) Structure of exotoxin A of *Pseudomonas aeruginosa* at 3.0-Angstrom resolution. *Proc. Natl. Acad. Sci. U.S.A. 83*, 1320–1324.
(8) Hwang, J., FitzGerald, D. J., Adhya, S., and Pastan, I. (1987) Functional domains of *Pseudomonas* exotoxin identified by deletion analysis of the gene expressed in *E. coli*. *Cell 48*, 129–136.
(9) Siegall, C. B., FitzGerald, D. J., and Pastan, I. (1990) Cytotoxicity of IL6–PE40 and derivatives on tumor cells expressing a range of interleukin 6 receptor levels. *J. Biol. Chem. 265*, 16318–16323.
(10) Siegall, C. B., Kreitman, R. J., FitzGerald, D. J., and Pastan, I. (1991) Antitumor effects of interleukin 6-*Pseudomonas* exotoxin chimeric molecules against the human hepatocellular carcinoma, PLC/PRF/5 in mice. *Cancer Res. 51*, 2831–2836.
(11) Kreitman, R. J., Siegall, C. B., FitzGerald, D. J. P., Epstein, J., Barlogie, B., and Pastan, I. (1992) Interleukin-6 fused to a mutant form of *Pseudomonas* exotoxin kills malignant cells from patients with multiple myeloma. *Blood 79*, 1775–1780.
(12) Studier, F. W., and Moffatt, B. A. (1986) Use of bacteriophage T7 RNA polymerase to direct selective high-level expression of cloned genes. *J. Mol. Biol. 189*, 113–130.
(13) Kreitman, R. J., Siegall, C. B., Chaudhary, V. K., FitzGerald, D. J., and Pastan, I. (1992) Properties of chimeric toxins with two recognition domains: Interleukin 6 and transforming growth factor α at different locations in *Pseudomonas* exotoxin. *Bioconjugate Chem. 3*, 63–68.
(14) Buchner, J., Pastan, I., and Brinkmann, U. (1992) A method for increasing the yield of properly folded recombinant fusion proteins: Single-chain immunotoxins from renaturation of bacterial inclusion bodies. *Anal. Biochem. 205*, 263–270.
(15) Batra, J. K., FitzGerald, D., Gately, M., Chaudhary, V. K., and Pastan, I. (1990) Anti-Tac(Fv)-PE40: A single chain antibody *Pseudomonas* fusion protein directed at interleukin 2 receptor bearing cells. *J. Biol. Chem. 265*, 15198–15202.
(16) Kreitman, R. J., Batra, J. K., Seetharam, S., Chaudhary, V. K., FitzGerald, D. J., and Pastan, I. (1993) Single-chain immunotoxin fusions between anti-Tac and *Pseudomonas* exotoxin: Relative importance of the two toxin disulfide bonds. *Bioconjugate Chem. 4*, 112–120.
(17) Chaudhary, V. K., Queen, C., Junghans, R. P., Waldmann, T. A., FitzGerald, D. J., and Pastan, I. (1989) A recombinant immunotoxin consisting of two antibody variable domains fused to *Pseudomonas* exotoxin. *Nature 339*, 394–397.
(18) Debinski, W., Puri, R. K., Kreitman, R. J., and Pastan, I. (1993) A wide range of human cancers express interleukin 4 (IL4) receptors that can be targeted with chimeric toxin composed of IL4 and *Pseudomonas* exotoxin. *J. Biol. Chem. 268*, 14065–14070.
(19) Chaudhary, V. K., FitzGerald, D. J., and Pastan, I. (1991) A proper amino terminus of diphtheria toxin is important for cytotoxicity. *Biochem. Biophys. Res. Commun. 180*, 545–551.
(20) Weigel, U., Meyer, M., and Sebald, W. (1989) Mutant proteins of human interleukin 2-Renaturation yield, proliferative activity and receptor binding. *Eur. J. Biochem. 180*, 295–300.
(21) Nesbitt, J. E., and Fuller, G. M. (1992) Dynamics of interleukin-6 internalization and degradation in rat hepatocytes. *J. Biol. Chem. 267*, 5739–5742.
(22) Lorberboum-Galski, H., Garsia, R. J., Gately, M., Brown, P. S., Clark, R. E., Waldmann, T. A., Chaudhary, V. K., FitzGerald, D. J. P., and Pastan, I. (1990) IL6–PE66^{4Glu}, a new chimeric protein cytotoxic to human-activated T lymphocytes. *J. Biol. Chem. 265*, 16311–16317.
(23) Kreitman, R. J., Chaudhary, V. K., Siegall, C. B., FitzGerald, D. J., and Pastan, I. (1992) Rational design of a chimeric toxin: an intramolecular location for the insertion of transforming growth factor α within *Pseudomonas* exotoxin as a targeting ligand. *Bioconjugate Chem. 3*, 58–62.